# PROCEEDINGS

## IX International Conference IcETRAN and LXVI ETRAN Conference

# ЗБОРНИК РАДОВА

## IX међународне конференције ИцЕТРАН и LXVI конференције ЕТРАН

Novi Pazar, Serbia, 6 - 9, June, 2022.
Нови Пазар 6 - 9. јуна 2022. године

ISBN 978-86-7466-930-3

# PROCEEDINGS

IX International Conference on Electrical, Electronic and Computing Engineering

## IcETRAN 2022

and

LXVI Conference on Electronics, Telecommunication, Computing, Automation and Nuclear Engineering

## ETRAN 2022

# ЗБОРНИК РАДОВА

IX међународна конференција за електротехнику, електронику и рачунарство

## ИцЕТРАН 2022

и

LXVI конференција за електронику, телекомуникације, рачунарство, аутоматику и нуклеарну технику

## ЕТРАН 2022

**Proceedings -** IX International Conference on Electrical, Electronic and Computing Engineering, IcETRAN 2022,
Novi Pazar, 6-9. June 2022

**Зборник радова -** LXVI Конференција за електронику, телекомуникације, рачунарство, аутоматику и нуклеарну технику,
Нови Пазар, 6-9.2022. године

Editor in Charge / Главни уредник
**Vladimir Katić / Владимир Катић**

Published by / **ETRAN Society, Belgrade, Academic Mind, Belgrade**
Издавачи / **Друштво за ЕТРАН, Београд и Академска мисао, Београд**

Production / Израда
**Academic Mind, Belgrade** / **Академска мисао, Београд**

Place and year of publication / Место и година издања
**Belgrade, 2022.** / **Београд, 2022.**

Circulation / Тираж
**200 copies** / **200 примерака**

**ISBN 978-86-7466-930-3**

**ETRAN – Society for electronics, telecommunication, computing, automatics and nuclear engineering**

**ЕТРАН - Друштво за електронику, телекомуникације, рачунарство, аутоматику и нуклеарну технику**

**Kneza Milosa 9/IV, 11000 Belgrade / Кнеза Милоша 9/IV, 11000 Београд**

**Phone / Телефон : +381 (0) 11 3233 957**

**E-mail / Е-пошта : office@etran.rs**

**www.etran.rs**

---

**ORGANIZERS - ОРГАНИЗАТОРИ**

**ETRAN Society, Belgrade / Друштво за ЕТРАН, Београд**

**State University of Novi Pazar, Serbia / Државни универзитет у Новом Пазару, Нови Пазар, Србија**

**University of Priština temporarily settled in Kosovska Mitrovica, Faculty of Technical Sciences, Serbia / Факултет техничких наука Косовска Митровица - Универзитет у Приштини са привременим седиштем у Косовској Митровици**

---

**SUPPORTED BY / ПОДРШКА**

**IEEE – Institute of Electrical and Electronics Engineers, USA**

**Power Electronics Society of Serbia / Друштво за енергетску електронику Србије**

**CIRED Serbia / CIRED Србија**

# INTRODUCTION PAPER
# /
# УВОДНИ РАД

ISBN 978-86-7466-930-3

# Konferencije ETRAN/IcETRAN kroz statistiku

Vladimir A. Katić, *Senior Member, IEEE,* Marko Jarnević, Dragomir Nikolić, Mirjana Jovanić

***Apstrakt*— Konferencija ETRAN je jedan od najstariji naučnih skupova u Srbiji, koji se neprekidno organizuje već 66 godina. Njeno međunarodno izdanje IcETRAN se sada približava prvoj deceniji postojanja. Obe konferencije uspešno organizuje Društvo za ETRAN, čiji kolektivni članovi su sve najznačajnije naučne i obrazovne institucije u Srbiji i Republici Srpskoj (BIH). U radu je prvo predstavljena struktura, kao i ključne teme, koje se na konferencijama razmatraju. Zatim su zajedno posmatrani odgovarajući, karakteristični statistički podaci o broju radova i autora. Oni su obrađivani u tri vremenska intervala, nešto širem (poslednjih 26 god., 1996.-2021. god.), srednjoročnom (poslednjih 9 god., 2014.-2022. god.), i nešto kraćem (poslednjih 4-5 god., 2018. – 2021(2). god.). Brojevi radova su analizirani agregatno, po pojedinačnim konferencijama, ali i detaljnije po tematskim sekcijama, dok su podaci o autorima vezivani za državu i instituciju zaposlenja, kao i za pol istraživača. Zaključeno je da ovi skupovi najčešće predstavljaju mesto prikazivanja naučnih rezultata istraživača iz akademske zajednice (fakulteta i instituta), a da je prisustvo privrede, vojnog i zdravstvenog sektora manje zapaženo. Takođe, najveći broj učesnika je iz Srbije i to sa tri najveća domaća fakulteta. Međutim, značajna je i međunarodna komponenta, kroz autore iz 31 zemlje. Učešće žena je popravljeno, ali još uvek nije adekvatno i iznosi 30%.**

***Ključne reči*— Konferencije ETRAN/IcETRAN, Naučno-stručni radovi, Statistika.**

## I. Uvod

Prve inicijative da se organizuje okupljanje inženjera, koji se bave elektronikom pojavile su se još daleke 1953. god. pod rukovodstvom dr Rajka Tomovića. Odbor za elektroniku uradio je sve pripremne aktivnosti i prva konferencija održana je od 7-11. juna 1955. god. [1, 2, 3]. U prvih par godina, konferencija je obuhvatala radove iz elektronike i srodnih disciplina, ali je već 1957. god. osnivanjem Saveznog centra za elektroniku, telekomunikacije i automatiku (ETA) oblast delovanja i zvanično proširena na telekomunikacije i automatiku. Naredne 1958. god. osnovan je Jugoslovenski komitet za ETAN, kada je uz pomenute tri oblasti dodata i nuklearna tehnika (ETAN).

Jugoslovenski komitet, kasnije Jugoslovenski savez za ETAN (od 1976. god.), pa republička Društva za ETAN (od 1980. god.) vodili su konferencije ETAN-a do 1992. god.

Vladimir A. Katić – Predsednik Društva za ETRAN, Univerzitet u Novom Sadu, Fakultet tehničkih nauka, Trg Dositeja Obradovića 6, 21000 Novi Sad, Srbija(e-mail: katav@uns.ac.rs)

Marko Jarnević – Firaso, Kneza Miloša 9/IV sprat, 11000 Beograd, Srbija (e-mail: marko@firaso.rs)

Dragomir Nikolić – Univerzitet u Novom Sadu, Fakultet tehničkih nauka, Trg Dositeja Obradovića 6, 21000 Novi Sad, Srbija (e-mail: nikolicd@uns.ac.rs)

Mirjana Jovanić – Društvo za ETRAN, Kneza Miloša 9/IV sprat, 11000 Beograd, Srbija (e-mail: etran.konferencija@gmail.com)

Društvo za elektroniku, telekomunikacije, računarstvo, automatiku i nuklearnu tehniku (Društvo za ETRAN), osnovano je 1993. god., kada je u tematske sadržaje konferencije uključeno i računarstvo, kao posebna sekcija [1]. To je rezultiralo promenom naziva iz ETAN u ETRAN. Društvo je nastavilo sa širenjem delatnosti i već 1994. god. je osnovana sekcija za elektroenergetiku (EE), a 1997 sekcija za metrologiju (ML).

Potreba za širom vidljivošću rezultata istraživanja u Srbiji dovela je do pokretanja međunarodne konferencije, IcETRAN (*International Conference on Electrical, Electronic and Computing Engineering*) 2014. god. sa istim tematskim okvirom, a na kojoj se predstavljaju radovi na engleskom jeziku u IEEE formatu. Od tada se konferencije ETRAN i IcETRAN odvijaju zajedno (paralelno) u istim terminima i na istoj lokaciji.

Trenutno ETRAN ima šesnaest sekcija, kojima su pokrivene sve moderne oblasti elektrotehnike. Karakteriše ga veliki broj individualnih, ali i kolektivnih članova (28 institucija i organizacija iz Srbije, Bosne i Hercegovine i Crne Gore). Ove 2022. god. održava se LXVI konferencija ETRAN-a, odnosno IX konferencija IcETRAN-a.

U literaturi se retko pojavljuju radovi u kojima je urađena statistička obrada naučne produkcije konferencija ETA, ETAN, ETRAN i IcETRAN. U publikaciji [1], dat je prikaz perioda od 2006. – 2015. god., s tim da su pojedine sekcije dale i celokupan pregled kretanja broja radova od svog osnivanja do 2015. god., dok je u [2] dat prikaz ranijih konferencija (1955-2014. god.), s tim da statistika nedostaje za period 1985-1996. god. U [4] je dat reprint svih radova u periodu 1955. – 2006. god., ali nema agregiranog statističkog prikaza, kao ni dela radova iz zbornika 1992. i 1993. god. i nekih ostalih godišta.

Neki podaci mogu se dobiti i iz uvodnih referata podnesenih na konferencijama ETRAN-a. Tako je na XL konferenciji u Budvi u junu 1996. god. prof. Milić Stojić, tadašnji predsednik ETRAN-a napisao: „Na proteklih 39 konferencija bilo je podneto ukupno 10.021 rad, koji su zatim publikovani na oko 70.000 stranica u 187 tomova zbornika radova. Na jubilarnoj XL Konferenciji očekuje se da će biti podneto 624 rada 1156 autora u okviru 15 stručnih komisija i 67 radnih sednica.“ [5].

Na sajtu ETRAN/IcETRAN konferencija dati su reprinti kompletnih zbornika sa poslednjih pet konferencija (2017.-2021. god.), a unos ranijih godišta je u toku [6]. Zbog kratkoće vremena i teškoće nabavke, autori ovog rada nisu bili u prilici da konsultuju ostalu literaturu vezanu za aktivnosti društva za ETAN/ETRAN, što ostaje kao zadatak za naredni period.

Cilj ovog rada je da predstavi sumirani pregled tematike i

 ISBN 978-86-7466-930-3

aktivnosti na obe konferencije (nacionalne i međunarodne) u tri vremenska intervala, nešto širem (poslednjih 26 god., 1996.-2021. god.), srednjoročnom (poslednjih 9 god., 2014.-2022. god.), i nešto kraćem (poslednjih 4-5 god., 2018. – 2021(2). god.), koristeći različite statističke prikaze broja radova i autora. Na taj način želi se ukazati na opšte pravce razvoja, na njihove trendove, ali i na segmente kojima je potrebno posvetiti veću pažnju i trud u budućnosti.

## II. KONFERENCIJE ETRAN/ICETRAN

Konferencije ETA/ETAN/ETRAN organizuju se godišnje, počevši od 1955. god. Prva i druga konferencija održane su u Beogradu 1955. i 1956. god., a nadalje su menjale lokacije, širom bivše Jugoslavije. Od 1992. god. održavaju se u Srbiji i Crnoj Gori, a od 2008. god. isključivo u Srbiji [2]. Od 2014. god. društvo za ETRAN svake godine organizuje dve paralelne konferencije, nacionalnu ETRAN i međunarodnu IcETRAN u nekom mestu u Srbiji. Najviše domaćinstava do sada ima Beograd 7 puta, Zlatibor 6 puta, pa Novi Sad i Niš po 4 puta. Ove 2022. god. ETRAN je prvi put u Novom Pazaru, kao mladom univerzitetskom centru.

Rad ETRAN/IcETRAN konferencija odvija se preko 16 sekcija, koje pokrivaju kompletnu oblast elektrotehnike i predstavljaju ključne teme svih konferencija. To su (po abecednom redu): Akustika (AK), Antene i prostiranja (AP), Automatika (AU), Biomedicinska tehnika (BT), Električna kola, električni sistemi i obrada signala (EK), Elektroenergetika (EE), Elektronika (EL), Metrologija (ML), Mikroelektronika i optoelektronika (MO), Mikrotalasna tehnika, tehnologije i sistemi (MT), Novi materijali (NM), Nuklearna tehnika (NT), Računarstvo (RA), Robotika i fleksibilna automatizacija (RO), Telekomunikacije (TE) i Veštačka inteligencija (VI).

Pored njih, na konferencijama se pojavljuju i radovi iz oblasti nastavne problematike, odnosno edukacije (EDU), kao i oni koji tematski obuhvataju interdisciplinarne oblasti,ili tematiku više struka, a koji su svrstani u specijalne sesije.

Na svakoj konferenciji, nekoliko radova ili predavanja se predstavljaju na plenarnim sednicama, kao uvodni ili *Key Note Lectures*. Takođe, u sklopu svake sekcije, prezentuju se pozvani radovi (*Invited Papers*) ili pozvana predavanja (*Invited Lectures*).

Uz prezentaciju radova, na konferencijama organizuju se i okrugli stolovi (*Pannel Sessions*) vezani za aktuelnu problematiku razvoja nauke u svetu ili Srbiji, kao i sednice posvećene pojedinim autorima.

## III. STATISTIKA BROJA RADOVA

Pregled broja radova po svim dosadašnjim konferencijama, kako ukupan, tako i po pojedinim sekcijama, prevazilazi okvire ovog rada, jer zahteva znatno više prostora za dijagrame, objašnjenja i komentare. Da bi se ipak dobio odgovarajući prikaz, autori su odlučili da se ograniče na statistiku broja radova u tri pomenuta vremenska intervala. Treba napomenuti da su za konferencije od 1996. god. do 2021. god. u statistiku uvršteni radovi, koji su ušli u Zbornik/Proceedings (prezentovani radovi), dok su za 2022. god. obuhvaćeni prihvaćeni radovi, koji su prošli duplu recenziju.

Na Sl. 1 prikazan je pregled kretanja broja radova na konferencijama ETRAN i IcETRAN u ovom periodu. Može se videti da je kvantitativno konferencija ETRAN krajem devedesetih godina prošlog veka predstavljala jedan od najvećih, ako ne i najveći naučni skup u Srbiji. Prema podacima za 1996. i 1997. god., XL i XLI konferencija održane u junu u Budvi i na Zlatiboru, respektivno, predstavile su čak 624, odnosno 622 naučna i stručna rada [2, 4].

U narednom periodu, broj radova polako opada, tako da se može zapaziti nekoliko kvantitativnih blokova vezanih za kretanje broja radova:

1996. – 1998. god.: Između 500 – 600+ radova, prosek 588,6
1999. – 2010. god.: Između 300 – 500 radova, prosek 352,5
2011. – 2019.god.: Između 200 – 300, prosek 269,3
2020. – 2022.god.: Između 100 – 200, prosek 158,3

Poslednji blok ukazuje da je sada broj radova dosta nizak, odnosno da odgovara nivou iz početnog perioda razvoja konferencije. Tek 1975. god. na XIX konferenciji u Ohridu broj radova je prešao obim od 200 radova i tu se zadržao sve do 2019. god.Ipak, stanje za konferenciju 2022. god. ohrabruje, jer je broj radova značajno povećan (+36%).

Međutim, sadašnje stanje nije na nivou reputacije konferencije(a) i upućuje da je potrebno uložiti dodatne napore na povećanju atraktivnosti konferencije, kvaliteta radova, širem povezivanju sa privredom i snaženju uticaja u naučnoj i stručnoj javnosti Srbije i sveta.


Sl. 1. Sveobuhvatni pregled broja radova na ETRAN/IcETRAN konferencijama 1996.-2022. god.

 ISBN 978-86-7466-930-3

### *A. Statistika radova 2014. – 2022. god.*

Iz razloga aktuelnosti i ovde će se posebno analizirati period 2014. – 2022. god. Karakteristika tog perioda je da se u njemu pojavljuju dve paralelne konferencije ETRAN, kao nacionalna i IcETRAN, kao međunarodna. To daje mogućnost autorima da svoje radove predstave na srpskom ili engleskom jeziku. Pored već pomenutih razloga internacionalizacije i bolje vidljivosti u inostranstvu, razlog za ovakvu odluku predsedništva ETRAN-a može se tražiti i u sve većem učešću naučnika iz Srbije na međunarodnim projektima, interesovanju svetskih naučnika za rezultate u Srbiji, intenziviranju značaja citiranosti za rangiranje naučnih radnika, ali i kao način snaženja uticaja i značaja konferencije u Srbiji i svetru.

Na Sl. 2, prikazan je „zumiran“ pregled broja radova sa slike 1, na obe konferencije u analiziranom periodu, ali prikazan odvojeno, odnosno uporedno po konferencijama. Ukupno je na konferenciji ETRAN predstavljeno 847 radova, dok na konferenciji IcETRAN 1239 radova, odnosno sve zajedno na obe konferencije 2086 radova. I ovde se može uočiti napredak u 2022. god.

Poređenjem dve konferencije, vidi se da se većina autora opredeljuje za konferenciju IcETRAN (59,4%), što ukazuje na potrebu dalje internacionalizacije konferencije. Ipak, značajan broj autora prikazuje svoje rezultate i na ETRAN-u, kao nacionalnom skupu, što je dobro jer podstiče razvoj domaće misli, usvajanje adekvatne terminologije na srpskom jeziku, odnosno umanjuje efekte anglikanizacije.

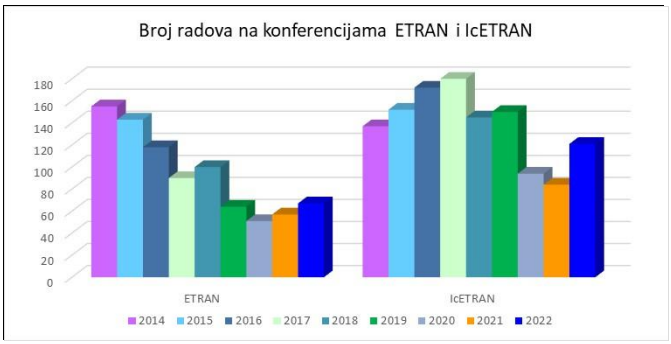


Sl. 2. Pregled broja radova na konferencijama ETRAN/IcETRAN u periodu 2014. – 2022. god.

### *B. Statistika radova po sekcijama (2018. – 2022. god.)*

Nešto bolji uvid u rezultate istraživanja može se dobiti ako se posmatra broj radova po pojedinim sekcijama. Međutim, s obzirom na broj sekcija, predstavljanje pomoću jedinstvenih dijagrama može biti nepregledno. Iz tog razloga, autori ovog rada odlučili su se da dodatno suze opseg posmatranja na poslednjih pet godina, odnosno na period od 2018. do 2022. god.

Na Sl. 3 predstavljen je broj radova po sekcijama u tom periodu. Vidi se da su najistaknutije bile sekcije za računarstvo (RT) i metrologiju (ML), zatim automatiku i obradu signala (AU), telekomunikacije (TE), akustiku (AK) i elektroenergetiku (EE). Kod nekih sekcija može se videti značajna redukcija aktivnosti (na primer, sekcije AK, AU, EK, EL, RT), kod nekih da su konferencije u 2020. ili 2021. god. bile kritične (na primer AP, EL, EK, MT), ali se kod većine zapaža oporavak u 2022. god. Ukupnom pozitivnom rezultatu za 2022. god. dodatno doprinose radovi u EDU sesiji i specijalnim sesijama, kao i predstavljanje međunarodnog projekta KALCEA.

### *C. Statistika radova po institucijama*

Na skupovima ETRAN/IcETRAN učestvuje veliki broj autora, najčešće sa univerziteta (fakulteta), naučnih instituta, privrede, ali i iz vojno-tehničkih i ustanova zdravstva. Naravno, mogući su i istraživački timovi kombinovani sa članovima iz različitih institucija. Kompletno sagledavanje prevazilazi obim ovog rada, pa je fokus stavljen na period 2018. – 2021. god.

Na Sl. 4 predstavljeno je učešće broja radova po grupisanim institucijama. Vidi se da su radovi autora sa univerziteta (fakulteta) bili najviše zastupljeni (59,0%), pa zatim radovi mešovitih timova (24,6%), istraživačkih grupa sa naučnih instituta (12,0%), te vojno-tehničkih ustanova (3,5%) i privrede (0,9%). Interesantno je da nije bilo većeg učešća radova autora isključivo iz zdravstvenih ustanova, odnosno oni su se pojavljivali u sklopu mešovitih timova.

Ovaj pregled pokazuje da su skupovi ETRAN/IcETRAN prvenstveno orijentisani na učesnike iz akademskog okruženja (fakulteta ili instituta), a da je prisustvo autora iz privrede i drugih institucija nedovoljno.

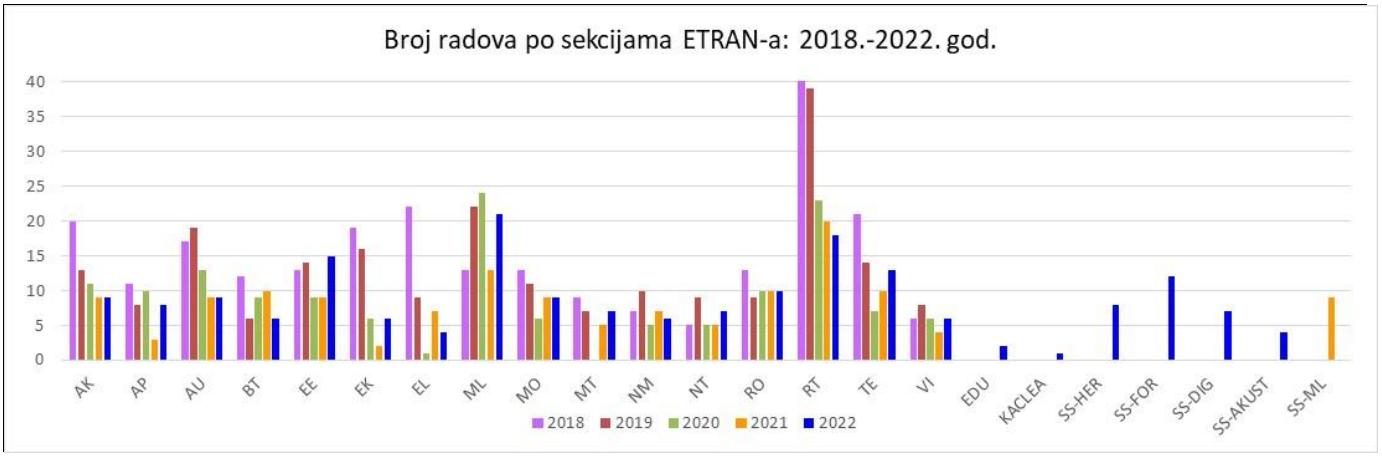


Sl. 3. Pregled broja radova po sekcijama u periodu 2018.-2022. god.


ISBN 978-86-7466-930-3

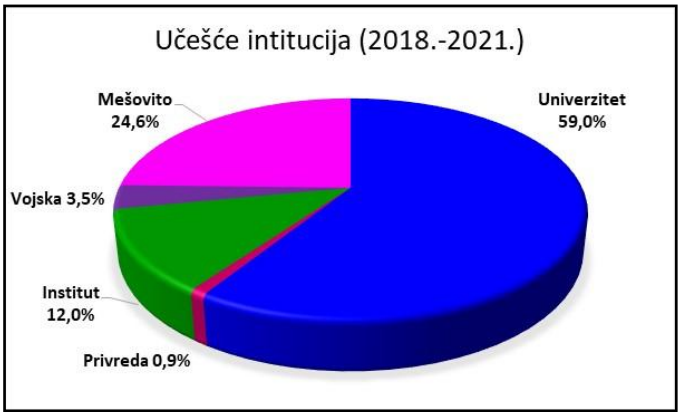


Sl. 4. Pregled učešća radova po institucijama za period 2018. – 2021. god.

## IV. STATISTIKA PO AUTORIMA

Zbog znatno složenije obrade, za statistiku po autorima koristiće se ograničeni vremenski interval od 4 odnosno 5 godina (2018. – 2021(2). god.). Na bazi iskustva i prethodnih podataka, može se odmah pretpostaviti da autori konferencijskih radova, odnosno učesnici ETRAN/IcETRAN konferencija uglavnom dolaze iz Srbije i iz akademskih institucija. Međutim, statistika ukazuje da su ove konferencije interesantne i za mnoge učesnike iz inostranstva i iz drugih institucija. Iz tih razloga interesantno je posmatrati i uporediti konferencije po nekim parametrima vezanim za autore. Ovde će se predstaviti statistika po državama iz kojih dolaze autori, odnosno u kojima se nalaze institucije i firme gde su zaposleni, zatim po pojedinačnim institucijama (mestu zaposlenja) autora, te po polu da bi se videla kakva je zastupljenost žena.

### A. *Autori iz inostranstva*

Da bi se potvrdila pomenuta pretpostavka, na Sl. 5 prikazano je procentualno učešće autora iz Srbije i iz drugih država u razmatranom periodu. Može se uočiti da velika većina, čak 92,1% dolazi iz Srbije. To je i očekivano, zbog nacionalnog karaktera konferencije ETRAN, ali i zbog toga što značajan broj autora je iz Srbije publikuju svoje rezultate na engleskom jeziku u okviru konferencije IcETRAN.

Ipak, detaljniji pregled autora pokazuje da preostalih 7,9% predstavljaju institucije iz čak 31 zemlje sveta. Da bi se jasnije videla njihova zastupljenost, na Sl. 6 predstavljena je statistika autora iz inostranih institucija. Može se uočiti da ih najviše dolazi iz Bosne i Hercegovine (uglavnom Republike

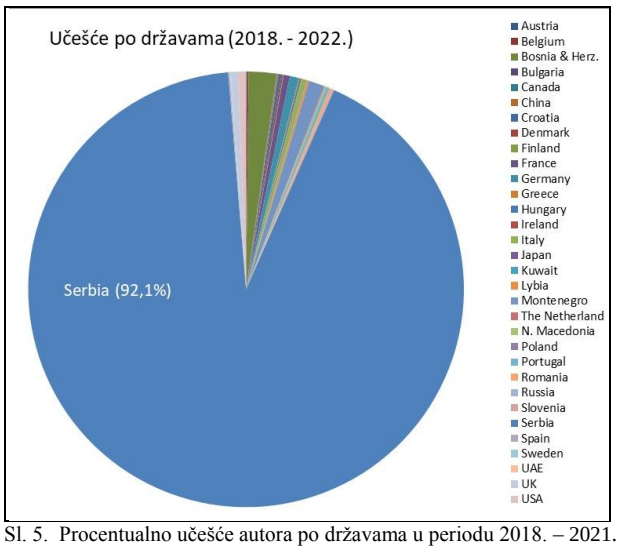


Sl. 5. Procentualno učešće autora po državama u periodu 2018. – 2021. god.

Srpske) i Crne Gore, pa zatim iz Nemačke, Velike Britanije (UK) i Sjedinjenih Američkih Država (USA). To ukazuje na dobru saradnju u regionu, jer su i autori iz Hrvatske, Slovenije i Severne Makedonije prisutni. Treba napomenuti da razlog za manje učešće tri poslednje pomenute države ex-Jugoslavije se može potražiti i u činjenici da one imaju svoje nacionalne konferencije, kojhe su potekle iz ETAN-a: KoREMA (bivša JUREMA), ELMAR (bivši ETAN u pomorstvu), ETAI i dr. Istaknuto prisustvo autora iz razvijenih, zapadnih zemalja je najvećim delom posledica aktivnosti naše naučne dijaspore, bilo u sklopu zajedničkih istraživanja sa autorima iz Srbije, bilo u sklopu timova sa svojih institucija.

### B. *Pregled po institucijama autora*

Već je pokazano da najviše radova dolazi od autorskih timova sa univerziteta ili instituta, ali da je značajno i učešće kombinovanih timova (Sl. 4). Iz tog pregleda se ne vidi jasno pripadnost institucijama pojedinačnih autora, pa je na Sl. 7 dat pregled učešća autora po institucijama grupisanim kao na Sl. 4 za period 2018. – 2021. god. Naravno, opet je najznačajnije prisustvo autora sa univerziteta (fakulteta) 70,0%, instituta 21,4%, ali se vidi i primetno učešće autora iz vojske 4,7%, privrede 3,4% i zdravstva 0,4%. Poređenjem sa Sl. 4 može se zaključiti da su radovi mešovitih timova najčešće rezultat saradnje istraživača sa univerziteta, odnosno instituta i privrede ili vojske, i nešto manje zdravstva.

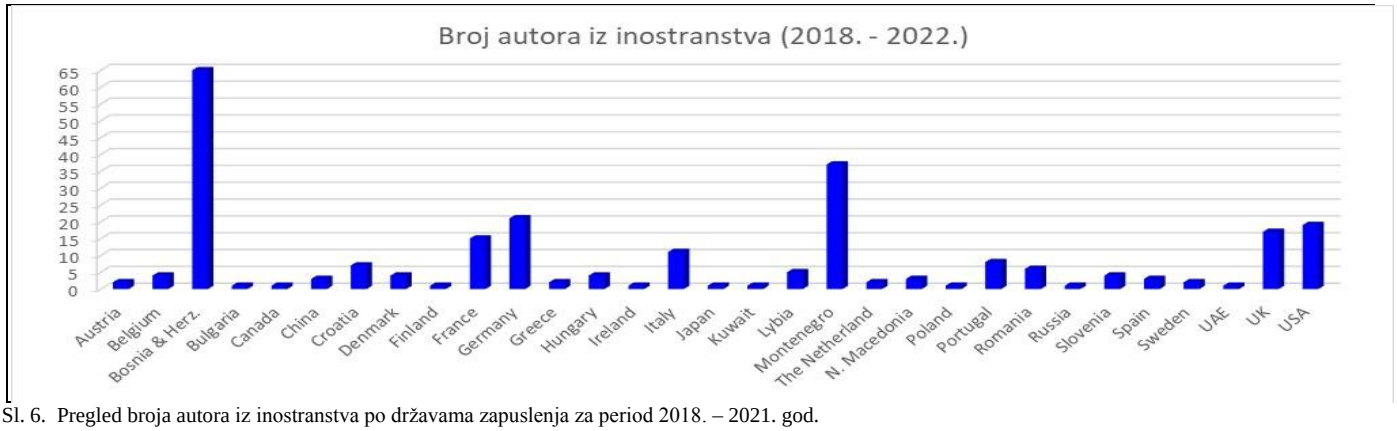


Sl. 6. Pregled broja autora iz inostranstva po državama zapuslenja za period 2018. – 2021. god.


ISBN 978-86-7466-930-3

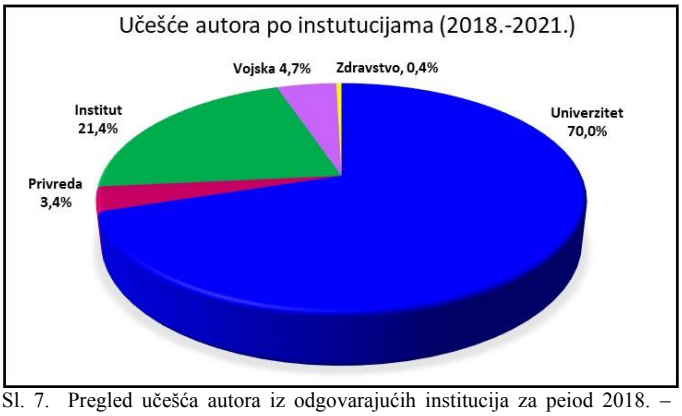


Sl. 7. Pregled učešća autora iz odgovarajućih institucija za peiod 2018. – 2021. god.

Pored pregleda po grupisanim institucijama, interesatno je analizirati mesta zaposlenja autora, tj. napraviti pregled učešća pojedinačnih institucija. Na Sl. 8 je dat ovakav pregled za period 2018.-2021. god., uz napomenu da su u obzir uzete samo one institucije čiji autori se pojavljuju bar 3 puta. Vidi se da je najveće učešće na konferencijama ETRAN/IcETRAN od strane autora sa Fakulteta tehničkih nauka iz Novog Sada (FTNNS), zatim sa Elektrotehničkog fakulteta u Beogradu (ETFBG), te Elektronskog fakulteta u Nišu (EFNI). Zatim ide Institut RT-RK iz Novog Sada (RTRK), Visoka škola elektrotehnike i računarstva strukovnih studije Beograd (VSEL), Fakultet tehničkih nauka iz Čačka (FTNCA), te grupa instituta: Institut za hemiju, tehnologije i metalurgiju iz Beograda (IHTM), Institut za nuklearne nauke Vinča (INNVIN), Institut Vlatacom Beograd (VLATA) i Institut Mihajlo Pupin iz Beograda (IMPBG).

Ovaj pregled potvrđuje da su skupovi ETRAN/IcETRAN prvenstveno orijentisani na učesnike iz akademskog okruženja, odnosno na autore sa fakulteta i instituta u Beogradu, Novom Sadu, Nišu i Čačku, ali je značajna i prisutnost autora iz specijalizovanih firmi (industrije), kao i iz inostranstva. Međutim, prisustvo autora iz privrede, te saradnja sa zdravstvom još uvek je nedovoljna.

### *C. Pregled broja autora prema polu*

U poslednje vreme sve više se govori i ulažu se dodatni napori da se poveća broj žena u inženjerskim strukama. Njihovo učešće postaje sve značajnije, pa je interesantna i statistika o njihovoj participaciji u naučnim radovima, koji se izlažu na ETRAN/IcETRAN konferencijama. Na Sl. 9 prikazan je pregled procentualnog učešća muškaraca i žena na ovim konferencijama u periodu 2018.-2021. god. Može se uočiti da je došlo do blagog povećanja učešća žena, odnosno da je ono sa 23,7% na konferencijama 2018. god. dostiglo 30% na konferencijama 2021. god. To je ohrabrujući trend, ali treba ulagati dodatne napore da se on održi.

## V. ZAKLJUČAK

Konferencija ETRAN, a sada i IcETRAN, u svom dugom postojanju prošle su kroz razne faze. Poslednjih godina uočljiv je rapidan pad broja radova i smanjeno interesovanje naučnika i istraživača. Šta su razlozi i uzroci ove negativne pojave svakako zahteva dublje analize, ali se oni mogu tražiti u sveukupnoj digitalizaciji naučne produkcije, pa i svih ostalih sfera rada i života, u specifičnim zahtevima vrednovanja naučnog rada gde je fokus stavljen na naučne časopise, u potrebi za većom dinamikom naučnog rada i produkcije, pa do uticaja ograničenja u finansiranju nauke, negativnim efektima pandemije virusa Korona-19 i dr.

Ovi skupovi najčešće predstavljaju mesto prikazivanja naučnih rezultata istraživača iz akademske zajednice (fakulteta i instituta), a prisustvo privrede, vojnog i zdravstvenog sektora treba intenzivirati. Takođe, najveći broj učesnika je iz Srbije i to sa tri najveća domaća fakulteta. Međutim, značajna je i međunarodna komponenta, kroz autore iz čak 31 zemlje. Učešće žena se popravlja, ali još uvek nije adekvatno i sada iznosi 30%.

Ovogodišnje konferencije, LXVI ETRAN i IX IcETRAN nagoveštavaju preokret i bolju budućnost ovih okupljanja. Broj radova značajno je porastao (+33%), kao i očekivano učešće istraživača. Konferencija je ponovo organizovana „u živo“, a postavljeni su osnovi za intezivnije pojavljivanje *hi-tech* privrede i veze sa naučno-tehnološkim parkovima. To ukazuje da osnovni razlozi okupljanja naučnika i istraživača, a to je neposredna razmena rezultata i iskustava, dolaženje do novih ideja i zajedničko druženje i dalje predstavljaju značajan motiv za učestvovanje. Ovo i ohrabruje na nove napore za poboljšanje značaja i organizacije konferencija, povećanje atraktivnosti, uvećanje učešća naučnika, istraživača i stručnjaka iz privrede, kao i mladih doktoranata, internacionalizaciju, povezivanje sa svetskim asocijacijama (IEEE, IFAC i dr.), kao i bolju vidljivost ovih konferencija u svetskoj i domaćoj naučnoj zajednici.

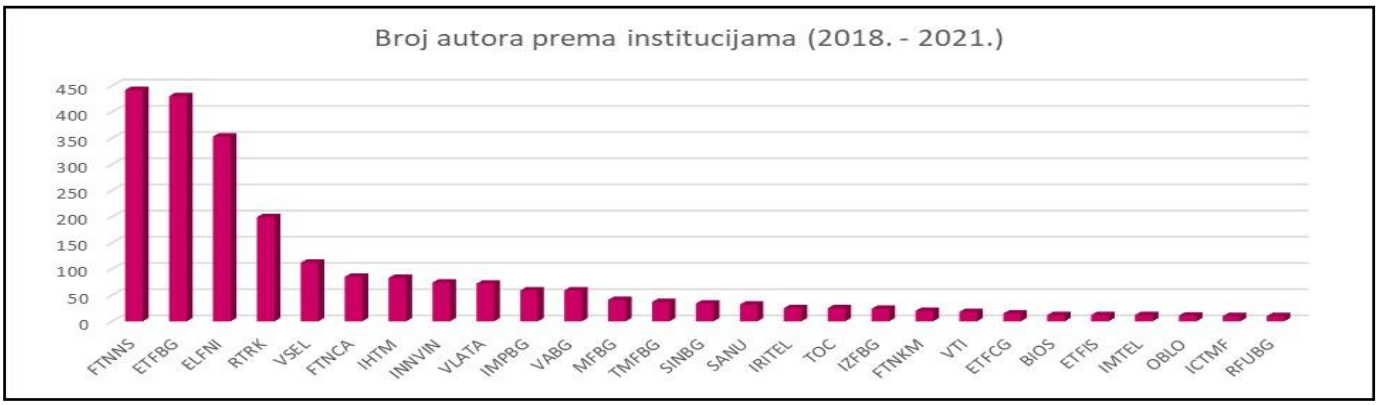


Sl. 8. Pregled broja autora prema institucijama za period 2018. – 2021. god.

 ISBN 978-86-7466-930-3

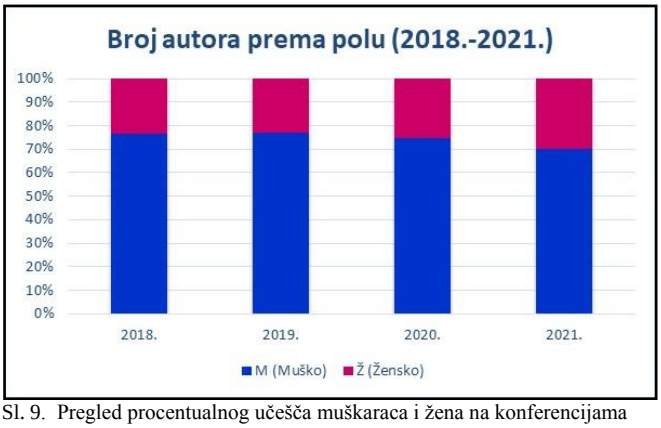


Sl. 9. Pregled procentualnog učešća muškaraca i žena na konferencijama ETRAN/IcETRAN u periodu 2018.-2021. god.

## LITERATURA

[1] ***, *„ET(R)AN Prvih šezdeset konferencija – Doprinos ravoju elektrotehničke struke“*, Uredili: B. Milovanović i Z. Jakšić, pp. 90-98, Beograd, Društvo za ETRAN i Akademska misao, 2016.

[2] M. R. Stojić, *„Društvo za ETAN/ETRAN 1953-2016“*, Akademska misao, Beograd, 2016.

[3] S. Ristić, „Dvadeset godina ETAN-a“, XVII konferencija ETAN, Novi Sad, jun 1973.

[4] B. Milovanović, B. Kovačević, Z. Jakšić, M. Jovanić i dr., *„e-TRAN Elektronski zbornik svih radova prvih pedeset konferencija ETAN/ETRAN 1955-2006“*, Beta verzija, DVD , Društvo za ETRAN, Beograd, 2006.

[5] M.R. Stojić, „Uticaj četrdeset konferencija ETRAN-a na razvoj naučne i stručne misli“, Plenarni rad po pozivu, Zbornik sa XL Konferencije za ETRAN, Budva, 1996., pp.3-6.

[6] https://www.etran.rs

## ABSTRACT

The ETRAN conference is one of the oldest scientific gatherings in Serbia, which has been organized continuously for 66 years. Its international edition IcETRAN is now approaching its first decade of existence. Both conferences are successfully organized by the Society for ETRAN, whose collective members are all the most important scientific and educational institutions in Serbia and the Republika Srpska (BIH). The paper first presents the structure, as well as key topics, which are discussed at conferences. Then, the corresponding, characteristic statistical data on the number of papers and authors were observed together. They were analyzed for three periods, a broader one (last 26 years, 1996-2021), a medium-term (last 9 years, 2014-2022), and a shorter one (last 4-5 years, 2018 – 2021(2)). The numbers of papers were analyzed in aggregate, but also by individual conferences and in more detail by thematic sections, while the data on the authors were related to the country and the institution of employment, as well as to the gender of researchers. It was concluded that these gatherings usually represent the place of presenting the scientific results of researchers coming from the academia (faculties and institutes) and that the presence of the ones from industry, military, or healthcare is less noticeable. Also, the largest number of participants is from Serbia, coming from the three largest national universities. However, the international component is also significant, through authors from 31 countries. The participation of women has been improved, but it is still not adequate and amounts to 30%. These data were the fundamentals to discuss the future development of both conferences.

## The ETRAN/IcETRAN ConferencesThrough Statistics

Vladimir A. Katić, Marko Jarnević, Dragomir Nikolić, Mirjana Jovanić

 ISBN 978-86-7466-930-3

# ACOUSTICS
# /
# АКУСТИКА
# (AKI/AK)

ISBN 978-86-7466-930-3

# Recent Advances on Perforated Panels for Sound Absorption Applications

Jesús Carbajo, Nicholas Xuanlai Fang and Sang-Hoon Nam

***Abstract*—Perforated panel sound absorbers have become one of the most promising passive noise control solutions not only because of their excellent sound absorption performance but also because of their high structural strength and durability. These features make them an interesting eco-friendly alternative to traditional porous fibrous media or foams, especially in those scenarios implying aggressive environmental agents (e. g. strong wind, heavy rain…) or severe working conditions (e. g. turbines, jet engines…). Many engineering applications of these systems can be found in practice ranging from noise barriers and room acoustics conditioning to the design of muffler devices and MRI scanners. This work briefly reviews the fundamentals of classical perforated panel sound absorbers and reports some recent advances in their use for sound absorption applications.**

***Index Terms*—Acoustics; sound absorption; perforated panels.**

## I. Introduction

Noise pollution is a problem of major concern because of the harmful effects on human health and the negative impact on the environment. In this context, the scientific community together with industrial partners and public authorities are working together on the development of systems that let reduce noise. Among these, passive sound absorbers have become one of the most-extended solutions, being the perforated panel sound absorbers of great interest due to their improved structural features when compared to conventional porous media. Although generally used as a protective covering for such media, when backed by an air cavity the resulting panel system may work as an acoustic resonator for sound absorption itself. To improve the low-frequency absorption performance and absorption bandwidth of these resonators, many authors have proposed different configurations throughout the years. Maa [1] proposed the use of panels whose perforations are sub-millimetric in size resulting in the so-called Micro-Perforated Panel (MPP) sound absorbers. Subsequently, he analyzed their wideband capabilities by using double-layer MPP arrangements [2]. Some other examples are the study of perforated panels with viscous energy dissipation enhanced by orifice design carried out by Randeberg [3], taking advantage of the vibrational response of thin perforated panels [4], the use of multiple sizes of holes investigated experimentally by Miasa et al. [5], or the parallel arrangement of MPPs [6]. All of these and many other studies served to a great extent as a reference to further developments on this topic, a brief review of the fundamentals of classical perforated panel sound absorbers, and a summary of some recent works being the main aim of this work.

Jesús Carbajo is with the Department of Physics, Systems Engineering and Signal Theory, University of Alicante, Carretera San Vicente del Raspeig s/n, 03690 San Vicente del Raspeig, Spain (e-mail: jesus.carbajo@ua.es).

Nicholas X. Fang and S-H. Nam are with the Department of Mechanical Engineering, Massachusetts Institute of Technology, Carretera San Vicente del Raspeig s/n, 02139 Cambridge (Massachusetts), USA (e-mails: {nicfang, shnam}@mit.edu).

## II. Classical Perforated Panel Sound Absorber

A perforated panel typically consists of a flat rigid surface with periodically arranged perforations such as circular holes or slits, the attenuation of sound being produced by viscothermal losses in these holes (i. e. viscous friction and thermal conduction in the inner air of the perforations). When backed by an air cavity and a rigid wall, a resonant sound absorber is achieved. Let us consider the schematic representation of a classical perforated panel sound absorber as that depicted in Fig. 1. The sound absorption performance of this perforated panel absorber for the case of circular perforations is mainly determined by the radius of the holes, $R$, the spacing between perforations, $b$, the panel thickness, $d$, and the backing air cavity depth, $D$. Note that the spacing between perforations can be directly related to the perforation rate in the case of periodically distributed perforations by $\phi = \pi R^2/b^2$. In brief, by reducing the radius of the holes the absorption bandwidth can be widened, whereas an increase in the panel thickness or the air cavity depth shifts the peak frequency to lower frequencies.

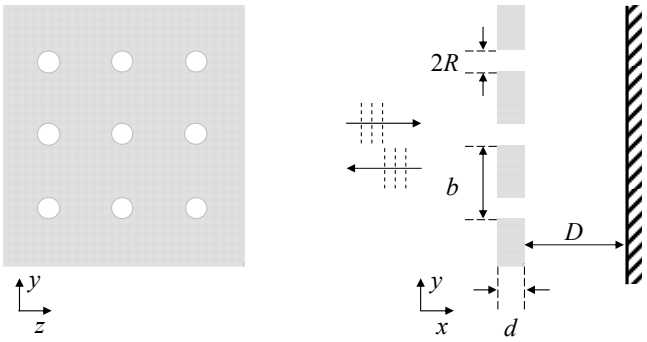


Fig. 1. Schematic representation of a classical perforated panel sound absorber. Left: frontal view. Right: lateral view.

Under plane wave incidence along the $x$-direction, the acoustic impedance $Z$ of the resonator system is given by

 ISBN 978-86-7466-930-3

$$Z = Z_{PP} - jZ_0 \cot\left(k_0 D\right). \quad (1)$$

where $Z_{PP}$ is the transfer impedance of the perforated panel and $D$ is the backing air cavity depth, being $Z_0$ and $k_0$ the characteristic impedance and wavenumber in air, respectively.

Once the acoustic impedance of the resonator is obtained, it is straightforward to calculate its sound absorption coefficient as

$$\alpha = 1 - \left|\frac{Z - Z_0}{Z + Z_0}\right|^2 . \quad (2)$$

Much research has been dedicated to determining the transfer impedance of perforated panels throughout the years. Based on early works by Crandall [7] and Rayleigh [8] on sound propagation in narrow tubes, several authors have proposed theoretical models that let predict the acoustic behavior of the whole resonator system [9]. Some relevant contributions are the end correction terms suggested by Ingard [10] to account for the finite thickness of the panels, the formulas for MPPs proposed by Maa [1], or the derivation of an equivalent fluid model as that proposed by Atalla and Sgard [11]. Moreover, some works have analyzed the acoustic properties of perforated panels at high sound pressure levels [12] or orifices under grazing flow conditions [13]. Unfortunately, the above models may present some limitations for the analysis of complex configurations (e. g. a panel with non-uniform perforations). Nevertheless, the high development of computers over the last decades has paved the way for implementations based on numerical methods such as the Finite Element Method (FEM) that allow dealing with those cases. Some recent examples are the use of Computational Fluid Dynamics (CFD) models for the analysis of tapered perforations [14] or the adoption of a full linearized Navier-Stokes formulation for the analysis of a non-homogeneous distribution of the perforations [15].

On the other hand, the acoustic characterization of such absorbers is an essential task both to assess the validity of a predictive model and to analyze extra dissipation phenomena (e. g. the structural resonances). One of the most extended methods to determine their sound absorption coefficient is the transfer function method, whose measurement procedure can be found in the ISO 10534-2 standard [16]. Alternatively, a transfer matrix approach as that described in detail in the ASTM E2611-09 [17] can be used to derive their transfer impedance. Given that the estimation of these acoustic indicators using a prediction model depends on a set of geometrical parameters, it is also common to obtain the values of the latter by using an optimization procedure (e. g. the Nelder-Mead direct search method [18]) that let obtain the best fit between the measured data and the theoretical predictions.

## III. Innovative Perforated Panel Sound Absorbers

Even though classical perforated panel sound absorbers may show an excellent sound absorption performance, apart from interesting aesthetical and structural features, there has been some representative research over the last years that not only show their great capabilities, but also the potential of these devices to be used in diverse scenarios. A representative selection of six of these research works is briefly outlined next.

### *A. Parallel-Arranged Extended Tubes (PPET)*

Perforated Panels with Extended Tubes (PPET) have been reported to significantly improve the sound absorption in the low frequencies. The use of extended tubes not only let increase the "effective length" of the panel but also achieves a wider bandwidth when combining parallel-arranged PPETs with different cavities (see Fig. 2a). A theoretical investigation into the performance of the PPET was carried out by Li et al. [19], serving this analysis to obtain an optimal design for practical application in the low-frequency range (120-250 Hz). For this purpose, an optimization procedure based on the simulated annealing algorithm was used to derive a configuration of four parallel-arranged PPETs in a constrained space of 100 mm. Experimental validation of the proposed design was performed by manufacturing a prototype which was tested using an impedance tube setup, results showing a reasonable agreement when compared to predictions.

### *B. Coiled Coplanar Air Chamber*

Most perforated panel sound absorbers have a total thickness comparable to the peak absorption wavelength, this being a drawback when designing absorbers for low frequencies. Li and Assouar [20] showed that by coiling up space into the air cavity of the perforated panel absorber an extremely low-frequency acoustic resonator can be achieved. The absorber system consisted of a metasurface composed of a perforated plate combined with a coiled air chamber formed with solid beams as depicted in Fig. 2b. Simulations based on fully coupled acoustic with thermodynamic equations and theoretical impedance analysis were carried out to further understand the underlying physic phenomena. The resulting metasurface possessed a deep subwavelength thickness down to a feature size of $\lambda/223$ achieving perfect sound absorption at 125.8 Hz for a total thickness of the system of 12.2 mm. Furthermore, perfect sound absorption was achieved at the design target frequency. The high efficiency of this type of structure and easy fabrication, when compared to labyrinthine metasurfaces, encourages their use in many applications.

### *C. Perforated Honeycomb-Corrugation*

Tang et al. [21] showed that an ultra-lightweight sandwich panel with perforated honeycomb corrugation in its core as shown in Fig. 2c can be an excellent sound absorber. By using small perforations on the top face sheet and the corrugation of a sandwich panel in the inner cavity, an improvement in both the sound absorption within the frequency band 250-2000 Hz and the mechanical performance of the structure (stiffness and strength) was achieved. Additionally, a theoretical model for sound

 ISBN 978-86-7466-930-3

absorption was used to show that wideband sound absorption performance can be also achieved if multiple acoustic resonators are introduced. The resulting multi-functional structure showed to be promising for many engineering applications requiring lightweight constructions with both great acoustic and mechanical properties.

### *D. Compressed and Micro-Perforated Metal*

As an alternative to typical perforated panels, Bail et al. [22] proposed a panel fabricated by compression and micro-perforation of a porous metal. The compressed and micro-perforated porous metal panel absorber let achieve better sound absorption than the un-compressed porous metal or a simply micro-perforated spring steel panel. A fourth-order polynomial function was proposed to express the superposition absorption effect resulting from the simultaneous action of the porous and micro-perforated structures. An analysis of the micro-morphology (see Fig. 2d) of the fabricated panel samples provided intuitive explanations of the improvement, which was attributed to the irregular micro-vias from the micro-pores to the micro-perforation.

### *E. Panel with Oblique Perforations*

A perforated panel design that uses perforations aligned obliquely to the panel surface as illustrated in Fig. 2e was proposed in a recent work by the authors [23]. Similar to the PPET, an increase of the "effective length" of the panel allow both improving the low-frequency sound absorption and dealing with limiting space constraints common in many practical scenarios. In doing so, not only a frequency shift of 730 Hz of the resonance frequency of the absorber towards low frequencies can be achieved but also an increase in the peak absorption amplitude provided the geometrical characteristics of the panel are properly chosen. A simple predictive model that relies on the fluid-equivalent theory was developed to investigate the acoustic properties of these absorbers, modified expressions for the geometrical tortuosity and flow resistivity being proposed. Measurements in an impedance tube over additive manufactured samples confirmed previous assertions showing a good agreement when compared to prediction data. Unlike coiled or labyrinthine solutions avoids addressing the air cavity design, which may pose an advantage in terms of further development for practical purposes.

### *F. Graded spherical perforations*

In a recent work by Sailesh et al. [24], the influence of spherical bubble perforations and their grading was investigated by preparing different samples with 3D printed biodegradable material. Both the sound absorption and sound transmission performance of these panel designs were assessed by using the impedance tube method and finite element numerical simulations (see Fig. 2f). Results for different sizes of the spherical bubbles and different types of patterns of graded perforations revealed an enhanced sound absorption performance in the low-frequency range up to 1000 Hz. The authors suggest that these solutions can be effectively used in soundproofing applications in the building and transportation sectors.

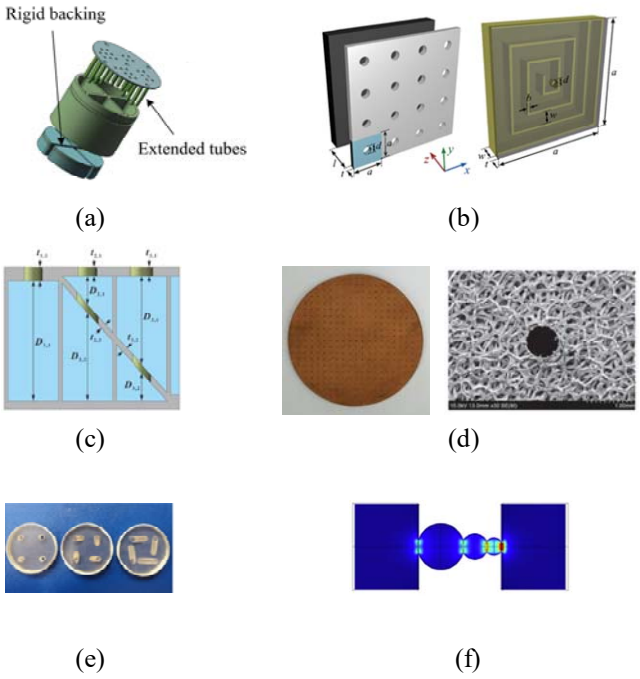


Fig. 2. Innovative perforated panel sound absorbers: (a) parallel-arranged extended tubes (PPET) [19]; (b) coiled coplanar air chamber [20]; (c) perforated honeycomb-corrugation [21]; (d) compressed and micro-perforated metal [22]; (e) panel with oblique perforations [23]; and (f) graded spherical perforations [24].

## IV. Conclusion

In summary, perforated panel sound absorbers show higher durability and structural strength capabilities than conventional porous media. These advantages make these resonator systems provide a wide range of possibilities in many research fields and disciplines of engineering. On the other hand, the incessant development of additive manufacturing techniques poses a new scenario for the conception of innovative designs like those reviewed in this work. In this regard, it may turn out of great interest to also develop new characterization procedures and perhaps to define additional absorption performance indicators. All the same, there is still a need for cost-effective fabrication processes that ease these fabrication procedures to be more extensively adopted in practice. Extending these techniques into the acoustic materials industry will presumably be a challenge to be faced in the forthcoming years.

## Acknowledgment

J. C. would like to thank the Organizing Committee of IcETRAN 2022 for the invitation to the Section of Acoustics and also express gratitude to dr. Dejan G. Ćirić for the proposal.

 ISBN 978-86-7466-930-3

## REFERENCES


[1] D. Y. Maa, "Theory and design of micro-perforated sound-absorbing constructions," *Scientia Sinca*, vol. *18,* pp. *55-71,* 1975.

[2] D. Y. Maa, "Microperforated-panel wideband absorbers," *Noise Control Eng J*, vol. *29,* no. *3,* pp. *77-84,* 1987.

[3] R. T. Randeberg, "Perforated panel absorbers with viscous energy dissipation enhanced by orifice design," Ph.D. dissertation, Trondheim, Norway, 2000.

[4] Y. Y. Lee, E. W. M. Lee, C. F. Ng, "Sound absorption of a finite flexible micro-perforated panel backed by an air cavity," *J Sound Vib*, vol. *287,* pp. *227-43,* 2005.

[5] I. M. Miasa, M. Okuma, G. Kishimoto, T. Nakahara, "An experimental study of a multi-size microperforated panel absorber," *J Syst Des Dyn*, vol. *1,* no. *2,* pp. *331-9,* 2007.

[6] C. Q. Wang, L. X. Huang, "On the acoustic properties of parallel arrangement of multiple micro-perforated panels with different cavity depths," *J Acoust Soc Am*, vol. *130,* pp. *208-18,* 2010.

[7] I. B. Crandall, *Theory of vibrating systems and sound,* New York, USA: Van Nostrand, 1926.

[8] L. Rayleigh, *Theory of Sound,* New York, USA: Dover Publications, 1945.

[9] J. F. Allard, N. Atalla, *Propagation of Sound in Porous Media. Modelling Sound Absorbing Materials,* Chichester, UK: John Wiley and Sons, 2009.

[10] K. U. Ingard, *Notes on sound absorption technology,* New York, USA: Noise control foundation, 1945.

[11] N. Atalla, F. Sgard, "Modeling of perforated plates and screens using rigid frame porous models," *J Sound Vib*, vol. *303,* pp. *195-208,* 2007.

[12] T. H. Melling, "The acoustic impedance of perforates at medium and high sound pressure levels," *J Sound Vib*, vol. *29,* no. *1,* pp. *1-65,* 1973.

[13] A. Cummings, "The effect of grazing turbulent pipe flow on the impedance of an orifice," *Acustica*, vol. *61,* pp. *233-42,* 1986.

[14] T. Herdtle, J. S. Bolton, N. N. Kim, J. H. Alexander, R. W. Gerdes, "Transfer impedance of microperforated materials with tapered holes," *J Acoust Soc Am*, vol. *134,* no. *6,* pp. *4752-62,* 2013.

[15] J. Carbajo, J. Ramis, L. Godinho, P. Amado-Mendes, J. Alba, "A finite element model of perforated panel absorbers including viscothermal effects," *Appl Acoust*, vol. *90,* pp. *1-8,* 2015.

[16] *Determination of sound absorption coefficient and impedance in impedance tubes*, ISO 10534-2, 1998.

[17] *Standard Test Method for Normal Incidence Determination of Porous Material Acoustical Properties Based on the Transfer Matrix Method*, ASTM E2611, 2019.

[18] J. A. Nelder, R. Mead, "A simplex method for function minimization," *Comput J*, vol. *7,* no. *4,* pp. *308-13,* 1965.

[19] D. Li, D. Chang, B. Liu, "Enhancing the low frequency sound absorption of a perforated panel by parallel-arranged extended tubes," *Appl Acoust*, vol. *102,* pp. *126-32,* 2016.

[20] Y. Li, B. M. Assouar, "Acoustic metasurface-based perfect absorber with deep subwavelength thickness," *Appl Phys Lett*, *063502,* 2016.

[21] Y. Tang, F. Li, F. Xin, T. J. Lu, "Heterogeneously perforated honeycomb-corrugation hybrid sandwich panel as sound absorber," *Mater Des*, vol. *134,* pp. *502-12,* 2017.

[22] P. Bai, X. Yang, X. Shen, X. Zhang, Z. Li, Q. Yin, G. Jiang, F. Yang, "Sound absorption performance of the acoustic absorber fabricated by compression and microperforation of the porous metal," *Mater Des*, vol. *167, 107637,* 2019.

[23] J. Carbajo, "Sound absorption of acoustic resonators with oblique perforations," *Appl Phys Lett*, vol. *116, 054101,* 2020.

[24] R. Sailesh, L. Yuvaraj, M. Doddamani, L. B. M. Chinnapandi, J. Pitchaimani, "Sound absorption and transmission loss characteristics of 3D printed bio-degradable material with graded spherical perforations," *Appl Acoust*, vol. *186, 108457,* 2022.


 ISBN 978-86-7466-930-3

# Real-time Speaker Independent Recognition of Bimodal Produced Speech

Boris Malčić, Vlado Delić, Jovan Galić and Nebojša Babić

***Abstract*—This paper presents the initial results in recognition of neutral speech and whispering in real-time, independent of a spea er. The speech database used for training is Whi- pe. The system for training and testing is based on the phin -4 recognition platform. The e periments in recognition showed average recognition accuracy of .2 (for normal speech) and .2 (for whisper). Compared to the recognition in controlled conditions, significant drop of the performance is observed in real-time recognition, for both speech modes.**

**eywords— peech recognition; Whi- pe speech database; phin -4; whispered speech.**

## I. Introduction

Recent advances in automatic speech recognition (ASR) systems have brought many benefits in man-machine speech interaction. Despite good performance in controlled conditions, relatively high sensitivity in adverse conditions is the main reason for low robustness and poor use in real-life scenarios [1-2]. Speech technologies are intended for commonly used modes of speech, i.e. normally phonated speech (normal speech). Other speech modalities include shouted speech, louder speech, soft speech and whisper. The parameters for distinction of these 5 modes are sound pressure level (SPL), sentence duration and silence percentage, frame energy distribution and spectral tilt [3]. Whispered speech is pronounced as an alternative to neutral speech for a number of reasons: when someone does not like to disturb others, when loud speech is prohibited or unpleasant, when the information to speak is secret, when someone wishes to hide identity etc. Also, whispered speech can be produced due to health problems (laryngitis or rhinitis) [4]. Whisper as a speech mode is characterized by a lack of glottal vibration, noisy excitation of the vocal tract and in general, the changes of the vocal tract structure. Recent studies demonstrated performance gain in whispered speech recognition using data augmentation techniques [5-6], denoising autoencoders [7], as well as voice conversion [8].

The goal of the research study presented in this paper is to present initial results in real-time speaker independent recognition of bimodal produced speech (isolated words in neutral speech and whisper) for Serbian. The ASR system for training and testing is based on CMU Sphinx platform [9]. The remainder of this paper is organized in the following manner. In Section 2 a short overview of Hidden Markov Models (HMM) is given. Section 3 presents a speech database, the training of the ASR system and experiment setup for testing. In Section 4 we give results of experiments as well as its discussion, whereas concluding remarks and direction for future studies are stated in Section 5.

Boris Malčić is with the Faculty of Electrical Engineering, University of Banja Luka, Department of Electronics and Telecommunications, Banja Luka, Patre 5, Bosnia and Herzegovina (e-mail: boris.malcic@etf.unibl.org), ( https://orcid.org/0000-0002-7476-5140).

Vlado Delić is with the Faculty of Technical Sciences, University of Novi Sad, Novi Sad, Serbia (e-mail: vdelic@uns.ac.rs), (https://orcid.org/0000-0002-4558-9918).

Jovan Galić is with the Faculty of Electrical Engineering, University of Banja Luka, Department of Electronics and Telecommunications, Banja Luka, Patre 5, Bosnia and Herzegovina (e-mail: jovan.galic@etf.unibl.org), (https://orcid.org/0000-0002-2487-7136).

Nebojša Babić is with the Faculty of Electrical Engineering, University of Banja Luka, Department of Informatics, Banja Luka, Patre 5, Bosnia and Herzegovina (e-mail: nebojsa.baabic@gmail.com).

## II. Hidden Markov Models

Modern ASR systems are inconceivable without Markov models that are combined with a model of a mixture of Gaussian distributions, or with deep neural networks that have become increasingly popular in recent times. The HMMs have become one of the most useful statistical methods for modeling speech signals [10]. Moreover, HMM is often defined by a parameter set $\mathbf{\Lambda} = (\mathbf{A}, \mathbf{B}, \boldsymbol{\pi})$ where are denoted: a transition probability matrix as $\mathbf{A} = [a_{ji}]$; an output probability matrix as $\mathbf{B} = [b_j(m)]$, $b_j(m) = P(X_t = o_m | x_t = j)$; and an initial state distribution matrix as $\boldsymbol{\pi} = [\pi_j]$. Furthermore, with a fully connected (ergodic) HMM, transition from any state to any other state is possible. On the other hand, due to the dynamic nature of the speech signal, in modern ASR systems, the serial structure dominates in which transition is possible only to a state with the index higher than the current one. An example of such structure is shown in Fig. 1 where the inactive states (null states) are shaded and located at the beginning and at the end of the sequence, while the output (ultimate) probabilities at the final moment $t = T$ (we observe a series of $T$ feature vectors) are defined by $\eta_j = P(x_T = j), 1 \leq j \leq M, \eta_j + \sum_{i=1}^{M} a_{ji} = 1, \forall j$ for a certain state sequence $\boldsymbol{X} = \{x_1, x_2, \dots, x_T\}$.

In HMM-based speech recognizers, model parameters can be obtained using the Viterbi algorithm in training and the expectation maximization (EM) algorithm. Improved values are obtained by the EM algorithm using the method of Lagrange multipliers to determine the local extremum of a multivariate function. This procedure is called the iterative Baum-Welch (BW) training algorithm. Moreover, it is

 ISBN 978-86-7466-930-3

important to emphasize that the BW algorithm does not guarantee reaching a global maximum but only a local one, and the iterative procedure is repeated while the joint probability of training data increases.

In order to be able to apply the previous discrete HMM methodology for speech signal recognition, continuously distributed HMMs have been introduced where the probabilities of emitting discrete symbols are changed as a function of the probability density of observations. Since the probability density function of any random variable can be approximated by the sum of *N* Gaussian random variables, the multivariate Gaussian mixtures are used in HMM recognizers.

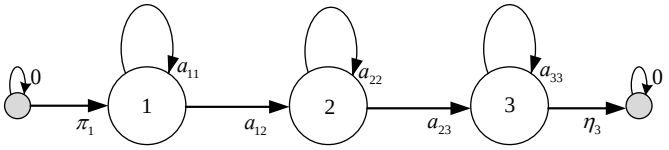


Fig. 1. An example of the serial left-right topology with 3 active states without the possibility of skipping a state

## III. System for Recognition

### *A. Speech database*

There are a relatively small number of languages with available speech databases created in modes other than neutral [11-13]. The Whi-Spe database was created for research activities needed for human-machine interaction in Serbian for bimodal produced speech [14]. In its initial form, the database contains recordings of 50 different words from 10 speakers (5 female and 5 male). The vocabulary of 50 words is divided in three groups: basic colors (6 words), numbers (14 words) and phonetically balanced words (30). Each word is repeated 10 times in both speech modes. Finally, the database includes 10.000 utterances (*wa* records) in a total duration of 2 hours. The sampling frequency of speech samples is 22050 Hz and 16 bits per sample (mono PCM *wa* format). More details about the database (recording, segmentation procedure, labeling and quality control) can be found in [14].

### *B. AS training system*

The task of the automatic speech recognition system (ASR) is to extract words from the speech signal in the order in which they are spoken. The block diagram of the ASR system based on HMM is shown in Fig. 2. Moreover, in section III c. we present a graphical interface of our program implemented in Java, and based on Fig. 2. First, in the feature extraction block, the speech signal is transformed into a series of feature vectors. The task of the feature extraction block is also to eliminate various variations caused by changes in speakers, ambience or channels. The task of the recognizer is to find the sequence of words that (according to a predetermined criterion) best corresponds to what was actually said.

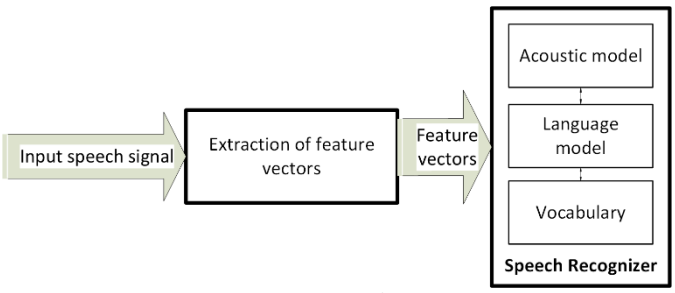


Fig. 2. The operation principle of a general ASR system

From a statistical point of view, the recognizer finds a string (i.e. $\widehat{W} = w_1, w_2, \dots, w_M$) of *M* words which maximizes a posteriori probability $P(W|X)$ where $\hat{X} = x_1, x_2, \dots, x_T$ is an array of *T* features. Namely, the language model describes the relationship between words taking into account the grammar of the language for which the recognizer is intended, while the description of the statistical point of view of speech behavior in the feature vector space is presented with an acoustic model. In ASR systems, the basic units for modeling are phonemes, and from their point of view in speech communications, the smallest acoustic unit that a person can perceive is a phoneme. In context-independent recognition, each phoneme is modeled independently, and that modeling unit is called a monophone. However, due to coarticulation, the pronunciation of a particular phoneme largely depends on neighboring phonemes, and then triphones (rarely biphones) are usually used, which are derived using the monophones in a way which takes into account the previous and next phonemes. When using the same, there is a need for a huge training database, which is also one of the main disadvantages of using triphones, and due to the relatively small Whi-Spe database used in this research paper, we only were able to train the acoustic model using the monophones.

Furthermore, let us now mention that speech recognition is divided into two phases: 1st phase of system training, 2nd phase of speech recognition or system testing. Common to both of these phases is that they need to perform feature vector extraction. In doing so, the feature vector should describe as adequately as possible the envelope of the amplitude spectrum of the spoken phoneme, because the information about the spoken phoneme is precisely contained in that envelope. In the training phase, we divided speech into frames (smaller segments) of 25 ms duration within which the speech signal can be considered quasi-stationary. Also, adjacent frames are shifted 10 ms to better track changes in the speech signal spectrum. The most commonly used features in speech recognition are the mel-frequency cepstral coefficients (MFCCs), and Fig. 3 presents the block diagram for the extraction of MFCC feature vectors.

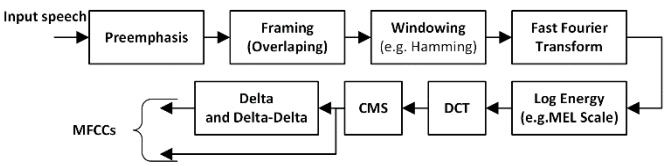


Fig. 3. Process for the MFCCs feature vector extraction

 ISBN 978-86-7466-930-3

Fig. 3. depicts that several steps need to be performed in the processing chain to extract MFCCs from the input speech signal. Some of these steps are Fast Fourier Transform (FFT) over speech signal frames. Next, the signal spectrum is passed through a filter bank (describing the operation of the basilar membrane) whose filters are distributed evenly on the mel-frequency scale. Furthermore, Discrete Cosine Transform (DCT) replaces inverse FFT and is used to calculate cepstral coefficients because the speech is a real signal and its amplitude spectrum is an even function. Then, to increase the robustness of the system, normalization with Cepstral Mean Subtraction (CMS) is performed, because by subtracting the mean value from Cepstral coefficients, a significant separation of excitation and transfer function of the vocal tract is achieved. This procedure is very useful in whisper recognition. Finally, with the last block in the processing chain on Fig. 3 we single out the dynamic features using which are better monitored the time characteristics of the speech signal, and that achieves less correlation between adjacent frames. For this purpose are used the so-called delta (Δ) features that represent the first derivative (rate of feature change) of static features, and also the delta-delta (ΔΔ) features that are obtained as a second derivative and represent the acceleration with which static features are changed.

In order to train the acoustic model for CMUSphinx, we followed in detail the procedure described in [15]. First, following the procedure all the necessary files (*an4.dic, an4.filler, an4.phone, an4 train.fileids, an4 train.transcription*) for training are created. For that purpose, the phonemes used in training the acoustic HMM for Serbian are presented in Table I. Next, in Table I phonemes {CC, CH, Dj, DZ, SH, ZH} are in Serbian {Ć, Č, Đ, Dž, Š, Ž}, and the notation Y is used for the phoneme SCHWA. Furthermore, an example of the phonetic transcription for only three words (of all 50 words in the Whi-Spe that are used in the process of training for the Serbian ASR system), is shown in Table II.

TABLE I
PHONEMES USED FOR MODEL TRAINING

| | | | | | | | |
|---|---|---|---|---|---|---|---|
| A | B | C | CC | CH | D | Dj | DZ |
| E | F | G | H | I | J | K | L |
| Lj | M | N | Nj | O | P | R | S |
| SH | T | U | V | Y | Z | ZH | SIL |

TABLE II
AN EXAMPLE OF PHONETIC TRANSCRIPTION FOR THREE WORDS

| Word | Phonetic transcription |
|---|---|
| CRNA | C Y R Y N A |
| TRI | T Y R I |
| ZGRADE | Z G Y R A D E |

Second, we prepared the directory **an4** (i.e. our appropriate directory where we created the *wa* subdirectory inside which are all *wa* records). In our case, 10,000 *wa* records are used from the training Whi-Spe database. After that, using the terminal, we positioned into the **an4**, and executed the command **sphin train -t an4 setup**.

The previous command created a subdirectories **an4** and **feat** in the directory **an4** and the subdirectory **feat** was not visible in the file system, but it was visible in the terminal which could be checked with the commands **ls** and/or **la**. Please note that in relation to the steps of the official instructions, it is important that in the **etc** directory (created previously) from our database (which we called **an4**) we store all the necessary files for training, namely: *an4.dic, an4.filler, an4.phone, an4 train.fileids, an4 train.transcription, sphin train.cfg*. Next, be sure to create a wav directory in the directory of the database (**an4**), and place in it all wav records. Furthermore, we need to modify the configuration file (**sphin train.cfg**) by replacing the following lines (paths) in the configuration file:

```
C G A DI home user Des top sphin -source an4 ;
C G P I T AI DI home user Des top sphin -source sphin train ;
```

Also, in the configuration file we need to set

```
(yes no) Train conte tually dependent models
C G CD T AI no ;
```

Moreover, this previously modified **sphin train.cfg**, and all other files from the **etc** file within **an4**, should be copied and moved to the **etc** folder within the folder **home user Des top sphin -source sphin train**. Finally, after all the previous preparation steps, we started the model training by calling **perl** scripts. Specifically, we go to the terminal in the **sphin train** folder which is inside the **sphin -source** directory (within that directory there are also **an4**, **sphin base** and **poc etsphin** directories which we prepared earlier). Next, we observed that differences in github's **sphin train** versions manifested by writing keyword **scripts** instead of the original **scripts pl** in the training commands, and by changing the numbers of **perl** scripts equivalent to those in the training internals sections [15], so for example instead of the command **perl scripts pl 1 .vector quantize slave. .pl** now it is necessary to write **sudo perl scripts 5.vector quantize slave. .pl**. The previous is mentioned because we pulled the edge CMU Sphinx toolkit packages from github, and not used the recommended (5prealpha) releases [16]. Finally, after being positioned in the **sphin train** directory, we executed the following commands in terminal for model training:

```
user ubuntu Des top sphin -source sphin train
sudo perl scripts .comp feat slave feat.pl
user ubuntu Des top sphin -source sphin train
sudo perl scripts .verify verify all.pl
```


ISBN 978-86-7466-930-3

```
user ubuntu Des top sphin -source sphin train
sudo perl scripts 5.vector quantize slave. .pl
user ubuntu Des top sphin -source sphin train
sudo perl scripts 2 .ci hmm slave convg.pl.
```

After executing the last command, we got the parameters of the Context Independent (CI) trained model as in Fig. 4.

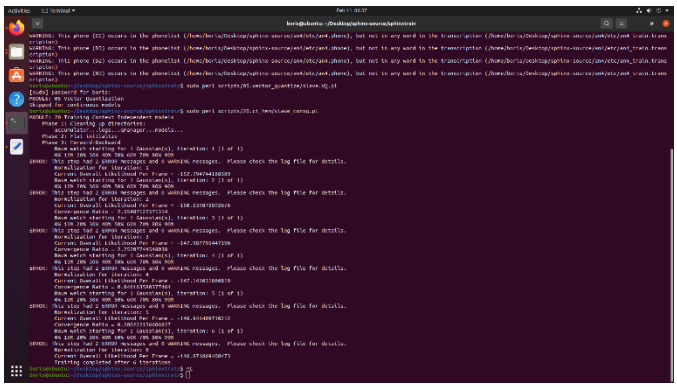

Fig. 4. An example of output **CI** training in the Ubuntu 20.04.3 LTS terminal

To sum up, we finally created new directories in **an4**, such as the **model parameters** directory within which is located directory **an4.ci cont** containing 7 files obtained during the training process, i.e.: **feat.params**, **mdef**, **mean**, **mi weights, noisedict, transition matrices**, **variances**. From the **feat.params** file is visible the number of filters in filterbank is 25. Then, as a feature vector, a 39-dimensional dynamic feature vector is used (13-static + Δ + ΔΔ). The number of Gaussian mixtures is 8. For each utterance, cepstral mean normalization (cmn) is performed. The number of monophones is 32 (of which 30 corresponding to the 30 phonemes in Serbian, then phoneme SCHWA and silence - SIL). As a result, the models of monophones are initialized with global mean value and variance (flat-start initialization). These all files in **an4.ci cont** represent the CI continuous HMM that will be used in the following section by the application for the process of testing.

### *C. AS recognition testing system*

Fig. 5. shows the main window of the interface. Labeled with numbers, the components are as follows: 1. Main menu, 2. The list of words available in the model but left out, 3. The list of words chosen for the test, 4. Buttons for managing lists 2 and 3, 5. Most commonly used commands available in the main menu, 6. Output console, and 7. Console-related commands.

The main menu holds all options needed to run the test, load the language model, overview of the used grammar and management of extra words and sentences for the test. The application is packaged with the language model, but also any other compatible language model can be tested through the application. By default, the list of available words is displayed using the language model's dictionary.

When loading the custom model, the user can choose whether to use a grammar definition instead of relying on the language model.

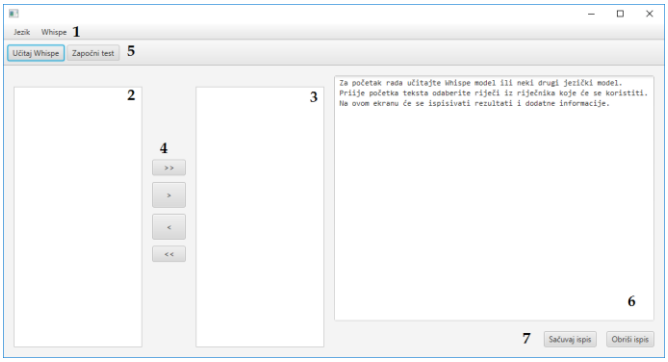


Fig. 5. The main window of the interface

As the list of available words loaded from the dictionary cannot match any but the most basic of grammars, the user can load sentences to use in the test. Each loaded sentence file is treated as a group of sentences where each sentence is one line in the text file. Each loaded file has the box (❒) icon next to the name to indicate that the selected keyword is actually a container of multiple test entries.

When the user wants to run a test, they have an option of shuffling and/or repeating the words multiple times. The user can also decide to save logs into a file instead of relying on the console for the test results. The console will show the results regardless of this setting. When performing many consecutive tests with the same settings, the user can instead provide the configuration through a file. When the file *testConfig.t t* is provided in the same directory as the application, the test settings step is skipped.

The test process screen is shown on Fig. 6. The test process aims to be as simple as possible. The left side of the window shows the instructions of what to pronounce. On each pronunciation, the next word or sentence is shown. The test can be stopped at any time for partial results. The right side of the window shows the test result logs. On each pronunciation, a line with a timestamp, the detected and the correct word will show. When the test is finished, the statistical result will also show, stating the overall accuracy. The console output can be saved or cleared at any time using the buttons below the console.

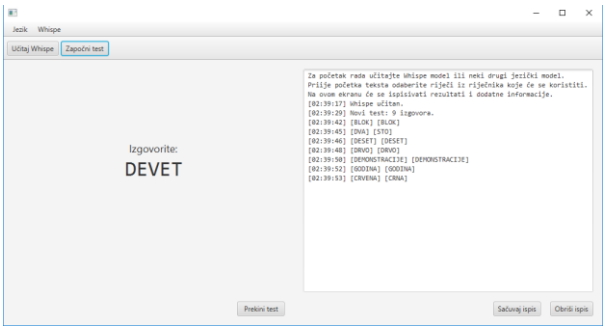


Fig. 6. The application window in the testing phase


ISBN 978-86-7466-930-3

## IV. RESULTS

The accuracy and correctness of speech recognition are tested on 10 people, i.e. 5 male testing examinees enumerated as {M1, M2, M3, M4, M5}, and 5 female examinees marked as {F1, F2, F3, F4, F5}. All the above respondents pronounced the words from Whi-Spe. The testing was performed in a room with SPL of 30-35 dB(A).

For this purpose, first the parameters of the HMM trained on the entire Whi-Spe for the normal speech, are loaded into the application, and then the testing scenario is repeated for the whisper speech. Exactly, these models are tested on all 10 examinees and this scenario is denoted as **full**. Then, we tested a new scenario denoted as **match** in which the parameters of HMMs were obtained by training only over part of the Whi-Spe (i.e. only on *female male* speakers in the database), and the obtained models for normal speech (n) and whisper (w) are tested only on 5 *female male* respondents, respectively. For all those models 8 Gaussian mixtures were used in the configuration file for the training. Next, for all different scenarios (*n full, n match, ..., w_match*), the obtained corresponding results for the accuracy (***Acc*** ), and the correctness ( ***rr*** ) are calculated in Table III and in Table IV, using the following expressions[17]

$$Corr[\%] = \frac{N-D-S}{N} \times 100\%, \quad (1)$$

$$Acc[\%] = \frac{N-D-S-I}{N} \times 100\%, \quad (2)$$

where: $N$ is the total number of words in the reference transcriptions, is the number of deletion errors, $S$ is the number of substitution errors, and $I$ is the number of insertion errors in each of the tested HMMs. From Table III it is calculated the mean value of recognition accuracy (*Acc_n full*) of 86.4% with a mean absolute deviation (MAD) equal to 3.52% in the case of normal speech recognition on female examinees in the case of a full scenario (i.e. *n full*), while for the whisper speech the mean *Acc_w full* is 62.8% with the average correctness (*Corr_w full*) of 90.8%. Furthermore, from Table IV, the mean of *Acc_n match* is 88% (mean value of *Corr_n match* is 93.6%) with MAD = 4% for testing the male examinees of normal speech for the **matched** (i.e. trained on utterances of male speakers, and tested on male examinees) case.

TABLE III
RESULTS OF SPEECH RECOGNITION ON FEMALE EXAMINEES FOR DIFFERENT SCENARIOS

| Examinee | F1 | F2 | F3 | F4 | F5 |
|---|---|---|---|---|---|
| *Acc_n full* [%] | 88 | 84 | 92 | 80 | 88 |
| *Acc_n match* [%] | 74 | 88 | 74 | 70 | 62 |
| *Acc_w full* [%] | 70 | 64 | 72 | 54 | 54 |
| *Acc_w match* [%] | 50 | 58 | 66 | 56 | 60 |
| *Corr_n full* [%] | 90 | 84 | 94 | 82 | 94 |
| *Corr_n match* [%] | 86 | 92 | 88 | 84 | 92 |
| *Corr_w full* [%] | 72 | 64 | 76 | 60 | 70 |
| *Corr_w match* [%] | 58 | 72 | 74 | 68 | 78 |

TABLE IV
RESULTS OF SPEECH RECOGNITION ON MALE EXAMINEES FOR DIFFERENT SCENARIOS

| Examinee | M1 | M2 | M3 | M4 | M5 |
|---|---|---|---|---|---|
| *Acc_n full* [%] | 94 | 84 | 88 | 74 | 90 |
| *Acc_n match* [%] | 84 | 86 | 84 | 94 | 92 |
| *Acc_w full* [%] | 76 | 58 | 72 | 62 | 80 |
| *Acc_w match* [%] | 76 | 76 | 82 | 62 | 80 |
| *Corr_n full* [%] | 98 | 94 | 90 | 78 | 94 |
| *Corr_n match* [%] | 94 | 94 | 88 | 96 | 96 |
| *Corr_w full* [%] | 80 | 62 | 76 | 68 | 80 |
| *Corr_w match* [%] | 80 | 84 | 86 | 64 | 88 |

Next, in the matched case for recognizing males' whispers the mean correctness is 80.4% with MAD = 6.72% and word error rate (WER) of 24.8%. Of course, in the case of the larger (with more different speakers) training database it would be logical to get better testing results in the match case, but for our research the relatively small Whi-Spe database was only available. Moreover, there is an evident reduction in real-time recognition accuracy compared to the controlled conditions (quiet environment and same recording equipment) in closed set speaker independent recognition based on HMM where accuracy was 98.3% (for neutral speech) and 96% (for whisper) [18]. As well, recognition of whisper in real-time is with significantly lower success than recognition of neutral speech. As can be seen from results in Tables 3 and 4, average recognition rate (accuracy and correctness) is higher for male speakers, but this is not statistically confirmed, despite the same training database. Variations among different speakers are high for both speech modes. For the determination of statistically significant parameters which contribute to high deviation of performance among speakers, a higher number of speakers is needed.

## V. CONCLUSION

Speech recognition of mode other than neutral is by all means a serious challenge for modern ASR systems. In this paper, the experiments on real-time speech recognition in normal and whisper mode for Whi-Spe speech database and HMM algorithm, are conducted. Obtained results suggest that for recognition in real world scenarios, the larger speech database is needed for training. Future studies will be focused on the analysis of data augmentation techniques in multimodal speech recognition. Finally, the further research will also be based on deep neural networks (DNNs) because using *n*-gram language model from randomly initialized DNN with lattice-free maximum mutual information is possible WER relative reduction around 25% with respect to the best HMMs based ASR system [19].

## ACKNOWLEDGEMENT

This research was supported by the Science Fund of the Republic of Serbia, #6524560, AI-S-ADAPT Ministry of

 ISBN 978-86-7466-930-3

Education, Science and Technological Development of Serbia: University of Novi Sad, Faculty of Technical Sciences (MPNTR - 451-03-68/2020-14/200156).

The authors would like to thank all examinees for participation in speech recognition tests.

## REFERENCES

[1] M. P. Fernández-Gallego, D. Toledano, A Study of Data Augmentation for ASR Robustness in Low Bit Rate Contact Center Recordings Including Packet Losses, Applied Sciences, vol.2, no. 3, 1580, 2022.

[2] J. Holms, W. Holms, *Speech Synthesis and ecognition*, Taylor & Francis, London, United Kingdom, 2001.

[3] C. Zhang, J. H. L. Hansen, "Analysis and classification of Speech Mode: Whisper through Shouted," Proceedings of Interspeech 2007, pp. 2289-2292, 2007.

[4] T. Ito, K. Takeda, F. Itakura, "Analysis and recognition of whispered speech," Speech Communication, vol. 45, no. 2, pp. 139–152, 2005.

[5] P. R. Gudepu, G. P. Vadisetti, A. Niranjan, K. Saranu, R. Sarma, M. Ali Basha Shaik, and P. Paramasivam. "Whisper Augmented End-to-End/Hybrid Speech Recognition System - CycleGAN Approach." *INTE SPEEC* , 2020.

[6] H. Hikaru, and C. Pajot, "Data Augmentation for ASR using CycleGAN-VC.", Computer Science, 2021.

[7] Đ. Grozdić, S. Jovičić, M. Subotić, "Whispered speech recognition using deep denoising autoencoder", Engineering Applications of Artificial Intelligence, vol. 59, pp 15-22, 2017.

[8] M. Cotescu, T. Drugman, G. Huybrechts, J. Lorenzo-Trueba, A. Moinet, Voice Conversion for Whispered Speech Synthesis, IEEE Signal Processing Letters, 2020.

[9] P. Lamere, P. Kwok, E. Gouvêa, B. Raj, R. Singh, W. Walker, M. Warmuth, P. Wolf, "The CMU SPHINX-4 Speech Recognition System", ICASSSP, 2003.

[10] X. Huang, A. Acero, H-W. Hon, *Spoken anguage Processing A Guide to Theory, Algorithm, and System e elopment,* 1st ed. New Jersey, USA, Prentice Hall PTR, 2001.

[11] P. X. Lee, D. Wee, H. S. Yin Toh, B. P. Lim, N. Chen, B. Ma, "Whispered Mandarin Corpus for Speech Technology Applications," Proceedings of Interspeech 2014, pp. 1598–1602, 2014.

[12] T. Tran, S. Mariooryad, C. Busso, "Audiovisual corpus to analyze whisper speech," presented at the International Conference on Acoustics, Speech and Signal Processing, pp. 8101–8105, 2013.

[13] F. Cummins, M. Grimaldi, T. Leonard, J. Simko, "The chains corpus: Characterizing individual speakers," Proceedings of International Conference on Speech and Computer SPECOM, St. Petersburg, Russia, pp. 421–435, 2006.

[14] B. Marković, S. T. Jovičić, J. Galić, Đ. Grozdić, "Whispered speech database: design, processing and application," In: Habernal, I., Matousek, V. (eds.), TSD 2013, LNAI 8082, Springer-Verlag Berlin Heidelberg, pp. 591–598, 2013.

[15] N. Shmyrev, 'Training an acoustic model for CMUSphinx'. [Online]. Available: https://cmusphinx.github.io/wiki/tutorialam/ . [Accessed: 11-Feb-2022].

[16] N. Shmyrev, 'CMU Sphinx downloads'. [Online]. Available: https://cmusphinx.github.io/wiki/download/ . [Accessed: 10-Feb-2022].

[17] S. Young, G. Evermann, M. Gales, T. Hain, D. Kershaw, X. Liu, G. Moore, J. Odell, D. Ollason, D. Povey, V. Valtchev, P. Woodland, *The T Book for T ersion 3.4* , Cambridge University Engineering Department, 2006. [Online]. Available: http://htk.eng.cam.ac.uk/prot-docs/htkbook.pdf .

[18] J. Galić, S. Jovičić, V. Delić, B. Marković, D. Šumarac Pavlović, Đ. Grozdić: "HMM-based Whisper Recognition Using μ-law Frequency Warping", SPIIRAS Proceedings, St. Petersburg Institute for Informatics and Automation of the Russian Academy of Sciences, ISSN 2078-9181 (print), ISSN 2078-9599 (online), Issue No. 3(58), pp. 27-52, 2018.

[19] V. Delić, Z. Perić, M. Sečujski, N. Jakovljević, J. Nikolić, D. Mišković, N. Simić, S. Suzić, and T. Delić, "Speech Technology Progress Based on New Machine Learning Paradigm," *Comput Intell Neurosci.*, 2019. [Online]. Available: https://www.ncbi.nlm.nih.gov/pmc/articles/PMC6614991/. [Accessed: 05-Apr-2022].

 ISBN 978-86-7466-930-3

# Feature Analysis for Industrial Product Sounds Using Discrete Meyer Wavelet

Đorđe Damnjanović, Dejan Ćirić and Dejan Vujičić

***Abstract*—The process of wavelet decomposition into approximation and detail coefficients is used in many research fields, especially when signal de-noising is in focus. Extraction of features of different signal types is also an area where wavelets are often mentioned. Different wavelet families provide interesting results in feature analysis and further classification. In that regard, a wavelet that has attracted a significant interest is discrete Meyer. This paper presents the usage of discrete Meyer wavelet for feature analysis of industrial product sounds. More than 100 sounds of 6 different industrial products are tested. The most representative results are given here.**

***Index Terms*—Audio feature analysis; Discrete Meyer wavelet; Approximation coefficients; Detail coefficients; Industrial product sound.**

## I. Introduction

Wavelets are often mentioned in literature as an algorithm that solved some problems in the Fourier transform [1-2]. If short time Fourier transform (STFT) and wavelet algorithms are compared, the window function are used in both cases for purpose of analysis and processing of signals. However, in the case of wavelets, window function is not of a fixed size. Width of the wavelet window can be changed as the transform is computed for every single spectral component, and that is the main difference in comparison with STFT [1-2].

Applicability of wavelets can be considered to be one of their advantages since a number of applications are made based on the wavelet algorithms. Some of them include echo cancelation, noise control, speech recognition, de-noising of audio and image signals, unknown system detection and others. Applications can be found in different fields, such as biomedical engineering, telecommunications, signal processing, computer engineering, etc [3-6].

The process of wavelet decomposition into approximation and detail coefficients (Fig. 1) is often used nowadays in feature extraction and analysis. Authors of this paper already presented the results of feature extraction method using wavelets for DC motor sounds in [7-9], where focus is on differences between non-faulty and faulty motors. In that regard, a lot of wavelet families are used, such as Haar, Daubechies, Coiflet, Symlet, biorthogonal, reverse biorthogonal and Meyer.

In the discrete wavelet processing, the decomposition process is done using the discrete wavelet transform (DWT), (see Fig. 1). This process is based on the use of low-pass (LP) and high-pass (HP) filters. Here, "A" stands for the approximation coefficients, "D" stands for the detailed coefficients and 2↓ is the down-sampling. Fig. 1 presents only decomposition up to level 2, but the whole process can be extended to a higher level of decomposition [4-5,10-11].

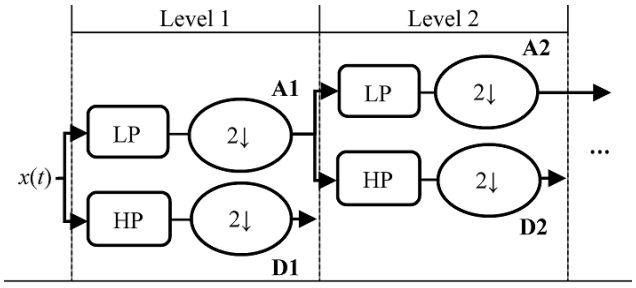


Fig 1. Block diagram of wavelet decomposition.

This paper presents usage of the discrete Mayer wavelet for the purpose of feature extraction from different industrial product sounds. More than 100 sounds organized into 6 different classes (categories) are tested: fan, gearbox, slider, toycar, toytrain and valve. Those sounds are taken from the DCASE 2021 challenge (task 2) [12]. The goal is to find certain similarities of the extracted features within the same class and certain differences among the classes in order to prepare the obtained features for future classification. The analysis is done in Matlab software package.

## II. Meyer Wavelet

In 1985, Yves Meyer developed the first nontrivial orthogonal wavelet basis. This wavelet is in-group of orthogonal wavelets where are also Daubechies, Coiflet and Symlet wavelets. The main idea was to define wavelet and scaling function in the frequency domain using trigonometric functions. Both wavelet and scaling functions are presented in (1) and (2) [11,13-15]:

$$\hat{\psi}(\omega)=\frac{1}{\sqrt{2\pi}}e^{j\frac{\omega}{2}}\begin{cases}\sin\left(\frac{\pi}{2}v\left(\frac{3}{2\pi}|w|-1\right)\right) & \frac{2\pi}{3}\le|\omega|\le\frac{4\pi}{3}\\ \cos\left(\frac{\pi}{2}v\left(\frac{3}{4\pi}|w|-1\right)\right) & \frac{4\pi}{3}\le|\omega|\le\frac{8\pi}{3}\\ 0 & |\omega|\notin\left[\frac{2\pi}{3},\frac{8\pi}{3}\right]\end{cases} \quad (1)$$

Đorđe Damnjanović is with the University of Kragujevac, Faculty of Technical Sciences Čačak, Svetog Save St. 65, 32000 Čačak, Serbia (e-mail: djordje.damnjanovic@ftn.kg.ac.rs).

Dejan Ćirić is with the University of Niš, Faculty of Electronic Engineering in Niš, Aleksandra Medvedeva 14, 18000 Niš, Serbia (e-mail: dejan.ciric@elfak.ni.ac.rs).

Dejan Vujičić is with the University of Kragujevac, Faculty of Technical Sciences Čačak, Svetog Save St. 65, 32000 Čačak, Serbia (e-mail: dejan.vujicic@ftn.kg.ac.rs).

 ISBN 978-86-7466-930-3

$$\hat{\varphi}(\omega)=\frac{1}{\sqrt{2\pi}}\begin{Bmatrix}1 & |\omega|\le\frac{2\pi}{3}\\ \cos(\frac{\pi}{2}v(\frac{3}{2\pi}|w|-1)) & \frac{2\pi}{3}\le|\omega|\le\frac{4\pi}{3}\\ 0 & |\omega|\ge\frac{2\pi}{3}\end{Bmatrix} \quad (2)$$

where the function $v$ can be changed for the purpose of obtaining different wavelets, for example as done in (3) [12,14]:

$$v(a)=a^4(35-84a+70a^2-20a^3), a\in[0,1]. \quad (3)$$

The wavelet function, presented in (1), is symmetrical around point 1/2, while the scaling function (2) is symmetrical around the point 0 [12-14]. What is also important to mention is that the Meyer wavelet is an indefinitely differentiable with infinite support. In Fig. 2, the discrete Meyer wavelet function (which is often used in software packages) is presented.

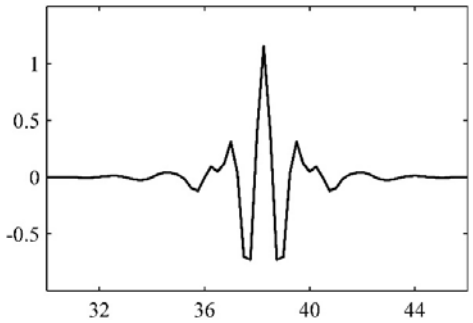


Fig 2. Discrete Meyer wavelet function.

## III. Methods of Analysis

Within the task 2 (Unsupervised anomalous sound detection for machine condition monitoring under domain shifted conditions) of DCASE 2021 challenge [12], a number of sounds of 7 different industrial machines (products) - fan, gearbox, pump, slide rail (slider), toycar, toytrain and valve are available. For each of the mentioned products, there are three datasets – development, additional training and evaluation datasets. The development dataset is split into three subsets, and in overall these development datasets contain more than 4000 sound samples of normal and anomalous operating product modes.

Among those sounds from the development datasets, about 100 sound samples from 6 classes – from all classes mentioned above except pump (approximately around 17 sounds per product) are chosen here for initial analysis. All sounds are recorded using the sampling frequency of 16 kHz. Length of the recorded signals is 10 s, and they include both the sounds of a machine and its associated equipment as well as environmental noise [12]. In this paper, the following abbreviations will be used: fan-f, gearbox-g, slider-s, toycar-tc, toytrain-tt, valve-v.

At the very beginning, all chosen sounds are analyzed in the time and frequency domain. Then, segmentation process is applied. Size of segments is 50 ms. In this paper, the overlap between neighbor segments of 50% (25 ms) is chosen like in some other previous papers [7-9,16]. Size of segments and overlap can vary from research to research. In some studies, authors propose no overlap between segments [17-18].

After segmentation, the signals are decomposed using the discrete Meyer wavelet. This wavelet is a unique wavelet in the sense that there are no more variations, as for instance in the Coiflet wavelet family, where there are 5 different types in Matlab or in the Symlet wavelet having 45 types, etc [19]. The Meyer wavelet is chosen here having in mind the previous authors' researches [8-9] where this wavelet gave interesting results. The detail coefficients obtained through the wavelet decomposition with different levels of decomposition (from 1 up to 8) are used for further analysis

At each decomposition level and for every segment, the absolute values of the detail coefficients are calculated, and then the mean value of these absolute values is obtained. The set of the mean values of the details coefficients generated in the described way is used as a representative audio feature (wavelet-based feature). In some researches, such as [7-9,20-21], it is presented that the standard deviation can also be used, but authors of this paper showed previously, see [8-9], that the results based on the mean values and standard deviation are similar. This is why the standard deviation is omitted here.

The analysis is carried out in Matlab software package. When the wavelet decomposition is in focus, it is worthwhile to mention a few functions: *wavedec* for wavelet decomposition, *appcoef* and *detcoef* for obtaining the approximation and detail coefficients, *abs* and *mean* for calculating absolute and mean values, respectively.

A specific measure (quantity) named feature difference is introduced in certain isolated cases. It is calculated as the mean value of a difference between wavelet-based features for different industrial products taken from all segments and normalized by the mean feature value [8-9]. This measure is used to indicate more closely the numerical differences among the obtained features in addition to what is shown graphically.

## IV. Results

The initial analysis starts with observation of signals in the time and frequency domain. In Fig. 3, six random audio signals (one from each type of the industrial products) are presented in the time domain. If the graphs are closely observed, it can be pointed out that differences between these signals are small. Thus, the time domain signals of fan and gearbox are very similar. The same is valid for the signals of slider, toycar and valve, although some more transients are present here. An exception is the signal of toytrain, which has a rather different shape and amplitude comparing to others. In the next four figures, lines associated to these products are plotted by the same color scheme as done in Fig. 3: red color for fan, blue color for gearbox, black color for slider, green color for toycar, magenta color for toytrain, cyan color for

 ISBN 978-86-7466-930-3

valve.

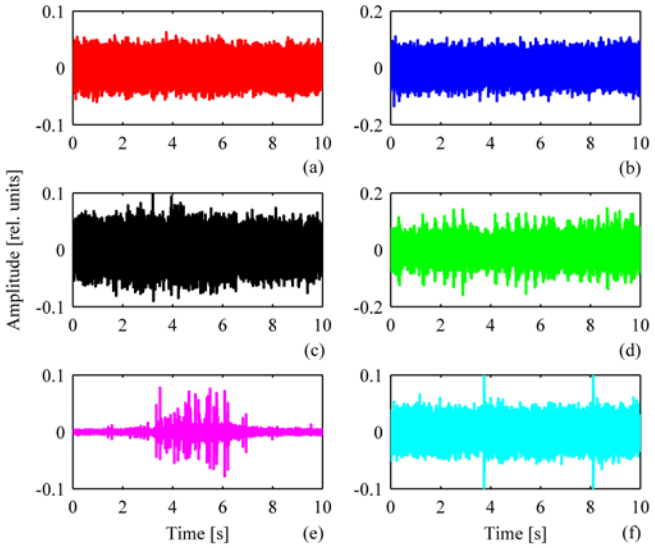


Fig 3. Audio signals (sounds) of industrial products in time domain: (a) fan, (b) gearbox, (c) slider, (d) toycar, (e) toytrain and (f) valve.

Spectra of the signals from Fig. 3 are presented in Fig. 4. In the frequency domain, the situation is rather different and differences between spectra are more prominent than in the time domain. Again, like in the time domain, the sound of toytrain product sound stands out from the others (see Fig. 4). The trend in spectra for all other products is similar in the frequency range above 125 Hz, where the maximum deviation of any spectra of these products is not greater than approximately 10 dB. On the other hand, the spectrum of toycar shows a significant rolloff below 125 Hz, which is not the case with spectra of other products.

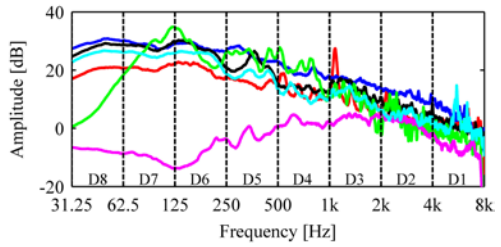


Fig 4. Spectra of audio signals (sounds) of industrial products (the same colors are used as in Fig. 3).

The results obtained in the frequency domain indicate a very favorable trend of what could happen when the signal decomposition by the discrete Meyer wavelet is done. In Fig. 4, the areas from D1 to D8 (from right to left) are also indicated. Those areas are related to the frequency ranges of the detail wavelet coefficients after decomposition at a particular level. Thus, the frequency range from 4 kHz to 8 kHz is correlated with the detail coefficients at the decomposition level 1 (D1). At the next decomposition level, the lower frequency range (up to 4 kHz) is split into two halves, so that the detail coefficients at the decomposition level 2 (D2) are extracted from the frequency range from 2 kHz to 4 kHz. This trend continues through the next decomposition levels [9] up to the last one, which is here the level 8. For all 8 decomposition levels, the related frequency ranges are given in Table I.

The illustration of the product sound characteristics in both time and frequency domain is given through the spectrograms presented in Fig. 5. The trend seen in the spectra given in Fig. 4 of the level reduction with frequency is also visible in the spectrograms. However, here some unique time-stamps of the signals are stressed, such as fluctuation in time of the slider or non-stationary amplitude of the toytrain.

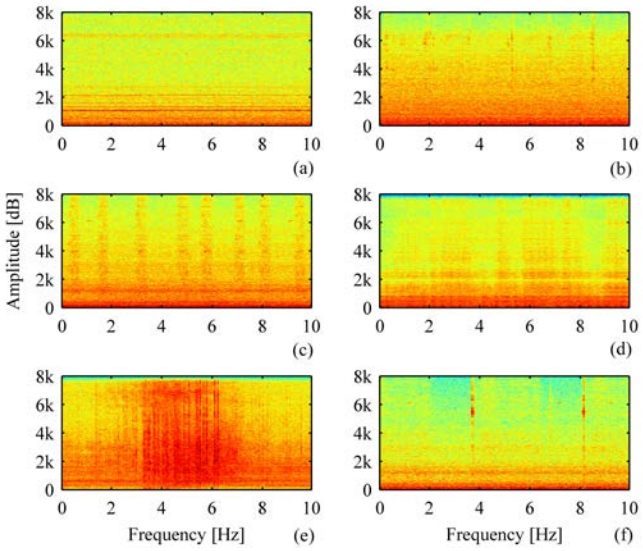


Fig 5. Spectrograms of audio signals (sounds) of industrial products: (a) fan, (b) gearbox, (c) slider, (d) toycar, (e) toytrain and (f) valve.

TABLE I
DEPENDENCE OF THE WAVELET DECOMPOSITION LEVEL TO THE FREQUENCY RANGE

| Decomposition level | Frequency range |
|---|---|
| 1 | 4 kHz – 8 kHz |
| 2 | 2 kHz – 4 kHz |
| 3 | 1 kHz – 2 kHz |
| 4 | 500 Hz – 1 kHz |
| 5 | 250 Hz – 500 Hz |
| 6 | 125 Hz – 250 Hz |
| 7 | 62.5 Hz – 125 Hz |
| 8 | 31.25 Hz – 62.5 Hz |

After analysis in the time and frequency domain, the chosen signals are decomposed using the discrete Meyer wavelet. Fig. 6 presents the values of the extracted wavelet-based feature for all six products, that is, signals whose time and frequency representations are given in Figs. 3, 4 and 5. All signals are segmented, wavelet decomposed and then the mean value of the absolute values of the obtained detail coefficients is calculated for each particular segment. At each decomposition level, some differences between the wavelet-based features (detail coefficients) of different products can be observed.


ISBN 978-86-7466-930-3

These differences are smaller for some decomposition levels and comparing certain products, while they are larger at some other levels and for some other products. Also, the stationarity of the features of different products is not the same, and it might be used as one more parameter for differentiating the products. The previously mentioned emphasizes the need to make a more detailed analysis between the signals and the detail coefficients (wavelet-based features).

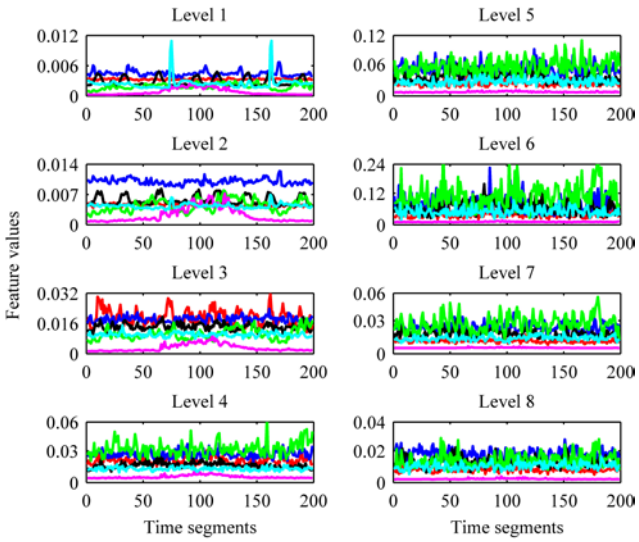


Fig 6. Wavelet-based features generated from the detail coefficients obtained after applying discrete Meyer wavelet to segmented signals and using the decomposition levels from 1 to 8.

In Tables II and III, the numerical values of the feature difference measure are summarized, where indexes in the numerical values represent the level of decomposition from which that specific case is obtained. These differences can be used to consider more closely the relations between particular products. Table II presents the feature differences between the products belonging either to the same class or different classes, where these differences are prominent. On the other hand, Table III presents the feature differences between the products where the differences are rather small when the products belong to the same class, but also when the products belong to different classes.

TABLE II
PROMINENT DIFFERENCES BETWEEN INDUSTRIAL PRODUCT SOUNDS REGARDING THE FEATURE DIFFERENCE MEASURE

| *Diff.* | f | g | s | tc | tt | v |
|---|---|---|---|---|---|---|
| f | $0.79_1$ | $1.12_2$ | $1.15_2$ | $1.35_7$ | $1.76_8$ | $1.01_2$ |
| g | $1.12_2$ | $0.86_4$ | $1.13_1$ | $1.32_1$ | $1.84_6$ | $1.24_4$ |
| s | $1.15_2$ | $1.13_1$ | $0.76_2$ | $1.31_6$ | $1.91_6$ | $0.85_1$ |
| tc | $1.35_7$ | $1.32_1$ | $1.31_6$ | $0.84_2$ | $1.91_7$ | $1.36_6$ |
| tt | $1.76_8$ | $1.84_6$ | $1.91_6$ | $1.91_7$ | $1.06_5$ | $1.73_8$ |
| v | $1.01_2$ | $1.24_4$ | $0.85_1$ | $1.36_6$ | $1.73_8$ | $1.03_3$ |

TABLE III
SMALL DIFFERENCES BETWEEN INDUSTRIAL PRODUCT SOUNDS REGARDING THE FEATURE DIFFERENCE MEASURE

| *Diff.* | f | g | s | tc | tt | v |
|---|---|---|---|---|---|---|
| f | $0.007_8$ | $0.005_2$ | $0.009_3$ | $0.008_1$ | $0.24_2$ | $0.004_5$ |
| g | $0.005_2$ | $0.002_2$ | $0.001_7$ | $0.005_2$ | $0.84_3$ | $0.002_4$ |
| s | $0.009_3$ | $0.001_7$ | $0.001_6$ | $0.03_2$ | $0.71_2$ | $0.001_2$ |
| tc | $0.008_1$ | $0.005_2$ | $0.03_2$ | $0.005_7$ | $0.53_2$ | $0.001_2$ |
| tt | $0.24_2$ | $0.84_3$ | $0.71_2$ | $0.53_2$ | $0.001_1$ | $0.5_2$ |
| v | $0.004_5$ | $0.002_4$ | $0.001_2$ | $0.001_2$ | $0.5_2$ | $0.007_8$ |

Analyzing Table II, it can be concluded that the smallest feature difference is obtained within the same class, that is going along the diagonal except for the product valve denoted as “v”, which has slightly smaller values for fan and slider meaning that this feature of the valve is more similar to the feature of those two products - fan and slider. But, in other products, it can be clearly seen that the features are much more similar within the class than between the classes.

The trend seen in Table II can not be seen in Table III where the features differences are rather small independently whether the compared products belong to the same class or different classes. The only exception is the product toytrain that has considerably larger feature differences when the product is compared to other product belonging to other classes. All these trends seen in the feature difference measure are in line with the noticed specific properties of spectra of these products.

Fig. 7 presents the feature differences from Tables II and III in the plot format. Differences having moderate values (called prominent differences) are given by blue curves, while small differences are given by red curves. Here, Fig. 7(b) presents only 6 cases randomly extracted from Tables II and III used to illustrate prominent and small differences between the classes. The values for prominent differences are smaller within the same class, Fig. 7(a) and diagonal elements of Table II, in comparison with the values between the classes, Fig. 7 (b). On the other hand, the values for small differences are rather small independently whether are calculated within the same class or between the classes except for the toytrain as discussed above. The latter shows that the differences of the wavelet-based feature between the classes can be small in some extreme cases representing minority of all cases.

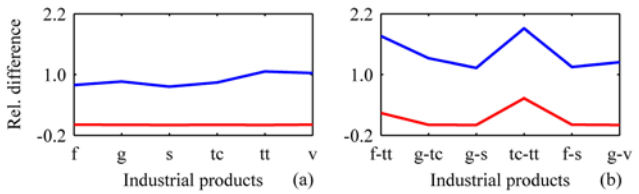


Fig 7. Differences between wavelet-based features (values of the feature difference measure): (a) prominent (blue) and small (red) differences between signals from same class, (b) prominent (blue) and small (red) differences between signals from different classes (products).

It is beneficial to look at the differences in the obtained detail coefficients (wavelet-based features) from different

 ISBN 978-86-7466-930-3

angles. As in all other cases of the wavelet-based features presented here, these features are obtained by applying the discrete Meyer wavelet to each signal segment. Fig. 8 presents prominent differences in the detail coefficients at some decomposition levels between the signals from same class (the same product type). The level of decomposition and class are indicated in the title of each graph, as it is also done for next figures of the same type. The blue curve is related to the first signal (product), while the red curve is related to the second signal (product). The presented differences are obvious, like the ones given in Table II.

A rather specific situation is presented for the toycar in Fig. 8, where the detail coefficients of these two toycar signals differ in a part of the segments (part of the signal), while this is not the case in the rest of the segments (rest of the signal) where the differences are negligible.

The opposite case is given in Fig. 9 presenting the negligible differences between the detail coefficients obtained from the signals belonging to the same class (the same type of industrial product). This figure can be used as a graphical confirmation of the results listed in Table III.

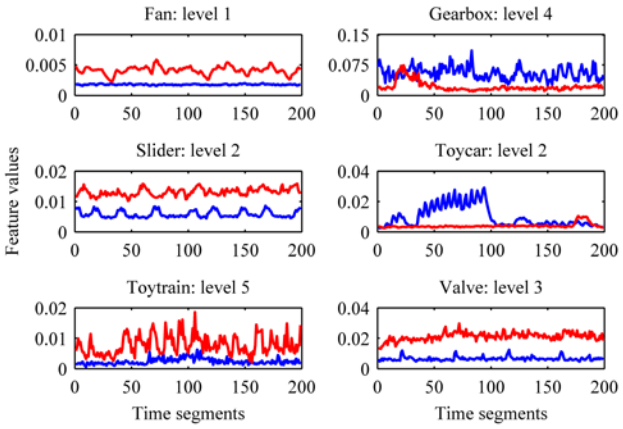


Fig 8. Wavelet-based features generated from the detail coefficients after applying discrete Meyer wavelet to segmented signals obtained for signals from the same class (type of industrial product); the case where the differences are obvious.

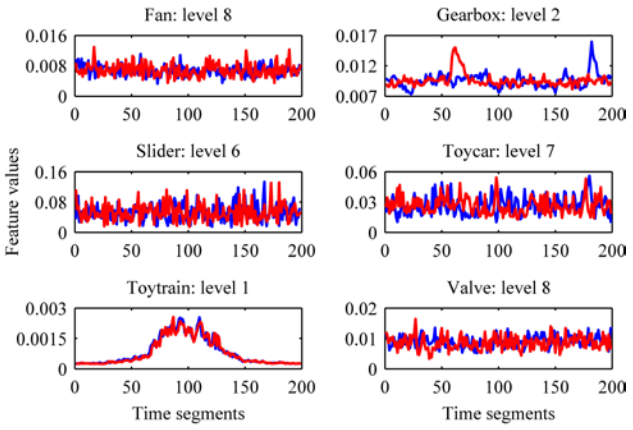


Fig 9. Wavelet-based features generated from the detail coefficients after applying discrete Meyer wavelet to segmented signals obtained for signals from the same class (type of industrial product); the case where the differences are negligible.

Fig. 10 presents some illustrative examples of the wavelet-based features - detail coefficients at particular levels of decomposition where the differences between the signals from different classes (types of industrial products) are obvious. Those difference are rather prominent, and they are greater than differences seen between the products belonging to the same class. Smaller differences between the detail coefficients (wavelet-based features) for signals from different classes (types of industrial products groups) are shown in Fig. 11. The found differences could not be considered to be negligible. They are smaller than those given in Fig. 10, but greater than those given in Fig. 9. What is also worth mentioning is that these wavelet-based features have some specific behavior along the time axis. For some of the classes (product types), such as the toytrain and toycar, it is not an easy task to find small differences between the wavelet-based features. These signals are not as stationary in time as other signals, and this is why their wavelet-based features show significant fluctuations of values along the time axis, that is, going through the segments.

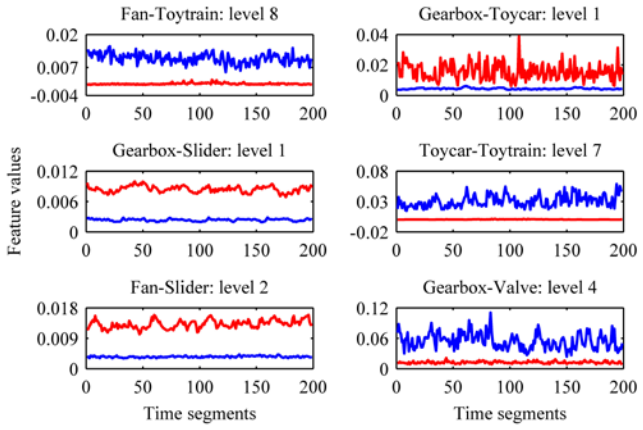


Fig 10. Wavelet-based features generated from the detail coefficients after applying discrete Meyer wavelet to segmented signals obtained for signals from different classes (types of industrial products) (extracted illustrative examples); the case where the differences are obvious.

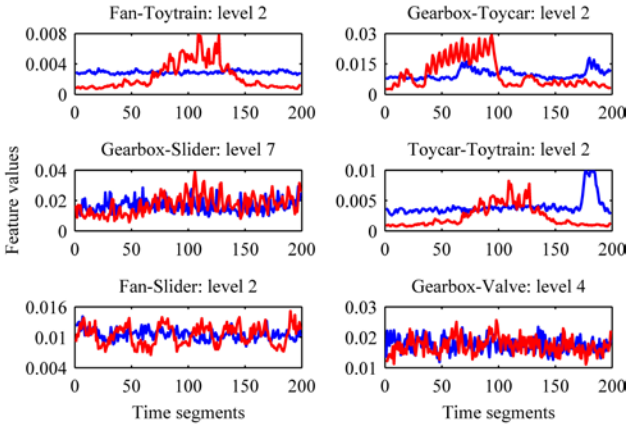


Fig 11. Wavelet-based features generated from the detail coefficients after applying discrete Meyer wavelet to segmented signals obtained for signals from different classes (types of industrial products) (extracted illustrative examples); the case where the differences are small.


ISBN 978-86-7466-930-3

Analyzing Figs. from 8 to 11, it can be concluded that the presented prominent differences between the wavelet-based features are related to the cases when the feature curves differ from each other, while the negligible differences are related to the cases where the feature curves are overlapped (or close to each other) in the majority of time segments.

## V. CONCLUSION

Wavelets represents a technique that is more and more popular nowadays in diverse application including audio feature extraction. Since there are a number of different wavelet families, it is a rather difficult task to select the most appropriate one for a particular purpose. This paper presents usage of the discrete Meyer wavelet in signal decomposition to approximation and detail coefficients, where the latter are used as the wavelet-based features. The goal is to get relevant audio features able to provide a large enough distinction among industrial products based on sound they generate.

More than 100 sound samples of industrial products (machines) belonging to six different classes are used in this study. The decomposition of every sound using the discrete Meyer wavelet goes from level 1 to level 8. All signals are first segmented, where the overlap between two segments is 50% of the segment length.

In this phase of the research, only manual numerical and graphical analysis is performed. The results show that the detail coefficients used as a wavelet-based feature provide a significant difference between the classes (types of industrial products) in majority of cases. Certain differences exist even between the sound samples from the same class, but typically they are smaller than the ones between the classes. Some illustrative examples showing small differences both within the same class and between different classes are identified and presented. This confirms that even when different industrial products are analyzed, it is possible to get very similar characteristics in the time and frequency domain, but also in the domain of audio features (in this case wavelet-based feature). This is why a more detailed analysis of statistics of the extracted wavelet-based features will be done in the next phase of the research.

## ACKNOWLEDGMENT

This study was supported by the Ministry of Education, Science and Technological Development of the Republic of Serbia (the results are parts of the Grant No. 451-03-68/2022-14/200132 with University of Kragujevac - Faculty of Technical Sciences Čačak and University of Niš - Faculty of Electronic Engineering) as well as by the Science Fund of the Republic of Serbia, 6527104, AI-Com-in-AI.

## REFERENCES

[1] M. Sifuzzaman, M. R. Islam, M. Z. Ali, “Application of wavelet transform and its advantages compared to Fourier transform”, Journal of Physical Sciences, vol. 13, pp. 121-134, 2009.

[2] R.J.E. Merry, “Wavelet Theory and Applications: a literature study”, Technische Universiteit Eindhoven, Eindhoven, June 7, 2005.

[3] S. Berry, “Practical wavelet signal processing for automated testing”, AUTOTESTCON, International Automatic Testing Conference, pp. 653-660, San Antonio, TX, USA, 30 Aug.-2 Sept. 1999.

[4] B. Ergen, “Signal and image denoising using wavelet transform”, Chapter 21 in: Advances in wavelet theory and their applications in engineering. Physics and Technology, In-Tech (2012), pp. 495–515.

[5] Đ. M. Damnjanović, D. G. Ćirić, B. B. Predić, “De-Noising of a Room Impulse Response by Applying Wavelets”, Acta Acustica United With Acustica, Journal of the European Acoustics Association (EAA) - International Journal on Acoustics, Vol. 104, No. 3, pp. 452 – 463, May/June 2018.

[6] G. Kaushik, H.P. Sinha, L. Dewan, “Biomedical signals analysis by dwt signal denoising with neural networks”, Journal of Theoretical and Applied Information Technology, Vol. 62, No.1, pp. 184 – 198, 10th April 2014.

[7] Đ. Damnjanović, D. Ćirić, Z. Perić, “Analysis of DC Motor Sounds Using Wavelet-Based Features”, Proceedings of the 6th International Conference on Electrical, Electronic and Computing Engineering “(Ic)ETRAN 2019”, Srebrno jezero, ISBN 978-86-7466-785-9, pp. 17-22, Serbia, June 3 - 6, 2019.

[8] Đ. Damnjanović, D. Ćirić, M. Miletić, D. Vujičić, “Usage of Different Wavelet Families in DC Motor Sounds Feature Analysis”, Proceedings of the 7th International Conference on Electrical, Electronic and Computing Engineering “(Ic)ETRAN 2020”, Belgrade, Niš, Novi Sad and Čačak, Serbia, pp. AKI 1.2.1-1.2.6., September 28 - 30, 2020.

[9] Đ. Damnjanović, D. Ćirić, Z. Perić, “Wavelet-Based Audio Features of DC Motor Sound”, FACTA UNIVERSITATIS, Series: Electronics and Energetics, vol. 34, no. 1, pp. 71–88, March 2021.

[10] M. Misiti, Y. Misiti, G. Oppenheim, J.-M. Poggi, Wavelet Toolbox for Use with MATLAB, COPYRIGHT 1997–2019 by The MathWorks, Inc.

[11] D. Radunović, Wavelets - from Math to Practice, Belgrade, Serbia: Springer with Academic Mind, 2009.

[12] IEEE AASP Challenge on Detection and Classification of Acoustic Scenes and Events (DCASE) 2021 (Task2): https://dcase.community/challenge2021/index.

[13] S. Mallat, A Wavelet Tour of Signal Processing, Academic Press, Elsevier Inc., October 9, 2008.

[14] V. V. Valenzuela, H. M. de Oliveira, “Close expressions for Meyer Wavelet and Scale Function”, XXXIII Simpósio Brasileiro de Telecomunicacoes SBrT 2015, January 2015.

[15] T. Xudong, L. Xinyuan, D. Yiqing, L. Jianru, “Design of Orthonormal Filter Banks based on Meyer Wavelet”, International Journal of Advanced Computer Science and Applications (IJACSA), Vol. 6, No. 7, 2015.

[16] M. C. Sezgin, B. Gunsel, G. K. Kurt, "Perceptual audio features for emotion detection", EURASIP Journal on Audio, Speech, and Music Processing, No. 16, pp. 1-21, 2012.

[17] A. Glowacz, "Diagnostics of direct current machine based on analysis of acoustic signals with the use of symlet wavelet transform and modified classifier based on words", Eksploatacja i Niezawodnosc – Maintenance and Reliability, vol. 16, no. 4, pp. 554-558, 2014.

[18] A. Glowacz, "DC Motor Fault Analysis with the Use of Acoustic Signals, Coiflet Wavelet Transform, and K-Nearest Neighbor Classifier", Archives of Acoustics, vol. 40, no. 3, pp. 321-327, 2015.

[19] The MathWorks, Inc., “Wavelet filters”. [Online]. Available: https://www.mathworks.com/help/wavelet/ref/wfilters.html

[20] G. Tzanetakis, G. Essl, P. Cook, "Audio Analysis using the Discrete Wavelet Transform", In Proceedings of the WSES International Conference Acoustics and Music: Theory and Applications (AMTA 2001), pp. 318-323, Skiathos, Greece, January 2001.

[21] Y. Shi, G. Wang, J. Niu, Q. Zhang, M. Cai, B. Sun, D. Wang, M. Xue, X. D. Zhang, "Classification of Sputum Sounds Using Artificial Neural Network and Wavelet Transform", International Journal of Biological Sciences, vol. 14, Issue 8, pp. 938-945, 2018.

 ISBN 978-86-7466-930-3

# Multidisciplinarnost u istraživanju slike i zvuka u sakralnom prostoru

Jelena Erdeljan, Ljubica Vinulović

***A stra t*— Multidisciplinarnost u istraživanju studija vizuelne ulture u poslednje dve decenije imala je ljučnu ulogu. ombinovanje metoda različitih naučnih oblasti poput istorije umetnosti, etnologije, istorije liturgi e,muzi ologije, digitalnih tehnologija i inženjerstva, posebno inženjera akustike doprinelo je potpunijem razumevanju odnosa oji su zvu i sli a imali u obli ovanju sa ralnog prostora srednjove ovne cr ve. njiga Bisere Penčeve *Ic ns nd ce Arc tect re and Ima nat n n ed e a Art*, pruža podatke o višegodišnjim istraživanjima odnosa sli e i zvu a i njihovoj ulozi u re reaciji autentičnog srednjovekovnog akustičnog ambijenta.**

***Ključne reči*—multidisciplinarnost; sli a; zvu ; sa ralni prostor; vizuelna ultura, auralnost**

## I. UVOD

Novija istraživanja vizuelne kulture tj. slike (*imago*), prevazilaze tradicionalne okvire ikonografskih pa i ikonoloških studija, koje su, izvesno, značajno doprinele njenom proučavanju. Ona danas uključuju široki opseg materijala koji se proučava kao što su predmeti vizuelne kulture, efemerni spektakli, film, televizija, opera, pozorište, multimedijalne instalacije, video igre, a oslanjaju se na metode i istraživačke postupke velikog broja disciplina – od istorije umetnosti preko studija kulture, performativnosti, do muzikologije i etnolmuzikologije, te psihologije muzike i kognitivnih neuro-nauka.

Knjiga profesorke Bisere Penčeve, profesorke istorije vizantijske umetnosti sa univerziteta Stenford (SAD), *Ikone uka* ( u originalu *Icons of Sound*: *oice, Architecture, and Imagination in Medie al Art*), predstavlja zbornik tekstova od izuzetnog značaja za proučavanje performativnosti tj. odnosa između slike i zvuka u sakralnom prostoru srednjovekovne crkve [1]. Eseji autora govore o višegodišnjim istraživanjima u okviru projekta profesorke Penčeve koji ona vodi od 2008. godine na Stenford Univerzitetu. Ključ istraživanja odnosa i slike i zvuka leži u multidisciplinarnom i interdisciplinarnom pristupu. Na projektu je okupljen tim vodećih stručnjaka iz različitih naučnih oblasti kao što su istorija umetnosti,etnologija, istorija liturgike, muzikologija, digitalne tehnologije i inženjerstvo, a posebno inženjeri koji se bave pitanjem akustike [2]. Njihova zajednička istraživanja doprinela su formiranju krajnjeg cilja projekta a to je kako umetnost i slika postaje oživotvorena putem zvuka i glasa. Merenja zvuka u crkvi Svete Sofije u Carigradu doprinela su jasnijem razumevanju na koji način se zvuk kretao kroz prostor crkve i kako se u vidu „vodopada“ odbijao od pojedinih tačaka u crkvi, na koji način je to oživljavalo mozaike i ono što je najvažnije, kako je to sadejstvo slike i zvuka imalo uticaj na doživljaj vernika [3]. Istraživanja na ovom projektu pokazala su da je putem zvuka slika prestajala da bude dvodimenzionalna i da je oživljavala pred očima vernika. Angažovanje profesionalnog hora Kapela Romana čiji su pojci pojali iz originalnih sačuvanih srednjovekovnih notnih zapisa omogućilo je ovom timu stručnjaka da rekreira autentičan akustični ambijent srednjovekovnih sakralnih prostora, pre svega sakralnog prostora Svete Sofije. Današnja dostignuća digitalne tehnologije omogućila su da se izvođenje liturgije i različitih služni služenih na originalnom grčkom jeziku snimi i postavi na youtube kako bi se ljudi mogli da osete deo autentične srednjovekovna atmosfere [4]. Istraživanja predstavljena u radovima obuhvataju izuzetno veliku geografsku širinu, od srednjovekovne Francuske, Španije i Italije do Vizantije i Jermenije. Hronološki raspon obuhvaćen u radovima je od 9. do 16. veka.

## II. METOD

Metodologija studije vizuelne kulture kombinovana je sa metodologijom studija muzikologije, istorije liturgike, etnologije i inženjeringa s obzirom na to da su njihovi rezultati a posebno rezultati muzikologije i inženjeriga opipljivi i empirijski ih je moguće izmeriti i zabeležiti [1]. Rezultati obrađeni u okviru ove knjige su čistoća zvuka, rasipanje zvučne energije, jačina zvuka i njegova reverberacija. Merenje, prikupljanje i obrada ovih podataka omogućilo je kreiranje akustičnog modela odabranih sakralnih prostora i stvaranje njihove auralne atmosfere, kao što je to slučaj sa Svetom Sofijom. Ova istraživanja omogućena su upravo uključivanjem hora Kapela Romana koji je pojao određene originalne srednjovekovne službe od kojih su neke od njih posebno pisane za Svetu Sofiju. Merenja su vršena tokom njihovog pojanja i istraživači su mogli da utvrde kojom brzinom zvuk putuje kroz prostor crkve, koja mu je jačina u određenim tačkama prostora kao i koliko traje revebreracija [3]. Ovakva istraživanja nisu mogla da budu obavljena bez uključivanja inženjera čija je uska specijalnost akustika. Njihova istraživanja spojena sa vizuelnom kuluturom su istoričari umetnosti, muzikolozi i istoričari liturgike stavili u

Jelena Erdeljan – Odeljenje za istoriju umetnosti, Filozofski fakultet, Univerzitet u Beogradu, Čika Ljubina 18–20, 11000 Beograd, Srbija (e-mail: jerdelja@f.bg.ac.rs).

Ljubica Vinulović – Odeljenje za istoriju umetnosti, Filozofski fakultet, Univerzitet u Beogradu, Čika Ljubina 18–20, 11000 Beograd, Srbija (e-mail: ljvinulovic91@gmail.com).

 ISBN 978-86-7466-930-3

kontekst i dali su im interpretaciju kako bi rekonstruisali i oživeli prošlost.

## III. GLAVNI REZULTATI

Knjiga je podeljena na tri „neopipljiva“ aspekta koji su međusobno povezani. To su liturgijski glas (liturgijsko pojanje), zvučni identitet prostora i reverberacija. Ova tri aspekta zajedno čine auralnu dimenziju sakralnog prostora koja komunicira sa slikama na zidu [2]. Tehnička merenja jačine zvuka i njegove reverberacije omogućila su da se rekonstruiše autentična atmosfera srednjovekovnih sakralnih prostora. Digitalni zapisi omogućili su da se ljudi bliže upoznaju sa akustikom srednjovekovnih prostora od kojih je danas veliki broj „gluv“ prostor s obzirom na to da se tu više ne vrše službe ili su oni pretvoreni u muzeje ili džamije kao što je to danas slučaj sa velikim brojem vizantijskih crkava. Sva istraživanja povezana su sa krajnjom svrhom liturgijskog pojanja i slika svete istorije u crkvi, a to je spasenje kroz realno Božije prisustvo koje se ogleda upravo u zvuku i slici. U ovom doživljaju su pored cula sluha, ogromnu ulogu imala i druga ljudska čula kao i ljudska psiha i moć imaginacije. Nekoliko radova fokusirano je na sferu imaginalnog i taktilnog, kao ključne aspekte za rekonstrukciju korelacije zvuka i slike a u cilju da se spasenje definiše u pojmu auralnosti koji omogućava da se Bog čuje [2].

Kroz radove se istražuje odnos između zvuka, umetnosti i arhitekture i njihovi zajednički uticaj na ljudsku imaginaciju i doživljaj sakralnog prostora [1,5]. Ključno pitanje ovih radova je koju je ulogu zvuk imao u pojanju u sakralnom prostoru i njegovom oblikovanju kao i u percepciji metafizičkog i aktiviranju veze između fizičke slike i imaginacije. Još od vremena autora iz ranog srednjeg veka kao što je Sveti Benedikt hor monaha koji poje predstavljao je odraz hora anđela. Pojanje u okviru sakralnog prostora simboliše prisustvo anđela kao i Boga koji prebiva u okviru crkve ili manastira. Na ovaj način su vernici istovremeno slušajući pojanje i gledajući slike ostvarivali kontakt sa Bogom.

Francisko Prado–Vilar jedan od autora posebno se u svom radu fokusirao na moć imaginacije i ulogu koji zvuk kako imaginarni tako i realni ima u tome [6]. Predmet njegovog istraživanje je takozvani Porta Francigena, severni portal hodočasničke crkve Santijago de Kompostela koji se nalazi u Galiciji na severu današnje Španije. Ova crkva u kojoj se čuvaju mošti Svetog Jakova Zavedejeva jednog od dvanaest Hristovih učenika u srednjem veku je pored Jerusalima i Rima predstavljao jednu od najvažnijih hodočasničkih tačaka i krajnji cilj hodočasnika na zapadu. Svoju pažnju je posebno fokusirao na mermerni stub. Na njemu su u vidu friza duž celog stuba u nekoliko registra predstavljene scene iz Odiseje. U pitanju je antička scena *Nostos* koja priča priču o Odisejevom povratku kući na rodnu Itaku i poteškoćama koje su zadesile Odiseja i njegovu posadu tokom putovanja. Na stubu je posebno istaknut Odisejev susret sa sirenama i morskim nemanima Scilom i Haribdom na uzburkanom moru. Stub je nekada činio sastavni deo severnog portala koji je predstavljao glavni ulaz za hodočasnike koji su dolazili na poklonjenje moštima Svetog Jakova. Predstave sa stuba komunicirale su sa scenama koje su se nalazile na timpanonu portala. To su Stvaranje Adama i Adamov izgon iz Raja kao i Blagovesti Bogorodici. Autor posebno ističe moć taktilnog u ljudskoj imaginaciji, s obzirom na to da su hodočasnici mogli da dodirnu stub i uzborkane talase mora koji su isklesani na njemu i na taj način da evociraju šum i miris mora. U tome im je umnogo pomagao prirodni ambijent i prirodni zvukovi jer se sama crkva nalazi na obali Atlantskog okeana. Realni šum i miris okeana bili su okidači za kontemplaciju vernika pred ovim portalom na kojem je noseća tema putovanje kući, koje u hrišćanskoj interpretaciji predstavlja putovanje čoveka u porazi za iskupljenjem čoveka, njegovo pomirenje i susret sa Bogom i povratak u Raj. U rekreaciji ovog susreta čoveka i Boga ključnu ulogu imao je zvuk vode, kiše i vetra koji je oživljavao Božiji glas i njegovo realno prisustvo u scenama na portalu. Ljudska čula zajedno sa slikom i zvukom kako prirodnim tako i imaginarnim oblikuje sakralni prostor u kojem se pred očima vernika prepliću realno i metafizičko.

## IV. ZAKLJUČAK

Uloga zvuka imala je ključnu ulogu u aktivaciji slike kreirajući na taj način sakralnu dramu u kojoj su uslgu imali pojci, svečtenici, slike na zidovima crkava i vernici koji su prosustvovali liturgiji i drugim sakralnim obredima za koje su pisane posebne službe. Odnos zvuka, slike i osvetljenja oživljavao je sakralni prostor u kojem prebiva Bog i Božija sila. Zvučna atmosfera srednjovekovnih crkava stvaranja je kroz pojanje i molitve. Slike i osvetljenje prostora predstavljale su neizostavni deo ove atmosfere. Tokom merenja utvrđeno je da su se određeni tonovi sa određenim slogovima odbijali od određenih tačaka na mozaicima ili freskama [3]. Na ovaj način su dodatno davali život ovim slikama. U sadejstvu zvuka sa osvetljenjem stvaran je pokret i tako su vernici pred svojim očima videli žive, oživotvorene svetitelje i postajali su realni svedoci svete istorije koja je predstavljena na zidovima crkve u vidu mozaika ili fresaka. Ova međusobna povezanost zvuka, slike i osvetljenja predstavlja štimung jednog sakralnog prostora.

## LITERATURA

[1] B. V. Pentcheva, *Icons of Sound oice, Architecture, and Imagination in Medie al Art*, 1th ed. New York, NY: Routl, 2021.

[2] B. V. Pentcheva, *Aural Architecture in By antium Music, Acoustic, and itual*, 1th ed. New York, NY: Routl, 2018.

[3] B. V. Pencheva, “The Glittering Sound of Hagia Sophia and Feast of the Ecalation of the Cross in Constantinople,” in *Icons of Sound oice, Architecture, and Imagination in Medie al Art*, ch. *3*, pp. 52–100, New York, NY: Routl, 2021.

[4] F. Prado–Vilar, “The Marble Tempest: Material Imagination, the Echoes of Nostos, and the Transfiguration of Myth in Romanesque Sculpture”, in Icons of Sound: Voice, Architecture, and Imagination in Medieval Art, ch. , pp. 152–205, New York, NY: Routl, 2021.

 ISBN 978-86-7466-930-3

[5] B. V. Pencheva, “Introduction,” in *Icons of Sound oice, Architecture, and Imagination in Medie al Art*, pp. 1–18, New York, NY: Routl, 2021.
[6] D. Howard, “Sound, Space, and the Sensory Perception: The Eastern Mass in the Liturgy of San Marco, Venice,” in *Icons of Sound oice, Architecture, and Imagination in Medie al Art*, ch. , pp. 135–151, New York, NY: Routl, 2021.

ABSTRACT

The multidisciplinary approach to the research in the field of study of visual culture has been prevalent over the last two decades. A combination of methods of various fields of research such as art history, ethnology, liturgical history, musicology, digital technologies and engineering, and in particular electrical and acoustical engineering, has contributed to a more encompassing understanding of the relation between image and sound in the shaping of the sacral space of medieval churches. The volume *Icons of Sound oice, Architecture and Imagination in Medie al Art* edited by Bissera Pentcheva offers insight into years of research in the field of correlation between image and sound and their role in the process of recreating authentic medieval acoustical (aural) ambiences and bringing the past back to the present.

**ultidisciplinary approach in the study of image and sound in sacral space**

Jelena Erdeljan and Ljubica Vinulović

 ISBN 978-86-7466-930-3

# Auralizacija sakralnih prostora i likovni programi: nove perspektive i mogućnosti istraživanja

Vuk Dautović, Jakov Đorđević

***Apstrakt*—Doživljaj prisustva svetosti bio je gotovo pretpostavljeno čulno iskustvo za srednjovekovne ljude. Poslednjih decenija istraživanja uloge svetla, mirisa i performativnih aspekata likovnih programa u dočaravanju prisustva svetosti unutar srednjovekovnih crkava omogućila su nove perspektive u razumevanju sakralne vizuelne kulture. Interdisciplinarna grupa naučnika okupljena oko projekta *Soundscapes of Byzantium* doprinela je jasnijem uvidu o važnosti zvuka kada je reč o oblikovanju vizantijskih sakralnih prostora istraživanjem auralizacije osam crkava u Solunu. Ne samo da je potvrđeno kako su promene u arhitekturi i likovnim programima išle paralelno sa promenama u bogosluženju i pojanju već je utvrđena i veza između likovnih programa i akustičkih karakteristika crkava.**

***Ključne reči*—auralizacija; sakralni prostor; obred; likovni program; multidisciplinarnost; zvučna slika.**

## I. Uvod

Pozitivistička podela na jasno definisane i kruto odvojene discipline odavno se pokazala nedovoljnom za sticanje saznanja iza kojih stoje složenija pitanja o ljudskoj prirodi, kreativnom delovanju i svetu imaginarnog. Pristup svetosti i doživljaj svetog već decenijama privlače pažnju naučnika koji nominalno ne pripadu isključivo krugu antropologa. Tako se istorija religioznog slikarstva pomerila od jednostavnog objašnjenja likovnih izvedbi njihovim svođenjem na „Bibliju za nepismene“, a istorija arhitekture sakralnih zdanja od potrebe za hronološkim praćenjem promena arhitektonskih formi kvalitativno okarakterisanih kroz prizmu napretka i stagnacije. Štaviše, kada je konkretno reč o crkvama, istraživanja poslednjih godina donose sve više rezultata koji opravdavaju novu perspektivu njihovog posmatranja kao multimedialnih instalacija. Pored osnovne funkcije pružanja mesta kolektivne molitve, crkve su podizane i oblikovane sa namerom da vernicima obezbede manifestaciju prisustva svetosti i čulno učešće u njoj.

Grupa naučnika okupljena na projektu *Soundscapes of Byzantium*, imajući u vidu da glas predstavlja osnovno sredstvo molitve, postavila je kao svoj osnovni predmet istraživanja ulogu zvuka u kreiranju sakralnih prostora Vizantijskog carstva. Ovaj interdisciplinarni tim predvođen Šeron Gerstel (profesorka vizantijske umetnosti i arheologije na Univerzitetu u Kaliforniji, Los Anđeles) i Krisom Kiriakakisom (direktor Imersivne audio laboratorije na Univerzitetu Južne Kalifornije) odabrao je osam srednjovekovnih crkava u Solunu kao polaznu tačku svog ispitivanja [1]. Budići da je reč o gradu sa drevnom istorijom koji i danas čuva mesta hrišćanske molitve još od kasnoantičkog razdoblja, Solun je pružio priliku za analizu akustičkih svojstava crkava različitih perioda hiljadugodišnjeg carstva, a time i razmatanje nove pretpostavke uslovljenosti promena u arhitekturi i slikarstvu uvođenjem novina u crvenom bogosluženju i stilu pojanja [1, 2].

Vuk Dautović – Filozofski fakultet, Univerzitet u Beogradu, Čika Ljubina 18-20, 11000 Beograd, Srbija (e-mail: vukdau@gmail.com).

Jakov Đorđević – Filozofski fakultet, Univerzitet u Beogradu, Čika Ljubina 18-20, 11000 Beograd, Srbija (e-mail: jakovdj@gmail.com).

## II. Pristup istraživanju

Istraživanje sprovedeno u okviru projekta *Soundscapes of Byzantium* počiva na merenju impulsnih odziva na različitim mestima unutar crkava. Odabir odgovarajućih pozicija za izvore zvuka i mikrofone za snimanje određivan je na osnovu nekoliko kriterijuma: 1) položaju specifičnih arhitektonskih formi koje potvrđeno doprinose oblikovanju posebnih akustičkih efekata; 2) pozicijama određenih likovnih predstava koje nagoveštavaju vezu sa crkvenim pojanjem; 3) mestima koja su posebno izdvojena u vizantijskim bogoslužbenim knjigama kao tačke odigravanja specifičnih obrednih radnji. Kako bi se postigla što objektivnija kvalifikacija, merenja su ponavljana svakog dana u isto vreme, obraćajući pažnju na eventualne promene prouzrokovane različitim temperaturama i vlažnošću prostora. Sprovedena analiza dobijenih podataka omogućila je razmatranje auralne atmosfere svake sakralne građevine ponaosob, ali i komparativno sagledavanje svih osam solunskih crkva. Takođe je pridata pažnja utvrđivanju čistoće zvuka i varijacijama koje uvodi izgovorena reč u odnosu na otpevan ton, kao i razlikama koje donosi izvedba soliste nasuprot horskom pevanju. Budući da je reč o pokušaju rekreiranja originalne estetike zvučne slike i njene sinergije sa likovnim programom i arhitektonskim karakteristikama prostora, psihoakustička razmatranja predstavljala su kranji cilj analize. Prikupljeni podaci upoređeni su sa opservacijama pojaca angažovanih na projektu baš kao i pažljivo pozicioniranih slušalaca. Najzad, empirijsko sagledavanje i pojedinačne impresije omogućile su novu perspektivu za preispitivanje opisa akustičkih doživljaja zabeleženih u vizantijskim izvorima [1-3].

 ISBN 978-86-7466-930-3

Ovim merenjima prethodila su jasno formulisana metodološka stanovišta koja su na teorijskom planu pripremila i uporedila različita znanja o shvatanju zvuka i njegovoj ulozi u oblikovanju verske stvarnosti. Pošavši od premise da je savremeni čovek izložen brojnim auditivnim doživljajima i da su muzika i zvuk prisutniji od tišine, za razliku od čoveka vizantijskog doba koji se sa muzikom i pevanjem u najveličajnijem vidu mogao sresti tokom bogosluženja u samim crkvama ali i tokom molitvenih procesija koje su hristijanizovale spoljni prostor, te tokom kojih su svi senzorni aspekti bili jednako važni, udruživši vizuelnost, auditivno i olfaktorno u performativnom činu krsnog hoda ili litije. Konačno sama crkva shvaćena je kao muzički instrument odnosno „rezonantna kutija“ koja zvuku kroz svoja akustička stvojstva daje konačan pečat [3, 5].

Teorijsko poznavanje tumačenja auditivnog, pre svega teoloških spisa i patristike istočne crkve uporedo je posmatrano sa akustičkim mogućnostima solunskih crkava shvatanih kao odraz „nebesa na zemlji“. Upravo je veza sa mističnom teologijom istočne crkve i poznavanje angelologije kao teološke discipline koja se bavi karakterom i prirodom bestelesnih nebesnih sila u fokus stavila zvuk kao neposredni emanator nevidljivog sveta, što potvrđuju brojni istorijski izvori. Važna ideja na kojoj počiva recepcija zvuka bogosluženja jeste učenje po kome se nebeska i zemaljska liturgija odvijaju istovremeno i jedinstveno na beskonačnom broju oltara. Pisanje savremenika, Solun XIV veka opisuje kao „još jedno nebo“, što je značajna polazišna osnova pri tumačenju akustičkih osobenosti njegovih hramova. Izvođenje crkvenih himni svetiteljima i pevanje psalama, karakteristični za svakodnevicu srednjevekovnog razdoblja pružali su u javnim manifestacijama pobožnosti priliku za „kolektivan emocionalni odušak“ naročito vezano za praznike povezane sa Hristovim Vaskrsenjem, te su glasnost i jauci jednako oblikovali auditivni svet medijevalnih ljudi. U tom smislu i sam grad koji je mogao biti prepešačen u vremensmom okviru od 45 minuta postaje svojevrstan muzički instrument ili rezonator u njemu proizvedenog kolektivnog zvuka [3] .

Znanja o vizantijskoj liturgici, i sve promene koje se tiču poretka molitava i pesama koje se tokom bogosluženja izvode jesu od značaja za šire tumačenje povezanosti likovnih programa i vizuelizacije izvođenja crkvenih pesama ili još detaljnije pojedinih trenutaka u liturgiji na njima prikazanih. Upravo je smeštanje određenih molitava poput *Trisvete pesme* u izabrani segment unutar sakralne topografije hrama stvaralo mogućnost da kroz načine komponovanja ali i akustička svojstva odbijanja zvuka efekte udvojenih glasova ili „anđeoskih horova“ [3, 5].

Naglašavanje muzike i auditivnog bilo je postignuto kreiranjem paralelnih narativnih scena u kojima su anđeli obučeni poput đakona sa ripidima i svicima izvodili određene molitve bivajući veza sa mističnom stvarnošću koja verniku iznova nudi „multimedijalni“ doživljaj bogosluženja. Ovakve slike javljaju se u brojnim umetničkim medijima od veza preko bogoslužbenih predmeta od metala i sveth slika, pojačavajući značaj vizuelno-auditivnog polja. Pomenuta uporišta u kulturno istorijskoj praksi vizantijskog sveta, himnografiji, liturgici te istoriji muzike i istoriji vizantijske umetnosti stavljena su u službu posmatranja crkvenog prostora kao akustičkog sistema koji prima glas kao zvučni impuls emitujuću zvuk koji je modifikovan akustičkim svojstvima same građevine. Upravo je kroz multidisciplinarnost ove vrste izvršena demonstracija načina na koje društveno-humanističke i tehničke nauke mogu doprineti polju episteme otvarajući unutar njega nove perspektive.

## III. NOVE PERSPEKTIVE

Uvođenje sve većeg broja svetiteljskih figura sa svitcima na kojima se čitaju odlomci stihova crkvene poezije, baš kao i pojava doslovne vizualizacije sastava crkvenog pesništva u vidu složenih kompozicionih rešenja i ciklusa, samo su neke od karakteristika oblikovanja likovnih programa crkava kasnijih epoha Vizantijskog carstva. Navedene predstave sa svojim naslikanim tekstovima neretko su korišćene za obeležavanje posebno važnih obrednih tačaka u hramu sa ciljem definisanja emocionalnog iskustva vernika koji prisustvuje službi. Gotovo dramski iscenirani prizori često su praćeni rečima zahvalnosti, tugovanja, radosti ili strahopoštovanja i njihovim čitanjem vernik bi ih prisvajao postajući učesnik u ritualnom rekreiranju događaja iz svete istorije prilikom liturgije. Monumentalna kompozicija Oplakivanja Hrista u crkvi Svetog Pantelejmona u Nerezima brižljivo dočarava ekspresije bola na licima aktera scene, podstičući empatiju posmatrača. Sa druge strane, figure svetih himnografa pod freskom drže u rukama poetske sastave čije čitanje ne samo da nagoveštava teološke premise ovog događaja već verbalizuje i poželjne emocionalne odgovore vernika. Međutim, budući da je reč o performativnim tekstovima, odnosno onima koji su čitani ili pevani naglas makar jednom u toku liturgijske godine, ispisane reči bile bi animirane glasom. Predstave svetih himnografa u crkvi u Nerezima nalaze se u severnoj pevnici i bile su delimično zaklonjene grupom pojaca koji su sa tog mesta pevali za vreme službe, uznoseći stihove svitaka u molitvenoj pesmi [4]. U paraklisu Hrista Hore u Carigradu, funerarnoj kapeli namenjenoj čuvanju uspomene na tu sahranjene preminule, zapadni travej nosi kupolu sa pandantifima na kojima su prikazani sveti sastavljači stihova čitanih prilikom komemorativnih službi [4]. Reči njihovih svitaka mogle su da se čuju prilikom izvedbe navedenih obreda. Stoga, likonvi programi vizantijski crkava mogli su da ukažu na konkretne prostorne tačke namenjene izvedbi pojanja, ali i na prirodu molitve, „režirajući“ pozicije okupljenih kao i njihov duhovni doživljaj [4, 5].

Kada je reč o „animiranju“ naslikanih figura, zanimljivo ispitivanje proizašlo je iz akustičke analize u crkvi Svetog Nikole Orfanosa u Solunu. Severni krak ophodnog broda originalno je bio zatvoren zidom sa zapadne strane obrazujući zasebnu kapelu prislonjenu uz jezgro crkve. Bogorodičin akatist, likovni ciklus sačinjen od ilustracija stihova himne posvećene Hristovoj majci, nekada je pokrivao sve zidove kapele izuzev istočnog zida. Danas su kompozicije Akatista

 ISBN 978-86-7466-930-3

opstale jedino na južnom zidu i to u registru koji teče neposredno iznad dva prolaza u glavnu crkvu – njen oltarski prostor i naos. Kako je reč o vizualizaciji pesničkog sastava, članove tima *Soundscapes of Byzantium* zainteresovao je odnos izvedbe pojaca i slike. Prva analiza bazirana je na ispitivanju akustičkih svojstava prostora na osnovu pojanja u samom severnom kraku ophodnog broda. Činjenica da je nekadašnja kapela izgubila originalni zid sa zapadne strane svakako je doprinela potpunoj promeni prvobitnog akustičkog okruženja i pokazalo se da je „nedostatak rezonancije podjednako nezadovoljavajuć i za pojce i slušaoce“ [4]. Premda je teško utvrditi originalnu zvučnost kapele, eksperiment pozicioniranja jednog pojca okrenutog prema istoku sa zapadne strane oltarske pregrade glavne crkve (mesta sa kojeg bi kretalo pojanje u pojedinim trenucima liturgijske službe), pokazao je da je svakako postojala svest o promišljanju akustičkih svojstava u sprezi sa osmišljavanjem likovnog programa. Istočni prolaz koji povezuje kapelu i crkvu pojačao je jačinu glasa koji je dolazio u kapelu. Na osnovu opisa iskustva prisustva bogosluženju iz izvora i dosadašnjih istraživanja kontemplativnog stanja monaha pred slikom, ukazala se mogućnost specifične zamisli pri planiranju programa: namera da se stvori utisak kao da pojanje dolazi od naslikanih figura Akatista koje su i prikazane kako pesmom proslavljaju mladog Hrista na prestolu nad lučnim prolazom [4].

Ovakve „zvučne slike“, odnosno predstave koje bi bile animirane glasom, prema istraživanju projekta *Soundscapes of Byzantium*, obeležavale su posebna mesta namenjena okupljanju kongregacije u okviru odgovarajuće službe. Nad ulazom u središnji deo naosa crkve Svetih Apostola u Solunu iz severnog kraka ambulatorijuma, koji je funkcionisao kao kapela Svetog Jovana Krstitelja, naslikana je kompozicija Božićnog tropara. Monumentalna freska obavija gornji deo lučnog prolaza prikazujući anđele koje se u pesmi spuštaju kroz otvorene nebeske vratnice i monahe koji poju podeljeni u dve grube pri dnu kompozicije (sa obe strane ulaza u naos). Kako su vizantijski pojci bili podeljeni u desnu i levu pevnicu, navedena predstava ne samo da je obeležavala mesto izvedbe službe na božićnom jutrenju, nakon čega bi svi ušli u naos, već je nudila i model okupljenima, poistovećujući posmatrače sa akterima scene. Slika je mogla da se čuje, a glasu je pružana vizija više duhovne stvarnosti gde su nebeske sile saučestvovale u obredu [4, 5].

Projekat *Soundscapes of Byzantium* uložio je posebne napore da razmotri da li je mistično tumačenje liturgije kao zajedničke službe neba i zemlje moglo da bude i doslovno opaženo čulom sluha putem postignutih akustičkih efekata [3]. Kupole, apside i svodovi, pored činjenice da prema stepenovanju svetosti predstavljaju prostore najviše sakralnosti, takođe su pojačavali i usmeravali glasove. Akustička svojstva apside doprinosila su čujnosti glasa sveštenika okrenutog prema istoku, a važnost prostora kupole i kao najrezonantnijeg dela crkve ogleda se u vizantijskim liturgijskim priručnicima koji daju instukcije da se posebni delovi službe upravo tu odigravaju [5]. Sprovedena akustička merenja na različitim pozicijama unutar solunskih crkava i psihoakustička razmatranja pružila su nove poglede kada je u pitanju sama percepcija. Zahvaljujući postojanju galerije sa pogledom na naos, crkva Proroka Ilije omogućila je uvud i u razlike prisustva bogosluženju kada se vernik nalazi na uzvišenom mestu. Utisak da je zvuk na galeriji čistiji i jasniji potvrđen je poređenjem impulsnih odziva. Iz toga proističe da su galerije, budući namenjene osobama višeg dostojanstva, omogućavale, pored neometanog pogleda na naos, i privilegovaniji položaj za slušanje [1]. Međutim, testiranjem zvuka solunskih crkva uočeni su i posebno zanimljivi akustički obrasci koje su pojci opisali kao prisustvo „bestelesnih glasova“ [3]. Prema opisu, čuli su melodijsku liniju za oktavu višu istovremeno sa sopstvenim pojanjem. Zapravo, u akustičkom smislu, ono što su čuli bio je prvi oberton iz niza kao posledicu reverberacije građevine. Zabeležen doživljaj sličan je vizantijskim teološkim opisima zajedničkog služenja liturgije nebeskih sila sa vernicima na zemlji [3].

## IV. ZAKLJUČAK

Premda je sagledavanje originalne auralizacije drevnih zdanja otežano zbog njihovih kasnijih prepravki, dogradnji i oštećenja, pri čemu je čest gubitak izvornog materijala sa svojim prirodnim svojstima reflektovanja i upijanja zvuka ostavio trajne posledice [2, 4], grupa predvođena Šeron Gerstel i Krisom Kiriakakisom donela je veoma važne rezultate i postavila dragocene smernice za buduća istraživanja. Komparativna ispitivanja osam crkava u Solunu potvrdila su visoku svest o važnosti akustike pri oblikovanje sakralnih prostora u Vizantijskom carstvu. Štaviše, promene u planu, obliku i likovnim programima vizantijskih crkava išle su paralelno sa promenama u bogosluženju i pojanju kao neraskidivi splet koji je trebalo da ostvari multisenzorno iskustvo učešća u svetosti [1, 2]. Nije slučajno da se novi tip pojanja sa mnoštvom ukrasa i težnjom ka apstrakciji pojavio u XIII veku – periodu kada počinju da se slikaju raskošne kompozicije inspirisane crkvenim pesništvom [1, 4, 5]. Projekat *Soundscapes of Byzantium* doneo je važan materijal za dalja komparativna istraživanja crkava na drugim područjima koja bi u budućnosti mogla da daju još detaljniji i dublji uvid u duhovne potrebe, kreativnost i svet imaginarnog srednjovekovnih ljudi, ali i da odrede preciznije karakteristike verske kulture na području Evrope.

## LITERATURA

[1] S. Antonopoulos, S. E. J. Gerstel, C. Kyriakakis, K. T. Raptis, J. Donahue, “Soundscapes of Byzantium,” *Speculum*, vol. 92, no. S1, pp. S321-S335, Oct., 2017.

[2] S. E. J. Gerstel, C. Kyriakakis, K. T. Raptis, S. Antonopoulos, J. Donahue, “Soundscapes of Byzantium: The Acheiropoietos Basilica and the Cathedral of Hagia Sophia in Thessaloniki,” *Hesperia*, vol. 87, no. 1, pp. 177-213, Jan.-Mar., 2018.

[3] S. E. J. Gerstel, C. Kyriakakis, S. Antonopoulos, K. T. Raptis, J. Donahue, “Holy, Holy, Holy: Hearing the Voices of Angels,” *Gesta*, vol. 6, no. 1, pp. 31-49, Spr., 2021.

[4] S. E. J. Gerstel, “Images in Churches in Late Byzantium: Reflections and Directions,” in *Visibilité et présence de l’image dans l’espace ecclesial*, ch. 6, pp. 93-120, Paris, France, Édit. de la Sorb., 2019.

 ISBN 978-86-7466-930-3

[5] S. E. J. Gerstel, “Monastic Soundspaces: The Art and Act of Chanting,” in *Resounding Images Medieval Intersections of Art, Music, and Sound*, ch. 6, pp. 135-152, Turnhout, Belgium, Brep., 2015.

ABSTRACT

The presence of the sacred was experienced by the senses in the Middle Ages. In the last decades, the research on the role of light, smell, and the performative aspects of pictorial programs in evoking the presence of holiness within the medieval churches provided new perspectives in understanding the sacral visual culture. The interdisciplinary group of scientists gathered around the project Soundscapes of Byzantium contributed to better insight into the importance that sound had in fashioning Byzantine sacred spaces by researching the auralization of the eight churches in Thessaloniki. It is not only attested that changes in architecture went hand in hand with the changes in liturgical rite and chanting but the connection between pictorial programs and acoustical characteristics of the churches has also been shown.

## Auralization of sacral spaces and pictorial programs: new perspectives and possibilities of research

Vuk Dautović, Jakov Đorđević

 ISBN 978-86-7466-930-3

# Istraživanje zvučnog ambijenta srpskih sakralnih prostora kao višemedijskog fenomena

Miomir Mijić, Miloš Bjelić, Dragana Šumarac Pavlović, Tatjana Miljković, Filip Pantelić

***Apstrakt* — Istraživanje zvučnih ambijenata u istorijskom kontekstu iznedrilo je posebnu oblast akustike nazvanu arheoakustika. Pored mnogih značajnih istorijskih objekata, tema takvih istraživanja bile su povremeno i akustičke karakteristike verskih prostora. Sintezom akustičkih, istorijskih i teoloških činjenica o srpskim sakralnim prostorima dolazi se do zaključka da je njihov koncept višemedijska tema u kojoj je zvuk samo jedna, mada važna komponenta. Da bi se dao smisao mogućnostima koje savremena akustička analiza može pružiti u tumačenju sakralnih prostora neophodno je izaći iz okvira fizike i posmatrati sadejstva zvuka sa ostalim korišćenim medijima kao što su slikarstvo, arhitekura, muzika, koreografija, svetlost. Ovaj rad razmatra mesto i ulogu akustike u kontekstu mogućih multidisciplinarnih istraživanja srpskih sakralnih prostora. Fokus se usmerava na nekoliki karakterističnih inženjerskih tema: na korelaciju impulsnih odziva i fizičkih formi sakralnih prostora, na auralizaciju zvučnog polja u njima kako bi se omogućilo izmeštanja istraživanja u laboratorijske uslove, na uticaj akustičkog ambijenta sa pozicije pojaca i sveštenika, kao i na akustičku karakterizaciju šireg fizičkog ambienta iz kojeg vernici ulaze u domen sakralnog prostora i u koji se iz njega vraćaju.**

***Ključne reči* — akustički ambijent; arheoakustika, crkve, impulsni odziv, sakralni prostor, *stage support***

## I. UVOD

Jednom prigodom neko je zanimljivo primetio da je istorija sve do dvadesetog veka zapravo bila nema. Zvuk je oko čoveka oduvek nastajao, ali i nestajao u istom trenutku, ostajući dostupan samo neposredno prisutnim oko mesta gde se javio. Zbog toga se istorijsko proučavanje nužno fokusiralo na artefakte koji traju u vremenu, na građevine, predmete i zapise, dok su zvuci koji su pratili život ljudi, kao i informacije koje su ti zvukovi nosili, ostali trajno nedostupni. Tek sa audiotehnikom, koja se pojavljuje na prelazu iz devetnaestog u dvadeseti vek, i njenim razvojem čovečanstvo i civilizacija počinju da ostavljaju reativno trajne zvučne otiske koji o minulim događajima i ljudskim odnosima svedoče na svoj način i pružaju dodatne informacije [1].

S razvojem novih tehničkih mogućnosti, neumitno se postepeno javilo zanimanje za akustičke fenomene i u istorijskom kontekstu, što je učinilo da se s vremenom izdvoji nova multidisciplinarna oblast nazvana „arheoakustika“. Njena najširа definicija kaže da se „arheoakustika bavi odnosima između ljudi i zvuka kroz istoriju“ [2]. Ilustrativna je i definicija koja naglašava upravo njenu multidisciplinarnost, i po kojoj se arheoakustika bavi „akustikom na arheološkim lokalitetima u različitim kulturama koristeći i kombinujući u svom pristupu fiziku, antropologiju i arhitekturu“ [3]. U tom kontekstu su i akustičke karakteristike srpskih crkvenih prostora povremeno bivale predmet istraživanja [4-10].

Pregledom naslova publikovanih radova u akustičkoj literaturi saznaje se da je arheoakustika došla u fokus istraživača krajem dvadesetog veka. To se može objasniti činjenicom da poslednje dekade prošlog veka koincidiraju sa eksplozivnim razvojem računara i raznih softverskih alata od značaj za tu oblast: za simulaciju zvučnog polja, za snimanje i analizu impulsnog odziva prostora, a kasnije i za auralizaciju. Postalo je jednostavno da se za razne istorijski značajne prostore dobije detaljna akustička karakterizacija. Ta mogućnost potoji čak i za prostore koji danas više ne postoje, samo ako su njihova geometrija i materijalizacija dovoljno detaljno dokumentovane.

U obilju danas dostupnih tehničkih mogućnosti nametnula se ideja traganja za širim smislom koju mogu dobiti izmerene ili izračunate akustičke informacije o prostoru, a koje su po pravilu predstavljene „autističnim“ numeričkim podacima. Naime, zvuk se uvek pojavljuje u nekom kontekstu i nosi informacije o tome koje čulo sluha čoveka dekoduje. Zvučne informacije se neumitno povezuju sa ostalim perceptivnim inputima koji se istovremeno stiču u moždanim centrima, pa je doživljaj čovekovog okruženja rezultat multisenzorske percepcije. U takvom kontekstu zvuk pod određenim okolnostima može dobiti jedan širi i složeniji smisao.

Možda najintrigantniji fenomen pojave zvuka javlja se u sakralnim prostorima. Crkvena služba koja se u njima odvija, sa vizuelnim dimenzijama prizora i narativom koji ih prati, tipičan su primer višemedijske forme koja kod ljudi aktivira mulitisenzorsku percepciju. U sakralnom prostoru zvuk je u sprezi sa drugim primenjenim medijima: slikarstvom, arhitekturom, svetlošću, muzikom, koreografijom. Da je u pitanju višemedijski efekat dokazuje, na primer, jasna razlika između doživljaja pri slušanja snimka nekog pojanja emitovanog s kućnog sistema za reprodukciju zvuka u atmosferi dnevne sobe i slušanja istog pojanja uz fizičko prisustvo službi u nekoj crkvi.

Miomir Mijić – Elektrotehnički fakultet, Univerzitet u Beogradu, Bulevar Kralja Aleksandra 73, 11020 Beograd, Srbija (e-mail: emijic@etf.rs).

Miloš Bjelić – Elektrotehnički fakultet, Univerzitet u Beogradu, Bulevar Kralja Aleksandra 73, 11020 Beograd, Srbija (e-mail: bjelic@etf.rs).

Dragana Šumarac Pavlović – Elektrotehnički fakultet, Univerzitet u Beogradu, Bulevar Kralja Aleksandra 73, 11020 Beograd, Srbija (e-mail: dsumarac@etf.rs).

Tatjana Miljković – Elektrotehnički fakultet, Univerzitet u Beogradu, Bulevar Kralja Aleksandra 73, 11020 Beograd, Srbija (e-mail: tm@etf.rs).

Filip Pantelić – Akademija tehničko.umetničkih strukovnih studija, Odsek Visoka škola elektrotehnike i računarstva, Vojvode Stepe 283, 11020 Beograd, Srbija (e-mail: filipp@viser.edu.rs).

 ISBN 978-86-7466-930-3

Razlika u doživljaju koja je u navedenom primeru prilično jasna objašnjava fenomen multisenzorske percepcije u sakralnim prostorima. Višemedijsku prirodu pravoslavne crkvene službe istoričari su razmatrali dokazujući da je u tome evidentno združeno dejstvo monumentalnog slikarstva na zidovima, zvuka pojanja i specifičnog akustičkog odziva prostora crkve koji nastaje pri takvoj zvučnoj pobudi [11]. Šaron Gerstel u jednom svom članku konstatuje: "U ovoj maloj crkvi zvuk pojanja, reči koje se izgovaraju i sakralne slike povezane su na neočekivani i sofisticiran način" [12]. Specifične efekte produžene reverberacije i mešanje različitih zvukova koji nastaju u atmosferi crkvene službe neki istoričari su prepoznavali kao „mešanje nebeskih i ljudskih glasova" [13].

U tehničkom domenu višemedijska priroda crkvene službe može se prepoznati kao najraniji pojavni oblik multimedijalnih događaja. Danas je savremena tehnologija, pogotovo ona najsofisticiranija, u multimedijalnim produkcijama prebacila poentu na tehnički spektakl, a ponekad i na spektakl tehnologije po sebi, ali sâm koncept događaja osmišljenog da podstakne multisenzorsku percepciju očigledno potiče od davnina.

Zvučna dimenzija crkvene službe zasniva se na ljudskom glasu i nekim specifičnim zvukovima koji prate određene radnje kao što su zvukovi posuda sa tamjanom, zvona, klepala. Neki istraživači srednjeg veka ukazuju da su Vizantinci bili pod uticajem zvuka i naglašavaju moguće psihološke dimenzije raznih zvučnih fenomena. U literaturi je zabeležen stav da je prijem zvuka kod publike bio faktor koji je uticao na organizaciju oslikavanja i postavljanje slika tematski povezanih sa pojanjem u određenim zonama crkve [13].

Sa aspekta fiziološke i psihološke akustike čulo sluha čoveka u predmodernom dobu bilo je isto kao i danas. To je suviše kratak vremenski period da bi evolucija unela neke fiziološke promene, što daje za pravo da se zaključci savremenih istraživanja primene i na tumačenja reakcija ljudi suočenih sa višemedijskim delovanjem sakralnih prostora u srednjem veku. Uprkos postepene promene karaktera zvučnih ambijenata, pre svega značajnom povećanju ukupnog nivoa buke u životnoj sredini nastalom od početka industrijskog doba, čulo sluha je centralno svojstvo ljudskog iskustva danas kao što je bilo i za srednjovekovnog čoveka.

Istraživanje zvučne komponente ambijenta sakralnih prostora ne može se odvojiti od njihove višemedijske prirode. To zahteva postavljanje pravih pitanja koja ne smeju biti rezultat isključivo inženjerskih shvatanja teme. Traganje za odgovorima otvara nekoliko važnih istraživačkih putanja. Prvo, to je utvrđivanje osnovnih karakteristika akustičkog odziva prostorija koji čine deo sakralnih prostora i njihovog odraza na subjektini doživljaj slušalaca. Za postojeće prostore do tog saznanja se može doći neposrednim snimanjem impulsnih odziva, a za prostore koji su vremenom devastirani ili potpuno uništeni do toga se može doći metodama simulacije zvučnog polja (ako postoje zapisi sa dovoljno informacija o njihovoj geometriji i materijalizaciji).

Drugo, to je stvaranje baze snimaka onoga što ljudi slušaju tokom službe, snimljenih na različitim mestima u crkvama različitih veličina i formi. Glavni cilj toga je stvaranje mogućnosti da se u laboratorijskim uslovima primenom auralizacije analizira priroda auditornih doživljaja u okvirima sakralnih prostora.

Treće, postoji izvestan uticaj zvučnog ambijenta na one koji pevaju, sveštenike, pojce i horove. U kontroli njihovog pevanog glasa oni se prilagođavaju onome kako sebe čuju, što zavisi od akustičkog odziva prostora. Povratna sprega koja neumitno postoji upravlja kontrolom glasa, a u ovom slučaju verovatno i na vokalnu interpretaciju.

Najzad, širi obuhvat sakralnih prostora, to jest ambijent u kome se nalaze verski objekti, ima neke svoje akustičke karakteristike. Tokom dolaska ljudi u crkvu one možda imaju ulogu u njihovoj pripremi za kompleksni doživljaj službe, a takođe predstavljaju ono što ih u zvučnom smislu dočekuje nakon završetka službe.

U ovom radu su detaljnije razmatrane četiri opisane istraživačke putanje u arheoakustičkom pristupu sakralnim prostorima i njihove veze sa tangentnim naučnim oblastima u kojim se analiziraju iste teme.

## II. IMULSNI ODZIVI SAKRALNIH PROSTORA

Od samog nastanka moderne akustike pre stotinak godina istraživanja su bila usmerena na pokušaje da se procesi u prostorijama na neki način numerički karakterišu, a sve sa ciljem da se u nekom sledećem koraku utvrde veze između dobijenih brojeva i dimenzija koje u subjektivnom doživljaju zvuka i estetike zvučne slike prepoznaje slušalac. Najveći zamah u tom domenu dalo je istraživanje koncertnih i operskih sala i pokušaji da se inženjerski izmerene veličine, što znači numerički pokazatelji, povežu sa subjektivnim doživljajem estetike onoga što slušalac čuje u sali tokom muzičkih izvođenja [14,15]. Saznanja o tome koja su stečena do danas predstavljaju dobru osnovu za istraživanje sakralnih prostora u kojima je zvuk element crkvene službe, i gde čulo sluha takođe na svoj kompleksan način vrednuje ono što prima.

Osnovni prikaz procesa u kome zvuk iz nekog izvora stiže do slušaoca je impulsni odziv prostora u kome se taj proces dešava. Zato prvi korak u istraživanju sakralnih prostora podrazumeva utvrđivanje karaktera impulsnog odziva u crkvama od interesa. Definicija impulsnog odziva podrazumeva da su u prostoru definišu pozicije izvora zvuka i prijemnika, a to su slušaoci. Njihove pozicije su relativno precizno određene liturgikom i arhitekturom crkve. Dva primera njihovih pozicija prikazani su na slici 1. Uzeti su primeri crkve Preobraženja u manastiru Pridvorica (12. vek) i crkve Vaszesenja Gospodnjeg u manastiru Mileševa (13. vek). Vidi se da postoji jasna podela na zonu u kojoj se nalaze potencijalni slušaoci i relativno lokalizovane pozicije izvora zvuka: pevnice, amvon i časna trpeza. To u izvesnom smislu pojednostavljuje pristup snimanju impulsnih odziva i svodi taj istraživački korak na relativno ograničen broj parova tačaka izvor zvuka – prijemnik zvuka.

## III. AURALIZACIJA AMBIJENTA SAKRALNIH PROSTORA

Auralizacija je termin koji je uveden kao analogija pojmu vizuelizacije, pa se može slikovito reći da je to „renderovanje" zvučnog polja [16]. Taj proces podrazumeva reprodukciju zvuka pomoću slušalica, jer je koncept zasnovan na pripremi binauralnih signala. Cilj auralizacije je da se kod slušaoca u laboratorijskim uslovima generiše auditorni događaj kakav bi

 ISBN 978-86-7466-930-3

doživeo u različitim prostorima kada bi se u njima fizički nalazio, slušajući pri tome zvučne sadržaje koji se mogu proizvoljno birati. Auralizacija omogućava rekonstrukciju onoga što se čuje u nekom prostoru bez potrebe da se u njemu fizički nalazi, i što je u istraživačkom smislu posebno važno, da se to preslušava proizvoljan broj puta.

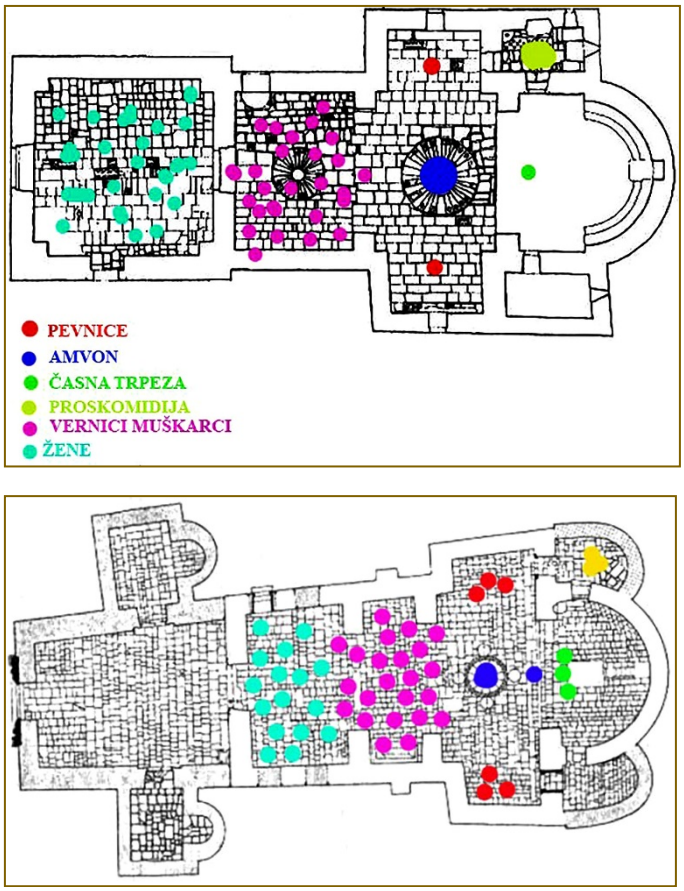


Sl.1. Osnova crkve Preobraženja u manastiru Pridvorica (gore) i crkve Vaznesenja u manastiru Mileševa (dole) sa naznačenim tačkama od značaja za snimanje impulsnih odziva.

Za auralizaciju je potrebno raspolagati binauralno snimljenim impulsnim odzivima prostora koji se želi predstaviti, a to znači sa signalima impulsnog odziva registrovanim na pozicijama levog i desnog uva neposredno prisutnog slušaoca. Takvi odzivi su označeni kao impulsni odzivi glave (HRTF – Head Related Transfer Function). Oni se u praksi dobijaju snimanjem impulsnog odziva pomoću veštačke glave ili pomoću takozvanih binauralnih mikrofona.

Veštačka glava je uređaj koji se izrađuje od tvrde gume ili sličnih materijala, i u geometrijskom smislu ima sve atribute ljudske glave [17]. Njene dimenzije i oblik kopiraju osnovnu formu prosečne ljudske glave utvrđene statistički, s posebno detaljno modelovanim ušnim školjkama. U unutrašnjosti veštačke glave, na poziciji ušiju, nalaze se mikrofoni čiji izlazni signali predstavljaju zvučne pritiske koji se javljaju na levom i desnom uvu slušaoca. Tako dobijeni signali sadrže u sebi uticaj glave kao prepreke, što je neophodno čulu sluha za dekodovanje prostornih dimenzija zvučnog polja. Veštačka glava se postavlja na stativ na poziciji gde se želi registrovati signal.

Binauralni mikrofoni su minijaiturni mikrofoni koji se postavljaju u uši poput slušalica kakve se koriste uz mobilne telefone. Kao i veštačka glava, oni daju signale koji odgovaraju onome što deluje na uši slušaoca kada se nalazi u nekom zvučnom polju. Razlika je samo u tome što se glava pravi prema statistički utvrđenim dimenzijama i sa pojednostavljenom geometrijom lica, a binauralni mikrofoni daju signale koji su personalizavani, jer se pri snimanju nalaze na realnoj osobi.

Pobuda prostora pri snimanju impulsnog odziva vrši se neusmerenim zvučnikom postavljenim na odabranoj poziciji realnog izvora zvuka, to jest sveštenika ili pojca. Preko njega se reproduku posebno pripremljeni veštački signali koji su označeni kao MLS i *sweep*, i koji su napravljeni numerički. Kroz odgovarajuću numeričku proceduru iz takvog procesa dobija se signal impulsnog odziva za odabrani par tačaka izvor zvuka – prijemnik, to jest zvučnik i veštačka glava.

U istraživanju sakralnih prostora, a posebno u multidisciplinarnom pristupu njihovoj višemedijskoj prirodi, auralizacija može biti značajan istraživački alat, posebno u slučaju istraživanja istovremenog dejstva više medija na čoveka. Takav alat se može koristiti u dva važna domena. Prvo, beleženjem akustičkog odziva u prostorima od interesa moguće je u laboratorijskim uslovima auralizacijom stvoriti kod slušaoca auditorni utisak kakav bi bio kada bi se nalazio u tom prostoru. Pri tome, moguće je napraviti binauralne snimke sa bilo kojim muzičkim i drugim signalima, kao što su glas sveštenika, pojanja sa pevnica, zvuk zveckanja kadionice ili sve zajedno. Napravljeni snimak može se reprodukovati proizvoljan broj puta i u proizvoljnim trenucima u laboratoriji ili na nekom drugom mestu.

Drugo, pomoću softverskih alata za modelovanje zvučnog polja moguće je akustički odziv, to jest HRTF, dobiti simulacijom prostora koji odavno više ne postoje. Za takav postupak potrebno je raspolagati sa dovoljno detaljnim grafičkim prikazima objekta, to jest arhitektonskim crtežima dobijenim nekim prethodnim istraživanjima, i informacijama o materijalizaciji svega što je u njegovom enterijeru izloženo zvučnom polju.

Korišćenje mogućnosti auralizacije u istraživanju sakralnih prostora zahteva, pored ostalog, i razradu jedne teorijske teme iz domena obrade signala. Naime, postoje okolnosti u kojim se slušaoci kreću kroz prostor, kao na primer tokom raznih procesija. U literaturi je nagoveštено da se u crkvama mogu očekivati promene karaktera akustičkog odziva po prostoru, što je na neki način potrebno predstaviti i u auralizaciji. Za takve namene potreban je algoritam za kontinualnu promenu HRTF po trajektoriji kojom se slušalac kreće pri zadatim položajima izvora zvuka. S obzirom da se snimanje impulsnog odziva po definiciji obavlja za nepomičan izvor zvuka i mikrofona dok traje sekvenca snimanja (interval vremena koji je potreban za određeni broj ponavljanja sekvenci MLS ili *sweep* signala), jasno je da se može raspolagati samo sa snimcima HRTF u diskretnom skupu parova tačaka. Za kvalitetnu auralizaciju onoga što se čuje pri kretanju kroz prostor crkve potrebno je istraživati mogućnosti morfinga, a to znači interpolacije oblika binauralnih impulsnih odziva za bilo koju kombinaciji položaja

 ISBN 978-86-7466-930-3

izvora zvuka i slušaoca, a na osnovu snimaka HRTF u konačnom broju tačaka duž zadate trajektorije.

## IV. Uticaj akustičkog ambijenta crkve na pevanje

U literaturi iz oblasti arheoakustike inicirano je pitanje doživljaja sopstvenog glasa onih koji pevaju u crkvama [11,13]. Primećeno je da u tradicionalnim formama pravoslavnih crkava postoji razlika u karakteru doživljaja zvuka kada se peva sa različitih pozicija. Ukazano je da promena položaja pevača ima ulogu u ukupnom doživljaju ambijenta kod slušalaca, ali da takođe postoji povratno dejstvo na doživljaj sopstvenog glasa onog ko peva. Tako na primer, u literaturi se za jednu crkvu konstatuje da je „nedostatak rezonance uznemiravao i pevače i slušaoce“ [11].

Sa takvim informacijama iz literature jasno je da istraživanje zvučnog ambijenta sakralnih prostora neminovno zahteva i analizu njihovih akustičkih karakteristika sa aspekta onoga što čuju pevači, to jest sveštenici, pojci i hor. To utiče na formiranje njihovog pevanog glasa, kao i na celovit pevački izraz. Tema za istraživanje u tom domenu treba da bude korelacija između arhitektonskih odlika crkve, njene veličine i forme, i subjektovnog doživljaja sopstvenog glasa pevača na različitim pozicijama u njoj.

I u ovom domenu istraživanja se mogu koristiti saznanjima iz akustičke teorije koncertnih i operskih sala. U postupcima za njihovo objektivno ocenjivanje definisan je i koristi se parametar nazvan „podrška“ i označava se sa ST (*Stage support*). On numerički odslikava u kojoj meri ambijent svojim odzivom deluje na izvor zvuka nekom formom povratne sprege i tako pomaže u formiranju i kontroli zvuka koji se stvara, pevanog ili pomoću muzičkog instrumenta. Postupak njegovog izračunavanja je standardizovan [18]. Dobija se iz impulsnog odziva snimljenog u postavci kada se zvučnik nalazi na mestu gde bi se nalazio izvora zvuka (u koncertnim salama to je na bini a u crkvama su to uobičajene pozicije sveštenika, pojaca i hora), a merni mikrofon se nalazi na rastojanju 1 m od akustičkog centra zvučnika. U karakterizaciji podrške najčešće se koristi takozvana „rana podrška“ $ST_{Early}$ koja po definiciji predstavlja odnos u decibelima reflektovane energije koja stiže u prvih 100 ms i energije direktnog zvuka, pa je:

$$ST_{Early} = 10log\left[\frac{\int_{0.020}^{0.100} h^2(t)dt}{\int_{0}^{0.010} h^2(t)dt}\right]$$

gde je $h(t)$ signal snimljenog impulsnog odziva, a $t = 0$ trenutak stizanja direktnog zvuka u njemu. Prema tome, postoji teorijski aparat i merna procedura da se istraživanje usmeri u tom pravcu. Za koncertne sale definisana je optimalna vrednost, preciznije donji prag koji vrednosti $ST_{Early}$ mora da prebaci da bi prostor bio zadovoljavajući za izvođače. Za okolnosti kakve postoje u crkvama tek predstoji utvrđivanje optimalnih vrednosti ovog parametra. Za to su potrebna merenja $ST_{Early}$ i ankete među pevačima o njihovim utiscima u kojoj bi oni vredovali različite pozicije za pevanje.

## V. Zvučni ambijent prostora u kome se nalaze sakralni objekti

Sastavni deo doživljaja sakralnih prostora je i zvuk ambijenta u širem smislu u kome se taj prostor nalazi. Realno je pretpostaviti da postoji razlika kada se nakon doživljaja službe izađe u bučnu ulicu sa mnoštvom zvučnih nadražaja koji privlače pažnju, što je upobičajeno u gradskim sredinama i uopšte u naseljima, i kada je to ambijent prirode kao u slučaju manastira i njihovog okruženja. Mesta gde je pozicionirana većina manastira još uvek okružuje manje-više očuvani mir i ambijent prirode.

Nesumnjivo je da takve ambijente karakteriše relativna tišina. Apsoluta tišina ne postoji, pa čulo sluha uvek registruje neke prisutne zvukove. Činjenica da su zvukovi takvih ambijenata vrlo niskih apsolutnih nivoa, otvara još i pitanje mikrofona s kojim bi se mogli registrovati za potrebe njihove naknadne analize. Za kvalitene uzorke signala tihih ambijenata neophodno je raspolagati s mikrofonima vrlo niskog nivoa sopstvenog šuma što, moguće je, izlazi iz okvira standardne opreme za audio snimanja.

Snimci ambijenata iz očuvanih okruženja omogućili bi da se u laboratorijskim uslovima ambijent ekstremne tišine, kakav postoji u anehoičnim i semianehoičnim prostorijama koje se uobičajeno koriste za psihoakustičke testove, obogati zvučnim sadržajem prirodne „tišine“ manistirskih ambijenata.

U evropskim naseljima tokom prethodnih vekova zvuci koje su ljudi slušali bili su različiti od današnjih. Promene su nastupile sa industrijskom revolucijom koja je donela motore i mehaničke sprave čiji rad generiše buku. Ipak, razlika je mnogo dublja od ekoloških tema o kojim se danas intenzivno govori. Dok danas ljudi pokušavaju da pobegnu od gradske buke, za stanovnike ranih gradova zvuk je služio kao ključni izvor informacija. Formirao je semiotički sistem, prenoseći vesti, pomažući ljudima da se lociraju u vremenu i prostoru i čineći ih delom „audijalne zajednice“ [2]. Zvuk je pomogao da se izgradi identitet i da se struktuiraju odnosi među ljudima. Evolucija ovog informacionog sistema odražava promene u društvenoj i političkoj organizaciji i u odnosu prema vremenu i urbanom prostoru. Zbog toga je u istraživanju istorijske dimenzije zvučnog ambijenta sakralnih prostora potrebno uložiti napor da se u izvesnoj meri rekonstruišu mogući ambijenti u kojima su se oni mogli nekada nalaziti.

## VI. Problem rekonstruisanih crkava

U istraživanjima akustičkog aspekta srpskih sakralnih prostora izvestan problem može nastati u crkvama koji su u relativno novije vreme rekontruisane. Materijali koji se pri tome koriste ili autorski stav onoga ko vodi rekonstrukciju mogu promeniti akustičke uslove u njima. To dalje može usmeriti današnja istraživanja u pogrešnom smeru jer je ambijent akustički izmenjen.

Primer toga može se videti u crkvi manastira Žiča. Prema kazivanju onih koji imaju auditivna iskustva sa tim prostorom pre i posle građevinskih intervencija, u crkvi su se nakon rekonstrukcijen u izvesnoj meri promenile akustičke karakteristike. Na žalost, nema rezutata akustičkih merenja iz perioda pre toga, ali se kroz diskusiju došlo do zaključka da je uzrok takve promene novi malter koji je upotrebnjen prilikom rekonstrukcije.

 ISBN 978-86-7466-930-3

Naime, crkve su sa aspekta akustičkog dizajna specifični prostori, jer u njima nema izrazito apsorpcionih površina, osim naroda koji se u njima okupi za vreme službe. Sve unutrašnje površine u crkvama su akustički „tvrde“, po pravilu malterisane radi oslikavanja, osim poda koji je pokriven kamenom. Takve tvrde površine dominantno određuju prepoznatljiv akustički odziv crkvenih prostora. Prema podacima iz literature, koeficijent apsorpcije malterisane površine na masivnom zidu je vrlo mali i može se očekivati da je u intervalu $\alpha = 0{,}05\text{-}0{,}07$ [19]. U odsustvu površina sa intenzivnom apsorpcijom, male varijacije vrednosti koeficijenta apsorpcije, čak samo na nivou druge decimale, mogu se značajnije odraziti na akustički odziv prostora.

Jednostavna numerička ilustracija može objasniti značaj karaktera maltera u crkvama. Zapremine starih srpskih crkava su u najvećem broju slučajeva u intervalu od 500 $m^3$ do 3000 $m^3$ [7]. Veće crkve su vrlo retke, dok manje od 500 $m^3$ nemaju očekivani akustički ambijent karakterističan za crkve. Uzimajući 1000 $m^3$ kao približnu sredinu tog intervala posmatranog u logaritamskoj razmeri i koristeći Sabinov obrazac za izračunavanje vremena reverberacije može se dobiti gruba procena kakvu promenu u akustičkom odzivu unosi promena maltera sa koeficijentom apsorpcije 0,05 na malter čija je vrednost 0,07. Pri tome su obe vrednosti veoma male u odnosu na vrednosti koeficiejnta apsorpcije ostalih materijala koji se koriste u zgradama. U proračunu se polazi od pretpostavke da je vreme reverberacije tog hipotetičkog crkvenog prostora 2 s, što je ranije utvrđeno kao estetski optimum za pravoslavni crkvenu službu [5,7]. Na osnovu toga je procenjena i rezidualna apsorpcija zvuka koju unose svi drveni predmeti, tkanine i druga uobičajena oprema enterijera u crkvama

Pojednostavljen akustički proračun pokazuje da će se vreme reverberacije samo promenom prirode maltera i njegove poroznosti, to jest povećanjem njegovog koeficijenta apsorpcije sa 0,05 na 0,07, smanjiti sa vrednosti 2 s na vrednost 1,7 s. To je promena koja se zapaža slušanjem. Realno je pretpostaviti da se vrednost koeficijenta apsorpcije maltera u srkvama može kretati i u širim granicama od ovih koje su usvojene u pojednostavljenom proračunu, pa se mogu dobiti i veće promene akustičkog odziva.

Prikazani proračun je krajnje aproksimativan, ali ukazuje na veliki značaj maltera za akustički odziv u okolnostima kada malterisane površine čine dominatnu apsorpciju u prostoriji, kao što je to u crkvama. U literaturi nisu nađeni podaci o apsorpcionim svojstvima starih maltera kakvi se nalaze u istorijski značajnim srpskim sakralnim građevinama. To je svakako jedna od tema koje zaslužuju detaljniju analizu i sasvim sigurno merenja na terenu. Problem u tome koji treba istraživački rešiti je što ne postoji standardizovani merni postupak za *in situ* merenja koeficijenta apsorpcije koji bi se mogao direktno primeniti. Posebno što se zahteva merenje izuzetno malih vrednosti.

Još jedan karakterističan slučaj od značaja za istraživanje zvučnog ambienta srpskih sakralnih prostora nalazi se u crkvi manstira Gradac, sazidanoj u 13. veku. Ona je izgrađena od poroznog kamena čije je nalazište u lokalnoj sredini. Fotografije površine jednog primerka tog kamena prikazana je na slici 2. Ovaj materijal zbog svoje poroznosti nesumnjivo ima značajno veći koeficijent apsorpcije od masivnog malterisanog zida kakav je uobičajen u crkvama. Ne postoje podaci o merenju apsorpcije ovakvog kamena, pa je to svakako još jedna tema za istraživanje.

Crkva manastrira Grdac bila je u stanju polurazrušenosti do njene rekonstrukcije. Princip koji je usvojen pri obnovi je da se svi novoizgrađeni delovi ne malterišu kako bi se jasno naglasila razlika između originalnog i novog [20,21]. Zbog toga je relativno velika unutrašnja površina crkve ostala sa vidljivim poroznim kamenom kao sa slike 2. Subjektivni utisak u prostoru ove crkve je akustička prigušenost neuobičajena za takve ambijente.

Slučajevi kao što je crkva manastira Gradac nakon njene rekonstrukcije očigledno ne odslikava očekivane akustičke karakteristike sakralnog prostora. Možda upravo takva crkva može biti pogodna za neka istraživanja u domenu višemedijske prirode u okolnostima redukovanog akustičkog sadržaja.

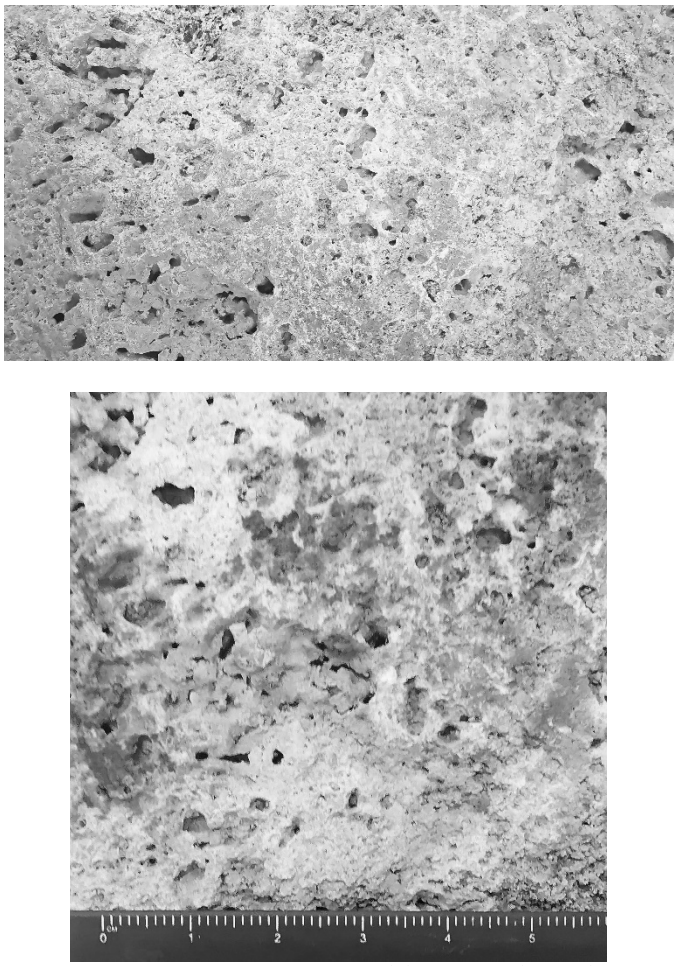

Sl.2. Izgled strukture kamena od koga je sačinjena unutrašnja površina crkve manastira Gradac: gore – izgled površine; dole – detalj sa razmernikom u cm da se može proceniti veličina poroznosti

## VII. ZAKLJUČAK

Celovito istraživanje zvučnog ambijenta srpskih sakralnih prostora u kojima nastaju multisenzorski doživljaji zahteva saradnju istraživača iz svih domena njihove višemedijske prirode. Ono u toj kompleksnosti pokreće nekoliko sasvim novih pitanja iz domena akustike prostorija i psihoakustike za

 ISBN 978-86-7466-930-3

čije je odgovore neophodan iskorak iz inženjerske rutine i uključivanje u multidisciplinarno posmatranje sakralnih prostora. U radovima istoričara postoji dovoljno naznaka za preciznije definisanje mogućih ciljeva istraživanja, a teorijske osnove iz oblasti akustike i obrade signala omogućavaju da se ostvari kvalitetativni pomak u metodologiji istraživačkog rada.

Primena auralizacije otvara nove mogućnosti za pouzdanije sagledavanje kompleksnih uticaja sakralnih prostora na prisutne ljude. Posebno je značajna činjenica da auralizacija omogućava premeštanje istraživanja u laboratoriju, gde je moguće postići kontrolu pobude i ponavljanje ispitivanja proizvoljan broj puta. Posebno je istraživački zanimljiv eventualni povratni uticaj akustičkog ambijenta na pevače, što bi dalo objašnjenja za neke pojave ranije konstatovane u istorijskoj literaturi.

## LITERATURA


[1] Miomir Mijić, "Audio industrija u Srbiji", Flogiston, 29/2021, Muzej nauke i tehnike, ISSN 0354-6640

[2] https://en.wikipedia.org/wiki/Archaeoacoustics

[3] A.González Menéndez "Archaeoacoustics: The Study of Acoustics at Archaeological Sites", OpenMind, 16 March 2020.

[4] M.Mijić, ″Acoustical characteristics of some Serbian Orthodox worship spaces″, 120th Meeting of Acoustical Society of America, abstrakt objavljen u Journal of Acoustical Society of America, Vol. 88, Supplement 1, 1990, S185

[5] M.Mijic, V. Banjac, ″O ulozi ugrađenih akustičkih rezonatora u srpskim crkvama na primeru Gornje crkve u Sremskim Karlovcima″, Građa za proučavanje spomenika kulture Vojvodine XX, Novi sad (1999) 87-104

[6] M.Mijic, D. Sumarac-Pavlovic, ″Acoustical characteristics of old wooden churches in Serbia", The Journal of the Acoustical Society of America Vol. 108, page 2648 (2000); https://doi.org/10.1121/1.4743873

[7] M.Mijić, ″Serbian orthodox church - An acoustical view″, ICA, Rim, 2-7 septembra 2001. 6C.09.04

[8] D.Šumarac Pavlović, „Uticaj geometrijskih karakteristika prostorije na njen akustički odziv″, Doktorska disertacija, Elektrotehnički fakultet u Beogradu, 2007.

[9] M.Mijic, D. Sumarac-Pavlovic, ″Acoustic resonators in serbian orthodox churches″, Proc. Forum Acusticum, Sevilla (2002) RBA-05-001-IP

[10] M.Mijić, D.Šumarac-Pavlović, „Acoustic Resonators in Serbian Orthodox Churches", poglavlje u monografiji „Collected Papers in Building Acoustics: Room Acoustics and Environmental Noise", Multi Science Publishing Co., London, 2010, 141-156

[11] Bissera V. Pentcheva, "Hagia Sophia and Multisensory Aesthetics", Gesta 50, no. 2 (2011): 93–111

[12] Sharon E. J.Gerstel, "Images in Churches in Late Byzantium", https://books.openedition.org/psorbonne/39781

[13] S.Gerstel C.Kyriakakis, S.Antonopoulos, K.Raptis, J.Donahue, "Holy, Holy, Holy: Hearing the Voices of Angels", Gesta 60, No. 1 (2021): 31–49

[14] L.Berananek, „Concert Halls and Opera Houses: Music, Acoustics, and Architecture", Springer (2004)

[15] Y.Ando, „Opera House Acoustics Based on Subjective Preference Theory", Springer (2015)

[16] M.Kleiner, B.I.Dalenbäck, P.Svensson, "Auralization-An Overview", JAES Vol.41 No.11, 1993, 861-875

[17] M.Mijić, „Audio sistemi", Akademska misao (2010)

[18] ISO 3382-1: Acoustics — Measurement of room acoustic parameters — Part 1: Performance spaces

[19] M.Mijić, „ELA 1 – Koeficijenti apsorpcije materijala", Laboratorija za akustiku Elektrotehničkog fakulteta u Beogradu, 1998.

[20] A.Jurišić, „Gradac – rezultati areoloških istraživanja", Republički zavod za zaštitu spomenika kulture, Beograd (1989)

[21] O.Kandić, The Monastery of Gradac", Republički zavod za zaštitu spomenika kulture, Beograd (1987)

[22] "Soundscapes of Byzantium", *Speculum*, Vol. 92, No. S1 October 2017, pp. S321-S335


## ABSTRACT


The study of soundscape in the historical context has given rise to a new field of acoustics called archaeoacoustics. In addition to many important historical buildings, the topic of such research was the acoustic characteristics of religious spaces, too. The synthesis of acoustic and historical facts about Serbian sacral spaces led to the conclusion that their concept is a multimedia topic in which sound is only one, although important component. In order to give meaning to the complex acoustic analysis results, one has to look beyond physics and recognize the interactions of sound with other applied media such as painting, architecture, music, light. This paper considers the place and role of acoustics in the context of possible multidisciplinary research of Serbian sacral spaces. The focus is on several characteristic topics: the correlation of impulse responses and physical forms of sacral spaces, the auralisation of the sound field in them to enable the relocation of research to laboratory ambient, the impact of the acoustic environment on the position of priests and chanters, as well as acoustic characterization the physical ambience from which people enter the sacred space and into which they come back.


**Research of the Serbian sacral space soundscape as a multimedia phenomenon**


Miomir Mijić, Miloš Bjelić, Dragana Šumarac Pavlović, Tatjana Miljković, Filip Pantelić


 ISBN 978-86-7466-930-3

# O ulozi akustičkih rezonatora u prostoru hrama Svetog Save u Beogradu

Dragana Šumarac Pavlović, Miomir Mijić, Jelena Erdeljan, Tatjana Miljković

***Apstrakt*— Akustički rezonatori su naprave od davnina korišćene u crkvama sa idejom da se pomoću njih na neki način kontroliše zvučni odziv prostora. Projekat hrama Svetog Save u Beogradu svojevremeno je predvideo ugradnju 476 posebno dizajniranih rezonatora da bi se umanjila očekivana reverberacija u njegovoj velikoj zapremini od 117.000 m$^3$. Tokom izrade mozaika kojim je oslikan hram tako veliki broj rezonatorskih otvora relativno velikog prečnika otežavao je montažu kamenih elemenata mozaika. Zbog toga se nametnulo pitanje njihove nužnosti i svrsishodnosti u hramu i pokrenuto je istraživanje realne efikasnosti ugrađenih rezonatora i rizika koje nosi njihovo eventualno zatvaranje. Tadašnja analiza je malo proširena i ukupni rezultati do kojih se došlo prikazani su u ovom radu.**

***Ključne reči* — akustički odziv; akustički rezonatori; crkve, Hram Svetog Save.**

## I. UVOD

Nesumnjivo najznačajniji sakralni objekat u Srbiji je hram Svetog Save. Izgrađen je na vrhu Vračarskog brda u Beogradu, pa zahvaljujući svom položaju, ali i fizičkoj monumentalnosti, dominira Beogradom i vidljiv je s velikog dela teritorije grada. Navodi se da je Hram po zapremini glavnog molitvenog prostora najveća aktivna pravoslavna crkva na svetu [1]. Njegova zapremina, preciznije unutrašnji vazdušni prostor, zauzima oko 117.000 m$^3$.

Aktivnosti na izgradnji hrama započete su još 1895. godine kada je u Beogradu osnovano „Društvo za podizanje hrama Svetog Save na Vračaru“. Društvo je 1905. godine raspisalo arhitektonski konkurs za idejno rešenje hrama. Zanimljivo je da su svi prispeli radovi, a prispelo ih je samo 5, odbačeni kao nedovoljno dobri. Nakon I svetskog rata Društvo je obnovilo rad i 1926. godine raspisan je novi konkurs. Kao najuspešniji proglašen je rad arhitekte Bogdana Nestorovića, pa je Društvo 1930. godine poverio izradu projekta arhitektama Nestoroviću i Aleksandru Deroku. Izgradnja hrama je konačno započela 15. septembra 1935. godine.

Od početka građevinskih radova do nemačke okupacije 1941. godine izgrađeni su temelji hrama i podignuti zidovi visine od 7 do 11 m. Stariji beograđani pamte takvo njegovo stanje sa poluizgrađenim zidovima od opeke. S Drugim svetskim ratom „Društvo za izgradnju hrama“ je prestalo da postoji.

Nastavak gradnje hrama započet je 1984. godine, a za novog arhitektu hrama imenovan je arhitekta Branko Pešić. Gradnja objekta je u građevinskom smislu završena 2004. godine. Međutim, radovi na unutrašnjem uređenju i dekoraciji dovršeni su značajno kasnije, da bi se otvaranje hrama ozvaničilo tek nedavno, krajem 2021. godine nakon završetka oslikavanja mozaikom i finalizacije većine prostora u hramu (iako se u njemu još uvek odvijaju građevinski i instalaterski radovi).

Svakako je zanimljivo da su u projektovanju hrama tokom osamdesetih godina dvadesetog veka projektanti razmatrali i akustičke aspekte. Kao akustički konsultant angažovan je Stevan Milosavljević. Tokom rada na projektu doneta je odluka da se kontrola akustičkog odziva prostora hrama realizuje pomoću akustičkih rezonatora, svakako imajući u vidu brojne informacije o njihovom postojanju u srednjovekovnim crkvenim prostorima. Neki od radova koji obrađuju tu temu pobrojani su u spisku literature na kraju ovog rada [2-9]. Činjenica je da radovi o rezonatorima u crkvama koji se mogu naći u raznorodnoj literaturi većim delom nisu inženjerski, preciznije akustičarski. Postoje brojni radovi koji su rezultat analiza koje su sprovodili arheolozi, istoričari umetnosti, arhitekte i drugi autori iz oblasti tangentnih sa akustikom.

Ideja o rezonatorima kao sredstvu za kontrolu akustičkog odziva u hramu inicirala je u vreme projektovanja opsežnu studiju o kojoj je pisao D.Kalić [10]. Dimenzije rezonatora prikazane u njegovom radu određene su na osnovu prethodno usvojene odluke o potrebnim rezonantnim frekvencijama u zadatom prostoru. Rezonatori imaju formu betonskih kocki sa okruglim otvorom na prednjoj strani. Primenjena su dva tipa rezonatora, manji i veći. Veći rezonatori imaju dužinu stranice 1,1 m i proračunom utvrđenu rezonatnu frekvenciju 125 Hz, a manji su sa stranicom 55 cm i proračunom utvrđenom rezonantnom frekvencijom 250 Hz. U hramu je projektom predviđeno ukupno 476 takvih rezonatora. Njihove pozicije su vidljive na fotografiji prikazanoj na slici 1. Rezonatori su postavljani u površine gornje zone hrama, u kupoli i svim bočnim svodovima, očigledno prema realnim mogućnostima ugradnje takvih relativno velikih kutija u građevinske strukture. Naime, na tim delovima građevinske konstrukcije hrama postoji dvostruka betonska ljuska. To je omogućilo da prisustvo nezavisnih celina kakve su kutije rezonatora ne ugrožavaju statiku objekta. Bliski poled na dva rezonatora u ugrađenom stanju prikazan je na slici 2.

Miomir Mijić – Elektrotehnički fakultet, Univerzitet u Beogradu, Bulevar Kralja Aleksandra 73, 11020 Beograd, Srbija (e-mail: emijic@etf.rs).

Dragana Šumarac Pavlović – Elektrotehnički fakultet, Univerzitet u Beogradu, Bulevar Kralja Aleksandra 73, 11020 Beograd, Srbija (e-mail: dsumarac@etf.rs).

Jelena Erdeljan – Filozofski fakultet, Univerzitet u Beogradu, Čika Ljubina 18-20, 11020 Beograd, Srbija (e-mail: @).

Tatjana Miljković – Elektrotehnički fakultet, Univerzitet u Beogradu, Bulevar Kralja Aleksandra 73, 11020 Beograd, Srbija (e-mail: tm@etf.rs).

 ISBN 978-86-7466-930-3

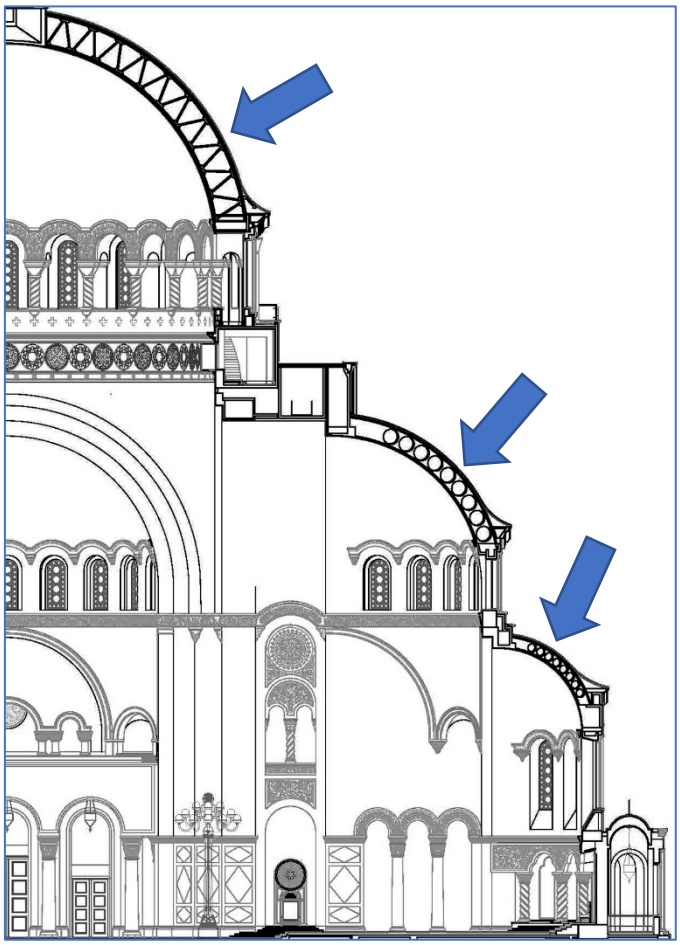

Sl.1. Gore - izgled unutrašnjosti hrama pre postavljanja mozaika sa vidljivom otvorima rezonatora oko kupole (fotografia je napravljena 2010. godine, to jest pre postavljanja mozaika); dole – označene pozicije dvostrukih betonskih struktura kupole i svodova vidljive u preseku u koje su ugrađeni rezonatori.

Oslikavanje hrama, a posebno odluka da se za to koristi mozaik kao tehnika, otvorilo je neke praktične probleme koji očigledno nisu uzeti u obzir pri projektovanju takve akustičke obrade prostora. Problemi su posledica činjenice da na unutrašnjim površinama hrama prostoje brojni, relativno veliki otvori rezonatora. Oni su potencijalno remetili strukuru slika, ali i komplikovali montažu teških obloga sa pripremljenim kamenim elementima mozaika. Zbog toga je pokrenuto pitanje provere svrsishodnosti i realnih dometa rezonatora u kontroli veoma duge reverberacije prostora hrama i procene akustičkog rizika koji nastaje ako se rezonatori eliminišu prekrivanjem njihovih otvora.

Sl.2. Bliski pogled na dva rezonatora u kupoli - levo je manji, a desno veći rezonator.

Da bi se razrešile nedoumice oko uticaja rezonatora i montaže mozaika inicirano je posebno istraživanje. Njegov cilj je bio da pomogne u donošenju strateških odluka u konačnom dovršavanju hrama. Istraživanje je obavljeno tokom 2010. godine, a u njemu su učestvovali članovi stručnog tima Laboratorije za akustiku Elektrotehničkog fakulteta u Beogradu. U analizama su korišćeni rezultati merenja akustičkog odziva hramu u zatečenom stanju i u njegovom numeričkom modelu pomoću rej-trejsing simulacije. Za sagledavanje novih aspekata analiziranog problema utrađene su u novije vreme neke dodatne analize. Rezultati su prikazani u ovom radu.

## II. KARAKTERISTIKE UGRAĐENIH REZONATORA

Prvi korak u istraživanju na temu mogućeg doprinosa ugrađenih rezonatora na akustički odziv hrama uključilo je proveru njhovih realno postignutih rezonantnih frekvencija. Podaci o tome prikazani u projektu dobijeni su proračunima koji uvek nose moguću grešku zbog nesavršenosti matematičkih modela [11-14]. S tim ciljem je organizovano *in situ* merenje rezonantnog odziva urađenih rezonatora.

Za tu namenu iskorišćena je dizalica sa platformom koja je u to vreme postojala u hramu i korišćena je za potrebe građevinskih radova. Dizalica je vidljiva na desnoj strani fotografije sa slike 1. Ona je omogućila da se ostvari dovoljno približavanje jednoj grupi rezonatora u kupoli i postavljanje zvučnog izvora i mernih mikrofona. S obzirom na njihovu poziciju u hramu, merenja su izvršena na rezonatorima koji su bili dohvatni sa platforme dizalice i prikazani su na slici 1.

Metodologija merenja rezonantnih svojstava ugrađenih rezonatora ilustrovana je na slici 3. Koncept merenja njihove rezonantne frekvencije i propusnog opsega ranije je razvijen za potrebe detaljne analize izvesnog broja rezonatora izvađenih iz srednjovekovnih srpskih crkava [15]. Za tu namenu korišćen je priručni širokopojasni izvor zvuka pozicioniran u zoni otvora ispitivanih rezonatora. Zvučni signal je registrovan sa dva merna mikrofona – jedan se nalazio u blizini otvora rezonatora i registrovao je pobudu rezonatora iz prostora hrama, a drugi je bio u unutrašnjosti rezonatora i u njemu registrovao odziv na

 ISBN 978-86-7466-930-3

primenjenu pobudu. Na osnovu razlike signala iz mikrofona u ove dve tačke dobijena je relativna promena nivoa zvuka po frekvencijama u rezonatoru, a koja nastaje kao posledica rezonantnog procesa. Dobijene rezonatne krive za dva tipa rezonatora ugrađena u hramu prikazane su na slici 4.

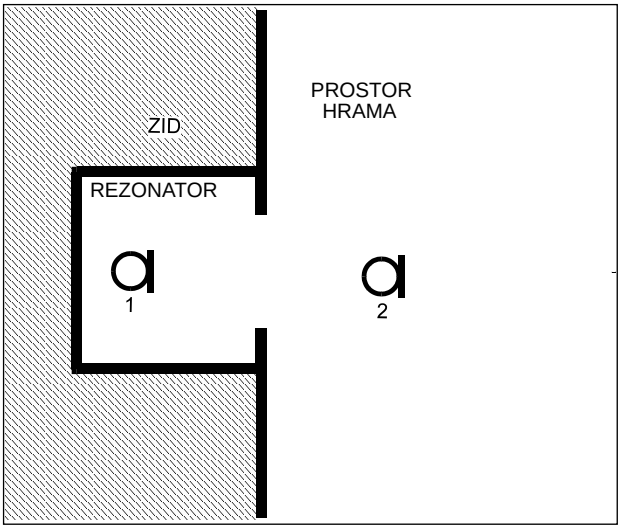


Sl.3. Šematski prikaz postupka merenja rezonantne frekvencije ugrađenih rezonatora: 1 – mikrofon u rezonatoru, 2 – mikrofon u prostoru ispred rezonatora

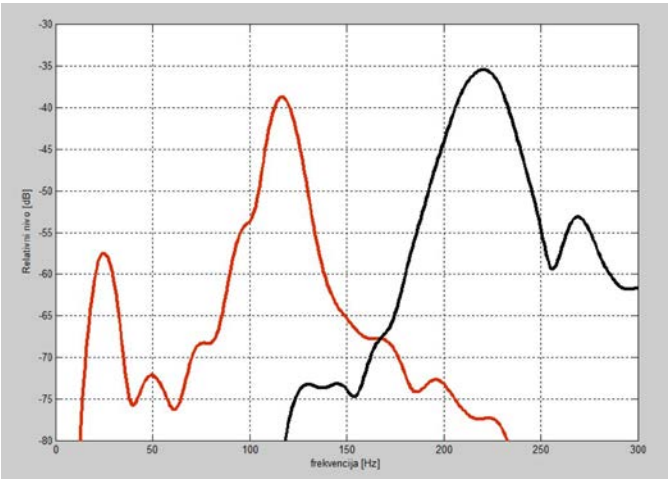


Sl.4. Odzivi dva tipa rezonatora ugrađena u kupoli hrama; odzivi su snimljeni metodologijom prikazanom na slici 2: crvena linija – veći rezonator, crna linija – manji rezonator.

Sa slike 4 se vidi da je snimljeni odziv analiziranih rezonatora na spoljašnju zvučnu pobudu karakterističan za rezonantni proces, Jasno se vidi da je njihova selektivnost relativno uska. Rezonantna frekvencija većeg rezonatora je bliska 125 Hz, kao što je bilo predviđeno projektom, a propusni opseg je oko 10 Hz. Rezonantna frekvencija manjeg rezonatora je oko 220 Hz (projektom je predviđeno 250 Hz), a propusni opseg je oko 20 Hz. To ukazuje da se njihov uticaj na zvučno polje može očekivati samo u okvirima njihovih propusnih opsega vidljivih na dijagramu. Činjenica je da se opseg delovanja rezonatora može širiti korišćenjem nekog apsorpsionog materijala, ali proširivanje selektivnosti rezonantnog procesa neumitno smanjuje eventualni efekat apsorpcije zvuka na rezonantnoj frekvenciji. Rezultat merenja sa slike 4 pokazuje da je sa aspekta akustičkog odziva u prostoru hrama eventualni dobitak takvom modifikacijom upitan.

## III. KARAKTERISTIKE ZVUČNE POBUDE KOJA SE JAVLJA U HRAMU

Potencijalni doprinos ugrađenih rezonatora u akustičkom odzuvu hrama, sa njihovim izmerenim rezonatnim odzivima, zavisi od zvučnih sadržaja koji se pojavljuje tokom službi. Da bi se to razjasnilo izvršena je frekvencijska analiza uzoraka zvučnih signala koji se pojavljuju tokom službe u srpskim pravoslavnim crkvama, i kojim se pobuđuje njihov prostor. Za analizu su uzeti liturgijsko pevanje hora i pojanje sa pevnice. Da bi rezultati takve analize bili primenjivi moraju se posmatrati izvorni akustički signali koje emituju glasovi kao zvučni izvori, to jest bez uticaja ambijenta koji promenama u frekvencijskom i vremenskom domenu utiče na karakter zvuka koji se čuje. Zbog toga su upotrebljeni snimci bliski anehoičnim, napravljeni u jednom ranijem istraživanju, pa su primenjeni i za potrebe ove analize. Pojanja su snimljena u crkvenom prostoru, ali sa vrlo bliskim mikrofonima. Na taj način je u dobijenom signalu potisnut uticaj ambijenta karakterističnog za crkve. Pevanje hora je snimljeno u relativno maloj prostoriji za probe koja je prigušena izvesnom količinom apsorpcionog materijala. Dugovremeni spektri šest uzoraka takvih signala prikazani su na slici 5.

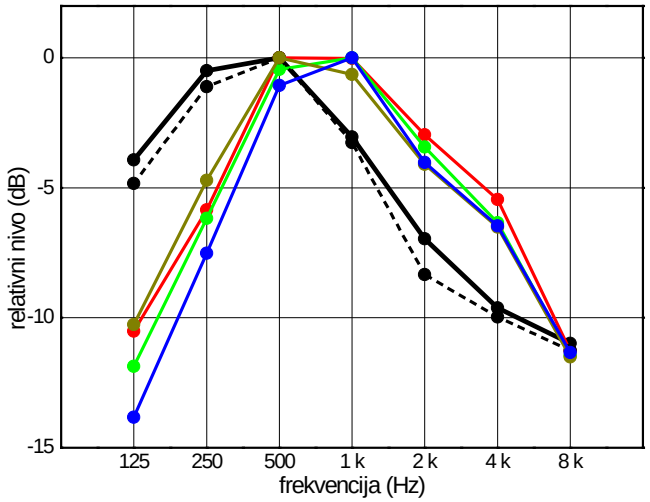


Sl.5. Dugovremeni spektri segmenata liturgije koju peva hor i pojanja grupe pojaca: crne linije – pojanje sa pevnice, obojene linije – pevanje hora.

Dijagrami sa slike 5 pokazuju karakter zvuka kojim se uobičajeno pobuđuje prostor pravislavnih crkava za vreme službe. Spektri u kome dominiraju muški glasovi, kao što je pojanje sa pevnice, imaju maksimum spektra u oktavi na 500 Hz, dok je u pevanju mešovitog hora maksimum energije u oblasti oktava sa centralnim frevencijama na 500 Hz i 1 kHz, i sa opadanjem relativnog nivoa ka višim i nižim frekvencijama.

Upoređujući dugovremene spektre sa slike 5 sa rezonantnim svojstvima akustičkih rezonatora prikazanim na slici 4, zaključuje se da su oni podešeni na frekvencije ispod oblasti u


ISBN 978-86-7466-930-3

kojoj se nalazi maksimum energije glasova, a to znači maksimum zvučne pobude crkvenog prostora tokom službe. Takav zaključak je apostrofiran i u ranijem istraživanju akustičkih rezonatora pronađenih u srednjovekovnim srpskim crkvama [15]. Ovakva činjenica ograničava moguće auditivne efekte koje oni mogu ispoljavati u srpskim pravoslavnim crkvama, pa i u hramu Svetog Save.

## IV. MERENJE U HRAMU PRE POSTAVLJANJA MOZAIKA

Da bi se utvrdilo realno stanje akustičkog odziva prostora hrama sa ugrađenim rezonatorima organizovano je merenje akustičkog odziva. Merenje je sprovedeno u dve seanse tokom 2010. godine. Bilo je to u fazi izgradnje hrama, kada je objekat u ugrađevinskom smislu bio završen, a pre početka većih radova na oslikavanju i ukrašavanju. Merenja su vršena tokom noći kada u njemu nije bilo posetilaca. Od dodatnih elemenata u hramu kojh neće biti u njegovom finalnom stanju tom prilikom su postojale skele u jednom delu prostora, manja količina građevinskog materijala ograđenog mrežama koja ih štiti i dizalica vidljiva na slici 1. Pod u to vreme nije bio popločan.

Merenje akustičkog odziva je izvršeno direktnom metodom, što znači da je za pobudu korišćen izvor impulsnog zvuka. U prostoru koji ima tako veliku zapreminu to je bio jedini dostupan način za njegovu pobudu neusmerenim zračenjem. Rezultat merenja vremena reveberacije prikazan je na slici 6, dobijen usrednjavanjem za nekoliko prijemnih i predajnih mesta u hramu.

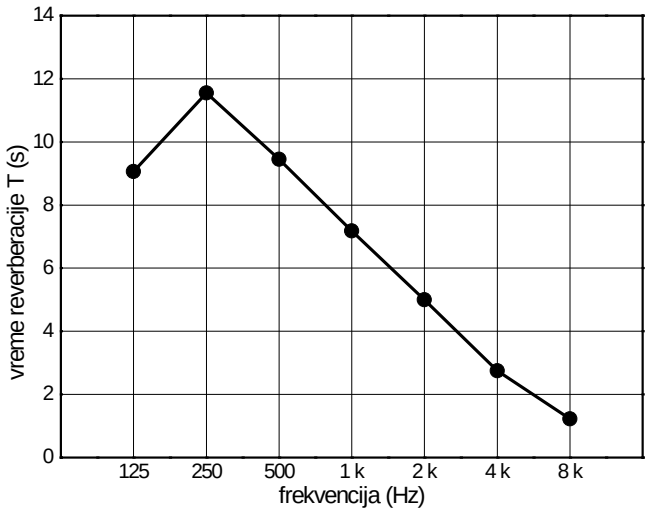


Sl.6. Rezultat merenja vremena reverberacije u hramu u fazi pre postavljanja mozaika.

Sa dijagrama na slici 6 može se uočiti nekoliko karakterističnih činjenica.

1. I pored postojanja rezonatora prostor hrama na nižim frekvencijama ima veliku vrednost vremena reverberacije, čak do 12 s u oktavi na 250 Hz. Vrednosti oko 10 s su konstatovane i u drugim tako velikim prostorima, kao na primer u Beogradskoj areni čija je unutrašnja zapremina oko 300.000 $m^3$ [16]

2. U hramu ne postoje površine koje bi mogli doprineti povećanoj apsorpciji na niskim frekvencijama. To bi teorijski mogle biti sve površine koje deluju kao mehanički rezonatori: drvene obloge, površine sa gipsanim pločama i slično. Činjenica je da u hramu postoje relativno velike površine vrata, podaščane zone i površine slične materijalizacije koje mogu u nekoj maloj meri doprineti apsorpciji najnižih frekvencija, ali je to po ukupnoj kvadraturi minorno u datoj zapremini. Zbog toga je pad vrednosti vremena reverberacije u oktavi na 125 Hz očigledna posledica delovanja rezonatora. Pa ipak, i pored svih tih uticaja vrednost vremena reverberacije je relativno velika, čak 9 s.

3. Uticaj rezonatora se u oktavi na 250 Hz iz nekih razloga ne primećuje, iako dijagram sa slike 3 pokazuje da je oko polovina od njhovog ukupnog broja podešena na frekvenciju koja se nalazi upravo u tom opsegu. Razlog tome može biti suviše uzak propusni opseg rezonatora u odnosu na ukupnu širinu oktave na 250 Hz koja je oko 170 Hz (od oko 180 Hz do oko 350 Hz). Njegov doprinos sa delovanjem u opsegu širine od samo 20 Hz očigledno se ne primećuje u usrednjenoj oktavnoj vrednosti vremena reverberacije.

4. Modelovanje funkcije usamljenog rezonatora ugrađenog u masivnom zidu pokazuje da je maksimalno moguća vrednost ekvivalentne apsorpcione površine koju on ispoljava [17]:

$$A = \frac{\lambda_0^2}{2\pi} \text{ [m}^2\text{]}$$

Ova vrednost se dostiže samo ako je dizajn rezonatora optimalan. To znači da će udeo rezonatora u ukupnoj apsorpciji prirodno da opada sa frekvencijom. To može biti objašnjenje manje vidljivosti uticaja rezonatora na vreme reverberacije u oktavi na 250 Hz u odnosu na oktavu na 125 Hz.

5. Monotoni pad vrednosti vremena reverberacije na višim frekvencijama jasno je određen uticajem disipacije u vazduhu, jer u enterijeru hrama nema poroznih materijala koji bi uneli takvu apsorpciju. To znači da je kriva vremena reverberacije u toj oblasti frekvencija u izvesnoj meri promenljiva u funkciji promene vlažnosti i temperature vazduha, ali da ima očekivani monotoni pad ka višim frekvencijama počev od oktave 250 Hz.

## V. ANALIZA MOGUĆEG DOPRINOSA REZONATORA U HRAMU SIMULACIJOM ZVUČNOG POLJA

Da bi se procenila mogućnost predikcije efekta ugrađenih rezonatora u prostoru hrama sprovedena je analiza proračunima. Za to su primenjena dva pristupa:

- simulacijom zvučnog polja u softverskom modelu njegove unutrašnjosti pomoću rej-trejsing analize i
- pomoću statističkog modela zvučnog polja koristeći poznatu Sabinovu formulu za vreme reverberacije u prostoriji.

Za potrebe rej-trejsing simulacije napravljen je model unutrašnjosti hrama čiji je izgled prikazan na slici 7. Unutrašnjim površinama dodeljene su procenjene vrednosti koeficijenta apsorpcije koristeći podatke iz literature [18]. Za potrebe proračuna posebno je izvršena procena vrednosti koeficijenta apsorpcije površina sa ugrađenim reznonatorima, tačnije izračunavanje njihove apsorpcione površine, da bi se to primenilo u ovim modelima.

Rezultat proračuna vremena reverberacije metodom rej-trejsinga i Sabinovom formulom prikazan je na slici 8. Radi

 ISBN 978-86-7466-930-3

poređenja, na dijagramu je ucrtan i rezultat merenja sa slike 6. Na osnovu ovih rezultata može se izvesti nekoliko važnih zaključaka.

1. U oktavi na 125 Hz izmerena vrednost vremena reverberacije poklapa se sa rezultatom proračunom za obe primenjene metode modelovanja.

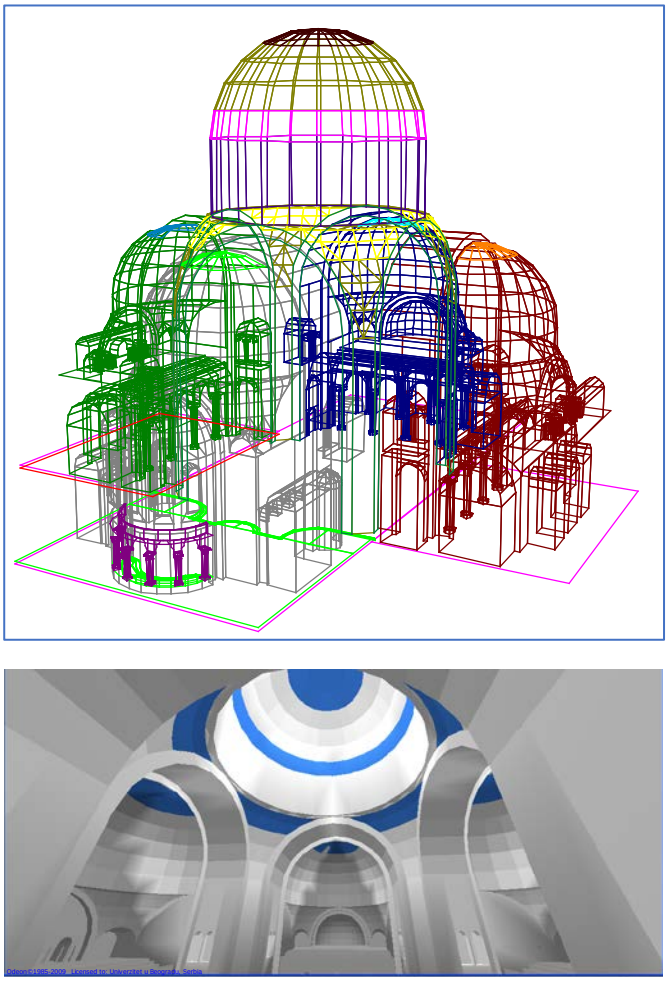

Sl.7. Izgled softverskog modela unutrašnjosti hrama u kome je izvršeno modelovanje zvučnog polja metodom *rej-trejsing*: gore – žičani model, dole – model sa unetom materijalizacijom gde je vrednost koeficijenta apsorpcije kodovana bojama.

2. U oktavi na 250 Hz izmerena vrednost vremena reverberacije se približno poklapa sa vrednostima izračunatim za slučaj hrama bez rezonatora. Preciznije, izmerena vrednost je između vrednosti dobijenih Sabinovom formulom i rej-trejsing simulacijom za slučaj bez rezonatora.

3. Na višim frekvencijama proračuni po obe metode premašuju izmerene vrednosti. To može biti posledica dva faktora: razlike u proceni disipacije u vazduhu i činjenice da u nedovršenom hramu neke površine ipak imaju izvesnu poroznost koja može imat uticaja na apsorpciju viših frekvencija, a što nije moglo biti sagledano u primenjenim proračunima.

## VI. MERENJA U ZAVRŠENOM PROSTORU HRAMA

Da bi se zaokružila slika o mogućim efektima rezonatora na akustički odziv hrama potrebno je izvršiti finalno merenje akustičkog odziva u njemu. Uslovi za takvo merenje su se steki tek nedavno, nakon finalizacije oslikavanja i nekih drugih bitnih detalja. Time su svi otvori ugrađenih rezonatora zatvoreni masivnim slojem materijala od koga je načinjen mozaik. Nažalost, sticajem raznih okolnosti organizacione prirode to merenje još uvek nije izvršeno.

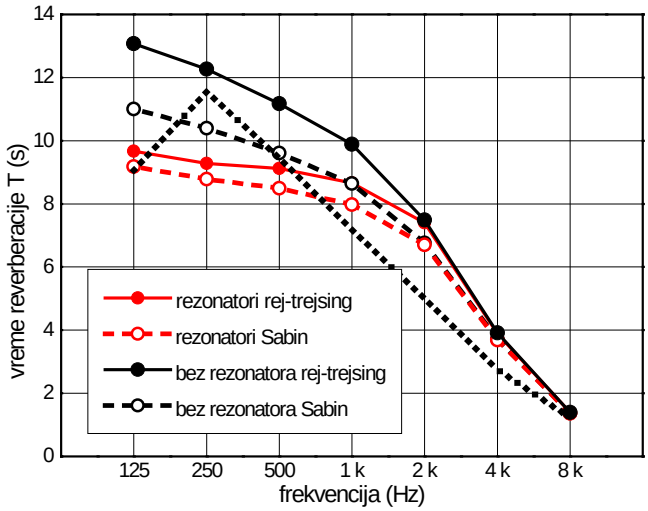


Sl.8. Rezultati proračuna vremena reverberacije u hramu za slučaj sa i bez uticaja ugrađenih rezonatora: proračuni su urađeni na dva načina: metodom rej-trejsing i pomoću Sabinove formule; tačkasto je ucrtan rezultat merenja u hramu.

## VII. ZAKLJUČAK

Iz analize uticaja akustičkih rezonatora u hramu Svetog Save u Beogradu proizašlo je nekoliko zaključaka koji se odnose na tu temu, ali i na šire aspekte akustike.

1. Pokazalo se da su rezonantne frekvencije primenjenih rezonatora ispod oblasti frekvencija gde se dominantno nalazi najveći dao energije glasova horskog pevanja i pojanja. To potvrđuje ranije zaključke koji su prizašli iz studije akustičkih rezonatora u srednjovekovnim srpskim crkvama.

2. Rezultati sprovedenih proračuna i njihovo poređenje sa rezultatima merenja u izgrađenom hramu pokazuju da postoji problem tačnosti modelovanja zvučnog polja i predikcije akustičkog odziva tako velikih prostora kao što je hram Svetog Save (117.000 $m^3$). Očigledno je da u projektovanju to zahteva posebnan istraživački pristup. Sličan zaključak je već ustanovljen prilikom projektovanja Beogradske arene [16].

3. U veoma velikim prostorima kao što je hram nemoguće je da se služba odvija bez primene sistema za ozvučavanje. Naime, ne postoje sredstva akustičkog dizajna prihvatljiva u kanonizovanom crkvenom prostoru koja bi mogla da vreme reverberacije svedu na optimalnu meru za takve ambijente (2-3 s) [7].

4. Savremena tehnologija daje mogućnost primene vrlo usmerenih zvučničkih sistema kakvi su danas uobičajeni u sistemima za ozvučavanje, koji kombinovani sa bliskim mikrofonima na sveštenicima i pojcima omogućavaju minimizaciju uticaja akustičkog ambijenta na ono što će se čuti


ISBN 978-86-7466-930-3

na pozicijama slušaoca. Na taj način danas je u izvesnom smislu eliminisana neophodnost podešavanja vremena reverberacije u vrlo velikim verskim prostorima kakav je hram, što se odražava i na eventualnu ideju o primeni rezonatora.

## LITERATURA


[1] https://hramsvetogsave.rs/
[2] M.Kayili, ″Use of cavity resonators in Anatolia since Vitruvius″, Prc. 7th International Congress on Sound and Vibration, Garmisch-Partenkirchen, 1621-8 (2000)
[3] T.Pretlove, ″Helmholtz resonators for the new Russian Orthodox church in London″, Acoustic Bulletin, London, January/February (1998)
[4] A.Carvalho, V.Desarnaulds, Y.Loerincik, ″Acoustic behavior of ceramic pots used in middle age worship spaces - a laboratory analysis″, Proc. 9th International Congress on Sound and Vibration, Garmisch-Partenkirchen, 1621-8 (2000)
[5] S.Nenadovic, ″Rezonatori u crkvama srednjovekovne Srbije″, Zbornik Arhitektonskog fakulteta Univerziteta u Beogradu (1960) sveska V
[6] M.Bajalovic-Hadzi-Pesic, ″Keramika u srednjovekovnoj Srbiji″, Muzej grada Beograda, (1981) 71-73
[7] M.Mijic, V. Banjac, ″O ulozi ugrađenih akustičkih rezonatora u srpskim crkvama na primeru Gornje crkve u Sremskim Karlovcima″, Građa za proučavanje spomenika kulture Vojvodine XX, Novi sad (1999) 87-104
[8] M.Mijic, D. Sumarac-Pavlovic, ″Acoustic resonators in serbian orthodox churches″, Proc. Forum Acusticum, Sevilla (2002) RBA-05-001-IP
[9] D.Kalic, ″Acoustic resonators in Serbian medieval churches ″, Proc. II Joint meeting of Greek and Yugoslav Acoustical Societies (1984), Proceedings, 91-97
[10] D.Kalić, ″Akustika hrama Svetog Save″, Izgradnja, No 1 (1993) 23-29
[11] J.Holtsmark, ″The absorption and diffusion of sound by resonators″, I Kommisjon hos Jacob Dybwad, Oslo (1946)
[12] A.K.Nielsen, ″Acoustic resonators of circular cross-section and with axyal symmetry″, Trans. of the Danish Academy of Technical Sciences, No 10 (1949)
[13] A.Alster, ″Improved calculation of resonant frequencies of Helmholtz resonators″, Journal of Sound and Vibration, Vol. 24, No 1 (1972) 63-85
[14] G.R.Bigg, ″The three dimensional cavity resonator″, Journal of Sound and Vibration, Vol. 85 (1982) 85-103
[15] Miomir Mijić, Dragana Šumarac-Pavlović, „Acoustic Resonators in Serbian Orthodox Churches“, poglavlje u monografiji „Collected Papers in Building Acoustics: Room Acoustics and Environmental Noise“, Multi Science Publishing Co., London, 2010, 141-156
[16] M.Mijić, Dragana Šumarac-Pavlović, ″Acoustic design of the Belgrade Arena hall″, FORUM ACUSTICUM, Budimpešta, 2005. Proceedings, 2399-2404
[17] U.Ingard, “On the Theory and Design of Acoustic Resonators”, JASA, Vol.25, NO 6 (1953) 1037-1061
[18] M.Mijić, „ELA 1 – Koeficijenti apsorpcije materijala“, Laboratorija za akustiku Elektrotehničkog fakulteta u Beogradu, 1998.


## ABSTRACT


Acoustic resonators are elements that have long been used in churches with the idea of using them to control the acoustic response of the worship space. The project of the Saint Sava temple in Belgrade included the installation of 476 specially designed resonators in order to reduce the expected reverberation. During the construction of the mosaic with which the temple was painted, such a large number of resonators with relatively large diameter of opening made it difficult to assemble the stone elements of the mosaic. Due to that, the question of their necessity and purposefulness in the temple arose. So, the research of the built-in resonators' real acoustic efficiency in the temple and the acoustical risk of their termination was initiated. The paper describes the results of the research and the achieved conclusions.


**On the role of acoustic resonators in the temple of Saint Sava in Belgrade**


Dragana Šumarac Pavlović, Miomir Mijić, Jelena Erdeljan, Tatjana Miljković


 ISBN 978-86-7466-930-3

# Optimizacija prostorne rezolucije mikrofonskog niza za merenje saobraćajne buke

Miodrag Stanojević, Miloš Bjelić, Tatjana Miljković

***Apstrakt* — Merenje saobraćajne buke mikrofonskim nizom omogućava određivanje ugaone raspodele incidentne energije buke na fasadi zgrada. Jedan od osnovnih parametara koji se zadaje u ovakvom merenju jeste ugaona rezolucija kojom se vrši odabiranje u prostornom domenu. S obzirom na računsku kompleksnost algoritma za prostorno-vremensku obradu signala mikrofonskog niza, optimizacija minimalne potrebne prostorne rezolucije omogućava značajno skraćivanje procesa izračunavanja. Merenja prikazana u ovom radu vršena su na četiri lokacije u urbanoj sredini. Lokacije se razlikuju u broju saobraćajnih traka, tipu saobraćaja, udaljenosti objekata, itd. Pretpostavka koja se istražuje u ovom radu jeste da je minimalna potrebna rezolucija mikrofonskog niza različita za svaku od ovih lokacija, i da je dominantno određena morfologijom urbane lokacije. Merenja su vršena mikrofonskim nizom koji čine 24 omnidirekciona mikrofona. Geometrija mikrofonskog niza je optimizovana za merenje saobraćajne buke.**

***Ključne reči* — mikrofonski niz, rezolucija, saobraćajna buka**

## I. Uvod

Merenje izvora zvuka mikrofonskim nizom omogućava eksperimentalno utvrđivanje ugaone raspodele incidentne energije [1]. Prilikom tumačenja rezultata ovakvih merenja neophodno je uzeti u obzir fizička ograničenja mikrofonskog niza, odnosno *beampattern* koga karakterišu dva ključna parametra: širina glavnog loba i potisnutost bočnih lobova. Ova dva parametra su frekvencijski zavisna i određena prvenstveno rasporedom mikrofona, odnosno geometrije mikrofonskog niza. Mikrofonski niz koji je korišćen za merenja prikazana u ovom radu je dvodimenzionalni niz sa 24 omnidirekciona mikrofona čija je geometrija optimizovana za frekvencijski opseg u kom se nalazi saobraćajna buka [2]. Algoritam za eksperimentalno određivanje ugaone raspodele incidentne energije polazi od određivanja doprinosa zvučne energije iz pojedinačnih tačaka zamišljene ekvidistantne mreže tačaka na koju je podeljen prostor ispred mikrofonskog niza. Određivanje doprinosa energije podrazumeva virtuelno usmeravanje glavnog loba mikrofonskog niza i pomeranje od tačke do tačke i merenje energije izlaznog signala. Virtuelno usmeravanje mikrofonskog niza (*beamsteering)* vrši se nakon usnimavanja 24-kanalnog signala mikrofonskog niza.

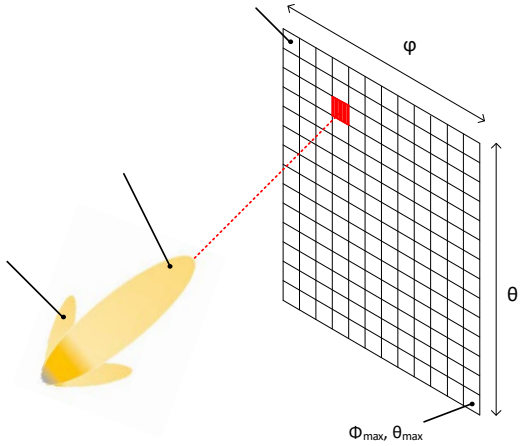


Sl. 1. Usmeravanje mikrofonskog niza – *beamsteering*. Zamišljeni grid tačaka skeniranja određenih azimutom (φ) i elevacijom (θ).

Imajući u vidu navedene nesavršenosti mikrofonskog niza (konačna širina glavnog loba i postojanje bočnih lobova koji nisu zanemarljivi), dobija se mapa prostorne raspodele energije koja predstavlja konvoluciju stvarne raspodela izvora zvuka i odziva mikrofonskog niza, stoga se ovakav rezultat naziva „prljava mapa“. Ova mapa služi kao osnov za dalju obradu koja podrazumeva set dekonvolucionih procedura koje imaju za cilj da dobijeni rezultat očiste od uticaja mikrofonskof niza. Dekonvolucioni algoritam koji se koristi u ovom istraživanju je DAMAS2 [3,4,5]. Nakon toga se moguće je odrediti gustinu verovatnoće energije po prostornim uglovima u odnosu na liniju upravnu na ravan fasade, koja služi za proračun izolacione moći pregrade.

Vremenski najzahtevniji postupak u opisanoj proceduri jeste dobijanje „prljave mape“. Razlog za to je iterativni postupak izračunavanja energetskih doprinosa koji podrazumeva izračunavanje za svaki par azimut-elevacija. S obzirom da je kompleksnost ovog procesa $O(n^2)$, smanjivanje rezolucije odabiranja donosi velike uštede u vremenu potrebnom za izračunavanje.

Pretpostavka koja se istražuje u ovom radu je da minimalna potrebna rezolucija zavisi od karakteristika urbane lokacije na kojoj se vrši merenje: da li je kanjon ulica, udaljenost saobraćajnih traka od fasade objekta (tzv. udaljenost ravni skeniranja *r*), postojanje raskrsnica i sl. Pretpostavlja se da će dominantan uzrok razlike u minimalnoj potrebnoj rezoluciji na različitim lokacijama biti različita udaljenost ravni skeniranja od fasade objekta na kojoj je postavljen mikrofonski niz. Međutim, istražena je eventualna zavisnost minimalne potrebne rezolucije od drugih parametara lokacije.

Miodrag Stanojević – Elektrotehnički fakultet, Univerzitet u Beogradu, Bulevar kralja Aleksandra 73, 11020 Beograd, Srbija (e-mail: miodragstanojevic@bitprojekt.co.rs).

Miloš Bjelić – Elektrotehnički fakultet, Univerzitet u Beogradu, Bulevar kralja Aleksandra 73, 11020 Beograd, Srbija (e-mail: bjelic@etf.rs).

Tatjana Miljković – Elektrotehnički fakultet, Univerzitet u Beogradu, Bulevar kralja Aleksandra 73, 11020 Beograd, Srbija (e-mail: tm@etf.rs).

 ISBN 978-86-7466-930-3

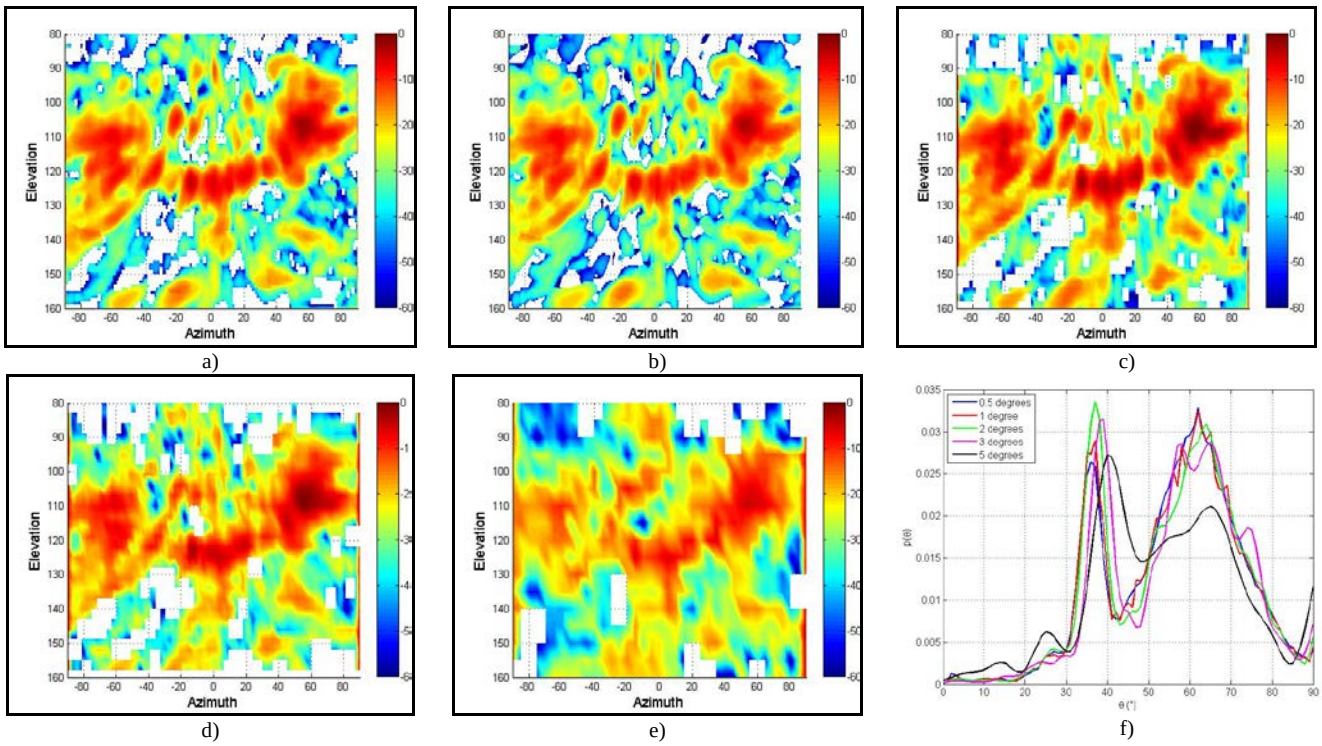


a) b) c) d) e) f)

Sl. 2. Raspodela incidentne energije po azimutu i elevaciji za događaj prolaska automobila za različite ugaone rezolucije (pomeraje po azimutu i elevaciji): a) $\Delta\varphi=\Delta\theta=0.5^o$, b) $\Delta\varphi=\Delta\theta=1^o$, c) $\Delta\varphi=\Delta\theta=2^o$, d) $\Delta\varphi=\Delta\theta=3^o$ i e) $\Delta\varphi=\Delta\theta=5^o$. Funkcija gustine verovatnoće incidentne energije za različite ugaone rezolucije.

Cilj istraživanja jeste dobijanje formule za određivanje minimalne potrebne rezolucije kojom se ulazi u proračun za datu lokaciju, kako bi se postigla maksimalna efikasnost algoritma i skratilo vreme izračunavanja.

## II. METODE

Na slici 2 prikazana je raspodela energije po azimutu i elevaciji za jedan prolazak automobila ispred fasade objekta, za različite vrednosti prostorne rezolucije odabiranja. Na slici f) prikazana je gustina verovatnoće incidentne energije po prostornim uglovima u odnosu na normalu na površinu fasade. Funkcija gustine verovatnoće prikazana je za jedan frekvencijski bin širine 1 Hz opseg oko centralne frekvencije 1000 Hz. Iz oba prikaza se može zaključiti da smanjivanje rezolucije do $\Delta\phi=\Delta\theta=3^o$ ne unosi značajnu grešku u određivanju funkcije gustine verovatnoće incidentne energije. Kako bi se sagledao uticaj na krajnji rezultat, neophodno je izvršiti analizu nad svim frekvencijskim binovima, odnosno proračunati prediktovanu vrednost izolacione moći fasadne pregrade koja je izložena buci sa ovakvom raspodelom [6].

Na slici 3 prikazana je proračunata prediktovana vrednost izolacione moći fasadne pregrade od betona debljine 20 cm. (Parametri pregrade $d=0.20$ m, $msp=2500$ kg/m$^3$, $c_l=3500$ m/s, $\eta_i=0.006$). Prikazane su frekvencijski zavisne vrednosti izolacione moći za rezolucije 1,2,3 i 5 stepeni, kao i teoretska vrednost proračunata za oblik raspodele incidentne energije $sin(2\theta)$. Na slici se može uočiti da su proračunate vrednosti u određenim frekvencijskim opsezima i do 8 dB za različite vrednosti ugaone rezolucije. Međutim, kada se posmatraju jednobrojne vrednosti izolacione moći (Tabela 1), uočava se da je razlika između različitih rezolucija sa kojima se ulazi u proračun zanemarljiva. U svim slučajevima izolaciona moć proračunata na osnovu realnih raspodela energije podmašuje teoretsku vrednost u frekvencijskom opsegu oko frekvencije koincidencije, a premašuje u opsegu iznad oko 300 Hz. Jednobrojne vrednosti izolacione moći proračunate na osnovu realnih raspodela energije premašuju teoretsku vrednost u svim slučajevima.

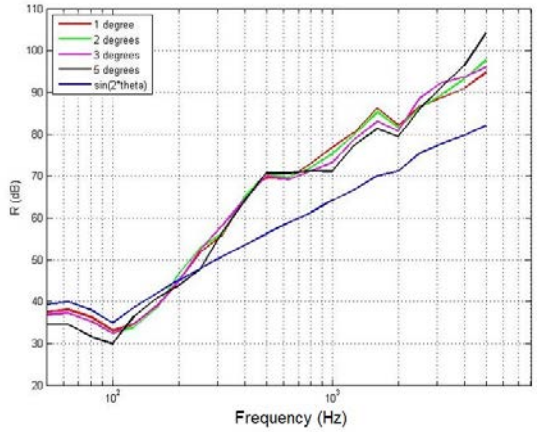


Sl. 3. Izolaciona moć fasadne pregrade za različite vrednosti ugaone rezolucije. Struktura pregrade – beton 20 cm.

| $\Delta\phi=\Delta\theta$ | $R'_w$ (dB) |
|---|---|
| $1^o$ | 60 |
| $2^o$ | 60 |
| $3^o$ | 59 |
| $5^o$ | 59 |
| $p(\theta)=sin(2\theta)$ | 58 |

Tabela 1. Jednobrojne vrednosti izolacione moći fasadne pregrade za različite vrednosti ugaone rezolucije. Struktura pregrade – beton 20 cm.

Prikazano poređenje izvršeno je na bazi jednog događaja na jednoj lokaciji u gradskoj sredini. Kako bi se izveli generalni zaključci analiza je proširena na veći broj lokacija, događaja i tipova događaja.


ISBN 978-86-7466-930-3

U prethodnim istraživanjima pokazano je da se prostorna raspodela energije na lokaciji može utvrditi analizom ključnih događaja, te da je globalna raspodela energije na lokaciji funkcija raspodela pojedinačnih događaja [7]. Stoga je analiza prikazana u ovom radu sprovedena nad setom od 10 ključnih događaja za četiri različite lokacije u gradskoj sredini. Pet događaja koji su predstavljaju pomeranje dominantnog zvučnog izvora na lokaciji (saobraćaj – automobili, trojelbusi autobusi) i pet događaja koji predstavljaju ambijentalni fon prisutan na lokaciji bez dominantnih izvora zvuka koji se izdvajaju po energiji.

## III. REZULTATI

Na slici 4 je prikazana razlika između maskimalne i minimalne dobijene vrednosti izolacione moći po frekvencijama za 10 događaja na lokaciji Bulevar Kralja Aleksandra.

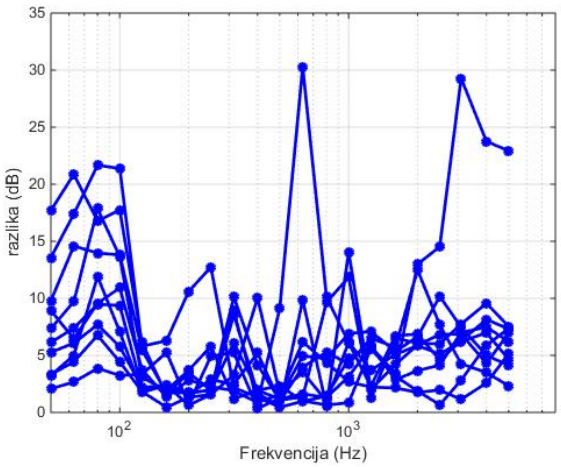


Sl. 4. Varijabilnost proračunate vrednosti izolacione moći za različite prostorne rezolucije. Lokacija – Bulevar Kralja Aleksandra

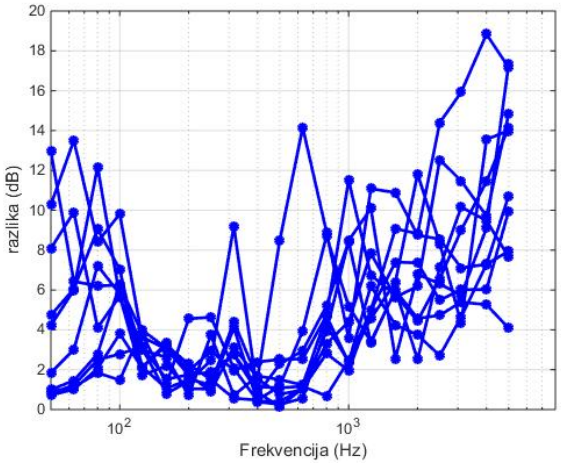


Sl. 5. Varijabilnost proračunate vrednosti izolacione moći za različite prostorne rezolucije. Lokacija – Cara Nikolaja II

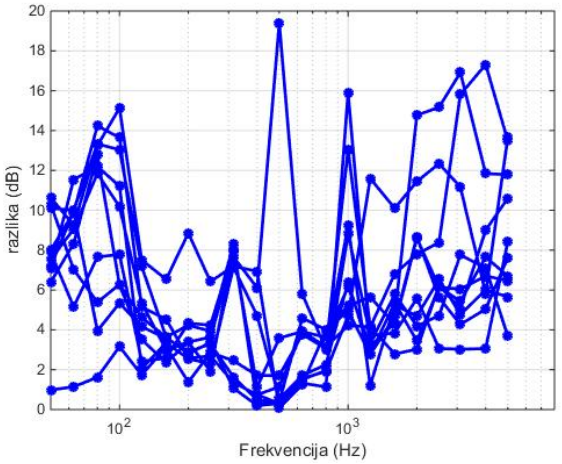


Sl. 6. Varijabilnost proračunate vrednosti izolacione moći za različite prostorne rezolucije. Lokacija – Ilije Garašanina

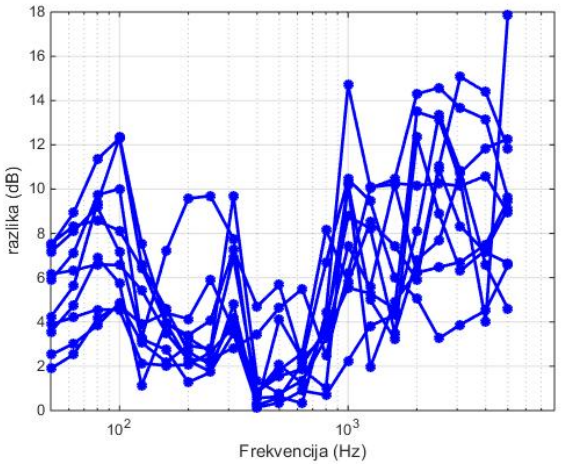


Sl. 7. Varijabilnost proračunate vrednosti izolacione moći za različite prostorne rezolucije. Lokacija – Molerova

## IV. DISKUSIJA

## ZAHVALNICA

Ovaj rad je realizovan u okviru projekta TR 36026 koga finansira Ministarstvo prosvete, nauke i tehnološkog razvoja Republike Srbije.

## LITERATURA

[1] M. Stanojević, M. Bjelić, D. Šumarac Pavlović, M. Mijić, Measurements of noise energy angular distribution at the building envelope using microphone arrays, Applied Acoustics, Vol 140, 283-287 (2018).

[2] M. Bjelić, M. Stanojević, D. Šumarac Pavlović, M. Mijić, „Microphone array geometry optimization for traffic noise analysis“, The Journal of the Acoustical Society of America, Vol 141(5), 3101-3104 (2017).

[3] T.F. Brooks, W.M. Humphreys, „A deconvolution approach for the mapping of acoustic sources (DAMAS) determined from phased microphone arrays“, *Journal of Sound and Vibration* 294.4, 856-879, 2006.

[4] R.P. Dougherty, „Extensions of DAMAS and Benefits and Limitations of Deconvolution in Beamforming“, *AIAA*, 2961.11, 2005.

[5] K. Ehrenfried, L. Koop, „A comparison of iterative deconvolution algorithms for the mapping of acoustic sources“, *AIAA journal*, 45.7:1584-1595, 2007.

[6] H. Kurtović, **“**Priručnik za proračun zvučne izolacije”. Beograd : Elektrotehnički fakultet, Laboratorija za akustiku, 1994.

[7] Miloš Bjelić, Miodrag Stanojević, Dragana Šumarac Pavlović, Miomir Mijić, Tatjana Miljković, Određivanje ostvarene vrednosti izolacione moći fasadnih pregrada na bazi izdvojenih karakterističnih

 ISBN 978-86-7466-930-3

događaja, Zbornik radova 64. Konferencije ETRAN, Beograd, Septembar 2020, str. AK2.2.1-AK1.2.6, ISBN: 978-86-7466-852-8.
[8]
[9] C.Brutel-Vuilmet, C.Guigou-Carter, M.Villot, „A Study of the Influence of Incidence Angle on Sound Reduction Index Using NAH-Phonoscopy. Acta Acustica United with Acustica, 2007;Vol. 93: 364–374.
[10] D. Šumarac Pavlović, F. Pantelić, S. Bojičić, M. Bjelić, „Airborne sound insulation of monolithic partition as a function of incidence angles“, Proc. Forum Acusticum, Krakow 2014.
[11] G.Vermeir, G.Geentjens, W.Bruyninckx, „Measurement and calculation experiences on façade sound insulation“, Proc INTER-NOISE 2004.
[12] ISO 140-5 „Acoustics - Measurement of sound insulation in buildings and of building elements – Part 5: Field measurements of airborne sound insulation of façade elements and façades“.
[13] M. Bjelić, M. Stanojević, D. Šumarac Pavlović, M. Mijić, „Određivanje uglova incidencije buke u urbanim sredinama“, ETRAN, Kladovo, jun 2017, Broj rada (zbornik radova CD): AK 1.1, ISBN: 978-86-7466-692-0.
[14] M. Bjelić, „Analiza ugaone raspodele incidentne energije spoljašnje buke primenom mikrofonskog niza“, Univerzitet u Beogradu, Elektrotehnički fakultet, Doktorska disertacija, jun 2018.
[15] M. Bjelić, M. Stanojević, D. Šumarac Pavlović, M. Mijić, T. Miljković, „Analiza ugaone raspodele incidentne energije spoljašnje buke u urbanim uslovima“, ETRAN, Palić, jun 2018, Zbornik radova 49-54, ISBN: 978-86-7466-752-1.
[16] M. Bjelić, „Analiza ugaone raspodele incidentne energije spoljašnje buke na fasadama zgrada u urbanim uslovima pomoću mikrofonskog niza“, 26th Telecommunications forum TELFOR 2018, Belgrade, November 2018, CD Proceedings paper No. 8.9., ISBN: 978-1-5386-7170-2.
[17] ISO 717-1:1996 „Acoustics – rating of sound insulation in buildings and of building elements – Part 1: Airborne sound insulation“.
[18] C. Buratti, E. Belloni, E. Moretti, **“**Façade noise abatement prediction: New spectrum adaptation terms measured in field in different road and railway traffic conditions“, Appl. Acoust. 2014;76:238–248.
[19] J. Hald and J. Christensen, „A novel beamformer array design for noise source location from intermediate measurement distances“, J. Acoust. Soc.Am. 112, 2448, DOI: 10.1121/1.4780077, (2002).
[20] M. Bjelić, M. Stanojević, D. Šumarac Pavlović, M. Mijić, „Dizajn mikrofonskog niza optimizovanog za monitoring saobraćajne buke“, ETRAN, Zlatibor, jun 2016, Broj rada (zbornik radova CD): AK 1.2, ISBN: 978-86-7466-618-0.
[21] U. Michel, “History of acoustic beamforming”, Berlin , 2006. Berlin Beamforming Conference.
[22] L. Beranek, “Noise Reduction. New York”: McGraw-Hill Book Company, Inc., 1960.
[23]

ABSTRACT

Measurements of the traffic noise using microphone arrays enables the determination of angular distribution of the incident energy on a building façade. One of the parameters which are set in such measurements is the spatial resolution. Considering high computational complexity of space-time algorithms for array signal processing, the optimization of required spatial resolution can reduce the computation process significantly. The measurements shown in this paper were performed on four urban locations. The locations differ in the number of traffic lanes, traffic types, distances to the surrounding buildings, etc. This paper examines the assumption that the minimal required resolution of the microphone array is different for each location, and is dominantly determined by the urban location morphology. The measurements were performed with a microphone array comprised of 24 omnidirectional microphones. The geometry of the microphone array is optimized for traffic noise measurements.

**Microphone array spatial resolution optimization for traffic noise measurements**

Miodrag Stanojević, Miloš Bjelić, Tatjana Miljković

 ISBN 978-86-7466-930-3

# Komparativna analiza akustičkih signala motora sa unutrašnjim sagorevanjem mapiranih u slike bazirane na spektrogramu

Marko Milivojčević, Emilija Kisić, Dejan Ćirić

***Apstrakt*—Motori sa unutrašenjm sagorevanjem kao i druge vrste motora i mašina pri svom radu generišu zvuk. On se karakteriše specifičnim svojstvima zavisno od vrste motora, moda rada, kao i stanja samog motora. Na osnovu zvuka moguće je izvući značajne informacije o motoru, uključujući i detekciju pogonskog goriva (benzina ili dizela). U tom kontekstu, u ovom radu je izvršena analiza akustičkih signala motora sa unutrašnjim sagorevanjem posle njihovog prebacivanja (mapiranja) u odgovarajuće slike i to spektrogram, hromagram, gamatonegram i tempogram. Kako sve ove slike imaju formu klasičnog spektrograma, one se u literaturi nazivaju slike bazirane na spektrogramu ili slične spektrogramu. Cilj analize je da se izvrši međusobno poređenje navedenih slika i da se ustanovi koja od njih najbolje prikazuje razliku između signala motora koje pokreće benzin i dizel gorivo. Analiza je izvršena nad bazom od 350 snimljenih signala kako bi se u nastavku istraživanja koristeći izabranu metodu mapiranja signala u slike izvršila klasifikacija pogonskog goriva sa što većom tačnošću pomoću tehnika dubokog učenja.**

***Ključne reči*—Akustičke karakteristike, audio zapis, vremenski domen, motori sa unutrašnjim sagorevanjem, spektrogram, hromagram, gamatonegram, tempogram.**

## I. Uvod

Sa razvojem modernih tehnologija i naprednih tehnika dubokog učenja, problemi automatizovane klasifikacije ili detekcije, kao što je prepoznavanje govora ili akustičkih signala, mogu se veoma uspešno rešiti ukoliko se izabere adekvatan algoritam mašinskog učenja i ukoliko se formira kvalitetna baza podataka na osnovu koje će se sistem obučiti.

Kada je reč o akustičkim signalima, njihovo prepoznavanje predstavlja veoma kompleksan zadatak i za čoveka, pre svega zbog nemogućnosti svih slušaoca da identično čuju odgovarajući signal što je uslovljeno različitim auditivnim karakteristikama svakog od slušaoca. Problem postaje još složeniji uzimajući u obzir da je na osnovu primljenog signala potrebno izvršiti klasifikaciju ili detekciju događaja upotrebom prethodno stečenog iskustva. "Treniranjem sluha", posebno u istom (radnom) okruženju, je moguće postići tačniju procenu događaja. Primena automatske klasifikacije/detekcije akustičkih signala za određenu vrstu događaja bi eliminisala nesavršenost čovekovog slušnog aparata, kao i elemente individualne subjektivnosti i manuelnog izvršavanja postupka klasifikacije/detekcije.

Činjenica da motori sa unutrašnjim sagorevanjem generišu zvuk prilikom svog rada, kao i da se taj zvuk perceptivno razlikuje u zavisnosti od pogonskog goriva, a sa dodatnom potrebom da se pogonska goriva klasifikuju iz ekoloških razloga [1], poslužila je kao motiv za razvoj sistema automatske klasifikacije baziran na audio snimcima rada motora.

U cilju realizacije jednog ovakvog sistema bilo je potrebno razviti akvizicioni sistem za prikupljanje audio signala. Ovi signali će formirati bazu uzoraka na osnovu koje će se sistem obučiti nekim od algoritama mašinskog, odnosno dubokog učenja. Pomenuti akvizicioni sistem za snimanje uzoraka koristi mikrofon pozicioniran u oblasti ispod motornog prostora putničkog vozila [2, 3] pošto se detektuje prisustvo vozila iznad mikrofona. Nakon toga, dodatnom obradom u vremenskom domenu vrši se izdvajanje režima praznog hoda motora. Kako je u režimu praznog hoda motora slušanjem utvrđena najveća razlika između pogonskih goriva, dodatna obrada je poslužila da se u banci uzoraka nađu samo audio zapisi takvog režima rada motora, pri čemu je detaljan prikaz postupka izdvajanja željenog režima rada motora prikazan u prethodnim fazama ovog istraživanja [4].

U ovom radu je izvršena komparativna analiza signala iz baze uzoraka mapiranjem signala u slike na bazi spektrograma. Osnovni motiv za analizu akustičkih signala mapiranih u slike bazirane na spektrogramu je visoka uspešnost klasifikacije na osnovu signala predstavljenih na ovaj način, videti na primer [5]. Krajnji cilj ovog istraživanja je izdvajanje onog prikaza koji daje dovoljno malu razliku unutar istog pogonskog goriva motora (benzin ili dizel), a ujedno najveću razliku između pogonskih goriva kako bi se u budućoj klasifikaciji pravilno formirala hijerarhija obeležja na osnovu kojih će se vršiti klasifikacija.

Rad je podeljen u više poglavlja. Karakteristični slučajevi prikupljenih audio signala i metode njihove obrade su prikazani u poglavlju gde je opisana metodologija. U poglavlju gde su opisani rezultati prikazani su karakteristični signali mapirani u slike u obliku spektrograma, hromagrama, gamatonegrama i tempograma. Zaključci komparativne analize dobijenih prikaza su sumirani u poglavlju koje sledi,

Marko Milivojčević – Akademija tehničko-umetničkih strukovnih studija Beograd, odsek: Visoka škola elektrotehnike i računarstva strukovnih studija, Vojvode Stepe 283, 11000 Beograd, Srbija (e-mail: markom@viser.edu.rs).

Emilija Kisić – Univerzitet Metropolitan, Beograd Fakultet informacionih tehnologija, Tadeuša Košćuška 63, 11000 Beograd, Srbija (e-mail: emilija.kisic@metropolitan.ac.rs).

Dejan Ćirić – Univerzitet u Nišu, Elektronski fakultet u Nišu, Aleksandra Medvedeva 14, 18000 Niš, Srbija (e-mail: dejan.ciric@elfak.ni.ac.rs).

 ISBN 978-86-7466-930-3

iza kojeg je dat spisak korišćene literature.

## II. METODOLOGIJA

Prikupljanjem audio signala generisanih radom motora sa unutrašnjim sagorevanjem u realnim uslovima formirana je baza od 350 uzoraka. Preslušavanjem baze i analizom vremenskog oblika signala izdvojen je po jedan karakterističan signal rada benzinskog i jedan signal rada dizel motora u režimu praznog hoda radi lakše ilustracije i predstavljanja rezultata.. Kao predstavnici svojih klasa ova dva signala su uporedno analizirana i mapirana u slike bazirane na spektrogramu. Vremenski oblici analiziranih uzoraka su prikazani na Sl. 1.

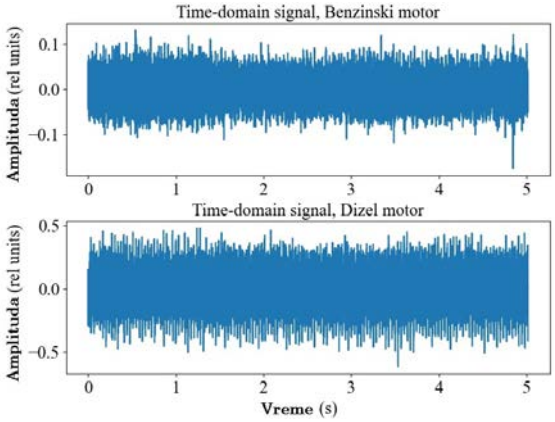


Sl.1. Vremenski oblik audio signala benzinskog i dizel motora

### A. Spektrogram

Jedna od tehnika za mapiranje akustičkih signala u sliku koja je korišćena u ovom radu je ona koja kao rezultat daje spektrogram. Ovakva vrsta slike je veoma pogodna reprezentacija signala, zato što se pomoću nje signal predstavlja u tri dimenzije: na horizontalnoj osi prikazuje se vreme, na vertikalnoj osi prikazuje se frekvencija, dok se amplituda predstavlja skalom boja. Spektrogram se može zamisliti kao grupa spektara signala poređanih jedan do drugog, gde je jačina spektralnih komponenti predstavljena intenzitetom boje. Spektrogram zapravo predstavlja kratkovremensku brzu Furijeovu transformaciju (eng. *short time fast Fourier transform*- STFT) [6], i računa se kao brza Furijeova transformacija (eng. *fast Fourier transform*-FFT) na pomerajućem prozoru podataka.

Osnovna ideja kod spektrograma jeste da se ceo signal podeli na segmente (okvire, odnosno frejmove, eng. *frame*) sa preklapajućim kratkovremenskim prozorima i da se zatim primeni FFT na svaki segment. Korišćenje spektrograma je veoma važno kod signala koji su kvazi-stacionarni, odnosno kod signala kod kojih postoji stacionarnost, ali samo na dovoljno kratkim odsečcima signala. Zbog toga, umesto standardne Furijeove transformacije koja transformiše signal iz vremenskog domena u frekvencijski domen (spektar), kod obrade akustičkih signala se uglavnom koristi vremenski kratkotrajna Furijeova transformacija. Njena glavna prednost jeste da se spektralna analiza sprovodi nad kratkim odsečcima signala kod kojih je zadovoljen uslov stacionarnosti.

Izdvajanje takvih odsečaka se sprovodi primenom vremenskih prozora, koji su različiti od nule samo za konačan skup indeksa. Množenjem ulaznog signala sa takvim vremenskim prozorom postavljenim na željeno mesto u signalu, dobija se novi signal takođe beskonačnog trajanja, ali čiji su uzorci jednaki nuli za sve indekse signala koji se nalaze izvan primenjenog vremenskog prozora.

Neka je akustički signal dužine $N$ odmeraka označen kao $s[n]$. Spektrogram akustičkog signala predstavlja funkciju i vremena i frekvencije što se može zapisati kao:

$$STFT[f,t] = \sum_{n=0}^{N-1} s[n] \cdot w[n] e^{-j2\pi fn} \quad (1)$$

gde $f$ predstavlja frekvenciju, $n$ vremenski argument spektrograma, a $w[n]$ je prozorska funkcija.

U ovom radu za računanje spektrograma signala korišćena je *stft* funkcija u okviru biblioteke *librosa* u programskom jeziku *Python*. Podela signala na segmente (okvire) je već implementirana unutar funkcije. Potrebno je definisati širinu prozora $W$, zatim korak analize $K$ (odnosno veličinu preklapanja prozora), kao i broj tačaka $M$ u kojima se računa Furijeova transformacija. Drugim rečima, funkcija *stft* deli akustički signal na preklapajuće okvire (gde se definiše širina prozora i veličina preklapanja), zatim za svaki od okvira računa FFT u onom broju tačaka koji se zada, a na spektrogramu se mogu pročitati informacije o vremenu, frekvenciji i amplitudi željenog signala. U ovom radu za širinu prozora je izabrano $W$=2048, preklapanje prozora je $K$=512, a broj tačaka za računanje Furijeove transformacije je $M$=2048. Izabrana prozorska funkcija je *Hann*-ova prozorska funkcija.

### B. Hromagram

Hromagram (hroma spektar) predstavlja veoma moćnu reprezentaciju audio signala u kojoj se ceo spektar projektuje na 12 binova koji predstavljaju 12 različitih polutonova (ili hroma) muzičke oktave [1].

Pošto se u muzici note koje su udaljene za tačno jednu oktavu doživljavaju kao posebno slične, poznavanje raspodele hroma čak i bez apsolutne frekvencije (tj. originalne oktave) može dati korisne muzičke informacije o zvuku, odnosno može otkriti uočenu muzičku sličnost koja nije vidljiva u originalnim spektrima.

Hromagram se dobija preslikavanjem diskretnih vrednosti dobijenih kratkotrajnom brzom Furijeovom transformacijom (STFT) audio signala u 12 hroma, odnosno prelaskom iz domena diskretnih frekvencija u domen diskretnih veličina hroma.

### C. Gamatonegram

Spektrogram je tradicionalna vremensko-frekvencijska vizualizacija, ali zapravo ima nekih važnih razlika u odnosu na to kako se zvuk analizira od strane ljudskog uva. Najznačajnija razlika je to što frekvencijski podopsezi uva postaju širi na većim frekvencijama, dok spektrogram ima

 ISBN 978-86-7466-930-3

konstantan propusni opseg na svim frekvencijama, odnosno u svim frekvencijskom opsezima (kanalima). Kako bi se ovo ograničenje prevazišlo može se koristiti *Gama-spektrogram*, zasnovan na primeni gamatone filtara, odnosno *gamatonegram* [8].

*Gamatone* filteri su dizajnirani tako da modeluju frekvencijski selektivne kohlea aktivacione odzive ljudskog unutrašnjeg uva [9], pri čemu izlaz filtra simulira frekvencijski odziv bazilarne membrane. *Gamatone* filtar je linearni filtar opisan impulsnim odzivom koji je proizvod gama raspodele i sinusoidalnog tona. Impulsni odziv filtra dat je sledećom jednačinom:

$$g[k] = k^{P-1}T^{P-1}e^{-2bkT\pi}\cos(2fkT\pi + \theta) \qquad (2)$$

gde je $k$ vreme, $P$ je red filtra, $T$ je perioda odabiranja, $b$ je propusni opseg filtra, $f$ je centralna frekvencija, a je $\theta$ faza nosioca. *Gamatone* filtri se koriste za modelovanje ljudskog slušnog sistema i sastoje se od niza filtara propusnika učestanosti. Banka *gamatone* filtara je formulisana kao ERB (eng. *equivalent rectangular bandwidth*) skala [10] na sledeći način:

$$ERB = 24.7\left(4.37\cdot 10^{-3} f + 1\right) \qquad (3)$$

Kako bi se generisao gamatonegram u ovom radu korišćen je toolbox razvijen od strane Ellis at al. [8], primenjen u programskom jeziku Python. Prvo je akustički signal transformisan u STFT spektrogram, kao što je gore opisano. Zatim je primenjeno *gamatone* ponderisanje $COE[F_{gam},F]$ na STFT kako bi se dobio gamatonegram:

$$GAM[F_{gam},T] = COE[F_{gam},F]\times STFT[F,T] \qquad (4)$$

gde je $F_{gam}$ rezolucija gamatonegrama (GAM spektrograma) i predstavlja broj gamatone filtara [11]. U ovom radu je broj gamatone filtara 64.

### *D. Tempogram*

Slično spektrogramu, tempogram se definiše kao vremenska-tempo reprezentacija, odnosno tempo datog signala koji zavisi od vremena [12]. Tempogram signala je reprezentacija koja sadrži informaciju o lokalnom tempu za svaki frejm audio sigala. Postoje dva tipa tempograma: Furijeov tempogram i autokorelacioni tempogram. Furijeov tempogram konvertuje frekvenciju u tempo (eng. *beat per minute* - BPM) naglašavajući harmonike, dok autokorelacioni tempogram konvertuje vremensko kašnjenje (sekunde) u tempo, ističući subharmonike. U ovom radu korišćen je ciklični tempogram pomoću *libros*-a biblioteke u Python programskom jeziku. Ciklični tempogram se dobija iz Furijeovog i autokorelacionog tempograma [12].

## III. REZULTATI ANALIZE

Kako je akvizicioni sistem razvijen tako da kao krajnji rezultat prikupljanja audio zapisa izdvaja i čuva samo režim praznog hoda motora, predmet analize nisu bili signali sa promenljivim režimom rada. Primenom predstavljenih metoda za analizu iz prethodnog poglavlja, mapiranje signala je realizovano na karakterističnim signalima dobijenim radom benzinskog i dizel motora isključivo u režimu praznog hoda čiji su vremenski oblici prikazani na Sl. 1.

Na Sl. 2. je prikazan spektrogram gde je nivo signala predstavljen u linearnoj razmeri, dok je na Sl. 3. takođe prikazan spektrogam istih signala pri čemu je snaga signala predstavljena u logaritamskoj razmeri.

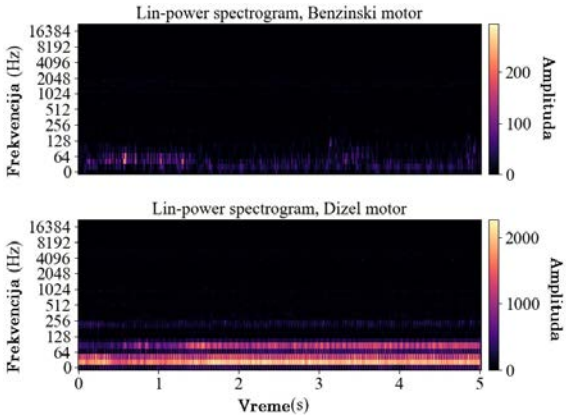


Sl. 2. Spektrogrami signala u linearnoj razmeri (*lin-power* spektrogrami)

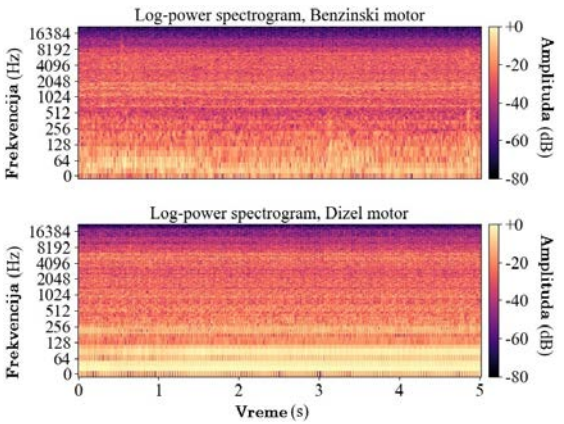


Sl. 3. Spektrogrami signala u logaritamskoj razmeri (*log-power* spektrogrami)

Analizom signala prikazanih u vidu spektrograma sa linearnom razmerom na Sl. 2. može se uočiti višestruka razlika signala između motora na benzin i dizel. Spektrogram benzinskog motora ima gotovo desetostruko niži nivo signala, dok spektrogram dizel motora pored višeg niva signala poseduje i izražene komponente na višim frekvencijama u odnosu na benzinski motor. Kod dizel motora se može uočiti neprekidnost spektrograma, posebno na osnovnoj učestanosti rada motora.

Prikazom ova dva signala u vidu spektrograma sa logaritamskom razmerom dobija se detaljniji prikaz spektralne raspodele signala, sl. 3. Na ovoj slici se takođe može uočiti viši nivo signala i veća gustina spektra dizel motora na nižim učestanostima. Pored ove osobine signala dobijenog radom dizel motora, koji odgovara percepciji slušaoca, da ovaj tip

 ISBN 978-86-7466-930-3

motora radi „dublje“, može se uočiti ravnomernija „popunjenost“ spektra sve do visokih frekvencija, dok se kod benzinskog motora posebno na približno 500 Hz može uočiti niži nivo signala. Kod signala generisanog radom benzinskog motora je i u oblasti visokih učestanosti, preko 10 kHz nivo signala niži, što odgovara percepciji slušaoca da prilikom dugog izlaganja buci dizel motora dolazi ranije do zamaranja slušaoca. Ova karakteristika generisanog zvuka se može potvrditi i analizom zvučne izolacije koja se ugrađuje na identičan tip putničkog vozila pokretanog različitim motorima, gde je zvučna izolacija dizel motora u najvećem broju slučajeva zbog komfora bolje izvedena.

Rezultat primene funkcija za određivanje hromagrama za izabrane karakteristične signale rada benzinskog i dizel motora u praznom hodu je prikazan na Sl. 4. Na dobijenom prikazu može se uočiti da je kod dizel motora zastupljenost različitih visina tj. klasa tonova kroz čitav opseg od svih dvanaest klasa, gotovo uniforman, pri čemu su najistaknutije klase D, D#, F# i A#, dok su kod benzinskog motora izražene klase F, F#, G i A. Na osnovu ovakvog prikaza signala moguće je uočiti da su kod benzinskog motora zastupljenije osnovne klase tonova dok su kod dizel motora zastupljenije povišene/snižene klase tonova.

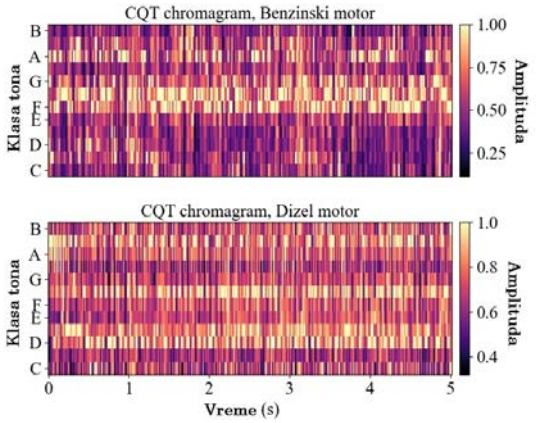


Sl. 4. Hromagram benzinskog i dizel motora

Primenom gamatone filtara prilikom proračuna spektrograma za posmatrane signale dobijen je gamatonegram koji je prikazan na Sl. 5. Na prikazanom gamatonegramu jasno je moguće uočiti razliku između dva pogonska goriva. Kod dizel motora nivoi signala su viši na svim frekvencijama, a posebno je istaknut opseg 4-8 kHz, kao i opseg niskih frekvencija gde se nalazi osnovna učestanost rada motora. Kod benzinskog motora je moguće uočiti veoma nizak nivo signala u opsegu ispod 1 kHz i iznad 10 kHz. Kako je gamatonegram posebno prilagođen ljudskom uvu, dobijeni prikazi odgovaraju percepciji „glasnijeg“ dizel motora bez obzira na mereni nivo signala instrumentom.

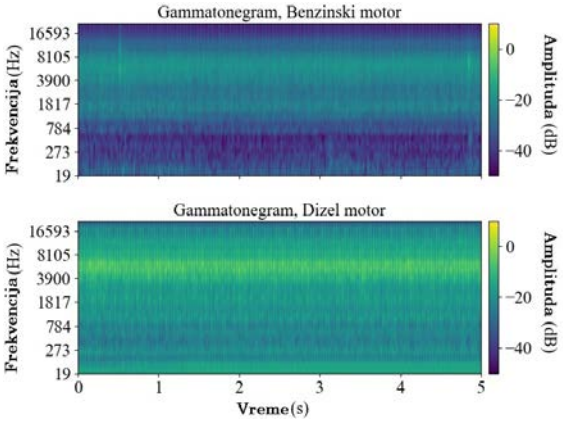


Sl. 5. Gamatonegram benzinskog i dizel motora

U okviru analize izabranih audio signala posebna pažnja je posevećena percepciji slušaoca koja se odnosi na utisak veće ili manje ujednačenosti rada motora odnosno doživljaja tempa rada motora. Rezultat proračuna tempograma u vremenu prikazan je na Sl. 6. Na prikazanom tempogramu su razlike između benzinskog i dizel motora veoma jasno vidljive. Kod dizel motora tempogram je jasno definisan kao posledica koncentracije energije signala u okolini odgovarajućih učestanosti, dok kod benzinskog motora postoji uniformna raspodela amplituda kroz čitav opseg frekvencija.

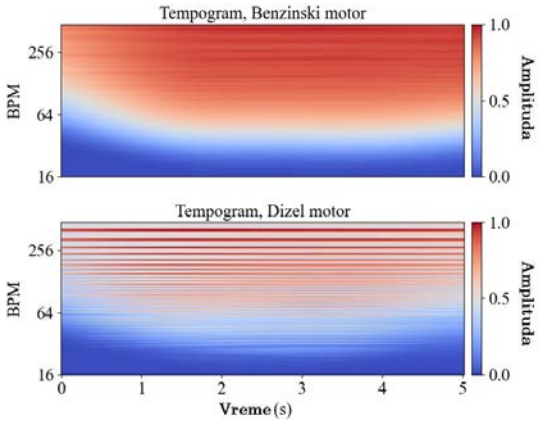


Sl. 6. Tempogram benzinskog i dizel motora

## IV. ZAKLJUČAK

Primenom akvizicionog sistema prilagođenog prikupljanju audio zapisa generisanih radom motora sa unutrašnjim sagorevanjem, prikupljeno je 350 uzoraka. Izvršeno je izdvajanje isključivo režima praznog hoda, kao režima u kome je slušaocu najjednostavnije da samo na osnovu zvuka utvrdi razliku između pogonskih goriva. Prikupljeni uzorci su analizirani u cilju pronalaženja i reprezentacije razlika koje bi omogućile primenu automatske klasifikacije upotrebom mašinskog i/ili dubokog učenja.

Prikupljanje uzoraka i klasifikacija se realizuju u realnim uslovima, što je stvorilo potrebu da se pronađu parametri na osnovu kojih će biti moguće razlikovati pogonska goriva bez obzira na okolnu buku. U ovom radu je korišćen metod mapiranja audio signala u slike bazirane na spektrogramu.


ISBN 978-86-7466-930-3

Odgovarajućim odabirom tipa prikaza kao i parametara izračunavanja dobijene su slike na kojima je moguće jasno uočiti razlike između pogonskih goriva.

U poglavlju rezultati su dati uporedni prikazi za benzinski i dizel motor na primeru dva karakteristična audio signala. Prikazani spektrogrami signala daju uočljivu razliku kako za prikaz u linearnoj tako i za prikaz u logaritamskoj razmeri, pri čemu prikaz u logaritamskoj razmeri daje mogućnost detaljnije analize nivoa signala po frekvencijama (Sl. 2 i 3). Za oba prikaza dizel motor ima veću energiju skoncentrisanu na nižim učestanostima. Mapiranjem signala u hromagram takođe su dobijene jasno uočljive razlike u pogledu pogonskih goriva (Sl. 4). Na osnovu hromagrama uočljivo je da dizel motor generiše zvuk gotovo podjednako zastupljen na svim klasama tonova, pri čemu su više istaknute klase povišenih/sniženih tonova u odnosu na benzinski motor gde su istaknutije kase osnovnih tonova. Generisanjem gamatonegrama moguće je uočiti razliku koja se pre svega odnosi na nivo signala u čitavom opsegu, koji je kod dizel motora evidentno viši (Sl. 5). Izračunavanjem tempograma (Sl. 6) moguće je kod dizel motora uočiti jasnu koncentraciju energije za odgovarajuće nivoe tempa, dok je kod benzinskog motora tempogram gotovo uniforman.

Dobijene razlike za izdvojene parametre pružaju mogućnost binarne klasifikacije pogonskih goriva što predstavlja nastavak ovog istraživanja i budući rad za koji je bilo neophodno izvršiti ovakvu analizu.

## ZAHVALNICA

Ovaj rad je realizovan zahvaljujući gospodinu Neđi Petijeviću ispred firme Novi Dom doo u Beogradu koji je omogućio pristup ulaznoj rampi podzemne garaže uz poštovanje svih bezbednosnih procedura. Ovaj rad je podržan od strane Ministarstva prosvete, nauke i tehnološkog razvoja Republike Srbije, evidencioni broj 451-03-68/2022-14/200102.

## LITERATURA

[1] G.P. Chossière, R.Malina, F. Allroggen, S. D. Eastham, R.L. Speth, S.R.H. Barrett, "Country- and manufacturer-level attribution of air quality impacts due to excess NOx emissions from diesel passenger vehicles in Europe", Atmospheric Environment, Volume 189, Pages 89-97, September 2018.

[2] M. Milivojčević, F. Pantelić, D. Ćirić, "Comparison of frequency characheristic of sound generated by internal combustion engines depending on fuel," Proc. 26th Noise and Vibration, Niš, Serbia, pp. 115-120, 6-7 December 2018.

[3] M. Milivojčević, F. Pantelić, D. Ćirić, "Pozicioniranje mikrofona prilikom snimanja audio karakteristika motora putničkih vozila" Proc. 63rd National Conference on Electrical, Electronic and Computing Engineering ETRAN, Srebrno Jezero, Serbia, pp. 58-62, 3-6 June 2019.

[4] M. Milivojčević, D Ćirić, „Izdvajanje značajnih akustičkih karakteristika motora sa unutrašnjim sagorevanjem" Proc. 64rd National Conference on Electrical, Electronic and Computing Engineering ETRAN, Belgrade, Serbia, 2020.

[5] D. Ćirić, Z. Perić, J. Nikolić, N. Vučić, "Audio Signal Mapping into Spectrogram-Based Images for Deep Learning Applications," 2021 20th International Symposium INFOTEH-JAHORINA (INFOTEH), 2021, pp. 1-6.

[6] F. A. Andrade, I. Esat, and M.N.M. Badi, "Gearbox fault detection using statistical methods, time–frequency methods (STFT and Wigner–Ville distribution) and harmonic wavelet-A comparative study," in Proceedings of the COMADEM '99, Chipping Norton, pp. 77–85, 1999.

[7] Mark A. Bartsch, Gregory H. Wakefield, "Audio thumbnailing of popular music using chroma-based representations," IEEE Trans. Multimedia, vol. 7, no. 1, pp. 96–104, 2005.

[8] Daniel PW Ellis, "Gammatone-like spectrograms," web resource: http://www.ee.columbia.edu/dpwe/resources/matlab/gammatonegram, 2009.

[9] Roy D Patterson, "Auditory filters and excitation patterns as representations of frequency resolution," Frequency selectivity in hearing, 1986.

[10] Brian R Glasberg and Brian CJ Moore, "Derivation of auditory filter shapes from notched-noise data," Hearing research, vol. 47, no. 1-2, pp. 103–138, 1990.

[11] Nguyen, Anh & Phan, Ben & Tran, Khoa & Nguyễn, Trường. (2020). Deep Learning Framework Applied for Predicting Anomaly of Respiratory Sounds..

[12] Grosche, Peter, Meinard Müller, and Frank Kurth. "Cyclic tempogram - A mid-level tempo representation for music signals." ICASSP, 2010.

## ABSTRACT

Internal combustion engines as well as other types of engines and machines generate sound during their operation. It is characterized by specific properties depending on the type of engine, operating mode, as well as the condition of the engine itself. Based on the sound, it is possible to extract important information about the engine, including the detection of fuel (gasoline or diesel). In that regard, in this paper, the analysis of acoustic signals of internal combustion engines is performed after their mapping into the appropriate images, namely spectrogram, chromagram, gammatonegram and tempogram. As all these images have the form of a classical spectrogram, they are called in the literature images based on a spectrogram or similar to a spectrogram. The aim of the analysis is to compare the above images and to determine which of them best shows the difference between the signals of the engine that runs on gasoline and diesel fuel. The analysis is performed on a database of 350 recorded signals, so that in the continuation of the research, using the selected method of mapping the signals into images, the fuel classification will be performed with the highest possible accuracy using deep learning techniques.

## Comparative analysis of acoustic signals generated by internal combustion engines mapped into spectrogram-based images

Marko Milivojčević, Emilija Kisić, Dejan Ćirić

 ISBN 978-86-7466-930-3

# Koeficijent inharmoničnosti tonova harfe – Specifičnost i problemi automatske procene

Tatjana Miljković, Miloš Bjelić, Jelena Ćertić, Dragana Šumarac Pavlović

***A stra t*— vaj rad bavi se ara terizacijom tona harfe i predstavlja nastavak istraživanja vezanih za ara terizaciju tonova žičanih instrumenata. ara terizacija tona harfe bazirana je pre svega na proceni oeficijenta inharmoničnosti. Inharmoničnost je svojstvo tonova žičanih instrumenata i ogleda se u odstupanju fre vencija parcijala od vrednosti celobrojnih umnožaka osnovne frekvencije. Preciznost automats og određivanja oeficijenta inharmoničnosti otežano je postojanjem "fantoms ih" parcijala oji su posledica različitih fizičkih procesa oji zavise od konstrukcije instrumenta, načina pobude, ao i materijala od kojih su žice napravljene. ao posledica onstru cije instrumenta i načina zatezanja žice, od harfe su veoma izraženi višestruki pikovi u spektru koji otežavaju automatsko izračunavanje koeficijenta inharmoničnosti. oeficijent je procenjen uz pomoć P D algoritma i upoređen sa vrednostima oje su procenjene uz pomoć namenski napravljenog alata za manuelnu procenu. rednosti oeficijenata za harfu upoređeni su sa vrednostima oeficijenta kod klavira i čembala.**

***Ključne reči*—Inharmoničnost parcijala, harfa, procena spe tra, „fantoms i" parcijali**

## I. UVOD

Muzički ton karakteriše diskretan spektar sa harmonijski raspoređenim komponentama na celobrojnim umnošcima osnovne frekvencije. Jedna od specifičnosti tonova žičanih instrumenata je pojava inharmoničnosti parcijala koja se ogleda u odstupanju frekvencija parcijala od harmonijskog niza. Ovo svojstvo je prisutno kod svih žičanih instrumenata, ali je kod nekih manje ili više izraženo. Konstrukcija instrumenta, dužina žice, materijal od koga je žica napravljena, način okidanja žice, kao i način pričvršćivanja i zatezanja dovode do različitih fizičkih procesa koji za posledicu imaju odstupanje frekvencija modova od pravilnog harmonijskog niza.

Druga osobina spektra tonova žičanih instrumenata je prisustvo parazitnih diskretnih komponenti koji su posledica više različitih faktora: sprezanja oscilovanja susednih žica, sprezanja oscilovanja žice sa drugim rezonantnim sistemima, kao i nelinearne pojave koje prouzrokuju pojavu takozvanih „fantomskih" parcijala [1-3]. U slučaju harfe koja je predmet analize u ovom radu, veoma su izraženi skoro svi nabrojani faktori koji kao posledicu imaju dodatne komponente u spektru tonova koje su tema brojnih istraživanja [1-5].

Usled transverzalnih vibracija javljaju se nelinarnosti u procesu oscilovanja koji kao posledicu imaju pojavu takozvanih „fantomskih" parcijala [3, 6]. Fantomski parcijali se pojavljuju kao zbirovi inharmoničnih parcijala nižeg reda ili kao dvostruke vrednosti parnih harmonika. Posledica dodatnih pikova u spektru u okolini inharmoničnih modova prouzrokuje amplitudsku modulaciju anvelope harmonika koja utiče na boju zvuka. Kod različitih žičanih instrumenata postoje manje ili više izraženi pojedini efekti koji utiču na formiranje prepoznatljive boje zvuka određenog instrumenta. Navedeni artefakti spektra dodatno usložnjavaju njegovu prirodu, što za posledice ima komplikacije prilikom procene koeficijenta inharmoničnosti.

U cilju karakterizacije tonova žičanih instrumenata na osnovu koeficijenta inharmoničnosti neophodno je obuhvatiti ceo registar instrumenta. S obzirom da se registri instrumenata razlikuju, kao i da ih čini mnoštvo tonova uglavnom od 80 do 100, potrebno je izvršiti automatizaciju procesa procene koeficijenta inharmoničnosti. U literaturi postoje različite metode i algoritmi za procenu koeficijenta inharmoničnosti [7,8,9]. Uglavnom se automatska procena koeficijenta inharmoničnosti zasniva na proceni diskretnih inharmonijskih parcijala u spektru. Procena takvih parcijala iz spektra tona često je otežana zbog prisustvu brojnih izraženih spektralnih komponenti u blizini inharmoničnih parcijala. U ovom radu razmatrani su specifičnosti automatske procene koeficijenata inharmoničnosti, kao i problemi koji su doveli do otežane realizacije automatske procene.

Rad je organizovan kako sledi. U drugom poglavlju rada prikazana je konstrukcija i način proizvođenja tonova različitih tonskih visina, kao i karakteristike spektra i vremenskog razvoja pojedinih parcijala tonova hafre. U trećem poglavlju prikazana su dva postupka za procenu koeficijenta inharmoničnosti. Jedan postupak zasniva se na automatskoj proceduri zasnovanoj na PFD (*Partial Fre uency e iation*) algoritmu sa procenom spektra na bazi AR (*Auto egressi e*) modela, a drugi postupak baziran je na manuelnoj proceni na bazi namenski napravljenog alata. U IV poglavlju prikazani su i diskutovani eksperimentalni rezultati proračuna koeficijenta inharmoničnosti za kompletan registar tonova harfe. Procena je izvršena za sve tri pozicije pedala kao i uporedna analiza automatskog i manuelnog postupka procene. Procenjene vrednosti koeficijenta inharmoničnosti za harfu upoređene su sa vrednostima dobijenim za klavir i čembalo koji su analizirani u prethodnim istraživanjima.

Tatjana Miljković – Elektrotehnički fakultet, Univerzitet u Beogradu, Bulevar Kralja Aleksandra 73, 11020 Beograd, Srbija (e-mail: tm@ etf.bg.ac.rs).

Miloš Bjelić – Elektrotehnički fakultet, Univerzitet u Beogradu, Bulevar Kralja Aleksandra 73, 11020 Beograd, Srbija (e-mail: bjelic@etf.bg.ac.rs).

Jelena Ćertić – Elektrotehnički fakultet, Univerzitet u Beogradu, Bulevar Kralja Aleksandra 73, 11020 Beograd, Srbija (e-mail: certic@ etf.bg.ac.rs).

Dragana Šumarac Pavlović – Elektrotehnički fakultet, Univerzitet u Beogradu, Bulevar Kralja Aleksandra 73, 11020 Beograd, Srbija (e-mail: dsumarac@etf.bg.ac.rs).

 ISBN 978-86-7466-930-3

## II. OSNOVNE KARAKTERISTIKE HARFE

### *A. onstrukcija harfe*

Harfa je instrument u obliku trostranog okvira, visokog oko 180 cm, sa nizom žica razapetih u uspravnoj ravni. Okvir harfe se sastoji iz 5 osnovnih delova. Osnovu instrumenta čini postolje, koje se još naziva pedalijera, jer su u njegovim stepenastim prorezima smešteni pedale za preštimavanje žica. Uspravno na postolju stoji šuplji stub, kroz čiju unutrašnjost prolaze čelične poluge koje povezuju pedale sa gornjim delom mehanizma za preštimavanje. Drugi krak okvira čini rezonantno telo, koje je takođe šuplje. Zaobljena strana rezonatora je okrenuta nadole i uglavom se izgrađuje od bukovog ili javorovog drveta.

Treću stranu okvira čini drveni vrat. Kroz vrat su provučene čivije – metalni zavrtnji koji drže gornje krajeve žica. Same žice su zakačene s leve strane, a sa desne strane se čivije mogu, posebnim ključem, zatezati ili otpuštati, čime se podešava osnovno štimovanje žica. Zajednicu sa vratom čini most, u kome se između dve mesingane ploče, nalazi gornji deo mehanizma za preštimavanje žica. Poluge ovog mehanizma, koje su kroz stub harfe povezane s pedalama u postolju, pokreću 90 bakarnih koturića postavljenih u dvostrukom nizu na spoljnoj levoj strani mosta. Svaki koturić ima po dva mala klina između kojih prolazi žica, a svaku žicu zahvataju po dva takva koturića [10]. Najniže dve do tri žice nemaju ove koturiće. Njihovi tonovi su vrlo retko u upotrebi, pa se pre sviranja štimovanje ključem podesi na onu tonsku visinu koja će biti potrebna. Na slici 1 prikazan je opisani sitem za preštimavanje žica na harfi. Takođe, na slici 1 se može uočiti kako se u postolju harfe nalaze 3 stepenasta proreza, koje označavaju da se pedale harfe mogu postaviti u 3 različita položaja.

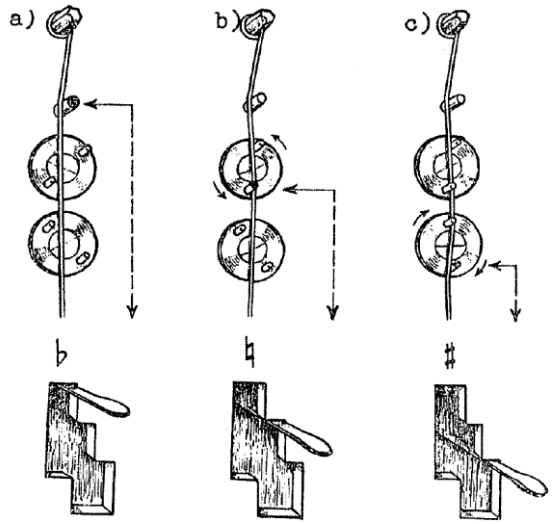


Sl. 1 Sistem preštimavanja žice na harfi; a) položaj 1 – otvorena žica, b) položaj 2 – jedanput skraćena žica, c) položaj 3 – dvaputa skraćena žica [10]

U gornjem položaju pedala je opuštena i ne deluje na gornji mehanizam, tako da klinovi koturića ne dotiču žicu i ona slobodno osciluje celom svojom dužinom. Ako se pedala pritisne i zakači u srednji položaj, taj se pritisak polugama prenosi do gornjeg od dva koturića i okreće ga za toliko, da njegovi klinovi zahvate žicu. U tom slučaju, njena aktivna dužina je skraćena, pa žica daje ton viši od osnovnog štimovanja za pola stepena. Pomeranjem u donji položaj, pedala pokreće, posredstvom poluga, i donji koturić, pa njegovi klinovi još više skrate dužinu žice i povise joj ton još za pola stepena. Opisanim postupkom, se iz svake žice mogu izvući po 3 tona različite visine. Time se postiže znatna ušteda u broju žica, što je za spretnost sviranja od velike važnosti.

Jedna pedala mehanizmom zahvata istovremeno žice istoimenih tonova u svim oktavama (npr. G1, G2, G3, G4 itd.) i zahvaljujući preštimavanju njihove hromatske varijante. Time je broj pedala sveden na 7. Oni su raspoređeni naspram leve i desne noge svirača i nose ime žica, koje kroz sve oktave, zahvataju [10]. Osnovno štimovanje harfe je dijatonski Ces-dur. Za ostvarenje te lestvice moraju sve žice da osciluju slobodno, celom dužinom, odnosno sve pedale moraju biti u gornjem položaju. Ako su sve pedale u srednjem položaju, dobija se C-dur, a donji položaj svih pedala daje Cis-dur. Kombinacijom različitih položaja pojedinih pedala može da da i bilo koju drugu lestvicu, osim naravno hromatske.

Tonski opseg harfe zahvata šest i po oktava: to je pri gornjem položaju pedala, od Ces1 do Ges7. Sa po 7 žica u okviru oktave, ukupan broj žica iznosi 46 ili 48. Orjentacija svirača u tolikom nizu žica olakšana je time, što su sve C žice obojene crveno, a sve F žice plavo. Dvanaest najnižih (najdužih) žica do As2 koje se još nazivaju bas žice imaju čelično jezgro, omotano metalnom niti; sledeći opseg od As2 do Es6 su žice od creva, i na kraju opsega od Fes6 do Ges7 žice su izgrađene od najlona.

### *B. remenske i spektralne karakteristike tono a harfe*

Harfa spada u žičane muzičke instrumente, gde se ton proizvodi trzanjem žice. Tako se i u spektru tonova harfe uočavaju pojave koje su karakteristične za žičane instrumente. Jedan od efekata je inharmoničnost koja se ogleda u odstupanju položaja parcijala od frekvencija koje su celobrojni umnožak osnovne frekvencije. Međutim, u spektru harfe, uočavaju se i druge pojave koje se ne mogu objasniti inharmoničnošću a koje otežavaju sistematsku, automatsku analizu karakteristika harfe kao tipa instrumenta i parametre koji bi opisali svaki pojedinačan instrument i omogućili objektivno poređenje instrumenata. Pojave kojima se može objasniti prisustvo artefakata u spektru signala harfe opisane su u literaturi i definišu se :

- kao posledice nelinearnosti [3,6] usled koje se javljaju komponente u spektru koje predstavljaju zbir harmonika.
- kao posledice pobuđivanja i drugih žica osim žice koja se okida [1,2] usled koje se „čuju“ i pri analizi spektra i vide komponente koje po frekvenciji odgovaraju parcijalima neke druge žice ili žica. Ova pojava opisana je posebno za hrafu i posledica je konstrukcije samog instrumenta.

Obe pojave mogu dovesti do toga da se u spektru signala pojave komponente, koje su po frekvenciji bliske nekom od osnovnih inharmoničnih parcijala. Pomenute komponente dovode do amplitudske modulacije parcijala. Na slici 2 prikazan je spektar jednog tona harfe sa detaljnijim prikazom spektra prvog i sedmog parcijala, kao i njihove vremenske obvojnice. Komponente su izdvojene primenom namenski napravljene banke filtara [11] na čijem su izlazu dostupni

 ISBN 978-86-7466-930-3

uskopojasni signali pojedinačnih parcijala. Sa slike 2 se može uočiti da u okolini sedmog harmonika postoji izražena dodatna spektralna komponenta koja menja anvelopu pacijala i dovodi do toga da se anvelopa sedmog parcijala značajno razlikuje od tipične anvelope čiji je predstavnik anvelopa prvog parcijala. U okviru ovog rada, pojave dodatnih komponenti u spektru su razmatrane jer ograničavaju mogućnost za automatsku procenu koeficijenta inharmoničnosti, o čemu će biti više reči u poglavljima III i IV.

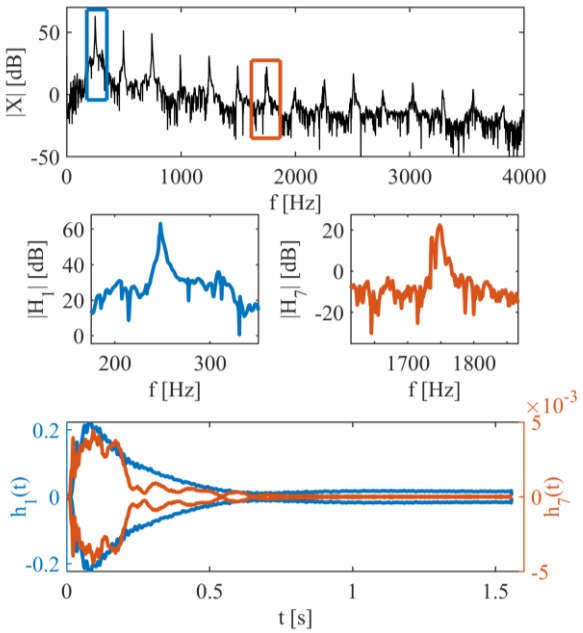


Sl. 2 Spektar tona Ces4 odsviranog na harfi sa prikazom vremenske obvojnice prvog i sedmog parcijala

## III. METODOLOGIJA ODREĐIVANJA KOEFICIJENTA INHARMONIČNOSTI

Nastanak zvuka kod žičanih instrumenata potiče od vibriranja žice. U zavisnosti od načina na koji se žica pobuđuje na vibriranje razlikujemo 3 podgrupe žičanih instrumenata (gudačke, trzane i udarne žičane instrumente). Bez obzira na različite podgrupe žičanih instrumenata, za sve tipove žičanih instrumenata kod kojih zvuk nastaje udarom žice ili njenim okidanjem, karakteristična je pojava inharmoničnosti parcijala. Izučavanjem prirode i fizičkih uzroka inharmoničnosti izvedena je zakonitosti po kojoj se može odrediti frekvencija inharmonijskih parcijala :

$$f_k = kf_0\sqrt{1+k^2B}, \qquad (1)$$

gde je $k$ redni broj harmonika, $f_0$ osnovna frekvencija tona, a $B$ koeficijent inharmoničnosti [12]. Za svaki ton postoji jedinstven koeficijent inharmoničnosti $B$ koji u izvesnoj meri na istom instrumentu varira sa promenom tonskih visina.

Procena $B$ zasniva se na proceni spektra i u literaturi su predloženi različiti algoritmi za njegovu automatsku procenu. [7,8,9]. U ovom radu za automatsku procenu koeficijenta inharmoničnosti $B$ razmatran je PFD algoritam [13]. Kako su automatskom procenom dobijene vrednosti $B$ koje neočekivano variraju sa promenom tonskih visina, paralelno je izvršena procena $B$ uz pomoć namenski napravljenog alata za manuelnu procenu.

### *A. Automatska procena koeficijenta inharmoničnosti na osno u PF algoritma*

PFD algoritam se može razmatrati kao algoritam koji se izvršava u dve etape. U prvoj etapi algoritma je neophodno izvršiti procenu spektra signala i odrediti prvih $k$ frekvencija parcijala analiziranog tona. Grupa Finskih naučnika koja je predložila PFD algoritam kao algoritam za automatsku procenu $B$, procenu spektra tona bazirala je na DFT ( *iscrete Fourier Transform*) metodi [13].

U prethodnim radovima pokazani su nedostaci takve metode za procenu spektra tonova[14,15]. Zbog navedenih nedostataka kao metod za procenu spektra predložen je AR model [15].

AR modelovanje podrazumeva da se na osnovu segmenata signala procene koeficijenti modela. Znajući koeficijente modela, za signale kod kojih su spektralne komponente izražene moguće je izvršiti procenu frekvencija spektralnih komponenti. Detaljni opis primenjenog AR modela prikazan je u radovima [16]. Krajnji rezultat metode AR modelovanja je procenjivanje frekvencija spektralnih komponenti na osnovu položaja dominantnih polova.

Druga etapa PFD je iterativni postupak koji se zasniva na izračunavanju devijacije frekvencije parcijala, gde se proračunava razlika niza frekvencija parcijala dobijenih iz procene spektra i odgovarajućeg niza frekvencija parcijala dobijenih na osnovu jednačine (1) za vrednost $B$ u tekućoj iteraciji. Na osnovu trenda devijacije frekvencije, potrebno je doneti odluku da li se vrednost koeficijenta $B$ smanjuje ili povećava [13]. Nakon određenog trenda devijacije moguće je modifikovati vrednost koeficijenta $B$ polaznog tona. Minimizacijom krive devijacije postiže se konvergencija algoritma. Konačni rezultat cele procedure predstavlja jednobroja vrednost koeficijenta inharmoničnosti $B$ za posmatrani ton.

### *B. Procena koeficijenta inharmoničnosti pomoću specijali o anog alata*

Sa ciljem da se detaljnije sagleda priroda spektra tonova realizovan je specijalizovani alat za analizu tonova muzičkih instrumenata. Alat je nastao kao unapređenje ranije realizovane komplementarne filtarske banke [11]. Razvijanje alata je sprovedeno u MATLAB okruženju kao grafički interfejs (slika 3). Osnovne karakteristike alata koje su implementirane odnose se na sledeće kontrole: učitavanje signala, filtriranje namenski projektovanom bankom usklađenom sa karakteristikama spektra, određivanje osnovne frekvencije signala i definisanje pozicije parcijala u odnosu na zadatu vrednost $B$ (prema formuli (1)), kao i uskopojasno filtriranje prema definisanim frekvencijama inharmonijskih parcijala**.** Uz pomoć dva klizača vrši se manuelno podešavanje koeficijenta inharmoničnosti $B$, za zadati broj parcijala.

Na slici 3 dat je prikaz interfejsa specijalizovanog alata, gde je učitan signal ton As2 odsviranog na harfi. Na prikazanom logaritamskom spektru, isprekidanim crvenim linijama čiji je

 ISBN 978-86-7466-930-3

broj određen brojem upisanim u polje „ukupno“ obeležene su pozicije parcijala tona. Pomeranjem klizača $f_0$ i $B$ menjaju se pozicije isprekidanih crvenih linija. U cilju što bolje procene koeficijenta $B$ neophodno je pozicionirati isprekidane crvene linije tako da odgovaraju vrhovima spektralnih komponenti parcijala analiziranog tona. Vrednosti $f_0$ i $B$ za koje se isprekidane linije najbolje poklapaju sa spektralnim komponentama tona proglašavamo za procenjene vrednosti osnovne frekvencije i koeficijenta inharmoničnosti analiziranog tona.

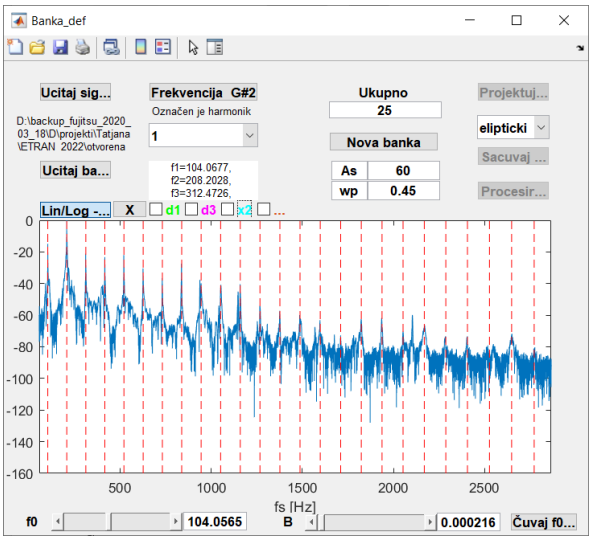

Sl. 3 Prikaz interfejsa alata za analizu pojedinačnih tonova muzičkih instrumenata

Detaljnijim uvidom u spektar posmatranog tona (slika 4) u opsegu od 1000 do 2000 Hz, može se uočiti postojanje spektralnih komponenti veoma frekvencijski bliskih parcijalima odsviranog tona. Pored postojanja udvojenih parcijala, još jedan od neregularnih spektralnih artefakta tona As2 jeste pojava veoma amplitudski izražene spektralne komponente između 2000 i 2200 Hz, koji se nalazi tačno na polovini između 19og i 20og harmonika tona As2. Navedeni fenomeni koji se pomoću specijalizovanog alata mogu uočiti u spektru tona otežavaju automatizaciju procene koeficijenta inharmoničnosti za ceo opseg tonova harfe.

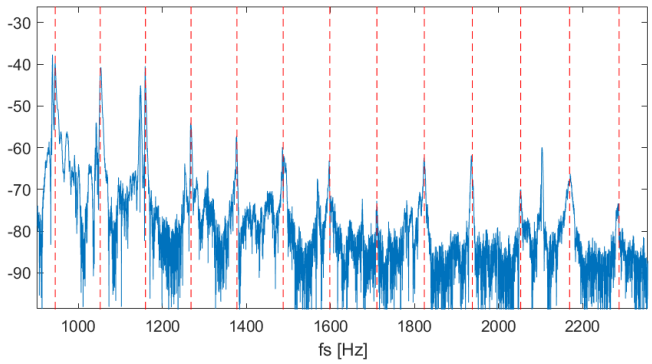

Sl. 4 Deo spektra tona As2 odsviranog na harfi

## IV. EKSPERIMENTALNI REZULTATI I DISKUSIJA

U prethodnom poglavlju izložene su dve metodologije za određivanje koeficijenta inharmoničnosti, automatska procena na osnovu PFD algoritma i procena pomoću specijalizovanog alata. Krajnji rezultat obe metodologije jeste vrednost koeficijenta inharmoničnosti za celokupni opseg harfe. Bazu čini 141 snimak tonova odsviranih na harfi. Snimljeni tonovi pokrivaju celokupni registar harfe, odnosno svih 47 žica su pobuđene za sva 3 položaja pedale. Tonovi harfe snimljeni su u prostorijama Fakulteta muzičke umetnosti u Beogradu.

### *A. omparacija re ultata koeficijenta inharmoničnosti algoritmom i pomoću alata*

Uticaj dve metodologije na procenu koeficijenta inharmoničnosti najbolje se može uočiti poređenjem trenda krive koeficijenta $B$. Na slici 5 dat je grafik koeficijenta inharmoničnosti $B$ za tonove harfe odsvirane za položaj 1 pedale, odnosno za slučaj kada je žica otvorena. Koeficijenti inharmoničnosti su dobijeni na osnovu dve metofologije, pomoću PFD algoritma i manuelno, odnosno pomoću specijalizovanog alata. Za tonove iz srednjeg i višeg registra harfe koeficijenti $B$ procenjeni na osnovu dve metodologije se ne razlikuju previše, dok za slučaj tonova iz nižeg registra dolazi do uočljivog razilaženja u vrednostima i to za red veličine. Glavni razlog za lošiju procenu koeficijenta inharmoničnosti na osnovu algoritma leži u kompleksnosti spektra tona harfe koji se odlikuje sa udvojenim parcijalima čije su vrednosti i frekvencijski i amplitudski veoma bliske, te se sam algoritam u odabiru spektralnih komponenti parcijala tona odluči za pogrešan.

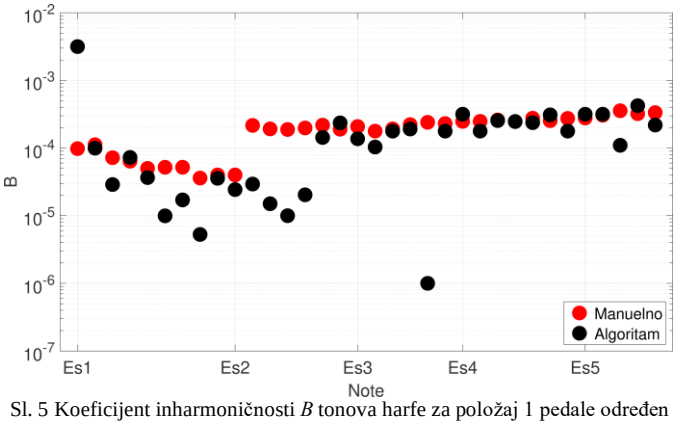

Sl. 5 Koeficijent inharmoničnosti $B$ tonova harfe za položaj 1 pedale određen algoritmom i pomoću specijlizovanog alata

### *B. Procena koeficijenta inharmoničnosti za različite položaje pedala harfe*

Na slici 6 prikazani su koeficijenti $B$ tonova odsviranih na harfi za sva tri položaja pedale. Trend krive koeficijenta $B$ očuvan je za sva tri položaja pedale. Za razliku od trenda krive koeficijenta $B$ koji je očuvan razlike u vrednostima koeficijenta $B$ za tonove iz nišeg registra u odnosu na vrednosti koeficijenta $B$ za tonove iz srednjeg i višeg registra postoji. Procenjene vrednosti koeficijenta $B$ kreću se u rasponu od $3{\cdot}10^{-4}$ do $2{\cdot}10^{-3}$. Veće vrednosti $B$ označavaju veću inharmoničnost, odnosno veće odstupanje inharmonijskih frekvencija u odnosu na očekivane frekvencije harmonijskog niza. Na osnovu skoka u vrednosti koeficijenta

 ISBN 978-86-7466-930-3

inharmoničnosti možemo zaključiti da na samu vrednost koeficijenta inharmoničnosti utiče značajno materijal od kojeg je žica napravljena, s obzirom da su tonovi iz nižeg registra proizvedeni na metalnim žicama, dok su tonovi iz srednjeg i višeg registra proizvedeni na crevnim i najlonskim žicama.

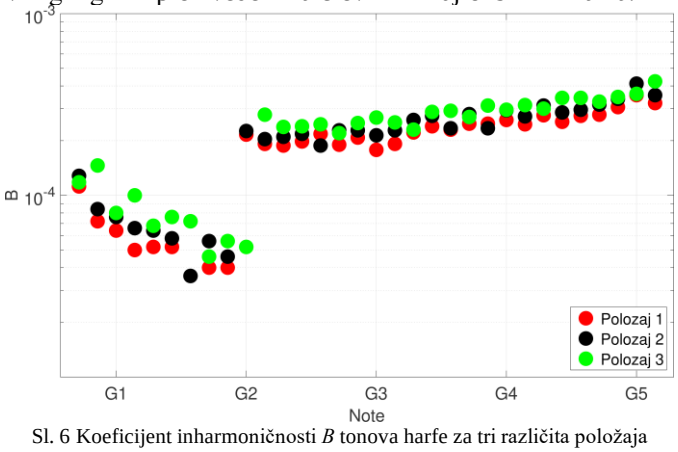


Sl. 6 Koeficijent inharmoničnosti *B* tonova harfe za tri različita položaja pedale

Još jedan od fenomena harfe kao muzičkog instrumenta se može uočiti iz krive koeficijenta inharmoničnosti prikazanog na slici 6. Iako postoje tonovi koji su enharmonski parovi (tonovi jednakih tonskih visina, ali različite notacije npr. Gis i As) njihovi koeficijenti inharmoničnosti se međusobno razlikuju. Razlog za razlike u vrednostima koeficijenta *B* se krije upravo u fizici nastanka tona. Iako su to tonovi istih osnovnih frekvencija, da bi se na harfi dobio ton As pedala se nalazi u položaju 1, žica je otvorena i kao takva osciluje, dok za slučaj tona Gis pedala se nalazi u položaju 3 i pomoću mehanizma sa dva koturića žica je skraćena na dva mesta za razliku od žice kada se pedala nalazi u položaju 1. S obzirom na fizičko skraćivanje žice, menjaju se i granični uslovi oscilovanja žice. Opisane razlike za enharmonski par tonova As2 i Gis2 mogu se uočiti i u prikazima njihovih spektara. Na slici 7 dat je prikaz tonova As2 i Gis2 odsviranih na harfi. Sa slike se može uočiti da na frekvencijama od 1000 Hz parcijali tonova As2 i Gis2 se razilaze za par Hz, što za posledicu ima različite vrednosti koeficijenta inharmoničnosti.

Osim razilaženja u frekvenciji inharmonijskih parcijala dolazi do pomeranja i „fantomskih“ parcijala koji su zavisni od osnovnih inharmonijskih parcijala.

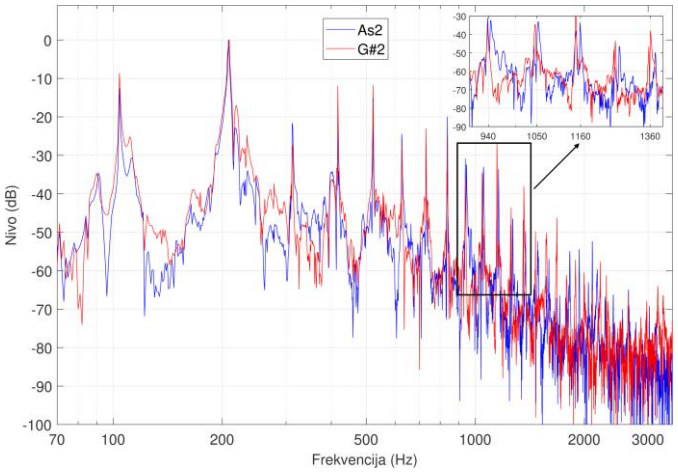


Sl. 7 Prikaz spektra tonova As2 i Gis2 odsviranih na harfi

### *C. Poređenje procenje rednosti koeficijenta inharmoničnosti a tono e harfe, klavira i čembala*

Koeficijent inharmoničnosti predstavlja kako kvalitativan tako i kvantitativan atribut tona žičanih muzičkih instrumenata. Sa ciljem opisivanja razlike između različitih klasa žičanih instrumenata izvršeno je poređenje koeficijenta inharmoničnosti tonova klavira, čembala i harfe. Na slici 8. prikazani su procenjeni koeficijenti inharmoničnosti za opseg tonova koji je zajednički za sva tri instrumenta, odnosno za tonove iz opsega od G1 do C6. S obzirom da se kod harfe ne može postići potpuna hromatika, kao kod klavira i čembala, pri izračunavanju koeficijenta inharmoničnosti tonova harfe, tonovi su birani tako da se njihove osnovne frekvencije slažu sa osnovnim frekvencijama tonova klavira i čembala. Takođe, koeficijenti *B* tonova harfe prikazani na grafiku određeni su pomoću specijalizovanog alata, a ne automatskom procedurom pomoću PDF algoritma. Na osnovu slike se može zaključiti da je trend krive koeficijenta inharmoničnosti za sva tri instrumenta očuvan. Vrednosti koeficijenta *B* tonova harfe iz nižeg registra se poklapaju sa vrednostima koeficijenta *B* klavira, što se objašnjava činjenicom da su žice od istog materijala, čak i poredive dužine. Takođe, činjenica da se u srednjem i višem registru vrednosti koeficijenata *B* harfe razlikuju i od koeficijenata *B* čembala i klavira može se opravdati različitim materijalom žice, gde su kod klavira i čembala žice metalne, a kod harfe od creva.

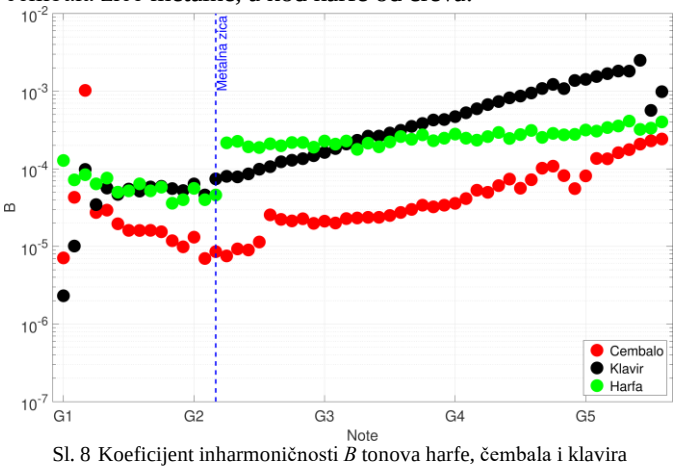


Sl. 8 Koeficijent inharmoničnosti *B* tonova harfe, čembala i klavira

Posledice različitih vrednosti koeficijenta inharmoničnosti za tonove klavira, čembala i harfe mogu se uočiti uporednom analizom spektra tonova pomenutih instrumenata. Na slici 9 dat je prikaz spektra tona iste frekvencije odsviranih na klaviru, čembalu i harfi. Na osnovu spektra signala može se uočiti da iako su tonovi istih frekvencija pozicije njihovih parcijala se razlikuju, što doprinosi različitim vrednositma koeficijenta inharmoničnosti. Takođe, poređenjem spektara tonova za tri navedena instrumenta može se zaključiti da je broj izraženih parcijala kod tona harfe manji u odnosu na broj izraženih parcijala klavira i čembala. Ta činjenica direktno utiče na vrednosti koeficijenata inharmoničnosti, s obzirom da se njegova vrednost procenjuje na osnovu frekvencija parcijala tonova, gde spektralno bogatstvo parcijala doprinosi niže procenjenoj vrednosti koeficijenta inharmoničnosti, a njihovo odsustvo utiče na povećanje procenjene vrednosti koeficijenta inharmoničnosti.

 ISBN 978-86-7466-930-3

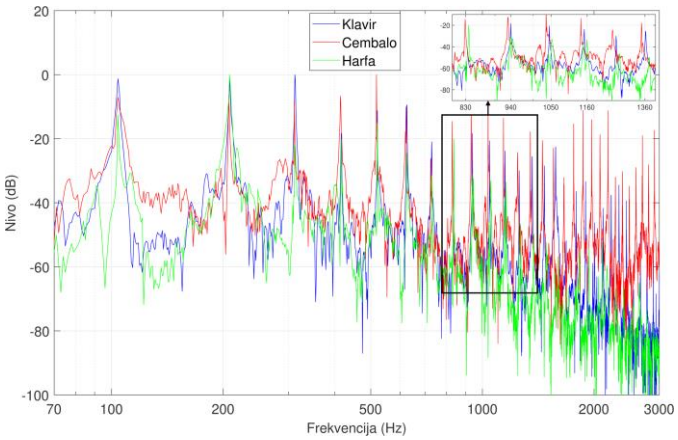


Sl. 9 Prikaz spektra tonova iste frekvencije odsviranih na klaviru, čembalu i harfi

## V. ZAKLJUČAK

U ovom radu razmatran je koeficijent inharmoničnosti tonova harfe kroz prizmu automatske procene i specifičnosti koje prati data problematika. Formirana je baza snimaka koja se sastoji od 141 tonova odsviranih na harfi. Harfa je izabrana kao instrument u cilju proširivanja prethodnog istraživačkog rada i upotpunjavanja do sada formirane baze tonova žičanih muzičkih instrumenata. Koeficijent inharmoničnosti je računat na osnovu automatske procedure pomoću modifikovanog PFD algoritma. Pokazano je da za pojedine tonove iz nižeg registra harfe dobijene vrednosti koeficijenta inharmoničnosti na osnovu automatske procedure nisu dobro procenjene. Iz tog razloga realizovan je specijalizovani alat za analizu audio signala, pomoću koga se manuelnom inspekcijom može proceniti koeficijent inharmoničnosti tonova žičanih instrumenata. Novonastali specijalizovani alat otvara nove istraživačke mogućnosti, gde će nastavak istraživanja podrazumevati savladavanje problema automatske procene. Pored toga, kreirani alat otvara mogućnosti za proširivanje samog istraživanja dodavanjem mogućnosti ne samo analize tonova žičanih muzičkih instrumenata, već i njihove sinteze.

## ZAHVALNICA

Ovaj rad je realizovan u okviru projekta TR36026 koji finansira Ministarstvo prosvete, nauke i tehnološkog razvoja Republike Srbije. Zahvaljujemo se profesorki dr um. Mileni Stanišić na pomoći pri formiranju baze snimaka neophodnoj za ovo istraživanje.

## LITERATURA

[1] J-L. Le Carrou, F. Gautier, E. Foltête, "Experimental study of A0 and T1 modes of the concert harp", *.Acoust.Soc.Am*., Vol. 121(1), pp.559-567, January 2007.
[2] J-L. Le Carrou, F. Gautier,R.Badeau, "Sympathetic String Modes in the Concert Harp", *Acta Acustica united with Acustica*, Vol. 95, pp. 744-752, 2009.
[3] Harold A. Conklin, Jr., "Generation of partials due to nonlinear mixing in a stringed instrument", *.Acoust.Soc.Am*., Vol. 105(1), pp.536-545, January 1999.
[4] V. Bucur, "About the acoustic and other non-destructive methods for the characterization of old historical string musical instruments – an overview", 22nd International Congress on Acoustics, ICA 2016, Buenos Aires – 5 to 9 September, 2016.
[5] V. Bucur, "Handbook of Materials for String Musical Instruments", ISBN: 978-3-319-32078-6 Springer,2016.
[6] Harold A. Conklin, Jr., "Piano strings and "phantom" partials", *.Acoust.Soc.Am*., Vol. 102(1), pp.536-545, July 1997.
[7] A.S. Galembo, and A. Askenfelt, A. "Signal representation and estimation of spectral parameters by inharmonic comb filters with application to the piano," IEEE Trans. Speech Audio Process, vol. 7, no.2, pp. 197–203, 1999.
[8] A. Askenfelt and A.S. Galembo, "Study of the spectral inharmonicity of musical sound," Acoust. Phys. vol. 46, no. 2, pp. 121–132, 2000.
[9] A. Klapuri, "Multiple fundamental frequency estimation based on harmonicity and spectral smoothness," IEEE Trans. Speech Audio Process, vol. 11, no. 6, pp. 184–194, 2003.
[10] D. Despić, *Muzički instrumenti*, Univerzitet umetnosti Beograd, 1979.
[11] J. Ćertić, D. Šumarac Pavlović, I. Salom, "Softverski paket za obradu i analizu audio signala", TELFOR 2010, pp. 1269-1272, Beograd, Nov.,2010
[12] H. Fletcher, E. D. Blackham, and R. Stratton, "Quality of piano tones", *. Acoust. Soc. Am*., vol. 34, no. 6, pp. 749–761, 1962.
[13] J. Rauhala, H.M. Lehtonen, V. Välimäki, "Fast automatic inharmonicity estimation algorithm"Acoust. Soc. Am., vol. 121, EL184, doi:10.1121/1.2719043, 2007
[14] T. Miljković, M. Bjelić, D. Šumarac Pavlović, J. Ćertić, "Analiza algoritma za procenu koeficijenta inharmoničnosti različitih klavira", Zbornik radova 64. Konferencije ETRAN, pp. AK1.2.1 - AK1.2.6, Beograd, Sep, 2020.
[15] T. Miljković, J.Damnjanović, J. Ćertić, D. Šumarac Pavlović, "Uticaj estimacije frekvencija harmonica na procenu koeficijenta inharmoničnosti čembala", Zbornik radova 65. Konferencije ETRAN, pp. 9 -14, Etno selo Stanišići, Sep, 2021.
[16] P.A.A. Esquef, M. Karjalainen, and V. Välimäki, "Frequency-Zooming ARMA Modeling for Analysis of Noisy String Instrument Tones", EURASIP J. Adv. Signal Process, pp. 953-967, 2003.

## ABSTRACT

This paper deals with the characterization of harp tones and presents continuation of research related to the string instruments characterization. The characterization of the harp tone is based primarily on the estimation of the inharmonicity coefficient. Inharmonicity is a property of the tones of string instruments and is reflected in the deviation of the partial frequencies from the integer multiple of the fundamental frequency. The accuracy of the automatic determination of the inharmonicity coefficient B is hampered by the existence of "phantom" partials which are consequences resulting from different physical processes that depend on the construction of the instrument, the excitation method, as well as the materials from which the strings are made. As a consequence of the instrument construction and the way the string is tightened, in harp multiple peaks in the spectrum are very pronounced, which makes it difficult to automatically calculate inharmonicity coefficient. The coefficient B was estimated using the PFD algorithm and compared with the values estimated using a purpose-built tool for manual estimation. The coefficient B values of the harp were compared with the values of the coefficient B of piano and harpsichord.

**Inharmonicity coefficient of harp tones - pecificity and problems of automatic estimation**

Tatjana Miljković, Miloš Bjelić, Jelena Ćertić, Dragana Šumarac Pavlović

 ISBN 978-86-7466-930-3

# Implementacija algoritama za kontrolu usmerenosti zvučničkog niza sa dva glavna loba na otvorenom hardveru

Tijana Đorđević, Stefan Aćimović, Miloš Bjelić

***A stra t*— ovom radu pri azana je implementacija softverski usmerenih zvučničkih sistema. Softverski i hardvers i implementirani usmereni zvučnički sistemi, osim što povećavaju nivo zvu a u zadatom pravcu, takođe dovode i do smanjenja reverberacije. U implementaciji korišćeni su zvučnički niz i procesor na kome se izvršavaju tri različita algoritma za obradu signala. Prvo rešenje podrazumeva usmeravanje zvuka ka jednoj zadatoj tački, a drugo i treće rešenje podrazumevaju usmeravanje zvuka ka dvema tačkama koje su proizvoljno zadate. Akcenat rada je na drugom i trećem rešenju koja se koriste u slučajevima kada želimo da obezbedimo pokrivanje dva pravca u auditorijumu. Pored tri nezavisna algoritma u radu je pri azana i simulacija pomoću koje je moguće predvideti dijagrame usmerenosti u sva tri slučaja. Rezultati algoritma vantifi ovani su merenjem dijagrama usmerenosti po 1 oktavnim frekvencijskim opsezima. Biće pomenuti detalji implementacije i pojedinosti na oje treba obratiti pažnju prili om rada sa hardvers om platformom ela. radu su izložena poboljšanja koja su dobijena korišćenjem dva, umesto jednog snopa zvu a.**

***Ključne reči*—hardvers a platforma ela, dijagram usmerenosti, softverska kontrola usmerenosti, zvučnički niz.**

## I. UVOD

Sa napretkom sistema za ozvučavanje i sa povećanjem zahteva korisnika sve je više istraživanja u oblasti softverski usmerenih zvučničkih sistema. Istorijski gledano pre ovih sistema nastali su sistemi koji su se na terenu podešavali tako što se od nekoliko zvučnika napravi niz koji je zakrivljen. Zakrivljenje niza omogućavalo je da se signali fazno usklade i da se maksimalna energija emituje u zadatom pravcu. Iako se ovi sistemi i danas koriste u mnogim aplikacijama, njihova nefleksibilnost je veliki problem. Potencijalno rešenje ovog problema može biti procesiranje signala koji se emituju na pojedinačnim zvučnicima. Glavna prednost ovih sistema je to što se usmeravanje zvuka može postići bez fizičkog pomeranja zvučnika. Promena željene tačke ka kojoj se fokusira zvuk može se uraditi bez menjanja položaja zvučnika. Zbog toga su ovi sistemi pogodni i za daljinsku kontrolu.

Tijana Đorđević – Elektrotehnički fakultet, Univerzitet u Beogradu, Bulevar kralja Aleksandra 73, 11020 Beograd, Srbija (e-mail: dt213283m@student.etf.bg.ac.rs).

Stefan Aćimović - Elektrotehnički fakultet, Univerzitet u Beogradu, Bulevar kralja Aleksandra 73, 11020 Beograd, Srbija (e-mail: as213306m@student.etf.bg.ac.rs).

Miloš Bjelić – Elektrotehnički fakultet, Univerzitet u Beogradu, Bulevar kralja Aleksandra 73, 11020 Beograd, Srbija (e-mail: bjelic@etf.rs).

Softverski usmereni zvučnički sistemi promenama kašnjenja signala za pojedinačne zvučnike usmeravaju zvuk ka željenoj tački. Ukoliko se signal ne procesira, maksimum će biti u osi koja je normalna na zvučnik, a pomenutim procesiranjem maksimum se pomera u željenom pravcu. Problem koji nastaje prilikom usmeravanja zvuka u jednom pravcu je izrazito jak bočni lob. Bočni lob se u mnogim slučajevima gotovo i ne razlikuje od glavnog loba. Na veličinu i širinu bočnog loba se ne može uticati, ona zavisi od frekvencije na kojoj se zvuk šalje, kao i rasporeda zvučnika na zvučničkom nizu. Teško je napraviti optimalnu geometriju zvučničkog niza koja bi za sve frekvencije podjednako dobro potiskivala bočne lobove U ovom radu će biti prikazana rešenja za softversko usmeravanje zvuka u jednom pravcu kao uvod u rešenja koja prikazuju pokrivanje dva pravca.

Do sada je u literaturi bilo pomena o implementaciji jednog loba [1]. U radu su prikazani dijagrami usmerenosti za 1/3 oktavne opsege čije su centralne frekvencije: 630 Hz, 1250 Hz, 2500 Hz i 4000 Hz. Takođe, neka istraživanja su se bavila i implementacijom algoritma za pokrivanje dva pravca [2], međutim, opseg signala koji je posmatran je ultrazvučni. Budući da će se ovi algoritmi koristiti za ozvučavanje, merenja u radu su izvršena u zvučnom opsegu. Za fokusiranje zvuka neophodan je zvučnički niz. Zvučnički nizovi se sastoje od nekoliko zvučnika raspoređenih na različite načine. Korišćeni su zvučnici koji su postavljeni duž y-ose i fokusiraju zvuk ka tački na željenoj visini. Zvučnički nizovi mogu biti sastavljeni od zvučnika sa različitim karakteristikama usmerenosti. Karakteristika pojedinačnih zvučnika utiče na formiranje dijagrama usmerenosti zvučničkog niza. Zvučnici koji se koriste u eksperimentu su kardioidni i to je neophodno implementirati u simulaciji.

Okosnicu ovog rada predstavlja implementacija sistema koji pokriva dva auditorijuma. Za ovu namenu dizajnirana su dva rešenja. Ideja prvog rešenja je da se polovina zvučnika koristi za usmeravanje signala ka jednoj tački, a druga polovina za usmeravanje signala ka drugoj tački. Budući da se za usmeravanje signala koristi samo polovina zvučnika, lobovi dijagrama usmerenosti će biti širi nego u slučaju kada usmeravanje vršimo sa svim zvučnicima. Drugo rešenje otklanja ovaj problem tako što koristi svih 8 zvučnika. Njegov glavni lob dijagrama usmerenosti za jedan pravac se praktično poklapa sa glavnim lobom u prvom slučaju kada se zvuk usmerava samo u jednom pravcu. U radu će biti prikazano poređenje rešenja kroz merne rezultate, kao i kroz simulaciju.

 ISBN 978-86-7466-930-3

Budući da se ovakvi sistemi koriste za ozvučavanje prostora neophodno je da oni rade u realnom vremenu. Ograničenje koje donosi ovaj zahtev je složenost algoritma. Poželjno je da algoritam bude što jednostavniji i da se odgovarajući parametri sistema prilikom izvršavanja algoritma na hardveru uzimaju iz memorije.

Primena pomenutih algoritama može biti u sistemima za ozvučavanje koncertnih sala, bioskopa i drugih objekata gde je neophodno pokrivanje dva pravca (parter i galerija). Takođe, moguće je da zvučnički niz bude ugrađen u TV i da u kućnim uslovima imitira *surround* sisteme.

## II. METODOLOGIJA

U nastavku će biti prikazana tri različita rešenja za softversko usmeravanje zvučnika. Kao što je pomenuto, osim algoritma koji će se izvršavati na procesoru razvijena je i simulacija za proveru rešenja. Simulacija se sastoji od programa koji generiše jedinični impuls za svaki pojedinačni zvučnik. Signal se posmatra u nekoj tački na mestu prijema i zbog toga je potrebno uračunati kašnjenje i slabljenje usled pređenog puta. Takođe, neophodno je uračunati i usmerenost pojedinačnih zvučnika koja zavisi od ugla, te signal sa svakog pojedinačnog zvučnika pomnožiti sa tom vrednošću. Ukupan signal u nekoj tački računa se kao zbir signala sa svih zvučnika. Da bi se dobio signal po 1/3 oktavnim opsezima neophodno je na kraju filtrirati ukupan signal.

### *A. smera anje zvuka ka jednoj tački u prostoru*

Prvo rešenje podrazumeva usmeravanje ka jednoj tački u prostoru. Da bi se ovo realizovalo neophodno je signale koji dolaze na ulaze Bela platforme obraditi i fazno uskladiti. Fazno usklađivanje ovih signala se vrši tako što se na različitim zvučnicima primeni različito kašnjenje. Kašnjenje zavisi od pozicije zvučnika i tačke ka kojoj se signal usmerava.

Računanje kašnjenja biće detaljno obrazloženo za ovo rešenje, a za ostala dva rešenja će biti pomenuta ograničenja i izmene. Na slici 1 prikazan je zvučnički niz i usvojeni koordinatni sistem. Centar koordinatnog sistema je sredina zvučničkog niza. Ugao $\varphi$ je ugao između -ose i prave koja spaja koordinatni početak i tačku A. Tačka A predstavlja tačku u kojoj je potrebno fokusirati zvuk. Rastojanje između tačke A i koordinatnog početka je D. Koordinate tačke A računaju se na osnovu sledećih izraza:

$$_A = \cdot\cos(\varphi) \quad (1)$$

$$y_A = \cdot\sin(\varphi) \quad (2)$$

Rastojanje između tačke A i zvučnika *i* računa se na sledeći način:

$$r_i = \sqrt{\left( _A - _i \right)^2 + \left( y_A - y_i \right)^2} \quad (3)$$

gde su $_i$ i $y_i$ koordinate pojedinačnih zvučnika.

Ukoliko fazno ne uskladimo pojedinačne zvučnike, signal sa zvučnika 1 će prvi stići do tačke, a potom redom signali sa zvučnika 2, 3 itd. Kako bi se fazno uskladili signali neophodno je primeniti kašnjenja na svakom signalu. Kašnjenja se računaju prema sledećem izrazu:

$$\Delta t_i = \frac{r_{\max} - r_i}{c} \quad (4)$$

$$r_{\max} = \max\{r_i\}, i = 1,2...N \quad (5)$$

gde je $N$ ukupan broj zvučnika, u ovom slučaju 8, a $c$ brzina prostiranja zvuka u vazduhu.

Problem prvog rešenja predstavljaju bočni lobovi. Prilikom usmeravanja signala veliki deo snage signala biva emitovan kroz bočni lob. Naredna rešenja zasnivaju se na dodavanju još jedne tačke ka kojoj će zvučnik usmeravati signal. Na ovaj način moguće je pokriti dva željena pravca zvukom. Primena se može naći u pokrivanju objekata koji se sastoje iz partera i balkona.

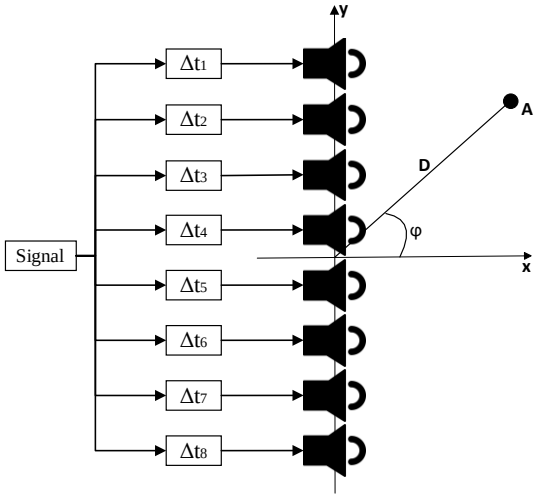


Sl. 1. Blok šema zvučničkog sistema za usmeravanje signala u jednom pravcu

### *B. smera anje uka ka d ema tačkama u prostoru sa odvojenim zvučnicima*

Drugo rešenje podrazumeva da se signali na prva četiri zvučnika i poslednja četiri zvučnika posebno obrađuju. Ovaj sistem prikazan je na slici 2.

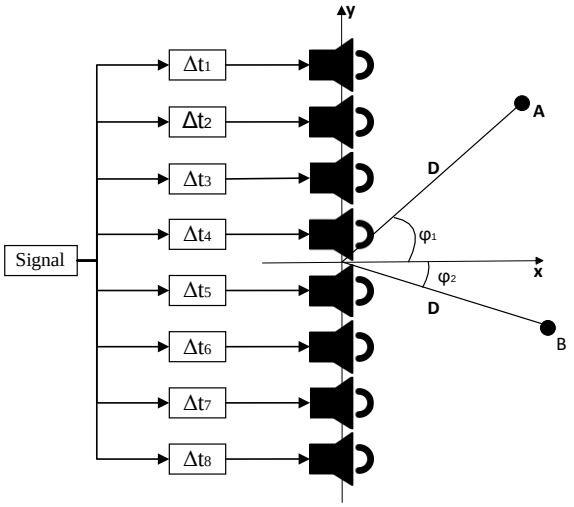


Sl. 2. Blok šema zvučničkog sistema za usmeravanje zvuka ka dvema tačkama sa odvojenim zvučnicima

Zvučnici označeni brojevima od 1 do 4 emituju zvuk ka tački A, a zvučnici označeni brojevima od 5 do 8 emituju

 ISBN 978-86-7466-930-3

zvuk ka tački B. Moguće je proizvoljno podesiti uglove $\varphi_1$ i $\varphi_2$, a oba ugla su iz opsega [-90˚,90˚]. Poželjno je da $\varphi_1$ bude veći od $\varphi_2$, jer je na taj način slabljenje signala minimalno, pošto je rastojanje između zvučnika i prijemnih tačaka minimalno. Kašnjenja se računaju pomoću izraza (5) sa razlikom kod $r_{ma}$. Maksimalna razdaljina računaće se pojedinačno za zvučnike označene sa 1 do 4 i pojedinačno za zvučnike označene sa 5 do 8.

Prilikom implementacije se umesto 8 zvučnika koristi samo 4 za usmeravanje ka jednoj tački. Posledica ovoga su značajno širi glavni lobovi nego u prvom slučaju. Ovaj problem pokušavamo da prevaziđemo u narednom rešenju tako što umesto 4 koristimo svih 8 zvučnika za obe tačke.

### *C. Usmeravanje zvuka ka dvema tačkama u prostoru sa kombinovanim zvučnicima*

U ovoj implementaciji koristiće se 8 zvučnika (slika 3) koji se usmeravaju ka dve nezavisne tačke.

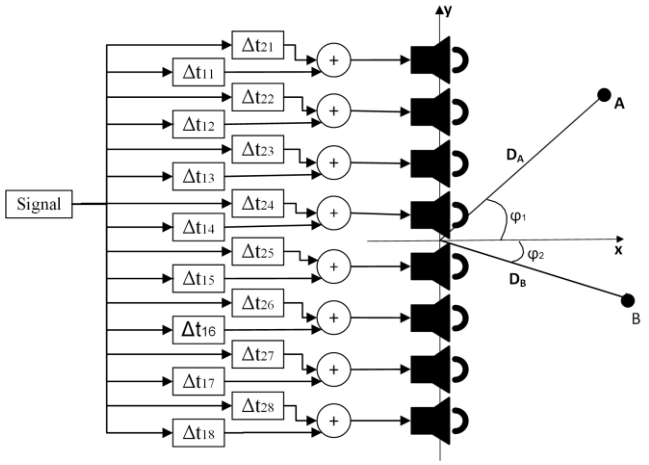


Sl. 3. Blok šema zvučničkog sistema za usmeravanje zvuka ka dvema tačkama sa kombinovanim zvučnicima

Signali sa ulaza Bela platforme se obrađuju za svaku tačku pojedinačno, nakon čega se signali sabiraju za svaki pojedinačni zvučnik. Kašnjenja se računaju pomoću izraza (5), tako što se prvo posmatraju rastojanja do tačke A, a potom do tačke B. Ovim postupkom dobijamo 2 seta kašnjenja, posebno za tačku A i posebno za tačku B. Ova kašnjenja se nezavisno primenjuju na ulazni signal, potom se zakašnjeni signali sabiraju. Klipovanje se javlja kada je signal koji se prosleđuje funkciji *analogWrite* veći od 1 ili manji od 0. Prilikom sabiranja neophodno je skalirati signale sa faktorom 0.5 kako ne bi došlo do klipovanja na Bela platformi. Faktor skaliranja iznosi 0.5 jer se sabiraju dva signala u opsegu [0,1].

## III. EKSPERIMENTALNA POSTAVKA

Prilikom realizacije ovog sistema korišćeni su: zvučnički niz, hardverska platforma Bela i računar. Signal se iz izvora audio signala vodi se na ulaz hardverske platforme Bela. U njoj se ulazni signal multiplicira 8 puta i svaka kopija se dalje nezavisno procesira i prosleđuje na odgovarajući pojačavač, a odatle na zvučnik.

### *A. Zvučnički ni*

Zvučnički niz koji je korišćen sastoji se od *Genius* SP-D150 zvučnika. On sadrži 12 zvučnika sa kardioidnom karakteristikom usmerenosti. Prilikom eksperimenta biće korišćeno samo 8 zvučnika jer je to maksimalan broj audio izlaza kod audio ekspandera na hardverskoj platformi Bela. Zvučnici se nalaze na rastojanju od 6 cm. Unutar zvučničke kutije su osim zvučnika smešteni i pojačavači. Pojačavači se napajaju iz jednosmernog izvora za napajanje napona 9 V. Frekvencijska karakteristika jednog zvučnika koji je ugrađen u sistem je približno ravna na frekvencijama većim od 300 Hz [3].

Pre samog eksperimenta neophodno je sprovesti kalibraciju zvučnika. Potrebno je normalizovati nivoe signala tako da svi zvučnici za istu pobudu emituju isti nivo signala. Na slici 4 prikazan je zvučnički niz.

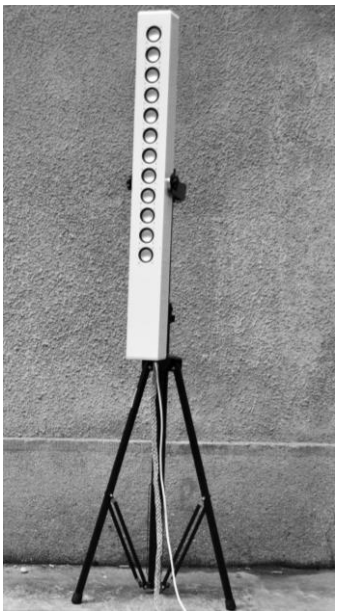

Sl. 4. Zvučnički niz

### *B. ard erska platforma Bela*

Hardverska platforma Bela je *open source single-board* uređaj za obradu signala. Bela se sastoji od platforme Beagle-Bone i namenske nadploče Bela. BeagleBone platforma je Linux kompatiblni sistem čiji je centralni deo ARM Cortex-A8 procesor sa 512MB RAM-a. Glavna prednost pri korišćenju Bele je malo kašnjenje koje će omogućiti da se reprodukcija zvuka odvija u realnom vremenu. Hardverska platforma Bela ima 2 stereo ulaza i 2 stereo izlaza za audio signal, zbog čega je neophodno koristiti audio ekspander [4]. Audio ekspander je dodatak koji povećava broj audio ulaza i izlaza. Na slici 5 prikazana je hardverska platforma Bela sa audio ekspanderom. Audio ekspander ima dodatne priključke na koje je moguće dovesti audio signal koji će nakon obrade biti prosleđen na analogne ulaze hardverske platforme Bela. Pre početka rada neophodno je povezivanje pojedinih pinova na audio ekspanderu. Konektori obezbeđuju vezu između audio ulaza ekspandera i analognih ulaza hardverske platforme Bela. Audio ulazi ekspandera su povezani sa


ISBN 978-86-7466-930-3

analognim ulazima hardverske platforme Bela, te će se ovom signalu pristupati uz pomoć funkcija *analog ead* , *analogWrite* i *analogWrite nce* .

Sl. 5. Hardverska platforma Bela sa audio ekspanderom

Korišćenje 8 audio izlaza uvodi dodatno ograničenje kada je u pitanju frekvencija odabiranja. Umesto 44.1 kHz, frekvencija odabiranja biće 22.05 kHz. Bela platforma podržava objektno-orijentisanu paradigmu. Jezik u kome je pisan algoritam je C++. Poznato je da su jezici C/C++ daleko brži od ostalih zbog mogućeg direktnog pristupa memoriji i njenim registrima. Ovo doprinosi brzini izvršavanja algoritma na hardverskoj platformi Bela koja je ključna za *real-time* sisteme. Jezici koji se mogu koristiti su *Csound* i *SuperCollider*, a grafički interfejs se može pisati u *a aScript*-u.

Ukoliko se u softveru ne izabere opcija za korišćenje audio ekspandera signal će biti u opsegu [0,1] i imaće jednosmernu komponentu od približno 0.44 V. To je posledica toga što Bela signale sa audio ekspandera čita kao analogne, a ne kao audio. Podešavanjima parametara na samoj platformi moguće je podesiti da ekspander automatski skalira signal sa [0, 1] na [-1, 1] i eliminiše jednosmernu komponentu.

Hardverska platforma Bela obrađuje blok po blok ulaznog signala i šalje ga na izlaz. Ovo Belu čini sistemom za obradu signala u realnom vremenu. Signal koji se pojavi na pinovima automatski se smešta u bafer, odakle biva iščitan uz pomoć pomenutih funkcija za analogne signale.

## IV. EKSPERIMENTALNI REZULTATI

Na slici 6 prikazani su rezultati simulacije za 1/3 oktavni frekvencijski opseg sa centralnom frekvencijom 1250 Hz za različite algoritme implementirane u ovom radu. Sa slike 6 a) se jasno vidi problem širine lobova kod rešenja u kom se koriste odvojeni zvučnici za formiranje dva glavna loba. Na slici 6 b) je rešenje sa kombinovanim zvučnicima kod koga možemo uvideti da rešava pomenuti problem.

Merenje je izvršeno u anehoičnoj sobi na Elektrotehničkom fakultetu. Za eksperiment je korišćen neusmereni merni mikrofon [5]. Snimane su vertikalna i horizontalna karakteristika usmerenosti zvučničkog niza. Mikrofonom je meren nivo zvuka u tačkama na zamišljenoj kružnici poluprečnika . Rezolucija merenja je 15˚.

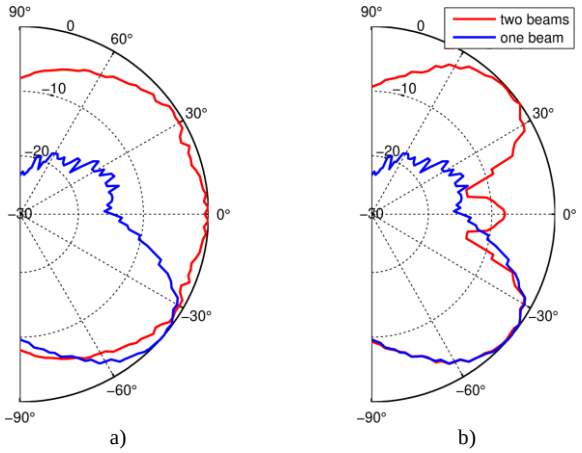


Sl. 6. Vertikalni dijagram usmerenosti zvučničkog niza na frekvenciji 1250 Hz za algoritam: a) sa odvojenim zvučnicima, b) sa kombinovanim zvučnicima.

Signal koji se šalje na procesor je MLS (Maximum-Length Sequence) sekvenca [6]. Poznato je da zvučnički nizovi kod kojih su zvučnici raspoređeni samo po jednoj dimenziji nisu u stanju da usmeravaju zvuk van te dimenzije. U eksperimentu zvučnik je postavljen vertikalno, te on nije u stanju da usmerava zvuk horizontalno. To je potvrđeno i u eksperimentima, horizontalni dijagram usmerenosti se ne menja korišćenjem algoritama za prostorno-vremensku obradu signala.

Na slici 7 prikazani su rezultati merenja pomenutih algoritama za različite opsege. Na slikama od a) do d) prikazani su dijagrami usmerenosti na različitim frekvencijama za prvo i drugo rešenje. Plavom bojom označeni su dijagrami usmerenosti za prvo, a crvenom bojom za drugo rešenje. U prvom rešenju signal se usmerava ka jednoj tački u prostoru koja se nalazi na rastojanju 2 m od centra zvučničkog niza i pod uglom od -45˚. Drugo rešenje predstavlja usmeravanje zvuka ka dve tačke sa odvojenim zvučnicima. Tačke se nalaze na rastojanju od 2 m pod uglovima od -45˚ i 45˚. Na slikama od e) do h) prikazani su dijagrami usmerenosti za prvo i treće rešenje. Plavom bojom je označen dijagram usmerenosti prvog, a crvenom trećeg rešenja. Treće rešenje podrazumeva usmeravanje signala ka dve tačke u prostoru sa svih 8 zvučnika. Tačke prema kojima se usmerava su identične kao i za prethodni slučaj.

Posmatrajući dijagrame usmerenosti za prvo rešenje dolazimo do određenih zaključaka. Merenja pokazuju da je zbog velike talasne dužine usmeravanje signala na niskim frekvencijama jedva primento. Na višim frekvencijama usmeravanje signala se povećava, ali se povećava i veličina bočnih lobova. Sa slika se može videti da su u opsegu 4000 Hz glavni i sporedni bočni lob gotovo jednaki. Usmeravanje signala ka jednoj tački dovelo je do neželjenog usmeravanja signala ka još jednoj tački u prostoru. Na ovaj način gubi se deo energije, budući da se ne emituje u željenom pravcu. Izgled bočnog loba zavisi od frekvencije i rastojanja između zvučnika na zvučničkom nizu, te na to ne možemo uticati.


ISBN 978-86-7466-930-3

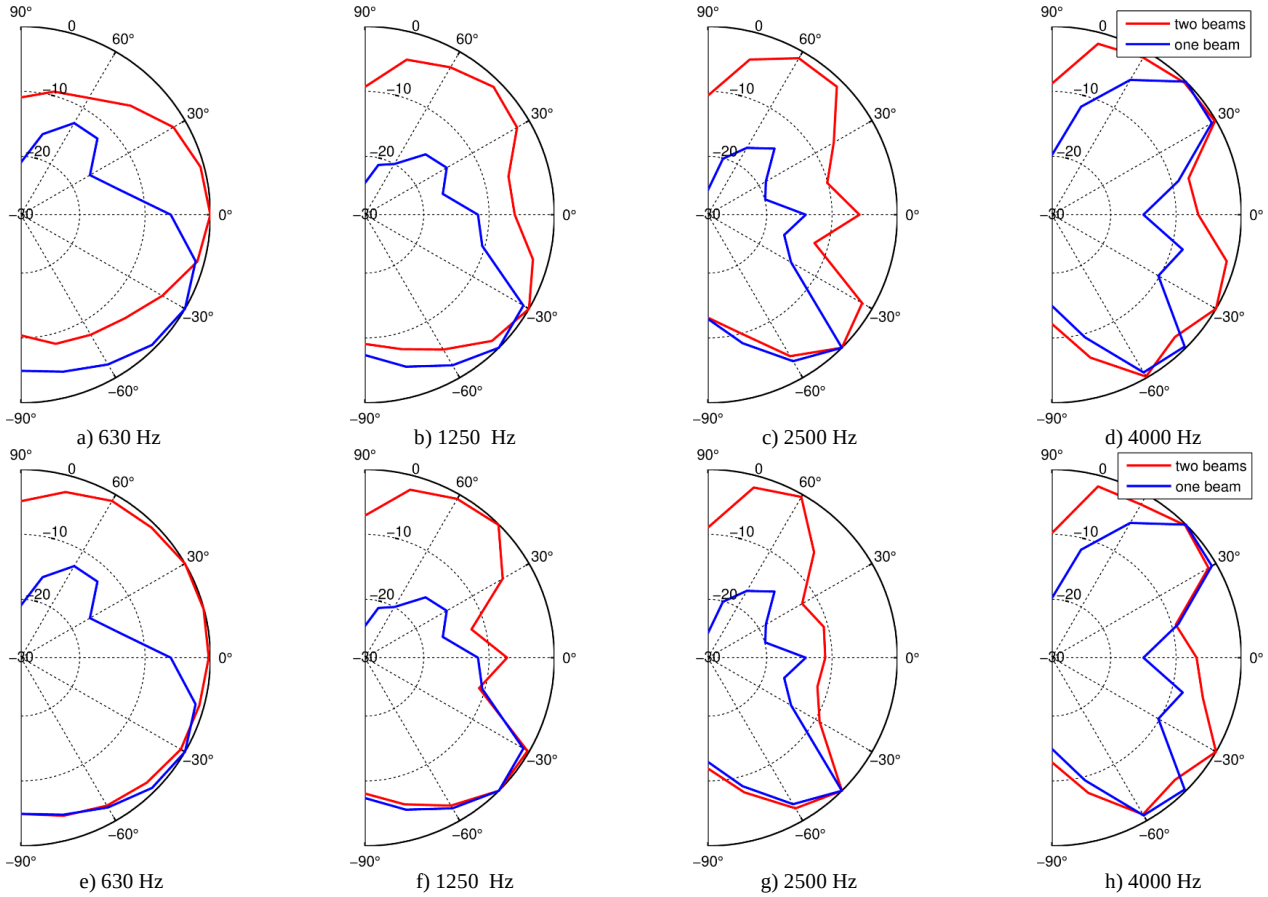


Sl. 7. Vertikalni dijagram usmerenosti zvučničkog niza u slučaju usmeravanja zvuka ka jednoj tački (plava boja) i u slučaju usmeravanja zvuka ka dvema tačkama sa odvojenim zvučnicima na frekvencijama a) 630 Hz b) 1250 Hz c) 2500 Hz i d) 4000 Hz i u slučaju usmeravanja zvuka ka dvema tačkama sa kombinovanim zvučnicima na frekvencijama e) 630 Hz f) 1250 Hz g) 2500 Hz i h) 4000 Hz

Drugo i treće rešenje pokazuju da je moguće istovremeno softverski uticati na pravce u kojima će se signal emitovati. Ova rešenja su primenjiva u situacijama kada želimo da direktnim zvukom pokrijemo više različitih auditorijuma. Kao i kod prvog rešenja na nižim frekvencijama usmerenost je relativno mala, a na višim frekvencijama se uočava jasna pojava dva loba pod uglovima od -45˚ i 45˚. Problem koji se javlja kod drugog rešenja jeste velika širina lobova na visokim učestanostima. Do smanjenja usmerenosti dovodi korišćenje samo polovine zvučnika. Treće rešenje koje je pomenuto rešava ovaj problem. Korišćenje svih osam zvučnika daje mogućnost boljeg usmeravanja signala. Možemo primetiti da su u ovom slučaju lobovi uži u odnosu na prethodni slučaj. Takođe, lobovi u ovom rešenju se gotovo podudaraju sa širinom glavnog loba iz prvog rešenja.

## V. Zaključak

Rezultati koji su dobijeni prikazuju da je moguće softverskom obradom signala upravljati širinom i pozicijom snopova signala. Pokazano je da je moguće dodati još jedan nezavisni snop signala bez kvarenja već postojećeg snopa. Takođe, rešen je problem koji se javlja prilikom korišćenja polovine zvučnika za usmeravanje zvuka ka dvema tačkama. Značaj dobijenih rezultata leži u činjenici da su ova rešenja primenjiva u praksi. Rezultati eksperimenata pokazuju dobro poklapanje sa rezultatima simulacije, čime je potvrđena validnost simulacionog modela.

Budući rad će obuhvatati rešenja kod kojih će se drugačije računati kašnjenja. Moguće je za konkretnu geometriju niza i konkretan frekvencijski opseg naći optimalna kašnjenja pomoću optimizacionog algoritma. Kašnjenja bi se razlikovala u zavisnosti od uslova koji bi se postavio. Neki od uslova bi mogli biti da odnos glavnih i bočnih lobova bude minimalan ili da širina lobova bude minimalna.

Na samom početku rada pomenuto je da je nemoguće u potpunosti eliminisati bočne lobove jer oni nisu samo posledica frekvencije na kojoj se signal šalje, već i geometrije niza. Još neka poboljšanja postojećih rešenja mogla bi se ogledati u tome da je moguće odrediti kojih 8 od 12 zvučnika je optimalno koristiti na zvučničkom nizu da bi se smanjio uticaj bočnih lobova. Takođe, problem bočnih lobova je moguće rešiti optimalnim rasporedom zvučnika na zvučničkom nizu, odnosno menjanjem geometrije niza.

## Zahvalnica

Ovaj rad je realizovan u okviru projekta TR 36026 koga finansira Ministarstvo prosvete, nauke i tehnološkog razvoja Republike Srbije.

 ISBN 978-86-7466-930-3

## LITERATURA

[1] M. Bjelić, A. Golubović, M. MihiGolubović, M. MihiGolubović, M. Mijić, "Realizacija zvučničkog sistema sa softverskom kontrolom usmerenosti," Beograd, Srbija, 2020

[2] Chuang Shi, Yoshinobu Kajikawa, Woon-Seng Gan, "Generating dual beams from a single steerable parametric loudspeaker", Osaka, Japan, 2015

[3] Miomir Mijić, Dragana Šumarac Pavlović, Miloš Bjelić, Miodrag Stanojević, Laboratorijski model zvučničkog stuba sa softverski kontrolisanom usmerenošću, Tehničko rešenje 2015

[4] Tehnička dokumentacija proizvođača, dostupno na: https://learn.bela.io/, pristupano 14.4.2022.

[5] Tehnička dokumentacija proizvođača: .http://www.nti-audio.com/Portals/0/data/en/MiniSPL-Measurement

[6] A. Mitra: On the Properties of Pseudo Noise Sequences with a Simple Proposal of Randomness Test, World Academy of Science, Engineering and Technology, International Scholarly and Scientific Research and Innovation, Vol. 2, No .9, 2008, pp. 631 – 636.



## ABSTRACT

This paper presents the implementation of software-oriented speaker systems. Software and hardware implemented directional speaker systems, in addition to increasing the sound level in a given direction, also lead to a reduction in reverberation. The implementation used a speaker array and a processor on which three different signal processing algorithms are executed. The first solution involves directing the sound to one set point, and the second and third solutions involve directing the sound to two points that are arbitrarily set. The emphasis of the paper is on the second and third solutions used in cases when we want to provide coverage of two directions in the auditorium. In addition to three independent algorithms, the paper also presents a simulation that can be used to predict directional diagrams in all three cases. The results of the algorithm were quantified by measuring the directivity diagrams in 1/3 octave frequency bands. The details of the implementation and the details to pay attention to when working with hardware Bela platform will be mentioned. The paper presents the improvements obtained by using two, instead of one sound beam.


## Implementation of spea er array directional control algorithms with two main lobes on open hardware

Tijana Đorđević, Stefan Aćimović, Miloš Bjelić

 ISBN 978-86-7466-930-3

# Optimizacija pozicija zvučnika u zvučničkom nizu

Stefan Aćimović, Tijana Đorđević, Miloš Bjelić

*Abstract*— **Optimizacioni algoritmi sve više nalaze primenu o raznim oblastima, kako nauke, tako i života. Uz analizu softverske kontrole usmerenosti zvučničkog sistema javila se i potreba za optimizacijom već postojećih rešenja. U ovom radu prikazano je kako se na više načina može doći do rešenja 2D optimizacione funkcije, gde se najbolje rešenja bira iz niza dovoljno dobrih. radu je pri azan algoritam za prostorno-vremensku obradu signala koji omogućava upravljanje dijagramom usmerenosti u verti alnoj ravni. Poboljšanje postojećih rezultata izvršeno je uz pronalaženje linearne pozicije 1 zvučnika u zvučničkom stubu, tako da njegov dijagram usmerenosti bude što usmereniji za određeni prostorni ugao i da je odnos glavnog i bočnih lobova što veći. a ove rezultate oristili su se parametri u vidu dva oeficijenta oji su dovoljno dobro opisivali kvalitet rešenja, tako što se svako rešenje smeštalo u funkciju, a nalaženje najboljih se sprovodilo preko Pareto fronta. Popunjavanje tačaka, odnosno rešenja dodatno se ubrzalo sa genetičkim optimizacionim algoritmom koji je u znatno manje iteracija doveo do jedna o dobrog rešenja kao i metod slučajnog generisanja potencijalnog rešenja.**

*Ključne reči* — **algoritmi, obrada signala, optimizacija, pareto front, genetički algoritam, softverska kontrola, usmerenost, zvučnički niz.**

## I. UVOD

Zvučnički sistemi koji se koriste u sistemima za ozvučavanje treba da prenesu zvučni sadržaj do slušalaca koji se nalaze u određenom delu prostora. Zvučna energija koja odlazi u deo prostora na kome nema slušalaca na otvorenom prostoru predstavlja gubitak, a u prostorijama ima negativne posledice na percepciju zvuka jer dodatno pobuđuje reverberacioni proces. Zbog toga se u sistemima za ozvučavanje koriste usmereni zvučnički sistemi da bi se najveći deo zvučne snage slao u prostor gde se nalaze slušaoci. Usmereni zvučnički sistemi podrazumevaju da se grupa zvučnika nalazi na jednoj lokaciji i da su koncentrisani u jedinstven sistem. U ovu grupu zvučničkih sistema, na primer, spadaju takozvani *ine array* sistemi, kod kojih se usmerenost postiže tako što je zvučnička skupina zakrivljena, to jest pojedinačni zvučnici se nalaze na različitim udaljenostima od mesta prijema [1].

Zvučnički nizovi čiji se dijagram usmerenosti obradom signala usmerava postaju sve popularniji i tema su ovog rada. Ideja rada je razmatranje načina kako da se gubitak zvučne energije minimizira. Rešenje koje se razmatra u ovom radu je optimizacija pozicija 16 zvučnika, koji stoje u istoj osi, ali na različitim rastojanjima. U sličnim radovima iz ove oblasti predstavljena su uglavnom rešenja sa uniformnom raspodelom zvučnika ili sa jednostavnijom računicom koja je vezana za liniju kašnjenja i odgovarajuću raspodelu zvučnika. Metod nalaženja najboljih pozicija zvučnika u zvučničkom stubu svodi se na tehnike optimizacije 2D funkcije i nalaženja skupa pogodnih rešenja koja zajedno čine pareto front. Baš zbog prirode problema koja zahteva da se dve stvari optimizuju, a koje su zavisne. Pareto front se uveo kao potencijalni alat za rešavanje ovog problema. U ovom radu je služio kao kriterijum za ocenjivanje skupa rešenja od kojih je odabrano ono najpovoljnije. Pošto Pareto front daje skup (front) rešenja gde je svako podjednako dobro, komparativnom metodom je utvrđeno koje rešenje je dovoljno dobro za predstavljeni problem [2].

Od celog fronta bira se jedino rešenje, tako da najmanje šteti uslovima optimizacije. Uslovi su da je odnos glavnog i bočnog loba što veći (što bi značilo da je gubitak energije manji) i da je širina glavnog loba što manja (odnosno da je što više moguće usmeriti zvučnički niz po svim oktavnim opsezima i za sve zadate uglove).

Metode optimizacije koje su se koristile u ovom radu jesu slučajno generisanje rešenja u pareto front, kao i genetički algoritam [3]. Oba algoritma se svode na skupinu koeficijenata koji na neki način opisuju trenutno rešenje i koliko dobro ono zadovoljava oba gore pomenuta uslova, zatim se od najboljih mogućih rešenja, koja su sastavljena u front, odabira najbolje moguće. Ovakvo rešenje proverava se za sve uglove od značaja, kao i da li se može fizički realizovati, odnosno da nema preklapanja jednog zvučnika preko drugog. Uglovi od značaju su nam oni uglovi koji se koriste i kada se fizički usmeravaju nizovi zvučnika na većim ili manjim prostorima, okvirna granica može biti od 30° do 60°. Metode provere svode se na poređenje već postojećih rešenja sa uniformnom raspodelom zvučnika, kao i na prethodna dobijena rešenja, kako preko algoritma, tako i preko drugih radova iz literature.

## II. METODOLOGIJA

### A. Zvučnički niz i dijagram usmerenosti

Za definisanje problema optimizacije potrebno je uvesti element koji je povoljan, tako da se lako može vršiti obrada nad njim u softverskom, a i da se rezultat može primeniti i u

Stefan Aćimović - Elektrotehnički fakultet, Univerzitet u Beogradu, Bulevar kralja Aleksandra 73, 11020 Beograd, Srbija (e-mail: as213306m@student.etf.bg.ac.rs).

Tijana Đorđević – Elektrotehnički fakultet, Univerzitet u Beogradu, Bulevar kralja Aleksandra 73, 11020 Beograd, Srbija (e-mail: dt213283m@student.etf.bg.ac.rs).

Miloš Bjelić – Elektrotehnički fakultet, Univerzitet u Beogradu, Bulevar kralja Aleksandra 73, 11020 Beograd, Srbija (e-mail: bjelic@etf.rs).

 ISBN 978-86-7466-930-3

hardverskom delu sistema. Metodologija koja je primenjena u ovom radu jeste menjanje relativnih pozicija svih 16 zvučnika, zatim računanje dijagrama usmerenosti koji se posle delom pretvara u koeficijente koji su služili za dalju optimizaciju.

Na slici 1 prikazana je pozicija zvučnička u uniformnom raspodelom pozicija zvučnika. Dimenzija zvučničkog niza koja je definisana u ovom radu je 2 metra. Na osnovu poznatih pozicija zvučnika i poznavanja njihovog dijagrama usmerenosti moguće je dobiti dijagram usmerenosti zvučničkog niza [4]. Adekvatnom obradom signala za pojedinačne zvučnike moguće je izvršiti usmeravanje glavnog loba u dijagramu usmerenosti za željeni prostorni ugao. Na slici 2 prikazan je izgled dijagrama usmerenosti uniformnog niza za određeni prostorni ugao [5].

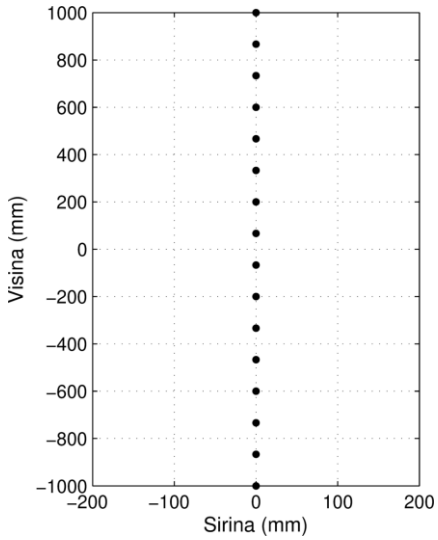


Sl. 1. Raspored zvučnika za uniformnu geometriju zvučničkog stuba

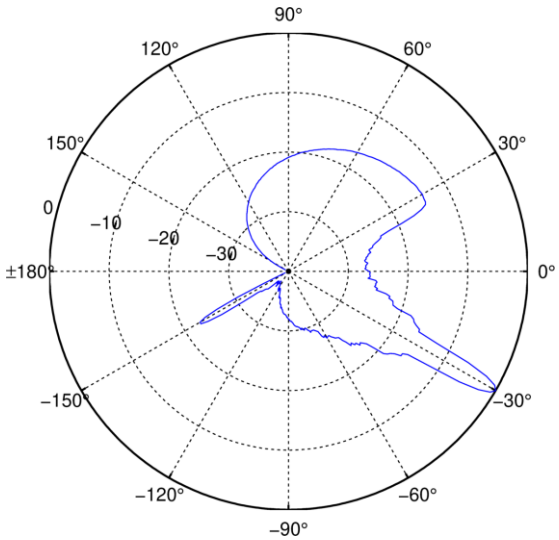


Sl. 2. Dijagram usmerenosti uniformnog zvučničkog niza za prostorni ugao -30° i 1/3 oktavni frekvencijski opseg 1250 Hz

Bočni lobovi predstavljaju problem u smislu gubitka energije, jer je cilj imati što usmereniji glavni lob [6], a idealno bi bilo da bočni lobovi budu maksimalno potisnuti. Kod uniformne raspodele zvučnika jasno se može videti da energija koju ima bočni lob samo oko 10 dB manja u odnosu na glavni lob za frekvencije već oko 1000 Hz, što se i vidi na Sl. 4. Sa povećavanjem frekvencije glavni i bočni lob postaju jednaku. Svaki rezultat koji za cilj ima da smanji odnos glavnog i bočnog loba čak i za 1 dB može se smatrati kao povoljnim rešenjem, jer je početna tačka odnosa lobova na nuli. Uz algoritme optimizacije dokazano je u radu da se bočni lob može smanjiti čak i do 10 dB.

### *B. Pareto front i slučajno generisana geometrija*

Kod pristupa slučajnog generisanja pozicija zvučnika u zvučničkom nizu pozicije su generisane iz skupa [-1, 1] metar, što su maksimalne dimenzije zvučničkog niza. Na osnovu dobijene geometrije izračunava se dijagram usmerenosti, usmeren za odrešeni prostorni ugao. Zatim je na osnovu dobijenog dijagrama moguće izračunati koeficijente sa kojima se opisuje širina glavnog loba, odnosno njegova usmerenost, kao i odnos glavnog i najvećeg bočnog loba. Koeficijenti se izračunavaju na osnovu sledećeg izraza:

$$\alpha = \begin{cases} 0.5 * \ [n], n \in \left[0, \frac{1}{3} * end\right] \\ [n], n \in \left[\frac{1}{3} * end, end\right] \end{cases}$$
$$\beta = \begin{cases} [n], n \in \left[0, \frac{1}{3} * end\right] \\ 0.5 * \ [n], n \in \left[\frac{1}{3} * end, end\right] \end{cases} \quad (1)$$

gde su $\alpha$ i $\beta$ koeficijenti kojima se opisuju frekvencijski koraci od po 50 Hz za odnos glavnog i bočnog loba, kao i usmerenost glavnog loba respektivno. Ovde se jasno vidi da postupak optimizacije zapravo zavisi od dva parametra koja nisu nezavisne, već zajedno prave potencijalnu skupinu rešenja koja se može predstaviti u 2D površi. Za rešavanje ovog problema uveden je Pareto front.

Pareto front (koji se takođe naziva Pareto granica ili Pareto skup), koristi se u višedimenzionoj optimizaciji i predstavlja skup svih Pareto efikasnih rešenja. Koncept se široko koristi u inženjerstvu. Omogućava se ograničenje pažnje na skup efikasnih izbora, te je umesto da se razmatra čitav opseg svakog parametra, pravljenje kompromisa u okviru ovog skupa jedna od stvari koje su neizbežne i neophodne.

Pareto front se može lako opisati kao pomoć u odabiru velikog niza kolača od kojih svaki ima određenu vrednost koliko je ukusan i koliko kalorija vredi. Te dve vrednosti su povezane i ne mogu se nezavisno menjati, obično što je kolač ukusniji, to više kalorija ima. Pareto front nam služi da od gomile kolača odaberemo nekoliko ili jedan koji će biti dovoljno sladak i imati onoliki broj kalorija koji možemo da pojedemo a da se ne osećamo loše. Za taj broj kalorija pareto nam sigurni može tvrditi da smo izabrali najslađi kolač i obrnuto, za kolač odabrane slatkoće nam može tvrditi da od ostalih kolača iste slatkoće, mi smo definitivno izabrali onaj sa najmanje kalorija.

Koeficijenti koji su primenjeni ovde dobijeni su empirijski gde se uz nekoliko eksperimenata dobilo saznanje o tome koji


ISBN 978-86-7466-930-3

je skup frekvencija više, a koji je manje važan za određivanje najbolje moguće pozicije zvučničkog niza.

Na slici 3 prikazan je skup rešenja koji se dobiju bilo za slučajno generisanje zvučničkog niza ili uz genetički algoritam. Svaka tačka predstavlja rezultat jedne geometrije koja se uz formulu koeficijenata stavlja na 2D *scatter* rezultat. Crvena linija predstavlja Pareto front odnosno sva rešenja koja su podjednako dobra. Cilj nam je da vrednosti na obe ose budu što manje, ali se uglavnom smanjivanjem jedne vrednosti povećava ona druga [7]. Za rešenja koja su povoljna ovom radu uzimao se kriterijum gde je značajnije imati smanjenje od 1 dB bočnog loba nego povećanje usmerenosti glavnom loba za 1˚. Apsica predstavlja rezultate koeficijenta koji opisuje usmerenost glavnog loba, dok ordinata predstavlja rezultate odnosa bočnog i glavnog loba. Na ovom primeru bi neko potencijalno rešenje bilo više prema desnoj strani Pareto fronta.

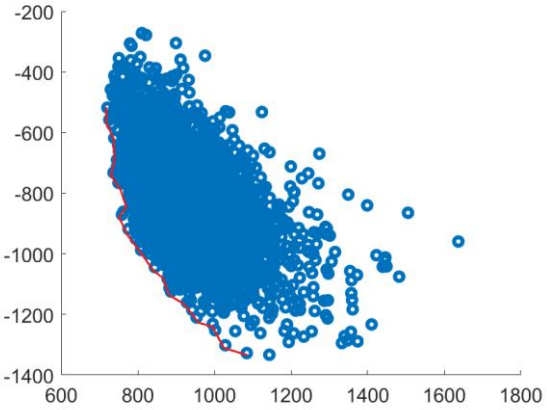


Sl. 3. Pareto front koji prikazuje povezanost oba uslova, širinu glavnog loba i odnos glavnog i bočnog loba zajedno sa koeficijentima.

### *C. Genetički algoritam*

Koeficijenti primenjeni u ovom pristupu dobijeni su empirijski gde se uz nekoliko eksperimenata dobilo saznanje o tome koji je skup frekvencija više, a koji je manje važan za određivanje najbolje moguće pozicije zvučničkog niza. Pored slučajne raspodele rešenja koristio se modifikovani genetički algoritam, čiji su osnovni principi uvek isti, ali se za ovaj problem algoritam u nekim delovima razlikuje od klasičnog pristupa. Genetički algoritam veoma je popularan optimizacioni algoritam i njegova rasprostranjenost i primena je velika. Od NASA antene koja prikuplja i šalje zrake određenih frekvencija sa najmanjim gubicima do svih omiljenih stvari koje možete staviti u kofer za avion, a da one ne prevaziđu određenu težinu [8].

Jasno je da se genetički algoritam koristi za traženje optimalnog rešenja od gomile ponuđenih uz dodatne uslove. Osnovni koraci genetičkog algoritma su sledeći:

- Nulta generacija (skup genoma)
- Fitnes funkcija
- *Crosso er* funkcija
- Odabir novih genoma
- Mutacija (opciono)
- Nova generacija

Algoritam radi po gore pomenutim tačkama, gde je nulta generacija zapravo populacija slučajno izabranih distanci zvučnika zvučničkog niza. Sam početak je isti kao i za generisanje slučajnih pozicija zvučnika. Fitnes funkcija ovde je predstavljena na način koliko dobro jedan genom, odnosno raspodela zvučničkog niza daje rezultat u vidu tačke pareto fronta. Svaki zvučnički niz nulte generacije prolazi kroz ovu funkciju. Nakon toga se odabiraju dva najbolja iz generacije i šalju se na *crosso er* funkciju. Jedinke, odnosno zvučnički nizovi koji se šalju na *crosso er* funkciju nazivaju se roditelji, a njihovi rezultati ukrštanja, deca. Roditelji se ukrštaju tako što se na slučajnom mestu prepolovi zvučnički niz i od tog mesta se zameni sa drugim rediteljem, isto tako se dešava i za drugog roditelja.

Nakon ovih rezultata odabiraju se ostali genomi koji će na neki način učestvovati u sledećoj generaciji. Tehnika koja je rađena u ovom radu jeste tehnika turnira, gde se nasumično biraju dva genoma, te onaj sa boljom fintes funkcijom ide u turnir, postupak se ponavlja, te se onda dva pobednika vode na *crosso er* funkciju, njihova deca se šalju u novu generaciju. Neki genomi generisani su ponovo slučajno i dodati u novu generaciju. Nakon toga postoji i opciona mutacija koja sa malom verovatnoćom menja jedan deo jednog slučajnog broja genoma, odnosno poziciju jednog od zvučnika u celom zvučničkom nizu. Tako se dobija nova generacija i ceo postupak se ponavlja ponovo kao i za nultu generaciju genoma.

## III. REZULTATI I DISKUSIJA

Na slici 4 su prikazani rezultati slučajnog rasporeda zvučnika i rasporeda zvučnika dobijenog genetičkim algoritmom.

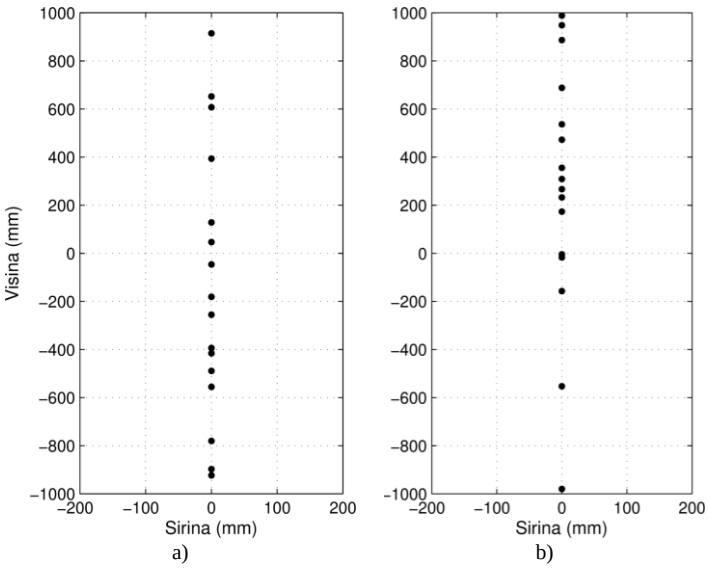


Sl. 4. Raspored zvučnika na osnovu rezultata algoritma: a) Slučajni raspored i b) Genetički algoritam

Na osnovu prikazanih geometrija izračunati su parametri pomoću kojih je moguće proceniti kvalitet rešenja: odnos glavnog i maksimalnog bočnog loba (MSL) i širina glavnog loba (BW). Ovi parametri izračunati su za frekvencijski opseg


ISBN 978-86-7466-930-3

od interesa i za prostorni ugao od -30 stepeni za glavni lob. Na slici 5 je prikazana frekvencijska zavisnost parametra koji predstavlja odnos glavnom i najvećeg bočnog loba.

Kod pristupa rešavanja gde su se pozicije zvučničkog niza sasvim slučajno generisale dobijene su znatno niže vrednosti bočnih lobova, za gotovo ceo frekvencijski opseg. Isti slučaj daje i genetički algoritam, što je bio cilj. U odnosu na uniformnu raspodelu jasno se vidi da slučajno generisanje daje daleko bolje rezultate za bilo koji frekvencijski opseg, a da time nije narušilo usmerenost glavnog loba, što znači da definitivno postoji kombinacija rasporeda zvučnika u zvučničkom nizu koja se može i hardverski realizovati, isti rezultat u odnosu na uniformnu raspodelu zvučnika vidi se i sa genetičkim algoritmom. Sa slike 5 se vidi da se za slučajno generisanje nešto bolji odnos lobova vidi na nižim frekvencijama, dok kod viših dominira genetički algoritam. Oba rešenja se mogu smatrati za dobrim, jer je razlika ovih rešenja između 1 dB do 2 dB u nekim frekvencijskim opsezima. Važna napomena je ta da je za generisanje rešenja slučajne raspodele bilo potrebno preko 200000 iteracija algoritma, dok se sličan rezultat postigao sa 1500 iteracija genetičkim algoritmom.

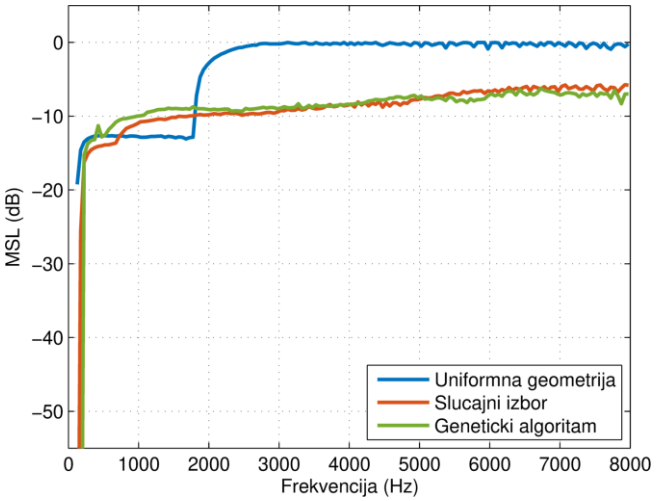


Sl. 5. Frekvencijska zavisnost nivoa bočnih lobova zvučničkog niza

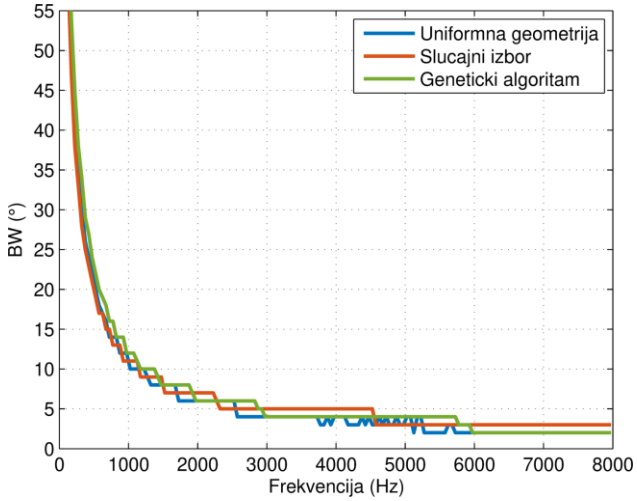


Sl. 6. Frekvencijska zavisnost nivoa bočnih lobova zvučničkog niza

Zvučnički niz dobijen slučajnim generisanjem pozicija zvučnika predstavlja daleko bolje rešenje od uniformne raspodele pozicija. Ovakvo rešenje može se dobiti uz veliki broj različitih rešenja i svođenja rezultata na front, bez ikakve dodatne optimizacije, koja bi ta rešenja dalje poboljšavala. Već sa ovim pristupom može se pokazati da za 16 zvučnika, sa kardioidnom usmerenosti postoje rešenja softverskog usmeravanja zvučnika takva da je u svim oktavnim opsezima od važnosti odnos glavnog i bočnog loba iznosi približno 10 dB. Prednost uniformne raspodele zvučnika je ta što na različitim uglovima usmerenosti ona daje jako malu širinu glavnog loba, što se može videti na prikazanom grafiku. Rešenje koje je dobijeno slučajnim generisanjem rešenja, ne samo da je bolje u smislu odnosa lobova, nego je i zadržalo visok nivo usmerenosti glavnog loba na svim frekvencijskim opsezima. Kao jedna od mera za izbor povoljnog rešenja bio je i kriterijum da je razlika bočnog i glavnog loba od dodatnih 2 dB znatno bitnija nego smanjenje usmerenosti glavnog loba za 2°.

Rezultati dobijeni genetičkim algoritmom su veoma slični rezultatima slučajne raspodele, samo što postoji jedna važna razlika razlika koja se ogleda u vremenu izvršavanja algoritma. Vreme koje je bilo potrebno računaru da dođe do optimalnog rešenja sa slučajnom raspodelom bilo je tri dana, dok je genetički algoritam došao do jednako dobrog rešenja za sat vremena.

## IV. ZAKLJUČAK

Dobijeni rezultati jasno prikazuju da su rešenja dobijena optimizacijom na oba načina daleko bolja od polaze situacije. Sa softverskom simulacijom je pokazano da se na različite načine može doći do rešenja koje u većini delova frekvencijskog spektra od značaja uspeva da suzbije bočni lob za čak 10dB, a da pritom ne šteti povećanju širine glavnog loba.

Budući radovi koji se zasnivaju na modernijim metodama optimizacije stoje na raspolaganju. Potrebno je uvesti dodatna ograničenja na algoritam, tako da se definitivno omogući i hardverska realizacija rešenja. Pored biranja najbolje pozicije zvučnika u zvučničkom nizu, takođe se javlja mogućnost da se odabiraju i najoptimalnija kašnjenja sa istim i sličnim algoritmima sa kojima se dolazilo do gore pomenutih rešenja.

Zbog fizike problema, na niskim frekvencijama je jako teško dodatno usmeriti glavni lob, a da to ne utiče na povećanje odnosa glavnog i bočnog loba, pogotovo na višim frekvencijama. Takođe se vidi i da se bočni lobovi nikada ne mogu potpuno suzbiti, te se gubitak energije može samo optimalno smanjiti. Ovaj rad samo otvara novo poglavlje u kome je optimizacija ponovo našla svoju primenu, a ostavlja skup mogućnosti i ideja kojima se ovakvi problemi mogu dodatno razložiti i potencijalno još bolje i efikasnije rešiti.

## ZAHVALNICA

Ovaj rad je realizovan u okviru projekta TR 36026 koga finansira Ministarstvo prosvete, nauke i tehnološkog razvoja Republike Srbije.


ISBN 978-86-7466-930-3

## REFERENCES


[1] L. C. Godara, "Application of antenna arrays to mobile communications. II. Beam-forming and direction-of-arrival considerations," in Proceedings of the IEEE, vol. 85, no. 8, pp. 1195-1245, Aug. 1997, doi: 10.1109/5.622504.

[2] A. Kesireddy, L. R. Garcia Carrillo and J. Baca, "Multi-Criteria Decision Making - Pareto Front Optimization Strategy for Solving Multi-Objective Problems," 2020 IEEE 16th International Conference on Control & Automation (ICCA), 2020, pp. 53-58, doi: 10.1109/ICCA51439.2020.9264536.

[3] S. D. Immanuel and U. K. Chakraborty, "Genetic Algorithm: An Approach on Optimization," 2019 International Conference on Communication and Electronics Systems (ICCES), 2019, pp. 701-708, doi: 10.1109/ICCES45898.2019.9002372.

[4] D. N. Swingler and R. S. Walker, "Line-array beamforming using linear prediction for aperture interpolation and extrapolation," in IEEE Transactions on Acoustics, Speech, and Signal Processing, vol. 37, no. 1, pp. 16-30, Jan. 1989, doi: 10.1109/29.17497.

[5] Array Signal Processing, NJ, Englewood Cliffs:Prentice-Hall, 1985.

[6] M. Bjelić, A. Golubović, M. MihiGolubović, M. MihiGolubović, M. Mijić, "Realizacija zvučničkog sistema sa softverskom kontrolom usmerenosti," Beograd, Srbija, 2020

[7] X. -B. Hu, M. Wang, X. -B. Hu and M. S. Leeson, "Calculating the complete pareto front for a special class of continuous multi-objective optimization problems," 2014 IEEE Congress on Evolutionary Computation (CEC), 2014, pp. 290-297, doi: 10.1109/CEC.2014.6900297.

[8] K. F. Man, K. S. Tang and S. Kwong, "Genetic algorithms: concepts and applications [in engineering design]," in IEEE Transactions on Industrial Electronics, vol. 43, no. 5, pp. 519-534, Oct. 1996, doi: 10.1109/41.538609.


## ABSTRACT


Optimization algorithms are increasingly being applied in various fields, both science and life. Along with the analysis of the software control of the direction of the speaker system, there was also a need to optimize the already existing solutions. In this paper, it is shown how the solution of the 2D optimization function can be reached in several ways, where the best solutions are chosen from a series of good enough ones. The paper presents an algorithm for spatial-temporal signal processing that enables control of the direction diagram in the vertical plane. For these results, parameters in the form of two coefficients were used, which described the quality of the solution well enough. Each solution was placed in a function, and finding the best was carried out via the Pareto front. Filling in the points, ie the solution, was additionally accelerated with the genetic optimization algorithm, which in significantly fewer iterations led to an equally good solution as the method of random generation of a potential solution.


**ptimization of a loudspea er system with software-controlled directivity**

Stefan Aćimović, Tijana Đorđević, Miloš Bjelić

 ISBN 978-86-7466-930-3

# Realizacija sistema za aktivnu kontrolu buke u cevi na otvorenom hardveru

Marija Ratković, Nebojša Kolarić, Miloš Bjelić

***A stra t*— A C (Acoustic oise Control) sistemi su neophodni u prostorijama gde se traži eliminisanje neželjenih zvu ova. ovom radu bavili smo se simulacijom i implementacijom na hardveru A C sistema u cevi. Testirani su adaptivni algoritmi ( iltered east ean quare) i ( ormalized iltered east ean quare). Algoritmi su poređeni po robusnosti sistema, neophodnom redu adaptivnog filtra i brzini onvergencije. simulaciji su ao test signali korišćeni: sinusoida, klipovana sinusoida i šum realnog ventilatora. zavisnosti od omple snosti test signala menjali su se parametri adaptivnog filtra. ezultati po azuju da je moguće potisnuti akustičku buku do određene granice u zavisnosti od omple snosti signala, ao i da je moguće ta ve algoritme implementirati na otvorenom hardveru.**

***Ključne reči*— A tivna ontrola bu e, adaptivni algoritmi, filtri, hardvers a implementacija, .**

## I. UVOD

Jedna od najuspešnijih primena *ANC Acoustic Noise Control* sistema je njihova implementacija u cevi [1]. Razlog tome je što veliki broj uređaja koji prave buku koriste cevi za njihovu primarnu namenu, samim tim jednostavno je implementirati ovakav sistem. Potiskivanje buke prouzrokovane šumom ventilatora, koji se nalaze u mnogim električnim uređajima kao što su transformatori, računari i sistemi za klimatizaciju, je jedna od najčešćih primena ovakvih sistema. Ovakvi akustički zvukovi mogu nepoželjno da utiču na čoveka, da ga psihički zamaraju i ometaju u radu.

U ANC sistemu, digitalni kontroler vrši obradu nad neželjenim signalom i na njegovom izlazu se generiše signal koji je iste amplitude a suprotne faze sa primarnom bukom koju želimo potisnuti. Superpozicijom ova dva zvučna signala na izlazu iz sistema (cevi) se formira zona koja je približna zoni tišine, potiskivanjem početnog šuma [2].

Tradicionalne metode za potiskivanje šuma, poput korišćenja apsorpcionih materijala imaju lošije performanse na niskim frekvencijama. Zbog toga je ANC predložen kao rešenje za taj problem, da bi se u kombinaciji sa zvučnim apsorberima što više smanjio neželjeni akustički šum. Primena ovakvog sistema pronalazi svoje mesto u prostorijama u kojima je neophodno obezbediti što veći nivo tišine, kao što su muzički studio, koncertne sale. Postići će se potiskivanje buke na niskim frekvencijama i doprineti klasičnim načinima potiskivanja buke. Konkretna buka na koju se misli su šumovi ventilatorskih sistema koji se koriste za protok vazduha u samim prostorijama. Samim tim što ove velike cevi kroz koje struji vazduh nije moguće zapušiti sa nekim akustičkim materijalom, neophodno je naći drugi način za postizanje tišine što nam omogućava ovakav način implementacije.

Ideja ovog rada je ispitivanje mogućnosti implementacije ovog sistema za adaptivnu obradu signala na realnom modelu korišćenjem otvorenog hardvera *Bela*, uz ispitivanje krajnjih mogućnosti hardvera i njegovih mogućnosti za primenu u realnim sistemima. Model na kom je sistem implementiran se sastoji od cevi sa zadebljanim zidovima, dva zvučnika i dva mikrofona, koji imaju za cilj da na što bolji način simuliraju realnu cev za ventilaciju kroz koju se prostiru ravanski talasi.

U literaturi [1] je opisana implementacija ovog sistema sa FxLMS (*Filtered east Mean S uare*) algoritmom [3]. Ovaj algoritam pruža stabilnost čitavom sistemu, što je njegova ključna prednosti u odnosu na poznati LMS *east Mean S uare* algoritam [4]. U ovom radu je ispitan FxLMS i zaključeno je da koeficijenti adaptivnog filtra sporo konvergiraju do svojih optimalnih vrednosti. Na osnovu toga je zaključeno da je potrebno upotrebiti drugi adaptivni algoritam [5]. Algoritam koji je približno jednostavan kao i FxLMS je NFxLMS (*Normali ed Filtered east Mean S uare*) [6]. On omogućava bržu konvergenciju koeficijenata, što je jako bitno prilikom implementacije ovog sistema na hardveru.

Krajnji cilj ovog istraživanja je ispitivanje za koji ulazni signal i koju kompleksnost algoritma je moguće realizovati ovakav sistem na hardveru. U radovima iz literature [7] je korišćena frekvencija odabiranja od 8 kHz, što je daleko manje od frekvencije koju je neophodno koristiti u realnom sistemu kako bi čitav sistem funkcionisao. Tokom testiranja sistema testirano je više frekvencija odabiranja, uz ograničenje da sa povećanjem frekvencije odabiranja raste kompleksnost. Posebna pažnja se obraća na maksimalno slabljenje koje će sistem u hardverskoj implementaciji obezbediti, i razlike u odnosu na slabljenje postignuto u simulaciji.

## II. METODOLOGIJA

### A. ANC

Aktivna kontrola buke je elektroakustički sistem koji potiskuje primarnu buku. Sistem je baziran na principu

Marija Ratković– Elektrotehnički fakultet, Univerzitet u Beogradu, Bulevar kralja Aleksandra 73, 11020 Beograd, Srbija (e-mail: rm180095d@student.etf.bg.ac.rs).

Nebojša Kolarić – Elektrotehnički fakultet, Univerzitet u Beogradu, Bulevar kralja Aleksandra 73, 11020 Beograd, Srbija (e-mail: kn180670d@student.etf.bg.ac.rs).

Miloš Bjelić – Elektrotehnički fakultet, Univerzitet u Beogradu, Bulevar kralja Aleksandra 73, 11020 Beograd, Srbija (e-mail: bjelic@etf.rs).

 ISBN 978-86-7466-930-3

superpozicije. Na slici 1. je prikazan model ANC-a. Sistem zahteva referentni mikrofon neophodan za prikupljanje referentnog signala koji potiče od izvora buke, a koji treba potisnuti. Na kraju cevi se nalazi mikrofon koji prikuplja zbirni signal primarne i sekundarne buke, odnosno skuplja ukupnu grešku. Sekundarna buka proizilazi iz sekundarnog zvučnika koji emituje signal tako da je suprotan primarnoj buci. To ima za cilj da anulira primarnu buku i na taj način stvara zonu tišine u tom okruženju. ANC kontroler podešava svoje parametre na osnovu signala skupljenih na primarnom i sekundarnom mikrofonu, kontroler je baziran na LMS adaptivnom algoritmu. Algoritam je zadužen da podešava koeficijente adaptivnog filtra tako da se greška na sekundarnom mikrofonu minimizira. Na izlazu iz kontrolera se generiše signal koji će biti reprodukovan na sekundarnom zvučniku, koji je jednak po amplitudi i suprotan po fazi sa primarnom bukom. Njihovim kombinovanjem dobija se potiskivanje obe buke.

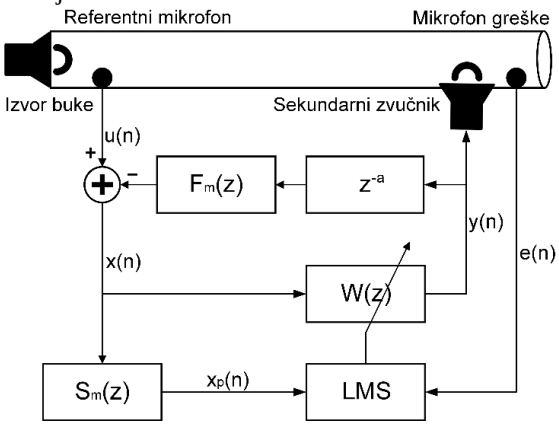


Sl. 1. Blok šema ANC sistema

*B. pis algoritma*

U ovom delu je detaljno objašnjen FxLMS algoritam [8], na osnovu blok šeme prikazane na slici 1. Impulsni odzivi modelovanih filtara, $S_m$ i $F_m$ , su određeni pomoću adaptivnog algoritma za identifikaciju nepoznatog sistema. Impulsni odzivi primarne i sekundarne putanje modelovani su funkcijom *fir2*, koja je ugrađena u Matlabu, Primarna buka na ulazu u referentni mikrofon koju treba potisnuti može biti izražena kao:

$$d(n) = P \times u(n) \tag{1}$$

gde $P$ predstavlja impulsni odziv primarnog puta od referentnog mikrofona do mikrofona greške, a $u\ n$ predstavlja odbirke signala na referentnom mikrofonu. $M$ predstavlja red filtra koji je modelovan od impulsnog odziva $P$. Za dalju obradu unutar LMS algoritma neophodno je obraditi ulazni signal $u\ n$ sa referentnog mikrofona.

U realizaciji ovog sistema se javlja problem akustičke povratne sprege koja potiče od sekundarnog zvučnika ka referentnom mikrofonu. Iz tog razloga neophodno je modelovanje još jednog impulsnog odziva $F$ koji podrazumeva tu putanju i koji utiče na ulazni signal.

$$(n) = u(n) - k(n) \tag{2}$$

gde $k\ n$ predstavlja signal koji je bio izlaz sekundarnog zvučnika zakašnjen za $a$ odbiraka, propušten kroz filtar reda koji je modelovan impulsnim odziv, $F_m$ [9].

$$k(n) = F_m \times y_{a'} \tag{3}$$

Broj odbiraka $a$ za koji treba zakasniti sekundarni signal je izračunat kao odnos dužine dela puta od sekundarnog zvučnika do referentnog mikrofona i brzine prostiranja zvuka. Tako dobijena vrednost u vremenu pomnožena je vrednošću frekvencije odabiranja kako bi se dobio potrebni broj odbiraka. Neophodno je uračunati i vreme kašnjenja samog hardvera, označeno sa $t_{Bela}$, pri implementaciji algoritma na hardveru.

$$a = (t - t_{Bela}) \times f_s \tag{4}$$

U simulaciji nije neophodno korišćenje ovog dela, jer nema reprodukcije sa sekundarnog signala na sekundarni mikrofon. Samim tim nema ni ometanja u vidi akustičke povratne sprege. Ipak u realnoj implementaciji neophodno je posvetiti pažnju ovom delu. Na osnovu izloženog Zaključuje se da je u simulaciji $k\ n$ =0.

Sekundarna putanja podrazumeva deo cevi od sekundarnog zvučnika do mikrofona greške, uz to ona obuhvata: digitalno analogni (D/A) konvertor, filter za rekonstrukciju, pojačavač, zvučnik i akustičku putanju od zvučnika do mikrofona greške, mikrofon, mikrofonski pretpojačavač i A/D konvertor. Neophodno je da ulazni signal pre ulaska u LMS algoritam bude propušten kroz model impulsnog odziva sekundarne putanje $S_m$ [10], reda N.

$$_p(n) = S_m \times \ _1' \tag{5}$$

gde je $_1$' ulazni signal za LMS algoritam, koji je jedan od parametara koji konfigurišu u relaciji za izračunavanje koeficijenata adaptivnog filtra, reda . Signal $y$ koji se reprodukuje na sekundarnom zvučniku dobija se propuštanjem signala $_p$ kroz adaptivni filtar $W$. Svaki od odbiraka se računa na sledeći način:

$$y(n) = W \times \ _2' \tag{6}$$

Sekundarna buka na mikrofonu greške $y_p(n)$, koja treba da potisne primarnu buku $d\ n$ , dobija se propuštanjem sekundarne buke sa sekundarnog zvučnika kroz filtar koji modeluje sekundarnu putanju $S$ i ima red N:

$$y_p(n) = S \times y' \tag{7}$$

Signal greške $e(n)$ je primljen na mikrofonu greške, i on predstavlja razliku primarne i sekundarne buke:

$$e(n) = d(n) - y_p(n) \tag{8}$$

U $F\ \ MS$ algoritmu koeficijenti adaptivnog filtra $W$ se u svakoj iteraciji optimizuju kako bi greška $e\ n$ bila što manja, računaju se na sledeći način:

$$w(n+1) = w(n) + \mu \times \ _p(n) \times e(n) \tag{9}$$

Parametar je konstantna male vrednosti koja se zadaje tako da konvergencija koeficijenata bude što brža. Ova vrednost ne sme biti prevelika da se optimalna vrednost ne bi preskočila u nekoj od iteracija. Algoritam bi trebalo da se izvrši onoliko puta koliko je potrebno da greška dostigne neku određenu, dovoljno malu vrednost. To će se postići kroz stalno menjanje koeficijenata filtra kako bi se što bolje prilagodila greška traženoj vrednosti.


ISBN 978-86-7466-930-3

U simulaciji je umesto FxLMS algoritma korišćen NFxLMS, kako bi koeficijenti brže iskonvergirali do optimalnih vrednosti [11]. Za NFxLMS se može koristiti manji red adaptivnog filtra što je ključni razlog za njegovo korišćenje u ovom radu, prilikom implementiranja na hardveru je potrebno smanjiti broj računskih operacija što se na ovaj način postiže. Jedina razlika između ova dva algoritma je što se drugačije računaju koeficijenti $w\ n\ 1$, tačnije promenljiv je korak adaptacije $n$. Koeficijenti NFxLMS alagoritma se računaju:

$$w(n+1) = w(n) + \mu(n) \times \ _p(n) \times e(n) \tag{10}$$

Parametar $n$ se izračunava kao:

$$\mu(n) = \frac{\mu}{s+\delta} \tag{11}$$

gde $\delta$ predstavlja malu proizvoljnu konstantu. Vrednost $s\ n$ je izraženo kao:

$$s(n) = \sum_{i=0}^{-1} \ _p(n-1)^2 \tag{12}$$

### C. Implementacija algoritma na realnom modelu

Algoritam je testiran na realnom modelu koji se sastoji od cevi dugačke približno jedan metar, dva zvučnika, primarnog i sekundarnog i dva mikrofona, kao što je prikazano na slici 2.

Sl. 2. Izgled korišćene cevi za hardversku implementaciju

Cev je dugačka 1 m, njen prečnik iznosi 7.5 cm. Korišćeni su širokopojasni zvučnici čija veličine membrane iznosi 3″. Korišćeni su neusmereni elektret mikrofoni. Cev ima rezonantne frekvencije, koje se mogu odrediti preko izraza:

$$f = \frac{c}{4\times} \tag{13}$$

gde je $c$ brzina zvuka u vazduhu koja iznosi približno 340 m/s, a je dužina cevi.

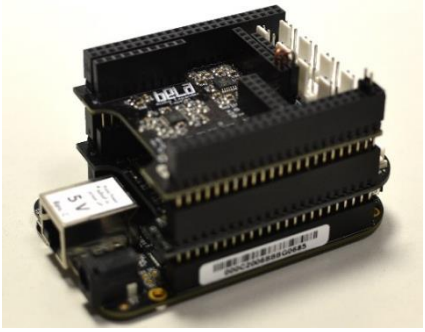

Sl. 3. Bela procesor

Za implementaciju algoritma korišćena je platforma Bela, koja predstavlja računarski sistem namenjen za obradu audio signala, bazira se na *BeagleBone* platformi. Izgled Bela procesora prikazan je na slici 3. Glavna karakteristika ovog procesora je malo kašnjenje kada se obrađuju audio signali i sistemi, kao što je ANC sistem. Korišćeni su dva audio ulaza i jedan audio izlaz koje Bela poseduje, sa frekvencijama odabiranja 22050 Hz. Primarni mikrofon i mikrofon greške su bili povezani na po jedan kanal ulaza, a sekundarni zvučnik je bio povezan na izlaz Bele. Primarni zvuk je generisan pomoću generatora, kojim su generisani signali različitih vremenskih oblika.

Adaptacija algoritma za generisanje sekundarnog zvuka izvršena je pomoću integrisanog razvojnog okruženja koje ovaj sistem poseduje. Razvojno okruženje bazirano je programskom jeziku C.

### . Modelo anje impulsnih od i a

U cevi je izvršeno snimanje svih potrebnih impulsnih odziva za softversku realizaciju (impulsni odziv primarne putanje, sekundarne, kao i putanje unazad od sekundarnog zvučnika do referentnog mikrofona). Kao što je ranije navedeno za konkretnu softversku implementaciju ovog sistema nije bio potreban impulsni odziv putanje unazad, *F*, ali će za hardversku implementaciju biti neophodan, zato je i on snimljen. Dobijene impulsne odzive je bilo neophodno modelovati, kako bi bili iskorišćeni u algoritmu.

U simulaciji ovi impulsni odzivi su bili modelovani FIR filtrima, korišćenjem ugrađenih funkcija, trudeći se da amplitudska i fazna karakteristika modela budu što sličnije originalnoj. Rezultati simulacija su zavisili od izabranih redova filtara. U zavisnosti od složenosti test signala neophodni redovi filtara su se menjali, od stotog pa sve do dve hiljaditog reda. U realizaciji u realnom vremenu na hardverskoj platformi ti redovi su preveliki i nije moguće koristiti ih. Zbog toga je bilo neophodno na drugi način modelovati tražene impulsne odzive.

Manji red filtara, do stotog reda, je dobijen modelovanjem impulsnih odziva preko paralelne veze IIR filtara drugog reda. Amplitudska karakteristika tako dobijenog modela je približno istog oblika kao i kod originalnog impulsnog odziva. Sa ovakvim modelima algoritam nije konvergirao, iz čega se zaključuje da amplitudska karakteristika nema veliki uticaj i da je mnogo bitnija fazna karakteristika koja se na ovaj način ne uzima u obzir.

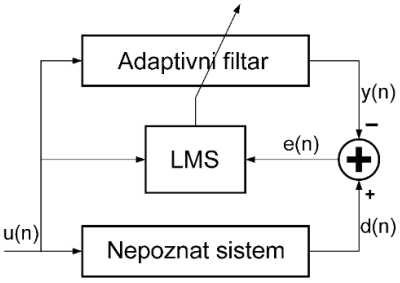


Sl. 4. Blok šema za prepoznavanje nepoznatog sistema

Kao optimalno rešenje za modelovanje ovih putanja, tako da red filtra bude dovoljno mali i da se fazna karakteristika na što bolji način modeluje, korišćenje adaptivni algoritam za prepoznavanje nepoznatog sistema. Principska blok šema sistema prikazana je na slici 4. Na ovaj način je očuvana i fazna i amplitudska karakteristika u onoj meri u kojoj je to neophodno kako bi čitav sistem funkcionisao. U simulaciji i u hardverskoj implementaciji su korišćeni isti modelovani filtri stotog reda.

 ISBN 978-86-7466-930-3

U hardverskoj implementaciji nije bilo potrebe modelovati primarnu putanju, jer će signal proći taj put i pretrpeće uticaj impulsnog odziva primarnog puta. Primarni signal koji treba potisnuti će biti pod uticajem zvuka sa sekundarnog zvučnika i to moramo izbeći. Zato je neophodno koristiti impulsni odziv putanje unazad kako bi uspeo da se generiše signal koji se pušta na sekundarnom zvučniku, koji je optimalan za potiskivanje primarnog signala.

## III. REZULTATI

### *A. e ultati simulacije*

Korišćeno je više različitih primera signala kao izvore buke na referentnom zvučniku, kako bi se ispitale performanse sistema. Za svaki od slučajeva je bilo potrebno koristiti različite redove adaptivnog filtra. Za složenije signale bilo je neophodno povećati red filtra, kako bi dobili što bolje potiskivanje zvuka sa referentnog zvučnika. Takođe, pored menjanja redova filtra neophodno je bilo podešavati i statički korak adaptacije . Pritom se mora obratiti pažnja da vrednost ne bude prevelika jer bi se preskočilo optimalno rešenje i filtar bi prooscilovao.

Prvi najjednostavniji primer na kome je isproban sistem je bila sinusoida koja je potisnuta u potpunosti, što se može videti sa slike 4. Na slici 4 je prikazan vremenski oblik originalnog signala na ulazu u mikrofon greške kada ne bi bilo ANC sistema i signal greške *e*, gde jasno uviđamo da postaje nula. Za ovaj primer bio je dovoljan da vrednost reda adaptivnog filtra bude =50, a korak adaptacije =0.001.

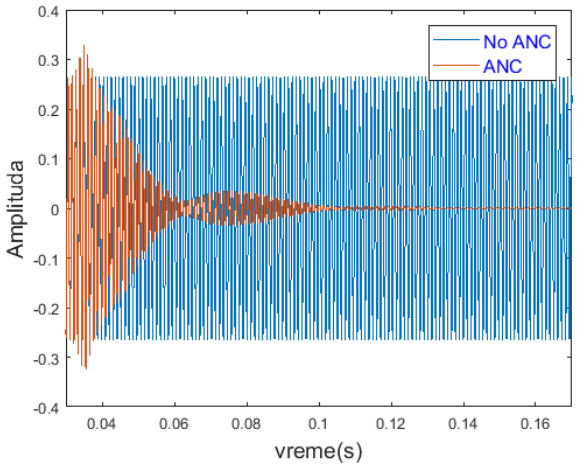


Sl. 4. Vremenski oblik originalnog i signala greške za sinusnu pobudu

Sledeći slučaj na kom je testiran sistem je „klipovana“ sinusoida. Ovaj signal je dobijen direktnom reprodukcijom signala na referentni zvučnik u cevi i njegovim snimanjem na primarnom i sekundarnom mikrofonu. Samim tim nije bilo potrebe propuštati ulazni signal kroz impulsni odziv *P*, jer je korišćen snimljeni primarni signal na mikrofonu greške. Ovaj signal je složeniji i nije se mogao potpuno potisnuti kao u prvom slučaju, ali se vidi na slici 5. da je dosta oslabljen. Koeficijenti teže konvergiraju jer je sam signal složeniji. Korišćen je red filtra =100, a =0,0005.

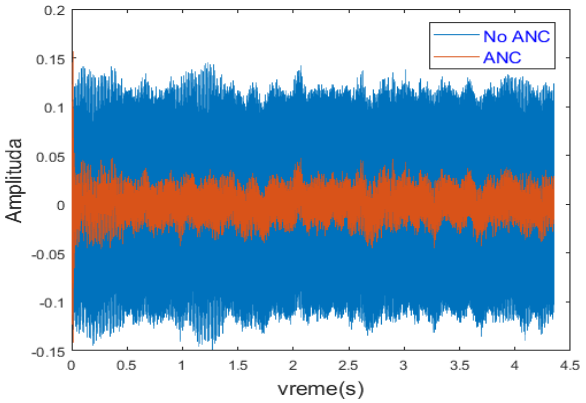


Sl. 5. Vremenski oblik originalnog i signala greške pobudni signal klipovane sinusoide

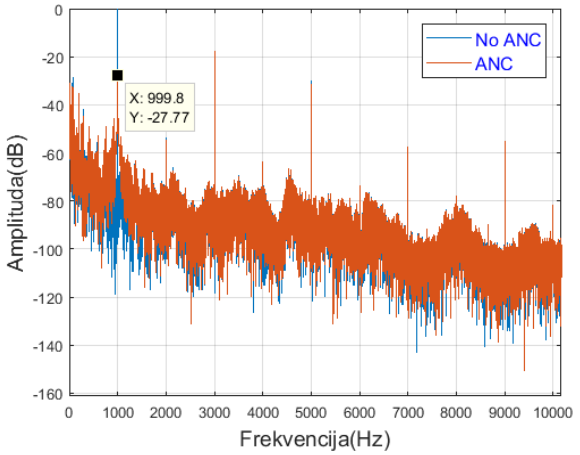


Sl. 6. Spektar originalnog signala i signala greške za šum oblika klipovane sinusoide

Kao što se vidi na slici 6. na kojoj su prikazani spektri originalnog i potisnutog signala najviše je potisnut osnovni harmonik i to za 27 dB. Pored potiskivanja prvog harmonika uočava se da na ostale harmonike algoritam nije imao uticaj i ne potiskuje ih. Najvažnije je upravo potiskivanje na osnovnoj frekvenciji što je upravo postignuto.

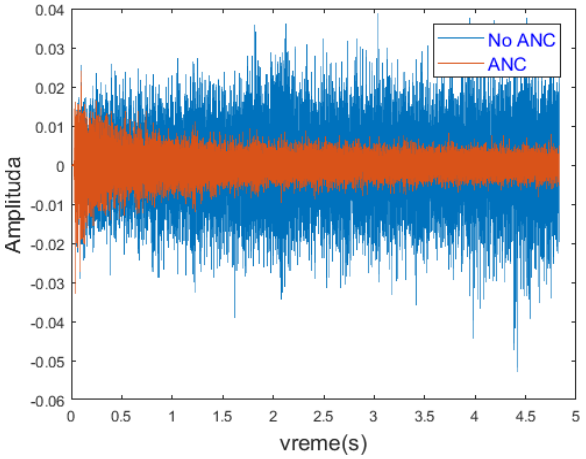


Sl. 7. Vremenski oblik originalnog signala i signala greške za šum ventilatoa

Najsloženiji širokopojasni signal koji je testiran je snimak ventilatora. Zbog same složenosti ovog signala potiskivanje je bilo najlošije, ali ipak postoji što se vidi na slici 6. Kada se


ISBN 978-86-7466-930-3

poredi signal bez ovog algoritma kada samo prođe kroz cev i signala greške kada se koristi algoritam, jasno se primećuje razlika da je signal oslabljen i to za 13 dB kada se koristi ANC. Zbog same složenosti signala algoritam mora biti kompleksniji kako bi koeficijenti konvergirali.Samim tim bilo je potrebno da red adaptivnog filtera bude veći i iznosi =700, korak adaptacije iznosi 0.002. Takođe, modelovana sekundarna putanja se adaptirala u odnosu na Gausov šum i red adaptivnog filtra za prepoznavanje nepoznatog sistema morao biti 600 da bi se dobro modelovala sekundarna putanja.

### *B. ard erska implementacija na Beli platformi*

Implementacije na hardveru su dosta zahtevnije od softverskih simulacije jer se mora voditi računa o nizu problema. Jedan od problema je na primer određeno vreme izvršavanja čitave obrade signala na jednom odbirku. Ovaj problem uvodi ograničenja odmah na početku i zahteva da redovi filtara (modelovanih i adaptivnog) budu što manji da bi obrada signala stigla da se izvrši za određeno vreme. Maksimalno dozvoljeno vreme obrade je $1/f_s$, gde je $f_s$ frekvencija odabiranja. To dovodi do nemogućnosti korišćenja složenijih i bržih adaptivnih algoritama od LMS-a, jer će biti povećan broj računskih operacija i samim tim duža obrada. Drugi problemi na koje se mora paziti su modelovanje adekvatnog kašnjenja, tako da izlaz sekundarnog zvučnika reprodukuje odbirak u trenutku kada isti taj odbirak stiže od primarnog zvučnika da bi oba signala superponirala i poništila. Ovo je rešeno tako što je izmereno rastojanje između referentnog mikrofona i sekundarnog zvučnika, koje iznosi =0.87 m. Pa je kašnjenje izračunato i iznosi $t$=2.55 ms. Nakon toga treba oduzeti kašnjenje koje je potrebno za propagaciju signala sa ulaza na izlaz (kašnjenje hardvera)Ovo vreme iznosi $t_{Bela}$=0.93 ms. Na kraju kako bi se dobio broj odbiraka, vreme $t_{Bela}$ je pomnoženo sa frekvencijom odabiranja:

$$samples = (t - tBela) \times fs = 35. \quad (15)$$

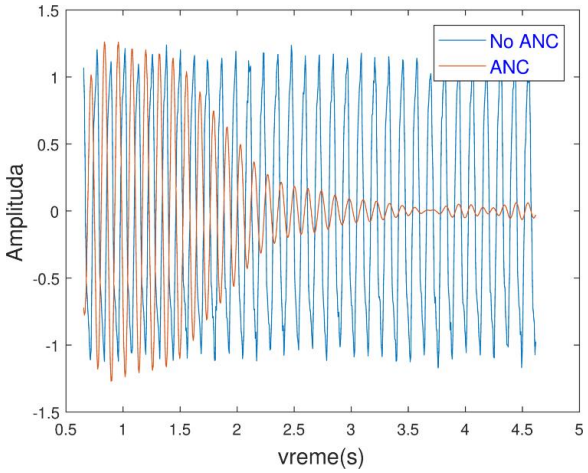


Sl. 8. Vremenski oblik originalnog signala i signala greške za sinusoidalnu pobudu za implementaciju na hardveru

Prvi signal koji je korišćen za testiranje sistema, korišćenjem generatora kao izvora, je sinusoida frekvencije 900 Hz. Na slici 8 prikazan je vremenski oblik sinusoide na ulazu u zvučnik i signala greške koji se prikuplja na mikrofonu greške. Jasno se primećuje da je sinusoida potisnuta u velikoj meri nakon 3.5 s.

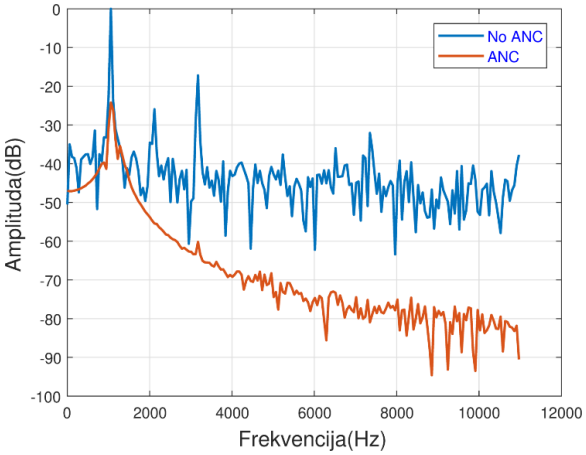


Sl. 9. Spektar originalnog signala i signala greške za sinusoidalnu pobudu za implementaciju na hardveru

Ako se poredi signal greške koji se dobija u softverskoj realizaciji (slika 4) i signal dobijen u hardverskoj realizaciji jasno se uviđa da hardversko rešenje ne potiskuje sinusoidalni signal u potpunosti. Na slici 9 prikazani su spektri originalnog signala i signala greške. Zaključuje se da je algoritam uspeo da potisne sinusoidu i oslabi je za 24 dB u odnosu na signal smetnje. Red adaptivnog filtra korišćen za ovaj test primer iznosio je =100, a koeficijent adaptacije =0.00002.

Drugi primer koji je testiran je signal klipovane sinusoide reprodukovan na referentnom zvučniku. Klipovana sinusoida je kompleksniji signal i teže je potisnuti ga. Na slici 10 su prikazani signali skupljeni na referentnom mikrofonu i na mikrofonu greške, gde jasno uviđamo da je uspešno potisnuta primarna buka. Red adaptivnog filtra neophodan da bi algoritam dobro radio je =100, a korak adaptacije =0.00008. Ovaj primer je uspešno potisnut i oslabljen za 20 dB, kao što se može videti na slici 11.

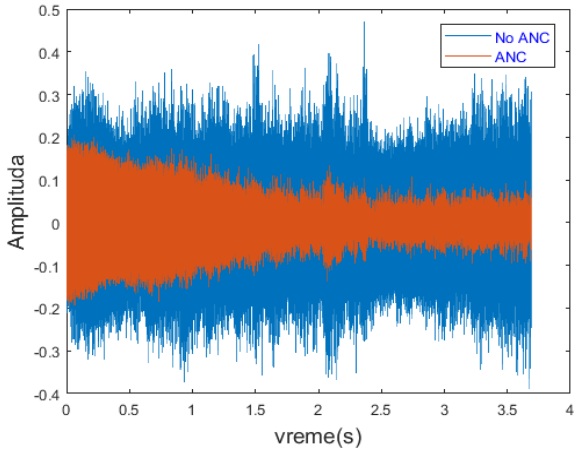


Sl. 10. Vremenski oblik originalnog signala i signala greške za klipovanu sinusoidalnu pobudu za implementaciju na hardveru

Algoritam na hardveru je testiran i za šum ventilatora, što je njegova suštinska primena, ali rezultat nije pozitivan. Šum ventilatora je mnogo složeniji signal od ova dva prethodno

 ISBN 978-86-7466-930-3

opisana, samim tim neophodno je da red filtra bude mnogo veći. Povećavanjem reda filtra povećava se i potrebno vreme za izvršavanje čitavog procesa i prevazići će se maksimalno vreme koje je moguće na hardveru. Cilj narednih istraživanja i obrađivanja ovog sistema će upravo biti optimizovanje algoritma tako da uspešno potiskuje šum ventilatora.

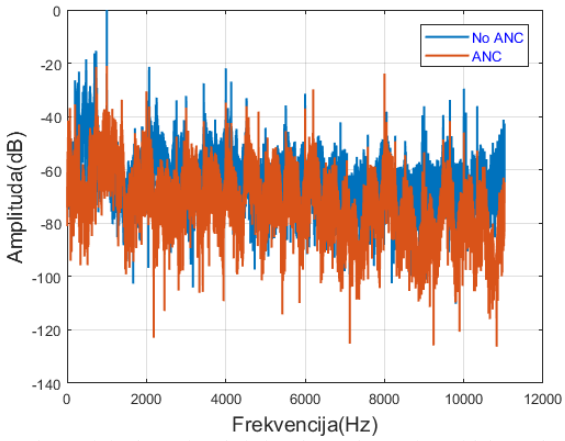


Sl. 11. Spektar originalnog signala i signala greške za sinusoidalnu pobudu za implementaciju na hardveru

## IV. ZAKLJUČAK

U ovom radu prikazana je implementacija ANC algoritma kroz softversku simulaciju i hardversku realizaciju. Softversko rešenje je jednostavnije implementirati jer predstavlja simulaciju realnog problema iz kojeg se izostavlja veliki broj spoljašnjih faktora koji otežavaju realizaciju sistema na hardveru. Implementacijom algoritma u softveru se dobijaju približno najbolja moguća rešenja kojima će se težiti u realnim sistemima. Jedna od najvećih razlika između ova dva načina testiranja algoritma je što implementacija na hardveru korišćenjem pravog modela mora biti u realnom vremenu. Postoji ograničeno vreme za koje algoritam mora biti izvršen, samim tim neophodno je smanjivati redove filtara modelovanih impulsnih odziva, kao i red adaptivnog filtra čime se gubi na performansama samog algoritma. Dodatne komplikacije koje se javljaju kad se implementira sistem na pravom modelu je kompenzacija kašnjenja koja potiče od samog procesiranja na platformi Bela, kao i pojava akustičke povratne sprege na koju se mora obrtati posebna pažnja. Takođe Bela hardver ima određena ograničenja, kao što su frekvencija odabiranja, kašnjenje koje se javlja prilikom obrade podataka, kao i maksimalno vreme za koje se mora izvršiti algoritam. Iz svih navedenih razloga zaključuje se da će finalna rešenja na realnom sistemu biti lošija, što se i vidi iz prikazanih rezultata. Kroz softversku implementaciju test signal sinusoide je oslabljen za 36 dB dok na realnom modelu pri reprodukciji signala sinusoide maksimalno slabljenje iznosi 24 dB. Može se videti da postoji razlika ali suštinski u oba slučaja sinusoidalna buka je potisnuta. Takođe za primer u kome je primarni signal klipovana sinusoida se vidi razlika u potiskivanju od 20 dB pri primeni na hardveru.

Buduća nadogradnja ovog rada će se kretati u smeru pronalaženja rešenja za potiskivanje realnog šuma ventilatora na realnom modelu u cevi. Rešenje tog problema predstavljalo bi primenu ANC sistema u svakodnevnom životu. Mogućnosti korišćenja ovakvih sistema bile bi u određenim prostorima gde je od velikog značaja potiskivanje spoljašnje buke na niskim frekvencijama, koja potiče od ventilatora, klima uređaja, ventilacionih sistema itd.

## ZAHVALNICA

Autori žele da se zahvale profesorki Jeleni Ćertić na korisnim savetima prilikom implementacije algoritama. Ovaj rad je realizovan u okviru projekta TR36026 koji finansira Ministarstvo prosvete, nauke i tehnološkog razvoja Republike Srbije.

## LITERATURA

[1] S. Sadeghi, J. Poshtan, M. Kahaei, “The simulation and implementation of an active noise control system in a laboratory duct”, European control conference, Cambridge, UK, pp. 1252-1256, 1-4. September, 2003.
[2] Stephen J. Elliott, „Signal Processing for Active Control“, Academic Press, 2001.
[3] S. M. Kuo, D. R. Morgan, „Active noise control: a tutorial review“, Proceedings of the IEEE, vol. 87, no. 6, pp. 943-973. 1999.
[4] B. Widrow, S. D. Stearns, “Adaptive Signal Processing”, Prentice Hall, New Jersey, 1985.
[5] M. T. Akhtar, W. Mitsuhashi, “Improving Performance of FxLMS Algorithm for Active Noise Control of Impulsive Noise”, Jr. Sound Vibr., vol. 327, No. 3-5, pp 647-656, Nov. 2009.
[6] M. T. Akhtar, W. Mitsuhashi, „A modified normalized FxLMS algorithm for active control of impulse noise“, 18th European Signal Processing Conference, Aalborg, Denmark, August 23-27, 2010.
[7] H. Lan, M. Zhang, W. Ser, „A weight-constrained FxLMS algorithm for feedforward Active noise control systems“, IEEE signal processing letters, vol. 9, No. 1, January, 2002.
[8] Simon Haykin, “Adaptive filter theory”, 4th ed. Upper Saddle River, New Jersey, 2002.
[9] Sen M. Kuo, Dennis R. Morgan, “Active Noise Control Systems-Algorithms and DSP Implementations”, John Wiley, 1996.
[10] Sakshi Gaur, V. K. Gupta, “A review on Filtered-x LMS algorithm”, International Journal of Signal Processing Systems vol. 4, No. 2, April 2016.
[11] I. T. Ardekani and W. Abdulla, “Study of convergence behaviour of real time adaptive active noise control systems,” in Proceedings of 2010 Asia Pacific Signal and Information Processing Association Annual (APSIPA) Summit and Conference, Biopolis, Singapore, 14-17 December 2010,
Pages 534-537.

## ABSTRACT

ANC (Acoustic Noise Control) systems are necessary in the premises where the elimination of unwanted sounds is required. In this paper, we have done simulation of ANC system in the duct and implementationon hardware. FxLMS (Filtered x Least Mean Square) and NFxLMS (Normalized Filtered x Least Mean Square) adaptive algorithms were tested, they were compared by robusntness, necessary order of adaptive filter and convergence rate. In the simulation were used: sinusoid, clipped sinusoid and fan noise. Depending on the complexity of the test signal the parameters of the adaptive filter have changed. The results show that it is possible to supress acoustic noise to a certain limit depending on the complexity of the signal.

**Acoustic noise control in a duct**

Marija Ratković, Nebojsa Kolarić, Milos Bjelić

 ISBN 978-86-7466-930-3

# ANTENNAS AND PROPAGATION
# /
# АНТЕНЕ И ПРОСТИРАЊЕ
# (API/АП)

ISBN 978-86-7466-930-3

# Application of Microwave Imaging for Brain Diagnostics

Marija Nikolic Stevanovic, Darko Ninkovic, Tushar Singh, Branislav Ninkovic, Miodrag Tasic, and Branko Kolundzija

***Abstract*— We present the application of the distorted Born iterative method for permittivity estimation of a realistic human phantom, which is an essential step in microwave medical diagnostics. Permittivity reconstruction is a difficult task due to the complexity of the electromagnetic model and the ill-posedness of the inverse scattering problems. Assuming that prior knowledge of the head anatomy is available from other imaging modalities, such as magnetic resonance imaging, we showed that electromagnetic tissue parameters could be accurately estimated even for tissues deeply located in the head. In our implementation of DBIM, we have gradually improved the estimation accuracy by initializing more complex models with results obtained for simpler models.**

***Index Terms*—Microwave imaging, inverse scattering, distorted Born iterative method, human phantoms.**

## I. Introduction

In the last decade, the application of microwaves in medical diagnostics has gained much attention. The advantages of medical microwave imaging (MMWI) are non-invasiveness, low cost, utilization of nonionizing radiation, and ease of portability. However, due to the relatively low resolution of MMWI, it is envisioned primarily as a complementary screening tool for medical applications [1]–[3].

The gold standards in medical diagnostics are magnetic resonance imaging (MRI), computed tomography (CT), and positron emission tomography (PET) [4], [5], which produce high-resolution images with well-resolved tissues. However, their application is usually limited to large medical centers due to their high cost, and they are not appropriate for bedside monitoring. Additionally, CT and PET scans utilize harmful ionizing radiation.

The essential elements of any MMWI system are an antenna array, a reconstruction algorithm based on inverse scattering, and a reliable efficient 3D electromagnetic solver. Additionally, realistic human models (phantoms) are necessary for designing and testing MMWI systems.

Microwave imaging algorithms are generally classified into two categories: qualitative and quantitative. The goal of qualitative algorithms in medical imaging is to detect possible lesions or other tissues changes between measurements. They cannot infer the electromagnetic properties of the changes; instead, they estimate their location and shape. Examples of qualitative imaging algorithms are truncated singular value decomposition (TSVD) [6] and the linear sampling method (LSM) [7]. In contrast, quantitative algorithms reconstruct the complex permittivity in the whole domain of interest. Since different tissues have different electromagnetic properties, permittivity maps are also images of particular body parts.

Solving quantitative algorithms is difficult due to the complex scattering phenomenon. They are non-linear and ill-posed, making them prone to false solutions and more computationally intensive than qualitative algorithms. Examples are the inexact Newton methods [8] and the distorted Born iterative method (DBIM) [9], [10].

In this paper, we study the application of the DBIM to the permittivity reconstruction of a realistic head phantom. Although the utilized method is well-established, there are only a few examples of its application to realistic 3D human models. The main reasons for this are the non-uniqueness of the solution, the lack of detailed anatomical models adapted for electromagnetic analysis, and the extremely long computational time. The goal of this work is to test the algorithm's ability to estimate tissues' permittivities. Thus, we assume that the tissue boundaries are available, e.g., from a prior MRI screening. To initialize the algorithm, we first compute the average permittivity of the head.

The paper is organized as follows. After the introduction, we explain the DBIM in Section II. Section III describes the numerical examples and presents the obtained results. Finally, in the concluding section, we summarize the obtained results and give guidelines for future work.

## II. Distorted Born Iterative Method

The goal of quantitative microwave imaging is to estimate the complex permittivity of the unknown object or the whole domain of interest. Fig. 1 illustrates a three-dimensional (3D) microwave imaging scenario consisting of an unknown non-magnetic inhomogeneous object, which occupies a volume $v'$ and has the permittivity $\varepsilon$. The object is located in a known non-magnetic background medium whose permittivity is $\varepsilon_b$.

M. Nikolic Stevanovic is with the School of Electrical Engineering, University of Belgrade, Serbia (e-mail: mnikolic@etf.bg.ac.rs).

D. Ninkovic is with the School of Electrical Engineering, University of Belgrade, Serbia (e-mail: darko@etf.bg.ac.rs).

T. Singh is with WIPL-D d.o.o. Belgrade, Serbia and the School of Electrical Engineering, University of Belgrade, Serbia (e-mail: tushar.singh@wipl-d.com).

B. Ninkovic is with WIPL-D d.o.o. Belgrade, Serbia (e-mail: branislav.ninkovic@wipl-d.com).

M. Tasic is with the School of Electrical Engineering, University of Belgrade, Serbia (e-mail: tasic@etf.bg.ac.rs).

B. Kolundzija is with WIPL-D d.o.o. Belgrade, Serbia and School of Electrical Engineering, University of Belgrade, Serbia (e-mail: branko.kolundzija@wipl-d.com)

 ISBN 978-86-7466-930-3

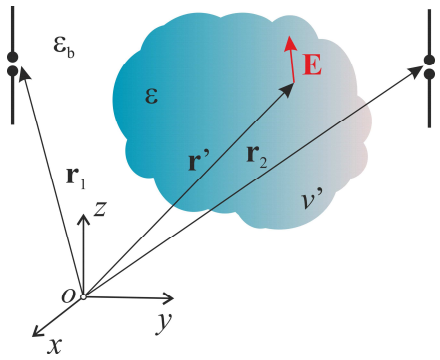


Fig. 1. Measurement scenario.

The measurements are taken by an array consisting of $M$ antennas, out of which only two are shown in Fig. 1. The differential transmission coefficient between the $i$-th and the $j$-th antenna due to the presence of the object is given by [11]:

$$\Delta s_{ji} = -\frac{\mathrm{j}\omega}{2a_i a_j}\int_{v'} \Delta\varepsilon(\mathbf{r}')\,\mathbf{E}^j(\mathbf{r}';\varepsilon_\mathrm{b})\cdot\mathbf{E}^i(\mathbf{r}';\varepsilon)\mathrm{d}v', \tag{1a}$$

$$\Delta s_{ji} = s_{ji}(\varepsilon) - s_{ji}(\varepsilon_\mathrm{b}),\ i,j=1,\ldots,M, \tag{1b}$$

$$\Delta\varepsilon(\mathbf{r}') = \varepsilon(\mathbf{r}') - \varepsilon_\mathrm{b}(\mathbf{r}') \tag{1c}$$

where $\omega$ is the angular frequency, $s_{ji}(\varepsilon)$ is the transmission coefficients computed (or measured) in the presence of the scatterer, $s_{ji}(\varepsilon_\mathrm{b})$ is the transmission coefficient computed when the object is removed and substituted by the background medium, $\mathbf{r}'$ is the position vector of a point inside the object, $\mathbf{E}^j(\mathbf{r}';\varepsilon_\mathrm{b})$ is the electric field vector produced by the $j$-th antenna at $\mathbf{r}'$ in the background medium (the incident field), $\mathbf{E}^i(\mathbf{r}';\varepsilon)$ is the electric field vector produced by the $i$-th antenna at $\mathbf{r}'$ when the object is present (the total field), $a_i$ and $a_j$ are the complex amplitudes of the incident power waves at the $i$-th and $j$-th port, respectively.

If the estimate of the target permittivity ($\hat{\varepsilon}$) is utilized instead of the background permittivity ($\varepsilon_\mathrm{b}$), (1) becomes

$$\Delta s_{ji} = -\frac{\mathrm{j}\omega}{2a_i a_j}\int_{v'} \Delta\varepsilon(\mathbf{r}')\,\mathbf{E}^j(\mathbf{r}';\hat{\varepsilon})\cdot\mathbf{E}^i(\mathbf{r}';\varepsilon)\mathrm{d}v', \tag{2a}$$

$$\Delta s_{ji} = s_{ji}(\varepsilon) - s_{ji}(\hat{\varepsilon}),\ i,j=1,\ldots,M, \tag{2b}$$

$$\Delta\varepsilon(\mathbf{r}') = \varepsilon(\mathbf{r}') - \hat{\varepsilon}(\mathbf{r}'). \tag{2c}$$

Since the object permittivity is unknown, the Born approximation is utilized, $\mathbf{E}^i(\mathbf{r}';\varepsilon)\approx\mathbf{E}^i(\mathbf{r}';\hat{\varepsilon})$. Thus, (2a) becomes

$$\Delta s_{ji} \approx -\frac{\mathrm{j}\omega}{2a_i a_j}\int_{v'} \Delta\varepsilon(\mathbf{r}')\,\mathbf{E}^j(\mathbf{r}';\hat{\varepsilon})\cdot\mathbf{E}^i(\mathbf{r}';\hat{\varepsilon})\mathrm{d}v'. \tag{3}$$

In the limit when $\hat{\varepsilon}\approx\varepsilon$, the left-hand side of (3) approaches zero. The equation (3) is fundamental for DBIM.

In order to apply DBIM, it is necessary to divide the domain of interest into smaller domains (voxels), $v_k$, $k=1,\ldots,L$. We assume that all voxels have the same volume $\Delta V$, which has to be sufficiently small so that the permittivity is approximately constant in each voxel. We use $\varepsilon_k$ and $\hat{\varepsilon}_k$ to denote the true and estimated complex permittivity of the $k$-th voxel.

DBIM is an iterative algorithm that needs to be initialized. If there is no prior knowledge about the permittivity of the inspected object, typically, the background permittivity is utilized, i.e., $\varepsilon_k^{(1)} = \varepsilon_{\mathrm{b},k}$, where $\varepsilon_{\mathrm{b},k}$ is the permittivity of the background medium in the $k$-th voxel and the superscript (1) denotes the iteration number. In the $i$-th iteration, the linear system of equations is

$$\Delta\mathbf{s}^{(i)} = \mathbf{L}^{(i)}\Delta\boldsymbol{\varepsilon}^{(i)}, \tag{4}$$

where $\Delta\mathbf{s}^{(i)}$ is a known vector whose elements are differences of the scattering parameters,

$$\Delta\mathbf{s}^{(i)} = \left[\Delta s_{1,1}^{(i)} \quad \Delta s_{1,2}^{(i)} \quad \cdots \quad \Delta s_{M,M}^{(i)}\right]^\mathrm{T}, \tag{5a}$$

$$\Delta s_{ij}^{(i)} = s_{ij}(\boldsymbol{\varepsilon}) - s_{ij}(\hat{\boldsymbol{\varepsilon}}^{(i)}),\ i,j=1,\ldots,M, \tag{5b}$$

$\hat{\boldsymbol{\varepsilon}}^{(i)}$ is the current permittivity estimate

$$\hat{\boldsymbol{\varepsilon}}^{(i)} = \left[\hat{\varepsilon}_1^{(i)} \quad \hat{\varepsilon}_2^{(i)} \quad \cdots \quad \hat{\varepsilon}_L^{(i)}\right]^\mathrm{T}, \tag{6}$$

$\mathbf{L}^{(i)}$ is the system matrix

$$\mathbf{L}^{(i)} = -\frac{\mathrm{j}\omega\Delta V}{2}\cdot \begin{bmatrix} \dfrac{\mathbf{E}^1(\mathbf{q}_1;\hat{\boldsymbol{\varepsilon}}^{(i)})\cdot\mathbf{E}^1(\mathbf{q}_1;\hat{\boldsymbol{\varepsilon}}^{(i)})}{a_1 a_1} & \cdots & \dfrac{\mathbf{E}^1(\mathbf{q}_L;\hat{\boldsymbol{\varepsilon}}^{(i)})\cdot\mathbf{E}^1(\mathbf{q}_L;\hat{\boldsymbol{\varepsilon}}^{(i)})}{a_1 a_1} \\ \dfrac{\mathbf{E}^1(\mathbf{q}_1;\hat{\boldsymbol{\varepsilon}}^{(i)})\cdot\mathbf{E}^2(\mathbf{q}_1;\hat{\boldsymbol{\varepsilon}}^{(i)})}{a_1 a_2} & \cdots & \dfrac{\mathbf{E}^1(\mathbf{q}_L;\hat{\boldsymbol{\varepsilon}}^{(i)})\cdot\mathbf{E}^2(\mathbf{q}_L;\hat{\boldsymbol{\varepsilon}}^{(i)})}{a_1 a_2} \\ \vdots & \cdots & \vdots \\ \dfrac{\mathbf{E}^M(\mathbf{q}_1;\hat{\boldsymbol{\varepsilon}}^{(i)})\cdot\mathbf{E}^M(\mathbf{q}_1;\hat{\boldsymbol{\varepsilon}}^{(i)})}{a_M a_M} & \cdots & \dfrac{\mathbf{E}^M(\mathbf{q}_l;\hat{\boldsymbol{\varepsilon}}^{(i)})\cdot\mathbf{E}^M(\mathbf{q}_L;\hat{\boldsymbol{\varepsilon}}^{(i)})}{a_M a_M} \end{bmatrix}, \tag{7}$$

and $\Delta\boldsymbol{\varepsilon}^{(i)}$ is an unknown vector

$$\Delta\boldsymbol{\varepsilon}^{(i)} = \left[\Delta\varepsilon_1^{(i)} \quad \Delta\varepsilon_2^{(i)} \quad \cdots \quad \Delta\varepsilon_L^{(i)}\right]^\mathrm{T}, \tag{8}$$

whose elements are the permittivity updates. The system (4) is solved by means of truncated singular value decomposition. The regularized solution is

$$\Delta\boldsymbol{\varepsilon}^{(i)} = \sum_{n=1}^{n_\mathrm{max}} \frac{1}{\sigma_i}\left(\mathbf{u}_n^\mathrm{H}\cdot\Delta\mathbf{s}^{(i)}\right)\mathbf{v}_n, \tag{9}$$

where $\mathbf{u}_n$, $\mathbf{v}_n$ are the singular vectors of matrix $\mathbf{L}^{(i)}$, $\sigma_i$ are the corresponding singular values, and $n_\mathrm{max}$ is the truncation index, obtained from the condition $10\log_{10}(\sigma_{n_\mathrm{max}}/\sigma_1) < -20$ dB. The permittivity estimate in the next iteration is obtained as


ISBN 978-86-7466-930-3

$$\hat{\boldsymbol{\varepsilon}}^{(i+1)} = \hat{\boldsymbol{\varepsilon}}^{(i)} + \Delta\hat{\boldsymbol{\varepsilon}}^{(i)}, \tag{9}$$

The iterative algorithm terminates when the magnitude of each member of the vector $\Delta\boldsymbol{\varepsilon}^{(i)}$ is smaller than some predefined value.

In some cases, prior knowledge about the tissue is available, i.e., from MRI scans. In these situations, we estimate the tissue permittivity, assuming that their surface boundaries are known. Thus, we can reduce the number of unknowns to the number of tissues. The measurement model becomes

$$\Delta\mathbf{s}^{(i)} = \mathbf{L}^{(i)}\mathbf{H}\,\Delta\boldsymbol{\varepsilon}^{(i)}, \tag{10}$$

where $\mathbf{H}$ is the transformational matrix of size $L\times N$, and $N$ is the number of tissues. The $(k,j)$ element of $\mathbf{H}$ is one if $v_k$ belongs to $j$-th domain and zero otherwise. The unknown vector is now

$$\Delta\boldsymbol{\varepsilon}^{(i)} = \left[\Delta\varepsilon_1^{(i)} \quad \Delta\varepsilon_2^{(i)} \quad \cdots \quad \Delta\varepsilon_N^{(i)}\right]^{\mathrm{T}}, \tag{11}$$

where $\Delta\varepsilon_j^{(i)}$ refers to the $j$-th domain.

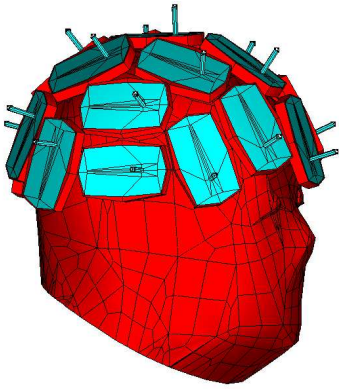

Fig. 2. Head model and the antenna array.

## III. Numerical Results

In order to test the DBIM algorithm, we considered a realistic head model derived from the NEVA woman model [12]–[14]. The antenna array consisted of 21 identical microstrip trapezoidal patch antennas described in [12]. The antennas were fed by coaxial cables as illustrated in Fig. 2. The operating frequency of the array was 1 GHz, as this frequency is found to be the optimal in terms of both penetration depth and resolution.

The forward simulations were computed using the full-wave electromagnetic solver WIPL-D Pro [15]. All results presented in this paper are generated using a desktop computer: Intel Core i7-9700 CPU @3 GHz, NVIDIA GeForce GTX 750 Ti GPU, with 32 GB of RAM under the Windows 10 operating system.

In the first example, the goal was to find the equivalent homogeneous head phantom, which is equivalent (in terms of scattering parameters) to the realistic head phantom comprising seven tissues (skin, fat, mucous membrane, skull, gray matter, white matter and cerebellum).

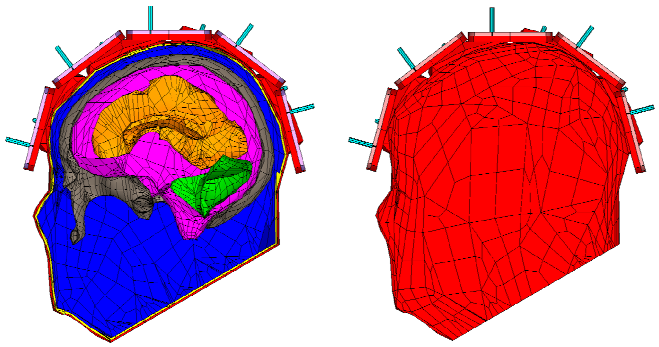

(a) (b)

Fig. 3. (a) Reference head model with seven tissues. (b) Equivalent homogeneous head model filled with the average tissue.

The head interior was divided into $L = 8676$ voxels. As there was only one domain (averaged tissue), the transformation matrix $\mathbf{H}$ was a column vector of size $L\times 1$ with all elements being equal to one. As the initial permittivity estimate, we used the value calculated by the standard averaging procedure $\varepsilon_{\mathrm{r}}^{(1)} = 41.47 - \mathrm{j}14.15$ [12]. After six iterations, the permittivity value converged to $\varepsilon_{\mathrm{r}}^{(6)} = 34.64 - \mathrm{j}12.68$. As a comparison, the gradient optimization [12] yielded for the average tissue permittivity $\varepsilon_{\mathrm{r}} = 34.68 - \mathrm{j}12.68$, which is almost the same result. The number of unknowns in the WIPL-D model (current coefficients) for this example was 24109, and an iteration lasted about 6 minutes.

In the second scenario, the goal was to reconstruct the permittivities of five tissues (skin, fat, mucous membrane, skull, and gray matter) from the head model shown in Fig. 4, assuming that the tissue boundaries are known. As the initial permittivity, we used the value obtained in the first experiment, $\varepsilon_{\mathrm{r}}^{(1)} = 34.64 - \mathrm{j}12.68$, for all tissues.

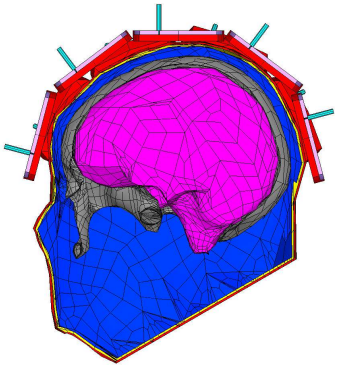

Fig. 4. Model with five tissues.

The WIPL-D model with five tissues has 48354 unknowns and each iteration lasted about 55 minutes. The results obtained after 20 iterations of the algorithm are shown in Table I. The true permittivities of tissues are given in the second column, and the estimated permittivities are shown in the third column. The last column indicates the number of voxels per each tissue.


ISBN 978-86-7466-930-3

TABLE I. ESTIMATION RESULTS FOR THE HEAD WITH FIVE TISSUES

| Tissue Name | $\varepsilon_r$ | $\varepsilon_r^{(20)}$ | Number of voxels |
|---|---|---|---|
| Skin | 45.71 – j15.84 | 45.79 – j15.82 | 3445 |
| Fat | 11.29 – j2.09 | 11.27 – j2.17 | 5086 |
| Mucous Membrane | 45.66 – j15.95 | 45.64 – j15.94 | 35340 |
| Grey Matter | 52.28 – j17.71 | 52.28 – j17.71 | 18267 |
| Skull Bone | 20.58 – j6.54 | 20.59 – j6.55 | 7179 |

In the last example, the goal was to reconstruct the permittivities of the head phantom with seven tissues (Fig. 3a), assuming that the tissue boundaries are known. Again, all elements of the vector $\boldsymbol{\varepsilon}^{(1)}$ were initialized with the averaged tissue value $\varepsilon_r = 34.64 - j12.68$. Firstly, we ran the algorithm with a smaller number of voxels for 20 iterations, and each of them lasted about 60 minutes. We used the obtained results as the initial guess for the permittivities for the next 10 iterations with an increased number of voxels. The execution time of each of those iterations was about 105 minutes. The number of unknowns in the WIPL-D model for this scenario was 60778. Table II shows the results obtained after all 30 iterations.

TABLE II. ESTIMATION RESULTS FOR THE HEAD WITH SEVEN TISSUES

| Tissue Name | $\varepsilon_r$ | $\varepsilon_r^{(30)}$ | Number of voxels |
|---|---|---|---|
| Skin | 45.71 – j15.84 | 45.69 – j15.85 | 463/3445 |
| Fat | 11.29 – j2.09 | 11.33 – j2.03 | 655/5086 |
| Mucous Membrane | 45.66 – j15.95 | 45.73 – j15.92 | 4480/35340 |
| Grey Matter | 52.28 – j17.71 | 52.42 – j17.91 | 1690/13285 |
| Skull Bone | 20.58 – j6.54 | 20.67 – j6.70 | 903/7179 |
| White Matter | 38.58 – j11.18 | 38.33 – j11.27 | 492/3864 |
| Cerebellum | 48.86 – j23.51 | 34.66 – j12.65 | 140/1118 |

The biggest error was obtained for the cerebellum permittivity, which is the smallest domain located deep inside the head. The estimated permittivity values are shown in Fig. 5 (dots at the end represent the true values). Moreover, it can be observed that the cerebellum permittivity has changed insignificantly. Thus, we ran additional 10 iterations of DBIM for estimating the permittivity of the cerebellum, while the permittivities of other six tissues were fixed to the values obtained after 30 iterations. Finally, the permittivity of the cerebellum converged closely to the true value ($\varepsilon_r^{(40)} = 48.80 - j23.51$).

## IV. CONCLUSION

We studied the capability of the DBIM to estimate the permittivities of tissues in realistic human head phantoms. We considered phantoms of different complexity and utilized the simplest model to initialize more elaborate ones. The permittivity was accurately estimated under the assumption that tissue boundaries are known. We will consider the case in which no prior knowledge is available in future work. However, voxel-based meshing has to be utilized in that case, which yields a significantly larger number of unknowns in the forward electromagnetic model and, consequently, increases the computational time enormously.

## ACKNOWLEDGMENT

This work was supported by the EMERALD project funded from the European Union's Horizon 2020 research and innovation program under the Marie Skłodowska-Curie grant agreement No. 764479.

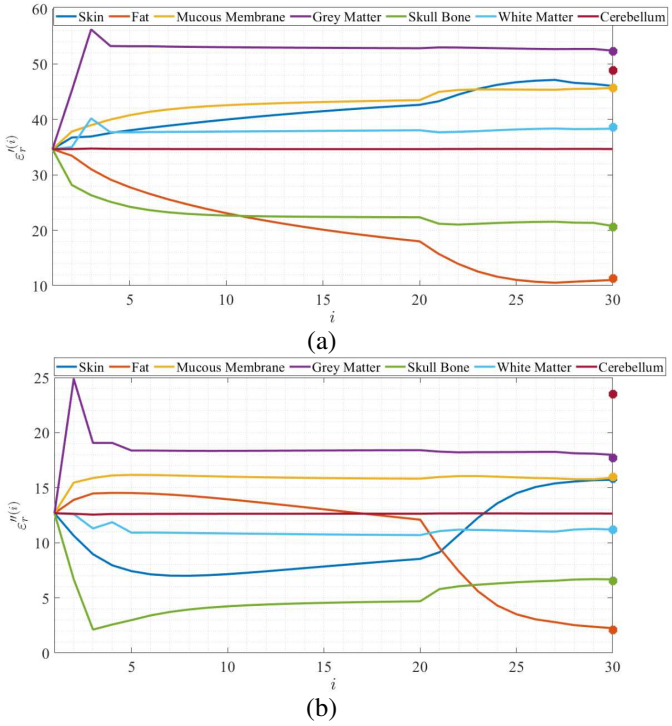


Fig. 5. Estimated permittivites of tissues for each iteration. (a) Real and (b) imaginary part of the complex permittivity.

## REFERENCES

[1] R. Chandra, H. Zhou, I. Balasingham and R. M. Narayanan, "On the Opportunities and Challenges in Microwave Medical Sensing and Imaging," *IEEE Transactions on Biomedical Engineering*, vol. 62, no. 7, pp. 1667-1682, July 2015.

[2] L. Crocco, I. Karanasiou, M. James, R. Conceição, "Emerging Electromagnetic Technologies for Brain Diseases Diagnostics, Monitoring and Therapy," *Springer*, Cham, Switzerland, 2018.

[3] R. Conceição, J. Mohr, M. O'Halloran, "An Introduction to Microwave Imaging for Breast Cancer Detection," Switzerland, Springer, 2018.

[4] G. Zhu, A. Bialkowski, L. Guo, B. Mohammed and A. Abbosh, "Stroke Classification in Simulated Electromagnetic Imaging Using Graph Approaches," *IEEE Journal of Electromagnetics, RF and Microwaves in Medicine and Biology*, vol. 5, no. 1, pp. 46-53, March 2021.

[5] A. S. M. Alqadami, A. Trakic, A. E. Stancombe, B. Mohammed, K. Bialkowski and A. Abbosh, "Flexible Electromagnetic Cap for Head

 ISBN 978-86-7466-930-3

Imaging," *IEEE Transactions on Biomedical Circuits and Systems*, vol. 14, no. 5, pp. 1097-1107, Oct. 2020.

[6] J. D. Shea, B. D. Van Veen and S. C. Hagness, "A TSVD Analysis of Microwave Inverse Scattering for Breast Imaging," *IEEE Transactions on Biomedical Engineering*, vol. 59, no. 4, pp. 936-945, April 2012.

[7] L. Crocco, I. Catapano, L. Di Donato and T. Isernia, "The Linear Sampling Method as a Way to Quantitative Inverse Scattering," *IEEE Transactions on Antennas and Propagation*, vol. 60, no. 4, pp. 1844-1853, April 2012.

[8] G. Bozza, C. Estatico, M. Pastorino, and A. Randazzo, "An Inexact Newton Method for Microwave Reconstruction of Strong Scatterers," in *IEEE Antennas and Wireless Propagation Letters*, vol. 5, pp. 61-64, 2006.

[9] L. Guo, N. Nguyen-Trong, A. AI-Saffar, A. Stancombe, K. Bialkowski and A. Abbosh, "Calibrated Frequency-Division Distorted Born Iterative Tomography for Real-Life Head Imaging," in IEEE Transactions on Medical Imaging, doi: 10.1109/TMI.2021.3132000.

[10] L. Guo, M. Khosravi-Farsani, A. Stancombe, K. Bialkowski and A. Abbosh, "Adaptive Clustering Distorted Born Iterative Method for Microwave Brain Tomography With Stroke Detection and Classification," in IEEE Transactions on Biomedical Engineering, vol. 69, no. 4, pp. 1512-1523, April 2022.

[11] Nikolova, N. Introduction to Microwave Imaging, EuMA High Frequency Technologies Series, Cambridge University Press, Cambridge.

[12] T. Singh et al., "New Method for Calculation of Average Electric Properties of Reference Head Phantom in Microwave Imaging," 2022 16th European Conference on Antennas and Propagation (EuCAP), 2022, pp. 1-5.

[13] S. N. Makarov, G. M. Noetscher, J. Yanamadala, M. W. Piazza, AU - S. Louie, A. Prokop, A. Nazarian, A. Nummenmaa "Virtual Human Models for Electromagnetic Studies and Their Applications," in *IEEE Reviews in Biomedical Engineering*, vol. 10, pp. 95-121, 2017, doi: 10.1109/RBME.2017.2722420.

[14] https://www.nevaelectromagnetics.com/

[15] WIPL-D Pro v17 [Online]. Available: http://www.wipl-d.com/.

 ISBN 978-86-7466-930-3

# Current distribution in a hollow cylindrical conductor influenced by a parallel filament

Dragan Filipović, Tatijana Dlabač

***Abstract*—This paper presents a rigorous solution for the current distribution in a hollow cylindrical conductor in the presence of a current filament placed outside the conductor. The currents are assumed low-frequency, time-harmonic, flowing in opposite directions. As a starting point, we chose a redholm-type integral equation for the current density whose solution is sought in the form of an infinite sum of the proper harmonics – the modified essel functions of the second ind and trigonometric functions. The un nown coefficients in the sum are determined by equating the coefficients standing with the corresponding functions on both sides of the integral equation. The method presented in the paper allows treatment of the cases when the filament is inside the conductor and or the currents have the same direction.**

***Index Terms*—current distribution; hollow conductor; filament; integral equation**

## I. INTRODUCTION

Determination of current distribution in a system of parallel cylindrical conductors with time-varying currents is a very complex problem since this distribution in each of the conductors is not only affected by its own electromagnetic field (skin effect), but also by the fields of all other conductors (proximity effect). There are very few cases where this problem can be solved in a closed form, so generally an implementation of various numerical methods is required. Among the most commonly used approaches to the combined skin and proximity effects we mention here: usage of Maxwell's equations in terms of the magnetic vector potential [1–4], method of integral equations [5–11], boundary integral equation formulation [12,13], method of model functions [14], etc.

In this paper we use an integral equation to solve in a closed form the problem of low-frequency current distribution in a cylindrical hollow conductor in the presence of an outer current filament, the currents being assumed sinusoidal and to flow in opposite directions. The solution is sought in the form of an infinite sum of proper harmonics with some unknown coefficients. These coefficients are found in a closed form by equating coefficients with the corresponding functions on both sides of the integral equation.

Dragan Filipović is with the Faculty of Electrical Engineering, University of Montenegro, 81000 Podgorica, Montenegro (e-mail: draganf@ucg.ac.me), (https://orcid.org/0000-0001-8652-0661)

Tatijana Dlabač is with the Maritime Faculty Kotor, University of Montenegro, 85330 Kotor, Montenegro (e-mail: tanjav@ucg.ac.me), (https://orcid.org/0000-0001-9473-5558)

## II. INTEGRAL EQUATION FOR THE CURRENT DENSITY IN A HOLLOW CYLINDRICAL CONDUCTOR IN THE PRESENCE OF A FILAMENT

Geometry of the problem is shown in Fig. 1. A current filament is parallel to a massive hollow cylindrical conductor of radii $a$ and $b$.

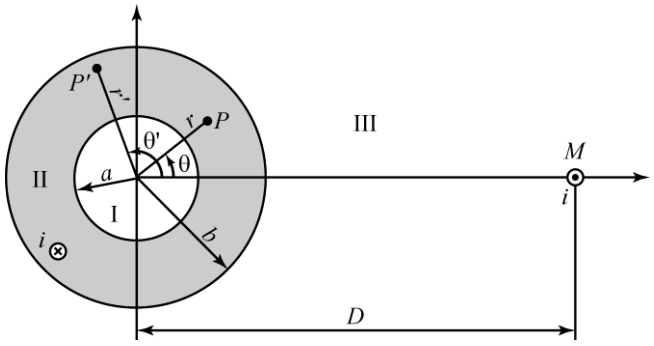


Fig. 1. Massive hollow cylindrical conductor and filament

The distance between the filament and the conductor axis is , and the parameters of the conductor are σ and $\mu_0$. Currents of equal r.m.s. $I$ and of frequency $f$ flow through the conductor and the filament in opposite directions. The objective is to find the current distribution in the massive conductor.

Following [5]-[6], [9], [11], we can write an integral equation for current density in the conductor:

$$(r,\theta) = \frac{k^2}{4\pi}\left[\int_S r' \quad (r',\theta')\ln\frac{r^2+r'^2-2rr'\cos(\theta-\theta')}{2}\,dr'\,d\theta' - I\ln\frac{r^2+\quad^2-2r\quad\cos\theta}{2}\right]+\quad , \tag{1}$$

where $k^2 = j\omega\mu_0\sigma$, is an unknown constant, and $S$ is the annulus $a \le r \le b$, $0 \le \theta \le 2\pi$.

Current density $(r,\theta)$ in (1) is subject to the condition:

$$\int_S (r,\theta) r\,dr\,d\theta = I. \tag{2}$$

## III. SOLUTION OF THE INTEGRAL EQUATION

Separation of variables in the wave equation for current density leads to the following particular solutions (harmonics): $I_n(kr)$, $_n(kr)$, $\cos n\theta$, $\sin n\theta$, where $I_n$ and $_n$ are

 ISBN 978-86-7466-930-3

modified Bessel functions. Symmetry requires that $(r,\theta)$ be an even function in θ, which eliminates $\sin n\theta$. Hence, an appropriate form of the solution of (1) is

$$(r,\theta)=\sum_{n=0}^{\infty}\left[A_n I_n(kr)+B_n \;\; {}_n(kr)\right]\cos n\theta \tag{3}$$

with some unknown coefficients $A_n$ and $B_n$. When (3) is substituted into (1), we obtain

$$\begin{aligned}&\sum_{n=0}^{\infty}\left[A_n I_n(kr)+B_n \;\; {}_n(kr)\right]\cos n\theta = \\ &=\frac{k^2}{4\pi}\sum_{n=0}^{\infty}A_n F_n(r,\theta)+\frac{k^2}{4\pi}\sum_{n=0}^{\infty}B_n G_n(r,\theta)+ \\ &+\frac{k^2 I}{2\pi}\sum_{n=1}^{\infty}\left(\frac{r}{}\right)^n\frac{\cos n\theta}{n}+\end{aligned} \tag{4}$$

where

$$F_n(r,\theta)=\begin{cases}\dfrac{4\pi}{k}\left[b\ln\dfrac{b}{}I_1(kb)-a\ln\dfrac{r}{}I_1(ka)\right]-\dfrac{4\pi}{k^2}\left[I_0(kb)-I_0(kr)\right], n=0\\ \left\{-\dfrac{2\pi}{nk}\left[b\left(\dfrac{r}{b}\right)^n I_{n-1}(kb)-a\left(\dfrac{a}{r}\right)^n I_{n+1}(ka)\right]+\dfrac{4\pi}{k^2}I_n(kr)\right\}\cos n\theta,\ n>0\end{cases} \tag{8}$$

$$G_n(r,\theta)=\begin{cases}\dfrac{4\pi}{k}\left[a\ln\dfrac{r}{} \;\; {}_1(ka)-b\ln\dfrac{b}{} \;\; {}_1(kb)\right]-\dfrac{4\pi}{k^2}\left[\;\; {}_0(kb)-\;\; {}_0(kr)\right], n=0\\ \left\{-\dfrac{2\pi}{nk}\left[a\left(\dfrac{a}{r}\right)^n \;\; {}_{n-1}(ka)-b\left(\dfrac{r}{b}\right)^n \;\; {}_{n-1}(kb)\right]+\dfrac{4\pi}{k^2} \;\; {}_n(kr)\right\}\cos n\theta,\ n>0\end{cases} \tag{9}$$

With $F_n$ and $G_n$ given by (8) – (9), we can equate the constant terms and the coefficients with ln ($r$/ , $r^n\cos n\theta$ and $r^{-n}\cos n\theta$ on both sides of (4), to get respectively

$$\begin{aligned}0=&A_0\left(kb\ln\frac{b}{}I_1(kb)-I_0(kb)\right)+\\ &+B_0\left(-kb\ln\frac{b}{} \;\; {}_1(kb)-\;\; {}_0(kb)\right)+\end{aligned} \tag{10}$$

$$0=-A_0 I_1(ka)+B_0 \;\; {}_1(ka) \tag{11}$$

$$0=-A_n I_{n-1}(kb)+B_n \;\; {}_{n-1}(kb)+\frac{kI}{\pi b}\left(\frac{b}{}\right)^n \tag{12}$$

$$0=A_n I_{n+1}(ka)-B_n \;\; {}_{n+1}(ka). \tag{13}$$

To determine the five unknown constants ($A_0$, $B_0$, $A_n$, $B_n$ and ) we need one more equation beside the four equations given by (10) - (13). This additional equation is obtained from (2) if we replace $(r, \theta)$ by (3). Then, we have

$$F_n(r,\theta)=\int_S r' I_n(kr')\ln\frac{r^2+r'^2-2rr'\cos(\theta-\theta')}{2}dr'd\theta' \tag{5}$$

$$G_n(r,\theta)=\int_S r' \;\; {}_n(kr')\ln\frac{r^2+r'^2-2rr'\cos(\theta-\theta')}{2}dr'd\theta' \tag{6}$$

and we made use of [15]

$$\ln\left(1+\frac{r^2}{2}-\frac{2r}{}\cos\theta\right)=-2\sum_{n=1}^{\infty}\left(\frac{r}{}\right)^n\frac{\cos n\theta}{n},\ \frac{r}{}<1. \tag{7}$$

The double integrals $F_n$ and $G_n$, given by (5) - (6), seemingly very complex, can be evaluated in a closed form. This is done in the Appendix for $F_n$; $G_n$ is found in the same way. Here we state the result.

$$\begin{aligned}I=&\int_0^{2\pi}d\theta\int_a^b r \;\; (r,\theta)dr=\\ &=\sum_{n=0}^{\infty}\int_0^{2\pi}\cos n\theta\int_a^b r\left(A_n I_n(kr)+B_n \;\; {}_n(kr)\right)dr= \\ &=A_0 2\pi\int_a^b rI_0(kr)dr+B_0 2\pi\int_a^b r \;\; {}_0(kr)dr.\end{aligned} \tag{14}$$

The integrals in (14) are readily evaluated by making the change of variables $kr=$ and using the identities [16]

$$I_0(\;)=(\;I_1(\;))'$$

$${}_0(\;)=-(\;\; {}_1(\;))'.$$

Hence (14) becomes

$$I=\frac{2\pi}{k}\left\{A_0\left[bI_1(kb)-aI_1(ka)\right]+B_0\left[a \;\; {}_1(ka)-b \;\; {}_1(kb)\right]\right\}. \tag{15}$$

Now, (11) and (15) can be solved for $A_0$ and $B_0$


ISBN 978-86-7466-930-3

$$A_0 = \frac{kI}{2\pi b}\frac{{}_1(ka)}{I_1(kb)\ {}_1(ka) - I_1(ka)\ {}_1(kb)} \tag{16}$$

$$B_0 = \frac{kI}{2\pi b}\frac{I_1(ka)}{I_1(kb)\ {}_1(ka) - I_1(ka)\ {}_1(kb)} \tag{17}$$

and $A_n$, $B_n$ are found from (12) - (13)

$$A_n = \frac{kI}{\pi b}\left(\frac{b}{}\right)^n \frac{{}_{n+1}(ka)}{{}_{n+1}(ka)I_{n-1}(kb) - {}_{n-1}(kb)I_{n+1}(ka)} \tag{18}$$

$$B_n = \frac{kI}{\pi b}\left(\frac{b}{}\right)^n \frac{I_{n+1}(ka)}{{}_{n+1}(ka)I_{n-1}(kb) - {}_{n-1}(kb)I_{n+1}(ka)}. \tag{19}$$

The remaining unknown can be determined from (10), (16) – (17), but it is of no importance.

Finally, (3) and (16) - (19) determine current density in the massive conductor

$$\begin{aligned}(r,\theta) &= \frac{kI}{2\pi b}\frac{{}_1(ka)I_0(kr) + I_1(ka)\ {}_0(kr)}{I_1(kb)\ {}_1(ka) - I_1(ka)\ {}_1(kb)} + \\ &+ \frac{kI}{\pi b}\sum_{n=1}^{\infty}\left(\frac{b}{}\right)^n \frac{{}_{n+1}(ka)I_n(kr) + I_{n+1}(ka)\ {}_n(kr)}{I_{n-1}(kb)\ {}_{n+1}(ka) - I_{n+1}(ka)\ {}_{n-1}(kb)}\cos n\theta.\end{aligned} \tag{20}$$

Physically, the first term on the right-hand side of (20) is due to the skin effect, and the infinite sum accounts for the influence of the filament (proximity effect).

The same method applies if the filament is inside the conductor. In this case $b/$ in the infinite sum in (20) should be replaced by $/b$.

Expression (20) may also be derived by using Maxwell's equations [4]. In this approach the magnetic vector potential is determined in media I, II and III (Fig. 1), which includes usage of appropriate boundary conditions on the interfaces $r=a$ and $r=b$. The approach in the present paper is much simpler –solving integral equation (1) does not involve any boundary conditions.

It may be shown that the particular cases $a = 0$ (massive conductor [6], [11]), and $b - a = d << a$ (thin tubular conductor [5], [9]), follow from (20). Derivation for the former case is straightforward; for the latter case, it requires usage of a few formulas that involve Bessel functions.

## IV. CONCLUSION

In this paper, we derived a closed-form solution for the current distribution in a hollow cylindrical conductor in the presence of a current filament placed outside the conductor. A solution of an integral equation for the current density is found in the form of an infinite sum of proper harmonics - the modified Bessel functions of the second kind and the trigonometric functions. A remarkable feature of the method used is that it does not involve any boundary conditions.

## APPENDIX

In this Appendix we prove (8), relation (9) is justified by the same procedure.

Let $n = 0$. Then

$$\begin{aligned}F_0(r,\theta) &= \int_0^{2\pi} a\theta' \int_a^b r' I_0(kr') \ln\frac{r^2 + r'^2 - 2rr'\cos(\theta-\theta')}{2}\,dr' = \\ &= \int_0^{2\pi} a\theta' \left[\int_a^r r' I_0(kr') \ln r^2 \frac{r^2 + r'^2 - 2rr'\cos(\theta-\theta')}{r^2\ \ 2}\,dr' + \int_r^b r' I_0(kr') \ln r'^2 \frac{r^2 + r'^2 - 2rr'\cos(\theta-\theta')}{r'^2\ \ 2}\,dr'\right] = \\ &= \int_0^{2\pi} a\theta' \left\{\int_a^r r' I_0(kr')\left[\ln\frac{r^2}{2} + \ln\left(1 + \frac{r'^2}{r^2} - 2\frac{r'}{r}\cos(\theta-\theta')\right)dr'\right] + \int_r^b r' I_0(kr')\left[\ln\frac{r'^2}{2} + \ln\left(1 + \frac{r^2}{r'^2} - 2\frac{r'}{r}\cos(\theta-\theta')\right)dr'\right]\right\} \\ &= \int_0^{2\pi} a\theta' \left[\ln\frac{r^2}{2}\int_a^r r' I_0(kr')dr - 2\int_a^r r' I_0(kr')\sum_{m=1}^{\infty}\left(\frac{r'}{r}\right)^m \frac{\cos m(\theta-\theta')}{m}\,dr' + \int_r^b r' \ln\frac{r'^2}{2} I_0(kr')dr' - 2\int_r^b r' I_0(kr')\sum_{m=1}^{\infty}\left(\frac{r}{r'}\right)^m \frac{\cos m(\theta-\theta')}{m}\,dr'\right]\end{aligned} \tag{A1}$$

where we used (7). We do not need to evaluate the integrals that include infinite sum, since $\cos m(\theta-\theta') = \cos m\theta\cos m\theta' + \sin m\theta\sin m\theta'$, and the subsequent integration in θ' gives zero, since $\int_0^{2\pi}\cos m\theta' d\theta' = \int_0^{2\pi}\sin m\theta' d\theta' = 0,\ m \geq 1$. The two remaining integrals are evaluated as follows

$$\int_a^r r' I_0(kr')dr' = \frac{1}{k^2}\int_{ka}^{kr} uI_0(u)du = \frac{1}{k}\left(rI_1(kr) - aI_1(ka)\right), \tag{A2}$$

where the change of variables $kr'=u$ and the identity

$$uI_0(u) = \left(uI_1(u)\right)',$$

were used. Similarly, by using integration by parts

 ISBN 978-86-7466-930-3

$$\int_r^b r'\ln\frac{r'^2}{2}I_0(kr')dr' = \frac{2}{k^2}\int_{kr}^{kb} u\ln\frac{u}{k}I_0(u)du =$$
$$= \frac{2}{k^2}\left[uI_1(u)\ln\frac{u}{k}\Big|_{kr}^{kb} - \int_{kr}^{kb} uI_1(u)\frac{du}{u}\right] =$$
$$= \frac{2}{k^2}\left(kb\ln\frac{b}{}I_1(kb) - kr\ln\frac{r}{}I_1(kr) - \int_{kr}^{kb} I_1(u)du\right) = \quad \text{(A3)}$$
$$= \frac{2}{k^2}\left[kb\ln\frac{b}{}I_1(kb) - kr\ln\frac{r}{}I_1(kr) - \left(I_0(kb) - I_0(kr)\right)\right]$$

since [16]

$$I_1(u) = I_0'(u).$$

Now, relation (8) for $n = 0$ follows from (A1) - (A3).

For $n \geq 1$

$$F_n(r,\theta) = \int_0^{2\pi}\cos n\theta' d\theta'\left[\ln\frac{r^2}{2}\int_a^r r'I_n(kr')dr' - \right.$$
$$-2\int_a^r r'I_n(kr')\sum_{m=1}^{\infty}\left(\frac{r'}{r}\right)^m\frac{\cos m(\theta-\theta')}{m}dr' + \quad \text{(A4)}$$
$$\left.+\int_r^b r'ln\frac{r'^2}{2}I_n(kr')dr' - 2\int_r^b r'I_n(kr')\sum_{m=1}^{\infty}\left(\frac{r}{r'}\right)^m\frac{\cos m(\theta-\theta')}{m}dr'\right]d\theta'$$

In this case, the integrals $\int_a^r r'I_n(kr')dr'$ and $\int_r^b r'\ln\frac{r'^2}{2}I_n(kr')dr'$ are irrelevant, since the subsequent integration in θ' gives zero $\left(\int_0^{2\pi}\cos n\theta' d\theta' = 0,\ n \geq 1\right)$, hence (A4) becomes

$$F_n(r,\theta) = -2\sum_{m=1}^{\infty}\frac{1}{mr^m}\int_0^{2\pi}\cos n\theta'\cos m(\theta-\theta')d\theta'\int_a^r r'^{m+1}I_m(kr')dr' - \quad \text{(A5)}$$
$$-2\sum_{m=1}^{\infty}\frac{r^m}{m}\int_0^{2\pi}\cos n\theta'\cos m(\theta-\theta')d\theta'\int_r^b r'^{-m+1}I_m(kr')dr'.$$

Only the term with $m = n$ should be kept in the infinite sums, since for $m \neq n$

$$\int_0^{2\pi}\cos n\theta'\cos m(\theta-\theta')d\theta' =$$
$$= \cos n\theta\int_0^{2\pi}\cos n\theta'\cos m\theta' d\theta' + \sin m\theta\int_0^{2\pi}\cos n\theta'\sin m\theta' d\theta' = 0,$$

due to orthogonality of the sine and cosine functions. As a consequence, (A5) simplifies to

$$F_n(r,\theta) = \left(-\frac{2\pi}{nr^n}\int_a^r r'^{n+1}I_n(kr')dr' - \right.$$
$$\left.-\frac{2\pi r^n}{n}\int_r^b r'^{-n+1}I_n(kr')dr'\right)\cos n\theta \quad \text{(A6)}$$

where we have taken into account that

$$\int_0^{2\pi}\cos n\theta'\cos n(\theta-\theta')d\theta' =$$
$$= \cos n\theta\int_0^{2\pi}\cos^2 n\theta' d\theta' + \sin n\theta\int_0^{2\pi}\cos n\theta'\sin n\theta' d\theta' = \pi\cos n\theta.$$

The change of variables $kr'=u$ and the relations [16]

$$u^{n+1}I_n(u) = \left(u^{n+1}I_{n+1}(u)\right)'$$
$$u^{-n+1}I_n(u) = \left(u^{-n+1}I_{n-1}(u)\right)'$$

enable to evaluate the two integrals in (A6)

$$\int_a^r r'^{n+1}I_n(kr')dr' = \frac{1}{k}\left(r^{n+1}I_{n+1}(kr) - a^{n+1}I_{n+1}(ka)\right) \quad \text{(A7)}$$

$$\int_r^b r'^{-n+1}I_n(kr')dr' = \frac{1}{k}\left(b^{-n+1}I_{n-1}(kb) - r^{-n+1}I_{n-1}(kr)\right). \quad \text{(A8)}$$

Finally, from (A6) - (A8)

$$F_n(r,\theta) = -\frac{2\pi}{nk}\left\{r\left[I_{n+1}(kr) - I_{n-1}(kr)\right] + b\left(\frac{r}{b}\right)^n I_{n+1}(kb) - \right.$$
$$\left.-a\left(\frac{a}{r}\right)^n I_{n+1}(ka)\right\}\cos n\theta =$$
$$= \left\{-\frac{2\pi}{nk}\left[b\left(\frac{r}{b}\right)^n I_{n-1}(kb) - a\left(\frac{a}{r}\right)^n I_{n+1}(ka)\right] + \frac{4\pi}{k^2}I_n(kr)\right\}\cos n\theta$$

since [16]

$$I_{n+1}(kr) - I_{n-1}(kr) = -\frac{2n}{kr}I_n(kr).$$

Therefore, the proof of (8) is completed.

## REFERENCES

[1] P. Rolicz: "Skin effect in a system of two rectangular conductors carrying identical currents", Electrical Engineering 82 (2000) 285-290 © Springer-Verlag 2000

 ISBN 978-86-7466-930-3

[2] P. Dokopoulos, D. Tampakis, "Eddy current in system of tubular conductors", IEEE Trans. on magnetics, vol. MAG-20, no. 5, pp 1971 - 1973, 1984.
[3] J. A. Tegopoulos, E. E. Kriezis, "Eddy current distribution in cylindrical shells of infinite length due to axial currents, Part I: Shells of one boundary", IEEE Trans. on Power Apparatus and Systems, vol. PAS-90, Issue:3 pp 1278 - 1286, 1971.
[4] J. A. Tegopoulos, E. E. Kriezis, "Eddy current distribution in cylindrical shells of infinite length due to axial currents, Part II: Shells of finite thickness", IEEE Trans. on Power Apparatus and Systems, vol. PAS-90, Issue:3 pp 1287 - 1294, 1971.
[5] H. B. Dwight, Electrical Coils and Conductors, Mc Graw-Hill, New York, 1945.
[6] C. Manneback, "An integral equation for skin effect in parallel conductors", J. Math. Phys., vol. 1, pp. 123–146, Apr. 1922.
[7] B. D. Popović, Z. D. Popović: "Method of determining power-frequency current distribution in cylindrical conductors", Proc. IEE, Vol. 119, no 5. May 1972, pp. 569-574.
[8] B. Popović, D. Filipović, "Theory of power-frequency proximity effect for strip conductors", Proc. IEE, Vol. 122, no 8. August 1975, pp. 820-823.
[9] D. Filipović, T. Dlabač, "A closed form solution for the proximity effect in a thin tubular conductor influenced by a parallel filament", Serbian Journal of Electr. Eng., vol. 7, no. 1, May 2010, 13-20
[10] Dlabač T., Filipović D., Plazinić M., "Integral Equation Method for Determining Current Distribution in a System of Parallel Conductors", Technics Technologies Education Management (ISSN:1840-1503), vol. 7, no. 4, 11/12, 2012.
[11] D. Filipović, T. Dlabač, "A closed form solution for the current density in a solid round conductor influenced by a filament", Proc. of the 54th ETRAN conference, Donji Milanovac, Serbia, 7 - 10 June 2010, (in Serbian).
[12] M. Cao, P.P. Biringer, "BIE formulation for skin and proximity effect problems of parallel conductors", IEEE Trans. on magnetics, vol. 26, no. 5, September 1990, pp 2768 - 2770.
[13] M. Cao, P.P. Biringer, "Asymmetry in bus bars due to proximity effects", J. Appl. Phys., vol. 67, no. 9, May 1990, pp. 4729-4731
[14] P. Silvester, "Skin effect in multiple and polyphase conductors", IEEE Trans. on Power Apparatus and Systems, vol. PAS-88, no. 3, pp. 231-238, March 1969.
[15] I. Gradshteyn and I. Ryzhik, Table of Integrals, Series, and Products, 7th ed. New York, NY, USA: Academic, 2007.
[16] H. Bateman, A. Erdelyi, Higher Transcedental Functions, vol. 2, Mc Graw-Hill, New York, 1953.

 ISBN 978-86-7466-930-3

# Jamming a Drone - EM Simulation of Simple EW and EW Countermeasures Scenarios

Tomislav Milošević

***Abstract*—The paper discusses electromagnetic simulations ( ) of an electronic warfare ( W) scenario where a drone is jammed using a continuous wave (CW) jammer. W countermeasures have been proposed based on calculated currents induced on specific parts of the drone critical for jamming effectiveness, such is antenna or wire in printed circuit board. All the simulations relate to widely used 2.4 G z frequency band.**

***Index Terms*—jamming, drone, anti-drone.**

## I. Introduction

VARIOUS types of drones exist on a consumer market spanning from pieces dedicated to sport or entertainment to high class devices capable to carry out complex tasks. Besides utilization of drones along with positive legislation, even drones with basic functionality can potentially be used for malicious activities in scenarios which are not socially tolerable or could even be harmful. For example, a very basic drone can be used by paparazzi in invading celebrities' privacy or by criminals and terrorists in compromising security of a potential target. Therefore, in parallel with development of the drones, various anti-drone systems have been developed as well.

This paper presents a scenario where a radio-controlled drone is flying within an active zone of an anti-drone system. Anti-drone system itself is simply a helix antenna with a reflector.

Communication systems in general may exhibit restricted or completely inhibited functionality when subjected to interference, jamming or outer EW measures [1], [2]. Described model of jamming system represents the class of anti-drone systems which uses a CW signal to jam the drone flight-control receiver. In order to reduce the effect of the jammer, simple passive countermeasures can be used. In general, passive countermeasures do not involve the emission of any signals or noise [1]. It will be shown that using the results of EM reconnaissance, a simple, partial shielding of the jamming sensitive parts of the drone can significantly reduce the effectiveness of the jamming. It is assumed that anti-drone system and the drone receiver both operate at 2.4 GHz, the frequency widely used for Wireless LAN [3].

The basic principle of an anti-drone system operation is to induce current – a strong jamming signal on the drone side and saturate the receiver. Also, it is possible that the anti-drone system induces current in the printed circuit board (PCB) which is a part of the drone electronic system causing the malfunctioning of onboard electronics. Addressing the practical side of anti-drone system as described, one can say that receiving of control signals through the drone receiver will be blocked and that additionally a spurious signal would be induced in the electronic circuits.

The effects of the jamming will be simulated using WIPL-D Pro, a full wave 3D electromagnetic Method-of-Moments (MoM) based software which applies Higher Order Basis Functions over bilinear surfaces combined with Surface Integral Equations [4]. The software considers the bilinear surfaces as nonplanar quadrilaterals defined uniquely by four vertices [5]. Thanks to the inherent property of MoM, the size of EM model and accordingly the complexity of the simulation does not increase with increased jammer-to-drone distance [4].

## II. Model of the Drone

The model of the drone is shown in the Fig. 1. It contains a camera mounted below the drone, which represents a payload of the drone. The drone with its payload is modeled as a dielectric object with the following dielectric properties: $\varepsilon_{rReal}$=2.2 and $\varepsilon_{rImag}$=-0.066. Beside the dielectric, the drone contains some metallic parts which are also shown in the Fig. 1. The "upper" metallic parts represent the monopole antenna with the ground plane. The monopole antenna is intended to be used for receiving flight control signals. The "lower" metallic parts represent a simplified PCB with a rectangular half-loop on it.

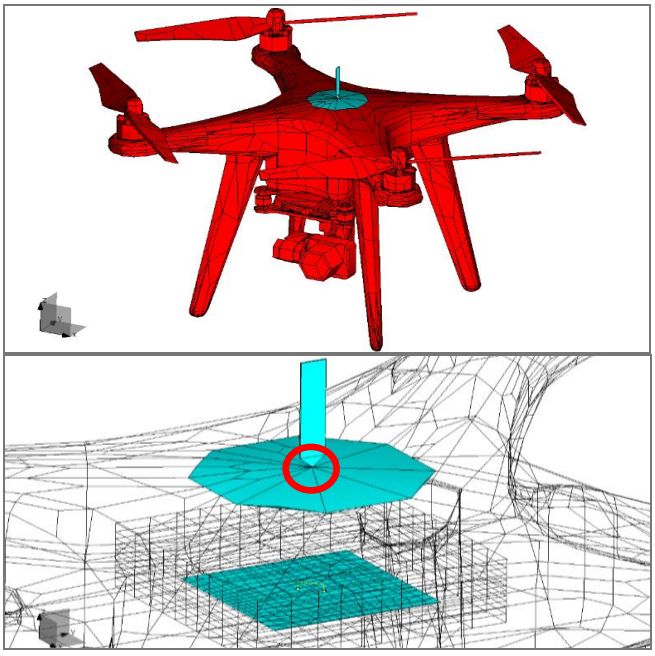

Figure 1. The model of the drone with the payload and the metallic parts of the drone.

Tomislav Milošević is with WIPL-D d.o.o., Gandijeva 7, 11073 Belgrade, Serbia (e-mail: tomislav.milosevic@wipl-d.com).

 ISBN 978-86-7466-930-3

Inducing the jamming current on the receiver will be monitored on the wire used to feed the monopole antenna. The wire is located at the very end of the antenna and it is encircled in red in Fig. 1.

The current induced in drone PCB is monitored on the grounded half-loop. Actually, as presented with markings outlined in the Fig. 2, the induced current is calculated over the "horizontal" wire. The dimensions of the metallic surface representing demonstration model of the PCB and the half-loop are also displayed in the Fig. 2.

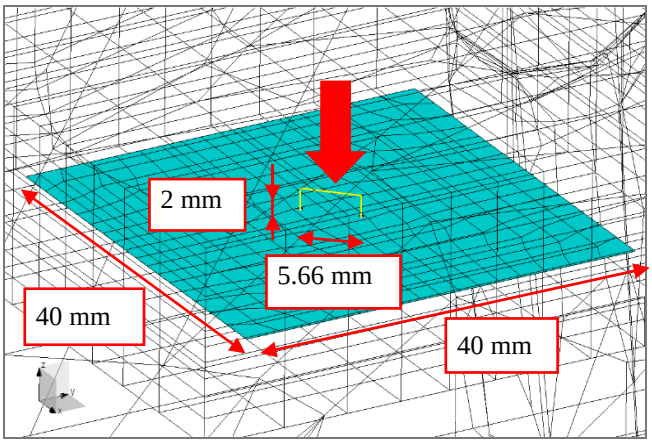


Figure 2. Demonstration model of the circuit board located within the drone.

It can be seen in the Fig. 3 that interior of the drone accommodates the described model of a PCB where onboard electronics is located. In other words, the metallic surface and the half-loop are immersed in the air box inside the drone dielectric.

The S-parameters and 3D radiation pattern[1] of the monopole antenna from Fig. 1 when the drone hovers above the PEC plane are shown in the Fig. 4.

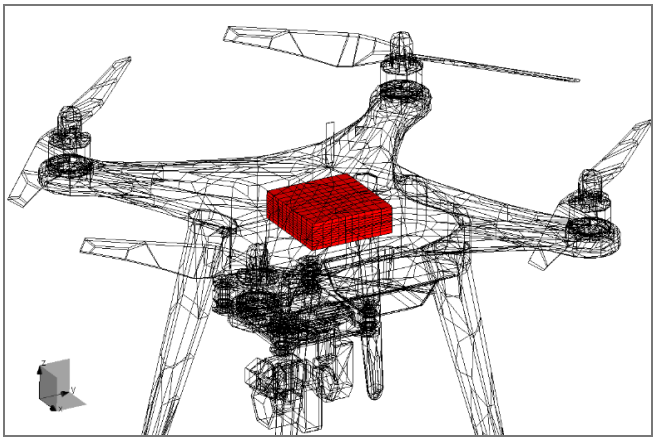

Figure 3. The air box in which the PCB with the half-loop is located.

## III. The Model of the Jammer

The simplified model of the jammer in the form of the EM gun only contains a helix antenna and an octagon reflector both located over the PEC ground plane. The details related to geometry of the EM gun structure are presented in the Fig. 5. The center of the antenna reflector is located at the height of 0.1 meter and the axis of the helix is oriented at elevation angle of 35°. The radiation pattern of the jammer antenna above PEC plane is also shown in the Fig. 5. It can be seen that the 3D radiation pattern is influenced by PEC presence and that the position of the antenna has been adjusted to boost the radiation at a sector of interest to a gain higher than 10 dB. The sector of interest covers elevation angles from approximately 9° to approximately 57°.

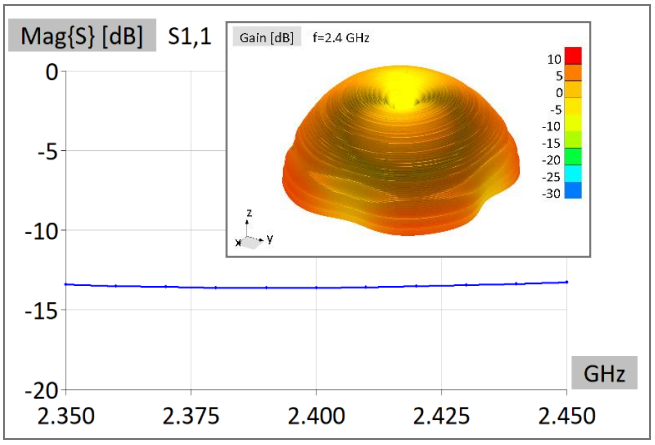


Figure 4. S-parameters and radiation pattern of the monopole mounted on the drone hovering above PEC plane.

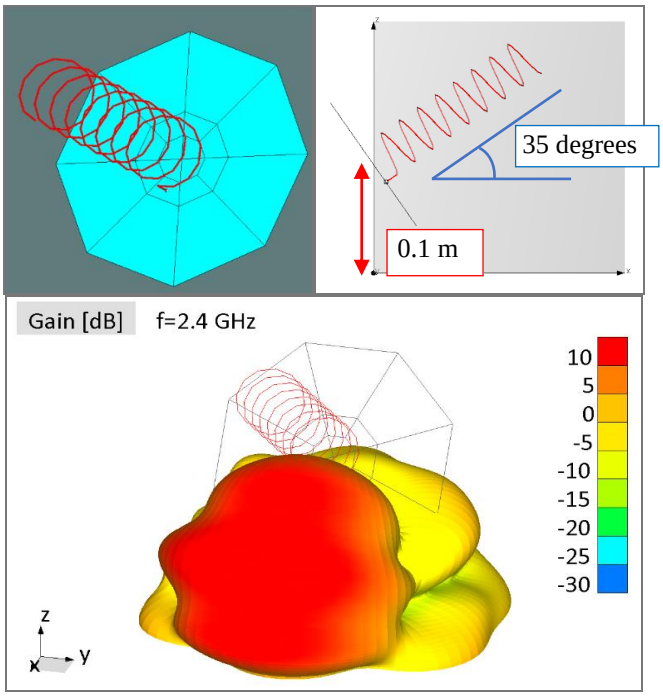


Figure 5. The model and the position of the jammer/EM gun over the PEC plane with 3D radiation pattern at 2.4 GHz.

## IV. Jamming Scenario

The particular jamming scenario is illustrated in the Fig. 6 in 3D view, bird's view, and side view, from top to bottom. Both, drone and anti-drone system are located above the ground modeled as a Perfect Electric Conductor (PEC) plane. It is assumed that the drone flies through the zone protected with the jammer along a straight line, which is a realistic assumption.

[1] In this paper, all *Gain* values are in dBi.


ISBN 978-86-7466-930-3

The top part of the Fig. 6 shows the direction of the antenna rotation starting from the lowest phi angle (phi = 0°) and the drone flight direction. The middle part of the figure explains the details related to the distance between the antenna and the drone, the angles of antenna rotation, and the drone flight direction. Finally, the lower part of the figure shows the side view of the jamming scenario.

The initial location of the drone is (x, y, z) = (15 m, 0 m, 5 m). The final location of the drone is (x, y, z) = (15 m, 25.98 m, 5 m). The jammer antenna is located in (x, y, z) = (0 m, 0 m, 0.1 m) as shown in Fig. 6 and it is being rotated from phi=0° to phi=60° (Fig. 6) keeping the elevation angle of 35°. This means that the monopole antenna mounted on the drone is constantly illuminated with the jammer signal during the described flight along the straight line. The helix antenna which is part of the jammer operates in axial mode at 2.4 GHz (see also Fig. 4 and $S_{11}$ of the monopole antenna mounted on the drone).

Induced current in the middle of the wire located in the root of the monopole antenna mounted on the drone is shown in the Fig. 7. The current induced in the middle of the wire which is part of the half-loop on the PCB is shown in the Fig. 8.

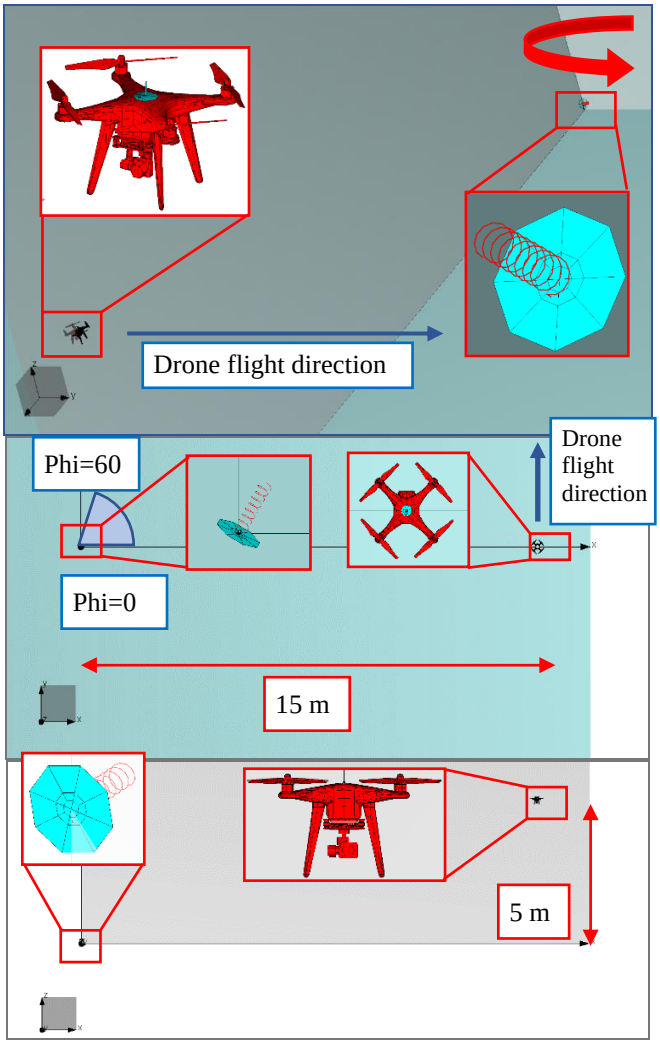


Figure 6. Investigated scenario in 3D, birds view, and side view, from top to bottom, respectively.

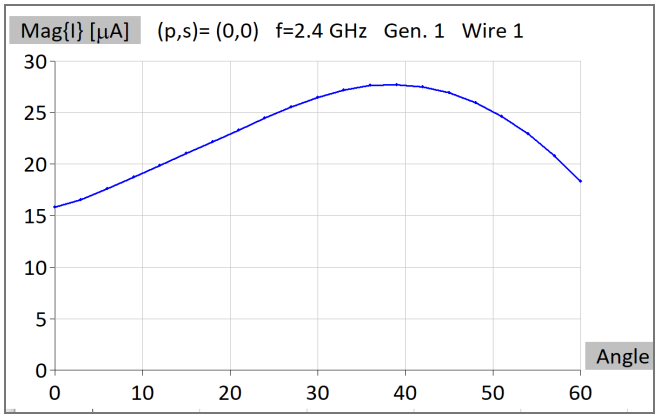


Figure 7. The current induced in the middle of the wire in the root of the monopole antenna.

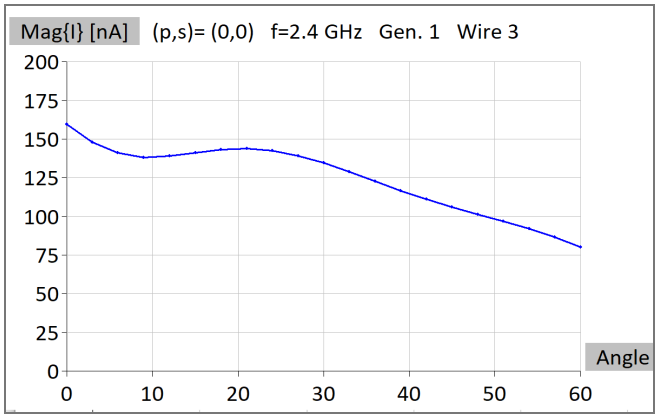


Figure 8. The current induced in the middle of the upper wire in the half-loop on PCB.

## V. Decreasing Jamming Effectiveness

The presumption of the successful jammer countermeasures is the reliable information of the exact position of the jammer which can be revealed by visual surveillance or EM reconnaissance.

In order to decrease jamming effectiveness, the drone can be modified using a simple, commonly available objects. The PBC area can be easily protected from the outer influence by enclosing it in full (could be a piece of food-wrapping aluminum foil), which is a straight-forward action. However, the antenna used for receiving control signals cannot be fully enclosed for obvious reasons, but, when the position of the jammer is known, it can be partially enclosed so that the covered part coincides with the direction where the jammer is located. The very simple enclosure will be considered here, the one comprising a smooth cylinder or conical object (could be a disposable paper cup). with a metalized part located towards the jammer as described (again, the metallization could simply be a piece of an aluminum foil).

The model of the modified drone is shown in the Fig. 9. The drone dielectric is being displayed in yellow in the upper part of this figure. The cup, with assumed relative dielectric constant of $\varepsilon_{rCupReal}$=3 is colored in blue. The metallic sheet representing the aluminum foil is in cyan and clearly visible in both parts of the Fig. 9. Mechanical connections which should be added to real-life drone


ISBN 978-86-7466-930-3

structure are excluded from this EM model, without losing the quality of approximation. Enclosing the PCB using thin metal sheet following a box shape displayed in Fig. 3 can be noticed in the lower part of the Fig. 9. More precise explanation of the scenario with metallic sheet is presented in Fig. 10 where the arrow points to the cup which is mounted on the top of the drone. In other words, the metallic sheet is positioned on the left side of the cup.

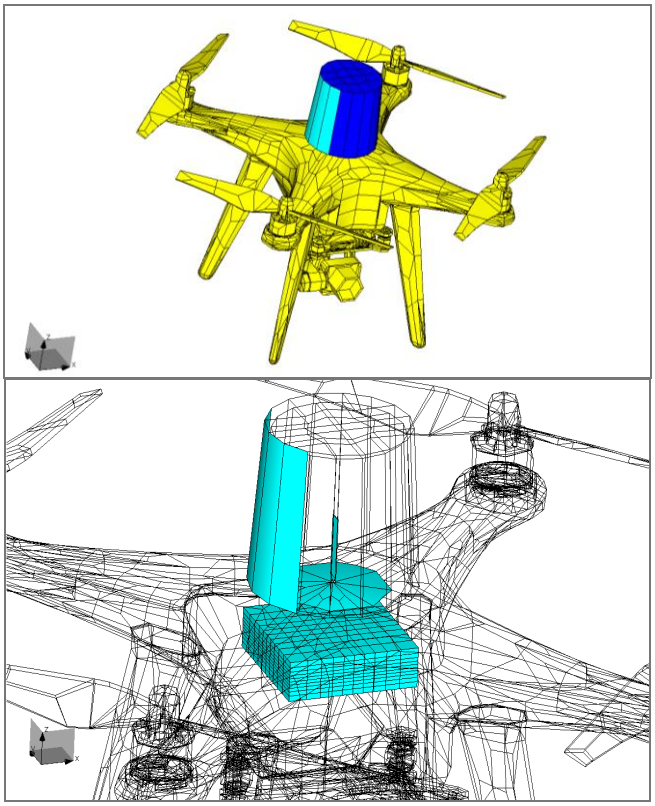

Figure 9. The drone with modifications and the metallic parts with enclosing of PCB.

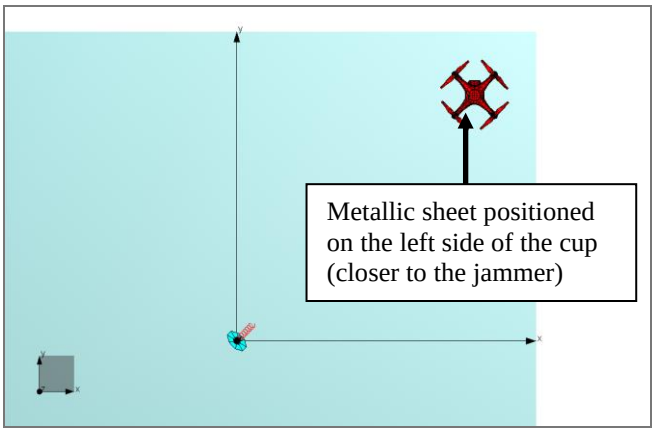


Figure 10. The position of the drone and the jammer with explained position of the metallic sheet. Not to be scaled.

The output results are displayed and compared in Figs 11-12. Fig. 11 displays comparison of the induced currents on the wire in the root of the antenna without the cup, with the cup and metallic sheet, and with the metallic sheet, only. It can be seen that without the metallic sheet attached to the cup, the level of induced current is the highest. Adding metallic sheet wrapped around the cup lower levels of induced currents are obtained. Similar result appears with the metallic sheet added and without the cup. This proves that metallic sheet mainly influences the jamming signal.

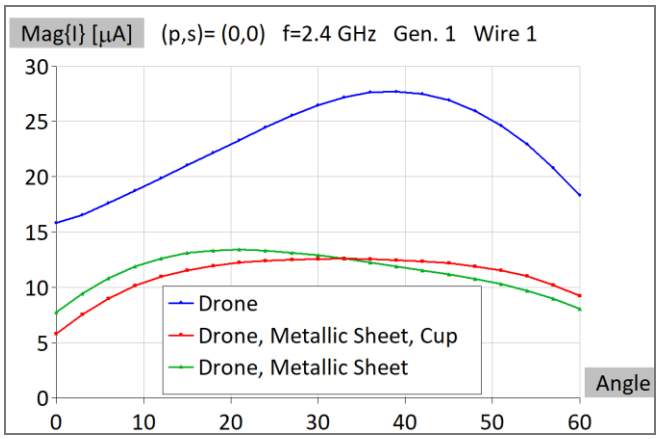


Figure 11. The comparison of currents induced in the middle of the wire in the root of the monopole antenna.

Fig. 12 displays comparison of currents on the PCB wire in three previously explained cases. The drop in level of the induced signal for shielded PCB is clearly noticeable.

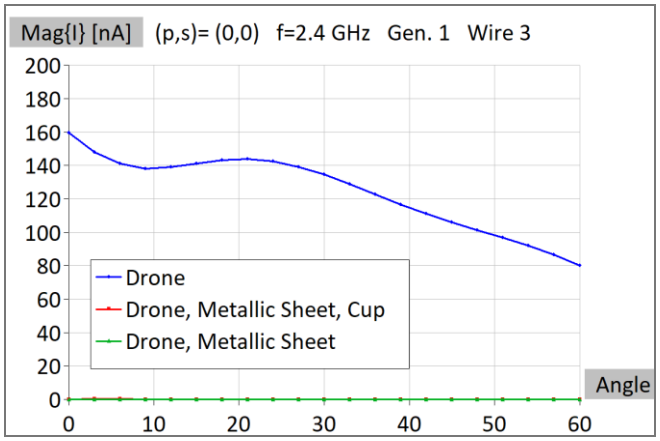


Figure 12. The comparison of currents induced in the middle of the upper wire in the half-loop on PCB

## VI. Computer Platform and Simulation Time

All scenarios were simulated using a MoM based software and dedicated sweeping tool rotating the jammer from angle phi=0° to phi=60° in 21 equidistant points and moving the drone in the appropriate direction. The most demanding simulation of the jammed drone with the metallic sheet and the cup required 16,761 elements and 36,060 unknowns. The simulation time per a single angle of rotation for the same model is about than 8 minutes. The computer used for carrying out the simulation is Intel® Xeon® Gold 5118 CPU @ 2.30GHz (2 processors) with 192 GB RAM and a GPU card NVIDIA GeForce GTX 1080 Ti. GPU card is used for both matrix fill-in and matrix inversion.


ISBN 978-86-7466-930-3

## VII. Conclusion

A scenario encompassing the drone and an anti-drone system in the form of an EM gun over the PEC ground plane has been investigated. The effectiveness of jamming is demonstrated by calculating the induced currents at 2.4 GHz. Also, basic countermeasures were presented based on simple modifications of the drone.

The main effect of the jamming comes from the saturation of the receiver. Such a result can be explained easily as the antenna is directly exposed to the jamming signal. It was shown that mounting metallic sheet between the jammer and the receiving monopole, using an auxiliary cylindrical object like a paper cup, can significantly reduce the effectiveness of the jammer signal.

The current induced in the PCB elements might cause malfunction of drone electronics but being significantly lower than the level of the current on the antenna connection, is of secondary importance to the jamming scenario. Furthermore, the countermeasures can be performed easier by enclosing critical area around the PCB.

As it has been confirmed that simple countermeasures can make the drone resilient to jamming from a single source, the counter-countermeasures should include the distribution of several jammers in different locations around the target as it makes the method of partial shielding impractical.

Utilization of a Method-of-Moments (MoM) based software, for calculation of the induced currents has been also demonstrated. The numerical results have been obtained with high efficiency on an affordable desktop machine.

Further investigation could include propagation effects, or adding some objects such as metallic fences or lampposts and their influence on jammer-to-drone link.

## References

[1] D. M. Pozar, Microwave Engineering, 2nd ed., USA, John Wiley & Sons, 1998.
[2] D. Banjac, Electronic Warfare in Anti-Aircraft Defense (in Serbian), Military Publishing and Media Center, Belgrade, 1986.
[3] J. L. Volakis, Antenna Engineering Handbook, 4th ed., USA: McGraw-Hill, 2007
[4] WIPL-D Software, WIPL-D d.o.o, Belgrade 2021. www.wipl-d.com
[5] B. M. Kolundzija, A. R. Djordjevic, Electromagnetic Modeling of Composite Metallic and Dielectric Structures, 1st ed. Norwood, Massachusetts, USA: Artech House, 2002.

 ISBN 978-86-7466-930-3

# Simulation Study of Voxel-Based Head Phantom for Medical Microwave Imaging

Mladjen Stevanetic, Branko Kolundzija, Tushar Singh, Marija Nikolic Stevanovic

***Abstract*—The paper describes the crucial role of phantoms in icrowave Imaging ( WI) for medical devices. Accurate modelling of numerical scenarios is crucial in designing, testing, and developing WI devices. Phantoms with appropriate tissue electrical properties are inevitable components of imaging scenarios. Therefore, high computing resources are required to develop such phantom, and simulation of such scenarios requires a more prolonged time. A defined blueprint is required to reduce the comple ity of such scenarios to use them effectively for WI purposes. In the given paper, a brief study of the three-dimension vo el model of the head is presented, where a unit cell is a cube with tissue-mimic ing properties. The phantom is developed on the WIP -D Pro simulation platform. urther, the vo els are grouped in the form of , where is the number of vo els on each a is. omogenization techniques are implemented on the grouped vo els and result in one big cube, the main building element of the electromagnetic model. The C simulation is performed with plane wave e citation for different values of , and the results are analyzed for convergence to the reference model. Also, the relative mean absolute deviation ( *A*) of the whole phantom as a result of the homogenization process is presented and its convergence is compared with the convergence of the mean deviation of simulated results.**

***Index Terms*— ead phantom; icrowave Imaging; o el odel; ubal**

## I. INTRODUCTION

BRAIN stroke has been one of the leading causes of death in humans over the last decade. Early-stage screening of stroke is a crucial step for diagnosis and treatment purposes [1]. Conventional technologies such as MRI, CT and X-ray are the gold standard for stroke detection due to accurate scanned results with high spatial resolution for clinical diagnosis. Although, these methods have several disadvantages, such as expensive procedures, low portability and ionizing radiation [2] – [3]. On the other hand, Microwave Imaging (MWI) is envisioned as a complementary tool to the imaging technologies for brain stroke detection. It is a low health risk, non-invasive, and cost-effective procedure [4] – [5].

Developing medical devices based on microwave imaging requires accurate electromagnetic modelling of imaging scenarios. The vital components of imaging scenarios are powerful EM simulation environment, anthropomorphic phantoms, tissue electrical properties and a measurement system. The simulation tool provides ease in modelling and accurate numerical analysis. The measurement system reduces to the antenna system around the organ of interest. Tissue mimicking properties help to understand the wave propagation through the human organ. Realistic human-like phantoms are crucial to understanding the complex structure of the organ with defined electrical properties. Modelling complex phantoms is the decisive factor for the accuracy and validation of the imaging scenario. Voxel and STL formats are widely available for designing phantoms [6]. The source format of the phantom is highly complex and requires efficient strategies to reduce the complexity of the structure while retaining accuracy.

The proposed study is focused on the study and accurate design of voxel based anatomically realistic head phantom for MWI purposes. The phantom data is usually derived from MRI images. The model is obtained from an online repository [7] in binary format. The 3D EM simulation platform WIPL-D Pro helps to transform the medical data into the 3D electromagnetic head model [8]. The unit structure of the actual phantom is a voxel or small cube with a side length of approximately 1 mm. The source file contains around 4 million such voxels. Each voxel has its own defined tissue properties. Simulation of such a model is very challenging. Therefore, with efficient procedures, the complexity is reduced. The voxels are grouped to form a big cube and then homogenization techniques are implemented on these big cubes. As mentioned, each voxel defined with one cube leads to a huge requirement of resources, therefore at the initial stage voxels are grouped using the parameter N, where N denotes the total number of voxels along each axis. The reference model is created with $N$=3. The homogenization is implemented using various mixing formulas [9]. A group of voxels with the given value of N is treated as one big cube, and its electrical property is derived from the averaging techniques. Implementing these methods significantly reduces the computational requirement and speeds up the simulation for EM analysis within the measurement system. In order to study the agreement between homogenization techniques and reduction in complexity, EM simulation is performed for various values of $N$ ranging from 3 to 12 voxels in each axis. The excitation is a plane wave for the bistatic RCS estimation. The deviation between the reference model and the model with higher values of $N$ gives the information on the accuracy of the simplification process in terms of % error. At the same time, the Relative Mean Absolute ( *MA*) differences between the reference model and other models (with $N$>3) give insight in the averaging process and its convergence.

The paper is divided into three main sections. Section II is about the voxel model and homogenization techniques,

Mladjen Stevanetic is with WIPL-D d.o.o. Belgrade, Serbia (e-mail: mladjen.stevanetic@wipl-d.com)

Branko Kolundzija is with WIPL-D d.o.o. Belgrade, Serbia and School of Electrical Engineering, University of Belgrade, Serbia (e-mail: branko.kolundzija@wipl-d.com).

Tushar Singh is with WIPL-D d.o.o. Belgrade, Serbia and School of Electrical Engineering, University of Belgrade, Serbia (e-mail: tushar.singh@wipl-d.com).

Marija Nikolic Stevanovic is with School of Electrical Engineering, University of Belgrade, Serbia (e-mail: mnikolic@etf.bg.ac.rs).

 ISBN 978-86-7466-930-3

Section III is focused on numerical results, and Section IV concludes the paper.

## II. Voxel Phantom and Homogenization

### A. o el phantom

The voxel phantom represents dispersive dielectric properties data of a part of the human body (organ(s)), as a result of the MRI (Magnetic Resonance Imaging) or CT (computed tomography x-ray) scans of respective human body part [7].

That scan outputs the grid of points, named voxels, distributed in three-dimensional volume that covers the scanned organ with a specific resolution. Each voxel brings different dielectric properties of tissue. Although some phantom use Cole-Cole and Debye parameters to present dielectric properties of the tissue [10] - [11], this type of phantom comes with the binary input that holds identifications of tissue types for each voxel. The number of voxels varies depending on organ size and scanning resolution from 2 to 20 million or more. The resolution or distance between voxels is considered around 0.5 mm or 1 mm. Some of the voxels contain information on the surrounding media, in our case it is air.

However, it is very challenging and still under research to simulate the entire model with millions of unknowns, defined with thousands of domains i.e., closed regions with the same dielectric properties. Today's most robust full MoM solver, WIPL-D, reinforced with the HOBFs and fully parallelized, still requires large simulation time for millions of unknowns. Therefore, we designed a simple procedure, built-in WIPL-D, for transforming the medical data to the electromagnetic model being simulated in a reasonable amount of time and providing valuable information for overall phantom analysis.

### B. omogeni ation

All the voxels are treated as small cubic volumes in space with specific dielectric constant values. Generally, these values are different for different voxels but are similar for the voxels of the same tissue type. In order to decrease the complexity of such a significant problem, we perform the averaging techniques on voxels. We create bigger cubic volumes that contain several voxels, taking the same number of voxels per each of the coordinate axes of a new, larger volume. If we treat one voxel as a small cube with a size equal to the resolution of the phantom, we create a big cube with N voxels per axis. Fig. 1 shows a preview of the Zubal head phantom [7] in two resolutions $N$=3 and $N$=8 on the WIPL-D Pro platform.

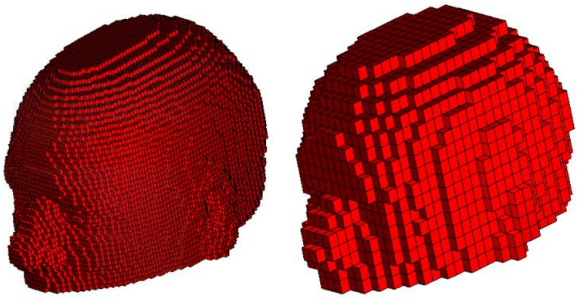

Fig. 1. Zubal anthropomorphic head phantom. Left, resolution $N$=3 and right, resolution $N$=8.

By increasing $N$, the resolution and therefore the complexity is gradually decreased, but the error due to averaging procedure is increased.

The new, big cube, represents a building element of the electromagnetic model. Its effective permittivity is obtained using mixing or averaging formulas applied to all the dielectric constant values of the voxels inside the same cube. These formulas were initially implemented for physical mixtures.

Standard averaging formula implements standard arithmetic mean:

$$\varepsilon_{eff} = \frac{\sum_{i=1}^{N^3} v_i * \varepsilon_i}{\sum_{i=1}^{N^3} v_i}, \quad (1)$$

where $\varepsilon_i$ is voxel dielectric constant and $v_i$ is voxel volume.

Lichtenecker formula is a logarithmic formulation of physical components of the mixture as shown below:

$$\ln(\varepsilon_{eff}) = \frac{\sum_{i=1}^{N^3} v_i * \ln(\varepsilon_i)}{\sum_{i=1}^{N^3} v_i}. \quad (2)$$

The formula has been established for biological materials such as human blood [12].

Looyenga equation is considered to be the most reliable formulation to predict the effective permittivity of the mixture [13] - [14]:

$$\varepsilon_{eff}^{(\frac{1}{M})} = \frac{\sum_{i=1}^{N^3} v_i * \varepsilon_i^{(\frac{1}{M})}}{\sum_{i=1}^{N^3} v_i}, \quad (3)$$

where $M = 2, 3$. Looyenga equation is considered up to third degree. All the formulas were implemented and the results of conversion of the phantom to the electromagnetic model as well as simulated results, and its comparison, were provided for each of the formulas. That is given in the next section.

Once the effective dielectric constant that represents averaged value of all the voxels permittivity inside a big cube is obtained, the second level of homogenization is applied. It implies all the big cubes being considered to define a finite number of the domains. Hence the number of big cubes is still significant, for example, more than 100000 in some cases, each cube cannot represent a separate domain. Therefore, all the cubes are divided into several groups, where, inside each group, a relative deviation of the effective dielectric constant is kept below some small threshold. In other words, the cubes in the group possess similar values of effective dielectric constant. One group defines one domain. The domain dielectric constant is a mean value of all effective dielectric constants within the group. The domain dielectric constant is assigned to all the cubes in the group as their new averaged value (new effective dielectric constant) because it is used in the electromagnetic simulation of the phantom. We called it "the assigned dielectric constant".

The number of the domains approximately goes from 100 to 300 for all the resolutions and all four mixing formulas considered in the paper. The higher the resolution (lower $N$)

 ISBN 978-86-7466-930-3

the number of domains generally decreasing and approaches to the number of different tissue types in the model. Each domain represents a closed region, and all the mesh elements, or big cubes' sides, inside the domain were removed to reduce complexity and thus the number of unknowns in the final model. Only domains' surface mesh elements took part in the MoM simulation.

The last part of big cubes' creation is the calculation of the deviation. For each cube, the deviation is calculated per the above-mentioned formulas. The formula used for averaging is also used for calculating deviation. The only difference is that part $\varepsilon_i$ in the above equations is changed with the $|\varepsilon_i - \varepsilon'_{eff}|$ which is the deviation of one small voxel. Therefore, the Lichtenecker method is given as

$$\ln(\delta) = \frac{\sum_{i=1}^{N^3} v_i * \ln |\varepsilon_i - \varepsilon'_{eff}|}{\sum_{i=1}^{N^3} v_i}, \quad (4)$$

standard and Looyenga method is

$$\delta^{(\frac{1}{M})} = \frac{\sum_{i=1}^{N^3} v_i * |\varepsilon_i - \varepsilon'_{eff}|^{(\frac{1}{M})}}{\sum_{i=1}^{N^3} v_i}, \quad (5)$$

where $M = 1, 2, 3$, $v_i$ is voxel volume and $\varepsilon'_{eff}$ is the assigned dielectric constant value.

Therefore, a mean deviation for each big cube is calculated as the mean absolute distance of each voxel in the cube from the assigned dielectric constant value, rather than the distance from the averaged value $\varepsilon_{eff}$.

### C. *Estimation of Error*

In the end, the deviation for the whole phantom is obtained from the particular deviations of big cubes. This value actually represents the error raised from the averaging procedure.

The error value is also calculated using a specific formula which is similar to the averaging process, so, either with standard, Lichtenecker or Looyenga procedure. Lichtenecker method

$$\ln(\Delta) = \frac{\sum_{j=1}^{K} V_j * \ln(\delta_j)}{\sum_{j=1}^{K} V_j}, \quad (6)$$

standard and Looyenga method

$$\Delta^{(\frac{1}{M})} = \frac{\sum_{j=1}^{K} V_j * \delta_j^{(\frac{1}{M})}}{\sum_{j=1}^{K} V_j}, \quad (7)$$

where $K$ is number of big cubes, $M = 1, 2, 3$, $\delta_j$ is the big cube deviation and $V_j$ is big cube volume. We can calculate the average value $A$ of the whole phantom using the Lichtenecker method

$$\ln(A) = \frac{\sum_{j=1}^{K} \sum_{i=1}^{N^3} v_{ji} * \ln|\varepsilon_{ji}|}{\sum_{j=1}^{K} \sum_{i=1}^{N^3} v_{ji}}, \quad (8)$$

standard and Looyenga method

$$A^{(\frac{1}{M})} = \frac{\sum_{j=1}^{K} \sum_{i=1}^{N^3} v_{ji} * |\varepsilon_{ji}|^{(\frac{1}{M})}}{\sum_{j=1}^{K} \sum_{i=1}^{N^3} v_{ji}}, \quad (9)$$

where $K$ is number of big cubes, $M = 1, 2, 3$, $v_{ji}$ is voxel volume of $i$-th voxel in the $j$-th big cube and $\varepsilon_{ji}$ is voxel dielectric constant of $i$-th voxel in the $j$-th big cube. The air voxels are omitted from the overall phantom.

Now, we can calculate the relative mean absolute error of the whole phantom as

$$RMA[\%] = \frac{\Delta}{A} * 100\,. \quad (10)$$

This value is provided at the end of the conversion process of the phantom to the electromagnetic model, ready for simulation.

The relative mean absolute deviation of simulated results is given by

$$RMA_{sim}[\%] = \frac{\frac{1}{n} * \sum_{i=1}^{n} |E_i^N - E_i^{Ref}|}{\frac{1}{n} * \sum_{i=1}^{n} |E_i^{Ref}|} * 100, \quad (11)$$

where $n$ is the number of directions for bistatic RCS far-field, here 73x37 for azimuth and elevation, $E_i^N$ is far-field for phantom with resolution $N$ and $E_i^{Ref}$ is far-field for the reference fantom.

## III. RESULTS

We used the Zubal head phantom for analysis. The full MoM electromagnetic simulations were performed in WIPL-D software.

Simulations in WIPL-D provide results for bistatic RCS in a number of space angles, with plane wave excitation. The results were provided for different resolutions $N$=3, 4… 12 and for all mixing formulas, Lichtenecker and Looyenga where $M$=1, 2, 3. We also provide the $MA$ values for all the conversions.

The phantom with the highest resolution, $N$=3, is taken as the reference result. At the operating frequency of 1 GHz, this phantom has 500000 unknowns with around 100 domains and the resolution is about 3.5 mm. Simulation time on the machine Intel(R) Xeon(R) CPU E5-2650 v4 @ 2.20GHz (2 processors), with 48 logical processors, 256 GB of RAM and 4 GPU cards NVIDIA GeForce GTX 1080Ti, is about 7.3 hours.

All other phantoms were compared to this reference phantom, mean deviation of the RCS far-field is calculated for each of them relative to the reference phantom i.e., $MA_{sim}$. In the same manner, the differences were provided for the $MA$ values too, relative to the reference phantom.

The next four figures present a comparison of $MA_{sim}$ and $MA$ relative to the reference phantom.


ISBN 978-86-7466-930-3

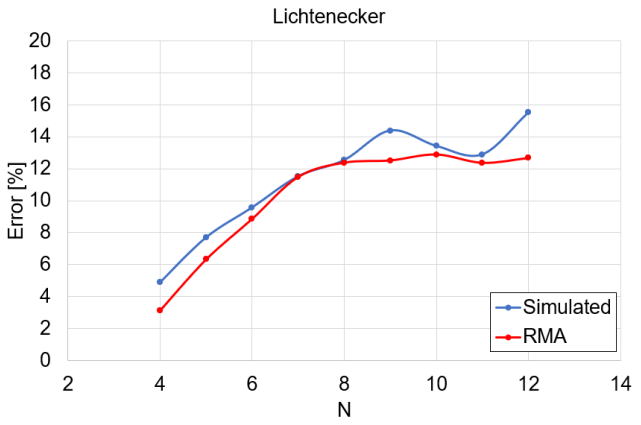


Fig. 2. Lichtenecker method. The Error for the blue trace represents the mean deviation of the RCS far-field relative to the reference phantom $N$=3 i.e., $MA_{sim}$. The Error for the red trace represents differences in $MA$ also relative to the reference phantom $N$=3. $N$ is resolution.

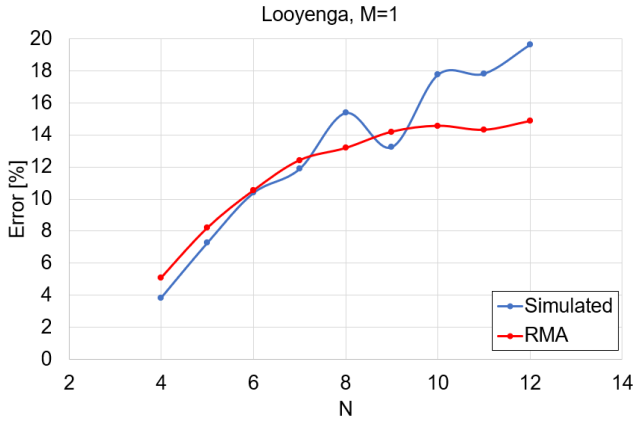


Fig. 3 Looyenga method, with $M$=1 degree. The Error for the blue trace represents the mean deviation of the RCS far-field relative to the reference phantom $N$=3 i.e., $MA_{sim}$. The Error for the red trace represents differences in $MA$ also relative to the reference phantom $N$=3. $N$ is resolution.

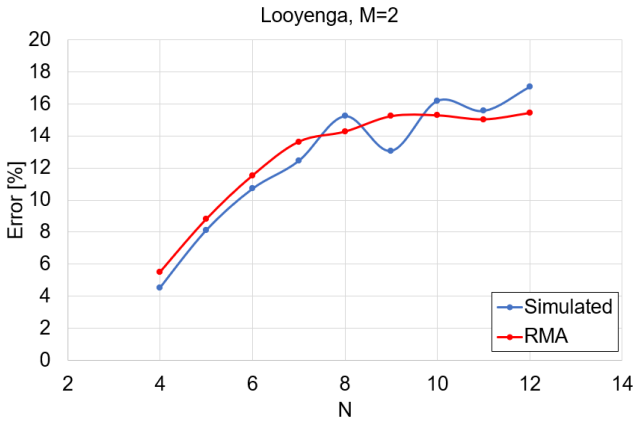


Fig. 4. Looyenga method, with $M$=2 degree. The Error for the blue trace represents the mean deviation of the RCS far-field relative to the reference phantom $N$=3 i.e., $MA_{sim}$. The Error for the red trace represents differences in $MA$ also relative to the reference phantom $N$=3. $N$ is resolution.

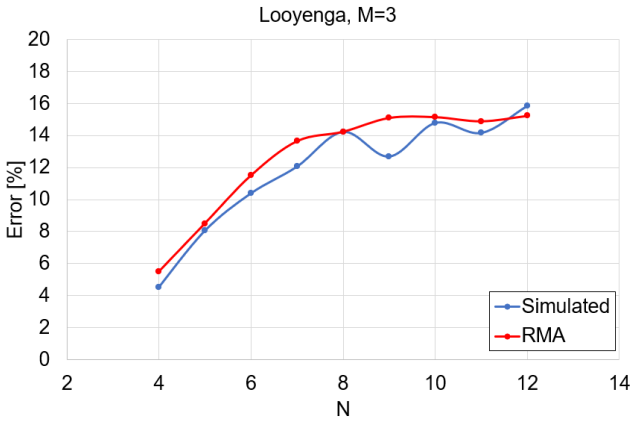


Fig. 5. Looyenga method, with $M$=3 degree. The Error for the blue trace represents the mean deviation of the RCS far-field relative to the reference phantom $N$=3 i.e., $MA_{sim}$. The Error for the red trace represents differences in $MA$ also relative to the reference phantom $N$=3. $N$ is resolution.

## IV. Conclusion

We present a novel technique for the conversion of large voxel phantoms by averaging and homogenization of the voxel data to the electromagnetic simulation ready model. The obtained model is suitable for analysis of the imaging scenario, with reasonable simulation time.

We've also shown the estimated error, or relative mean absolute value $MA$, as a result of the simplification process. A comparison in error behavior between $MA$ and simulated RCS results is provided. It can be seen that the $MA$ expresses very similar behavior with the mean deviation in simulated results, for different resolutions, relative to some phantom of a very high resolution taken as the reference. The estimated convergence of the $MA$ can serve as a guide of anticipating the characteristics of the phantom before performing electromagnetic simulation itself.

## References

[1] S. Mustafa, B. Mohammed and A. Abbosh, "Novel Preprocessing Techniques for Accurate Microwave Imaging of Human Brain," in IEEE Antennas and Wireless Propagation Letters, vol. 12, pp. 460-463, 2013

[2] A.S. M. Alqadami, A. Trakic, A. E. Stancombe, B. Mohammed, K. Bialkowski and A. Abbosh, "Flexible Electromagnetic Cap for Head Imaging," in IEEE Transactions on Biomedical Circuits and Systems, vol. 14, no. 5, pp. 1097-1107, Oct. 2020, doi: 10.1109/TBCAS.2020.3025341.

[3] Zhao Wang, Eng Gee Lim, Yujun Tang, Mark Leach, "Medical Applications of Microwave Imaging", The Scientific World Journal, vol. 2014, Article ID 147016, 7 pages, 2014. https://doi.org/10.1155/2014/147016.

[4] M. Pastorino, A. Randazzo, Microwave Imaging Methods and Applications, in *Artech ouse*, 2018.

[5] L. Crocco, I. Karanasiou, M. James, R. Conceição, "Emerging Electromagnetic Technologies for Brain Diseases Diagnostics, Monitoring and Therapy," *Springer*, Cham, Switzerland, 2018.

[6] S. N. Makarov, G. M. Noetscher and A. Nazarian, Low-Frequency Electromagnetic Modeling for Electrical and Biological Systems Using Matlab, *ohn Wiley Sons*, Inc, 2016

[7] The Zubal Phantom – http://noodle.med.yale.edu/zubal/

[8] WIPL-D software suite (WIPL-D Pro v17 & Pro CAD 2020), WIPL-D d.o.o, Belgrade, 2020.

[9] T. Singh, M. Stevanetic, M. Stevanovic and B. Kolundzija, "Homogenization of Voxel Models using Material Mixing Formulas," 2020 14th European Conference on Antennas and Propagation (EuCAP), 2020, pp. 1-4.

[10] Zastrow E, Davis SK, Lazebnik M, F. Kelcz, B. D. Van Veen, and S. C. Hagness, Database of 3D grid-based numerical breast phantoms for

 ISBN 978-86-7466-930-3

use in computational electromagnetics simulations. Madison (WI): University of Wisconsin-Madison; c2014. [cited 2014 Sep 21]. Available at: https://uwcem.ece.wisc.edu/phantomRepository.html.

[11] M. Lazebnik, L. McCartney, D. Popovic, C. B. Watkins, M. J. Lindstrom, J. Harter, S. Sewall, A. Magliocco, J. H. Booske, M. Okoniewski, and S. C. Hagness, "A large-scale study of the ultrawideband microwave dielectric properties of normal breast tissue obtained from reduction surgeries," Physics in Medicine and Biology, vol. 52, pp. 2637-2656, April 2007.

[12] Ray Simpkin, "Derivation of Lichtenecker's Logarithmic Mixture Formula From Maxwell's Equations," IEEE Transactions on Microwave Theory and Techniques, Vol. 58, No. 3, March 2010.

[13] S.O. Nelson, "Measurement and Computation of Powdered Mixture Permittivities," Proceedings of the 17th IEEE Instrumentation and Measurement Technology Conference, DOI: 10.1109/IMTC.2000.848661.

[14] Kimmo Kalervo Kärkkäinen, Ari Henrik Sihvola, and Keijo I. Nikoskinen, "Effective Permittivity of Mixtures: Numerical Validation by the FDTD Method," IEEE Transactions on Geoscience and Remote Sensing, Vol. 38, No. 3, May 2000 1303.

 ISBN 978-86-7466-930-3

# Radome Shape Impact on Automotive Radar Sensor Operating at 79 GHz

Nebojša Pupavac and Miodrag Tasić, *Member, IEEE*

***Abstract*—At high frequencies radome ( adar Dome) degrades the automotive radar performance significantly. To gain better understanding of this phenomenon the radome shape and its impact on radiation pattern of the radar antenna array is analyzed in this paper. To analyze the impact of the radome shapes, an array of printed antennas is simulated with two different radome shapes and compared against the radiation pattern simulated without any radome. A simple single patch antenna for G z is designed using WIP -D software platform, which was used for simulation of the antenna array with and without radome.**

***Index Terms*— adome; radar sensor; antenna array; patch antenna.**

## I. Introduction

A radome (radar dome) is a protective shield that encloses mmWave radar sensors and the antenna. It protects the antennas and electronics from external environment effects. The radome should be designed to minimally attenuate the electromagnetic signals transmitted and received by the antennas and as such should effectively be transparent to radio waves.

Since short range automotive radars work in 77-81 GHz frequency range [1], wavelengths of radar signals are rather small (3.75 mm at 80 GHz). This can cause significant interactions between radar signals and the plastic parts of the vehicle (painted bumper) and/or used radome, resulting in unpredictable error in the angle of arrival estimation [2]. Sometimes a calibration of the system can include the radar itself [3], but in the most cases radome is designed separately, with a goal to minimize reflections [4].

Although there are some general guidelines for automotive radar design [5], an electromagnetic simulation is necessary step in this process. In this paper we present results of the electromagnetic simulations for two radomes scenarios: spherical radome and rectangular radome, covering microstrip patch array. We will compare radiation patterns of these two systems with the radiation pattern of the microstrip patch array without the radome. The results can be used as a starting point in finding the optimal radome shape for a particular automotive radar design.

Nebojša Pupavac is with the School of Electrical Engineering, University of Belgrade, 73 Bulevar kralja Aleksandra, 11020 Belgrade, Serbia (e-mail: nebojsapupavac@gmail.com), (https://orcid.org/0000-0001-7851-7649)

Miodrag Tasić is with the School of Electrical Engineering, University of Belgrade, 73 Bulevar kralja Aleksandra, 11020 Belgrade, Serbia (e-mail: tasic@etf.bg.ac.rs), (https://orcid.org/0000-0002-8356-1190)

## II. Guidelines for Radome Design

Since the most radomes are designed out of perfect dielectric material (with the relative permeability equal to 1, and the conductivity which is close to 0), main parameters for selecting appropriate material are relative permittivity and the loss tangent. The lower loss tangent provides the smaller attenuation by the radome, and overall smaller effect of the radome on the antenna performance. In finding optimal relative permittivity and a shape of the radome, the electromagnetic theory of time-harmonic electromagnetic fields for the plane-wave assumption can be used.

Electromagnetic wave reflections occur at the boundaries of the plane of mismatch. The plane of mismatch is the boundary of two domains with different dielectric permittivity. The interaction of the electromagnetic wave at the boundaries leads to the reflection and transmission of waves, quantized in terms of reflection coefficient ,

$$= \frac{\sqrt{\varepsilon_{r1}} - \sqrt{\varepsilon_{r2}}}{\sqrt{\varepsilon_{r1}} + \sqrt{\varepsilon_{r2}}}, \tag{1}$$

and transmission coefficient $T$,

$$T = \frac{2\sqrt{\varepsilon_{r1}}}{\sqrt{\varepsilon_{r1}} + \sqrt{\varepsilon_{r2}}}. \tag{2}$$

Expressions (1) and (2) hold for an incident plane wave normal to the infinite flat boundary between the domains with relative permittivities $\varepsilon_{r1}$ and $\varepsilon_{r2}$ [6]. These expressions indicate that lower relative permittivity of radome dielectric material causes lower degradation of radar performance (since the other domain is air, with relative permittivity close to 1). However, optimal radome material needs to provide adequate mechanical characteristics, and the boundary in the general case is not a flat surface. Therefore, the selection of the dielectric material is always a tradeoff.

The radome thickness is particularly important for optimal performance of the automotive radar sensors. To avoid reflection at the radome wall, its thickness should be equal to an integer multiple, $n$, of the half of the wavelength in the radome [6]:

$$t_{opt} = n\frac{c_0}{2f_r\sqrt{\varepsilon_r}}, \tag{3}$$

 ISBN 978-86-7466-930-3

where $c_0$ is speed of light in vacuum, $\varepsilon_r$ is relative permittivity of radome material, and $f_r$ is central frequency.

Typical parameters for the radome materials are shown in Table I. For radome shape analyses PTFE is selected as optimal solution which could be fabricated and tested to confirm simulation results presented in this paper. For $\varepsilon_{rPTFE} = 2$ and $f_r = 79\,\text{GHz}$, the optimal thickness of radome material from (3) is obtained for $n = 2$, $t_{opt} = 2.68\,\text{mm}$ (since the radome has to be at least 2 mm thick). Note that (3) is valid for electromagnetic plane waves at infinite flat boundary.

TABLE I
TYPICAL RADOME MATERIALS

| aterial | elative Permittivity ($\varepsilon_r$) | oss tangent tg(δ) |
|---|---|---|
| Polycarbonate | 2.9 | 0.012 |
| ABS | 2.0-3.5 | 0.0050-0.019 |
| PEEK | 3.2 | 0.0048 |
| PTFE | 2 | <0.0002 |
| Plexiglass | 2.6 | 0.009 |
| PE | 2.3 | 0.0003 |
| PBT | 2.9-4.0 | 0.002 |

The optimal distance between the antenna and the internal surface of the radome helps to minimize the effects of reflections caused by the radome. These effects become minimal if the waves returned to the antenna are in phase with the transmitted waves. So, the optimal distance between antenna and radome is [5]:

$$d_{opt} = m\frac{c_0}{2f_r}. \tag{4}$$

For $m = 7$ we have $d_{opt} = 13.29\,\text{mm}$. A spherical radome in that case would have inner diameter of $26.58\,\text{mm}$, which is sufficient to cover the whole automotive radar sensor, including all necessary components.

## III. ANTENNA DESIGN

We will model typical automotive radar sensors at 79 GHz, with four microstrip patch antennas. The layout of the single patch antenna is shown in Fig. 1. A substrate thickness is $t = 127\,\mu\text{m}$, with relative permittivity $\varepsilon_r = 3$, and loss tangent $\tan\delta = 0.0017$.

The patch width ($W$) and length ( ) are calculated using the standard approximation [7],

$$W = \frac{c_0}{2f_r\sqrt{\frac{\varepsilon_r+1}{2}}}, \tag{5}$$

$$= \frac{c_0}{2f_r\sqrt{\varepsilon_{eff}}}, \tag{6}$$

where $\varepsilon_{eff}$ is given by

$$\varepsilon_{eff} = \frac{\varepsilon_r+1}{2} + \frac{\varepsilon_r-1}{2}\left(1+12\frac{t}{W}\right)^{-\frac{1}{2}}. \tag{5}$$

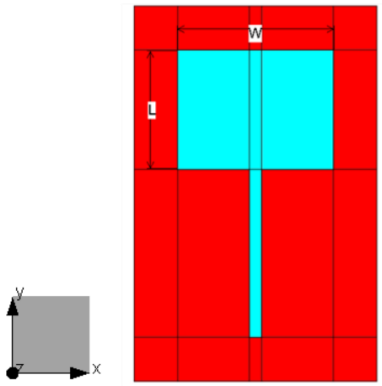


Fig. 1. Single rectangular patch antenna.

Antenna matching is achieved by adjusting the length of 0.1 mm wide feeding line using software package for electromagnetic modeling WIPL-D Pro [8]. Parameter $s_{11}$ over desired frequency bandwidth is shown in Fig. 2, whereas radiation pattern in H-plane and E-plane is shown in Fig. 3.

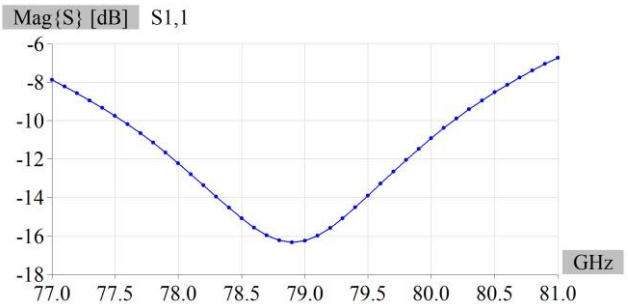


Fig. 2. Parameter $s_{11}$ for a single microstrip patch antenna.

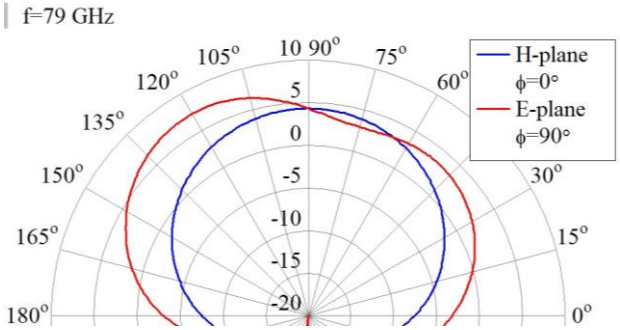


Fig. 3. Radiation pattern (Gain in dB) for a single microstrip patch antenna.


ISBN 978-86-7466-930-3

Typical automotive radar sensors at 79 GHz are using 3 Tx and 4 Rx antennas. In this simulation only Rx antenna is simulated. It is made of four single microstrip patch antennas shown in Fig. 1, with λ/2 spacing, as shown in Fig. 4.

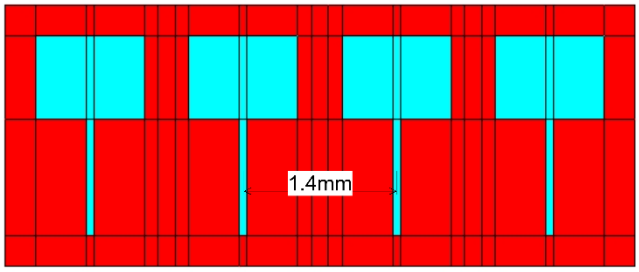


Fig. 4. Antenna Array with λ/2 spacing.

Since the array is symmetrical, only first two antennas (from left to right) are connected to generators, G1 and G2. The third and fourth antennas are symmetrical, so it is assumed that inner antennas have identical, but mirrored radiation pattern, as well as the outer antennas.

Fig. 5 shows that H-plane radiation patterns of both inner and outer antenna are deformed compared to the radiation pattern of a single antenna from Fig. 3 (where H-plane radiation pattern was symmetrical). Inner antenna deformation is less significant because it is surrounded by identical antennas from both left and right side.

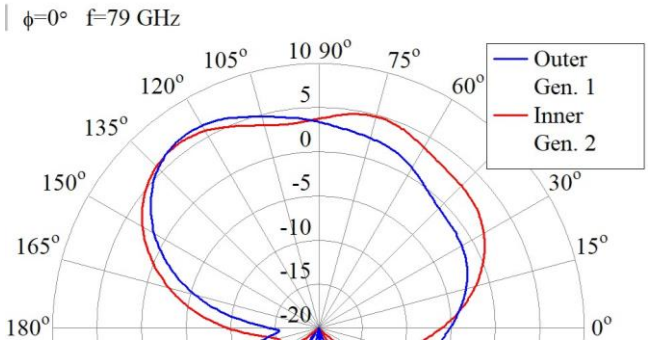


Fig. 5. Inner and Outer Antenna Radiation Patterns in H-plane.

## IV. Antenna Array With Radome

Antenna array with a spherical radome of radius $d_{\text{opt}} + t = 13.42$ mm, with the center in the center of the array, is shown in Fig. 6.

Antenna array with a rectangular radome, with the same distance from the antenna array, having square cross section with the same width as the sphere radome diameter is shown in Fig. 7.

Both radomes are made from the material with relative permittivity 2 and thickness $t_{\text{opt}} = 2.68$ mm.

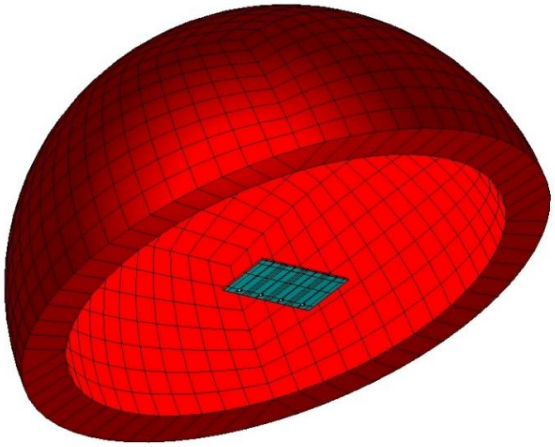

Fig. 6. Antenna array with the spherical radome.

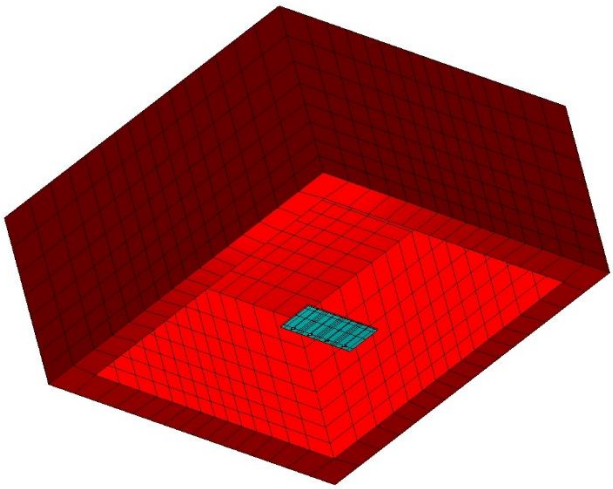

Fig. 7. Antenna array with the rectangular radome.

The electrical distance through the radome in boresight is equivalent to the thickness of the radome wall. The radome wall thickness $t_{\text{opt}}$ is designed to cancel reflections from the radome, but in the case of normal incidence of the electromagnetic plane wave on infinite flat boundary Therefore, at boresight of the radome, the reflections at the inner wall will mainly cancel, resulting in low net reflections.

In the case of a rectangular (flat) radome, when moving away from the boresight to higher grazing angles of arrival, the distance traveled by the mmWave signal is greater than "optimal thickness", as illustrated in Fig. 8. This causes multiple reflections at the radome interface boundary resulting in ripples in the antenna radiation patterns and leading to nulls. These ripples and nulls can cause inconsistency in the detection of the objects at higher grazing angles resulting in angle estimation errors.

In the case of the spherical radome, the radome performance at different grazing angles will be more similar to the performance at boresight.

 ISBN 978-86-7466-930-3

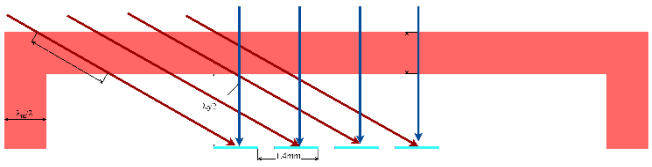

Fig. 8. Cross sectional view of the rectangular radome and the antenna array.

Radiation patterns of the outer antenna in E-plane, without a radome, and with spherical and rectangular radomes are shown in Fig. 9, whereas the similar graph for the inner antenna is shown in Fig. 10.

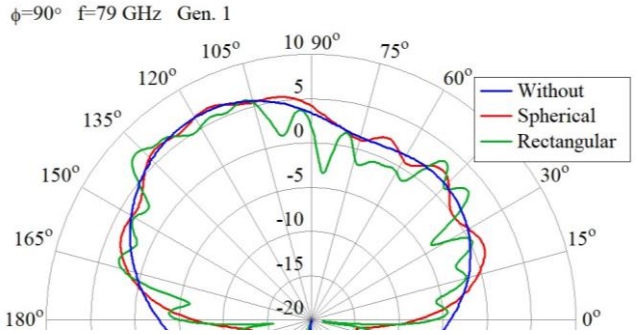


Fig. 9. Outer antenna radiation pattern in E-plane.

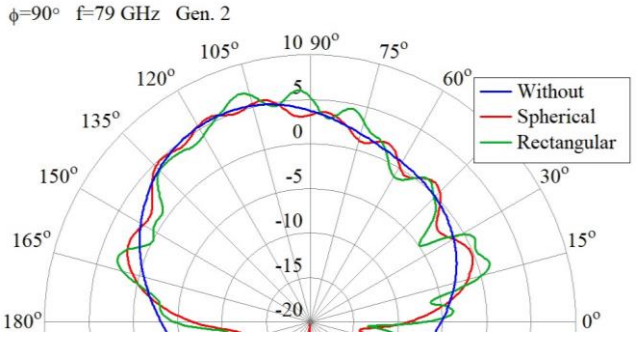


Fig. 10. Inner antenna radiation pattern in E-plane.

Radiation patterns of the outer antenna in H-plane, without a radome, and with spherical and rectangular radomes are shown in Fig. 11, whereas the similar graph for the inner antenna is shown in Fig. 12.

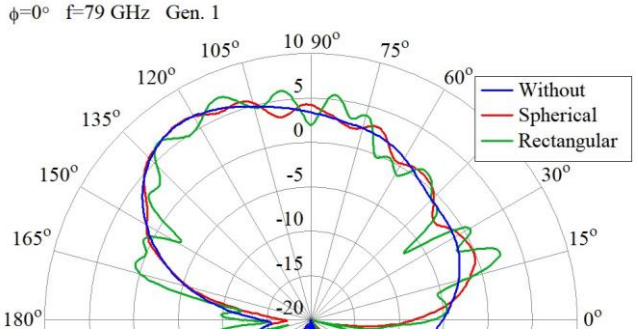


Fig. 11. Outer antenna radiation pattern in H-plane.

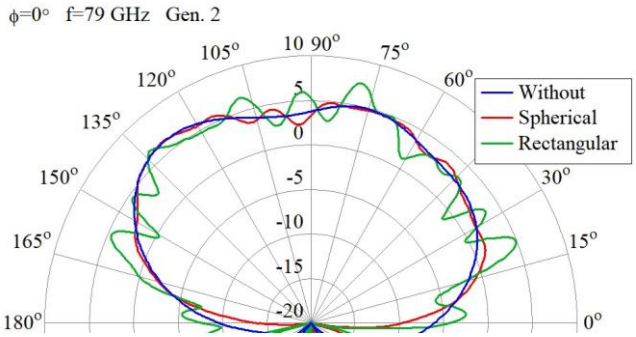


Fig. 12. Inner antenna radiation pattern in H-plane.

The radiation pattern from 180° to 360° is not interesting for the radar performance, also the simulation result is not relevant as the model doesn't include the complete PCB which is in realty much larger and has many components which are not modeled and neglected for the antenna simulation.

For the most applications azimuth angle of arrival estimation is more important. Therefore, the radiation patterns for H-plane (azimuth plane) are also shown in Cartesian system, in Figs. 13 and 14, to emphasize the ripples caused by radomes and to show the difference between the two radome shapes. Expected field of view of the automotive sensor is around ±60°, so antenna patterns from 15° to 165° are shown.

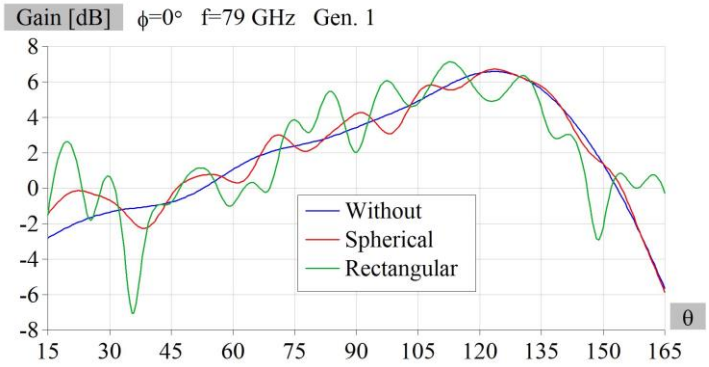


Fig. 13. Outer antenna radiation pattern in H-plane (Cartesian).

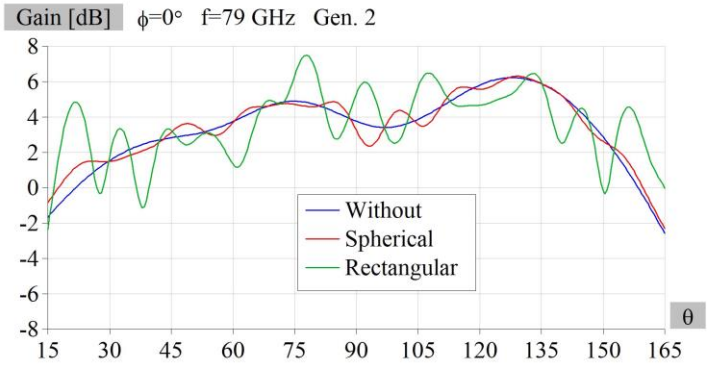


Fig. 14. Inner antenna radiation pattern in H-plane (Cartesian).


ISBN 978-86-7466-930-3

## V. CONCLUSION

The aim of these simulations was to show weather the radome shape could improve automotive radar sensor performance and if it makes sense to invest in designing more complicated radome shapes compared to the most common rectangular design. The simplified model comprising of only 4 Rx antennas (typically mmWave sensors are using 4 Rx and 3 Tx antennas) is showing that spherical radome has significantly reduced ripples compared to the flat radome.

Also, the spherical radome cannot fulfill half wavelength conditions for each antenna, so some of the ripples still appear comparing to the scenario without a radome.

Main influence of the above-mentioned ripples is the degradation of the radar performance by means of angle of arrival estimation and the maximal detection range. To confirm the simulation results, a realistic antenna array with both Rx and Tx antennas should be measured using Vector Network analyzer (VNA) and referent (horn) antenna using different radomes. Also, the complete mmWave sensor with the identical antenna array and targets at different angle of arrival could be tested to indicate the angle estimation accuracy degradation introduced by different radomes and compared with the radar simulation results.

## REFERENCES

[1] K. M. Strohm, H. L. Bloecher, R. Schneider and J. Wenger, "Development of future short range radar technology," *European adar Conference, 2005. E A 2005.*, 2005, pp. 165-168.

[2] M. M. S. Hossain *et al*., "Wideband Radomes for Millimeter-Wave Automotive Radars," in *IEEE Transactions on Antennas and Propagation*, vol. 70, no. 2, pp. 1178-1186, Feb. 2022.

[3] S. Buitrago, S. Blanch and J. Romeu, "Automotive radar and radome calibration to improve the direction of arrival detection performance," *12th European Conference on Antennas and Propagation EuCAP 201* , 2018, pp. 1-5.

[4] F. Fitzek and R. H. Rasshofer, "Automotive Radome Design - Reflection Reduction of Stratified Media," in *IEEE Antennas and Wireless Propagation etters*, vol. 8, pp. 1076-1079, 2009.

[5] C. K., H. U. R. M. and G. P. Authors, “mmWave Radar Radome Design Guide,” TI, Dallas, Texas, USA, 2021.

[6] A. Đorđević, *Elektromagnetika*, Akademska misao, Beograd,2008.

[7] A. Pandey, *Practical Microstrip and Printed Antenna esign*, Artech House. 2019.

[8] https://wipl-d.com/products/wipl-d-pro/.

 ISBN 978-86-7466-930-3

# Implementing Gradient Model for Surface Roughness in WIPL-D

Milan P. Radović, Aleksandar Z. Golubović *Student Member, IEEE* and Miloš M. Jovičić

***Abstract*—The implementation of gradient method for surface roughness correction in WIPL-D software package is presented. Surface roughness model is tested on modified ring resonator model. Finally, simulation results from WIPL-D and CST Studio Suite are compared.**

***Index Terms*—surface roughness, gradient model, effective conductivity, WIPL-D, ring resonator, surface impedance**

## I. Introduction

MODERN automotive radar systems are often developed in mm-Wave technology [1],[2] and require precise design and manufacturing. Hence, accurate full-wave electromagnetic modeling of such systems has an immense importance in development. To that aim, many electromagnetic effects, that are negligible at lower frequencies, should be taken into consideration at higher frequencies. One of such effects is surface roughness of conductors.

In this case study, gradient method [3] for surface roughness approximation is implemented in WIPL-D software package [4]. The implementation is tested on a model of modified ring resonator [5]. The results are then compared to the results acquired by CST Studio Suite [6].

Skin effect is a tendency of alternating currents to concentrate on the surfaces of conductors, and exponentially drop with conductor depth. It is a result of opposing Eddy currents induced by the changing magnetic fields. If a cylindrical wire-like conductor is observed, the countering Eddy currents will be strongest along the center of the cylinder and drop towards the surface. This will create a characteristic current density profile in the conductor, as shown in Fig. 1. With higher frequencies, currents are more concentrated at the surface of the conductor. We define skin depth, $\delta$, as the depth at which the current density drops to $\frac{1}{e}$ of it's value (around $36.7\%$)

Skin depth is given by [7]

$$\delta = \sqrt{\frac{2\rho}{\omega\mu}}\sqrt{\sqrt{1+(\rho\omega\varepsilon)^2}+\rho\omega\varepsilon}, \qquad (1)$$

Milan P. Radović is with the School of Electrical Engineering, University of Belgrade, 73 Bulevar kralja Aleksandra, 11020 Belgrade, Serbia and with NOVELIC d.o.o., Veljka Dugosevica 54/B5, 11000 Belgrade, Serbia (e-mail: milan.radovic@novelic.com).

Aleksandar Z. Golubović is with the School of Electrical Engineering, University of Belgrade and with NOVELIC d.o.o. (e-mail: aleksandar.golubovic@novelic.com).

Miloš M. Jovičić is with NOVELIC d.o.o. (e-mail: milos.jovicic@novelic.com)

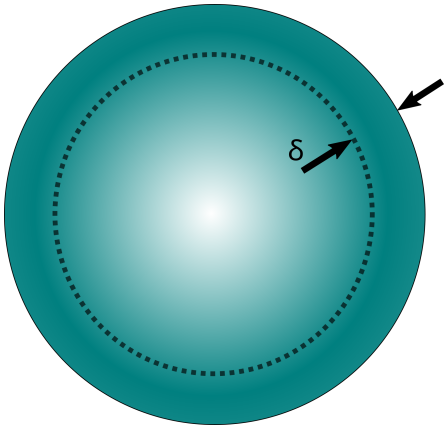


Fig. 1: Illustration of current density and the skin depth.

where $\rho$ is the specific electrical resistance, $\omega$ is the angular frequency of current , $\mu$ is the permeability of the conductor and $\varepsilon$ permittivity. At frequencies of interest, (1) can be approximated by

$$\delta = \sqrt{\frac{2}{\sigma\omega\mu}}. \qquad (2)$$

At low frequencies, the skin depth is larger than the imperfections of the conductor surface. Therefore, when modeling conductors for electromagnetic analysis it is common to approximate the surface of the conductor as ideally flat. However, at high frequencies the skin depth is small enough that it is of comparable size to the roughness of the surface ( $0.23$ μm at 80 GHz). The rough surface of the conductor and the comparable skin depth qualitatively make the current paths longer. At microscopic levels, the roughness structures are electrically larger causing resonant frequencies to shift lower. Additionally, longer current paths will induce larger resistive losses.

We define $R_q$ as the root mean square average of the profile height deviations from the mean line of ideal surface. Different copper deposition methods will yield different surface profiles with different $R_q$. Some of the most widely used copper profiles are [8] STD (Standard foil, $R_q = 5-10$ μm), HPF (High Performance Foil, $R_q = 10-15$ μm), RTF (Reverse Treated Foil, $R_q = 3-6$ μm), VLP (Very Low Profile, $R_q = 3-6$ μm), HVLP (Hyper Very Low Profile, $R_q = 1-3$ μm) and ULP (Ultra Low Profile, $R_q = 0.5-1$ μm), which are shown in Fig. 2. At 1 GHz, the skin depth is $2$ μm and is considerably smaller than most copper profile $R_q$. Since

 ISBN 978-86-7466-930-3

most of the high frequency current will be conducted trough irregular boundary surface, it is important to realistically model and correct for the effects which the rough surface will induce.

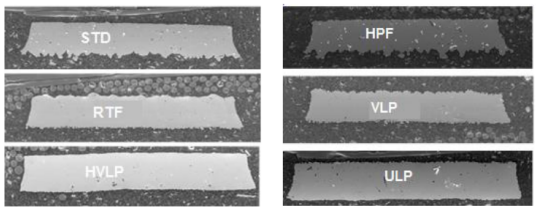


Fig. 2: Microscopic images of common copper deposition profiles.

## II. Gradient Method

The gradient method relies on the fact that the surface profile can be described as a conductivity gradient, from conducting copper to non-conductive dielectric.

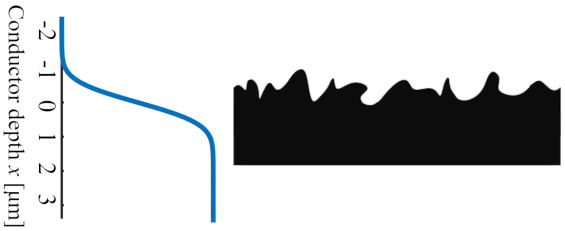


Fig. 3: An example of conductor surface profile and its cumulative distribution function.

It is evident from [3] that the conductivity, $\sigma(x)$, is a cumulative distribution function of $x$

$$\sigma(x) \propto CDF(x). \tag{3}$$

Cumulative distribution function is given as the integral of probability distribution function over the entire $x$ domain

$$CDF(x) = \int_{-\infty}^{x} PDF(u)\mathrm{d}u. \tag{4}$$

We approximate the probability distribution function with a normal Gauss distribution

$$PDF(x) = \frac{1}{R_q\sqrt{2\pi}} \mathrm{e}^{\frac{-x^2}{2R_q^2}}. \tag{5}$$

Finally, the conductivity function can be written as

$$\sigma = \sigma_0 CDF(x) = \sigma_0 \int_{-\infty}^{x} \frac{1}{R_q\sqrt{2\pi}} \mathrm{e}^{\frac{-u^2}{2R_q^2}} \mathrm{d}u. \tag{6}$$

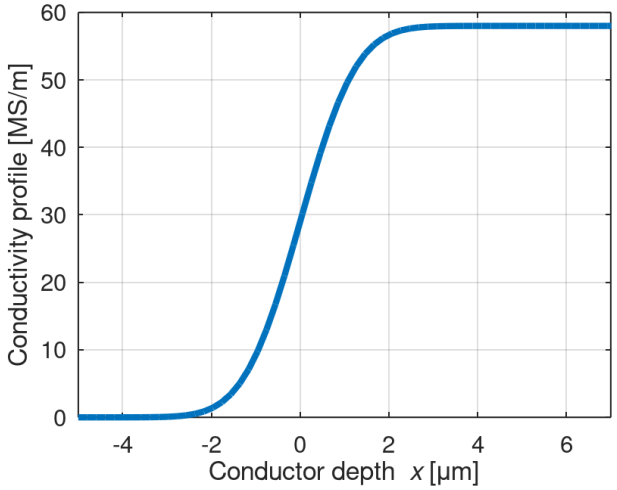


Fig. 4: Conductivity profile of copper surface for $R_q = 1$ μm.

Next, wave equations are derived with additional term that corresponds to variable conductivity due to surface roughness [3]

$$\frac{\partial^2 B_y}{\partial x^2} - \mathrm{j}\omega\mu_0\sigma B_y - \frac{\partial}{\partial x}\ln(\sigma(x))\frac{\partial B_y}{\partial x} = 0, \tag{7}$$

where $B$ is magnetic flux density vector. It should be noted that when the conductivity profile is constant, (7) simplifies down to classical Helmholtz equation which is analytically solvable. However, (7) needs to be numerically solved.

Finite differences method is used to solve (7) for $B_y$. The results are presented in Fig. 5.

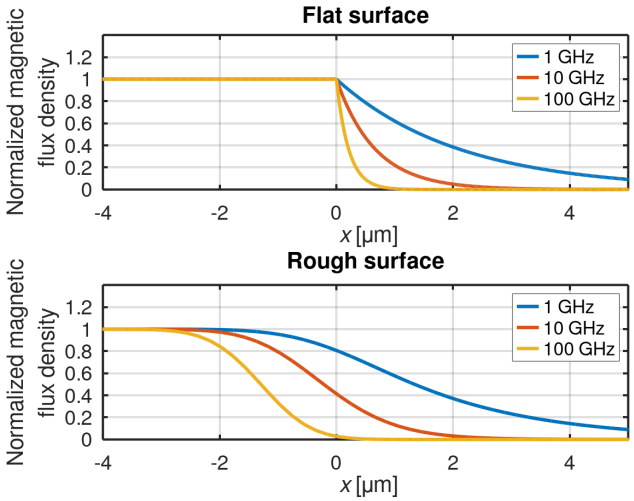


Fig. 5: Comparison of magnetic flux density $y$ component for flat and rough surface ($R_q = 1$ μm).

.


ISBN 978-86-7466-930-3

The change in magnetic flux density is gradual and not sharp as in the flat approximation, which is more in accordance to the real scenario. Knowing the magnetic flux density it is possible to find the current density distribution given by Fig. 6

$$J_z = \frac{1}{\mu_0}\frac{\partial B_y}{\partial x}. \tag{8}$$

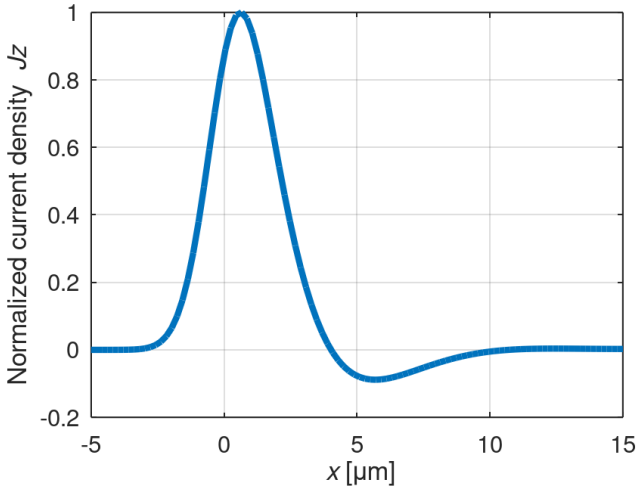


Fig. 6: Normalized current density distribution.

## III. Effective Conductivity

The power density of the conductor surface is given by [3]

$$P_{\mathrm{d}} = \int_{\sigma>0} \frac{|J|^2}{2\sigma(x)}\mathrm{d}x. \tag{9}$$

Consider another conductor with a flat surface that has the same power density as observed rough surface conductor. Its conductivity profile will be a step function

$$\sigma(x) = \begin{cases} \sigma_{\mathrm{eff}}, x < 0 \\ 0, x > 0 \end{cases}. \tag{10}$$

By equalizing the two power distributions, we can calculate the effective conductivity that a flat conductor will need to have, in order to the reproduce the same power distribution as a rough surfaced one

$$\int_{\sigma>0} \frac{|J_{\mathrm{rough}}|^2}{2\sigma(x)}\mathrm{d}x = \int_{\sigma>0} \frac{|J_{\mathrm{flat}}|^2}{2\sigma_{\mathrm{eff}}}\mathrm{d}x. \tag{11}$$

Finally, effective conductivity for different $R_q$ values is numerically computed (7).

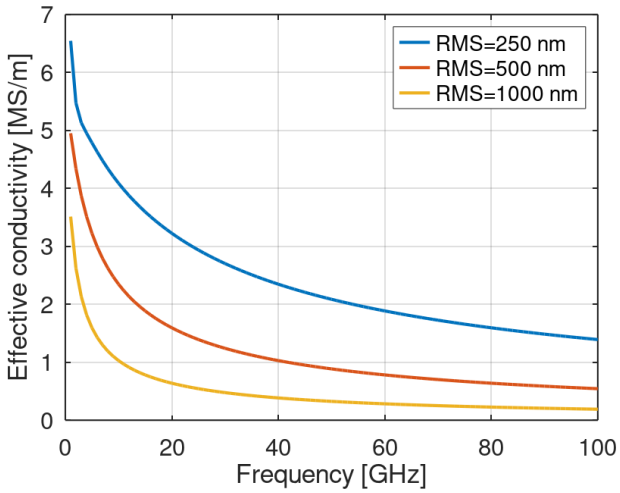


Fig. 7: Comparison of effective conductivity in function of frequency for different values of $R_q$.

## IV. Effective Permeability

Previous method models the resistive losses that will be induced from the surface roughness, however, due to different surface profile the conductor will have different reactive losses.

Similarly to previous modeling of effective conductivity, we will model an effective permeability to account for reactive losses. We observe another conductor with identical magnetic field energy distribution, however, with effective permeability. Equalizing the two energy distributions we can calculate the effective permeability as

$$\int_{\sigma>0} \frac{|B_{y,\mathrm{rough}}|^2}{2\mu_0\mu_{\mathrm{r}}}\mathrm{d}x = \int_{\sigma>0} \frac{|B_{y,\mathrm{flat}}|^2}{2\mu_0\mu_{\mathrm{r,eff}}}\mathrm{d}x. \tag{12}$$

By numerically solving, we yield (Fig. 8):

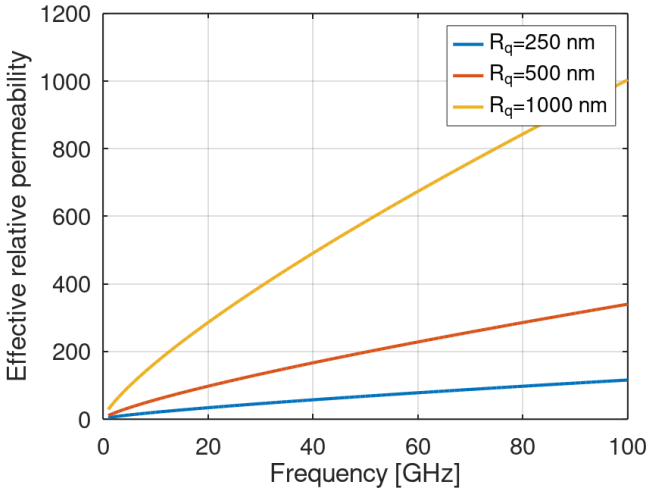


Fig. 8: Comparison of effective permeability in function of frequency for different values of $R_q$.


ISBN 978-86-7466-930-3

## V. Implementation and Results

By obtaining both conductivity and permeability, we can model both resistive and reactive losses. The software package WIPL-D can model distributed loadings with surface impedance, hence we need to translate our parameters into surface impedance as,

$$Z_s = R_s + jX_s = \frac{1}{\sigma_{eff}\delta(\sigma_{eff})} + \frac{1}{\sigma_0\delta(\mu_{r,eff})}. \quad (13)$$

We model a modified ring resonator in both WIPL-D and CST Studio Suite for the purposes of result comparison (Figure 9). In CST we use the surface roughness method provided with the software, while in WIPL-D we use the frequency table function to implement the surface impedance into the model.

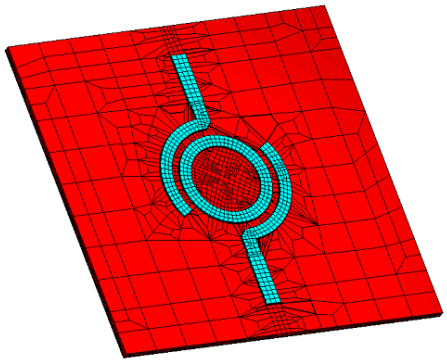

(a)

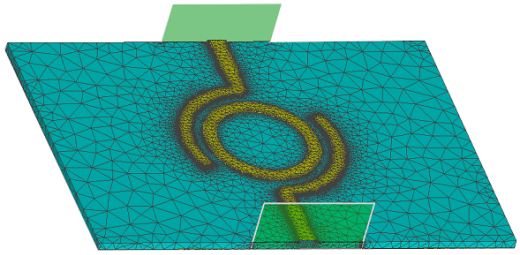

(b)

Fig. 9: a) Ring resonator model in WIPL-D and b) ring resonator model in CST

Since CST uses gradient method that accurately model surface roughness, matching of results obtained by CST and WIPL-D will prove a successful implementation of gradient method in WIPL-D.

The comparison of simulated reflection coefficient for both flat and rough surface of modified ring resonator is shown in 10. From these figures we can observe that there is an excellent matching between the results, thus the gradient method is successfully implemented in WIPL-D.

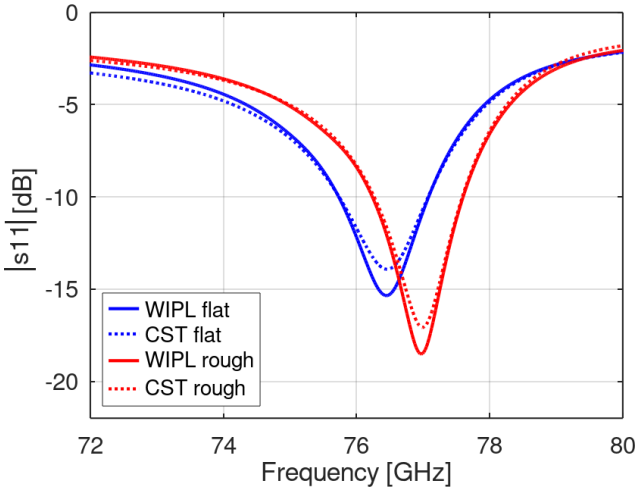


Fig. 10: Comparison of $s_{11}$ for CST and WIPL-D.

## VI. Conclusion

Gradient method for surface roughness estimation is implemented in WIPL-D and tested on modified ring resonator model. Results match the ones obtained using CST Studio Suite, thus gradient model implementation is corroborated. This method can be utilized in WIPL-D, for mm-Wave designs, where surface roughness is crucial.

## References

[1] Baolong Jian, Jing Yuan, and Qiqin Liu. “Procedure to Design a Series-fed Microstrip Patch Antenna Array for 77 GHz Automotive Radar”. In: *2019 Cross Strait Quad-Regional Radio Science and Wireless Technology Conference (CSQRWC)*. 2019, pp. 1–2.

[2] Sungjun Yoo et al. “Patch Array Antenna Using a Dual Coupled Feeding Structure for 79 GHz Automotive Radar Applications”. In: *IEEE Antennas and Wireless Propagation Letters* 19.4 (2020), pp. 676–679.

[3] Gerald Gold and Klaus Helmreich. “A Physical Surface Roughness Model and Its Applications”. In: *IEEE Transactions on Microwave Theory and Techniques* 65.10 (2017), pp. 3720–3732.

[4] WIPL-D. https://wipl-d.com.

[5] Piotr Jankowski-Mihułowicz et al. “Determination of the Material Relative Permittivity in the UHF Band by Using T and Modified Ring Resonators”. In: *International Journal of Electronics and Telecommunications* 62 (June 2016).

[6] CST Studio Suite. https://www.3ds.com/products-services/simulia/products/cst-studio-suite.

[7] Vander Vorst Andre; Rosen Arye; Kotsuka Youji. *RF/Microwave Interaction with Biological Tissues.* Wiley-Interscience, p. 41.

[8] Aleksei V. Rakov et al. “Quantification of Conductor Surface Roughness Profiles in Printed Circuit Boards”. In: *IEEE Transactions on Electromagnetic Compatibility* 57.2 (2015), pp. 264–273.

 ISBN 978-86-7466-930-3

# The Ability to Minimize a New Type of Moderate-Bandwidth Microwave Filter

Dušan Nešić, *Member, IEEE*, Tomislav Milošević

***Abstract*—An example of minimizing the width of a microwave filter structure by bending the stubs and reducing the number of required via holes is presented in this paper. It is shown that the filter area can be reduced near 2 times after bending the stubs. EM model of minimized structure is presented and compared with common filter design.**

***Index Terms*—Microwave filter, Minimization, Microstrip.**

## I. Introduction

WIDE bandpass filters (WBPFs) are important components found in microwave circuits [1-8]. Their purpose is to suppress DC components of the signal as well as low frequency signal components. This suppression is achieved by combing coupling and short-circuiting stubs [1-4] or by only short-circuiting stubs [5-8]. Also, the defective ground structure (DGS) or multilayers can be also used with the same purpose [1,4].

Fig. 1 shows an infinite periodical series of identical T-cells with a short-circuited stub and uniform lines implemented in microstrip technology. Here, $Z$ and $Z_s$ represent characteristic impedances of the base line $\theta$ and stub $\theta_s$. $\theta$ is electrical length given as the phase for a given frequency or wavelength ($\theta=2\pi L/\lambda$). Central passband frequency $f_c$ corresponds to $\theta_s = \pi/2$ i.e., $L = \lambda_c/4$. $\lambda_c$ is wavelength for the frequency $f_c$.

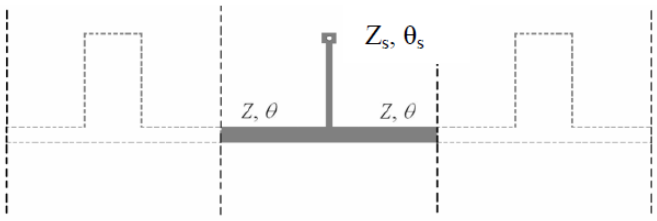


Fig. 1. Scheme of one cell within a filter in microstrip technology.

In [9, 10] relation $\theta_s = 2\theta$ was chosen to eliminate ripples in the stopband. For that relation optimized $S_{11}$-parameters are for $Z = 50\ \Omega$ for all values of $Z_s$. Calculated design curve of $Z_s$ on the relative bandwidth (*RBW*) is presented in Fig. 2.

The film for fabrication (etching) for 4-cells filter with the dimensions is outlined in Fig. 3 [10]. Central frequency is 3 GHz while used substrate is FR-4 with $\varepsilon_r = 4.3$. *RBW* is 100% (1.00) for $Z_s = 60.5$ Ohms. The dimensions of the metallization (black surfaces in the Fig. 3) are 15 μm (0.015 mm) wider on both sides (2 x 15 μm) in order to compensate the lateral etching.

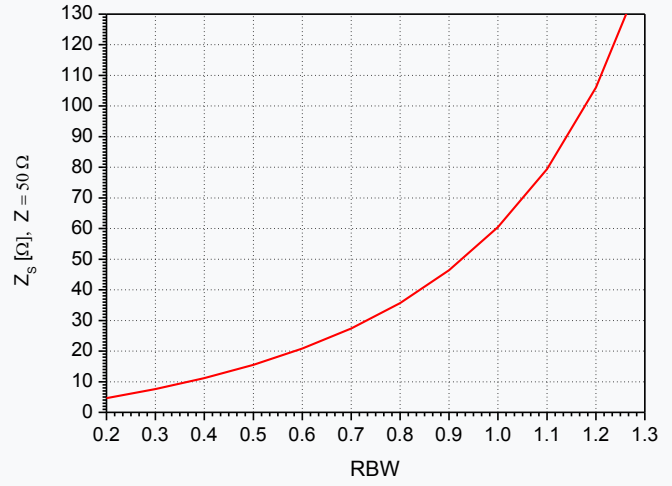


Fig. 2. Design curve of $Z_s$ depending on *RBW* for Z = 50 Ω [9, 10].

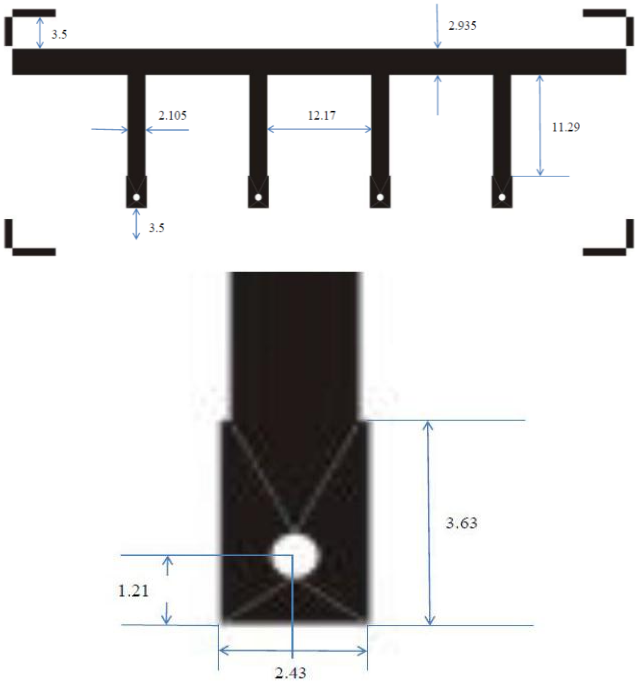


Fig. 3. Dimensions of the film used for etching in mm. Hole radius is equal to 0.385 mm (0.4 mm – 0.015 mm) [10].

Dušan Nešić is with Centre of Microelectronic Technologies, Institute of Chemistry, Technology and Metallurgy, University of Belgrade, Njegoševa 12, 11000 Belgrade, Serbia (e-mail: nesicad@nanosys.ihtm.bg.ac.rs).

Tomislav Milošević is with WIPL-D d.o.o., Gandijeva 7, 11073 Belgrade, Serbia (e-mail: tomislav.milosevic@wipl-d.com)

 ISBN 978-86-7466-930-3

One of the problems with all structures, including filters, is minimization. Here, one cell has an area of about $\lambda_c^2/16$ ($\lambda_c$ is wavelength for the central passband frequency $f_c$). The area can be reduced by bending the stubs and connecting the pair of stubs to one via [8].

## II. MINIMIZATION

Bending the stubs and connecting a pair of stubs to one via is possible according to the relation $\theta_s = 2\theta$. Actually, the length of one stub is approximately the same as the length of a line between the stubs, see Fig. 3. The EM model of the commonly used filter (the model without bending stubs) and the model of the filter with bent stubs are all presented in the Fig. 4 in Program Package WIPL-D [11]. After bending, the area of the filter is reduced near 2 times. The comparison of calculated S-parameters is given in the Fig. 5. A good agreement between the results can be noted.

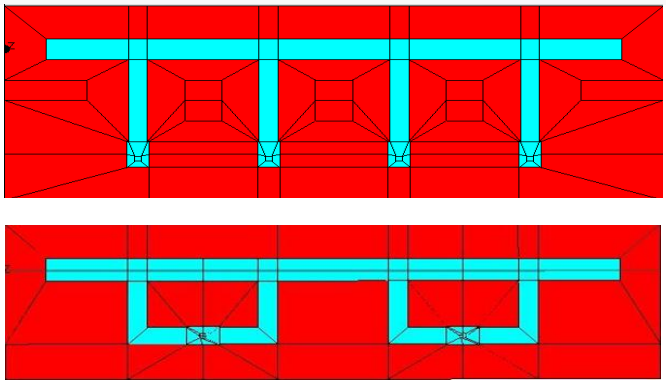

Fig. 4. Commonly used model and the model with bending of the stubs.

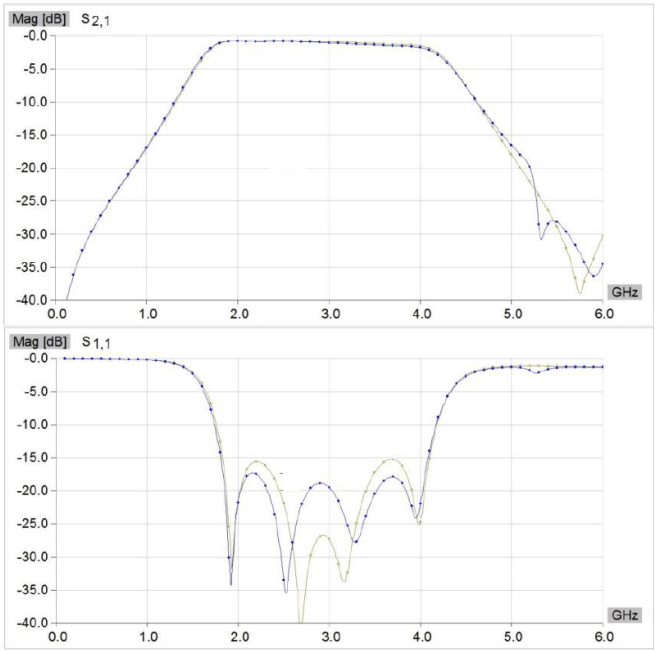


Fig. 5. The comparison between the S-parameters of the commonly used model and the model with bent stubs which are displayed in Fig. 4. No bending (yellow); Bending (blue).

The solution with low Zs values, i.e. implementation with wide microstrip stubs, can be realized as a parallel connection of branches with two times higher Zs. The EM model for 2 times lower Zs than the model presented in Fig. 4 ($Zs = 60.5\ \Omega / 2 = 30.25\ \Omega$) is outlined in Fig. 6 in Program Package WIPL-D [11]. That way the filter achieves relative bandwidth of about 75% (0.75) according to Fig. 2. It is accompanied by the model with bending stubs.

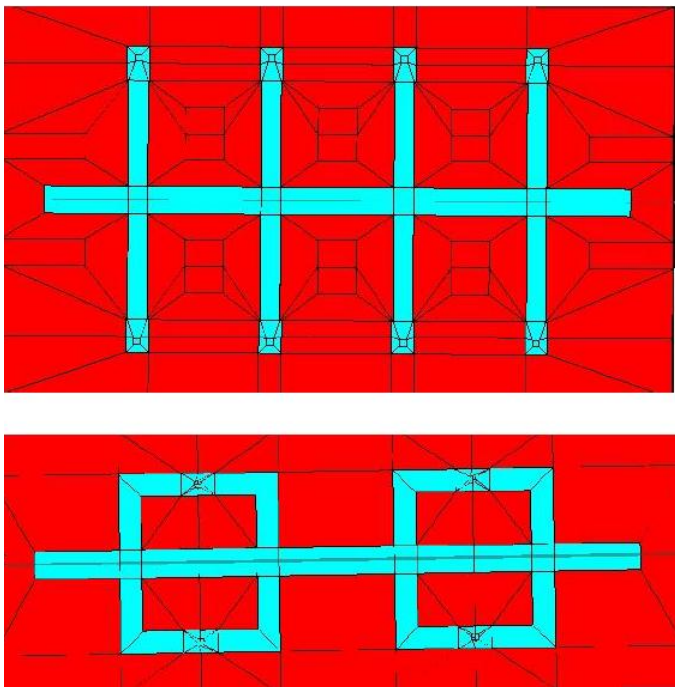

Fig. 6. EM model of the filter with parallel connection of stubs with twice higher Zs and the model with bent stubs.

The comparison between the S-parameters of the model without and the model with bending is shown in Fig. 7. It can be seen that, if the parameter $S_{21}$ is observed, the model with stub bending gives a bit "worse", but still acceptable result in the higher frequency stop-band. The filter area is also reduced near 2 times.

## III. CONCLUSION

An example of minimizing the width of the filter structure by bending the branches as well as reducing the number of required holes for vias was presented. A solution applying low impedances, i.e., wide microstrip lines of branches, was also given, as a parallel connection of branches with twice as large $Z_s$. It is accompanied with a model with bending of branches and minimization.

It can be seen that minimization of the filters was performed successfully and that responses of the filters after bending the stubs are almost the same as the response of the commonly designed filters.


ISBN 978-86-7466-930-3

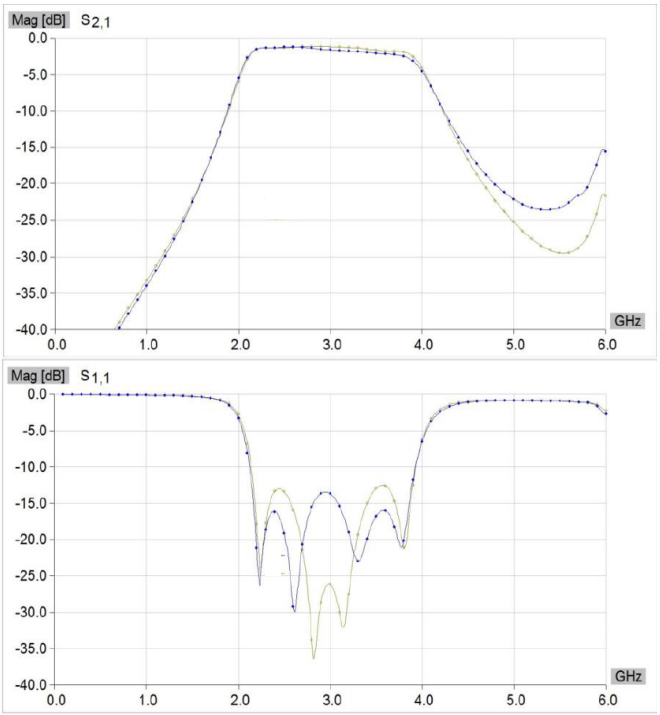


Fig. 7. The comparison of the S-parameters of the model without and with bending in Fig. 6. No bending (yellow); Bending (blue).

## ACKNOWLEDGMENT

This work was financially supported by Ministry of Education, Science and Technological Development of the Republic of Serbia (Grant No. 451-03-68/2022-14/200026).

## REFERENCES

[1] Z.-C. Hao and J.-S. Hong, "Ultrawideband filter technologies," *IEEE Microwave Magazine*, vol.11, no.4, pp.56-68, 2010.

[2] R. Zhang and D. Peroulis, "Planar Multifrequency Wideband Bandpass Filters With Constant and Frequency Mappings," *IEEE Transactions on Microwave Theory and Techniques*, vol.66, no.2, pp.935-942, 2018.

[3] R. Zhang, S. Luo, L. Zhu, "A New Synthesis and Design Method for Wideband Bandpass Filters with Generalized Unit Elements," *IEEE Transactions on Microwave Theory and Techniques*, vol. 65, no. 3, pp. 815-823, 2017.

[4] L.-T. Wang, Y. Xiong and M. He (2019), "Review on UWB Bandpass Filters, UWB Technology - Circuits and Systems," Mohamed Kheir, Intech Open, DOI: 10.5772/intechopen.87204. Available from: https://www.intechopen.com/books/uwb-technology-circuits-and-systems/review-on-uwb-bandpass-filters.

[5] M. S. Razalli, A. Ismail, M. A. Mahd and M. N. Hamidon, "Compnact Configuration Ultra- Wideband Microwave Filter Using Quarter-Wave Length Short-Circuited Stub," *Proceedings of Asia-Pacific Microwave Conference 2007*.

[6] J.-S. Hong and H. Shaman, "An Optimum Ultra-Wideband Microstrip Filter," *Microwave and Optical Technology Letters*, vol. 47, no. 3, pp.230-233, 2005.

[7] M. S. Razalli A. Ismail, M. A. Mahdi and M. N. Hamidon, "Ultra-Wide Band Microwave Filter Utilizing Quarter-wavelength Short-Circuited Stubs," *Microwave and Optical Technology Letters*, Vol. *50*, no. 11, pp. 2981-2983, 2008.

[8] M. S. Razalli, A. Ismail, M. A. Mahdi and M. N. Hamidon, "Compact Ultra-Wide Band Microwave Filter Utilizing Quarter-Wave Length Short Circuited Stubs with Reduced Number of Vias," *Microwave and Optical Technology Letters*, vol. 51, no. 9, pp. 2116-2119, 2009.

[9] D. A. Nesic, One new solution of algorithm for wide bandpass filters, 2020 28th Telecommunications Forum, TELFOR 2020 – Proceedings

[10] D. Nesic, and T. Milosevic, Application of a New Algorithm for the Wide Bandpass Filters, TELSIKS 2021

[11] *Program Package* WIPL-D Pro v18 (*WIPL-D d.o.o, Belgrade 2022. www.wipl-d.com*)

 ISBN 978-86-7466-930-3

# AUTOMATION
# /
# АУТОМАТИКА
# (AUI/АУ)

ISBN 978-86-7466-930-3

# The Improved GM PHD algorithm for Multi-Target Radar Tracking

Zvonko Radosavljević, Dejan Ivković and Branko Kovačević

***Abstract*—Gaussian mixture probability hypothesis density (GM PHD) is a modern nonlinear algorithm for tracking multiple targets in a clutter environment. It is accompanied by known problems that are primarily related to the impossibility of associating the measurement of existing targets and determining the quality of the tracks. For this purpose the automatics track initialization by known 'two point initialization' was introduced. Difference of successive measurements from two radar antenna revolutions is compared with the threshold, which depends on the velocity of the target. The paper proposes to improve the algorithm by introducing the probability of the existence of a target and to reject false tracks. The results of intensive simulations of tracking multiple radar targets have shown the justification for the application of the proposed algorithms.**

***Index Terms*—Target tracking, probability hypothesis density, track while scan (TWS) radars.**

## I. INTRODUCTION

Multi-target tracking in clutter, assuming linear target trajectory propagation and linear target measurement equation, naturally leads to a Gaussian mixture (GM) target tracking solution. As the origin of measurements is uncertain, both true tracks (which follow targets) and false tracks (which do not) exist [1].

The random finite sets (RFS) are representations of multi-target states and multi-target measurements. The modeling of multi-target dynamics using random sets leads to algorithms which incorporate track initiation and termination, a procedure that has mostly been performed separately in tracking algorithms. The first systematic treatment of multi-sensor multi-target filtering, as part of a unified framework for data fusion using random set theory was finite set statistics (FISST). The alternative to optimal multi-target filtering is the Probability Hypothesis Density (PHD) filter [2], [3], [4]. It is a recursion propagating the 1st moment, called the intensity function or PHD, associated with the multi-target posterior.

A Gaussian mixture, consisting of a weighted sum of Gaussian PDF, each with different means and covariance's, is the natural form of the PDF of target state. Using such a structure, a mixture component is created for every possible association, using every possible pairing of targets and measurements with the mean and covariance calculated assuming that the particular hypothesis is true, and the weight calculated to represent the probability that the particular hypothesis is true. The serious problem in multi-target tracking is the unknown association of measurements with appropriate targets [5], [6]. Moreover, the data association problem makes up the growth of the computational load in multi target tracking algorithms. Recently, multi-target tracking formulations involve explicit associations between measurements and targets

The Gaussian Mixture Probability Hypothesis Density Filter (GM-PHD Filter) provided a closed form solution to the PHD filter recursion for multiple target tracking [7]. The posterior intensity function is estimated by a sum of weighted Gaussian components whose means, weights and covariances can be propagated analytically in time. In particular, the means and covariances are propagated by the Kalman filter.

The original Gaussian Mixture PHD filter algorithm provided a means of estimating the number of targets and their states at each point in time. The method for determining the targets simply used the weights of the Gaussian components and did not take into account tempo al continuity. We show that if a target is not detected for each iteration, the Gaussian components can still track the targets in the presence of some missed detections. The trajectory of the target in the past, before it has been detected, can also be determined by keeping the trajectories of each of the Gaussian components. The original formulation of the GM PHD filter allowed targets to be spawned from existing targets [8].

The paper proposes and tests the improved GMPHD algorithm with automatic track initialization (ATI) via 'two point methodology'. Each incoming measurement (from the previous scan) is paired with each incoming measurement from the current scan in order to examine the possibility of initializing a new trace based on the knowledge of the maximum speed of movement of the targets [9].

Rest of papers is organized as follows. Second chapter is dedicated basic problem statements, which precedes Third chapter, which brief decrypted GM PHD algorithm. Results of experiments are given by Fourth chapter. Final conclusions are given by the Fifth chapter.

## II. PROBLEM STATEMENTS

Consider the target tracking scenario with two dimensions. Also, consider the tracking algorithm with two parameters:

Zvonko Radosavljević and Dejan Ivković is with the Millitary Technical Institute, Belgrade, Ratka Resanovica bb, 11030 Belgrade, Serbia (e-mail: zvonko.radosavljevic@gmail.com and divkovic555(@)gmail.com).

Branko Kovačević is with the School of Electrical Engineering, University of Belgrade, 73 Bulevar kralja Aleksandra, 11020 Belgrade, Serbia (e-mail: kovacevic_b@etf.rs ).

 ISBN 978-86-7466-930-3

probability of detection ($P_D$) and clutter density. The clutter density is depending on target dynamics and characteristic of sensor. Generally, clutter is defined by number of selection measurement from size of selection gate. At begin, consider the target state $x_k \in R^{n_z}$ at time interval *k*. The dynamic target trajectory state models at the time *k* are given by the:

$$x_k = Fx_{k-1} + \nu_k \quad (1)$$

where F is the propagation matrix, $\nu_k$ is a zero mean and white Gaussian sequence with covariance *R*. At each scan the sensor returns a random number of random target and clutter measurements. At time *k*, one sensor delivers a set of measurements $z_k = \{z_{k,j}\}_{j=1}^{M_k}$ track out of which a set of measurements are selected for track update. Converted target measurement *y* is given by [10] :

$$y_k = Hx_k + w_k \quad (2)$$

where *H* is measurements matrix and the measurements noise $w_k$ is zero mean and white Gaussian sequence. A measurements of target is present in each scan with a probability of detection $P_D$ . Clutter measurements follow the Poisson distribution characterized at location by clutter measurements density $\rho_k(y)$ [ 11].

At time $k$ a set of $m(k)$ measurements $Y(k) = \{y_i(k)\}_{i=1}^{m(k)}$ are detected, where each measurement either originate from one of *n* known linear measurement models or is a false detection. The sequences $\nu(k)$ are mutually independent and uncorrelated with the process noise.

### A. *Finite Sets statistics*

Finite set statistics is the concept of belief-mass functions, which are non adaptive generalizations of probability mass functions and are equivalent to probability mass function on certain abstract topological spaces. The multi-target state and multi-target measurement at time k are represented as finite subsets $X_k$ and $Z_k$, respectively.

The models of motion of the multi-target system using a randomly varying RFS is given by the [12]:

$$\Gamma_k = \Phi_k[X_{k-1}, V_{k-1}] \cup B_k[X_{k-1}] \quad (3)$$

where $\Phi_k[X_{k-1}]$ represents the dynamics of the existing targets, $X_{k-1}$ is the random set of the state vectors of the random number of targets, and $V_{k-1}$ denotes the system process noise, while $B_k[X_{k-1}]$ represents the process of target birth.

## III. THE GAUSSIAN MIXTURE PHD FILTER ALGORITHM

In this section, we describe the linear-Gaussian multiple target model and the recently developed Gaussian Mixture PHD filter. The multiple target models for the PHD recursion is described here. Each target follows a linear Gaussian dynamical model [13],

$$f_{k|k-1}(x|\xi) = N[x; F_{k-1}(\xi), Q_{k-1}] \quad (4)$$

$$g_k(y|x) = N[y; H_k(x), R_k] \quad (5)$$

where $N(.;m,P)$ denotes a Gaussian density with mean *m* and covariance *P*, $F_{k-1}$ is the state transition matrix, $Q_{k-1}$ is the process noise covariance, $H_k$ is the observation matrix and $R_k$ is the observation noise covariance. The survival $p_{Sk}(x) = p_{S,k}$ and detection $p_{Dk}(x) = p_{D,k}$ probabilities are state independent. The intensities of the spontaneous birth and spawned targets are Gaussian mixtures,

$$\gamma_k(x) = \sum_{i=1}^{J_\gamma(k)} w_{\gamma k}^i N[x; m_{\gamma k}^i, P_{\gamma k}^i] \quad (6)$$

$$\beta_{k|k-1}(x|\varsigma) = \sum_{j=1}^{J_\beta(k)} w_{\beta k}^j N[x; F_{\beta k-1}^j(\varsigma) + d_{\beta k-1}^j Q_{\beta k-1}^j] \quad (7)$$

where $J_{\gamma k}, w_{\gamma k}^i, m_{\gamma k}^i, P_{\gamma k}^i$, $i = 1,..., J_\gamma(k)$ are given model parameters that determine the shape of the birth intensity, similarly, $J_{\beta k}, w_{\beta k}^j, F_{\beta k-1}^j, d_{\beta k-1}^j$ and $Q_{\beta k-1}^j$ $j = 1,..., J_\beta(k)$ determine the shape of the spawning intensity of a target with previous state.

### A. *Algorithm steps*

#### *1 Prediction step*

Under the assumptions that each target follows a linear Gaussian dynamical model, the survival and detection probabilities are constant, the intensities of the birth and spawned targets are Gaussian mixtures, and that the posterior intensity at time *k-1* is a Gaussian mixture of the form [14]

$$D_{k-1|k-1}(x) = \sum_{i=1}^{J(k-1)} w^i{}_{k-1} N[x; m^i{}_{k-1}, P^i{}_{k-1}] \quad (11)$$

Then the predicted intensity to time *k* is also a Gaussian mixture, and is given by

$$D_{k|k-1}(x) = D_{S\,k|k-1}(x) + D_{\beta\,k|k-1}(x) + \gamma_k(x) \quad (12)$$

where $D_{S\,k|k-1}(x)$ is the PHD of existing targets, $D_{\beta\,k|k-1}(x)$ is the PHD for spawned targets, and $\gamma_k(x)$ is the PHD of spontaneous birth targets.

The density for existing targets, $D_{S\,k|k-1}(x)$, is determined from the linear Gaussian model using the Kalman prediction equations,


ISBN 978-86-7466-930-3

$$D_{S\,k|k-1}(x) = p_{S\,k} \sum_{j=1}^{J(k-1)} w^{j}{}_{k-1} N[x; m^{j}_{S\,k|k-1}, P^{j}_{S\,k|k-1}] \quad (13)$$

where

$$m^{j}_{S\,k|k-1} = F_{k-1} m^{j}{}_{k-1} \quad (14)$$

$$P^{j}_{S\,k|k-1} = Q_{k-1} + F_{k-1} P^{j}{}_{k-1} F^{T}{}_{k-1} \quad (15)$$

and similarly for the spawned target density,

$$D_{\beta\,k|k-1}(x) = \sum_{j=1}^{J(k-1)} \sum_{l=1}^{J_{\beta}(k)} w^{j}{}_{k-1} w^{l}_{\beta} N[x; m^{j,l}_{\beta\;k|k-1}, P^{j,l}_{\beta\;k|k-1}] \quad (16)$$

where

$$m^{j,l}_{\beta\;k|k-1} = F^{l}_{\beta\,k-1} m^{j}{}_{k-1} + d^{l}_{\beta\,k-1} \quad (17)$$

$$P^{j,l}_{\beta\;k|k-1} = Q^{l}_{\beta\,k-1} + F^{l}_{\beta\,k-1} P^{j}{}_{k-1} (F^{l}_{\beta\,k-1})^{T} \quad (18)$$

***2 Update step***

Under the above assumptions, and that the predicted intensity to time *t* is a Gaussian mixture of the form [15]

$$D_{k|k-1}(x) = \sum_{i=1}^{J(k|k-1)} w^{i}{}_{k|k-1} N[x; m^{i}{}_{k|k-1}, P^{i}{}_{k|k-1}] \quad (19)$$

Then the posterior intensity at time *k* is also a Gaussian mixture, and is given by

$$D_{k|k}(x) = [1 - p_{D\,k}] D_{k|k-1,}(x) + \sum_{y \in Y^{k}} \sum_{j=1}^{J(k|k-1)} w^{j}{}_{k}(y) \quad N[x; m^{j}{}_{k|k}(y), P^{j}{}_{k|k}] \quad (20)$$

where the weights are calculated according to the closed form PHD update equation,

$$w^{j}{}_{k}(y) = \frac{p_{D\,k} w^{i}{}_{k|k-1} N[y; H_{k} m^{j}{}_{k|k-1}, R_{k} + H_{k} P^{j}{}_{k|k-1} H^{T}{}_{k}]}{K_{k}(y) + p_{D\,k}) \sum_{l=1}^{J(k|k-1)} w^{l}{}_{k|k-1} N[y; H_{k} m^{l}{}_{k|k-1}, R_{k} + H_{k} P^{l}{}_{k|k-1} H^{T}{}_{k}]} \quad (21)$$

and the mean and covariance are updated with the Kalman filter update equations,

$$m^{j}{}_{k|k}(y) = m^{j}{}_{k|k-1}(y) + K^{j}{}_{k}[y - H_{k} m^{j}{}_{k|k-1}(y)] \quad (22)$$

$$P^{j}{}_{k|k} = [I - K^{j}{}_{k} H_{k}] P^{j}{}_{k|k-1} \quad (23)$$

$$K^{j}{}_{k} = P^{j}{}_{k|k-1} H^{T}{}_{k} [H_{k} P^{j}{}_{k|k-1} H^{T}{}_{k} + R_{k}]^{-1} \quad (24)$$

*B. GMPHD practical implementation of algorithm*

At begin, we given weights, mean and covariance of the each track:

$$\{w^{(i)}{}_{k-1}, m^{(i)}{}_{k-1}, P^{(i)}{}_{k-1}\}_{i=1}^{J(k-1)}$$

At each scan we given measurement set $Z(k)$, from the radar sensor .

Step 1: **Prediction for birth targets**

$i = 0.$

***for j=1,…,*** $J_{\gamma}(k)$

***i=i+1.***

$$w^{(i)}{}_{k|k-1} = w^{(j)}_{\gamma\;k},$$

$$m^{(i)}{}_{k|k-1} = m^{(j)}_{\gamma\;k}$$

$$P^{(i)}{}_{k|k-1} = P^{(j)}_{\gamma\;k}$$

***End***

***for j=1,…,*** $J_{\beta}(k)$

***for l=1,…,*** $J(k-1)$

***i=i+1.***

$$w^{(i)}{}_{k|k-1} = w^{(l)}{}_{k-1} w^{(j)}_{\beta\;k}$$

$$m^{(i)}{}_{k|k-1} = d^{(j)}_{\beta\;k-1} + F^{(j)}_{\beta\;k-1} m^{(l)}{}_{k-1}$$

$$P^{(i)}{}_{k|k-1} = Q^{(j)}_{\beta\;k-1} + F^{(j)}_{\beta\;k-1} P^{(l)}{}_{k-1} (F^{(j)}_{\beta\;k-1})^{T}$$

***end***

***end***

Step 2: **Prediction for existing targets**

***for j=1,…,*** $J(k-1)$

***i=i+1.***

$$w^{(i)}{}_{k|k-1} = p_{S\,k} w^{(j)}_{\gamma\;k-1},$$


ISBN 978-86-7466-930-3

$$m^{(i)}_{k|k-1} = F_{k-1} m^{(j)}_{\gamma\ k-1}$$

$$P^{(i)}_{k|k-1} = Q_{k-1} + F_{k-1} P^{(j)}_{k-1} (F_{k-1})^T$$

***end***

$$J(k|k-1) = i$$

Step 3: **Construction of PHD update components**

***for j=1,…,*** $J(k|k-1)$

$$\eta^{(j)}_{k|k-1} = H_k m^{(j)}_{k|k-1}$$

$$S^{(j)}_k = R_k + H_k P^{(j)}_{k|k-1} H^T_k$$

$$K_k = P^{(j)}_{k|k-1} H^T_k [S^{(j)}_k]^{-1}$$

$$P^{(j)}_{k|k} = [I - K^{(j)}_k H_k] P^{(j)}_{k|k-1}$$

***end***

Step 3: **(Update)**

***for j=1,…,*** $J(k|k-1)$

$$w^{(j)}_k = (1 - p_{D,k}) w^{(j)}_{k|k-1},$$

$$m^{(j)}_k = m^{(j)}_{k|k-1},$$

$$P^{(j)}_k = P^{(j)}_{k|k-1}$$

***end***

***l=0.***

***for each*** $y \in Y^k$

***l=l+1,***

***for j=1,…,*** $J(k|k-1)$

$$w^{(lJ(k|k-1)+j)}_k =$$

$$p_{Dk} w^{(j)}_{k|k-1} N(y; \eta^{(j)}_{k|k-1}, S^{(j)}_k)$$

$$m^{[lJ(k|k-1)+j]}_k =$$

$$= m^{(j)}_{k|k-1} + K^{(j)}_k [y - \eta^{(j)}_{k|k-1}]$$

$$P^{[lJ(k|k-1)]}_k = P^{(j)}_{k|k}$$

***End***

$$w^{[lJ(k|k-1)+j]}_k = \frac{w^{[lJ(k|k-1)+j]}_k}{\mathrm{K}^{(y)}_k + \sum_{i=1}^{J(k|k-1)} w^{[lJ(k|k-1)+i]}_k}, \; j = 1,\ldots, J(k|k-1)$$

***end***

$$J(k) = lJ(k|k-1) + J(k|k-1)$$

***Output*** $\{w^{(i)}_k, m^{(i)}_k, P^{(i)}_k\}_{i=1}^{J(k)}$

C. *Output Calculation*

Finally, we can calculate the output state estimate and covariance (for output purpose only):

$$\hat{x}_{k|k} = \sum_{l=1}^{Np} w^l_k x^l_k \tag{25}$$

$$P_k = \left( \sum_{l=1}^{Np} w^l_k \cdot x^l_k \cdot x^{l\,T}_k \right) - \hat{x}_k \cdot \hat{x}^{\,T}_k \tag{26}$$

## IV. RESULTS OF EXPERIMENT

For the purpose of simulations, we propose a two-dimensional scenario (Fig. 1) with an unknown crossing and time varying number of targets in clutter over the region [−500; 500] × [−500; 500]. The state $\boldsymbol{x}_k = [\, x_k\ v_{xk}\ y_k\ v_{yk}\,]^T$, of each target consists of position ($x_k$; $y_k$) and velocity ($v_{xk}$; $v_{yk}$), while the measurement is a noisy version of the position [16].

Each target has survival probability $p_{S;k}$ = 0,9, detection probability $p_{D;k}$=0,99 and follows the linear Gaussian dynamics. Each simulation experiment consists of a number of simulation runs. In each simulation run, targets will repeat their trajectories. The measurements are generated independently. Each algorithm uses the same set of measurements. False tracks may be initiated using target measurements, either in a conjunction with a clutter measurement, or by using measurements from different targets in different scans. The sampling period of radar sensor is *T=1s*. Duration of the scenario is 70 scans. The implemented GM-PHD is evaluated by Monte Carlo (MC) simulations over representative 2-dimensional test scenario. A target motion scenario (Fig.2) includes non-maneuvering flights modes. Dimension of terrain surveillance is x=500m and y=500m.

Transition matrix and process noise matrix are given by:

$$F = \begin{bmatrix} 1 & T & 0 & 0 \\ 0 & 1 & 0 & 0 \\ 0 & 0 & 1 & T \\ 0 & 0 & 0 & 1 \end{bmatrix}, \quad Q_k = q \begin{bmatrix} T^3/3 & T^2/2 & 0 & 0 \\ T^2/2 & T & 0 & 0 \\ 0 & 0 & T^3/3 & T^2/2 \\ 0 & 0 & T^2/2 & T \end{bmatrix} \tag{27}$$

respectively. Measurements matrix and measurements noise matrix is given by:


ISBN 978-86-7466-930-3

$$H = \begin{bmatrix} 1 & 0 & 0 & 0 \\ 0 & 0 & 1 & 0 \end{bmatrix}, \quad R_k = \begin{bmatrix} \sigma_x^2 & 0 \\ 0 & \sigma_y^2 \end{bmatrix} \tag{28}$$

respectively.

For the purpose of performance testing tracking targets, we propose Wasserstein distance diagram.

*A. Wasserstein distance:*

The Wasserstein distance from theoretical statistics was adopted as a means of defining a performance metric for multi target distances which penalizes when the estimate of the number of targets is incorrect. When the number of targets is estimated correctly, the Wasserstein distance is the same as the Hausdor distance but the Hausdor does not penalise for incorrectly estimating the number of targets. This metric has been used for assessing the performance of the PHD filter.

Let $X_t$ and $Y_t$ be the finite sets of target states and estimated target states at time interval *k*.. The $L^P$ Wasserstein distance between the two sets is defined as:

$$d_P^W(X_t, Y_t) = \inf_C \Big( \sum_{x_t \in X_t} \sum_{\hat{x}_j \in \hat{X}_t} C_{ij} d(x_i, \hat{x}_j)^P \Big)^{1/P} \tag{29}$$

where C is an $|X_t| \times |\hat{X}_t|$ matrix $\{C_{ij}\}$ such that $\forall i = 1...|X_t|, j = 1...|\hat{X}_t|$:

$$\sum_{i=1}^{|X_t|} C_{ij} = \frac{1}{|\hat{X}_t|}, \sum C_{ij} = \frac{1}{|X_t|}, C_{ij} \geq 0 \tag{30}$$

The $L^{\infty}$ Wasserstein distance is defined as:

$$d_{\infty}^W(X_t, \hat{X}_t) = \inf_C \max_{xi \in X_t, \hat{x}_j \in \hat{X}_t} C_{ij} d(x_i, \hat{x}_j) \tag{31}$$

Where $\tilde{C}_{ij} = 1$ if $C_{ij} > 0$ and $\tilde{C}_{ij} = 0$ if $C_{ij} = 0$

*B. Two point differencing initializations*

Initialization with the difference of successive observations (Two point differentiation initializing) uses measurements located in the 'window' of the trace from two successive scans to initialize the trace. This procedure is repeated for all measurements from the scan k-1 . Consider such a measurement $z_{k-1,j}$. The new trace is initialized by measurement $z_{k-1,j}$ and each selected measurement $z_{k,i}$, forming a Gaussian probability density function with the mean value given as:

$$\hat{x}_k^{(2)} = \begin{bmatrix} z_{k,i} \\ \dfrac{z_{k,i} - z_{k-1,j}}{\Delta T_k} \end{bmatrix} \tag{32}$$

where $\Delta T_k$ one is the period of rotation of the radar antenna. Since there is no a priori knowledge of the target speed, it can be modeled through a uniform distribution of a priori pdf measurements. At the moment k, the Np particles of the mean value $\hat{x}_k^{(2)}$ are initialized, as well as the symmetric and semi-finite covariance matrices $P_{(2|2)}$ which correspond to the normal distribution of several variables (Figure 1):

$$x_k^p = N[\hat{x}_k^{(2)}; P_{(2|2)}] \tag{33}$$

where the initial covariance error of the condition is calculated under the assumption that there is no process noise [24]:

$$P_{(2|2)} = \begin{bmatrix} R_k & R_k / T \\ R_k / T & 2R_k / T^2 \end{bmatrix} \tag{34}$$

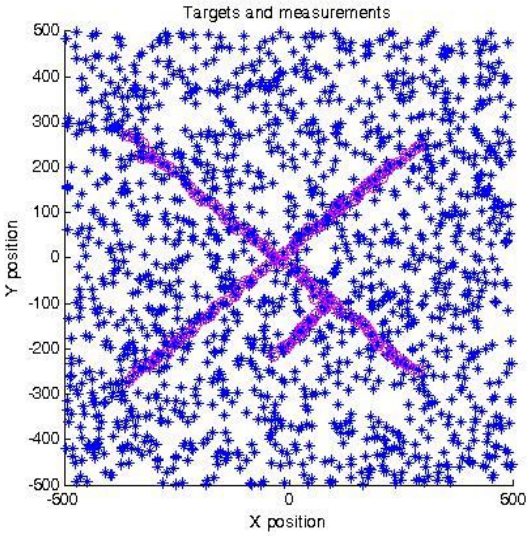


Fig. 1. Simulation scenario: targets and measurements .

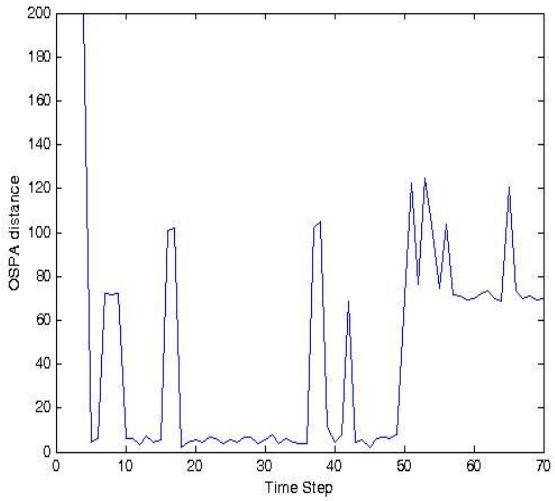


Fig. 2. Wasserstein distance metric (OSPA diagram)

 ISBN 978-86-7466-930-3

Simulation results (OSPA diagram- Fig. 2) show good performance for tracking two crossing targets with one spawned targets, from scan 50 (Fig. 1). Blue dots (measurements) and magenta circle (targets) show good initializing and tracking targets in heavy clutter environments.

## V. CONCLUSION

An improved GM PHD algorithm for radar sensor approaches has been presented for tracking multiple targets in high clutter density which has the ability to estimate the number of targets, track the trajectories of the targets over time, operate with missed detections and give the trajectories of the targets in the past once a target has been identified. It has been shown to outperform the ability to operate in clutter with fewer false tracks and can initiate and eliminate targets more accurately.

Future research should better determine the association of radar received measurements with existing targets as well as automatic initialization of targets. The theoretical constraints of the proposed tracking algorithm have been discussed in the case of crossing targets. It is anticipated that the problem of retaining the correct target identity in this scenario can be resolved by considering the previous trajectories of targets.

Especially, the proposed algorithm will be tested in practice on the example of video tracking [17, 18].

## REFERENCES

[1] S. Blackman, Multiple Target Tracking with Radar Applications. Artech House, Norwood, 1986.

[2] Challa S., Evans R., Morelande M., Mušicki D.: Fundamentals of Object Tracking, Cambridge University Press 2011

[3] R. Mahler, “Multitarget Bayes filtering via first-order multitarget moments,” IEEE Trans. Aerosp. Electron. Syst., vol. 39, no. 4, pp. 1152–1178, Oct. 2003.

[4] O. Erdinc, P. Willet, and Y. Bar-Shalom. Probability Hypothesis Density Filter for Multitarget Multisensor Tracking. Proc. FUSION 2005.

[5] B. Vo and W. K. Ma. The Gaussian Mixture Probability Hypothesis Density Filter. IEEE Transactions on Signal Processing, 2006.

[6] B. Vo, S. Singh, and A. Doucet, “Sequential Monte Carlo methods for multi target filtering with random finite sets,” IEEE Trans. Aerosp. Electron.Syst., vol. 41, no. 4, pp. 1224–1245, Oct. 2005.

[7] D. Clark and J. Bell, “Convergence results for the particle PHD filter,” IEEE Trans. Signal Process., vol. 54, no. 7, pp. 2652–2661, Jul. 2006.

[8] R. Mahler. Multi-target Bayes filtering via first order multi target moments. IEEE Transactions on Aerospace and Electronic Systems, 39, No.4:1152-1178, 2003.

[9] K. Panta, B. Vo, S. Singh, and A. Doucet. Probability hypothesis density filter versus multiple hypothesis tracking. Proceedings of SPIE, Volume 5429 Signal Processing, Sensor Fusion, and Target Recognition XIII, Ivan Kadar, Editor, August 2004, pp. 284-295.

[10] Z. Radosavljević, T.L. Song, B.Kovacevic, Linear Multi-Target IPF Algorithm for Automatic Tracking, Scientific Technical Review, 2016,Vol.66,No.1,pp.3-10, Belgrade 2016.

[11] Z. Radosavljević, D. Mušicki, B. Kovačcević, W. C. Kim, and T. L. Song, Integrated particle filter for target tracking in clutter, IET proceedings on Radar Sonar and Navigation, DOI: 10.1049/iet-rsn.2014.0341 , Print ISSN 1751-8784, May, 2015.

[12] T. L. Song, D. Mušicki, D.S. Kim and Z.Radosavljević, Gaussian mixtures in multi-target tracking: a look at Gaussian mixture probability hypothesis density and integrated track splitting, IET proceedings on Radar Sonar and Navigation, Vol 6, no 5, pp. 359-364, June 2012.

[13] B. Kovačević, Z. Radosavljević and D. Ivković, "The Interacting Multiple Model GM PHD for Single Target Tracking", Proc. of 64. International Conference IcETRAN 2020, Belgrade, September 28.-29., 2020.

[14] Z. Radosavljevic,D. Musicki, B. Kovacevic, W.C. Kim and T. L. Song, ‘Integrated Particle Filter for Target Tracking’, Proceedings of International Conference on Electronics, Information and Communications (ICEIC). Kota Kinabalu, Malesya, Januar 2014.

[15] Z. Radosavljevic, D. Paunovic, D. Ivkovic, D. Nikolic, An Efficient Solid State VHF Band Radar Transimitter,, 6th International Scientific Conference on Defensive Technologies OTEH 2014, Belgrade, 2014.

[16] Z. Radosavljevic, D. Musicki, Limits of target tracking in heavy clutter, ASIA-Pacific International Conference of Synthetic Aperture Radar APSAR 2011, Seoul, Republic of Korea., 2011.

[17] Z. Fu, F. Angelini, J. Chambers, and S. M. Naqvi, “Multi-Level Cooperative Fusion of GM-PHD Filters for Online Multiple Human Tracking,” IEEE trans. Multimedia. (Early Access), Mar. 2019.

[18] N. L. Baisa and A. Wallace, “Development of a n-type GM-PHD filter for multiple target, multiple type visual tracking.” J. Vis. Commun. Image Represent., vol. 59, pp. 257–271, 2019

 ISBN 978-86-7466-930-3

# Four-Stage Recursive Least Squares Algorithm for CARARMA Systems

Nasar Aldian Ambark Shashoa(1), *Senior Member, IEEE*, Ahmed J. Abougarair(2), Abdulhakim Amer Agll(3) and Abdurrezag S. Elmezughi(4)
(1) Department of Electrical and Computer Engineering, Libyan Academy
(2) Department of Electrical and Electronic Engineering, University of Tripoli
(3) Department of Mechanical and Industrial Engineering,University of Tripoli and Embry-Riddle Aeroneutical University Worldwide
(4) Department of Computer Engineering, Azzaytuna University

***Abstract*—this paper derives four -stage recursive least squares parameter estimation algorithm for Controlled Autoregressive Autoregressive Moving Average (CARARMA) systems. By applying the decomposition technique, (CARARMA) system decompose into four subsystems, which contain one parameter vector each. Compared with the recursive generalized least squares algorithm, the proposed algorithm improves the accuracy of estimated parameters and decrease the computational burden. The simulation example is given to indicate the efficiency of the proposed algorithm**.

***Keywords— parameter estimation, decomposition technique,* computational burden, *(Q-Q) plot, estimation error.***

## I. INTRODUCTION

The modeling of manufacturing systems plays a critical function in system analysis and control. System identification is fundamental for structuring the systems mathematical models and parameter estimation is the basis of system identification [1]. In the past decades, researchers have done a lot of research work on parameter estimation methods such as the iterative algorithms, the maximum likelihood methods, the filtering technique, multiple-stage algorithms and so on. Multi-stage least squares identification algorithm is recently employed for parameter estimation of various system models. The main contribution in this technique is to reduce the computational load. The computational load is a significant feature of the recursive algorithms. Low computational load can help the recursive algorithms realize best performances in the systems. The computational efficiency in least squares [2]. The main idea is based on the decomposition technique that can split the main identification system into few small-size subsystems, so as to enhance the computational efficiency and easy to solve. Four-Stage Recursive Least Squares Algorithm is proposed for CARARMA Systems. The decomposition technique is using in this algorithm to reduce the Computational burden. The layout of the rest of this article is arranged as follows.Section 2 derives four-stage recursive identification algorithm. Section 3 presents recursive generalized extended least squares algorithm. Section 4, a illustrative example is given to demonstrate the performance of this algorithm. Finally, the conclusions are offered in section 5.

## II. FOUR-STAGE RECURSIVE IDENTIFICATION ALGORITHM

Consider linear, time-invariant, discrete-time system [3] as shown in fig. 1, described by (CARARMA), which can be expressed as:

$$A(z)y(k) = B(z)u(k) + \frac{D(z)}{C(z)}v(k) \tag{1}$$

where

$\{u(\mathrm{k})\}$ and $\{\mathrm{y(k)}\}$ are the input and output, $\{v(\mathrm{k})\}$ is the white noise sequence with zero mean and unit variance $\sigma^2$ [9] and $\mathrm{A(z)}, \mathrm{B(z)}, \mathrm{C(z)}$and $\mathrm{D(z)}$ are polynomials in the unit backward shift operator z [4].

$$A(z) = 1 + \sum_{i=1}^{n_a} a_i z^{-i}$$

$$B(z) = \sum_{i=1}^{n_b} b_i z^{-i}$$

$$C(z) = 1 + \sum_{i=1}^{n_c} c_i z^{-i}$$

$$D(z) = 1 + \sum_{i=1}^{n_c} d_i z^{-i}$$

The equation (1) can be rewritten as:

$$y(k) = [1 - A(z)]y(k) + B(z)u(k) + w(k) \tag{2}$$

$w(k)$ is defined as

$$w(k) = [1 - C(z)]w(k) + D(z)v(k) \tag{3}$$

 ISBN 978-86-7466-930-3

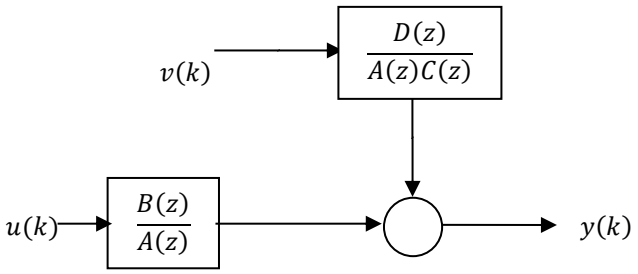


Fig. 1. CARARMA Model.

The parameter vector $\{\theta_1, \theta_2, \theta_3, \theta_4\}$ and the information vectors $\{\varphi_1(k), \varphi_2(k), \varphi_3(k), \varphi_4(k)\}$ are defined as:

$$\theta_1 := [a_1, a_2, \dots, a_{n_a}]^T$$

$$\theta_2 := [b_1, b_2, \dots, b_{n_b}]^T$$

$$\theta_3 = [c_1, c_2, \dots, c_{n_c}]^T$$

$$\theta_4 := [d_1, d, \dots, d_{n_d}]^T$$

$$\varphi_1(k) = [-y(k-1), -y(k-2), \dots, -y(k-n_a)]^T$$

$$\varphi_2(k) = [u(k-1), u(k-2), \dots, u(k-n_b)]^T$$

$$\varphi_3(k) = [-w(k-1), -w(k-2), \dots, -w(k-n_c)]^T$$

$$\varphi_4(k) = [v(k-1), v(k-2), \dots, v(k-n_d)]^T$$

Then,

$$y(\mathrm{k}) = \varphi_1{}^T(k)\theta_1 + \varphi_2{}^T(k)\theta_2 + w(k) \quad (4)$$

$$w(k) = \varphi_3{}^T(k)\theta_3 + \varphi_4{}^T(k)\theta_4 + v(k) \quad (5)$$

Using equation (5), equation (4) can be written as [5].

$$y(k) = \varphi_1{}^T(k)\theta_1 + \varphi_2{}^T(k)\theta_2 + \varphi_3{}^T(k)\theta_3 + \varphi_4{}^T(k)\theta_4 + v(k)$$

$$y(k) = \varphi^T(k)\theta + v(k) \quad (6)$$

$$\varphi^T(k) = [\varphi_1{}^T(k)\ \varphi_2{}^T(k)\ \varphi_3{}^T(k)\ \varphi_4{}^T(k)]$$

$$\theta = [\theta_1\ ; \theta_2; \theta_3; \theta_4]$$

The basic principle in this work is to decomposed the identification system in equation (6) into four subsystems, and the parameters of each subsystem are estimated separately [6].

Define four intermediate output variables:

$$y_1(k) = y(k) - \varphi_2{}^T(k)\theta_2 - \varphi_3{}^T(k)\theta_3 - \varphi_4{}^T(k)\theta_4, \quad (7)$$

$$y_2(k) = y(k) - \varphi_1{}^T(k)\theta_1 - \varphi_3{}^T(k)\theta_3 - \varphi_4{}^T(k)\theta_4, \quad (8)$$

$$y_3(k) = y(k) - \varphi_1{}^T(k)\theta_1 - \varphi_2{}^T(k)\theta_2 - \varphi_4{}^T(k)\theta_4, \quad (9)$$

$$y_4(k) = y(k) - \varphi_1{}^T(k)\theta_1 - \varphi_2{}^T(k)\theta_2 - \varphi_3{}^T(k)\theta_3, \quad (10)$$

This system can be decomposed into the following four subsystems:

$$y_i(k) = \varphi_i^T(k)\theta_i + v(k), \quad i = 1,2,3,4. \quad (11)$$

Define the cost functions:

$$J_i(\theta_i) := \sum_{j=1}^{k} [y_i(j) - \varphi_i{}^T(j)\theta_i]^2, \quad i = 1,2,3,4.$$

Let $\hat{\theta}(k) = [\hat{\theta}_1(k)\ ; \hat{\theta}_2(k); \hat{\theta}_3(k); \hat{\theta}_4(k)]$ be the estimate of $\theta = [\theta_1\ ; \theta_2; \theta_3; \theta_4]$ .Also, let the partial derivatives of $J_i(\theta_i), i = 1,2,3,4$ with respect to $\theta_i$ be zero

$$\frac{\partial J_i(\theta_i)}{\partial \theta_i} = -2\varphi_i(j) \sum_{j=1}^{k} [y_i(j) - \varphi_i{}^T(j)\hat{\theta}_i(k)] = 0 \quad (12)$$

Then, the following RLS algorithm can be obtained:

$$\hat{\theta}_i(k) = \hat{\theta}_i(k-1) + L_i(k)\big[[y_i(k) - \varphi_i{}^T(k)\hat{\theta}_i(k-1)\big] (13)$$

$$L_i(k) = P_i(k-1)\varphi_i(k)[1 + \varphi_i{}^T(k)P_i(k-1)\varphi_i(k)]^{-1},$$

$$P_i(k) = [I - L_i(k)\varphi_i{}^T(k)]P_i(k-1),$$

$$P_i(0) = p_0 I, \ \ i = 1,2,3,4$$

Substituting equations (9, 10, 11and12) into equation (13) [7].

$$\hat{\theta}_1(k) = \hat{\theta}_1(k-1) + L_1(k)\big[y(k) - \varphi_2{}^T(k)\theta_2 - \varphi_3{}^T(k)\theta_3 - \varphi_4{}^T(k)\theta_4 - \varphi_1{}^T(k)\hat{\theta}_1(t-1)\big] \quad (14)$$

$$\hat{\theta}_2(k) = \hat{\theta}_2(k-1) + L_2(k)\big[y(k) - \varphi_1{}^T(k)\theta_1 - \varphi_3{}^T(k)\theta_3 - \varphi_4{}^T(k)\theta_4 - \varphi_2{}^T(k)\hat{\theta}_2(k-1)\big] \quad (15)$$

$$\hat{\theta}_3(k) = \hat{\theta}_3(k-1) + L_3(k)\big[y(k) - \varphi_1{}^T(k)\theta_1 - \varphi_2{}^T(k)\theta_2 - \varphi_4{}^T(k)\theta_4 - \varphi_3{}^T(k)\hat{\theta}_3(k-1)\big] \quad (16)$$

$$\hat{\theta}_4(k) = \hat{\theta}_4(k-1) + L_4(k)\big[y(k) - \varphi_1{}^T(k)\theta_1 - \varphi_2{}^T(k)\theta_2 - \varphi_3{}^T(k)\theta_3 - \varphi_4{}^T(k)\hat{\theta}_4(k-1)\big] \quad (17)$$

Although the all RLS sub-algorithms are derived for calculating $\hat{\theta}_1(k), \hat{\theta}_2(k), \hat{\theta}_3(k)\ and\ \hat{\theta}_4(k)$ . They are unattainable to be completed, because the right-hand sides all RLS sub-algorithms include the unknown parameters$\theta_1, \theta_2, \theta_3\ and\ \theta_4$. In order to handles this issue; the parameters $\theta_i\ \ i = 1,2,3,4$ are replaced with $\hat{\theta}_i(k-1)$ [8].

Then, $\hat{\theta}_1(k), \hat{\theta}_2(k), \hat{\theta}_3(k)\ and\ \hat{\theta}_4(k)$ can be calculated by

$$\hat{\theta}_1(k) = \hat{\theta}_1(k-1) + L_1(k)\ \big[y(k) - \varphi_2{}^T(k)\hat{\theta}_2(k-1) - \varphi_3{}^T(k)\hat{\theta}_3(k-1) - \varphi_4{}^T(k)\hat{\theta}_4(k-1) - \varphi_1{}^T(k)\hat{\theta}_1(k-1)\big]$$

$$= \hat{\theta}_1(k-1) + L_1(k)\big[y(k) - \varphi^T(k)\hat{\theta}(k-1)\big] \quad (18)$$

$$\hat{\theta}_2(k) = \hat{\theta}_2(k-1) + L_2(k)\big[y(k) - \varphi_1{}^T(k)\hat{\theta}_1(k-1) - \varphi_3{}^T(k)\hat{\theta}_3(k-1) - \varphi_4{}^T(k)\hat{\theta}_4(k-1) - \varphi_2{}^T(k)\hat{\theta}_2(k-1)\big]$$

 ISBN 978-86-7466-930-3

$$= \hat{\theta}_2(k-1) + L_2(k)\left[y(k) - \varphi^T(k)\hat{\theta}(k-1)\right] \quad (19)$$

$$\hat{\theta}_3(k) = \hat{\theta}_3(k-1) + L_3(k)\left[y(k) - {\varphi_1}^T(k)\hat{\theta}_1(k-1) - {\varphi_2}^T(k)\hat{\theta}_2(k-1) - {\varphi_4}^T(k)\hat{\theta}_4(k-1) - {\varphi_3}^T(k)\hat{\theta}_3(k-1)\right],$$

$$= \hat{\theta}_3(k-1) + L_3(k)\left[y(k) - \varphi^T(k)\hat{\theta}(k-1)\right] \quad (20)$$

$$\hat{\theta}_4(k) = \hat{\theta}_4(k-1) + L_4(k)\left[y(k) - {\varphi_1}^T(k)\hat{\theta}_1(k-1) - {\varphi_2}^T(k)\hat{\theta}_2(k-1) - {\varphi_3}^T(k)\hat{\theta}_3(k-1) - {\varphi_4}^T(k)\hat{\theta}_4(k-1)\right]$$

$$= \hat{\theta}_4(k-1) + L_4(k)\left[y(k) - \varphi^T(k)\hat{\theta}(k-1)\right] \quad (21)$$

Notice that the right-hand sides of equations (18)–(21) include the unknown information vectors $\varphi_3(k)$ which contains the unknown inner variables $w(k-i)$ and $\varphi_4(k)$ which contains unknown inner variables $v(k-i)$, so that, this algorithm cannot be performed [9]. Replacing $w(k-i)$ and$v(k-i)$ with their estimates $\hat{w}(k-i)$ and $\hat{v}(\mathrm{k-i})$, and $\hat{\varphi}_3(k), \hat{\varphi}_4(k)$ are written as

$$\hat{\varphi}_3(k) = [-\hat{w}(k-1), -\hat{w}(k-2), \dots, -\hat{w}(k-n_c)]^T \quad (22)$$

$$\hat{\varphi}_4(k) = [\hat{v}(k-1), \hat{v}(\mathrm{k-2}), \dots, \hat{v}(\mathrm{k-n_d})]^T \quad (23)$$

$$\hat{\varphi}(k) = [\varphi_1, \varphi_2, \hat{\varphi}_3, \hat{\varphi}_4]^T$$

Where,

$$\hat{w}(k) = y(k) - {\varphi_1}^T(k)\hat{\theta}_1 - {\varphi_2}^T(k)\hat{\theta}_2 \quad (24)$$

$$\hat{v}(k) = \hat{w}(k) - {\hat{\varphi}_3}^T(k)\hat{\theta}_3 - {\hat{\varphi}_4}^T(k)\hat{\theta}_4 \quad (25)$$

Thus, Four-Stage Recursive Least Squares Algorithm for CARARMA Systems is summarize as:

$$\hat{\theta}_1(k) = \hat{\theta}_1(k-1) + L_1(k)\left[y(k) - \hat{\varphi}^T(k)\hat{\theta}(k1)\right] \quad (26)$$

$$L_1(k) = P_1(k-1)\varphi_1(k)[1 + {\varphi_1}^T(k)P_1(k-1)\varphi_1(k)]^{-1} \quad (27)$$

$$P_1(k) = [I - L_1(k){\varphi_1}^T(k)]P_1(k-1) \quad (28)$$

$$\varphi_1(k) = [-y(k-1), -y(k-2), \dots, -y(k-n_a)]^T \quad (29)$$

$$\hat{\theta}_2(k) = \hat{\theta}_2(k-1) + L_2(k)\left[y(k) - \hat{\varphi}^T(k)\hat{\theta}(k-1)\right] \quad (30)$$

$$L_2(k) = P_2(k-1)\varphi_2(k)[1 + {\varphi_2}^T(k)P_2(k-1)\varphi_2(k)]^{-1} \quad (31)$$

$$P_2(k) = [I - L_2(k){\varphi_2}^T(k)]P_2(k-1) \quad (32)$$

$$\varphi_2(k) = [u_1(k-1), u_1(k-2), \dots, u_1(k-n_1)]^T \quad (33)$$

$$\hat{\theta}_3(k) = \hat{\theta}_3(k-1) + L_3(k)\left[y(k) - \hat{\varphi}^{\mathrm{T}}(k)\hat{\theta}(k-1)\right] \quad (34)$$

$$L_3(k) = P_3(k-1)\hat{\varphi}_3(k)\left[1 + {\hat{\varphi}_3}^T(k)P_3(k-1)\hat{\varphi}_3(k)\right]^{-1} \quad (35)$$

$$P_3(k) = \left[I - L_3(k){\hat{\varphi}_3}^T(k)\right]P_3(k-1) \quad (36)$$

$$\hat{\varphi}_3(k) = [-\hat{w}(k-1), -\hat{w}(k-2), \dots, -\hat{w}(k-n_c)]^T \quad (37)$$

$$\hat{\theta}_4(k) = \hat{\theta}_4(k-1) + L_4(k)\left[y(k) - \hat{\varphi}^T(k)\hat{\theta}(k-1)\right] \quad (38)$$

$$L_4(k) = P_4(k-1)\hat{\varphi}_4(k)\left[1 + {\hat{\varphi}_4}^T(k)P_4(k-1)\hat{\varphi}_4(k)\right]^{-1} \quad (39)$$

$$P_4(k) = \left[I - L_4(k){\hat{\varphi}_4}^T(k)\right]P_4(k-1) \quad (40)$$

$$\hat{\varphi}_4(k) = [\,\hat{v}(k-1), \hat{v}(\mathrm{k-2}), \dots, \hat{v}(\mathrm{k-n_d})]^T \quad (41)$$

## III. The Recursive Generalized Least Squares Algorithm

In order to demonstrate the features of the Four-Stage -RLS algorithm, the following discuss recursive generalized extended least squares (RGELS) algorithm [10]. As we all know, (RGELS) algorithm can identify CARARMA Systems. The main issue is to replace $w(k-i)$ and $v(k-i)$ with their estimates in the information vector. Finally, (RGLS) algorithm can obtained and the estimated parameter vectors of CARARMA model can be calculated as [11].

$$\hat{\theta}(k) = \hat{\theta}\,(k-1) - L(k)\,[y(k) - \hat{\varphi}\,(k)^T\,\hat{\theta}(k-1)] \quad (42)$$

$$L(k) = \frac{P(k-1)\hat{\varphi}\,(t)}{1 + \hat{\varphi}^T(k)P(k-1)\hat{\varphi}\,(k)} \quad (43)$$

$$P(k) = [I - L(k)\hat{\varphi}^T(k)]\,P(k-1). \quad (44)$$

$$\hat{\varphi}(k) = [\varphi_s(k)\ \ \varphi_n(k)]^T,\ \hat{\theta}(k) = [\hat{\theta}_s(k)\,;\hat{\theta}_n(k)] \quad (45)$$

$${\varphi_{\mathrm{s}}}^T(k) = [-y(k-1), -y(k-2), \dots, -y(k-\ na), u(k\ -1), u(k-2), \dots, u(k-n_b)] \quad (46)$$

$${\varphi_{\mathrm{n}}}^T(k) = [-w(k-1), -w(k-2), \dots, -w(k-\ n_c), v(k\ -1), v(k-2), \dots, v(k-n_d)] \quad (47)$$

$$\hat{w}(k) = y(k) - {\varphi_{\mathrm{s}}}^T(k).\,\hat{\theta}_s(k) \quad (48)$$

$$\hat{v}\,(k) = y(k) - \hat{\varphi}^T(k)\hat{\theta}(k) \quad (49)$$

$$\hat{\theta}_s(k) = \left[\hat{a}_1(k), \hat{a}_2(k), \dots, \hat{a}_{n_a}(k), \hat{b}_1(k), \hat{b}_1(k), \dots, \hat{b}_{nb}(k)\right] \quad (50)$$

$$\hat{\theta}_n(k) = \left[\hat{c}_1(k), \hat{c}_2(k), \dots, \hat{c}_{n_c}(k), \hat{d}_1(k), \hat{d}_1(k), \dots, \hat{d}_{nd}(k)\right] \quad (51)$$

## IV. Simulation Results

The effectiveness of Four-Stage -RLS algorithm has been checked on samples generated by the following (CARARMA) model:

$$\mathrm{A}(z)y(k) = B(z)u(k) + \frac{D(z)}{C(z)}v(k)$$

$$A(z) = 1 + 0.72z^{-1} + 0.81z^{-2}$$

$$B(z) = 0.22z^{-1} + 0.33z^{-2}$$

$$C(z) = 1 + 0.65z^{-1}$$

$$D(z) = 1 + 0.55z^{-1}$$

 ISBN 978-86-7466-930-3

$$\theta = [a_1, a_2, b_1, b_2, c_1, d_1]^T,$$

$$= [0.72, 0.81, 0.22, 0.33, 0.65, 0.55]^T,$$

The input $u(k)$ adopts a persistent excitation sequence with $m = 0$ and $\sigma = 1$, while $v(k)$ is a white noise sequence with $m = 0$ and $\sigma = 0.3^2$.
Quantile-quantile (Q-Q) plot and estimation error have been used in order to evaluate the performance of the proposed algorithm.

### *A. Quantile-quantile (Q-Q) plot*

Quantile-quantile (Q-Q) plot is a diagnostic tool, which is widely used to assess the distributional similarities and differences between two independent univariate samples. It is also used to determine how well a specified probability distribution fits a given sample [12].

The following steps create a Quantile-Quantile-plot (Q-Q-plot)

**1.** Rank your data in ascending order: $x_1, \ldots\ldots, x_n$

**2.** For each data point $x_i$ compute the empirical percentiles $\rho_i$ of data points smaller than or equal to $x_i$ ,i.e

$$\rho_i = \frac{i}{n}$$

**3.** Define a theoretical matching normal distribution as the normal distribution with the same mean and variance as the sample.

**4.** For each percentile $\rho_i$ find the corresponding quantile $y_i$ in the theoretical normal distribution.

**5.** Plot $y_i$ against $x_i$

**6.** If $x_i = y_i$ for all $i$ we get a straight line indicating that $x_i$'s are normally distributed [13].

### *B. The estimation error*

The estimation error is determined as [14].

where

$$\delta = \sqrt{\frac{\|\hat{\theta}_1 - \theta_1\|^2 + \|\hat{\theta}_2 - \theta_2\|^2 + \|\hat{\theta}_3 - \theta_3\|^2 + \|\hat{\theta}_4 - \theta_4\|^2}{\|\theta_1\|^2 + \|\theta_2\|^2 + \|\theta_3\|^2 + \|\theta_4\|^2}} \qquad (40)$$

As it's known, when the parameter estimation errors become smaller with the sequences increasing, the accuracy of the estimated parameters is increased.

Four-Stage -RLS algorithm and (RGELS) algorithm have been applied to estimate the parameters of the system and the estimation errors for these algorithms versus sequences (k) are shown in Fig. 2.

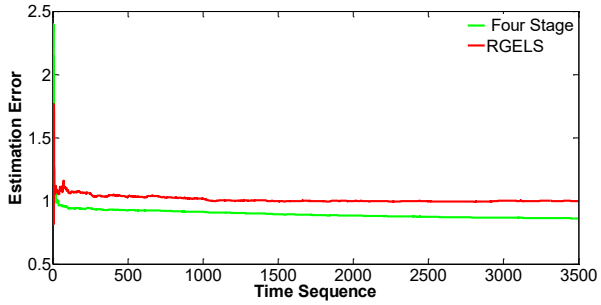


Fig. 2. Four-Stage -RLS and (RGELS) estimation errors versus *k*

The figure demonstrates that Four-Stage -RLS algorithm can achieved more accurate estimates than the (RGELS) algorithm.
Fig. 3 shows Q-Q plots for a residuals generation of Four-Stage -RLS algorithm (blue color) and (RGELS) algorithm (red color) which are tested in comparison with the standard normal distribution (black color) to determine the extent of the quantiles match.

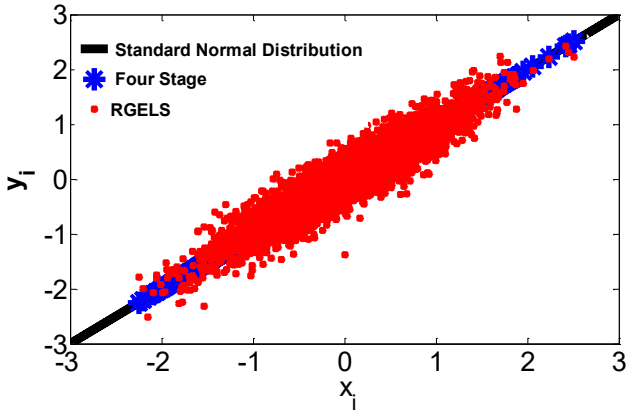


Fig. 3 Q-Q plots for a residuals generation of Four-Stage -RLS algorithm " blue color" and (RGELS) algorithm" red color".

The figure offers that, the result of the Four-Stage -RLS algorithm matches more closely along standard normal distribution than the result of the (RGELS) algorithm. This result indicates that the proposed algorithm is more effective than (RGELS) algorithm.

The estimated output and the true output of Four-Stage -RLS algorithm are plotted in Fig. 4.

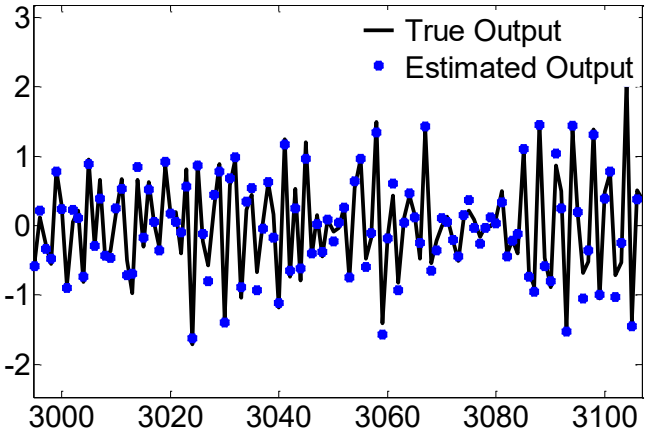


Fig. 4 The estimated output and the true output of Four-Stage -RLS algorithm


ISBN 978-86-7466-930-3

The figure illustrate that estimated output is close to the true output, which means the estimated model can fit the validation data well [10].

## V. CONCLUSIONS

In this paper, Four-Stage recursive identification algorithm is derived. Through a simulation results, it is shown that the proposed algorithm has some advantages, in comparison with (RGLES) algorithm. Four-Stage -RLS improves the accuracy for estimated parameters, and has higher computational efficiency than (RGLES) algorithm. The proposed technique in this article can be extended to study the parameter estimation algorithm of (MISO) and (MIMO) systems with colored noise.

## REFERENCES

[1] Y. Ji and Z. Kang "Three-stage forgetting factor stochastic gradient parameter estimation methods for a class of nonlinear systems," Int J Robust Nonlinear Control, 2020.

[2] M. Junxia, C.Jing, D. Feng"Filtering Based Multi-Stage Recursive Least Squares Parameter Estimation Algorithm for Input Nonlinear Output-Error Autoregressive Systems," 35th Chinese Control Conference, July 27-29, 2016, Chengdu, China.

[3] F. Fraccaroli, A. Peruffo, and M. Zorzi, "A New Recursive Least-Squares Method with Multiple Forgetting Schemes," arXiv, pp.1503.07338v1 [math.OC], 2015.

[4] F.Ding, YanjiaoWang and J.Ding "Recursive least squares parameter identification algorithms for systems with colored noise using the filtering technique and the auxilary model," Digital Signal Processing, 2014.

[5] W. Wang, F. Ding and J.Dai "Maximum likelihood least squares identification for systems with autoregressive moving average noise," Applied Mathematical Modelling, pp.1842–1853, 2012.

[6] M. A. Arwin and N. A. Shashoa, " Extended Three-Stage Recursive Least Squares Identification Algorithm for multiple-input single-output CARARMA Systems," 2021 IEEE International IOT, Electronics and Mechatronics Conference (IEMTRONICS). Canada, April, 2021.

[7] Y. Guo, L. Wan, L. Xu, F. Ding, A. Alsaedi, and T. Hayat " Two-stage Recursive Least Squares Parameter Estimation Algorithm for Multivariate Output-error Autoregressive Moving Average Systems," International Journal of Control, Automation and Systems. pp. 1547-1557, 2019.

[8] H. Xu1, F. Ding, M.Gan and E Yang "Two-stage recursive identification algorithms for a class of nonlinear time series models with colored noise," Int J Robust Nonlinear Control, 2020.

[9] H. Duan, J. Jia, M.Gan and R. Ding "Two-stage recursive least squares parameter estimation algorithm for output error models," Mathematical and Computer Modelling, 2011.

[10] F. Chen and F. Ding, "Recursive Least Squares Identification Algorithm for Multiple-Input Nonlinear Box-Jenkins Systems Using Maximum Likelihood Principle", Journal of Computational and Nonlinear Dynamics Vol. 11, 2016.

[11] D. Meng and F. Ding, "Model Equivalence-Based Identification Algorithm for Equation-Error Systems with Colored Noise", Algorithms. pp. 280-291, 2015.

[12] S. Dhar, P. Chaudhuri and B. Chakraborty, Multivariate quantile-quantile plots and related tests using spatial quantiles.Theoretical Statistics and Mathematics Unit, Indian Statistical Institute,Calcuttaand School of Mathematics, University of Birmingham.

[13] H. Støvring, Q-Q plots, Biostatistics Department of Public Health, Aarhus University, spring 2010.

[14] B.Baoa, Y. Xua, J. Shengb and R. Ding"Least squares based iterative parameter estimation algorithm for multivariable controlled ARMA system modelling with finite measurement data," Mathematical and Computer Modelling, 2011.

 ISBN 978-86-7466-930-3

# Consensus on the Auxiliary Variables in Distributed Gradient-Based Temporal Difference Algorithms

Miloš S. Stanković, Marko Beko, Nemanja Ilić and Srdjan S. Stanković

***Abstract*—In this paper we discuss important properties of two novel distributed algorithms for iterative multi-agent off-policy learning of linear value function approximation in Markov Decision Processes (MDP). The algorithms are derived using the off-policy Gradient Reinforcement Learning (GRL) methodology, together with linear dynamic consensus iterations over an underlying inter-agent communication network represented by directed graphs. The proposed algorithms are entirely decentralized, offering new possibilities for choosing different behavior policies while evaluating one single target policy. The presented algorithms formally differ only in the way of applying consensus iterations to the so-called auxiliary variables. The presented proof of weak convergence of both algorithms represents a firm basis for deriving relevant conclusions concerning the role of the consensus iterations. It is shown that the algorithm utilizing consensus on the auxiliary variables shows slightly inferior asymptotic properties, but can provide a higher convergence rate. The figure of merit of each of the algorithms is presented and discussed using the theoretical results obtained under generally nonrestrictive assumptions.**

## I. Introduction

Decentralized multi-agent decision making algorithms have recently gained much popularity due to their high effectiveness in dealing with uncertain and dynamic environments typical for the emerging areas of Cyber-Physical Systems (CPS) and Internet of Things (IoT). Numerous distributed estimation, optimization and adaptation methods have been successfully developed using recursive collaborations aimed at achieving a consensus on variables of interest (e.g. [1]–[15] and references therein).

Reinforcement learning (RL) is a general methodology for decision making in uncertain environments based on models in the form of Markov Decision Process (MDP) based on utilization of approximate dynamic programming [16], [17]. A very important issue in this domain is the problem of approximation of the value function under very large state space and the presence of a discrepancy between the behavior policy of an agent and a policy that is currently targeted for evaluation (off-policy learning, e.g. [18]). Recently, in [19]–[22] several fast gradient-based algorithms for temporal-difference (TD) learning have been proposed. Distributed and multi-agent RL methods have become very popular very recently (see, e.g. [1], [23]–[25] and references therein). Different setups have been adopted in a number of recent works [26]–[32].

In this paper we shall present and discuss two distributed algorithms for *iterative multi-agent off-policy learning* of linear approximation of the value function in MDPs [1]. The algorithms represent generalizations of the recently proposed single agent off-policy gradient algorithm GTD2($\lambda$) [1], [19]–[21], incorporating a distributed consensus scheme operating over a network of typically sparsely connected agents. Another important property of the algorithms is that the local recursions of each agent can be based on eligibility traces [20], [21], where each agent may choose different $\lambda$ parameters. We provide a firm theoretical background in the form of a proof that the parameter estimates *weakly converge* to consensus points [1], [19], [28], [29], [31], [33], under nonrestrictive connectivity assumption on the topology of the underlying digraph and on the state-visiting distributions of the agents (their behavior policies). The main focus of this paper is placed on the dilemma whether or not to apply consensus to the *auxiliary variables* in the DGTD2($\lambda$)-type algorithms with one-time-scale (see [19], [28], [31]). Notice that the paper [33] deals with the basically two-time-scale algorithms of DGTDC($\lambda$)-type. The given analysis will be exclusively concerned with the limit points of the mean asymptotic ODEs: in this sense the behavior of the estimates for large, but finite $t$, including the derivation of the corresponding ODEs, can be found in [1], [33]. The limit sets are analyzed by formulating appropriate Lyapunov functions, following the line of thought of [21]. A discussion on role of convexification of the auxiliary variables is provided apart, showing that the two algorithms converge to the same limit points only in special cases. Application of consensus to the auxiliary variables causes, in principle, inferior asymptotic performance, having in mind that the implicitly imposed constraint increases the achievable estimation error. On the other hand, introduction of consensus can contribute to the overall convergence rate at the global level; however, the global convergence rate depends largely on the network connectivity.

The paper is organized as follows. In Section II we formulate the problem and define the algorithms. In Section III a rigorous weak convergence analysis is presented focused on the limit points, while Section IV is devoted to a general discussion on the application of consensus to the auxiliary variables in the DGTD2($\lambda$) algorithms.

M. S. Stanković is with Singidunum University, Belgrade, Serbia; and Vlatacom Institute, Belgrade, Serbia; e-mail: milstank@gmail.com.

M. Beko is with Instituto de Telecomunicações, Instituto Superior Técnico, Universidade de Lisboa, Lisbon, Portugal; and Faculty of Information Technology and Engineering, University Union Nikola Tesla, Belgrade, Serbia; e-mail: beko.marko@gmail.com.

N. Ilić is with College of Applied Technical Sciences, Kruševac, Serbia; and Vlatacom Institute, Belgrade, Serbia; e-mail: nemiliexp@yahoo.com.

S. S. Stanković is with School of Electrical Engineering, University of Belgrade, Serbia; e-mail: stankovic@etf.rs.

This research was supported by the Science Fund of the Republic of Serbia, Grant #6524745, AI-DECIDE.

 ISBN 978-86-7466-930-3

## II. Distributed Gradient Temporal Difference Algorithms

### A. Problem Formulation. Definition of the Algorithm

Consider *N autonomous agents* learning linear approximation to the *state value function* for a given policy in an MDP (denoted as $\mathrm{MDP}^{(0)}$), using observations of sample transitions in additional $N$ *independent* MDPs, denoted as $\mathrm{MDP}^{(i)}$, $i = 1, \ldots, N$. Assume a finite state space $\mathcal{S} = \{1, \ldots, M\}$, and that $\mathrm{MDP}^{(0)}$ has the transition matrix $P$, and $\mathrm{MDP}^{(i)}$ the transition matrices $P^{(i)}$, $i = 1, \ldots, N$; these chains are induced by $\pi$ and $\pi^{(i)}$, and referred to as the *target policy* and *behavior policies*, respectively. We are, therefore, dealing with a *cooperative off-policy learning* problem [1], [16], [18], [31].

We introduce the one-stage *reward function* $r_\pi : \mathcal{S} \to \mathcal{R}$, specifying the expected reward at each state $s \in \mathcal{S}$, where $\mathcal{R}$ is the set of real numbers [16], [21]. The associated discounted *total reward criterion* (*value function*), with the state dependent discount factors $\gamma(s) \in [0, 1]$, $s \in \mathcal{S}$, is given by

$$v_\pi(s) = E_s^\pi\{r_\pi(S_0) + \sum_{n=1}^{\infty} \gamma(S_1)\gamma(S_2)\cdots\gamma(S_n) \cdot r_\pi(S_n)\}, \tag{1}$$

where $E_s^\pi\{\cdot\}$ indicates the expectation w.r.t. to the Markov chain $\{S_n\}_{n>0}$ induced by $\pi$, with the initial state $S_0 = s$. Denote by $\Gamma$ the $M \times M$ diagonal matrix with $\gamma(s)$ as diagonal entries and $v_\pi = [v_\pi(s_1) \cdots v_\pi(s_M)]^T$.

We assume the following [21]:

(A1) a) $P$ is such that $I - P\Gamma$ is nonsingular; b) $P^{(i)}$ is irreducible and for all $s, s' \in \mathcal{S}$ $P_{ss'}^{(i)} = 0 \Rightarrow P_{ss'} = 0$, $i = 1, \ldots, N$.

By the MDP theory [1], [16], [21], [34], $v_\pi$ uniquely satisfies the *Bellman equation* $v_\pi = r_\pi + P\Gamma v_\pi$ (see e.g. [21], [34]). Within the framework of the *temporal-difference* (TD) algorithms, it is usual to consider the Bellman equation depending on the so-called *λ-parameters*, procedurally introduced by the so-called *eligibility traces*. In this sense, $v_\pi = T^{(\lambda)}v_\pi$ is considered as a *generalized Bellman equation*, where $T^{(\lambda)}v = r_\pi^\lambda + P^{(\lambda)}v$, $\forall v \in R^{|S|}$, is the *generalized Bellman operator* for a vector $r_\pi^{(\lambda)}$ and a substochastic matrix $P^{(\lambda)}$ [16], [21].

Let $\phi : S \to R^p$ be a function that maps each state to a $p$-dimensional feature vector $\phi = [\phi_1 \cdots \phi_p]^T$; let the subspace spanned by feature vectors $\phi$ be $\mathcal{L}_\phi$. In general, TD algorithms look for some function $v \in \mathcal{L}_\phi$ that satisfies $v \approx T^{(\lambda)}v$. We assume that the approximation functions are parameterized as $v(s) = \phi(s)^T\theta$, $s \in \mathcal{S}$ using parameters $\theta \in \mathcal{R}^p$, so that the algorithms learn the vector $\theta$. If we define the $M \times p$ matrix $\Phi$ as a matrix composed of p-vectors $\phi(s)$ as row vectors, we have $v_\theta = \Phi\theta$.

In order to construct a distributed algorithm for finding an approximation function $v_\theta \in \mathcal{L}_\phi$ by using observations from $\mathrm{MDP}^{(i)}$, $i = 1, \ldots, N$, we define the following *global objective function*

$$J(\theta) = \sum_{i=1}^{N} q_i J_i(\theta) = \frac{1}{2}\sum_{i=1}^{N} q_i \|\Pi_{\xi_i}(T^{(\lambda_i)}v_\theta - v_\theta)\|_{\xi_i}^2, \tag{2}$$

where $J_i(\theta)$ are the *local objective functions*, $q_i > 0$ the *a priori* defined weighting coefficients, $\lambda_i$ is the local $\lambda$-parameter and $\Pi_{\xi_i}$ denotes the projection onto the subspace $\mathcal{L}_\phi$ w.r.t. the weighted Euclidean norm $\|v\|_{\xi_i}^2 = \sum_{s\in\mathcal{S}} \xi_{i;s} v(s)^2$ for a positive $M$-dimensional vector $\xi_i$ with components $\xi_{i;s}$ (see [21], [31]). In accordance with [21], [34], we take $\xi_i$ to be the invariant probability distribution for the local Markov chain $\mathrm{MDP}^{(i)}$, with the transition matrix $P^{(i)}$ induced by $\pi^{(i)}$ ($\xi_i^T P^{(i)} = \xi_i^T$). It follows that

$$\nabla J(\theta) = \sum_{i=1}^{N} q_i(\Phi^T\Xi_i(P^{(\lambda_i)} - I)\Phi)^T w_i(\theta), \tag{3}$$

where $\Xi_i$ is an $M \times M$ diagonal matrix with the components of $\xi_i$ on the diagonal, and $w_i(\theta)$ the unique solution (in $w_i$) of the equation

$$\Phi w_i = \Pi_{\xi_i}(T^{(\lambda_i)}v_\theta - v_\theta), \tag{4}$$

assuming that $w_i \in \mathrm{span}\{\phi(S)\}$.

In the off-policy scenario, we introduce the local *importance sampling ratios* $\rho_i(s, s') = P_{ss'}^i / P_{ss'}$ for $s, s' \in \mathcal{S}$, $i = 1, \ldots, N$; denote $\rho_i(n) = \rho_i(S_n, S_{n+1})$, as well as $\gamma(n) = \gamma(S_n)$ [21], [34]. The local *temporal-difference term* is defined by

$$\delta_i(v_\theta; n) = \rho_i(n)(R(n+1) + \gamma(n+1)v_\theta(S_{n+1}) - v_\theta(S_n)). \tag{5}$$

The local *eligibility trace vectors* $\{e_i(n)\}$ are generated by

$$e_i(n) = \lambda_i(n)\gamma(n)\rho_i(n-1)e_i(n-1) + \phi(S_n), \tag{6}$$

where $\lambda_i(n) \in [0, 1]$ are the local *λ-parameters*, $i = 1, \ldots, N$ [21], [34].

The distributed algorithms for learning linear approximation to the state value function for a given policy $\pi$ we are going to analyze consist of two main parts: 1) *local parameter updates* based on the *gradient descent* methodology using local state transition observations from $\mathrm{MDP}^{(i)}$, and 2) interchange of the current parameter estimates aimed at achieving *consensus* between the agents. The local parameter updates are defined by

$$\begin{aligned}\theta_i'(n) =& \theta_i(n) + \alpha_i(n)q_i\rho_i(n)(\phi(S_n) \\ &- \gamma(n+1)\phi(S_{n+1}))e_i(n)^T w_i(n)\end{aligned} \tag{7}$$

$$\begin{aligned}w_i'(n) =& w_i(n) + \beta_i(n)(e_i(n)\delta_i(v_{\theta_i(n)}; n) \\ &- \phi(S_n)\phi(S_n)^T w_i(n))\end{aligned} \tag{8}$$

where $v_{\theta_i(n)} = \Phi\theta_i(n)$; $\theta_i(0)$ is chosen arbitrarily, while for $w_i(0)$ and $e_i(0)$ we have $w_i(0)$, $e_i(0) \in \mathrm{span}\{\phi(S)\}$ [21]. Notice that the algorithm incorporates the *auxiliary variables* $w_i(n)$ and $w_i'(n)$; their role is essential for this paper [19], [21].

The second, communication part of the algorithm performs the following convexification w.r.t. the approximation parameter $\theta$, leaving local auxiliary parameters unchanged, *i.e.*,

$$\theta_i(n+1) = \sum_{j=1}^{N} a_{ij}(n)\theta_j'(n), \qquad w_i(n+1) = w_i'(n), \tag{9}$$

where $a_{ij}(n)$ are random variables, elements of a random matrix $A(n) = [a_{ij}(n)]$ [11], [31], [35]. If one adopts that the

 ISBN 978-86-7466-930-3

available $N$ MDP's are connected by communication links in accordance with a directed graph $\mathcal{G} = (\mathcal{N}, \mathcal{E})$, where $\mathcal{N}$ is the set of nodes and $\mathcal{E}$ the set of arcs, then matrix $A(n)$ has zeros at the same places as the graph adjacency matrix $A_G$ and is *row-stochastic, i.e.*, $\sum_{j=1}^{N} a_{ij}(n) = 1$, $i = 1, \ldots, N$, $\forall n \geq 0$. The algorithm (7), (8) incorporating consensus only w.r.t. $\theta$ according to (9) will be denoted as AlgA.

We also consider a modification of AlgA, denoted as AlgB, obtained by applying convexification to both $\theta_i$ and $w_i$, $i = 1, \ldots, N$, in such a way that the second relation in (9) becomes

$$w_i(n+1) = \sum_{j=1}^{N} a_{ij}(n) w'_j(n). \tag{10}$$

A comparative analysis of AlgA and AlgB is in the main focus of this paper.

## III. Convergence Analysis

### A. Prerequisites

*1) Choice of $\lambda$-parameters:* The results given below are applicable to both *state-dependent* and *history-dependent* $\lambda_i$. In the first case, we have simply $\lambda_i(n) = \lambda_i(S_n)$ for a given function $\lambda_i : \mathcal{S} \to [0, 1]$, while in the second case $\lambda_i(n) = \lambda(y_i(n), e_i(n-1))$, $y_i(n) = f(y_i(n-1), S_n)$, where $y(n)$, $n \geq 0$, is a memory state summarizing the history of the past states up to time $n$ (see [21], [34]).

Different choices of $\lambda_i$ lead to different generalized Bellman operators. For example, in the case of state-dependent $\lambda_i$, we have:

$$T^{(\lambda_i)} v = (I - P\Gamma\Lambda_i)^{-1} r_\pi + (I - P\Gamma\Lambda_i)^{-1} P\Gamma(I - \Lambda_i)v, \tag{11}$$

where $\Lambda_i$ is an $M \times M$ diagonal matrix with entries $\lambda_i(s)$; therefore, we have $P^{(\lambda_i)} = (I - P\Gamma\Lambda_i)^{-1} P\Gamma(I - \Lambda_i)$. For the history-dependent $\lambda_i$-parameters, the formulation is more complex [21], [34] (the details are out of the scope of this paper).

*2) Properties of the State-Trace Processes:* Under the behavior policies $\pi^{(i)}$, the *state-trace processes* are defined as $\{S_n, e_i(n)\}$. These state-trace processes are Markov chains with the weak Feller property [21], [34]. Let $Z_i(n) = (S_n, e_i(n), S_{n+1})$. We have the following important result [21], [34]: a) the state-trace weak Feller-Markov chain process $Z_i(n)$ has a unique invariant probability measure $\zeta_i$; for each initial condition the *occupation probability measure* converges weakly to $\zeta_i$ [21, Theorem 2.1(i)]; b) if $E_{\zeta_i}$ denotes the expectation of the stationary state-trace process with initial distribution $\zeta_i$, then $E_{\zeta_i}\{\|f(Z_0)\|\} < \infty$ and $\frac{1}{n}\sum_{j=0}^{n-1} f(Z_i(j))$ converges to $E_{\zeta_i}\{f(Z_i(0))\}$ in mean and a.s., where $f(z)$ is a Lipschitz continuous function in the trace variable $e$ [21, Theorem 2.1(ii)].

The results a) and b) are used to prove the following:
1) $E_{\zeta_i}\{\phi(S_0)\phi(S_0)^T\} = \Phi^T \Xi_i \Phi$;
2) $E_{\zeta_i}\{e_i(0)\ \delta_i(v; 0)\} = \Phi^T \Xi_i (T^{(\lambda_i)} v - v), \quad \forall v \in \mathcal{R}^M$
3) $E_{\zeta_i}\{e_i(0)\rho_i(0)(\phi^j(S_0) - \gamma(1)\phi^j(S_1))\} = \Phi^T \Xi_i (I - P^{(\lambda_i)})\Phi_j, \quad 1 \leq j \leq p$;
4) $E_{\zeta_i}\{e_i(0)\rho_i(0)(1 - \lambda_i(1))\gamma(1)\phi^j(S_1)\} = \Phi^T \Xi_i P^{(\lambda_i)} \Phi_j$, $1 \leq j \leq p$;

where $\phi^j(\cdot)$ is the $j$-th component of $\phi(\cdot)$ and $\Phi_j$ the $j$-th column vector of $\Phi$ [21, Proposition 2.1].

Under (A1), the results from [21, Proposition 2.2] also show that the sequences of traces $\{e_i(n)\}$ satisfy the condition $E\{\|e_i(n) - \hat{e}_i(n)\|\} \leq c(n)$, where $c(n) \to 0$ when $n \to \infty$, while $\{e_i(n)\}$ and $\{\hat{e}_i(n)\}$ are obtained using the same trajectory of states, but with different initial conditions $e_i(0)$ and $\hat{e}_i(0)$. Also, $\{e_i(n)\}$ is uniformly integrable, and, consequently, the random variables $\{Z_i(n)\}$, $n \geq 0$, are tight [36].

Let

$$g_i(\theta_i, w_i, Z_i) = \rho_i(s, s')(\phi(s) - \gamma(s')\phi(s'))e_i^T w_i \tag{12}$$

and

$$k_i(\theta_i, w_i, Z_i) = e_i \bar{\delta}_i(s, s', v_{\theta_i}) - \phi(s)\phi(s)^T w_i, \tag{13}$$

where $\bar{\delta}_i(s, s', v_{\theta_i}) = \rho_i(s, s')(r(s, s') + \gamma(s')v_{\theta_i}(s') - v_{\theta_i}(s))$. We also have:

$$\begin{aligned} \bar{g}_i(\theta_i, w_i) &= E_{\zeta_i}\{g_i(\theta_i, w_i, Z_i(0))\} \\ &= (\Phi^T \Xi_i (I - P^{(\lambda_i)})\Phi)^T w_i, \end{aligned} \tag{14}$$

$$\begin{aligned} \bar{k}_i(\theta_i, w_i) &= E_{\zeta_i}\{k_i(\theta_i, w_i, Z_i(0))\} \\ &= \Phi^T \Xi_i (T^{(\lambda_i)} v_{\theta_i} - v_{\theta_i}) - \Phi^T \Xi_i \Phi w_i, \end{aligned} \tag{15}$$

and

$$\bar{g}_i(\theta_i, w_i(\theta_i)) = (\Phi^T \Xi_i (I - P^{(\lambda_i)})\Phi)^T w_i(\theta_i). \tag{16}$$

Comparison with (3) shows that $\bar{g}_i(\theta_i, w_i(\theta_i) = -\nabla J_i(\theta_i)$.

Based on the above definitions and the results from [21], we have the following important ergodic properties:

*Lemma 1 ( [21]):* Under (A1), the following holds for each $\theta_i$ and $w_i$ and each compact set $D_i \subset \mathcal{Z}_i$:
a) $\lim_{m,n\to\infty} \frac{1}{m}\sum_{s=n}^{n+m-1} E_n\{k_i(\theta_i, w_i, Z_i(s+1)) - \bar{k}_i(\theta_i, w_i)\} I(Z_i(n) \in D_i) = 0$ in mean,
b) $\lim_{m,n\to\infty} \frac{1}{m}\sum_{s=n}^{n+m-1} E_n\{g_i(\theta_i, w_i, Z_i(s+1)) - \bar{g}_i(\theta_i, w_i)\} I(Z_i(n) \in D_i) = 0$ in mean,
c) $\lim_{m,n\to\infty} \frac{1}{m}\sum_{s=n}^{n+m-1} E_n\{g_i(\theta_i, w_i(\theta_i), Z_i(s+1)) - \bar{g}_i(\theta_i, w_i(\theta_i))\} I(Z_i(n) \in D_i) = 0$ in mean,
where $E_n\{\cdot\}$ denotes the conditional expectation given the history $(Z_i(0), \cdots, Z_i(n))$ and $I(\cdot)$ denotes the indicator function.

### B. Global Model

Let $X(n) = [\Theta(n)^T \vdots W(n)^T]^T$, $\Theta(n) = [\theta_1(n)^T \cdots \theta_N(n)^T]^T$, $W(n) = [w_1(n)^T \cdots w_N(n)^T]^T$; similarly, $X'(n) = [\Theta'(n)^T \vdots W'(n)^T]^T$, together with the corresponding vector components. Then, we have for AlgA the following global model at the network level

$$\begin{aligned} X'(n) &= X(n) + \Gamma(n)F(X(n), n), \\ X(n+1) &= \mathrm{diag}\{(A(n) \otimes I_p), I_{Np}\} X'(n), \end{aligned} \tag{17}$$

where $\otimes$ denotes the Kronecker's product, while $\Gamma(n) = \mathrm{diag}\{\alpha_1(n), \ldots, \alpha_N(n), \beta_1(n), \ldots, \beta_N(n)\} \otimes I_p$,

$$F(X(n), n) = [F^\theta(X(n), n)^T \vdots F^w(X(n), n)^T]^T,$$

$$\begin{aligned} F^\theta(X(n), n) = [&q_1 g_1(\theta_1(n), w_1(n), Z_1(n))^T \cdots \\ &q_N g_N(\theta_N(n), w_N(n), Z_N(n))^T]^T, \end{aligned}$$


ISBN 978-86-7466-930-3

$$F^w(X(n),n) = [k_1(\theta_1(n), w_1(n), Z_1(n))^T + e_1(n)^T\omega_1(n+1)\cdots k_N(\theta_N(n), w_N(n), Z_N(n)) + e_N(n)^T\omega_N(n+1)]^T$$

with $g_i(\cdot)$ defined by (12).

Introduce dummy variables $X = [\Theta^T \vdots W^T]^T$, together with $\bar{F}(X) = [\bar{F}^\theta(\Theta, W)^T \vdots \bar{F}^w(\Theta, W)^T]^T$, $F^\theta(\Theta,\ W) = [q_1\bar{g}_1(\theta_1, w_1)^T \cdots q_N\bar{g}_N(\theta_N, w_N)^T]^T$, with $\bar{g}_i(\cdot,\cdot)$ defined by (14), $F^w(\Theta, W) = [\bar{k}_1(\theta_1, w_1)^T \cdots \bar{k}_N(\theta_N, w_N)^T]^T$, with $\bar{k}_i(\cdot,\cdot)$ defined by (15).

In the case of AlgB, we have a slightly modified model (17): instead of $\mathrm{diag}\{(A(n)\otimes I_p), I_{Np}\}$ in the second relation in (17), we have $\mathrm{diag}\{(A(n) \otimes I_p), (A(n) \otimes I_p)\}$, as a consequence of consensus w.r.t. $w_i$.

### C. Communication Part of the Algorithm

The result of this subsection is a slight generalization of the results in [5], based on [11].

Define $\Psi(n|k) = A(n)\cdots A(k)$ for $n \geq k$, $\Psi(n|n+1) = I_N$. Let $\mathcal{F}_n$ be an increasing sequence of $\sigma$-algebras such that $\mathcal{F}_n$ measures $\{X(k), k \leq n, A(k), k < n\}$.

(A2) There is a scalar $\alpha_0 > 0$ such that $a_{ii}(n) \geq \alpha_0$, and, for $i \neq j$, either $a_{ij}(n) = 0$ or $a_{ij}(n) \geq \alpha_0$.

(A3) There are a scalar $p_0 > 0$ and an integer $n_0$ such that $P_{\mathcal{F}_n}\{$agent $j$ communicates to agent $i$ on the interval $[n, n+n_0]\} \geq p_0$, for all $n$ and $i = 1,\ldots N$, $j \in \mathcal{N}_i$.

(A4) The digraph $\mathcal{G}$ is strongly connected.

According to [5], [11], it is possible to show that (A2)-(A4) imply that $\Psi(k) = \lim_n \Psi(n|k)$ exists w.p.1; moreover, its rows are equal and $E\{|\Psi(n|k) - \Psi(k)|\}$, $E_{\mathcal{F}_n}\{|\Psi(n|k) - \Psi(k)|\} \to 0$ geometrically as $n-k \to \infty$, uniformly in $k$ and $\omega$ (w.p.1). In addition, $E_{\mathcal{F}_n}\{\Psi(n|k)\}$ converges to $\Psi(k)$ geometrically, uniformly in $\omega$ and $k$, as $n \to \infty$.

### D. Convergence Proofs

(A5) Sequence $\{A(n)\}$ is independent of the processes in MDP$^i$, $i = 1,\ldots,N$.

(A6) There is a $N\times N$ matrix $\bar{\Psi}$ such that $E\{|E_k\{\Psi(n)\} - \bar{\Psi}|\} \to 0$ as $n-k \to \infty$, which, under the conditions of Lemma 1, has the form

$$\bar{\Psi} = \begin{bmatrix} \bar{\psi_1} & \cdots & \bar{\psi_N} \\ & \cdots & \\ \bar{\psi_1} & \cdots & \bar{\psi_N} \end{bmatrix} = \begin{bmatrix} \hat{\Psi} \\ \vdots \\ \hat{\Psi} \end{bmatrix},$$

where $\sum_i \bar{\psi}_i = 1$ ($|\cdot|$ denotes the infinity norm).

(A7) Sequence $\{X(n)\}$ is tight.

*1) AlgA):*

*Theorem 1:* Let (A1)–(A7) hold. Let $X^\alpha(n)$ be generated by AlgA, (7), (8), (9), with $\beta_i(n) = \alpha_i(n) = \alpha$ and define for $t \geq 0$, $t \in \mathcal{R}$, $X^\alpha(t) = X(n)$ for $t \in [(n-n_\alpha)\alpha, (n-n_\alpha+1)\alpha)$. Let $w_i^\alpha(0) = w_{i,0}^\alpha$, $e_i(0) = e_{i,0} \in \mathrm{span}\{\phi(S)\}$. Then, for any integers $n'_\alpha$ such that $\alpha n'_\alpha \to \infty$ as $\alpha \to 0$, there exist positive numbers $\{T_\alpha\}$ with $T_\alpha \to \infty$ as $\alpha \to 0$ such that for any $\epsilon > 0$

$$\limsup_{\alpha\to 0} P\{(X^\alpha(n'_\alpha + k)) \notin N_\epsilon(\bar{\Sigma}) \text{ for some } k \in [0, T_\alpha/\alpha]\} = 0, \quad (18)$$

$i = 1,\ldots,N$, where $N_\epsilon(\cdot)$ denotes the $\epsilon$-neighborhood, while $\bar{\Sigma} = \bar{\Sigma}_\theta \times \cdots \bar{\Sigma}_\theta \times \bar{\Sigma}_{w_1} \times \cdots \bar{\Sigma}_{w_N}$ is the set of points $\bar{\theta},\ldots,\bar{\theta},\bar{w}_1,\ldots,\bar{w}_N$ satisfying

$$\begin{aligned} \sum_{i=1}^N \bar{\psi}_i q_i G_i^T \bar{w}_i &= 0, \\ G_1\bar{\theta} + b_1 - H_1\bar{w}_1 &= 0, \\ &\vdots \\ G_N\bar{\theta} + b_N - H_N\bar{w}_N &= 0, \end{aligned} \quad (19)$$

where $G_i = \Phi^T\Xi_i(P^{(\lambda_i)} - I)\Phi$, $b_i = \Phi^T\Xi_i r_\pi^{(\lambda_i)}$, $r_\pi^{(\lambda_i)}$ is a constant $M$-vector in the affine function $T^{(\lambda_i)}(\cdot)$, while $H_i = \Phi^T\Xi_i\Phi$, $i = 1,\ldots,N$.

*Proof:* The proof is based on [1], [33] and the general results from [5], [11], [36]. In order to apply the proof of Theorem 3.1 in [5], it is essential to verify whether the basic assumptions from [5] concerning $F(X(n), n)$ hold in our case. We can easily conclude that Lemma 1 implies that the assumptions (C3.2) and C(3.3') from Section 3 in [5] hold. Following further [5], it follows that the Skorokhod embedding implies that we have the limit process $X^\alpha(\cdot) \to X(\cdot)$, where $\dot{X} = \mathrm{diag}\{\bar{\Psi}\otimes I_p, I_{Np}\}\bar{F}(X)$ [5]. By Lemma 1 and (A6), all the rows of $\bar{\Psi}$ are equal. Consequently, $\Theta(\cdot) = [\theta(\cdot)^T \cdots \theta(\cdot)^T]$, $\forall\theta(\cdot) \in \mathcal{R}^p$, implying that $\dot{\theta} = \bar{\psi}_1 q_1\bar{g}_1(\theta, w_1) + \cdots + \bar{\psi}_N q_N\bar{g}_N(\theta, w_N)$; we also have $\dot{w}_1 = \bar{k}_1(\theta, w_1), \ldots \dot{w}_N = \bar{k}_N(\theta, w_N)$, having in mind that consensus is not applied to the auxiliary variables.

In order to prove (18), we study the limit set

$$E = \cap_{\tau\geq 0}\mathrm{cl}\{\theta(t), w_1(t), \ldots, w_N(t) | \theta(0), w_1(0), \ldots, w_N(0) \in \mathcal{R}^{(N+1)p}, t \geq \tau\}. \quad (20)$$

where $\mathrm{cl}\{\cdot\}$ denotes the closure of a given set. Following [21] ( Proposition 4.1), we introduce the Lyapunov function

$$V(\theta, w_1, \ldots w_N) = \frac{1}{2}\|\theta - \bar{\theta}\|^2 + \frac{1}{2}\sum_{i=1}^N q_i\bar{\psi}_i\|w_i - \bar{w}_i\|^2, \quad (21)$$

where $\bar{\theta}$ and $\bar{w}_i$ are given by (19). We have directly

$$\begin{aligned} \dot{V}(\theta, w_1, \ldots w_N) =& \langle\theta - \bar{\theta}, -\sum_{i=1}^N q_i\bar{\psi}_i G_i^T w_i\rangle \\ &+ \sum_{i=1}^N q_i\bar{\psi}_i\langle w_i - \bar{w}_i, G_i\theta + \bar{g}_i - \bar{H}_i w_i\rangle \\ =& -\sum_{i=1}^N q_i\bar{\psi}_i\langle w_i - \bar{w}_i, H_i(w_i - \bar{w}_i)\rangle. \end{aligned} \quad (22)$$

Therefore, $\dot{V}(\theta, w_1, \ldots w_N) < 0$ for $w_i \in \mathrm{span}\{\phi(S)\}$ and $w_i \neq \bar{w}_i$, implying that $\hat{w}_i = \bar{w}_i$ if $[\hat{\theta}^T\hat{w}_1^T \ldots \hat{w}_N^T]^T \in$

 ISBN 978-86-7466-930-3

$E$ and $\hat{w}_i \in \text{span}\{\phi(S)\}$, $i = 1, \dots, N$. Similarly, if $[\hat{\theta}^T \bar{w}_1^T \dots \bar{w}_N^T]^T \in E$, then $\hat{\theta} = \bar{\theta}$. In such a way we conclude that for initial conditions $w_i(0) \in \text{span}\{\phi(S)\}$ the limit set $E$ is indeed the set $\bar{\Sigma}$ of points satisfying (19).

The steps remaining to prove (18) are standard for the stochastic approximation theory (see [1], [21], [36]). ■

*2) AlgB):*

*Theorem 2:* Let (A1)–(A7) hold. Let $X^\alpha(n)$ be generated by AlgB (7), (8), (9) and (10), with $\beta_i(n) = \alpha_i(n) = \alpha$, and let both $w_i^\alpha(0) = w_{i,0}^\alpha$ and $e_i(0) = e_{i,0} \in \text{span}\{\phi(S)\}$. Then, for any integers $n'_\alpha$ such that $\alpha n'_\alpha \to \infty$ as $\alpha \to 0$, there exist positive numbers $\{T_\alpha\}$ with $T_\alpha \to \infty$ as $\alpha \to 0$ such that for any $\epsilon > 0$

$$\limsup_{\alpha \to 0} P\{ \begin{bmatrix} \theta_i^\alpha(n'_\alpha + k) \\ w_i^\alpha(n'_\alpha + k) \end{bmatrix} \notin N_\epsilon(\bar{\Sigma}) \text{ for some } k \in [0, T_\alpha/\alpha]\} = 0, \quad (23)$$

$i = 1, \dots, N$, where $N_\epsilon(\cdot)$ denotes the $\epsilon$-neighborhood, while $\bar{\Sigma} = \bar{\Sigma}_\theta \times \bar{\Sigma}_w$ is the set of points $\bar{x} = [\bar{\theta}^T \bar{w}^T]^T \in \mathcal{R}^{2p}$ satisfying

$$\bar{G}\bar{\theta} + \bar{g} - \bar{H}\bar{w} = 0, \quad \bar{G}^T \bar{w} = 0, \quad (24)$$

where $\bar{G} = \sum_{i=1}^N \bar{\psi}_i q_i \Phi^T \Xi_i (P^{(\lambda_i)} - I)\Phi$, $\bar{b} = \Phi^T \sum_{i=1}^N \bar{\psi}_i q_i \Xi_i r_\pi^{(\lambda_i)}$, $r_\pi^{(\lambda_i)}$ is a constant $M$-vector in the affine function $T^{(\lambda_i)}(\cdot)$, while $\bar{H} = \sum_{i=1}^N \bar{\psi}_i q_i \Phi^T \Xi_i \Phi$.

*Proof:* AlgA differs from AlgB only in the communication part of the algorithm. Formally, the procedure of the proof remains the same as in Theorem 1, after replacing $\text{diag}\{(A(n) \otimes I_p), I_{Np}\}$ by $\text{diag}\{(A(n) \otimes I_p), (A(n) \otimes I_p)\}$. This implies that, asymptotically, instead of $\text{diag}\{(\hat{\Psi} \otimes I_p), I_{Np}\}$ we have now $\text{diag}\{(\hat{\Psi} \otimes I_p), (\hat{\Psi} \otimes I_p)\}$. In this sense, we obtain $X(\cdot) = [\theta(\cdot)^T \cdots \theta(\cdot)^T w(\cdot)^T \cdots w(\cdot)^T]^T$, where $\theta(\cdot)$ and $w(\cdot)$ satisfy the following ODE:

$$\begin{bmatrix} \dot{\theta} \\ \dot{w} \end{bmatrix} = \bar{\psi}_1 q_1 \begin{bmatrix} \bar{g}_1(\theta, w) \\ \bar{k}_1(\theta, w) \end{bmatrix} + \cdots + \bar{\psi}_N q_N \begin{bmatrix} \bar{g}_N(\theta, w) \\ \bar{k}_N(\theta, w) \end{bmatrix} \quad (25)$$

The limit points (24) follow from (25), according to Theorem 1. Namely, we define the Lyapunov function

$$V(\theta, w_1, \dots w_N) = \frac{1}{2}\|\theta - \bar{\theta}\|^2 + \frac{1}{2}\|w - \bar{w}\|^2, \quad (26)$$

where $\bar{\theta}$ and $\bar{w}$ are given by (24) and obtain for the derivative that

$$\begin{aligned} \dot{V}(\theta, w) &= \langle \theta - \bar{\theta}, \bar{G}^T w \rangle + \langle w - \bar{w}, \bar{G}\theta + \bar{b} - \bar{H}w \rangle \\ &= -\langle w - \bar{w}, \bar{H}(w_- \bar{w}) \rangle. \end{aligned} \quad (27)$$

Therefore, $\dot{V}(\theta, w) < 0$ for $w_i \in \text{span}\{\phi(S)\}$ and $w \neq \bar{w}$, implying that $\hat{w} = \bar{w}$ if $[\hat{\theta}^T \hat{w}^T]^T \in E$ and $\hat{w} \in \text{span}\{\phi(S)\}$. In the same way, if $[\hat{\theta}^T \bar{w}^T]^T \in E$, then $\hat{\theta} = \bar{\theta}$. Consequently, for the initial conditions $w_i(0) \in \text{span}\{\phi(S)\}$, the limit set of ODE (25) is the set $\bar{\Sigma}$ satisfying (24). ■

## IV. Discussion

The preceding section has been devoted to the weak convergence of the proposed distributed temporal difference learning algorithms. The role of convexification of $w_i$ remains to be clarified. It is clear, from the definition of the criterion function (2) and the algorithm construction, that AlgA follows from the basic local relations (4), providing for all $i$ unique solutions $w_i(\theta)$ for all $\theta$. However, AlgB is based on the introduction of an additional constraint that $w_1(\theta) = \cdots = w_N(\theta) = w(\theta)$, where $w(\theta)$ is the unique solution of

$$\Phi^T (\sum_{i=1}^N \bar{\psi}_i q_i \Xi_i) \Phi w(\theta) = \sum_{i=1}^N \bar{\psi}_i q_i \Pi_{\xi_i} (T^{(\lambda_i)} v_\theta - v_\theta). \quad (28)$$

It is straightforward to observe from (28) that we have for any given $\theta$

$$\Phi^T (\sum_{i=1}^N \bar{\psi}_i q_i \Xi_i) \Phi w(\theta) = \sum_{i=1}^N \bar{\psi}_i q_i \Phi \Xi_i \Phi w_i(\theta). \quad (29)$$

This property is verified by the above theorems.

Consequently, convergence points of $\theta$ are different for these two cases. In order to get a clearer insight, assume that $\det H_i \neq 0$. Then, for AlgA we have

$$\sum_{i=1}^N \bar{\psi}_i q_i G_i^T w_i(\theta) = \sum_{i=1}^N \bar{\psi}_i q_i G_i^T [H_i^{-1}(G_i\theta + b_i)] = 0, \quad (30)$$

resulting in

$$\sum_{i=1}^N \bar{\psi}_i q_i G_i^T H_i^{-1} G_i \theta = \sum_{i=1}^N \bar{\psi}_i q_i G_i^T H_i^{-1} b_i = 0, \quad (31)$$

while for AlgB we obtain

$$\bar{G}^T \bar{H}^{-1} \bar{G}\theta = \bar{G}^T \bar{H}^{-1} \bar{b}. \quad (32)$$

Notice that in the case of equal $\lambda$-parameters and equal behavior policies for all the agents, both algorithms provide the same solution.

It is difficult to make any general conclusion about the relative advantage of one of the two presented algorithms. It is to be noticed that this issue has not been directly treated in the literature; all the examples of distributed TD algorithms subsume that the consensus operator is applied to both $\theta$ and $w$, without mentioning any alternative (*e.g.*, [28] with the references therein). As far as the limit points of the corresponding ODEs are concerned, it should be noticed that a better approximation could be, in general, expected when consensus is not applied to $w$. Our experience confirms this statement; however it does not show any significant difference from this point of view. In some cases it could be expected that the application of consensus to $w$ may improve the convergence rate of the algorithm. It is hard to draw any definite conclusion, in general, having in mind that connectedness of the underlying network can play an essential role from this point of view. A comprehensive Monte Carlo analysis could practically resolve the remaining dilemmas. It would be also interesting to analyze the discussed problem in the two-time-scale cases (see [1]).

 ISBN 978-86-7466-930-3

## V. Conclusion

In this paper we have presented and discussed two novel algorithms for distributed off-policy gradient-based value function approximation within a collaborative multi-agent reinforcement learning setting. The algorithms are based on an integration of linear dynamic consensus schemes into local gradient-based recursions, involving the so called *auxiliary variables*. We presented rigorous proofs that, under nonrestrictive assumptions, the parameter estimates weakly converge to consensus. Based on these proofs, a discussion is provided of the incorporation of consensus w.r.t. auxiliary variables, defining clearly the figure of merit of the alternative approaches.

## References


[1] M. S. Stanković, M. Beko, and S. S. Stanković, "Distributed value function approximation for collaborative multi-agent reinforcement learning," *IEEE Trans. Control Networked Systems*, vol. (Early Access), 2021.

[2] M. S. Stanković, S. S. Stanković, and D. M. Stipanović, "Consensus-based decentralized real-time identification of large-scale systems," *Automatica*, vol. 60, pp. 219–226, 2015.

[3] J. N. Tsitsiklis, "Problems in decentralized decision making and computation," Ph.D. dissertation, Dep. Electrical Eng. Comput. Sci., M.I.T., Cambridge, MA, 1984.

[4] J. N. Tsitsiklis, D. P. Bertsekas, and M. Athans, "Distributed asynchronous deterministic and stochastic gradient optimization algorithms," *IEEE Trans. Autom. Control*, vol. 31, pp. 803–812, 1986.

[5] H. J. Kushner and G. Yin, "Asymptotic properties of distributed and communicating stochastic approximation algorithms," *SIAM J. Control Optim.*, vol. 25, pp. 1266–1290, 1987.

[6] A. Nedić and A. Ozdaglar, "Distributed subgradient methods for multi-agent optimization," *IEEE Trans. Autom. Control*, vol. 54, pp. 48–61, 2009.

[7] P. Bianchi, G. Fort, and W. Hachem, "Performance of a distributed stochastic approximation algorithm," *IEEE Trans. Inf. Theory*, vol. 59, pp. 7405–7418, 2013.

[8] M. S. Stanković, S. S. Stanković, and K. H. Johansson, "Distributed time synchronization for networks with random delays and measurement noise," *Automatica*, vol. 93, pp. 126 – 137, 2018.

[9] A. Nedić and A. Olshevsky, "Distributed optimization over time-varying directed graphs," *IEEE Trans. Autom. Control*, vol. 60, pp. 601 – 615, 2015.

[10] S. Tu and A. Sayed, "Diffusion strategies outperform consensus strategies for distributed estimation over adaptive networks," *IEEE Trans. Signal Process.*, vol. 60, pp. 6217–6233, 2012.

[11] M. S. Stanković, N. Ilić, and S. S. Stanković, "Distributed stochastic approximation: Weak convergence and network design," *IEEE Trans. Autom. Control*, vol. 61, no. 12, pp. 4069–4074, 2016.

[12] N. Ilić, S. S. Stanković, M. S. Stanković, and K. H. Johansson, "Consensus based distributed change detection using generalized likelihood ratio methodology," *Signal Processing*, vol. 92, no. 7, pp. 1715 – 1728, 2012.

[13] M. S. Stanković, S. S. Stanković, K. H. Johansson, M. Beko, and L. M. Camarinha-Matos, "On consensus-based distributed blind calibration of sensor networks," *Sensors*, vol. 18, no. 11, 2018.

[14] M. S. Stanković, K. H. Johansson, and D. M. Stipanović, "Distributed seeking of Nash equilibria with applications to mobile sensor networks," *IEEE Trans. Autom. Control*, vol. 57, no. 4, pp. 904–919, 2012.

[15] S. S. Stanković, M. Beko, and M. S. Stanković, "Nonlinear robustified stochastic consensus seeking," *Systems & Control Letters*, vol. 139, p. 104667, 2020.

[16] R. S. Sutton and A. G. Barto, *Reinforcement learning: An introduction*. MIT press Cambridge, 1998.

[17] D. P. Bertsekas and J. Tsitsiklis, *Neuro-Dynamic Programming*. Athena Scientific, 1996.

[18] D. Precup, R. S. Sutton, and S. Dasgupta, "Off-policy temporal-difference learning with function approximation," in *Proc. 18th Int. Conf. on Machine Learning*, 2001, pp. 417–424.

[19] R. S. Sutton, H. R. Maei, D. Precup, S. Bhatnagar, D. Silver, C. Szepesvári, and E. Wiewiora, "Fast gradient-descent methods for temporal-difference learning with linear function approximation," in *Proc. 26th Int. Conf. on Machine Learning*, 2009, pp. 993–1000.

[20] M. Geist and B. Scherrer, "Off-policy learning with eligibility traces: A survey," *Journal of Machine Learning Research*, vol. 15, pp. 289–333, 2014.

[21] H. Yu, "On convergence of some gradient-based temporal-differences algorithms for off-policy learning," *arXiv:1712.09652*, 2017.

[22] B. Dai, A. Shaw, L. Li, L. Xiao, N. He, J. Chen, and L. Song, "SBEED: Convergent reinforcement learning with nonlinear function approximation," *arXiv:1712.10285*, 2017.

[23] L. Busoniu, R. Babuska, and B. De Schutter, "A comprehensive survey of multiagent reinforcement learning," *IEEE Transactions on Systems, Man, and Cybernetics, Part C: Applications and Reviews*, vol. 38, no. 2, pp. 156–172, 2008.

[24] J. K. Gupta, M. Egorov, and M. Kochenderfer, "Cooperative multi-agent control using deep reinforcement learning," in *Autonomous Agents and Multiagent Systems*, G. Sukthankar and J. A. Rodriguez-Aguilar, Eds. Cham: Springer International Publishing, 2017, pp. 66–83.

[25] A. OroojlooyJadid and D. Hajinezhad, "A review of cooperative multi-agent deep reinforcement learning," *arXiv:1908.03963*, 2019.

[26] A. Mathkar and V. S. Borkar, "Distributed reinforcement learning via gossip," *IEEE Trans. Autom. Control*, vol. 62, no. 3, pp. 1465–1470, 2017.

[27] S. Kar, J. M. Moura, and H. V. Poor, "QD-Learning: A collaborative distributed strategy for multi-agent reinforcement learning through consensus + innovations," *IEEE Trans. Signal Proc.*, vol. 61, no. 7, pp. 1848–1862, 2013.

[28] S. V. Macua, J. Chen, S. Zazo, and A. H. Sayed, "Distributed policy evaluation under multiple behavior strategies," *IEEE Trans. Autom. Control*, vol. 60, no. 5, pp. 1260–1274, 2015.

[29] D. Lee, H. Yoon, and N. Hovakimyan, "Primal-dual algorithm for distributed reinforcement learning: Distributed GTD," in *IEEE Conf. Decision and Control*, 2018, pp. 1967–1972.

[30] Y. Zhang and M. M. Zavlanos, "Distributed off-policy actor-critic reinforcement learning with policy consensus," *arXiv:1903.09255*, 2019.

[31] M. S. Stanković and S. S. Stanković, "Multi-agent temporal-difference learning with linear function approximation: Weak convergence under time-varying network topologies," in *2016 American Control Conference (ACC)*, 2016, pp. 167–172.

[32] T. Doan, S. Maguluri, and J. Romberg, "Finite-time analysis of distributed TD(0) with linear function approximation on multi-agent reinforcement learning," in *Proc. Int. Conf. Machine Learning*, 2019, pp. 1626–1635.

[33] M. S. Stanković, M. Beko, N. Ilić, and S. S. Stanković, "Distributed multi-agent reinforcement learning algorithm based on gradient correction," in *Proc. IcETRAN Conference*, 2020.

[34] H. Yu, A. Mahmood, and R. Sutton, "On generalized Bellman equations and temporal-difference learning," *Journal of Machine Learning Research*, vol. 19, pp. 1–49, 2019.

[35] S. S. Stanković, M. S. Stanković, and D. M. Stipanović, "Decentralized parameter estimation by consensus based stochastic approximation," *IEEE Trans. Autom. Control*, vol. 47, pp. 531–543, 2011.

[36] H. J. Kushner and G. Yin, *Stochastic Approximation and Recursive Algorithms and Applications*. Springer, 2003.


 ISBN 978-86-7466-930-3

# Application of Subtractive Clustering in Data Processing

Boris Barišić, Aleksandra Krstić, Sanja Vujnović, Željko Đurović

***Abstract*—The problem of data clustering is still in development and various approaches to solving it are being proposed, all of which have different success rates. ne of the nonparametric clustering methods is subtractive clustering. The success of this algorithm largely depends on tuning its parameters. In this paper we give a theoretical analysis of different suggestions for choosing their values. ased on probability theory, we e amined the impact of dimensionality and number of samples on the clustering radius. y conducting a controlled e periment with nown sample distributions, the performance of this algorithm with suggested parameters is tested, as well as its robustness.**

***Index Terms*—subtractive clustering, parameters tuning, classification, data processing**

## I. Introduction

For a large number of classification problems we do not have adequate a priori knowledge and therefore we are not able to generate an appropriate training set. Starting with Charles Darwin and his systematization of animals and plants into genera, species, families etc. up until the development of systems based on various forms of artificial intelligence, the man has attempted to improve clustering techniques.

Nonparametric clustering methods do not consider optimization criteria or data distributions. They are based on implementing different ways to locate 'valleys' or 'hills' in the probability density function of the data as a natural border between different classes.

In 1992. Yager and Filev suggested *mountain clustering* as one of the techniques [1]. The method is based on dividing the entire data space into a dense grid of small hypercubes whose vertices are potentially cluster centers. The potential i.e., the *mountain* function is then calculated for each vertex as a measure of sample density in its surrounding. Clearly the potential for the vertex to be a cluster center increases with the number of samples surrounding it. The core idea of this method is the following: after finding the first cluster center, potentials of all vertices are reduced inversely proportional to the distance from the vertex to the cluster center. For vertices closer to the center, the potential reduces more. The next cluster center is chosen as the vertex with the highest potential (after reduction). This method of finding cluster centers repeats until the potential in all vertices falls beneath a certain threshold.

Even though it was imagined as a very simple method, its numerical complexity grows exponentially with sample dimensionality due to a large number of hypercubes in the grid. In 1994. Chiu suggested a modification of this algorithm called subtractive clustering [2].

## II. Theoretical analysis

### A. Algorithm

The idea of *subtracti e* clustering is that every sample in the dataset can be a cluster center. Due to this starting assumption of considering only given samples as cluster centers, the complexity of this algorithm is practically linear.

Samples are assigned a certain density based on which the cluster centers are found during the iterative procedure. Aside from considering a smaller dataset than *mountain* clustering, calculating the density function implies the squared distance between samples, so there is no need for determining the square root.

Based on the description given in [2], the algorithm is comprised of a few steps:

*Step 0* For each of $N$ samples we calculate the value of the initial density $D_i^1$ according to equation (1),

$$D_i^1 = \sum_{j=1}^{N} e^{-\frac{\|X_i - X_j\|^2}{(r_a/2)^2}}, i = \overline{1,N} \tag{1}$$

where $r_a$ is a positive constant called the clustering radius.

*Step 1* Based on initial density values we determine the first cluster center $X_c^1$:

$$X_c^1 = \arg\{\max_{i=1,N} D_i{}^1\} \tag{2}$$

*Step 3* Having found the first cluster center, we start the iterative procedure of finding other cluster centers. Since the first center is already found, let the iteration counter start at $k = 1$.

*Step 4* We increment the counter to $k = k + 1$ and eliminate the influence of samples near the previously found center by modifying their density function:

$$D_i^k = D_i^{k-1} - D_c^{k-1} e^{-\frac{\|X_i - X_c^{k-1}\|^2}{(r_b/2)^2}}, i = \overline{1,N} \tag{3}$$

Boris Barišić – School of Electrical Engineering, University of Belgrade, Bulevar Kralja Aleksandra 73, 11020 Belgrade, Serbia (e-mail: boris.barisic@ etf.bg.ac.rs).

Aleksandra Krstić – School of Electrical Engineering, University of Belgrade, Bulevar Kralja Aleksandra 73, 11020 Belgrade, Serbia (e-mail: amarjanovic@ etf.bg.ac.rs).

Sanja Vujnović – School of Electrical Engineering, University of Belgrade, Bulevar Kralja Aleksandra 73, 11020 Belgrade, Serbia (e-mail: svujnovic@etf.bg.ac.rs).

Željko Đurović – School of Electrical Engineering, University of Belgrade, Bulevar Kralja Aleksandra 73, 11020 Belgrade, Serbia (e-mail: zdjurovic@etf.bg.ac.rs).

 ISBN 978-86-7466-930-3

$D_i^k$ is the new density function value, and $D_i^{k-1}$ is the previous one. $D_c^{k-1}$ is the maximum density from the previous iteration, and $X_c^{k-1}$ is the cluster center found also in the previous iteration. Parameter $r_b$ represents a new clustering radius.

*Step 5* Based on the newly modified values of density functions we choose a k[th] cluster center $X_c^k$:

$$X_c^k = \arg\{\max_{i=\overline{1,N}} {D_i}^k\} \tag{4}$$

*Step* We check whether $D_c^k$ i.e., the density of samples in radius $r_b$ of k[th] cluster center satisfies:

$$D_c^k \leq \delta D_c^1 \tag{5}$$

If the given condition is not satisfied, we go back to step 4, and if it is, the algorithm ends. Parameter $\delta$ is a positive value smaller than 1 and it is called the clustering threshold.

*B. Parameter tuning*

The success of clustering largely depends on choosing the values for $r_a$, $r_b$ and $\delta$. Clustering radiuses $r_a$ and $r_b$ should in some way incorporate the information on how samples are scattered around cluster centers.

A great number of scientists and engineers have put their knowledge and experience into determining clear and straight-forward recommendations for choosing the values of parameters involved in clustering. Unfortunately, most of them so far have turned out to be inefficient and inapplicable in most cases. In [3] it is suggested and in [4] analyzed that the parameter $r_a$ should be chosen according to:

$$r_a = \left\{\frac{1}{4}\left[\max\{\|X_i - X_j\|\} + \min\{\|X_k - X_l\|\}\right]\right\}^{\beta} \tag{6}$$

where $i, j, k, l = \overline{1, N}$, and $N$ the total number of samples available. Parameter $\beta$ should serve as amortization for extreme values of maxima which come from potential outliers [3].

We will perform an analysis on how the theoretical probability density function (pdf) of $r_a$ changes according to $N$ and dimensionality $n$. First, we consider a one-dimensional case ($n = 1$). Let samples from all clusters have a Gaussian joined probability density function $\mathcal{N}(m, \sigma^2)$. For the sake of simplicity, we will consider the minimum value to be neglectable in respect to the maximum value, as well as the parameter $\beta = 1$. Samples $X_i$ and $X_j$ then become independent identically distributed random variables, and parameter $r_a$ becomes a random variable $R_a$ for which the following holds:

$$R_a = \max\{|X - Y|\} \tag{7}$$

Random variable $Z = X - Y$ will then also have a Gaussian pdf with parameters $\mathcal{N}(0, 2\sigma^2)$, as it is a subtraction of two Gaussian variables. The absolute value of this variable $U = |Z|$ will have a cumulative distribution function (cdf):

$$F_U(u) = P(U \leq u) = P(|Z| \leq u) = P(-u \leq Z \leq u)u_H(u) \tag{8}$$

i.e. the following will hold:

$$F_U(u) = (2F_Z(u) - 1)u_H(u) \tag{9}$$

where $u_H(u)$ represents a Heaviside unit step function.

Now we can easily obtain the probability density function of the random variable $U$:

$$f_U(u) = 2f_Z(u)u_H(u) \tag{10}$$

If the total number of samples in our dataset is $N$, then there are $N_U = \binom{N}{2} = \frac{N(N-1)}{2}$ values which can be calculated as $U = |X - Y|$ and let these values be $U_1, \dots, U_{N_U}$. Let us form an array $U_{(1)}, \dots, U_{(N_U)}$, whose elements are variables $U_1, \dots, U_{N_U}$ in a non-declining order. $U_{(1)}$ is the minimum, and $U_{(N_U)}$ the maximum calculated value. If we want to determine the cdf $F_{U_{(k)}}(u)$ for $U_{(k)}$, we will notice that the event of $\{U_{(k)} \leq u\}$ occurs if and only if the k[th] value is not bigger than $u$, meaning that at least $k$ of $N_U$ random variables $U_1, \dots, U_{N_U}$ have a value less than or equal to $u$. Imagine we have $N_U$ Bernoullie's experiments, with every experiment testing whether the event $\{U_{(k)} \leq u\}$ (success) occured or not [5]. The probability of success is equal to $P(U_{(k)} \leq u) = F_U(u)$, and the probability of at least $k$ successes occuring in $N_U$ experiments is:

$$F_{U_{(k)}}(u) = P(U_{(k)} \leq u) = \sum_{i=k}^{N_U} \binom{N_U}{i} F_U^i(u)(1 - F_U(u))^{N_U - i} \tag{11}$$

Since the object of our analysis is the maximum value of $|X - Y|$ i.e. $R_a = U_{(N_U)}$, by replacing $k$ with $N_U$ we get:

$$F_{R_a}(r_a) = \left(F_U(r_a)\right)^{\frac{N(N-1)}{2}} \tag{12}$$

The pdf for the parameter $R_a$ is:

$$f_{R_a}(r_a) = \frac{N(N-1)}{2}\left(F_U(r_a)\right)^{\frac{N(N-1)}{2} - 1} f_U(r_a) \tag{13}$$

Let us assume now that our samples are n-dimensional. Let samples $\boldsymbol{X_i}$ and $\boldsymbol{X_j}$ be independent identically distributed vectors whose pdf is $\mathcal{N}(\boldsymbol{M}, \boldsymbol{\Sigma})$. We will additionally assume that their variances along all dimensions are equal and not correlated, i.e. that the covariance matrix has the form $\boldsymbol{\Sigma} = \sigma^2 \boldsymbol{I}$, where $\boldsymbol{I}$ is the identity matrix.

The Euclidian norm $V = \|\boldsymbol{X} - \boldsymbol{Y}\|$ is calculated as

$$V = \sqrt{\sum_{i=1}^{n} (X_i - Y_i)^2} = \sqrt{\sum_{i=1}^{n} Z_i^2} \tag{14}$$

where $Z_i$ is the random variable $Z_i = X_i - Y_i$. We previously showed that the distribution of $Z_i$ will be $\mathcal{N}(0, 2\sigma^2)$, which means that $\frac{Z_i}{\sqrt{2}\sigma}$ will have a Gaussian pdf $\mathcal{N}(0,1)$. We can determine the distribution of random variable

 ISBN 978-86-7466-930-3

$$V = \sqrt{2}\sigma \sqrt{\sum_{i=1}^{n} \left(\frac{Z_i}{\sqrt{2}\sigma}\right)^2} \tag{15}$$

using the results known from probability theory, which state that the square root of the sum of squares of $n$ independent identically distributed variables with distribution $\mathcal{N}(0,1)$ will have a $\chi$ distribution with $n$ degrees of freedom [6]. Therefore, the cdf of random variable $V$ will be:

$$F_V(v) = \frac{\gamma\left(\frac{n}{2}, \frac{v^2}{4\sigma^2}\right)}{\Gamma\left(\frac{n}{2}\right)} u_H(v) \tag{16}$$

where $\Gamma$ is the gamma function, and $\gamma$ is the lower incomplete gamma function.
The pdf of random variable $V$ is:

$$f_V(v) = \frac{v^{n-1}}{2^{n-1}\sigma^n \Gamma\left(\frac{n}{2}\right)} e^{-\frac{v^2}{4\sigma^2}} \cdot u_H(v) \tag{17}$$

Results given in equations (12) and (13) also hold for the distribution of the maximum value of random variable $V$ with arbitrary dimensionality $n$.

Fig. 1 shows the probability density function of random variable $R_a$ for different dimensionalities $n$ and different number of samples $N$. We can see that the clustering radius can be affected by changes in both parameters. Larger dimensionality $n$ results in more additions when calculating the norm, which expectedly also results in larger values of clustering radius. On the other hand, having more samples (larger $N$) increases the chance of extrema appearing, i.e. the chance of having samples which are far away from each other, which has a bigger clustering radius as a result.

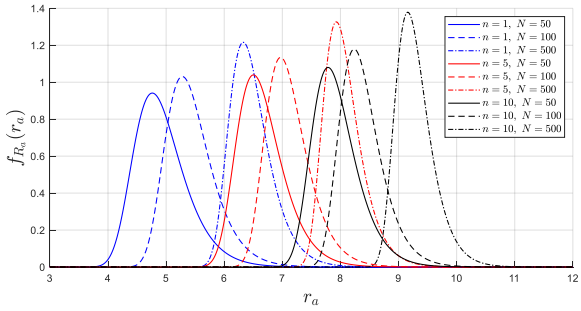


Fig. 1. Probability density function of random variable $R_a$ which represents maximum of Euclidian norm between two samples.

It is also meaningful to analyze how the mathematical expectation $m_{R_a}$ and variance $\sigma^2_{R_a}$ of the pdf of variable $R_a$ change depending on sample number $N$ and dimensionality $n$. Both statistics have been calculated using numerical integration of pdf in equation (13) and the results are shown in Fig. 2 and Fig. 3. Mathematical expectation and variance increase with the increase of $n$. On the other hand, larger number of samples increases the mathematical expectation, but decreases variance.

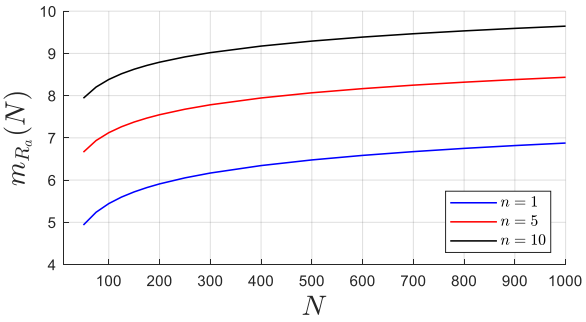


Fig. 2. Mathematical expectation $m_{R_a}$ of random variable $R_a$ depending on dimensionality $n$ and number of samples $N$.

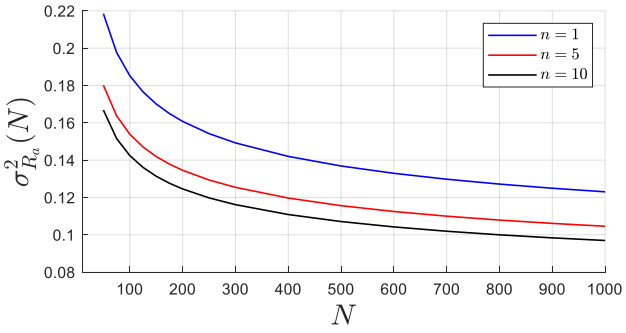


Fig. 3. Variance $\sigma^2_{R_a}$ of random variable $R_a$ depending on dimensionality $n$ and number of samples $N$.

In the beginning of this analysis, we assumed that parameter $\beta = 1$, which does not have to be the case in general. Let us introduce a random variable $W = R_a^{\beta}$ to show how parameter $\beta$ affects the clustering radius. We can easily obtain the cdf for random variable $W$:

$$F_W(w) = P\left(R_a^{\beta} \le w\right) = P\left(R_a \le w^{\frac{1}{\beta}}\right) = F_{R_a}\left(w^{\frac{1}{\beta}}\right) u_H(w) \tag{18}$$

as well as its pdf:

$$f_W(w) = \frac{1}{\beta} w^{\frac{1}{\beta}-1} f_{R_a}\left(w^{\frac{1}{\beta}}\right) u_H(w) \tag{19}$$

For a constant number of samples $N = 100$ and various values of $\beta$, the pdf of $W$ is calculated and shown in Fig.4. We can see that by changing the value of $\beta$ by $\pm 30$ % in respect to the unit value, we make a great impact on the expected value of clustering radius, as well as its variance.

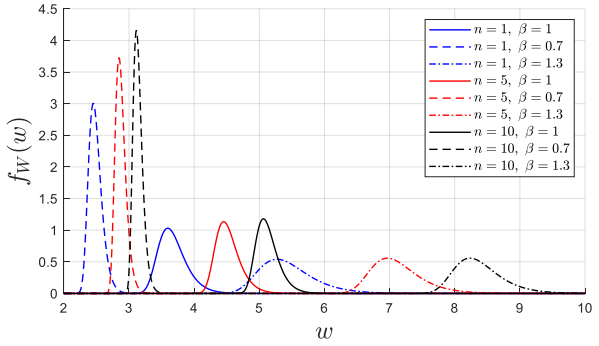


Fig. 4. Probability density function of random variable $W = R_a^{\beta}$ depending on dimensionality of samples $n$ and parameter value $\beta$. $W$ represents maximum of Euclidian norm between two samples to the power of $\beta$.


ISBN 978-86-7466-930-3

### C. *Classification accuracy*

Performance of clustering algorithm is tested on two-dimensional samples from 5 classes, distributed normally with different covariance matrices.

The main goal of clustering is to find centers of all classes and then test how accurate the classification is. Since the dataset is synthetically generated and all classes and covariance matrices are known, we decided to determine which class a sample belongs to by calculating the statistical distance according to equation (20),

$$d_i^2 = \left(X - X_{c_i}\right)^T \Sigma_{c_i}^{-1} \left(X - X_{c_i}\right) \tag{20}$$

where $d_i$ is the statistical distance of sample $X$ to $i^{\text{th}}$ class, whose center is in $X_{c_i}$, and covariance matrix is $\Sigma_{c_i}$. For each sample the statistical distance to all found centers is calculated, and then the sample gets placed in the class for which the distance is minimal. Classification accuracy is finally measured as a percentage of accurately classified samples.

## III. RESULTS AND DISCUSSION

We generated 300 samples for each of the 5 classes. As previously mentioned, each class is normally distributed. Clustering radius $r_a$ is determined according to (6), and parameter $\beta = 0.5$ [3]. As suggested in [2], the new clustering radius $r_b$ is $r_b = 1.5r_a$. Clustering threshold $\delta$ is manually tuned for the algorithm to detect the right number of clusters.

Figure 6. shows all classes and centers which were detected by subtractive clustering.

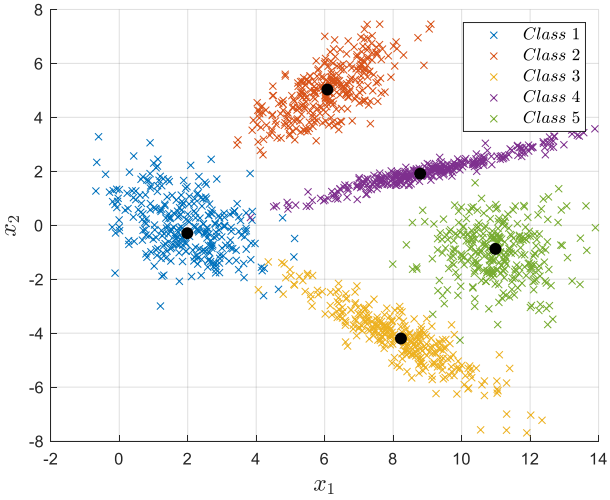


Fig. 5. Sample distribution among classes and corresponding cluster centers found.

To test the sensitivity of the algorithm (with said parameter values) the experiment was repeated 500 times. For each experiment the clustering radius $r_a$ is determined separately. The histogram of the number of detected cluster centers in 500 experiments is given in Fig. 6.

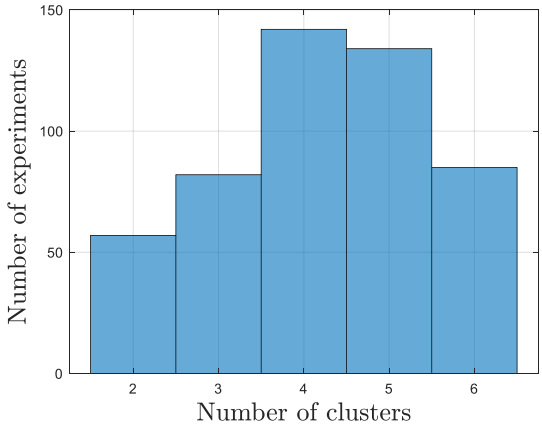


Fig. 6. Histogram of the number of detected cluster centers.

For experiments in which the detected number of centers is correct, i.e. 5, we calculated the classification accuracy as mentioned earlier. Figure 7. shows the histogram of classification accuracy.

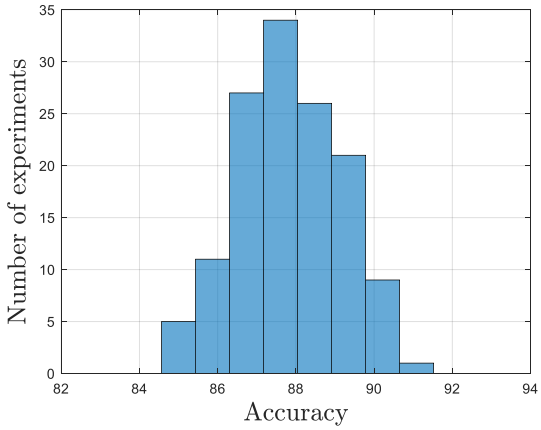


Fig. 7. Histogram of classification accuracy.

In 134 out of 500 experiments the algorithm has managed to detect all cluster centers. The average accuracy in these experiments is 88 %.

Finally, it is also interesting to see how the new cluster radius $r_b$ affects the success of finding cluster centers. We choose o $r_b$ according to:

$$r_b = \varepsilon r_a \tag{21}$$

where $\varepsilon$ is a positive constant called the squash factor. Various papers give different suggestions regarding the value of $\varepsilon$, depending on the practical use of the algorithm. Based on [7] and [8] $\varepsilon$ should be in an interval of $\varepsilon \in [1, 1.5]$.

We generated the same number of samples with the same distribution as before, and for each of the experiments we tested the success of the algorithm by changing $\varepsilon$ from 1 to 1.5 with the step $\Delta\varepsilon = 0.05$. The experiment was repeated one hundered times. Histogram of the number of centers found depending on $\varepsilon$ is shown in Fig. 8.


ISBN 978-86-7466-930-3

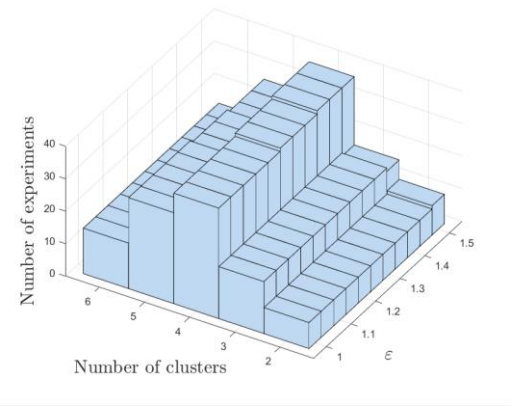


Fig. 8. Histogram of the number of cluster centers found depending on $\varepsilon$.

## IV. Conclusion

In this paper we analyzed both theoretically and experimentally the technique of subtractive clustering, as well as suggestions for tuning its parameters. Values of parameters $r_a$, $r_b$ and $\delta$ significantly affect the success of clustering. We observed that even with various suggestions on how to choose the values, the algorithm does not always perform well on different sets with the same distribution.

However, even if we assume that parameters $r_a$ and $r_b$ are tuned correctly, there are no theoretical propositions on choosing the threshold value $\delta$, which has a great impact on the number of clusters found. In case of samples with dimensions $n = 1, 2, 3$ we can visualize the dataset and assess whether the cluster centers have been found correctly. Nevertheless, in most cases the dimensions will be significantly bigger and there would be no unique way to rate the success of the algorithm.

One of the methods to further enhance the algorithm and propose a uniform way for choosing parameter values would be to separately consider the maximum scattering along each of the axis. For example, if we have two-dimensional samples where the variance along one axis is much larger than the other and classes are near to each other, determining the density in the radius as the maximum quadratic norm of two samples, would lead to poor results.

Though the simplicity of subtractive clustering is its big advantage, the results are not ideal. That being said, it can be used as a preprocessing technique for other more sophisticated methods.

## References

[1] R. R. Yager and D. P. Filev. "Approximate clustering via the mountain method". *IEEE Transactions on systems, man, and Cybernetics*: pp. 1279-1284, 1994.

[2] S. L. Chiu, "Fuzzy model identification based on cluster estimation", *ournal of Intelligent fu y systems,* vol. 2, no. 3, pp. 267-278, 1994.

[3] X. Cui, S. Liu, and L. Jia, "An improved method of semantic driven subtractive clustering algorithm", in *2015 IEEE 5th International Conference on Electronics Information and Emergency Communication*, pp. 232-235, IEEE, 2015.

[4] M. M. Milošević, "Speaker identification in conditions of emotional speech", Ph.D. dissertation, Signals and Systems, University of Belgrade, Belgrade, Serbia, 2020.

[5] M. Merkle, "Random variabiles", *Probability and statistics for engineers and engineering students* [in Serbian], Belgrade, Serbia, Akademska misao, 2016, ch. 3, sec. 3.6, pp. 81–82.

[6] M. Merkle, "Some important distributions", *Probability and statistics for engineers and engineering students* [in Serbian], Belgrade, Serbia, Akademska misao, 2016, ch. 7, sec. 7.2, pp. 157–159.

[7] K. Demirli, S. Cheng, and P. Muthukumaran, "Subtractive clustering based modeling of job sequencing with parametric search", *Fu y Sets and Systems*, vol. 137, no. 2, pp. 235-270, 2003.

[8] X.-x. Jing, L. Zhan, H. Zhao, and P. Zhou, "Speaker recognition system using the improved gmm-based clustering algorithm", in 2010 International Conference on Intelligent Computing and Integrated Systems, pp. 482-485, IEEE, 2010.

 ISBN 978-86-7466-930-3

# Arduino based online laboratory platform for digital control systems analysis and design

Vladimir Mitić, Vladimir Sibinović, Snežana Đorđević, Boban Veselić

***Abstract*— This paper presents a laboratory platform with remote access for e ercising digital control systems analysis and design. The laboratory environment utilizes three types of standard control systems positional servosystem, velocity servosystem and temperature regulation system. It also has online access through a standard Web browser that enables remote e ecution, visualization and data acquisition. tudents can perform different variety of e periments, ranging from bachelor to master level studies. They can wor independently or collaborate within a group with multiuser access to the platform. The laboratory platform is designed a way to be applicable to any regulation system with implemented communication protocols.**

***Index Terms*— aboratory platform, remote access, digital control theory, Arduino.**

## I. Introduction

The previous two years, because of the pandemic outbreak, introduced remote learning to all levels of education. While this type of learning is not new, it was never before used at such an extent and for a large number of topics.

Remote laboratories were always popular in engineering education, but their popularity has grown rapidly in recent years. With the development of different technologies, e.g., Internet-of-things, more and more researchers turn to developing remote laboratories for different topics.

The results presented in this paper stemmed from the efforts, started a long time ago, trying to modernize old laboratory teaching platforms that were used to explain control system fundamentals to students. The possibility of remote access to the laboratory setup was a priority from a very beginning. Remote experiments offer more flexibility both for teachers and students, and some experiments were performed at the Faculty of Electronic Engineering in Niš more than 10 years ago [1].

Gaining experience in that field over the years, the authors started developing a new laboratory platform for teaching control system fundamentals. With flexibility and simplicity, as the main guiding principles, a new platform has been designed for teaching digital control systems analysis and design. Remote access to the platform requires from a student to only have a device with internet access. On the other hand, the platform can be built using off the shelf components that are inexpensive.

The paper is organized as follows. Section II presents the hardware system design, while Section III describes the software architecture of the system Section IV shows the educational possibilities and potentials of the realized laboratory platform and demonstrates its ease of use through some examples of laboratory exercises.

## II. Hardware architecture

Arduino Due development board has been chosen to be the key component of the laboratory platform. Arduino is an open-source development environment that has become ubiquitous in education, from the primary schools all the way to the universities. Arduino platform provides different inexpensive development boards, that can be used for teaching different topics like programming [2], robotics [3], physics [4], etc. Arduino Due has an Atmel SAM3X8E Arm Cortex-M3 microcontroller, which uses a 32-bit RISC processor operating at the maximum frequency of 84 MHz. This gives the platform adequate processing power and enables further development of the system. It also has plenty of general-purpose input/outputs (GPIOs) for connecting other parts of the system. The main disadvantage is that this system is 3.3V transistor-transistor logic (TTL) and requires logic level converters to work with components having 5V TTL.

In order to be able to create a set of different laboratory exercises, the three standard control systems have been implemented: positional and velocity servosystems using DC motors, and temperature regulation system using heating elements.

### *A. Positional and elocity ser osystem*

The positional and velocity servosystems were realized using Crouzet 82830010 DC motor that has the nominal power output of 33W. A gearbox with the ratio of 12.25 is coupled with the motor for the positional servosystem, for more accurate angular position control. An absolute magnetic encoder with 4096 increments per revolution is chosen for position measuring. These measurements are also used for the angular speed estimation of the motor shaft [5]. This was chosen as the most inexpensive solution with the highest resolution. Since the encoder is absolute, a lot of attention has been dedicated to detecting the zero-crossing condition, especially when operating on high speeds. The motor speed is estimated using simple Euler derivative approximation, which means that for small sampling periods the speed signal can be noisy. According to the predicted motor current requirements, Pololu VNH5019 motor driver has been chosen. A custom printed circuit board (PCB) was designed

Vladimir Mitić is with the Faculty of Electronic Engineering, University of Niš, Aleksandra Medvedeva 14, 18000 Niš, Serbia (e-mail: vladimir.mitic@elfak.ni.ac.rs)
Vladimir Sibinović is with the Faculty of Electronic Engineering, University of Niš, Aleksandra Medvedeva 14, 18000 Niš, Serbia (e-mail: vladimir.sibinovic@elfak.ni.ac.rs)
Snežana Đorđević is with the Faculty of Electronic Engineering, University of Niš, Aleksandra Medvedeva 14, 18000 Niš, Serbia (e-mail: snezanadjordjevic@elfak.rs)
Boban Veselić is with the Faculty of Electronic Engineering, University of Niš, Aleksandra Medvedeva 14, 18000 Niš, Serbia (e-mail: boban.veselic@elfak.ni.ac.rs)

 ISBN 978-86-7466-930-3

and manufactured for easy component interconnection and system replication. All the required mechanical components were designed and 3D printed with the special care for safety and transferability. A photo of the laboratory setup is displayed in Fig. 1.

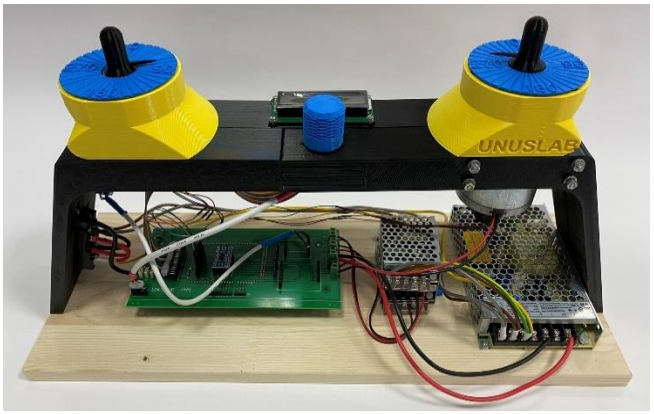


Fig. 1. Velocity servosystem laboratory platform.

A power supply port, an USB port for communication and an USB port for Arduino programming are located in the left-hand side of the platform. The power supplies are integrated into the platform, in the right-hand side, so only a standard PC power cable is needed for powering the system. The laboratory setup was designed to operate both in the stand-alone mode (controlled using the knob and display in the middle) and with usage of a computer. The referent speed/position is selected using the pointer on the left, and the motor rotation is observed using the pointer on the right.

### *B. Temperature regulation of a thermal process*

Temperature regulation system consists of a ceramic resistor with 2.7 Ω resistance and maximum power output of 10 W. It has the role of a control object whose temperature needs to be regulated. A strong MOSFET transistor serves as the actuator of the system, and it allows current switching trough the resistor. The feedback is realized using an analog temperature sensor that is amplified to achieve the highest resolution for the temperature range of 0 $^0$C – 100 $^0$C. A photo of the temperature regulation platform is shown in Fig. 2.

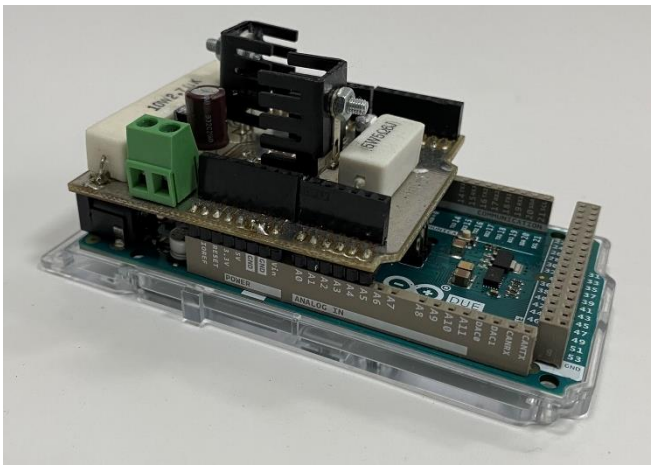

Fig 2. Temperature regulation system

The system also has a secondary ceramic resistor, that has the resistance of 5.6 Ω and maximum power dissipation of 5 W. The resistors represent two different heating elements, that can be utilized either separately or together. This provides flexibility to the platform to be able to emulate different thermal processes.

## III. SOFTWARE ARCHITECTURE

The software architecture consists of three parts: (i) real-time control system implemented on the Arduino DUE, (ii) server that generates the user interface (UI) and (iii) a bridge application that connects the previous two. The system block diagram is given in Fig. 3.

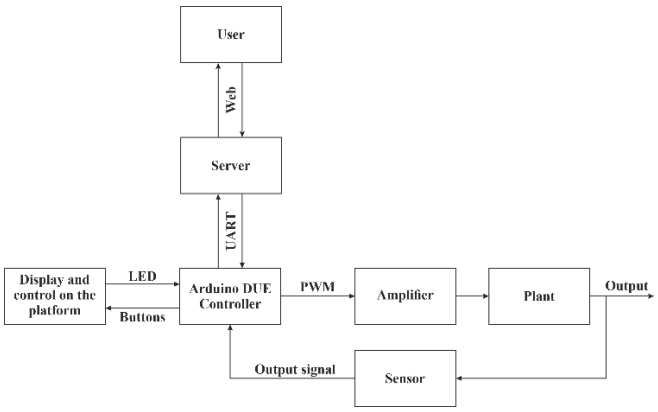


Fig 3. Block diagram of the system.

### *A. Communication protocols*

The real-time control system communicates with the bridge application using universal asynchronous receiver-transmitter (UART) protocol. UART messages are optimized for the minimization of number of bytes, which means that they need to be decoded and passed to the server. This is implemented because of the limited transmission speed of the protocol with really large amount of data (e.g., plot data). The bridge application decodes the UART data and generates Java Script object notation (JSON) messages that are transferred to the server via WebSocket protocol. The communication is organized using a master-slave type of protocol where the server is the master, and the Arduino is the slave. Every message from the server generates a response from the Arduino so any communication error can be easily recognized. If no response is generated retransmission feature has been implemented as well. This provides reliable communication between system components.

### *B. eal-time control system*

The real-time control system consists of three main parts: 1) control loop, 2) communication handler and 3) display handler.

#### *1 Control loop*

The control loop must have a real-time component, executed every 4 ms by generating the timer interrupt. It handles the sensor readings for the reference and the output signal, calculate the control signal according to the applied control algorithm, converts that signal from voltage to PWM and forwards it to the selected driver. The control loop can be set to be executed with a longer sampling period, which is the integer product of 4 ms. This enables changing the sampling period of the system. This feature is useful for the experiments that analyze the effects of the sampling period size on a digital control system, as well as for the systems that

 ISBN 978-86-7466-930-3

are considerably slower, such as the temperature regulation system. Several digital control laws can be employed for the control signal calculation. The implemented standard digital controllers are: PD, PID, PID AW, I-P, I-PD and universal controller. PD controller can be used for realization of P controller, by setting the derivative gain to zero. The same goes for PID controller that can be used for the realization of PI controller. PID AW represents the standard PID controller with anti-windup mechanism. I-P and I-PD controllers denote controllers with relocated P and PD actions, respectively. The implemented universal controller can represent any second-order (or less) discrete-time transfer function described by

$$G(z) = \frac{b_2 z^2 + b_1 z + b_0}{a_2 z^2 + a_1 z + a_0} \quad (1)$$

This means that virtually any linear digital controller (up to the second-order) can be tested on the given system.

It is also envisaged that the control signal can be formed using state feedback control approach. In order to implement the state feedback control loop, it is necessary to use the state-space representation of the control plant. The state variables required for the state feedback control can be obtained directly by measuring, or by using state estimation. For this reason, a predictive state observer, a current state observer and a Kalman estimator (filter) were also implemented. The software is realized in a such manner that the real-time simultaneous switching between the controllers can be done. This offers the students the possibility to compare the efficiencies of various controllers.

The desired reference signal can be obtained manually from the user or as the output of the built-in signal generator. The implemented signal generator can generate real-time step, ramp, parabolic, pulse, sine and sawtooth signals. The signal parameters can be arbitrary set and the switching between signals can be done in real-time.

*2 Communication handler*

The communication handler manages receiving a message, its decoding and generating and sending the corresponding response. The communication handler has various types of error checking, starting from incorrect number of bytes to incorrect data or data types. The number of system parameters that can be changed through the communication handler is 70. This means that every controller gain, every signal generator parameter and every other control loop parameter can be changed by the user through the Web UI. The communication handler is responsible for generating and sending the plot data, which consists of the timestamp, referent signals, output signals, and control signals. The time period of the plot data sending is defined as a user settable parameter, enabling the user to appropriately adjust the plot figure as needed.

*3 isplay handler*

The display handler controls the information presented on the display and the knob that is used for moving through the menus. The display information is useful when performing experiments in the stand-alone mode (not connected to a computer). Still, for the full functionality of the system the Web UI should be used.

### *C. Web I*

The Web UI is accessible through any Web browser with no special requirements. When granted the access to the platform by the system administrator, the user establishes the connection to the Web UI by typing in the Web address as shown in [6]. Multiple users can access the platform at the same time which enables working in groups, where the members don't need to be in the same location. This has proven to be a useful option, since the pandemic has separated students from each other. The first batch of students that used the laboratory had positive feedback on the look and usability of the Web UI. When accessing the provided Web page, a login screen firstly appears. After entering the correct login information, the control page is shown. The control page is dynamically changing the displayed parameters based on the selected options. Fig. 4. shows the overview of the control page.

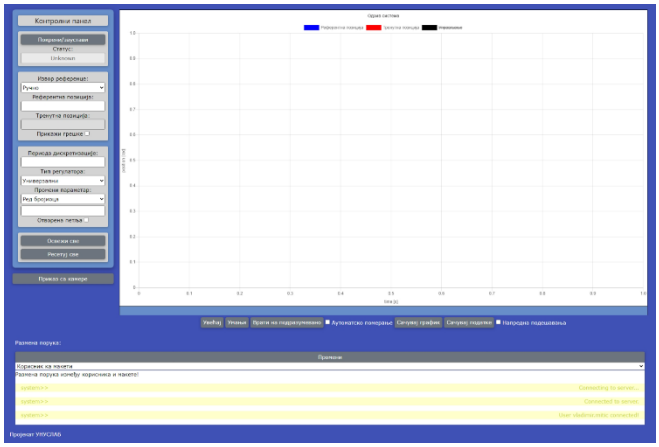

Fig. 4. The control page of the Web UI.

The control page consists of the 1) control panel on the left, 2) control chart on the right and a 3) message panel on the bottom.

*1 Control panel*

The control panel is used for starting and stopping the system and for system parameter manipulation. It is divided into four sections. The first section consists of the *Start Stop* button and a system status indicator. The possible system statuses are: Unknown, Stopped, Running and Disconnected. The statuses are described in Table 1.

TABLE I
SYSTEM STATUS DESCRIPTION

| Status | Description |
|---|---|
| Unknown | The bridge application is not responding. |
| Stopped | Control loop is disabled, and plot data sending is stopped. |
| Running | Control loop is enabled, and new plot data is being displayed. |
| Disconnected | Connection with the server is terminated, the page should be refreshed |

The second section is intended for reference signal control and output signal display. A dropdown list is used for selecting if the reference signal is entered manually or if it is connected to the signal generator. If a signal generator is selected, the corresponding signal parameters are displayed and can be changed. When the state feedback control is enabled, two input fields are displayed. One for each referent

 ISBN 978-86-7466-930-3

state, and two display fields for each measured state variable. A *Show trend* checkbox displays three new fields, showing the current error, the error derivative and the error integral.

The third section is intended for setting the control loop. The first adjustable parameter is the system sampling period. A dropdown list is used for selecting the loop type and controller type. Loop type can be the standard negative feedback or the state feedback. Controller type is used for selecting one of the implemented digital controllers, explained in the previous section. When selecting the desired controller, corresponding parameters of that controller are displayed and can be tuned. Finally, there is a check box for selecting open or closed control loop. This is mostly useful in system identification exercises.

The fourth section consists of two buttons, one for refreshing of all parameters and one for resetting the all parameters to their default values. Below the control panel, there is a button that is used for displaying the webcam image. It opens a new tab that will display a livestream of the laboratory platform that is obtained via a webcam, which is mounted above the platform.

*2 Control chart*

The control chart is an interactive chart that can be manipulated in various ways by the user. Signal manipulation can be accomplished on the chart itself. Every signal on the chart can be hidden or shown by clicking on the signal name. Every point on the chart can be displayed in detail by hovering the mouse pointer over it. Additional controls for manipulating the chart are located directly below it. They consist of the following buttons: *Zoom in*, *Zoom out*, *eset iew* buttons and *Auto-scroll* checkbox for closer observations of the response, *Sa e graph* and *Sa e data* buttons for storing the response and an *Ad anced settings* checkbox. *Sa e graph* button stores the presented response as an "Graph.png" file while the *Sa e data* button stores the response in a "data.csv" file. Every row in the file represents one timeseries, and every column one signal. This makes the data easily readable, and importable into various software packages (like Matlab) for further detailed analysis. The *Ad anced settings* checkbox displays three new input fields: *Plot ac uisition period*, *Number of seconds to store* and *Number of samples to store*. *Plot ac uisition period* defines the period at which the platform sends the data to the user. This period can be different to the control sampling period if we do not need so much data collected and displayed. *Number of seconds to store* defines the timespan that is shown on the chart and that will be stored with the save button. *Number of samples to store* represents the number of timeseries points that is displayed and stored. Because these two fields affect the same property (timespan of the plot), only one of them should be changed.

With this kind of interactive control chart, it is obvious that it alone is sufficient for any standard system analysis, which is done when executing a laboratory exercise. This enables the students to observe the experiment, notify and immediately correct any unexpected system behavior.

*3 Messaging system*

The messaging system is a feature that is designed for student groups that are scattered in different places. Using the toggle button on the top of the messaging panel, different types of messaging channels can be selected. Firstly, there is the *ser-de ice* channel that is used for verifying that all the parameters are set correctly. Secondly, there is the *ser-user* channel which is organized in a standard chat form and enables students to collaborate more effectively while performing the given task.

## IV. LABORATORY EXERCISES

The realized laboratory platforms have a lot of teaching potential for the students, and they can provide practical engagement for students to better learn and understand control theory. First, students can learn about system identification techniques for different types of control plants. For example, students can record the step response of the system by removing the feedback loop and setting the digital controller to PD with the gains $k_p = 1$, $k_d = 0$. In this way, the value of the referent signal is directly passed to the plant. They can save the response data and use Matlab for system identification. By performing this on the servosystems, they learn about first- and second-order transfer function identification. In case of the thermal plant, they can learn about identifying a system with transport delay.

The second set of experiments are devoted to time-discretization process and signal reconstruction in digital control systems. Students can observe the effects of the sampling period selection on a system performance. They can experimentally determine critical gain and critical frequency when system reaches stability margin, Fig. 5. Also, they can calculate steady state errors to different input signals and experimentally validate them.

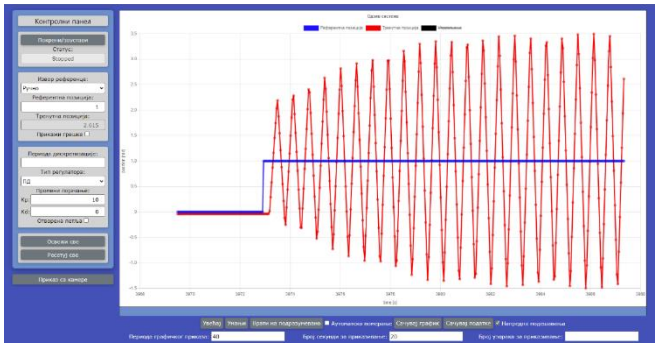

Fig 5. Experimentally determining the critical gain and frequency of a closed loop system.

When it comes to digital control systems design, the implemented digital controllers give the students a lot of possibilities. Starting from standard control loops, they can design P, PI, PD, PID controllers, lead-lag compensators and compare the system responses that they provide. Also, the students can experience some issues related to practical implementation of a control system. One of them is the saturation of the applied control signal, which can greatly affect the performance of a system. Consequently, possibilities are envisaged to implement digital controllers with relocated P and D actions that can reduce control signal peaks, as well as to enhance a control system with an anti-windup structure. The latter is crucial for temperature regulation system because of the large integrator windup produced by the dynamic properties of the system as well as the present transport delay, Fig. 6.

The state feedback control structure implementation widens even more the learning possibilities of the platform.

 ISBN 978-86-7466-930-3

By designing the state feedback controller, students get a better understanding of the state-space representation of a system and its practical usage. The implemented prediction state observer, current state observer and Kalman estimator, as a special type of current state observer, offers possibilities to students to try their design and get insight into state estimation and its possible usages. An example of application of current state observer in state feedback control is given in Fig. 7.

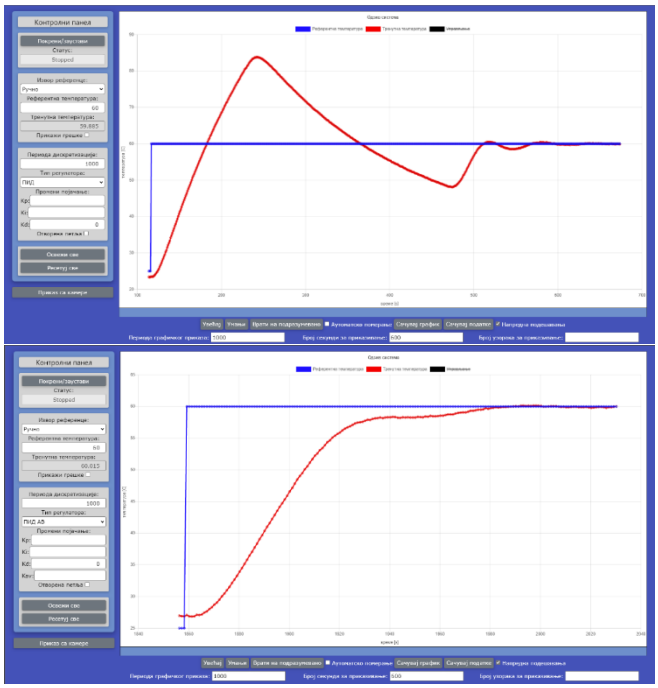

Fig. 6. Temperature regulation system without anti-windup structure (top), and with it (bottom).

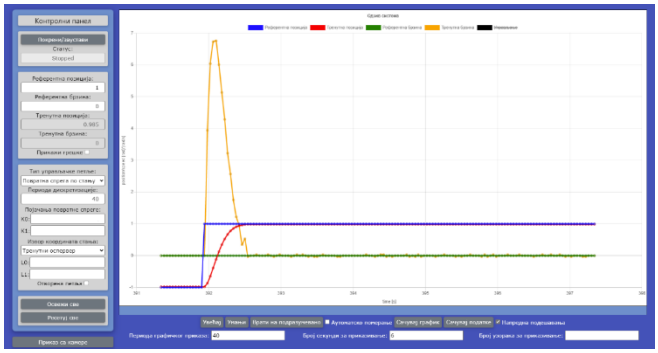

Figure 7. State feedback control implemented with current state observer.

## V. Conclusion

The designed laboratory platform represents a universal solution for teaching of different types of digital control systems. User friendly and modern UI makes it very easily understandable for students. Its inexpensiveness makes it a viable option for a lot of educational facilities. The applied motors and drivers can be easily replaced with any motor power and driver combination, without losing any of the functionality of the exercises. The Arduino microcontroller used here enables for realization of even more complex control loops, which can be useful to students at a higher educational level. The scalability of the system makes it work with any digital system with UART protocol and this type of communications handler. The special value of this platform is the possibility of remote access and performing laboratory exercises from a distant location, which was especially useful for students in a pandemic. Future work will be directed to introduction a cooling element to the temperature regulation system, implementing force feedback loops as well as a cascaded control system with the positional outer loop and velocity inner loop for jerk reduction. This will broaden the possible systems for which students can design and test different control structures.

## Acknowledgment

Part of this research was financed by the Serbian Ministry of Education, Science and Technological Development of the Republic of Serbia.

## References

[1] M.B. Naumović, D. Živanović: “Remote Experiments in Control Engineering Education Laboratory”, International Journal of Online Engineering, ISSN: 1861-2121, vol. 4, No. 2, 2008, pp. 48-53.

[2] I.Perenc, T. Jaworski, P. Duch, “Teaching programming using dedicated Arduino Educational Board”, Computer Applications in Engineering Education, Vol. 27. Issue 4, July 2019, pp 943-954.

[3] F.A. Candelas, G.J. García, et. al., “Experiences on using Arduino for laboratory experiments of Automatic Control and Robotics”, IFAC-PapersOnLine, Vol 48, Issue 29, 2015, pp 105-110.

[4] J Kinchin, “Using an Arduino in physics teaching for beginners”, Physics Education, Vol 53, No 6, 2018

[5] AEAT-6010/6012 Magnetic Encoder, https://docs.broadcom.com/docs/AV02-0188EN

[6] http://25.49.3.248:8080/WebPSAU_Position/

 ISBN 978-86-7466-930-3

# Implementation of the New Curricula in Smart Products and Services Engineering

Marko T. Milojković, Dragan S. Antić, *Senior Member*, Saša S. Nikolić and Nebojša S. Jotović

***Abstract*— Education system proved to have a challenge to cope with today's world of accelerated development of new technologies and ever changing industry. New paradigm dictates not only new teaching contents, but whole new holistic approach to the education of engineers, especially in the field of development of smart products and services. A group of professors from the University of Niš (Faculties of Electronic and Mechanical Engineering) developed a new teaching module named "Smart Products and Services Engineering" and successfully applied for funding from European Education and Culture Executive Agency in the scope of Jean Monnet Erasmus+ project call. Raising the level of knowledge and skills of students in the field of smart products and services should further encourage the development of a modern educational system in one of the most important areas of technology.**

***Index Terms*—Smart products, smart services, engineering education.**

## I. Introduction

The advancement of information and communication technologies is emerging at such a pace that they are increasingly penetrating traditional industries, changing products, processes, organizations, business models and entire value chains. Existing products are transformed into smart products [1], [2] which can intelligently communicate with other smart products and react autonomously to changes in their environment. Smart products are expanding into smart services or smart service systems. Designers today must quickly and flexibly integrate new trends and standards into their solutions. Therefore, the application of modern efficient engineering of the new generation of smart products and services, characterized by high interdisciplinarity, networking, complexity and heterogeneity, is more than necessary. Today, it is convenient to consider a holistic approach to engineering, where, in addition to the development of products and services, their complete life cycle is also taken into account. The components of holistic engineering are the models and methods used in the development process, IT tools, information models and organizational structures, united by human resources with appropriate competencies. The key competence of development engineers is creativity, because it enables successful innovations, i.e. the development of creative and market-competitive products. All these modern tendencies dictate a new approach to education of engineers in the field of smart products and services [3], [4], [5].

Marko T. Milojković, Dragan S. Antić, Saša S. Nikolić and Nebojša S. Jotović are with the University of Niš, Faculty of Electronic Engineering, Department of Control Systems, Aleksandra Medvedeva 14, 18000 Niš, Serbia (e-mails: {marko.milojkovic, dragan.antic, sasa.s.nikolic, nebojsa.jotovic}@elfak.ni.ac.rs).

With the goal to enable master students of technical faculties to acquire adequate competencies in the application of methods, models and IT tools in the efficient engineering of smart products and services, group of professors from the University of Niš successfully applied for funding from EACEA (European Education and Culture Executive Agency). Concrete project application was for Erasmus+ programme call Jean Monnet Actions in the field of Higher Education: Modules, with the project named "Smart Products and Services Engineering" (acronym SPaSE) 101047566-JMO-2021-HEI-TCH-RSCH. Project team consists of ten professors from two faculties: six from the Faculty of Electronic Engineering and four from the Faculty of Mechanical Engineering. Project duration is December 2021 - November 2023 (36 months), and during that time, project team is obligated to hold teaching module dedicated to Smart Products and Services Engineering for three generations of students. Students applicable for the module will be the students from technical faculties who already finished basic level of studies (either master students or working persons).

## II. Project Objectives

Main objectives of the project "Smart Products and Services Engineering" (SPaSE) are:

- Acquiring the necessary knowledge and skills by the master students of technical faculties in the field of innovation and creative techniques for the development of smart market-competitive products and services.
- Mastering the methods, models and IT tools applicable in efficient engineering of the new generation of smart products and services.
- Transfer of acquired engineering competencies in the field of smart products and services to the business entities in the region.
- More efficient use of available human resources and faster integration of the region in the application of European achievements in this area.

Project aims to contribute to the acquisition of professional competencies and innovative readiness in the field of smart product development both in educational institutions and in economic entities in the region. New student teaching module will be the focal point, where the students will learn the basics of Industry 4.0 (I4.0), application of creativity and innovation in product development, basics of digital product development, application of artificial intelligence, sensor

 ISBN 978-86-7466-930-3

technologies and business models I4.0. Special attention will be paid to the development of relevant competencies [6]: professional, methodological, and social. Students will work in teams on practical projects where they will be able to strengthen creativity and teamwork.

Besides teaching part, project team will have numerous related activities oriented toward teaching and scientific community as well as toward local business entities in the field of smart products and services. A lot of events are planned like: round tables with business, workshops, study visits, writing research papers as well as a handbook on smart products and services. All these activities will help reaching the project specific objectives:

O1: Raising the level of knowledge and skills in the field of smart products and services

O2: Efficient application of methods and IT tools for engineering a new generation of smart products and services

O3: Application of creative and innovative techniques, which provides an opportunity for multidisciplinary application of advanced technologies

O4: Strengthening human and institutional resources in the field of research and development

O5: Encouragement to development of a modern educational system in one of the most important areas of technology

O6: Encouragement to strengthen the competitiveness of the national economy

O7: Increasing the technological readiness of educational institutions and economic entities for Serbia's integration into the EU.

## III. Module Composition

Jean Monnet Module "Smart Products and Services Engineering" is composed of 11 courses with 118 school hours of teaching in total. Module is organized in 15 weeks (3 months), two teaching days in a week, with 4 hours teaching blocks.

C1. Introduction to European integration and legislation in the field of smart engineering (6 teaching hours). The main goal is to enhance the existing theoretical understanding of legal, economic, political, and social aspects of European integration. The lectures are based on the interdisciplinary approach regarding the European integration process and its benefits, law, and future aspects with emphasize on the field of smart engineering.

C2. I 4.0: Smart products and services engineering (12 teaching hours). The main goal of the course is to master the knowledge and skills for the efficient application of engineering of the new generation of smart products and services. As part of the course, students will study basic approach in product design and development, modular principle in product development, Industry 4.0 and Reference Architecture Model for Industry 4.0 - RAMI 4.0, holistic approach in product development, smart product and service development models [7], [8].

C3. Creativity and innovation in product development (12 teaching hours). The main aim of this course is for students to master creative skills and competencies and also to present them innovative techniques which will be helpful in developing of future smart products and services [9].

C4. Digital product development (12 teaching hours). The course program will train students to independently use state of the art technologies and methods in the process of development of digital products. The acquired knowledge will enable students to create and holistically administer information, documents and resources in the digital product development process, thus fostering innovation [10].

C5. 3D CAD construction (10 teaching hours). Getting the knowledge about the basic geometrical objects and their relative positions and sections, developing surfaces, as well as the vector analysis and computing graphics. The focus of the course is on parametric design and the proper use of CAD software to produce 3D models, engineering parts, and documentation [11].

C6. Information technology (12 teaching hours). Introduction to the basic IT principles, methods, and techniques. The ultimate goal is the IT education of IT experts, capable of application of information technologies in the industry at all stages during the development of software solutions [12], [13].

C7. Artificial intelligence (12 teaching hours). The aim of course is to introduce the concepts and algorithms at the foundation of modern artificial intelligence, and explore the ideas that give rise to smart products and services. Through real world examples, students will gain knowledge to recognize and apply main tools and algorithms of AI and machine learning with the special emphasize on multilayer artificial neural networks (deep learning) [14], [15].

C8. Big data and data analytics (12 teaching hours). Upon completion of this course the students should become familiar with the principles of Big data and data analytics, gain understanding of the basic tools and techniques for data collection, processing and analysis. The desired outcome is to stimulate the students to adapt EU legislative in this area and apply main tools and algorithms of these concepts in design of simple smart products and services [16], [17].

C9. Internet and sensing technology (12 teaching hours). This course aims to provide an overview of technologies focusing on the Internet of Things and Industrial Internet of Things. Besides fundamentals and operational principles, the emphasize will be on introducing legal EU requirements and frameworks for building secure and reliable systems, opportunities and challenges, successful real-world practices, and efficient internet and sensing applications [18].

C10. Digital twins (10 teaching hours). Digital twin fundamentals, which integrate the internet of things, artificial intelligence, and software programming, will be introduced as a virtual representation of an object or system during its lifecycle, which is updated from real-time data and uses simulation, machine learning, and reasoning to help decision-making [19].

C11. Business models I4.0 (8 teaching hours). This course will be focused on analysing business model characteristics

 ISBN 978-86-7466-930-3

for Industry 4.0, providing an in-depth perspective of companies' processes, structures, and tools for business model innovation. The course will also provide insight in EU good practices and competencies for business model innovation in the course of Industry 4.0 [20].

## IV. CONCLUSION

This paper presented main aspects of newly designed student module at the University of Niš, named "Smart Products and Services Engineering". Module implementation is financially supported by European Education and Culture Executive Agency (EACEA) under the umbrella of Jean Monnet Erasmus+ project call. Module is jointly designed by professors from two faculties – Faculty of Mechanical Engineering and Faculty of Electrical Engineering. Module "Smart Products and Services Engineering" is composed of 11 courses with 118 school hours of teaching in total, organized during 15 weeks (3 months), two teaching days in a week, with 4 hours teaching blocks. Topics to be mastered are: Introduction to European integration and legislation in the field of smart engineering, I4.0: Smart products and services engineering, Creativity and innovation in product development, Digital product development, 3D CAD construction, Information technology, Artificial intelligence, Big data and data analytics, Internet and sensing technology, Digital twins, Business models I4.0.

Besides the main goal of the project which is acquiring the necessary knowledge and skills by the master students of technical faculties in the field of innovation and creative techniques for the development of smart market-competitive products and services and mastering the methods, models and IT tools applicable in efficient engineering of the new generation of smart products and services, project has several additional goals. Most important ones are the transfer of acquired engineering competencies in the field of smart products and services to the business entities in the region as well as more efficient use of available human resources and faster integration of the region in the application of European achievements in this area. In order to achieve all these goals, project anticipates besides teaching part, numerous related activities oriented toward teaching and scientific community as well as toward local business entities in the field of smart products and services. A lot of events are planned like: round tables with business, workshops, study visits, writing research papers as well as a handbook on smart products and services.

## ACKNOWLEDGMENT

Funded by the European Union under project Smart Products and Services Engineering (SPaSE) 101047566-ERASMUS-JMO-2021-MODULE. Views and opinions expressed are however those of the author(s) only and do not necessarily reflect those of the European Union or EACEA. Neither the European Union nor the granting authority can be held responsible for them.

## REFERENCES

[1] V. Miltenović and D. Antić, "Smart Products and Services Engineering,"University of Niš, Niš, Serbia, 2020.
[2] V. Miltenović and N. Marjanović, "Development of innovative and smart products - opportunities and challenges," Proceedings of the 9th International Scientific Conference-Research and Development of Mechanical Elements and Systems, Kragujevac, S. 11-21, 5-7, September, 2019.
[3] V. Miltenović and V. Đorđević, "Excellence, relevance and efficient application of research results at university and institutes from the standpoint of economy developing," Proceedings of the International Symposium Machine and Industrial Design in Mechanical Engineering (KOD), Novi Sad, Serbia, vol. 393, 6-8 June 2018.
[4] G. K. Fomunyam, "Education and the fourth industrial revolution: challenges and possibilities for engineering education," International Journal of Mechanical Engineering and Technology, vol. 10, no. 6, pp. 271–284, 2019.
[5] S. Coskun, Y. Kayıkc, and E. Gençay, "Adapting engineering education to Industry 4.0 vision," Technologies, vol. 7, no. 1, pp. 1–10, 2019.
[6] A. Miltenović, M. Banić. and V. Miltenović, "Importance and role of competence in professional career of product develop engineers," Proceedings of the 7th International Conference on Manufacturing Science and Education - MSE 2015, Sibiu, Romania, June 3-6, 2015.
[7] Platform Industrie 4.0: Reference Architectural Model Industrie 4.0 (RAMI 4.0). Available online: https://www.plattform-i40.de/I40/Redaktion/DE/Downloads/Publi-kation/rami40-eine-einfuehrung.pdf?__blob=publicationFi le&v=10 (Stand: 3.5.2018).
[8] M. Abramovici, Engineering smarter Produkte und Services Platform Industrie 4.0. Studie, Deutsche Akademie der Technikwissenschaften. München, 2018.
[9] V. Miltenović, R. Mitrović, N. Burkardt, S. Stefanov, A. Miltenović, M. Banić, and M. Tica, Innovation management (in Serbian). University of Nis, Faculty of Mechanical Engineering, (2017).
[10] European Commission, 2021. 2030 Digital Compass: the European way for the Digital Decade. Available online: https://eur-lex.europa.eu/legal-content/en/TXT/?uri=CELEX%3A52021DC0118
[11] Z. Jeli B. Popokonstantinovic, and Stojicevic M., "Usage of 3D Computer Modelling in Learning Engineering Graphics," In Virtual Learning, InTechOpen, pp. 49–70.
[12] G. Gay and R. Blades, Information Technology, Oxford Information Technology for CSEC, 3rd edition, 2019.
[13] Introduction to Computers and Information Technology, Prentice Hall, 2011.
[14] S. J. Russell and P. Norvig, Artificial Intelligence: A Modern Approach, 3rd edition, 2015.
[15] European Commission, 2020. On Artificial Intelligence - A European approach to excellence and trust. Available online: https://ec.europa.eu/info/publications/white-paper-artificial-intelligence-european-approach-excellence-and-trust_en
[16] European Commission, 2020. A European strategy for data. Available online: https://eur-lex.europa.eu/legal-content/EN/TXT/?qid=1593073685620&uri=CELEX:52020DC0066
[17] B. Marr, Big Data: Using SMART Big Data, Analytics and Metrics To Make Better Decisions and Improve Performance, John Wiley & Sons, 2015.
[18] G. Veneri and A. Capasso, Hands-On Industrial Internet of Things: Create a powerful Industrial IoT infrastructure using Industry 4.0, Packt Publishing Ltd, 2018.
[19] F. Tao, M. Zhang, and A.Y.C. Nee, Digital Twin Driven Smart Manufacturing, 1st Edition, Academic Press, 2019.
[20] T. Döbler, B. Sniderman, M. Mahto, and C. Ahrens, Driving innovation and new business models through Industry 4.0, Deloitte insights, 2020.

 ISBN 978-86-7466-930-3

# Denoising the open-loop step response using an encoder-decoder convolutional neural network

Natalija Đorđević, Nenad Džamić, Aleksa Stojić, Goran Kvaščev

***Abstract*—Denoising signals is used as a preprocessing step for all signal processing. ncoder-decoder neural networ s are often proposed as a method of denoising 1D and 2D signals, because of their ability to e tract essential features from the signal and then recreate it without noise. In this paper we propose a simple architecture of a convolutional neural networ for denoising step responses of systems with different open-loop transfer function. The networ is trained on synthetic data with added noise of different distributions, then tested on a portion of synthetic data and real-life step responses.**

***Index Terms*— denoising, encoder-decoder, convolutional neural networ , step response**

## I. INTRODUCTION

Signal denoising is an important preprocessing step in every type of signal processing. Even though many observations can be made on generated pure signals, real-life signals always come with a certain amount of noise. For any signals measured on electrical circuits, noise cause can be the imperfect design or layout of the circuit itself, faulty components, close proximity to other electrical equipment, environmental causes etc. However, even if causes are known, the behavior of noise is unpredictable and rarely fits into a specific probability density function. Having a denoising method that would be applicable to different types of signals and noises would be of great importance for signal processing.

In the paper [1], authors used deep recurrent denoising neural networks to denoise ECG signals and improve signal-to-noise ratio of signal from -8.82dB to 7.71dB. They used a synthetic dataset with added noise. Medical signals such as ECG are of great importance, which shows in the number of papers that deal with their denoising. Once again, a convolutional neural network proves efficient with ECG signals in [2]. Seismic data is one of the representatives of noisy real-life data, and effective use of deep convolutional neural networks for denoising of synthetic seismic data can be seen in [3]. Using a convolutional network for denoising images with Gaussian noise is also proposed in [4]. There is not a single specific architecture for denoising convolutional networks that is superior, and a useful comparison of different kinds is given in [5]. However, one structure seems to be mentioned for multiple purposes, and it is the encoder-decoder structure. The authors in [6] suggest the use of an autoencoder for medical image denoising, which served as an initial inspiration to use encoder-decoder networks for 1D signals. Application of the encoder-decoder structure on denoising micro seismic signals is shown in [7].

In this paper we have trained an encoder-decoder neural network to denoise a step response of an open-loop system. This particular structure seemed promising and in various papers was proven to perform well in denoising for different purposes. Its great advantage is that it does not have strict limitations on the results it can produce. There are however many things that have an effect on its performance, such as the architecture, hyperparameters, the dataset etc. In this paper we attempted to make a structure that is not complicated, but performs well, as well as to generate a dataset that is informative enough for our neural network. The reason that the step response signal was chosen is its importance in observing how industrial processes react to a change in reference value. Without diving into the details of which processes each system represents, we will define their behavior only by their open-loop transfer functions.

## II. DATASET SYNTHESIS

Collecting data for neural networks can be expensive and time-consuming. In order for our dataset to be as diverse as possible and simultaneously to represent many industrial processes, we used equation (1) as a general form for our open-loop transfer function. [8].

$$G(s) = \frac{e^{-\theta_d s}(1-\alpha s)}{(s+1)^n} \quad (1)$$

Parameter $\theta_d$ represents transport delay which is the amount of time that our system needs to react to a change in reference value. The measure $1/\alpha$ represents the position of a zero in the right half-plane. The system in which $\alpha$ is not equal to zero is called the non-minimum phase system and in its step response we can see an initial dip in value before a rise towards the reference value. An example is shown in Fig.1. Finally, the parameter $n$ refers to the order of the system which, in general, dictates the dynamic of the system.

Natalija Đorđević is a teaching associate at the Signals and systems department at the School of Electrical Engineering, University of Belgrade, 73 Bulevar kralja Aleksandra, 11020 Belgrade, Serbia (e-mail: natalija.djordjevic@etf..bg.ac.rs)

Nenad Džamić is with the School of Electrical Engineering, University of Belgrade, 73 Bulevar kralja Aleksandra, 11020 Belgrade, Serbia (e-mail: dn213336m@student.etf.bg.ac.rs)

Aleksa Stojić is a teaching associate at the Signals and systems department at the School of Electrical Engineering, University of Belgrade, 73 Bulevar kralja Aleksandra, 11020 Belgrade, Serbia (e-mail: aleksa.stojic@etf..bg.ac.rs)

Goran Kvaščev is a associate professor at the Signals and systems department at the School of Electrical Engineering, University of Belgrade, 73 Bulevar kralja Aleksandra, 11020 Belgrade, Serbia (e-mail: kvascev@etf..bg.ac.rs)

 ISBN 978-86-7466-930-3

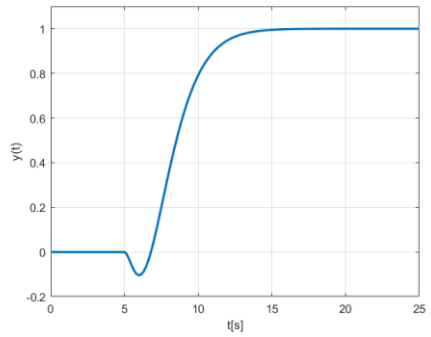


Fig. 1. Step response for a non-minimum phase system with parameters: $\theta_d = 5, n = 3, \alpha = 1$.

Convolutional neural networks are known for needing a large training set to perform well. These parameters can drastically change the output of the system which means that, in order to get a diverse dataset, we should try as many combinations as possible. We generated pure step responses for transfer functions which include parameter values given in Table I. Each signal has a duration of 25s and is sampled with a step size of 0.1s, making it 251 samples long.

TABLE I
TRANSFER FUNCTION PARAMETER VALUES

| | Minimum value | Maximum value | Step size |
|---|---|---|---|
| $\theta_d$ | 0 | 10 | 0.2 |
| $\alpha$ | 0 | 2 | 0.05 |
| n | 1 | 8 | 1 |

To every pure signal we generated, we added three types of noise. Given that real-life noise rarely fits into one specific probability density function, feeding different types of noise to our neural network seemed as a good way to have it generalize well after it is trained. The three types of noise added are Gaussian white noise, uniform noise and noise with Rayleigh distribution. All three types of noise have a standard deviation of 0.05. Probability density functions are given in equations (2), (3) and (4), respectively and shown in Fig.2.

$$p(x) = \frac{1}{\sigma\sqrt{2\pi}} e^{-0.5\left(\frac{x}{\sigma}\right)^2};\ \sigma = 0.05 \tag{2}$$

$$p(x) = \begin{cases} 10/\sqrt{3}, & x \in \{-0.05\sqrt{3}, 0.05\sqrt{3}\} \\ 0, & x \notin \{-0.05\sqrt{3}, 0.05\sqrt{3}\} \end{cases} \tag{3}$$

$$p(x) = \frac{x}{\sigma^2} e^{-x^2/(2\sigma^2)},\ \sigma = 0.05\sqrt{\frac{2}{4-\pi}} \tag{4}$$

The expected value of the Rayleigh distribution given in equation (4) is a positive non-zero value, so to avoid having an offset in our noise we subtracted the expected value.

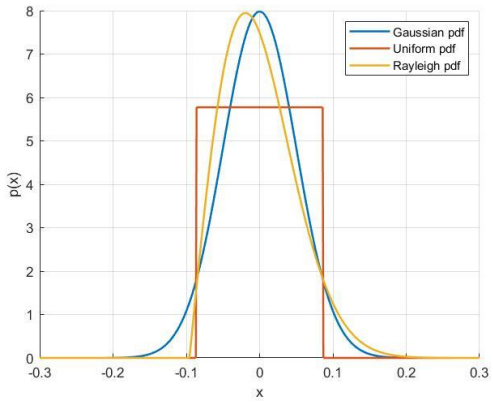


Fig. 2. Comparing three different noise probability density functions.

Final dataset has 50184 samples and 25% percent of it is intended for testing, while the rest is used for training. The test set consists of all step responses for systems of order 4 and 5, while all other orders belong to the training set. This will allow us to test our network on system orders that it has not encountered during training.

## III. ARCHITECTURE AND TRAINING OF NEURAL NETWORK

When the term ‘denoising’ is mentioned in the context of neural networks, the autoencoder neural networks are usually suggested as an appropriate architecture. The idea behind them is to have an encoder part of the network, whose role is to extract features from the given input, followed by the decoder part, which tries to recreate the input from the features. Autoencoder networks are a type of unsupervised learning, because the desired output is the same as the input, therefore the input/output pair is not explicitly given during training. These networks served as an inspiration for this paper and creating the encoder-decoder architecture.

Encoder-decoder neural networks fall into the category of convolutional networks and the term ‘convolutional’ refers to the method of feature extraction. Let us consider that the input is a 2D matrix, such as a photograph. The dimensions of the photograph tend to be quite large and if we were to feed it to a regular fully-connected neural network, we would have too many trainable parameters. This would imply a huge amount of time to train and a lot of unnecessary computational resources. Also, each pixel itself might not carry as much information about the photograph as their relations do. So instead of treating individual pixels as separate entities, the idea behind convolutional neural networks is to have filters in the form of kernels (matrices with smaller dimensions) whose parameters are to be learned, which in convolution with the input would produce something more informational. Convolution is simply ‘sliding’ the kernel across the photo and multiplying it with appropriate submatrix of the photo. This way, instead of trying to learn a million neurons, the network has to learn filters which would extract meaningful features. The general advantage of neural networks is that it is not necessary for us to have insight into exactly what these filters are and what features they extract, but only how well the output is decoded using those features.

 ISBN 978-86-7466-930-3

Convolution can also be done with 1D inputs, such as various forms of signals. The principal of convolution stays the same and the kernel is now a vector instead of a matrix. As previously mentioned, the aim of this project is to use a convolutional encoder-decoder network to denoise a step response of an open-loop system.

For this purpose we used *python* and the *tensorflow* library. It allows users to build a sequential neural network model by adding desired layers one-by-one.

For the encoder part of the network, we followed a standard structure of convolutional networks which implies alternatively adding convolutional layers and pooling layers. Convolutional layers learn kernel parameters and produce a convolution of the input with the kernel. It is common practice to have kernels with small dimensions, so in every convolutional layer we used kernels of size 5 (vectors of length 5). Every convolutional layer we added is followed by a *ma -pooling* layer, whose role is to cut down the dimensions. It takes subvectors (of the specified size) of the input and produces an output which is the maximum value of the subvector. If the size is properly defined, we get the effect of having less computation needed, without any crucial loss in information.

The decoder part of the network has the inverse structure of the encoder part. Therefore, all convolutional layers are replaced with transposed convolutional layers. They perform deconvolution, which is an inverse operation to convolution. Opposite of *ma -pooling* layers are *upsampling* layers. They once again make the dimensions larger by repeating the values of their input a specified amount of times. It is easy to notice that the output of the *upsampling* layers will not be exactly the same as the input of *ma -pooling* layers.

The final architecture we chose is the simplest one that performed well. Details of its structure are shown in Table II. and Fig. 3.

TABLE II
ARCHITECTURE OF NEURAL NETWORK

| Layer type | Kernel size | Output shape |
|---|---|---|
| Convolutional | 5 | (1, 247, 128) |
| Max-pooling | 2 | (1, 124, 128) |
| Convolutional | 5 | (1, 120, 64) |
| Max-pooling | 2 | (1, 60, 64) |
| Transposed convolutional | 5 | (1, 64, 64) |
| Upsampling | 2 | (1, 128, 64) |
| Transposed convolution | 5 | (1, 132, 128) |
| Upsampling | 2 | (1, 264, 128) |
| Convolutional | 5 | (1, 264, 1) |
| Cropping | / | (1, 251, 1) |

The activation function for all layers is ReLU, except for the output layer whose activation function always depends on what the network is trying to predict. Since in our case we are doing regression, the adequate activation function is linear. The metric used to access the performance is mean-squared error, also suitable for regression.

When training a neural network it is necessary to make sure not to overfit it to the training data. Overfitting is a term used to describe the behaviour of a network that performs very well on training data, but has problems with data that it has not encountered during training, i.e. it generalizes poorly. One method to prevent overfitting we already implicitly implemented by making a large training dataset. Having a diverse dataset with many samples decreases the chances of overfitting. We also added a kernel constraint with value 3 to every layer, which stops parameters from rising above the given value. Popular method to avoid overfitting is also adding *dropout* layers after convolutional layers. Their role is to remove certain neurons with a specified rate and have them not impact the output. Adding *dropout* layers did not make the network perform better, so they were left out. 20% of samples in the dataset were used for validation. Finally, the network was trained for 7 epochs in mini-batches of size 32.

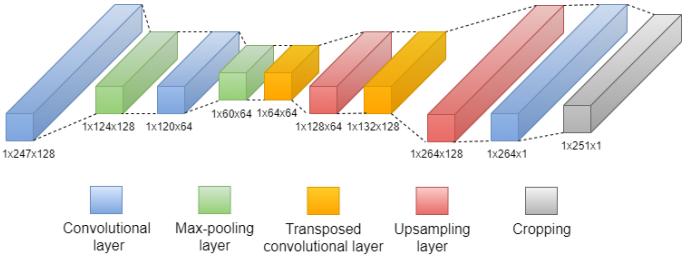


Fig. 3. Neural network architecture

The optimizer used is *Adam* optimizer, which is a type of a stochastic gradient descent algorithm. It is known for keeping track of the first and second momentum to provide quicker and more stable convergence. Its primary hyperparameters are learning rate, $\beta_1$ and $\beta_2$. We used stochastic grid-search to find optimal hyperparameter values and they are: learning rate = 0.0005, $\beta_1 = 0.9$ and $\beta_2 = 0.99$.

## IV. RESULTS

The network was first tested on a generated test set mentioned in chapter II. Average mean-squared error (mse) on the entire test set and on separate noise types are shown in Table III. In Fig. 5 the average values and standard deviations of mse for each of the noises are shown. Gaussian noise has the highest error, however all three have values bellow $9e^{-5}$. One more metric to asses the denoising process is comparing the signal-to-noise ratios (SNR) of signals before and after denoising. The average SNR for all types of noise was 53.5dB in the beginning. Signal-to-noise ratios after denoising are given in Table III.


ISBN 978-86-7466-930-3

TABLE III
MEAN-SQUARED ERROR FOR DIFFERENT NOISE TYPES

| | MSE | SNR (dB) |
|---|---|---|
| Gaussian noise | $8.84e^{-5}$ | 87.8 |
| Uniform noise | $8.14e^{-5}$ | 88.6 |
| Rayleigh noise | $7.21e^{-5}$ | 89.9 |
| Entire test set | $8.06e^{-5}$ | 88.8 |

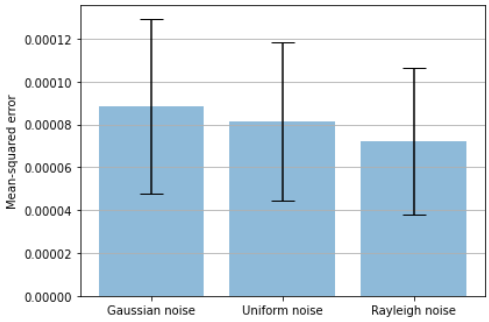


Fig. 4. Means and standard deviations of mean-squared errors for each noise

In Fig 5A. there are three representative step responses: one for each of the three types of noises. Based on observing, the output of the network seems to follow the signal dynamic well. Judging by the mean-squared error and Fig. 5A, Gaussian noise is the most difficult to remove, while Rayleigh noise seems the easiest to remove.

Next step was to test our network in a real-world environment to see how it handles a step response with noise which does not specifically match any distribution. The system we tested on was a handmade dryer that consists of a chamber on a metal surface and it has three platinum temperature sensors and one sensor which measures the airflow. The chamber is 1m long and has a heater of 400W and a ventilator on one side. Since airflow is not steady and turbulence occurs, the signal we captured is very noisy. In Fig 5B. there are three different original signals of airflow, as well as their denoised version. The results are satisfactory considering the amount of noise and the fact that the exact transfer function was not included in the training set.

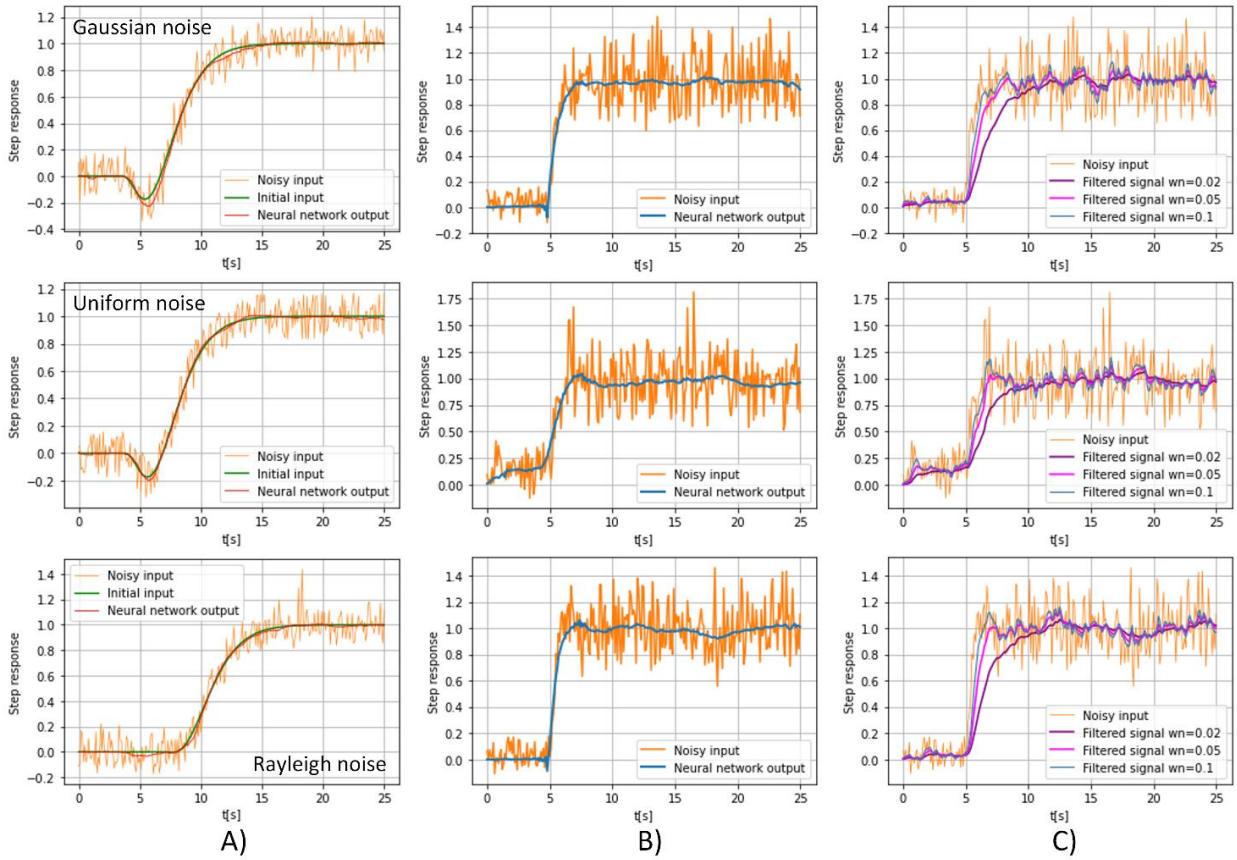


Fig. 5. Step responses before and after denoising. A) synthetic data, B) airflow signal after neural network, C) airflow signal filtered with Butterworth filter

To compare our results with classical filtering methods, we give the same noisy inputs but filtered with a first order Butterworth filter with different normalized frequencies in Fig. 5C. We see that in order to not compromise the dynamic of the signal, we have to settle for less noise removal. The neural network we trained gives better results in terms of removing noise, but still following the dynamic. The comparison we did gives us an insight into why using a neural network for denoising could be a justified option. Conventional filtering methods often have to make sacrifices in terms of degrading

 ISBN 978-86-7466-930-3

some other signal characteristics. Even though the structure of the neural network is not necessarily simple for all purposes, it is very flexible, and if we feed it the right amount of input data to learn from, the results it yields can be satisfactory in many ways.

## V. CONCLUSION

The architecture of neural network used in this paper shows great potential for signal denoising. The proposed general form of transfer function in equation (1) also proved to be enough for the network to be able to follow the step response dynamic well. The next step in improving performance and extending it to other signals can move in a couple of directions. Having a training set with more noise distributions would also help the network generalize even better. Next possible extension could be having step responses with added disturbances at different moments in time in our dataset, as well as creating open-loop transfer functions in a more generalized form.

## ACKNOWLEDGMENT

The paper was co-funded by the Ministry of Education, Science, and Technological Development of the Republic of Serbia. This year's contract number is 451-03-68/2022-14/200103.

## REFERENCES

[1] Antczak, Karol. "Deep recurrent neural networks for ECG signal denoising." *ar i preprint ar i 1 0 .11551* (2018).

[2] Arsene, Corneliu TC, Richard Hankins, and Hujun Yin. "Deep learning models for denoising ECG signals." *201 2 th European Signal Processing Conference E SIPC* . IEEE, 2019.

[3] Zhu, Weiqiang, S. Mostafa Mousavi, and Gregory C. Beroza. "Seismic signal denoising and decomposition using deep neural networks." *IEEE Transactions on Geoscience and emote Sensing* 57.11 (2019): 9476-9488.

[4] Murali, Vineeth, and P. V. Sudeep. "Image denoising using DnCNN: an exploration study." Advances in Communication Systems and Networks. Springer, Singapore, 2020. 847-859.

[5] Thakur, R. S., Yadav, R. N., & Gupta, L. (2019). State-of-art analysis of image denoising methods using convolutional neural networks. *IET Image Processing*, *13*(13), 2367-2380.

[6] Gondara, Lovedeep. "Medical image denoising using convolutional denoising autoencoders." *201 IEEE 1 th international conference on data mining workshops IC MW* . IEEE, 2016

[7] Zhang, Hang, et al. "Microseismic signal denoising and separation based on fully convolutional encoder–decoder network." *Applied Sciences* 10.18 (2020): 6621.

[8] Goran Kvaščev. "Dalji razvoj i uporedna analiza procedura za eksperimentalno projektovanje i podešavanje industrijskih regulatora" Magister's thesis, 2005.

 ISBN 978-86-7466-930-3

# Single Screw Extruder Temperature Control Using PLC and HMI in Cable Production Process

Igor Kocić, Saša S. Nikolić, Aleksandra Milovanović, Darko Mitić, Petar Đekić and Nikola Danković

***Abstract*— In this paper it is developed and described the control software for the temperature regulation of the extruder zones with the mutual influence of zones. Extruder zone temperature control realized using Siemens PID_Temp block FB1132. PID_Temp block does not take into account the interaction of zones. This effect can only be taken into account if all zones are adjusted at the same time. The temperature process of the extruder was identified with an emphasis on the mutual influence of the zones. After that, a simulation was performed in Matlab and Simulink, and the results were experimentally verified using Siemens' LSim_LIB_V3_0_0 library and in a real process.**

***Index Terms*— Extrusion, zone temperature identification, PID Temp controller, PID tuning.**

## I. Introduction

Extrusion [1, 8] of plastics and rubber is basically a continuous process. The starting raw material is usually in powder or granules, while in the case of rubber extruders it can also be in the form of a belt. The raw material moves from the basket under the action of gravity towards the feeder, and then enters the cylinder. A screw is placed in the cylinder, which transports the mass in advance under the action of the drive, the mass is further heated, homogenized and finally formed into the desired shape by passing through the tool. The machine in which this process takes place is called an extruder. Single-screw extruders have a huge application in polymer processing, they are simple constructions, have good technical performance, they are cheaper than multi-screw extruders.

Extruder temperature control is a problem that occurs very often in the industry. The main goal of temperature control is to maintain the set temperature. The extruder [1] consists of three basic units:

1. feed zone,
2. melting (compression) zone, and
3. pumping zone

In Section II we analysis the mutual influence of zones in terms of heat transfer from zone to zone on real extruder. Based on the recorded characteristics for zones 1, 2 and 3, a model of the mutual influence of the zones was made. Based on the zone influence model, the synthesis of the temperature controller was performed in Section III using the Siemens PID Temp controller and software was written in SCL for the simultaneous setting of the PID parameters of the zone controller. In chapter four, a check of the controller operation was performed using the Siemens simulation library LSim_LIB_V3_0_0.

Igor Kocić, Saša S. Nikolić, Aleksandra Milovanović, Darko Mitić, and Nikola Danković are with the University of Niš, Faculty of Electronic Engineering, Department of Control Systems, Aleksandra Medvedeva 14, 18000 Niš, Serbia (e-mails: {igor.kocic, sasa.s.nikolic, aleksandra.milovanovic, darko.mitic, nikola.dankovic}@elfak.ni.ac.rs)

Petar Đekić is with The Academy of Applied Technical and Preschool Studies-Niš, Aleksandra Medvedeva 20, Niš, Serbia, e-mail: petar.djekic@akademijanis.edu.rs

## II. Extruder Zone Temperature Identification

Figure 1 shows a diagram of a single-screw extruder [1] with nine zones. The basic parts of each extruder are hopper, barrel, screw and head with tool. Each zone of the extruder has its own heating heater, if necessary a cooling fan and a sensor that measures the current temperature value. In addition to measuring the temperature, the melting pressure is also measured at the place where the tool is located. Zones 1 to 5 have heater and cooler, zones 6 to 9 have only heater, cooling is done by the influence of ambient temperature.

It is noticed that zones 2, 3, ..., 8 are inner zones, and zones 1 and 9 are outer zones, and therefore the character of heat dissipation is different.

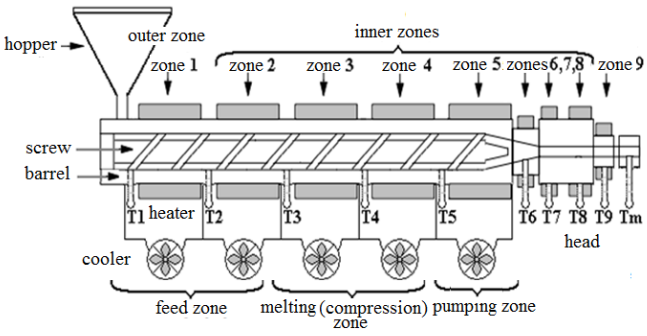


Fig. 1. Diagram of a single-screw PVC extruder

In determining the mutual influence of the zones, we started from the assumption that the control object in this case is the extruder cylinder is homogeneous and isotropic, which is correct because it is made of the same material. The influence of the heater and fan transmission function has not been considered.

In the general case, the temperature field of the extruder cylinder is non-stationary and can be described by the

 ISBN 978-86-7466-930-3

following equation [4, 8]:

$$T = f(x, y, z, t) \tag{1}$$

When heating, the temperature at the measuring points changes over time (2), for isotropic materials, Fourier's law [8] of heat conduction applies (3), where $Q$ is the amount of heat, $S$ is the area, $dQ/dS$ is the specific heat flux, and $\lambda$ is the heat conduction coefficient:

$$\frac{\partial T}{\partial t} \neq 0 \tag{2}$$

$$dQ = -\lambda \nabla(T) dS dt. \tag{3}$$

If we take into account that the temperature changes over time, which is the case, we get a partial differential equation of parabolic type:

$$\frac{\partial T}{\partial t} = a \frac{\partial^2 T}{\partial x^2} \tag{4}$$

For further simplification, it is assumed that the temperature at the measuring points is equal to the temperature of the entire section, the temperature of the section is considered to be the temperature of the extruder zone. In this way, we consider sections to be isothermal surfaces. For the of further simplification, we will consider that the temperature is transferred only along the x axis ($x>>y$, z in practice the ratio of length and diameter of the cylinder in PVC extruders is large) Fig. 2 and that it is a stationary temperature field. At the time of temperature measurement at the zone boundaries, we can consider it constant.

If we now observe the part of the cylinder between the temperature measurement points of zone 1 (T1) and zone 2 (T2) and consider that these temperatures are constants, and then the following applies to the temperature field Eqs. (4) and (5) reduces to (6) where a is thermal diffusion coefficient:

$$\frac{\partial T}{\partial t} = a\left(\frac{\partial^2 T}{\partial x^2} + \frac{\partial^2 T}{\partial y^2} + \frac{\partial^2 T}{\partial z^2}\right) \tag{5}$$

$$\frac{\partial T}{\partial t} = 0 \ , \frac{\partial T}{\partial y} = 0, \frac{\partial T}{\partial y} = 0 \tag{6}$$

$$a \frac{\partial^2 T}{\partial x^2} = 0 \tag{7}$$

$$\frac{\partial T}{\partial x} = const. \tag{8}$$

By integrating (7) and taking the boundary conditions T(0)=T1, T(L)=T2, where L is the distance from the temperature measurement point T1 to T2, we get that the temperature in x coordinates changes according to (8):

$$T(x) = T_1 - \frac{T_1 - T_2}{L} x \tag{9}$$

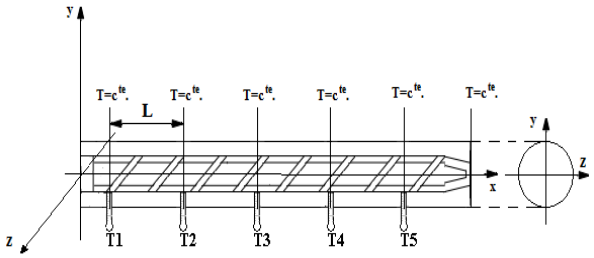


Fig. 2. Extruder cylinder (barrel) in *x*, *y*, *z* coordinate system observed along the x axis

When performing the above equation, we started from the assumption that T1>T2, that only zone 1 is heated, and zone 2 is not. In order to determine the mutual influence of the zones, measured was applied on real Royle 4 1/2" extruder during heating and cooling, heating of zone 1 was done first, where the temperatures in zones 1 and 2 were measured, zone 2 was not heated. The ambient temperature at which the experiment was performed is Ta=17°C. Fig. 3 shows the influence of zone 1 on zone 2 as well as the temperature difference between zones 1 and 2.

The extruder was then cooled to ambient temperature. Only zone 2 was heated and the characteristics of zone 2 were recorded. Then the extruder was cooled, and zones 1, 2 and 3 were heated, and the temperature characteristics of zones 1, 2 and 3 were recorded at the same time so that the mutual influence of zones could be considered. Fig. 5.a shows the characteristics of only zone 2 which is heated by itself and Fig. 5.b shows the characteristics of zones 1, 2 and 3 which are heated at the same time. The extruder is heated to a temperature of 100 ° C, which corresponds to a time of about 25 min. Ambient temperature $T_a$=17°C.

The Matlab software package was used to draw the temperature characteristics of the characteristic zones.

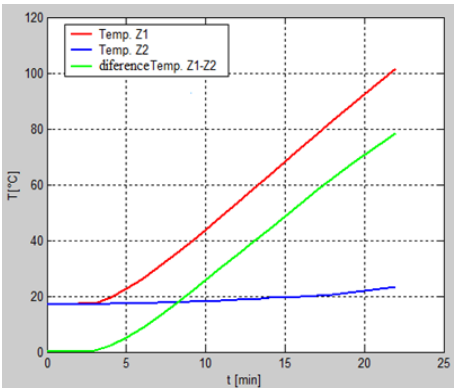


Fig. 3. Influence of Zone 1 to Zone 2


ISBN 978-86-7466-930-3

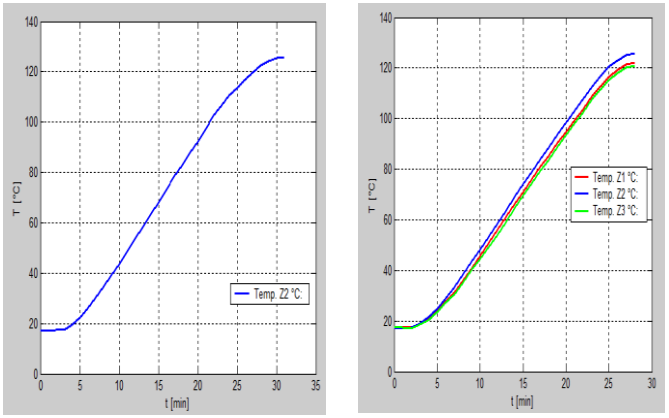


Fig. 4. Characteristics of heated

From Fig. 4 it is clearly seen that the heat transfer from zones 1 and 3 directly affects the temperature of zone 2. In Fig. 5.b we notice that the temperature of zone 1 is slightly higher than the temperature of zone 3, the reason is that zone 1 is the outer zone , and its adjacent zone is the feeder zone whose mass is less than zone 4. Zone 4 is not heated, so part of the heat from zone 3 passed to it.

In identifying and determining the process model, we started from the FOPDT model (9), which approximated the process, starting from the assumption that the transfer function of the object that controls astatism is zero. The parameters of the model are determined on the basis of the bounce response in the open coupling. The moment when the bounce trigger is brought is considered as the zero moment. Based on the recorded characteristics, the dead time $T_u$, the time constant $T_u$ and the gain $K$ were determined using the Küpfmüller method [10], so the model of the heating process for all three zones is described by the transfer function:

$$G_{ob}(s) = \frac{k_{ob}}{1+sT_{ob}} e^{-sT_u} \qquad (10)$$

To determine the parameters $T_u$ and $T_{ob}$, a program was written in Matlab. Table gives the values first only for zone 2 when only it is heated, and then for zones 1, 2 and 3 that are heated at the same time.

TABLE I
HEATING ZONE 2 ONLY, AND ZONE 1, 2, 3

| | only zone 2 is heated | zone 1, 2, 3 are heated at the same time | | |
|---|---|---|---|---|
| | zone 2 | zone 1 | zone 2 | zone 3 |
| $T_u$[min] | 5.5882 | 5.05769 | 4.214 | 5.117 |
| $T_{ob}$[min] | 21.098 | 16.654 | 16.214 | 17.153 |
| $K_{ob}$ | 0.869 | 0.912 | 0.945 | 0.902 |

Based on the measurements, it is clear that the times $T_u$ and $T_{ob}$ for zone 2 are higher when only zone 2 is heated. It can also be seen that when zones 1, 2, 3 are heated, that zone 2 reaches the temperature the fastest, where the impact of zone 1 and zone 3 on zone 2 is observed.

FOPDT models of zones 1, 2 and 3 were used for the initial analysis of the process. For further analysis, an attempt was made to determine the $PT_2$ model based on the Streitz approximation through two points [3]. The $PT_2$ process model is given in (11) where $K$ are the gain of the object, and $T_2$ are the time constants of the $PT_2$ model.

$$G_{ob}(s) = \frac{k_{ob}}{(1+sT_1)(1+sT_2)} \qquad (11)$$

If the analysis of the ratio $T_{ob}/T_u$ from table I according to table II ($T_{ob}/T_u$<9,65) is performed, it is concluded that it is impossible to determine the characteristics of the process described by the $PT_2$ model according to Streitz's identification method [3]. After that, models were determined for all three zones based on the $PT_N$ model (12), where $T$ is the process time constant, n is the order of the $PT_N$ model, $T_{ob}$ is the object gain taken from the FOPDT model [3]:

$$G_{ob}(s) = \frac{k_{ob}}{(1+sT)^n} \qquad (12)$$

TABLE II
RELATIONSHIP BEETWEN FOPTD AND PTN MODEL

| n | 1 | 2 | 3 | 4 | 5 | 6 | 7 |
|---|---|---|---|---|---|---|---|
| $T_{ob}/T_u$ | | 9.65 | 4.59 | 3.13 | 2.44 | 2.03 | 1.75 |
| $T_{ob}/T$ | 1 | 2.718 | 3.695 | 4.463 | 5.119 | 5.699 | 6.226 |
| $T_u/T$ | 0 | 0.282 | 0.805 | 1.425 | 2.1 | 2.811 | 3.549 |

Based on that, a model of the third order process is made for all three zones. To calculate the time constant of the $PT_N$ model, a program was written in Matlab. The time constants $T$ for the sweater zones are given in Table III.

TABLE III
VALUE OF THE TIME CONSTANT OF THE PTN MODEL

| | only zone 2 is heated | zone 1,2,3 are heated at the same time | | |
|---|---|---|---|---|
| | zone 2 (n=3) | zone 1 (n=3) | zone 2 (n=3) | zone 3 (n=3) |
| T [min] | 5.710 | 4.507 | 4.3887 | 4.643 |

Figure 5a shows the temperature difference $T_{z2}-T_{z1}, T_{z2}-T_{z3}$ and Fig. 5b analyzes the influence of zone 1 on zone 2 according to the equation $(T_{z2}-T_{z1})/T_{z2}$ and the influence of zone 3 on zone 2 according to the equation $(T_{z2}-T_{z3})/T_{z2}$.

The mutual influence of the zones during the simultaneous heating of zones 1, 2 and 3 is the greatest during the transition process when it moves up to 8%, after that it decreases and moves in up to 4% Fig. 5.


ISBN 978-86-7466-930-3

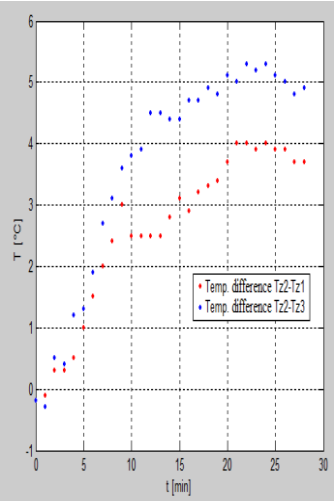


Fig. 5a.

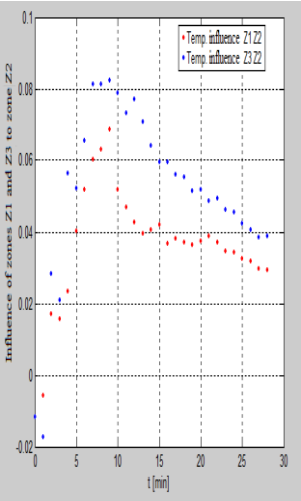


Fig. 5b.

Fig. 5. Influence of zones Z1 and Z3 on zone Z2

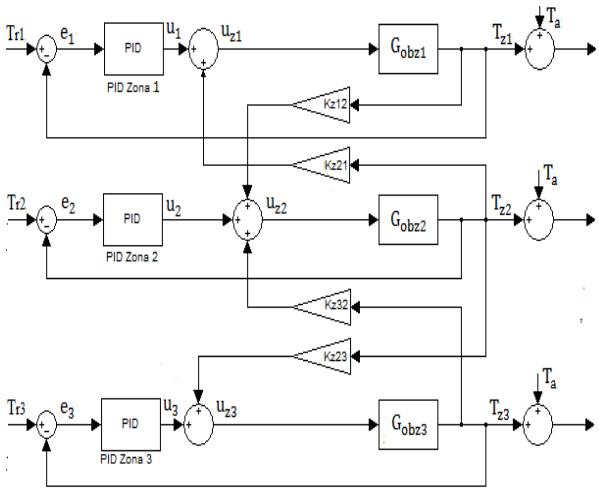


Fig. 6. Model of mutual influence of zones

It is noticed that the temperature difference between zone 2 and zone 3 is greater than between zone 2 and zone 1, the reason is that zone 1 is an external zone, and adjacent to zone 3 is zone 4 which is not heated, so part of the heat is removed from zone 3 to zone 4. Fig. 6 shows a model of the mutual influence of zones.

The equation (13) [9, 10] applies to the simulation model of the impact of zones 1 and 3 on zone 2:

$$T_{z2}(s) = G_{obz2}\left(u_2 + k_{z12}T_{z1} + k_{z32}T_{z3}\right) \qquad (13)$$

In general, applies equation (14), where ($i$ = 1,…,$n$) is denoted by observed zone:

$$T_{zi}(s) = G_{obzi}\left(u_2 + k_{z(i-1)i}T_{z(i-1)} + k_{z(i+1)i}T_{z(i+1)}\right) \qquad (14)$$

When it is taken into account that zone 2 affects zones 1 and 3, can applies equation (15) [9,10] where the coefficient $K_{z2z2}$ takes into account that part of the energy of zone 2 is spent on heating zones 1 and 3.

$$T_{z2}(s) = G_{obz2}\left(u_2 + k_{z12}T_{z1} + k_{z32}T_{z3} - k_{z2z3}T_2\right) \qquad (15)$$

When simulating the mutual influence of zone heating, all zones are identified separately. This means that it is necessary to heat only the observed zone, make its model, cool it and its neighboring zones. Repeat the procedure for all zones observed. In this way, the coefficient $K_{z22}$ can be determined by comparing the influences when the heated zones are individually and all at once, so model (14) is applied for the simulation.

## III. SYNTHESIS TEMPERATURE CONTROLLER

Zone temperature controler is realized using a Siemens PID_Temp block FB1132 [10] with anti windup function and adjustable weight coefficients for proportional and integral action which is a continuous PID controller designed for heating and cooling applications, where y is output of PID controller, $K_p$ proportional gain, $b$ weight coefficient of proportional action, w set value, x measured value, $T_i$ time constant of integral action, $T_d$ time constant of differential action, and time delay differential action, $c$ weighting coefficient of differential action.

$$y = k_p\left[(bw - x) + \frac{1}{T_i s}(w - x) + \frac{T_d s}{aT_d s + 1}(cw - x)\right]. \qquad (16)$$

The PIDT controller (Siemens PID temperature controller block) (16) is integrated within the PID_Temp block [10]. The configuration and algorithm for setting the parameters of the PID_Temp block parameters is performed using the TIA Portal, where one instance is created for each control loop. For zone i, InstPIDTemp(i) is assigned a data block specifically DB(i) within which all settings for that instance are stored. Instances are called from the OB30 block (cyclic interupt) Fig. 7 whose call time is set to 0.1s.

The PID_Temp block has two setup algorithms: pretuning and Fine Tune. For both tuning algorithms from TIA Portal software Siemens does not give a closer explanation of which criterion it uses to obtain parameters. Specifies only the necessary conditions for executing tuning algorithms.


ISBN 978-86-7466-930-3

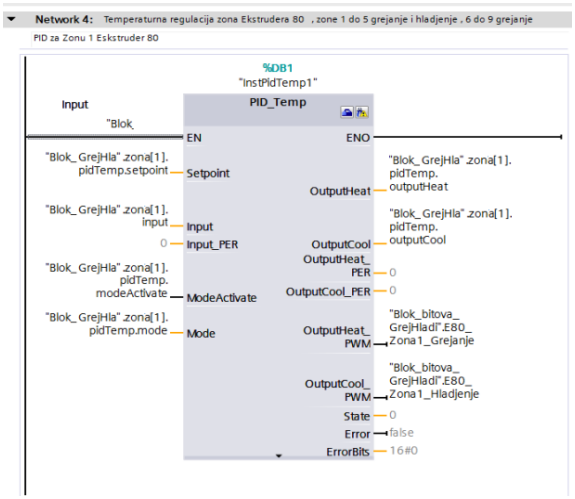


Fig. 7. Calling InstPIDTemp1 from OB30 block for zone 1

The disadvantage of individual adjustment of zones [11, 14] is reflected in the fact that the mutual influence of zones through thermal coupling is not fully taken into account. For this reason, software has been developed to simultaneously enable the setting of all zones from the HMI panel.

Before switching on the pre-tuning, the temperatures of the operating points of all zones are set, which must be higher than the current temperature, it is best to start from the ambient temperature. The inactive PID mode is selected for all zones. When performing pre-tuning, the heating pre-tuning is performed first, the cooling of the zones is temporarily switched off so that one of the zones does not adjust the heating parameters and its adjacent zones have completed the adjustment and switched to cooling mode. This creates a false temperature coupling. When the setting of the heating parameters is completed, the setting of the cooling parameters for all zones is switched on.

## IV. Experimental Results

Experimental results were obtained using Royle 4_1/2" extruder for PVC insulation and Siemens library LSim_LIB_V3_0_0 [15], Siemens PLC type S7 1500 3PN/DP, HMI 1500 Comfort series. The simulation of the interaction of zones 1, 2 and 3 was implemented in the software using the model of the interaction of zones by (14), Fig. 8.

The zone transfer functions are simulated by the Siemens function to simulate the third-order process LSIM_PT3. Simulation software was written in SCL. Part of the Zone 2 simulation software is shown in Fig. 8.

The transfer function (12) was realized using the LSim_PT3 block. At the input of the block Block_Zone2 are the control signals from the PID block (InstPidTemp2) of zone 2 and the coefficients of mutual influence of the zones. In the function block Block_Zone2, a program is written that realizes the equation of influence of zone 1, 3 on zone 2 (13). The value thus obtained is fed to the input of the block LSim_PT3_Zone 2, at the output of which the value for the temperature of zone 2 is obtained.

In the theoretical part, only heating is considered, and here the results for heating and cooling are given, Table IV. The simulation program is called from the OB30 object block with a selection period of 0.1 s. In Fig. 9 shows the response ratio of the calculated PID controller according to the $PT_3$ model and the controller obtained using the PLC simulation library for zone 1. The time to reach the desired temperature of the extruder zones is completely satisfactory. given the mass of the extruder cylinder.

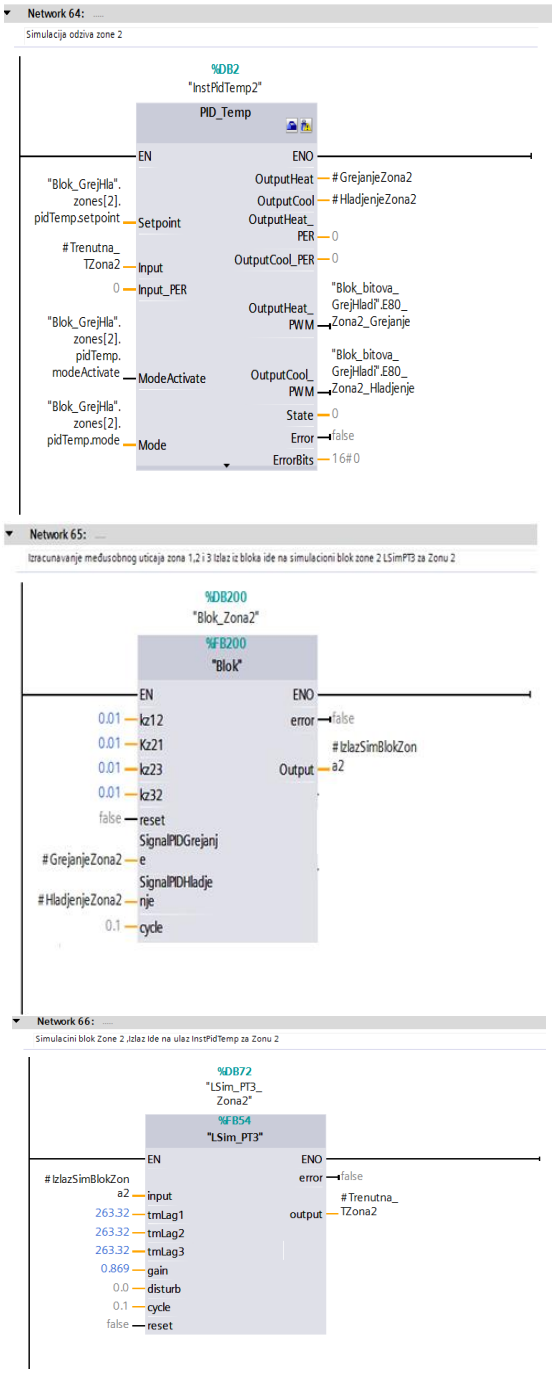


Fig. 8. Part of software for simulation of zone 2

 ISBN 978-86-7466-930-3

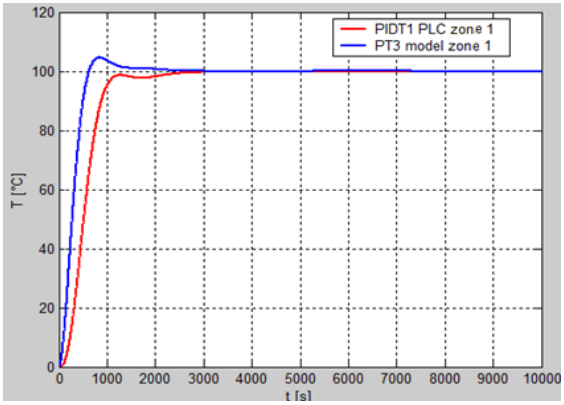


Fig. 9. Response characteristics of the calculated PID controller for $PT_3$ model and PIDT1 for Zone1 obtained by simulation using a PLC controller and a simulation library

TABLE IV
PID HEATING AND COOLING PARAMETERS OBTAINED USING SIMULATION ON PLC

| | PID heating parameters | | |
|---|---|---|---|
| | Zone 1 | Zone 2 | Zone 3 |
| Kr | 2.2338 | 2.1643 | 2.2562 |
| Ti | 816.98 | 756.866 | 875.896 |
| Td | 163.5282 | 158.118 | 167.8306 |
| a | 0.1 | 0.1 | 0.1 |
| b | 0.8 | 0.8 | 0.8 |
| c | 0 | 0 | 0 |
| | PID cooling parameters | | |
| | Zone 1 | Zone 2 | Zone 3 |
| Kr | 5.7454 | 5.7056 | 5.7557 |
| Ti | 317.126 | 273.652 | 359.381 |
| Td | 118.5414 | 114.6287 | 122.3443 |
| a | 0.1 | 0.1 | 0.1 |
| b | 0.8 | 0.8 | 0.8 |
| c | 0 | 0 | 0 |

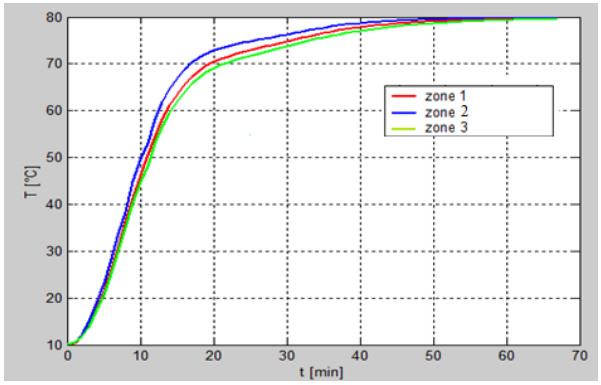


Fig. 10. Response characteristics zones 1, 2, 3 using simulation library

Figure 10 shows the real characteristics obtained by drawing in Matlab, based on the data collected by recording the temperatures of all three zones by entering in the DB block of the PLC during the simulation using the $PT_3$ SIM library.

## V. CONCLUSION

This paper presents zone temperature controler of extruder zones with special reference to the mutual influence of extruder zones. A model of mutual influence of zones is given, a simulation is done in TIA Portal.

It has been shown that the mutual influence of the zones during the simultaneous heating of the zones is greatest during the transition process when it moves up to 8%, after that it decreases and moves up to 4%.

The paper develops software for simultaneous adjustment of parameters of all extruder zones, as well as for adjustment of individual zones. The big advantage is that the software enables the adjustment of extruder zones from the HMI panel and not only from the TIA Portal software package.

## REFERENCES

[1] J.R. Wagner, E.M. Mount, and H.F. Giles, Extrusion: The Definitive Processing Guide and Handbook. USA, 2013.
[2] A. Visioli, Practical PID Control, Springer, London, UK, 2006.
[3] H. Uhbehauen and G. P. Rao, Identification of Continuous- time Systems, North-Holland Publishing Co., 1987.
[4] B.R. Tibbetts and J.T.-Y. Wen, “Extrusion Process Control: Modeling Identification, and Optimization,” IEEE Transactions on control Systems technology, vol. 6, no. 2, pp. 134-145, 1998.
[5] J.G. Ziegler and N.B. Nichols, “Optimum settings for automatic controllers,” Trans. ASME, no 64, pp 759-768, 1942.
[6] P. Isermann, “Results on the simplification of dynamic process models,” International Journal of Control, vol. 19, no. 1, pp. 149-159, 1973.
[7] M. Maksimović, Tehnološke operacije, Tehnološki fakultet Banja Luka, 2007.
[8] Multi-Zone Control with "PID_Temp”, https://cache.industry.siemens.com/dl/files/463/109740463/att_993000/v1/109740463_PidTemp_MultiZone_DOC_V11_en.pdf
[9] Function Manual: SIMATIC S7-1200, S7-1500 PID Control, https://support.industry.siemens.com/cs/document/100746401/pid-control-with-pid_compact-for-simatic-s7-1200-s7-1500?dti=0&lc=en-AR
[10] S.L. Crabtree, M. A. Spalding, and C. L. Pavlicek, “Single screw extruder zone temperature selection for optimized performance,” pp. 1410-1415, 2008.
[11] .J.G. Gonzales and M. Chimal, “Adaptive temperature controller for plastic extrusion process, Laboratoire d'Informatique, de Robotique et de Microélectronique de Montpellier (LIRMM), 2020.
[12] C.-C. Yu, Auto Tuning of PID Controllers, Springer, London, 2006.
[13] C. Abeykoon, K. Li, M. McAfee, P.J. Martin, and G.W. Irwin, “Extruder melt temperature control with fuzzy logic, IFAC Proceedings, vol. 44, no. 1, pp. 8577-8585, 2011.
[14] Manual: 79047707_LSim_DOC_V3_0_0_en, https://www.scribd.com/document/441305559/79047707-LSim-DOC-V3-0-0-en
[15] Function Manual: SIMATIC S7-1200, S7-1500 PID Control.

 ISBN 978-86-7466-930-3

# Upravljanje nivoom vode i pumpama upotrebom SMS poruka

Igor Kocić, Zoran Jovanović, *Elektronski fakultet u Nišu*

***Apstrakt*— U radu je opisano daljinsko upravljanje pumpama za dopremanje vode za potrebe proizvodnog procesa upotrebom Siemens Logo PLC kontrolera i odgovarajućih GSM modula. Radi povećanja pouzdanosti rada sistema komunkacija se obavlja dvojako upotrebom SMS poruka i žičane veze. Projektovan je i realizovan softver i hardver za obe vrste komunikacije, kao i softver za HMI panel kojim se vrši upravljanje i nadzor rada celog postrojenja.**

***Ključne reči*— Logo PLC, CMR modul, SMS, sekvencijalno upravljanje**

## I. UVOD

U sistemima za upravljanje na daljinu tradicionalno se koristila prosta žičana veza. Osnovni nedostatak takvih sistema javlja se u slučaju prekida kabla u komandnom kolu.
U tom slučaju se u potpunosti gube informacije o sistemu upravljanja na udaljenoj lokaciji. U novije vreme žičana veza se menja radio vezom, čime je pouzdanost takvog sistema značajno povećana. Sa razvojem mobilne telefonije i interneta ostvarena je mogućnost upravljana na daljinu sa velikom pouzdanošću.
Zbog potrebe povećanja pouzdanosti sistema u radu razvijen je upravljački softver i hardver za upravljanje nivoom vode u bazenima upotrebom SMS poruka. Pogodnim algortimom sekvencijalnog upravljanja ostvareno je upravljanje pumpama i nivoom vode u rezervoaru.

U slučaju otkaza mobilne mreže softver omogućava automatski prelaz na žičanu vezu i obrnuto. Postojeću žičanu vezu operater može uključiti ručno u svakom trenutku.

## II. APLIKACIJA-OPIS HARDVERSKOG I SOFTVERSKOG REŠENJA

Na Sl.1. je dat šematski prikaz lokacije postrojenja, uređaja i opreme. Postrojenje je smešteno na dve udaljene lokacije. Glavni upravljački centar se nalazi u fabrici, a vodozahvat se nalazi na oko 2 km od fabrike. Lokacija bazena je nazvana: "Lokacija 2", a lokacija vodozahvata sa pumpnim postrojenjem nazvana je: "Lokacija 1".
U radu će se nadalje koristiti ovi nazivi. Sistem se sastoji od glavnog upravljačkog centra gde su ujedno nalaze bazeni sa sistemom za merenje nivoa vode i udaljenog pumpnog postrojenja u kome su instalirani frekvencijski regulatori kojima se obavlja pokretanje pumpi i regulacija pritiska u cevovodu i sistem za zaštitu od prevelikog pritiska na cevovodu.

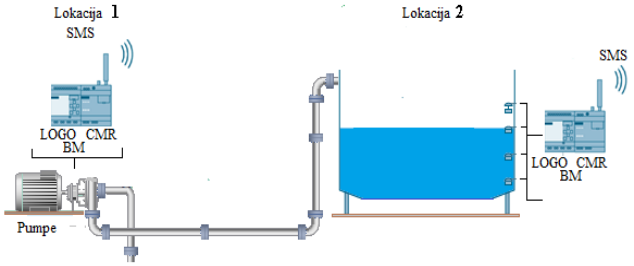


Sl.1. Šematski prikaz procesa daljinskog upravljanja pumpnim postrojenjem

Kašnjenje upravljačkih signala nije od velikog značaja jer su bazeni za vodu velikog kapaciteta. Na obe lokacije se nalaze po jedan PLC kontroler serije LOGO sa komunikacionim modulima tip CMR2020 [2].
Na Sl.2 prikazana je topologija GSM mreže preko koje se obavlja komunikacija SMS porukama.

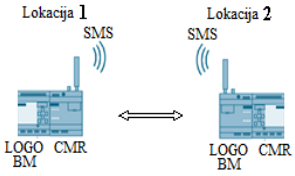


Sl.2. Topologija mobilne mreže, komunikacija SMS porukama

CMR modul za GSM/GPRS komunikaciju ima široku vrstu primena. Neki od mogućih slučajeva upotrebe su sledeći:

1. Mobilna bežična komunikacija bez LOGO PLC kontrolera,
2. Mobilna bežična komunikacija sa LOGO PLC kontrolerom,
3. Određivanje položaja (GPS).

U svaki CMR modul instalirane su SIM kartice i podešeni potrebni parametri dobijeni od strane mrežnog operatera. Svaki CMR modul povezan je na LOGO PLC [1]. LOGO PLC je sa CMR modulom povezan pomoću lokalne Ethernet mreže. CMR modul koristi omnidirekcionu antenu za mreže tipa GSM (2G), UMTS (3G) i LTE (4G) [2]. Time je omogućeno slanje i primanje SMS poruka povezanih sa događajima koji su programirani u LOGO PLC kontroleru, i pokretanje akcija i slanje informacija o statusu pomoću SMS poruka.
Podešavanje CMR modula obavlja se pomoću internet pretraživača unošenjem default adrese. Nakon inicijalnog podešavanja adrese su promenjene.

Igor Kocić – Elektronski fakultet, Univerzitet u Nišu, Aleksandra Medvedeva 14, 18000 Niš, Srbija (e-mail: igkocic@ gmail.com).
Zoran Jovanović – Elektronski fakultet, Univerzitet u Nišu, Aleksandra Medvedeva 14, 18000 Niš, Srbija (e-mail: zoran.jovanovic@elfak.ni.ac.rs).

 ISBN 978-86-7466-930-3

Podešavanje CMR modula se sastoji iz sledećih koraka:

1.Podešavanje parametara mobilne i lokalne Ethernet mreže.
2.Podešavanje parametara za SMS poruke.
3.Podešavanje korisnika i grupa korisnika.
4.Podešavanje poruka, akcija, definisanje ulaza, izlaza, događaja, alarmnih i poruka greške.
5.Definisanje poruka i akcija slanja i prijema poruka.

Na Sl.3 prikazan je glavni konfiguracioni ekran CMR modula. Svakom od modula dodeljena su imena i lokalne Ethernet adrese. Podešavanje mobilne mreže obavljeno je unosom PIN koda SIM kartice, broja kartice i aktivacijom interfejsa za komunikaciju preko mobilne mreže. Takođe moguća je komunikacija i sa uređajima koji su u drugoj zemlji uključenjem Roming opcije.

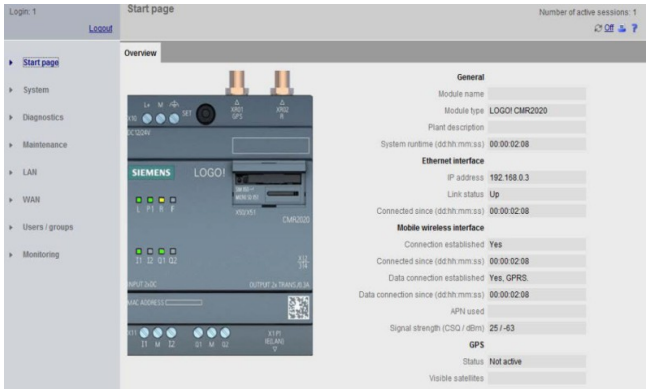


Sl.3. Glavni konfiguracisjki ekran CMR modula

Primer sintakse SMS poruka dat je ispod u formi:

<Password>;LOGO=VM<Address>,<Value>,<Data type>.

Password predstavlja lozinku za komande tipa write "pisanje", čime je ostvarena dodatna zaštita od neovlašćenog slanja poruka.

LOGO=VM<Address> predstavlja lokalnu adresu u memoriji LOGO PLC , <Value> predstavlja vrednost koja se šalje ili prima, Data type je tip podatka koji se šalje ili prima.

SMS poruka komande upisa u LOGO PLC na adresu memorjske lokacije VM0 data je u formi:
SMSupis;LOGO=VM0,50,WORD.
Izvršavanjem ove komande u registar VM0 LOGO PLC kontrolera upisuje se vrednost 50.

Podešavanje korisnika i grupa korisnika obavljeno je unosom imena korisnika, lozinke, broja telefona korisnika i dozvolom za čitanje i slanje SMS poruka prema CMR modulu. Napravljene su dve grupa korisnika, prva dobija samo poruke o alarmima, a druga grupa pored alarmnih poruka ima dodeljene privilegije isključenja ili uključenja delova postrojenja u normalnom radu ili interventno.

Podešavanje poruka i akcija na događaje urađeno je dodelom ID broja poruke, imenom poruke i akcije kojom se šalje određena poruka.
Ako je nivo u bazenu nizak šalje se poruka čija je sintaksa:

SMSupis;LOGO=VM0,10,WORD.
Za slučaj greške komunikacije korisnicima se šalje poruka:

Text: ! 'Error: Stanica na Lokaciji 1 nedostupna.'.

Ako je detektovana greška nivoa šalje se poruka :
Text: ! 'Error: Signal nivoa nije u redu. Senzor ili kabl je neispravan.'

Lokalne Ethernet adrese uređaja su redom:

1. PLC LOGO 8.2 Lokacija 2 bazen 192.168.0.103,
2. CMR modul 192.168.0.21,
3. PLC LOGO 8.2 Lokacija 1 vodozahvat 192.168.0.104,
4. CMR modul 192.168.0.11,
5. Touch HMI Panel KTP400 192.168.0.232

Na ovaj način omogućen je pristup mreži sa bilo koje od dve lokacije upotrebom mrežnih rutera.

Na lokaciji 2 upotrebom senzora za detekciju nivoa vrši se detekcija nivoa u više tačaka. Od interesa je minimalni i maksimalni nivo.
Kada nivo vode u tankovima padne ispod minimalne vrednosti vrši se uključenje pumpi za dopremanje vode. Isključenje pumpi vrši se u dva slučaja:

1. radni uslov isključenja, kad je dostignut željeni nivo vode u tankovima,
2. havarijsko isključenje, koje se obavlja ako se pritisak u cevovodu poveća iznad određene vrednosti.

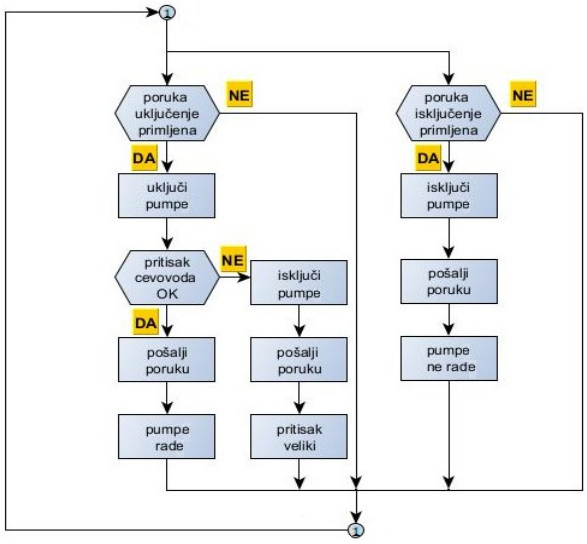


Sl.5. Deo algoritma rada udaljenog postrojenja upotrebom SMS poruka(lokacija 1)


ISBN 978-86-7466-930-3

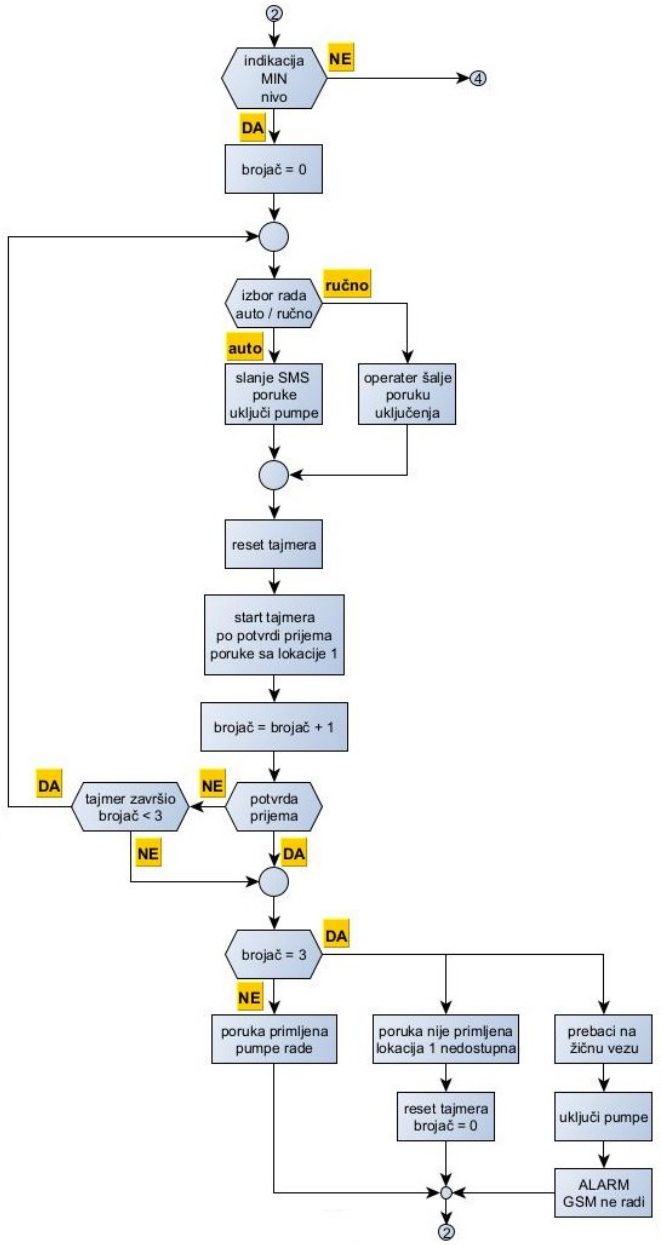


Sl.5. Deo algoritma rada postrojenja upotrebom SMS poruka pri indikaciji minimalnog nivoa (lokacija 2)

Pored automatskog rada, postrojenje može da radi i u ručnom režimu, kada se uključenje ili isključenje obavlja pomoću HMI panela i relejnom komandom ili SMS porukama koje šalju operateri koji za to imaju definisane privilegije. Postrojenje može da radi i upotrebom "stare" žičane veze, pod uslovom da je SMS komunikacija isključena.

Neki od ulaza, izlaza koji se koriste na LOGO PLC na lokaciji 2 su redom:

1. I1 minimalni nivo,
2. I2 nivo 2,
3. I3 nivo 3,
4. I4 maksimalni nivo,
5. I5 izbor rada ručno ili automatski,
6. I6 izbor SMS ili žičana veza,
7. I7 greška komunikacije,
8. Q1 signal greške komunikacije,
9. Q2 signal indikacije greške usled prevelikog pritiska

Neki od ulaza, izlaza koji se koriste na LOGO PLC na lokaciji 1 su redom:

1. I2 dozvola rada,
2. I4 senzor pritiska (presostat),
3. Q1 uključenje isključenje pumpe.

Na Sl.4. prikazan je deo upravljačkog algoritma za uključenje, isključenje pumpi u udaljenom postrojenju. U slučaju povećanja pritiska u cevovodu senzor pritiska (presostat) isključuje pumpe.

Na Sl.5. prikazan je deo upravljačkog algoritama postrojenja kada je nivo niži od minimalnog. U slučaju da se pojavi greška ili prekid u komunikcionom protokolu koji se trenutno koristi automatski se izvrši prelaz sa trenutnog na žičani tip komunikacije (žičanu vezu). Ako je trenutno aktivna SMS, prebacivanje se obavlja na žičanu vezu.
Softver za komunikaciju SMS porukama napisan je upotrebom Simensovog LOGO!Soft Comfort V8.2 alata za programiranje LOGO PLC kontrolera.

Na Sl.6 dat je deo softvera koji se odnosi na slanje poruka za uključenje i isključenje pumpi u udaljenom pumpnom postrojenju (lokacija 1), kao i dela za prijem i obradu poruka koje šalje udaljeno postrojenje.

Kada nivo vode padne ispod minimalnog nivoa sa lokacije 2 šalje se prva SMS poruka. U slučaju fluktuacije nivoa usled talasanja vode a koja može uticati na sondu za signal minimalnog nivoa, signal aktivacije slanja poruke se filtrira upotrebom tajmera sa kašnjenjem od 10s instrukcije za detekciju rastuće ivice. Obezbeđeno da se svaki zahtev za slanje izvrši jedanput. Nakon slanja poruke aktivira se tajmer kojim je definisano maksimalno vreme potrebno da udaljeno pumpno postrojenje kojom je poslata poruka odgovori (60 s). Ovo vreme eksperimentalno je definisano tako da ne utiče na regulaciju nivoa. Ako vreme za odgovor istekne ista poruka se šalje i drugi put. Ukoliko odgovor sa udaljene lokacije 1 i u tom slučaju ne stigne, automatski se šalje poruka lokacija 1 je neaktivna. Poruka greške se ispisuje na HMI panel i šalje SMS poruka na brojeve koji su konfigurisani u CMR modulu. Komunikacija se automatski prebacuje na žičanu vezu. U režimu ručnog rada operater nadgleda rad postrojenja upotrebom HMI panela i odlučuje kada će da uključi ili isključi pumpe.

 ISBN 978-86-7466-930-3

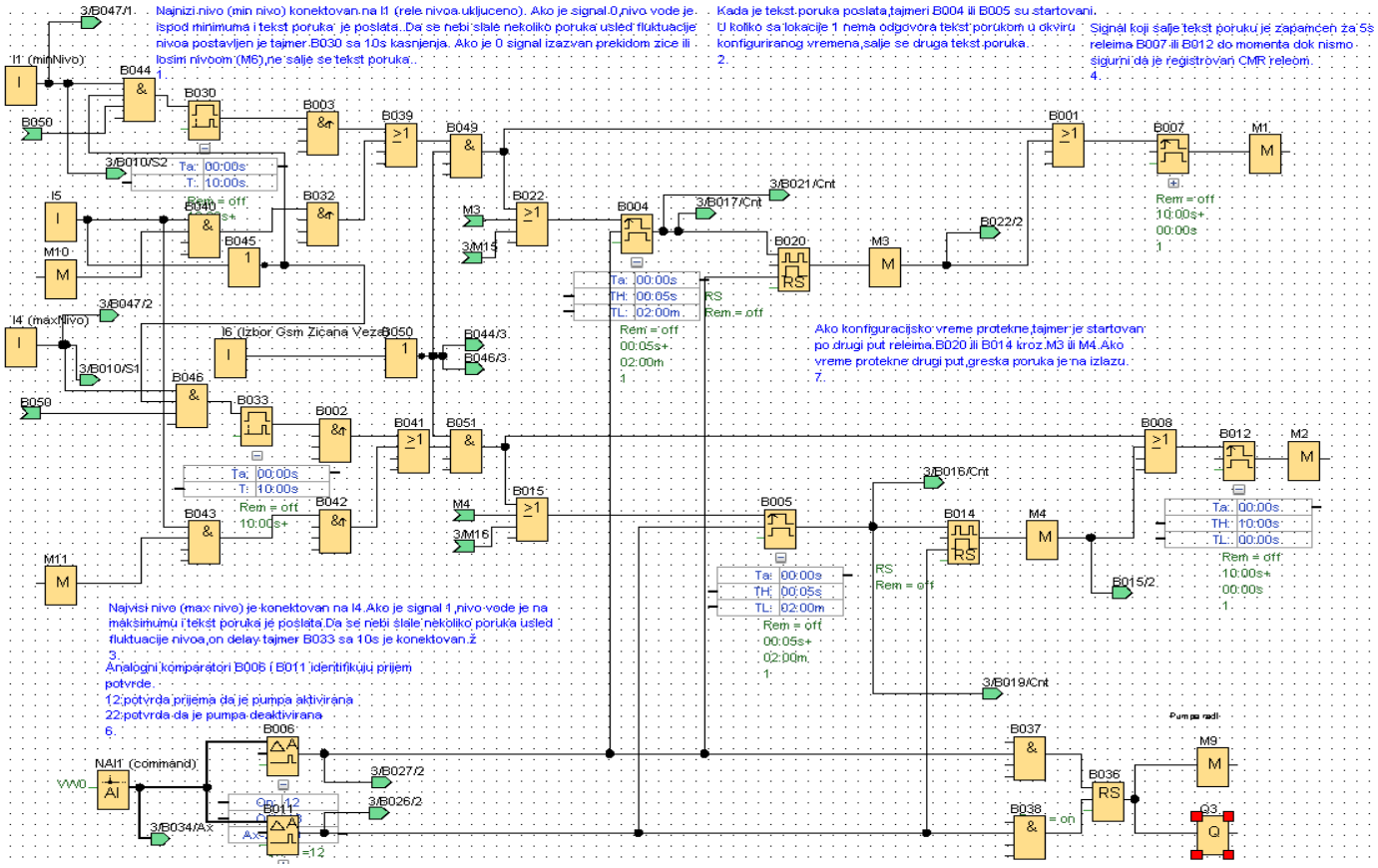


Sl.6. Deo softvera za slanje i prijem poruka za uključenje, isključenje i indikaciju rada pumpi pumpnog postrojenja

Deo softvera koji se koristi za uključenje isključenje pumpi na udaljenoj lokaciji 1 dat je na Sl.7. Poruka koja je primljena se poredi komparatorima B006 i B002. U koliko je primljena poruka koja se nalazi u registru VM0=10 na Logo PLC kontroleru se uključuje izlaz Q1 koji aktivira frekvencijski regulator za kontrolu rada pumpi. Odmah po prijemu vrši se slanje SMS poruke sa vrednosti '11' prema lokaciji 2 koji nosi informaciju da su pumpe startovane.

Ukoliko je primljena poruka VM0=20 izlaz Q1 se isključuje čime se rad frekfentnog regulatora a samim tim i pumpi stopira. Po prijemu te poruke prema lokaciji 2 šalje se poruka sa vrednošću '22' pumpa isključena. Ukoliko se iz nekog razloga pritisak na cevovodu poveća senzor pritiska (presostat) detetektuje nedozvoljenu vrednost pritiska, obavlja se havarijsko isključenje frekvencijskog regulatora pumpi. Prema lokaciji 2 šalje se poruka sa vrednošću '13', uključuje se alarm sa informacijom da je izvršeno havarisjko isključenje pumpi, pritisak povećan pumpe isključene. Takođe se šalje i SMS poruka operateru koji dalje preduzima potrebne mere.

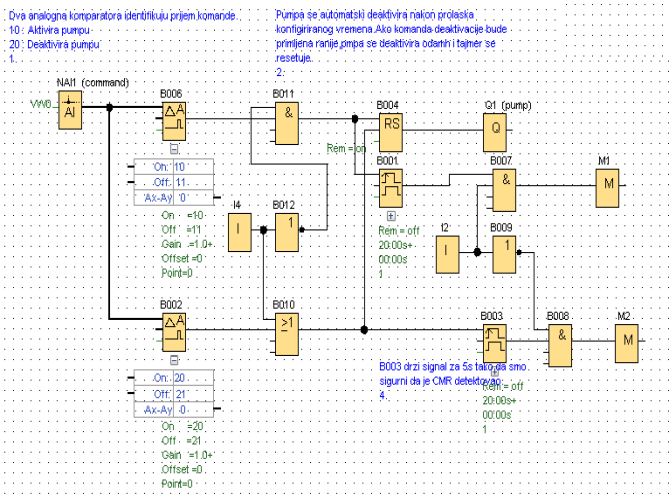


Sl.7. Deo softvera za uključenje isključenje pumpi u udaljenom pumpnom postrojenju

## III. REALIZACIJA UPRAVLJAČKE APLIKACIJE ZA UPRAVLJANJE NIVOOM VODE U REZERVOARU

Sekvencijalno upravljanje nivoom vode u bazenu na lokaciji 2 obavljeno je izradom dva upravljačka ormana za prenos poruka upotrebom SMS poruka i ormana sa relejnom logikom, kao i ormanom sa frekfentnim regulatorom koji upravlja radom pumpi.


ISBN 978-86-7466-930-3

Na Sl.8 prikazan je upravljački orman na lokacijama 1 i 2 .

Sl.8. Upravljački ormani za upravljanje nivoom vode

U svakom od njih je postavljen po jedan LOGO PLC sa komunikacionim CMR modulom i S7 1200 PLC kontrolerom koji upravlja radom postrojenja pomoću zičane veze.
Na Sl.9 prikazan je HMI panel za nadzor postrojenja.

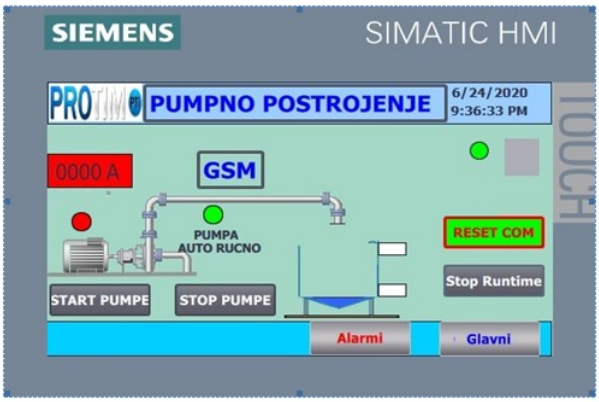


Sl.9. Prikaz HMI panela pri SMS komunikaciji

## IV. ZAKLJUČAK

Za realizaciju ovakve vrste upravljačkih zadataka godinama se koristila samo žičana veza i prosta relejna logika. Izrade žičane veze za velike udaljenosti obično se realizuje u momentu izrade cevovoda, kada se paraleleno sa cevima polažu komunikacioni i napojni kablovi do udaljenje lokacije. U slučaju otkaza, oštećenja komuniakcionih veza potrebno je ponovo otkopati deo trase kako bi se otkrio prekid u komunikaciji, što iziskuje značajna sredstva. U novije vreme sve češće se koristi komunikacija SMS porukama upotrebom mreže mobilne telefonije. U radu je pored softvera i hardvera razvijenog za komunikaciju SMS porukama razvijen i deo softvera i hardver za komunikaciju preko žičane veze. Time je mogućnost otkaza sistema smanjena.

## LITERATURA

[1] Logo_e, Manal Edition 06/2003, https://www.google.com/url?esrc=s&q=&rct=j&sa=U&url=https://cache.industry.siemens.com/dl/files/461/16527461/att_82564/v1/Logo_e.pdf&ved=2ahUKEwjm-qqJz9n3AhUBlmoFHboXDvoQFnoECAkQAg&usg=AOvVaw07CoQzjU-TKxPeO7uedRlp
[2] SIMATIC NET LOGO! - Industrial Ethernet, LOGO! CMR2020, LOGO! CMR2040, Operating instruction, 05/2015, C79000-G8976-C356-02, https://cache.industry.siemens.com/dl/files/268/103657268/att_850514/v1/BA_LOGO-CMR2020-CMR2040_76_en-US.pdf
[3] SIMATIC, S7-1200 Programmable controller, System Manual, V4.3.0 02/2019, A5E02486680-AM ,https://cache.industry.siemens.com/dl/files/129/109764129/att_974298/v1/s71200_system_manual_en-US_en-US.pdf
[4] Hans Berger, Automating with SIMATIC S7-1200, Publicis,2nd edition (June 10, 2013)
[5] J.F. DiMarzio, Rutiranje, Kompjuter biblioteka, 2002
[6] M. Fallahnejad, A new algorithm for connecting between LOGO and labview software, January 2012
[7] G.Kozoris, M. Papoutsidakis, A. Chatzopoulos, Electropneumatic Positioning System Control With The Legendary LOGO! PLC, December 2017
[8] L. Fang, Application of PLC technology in electrical engineering and automation control, January 2017

## ABSTRACT

The paper describes the remote control of water supply pumps for the needs of the production process using Siemens Logo PLC controllers and appropriate GSM modules. In order to increase the reliability of the system, communication is performed in two ways using SMS messages and wired connection. Software and hardware for both types of communication were designed and implemented, as well as software for the HMI panel which manages and supervises the operation of the entire plant.

**Water level and pump control using SMS messages**

Igor Kocić, Zoran Jovanović

 ISBN 978-86-7466-930-3

# BIOMEDICAL ENGINEERING
# /
# БИОМЕДИЦИНСКА ТЕХНИКА
# (BTI/БТ)

ISBN 978-86-7466-930-3

# AGILIS: Restoring Functional Grasping in Individuals with Tetraplegia using Epineural Electrodes

Christine Azevedo Coste, Charles Fattal, Lucie William, *Member, IEEE*, Lucas Fonseca, *Member, IEEE*, Arthur Hiairrassary, David Andreu, Antoine Geffrier, Jacques Teissier and David Guiraud, *Member, IEEE*

***Abstract*— We propose a novel approach to restore grasping in individuals with complete tetraplegia using epineural stimulation. Two multi-contact cuff electrodes were positioned around radial and median nerves in 2 volunteers during a surgery. The electrodes were maintained for 28 days. A user interface allowed triggering pre-programmed stimulation sequences on demand by executing stereotyped movements or by contracting voluntarily muscle on the contralateral shoulder. The stimulation selectivity obtained with the epineural electrodes was sufficient to obtain functional palmar and key pinch grip.**

***Index Terms*—Functional Electrical Stimulation (FES), Tetraplegia, Neural electrodes.**

## I. Introduction

Functional electrical stimulation (FES) is a means of restoring upper limb function in people with complete tetraplegia when functional tendon surgery or nerve transfer is not an option [1].

Intramuscular and epimysial electrodes have been used in the past to restore grip [2,3]. A disadvantage of this approach is the need for one electrode and one cable per muscle to be activated. Miniature, self-contained implant designed to be injected in or near muscles have also been proposed to avoid cables [10].

In the AGILIS approach, we propose to use 1 epi-neural electrode per nerve to activate the different muscles to reduce the number of implanted electrodes [4]. The cuff electrodes were designed to be self-adjusting to nerve diameter.

The objectives of the study we present here were to: 1) evaluate the safety of the procedures of implanting 2 cuff electrodes around the median and radial nerves respectively and maintaining them for 28 days, 2) evaluate the ability of the solution to elicit a functional grip in two participants with complete tetraplegia.

Christine Azevedo Coste is with Inria, University of Montpellier, France (e-mail: Christine.Azevedo@inria.fr), (https://orcid.org/0000-0002-7379-8004)

Charles Fattal is with Rehabilitation Center Bouffard-Vercelli USSAP, Perpignan, France, (https://orcid.org/0000-0002-3042-0941)

Lucie William with Inria, University of Montpellier, France,

Lucas Fonseca is with with Inria, University of Montpellier, France, (https://orcid.org/0000-0002-7255-5916)

Arthur Hiairrassary is with Neurinnov, Montpellier, France.

David Andreu is with Neurinnov, Montpellier, France.

Antoine Geffrier is with University Hospital Center Pontchaillou, Rennes, France. He was previously with APHP, Paris France.

Jacques Teissier is with Surgical Clinic OrthoSud, Montpellier, France.

David Guiraud is with Inria, University of Montpellier, France and Neurinnov, Montpellier, France.

## II. Methods

Two volunteers with complete C4 tetraplegia, AIS A were included. They signed an informed consent. The study was approved by the National Ethics Committee (ClinicalTrials.gov ID NCT04306328).

The electrodes were placed during an initial surgical procedure and explantation surgery took place 28 days later. 2 multi-contact spinal electrodes (CorTec GmbH Freiburg Germany) were wrapped around the nerves above the elbow. Each electrode was connected to a percutaneous cable to connect the multi-source external stimulator (STIMEP, INRIA, Montpellier) [8]. The stimulator was controlled from a computer (Figure 1).


Fig. 1. AGILIS approach principle: 2 multi-contact cuff electrodes are wrapped around radial and median nerves. Percutaneous cables are connected on demand to an external pulse generator. Stimulation configuration patterns are pre-programmed to elicit hand opening/closing. The user controls contralateral shoulder movements or muscle contraction to send commands to the stimulator software: hand opening, palmar or key pinch grip…

Two control interfaces were tested to allow the user to trigger the pre-programmed stimulation patterns: 1) the participant used stereotyped voluntary shoulder movements of the contralateral limb captured by 1 IMU, 2) the participant used voluntary contractions of 2 muscles of the contralateral limb

 ISBN 978-86-7466-930-3

captured by 2 EMGs (trapezius and platysma). A finite state machine (FSM) was defined to associate user commands (EMG threshold detection or predefined movement recognition (IMU)) with actions depending on the current state of the FSM [6].

Various measurements were made wireless sensors (Delsys, Natick, MA) and offline processed using: electromyography (EMG), forces applied to objects (resistive force sensors (FSR)), movements (inertial measurement units (IMU)). The kinematics of the movements were also analysed (Leap Motion, Inc, San Francisco, California). FES-induced evoked muscle contractions (eEMG) were also acquired and post-processed to extract recruitment curves [9].

## III. Results

Both participants were able to perform object grasping tasks using two types of grasp (key pinch and digito-palmar). Participant 1 was able to use both control interface modalities (muscle contraction and voluntary movements). Participant 2, due to a significant fatigability of the shoulder muscles, was able to use only voluntary shoulder movements to trigger the stimulation sequences, but in a rather non-robust manner, which led us to propose a third solution based on occipital contactors. Some results have been published in a recent article [7]. Additional results will be detailed during the presentation at the conference.

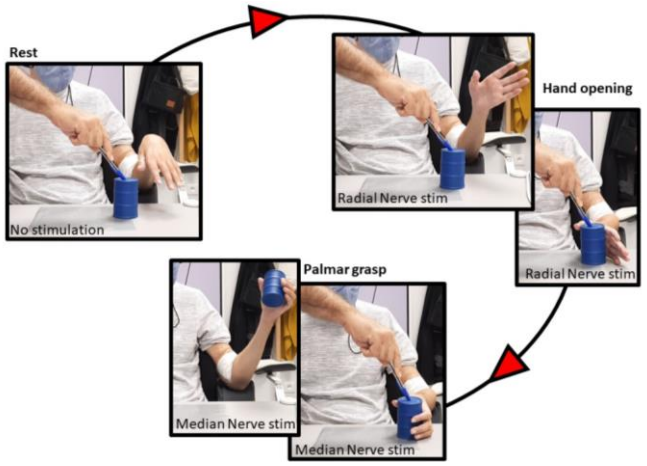


Fig. 2. Example of a sequence of movements for gripping a foam cylinder. The participant triggers the stimulation of the radial nerve which causes the hand to open (extension of fingers and wrist), he positions his hand on the object and then triggers the stimulation of the median nerve which causes the fingers to close around the object which he can then move.

## IV. Conclusion

This preliminary study is a further step in the validation of the AGILIS approach which suggests the feasibility of a solution for grip restoration that minimises surgical complexity. Less than 2 hours were required to place the 2 multi-contact epineural electrodes with percutaneous cables around the radial and median nerves. These two electrodes associated with the electrical stimulator allow the injected currents to be controlled to achieve selective activation of the nerve fascicles. Two separate taps could be activated and associated with reproducible configurations (active electrode poles and stimulation parameters). The behaviour of the electrodes remained stable during the implantation period (28 days). Further studies are needed to strengthen the results.

## Acknowledgment

The authors would like to thank the two volunteers, as well as Mrs Caralp and Mrs Porra (OT), Mr Panel and Mr Ferrer (PT), and the health care teams responsible for daily care. This study was supported by grants from the EIT Health, the Occitanie Region and the ERC MSCA.

## References

[1] van Zyl, N., Hill, B., Cooper, C., Hahn, J., and Galea, M.P. Expanding traditional tendon-based techniques with nerve transfers for the restoration of upper limb function in tetraplegia: a prospective case series. *Lancet* 394, 565–575, 2019.

[2] Hoshimiya, N., and Handa, Y. A master-slave type multi-channel functional electrical stimulation (FES) system for the control of the paralyzed upper extremities. *Automedica*, 209–220, 1989.

[3] Keith, M.W., Peckham, P.H., Thrope, G.B., Stroh, K.C., Smith, B., Buckett, J.R., Kilgore, K.L., and Jatich, J.W. Implantable functional neuromuscular stimulation in the tetraplegic hand. *J Hand Surg Am* 14, 524–530, 1989.

[4] Tigra, W., Dali, M., William, L., Fattal, C., Gélis, A., Divoux, J.-L., Coulet, B., Teissier, J., Guiraud, D., and Azevedo Coste, C. Selective neural electrical stimulation restores hand and forearm movements in individuals with complete tetraplegia. *J Neuroeng Rehabil*, 2020.

[5] Tigra, W., Navarro, B., Cherubini, A., Gorron, X., Gelis, A., Fattal, C., Guiraud, D., and Azevedo Coste, C. A Novel EMG Interface for Individuals with Tetraplegia to Pilot Robot Hand Grasping. *IEEE Trans Neural Syst Rehabil Eng* 26, 291–298, 2018

[6] Fonseca, L., Tigra, W., Navarro, B., Guiraud, D., Fattal, C., Bó, A., Fachin-Martins, E., Leynaert, V., Gélis, A., and Azevedo-Coste, C. Assisted Grasping in Individuals with Tetraplegia: Improving Control through Residual Muscle Contraction and Movement. *Sensors (Basel)*, 2019.

[7] Fattal C., Teissier J., Geffrier A., Fonseca L., William L., Andreu D., Guiraud D., Azevedo-Coste C. Restoring Hand Functions in People with Tetraplegia through Multi-Contact, Fascicular, and Auto-Pilot Stimulation: A Proof-of-Concept Demonstration. *Journal of Neurotrauma*, 2022.

[8] Guiho T., López-Alvarez V., Cvancara P., Hiairrassary A., Andreu D., Stieglitz T., Navarro X., Guiraud D., New Stimulation Device to Drive Multiple Transverse Intrafascicular Electrodes and Achieve Highly Selective and Rich Neural Responses, *Sensors*, 2021.

[9] William L., Dali M., Azevedo Coste C., Guiraud D. A method based on wavelets to analyse overlapped and dependant M-Waves, *Journal of Electromyography and Kinesiology*, 2022.

[10] Popovic D, Baker LL, Loeb GE. Recruitment and comfort of BION implanted electrical stimulation: implications for FES applications. IEEE Trans Neural Syst Rehabil Eng. 2007.

 ISBN 978-86-7466-930-3

# A Device for Monitoring Physiological Parameters and Electrotactile Stimulation

Bojan Jorgovanović, Matija Štrbac, Miloš Kostić, Vojin Ilić, Nikola Jorgovanović

***Abstract* — This wor stems from a research and innovation action financed under ecure societies programme of the European Union's Horizon 2020 framewor . pecifically, the aim is to develop an easy-to-use wearable system for enhancing situational awareness of first responders deployed in e treme environments by providing tactile feedbac on the ris factors that can lead to rapid deterioration of their health or operation capabilities. or this purpose, an unobtrusive system was designed to acquire, process, and analyse the data from a battery of novel biosensors and generate actionable information about assessed health ris s, in real-time. Aptly named I T , it leverages electrotactile stimulation to continually convey this information to the first responder wearing it, leveraging the sense of touch. It effectively e pands first responders' sensory bandwidth to include the "feeling" of changes in critical parameters that are not within the reach of human senses, li e the ionic imbalance, the lactate level or physiological strain, much before they manifest through symptoms of e haustion, heatstro e or hypothermia. The developed system further incorporates means for transmitting information to the command centre, where it can be analysed and visualised through a mission specific decision support system, allowing for a more efficient and safer data-driven team management.**

***Index Terms*— lectrotactile stimulation; irst responders; Wearable acquisition unit**

## I. Introduction

SIXTHSENSE is a multidisciplinary innovation and research action with the overall aim to significantly improve efficacy and safety of first responders' deployment in hazardous environments by optimising on-site team coordination and mission execution.

Bojan Jorgovanović is with the Faculty of Technical Sciences, University of Novi Sad, Trg Dositeja Obradovića 6, 21000 Novi Sad, Serbia and Global Electronic Solutions doo, Cara Dušana 75, 21000 Novi Sad, Serbia (e-mail: bojan.jorgovanovic@uns.ac.rs).

Matija Štrbac is with Tecnalia Serbia doo, Deligradska 9, 11000 Belgrade, Serbia (e-mail: matija.strbac@tecnalia.com).

Miloš Kostić is with Tecnalia Serbia doo, Deligradska 9, 11000 Belgrade, Serbia (e-mail: milos.kostic@tecnalia.com).

Vojin Ilić is with the Faculty of Technical Sciences, University of Novi Sad, Trg Dositeja Obradovića 6, 21000 Novi Sad, Serbia and Global Electronic Solutions doo, Cara Dušana 75, 21000 Novi Sad, Serbia (e-mail: vojin@uns.ac.rs).

Nikola Jorgovanović is with the Faculty of Technical Sciences, University of Novi Sad, Trg Dositeja Obradovića 6, 21000 Novi Sad, Serbia and Global Electronic Solutions doo, Cara Dušana 75, 21000 Novi Sad, Serbia (e-mail: nikolaj@uns.ac.rs).

Between the booming EU economy and the climate change, the number and consequences of disasters occurring in inaccessible rural areas is on a constant rise. First responder deployments in extreme conditions such as fighting wildfires or alpine search and rescue missions have gone from exceptional to regular events in only a couple of decades. As this trend is likely to continue, the risks for wellbeing of the engaged first responders continue to grow. To avoid the loss of life or lasting consequences on the first responders' health, it is important that the key physiological parameters of deployed operatives are monitored in a way that provides timely and actionable information, without hindering their operational capacity [1]. One way to achieve gathering such data and providing feedback is to use a device which could monitor the first responder's physiological parameters and use electrotactile stimulation as a way of conveying a message [2, 3].

At this point, a device that could do both data acquisition and analysis and give feedback to the first responder via stimulation is not available on the market, so it was necessary to develop one. The device presented in this paper is named the Alpha Mobile Device (AMD). The AMD is a system for multimodal data acquisition and control of electrotactile feedback stimulation. The aim of the AMD design was to enable synchronised electrotactile stimulation and acquisition from multiple sensors in a modular and scalable way that enables the inclusion of existing, developed and emerging sensors. The AMD design provides compactness, low power consumption, small overall dimensions and robustness with a main goal to develop a real mobile and wearable system.

## II. Architecture of the AMD

The AMD was based on the STM32H743VIT6 microcontroller by ST Microelectronics. This ARM microcontroller has plenty of integrated peripheral modules which can work with very little or no processor core supervision. Furthermore, the STM32H743VIT6 microcontroller includes enhanced power management which provided all necessary power down or sleep operating modes in order to reduce power consumption.

The AMD needed to encompass 3 functionalities - data acquisition, electrotactile stimulation and communication. A block diagram of the AMD is shown in Figure 1.

 ISBN 978-86-7466-930-3

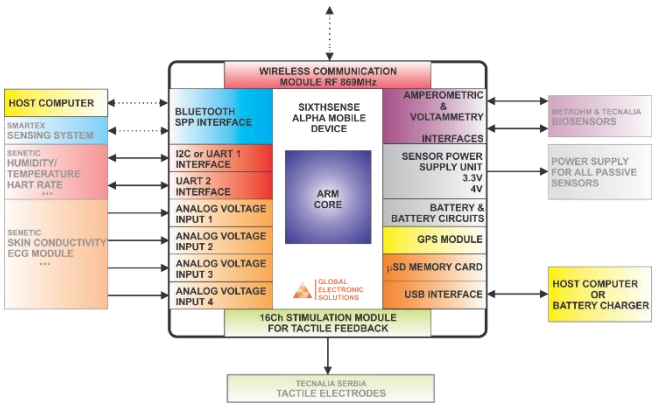


Figure 1. Block diagram of the AMD

### *A. ata ac uisition*

The AMD is equipped with interfaces for acquisition data from following type of sensors:

- Analog sensors with voltage output
- NTC thermistor sensor for temperature measurement
- Electrochemical sensors – Biosensors
- Digital wired sensors with USART interfaces
- Digital wired sensor with I2C interface
- Wireless connected sensor system with Bluetooth SPP interface
- GNSS sensor

The AMD is equipped with four voltage analogue inputs. Analogue voltage input 1 is also equipped with a precise current source which provides a constant current flow of 100µA to pin 13 of the sensor connector. This construction allows temperature measurement using the precise 10kΩ NTC thermistor connected between analogue ground and AIN_0. The other three analogue inputs are standard voltage inputs. By default, all four analogue inputs are connected to the internal 16-bit ADC of the microcontroller with a sampling rate of 1KSPS. If it turns out that the accuracy of the internal ADC is not satisfactory each input can be independently rerouted to a high speed and high accuracy ADC of the AD5941 by SMD jumpers on the PCB.

The AMD is equipped with two inputs for electrochemical sensors (biosensors). This interface is based on the single channel electrochemical front end circuit, AD5941, by Analog Devices. The electrochemical sensor interface can be set to operate in the following modes:

- Amperometric
- Chronoamperometric
- Cyclic Voltammetry

### *B. Electrotactile stimulation*

This functionality is intended for conveying messages to the first responder wearing the device through electrotactile stimulation. The device is designed to be compatible with multi-pad electrodes [4] designed and produced by Tecnalia Serbia doo. The AMD stimulation unit consists of the following blocks:

- DC/DC step-up voltage converter
- Biphasic current source
- Switch area (output demultiplexer)
- Control unit
- Battery and interfaces

The purpose of the DC/DC step-up converter is to provide voltage which is high enough to enable current flow through relatively high electrode-skin interface impedance. The manufactured DC/DC converter for the AMD is capable to boost battery voltage to voltage a level of up to 150V. This converter is based on a modified boost topology with coupled coils, and this design is confirmed in a number of different electrical stimulators previously developed by Global Electronic Solutions. The converter output voltage can be pre-set by the programme of the control unit. This flexibility is very important especially for the Alpha system in order to find the optimal voltage level in real life tests.

Biphasic Current source is based on current controlled H-bridge topology which is capable to create an either monophasic or biphasic current pulse. The amplitude of the current pulse is controlled by a control loop which is integrated into the H-bridge. This approach reduces the number of components and overall module dimensions. The set-point of the pulse amplitude is set by the control unit via a 16-bit D/A converter with standard SPI interface.

The Switch area includes a high-voltage switching circuit that allows multiplexing a signal from the H-bridge and driving it to one or more of the 16 output channels. Only one pole of the current source (cathode) can be distributed to any of the 16 electrode pads while the other pole (anode) is connected to a single predefined electrode pad, known as the unipolar stimulation topology.

The Alpha prototype will be based on ST Electronics' high performance ARM microcontroller (MCU). Only a small part of this microcontroller's resources are intended for the operation of the stimulator subsystem, while a bigger part will be used for the sensor data acquisition module. According to that, the part of the MCU which acts as the Stimulator control unit has the following important functionalities:

- Stimulation pulses waveform timing control
- Stimulation pulses amplitude control
- Stimulation pulse distribution to the pads of the multi-pad electrode
- Execution of the predefined electrotactile stimulation schemes

Beside the subsystems intended exclusively for the stimulator subsystem, there are two other common parts of the Alpha prototype which are necessary for the functioning of the stimulator subsystem and those parts are also integrated in the realized stimulator prototype:

- Battery and a battery electronic circuit
- Communication interfaces

The manufactured prototype is powered by Li-poly rechargeable battery. Battery charging, battery protection and battery monitoring electronic circuits are an integral part of the stimulator prototype. The manufactured device has Bluetooth

 ISBN 978-86-7466-930-3

and isolated USB interfaces. The following functionalities are realized via both communication channels:

- Setting all stimulation parameters (pulse width, pulse rate, pulse amplitude, active output channels)
- Starting/Stopping the stimulation
- Creating stimulation schemes
- Programming via a bootloader application

The device is also equipped with two multicolour LEDs indicating battery status, communication and stimulator activity. A block diagram of the stimulator is shown in Figure 2.

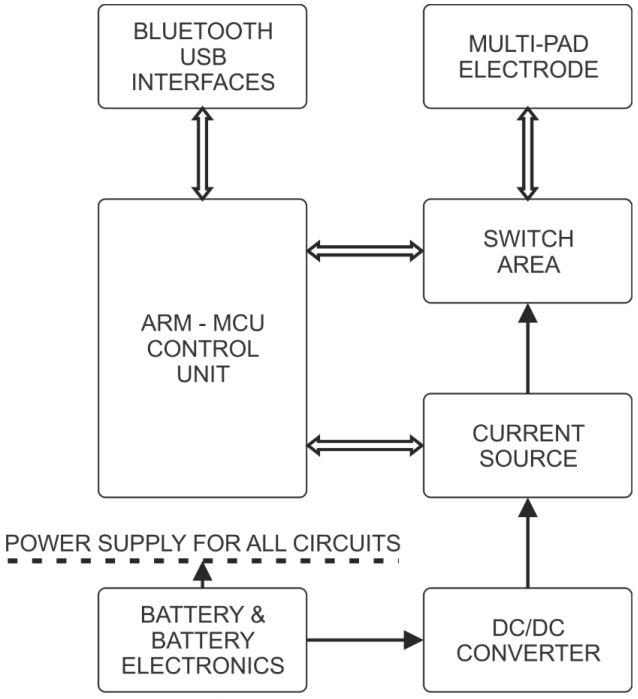


Figure 2. Block diagram of the AMD stimulator

### C. Communication

The AMD is equipped with a narrow band RF communication channel for duplex communication between the first responder and the command centre. The communication is based on the GES-RF869 communication module produced by Global Electronic Solutions. The GES-RF869 is a radio module which is in compliance with ETSI EN 300 220-1. This module provides the possibility of exchanging small packets of data, up to 100 Bytes, with low speeds, in a relatively simple way. It works on an operational frequency band ranging from 869,400MHz-869,650MHz which enables it to have radiated power of up to 27dBm (500mW). It provides duty cycle control and obeys the 10% duty cycle restrictions for the 869,400MHz-869,650MHz frequency band. It offers multiple radio communication channels inside the operational frequency band and the possibility of configuring the transmit power. In order to optimize power consumption and communication range the transmit power can be set between 10mW and 500mW. The ISM standalone antenna by Molex is integrated inside of the AMD enclosure.

## III. Results

The stimulator was tested on a circuit which resembles the electronic properties of the electrode-tissue interface and the signals were recorded using an oscilloscope. The waveform of the stimulation current is recorded at the serial resistor $R_S$ by voltage input of the oscilloscope. The resistance of $R_S$ is 1kΩ, so 1V at the recorded waveform corresponds to 1mA of measured current. A block diagram of the equipment used for testing the stimulator is shown in Figure 3.

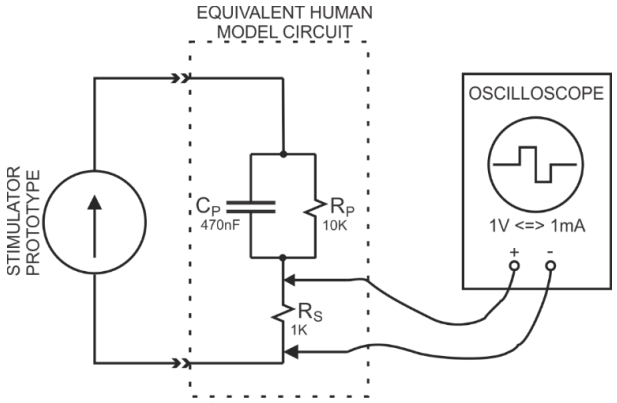


Figure 3. Block diagram of the test equipment

The waveform of a biphasic pulse generated by the AMD stimulator is shown in Figure 4. The pulse width of the generated stimulation pulse is 250µs, and the amplitude is 5mA.

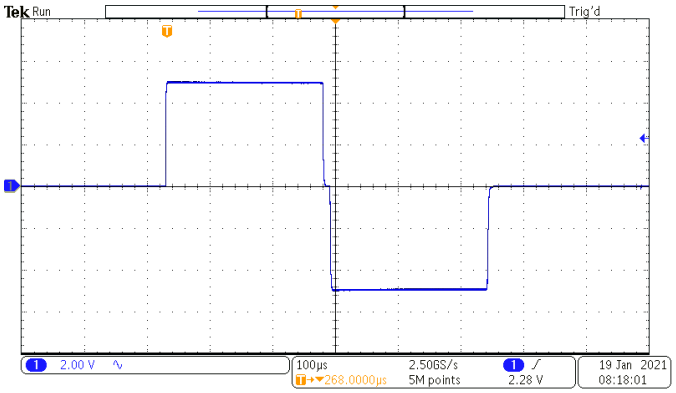


Figure 4. Stimulation pulse biphasic charge compensated test

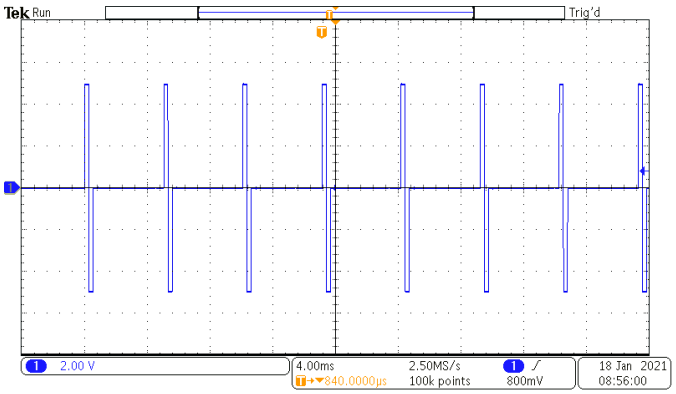


Figure 5. Stimulation pulse train


ISBN 978-86-7466-930-3

A stimulation pulse train generated by the AMD stimulator is shown in Figure 5. The frequency of the pulse train is 200pps and each pulse has the same stimulation parameters as the pulse shown in Figure 4.

## IV. Conclusion

The AMD device was designed and produced for the purposes of the SIXTHSENSE project. It has since been successfully tested in two field trials performed by first responders. The functionality of acquiring data was used for collecting physiological data about the first responders from various sensors. These data were both logged on an integrated µSD card and transmitted to a command centre which was realised through the communication functionality. Through electrotactile stimulation, the first responders were notified if certain parameters were out of regular boundaries. Feasibility tests in the field trials proved that the realized specifications of the voltage converter and the current source provided a sufficient range of stimulation levels for the tactile communication over multi-array electrodes placed on the torso of the user during physical activity, i.e. skiing and walking. The accuracy of the stimulation pulses shown in Figures 4 and 5 is satisfactory for electrotactile stimulation and the pulse amplitude error with respect to the set point value is negligible. Furthermore, initial tests proved that flexibility provided through the creation of stimulation patterns, which consider change of the active electrode pad and stimulation frequency, allow the generation of a large number of feedback messages. Given the number of different interfaces integrated in the device, it can also be used outside the scopes of the SIXTHSENSE project. The mentioned interfaces allow the device to communicate with both analogue and digital sensors of many types which makes it suitable for different kinds of tests and experiments. Furthermore, the powerful STM32H743VIT6 microcontroller used as the core of the device can even be used for certain signal processing applications or for running more complex algorithms than the ones used in this project.

## Acknowledgment

This work has received funding from the European Union's Horizon 2020 research and innovation programme under grant agreement No 883315.

## References

[1] R. Gasaway, Situational Awareness for Emergency Response, 2013.

[2] M. A. Garenfeld, N. Jorgovanović, V. Ilić, M. Štrbac, M. Isaković, J. L. Dideriksen and S. Došen, "A compact system for simultaneous stimulation and recording for closed-loop myoelectric control," *ournal of NeuroEngineering and ehabilitation,* 2021.

[3] M. Štrbac, M. Isaković, J. Malešević, G. Marković, S. Došen, N. Jorgovanović, G. Bijelić and M. Kostić, "Electrotactile Stimulation, A New Feedback Channel for First Responders," 2021.

[4] A. Popović-Bijelić, G. Bijelić, N. Jorgovanović, D. Bojanić, M. B. Popović and D. B. Popović, "Multi-Field Surface Electrode for Selective Electrical Stimulation," 2005.

 ISBN 978-86-7466-930-3

# Deep Neural Network Approach for Artifact Detection in Raw ECG

Tanja Boljanić, Jovana Malešević, Goran Kvaščev

***Abstract*— lectrocardiography is a non-invasive technique for monitoring the electrical activity of the heart, and its analysis can detect and then prevent many health problems. Alterations that are not related to cardiac electrical activity represent artifacts in signal and should be minimized in order to correctly interpretate the signal. This is of great importance in wearable systems for electrophysiological monitoring that have numerous applications in healthcare and fitness. This paper presents how to build a classification model to detect artifacts in electrocardiogram ( CG) signal using deep neural networ . The ong hort-Term emory ( T ) networ was proposed for classifying 1 -s single-channel CG segments as *a d* and *Art act* Data set consists of 1 ,2 1 raw CG samples. The results show that the proposed method can classify the data with the accuracy of .1 , i.e., efficiently deal with acceptance of good ( . ) and rejection of poor ( .1 ) CG quality.**

***Index Terms*— CG; Deep eural etwor ; T , Classification odel**

## I. Introduction

ELECTROCARDIOGRAPHIC (ECG) artifacts are alterations that are not related to cardiac electrical activity. The artifacts could be caused by the unexpected motion intensity, loss of electrode-skin contact or movements of different part of the system such as cables. Additionally, some of the common noises that appear in the ECG signal are electromyogram (EMG) noise and baseline drift due to breathing or sudden movement, and such noises can be easily removed using various filtering approaches. The problem occurs if the artifacts last too long, and completely compromise the shape of the signal. Then, the current physical state of the subject could be misinterpreted. That is why it is of great importance to identify these types of artifacts and ignore the parts of the signal in which they appear. This is especially referring to the wearable systems for electrophysiological monitoring that are used for healthcare or fitness where health condition of the subjects is further decided based on the parameters extracted from the ECG signal. Since the subjects perform various physical activity, the quality of the ECG signal even more decreases. As predictions of the physical state are given in the real time, the artifacts detection as well as the other algorithms should be performed automatically.

Lui et al. [1] developed a wearable system for early detection of cardiovascular diseases and used machine learning algorithm for classifying ECG segments as acceptable and unacceptable for further analysis. Using Support Vector Machine (SVM), they could exclude unacceptable segments with an accuracy of 96.4%.

Neural networks are widely used for classification of different types of artifacts or arrhythmias in ECG signal [2-7]. Saadatnejad at al. [2] proposed a method consisting of wavelet transform and multiple recurrent neural networks for classifying arrhythmias in continuous cardiac monitoring on wearable devices. Deep network with wavelet sequences as input was used for classification of five heartbeat signals, resulting in high recognition performance [3]. Six common types of urgent arrhythmias are classified using deep neural network with an overall accuracy of 81% [4]. Deep learning algorithms were also used to classify shockable versus non-shockable rhythms in the presence and absence of cardiopulmonary resuscitation (CPR) artifact for automated external defibrillators [5]. Chauhan and Vig used deep recurrent neural network architecture with Long Short Term Memory (LSTM) units to detect abnormal and normal signals in ECG data [6]. The data included four different types of abnormal beats and the proposed detection system provided 96.5% performance.

The aim of the presented work is to develop a system that can automatically identify artifacts in ECG signals. We propose deep learning method for classification of unwanted artifacts and ECG signal that could be further processed, as we believe that these differences in signal could be reliably detected by a properly trained neural network.

Section II contains the method, including data preparation, and an explanation of used algorithm with the configuration of its parameters. The results are presented and discussed in section III, while the conclusion is attached in the final section.

## II. The Method

The proposed algorithm is implemented in the Matlab R2019b software installed in a Windows 10 Pro platform, using the Signal Processing and Deep Learning toolboxes. The computer that was used is equipped with NVIDIA GeForce RTX 3060 graphics processing unit.

### *A. ataset and Implementation*

Dataset that was used in this study was collected by Tecnalia Serbia during the field trials within SIXTHSENSE

Tanja Boljanić and Goran Kvaščev are with the School of Electrical Engineering, University of Belgrade, 73 Bulevar kralja Aleksandra, 11020 Belgrade, Serbia (e-mail: tanja.boljanic@gmail.com )

Tanja Boljanić and Jovana Malešević are with the Tecnalia Serbia Ltd, Deligradska 9, 11000 Belgrade, Serbia

 ISBN 978-86-7466-930-3

project [8] in Bormio, Italy. The sensing module based on a multi-electrode array (MEA) for ECG recording was placed below the left major pectoralis. The MEA contains two recording and one referent electrode. The module provides conditioning and A/D conversion of the signal, and it is connected to the sensor for data acquisition via the flat cable. Described prototype was developed for research purposes within the project. This dataset comprises one-lead ECG recordings from 12 mountain rescuers that were performing the rescue task (male/female, 11/1, age (mean ± std), 31.7 ± 6.0 year). The length of the ECG signals ranges from 90 to 200 min with the average of 150 min, and the sampling rate is 1000 Hz. The signal contains motion artifacts due to the unexpected motion intensity and motion state, and the noises due to the change of relative displacement between electrode and skin, as well as the artifacts due to the cable movements. These noises have typical characteristics as transient high amplitude impulse and signal saturation. In order to utilize the automatic identification of the artifacts in signal, the ECG was visually inspected and we manually selected segments that are extremely noisy.

All signals were divided into 10-s segments, with total of 7,517 valid ECG and 2,714 segments labeled as signal with artifacts (7,517 + 2,714 = 10,231). Artifact segments are selected so that more than a half of the segment contain pure noise resulting in visually undetectable QRS complexes. An example of signal's both classes is presented in Fig. 1.

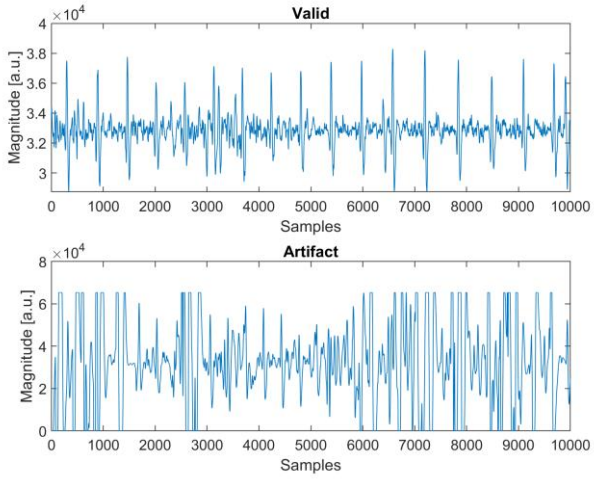


Fig. 1. The example of 10-s ECG segments: a segment without artifacts ( *alid*, top) and a segment with artifacts (*Artifact*, bottom)

The raw data segments were divided into two sets: 90% and 10% for the training and testing, respectively. Both classes were randomly divided into these two sets. Since 73.5% of the dataset are valid segments, a classifier would learn that it can achieve a high accuracy simply by classifying all signals as *alid.* To avoid this bias, the *Artifact* signal was augmented so that there is the same number of *alid* and *Artifact* signals. This is one form of data augmentation used in deep learning, known as oversampling [9]. *Artifact* signals were augmented after splitting data into two sets, hence the data from the test set are not included in the training set. At the end, the distribution between *alid* and *Artifact* signals was evenly balanced, as showed in Table I.

### *B. Proposed eep Neural Network*

Deep Neural Networks (DNN) are one type of model for machine learning that is subfield of artificial inteligence (AI) [10]. The appropriate deep learning algorythm depends on the task and the available data. Long short-term memory (LSTM) networks are the most commonly used variation of recurrent neural networks (RNN) that are well situated to study sequence and time-series data [11].

TABLE I
THE DIVISION OF THE ENTIRE DATASET INTO TRAINING AND TESTING SETS

| Classes | The original number of 10-s segments | Number of 10-s segments after leveling | |
|---|---|---|---|
| | | Training | Test |
| *alid* | 7,517 | 6,765 | 752 |
| *Artifact* | 2,714 | 6,765 | 271 |

The LSTM network can effectively learn long-term relationships between time steps of a sequence. It consists of an input gate, forget gate, output gate and cell unit. The cell remembers values over arbitrary time intervals, and the gates regulate the flow of information into and out of the cell. Input gate protects the unit from irrelevant input events, while the forget gate controls when to forget previous memory contents. The output gates controls the output flow. Graphical representation of an LSTM unit is presented in Fig. 2. The LSTM network can look at the time sequence in the forward direction and in both forward and backward directions, which is than called bidirectional LSTM (BiLSTM). This is useful when there is need to learn from the complete time series at each time step.

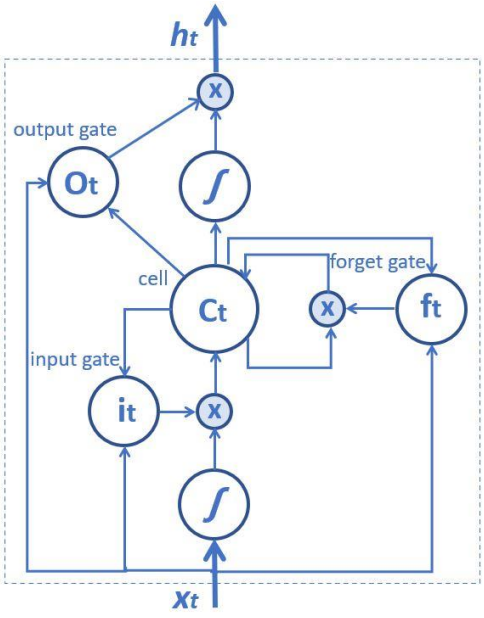


 ISBN 978-86-7466-930-3

Fig. 2. LSTM block diagram. The variables are: $x_t$ – input vector to the LSTM unit, $i_t$ – input gate's activation vector, $f_t$ – forget gate's activation vector, $o_t$ – output gate's activation vector, $c_t$ – cell state vector, $h_t$ – output vector of the LSTM unit.

### C. Network Parameter Configuration

LSTM network was proposed for ECG classification. The network parameters were selected experimentally or following the other studies [9,12,13]. The bidirectional LSTM (BiLSTM) with 200 hidden units was used, as it looks at the sequence in both directions – backwards and forward, which is important when network should learn from full-time series at each time step. Sequence input was set to one dimension, because the input signal is only the amplitude of raw ECG. Two classes were specified by including a fully connected layer of size 2. The last two layers were softmax and classification layer with cross-entropy loss function. The adaptive moment estimation algorithm (ADAM) was used as the optimization method. Architecture of a network is summarized in Table II. The layer information from the table includes the layer type, the size and format of the layer activations, and the size of learnable parameters.

TABLE II
THE DETAILED INFORMATION FOR EACH LAYER OF THE PROPOSED NETWORK MODEL

| Name | Type | Activations | Learnables |
|---|---|---|---|
| *input* | Sequence input | 1 | - |
| *Bi STM* | BiLSTM | 400 | InputWeights 1600x1<br>RecurrentWeights 1600x200<br>Bias 1600x1 |
| *fc* | Fully Connected | 2 | Weights 2x400<br>Bias 2x1 |
| *softma* | Softmax | 2 | - |
| *output* | Classification Output | - | - |

The BiLSTM layer has the following parameters: initial learning rate = 0.01, mini-batch size = 150, epoch = 10, gradient threshold = 1, sequence length = 1000, dropout = 0. Number of epochs in the number of passes through the training data, and increasing this number wasn't resulting in better classification accuracy. Mini-batch size is the number of signals that neural network looks at a time, while the signal is broken into smaller sequences (sequence length) so that the computer does not run out of the memory. Dropout layer was not used as the previous studies showed that it did not increase the network generalization ability [9,12].

## III. RESULTS AND DISCUSSION

The ECG data were classified using the LSTM network and performance measures of the model were evaluated using a confusion matrix. Confusion matrixes that are obtained after the training and testing process are presented in Fig. 4-5.

A row-normalized row summary represents the percentages of correctly and incorrectly classified observations for each true class, while a column-normalized column summary represents the same thing but for each predicted class. In order to report performance results for binary classification of *alid* and *Artifact* ECG, five statistical metrics are extracted from the confusion matrix and presented in Table III: accuracy, sensitivity, specificity, precision and F1-score.

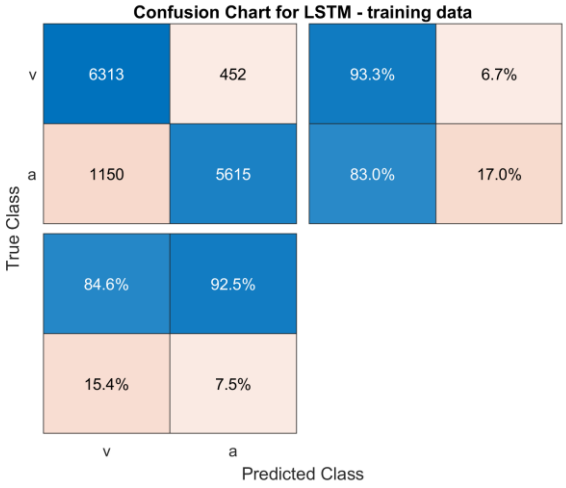


Fig. 4. Confusion matrix for the training set of the LSTM with a raw ECG. The axes labels represent the class labels, *alid* - "v" and *Artifact* - "a".

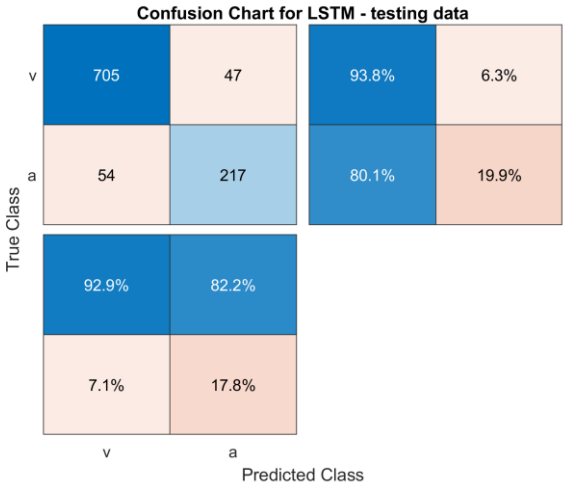


Fig. 5. Confusion matrix for the test set of the LSTM with a raw ECG. The axes labels represent the class labels, *alid* - "v" and *Artifact* - "a".

The LSTM accuracy for the training set was 88.2%, while for the testing set it was 90.1%. The accuracy is the proportion of correctly classified ECG segments of all ECG segments. Sensitivity calculates the number of correctly classified valid ECG segments out of the total samples in the class, while the specificity calculates the number of correctly classified artifact ECG segments out of the total samples in the mentioned class. The precision calculates the number of true positives out of the positive classified classes. Finally, F1-score is the harmonic mean of both the precision and sensitivity measures and it is used as an overall score on how well the model is performing.


ISBN 978-86-7466-930-3

TABLE III
EVALUATION METRICS FOR A CLASSIFICATION TEST

| | |
|---|---|
| Accuracy | 90.1% |
| Sensitivity | 93.8% |
| Specificity | 80.1% |
| Precision | 92.9% |
| F1-score | 93.3% |

The time consumption for training was 53 min, which is acceptable, considering the large database that included more than 10,000 ECG segments (a 10-s duration for each segment). Segments of 10 seconds was used, because most of the ECG monitors display and analyze such signal duration, and Hajeb-M et al. [5] reported that 8 s segments is the best choice for classification accuracy. As mentioned in the method section, we selected the segments of ECG signal that are extremely noisy as *Artifact* signals. In practical applications, it would be of interest to observe not only the signals that are incredibly noisy, but rather signals with various degrees of noise, and it will be considered in the future work. Network parameters that are used are the optimal one for this type of dataset. Other options did not help the network to improve the classification accuracy. Some of the changes that were performed are decreasing the learning rate and the mini-batch size, and increasing the number of epochs.

The overall accuracy of 90.1% indicates that the proposed model could provide accurate prediction on a raw ECG data. By observing the sensitivity and specificity values, it can be seen that performed model recognizes valid ECG segments better than artifacts.

Similar study [9] that was also using LSTM network on raw ECG data showed the accuracy of 70.8%. Chen et al. [4] developed a classification model for six types of urgent arrhythmias combining CNN (Convolutional Neural Network) and LSTM with accuracy of 81.0%, sensitivity of 82.0% and specificity of 97.0%. Combination of CNN and LSTM was also used by Liang et al. [14], who verified the classification accuracy on three different datasets of raw ECG signals and obtained F1-scores of 85.0%, 80% and 82.6%. For detection of shockable rhythms in the presence and absence of cardiopulmonary resuscitation (CPR) artifact, Hajeb-M et al. applied deep-learning algorithm using convolutional layers, residual networks and BiLSTM [5]. The sensitivity, specificity, accuracy and F1-score were 95.2%, 86.0%, 88.1% and 83.5%, respectively.

## IV. CONCLUSION

Automatic detection of artifacts in ECG signal is important goal in wearable monitoring systems in order to accurate determine subject's physical state. This work proposes to use deep learning technique for classifying ECG signal. LSTM network was used on a raw ECG signal that was divided into 10-s segments. The classification accuracy of 90.1% indicate that the proposed model shows promising results. The future work will include more data to improve the training of the neural network. Also, ECG signals with various degrees of noise will be considered. One of the possible applications of this research could be within the SIXTHSENSE project, to improve the existing algorithm for determining the heart rate signal from the ECG of the first responders (mountain rescuers and firefighters).

## ACKNOWLEDGMENT

The authors would like to acknowledge that this research was supported by the Ministry of Education, Science and Technological Development of the Republic of Serbia (contract 451-03-68/2022-14/200103).

The work in this study was also performed within the SIXTHSENSE project, which has received funding by European Union's Horizon 2020 research and innovation programme under grant agreement No 883315.

## REFERENCES

[1] Liu, C., Zhang, X., Zhao, L., Liu, F., Chen, X., Yao, Y., & Li, J. (2018). Signal quality assessment and lightweight QRS detection for wearable ECG SmartVest system. *IEEE Internet of Things ournal*, (2), 1363-1374.

[2] Saadatnejad, S., Oveisi, M., & Hashemi, M. (2019). LSTM-based ECG classification for continuous monitoring on personal wearable devices. *IEEE journal of biomedical and health informatics*, *24*(2), 515-523.

[3] Yildirim, Ö. (2018). A novel wavelet sequence based on deep bidirectional LSTM network model for ECG signal classification. *Computers in biology and medicine*, , 189-202.

[4] Chen, Y. J., Liu, C. L., Tseng, V. S., Hu, Y. F., & Chen, S. A. (2019, May). Large-scale classification of 12-lead ECG with deep learning. In *201 IEEE EMBS International Conference on Biomedical ealth Informatics B I* (pp. 1-4). IEEE.

[5] Hajeb-M, S., Cascella, A., Valentine, M., & Chon, K. H. (2021). Deep Neural Network Approach for Continuous ECG-Based Automated External Defibrillator Shock Advisory System During Cardiopulmonary Resuscitation. *ournal of the American eart Association*, *10*(6), e019065.

[6] Chauhan, S., & Vig, L. (2015, October). Anomaly detection in ECG time signals via deep long short-term memory networks. In *2015 IEEE International Conference on ata Science and Ad anced Analytics SAA* (pp. 1-7). IEEE.

[7] Attia, Z. I., Kapa, S., Lopez-Jimenez, F., McKie, P. M., Ladewig, D. J., Satam, G., ... & Friedman, P. A. (2019). Screening for cardiac contractile dysfunction using an artificial intelligence–enabled electrocardiogram. *Nature medicine*, *25*(1), 70-74.

[8] https://sixthsenseproject.eu/

[9] Kłosowski, G., Rymarczyk, T., Wójcik, D., Skowron, S., Cieplak, T., & Adamkiewicz, P. (2020). The use of time-frequency moments as inputs of lstm network for ecg signal classification. *Electronics*, (9), 1452.

[10] Goodfellow, I., Bengio, Y., & Courville, A. (2016). *eep learning*. MIT press.

[11] Patterson, J., & Gibson, A. (2017). *eep learning A practitioner s approach*. " O'Reilly Media, Inc.".

[12] Gao, J., Zhang, H., Lu, P., & Wang, Z. (2019). An effective LSTM recurrent network to detect arrhythmia on imbalanced ECG dataset. *ournal of healthcare engineering*, *201* .

[13] Kim, B. H., & Pyun, J. Y. (2020). ECG identification for personal authentication using LSTM-based deep recurrent neural networks. *Sensors*, *20*(11), 3069.

[14] Liang, Y., Yin, S., Tang, Q., Zheng, Z., Elgendi, M., & Chen, Z. (2020). Deep learning algorithm classifies heartbeat events based on electrocardiogram signals. *Frontiers in Physiology*, 1255.

 ISBN 978-86-7466-930-3

# Inhibition Potency of Terpyridine Metal Complexes toward Penicillin-Binding Protein 1A

Svetlana Jeremić, Enisa Selimović, Milan Dekić, and Tanja Soldatović

***Abstract*—The potency of copper(II) and zinc(II) terpyridine complexes to inhibit penicillin-binding protein 1A (PBP1a) was investigated by *in silico* methods. The geometries of ligands are optimized using DFT calculations. In order to estimate the binding sites, inhibition constants and binding energies between ligands and PBP1a protein, molecular docking analysis is performed. The inhibition potency of examined terpyridine metal complexes is compared with the inhibition potency of lactivicin, an antibiotic already used in the treatment of Gram-negative and Gram-positive bacteria. Performed docking analysis indicated that investigated terpyridine metal complexes show higher inhibition potency toward PBP1a protein than lactivicin. The results identified these complexes as potential antimicrobial agents for further *in vitro* experiments.**

***Key words* — copper(II) terpyridine; zinc(II) terpyridine; penicillin-binding protein 1A; lactivicin; molecular docking analysis.**

## I. Introduction

Antibiotics have transformed medicine by changing the outcome of bacterial infections. Since the discovery of penicillin by Sir Alexander Fleming in 1928, antibiotics extend expected life spans for almost 25 years in the USA and have had similar beneficial effects worldwide. Nevertheless, the emergence of resistant microorganisms endangering the efficacy of antibiotics - bacterial infections have again become a threat due to the resistance that has been seen to nearly all antibiotics that have been developed. This has been attributed to the overuse and misuse of antibiotics, as well as a lack of new drug development, urging to renew efforts in the research of new antimicrobials and investigation of their mechanism of action [1].

Epidemic antibiotic resistance has been described in numerous pathogens, including common respiratory pathogens such as *Streptococcus pneumoniae*. This pathogen causes pneumonia, otitis media, and sepsis, and has been responsible for over one million yearly deaths worldwide [2]. Presently, 25% of all invasive strains are resistant to penicillin, amoxicillin, and cephalosporins [3, 4].

Svetlana Jeremić is with the Department of Natural Sciences and Mathemathics, The State University of Novi Pazar, 9 Vuka Karadžića, 36300 Novi Pazar, Serbia (e-mail: sjeremic@np.ac.rs).

Enisa Selimović is with the Department of Natural Sciences and Mathemathics, The State University of Novi Pazar, 9 Vuka Karadžića, 36300 Novi Pazar, Serbia (e-mail: eselimovic@np.ac.rs).

Milan Dekić is with the Department of Natural Sciences and Mathemathics, The State University of Novi Pazar, 9 Vuka Karadžića, 36300 Novi Pazar, Serbia (e-mail: mdekic@np.ac.rs).

Tanja Soldatović is with the Department of Natural Sciences and Mathemathics, The State University of Novi Pazar, 9 Vuka Karadžića, 36300 Novi Pazar, Serbia (e-mail: tsoldatovic@np.ac.rs).

In the last few decades we have seen a dramatic increase in the number of β-lactam antibiotics and understanding of their mechanism in inhibition of peptidoglycan biosynthesis. Peptidoglycan component of bacterial cell wall consists of polymerized chains of repeating disaccharide subunits (N-acetylglucosamine and N-acetylmuramic acid cross-linked by stem pentapeptides), whose function is to provide cellular shape and maintain osmotic pressure [5]. Both the polymerization of disaccharide subunits and peptide cross-linking reactions are catalyzed by penicillin-binding proteins (PBPs), membrane-associated enzymes essential for cell division and daughter cell formation. PBPs possess the ability to covalently bind β-lactam antibiotics [6]. All enterobacteria appear to possess a similar spectrum of PBPs differing in molecular weight and affinity for β-lactams [7]. The high molecular-weight (HMW) PBPs (PBP1a/1b, PBP2, and PBP3) are physiologically important bifunctional enzymes that catalyze the final stages of peptidoglycan synthesis [6].

In Gram-positive bacteria, such as *S. pneumoniae*, the cell wall is composed mostly of peptidoglycan. *S. pneumoniae* has six PBPs, three of which are bifunctional - PBP1a, PBP2a, and PBP1b [8]. A PBP1a is essential for cell viability. This protein plays a key role in the formation of the cell septum during the bacterial division cycle and is involved in homologous DNA recombination mechanism, repair, and chromosome segregation [2]. To date, the mechanism used by bifunctional PBPs in the development of β-lactam resistance has remained unknown [2]. X-ray studies of soluble forms of pneumococcal PBP1a, both in apo (an inactive form, with no bounded ligand) as well as in antibiotic-bound forms, demonstrate that this protein contains three domains – the central transpeptidase domain flanked N-terminally by a GT/TP interdomain linker region, and C-terminally by a small, β-sheet rich unit. The active site of PBP1a is unusually narrow, suggesting that ligands must initially be threaded into the gorge to be recognized [2].

The search for effective inhibitors of PBP1a protein indicated that among the molecules with significant inhibitory affect there are different metal complexes of 2,2′:6′,2″-terpyridine molecule. The 2,2′:6′,2″-terpyridine (terpy) ligand is tridentate, nearly coplanar, $N_3$ donor ligand. It has been recognized as a useful ligand for transition metal and rare earth metal ions in inorganic chemistry. Square-planar, square-pyramidal and octahedral metal complexes with terpy ligands have been reported to be of great biological interest [9, 10, 11].

The biologically important metal ions copper(II) and zinc(II) have the ability to coordinate into different

 ISBN 978-86-7466-930-3

geometries depending on the specific arrangement of donor atoms in biomolecules, but strong π-acceptor ability of the tridentate chelate 2,2′:6′,2′′-terpyridine stabilizes the square-pyramidal geometry [10]. Different substituted terpyridene molecules generate complexes with copper(II) and zinc(II) ions, that exert anti-microbial, anti-bacterial, anti-fungal, anti-proliferative and inhibitory activity. For example, terpyridine complexes of Cu(II) and Zn(II), and especially complexes of $Cu(TTP)Cl_2$ and $Zn(TTP)Cl_2$ (TTP is 4 -[*p*-tolyl]- 2,2′:6′,2′′-terpyridine) are efficient inhibitors of furin. Furin, a human subtilisin-related proprotein convertase (SPC), is emerging as an important pharmaceutical target because it processes vital proteins of many aggressive pathogens. Inhibition is irreversible, competitive with substrate, and affected by substituents on the chelate. The free chelates are not inhibitors [12]. Complexes of terpyridine-based ligands with Zn(II) as a central metal ion has also shown significant inhibitory activity against B-DNA molecule and similar double helixes, as against penicillin binding protein 2a [9]. This fact indicated the importance of examining the possibility of complexes of terpyridine with Cu(II) and Zn(II) to inhibit PBPa1 protein, which is known to be a protein of great importance in the development of bacteriological infections.

## II. Methodology Section

The inhibition potency of copper(II) and zinc(II) terpyridine complexes toward penicillin-binding protein 1A (PBP1a) is investigated using molecular docking analysis. The structures of terpyridine metal complexes are optimized using M06-2X functional [13] in combination with 6-311++G(d,p) basis set implemented in Gaussian 09 program package [14]. Molecular docking simulations were carried out using AutoDock 4.0 software [15]. The three-dimensional (3D) crystal structure of PBP1a protein was downloaded from the Protein Data Bank (PDB ID: 2C6W) [2]. The protein structure is released from the co-crystallized ligand, water molecules, and co-factors and prepared for docking simulations using Discovery Studio 4.0 [16]. The affinity maps of the target protein are established using AGFR (AutoGridFR) software [17]. According to AGFR, binding site with the lowest expected binding energy is grid box with dimensions 98.799Å x 35.214Å x 55.068Å in -x, -y, and -z directions. A grid point spacing of 0.375 Å was used for auto grid runs. The addition of polar hydrogen atoms and the calculation of Kollman charges are done by using AutoDockTools (ADT) graphical interface. The ligands are set to be flexible, while the structure of protein remains standing as rigid. The Lamarckian Genetic Algorithm (LGA) is used for protein-ligand flexible molecular docking simulations. Calculations are performed at a temperature of 298.15 K. Analysis of molecular docking simulation results and visualizations of predicted protein-ligand interactions are performed using BIOVIA Discovery Studio [16].

## III. Results and Discussions

Molecular docking analysis is a useful and widely used method for predicting the inhibitory activity of biologically active compounds. Terpyridine metal complexes possess significant anti-bacterial, anti-fungal and anti-cancerous activity [9, 10]. Moreover, recent research has shown that complexes of terpyridine and some its derivatives with different metals show significant inhibitory activity against various protein molecules [18, 19]. Since terpyridine complexes of Cu(II) and Zn(II) are already selected as potential agents against different disease, here is investigated their potency to inhibit PBP1a protein. PBP1a protein is membrane-associated enzyme that plays essential roles in the peptidoglycan biosynthetic process [2]. In this way it enables the proliferation of bacteria *Streptococcus pneumoniae*. The infection caused by this pathogen have been treated with β-lactam antibiotics for almost a century, but the proliferation of strains that are highly resistant to such drugs is a problem of worldwide concern. Although *S. pneumoniae* has six penicillin-binding proteins, PBP1a is essential for the development of high-level resistance to penicillins and cephalosporins [2]. Therefore, the development of agents that enable the inhibition of this protein is of particular interest.

In order to be able to compare the inhibitory activity of terpyridine metal complexes with an activity of a compound already used for these purposes, the inhibitory potency of the drug lactivicin was also examined. Lactivicin is compound that shows moderate activity against Gram-negative and high activity against Gram-positive bacteria. The mechanism of its activity is based on the binding to PBPs and violation of its structure [20]. Structures of copper(II) terpyridine complex, zinc(II) terpyridine complex and lactivicin are shown in Fig. 1.

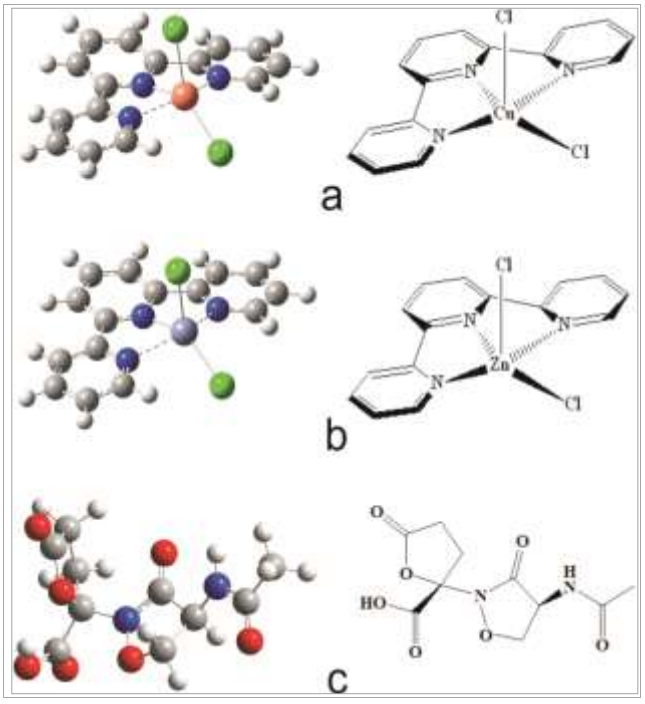


Fig. 1. 2D structures (right) and optimized structures (left) of copper(II) terpyridine complex (a), zinc(II) terpyridine complex (b) and lactivicin (c).

The evaluation of the inhibitory nature of ligand according to PBP1a was performed using molecular docking study. At the beginning of the research, the pockets and binding sites of the targeted protein were determined using the AGFR software [17]. All three estimated ligands showed

 ISBN 978-86-7466-930-3

the highest activity against protein at the same position. Grid box with dimensions 98.799Å x 35.214Å x 55.068Å in -x, -y, and -z directions, and with spacing of 0.375 Å is predicted. For all three estimated ligands it comprises the same pocket of the polypeptide chain (Fig.2).

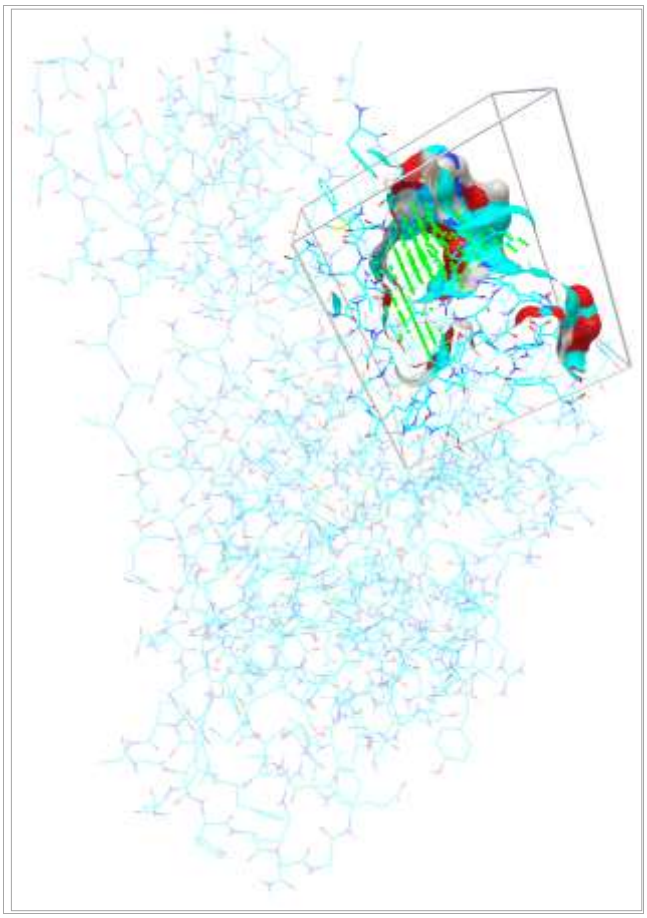

Fig. 2. The location of the most probable binding site of PBP1a for all three estimated ligands.

After configuring and computing affinity maps for a receptor-protein interactions, the one with the lowest binding energy was used for AutoDock4 calculations. Ten different conformations of protein-ligand complexes are set for molecular docking simulations. It should be emphasized that only one conformation has been accomplished when as ligand is used any of estimated terpyridine metal complexes. It can be explained by the complete rigidity of the ligand structure. On the other side, flexible structure of lactivicin allowed formation of ten protein-ligand complexes. The complex conformation that possesses the lowest binding energy was selected for further analysis.

TABLE I

THE IMPORTANT THERMODYNAMICAL PARAMETERS FROM MOLECULAR DOCKING SIMULATIONS BETWEEN PENICILLIN-BINDING PROTEIN 1A (PBP1A) (PDB ID: 2C6W) AND SELECTED COMPOUNDS

| Ligand | $\Delta G_{bind}$ (kcal/mol) | Ki (μM) |
|---|---|---|
| $[CuCl_2(terpy)]$ | -6.66 | 13.11 |
| $[ZnCl_2(terpy)]$ | -6.62 | 13.99 |
| lactivicin | -5.48 | 95.46 |

The inhibitory potency of preferred compounds can be estimated based on the thermodynamical parameters obtained by statistical mechanical analysis. Values of the free energy of binding ($\Delta G_{bind}$) expressed in kcal/mol and inhibition constant (Ki) expressed as micromolar concentration, are presented in Table 1. The lowest binding energy indicates to the easiest binding possibility of the investigated ligand. Low values of the inhibition constant indicate that a low concentration of inhibitor is required in order to inhibit the activity of the observed protein. Both $\Delta G_{bind}$ and Ki indicate that the highest inhibition potency shows Cu(II)-terpyridine complex. Somewhat lower inhibition potency has Zn(II)-terpyridine complex, while lactivicin shows the least.

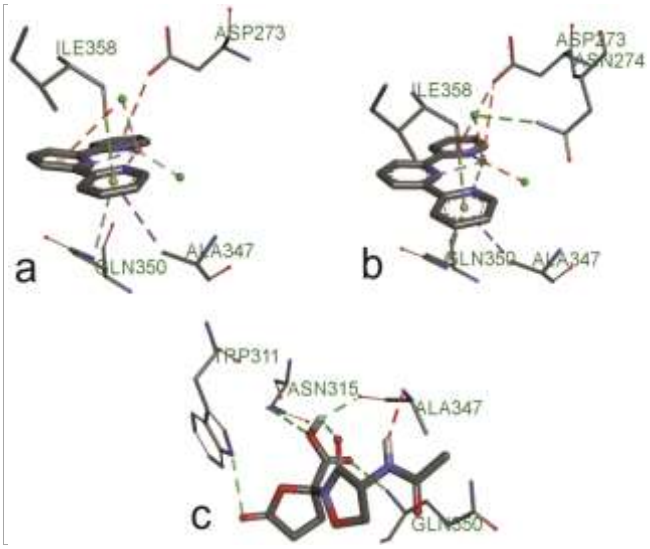


Fig. 3. Docking positions of the Cu(II)-terpyridine complex (a), Zn(II)-terpyridine complex (b) and lactivicin (c), with PBP1a protein.

Each of the three considered ligands achieves at least four protein-ligand interactions. PBP1a protein interact with Cu(II)-terpyridine complex forming π – anion electrostatic interaction via Asp273, then π – lone pair interaction via Ile358, π – donor hydrogen bond via Gln350, and π – σ interaction via Ala347. The interactions achieved by Zn(II)-terpyridine complex with PBP1a are the same as those achieved by the complex with copper, except that Zn-complex achieves another additional conventional hydrogen bond via Asn274 amino acid of PBP1a. Lactivicin generates with the protein four conventional hydrogen bonds, via the amino acids Trp311, Asn315, Ala347 and Gln350. It can be seen that all three ligands interact with PBP1a via Ala347 and Gln350 (Fig. 3). As it can be concluded, the number of ligand-protein interactions is not the only parameter that affects to the strength of inhibition, but it is also the type of interactions. Although conventional hydrogen bonds are among the most significant interactions in protein inhibition, the effect of interactions involving π–electrons derived from terpyridine should not be overlooked.

## IV. CONCLUSIONS

Metal complexes of terpyridine are known as compounds with significant anti-bacterial, anti-fungal and anti-

 ISBN 978-86-7466-930-3

cancerous activity [9, 10]. On the other hand, there are numerous infections caused by bacteria *Streptococcus pneumonia*. Penicillin binding proteins (PBPs) play a key role in the proliferation of this bacterium [2]. Therefore, the device of molecules that would lead to the inhibition of this protein could significantly contribute to the treatment of infections caused by *S. pneumonia*.

The potency of Cu(II)-terpyridine complex and Zn(II)-terpyridine complex to inhibit penicillin-binding protein 1A (PBP1a) is investigated in this purpose. Due to it molecular docking simulations are performed. Inhibition potency of $[CuCl_2(terpy)]$ and $[ZnCl_2(terpy)]$ are compared with inhibition potency of lactivicin, molecule that is already used in the treatment of *S. pneumonia*.

The analysis of results obtained by molecular docking simulations indicated that the highest inhibition potency express Cu(II)-terpyridine complex, while Zn(II)-terpyridine complex shows somewhat lower inhibition potency. Both estimated complexes possess higher inhibition potency than lactivicin. All three investigated ligands react with PBP1a at the same reaction position, and in some cases, via the same amino acids of protein. All ligands generate at least four interactions with protein, among the most important are conventional hydrogen bonds, and interactions involving π–electrons from terpyridine.

Comparing inhibition potency of $[CuCl_2(terpy)]$ and $[ZnCl_2(terpy)]$ with inhibition potency of some other complexes of terpyridine and its derivatives with different metals [18, 19], it can be seen that here investigated complexes possess similar or higher inhibition potency toward here estimated protein.

The results of the docking analysis conducted in this study provide significant preliminary results related to the inhibitory activity of the complexes tested here. With all this in mind, the herein discussed metal complexes may be considered as potential agents in the treatment of bacterial infections. Among further studies of the biological activity of the terpyridine complex, *in vivo* studies are certainly the most important.

## ACKNOWLEDGMENT

This research was supported by the Serbian Ministry of Education, Science, and Technological Development (Agreement No. 451-03-68/2022-14/200252).

## REFERENCES

[1] C. L. Ventola C. L., "The antibiotic resistance crisis: part 1: causes and threats," *P T.*, vol. *40*, no. *4*, pp. *277-283*, Apr. 2015.

[2] C. Contreras-Martel, V. Job, A. M. Di Guilmi, T. Vernet, O. Dideberg, A. Dessen, "Crystal structure of penicillin-binding protein 1a (PBP1a) reveals a mutational hotspot implicated in beta-lactam resistance in Streptococcus pneumoniae," *J. Mol. Biol.*, vol. *355*, no. *4*, pp. *684-696*, Nov. 2005.

[3] C. Doit, C. Loukil, F. Fitoussi, P. Geslin, E. Bingen, "Emergence in France of multiple clones of clinical Streptococcus pneumoniae isolates with high level resistance to amoxicillin," *Antimicrob. Agents Chemother.* vol .*43*, no. *6*, pp. *1480-1483*, Jun 1999.

[4] T. J. Coffey, M. Daniels, L. K. McDougal, C. G. Dowson, F. C. Tenover, B. G. Spratt, "Genetic analysis of clinical isolates of Streptococcus pneumoniae with high-level resistance to expanded-spectrum cephalosporins," *Antimicrob. Agents Chemother.*, vol. *39*, no. *6*, pp. *1306-1313*, Jun 1995.

[5] J. V. Holtje, "Growth of the stress-bearing and shape-maintaining murein sacculus of *Escherichia coli*," *Microbiol. Mol. Biol. Rev.*, vol. *62*, no. *1*, pp. *181-203*, Mar. 1998.

[6] R. Fontana, G. Cornaglia, M. Ligozzi, A. Mazzariol, "The final goal: penicillin-binding proteins and the target of cephalosporins," *Clin. Microbiol. Infect.*, vol. *6*, no. *3*, pp. *34-40*, Jan. 2000.

[7] N. A. Curtis, D. Orr, G. W. Ross, M. G. Boultan, "Competition of beta-lactam antibiotics for the penicillin-binding proteins of *Pseudomonas aerogenes, Proteus rettgeri, and Escherichia coli*. Companion with antibacterial activity and effects upon bacterial morphology," *Antimicrob. Agents. Chemother.*, vol. *16*, no. *3*, pp. *325-328*, Sep. 1979.

[8] C. Goffin, J. M. Ghuysen, "Multimodular penicillin-binding proteins: an enigmatic family of orthologs and paralogs," *Microbiol. Mol. Biol. Rev.*, vol. *62*, no. *4*, pp. *1079-1093*, Dec. 1998.

[9] E. U. Mughal, M. Mirzaei, A. Sadiq, S. Fatima, A. Naseem, N. Naeem, N. Fatima, S. Kausar, A. Ali Altaf, M. N. Zafar, B. A. Khan, "Terpyridine-metal complexes: effects of different substituents on their physico-chemical properties and density functional theory studies," *R. Soc. Open Sci.*, vol. *7*, no. *11*, pp. e*201208*, Nov. 2020.

[10] E. Selimović, S. Jeremić, B. Ličina, T. Soldatović, "Kinetics, DFT study and antibacterial activity of zinc(II) and copper(II) terpyridine complexes," *J. Mex. Chem. Soc.*, vol. 62, no. *1*, pp. *1-18*, Mar. 2018.

[11] J. Li, R. Liu, J. Jiang, X. Liang, L. Huang, G. Huang, H. Chen, L.Pan, Z. Ma, "Zinc(II) Terpyridine Complexes: Substituent Effect on Photoluminescence, Antiproliferative Activity, and DNA Interaction," *Molecules*., vol. *24*, no. *24*, pp. *4519-4546*, Dec. 2019.

[12] P. Podsiadlo, T. Komiyama, R. S. Fuller, O. Blum, "Furin inhibition by compounds of copper and zinc," *J. Biolog. Inorg. Chem*., vol. 279, no. 35, pp. 36219-36227, Aug. 2004.

[13] Y. Zhao, D. G. Truhlar, "The M06 suite of density functionals for main group thermochemistry, thermochemical kinetics, noncovalent interactions, excited states, and transition elements: two new functionals and systematic testing of four M06- class functionals and 12 other functionals," *Theor. Chem Acc*., vol. *120*, no. *1-3*, pp. *215-241*, Jan. 2008.

[14] M. J. Frisch, G. W. Trucks, H. B. Schlegel, G. E. Scuseria, M. A. Robb, J. R. Cheeseman, G. Scalmani, V. Barone, G. A. Petersson, H. Nakatsuji, X. Li, M. Caricato, A. Marenich, J. Bloino, B. G. Janesko, R. Gomperts, B. Mennucci, H. P. Hratchian, J. V. Ortiz, A. F. Izmaylov, J. L. Sonnenberg, D. Williams-Young, F. Ding, F. Lipparini, F. Egidi, J. Goings, B. Peng, A. Petrone, T. Henderson, D. Ranasinghe, V. G. Zakrzewski, J. Gao, N. Rega, G. Zheng, W. Liang, M. Hada, M. Ehara, K. Toyota, R. Fukuda, J. Hasegawa, M. Ishida, T. Nakajima, Y. Honda, O. Kitao, H. Nakai, T. Vreven, K. Throssell, J. A. Montgomery, Jr., J. E. Peralta, F. Ogliaro, M. Bearpark, J. J. Heyd, E. Brothers, K. N. Kudin, V. N. Staroverov, T. Keith, R. Kobayashi, J. Normand, K. Raghavachari, A. Rendell, J. C. Burant, S. S. Iyengar, J. Tomasi, M. Cossi, J. M. Millam, M. Klene, C. Adamo, R. Cammi, J. W. Ochterski, R. L. Martin, K. Morokuma, O. Farkas, J. B. Foresman, D. J. Fox, Gaussian 09, Revision A.02, Gaussian, Inc., Wallingford CT, 2016.

[15] G. M. Morris, R. Huey, W. Lindstrom, M. F. Sanner, R. K. Belew, D. S. Goodsell, A. J. Olson, "AutoDock4 and AutoDockTools4: Automated docking with selective receptor flexibility," *J. Comput. Chem*., vol. *30*, no. *16*, pp. *2785-2791*, Dec. 2009.

[16] D. S. Biovia, Discovery studio modeling environment, 2017.

[17] Y. Zhang, S. Forli, A. Omelchenko, M. F. Sanner, "AutoGridFR: improvements on AutoDock affinity maps and associated software tools," *J. Comput. Chem*., vol. *40*, no. *32*, pp. *2882-2886*, Dec. 2019.

[18] E. U. Mughal, M. Mirzaei, A. Sadiq, S. Fatima, A. Naseem, N. Naeem, N. Fatima, S. Kausar, A. Ali Altaf, M. N. Zafar, B. A. Khan, "Terpyridine-metal complexes: effect of different substituents on their physic-chemical properties and density functional theory studies," *Roy. Soc. Open Sci*., vol. *7*, no. *11*, *e201208*, May 2022.

[19] X. Liang, J. Jiang, X. Xue, L. Huang, X. Ding, D. Nong, H. Chen, L. Pan, Z. Ma, "Synthesis, characterization, photoluminescence, anti-tumor activity, DFT calculations and molecular docking with proteins of zinc(II) halogen substituted terpyridine compounds," *Dalton Trans.*, vol. *48*, pp. *10488-10504*, Dec. 2019.

[20] Y. Nozaki, N. Katayama, S. Harada, H. Ono, H. Okazaki, "Lactivicin, a naturally occurring non-beta-lactam antibiotic having beta-lactam-like action: biological activities and mode of action," *J. Antibiot.*, vol. 4*2*, no. *1*, pp. *84-93*, Jan. 1989.

 ISBN 978-86-7466-930-3

# GT Analyzer – A Basic Tool for Handwriting Movement Data

Vladimir Džepina, Nikola Ivančević, Vera Miler-Jerković, Blažo Nikolić, Dejan Stevanović, Jasna Jančić and Milica M. Janković, *Member*, IEEE

***Abstract*—In the presence of neurological and psychiatric diseases, sensorimotor and cognitive skills tend to deteriorate. One of the daily activities that could be easily affected is handwriting. In this paper, we present the open-source software GT Analyzer, developed for visual analysis and feature extraction of the handwriting data acquired by graphic tablet. Data is acquired while patients are working on graphic tasks developed by clinicians. Visual and feature analysis of handwriting data could be of great use in establishing a correct diagnosis or in following the changes during medical therapies for neurological and psychiatric diseases. Furthermore, extracted features can be used later in statistical tools, to improve the classification and determination of therapeutic effects to a greater extent.**

***Index Terms*—handwriting; graphic tablet; depression; Parkinson's disease; open-source**

## I. Introduction

Handwriting is a complex motor task consisting of both cognitive and motor processes interplaying together [1, 2]. Computer analysis of handwriting, using a digital writing tablet, has shown its usefulness in clinical studies in the fields of neurology, psychiatry and neuropsychology in both adults and children [3]. Data obtained from handwriting analysis could help clinicians to establish correct diagnosis e.g. in Parkinson's disease and Parkinsonism [4-6], or to track changes in motor functioning and the influence of therapy on it in depression in adult subjects [7] or in attention deficit hyperactivity disorder/ADHD in children [8].

The summary of computer analysis of handwriting is that clinicians are giving patients several specially designed drawing and/or writing tasks, which they have to draw or write on a graphic tablet [2, 3, 4, 6]. During the task, the tablet is acquiring the position of the pen and the pressure with which the pen is pressed on the tablet [2]. Both on-surface and in-air handwriting movements can be analyzed [6]. After the task is completed, acquired data can be operationalized through kinematic handwriting features [2, 4].

This system is favored as it has low complexity of installment, has great ease of use for both patients and clinicians and has low chances of errors while performing the task. Also, kinematic handwriting features acquired using writing tablets show high test-retest reliability [2].

Our previous research [3, 6, 8-10] in the field of handwriting analysis has shown a great need for an open-source, user-friendly software suitable for data acquisition alongside the application software that will be used for later exploration of acquired data. This could help make the research methodology more uniform and to ease data exchange and comparison between different studies.

The aim of this paper is to present a novel, user-friendly, open-source interface for reading, visualization and analysis of data that was acquired during different graphic tasks on digital graphic tablets. This software also stresses out the importance of visual analysis of extracted handwriting features.

The flowchart of the implemented interface and software options are presented in Section II. The software functionality is demonstrated through examples from two different datasets in Section III. A brief overview of software advantages and usage options is presented in the Conclusion section.

## II. The Method

Graphic Task Analyzer (GT Analyzer) is an open-source application that enables the reading of recorded pen position ($X$,$Y$) and pen pressure ($p$) data from digital graphic tablets, a simple preview of calculated kinematic features of handwriting over time and export of 173 standard kinematic handwriting features, Fig. 1. An example of visualization for ($X$,$Y$,$p$) input sequence for three drawn figures (figure separators are marked by green arrows) is also presented in Fig. 1.

Vladimir Džepina is with the School of Electrical Engineering, University of Belgrade, Bulevar kralja Aleksandra 73, 11020 Belgrade, Serbia (e-mail: dzepina.vladimir@gmail.com).

Nikola Ivančević is with the Clinic of Neurology and Psychiatry for Children and Youth, Faculty of Medicine, University of Belgrade, Serbia (email: ivancevicsd@gmail.com).

Vera Miler-Jerković is with the Innovation Center, School of Electrical Engineering, University of Belgrade, Bulevar kralja Aleksandra 73, 11120 Belgrade, Serbia (e-mail: vera.miler@etf.bg.ac.rs).

Blažo Nikolić is with the Clinic of Neurology and Psychiatry for Children and Youth, Faculty of Medicine, University of Belgrade, Serbia (e-mail: blazonikolic87@gmail.com).

Dejan Stevanović is with the Clinic of Neurology and Psychiatry for Children and Youth, Faculty of Medicine, University of Belgrade, Serbia, Gillberg Neuropsychiatry Centre, Institute of Neuroscience and Physiology, Sahlgrenska Academy, University of Gothenburg, Sweden (email: stevanovic.dejan79@gmail.com).

Jasna Jančić is with the Clinic of Neurology and Psychiatry for Children and Youth, Faculty of Medicine, University of Belgrade, Serbia (e-mail: jasna.jancic.npk@gmail.com).

Milica M. Janković is with the School of Electrical Engineering, University of Belgrade, Bulevar kralja Aleksandra 73, 11020 Belgrade, Serbia (e-mail: piperski@etf.bg.ac.rs).

 ISBN 978-86-7466-930-3

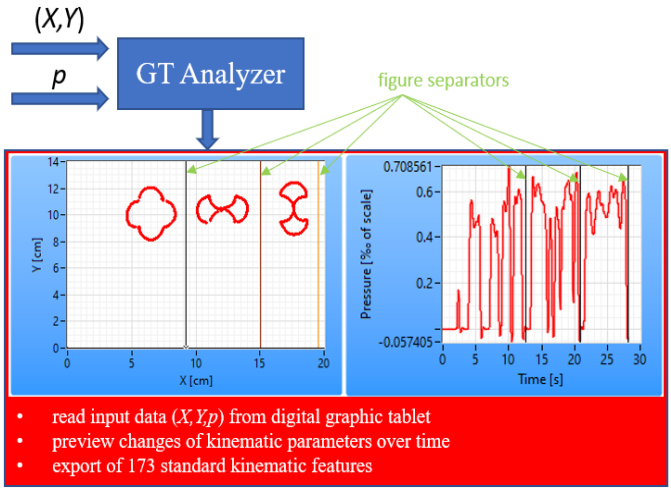


Fig. 1. GT Analyzer software options with preview example of input data (coordinate pair $(X,Y)$ and pressure $p$ of the pen tip)

### A. *Software description*

The application was developed in the LabVIEW 2019 environment (National Instruments, Texas, USA). The code of the software is available at the following Github link: https://github.com/MagnumSinum/GT-Analyzer/blob/main/GT%20Analyzer%20source%20code.rar

### B. *Kinematic features*

For each $(X,Y,p)$ input sequence, the algorithm calculates the 1st, 2nd and 3rd derivatives. The 1st derivatives of $X(t)$ data and $Y(t)$ data correspond to the velocity $V_x(t)$ and $V_y(t)$, respectively. The total velocity $V = \sqrt{V_x^2 + V_y^2}$ was also calculated. The 1st derivative of $p(t)$ data corresponds to $dp(t)/dt$. The 2nd derivatives of $X(t)$ data and $Y(t)$ data correspond to the acceleration $A_x(t)$ and $A_y(t)$, respectively. The total acceleration $A(t)$ corresponds to the 1st derivative of $V(t)$. The 2nd derivative of $p(t)$ data corresponds to $d^2p(t)/dt^2$. The 3rd derivatives of $X(t)$ data and $Y(t)$ data correspond to the jerk $J_x(t)$ and $J_y(t)$, respectively. The total jerk $J(t)$ corresponds to the 2nd derivative of $V(t)$. The 3rd derivative of $p(t)$ data corresponds to $d^3p(t)/dt^3$. The list of implemented statistical handwriting features is presented in Table 1.

TABLE I THE LIST OF STATISTICAL HANDWRITING FEATURES

| Data | Statistical feature |
|---|---|
| $X(t),Y(t),p(t),$ $V_x(t),V_y(t),$ $V(t),$ $dp(t)/dt,$ $A_x(t),A_y(t),$ $A(t),$ $d^2p(t)/dt^2,$ $J_x(t),J_y(t),$ $J(t),$ $d^3p(t)/dt^3$ | Median value |
| | Mean value |
| | Standard deviation |
| | Variance |
| | Coefficient of variation |
| | Maximum value |
| | Minimum value |
| | 10th percentile |
| | 25th percentile |
| | 75th percentile |
| | 90th percentile |
| *Total variables =15* | *Total number of features=11* |

For each figure, 8 kinematic features, so-called "figure features" were calculated. The list of figure features is presented in Table 2.

TABLE II THE LIST OF FIGURE FEATURES

| Abbreviation | Figure feature |
|---|---|
| FL [cm] | Figure length |
| FT [s] | Figure drawing time |
| FS [cm/s] | Figure drawing speed |
| NCV [n.u.] | Number of changes in velocity |
| RNCV [n.u.] | Number of changes in velocity relative to figure drawing time (NCV/FT) |
| NST [n.u.] | Time spent during drawing on-surface or in-air normalized by the figure drawing time (ON-SURFACE TIME/FT or IN-AIR TIME/FT) |
| NCA [n.u.] | Number of changes in acceleration |
| RNCA [$s^{-1}$] | Number of changes in acceleration relative to figure drawing time (NCA/FT) |

### C. *Implementation details*

The expected input file format for GT Analyzer tool is a textual file with 3 columns, each column corresponding to $X(t)$, $Y(t)$ and $p(t)$ data respectively, obtained by the data acquisition software from the digital graphic tablet. Expected units of the position data $(X,Y)$ are meant to be $10^{-5}$ m. The pressure data $p(t)$ is unitless because it is expected to be expressed relative to the full pressure scale of the digital graphic tablet. Also, it is expected that in the input file name first 4 characters are reserved for the subject ID and the last single digit in the file name is reserved for the number of the performed task by the subject. Each task could include up to eight figures.

Within the GT Analyzer tool, the following setting parameters could be selected:

- input file name (two file names could be selected at once in order to compare results for two subjects (e.g. patient vs. healthy data))
- input folder name (with several input files) for the automatic analysis and export of all kinematic features to one excel file per task.
- sample rate (performed by the data acquisition software used for $(X,Y,p)$ data recording from the digital graphic tablet)
- lower cut-off frequency that will be performed in $(X,Y)$ data processing by the 3rd order low pass Butterworth filter, the default value is set to 2 Hz
- NCV tolerance (minimal difference between two time-adjacent samples of $V(t)$ to count it as a change in velocity, the default value is set to 0.1 cm/s)
- NCA tolerance (minimal difference between two time-adjacent samples of $A(t)$ to count it as a change in acceleration, the default value is set to 1 $cm/s^2$)
- *Width* parameter (the number of consecutive data points to be used in the quadratic least-squares fit when the tool is determining local minimums on $V_y$ – local minimums on $V_y$


ISBN 978-86-7466-930-3

separate different strides within the figure)

- *Threshold* parameter (maximum value of local minimums that will be accepted when the tool is determining local minimums on $V_y$).

After the adjustment of parameters, the user can perform the following actions:

- DISPLAY DATA: Process (*X,Y,p*) input sequence from input files – extraction of all features defined in *Section II B Kinematic features*. Display (*X,Y*) data on XY graph, as well as a display of temporal graphics for *p(t), $V_y$(t), V(t), A(t)* and *J(t)* from two selected input files. The software differentiates (*X,Y,p*) samples when the pen was on the surface or in-air and represents it with red and blue color, respectively. Stride ends (found local minimums on $V_y$) are presented by green circles on *$V_y$(t), V(t), A(t)* and *J(t)* graphics.
- SAVE LIMITS: Figure separators (separators between data for different figures in one task) could be set using cursors on XY graphs (up to eight) and the cursor limits could be saved for each task.
- EXPORT LOADED DATA: Extracted kinematic features could be saved in one .xls file per each selected input file.
- EXPORT FOLDER DATA: Extracted kinematic features could be saved in one .xls file for each file within the selected input folder.

All settings and actions can be repeated while the GT Analyzer application is still running.

### *D. Dataset description*

Two different datasets acquired during graphic tablet tasks have been used to present the functionality of the GT Analyzer software:

- PaHaW adult subjects dataset, presented by Drotar and others [4] - labeled as DS1,
- pediatric subjects dataset used in the Doctoral dissertation of Ivančević N. D. [9] - labeled as DS2.

One pair from each dataset (one healthy and one diseased subject from DS1 and DS2, paired by gender and handedness), was selected to demonstrate the GT Analyzer interface. From DS1, the subject ID 6 (diagnosed with Parkinson's disease) and the healthy subject ID 26 were selected for the "drawing a spiral". During this task, the subject starts the drawing from the center of the spiral. From DS2, the subject ID 17, diagnosed with pediatric-onset major depressive disorder (drug-naive), and the healthy subject ID 25 were selected for the writing of two figures of the consecutive cursive letter "l": 1) figure 1 was drawn in the large rectangle 40x160 mm and 2) figure 2 was drawn in the small rectangle 9x160 mm.

Data acquisition for both DS1 (sample rate 100 Hz) and DS2 (sample rate 200 Hz) was performed using a digital graphic tablet Wacom Intous4 XL (Wacom Europe GmbH, Krefeld, Germany) with the cordless pen that enables on-surface and in-air handwriting. Custom-made data acquisition *LabHand* [10] previously developed in the LabVIEW environment, the same environment as for the GT Analyzer, was used for the data recording.

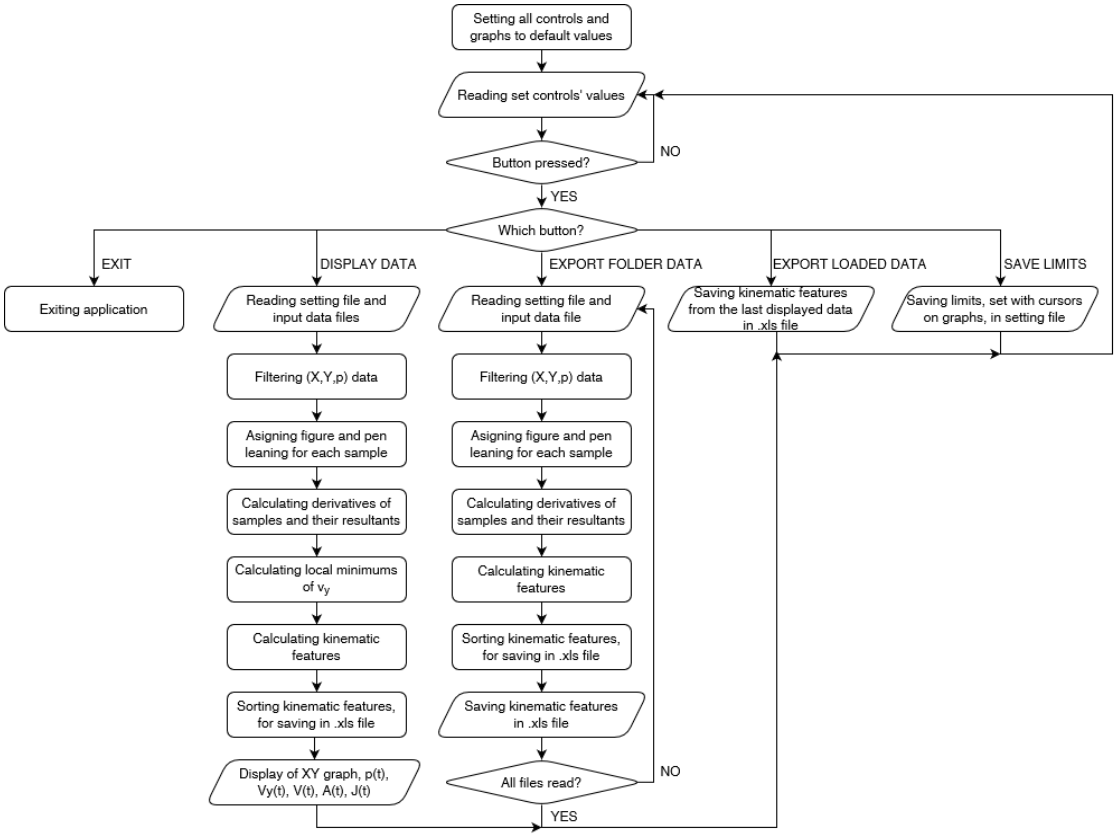


Fig. 2. GT Analyzer flowchart

 ISBN 978-86-7466-930-3

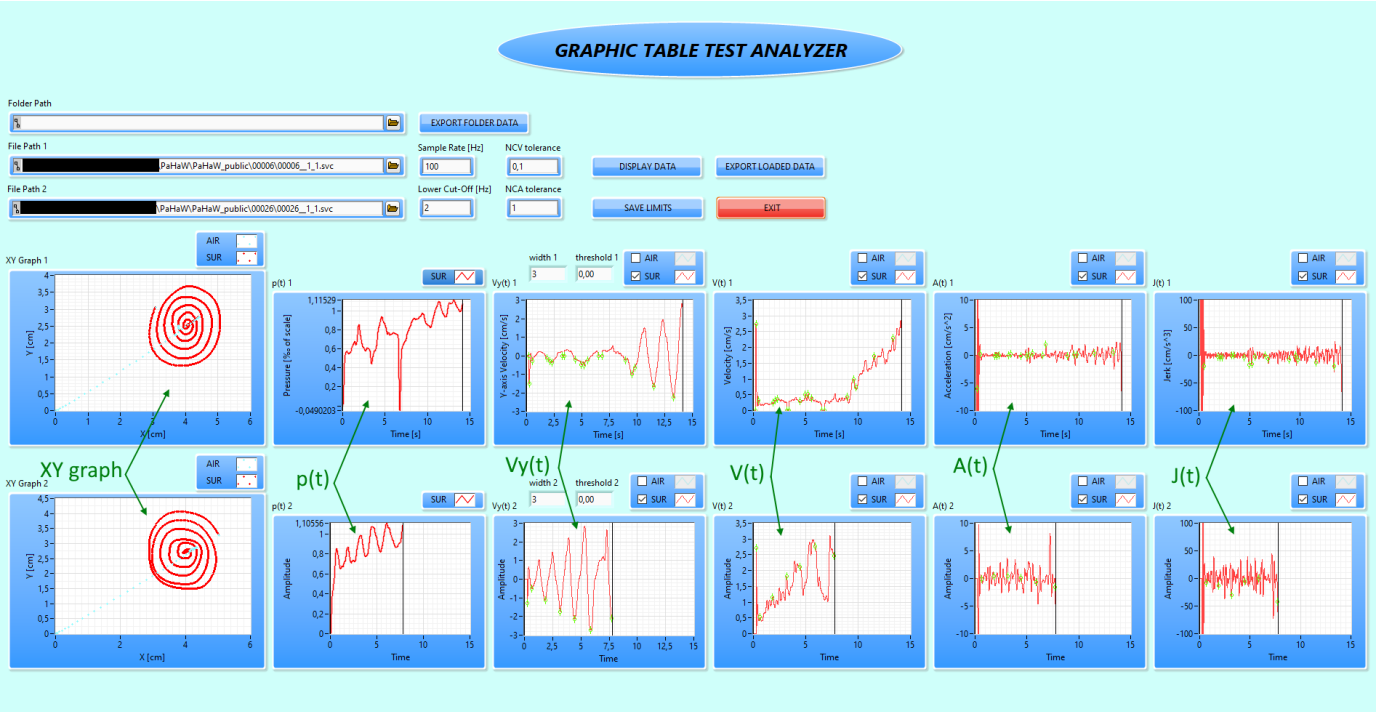


Fig. 3. An example of GT Analyzer interface from DS1 for "drawing a spiral" task (top graphics of subject ID 6 diagnosed with Parkinson's disease and bottom graphics of healthy subject ID 26)

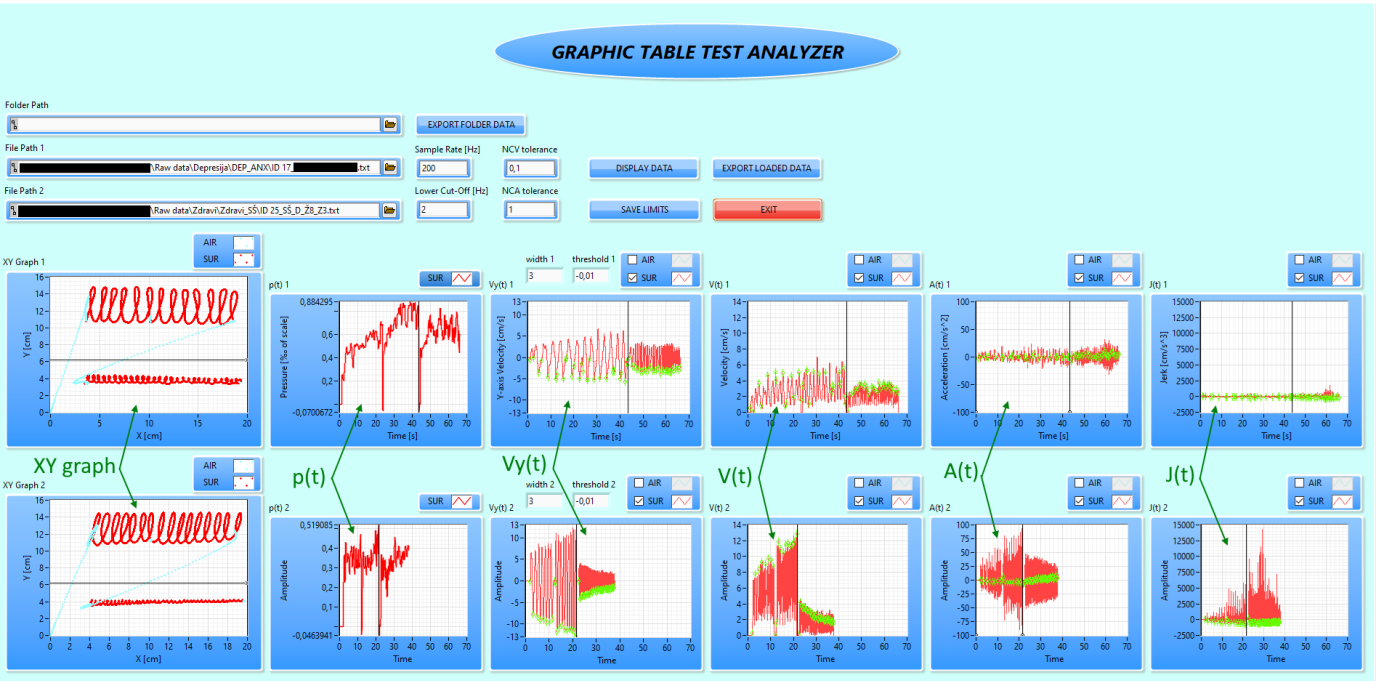


Fig. 4. An example of GT Analyzer interface from DS2 for writing two figures: the cursive letter "l" in 1) large rectangle and 2) small rectangle (top graphics of subject ID 17 diagnosed with major depressive disorder and bottom graphics of healthy subject ID 25)

## III. Results

Two examples of the GT Analyzer interface after loading selected subjects from DS1 and DS2 (see *Section II D. Dataset description*) are presented in Fig. 3 and Fig. 4, respectively

In Fig. 3, it is evident that the subject with Parkinson's disease needs more time to finish a task and that he had trouble at the beginning of the task, where fine movements are hampered due to micrographia seen in Parkinson's disease This resulted in a significant increase in local minimums of $V_y$. Both facts are expected from patients with Parkinson's disease [11].

In Fig. 4, there is a similarity in pressure graphs for the patient with depression and the healthy subject. Both subjects

 ISBN 978-86-7466-930-3

took a break in a similar place while writing the first part of the task (cursive letter "l" in a large rectangle), which is represented as a pressure drop. That is also evident on the XY graph where the blue line presents in-air movement. One of the main kinematic descriptors of depression, psychomotor slowing/retardation, is more pronounced with larger scale movements. That is why a drop in speed amplitude and a significant increase in writing duration are evident in the subject with depression while writing the first part of the task [12].

## IV. Conclusion

In this paper, a novel application for visual analysis of handwriting (drawing) tasks is presented. This user-friendly, open-source, clinically validated interface with implemented all standard kinematic features for handwriting analysis has the potential of helping users visually determine differences between healthy and diseased subjects. Furthermore, it can export the conventional kinematic features that can be used later in statistical analysis or classification procedures. The developed analysis software could be integrated with the previously developed data acquisition *LabHand* [10] software as a unique package for the overall handwriting data acquisition, analysis and kinematic feature extraction.

Future work will be focused on greater flexibility and compatibility of the application, as well as on defining and adding new features that will be used for an automatic distinction between different subject groups, including patients with different neurological or psychiatric disorders.

## Acknowledgment

The research was supported by the Ministry of Education, Science and Technological Development of the Republic of Serbia (contract 451-03-68/2022-14/200103).

## References

[1] S. Palmis, J. Danna, J-L. Velay & M. Longcamp, "Motor Control of Handwriting in the Developing Brain: A Review", *Cognitive Neuropsychology*, vol. 34, no. 3-4, pp. 187-204, Sep 2017.

[2] R. Mergl, P. Tigges, A. Schröter, H. Möller & U. Hegerl, "Digitized analysis of handwriting and drawing movements in healthy subjects: methods, results and perspectives", *Journal of Neuroscience Methods*, vol. 90, no. 2, pp. 157–169, Aug 1999.

[3] N. Ivančević, M. Novičić, V. Miler – Jerković, M. Janković, D. Stevanović, B. Nikolić, B. M. Popović & J. Jančić, "Does handedness matter? Writing and tracing kinematic analysis in healthy adults", *Psihologija*, vol. 52, no. 4, pp. 413–435, Jan 2019.

[4] P. Drotár, J. Mekyska, I. Rektorová, L. Masarová, Z. Smékal, & M. Faundez-Zanuy, " Evaluation of handwriting kinematics and pressure for differential diagnosis of Parkinson's disease", *Artificial Intelligence in Medicine*, vol. 67, pp. 39–46. Feb 2016.

[5] P. Drotár, J. Mekyska, I. Rektorová, L. Masarová, Z. Smékal, & M. Faundez-Zanuy, "Analysis of in-air movement in handwriting: A novel marker for Parkinson's disease", *Computer Methods and Programs in Biomedicine*, vol. 117, no. 3, pp. 405–411, Dec 2014.

[6] V. Miler Jerkovic, V. Kojic, D. N. Miskovic, T. Djukic, V.S. Kostic & M. B. Popovic, "Analysis of on-surface and in-air movement in handwriting of subjects with Parkinson's disease and atypical parkinsonism", *Biomedical Engineering / Biomedizinische Technik*, vol. 64, no. 2, pp 187-194, Apr 2019.

[7] R. Mergl, O. Pogarell, G. Juckel, J. Rihl, V. Henkel, T. Frodl, F. Müller-Siecheneder, M. Karner, P. Tigges, A. Schröter & U. Hegerl, "Hand-motor dysfunction in depression: characteristics and pharmacological effects", *Clinical EEG and neuroscience*, vol. 38, no. 2, pp. 82–88, Apr 2007.

[8] N. Ivančević, V. Miler-Jerković, D. Stevanović, J. Jančić, M. B. Popović, "Writing kinematics and graphic rules in children with ADHD", *Serbian Archives of Medicine*, vol. 148, no. 7-8, pp. 462-468, Jan 2020.

[9] N. Ivančević, "Kinematic analysis of handwriting in neurological, psychiatric and neurodevelopmental disorders of childhood and adolescence", Ph.D. dissertation, Biomedical engineering and technologies, University of Belgrade, Belgrade, Serbia 2021.

[10] V. Miler Jerković, V. Kojić, M. B. Popović, "An Information and Reliability Analysis of handwriting Kinematics", 2nd International Conference on Electrical, Electronic and Computing Engineering IcETRAN, Silver Lake, Serbia, pp. 1-4. 8-11 June 2015.

[11] E. J. Smits, A. J. Tolonen, L. Cluitmans, M. van Gils, B. A. Conway, R. C. Zietsma, K. L. Leenders & N. M. Maurits, "Standardized Handwriting to Assess Bradykinesia, Micrographia and Tremor in Parkinson's Disease", *PLoS ONE*, vol. 9, no. 5, pp. 1-8, May 2014.

[12] D. Bennabi, P. Vandel, C. Papaxanthis, T. Pozzo, E. Haffen, "Psychomotor retardation in depression: a systematic review of diagnostic, pathophysiologic, and therapeutic implications", *Biomed Res Int*., pp. 1-18, Oct 2013

 ISBN 978-86-7466-930-3

# Morphological parameters assessment with a depth camera based measurement system

Olivera Tomašević, Luka Mejić, Darko Stanišić, Nikolina Maravić

***Abstract*—Lately, depth cameras are being widely used for computer vision applications such as human pose estimation, activity recognition, object and people tracking, 3D mapping and localization. Possibilities for depth sensing integration in economy sectors like agriculture and healthcare services are growing as researchers are stating numerous advantages in contactless measurements done by robust low-cost depth camera systems. In this paper, we discuss an application of two different depth-sensing technologies for morphological parameters assessment.**

***Index Terms*— Morphological parameters, active depth-sensing technology, Intel RealSense.**

## I. INTRODUCTION

Since computer vision has largely been concerned with obtaining 3D information from 2D images, the invention of low-cost commercial depth sensing cameras made a significant contribution to solving computer vision problems. Derived 3D depth map allowed segmentation of the scene into foreground and background, which facilitated identification and tracking of simple objects. This opened new opportunities for many practical computer vision applications such as human pose estimation [1], activity recognition [2], object and people tracking [3], 3D mapping and localization [4].

Depth maps and resulting 3D reconstructions of objects acquired in real time also enabled non-contact measurement of objects' morphological properties. Researchers have been assessing objects' static properties such as size [5] and volume [6], and dynamic such as breathing patterns [7] in conditions of clinical interest. With this application, depth sensing is likely to gain significant role in economic sectors such as agriculture and healthcare services, but also in industrial and clothing design, and ergonomics.

Namely, in [8] it was concluded that when it came to body measurement, depth camera acquired results close to real data, and as a more affordable method, it could be an appropriate alternative to high cost laser scanner. In similar fashion, in [9] the depth camera based body measurement was shown to be an efficient approach for anthropometric data collection, and in [10] it was demonstrated that low-cost depth camera based system could be used for rapid and robust tracking of body shapes and anthropometric changes in children.

Contactless measurement of body size and volume has also been described as an innovative tool for making management decisions for livestock. In [11], the authors demonstrated an accurate body measurement system based on Microsoft Kinect v2 camera, which was applied to livestock. They successfully validated the quality of generated model against manually measured body references such as height, depth, length, and girth of certain body parts. Similarly, in [12], the authors presented the measurement of body parameters such as linear and integral characteristics along directional lines and local areas, geodesic distances and perimeters of cross sections. While in [13], the measurement system was also based on Microsoft Kinect sensor, the aim was the livestock's growth assessment through the repetitive analysis of 3D models of their certain body portions.

In a similar manner, and in order to optimize the harvesting by the growth state and crop yield assessment, researchers have been measuring structural parameters of fruits and vegetables. For instance, from the segmented lettuce point clouds in [14], they extracted the volume, surface area, leaf cover area, height predictors, and correlated them to the fresh weight. Analysis showed that the calculated surface areas correlated strongly with measured fresh weight. With the similar aim, in [15] the authors used a Microsoft Kinect sensor and reported that accuracy of the 3D models of cauliflower crops deviated from the ground truth measures by less than 2 cm in diameter/height, while the fruit volume estimation showed an error below 0.6% overestimation.

When it comes to expected measurement accuracy, it immensely depends on the choice of depth-sensing technology and application context, particularly lighting conditions and working distance. Namely, depth-sensing technology has been developing for many years in several different forms. Stereo [16] may be the most basic approach for acquiring 3D depth maps. It is a "passive" depth sensing method that uses two or more standard RGB cameras, and calculates depth by finding correspondences between image points. In contrary, "active" [17] approaches use their own light sources, and can potentially overcome the limitations of passive stereo, such as large textureless surfaces and low light levels.

As revised in [18], on the market there are several representatives of state-of-the-art active depth-sensing solutions. Intel RealSense product line is one of them. It supports active depth-sensing technologies that marked the last decade: structured (coded) light (SL), active IR stereo (AIRS), and time-of-flight (TOF). In this paper, we discuss the measurement of morphological parameters using two

Olivera Tomašević is with the Faculty of Technical Sciences, University of Novi Sad, Trg Dositeja Obradovića 6, 21000 Novi Sad, Serbia (e-mail: olivera.tomasevic@uns.ac.rs).

Luka Mejić is with the Faculty of Technical Sciences, University of Novi Sad, Trg Dositeja Obradovića 6, 21000 Novi Sad, Serbia (e-mail: mejic@uns.ac.rs).

Darko Stanišić is with the Faculty of Technical Sciences, University of Novi Sad, Trg Dositeja Obradovića 6, 21000 Novi Sad, Serbia (e-mail: darkos@uns.ac.rs).

Nikolina Maravić is with the Faculty of Technical Sciences, University of Novi Sad, Trg Dositeja Obradovića 6, 21000 Novi Sad, Serbia (e-mail: nikolina.maravic@uns.ac.rs).

 ISBN 978-86-7466-930-3

different Intel RealSense solutions, which we find suitable for close range applications.

The paper is organized as follows. First, we describe the acquisition system and software, then we look at the expected accuracy depending on the chosen device, and in the end, we propose methods for morphological parameters assessment based on a point cloud data.

## II. THE METHOD

### A. Acquisition system

Namely, Intel RealSense has produced depth cameras through three different series: SR300, D400, and L500. Each series represents a distinct depth sensing technology. What separates them is their ideal operating parameters, along with differences in how accurate the depth information is in different situations [19]. As SR300 and D400 series allow measurements of similar distance ranges, we opted to incorporate a representative of each in our acquisition system, independently.

SR305 camera is Intel RealSense's only representative of SR300 series [20], and thus it's only representative of structured light technology. The camera uses patterned light to determine depth within the scene, thus it is ideal for use in indoor, controlled lighting situations. It is also intended for very short-range applications under one meter, but its operating range goes even up to 2m. It utilizes rolling shutter technology, has a field of view (FOV) of 71.5° x 55° and will provide up to 640×480 resolution depth images at 60 fps.

D435i camera is one of Intel RealSense's representatives that belong to D400 series [21]. It is based on active IR stereo, which uses stereo vision to calculate depth, but also projects an invisible infrared pattern to improve depth accuracy in scenes with low texture. Taken that it is based on stereovision, it is expected to perform equally well in both indoor and outdoor environments. It has an ideal operating range of 0.3m to 3m. It utilizes global shutter technology, has a wide field of view of 85.2° x 58°, and provides up to 1280 x 720 resolution depth images at 90 fps. Since depth camera D435 is another representative in the series that only differs in IMU presence, in the following text we will use the term D435, as equally.

For the purposes of visualization, Intel has developed specialized tools such as Intel RealSense Viewer and Intel RealSense Depth Quality Tool, but has also developed an open source SDK [22] that supports various platforms and programming languages, thus enabling us to build applications for data acquisition and processing adapted to our needs.

### B. Acquisition software

Software for data acquisition on PC is written in Matlab (ver. R2021a, MathWorks, USA). It allows acquisition parameters setting, acquisition and processing, and visualization.

Acquisition parameters refer to stream configuration and depth property settings. These parameters are supported by the SDK library, which allows the configuration of the camera with a number of internal settings.

Stream configuration implies settings like stream type, stream format, stream resolution, and sampling frequency. Stream types refer to different types of data provided by RealSense devices. In order to get point cloud that contains RGB information for every data point, our software allowed acquisition of both, depth frame, i.e. data from depth sensor, and color frame, i.e. image from embedded RGB camera. These were thereafter aligned in order to get final point cloud representation of the scene. Available stream format, which identified binary data encoding within a frame, was set to a predefined value, which depended on a type of a stream.

Sampling frequency can take several different predefined values. In cases of dynamic parameter assessment, the sampling frequency value also determined the time resolution of dynamic morphological parameters. Thus, in cases when official documentation did not recommend any value that would ensure good quality depth, we set the highest possible value that still allowed depth and RGB frame alignment. The same applied to stream resolution parameters.

In order to get good quality depth data, we set specific values to a combination of depth property parameters such as depth projector power, accuracy, filter option and depth preset setting. The values were set specifically to achieve as better depth accuracy as possible.

Depth preset setting is a working mode that implies predefined settings for all the depth property parameters that official documentation offers as optimal for certain conditions. Considering that we were after high accuracy mode, if it was supported for given device, we opted for high accuracy preset.

In case of SR305 device, depth accuracy was set through the depth property parameter of the same name, which defined the number of patterns projected per frame. In case of D435 device, high depth accuracy was achieved through the high accuracy preset, which set high confidence threshold value of depth.

Intel SDK library includes post-processing filters to enhance the quality of depth data and reduce noise levels. When done in real time, it negatively affects the temporal resolution of the acquired frames, which should be taken in consideration when assessing dynamic parameters of an object.

As recommended in [23], images acquired with SR305 camera were filtered with default depth filter, which had moderate smoothing effects.

### C. Expected accuracy

As said before, expected measurement accuracy immensely depends on application context, particularly lighting conditions and working distance. However, even when these conditions are met in accordance to camera specifications, 3D reconstructed model is still very likely to contain inaccurate, i.e. dimensions that differ from ground truth.

Depth error of SR305 camera is described in [23]. The systematic distance inhomogeneity in case of this camera brings two main systematic error components increasing with distance: non-planarity and depth offset. Non planarity can be explained through error map between the target plane and multiple point clouds acquired with increasing distance from the plane itself, while depth offset can be approximated by a parabolic function with a high coefficient of determination. For instance, for distance of 65 cm, depth offset is somewhat larger than 12 mm.

The error inherent in SR305 camera acquisition is perhaps best portrayed through evaluation of the error introduced in

 ISBN 978-86-7466-930-3

measuring a flat surface that compares SR305 camera model with D415 camera model from D400 series. The comparison can be found in [24]. Namely, D415 has a considerably lower error both in terms of planarity and of distance accuracy.

D435 camera is, on the other hand, a lot more similar to D415 camera - they use the same vision processor to provide RGB-D data. The main difference lays in depth quality, which is usually portrayed through RMS error - the depth noise for a localized plane fit to the depth value. Comparison between the two models can be found in [25]. Namely, the depth RMS error scales as the square of the distance away from the camera, in both cases. However, due to the wider FOV, the smaller baseline, and the smaller sensor resolution, the D435 has more depth noise at any given range. At the same time, this model benefits from having smaller minimum operation distance, which allows acquisition at shorter distances, and global, as opposed to rolling, shutter sensor, so is expected to be more accurate when dealing with dynamic scenes.

### *D. Data acquisition and processing*

The acquisition was performed indoors under artificial lighting conditions. Chosen camera was fixed at a distance of about 50 cm from the horizontal table top on which objects of interest were placed. It was taken into account that placed object should be in the camera's field of view and that all its interest points should also be within the recommended range of distances for a given camera type.

In the case of SR305 camera, RGB-D images were acquired in resolution of 640x480, and with sampling frequency of 60 Hz, and in the case of D435, they were acquired in resolution of 848x480, and with sampling frequency of 30 Hz. Upon the start of acquisition, the first couple of frames were discarded to allow the camera time to settle.

The steps we found useful in the process of parameters extraction were the following:

- points selection within a region of interest in the point cloud so as to lower the computational recources needed for further processing steps
- potential selection of markers that would be used for parameter assessment
- potential rigid transformations so as to align the direction of markers propagation with a certain axes of the camera local coordinate system
- potential plane fitting through the table surface so as to assess camera tilt relative to the table, and perform appropriate tilt correction through rigid transformations
- calculation of the distance between markers based on Euclidean distances between the each two nearest adjacent points
- calculation of surface area in a region of interest based on Delaunay triangulation [26] of point cloud data
- extraction of cross sections defined by the markers trajectory
- calculation of the cross-section area
- in the cases of dynamic parameters assesment, tracking of marker koordinates over succesive frames

## III. RESULTS

The point cloud acquisition and calculation of morphological parameters is demonstrated on the cropped RGB-D image of a human body torso. Fig. 1 contains RGB-D image acquired with SR305 (on the left), and with D435 camera (on the right), respectively.

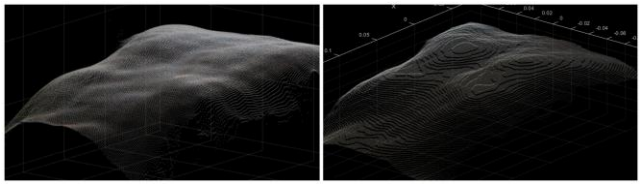

Fig. 1. Cropped RGB-D image of a human body torso captured with SR305 (on the left) and D435 (on the right).

In the case of D435, different levels of depth values are obvious. More specifically, we acquired depth maps with resolution of 1mm, which is a default depth unit of underlying vision processor. In the case of SR305, depth unit is a lot smaller (0.000125 m), thus its depth resolution is higher, as can also be noted in the figure. Other than on visual representation, these differences did not have any significant affect on parameters assessment methods. They are processed in the same manner, and results are stated in the following figures.

Fig. 2 contains example of static morphological parameters derivation based on trajectories in certain directions. Resulting cross-sections are visible in the point cloud (on the left), and isolated so that their length could be assessed (on the right). Top row refers to measurements based on SR305 camera, while bottom row refers to D435 camera. As previously stated, the cross-section lengths were estimated by the calculation of Euclidian distances between the each two nearest adjacent points.

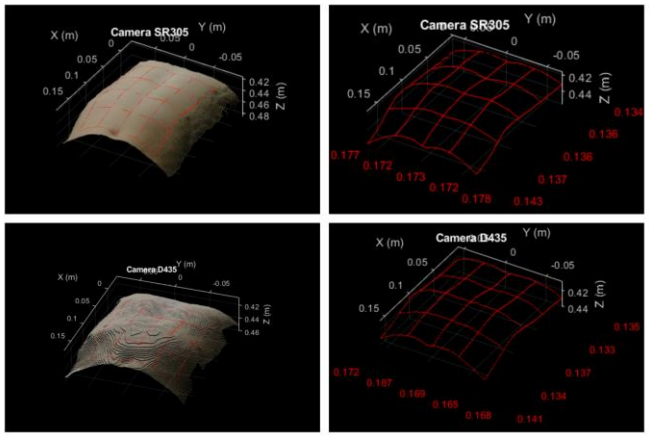


Fig. 2. Static morphological parameters derivation: cross-sections marked in a point cloud (on the left), and extracted cross-sections (on the right) along with their calculated dimensions.

Due to the anatomical planes in which they are located, these cross-sections are referred to as transverse and sagittal cross-sections, respectively. They depended on the marker positions, which were set on nipples and navel, by the user selection. Transverse cross-sections were defined based on direction on which the nipples were lying, and they were equidistantly distributed between the level of the nipples and level of the navel. Sagittal cross-sections were perpendicular with respect to them. The outermost positions of the sagittal cross-sections were left and right nipple location, respectively.

 ISBN 978-86-7466-930-3

These measurements were rounded to a precision of 1 mm. As can be seen on Fig. 2, there are certain differences in the cross-section length measurements that depend on the used camera. They are most prominent in sagittal sections and amount the most in the case of difference of 10 mm in favor of SR305 camera for the outermost left sagittal cross-section (from the perspective of the respondent). We assume that significant part of this difference lays in depth-offset error of camera SR305, which reportedly [23] takes out around 4 mm for the object distance of 400 mm, and 5.433 mm for the object distance of 450 mm.

Extracted cross-sections and their dimensions may indicate local torso characteristics. On the other hand, the object, the torso in this case could also be described globally by parameters such as surface area and volume. An example of surface area calculation is given in Fig. 3. Figure represents marked surface in the region of interest defined by the same markers that defined cross-sections: locations of nipples and navel. The area was estimated on tridimensional polygon mesh generated with Delaunay triangulation applied to the point cloud data illustrated in Fig 4. The resulting surface area is calculated upon all the areas of triangles at the base of the resulting mesh.

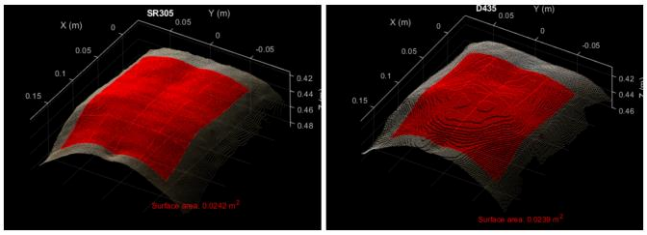


Fig. 3. Static morphological parameters derivation: marked surface in the region of interest – SR305 image (on the left), and D435 image (on the right) along with their respective results.

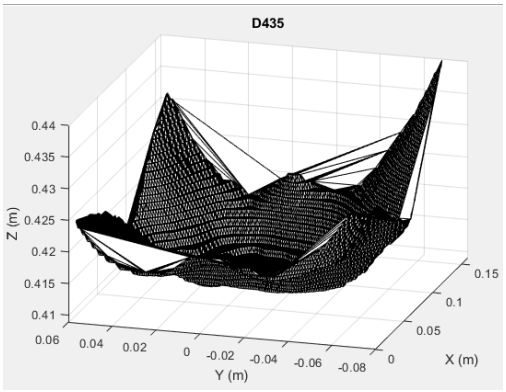


Fig. 4. Tridimensional polygon mesh calculated on the point cloud region of interest. This specific example refers to RGB-D image acquired with camera D435.

As Fig. 3 indicates, the image from SR305 camera resulted in slightly higher value of surface area parameter – 0.0242 $m^2$ as opposed to 0.0239 $m^2$ that resulted from D435 acquisition. This is in accordance with the conclusion regarding the length of the cross-sections acquired with these cameras.

Considering that demonstrated parameters can directly allow estimating of the dimensions of either torso or its parts, non-contact measurements of this type could have a purpose in clinical practice.

## IV. Discussion

Results above show that visual representation of the scene did not vary significantly depending on the used camera. However, there are certain differences in their performance. Namely, results confirm the higher resolution of camera SR305 compared to D435 model (see Fig. 1). Considering that SR305 is capable of detecting depth with a higher resolution than D435, if the morphological characterization of fine details within small samples was at task, it could be expected that SR305 would be able to better reconstruct the object model, and thus would allow drawing contours that might not be visible in the acquisition with D435 camera.

On the other hand, SR305 has non-planarity and depth offset issues that contraindicate its use in precise measurement systems. As previously stated, in terms of planarity and distance accuracy, SR305 is outperformed by D400 series representatives.

When it comes to D400 series, D415 has more precision than D435. This regularity is accounted to the larger field of view of D435 camera. However, considering that D435 is better suited for dynamic scenes than D415, it could be expected that both these representatives of D400 be equally used in applications concerning morphological parameters assessment.

## V. Conclusion

The aim of this study was to demonstrate derivation of morphological parameters with different depth sensing technologies. We discussed acquisition parameters that would allow good depth in static, as well as in dynamic scenes, and gave an example of static parameters calculation that could have a purpose in clinical practice.

As we discussed two different acquisition systems, we can conclude that for this type of application, one should use D400, rather than SR300 series, as it is more likely to provide sufficiently reliable measurements for the task at hand.

## References

[1] Marin-Jimenez, M.J., Romero-Ramirez, F.J., Munoz-Salinas, R. and Medina-Carnicer, R., 2018. 3D human pose estimation from depth maps using a deep combination of poses. *Journal of Visual Communication and Image Representation*, *55*, pp.627-639.

[2] Park, S.U., Park, J.H., Al-Masni, M.A., Al-Antari, M.A., Uddin, M.Z. and Kim, T.S., 2016. A depth camera-based human activity recognition via deep learning recurrent neural network for health and social care services. *Procedia Computer Science*, *100*, pp.78-84.

[3] Zhou, Q.Y. and Koltun, V., 2015. Depth camera tracking with contour cues. In *Proceedings of the IEEE Conference on Computer Vision and Pattern Recognition* (pp. 632-638).

[4] Schubert, S., Neubert, P. and Protzel, P., 2017, July. Towards camera based navigation in 3d maps by synthesizing depth images. In *Annual Conference Towards Autonomous Robotic Systems* (pp. 601-616). Springer, Cham.

[5] Vo-Le, C., Van Muoi, P., Son, N.H., Van San, N., Duong, V.K. and Huyen, N.T., 2021, January. Automatic Method for Measuring Object Size Using 3D Camera. In *2020 IEEE Eighth International Conference on Communications and Electronics (ICCE)* (pp. 365-369). IEEE.

[6] Dellen, B. and Rojas Jofre, I.A., 2013. Volume measurement with a consumer depth camera based on structured infrared light. In *Proceedings of the 16th Catalan Conference on Artificial Intelligence, poster session* (pp. 1-10).

[7] Kotoku, J.I., Kumagai, S., Uemura, R., Nakabayashi, S. and Kobayashi, T., 2016. Automatic Anomaly Detection of Respiratory Motion Based on Singular Spectrum Analysis. *International Journal of Medical Physics, Clinical Engineering and Radiation Oncology*, *5*(01), p.88.

 ISBN 978-86-7466-930-3

[8] Yüksel, H. and Oktav, M.B., 2020. Analyses of body measurement with depth image data using motion capture sensor. *Industria Textila*, *71*(6), pp.530-537.
[9] Lin, Y. L., Wang, M. J. and Wang, B., 2015. Body dimension measurements using a depth camera. *New ergonomics perspective* (pp. 367-371), CRC Press/Balkema.
[10] Park, B.K., Lumeng, J.C., Lumeng, C.N., Ebert, S.M. and Reed, M.P., 2015. Child body shape measurement using depth cameras and a statistical body shape model. *Ergonomics*, *58*(2), pp.301-309.
[11] Ruchay, A., Kober, V., Dorofeev, K., Kolpakov, V. and Miroshnikov, S., 2020. Accurate body measurement of live cattle using three depth cameras and non-rigid 3-d shape recovery. *Computers and Electronics in Agriculture*, *179*, p.105821.
[12] Ruchay, A.N., Dorofeev, K.A., Kalschikov, V.V., Kolpakov, V.I. and Dzhulamanov, K.M., 2019, October. A depth camera-based system for automatic measurement of live cattle body parameters. In *IOP Conference Series: Earth and Environmental Science* (Vol. 341, No. 1, p. 012148). IOP Publishing.
[13] Pezzuolo, A., Guarino, M., Sartori, L. and Marinello, F., 2018. A feasibility study on the use of a structured light depth-camera for three-dimensional body measurements of dairy cows in free-stall barns. *Sensors*, *18*(2), p.673.
[14] Mortensen, A.K., Bender, A., Whelan, B., Barbour, M.M., Sukkarieh, S., Karstoft, H. and Gislum, R., 2018. Segmentation of lettuce in coloured 3D point clouds for fresh weight estimation. *Computers and Electronics in Agriculture*, *154*, pp.373-381.
[15] Andujar, D., Ribeiro, A., Fernandez-Quintanilla, C. and Dorado, J., 2016. Using depth cameras to extract structural parameters to assess the growth state and yield of cauliflower crops. *Computers and Electronics in Agriculture*, *122*, pp.67-73.
[16] Flusser, B.Z.J.: Image registration methods: a survey. Image Vis. Comput. 21(11), 977–1000 (2003)
[17] Krig, S., 2014. *Computer vision metrics: Survey, taxonomy, and analysis* (p. 508). Springer nature.
[18] Giancola, S., Valenti, M. and Sala, R., 2018. *A survey on 3D cameras: Metrological comparison of time-of-flight, structured-light and active stereoscopy technologies*. Springer Nature.
[19] Intel® RealSense™ Depth and Tracking Cameras, 2019. *Which Intel RealSense device is right for you? (Updated June 2020)*. [online] Available at: https://www.intelrealsense.com/which-device-is-right-for-you/ [Accessed 15 May 2022].
[20] Intel ® RealSense TM Depth Camera SR300 Series Product Family Datasheet Intel ® RealSense™ Depth Camera SR305, Intel ® RealSense™ Depth Module SR300 Revision 002, 2019. [online] Available at: https://www.intelrealsense.com/wp-content/uploads/2019/07/RealSense_SR30x_Product_Datasheet_Rev_002.pdf [Accessed 15 May 2022].
[21] Intel ® RealSense TM Product Family D400 Series Datasheet Intel ® RealSense™ Vision Processor D4, Intel, n.d. [online] Available at: https://www.intelrealsense.com/wp-content/uploads/2022/04/Intel-RealSense-D400-Series-Datasheet-April-2022-v2.pdf?_ga=2.226817501.1950346234.1651486981-1661064436.1599063643 [Accessed 15 May 2022].
[22] Intel® RealSense™ Depth and Tracking Cameras, n.d. *Intel RealSense SDK 2.0 – Intel RealSense Depth and Tracking cameras*. [online] Available at: https://www.intelrealsense.com/sdk-2/.
[23] Carfagni, M., Furferi, R., Governi, L., Servi, M., Uccheddu, F. and Volpe, Y., 2017. On the performance of the Intel SR300 depth camera: metrological and critical characterization. *IEEE Sensors Journal*, *17*(14), pp.4508-4519.
[24] Carfagni, M., Furferi, R., Governi, L., Santarelli, C., Servi, M., Uccheddu, F. and Volpe, Y., 2019. Metrological and critical characterization of the Intel D415 stereo depth camera. *Sensors*, *19*(3), p.489.
[25] Intel® RealSense™ Developer Documentation, n.d. *Tuning depth cameras for best performance*. [online] Available at: https://dev.intelrealsense.com/docs/tuning-depth-cameras-for-best-performance.
[26] www.mathworks.com. n.d. *Delaunay triangulation in 2-D and 3-D - MATLAB*. [online] Available at: https://www.mathworks.com/help/matlab/ref/delaunaytriangulation.html [Accessed 15 May 2022].

 ISBN 978-86-7466-930-3

# POWER ENGINEERING
# /
# ЕЛЕКТРОЕНЕРГЕТИКА
# (EEI/EE)

ISBN 978-86-7466-930-3

# Overview of measuring methods and equipment for calibration of instrument transformers

Dragana Naumović-Vuković, *Member, IEEE*

***Abstract*— Instrument transformers are an important and inevitable element of AC current and voltage measurement techniques. They have been in use for more than a century. In parallel with the development of technical characteristics and improvement of instrument transformers measurements, the measurement methods and measuring equipment developed too. The significant parts of the development in this field are measuring methods, measuring devices, and systems for testing the accuracy of measuring transformers. The measurement accuracy is the most important characteristic of instrument transformers since that is the important factor in the accurate billing of electricity. The tradition in the field of testing instrument transformer's accuracy at the Electrical Engineering Institute Nikola Tesla is more than 60 years long. From the very beginning, the experts of the Institute have been active participants in the development of this field, both domestically and internationally. They have contributed to the development of measuring systems and standards for testing and calibration of instrument transformers, which have found application in laboratory calibration of the national metrology laboratories, as well as in industry. This paper provides an overview of the development of measuring methods for testing and calibration of instrument transformers, as well as a wide range of measuring devices and standards based on different measuring methods. The concrete application of measuring methods in the field of calibration in national institutes of metrology and research metrological laboratories is presented. The paper also presents the application of different measuring devices and systems in the industry, for intermediate and final control of measuring transformers as products in the instrument transformer manufacturers. A special review in this paper is dedicated to the contribution of the experts of the Electrical Engineering Institute Nikola Tesla in this field.**

***Index Terms*—Instrument transformers, accuracy, measuring methods, calibration, standard transformers**

## I. INTRODUCTION

Instrument transformers are unavoidable elements in the electric circuits and systems for measuring alternating voltage, current, power and energy. Their role is to adjust (transform) the real values of voltage and current (voltages of several hundred and thousands of volts and currents of several hundred to thousands of amperes) to the appropriate optimal levels of measuring, control and protection systems. Furthermore, galvanic separation of the working energy system from the metering and protection system achieves by them.

Dragana Naumović-Vuković is with the Electrical Engineering Institute Nikola Tesla, University of Belgrade, Koste Glavinića 8a, 11000 Belgrade Serbia (e-mail: dragananv@ieent.org), (https://orcid.org/0000-0002-8334-4452).

The electric voltage, current, power and energy measurement, as well as regulation and protection in power facilities, cannot be imagined without the use of instrument transformers.

According to their purpose instrument transformers are divided in two main groups: measuring instrument transformers and protective instrument transformers. In this paper emphasis is on instrument transformers for a measuring purpose.

Their role in the billing metering of electricity is especially important, where the overall accuracy of energy measurement directly depends on the accuracy of measuring transformers [1]. In the production - transmission - distribution chain, electricity is measured at least three times. Therefore, it is also financial interest, especially in the conditions of a deregulated market, to measure energy with the least possible error. Consequently, measuring transformers as well as electricity meters belong to legal metrology. Legal metrology regulations and domestic and international standards precisely define the conditions of application, calibration, as well as the deadlines for periodic review of these types of measuring instruments [2, 3, 4, 5, 6, 7].

The main direction of development of measuring transformers, in addition to improving their reliability, is to reduce the error of transformation of primary quantities into secondary ones. Improving the accuracy of instrument transformers is conditioned by the development of measuring methods and devices for measuring and determining its errors. Historically, the subject of measuring transformers dates back to the beginning of the twentieth century [8, 9]. The development of measuring methods and devices for errors measurement of measuring transformers depended primarily on the technical and technological capabilities of the time in which it took place. Consequently, the first methods and devices were based on a square electrometer [10, 11]. Modern devices have been developed on the most modern microprocessor technologies and virtual instrumentation [12, 13, 14, 15, 16].

The EEINT has the international reputation in the development and application of devices and systems for accuracy testing of instrument transformers for more than 60 years. Devices for accuracy testing of measuring transformers based on different measuring methods, developed at the EEINT, have been used in all manufactories for instrument transformers in the former Yugoslavia, as well as in many other testing laboratories of distribution companies and transmission networks. These devices have shown a number of advantages over other solutions, especially in the on-site

 ISBN 978-86-7466-930-3

testing of measuring transformers, in factory serial quality control, as well as the most accurate measurements [17, 18].

New generations of devices for accuracy testing of the instrument transformers, developed at the EEINT in the last ten years, have been used at the folloving manufacturers: MINEL -FEPO Zrenjanin (Serbia), FMT - Factory of instrument transformers Zajecar (Serbia), "Energoinvest" (Bosnia and Hercegovina), EMO-Ohrid (Macedonia), Končar – Instrument Transformers (Croatia), MBS - Instrument transformers (Germany). In the EEINT special attention is paid to the development of measuring devices for application in the most accurate measurement in this field. Such measuring systems have been developed and made for the National Research Council of Canada (NRC) and the Hydro Qebek High Voltage Testing Laboratory, also in Canada.

## II. COMPLEX ERROR

Electric voltage and current are vector quantities. Therefore, their complex transformation error is defined by ratio (amplitude) error and phase displacement. Like any measurement transformation, this one is also followed by certain errors. In a case of vector quantities, discrepancy from the ideal transformation is characterized by a complex error G. The complex error of measuring current and voltage transformers is defined as the fundamental harmonic of current, i.e., voltage. The complex error includes the ratio (amplitude) error, $g$, and the phase displacement, $\delta$, expressed in mathematical form:

$$\underline{G} = g + j\delta \tag{1}$$

Ratio error of current transformer $g$ in %, in accordance to standard [4] is defined as:

$$g = \frac{K_N \cdot I'' - I'}{I'} \cdot 100 \tag{2}$$

where $K_N$ is the rated transformation ratio.

The phase displacement $\delta$ in min (1%=34.4min=1crad), is defined as the phase shift of the secondary current $I''$ in relation to the primary current $I'$ [4].

The ratio error and phase displacement of the current transformer are defined by its:

- constructive and technological parameters: material, shape and dimensions of the magnetic circuit, number of ampere-turns, length and cross-section of the wire, geometry of the primary and secondary winding;
- operating parameters: secondary load, ratio of measured current to rated, frequency, distortion and shape of measured primary current;
- ambient conditions: temperature and pressure.

The ratio error of voltage transformer $g$ in (%), in accordance to standard [5] is defined as:

$$g = \frac{K_N \cdot U'' - U'}{U'} \cdot 100 \tag{2}$$

where $K_N$ is rated transformation ratio

The phase displacement $\delta$ in (min), of voltage transformers is defined as the phase shift of the secondary voltage $U''$ in relation to the primary voltage $U'$. The ratio error and phase displacement of the voltage transformer are also defined by its constructive, technological, operating parameters and ambient condition.

The main difference between current and voltage transformers is that the initial design parameter in current transformers is the magnetic excitation force, while in voltage transformers this is the magnetic induction. However, in the constructive, technological and physical sense, there are significant differences between current and voltage transformers, which results from different operating modes. The current transformer operates in the short-circuit mode, and the voltage transformer in the idling mode.

The functional connections between parameters and ratio error and phase displacement are known. Therefore, it is possible to analytically calculate their values for a given current or voltage transformer, which is usually done during design.

The main parameters in designing current and voltage transformers as well as in declaring their errors (accuracy classes) are secondary burden and reference currents and voltages. The limits of errors for declared classes by standard, for current measuring transformers are defined in accordance to percentage of rated currents (i.e., reference currents) and for secondary burden between ¼ and rated value [4]. In the same way, the limits of errors for declared classes for voltage measuring transformers are defined in accordance to percentage of rated voltage (i.e., reference voltage) and also for secondary burden between ¼ and rated value [5]. This method of errors declaring corresponds to their nonlinear character. The accuracy class of measuring transformer directly affects its application.

However, the true (more accurate) error values are obtained only by measuring the accuracy of the measuring transformer.

## III. THE MEASURING METHODS AND DEVICES FOR ACCURACY TESTING

From the early beginning of the application of measuring transformers, back in 1892, [19], there was a need for their accuracy testing. The errors of these first current transformers were in the order of about 3% for ratio error and approximately 200 minutes for phase displacement [8]. In that time, these errors had been determined by direct measurement of primary and secondary currents and phase shift. In addition to the error of the measurement method, limitations have also appeared in the application of analog measuring instruments [20]. For example, the limits of current measurement with analog measuring instruments were 200A. Appropriate shunts and pre-resistors were used for currents higher than this value.

With the rapid technological development, the applications

 ISBN 978-86-7466-930-3

of precise standard measuring transformers [21] have begun. With the progress in the production and application of new magnetic materials, in the thirties of the last century, the errors of measuring transformers have been reduced to 0.1% and 5min [22].

A. *Classical methods and devices for accuracy testing of instrument transformers*

The first methods for accuracy testing of instrument transformers appeared at the beginning of the last century [23, 24, 25]. The most important methods, whose influences extend to the present days, are compensation, differential and current comparator methods.

The compensation method, Fig 1, is basically a direct comparison of two alternating voltages generated on precision reference shunts (for current transformer testing) or voltage dividers (for voltage transformers testing), one in the primary circuits and the other in the secondary circuits of the transformer under test, ($T_X$).

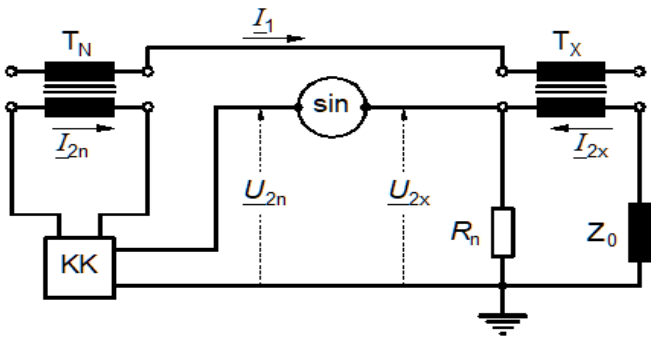


Fig.1. Compensation method for current transformer accuracy testing [17].

The compensating method was usually used in laboratory testing. The main reason for that is demand for satisfactory high accuracy of the elements that is incorporated in complex compensator (precise resistors and voltage dividers), and that are also temperature and time stable. In addition, there is also a problem of additional load in secondary circuits of transformer under test that is not negligible. The main advantage of this method is the ability to accuracy testing of the instrument transformers of non-standard transformation ratio.

The differential method is attributed to F. B. Silsbee and is related to 1917 [23]. This method was perfected by Hole (W. Hohle) in 1934 [26]. The essence of this method, Fig. 2, is to measure the differences between two quantities. In this method the secondary voltages (or currents) of the device under test (current or voltage transformer), ($T_X$) and of the standard transformer ($T_N$) of approximately equal transformation ratios are compared. In order to achieve comparison as accurate as possible, the standard current transformer should have a negligibly error.

The basic elements of the devices for accuracy testing based on differential and compensational methods are complex compensator (KK) and selective zero indicator (SIN), Fig. 1, and Fog. 2.

Around 1930, measuring devices based on the compensation method and the complex compensator [27, 28] appeared. The best accuracy of such early commercial devices was about 0.02% and 2 min. There are many solutions of complex compensators, but from the point of view of accuracy testing of instrument transformers, the most significant is certainly the work of scientists Schering and Alberti [24].

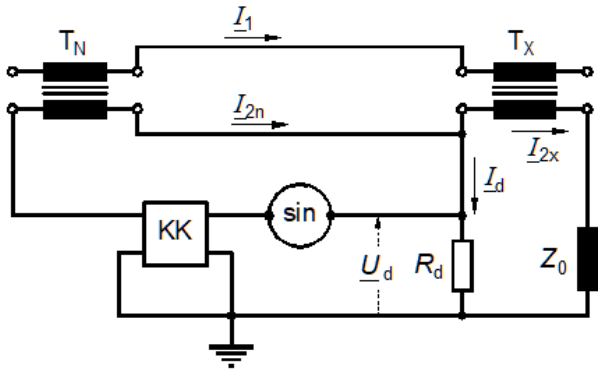


Fig.2. Differential method for current transformer accuracy testing [17].

Measuring device, so-called Hole's compensator based on differential method has also found wide practical application [29].

With the selective zero indicator, the equality of two voltages is determined at a certain (basic) frequency. This implies two requirements: indicator should be sufficiently sensitive to the basic measured voltage and also insensitive to parasitic (disturbing) voltages as well as to higher harmonics of the measured voltage. Two types of selective zero indicators have been used: a classic solution with a vibrating galvanometer and an electronic zero indicator.

Technological improvements and modifications of this compensator and selective indicators, made in the 1930s, especially in the late 1960s, made these instruments indispensable in the laboratories for testing and calibration of measuring transformers, for a long time during the last century.

The third, important measuring method that has remained until today is based on the application of a current comparator. The idea of the current comparator was first presented in 1917 by the American physicist Baker [25]. He suggested measurement of the difference between the two currents by using windings on a magnetic core. The current comparator with a compensating winding was first used in 1930 by the English scientist Bruges [30], and the German physicist Reihe used it as a test device for the accuracy testing of current transformers [31]. This, therefore, long-known but, then technically and technologically imperfect method, experienced its reaffirmation in several metrological laboratories in the 1950s. The current comparator was first used in the comparison of alternating currents, and later for accurate measurement of resistance, capacity, etc. The

 ISBN 978-86-7466-930-3

Electrical Engineering Institute Nikola Tesla (EEINT), mostly thanks to Ilija Obradovic, Petar Miljanic and Srdjan Spiridonovic, is the pioneers in this field. The first device for measuring the accuracy of current transformers is being realized then. This work, which have been continued to these days, is marked by a series of successful results and articles The very name "current comparator", today is internationally accepted technical term, first appeared in the works of experts from the EEINT [32].

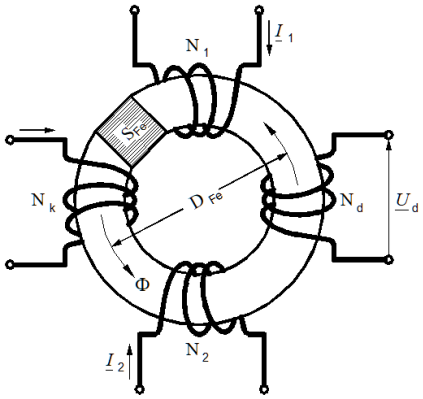


Fig.3. A simplified scheme of current comparator [35].

Significant progress in the construction and manufacture of current comparators has been achieved through the joint work of associates of the Canadian NRC (National Research Council) and the EEINT [33].

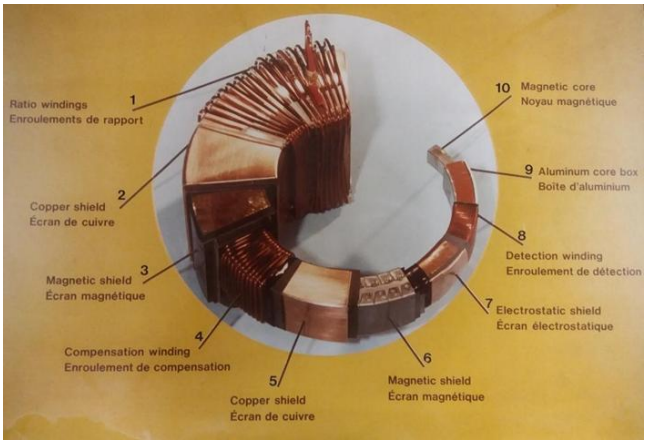


Fig.4 The structure of current comparator [17].

An ideal transformer is a transformer for which the equality of magnetomotive force applies [33]. In reality, a part of the primary magnetomotive force is spent on magnetizing of the core and losses in it. This is the main reason for the error of the current measuring transformer. If the magnetic flux in the core is artificially reduced to zero, then the current transformer becomes ideal. In that way the comparison of the currents reduces to the turn ratio of primary and secondary windings. This ratio is stable during the time and insensitive by temperature changes. This gives the possibility of a very accurate comparison of two alternating currents, which is the basic idea of the current comparator [34].

Fig. 3 shows simplified scheme of a current comparator. To measure the magnetic flux in the core of the current comparator, the detection coil $N_d$ is used, and compensating coil $N_k$ brings the magnetic flux to zero [35]. Practical realization of current comparator is more complex as shown in Fig. 4.

With carefully construction and realization of current comparators, it is possible to achieve its ratio error within the range from $10^{-6}$ to $10^{-7}$, and the phase displacement in the order of 0.01 min.

*B. The recent methods and devices for accuracy testing of instrument transformers*

In the last years of the 20th century, with the application of modern electronic solutions and microcomputer techniques, measuring methods and devices for accuracy testing of instrument transformers have been significantly improved [36, 37]. Possibilities and advantages of PC hardware and software support are not only in the field of increasing efficiency, or reliability of work, but also in increasing measurement accuracy. Modern devices are based on the general tendency in electronics that the processing of the measuring signal is realized in digital form. The differences between the individual solutions of these devices are most often in the way of further digital processing of measuring signals [17, 38, 39, 40, 41].

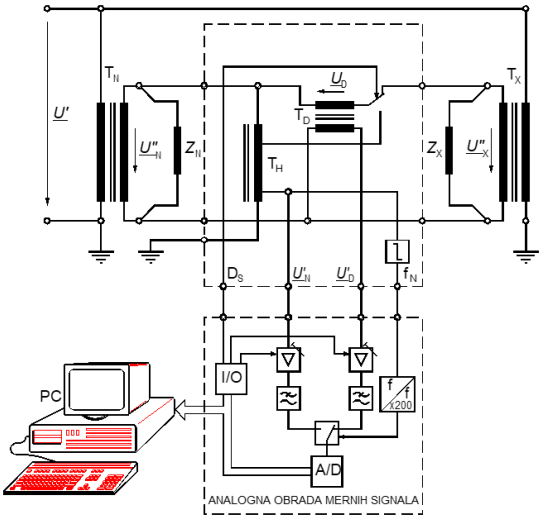


Fig. 5 The structure of DFT measuring method developed by PTB [46].

The application of the measuring method of discrete Fourier transformation (DFT) for the accuracy testing of measuring transformers originates from the laboratory for measuring transformers of the National Metrology Institute of Germany (PTB) which has a long tradition in the field of metrology, even from the early beginning in 1877 [42]. This laboratory has developed several important measuring devices for accuracy testing of the measuring transformers, known as: Schering-Alberti's [24], Hole's [26] and Keller's compensator [43]. PTB experts have significantly contributed to the development of measuring methods and measuring techniques

 ISBN 978-86-7466-930-3

in the field of measuring transformers. As a result of recent research in PTB, the method of discrete Fourier transform was applied, first for testing the accuracy of current measuring transformers [44], and later for testing voltage measuring transformers [45].

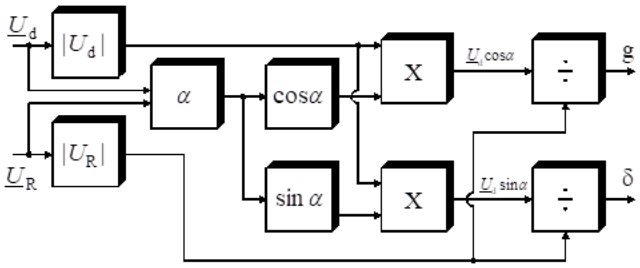


Fig. 6 The structure of measuring method based on orthogonal voltage components [48].

The structure of DFT measuring method developed by PTB experts is shown on Fig. 5 [46]. The device for accuracy testing of instrument transformers based this method, Fig. 5, have following characteristics: measurement range of ± 0,2 % and ± 2 % for ratio error, ± 0,2 crad and ± 2 crad for phase displacement; resolution of 0.000001%, accuracy ± 0,5 % of measuring value and ± 0,05 % of measuring range. This device was capable to measure in a full range from 1% to 200% of rated current, i.e., of rated voltage.

The structure of measuring method based on orthogonal voltage components is shown in Fig. 6

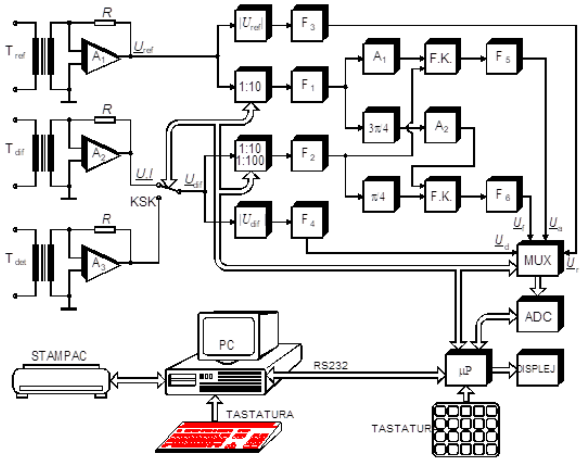


Fig. 7 Block scheme for device for instrument transformer accuracy testing, type INST-2A [47].

Basically, this is a differential method that enables measurement of fundamental harmonic of two voltages and its phase angle, but with some original solutions [47, 48]. The device based on this method is shown in Fig. 7. Novel solution of current-voltage transformer was applied for both differential and detection voltage, as well as for reference voltage. In this way, the adjustment of voltage measured signals to the optimal level was achieved, with minimal degradation of basic signals, and the conversion of current measuring signals into voltages. This initial level of analog processing of measuring signals is very important for the overall accuracy of the device. The second improvement is in electronic bloc that is applied phase regulated rectifier which makes phase shift between $\underline{U}_r$ and $\underline{U}_d$. The phase shift of π/2 by this phase rectifier is obtained as discrepancy between phase shift of 3π/4 for $\underline{U}_r$ and phase shift of 3π/4f or $\underline{U}_d$ [48]. Another recent improvement of differential measuring method is two phase conversion method [49]. The method is based on the measurement of phase angles between three relevant voltages, Fig. 8. The measured ratio error and phase displacement are than presented as a function of two angles. Structure scheme presented in Fig.8 consist of commercial dual channel power analyzer, electronic module and PC. The electronic module integrates: an amplifier, two summing circuits, circuits for π/2 phase shift and multiplexer. The input voltages $U_R$ and $U_d$ are subjected to relatively simple analog processing in the electronic module, and as such, are brought through multiplexer to a dual-channel power analyzer. The PC manages the operation of the electronic module and the dual power analyzer according to the given program [39, 49, 50].

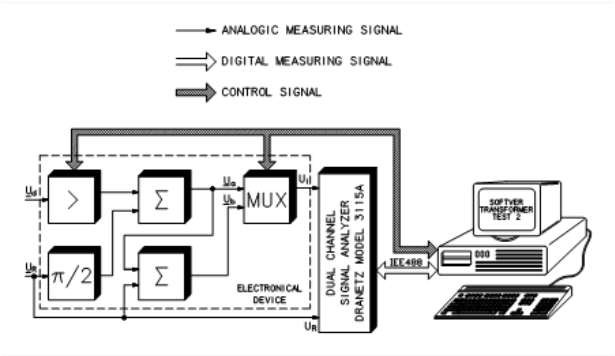


Fig. 8 The structure scheme of two phase conversion method realization [49]

## IV. EEINT'S METHODS AND DEVICES

Measuring systems for accuracy testing instrument transformers based on measuring methods mentioned above usually consist of: standard current/voltage transformer, standard current/voltage burden, device for accuracy testing and measuring transformer under test.

In this field of measurement, methods that are used for testing and calibration purpose are basically the same. The difference is in the accuracy of the standard transformer and the device for accuracy testing which is applied [51].

The experts from EEINT continuously follow the development in this field. Devices for accuracy testing of instrument transformers based on different measuring methods as well as standard transformers developed at the EEINT, have been used for manufactory testing, on-site testing in the power and distribution facilities and for calibration in national metrology laboratories.

The first devices for current and voltage measuring transformer testing were developed in seventeens in last century, Fig. 9. These measuring systems are based on current

 ISBN 978-86-7466-930-3

comparator methods.

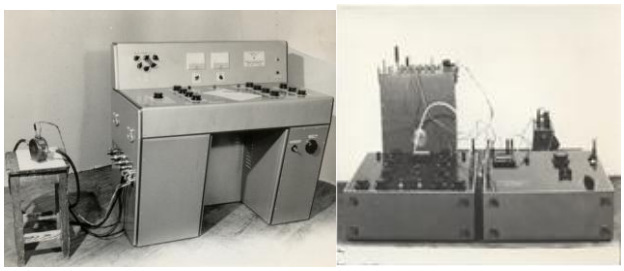

Fig. 9 Devices for current measuring transformer accuracy testing, type KSK-6 (1965) and KSK-7 (1968), respectively.

For accuracy testing of measuring voltage transformers EEINT experts developed measuring system type NIT-2p applied both for laboratory and on-site testing in distribution facilities, Fig 10. The system is based on classical differential method for accuracy testing of voltage transformers that assumed comparison between voltage transformer under test and standard voltage transformer. In that case transformer under test and standard transformer had to have the same transformation ratio.

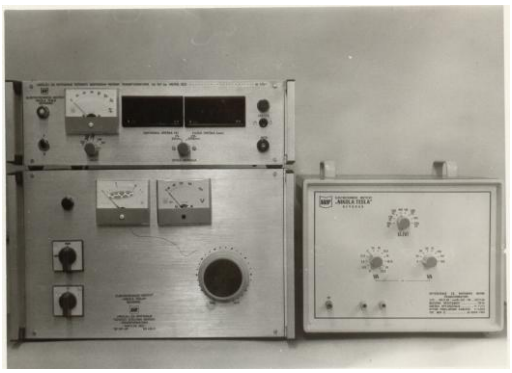

Fig. 10 System for voltage transformers accuracy testing, type NIT-2p (1981.)

With the development of instrument transformers industry in former Yugoslavia, the need for faster and more efficient routine accuracy testing appeared. This demand is satisfied with development of first automatic systems for accuracy testing of current transformers [52, 53], shown in Fig 11 and Fig 12.

Fig. 11 System for automatic accuracy testing of current measuring transformer, type ASK-1 [52]

Fig. 12 System for automatic accuracy testing of current measuring transformer, type ASK-2 [53]

Automatic systems for routine testing of measurement current transformers have been further developed together with new technological achievements. Together with ISKRA AMESI, Slovenia, in 2012, EEINT realized robotized system for routine testing of current transformer, Fig 13. Among the other routine tests according to standard [2], this system can perform accuracy testing of 7 current transformers synchronously. EEINT developed and manufacture the standard transformer, standard burden and device for accuracy testing based modified differential method and multiplexing concept [54].

Fig. 13 Robotized system for current transformers accuracy testing in MBS factory Germany (2012.) [54]

Three years later, for Instrument transformers factory FMT Zajecar, EEINT developed and made device for simultaneously testing of 3 current transformers [55], Fig. 14.

Fig. 14 Automatic device for accuracy testing of 3 current transformers simultaneously [55]

Based on the experience in the realization of different measuring devices in this field, in 2001, EEINT was designed and built a mobile laboratory for on-site accuracy testing of measuring transformers, Fig 15. This mobile laboratory was


ISBN 978-86-7466-930-3

used by “Elektrostopanstvo”, Macedoni, for accuracy testing of measuring transformers in the distribution facilities [56].

Fig. 15 Mobile laboratory for accuracy testing of measuring transformers [56]

Experts from EEINT have made a special contribution to the development of standards and high-precision devices for use in national metrology laboratories. Standard current transformer with electronic compensation of errors type EST-3000 [57] was designed and made together with device for measuring transformers accuracy testing, type INST-2A [47] for Directorate for Measures and Precious Metals (DMDM). This system represents the national standard of Serbia in the field of measuring transformers.

In period from 2016 to 2019 in EEINT three high accuracy systems developed for the needs of National metrology institutes of Canada (NRC) and Singapore (A*Star), as well as for laboratory of power transmission system of Quebec (Hydro Quebec), Canada. In these measuring systems, a differential method with a special construction of a standard transformer and measuring device was applied [58]. The high accuracy of the standard transformer was achieved by an unconventional two stage design. The transformer's detection core is made of high permeability magnetic material, whereas the working core is made of a standard magnetic material for current transformers. The primary and secondary windings are evenly wound around the cores and magnetically and electrostatically shielded. The compensation winding is not connected to the secondary winding but instead to a separate differential transformer winding. This way, the $N_{sc}$ winding of the Ts transformer is not burdened with a voltage created by the full secondary current $I_{ss}$ and the $N_{ds}$ winding impedance, but with a significantly smaller voltage created by a small compensation current $I_{sc}$ and the $N_{dc}$ winding impedance, Fig 16. This makes the impedance seen by the $N_{sc}$ winding smaller and the compensation much thus more effective. This improvement leads to at least two to three times lower measurement errors [58]. The system is verified by simultaneously comparison with NRC system for current transformer accuracy testing – national standard of Canada. The obtained discrepancies in ratio and phase errors were within a few μA/A or μrad, respectively. Practical realization of mentioned measuring system is shown in Fig. 17. The method of simultaneously comparison is developed and firstly applied at EEINT [59].

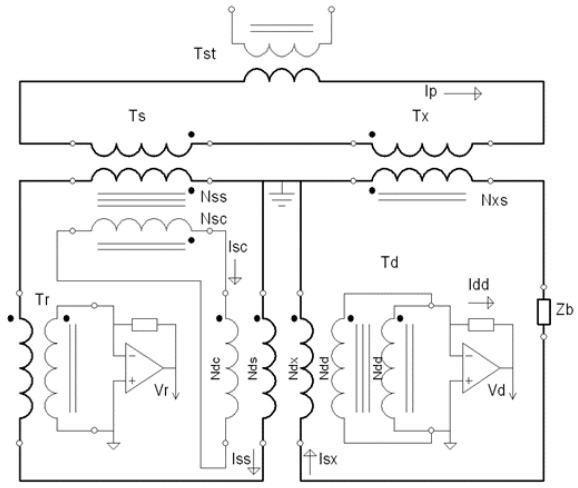


Fig. 16 Block diagram of the differential CT calibration system with special construction of two stage standard transformer $T_s$ and differential $T_d$ transformers [58]

## V. NEW GENERATION OF MEASURING TRANSFORMERS

Digitalization of distribution and power facilities is the process that is part of much large movement, the Industrial Revolution 4.0 conventional transformers are no longer suitable for use in such systems. Therefore, new generations of current and voltage transformers and sensors have been developed that can be applied in digitized distribution and power facilities [60, 61, 62]. New types of measuring transformers and sensors require the development of new suitable measuring methods and devices for their testing. Some new proposals for accuracy testing of new generation of instrument transformers, so-cold low power instrument transformers are given in serial of EN/IEC standards [60]. It can be noted that these international standards recommend in the use of current comparators as a part of some proposed measuring systems for accuracy testing of low power instrument transformers.

Fig. 17 Practical realization of NRC measuring system for accuracy testing of current transformer

## VI. CONCLUSION

The measurement accuracy is the most important characteristic of measuring transformers since that is the important factor in the accurate measurement of the high

 ISBN 978-86-7466-930-3

voltage and currents. The billing of electricity, as well as the power measurement at low power factors, is the explicit examples where accuracy of instrument transformers has very important role. The need for accurate measurement current and voltage by measuring transformers influenced both the improvement of their characteristics and the development of methods for determining their accuracy. The accuracy of measuring methods and measuring equipment for the accuracy testing of measuring transformers has improved along with technological progress.

This paper presents a historical overview of the development of measuring methods and devices in the field of measuring transformers. Also, the paper presents the most important trends in the development of measuring methods and devices for different applications. The systems for accuracy testing of measuring transformers in manufacturing process as well as high accuracy equipment for laboratory calibration of standard transformers are presented. Special attention was given to the contribution of EEINT experts in this field, both in the past and present.

## ACKNOWLEDGMENT

Autor would like to thank dr. Slobodan Skundric for very useful discussion and suggestions regarding to topics that are presented in this paper.

## REFERENCES

[1] S. Škundrić, D. Naumović-Vuković, D .Kovačević, “The Role and Importance of Instrument Transformers in Electrical Quantity measurements”, JUKO CIRED, Herceg Novi, 2004.
[2] Rule book of instrument transformers applied in the billing metering of electricity, "Official Journal RS", No. 66/15
[3] Instrument transformers – Part 1: General requirements, EN 61869-1: 2009
[4] Instrument transformers – Part 2: Additional requirements for current transformers, EN 61869-2:2012
[5] Instrument transformers – Part 3: Additional requirements for inductive voltage transformers, EN 61869-3: 2011
[6] Instrument transformers – Part 4: Additional requirements for combine transformers EN 61869-4: 2013
[7] Instrument transformers – Part 5: Additional requirements for capacitive voltage transformers EN 61869-5: 2011
[8] P. G. Agnew and T.T. Fitch, "The determination of the constants of instrument transformers", *Bull. Bureau Standards*, vol.6, pp.281-299, April 1909.
[9] H. B. Brooks and F.C. Holtz, "The two-stage current transformer", *Trans. Amer. Inst. Elect. Eng*., Vol. XLI, pp. 382-393, Jun, 1922.
[10] F. B. Silsbee, "A method for testing current transformers", *Bull. Bureau Standards*, vol.14, pp.317-329, July 1917.
[11] A. H. M. Arnold, "Current transformer testing", *J. Inst. Elect. Eng*., vol. 74, No. 449, pp. 424-437, May 1934.
[12] G. Rietveld, L. Jol, H. E. van den Brom and E. So, "High-current CT calibration using a sampling current ratio bridge", *IEEE Trans. Instrum. Meas*. vol. 62, No. 6, pp. 1693-1698, Jun. 2013.
[13] E. Mohns, J. Meisner, G. Roeissle and M. Seckelmann, "A wideband current transformer bridge", *IEEE Trans. Instrum. Meas*. vol. 63, No. 10, pp. 2322-2329, Jun. 2013.
[14] E. Mohns, G. Roeissle, S. Fricke, F. Pauling, "An AC Current Transformer Standard Measuring System for Power Frequencies", IEEE Trans. on Instrumentation and Measurement, Vol. 66, Issue 6, pp. 1433-1440, 2017.
[15] E. Mohns, S Fricke, F. Pauling, "An AC power amplifier for testing instrument transformer test equipment", Conference on Precision Electromagnetic measurements, CPEM2016, 2016.
[16] S. Siegenthaler, C. Mester, "A Computer - Controlled Calibrator for Instrument transformer Test Sets", IEEE Trans. on Instrumentation and Measurement, Vol. 66, Issue 6, pp. 1184-1190, 2017.
[17] S.Škundrić, F. Smak, S. Spiridonović, N. Pandurović, D. Kovačević, "Modern methods and devices for testing of measuring transformers“ Study arranged for the United Electric Power Industry of Serbia, Electrical Engineering Institute „Nikola Tesla“, Belgrade, 1990.
[18] S. Škundrić, D. Kovačević, D. Naumović-Vuković, „The role and importance of Software Application in Instrument Transformers Accuracy Testing“, IMEKO XVIII World Congress, Rio de Janeiro, Brazil, September, 2006.
[19] S. Spiridonović, S. Škundrić, "Current measuring Transformers", Proceedings - Conference on instrument transformers in power engineering, 1996.
[20] G. Keinath, "Fehlergroben des Stromwandlers", ATM, (Z224-1), 1932.
[21] G. Keinath, "Stromwandler mit Hochter Genauigkeit, ATM, (Z20-4), 1932
[22] G. Keinath, "Hochmagnetische Legirungen", ATM, (Z913-3), 1932
[23] F. B. Silsbee, "A method for testing current transformers", *Bull. Bureau Standards*, vol.14, pp.317-329, July 1917.
[24] H. Schering, E. Alberti, Eine einfache Methode zur Prufung von Stromvandlern, Arch. Elektrotechn, Bd. 2, pp. 236-237, 1914.
[25] H.S. Baker, "Current Transformer Ratio and Phase Error by Test Ring Method", AIEE Proc., Vol. XXXVI, pp.1173, 1917
[26] W. Hohle, Neure Stromwandler - Prufeinrictungen, ATM, (Z224-4), 1934
[27] W. Geyger, "Wechelstrom - Kompensatoren", ATM, (J94-1), 1932.
[28] W. Geyger, "Wechelstrom - Kompensatoren", ATM, (J94-9), 1937.
[29] W. Hohle, "Messwandler - Prufeinrichtungen", Arch. Elektrotechn., Bd27, pp849, 1933.
[30] W.E. Bruges, "Method of Testing Current Transformers", Jurnal IEVE, Vol. 68, pp.305, 1930.
[31] W. Reiche, "Stromwoundler Hochster Genauikeit", VDE Fachberichte, 1935.
[32] I. Obradovic, P. Miljanic, S. Spiridonovic, "Prufung von Stromwandler mittls eines Stromkomparators und eines elektrischen Hilfssystems", *ETZ-A*, H.19, pp.699-701., 1957.
[33] P. N. Miljanic, N. L. Kusters and W. J. Moore, "The development of the current comparator, a high-accuracy A-C ratio measuring device", Trans. Amer. Inst. Elect. Eng. I, Commun. Electron., vol 81, no.5, pp.359-368, Nov. 1962.
[34] W.J.M. Moore and P.N. Miljanic, “The Current Comparator”, Peter Peregrines Ltd., ISBN 0 86341 112 6, 1988.
[35] S. Škundrić, D. Kovačević, D. Naumović-Vuković, S. Milosavljević, „ Application of current comparator for testing the accuracy of standards and conventional transformers in measuring groups“, „Power systems: operation, management, testing, measurement“, Monography, Electrical Engineering Institute „Nikola Tesla“, Belgrade, 2006. (ISBN 86-83349-06-3, ISBN 978-86-83349-06-07 a) Power Systems COBISS.SR-ID 136938252
[36] E. Mohns, J. Meisner, G. Roeissle and M. Seckelmann, "A wideband current transformer bridge", *IEEE Trans. Instrum. Meas*. vol. 63, No. 10, pp. 2322-2329, Jun. 2013.
[37] G. Rietveld, L. Jol, H. E. van den Brom and E. So, "High-current CT calibration using a sampling current ratio bridge", IEEE Trans. Instrum. Meas. vol. 62, No. 6, pp. 1693-1698, Jun. 2013.
[38] E. Mohns, G. Roeissle, S. Fricke, F. Pauling, "An AC Current Transformer Standard Measuring System for Power Frequencies", IEEE Trans. on Instrumentation and Measurement, Vol. 66, Issue 6, pp. 1433-1440, 2017
[39] S. Škundrić, V. Radenković, D. Kovačević, F. Smak, S. Mikičić, Testing of Instrument Transformers with non-standard rations, XXIV IMEKO World Congress, Tampere, 1997.
[40] S. Škundrić, F.Smak, D. Kovačević, S. Mikičić, The Testing of the Instrument Transformers Accuracy Calass in Power Plants, Universities Power Engineering Copnference, Crete, 1996.
[41] S. Škundrić, F. Smak, S. Vukovojac, D. Kovačević, “The Microprocessor based device for testing of measuring transformers”, Proceedings, 14. JUKEM, Sarajevo, 1990.
[42] www.ptb.de
[43] A. Keller, "Neuzeitliche Messwandler - Prufeinrictungen nach dem Differentialvervahren, ETZ-a, pp. 105-108, 1953
[44] A. Braun, "Elektronischer Vektormesser fur die Komplexe Wechselstrommesstechnik", TM50, H.10, pp. 372-377, 1985.

 ISBN 978-86-7466-930-3

[45] A. Braun, H. Moser, "Rechnergesteuerter Massplatz yur Lakibrierung von Normalsoannungswandlern" PTB Miteilungen, pp. 298-302, 1989.
[46] G. Ramm, H. Moser, Eine neuartige, rechnergesteuerte und sebstkalibrierende Stromwandler-Messeinrichtung. PTB-Miteilungen Bd.105, H4, s.263-271, 1995
[47] F. Smak, S. Škundrić, S. Vukovojac, D. Kovačević, M. Korolija „The Modern device for testing of instrument transformers, type INST-2A“, Conference: Transformers in power engineering, Belgrade 1996.
[48] S. Škundrić, V. Radenković, „Electronic phase reversal of the measuring signal by π/2 in measuring transformer testing devices“, Conference ETRAN, Budva 1996.
[49] S. Škundrić, V. Radenković, Instrument Transformers Accuracy Testing by the Two-Phase Conversion Method, Electrical Engineering, H4, pp. 326-328, 1998.
[50] S. Škundrić, V. Radenković, Instrument Transformers in Contemporary Electronic Instruments, VI International SAUM Conference, Niš, 1995.
[51] E. Mohns, P. Rather, “Test equipment and its effect on the calibration of instrument transformers”, Journal of Sensors and Sensor Systems, No.7, pp339-347, 2018., https://doi.org/10.5194/jsss-7-339-2018
[52] N. Pandurović, D. Miličević, S. Škundrić, “A System for Automatoc Testing of Instrument Current Transformer Accuracy”, III Conference for Electricity Supply, London, 1977.
[53] S. Škundrić, D. Kovačević, F. Smak, S. Vukovojac, “”Computer-controlled system for automatic testing of accuracy of measuring current transformers, Proceedings of the Electrical Engineering Institute "Nikola Tesla", Vol. 9., Belgrade 1991.
[54] Dragana Naumovic - Vukovic, Slobodan Skundric, Aleksandar Zigic, The Device for Simultaneously Accuracy Testing of Current Transformers, Journal of Physics Conference Series 1065(5):052017, IOP Publishing, vol. 1065, pp. 1 - 4, issn: 1742-6596, Belfast, 3. - 6. Sep, 2018.
[55] D. Naumovic Vukovic, S. Skundric, A. Zigic, Three channels device for current transformers accuracy testing, Proceedings of 19th International Symposium on Power Electronics -Ee2017, Power Electronics Society, Faculty of Technical Science Novi Sad, Electrical Engineering Institute Nikola Tesla Belgrade, pp. 1 - 4, doi: 9781538635025/17/$31.00@2017IEEE, isbn: 978-86-7892-980-9, Novi Sad, 19. - 21. Oct, 2017.
[56] S. Skundric, D. Kovacevic, “Contribution to the teaching about measurement”, Conference MAKO-CIGRE, Ohrid 2005.
[57] F. Smak, S. Škundrić, D. Kovačević, M. Korolija, “Standard current transformer with electronic error compensation for primary currents up to 3000 A”, Conference on instrument transformers in power engineering, Belgrade 1996.
[58] B. Djokic, H. Parks, N. Wise, D. Naumovic Vukovic, S. Skundric, A. Zigic, V Poluzanski, A Comparison of Two Current Transformer Calibration Systems at NRC Canada, IEEE Transactions on Instrumentation and Measurement, IEEE Instrumentation and Measurement Society, vol. 66, no. 6, pp. 1628 - 1635, issn: 0018-9456, doi: 10.1109TIM.2017.2631739, 2017.
[59] D. Naumovic-Vukovic, “The Recent Contribution to Calibration of Current Transformers”, PhD Thesis, University of Novi Sad, Faculty of Technical Science, 2018.
[60] Instrument transformers – Part 6: Additional general requirements for low power instrument transformers EN 61869-6: 2016
[61] Instrument transformers – Part 10: Additional requirements for low-power passive current transformers EN 61869-10: 2018.
[62] Instrument transformers – Part 11: Additional general requirements for low-power passive voltage transformers EN 61869-11: 2018.

 ISBN 978-86-7466-930-3

# Effects of cryptocurrency mining rig operation on power quality in LV distribution network

Vladimir A. Katić, *Senior Member, IEEE,* Zoltan J. Čorba, *Member, IEEE,* Aleksandar M. Stanisavljević, *Member, IEEE*

***Abstract*—The paper presents the influence of power supply units of a cryptocurrency mining rig on the power quality in a standard low-voltage network. Measurement and monitoring of the power quality indices of one mining rig with an optimized power of 1000W were performed. For comparison, the results of power quality measurement of a group of desktop computers (PC cluster) from a computer centre are presented. It has been observed that the mining rig had a smaller impact on power quality (harmonics) than the PC cluster, but that they represent a significantly higher and almost constant power demand.**

***Index Terms*—Cryptocurrency mining rig; PC cluster; Power quality; Measurements.**

## I. Introduction

Widespread use of computers, computer equipment, various digital electronic and mobile devices, consumer electronics, and household appliances, as well as other nonlinear systems based on energy electronic converters, has led to reports of distorted current waveforms in the network, i.e., occurrences of harmonics [1]. The consequence was a reduction in the power quality and the possibility of the appearance of some negative effects on other interconnected loads (linear), but also on the above-mentioned nonlinear ones. Computers and computer equipment are a special problem due to their frequent concentration in large groups (clusters) [2]. As individual loads, they draw pulse current waveforms from the network with a very high level of distortion, so the total harmonic distortion of this current (THDI) may reach more than 120% [1,2]. However, due to group work in different modes, with different individual parameters (diversity factor), as well as due to the phenomenon of harmonic cancellation and attenuation the THDI of a PC cluster is ranged between 30-40% [2,3]. Furthermore, as their power demand is low in relation to the short-circuit power at the connection point, these values are within the limits stipulated by the international standard IEC 61000-3-4 [1,4].

However, in recent years, the use of cryptocurrencies (Bitcoin, Ethereum, Tether, etc.) is growing, as well as the need to verify their transactions on a public digital ledger (public digital book) known as the blockchain. As this process will also create new cryptocurrency values it is called the Bitcoin, or more generally, the cryptocurrency mining [5]. Unlike individual PCs or their groups (PC clusters) where the power varies during operation, cryptocurrency mining is performed with almost constant power, i.e., with a constant engagement of microprocessor resources. In this case, two problems arise. One is the power demand or efficient operation of the device, i.e., its electricity consumption, and the other is the impact on the power quality in the connected network [6,7]. It should be noted that these devices are of low rated power, so they are connected to a low-voltage single-phase network, i.e., one cryptocurrency mining rig represents a set of 6 graphics cards, which are powered via one or two power supply units. The response to both mentioned problems depends on the quality of the rig, i.e., the optimization of its operation, as well as the construction of the power supply (AC/DC converter with PFC).

There are many papers in the scientific literature that treat the first problem, and a lot of articles and reviews on professional sites (blogs) and journalism are dedicated to that. For the sake of objectivity, only those papers that have been published in the reference scientific literature will be considered here [6-11]. The impact of increasing network losses as a result of the operation of these devices was mainly considered in [6], long-term trends related to changes in the amount of energy per transaction in [8], the cost-effectiveness of mining concerning electricity prices in certain countries and environmental factors in [9], and mining of other cryptocurrencies, beside of Bitcoin in [10]. The issue of the effects on the power quality was less prominent and not researched in more detail. Some results presented in [7] show that such a low interest was a consequence of the higher quality power supply unit applications than in standard PCs, so the recorded current distortion had been less than THDI<10% [7]. However, in the case of larger cryptocurrency mining operations, the distortion of electricity may be more significant, even beyond the standards' permissible limits. This was observed in [11], but more detailed measurements and analyses have not been performed.

This paper aims to present the impact of the cryptocurrency mining rigs, i.e., their power supply units, on the power quality in a low-voltage distribution network and to compare it with the effects of conventional desktop (PC) computers. To enable this, the results of multi-day measurements were used, as well as the appropriate analysis of the measured results in the time and frequency domain.

Vladimir A. Katić – Univerzitet u Novom Sadu, Fakultet tehničkih nauka, Trg Dositeja Obradovića 6 21000 Novi Sad, Srbija (e-mail: katav@uns.ac.rs), (https://orcid.org/0000-0002-0138-8807).

Zoltan J. Čorba – Univerzitet u Novom Sadu, Fakultet tehničkih nauka, Trg Dositeja Obradovića 6 21000 Novi Sad, Srbija (e-mail: zobos@uns.ac.rs)

Aleksandar M. Stanisavljević – Univerzitet u Novom Sadu, Fakultet tehničkih nauka, Trg Dositeja Obradovića 6 21000 Novi Sad, Srbija (e-mail: acas@uns.ac.rs), (https://orcid.org/0000-0002-7156-3869).

 ISBN 978-86-7466-930-3

## II. MEASUREMENTS OF POWER QUALITY INDICES

Professional device C.A. 8332 by Chauvin Arnoux [12] was used to measure electricity quality indices, which follow the European standard EN 50160 [1,4]. The measurements were performed over a period of seven days, continuously at the place of connection of the device, i.e., at the busbars of the distribution cabinet in the low voltage network. The power quality indices of a PC cluster placed in the computer centre and a cryptocurrency mining rig were measured. The measured values included the effective value of voltage and current, frequency, power, power factor (PF), flicker, harmonics of voltage and current, and k-factor. However, due to limited space, only the most significant measurement results will be presented here, namely, those related to work efficiency (active P, reactive Q, distortive D, and apparent power S, as well as PF), i.e., electricity consumption (kWh, kVAh), and the impact on the power quality (total harmonic distortion of voltage and current, THDU, THDI).

### *A. Measurement results for the computer centre*

As part of the activities on the subject of master's academic studies "Quality of electricity", measurements of power quality indices are regularly conducted on the internal network of the Faculty of Technical Sciences. For the purposes of this paper, obtained measurement results at the distribution cabinet of the computer centre during November/December 2019 will be used. Fig. 1 shows the measuring point, and Fig. 2 shows the waveform of the voltage and current of the single-phase network. In the line shown, 42 computers are connected, which have different power supply units HP Lite-On PA 1181-7 and Fujitsu D12-250 P1A with powers of 180 W and 250W, respectively. During the measurement, not all of them were turned on, that is, 28 computers were working continuously. The operation of these computers is characterized by high current distortion (Fig. 2), so in addition to active and reactive power, there is also distortion power.

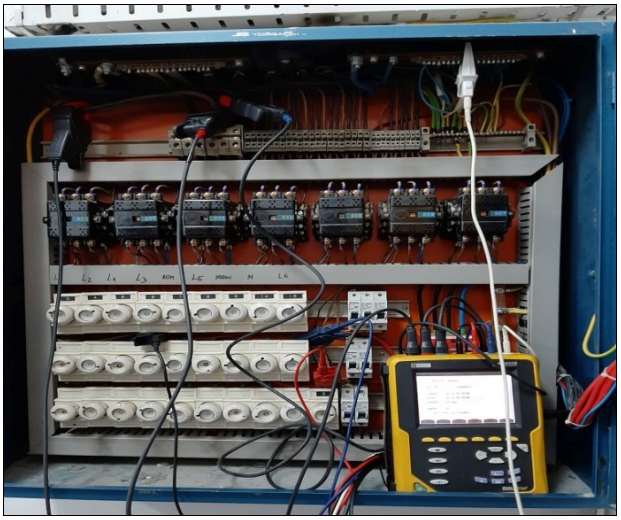

Fig. 1. Photo of measurement location during measurement at the computer centre

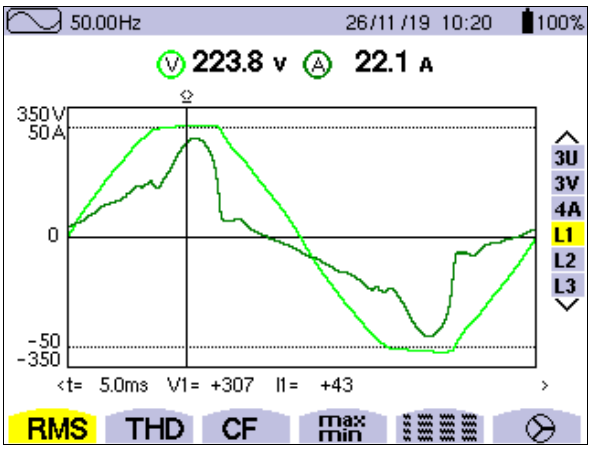


Fig. 2. Voltage and current waveforms of a single phase at the computer centre

Fig. 3 (up) shows the variation of the apparent (S), active (P), and reactive (Q) power, as well as distortion power (D) during a one-week measurement, while Fig. 3 (down) shows their statistical analysis. It can be seen that over 50% of the time computers work in standby (idle) mode, that they are capacitive as the reactive power is Q<0 (this can be also seen from Fig. 2, where the current waveform precedes the voltage one), and that the measured distortion power (D) is negligible. In addition, the measured power factor (PF) presented in Fig.4 indicates significant effects of the PC supply unit capacitance, but also the current harmonic distortion. Fig. 4 shows its variation during the one-week measurement and the statistical analysis. It can be seen that PF was below 0.95 all the time, which indicates a potential problem. In order to better understand all statistical values, Table I gives the most significant results of statistical analysis for all types of power (S, P, Q, and D), as well as for the power factor. It can be seen that power demand is much higher than average power, which shows variation in computers usage.

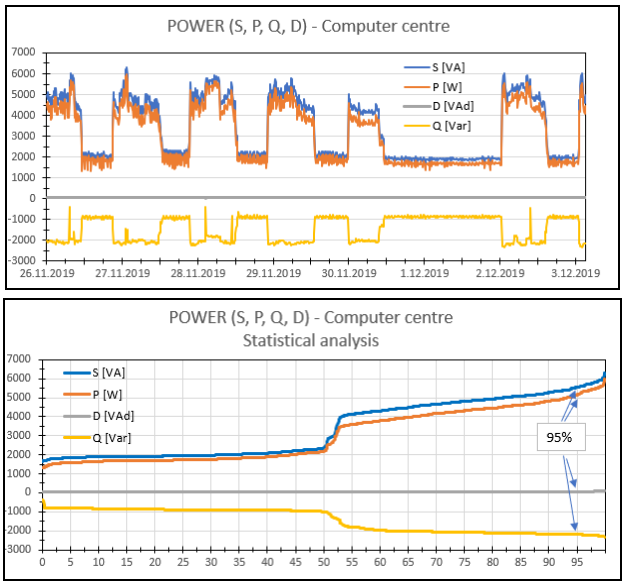


Fig. 3. Variation of the computer centre power demand during one-week measurements: time wave-form (up) and statistical analysis (down)


ISBN 978-86-7466-930-3

TABLE I
STATISTICS FOR POWER (S,P,Q,D) AND POWER FACTOR OF THE COMPUTER CENTRE

| Power | Mini-mum | Median (50%) | Average | 95% value | Maximum |
|---|---|---|---|---|---|
| S [kVA] | 1657.3 | 2348.4 | 3373.1 | 5544.1 | 6290.9 |
| P [kW] | 1337.2 | 2180.7 | 3029.3 | 5157.8 | 5992.5 |
| Q [kVAr] | -381.1 | -995.6 | -1448.4 | -2195.3 | -2328.4 |
| D [kVAd] | 39.2 | 50.9 | 58.6 | 73.7 | 75.7 |
| PF | 0.79 | 0,89 | 0,889 | 0,936 | 0,952 |

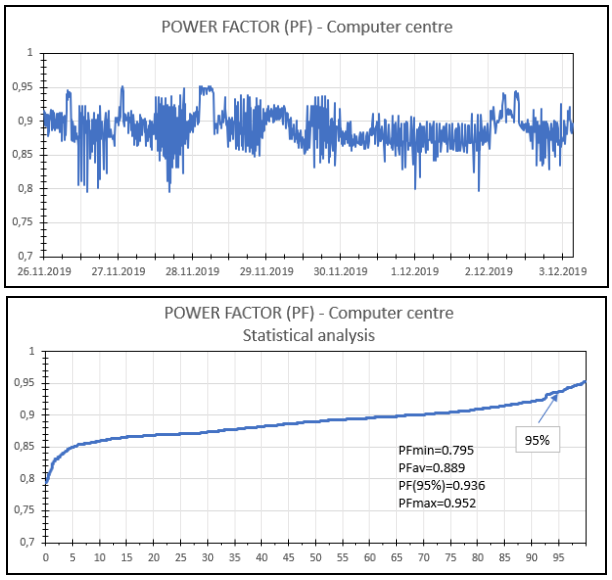


Fig. 4. Variation of the computer centre power factor during one-week measurements: time wave-form (up) and statistical analysis (down)

The observed waveforms of current and voltage (Fig. 2) indicate the existence of harmonic distortion, which is pronounced in the current pulsed waveshape, while in voltage it can be seen as a "flattened top" of the sinusoid. Both distortions are a consequence of the operation of power supply units (in PC and the monitor), which are usually realized as a diode bridge rectifier with a capacitive filtering (for "ironing" of the DC voltage) and additional DC/DC converter (for obtaining different voltage levels). Due to the parallel operation of a large number of computers, the mentioned phenomenon of harmonic cancellation and attenuation is present, so the values of THDI and individual harmonic distortion of the current (HDI) are less than in the case of individual computers. Figs. 5 and 6 show the variation of the THDU (Fig. 5) and THDI (Fig. 6) during one-week measurements. If the results are compared with Fig. 3, it can be seen that the distortions are smaller in the standby ("night" mode) (THDU≈2.2%; THDI≈22%), and that they increase during the working days when the PCs are in active use (THDU≈2.8%; THDI≈45%).

### *B. Measurement results of cryptocurrency mining rig*

Cryptocurrency mining uses a dedicated computer assembly (rig) consisting of a power supply unit, mainboard, and graphics cards. Fig. 7 shows an illustrated block diagram of this device. A set of six graphic card units (GCU) were in operation during the measurement, which was powered by two high-quality power supplies: HPE model "ProLiant" DL580 G7 (1200W, Platinum, η=94%) and "Be Quiet!" model Straight Power 11 (650 W, Platinum, η=94%) connected to a single-phase network (230V, 50 Hz). The maximum power of both supplies is 1850W, but they are optimized to work on 1000W. Fig. 8 shows the photo of the treated rig and the location where C.A 8332 was connected.

The main characteristic of the rig´s operation is the constant engagement of the GCU processor, which leads to higher electricity consumption, but also significant thermal losses. For this reason, applied power supply units are of high efficiency (94% -95%), but also with a more complex schematic. They have an additional power factor correction (PFC) unit, which enables close to unity power factor, but also contributes to the significant reduction of harmonic distortion.

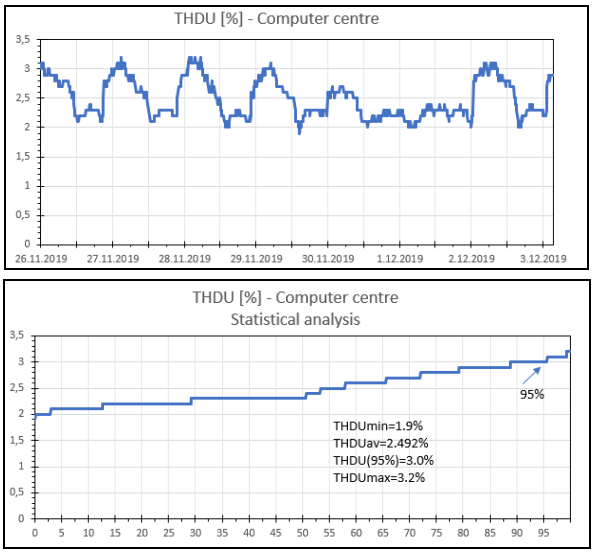


Fig. 5. Variation of the computer centre THDU during one-week measurements: time wave-form (up) and statistical analysis (down)

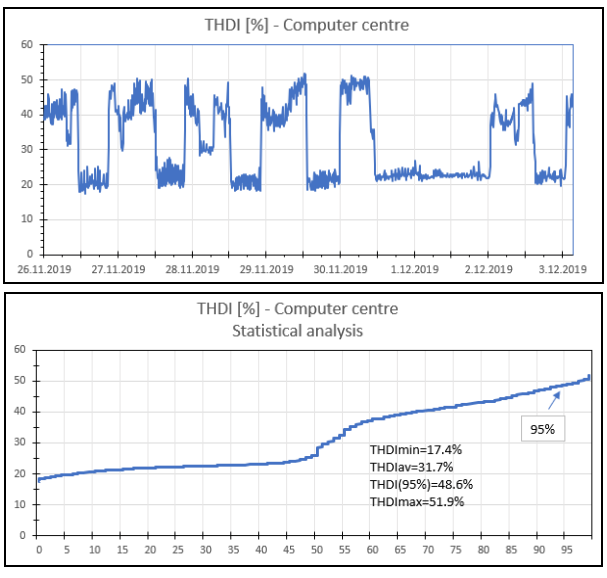


Fig. 6. Variation of the computer centre THDI during one-week measurements: time wave-form (up) and statistical analysis (down)


ISBN 978-86-7466-930-3

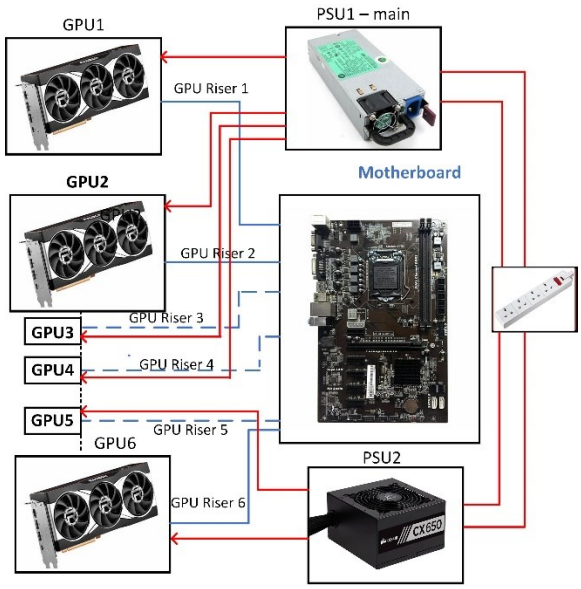


Fig. 7. Block scheme of the cryptocurrency mining rig

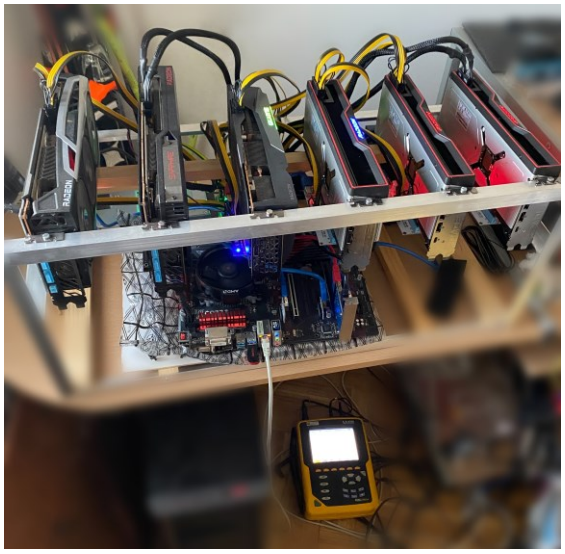

Fig. 8. Photo of measurement location during cryptocurrency mining rig measurement

The measurement results are shown in Figs. 9-14. Fig. 9 shows the waveforms of voltage and current, which are characterized by the flatness of the sinusoidal top and very low current distortion and displacement. Fig. 10 shows the measurement results for different types of power, while Fig. 11 the power factor. It can be seen that there were some short periods with lower power demand, which corresponds to some problems with the Internet and shutting down at the end of the measurement. In order to better understand the statistical values, Table II gives the most significant results of statistical analysis of measured power and power factors for the cryptocurrency mining rig. It can be noticed that the rig works with practically constant power and a close to unity power factor (0.988).

Figs. 12 and 13 show the results of the voltage and current harmonic distortion of the cryptocurrency mining rig. The variation of the THDU during one-week measurements is shown in Fig. 12, while the THDI is in Fig. 13. A low voltage and current distortion can be observed. However, significant increases in current distortion can be observed during the measurement and at the end (Fig.13). These are the periods when there was a significant reduction in processor activity of the GCU i.e., in the mining, when the system operates with lower power (see Fig. 10) and outside the optimal parameters. However, these periods do not significantly affect the overall assessment of current distortion.

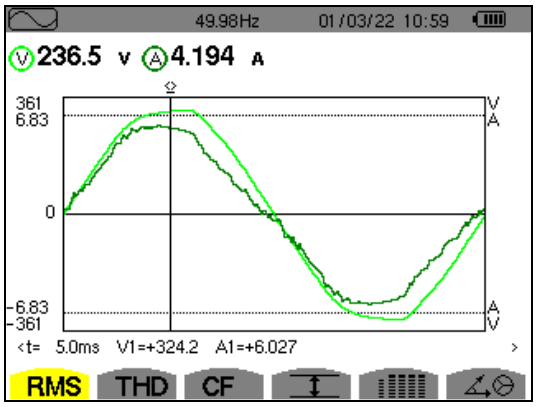


Fig. 9. Voltage and current waveforms of the cryptocurrency mining rig

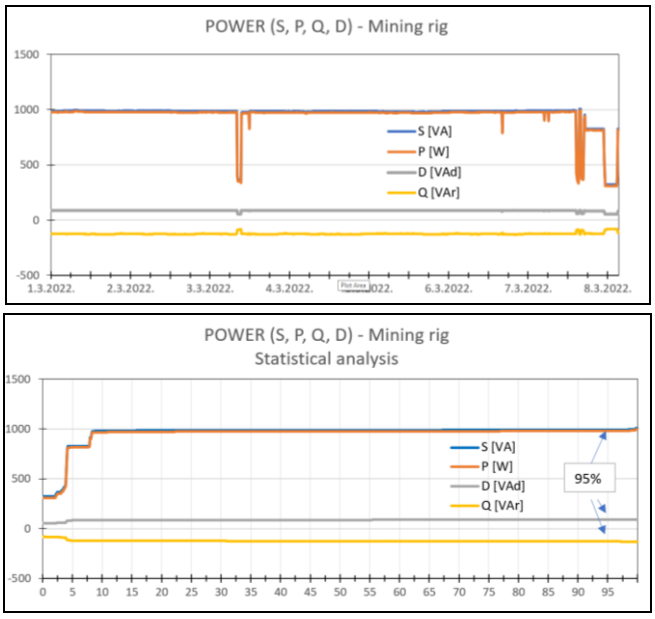


Fig. 10. Variation of the cryptocurrency mining rig power demand during one-week measurement: time wave-form (up) and statistical analysis (down)

## III. Discussion

### A. Comparison of PC cluster and Mining rig by distortion

Commercial PCs, which are widespread and present in many locations are well-known as current and voltage distortion sources in low voltage distribution networks [1]. If they are clustered, the distortion is much less than if a single one is considered [2]. Yet, the current harmonic distortion limits stipulated by international standards are not surpassed.


ISBN 978-86-7466-930-3

Still, the voltage distortion is increased (depending on the power demand of the PC cluster) and may contribute to the appearance of some negative effects at other connected loads. The remaining problems are high and distorted current in the neutral conductor and poor power factor.

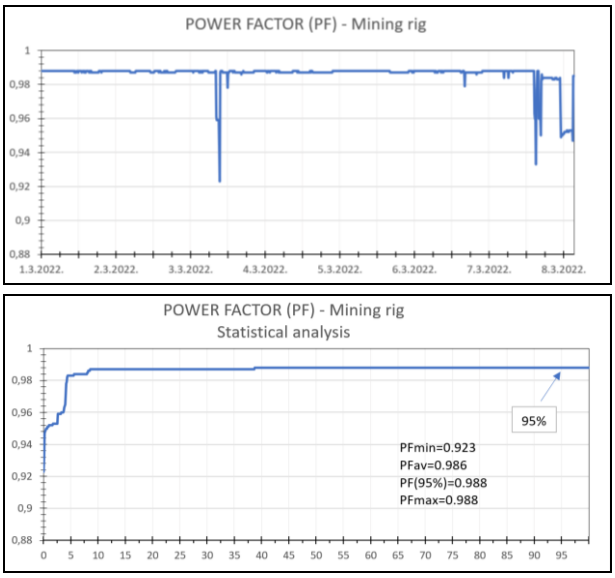


Fig. 11. Variation of the cryptocurrency mining rig power factor during one-week measurements: time wave-form (up) and statistical analysis (down)

TABLE II
STATISTICS OF POWERS (S,P,Q,D) AND POWER FACTOR OF THE CRYPTOCURRENCY MINING RIG

| Power | Mini-mum | Median (50%) | Average | 95% value | Maximum |
|---|---|---|---|---|---|
| S [VA] | 323.8 | 987.8 | 956.1 | 992.7 | 1007.0 |
| P [W] | 308.4 | 975.7 | 943.9 | 980.9 | 994.9 |
| Q [VAr] | -81.3 | -125.4 | -123.9 | -128.6 | -1431.3 |
| D [VAd] | 53.3 | 87.8 | 86.3 | 88.5 | 89.6 |
| PF | 0.923 | 0.988 | 0.986 | 0.988 | 0.988 |

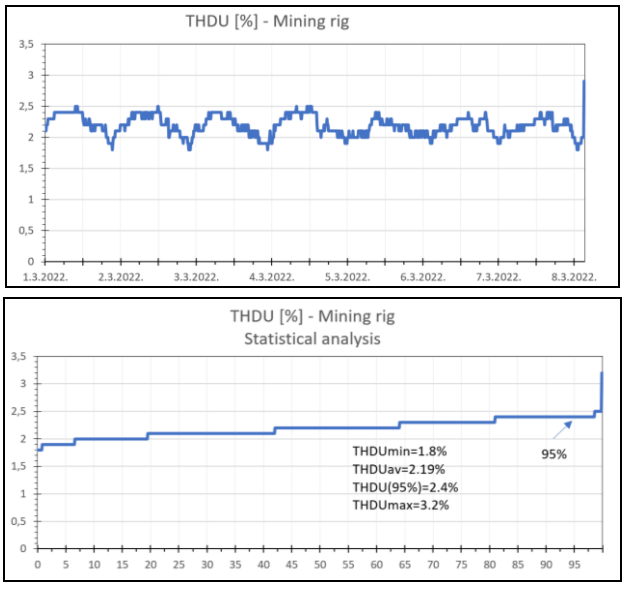


Fig. 12. Variation of the cryptocurrency mining rig THDU during one-week measurements: time wave-form (up) and statistical analysis (down)

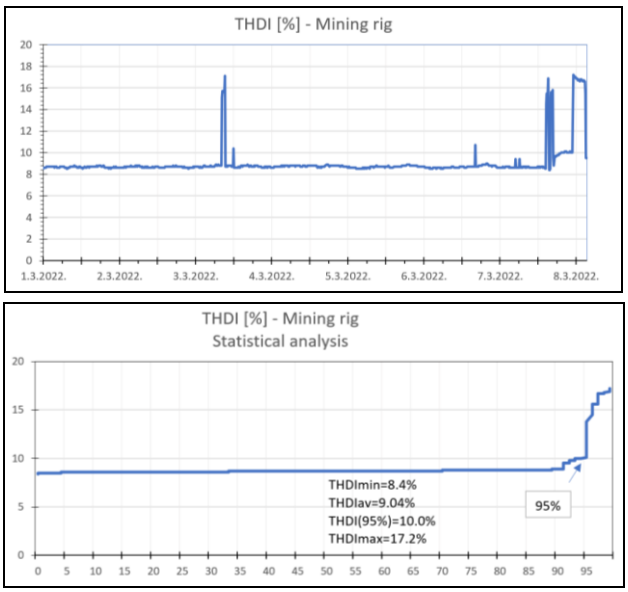


Fig. 13. Variation of the cryptocurrency mining rig THDI during one-week measurements: time wave-form (up) and statistical analysis (down)

In the case of the connection of the cryptocurrency mining rig to the low voltage distribution network the measured harmonic distortion factors and power factor are good and in accordance with international standards. It shows that the power supply units of the rig are carefully selected to enable optimum operation.

Table III shows a comparison of main power quality indicators recorded during measurements of the PC cluster and the cryptocurrency mining rig. It can be seen that the cryptocurrency mining rig has superior performance. Such a conclusion is not a surprise as the power supply units of the mining rig are of much higher quality than the ones of the PC in the cluster.

TABLE III
COMPARISON OF DISTORTION FACTORS AND POWER FACTORS OF THE PC CLUSTER AND THE MINING RIG

| | THDU (95%) | THDU (Max.) | THDI (95%) | THDI (Max) | PF 95% | PF (Max) |
|---|---|---|---|---|---|---|
| PC cluster | 3.0% | 3.2% | 48.6% | 51.9% | 0,936 | 0,952 |
| Mining rig | 2.4% | 3.2% | 10.0% | 17.3% | 0.988 | 0.988 |

### *B. Comparison of PC cluster and Mining rig by power and electricity consumption*

The PC cluster and the cryptocurrency mining rig comparison by power demand and electricity consumption is more interesting. The measurement results show that the power demand of the cryptocurrency mining rig is much higher. Moreover, it is constant over time, so the low-voltage distribution network may see it as a high (~1000W) load of a resistive nature (like some heater).

Fig. 14 (up) shows a comparison of a PC cluster and the cryptocurrency mining rig's active power demand. The power demand of the PC cluster is downsized to the one comparable with the cryptocurrency mining rig (~1000 W). Fig.14 (down)


ISBN 978-86-7466-930-3

shows the same comparison, but regarding the electricity consumption. It can be seen that the power demand of the cryptocurrency mining rig was in some periods much higher, while in others similar to the PC cluster. Regarding electricity, the consumption was much higher (almost twice).

### *C. Effects on voltage distortion (THDU)*

Considering the above observations, it is rational to assume that the operation of the PC cluster, as well as the cryptocurrency mining rig, may have some effects on the low-voltage distribution network voltage harmonics. From Fig.5 it can be seen that there is a high difference between the voltage harmonic levels during the night (PCs are in idle mode) and during the day. It can be estimated that the PC cluster operation increase voltage harmonics from $THDU_{night}$=2.3% to $THDU_{day(95\%)}$=3.0%, i.e., for 30%, up to $THDU_{day(max)}$=3.2%, i.e., for almost 40%.

In the case of the cryptocurrency mining rig, there are no differences between night and day, so it is difficult to estimate the rig´s effect on voltage harmonics. Still, from Figs.10 and 14, it can be noticed some periods with low power operation (when the mining process has been ended and the rig had continued operation in an idle mode), i.e., with a reduced effect on voltage harmonics. Therefore, observing corresponding Fig.12 it can be estimated that the cryptocurrency mining rig operation increase voltage harmonics from $THDU_{min}$=1.8% to $THDU_{day(95\%)}$=2.4%, i.e., for around 33%, up to $THDU_{day(max)}$=3.2%, i.e., 78%!

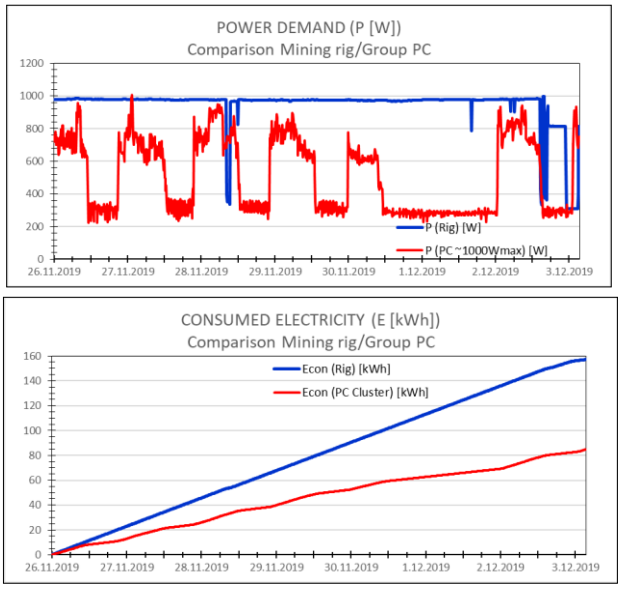


Fig.14. Comparison of the cryptocurrency mining rig and a PC cluster of the same size: of power demand (up) and consumed electricity (down)

## IV. CONCLUSION

The paper presents research results of the cryptocurrency mining rig's effects on the power quality at the low-voltage distribution network. The most important power quality indices obtained during one-week measurements are recorded and discussed. For comparison, similar research has been worked out for a PC cluster.

The research results show that cryptocurrency mining rig has higher power demand and electricity consumption than the similar-sized PC cluster. The power factor is much better (close to unity) than the PC cluster has (below 0.95). It has a lower effect on current distortion (THDI), while the effects on voltage distortion (THDU) are similar to the PC cluster ones.

However, the THDU of the cryptocurrency mining rig might increase significantly if more rigs are connected at the same bus and endangered power (voltage) quality for other loads. Further research will be focused on this problem.

## ACKNOWLEDGEMENT

This work was supported by the Republic of Serbia, Ministry of Education, Science, and Technological Development, through the Integrated and Interdisciplinary Research project entitled “Innovative Scientific and Artistic Research from the Faculty of Technical Sciences Activity Domain” under Grant No. 451-03-68/2022-14/200156.

## REFERENCES

[1] V.A. Katić, *“Kvalitet električne energije – viši harmonici”*, Monografija, Br. 6, Fakultet tehničkih nauka, Novi Sad, Srbija, 2002.

[2] V.A. Katić, S.V. Mujović, V.M. Radulović, J.S. Radović, “The Impact of the Load Side Parameters on PC Cluster’s Harmonics Emission”, *Advances in Electrical and Computer Engineering*, Vol. 11, No. 1, 2011, pp.103-110. https://doi.org/10.4316/AECE.2011.01017

[3] L. Michalec, M. Jasinski, T. Sikorski, Z. Leonowicz, L. Jasinski and V. Suresh, „Impact of Harmonic Currents of Nonlinear Loads on Power Quality of a Low Voltage Network – Review and Case Study”, *Energies*, 2021 Vol. 14, Paper #3665, Open Access, https://doi.org/10.3390/en14123665

[4] V.A. Katic, „Network Harmonic Pollution - A Review and Discussion of International and National Standards and Recommendations”, 3rd Inter. Power Electronic Congress - CIEP '94, Puebla, Mexico, 21-25 Aug. 1994, https://doi.org/10.1109/CIEP.1994.494413

[5] U. Mukhopadhyay, A. Skjellum, O. Hambolu, J. Oakley, L. Yu, and R. Brooks, „A Brief Survey of Cryptocurrency Systems“, 2016 14th Conference on Privacy, Security and Trust (PST), Auckland, New Zealand, 12-14. Dec. 2016, https://doi.org/10.1109/PST.2016.7906988

[6] D. Stevanović, M. Andrejević Stošović, M. Dimitrijević, and P. Petković, “Utility losses due to cryptocurrency mining”, 10th Conf. on ICT Innovations, 2018, Web Proceedings, pp.27-36. https://proceedings.ictinnovations.org/attachment/paper/479/utility-losses-due-to-cryptocurrency-mining.pdf

[7] K.A. Wheeler, A.W. Bowers, C.H. Wong, J.Y. Palmer, and X. Wang, “A Power Quality and Load Analysis of a Cryptocurrency Mine”, 2018 IEEE Electrical Power and Energy Conference (EPEC), Toronto, Canada, 10-11 Oct. 2018, https://doi.org/10.1109/EPEC.2018.8598358

[8] Y-D. Song and T. Aste, “The Cost of Bitcoin Mining Has Never Really Increased”, *Frontiers in Blockchain*, 22 October 2020, Vol. 3, Article 565497, https://doi.org/10.3389/fbloc.2020.565497

[9] S.L.N. Alonso, J. Jorge-Vázquez, M.Á.E. Fernández, and R.F.R. Forradellas, “Cryptocurrency Mining from an Economic and Environmental Perspective. Analysis of the Most and Least Sustainable Countries”, *Energies*, 2021 Vol. 14, Paper #4254, Open Access, https://doi.org/10.3390/en14144254

[10] U. Gallersdorfer, L. Klaasen, and C. Stoll, “Energy Consumption of Cryptocurrencies Beyond Bitcoin”, *Joule*, Vol. 4, pp. 1839–1851, 2020, https://doi.org/10.1016/j.joule.2020.07.013

[11] I. Bitir-Istrate, C. Gheorghiu, and M. Gheorghiu, “The transition towards an environmental sustainability for Cryptocurrency mining”, E3S Web of Conferences, Vol. 294, 2021 6th Int. Conf. on Sustain. and Renewable Energy Eng., https://doi.org/10.1051/e3sconf/202129403004

[12] ***, “Qualistar+ C.A 8332”, Chauvin Arnoux, Datasheet, http://qualistar.chauvin-arnoux.com/en

 ISBN 978-86-7466-930-3

# Prediction of voltage dips characteristics in IEEE 13-bus test grid using harmonic footprint

Aleksandar M. Stanisavljević, *Member, IEEE,* and Vladimir A. Katić, *Senior Member, IEEE*

***Abstract*—In this paper, the method of harmonic footprint (HF), as a significant feature of voltage dip is applied for a dip characterization. The dips are generated using an internationally verified test grid, the IEEE 13-bus test grid. First, the method of the HF is presented and described. Then, the IEEE 13-bus test grid modified by adding the distributed generators (wind or solar power) is described. Faults were simulated in the test network, and the values of the HF parameters were determined. The results were used for the voltage dips characteristics prediction. The results of simulation and prediction were compared and the mutual deviation (error) was determined. It is shown that the HF can be used for the early voltage dips characteristic prediction and further applied for training a deep-learning algorithm. Some limitations have been observed and their mitigation will be a topic of future research.**

***Index Terms*—Electric power quality, Voltage Dips, Harmonic footprint, Test grids**

## I. Introduction

In recent years, power quality issues have become more relevant, and significant attention had been paid to the related topics. In addition to the quality of delivery, the quality of delivered electrical energy is also important, which is often recognized as the quality of voltage. Voltage dips or sags are a consequence of disturbances in the operation of the power system and may have serious negative effects on industrial loads and connected distributed generation (DG) [1]. Particularly inconvenient are outages of industrial plants or the shutdown of small power plants in the distribution network, which can have major financial consequences. For these reasons, great research efforts are focused on the rapid detection and successful characterization of voltage dips [2, 3] and techniques of its compensation [4].

One of the successful methods for the dip's characterization is the application of harmonic footprint [5]. It provides the possibility for early characterization of a voltage dip so that in the first phase of fault its characteristics can be predicted with high probability [5, 6, 7]. For the sake of more accurate categorization and faster response, it is convenient to apply some of the methods of artificial intelligence, i.e., machine learning or deep learning [8, 9]. However, the main problem is the training, i.e., providing a huge number of adequate and different cases of voltage dips. Voltage dips occurrence in real grids is relatively rare, so long-term measurements are needed, which is costly and requires specialized equipment. Therefore, the use of synthetic dips based on mathematical calculations or simulated ones, based on the response from the grid simulation model are possible solutions.

This paper aims to test the application of the harmonic footprint method for the prediction of the voltage dip characteristics and to discuss such an approach for training a deep learning algorithm. The testing is based on recognizable and internationally verified references or test grids [10]. First, the method of harmonic imprinting is presented and described. Then, the IEEE 13-bus test grid is described, which is modified by additional distributed generators (wind and solar power plants). Faults were simulated in the test grid, and the values of the harmonic footprint parameters were determined for the various types of voltage dips thus obtained. The results of modeling and prediction of the voltage dips characteristics were compared and the mutual deviation (error) was determined.

## II. Harmonic Footprint

It is generally known that voltage dips are a consequence of faults in the network, high-power motor drive starting, or power transformer energizing [1]. During these events, a sudden rise of current may be observed, which distorts the voltage waveform all over a huge area of the grid. If the Fourier transformation is performed, the second and several other low-order harmonics may be noticed [1, 5]. If they are traced as a group, which consists of the 2nd, the 3rd, then 5th, and the 7th harmonics, and monitored throughout a voltage dip, a specific waveform may be observed [5]. It was named harmonic footprint (HF) [5]. Its mathematical representation is:

$$HF = \frac{\sqrt{\sum_{n=2,3,5,7} U_n^2}}{U_1^2} \cdot 100 \quad [\%] \tag{1}$$

where $n$ is harmonic order, and $U_n$ is r.m.s. value of the *n-th* harmonic.

The harmonic footprint is an important feature of a voltage dip. It appears at each voltage dip transition state, i.e., at the start of the dip and its end. Additionally, the HF may be recorded if the dip progresses from single-ground one to two-phase to ground or if some other voltage transition occurs. It

Aleksandar M. Stanisavljević with the University of Novi Sad, Faculty of Technical Sciences, Trg Dositeja Obradovića 6, 21000 Novi Sad, Serbia (e-mail: acas@uns.ac.rs).

Vladimir A. Katić is with the University of Novi Sad, Faculty of Technical Sciences, Trg Dositeja Obradovića 6, 21000 Novi Sad, Serbia (e-mail: katav@uns.ac.rs).

 ISBN 978-86-7466-930-3

can be obtained in a few milliseconds, so the HF method represents one of the fastest tools [11].

The main parameters of an HF are its initialization (start-up), maximum value (MHF), and width (wHF). They may be used for voltage dip detection (start-up moment) and prediction of voltage dip magnitude (depth), and duration, i.e., for fast and accurate characterization [5, 6, 7]. The HF and its parameters are presented graphically in Fig.1.

The HF method was tested with voltage dips recorded in various real distribution grids, and the configurations of the different distribution grids did not significantly affect the accuracy of the algorithm [5, 6, 7]. Furthermore, it can be noted that stochastic quantities, like fault resistance and fault inception angle, have some influences on the HF, but their effects are combined with the distance from the fault (line impedance between the fault location and voltage dip recording point). Generally, the total impedance has an inversely proportional effect, i.e., if it is higher, the HF is usually of a smaller value. The fault inception angle does not influence the precision of the method, as it is tested with real faults, which had different fault inception angles.

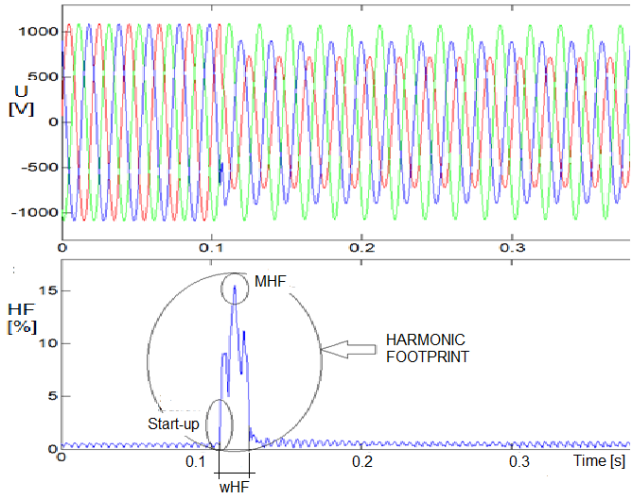


Fig.1.Harmonic footprint characteristics

## III. MODIFIED IEEE 13-BUS TEST GRID

There are several different test grids available for the simulations of voltage disturbances in a grid [10]. In this paper, the IEEE 13-bus test grid will be used. It represents a sample of the North American distribution grid consisting of three-phase lines, with two-phase and single-phase ones close to the ends of feeder laterals (load side). The supply voltage is 155 kV, while the distribution voltage is 4.16 kV. The grid is loaded with constant current, constant impedance, and constant power consumers, so that the total load is 3.466 MW. Unity power factor is assumed.

The test grid was modified with the addition of DGs, to make a better representation of a modern distribution grid. The optimal DG size is 2.5 MW connected at bus #633 [12], but in this paper, it will not be concentrated. A 2 MW wind plant was added at bus #633, and a 0.5 MW solar PV system at bus #652. The wind plant consists of four wind generators of 0.5 MW each interconnected with the grid via a power transformer and a one-kilometer-long power line. The solar PV plant is an on-grid solar PV system of 0.5 MW connected to the grid at bus #652 via a power transformer, which is further connected to the mainline at bus #648 via a 2 km line. These plants are dispatchable, but also comply with low-voltage ride-through (LVRT) requirements [13]. Therefore, they can support the grid during the duration of a voltage dip.

The IEEE 13-bus test grid is available as the Matlab/Simulink simulation model in [14]. Its modification is also done in Matlab/Simulink and its one-line diagram is presented in Fig.2.

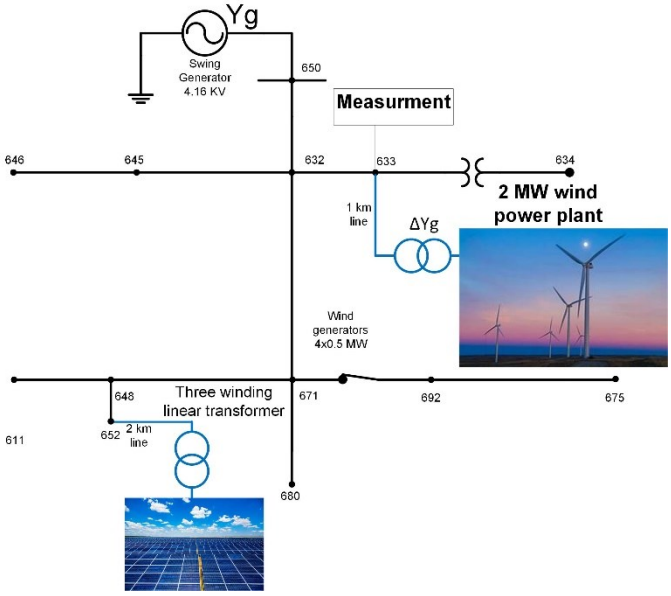


Fig.2. Modified IEEE 13-bus test grid with added DGs

## IV. VOLTAGE DIPS SIMULATIONS

The simulated voltage dips are the result of hypothetical faults in the test grid. The faults are generated at buses #692, #633, and #671 with a rated voltage of 4.16 kV. Different faults are simulated: single-phase to the ground (line-to-ground), two-phase faults (line-to-line), and a three-phase to the ground.

The voltage dips are measured (recorded) at bus #633. Two main features are monitored, the magnitude of voltage dip (MoVD) and duration.

The magnitude of a voltage dip represents the voltage during the dip as a percentage of the rated voltage, i.e., it is defined as:

$$MoVD = \frac{U_{rem.}}{U_r} \cdot 100 \ [\%] \qquad (2)$$

where $U_{rem}$ is the remaining voltage during the voltage dip at the observing bus and $U_r$ is the rated voltage.

The duration of a voltage dip is defined as a period when the voltage at the observing bus is lower than $0.9U_r$.


ISBN 978-86-7466-930-3

Fig. 3 shows an example of the single-phase (line-to-ground) voltage dip recorded at bus #633. The fault occurred on line 1 (L1, the blue line) at bus #671. As the result, the voltage at observing bus #633 suddenly decreases from the rated to 5% of the rated, i.e., the MoVD=5%. The voltages of the other two lines (L2, the red one, and L3, the green one) experience voltage swells, i.e., increased by around 15%. The duration of the voltage dip was 0.16 seconds. After that, the fault was cleared and all voltages returned to the rated values. It can be easily observed that significant voltage distortion occurred during the voltage transient states, i.e., when a fault and corresponding voltage dip initiated (started) and when it ended. In these periods the HF appears, and it can be calculated and recorded.

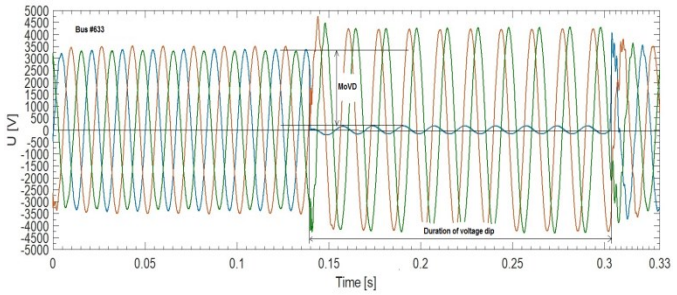


Fig. 3. Single-phase voltage dip recorded at bus #633.

Beside the single-phase to the ground (line-to-ground) fault and corresponding voltage dip presented in Fig. 3, six more cases of different faults were simulated. They are presented in Table I. It can be seen that three single-phase to the ground faults which occurred on the busses #692, #671, and #648 were simulated, together with the additional three phase-to-phase (line-to-line) faults on the same busses and one three-phase to the ground on bus #643. In total, seven faults were tested.

The recorded voltage dips on bus #633 were also summarized in Table I. It shows the main characteristics of the simulated voltage dips, their magnitude (given by MoVD), and their duration. It can be seen that for single-phase to the ground faults the MoVDs are very small, as well as for the three-phase to the ground fault, while in cases of phase-to-phase faults the MoVD values are around 50%.

## V. HARMONIC FOOTPRINT PARAMETERS DETERMINATION

The harmonic analysis of the tested voltage dips resulting in their harmonic footprint was performed. An example of the HF for the case of the voltage dip presented in Fig. 3 (fault No.2 in Table I) is shown in Fig. 4. It can be seen that there are two HFs, one at the beginning of the dip and the other at its end. For further analysis, the first one will be considered. Specific parameters of the harmonic footprint can be distinguished, its MHF and wHF. For the voltage dip characterization, the MHF is important. It can be seen that the MHF value in this case (single-phase to the ground fault) is 36%.

A similar analysis is done for all other recorded voltage dips cases. Due to limited space, the HF diagrams for the other cases will not be shown here. The results for the MHF are presented in Table I (column to the right). It can be seen that in the cases of the low MoVD values (deep voltage dips) the MHF values are above 30%, while for the higher MoVDs the MHF is lower.

TABLE I
SIMULATED VOLTAGE DIPS CHARACTERISTICS

| No. | Type of faults / Voltage dip characteristics | MoVD [%] | Duration [s] | MHF [%] |
|---|---|---|---|---|
| 1 | Single-phase to the ground at bus #692 | 7 | 0.18 | 37 |
| 2 | Single phase to ground at bus #671 | 5 | 0.16 | 36 |
| 3 | Single-phase to the ground at bus #648 | 8 | 0.20 | 35 |
| 4 | Phase A and B at bus #692 | 48 | 0.30 | 24 |
| 5 | Phase A and C at bus #671 | 49 | 0.33 | 25 |
| 6 | Phase C and B at bus #648 | 62 | 0.50 | 18 |
| 7 | Three-phase to ground at bus #643 | 9 | 0.80 | 32 |

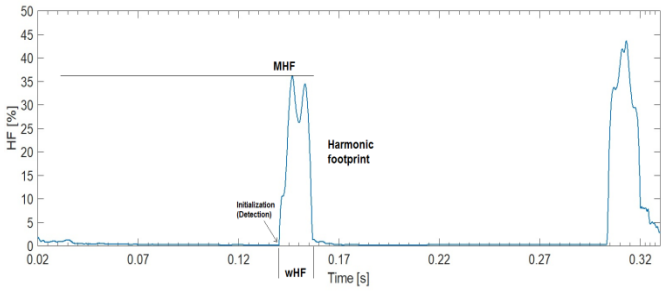


Fig. 4. The HF for the case of the single-phase voltage dip recorded at bus #633 for fault No. 2 in Table I

## VI. ESTIMATION OF THE VOLTAGE DIPS CHARACTERISTICS

The obtained HF parameters can be used for the early prediction of the voltage dip characteristics, its magnitude (MoVD), and its duration. These characteristics can be predicted using the maximum value of the HF (MHF) according to the expressions given in [6, 7].

The prediction function calculates voltage magnitude as a function of the maximum value of the HF:

$$MoVD^* = f(MHF) \tag{3}$$

where $MoVD^*$ is the predicted value of the voltage dip magnitude, and $MHF$ is a global maximum of the HF during the first transient stage. The voltage dip magnitude can be calculated using the following expression [6]:

$$\log_{10}(MoVD^*) = 1.913 + 0.00284 \cdot MHF + \\ + 0.000036 \cdot MHF^2 - 0.000024 \cdot MHF^3 \tag{4}$$

The results of the calculations are presented in Table II. For the generated faults (Table I) the values of the predicted MoVD* are presented in the second column of Table II. For comparison, the simulated (recorded) MoVD values are given


ISBN 978-86-7466-930-3

in the third column (repeated from Table I). It can be seen that predicted values are close to the actual (simulated) ones. The absolute errors of prediction are given in the third column of Table II. It can be seen that these errors are below 9 percent. The average absolute error of the prediction is 4.2%, while r.m.s. error is 5.12%. It can be concluded that the prediction can be successfully performed with an acceptable error of prediction.

For prediction of the voltage dip duration, the method presented in [7] is used. The method uses the *MHF* values to calculate the probability function *f(MHF)* [7]:

$$f(MHF) = (1 + e^{9.15 - 0.2320 MHF})^{-1} \quad (5)$$

The probability function determines the probability of the voltage dip duration being predicted as momentary or temporary. It is a sigmoid function, so two zones (momentary or temporary) can be distinguished easily. If the *f(MHF)* is less than 0.4, which corresponds to MHF<37.7% the voltage dip is momentary, i.e., less than 3 seconds. If the *f(MHF)* is above 0.6 (MHF>41.2%) then the voltage dip is temporary, i.e., longer than 3 s. In between is uncertainty or border zone, where both solutions are possible.

The probability function is calculated for the obtained MHF values and presented in Table III. It can be seen that for all observed cases of the voltage dips predicted duration was "momentary", i.e., less than 3 s, which is in accordance with the actual duration. Therefore, the prediction was true.

TABLE II
VOLTAGE DIPS MAGNITUDE PREDICTION AND PREDICTION ERROR

| Fault No. | Predicted MoVD* [%] | Simulated MoVD [%] | Absolute Error [%] |
|---|---|---|---|
| 1 | 7.11 | 7 | 0.11 |
| 2 | 8.75 | 5 | 3.75 |
| 3 | 10.65 | 8 | 2.65 |
| 4 | 46.79 | 48 | 1.21 |
| 5 | 42.81 | 49 | 6.19 |
| 6 | 68.52 | 62 | 6.52 |
| 7 | 17.96 | 9 | 8.96 |
| The average absolute error of prediction | | | 4.20 |
| Root mean squared error | | | 5.12 |

TABLE III
VOLTAGE DIPS DURATION PREDICTION AND PREDICTION ACCURACY

| Fault No. | Probability function *f(MHF)* | Predicted VD DURATION [S] | Simulated VD DURATION [s] | Prediction accuracy |
|---|---|---|---|---|
| 1 | 0.362 | Momentary (<3s) | 0.18 | TRUE |
| 2 | 0.311 | Momentary (<3s) | 0.16 | TRUE |
| 3 | 0.263 | Momentary (<3s) | 0.20 | TRUE |
| 4 | 0.027 | Momentary (<3s) | 0.30 | TRUE |
| 5 | 0.034 | Momentary (<3s) | 0.33 | TRUE |
| 6 | 0.001 | Momentary (<3s) | 0.50 | TRUE |
| 7 | 0.101 | Momentary (<3s) | 0.80 | TRUE |

## VII. DISCUSSION

The harmonic footprint presents a unique feature of a voltage dip, which may be used for the prediction of its characteristics. Moreover, it offers the possibility of dip detection and obtaining its early characterization. The presented results show that the simulated voltage dips have been analyzed adequately and that the predicted characteristics are true and acceptable regarding prediction error.

The predicted dip magnitudes correspond to the simulated ones with the r.m.s. error of 5.12%, which is acceptable in engineering practice. The predicted dip durations were true, but the prediction was limited to only two options – momentary (less than 3 s) and temporary (more than 3 s). Additional problem is that the HF is not able to predict the exact duration of voltage sag, so the whole period of voltage sag should be recorded. In that case, the two HFs should be calculated (at the beginning and the end of a voltage dip) and their detection times compared (see Fig.4). Other possible solutions will be sawn in future research.

The results also show that simulated voltage dips may be used for creating a database for the training of a deep learning algorithm. Available reference or test grids (IEEE or others) are adequate and suitable, so many different cases may be simulated.

Still, the number of simulated cases is limited, as for the deep-learning algorithm or any other machine learning one high number of input data is needed. One solution is to use the test grids with more buses (feeders) where there are more options to generate the faults and obtain voltage dips. There are other options and they will be the topic of future research.

## VIII. CONCLUSION

The voltage dips characterization is an important task for modern industrial or other loads, as well as for distributed generation and protection of the distribution network. The use of artificial intelligence and deep-learning algorithms for solving this task proved a good solution but require a huge database for the algorithm training process.

In previous papers, the authors have presented that the harmonic footprint, as a voltage dip feature, can be successfully implemented for the prediction of voltage dip characteristics. These results were based on the measurement results obtained in the real grid.

The result of this paper shows that simulation in the referenced test grids can be also used for that purpose. The harmonic footprint has been successfully applied for a voltage dip early characterization. It proves that such an approach can be also applied for the generation of an artificial (simulated) set of voltage dip cases (characteristics) and used for deep-learning algorithm training. Some limitations of this method have been observed, so future work will focus on their mitigation.

## ACKNOWLEDGMENT

This work was supported by the Republic of Serbia, Ministry of Education, Science, and Technological Development, through the Integrated and Interdisciplinary Research project entitled "Innovative Scientific and Artistic Research from the Faculty of Technical Sciences Activity

 ISBN 978-86-7466-930-3

Domain" under Grant No. 451-03-68/2022-14/200156.

## REFERENCES

[1] M.H.J. Bollen, *Understanding Power Quality Problems – Voltage Sags and Interruptions*, IEEE Press - Series on Power Engineering, New York, USA., 2000.

[2] P. Khetarpal and M.M. Tripathi, "A critical and comprehensive review on power quality disturbance detection and classification, "*Sustainable Computing: Informatics and Systems*, Vol.28, Paper #100417,2020.

[3] A.E.L. Rivas and T. Abrao, "Faults in smart grid systems: Monitoring, detection, and classification," *Electric Power Systems Research*, Vol.189, Paper #106602, pp.1-26, 2020.

[4] A.H. Soomro, A.S. Larik, M.A. Mahar, A.A. Sahito, A.M. Soomro, and G.S. Kaloi, "Dynamic Voltage Restorer - A comprehensive review", *Energy Reports*, Vol. 7, pp. 6786-68905, 2021.

[5] V.A. Katić and A.M. Stanisavljević, "Smart Detection of Voltage Dips Using Voltage Harmonics Footprint," *IEEE Trans. Ind. Applications,* vol. 54, no. 5, pp. 5331–5342, 2018.

[6] A.M. Stanisavljević and V.A. Katić, "Magnitude of Voltage Sags Prediction Based on the Harmonic Footprint for Application in DG Control System," *IEEE Trans. Ind. Electronics*, vol. 66, no. 11, pp.8902–8912, 2019.

[7] A.M. Stanisavljević, V.A. Katić, and S.Lj. Milićević, "A method for real-time prediction of the probability of voltage sag duration based on harmonic footprint," *IEEE Access*, Vol.10, pp.23757-23774, 2022.

[8] A.K. Ozcanli, F. Yaprakdal, and M. Baysal, "Deep learning methods and applications for electrical power systems: A comprehensive review," *Int. Journal of Energy Research*, Vol.44, pp.7136-7157, 2020.

[9] R. Turović, D. Dragan, G. Gojić, V.B. Petrović, D.B. Gajić, A.M. Stanisavljević, and V.A. Katić, "An End-to-end Deep Learning Method for Voltage Sag Classification," *Energies*, Vol.15, Paper #2898, pp.1-22, 2022.

[10] A.M. Stanisavljević, V.A. Katić, B.P. Dumnić, and B.P. Popadić, "A brief overview of the distribution test grids with a distributed generation inclusion case study," *Serbian Journal of Electrical Engineering*, Vol.15, No.1, pp.115-129, 2018.

[11] A. Usman and M.A. Choudhry, "An Efficient and High-Speed Disturbance Detection Algorithm Design with Emphasis on Operation of Static Transfer Switch," *Advances in Electrical and Computer Engineering*, Vol. 21, No. 2, pp.87-98, 2021.

[12] M. Shaaban and J.O. Petinrin, "Sizing and sitting of distributed generation in distribution systems for voltage improvement and loss reduction," *Intern. Journal of Smart Grid and Clean Energy*, Vol.2, No.3, pp.350-356, Oct. 2013.

[13] R. Hiremath and T. Moger, "Comprehensive review on low voltage ride-through capability of wind turbine generators," *Int. Trans. on Electrical Energy Systems*, Vol.30, Paper #e12524, pp.1-26, 2020.

[14] https://www.mathworks.com/help/physmod/sps/ug/ieee-13-node-test-feeder.html;jsessionid=0abf70e84f19a1618f96de0a91e3

 ISBN 978-86-7466-930-3

# Optimal Power Dispatch in Distribution Networks with PV Generation and Battery Storage

Jordan Radosavljević, Miloš Milovanović, Nebojša Arsić, Andrijana Jovanović, Bojan Perović and Jovan Vukašinović

***Abstract*—Numerous researchers in the last two decades have intensively dealt with various aspects of the integration of renewable energy sources (RES) into distribution networks (DNs). It has been shown that optimal planning and operation of RES can achieve positive effects, both in terms of technical performance of the system, and from the environmental and economic aspects. However, the uncontrollability and stochastic nature of wind speed and solar irradiance as the primary sources of RES remained their main shortcomings. The energy crisis that has been present lately imposes the need for much more flexible use of RES. This means finding technically efficient and economically acceptable solutions for energy storage, in order to fully exploit the potential of RES integrated into the system. This paper deals with the issues of the optimal operation and management of rechargeable batteries for energy storage in DNs with PV generation.**

***Index Terms*—Distribution networks, Renewable energy sources, Battery energy storage, Optimal power flow**

## I. INTRODUCTION

In the last twenty years, we have witnessed the expansion of renewable energy sources (RES), primarily wind and solar photovoltaic (PV) power plants. The development and application of these technologies have several causes. First of all, it is the constant growth of the electricity consumption and need for new generation capacities. Another, no less important cause, is the ultimative request to limit the use thermal power plants in order to reduce global warming due to $CO_2$ emissions. In addition, the deregulation and liberalization of electricity market and preferential prices for green energy have contributed rapid growth of RES in the last two decades [1].

Jordan Radosavljević is with the Faculty of Technical Sciences, University of Priština in Kosovska Mitrovica, 7 Knjaza Miloša, 38220 Kosovska Mitrovica, Serbia (e-mail: jordan.radosavljevic@pr.ac.rs).

Miloš Milovanović is with the Faculty of Technical Sciences, University of Priština in Kosovska Mitrovica, 7 Knjaza Miloša, 38220 Kosovska Mitrovica, Serbia (e-mail: milos.milovanovic@pr.ac.rs).

Nebojša Arsić is with the Faculty of Technical Sciences, University of Priština in Kosovska Mitrovica, 7 Knjaza Miloša, 38220 Kosovska Mitrovica, Serbia (e-mail: nebojsa.arsic@pr.ac.rs).

Andrijana Jovanović is with the Faculty of Technical Sciences, University of Priština in Kosovska Mitrovica, 7 Knjaza Miloša, 38220 Kosovska Mitrovica, Serbia (e-mail: andrijana.jovanovic@pr.ac.rs).

Bojan Perović is with the Faculty of Technical Sciences, University of Priština in Kosovska Mitrovica, 7 Knjaza Miloša, 38220 Kosovska Mitrovica, Serbia (e-mail: bojan.perovic@pr.ac.rs).

Jovan Vukašinović is with the Faculty of Technical Sciences, University of Priština in Kosovska Mitrovica, 7 Knjaza Miloša, 38220 Kosovska Mitrovica, Serbia (e-mail: jovan.vukasinovic@pr.ac.rs).

Wind and solar technology is becoming cheaper year by year [2], which makes it widely available. There are wind and solar power plants with installed capacity of several hundred MW connected to the transmission network. In addition, there has long been a trend of building smaller so-called distributed energy sources from several kW to several MW, which are integrated into distribution networks (DNs).

A large number of papers have been written on the topic of the distributed energy sources. Various aspects in their planning, operation and control have been explored. It has been shown that optimal planning and control can maximize their positive effects, such as reducing power losses, improving voltage profiles, increasing the supply reliability in DNs, reducing greenhouse gas emissions, etc. However, the uncontrollability and stochastic nature of wind speed and solar irradiance as primary sources of RES remained their main shortcomings.

The energy crisis that has been present recently, imposes the need for much more flexible use of RES. This means finding (using) technically efficient and economically acceptable solutions for energy storage, in order to fully use the potential of RES integrated into the DN.

There is no way to directly store active electricity. There are more or less developed technologies and solutions for indirect storage of the electricity, i.e. converting the electricity into another type of the energy that can be stored in a certain medium. The energy stored in this way is, when necessary, converted back into the electricity, which is injected into the transmission or distribution system.

At the level of DNs, the battery energy storage systems (BESS) are imposed as a solution. For their application in DNs with significant penetration level of RES, type WT and PV, it is necessary to solve two questions beforehand. The first one refers to the optimal planning of the BESS, which includes the choice of capacity, rated power and location in the DN. The second one is the optimal exploitation, i.e. determination of the BESS operation mode in a given period of time, usually 24 h. This implies defining the charging/discharging regime, i.e. the time schedule and the charging/discharging power of the BESS in accordance with the adopted function that it should perform in the DN. These functions can be [3-7]: (i) providing energy management and optimal power flow for reducing the cost for electricity, minimizing power losses, and improving the power quality, (ii) enable/facilitate the

 ISBN 978-86-7466-930-3

realization of smart grids, (iii) meeting peak electrical load demands, (iv) increasing the reliability of power supply. The mode of operation of the BESS is determined taking into account variable load, as well as the variable and stochastic power of RES (PV and WT).

In essence, this is a problem of optimal power dispatch in DNs. Given the specificity of the BESS, i.e. the limitation related to the state of charge (SoC), which directly affects the battery status in the next time segment (charging/discharging and power level), the problem of optimal power dispatch must be observed in a certain (given) time horizon, usually a period of 24 hours. Therefore, the problem of optimal power dispatch becomes a dynamic problem on a certain time horizon. The solution of this problem is performed by time segments (e.g. from 1 to 24 h), where the solution in a given segment ($t$) is conditioned by the solution obtained for the previous segment ($t$-1).

This paper presents a two-stage procedure for optimal dispatch of active and reactive power in DNs with PV sources and BESS. In the first stage, the optimal active power dispatch in DN is determined, based on the classical model of dynamic economic dispatch with neglected power losses. The aim is minimizing costs for electricity from the source (upstream) grid. After that, the problem of optimal reactive power dispatch in DN is solved to minimize energy losses and voltage deviation.

## II. Models of PV, Load and Battery Storage

### A. PV Model

The power generated by a PV unit is dependent on the solar irradiance. Beta PDF is suitable to modeling the stochastic nature of the solar irradiance. The solar irradiance measurements are made available with the sampling time of 1-10 min. Therefore, the mean and standard deviation of the solar irradiance can be calculated from measured data which correspond to the certain time interval $\tau$ (e.g. 1 h). Based on the mean and standard deviation of the solar irradiance, the shape parameters of Beta PDF can be calculated [8].

To realize Beta PDF in discrete form, the time interval $\tau$ is divided into $N_s$ states, where the corresponding solar irradiance and probability for each state ($g = 1 \div N_s$) can be calculated. The output power of PV is then estimated taking into account the probabilities of all solar irradiance states in the observed time interval, as explained in [8,9].

### B. Load Model

It is assumed that the load diagram is the same for active and reactive power. The load is assumed to be a random variable following the same normal PDF within each hour of a given daily load diagram.

To realize the normal PDF load function, the hour $t$ is divided into $N_L$ states, and the corresponding loads and probabilities for each state ($g = 1: N_L$) are calculated.

The level of the load in the certain time segment $t$ is determined based on the probability of all possible conditions within that hour [9].

### C. BESS Model

The BESS model is conditioned by a continuous change in the state of charge ($SoC$). This means that the value of the $SoC$ at a given time-hour ($t$) depends on its value in the previous time segment ($t$-$\Delta t$ or $t$-1). Mathematically, this can be expressed as follows [10]:

$$SoC(t) = SoC(t - \Delta t) + \Delta SoC\,, \tag{1}$$

$$\Delta SoC = \frac{P_{bat}(t-1)\cdot \Delta t}{C_B}\,, \tag{2}$$

where $C_B$ is the total capacity of the battery, $\Delta t$ is the time segment (1 h), and $P_{bat}$ is the power of the battery.

BESS mode means the time schedule and dynamics of charging/discharging of the battery during the considered time period (e.g. 24 h). The mode of the operation of the BESS in each time segment of the observed period is determined in accordance with the adopted function of the BESS in the DN. This can be, for example, minimizing the cost for electricity from the source grid, reducing peak loads, maximizing the use of the energy from RES to supply local loads in the DN, etc. The power of the BESS at time $t$ depends on the adopted battery mode operation. At the same time, the following limits must be met:

$$-P_{bat,n} \le P_{bat}(t) \le P_{bat,n}\,, \tag{3}$$

$$SoC^{\min} \le SoC(t) \le SoC^{\max}\,, \tag{4}$$

where $SoC^{\min}$ and $SoC^{\max}$ are the predefined minimum and maximum charge levels, respectively, and $P_{bat,n}$ is the rated power of the BESS.

## III. Optimal Active Power Dispatch

It seems that the minimization of the cost for electricity from the source grid is most appropriate function of BESS in the DN:

$$Cost = \sum_{t=1}^{24} P_g(t)\cdot C_{en}(t)\,, \tag{5}$$

where $P_g(t)$ is the active power from/to the source grid at the hour $t$, $C_{en}(t)$ is the electricity price in the hour $t$.

This means that during periods of the day when the electricity price is low, the BESS is used to store the energy from RES and the source grid, working in the charging mode. During periods of the day with a high price of the energy from the source grid, the BESS is used as an additional power source, i.e. it operates in the discharge mode. It is assumed that the electricity price from the source grid changes during the day according to a predetermined diagram, i.e. the electricity price is known in each time segment (hour) of the considered time period.

It is clear that in the charging mode BESS behaves as a

 ISBN 978-86-7466-930-3

load, and that according to the adopted reference directions the battery power is positive, and in the discharge mode BESS acts as a generator in the DN and the power $P_{bat}$ is negative. In order to define the terms "high price" and "low price", it is assumed that the electricity price at a given time $t$ is high if it is higher than the mean price in the observed time period (day), and that the electricity price at the given time $t$ is small if it is less than the mean value of the electricity price in the considered period.

In order to define the charging/discharging power of the BESS, i.e. to define the value of $P_{bat}(t)$, the principle was adopted is that the greater difference in the energy price at a given moment $t$, $C_{en}(t)$, in relation to the mean electricity price during the day, it is also the higher power of the battery $P_{bat}(t)$ in relation to the rated power of the battery $P_{bat,n}$. Therefore, the BESS mode at the time $t$ can be defined as follows:

$$P_{bat}(t)=\begin{cases} 0 & \text{if} \quad SoC(t)=SoC_{\max} \\ & \text{and} \quad SoC(t)=SoC_{\max} \\ a_f(t)\cdot P_{bat,n} & \text{if} \quad C_{en}(t)\le C_{en,sr} \\ & \text{and} \quad SoC_{\min}\le SoC(t)<SoC_{\max} \\ 0 & \text{if} \quad C_{en}(t)>C_{en,sr} \\ & \text{and} \quad SoC(t)=SoC_{\min} \\ -a_f(t)\cdot P_{bat,n} & \text{if} \quad C_{en}(t)>C_{en,sr} \\ & \text{and} \quad SoC_{\min}<SoC(t)\le SoC_{\max} \end{cases} \tag{6}$$

where the coefficient $a_f$ shows the difference in the electricity price at the time $t$ from the mean value during the observed day:

$$a_f(t)=\frac{\left|C_{en}(t)-C_{en,mean}\right|}{C_{en,\max}}, \tag{7}$$

$C_{en,mean}$ and $C_{en,\max}$ are mean and maximum electricity price during the day, respectively.

The constraint related to the power balance in the DN for each time interval $t$, without considering power losses, can be expressed as folows:

$$P_g(t)=P_{load}(t)-P_{PV}(t)+P_{bat}(t), \tag{8}$$

where $P_{load}(t)$ is the total power of loads in the DN at the hour $t$, $P_{PV}(t)$ is the total power generation of PV sources at the hour $t$, while $P_{bat}(t)$ is the power of the BESS at the hour $t$ determined according to (6).

The DN operating conditions are defined through the predicted daily load curve and PV source generation profile. In this model, the power losses in the DN are not taken into account, nor the cost of the BESS operation, and the cost of the PV generation.

## IV. Optimal Distribution of Reactive Powers

PV sources and BESS are connected to the DN through three-phase inverters. Inverters have the ability to control the reactive power. Assuming that the rated power of the corresponding inverter is slightly higher (e.g. 10%) than the rated power of the PV source and BESS, it means that inverters can be used as an additional control resource in the DN. It is clear that the range of the reactive power is determined by the rated apparent power of the inverter and the active power that is transmitted through the inverter at a given moment. This can be expressed by the following relation [10]:

$$Q_{inv}^{\max}(t)=\pm\sqrt{S_{inv,n}^2-P_{PV}^2(t)}, \tag{9}$$

where $Q_{inv}^{\max}(t)$ is the maximum (minimum) reactive power of the inverter at the time $t$, $S_{inv,n}$ is the rated power of the inverter, and $P_{PV}(t)$ is the active power of the PV source at the time $t$. Equation (9) also applies to the BESS.

The optimal reactive power dispatch can be considered as a problem of determining the optimal values of the reactive powers of inverters with a certain objective function, such as minimizing power loss and/or voltage deviation in DN. Mathematically, this can be formulated as follows:

$$\min\ F(\mathbf{x},\mathbf{u}), \tag{10}$$

with constraints:

$$g(\mathbf{x},\mathbf{u})=0, \tag{11}$$

$$h(\mathbf{x},\mathbf{u})\le 0, \tag{12}$$

$$\mathbf{u}\in\mathbf{U}, \tag{13}$$

where $\mathbf{x}$ is the vector of dependent variables, $\mathbf{u}$ is the vector of control variables, and $F$ is the objective function.

The vector of dependent variables $\mathbf{x}$ consists of the slack bus power ($P_0$), load bus voltages ($V_L$), and line loadings ($S_l$). On the other hand, the vector of control variables $\mathbf{u}$ consists of the inverters reactive powers ($Q_{inv}$), and slack bus voltage ($V_0$). The equality constraints (11) are the typical nonlinear power flow equations. Inequality constraints (12) are the functional operating constraints, such as: slack bus active power limits, load bus voltage limits, and branch flow limits. Constraints (13) define the feasibility region of the problem control variables, i.e. inverter reactive power limits, and slack bus voltage limits.

It is worth mentioning that the control variables are self-constrained. The inequality constraints of dependent variables are incorporated in the objective function (10) as quadratic penalty terms [11].

To solve this nonlinear optimization problem with constraints, a large number of classical and metaheuristic methods are available. In this paper, the hybrid metaheuristic method PSOS-CGSA was applied [12].

 ISBN 978-86-7466-930-3

## V. Simulation Results

The proposed procedure was applied to a modified IEEE 69-bus test system [13]. Modification of the original IEEE 69-bus system is reflected in the fact that in buses 16 and 61, according to the results in [1], are connected PV sources, as shown in Fig. 1. Both PV sources have the same rated power of 1.8 MW, and they are connected to the network through inverters whose apparent powers are 10% higher than the rated powers of the PV sources. In the bus 4 is connected a BESS, rated power of 2 MW, and capacity of 8 MWh. The apparent power of the BESS converter is also 10% higher than the rated power of the BESS.

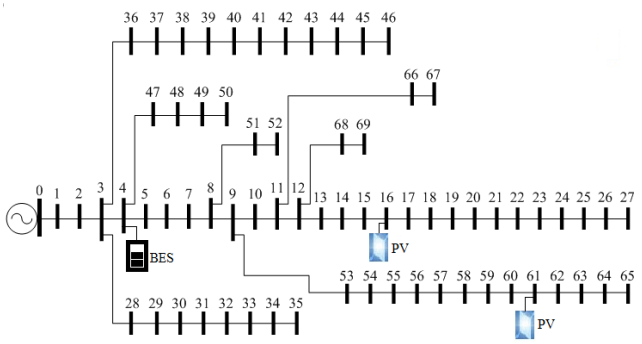


Fig. 1. Single-line diagram of the modified IEEE 69-bus test system.

It is assumed that all loads have the same daily load diagram, as shown in Fig. 2. The rated powers of loads are given in [13]. Also, it was adopted that the change of the solar irradiation is the same in the whole area of the DN, so that the powers of both PV sources change according to the same dynamics during the day, as in Fig. 2. The procedure for determining the optimal active power dispatch was carried out according to the algorithm described in Section III. The daily diagram of the change in the energy price from the source grid, expressed in p.u., is also shown in Fig. 2. The base energy price is 100 €/MWh [14]. It was adopted that $SoC_{min}$ is 30%, $SoC_{max}$ is 100%, and the initial state of charge is 30%.

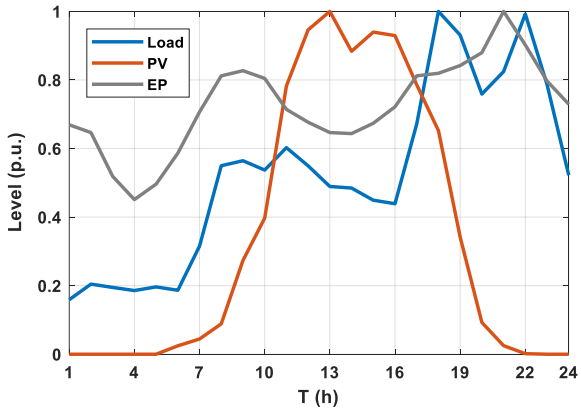


Fig. 2. Load, PV generation, and energy price (EP) profiles.

After determining the optimal active power dispatch, the procedure for determining the optimal reactive power dispatch was carried out for three types of the objective function, as follows:

- Case 1: Minimization of energy losses during the day
- Case 2: Minimization of load buses voltage deviation
- Case 3: Simultaneously minimization of energy losses and voltage deviation

It was adopted that the allowable voltage limits at load buses are from 0.95-1.05 p.u. The voltage magnitude at the slack bus is considered in the range 0.9 -1.1 p.u., whereas the reactive power limits of the inverters are changeable, according to (9).

### A. Optimal Active Power Dispatch

In order to compare the results, the base case was adopted when PV sources are connected to the DN but there is no the BESS. Fig. 3 shows the costs for electricity from the source grid in the case when there is no the BESS and in the case when there is the BESS with the optimal active power dispatch obtained according to the algorithm described in Section III.

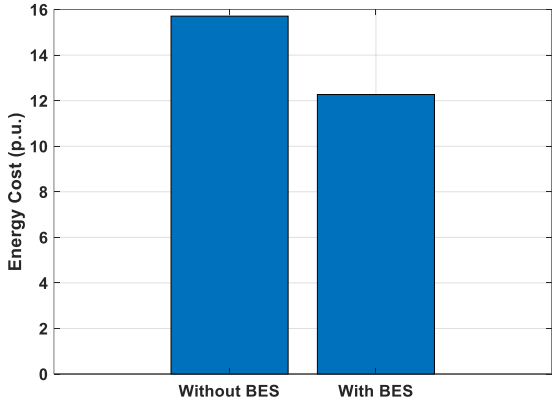


Fig. 3. Comparison of costs for energy purchased from the source grid.

As results of the optimal active power dispatch, daily diagrams of the active power and SoC of the BESS were obtained, as shown in Figs. 4 and 5, respectively.

Based on the results in Figure 3, it is clear that the integration of BESS and application of the proposed algorithm for optimal active power dispatch lead to a significant reduction in costs for electricity from the source grid. This conclusion is derived with the notation that the operating costs of the PV source and the BESS were not considered in this case.

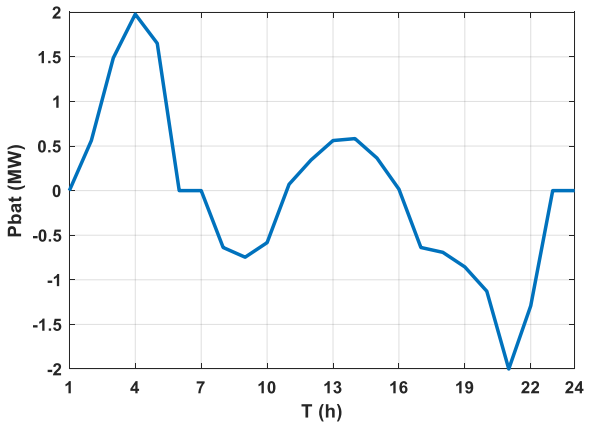


Fig. 4. The power change of the battery during the day.


ISBN 978-86-7466-930-3

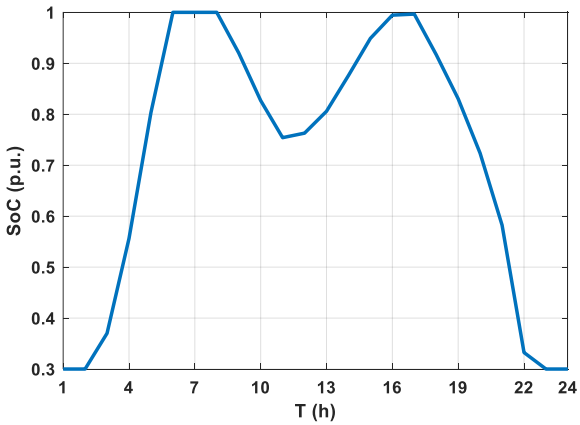


Fig. 5. The $S_OC$ change of the battery during the day.

### B. *Optimal Distribution of Reactive Powers*

The results of the optimal reactive power dispatch are given in Table I. The base case is taken when PV sources and BESS operate with unity power factor, and the slack bus voltage is equal to 1 p.u. The table shows the values of the active energy losses during the day ($W_{loss}$), the sum of voltage deviations at load buses during the day ($\Delta V_{pq}$) and the maximum values of voltage deviations during the day in the whole DN. It is obvious that the proposed approach for the optimal reactive power dispatch in Case 1 achieves a significant reduction in energy losses, and in Case 2 a reduction in voltage deviations in the network. As expected, a compromise solution was obtained in Case 3. The optimal values of the control variables for Case 1 and Case 3 are shown in Figs. 6 and 7, respectively.

TABLE I
RESULTS OF THE OPTIMAL DISTRIBUTION OF REACTIVE POWERS

| | Case | | | |
|---|---|---|---|---|
| | Base case | Case 1 | Case 2 | Case 3 |
| $W_{loss}$ (MWh) | 2.33 | 2.04 | 2.93 | 2.15 |
| sum($\Delta V_{pq}$) (p.u.) | 22.60 | 57.19 | 16.88 | 19.78 |
| max($\Delta V_{pq}$) (p.u.) | 0.09 | 0.05 | 0.05 | 0.05 |

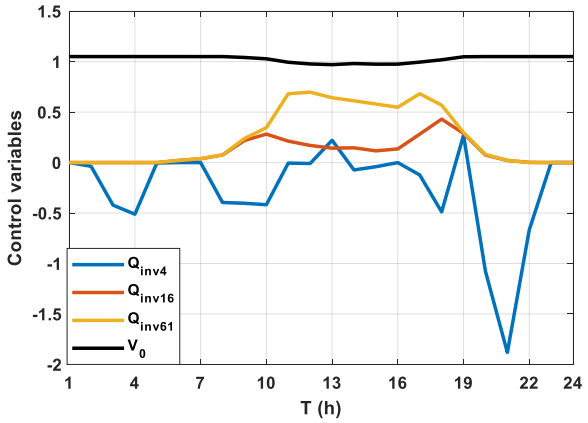


Fig. 6. Optimal values of control variables in Case 1.

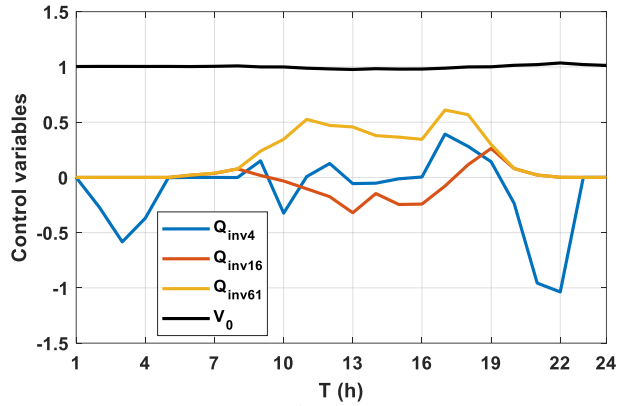


Fig. 7. Optimal values of control variables in Case 3.

The voltage profiles of the DN for the 24-hour period corresponding to the optimal active/reactive power dispatch for Cases 1-3 are shown in Figs. 8-10, respectively.

Based on these results, it can be seen a significant voltage deviation for Case 1 compared to the base case and Cases 2 and 3. This is a consequence of presenting loads with the constant power model; to minimizing the power losses in Case 1, control variables are optimized so that load voltages have higher values within the permissible limits to minimize branch currents, and thus power losses in the DN.

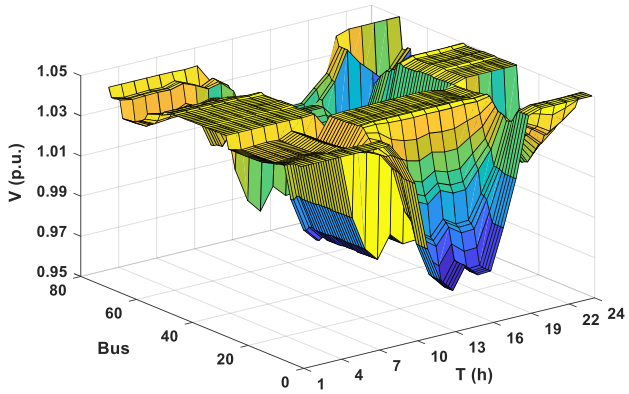


Fig. 8. Voltage profiles for Case 1.

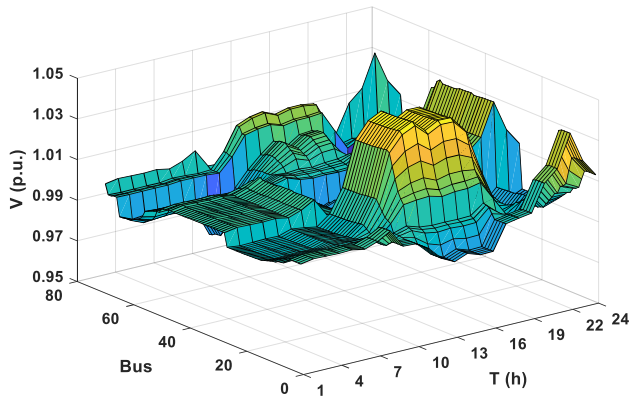


Fig. 9. Voltage profiles for Case 2.


ISBN 978-86-7466-930-3

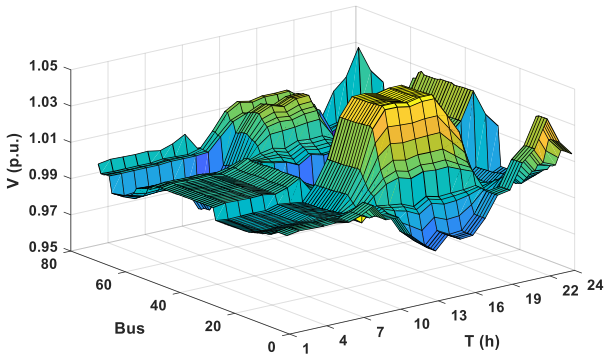


Fig. 10. Voltage profiles for Case 3.

## VI. CONCLUSION

In this paper, a two-stage active/reactive power dispatch approach for DNs with high penetration of PV generation and BESS has been considered. The proposed procedure has been tested on the IEEE 69-bus test system with two PV sources and one BESS. The simulation results lead to conclusions that can be summarized as follows:

- Integration of BESS and application of proposed algorithm for optimal active power dispatch lead to a significant reduction in costs for electricity from the source grid. In this particular case, the results showed that it is possible to achieve a reduction in the energy cost by about 22%, compared with the base case without BESS.
- It has been shown that PV and BESS inverters can serve as additional control resources for reactive power. By applying the proposed algorithm for optimal reactive power dispatch, a significant reduction in active power losses and voltage deviations in DNs can be achieved. Specifically, in comparison with the base case, the solutions obtained by the proposed algorithm provide a reduction in energy losses of 12.45% for Case 1, and a reduction in voltage deviations of 25.31% for Case 2.

## ACKNOWLEDGMENT

This work was supported by the Ministry of Education, Science and Technological Development of the Republic of Serbia under Grant TR 33046 and ERASMUS + project: “Knowledge triangle for a low carbon economy (KALCEA)”.

## REFERENCES

[1] J. Radosavljević, N. Arsić, M. Milovanović, A. Ktena, “Optimal placement and sizing of renewable distributed generation using hybrid metaheuristic algorithm,” *Journal of Modern Power Systems and Clean Energy*, vol. 8, no. 3, pp. 499-510, 2020

[2] IRENA, “Renewable Power Generation Costs in 2020,” International Renewable Energy Agency, Abu Dhabi, 2021

[3] X. Luo, J. Wang, M. Donner, J. Clarke, “Overview of current development in electrical energy storage technologies and application potential in power system operation”, *Applied Energy*, vol. 137, pp. 511-536, 2015

[4] C. Tang, J. Xu, Y. Sun, S. Liao, F. Zhang, L. Ma, “Stochastic battery energy storage scheduling considering cell degradation and distributed energy resources,” *International Transactions on Electrical Energy Systems*, vol. 29, no. 7, e12028, 2019

[5] K. Das, A. L. T. P. Grapperon, P. E. Sorensen, A. D. Hansen, “Optimal battery operation for revenue maximization of wind-storage hybrid power plant,” *Electric Power System Research*, vol. 188, pp. 106-631, 2020

[6] M. Ahmadi, O. B. Adewuyi, M. Sayed, S. M. S. Danish, P. Mandal, A. Yona, T. Senjyu, “Optimum coordination of centralized and distributed renewable power generation incorporating battery storage system into the electric distribution network,” *Electrical Power and Energy Systems*, vol. 125, pp. 106-458, 2021

[7] J. Radosavljević, “Voltage regulation in LV distribution networks with PV generation and battery storage,” *Journal of Electrical Engineering*, vol. 72, no. 6, pp. 356-365, 2021

[8] J. Radosavljević, N. Arsić, S. Štatkić, “Dynamic Economic Dispatch Considering WT and PV Generation using Hybrid PSOS-CGSA Algorithm”, 2021 20th International Symposium INFOTEH-JAHORINA (INFOTEH), East Sarajevo, Bosnia and Herzegovina, vol. no, pp. 1-6, 17-19 March, 2021

[9] Z. Ullah, S. Wang, J. Radosavljević, J. Lai, A Solution to the Optimal Power Flow Problem Considering WT and PV Generation, IEEE Access, Vol. 7, 2019., pp. 46763-46772.

[10] A. Ali, K. Mahmoud, D. Raisz, and M. Lehtonen, “Probabilistic approach for hosting high PV penetration in distribution systems via optial oversized inverter with watt-var functions,” *IEEE Systems Journal*, vol. 15, no. 3, pp. 684-693, 2021

[11] J. Radosavljević, M. Jevtić, M. Milovanović, “A solution to the ORPD problem and critical analysis of the results,” *Electrical Engineering*, vol. 100, no. 1, pp. 253-265, 2018

[12] Z. Ullah, M. R. Elkadeem, S. Wang, J. Radosavljević, “A Novel PSOS-CGSA Method for State Estimation in Unbalanced DG-integrated Distribution Systems,” *IEEE Access*, vol. 8, pp. 113219-113229, 2020

[13] N. Ranjan, B. Venkatesh, D. Das, “Voltage stability analysis of radial distribution networks,” *Electric Power Components and Systems*, vol. 23, no. 2, pp. 129-135, 2001

[14] M. Giuntoli, M. Subasic, S. Schmitt, “Control of distribution grids with storage using nested Benders’ decomposition,” *Electric Power Systems Research*, vol. 190, pp. 1-6, 2021

 ISBN 978-86-7466-930-3

# Modeling of High-Voltage Induction Machines with Fallen-out Magnetic Slot Wedges

Milica Banović, Kristina Vujkov, *Student Member, IEEE*, Mladen Terzić, *Member, IEEE*, Dejan Jerkan, *Member, IEEE*

***Abstract*— lectrical machines of medium to high voltage range are commonly fabricated with wide stator slot openings which often lead to the increase of noise, vibrations and power losses. The use of magnetic slot wedges is intended to minimize these effects.**

**posure to high magnetic and mechanical forces may cause magnetic wedge fall-outs. In this paper, a dynamical model of an induction machine was developed in order to investigate the influence of stator slot magnetic wedge failures on the machine's performance. Through observation of the machine's terminal quantity disturbances, the model demonstrated remar able differences in steady-state rated operation, regarding stator line currents, rotor loop currents and generated electromagnetic toque, in case of healthy and faulty machine.**

***Index Terms*—induction machine; magnetic slot wedges; finite element analysis; CCA; motor faults.**

## I. Introduction

Induction machines (IMs) designed for use in modern drives and industry must cope with ever-growing demands for increased efficiency and high performance. Furthermore, there are strong requirements for the reduction of noise pollution and vibrations which represent one of the most common issues in today's motor drives. For high and medium voltage IMs, it is reported that wide open stator slots are the main cause of those issues [1-3]. A well-known means to mitigate suggested problems in medium and high voltage motors is to install magnetic stator slot wedges.

Most magnetic slot wedges are made from iron powder (~ 75%), glass fabric and epoxy resin binders, and therefore, have larger relative permeability (less than 10) compared to epoxy edges [4]. Their higher relative permeability compared to classical non-magnetic wedges reduces the flux fluctuations on the rotor core surface and decreases the effective air gap width. The smoothened flux [6] in the air gap reduces the surface core losses, acoustic noise and improves the torque characteristics [4, 5]. Therefore, magnetic slot wedges also improve motor efficiency, power factor and power density.

Since the iron powder in the magnetic wedges makes them mechanically weakened, they are more prone to failures (fall-outs) caused by exposure to high magnetic and mechanical forces. There are many cases of wedge failures in medium (high) voltage motors (above 3.3 kV) reported, where up to 50% of the wedges were lost within 3 years of service [4].

Magnetic wedge fall-outs impact the machine's performance and are observable through the IM terminal quantity disturbances. Numerical modeling of this phenomenon may be used as a starting point for the evaluation of this type of fault and investigation of reliable fault indicators.

For this purpose, a dynamical model of an IM, based on Multiple Coupled Circuit Approach (MCCA) and Finite Element Analysis (FEA) analysis [7-9] is developed in Section II. FEA calculations of IM inductances for the healthy and faulty machine are illustrated and discussed in Section III and then used for MCCA model inductance matrices formation. MCCA model simulation results, presented in Section IV clearly demonstrate the influence of magnetic slot wedge fall-outs through unbalanced stator line currents, distorted rotor bar currents and increased torque pulsation. Conclusion of this paper with further research topics suggestions is given in Section V.

## II. Mathematical Representation of Mcca Model Of Squirrel-Cage Induction Motor

MCCA model of squirrel-cage IM is used to model energy conversion process in the machine, taking into account higher-order harmonic components in the magnetic field, induced voltages and currents. The nonsinusoidal electromagnetic field in the machine can be incorporated effectively by the rotor position-dependent variation of elements in MCCA model inductance matrices.

In this paper, the inductance matrix is reconstructed using series of linear 2-D FEA magneto-static simulations [7]. Discrete values of inductances obtained by this method are then represented via Fourier series, allowing the choice of harmonic components from the series which will be afterward used in the MCCA model.

The squirrel-cage rotor can be represented as identical and equally spaced rotor loops. Rotor loop consists of two neighboring rotors bars and adjacent end-ring segments. Fig. 1 shows three neighboring rotor loops (detail of rotor cage).

Milica Banović is with the School of Electrical Engineering, University of Belgrade, 73 Bulevar kralja Aleksandra, 11020 Belgrade, Serbia (e-mail: banovicmilicaa@gmail.com).

Kristina Vujkov is with the Faculty of Technical Sciences, University of Novi Sad, Trg Dositeja Obradovića 6, 21101 Novi Sad, Serbia (e-mail: kristina.vujkov@uns.ac.rs).

Dejan Jerkan is with the Faculty of Technical Sciences, University of Novi Sad, Trg Dositeja Obradovića 6, 21101 Novi Sad, Serbia (e-mail: dejan.jerkan@uns.ac.rs).

Mladen Terzić is with the School of Electrical Engineering, University of Belgrade, 73 Bulevar kralja Aleksandra, 11020 Belgrade, Serbia (e-mail: terzic@etf.bg.ac.rs).

 ISBN 978-86-7466-930-3

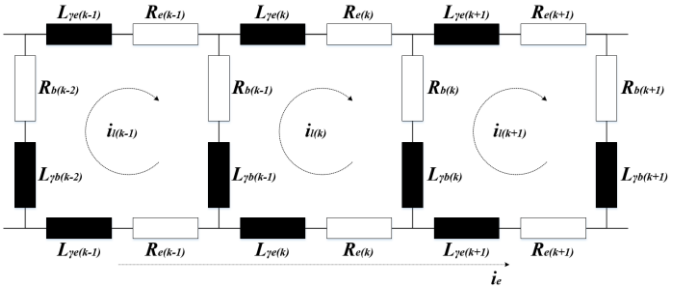


Fig. 1. Detail of squirrel-cage electrical circuit.

The mathematical model of the squirrel-cage IM can be formulated as:

$$\boldsymbol{V} = \boldsymbol{RI} + \frac{d}{dt}(\boldsymbol{LI}). \tag{1}$$

Voltage vector $\boldsymbol{V}$ consists of stator ($\boldsymbol{V_s}$) and rotor ($\boldsymbol{V_r}$) voltage vectors:

$$\begin{aligned} &\boldsymbol{V} = [\boldsymbol{V_s}\ \boldsymbol{V_r}]^T, \\ &\boldsymbol{V_s} = [v_a \quad v_b \quad v_c], \quad , \\ &\boldsymbol{V_r} = [0 \quad 0 \ldots 0 \quad 0]_{n_B+1.} \end{aligned} \tag{2}$$

where $v_a$, $v_b$, and $v_c$ are three stator voltages and $n_B$ is the number of rotor bars. There are $(n_B + 1)$ rotor voltages equal to zero for $(n_B + 1)$ independent current loops in the rotor cage which stand for $n_B$ rotor bars and two end rings. Likewise voltage vector $\boldsymbol{V}$, current vector $\boldsymbol{I}$ in (1) consists of stator ($\boldsymbol{I_s}$) and rotor ($\boldsymbol{I_r}$) current vectors:

$$\begin{aligned} &\boldsymbol{I} = [\boldsymbol{I_s}\ \boldsymbol{I_r}]^T, \\ &\boldsymbol{I_s} = [i_a \quad i_b \quad i_c], \quad . \\ &\boldsymbol{I_r} = [i_{l1} \quad i_{l2} \ldots i_{ln_B} \quad i_e]_{n_B+1,} \end{aligned} \tag{3}$$

where $\boldsymbol{I_s}$ is the stator current vector for three stator phase windings $i_a$, $i_b$, and $i_c$. Rotor current vector $\boldsymbol{I_r}$ includes $n_B$ rotor loops currents $i_{r1}$, $i_{l2}$, …, $i_{ln_B}$ and one end-ring current $i_e$.

Diagonal 3x3 stator resistance matrix $\boldsymbol{R_s}$ and rotor resistance symmetrical matrix $\boldsymbol{R_r}$ comprise resistance matrix $\boldsymbol{R}$ from (1):

$$\begin{aligned} &\boldsymbol{R} = \begin{bmatrix} \boldsymbol{R_s} & \\ & \boldsymbol{R_r} \end{bmatrix}, \\ &\boldsymbol{R_s} = \begin{bmatrix} R_s & & \\ & R_s & \\ & & R_s \end{bmatrix}, \\ &\boldsymbol{R_r} = \begin{bmatrix} R_{l1} & -R_{b2} & \ldots & -R_{bn_B} & -R_{e1} \\ -R_{b1} & R_{l2} & \ldots & 0 & -R_{e2} \\ \vdots & \vdots & \ldots & \vdots & \vdots \\ \vdots & \vdots & \ldots & \vdots & \vdots \\ 0 & 0 & \ldots & -R_{bn_B} & -R_{e(n_B-1)} \\ -R_{b1} & 0 & \ldots & R_{ln_B} & -R_{en_B} \\ -R_{e1} & -R_{e2} & \ldots & -R_{en_B} & \sum_{i=1}^{N_B} R_{ei} \end{bmatrix}_{(n_B+1)\mathrm{x}(n_B+1)} \end{aligned} \quad , \tag{4}$$

where $R_{lk}$ represents resistance of rotor $k$ loop, defined as $R_{lk} = R_{bk} + R_{b(k+1)} + 2R_{ek}$ with $R_{bk}$ as $k$ bar resistance and $R_{ek}$ end-ring $k$ segment resistance.

Interaction between neighboring rotor loops and end-ring segments shown in Fig. 1 are reflected in the resistance matrix $\boldsymbol{R_r}$. Voltage equation for arbitrarily $k$ rotor loop ($1 < k \leq N_B$) (Fig. 1) has the following form:

$$\begin{aligned} R_{ek} i_{rlk} + R_{bk}\left(i_{rlk} - i_{rl(k+1)}\right) + R_{ek}(i_{rlk} - i_e) - \\ R_{b(k-1)}\left(i_{rl(k-1)} - i_{rlk}\right) + \frac{d\Psi_{\mathrm{rlk}}}{dt} = 0, \end{aligned} \tag{5}$$

It can be noticed that negative elements in the matrix $\boldsymbol{R_r}$ (4) result from interactions between neighboring rotor loops and end ring.

Rotor bar current $i_{bk}$ can be expressed through neighboring rotor loop currents as follows:

$$i_{bk} = i_{lk} - i_{l(k+1)}. \tag{7}$$

Inductance matrix $\boldsymbol{L}$ is a periodic function of rotor angular position $\theta$, and it consists of four sub-matrices:

$$\boldsymbol{L}(\theta) = \begin{bmatrix} \boldsymbol{L_{ss}}(\theta) & \boldsymbol{L_{sr}}(\theta) \\ \boldsymbol{L_{rs}}(\theta) & \boldsymbol{L_{rr}}(\theta) \end{bmatrix}. \tag{8}$$

Stator inductance matrix $\boldsymbol{L_{ss}}$ is $\theta$-dependent 3x3 matrix which defines magnetic coupling between stator phases:

$$\boldsymbol{L_{ss}}(\theta) = \begin{bmatrix} L_a & M_{ab} & M_{ac} \\ M_{ba} & L_b & M_{bc} \\ M_{ca} & M_{cb} & L_c \end{bmatrix}. \tag{9}$$

Rotor inductance matrix $\boldsymbol{L_{rr}}$ is a $(n_B + 1)$x$(n_B + 1)$ position-varying matrix generated similarly to rotor resistance matrix with one major difference; any rotor loop is magnetically coupled with all the other loops and generally there are no zero elements in it:

$$\boldsymbol{L_{rr}}(\theta) = \begin{bmatrix} L_{l1} & \ldots & M_{r1n_B} - L_{bn_B} & -L_{\gamma e1} \\ M_{r21} - L_{b1} & \ldots & M_{r2n_B} & -L_{\gamma e2} \\ \vdots & \ldots & \vdots & \vdots \\ \vdots & \ldots & \vdots & \vdots \\ M_{r(n_B-1)1} & \ldots & M_{r(n_B-1)n_B} - L_{bn_B} & -L_{\gamma e(n_B-1)} \\ M_{rn_B1} - L_{b1} & \ldots & L_{ln_B} & -L_{en_B} \\ -L_{e1} & \ldots & -L_{en_B} & \sum_{i=1}^{n_B} L_{ei} \end{bmatrix}. \tag{10}$$

Rotor $k$ loop inductance $L_{lk}$ ($1 \leq k \leq n_B$) is defined as $L_{lk} = L_k + L_{\gamma bk} + L_{\gamma b(k+1)} + 2L_{\gamma ek}$, where $L_k$ is $k$ loop self-inductance, $L_{\gamma bk}$ is rotor $k$ bar leakage inductance, and $L_{\gamma ek}$ is rotor end-ring $k$ segment leakage inductance. Mutual inductances between arbitrary rotor loops $m$ and $n$ are labeled as $M_{rmn}$ ($1 \leq m, n \leq n_B \wedge m \neq n$).

Stator-rotor inductance matrix $\boldsymbol{L_{sr}}$ is defined as:


ISBN 978-86-7466-930-3

$$\boldsymbol{L_{sr}}(\theta) = \begin{bmatrix} M_{al1} & M_{al2} & \dots & M_{al_{n_B}} & 0 \\ M_{bl1} & M_{bl2} & \dots & M_{bl_{n_B}} & 0 \\ M_{cl1} & M_{cl2} & \dots & M_{cl_{n_B}} & 0 \end{bmatrix}, \quad (11)$$

Mutual inductance between arbitrarily stator phase $x$ and rotor loop $k$ is labeled as $M_{xlk}$, where $x \in \{a, b, c\}, 1 \leq k \leq n_B$. Rotor-stator inductance matrix $\boldsymbol{L_{rs}}$ can be derived from (11), by transposition of stator-rotor inductance matrix $\boldsymbol{L_{rs}} = \boldsymbol{L_{sr}^T}$.

The calculation of torque $T_e$ in the MCCA model is based on the virtual work principle ($p$ is pole pairs number):

$$T_e = \frac{1}{2} p \begin{bmatrix} \boldsymbol{I_s} \\ \boldsymbol{I_r} \end{bmatrix}^T \frac{d}{d\theta} \left( \begin{bmatrix} \boldsymbol{L_{ss}} & \boldsymbol{L_{sr}} \\ \boldsymbol{L_{rs}} & \boldsymbol{L_{rr}} \end{bmatrix} \right) \begin{bmatrix} \boldsymbol{I_s} \\ \boldsymbol{I_r} \end{bmatrix}. \quad (12)$$

## III. Inductance Calculation of Healthy and Faulty IM

After derivation of MCCA model in Section II, inductance calculation method shall be presented in the following. Modeled induction machine is a 2-pole, 6 kV high voltage motor with rated output power of 1.03 MW (detailed machine data are given in Appendix). Magnetic slot wedges of relative permeability 5 are used to close stator slot openings.

Linear magneto-static 2-D FEA simulations are used to compute discrete values of machine's inductances relative to absolute rotor angular position. Saturation effect is neglected. In the calculated inductance waveforms, only harmonics provoked by geometry variations and presence/absence of the magnetic wedges are investigated. These harmonics are independent from saturation-induced harmonics and can be treated separately.

In order to obtain self- and mutual inductances of an arbitrary winding for a fixed rotor position, only the winding itself is supplied with 1 A direct current. After single magneto-static simulation is completed, flux linkages of all windings in the machine are determined and used for single discrete value inductance calculation. Next magneto-static simulation is performed in the same manner after fixed-valued angle increment of rotor position. The value of angle increment determines the precision of inductances waveforms.

One full revolution of rotor is necessary for complete inductance matric reconstruction. Derived discrete waveforms are then represented with Fourier series coefficients in the MATLAB&Simulink model.

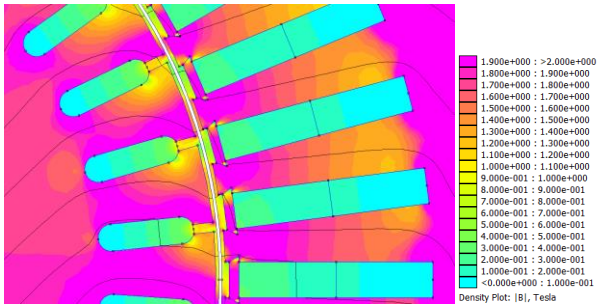


Fig. 2. Discrete magneto-static simulation of healthy IM

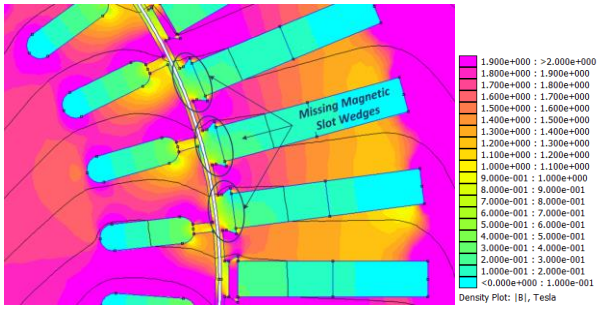


Fig. 3. Discrete magneto-static simulation of faulty IM (three consecutive fallen-out wedges)

Detail of magneto-static simulation for healthy and faulty IM is given in Fig. 2 and Fig. 3, respectively. The analyzed fault is modeled by three consecutive completely fallen-out wedges. As can be seen from the figures magnetic flux lines crossing the air gap from rotor to stator have significantly more homogeneous flow in the healthy motor compared to the one with missing wedges. Represented local distortion of flux lines will lead to deformation of machine inductances in case of fault occurrence.

Stator phase *A* self-inductance as a function of rotor angular position is shown in Fig. 4. Minor oscillations around the constant value of stator self-inductance are the result of air gap equivalent permeability variations caused by rotor slotting. Since analyzed IM has 36 rotor slots all three stator self-inductances have identical waveforms and their minor oscillations are in phase.

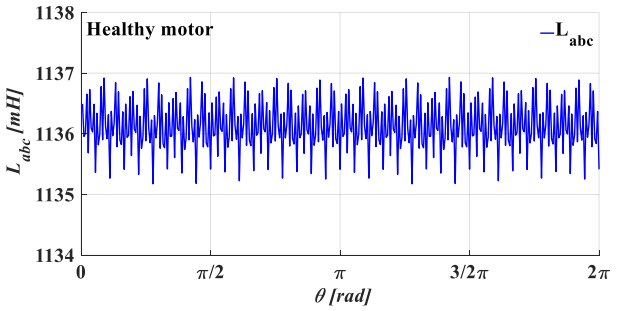


Fig. 4. Stator phase A self-inductance waveform – healthy motor

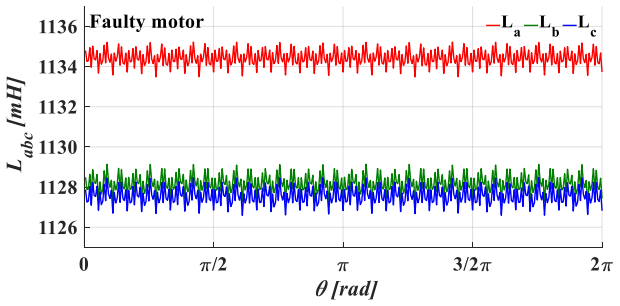


Fig. 5. Stator phases self-inductances waveform – faulty motor

In case of fallen-out wedges, the balance of stator


ISBN 978-86-7466-930-3

windings is corrupted. This leads to different mean values of stator self inductances for phase *A*, *B*, and *C*. Modeled missing wedges are in close vicinity of phase *B* and *C* winding axes. Lack of ferromagnetic material caused by fallen-out magnetic wedges decreases inductances of most affected windings - Fig. 5.

Similar phenomena can be observed in stator mutual inductance waveforms. All stator mutual inductances are identical in case of healthy motor (Fig. 6), while in the event of fault (Fig. 7), all mutual inductances suffer in mean value reduction. Mutual inductances involving phase *A* are less influenced by the fault, as expected.

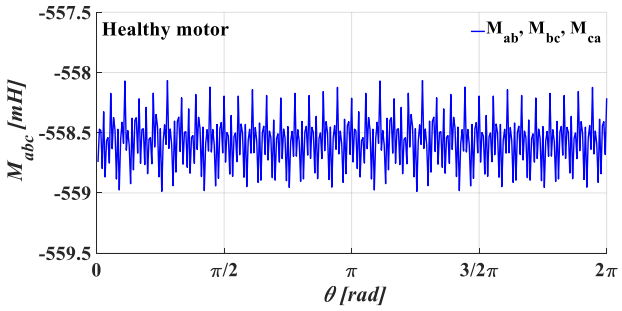


Fig. 6. Stator phases mutual inductances waveform – healthy motor

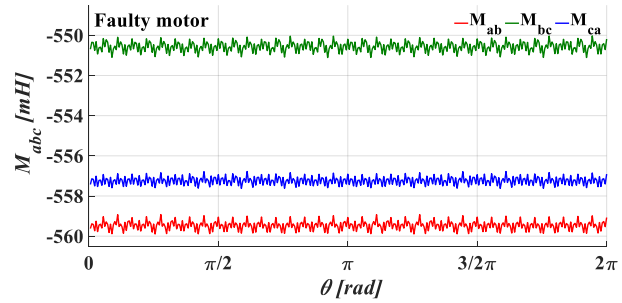


Fig. 7. Stator phases mutual inductances waveform – faulty motor

Stator-rotor inductances of IM are the main contributors to torque generation. For healthy motor, they are symmetrical, alternating, rotor angular position-dependent functions with characteristic trapezoidal shape (Fig. 8 – blue line). Therefore, spectrum of trapezoidal inductance signal contains only odd higher-order harmonics (Fig. 9 – blue bars). However, in the presence of slot wedge faults, a local dip in the waveform is formed each time specific rotor loop passes by stator slots with missing wedges (Fig. 8 – red line). As a result, new even harmonic components in the Fourier series appear (Fig. 9 – red bars). These additional components will further induce characteristic harmonics in flux linkages and consequently, in induced voltages and currents. This will affect torque production by causing unwanted pulsations.

The fallen-out magnetic slot wedges also have impact on rotor inductance matrix. Similar to stator inductances, rotor inductances in the healthy machine are fairly constant quantities with small oscillations around the mean value. These oscillations are the consequences of stator slotting. Slot wedges reduce these oscillations by making stator inner circumference more magnetically uniformed.

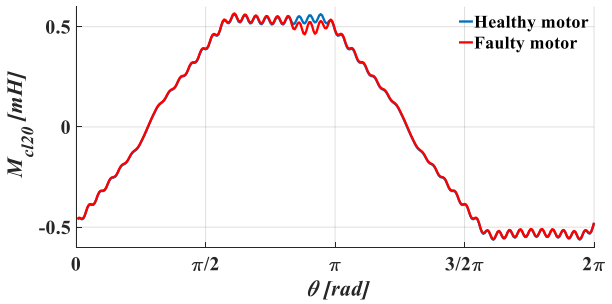


Fig. 8. Mutual inductance between stator phase C and rotor loop 20

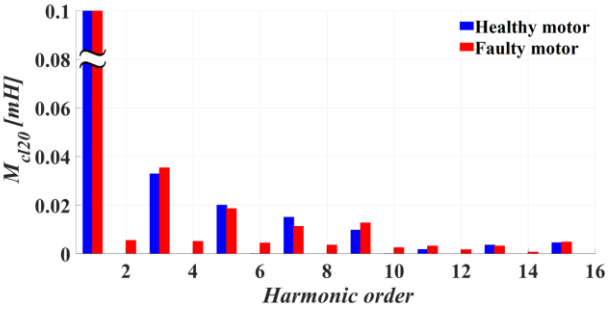


Fig. 9. Mutual inductance between stator phase C and rotor loop 20 - Fourier series coefficients

In Fig. 10 blue line illustrates rotor loop self-inductance waveform in healthy motor. There are exactly 48 oscillations in one rotor revolution due to the number of stator slots. When slot wedges are missing stator magnetic uniformity is lost which will locally diminish rotor self-inductance just as rotor loop passes by faulty slots. Since three neighboring slots are impacted by the fault, there will be three more prominent oscillations combined with lower mean value in the inductance waveform (Fig. 10 – red line).

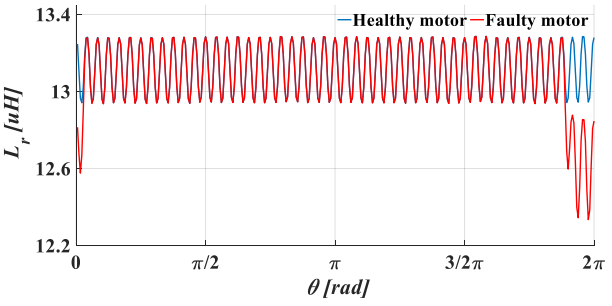


Fig. 10. Rotor loop self-inductance

A detail of rotor self-inductance spectrum, both for healthy and faulty motor, is shown in Fig. 11. In order to emphasize the emergence of additional spectral components, dominant mean value is excluded from the figure. Despite their small magnitudes, higher-order components have a significant impact on the energy conversion process which will be


ISBN 978-86-7466-930-3

illustrated and discussed in the next Section.

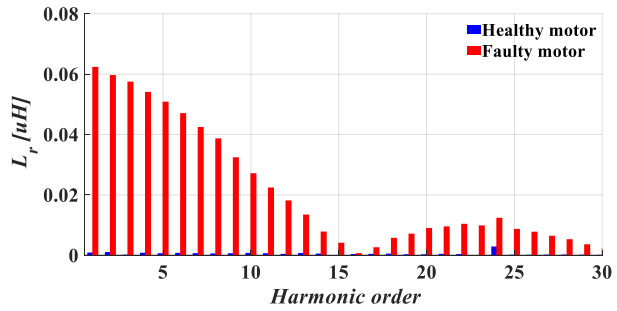


Fig. 11. Rotor loop self-inductance – spectrum with mean value excluded

As the last characteristic example of the magnetic wedge fall-outs impact on machine's inductances, mutual inductance between arbitrarily chosen rotor loops is shown in Fig. 11 (healthy machine in blue and faulty in red line). Magnetic coupling between two rotor loops subjects to complex mechanisms of flux lines formation and it is dependent on relative rotor position and the mutual position of the loops themselves. The situation grows even more puzzling when slot wedge fault is present, as observable in Fig. 11- red line.

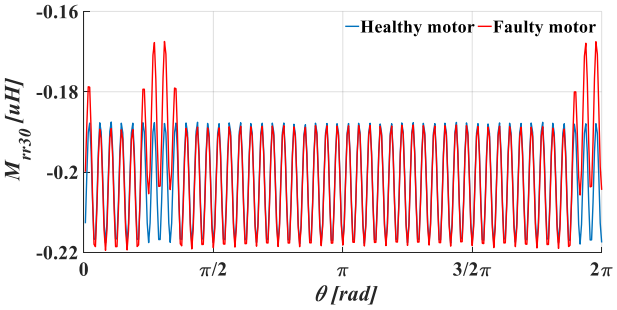


Fig. 12. Mutual inductance between first and 31st rotor loop

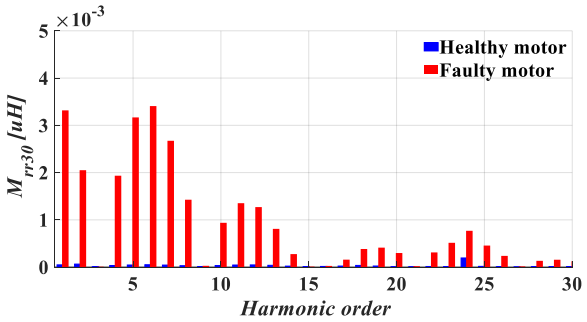


Fig. 13. Mutual inductance between first and 31st rotor loop – spectrum with mean value excluded

Singled out higher-order components of the mutual inductance between first and 31st rotor loop, shown in Fig. 13 are compliant with the expected increase in number and magnitude of additional components in the spectrum, similar to elaborated phenomena in Fig. 11.

## IV. Simulation Results

Based on FEA calculation of machine's inductances presented in Section III and MCCA model derived in Section II MATLAB&Simulink model of the machine under investigation (Appendix) was developed.

The output of FEA computations i.e. waveforms of machine inductances are firstly represented with Fourier series coefficients. These coefficients are then used for the formation of time and position varying inductance matrices of dynamic MCCA machine model. Inductances independent from geometry variations which cannot be calculated using 2-D representation of the machine: stator end-winding and rotor end-ring leakage inductances are added to the MCCA model inductance matrices as constant values. Their values are provided from separate simulations performed using commercial FEA software with such built-in options. MCCA model is able to simulate transient behavior of the machine under arbitrary supply and loading conditions, similar to conventional $dq$ models, but with much more insight into construction-dependent properties of the specific machine.

Stator line currents during steady-state operation under the rated load of healthy machine are illustrated in Fig. 14. The machine was supplied from three-phase balanced voltage source of 6 kV at rated frequency of 50 Hz. Rated speed of the machine was 2985 rpm, rated torque 3.23 kNm and rated output power 1.03 MW. As expected, line currents are balanced in the case of healthy machine.

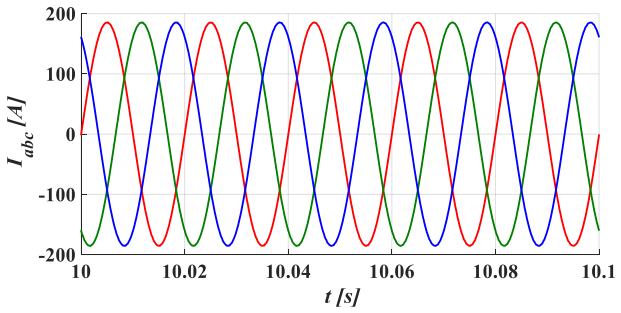


Fig. 14. Stator line currents under full load – healthy machine

Under the same supply and loading conditions, but with magnetic wedge fault present, unbalance in stator line currents is clearly visible in Fig. 15. Fallen-out magnetic wedges led to unbalanced inductances of stator phase windings (Fig. 5 and 7) which consequently caused noticeable imbalance in the currents as well.

Fig. 16 shows differences between arbitrary rotor loop current waveforms in case of the healthy and faulty machine. It is noticeable that, in the event of fault, rotor loop current waveform will contain more prominent oscillations which were expected as the result of emergence of additional components in the inductance spectrum of the faulty machine.


ISBN 978-86-7466-930-3

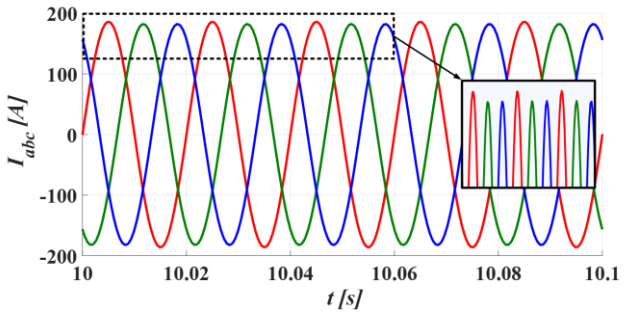


Fig. 15. Stator line currents under full load – faulty machine

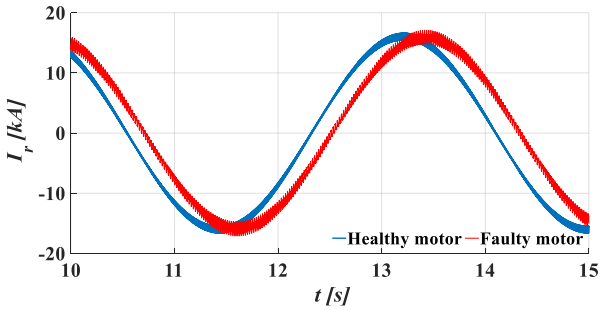


Fig. 16. Current waveform of arbitrary rotor loop under full load

Parasitic torque pulsations are direct outcome of increased oscillations in the machine inductances and currents. In the Fig. 17, the machine toque waveform is illustrated for rated operational mode with and without fault. Increased torque pulsations may provoke an unwanted mechanical response from the machine which could reflect on the level of noise and vibrations. Exceeding level of vibration can have great impact on bearing deterioration, may cause cracks in the winding insulation and tightness of the lamination stack.

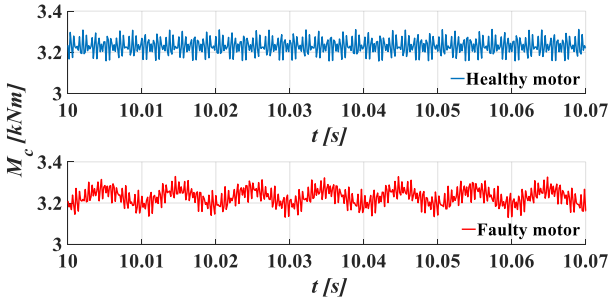


Fig. 17. Rated electromagnetic torque

## V. Conclusion

In this paper MCCA model of high voltage squirrel-cage induction machine is used to investigate the influence of stator slot magnetic wedge failures on machine's performance. Series of magneto-static FEA simulations illustrated differences in waveforms of characteristic inductances of the machine in case of healthy machine and the machine with three consecutive fallen-out stator magnetic wedges. FEA results provided input data for MCCA inductance matrices formation, using the Fourier series coefficient. Through observation of the machine's terminal quantity disturbances, performed simulations in MATLAB&Simulink dynamic MCCA model of IM demonstrated remarkable differences in steady-state rated operation, regarding stator line currents, rotor loop currents and generated electromagnetic toque. Further research may include targeted thorough analysis of the terminal quantities in the interest of reliable and non-invasive detection of fallen-out wedges.

## Appendix

TABLE I
Motor Parameters

| | |
|---|---|
| *ated Power* | *1.03 MW* |
| *ated Speed* | *2 5 rpm* |
| *ated Tor ue* | *3.23 kNm* |
| *ated oltage* | *k* |
| *Number of Stator Slots* | *4* |
| *Number of otor Slots* | *3* |
| *Stator Inner uter iameter* | *430 0 mm* |
| *Air Gap Width* | *4 mm* |
| *amination Stack ength* | *5 mm* |

## References

[1] G. Stojicic, M. Vasak, N. Peric, G. Joksimovic and T. M. Wolbank, "Detection of partially fallen-out magnetic slot wedges in inverter fed AC machines under various load conditions," 2012 IEEE Energy Conversion Congress and Exposition (ECCE), 2012, pp. 4015-4020.

[2] G. Stojičić et al., "A method to detect missing magnetic slot wedges in AC machines without disassembling," IECON 2011 - 37th Annual Conference of the IEEE Industrial Electronics Society, 2011, pp. 1698-1703.

[3] G. Stojicic, M. Vasak, N. Peric, G. Joksimovic and T. M. Wolbank, "Detection of partially fallen-out magnetic slot wedges in inverter fed AC machines under various load conditions," 2012 IEEE Energy Conversion Congress and Exposition (ECCE), 2012, pp. 4015-4020.

[4] K. W. Lee et al., "Detection of Stator-Slot Magnetic Wedge Failures for Induction Motors Without Disassembly," in IEEE Trans. on Industry Applications, vol. 50, no. 4, pp. 2410-2419, July-Aug. 2014.

[5] Shuping Wang, Zhengming Zhao, Liqiang Yuan and Buyao Wang, "Investigation and analysis of the influence of magnetic wedges on high voltage motors performance," 2008 IEEE Vehicle Power and Propulsion Conference, 2008, pp. 1-6.

[6] H. Mikami, K. Ide, K. Arai, M. Takahashi and K. Kajiwara, "Dynamic harmonic field analysis of a cage type induction motor when magnetic slot wedges are applied," in IEEE Trans. on Energy Conversion, vol. 12, no. 4, pp. 337-343, Dec. 1997.

[7] D. G. Jerkan, D. D. Reljić and D. P. Marčetić, "Broken Rotor Bar Fault Detection of IM Based on the Counter-Current Braking Method," in IEEE Trans. on Energy Conversion, vol. 32, no. 4, pp. 1356-1366, Dec. 2017.

[8] Xiaogang Luo, Yuefeng Liao, H. A. Toliyat, A. El-Antably and T. A. Lipo, "Multiple coupled circuit modeling of induction machines," in IEEE Trans. on Industry Applications, vol. 31, no. 2, pp. 311-318, March-April 1995.

[9] M. Ojaghi, M. Sabouri and J. Faiz, "Performance Analysis of Squirrel-Cage Induction Motors Under Broken Rotor Bar and Stator Inter-Turn Fault Conditions Using Analytical Modeling," in IEEE Trans. on Magnetics, vol. 54, no. 11, pp. 1-5, Nov. 2018, Art no. 8203705.

 ISBN 978-86-7466-930-3

# Time-domain Simulation of Electric Circuit with Nonlinear Hysteretic Inductor

Srđan Divac and Branko Koprivica

***Abstract*—The aim of this paper is to present a method for simulation of electric circuits with nonlinear inductor with hysteresis in time domain. The method is based on solving equation derived from Kirchhoff's law of the considered electric circuit through a series of successive iterations. Electric circuit consisting of AC voltage source connected in series with linear resistor, linear inductor and nonlinear inductor with hysteresis has been considered. Simulations have been performed for four cases of the considered electric circuit – without linear elements, with one and both linear elements, for sinusoidal voltage source amplitudes from 2 V to 10 V with the step of 2 V. Detailed simulation procedure, measurement and simulation results, as well as adequate discussion, have been presented.**

***Index Terms*—Simulation method, electric circuit, nonlinear inductor, magnetic hysteresis, time domain.**

## I. Introduction

SOLVING an electric circuit with nonlinear inductor with hysteresis is very challenging due to the appearance of higher harmonics in the electric current, due to distorted waveform of the magnetic field (strength) of considered inductor [1]. Methods used in power engineering are commonly obtained by substituting the inductor with an equivalent *RL* circuit (consisting of a single nonlinear inductor represented by magnetising curve in parallel with linear or nonlinear resistor to represent hysteresis power loss) and solving the circuit [2]. However, this method cannot accurately solve electric circuits in time domain. Better results in time domain can be obtained by varying the resistance and the inductance of the elements in time, as proposed by De Leon [3]. More complex solutions of the electric circuit implement the use of one of the hysteresis models to represent the inductor with hysteresis [4]. Some of the commonly used models are: Preisach [5], Jilles-Atherton [6], Neural Network based models [7] and others. This method gives better results in time domain but the mathematics behind the model itself can be quite complex and its parameters difficult to obtain.

Presented simulation method is based on solving equation derived from Kirchhoff's law for the considered electric circuit through series of successive iterations. Electric circuit consisting of AC voltage source connected in series with linear resistor, linear inductor and nonlinear inductor with hysteresis. Influence of the inductor with hysteresis has been accounted for by calculating circuit current from dynamic magnetic field waveform $H_{dyn}(t)$ of the inductor. Dynamic field $H_{dyn}(t)$ has been obtained by following the simulation method for dynamic hysteresis loops and rate-independent property of the quasistatic hysteresis loops [8, 9]. This has been done by considering three components of $H_{dyn}(t)$ - quasistatic field $H_{qs}(t)$, eddy current field $H_{eddy}(t)$ and excess field $H_{exc}(t)$ [10].

Measurements of the magnetic field waveform $H(t)$ and magnetic flux density waveform $B(t)$ have been made using the measurement method based on data acquisition with PC [1]. Waveforms have been measured at frequency of 1 Hz for amplitudes of sinusoidal $B(t)$ from 0.2 T to 1.6 T with measurement step of 0.2 T. Also, measurement has been made at frequency of 50 Hz for sinusoidal $B(t)$ with the amplitude of 1 T. This measurement has been used for calculation of phenomenological parameters of $H_{exc}(t)$ by fitting the calculated excess power loss to measured excess loss. Fitting has been performed using the criteria of least root mean square deviation (RMSD [11, 12]) between excess power loss.

Simulations have been made for four cases of the considered electric circuit - without linear elements, with one and both elements, for sinusoidal input voltage with amplitudes from 2 V to 10 V with the step of 2 V.

A description of the simulation procedure, presentation of measurement and simulation results, as well as adequate discussion have been given in the paper.

## II. Measurement Results

Measurements of magnetic field $H(t)$ and magnetic flux density $B(t)$ waveforms have been performed by using measurement method based on data acquisition and PC [1]. Measurements have been made with toroidal shaped sample made of electrical steel sheet 27PH100 (manufactured by POSCO). Parameters of used toroidal sample can be found in Table I. All measurements have been made with 1000 data points.

TABLE I
Parameters of the Toroidal Sample

| | | | |
|---|---|---|---|
| $N_1$ | 175 | $r_1$ [mm] | 45 |
| $N_2$ | 60 | $r_2$ [mm] | 52.5 |
| $l_c$ [m] | 0,306 | $m$ [kg] | 0.241 |
| $S$ [mm$^2$] | 102,80 | $w$ [mm] | 15 |

A set of quasistatic hysteresis loops has been measured at

Srđan Divac – Faculty of technical sciences Čačak, University of Kragujevac, Svetog Save 65, 32000 Čačak, Serbia, (e-mail: srdjan.divac@ftn.kg.ac.rs).

Branko Koprivica – Faculty of technical sciences Čačak, University of Kragujevac, Svetog Save 65, 32000 Čačak, Serbia, (e-mail: branko.koprivica@ftn.kg.ac.rs).

 ISBN 978-86-7466-930-3

frequency of 1 Hz for controlled sinusoidal shape of $B(t)$ (voltage induced at the secondary winding). Measurements have been made for $B(t)$ amplitudes ranging from 0.2 T to 1.6 T with step of 0.2 T. The obtained hysteresis loops are presented in Fig. 1. Also, $H(t)$ and $B$(t) have been measured at 50 Hz and 1 T to obtain a dynamic hysteresis loop needed for calculation of phenomenological parameters of $H_{exc}(t)$. This hysteresis loop is shown in Fig. 1 as dashed line.

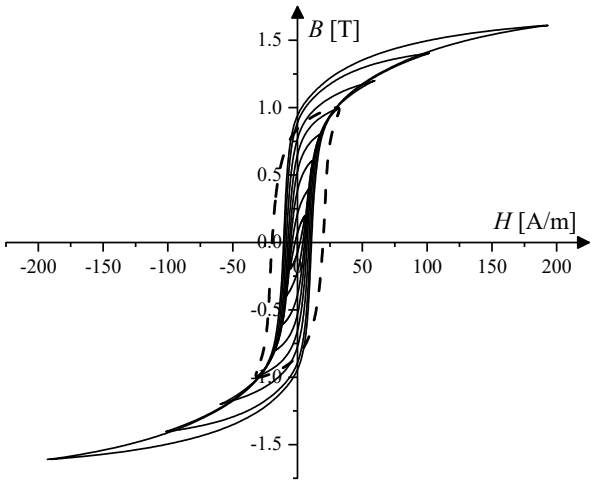


Fig. 1. Measured hysteresis loops for sinusoidal shape of $B(t)$.

## III. SIMULATION PROCEDURE

Considered electric circuit consisting of voltage source $u(t)$ in series with linear resistor $R$, linear inductor $L$ and nonlinear inductive element exhibiting hysteretic properties $L_h$ is presented in Fig. 2.

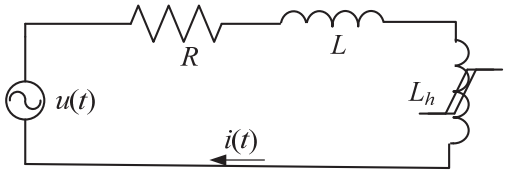


Fig. 2. Electric AC circuit with linear $R$ and $L$ elements and nonlinear $L_h$ element with hysteresis.

Solving of this circuit means the calculation of its electric current $i(t)$, which depends on elements $R$, $L$ and $L_h$ and their characteristics. Obtaining dynamic solution is complicated due to the nonlinear and hysteretic characteristic of $L_h$. Its characteristic is usually represented with the dynamic hysteresis loops (the dynamic magnetic field $H_{dyn}(t)$ and magnetic flux density $B(t)$).

### A. Calculation of dynamic magnetic field $H_{dyn}(t)$

Dynamic magnetic field $H_{dyn}(t)$ can be obtained by calculating its quasistatic $H_{qs}(t)$, eddy current $H_{eddy}(t)$ and excess $H_{exc}(t)$ components, and summing them up [10, 12]:

$$H_{dyn}(t) = H_{qs}(t) + H_{eddy}(t) + H_{exc}(t) \qquad (1)$$

Calculation of $H_{qs}(t)$ requires two steps. First, quasistatic field $H_{int}(t)$ needs to be calculated for sinusoidal $B(t)$, $B_{int}(t)$, with the amplitude $B_{max}$ of interest. So, $N$ harmonic components (amplitudes and phases) of measured quasistatic $H(t)$ need to be calculated at particular amplitudes of $B(t)$ for each measured quasistatic loop, Fig. 1. For new $B_{max}$ of interest, $N$ new harmonics of $H_{int}(t)$ can be calculated by linear or higher order polynomial interpolation of previously calculated harmonics [8]. Further, $H_{int}(t)$ and a new quasistatic hysteresis loop formed by $H_{int}(t)$ and sinusoidal $B_{int}(t)$ can be obtained. In the second step, a general solution for $H_{qs}(t)$ for non-sinusoidal $B(t)$, $B_{Lh}(t)$, with the amplitude of $B_{max}$, can be obtained by using inverted hysteresis loop $H_{int}(B_{int})$, which can be considered as rate-independent (having fixed shape) at the frequency of 1 Hz. The shape of that hysteresis loop is only determined by the amplitudes of $H(t)$ and $B(t)$ and not by the shape of their waveforms [9]. Thus, $H_{qs}(t)$ can be obtained by reconstructing data points for $B_{Lh}(t)$ over data points for $H_{int}(B_{int})$ [13]. This procedure is illustrated in Fig. 3.

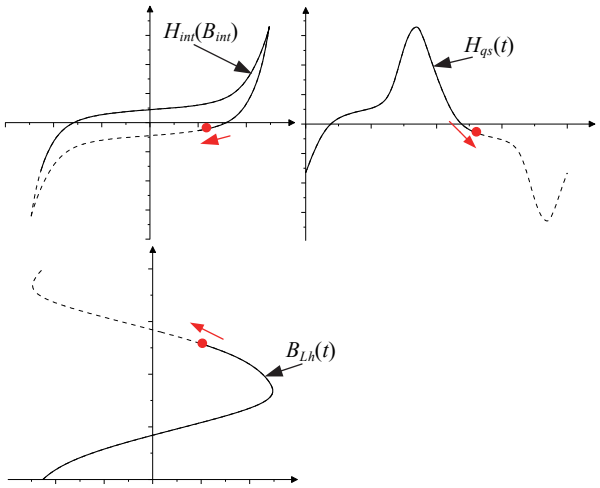


Fig. 3. Illustration of obtaining $H_{qs}(t)$ by reconstructing of non-sinusoidal $B_{Lh}(t)$ over the quasistatic hysteresis loop $H_{int}(B_{int})$.

Calculation errors may occur during this step due to the phase difference between $B_{Lh}(t)$ and $B_{int}$(t). This phase difference can be taken into account by delaying $B_{Lh}(t)$ for the period of $\Delta t$, $B_{Lh}(t+\Delta t)$, and proceed further with the calculations. Delaying period should be chosen so that the minimum and maximum values of $B_{Lh}(t+\Delta t)$ occur at the same time as for $B_{int}(t)$. Resulting $H_{qs}(t+\Delta t)$ should be delayed for the period of $-\Delta t$ to obtain $H_{qs}(t)$.

Waveform of $H_{eddy}(t)$ can be calculated from well-known analytical expression [10]:

$$H_{eddy}(t) = \frac{\sigma d^2}{12}\frac{\mathrm{d}B_{Lh}(t)}{\mathrm{d}t}, \qquad (2)$$

where σ is the conductivity of steel sheet and $d$ is its thickness.


ISBN 978-86-7466-930-3

Calculation of $H_{exc}(t)$ can be made using the following expression [10]:

$$H_{exc}(t)=\frac{n_0V_0}{2}\left(\sqrt{1+\frac{4\sigma GS}{{n_0}^2V_0}\frac{\mathrm{d}B_{Lh}(t)}{\mathrm{d}t}}-1\right), \quad (3)$$

where $G$ is equal to 0.1356 and $n_0$ and $V_0$ are phenomenological parameters of material.

Consideration of hysteresis loop measured at 1 Hz as rate-independent is not completely correct (accurate), as there would always exist some difference between such loop and true static loop due to the existence of the dynamic components of the field ($H_{eddy}(t)$ and $H_{exc}(t)$). Dynamic components at 1 Hz participate with several percent in the quasi-static field and power loss under sinusoidal and non-sinusoidal conditions [14]. However, these components are much smaller at 1 Hz than at 50 Hz, considered in the simulations. Accordingly, the accuracy of the simulation would not be significantly affected with such consideration (approximation).

It should be noted that all quantities measured and calculated (magnetic field and flux density) are averaged for the considered mean magnetic path length and cross-section area of the toroidal sample. Actually, these quantities vary with the radial distance from the sample longitudinal axis (over the radius). However, the variations are not too high when the outer to inner radius ratio ($r_2$/ $r_1$) is low, as in the case of used sample (see Table I). The results of the simulation relate to the sample as a whole, as a part of the considered electric circuit, neglecting inhomogeneity of the magnetic field, which is acceptable in most of the practical applications. Accordingly, expressions (2) and (3) do not depend on the toroid dimensions (radiuses $r_1$ and $r_2$ and width $w$).

### *B. Iterative procedure*

Proposed iterative algorithm for solving the circuit presented in Fig. 2 can be divided into the following steps:

1) calculating of the voltage at $L_h$ for ($i$+1)-th iteration, $u_{Lh,i+1}(t)$, using II Kirchhoff's law [15]:

$$u_{Lh,i+1}(t)=u(t)-Ri_i(t)-L\frac{\mathrm{d}i_i(t)}{\mathrm{d}t}, \quad (4)$$

where $i_i(t)$ is the current derived from $i$-th iteration, $t$ is the time, $R$ and $L$ are the resistance and inductance of the considered linear elements,

2) calculation of $B_{Lh,i+1}(t)$ from $u_{Lh,i+1}(t)$ using Faraday's law [15], as follows:

$$B_{Lh,i+1}(t)=\frac{1}{N_1S}\int_0^t u_{Lh,i+1}(t)\mathrm{d}t, \quad (5)$$

where $N_1$ is the number of turns in the magnetising coil and $S$ is the cross-section area of magnetic core of $L_h$,

3) calculation of $H_{dyn,i+1}(t)$ for non-sinusoidal $B_{Lh,i+1}(t)$ using the procedure explained in subsection A,

4) calculation of $i_{i+1}(t)$ using Ampere's law [15]:

$$i_{i+1}(t)=\frac{H_{dyn,i+1}(t)}{N_1}l_c, \quad (6)$$

where $l_c$ is the mean magnetising path length of $L_h$,

5) steps 1-4 should be repeated until condition (7) is met:

$$\frac{\max\{|i_i(t)|\}-\max\{|i_{i+1}(t)|\}}{\max\{|i_{i+1}(t)|\}}100\%<\varepsilon, \quad (7)$$

where ε is predetermined limit, which is not so rigorous.

Iterative procedure starts with $i_0(t)$=0 A for each time sample of $t$>0 and amplitude of $u(t)$ factorised by $K$>1 to minimise the oscilations and time shifts between iterations, such that:

$$U_{m,k}=\frac{U_m}{K}k, \quad (8)$$

where $k$=1, 2, 3,…, $K$. Solution of the $k$-th step is the new initial condition $i_k(t)$ for the ($k$+1)-th step. The value of $K$ should be chosen high enough to allow for good convergence of the iterative procedure, but low enough to keep required computation time acceptable.

After finishing the iterative procedure, obtained waveforms of $H_{dyn}(t)$ and $B_{Lh}(t)$ can be used to plot dynamic hysteresis loop of $L_h$. Also, the specific power loss of $L_h$ (corresponding to the area of the dynamic hysteresis loop), expressed in W/kg, can be calculated as:

$$P_s=\frac{1}{mT}\int_0^T u_{L_h}(t)i(t)\mathrm{d}t=\frac{Sl_c}{mT}\int_0^T\frac{\mathrm{d}B_{L_h}(t)}{\mathrm{d}t}H_{dyn}(t)\mathrm{d}t, \quad (9)$$

where $T$=1/$f$ is the period and $m$ is the mass.

## IV. SIMULATION RESULTS

Four cases of the electric circuit presented in Fig. 2 have been considered:

I. with $R$=0 Ω and $L$=0 H;
II. with $R$=48 Ω and $L$=0 H;
III. with $R$=0 Ω and $L$=20 mH and
IV. with $R$=48 Ω and $L$=20 mH.

A sinusoidal voltage source with $U_m$ from 2 V to 10 V with the step of 2 V and frequency of 50 Hz has been used for all performed simulations. All simulations have been made using 1000 data points.

Other, lower or higher frequencies can also be used in simulations. However, the frequency of 50 Hz is of particular importance, as it is used as the working frequency in most of the basic electric circuits, as considered one. Consideration of higher frequencies would also be interesting for some advanced applications of electric machines and drives, power

 ISBN 978-86-7466-930-3

electronics and other. However, that is beyond of the scope of this paper.

Total of $N$=35 harmonics of measured quasistatic $H(t)$ have been used during the 4th step of the simulation process. This number of harmonics has been found to be optimal in case of $U_m$=10 V, therefore, less harmonics could be used for lower $U_m$.

Parameters of the electrical steel σ and $d$, used to calculate the magnetic field of eddy currents in (2), have been provided by the manufacturer and amount 2083 kS/m and 0.27 mm, respectively. Other parameters of the material given by the producer are: density ρ=7650 kg/m$^3$, $B_{max}$=1.90 T for $H_{max}$=800 A/m, specific power loss at 50 Hz is 0.72 W/kg for 1.5 T and 0.95 for 1.7 T, maximum of the relative permeability is around 70000 for static fields, coercive field goes up to 10 A/m for static field and up to 25 A/m for field at 50 Hz under sinusoidal $B(t)$.

Parameters $n_0$=908 and $V_0$=0.08 A/m in (3) have been obtained by fitting the excess power loss caused by $H_{exc}(t)$ for sinusoidal shape of $B(t)$ at 1 T to the excess power loss calculated from measurements for the same $B(t)$ [12], taking into account both hysteresis and dynamic loss (given by the hysteresis loops measured at 1 Hz and 50 Hz) and eddy current loss calculated using $H_{eddy}(t)$ given by (2) at 50 Hz. Fitting has been performed using the criteria of RMSD between excess power loss produced by fitted and calculated excess magnetic field. Both parameters have been kept constant in all performed simulations.

Predetermined limit ε has been set to 0.5%. This value has been chosen in order to obtain best convergence of the simulation procedure. Parameter $K$ has been set to 30 to obtain best solutions in case III for $U_m$=10 V and has been kept at this value for all simulations. It has been found that total number of iterations for $K$ steps is 36, 30, 31 and 30, for each of the considered cases at $U_m$=10 V, respectively.

Results for $i(t)$ for case IV of electric circuit for all considered values of $U_m$ are presented in Fig. 4.

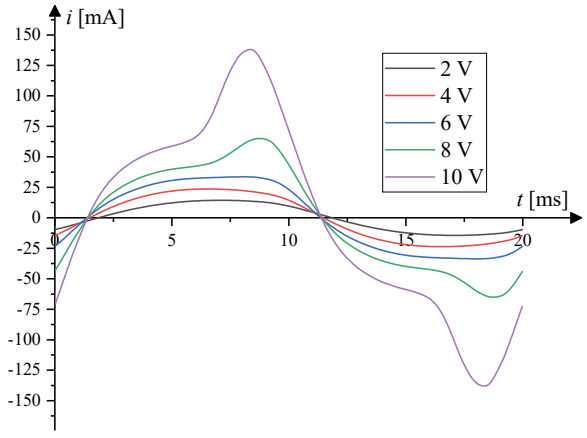


Fig. 4. Simulated $i(t)$ waveforms for the case of $R$=48 Ω and $L$=20 mH, for all considered values of $U_m$.

Influence of linear circuit elements $R$ and $L$ to the solution of the circuit for considered cases I-IV is better seen in observing the hysteresis loops of $L_h$ than in observing $i(t)$. Therefore, a number of simulated hysteresis loops has been constructed and the loops have been compared to observe such influence.

Simulated hysteresis loops for each of the considered cases of circuit and all values of $U_m$ are presented in Fig. 5-8, respectively. Scales are the same in all these figures for better illustration of $R$ and $L$ influence.

It can be seen that in all of the presented cases simulated hysteresis loops for lower $U_m$ are fully encompassed by the hysteresis loops of higher $U_m$. This is in accordance with the hysteresis theory which states that hysteresis loops obtained for higher voltages, under same conditions, should encompass the ones at lower voltages [10].

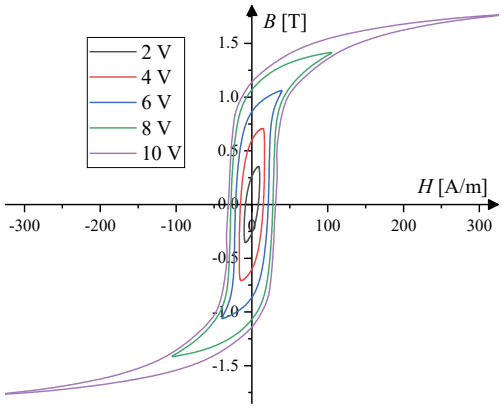


Fig. 5. Simulated hysteresis loops for the case of $R$=0 Ω and $L$=0 mH, for all considered values of $U_m$.

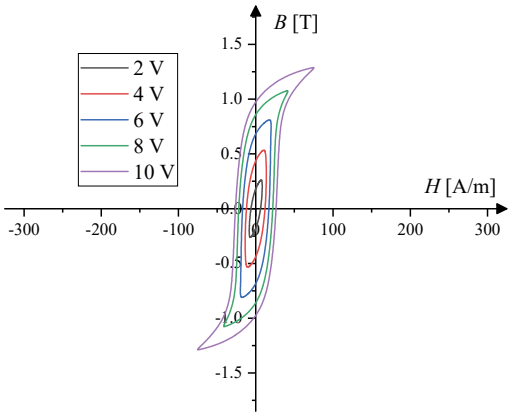


Fig. 6. Simulated hysteresis loops for the case of $R$=48 Ω and $L$=0 mH, for all considered values of $U_m$.

Hysteresis loops for all considered cases of electric circuit at particular values of $U_m$ are presented in Fig. 9-13, respectively.

At lower voltages, Figs. 9 and 10, the used electrical steel exhibits almost linear behaviour, therefore resulting in almost elliptical loops and sinusoidal $i(t)$. This limits the influence of $L$ in (4) since its voltage is proportion to the rate of change of $i(t)$. Also, adding $R$ in the electric circuit results in lover voltage levels at $L_h$. Its influence is more noticeable than the $L$'s, since the voltage over the resistor is proportional to the $i(t)$.


ISBN 978-86-7466-930-3

Simulations at higher voltages, Figs. 11-13, show greater influence of nonlinearity of the material, causing the significant peaks in the $i(t)$. Influence of $L$ is more prominent under these conditions, resulting in smoother $i(t)$ in case III than in case I by effectively lowering its peaks. Choking of the current [15] is less prominent in case IV since in this case linear $R$ causes lower voltage levels at $L_h$-lesser influence of nonlinearity on the shape of $i(t)$, making it smoother.

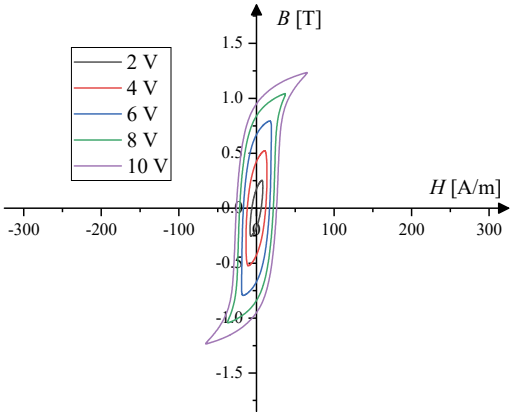


Fig. 7. Simulated hysteresis loops for the case of $R$=0 Ω and $L$=20 mH, for all considered values of $U_m$.

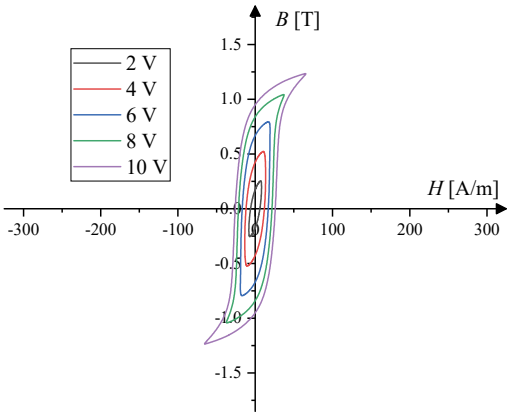


Fig. 8. Simulated hysteresis loops for the case of $R$=48 Ω and $L$=20 mH, for all considered values of $U_m$.

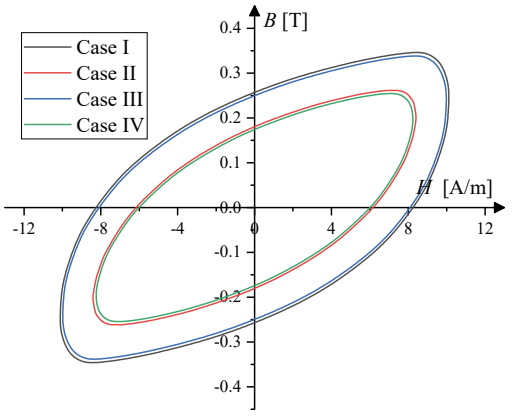


Fig. 9. Simulated hysteresis loops for $U_m$=2 V for all considered cases of electric circuit.

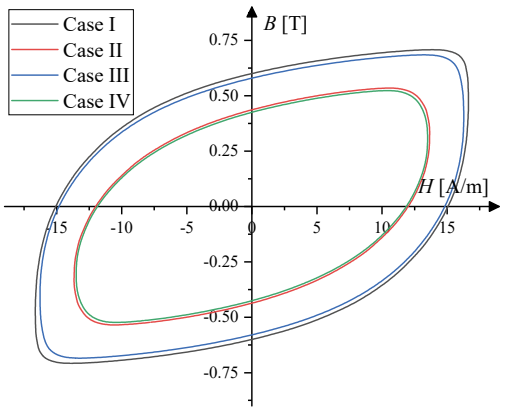


Fig. 10. Simulated hysteresis loops for $U_m$=4 V for all considered cases of electric circuit.

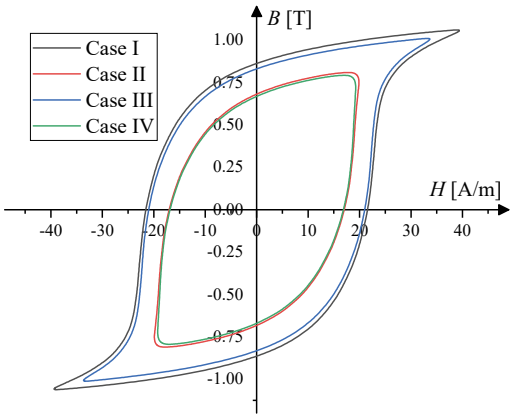


Fig. 11. Simulated hysteresis loops for $U_m$=6 V for all considered cases of electric circuit.

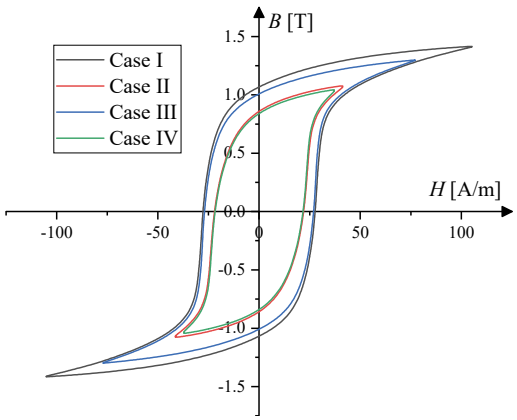


Fig. 12. Simulated hysteresis loops for $U_m$=8 V for all considered cases of electric circuit.

According to the results presented, simulation method presented could be suitable for solving electric circuits with $L_h$ for sinusoidal $u(t)$ in the steady state time domain. The simulation method presented has not been tested in simulation of transient processes.


ISBN 978-86-7466-930-3

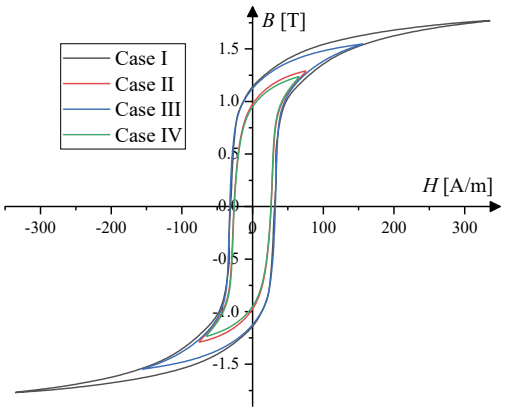


Fig. 13. Simulated hysteresis loops for $U_m$=10 V for all considered cases of electric circuit.

## V. CONCLUSION

A simulation method for solving electric circuits with nonlinear inductor with hysteresis in time domain has been resented in this paper. The considered electric circuit consisted of AC voltage source connected in series with linear resistor, linear inductor and nonlinear inductor with hysteresis. Proposed calculation procedure has been based on solving an equation derived from Kirchhoff's law through series of successive iterations. Influence of the inductor with hysteresis has been accounted for by calculating current in the electric circuit from its $H_{dyn}(t)$ corresponding to the $B_{Lh}(t)$ from iteration. Waveform of $H_{dyn}(t)$ has been calculated as the sum of its quasistatic, eddy current and excess magnetic field components. Each component has been calculated separately for the considered $B_{Lh}(t)$.

Measurements have been made for $H(t)$ at low frequency of 1 Hz for sinusoidal shape of $B(t)$ for amplitude from 0.2 T to 1.6 T with the measurement step of 0.2 T. Also, measurements have been made at 50 Hz for the sinusoidal $B(t)$ of 1 T.

Simulations have been performed for sinusoidal voltage source with the amplitudes from 2 V to 10 V with the step of 2 V. Also, four cases of the electric circuit have been considered for each of the voltages-without, with one and with both linear elements. Based on the simulation result and their discussion, it can be concluded that the presented simulation method could be suitable for solving electric circuits with nonlinear inductors with hysteresis in steady state time domain.

## ACKNOWLEDGMENT

This study was supported by the Ministry of Education, Science and Technological Development of the Republic of Serbia, and these results are parts of the Grant No. 451-03-68/2022-14/200132 with University of Kragujevac - Faculty of Technical Sciences Čačak.

## REFERENCES

[1] B. Koprivica, A. Milovanović, M. Đekić, "Effects of Wound Toroidal Core Dimensional and Geometrical Parameters on Measured Magnetic Properties of Electrical Steel", Serbian Journal of Electrical Engineering, vol. 10, no. 3, pp. 459-471, Oct. 2013.

[2] A. Rezaei-Zare, R. Iravani, "On the Transformer Core Dynamic Behavior During Electromagnetic Transients", *IEEE Transactions on Power Delivery*, vol. *25*, no. *3*, pp. *1606-1619*, July 2010.

[3] F. G. Montoya, F. De Leon, F. Arrabal-Campos, A. Alcayde, "Determination of Instantaneous Powers from a Novel Time-Domain Parameter Identification Method of Non-Linear Single-Phase Circuits", *IEEE Transactions on Power Delivery* (Early Access), Dec. 2021.

[4] J. H. B. Deane, "Modelling the Dynamics of Nonlinear Inductor Circuits", *IEEE Transactions on Magnetics*, vol. *30*, n0. *5*, pp. *2795 – 2801*, Sept. 1994.

[5] I. D. Mayergoyz, "*Mathematical Models of Hysteresis and Their Applications*", Elsevier Science, New York, USA, 2003.

[6] A. R. P. J. Vijn, O.Baas, E. Leepelaars, "Parameter Estimation for the Jiles–Atherton Model in Weak Fields", *IEEE Transactions on Magnetics*, vol. *56*, no. *4*, April 2020.

[7] A. S. Q. Antonio, F. R. Fulginer, A. Laudani, A. Faba, E. Cardelli, "An Effective Neural Network Approach to Reproduce Magnetic Hysteresis in Electrical Steel Under Arbitrary Excitation Waveforms", *Journal of Magnetism and Magnetic Materials,* vol. *528*, June 2021.

[8] S. Divac, B. Koprivica, "Simulation of Dynamic Hysteresis Loops for Toroidal Sample for Sinusoidal Shape of Magnetic Flux Density", 21st International Symposium INFOTEH-JAHORINA, 16-18. March 2022.

[9] D. Makaveev, L. Dupre, M. De Wulf, J. Melkebeek, "Modelling of Rate-Independent Hysteresis with Feed-Forward Neural Networks", Conf. Proc. Neural Networks and Appl., Interlaken, Switzerland, pp. 3451-3456, Feb. 2002.

[10] G. Bertotti, "*Hysteresis in Magnetism for Physicists, Material Scientists and Engineers*", Academic Press, New York, USA, 1998.

[11] C. D. Schunn, D. Wallach, "Evaluating Goodness-of-Fit in Comparison of Models to Data", pp. *115-135*, 2005. In W. Tack (Ed.), Psychologie der Kognition: Reden and Vorträge anlässlich der Emeritierung von Werner Tack, Saarbrueken, Germany, University of Saarland Press.

[12] B. Koprivica, S. Divac, "Analysis and Modeling of Instantaneous Magnetizing Power of Ferromagnetic Core in Time Domain", *IEEE Magnetic Letters*, vol. *12*, p. *2103505*, Sept. 2021.

[13] J. Takacs, "Hysteresis Loop Reversing by Applying Langevin Approximation", *The International Journal for Computation and Mathematics in Electrical and Electronic Engineering*, vol. *36*, no. *4*, July 2017.

[14] M. De Wulf, L. Dupre, J. Melkebeek, "Quasistatic Measurements for Hysteresis Modeling", Journal of Applied Physics, vol. 87, no. 9, pp. 5239-5241, May 2000.

[15] K. L. Kaiser, "*Electromagnetic Compatibility Handbook*", CRC Press, New York, USA, 2004.

 ISBN 978-86-7466-930-3

# A Comparative Analysis of Three-Phase Phase-Locked Loops for Grid-Connected Systems

Filip Bakić, Lazar Stojanović, Katarina Obradović, Emilija Lukić

***Abstract*—In renewable power generation system, synchronization of the inverter and the power grid is essential for the stable control of grid-connected inverters. Phase-Locked Loops (PLL) are widely used for grid synchronization due to simple implementation and robust performance against the grid disturbances. The main goal of this paper is to present a survey of the comparative performance evaluation among the synchronous reference frame PLL (SRF-PLL), Lag-PLL, stationary-frame based enhanced PLL (SF-EPLL) and double second-order generalized integrator PLL (DSOGI-PLL) under disturbances such as frequency changes, voltage sags and harmonic distortion. System structures and working principles are presented. Moreover, the parameters design for each algorithm are proposed. Dynamic analysis and experimental results of steady state performance of PLLs are observed and compared to verify and validate theoretical comparative analysis.**

***Index Terms*—Phase-locked loop, grid synchronization, frequency estimation, three-phase**

## I. Introduction

Over the past couple of decades, there is a clear trend of switching from fossil fuels to renewable energy sources (RES) in electricity production. Furthermore, distributed generation (DG) of RES and their wide prevalence created a possibility to work independently from the grid i.e. in islanded mode, but also as generating units that inject active or reactive power directly to the grid. Many such grid-tied solutions rely on the proper usage of DC-AC power converters in order to successfully connect to the power system. Hence, advancing both hardware and control solutions has become a great deal.

The process of connecting the inverter to the grid is called synchronization of the inverter. In order to achieve successful synchronization, it is important that amplitude, phase and the frequency of the inverter's and the grid's voltages are precisely determined. In case of small DG such as rooftop solar PV systems intended to connect to weak distribution grid, parameters and quality of grid's voltage can vary significantly due to constant change of load. Thus, robust, efficient and precise controlling scheme becomes even more important.

The research work for the most suitable way for synchronizing inverters with the grid has resulted in numerous solutions. In general, all these methods could be classified as either single phase or three-phase based methods. Some of them, such as open transition transfer, are less applicable due to reduced reliability of the power system. On the other side, others, such as passive synchronization, imply usage of synchoncheck relay for synchronization check of voltage, frequency and phase [1]. Although passive synchronization methods do not require control mechanism, using this type of synchronization results in longer reconnecting process. Nevertheless, the most commonly used synchronization method is active synchronization. With implementation of controlling mechanisms, synchronization can be done by controlling the frequency and voltage. The most acknowledged concepts nowadays are Frequency Locked Loop [2], Droop Control [3], [4] and Phase Locked Loop (PLL). Due to simplicity, robustness and effectiveness in various grid conditions, PLL is the most commonly used synchronization method. To improve PLL performances under various grid conditions, numerous modifications have been done, such as Synchronous Reference Frame PLL (SRF-PLL) [5], enhanced PLL (EPLL), fixed-reference frame PLL (FRF-PLL) [6], Lag-PLL, SF-EPLL and DSOGI-PLL [7] .

In this paper, multiple PLL solutions are introduced and discussed. In the third paragraph PLL algorithms Synchronous Reference Frame PLL (SRF-PLL), Lag-PLL, SF-EPLL and DSOGI-PLL are analyzed. Then, Paragraph IV The process of selection of the adequate parameters for each algorithm is explained. Finally, experimental results were conducted on real prototype of grid-connected inverter.

## II. Generalized structure of PLL

Basic structure of every PLL can be organized in three sections, Fig. 1:

1) Phase detector (PD): It compares generated signal with desired one and generates corresponding error. For three-phase systems, voltages $u_{abc}$ in a stationary reference frame are transformed in a synchronous rotating frame, where sinusoidal voltages are represented as DC values $u_{dq}$.
2) Low-Pass filter (LPF): Some phase detectors generate undesired high frequency signals that need to be filtered. For three-phase systems, LPF is often designed as PI controller which input is $q$ component of the voltage. The goal for PI controller is to bring $q$ component to zero. This will ensure that phase is aligned with $d$ axis.
3) Voltage controlled oscillator (VCO): After the angular frequency is estimated, it is integrated to get phase. This phase is then sent to phase detector to finish one iteration of PLL.

Filip Bakić is master student in School of Electrical Engineering, University of Belgrade (email: filip543bakic@gmail.com)
Lazar Stojanović is master student in School of Electrical Engineering, University of Belgrade (email: lazastojanovic99@gmail.com)
Katarina Obradović is master student in School of Electrical Engineering, University of Belgrade (email: obradovick15@gmail.com)
Emilija Lukić is master student in School of Electrical Engineering, University of Belgrade (email: emilija.lukic505@gmail.com)

 ISBN 978-86-7466-930-3

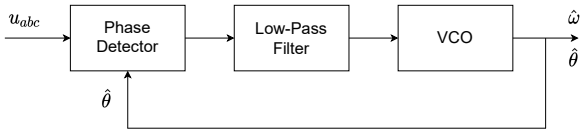


Fig. 1. Basic structure of PLL

## III. Overview of the Three-Phase PLL Algorithms

### A. SRF-PLL

Synchronous Reference Frame PLL is one of most commonly used algorithm due to its low complexity and easy digital realization. Conventional scheme of the SRF-PLL is shown on Fig.2. Phase detector is cascade Clark (1) and Park (2) transformation. Angle used in Park transformation $\theta$ is one estimated from algorithm in previous cycle.

$$T_{abc/\alpha\beta} = \begin{bmatrix}\alpha\\ \beta\end{bmatrix} = \frac{2}{3}\begin{bmatrix}1 & -\frac{1}{2} & -\frac{1}{2}\\ 0 & \frac{\sqrt{3}}{2} & -\frac{\sqrt{3}}{2}\end{bmatrix}\begin{bmatrix}a\\ b\\ c\end{bmatrix} \tag{1}$$

$$T_{\alpha\beta/dq} = \begin{bmatrix}d\\ q\end{bmatrix} = \begin{bmatrix}\cos(\theta) & \sin(\theta)\\ -\sin(\theta) & \cos(\theta)\end{bmatrix}\begin{bmatrix}\alpha\\ \beta\end{bmatrix} \tag{2}$$

The goal of this PLL is to bring $q$ component to zero and align the voltage vector with $d$ axis. It is achieved by utilizing PI controller which output is angular frequency. A stationary value of frequency is added to ensure faster phase tracking. Frequency is then integrated to obtain phase, which is then used in PD.

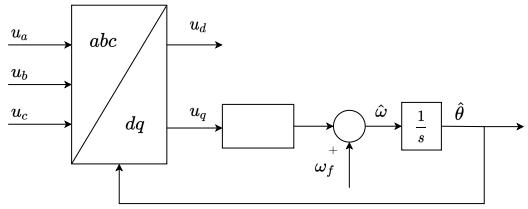


Fig. 2. Scheme of SRF-PLL

### B. Lag-PLL

Another implementation of the PLL is shown in Fig.3 as proposed in [8] and referred as Lag-PLL, is derived from SRF-PLL by passing $u_q$ through low-pass filter prior to the PI regulator. The intention of signal filtering is to improve PLL performance when sensing noise and higher harmonics are present in grid voltages.

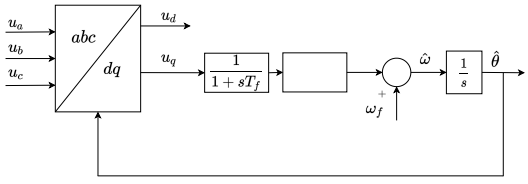


Fig. 3. Scheme of Lag-PLL

### C. SF-EPLL

Since standard EPLL algorithm is implemented in a three-phase stationary it is relatively complex due to trigonometric and multiplying operations, the presented algorithm reduces complexity by transforming voltages in $\alpha\beta$ frame. Fig.4 shows the three-phase implementation of the enhanced PLL which was proposed in [9]. Besides estimating phase and frequency, EPLL add amplitude loop in PLL scheme. After the three-phase signals are transformed into $u_\alpha$ and $u_\beta$ are subtracted by the estimated components $y_\alpha$ and $y_\beta$ to obtain the estimated errors $e_\alpha$ and $e_\beta$. Amplitude and frequency error are defined as

$$e_v = e_\alpha sin(\tilde{\theta}) + e_\beta sin(\tilde{\theta} - 90°) \tag{3}$$

$$e_w = e_\alpha cos(\tilde{\theta}) - e_\beta cos(\tilde{\theta} - 90°) \tag{4}$$

They are, respectively, integrated to obtain amplitude and passed to the PI controller for frequency estimation. By integrating $\tilde{\omega}$ estimated angle is obtained.

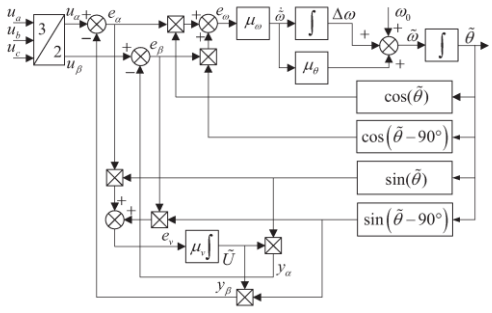


Fig. 4. Scheme of SF-EPLL [9]

### D. DSOGI-PLL

Instead of filtering q component, DSOGI algorithm is designed in a way to prefilter $\alpha\beta$ components. Besides that, by dual integration, it is able to conserve information from positive sequenced harmonics by canceling negative sequenced harmonics in $u'_\alpha$ and $u'_\beta$ by dividing with 2 voltage amplitude is preserved. Then $u'_\alpha$ and $u'_\beta$ are transformed in $dq$ components which further can be pass to standard SRF-PLL for frequency and phase estimation.

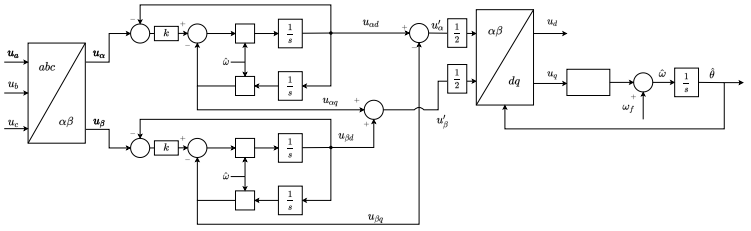


Fig. 5. Scheme of DSOGI-PLL


ISBN 978-86-7466-930-3

## IV. Selection of Parameters

### A. SRF-PLL

Because of nonlinear structure of phase detector analysis and parameters selection would be complicated so model is linearized Fig. 6. From the obtained linear model, we can select parameters of PI controller to achieve desired response. Open loop transfer function is equal to:

$$W_{open}(s) = \frac{\varphi_{PLL}}{\varphi_{grid}} = \frac{sK_pK_{pd} + K_iK_{pd}}{s^2} \tag{5}$$

from which closed loop function is equal to:

$$W_{close}(s) = \frac{sK_pK_{pd} + K_iK_{pd}}{s^2 + sK_pK_{pd} + K_iK_{pd}} \tag{6}$$

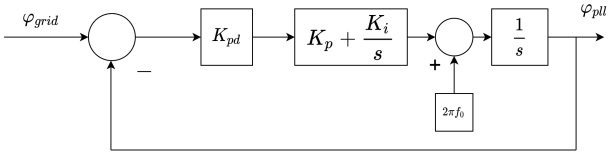


Fig. 6. Linearized model of SRF PLL

Where $K_p$, $K_i$ are parameters of PI controller and $Kpd$ represents amplitude of three-phase voltage. Selecting of parameters $K_p$ and $K_i$ is done to achieve desired bandwidth and damping by selecting coefficients to meet standard second order polynomial.

$$s^2 + 2\xi\omega_n s + \omega_n^2 = s^2 + sK_pK_{pd} + K_iK_{pd} \tag{7}$$

From where we can obtain parameters as:

$$K_i = \frac{\omega_n^2}{K_{pd}},\ K_p = \frac{2\xi\omega_n}{K_{pd}} \tag{8}$$

in this study, we chose $\xi = 1$ and $w_n = 37.7$ rad/s which corresponds with desired closed loop bandwidth of 6 Hz and absence of oscillations in response.

### B. LAG-PLL

The idea of this PLL is to better filter higher harmonics than SRF. Since it only differs from SRF in added filter, we can use $K_i$ and $K_p$ used for SRF PLL. $T_f$ is selected to minimize effect on system response. Open loop transfer function is equal to:

$$W_{open}(s) = \frac{\varphi_{PLL}}{\varphi_{grid}} = \frac{sK_pK_{pd} + K_iK_{pd}}{s^3T_f + s^2} \tag{9}$$

To find poles positions of closed loop in depending on $T_f$ we used modified transfer function $W_{mod}$

$$W_{mod}(s) = \frac{T_f s^3}{s^2 + sK_pK_{pd} + K_iK_{pd}} \tag{10}$$

because closed loop poles for both transfer functions are the same. Poles position with respect to different value of $T_f$ is shown in Fig. 7.$T_f$ must be small enough to not interfere with system dynamics and large enough to filter higher harmonics. As a good compromise, $T_f$ is selected to filter dynamics over 100Hz so $T_f = \frac{1}{200\pi}$.

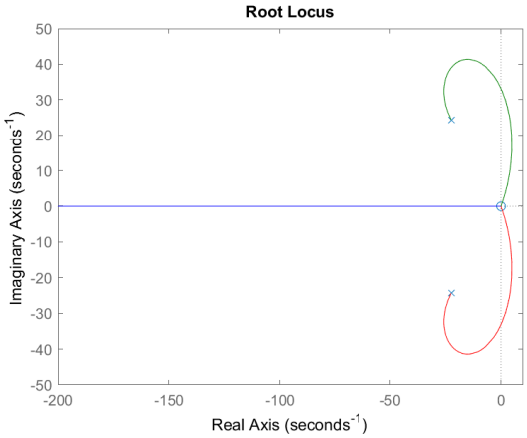


Fig. 7. Pole position for different values of $T_f$

### C. DSOGI

Filtering power of dual integrator is determined by parameter, $k$ which can we see in transfer functions from $u_\alpha$ to $u_{\alpha d}$ and $u_\alpha$ to $u_{\alpha q}$

$$G_d(s) = \frac{u_{\alpha d}}{u_\alpha} = \frac{k\omega_1 s}{s^2 + k\omega_1 s + \omega_1^2} \tag{11}$$

$$G_q(s) = \frac{u_{\alpha q}}{u_\alpha} = \frac{k\omega_1^2}{s^2 + k\omega_1 s + \omega_1^2} \tag{12}$$

transfer functions from $u_\beta$ to $u_{\beta d}$ and $u_\beta$ to $u_{\beta q}$ are the same.

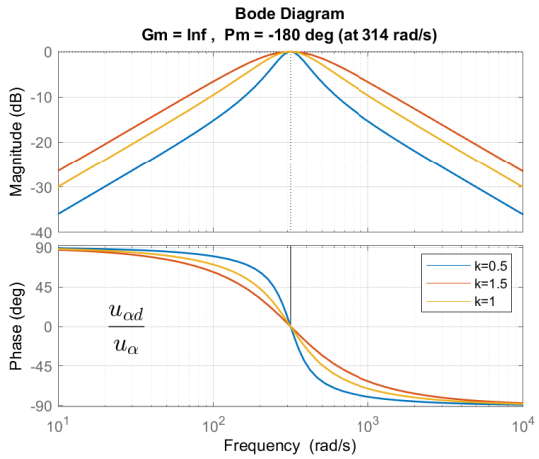


Fig. 8. Bode plot $G_d$ in function of $k$

As it is shown on Fig. 8 and Fig. 9 increasing $k$ give better attenuation of harmonics but also causes higher overshoot and greater settling time of estimation. For best trade-off $k = 1$ is selected. Parameters of PI controller $K_i$ and $K_p$ are same as in SRF and Lag-PLL.

### D. SF-EPLL

For this PLL parameters for amplitude and frequency estimation can be chosen separately. For amplitude loop time


ISBN 978-86-7466-930-3

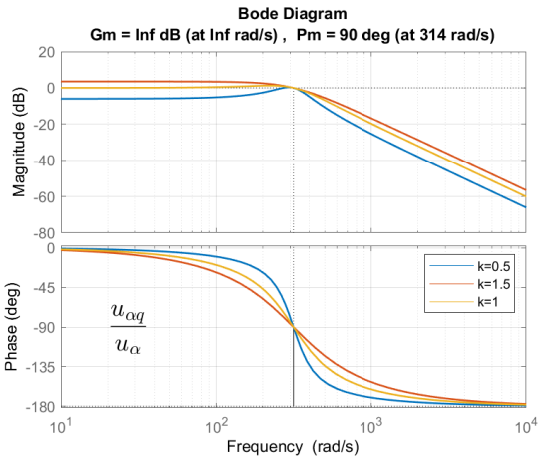


Fig. 9. Bode plot of $G_q$ in function of $k$

constant of response is the same as $1/\mu_v$, from setting time of 50ms and $T_{sett} = 5/\mu_v$ we chose $\mu_v = 100$. Dynamic model of this PLL are provided in [9] from where $\mu_\theta = 2\xi/w_n$ and $\mu_\omega = w_n/\mu_\theta/U$ where $U$ is estimate amplitude of grid voltage.

## V. Simulation Results

Modeling of different PLLs and simulation is done by using Matlab and Simulink software.

Dynamic response of different PLLs is examined by step frequency change. As shown in Fig. 10 PLLs have similar rise time which means that regulation bandwidth is roughly the same. Despite, $\psi = 1$ overshoot is present due to the presence of dominant zero. Difference in overshoot is not crucial for performance of PLL.

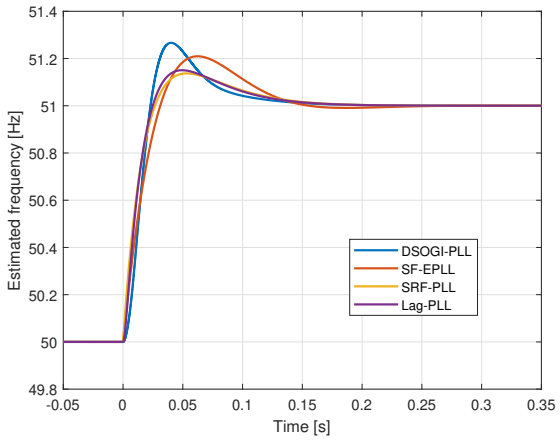


Fig. 10. Response on step frequency change

Unbalanced three-phase system is a problem for PLLs because it introduces ripple in frequency estimation. Unbalanced grid voltage used for simulation is shown in Fig. 11. Unbalanced grid conditions have the largest impact on SRF PLL. On the other hand, DSOGI is unaffected by distortions.

TABLE I
Performance comparison on step frequency change

| PLL | Overshoot [%] | 2% settling time [s] |
|---|---|---|
| SRF | 13.70 | 0.143 |
| Lag | 15.05 | 0.140 |
| SF-EPLL | 20.95 | 0.138 |
| DSOGI | 26.65 | 0.130 |

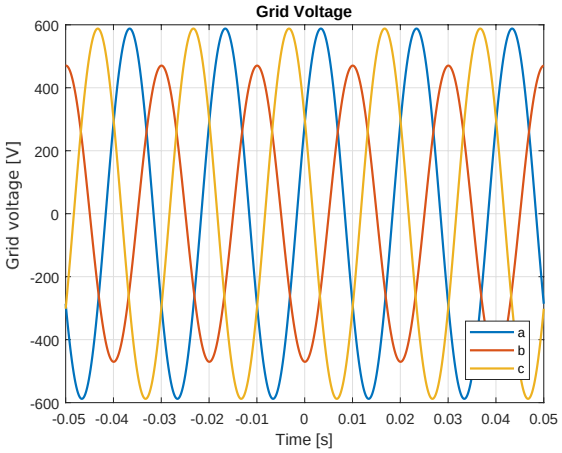


Fig. 11. Unbalanced grid voltage during simulation

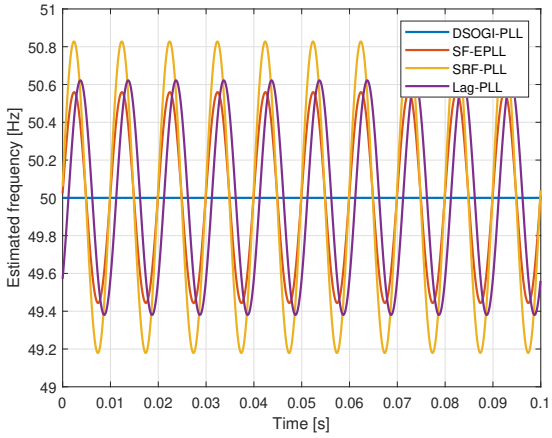


Fig. 12. Frequency estimation

TABLE II
Performance comparison in unbalanced conditions

| PLL | Steady oscillation amplitude [Hz] |
|---|---|
| SRF | 0.828 |
| Lag | 0.622 |
| SF-EPLL | 0.560 |
| DSOGI | 0 |

## VI. Experimental Results

Experimental results were conducted of grid-connected inverter prototype. The prototype was designed for a grid with 208 V line voltage, so tests were conducted on that voltage. The algorithm is implemented on TMS320F28379D microcontroller. Experimental setup is shown on Fig. 13. The idea of this test is to show influence of real implementation


ISBN 978-86-7466-930-3

and grid conditions on performance of PLL algorithms. Grid voltage with THD of 3.67% is shown on Fig. 14. Performance of different algorithms can be seen on Fig. 15 and Table III.

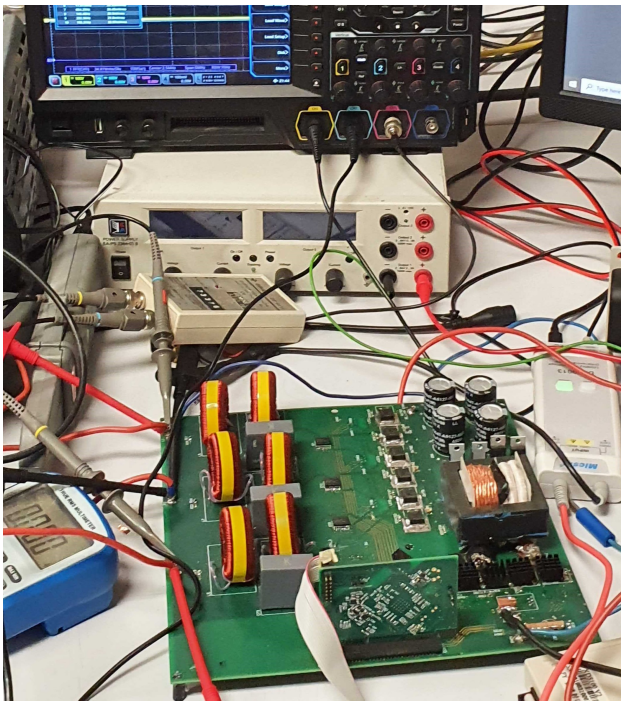

Fig. 13. Experimental setup

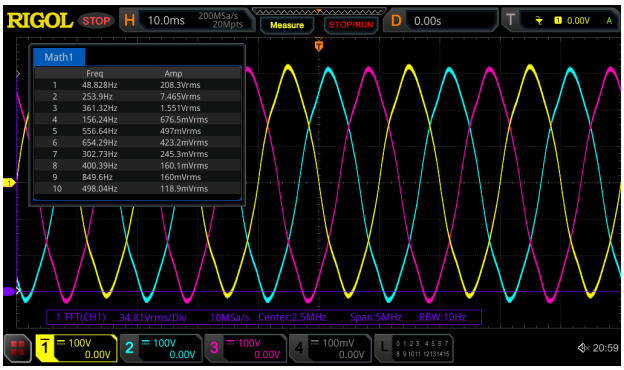


Fig. 14. Grid voltage

TABLE III
PERFORMANCE COMPARISON IN EXPERIMENTAL CONDITIONS

| PLL | Maximum error [Hz] | Mean error [Hz] |
|---|---|---|
| SRF | 0.771 | 0.439 |
| Lag | 0.675 | 0.4153 |
| SF-EPLL | 0.509 | 0.2930 |
| DSOGI | 0.357 | 0.224 |

## VII. CONCLUSION

Analysis and performance comparison of four three-phase PLL structures have been simulated and tested on real prototype. From the presented comparison, it is found that DSOGI-PLL has the best performance in all three scenarios, providing

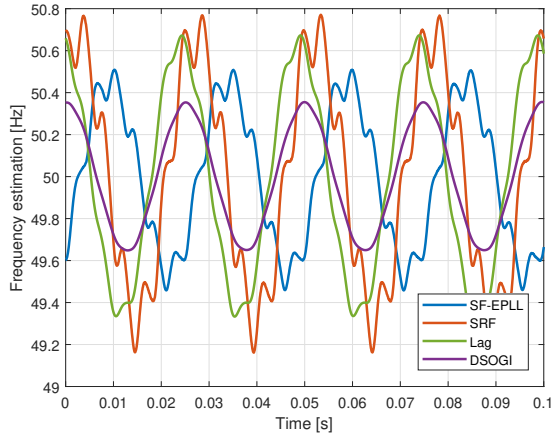


Fig. 15. Frequency estimation

the most accurate frequency estimation. Worst results are obtained with SRF-PLL which was expected knowing that all other PLLs presents modification of this algorithm in desire to achieve better performance. Future analysis will focus on quality of current injected to grid by inverter knowing the dynamic and performance of frequency estimation, which is essential for accurate grid synchronization.

## ACKNOWLEDGMENT

We are grateful to Laboratory of the Digital Drive Control in the School of Electrical Engineering, University of Belgrade for testing equipment. Also, we are grateful to all H-Bridges team members for developing and implementation of this prototype.

## REFERENCES

[1] N. Lidula and A. Rajapakse, "Voltage balancing and synchronization of microgrids with highly unbalanced loads," in *Renew. Sustain.Energy Rev.*, vol. 31, 2014, pp. 907–920.

[2] L. Widanagama Arachchige and A. Rajapakse, "Voltage balancing and synchronization of microgrids with highly unbalanced loads," *Renewable and Sustainable Energy Reviews*, vol. 31, pp. 907–920, 03 2014.

[3] C. Jin, M. Gao, X. Lv, and M. Chen, "A seamless transfer strategy of islanded and grid-connected mode switching for microgrid based on droop control," in *2012 IEEE Energy Conversion Congress and Exposition (ECCE)*, 2012, pp. 969–973.

[4] Y. Jia, D. Liu, and J. Liu, "A novel seamless transfer method for a microgrid based on droop characteristic adjustment," in *Proceedings of The 7th International Power Electronics and Motion Control Conference*, vol. 1, 2012, pp. 362–367.

[5] A. Bellini, S. Bifaretti, and F. Giannini, "A robust synchronization method for centralized microgrids," *IEEE Transactions on Industry Applications*, vol. 51, no. 2, pp. 1602–1609, 2015.

[6] M. Martinez-Montejano, G. Escobar, and R. Torres-Olguin, "Fixed reference frame phase-locked loop (frf-pll) for unbalanced line voltage conditions," in *2008 IEEE Power Electronics Specialists Conference*, 2008, pp. 4723–4728.

[7] X. Wang, "Optimization strategy of dsogi-pll precision under harmonic interference conditions," in *2020 IEEE Sustainable Power and Energy Conference (iSPEC)*, 2020, pp. 852–857.

[8] A. Ortega and F. Milano, "Comparison of different pll implementations for frequency estimation and control," in *2018 18th International Conference on Harmonics and Quality of Power (ICHQP)*, 2018, pp. 1–6.

[9] F. Wu, L. Zhang, and J. Duan, "A new two-phase stationary-frame-based enhanced pll for three-phase grid synchronization," *IEEE Transactions on Circuits and Systems II: Express Briefs*, vol. 62, no. 3, pp. 251–255, 2015.

 ISBN 978-86-7466-930-3

# Parameter estimation of induction motors using Wild Horse Optimizer

Jovan Vukašinović, Miloš Milovanović, Nebojša Arsić, Jordan Radosavljević, Saša Štatkić, Bojan Perović and Andrijana Jovanović

***Abstract*—In this paper, a new metaheuristic algorithm called the Wild Horse Optimizer (WHO) is for the first time proposed for estimation of the equivalent circuit parameters of the single-cage induction motors. The parameters of the motors are found as a result of the error minimization function between the calculated and manufacturer data. Simulation results obtained using the WHO algorithm are compared to the results obtained using other optimization methods applied in solving the induction motor parameter estimation problem. The performances of the methods are evaluated using the motors of different powers (i.e. 5 HP and 40 HP), based on the statistical analysis of the results obtained in several independent runs of the methods. It is shown that the proposed WHO algorithm has better performance, i.e. it is able to provide quality solutions with faster convergence speed and better statistical indicators.**

***Index Terms*—Induction motors, Parameter estimation, Optimization, Metaheuristic, Wild Horse Optimizer (WHO)**

## I. INTRODUCTION

Induction motors are the most widespread electric motors in the world, and as such they represent one of the largest consumers of the electricity. Today, induction motors consume between 35% and 40% of the world's total electricity production. Knowing the parameters of the equivalent circuit of an induction motor is of great importance for drive control processes, as well as for fault diagnosis of the induction motor.

Classical methods for determining the parameters of the equivalent circuits of induction motors are based on no-load and short-circuit experiments. Because these tests are very difficult to perform in cases where the motor is already connected to a mechanical load, these methods are not always easily applicable in industry. For these reasons, in the recent years, many analytical and optimization methods have been proposed to estimate the parameters of induction motors. Some of the commonly used methods for estimation the parameters of induction motors that can be found in the literature are: Particle Swarm Optimization (PSO) [1], Genetic Algorithm (GA) [2], Charged System Search (CSS) [3], hybrid GA and PSO (HGAPSO) [4], Gravitational Search Algorithm (GSA) [5], hybrid Phasor Particle Swarm Optimization and Gravitational Search Algorithm (PPSOGSA) [6], and Shuffled Frog Leaping Algorithm (SFLA) [7].

In this paper, the Wild Horse Optimizer (WHO) [8] is for the first time proposed for estimating the single-cage induction motors parameters. It could be regarded as the main contribution of the paper. In the scientific literature, there is no research that deals with the direct application of the WHO algorithm for solving any problem of induction motor parameter estimation. The WHO algorithm has shown very good results in solving different complex benchmark functions, as pointed out in [8], and practical engineering problems, such as the problems of the parameter estimation of diode PV models [9], static/dynamic PV models [10], and damage identification in steel plates [11]. For this reason, the authors of this paper have decided to use the WHO algorithm.

## II. PROBLEM FORMULATION

In order to optimize the values of the electrical parameters, the formulation of the objective function is required. In this case the objective function has the following form [7]:

$$OF = F_1^2 + F_2^2 + F_3^2 + F_4^2, \tag{1}$$

where

$$F_1 = \frac{T_{fl.cal} - T_{fl.mf}}{T_{fl.mf}}, \tag{2}$$

$$F_2 = \frac{T_{st.cal} - T_{st.mf}}{T_{st.mf}}, \tag{3}$$

$$F_3 = \frac{T_{\max.cal} - T_{\max.mf}}{T_{\max.mf}}, \tag{4}$$

Jovan Vukašinović is with the Faculty of Technical Sciences, University of Priština in Kosovska Mitrovica, 7 Knjaza Miloša, 38220 Kosovska Mitrovica, Serbia (e-mail: jovan.vukasinovic@pr.ac.rs).

Miloš Milovanović is with the Faculty of Technical Sciences, University of Priština in Kosovska Mitrovica, 7 Knjaza Miloša, 38220 Kosovska Mitrovica, Serbia (e-mail: milos.milovanovic@pr.ac.rs).

Nebojša Arsić is with the Faculty of Technical Sciences, University of Priština in Kosovska Mitrovica, 7 Knjaza Miloša, 38220 Kosovska Mitrovica, Serbia (e-mail: nebojsa.arsic@pr.ac.rs).

Jordan Radosavljević is with the Faculty of Technical Sciences, University of Priština in Kosovska Mitrovica, 7 Knjaza Miloša, 38220 Kosovska Mitrovica, Serbia (e-mail: jordan.radosavljevic@pr.ac.rs).

Saša Štatkić is with the Faculty of Technical Sciences, University of Priština in Kosovska Mitrovica, 7 Knjaza Miloša, 38220 Kosovska Mitrovica, Serbia (e-mail: sasa.statkic@pr.ac.rs).

Bojan Perović is with the Faculty of Technical Sciences, University of Priština in Kosovska Mitrovica, 7 Knjaza Miloša, 38220 Kosovska Mitrovica, Serbia (e-mail: bojan.perovic@pr.ac.rs).

Andrijana Jovanović is with the Faculty of Technical Sciences, University of Priština in Kosovska Mitrovica, 7 Knjaza Miloša, 38220 Kosovska Mitrovica, Serbia (e-mail: andrijana.jovanovic@pr.ac.rs).

 ISBN 978-86-7466-930-3

$$F_4 = \frac{pf_{fl.cal} - pf_{fl.mf}}{pf_{fl.mf}}. \quad (5)$$

In (1) – (5) variables have the following meaning: *OF* is the objective function, $F_i$ ($i$ = 1,2,…,4) is the $i$-th component of the objective function (i.e., it is an error between the calculated and manufacturer value), $T$ is a torque, $I$ is a current, *pf* is a power factor, subscripts *st*, *fl* and max correspond to the start load, full load, and maximum load, respectively. Also, subscripts *cal* and *mf* are used for the calculated and manufacturer data.

According to Fig. 1, the stator ($\underline{I}_s$) and rotor ($\underline{I}_r$) currents in terms of slip ($s$) can be calculated using the following equations:

$$\underline{I}_s(s) = \frac{\underline{V}_{ph}}{R_s + jX_s + \underline{Z}_p(s)}, \quad (6)$$

$$\underline{I}_r(s) = \frac{\underline{Z}_p(s) \cdot \underline{I}_s(s)}{\frac{R_r}{s} + jX_r}, \quad (7)$$

where $\underline{V}_{ph}$ is the stator phase voltage, $R_s$ is the stator resistance, $R_r$ is the rotor resistance, $X_s$ is the stator leakage reactance, $X_r$ is the rotor leakage reactance, and $X_m$ is the magnetizing leakage reactance.

The equivalent impedance ($\underline{Z}_p$) and Thevenin's equivalent impedance ($\underline{Z}_{Th}$) are:

$$\underline{Z}_p(s) = \frac{1}{\frac{1}{jX_m} + \frac{1}{\frac{R_r}{s} + jX_r}}, \quad (8)$$

$$\underline{Z}_{Th} = R_{Th} + jX_{Th} = \frac{1}{\frac{1}{R_s + jX_s} + \frac{1}{jX_m}}. \quad (9)$$

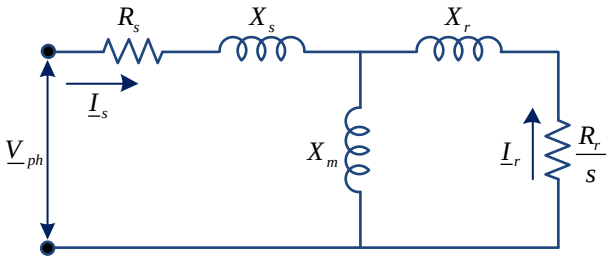


Fig. 1. One phase steady-state equivalent circuit of a single-cage three-phase induction motor.

The torque in terms of slip can be obtained by using the following equation:

$$T(s) = \frac{3p}{\omega_s}\left[I_r(s)\right]^2 \frac{R_r}{s}. \quad (10)$$

Thus, $T_{fl} = T(s_{fl})$, $T_{st} = T(1)$, and $T_{\max} = T(s_{\max})$, where the maximum torque slip ($s_{max}$) is given by (11).

$$s_{\max} = \frac{R_r}{\sqrt{R_{Th}^2 + \left(X_{Th} + X_r\right)^2}}. \quad (11)$$

The apparent, active and reactive powers are:

$$\underline{S}(s_{fl}) = 3 \cdot \underline{V}_{ph} \cdot \left[\underline{I}_s(s_{fl})\right]^*, \quad (12)$$

$$P_{fl} = \mathrm{Re}\left\{\underline{S}(s_{fl})\right\}, \quad Q_{fl} = \mathrm{Im}\left\{\underline{S}(s_{fl})\right\}. \quad (13)$$

Finally, the power factor can be calculated:

$$pf_{fl} = \arctan\left(\frac{Q_{fl}}{P_{fl}}\right). \quad (14)$$

According to [6, 7], the following constraints are taken into account:

$$R_s, R_r, X_s, X_r, X_m > 0, \quad (15)$$

$$X_s = X_r. \quad (16)$$

## III. Solution Method

The WHO algorithm [8] is a recently proposed metaheuristic algorithm developed by Naruei and Keynia. This algorithm is inspired by the social life behavior of wild horses in the nature. Wild horses exhibit different group behaviors, such as grazing, chasing, mating, dominance and leadership.

The WHO algorithm consists of the following steps [8]:

### *A. Creating an Initial Population and Forming Horse Groups, and Selecting Leaders*

The WHO begins with an initial population of $N$ agents, $\mathbf{POP}(1) = \left[\mathbf{X}_1(1), \mathbf{X}_2(1), ..., \mathbf{X}_N(1)\right]^T \subseteq \mathbf{U}$. In the initial iteration, the $i^{\text{th}}$ agent $\mathbf{X}_i(1)$ can be expressed as: $\mathbf{X}_i(1) = \left[X_i^1(1), ..., X_i^d(1), ..., X_i^n(1)\right]$, where $X_i^d$ is the position of the $i^{\text{th}}$ agent in the $d^{\text{th}}$ dimension, $n$ is the dimension of the problem, while $\mathbf{U}$ is the space of possible solutions. The initial population is divided into several groups. Each group has only one leader (stallion) and one or more mares and foals.

### *B. Grazing of Horses*

The following equation is used to simulate the grazing:

$$\mathbf{X}_{i,G}^j(t+1) = 2 \cdot \mathbf{Z}(t) \cdot \cos\left(2 \cdot \pi \cdot R \cdot \mathbf{Z}(t)\right) \times \times \left(\mathbf{Stallion}^j(t) - \mathbf{X}_{i,G}^j(t)\right) + \mathbf{Stallion}^j(t) \quad (17)$$

where $\mathbf{X}_{i,G}^j(t)$ and $\mathbf{X}_{i,G}^j(t+1)$ are the current position and new position of the foal or mare, respectively; $t$ is the current iteration; $t + 1$ is the next iteration; $\mathbf{Stallion}^j(t)$ is the current position of the stallion; $R$ is a uniform random number between [-2,2], and $\mathbf{Z}(t)$ is an adaptive mechanism described in [8].


ISBN 978-86-7466-930-3

*C. Horse Mating Behavior*

To simulate the departure and mating of horses, the following formula can be used:

$$\mathbf{X}_{G,k}^{p} = \text{crossover}\left(\mathbf{X}_{G,i}^{q}, \mathbf{X}_{G,j}^{z}\right);\ \ i \neq j \neq k; \quad p = q = \text{end};\ \ \text{crossover} = \text{mean} \tag{18}$$

where $\mathbf{X}_{G,k}^{p}$, $\mathbf{X}_{G,i}^{q}$ and $\mathbf{X}_{G,j}^{z}$ are the positions of horses *p*, *q* and *z* from groups *k*, *i* and *j*, respectively.

*D. Leadership and Leading the Group by the Leader*

The mathematical model of leading the group by the stallion can be described by (19).

*E. Exchange and Selection of Leaders*

In this step, the leaders of the groups – stallions are selected. Firstly, to preserve the stochastic nature of the algorithm, the leaders are selected randomly. In the later stages of the iteration process, the leaders are selected based on their fitness values using (20).

$$\mathbf{Stallion}_{G,i}(t+1) = \begin{cases} 2\cdot\mathbf{Z}(t)\cdot\cos\left(2\cdot\pi\cdot R\cdot\mathbf{Z}(t)\right)\times\left(\mathbf{WH}(t)-\mathbf{Stallion}_{G,i}(t)\right)+\mathbf{WH}(t) & \text{if}\ \ R_2 > 0.5 \\ 2\cdot\mathbf{Z}(t)\cdot\cos\left(2\cdot\pi\cdot R\cdot\mathbf{Z}(t)\right)\times\left(\mathbf{WH}(t)-\mathbf{Stallion}_{G,i}(t)\right)-\mathbf{WH}(t) & \text{if}\ \ R_2 \leq 0.5 \end{cases}, \tag{19}$$

$$\mathbf{Stallion}_{G,i}(t+1) = \begin{cases} \mathbf{X}_{G,i}(t+1) & \text{if}\ \ \text{cost}\left(\mathbf{X}_{G,i}(t+1)\right) < \text{cost}\left(\mathbf{Stallion}_{G,i}(t)\right) \\ \mathbf{Stallion}_{G,i}(t) & \text{if}\ \ \text{cost}\left(\mathbf{X}_{G,i}(t+1)\right) \geq \text{cost}\left(\mathbf{Stallion}_{G,i}(t)\right) \end{cases}. \tag{20}$$

In (19) and (20), **WH**(*t*) presents the position of the water hole (i.e. the global best position). More details about the WHO algorithm can be found in the paper [8].

As for any other optimization problem, a potential solution can be presented by a vector consisting of a combination of control variables, i.e., in this case, corresponding induction motor parameters. The electrical parameters of the single-cage motors are the following: $R_s$, $R_r$, $X_s$, $X_r$, and $X_m$. Generally, it is supposed that the stator and rotor leakage reactances are equal: $X_s = X_r$. Therefore, the position of the agent *i* can be defined as follows:

$$\mathbf{X}_i = \left[R_{s,i}, R_{r,i}, X_{s,i}, X_{m,i}\right]. \tag{21}$$

The flowchart of the WHO algorithm is given in Fig. 2.

## IV. Simulation Results and Discussion

The proposed WHO method is tested on two three-phase single-cage induction motors. The manufacturer data of the test motors are shown in Table I.

TABLE I
MANUFACTURER DATA OF THE TEST MOTORS [6,7]

| Parameters | Values | |
|---|---|---|
| Rated power $P_n$ (HP) | 5 | 40 |
| Rated voltage $U_n$ (V) | 400 | 400 |
| Rated frequency $f_n$ (Hz) | 50 | 50 |
| Starting current $I_{st}$ (A) | 22 | 180 |
| Full-load current $I_{fl}$ (A) | 8 | 45 |
| Number of pole pairs *p* | 2 | 2 |
| Starting torque $T_{st}$ (N·m) | 15 | 260 |
| Full-load torque $T_{fl}$ (N·m) | 25 | 190 |
| Maximum torque $T_{max}$ (N·m) | 42 | 370 |
| Full-load power factor $pf_{fl}$ | 0.8 | 0.8 |
| Slip at full load $s_{fl}$ | 0.07 | 0.09 |

The following parameter ranges are considered:

- For the motor of 5 HP:

$$0.1 \leq R_s \leq 5,\ 1 \leq X_s \leq 15,\ 50 \leq X_m \leq 150,$$
$$0.5 \leq R_r \leq 10,\ 1 \leq X_r \leq 15$$

- For the motor of 40 HP:

$$0.01 \leq R_s \leq 0.5,\ 0.1 \leq X_s \leq 2,\ 5 \leq X_m \leq 15,$$
$$0.05 \leq R_r \leq 1,\ 0.1 \leq X_r \leq 2$$

The algorithm was developed in the MATLAB computing environment. To examine the effectiveness of the proposed WHO algorithm, the same problem was solved using the PPSOGSA algorithm [6] (which proved to be effective in solving problems in this area). The obtained results are compared with those obtained using the other methods reported in the literature.

The algorithms are implemented with the following control parameters: for the PPSOGSA [6], $c_1$ and $c_2$ are set to 2, $\alpha$ is set to 25, and $G_0$ is set to 1; for the WHO [8], the crossover process is carried out using the mean value of corresponding group members (mean crossover type), crossover percentage is set to 0.1, and the percentage of stallions in the total population (*PS*) is set to 0.2. For both algorithms, the population size (*N*) and the maximum number of iterations ($t_{max}$) are set to 300 and 100, respectively.

The results of WHO and PPSOGSA are obtained after fifty consecutive test runs. The best results achieved over these runs are presented in Tables II and III. Also, the tables show the results obtained by other optimization methods. The corresponding steady-state equivalent circuit electrical parameters of the test motors are presented in Table IV.

By comparing the results from Tables II and III, it can be seen that the values of the objective function (*OF*) obtained with the WHO are lower than those obtained by other methods, except the MSFLA [7] for the motor of 5 HP. In [7], a larger range of control variables was taken into consideration, i.e. the optimal value of the stator resistance was 0.0037 Ω, which is far less than the value of 0.3 Ω obtained by the WHO, as presented in Table IV; that may be a possible reason why the *OF* value obtained using the MSFLA is less than the value obtained by the WHO.

The convergence profiles of the WHO and PPSOGSA for the motors of 5 HP and 40 HP are shown in Figs. 3 and 4, respectively. The figures indicate that the proposed WHO algorithm converges to the optimal solution in lower iterations in comparison to the PPSOGSA algorithm.

 ISBN 978-86-7466-930-3

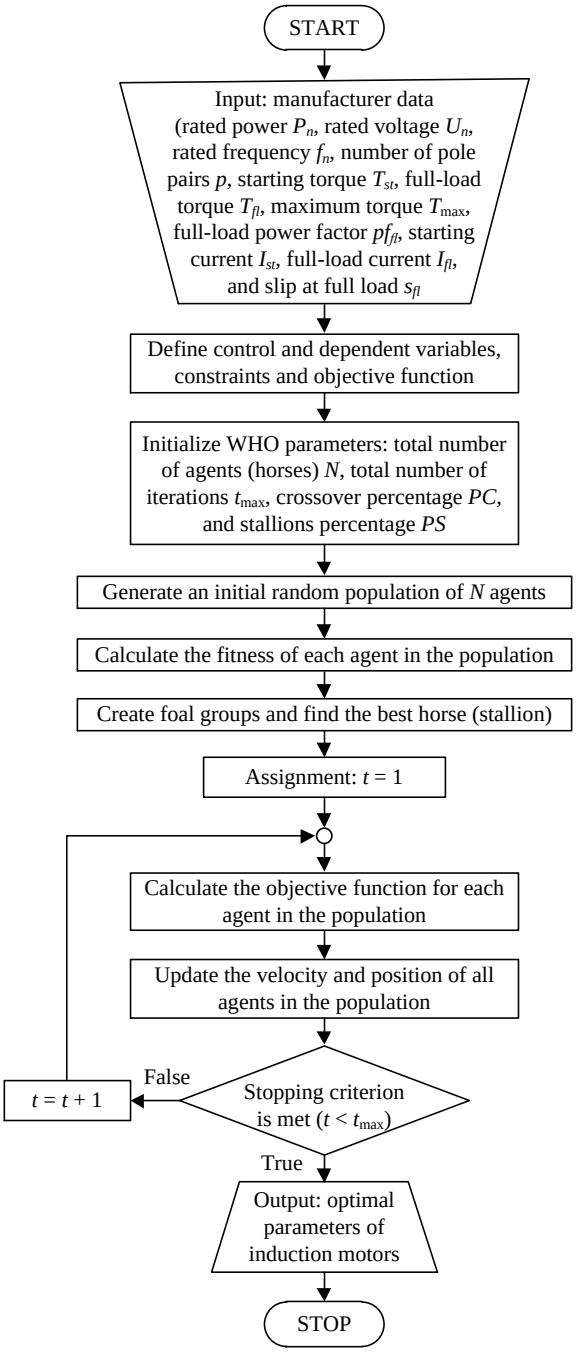


Fig. 2. The flowchart of the WHO algorithm in solving the induction motor parameter estimation problem.

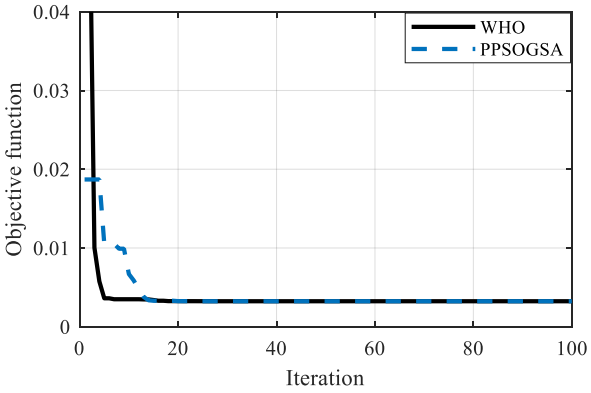


Fig. 3. Convergence profiles obtained for the motor of 5 HP.

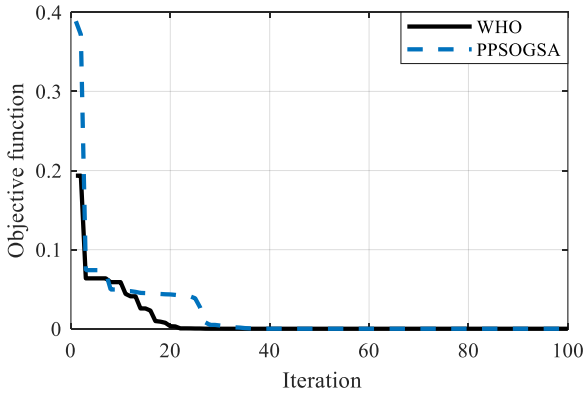


Fig. 4. Convergence profiles obtained for the motor of 40 HP.

Torque-slip characteristics of the motors of 5 HP and 40 HP obtained using the WHO algorithm are presented in Figs. 5 and 6, respectively. From these figures, it is evident that the results obtained by the WHO are in very good agreement with the manufacturer values.

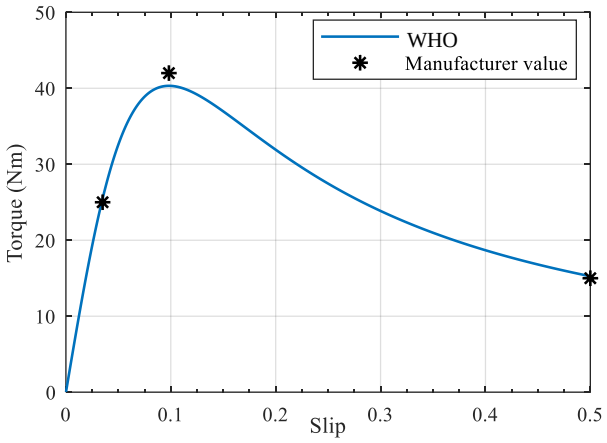


Fig. 5. Torque versus slip curve for the motor of 5 HP.

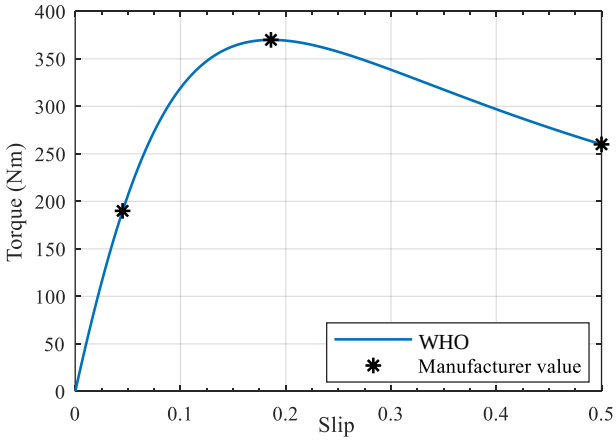


Fig. 6. Torque versus slip curve for the motor of 40 HP.

The statistical parameters of the results (i.e. minimum, maximum and mean values of the objective function, as well as the standard deviations) obtained by the WHO and PPSOGSA over fifty runs for the both test motors are presented in Table V. The results from Table V show that the proposed WHO algorithm is more robust compared to the PPSOGSA. From the aspect of running, the running time of the WHO is a little shorter than the time of the PPSOGSA.


ISBN 978-86-7466-930-3

TABLE II
A COMPARISON OF THE RESULTS OBTAINED BY THE PROPOSED METHOD AND OTHER METHODS FOR THE MOTOR OF 5 HP

| Parameter | Manufacturer data | PSO [7] | | SFLA [7] | | MSFLA [7] | | PPSOGSA | | WHO | |
|---|---|---|---|---|---|---|---|---|---|---|---|
| | | Reported result | Error (%) | Reported result | Error (%) | Reported result | Error (%) | Obtained result | Error (%) | Obtained result | Error (%) |
| $T_{st}$ (Nm) | 15 | 15.3465 | 2.31 | 15.4939 | 3.29 | 15.2725 | 1.82 | 15.3029 | 2.02 | 15.2987 | 1.99 |
| $T_{fl}$ (Nm) | 25 | 25.5692 | 2.28 | 25.6484 | 2.59 | 25.5541 | 2.22 | 25.6067 | 2.43 | 25.5979 | 2.39 |
| $T_{max}$ (Nm) | 42 | 39.0047 | –7.13 | 40.7390 | –3.00 | 40.3870 | –3.84 | 39.9683 | –4.84 | 40.0016 | –4.76 |
| $pf_{fl}$ | 0.8 | 0.7888 | –1.40 | 0.7710 | –3.63 | 0.7991 | –0.11 | 0.8000 | 0.00 | 0.8000 | 0.00 |
| *OF* | / | 0.006334059* | | 0.003972333* | | 0.002297462* | | 0.003336732 | | 0.003232706 | |

*Recalculated value

TABLE III
A COMPARISON OF THE RESULTS OBTAINED BY THE PROPOSED METHOD AND OTHER METHODS FOR THE MOTOR OF 40 HP

| Parameter | Manufacturer data | PSO[7] | | SFLA [7] | | MSFLA [7] | | PPSOGSA | | WHO | |
|---|---|---|---|---|---|---|---|---|---|---|---|
| | | Reported result | Error (%) | Reported result | Error (%) | Reported result | Error (%) | Obtained result | Error (%) | Obtained result | Error (%) |
| $T_{st}$ (Nm) | 260 | 261.1978 | 0.46 | 260.3347 | 0.13 | 259.5611 | −0.17 | 259.9991 | −0.00 | 260.00 | 0.00 |
| $T_{fl}$ (Nm) | 190 | 188.9053 | −0.58 | 193.5212 | 1.85 | 190.6352 | 0.33 | 189.9865 | −0.01 | 190.00 | 0.00 |
| $T_{max}$ (Nm) | 370 | 360.8307 | −2.48 | 365.0454 | −1.34 | 370.8140 | 0.22 | 370.0364 | 0.01 | 370.00 | 0.00 |
| $pf_{fl}$ | 0.8 | 0.7883 | −1.46 | 0.7860 | −1.75 | 0.7995 | −0.06 | 0.7999 | −0.00 | 0.80 | 0.00 |
| *OF* | / | 0.000882452* | | 0.000830679* | | $1.92569\times10^{-5}$* | | $3.03638\times10^{-8}$ | | 0 | |

*Recalculated value

TABLE IV
ELECTRICAL PARAMETERS OF INDUCTION MOTORS OBTAINED BY THE PROPOSED METHOD AND OTHER METHODS

| Parameter | Motor of 5 HP | | | | | Motor of 40 HP | | | | |
|---|---|---|---|---|---|---|---|---|---|---|
| | PSO [7] | SFLA [7] | MSFLA [7] | PPSOGSA | WHO | PSO [7] | SFLA [7] | MSFLA [7] | PPSOGSA | WHO |
| $R_s$ (Ω) | 0.9872 | 0.0008 | 0.0037 | 0.3300 | 0.3000 | 0.3555 | 0.3437 | 0.2707 | 0.2694 | 0.2778 |
| $X_s$ (Ω) | 5.3785 | 5.5847 | 5.7202 | 5.6667 | 5.6771 | 0.4353 | 0.4345 | 0.4773 | 0.4842 | 0.4797 |
| $X_m$ (Ω) | 77.042 | 77.9101 | 94.1401 | 91.5892 | 91.9613 | 6.4223 | 6.2629 | 7.5432 | 7.7277 | 7.6037 |
| $R_r$ (Ω) | 2.0322 | 2.1330 | 2.1818 | 2.1526 | 2.1574 | 0.3455 | 0.3360 | 0.3573 | 0.3631 | 0.3611 |
| $X_r$ (Ω) | 5.3785 | 5.5847 | 5.7202 | 5.6667 | 5.6771 | 0.4353 | 0.4345 | 0.4773 | 0.4842 | 0.4797 |

TABLE V
STATISTICAL PARAMETERS AND EXECUTION TIMES OF WHO AND PPSOGSA METHODS

| Power (HP) | Method | Minimum | Maximum | Mean | Standard deviation | Execution time [s] |
|---|---|---|---|---|---|---|
| 5 | PPSOGSA | 0.00334 | 0.00348 | 0.00338 | 0.00024 | 1.89 |
| | WHO | 0.00323 | 0.00323 | 0.00323 | 0 | 1.73 |
| 40 | PPSOGSA | $3.0364\times10^{-8}$ | 0.04491 | 0.00389 | 0.01151 | 1.46 |
| | WHO | 0 | 0.00592 | 0.00041 | 0.00154 | 1.35 |

## V. CONCLUSION

The main conclusions that can be drawn from the presented results and discussion of them are the follows:

- By comparing the results obtained using the WHO algorithm with those obtained using other algorithms (i.e. using the PSO, SFLA, MSFLA, and PPSOGSA algorithms), it is found that the WHO provides effective, robust and high-quality solutions.
- It is shown that the results obtained by the WHO algorithm are in very good agreement with the manufacturer data. The maximum relative deviations are less than 5%.
- The average running time of the WHO algorithm for both test motors was less than 2 s. This means that the calculation speed of the WHO algorithm is high.
- It is found that the WHO algorithm has better performance than the PPSOGSA algorithm in terms of the solution quality and convergence speed.

## ACKNOWLEDGMENT

The research for this article was carried out with ERASMUS + project: “Knowledge triangle for a low carbon economy (KALCEA)” and with scientific project the TR 33016 – “Research, development and implementation of programs and procedures Energy efficiency of electric drives” funded by the Ministry of Education, Science and Technological Development of the Republic of Serbia.

 ISBN 978-86-7466-930-3

## REFERENCES


[1] V. P. Sakthivel, R. Bhuvaneswari, S. Subramanian, "Multi-objective parameter estimation of induction motor using particle swarm optimization," *Engineering Applications of Artificial Intelligence*, vol. 23, iss. 3, pp. 302-312, 2010

[2] I. Kostov, V. Spasov, V. Rangelova, "Application of genetic algorithms for determining the parameters of induction motors," *Technical Gazette*, vol. 16, no. 49, pp. 49–53, 2009

[3] A. I. Canakoglu, A. G. Yetgin, H. Temurtas, M. Turan, "Induction motor parameter estimation using metaheuristic methods," *Turkish Journal of Electrical Engineering & Computer Sciences*, vol. 22, pp. 1177-1192, 2014

[4] H. R. Mohammadi, A. Akhavan, "Parameter estimation of three-phase induction motor using hybrid of genetic algorithm and particle swarm optimization," *Journal of Engineering*, vol. 2014, pp. 198-204, 2014

[5] O. Avalos, E. Cuevas, E. Cuevas, "Induction Motor Parameter Identification Using a Gravitational Search Algorithm," *Computers*, vol. 5, no. 6, 2016

[6] J. Vukasinović, M. Milovanović, N. Arsić, J. Radosavljević, S. Statkić, "Parameters estimation of double-cage induction motors using a hybrid metaheuristic algorithm," 21st International Symposium INFOTEH-JAHORINA (INFOTEH) East Sarajevo, Bosnia and Herzegovina, pp. 1-6, March 16-18, 2022

[7] I. Perez, M. Gomez-Gonzalez, F. Jurado, "Estimation of induction motor parameters using shuffled frog-leaping algorithm," *Electrical Engineering*, vol. 95, iss. 3, pp. 267-275, 2012

[8] I. Naruei, F. Keynia, "Wild horse optimizer: a new meta-heuristic algorithm for solving engineering optimization problems," *Engineering with Computers*, vol. no, pp. no, 2021

[9] A. Ramadan, S. Kamel, I. B. M. Taha, M. Tostado-Véliz, "Parameter estimation of modified double-diode and triple-diode photovoltaic models based on wild horse optimizer," *Electronics*, vol. 10, no.18, pp. 1-19, 2021

[10] A. Ramadan, S. Kamel, M. H. Hassan, M. Tostado-Véliz, "Parameter estimation of static/dynamic photovoltaic models using a developed version of eagle strategy gradient-based optimizer," *Sustainability*, vol. 13, no. 23 pp. 1-29, 2021

[11] S. Khatir, M. A. Wahab, S. Tiachacht, C. L. Thanh, R. Capozucca, E. Magagnini, B. Benaissa, "Damage identification in steel plate using FRF and inverse analysis," *Frattura ed Integrità Strutturale*, vol. 58, pp. 416-433, 2021


 ISBN 978-86-7466-930-3

# Damper Winding Inductances Calculation by Winding Function Approach

Aldin Kajević, Gojko Joksimović, *Senior Member, IEEE*

***Abstract*—The paper presents a procedure for dq model parameters calculation of a synchronous turbogenerator using winding function theory, with special emphasis on the damper winding. The advantage of this procedure is that the real spatial distribution of all windings in the machine is taken into account, therefore, taking into account all spatial harmonics simultaneously. A real synchronous turbogenerator of type TBB-200-2A was analyzed as a case study.**

***Index Terms*—Damper winding, Inductance, Synchronous machine, Turbo-generator, Winding function.**

## I. Introduction

Mathematical model of synchronous machine projected on two mutually orthogonal axes, *dq* model, is the most common dynamic model of synchronous machine, [1], [2]. Although the model itself is often found in the literature, in rare cases attention is paid to determining the parameters that appear in the model itself. Additionally, model parameters are most often given in unit values. The key parameters of the model that are at the same time the most demanding to determine are the self and mutual inductances of the windings. Analytical expressions that assume an ideal, sinusoidal spatial distribution of windings are often used when determining these parameters, or, which is the same, only the fundamental harmonic of the real spatial winding distribution is taken into account, [3], [4]. In this paper, using the theory of the winding functions, [5], [6], [7], [8], all spatial harmonics of the magnetomotive force (mmf) of the real winding are taken into account simultaneously.

The generic synchronous machine is characterized by the existence of three symmetrical armature phase windings as well as the field and damper winding on the rotor.

The paper presents a methodology that allows direct and fairly intuitive determination of self and mutual inductances of windings, inductances that appear as parameters of the *dq* model of the machine. The first step in order to calculate inductances is to determine the winding functions of the stator windings and the damper windings of the machine in the natural frame of reference. However, the following convention should be introduced here: in order to avoid rugged constructions as "winding function of field winding" or "winding function of stator phase winding", etc. a simpler sentence construction will be used – simply "field winding function" or "damper winding function" or "stator phase winding function". When the winding functions are known, then in the case of stator phase windings, their equivalent winding functions are determined in a rotating *dqn* reference frame fixed to the rotor. The role of these functions is twofold. Firstly, they enable obtaining self and mutual inductances of the stator windings directly in the *dqn* system. Secondly, their existence enables, in combination with the damper winding functions along the *d* and *q* axes, the direct calculation of its mutual inductances. The procedure for obtaining the damper winding functions along the *d* and *q* axes is also presented in this paper and these functions represent one of the main results of this paper.

The whole procedure is illustrated on the example of a synchronous turbogenerator of type TBB-200-2A. As a final result, all self and mutual inductances that appears as the parameters of the *dq* model are determined. A comparison of the obtained parameters concerning the stator windings with the factory data of the generator was performed and a high degree of agreement was observed.

Aldin Kajević is with the Faculty of Electrical Engineering, University of Montenegro, Cetinjski put b.b, 81000 Podgorica, Montenegro (e-mail: Aldin.Kajevic@ucg.ac.me)

Gojko Joksimović is with the Faculty of Electrical Engineering, University of Montenegro, Cetinjski put b.b, 81000 Podgorica, Montenegro (e-mail: Gojko.Joksimovic@ucg.ac.me), (https://orcid.org/0000-0002-2764-1540)

## II. DQ Model of Synchronous Machine

The voltage equations of a synchronous turbogenerator in matrix form are given below, [1]. The indexes *a*, *b* and *c* are associated with the values concerning the three phase windings of the stator, in the natural (*abc*) frame of reference. The indexes *d* and *q* are associated with the damper winding along the *d* and *q* axes, respectively. Index *f* refers to the field winding. The indexes *s* and *r* refer to the stator and rotor, respectively.

$$[U_{abcs}] = [R_s][i_{abcs}] + \frac{d}{dt}[\psi_{abcs}] \quad (1)$$

$$[U_{dqfr}] = [R_r][i_{dqfr}] + \frac{d}{dt}[\psi_{dqfr}] \quad (2)$$

The equations of magnetic coupling for the stator and rotor windings, in matrix form, are:

$$[\psi_{abcs}] = [L_{abcs}][i_{abcs}] + [L_{abcsr}][i_{dqfr}] \quad (3)$$

 ISBN 978-86-7466-930-3

$$\left[\psi_{dqfr}\right]=\left[L_{abcsr}\right]^{T}\left[i_{abcs}\right]+\left[L_{dqfr}\right]\left[i_{dqfr}\right] \quad (4)$$

Vectors of voltages, currents and fluxes that appear in the previous expressions together with the matrices of inductance and resistance are given in the Appendix. The same will be done with the vectors and matrices in the continuation of the work.

It is now necessary to transform the previous equations from the natural (*abc*) frame of reference to the rotating *dqn* coordinate system. The transformation will be done using the transformation matrix [$T(\theta)$]. The angle θ in the transformation matrix is the angle that the rotating reference frame, fixed to the rotor, occupies at a certain point in time in relation to the reference, i.e. initial position. For a coordinate system that rotates with an arbitrary angular velocity ω, assuming that the initial angle is equal to zero, at time $t$=0, the following holds:

$$\theta=\omega t \quad (5)$$

After the transformation of equations, procedure of which will not be presented in detail here, the following equations are obtained in the *dqn* system,

$$\left[U_{dqns}\right]=\left[R_s\right]\left[i_{dqns}\right]+\frac{d\left(\left[\psi_{dqns}\right]\right)}{dt}+\left[\omega x\right]\left[\psi_{dqns}\right] \quad (6)$$

$$\left[U_{dqfr}\right]=\left[R_r\right]\left[i_{dqfr}\right]+\frac{d}{dt}\left[\psi_{dqfr}\right] \quad (7)$$

$$\left[\psi_{dqns}\right]=\left[L_{dqns}\right]\left[i_{dqns}\right]+\left[L_{dqnsr}\right]\left[i_{dqfr}\right] \quad (8)$$

$$\left[\psi_{dqfr}\right]=\frac{3}{2}\left[L_{dqnsr}\right]^{T}\left[i_{dqns}\right]+\left[L_{dqfr}\right]\left[i_{dqfr}\right] \quad (9)$$

where:

$$\left[L_{dqns}\right]=\left[T(\theta)\right]\left[L_{abcs}\right]\left[T(\theta)\right]^{-1} \quad (10)$$

$$\left[L_{dqnsr}\right]=\left[T(\theta)\right]\left[L_{abcsr}\right] \quad (11)$$

## III. WINDING FUNCTIONS IN DQ SYSTEM, INDUCTANCES AND METHOD OF THEIR DETERMINATION

The stator winding functions in the *dqn* system are given in expression (12). There $N_a(\theta_m)$, $N_b(\theta_m)$ and $N_c(\theta_m)$ are the stator phase windings functions in the natural frame of reference, and $\theta_m$ is the mechanical angle.

In addition to the previously listed winding functions, it is necessary to determine the function of the field winding $N_{fr}(\theta_m)$, as well as the damper winding functions along the *d* and *q* axes, $N_{dr}(\theta_m)$ and $N_{qr}(\theta_m)$, respectively. All these functions will be determined in the following by applying the winding function theory on the example of a real synchronous turbogenerator of type TBB-200-2A.

When the winding functions for all windings are determined then self and mutual inductances in the model matrices can be obtained by numerical integration. Some of the inductances in the matrices [$L_{dqns}$], [$L_{dqnsr}$] and [$L_{dqfr}$] are given by expressions (15) - (20), just for illustration purposes.

$$N_{ds}=\frac{2}{3}\left(N_a(\theta_m)\sin(\theta)+N_b(\theta_m)\sin\left(\theta-\frac{2\pi}{3}\right)+N_c(\theta_m)\sin\left(\theta+\frac{2\pi}{3}\right)\right) \quad (12)$$

$$N_{qs}=\frac{2}{3}\left(N_a(\theta_m)\cos(\theta)+N_b(\theta_m)\cos\left(\theta-\frac{2\pi}{3}\right)+N_c(\theta_m)\cos\left(\theta+\frac{2\pi}{3}\right)\right) \quad (13)$$

$$N_{ns}=\frac{\sqrt{2}}{3}\left(N_a(\theta_m)+N_b(\theta_m)+N_c(\theta_m)\right) \quad (14)$$

$$L_{dsds}=\frac{3\mu_0 rl}{2g}\int_0^{2\pi}N_{ds}^2(\theta_m,\theta)d\theta_m \quad (15)$$

$$L_{dsqs}=\frac{3\mu_0 rl}{2g}\int_0^{2\pi}N_{ds}(\theta_m,\theta)N_{qs}(\theta_m,\theta)d\theta_m \quad (16)$$

$$L_{dsdr}=\frac{\mu_0 rl}{g}\int_0^{2\pi}N_{ds}(\theta_m,\theta)N_{dr}(\theta_m,\theta_r)d\theta_m \quad (17)$$

$$L_{dsqr}=\frac{\mu_0 rl}{g}\int_0^{2\pi}N_{ds}(\theta_m,\theta)N_{qr}(\theta_m,\theta_r)d\theta_m \quad (18)$$

$$L_{drdr}=\frac{\mu_0 rl}{g}\int_0^{2\pi}N_{dr}^2(\theta_m,\theta)d\theta_m \quad (19)$$

$$L_{drqr}=\frac{\mu_0 rl}{g}\int_0^{2\pi}N_{dr}(\theta_m,\theta)N_{qr}(\theta_m,\theta_r)d\theta_m \quad (20)$$

etc.

## IV. STATOR PHASE WINDING AND FIELD WINDING FUNCTIONS

The synchronous generator of type TBB-200-2A is a turbogenerator that is cooled by water and hydrogen. Its rated active power is 200 MW, rated voltage is 15.75 kV, rated frequency 50 Hz. It is a two-pole generator. On the stator of this generator, there exists 60 slots in which the stator winding is manufactured. The stator winding consists of three symmetrical phase windings. Each phase winding additionally consists of two half-windings connected in parallel. The phase windings are connected in star conection. Due to the existence of two parallel connected half-windings, this conection is also known as a double star conection. The three-phase stator winding consists of sixty coil groups with one coil, or twenty coils per phase - ten per half-winding. In Fig. 1 all slots and all coil groups on the stator and rotor are shown and numbered. On the stator, the shades of red represent the conductors of the phase A winding. More intense red color shows the first and lighter one the second half-winding. The other two phases are represented by shades of yellow and green - phase B in yellow and phase C in green. All slots, coil

 ISBN 978-86-7466-930-3

groups are clearly numbered and the adopted reference directions of currents and mechanical angle are shown. Based on the previous data, the functions of the phase windings can be determined, [5]-[8]. Thus, the winding function of phase A is given in Fig. 2.

Field and damper winding are mounted in 36 rotor slots. The rotor slot pitch is $\tau_r=2\pi/52$. The field winding consists of 18 coil groups, and each coil group consists of seven coils. Coil groups of the field winding are marked in green and red on the rotor, Fig. 1. Damper winding consists of conductive wedges made of aluminum alloy which close the slots in which the field winding is located. These bars are short-circuited on the front and back sides by a conductive tension rings. They are shown in blue in Fig. 1 The waveform of the field winding function is given on Fig. 3 – that is at the same time the waveform of the field winding mmf for a unit current, [1].

The functions of the fictive stator windings in the rotating frame of reference fixed to the rotor are obtained from the original functions of the phase windings using expresions (12)-(14). The winding functions obtained in this way, under the *d* and *q* axes, are given in Fig. 4 for the case $\theta=0^o$.

All of these functions will be used in the following paragraphs to calculate the inductances that appear in the *dq* model.

The function of the field winding that is located on the rotor does not need to be reduced because the rotating frame of reference is already fixed to the rotor. The magnetic axis of this winding is the *d* axis, Fig. 1.

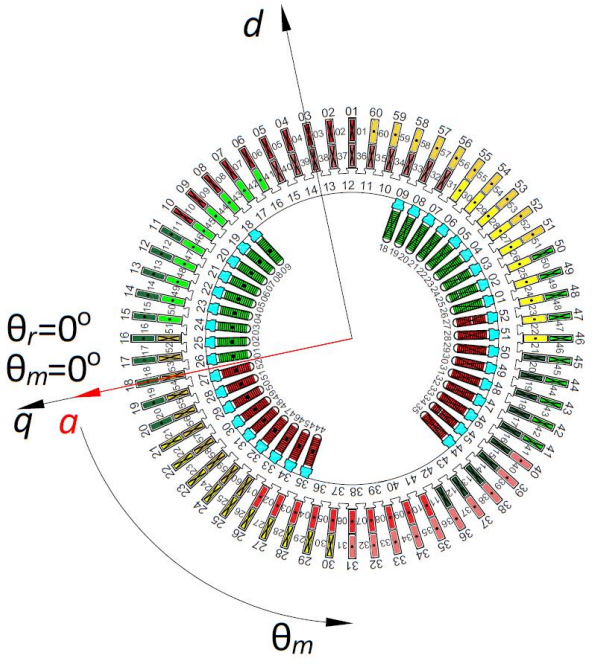


Fig.1. Design of phase, field and damper windings of the TBB-200-2A turbogenerator

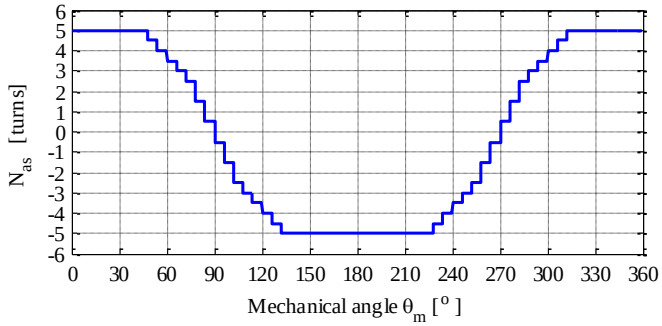


Fig.2. Stator phase A - winding function

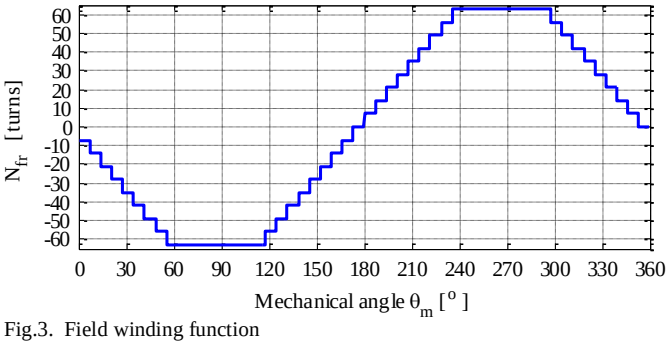


Fig.3. Field winding function

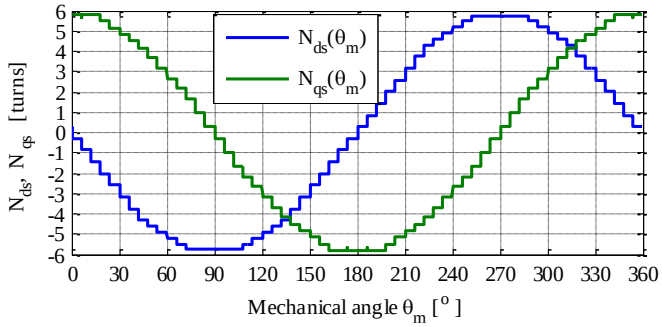


Fig.4. Fictive stator winding functions reduced to a rotating frame of reference, $\theta=0^o$

## V. DAMPER WINDING FUNCTIONS

Structurally, the damper winding consists of conductive bars located in the top of the rotor slots. These bars are short-circuited on the front and back sides by the conductive tension rings. From the construction of the damper winding itself, it is clear that the same currents do not flow in short-circuited conducting bars, which, at first glance, makes this winding complicated for analysis using the concept of winding function. Namely, in order to be able to apply the definition of the winding function, it is necessary that one and the same current flows through that winding, [1]. This condition is met for armature phase windings and the field winding. This difficulty in determining the function of the damping winding can be overcome by taking into account some assumptions and neglections. As the bars on the rotor are short-circuited, currents in them are induced as a result of time-varying magnetic flux generated by currents in the phase windings of the stator. Due to the symmetry of the phase windings, it is sufficient to observe the case of induced currents resulting from the magnetic flux generated by one of the armature

 ISBN 978-86-7466-930-3

phase windings. The phase A winding will be observed here. Based on the currents induced in the bars as a consequence of the current in the phase winding, a usable damper winding function along the *d* and *q* axes can be obtained.

In order to determine the function of the damper winding along the *d* axis, Fig. 5 shows the developed scheme of the damper winding for the case when the *d* axis is in the same position as the axis of the phase A winding, i.e. the *d* axis is below the maximum value of fundamental harmonic of winding A mmf wave.

The $N_{as}$ function shown in red in Fig. 5 represents the fundamental harmonic of the phase A winding function. Multiplying function $N_{as}(\theta_m)=N_m\cos(\theta_m)$ by the sinusoidal current in the winding, $I_a\sin(\omega_e t)$, gives a pulsating mmf. As the air-gap in the turbogenerator is uniform (ignoring the stator and rotor slots), the magnetic flux density wave created by the phase A winding will also be sinusoidal along the rotor circumference. Due to the existence of symmetry, the induced currents in bars 1 and 1' are the same but of opposite polarity, so these two bars can be considered as one fictious coil. The same situation is with 2-2', 3-3' pair of bars, etc. which are under same pole. The magnetic fluxes coupled by these fictitious coils are given by the following expressions,

$$\phi_{11'}=\frac{2\mu_0 N_m I_a r l \sin(9z/2)}{g}\sin(\omega_e t) \qquad (21)$$

$$\phi_{22'}=\frac{2\mu_0 N_m I_a r l \sin(11z/2)}{g}\sin(\omega_e t) \qquad (22)$$

etc.

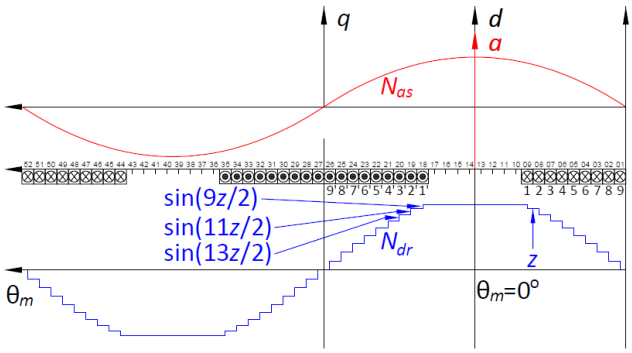


Fig.5. Damper winding function along the *d* axes

What can be seen from the previous expressions is the fact that the fluxes in the fictious coils differ only by the factors sin(9z/2), sin(11z/2), ... This difference is due to the difference in the area occupied by these coils, or differences in coil step. The induced electromotive forces in them differ for the same factors. The resistance and leakage inductance of each bar is the same. The resistance and leakage inductance of the ring segments connecting the two bars of the fictitious coil is different for each coil due to the difference in length. However, as the resistance and leakage inductance of the ring segments are usually very small, [1], around thousend times smaller than values for bars, they will not be considered here. As a consequence of the previously mentioned neglection, the currents in the fictitious windings will be the ratio of the induced electromotive force and the double impedance of the bar. Based on the above, it is concluded that the currents will differ only by the factors sin(9z/2), sin(11z/2), ..., too. Now the damper winding can be viewed as a fictive, concentrated winding through whose coils flows the same current. However, each coil has a number of conductors that differs by a factor of sin(9z/2), sin(11z/2), ... etc. In this way the mmf of the damper winding remains unchanged. The damper winding function obtained in this way is sketched in Fig. 5, in blue. Fig. 7 shows the exact shape of the damper winding function along the *d* axis, for the analysed machine, taking the position of the *q* axis as the starting position for the mechanical angle when it is in the same position as the phase A winding axis, $\theta_r=0^o$.

The procedure for obtaining the damper winding function along the *q* axis is similar to the previous procedure. Now, Fig. 6, *q* axis is placed in a position that coincides with the magnetic axis of the phase A winding. Due to the obvious symmetry the currents induced in bars 1 and 1' are the same in magnitude but opposite in direction, so these two bars can be viewed as a fictive coil. The situation is similar with other pairs of bars 2-2', 3-3', etc. The magnetic fluxes coupled by these fictive coils are:

$$\phi_{11'}=\frac{2\mu_0 N_m I_a r l \sin(z/2)}{g}\sin(\omega_e t) \qquad (23)$$

$$\phi_{22'}=\frac{2\mu_0 N_m I_a r l \sin(3z/2)}{g}\sin(\omega_e t) \qquad (24)$$

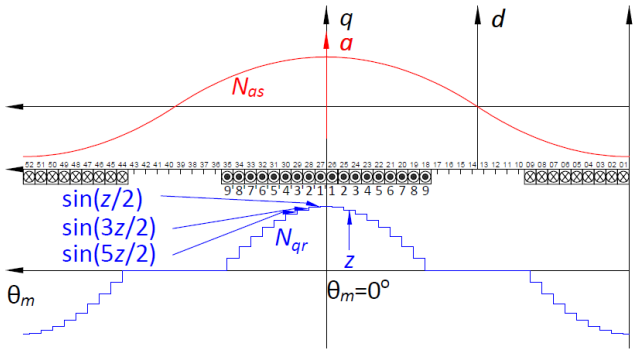


Fig.6. Damper winding function along the *q* axes

Now the factors are sin(z/2), sin(3z/2), etc. As before, ignoring the impedances of the ring segments that connect the corresponding bars, one can conclude that the currents will differ from each other only by the factors sin(z/2), sin(3z/2), etc. Now the damper winding along the *q* axis can be considered as fictitious concentrated winding through whose coils the same current flows, but each of the coils has different number of conductors. In this way the mmf of the damper winding remains unchanged. The function of the damper winding along the *q* axis is sketched in Fig. 7 in blue. Fig. 8 gives the exact waveform of the damper winding function along the *q* axis, for the analyzed machine and for the adopted reference directions from Fig. 1.


ISBN 978-86-7466-930-3

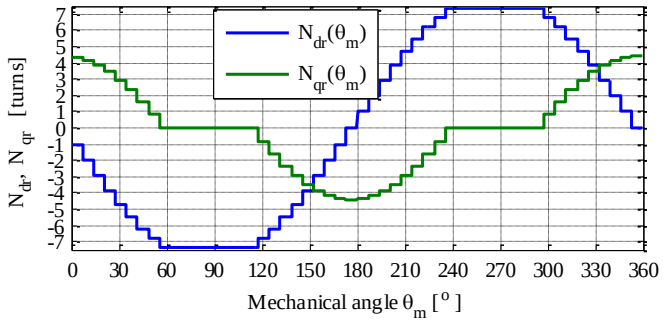


Fig.7. Damper winding functions along the *d* and *q* axes

## VI. Results

The winding functions defined in the previous paragraphs enable the determination of all inductances that appear in the equations of the *dq* model. As the rotating frame of reference is fixed to the rotor all the inductances of the model are constant valued. The values of inductances obtained on the example of the analyzed generator are given in Table I.

TABLE I
CALCULATED INDUCTANCES FOR ANALYSED MACHINE

| $L_{dsds}$ | $L_{qsqs}$ | $L_{dsqs}$ | $L_{dsns}$ | $L_{qsns}$ | $L_{dsdr}$ | $L_{qsqr}$ | $L_{dsqr}$ |
|---|---|---|---|---|---|---|---|
| mH | mH | mH | mH | mH | mH | mH | mH |
| 6.6 | 6.6 | 0.0017 | 0.0 | 0.0 | 5.9 | 2.65 | 0.16 |
| $L_{qsdr}$ | $L_{dsfr}$ | $L_{qsfr}$ | $L_{drdr}$ | $L_{qrqr}$ | $L_{drqr}$ | $L_{drfr}$ | $L_{qrfr}$ |
| mH | mH | mH | mH | mH | mH | mH | mH |
| –0.36 | 48.8 | –2.95 | 8.0 | 1.8 | 0.0 | 65.9 | –0.0023 |

What can be noticed from the previous Table is that there is a certain magnetic coupling between those windings that are located on orthogonal axes (except on the fictitious *n* axis which is normal to the plane formed by the *d* and *q* axes). This magnetic coupling is, however, very weak, as illustrated by the obtained values of the mutual inductances of the windings along these axes: $L_{dsqs}$, $L_{dsqr}$, $L_{qsdr}$, $L_{qsfr}$ and $L_{qrfr}$. The existence of these mutual inductances is a consequence of higher spatial harmonics which are taken into account by the winding functions.

By adding the leakage inductance of armature phase winding, which for this generator is 0.5 mH to the inductance $L_{dsds}$, synchronous inductance along the *d* axis is 7.1 mH. Multiplying this value by the electric angular frequency results in a synchronous reactance along the *d* axis of this generator: $X_d$ =2.2305 Ω. By dividing this reactance with the base impedance of the generator, $Z_b$=1.0556 Ω, unit value of synchronous reactance along the *d* axis can be obtained: $x_d$=2.113. The unit value of synchronous reactance given in the "passport" of this generator is $x_d$ =2.106. This very good match, testifies to the usefulness of this procedure in determining the parameters of the *dq* model.

## VII. Conclusion

The method of determining the parameters of the *dq* model of a synchronous generator using winding function theory is presented in this paper. The procedure enables direct obtaining of parameters without the need for a large number of mathematical manipulations over matrix equations. The method of determining the functions of the damper winding along the *d* and *q* axes, which enables its modeling, is also presented. The procedure is illustrated on a real synchronous turbogenerator of type TBB-200-2A.

Plan for future research is to develop software that will enable obtaining electromagnetic torque, stator, field and damper windings curents in the time domain using the parameters obtained by the explained procedure.

## Appendix

$$[U_{abcs}]=[U_{as}\quad U_{bs}\quad U_{cs}]^T$$

$$[U_{dqfr}]=[U_{dr}\quad U_{qr}\quad U_{fr}]^T$$

$$[i_{abcs}]=[i_{as}\quad i_{bs}\quad i_{cs}]^T$$

$$[i_{dqfr}]=[i_{dr}\quad i_{qr}\quad i_{fr}]^T$$

$$[R_s]=\begin{bmatrix} r_s & 0 & 0\\ 0 & r_s & 0\\ 0 & 0 & r_s\end{bmatrix}$$

$$[R_r]=\begin{bmatrix} r_{dr} & 0 & 0\\ 0 & r_{qr} & 0\\ 0 & 0 & r_{fr}\end{bmatrix}$$

$$[L_{abcs}]=\begin{bmatrix} L_{asas}+L_{ls} & L_{asbs} & L_{ascs}\\ L_{asbs} & L_{bsbs}+L_{ls} & L_{bscs}\\ L_{ascs} & L_{bscs} & L_{cscs}+L_{ls}\end{bmatrix}$$

$$[L_{abcsr}]=\begin{bmatrix} L_{asdr} & L_{asqr} & L_{asfr}\\ L_{bsdr} & L_{bsqr} & L_{bsfr}\\ L_{csdr} & L_{csqr} & L_{csfr}\end{bmatrix}$$

$$[L_{dqfr}]=\begin{bmatrix} L_{drdr} & L_{drqr} & L_{drfr}\\ L_{drqr} & L_{qrqr} & L_{qrfr}\\ L_{drfr} & L_{qrfr} & L_{frfr}\end{bmatrix}$$

$$[T(\theta)]=\frac{2}{3}\begin{bmatrix} \sin(\theta) & \sin\left(\theta-\frac{2\pi}{3}\right) & \sin\left(\theta+\frac{2\pi}{3}\right)\\ \cos(\theta) & \cos\left(\theta-\frac{2\pi}{3}\right) & \cos\left(\theta+\frac{2\pi}{3}\right)\\ \frac{1}{\sqrt{2}} & \frac{1}{\sqrt{2}} & \frac{1}{\sqrt{2}}\end{bmatrix}$$

$$[\omega x]=\begin{bmatrix} 0 & -\omega & 0\\ \omega & 0 & 0\\ 0 & 0 & 0\end{bmatrix}$$

$$[U_{dqns}]=[T(\theta)][U_{abcs}]$$

$$[i_{dqns}]=[T(\theta)][i_{abcs}]$$


ISBN 978-86-7466-930-3

$$\left[\psi_{dqns}\right]=\left[T\left(\theta\right)\right]\left[\psi_{abcs}\right]$$

$$\left[L_{dqns}\right]=\begin{bmatrix} L_{dsds}+L_{ls} & L_{dsqs} & L_{dsns} \\ L_{dsqs} & L_{qsqs}+L_{ls} & L_{qsns} \\ L_{dsns} & L_{qsns} & L_{nsns}+L_{ls} \end{bmatrix}$$

$$\left[L_{dqnsr}\right]=\begin{bmatrix} L_{dsdr} & L_{dsqr} & L_{dsfr} \\ L_{qsdr} & L_{qsqr} & L_{qsfr} \\ L_{nsdr} & L_{nsqr} & L_{nsfr} \end{bmatrix}$$

## REFERENCES


[1] T. A. Lipo, "Analysis of synchronous machines", CRC Press, 2012.

[2] I. Boldea, S. A. Nasar, "Synchronous generators", CRC Press, 2006.

[3] T. A. Lipo, "Introduction to ac machine design", IEEE Press, John Wiley & Sons, Hoboken, New Jersey, 2017.

[4] S. Vukosavić: "Električne mašine", Akademska misao, Beograd, 2010.

[5] G. Joksimović, M. Đurović, J. Penman, "Cage rotor mmf – winding function approach", IEEE Power Engineering Review, vol. 21, no. 4, pp. 64-66, April 2001.

[6] G. Joksimović, "AC winding analysis using winding function approach", International Journal of Electrical Engineering Education, Manchester University Press, vol. 48, no. 1, pp. 34-52(19), January 2011.

[7] E. S. Obe, "Direct computation of ac machine inductances based on winding function theory", Energy Conversion Management, vol. 50, no. 3, pp. 539–542, 2009.

[8] G. Joksimović, E. Levi, A. Kajević, M. Mezzarobba, A. Tessarolo, "Optimal selection of rotor bar number for minimizing torque and current pulsations due to rotor slot harmonics in three-phase cage induction motors", *IEEE Access*, vol. 8, pp. 228572-228585, 2020.


 ISBN 978-86-7466-930-3

# Inteligentni DTC algoritam sa automatskom reorganizacijom u zavisnosti od ripla momenta

Marko Rosić

***A stra t* — ad prezentuje ara teristi e algoritma dire tne ontrole momenta bazirane na dis retizovanim napons im intenzitetima sa mogućnošću automats e modifi acije u cilju ograničenja ripla (pulsacija) momenta ispod njegove definisane ma simalno dozvoljene vrednosti u pogonu. Algoritam je baziran na onvencionalnoj prekidač oj tabeli sa proizvoljnim brojem dis retizovanih napons ih intenziteta omogućavajući na taj način veću prostornu rezoluciju naponskih vektora u αβ ravni i rezultujući manjim intenzitetom ripla momenta. roj raspoloživih napons ih intenziteta (ve tora) može biti jednostavno definisan ili izmenjen bez potrebe za odgovarajućom izmenom prekidač e tabele. zavisnosti od definisanog broja napons ih intenziteta odgovarajuće izmene upravljačke stru ture algoritma su automatizovane, čineći ovaj algoritam jednostavnim, efi asnim i pogodnim za implementaciju u pametnim pogonima oje zahteva ubrzano dolazeća Industrija 4. . sperimentalna verifi acija rezultata na digitalnoj platformi 2 5, potvrđuje značajnu redu ciju ripla momenta asinhrone mašine u zavisnosti od broja napons ih intenziteta istovremeno zadržavajući jednostavnost, efi asnosti i dobre dinamičke osobine DTC pogona sa asinhronom mašinom.**

***Ključne reči*—direktna kontrola momenta, asinhrona mašina, automats a modifi acija algoritma, pametni pogon, Industrija 4. , ripl momenta, indu ovana , 2 5.**

## I. UVOD

Principi konvencionalne direktne kontrole momenta (cDTC) su dobro poznati i prezentovani u brojnoj naučnoj i stručnoj literaturi. Jednostavnost i dobre dinamičke osobine ovog vida kontrole čine ga i dalje aktuelnim u savremenim industrijskim pretvaračima. Kada se radi o metodama DTC zasnovane na prekidačkim tabelama, ripl momenta kao najveći nedostatak ove metode, pored ostalog, u najvećoj meri zavisi od broja raspoloživih naponskih vektora. Sa povećanjem broja raspoloživih naponskih vektora, korišćenjem invertora sa više nivoa ili kombinacije aktivnih naponskih vektora, DTC algoritmi zahtevaju definisanje nove, složenije prekidačke table koja zavisi od broja aktivnih naponskih vektora i brzine obrtanja motora [1, 2].

Sa druge strane, savremeni upravljački algoritmi, pored osnovnog dela, zahtevaju implementaciju i brojnih pratećih algoritamskih struktura kao što su estimacija parametara mašine u toku rada, self-tuning metode, napredni estimatori fluksa, opserveri stanja, kompenzacija efekta mrtvog vremena [3-5], itd. Iako ovi prateći algoritmi doprinose kvalitetu i stabilnosti pogona u širokom opsegu radnih brzina i režima rada, oni povećavaju ukupno proračunsko vreme algoritma ($T_s$ ≈ 50-100 μs) smanjujući frekvenciju izvršavanja algoritma odnosno ograničavaju propusni opseg regulisane veličine. Iz tog razloga potrebno je da glavni deo algoritma bude što je moguće jednostavniji i manje vremenski zahtevan kako se ne bi umanjile dinamičke karakteristike sistema.

Industrija 4.0 takođe zahteva razvoj inteligentnih elektromotornih pogona sposobnih da izvrše samo evaluaciju, procenu stanja i životnog veka, autodetekciju kvara itd. [6-7]. Iz tog razloga upravljački algoritmi sa jedne strane treba da imaju sposobnost brze optimizacije i modifikacije u toku rada, a sa druge strane proračunsku jednostavnost i efikasnost koja ostavlja dovoljno prostora za implementaciju pomenutih pratećih kompenzacionih algoritamskih struktura.

Imajući u vidu navedeno, postoji potreba za robusnim, što jednostavnijim algoritmima, kao što je cDTC, sa visokim dinamičkim osobinama i malim riplom struje / momenta. Ovaj rad prezentuje karakteristike DTC algoritma baziranog na prekidačkoj tabeli sa mogućnošću njegove automatske adaptacije u cilju smanjenja ripla momenta, a u zavisnosti od broja raspoloživih diskretizovanih naponskih intenziteta (DVI). Definisanje broja naponskih intenziteta moguće je ručno (od strane korisnika) ili automatski, u zavisnosti od definisane maksimalne vrednosti ripla momenta u pogonu i ne zahteva izmene konvencionalne prekidačke tabele.

## II. TEORIJSKA POZADINA DVI-DTC ALGORITMA

DVI-DTC metod baziran je na primeni više diskretizovanih naponskih intenziteta u svakom od šest osnovnih pravaca kod standardnog naponskog invertora kao što je prikazano na Sl.1.

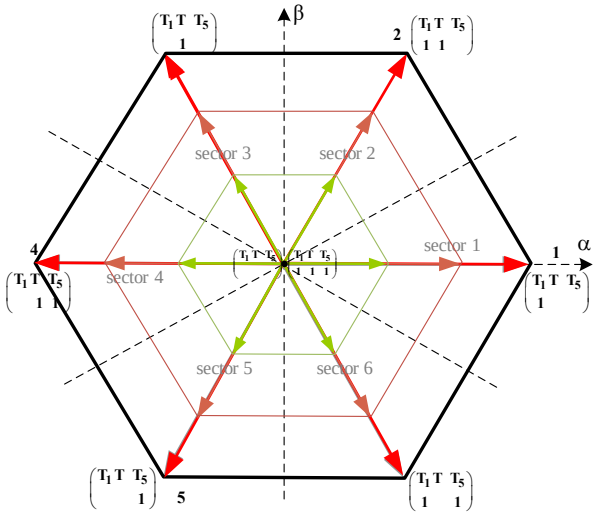


Sl. 1. Rezolucija naponskih vektora u αβ ravni sa definisana 3 naponska int.

Marko Rosić – Fakultet tehničkih nauka Čačak, Univerzitet u Kragujevcu, Sv. Save 65, 32000 Čačak, Srbija (e-mail: marko.rosic@ftn.kg.ac.rs).


ISBN 978-86-7466-930-3

U zavisnosti od definisanog broja naponskih intenziteta formira se odgovarajući komparator momenta. Komparator fluksa i prekidačka tabela (Tabela I) ostaju isti kao kod cDTC nezavisno od broja naponskih intenziteta . Ova osobina DVI-DTC omogućava da se broj naponskih vektora može jednostavno definisati ili promeniti bez potrebe za izmenom prekidačke tabele, kao što je to slučaj u [2, 8] gde je potrebno definisati novu prekidačku tabelu pri svakoj promeni broja raspoloživih naponskih intenziteta (vektora).

TABELA I – KONVENCIONALNA PREKIDAČKA TABELA

| $\psi$ | $T$ | | |
|---|---|---|---|
| | 1 | 0 | -1 |
| 1 | k+1 | 7 or 8 | k-1 |
| -1 | k+2 | 7 or 8 | k-2 |

Izmene u broju naponskih intenziteta $n$ kod DVI-DTC zahtevaju samo redefinisanje granica novog komparatora momenta $T_{ba}$, koja se može izvršiti prema (1).

$$T_{ba} = \frac{T_{ba\_c}}{3} \cdot i = \frac{T_{ba\_c}}{3} \cdot (2 \cdot n + 1) \qquad (1)$$

Negativan efekat indukovane elektromotorne sile (EMS) na inkremente momenta pri visokim (dokumentovan u [9]) može se jednostavno kompenzovati prema (2).

$$\begin{aligned} \mathbf{u}_{s\,\text{new}} &= \mathbf{u}_s + \mathbf{u}_{\text{add.}} \\ &= \mathbf{u}_s + j\omega\boldsymbol{\psi}_s = u_{\alpha s} + ju_{\beta s} + j\omega\left(\psi_{\alpha s} + j\psi_{\beta s}\right) \\ &= \underbrace{u_{\alpha s} - \omega\psi_{\beta s}}_{\text{Re}(\mathbf{u}_{s\,\text{new}})} + j\underbrace{(u_{\beta s} + \omega\psi_{\alpha s})}_{\text{Im}(\mathbf{u}_{s\,\text{new}})} \end{aligned} \qquad (2)$$

Vrednost indukovane EMS potrebno je dodati prethodno izabranom naponskom vektoru odgovarajućeg intenziteta (kao izlaza iz komparatora momenta) formirajući rezultujući naponski vektor, kao što je to prikazano na slici 2. Blok dijagram DVI-DTC algoritma prikazan je na slici 3, gde su zelenom bojom obeleženi delovi koji su izmenjeni u odnosu na cDTC.

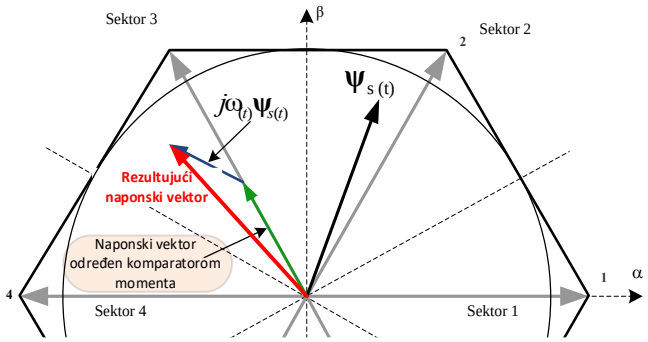


Sl. 2. Kompenzacija EMS i formiranje rezultujućeg naponskog vektora

Broj definisanih naponskih intenziteta teorijski može varirati od 2 pa do maksimalnog broja ograničenog brojačem DSP. Ipak, u [10] pokazano je da ripl momenta eksponencijalno opada sa povećanjem broja naponskih intenziteta i da je sa 6 naponskih intenziteta ripl smanjen 8 puta u poređenju sa riplom momenta koji se ima kod cDTC.

DVI-DT može biti dalje unapređen definisanjem više pravaca (8, 12, 16 ili više) naponskih vektora dalje povećavajući prostornu rezoluciju vektora statorskog napona. U tom slučaju bilo bi potrebno modifikovati prekidačku tabelu u zavisnosti od definisanog broja pravaca. Ipak, rezultati prezentovani u [11] pokazuju da stepen smanjenja ripla momenta kod DT algoritama baziranih na prekidačkim tabelama ne zavisi u velikoj meri od izabranog pravca naponskog vektora koliko od njegovog intenziteta. Stoga, zadržavanje konvencionalne prekidačke table sa 6 aktivnih naponskih vektora se čini opravdanim. Zahvaljujući odsustvu koordinatnih transformacija, složenih matematičkih operacija, PI regulatora itd., DVI-DTC algoritam ima veoma malo vreme izvršavanja i zadržava visoke dinamičke osobine karakteristične za cDTC. Navedene osobine promovišu DVI-DTC algoritam kao pogodnog kandidata za implementaciju u savremenim upravljačkim sistemima koji zahtevaju širok propusni opseg po momentu i kontrolu maksimalnog intenziteta ripla momenta u pogonu.

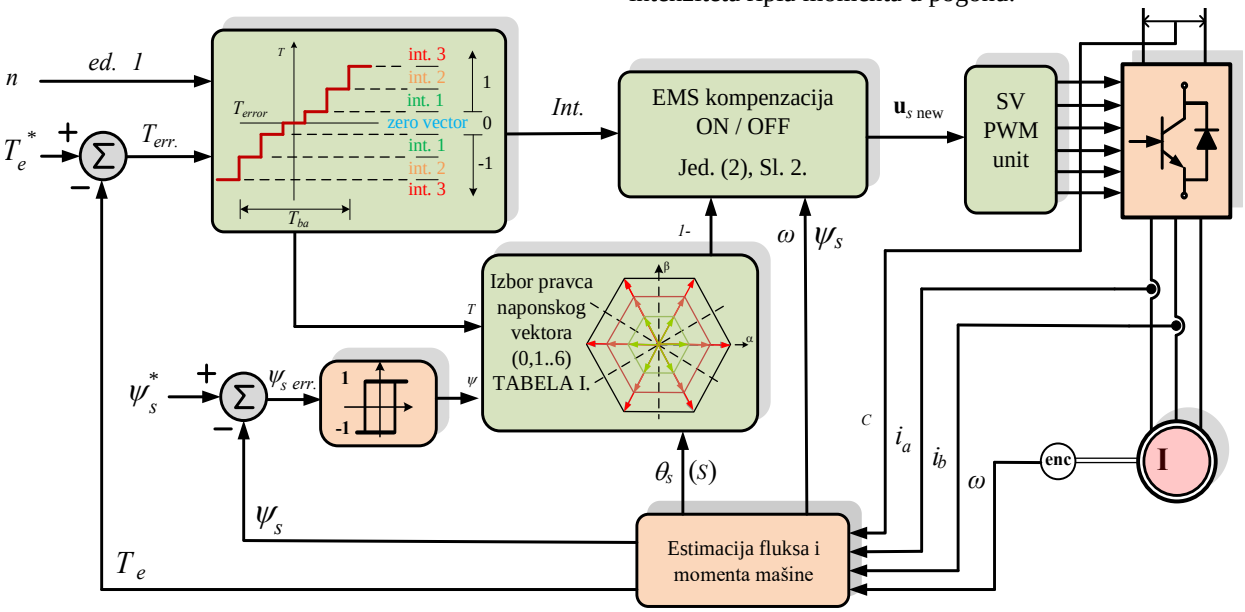


Sl. 2. Blok struktura DVI-DTC algoritma


ISBN 978-86-7466-930-3

## III. AUTOMATSKA MODIFIKACIJA DVI-DTC ALGORITMA

U cilju adekvatnog smanjenja ripla momenta, broj diskretizovanih naponskih intenziteta može biti definisan na dva načina:

- Od strane korisnika (ručno) ili
- Automatski, od strane algoritma, bazirano na estimiranim vrednostima momenta i ripla.

Na početku algoritma korisnik definiše broj naponskih intenziteta *n,* na osnovu koga se DVI-DTC algoritam dalje modifikuje pre starta. Pored ovoga, potrebno je definisati i maksimalno dozvoljeni intenzitet ripla momenta u pogonu $\Delta T_{ma}$ , kao i broj uzoraka estimiranog momenta *m* na osnovnu koga će biti određen trenutna vrednost ripla momenta. Ukoliko je ripl momenta veći od definisane vrednosti $\Delta T_{ma}$ , broj naponskih intenziteta se uvećava za jedan i algoritam nanovo modifikuje pre sledećeg starta. Slika 3 daje prikaz kompletnog algoritma inteligentnog DVI-DTC algoritma.

Inteligentni DVI-DTC algoritam je podeljen na 5 sekcija. U sekciji I zahteva se definisanje inicijalnih karakteristika pogona kao što su početni broj naponskih intenziteta i opcija kompenzacije EMS (uključena ON ili isključena OFF) od strane korisnika. Takođe u sekciji I definišu se i vrednosti za $\Delta T_{ma}$ i *m* potrebne za analizu ripla momenta u sekciji IV.

Kao što je rečeno, uvećanje broja naponskih intenziteta ne zahteva izmene u prekidačkoj tabeli. Dalja automatska modifikacija algoritma svodi se na sledeća dva koraka:

- predefinisanje odgovarajućih naponskih intenziteta u SVPWM jedinici i
- modifikacije granica komparatora momenta sa *n* nivoa.

Ova dva koraka, definisana u sekciji II, predstavljaju glavni deo automatske modifikacije DVI-DTC algoritma. Jednostavna automatizovana modifikacija u dva koraka omogućena je zahvaljujući raspregnutom izboru pravca i (prekidačka tabela) i intenziteta (komparator momenta sa *n* nivoa) kao glavnoj prednosti DVI-DTC algoritma.

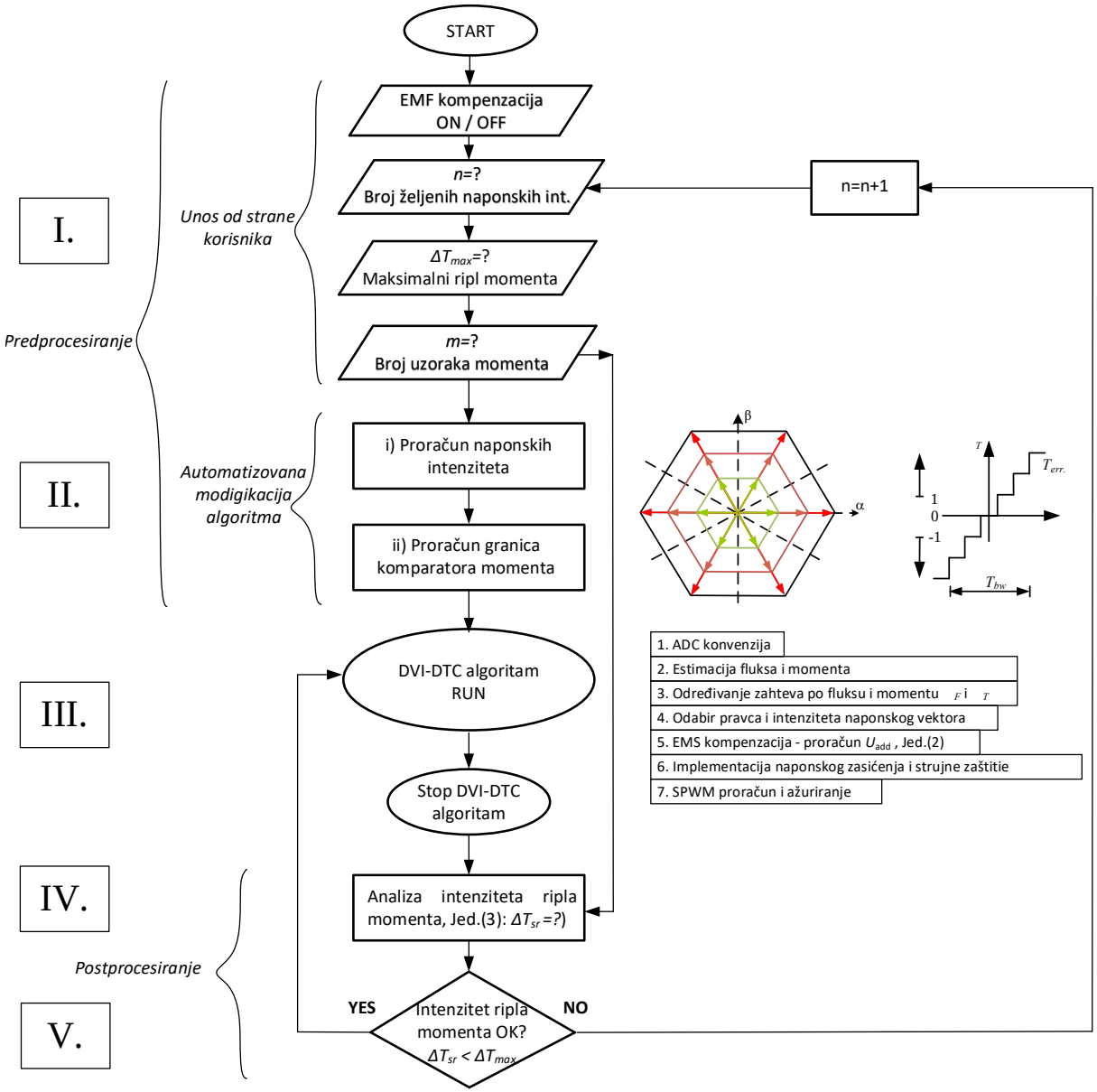


Sl. 3. Inteligentni DVI-DTC algoritam


ISBN 978-86-7466-930-3

Predefinisanje odgovarajućih naponskih intenziteta podrazumeva podelu punog opsega SVPWM generisanog naponskog vektora na jednake delove. Izuzimajući oblast nadmodulacije i negativan efekat mrtvog vremena, maksimalni intenzitet naponskog vektora generisanog uz SVPWM ograničen je radijusom upisanog kruga u heksagon koga formiraju šest aktivnih naponskih vektora (Sl.1), što predstavlja 86.7% od intenziteta maksimalnog naponskog vektora. Dalje se ovaj intenzitet deli na jednake delove na osnovu čega se definišu odgovarajuća vremena vođenja prekidačkih elemenata kod SVPWM. Odgovarajući komparator momenta i njegove granice određene su prema (1) ravnomernom raspodelom nivoa komparatora i odgovarajućih naponskih intenziteta u okviru širine komparatora $T_{ba}$.

Kako se opisane sekcije algoritma I i II izvršavaju pre starta glavnog dela DVI-DTC algoritma definisani su kao predpocesiranje. Ovo omogućava da glavni deo algoritma (sekcija III) zadrži proračunsku jednostavnost sličnu kao kod cDTC. Glavni deo DVI-DTC algoritma startuje sa ADC konverzijom statorskih struja i prikazan je na slici 3 koracima od 1 do 7.

Postprocesiranje odnosi se na sekcije IV i V koji se realizuju nakon zaustavljanja glavnog dela DVI-DTC algoritma. Ovaj deo zadužen je za analizu rezultata (ripla momenta) i odgovarajuće donošenje odluka u sekciji V. Ukoliko je rezultujući ripl momenta u okviru definisanih granica DVI-DTC algoritam može biti startovan opet. U suprotnom, broj definisanih naponskih intenziteta će biti uvećan u okviru sekcije I. Ova petlja (od sekcije V do sekcije I) omogućava uvećanje broja predefinisanih naponskih vektora za jedan nakon čega se na odgovarajući način algoritam automatski modifikuje u sekciji II. Odluka da li trenutna vrednost ripla momenta zadovoljava maksimalno definisanu vrednost $\Delta T_{ma}$ (definisanu od strane korisnika u sekciji I) donosi se na osnovu proračuna procentualne srednje vrednosti ripla momenta $\Delta T_{sr}$ u odnosu na nominalnu vrednost momenta motora $T_n$ prema (3).

$$\Delta T_{sr} = \frac{\sqrt{\frac{1}{m}\sum_{=1}^{m}\left(T - T_{ref.}\right)^2}}{T_n} \cdot 100 \quad [\%] \qquad (3)$$

Gde je $m$ broj semplova estimiranog momenta prikupljenih u cilju analize ripla momenta $T$, a $T_{ref.}$ predstavlja aktuelnu referentnu vrednost momenta. U cilju što objektivnije ocene srednje vrednosti ripla momenta $\Delta T_{sr.}$, i odabira odgovarajućeg broja potrebnih naponskih intenziteta, potrebno je da budu ispunjeni sledeći uslovi:

- kompenzacija EMS mora biti uključena (ON)
- broj semplova estimiranog momenta $m$ treba da obuhvata vrednosti momenta pri konstantnoj referentnoj vrednosti momenta.

Ova dva uslova obezbeđuju eliminisanje greške momenta kao posledice uticaja EMF (naročito pri visokim brzinama) i trenutne greške momenta koja se javlja kao posledica nagle promene referentne vrednosti i kašnjenja usled ograničene dinamike odziva momenta kao i kašnjenja usled digitalne implementacije.

Očigledno, ova petlja zahteva da DVI-DTC algoritam najpre bude stopiran sa svakom novom iteracijom sve dok uslov maksimalnog ripla momenta ne bude ispunjen (sekcija V). Razlog ovome leži u činjenici što su delovi algoritma koji nisu prioritetni izmešteni u predprocesiranje i postprocesiranje i kao takvi pogodni su za implementaciju zajedno sa drugim *self-tuning* algoritmima opisanim u uvodu. Sa druge strane, ovim je omogućeno očuvanje jednostavnosti glavnog dela DVI-DTC algoritma.

Automatska regulacija ripla momenta moguća je i bez zaustavljanja DVI-DTC pogona u slučaju kada se sekcije I, II, IV i V izvršavaju paralelno sa sekcijom III. Ovo bi zahtevalo implementaciju ovih delova koda koji se izvršavaju sa manjom frekvencijom kao što su poziciona ili brzinska petlja. Drugi način odnosi se na implementaciju ovih delova u posebne delove koji se izvršavaju na zahtev korisnika ili nadređene upravljačke strukture.

DVI-DTC algoritam pretenduje da pokaže svoj pun potencijal sa višefaznim mašinama i odgovarajućim višefaznim pretvaračima gde mogu biti implementirani ne narušavajući originalnu jednostavnost. Prirodno veća prostorna rezolucija naponskog vektora kod višefaznih pretvarača može biti dalje umnožena uvođenjem diskretizovanih naponskih intenziteta što bi dovelo većeg stepena redukcije ripla momenta. Takođe implementacija DVI-DTC algoritma sa višefaznim mašinama bi omogućila unapređenje robusnosti i otpornosti sistema (eng. *fault tolerant*) na potencijalne kvarove na pojedinačnim fazama.

## IV. EKSPERIMENTALNI REZULTATI

DVI-DTC algoritam implementiran je i testiran na MSK28335 DSP digitalnoj platformi u EMPA laboratoriji Fakulteta tehničkih nauka u Čačku. DSP platforma sastoji se od TMS320F28335 procesora sa pokretnom tačkom, 150 MHz, konvencionalnog naponskih invertora sa 6 IGBT 750 W i 310 V DC kolom. Eksperimentalna platforma je prikazana na slici 4 dok su podaci motora dati u prilozima.

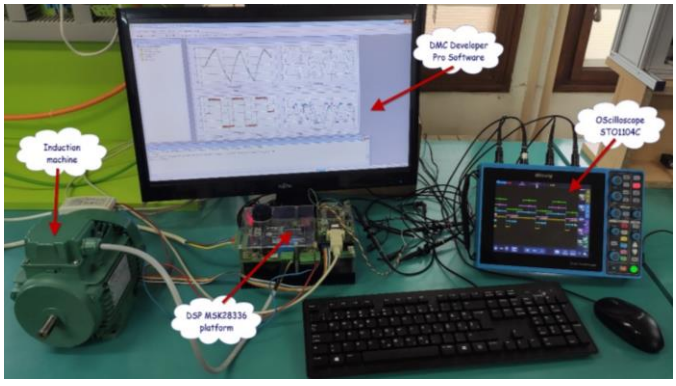


Sl. 4. Eksperimentalna postavka sa merenjem vremena izvršavanja

Prekidačka frekvencija je definisana na 20kHz, ostavljajući na raspolaganju $T_s$ 50 μs za izvršenje DTC algoritma.


ISBN 978-86-7466-930-3

Estimacija fluksa realizovana je sa *Gopinath* fluks opserverom [12] koji kombinuje strujni i naponski model mašine. Osciloskop STO1104C je korišćen za snimanje vremena izvršavanja pojedinih DVI-DTC algoritma praćenjem digitalnog izlaza procesora koji pri startu praćenog dela algoritma daje logičku nulu a pri završetku se opet vraća na nivo logičke jedinice. Vremena trajanja cDTC i DVI-DTC su snimljena i prikazana na slici 5.

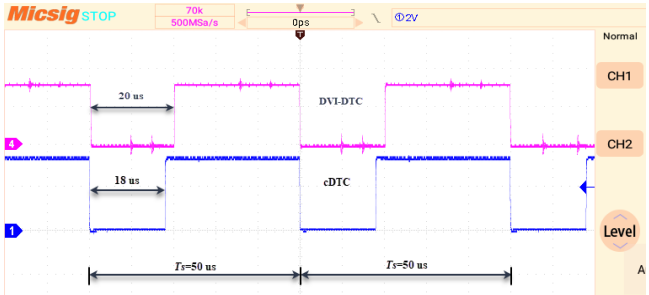


Sl. 5. Vremena izvršavanja DVI-DTC (gore) i cDTC algoritama (dole)

Slika 5 potvrđuje da glavni deo DVI-DTC algoritma zahvaljujući svojoj jednostavnosti ima oko 2 μs (≈10%) duže vreme izvršavanja u poređenju sa cDTC. Pri aktiviranju kompenzacije EMS (ON), ovo vreme izvršavanja DVI-DTC produžava se oko 7 μs kao što je prikazano na slici 6.

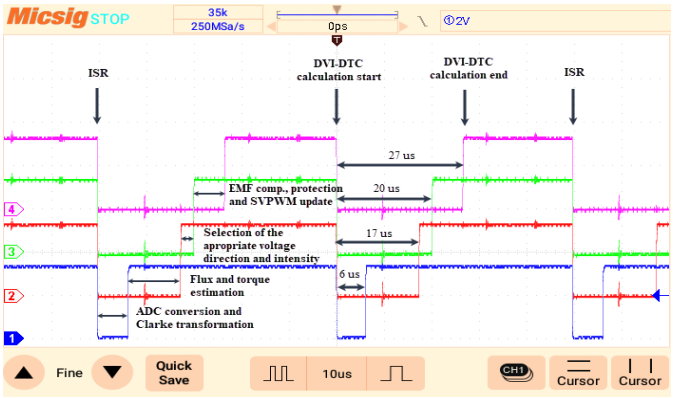


Sl. 6. Vremena izvršavanja delova DVI-DTC algoritma (sekcija III) sa uključenom kompenzacijom EMS

Eksperimentalni rezultati DVI-DTC sa 3, 4, 5 i 6 naponskih intenzitete sa ili bez kompenzacije indukovane EMS prikazani su na slici 7. Vremenska osa odgovara uzorkovanju rezultata na 1 ms. Na brzinskoj osi 15 pulseva odgovara brzini od 900 $min^{-1}$ dok je osa momenta izražena u Nm. Rezultati prikazani na slici 7 potvrđuju da se ripl momenta značajno smanjuje sa rastom broja definisanih naponskih intenziteta.

## V. ZAKLJUČAK

Ovaj rad prezentuje inteligentni DTC algoritam baziran na diskretizovanim naponskim intenzitetima koji ima mogućnost se automatske adaptacije u zavisnosti od intenziteta ripla momenta. Odgovarajući broj naponskih intenziteta može biti definisan od strane korisnika ili automatski kroz iterativni postupak u cilju zadovoljenja definisanom maksimalnog ripla momenta u pogonu. Originalna jednostavnost i dobre dinamičke osobine koje karakterišu cDTC su zadržane kod DVI-DTC. Dobijeni eksperimentalni rezultati potvrđuju proračunsku jednostavnost DVI-DTC algoritma u poređenju sa konvencionalnom DTC i značajno smanjenje ripla momenta sa porastom broja predefinisanih diskretizovanih naponskih intenziteta. Navedene karakteristike DVI-DTC sa mogućnošću automatske modifikacije u cilju redukcije ripla momenta čine ovaj metod kontrole pogodan za implementaciju u pametnim pogonima sledeće generacije.

## DODATAK

TABELA II - PARAMETRI ASINHRONOG MOTORA SIEBER LS71

| | | | |
|---|---|---|---|
| $_n$ [V] | 400 | $_s$ [Ω] | 24.6 |
| $I_n$ [A] | 0.95 | $_r$ [Ω] | 16.1 |
| $_n$ [W] | 370 | $_m$ [H] | 1.46 |
| $n_n$ [$min^{-1}$] | 2860 | $_s$ [H] | 1.48 |
| [p.p.] | 1 | $_r$ [H] | 1.48 |

## ZAHVALNICA

Prikazani rezultati predstavljaju deo aktivnosti u okviru projekta pod ugovornim br. 451-03-68/2022-14/200132 zaključenog između Ministarstva prosvete nauke i tehnološkog razvoja Republike Srbije i Fakulteta tehničkih nauka u Čačku, Univerzitet u Kragujevcu.

## LITERATURA

[1] D. Mohan, X. Zhang, and G. H. Beng Foo, "Generalized DTC Strategy for Multilevel Inverter Fed IPMSMs with Constant Inverter Switching Frequency and Reduced Torque Ripples", *IEEE Trans. on Ener. Con* . vol. 32, no. 3, pp. 1031–1041, 2017.

[2] Casadei D, Serra G, Tani A., "Implementation of a direct control algorithm for induction motors based on discrete space vector modulation", *IEEE Trans. on .P. Elec.*, vol. 15, no. 4, pp.769-777, 2012.

[3] M. Holakooie, M. Ojaghi, A. Taheri, "Direct Torque Control of Six-Phase Induction Motor with a Novel MRAS-Based Stator Resistance Estimator", *IEEE Trans. on Ind. El.*, vol. 65, no.10, pp.7685-7696, 2018

[4] M. N. Uddin, M. Hafeez and N. A. Rahim, "Self-tuned NFC and adaptive torque hysteresis-based DTC scheme for IM Drive", *Proc. of the IEEE Industry Applications Society Annual Meeting*, pp. 1-8, 2011.

[5] L. Q. Zhou, "A new dead-time compensation method on direct torque control system based on DSP", *Proc. of the 4th IEEE Conference on Industrial Electronics and Applications*, pp. 2359-2362, 2009.

[6] M. N. S. K. Shabbir, X. Liang and S. Chakrabarti, "An ANOVA-Based Fault Diagnosis Approach for Variable Frequency Drive-Fed Induction Motors", *IEEE Trans. on Ener. Con* ., vol. 36, no. 1, pp. 500-512, 2021.

[7] S. Shi, Y., et al., "Moving Integration Filter-Based Open-Switch Fault-Diagnosis Method for Three-Phase Induction Motor Drive Systems", *IEEE Trans. on Tr. Electr.*, vol. 6, no. 3, pp. 1093-1103, 2020.

[8] S. Suresh and R. P. P., "Virtual Space Vector-Based Direct Torque Control Schemes for Induction Motor Drives", *IEEE Transactions on Industry Applications*, vol. 56, no. 3, pp. 2719-2728, 2020.

[9] M. Rosic, M. Bjekic, M. Bebic and B. Jeftenic, "Electromotive force compensation in direct torque control with discretized voltage intensities", *Proc. of the 4th International Symposium on En ironmental Friendly Energies and Applications EFEA* , pp. 1-6, 2016

[10] M. Rosić, S. Antić, M. Bebić, "Improvements of torque ripple reduction in DTC IM drive with arbitrary number of voltage intensities and automatic algorithm modification", *Turk. our. of El. Eng. Comp. Sci.*, vol. 29, no.2, pp. 687-703, 2021.

[11] Arumugam S, Thathan M., "Novel switching table for direct torque controlled permanent magnet synchronous motors to reduce torque ripple", *our. of Power Electr.*, vol. 13 no. 6, pp. 939-954, 2013.

[12] West, N. T., and Lorenz, R. D., "Digital Implementation of Stator and Rotor Flux-Linkage Observers and a Stator-Current Observer for Deadbeat Direct Torque Control of Induction Machines", *IEEE Transactions on Industry Applications*, vol. 45, no. 2, pp.729-736, 2009.

 ISBN 978-86-7466-930-3

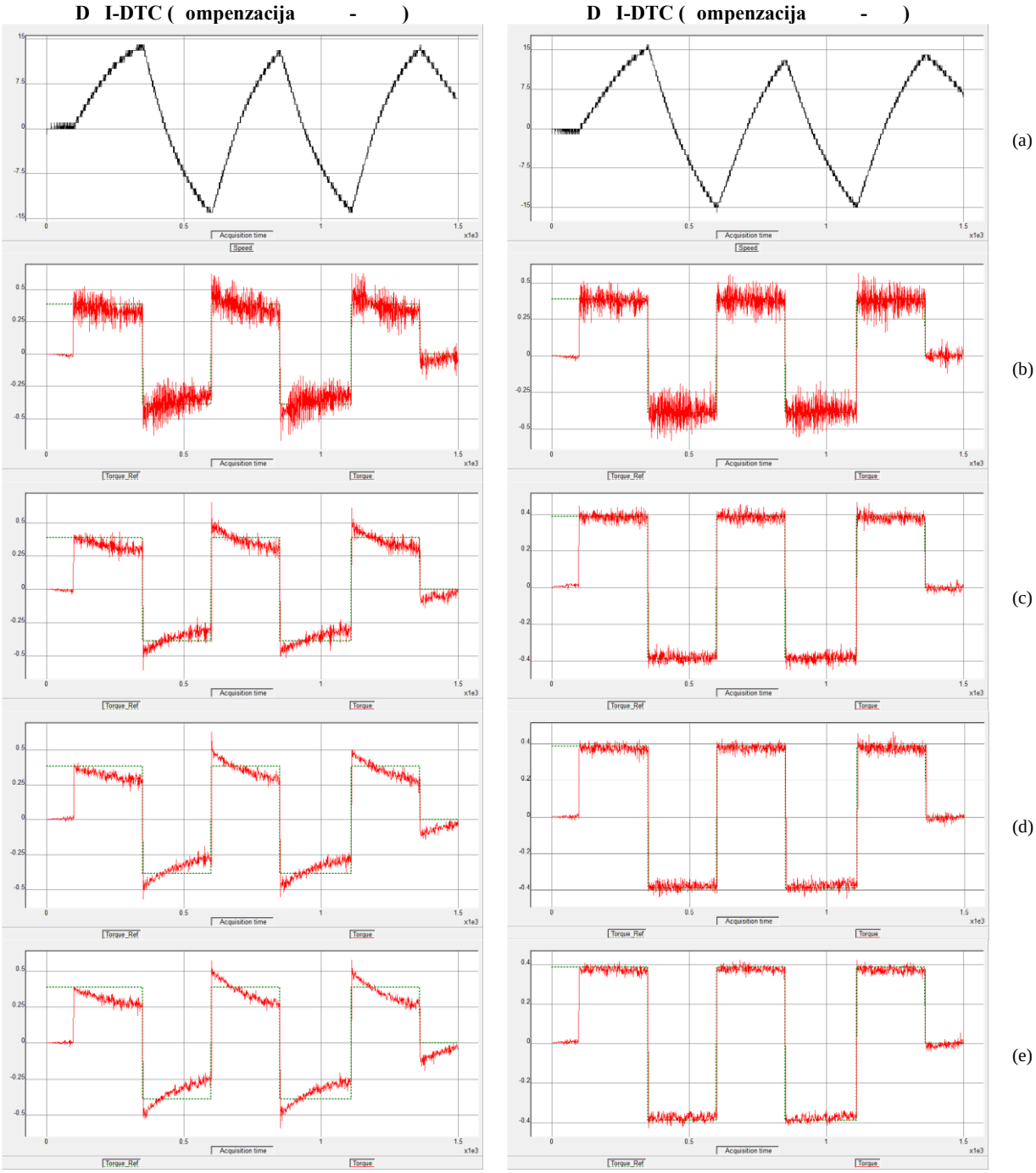


Sl. 7. Brzina (a) i estimirani moment (b) kod DVI-DTC sa 3 (b), 4 (c), 5 (d) i 6 (e) naponskih intenziteta sa i bez kompenzacije indukovane EMS


## ABSTRACT

The paper presents characteristic of direct torque control method based on discretised voltage intensities with possibilities of automatic algorithm modification in terms of torque ripple reduction. The algorithm uses the conventional switching table with an arbitrary number of discretized voltage intensities allowing higher space-voltage resolution and consequently lower torque ripple. The number of available voltage intensities can be easily changed without the need to modify the conventional switching table. Depending on the number of defined, discretized voltage intensities corresponding algorithm structures are automatized, making this kind of control method simple, effective, and suitable for upcoming smart drives in the rapidly growing industry 4.0. Experimental validation presented in the paper confirms improvements in torque ripple reduction retaining the simple and time-effective control structure of the induction machine DTC drive.


**Intelligent DTC algorithm with automatic reorganisation based on the torque ripple intensity**

Marko Rosić

 ISBN 978-86-7466-930-3

# Primjena električnih vozila za smanjenje deficita snage u sistemu

Uroš Ognjenović[1], Saša Mujović[1], Lazar Šćekić[1]
[1]Univerzitet Crne Gore, Elektrotehnički fakultet, Bulevar Dž. Vašingtona bb, Podgorica, Crna Gora

***Apstrakt*—Električna vozila (EVs – electric vehicles) su jedan od vodećih trendova u svijetu kada je u pitanju održivi razvoj i smanjenje emisije štetnih gasova. Prodor električnih vozila u elektroenergetski sistem znači povećano opterećenje, ali i omogućava plansko punjenje i pražnjenje ovih vozila uz benefit po sistem i korisnike električnih vozila. U ovom radu analizirana je primjena planskog punjenja i pražnjenja električnih vozila zasnovana na metodi igara na sreću, u cilju smanjenja deficita snage u sistemu.**

***Ključne riječi*—električna vozila; agregator; plansko pražnjenje; plansko punjenje**

## I. UVOD

Električna vozila cjelokupnu snagu ili jedan njen dio obezbjeđuju iz električne mreže i dijele se na potpuno električna vozila (AEVs – all-electric vehicles) i hibridna vozila (PHEVs – plug-in hybrid electric vehicles). Potpuno električna vozila su pokretana od strane jednog ili više električnih motora. Energiju obezbjeđuju punjenjem sa električne mreže i njenim čuvanjem u baterijama. Ne troše fosilna goriva i ne proizvode toksične gasove niti gasove sa efektom staklene bašte. Hibridna vozila koriste baterije za napajanje električnog motora, ali pored toga posjeduju i motor sa unutrašnjim sagorijevanjem (ICE – internal combustion engine).

Nagli rast interesovanja za razvoj električnih vozila je dobrim dijelom rezultat negativnog uticaja na životnu sredinu usljed industrijskog razvoja, konflikta u zemljama izvoznicama nafte na Bliskom Istoku i sa tim u vezi visokom cijenom nafte. Finansijska ulaganja i podsticaji za razvoj i posjedovanje električnih vozila su zasnovani na percepciji da su električna vozila ekološki prihvatljiv vid transporta u budućnosti.

Električna vozila su tek na početku svog ubrzanog razvoja i prodora na tržište (iako je prvo električno vozilo proizvedeno davne 1832.) što znači da će međusobni uticaj električnih vozila i EES-a (elektroenergetskog sistema) da raste u narednom periodu što potvrđuju sledeće zanimljivosti:

- 2,6% prodatih automobila u svijetu u 2019. su bila električna vozila, što predstavlja značajan porast u odnosu na 2017. kada je taj udio bio 1%.
- Norveška planira da u potpunosti izbaci iz upotrebe vozila sa motorom sa unutrašnjim sagorijevanjem do 2025., dok Francuska i Velika Britanija to planiraju da urade do 2040.
- Broj stanica za punjenje u Holandiji je u februaru 2020. iznosio nešto više od 37.000 (jedna stanica na 459 stanovnika) što Holandiju pozicionira na prvo mjesto u svijetu.
- Od ukupne potrošnje energije u Sjedinjenim Američkim Državama u 2005. u iznosu od 29.000 TWh, 28% odnosno 4.953 TWh je utrošeno u sektoru transporta. Ukoliko se pretpostavi da je ova energija utrošena isključivo u automobilima, dolazi se do zaključka da bi SAD trebalo da obezbijede energiju koja je veća od njene ukupne godišnje proizvodnje električne energije u istoj godini (4.055 TWh) za potpuni prelazak na električna vozila.

Imajući u vidu mogućnost kontrolisanog punjenja i pražnjenja, električna vozila se mogu posmatrati kao pokretni upravljivi sistemi za skladištenje električne energije. Interes korisnika električnih vozila je razlika između cijene električne energije predate u mrežu i cijene električne energije za punjenje. Kao rezultat učešća u V2G, dolazi do degradacije baterije tako da novčane naknade korisnicima moraju biti veće od troškova usljed degradacije baterije.

Ostatak rada je organizovan na sledeći način. U drugom poglavlju je objašnjen problem planskog pražnjenja vozila. Metod igara na sreću, proces aukcije i benefit korisnika su opisani u trećem poglavlju. Rezultati proračuna potencijala upotrebe električnih vozila za smanjenje deficita snage u primorskoj regiji Crne Gore su dati u poglavlju broj četiri. Peto poglavlje sumira ovaj rad. Na kraju rada je dat spisak korišćene literature.

## II. ELEKTRIČNA VOZILA U ELEKTROENERGETSKOM SISTEMU

Istraživanja pokazuju da su špic sati za dolazak na posao električnim vozilom između 7:00 i 8:00 i da je vrijeme punjenja tokom radnih sati. Špic sati za povratak sa posla električnim vozilom su između 17:00 i 19:00 i vrijeme punjenja je između 19:00 i 6:00 narednog dana. Dakle, električno vozilo se može povezati na mrežu dva puta dnevno [1]. Pored toga, više od 90% vozila je parkirano negdje i 50% kod kuće tokom dana, što otvara mogućnost za ispomoć električnoj mreži ukoliko postoji odgovarajući stimulans [2]. Konkretno, zabrana prodaje automobila na benzin i dizel koja je predložena u nekim zemljama će promovisati prodor električnih vozila, tako da imaju veliki potencijal kao kontrolisano opterećenje [3].

Obzirom da se električna vozila mogu posmatrati kao distribuirani izvor energije i kao opterećenje koje može biti planirano, stvorena je ideja o sistemu vozilo-ka-mreži (V2G –

Uroš Ognjenović – Elektrotehnički fakultet, Univerzitet Crne Gore, Džordža Vašingtona bb, 81000 Podgorica, Crna Gora (e-mail: urosognjenovic@gmail.com).
Saša Mujović – Elektrotehnički fakultet, Univerzitet Crne Gore, Džordža Vašingtona bb, 81000 Podgorica, Crna Gora (e-mail: sasam@ucg.ac.me).
Lazar Šćekić – Elektrotehnički fakultet, Univerzitet Crne Gore, Džordža Vašingtona bb, 81000 Podgorica, Crna Gora (e-mail: slazar@ucg.ac.me).

 ISBN 978-86-7466-930-3

vehicle-to-grid). U V2G sistemu, energija može da teče između električne mreže i električnog vozila [1].

Za koordinaciju punjenja i pražnjenja električnih vozila se koristi agregator. Agregator je centralni entitet koji koordiniše i planira status električnih vozila. Očekuje se da će u budućnosti većina električnih vozila biti povezana na Internet preko VANET-a (Vehicular ad hoc network – Bežična ad-hok mreža), Wi-Fi-ja ili mobilne mreže. Električna vozila mogu da prenose informacije kao što je tip vozila, kapacitet baterije, neophodno punjenje, ruta, itd. agregatoru [4]. Sva električna vozila karakteriše i status napunjenosti (SoC – State of Charge) koji je nivo napunjenosti u odnosu na kapacitet baterije (između 0% i 100%).

Za određivanje uticaja električnih vozila na elektroenergetski sistem neophodno je razumjeti različite statuse koje električna vozila mogu imati u bilo kom trenutku. Razlikuje se 5 statusa [5]:

- Električna vozila na punjenju: Električna vozila su priključena na mrežu i preuzimaju energiju za punjenje njihovih baterija.
- Električna vozila u V2G sistemu: Električna vozila predaju energiju mreži.
- Električna vozila kao eksplicitna rezerva: Električna vozila su priključena na mrežu, ali ne preuzimaju niti injektiraju energiju u mrežu. U ovom slučaju, električna vozila mogu započeti proces punjenja ili pražnjenja na zahtjev agregatora, uzimajući u obzir trenutno stanje baterije.
- Električna vozila koja se koriste za transport. U ovom modu električna vozila nijesu priključena na mrežu, već se koriste za transport i troše energiju skladištenu u baterijama.
- Neiskorištena električna vozila: Električna vozila su priključena na mrežu, ali agregator odlučuje da ne koristi ova vozila za punjenje, V2G niti kao rezervu.

## III. METOD IGARA NA SREĆU

Za učešće u V2G sistemu se primjenjuje mehanizam aukcije po prvoj cijeni (first-price auction). Pobjednici aukcije su učesnici koji su dali najviše ponude i oni plaćaju iznose koje su ponudili. Kao benefit ostvaruju razliku između cijene električne energije za punjenje električnih vozila i ponude, sa jedne strane, i cijene električne energije predate u mrežu, sa druge strane. Učesnici aukcije nisu upoznati sa ponudama drugih učesnika (sealed-bid auction – aukcija sa zatvorenim ponudama). Potrošači, odnosno učesnici aukcije koji ne žele da pobijede na aukciji i time učestvuju u V2G sistemu, mogu da daju ponudu za koju vjeruju da neće biti najviša. Time se obezbjeđuje autonomija – potrošači bi trebalo da sami odlučuju da li da učestvuju u V2G poređenjem benefita V2G i mobilnosti [3].

Aukcija se vrši za svaki 60-minutni interval pojedinačno za naredni dan. Na osnovu prognoze proizvodnje i potrošnje za naredni dan, $P_{pro}(t)$ i $P_{pot}(t)$, se određuje deficit snage po satima $P_{def}(t)$, gdje je $t$ indeks intervala ($t \in \{1,2,...,T\}$, gdje je $T$ poslednji interval). Ovaj podatak se koristi za dobijanje podataka o idealnom broju idealnih vozila (idealna vozila su vozila čiji status baterije omogućava predaju određene količine energije mreži tokom odgovarajućeg intervala pri određenoj snazi) $N_{ide}(t)$ koja bi predala električnu energiju sistemu. Ukoliko su sva električna vozila istih karakteristika, $N_{ide}(t)$ se dobija po formuli:

$$N_{ide}(t) = floor(\frac{P_{def}(t)}{P_{pra}}), t = 1,2,..., T, \quad (1)$$

gdje je $P_{pra}$ snaga kojom električna vozila predaju električnu energiju mreži [kW]. Floor($P_{def}(t)/P_{pra}$) označava prvu manju cijelu vrijednost količnika $P_{def}(t)/P_{pra}$ – zaokruženu vrijednost.

V2G se realizuje kada se, na osnovu prognoze proizvodnje i potrošnje električne energije za naredni dan ustanovi da se makar u jednom od intervala javlja deficit snage $P_{def}(t)$ i kada je taj deficit veći od $P_{pra}$. Ovaj uslov se može predstaviti relacijom:

$$\sum_{t=1}^{T} N_{id}(t) \geq 1. \quad (2)$$

Neka se u nekom EES-u nalazi $N$ električnih vozila. Broj vozila $N_{ide}(t)$ za određeni interval može biti veći, jednak, ili manji od stvarnog broja vozila u sistemu. U slučaju da je $N_{ide}(t)$ veće od ili jednako $N$, svi korisnici električnih vozila mogu da učestvuju u V2G, čime se gubi potreba za održavanjem aukcije u odgovarajućem intervalu. U ovoj situaciji, agregator određuje vrijednost po kojoj se električna energija otkupljuje od korisnika električnih vozila. Ova vrijednost se određuje po relaciji:

$$C_{otk} = k_1 C_{maks}, \quad (3)$$

gdje je:

$C_{otk}$ – cijena otkupljene električne energije od potrošača [EUR/kWh]

$k_1$ – koeficijent kojim se obezbjeđuje benefit potrošaču u najnepovoljnijem slučaju kada je električno vozilo punjeno tokom perioda maksimalne cijene električne energije i koji je veći od 1 (npr. 1,1), za slučaj kada je $N_{ide}(t)$ veće od jednako $N$.

$C_{maks}$ – maksimalna cijena električne energije tokom dana [EUR/kWh]

Kada je $N_{ide}(t)$ manje od $N$, odnosno kada je deficit u sistemu moguće pokriti sa brojem vozila koji je manji od stvarnog broja vozila u sistemu, održava se aukcija kako bi se odredio broj korisnika električnih vozila koji žele da učestvuju u V2G. Da bi korisnici električnih vozila ostvarili benefit pri učestvovanju u aukciji, moraju biti upoznati sa cijenom otkupa električne energije koja se može razlikovati od slučaja kada je $N_{ide}(t)$ veće od ili jednako $N$. Na osnovu ovog podatka, određuje se maksimalna moguća ponuda korisnika *maksPonuda* [EUR] koja donosi benefit po relaciji:

$$maksPonuda = floor(P_{pra}(k_2 - 1)C_{maks}), \quad (4)$$

gdje je $k_2$ koeficijent kojim se obezbjeđuje benefit potrošaču, za slučaj kada je $N_{ide}(t)$ manje od $N$.

U realnosti, električna vozila nisu idealna, već ih karakteriše SoC između 0% i 100% što direktno utiče na

 ISBN 978-86-7466-930-3

mogućnosti isporuke električne energije mreži. Štaviše, usljed degradacije baterije, ne preporučuje se punjenje iznad 80% za model Nissan Leaf. Uvodi se i zahtjev da baterija nijednog električnog vozila ni u jednom trenutku ne smije da dostigne status napunjenosti manji od $b$ kapaciteta baterije [r.j. – relativne jedinice] čime jedan dio korisnika automatski gubi mogućnost za učešće u V2G, a koji je rezultat upotrebe električnih vozila u prethodnom periodu (ovaj uslov se može eliminisati ako se uzme da je $b$ jednako nuli što znači da se električna vozila mogu potpuno isprazniti ako se koriste za ispomoć mreži). Ovaj uslov se uvodi usljed činjenice da je glavna uloga električnih vozila transport pa se podrazumijeva da se baterija ne smije potpuno isprazniti. Neka je $EV$ niz kapaciteta baterija svih električnih vozila u sistemu. Uslov za određivanje niza potencijalnih električnih vozila $EV_{pot}$, dužine $N_{pot}$, od svih vozila u sistemu, za učešće u planskom pražnjenju je sledeći:

$$EV(n) \geq bE_{bat} + P_{pra}, n = 1,2,\ldots,N \quad (5)$$

gdje je $E_{bat}$ kapacitet baterije [kWh].

Dakle, električna vozila koja mogu da učestvuju u V2G su ona vozila koja imaju skladištenu minimalnu količinu energije plus količinu energiju koju mogu predati mreži tokom jednog sata pri snazi pražnjenja $P_{pra}$. Od niza svih električnih vozila u sistemu se dobija niz potencijalnih vozila $EV_{pot}$ čija je dužina $N_{pot}$ manja od ili jednaka $N$. Ovaj niz sadrži podatke o vozilima u sistemu koja zadovoljavaju (5).

Treba imati u vidu da vozila $EV_{pot}(j)$ ($j$=1,2,...,$N_{pot}$) zadovoljavaju (5) samo za prvi interval posmatranog dana. Na kraju tog intervala, a u zavisnosti od upotrebe električnog vozila (punjenje, plansko pražnjenje, vožnja, itd.), električna vozila karakteriše SoC koji se razlikuje od SoC na početku intervala. Dakle, (5) je neophodno provjeriti za svaki od intervala za posmatrani dan.

Obzirom da se aukcija održava za naredni dan, tačni SoC električnih vozila u $t$-om intervalu nije poznat ni agregatoru ni korisniku. Međutim, SoC na početku dana se za proračune može opisati normalnom raspodjelom $N$(0,6, 0,01) [1].

Iz niza $EV_{pot}$, na osnovu ponuda učesnika aukcije za učešće u V2G za odgovarajući interval, agregator određuje niz dobitnika aukcije $EV_{dob}$. Ovi korisnici su dužni da u datom intervalu obezbijede dogovorenu količinu energije mreži. U slučaju da korisnik, koji je pobijedio na aukciji za određeni interval, odluči da isključi vozilo sa mreže tokom tog istog intervala, što se u praksi može desiti, dužan je da plaća penale čiji iznos određuje sistem operator i čiji detalji su precizirani u ugovoru između ove dvije strane.

Obzirom na ograničeni kapacitet baterije, korisnici električnih vozila nisu u mogućnosti da učestvuju u V2G u svim mogućim intervalima. Za svakog pobjednika agregator vrši proračun dostupnog kapaciteta kako bi se odredio zahtijevani plan pražnjenja. Ukoliko agregator odredi da u $k$-tom ($k$=1,2,...,$T$) intervalu dobitnik aukcije nije u mogućnosti da učestvuje u V2G, provjerava se da li je u t-im ($t$=1,2,...,$k$-1) intervalima moguće dopuniti električno vozilo energijom neophodnom za učešće u planskom pražnjenju u $k$-tom intervalu. Opcije su sledeće:

- Ukoliko to jeste moguće, korisnik donosi odluku da priključi vozilo na mrežu u zahtijevanom intervalu ili da se povuče iz aukcije. U slučaju da odluči da se povuče iz aukcije, prvi gubitnik aukcije dobija priliku da učestvuje V2G.
- Ukoliko to nije moguće, prvi gubitnik aukcije dobija priliku da učestvuje u V2G.
- Agregator automatski isključuje datog korisnika iz planskog pražnjenja za posmatrani interval i prvi gubitnik aukcije dobija priliku da učestvuje u V2G.

Pored određivanja plana pražnjenja, agregator može kao izlazni podatak da daje i dostupni kapacitet baterije u nekom trenutku, što bi korisnicima olakšalo planiranje upotrebe električnog vozila.

Za interakciju između agregatora (sistema) i korisnika električnih vozila je neophodno izgraditi odgovarajuću komunikacionu infrastrukturu.

## IV. NUMERIČKI REZULTATI

Posmatra se EES Crne Gore. Elektrane od velikog značaja za EES Crne Gore i njihove karakteristike su prikazane u tabeli I.

TABELA I
Velike elektrane u EES-u Crne Gore

| Elektrana | Tip | Instalisana snaga [MW] |
|---|---|---|
| HE Piva | Akumulaciona hidroelektrana | 342 |
| HE Perućica | Protočna hidroelektrana | 307 |
| TE Pljevlja | Termoelektrana na ugalj | 210 |
| VE Krnovo | Vjetroelektrana | 72 |
| VE Možura | Vjetroelektrana | 46 |

EES Crne Gore je pretežno hidro sistem sa instalisanom snagom velikih hidroagregata od 649 MW što predstavlja 66,43%, odnosno približno dvije trećine ukupnih kapaciteta (nisu uračunate male hidroelektrane).

Ljetnje mjesece u EES-u Crne Gore karakteriše naročito povećanje opterećenja u južnoj regiji kao rezultat izraženih turističkih aktivnosti. Na slici 1 je dat dijagram opterećenja konzuma, a na slici 2 proizvodnja proizvodnih jedinica Crne Gore na dan 27.07.2020.

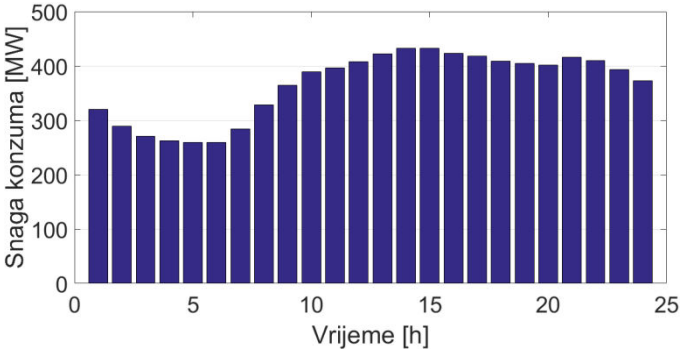


Sl. 1. Konzum Crne Gore na dan 27.07.2020. (izvor ENTSO-E Transparency)


ISBN 978-86-7466-930-3

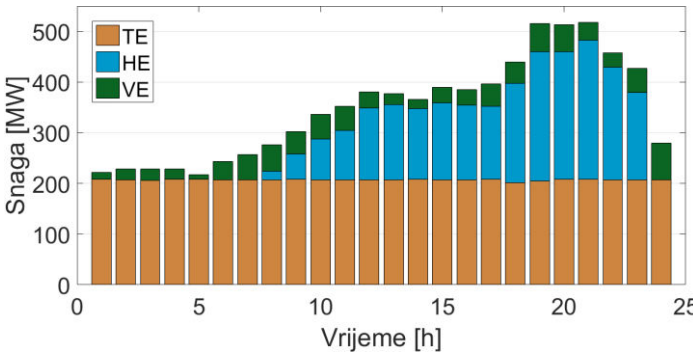


Sl. 2. Proizvodnja na dan 27.07.2020. (izvor ENTSO-E Transparency)

Na osnovu podataka sa slike 1 i 2 se zaključuje sledeće:

– TE Pljevlja tokom cijelog 24-časovnog perioda radi sa snagom koja je približno jednaka njenoj instalisanoj snazi od 210 MW i ta snaga se kreće u opsegu od 201 MW do 208 MW. Maksimalno se koristi raspoloživa snaga TE i tokom cijelog dana se javlja opterećenje koje je veće od tehničkog minimuma TE Pljevlja pa se ne javlja potreba za isključenje date elektrane sa mreže.
– Energija vjetra se koristi u onoj mjeri u kojoj je to moguće – teži se što boljem iskorišćenju raspoložive energije.

Na slici 3 dat je bilans snaga u EES-u Crne Gore na dan 27.07.2020.

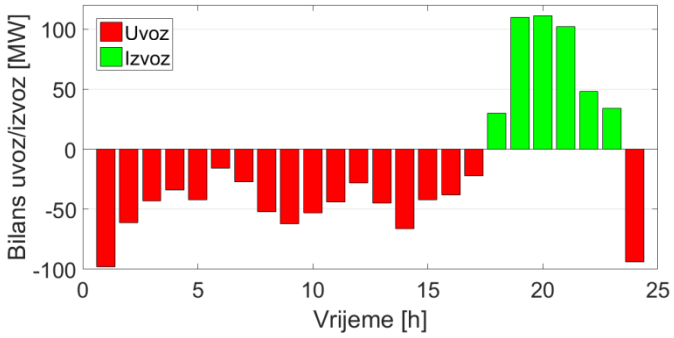


Sl. 3. Bilans snaga uvoz/izvoz na dan 27.07.2020.

Električna energija se uvozi u periodu između 00:00 i 17:00, kao i između 23:00 i 00:00, dok se izvozi u periodu između 17:00 i 23:00 časa. Višak proizvodnje u sistemu tokom ovog perioda se može iskoristiti za punjenje električnih vozila, koja se u preostalim intervalima (kada se javlja manjak snage) mogu ponašati kao generatori električne energije. Izvezena količina električne energije tokom posmatranog dana iznosi 435 MWh, dok je uvezena količina približno dva puta veća i iznosi 867 MWh.

Ukoliko se uvede pretpostavka da, od ukupne nedostajuće količine energije, odnosno snage, 30% otpada na južnu regiju, dolazi se do podataka o deficitu snage prikazanih na slici 4.

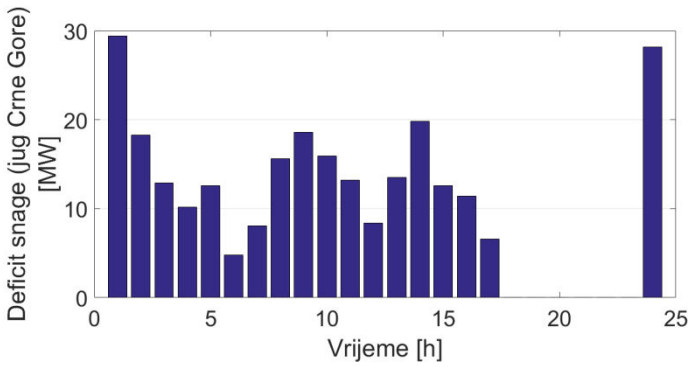


Sl. 4. Nedostajuća snaga u južnoj regiji Crne Gore na dan 27.07.2020. (aproksimacija od 30% ukupne nedostajuće snage u EES-u)

Na osnovu ovih podataka, ukupna nedostajuća količina energije u južnoj regiji Crne Gore na dan 27.07.2020. je 260,1 MWh (približno 260 MWh), a prosječna nedostajuća snaga je 14,45 MW. Nedostajuća količina energije bi mogla biti nadoknađena iz baterija električnih vozila za šta bi bilo neophodno priključiti na mrežu 5.200 vozila sa kapacitetom baterija 50 kWh i potpuno ih isprazniti. Međutim, električna vozila se koriste za transport tako da se uzima u obzir da ni u jednom trenutku ni jedno električno vozilo ne smije biti u potpunosti ispražnjeno. Time se zaključuje da u EES-u Crne Gore, tj u južnoj regiji, treba da postoji 6.500 električnih vozila sa baterijama kapaciteta 50 kWh koje ni u jednom trenutku ne padaju ispod stanja napunjenosti od 20%, odnosno 10 kWh, kako bi se pokrio deficit električne energije. U 2019. je u gradovima južne regije Crne Gore registrovano ukupno 66.410 vozila (Bar 17.232; Budva 11.922; Kotor 9.961; Tivat 7.397; Ulcinj 7.781; Herceg Novi 12.117) tako da se zaključuje da svako deseto vozilo treba da bude električno sa odgovarajućim karakteristikama.

U proračunu potencijala upotrebe električnih vozila u V2G sistemu u EES-u Crne Gore posmatraju se četiri stepena prisustva električnih vozila u južnoj regiji i to: 1.000 vozila, 5.000 vozila, 10.000 vozila i 20.000 vozila. Smatra se da su sva vozila istih karakteristika i to:

– Baterije su kapaciteta 50 kWh
– Snaga punjenja je 10 kW
– Snaga pražnjenja je 5 kW

Koeficijenti $k_1$ i $k_2$ su 1,1 i 1,2, respektivno. Na osnovu (5), minimalna količina energije neophodne za učešće u V2G, sa koeficijentom $b$=0,2, je 15 kWh.

SoC na početku dana se opisuje normalnom raspodjelom sa koeficijentima $\mu$=0,6 i $\sigma$=0,1. Zaključuje se da 99,87% vozila ispunjava (5), što nema značajniji uticaj na sistem (u odnosu na slučaj kada bi 100% vozila ispunjavala dati uslov), ali je poželjno voditi računa o pomenutom uslovu radi maksimalne udobnosti korisnika koji električno vozilo koriste prije svega za transport.

Po dvotarifnom modelu u Crnoj Gori, maksimalna cijena električne energije je jednaka cijeni električne energije tokom perioda visoke tarife i iznosi približno 0,103 EUR/kWh.

Električna vozila nijesu generatori električne energije, već pokretne baterije za njeno skladištenje. Dakle, pored V2G sistema, mora se uzeti u obzir i pitanje punjenja električnih

 ISBN 978-86-7466-930-3

vozila tokom posmatranog dana sa ciljem bolje procjene njihovog uticaja na sistem. Iz ovog razloga, za svaki stepen prisustva električnih vozila se posmatraju dva podslučaja:

1. Kada korisnici električna vozila pune onda kada žele.
2. Kada korisnici električna vozila pune u periodu viška snage u sistemu.

Svi proračuni koji zavise od odluka potrošača koje imaju dva ishoda su izvedeni upotrebom funkcije koja nasumično generiše date odluke (npr. da li napuniti vozilo u posmatranom intervalu ili ne).

U tabelama II i III prikazani su rezultati proračuna za 8 posmatranih slučajeva. Date veličine su sledeće:

- Deficit energije u sistemu sa električnim vozilima [MWh] i u odnosu na deficit energije u originalnom sistemu [%]
- Suficit energije u sistemu sa električnim vozilima [MWh] i u odnosu na suficit energije u originalnom sistemu [%]
- Prosječna zarada planskog pražnjenja [EUR/kWh]
- Prosječna energija vozila na kraju dana [kWh]
- Prosječno pokrivanje deficita snage po satima [%] daje podatak o učešću električnih vozila u pokrivanju nedostatka snage u sistemu. Negativna vrijednost označava povećanje prosječnog pokrivanja deficita i javlja se isključivo kada korisnici vozila pune kada žele
- Prosječno pokrivanje suficita snage po satima [%] daje podatak o učešću električnih vozila (punjenju) u preuzimanju viška snage u sistemu

TABELA II
Rezultati proračuna (prvi dio)

| Broj vozila | Deficit energije [MWh] ([%]) | Suficit energije [MWh] ([%]) | Prosječna zarada pražnjenja [EUR] |
|---|---|---|---|
| 1.000 (1.) | 258,62 (99,43) | 425,39 (97,79) | 0,0103 |
| 1.000 (2.) | 239,64 (92,14) | 416,6 (95,77) | 0,0102 |
| 5.000 (1.) | 259,03 (99,59) | 390,50 (89,77) | 0,0097 |
| 5.000 (2.) | 158,30 (60,86) | 338,24 (77,75) | 0,0098 |
| 10.000 (1.) | 305,88 (117,60) | 378,82 (87,08) | 0,0097 |
| 10.000 (2.) | 61,325 (23,57) | 254,97 (58,61) | 0,0096 |
| 20.000 (1.) | 444,45 (170,87) | 374,50 (86,09) | 0,0096 |
| 20.000 (2.) | 0,025 (0,0096) | 141,33 (32,49) | 0,0097 |

TABELA III
Rezultati proračuna (drugi dio)

| Broj vozila | Prosječna energija vozila na kraju dana [kWh] | Prosječno pokrivanje deficita snage po satima [%] | Prosječno pokrivanje suficita snage po satima [%] |
|---|---|---|---|
| 1.000 (1.) | 38,13 | -0,15 | 3,03 |
| 1.000 (2.) | 27,94 | 9 | 6 |
| 5.000 (1.) | 38,6690 | -9,58 | 13,84 |
| 5.000 (2.) | 28,9750 | 34,79 | 31,05 |
| 10.000 (1.) | 40,1900 | -43,62 | 17,58 |
| 10.000 (2.) | 28,1195 | 65,06 | 42,86 |
| 20.000 (1.) | 42,2390 | -106,37 | 18,71 |
| 20.000 (2.) | 31,6760 | 99,95 | 66,27 |

Na osnovu podataka iz tabela II i III se zaključuje sledeće:

- Uvođenjem električnih vozila u sistem se povećava deficit snage u sistemu kada korisnici električna vozila pune onda kada to smatraju za shodno (slučajevi 1.), a pritom ne dolazi do značajnijeg smanjenja suficita što je rezultat ravnomjernog punjenja vozila tokom cijelog dana.
- Kada se V2G kombinuje sa planskim punjenjem (slučajevi 2.), dolazi do znatnog smanjenja deficita snage sa povećanjem prisustva električnih vozila u sistemu.
- Prosječna energija skladištena u baterijama električnih vozila na kraju dana u slučajevima 2. iznosi u prosjeku 29,21 kWh, odnosno 97,37% prosječnog kapaciteta energije na početku dana, što govori da je V2G sistem u kombinaciji sa planskim punjenjem održiv i kada se primijeni na periode duže od jednog dana. U proračunima međutim nije uzeto u obzir korišćenje električnih vozila za prevoz, odnosno smanjenje dostupne energije u baterijama električnih vozila tokom dana.
- Kombinovanje V2G sistema i planskog punjenja pozitivno utiče na sistem, jer u suprotnom električna vozila praktično međusobno izmjenjuju električnu energiju (kada jedno električno vozilo predaje energiju mreži, drugo se puni, pa je uticaj na sistem manji nego kada bi se punjenje električnih vozila prebacilo u interval viška snage u sistemu).

Na slici 5 dat je prikaz deficita snage na jugu Crne Gore po satima i ukupan deficit u sistemu sa 10.000 električnih vozila koja se pune tokom perioda viška snage (slučaj 2.).


ISBN 978-86-7466-930-3

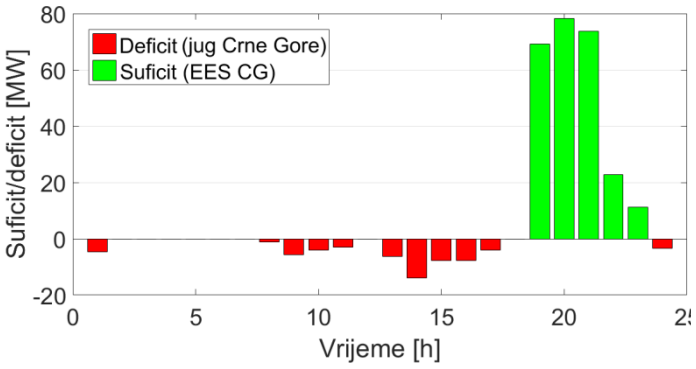


Sl. 5. Deficit snage na jugu Crne Gore i ukupni suficit u sistemu sa 10,000 (2.) električnih vozila na dan 27.07.2020.

Poredeći podatke sa slike 5 i podatke sa slike 3 i 4, zaključuje se da je deficit snage na jugu Crne Gore (pretpostavka o 30% deficita snage na nivou EES-a) značajno smanjen uvođenjem plana planskog pražnjenja vozila. U periodu između 1 i 6 časova u jutarnjim satima bilans snaga je jednak nuli. Primjećuje se i da je uticaj električnih vozila manji u kasnijim satima usljed pretpostavke da se električna vozila tokom posmatranog dana pune isključivo tokom perioda viška snage u sistemu, kada opet dostižu minimalnu količinu energije za učešće u V2G. Suficit snage u sistemu u periodu između 17 i 23 časa je takođe smanjen planskim punjenjem vozila. U intervalu između 17 i 18 časova se u potpunosti absorbuje višak proizvodne snage.

U proračunima o mogućem učešću električnih vozila u EES-u Crne Gore je zanemareno postojeće stanje. Naime, u 2018. godini je, od ukupnog broja registrovanih vozila od oko 235.000, registrovano tek nešto više od 100 električnih vozila, odnosno približno 0,043 %. Poredeći ovaj podatak i podatak o neophodnom broju vozila za pokrivanje nedostajuće snage u južnoj regiji Crne Gore, zaključuje se da se broj električnih vozila u ovoj regiji mora uvećati više od 300 puta.

Glavni uslov za prodor električnih vozila na tržište Crne Gore je uvođenje podsticajnih mjera za njihovu kupovinu i posjedovanje poput ukidanja poreza pri kupovini, besplatne registracije i parkinga, kao i izgradnje mreže stanica za punjenje. Pritom treba imati u vidu da su električna vozila još uvijek znatno skuplja od tradicionalnih vozila sa motorom sa unutrašnjim sagorijevanjem i da je kupovna moć građana Crne Gore znatno manja od kupovne moći zemalja koje su lideri u prelasku na električna vozila.

## V. ZAKLJUČAK

U ovom radu je obrađen problem primjene električnih vozila kao pokretnih upravljivih sistema za skladištenje električne energije i predaju energije mreži (V2G sistem) sa osvrtom i na pitanje planskog punjenja električnih vozila, a sa ciljem smanjenja deficita snage u sistemu. Izvedeni su proračuni za različite nivoe prisustva električnih vozila u elektroenergetskom sistemu Crne Gore za tipičan ljetnji dan koji karakteriše relativno visoko opterećenje tokom cijelog dana i smjena intervala manjka i viška proizvodne snage u sistemu.

Iako V2G sistem dobija puni smisao kada se električna vozila pune tokom perioda niskih opterećenja i predaju energiju mreži tokom vrhova opterećenja, ovaj rad tretira pitanje upotrebe električnih vozila za davanje ispomoći sistemu onda kada mu je to potrebno, nezavisno od doba dana i trenutnog opterećenja. Za primjenu V2G sistema za pokrivanje deficita snage u realnim uslovima je neophodno uzeti u obzir brojne faktore koji utiču na stepen ispomoći mreži kao što su: prisustvo vozila u EES-u i očekivani udio ovih vozila u budućnosti, upotreba električnih vozila za transport i matematički modeli koji opisuju ovaj mod, održivost, odnosno ekonomska isplativost otkupa električne energije od korisnika električnih vozila, itd.

## LITERATURA

[1] H. Fu, Y. Han, J. Wang, Q. Zhao, "A Novel Optimization of Plug-In Electric Vehicles Charging and Discharging Behaviors in Electrical Distribution Grid", *J. Electr. Compute. Eng.*, vol. *2018*, no *1-9*, Aug., 2018.

[2] D. Wu, D. C. Aliprantis, K. Gritza, "Electric Energy and Power Consumption by Light-Duty Plug-in Electric Vehicles", *IEEE Trans. Power Syst.: A Publication of the Power Engineering Society*, vol. *26*, no *2*, pp. *738-746*, Jun., 2011.

[3] H. Kikusato, Y. Fujimoto, S.-I. Hanada, D. Isogawa, S. Yoshizawa, H. Ohashi, Y. Hayashi, "Electric Vehicle Charging Management Using Auction Mechanism for Reducing PV Curtailment in Distribution Systems", *IEEE Trans. Sustain. Energy*, vol. *11*, no. *3*, pp. *1394-1403*, Jul., 2019.

[4] J. C. Mukherjee, A. Gupta, "Distributed Charge Scheduling of Plug-In Electric Vehicles Using Inter-Aggregator Collaboration", *IEEE Trans. Smart Grid*, vol. *8*, no. *1*, pp. 331-341, Jan., 2016.

[5] M. A. Ortega-Vazquez, F. Bouffard, V. Silva, "Electric Vehicle Aggregator/System Operator Coordination for Charging Scheduling and Services Procurement", *IEEE Trans. Power Syst.: A Publication of the Power Engineering Society*, vol. *28*, no. *2*, pp. *1806-1815*, May, 2013.

## ABSTRACT

EVs (electric vehicles) are one of the leading trends in the world when it comes to sustainable growth and reducing impact on the environment. EV penetration in power systems means an increased load, but it allows for planned charging and discharging which benefit both the system and the owners of EVs. This paper proposes the use of planned charging and discharging of EVs based on game theory, with the aim to reduce the power deficit in a system.

*Index terms*—electric vehicles; aggregator; planned discharging; planned charging

**Use of Electric Vehicles for Reduction of Power Deficit in System**

Uroš Ognjenović, Saša Mujović, Lazar Šćekić

 ISBN 978-86-7466-930-3

# Realizacija laboratorijskog sistema za bežični prenos energije

Dejan Janjić, Alenka Milovanović i Branko Koprivica

***Apstrakt*—Cilj ovog rada je prikaz teorijskih osnova i realizacije laboratorijskog sistema za bežični prenos električne energije. Na početku će biti razmotreni osnovni principi induktivnog i rezonantnog bežičnog prenosa energije i biće navedene njihove osnovne prednosti i mane. Dalje, biće detaljnije opisana rezonantna metoda realizovanog sistema, uključujući: šemu veza i opis principa rada predajnog i prijemnog dela sistema, tehničke podatke, prikaz realizovanog laboratorijskog sistema, kao i rezultate merenja i odgovarajuću analizu.**

***Ključne reči*—Bežični prenos energije; rezonantna metoda; rezonantna frekvencija, redno-paralelna kompenzacija.**

## I. Uvod

Metodologiju za bežični prenos električne energije je predložio Nikola Tesla, krajem 19. veka [1, 2]. Prve realizacije takvih sistema se javljaju na početku 21. veka, kada MIT realizuje prenos električne energije na rastojanje od 2 m za napajanje sijalice [3], kao i INTEL [4], a SONY predstavlja prvi bežični televizor [5]. Bežični prenos energije je sada već realnost koja se dalje razvija kroz različite primene, u medicini, robotici, za napajanje kućnih uređaja ili punjenje baterija prenosnih uređaja, električnih bicikli i mopeda, a očekuje se da će uskoro ući u primenu i bežični sistemi za punjenje električnih automobila.

Dosadašnja istraživanja u Srbiji u oblasti bežičnog prenosa električne energije (koliko je autorima poznato) odnose se na analizu i izradu Teslinog transformatora, ali ne i na realizacije sistema za napajanje uređaja [6, 7].

U ovom radu će biti date osnove teorije bežičnog prenosa energije bazirane na induktivnoj i rezonantnoj metodi i biće analizirane njihove prednosti i nedostaci. Zatim će biti analizirana rezonantna metoda sa redno-paralelnom kompenzacijom, koja se dobija dodavanjem kondenzatora [8]. Biće prikazana i praktična realizacija sistema, kao i rezultati merenja dobijeni u toku testiranja sistema.

## II. Osnovi bežičnog prenosa energije

Postoje dve glavne tehnologije koje se trenutno koriste za implementaciju bežičnog prenosa energije:

- induktivna i
- rezonantna.

Obe tehnologije rade po principu sprezanja predajnog i prijemnog namotaja u bliskom elektromagnetskom polju i koriste magnetsku spregu da prenesu električnu energiju. Glavna razlika je u tome koliko su namotaji međusobno udaljeni i da li su izrađeni tako da se javlja rezonancija ili ne, kao što je prikazano na Slici 1.

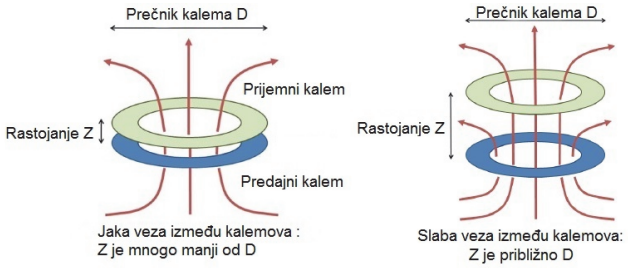


*a*) *b*)

Sl. 1. Ilustracija položaja kalemova za *a*) induktivnu i *b*) rezonantnu metodu.

Induktivni prenos energije podrazumeva blisku magnetsku spregu između predajnog kalema i prijemnog kalema na relativno malom rastojanju, reda nekoliko milimetara ili centimetara. Ovaj prenos energije se naziva i prenos energije sa jakom spregom. Predajni kalem je povezan na izvor naizmeničnog napona (najčešće u opsegu 100-400 kHz) koji generiše naizmeničnu struju kroz kalem i tako stvara magnetsko polje. Promenljivo magnetsko polje predajnog kalema se obuhvata prijemnim kalemom u kojem se indukuje naizmenični napon po Faradejevom zakonu, a samim tim i struja prijemnika. Količina prenete energije/snage se kontroliše promenom frekvencije napona u predajnom kalemu. Ova vrsta prenosa električne energije se može uporediti sa prenosom energije pomoću transformatora sa magnetskim jezgrom.

Rezonantna metoda prenosa električne energije se zasniva na magnetskoj rezonanciji između predajnog i prijemnog kalema. Predajni i prijemni kalem mogu biti i više desetina puta udaljeniji nego kod induktivnog prenosa, što karakteriše slabo spregnute kalemove za bežični prenos energije. Ova vrsta prenosa električne energije se može uporediti sa radio prenosom.

Rezonantni bežični prenos energije ima brojne prednosti u odnosu na induktivni, kao što su:

1. veće rastojanje između predajnog i prijemnog kalema,
2. veće osno odstupanje između predajnog i prijemnog kalema koji ne moraju biti postavljeni u osi, kao što je slučaj sa induktivnim prenosom,

Dejan Janjić – Tehnički remontni zavod Čačak, Dr Dragiše Mišovića 167, 32000 Čačak, Srbija (e-mail: dzandz@gmail.com).

Alenka Milovanović – Univerzitet u Kragujevcu, Fakultet tehničkih nauka u Čačku, Svetog Save 65, 32000 Čačak, Srbija (e-mail: alenka.milovanovic@ftn.kg.ac.rs).

Branko Koprivica – Univerzitet u Kragujevcu, Fakultet tehničkih nauka u Čačku, Svetog Save 65, 32000 Čačak, Srbija (e-mail: branko.koprivica@ftn.kg.ac.rs).

 ISBN 978-86-7466-930-3

3. jedan predajni kalem može preneti energiju/snagu na više prijemnih kalemova, dok induktivni prenos zahteva više predajnih kalemova, što omogućava prenos snage na više uređaja sa različitim opterećenjima (uređaji sa različitom snagom).

Nedostatak rezonantnog prenosa u nekim slučajevima je niža efikasnost u poređenju sa induktivnim prenosom. Razlog je to što se veći deo polja rasipa oko prijemnog kalema, zbog povećane udaljenosti, što nije slučaj kod induktivne metode.

## III. REZONANTNA METODA SA KOMPENZACIJOM

Za razliku od induktivne metode, rezonantna metoda se zasniva na postojanju reaktivnih (induktivnih i kapacitivnih) delova u predajnom i prijemnom kalema, kako bi sistem radio u rezonantnim uslovima. Zbog dimenzija kalemova, parazitna kapacitivnost nije dovoljna da obezbedi rezonanciju u radnom opsegu frekvencija, određenog primenom sistema za bežični prenos. U skladu sa tim, za postizanje rezonancije u željenom opsegu frekvencija potrebno je na predajnoj i prijemnoj strani dodati reaktivne elemente (najčešće kondenzatore), što se karakteriše kao dodatna kompenzaciona mreža. Tako se mogu realizovati redno-redna, redno-paralelna, paralelno-redna i paralelno-paralelna kompenzaciona metoda.

Šema veza rezonantnog kola sa redno-paralelnom kompenzacijom je prikazan na Slici 2.

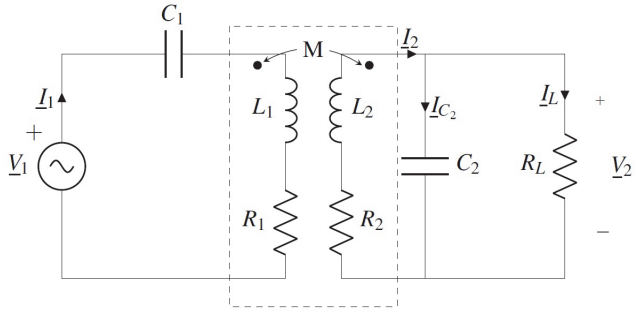


Sl. 2. Šema veza rezonantnog kola sa redno-paralelnom kompenzacijom.

Za spregnuto kolo sa Slike 2 se mogu napisati sledeće jednačine po I i II Kirhofovom zakonu i to:

$$\underline{V}_1 = \left(R_1 + \mathrm{j}\omega L_1 + \frac{1}{\mathrm{j}\omega C_1}\right)\underline{I}_1 - \mathrm{j}\omega M\underline{I}_2\,, \tag{1}$$

$$\underline{V}_2 = -\left(R_2 + \mathrm{j}\omega L_2\right)\underline{I}_2 + \mathrm{j}\omega M\underline{I}_1 = R_L\underline{I}_L = \frac{\underline{I}_{C_2}}{\mathrm{j}\omega C_2}\,, \tag{2}$$

$$\underline{I}_2 = \underline{I}_{C2} + \underline{I}_L\,, \tag{3}$$

$$\underline{I}_2 = \mathrm{j}\omega R_L C_2 \underline{I}_L\,, \tag{4}$$

gde je ω kružna učestanost i $\mathrm{j}^2 = -1$.

Izjednačavanjem imaginarnog dela ulazne impedanse:

$$\underline{Z}_{ul} = \frac{\underline{V}_1}{\underline{I}_1} = \left(R_1 + \mathrm{j}\omega L_1 + \frac{1}{\mathrm{j}\omega C_1}\right) + \frac{\omega^2 M^2\left(\mathrm{j}\omega C_2 R_L + 1\right)}{R_L + \left(R_2 + \mathrm{j}\omega L_2\right)\left(\mathrm{j}\omega C_2 R_L + 1\right)}\,, \tag{5}$$

sa nulom, može se odrediti rezonantna učestanost kola $\omega_r$.

Međutim, u praksi se rezonantna učestanost podešava pomoću parametara prijemnog kola (induktivnosti $L_2$ prijemnog kalema i kompenzacione kapacitivnosti $C_2$) tako da ona bude jednaka:

$$\omega_r = \frac{1}{\sqrt{L_2 C_2}}\,. \tag{6}$$

Kada kolo radi u režimu rezonancije važe sledeći izrazi [8]:

$$\omega_r L_1 - \frac{1}{\omega_r C_1} \approx \frac{\omega_r M^2}{L_2}\,, \tag{7}$$

$$C_1 \approx \frac{L_2^2 C_2}{L_1 L_2 - M^2}\,. \tag{8}$$

Izrazom (8) je približno određena vrednost kompenzacione kapacitivnosti $C_1$ za odabranu induktivnost predajnog kalema $L_1$. U slučaju kada je međusobna induktivnost $M$ mnogo manja od induktivnosti kalemova, odnos kapacitivnosti $C_1$ i $C_2$ će biti približno srazmeran odnosu induktivnosti $L_2$ i $L_1$.

## IV. REALIZACIJA LABORATORIJSKOG SISTEMA

Sistem za bežični prenos energije rezonantnom metodom sa redno-paralelnom kompenzacijom (Slika 1) je realizovan u laboratorijskim uslovima. Sistem se sastoji od: 1) ispravljača naizmeničnog napona 230 V, 50 Hz, 2) pretvarača stalnog napona u naizmenični napon više frekvencije realizovan kao mostni invertor sa MOSFET tranzistorima [9], 3) predajnog kalema sa kompenzacionim kondenzatorom, 4) prijemnog kalema sa kompenzacionim kondenzatorom, 5) ispravljača naizmeničnog napona više frekvencije realizovanog kao Grecov spoj sa brzim diodama i kondenzatorom [9] i 6) aktivnog opterećenja (sijalica sa užarenim vlaknom). Blok šema ovog sistema je prikazana na Slici 3, a odgovarajuće fotografije na Slici 4.

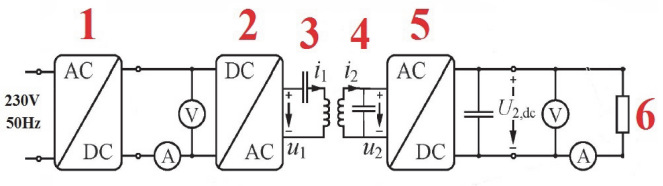


Sl. 3. Blok šema sistema za bežični prenos energije.

Sistem radi tako što se priključni napon od 230 V, 50 Hz ispravlja pomoću ispravljača 1 i na njegovom izlazu podešava na nivo od 30 V do 50 V, a zatim se taj stalni napon dovodi na ulaz DC u AC pretvarača 2 koji na svom izlazu generiše pravougaoni impulsni napon $u_1$ amplitude 30-50 V u opsegu frekvencija od 15 kHz do 120 kHz. Tako generisani napon se dovodi na rednu vezu predajnog kalema i kompenzacionog kondenzatora 3. Na izlazu prijemnog kalema 4 se indukuje naizmenični napon $u_2$ maksimalne amplitude 250-300 V za odabrano opterećenje, frekvencije jednake frekvenciji napona priključenog na predajni kalem 3. Indukovani naizmenični napon se ispravlja pomoću ispravljača 5 i priključuje na prijemnik 6. Ispravljanje napona $u_2$ je potrebno za većinu praktičnih primena, kao što su napajanje elektronskih uređaja ili punjenje njihovih baterija.


ISBN 978-86-7466-930-3

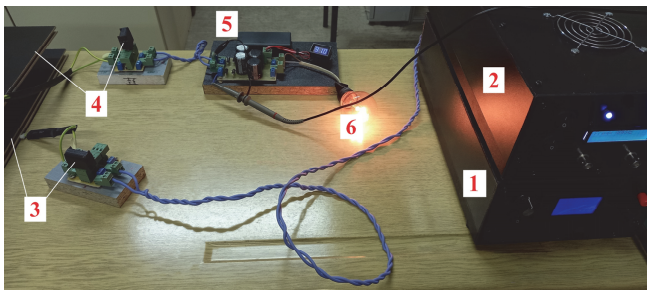


*a*)

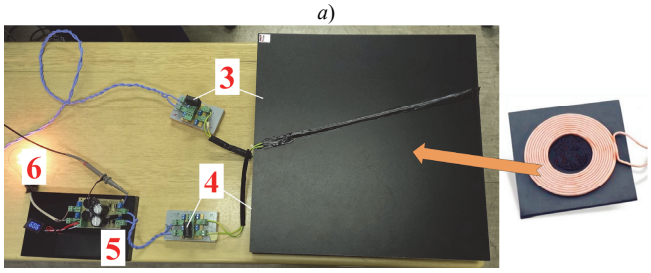


*b*)

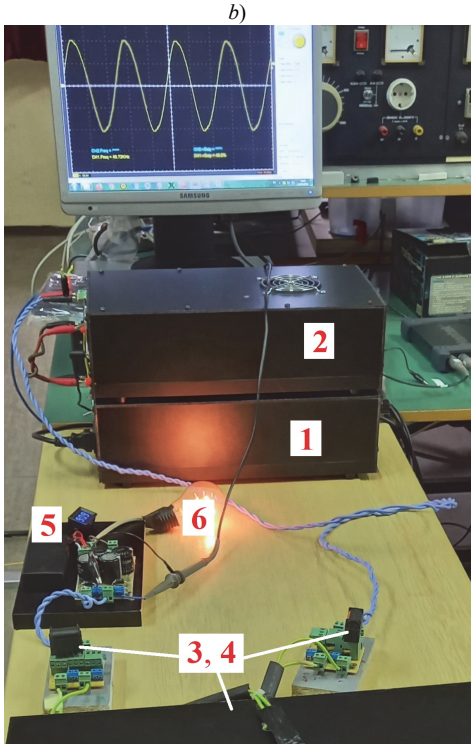


*c*)

Sl. 4. Fotografije realizovanog laboratorijskog sistema i kalema.

Predajni i prijemni kalem su namotani tako da imaju iste dimenzije i induktivnost, pa su i kompenzacioni kondenzatori izabrani tako da imaju istu kapacitivnost (zanemarujući uticaj međusobne induktivnosti). Podaci o dimenzijama i električnim parametrima sistema su date u Tabeli I.

TABELA I
PARAMETRI SISTEMA

| | |
|---|---|
| Unutrašnji prečnik kalemova | 375 mm |
| Spoljašnji prečnik kalemova | 440 mm |
| $L_1$, $L_2$ | 100 μH |
| $C_1$, $C_2$ | 300 nF |

Na osnovu izraza (6) i vrednosti parametara $L_2$ i $C_2$ datih u Tabeli 1 određena je rezonantna frekvencija sistema, koja iznosi približno 29,06 kHz.

## V. REZULTATI ISPITIVANJA SISTEMA

Ispitivanje rada realizovanog sistema za bežični prenos energije je urađeno sa aktivnim opterećenjem, sa jednom ili dve redno vezane sijalice sa užarenim vlaknom od po 100 W. Kalemovi su bili postavljeni na međusodnom rastojanjima od 7 cm do 23 cm.

Merenja napona su vršena pomoću četvorokanalnog USB osciloskopa Hantek 6074 DB. Mereni su stalni naponi na izlazu ispravljača 1, pravougaoni impulsni napon $u_1$ na izlazu pretvarača 2 i naizmenični napon $u_2$ na krajevima prijemnog kalema 4. Dodatno, digitalnim voltmetrom je meren stalni napon na izlazu ispravljača 5, što je i napon prijemnika 6.

Na Slici 5 su prikazani snimci ekrana pri merenju napona na pretvaraču 2 i prijemnom kalemu 4.

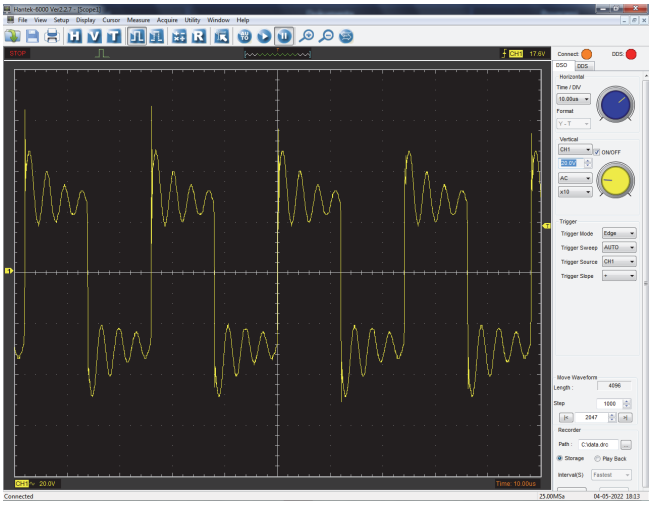

*a*)

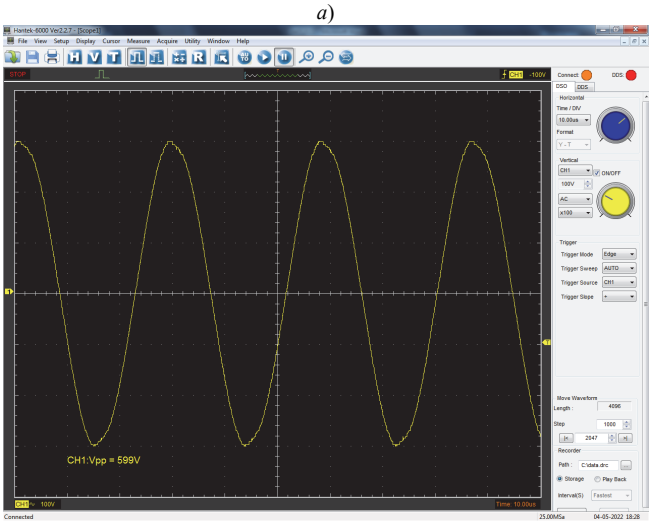


*b*)

Sl. 5. Snimci ekrana pri merenju osciloskopom: *a*) napon $u_1$ na pretvaraču 2 i *b*) napon $u_2$ na prijemnom kalemu 4.

Uočava se da napon $u_1$ nema sasvim pravougaoni oblik, što je posledica oscilatornog karaktera struje kroz kalem $L_1$ i


ISBN 978-86-7466-930-3

kondenzator $C_1$ koji su priključeni na taj napon. Sa druge strane napon $u_2$ ima skoro pravilan sinusoidalan oblik, a frekvencija mu je jednaka frekvenciji napona $u_1$.

U Tabeli 2 su dati rezultati merenja stalnog napona $U_2$ i struje $I_2$ prijemnika, kao i ostvarene aktivne snage $P_2$. Prijemnik je realizovan rednom vezom dve sijalice sa užarenim vlaknom naznačene snage od 100 W.

TABELA II
REZULTATI MERENJA

| $I_2$ [A] | $U_2$ [V] | $P_2$ [W] |
|---|---|---|
| 0,1 | 14,8 | 1,48 |
| 0,2 | 82,0 | 16,4 |
| 0,3 | 193,0 | 57,9 |
| 0,4 | 334,0 | 155,6 |

Detaljnije ispitivanje rada sistema su izvršena sa ciljem određivanja rezonantne učestanosti sistema merenjem napona na prijemniku za različite frekvencije izlaznog napona pretvarača 2. U toku ovakvog merenja se može očekivati da će se najveći napon izmeriti onda kada frekvencija napona pretvarača 2 odgovara rezonantnoj učestanosti sistema. S obzirom na to da je izračunata rezonantna frekvencija približno jednaka 29 kHz, ispitivanja su vršena u frekventnom opsegu od 25 kHz do 35 kHz.

Promena izmerenog napona sa frekvencijom za tri međusobna rastojanja između kalemova je prikazana na Slici 6. Strelicom je označen vrh rezonantne krive, na frekvenciji od 29,57 kHz, dobijene za najveće rastojanje između kalemova. Dobijena vrednost rezonantne frekvencije je veoma bliska proračunatoj vrednosti (29,06 kHz). Na manjim rastojanjima dolazi do razdvajanja maksimuma, koji se postižu za dve frekvencije, jednoj manjoj i jednoj većoj od proračunate. Razlika frekvencija za koje se postižu maksimumi se povećava sa smanjenjem rastojanja između kalemova. Ova pojava je povezana sa vrednošću međusobne induktivnosti $M$, koja se povećava sa smanjenjem rastojanja, pa se povećava i njen uticaj na vrednost rezonantne frekvencije, odnosno učestanosti $\omega_r$, približno određenu izrazom (7).

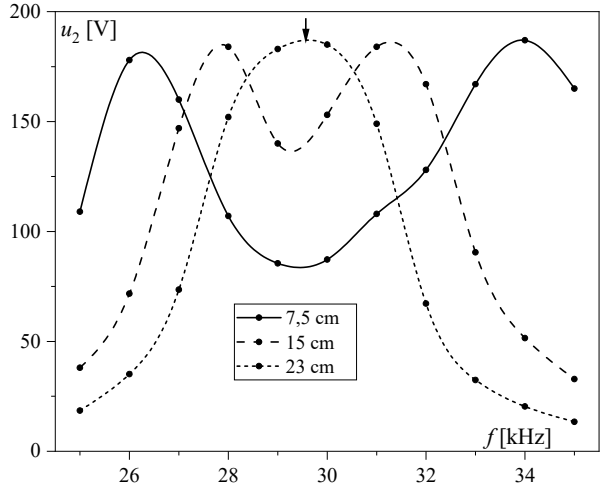


Sl. 6. Promena napona na prijemnom kalemu sa frekvencijom.

## VI. ZAKLJUČAK

U ovom radu su dati osnovi metodologije bežičnog prenosa električne energije pomoću spregnutih kalemova i pri tome su ukratko analizirane prednosti i nedostaci induktivne i rezonantne metode. Detaljnije je analiziran slučaj rezonantnog kola sa redno-paralelnom kompenzacijom i određena je rezonantna učestanost kola za poznate parametre kalemova i kompenzacionih kondenzatora. Proračunom je utvrđeno da rezonantna frekvencija iznosi približno 29 kHz.

U radu je prikazana i realizacija laboratorijskog sistema za bežični prenos energije rezonantnim kolom sa redno-paralelnom kompenzacijom. Sistem je testiran u frekventnom opsegu 25-35 kHz, bliskim proračunatoj rezonantnoj frekvenciji. Pri tome su mereni naponi na predajnom i prijemnom kalemu. Rad sistema na frekvencijama od 15 kHz do 120 kHz omogućava njegovo ispitivanje u skladu sa međunarodnim standardima (IEC, ISO, SAE i drugi) u oblasti bežičnog prenosa energije.

Detaljnije ispitivanje sistema je izvršeno za tri međusobna rastojanja između kalemova, pri čemu je meren napon na prijemnom kalemu u odabranom frekventnom opsegu. Pokazana je promena tog napona sa frekvencijom za tri slučaja i utvrđeno je da se maksimum može postići za dve frekvencije kada je rastojanje relativno malo i kada je uticaj međusobne induktivnosti značajan. Sa povećanjem rastojanja se smanjuje uticaj međusobne induktivnosti, pa se maksimum napona dobija na frekvenciji vrlo bliskoj proračunatoj rezonantnoj frekvenciji.

Realizovani laboratorijski sistem za bežični prenos energije će poslužiti kao osnova za nova istraživanja u oblasti koja je veoma aktuelna u svetu, a koja je još uvek nedovoljno istražena. Cilje daljih istraživanja će biti nalaženja novih praktičnih primena bežičnog prenosa energije u elektroenergetici.

## ZAHVALNICA

Istraživanja prezentovana u ovom radu su delimično finansirana sredstvima Ministarstva prosvete, nauke i tehnološkog razvoja RS, ugovor br.451-03-68/2022-14/200132 čiji je realizator Fakultet tehničkih nauka u Čačku - Univerziteta u Kragujevcu.

## LITERATURA

[1] N. Tesla, "System of Transmission of Electrical Energy," Patent No. 645,576, March 1900.
[2] A. Marinčić, Z. Civrić, B. Milovanović, "Nikola Tesla's Contributions to Radio Developments," *Serb. J. Electr. Eng.*, vol. *3,* no. *2,* pp. *131-148,* Nov. 2006.
[3] https://news.mit.edu/2007/wireless-0607.
[4] https://geekologie.com/2008/08/intel-demonstates-wireless-pow.php.
[5] https://www.sony.com/en/SonyInfo/News/Press/200910/09-119E/.
[6] R. Radetić, *Teslin transformator: teorija i praksa,* Niš, Srbija: Agencija Eho, 2019.
[7] J. M. Cvetić, "Tesla's High Voltage and High Frequency Generators with Oscillatory Circuits," *Serb. J. Electr. Eng.*, vol. *13,* no. *3,* pp. *301-333,* Oct. 2016.
[8] A. Triviño-Cabrera, J. M. González-González, J. A. Aguado, *Wireless Power Transfer for Electric Vehicles: Foundations and Design Approach,* Cham, Switzerland: Springer Nature, 2020.
[9] R. Radetić, *Tranzistorski pretvarači,* Bor, Srbija: Grafomed, 2006.

 ISBN 978-86-7466-930-3

ABSTRACT

The aim of this paper is to present the theoretical foundations and realization of the laboratory system for wireless transfer of electric energy. At the beginning, the basic principles of inductive and resonant wireless energy transfer will be considered and their basic advantages and disadvantages will be stated. Further, the resonant method of the implemented system will be described in more details, including the connection scheme and description of the principles of operation of the transmitting and receiving part of the system, its technical data, presentation of the implemented laboratory system, as well as measurement results and appropriate analysis.

**Realization of laboratory system for wireless energy transmission**

Dejan Janjić, Alenka Milovanović i Branko Koprivic

 ISBN 978-86-7466-930-3

# Pravci istraživanja u elektroenergetici kroz tematsku orijentaciju radova sa skupova CIRED Srbija i ETRAN/IcETRAN

Zoran J. Simendić i Vladimir A. Katić, *Senior Member, IEEE*

***Apstrakt*—U radu su razmatrani pravci istraživanja kroz radove na dva značajna naučno-stručna skupa, koja se održavaju u Srbiji, savetovanje CIRED Srbija i konferencije ETRAN/IcETRAN. Detaljnije je predstavljena struktura oba skupa, kao i ključne teme, koje se na njima razmatraju. Kod savetovanja CIRED Srbije teme su vezane za problematiku elektrodistribucije, preko stalnih studijskih komiteta i njihovih preferencijalnih tema, dok su kod konferencija ETRAN/IcETRAN one vezane i pokrivaju kompletnu oblast elektroenergetike. Na bazi toga razmatrana je zainteresovanost učesnika ovih skupova za predstavljanje svojih rezultata kroz brojnost prezentovanih naučno-stručnih radova u odgovarajućim tematskim oblastima. Zaključeno je da su najzastupljenije teme iz oblasti generisanja električne energije, distribuirane proizvodnje, primene obnovljivih izvora energije, priključenja električnih vozila, te upravljanja takvom proizvodnjom i pridruženim merenjima. Ovo ukazuje da istraživači u Srbiji obrađuju najnovije prodore u nauci i struci, te da razmatrani skupovi daju adekvatan prikaz o najnovijim dostignućima iz ovih oblasti.**

***Ključne reči*—Pravci istraživanja, Naučno-stručni radovi, Savetovanje CIRED Srbija, Konferencije ETRAN/IcETRAN.**

## I. Uvod

Elektroenergetski sistem u Srbiji je obuhvaćen delovanjem tri velika državna preduzeća, Elektroprivreda Srbije (EPS), Elektromreže Srbije (EMS) i Elektrodistribucija Srbije (ODS), koja su proistekla i ranijeg centralizovanog sistema EPS-a. Pored toga niz privatnih domaćih i stranih kompanija se bavi proizvodnjom električne energije uglavnom na bazi obnovljivih izvora, kao i proizvodnjom i ugradnjom elektroenergetske opreme. Takođe, niz firmi se bavi projektovanjem i izgradnjom elektroenergetskih objekata i mreže. U svim ovim preduzećima radi impozantan broj inženjera i tehničara, kao i veći broj magistara i doktora nauka. S druge strane, rad i tehnički napredak ovih firmi neraskidivo su vezani za usvajanje i primenu novih tehničkih i tehnoloških rešenja, stručnih inovacija i originalnih tehničkih unapređenja i patenata. Sve to motiviše zaposlene, odnosno pruža dobru osnovu za prikazivanje postignutog na redovnim dvogodišnjim savetovanjima sa regionalnim učešćem CIRED Srbije. Na njima se uglavnom prikazuju radovi iz oblasti elektrodistribucije, odnosno vezani za rad, planiranje i održavanje elektrodistributivnih mreža. Ova savetovanja organizuje udruženje CIRED Srbije, koje je nacionalni komitet u sklopu međunarodnog udruženja CIRED sa sedištem u Liježu (*Liege*), Belgija [1].

Društvo za elektroniku, telekomunikacije, računarstvo, automatiku i nuklearnu tehniku (Društvo za ETRAN), kao jedno od najstarijih društava iz oblasti elektrotehnike u Srbiji, koje ove godine organizuje svoju LXVI konferenciju, od 1994. godine neguje sekciju Elektroenergetika [2]. U njoj se uglavnom prezentuju radovi iz akademskog okruženja, odnosno od strane autora sa univerziteta u Beogradu, Novom Sadu, Nišu i Kragujevcu. Od 2014. god. ETRAN ima i svoje međunarodno izdanje, IcETRAN (International Conference on ETRAN), na kom se predstavljaju radovi na engleskom jeziku. Na obe konferencije se prikazuju radovi iz svih oblasti elektroenergetike, ali je najčešća tematika vezana za elektroenergetske mreže, industrijsku elektroenergetiku i električne potrošače.

Cilj ovog rada je da predstavi pregled stručne problematike i glavnih tema istraživanja iz oblasti elektroenergetike u Srbiji u poslednjih sedam godina (2014. – 2021. god.) čiji rezultati su predstavljeni na savetovanjima CIRED Srbije, odnosno konferencijama ETRAN/IcETRAN. Na taj način autori žele da ukažu na moguću spregu istraživača sa univerziteta i iz privrede u formulisanju najboljih rešenja za rad elektrodistributivnog sistema.

## II. Savetovanja CIRED Srbija

Savetovanje CIRED Srbija održavaju se dvogodišnje, svake parne godine i na njima se okupi oko 500 učesnika iz zemlje i regiona. Pored naučno-stručnog dela u kom se izlaži prijavljeni radovi, organizuje se i velika izložba kompanija i preduzeća iz oblasti, kao i tematski okrugli stolovi. Tako struktuirano, savetovanje je pre svega namenjeno stručnjacima iz privrede, koji na njemu mogu da vide najnovija tehnička i tehnološka dostignuća, kao i da dobiju pregled naučnih istraživanja u oblasti. Pored toga, značajno je prisustvo i prezentacije istraživača sa univerziteta i naučnih instituta, kroz koje se mogu videti i pravci istraživanja i moguće primeene u praksi.

Rezultati istraživanja prikazani u naučnim ili stručnim radovima (referatima ili informacijama) svrstani su tematski

Zoran J. Simendić – Predsednik CIRED Srbija, Elektrodistribucija Srbije d.o.o. Beograd, Ogranak Elektrodistribucija Sombor, Apatinski put bb, 25101 Sombor, Srbija (e-mail: Zoran.Simendic@epsdistribucija.rs)

Vladimir A. Katić – Predsednik Društva za ETRAN, Univerzitet u Novom Sadu, Fakultet tehničkih nauka, Trg Dositeja Obradovića 6, 21000 Novi Sad, Srbija (e-mail: katav@uns.ac.rs)

 ISBN 978-86-7466-930-3

prema preferencijalnim temama. Ove teme za svako savetovanje definišu odgovarajući studijski komiteti CIRED Srbije. Postoji šest stalnih studijskih komiteta (STK), čije delovanje obuhvata najaktuelnije teme vezane za savremene elektrodistributivne sisteme. To su:

STK 1 – Komponente mreža,

STK 2 – Kvalitet električne energije u elektrodistributivnim sistemima,

STK 3 – Zaštita i upravljanje elektroenergetskim mrežama,

STK 4 – Distribuirana proizvodnja i efikasno korišćenje električne energije,

STK 5 – Planiranje distributivnih sistema, i

STK 6 – Tržište električne energije i deregulacija.

*A. Preferencijalne teme CIDER Srbija 2022*

Preferencijalne teme (PFT) daju bliže odrednice tematike referata i definišu se u skladu sa razvojem nauke i struke. Za ovogodišnje savetovanje CIRED Srbija 2022 predložene preferencijalne teme obuhvataju sledeće problematike navedenih studijskih komiteta (ovde su teme navedene u skraćenom obliku, a kompletne se mogu naći u [1]):

STK 1:

- PFT 1.1 - Savremene konstrukcije, primena novih tehničkih rešenja i održavanje komponenti elektrodistributivnih mreža;
- PFT 1.2 - Testiranje, monitoring, dijagnostika i strategija održavanja komponenti elektrodistributivnih mreža;
- PFT 1.3 - Modelovanje i primena savremenih softverskih alata za analizu komponenti elektrodistributivnih mreža;
- PFT 1.4 - Uticaj komponenti elektrodistributivnih mreža na životnu i radnu sredinu;
- PFT 1.5 - Tehnička regulativa iz domena komponenti elektro-distributivnih mreža.

STK 2:

- PFT 2.1 - Kvalitet isporuke i kvalitet isporučene električne energije – uzroci, prostiranje, imunitet, eliminisanje, analize, iskustva;
- PFT 2.2 - Uređaji i metode za merenje i praćenje parametara kvaliteta električne energije (dijagnostičke metode, oprema, postupci i sl.);
- PFT 2.3 - Domaća i evropska tehnička regulativa o kvalitetu električne energije (standardizacija, tehnički propisi i postupci);
- PFT 2.4 - Uticaj distribuiranih generatora na kvalitet električne energije (naponski nivoi, struje kratkih spojeva, harmonici, podrška mreži – LVRT i sl.);
- PFT 2.5 - Uslovi priključenja nelinearnih potrošača i distribuiranih generatora, elektromagnetna kompatibilnost, bezbednost i interferencija;
- PFT 2.6 - Uticaj nedovoljnog kvaliteta u mreži na rad potrošača ili distribuiranih generatora (tehnički problemi, energetska efikasnost, pouzdanost, finansijski efekti, odnosi sa potrošačima...);
- PFT 2.7 - Prenaponi i zaštita od prenapona u distributivnim mrežama, poremećaji u uzemljenju i uticaj na kvalitet električne energije i druge povezane teme.

STK 3:

- PFT 3.1 - Ekploatacija (Strategije održavanja i procena stanja, tehnike i alati za upravljanje radnom snagom, zahtevi u pogledu upravljanja podacima, strategije upravljanja kriznim situacijama, eksploatacija industrijskih mreža);
- PFT 3.2 - Zaštita (Strategije pri zameni i rekonstrukciji zaštite, sistemi za nadzor i upravljanje u transformatorskim stanicama, uticaj distribuirane proizvodnje, nove zaštitne šeme i funkcije, simulacioni modeli, alati i nove funkcije, aspekti pouzdanosti, ispitivanje relejne zaštite, funkcija i sistema, analiza pojave kvarova i registrovanih zapisa);
- PFT 3.3 - Upravljanje i komunikacije (Automatizacija ED mreža, upravljanje u tržišnim uslovima, primena energetskih aplikacija, uvođenje sistemskih usluga, regulacija napona u SN i NN mrežama, primena komunikacionih sistema, sigurnosni aspekti pristupa informacijama, komunikacione tehnike i protokoli za realizaciju inteligentnih mreža, međusobna zavisnost).

STK 4:

- PFT 4.1 - Integracija i upravljanje distribuiranih izvora električne energije (DER) u distributivnim mrežama (Aktivno upravljanje sa distribuiranim izvorima električne energije, Upravljački algoritmi i filozofije, Prognoza proizvodnje iz obnovljivih izvora, Analiza mogućnosti priključenja distribuiranih izvora, Mikro-mreže, Električna vozila);
- PFT 4.2 - Uloga DER u poslovnim procesima u distributivnim sistemima (Koordinacija i upravljanje DER, Dobiti od skladišta električne energije i različitih strategija upravljanja, aktivno upravljanje DER u cilju optimizacije rada, uloga u unapređenju otpornosti distributivnih mreža, upravljanje opterećenjem);
- PFT 4.3 - Efikasno korišćenje električne energije (Smanjenje gubitaka, unapređenje efikasnosti distributivnih sistema, isporuka održive energije sa niskom emisijom gasova staklene bašte);
- PFT 4.4 - Pametna brojila i sistemi za daljinsko očitavanje i upravljanje brojilima (Korišćenje informacija sa pametnih brojila, analitika i studije slučaja, analiza troškova i dobiti).

STK 5:

- PFT 5.1 - Predviđanje potrošnje i proizvodnje distribuiranih izvora;
- PFT 5.2 - Pokazatelji kvaliteta mreža: zahtevi, rezultati i poređenje;
- PFT 5.3 - Strukture mreža i kriterijumi za planiranje mreža;
- PFT 5.4 - Metode za planiranje;
- PFT 5.5 - Strategije za investiranje.

STK 6:

- PFT 6.1 - Otvaranje tržišta električne energije i restrukturiranje elektroprivrede u regionu, praksa i iskustva;
- PFT 6.2 - Regulacija, modeli regulacije, uloga regulatora, izmene i unapređenja;
- PFT 6.3 - Učesnici tržišta električne energije, modeli

 ISBN 978-86-7466-930-3

snabdevanja i modeli tržišta;
PFT 6.4 - Distribuirani izvori energije u konkurentnim uslovima otvorenog tržišta.

*B. Tematska struktura naučnih radova*

CIRED savetovanja održavaju se od 1998. god., a ove 2022. god. se proslavlja 25 godina. U tom periodu održano je 12 savetovanja i predstavljeno 1449 radova u formi referata i stručnih informacija, odnosno u proseku po 121 rad po savetovanju [1, 3]. Na slici 1 prikazan je pregled prikazanih radova po godinama u kojima su održana savetovanja. Može se videti da broj radova se polako menja (opada), ali da se na poslednjih nekoliko savetovanja ustalio na oko 110 radova, što ukazuje na promenu aktivnosti istraživača u ovoj oblasti. Interesantno je uočiti da pandemija Korona-19 virusa nije ostavila posledice na broj radova, ali da je usled nje 12. savetovanje iz 2020. god. pomereno u 2021. god.

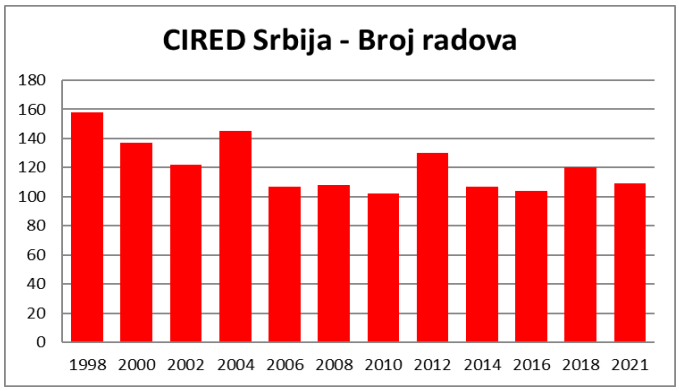


Sl. 1. Pregled broja radova na savetovanjima CIRED Srbija (ranije JUKO CIRED) od 1998. – 2021. god.

Međutim, da bi se dobila adekvatna slika tematske orijentacije istraživača u Srbiji kroz prezentovane radove na savetovanju CIRED Srbija, koja bi pravilno odslikavala postojeće stanje istraživanja u Srbiji, sužen je obim posmatranja. U obzir je uzet period poslednjih sedam godina (2014. god. – 2021. god.) u kom su održana četiri savetovanja na kojima je ukupno referisano 440 radova, informacija i referata na forumu „Smart grids“. U tom periodu su predstavljeni radovi razvrstani po studijskim komitetima, da bi se uočili dominantni pravci istraživanja. Na slici dva prikazan je broj radova po studijskom komitetu na poslednja četiri savetovanja. Može se uočiti da su najviše bile zastupljeni radovi iz tematike STK 1 (ukupno 100 rada), pa onda STK 3 (82 rada) i STK 4 (74 rada), dok su manje zastupljeni radovi iz oblasti STK 5 (59 radova), STK 2 (58 radova) i STK 6 (45 radova), dok je forum „Smart grids“ okupio još 22 rada.

## III. KONFERENCIJE ETRAN/ICETRAN

Društvo za ETRAN se sastoji od 16 tematskih sekcija, koje pokrivaju kompletnu oblast elektrotehnike i to: Akustika (AK), Antene i prostiranja (AP), Automatika (AU), Biomedicinska tehnika (BT), Električna kola, električni sistemi i obrada signala (EK), Elektroenergetika (EE), Elektronika (EL), Metrologija (ML), Mikroelektronika i optoelektronika (MO), Mikrotalasna tehnika, tehnologije i sistemi (MT), Novi materijali (NM), Nuklearna tehnika (NT), Računarstvo (RA), Robotika i fleksibilna automatizacija (RO), Telekomunikacije (TE), Veštačka inteligencija (VI). Društvo svake godine organizuje dve paralelne konferencije (nacionalnu ETRAN i međunarodnu IcETRAN), a prosečan broj radova je oko 200. Na ovim konferencijama autori uglavnom dolaze sa naučno-obrazovnih (univerziteta, fakulteta) i naučno-istraživačkih (instituta) institucija, odnosno iz akademskog okruženja, dok je prisustvo i doprinosi učesnika iz privrede znatno ređe.

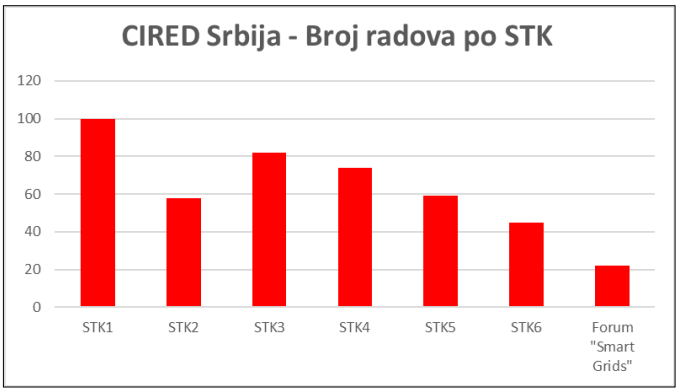


Sl. 2. Pregled ukupnog broja radova po studijskim komitetima (tematskim celinama) u periodu 2014.-2021. god.

Dok su savetovanja CIRED Srbija u celosti posvećena elektroenergetici, konferencije ETRAN/IcETRAN tek u jednom segmentu, kroz aktivnost sekcije Elektroenergetika pokrivaju ovu oblast. Međutim, konferencije se odvijaju svake godine, pa se u poređenju sa savetovanjima CIRED Srbija mogu predstaviti nešto aktuelniji radovi. Do sada je na sekciji prezentovano 456 radova, s tim da je na konferencijama ETRAN bilo 414 radova, a na IcETRAN 42 rada. Na slici 3 prikazan je pregled broja radova u periodu od formiranja sekcije 1994. god. do 2021. god. [2, 4]. Može se uočiti sličan opadajući trend, kao i kod CIRED Srbija savetovanja, s tim da se ovde prosečan broj radova 16,3, ali se poslednjih godina ustalio (spustio) na oko 10.

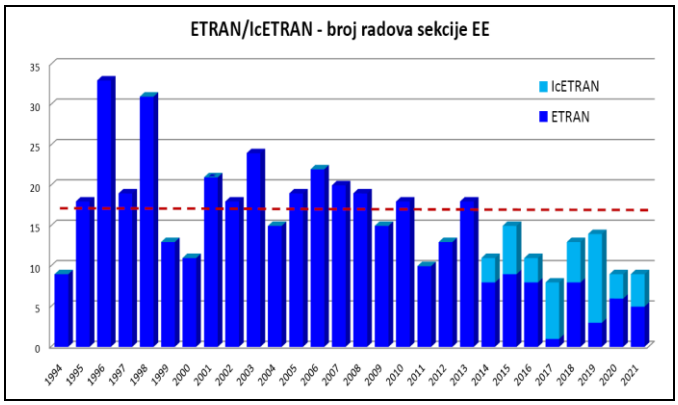


Sl. 3. Pregled broja radova na sekciji Elektroenergetika na konferencijama ETRAN i IcETRAN od 1994. – 2021. god.


ISBN 978-86-7466-930-3

Iz razloga aktuelnosti i ovde će se posebno analizirati period 2014. – 2021. god. Karakteristika tog perioda je da se u njemu javlja IcETRAN konferencija (počinje od 2014. god.), kao međunarodna konferencija i ETRAN, kao nacionalna. To daje mogućnost autorima da svoje radove predstave na jednoj od ove dve paralelne konferencije u zavisnosti kom auditorijumu žele da predstave svoje rezultate. Na slici 3 se može videti odnos radova na ove dve konferencije, koji se kreće u proseku 1,14:1 (53,3% i 46,7%).

Radovi na sekciji EE konferencija ETRAN/IcETRAN uglavnom su deljeni u dve oblasti: elektroenergetski sistemi i industrijska elektroenergetika. Međutim, da bi se bolje sagledala njihova tematska orijentacija i uskladila sa onom sa savetovanja CIRED Srbija, urađena je detaljnija klasifikacija. Kriterijum je bila uža tematika rada utvrđena kroz naslov, ključne reči i abstrakt. Sad su radovi svrstani su u osam tematskih oblasti:

EE-T1: Električne mreže (prenosne i distributivne), mikromreže i pametne mreže (smart grids);
EE-T2: Kvalitet električne energije, prenaponi i kompenzacija;
EE-T3: Elektroenergetska oprema, zaštita i informacioni sistemi;
EE-T4: Generatori, obnovljivi izvori energije (DER), električna vozila, te upravljanje proizvodnjom i merenje;
EE-T5: Električne mašine i transformatori (modelovanje, kvarovi, gubici, održavanje i sl.);
EE-T6: Elektromotorni pogoni (modelovanje, regulacija brzine, dinamika i sl.);
EE-T7: Energetska elektronika (energetski elektronski pretvarači, filteri, upravljački sklopovi i sl.);
EE-T8: Edukacija i ostalo.

Može se uočiti da se prve četiri oblasti (EE-T1 – EE-T4) više-manje poklapaju sa oblastima delovanja studijskih komiteta STK 1 – STK 4, dok su ostale van toga. Isto tako, radovi iz oblasti preostalih studijskih komiteta (STK 5 i STK 6) generalno nisu zastupljeni na konferencijama ETRAN/IcETRAN, pa su u slučaju eventualnog pojavljivanja svrstani pod ostalo, odnosno u EE-T8.

Na slici 4 prikazan je pregled broja radova na konferencijama ETRAN/IcETRAN svrstanih u skladu sa gornjom listom tematskih oblasti. Može se primetiti da su po broju radova tematske oblasti EE-T4 i EE-T5 dominantne, da su izražene teme iz oblasti EE-T7, EE-T1 i EE-T2, dok su oblasti EE-T6 i EE-T3 manje zastupljene. Dakle, na ovim konferencijama najčešće su bili izlagani radovi vezani za električne generatore, obnovljive izvore energije (DER), električna vozila, upravljanje proizvodnjom i merenjem, kao i vezane za električne mašine i transformatore, pa i energetsku elektroniku (energetske elektronske pretvarače) i filtere.

## IV. Pravci istraživanja u Srbiji

Na osnovu podataka sa slika 2 i 4 može se videti da su istraživači u Srbiji najviše bili zaokupljeni temama iz oblasti STK 1 (Komponente mreža), STK 3 (Zaštita i upravljanje elektroenergetskim mrežama) i STK 4 (Distribuirana proizvodnja i efikasno korišćenje električne energije), odnosno EE-T4 (Generatori, obnovljivi izvori energije (DER), električna vozila, te upravljanje proizvodnjom i merenje), EE-T5 (Električne mašine i transformatori) i EE-T7 (Energetska elektronika, energetski elektronski pretvarači i filteri). U tim oblastima, ukupno je prikazano 58,2% radova savetovanja CIRED Srbija, odnosno 62,1% radova sa konferencija ETRAN/IcETRAN. S obzirom na datu tematiku i pomenuto preklapanje tema, može se zaključiti da je fokus autora na obe konferencije u periodu 2014. god. – 2021. god. bio usmeren na različite teme, osim u slučaju problematike izučavane u STK 4, odnosno EE-T4. To opravdava organizaciju oba skupa, ali i ukazuje na zone daljeg profilisanja.

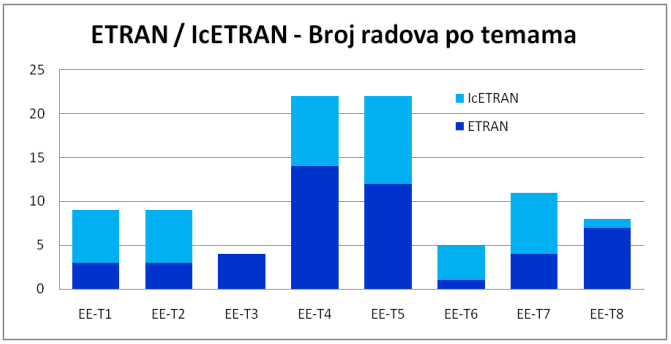


Sl. 4. Pregled broja radova sekcije Elektroenergetika na ETRAN/IcETRAN konferencijama u periodu 2014.-2021. god. svrstanih po oblastima

Dublja analiza radova iz tih oblasti može ukazati na specifičnu tematiku, kao i njenu moguću tehnološku vrednost i aplikativnost u srpskoj industriji.

### *A. Pravci istraživanja i broj radova*

U skladu sa gornjim zaključkom, dublje je analizirana produkcija po preferencijalnim temama pojedinih STK sa savetovanja CIRED Srbija, odnosno subtemama tematskih oblasti na konferencijama ETRAN/IcETRAN.

U studijskim komitetima STK 1, STK3 i STK4 na savetovanjima CIRED Srbija ponuđeno je ukupno 12 preferencijalnih tema (STK1=5, STK3=3 i STK4=4), s tim što je kod STK3 za savetovanje 2022. god. njihov broj znatno uvećan, pa su ovde one agregirane pod tri glavne. Na slici 5 prikazano je ukupno učešće radova po PFT za pomenuta tri STK u periodu 2014.-2021. god. Može se videti da su najistaknutije preferencijalne teme PFT 4.1, PFT 1.2 i PFT 3.3. Pored toga, istaknute su (sa više od 25 radova) teme PFT 4.2 i PFT 3.1.

Na osnovu toga može se zaključiti da su savetovanjima CIRED Srbija najčešće prezentovani rezultati istraživanja po temama Integracija i upravljanje distribuiranih izvora električne energije (DER) u distributivnim mrežama, Testiranje, monitoring, dijagnostika i strategija održavanja komponenti elektrodistributivnih mreža, Upravljanje i komunikacije u distributivnim mrežama, kao i teme Uloga DER u poslovnim procesima u distributivnim sistemima i Ekploatacija distributivnih mreža.


ISBN 978-86-7466-930-3

Što se tiče istaknutih tema iz elektroenergetike na konferencijama ETRAN/IcETRAN, sa slike 4 vidi se da se radi o temama EE-T4, EE-T5 i EE-T7, čiji sadržaj je naveden ranije. Po broju radova, konferencije ETRAN/IcETRAN nešto su skromnije od savetovanja CIRED Srbija, pa dalja parcelizacija ne bi bila svrsishodna.

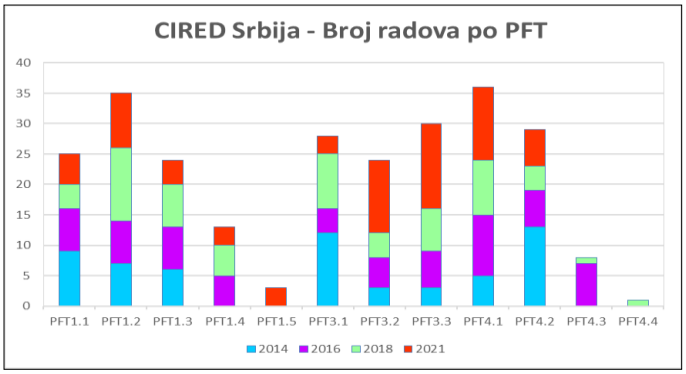


Sl. 5. Pregled broja radova sa savetovanje CIRED Srbija sortiranih po preferencijalnim temama za STK1, STK3 i STK4 u periodu 2014.-2021. god.

### *B. Pravci istraživanja i nagrađeni radovi*

Oba skupa nagrađuju najistaknutije radove po STK-ovima, odnosno po sekcijama. Nagrade se dodeljuju i mladim autorima, kao podsticaj u njihovom razvoju. Uglavnom se radi o radovima koji su ostavili najbolji utisak, prikazuju rezultate naprednih istraživanja ili neka istaknuta tehnička rešenja. U skladu sa prethodnim posmatrane su teme nagrađenih radova iz STK1, STK3 i STK4, odnosno sa sekcije EE.

Kod savetovanja CIRED Srbija u posmatranom periodu STK1 je dodelio dve nagrade za radove u sklopu PFT1.2, a dve za PFT1.3, kod STK3 dve nagrade su bile u PFT 3.2, a po jedna PFT3.1 i PFT3.3, dok su kod STK4 tri nagrađena rada bila iz PFT4.1, a jedan iz PFT4.2. Ovo u potpunosti odgovara prethodnom zaključku o glavnim pravcima istraživanja za STK1 i STK4, dok delimično za STK3.

Kod konferencija ETRAN/IcETRAN nagrađeni radovi su bili iz tematskih oblasti EE-T5 sa pet radova, EE-T4 sa tri rada, EE-T1 i EE-T2 sa po dva rada i iz EE-T6 i EE-T7 sa po jednim nagrađenim radom. Vidi se da se ovo poklapa sa ranijim zaključkom o najpopularnijim temama.

### *C. Ključni pravci istraživanja*

Poređenjem rezultata o najčešćim temama radova sa skupova CIRED Srbija i ETRAN/IcETRAN u periodu 2014.-2021. god., može se uočiti skoro potpuno poklapanje najpopularnije PFT 4.1 od STK4 i najzastupljenije teme EE-T4. To ukazuje da je i interesovanje akademske i stručne javnosti usmereno na istraživanja iz oblasti generisanja električne energije, distribuirane proizvodnje, primene obnovljivih izvora energije, priključenja električnih vozila, te upravljanja takvom proizvodnjom i pridruženim merenjima.

## V. ZAKLJUČAK

Posmatranjem tematike radova sa dva skupa, koja prezentuju rezultate istraživanja iz oblasti elektroenergetike, savetovanje CIRED Srbija i konferencije ETRAN/IcETRAN, razmatrani su glavni pravci istraživanja u Srbiji.

Po prirodi, prvi skup je nacionalnog karaktera sa međunarodnim učešćem (radovi su na srpskom jeziku sa dodatim naslovom i abstraktom na engleskom ili kompletno na engleskom jeziku, ako se radi o nekim stranim učesnicima), konferencija ETRAN je takođe nacionalnog tipa (radovi su na srpskom jeziku sa dodatim naslovom i abstraktom na engleskom jeziku), dok je konferencija IcETRAN čisto međunarodna (radovi su na engleskom jeziju u IEEE formatu).

Po svojoj naučno-stručnoj orijentaciji, koncepciji i strukturi, prvi skup je u potpunosti orijentisan na oblasti elektroenergetike, odnosno preciznije na oblast elektrodistributivnih sistema, dok se na druga dva razmatraju rezultati iz kompletne elektrotehnike, pa je tek u jednom segmentu posvećen elektroenergetici, u sklopu istoimene sekcije.

Po svojoj nameni i učesnicima, prvi je generalno namenjen stručnoj i akademskoj javnosti, dok je druga dva u najvećem broju okuplja učesnike sa univerziteta i naučnih instituta. Pored toga, gro autora je iz Srbije, ali je značajno i učešće autora iz inostranstva.

Na bazi ove komparacije, može se zaključiti da su ova dva skupa kompatibilna i da mogu poslužiti za dobijanje predstave o glavnim pravcima istraživanja.

U posmatranom periodu od 2014. god. do 2021. god. u kom su održana četiri savetovanja i osam konferencija uočeno je da postoji odgovarajuća bliža tematika, koja je najzastupljenija na oba skupa i koja ukazuje na glavni pravac istraživanja u Srbiji. Ona se odnosi, odnosno upravljena je na istraživanja iz oblasti generisanja električne energije, distribuirane proizvodnje, primene obnovljivih izvora energije, priključenja električnih vozila, te upravljanja takvom proizvodnjom i pridruženim merenjima.

Autori su uvereni da bi se slični zaključci mogli doneti i za druge (slične) konferencije u Srbiji i svetu. Ovo ukazuje da istraživači u Srbiji tretiraju najnovije prodore u nauci i struci, te da razmatrani skupovi mogu da posluže za dobijanje dobrog uvida o najnovijim dostignućima iz oblasti elektroenergetike u svetu.

## LITERATURA

[1] Simendić Z. i dr., *„Dvadeset godina rada srpskog nacionalnog komiteta CIRED Srbija“*, Monografija, Novi Sad, Srpski nacionalni komitet CIRED Srbija, 2017.

[2] Katić V., „Elektroenergetika“, u knjizi *„ET(R)AN Prvih šezdeset konferencija – Doprinos ravoju elektrotehničke struke“*, Uredili: B. Milovanović i Z. Jakšić, pp. 90-98, Beograd, Društvo za ETRAN i Akademska misao, 2016.

[3] http://www.ciredserbia.org.rs

[4] https://www.etran.rs

## ABSTRACT

The paper discusses the directions of research through papers at two important scientific and professional gatherings, which are held in Serbia, the CIRED Serbia conference and the ETRAN/IcETRAN conferences. The structures of the both are presented in more detail, as well as the key topics discussed in them. At the CIRED Serbia

 ISBN 978-86-7466-930-3

conference, topics are related to the issue of electricity distribution, through standing study committees and their preferential topics, while at the ETRAN / IcETRAN conferences, they are related to and cover the entire field of electricity. Based on that, the interest of the participants in these gatherings was discussed through the number of presented scientific and professional papers for the relevant thematic areas. It was concluded that the most common topics are in the field of electricity generation, distributed generation, application of renewable energy sources, a connection of electric vehicles, and control of such generation and associated measurements. This indicates that researchers in Serbia are treating the latest breakthroughs in science and profession, and that the considered conferences give an adequate overview of the latest achievements in this fields.

## Directions of research in electrical power engineering through thematic orientation of papers from CIRED Serbia and ETRAN/IcETRAN conferences

Zoran J. Simendić and Vladimir A. Katić

 ISBN 978-86-7466-930-3

# ELECTRIC CIRCUITS AND SYSTEMS AND SIGNAL PROCESSING

# /

# ЕЛЕКТРИЧНА КОЛА, ЕЛЕКТРИЧНИ СИСТЕМИ И ОБРАДА СИГНАЛА

## (ЕКІ/ЕК)

ISBN 978-86-7466-930-3

# A method for laser rangefinder reticle position calibration in a multi-sensor imaging system

Saša Vujić, *Member, IEEE*, Miloš Radisavljević, *Member, IEEE*, Dragana Perić, *Senior Member, IEEE* and Branko Livada, *Senior Member, IEEE*

***Abstract*— A method for laser rangefinder reticle position calibration in a multi-sensor imaging system is presented. This method was developed to provide system control software with proper parameters used for LRF reticle position, for all imagers and for different field of view configurations of those imagers in a typical multi-sensor imaging system. The importance of reticle position calibration and accuracy is explained, and error calculated. A prerequisite for laser rangefinder reticle position calibration is to perform each imager calibration and the multi-sensor imaging system optical axes rectification. The method is straight forward, fast and reliable. Details of the method are described and experimental verification of results obtained after the calibration are given.**

***Index Terms*—laser rangefinder; LRF; reticle calibration; multi-sensor imaging system; electro-optical system; long-range surveillance.**

## I. Introduction

Multi-sensor imaging systems (MSIS) with zoom lenses are used for surveillance with number of technical, technological and application challenges [1], and also for other applications where observed object of interest (target) distance is important, e.g. target geolocation. These MSIS' functionalities are related with the use of laser rangefinders (LRF) and their proper integration within the MSIS [2], [3]. A control station – operator's console, which provides a user interface to MSIS sensors data, is another important part of MSIS [4]. In order to create a usable system it is necessary to provide a system operator with possibility to accurately point with LRF beam to desired object of interest. For this purpose it is necessary to determine control software parameters used for LRF reticle positioning. With properly determined parameters control software displays the LRF reticle at the right place and operator is able to direct the MSIS, i.e. the LRF beam to target, for any selected field of view (FOV).

Saša Vujić is with the Vlatacom Institute of High Technologies, 5 MilutinaMilankovića Blvd., 11070 Belgrade, Serbia (e-mail: sasa.vujic@vlatacom.com), and with the Belgrade Metropolitan University, Tadeuša Košćuška 63, 11000 Beograd, Serbia

Miloš Radisavljević is with the Vlatacom Institute of High Technologies, 5 Milutina Milankovića Blvd., 11070 Belgrade, Serbia (e-mail: milos.radisavljevic@vlatacom.com), and with the Belgrade Metropolitan University, Tadeuša Košćuška 63, 11000 Beograd, Serbia

DraganaPerić is with the Vlatacom Institute of High Technologies, 5 Milutina Milankovića Blvd., 11070 Belgrade, Serbia (e-mail: dragana.peric@vlatacom.com).

Branko Livada is with the Vlatacom Institute of High Technologies, 5 Milutina Milankovića Blvd., 11070 Belgrade, Serbia (e-mail: branko.livada@vlatacom.com).

This work is continuation of work published in [2] and [3], where LRF integration, LRF reticle integration and camera calibration are described. In available literature there are also other articles related to these topics [5-12], however, the details and methods about how to determine control software parameters used for LRF reticle positioning are not readily available, and therefore we are not able to make any comparison with other calibration methods in the sense of complexity and accuracy.

In this work the main research issue was to establish the correlation between LRF beam, images from different imagers and for any FOV, and reticle which is shown on display. Furthermore, the particular goal was to define a method for determining control software parameters used for LRF reticle position.

In this paper in section II we describe a typical electro-optical MSIS architecture and basic functionalities, in section III some zoom lens properties, in section IV we explain the importance of LRF reticle position calibration and its accuracy, in section V we list prerequisites for LRF reticle calibration, in section VI we present a method for LRF reticle position calibration in a multi-sensor imaging system, in section VII we summarize results of the method experimental verification, and in section VIII we give the conclusion.

## II. Electro-optical multi-sensor system architecture and basic functionalities

Multi-sensor imaging systems (MSIS) are used for surveillance, observed object geolocation and other applications [13], [14]. Each of those systems comprises an electro-optical head with integrated sensors mounted on a gimbal, and remote operator's console with application software for monitoring and control [4].

A typical MSIS with MWIR thermal imager, visible light imager and a LRF mounted on a gimbal is shown in Fig. 1.

Fig. 1. Multi-sensor imaging systems with laser rangefinder.

The sensors that those systems usually comprise [1] are

 ISBN 978-86-7466-930-3

midwave infrared (MWIR) or longwave infrared (LWIR) thermal imagers with continuous zoom optics, visible light imagers with continuous zoom optics, short-wave infrared (SWIR) imagers with continuous zoom optics, laser rangefinders (LRF), positioning sensors and orientation sensors. Such systems are capable of measuring the line of sight distance from the electro-optical head with sensors to some object of interest, by using a LRF, and are also capable to accomplish many other more advanced tasks, e.g. calculating observed object of interest geolocation, based on known data about MSIS position, orientation and observed object distance [15-17].

A MSIS operator uses such a system through an operator's console with input and output devices, via a graphical user interface (GUI) which is a part of a software application for monitoring and control installed on the operator's console [4]. The operator's console can be in different forms, with one or more displays as output device, and with joystick, touchpad, trackball, touchscreen, keyboard or mouse as input device. An example of operator's console is shown in Fig. 2.

Fig. 2. Multi-sensor imaging system operator's console with three displays.

The GUI provides video streams for each of the integrated imagers, as well as other data, statuses and controls for MSIS functionalities. Depending on the selected operator's console for the particular application, the GUI is usually optimized to provide the best possible usability in a given scenario. An example of GUI with two video streams, map, statuses and controls is shown in Fig. 3.

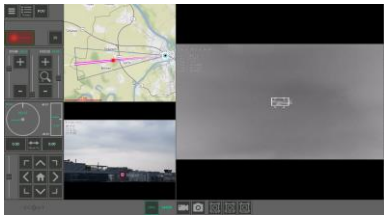

Fig. 3. Graphical user interface (GUI) of an operator's console, with two video streams, map, statuses and controls.

For each of the video streams there is an option to display a LRF reticle which shows the operator where the LRF beam is aiming. A video stream with reticle is shown in Fig. 4.

In order to bring such a system into the function there is a need to perform calibrations on different levels, including the continuous zoom imagers' calibration. One of the calibration tasks is to perform a calibration of LRF reticle position coordinates, for each imager, for different zoom levels. Before performing this reticle position calibration it is necessary to perform optical axes alignment to set up the axes of all imagers and LRF to be parallel to each other (a process called optical axes rectification, or boresighting).

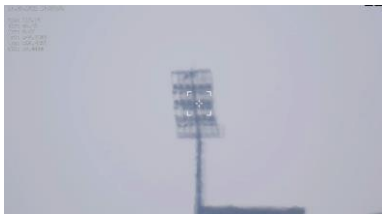

Fig. 4. Video stream with LRF reticle (object distance 4320m).

The optical axes rectification process is performed by means of precise mechanical positioning of structures holding optical elements. The optical axis rectification process is performed with zoom optics set in high end position, which gives a narrow field of view (NFOV), in order to achieve better accuracy. However, other fields of view (FOV) are also of interest and in order to provide a proper alignment of reticle for different zoom levels (different FOVs) there is a need to calibrate reticle position for different zoom levels due to an inherent characteristic of zoom lens to have deviation of optical axis from the ideal one when changing the zoom level. Therefore, the process of optical axis rectification does not have to be perfect and several pixels displacement can be allowed. Those displacements can be compensated by means of precision positioning of reticle in the image, i.e. in each frame of the video streams. The size of the reticle corresponds to the solid angle of the LRF beam. A typical LRF reticle, as drawn on visible light imager is show in Fig. 5.

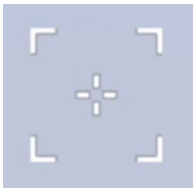

Fig. 5. LRF reticle as shown on screen

The process of reticle position coordinates calculation for all imagers and for different FOVs is time consuming and requires highly skilled operators and their high concentration, with high risk of making mistakes during the process. Therefore, in Vlatacom Institute we developed a method for LRF reticle position calibration such that the whole process is straight forward, fast and not prone to random errors.

## III. ZOOM LENS PROPERTIES

Zoom lenses are very popular in modern multi-sensor imaging systems used in long-range surveillance and related applications. They provide flexibility and controllability for different missions and use cases. Zoom lenses provide users with a functionality to observe areas with any FOV angle, from a wide field of view (WFOV) to NFOV, and also to focus objects on different distances from minimal object distance (MOD), to infinite distance, for any FOV. Some of

 ISBN 978-86-7466-930-3

the basic properties of each zoom lens are minimal and maximal focal length - $f_{min}$ and $f_{max}$, f-number - N, WFOV, NFOV and MOD. There are also many others which define lens optical characteristics and electro-mechanical interfacing.

WFOV and NFOV of imager depend on imaging sensor size and minimal/maximal lens focal lengths. WFOV, NFOV of two MSIS, C330 and C1000, are given in Table I.

TABLE I
CONTINUOUS ZOOM LENS PARAMETERS OF TWO THERMAL AND TWO VISIBLE LIGHT IMAGERS

| Lens\Par. | WFOV [°] | NFOV [°] | $f_{min}$ [mm] | $f_{max}$ [mm] |
|---|---|---|---|---|
| C330-VIS | 36 | 3.5 | 16 | 160 |
| C330-TH | 35.4 | 1.67 | 16 | 330 |
| C1000-VIS | 21 | 0.55 | 20 | 800 |
| C1000-TH | 18 | 0.75 | 40 | 1000 |

The thermal imager resolution is 640 x 480 with pixel size of 15 μm for C330-TH, and 1280 x 1024 with pixel size of 10 μm for C1000-TH.

One of the important properties is back focal length (BFL), also known as flange focal distance (FFD), flange focal depth (FFD), flange back distance (FBD), flange focal length (FFL). BFL defines the position of the zoom lens focal plane distance, where the imaging sensor plane should be placed, and the lens mounting reference plane. The adequate distance of the imaging sensor will result in the a possibility to focus objects from MOD to infinite distance, for any FOV from WFOV to NFOV. A typical test target used for back focus calibration, USAF 1951, is show in Fig. 6.

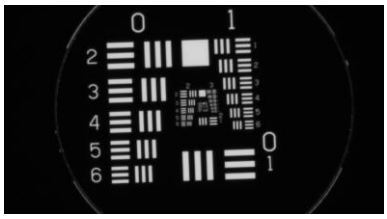


Fig. 6. USAF 1951 test target used for back focus calibration.

The zoom lens functionality is based on moving mechanisms which inherently involve lens elements displacements relatively to their ideal positions. For this reason it is necessary to perform additional zoom lens calibration for proper alignment of LRF reticle with LRF beam [17-21].

All these calibrations are necessary for successful LRF integration in any MSIS [2], [3].

Instantaneous field of view or (IFOV) is an important parameter which determines how much a single pixel can see in terms of FOV, depends on pixel size and focal length and equals IFOV = Pixel Size / Focal Length. With zoom lenses IFOV changes with FOV from wide IFOV($f_{min}$) to narrow IFOV($f_{max}$) angle.

## IV. THE IMPORTANCE OF RETICLE CALIBRATION AND ITS ACCURACY

The LRF beam is quite narrow with Gaussian distribution [2] and in tested systems it is circular in shape with divergence angle of 700 μrad in case of MSIS C330, and 250 μrad in case of MSIS C1000. Both are eye safe with 1,54 μm wavelength. The maximal measurement ranges are 20 km and 39 km, with range measurement accuracy of ±5 m, and ±1 m respectively. The minimal IFOV (at NFOV) in tested systems is 32 μrad in case of MSIS C330, and 5 μrad in case of MSIS C1000. For these cases the LRF beam divergence is 22 to 50 pixels.

If the LRF reticle was not well aligned with the LRF beam the LRF functionality would be lost, due to the fact that LRF beam would miss the target, i.e. it would not hit the area where the MSIS operator is targeting with the reticle, resulting in a wrong measured data, or no measurement at all. If the reticle was quite well aligned with the beam, but not perfectly, it would be possible to measure the object distance, but for any mistake or deviation in misalignment between the reticle and LRF beam an added error in geolocation calculation [16] would be made. With MSIS C330, at 10 km distance, the error introduced with reticle misalignment is 0,32 m for each pixel of reticle displacement. Therefore, the accuracy of reticle positioning is important for such systems. In a simplified model of MSIS, the LRF beam is an ideal line corresponding to the center of the reticle shown on the screen. However, in real case the center of LRF beam will not match ideally to the reticle center, as shown in Fig. 7.

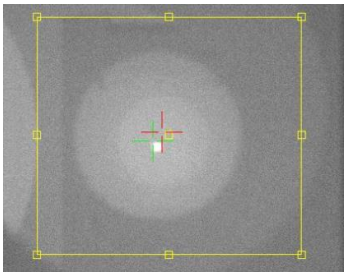

Fig. 7 Displacement of reticle and LRF

For some real MSIS and long distances at which these systems are used, the error that is made due to the reticle displacement can be significant. The error in geolocation calculation for one pixel of reticle displacement on real systems for four different imagers given in Table I, at distances of 1, 2, 5, 8 and 10 km, are given in Table II.

TABLE II
ERROR IN GEOLOCATION CALCULATION FOR ONE PIXEL OF RETICLE DISPLACEMENT AT DISTANCES OF 1, 2, 5, 8 AND 10 KM, IN MM

| Error in mm | Distance | | | | |
|---|---|---|---|---|---|
| Imager | 1km | 2km | 5km | 8km | 10km |
| C330-VIS | 32 | 64 | 159 | 255 | 318 |
| C330-TH | 46 | 91 | 228 | 364 | 455 |
| C1000-VIS | 5 | 10 | 25 | 40 | 50 |
| C1000-TH | 10 | 20 | 51 | 82 | 102 |


ISBN 978-86-7466-930-3

The error in geolocation calculation at object distance of 10 km, for 1, 2, 5, 8 and 10 pixels of reticle displacement on real systems for four different imagers given in Table I, are given in Table III.

TABLE III
ERROR IN GEOLOCATION CALCULATION AT 10KM DISTANCE FOR RETICLE DISPLACEMENTS OF 1, 2, 5, 8 AND 10 PIXELS, IN M

| Error in m | Displacement | | | | |
|---|---|---|---|---|---|
| Imager | 1 px | 2 px | 5 px | 8 px | 10 px |
| C330-VIS | 0,32 | 0,64 | 1,59 | 2,54 | 3,18 |
| C330-TH | 0,46 | 0,91 | 2,28 | 3,64 | 4,55 |
| C1000-VIS | 0,05 | 0,10 | 0,25 | 0,40 | 0,50 |
| C1000-TH | 0,10 | 0,20 | 0,51 | 0,82 | 1,02 |

## V. THE PREREQUISITES FOR LRF RETICLE CALIBRATION

A prerequisite for LRF reticle calibration is to perform each imager "zoom to FOV" calibration [2]. Depending on non-linearity of imager lens characteristic it is necessary to decide the number and value of discrete zoom lens positions for which the reticle will be calibrated. For all other zoom lens positions, in between the selected discrete positions, the reticle position will be calculated during the run time in the software application, using piecewise-linear approximation.

Furthermore, it is necessary to perform MSIS optical axes rectification, by means of precise mechanical positioning of structures holding optical elements, which is usually performed in NFOV setup for each imager. This way we will ensure that the calibrated MSIS will have the full correspondence of each imager reticle presenting the area where the LRF beam is aiming. In the ideal case the beam central line will correspond to each reticle central point. When the optical axes are nearly parallel, which can be observed and confirmed with use of collimator (few pixels displacement can be tolerated), a procedure of LRF reticle position calibration can be started.

It is necessary to perform the described procedure for each of the imagers contained in the MSIS. The sequence of the imagers' reticle calibration is irrelevant. Therefore the procedure can be started with any of the imagers that are contained in the MSIS. A MSIS set up in front of the collimator for rectification of visible light imager with LRF is presented in Fig. 8.

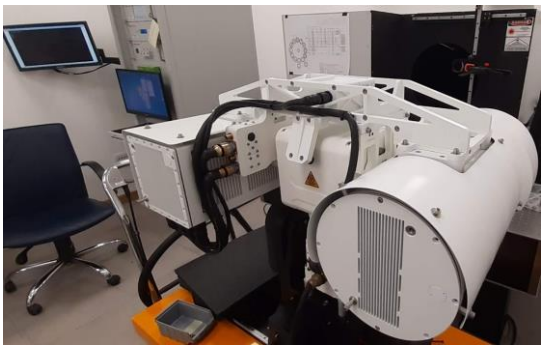

Fig. 8 A MSIS set up for rectification of visible light imager in front of the collimator

If the LRF is equipped with properly aligned visible light boresighting LED source, it can be used to make LRF reticle calibration, instead of LRF emitter. In that case instead of capturing videos a single image can be captured for each FOV. The same method can be used for LRF devices that can operate in continuous measurement mode (CMM). A single image will be sufficient for determining of LRF beam central point.

## VI. A METHOD FOR LRF RETICLE POSITION CALIBRATION IN A MULTI-SENSOR IMAGING SYSTEM

Within this method there are four stages to be completed. In the first stage the raw data should be captured, then in the second stage the position of LRF beam in the target should be determined, for each FOV. In the third stage the reticle calibration parameters should be calculated, and finally in the fourth stage the calibration parameters should be entered into software application that draws the reticle in the video stream.

For the first stage we need a device under test (DUT), in this case a selected imager, and an appropriate collimator for the selected imager's maximal focal length. In Fig. 9 an image taken with visible light imager of LRF firing in a target is shown.

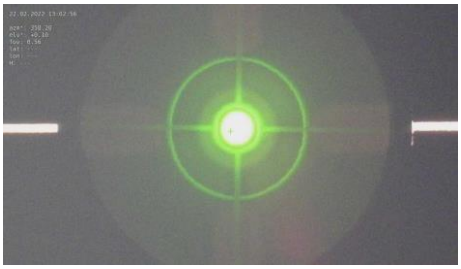

Fig. 9. Image taken with visible light imager of LRF firing in a target

All steps of the first stage are shown in block diagram in Fig. 10.

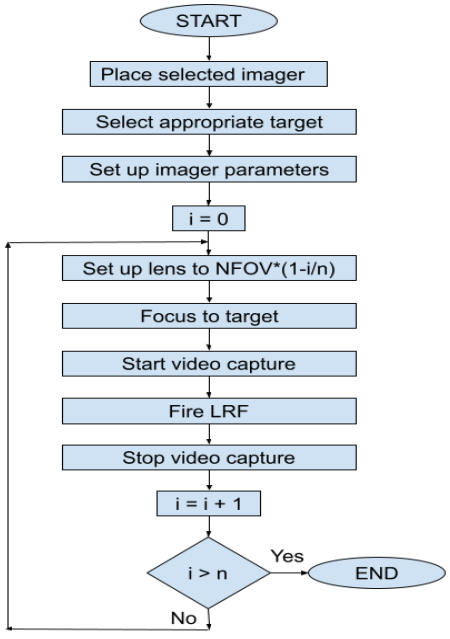


Fig. 10. Block diagram for first stage of the LRF calibration


ISBN 978-86-7466-930-3

The procedure is then repeated for each of the imagers contained in the MSIS.

When all videos are captured, for all imagers, then the first stage of this process is finished and the second stage can start. In the second stage for each captured video from the first stage we extract a frame in which the LRF beam is clearly visible. From that frame we determine the central coordinates of the LRF beam relatively to the image center.

In Fig. 11 an image taken with visible light imager of LRF firing in a target is shown.

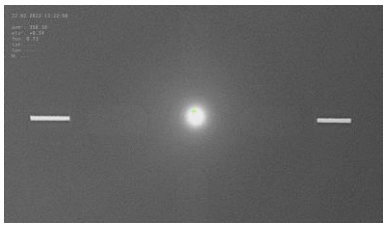

Fig. 11. Image taken with thermal imager of LRF firing in a target

For small angles close to NFOV the displacement from the image central coordinates to the LRF beam central coordinates depend on precision of optical axes rectification performed in previous stage. For wider angles closer to WFOV the displacement of LRF beam central coordinates depend on lens' construction. That can be seen also on the Fig. 12 where the reticle displacement in pixels for visible light and thermal imager are shown, for x and y axes. In case of visible imager the displacements are in range from 0 to 29 pixels in x axis, and from -6 to 29 pixels in y axis. In case of thermal imager the displacements are in range from -7 to 4 pixels in x axis, and from -1 to -12 pixels in y axis. In this case the displacements are higher for visible light imager due to the fact that its IFOV is twice smaller then in thermal imager.

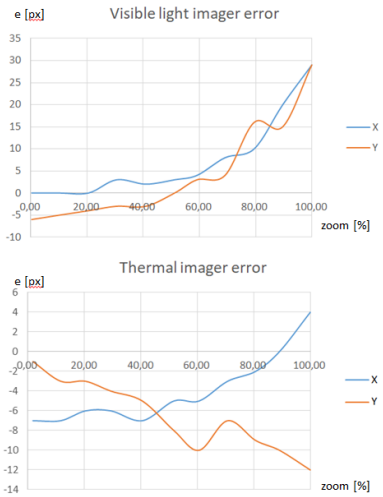


Fig. 12. Reticle displacement in pixels for visible light and thermal imager

When we have central coordinates for all imagers for each selected FOV, then in stage three we calculate reticle positioning parameters. As a result we have x and y reticle positioning parameters for each imager.

Finally, in stage four, the reticle positioning parameters can be entered into the software application that draws the reticle in the video stream.

By default, without the calibration, the reticle is drawn in the center of the video stream for any FOV. Only after the calibration parameters are entered the reticle will be drawn displaced to the image center, corresponding to the relative displacement of the LRF beam for any selected FOV.

## VII. RESULTS OF EXPERIMENTAL VERIFICATION

The proposed method for LRF reticle position calibration has been verified in real conditions using available MSIS. The MSIS has been placed on the rooftop of the building from where there is a good view on existing remote objects.

Fig. 13. A heating plant chimney at 8km distance used to verify the x-axis deviations of the reticle, in thermal and visible imager

The most appropriate objects for verification of LRF beam correspondence with reticle position on the screen are those objects which have large and sharp edges. It is important to use remote objects on relatively long distances, in order to minimize error due to non-coaxial quasi parallel axes of


ISBN 978-86-7466-930-3

imagers and LRF.

In this particular case a heating plant chimney at 8km distance was used to verify the x-axis deviations of the reticle from the ideal case in NFOV. Images taken with thermal and visible light imagers are shown in Fig. 13.

For verification of y-axis a rooftop heliport structure with upper and lower limits, at the distance of 620m was used as shown in Fig. 14.

Fig. 14. A rooftop heliport structure with upper and lower limits, at the 620m distance, used to verify the y-axis

Several LRF measurements have been accomplished in order to confirm where the LRF beam is really aiming and to verify the good correspondence with the LRF reticle on the screen. It has been shown that deviation is equal to 2 pixels in thermal imager, which in this case corresponds to 0.1 mrad, and 3 pixels in color imager, which in this case corresponds to 0.15 mrad.

Furthermore, it has been shown that for other FOVs reticle deviation from the ideal one is similar in pixel size, but is lower in angle, due to larger FOV angles.

## VIII. CONCLUSION

The described method was implemented to provide straight forward, fast and reliable process of reticle position calibration. The calibration process is complex but with this method it is straight forward, and can be performed by trained personnel. It is fast allowing efficient use of expensive equipment. Furthermore, it is reliable resulting in high process efficiency. However, there is a need for further work on additional improvements in process of reticle calibration. The further work will focus on automatic extraction of LRF spot central coordinates based on image processing techniques which can be applied on the same images taken during the reticle calibration process.

## ACKNOWLEDGMENT

Authors would like to thank Vlatacom Institute for equipment and support which enabled continuous work and improvements in the field of electro-optics. This work was undertaken within the Vlatacom Institute project P157.

## REFERENCES

[1] D. Perić, B. Livada, „Technical, technological and application limitations of the electro-optical surveillance systems“, 8th International Conference on Defensive Technologies, OTEH 2018, Belgrade, Serbia, 11-12 October 2018

[2] B. Livada, D. Perić, M. Perić, „Challenges of Laser Range Finder Integration In Electro-Optical Surveillance System“, 4th International Conference on Electrical, Electronic and Computing Engineering IcETRAN 2017, Kladovo, Serbia, June 05 – 08, 2017

[3] B. Tomić, D. Perić, M. Radisavljević, S. Vujić, „Reticle Integration and Camera Calibration in Multi Sensor Surveillance Systems“, 8th International Conference on Defensive Technologies, OTEH 2018, Belgrade, Serbia, 11-12 October 2018

[4] D. Perić, S. Vujić, B. Livada, „Multi-sensor system operator's console: Towards structural and functional optimization“, 7th International Conference on Defensive Technologies, OTEH 2016, Belgrade, Serbia, 6-7 October 2016

[5] S. M. Ayaz, M. Y. Kim, J. Park, Survey on zoom-lens calibration methods and techniques", Machine Vision and Applications, July 2017

[6] A. Pennisi, D. Bloisi, C. Gaz, L. Iocchi, D. Nardi, "Novel Patterns and Methods for Zooming Camera Calibration", Journal of WSCG, Volume 21, Number 1, 2013, pp. 59-67

[7] Z. Wu, and R. J. Radke, "Keeping a Pan-Tilt-Zoom Camera Calibrated", IEEE Transactions on Pattern Analysis and Machine Intelligence, November 2012

[8] S. Upadhyay, S.K.Singh, M. Gupta, A. K. Nagawat, "Linear and Non-linear Camera Calibration Techniques", Journal of Global Research in Computer Science, Volume 2, No. 5, April 2011

[9] B. Wu, H. Hu, Q. Zhu, and Y. Zhang, "A Flexible Method for Zoom Lens Calibration and Modeling Using a Planar Checkerboard", Photogrammetric Engineering & Remote Sensing, Vol. 79, No. 6, June 2013, pp. 555–571

[10] Z. Wang, J. Mills, W. Xiao, R. Huang, S. Zheng and Z. Li, "A Flexible, Generic Photogrammetric Approach to Zoom Lens Calibration", Remote Sens. 2017, 9, 244

[11] S. Zheng, Z. Wang, R. Huang, "Zoom lens calibration with zoom- and focus-related intrinsic parameters applied to bundle adjustment", ISPRS Journal of Photogrammetry and Remote Sensing 102 (2015), pp. 62–72

[12] Reg G. Willson, S. A. Shafer, "What is the center of the image?", J. Opt. Soc. Am. A ,/ Vol. 11, No. 11/, November 1994

[13] J. Y. Dufour (Editor), Intelligent Video Surveillance Systems. ISTE Ltd. London and John Wiley & Sons Inc., New York, 2013

[14] A. K. Maini, Lasers and Optoelectronics: Fundamentals, devices and applications, John Wiley and Sons, Chicheste,. UK, 2013

[15] J. A. Ross, B. R. Geiger, G. L. Sinsley, J. F. Horn, L. N. Long, and A. F. Niessner: " Vision-Based Target Geolocation and Optimal Surveillance on an Unmanned Aerial Vehicle", AIAA Paper 2008-7448, AIAA Guidance Navigation and Control Conference, Honolulu, Hawaii, 2008

[16] Livada, B.; Vujić, S.; Radić, D.; Unkašević, T.; Banjac, Z. Digital Magnetic Compass Integration with Stationary, Land-Based Electro-Optical Multi-Sensor Surveillance System. Sensors 2019, 19, 4331. https://doi.org/10.3390/s19194331

[17] B. Livada, S. Vujić, „Target position CEP50 estimation using electro-optical multisensory surveillance system", 8th International Conference on Defensive Technologies, OTEH 2018, Belgrade, Serbia, 11-12 October 2018

[18] D.C. Dilworth, "A zoom lens from scratch: the case for number crunching", Proc. SPIE 9947, Current Developments in Lens Design and Optical Engineering XVII, 994702 (27 September 2016)

[19] R. N. Youngworth and E. I. Betensky, "Fundamental Consideration for zoom lens Design (tutorial)", Proc. SPIE, Vol. 8488, Zoom Lenses IV, 2012

[20] Rowlands, D. Andrew, Field guide to photographic science, SPIE Press, Bellingham, USA, 2020

[21] S. Zhou and L. Jiang: "A modern description of Rayleigh's criterion", Phys. Rev. A , 99, 013808, 2019.

 ISBN 978-86-7466-930-3

# Linear regression in RR-RT domain for cardiac cycle evaluation

Milan S. Milivojević, *Student Member, IEEE*, Ana Gavrovska, *Member, IEEE* and Dragi Dujković, *Member, IEEE*

***Abstract*—Analysis of cardiac variability is of great importance for numerous applications. Among them are the ones based on electrocardiograms where detection of distorted signals during the acquisition process can be performed as well as discrimination of pathological records due to various diseases. ne way of presenting the cardiac variability relates to parameters derived from the time duration of the respective segments within the electrocardiogram cycle as well as their relationships. In this paper, cardiac cycle evaluation is performed in the domain of time features for the assessment of cardiac variability using the linear regression procedure. The calculated quotient shows the possibility to be useful in terms of error polarity.**

***Index Terms*— lectrocardiogram ( CG), cardiac cycle, pea , T wave, quotient, linear regression.**

## I. INTRODUCTION

The cardiac cycle is a series of pressure changes that take place within the heart. These pressure changes result in the movement of blood through different chambers of the heart and the body as a whole. They originate as conductive electrochemical changes within the myocardium that result in the concentric contraction of cardiac muscle [1]. The cardiac cycle can be divided into two phases: the systole phase and the diastole phase. During the systole phase heart muscle contracts and blood is pumped into the arteries. For electrocardiogram (ECG) this phase is manifested in the form of QRS complex appearance (associated with ventricular depolarization) and T waves (ventricular re-polarization). Diastole phase follows systole and represents relaxation of the heart muscle where the heart is filled with blood. Diastole can be identified on the electrocardiogram through the appearance of the P wave, which is further related to atrial depolarization [2].

Besides standard analysis of RR intervals (time intervals between successive R peaks), cardiac variability can be observed through intervals that describe the phase of diastole or systole. The characteristic points that divide the cardiac cycle into two phases are the R peak and the end of the T wave. There are different variants of interval definitions in the literature that are specific for these phases, which also include Q or S wave [3]. Since detection of the maximum within a cycle (R peak) is the basic procedure in ECG signal processing, R peak is taken as the point that defines the boundary between systole and diastole. Therefore, RT and corresponding difference between RR and RT intervals are considered to be suitable for the ventricular systole and ventricular diastole phases. Appropriate relationships derived from these intervals are the basis for the evaluation of cardiac cycles in electrocardiogram signal.

The golden ratio or cross-section represents a constant $\phi$ with an approximate value of 1,6180339887… This relationship has been known since ancient times as a principle in art from antiquity through the Renaissance to the present day. However, it is interesting that this relationship can be found in nature in organic and inorganic structures. Mathematical definition of the golden ratio ranges from the inherent geometric definition to the definition that includes extended fractions and series [4].

In this paper, a linear regression is performed in the domain of ECG time intervals (RR and RT intervals) in order to differentiate cases, like male and female individuals. Signals are taken from publically available Physionet data which includes healthy volunteers. A comparison of calculated direction coefficients obtained by the regression procedure with the reference representing the golden ratio constant is performed.

The work is organized into five sections. Section II presents the materials and methods applied in the paper. In Section III the experimental analysis is described. The results of the analysis are given in Section IV. Finally, Section V presents a conclusion with a note on further work.

## II. MATERIAL AND METHODS

### *A. Golden atio efinition*

Fibonacci array can be defined as a collection of elements where each array element value equals to the sum of the previous two elements of the array. Initial values of the first two members of the sequence are equal to 1. If limit value of the quotient of two consecutive members of the Fibonacci sequence is observed, a constant, here noted as $\phi$, can be defined. This is illustrated in Fig. 1.

This constant describes the golden ratio [5]:

$$\lim_{n\to\infty}\frac{[n+1]}{[n]}=\phi=1.61803399... \quad (1)$$

Milan Milivojević is with the University of Belgrade School of Electrical Engineering, Bulevar kralja Aleksandra 73, 11120 Belgrade, Serbia (e-mail: milansmilivojevic@gmail.com), and the Academy of Technical and Art Applied Studies Belgrade, Department School of Information and Communication Technologies, Zdravka Čelara 16, 11000 Belgrade, Serbia (e-mail: milan.milivojevic@ict.edu.rs) (https://orcid.org/0000-0001-6814-9520).

Ana Gavrovska is with the University of Belgrade - School of Electrical Engineering, Bulevar kralja Aleksandra 73, 11120 Belgrade, Serbia (e-mails: anaga777@gmail.com; anaga777@etf.rs), (https://orcid.org/0000-0003-2740-2803).

Dragi Dujković is with the University of Belgrade - School of Electrical Engineering, Bulevar kralja Aleksandra 73, 11120 Belgrade, Serbia (e-mail: dragi@etf.rs).

 ISBN 978-86-7466-930-3

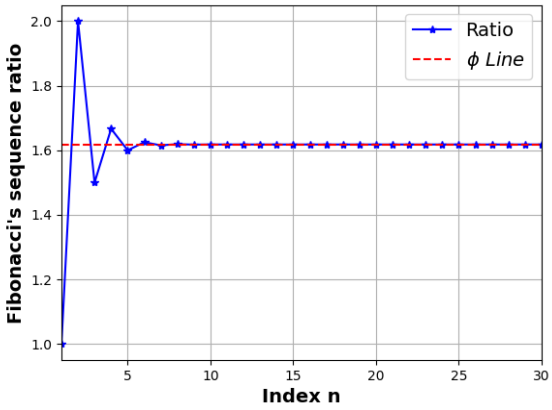


Fig. 1. Fibonacci sequences convergences.

The constant value ϕ can also be reached geometrically by dividing a segment into two parts. Let the lengths of the first and the second segment be noted as *a* and *b*, respectively. The segments are said to make a golden ratio if the ratio is as:

$$\frac{a+b}{a} = \frac{a}{b} = \phi . \tag{2}$$

The previous equation can be written in the form of the golden ratio characteristic equation:

$$\phi^2 - \phi - 1 = 0 \tag{3}$$

where solution leads to the exact value of the constant ϕ which is also equal to the positive solution of the quadratic equation:

$$\phi = \frac{1+\sqrt{5}}{2} . \tag{4}$$

### *B. ataset*

PhysioBank is a large and growing archive of digital recordings of physiological signals and corresponding data for biomedical and similar research. In this paper ECG-ID Database from Physionet is used for the analysis [6].

The database contains 310 ECG recordings, obtained from 90 individuals. Each record contains one electrocardiogram channel of twenty seconds duration and 12-bit resolution with 500Hz sampling frequency. The signal amplitude is within interval from -10mV to +10mV. The records were obtained from volunteers (44 men and 46 women aged from 13 to 75 years). The number of records per each person varies from two (collected during one day) to twenty (collected periodically over 6 months). The raw ECG signals are rather noisy and contain both high and low frequency noise components. Each record includes both raw and filtered signals. In the simulation presented in this paper only raw ECG signal are used [7].

### *C. Software Tools*

For the purposes of this work, Python 3 programming language is used, as well as the corresponding libraries, among which the Neurokit2 library stands out. NeuroKit2 is an open-source, community-driven, and user-centered Python package for neurophysiological signal processing. It provides a comprehensive suite of processing routines for a variety of bodily signals like ECGs [8].

## III. EXPERIMENTAL ANALYSIS

Within electrocardiogram (ECG) signal, three basic parts can be distinguished: P wave, QRS complex and T wave. Sometimes U wave is also visible. These waves are result of non-homogeneities of action potentials throughout the heart. They are directly related to the start time of depolarization and the time course of the action potential. The waves Q, R and S are manifestation of the depolarization in the two ventricles, while the waves T and U are consequence of the repolarization process in the ventricles [9].

Depending on the application, appropriate features can be extracted from the signal itself. In this paper, the focus is on finding the appropriate relations of the golden section, where temporal features are found [10].

Here, electrocardiogram signals from different volunteers are analyzed. Each signal is preprocessed, and this is followed by the detection of characteristic points. Based on the detected points, the corresponding time intervals (timestamps) are found as valuable features expressed in seconds. Based on two time intervals that are selected for each cardiac cycle, quotient value is estimated using the appropriate definition as well as in the form of direction coefficient obtained using the linear regression procedure. The values of this quotient are compared with the value given by the golden ratio constant.

### *A. Preprocessing*

As a first step, pre-processing of the original ECG signal was performed to remove unwanted signal components. These components primarily include muscle noise, 50 Hz network noise, and baseline deviation [11]. Noisy raw signals are chosen to observe practical importance of the ratio base relations between the waves. In order to suppress the interferences, a band-pass filter with a finite impulse response and a zero phase has been applied. The lower and upper bandwidth limits have been set to 0.3 Hz and 45 Hz, respectively. In Fig. 2 examples of raw signal from ECG-ID database and preprocessed signal are presented.

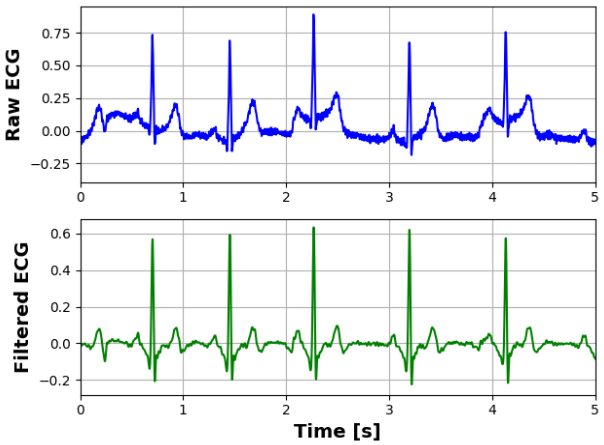


Fig. 2. Raw and preprocessed ECG signal.

### *B. ECG based inter al determination by characteristic point detection*

After the preprocessing step, characteristic points in time domain are found. Namely, for the experimental analysis

 ISBN 978-86-7466-930-3

two characteristic points are detected: R peaks and the moment corresponding to the end of the T wave (T wave offsets). The detection of these points is based on the wavelet method using functions from the Neurokit2 library [12]. The time intervals between two consecutive R maxima define the sequence of RR intervals.

For each RR interval, an additional time interval RT is found. It corresponds to the difference between the time moments of the end of the T wave and the corresponding R maximum. Since R peaks are relatively easy to detect T wave offsets can be considered also as fiducial points for further analysis. Figure 3 illustrates the detection of characteristic points in Fig.3 (a) as well as the determination of RR and RT time intervals based on detected characteristic points in Fig.3 (b).

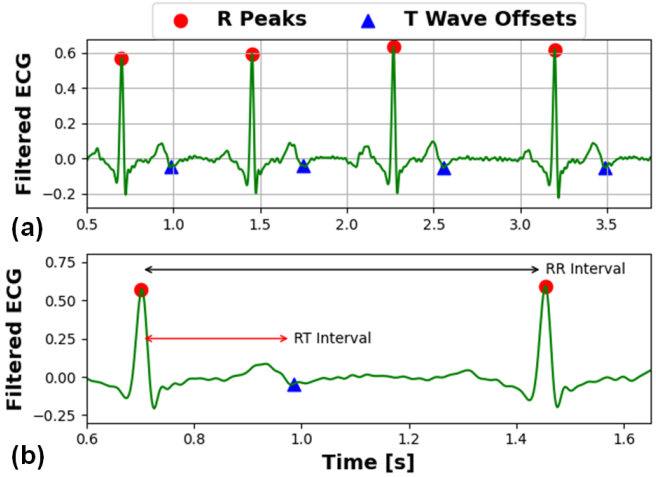


Fig. 3. (a) Detected ECG fiducial points (R peaks and T Wave offsets) and (b) corresponding time intervals (RR and RT intervals).

### C. *uotient based cardiac cycle description*

Having in mind available characteristic fiducial points a cardiac cycle can be described using a quotient based on RR and RT intervals. In this paper, quotient noted as $r$ can be defined as:

$$r = \frac{- \quad T}{T} \sim \phi \,. \tag{5}$$

This quotient can be find in the literature as the ratio of the diastolic and systolic phases of a cardiac cycle, where it is further averaged at the level of the cardiac cycle [13]. Moreover, RR interval can be expressed as a function of RT interval by applying the quotient:

$$= \quad T \cdot \left(1 + r\right). \tag{6}$$

In that case the slope is equal to the value of the ratio increased by one, and can be used as a mathematical model of cardiac behavior.

### . *Statistical e aluation of the uotient based cardiac cycle description*

For each set of points a well known linear regression is performed and the direction coefficient, noted as $k$, is estimated. Also, for each coefficient calculated in this way, the relative error is estimated, and the value $1 + \phi$ is taken as the correct value. The error value is calculated based on the formula:

$$\delta = \frac{r - \phi}{\phi} \cdot 100\% = \frac{k - 1 - \phi}{\phi} \cdot 100\% \tag{7}$$

where constant in the proportion of the golden section is taken as the reference value $\phi$ [14]. In this case, the modified relative error stores information about the sign of deviation from the golden ratio. The value of the quotient $r$ and the line direction coefficient obtained by linear regression are connected by a unique connection. Since there are several signals per each volunteer, in the second step averaging of the quotient values for a volunteer from the ECG ID database is performed.

## IV. RESULTS

Analysis was performed for signals from ECG ID database. After the described preprocessing, the detection of characteristic points and determination of RR and RT intervals for each cardiac cycle was performed. For each volunteer, ECG signals were recorded in several iterations meaning data was collected for a patient several times independently. Each calculated duration of RR and RT interval within a cycle make an ordered pair (RT, RR) representing a point in the RT-RR diagram. Figure 4 shows a set of all points for one volunteer from the ECG ID database, with all values observed for heart cycles from all iterations of signal recording as a single set. A linear regression procedure was performed on the set while forcing the passage of the regression line through zero (fit intercept is zero). As a result of linear regression, the direction coefficient k was obtained, which is equal to $1 + r$ on the basis of (6). This value is compared to a value of $1 + \phi$ where the constant $\phi$ corresponds to the golden ratio. The relative error in this case of the golden ratio is 1.14%.

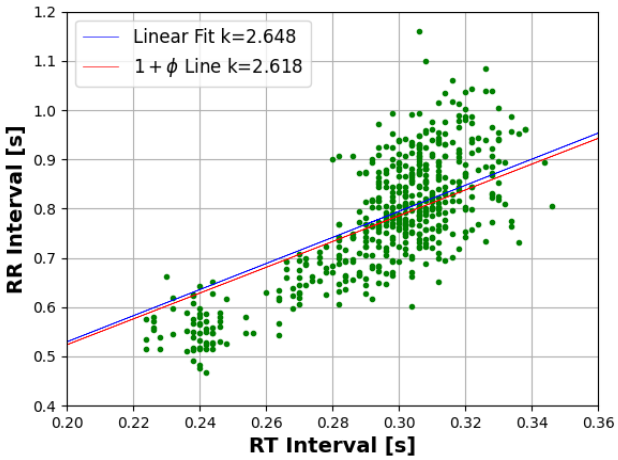


Fig. 4. Linear regression over points whose coordinates represent RR and RT values of cardiac cycles corresponding to a patient from ECG ID dataset.

In the second step, the quotient $r$ is averaged after iteration for the same volunteer. In this way, each iteration corresponds to one ratio of the averaged quotient. Figure 5 shows histogram of the averaged values of the quotient $r$. The histogram was fitted according to the Gaussian distribution, and the parameters and $\sigma$ were determined, which correspond to mean value and standard deviation, respectively. By comparing the mean value with respect to the value of $\phi$, a relative error value of 2.35% was obtained.

The procedure that involves determining the set in the RT-RR plane was repeated for volunteers. In Fig. 6 several

 ISBN 978-86-7466-930-3

individuals from the ECG ID database (two males and two females) are shown through corresponding sets.

After the calculation of error values, it can be noted that for males negative values are obtained, while for females this value is positive. There has also been some separation in terms of points belonging to different volunteers, which means that it is possible to differentiate individuals of different sex to some extent on the basis of quotient calculation. In the experimental analysis this is obtained for around 80% cases of samples that belong to female volunteers and around 70% cases belonging to male individuals. This can be considered to be a good starting point for further research.

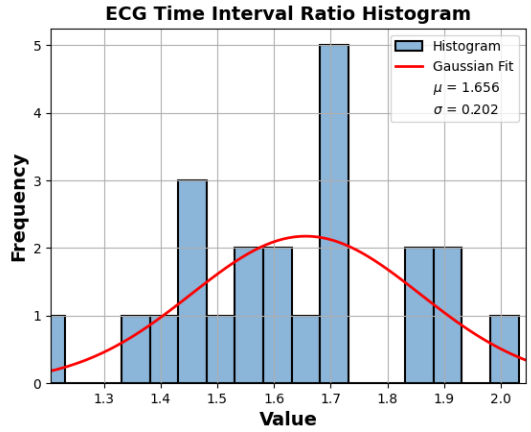


Fig. 5. Histogram representation and fitted normal distribution for averaged ratio values for a volunteer from the ECG ID database.

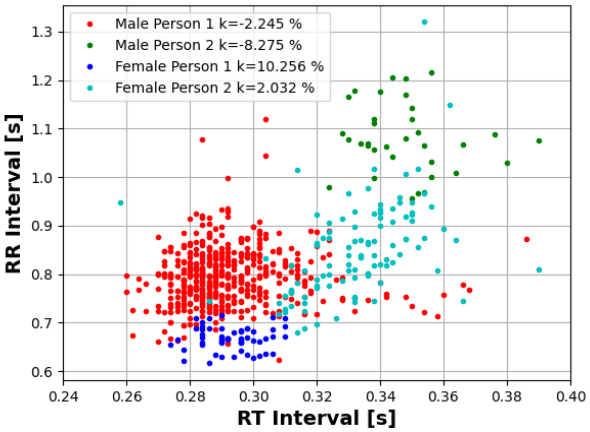


Fig. 6. Calculated RT and RR values in RT-RR domain for several volunteers.

## V. Conclusion

In this paper, the analysis of cardiac cycles is performed through the consideration of a relationship that exists between RR and RT intervals. The linear regression procedure used to estimate the direction coefficient, describes the proportionality between two quantities quite well. The estimated direction coefficients are related to the corresponding quotient of the diastolic and systolic portions in ECG signal. Errors of the coefficient deviation from the reference constant are calculated and here, for healthy individuals, the results showed minimal deviations. Also, signals belonging to volunteers of different sex are observed in order to analyze the usefullness of the quotient. It is noticed in the experimental analysis that the error values between the calculated quotient and the "golden ratio" have common case of different signs depending on the gender.

This paper is an initial study to test the hypothesis of whether the corresponding relationships within the ECG signal follow the "golden ratio" for further use and experiments. In the next steps, it is necessary to analyze the bases on a wider scale, where we would also analyze the signals that are pathologically altered due to cardiovascular diseases.

## Acknowledgment

This work is written during the research supported by the Ministry of Education, Science and Technological Development, Republic of Serbia, No. 2022/200103, and supported by the Academy of Technical and Art Applied Studies Belgrade, Department School of Information and Communication Technologies.

## References

[1] J. D. Pollock and A. N. Makaryus, "Physiology, Cardiac Cycle," *StatPearls*, Oct. 2021, Accessed: Apr. 14, 2022. [Online]. Available: https://www.ncbi.nlm.nih.gov/books/NBK459327/.

[2] T. Waselius, J. Wikgren, H. Halkola, M. Penttonen, and M. S. Nokia, "Learning by heart: Cardiac cycle reveals an effective time window for learning," . *Neurophysiol.*, vol. 120, no. 2, pp. 830–838, Aug. 2018, doi:10.1152/JN.00128.2018/ASSET/IMAGES/LARGE/Z9K0071846710007.JPEG.

[3] C. Ciucurel, L. Georgescu, and E. I. Iconaru, "ECG response to submaximal exercise from the perspective of Golden Ratio harmonic rhythm," *Biomed. Signal Process. Control*, vol. 40, pp. 156–162, Feb. 2018, doi: 10.1016/J.BSPC.2017.09.018.

[4] I. Ilić, M. Stefanović, and D. Sadiković, "MATHEMATICAL DETERMINATION IN NATURE-THE GOLDEN RATIO," doi: 10.5633/amm.2018.0317.

[5] W. T. Dobrosielski, J. Szczepański, and H. Zarzycki, "A Proposal for a Method of Defuzzification Based on the Golden Ratio—GR," *Ad . Intell. Syst. Comput.*, vol. 401, pp. 75–84, 2016, doi: 10.1007/978-3-319-26211-6_7.

[6] A. L. Goldberger *et al.*, "PhysioBank, PhysioToolkit, and PhysioNet," *Circulation*, vol. 101, no. 23, Jun. 2000, doi: 10.1161/01.CIR.101.23.E215.

[7] ECG database, "ECG-ID Database v1.0.0." https://physionet.org/content/ecgiddb/1.0.0/ (accessed Apr. 10, 2022).

[8] D. Makowski *et al.*, "NeuroKit2: A Python toolbox for neurophysiological signal processing," *Beha . es. Methods*, vol. 53, no. 4, pp. 1689–1696, Aug. 2021, doi: 10.3758/S13428-020-01516-Y/TABLES/3.

[9] A. Rashkovska, and V. Avbelj, "Signal processing methods for ST variability assessment in ECG," In *2013 3 th International Con ention on Information and Communication Technology, Electronics and Microelectronics MIP* , pp. 331-334, IEEE, 2013. https://ieeexplore.ieee.org/document/6596277 (accessed Apr. 12, 2022).

[10] C. Li, C. Zheng, and C. Tai, "Detection of ECG characteristic points using wavelet transforms," *IEEE Trans. Biomed. Eng.*, vol. 42, no. 1, pp. 21–28, 1995, doi: 10.1109/10.362922.

[11] L. Maršánová *et al.*, "ECG features and methods for automatic classification of ventricular premature and ischemic heartbeats: A comprehensive experimental study," *Sci. ep.*, vol. 7, no. 1, Dec. 2017, doi: 10.1038/S41598-017-10942-6.

[12] J. P. Martínez, R. Almeida, S. Olmos, A. P. Rocha, and P. Laguna, "A Wavelet-Based ECG Delineator Evaluation on Standard Databases," *IEEE Trans. Biomed. Eng.*, vol. 51, no. 4, pp. 570–581, Apr. 2004, doi: 10.1109/TBME.2003.821031.

[13] M. Ibranovic and A. Omerbasic, "View of The Human Heart: Deviating from the Golden Ratio and Diagnosing Disease," *American Academic Scientific esearch ournal for Engineering, Technology, and Sciences*, *0*(1), pp. 73-79, 2021. https://asrjetsjournal.org/index.php/American_Scientific_Journal/article/view/6889/2415 (accessed Apr. 10, 2022).

[14] C. J. Kat and P. S. Els, "Validation metric based on relative error," *Mathematical and Computer Modelling of ynamical Systems*, vol. 18, no. 5, pp. 487–520, Oct. 2012, doi: 10.1080/13873954.2012.663392.

 ISBN 978-86-7466-930-3

# Application of Bayes and knn classifiers in tumor detection from brain MRI images

Marta Mirkov and Ana Gavrovska, *Member, IEEE*

***Abstract*— Automatic detection of regions of interest is of great importance in computer-aided diagnosis systems. Magnetic Resonance Imaging (MRI) of head due to good soft-tissue contrast is widely used for brain tumor detection showing potential anomalies that indicate the need for further treatment. Current algorithms for processing and classification of medical images often involve complex designs of deep learning that require significant hardware resources and considerable execution time in order to assist doctors in detecting diseases. This may lead to labeling more complex cases in brain tumor detection. In this paper, statistical features are considered with application of Bayes and kNN classifiers showing comparable results having in mind publicly available brain tumor detection database.**

***Index Terms*— Magnetic Resonance Imaging, brain tumor detection, segmentation, feature extraction, machine learning.**

## I. Introduction

Today, depending on the need, various medical imaging modalities are used: X-ray, fluoroscopes, mammography, computer tomography (CT) devices as well as devices based on nuclear medicine techniques – Positron Emission Tomography (PET) and Single Photon Emission Tomography (SPECT). However, equipment that does not require ionizing radiation can be used for computer-aided diagnosis systems. Magnetic Resonance Imaging (MRI) scanners employ strong magnetic fields and magnetic field gradients to generate images of the organs or the whole body, and are found very useful in diagnostics. For example, according to the World Health Organization (WHO), cancer is the second leading cause of death [1]. Cancer detection from biopsy procedures is a painful process for patients, and therefore appropriate medical imaging modalities can facilitate this procedure [2].

Images obtained from MRI scanners show satisfying soft-tissue contrast, which is suitable for brain imaging. They provide a good visualization of the posterior cranial fossa, which contains the brain stem and cerebellum. The contrast between gray and white matter makes MRI the best choice for diagnosing many central nervous system conditions, including demyelinating diseases, dementia, cerebrovascular disease, infectious disease, Alzheimer's disease, and epilepsy [3]. Since many images are taken in milliseconds, it shows how the brain reacts to different stimuli, thus enabling doctors to study the brain's functional and structural abnormalities.

In this paper, statistical feature extraction and application of two classifiers will be observed, where the aim is to create a simple algorithm for brain tumor detection [4]-[9]. One of the motivations is usefulness of texture related features in MRI images [10]. Also, one of the famous examples of hypothesis testing is the Bayes test [5], which will be implemented here, and compared to knn (k-nearest neighbors) approach [7] based on revising hand-crafted statistical features.

The paper is organized as follows. After the introduction, in Section II related work is presented. It considers traditional statistical feature extraction and machine learning usage in brain tumor detection. Steps in the experimental analysis performed in this paper are explained in Section III, where further details for feature extraction are given in Section IV. Section V is dedicated to classifiers design and performance evaluation. Obtained results and conclusion are given in Section VI and Section VII, respectively.

## II. Related work

The brain tumor is an abnormal growth of cancer cells in the brain which disrupts the work of functional cells. Early detection and rapid diagnosis of tumors can help save the patient's life. Mathematical and software tools can be very successful in detecting brain abnormalities. Thus, related work is oriented towards statistical feature extraction and machine learning methods used in brain tumor detection.

Statistical features are found useful in machine learning and medical image segmentation and classification [10]-[12]. Particularly, in brain tumor detection texture is one of the most valuable features in designating the image appearance [10], [13]. It can be described statistically for the purpose of distinguishing image characteristics by the spatial allotment of gray levels. The most popular mathematical representation of image texture is co-occurrence matrix. For example, in the Gray Level Co-occurrence Matrix (GLCM), the spatial relationship of pixels is considered to examine the texture by using statistical methods. Four features can be extracted and found useful as in [10], [13]-[14]: energy, correlation, contrast, homogeneity. Namely, these features are used for extracting features and forwarding it to neuro-fuzzy models and, generally, machine and deep learning methods [15]-[18]. In [13] support vector machines are applied as classifier, where in [18] authors implemented deep convolutional neural network, and one of the publicly available datasets for brain tumor detection [19]. Using hand-crafted features are still valuable for obtaining satisfying results in brain tumor detection and more parameters may give better results. On the other hand, smaller dimension of the feature vector is important for algorithm execution, especially in the cases

Marta Mirkov is with the University of Belgrade - School of Electrical Engineering, Bulevar kralja Aleksandra 73, 11120 Belgrade, Serbia (e-mail: marta.mirkov@gmail.com).

Ana Gavrovska is with the University of Belgrade - School of Electrical Engineering, Bulevar kralja Aleksandra 73, 11120 Belgrade, Serbia (e-mails: anaga777@gmail.com ; anaga777@etf.rs ).

 ISBN 978-86-7466-930-3

where there is no need for higher complexity according to tested dataset. In this paper, Bayes and knn classifier are analyzed for classification model implementation using [19].

## III. Experimental analysis

The cancer tissue is expected to stand out from the normal part of image, but the question of choice of MRI features still remains. The experimental analysis performed here consists of:

- tumor segmentation based on labeled regions in images,
- hand-crafted feature extraction,
- classification and evaluation of results on available dataset.

The proposed work is tested with Brain MRI Images for Brain Tumor Detection dataset [19], containing 98 brain MRI images with healthy tissue and 155 brain MRI images with cancer tissue. Among features for segmentation task solidity of labeled regions is applied. Having in mind traditional hand-crafted features for classification: energy, correlation, contrast and homogeneity, two classifiers are tested in initial phase. Based on preliminary segmentation analysis, two additional statistical features are added for the binary classification. Both tested classifiers, Bayes and knn, are evaluated on the test set, which is made from 30 % of the whole dataset selected in a random manner, where the rest was used for the training set. For performance evaluation true positive rate (TPR), true negative rate (TNR) and balanced accuracy (BACC) are calculated as in (1)-(3), respectively:

1) *True Positive Rate- TPR*

$$Sensitivity = \frac{TP}{P}, \quad (1)$$

where TP represents true positive, the number of samples that were positive and detected as positive, and P represents the whole set of positive samples;

2) *True Negative Rate- TNR*

$$Specificity = \frac{TN}{N}, \quad (2)$$

where TN represents true negative, the number of samples that were negative and detected as negative, and N represents the whole set of negative samples;

3) *Balanced Accuracy- BACC*

$$BACC = \frac{TPR + TNR}{2}. \quad (3)$$

## IV. Proposed tumor segmentation

Proposed brain tumor segmentation is consisted of several steps. Firstly, MRI image is preprocessed using: high-pass filtering and image intensity adjustment, and then, after image binarization, connected regions are labeled. Finally, solidity is implemented for tumor segmentation.

### A. MRI image preprocessing and labeling

High-frequency filtering highlights sudden changes in the image by passing high-frequency components [4]. A fifth order Gaussian HP filter with cutoff frequency of 55 Hz was used. Although MRI images provide good tissue contrast, adjusting image intensity is important for tumor segmentation. By saturating the bottom 2% and the top 1% of all pixel values the grayscale range of image is shortened and the contrast is enhanced, and therefore it highlights tumor areas.

Because the image contrast is adjusted, the histogram of the image has a bimodal distribution with a deep and sharp valley between the two peaks, which enabled using Otsu's method for automatic thresholding [4]. Finally, binary image has different white regions where some of them might represent tumor tissue. Pixels are connected and are part of one region if their edges touch. Two adjacent pixels are part of the same object if they are both of the same intensity and are connected along all directions.

### B. Solidity characterization

For each labeled region, solidity can be calculated. Solidity is a measurement of the overall concavity of a particle. It is defined as the image area divided by the convex hull area. As the object form digresses from a closed circle, the convex hull area increases, and the calculated solidity decreases. Images with high solidity are more likely to contain tumor regions [13, 23]. A tumor can successfully be detected by comparing the calculated solidity of the labeled image with a higher value (closer to 1). In this case, the tumor is detected if solidity is higher than 0.6. When this area represents a tumor, it is the region or candidate with more white pixels, and when there is no tumor tissue on the image, some small regions can still be extracted. It may be assumed that differences between healthy and tumor tissue can be provided using features that describe the area and shape of this extracted region.

## V. Statistical hand-crafted features

GLCM is created by calculating how often a pixel with grayscale intensity value $i$ occurs horizontally adjacent to a pixel with the value $j$. Offset isn't used for defining pixel spatial relationships. The number of gray levels in the image determines the size of the GLCM. Scaling to 8 gray levels is used to reduce the number of intensity values in an image, so the size of GLCM is 8x8 pixels. The traditional statistical hand-crafted features extracted from GLCM are: energy, correlation value, contrast and homogeneity.

Energy estimates the sum of squared elements from GLCM and represents feature 1:

$$Energy = \sum_{i,j=0}^{N-1} p^2(i,j), \quad (4)$$

where N represents the number of pixels in image, $i$ and $j$ the location of pixel, and $p\,(i,j)$ the intensity of the pixel at the location $(i,j)$.

The mentioned pixel pairs are then estimated using joint probabilities. It gives linear dependency of the gray levels of neighboring pixels. In general, it ranges from [-1,1]:

$$Correlation = \sum_{i,j=0}^{N-1} \frac{(i-\mu x)(j-\mu y)p(i,j)}{\sigma_x \sigma_y}, \quad (5)$$

where $\mu_x$, $\mu_y$, are the means and $\sigma_x$ and $\sigma_y$ are the standard deviations of $P_x$ and $P_y$, respectively. Note that $P_x(i)$ is the $i$th entry in the marginal-probability matrix obtained by summing the rows of $P(i, j)$ and $P_y(i)$ is the $i$th entry in the marginal-probability matrix obtained by summing the rows of $P(i, j)$.

Contrast value (feature 3) estimates the local variations, i.e. sum of square variance, as in (6):

$$Contrast = \sum_{i,j=0}^{N-1} |i-j|^2\, p(i,j). \quad (6)$$

The fourth feature, homogeneity, estimates the closeness of distributed pixels.

 ISBN 978-86-7466-930-3

$$Homogenity = \sum_{i,j=0}^{N-1} \frac{p(i,j)}{1+|i-j|}. \quad (7)$$

These four features are applied in brain tumor detection, but having in mind the segmentation task, in combination with two more features like the number of white pixels (feature 5) and skewness (feature 6), one may assume further improvements can be obtained. The number of white pixels in the segmented images are expected to increase the accuracy results. Also, some additional statistical parameters can be great indicators of tissue condition. Skewness represents a measure of the asymmetry of the probability distribution [20]. It can be expected that umor tissue has much higher skewness than healthy tissue, thus it is also a reliable feature for classification.

## VI. Bayes and knn Classifiers and Evaluation of the Results

### A. Bayes classifier

For implementing Bayes classifier, it is necessary to define the posterior probabilities $q_i(X)$ which represent the conditional probability that the sample X comes from the class $\omega_1$ if its exact realization is known. Using the Bayes theorem, these probabilities can be calculated if priori probabilities of occurrence of class $p_i$ and posterior density probability functions of measured vectors $q_i(X)$ are known [5], [11]. In this case, the first class represents images with tumor tissue, and the second represents healthy tissue. A simple decision rule can be made based on conditional probabilities:

$$q_1(X) > q_2(X) \Rightarrow X \in \omega_1 \quad (8)$$

$$q_2(X) > q_1(X) \Rightarrow X \in \omega_2 \quad (9)$$

Although the probability density functions of the classes are not known, it can be assumed that, if there is a large number of samples, they can be taken as Gaussian (according to the central limit theorem) [6]:

$$f(x) = \frac{1}{|\Sigma|^{1/2}(2\pi)^{n/2}} e^{-(X-M)^T \Sigma^{-1}(X-M)} \quad (10)$$

where $n$ represents the dimension of the vector $X$, $M$ the mathematical expectation of the vector $X$, and $\Sigma$ the covariance matrix of the feature vector. These values for both classes are obtained from the training set. For both classes, feature vectors are formed for classification.

### B. k nearest neighbors Classifier

The most common issue in practice is information missing needed for classification based on hypothesis testing, so one may resort to non-parametric classification. One of the most popular methods is k nearest neighbors or knn. The algorithm classifies the observation point in relation to how the neighbors are classified. In the knn algorithm, k is a parameter that indicates the number of nearest samples involved in the classification [7], [21].

In Fig. 1, a new green sample that needs to be classified can be observed. The full circle in the figure represents the case when k=3: the neighbors are one blue square and two red triangles. Since there are more triangles, the green circle sample is assigned to the same class as the triangles.

However, if four is taken for k, the green circle will be classified into the blue squares class because there are more of them in the region. In conclusion, k is an essential parameter for successful classification [21]. Also, the success of the classification depends on which methods are used for defining what the nearest neighbors are. Some of the methods that are going to be considered in this paper are Euclidean, Chebyshev, Mahalanobis distance, and cosine similarity [22].

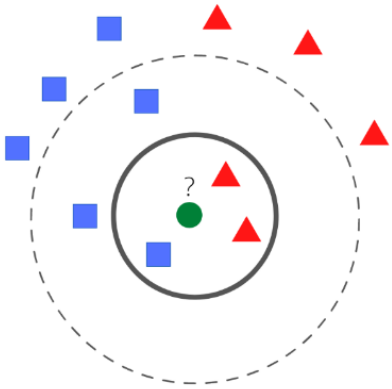


Fig. 1. Graphical representation of knn method, where green circle sample needs to be assigned to blue rectangle or red triangle class.

### C. Evaluation

On proposed tumor segmentation steps and feature extraction, results of Bayes and knn classifiers will be shown, as well as the influence of feature vector dimension on results. The performance will be evaluated using confusion matrices and metrics described by (1)-(3).

The confusion matrix for this classification consists of two columns and two rows. Each row of the matrix represents the instances in an actual class, while each column represents the instances in a predicted class. Images with tumor tissue are labeled as ‘positive’, and healthy tissues are labeled as ‘negative’. Four and six features are tested to observe the effects on the results using Bayes and knn classifiers. The effect of the distance type and different values of k (1 to 40) on accuracy have been also analyzed.

## VII. Experimental Results

### A. Preliminary segmentation and feature inspection results

Preliminary segmentation results are show in Fig. 2 and Fig. 3. It can be observed that tumor is correctly detected in Fig. 2 for cancer tissue example. In the image with healthy tissue in Fig.3, small regions which are not tumor are segmented as one (false) candidate. Segmented image that contains a tumor has larger white area extracted, as it can be seen in Fig. 2 and Fig. 3, so this can be also used as an effective feature that provides good separability.

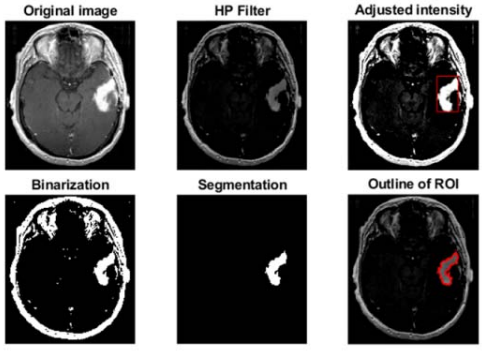


Fig.2. Results of segmentation for cancer tissue


ISBN 978-86-7466-930-3

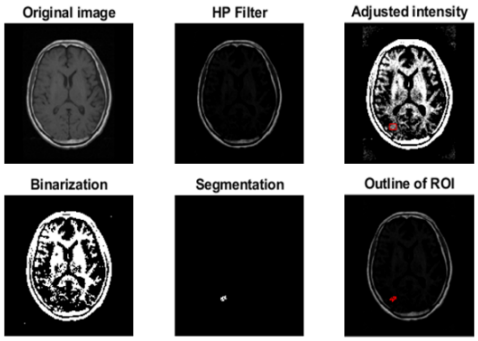


Fig. 3. Results of segmentation for normal tissue

Using the first four hand-crafted features may not be enough for high accuracy results. Adding two more features (feature 5 and feature 6) can improve results. From Fig.3 some of the separability inspection results can be seen.

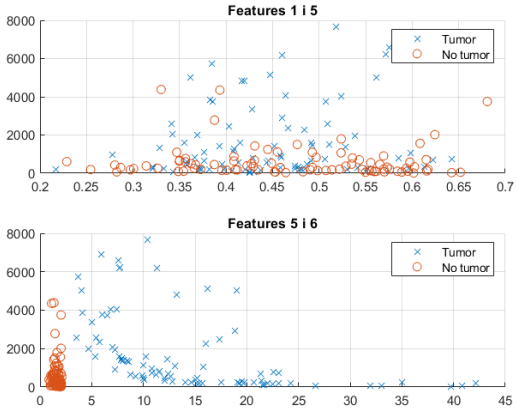


Fig. 4. Some of the separability inspection results of the selected features.

### *B. Classification results using proposed method*

Classification results with only traditional or texture related features using Bayes classifier did not give expected results, as presented in Table I. Similarly is obtained for knn classifier and it is presented in Table II. For higher accuracy results, these classifiers require more information obtained through using additional features.

TABLE I
RESULTS OBTAINED WITH BAYES CLASSIFIER

| Metric | TPR | TNR | BACC |
|---|---|---|---|
| Traditional four feature approach | 71.4 % | 82.6 % | 75.8 % |
| **The proposed method** | 96.6 % | 100 % | 98.3 % |

TABLE II
RESULTS OBTAINED WITH KNN CLASSIFIER

| Metric | TPR | TNR | BACC |
|---|---|---|---|
| Traditional four feature approach | 89.6 % | 65.5 % | 77.6 % |
| **The proposed method** | 100 % | 96.5% | 98.2 % |

In the case of knn and four feature selection, the accuracy is highest for the Chebyshev distance, which is achieved for k = 39. This is illustrated in Fig. 5. These results are not suitable for practice and two additional features are applied to feature vector. The accuracy in the case with more features is highest for the cosine similarity and the best case is secured with lower number of neighbours (k = 3), which can be seen in Fig. 6, where smaller number of neighbours is a better choice.

For medical image classification, sensitivity is aimed to be high because of the need for all positives to be recognized correctly. Specificity should not be low because many false alarms are undesirable.

It is proven that only four texture related features cannot provide expected results, and adding two more features improves results. Feature vector still contains relatively small number of elements. In further experiments it is shown that the kNN algorithm with more features provides reliable results for all parameters, and compared to the Bayes classifier, it provides better sensitivity for both cases (with the lower and higher number of features), which can be seen in Table III. Slightly higher results in overall evaluation are obtained for knn for the proposed method.

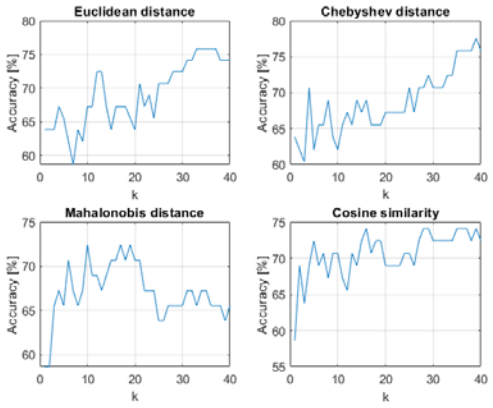


Fig. 5. Accuracy versus parameter k for four types of distances for four feature approach.

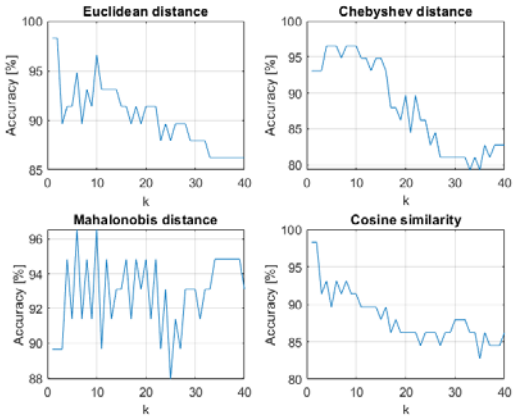


Fig. 6. Accuracy versus parameter k for four types of distances for proposed approach.

## VIII. CONCLUSION

The proposed tumor segmentation in MRI head images provided an excellent base for analyzing the tumor classification methods. The proposed classification method gives surprisingly good results compared to the other methods based on machine learning tested on the same dataset. The advantage of the proposed method lies in less demanding hardware resources where traditional classification methods are used. A more diverse selection of features can further increase accuracy. Since the knn method stood out as a method with high accuracy, it is possible to test other selections and analyze the types of distances by

 ISBN 978-86-7466-930-3

which the classification is performed.

A possible improvement of the model would also be classifying different types of tumors and labeling more complex cases in brain tumor detection. Such data labeling for classification improvements would require help from the experts.

## ACKNOWLEDGMENT

This work is written during the research supported and partially funded by the Ministry of Education, Science and Technological Development, Republic of Serbia. No. 2022/200103.

## REFERENCES

[1] H. Ritchie and M. Roser, “Causes of Death,” Published online at OurWorldInData.org. Retrieved from: 'https://ourworldindata.org/causes-of-death', 2018.

[2] S. Webb, *The physics of medical imaging*, Taylor and Francis Group, Country: USA, 1988. https://doi.org/10.1201/9780367805838

[3] R.A. Sadek, “An improved MRI segmentation for atrophy assessment,” *International Journal of Computer Science Issues* (IJCSI) vol. 9, no. 3, pp. 569-574, 2012.

[4] M. Popović, *Digitalna obrada slike,* Akademska misao, Serbia, 2006.

[5] B. Efron, “Bayes' theorem in the 21st century,” *Science*, vol. 340, no. 6137, pp. 1177-1178, 2013.

[6] S.G. Kwak, and J.H. Kim, “Central limit theorem: the cornerstone of modern statistics,” *Korean journal of anesthesiology*, vol. 70, no. 2, pp. 144-156, 2017.

[7] G. Guo, H. Wang, D. Bell, Y. Bi, and K. Greer, “Knn model-based approach in classification,” OTM Confederated International Conferences “On the Move to Meaningful Internet Systems,” pp. 986-996, 2003. Springer, Berlin, Heidelberg.

[8] S. A. Medjahed, “A comparative study of feature extraction methods in images classification,” *International journal of image, graphics and signal processing* vol. 7, no. 3, pp. 16-23, 2015.

[9] P. Nair, and I. Nair, “Classification of medical image data using k nearest neighbor and finding the optimal k value,” *International journal of scientific & technology research*, vol. 9, no. 4, pp. 221-226, 2020.

[10] P.K. Bhagat, P. Choudhary, and K.M. Singh, “A comparative study for brain tumor detection in MRI images using texture features,” Chapter 13: In Advances in ubiquitous sensing applications for healthcare, *Sensors for Health Monitoring*, Academic Press, vol. 5, pp. 259-287, 2019. https://doi.org/10.1016/B978-0-12-819361-7.00013-0

[11] K. Fukunaga, *Introduction to statistical pattern recognition*, (2nd ed.), Academic Press Professional, Inc., USA. 1990.

[12] J. Jaidip, N. Patil, C. Kala, K. Pandey, A. Agarwal and A. Pradhan. "Statistical characterization of tissue images for detection and classification of cervical precancers." arXiv preprint arXiv:1112.4298 2011.

[13] K. K. Kumar, M. Devi T, and S. Maheswaran “An Efficient Method for Brain Tumor Detection Using Texture Features and SVM Classifier in MR Images*.” Asian Pacific journal of cancer prevention* :APJCP vol. 19, pp. 2789-2794, 26 Oct. 2018, doi: 10.22034/APJCP.2018.19.10.2789

[14] M. Domingo, and D. Filbert. "Classification of potential defects in automated inspection of aluminium castings using statistical pattern recognition," *8th European Conference on Non-Destructive Testing* (ECNDT 2002), pp.1-10, 2002.

[15] T.M. Hsieh, Y. M. Liu, CC Liao, F. Xiao, I-J. Chiang, J-M. Wong, "Automatic segmentation of meningioma from non-contrasted brain MRI integrating fuzzy clustering and region growing", BMC Med Inform Decis Mak 11, 54, 2011. https://doi.org/10.1186/1472-6947-11-54

[16] K. Sharma, A. Kaur, and S. Gujral, “Brain tumor detection based on machine learning algorithms,” *International Journal of Computer Applications* 103.1, pp. 7-11, 2014.

[17] R. Ranjbarzadeh, B. Kasgari, S. J. Ghoushchi, S. Anari, M. Naseri, M. Bendechache, "Brain tumor segmentation based on deep learning and an attention mechanism using MRI multi-modalities brain images", Sci Rep 11, 10930, 2021. https://doi.org/10.1038/s41598-021-90428-8

[18] A. Çinar, and M. Yildirim, "Detection of tumors on brain MRI images using the hybrid convolutional neural network architecture," *Medical hypotheses*, *139*, 109684, 2020.

[19] Brain MRI images for brain tumor detection dataset: https://www.kaggle.com/navoneel/brain-mri-images-for-brain-tumor-detection

[20] H. J. Baek, H. S. Kim, N. Kim, Y. J. Choi, Y. J. Kim. "Percent change of perfusion skewness and kurtosis: a potential imaging biomarker for early treatment response in patients with newly diagnosed glioblastomas." *Radiology* vol. 264, no. 3, pp. 834-843, 2012.

[21] I. K. Preeti Nair, “Classification of medical image data using k nearest neighbor and finding the optimal k value,” *International journal of scientific technology*, volume 9, 2020.

[22] R. Ehsani, and F. Drabløs, "Robust Distance Measures for k NN Classification of Cancer Data," *Cancer informatics*, *19*, 1176935120965542, 2020.

[23] M. A. Javid, S. A. Buzdar, "A novel computer aided diagnostic system for quantification of metabolites in brain cancer," *Biomedical Signal Processing and Control*, Volume 66,102401, 2021. https://doi.org/10.1016/j.bspc.2020.102401

 ISBN 978-86-7466-930-3

# From puppet-master creation to false detection

Ana Pantelić and Ana Gavrovska, *Member, IEEE*

***Abstract*— Nowadays, many issues in society are affected by the misuse of deepfakes. One can say that we came to a point when prior knowledge of image processing is not a requirement for deepfake creation. With different motives, in a short period, and with limited resources, many deepfakes can appear on the internet. That brings us to testing that hypothesis of how easy and how fast someone can make a deepfake. In this paper several puppet-master creations are made for experimental purposes. In the aftermath of deepfake creation, an off-shelf available deepfake detection algorithm is applied for the detection analysis which is expected not to be universal solution for every type of deepfake realization. This brings us to high false detection, where specific cases are considered in this paper, like closed eye and head shape effects.**

***Index Terms*— Deepfake, puppet-master, deep learning, closed eye, head shape, false detection.**

## I. INTRODUCTION

Technologies are rapidly evolving, and the challenges due to hardware limitation are becoming obsoleted. On the other side, different associations are trying to solve technical issues through hackathons with solutions in the interest of society. One of those issues is the detection of deepfakes [1]-[3].

DeepFakes are getting easier to produce and harder to detect. DeepFake can be considered as altering approach based on artificial intelligence and deep learning architecture. Moreover, there are different types of deepfakes, where deepfake can be often described as a synthetic switch of identities of two persons, for example in a video sequence. Namely, there are different types of deepfakes like: face-swap, entire face synthesis, puppet-mastery, and lip-syncing [4]. It is highly used in revenge pornography, and based on DEEPTRACE research [5]-[6], in September 2019, 96% of deepfake videos belong to pornographic content, where the victims are widely women. There are also widely used for politicians and public figures. With available software tool almost everyone can generate a deepfake or deepface using recorded video and an image of a taget person.

In this paper a puppet-master creation as a popular method for deepfake creation is applied. Here, performed steps for creating a deepfake is explained. Moreover, one of the methods for deepfake detection is implemented in order to observe false detections. One may have in mind that the algorithm taken for experimental analysis is not selected purposely, but in a random manner from available recent solutions, in order to observe expected false detections. It is to expect that the detection method is not prepared for dealing with each type of deepfakes and scenarios. Thus, the motivation of this work is to perform popular deepfake generation and observe what would happen if a deepfake creation approach is not directly connected to some of the state-of-the art solutions focusing on specific details like edges around important face parts like: mouth, eye and similar.

The paper is organized as follows. After introduction, in Section II we give a brief description of popular deepfake creation and detection. Section III is dedicated to simulations for puppet-master creation and for neural network based detection without taking into account the type of creation. This is followed by the experimental results and discussion related to observed detection results in Section IV. Final conclusions are given in Section V.

Ana Pantelić is with the University of Belgrade - School of Electrical Engineering, Bulevar kralja Aleksandra 73, 11120 Belgrade, Serbia (e-mail: anaapantelic@gmail.com).

Ana Gavrovska is with the University of Belgrade - School of Electrical Engineering, Bulevar kralja Aleksandra 73, 11120 Belgrade, Serbia (e-mails: anaga777@gmail.com; anaga777@etf.rs).

## II. DEEPFAKE CREATION AND DETECTION

One of the most popular ways of creating deepfake is GAN (Generative Adversarial Network) [7]-[8]. GAN is an algorithm with two opposed neural networks that generate new, synthetic data that can pass as regular data. Neural networks and, generally, machine learning tools show the ability to mimic the human brain by learning, memorising and making the data they acquire in general. Typical deepfake algorithms for generating data are X2Face and First order motion model [2]-[3], [9].

In this paper, the neural network starts with the Monkey-Net neural network [10], and advance it to the First order motion model for image animation [9]. The First order motion model presents a fast and effective way of creating a deepfake with better results than advanced animation processing software.

Puppet-master deepfake creation is one of the modest and popular methods for making a deepfake. It shows how realistic the results can be, where the artefacts are still seen by human eye especially in video material. So, this method for creating a deepfake has its positive and negative sides. Artefacts are observable and this can be negative experience for the creater. This is also a positive information since we can still believe that we can distinguish true or false video story.

For deepfake detection, one has to be aware of the algorithm used for deepfake creation. Taking into consideration that the person who published a deepfake won't leave a piece of information related to origin or source or used tools for deepfake design, the common decision is that the detection from practial point of view will be applied to images cropped/grabbed from the video.

The main focus of detection of a deepfake are face parts like eyes and mouth, and head movement. Deepfake may be recognized on irregular pixel weight at the edges of the mentioned regions after training the neural network that detects them. One of the state-of-the art models based on such detection is Meso-4 model [11]-[12]. It is based on convolutional neural network and represents an efficient tool for dealing with particular types of visual modifications.

 ISBN 978-86-7466-930-3

Here, it is used as only one of the solutions for observing how can some deepfake examples created by the First order motion model be detectable as deepfakes and what are the cases when one may get high number of false detections, when deepfake frames are passed as regular images.

## III. SIMULATION

### A. *Steps for creating a deepfake*

Here, preparations for the deepfake creating is filming a video of 256×256 px, that is frontal with simple backround. Next to that, an image of a person we want to switch the identity with is chosen. The selected image is also frontal with simple backround and with the lack of face-covering details. In this paper Google Colaboratory with python script are used for experimental purposes [13]-[14].

First order motion model for image animation is upgraded convolutional neural network based on Monkey-Net-u [9], [11]. Monkey-Net codes information of movement through keypoints that are pretrained and self-observed. Down side of this neural network is possibly that, while following the trajectory of keypoints in faster movements, missing spots in image can appear. To solve that missing spot, affine transformation is used to perserve the propotion of the line and collinearity between dots. While it perserves propositions between lines and dots, affine transformation doesn't perserves all the angles. To have a clear overview, the improved parts of Monkey-Net are: keypoints aren't just detected but they are self-controled, which will add the adaptability on the targeted image; the generator of occlusion is added that gives a mask based on the parts that are not initially visible; it improved the visual domain of the puppet in general. In Fig. 1 simulation steps for creating a puppet deepfake are shown. If we follow from the video of the puppet, the keypoints are generated and local affine transformation is applied and collected. Until it comes to dense motion, from the source image we encode all the needed features and by warp operation the parts of process are connected. This is followed by occlusion map and decoder that brings the final creation result.

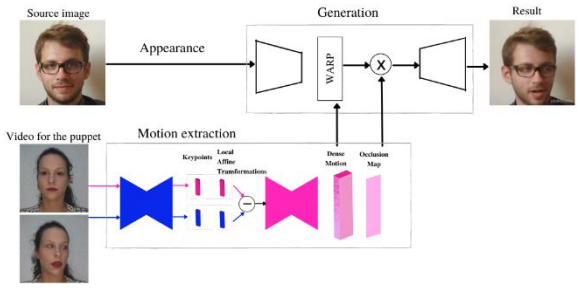


Fig. 1. Simulation steps for creating a puppet deepfake.

### B. *A deepfake detection model*

For the need of deepfake detection, a pretrained convolutional neural metwork MESO-4 model is used [12]. The architecture of the model is shown in Fig. 2. It is constructed of four convolutional blocks and one hidden layer. It recognizes the vertical and horizontal lines; applies batch normalization; uses the convolutional matrix with a task to bring all the important edges like edge of the lips, shape of the head or edges of the eyes; it employs pooling layer that will pick the pixel with dominating characteristics. Based on the pixel the reducing of spatial size of convolutional operations is possible. To improve the generalization, in the addition to the normalization of the batch, ReLU (Rectified Linear Unit) which introduces nonlinearity is applied.

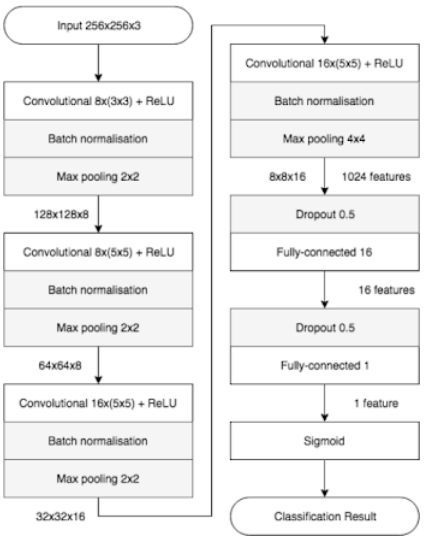


Fig. 2. Meso-4 architecture, where layers and parameters are displayed in rectangles [12].

### C. *False detection counting in a puppet related data*

We wanted to see if the head movement and misshapes of the head will be detected by Meso-4 neural network. That is the reason we produced the video with head movement on both sides (left and right), and then abruptly moved to one of the sides. Furthermore, the idea is to make mouth and eyes to seem natural in a deepfake, so the person often blinks. When making mouth movements, the mouth is moved naturally without exaggeration.

## IV. EXPERIMENTAL RESULTS

### A. *Experimental results for created deepfakes and false detection*

Three deepfake videos are made with source images of university assistant, public figure, and politician. One of the created deepfakes for a public figure is shown in Fig. 3.

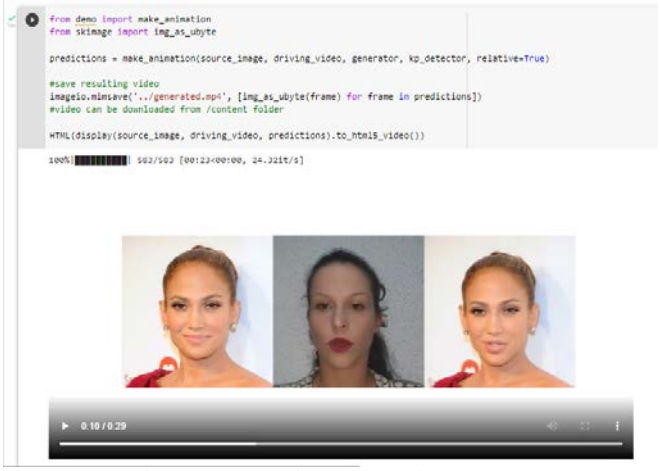


Fig. 3. One of the created deepfakes. From left we have source image, video for the puppet and the end result.


ISBN 978-86-7466-930-3

The results were satisfying, with expected characteristics of puppet-mastery. The process resulted in a source image that was following all the given movements of head, eyes, and lips.

For the detection task both original and deepfake frames are used. Totally, 461 images are tested whether they are real or not, giving for original examples satisfying results as shown in Fig. 4. Predicted likelihood is close to 1 which means that labeling is performed in adequate manner. Correct prediction can be noticed and it proves that the result is true.

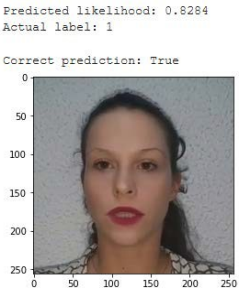


Fig. 4. The result of the detection. If the predicition is closer to one it means it sees it as real, and next to that it proves it predicition as True or False.

At first glance, a lot of images that are real are also detected as real, but unsatisfactory results are shown for deepfakes. The summary of obtained results is given in Fig.5. Out of 110 real images, 94 real cases are detected. On the other hand, high percentage is found for false detections where deepfake frame is considered real. In the experiment it is found that we have around 82.33% of chances for misinterpreting a deepfake image as real, and around of 14.5% of misinterpreting a real as a deepfake. The high false detection exists as it was expected.

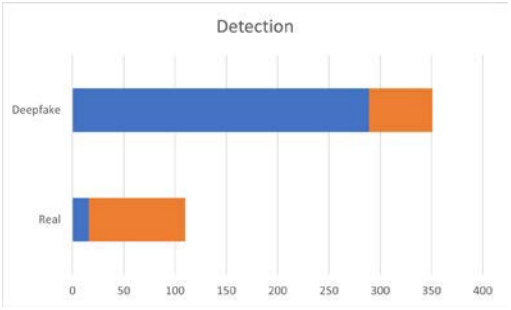


Fig. 5. The summary of detection. The blue colour presents the number of falsely detected images. Out of 351 deepfake images, 289 are detected real.

### *B. Further analysis on accurate results*

When observing accurate real results it was noticed that the probability of images with closed eyes, and when the head is curved, is close to 0.5, which means that there is a significant level of doubt. Similarly is noticed with cases where errors occurred, i.e. when real images are detected as deepfakes. The probability of around 50% can be interpreted as random class selection.

In Fig. 6 examples of true predictions are presented, where one of the examples show lower predicted likelihood. This is the case where eyelids and pupils are not visible while blinking. On the other hand, when eyelids and pupils are visible and when there is less blur around the face, there is a higher probability that the detected image is real.


Fig. 6. Examples of True predicitions.

There are frames that are detected as deepfake and similar pattern can be recognized as in Fig. 7.


Fig. 7. Real images detected as deepfake

It can be noted that there are frames in Fig. 7. where pupils and irises are not visible, as well as where there is a greater curvature of the head. In these cases Meso-4 has detected that there is a chance that it is a deepfake. Also, it is important to note that most predictions are around 0.4 and that the probability leans towards deepfake, mostly where the eyes are closed and the head is tilted. The results of the experiment were best shown on the targeted personalities with similar facial symmetry as in the video used for the puppet.

The script for the puppet video had slow head movements to one side and then to the other, and then it abruptly moved to one side to see the artefact mentioned in the works for Monkey-Net and the First Order Motion Model. The appearance of this artefact was expected, and the artefact appeared in the results. For a better solution, photos from other angles should be found for the target person, which would improve the occlusion - in the sense that the focus is placed on the other eye (which should not be visible) or the whole part of the face that should be covered, and a 3D model, which is not obtained here due to the different shape of the person's head in the original. As for the background, the improved occlusion gave favourable results. Also, on several clippings, an artefact was obtained, which was conceptually mitigated, and that is the disappearance of parts of the image/person, as shown in Fig.8.

Fig. 8. Image with the disappeared part of the image


ISBN 978-86-7466-930-3

Accurate results are obtained in this case, and a significant number of cases, as shown in Fig.9. It can be immediately noticed that the third of the displays are around 0.4 probabilities. All detected images have distorted heads and artefacts due to movement, i.e. tracking the trajectory of key points on the face of different symmetry in the 3D model or they have their eyes closed.

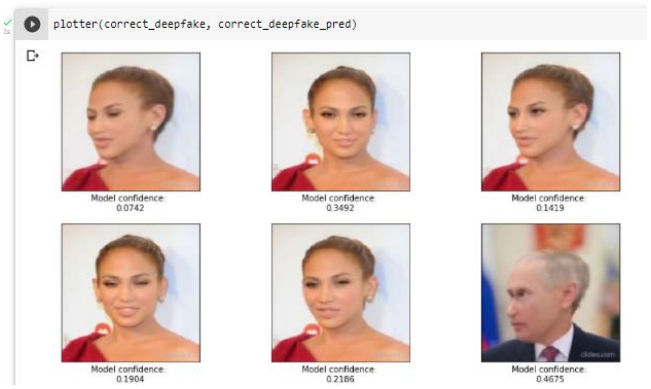


Fig. 9. Examples of images that are deepfakes, and detected as deepfakes

## C. *Analysis of false detection results*

Here, of the greatest importance are images that are detected as real, and these are images from deepfake videos.

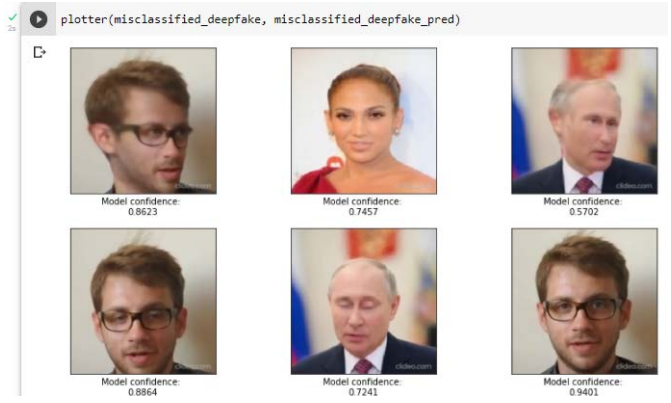


Fig. 10. Examples of images that are deepfakes and detected as real.

Three specific cases can be observed where there is a space for further improvements:
- mouth/lip movements,
- head movements and
- eye movements

Speaking of mouth movements, Fig.11, satisfactory results were obtained in creating a puppet, where the targeted persons followed the movements and had a tooth display at the appropriate moments. All lip movements that were observed in isolation from other movements contributed to the reality of deepfake and false detection. The lips are mostly in motion with teeth or collected. Compared to well-detected lips, every fifth well-detected mouth as a deepfake has a deformity along with the head. So one can say that lips are one of the parts where there is a need for a better detection.

Slow head movements to one side and then the other, and then abruptly movement to one side is a significant process, Fig.12. All the end movements are recognized as real images, in a manner that if the head is still, meaning in one place for more than one second without motion blur, the image will be detected as real. Furthermore, the detector sees even distinguished distortions of the head and face as realistic images. This is noticed in nearly 33% of false detected images. Moreover, it is very likely to have errors in differentiation when real images are frontal with clear head movement, while eyes are visible and lips in motion or collected. Those characteristics are visible in around 97% of all images that are deepfake and marked as real.

Fig. 11. Images with mouth movement

Fig. 12. Examples of frontal, right, left and right side (column-wise).

The most relevant results in terms of authenticity are in creating obtained by tracking eye movements, Fig.13. It can be considered the most difficult case in the creation process. False detection occurred in the eye related situations when the eyes are fully visible or when the iris and pupil are visible. Also, false detection is present when the eyes have a proportional distance between the pupils concerning the position of the face. This is shown in the most majority of images/frames, around 99%.

Fig. 12. Examples of eye movement.


ISBN 978-86-7466-930-3

## V. CONCLUSION

Based on the results of the experiments, it can be concluded that the creation of fast and efficient deepfake still meets the need for additional training of neural networks that map key points and where trajectories needs to be adapted to different head shapes so that the appearance of deepfake is invisible to the human eye. It is important to emphasize that the results completely coincided with the results from the paper [9]. It is believed that further training of such neural networks can lead to even more adaptable results.

On the other hand, the selected detection was not the best example for a given set of images which is shown through a variety of false detection results. This can be attributed to the fact that the detection follows certain edges and looks for dominant characteristics that were not the focus in creating the deepfake, such as eye details. Therefore, it is suggested that the type of detection should be adapted to specific type of deepfake. The importance of focusing on deepfake detection, and particularly eye movement, is emphasized which must be adapted to all new ways of creating deepfake videos.

In future work, we would focus on better detection of the misshaped head, as well as different tools for recognition of lip-syncing and eye tracking.

## ACKNOWLEDGMENT

This work is written during the research supported and partially funded by the Ministry of Education, Science and Technological Development, Republic of Serbia. No. 2022/200103.

## REFERENCES

[1] A.M. Almars, "Deepfakes detection techniques using deep learning: a survey," *Journal of Computer and Communications*, vol. 9, no. 5, pp. 20-35, May 2021.

[2] J.T. Hancock, and J.N. Bailenson, "The social impact of deepfakes," *Cyberpsychology, behavior, and social networking*, vol. 24, no. 3, pp. 149-152, 2021.

[3] M. Đorđević, M. Milivojević, and A. Gavrovska, "DeepFake video production and SIFT-based analysis," *Telfor Journal*, vol. 12, no. 1, pp. 22-27, 2020.

[4] M. Masood, M. Nawaz, K.M. Malik, A. Javed, and A. Irtaza, "Deepfakes Generation and Detection: State-of-the-art, open challenges, countermeasures, and way forward," *arXiv preprint arXiv:2103.00484*, 2021.

[5] C. Gosse, and J. Burkell, "Politics and porn: how news media characterizes problems presented by deepfakes," *Critical Studies in Media Communication*, vol. 37, no. 5, pp. 497-511, 2020.

[6] J.P. Dasilva, K.M. Ayerdi, and T.M. Galdospin, "Deepfakes on Twitter: Which Actors Control Their Spread?," *Media and Communication*, vol. 9, no. 1, p. 301-312, 2021.

[7] L. Guarnera, O. Giudice, and S. Battiato, "Deepfake detection by analyzing convolutional traces," In *Proceedings of the IEEE/CVF Conference on Computer Vision and Pattern Recognition Workshops*, 14-19 June, 2020. Doi: 10.1109/CVPRW50498.2020.00341

[8] C. Yang, L. Ding, Y. Chen, and H. Li, "Defending against gan-based deepfake attacks via transformation-aware adversarial faces," In *2021 International Joint Conference on Neural Networks* (IJCNN) IEEE, pp. 1-8, July 2021.

[9] A. Siarohin, S. Lathuilière, S. Tulyakov, E. Ricci, and N. Sebe, "First order motion model for image animation," *Advances in Neural Information Processing Systems* 32, 2019.

[10] M.T. Jafar, M. Ababneh, M. Al-Zoube, and A. Elhassan, "Forensics and analysis of deepfake videos," In *2020 11th international conference on information and communication systems* (ICICS) IEEE, pp. 053-058, April 2020.

[11] A. Siarohin, S. Lathuilière, S. Tulyakov, E. Ricci, and N. Sebe. "Animating arbitrary objects via deep motion transfer," In *CVPR*, pp. 2377-2386, 2019.

[12] D. Afchar, V. Nozick, J. Yamagishi, and I. Echizen, "Mesonet: A compact facial video forgery detection network," *10th IEEE International Workshop on Information Forensics and Security*, (WIFS) 2018. https://doi.org/10.1109/WIFS.2018.8630761

[13] Google Colab, https://colab.research.google.com/

[14] Python, https://www.python.org/

 ISBN 978-86-7466-930-3

# Kvarcni kristalni filtar frekvencije 35.4 MHz zasnovan na trećem overtonu

Dragi Dujković, Ana Gavrovska, Lenkica Grubišić, Snežana Dedić-Nešić, Irini Reljin, Ivan Popović

***A stra t*— a savremene tele omuni acije, posebno digitalne, veoma je važno oristiti valitetne omponente za prijem, predaju i prenos signala. Među najbitnijim omponentama u ta vim sistemima su ristalni filtri, oji su i često korišćene komponente. ovom radu je opisan ristalni filtar 5,4 z zasnovan na ristalnoj jedinki trećeg overtona, ao i korišćene tehničke karakteristike.**

***Ključne reči*— ristali, filtri, proje tovanje, overton, tehničke ara teristi e.**

## I. UVOD

Potrebno je imati u vidu da mogućnost projektovanja i realizacije kristalnih filtara prema konkretnom zahtevu korisnika pruža pogodnosti u ispunjenju različitih zahteva u pogledu centralne frekvencije filtra, širine propusnog opsega i selektivnosti, toka amplitudske i fazne karakteristike u propusnom opsegu. Mogući su i mnogi specifični zahtevi vezani za klimomehaničke karakteristike, intermodulaciju i druge karakteristike koje diktira primena filtra u specifičnim uslovima. Mali je broj proizvođača koji pružaju mogućnost realizacije kristalnih filtara na osnovu konkretnih zahteva korisnika. Uglavnom se proizvodnja zasniva na realizaciji kataloških tipova filtara [1-7].

U ovom je radu realizovan novi tip kristalnog filtra na frekvenciji 35.4 MHz. Projektovan je filtar koji obezbeđuje ispunjenje postavljenih zahteva. Proračunom filtra definisani su elementi ekvivalentne električne mreže i zahtevi za kristalne jedinke. Ovde zahtevi za kristalne jedinke obuhvataju: dozvoljeni nivo neželjenih rezonancija; frekvencije kristalnih jedinki; dozvoljeno odstupanje frekvencije kristala na sobnoj temperaturi i u radnom temperaturnom opsegu; vrednosti parametara kristalne jedinke; serijsku i paralelnu kapacitivnost; faktor dobrote kristala.

Postupak proizvodnje primenjen u realizaciji ovih filtara može da se uvede u proces proizvodnje svih tipova kristalnih filtara koji imaju slične zahteve u pogledu strogo definisanih električnih karakteristika.

Mogu se razmatrati sledeći iazazovi: ostvarivanje što većeg slabljenja u nepropusnom opsegu filtra i što manjeg slabljenja u propusnom opsegu filtra. Zajedno sa navedenim razmatranjem odvijao se razvoj kristalnih jedinki koje imaju ostvarene sve parametare koje je odredilo projekatvanje filtra. Posebno je vođeno računa o uslovu da se ostvari što veći - faktor i što veći faktor potiskivanja neželjenih rezonancija.

Q faktor je bezdimenzioni parametar koji opisuje koliko je oscilator ili rezonator nedovoljno prigušen. Približno se definše kao odnos početne energije rezonatora i energije izgubljene u jednom krugu ciklusa oscilovanja. Faktor potiskivanja neželjenih rezonancija je logaritam odnosa amplituda neželjenih signala i signala na centralnoj frekvenciji rezonatora.

Uporedo sa tim je urađena i analiza svih komponenata koji se ugrađuju u filtar i proveren njihov uticaj na osetljivost filtra u pogledu funkcionisanja u radnom temperaturnom opsegu i pri zadatim uslovima rada [10-11].

Rad je organizovan na sledeći način. U drugoj glavi dat je kratak osvrt na potrebe za realizacijom ovakvih filtara. Treća glava je posvećena samom projektovanju filtara. Kristalne jedinke su opisane, kao i njihova realizacija u glavi četiri. Na kraju, u petoj glavi nalazi se zaključak.

## II. REALIZACIJA FILTARA TRAŽENIH KARAKTERISTIKA

Zahtevane električne karakteristike filtara su direktno povezane sa namenom samog uređaja, a to određuje oblik amplitudske i fazne karakteristike u propusnom opsegu, centralnu frekvenciju filtra, širinu propusnog opsega i selektivnost.

Pored osnovnih karakteristika postoje i karakteristike koje u zavisnosti od toga u kakvim uslovima rada uređaj funkcioniše imaju zahteve koji se odnose na vibracije, udare, potrese, temperaturu, pritisak, vlagu. To su tzv. klimomehanički uslovi rada, ali postoji i dosta drugih specifičnih zahteva.

Ovi kristalni filtri, koji se prema traženoj specifikaciji ne mogu pronaći u katalozima proizvođača, zahtevaju kompletan razvoj uz odgovarajući projekat filtra prema postavljenim zahtevima.

Važna je potreba da se mogu realizovati kristalni filtri na osnovu specifičnih zahteva korisnika. To zahteva razvoj novih tehnoloških postupaka pri proizvodnji, kao i projektovanje filtara i njihovih komponenata. Zbog toga se većina proizvođača bavi proizvodnjom kataloških tipova filtara sa standardnim karakteristikama i komponentama [4–12].

Dragi Dujković – Univerzitet u Beogradu - Elektrotehnički fakultet, , Bulevar Kralja Aleksandra 73, 11120 Beograd, Srbija (e-mail: *dragi etf.bg.ac.rs*).

Ana Gavrovska – Univerzitet u Beogradu - Elektrotehnički fakultet, , Bulevar Kralja Aleksandra 73, 11120 Beograd, Srbija (e-mail: *anaga etf.bg.ac.rs*).

Lenkica Grubišić – Institut Mihajlo Pupin, Volgina 15, 11060 Beograd, Srbija (e-mail: *lenka pie o.imp.bg.ac.rs*).

Snežana Dedić-Nešić– Institut Mihajlo Pupin, Volgina 15, 11060 Beograd, Srbija (e-mail: *sne anadn gmail.com*).

Irini Reljin – Univerzitet u Beogradu -Elektrotehnički fakultet, Bulevar Kralja Aleksandra 73, 11120 Beograd, Srbija (e-mail: *irinitms etf.bg.ac.rs*).

Ivan Popović – Univerzitet u Beogradu -Elektrotehnički fakultet, Bulevar Kralja Aleksandra 73, 11120 Beograd, Srbija (e-mail: *poppo ici etf.bg.ac.rs*).

 ISBN 978-86-7466-930-3

## III. PROJEKTOVANJE FILTARA

Na osnovu liste tehničkih zahteva koja je prikazana u tabeli I, završen je projekat željenog filtra. Takođe, na osnovu zahteva u pogledu oblika amplitudske karakteristike u propusnom i nepropusnom opsegu određuje se red filtra i sama mreža koja ispunjava postavljene zahteve. Na slici 1 prikazana je šema jednog filtra. Prilikom proračuna parametara i projektovanja filtra mora se voditi računa i o tolerancijama komponenata koje se ugrađuju u filtar kako bi bile ispunjene tražene karakteristike.

Na osnovu predviđenih gubitaka u mreži, završen je proračun filtra, određena je električna šema i definisani su zahtevi vezani za kristalne jedinke. Projektovanjem filtra moraju se tačno definisati svi parametri kristalnih jedinki, njihove vrednosti i tolerancije. Proračunavaju se i parametri kao što su frekvencija kristala, serijske i paralelne kapacitivnosti kristala i podešenosti frekvencije na sobnoj temperaturi. Takođe se definišu i maksimalna dozvoljena odstupanja frekvencija kristala u radnom temperaturnom opsegu filtra.

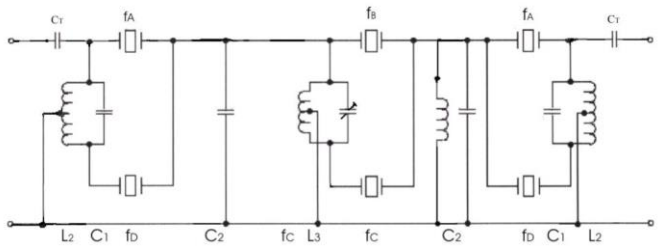


Sl. 1. Električna šema kristalnog filtra.

Prema datim zahtevima urađen je projekat filtra 6-og reda uz Chebyshev aproksimaciju. Razvijene su kristalne jedinke AT-reza sa malim odstupanjem frekvencije (lista tehničkih podataka tačka 8) u širokom temperaturnom opsegu koje ispunjavaju zadate zahteve u vidu položaja i potisnutosti sporednih rezonancija.

Potrebno je napomenuti i da se projektovanjem filtra oodređuju i vrednosti parametara ostalih elemenata, kao što su otpornici, kalemovi i kondenzatori, a takođe i njihov raspored na štampanoj ploči.

Mora se uzeti u obzir da filtri rade na visokim frekvencijama, gde prisustvo parazitnih kapacitivnosti značajno utiče na karakteristike filtara, tako da je raspored elemenata od izuzetnog značaja u podešavanu vrednosti selektivnosti i slabljenja u nepropusnom opsegu filtra [1-5].

## IV. PRISTUP ZASNOVAN NA KRISTALNIM JEDINKAMA I REALIZOVANI KRISTALNI FILTAR

Projektovani filtar ima relativno slabljenje u propusnom opsegu od ±4.25 kHz koje je manje od 3dB. Izvan frekvencijskog opsega od ±20 kHz slabljenje je veće od 60 dB . U širem opsegu frekvencija, do ±5 MHz, relativno slabljenje je veće od 60 dB.

Minimalno pogonsko slabljenje filtra je manje od 6 dB. Ulazna i izlazna otpornost filtra iznose 50 Ω. Radni temperaturni opseg filtra je -10º C do +60 ºC. Temperaturni opseg skladištenja, odnosno opseg temperatura u kojima filtar neće promeniti karakteristike dok se čuva u skladištu je -40 ºC do +85 ºC.

Filtar je smešten u kućište dimenzija (38,4×18.2×15.9) mm. Detalji svih tehničkih karakteristika filtra su dati u Tabeli I.

Nizom eksperimenata ustanovljen je povećan škart usled lomova na mašinama za glačanje i poliranje pri obradi pločica čiji je odnos prečnika i debljine $\Phi/t$>100. S obzirom da kvarcna pločica prečnika $\Phi$=5 mm, frekvencije 35.4 MHz osnovne učestanosti, ima odnos prečnika i debljine $\Phi/t$=106.38 pristupilo se realizaciji kristala trećeg overtona čiji je $\Phi/t$=35.46 čime je, sa druge strane zadovoljen uslov za planparalelni (PP) oblik pločica trećeg overtona ($\Phi/t$>35).

Overton je pojava odziva na rezonatoru koja je na frekvenciji 3, 5 ili 7 puta većoj od osnovne frekvencije rezonatora. Ova pojava se koristi da bi se postigle veće frekvencije rada kristalnog rezonatora.

U projektu mikrominijaturnih kristalnih jedinki trećeg overtona učestanosti 35.4MHz vodilo se računa o prečniku elektrode d=1.63mm i debljini nanetog filma t = 2,9x10-7m zbog zahteva za položaj i potisnutost sporednih rezonancija. S obzirom da se radi o tankim filmovima kao elektrodni materijal koristićen je aluminijum. Podešavanje frekvencije je hemijsko u sodi i anodnom oksidacijom. Sve kristalne jedinke su posle grupnog naparavanja i cementiranja stajale na vazduhu 24h radi formiranja stabilnog prirodnog oksidnog sloja. Kvarcne pločice su planparalelne (PP) prečnika Φ=5 mm i realizovane su od kvarca faktora dobrote Q>1.8 x10^6 bez strukturnih defekata i grešaka pakovanja. Kristalne jedinke montirane su u držač tipa RW-HC45.

Realizovane kristalne jedinke AT-reza zadovoljavaju zahteve za položaj i potisnutost sporednih rezonancija i dozvoljeno odstupanje frekvencije u radnom temperaturnom opsegu.

Na slici 2 prikazan je realizovani filtar. Filtar je smešten u standardno kućište koje je prikazano na slici 3.

Sl. 2. Realizovani kristalni filtar.


ISBN 978-86-7466-930-3

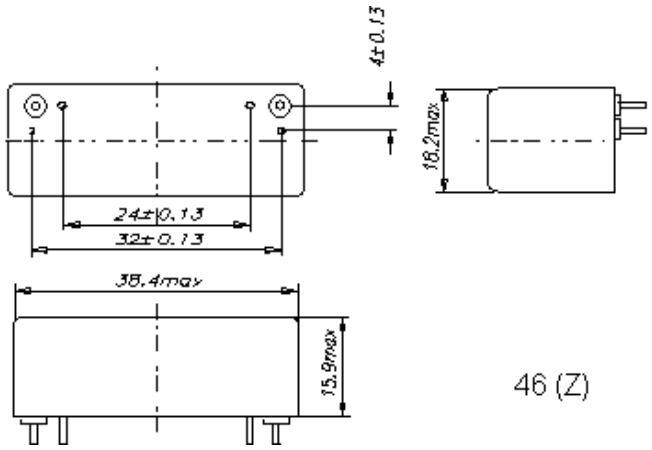


Sl. 3. Kućište filtra.

Ispitivanje filtara koje je izvršeno na sobnoj temperaturi i u radnom temperaturnom opsegu od -10˚C do +60˚C urađeno je na analizatoru spektra HP 8568A. Merenjima je utvrđeno da filtar zadovoljava tražene električne karakteristike.

Rezultati merenja amplitudske karakteristike filtra na sobnoj temperaturi prikazani su u dijagramima na slici 4.

Lista tehničkih podataka za kristalne jedinke za filtre 35,4 MHz je sledeća:

1. Kućište RW-HC45
2. 
3. frekvencija $f_1$ = 35392.53 kHz<br>$f_2$ = 35401.27 kHz<br>$f_1$ = 35393.73 kHz<br>$f_2$ = 35400.07 kHz
4. -faktor > 120000
5. dinamička kapacitivnost $C_1$ = 380 apF ± 10%
6. paralelna kapacitivnost $C_o$ = 1 pF ± 5%
7. dinamička otpornost $_1$ < 90 Ω
8. podešenost *df f*=±5 ppm
9. odstupanje *df f*=±15 ppm
10. starenje *df f*=1 ppm/god
11. radni temperaturni opseg -10÷+90˚C
12. neželjene rezonancije A. $f_0$+70 kHz–bez $f_n$

TABELA I

TEHNIČKE KARAKTERISTIKE FILTARA

| ***ara ter st e*** | ***redn st*** |
|---|---|
| Centralna frekvencija(CF) | 35,4 MHz |
| Širina propusnog opsega na 2 dB | ± 3 kHz |
| Širina propusnog opsega na 3 dB | ± 4.25 kHz |
| Talasnost u propusnom opsegu | 2 dB max u opsegu ± 7.5 kHz |
| Širina nepropusnog opsega na 60 dB | ± 20 kHz max |
| Relativno slabljenje u nepropusnom opsegu | 60 dB min za ± 5 MHz |
| Minimalno pogonsko slabljenje | 6 dB max |
| Ulazna impedansa | 50 Ω |
| Izlazna impedansa | 50 Ω |
| Radni temperaturni opseg | -10 ºC до +60 ºC |
| Temperaturni opseg skladištenja | -40 ºC до +85 ºC |

## V. ZAKLJUČAK

Pored proračuna i realizacije kristalnog filtra, razvijena je i nova kristalna jedinka. Ovakvi kristalni filtri predstavljaju novi proizvod, jer su u njemu korišćene nove tehnologije i nove komponente. Ovi proizvodi imaju širok dijapazon primena i veliku upotrebnu vrednost i ističu se svojom cenom i svojim kvalitetom, tako da se mogu smatrati konkurentnim na tržištu. Navedene karakteristike i konkurentnost na tržištu daju perspektivu razvoju novih elektronskih sklopova i proizvoda zasnovanih na kristalnim jedinkama.

U daljem razvoju ovih i sličnih uređaja treba ići na usvajanje novih tehnologija izrade kristalnih jedinki i upotrebe novih i kvalitetnijih komponenti u kolu elektronskih sklopova novih uređaja.

## ZAHVALNICA

Istraživanja opisana u ovom radu su finansirana od strane Ministarstva za obrazovanje, nauku i tehnološki razvoj Republike Srbije. Broj ugovora 451-03-68/2022-14/200103

 ISBN 978-86-7466-930-3

## LITERATURA


[1] S. Dedić-Nešić "Prilog projektovanju kristalnih filtara sa linearnom faznom karakteristikom", magistarska teza, Elektrotehnički fakultet, Univezitet u Beogradu, 1991.

[2] R. G. Kinsman, "A history of crystal filters," in Proc. of the 1998 IEEE Int. Frequency Control Symposium, pp. 563-570, 1998.

[3] H. J. Blinchikoff, A. I. Zverev "Filtering in the Time and Frequency Domains" John Wiley and Sons, Inc, 1976.

[4] D. S. Humpherys "The Analysis, Design and Synthesis of Electrical Filters" Prentice Hall, Englewood Clifs, N.J. 1970.

[5] S. Dedić-Nešić, D. Dujković, L. Grubišić, I. Reljin, B. Reljin, "Novi visokokvalitetni 90.1105 MHz filtri za komunikacije u rudnicima," ETRAN, 2010.

[6] D. Dujković, B. Reljin, S. Dedić-Nešić, L. Grubišić, D. Jevtić, "Novi kristalnih filtar F121," ETRAN, 2012.

[7] D. M. Dujković, S. Dedić–Nešić , L. Grubišić, A. Gavrovska, and I. Reljin, "High-quality crystal filter: Design and realization," *Telfor* ., vol. 5, no. 2, pp. 118–122, 2013.

[8] L. Grubišić, S. Dedić–Nešić, D. M. Dujković, , B. Reljin, "Novi tip kristalne jedinke za filtre namenjene za rad u posebnim klimo mehaničkim uslovima", ETRAN, 2012, EK2.6-1-4, Banja Vrućica 2011.

[9] D. Dujković, S. Dedić Nešić, L. Grubišić, B. Reljin, I. Reljin, "Crystal Filter 50 MHz for Applications in Specific Environmental Conditions," in Proc. 10th Int. Conf. on Telecommunication in Modern Satellite Cable and Broadcasting Services (TELSIKS), 2011, vol. 1. pp. 253-256, Nis, Serbia, 2011.

[10] D. M. Dujković, S. Dedić Nešić, L. Grubišić, M. Paskaš, and Irini Reljin, "New 76.8375 MHz Crystal filter Based on Third overtone Crystal units," 28th Telecommunications forum TELFOR 2020, pp.177-180, 2020.

[11] D. M. Dujković, I. Reljin, L. Grubišić, S. Dedić–Nešić, and A. Gavrovska, "Kristalni filtri za opseg frekvencija 150-170MHz," ETRAN, EK 1-1, pp. 213-216, Stanišići 2021.

[12] D. M. Dujković, S. Dedić–Nešić, L. Grubišić, I. Reljin, and A. Gavrovska, "New stop band 48 MHz crystal filter," Telfor Proceedings, pp. 249-252, Belgrade 2021.


## ABSTRACT


In modern telecommunications, especially digital, it is very important to use quality components for receiving, sending and transmitting signals. Among the most valuable components are crystal filters, which are also commonly used components. The paper describes a 35.4 MHz crystal filter based on crystalline units of the third overtone and applied technical characteristics.


**uartz crystal filter 5.4 z based on crystalline units of the third overtone**


Dragi Dujkovic, Ana Gavrovska, Lenkica Grubisic, Snezana Dedic-Nesic, Irini Reljin


 ISBN 978-86-7466-930-3

FILTER - TEST RECORD

| | | | | | |
|---|---|---|---|---|---|
| 1. nominal centre freq. | fc | : | 35.400000 MHz | | |
| 2. delta fc | | : | -306 Hz | | |
| 3. bandwidth | at 2.0 dB | : | 10.879 kHz | | |
| | w.r.t. fc | : | -5.745 kHz | | +5.133 kHz |
| 4. ripple | | : | 0.00 dB | in fm +/- | 3.000 kHz |
| 5. transducer attenuation | | : | 2.6 dB | | |
| 6. attenuation at fc | | : | 2.6 dB | | |
| 7. stop bandwidth | at | : | 60.0 dB | | |
| | at fc | : - | 14.498 kHz | + | 15.713 kHz |
| 8. ultimate attenuation | >= | : | 79.6 dB | | |
| | from | : | 30.400000 MHz | to | 35.380000 MHz |
| | >= | : | 90.6 dB | | |
| | from | : | 35.420000 MHz | to | 40.400000 MHz |

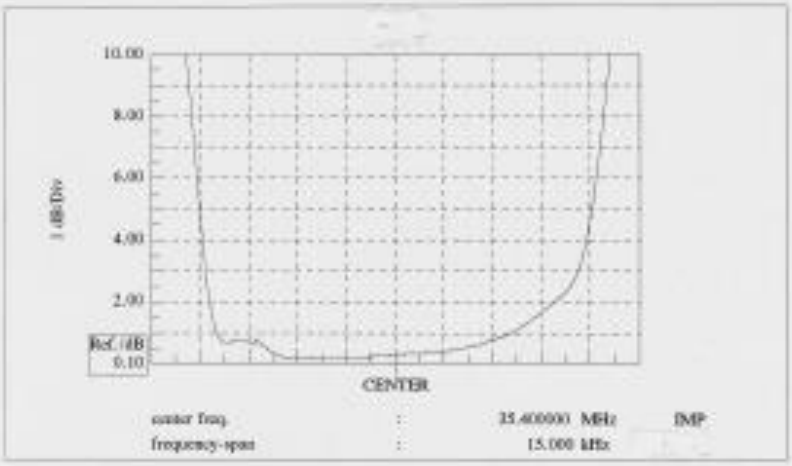


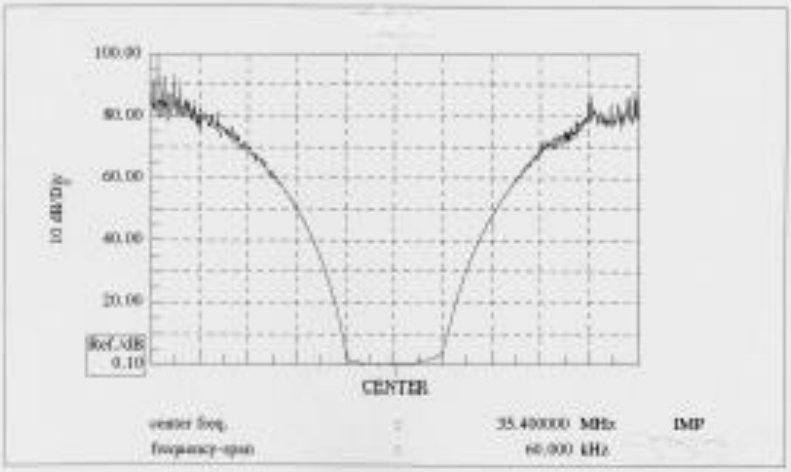


Sl. 4. Rezultati merenja amplitudske karakteristike filtra 35,4 MHz na sobnoj temperaturi.


ISBN 978-86-7466-930-3

# Primena vremensko-frekvencijskih metoda kod analize spektra u kognitivnom radiju

Nenad Stojanović, Milenko Andrić, Dimitrije Bujaković, Boban Bondžulić i Vladimir Ristić

***Apstrakt*—U radu je izvršena analiza primene tri metode vremensko-frekvencijske analize signala za potrebe analize spektra kod kognitivnog radija. Analiza je sprovedena modelovanim i realnim signalima za aditivni beli Gausov šum različitog odnosa signal/šum. Performanse metoda su analizirane kroz promene odnosa signal/šum i praga detekcije, određivanjem verovatnoće lažnog alarma, verovatnoće propuštene detekcije i verovatnoće ispravne detekcije. Pokazano je da se metode vremensko-frekvencijske analize signala mogu efikasno koristiti za potrebe analize spektra uz odgovarajuću optimizaciju parametara.**

***Ključne reči*—Frekvencijsko skakanje, kognitivni radio, vremensko-frekvencijska analiza spektra.**

## I. Uvod

EKSPONENCIJALNI rast broja bežičnih uređaja i sistema prenosa, kao i zahtevi korisnika za većim brzinama prenosa i boljem kvalitetu usluge, uticali su na sve izraženije probleme kod dodele spektra i uopšte pristupu radio spektru. Jedno od rešenja predstavlja kognitivna radio tehnologija, čiji je cilj da poveća spektralnu efikasnost koristeći delove sprektra koje ne koristi primarni korisnik za prenos signala sekundarnih korisnika [1]. Sekundarni korisnici određenog spektralnog opsega ni u kom slučaju ne smeju ometati primarne korisnike. U tom cilju, ovako koncipiran pristup radio spektru, odnosno upravljanju spektrom (eng. *Spectrum Management*) se sastoji iz četiri koraka [2]:

- analiza spektra (eng. *Spectrum Sensing*),
- donošenje odluka (eng. *Spectrum Decision*),
- deljenje spektra (eng. *Spectrum Sharing*) i
- mobilnost spektra (eng. *Spectrum Mobility*).

Kognitivni radio se može definisati kao unapređeni softverski definisani radio, sa ostvarenom sposobnosti učenja i zaključivanja, odnosno kognitivnost [3]. Jednu od definicija dao je i američki FCC (*Federal Communication Commision*) po kojem kognitivni radio predstavlja bežični uređaj koji dinamički detektuje neiskorišćene delove spektra i koristi ih tako da ni na koji način ne ometa primarne korisnike u tom opsegu [4].

Najvažnija funkcija kognitivnog radija je analiza spektra, pri čemu je osnovni izazov analize spektra detekcija signala male snage sa malom verovatnoćom propuštene detekcije u uslovima niskog odnosa signal/šum (eng. *Signal to Noise Ratio*, SNR). Postoji više različitih klasifikacija tehnika za analizu spektra [5, 6, 7]. Jedna od najčešće korišćenih je podela na: tehnike analize spektra za detekciju primarnih predajnika, tehnike analize spektra za detekciju primarnih prijemnika i tehnike analize spektra zasnovane na temperaturi interferencije.

Vremensko-frekvencijske metode analize signala se koriste za analizu spektra kognitivnog radija [8]. U [9] je izvršena analiza spektra kada je primarni signal digitalna televizija, odnosno OFDM (*Orthogonal Frequency Division Multiplexing*) signal. Autori u [10] predlažu modifikaciju vremensko-frekvencijskih metoda za analizu spektra u prisustvu OFDM signala. U [11] su autori pored OFDM signala, razmatrali i signal sa frekvencijskim skakanjem. Analiza spektra radio sistema TETRA (*Terrestial Trunked Radio*) je predložena u [12]. Karakteristika svih navedenih radova je korišćenje modelovanih signala za analizu spektra kognitivnog radija.

Slična analiza spektra vrši se tokom elektronskog rata u cilju prikupljanja informacija, ali bez potrebe za iskorišćenjem spektralnih šupljina. Kod ovakvih sistema neke od osnovnih funkcija su detekcija izvora zračenja, klasifikacija i identifikacija emitera, određivanje lokacije emitera i njegovo praćenje. Sve ove funkcije potrebno je obavljati u veoma kompleksnom okruženju u realnom vremenu.

U ovom radu su analizirane metode vremensko-frekvencijske analize signala za potrebe analize spektra kognitivnog radija. Razmatran je signal sa frekvencijskim skakanjem koji se često koristi u vojnim radio sistemima. Frekvencijsko skakanje predstavlja tehniku prenosa koja se zasniva na skokovitoj promeni frekvencije nosioca u širem opsegu nego što je to neophodno [13]. Za potrebe analize razvijen je simulacioni model, a takođe su korišćeni i snimljeni realni signali iz baze signala [14].

Ostatak rada je organizovan na sledeći način. U drugom delu rada ukratko su opisane korišćene metode za vremensko-frekvencijsku analizu signala. U trećem delu rada opisana je

Nenad Stojanović – Vojna akademija, Univerzitet odbrane u Beogradu, Veljka Lukića Kurjaka 33, 11000 Beograd, Srbija (e-mail: nivzvk@hotmail.com).

Milenko Andrić – Vojna akademija, Univerzitet odbrane u Beogradu, Veljka Lukića Kurjaka 33, 11000 Beograd, Srbija (e-mail: andricsmilenko@gmail.com).

Dimitrije Bujaković – Vojna akademija, Univerzitet odbrane u Beogradu, Veljka Lukića Kurjaka 33, 11000 Beograd, Srbija (e-mail: dimitrijebujakovic@gmail.com).

Boban Bondžulić – Vojna akademija, Univerzitet odbrane u Beogradu, Veljka Lukića Kurjaka 33, 11000 Beograd, Srbija (e-mail: bondzulici@yahoo.com).

Vladimir Ristić – Vojna akademija, Univerzitet odbrane u Beogradu, Veljka Lukića Kurjaka 33, 11000 Beograd, Srbija (e-mail: vladarist@gmail.com).

 ISBN 978-86-7466-930-3

metodologija analize spektra. Analiza modelovanih signala sa frekvencijskim skakanjem je data u četvrtom poglavlju, dok je u petom izvršena analiza realnih, akviziranih signala sa frekvencijskim skakanjem. U poslednjem odeljku dati su najvažniji zaključci i budući pravci istraživanja.

## II. METODE VREMENSKO-FREKVENCIJSKE ANALIZE SIGNALA

Najčešće korišćena vremensko-frekvencijska predstava signala je spektrogram. Spektrogram predstavlja energetsku verziju vremenski zavisne Furijeove transformacije (eng. *Short-time Fourier Transform*, STFT). STFT je definisana kao [15]:

$$STFT(n,k)=\sum_{m=-N/2}^{N/2} w(m)x(n+m)e^{-j(2\pi/N)mk}, \quad (1)$$

gde su $x(n+m)$ signal koji se analizira, $w(m)$ prozorska funkcija, dok je broj tačaka za izračunavanje Furijeove transformacije $N+1$. Spektrogram je definisan kao:

$$SPEC(n,k)=\left|STFT(n,k)\right|^2. \quad (2)$$

Vremenska i frekvencijska rezolucija određene su dužinom prozorske funkcije. Smanjenjem dužine prozora dobija se bolja vremenska rezolucija čime se negativno utiče na frekvencijsku rezoluciju. Povećanjem dužine prozora, smanjuje se vremenska rezolucija, ali se poboljšava predstava signala u frekvencijskom domenu. Prozori se međusobno mogu preklapati ili ne. Povećanjem preklapanja prozora poboljšava se vremenska rezolucija [16].

Vignerova vremensko-frekvencijska distribucija (eng. *Wigner Distribution*) je razvijena kao optimalna za predstavu jednokomponentnih linearno frekvencijski modulisanih signala u vremensko-frekvencijskom domenu. Pri analizi višekomponentnih signala, pojavljuju se komponente koje se ne nalaze u originalnom signalu, što predstavlja jedan od nedostataka ove transformacije. Kompleksnost izračunavanja ove distribucije je veoma velika, što je još jedan nedostatak. Pseudo Vigner-Vilova vremensko-frekvencijska distribucija signala (eng. *Pseudo Wigner-Ville Distribution,* PWV) predstavlja Vignerovu raspodelu analitičkog signala i može se predstaviti primenom STFT kao [17]:

$$\begin{aligned} WD(n,k)&=\sum_{i=-N/2}^{N/2} STFT(n,k+i)STFT^*(n,k-i)= \\ &=\left|STFT(n,k)\right|^2+2\,\mathrm{Re}\left\{\sum_{i=1}^{N/2} STFT(n,k+i)STFT^*(n,k-i)\right\} \end{aligned}, \quad (3)$$

gde je sa * označena konjugovano kompleksna vrednost. Poređenjem (2) i (3) uočava se da kod Vignerove raspodele postoji dodatni član koji povećava broj računskih operacija i time povećava složenost ovog algoritma u odnosu na spektrogram.

U cilju postizanja kompromisa između Vignerove raspodele i spektrograma, uz iskorišćenje prednosti koje daje Vignerova raspodela u smislu predstave signala i smanjenja računarske složenosti što je karakteristika spektrograma, predložen je S-metod, koji se definiše kao [18]:

$$SM_L(n,k)=\sum_{i=-L}^{L} STFT(n,k+i)STFT^*(n,k-i), \quad (4)$$

gde je $L$ frekvencijska dužina prozora. Za slučaj kada je $L=0$, S-metod predstavlja spektrogram, dok je za slučaj kada je $L=N/2$, S-metod zapravo pseudo Vignerova raspodela [17].

## III. ANALIZA SPEKTRA KORIŠĆENJEM VREMENSKO-FREKVENCIJSKIH METODA

U ovom istraživanju predložena je analiza spektra kognitivnog radija. Analiza spektra izvršena je na osnovu dve hipoteze:

$$\begin{aligned} H_0&: y[n]=z[n], n=1,...,N \\ H_1&: y[n]=x[n]+z[n], n=1,...,N \end{aligned}, \quad (5)$$

gde je $y[n]$ signal čiji se spektar analizira, $x[n]$ je signal primarnog korisnika, dok je $z[n]$ aditivni beli Gausov šum. Hipoteza $H_0$ je tačna kada u analiziranom spektru nema prisustva signala primarnog korisnika, dok je hipoteza $H_1$ tačna kada postoji primarni signal.

Analiza spektra se sprovodi kroz sledeće korake:

1. realizacija vremensko-frekvencijske analize spektra korišćenjem neke od opisanih metoda (spektrogram, S-metod za $L=2$ i pseudo Vigner-Vilova raspodela),
2. poređenje amplituda spektralnih komponenti sa pragom detekcije u svakom vremenskom binu i
3. donošenje odluke da li postoji primarni signal u određenom vremenskom intervalu i ako postoji koji deo spektra zauzima.

Analiza efikasnosti rada kognitivnog radija realizovana je kroz verovatnoće ispravne detekcije ($P_d$), lažnog alarma ($P_{fa}$) i propuštene detekcije ($P_{miss}$). Određivanje da li je signal primarnog korisnika ispravno detektovan vršeno je po vremenskim binovima, koji su određeni brojem odbiraka korišćenim za izračunavanje spektra nekom od opisanih vremensko-frekvencijskih metoda. Analiza je sprovedena za slučaj kada se u radio spektru javlja emisija samo jednog primarnog korisnika.

Određivanje definisanih verovatnoća vršena je po vremenskim binovima prema sledećem:

- ukoliko je detektovan signal u frekvencijskom opsegu u kojem je i emitovan, izvršena je uspešna detekcija,
- ukoliko nije detektovan signal kada nije ni bilo emisije, izvršena je uspešna detekcija,
- ukoliko je detektovan signal u nekom frekvencijskom opsegu u kome primarni korisnik nije vršio emisiju, došlo je do pojave lažnog alarma,
- ukoliko primarni signal nije detektovan u opsegu u kome je postajala emisija došlo je do propuštene detekcije,

 ISBN 978-86-7466-930-3

– ukoliko je detektovano više signala, od kojih je jedan signal primarnog korisnika, izvršena je uspešna detekcija,
– ukoliko je detektovano više signala, ali nijedan od njih nije u opsegu gde je emitovan primarni signal, došlo je do propuštene detekcije,
– ukoliko je detektovano više signala, a primarni korisnik nije vršio emisiju, došlo je do pojave lažnog alarma,

Testiranja su vršena Monte-Karlo simulacijama, pri čemu je zbog slučajnog procesa u kanalu izazvanog aditivnim belim Gausovim šumom, postupak ponavljan 100 puta, nakon čega je vršeno usrednjavanje rezultata. Izabran broj ponavljanja testova je u skladu sa [11]. Analizirani su spektri modelovanog signala i spektri realnog signala sa sporim frekvencijskim skakanjem primenom spektrograma, S-metoda za $L$=2 i pseudo Vigner-Vilove distribucije.

## IV. Analiza spektra modelovanog signala

Za potrebe analize razvijen je simulacioni model radio sistema prenosa sa frekvencijskim skakanjem koji predstavlja signal primarnog korisnika. Modelovani sistem koristi opseg od 30-80 MHz sa sporim frekvencijskim skakanjem, tako da se tokom jednog skoka prenosi 50 informacionih simbola. Korišćen je BFSK (*Binary Frequency Shift Keying*) modulacioni postupak. Generisani signal je trajanja nešto više od dve sekunde. Snaga aditivnog belog Gausovog šuma menjana je promenom njegove varijanse.

Na Sl. 1 prikazane su verovatnoće lažnog alarma i propuštene detekcije u odnosu na SNR za tri analizirane metode vremensko-frekvencijske analize signala (spektrogram, S-metod za $L$=2 i pseudo Vigner-Vilova distribucija). Tokom analize, korišćeno je 128 odbiraka ($N$=128) za potrebe analize spektra sa preklapanjem 50%. Hamingov (*Hamming*) prozor je korišćen. Prag detekcije je postavljen na 50% maksimalne vrednosti snage simuliranog signala primarnog korisnika.

Analizom Sl. 1 se može uočiti da za pozitivne vrednosti SNR gotovo da nema slučajeva propuštene detekcije i lažnog alarma. Smanjenjem SNR, dolazi do porasta verovatnoća lažnog alarma i propuštene detekcije u intervalu od -10 do 0 dB. Kod verovatnoća propuštene detekcije, spektrogram i S-metod imaju rast, a nakon toga, za još niže vrednosti SNR, ponovo pad i vraćanje na vrednosti približno jednake nuli. Kod PWV takođe postoji ovaj rast verovatnoće propuštene detekcije, ali je on zanemarljiv u odnosu na vrednosti dobijene korišćenjem druge dve metode. Pad ovih vrednosti se javlja zbog povećane snage šuma pa je detekcija signala češća, te stoga raste verovatnoća ispravne detekcije. Korišćenjem spektrograma i S-metoda, verovatnoće lažnog alarma za vrednosti SNR niže od -10 dB daju konstantnu vrednost, od oko 0.2. Verovatnoća lažnog alarma kod PWV raste postepeno dok ne dostigne vrednost približno jedinici. Kod PWV, zbog velike rezolucije detektovan je veliki broj spektralnih komponenti šuma, kao i međukomponenti signala primarnog korisnika, pa je verovatnoća lažnog alarma veća nego što je to slučaj kod druge dve metode.

Kako je u otežanim uslovima rada teško svesti verovatnoće lažnog alarma i propuštene detekcije na nulu, sa stanovišta realizacije kognitivnog radija povoljnije je obezbediti veću verovatnoću lažnog alarma u odnosu na verovatnoću propuštene detekcije. Smanjivanjem verovatnoće propuštene detekcije mogućnost ometanja primarnog korisnika svodi se na minimum.

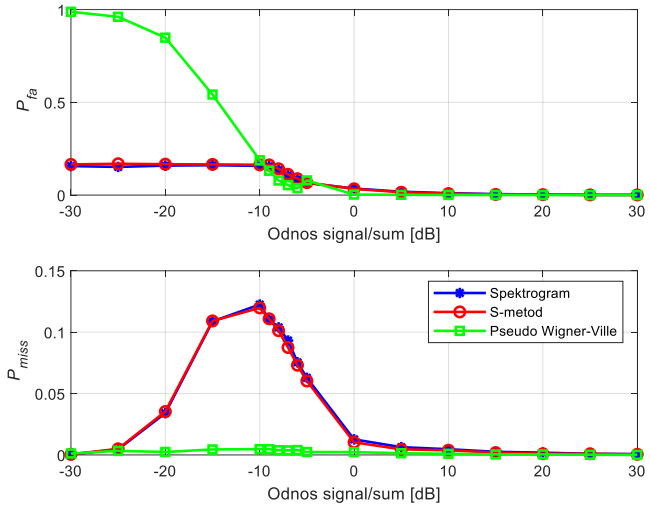


Sl. 1. Verovatnoća lažnog alarma i verovatnoća propuštene detekcije u zavisnosti od odnosa signal/šum kod simuliranog primarnog signala.

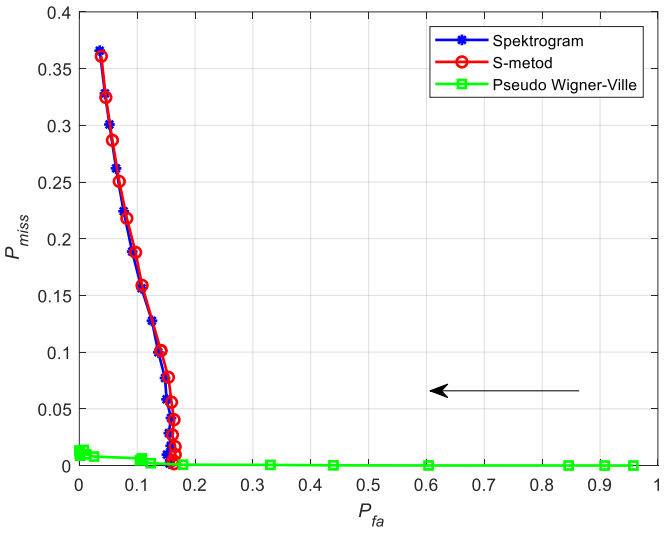


Sl. 2. Odnos verovatnoće propuštene detekcije i verovatnoće lažnog alarma za različite vrednosti praga detekcije kod simuliranog primarnog signala.

Na Sl. 2 prikazan je odnos verovatnoće propuštene detekcije u odnosu na verovatnoću lažnog alarma za sve tri analizirane metode vremensko-frekvencijske analize signala. Krive na Sl. 2 dobijene su za konstantnu vrednost SNR od -8 dB i dužinu prozora od 128 odbiraka, sa preklapanjem 50%. Promenom praga detekcije od 10% do 90% maksimalne vrednosti snage primarnog signala menjaju se odnosi verovatnoće lažnog alarma i verovatnoće propuštene detekcije. Vrednost SNR od -8 dB je uzeta jer se u tom


ISBN 978-86-7466-930-3

intervalu vrednosti SNR narušava primarni signal dovoljno da se može testirati efikasnost metoda pri radu u otežanim uslovima. Za niske vrednosti praga detekcije, povećava se verovatnoća lažnog alarma, a smanjuje verovatnoća propuštene detekcije i obrnuto. Spektrogram i S-metod su pokazali približno slične rezultate, dok je primenom PWV ostvarena mala verovatnoća propuštene detekcije za različite vrednosti praga detekcije. Ipak, iako PWV ima malo propuštenih detekcija, veliki broj detekcija lažnog alarma onemogućava korišćenje spektra od strane sekundarnih korisnika. Strelica na slici pokazuje smer povećanja praga detekcije.

## V. ANALIZA SPEKTRA REALNOG SIGNALA

Testiranje mogućnosti primene vremensko-frekvencijskih metoda analize signala u kognitivnom radiju izvršeno je na realnim signalima iz dostupne baze prikupljenih telekomunikacionih signala [14]. Navedena baza je, prema saznanjima autora, jedina dostupna baza telekomunikacionih signala u razmatranom opsegu učestanosti, a da je pogodna za vremensko-frekvencijsku analizu signala, s obzirom da je primarna namena korišćene baze klasifikacija različitih modulacionih postupaka i tehnika prenosa. Signali su prikupljani pomoću analizatora spektra koji je bio kablom direktno povezan sa radio uređajem kao generatorom signala, čime je pojava šuma prilikom snimanja signala bila smanjena u najvećoj mogućoj meri. U bazi signala postoji nekoliko različitih tipova modulisanih signala, a za potrebe analize u ovom radu korišćeni su samo signali sa frekvencijskim skakanjem. Snimljeni signali su trajanja nešto dužeg od dve sekunde. Radio uređaj je podešen tako da koristi opseg od 30 do 80 MHz za potrebe prenosa frekvencijskim skakanjem. Uređaj koristi 8-CPFSK (*Continuous Phase FSK*) modulaciju. U skladu sa brzinom promene frekvencije nosioca, uređaj podržava samo sporo frekvencijsko skakanje.

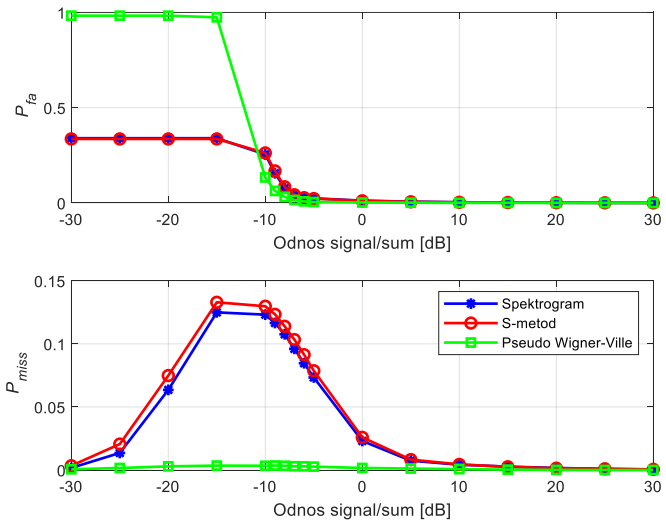


Sl. 3. Verovatnoća lažnog alarma i verovatnoća propuštene detekcije u zavisnosti od odnosa signal/šum kod realnog primarnog signala.

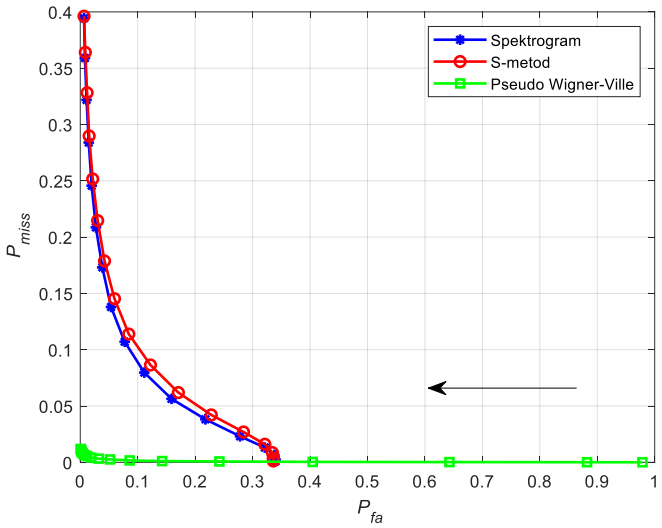


Sl. 4. Odnos verovatnoće propuštene detekcije i verovatnoće lažnog alarma za različite vrednosti praga detekcije kod realnog primarnog signala.

Na Sl. 3 su prikazane verovatnoće lažnog alarma i propuštene detekcije u zavisnosti od SNR, gde su korišćeni isti parametri za vremensko-frekvencijske metode kao i kod modelovanih signala. Dobijeni rezultati su veoma slični u odnosu na slučaj analize modelovanih signala prikazanih na Sl. 1. Dobijene vrednosti za verovatnoću propuštene detekcije su gotovo identične u slučaju modelovanih i realnih signala. Kod verovatnoće pojave lažnog alarma, korišćenjem PWV, za više vrednosti SNR u odnosu na modelovani signal, dostiže se verovatnoća bliska jedinici. Spektrogram i S-metod za niske vrednosti SNR dostižu vrednosti verovatnoće lažnog alarma oko 0.4, što je nešto više nego kod modelovanog signala. Na ovu razliku utiče i šum koji se javio tokom snimanja signala. I na ovoj slici strelica pokazuje smer povećanja praga detekcije.

Sl. 4 ilustruje odnos verovatnoće propuštene detekcije u odnosu na verovatnoću lažnog alarma, za prozor dužine 128 odbiraka uz 50% preklapanja, SNR=-8 dB i za različite vrednosti praga detekcije u istom opsegu kao i kod modelovanih signala. Dobijene krive su veoma slične kao pri analizi modelovanih signala, uz neznatno više vrednosti verovatnoća lažnog alarma i propuštene detekcije u slučajevima primene spektrograma i S-metoda. Primenom PWV ostvarena je mala verovatnoća propuštene detekcije, čime će se postići neometan rad primarnog korisnika.

Na Sl. 5 dat je uporedni prikaz vremensko-frekvencijskih distribucija realnih i simuliranih signala. Slike su prikazane za slučaj kada je SNR=-8 dB, prag detekcije postavljen na 50% amplitude primarnog signala, a broj odbiraka za analizu spektra je 128 uz polovinu odbiraka koji se preklapaju u sledećem intervalu analize. Na slikama je prikazan samo deo vremena signala, u trajanju od oko 100 ms, zbog preglednosti. Sa slika se jasnije uočavaju promene frekvencija nakon određenog vremena korišćenjem spektrograma i S-metode, bilo da su u pitanju modelovani ili realni signali, uprkos niskoj vrednosti SNR. Korišćenjem PWV, uprkos većoj rezoluciji, zbog pojave međuspektralnih komponenti, energija signala je rasuta i ne mogu se uočiti tačne frekvencije signala


ISBN 978-86-7466-930-3

tokom određenih vremenskih perioda. Iz tog razloga je češća pojava lažnih alarma kod PWV nego kod spektrograma i S-metode. Nešto kvalitetnija rezolucija za isti period prikaza signala dobijen je kod modelovanog signala zbog veće frekvencije odabiranja prilikom generisanja signala u odnosu na frekvenciju odabiranja prilikom snimanja realnih signala. Kod modelovanih signala, uočavaju se dve noseće frekvencije u zavisnosti od poslatog simbola, u toku jednog skoka zbog korišćenja BFSK modulacije.

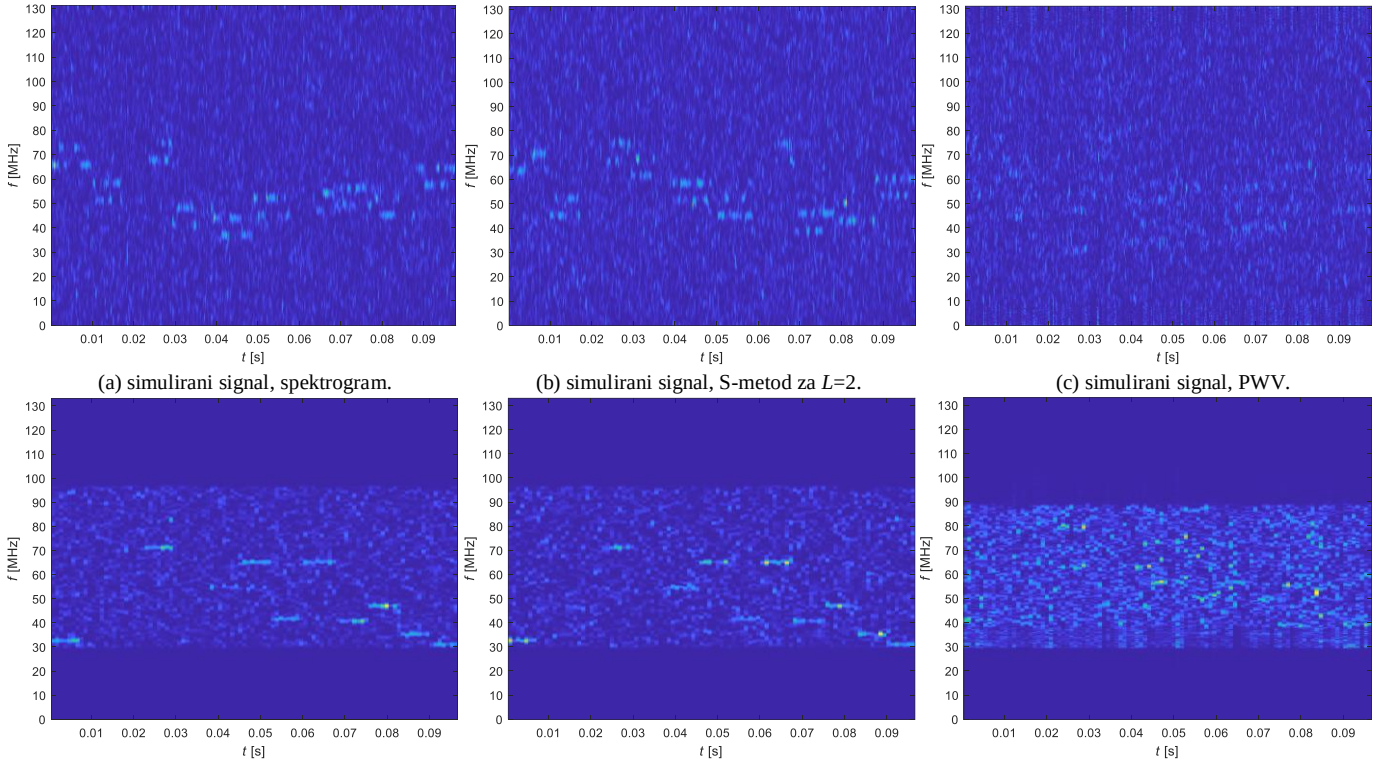


(a) simulirani signal, spektrogram. (b) simulirani signal, S-metod za $L$=2. (c) simulirani signal, PWV.

(d) realni signal, spektrogram. (e) realni signal, S-metod za $L$=2. (f) realni signal, PWV.

Sl. 5. Vremensko-frekvencijski prikaz simuliranog i realnog signala za SNR = -8 dB.

## VI. Zaključak

U radu je izvršena analiza mogućnosti upotrebe tri metode vremensko-frekvencijske analize signala kognitivnog radija prilikom analize spektra. Za potrebe analize, metode su testirane na modelovanom signalu i snimljenom realnom signalu frekvencijskog skakanja.

Utvrđeno je da dobre performanse za potrebe analize spektra kod kognitivnog radija pokazuje pseudo Vigner-Vil zbog veoma male verovatnoće propuštene detekcije. Ipak, zbog svoje računarske složenosti nije pogodan za implementaciju u sistemima koji za cilj imaju rad u realnom vremenu. Spektrogram je pokazao performanse koje bi bile zadovoljavajuće uz određenu optimizaciju pre svega u broju odbiraka korišćenih za analizu spektra, jer je moguće postići male verovatnoće propuštene detekcije uz male verovatnoće lažnog alarma, čime bi se pored efikasne analize spektra uspešno mogla odvijati i emisija kognitivnog radija. S-metod je metoda koja bi mogla biti dodatno istražena i testirana, radi optimalnog izbora parametra $L$ u cilju dostizanja male verovatnoće propuštene detekcije i male verovatnoće lažnog alarma kod nepovoljnog odnosa signal/šum, čime bi se postigla visoka verovatnoća ispravne detekcije kao kod pseudo Vigner-Vila i što niža računarska efikasnost kao kod spektrograma, što su i ciljevi daljeg istraživanja. Pokazano je da se adekvatnim modelovanjem može realizovati pogodno testno okruženje radi utvrđivanja performansi vremensko-frekvencijskih metoda analize signala.

U budućem radu planirana je implementacija predložene metode analize spektra na hardversku platformu softverski definisanog radija sa akcentom na optimalan izbor parametra $L$ kod S-metode. Dalje unapređenje analize spektra je moguće tako što će se nakon detekcije vršiti analiza karakteristika detektovanog signala sa karakteristikama očekivanog signala u cilju klasifikacije.

## Zahvalnica

Ovo istraživanje je deo projekta VA-TT/3/20-22, podržanog od strane Ministarstva odbrane Republike Srbije.

## Literatura

[1] G. Staple, K. Werbach, “The end of spectrum scarcity [spectrum allocation and utilization],” *IEEE Spectrum*, vol. *41*, no. *3*, pp. *48-52*, 2004.

 ISBN 978-86-7466-930-3

[2] I. F. Akyildiz, W. Y. Lee, M. C. Vuran, S. Mohanty, "A survey on spectrum management in cognitive radio networks," *IEEE Communications Magazine*, vol. *46*, no. *4*, pp. *40-48*, 2008.
[3] J. Mitola and G. Q. Jr. Maquire, "Cognitive Radio: making software radios more personal," *IEEE Personal Communications*, vol. *6*, no. *4*, pp. *13-18*, 1999.
[4] FCC-03-322, "Facilitating opportunities for flexible, efficient, and reliable spectrum use employing cognitive radio technologies," ET Docket, No. 03-108, December, 2003.
[5] M. Jaiswal, A. K. Sharma, V. Singh, "A survey on spectrum sensing techniques for cognitive radio," *Conference on Advances in Communication and Conrol Systems 2013*, pp. *647-660*. IEEE. 2013.
[6] M. Subhedar, G. Birajdar, "Spectrum sensing technique in cognitive radio networks: A survey," *International Journal of Next-Generation Networks*, vol. *3*, no. *2*, pp. *37-51*, June 2011.
[7] T. Yücek, H. Arslan, "A survey of spectrum sensing algorithms for cognitive radio applications," *IEEE Communications Surveys & Tutorials*, vol. *11*, no. *1*, pp. *116-130*, 2009.
[8] B. Boashash, *Time-frequency signal analysis and processing*, Elseiver LTD, 2016.
[9] W. Guibene, A. Hayar, "Joint time-frequency spectrum sensing for cognitive radio," In *International Symposium on Applied Sciences in Biomedical and Communication Technologies (ISABEL 2010)*, pp. *1-4*. IEEE. 2010.
[10] S. Monfared, A. Taherpour, T. Khattab, "Time-frequency compressed spectrum sensing in cognitive radios," In *Global Communications Conference GLOBECOM 2013*, pp. *1088-1094*. IEEE. 2013.
[11] F. Javed, A. Mahmood, "The use of time frequency analysis for spectrum sensing in cognitive radios," In *4-th International Conference on Signal Processing and Communication Systems*, pp. *1-7*. IEEE. 2010.
[12] S. M. Hiremath, S. K. Patra, A. K. Mishra, "Hard-combined cooperative spectrum sensing using time-frequency method," *In 5th International Conference on Wireless Communications, Vehicular Technology, Information Theory and Aerospace & Electronic Systems*, Hyderabad, India, 13-16. December 2015.
[13] D. Torrieri, *Principles of spread-spectrum communication systems*, Springer 2015.
[14] J. Bajčetić, D. Mikluc, "Novel method in robust radio communication emission classification," *Proceedings of the 8th Small Systems Simulation Symposium 2020*, pp. *111-116*. Niš, Serbia, February 12-14, *2*020.
[15] Lj. Stanković, M. Daković, T. Thayaparan, *Time-frequency signal analysis – with applications*, Artech House, 2013.
[16] D. Bujaković, M. Andrić, B. Bondžulić, S. Mitrović, S. Simić, "Time-frequency distribution analyses of ku-band radar Doppler echo signals," *Frequenz*, vol. *69*, no. *3-4*, pp. *119-128*, 2015.
[17] T. Thayaparan, Lj. Stanković, I. Đurović, "Micro-Doppler-based target detection and feature extraction in indoor and outdoor environments," *Journal of the Franklin Institute*, vol. *345*, no. *6*, pp. *700-722*, 2008.
[18] Lj. Stanković, "A measure of some time-frequency distributions concentration," *Signal Processing*, vol. *81*, no. *3*, pp. *621-631*, 2001.

ABSTRACT

The paper analyzes the application of three time-frequency signal analysis methods for spectrum sensing in cognitive radio. The analysis was performed based on simulated and real signals for additive white Gaussian noise of different signal-to-noise ratios. The performance of the methods is analyzed through changes in the signal to noise ratio and the detection threshold, determining the probability of false alarm, the probability of missed detection and the probability of correct detection. It is shown that the methods of time-frequency signal analysis can be efficiently used for spectrum sensing with appropriate parameter optimization.

## Spectrum Sensing in Cognitive Radio Using Time-Frequency Signal Analysis Tools

Nenad Stojanović, Milenko Andrić, Dimitrije Bujaković, Boban Bondžulić, Vladimir Ristić

 ISBN 978-86-7466-930-3

# ELECTRONICS
# /
# ЕЛЕКТРОНИКА
# (ELI/ЕЛ)

ISBN 978-86-7466-930-3

# A Gigabit Ethernet Media Access Controller for TCP/UDP Radar Data Streaming and Visualization

Vukan D. Damnjanović, *Student Member, IEEE*, and Vladimir M. Milovanović, *Senior Member, IEEE*

***Abstract*—A design of a gigabit Ethernet media access controller implemented using Verilog hardware description language is depicted in this paper. The proposed digital hardware module can be utilized for establishing client-server connections over a computer network with a PC, an FPGA-based board or some other separate piece of hardware. It allows users to perform network data transfers using either TCP or UDP communication protocols, in both directions. Data is transmitted to or received from a predefined Internet Protocol address utilizing packets of predefined size, in a format suitable for the corresponding protocol, with a packet header providing the receiving end with the information about the packet itself. The described design is able to achieve network throughput rates that exceed 110 MB/s making it suitable for systems and applications that require high-speed data streaming, such as the system for radar data streaming and PC visualization depicted in the latter part of the paper. Besides that, it can be used in a wide range of applications developed on systems containing boards and devices with the Ethernet 8P8C port as an integral part. The implemented design has been thoroughly tested using a combination of a commercial FPGA development kit and the PC-run Python applications. It was verified and confirmed that the design meets the expectations regarding both the specified functionality and performance.**

***Index Terms*—Gigabit Ethernet MAC, data streaming, UDP and TCP protocols, PC data visualization, Verilog hardware description language.**

## I. Introduction

During the last couple of decades, there is a growing trend for the amount of different devices used in the systems and applications in practically all the spheres of the IT industry. The same also applies for the systems used for collecting data, such as some sensor-based systems or radar systems. They are becoming more complex, consisting of more devices with more information needed to be carried. Whether it is because of the insufficient available resources, some environmental limitations, inappropriate system topology or something else, the data-collecting devices are often unable to perform the complete cycle of information extraction, processing and utilization relying only on themselves. Therefore, at some point of the cycle, it is necessary that the data is transferred to another device (or devices) so the system can work properly and fulfill its purpose. In most cases, those devices are PCs, due to their abilities and versatility.

Vukan D. Damnjanović is with the School of Electrical Engineering, University of Belgrade, Bulevar kralja Aleksandra 73, 11120 Belgrade, Serbia and also with NOVELIC d.o.o., Veljka Dugoševića 54/B5, 11060 Belgrade, Serbia (e-mail: vukan.damnjanovic@novelic.com).

Vladimir M. Milovanović is with the Department of Electrical Engineering, Faculty of Engineering, University of Kragujevac, Sestre Janjić 6, 34000 Kragujevac, Serbia (e-mail: vlada@kg.ac.rs).

The need for these data transfers is especially emphasized on the distinguished group of systems - real-time systems, where the information acquirement, extraction and/or presentation is performed constantly at relatively high rate [1]. That implies that the data transfers from one platform to the other needs to be performed in the same manner. The amount of data that needs to be transferred and the transfer rate differ from system to system and can vary significantly, which includes some large numbers as well.

In order to achieve the ability of performing these transfers, a vast number of mechanisms have been developed during the years. They can rely on different technologies and all of them have their advantages and disadvantages. Among the most common and popular ones is definitely Ethernet [2].

Ethernet is, technically speaking, a family of wired computer networking technologies, but it usually refers to the most common type of Local Area Networks (LANs) - a connected network of computers (or, to be more precise, devices) in a small area[1]. Devices possessing the Ethernet port and connected through it to the network are able to perform data transfers with other connected devices by following the series of standardized protocols and rules [3]. Ethernet has been developing and improving during the years. It is currently one of the fastest communication technologies.

Computer networks using Ethernet consists of several abstraction layers [4]. In order for the whole mechanism to work correctly, rules for each one of them have to be applied. Following those rules is often managed by some kind of the processing unit, in devices that poses one, but in ones that do not, such as an FPGA-based board, it might be challenging to achieve the flawless operation of the system. The gigabit Ethernet media access controller from this paper's topic is created so that the Ethernet ports can be utilized for preforming data transfers without engaging any kind of processing unit.

This paper, in its first part, gives the quick overview of the data streaming protocols used in the gigabit Ethernet media access controller module, as well as the detailed description of the module's design, along with the description of its implementation using Verilog Hardware Description Language (HDL). In the second part of the paper, obtained testing results and performances are provided with the example of one of the systems which the module was tailored for in the first place.

[1]Computer networks is a large field in network sciences and a lot could be written about it, but the information provided is sufficient for the comprehension of the content of this paper.

 ISBN 978-86-7466-930-3

## II. A Gigabit Ethernet Media Access Controller and Data Transfer Protocols

A gigabit Ethernet media access controller is a digital component which allows the user to perform data transfers between itself and some other module or device. Basically, the implemented module allows the user to send and receive the data to and from the specified address on the network belonging to some other device. In order for it to work properly, the module requires that the Ethernet port along with the gigabit Ethernet transceiver exist on the device. It is used to set up the transceiver for working in the appropriate mode at the beginning of the application and then to send (or receive) data through the Gigabit Media-independent interface (GMII) to the transceiver [5] and through the port to the network and the rest of the system. Data is fragmented and transferred in packets, where every packet is of the same length and consists of a header and data itself.

### A. Ethernet Abstraction Layers

Currently, two different versions of this module exist: one that supports transfers (receive and transmit) using Transmission Control Protocol (TCP) [6] and another that supports transfers using User Datagram Protocol (UDP) [7]. Those two protocols are parts of the Ethernet transport layer, one of the abstraction layers mentioned in the previous section. This layer provides the end-to-end communication services for applications. This module also secures that the device is working in accordance with two other abstraction layers: link layer, which provides the link to a physical connection of the host, and internet layer, which serves as a bridge between link and transport layer [4]. The fourth and final layer - application layer, can be implemented on the PC or on some other device.

The controller module implements the network link layer by applying the Address Resolution Protocol (ARP) [8]. It sends a message in the appropriate format that provides the physical MAC address of the Ethernet port when another device on the network asks for it.

The internet layer regulates that every message or packet in the network end up at the appropriate destination. The primary protocols for the internet layer are the Internet Protocol (IP). This protocol assigns an IP address to every device on the network, which allows a packet to find its way to the destination. The implemented module utilizes the IP protocol version 4 (IPv4).

The Ethernet transport layer, as mentioned before, is implemented using either TCP or UDP protocol. This layer provides services to the network, such as connection-oriented communication, reliability, flow control etc.

### B. TCP and UDP Protocols

TCP is a more complex protocol than UDP. It is connection-oriented with built-in systems checking for errors and guaranteeing that data will be delivered in the order it was sent. The connection firstly needs to be established, then maintained, and finally terminated, making it a more reliable protocol. All of this, however, requires larger overheads in data packets, which reduces its speed and efficiency. On the other hand, UDP is a simpler, connectionless protocol, faster and more efficient, but it does not provide any recovery options when a data error occurs or when a packet is lost [1].

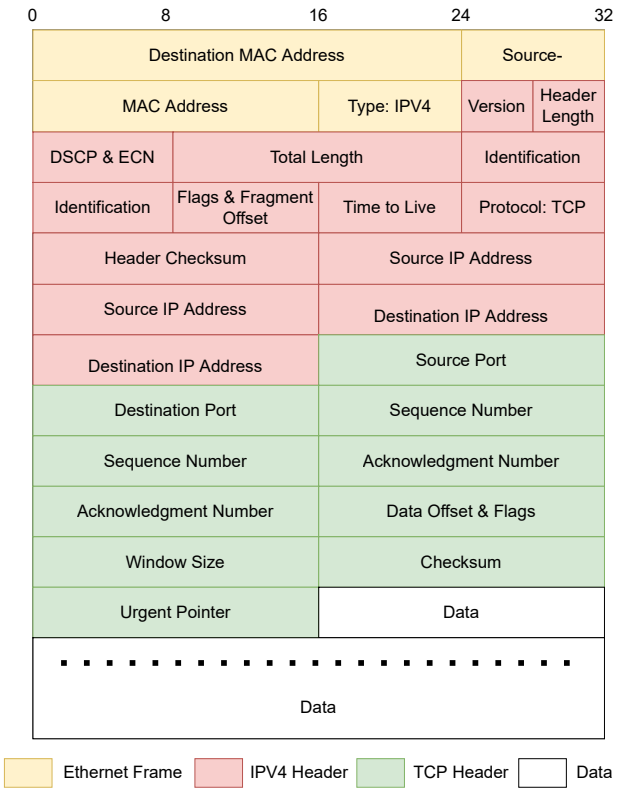


Fig. 1. A structure of data packets of the TCP protocol used in the design.

A structure of data packets of the TCP protocol used in the design is shown in Fig. 1. This type of format allows three network layers to be implemented: the link layer implementation is marked in yellow, the IPv4 header representing the internet layer is marked in red and the TCP header, as a part of the transport layer is marked in green [9]. The link layer carries the information about MAC addresses and the used IP protocol. The IPv4 header has the fields for various information, such as the IP addresses, packet identification number, packet length, header length, used transport layer protocol, the IPv4 header checksum value etc. The TCP header, besides the port numbers, holds the information necessary for establishing, maintaining and terminating the TCP connections, detecting and recovering from errors, flow controlling etc.

The main fields for enabling the TCP to have the connection-oriented communication are sequence number, acknowledgment number, flags and checksum. The sequence number is a 32-bit wide field that carries the number that identifies the first data octet in the packet. The acknowledgment number is also a 32-bit wide field, and it represents a response from the receiving end. It has the value of the next expected sequence number. If the first packet that has


ISBN 978-86-7466-930-3

arrived had the sequence number of 1 and the N bytes of data have arrived, then the acknowledgment number in the response would be $1 + N$. This mechanism ensures that the order of the received packets is preserved and that there is no packet or data missing. The flag fields have the purpose to indicate that some functionality is being used. There are six flags in total indicating different things: URG - the urgent pointer field is significant, ACK - the acknowledgment number field is significant, PSH - push functionality, RST - reset the connection, SYN - synchronize sequence numbers, FIN - no more data from sender. Basically, to run a TCP connection, only three flags are needed: SYN flag for establishing it, FIN flag for terminating it and ACK flag for acknowledging every received data packet during the connection's life. The checksum field is used for detecting if there is an error in the received data. It has a width of 16 bits, and it is the 16 bit one's complement of the one's complement sum of all 16 bit words in the header and text (only the TCP header and some field of the IPv4 header are included).

In Fig. 2, a diagram that depicts establishing, maintaining and terminating a TCP connection between a client and a server is shown. A client is called a device that initiates the connection and a server is a device that accepts it. Even though it is more usual for the server to send data and for the client to accepts it, it is the other way around in the example shown in Fig. 2. The client initiates the connection by sending a packet with the SYN flag active. The server responds with SYN and ACK flag, which the client acknowledges. At that point, the connection is established. The client then sends N bytes of data in each one of X sent packets, and the server responds for every packet received. Note that it is not necessary for the server to respond to every packet individually. It could also wait for all the packets to arrive and then to acknowledge the reception of them by sending the final acknowledgment number along with the ACK flag. After all the packets are sent, the client expresses the wish to end the communication, which the server accepts and the connection is then terminated.

The UDP data packet structure used in the design is similar to the one used for the TCP protocol. In fact, the only thing that differs is the transport layer protocol header. As mentioned before, the UDP does not provide the possibility of connection-oriented communication, flow control etc. so the UDP header has fewer fields than the TCP header. It only carries the information on the port numbers, packet length and the checksum value. The UDP protocol does not support or require the acknowledgement of the received packets. It straight-forwardly goes to the formation of the following packet, after the previous one has been sent.

## III. The Implementation of the Controller

Previously depicted gigabit Ethernet media access controller have been implemented using Verilog HDL. Its design has been thoroughly tested using standard verification and implementation paths for FPGA design flow. The design is made available [10] by the authors for public use as a free and open-source hardware library.

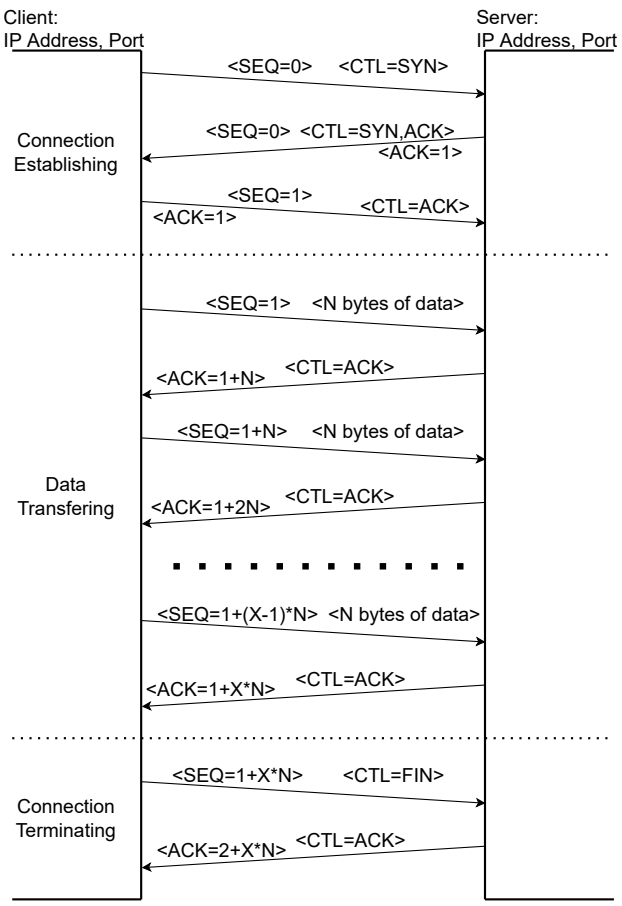


Fig. 2. A diagram that depicts establishing, maintaining and terminating a TCP connection between a client and a server.

The implemented design of the gigabit Ethernet media access controller is relatively complex. It can be divided into several mutually connected submodules, with some of them communicating with the outer world as well, through one of the module interfaces. A block diagram of the module with its submodules and interfaces is depicted in Fig. 3. In this section, descriptions of every individual submodule, implemented interfaces to the outer world and the way the module communicates with other devices will be provided.

### A. Design Interfaces

As it can be seen from Fig. 3, the implemented gigabit Ethernet media access controller has four interfaces. The first one is the AXI Stream interface. The purpose of this interface is to continuously collect data needed to be sent between the devices on the network. The direction of the interface can be both input and output, depending on the fact whether the module is receiving data from some other device, or sending it to the network. The second interface of the implemented module is the AXI4 memory-mapped interface. This interface is used to write values to the memory-mapped configuration registers of the controller, as well as to read status values from it. The next interface is the Reduced

 ISBN 978-86-7466-930-3

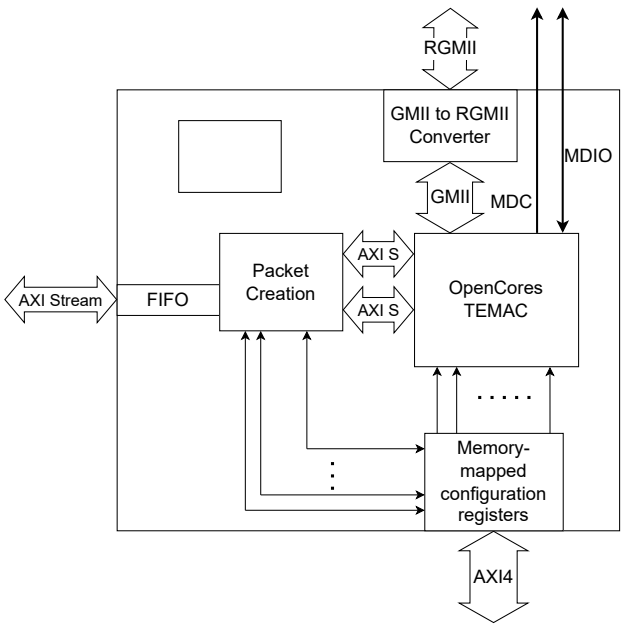


Fig. 3. A block diagram of the implemented module with its submodules and interfaces.

Gigabit Media-independent interface (RGMII), a version of the already mentioned GMII interface. Its role is to communicate with the Ethernet physical layer transceiver that controls the Ethernet port. The last interface is the Serial Management Interface (SMI), also known as Media-Independent Interface Management (MIIM). It is a serial interface used for configuration of the Ethernet physical layer transceivers. In the following paragraphs, the functionality and implementation of every submodule of the controller design will be described.

### *B. Design Clock Domains*

The whole design can be divided into four clock domains. The frequency of the input clock equals 100 MHz, and it drives the clock generator block that creates all other clocks in the module. These four clock domains are the user clock domain, the RGMII physical layer clock domain, the MIIM management interface clock domain and the AXI4 memory-mapped clock domain. The RGMII physical layer clock domain operates at the frequency of 125 MHz, and it is the only mandatory value for all the clock frequencies in the design. The frequency of the MIIM clock domain clock is run-time configurable. Its value depends on the value stored in one of the memory-mapped registers, and it equals the value of the AXI4 memory-mapped clock frequency divided by the register value. The MIIM clock frequency must not exceed 2.5 MHz. The AXI4 memory-mapped clock frequency is the frequency on which the memory-mapped configuration registers and the AXI4 bus operate. It has to be equal to the frequencies of the other memory-mapped devices connected to the bus, and in this version of the design it equals 10 MHz.

### *C. Design Submodules*

The OpenCores Tri-mode Ethernet Media Access Controller (TEMAC) is one of the most important submodules in the design. It is a modified version of an open-source controller downloaded from the OpenCores website [11]. The module has a ”Tri-mode” phrase in its name because, apart from being a gigabit controller, it can also operate as a 100-megabit or 10-megabit. However, in the proposed design, it is utilized solely as a gigabit version. The TEMAC module has several functionalities and five interfaces: an output and an input AXI Stream interfaces, a GMII interface, a MIIM interface and an input interface that provides the module with the memory-mapped register data. Its main function is to convert streaming data-to-be-sent from the input streaming native interface to the output GMII interface and data-to-be-accepted from the input GMII interface to the output streaming native interface. These two native interfaces are converted to the AXI Stream interfaces using the submodule wrapper. For these GMII-to-Stream conversion processes, the module instantiates two dual port block RAMs to serve as asynchronous FIFOs for getting the data from both sides. The finite-state machines (FSMs) control the flow for both directions, from 32-bit streaming data synchronized on the user clock, to 8-bit GMII data synchronized on the GMII clock (or vice versa). The submodule and the exact way it will operate can be set up by reading the input values from the memory-mapped configuration registers. Depending on some of those values, it also generates the MIIM signals for the Ethernet physical layer transceiver configuration.

The GMII to RGMII converter adapts the GMII interface signal to the needed RGMII interface signal. Basically, the RGMII signals are used instead of the GMII signals in order to reduce the number of the occupied output pins. Total number of utilized output pins is halved (12 instead of 24). It is achieved by running half as many data lines at a double speed, time multiplexing the signals and by eliminating non-essential signals. Output pins operate with double data rate (DDR) instead of single data rate (SDR), with the same clocking frequency of 125 MHz. Receiving pins are synchronized to the external clock provided by the Ethernet physical layer transceiver, while transmitting pins are synchronized to the internally generated clock. The clock generating block creates two different 125 MHz clocks with the 90 degrees phase difference, one for the output clock pin itself and the other for the synchronizing of the data and control lines, so that the setup and hold times of the output DDR pins are as large as possible.

The memory-mapped configuration registers module is a submodule whose function is to be accessible from the AXI4 interconnect bus and the rest of the system through the AXI4 memory-mapped interface and to provide the rest of the submodules inside the controller with the written values. It also has a task to inform the OpenCores TEMAC submodule to generate the signals in the MIIM interface. It has numerous registers and here are the most important ones:

 ISBN 978-86-7466-930-3

- `Physical address` - Value of the address of the Ethernet physical layer transceiver.
- `No preamble` - Indicator whether the transmitting packets will have the preamble to precede them.
- `Clock divider` - Value used to calculate the frequency of the MIIM interface clock.
- `Packet size` - Number of bytes in one data packet, can be up to 1500.
- `PHY data` - Data value to be written to one of the Ethernet transceiver registers.
- `PHY register address` - Register address inside the Ethernet transceiver to which data will be written.
- `PHY write enable` - Indicator that a write operation should be performed through the MIIM interface.

The packet creation submodule is responsible for implementing all the network abstraction layers and protocols in the design. This submodule has several tasks in its jurisdiction. It wraps the data arrived from the streaming interfaces with the appropriate header and calculates all the values for the header fields. It also accepts data packages arrived from the network and checks if they are addressed to this module and creates and sends the response if it is needed. IP addresses, MAC addresses and port numbers for both the client and the server side in this design are hard-coded. For both TCP and UDP versions of the module, this submodule always checks if there is an ARP request sent to the network. If the asked IP address is the one belonging to this module and the ARP format of the message is correct, an ARP response packet is created and sent providing the information about this module's MAC address. Creation of the UDP packets is not too complicated, considering that every field of the header except the identification field is a constant value. The packet creation submodule receives the streaming data and forwards it to the OpenCores TEMAC submodule, except for the occasions when the previous packet has ended and when the header fields are needed to be sent. The end of packet is indicated by sending the active high value for the AXI Stream data last signal.

The situation for the TCP version of the design is a bit more complex. The creation of the header is not as straight-forward as in the UDP version, and the communication between the devices on the network is more complicated. The packet creation submodule calculates the value for several fields for every sent packet, such as the sequence and acknowledgment number, checksum value, flags etc. When the application starts, it sends the synchronization request packet, as depicted in Fig. 2. Then it waits for the response and acknowledges it if the response has the appropriate form and values, and starts creating data packets and streaming data. At the end of the application, it waits for the data acknowledgment message, and then it terminates the connection as described in the previous section.

## IV. Testing Results and Streaming Radar Data Visualization Example

In this section, the design testing flow will be presented. During these tests, the functionality of the design was verified,

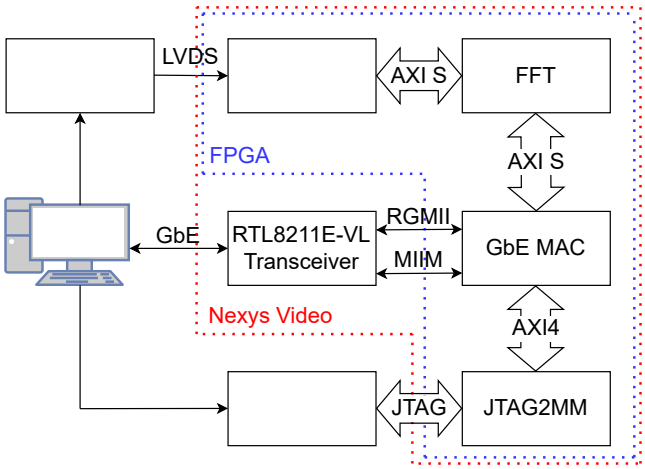


Fig. 4. A simplified block diagram of the complete radar data PC visualization system.

performances and resource utilization were measured, and the design validity is shown as it is used in the example system for radar data visualization. The first step in the design testing flow were the software simulations in the form of the testbench files written in Verilog and VHDL languages.

The next step is the implementation and verification of the design on an FPGA-based development board. A Digilent's Nexys Video board with Xilinx Artix-7 FPGA family is used for it. Nexys Video development board has the Realtek RTL8211E-VL Gigabit Ethernet Transceiver [5] as an integral part of it, making it suitable for the depicted design. For the design testing, some additional features were needed. An open-source JTAG-to-memory-mapped bus master bridge [12] for accessing the memory-mapped register space was used. An alternative for it can be Xilinx's JTAG-to-AXI4 Master module [13]. Write data transactions through AXI4 memory-mapped interface are initiated from the PC using the Python PyFTDI library and the FTDI's cable containing the FT232H chip [14]. Also, a server was run on the PC in order to generate responses for the arrived packets and to send data to the board. For running the server, Socket Python library was used. The arrived packets can be verified by utilizing software for the network packet monitoring, such as Wireshark [15]. Moreover, packets with previously defined data were sent from the board and checked on the PC using Pyhton scripts, therefore proving the correctness of the proposed design. All the examples and testing systems presented in this paper use 1066-byte long packets (52 bytes for the header and 1024 data bytes).

During the hardware implementation testing, data throughput measurements were done. It was proven that the design meets the performance expectations with the maximal data throughput of around 110 MB/s for both TCP and UDP design versions, making it around 90% of theoretically ideal value of 125 MB/s or 1 Gb/s. The resource utilization is moderate, but with less than 10% utilization for all the resource types and with the possibility to reduce it even more.


ISBN 978-86-7466-930-3

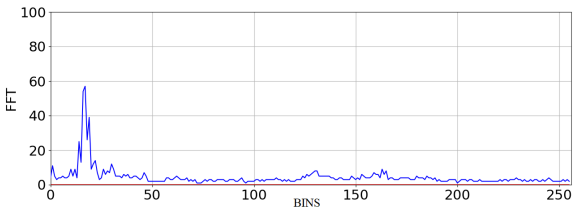


Fig. 5. An example of the radar data plot using Python libraries.

### A. Streaming Radar Data Visualization Example

The implemented design of the gigabit Ethernet media access controller, due to the extensive usage of computer networks and its functionality, could find its way into a wide range of different systems. In this subsection, a system for the TCP radar data streaming and PC visualization, one of the mentioned example systems, will be presented.

A simplified block diagram of the radar data visualization system is given in Fig. 4. The system is used to continuously collect data from the radar board, have the incoming streaming data processed (fast Fourier transformation) on the FPGA-based development board, and send it using the gigabit Ethernet to the PC, where the arrived data is plotted. The PC is showing the live display of the distance between the radar board and the detected targets. An example of such a display can be seen in Fig. 5. It should be emphasized that all the processing and data transferring is realized completely in hardware, without involving any kind of processing unit.

For the radar board, Texas Instruments' AWR2243 BOOST [16], along with the MMWAVE-DEVPACK and FMC-ADC-ADAPTER, is chosen. The output is in the form of the Low-Voltage Differential Signaling (LVDS) lines [17] containing radar data, clock and frame clock. Those LVDS lines are connected to the FPGA pins on the Nexys Video board, and they are received and converted to the 32-bit AXI Stream interface. The logic behind this conversion is not relevant for the matter and therefore not elaborated. The AXI Stream data is then driven to the input of the open-source fast Fourier Transformation processor module [18] available to simultaneously perform the processing and stream the output data to the gigabit Ethernet media access controller from the topic of this paper. The TCP packets are created there and sent to the PC through the gigabit Ethernet, where there is a Python script running the server and receiving and plotting data acquired from the Ethernet port using the Python's Matplotlib library. The radar board is previously configured using the MMWAVE Studio software [17] for the PC and the USB interface, as is the gigabit Ethernet MAC module using the JTAG-to-memory-mapped bus master bridge, depicted in the previous section.

## V. Conclusion

In this paper, a design of the gigabit Ethernet media access controller for the UDP and TCP data streaming implemented using Verilog HDL is proposed. This module can be used in a wide range of different systems, due to the nowadays' constant presence of the computer networks in many industrial spheres. One of those systems, or the system for the processed radar data PC visualization to be more precise, is depicted in this paper as well.

The generated instances of the JTAG to memory-mapped bus master bridge were tested and verified by both using software simulations and mapping onto a commercial FPGA development board, proving the correct functionality of the design. The hardware implementation also proved the competitiveness of the design in terms of performances, having the data throughput of over 110 MB/s.

It should be noted that this is only the first version of the design, and there is still a lot of space for improvement and for broadening the functionality of the module. Making it more parameterizable, completely run-time configurable, having better mechanisms to recover from data loss or error etc. are just some of the things that could be and hopefully will be improved in some future versions.

## Acknowledgements

The authors would like to thank NOVELIC d.o.o. for financially and logistically supporting the work on this project.

## References

[1] S. Tibor, P. Dukán, B. Odadžíc, and O. Péter, "Realization of reliable high speed data transfer over udp with continuous storage," in *2010 11th International Symposium on Computational Intelligence and Informatics (CINTI)*, 2010, pp. 307–310.
[2] *The Ethernet*. Digital Equipment Corporation, Intel Corporation, Xerox Corporation, 1982, a Local Area Network, Data Link Layer and Physical Layer Specifications.
[3] V. Cerf and R. Kahn, "A protocol for packet network intercommunication," *IEEE Transactions on Communications*, vol. 22, no. 5, pp. 637–648, 1974.
[4] I. E. T. Force, "Requirements for internet hosts – communication layers," in *RFC*, October 1989.
[5] *Integrated 10/100/1000M Ethernet Transceiver*, version 1.6 ed., Realtek, April 2016, track ID: JATR-3375-16.
[6] "Transmission control protocol," in *RFC*. Information Sciences Institute, University of Southern California, 1981, no. 793.
[7] J. Postel, "User datagram protocol," in *RFC*, 1980, no. 768.
[8] D. C. Plummer, "An ethernet adress resolution protocol," in *RFC*, 1982, no. 826.
[9] W. Zhang, Z. Wei, X. He, P. Qiao, and G. Liang, "The design of high speed image acquisition system over gigabit ethernet," in *2010 IEEE International Conference on Wireless Communications, Networking and Information Security*, 2010, pp. 111–115.
[10] V. D. Damnjanović and V. M. Milovanović, "Gigabit ethernet mac," www.github.com/milovanovic/gbemac, accessed: 2022/04/15.
[11] OpenCores, "Tri-mode ethernet mac," www.opencores.org/projects/ethernet_tri_mode/, accessed: 2022/04/15.
[12] V. D. Damnjanović and V. M. Milovanović, "A chisel generator of jtag to memory-mapped bus master bridge for agile slave peripherals configuration, testing and validation," in *2021 IcETRAN Proceedings*. ETRAN Society, Belgrade, 2021, pp. 239–244.
[13] *JTAG to AXI Master v1.2*, Pg174 ed., Xilinx, February 2021.
[14] *FT232H*, version 2.0 ed., FTDI, document No.: FT000288 Clearance No.: FTDI 199.
[15] U. L. R. Sharpe, E. Warnicke, *Wireshark User's Guide*, (version 3.7) ed.
[16] *AWR2243 Single-Chip 76- to 81-GHz FMCW Transceiver*, Texas Instruments, February 2020.
[17] *DCA1000EVM Data Capture Card*, Texas Instruments, May 2018.
[18] V. M. Milovanović and M. L. Petrović, "A highly parametrizable chisel hcl generator of single-path delay feedback fft processors," in *2019 IEEE 31st International Conference on Microelectronics (MIEL)*, 2019, pp. 247–250.

 ISBN 978-86-7466-930-3

# ANN model for one day ahead Covid-19 prediction

Jelena Milojković, Miljana Milić, and Vančo Litovski

*Abstract*— **One-day-ahead prediction of number of COVID-19 infected patients is presented in this paper. The study is relying on the data available in [1]. A model of artificial neural network (ANN) was developed and used with only the most recent data taken into account. We believe that only a few data from the near past is important for this type of prediction. ANNs have been proven as a very reliable method for the real time prediction systems. In our previous work in prediction electricity consumption [2] and traffic prediction [3], we obtained small prediction error. That encouraged us to conduct the research described in this work. The absence of the trend and the seasonal component in the given time series, made the prediction task more difficult. However, we have obtained good results, which could encourage the application of the model in health management to make better decision in control and prevention of the occurrence of a pandemic.**

***Index Terms*—Covid-19, number of infected, artificial neural network, short-term prediction.**

## I. Introduction

Global pandemic, named COVID-19, created his first wave of infection in China in the Wuhan province [4]. It has started in December 19 and continued to the present days. By the World Health Organization (WHO), the virus has affected populations worldwide, and its rapid spread is a universal concern. The high rate of spread as well as the high chance of transmission is still not effective, even with engaging all recommended prevention and implemented control strategies (isolation, detection tests and prophylactic measures). They still have limited effect in preventing or stopping the spread of the virus worldwide [5]. Since its first reporting at the end of December 2019. until 28.04.2022, over 508 million people have been infected, around 500 million people recovered, and 6 227 291 people died due to pandemic [6]. Basic and most important fact of COVID-19 is that it is spreading rapidly by a human-to-human transmission; where about 20% infected subjects are without symptom. The main characteristics of COVID-19 pandemics are high infection rate, incubation period, patients to be contagious during the incubation period, and symptomatic infection [7]. The elderly people and those who have weakened immune systems as well as people with special health conditions such as cancer, hypertension, severe asthma, cardiovascular disease, lung conditions, heart disease, diabetes, neurological conditions, HIV/AIDS infection, pregnancy and high weight are more vulnerable to the serious effects of this pandemic [8]. Based on this we can conclude that a global pandemic like Covid-19 has a high negative impact on the population health, social–cultural activities and global economy [9]. For this reason, it is necessary to develop models to predict the course of events during a pandemic outbreak. In our paper, we used ANN adapted to predict the number of infected on a daily basis. The developed model will help decision-makers, doctors and medical assistants to prepare and understand the magnitude of the risk and take appropriate measures to prevent major leaps. Forecasting tools can also help to assess the extent of risk in a timely manner and make the necessary preparations.

According to the research in the field of Covid-19 prediction by statistical methods, in order to achieve a satisfactory prediction, a basic prediction period of several hundred samples must be used [10, 11]. In the case when we have a set of data of several dozen samples, then time series is presented as a set of trends, random and seasonal components; these models also have a very limited number of parameters. In some cases, even some time series with a striking trend and seasonal component can be predicted with a smaller base period [12]. Actually, the amount of data available in this case is large enough to apply any other prediction method [13, 14, 15], but looking at a diagram curve representing the number of infected patients in one year, we easily recognize that past values of the infected patients are not very helpful when prediction is considered. Accordingly, we propose the problem of prediction of the infected case number in the next day to be performed as a deterministic prediction based on very short time series.

## II. Previous related work

The research in Covid -19 pandemic related with infected case number we describe here is based on our previous results in development and the application of ANN.

In our paper [16] we can see the evaluation of the idea about ANN structures dedicated to short term prediction. First, we will here briefly illustrate the development of two complex ANN structures, which started with a simple one-input-one-output feed-forward ANN.

We first got involved in the ANN based prediction when solving a problem of electronic waste management in Serbia [17]. It came out that there was no systematic way of forecasting the amount of electronic waste to be found in the literature. The main reason for that was the lack of data for a longer period in the past. That inspired us to start with the

Jelena Milojković, Miljana Milić and Vančo Litovski are with the Faculty of Electronic Engineering, University of Niš, Aleksandra Medvedeva 14, 18000 Niš, Serbia (e-mail: jelena.milojkovic@elfak.ni.ac.rs, miljana.milic@elfak.ni.ac.rs, vanco.litovski@elfak.ni.ac.rs).

 ISBN 978-86-7466-930-3

implementation of ANNs that are known as universal approximators. Namely, by using the ANN for approximation of a function represented by a set of equidistantly taken samples one automatically solves one of the biggest problems in approximation: the choice of the approximating function. Furthermore, ANNs are known as very successful interpolators which is frequently defined as a generalization property of ANNs. One had to investigate if ANNs could also extrapolate.

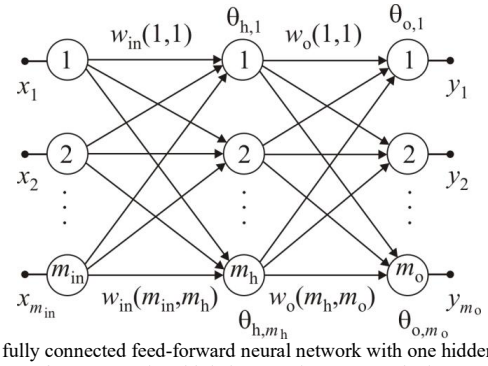


Fig.1. A fully connected feed-forward neural network with one hidden layer of neurons and multiple input and output terminals

This research was conducted in [18]. One fully connected feed-forward neural network is depicted in Fig. 1. To predict the amounts of electronic waste we have implemented a feed-forward ANN, named feed-forward accommodated for prediction - FFAP. The efficiency and good accuracy of the FFAP network inspired us to enter the problem of prediction for consumption of electrical power. There we were confronted with two types of periodicity (daily and weekly) where we have created new structure named Extended FFAP - EFFAP [19].

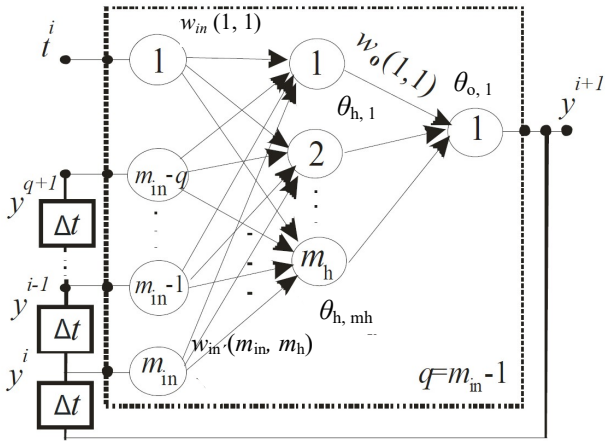


Fig. 2. Time controlled recurrent ANN - TCR

To improve the performance of the ordinary feed-forward ANN, in [20], we examined the capacities of time delayed ANN and evolved to a time controlled recurrent – (TCR) neural network depicted in Fig. 2. The prediction results obtained by the TCR ANN were equally good as those obtained by the FFAP ANN. That was confirmed in its application of prediction in microelectronics [21]. Using similar procedure to FFAP, we have formed a new structure named ETCR (Fig. 3). Two such ANN models we have also applied for prediction of electric power consumption and traffic [2, 3, 22].

## III THE METHOD

The basic neural network structure is shown in Fig. 1. It was proven that only one hidden can be sufficient for prediction problem [23] that is the subject of this research. In this figure input layer is denoted with “in”, hidden layer with “h”, and output layer with “o”. The set of weights, $w(k, l)$, connects the input and the hidden layer, where we have: $k$=1,2,..., $m_{in}$, $l$=1,2,..., $m_h$, while for the set that connects the hidden and output layer we have: $k$=1,2,...$m_h$, $l$=1,2,..., $m_o$. The threshold levels θ, are here designated with $\theta_{x,r}$, ($r$= 1, 2, …, $m_h$ or $r$= 1, 2, …, $m_o$), with $x$ standing for “h” for hidden or “o” for the output layer. The input layer neurons are only delivering the signals, and the hidden layer neurons are activated by a sigmoidal activation (logistic) function. At the end, the output layer neurons have a linear activation function. A variant of the steepest-descent minimization algorithm is applied during the ANN training [24].

To obtain the number of hidden neurons, $m_h$, a procedure based on proceedings given in [25] is applied. In prediction of time series, in that case, a samples dataset is available (acquired in every two hours) which means that only one input signal is enough, and that is the discretized time. According to equation (1) only one output value is predicted at a time, which means that only one output is required, too. Network’s output signals are consumed average power for a period of two hours.

For the implementation of the architecture in Fig. 1, (one input and one output terminal), the following time series would have to be learned: $(t_i, f(t_i))$, $i$=1,..., $m$.

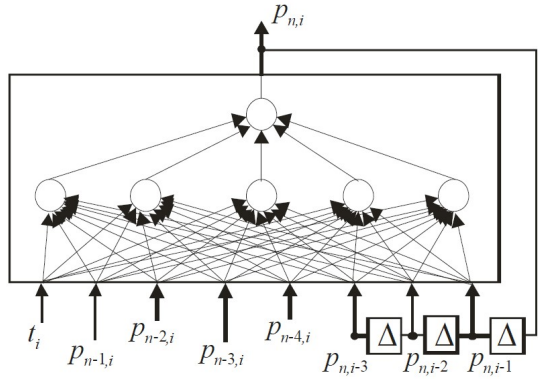


Fig. 3. ETCR. Extended time controlled recurrent ANN

To solve this problem, two new architectures were suggested as the possible solutions. They appeared to be the most convenient for the forecasting problem that is based on the short prediction base period [20]. However, these architectures had to be properly accommodated, due to the availability of data related to previous weeks.

The first network, referred to as a *time controlled recurrent* - TCR, Fig. 2 was derived from the basic time delayed recurrent ANN [26]. The structure has a recurrent architecture

 ISBN 978-86-7466-930-3

where time is the input variable, and it controls the predicted value. This structure is then extended, in order to allow that the values for the power consumption at a given time per day, and the values for the same days in three previous weeks, control the output. Consequently, the word *extended* had to be appended. The final architecture is depicted in Fig. 3, and is referred to as the Extended Time Controlled Recurrent (ETCR) architecture. It would be very useful to use the advantages of the ANNs' generalization property and the efficiency of the recurrent structure. This network learns a set in which the output value is controlled by the present time and its own previous instances of the average power consumption for a two hour period in a given day of the week:

$$p_{n,i}=f(t_i,\ p_{n,i-1},\ p_{n,i-2},\ p_{n,i-3},\ p_{n-1,i},\ p_{n-2,i},\ p_{n-3,i}),\quad i=3,\ \ldots,\ m. \qquad (1)$$

where $n$ stand for the number of the week (in the month or in the year). In that way the values designated with $n$ are from the current week, while the values indexed $n$-$j$, $j$=1,2,3, are from the previous weeks. The designation "$i$" stands for the $i$-th sample in the selected day. The actual value $p_{n,i}$ is unknown and should be predicted.

The second architecture is referred to as a *feed forward accommodated for prediction* (FFAP) and is shown in Fig. 4. The idea here was to push the neural network to learning the same data window several times simultaneously but shifted in time. It is expected that the previous responses of the function will have larger impact to the $f(t)$ mapping. The architecture has one input terminal - $t_i$. The approximation $y_{i+1}$ is obtained at the *future* terminal *Output*3. For multiple-step ahead predictions the future terminal can be considered as a vector. The *present* value $y_i$ is represented at the terminal *Output*2. *Output*1 has to learn the *past* value i.e. $y_{i-1}$. *Output*1 may also be considered as a vector if we need to control the mapping using a *set* of previous values. The functionality of the network could be expressed as

$$\{y_{i+1},\ y_i,\ y_{i-1},\ y_{i-2}\} = \mathbf{f}\,(t_i)\,, \qquad i=3,\ \ldots,m, \qquad (2)$$

where *Output*1={ $y_{i-1}$, $y_{i-2}$}. This indicates that one future, one present and two previous responses are to be learned.

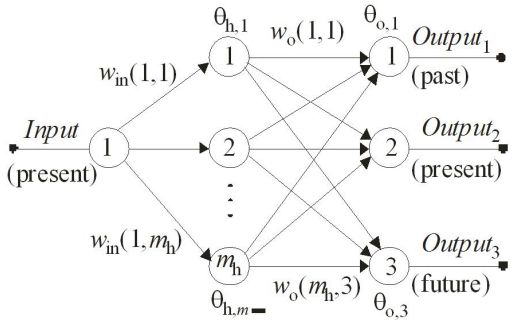


Fig. 4. FFAP. Feed forward ANN structure accommodated for prediction

According to our experience, the FFAP architectures produce more accurate forecasts than the TCR. However, it is a common practice to implement both of them for each forecasting problem and use the results obtained as a reference to each other when choosing the forecast that makes most sense. In this way, we could easily detect and avoid those solutions that represent local minima in the optimization process during the training of the ANN.

In the case of power consumption we have extended the FFAP architecture exactly in the same way as for the TCR architecture. The approximation function could then be written as

$$\{p_{n,i+1},\ p_{n,i},\ p_{n,i-1},\ p_{n,i-2},\ p_{n,i-3}\} = f(t_i,\ p_{n-1,i},\ p_{n-2,i},\ p_{n-3,i},p_{n-4,i})\,,\quad i=4,\ \ldots,m. \qquad (3)$$

The obtained network can estimate the future (unknown) values $p_{n,i+1}$, using the data for:

- the actual time $t_i$,
- the actual consumption $p_{n,i}$,
- the past consumption values for the given day in $n$–th week ($p_{n,i-k}$, $k$=1,2,3),
- and the past consumption values for the same day and actual time of the previous weeks ($p_{n-j,i}$, $j$=1,2,3,4).

The new architecture is referred to as an *extended feed forward accommodated for prediction* (EFFAP), and is shown Fig. 5.

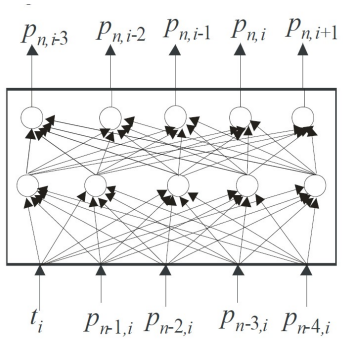


Fig. 5. EFFAP. Extended feed-forward accommodated for prediction ANN

## IV. Main Results

Having in mind the nature of the available data we have decided to implement the ETCR structure. A network with 6 hidden neurons was used while 8 previous samples were exploited for prediction.

The procedure could be described with the following steps. Having in mind the random choice of the initial values of the ANN's parameter for training, and the fact that for every such a choice local minima are reached after convergence, we have decided to repeat the prediction for every new day ten times. In that way 10 potential predictions were produced. Then, in order to make a better choice, those with a value above 80% and below 20% of the average were discarded. The final accepted prediction was the average of the rest.

Fig. 6 depicts the prediction results for a 50 day period in the summer of 2021. As can be seen errors not larger than 5% were obtained. This is in accordance with our previous results and, of course, with our expectations.

 ISBN 978-86-7466-930-3

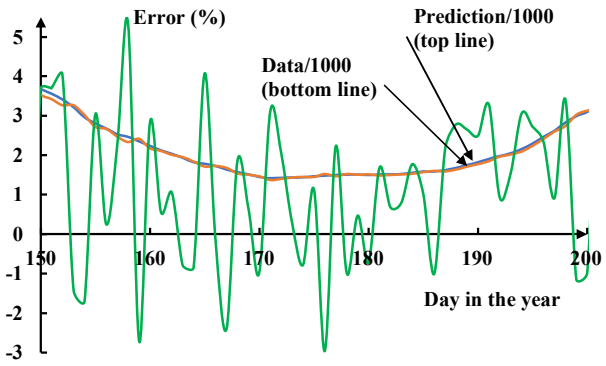


Fig. 6. Prediction results for a 50 day period in the summer of 2021.

## V. CONCLUSION

Based on our 30 years long experience in implementation of ANN in various aspects of technological and social life, we have implemented ANNs for prediction of COVID-19. The results obtained are, in our opinion satisfactory and encouraging for further improvement. That means implementation of other structures as described in the bulk of the paper.

## ACKNOWLEDGMENT

This work has been supported by The Ministry of Education, Science and Technological Development of the Republic of Serbia under the contract No. 451-03-68/2022-14/ 200102 of February, 04. 2022.

## REFERENCES

[1] https://www.worldometers.info
[2] J. Milojković, , V. Litovski, "One Month Ahead Prediction of Suburban Average Electricity Load", Proceedings of 2nd International Conference IcETRAN, Srebrno Jezero, Jun, 2015., ELI2.2, ISBN 978-86-80509-71-6.
[3] J. Milojković, D. Topisirović, M. Milić, M. Stanojević, "Short term local road traffic forecast using feed-forward and recurrent ANN", Facta Universitates, Working and Living Environmental Protection, Vol. 13, No 1, 2016, pp.1-12.
[4] C. Wang, P.W.Horby, F.G. Hayden, G.F. Gao, "A novel coronavirus outbreak of global health concern", The Lancet, Volume 395, Issue 10223,15–21 February 2020, Pages 470-473.
[5] Forecast of the outbreak of COVID-19 using artificial neural network: Case study Qatar, Spain, and Italy, 2021 Aug; 27:104484. doi: 10.1016/j.rinp.2021.104484. Epub 2021 Jun 21.
[6] https://covid19.who.int/
[7] P. Wang, J. A. Lu, Y. Jin, M. Zhu, L. Wang, S. Chen, "Statistical and network analysis of 1212 COVID-19 patients in Henan", China, Int. J. Infect. Dis. (2020). Published online 2020 Apr 24. doi: 10.1016/j.ijid.2020.04.051
[8] M. A. Turk, S. D. Landes, M. K. Formica, K. D. Goss, "Intellectual and developmental disability and COVID-19 case-fatality trends: TriNetX analysis", Disability and Health Journal, Volume 13, Issue 3, July 2020, 100942
[9] Y. Kuvvetly, M. Deveci, T. Paksoy, H. Garg, "Predictive analytics model for COVID-19 pandemic using artificial neural networks", Decision Analytics Journal, Volume 1,November 2021, 100007
[10] A. S. Ahmar, E. B. del Maj, "SutteARIMA: Short-term forecasting method, a case: Covid-19 and stock market in Spain", Science of the total environment, Vol. 729, No.10, August 2020, 138883.
[11] M. A. A. Al-qanes at all, "Optimization Method for Forecasting Confirmed Cases of COVID-19 in China", Journal of clinical Medicine, Vol. 9, no. 3, doi. 10.3390/jcm9030674.
[12] A. S., Mandel', "Method of Analogs in Prediction of Short Time Series: An Expert-statistical Approach", Automation and Remote Control, Vol. 65, No. 4, April 2004, pp. 634-641
[13] A.L.Bertozi, E.Franco, G.Mohler, D. Sledge, The challenges of modeling and forecasting the spread of COVID-19, PNAS, July 2, 2020, Vol.117 No.29, 16732-16738
[14] N. Balak at all., A simple mathematical tool to forecast COVID-19 cumulative case numbers, Clinical Epidemiology and Global Health, Vol. 12, October–December 2021, 100853
[15] Long-term forecasting of the COVID-19 epidemic, Dynamic Causal Modelling, UCL, UK, https://www.fil.ion.ucl.ac.uk/spm/covid-19/
[16] J. Milojković, and V. B. Litovski, "On the method development for electricity load forecasting", Proceedings of 1st International Conference on Electrical, Electronic and Computing Engineering, IcETRAN 2014, Vrnjačka Banja, Serbia, June 2 – 5, 2014, ISBN 978-86-80509-70-9
[17] J. Milojković, and V. B. Litovski, "Procedures of prediction of quantities of electronic computer waste", Tehnika (Elektrotehnika), Vol.56, No. 1, pp. E.7-E.16.(In Serbian), 2007.
[18] J. Milojković, and V. B. Litovski, "New procedures of prediction for sustainable development", 51th Conference of ETRAN, Herceg Novi, 04-08 Jun, 2007, Proc. on CD, EL1.8. (In Serbian).
[19] J. Milojković, and V. B. Litovski, "Short-term forecasting of electricity load using recurrent ANNs", 15th International Symposium On Power Electronics – Ee2009, Novi Sad, Serbia, ISSN Paper No. T1-1.7, 2009.
[20] J. Milojković, and V. B. Litovski, "Comparison of Some ANN Based Forecasting Methods Implemented on Short Time Series", 9th Symp. on Neural Network Applications in Electrical Eng., NEUREL-2008, pp. 179-179, Belgrade, 2008
[21] J. Milojković, and V. B. Litovski, "Prediction in Electronics based on limited information", Proc. of the 8th WSEAS Int. Conf. on Electronics, Hardware, Wireless And Optical Communications, EHAC'09, Cambridge, UK, pp. 33-38, February 2009
[22] M. Milić, J. Milojković, I. Marković, P. Nikolić, "Concurrent, Performance-Based Methodology for Increasing the Accuracy and Certainty of Short-Term Neural Prediction Systems", Computational Intelligence and Neuroscience, Vol. 2019, 1687-5265, doi:10.1155/2019/9323482, April, 2019.
[23] T. Masters, "Practical Neural Network Recipes in C++", *Academic Press,* San Diego, 1993
[24] Z. Zografski, "A novel machine learning algorithm and its use in modeling and simulation of dynamicalb systems", in Proc. of 5th Annual European Computer Conference, COMPEURO '91, Hamburg, Germany, 1991, pp. 860-864.
[25] E. B. Baum and D. Haussler, "What size net gives valid generalization", Neural Computing, 1989, Vol. 1, pp. 151-160.
[26] J. Milojković, and V. B. Litovski, "Short-term forecasting of electricity load using recurrent ANNs" 15th International Symposium On Power Electronics - Ee2009, Novi Sad, Paper No. T1-1.7, pp. 1-5, October 28th – 30th 2009

 ISBN 978-86-7466-930-3

# Equivalent Electromechanical Model of a Composite Ultrasonic Transducer

Igor Jovanović and Dragan Mančić

*Abstract*— **This paper presents an original one-dimensional model of a high-power composite ultrasonic transducer with a new structure. The equivalent circuit method is used for a model that can accurately depict the characteristics of the composite ultrasonic transducer and enable its efficient performance evaluation. The proposed model is verified by comparing the modeled dependencies of input electrical impedance vs. frequency with the experimental results. The equivalent circuit developed in this work can facilitate the design and analysis of complex composite transducer structures.**

*Index Terms*— **High-power ultrasound, Composite ultrasonic transducer, One-dimensional modeling.**

## I. Introduction

The piezoelectric ultrasonic transducer is a device that converts desired electrical signals to ultrasonic waves. The applications of high-intensity ultrasonic waves are based on the adequate exploitation of the non-linear effects associated with high amplitudes, such as the radiation pressure, streaming, cavitation, dislocation in solids, etc. [1].

An ultrasonic transducer is a widely used high-power electromechanical transducer for ultrasonic cleaning, ultrasonic liquid processing, and ultrasonic sonochemistry. There are increasingly needed high-power ultrasonic radiators with large amounts of power radiating surfaces. The development of various power ultrasound applications requires ultrasonic transducers with more significant maximum vibration velocity, energy efficiency, and lower temperature rise [2]. Ultrasonic transducer, which consists of piezoceramic and metal rings, has a low resonant frequency (considering the size of the transducer) and a high-quality factor.

Recent research in the field of powerful ultrasound aims to optimize the design of ultrasonic transducers by numerical and analytical modeling methods and the use of precise devices for measuring vibration, mechanical displacement, and stress [3].

The finite element method (FEM) has been a commonly used numerical modeling method to analyze acoustic characteristics of ultrasonic transducers. As a representative work on the use of the FEM, Kagawa and Yambuchi used this method to assess the effect of dimension and material on the resonance frequency of an ultrasonic transducer [4]. In [5], the finite element technique is used for polymer characterization. Wang et al. used FEM to evaluate the output displacement directions of a composite transducer [6]. In addition, FEM is used to evaluate the effect of structural parameters on the output displacement of an ultrasonic transducer [7]. Lin et al. used FEM to evaluate the composite transducer's radial radiation acoustic field distribution [8].

The need for extensive computing resources and long analysis time constitutes the main disadvantage of the FEM [9]. The FEM typically requires a long analysis time and considerable computational resources despite its widespread usage. Therefore, there is a strong need for a more efficient method for analyzing the performance characteristics of the ultrasonic transducer with high accuracy.

The most widely used analytical modeling approach for ultrasonic transducers found in literature is an application of one-dimensional theory using equivalent electromechanical circuits [10]. The equivalent circuit is a method that can analyze the acoustic characteristics of transducers more simply and efficiently than the FEM [9]. It has been utilized to design and analyze various transducers [11].

In their simplest form, ultrasonic transducers are represented by one-dimensional models that represent networks with one electrical and two mechanical approaches. However, when the modeling considers the influence of other parameters (influence of bolt, electrodes, insulators, various electrical connections, prestress, loads, power, etc.) of the transducer, there is an increase in the number of electrical and mechanical approaches in the electromechanical equivalent circuit [10]. Additionally, in the [12], it has been confirmed that using equivalent electromechanical circuits is still possible to model more complex transducer constructions with reasonable accuracy.

Therefore, the composite transducer with a new structure, analyzed in this paper, is presented in the simplest form as a network with two electrical and two mechanical approaches.

## II. Analytical One-Dimensional Modelling of Composite Transducer

A new structure of the composite transducer is shown in Fig. 1(a). The composite transducer contains a central mass (2) placed between the two active layers of the transducer ($PZT_{1,2}$ and $PZT_{3,4}$) and two metal endings (1 and 3) connected to the central mass by two central bolts.

Igor Jovanović is with the University of Niš, Faculty of Electronic Engineering, 14 Aleksandra Medvedeva, 18000 Niš, Serbia (e-mail: igor.jovanovic@elfak.ni.ac.rs), (https://orcid.org/ 0000-0001-7912-9154).

Dragan Mančić is with the University of Niš, Faculty of Electronic Engineering, 14 Aleksandra Medvedeva, 18000 Niš, Serbia (e-mail: dragan.mancic@elfak.ni.ac.rs).

 ISBN 978-86-7466-930-3

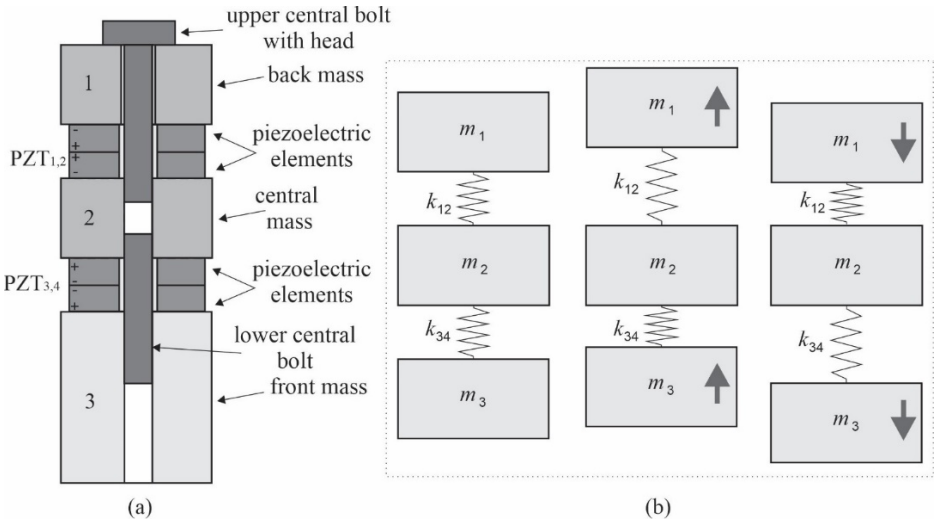


Fig. 1. The composite transducer with a new structure (a), represents of the simplest oscillatory structure of composite transducer (b).

Due to the mutually opposite polarization of the active piezoelectric elements connected to the same power supply, the masses in such a construction oscillates in the manner shown in Fig. 1(b). The three masses constituting this system are $m_1$, $m_2$, and $m_3$ (it is assumed in Fig. 1(b) that the masses are equal to each other), while $k_{12}$ and $k_{13}$ are the stiffness constant.

In its simplest form, the proposed composite transducer is a simple mechanical combination of two half-wave ultrasonic transducers with a sandwich structure that oscillates in the thickness direction (two Langevin-type transducers) [13].

Since the metal endings in the proposed structure are not of the same material, the composite transducer is not bidirectional. The proposed composite transducer has greater flexibility in operation than conventional transducers, which is reflected, among other things, in the possibility of independent excitation of the upper and lower active layer with different signals.

In this paper, modelling of the realized composite transducer with new structure, which represents a special unidirectional composite ultrasonic transducer, is performed. Prestressing the structure is achieved using two central bolts that are in contact with the central mass. The proposed model was adapted based on the structures of the composite transducer and shown as an equivalent electromechanical circuit shown in Fig. 2.

Elements of electromechanical circuits corresponding to isotropic and asymmetric metal parts made of different materials are calculated as:

$$Z_{i1} = jZ_{ci}tg\frac{k_i l_i}{2} \tag{1}$$

$$Z_{i2} = \frac{-jZ_{ci}}{\sin(k_i l_i)} \tag{2}$$

wherein $Z_{ci}=\rho_i v_i P_i$ and $k_i=\omega/v_i$ (for i=1, 2, and 3) are characteristic impedances and the corresponding wave numbers. $\rho_i$ are densities, $l_i$ and $P_i$ are lengths and surface areas of the cross-sections, and $v_i$ are the velocities of longitudinal ultrasonic waves propagation through the corresponding elements.

Elements of the circuit shown in Fig. 2 correspond to the piezoceramic rings in the upper active layer ($PZT_{12}$), and the piezoceramic rings in the lower active layer ($PZT_{34}$). These elements are determined as:

$$Z_{p1} = jZ_{cp}tg\frac{nk_p l_p}{2} \tag{3}$$

$$Z_{p2} = \frac{-jZ_{cp}}{\sin(nk_p l_p)} \tag{4}$$

wherein $Z_{cp}=\rho_p v_p P_p$ and $k_p=\omega/v_p$ are characteristic impedances and corresponding wave numbers, respectively. $\rho_p$, $l_p$, $P_p$ are densities, lengths, and surface areas of the piezoceramic cross-sections, $v_p$ are velocities of longitudinal ultrasonic waves propagation, respectively. The input electric voltages and currents are marked as $V$, $I_{12}$, and $I_{34}$.

The piezoceramic models consist of capacitance $C_0=n\varepsilon_{33}{}^S P_p/l_p$, and ideal transformers with transmission ratios $N=h_{33}C_0/n$, wherein $n$ is the number of piezoceramic rings per active layer ($n$=2). The piezoelectric properties of the transducer active layers are represented by the piezoelectric constant $h_{33}$ and the relative dielectric constant of the pressed ceramic $\varepsilon_{33}{}^S$.

Piezoceramic rings are mechanically connected in series with central mass, back and front endings. Back and front endings are closed with acoustic impedances $Z_R$ and $Z_E$, which are in this case negligible because experimental measurements were conducted with unloaded transducers oscillating in the air.

 ISBN 978-86-7466-930-3

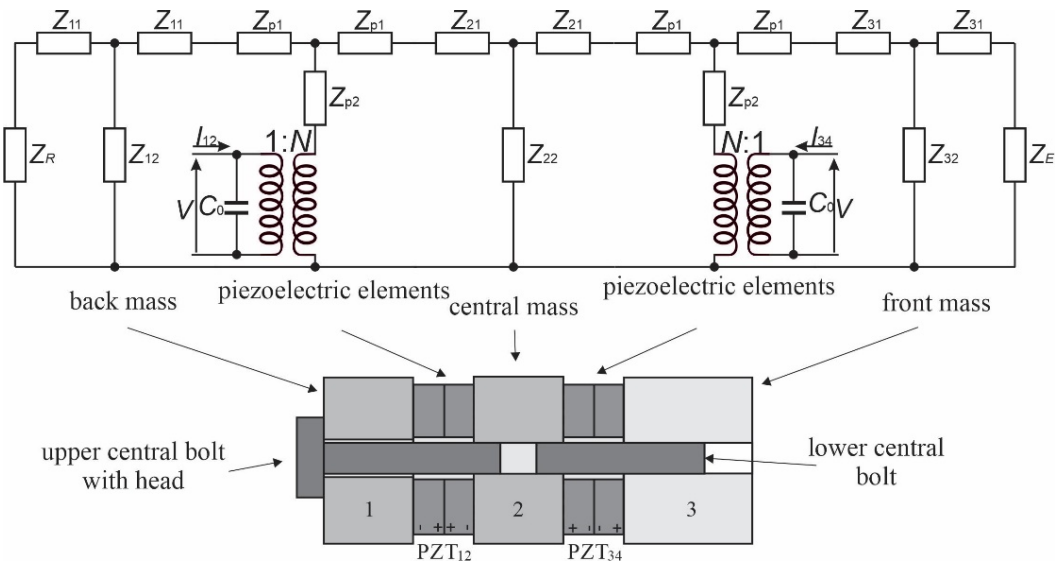


Fig. 2. One-dimensional model of the composite transducer.

Based on Eqs. (1-4) it is obvious that the transducer frequency response depends on the material characteristics of its constituting parts and their geometric dimensions.

In the proposed transducer model, it is assumed that the circuit elements are ideal, i.e. they do not have losses. Losses can be included if piezoelectric constants and constants of elasticity of the transducer metal parts are in the form of complex numbers, in which the imaginary parts represent losses.

## III. SIMULATION AND EXPERIMENTAL RESULTS

Table 1 shows the dimensions of the individual composite transducer. Dimensions of the exciting piezoceramic rings are Ø38/Ø13/6.35 mm, and rings are made of PZT8 piezoceramic equivalent material [14]. $L_i$ is the length, $a_i$ and $b_i$ are the outer and inner diameters of the corresponding $i$-th element.

The front ending is made of a dural, while the back ending and the central mass are made of steel with the standard material properties.

TABLE I
DIMENSIONS OF COMPOSITE TRANSDUCER USED IN EXPERIMENTAL ANALYSIS

| Dimension [mm] | Composite transducer |
|---|---|
| $L_1=L_2$ | 11 |
| $L_3$ | 37 |
| $a_1=a_2=a_3$ | 40 |
| $b_1=b_3$ | 9 |
| $b_2$ | 8 |

There is a similarity between the modeled and experimental dependences, as shown in Fig. 2. Since it is a composite transducer with a larger ratio of length and transverse dimensions, the proposed one-dimensional model gives satisfactory results during transducer analysis in the first resonant mode.

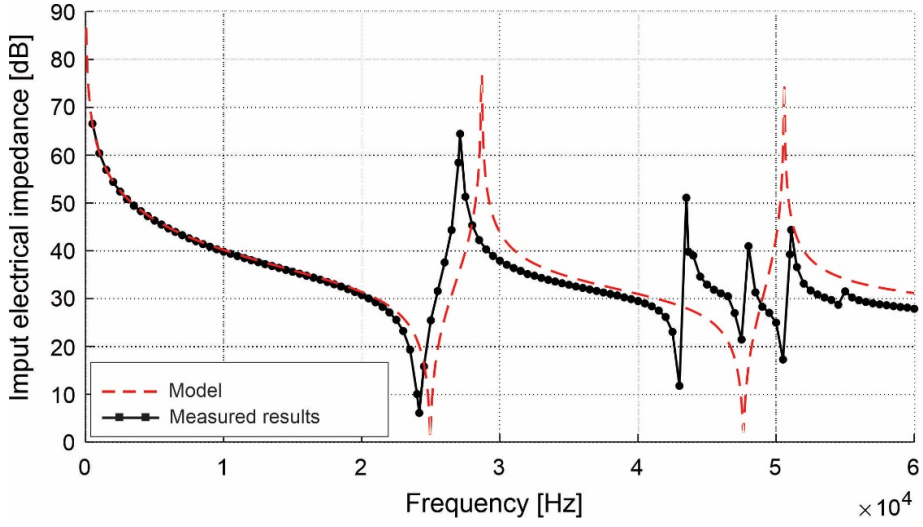


Fig. 3. Input electrical impedance vs. frequency for the proposed composite transducer

 ISBN 978-86-7466-930-3

The measured resonant frequency of the fundamental resonant mode is 24.95 kHz. The calculated resonant frequency using the proposed model is 24.95 kHz, where the error made by the one-dimensional model in determining this resonant frequency is 3.27%. When it comes to the antiresonant frequency, the measured value is 27.12 kHz, while the model calculated 28.7 kHz, i.e., the error made by the model is 5.83%. The proposed model can predict the general shape of the second resonant mode but with significant error. The measured resonant frequency of the second resonant mode is 43 kHz, while the resonant frequency obtained by the model is 47.65 kHz (the error is 10.81%).

This model allows only the thickness resonant modes to be predicted and, therefore, does not consider the inevitable radial resonant modes. One-dimensional models are generally not suitable for determining resonant frequencies of thickness oscillations that are close to resonant frequencies of radial oscillations. In the case shown, when the model does not predict the third and fourth modes, the calculated resonant frequencies for the first two modes are always higher than the measured ones. If a model that considers both the third and fourth modes were used, the first two modes would be moved to lower frequencies.

## IV. CONCLUSION

In this study, an equivalent circuit was developed for accurate analysis of the acoustic characteristics of an ultrasonic transducer over a wide frequency range.

Eqs. (1-4) confirm that the frequency characteristics of transducers in one-dimensional theory depend on the material characteristics of the components of composite transducers and their geometric dimensions.

In practice, one-dimensional modeling is most often used due to the great flexibility and efficient implementation of the model. The flexibility and efficiency of one-dimensional models come to the fore in the analysis of transducers operation, which includes a large number of parameters.

The proposed one-dimensional model of composite transducer does not include mechanical and electrical losses in the material. However, losses can be analyzed if the piezoelectric constants and the elastic constants of the metal parts of the converter are represented in complex numbers, where their imaginary parts represent losses.

## ACKNOWLEDGMENT

This work has been supported by the Ministry of Education, Science and Technological Development of the Republic of Serbia, contract no. 451-03-68/2022-14/200102.

## REFERENCES

[1] Y. Yao, Y. Pan, S. Liu, “Power ultrasound and its applications: A state-of-the-art review,” *Ultrasonics - Sonochemistry*, vol. 62, 104722, 2020.

[2] X. Lu, J. Hu, H. Peng, Y. Wang, “A new topological structure for the Langevin-type ultrasonic transducer,” *Ultrasonics*, vol. 75, pp. 1–8, 2017.

[3] D. Chen, L. Wang, X. Luo, C. Fei, D. Li, G. Shan, Y. Yang, “Recent Development and Perspectives of Optimization Design Methods for Piezoelectric Ultrasonic Transducers,” *Micromachines*, vol. 12, no. 7, 779. 2021.

[4] Y. Kagawa, T. Yambuchi, “Finite element simulation of a composite piezoelectric ultrasonic transducer,” *IEEE Trans. Sonics Ultrasonics*, vol. 26, no. 2, pp. 81–88, 1979.

[5] F. Wolf, T. Lahmer, L. Bahr, A. Hauck, A. Sutor, R. Lerch, M. Kaltenbacher, “Finite element modeling of ultrasonic transducer by utilizing an inverse scheme for the determination of its material parameters,” 2008 IEEE International Ultrasonics Symposium, Beijing, China, 2-5 November, 2008.

[6] L. Wang, J. A. Wang, J. M. Jin, L. Yang, S.W. Wu, C. Zhou, “Theoretical modelling, verification, and application study on a novel bending-bending coupled piezoelectric ultrasonic transducer,” *Mechanical Systems and Signal Processing*, vol. 168, 108644, 2022.

[7] F. Wang, H. Zhang, C. Liang, Y. Tian, X. Zhao and D. Zhang, “Design of High-Frequency Ultrasonic Transducers With Flexure Decoupling Flanges for Thermosonic Bonding,“ *IEEE Transactions on Industrial Electronics*, vol. 63, no. 4, pp. 2304-2312, 2016.

[8] S. Lin, L. Xu,W. Hu, “A new type of high-power composite ultrasonic transducer,” *Journal of Sound and Vibration*, vol. 330, pp. 1419–1431, 2011.

[9] H. Shim, Y. Roh, “Development of an Equivalent Circuit of a Cymbal Transducer,“ *IEEE Sensors Journal*, vol. 21, no. 12, pp. 13146-13155, 2021.

[10] I. Jovanović, U. Jovanović, D. Mančić, “General One-Dimensional Model of a New Composite Ultrasonic Transducer”, Proceedings of the 7th Small Systems Simulation Symposium 2018, Niš, Serbia, pp. 50-54, 12-14 February 2018.

[11] D. Mančić, I. Jovanović, M. Radmanović, Z. Petrušić, “Comparison of one-dimensional models of ultrasonic sandwich transducers” – in Serbian, Proceedings of the XXII Noise and Vibration, Niš, Serbia, pp. 119-127, 20-22. October 2010.

[12] I. Jovanović, D. Mančić, U. Jovanović, M. Prokić, “A 3D model of new composite ultrasonic transducer“, *Journal of Computational Electronics*, vol.16, no. 3, pp.977-986, 2017.

[13] P. Langevin, French Patent Nos: 502913 (29.5.1920); 505703 (5.8.1920); 575435 (30.7.1924).

[14] *Properties of Piezoelectricity Ceramics*, Technical Publication TP-226, Morgan Electro Ceramics.

 ISBN 978-86-7466-930-3

# Hardware Realization of Nearest Neighbour Search Algorithm over an In-Memory Pre-Stored $k$-d Tree

Aleksandar Z. Kondić, *Student Member, IEEE*, and Vladimir M. Milovanović, *Senior Member, IEEE*

***Abstract*—Nearest neighbour search is a fundamental statistical classification algorithm with widespread use in artificial intelligence (AI) sub-fields such as machine learning, computer vision, and robotics. Considering the shift in host platforms running AI algorithms from general-purpose computers to specialized hardware implementations, a parameterizable design generator of special purpose hardware instances that perform nearest neighbour search is proposed, captured inside Chisel hardware construction language, and validated on an FPGA platform. Based on an algorithm of nearest neighbour search that traverses a k-dimensional tree pre-stored inside read-only memory (ROM), the generator provides parameters for configuring the structure and volume of the tree and the points stored within it.**

***Index Terms*—Nearest neighbour search, hardware implementation, Chisel hardware construction language, k-dimensional tree.**

## I. Introduction

Nearest neighbour search is an algorithm which, for a given input point, finds a point closest to it among a set of points. It is useful for solving classification problems, which are especially prevalent in artificial intelligence (AI) subfields such as machine learning, computer vision [1], and robotics [2].

With artificial intelligence algorithms being increasingly shifted from general-purpose computers to dedicated hardware instances as a consequence of the need for increased computational power [3], various hardware implementations of classic AI algorithms targeting different platforms have appeared. The Nearest Neighbour Search (NNS), along with its variants, the Approximate Nearest Neighbour (ANN) and $k$-Nearest Neighbours ($k$-NN) algorithms, are no exceptions.

Considering field programmable gate arrays (FPGAs) as a hardware implementation platform of choice, there are various incarnations of the above mentioned algorithms. They are usually described and implemented either in the form of pure register-transfer level (RTL) [4], [5], high-level synthesis (HLS) [6], [7], or Open Computing Language (OpenCL) [8], [9] code. An alternative to these approaches is to write the behavioral code in an RTL-like form but utilizing a higher level hardware design language instead. One such language is Chisel [10], which is embedded in the Scala programming language, enabling its users to write RTL instance generators while providing benefits of both functional and object-oriented programming paradigms. This paper proposes an implementation of the nearest neighbour search algorithm in Chisel using an agile [11] digital design methodology.

An effective implementation of the nearest neighbour search algorithm should presumably work for a large number of pre-defined points as potential output points for a given input point. For such an implementation to be efficient in terms of resource utilization for a target hardware platform such as FPGA, the points need to be stored inside a memory module. This naturally implies that the digital logic may have access only to a limited number of pre-stored points per clock cycle. Therefore, it is desirable to minimize the number of memory accesses for a given input point while obtaining the correct solution.

This is the same problem that a purely software implementation of a nearest neighbour search algorithm on a processor would have. To minimize the amount of time needed to process an input point, an efficient algorithm with a desirable run-time complexity needs to be chosen. While the simplest solution would be to run an exhaustive search of the entire memory containing pre-defined points to find a point with the minimal distance from the input point—yielding a linear run-time complexity—more efficient algorithms exist.

Similar problems were encountered in the field of computer graphics. In order to ensure the rendering of a scene in a timely manner, it was necessary to retrieve relevant spatial data of the scene efficiently. A technique named *binary space partitioning* (BSP) was developed to solve this problem, mainly implemented through a tree data structure [12]. The technique entails recursively subdividing space into two parts along a hyperplane. When a given point or polygon is queried, the search is performed only in the sub-spaces where it could possibly be located, thus reducing the search domain.

Space partitioning is a general method of subdividing space in a defined manner until a certain condition is satisfied. There are multiple implementations of this method in the form of different tree structures with specific criteria on how a space is divided into sub-spaces and under which conditions. Examples of some tree structures that perform space partitioning are $k$-d trees, quadtrees, and octrees. Concerning the nearest neighbour search problem, some of the appropriate data structures that can be used are $R$-trees and $k$-dimensional trees.

The principal data structure driving this particular implementation of the nearest neighbour search algorithm is the $k$-dimensional tree, or $k$-d tree for short. A $k$-d tree is essentially a binary search tree that contains multi-dimensional points and is traversed based on the value of one of the coordinates of the input point at each node in the tree.

Aleksandar Z. Kondić was with the Faculty of Engineering, University of Kragujevac, Sestre Janjić 6, Kragujevac, Serbia (e-mail: konda@uni.kg.ac.rs).

Vladimir M. Milovanović is with the Department of Electrical Engineering, Faculty of Engineering, University of Kragujevac, Sestre Janjić 6, 34000 Kragujevac, Serbia (e-mail: vlada@kg.ac.rs).

 ISBN 978-86-7466-930-3

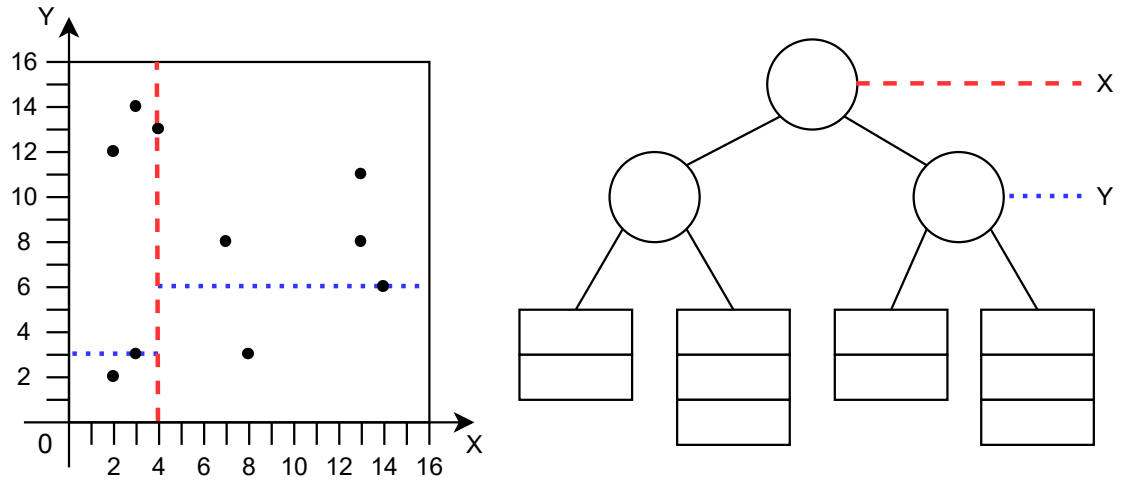


Fig. 1. An illustrative example of a $k$-dimensional tree (with $k = 2$ to simplify the drawing) and the two-dimensional space partitioning it performs.

Each node of the $k$-d tree contains a value by which the hyperspace it belongs to is split into two. The dimension in which the split is performed corresponds to the node's depth in the tree, which repetitively cycles from the last dimension to the first when the depth of the node becomes greater than the dimensionality of the points stored inside the tree. All child points that have the value of the coordinate in the corresponding dimension less than the node's stored value are part of the left sub-tree, while the child points with the corresponding coordinate's value greater than the value in the node are part of the right sub-tree. In the case of a child point having an equal corresponding coordinate value to the value of the node—due to the nature of the nearest neighbour search algorithm—it may belong to either of the sub-trees.

The average run-time complexity of the nearest neighbour search algorithm over a $k$-dimensional tree is $\mathcal{O}(m + \log_2 n)$, where $n$ is the number of nodes in the tree and $m$ is the average number of points contained in a leaf node.

## II. A $k$-D Tree-Based Hardware Implementation

The primary purpose and the use scenario of the proposed implementation is to execute the nearest neighbour search algorithm over a $k$-dimensional tree. The tree structure, along with the points it contains is assumed to be constructed and stored beforehand inside some form of a read-only memory (ROM). In the case of an FPGA platform the ROM is in the form of a single-port block RAM and mimics the static RAM.

This implementation uses a variant of the $k$-dimensional tree in which the number of nodes in the tree is not necessarily equal to the number of points. The points are, after a proper traversal through the $k$-d tree, stored in the leaf nodes. A leaf node may contain more than one point. An example $k$-dimensional tree of this kind is shown in Fig. 1, along with an illustration of how the tree partitions a two-dimensional space (but in general it can be an arbitrary $k$-dimensional hyperspace).

The nearest neighbour search algorithm finds the closest point to the query point by first performing a traversal of the $k$-d tree until reaching a leaf node. When visiting a node, the value of the query point's coordinate in the dimension corresponding to the node's depth is checked against the value in the node. If the value is smaller, traversal proceeds to the left sub-tree. Otherwise, traversal proceeds to the right sub-tree. When reaching a leaf node, all of the points in the leaf node are checked, calculating the distances between them and the query point. The current closest point, along with its distance to the query point, are stored inside dedicated registers which are updated when a closer point is found.

After exhausting all of the points in a leaf node, the search algorithm traverses backwards, that is up the tree and checks if the hypersphere around the current closest point with the radius equal to its distance from the query point intersects the node's splitting hyperplane. If so, a closer point to the query point may exist on the other side of the splitting hyperplane, so the search algorithm proceeds by traversing down the sub-tree contained in the node's unvisited child, until reaching a leaf node again. This process is repeated until the algorithm terminates when it is guaranteed to yield a point stored within the $k$-dimensional tree with the minimal distance from the query point.

For the purposes of this work, the structure of the $k$-dimensional tree and the points it contains are stored in two separate memories (or two non-overlapping memory segments). The memory used to store information about the points contains coordinates of each point. The points inside this particular memory (segment) are arranged in such a way that the points belonging to the same leaf node of the $k$-dimensional tree occupy consecutive memory locations.

Memory containing the tree structure stores the properties of each node. The following properties are stored: an indicator bit of whether the node is a leaf node, the discriminating value stored inside the node for tree traversal (valid only for non-leaf nodes), the starting address in the points ROM and the

 ISBN 978-86-7466-930-3

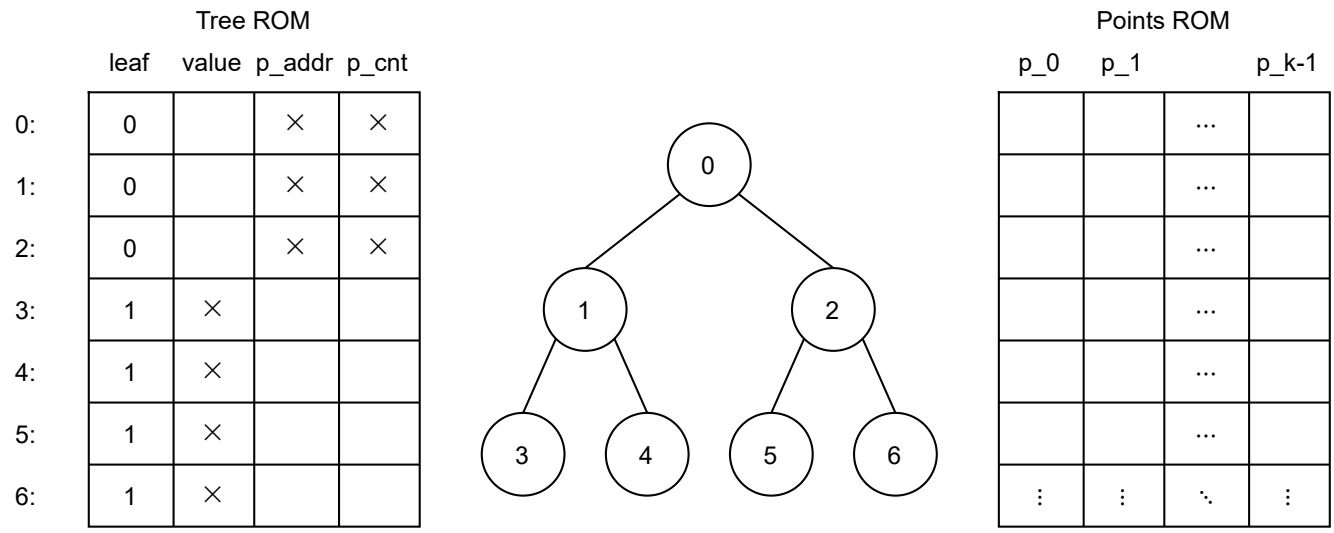


Fig. 2. Memory layout of a $k$-dimensional tree showing the associated Tree ROM and Points ROM structures over which the NNS realization operates.

number of points contained in the node (valid only for leaf nodes). A node at location $n$ in the tree ROM has its left and right children at locations $2n + 1$ and $2n + 2$, respectively. With this it is assumed that the stored $k$-d tree is balanced. It is possible to construct a balanced $k$-d tree from an arbitrary set of points as long as the points with the same coordinate value as the discriminating value in the node may be stored in either of the node's child sub-trees. In particular use cases of interest this discriminating value is actually the median value of relevant coordinates of the points being considered during $k$-d tree construction. The described memory layout is illustrated in Fig. 2.

The tree traversal algorithm is recursive. Traversal is performed in a depth-first manner, that is similar to the depth-first search algorithm (DFS), which is also recursive. The DFS algorithm, starting at the root of the tree, visits its child nodes in a pre-defined order. When visiting one of the child nodes, another instance of the DFS algorithm is started on the node, running more instances of the DFS algorithm on its children if it has any. Once an instance of the DFS algorithm for one child node terminates, the same process is repeated for the other. Therefore, by the time DFS starts visiting the root node's second child, the entirety of the sub-tree rooted in its first child will have already been explored.

An example of the order of traversal of binary tree nodes in the depth-first search algorithm is shown in Fig. 3. Non-leaf tree nodes are each visited a total of three times in order to visit the subtree rooted in their second child after visiting the first, and to potentially traverse back up to the parent node.

Each non-leaf node's left child is first explored, followed by the right child. The primary characteristic of DFS is that after visiting the leaves, it traverses back up the tree in order to traverse down unvisited sub-trees, repeating this process until the entire tree is explored.

A $k$-d tree traversal is essentially a variation on DFS tree traversal. The difference with $k$-d tree traversal is that the order of the children visited depends on the query point for which the closest point is to be found. The left child is first visited if the query point is on the "left" side of the splitting hyperplane represented by the node, otherwise the right child is first visited. Also, if the first child node's closest point is at a distance shorter than or equal to the distance of the query point from the splitting hyperplane, the second child is not explored. Unlike depth-first search, with $k$-d tree search the entire tree may not necessarily be explored.

A tree traversal over an example $k$-d tree is illustrated in Fig. 4. The query point for which to find the closest point is $(5, 3)$. In this example, during the traversal three out of the four leaf nodes were visited. The metric used to calculate the distance between two points (or between the query point and a splitting hyperplane) is the squared Euclidean distance.

Software implementations of recursive algorithms may make use of recursive function calls, which are realized on a call stack, or allocate a stack structure specifically to store their data and implement the algorithm as a non-recursive function. In this case only the second option is viable, so the stack data structure is actually implemented as an array of registers. A separate dedicated register is used to store a pointer that keeps track of the position of the top of the stack in the array.

## III. Design Generator of the $k$-d Tree-Based NNS

The previously described accelerator has been implemented as a parameterized RTL design generator in Chisel 3 hardware construction language. The generator has been extensively tested by following standard Chisel verification and implementation paths for FPGA design workflows. As a hardware library it is freely available for public use [13]. The next few paragraphs are elaborating on different generator parameters, as well as modes of operation of the module.

 ISBN 978-86-7466-930-3

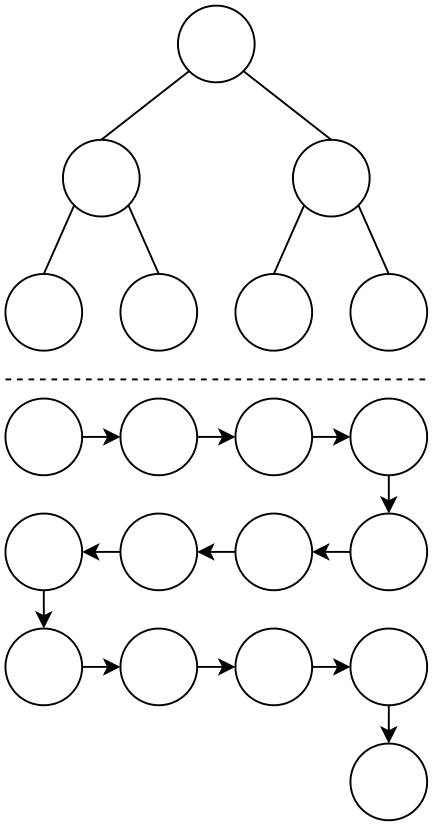

Fig. 3. An example of the order of nodes traversed in a binary tree using depth-first search.

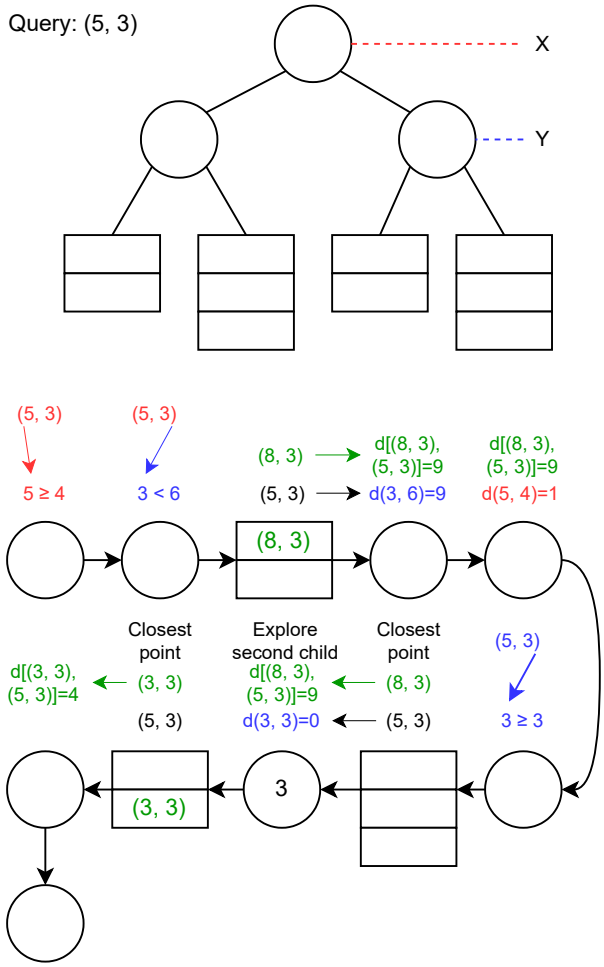


Fig. 4. An example of the order of nodes traversed in a $k$-d tree when finding the closest point to the query point $(5, 3)$.

### A. Generator Parameters

Parameterizable properties of the design pertain mainly to the structure of the $k$-dimensional tree itself and its points.

The values of point coordinates are signed integers with a specified bit width, which is one of the parameters of the design generator. Another generator parameter is the number of dimensions of each point. The total size of the points ROM is inferred from the bit width of its unsigned integer addresses, which is specified as a yet another generator parameter. These three parameters make up the structure of the points ROM.

Concerning the structure of the tree ROM, each location contains one bit indicating whether the node is a leaf, a signed integer representing the discriminator value of a node (in our use cases referred to as the *median*), and two unsigned integers representing the location and count of points inside the points ROM. The bit width of the discriminator is the same as the bit width of the points' individual coordinates, while the bit width of the location and count of points is the same as the bit width of the addresses in the points ROM. The size of the tree ROM, along with the bit width of its addresses is inferred from a generator parameter specifying the maximum depth of the tree. The number of nodes in the tree may be arbitrary though, as the nearest neighbour search algorithm assumes that nodes marked as leaves in the tree ROM do not have children.

### B. Modes of Operation

To keep track of the nodes visited for the purposes of traversing back up the tree after visiting a leaf node, a stack structure is implemented as an array of registers. Three distinct values are pushed onto the top of the stack to aid with the execution of $k$-d tree search:

- *Address of the node in tree ROM* – this is the main piece of data used to keep track which tree node to visit next.
- *The child of the node to visit next* – a single bit that determines whether to visit the first or the second child of the node during tree traversal. A value of 0 corresponds to visiting the first child, while a value of 1 corresponds to visiting the second child. When the value is 1, first the distance of the current closest point to the query point is compared to the distance of the query point to the splitting hyperplane of the node (the median value of the node in this case). If the distance of the closest point to the query point is not greater, the second child is not visited.
  Since after visiting the second child of a node there is nothing left to process, the current node visited is popped from the stack before the second child node is pushed


ISBN 978-86-7466-930-3

onto the stack. More precisely, the value at the top of the stack, which currently contains data about the current node being visited, is simply replaced with the data of its second child. In case the second child node is not to be visited, the current node is popped from the stack.

- *The depth of the node in the tree* – This information is used for calculating the distance of the current closest point from the splitting hyperplane. The value of the depth directly maps to which coordinate of the current closest point to compare to the stored node median and is also used to determine the coordinate of the query point to compare to the median value during tree traversal.
  While the depth of the node can be calculated from its index (memory address) in the tree ROM, it is simpler to just push onto the stack the current depth value of the node incremented by one when pushing child nodes. The depth value does not exceed the dimensionality of the points in the tree as it cycles between 0 and $k-1$.

Since the first node to process when a new query point is given is always the root of the tree (address 0 in tree ROM), whose depth is 0, and the next node to process is always its first child, the stack is always initialized to contain these values as the sole element of the stack before processing a new point.

At each clock cycle, the values at the top of the stack are retrieved, which mostly determine the mode of operation of the module. The relevant modes of operation are as follows:

- *Leaf processing* – this mode is active when the indicator for whether the current node is a leaf has the value 1. The values at the top of the stack are not used in this case. At each clock cycle, a counter indicating how many points were visited in the points ROM is incremented until reaching the value in tree ROM that indicates how many points a leaf node has. After that, the counter is reset to 0 and the current node is popped off the stack.
  The value of the counter is added to the starting address of the node's points in the points ROM, yielding an address of each point to be retrieved from the points ROM. The distance of each point is compared to the current minimal distance from the query point. In case it is smaller, both registers containing the closest point and its distance from the query point are updated accordingly.
  Since there is a delay of a few clock cycles due to memory access in the points ROM and distance calculations using registers to decrease the length of logic paths, once the points counter is set to 0, a "delay" counter is also initialized to 2. Each clock cycle the value of this counter is decremented until it reaches 0, regardless of the mode of operation. The module may not produce a valid result on its output while the value of this counter is greater than 0, even if there are no remaining nodes left in the tree to process for a given query point.
- *Tree traversal, first child node being next* – This mode is active when the current node is not a leaf (explained above) and the value of the child indicator at the top of the stack is 0. The appropriate query point coordinate is compared to the median value of the node to determine which of the left and right children is the first child to be visited. After that, the corresponding first child node is pushed onto the stack.
- *Tree traversal, second child node potentially being next* – This mode is active when the current node is not a leaf and the value of the child indicator is 1. The stored current minimal distance from the query point is compared to the distance of the query point's appropriate coordinate from the median value of the node. If the current minimal distance is not greater, the second child of the node will not be visited, and the current node is popped off the stack. Otherwise, values at the top of the stack are replaced with the values corresponding to the second child node.
  Since the median distance calculation also uses a register in order to decrease the length of logic paths, the result of this calculation is available in the next clock cycle. Therefore, a special one-bit register is set to signify that this mode of operation is still in progress. In the next clock cycle this register is reset, and the rest of the operations are performed as described.
- *Final phase of the algorithm* – active when the node stack is empty. While the value of the previously described "delay" counter is greater than 0, no additional operations are performed. Once the value of the counter reaches 0, the output valid signal of the module is set to 1, while the output point is simply a set of wires connected to the register storing the current closest point to the input point. The initial values of the stack are pushed onto the empty stack to prepare the processing of the next input point.

The block diagram in Fig. 5 depicts the generator's design. The inputs and outputs of this design adhere to the Ready/Valid handshaking protocol. Apart from the *ready* and *valid* signals, both the input and the output consist of a single $k$-dimensional point represented as a series of $k$ signed integers depicting their respective coordinate values. The dimensionality of these points, along with the structure of the point and tree ROMs, depend on the generator's parameters.

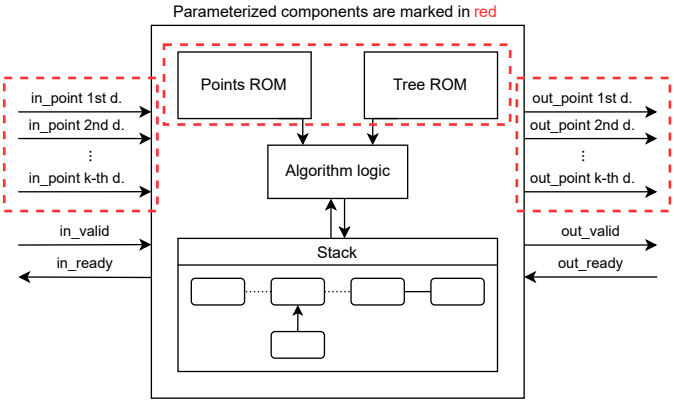


Fig. 5. Interface of the implemented Chisel design showing its input, output, and internals.

 ISBN 978-86-7466-930-3

## IV. Implementation and Testing Results

Testing of the generator is also performed using testing facilities provided by Chisel, i.e. *ChiselTest*. All generator parameters are randomized during testing, and the ROMs are also populated by appropriate randomly generated $k$-dimensional trees. The output of generated instances for random inputs is compared against the output of a $k$-d tree golden model written in Scala. The distances of the outputs of Chisel instances are compared with the distances of the outputs produced by the respective Scala golden model class instances.

The Scala golden model of the $k$-dimensional tree has also undergone rigorous testing. A list of random points is generated after selecting a random number of dimensions for the points. From the list of points and the desired number of tree nodes an instance of the golden model class is created.

This "golden model" instance is then supplied with random points as input. The output point's distance from the input point is compared to the distance of the closest point to the input point from the list of points in the tree, which is obtained by applying a simple brute-force exhaustive search algorithm. Due to the order of nodes and points traversed not being the same for the $k$-d tree model and the brute-force algorithm, only distances of the respective closest points to the input point are compared.

For additional testing and real in-hardware validation, various instances obtained from the design generator have been synthesized and implemented onto a commercially available FPGA development board. The board in question is Digilent's Arty A7 with Xilinx's Artix-7 FPGA family. All instances have been synthesized for a 100 MHz target clock frequency.

Resource utilization for the different generated instances is shown in Table I. Slice LUT utilization is most influenced by the bit width of the coordinates and $k$, the dimensionality of the points. A more minor effect on slice LUT utilization is exerted by the sizes of the point and tree ROMs. The number of slice registers seems to be mostly influenced by the bit width of the coordinates, followed by the dimensinoality of the points. Number of dimensions $k$ has an influence on both Block RAM Tile and DSP multiplier counts, although the greatest influence on the number of DSP multipliers is exerted by point coordinate data bit width.

TABLE I
FPGA Resource Utilization for Generated Design Instances

| Generator Instance Parameters | | | | FPGA Resources | | | |
|---|---|---|---|---|---|---|---|
| Data Width | Nodes | Points | $k$ | Slice LUTs | Slice Regs | BRAM Tiles | DSP muls |
| 8 bits | 31 | 100 | 3 | 728 | 272 | 1 | 3 |
| 16 bits | 31 | 100 | 3 | 383 | 288 | 1.5 | 7 |
| 24 bits | 31 | 100 | 3 | 528 | 444 | 1.5 | 11 |
| 32 bits | 31 | 100 | 3 | 706 | 412 | 1 | 19 |
| 16 bits | 7 | 100 | 3 | 334 | 287 | 1.5 | 7 |
| 16 bits | 15 | 100 | 3 | 328 | 288 | 1.5 | 7 |
| 16 bits | 63 | 100 | 3 | 339 | 288 | 1.5 | 7 |
| 16 bits | 31 | 50 | 3 | 326 | 271 | 1.5 | 7 |
| 16 bits | 31 | 200 | 3 | 372 | 311 | 1.5 | 6 |
| 16 bits | 31 | 100 | 2 | 339 | 232 | 1 | 6 |
| 16 bits | 31 | 100 | 4 | 381 | 337 | 1.5 | 8 |
| 16 bits | 31 | 100 | 5 | 453 | 393 | 2 | 9 |

## V. Conclusion

An approach to implementing a nearest neighbour search algorithm on an FPGA hardware platform has been explored. One of the key characteristics in this approach is in using a pre-stored $k$-dimensional tree to perform nearest neighbour search operations. Another is in using the Chisel hardware design language to create a generator of instances that can accommodate $k$-d trees with different structure parameters.

A variety of instances have undergone testing and additional verification by implementing them on a commercial FPGA development board. Apart from testing and verification, some consideration has also been given to their utilization of resources. This paper proves on an example case of the nearest neighbour search algorithm that parameterizable design generators can be used to produce instances of AI and machine learning hardware modules as an alternative to using CPU-based implementations.

## References


[1] O. Boiman, E. Shechtman, and M. Irani, "In defense of nearest-neighbor based image classification," in *2008 IEEE conference on computer vision and pattern recognition*. IEEE, 2008, pp. 1–8.

[2] A. Bewley and B. Upcroft, "Advantages of exploiting projection structure for segmenting dense 3d point clouds," in *Australian Conference on Robotics and Automation*, vol. 2, 2013.

[3] M. A. Talib, S. Majzoub, Q. Nasir, and D. Jamal, "A systematic literature review on hardware implementation of artificial intelligence algorithms," *The Journal of Supercomputing*, vol. 77, no. 2, pp. 1897–1938, 2021.

[4] M. A. Mohsin and D. G. Perera, "An fpga-based hardware accelerator for k-nearest neighbor classification for machine learning on mobile devices," in *Proceedings of the 9th International Symposium on Highly-Efficient Accelerators and Reconfigurable Technologies*, 2018, pp. 1–7.

[5] T. Ito, Y. Itotani, S. Wakabayashi, S. Nagayama, and M. Inagi, "A nearest neighbor search engine using distance-based hashing," in *2018 International Conference on Field-Programmable Technology (FPT)*. IEEE, 2018, pp. 150–157.

[6] Z.-H. Li, J.-F. Jin, X.-G. Zhou, and Z.-H. Feng, "K-nearest neighbor algorithm implementation on fpga using high level synthesis," in *2016 13th IEEE International Conference on Solid-State and Integrated Circuit Technology (ICSICT)*. IEEE, 2016, pp. 600–602.

[7] A. Lu, Z. Fang, N. Farahpour, and L. Shannon, "Chip-knn: A configurable and high-performance k-nearest neighbors accelerator on cloud fpgas," in *2020 International Conference on Field-Programmable Technology (ICFPT)*. IEEE, 2020, pp. 139–147.

[8] J. Zhang, S. Khoram, and J. Li, "Efficient large-scale approximate nearest neighbor search on opencl fpga," in *Proceedings of the IEEE Conference on Computer Vision and Pattern Recognition*, 2018, pp. 4924–4932.

[9] F. B. Muslim, A. Demian, L. Ma, L. Lavagno, and A. Qamar, "Energy-efficient fpga implementation of the k-nearest neighbors algorithm using opencl." in *FedCSIS (Position Papers)*, 2016, pp. 141–145.

[10] J. Bachrach, H. Vo, B. Richards, Y. Lee, A. Waterman, R. Avižienis, J. Wawrzynek, and K. Asanović, "Chisel: Constructing hardware in a scala embedded language," in *DAC Design automation conference 2012*. IEEE, 2012, pp. 1212–1221.

[11] Y. Lee, A. Waterman, H. Cook, B. Zimmer, B. Keller, A. Puggelli, J. Kwak, R. Jevtic, S. Bailey, M. Blagojevic *et al.*, "An agile approach to building risc-v microprocessors," *ieee Micro*, vol. 36, no. 2, pp. 8–20, 2016.

[12] H. Fuchs, Z. M. Kedem, and B. F. Naylor, "On visible surface generation by a priori tree structures," in *Proceedings of the 7th annual conference on Computer graphics and interactive techniques*, 1980, pp. 124–133.

[13] A. Kondić and V. Milovanović, "Hardware realization of nearest neighbour search algorithm over an in-memory pre-stored k-d tree," www.github.com/milovanovic/nns, accessed: April 15, 2022.


 ISBN 978-86-7466-930-3

# METROLOGY
# /
# МЕТРОЛОГИЈА
# (MLI/МЛ)

ISBN 978-86-7466-930-3

# An Intercomparison of the Broadband Electrical Field Meter NARDA NBM 550

Nenad Munić, Aleksandar M. Kovačević, Nenko Brkljač, Ljubiša Tomić

***Abstract*— This paper presents the intercomparison of five broadband electric field meters from the three laboratories. The Intercomparison was performed in broadband frequency range at different level of the electric field meter. The measurement results were compared using the z-score criteria. The intercomparison was performed with the aim of confirming the accuracy of broadband electric field meters, until the realization of calibration in an accredited metrology laboratory.**

***Index Terms* — Intercomparison, Broadband Electric Field Meter, z-score, Calibration.**

## I. Introduction

DIFFERENT measuring equipment can be used during the tests. Their accuracy can significantly affect the reliability of the measurements. Therefore, the measuring equipment must be calibrated before use [1]. In doing so, each laboratory must establish a program and procedure for calibrating its measuring equipment. Due to all the above, the Technical Testing Center (TTC) [2], a specialized military scientific research institution, in accordance with the requirements of the quality management system [3], developed a Procedure [4] for periodic calibration of measuring equipment.

One of the ways to determine and review the deadline for periodic calibration of measuring equipment are intermediate checks [1, 4]. In that case, the method of checking certain metrological characteristics of measuring equipment between two calibrations is used, in one of the following ways: a) using a references instrument; b) using a specially designed test device; c) participation in interlaboratory comparisons; e) participation in intercomparison.

Participation in intercomparison is one of the requirements for laboratories that are entering the accreditation process or have already been accredited [5]. Positive results of intercomparison are confirmation of the accuracy of measurements performed in the laboratory and the competence of that laboratory.

Intercomparison of meters is performed at the request of the user of the meter. In doing so, the intercomparison is performed by the laboratory user of the meter, and if necessary, other laboratories and the competent metrological laboratory can also participate [4]. Measurement intercomparison means the comparison of metrological characteristics of meters of the same type and approximately the same measurement uncertainty under established conditions.

Due to the complicated procedure of calibration in foreign accredited metrological laboratories, and for the needs of measuring in the field of electromagnetic compatibility (EMC), the Department of Electromagnetic Compatibility and Environmental Impacts in TTC initiated and organized intercomparison of broadband EM field meter NBM-550 with other broadband electric field S.A 43, manufactured by CHAUVIN ARNOUX [6].

In the meantime, the number of intercomparison participants increased, at the request of laboratories dealing with risk assessments at workplaces and in the work environment, (non-ionizing radiation), the Institute of Occupational Medicine of the Military Medical Academy (MMA) [7] and the Military Hospital in Nis [8]. A total of five meters from three laboratories were used in this intercomparison.

Intercomparison was performed for two cases: in the first case when setting defining value of electric field from the frequency range of meter and in the second case by measuring several different values of electric field at a certain frequency. Measurement results were compared using the z-score criterion.

The goal of the intercomparison is to extend the use of the broadband EM field meter NBM-550, manufactured by NARDA, until the realization of calibration in an accredited metrological laboratory. Namely, the aim of processing the results of intercomparison of these measures is to analyze the results according to the criteria for measures of the same type and approximately the same measurement uncertainty, under established conditions, then to determine the acceptability of results, and thus confirm their applicability to measure electric field strength.

## II. Intercomparison Conditions

The intercomparison was performed in the Faraday cage of the Technical Experimental Center, as shown in Fig. 1.

The subject of intercomparison are broadband EM field meters, as follows:

– Narda NBM-550, s/n: B-0503, with antenna (sensor) EF0391, s/n: A-0610 (Sen 1);
– Narda NBM-550, s/n: B-0594 with antennas (sensors):

Nenad Munić, , Nenko Brkljač, Ljubiša Tomić– Tehnički opitni centar, Generalštab Vojske Srbije, Vojvode Stepe 445, 11000 Beograd, Srbija (email: nenadmunic@yahoo.com).

Aleksandar M. Kovačević– Fakultet tehničkih nauka Čačak, Univerzitet u Kragujevcu (email: aleksandarkovacevic1962@yahoo.com).

 ISBN 978-86-7466-930-3

- EF0391, s/n: A-0700 (Sen 2);
- EF6091, s/n: 01084 (Sen 3);

– Narda NBM-550, s/n: H-0386 with antennas (sensors):
- EF0691, s/n: H-0550 (Sen 4);
- EF5091, s/n: 01606 (Sen 5);

Fig. 1. Electric field strength measurement with electric field meter, transmitting Ultra log antenna.

Fig. 2. NBM-550, „NARDA“ [6].

Intercomparison was performed by comparing the measured values of the electric field of different antennas (sensors) of EM field meters for the case when changing:
- transmission signal frequency (constant transmission power level),
- transmission signal strength (fixed transmission frequency).

EM field meters NBM-550, with its corresponding antenna (EF0391, EF6091 or EF5091), are mounted on a non-conductive styrofoam bracket mounted on a conductive table in a Faraday cage at a distance of 1.45 m from the transmitting antennas: Ultra log antennas (Fig. 1) or double-crest antennas (Fig. 3). The height of the transmitting antennas of 1.385 m corresponds to the height at which the antenna of the EM field meter is located.

Fig. 3. Electric field strength measurement with electric field meter, double-ridge transmitting antenna.

The NBM-550 meter is controlled by an application installed on a PC, NBM-TS PS Transfer software V 2.1.1. EM field meters are connected via a suitable optical cable and converter to a PC to monitor the value of the electric field.

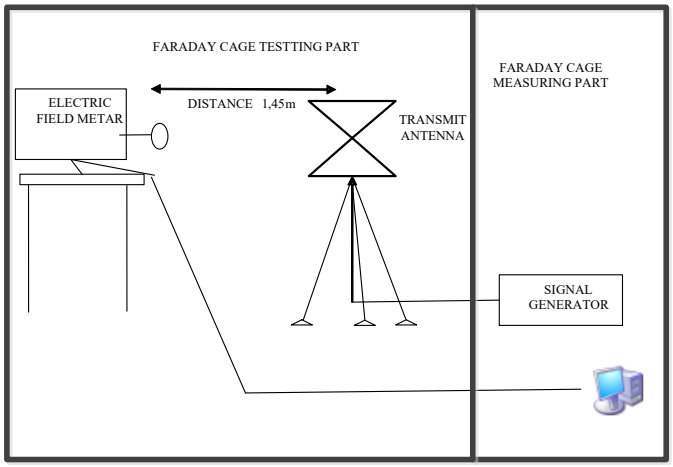


Fig. 4. Block diagram of measuring the strength of electric field, for different frequencies and fixed power level of signal generator.

The measurement is first performed when the excitation frequency is variable, by setting the transmit power level to the maximum value allowed by the signal generator. The block diagram of measuring the value of the electric field strength with the NBM-550 "NARDA" meter, in case when

 ISBN 978-86-7466-930-3

the frequency of the excitation signal was being changing is shown in Fig. 4.

For fixed frequency measuring, a signal amplifier was used while the excitation power level changed. The operating frequency is determined in the previous measurement by selecting the frequency from the middle of the measuring range at which the highest values of the electric field were achieved. In this case, the frequency of 600 MHz is selected. The block diagram of this measurement is shown in Fig. 5.

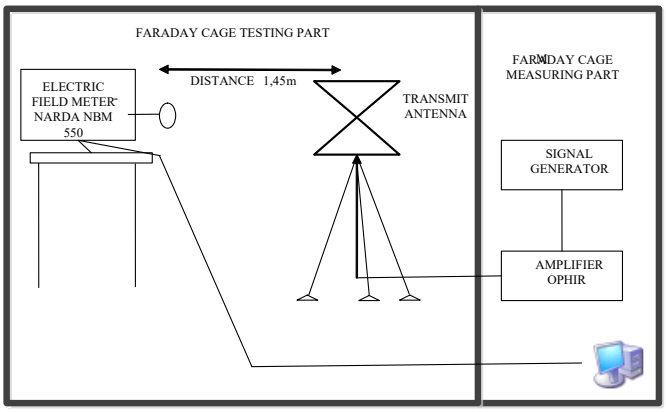


Fig. 5. Block diagram of measuring the strength of electric field, for different values of power levels and at a fixed frequency of signal generator.

The following measuring instruments and equipment were used for testing purposes:

- Broadband EM field meters NBM-550, "NARDA", listed in Chapter II,
- Signal generator SMB100, R&S, s/n. 1406.6000K03-178572-eW,
- RF amplifier 5126, „OPHIR“, from 20 MHz to 1000 MHz, s/n. 1020,
- ULTRALOG antenna HL562, R&S, ser. num. 1000324
- double-ridge antenna 960001, AILTECH, ser. br. 2097,
- Optical cable, 115200 Bd, length of 20 m,
- Cables RG-214/U (N-N), length of 10 m and 1,5 m,
- Wooden stand (tripod).
- Laptop with NBM-TS PS Transfer software V 2.1.1

At the same time, the characteristics of the measuring equipment meet the prescribed standards [9, 10].

Environmental conditions:

- temperature: 24 °C ± 2 °C,
- relative humidity:50 % ± 15 %.

## III. INTERCOMPARISON CRITERIA

As a criterion for evaluating the results of intercomparison, taking into account all the specifics of the measurement, the z-score was adopted, in accordance with the standard ISO 13528: 2005 [9, 10]. As five test samples participated in the comparison, the mean value of the test results for all samples was taken as the assigned (reference) value $X_{\text{ref}}$. The z-score should indicate whether the measured value deviates significantly from the assigned value, in our case from the mean value of the test results, taking into account the standard deviation $\sigma$.

The z-score is calculated as follows [10]:

$$z_i = \frac{x_{\text{lab}i} - X_{\text{ref}}}{\sigma}, i = 1, 2, \ldots, 5. \quad (1)$$

where:

$x_{\text{lab}_i}$ test results for each sample (i = 1, 2, ... , 5);

$X_{\text{ref}}$ the assigned (reference) value is the mean value of the test results of all samples,

$$x_{\text{ref}} = \frac{\sum_{i=1}^{n} x_{lab_i}}{n}, \text{ n = 5 ;} \quad (2)$$

$\sigma$ standard deviation for non-repeat testing,

$$\sigma = \sqrt{\frac{\sum_{i=1}^{n} (x_{lab_i} - x_{\text{ref}})^2}{n}}, \text{ n = 5.} \quad (3)$$

The z-score coefficient can be positive or negative and determines the number of standard deviations of the data set from the arithmetic mean. A negative result indicates a value less than the mean, and a positive result indicates a value greater than the mean, with the average of each z-score weighing to zero.

The value of z-score is interpreted as follows:

- A result that gives $|z| \leq 2{,}0$ is considered to be acceptable;
- A result that gives $2{,}0 < |z| < 3{,}0$ is considered to give a warning signal;
- A result that gives $|z| \geq 3,\ 0$ is considered to be unacceptable (or action signal) and the participants should be advised to check their measurement procedures following warning signals in case they indicate an emerging or recurrent problem [10].

## IV. RESULTS OF INTERCOMPARISON

The results of intercomparison at a given maximum signal level of the signal generator and different frequency values are shown in Table I. Based on the results obtained from Table I and the calculation of mean and standard deviation, and using formula (1) obtained values of z-score coefficient, shown in Table II.

TABLE I
RESULTS OF MEASUREMENT THE STRENGTH OF ELECTRIC FIELD, FOR DIFFERENT FREQUENCIES AND FIXED POWER LEVEL OF SIGNAL GENERATOR

| $f$ (MHz) | $E_{\text{sen1}}$ (V/m) | $E_{\text{sen2}}$ (V/m) | $E_{\text{sen3}}$ (V/m) | $E_{\text{sen4}}$ (V/m) | $E_{\text{sen5}}$ (V/m) |
|---|---|---|---|---|---|
| 100 | 5,59 | 5,63 | 4,409 | 5,954 | / |
| 200 | 6,176 | 6,194 | 4,696 | 6,272 | / |
| 300 | 17,89 | 17,68 | 15,26 | 18,36 | 15,52 |
| 400 | 16,93 | 17,14 | 14,93 | 15,77 | 16,15 |


ISBN 978-86-7466-930-3

| $f$ (MHz) | $E_{sen1}$ (V/m) | $E_{sen2}$ (V/m) | $E_{sen3}$ (V/m) | $E_{sen4}$ (V/m) | $E_{sen5}$ (V/m) |
|---|---|---|---|---|---|
| 500 | 10,45 | 11,02 | 8,529 | 9,725 | 7,103 |
| 600 | 22,14 | 21,7 | 21,27 | 21,9 | 21 |
| 700 | 11,92 | 13 | 11,2 | 12,56 | 9,8 |
| 800 | 7,73 | 7,654 | 5,118 | 7,465 | 5,18 |
| 900 | 18,48 | 19,01 | 19,46 | 21,5 | 16,14 |
| 1000 | 20,54 | 20,81 | 18,83 | 21,71 | 19,11 |
| 1200 | 12,89 | 13,05 | 12,84 | 14,84 | 10,52 |
| 1400 | 10,5 | 9,947 | 6,758 | 9,835 | 5,836 |
| 1600 | 10,85 | 10,55 | 8,499 | 10,34 | 5,912 |
| 1800 | 8,366 | 9,512 | 8,485 | 8,831 | 8,154 |
| 2000 | 11,61 | 12,05 | 12,78 | 12,11 | 12,23 |
| 2200 | 11,58 | 10,89 | 4,124 | 10,18 | 4,918 |
| 2400 | 9,145 | 8,299 | 12,26 | 10,23 | 13,45 |
| 2600 | 5,356 | 3,989 | 2,642 | 4,322 | 2,234 |
| 2800 | 11,76 | 9,156 | 7,031 | 10,57 | 5,24 |
| 3000 | 7,669 | 6,529 | 7,422 | 7,858 | 5,421 |
| 3500 | / | / | 6,643 | 10,07 | 4,511 |
| 4000 | / | / | 5,906 | 13,16 | 4,112 |
| 4500 | / | / | 10,41 | 6,313 | 8,919 |
| 5000 | / | / | 5,396 | 6,085 | 4,136 |
| 5500 | / | / | 6,942 | 6,548 | 5,377 |
| 6000 | / | / | 4,875 | 5,005 | 3,158 |
| 7000 | / | / | 2,041 | / | 1,287 |
| 8000 | / | / | 3,957 | / | 2,921 |
| 9000 | / | / | 2,436 | / | 3,427 |
| 10000 | / | / | 1,58 | / | 2,756 |
| 11000 | / | / | 0,6134 | / | 1,72 |
| 12000 | / | / | 0,8626 | / | 2,786 |
| 13000 | / | / | 0,258 | / | 2,819 |

TABLE II
RESULTS OF Z-SCORE, FOR DIFFERENT FREQUENCIES AND FIXED POWER LEVEL OF SIGNAL GENERATOR

| $f$ (MHz) | $z_{sen1}$ | $z_{sen2}$ | $z_{sen3}$ | $z_{sen4}$ | $z_{sen5}$ |
|---|---|---|---|---|---|
| 100 | 0,330 | 0,399 | -1,681 | 0,951 | / |
| 200 | 0,518 | 0,546 | -1,729 | 0,664 | / |
| 300 | 0,735 | 0,572 | -1,305 | 1,100 | -1,103 |
| 400 | 0,930 | 1,192 | -1,563 | -0,516 | -0,042 |
| 500 | 0,772 | 1,178 | -0,595 | 0,256 | -1,610 |
| 600 | 1,296 | 0,236 | -0,800 | 0,718 | -1,451 |
| 700 | 0,198 | 1,158 | -0,440 | 0,767 | -1,684 |
| 800 | 0,908 | 0,845 | -1,247 | 0,689 | -1,195 |
| 900 | -0,253 | 0,053 | 0,3143 | 1,496 | -1,610 |
| 1000 | 0,314 | 0,564 | -1,268 | 1,398 | -1,009 |
| 1200 | 0,045 | 0,161 | 0,008 | 1,465 | -1,680 |
| 1400 | 1,015 | 0,723 | -0,958 | 0,664 | -1,444 |
| 1600 | 0,874 | 0,712 | -0,394 | 0,599 | -1,792 |
| 1800 | -0,639 | 1,773 | -0,388 | 0,339 | -1,085 |
| 2000 | -1,452 | -0,282 | 1,660 | -0,122 | 0,196 |
| 2200 | 1,026 | 0,807 | -1,334 | 0,583 | -1,083 |
| 2400 | -0,798 | -1,239 | 0,825 | -0,232 | 1,445 |
| 2600 | 1,446 | 0,246 | -0,936 | 0,538 | -1,295 |
| 2800 | 1,275 | 0,171 | -0,729 | 0,771 | -1,488 |
| 3000 | 0,763 | -0,499 | 0,489 | 0,972 | -1,726 |
| 3500 | / | / | -0,188 | 1,308 | -1,119 |
| 4000 | / | / | -0,465 | 1,389 | -0,923 |
| 4500 | / | / | 1,100 | -1,319 | 0,219 |
| 5000 | / | / | 0,235 | 1,089 | -1,325 |
| 5500 | / | / | 0,982 | 0,389 | -1,372 |
| 6000 | / | / | 0,62 | 0,78 | -1,41 |

The results of the intercomparison of the measurement of the electric field value with the NARDA NBM-550 meter, for different values of the power level at a fixed frequency of the signal generator, are shown in Table III. Based on the results obtained from Table III and the calculation of the mean and standard deviation, and using formula (1), the values of the z-score coefficient were obtained, which are shown in Table IV.

TABLE III
RESULTS OF MEASUREMENT THE STRENGTH OF ELECTRIC FIELD, FOR DIFFERENT VALUES OF POWER LEVELS AND AT A FIXED FREQUENCY OF SIGNAL GENERATOR

| $P_{gen}$ (dBm) | $E_{sen1}$ (V/m) | $E_{sen2}$ (V/m) | $E_{sen3}$ (V/m) | $E_{sen4}$ (V/m) | $E_{sen5}$ (V/m) |
|---|---|---|---|---|---|
| -20 | 5,016 | 5,212 | 5,215 | 5,947 | / |
| -15 | 8,879 | 9,202 | 9,362 | 10,58 | 2 |
| -10 | 15,62 | 16,29 | 17,02 | 18,69 | 14,66 |
| -5 | 27,88 | 28,66 | 31,99 | 32,99 | 30,15 |
| 0 | 50,4 | 51,33 | 61,92 | 58,16 | 55,56 |
| 5 | 90,37 | 92,69 | 114,6 | 104,1 | 94,89 |
| 10 | 161,1 | 161,1 | 203,5 | 189,7 | 167,2 |
| 15 | 255,1 | 253,3 | 309,7 | 310,9 | 262,1 |

TABLE IV
RESULTS OF *Z-SCORE,* FOR DIFFERENT VALUES OF POWER LEVELS AND AT A FIXED FREQUENCY OF SIGNAL GENERATOR

| $P_{gen}$ (dBm) | $z_{sen1}$ | $z_{sen2}$ | $z_{sen3}$ | $z_{sen4}$ | $z_{sen5}$ |
|---|---|---|---|---|---|
| -20 | 0,341 | 0,431 | 0,433 | 0,771 | / |
| -15 | 0,286 | 0,391 | 0,444 | 0,842 | -1,964 |
| -10 | -0,614 | -0,121 | 0,414 | 1,641 | -1,319 |
| -5 | -1,270 | -0,866 | 0,857 | 1,375 | -0,095 |
| 0 | -1,184 | -0,967 | 1,505 | 0,627 | 0,020 |
| 5 | -1,001 | -0,742 | 1,707 | 0,533 | -0,496 |
| 10 | -0,901 | -0,901 | 1,576 | 0,770 | -0,544 |
| 15 | -0,877 | -0,945 | 1,194 | 1,239 | -0,611 |

Table V gives the budget of measurement uncertainty of electric field strength measurement, measuring instruments NBM-550 "NARDA". For the stated influential quantities (sources of measurement uncertainty), the estimation of measurement uncertainty was performed on the basis of data


ISBN 978-86-7466-930-3

from the manufacturer's specification and calibration certificates.

TABLE V
UNCERTAINTY MEASUREMENT BUDGET FOR THE CASE OF MEASURING THE STRENGTH OF THE ELECTRIC FIELD WITH THE METER NBM-550 „NARDA [6]

| Uticajna veličina $X_i$ | Procena $X_i$ ($x_i$) | | Standardna nesigurnost $u(x_i)$ | Koeficijent osetljivosti $c_i$ | Doprinos standardnoj nesigurnosti $u_i(y)=c_i\,u(x_i)$ |
|---|---|---|---|---|---|
| | Vrednost (dB) | Funkcija raspodele | | | |
| Merni prijemnik: Tačnost prijema sinusnog signala | ±3,0 | normalna $k = 2$ | 1,5 | 1 | 1,5 |
| Antena – merni prijemnik | +0,9 −1,0 | U-oblika $k = 1,414$ | 0,67 | 1 | 0,67 |
| Korekcije mernog prostora | | | | | |
| Nesavršenost mernog prostora | ±4,0 | trougaona $k = 2,449$ | 1,63 | 1 | 1,63 |
| Varijacije mernog rastojanja | ±0,2 | pravougaona $k = 1,732$ | 0,1 | 1 | 0,1 |
| Visina antenskog postolja na kome se nalazi merni prijemnik | ±0,1 | normalna $k = 2$ | 0,05 | 1 | 0,05 |
| | | | | | |
| Ponovljivost sistema merenja (tip **A**) | ±0.006910 | Standardna devijacija | 0.006910 | 1 | 0.006910 |
| Kombinovana standardna nesigurnost $u_c(y)$ | | normalna | $u_c(y) = \sqrt{\sum_i u_i^2(y)}$ | | 2,3 |
| Proširena merna nesigurnost $U$ | | нормална $k_p = 2$ | $U = k_p u_c(y)$ | | **4,63 dB** |

## V. CONCLUSION

Due to the complicated procedure of calibration in foreign metrological laboratories, and due to the need to confirm the accuracy of five EM field meters NBM-550, the Department of Electromagnetic Compatibility and Environmental Impacts in TTC, initiated and organized intercomparison. The intercomparison was also attended by laboratories that deal with risk assessments at workplaces and in the work environment, from the point of view of non-ionizing radiation, the Institute of Occupational Medicine of the Military Medical Academy and the Military Hospital in Nis.

The result of intercomparison according to frequencies and electric fields strength is represented by the numerical value of the z-score model in Tables 3 and Table 5. Based on the presented results, we conclude that the values of z-score, $|z| \leq 2$ and that the results are satisfactory (acceptable), and no corrective measures are needed. This shows that the deviations in the measurements, the values of the electric field between the five meters are acceptable in the entire frequency range of the meters.

The goal of the intercomparison, which was to extend the use of the broadband EM field meter "NARDA" NBM-550, until the realization of calibration in the accredited metrology laboratory is fulfilled. NBM-550 "NARDA" meters can be used to measure the strength of the electric field, until the realization of calibration in an accredited metrological laboratory.

Based on the above and the analysis of the conducted procedure and the results of the comparison of meters, it can be concluded that the conducted intercomparison procedure is currently sufficient to consider the metrological characteristics of NBM-550 "NARDA", but not metrological confirmation in terms of SRPS ISO / IEC 17025: 2006.

## REFERENCES


[1] Opšti zahtevi za kompetentnost laboratorija za ispitivanje i laboratorija za etaloniranje, SRPS ISO/IEC 17025:2017/Ispr.1:2018.
[2] http://www.toc.vs.rs.
[3] *Sistemi menadžmenta kvalitetom — Zahtevi, SRPS ISO 9001:2015.*
[4] *Procedura za preispitivanje rokova periodičnog etaloniranja merne opreme TOC,* Interni dokument B.00.081, TOC, 2005.
[5] *Pravila o učešću u programima za ispitivanje osposobljenosti i međulaboratorijskim poređenjima, ATS-PA02, Akreditaciono telo Srbije, Beograd, jul 2021.*
[6] *Aleksandar M. Kovačević, Ljubiša Tomić, Nenad Munić, Veljko Nikolić „Interkomparacija širokopojasnog merača električnog polja“, ETRAN 2016.*
[7] *http://www.vma.mod.gov.rs/*
[8] *http://www.vbnis.mod.gov.rs/*
[9] *Conformity assessment – General requirements for proficiency testing, ISO/IEC 17043:2010,*
[10] *Statistical methods for use in proficiency testing by interlaboratory comparisons, ISO 13528:2005.*


 ISBN 978-86-7466-930-3

# LiDAR measurements in Maritime transport safety and navigation of the deep seafloor

Dijana Džever, Marjan Urekar, *Member, IEEE*

***Abstract*— This paper provides an insight into how LiDAR can be applied for the benefit of shipping, sea and ocean traffic, as well as for navigation and detection of the deep seafloor. The current measuring and control methods of this sensor are presented along with the used equipment. The principles of sensor operation are described. The aim of this paper is to emphasize the future applications of LiDAR in ocean transport and its safety, as well as the detection and visualization of the underwater world and its hidden objects.**

***Index Terms*—**LiDAR; maritime; safety; seafloor; sensor; airborne; shipping; bathymetry; laser.

## I. INTRODUCTION

Nowadays, LiDAR (*Light Detection and Ranging*) is widely used in order to examine various properties of the atmosphere, in autonomous driving and many other aspects such as mapping and topography. LiDAR's possibilities in autonomous driving are highly evolving these days but, if we think about the other types of traffic such as oceanic transport, or transportation and navigation in general, we can see that it is not developed and utilized enough to fulfill the needs for a safer transport. This topic is possibly disregarded because of the limitations in the underwater use, which seem to cause more issues regarding its development, in comparison to LiDAR's use in the atmosphere and earth's surface. In this paper, the discussion on how LiDAR can be used to benefit shipping, navigation, autonomous navigation, present weather measurements and detection, is made and some proposals are given. The scope of this work is to present the multiple usages that LiDAR can offer in shipping together with a total proposed solution for the deep seafloor and underwater world detection. New and unfamiliar usages of LiDAR that could change the future in many ways are given some thought. I would like to emphasize the possibility of LiDAR's role in coastline protection, biological analysis of deep seafloor species, animals, algae's and other water plants and sea sponges. Also, one of the interesting applications are detection of water salinity levels and the analysis of chemical properties of underwater minerals. Later, we will mention a few more applications of LiDAR with their advantages, that could bring humanity more knowledge regarding the underwater world.

Dijana Džever – Fakultet tehničkih nauka, Univerzitet u Novom Sadu, Trg Dositeja Obradovića 6, 21000 Novi Sad, Srbija (e-mail: dzeverdijana@gmail.com).

Marjan Urekar – Fakultet tehničkih nauka, Univerzitet u Novom Sadu, Trg Dositeja Obradovića 6, 21000 Novi Sad, Srbija (e-mail: urekarm@uns.ac.rs).

## II. WORKING PRINCIPLE OF LIDAR SENSOR

LiDAR represents a digital optical measuring device for the detection and range of light. It is a remote sensing method that uses light in the form of a pulsed laser beam to measure the range, more precisely the variable distance to Earth. This sensor emits laser output pulses that have variable frequencies and intensity, while pulsed rays pass through the project area. Outgoing impulses are reflected from the surface objects and from the ground, and later, they are detected and captured by the sensor itself. The time delay between transmission and detection of each feedback pulse provides the distance from the sensor to the surface object, producing its 3D model [8].

In general, when we speak about the working principle of LiDAR, it is similar to EDMI devices [17], where a pulse, continuous wave or laser is fired from a transmitter, and later the reflected energy is captured.

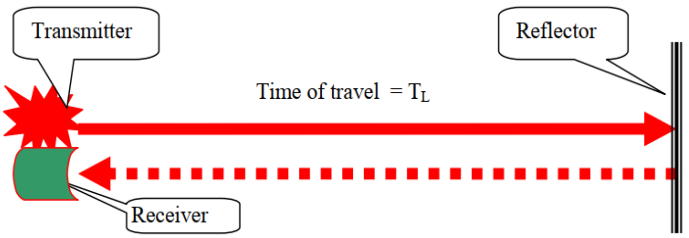


Fig. 1. Range measurement using laser principle [8]

The measuring distance from the transmitter and the reflector is determined by calculating the time of travel ($T_L$ / ToT). In some specific cases, the role of the reflector can be some natural object or an artificial reflector such as a prism. A laser pulse is emitted from an aircraft, to measure the terrain elevation from the time between emission and reception of reflected pulses. Measuring distance provides the coordinates (x, y, z) of the reflector.

 ISBN 978-86-7466-930-3

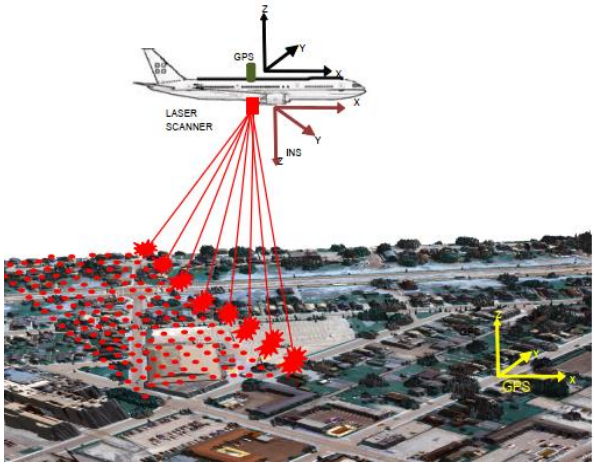


Fig. 2. LiDAR topographic system [8]

Flow diagram below indicates implemented sensors of various kinds in a LiDAR instrument, as well as the computation steps which form the ground and underwater coordinates.

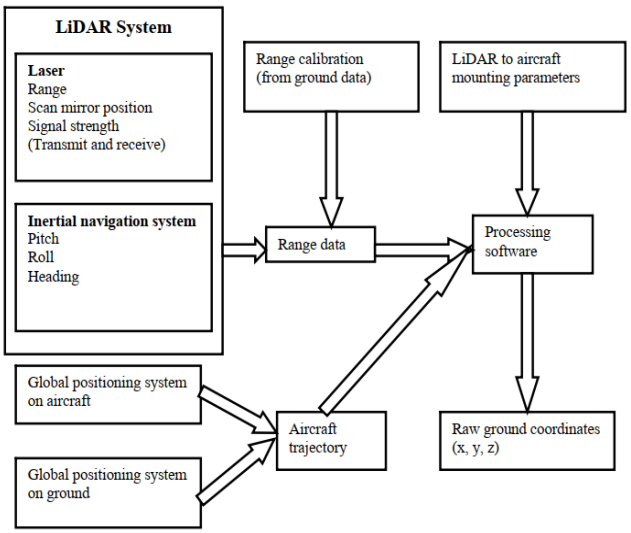


Fig. 3. An illustration of flow diagram used for computation of the ground coordinates [8]

## III. AIRBORNE TOPOGRAPHIC LIDAR

Airborne LiDAR System or ALS which stands for Airborne Laser Scanning represent a remote sensing technique used to measure the distance to an object. The basic principle of measuring distance to an object using this type of LiDAR is by determining the time of flight for an emitted laser beam. Basically, a laser pulse is emitted from an aircraft in order to measure the terrain elevation, which is derived from the time between emission and reception of reflected pulses. Then, the x, y, and z coordinates are registered through laser altimetry. Technologies on which LiDAR relies for its operation on are Global Positioning System (GPS) and Inertial Measurement Unit (IMU). The importance of these technologies plays the crucial part in airborne LiDAR scanning because it provides LiDAR with the location and orientation of the remote sensor which is located on the airborne platform. This technique has a special application in shallow waters.

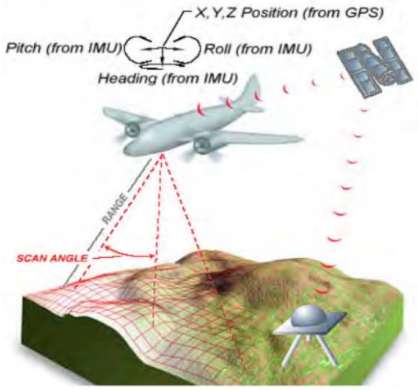


Fig. 4. Airborne LiDAR technology in the process of providing the location of the airborn platform, using a laser beam, GPS and IMU systems [7]

### A. *Bathymetric LiDAR*

When there is a need for scanning water bodies or even some ocean traffic points such as bridges, piers, dams and other infrastructure, topographic LiDAR does not complete this task. In order to accomplish sensing of these areas and objects, bathymetric LiDAR is commonly used. The main difference between these two types of LiDAR sensors is that a bathymetric LiDAR has the ability to shoot green laser pulses, while every other component of the bathymetric LiDAR is the same as the topographic one.

The basic principle implies the action of the pulses penetrating the water surface and then returning back to the sensor which is attached to the airborne vehicle. Estimated depth of the water and water bodies is attained by processing the collected data. As it is mentioned already, a laser pulse is transmitted to the water surface, where a portion of the energy is recaptured back to the optical receiver. The remainder of the pulse continues to penetrate to the water bottom through the water column and later, is reflected back to the receiver. Two main factors that defines the maximum depth penetration for a laser are water clarity and bottom reflection. LiDAR can measure various depths from 0.9 m to 40 m with a vertical accuracy of ±15 cm and horizontal accuracy of ±2.5 m, depending on the water clarity. It is important to mention that the elapsed time between the bottom pulses and the received surface allows determination of the water depth.

 ISBN 978-86-7466-930-3

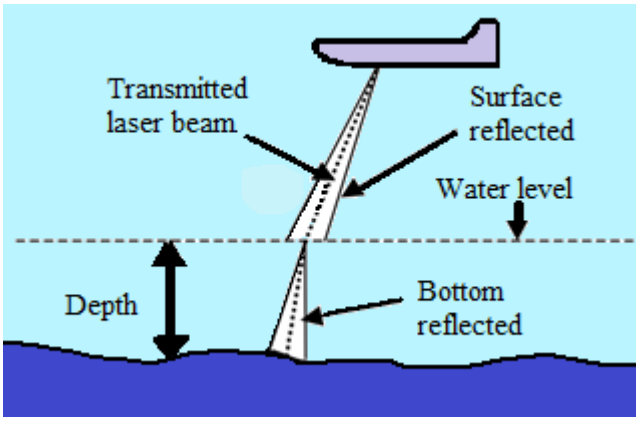


Fig. 5. Basic principle of bathymetric LiDAR [8]

Among all of those parameters mentioned before, water turbidity [18] is the most important one. It is defined as a factor caused by suspended or dissolved particles in water. Those particles scatter light in the water, making it appear cloudy. As far as water penetration is concerned, it is equal to two to three times the Secchi depth [19], which means three times the penetration depth of natural sunlight in a given water column. To be able to compute the water depth, the bottom and surface signals should be clearly distinctive, but in case of shallow depths, these signals overlap. This situation makes determination of the water depth unavailable.

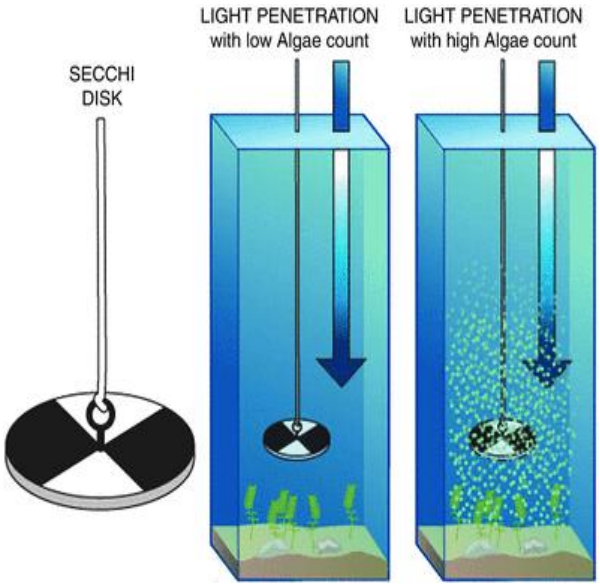


Fig. 7. Display of Secchi disk which is used to measure water clarity [19]

*B. Bathymetric LiDAR Sensor Characteristics*

When we discuss modern bathymetric LiDAR sensors, it should be noted that it can measure topography in addition to bathymetry, which is a double feature and a great advantage over a traditional topographic LiDAR sensor. It can measure both shallow and deep water systems.

The limit for shallow water is < 10 m and the lower limit for deep water systems is > 10 m. Characteristics of the shallow water systems are a higher measurement frequency, they have a higher resolution, and they have less laser power per pulse and smaller laser footprint diameter. A smaller receiver FOV (field of view) is also characteristic for them and they can only measure water depths within the visible water column. Opposite to this, the deep-water bathymetric LiDAR systems have a lower measurement frequency, low resolution, and they use more laser power per pulse. Also, a larger receiver field of view and a larger laser footprint is used within deep water LiDAR systems.

Depth penetration capability of the laser varies in between 2.0 to 3.0 times the Secchi depth measurement, as it was mentioned before. It is common for survey operators to utilize both sensors for shallow and deep water systems simultaneously, in order to achieve maximal coverage and detail. It is managed by combining those sensors in twin optical port survey aircraft.

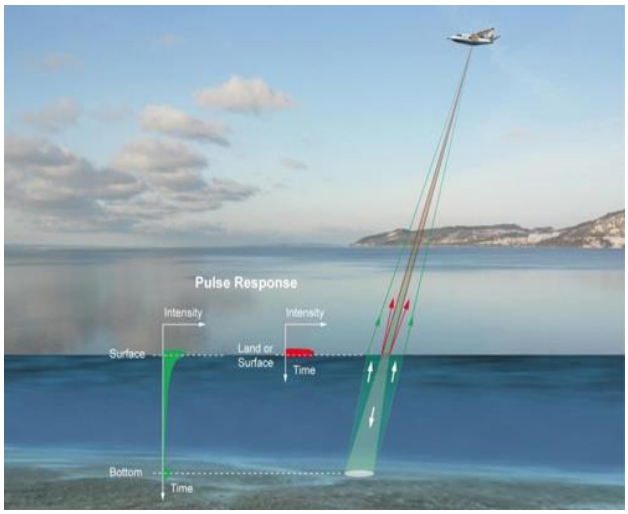


Fig. 6. Illustration of bathymetric LiDAR measurement [17]

We can see that the most important factor when bathymetric LiDAR systems are employed, is its laser energy per pulse, because the laser power represents the strongest influence on depth penetration, when it's combined with the pulse duration. This is important because the combination of high laser power and pulse duration, can provide us with a result even in deeper water column penetration. All of this mentioned influences a full insonification of the seabed, besides the fact that a high resolution laser's energy per pulse and low measurement frequency will result in a lower point density.

 ISBN 978-86-7466-930-3

### C. *Advantages and disadvantages of bathymetry*

In comparison to methods of topographic data collection such as land surveying, GPS, interferometry, and photogrammetry, LiDAR technology has some great advantages. Over time, LiDAR technology is rapidly improving, as well as its sensors characteristics. Some of them are listed below:

- Higher accuracy and data density
- Fast acquisition and processing
- Minimum human dependence
- Weather/Light independence (not dependent on the sea state)
- Canopy penetration possibilities
- Additional data storage
- High costs
- Fast method (up to 70 $km^2$ per hour over large linear areas)
- Reflectivity gives information on seafloor characteristics

Also, like every other sensor or detector used nowadays, these sensors have some disadvantages likewise. With that being said, some disadvantages of the LiDAR sensor are:

- Aircraft usage is weather dependent
- Applicable in clear shallow water only
- Less resolution than multibeam unless resolution survey is very high
- Limited penetration in high turbidity areas such as sandy shores
- Hard to use in shallow water depths ( < 0.5 m)

## IV. ENVIRONMENTAL CONSIDERATIONS

All of the external environmental effects can impact the water column in bathymetric LiDAR measurements. It makes them more sensitive and can lead to data errors, gaps, bad measurement quality and reduced data coverage. It can produce problems and increase cost. Preparations for a successful bathymetric LiDAR survey and measurements, imply numerous factors that needs to be considered in order to minimize unfavorable impacts. These include tides, turbidity, vegetation condition, sea state, ground control accessibility, traffic controls and last but not least weather conditions for flying the aircraft. Important conditions which impact shallow-water laser penetration from bathymetric LiDAR sensors, need to be properly understood and managed before measurement and processing of data. One major hindrance for this process is water clarity, which can either be satisfactory or insufficient. The lack of water clarity can cause great problems for the bathymetric LiDAR sensor. Furthermore, there are other factors that can disrupt the sensor, such as sea grass, low-reflectance and high turbidity.

Considerations of environmental factors and individual characteristics of the system are very important when selection and employment of LiDAR is in focus. Some important attributes and points of a best system for a survey are environment, survey area, sensor availability and project requirements. Point density, coverage, maximum depth, final product requirements and intended purpose for the data are some of the most important aspects that determine the choice of sensor. Even when the choice is the right one, the knowledge and experience of the operator is the key to a successful survey.

## V. AUTONOMOUS SHIPPING

Since LiDAR is not very widespread and investigated around the world, so it had recently paved a path towards a better understanding and greater investigation as well as exploration. We are surrounded by deep waters and oceans that are considered as mysterious areas in the manner of exploration, even in the 21st century with all of technological opportunities and achievements.

Exploration of deep oceans is a complex process. Maritime transport requires knowledge of terrestrial parameters, climate change and accurate weather forecasts in order to ensure safe trips. In addition, all of these conditions need to be fulfilled to achieve accurate LiDAR measurements. Protecting marine and coastal environment, bridges and various objects, is considered as one of the more important tasks of this sensor. However, it can serve for the purpose of updating nautical charts, cable landing sites which are connected to undersea fiber communication projects and off-shore wind farms.


Fig. 8. EchoBoat-240 seafloor system [13]

EchoBoat-240 Unmanned Surface Vessel dockside will eventually be demonstrated by Seafloor Systems. It excels in mapping shallow bodies of water. EchoBoat-240 has navigation abilities that led it into the real of fully-autonomous vehicles. A portable multibeam survey vessel will be displayed by the Seafloor System as a new platform which combines heightened portability and high-resolution data quality of a multibeam sonar.

 ISBN 978-86-7466-930-3

Predictions assume that LiDAR will be crucial in mapping and monitoring of coastlines which could bring us many new improvements in safety transport, investigation of the seafloor and even in ecology.

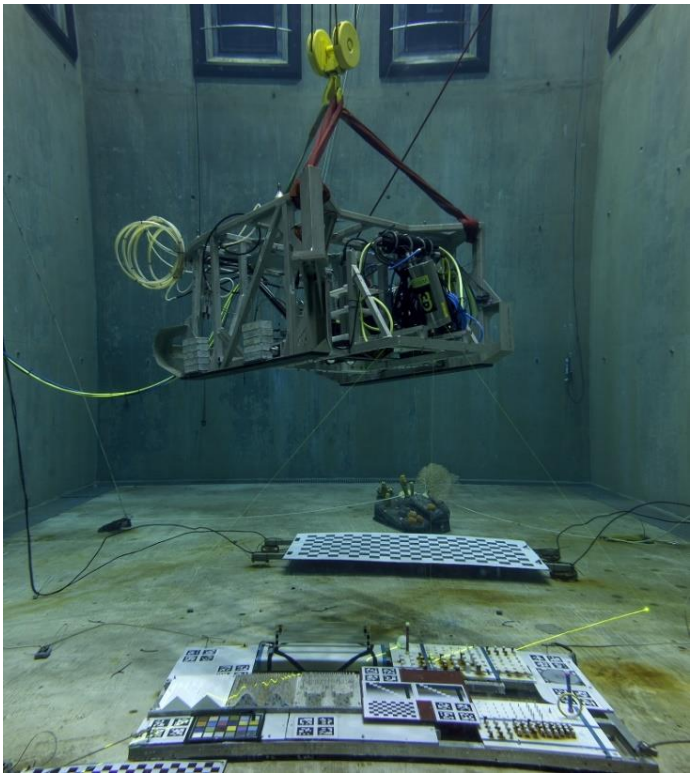

Fig. 9. Wide Swath Subsea LiDAR system in a test tank flown at a low altitude to achieve much higher resolutions than systems imaging from further off the bottom [2]

The Wide Swath Subsea LiDAR sensor, called WiSSL is able of mapping large areas at a 1 cm resolution. Its lasers are capable of pulsing 40,000 times per second in order to produce discrete surroundings. 90 degree vide field of view is made possible due to the WiSSL being equipped with two optical heads. With that being said, it is possible to achieve full bottom coverage at a maximum velocity of 1 m/s. Therefore, it is concluded that WiSSL is the first subsea LiDAR optimized for efficient mapping in the deep ocean [2].

Automated guided vehicles that are capable of providing real-time position data on port infrastructure, people, and objects, have one of the important roles in LiDAR application. The role of LiDAR sensors is to provide and enhance predictability and reliability, being a valuable component to port equipment. It can also improve efficiency and reduce risks and costs in marine transport and seafloor exploration processes.


Fig. 10. This photo shows launching the ROV Ventana into the ocean [2]

## VI. CURRENT APPLICATIONS IN MARITIME TRANSPORT

One of the newest applications regarding maritime transport and safety is helicopter-mounted laser that scans and detects underwater mine targets. The US Navy is the first user of this system which brings faster detection and a wider FOV to countermine investigating missions.

LiDAR type that enables high-speed shallow water mine detection and efficient results and data processing, is called Airborne Laser Mine Detection System. When echo is returned to the sensor, the data is collected, and next step is choosing the method of destroying the mine. For example, a detected mine can be either destroyed or brought out and transported to another place safety. Cameras underneath an aircraft are receiving reflections of emitted laser beams, from the water and later, processed reflections produce images that are displayed on an airborne console.

This system can work either in day or at night, regardless of light conditions, and without worrying about submerged equipment. This action can provide identification of objects on the bottom of the ocean and pursue attack with a much lower risk of mine-attack and mine explosion.

 ISBN 978-86-7466-930-3

Fig. 11. An illustration of Stanford's photoacoustic airborne sonar system [3]

## VII. CONCLUSION

LiDAR is currently experiencing an expansion. The contribution and value of this technology can change the future in which we will live. Changes in humanity are inevitable if we want to live longer and healthier, as well as save the planet. This sensor can help us succeed in that with its techniques that could provide us with data on inaccessible parts of the planet. Opportunities for research and protection of nature and humankind, transportation development among other things are growing as LiDAR becomes more effective, widespread and autonomous.

In this paper, the emphasis was put on safer maritime traffic and transport, as well as on the research of sea floor and hidden or buried objects. Airborne LiDAR can help improve coastal operations, along with signalling other ships at sea of a potential hazard detected by the sensor. That hazard could be a natural obstacle or perhaps an underwater mine, even a bridge that is not visible at night under some circumstances. Given that climate change is beginning to seriously threathen the planet, contributing towards the battle against climate change is necessary, and this could be achieved with the benefits of Industry 4.0 and novel measurement techniques and analysis.

A future application of this sensor, could be to help in the removal of carbon dioxide from the oceans. Using this technology, we can direct laser beams to determine where heavy seaweed is cultivated and enrich the water with alkaline compounds that would equalize the pH levels. By doing this, we can accelerate the restoration of underwater ecosystems, and remove excess carbon dioxide from water via electrochemical purification. In addition, another potential use can be found in analysis of seafloor and underwater rocks, minerals and various underwater species. One more idea worth mentioning is submarine and hazardous liquid detection, such as oil spills.It would be delightful to see the industry reap the benefits of this development, as that would provide additional valuable information to the end user. It is certain that LiDAR technology is already benefiting from open data, artificial intelligence and machine learning. These advantages should be utilized as much as possible as an overture to the solution for the near future.

## REFERENCES


[1] J.Van Rens, *"The Future of Lidar is Critical to the Future of Our World"*, gim-international.com.

[2] Monterey Bay Aquarium Research Institute, "Visualizing fine details of the deep seafloor", annualreport.mbari.org.

[3] C. Konowe, "Lidar Helps to illuminate the Future of Oceans", marinetechnologynews.com.

[4] N.D. Quadros, "Technology in Focus: Bathymetric Lidar", gim-international.com.

[5] "The Different Types of LiDAR Systems", lidarradar.com

[6] K. Osborn, "BANG: The Navy PLans To Detect Sea Mines Using Lasers", nationalinterest.org

[7] "Airborne Topographic LiDAR Help", ez-pdh.com

[8] B. Lohani. "Airborne Altimetric LiDAR: Principle, Data collection, processing and Applications", Dept.of Civil Engineering, IIT Kanpur, India. home.iitk.ac.in/~blohani/LiDARSchool2008/Downloads/LiDAR_notes/LiDAR_Full_Notes.pdf

[9] "LiDAR", splashcos.org, splashcos.org/sites/splashcos.org/files/downloads/9_Lidar.pdf

[10] A. Pantazis, "LIDARs Usage in Maritime Operations and ECO – Autonomous Shipping, for Protection, Safety and Navigation for NATO allies Awareness", National Technical Univ. of Athens, Greece. cmre.nato.int/msaw-2019-home/msaw2019-papers/1376-msaw2019-pantazis-lidarsusageinmaritimeoperationsandecoautonomousshippingforprotectionsafetyandnavigationfornatoalliesawareness/file

[11] "Surveillance of MARiTime surroundings through lasER technology" cordis.europa.eu/project/id/718624

[12] M.Melin, A.C. Shapiro, P.Glover-Kapfer."LIDAR for ecology and conservation", wwf.org.uk. wwf.org.uk/sites/default/files/2019-04/Lidar-WWF-guidelines.pdf

[13] C. Konowe, "*To Clear the Air:* Look Beneath The Waves", magazines.marinelink.com magazines.marinelink.com/nwm/MarineTechnology/202203/#page/6

[14] Neuvition, "LiDAR-based Ship Safety Driving Assistance System", neuvition.com neuvition.com/video/ship.html

[15] "An Airborne Sonar System for Underwater Remote Sensing and Imaging", Stanford University,airbornesonar.sites.stanford.edu/

[16] "Airborne LIDAR", Photomapping.com.au, photomapping.com.au/airborne-lidar

[17] "Lidar sheds light on ocean health", Electrooptics.com, Issue: June 2021. electrooptics.com/feature/lidar-sheds-light-ocean-health

[18] "Turbidity: Description, Impact on Water Quality, Sources, Measures – A General Overview", Minnesota Pollution Control Agency, Water Quality/Impaired Waters #3.21, March 2008. pca.state.mn.us/sites/default/files/wq-iw3-21.pdf

[19] M.D. Harrison, "Secchi Disk", Springer. link.springer.com/referenceworkentry/10.1007/978-94-017-8801-4_123


## ACKNOWLEDGMENT

This paper is supported by the Faculty of Technical Sciences in Novi Sad, Department of Energy Electronics and Telecommunications, under the grant MPNTR 200156: "Innovative scientific and artistic research in the field of FTN activities ".

 ISBN 978-86-7466-930-3

# Dvokoračna segmentna linearizacija kao deo mernog lanca termopara

Dragan Živanović, Milan Simić, Milica Stojanović i Dragan Denić

***A stra t*— ad pri azuje implementaciju dvokoračne segmentne metode linearizacije za smanjenje greške apro simacije termoparova. prvom delu je opisana softvers a obrada mernog signala pretvarača sa termoparom. valuaciju linearizacionih funkcija i analizu aproksimacionih grešaka vrši softvers i pa et virtuelne instrumentacije ab I W. snovni princip ove metode je da se apscisa prenosne fun cije prvo transformiše pomoću tabela za segmentnu linearizaciju na takav način da se opseg ulaznih vrednosti proširuje na opsezima na kojima je nelinearnost karakteristike značajna, a zatim se vrši standardna linearizacija po segmentima. a ovaj način, primena dvokoračne metode linearizacije na jedna im segmentima ima isti efe at ao i primena linearizacije na nejedna im segmentima. a date primere prenosnih fun cija termoparova, predložena metoda daje značajno manju grešku aproksimacije, uz jednaku potrošnju memorije za linearizacione tabele. Jednostavna softverska implementacija ovog dvokoračnog metoda linearizacije omogućava da se primenjuje u mernim pretvaračima mikrokontrolera male procesors e snage, umesto standardne segmentne linearizacije.**

***Ključne reči*— Dvokoračna linearna aproksimacija, prenosna funkcija termopara, smanjenje aproksimacione greške, virtuelna instrumentacija.**

## I. UVOD

Nelinearna prenosna karakteristika senzora u inteligentnim mernim pretvaračima može se kompenzovati brojnim metodama zasnovanim na hardveru i softveru. Polinomna aproksimacija je standardni metod koji se koristi za linearizaciju prenosne funkcije termoparova. Jednačine pogodne za linearizaciju prenosne karakteristike svakog tipa termopara definiše NIST i BIPM u obliku polinomne aproksimacije osmog ili većeg reda, za više (do 5) segmenta linearizacije, sa veoma malom greškom aproksimacije [1, 2]. Ako je dozvoljena greška linearizacije manja od 1%, a prenosna funkcija izrazito nelinearna, potreban je veći broj segmenata kako bi se prenosna karakteristika linearizovala, pa samim tim i polinom većeg stepena, ukoliko se koristi polinomna aproksimacija [4]. Dozvoljena greška termopara, dobijena u procesu proizvodnje i prouzrokovana starenjem pri upotrebi, je značajno veća [3], preko 1 °C. To znači da je za linearizaciju karakteristike moguće uspešno koristiti i polinomne funkcije [4], ili splajn funkcije [5] nižeg reda.

U radu [6] predložena je metoda progresivne polinomne kalibracije, gde se polinom određuje direktno, na osnovu mernih kalibracionih tačaka, što je posebno pogodno ukoliko prenosna karakteristika nije poznata. Sve nesavršenosti mernog sistema se zatim kompenzuju u istoj proceduri.

U nekoliko radova [7, 8] su, kao metode za linearizaciju, predložene veštačke neuronske mreže (Artificial Neural Networks - ANN). ANN metode su pogodne jer je moguće uzeti u obzir nesavršenost mernog sistema, kao i veličine koje utiču na merenje, poput temperature hladnog kraja [9].

Ukupni troškovi memorije i procesorske snage su veoma važni aspekti pri izboru optimalne metode linearizacije za određene primene. Za izračunavanje optimalnih koeficijenata linearizacije na osnovu poznatih funkcija ili kalibracionih tačaka, može se koristiti personalni računar (PC). Ako se za izračunavanje koriste resursi PC - a, kompleksnost algoritma ne predstavlja ograničenje. S druge strane, merni pretvarači obično imaju značajno male resurse u vidu memorije i procesorske snage, pa je veoma važno izabrati metodu za linearizaciju koja ne zahteva veliku memoriju i procesorsku snagu [10-12]. Kada mikroprocesor ima mogućnost povezivanja više ulaza ili direktnog multipleksiranja većeg broja senzora na ulazu, još je važnije odabrati metodu linearizacije koja zahteva mali broj mikroprocesorskih ciklusa za izračunavanja.

U mnogim aplikacijama može biti korisno da se izračunavanja vrše u celobrojnoj matematici, što je kompatibilno sa linearnom segmentnom aproksimacijom. Implementacijom aritmetike sa podacima koji se pamte u formatu sa pokretnim zarezom, može se zauzeti i do 1 KB memorije, što je dovoljno memorije da se zapamti do 500 segmenata u linearizacionoj tabeli sa celobrojnim tipom podataka [12]. Kako je proračun brži ukoliko se koristi celobrojni tip podataka, segmentna linearizacija koja koristi cele brojeve je efikasnija za korišćenje u odnosu na polinomnu aproksimaciju, i pogodna za implementaciju u mikrokontroleru za različite tipove senzora. Takođe je pogodna i za dvodimenzionalnu segmentnu linearizaciju (površinska), kada konačni rezultat zavisi od dve promenljive.

Linearizaciona metoda se u mnogim radovima kombinuje sa praktičnim implementacijama mernog sistema pretvarača

Dragan Živanović - Univerzitet u Nišu, Elektronski fakultet u Nišu, Aleksandra Medvedeva 14, 18000 Niš, Srbija (e-mail: dragan.zivanovic@elfak.ni.ac.rs).

Milan Simić - Univerzitet u Nišu, Elektronski fakultet u Nišu, Aleksandra Medvedeva 14, 18000 Niš, Srbija (e-mail: milan.simic@elfak.ni.ac.rs).

Milica Stojanović - Univerzitet u Nišu, Elektronski fakultet u Nišu, Aleksandra Medvedeva 14, 18000 Niš, Srbija (e-mail: milica.stojanovic@elfak.ni.ac.rs).

Dragan Denić - Univerzitet u Nišu, Elektronski fakultet u Nišu, Aleksandra Medvedeva 14, 18000 Niš, Srbija (e-mail: dragan.denic@elfak.ni.ac.rs).

 ISBN 978-86-7466-930-3

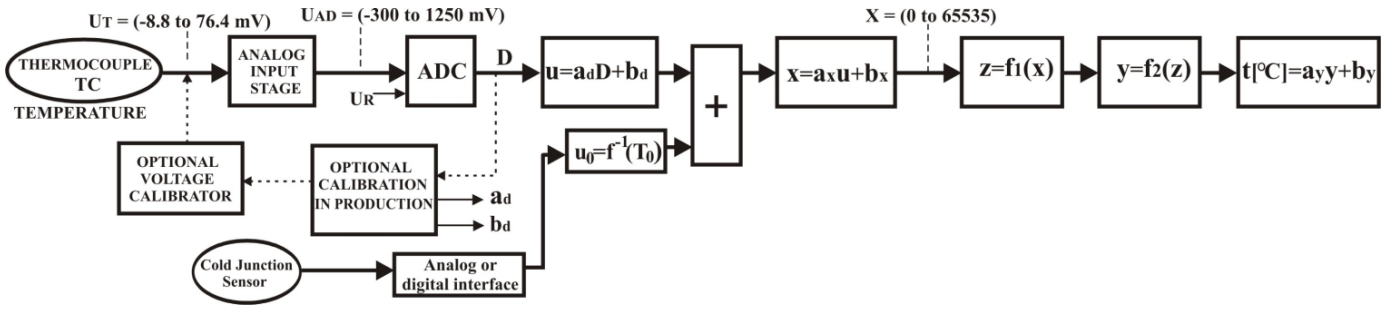


Sl. 1. Protok signala unutar mernog pretvarača sa termoparom

[6, 7, 9, 11, 14].

Radovi [11, 15] daju dobru komparativu analizu primena većeg broja metoda linearizacije. U radovima [15, 16, 17] prikazana je hardverska implementacija segmentne linearizacije.

Pri poređenju metoda, pored tačnosti aproksimacije, treba uporediti potrošnju memorijskog prostora i brzinu odziva, a sve ovo dosta zavisi i od posmatrane prenosne karakteristike.

## II. ULAZNI STEPEN TERMOPARA

Termoparovi se često koriste kao temperaturni senzori, zbog brzog odziva, robusne konstrukcije i temperaturnog opsega od -270 °C do 2500 °C, značajno šireg nego kod otpornih i poluprovodničih senzora [18, 19]. Nedostatak primene termoparova jeste nelinearnost prenosne karakteristike, kao i uticaj temperature hladnog kraja termopara na merenje.

Dve metalne žice, različitih termoelektričnih karakteristika su spojene na jednom kraju, koji je izložen visokim temperaturama, obično mnogo višim od drugog, otvorenog, kraja. Naponska razlika između žica na otvorenom kraju će zavisiti od materijala od kojeg su napravljene žice, kao i od temperature na oba kraja termopara. Tabela sa termoelektričnim naponima standardnih termoparova se daje pod pretpostavkom da se otvoreni kraj termoparova nalazi na temperaturi od 0 °C. Izvan oblasti sa visokim temperaturama, krajevi termopara mogu se produžiti korišćenjem jeftinijih kompenzacionih kablova, koji će omogućiti da se termopar poveže sa elektronikom. Kako bi se merila temperatura na vrućem kraju, temperatura na otvorenom ("hladnom") kraju mora biti poznata. [9, 20]. Za rešavanje problema kompenzacije hladnog kraja, u praktičnim realizacijama se dodaje temperaturni senzor sa boljom tačnošću, ali sa mnogo manjim temperaturnim opsegom, na primer, otporni senzori PT100, ili poluprovodnički senzor TMP275, povezan pomoću I2C digitalnog interfejsa.

Dodatni senzor temperature mora biti smešten veoma blizu hladnog kraja termopara, po mogućstvu u termoizolovanoj komori sa konektorom. Tipičan postupak linearizacije prenosne karakteristike termopara uključuje konverziju temperature hladnog spoja $T_0$, na napon $U_0$, korišćenjem funkcije $U_o = f(T_0)$. U sledećem koraku, napon $U_0$ treba dodati izlaznom naponu termopara $U_T$, zatim se inverznom funkcijom dobijeni napon konvertuje u temperaturu pomoću funkcije $T = f^{-1}(U_T + U_0)$ [9, 20]. Zbog nelinearnosti karakteristike termopara, direktno dodavanje temperature hladnog kraja inverznoj funkciji napona termopara nije tačno, jer traženo $T = f^{-1}(U_T + f(T_0))$ nije isto što i $T = f^{-1}(U_T) + T_0$.

Blok dijagram na Sl. 1. prikazuje algoritam softverske obrade signala u mernom pretvaraču, pogodnom za merenje sa različitim tipovima termopara. Odnos između rezultata ADC konverzije i ulaznog napona je isti za sve tipove termopara. Uobičajeno, u toku procesa proizvodnje pretvarača, neophodno je podesiti koeficijente $a_d$ i $b_d$ kako bi se izvršila kalibracija. Nakon toga, vrednost napona termopara treba uvećati za vrednost napona hladnog kraja senzora. Kako bi se pojednostavio postupak linearizacije za različite tipove termoparova i smanjila greška u celobrojnim proračunima, signal se zatim skalira tako da pokrije maksimalan opseg korišćenjem neoznačenih int16 promenljivih, od 0 do 65535, za opseg napona za izabrani tip termopara i temperaturni opseg.

Sledeći korak je primena inverzne funkcije za određeni tip termopara. U datom blok dijagramu, ova inverzna funkcija je podeljena na funkcije $f_1$ i $f_2$, prema predloženoj dvokoračnoj metodi linearizacije. Konačno, izračunata celobrojna vrednost temperature u opsegu od 0 do 65535 se konvertuje u konačni rezultat u formatu sa fiksnom decimalnom tačkom, a koeficijenti $a_y$ i $b_y$ (različiti za svaki tip termopara) obezbeđuju da rezultat bude predstavljen u obliku yyyy.y[°C].

## III. METOD DVOKORAČNE LINEARNE APROKSIMACIJE PRIMENJEN NA STANDARDNE TIPOVE TERMOPAROVA

Glavni cilj korišćenja metode dvokoračne segmentne linearne aproksimacije, koja je prvi put predstavljena u ranije objavljenim radovima [12, 13, 21,], jeste izvođenje svih izračunavanja pomoću celobrojne aritmetike, kao i da se izbegne određivanje kom segmentu pripada ulazna vrednost, koja je obavezna kod metoda koje koriste podelu na nejednake segmente.

Nelinearna prenosna karakteristika se može aproksimirati pomoću više linearnih segmenata, pri čemu se zahteva da su linearni segmenti povezani, kako bi se obezbedilo da dobijena linearizovana karakteristika bude kontinualna.

Kod segmentne linearizacije, apscisa se deli na jednake segmente. Kako bi se smanjila greška aproksimacije, potrebno je povećati broj segmenata u delu u kome je prenosna karakteristika jako nelinearna. To dovodi do nejednakih veličina segmenata. Razlika u veličini segmenata dovodi do usporavanja metode linearizacije.


ISBN 978-86-7466-930-3

Jedan od načina da se zadrži mali broj potrebnih segmenata, a da se pri tom ne uspori proces linearizacije korišćenjem segmenata nejednake veličine, je korišćenje dvokoračne metode linearizacije, predložene u radu [12]. Kod ove metode, prvo se određuju delovi prenosne karakteristike u kojima je izražena nelinearnost. Zatim se vrši transformacija X – ose, tako što se segmenti u kojima je nelinearnost izražena razvuku u odnosu na ostatak karakteristike. Za transformaciju X – ose se takođe primenjuje segmentna linearizacija. Zatim se, na tako transformisanu karakteristiku, ponovo primenjuje segmentna linearizacija. Na taj način se smanjuje greška aproksimacije. Transformacija X – ose je ovde izvedena na drugačiji način u odnosu na postupak iz rada [12], korišćenjem iterativnog postupka.

Predloženi metod se može primeniti na različite tipove senzora. Glavni zahtev prilikom vršenja linearizacije jeste da greška aproksimacije bude manja od granične vrednosti greške, definisane NIST i BIPM standardima za termoparove [1, 2]. Konačna greška linearizacije u ovom radu će biti računata kao maksimalna razlika između vrednosti ordinate aproksimirane funkcije i vrednosti ordinate koja se dobija primenom inverzne polinomne funkcije koju definiše NIST, na celom opsegu vrednosti napona, za određeni tip termopara. Cela procedura, sa odgovarajućim grafičkim prikazima, se vrši korišćenjem razvijenih softverskih algoritama u programskom okruženju LabVIEW. Na Sl. 2. dat je Front panel virtuelnog instrumenta LabVIEW na kome je predstavljena normalizovana, inverzna, prenosna karakteristika termopara tipa E.

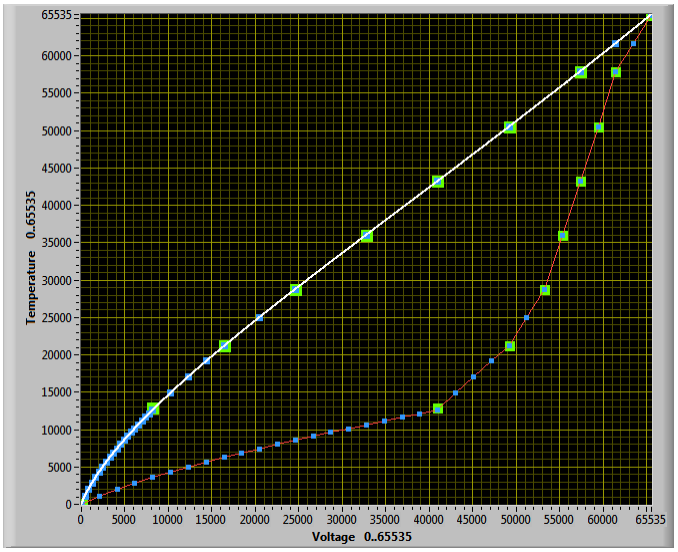


Sl. 2. Front panel LabVIEW – a, prikaz normalizovane, inverzne prenosne karakteristike termopara E tipa (bela linija) i karakteristika sa transformisanom X – osom (crvena linija)

Zelene tačke na graficima odgovaraju početnoj podeli bele (početne) prenosne karakteristike na osam segmenata. Crvena prenosna karakteristika, nakon zamene X – ose sa Z, postaje $Y = f(Z)$. Ova prenosna karakteristika je podeljena na 32 jednaka segmenta, deljenjem apscise, Z – ose (plave tačke). Vraćanjem plavih tačaka sa crvene na belu karakteristiku, može se uočiti da je praktično postignuta segmentna linearizacija sa podelom X – ose na nejednake segmente.

Konačno, linearizacija inverzne prenosne karakteristike termopara i izračunavanje temperature na osnovu normalizovane vrednosti ulaznog napona, vrši se prema relaciji:

$$Y = f_2(Z) = f_2(f_1(X)) = f_T(X) \quad (1)$$

Na Sl. 3. je prikazana funkcija $Z = f_1(X)$ koja transformiše X – osu na osam jednakih segmenata u opsegu od 0 do 65535.

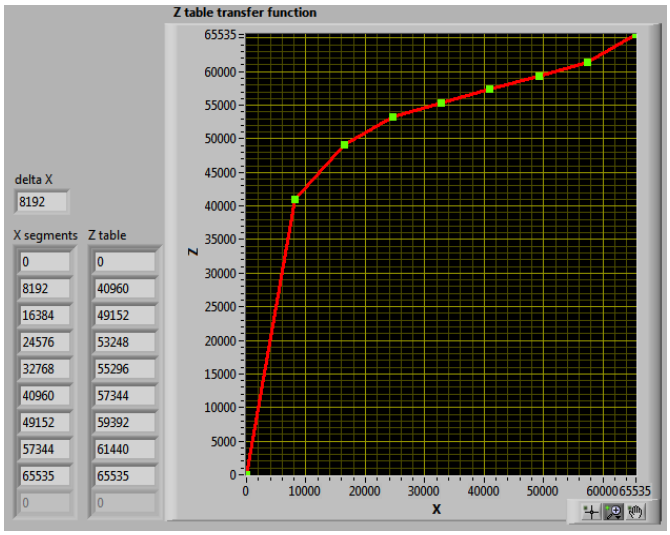


Sl. 3. Transformacija X – ose na 8 jednakih segmenata

Na Sl. 4. je dat prikaz LabVIEW blok dijagrama pomoću koga se vrše izračunavanja potrebna za primenu dvokoračne segmentne metode linearizacije karakteristike termopara, uključujući i računanje greške aproksimacije. U petljama se vrši iterativni postupak kako bi se dobile vrednosti potrebne za formiranje linearizacionih tabela. Ulazni parametri ove petlje su: broj segmenata u prvoj linearizacionoj tabeli, M, maksimalna dozvoljena greška aproksimacije (TargetError[°C] u LabVIEW blok dijagramu) i maksimalni dozvoljeni broj segmenata u drugoj linearizacionoj tabeli (MaxN). Petlja će se zaustaviti u iteraciji u kojoj je ispunjen jedan od dva uslova.

Na levoj strani blok dijagrama se bira jedan tip termopara, i u zavisnosti od izabranog tipa termopara, selektuje se odgovarajući opseg ulaznog napona. Zatim se, korišćenjem funkcije koju definiše NIST za polinomnu aproksimaciju, formira 65535 para tačaka napona i temperatura koje se nalaze u odgovarajućem opsegu, a nakon toga se vrednosti napona i temperature normalizuju na opseg od 0 do 65535.

Nelinearna prenosna karateristika se deli na M jednakih segmenata, deljenjem X – ose, i određuju se segmenti u kojima je karakteristika izrazito nelinearna. Svaka tačka na X – osi se može izračunati kao $X_i = \Delta X \times i$, za $i$=0, ..., M, pri čemu je veličina segmenata određena kao

 ISBN 978-86-7466-930-3

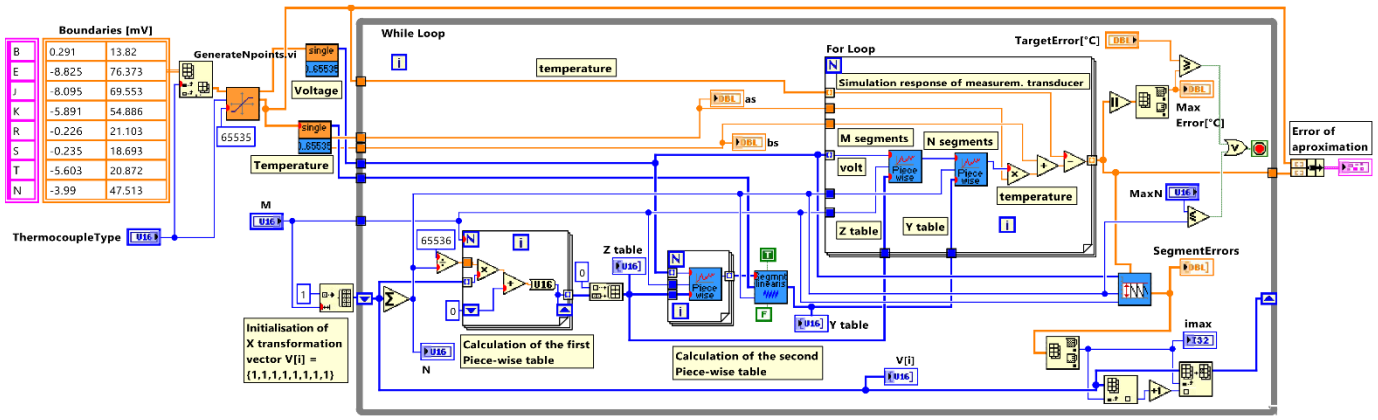


Sl. 4. LabVIEW blok dijagram koji prikazuje iterativni postupak za određivanje linearizacionih tabela za dvokoračni metod linearizacije i konačne greške aproksimacije

$$\Delta X = \frac{65535}{M} \tag{2}$$

Zatim se vrši transformacija X – ose, tako što se segmentni u kojima je karakteristika izrazito nelinearna, razvuku, tj. formira se Z – osa, $Z_i = f_1(X_i)$.

$$Z_0 = 0, Z_i = Z_{i-1} + \mathrm{V}[i]\Delta Z \tag{3}$$

Veličina segmenata na Z – osi, ΔZ, se izračuna pomoću jednačine:

$$\Delta Z = \frac{65535}{N} \tag{4}$$

U prvoj linearizacionoj tabeli je definisan vektor transformacije X – ose, V[i], tj. niz koeficijenata u (3). Ukoliko se izabere M=8 segmenata za formiranje prve linearizacione tabele, početna vrednost ovog vektora će biti $V[i] = \{1, 1, 1, 1, 1, 1, 1, 1\}$. Ovo znači da će druga linearizaciona tabela imati po jedan segment u svakom od osam naponskih opsega. Tokom iterativnog procesa, vektor V[i] se menja tako što se element vektora, kome odgovara segment sa izrazitom nelinearnošću, povećava.

Vektor transformacije X – ose, koji odgovara termoparu sa Sl. 3., nakon finalne iteracije će biti $V[i] = \{20, 4, 2, 1, 1, 1, 1, 2\}$. Suma svih elemenata vektora V[i] je 32, ukoliko je izabrana vrednost za N=32, tj. ukoliko je izabrano da se za drugu segmentnu linearizaciju apscisa podeli na 32 segmenta.

U ovom primeru, koristeći $V[i]$ prema (3), parametri u Z tabeli se računaju na sledeći način:

$$\begin{aligned}
&Z_0 = 0,\\
&Z_1 = Z_0 + 20\Delta Z,\\
&Z_2 = Z_1 + 4\Delta Z = 20\Delta Z + 4\Delta Z = 24\Delta Z,\\
&Z_3 = Z_2 + 2\Delta Z = 24\Delta Z + 2\Delta Z = 26\Delta Z,\\
&Z_4 = Z_3 + \Delta Z = 26\Delta Z + \Delta Z = 27\Delta Z,\\
&Z_5 = Z_4 + \Delta Z = 27\Delta Z + \Delta Z = 28\Delta Z,\\
&Z_6 = Z_5 + \Delta Z = 28\Delta Z + \Delta Z = 29\Delta Z,\\
&Z_7 = Z_6 + \Delta Z = 29\Delta Z + \Delta Z = 30\Delta Z,
\end{aligned} \tag{5}$$

$$Z_8 = Z_7 + 2\Delta Z = 30\Delta Z + 2\Delta Z = 32\Delta Z.$$

Transformisane X vrednosti, odnosno Z vrednosti, su izračunate na celom radnom opsegu, pomoću Z tabele (prve linearizacione tabele). Zatim se analizira inverzna kriva, tj. funkcija koja predstavlja transformisanu X – osu, kako bi se odredila 32 segmenta u drugom koraku linearizacije. Segmentna linearizacija koja se izvodi u drugom koraku je realizovana unutar Sub VI bloka, na isti način kao i određivanje vrednosti na osnovu prve linearizacione tabele, koja je u blok dijagramu nazvana “Segment Linearis” i “Pice_Wise”.

U desnom delu blok dijagrama nalazi se “For Loop” koja daje simulaciju odziva pretvarača, na osnovu linearizacionih tabela Z i Y. Na ulazu Sub VI se dovodi ulazni napon, čija je vrednost normalizovana na opsegu od 0 do 65535, i segmentna linearizacija se izvodi dva puta kako bi se aproksimirala inverzna prenosna karakteristika. Na kraju, dobijena vrednost se skalira na početni opseg temperature. Kako bi se izvršilo poređenje dobijene vrednosti sa vrednošću koju daje polinom koji propisuje NIST, računa se greška aproksimacije. Traženjem maksimalne greške aproksimacije na svakom od osam segmenata, u blok dijagramu se formira vektor “SegmentErrors”.

U donjem delu blok dijagrama, nalazi se funkcija čiji je zadatak da odredi u kom od osam segmenata je greška najveća. Kada se odredi segment sa najvećom greškom, “imax”, iterativni postupak povećava za jedan element vektora V[imax]. Petlja, u narednoj iteraciji, koristi izmenjenu vrednost vektora V[i].

U primeru termopara tipa E, početne greške segmenta u stepenima Celzijusovim, za svaki od osam segmenata su 20.274, 6.3, 1.482, 0.535, 0.168, 0.227, 0.332 i 0.476, kao što se može videti na Sl. 5. Može se primetiti da je najveća greška aproksimacije u prvom segmentu, i iznosi 20.274 °C. Dakle, vektor V[i] će u prvoj iteraciji da postane {2,1,1,1,1,1,1,1}. Nastavljajući iterativni postupak, dobija se krajnja vrednost za vektor V[i] = {20,4,2,1,1,1,1,2}.

Primenom dvokoračnog segmentnog metoda linearizacije, dobija se maksimalna greška na celom radnom opsegu od 0.303 °C. Upoređivanjem greške koja se dobija primenom metode dvokoračne segmentne linearizacije, korišćenjem prvo

 ISBN 978-86-7466-930-3

8, a zatim 32 segmenta, i metode segmentne linearizacije koja koristi 40 segmenata, zaključuje se da je greška smanjena 6 do 10 puta. Konačna greška aproksimacije za termopar tipa E je smanjena sa 2.95 °C na 0.303 °C, primenom metode dvokoračne segmentne linearizacije.

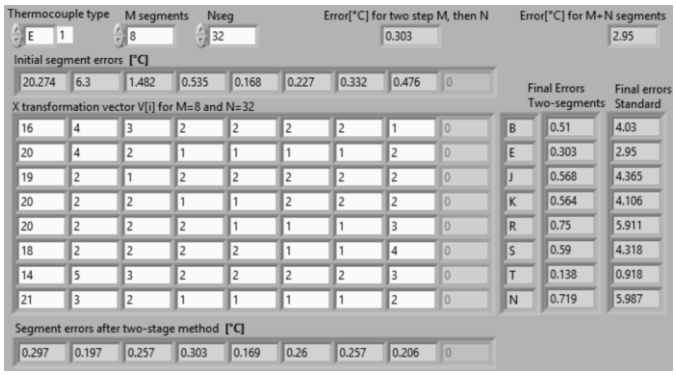


Sl. 5. Front panel sa koeficijentima prve linearizacione tabele i konačnim greškama, dobijenim primenom dvokoračne segmentne linearizacione metode koja koristi prvo 8, a zatim 32 segmenta i standardne segmentne aproksimacije sa 40 segmenata, za osam tipova termoparova,

Kako bi se izvršilo bolje poređenje metoda segmentne linearizacije i dvokoračne segmentne linearizacije, u tabeli 1 su date dobijene vrednosti greške aproksimacije za termopar tipa E, koje daju ove metode, za odabrane različite vrednosti broja segmenata M i N. Može se uočiti da povećanje broja segmenata, blago povećava prednost metode dvokoračne segmentne linearizacije, u odnosu na standardnu metodu sa M+N brojem segmenata.

Na Sl. 6. dat je Front panel na kome je prikazana greška aproksimacije dobijena primenom ove dve metode za termopar tipa E. Kriva označena belom bojom predstavlja grešku aproksimacije dobijenu korišćenjem standardne segmentne metode aproksimacije korišćenjem 40 segmenata. Kriva označena crvenom bojom predstavlja grešku aproksimacije koja je dobijena primenom dvokoračne segmentne metode linearizacije, korišćenjem prvo 8, a potom 32 segmenta. Može se primetiti da se primenom dvokoračne

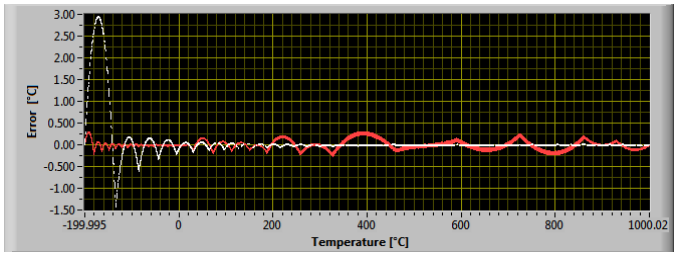


Sl. 6. Greška aproksimacije dobijena primenom standardne metode linearizacije korišćenjem 40 segmenata (bela) i dvokoračne metode linearizacije korišćenjem prvo 8, zatim 32 segmenta (crvena), prikazana na Front panelu u LabVIEW

metode linearizacije značajno smanjuje greška aproksimacije.

Treba još napomenuti da je važno obratiti pažnju prilikom odabira vrednosti za M. Ukoliko je M malo, javlja se velika greška, a ako je suviše veliko, ne ostaje dovoljan broj segmenata za drugi korak linearizacije. Vrednost M je najbolje uzeti kao $M = (N + M)/4$, jer će u tom slučaju vrednost M biti u obliku $2^k$. U svakom slučaju, dobijena greška je manja nego u slučaju primene standardne liearizacione metode.

Još jedna prednost ove metode jeste u tome što, ukoliko se ne koristi ceo temperaturni opseg termopara, već uži radni deo opsega, princip dvokoračne segmentne linearizacije je isti. Zadati opseg se na početku normalizuje na opseg od 0 do 65535, i primenjuje se linearizacija na prethodno opisan način. Smanjenje opsega će olakšati linearizaciju, jer se do željene tačnosti dolazi sa manjim brojem segmenata.

Uzimajući u obzir i druge izvore grešaka u mernom sistemu, vrednost greške od 0.2 °C se može opravdano uzeti za cilj za dati dvokoračni segmentni linearizacioni metod. U tabeli 2 je prikazan potreban broj segmenata za sve tipove termoparova kako bi se postigla greška aproksimacije od 0.2 °C, primenom standardne metode segmentne linearizacije i metode dvokoračne segmentne linearizacije.

TABELA I
GREŠKE APROKSIMACIJE TERMOPARA TIPA E DOBIJENE PRIMENOM METODE SEGMENTNE LINEARIZACIJE I DVOKORAČNE SEGMENTNE LINEARIZACIJE

| Vrednosti parametara M i N (broj segmenata) | Greška aproksimacije | |
|---|---|---|
| | Standardna linearizaciona metoda, M+N segmenata | Dvokoračna segmentna linearizaciona metoda, M, zatim N, segmenata |
| M=8, N=32 | ΔT=2.95 °C | ΔT=0.303 °C |
| M=8, N=48 | ΔT=1.79 °C | ΔT=0.144 °C |
| M=8, N=64 | ΔT=1.20 °C | ΔT=0.096 °C |
| M=16, N=32 | ΔT=2.26 °C | ΔT=0.220 °C |
| M=16, N=48 | ΔT=1.44 °C | ΔT=0.101 °C |
| M=16, N=64 | ΔT=1.00 °C | ΔT=0.075 °C |

TABELA 2
POTREBAN BROJ SEGMENATA KAKO BI SE DOBILA GREŠKA OD 0.2 °C, ZA SVE TIPOVE TERMOPAROVA

| Tip termopara | Standardni linearizacioni metod | Dvokoračni linearizacioni metod | |
|---|---|---|---|
| | N= | M=8, N= | M=16, N= |
| B | 215 | 52 | 46 |
| E | 196 | 43 | 35 |
| J | 270 | 53 | 42 |
| K | 250 | 52 | 42 |
| R | 330 | 70 | 51 |
| S | 260 | 59 | 46 |
| T | 92 | 27 | 26 |
| N | 342 | 64 | 47 |


ISBN 978-86-7466-930-3

## IV. ZAKLJUČAK

Linearizacioni metod predstavljen u ovom radu, implementiran je na osnovu dvokoračne segmentne linearizacione metode predložene u radu [12]. Opisani metod je pogodan za primenu kod termoparova, s obzirom na nelinearnost njihove prenosne karakteristike.

Predloženi dvokoračni segmentni linearizacioni metod, u poređenju sa standardnom segmentnom linearizacionom metodom, za dat primer nelinearne prenosne karakteristike termopara, daje manju grešku aproksimacije 6 do 13 puta, sa sličnim vremenom izvršenja i jednakom potrošnjom memorije za čuvanje linearizacionih tabela.

Prikazana linearizaciona metoda se lako može primeniti korišćenjem celobrojne aritmetike, što smanjuje broj procesorskih ciklusa potrebnih za izvođenje proračuna, kao i memorijskog prostora potrebnog za pamćenje linearizacionih tabela, za razliku od polinomne aproksimacije. Primena dvokoračnog segmentnog linearizacionog metoda je prikazana na primeru termopara, ali se može primeniti za linearizaciju nelinearne prenosne karakteristike i drugih senzora.

## LITERATURA


[1] Burns G, Scroger M, Strouse G, at al. NIST Monograph 175: Temperature-Electromotive Force Reference Functions and Tables for the Letter-Designated Thermocouple Types Based on the ITS-90, April 1993.

[2] Bedford R, Bonnier G, Maas H, Pavese F. Techniques for approximating the ITS-90, monograph BIPM, Bureau International des Poids et Mesures. Se`vres, France, 1990.

[3] Measuresoft. DATASCAN 7000 distributed data acquisition system thermocouple accuracy, datascan.measure-soft.com/docs/TC.pdf (accessed November 2019).

[4] Chen A and Chen C. Evaluation of piecewise polynomial equations for two types of thermocouples. *Sensors* 2013; 13(12): 17084–17097.

[5] Wang X, Wei G and Sun J. Free knot recursive B-spline for compensation of nonlinear smart sensors. *Measurement* 2011; 44(5): 888–894.

[6] Nadi M, Margo C, Kouider M, at al. Embedded system design and implementation of standard auto-calibrated measurement chain. *International ournal on Smart Sensing and Intelligent Systems* 2008; 1(1): 21-33.

[7] Danismana K, Dalkirana I and Celebib FV. Design of a high precision temperature measurement system based on artificial neural network for different thermocouple types. *Measurement* 2006; 39(8): 695–700.

[8] Rivera J, Carrillo M, Chaco´n M, et al. Self-calibration and optimal response in intelligent sensors desig based on artificial neural networks. *Sensors* 2007; 7(8): 1509–1529.

[9] Dey D and Munshi S. A new intelligent scheme for simultaneous cold junction compensation and linearization of thermocouples. *eonardo Electron Pract Technol* 2011; 19: 13–28.

[10] Bengtsson LE. Lookup table optimization for sensor linearization in small embedded systems. *ournal of Sensor Technology* 2012; 2(4): 177-184.

[11] Erdem H. Implementation of software-based sensor linearization algorithms on low-cost microcontrollers. *ISA Transactions* 2010; 49(4): 552-558.

[12] Živanović D, Arsić M and Đorđević J. Two-stage piece-wise linearization method. ***Internat na rna** of **de n** and **m at n*** 2004; 24(2): 85-89.

[13] Živanović D, Simić M. Two-stage segment linearization as part of the thermocouple measurement chain. *Measurement and Control* 2021; 54(1-2) 141–151

[14] Sarma U and Boruah PK. Design and development of a high precision thermocouple based smart industrial thermometer with on line linearisation and data logging feature. *Measurement* 2010; 43(10): 1589-1594.

[15] Islam T and Mukhopadhyay SC. Linearization of the sensors characteristics: a review. *International ournal on Smart Sensing and Intelligent Systems,* 2019, 12(1):1-21

[16] Živanović D, Lukić J and Denić D. A novel linearization method of sin/cos sensor signals used for angular position determination. *ournal of Electrical Engineering Technology - EET* 2014; 9(4): 1437-1445.

[17] Jovanović J and Denić D. A cost-effective method for resolution increase of the two-stage piecewise linear ADC used for sensor linearization. *Measurement Science e iew* 2016; 16(1): 28-34.

[18] JUMO GmbH & Co. KG. Data sheet 90.1000, Construction and application of thermocouples, www.jumo.net/ attachments/JUMO/attachmentdownload?id=4121 (2009, pristupljeno mart 2022).

[19] Texas Instruments. TI designs, Optimized sensor linearization for thermocouple, www.ti.com/lit/ug/tidua11a/tidua11a.pdf (2015, pristupljeno, mart 2022).

[20] Duff M and Towey J. Two ways to measure temperature using thermocouples feature simplicity, accuracy and flexibility. *Analog ialogue* 2010; 44(10): 1–6.

[21] Živanović D, Arsić M, Đorđević J, et al. Two stages piece-wise linearization method for intelligent transducers. In: *International scientific conference—ICEST 2003*, Sofia, Bulgaria, December 2003, pp.383–386.


## ABSTRACT


The paper presents the implementation of a two - stage piece - wise linearization method to reduce the thermocouple approximation error. The first part describes the software processing of the measuring signal of the transducer with a thermocouple. Evaluation of linearization functions and analysis of approximation errors is performed by the LabVIEW virtual instrumentation software package. The basic principle of this method is to first transform the abscissa of the transfer function using a linear segment look - up table in such a way that the range of input values expands to the ranges where the nonlinearity of the characteristic is significant, and then standard piece - wise linearization is performed. In this way, the application of the two-stage linearization method on equal segments has the same effect as the application of linearization on unequal segments. For the given examples of transfer functions of thermocouples, the proposed method gives a significantly smaller approximation error, with equal memory consumption for look - up tables. The simple software implementation of this two-stage linearization method allows it to be used in low calculation power microcontroller measurement transducers, instead of standard piece - wise linearization.


**Two-stage segment linearization as part of the thermocouple measurement chain**


Dragan Živanović, Milan Simić, Milica Stojanović and Dragan Denić


 ISBN 978-86-7466-930-3

# Poređenje merenja brzine vetra anemometrom sa šoljicama i ultrasoničnim anemometrom na vetroturbini

Robert Fajhner, Marjan Urekar, *Member*, IEEE

***A stra t* – Ovaj rad se bavi poređenjem performansi anemometra sa šoljicama i ultrasoničnog anemometra, instrumenata za merenje brzine vetra na jednoj od vetroturbina u vetropar u Alibunar. Podaci korišteni u analizi pribavljeni su putem CADA sistema vetropar a Alibunar.**

***Ključne reči* vetar; brzina vetra; anemometar; vetroturbina**

## I UVOD

U današnje vreme, potreba za merenjem brzine vetra je prisutna u mnogim sferama privrede. Prvenstveno za potrebe metereologije, u cilju praćenja vremenskih prilika i ocene zagađenosti vazduha, zatim za sisteme reagovanja u vanrednim situacijama, avionski saobraćaj kao i energetiku. U vetroenergetici, podaci o izmerenoj vrednosti brzine vetra koriste se za planiranje budućih projekata vetroparkova ali i za upravljanje radom postojećih vetroturbina.


Sl. 1. Blok dijagram mernog sistema vetroturbine

Anemometar je uređaj koji se koristi za merenje brzine vetra. Naziv potiče od ’anemos’, što je starogrčka reč za 'vetar'. Iako je reč izvedena iz starogrčkog, nismo bili u mogućnosti izmeriti brzinu vetra sve do 1450. godine kada je Leon Battista Alberti izumeo prvi mehanički anemometar – sa klatnom, koji se sastojao od ravnog diska koji se slobodno okreće oko horizontalne ose u svojoj ravni i iznad svog centra gravitacije, ceo sklop je bio usmeren u pravcu vetra pomoću vetrokaza (kasnije je ovaj izum pripisan Robert Hook-u 1667.godine). Poznatiji anemometar je anemometar sa šoljicama, koji je 1846. izumeo irski astronom Thomas Romney Robinson. Vetar je uzrokovao da se šoljice-lopatice rotiraju vodoravno, što je pomeralo niz točkića-zupčanika koji bi pokazivali brzinu vetra. Originalni anemometar koji je on postavio na opservatoriji (sa 4 lopatice), gde je radio eksperimente, još uvek stoji na tom mestu. Njegov dizajn se i danas koristi , naravno uz moderne materijale i drugačije načine prenosa informacije o samoj brzini vetra. Najnovija tehnologija anemometra je ultrasonični anemometar, koji je izumljen 1994. godine. Ova tehologija se i dalje razvija, i kao rešenje za merenje brzine vetra je najzastupljenija u svetu (pored informacije o brzini vetra, ultrasonični anemometar može još da daje informacije o pravcu vetra, temperaturi).

Kroz ovaj rad, porediće se izmerene vrednosti vetra mehaničkog anemometra (sa šoljicama) i ultrasoničnog anemometra, koji se koriste u mernom sistemu vetroturbina, u vetroparku Alibunar, u različitim temperaturnim uslovima, pri različitim izmerenim brzinama vetra.

Robert Fajhner – Fakultet tehničkih nauka, Univerzitet u Novom Sadu, Trg Dositeja Obradovića 6, 21000 Novi Sad, Srbija (e-mail: rfajhner@gmail.com).
Marjan Urekar – Fakultet tehničkih nauka, Univerzitet u Novom Sadu, Trg Dositeja Obradovića 6, 21000 Novi Sad, Srbija (e-mail: urekarm@uns.ac.rs).

## II KARAKTERISTIKE MERNIH UREĐAJA

Mehanički anemometar je proizvod kompanije Thies, model 4.3519.00. sa 3 lopatice [1], i služi za merenje

Sl. 2. Anemometar sa šoljicama Thies 4.3519.00. [9]

horizontalne brzine vetra. Uređaj je napravljen od materijala otpornih na koroziju. Kućište je napravljeno od eloksiranog aluminijuma i nerđajućeg čelika, dok su lopatice izrađene od ojačanog fiberglasa. Na izlazu iz anemometra je signal u opsegu 2–630 Hz (optoelektrični princip merenja brzine vetra) koji se pretvara putem integrisanog mernog pretvarača u analogni signal oblika 4-20 mA. Optoelektrični princip zasniva se na slanju LED svetla kroz kodni prsten prema foto prijemniku, na osnovu kojeg se formiraju električni impulsi. Merni opseg je od 0,5 m/s do 50 m/s, sa rezolucijom od 0,1

 ISBN 978-86-7466-930-3

m/s. Tačnost uređaja je definisana na intervalu: za vrednosti vetra 0,5 – 17 m/s, tačnost je +/- 0,5 m/s; za vrednosti 17-50 m/s, tačnost je +/-3% od merene vrednosti.

Ultrasonični anemometar je proizvela, takođe, kompanije Thies, model 2D 4.382x. sa dva para, naspramnih ultrazvučnih pretvarača, na rastojanju od 200 mm [2]. Izlazni signal može biti digitalni i/ili analogni. Anemometar pouzdano radi pri temperaturama od -50°C do +70°C. Merni opseg brzine vetra je 0,01 – 75 m/s (prag detekcije je 0,01 m/s). Što se tiče tačnosti merenja brzine vetra, za brzine do 5 m/s, tačnost je +/- 0,1 m/s, dok za brzine vetra preko 5 m/s, tačnost je +/- 2 % od merene vrednosti [3]. Zbog svoje kontrukcije (otporni materijali, nema pokretnih delova) redovna kalibracija usled starenja nije potrebna.

Sl. 3. Ultrasonični anemometar Thies 2D [2]

Greške u merenju se javljaju usled mehaničkih deformacija nosača pretvarača, odnosno promene dužine mernog puta između ultrasoničnih pretvarača. Uticaji pravca strujanja vazduha i turbulencije su kompenzovani u procesu računanja.

## III ODREĐIVANJE VREDNOSTI BRZINE VETRA

Merene vrednosti brzine vetra se šalju u digitalnom obliku upravljačkom sistemu vetroturbine. Operacije izračunavanja brzine vetra se izvršavaju u elektronskom sklopu dnevnika izmerenih vrednosti (data logger).

Kod anemometra sa šoljicama, preko data logger-a, dobijene vrednosti se uzorkuju (u kratkom vremenskom intervalu 10 ms) i tako dobijene vrednosti se dalje koriste u proračunima brzine vetra, u upravljačkom sistemu. Ove vrednosti se usrednjavaju na intervalima 50 ms, 100 ms, 500 ms, 1s, 10s, 30s i 600s, u pokretnom smislu i kao promenljive koriste u drugim operacijama kontrolnog sistema. Proračuni u pokretnom smislu se izvršavaju tako da se ‘najstarija’ merena vrednost zameni najskorijom merenom vrednošću, i ponovo izračuna srednja vrednost. Prilikom produkcije električne energije, u proračunima vrednosti brzine vetra mora da se uključi uticaj turbulencije rotirajućih elisa i vibracija gondole koji utiču na izmerene brzine vetra. Kroz te faktore se linerazuje jednačina po kojoj se vrednost brzine vetra računa i povećava preciznost mernog uređaja:

$$v_v = Af_s + B \tag{1}$$

Merena brzina vetra je $v_v$ u [m/s], $f_s$ je frekvencija generisanog signala na izlazu anemometra [Hz], a $A$ i $B$ koeficijenti dobijeni prilikom kalibracije samog anemometra [4]. Linearna zavisnost izmerene brzine kod anemometra sa lopaticma je i dokazana u laboratorijskim ispitivanjima [5]. Prilikom kalibracije navedenog tipa anemometra sa lopaticama izračunata je merna nesigurnost uređaja σ=2,04% [6].

Kod ultrasoničnog anemometra, proces merenja vrednosti vetra i njeno usrednjavanje je drugačije. Dve putanje na kojima se vrši merenje su međusobno upravne. Pretvarači rade i kao predajnici i kao prijemnici. Elektronski kontrolni sistem anemometra bira pravac i smer merenja, i u jednoj sekvenci merenja (2,5ms pri temperaturi 20°C) izvrše se 4 individualna merenja u sva četiri smera (S-N,W-E,N-S,E-W) mernih putanja. Brzina zvuka značajno zavisi od temperature vazduha, međutim pošto se merenje brzine prostiranja zvuka obavlja duž oba pravca merenja, i u oba smera, time se isključuje uticaj temperature na merenje.

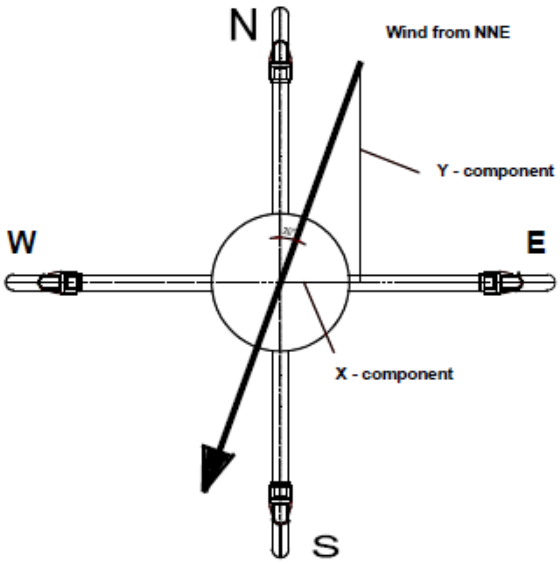


Sl. 4. Princip merenja ultrasoničnog 2D anemometra [3]


ISBN 978-86-7466-930-3

Merene vrednosti brzine prostiranja daju dve komponente vektora brzine vetra (X i Y), koje DSP anemometra pretvara u polarne koordinate, na osnovu kojih se u potpunosti rekontsruiše vektor brzine vetra. Usrednjavanje merenih vrednosti se odvija svakih 20ms, u pokretnom smislu kao i kod mehaničkog anemometra. Ove srednje vrednosti se ponovo preračunavaju na intervalima 100ms, 500ms, 1s, 10s, 30s i 600s. Pojedinačna horizontalna komponenta brzine vetra $u$ [m/s] može se aritmetički izračunati kao:

$$u = \frac{c^2}{2 f_z d} \tag{2}$$

gde je $c$ – brzina prostiranja zvučnog talasa koji se šalje između ultrasoničnih pretvarača; $f_z$ – frekvencija tog zvučnog talasa; a $d$ – rastojanje između pretvarača. Izračunata vrednost brzine vetra $v_v$ [m/s] je :

$$v_v = \sqrt{{u_x}^2 + {u_y}^2} \tag{3}$$

gde su $u_x$ i $u_y$ komponente vektora brzine vetra. Prilikom testiranja navedenog tipa 2D ultrasoničnog anemometra izračunata je merna nesigurnost uređaja σ=2% [7].

## IV POREĐENJE RADA MERNIH UREĐAJA

U svrhu analize rada mernih uređaja, upotrebljeni su podaci iz memorije jedne od vetroturbina iz vetroparka Alibunar, pri čemu se vodilo računa da se uzmu u obzir različiti vremenski uslovi (brzina vetra i spoljna temperatura). Podaci u dalje navedenim tabelama predstavljaju izmerene i usrednjene desetominutne vrednosti brzine vetra, u toku jednog dana (vremena su birana nasumično). Zbog značajno boljih karakteristika i nedostatka referentnog mernog instrumenta na koji ne bi uticali postojeći spoljni faktori, merenja ultrasoničnog anemometra će se smatrati referentnim.Veličine koje se navode u tabelama su: $_1$ – brzina izmerena anemometrom sa lopaticama; $_2$ – brzina izmerena ultrasoničnim anemometrom; $\Delta v$ – razlika između izmerenih brzina i - relativna greška u odnosu na referentnu vrednost.

U Tabeli I, prikazani su podaci iz 10. januara 2021. Na prvi pogled, lako se uočavaju drastične razlike između merenja mehaničkog i ultrasoničnog anemometra. Promene spoljne temperature su relativno male (manje od 1°C), dok razlike u merenim brzinama variraju od 2,32 m/s do 3,71 m/s (što daje grešku preko 40% u odnosu na referentnu vrednost). Uzrok greške je relativno niska spoljna temperatura (nekoliko dana je bila temperatura konstantno ispod 0°C), što je skoro dovelo do smrzavanja mehaničkog anemometra. Za ova merenja, mehanički anemometar ne ispunjava navedene tačnosti od strane proizvođača.

U Tabeli II, prikazani su izmerene vrednosti vetra od 25.01.2022. Opseg promene spoljne temperature se malo povećao, ali je i dalje na ivici temperature mogućeg smrzavanja anemometra sa lopaticama. Iz izmerenih vrednosti brzine vetra se vidi da se greška mehančkog anemometra smanjila (sad je do 16% merene vrednosti) ali se nalazi u granicama koje navodi proizvođač.

TABELA I MERENJE BRZINE VETRA PRI SPOLJNOJ TEMPERATURI OD -2,8°C DO -3,5°C

| VREME | $_1$ [m/s] | $_2$ [m/s] | $\Delta v$ [m/s] | |
|---|---|---|---|---|
| 20:10 | 3,720 | 6,769 | 3,049 | 39,25 |
| 17:40 | 3,859 | 6,960 | 3,101 | 44,54 |
| 14:30 | 2,960 | 5,280 | 2,320 | 43,94 |
| 11:30 | 3,950 | 7,110 | 3,160 | 44,44 |
| 09:40 | 3,670 | 6,420 | 2,750 | 42,83 |
| 08:00 | 4,349 | 8,029 | 3,680 | 45,83 |
| 06:30 | 4,590 | 7,989 | 3,399 | 42,54 |
| 04:20 | 5,170 | 8,869 | 3,699 | 41,71 |

TABELA II MERENJE BRZINE VETRA PRI SPOLJNOJ TEMPERATURI OD -3,3°C DO 1,6°C

| VREME | $_1$ [m/s] | $_2$ [m/s] | $\Delta v$ [m/s] | |
|---|---|---|---|---|
| 22:10 | 3,259 | 3,660 | 0,401 | 10,95 |
| 20:20 | 3,130 | 3,519 | 0,389 | 11,05 |
| 18:10 | 1,559 | 1,860 | 0,301 | 16,18 |
| 15:50 | 2,359 | 2,779 | 0,420 | 15,11 |
| 12:10 | 2,920 | 3,309 | 0,389 | 11,76 |
| 09:30 | 2,960 | 3,329 | 0,369 | 11,08 |
| 06:50 | 5,448 | 5,931 | 0,483 | 8,14 |
| 04:00 | 4,260 | 4,710 | 0,450 | 9,55 |

U Tabeli III (vrednosti merene 19.02.2022.) prikazani su uslovi temperature iznad nule odnosno ukupni porast spoljne temperature od 5,6°C u toku dana, pri vetrovima do 5 m/s. Vrednost relativne greške mehaničkog anemometra se i dalje smanjuje (ispod 10%).

TABELA III MERENJE BRZINE VETRA PRI SPOLJNOJ TEMPERATURI OD 4,2°C DO 9,8°C

| VREME | $_1$ [m/s] | $_2$ [m/s] | $\Delta v$ [m/s] | |
|---|---|---|---|---|
| 22:00 | 2,589 | 2,849 | 0,260 | 9,12 |
| 20:10 | 2,599 | 2,880 | 0,281 | 9,76 |
| 18:00 | 4,428 | 4,659 | 0,231 | 4,96 |
| 15:50 | 1,848 | 1,960 | 0,112 | 5,71 |
| 13:20 | 1,210 | 1,230 | 0,020 | 1,63 |
| 10:00 | 0,989 | 1,041 | 0,052 | 4,99 |
| 07:00 | 1,191 | 1,230 | 0,039 | 3,17 |
| 03:40 | 0 | 0,280 | 0,280 | 100 |


ISBN 978-86-7466-930-3

Zanimljivo je primetiti podatak kada mehanički anemometar ne detektuje vetar (brzina 0,28 m/s), što se u potpunosti slaže sa specifikacijom instrumenta.

Tabela IV prikazuje vrednosti izmerene brzine vetra za slučaj iste promene spoljne temperature (od 5,6°C), pri nešto višoj spoljnoj temperaturi u odnosu na Tabelu III. Podaci su od 13.03.2022. U ovom slučaju, izmerene brzine vetra su mnogo veće ( preko 5 m/s), i može se zaključiti da se relativna greška merenja mehaničkog anemometra još više smanjila (manje od 2%) u odnosu na referentnu vrednost.

TABELA IV MERENJE BRZINE VETRA PRI SPOLJNOJ TEMPERATURI OD 9,5°C DO 15,1°C

| VREME | $_1$ [m/s] | $_2$ [m/s] | $\Delta v$ [m/s] | |
|---|---|---|---|---|
| 22:40 | 10,729 | 10,699 | 0,030 | 0,28 |
| 20:20 | 7,597 | 7,689 | 0,092 | 1,19 |
| 18:30 | 10,792 | 10,890 | 0,098 | 0,90 |
| 16:00 | 10,010 | 10,069 | 0,059 | 0,58 |
| 14:10 | 8,810 | 8,890 | 0,080 | 0,90 |
| 12:00 | 8,100 | 8,100 | 0,000 | 0 |
| 09:20 | 5,309 | 5,400 | 0,091 | 1,68 |
| 06:10 | 11,147 | 11,189 | 0,042 | 0,37 |

U Tabeli V i Tabeli VI prikazane su brzine vetrova izmerene pri spoljnim temperaturama preko 20 °C ( Tabela V sadrži podatke od 01.08.2020. a Tabela VI od 03.07.2020.).

TABELA V MERENJE BRZINE VETRA PRI SPOLJNOJ TEMPERATURI OD 26,1°C DO 34,7°C

| VREME | $_1$ [m/s] | $_2$ [m/s] | $\Delta v$ [m/s] | |
|---|---|---|---|---|
| 22:50 | 8,039 | 8,060 | 0,021 | 0,26 |
| 20:50 | 9,707 | 9,710 | 0,003 | 0,03 |
| 18:40 | 5,059 | 5,059 | 0 | 0 |
| 16:20 | 9,010 | 9,020 | 0,010 | 0,11 |
| 13:30 | 7,789 | 7,771 | 0,018 | 0,23 |
| 11:20 | 7,420 | 7,409 | 0,011 | 0,15 |
| 08:00 | 10,102 | 10,149 | 0,047 | 0,46 |
| 05:30 | 9,770 | 9,770 | 0 | 0 |

TABELA VI MERENJE BRZINE VETRA PRI SPOLJNOJ TEMPERATURI OD 23,4°C DO 31,1°C

| VREME | $_1$ [m/s] | $_2$ [m/s] | $\Delta v$ [m/s] | |
|---|---|---|---|---|
| 23:20 | 3,970 | 4,028 | 0,058 | 1,43 |
| 21:50 | 2,700 | 2,710 | 0,010 | 0,37 |
| 19:10 | 3,970 | 4 | 0,030 | 0,75 |
| 16:20 | 2,799 | 2,838 | 0,038 | 1,33 |
| 13:00 | 2,430 | 2,460 | 0,030 | 1,21 |
| 10:20 | 1,379 | 1,379 | 0 | 0 |
| 06:00 | 4,559 | 4,610 | 0,051 | 1,10 |
| 02:20 | 7,050 | 7,130 | 0,080 | 1,12 |

U ovim tabelama obuhvaćene su vrednosti brzine vetra do 5 m/s i preko 5 m/s. Kao što se iz priloženog vidi, merene vrednosti mehaničkog anemometra se često podudaraju sa merenim vrednostima ultrasoničnog anemometra ili odstupaju manje od 1,5% merene vrednosti brzine vetra.

## V ZAKLJUČAK

Kroz analizu prikupljenih podataka o izmerenim brzinama vetra, uočio sam da mehanički anemometar ne ispunjava karakteristike date od strane proizvođača u slučajevima konstantne temperature ispod 0°C (skoro zamrzavanje anemometra). Velike razlike u merenjima predstavljenih uređaja daje indikaciju kontrolnom sistemu vetroturbine o

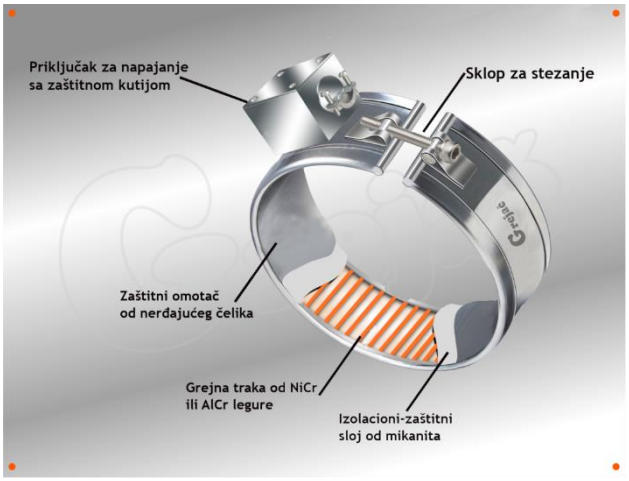


Sl. 4. Pojasni grejač [10]

mogućnosti stvaranja leda na elisama vetroturbine, koje može

biti veoma opasno po okolinu.Ova pojava inicira aktivaciju drugih podsistema vetroturbina kao što je zagrevanje elisa vetroturbine u cilju prevencije formiranja leda na njima. Takođe, potrebno je izvršiti neke modifikacije u sistemu merenja anemometra sa šoljicama, u cilju pružanja tačnijih izmerenih vrednosti brzine vetra.

Jedan od načina bio mogao biti tretiranje mehaničkih delova anemometra premazom ili sprejem protiv zamrzavanja, da se led ne bi hvatao za njih. Drugi način bi mogao biti dodavanje pojasnih grejača oko samog anemometra, koji bi mogao sprečiti smrzavanje osovine i ležajeva.

Sa druge strane, promenom metode za obradu signala koji generiše anemometar sa šoljicama mogla bi se smanjiti merna nesigurnost instrumenta. Umesto klasične metode uzorkovanja koja se koristi u današnjim mernim instrumentima, primenom stohastičke digitalne merne metode ovo bi bilo izvodljivo [8].


ISBN 978-86-7466-930-3

## ZAHVALNICA

Zahvaljujem se kompaniji Siemens Gamesa Renewable Energy na pruženoj podršci u stvaranju i razrađivanju ideje za ovaj rad. Ovaj rad je podržan od strane Fakulteta tehničkih nauka u Novom Sadu, Departmana za energetiku, elektroniku i telekomunikacije, u okviru realizacije projekta MPNTR 200156: 'Inovativna naučna i umetnička ispitivanja iz domena delatnosti FTN-a' .

## LITERATURA

[1] Opis uređaja ;https://www.thiesclima.com/pdf/en/Products/Wind-Compact/?art=300
[2] Opis uređaja https://www.thiesclima.com/pdf/en/Products/Wind-Ultrasonic-Anemometer/?art=145
[3] Uputstvo Instruction for use Ultrasonic anemometer Thies 2D
[4] S. Pindado, J. Cubas, F. Sorribes-Palmer ''TheCupAnemometer,a Fundamental Meteorological Instrument for the Wind Energy Industry. Research at the IDR/UPM Institute'', Madrid, Španija, 12. Novembar 2014.
[5] S. Pindado, E. Vega, A. Martínez, E. Meseguer, S. Franchini, I. Pérez '' Analysis of calibration results from cup and propeller anemometers. Influence on wind turbine Annual Energy Production (AEP) calculations'' Wind Energy, januar 2011.
[6] 40C Anemometer Uncertainty AppNote, 6. Februar 2015.
[7] T. Lipecki, P. Jaminska-Gadomska, A. Sumore '' Influence of Ultrasonic Wind Sensor Position on Measurement Accuracy under Full-Scale Conditions'', Lublin, Poljska, 02. Oktobar 2020.
[8] B. Ličina ''Metoda merenja snage i energije vetra zasnovana na merenju na intervalu'', doktorska disertacija, Elektrotrhničko i računarsko inženjerstvo, Fakultet tehničkih nauka, Novi Sad, 12. Jun 2016.
[9] Slika preuzeta iz katolga proizvoda kompanije Thies '' THIES-catalog-wind-e-9-2014''
[10] Slika preuzeta sa https://grejac.com/grejaci/pojasni-grejaci

## ABSTRACT

This paper compares the performance of a mechanical anemometer with cups and an ultrasonic anemometer, instruments for measuring wind speed on one of the wind turbines in the Alibunar windfarm. The data used in the analysis were obtained through the SCADA system of the Alibunar windfarm.

**Comparison wind speed measurements with cup anemometer and ultrasonic anemometer on the wind turbine**

Robert Fajhner, Marjan Urekar, *Member*, IEEE

 ISBN 978-86-7466-930-3

# Primena linearnog niza fotodetektora kod optičkih pseudoslučajnih pozicionih enkodera

Ivana Ranđelović, Dragan Denić, Goran Miljković i Aleksandar Jocić

***Apstrakt*—Precizno i pouzdano merenje ugaone pozicije je zahtev mnogih savremenim pokretnih sistema u industriji i drugim oblastima. Pseudoslučajni optički apsolutni enkoderi nude dobru rezoluciju, ali i pouzdanost i fleksibilnost u radu. U radu se analizira primena linearnog niza fotodetektora za paralelno očitavanje pseudoslučajnog koda pri čemu se dobija pravi apsolutni enkoder, koji za razliku od klasičnog ima jednu kodnu traku nezavisno od rezolucije. Razmatraju se karakteristike primenjenog senzora kao i ograničenja njegove primene za očitavanje pseudoslučajnog koda. Kako bi se izbegle greške prilikom projektovanja diska enkodera predlaže se metoda njegove provere nakon projektovanja bazirana na obradi slike. Takođe, moguća je i provera kvaliteta diska nakon njegove realizacije.**

***Ključne reči*—Pseudoslučajni pozicioni enkoder, merenje pozicije, paralelno očitavanje pseudoslučajnog koda, integrisani linearni niz fotodetektora.**

## I. Uvod

Pseudoslučajni optički enkoderi predstavljaju dobro rešenje za precizno i pouzdano merenje ugaone pozicije u različitim pokretnim sistemima u industriji, računarskim periferijama, antenama, kamerama, itd. Na tržištu se mogu naći kao obrtni i linearni pozicioni enkoderi visokih rezolucija. Pseudoslučajni pozicioni enkoderi, kao poseban tip apsolutnih enkodera, imaju manji broj kodnih traka, manji broj optičkih čitača, bolju pouzdanost i fleksibilnost. Pri samoj realizaciji pseudoslučajnog enkodera, obrtnog ili linearnog, potrebno je naneti pseudoslučajni binarni kod na disk ili traku enkodera i izvršiti odabir optičkog čitača, zatim definisati način očitavanja pseudoslučajnog koda [1], razmotriti metode skeniranja koda [2] kao i metode konverzije pseudoslučajnog u prirodni kod [3]. Dodatni kvalitet pseudoslučajnih enkodera koji im daje i veliku prednost u odnosu na klasične enkodere, jeste detekcija grešaka očitavanja koda. Korisniku se pruža dodatna informacija koja potvrđuje ispravnost informacije o poziciji sistema.

Pseudoslučajni apsolutni enkoderi imaju jednu kodnu traku sa pseudoslučajnom binarnom sekvencom, koja se može očitavati serijski i paralelno. Prilikom određivanja ugaone pozicije kod pseudoslučajnih apsolutnih enkodera se koristi „osobina prozora“ pseudoslučajne sekvence rezolucije $n$, pri čemu kada se očitaju $n$ susednih bitova; oni predstavljaju jedinstvenu kodnu reč iz koje se može dobiti informacija o poziciji. Kodne reči su raspoređene longitudinalno, pri čemu prvih ($n$-1) bita tekuće kodne reči su identični sa poslednjih ($n$-1) bita prethodne kodne reči. Tačnije, dve susedne kodne reči razlikuju se u samo jednom bitu. Pseudoslučajna binarna sekvenca maksimalne dužine $2^n$-1 se može generisati primenom pomeračkog registra od $n$-flip flopova i odgovarajuće povratne sprege. Ovako generisana pseudoslučajna binarna sekvenca sadrži $2^n$-1 različitih kodnih reči dužine $n$. Da bi se očitao pseudoslučajni binarni kod može se koristiti jedan ili dva detektora, a da se kodna reč formira u pomeračkom registru, ili se može koristiti linearni niz $n$ detektora pri čemu se paralelno očitavaju svih $n$ bitova u svakom trenutku [4, 5].

U radu se predlaže očitavanje pseudoslučajnog binarnog koda primenom optičkog modula sa integrisanim nizom fotodetektora. Radi se o metodi paralelnog očitavanja koda primenom senzora TCD1254GFG kompanije Toshiba koja je objašnjena u prvom delu rada. U drugom delu rada su razmatrana ograničenja prilikom primene ovog senzora za očitavanje pseudoslučajnog koda kod optičkog obrtnog pseudoslučajnog enkodera. U trećem delu rada je predstavljen postupak provere ispravnosti projektovanja i iscrtavanja pseudoslučajnih kodnih traka na tehničkom crtežu kao i provera samog diska nakon izrade a pre ugradnje.

## II. Metoda paralelnog očitavanja pseudoslučajnog binarnog koda

Kako bi se realizovao apsolutni pseudoslučajni enkoder, koji ne bi zahtevao inicijalno kretanje prilikom startovanja [1], može se primeniti linearni niz fotodetektora za očitavanje pseudoslučajnog koda sa diska enkodera. Inicijalno kretanje pokretnog mernog sistema je potrebno kod pseudoslučajnog enkodera sa serijskim očitavanjem koda kako bi se formirala prva validna kodna reč nakon startovanja mernog sistema. Takođe, ukoliko dođe do prekida napajanja enkodera ili se detektuje greška u merenju pozicije potrebno je inicijalno kretanje radi formiranja pseudoslučajne kodne reči.

Metod paralelnog očitavanja pseudoslučajnog binarnog koda može se postići primenom CCD senzora sa linearnim nizom fotodetektora.

Na slici 1 prikazan je rad pseudoslučajnog apsolutnog enkodera primenom metode paralelnog očitavanja koda [6], pri čemu se jedne strane kodne trake nalazi izvor svetlosti dok je sa druge strane linearni niz fotodetektora. Kodna traka je

Ivana Ranđelović – Elektronski fakultet, Univerzitet u Nišu, Aleksandra Medvedeva 14, 18000 Niš, Srbija (e-mail: ivana.randjelovic@elfak.ni.ac.rs).
Dragan Denić – Elektronski fakultet, Univerzitet u Nišu, Aleksandra Medvedeva 14, 18000 Niš, Srbija (e-mail: dragan.denic@elfak.ni.ac.rs).
Goran Miljković – Elektronski fakultet, Univerzitet u Nišu, Aleksandra Medvedeva 14, 18000 Niš, Srbija (e-mail: goran.miljkovic@elfak.ni.ac.rs).
Aleksandar Jocić – Elektronski fakultet, Univerzitet u Nišu, Aleksandra Medvedeva 14, 18000 Niš, Srbija (e-mail: aleksandar.jocic@elfak.ni.ac.rs).

 ISBN 978-86-7466-930-3

sastavljena od prozirnih i neprozirnih polja, širina svakog polja odnosno, pseudoslučajnog bita, veća je od širine fotoelemenata linearnog niza fotodetektora kako bi bilo moguće očitavati bitove pseudoslučajnog koda. Da bi se odredila apsolutna pozicija pseudoslučajnog enkodera neophodno je očitati *n* uzastopnih bitova sa pseudoslučajne kodne trake. Svaki pseudoslučajni bit očitava se sa kodne trake uz pomoć *m* fotodetektora. Primera radi, prikazan je 6-bitni pseudoslučajni binarni kod …101011… i linearni niz fotodetektor gde je broj fotodetektora koji očitava jedan bit *m*=8. Nakon primene linearnog niza fotodetektora, sa pseudoslučajne kodne trake dobija se sledeći niz na izlazu sistema za očitavanje koda

..1111111000000001111111100000000111111111111111...

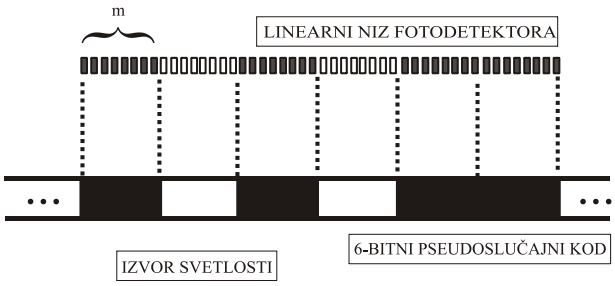


Sl. 1. Očitavanje pseudoslučajnog koda primenom metode paralelnog očitavanja koda

Rezolucija i tačnost očitavanja pseudoslučajnog koda zavise od karakteristika linearnog niza fotodetektora. Najvažniji parametri senzorskog modula sa lineranim nizom fotodetektora su: razmak između fotodetektora, broj fotodetektora, veličina fotodetektora, tip fotodetektora, napon napajanja, dodatne zaštite na primer u vidu elektronskog zatvarača ("electronic shutter") koji izlazni napon održava konstantnim bez obzira na varijacije intenziteta svetlosti. Kompanije kao što su iC-Haus GmbH [7], Hamamatsu company [8], Sensors Unlimited [9], Taos [10], Toshiba [11] samo su neki od prozvođača komercijalnih linearnih nizova fotodetektora. sa različitim širinama fotoosetljivog elementa koji su reda 400 μm, 100 μm, 50 μm, 25 μm, itd.

U radu se koristi optički modul TCD1254GFG kompanije Toshiba (slika 2), koji sadrži 2500 fotodetektora, dimenzije fotodetektora su 5.25 μm × 64 μm sa razmakom između fotodetektora 5,25 μm. Može se uočiti i da je sama dimenzija optičkog modula svega 13,371 mm.

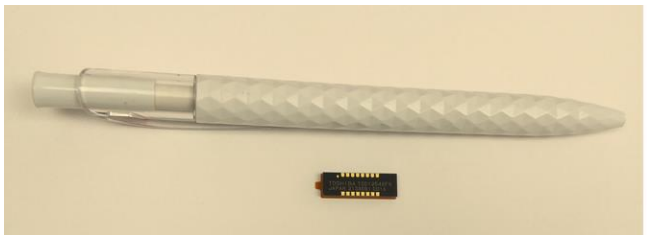

Sl. 2 Fotografija optičkog modula Toshiba TCD1254GFG

## III. ANALIZA PRIPREME LINEARNOG NIZA FOTODETEKTORA KOD PSEUDOSLUČAJNIH ABSOLUTNIH ENKODERA

Optički modul Toshiba TCD1254GFG sa 2500 foto elemenata može raditi na frekvencijama od -4 MHz, vreme jednog očitavanja svih piksela senzora je 10 ms. Vrednost napona napajanja senzorskog modula iznosi 4 V.

Analiziraće se primena prethodno opisanog senzora, linearnog niza fotodetektora, za očitavanje pseudoslučajnog koda različite rezolucije. Najpre se senzor koristi za očitavanje 16-bitnog pseudoslučajnog koda, pri čemu se svaki bit očitava sa 8 fotodetektora (piksela), slika 3a. Za očitavanje ovog koda iz senzora bi se koristio sledeći broj piksela

$$16 \text{ bita x } 8 \text{ piksela} = 128 \text{ piksela}$$

Zatim, ako se koristi za očitavanje 8-bitnog pseudoslučajnog koda, pri čemu se svaki bit očitava sa 64 piksela, broj upotrebljenih piksela iz senzora iznosi, slika 4b:

$$8 \text{ bita x } 64 \text{ piksela} = 512 \text{ piksela}$$

Potreban prečnik diska enkodera koji bi bio odgovarajući za očitavanje pseudoslučajnog koda definisane rezolucije prethodno predstavljenim senzorom bi bio:

a) za slučaj 16-bitnog koda dužine $2^{16} - 1 = 65535$ bita

$$5.25 \text{ μm x } 8 \text{ piksela x } 65535 \text{ bita} = 2\, r_{16}\, \pi$$
$$2\, r_{16} = 876.582 \text{ mm}$$

Može se uočiti da je prečnik diska suviše veliki za praktičnu primenu.

b) za slučaj 8-bitnog koda dužine $2^8 - 1 = 255$ bita

$$5.25 \text{ μm x } 64 \text{ piksela x } 255 \text{ bits} = 2\, r_8\, \pi$$
$$2\, r_8 = 27.286 \text{ mm}$$

Sada je prečnik diska enkodera pogodan za praktičnu primenu.

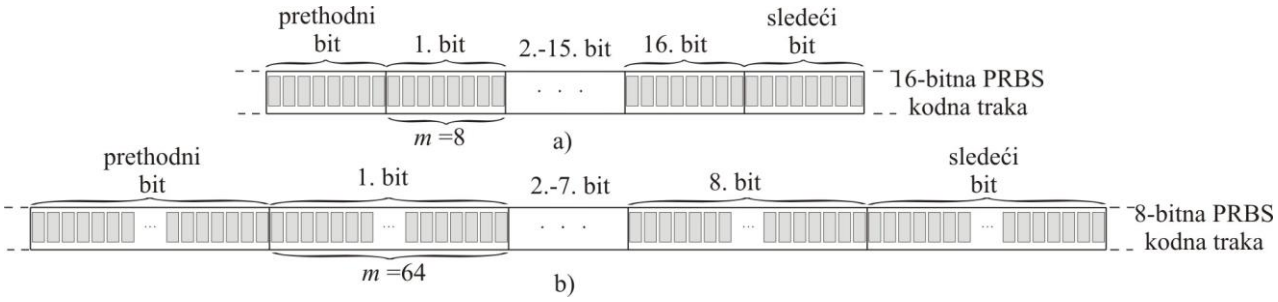


Slika 3. Paralelno očitavanje pseudoslučajnih kodova različite rezolucije

 ISBN 978-86-7466-930-3

Može se zaključiti da je sa povećanjem rezolucije pseudoslučajnog koda potreban veći prečnik diska enkodera, potrebno je naći kompromisno rešenje između broja fotodetektora koji će se koristiti za očitavanje jednog bita i rezolucije pseudoslučajnog koda.

Princip merenja ugaone pozicije kod ovako projektovanih pseudoslučajnih absolutnih enkodera je baziran na određivanju grube pozicije koja ima istu rezoluciju kao pseudoslučajna binarna sekvenca, kao i na povećanju rezolucije merenjem fine pozicije na osnovu očitavanja istog bita pseudoslučajnog koda sa $m$ susednih fotodetektora. Definiše se kodna reč koja predstavlja nultu poziciju enkodera prilikom njegovog montiranja na osovinu motora. Očitava se izlaz senzora, linearnog niza fotodetektora, ukoliko se dobije ista sekvenca nula i jedinica, ponavlja se očitavanje zato što nije bilo kretanja. Zatim se vrši detekcija redoslednih brojeva fotodetektora koji definišu prelaze između nizova nula i jedinica. Broj fotodetektora $m$ lineranog niza fotodetektora kojim se očitava jedan bit pseudoslučajnog koda je definisan prilikom projektovanja enkodera. Broj očitanih uzastopnih nula ili jedinica po jednom bitu koda na izlazu senzora će varirati u industrijskim uslovima rada enkodera od definisanog broja. Analizom sekvence nula i jedinica u izlaznom signalu, na osnovu redoslednih brojeva, definišu se granice bita i određuje se fina pozicija. Ako nema skoka fine pozicije od vrednosti 0 do vrednosti ($m$-1) i obrnuto, daje se informacija o tekućoj poziciji. Kada se javi skok fine pozicije određuje se smer rotacije i rekonstruiše se kodna reč, a zatim se konvertuje iz pseudoslučajnog u prirodni kod. Očitavanje jednog bita pseudoslučajne binarne sekvence sa $m$ fotodetektora je iskorišćen za povećanje rezolucije merenja ugaone pozicije u odnosu na samu rezoluciju pseudoslučajne binarne sekvence.

Pseudoslučajni absolutni enkoder je složena opto-elektro-mehanička komponenta koja je u industriji pod različitim spoljašnjim negativnim uticajima. Neki od izvora grešaka su ekscentricitet i eliptičnost diska enkodera, zaprljanje kodne trake, neprecizno odštampana kodna traka, vibracije, temperatura, itd. Zakrivljenje kodne trake i nejednako osvetljenje fotodetektora na ivicama kodnih bitova može takođe doprineti greškama očitavanja koda, slika 4.

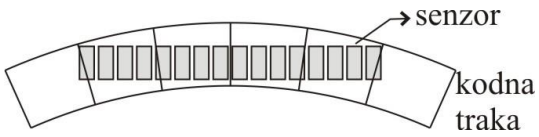


Sl. 4. Izvor greške očitavanja koda

## IV. PROVERA ISPRAVNOSTI PSEUDOSLUČAJNOG KODA DISKA POZICIONOG ENKODERA

Fizička realizacija diska pozicionog enkodera podrazumeva niz postupaka pri kojima je moguće uneti greške, koje dalje mogu dovesti do nefunkcionalnosti krajnjeg uređaja. Greške mogu biti unete u fazi iscrtavanja pseudoslučajnih traka u softveru za generisanje grafičkih prikaza, ali i u fazama fizičke izrade diska.

Prilikom izrade crteža, pseudoslučajna sekvenca bitova se interpretira tamnim (neprozirnim) (logička nula) i svetlim (prozirnim) (logička jedinica) poljima. S obzirom na to da pseudoslučajna sekvenca može imati veliku dužinu (npr. 1024, što odgovara rezoluciji od 10 bita), i da operater manuelno popunjava predviđena polja, postoji velika mogućnost pogrešnog unosa vrednosti bita. Ne postoji mogućnost automatskog (programiranog) iscrtavanja pseudoslučajnih sekvenci "nula" i "jedinica" u *vector graphics* formatu. Eventualna greška u ovoj fazi, koja bi bez provere bila otkrivena tek nakon ugradnje diska u uređaj, dovela bi do nepotrebnih troškova izrade diska kao i gubitka vremena. Kako postoji velika verovatnoća pojave greške u ovoj fazi izrade diska, neophodno je izvršiti pouzdanu proveru njegove ispravnosti.

Faza fizičke izrade diska podrazumeva niz aktivnosti kao što su izrada filma, fotolitografiju i ecovanje. Izrada filma se vrši tehnologijom koja poržava rezoluciju od 60 μm. U fotolitografskom postupku nejasne konture tamnih i svetlih polja, mogu nastati u slučaju nepravilnog postavljanja folije filma sa crtežom kodnih traka na pločicu diska (potrebno je da strana filma na kojoj je štampa bude uz površinu pločice pri osvetljavanju UV zracima kako ne bi došlo do rasipanja UV zraka na ivicama tamnih polja i pojave nejasnih kontura na samom disku). Nakon fotolitografije vrši se ecovanje. Usled nepreciznosti ovih postupaka može doći do promene dimenzija tamnih i svetlih polja, gubitka oštrine ivica polja, kao i njihovog pomeranja, usled čega kasnije pri korišćenju diska može doći do očitavanja pogrešne informacije. Zato se predlaže pouzdana provera ispravnosti diska i nakon ove faze.

Disk 10-bitnog ($n$ = 10) pseudoslučajnog enkodera sadrži 3 koncentrične trake, slika 5. Spoljna traka je inkrementalna traka dužine $2^{n+1}$ = 2048 bita (naizmenično poređanih "nula" i "jedinica"). Dve unutrašnje trake su pseudoslučajne trake dužine $2^n$ = 1024 bita.

Sl. 5. Izgled dela diska pseudoslučajnog pozicionog enkodera

Za pouzdanu proveru ispravnosti iscrtanih pseudoslučajnih traka iskorišćena je mogućnost da se slika tj. fajl u *bitmap* formatu, u programu MATLAB [12] može jednoznačno predstaviti matricom čiji elementi nose informaciju o

 ISBN 978-86-7466-930-3

pikselima slike. Dimenzije matrice odgovaraju dimenzijama slike izražene u broju piksela. *Bitmap* fajl mora biti pripremljen u *grayscale* modu, što za posledicu ima predstavljanje piksela, tj. elemenata matrice, celim brojevima u opsegu [0, 255]. Elementi matrice (slike) mogu biti predstavljeni samo vrednostima 0 i 1, ali zbog vizuelizacije potreban je i "sivi" piksel, odnosno, zadržan je dati opseg. Vrednošću 0 predstavlja se potpuno crni piksel, vrednošću 255 predstavlja se potpuno beli piksel, dok se vrednošću 128 predstavlja sivi piksel.

Potrebno je poznavati koordinate centra diska enkodera $(X_0,Y_0)$, kao i poluprečnike koncentričnih kružnica kojima su ograničene kodne trake. Predviđeno je inicijalno softversko određivanje ovih parametara.

Analiza *bitmap* fajla crteža kodnih traka, predstavljenih matricom na prethodno opisani način, vrši se očitavanjem vrednosti piksela po kružnoj putanji određenog poluprečnika sa centrom u $(X_0,Y_0)$. S tim u vezi, analiza se svodi na ispitivanje elemenata matrice primenom polarnih koordinata $(r, \varphi)$. Ceo krug (360˚) se deli na $P=100\cdot 2^{n+1}$ ravnomerno raspoređenih tačaka sa polarnim koordinatama $(r, \varphi_i)$ $i=1, ..., P$. Zatim se polarne koordinate transformišu u Dekartove koordinate $(x_i,y_i)$ u kojima se ispituje vrednost elementa matrice. Može se uočiti da je za rezoluciju uzorkovanja uzet ugao koji je 100 puta manji od ugla koji na disku zauzima „bit" sa najmanjom ugaonom širinom (u ovom slučaju „bit" na inkrementalnoj traci). Ovako određena rezolucija uzorkovanja obezbeđuje pouzdanu detekciju prelaza između bitova na inkrementalnoj traci.

Na slici 5. prikazan je detalj traka enkodera. Pri detektovanom prelazu kod inkrementalne trake, za isti ugao na kome je detektovan prelaz $\varphi_i$ očitava se piksel - elemenat matrice na polupečnicima koji odgovaraju sredinama pseudoslučajnih traka. Očitani pikseli svih traka su na slici 5. predstavljeni sivom bojom. U zavisnosti od vrednosti elementa matrice ustanovljava se da li bit pseudoslučajne trake nosi informaciju o logičkoj nuli ili logičkoj jedinici. Ove vrednosti se pamte u posebnim nizovima u programu. Nakon očitavanja svih bitova pseudoslučajnih traka, sadržaj ovih nizova se poredi sa tačnim pseudoslučajnim kodom koji se učitava preko ulaznog fajla i određuje da li postoji greška u njenoj poziciji.

## IV. Zaključak

U radu se predlaže očitavanje pseudoslučajnog binarnog koda primenom optičkog modula sa integrisanim nizom fotodetektora primenom metode paralelnog očitavanja koda. Razmatrana su ograničenja prilikom primene senzora TCD1254GFG kompanije Toshiba za očitavanje pseudoslučajnog koda kod optičkog obrtnog pseudoslučajnog enkodera. Analizirani su parametri kao što su prečnik diska i rezolucija enkodera u cilju nalaženja kompromisnog rešenja. Istaknuti su i neki od izvora grešaka u samoj realizaciji enkodera. Dat je i postupak provere ispravnosti projektovanja i iscrtavanja pseudoslučajnih kodnih traka na tehničkom crtežu kao i provera samog diska nakon izrade pre same ugradnje. U cilju daljeg razvoja predloženog rešenja potrebno je ispitati mogućnost primene drugih softverskih paketa koji bi doveli do ovakvih rezultata.

## Zahvalnica

Ovaj rad je podržan od strane Ministarstva prosvete, nauke i tehnološkog razvoja Republike Srbije. (Ugovor o realizaciji i finansiranju naučnoistraživačkog rada NIO u 2022. godini, evidencioni broj 451-03-68/2022-14/200102).

## Literatura

[1] M. Arsić, D. Denić, "New pseudorandom code reading method applied to position encoders", Electronics Letters, vol.29, pp. 893-894, 1993.
[2] D. Denić, G. Miljković, "Code reading synchronization method for pseudorandom position encoders", Sensors and Actuators A-Phys. vol. 150, pp. 188-191, 2009.
[3] D. Denić, I. Stojković, "Pseudorandom/natural code converter with parallel feedback logic configuration", Electronics Letters, vol. 46, pp. 921-922, 2010.
[4] J.T.M. Stevenson and J.R. Jordan, "Absolute position measurement using optical detection of code patterns", J. Phys E. Sci. Instrum. 21, pp. 1140-1145, 1988.
[5] H. Khalfallah, E.M. Petriu, F.C.A. Groen, "Visual position recovery for an automated guided vehicle", IEEE Trans. Instrument and Measurement, vol. 41, no. 6, pp. 906-910, 1992.
[6] D. Denić, I. Ranđelović, M. Rančić: "High-resolution pseudorandom encoder with parallel code reading", Electronics and electrical engineering Nr 7(56), Kaunas, Litvania, pp. 9-14, 2004.
[7] www.ichaus.com
[8] www.hamamatsu.com
[9] www.sensorsinc.com
[10] www.taosinc.com
[11] www.toshiba.com
[12] www.mathworks.com

## Abstract

Accurately and reliable measurement of angular position is a requirement of many modern moveable systems in industry and other fields. Pseudorandom optical absolute encoders offer good resolution as well as reliability and flexibility in operation. The paper analyses the application the linear array of photodetectors for parallel pseudorandom code reading to obtain a true absolute encoder, which, unlike the classical one, has one code track regardless of resolution. The characteristics of the applied sensor are considered, as well as the limitations of its application for pseudorandom code reading. In order to avoid errors when designing the encoder disk, a method of its verification after design based on image processing is proposed. Also, it is possible to check the quality of the disk after its realization.

**Application of linear array of photodetectors in optical pseudorandom position encoders**

Ivana Ranđelović, Dragan Denić, Goran Miljković i Aleksandar Jocić

 ISBN 978-86-7466-930-3

# Ponovljivost rezultata merenja nivoa električnog polja EM smetnji

Aleksandar M. Kovačević, Nenad Munić

***Apstrakt*—Ponovljivost rezultata merenja nivoa električnog polja EM smetnji, tokom vremena, na jednom uređaju informacione tehnologije, treba da omogući donošenje konačne odluke o usaglašenosti uređaja. Istovremeno, ponovljivost rezultata navedenih merenja treba da omogući akreditovanoj laboratoriji da preispita svoje rezultate ispitivanja radi obezbeđenja njihove validnosti.**

***Ključne reči*—Validnost; ponovljivost; merenje; električno polje smetnji.**

## I. Uvod

ELEKTRONSKA oprema se danas smatra kritičnim projektnim elementom sredstava i sistema naoružanja i vojne opreme (NVO). Pri tome, savremene telekomunikacione uređaje karakteriše s jedne strane velika snaga ultraširokopojasnih predajnika, a sa druge strane osetljivost prijemnika [1]. Pored toga, tome doprinosi i veoma brz razvoj informatičke tehnike, tako da postaje sasvim jasno da ispravan rad svakog uređaja ponaosob i svih zajedno nije moguć bez analize međusobnih elektromagnetskih uticaja.

U Tehničkom opitnom centru [2], specijalizovanoj vojnoj naučnoistraživačkoj ustanovi, u okviru Odeljenja za elektromagnetsku kompatibilnost i uticaje okoline, već više decenija se obavljaju ispitivanja elektromagnetske kompatibilnosti (EMC) sredstava i sistema NVO prema standardima posebne namene (Standardi odbrane Republike Srbije – SORS) [3-5]. Takođe, za potrebe ispitivanja se koriste i drugi vojni standardi od kojih je najpoznatiji MIL-STD-461 [6].

Pored toga, Odeljenje za elektromagnetsku kompatibilnost i uticaje okoline je akreditovano u oblasti ispitivanja elektromagnetske kompatibilnosti (u daljem tekstu Odeljenje za EMC i uticaje okoline), pa je u obavezi da u sklopu obezbeđenja validnosti rezultata ispitivanja redovno vrši sledeće aktivnosti: funkcionalnu proveru merne opreme i opreme za ispitivanje, međuprovere ključne merne opreme, ponavljanje ispitivanja korišćenjem istih metoda i sl. [7].

Veliki broj ponavljanja ispitivanja karakteristika EMC nije uvek moguć, ali u nekim situacijama može biti opravdan (npr. kada se izmerena vrednost menja i po frekvenciji i po amplitudi), jer se nakon navedenih ispitivanja treba da donese odluka o usaglašenosti uređaja [8].

U ovom radu je prikazano ponavljanje merenja nivoa električnog polja EM smetnji na jednom sredstvu NVO (uređaj informacione tehnologije), tokom vremena, radi donošenja konačne odluke o usaglašenosti uređaja (usvajanje uređaja u naoružanje Vojske). Istovremeno, navedeno ponavljanje je omogućilo akreditovanoj laboratoriji da preispita rezultate svojih ispitivanja radi njihove validnosti [7]. Merenja nivoa električnog polja EM smetnji su obavljena na jednom uređaju informacione tehnologije (u daljem tekstu IT uređaj) prema standardima SORS 1029/89 i SORS 1762/89 [3, 4].

## II. Uslovi ispitivanja

Merenja nivoa električnog polja EM smetnji su obavljena na jednom IT uređaju prema standardima [3, 4]. IT uređaj predstavlja laptop računar i robustan (eng. rugged) AC/DC adapter za napajanje iz izvora naizmenične struje.

Ispitivanje je izvršeno u opsegu od 30 MHz do 300 MHz, sa odgovarajućom prijemnom antenom (bikonusna antena), koja je postavljena na rastojanje 1 m od IT uređaja, na visini 1,2 m od poda Faradejevog kaveza. IT uređaj je postavljen na sto, visine 80 cm, i priključen AC/DC adapterom, preko ekvivalentne mreže i razdvojnog transformatora, na mrežu za napajanje. Pri tome, drveni sto je bio dimenzija: dužina 1 m, širina 1 m i visina 0,8 m, na kome se nalazi referentna provodna ploča (od bakra), dužine 2,6 m i širine 1 m (površina ploče 2,6 $m^2$), pri čemu je ploča savijena pod pravim uglovima na dva mesta (Sl. 1).

Sl. 1. Ispitivanje nivoa električnog polja EM smetnji.

Aleksandar M. Kovačević – Fakultet tehničkih nauka, Univerzitet u Kragujevcu, Svetog Save 65, 32000 Čačak, Srbija (e-mail: aleksandar.kovacevic@ftn.kg.ac.rs). Nenad Munić – Tehnički opitni centar, Generalštab Vojske Srbije, Vojvode Stepe 445, 11000 Beograd, Srbija (e–mail: nenadmunic@yahoo.com).

 ISBN 978-86-7466-930-3

Robustni adapter i kabl su odvojeni od provodne površine izolacionom podlogom dimenzija 1,8 m x 0,5 m, debljine 3 cm, koja je postavljena iza uređaja na rastojanju od 15 cm. Rastojanje između ekvivalentne mreže i IT uređaja je iznosilo 60 cm. Na uređaju je emitovano više paralelnih multimedijalnih sadržaja.

Pre početka merenja nivoa električnog polja EM smetnji izvršena je kontrola smetnji okoline kada je IT uređaj isključen (nivo smetnji ambijenta).

Merenje električnog polja EM smetnji vrši se tako što se mernim prijemnikom (meračem polja) pretraži zadati frekvencijski opseg, i merenje obavi na najmanje 3 frekvencije po oktavi na kojima je nivo EM smetnji najveći. Pri tome, beleži se najveća vrednost električnog napona. Pored toga, merenja treba obaviti i na kritičnim frekvencijama za ispitivano sredstvo (npr. frekvencija lokalnog oscilatora, međufrekvencija itd.) [4]. U ovom slučaju, korišćen je vršni – Pk (eng. Peak) detektor analizatora spektra.

Za navedena merenja korišćena su sledeća merna sredstva i oprema:

- EMC analizator spektra E7402A, Agilent, od 100 Hz do 3 GHz;
- Bikonusna antena SAS-542, A.H. Systems, od 20 MHz do 330 MHz;
- Ekvivalentna V-mreža ENV216, R&S;
- Stoni računar ASUS sa aplikacijom za automatizaciju merenja (EMC Measurement Application E7415A);
- RF limiter 11867A, Agilent;
- Razdvojni transformator MA 4801, ISKRA;
- Kabl RG-214/U.

Pre početka ispitivanja je konstatovano da je navedena merna oprema metrološki ispravna jer ima prihvatljivu metrološku sledivost, koju prate dokumenta o pregledu, odnosno isprave o usaglašenosti merne opreme sa propisanim zahtevima, a u skladu sa Pravilnikom o metrološkoj delatnosti u oblasti odbrane [9].

Uslovi okoline:

- temperatura okoline: 23°C ± 2°C,
- relativna vlažnost vazduha: 50% ± 15%.

## III. KRITERIJUM ZA OCENU REZULTATA MERENJA

Nivo električnog polja EM smetnji u zadatom frekvencijskom opsegu treba da bude manji od graničnih vrednosti [3]. S obzirom da IT uređaj nije ispunio zahteve standarda u frekvencijskom opsegu od 30 MHz do 300 MHz, nakon nekoliko meseci je izvršeno ponavljanje merenja na istom uređaju. Naime, ponavljanje merenja nivoa električnog polja EM smetnji na istom IT uređaju, trebalo je da omogući donošenje konačne odluke o usaglašenosti uređaja (usvajanje uređaja u naoružanje Vojske).

Pri tome, razmatrane su one frekvencije na kojima je nivo električnog polja EM smetnji bio iznad graničnih vrednosti. Kao kriterijum za ocenu rezultata merenja je uzeto da razlika u dobijenim vrednostima između ta dva merenja bude u granicama merne nesigurnosti $U_m$ – proširena merna nesigurnost merenja nivoa električnog polja EM smetnji (za faktor proširenja ili prekrivanja $k = 2$).

## IV. REZULTATI MERENJA

Grafički prikaz rezultata merenja nivoa električnog polja EM smetnji (rezultati I) je dat na Sl. 2.

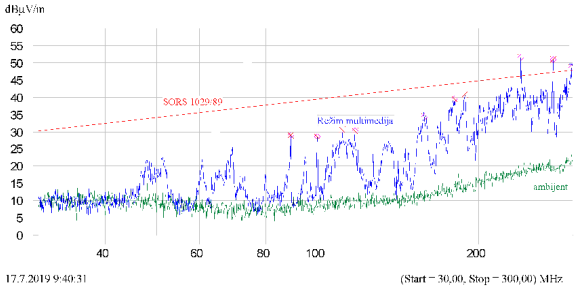


Sl. 2. Grafički prikaz rezultata merenja nivoa električnog polja EM smetnji (rezultati I).

Na osnovu Sl. 2 može se konstatovati da IT uređaj, u režimu multimedija, generiše električno polje EM smetnji iznad dozvoljene granične vrednosti [3], i to na 3 frekvencije: 255 MHz, 272 MHz i 298 MHz. Pri tome, maksimalno premašenje iznosi 5 dB (na frekvenciji od 255 MHz).

Nakon nekoliko meseci, izvršeno je ponavljanje merenja na istom uređaju u frekvencijskom opsegu od 30 MHz do 300 MHz. Grafički prikaz rezultata merenja nivoa električnog polja EM smetnji (rezultati II) je dat na Sl. 3.

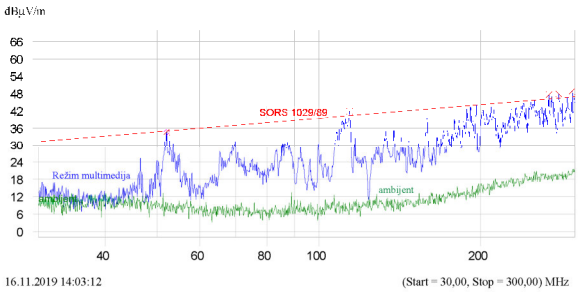


Sl. 3. Grafički prikaz rezultata merenja nivoa električnog polja EM smetnji (rezultati II).

Na osnovu Sl. 3 može se konstatovati da IT uređaj, u režimu multimedija, generiše električno polje EM smetnji iznad dozvoljene granične vrednosti [3], i to na 5 frekvencija: 55 MHz, 120 MHz, 260 MHz, 270 MHz i 295 MHz. Pri tome, maksimalno premašenje iznosi 2 dB (na frekvenciji od 295 MHz).

Proširena merna nesigurnost, $U_m$, za merenje nivoa električnog polja EM smetnji ($k = 2$), kada se za merenje koristi bikonusna antena, iznosi 5,3 dB i u skladu je sa preporukama standarda CISPR 16-4-2:2018 [10]. Pri tome, obračun merne nesigurnosti za električno polje EM smetnji

 ISBN 978-86-7466-930-3

dat je detaljno u internoj Proceduri za određivanje merne nesigurnosti kod ispitivanja EMC [11].

Na osnovu dobijenih rezultata (Sl.2 i Sl.3) i postavljenog kriterijuma, konstatovana je ponovljivost rezultata ispitivanja, odnosno ponovljivost smetnji na približno istim frekvencijama. Razlog manjih odstupanja, može biti razlika u napunjenosti baterije IT uređaja, odnosno struji punjenja u trenutku ispitivanja. Pored toga, utvrđeno je da je razlika u dobijenim vrednostima u granicama merne nesigurnosti, tako da je obezbeđena validnost rezultata merenja.

## V. ZAKLJUČAK

U Tehničkom opitnom centru, specijalizovanoj vojnoj naučnoistraživačkoj ustanovi, u okviru Odeljenja za elektromagnetsku kompatibilnost i uticaje okoline, već više decenija se obavljaju ispitivanja elektromagnetske kompatibilnosti (EMC) sredstava i sistema NVO prema standardima posebne namene (SORS).

Kako je Odeljenje za EMC i uticaje okoline akreditovano u oblasti ispitivanja elektromagnetske kompatibilnosti, u obavezi je da u sklopu obezbeđenja validnosti rezultata ispitivanja redovno vrši funkcionalnu proveru merne opreme i opreme za ispitivanje, međuprovere ključne merne opreme, ponavljanje ispitivanja korišćenjem istih metoda i sl.

U ovom radu je prikazano ponavljanje merenja nivoa električnog polja EM smetnji, u frekvencijskom opsegu od 30 MHz do 300 MHz, na jednom IT uređaju (sredstvo vojne opreme), tokom vremena, radi donošenja konačne odluke o usaglašenosti uređaja (usvajanje uređaja u naoružanje Vojske). Pri tome, navedeno ponavljanje je omogućilo akreditovanoj laboratoriji da preispita rezultate svojih ispitivanja radi njihove validnosti.

Na osnovu dobijenih rezultata, konstatovana je ponovljivost rezultata ispitivanja na približno istim frekvencijama. Razlog manjih odstupanja, može biti razlika u napunjenosti baterije IT uređaja, odnosno struji punjenja u trenutku ispitivanja. Pored toga, utvrđeno je da je razlika u dobijenim vrednostima u granicama merne nesigurnosti, tako da je obezbeđena validnost rezultata merenja.

## LITERATURA


[1] C.R. Paul, *Introduction to Electromagnetic Compatibility*, second ed., Wiley, New York, 2006.

[2] http://www.toc.vs.rs.

[3] *Elektromagnetske smetnje*, *ZAHTEVI,* SORS 1029/89, Biro za standardizaciju i metrologiju u JNA, 1989.

[4] *Elektromagnetske smetnje*, *MERENJA,* SORS 1762/89, Biro za standardizaciju i metrologiju u JNA, 1989.

[5] *Elektromagnetska kompatibilnost*, SORS 4077/89, Biro za standardizaciju i metrologiju u JNA, 1989.

[6] *Requirements for the Control of Electromagnetic Interference Characteristics of Subsystems and Equipment*, MIL-STD-461F, Department of Defense, USA, 2007.

[7] *Opšti zahtevi za kompetentnost laboratorija za ispitivanje i laboratorija za etaloniranje*, SRPS ISO/IEC 17025, ISS, 2017.

[8] A. Kovačević, V. Jokić, P. Osmokrović, "Utvrđivanje usaglašenosti pri merenju smetnji provođenja kada merni prijemnik pokazuje promenljive vrednosti koje su bliske granici", Zbornik radova 55. konferencije ETRAN-a, Banja Vrućica, Teslić, str. ML1.1-1-4, 6-9.06.2011.

[9] *Pravilnik o metrološkoj delatnosti u oblasti odbrane*, Službeni vojni list br. 19, Ministarstvo odbrane Republike Srbije, 2018.

[10] *Specification for radio disturbance and immunity measuring apparatus and methods – part 4–2: Uncertainties, statistics and limit modeling – Measurement instrumentation uncertainty*, CISPR 16-4-2, IEC, 2018.

[11] *Procedura za određivanje merne nesigurnosti kod ispitivanja EMC*, Interni dokument, TOC, 2018.



## ABSTRACT

The repeatability of EM interference electric field level measurement results, over time, on an information technology device, should enable a final decision on the conformity of the device. At the same time, the repeatability of the results of these measurements should allow the accredited laboratory to review its test results to ensure their validity.


**Repeatability of EM interference electric field level measurement results**

Aleksandar M. Kovačević, Nenad Munić

 ISBN 978-86-7466-930-3

# Pregled elektrogastrografske metode

Jelena Đorđević Kozarov, Platon Sovilj, *Member, IEEE*, Marjan Urekar, *Member, IEEE*, Milan Šaš i Miroljub Pešić

***A stra t* — le trogastrografija ( GG) je neinvazivna elektrofiziološka tehni a oja se oristi za snimanje električne a tivnosti želuca pomoću ele troda postavljenih na abdomen. GG se do sada najviše oristio u kliničkim studijama i dijagnostici u gastroenterologiji, ali se sve više javlja interesovanje za naučno istraživanje GG metode u oblasti biomedicine i psihofiziologije. Cilj ovog rada je da se, na osnovu postojeće literature, prikažu osnovne fiziološke ara teristi e EGG signala, kao i mogući načini snimanja i obrade ovih signala.**

***Ključne reči* — le trogastrografija; Gastrični spori talasi; Gastrointestinalni motilitet; Mioelektričnost.**

## I. UVOD

ELEKTROGASTROGRAFIJA je neinvazivna tehnika za snimanje mioelektrične aktivnosti želuca pomoću površinskih elektroda postavljenih na abdominalnu kožu u predelu želuca. Signal snimljen elektrogastrografijom naziva se elektrogastrogram (EGG) [1-5]. Tokom prve polovine dvadesetog veka, elektrogastrogram (EGG) su nezavisno otkrila tri naučnika: Valter Alvarez (gastroenterolog, 1922) [6,7], Harison Tumpeer (pedijatar, 1926, 1932) [7-9] i R.C. Davis (psihofiziolog, 1950) [10,11]. Počevši od 1974. godine, kada su istraživači Stevens i Vorrall (1974) prvi primenili tehniku spektralne analize na EGG [12], a potom 1975. istraživači u Engleskoj objavili brojne studije o frekvencijskoj analizi EGG signala, došlo je do velikog napretka u tehnikama analize EGG signala [13-15].

Zbog svoje neinvazivne prirode i sve većeg napretka tehnike snimanja EGG-a, kao i moguće računarske analize snimljenog signala, EGG je postao veoma atraktivan alat za proučavanje elektrofiziologije želuca i patofiziologije poremećaja motiliteta želuca, pa se trenutno koristi i u naučnim i u kliničkim istraživanjima [16-19].

Da bi se procenilo da li je EGG signal koristan kao istraživačko i/ili kliničko sredstvo, najpre treba u potpunosti razumeti šta se može meriti pomoću EGG-a i kako bi EGG trebalo da bude snimljen, interpretiran i analiziran. U tu svrhu, u ovom radu je najpre opisana elektrofiziologija želuca, odnosno mioelektrična aktivnost želuca koja se može meriti korišćenjem površinskih elektroda, a potom su opisani i karakteristični parametri EGG signala. S obzirom da se za snimanje EGG signala koriste površinske elektrode, EGG signal je osetljiv na artefakte pokreta, kao i na električne signale drugih unutrašnjih organa, te su u ovom radu opisani tehnički detalji pravilnog merenja EGG signala u cilju sprečavanja artefakata. Na kraju rada je dat pregled primene EGG-a, uključujući primenu EGG-a za proučavanje elektrofiziologije želuca, upotrebu EGG-a u proceni efekta intervencije i klinički značaj EGG-a kod pacijenata sa simptomima koji ukazuju na želudačnu disfunkciju.

Jelena Đorđević Kozarov – Elektronski fakultet, Univerzitet u Nišu, A. Medvedeva 14, 18000 Niš, Srbija (e-mail: kozarov@elfak.ni.ac.rs).
Platon Sovilj – Fakultet tehničkih nauka, Univerzitet u Novom Sadu, Trg Dositeja Obradovića 6, 21000 Novi Sad, Srbija (e-mail: platon@uns.ac.rs).
Marjan Urekar – Fakultet tehničkih nauka, Univerzitet u Novom Sadu, Trg Dositeja Obradovića 6, 21000 Novi Sad, Srbija (e-mail: urekarm@uns.ac.rs).
Milan Šaš – Fakultet tehničkih nauka, Univerzitet u Novom Sadu, Trg Dositeja Obradovića 6, 21000 Novi Sad, Srbija (e-mail: milansas@uns.ac.rs).
Miroljub Pešić – Elektronski fakultet, Univerzitet u Nišu, Aleksandra Medvedeva 14, 18000 Niš, Srbija (e-mail: miroljub.pesic@elfak.ni.ac.rs)

## II. ELEKTROFIZIOLOGIJA ŽELUCA

EGG se definiše kao snimanje mioelektrične aktivnosti glatkih mišića želuca pomoću elektroda pričvršćenih na kožu abdomena. EGG predstavlja bezbolan test kojim se određuje električna aktivnost u stomaku, pre, tokom i posle jela.

Radi lakšeg razumevanja rada želuca, na Sl. 1 su prikazani njegovi delovi:

- fundus je rezervoar za hranu,
- korpus - proizvodi se enzim pepsin,
- gastrični pejsmejker se nalazi na velikoj krivini korpusa i generiše električne impulse,
- antrum - proizvodi se hormon gastrin i tu se vrši mešanje i mlevenje hrane,
- pilorus je ventil između želuca i dvanaestopalačnog creva.

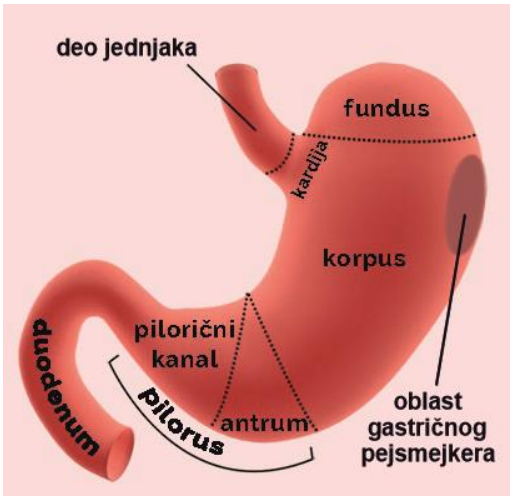


Sl. 1. Delovi želuca.

Gastrični pejsmejker generiše električni signal svakih 20 s, koji se širi ka antrumu, i kao odgovor na kalorijski izazov ili lek, stvara snažne peristaltičke kontrakcije koje guraju antralni sadržaj ka pilorusu i pomažu u mlevenju i mešanju hrane.

 ISBN 978-86-7466-930-3

### *A. Normalna mioelektrična akti nost želuca*

Mioelektrična aktivnost želuca sastoji se od sporih talasa i šiljastih (spajk) potencijala (Sl. 2) [3]. Spori talas se još naziva i aktivnost električne kontrole, dok se šiljasti potencijali nazivaju akcioni potencijali [20,21]. Frekvencija normalnih sporih talasa u želucu iznosi približno 3 ciklusa u minuti (cpm) kod ljudi [22-24] i 5 cpm kod pasa [25,26], dok je amplituda od 50 μV do 500 μV. Gastrični spori talas određuje maksimalnu frekvenciju i propagaciju želudačnih kontrakcija. Šiljasti potencijali se smatraju električnim parom želudačnih kontrakcija, odnosno kontrakcija želuca nastaje kada je spori talas praćen šiljastim potencijalima.

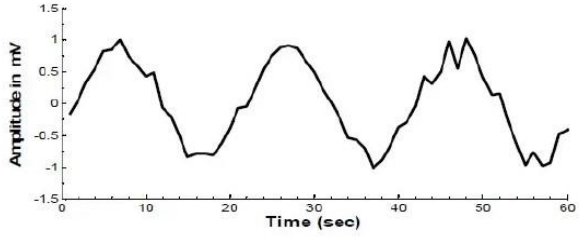


Sl. 2. Normalna mioelektrična aktivnost želuca.

### *B. Gastrična aritmija i abnormalni spori talasi*

Mioelektrična aktivnost želuca može se promeniti ili postati abnormalna u bolesnim stanjima ili nakon operativnih zahvata ili spontano. Abnormalna mioelektrična aktivnost želuca uključuje želudačnu aritmiju, abnormalno sporo širenje talasa (bradigastrija) i abnormalno povećanje brzine električne aktivnosti (tahigastrija). Normalna frekvencija gastričnog sporog talasa kod ljudi je oko 2-4 cpm, dok je bradigastrija u opsegu 0.5-2.0 cpm, a tahigastrija u opsegu 4-9 cpm. Ukoliko se dominantna frekvencija ne može odrediti, u pitanju je želudačna aritmija. Bradigastrija i tahigastrija mogu biti povezani sa mučninom, gastroparezom, sindromom iritabilnog creva.

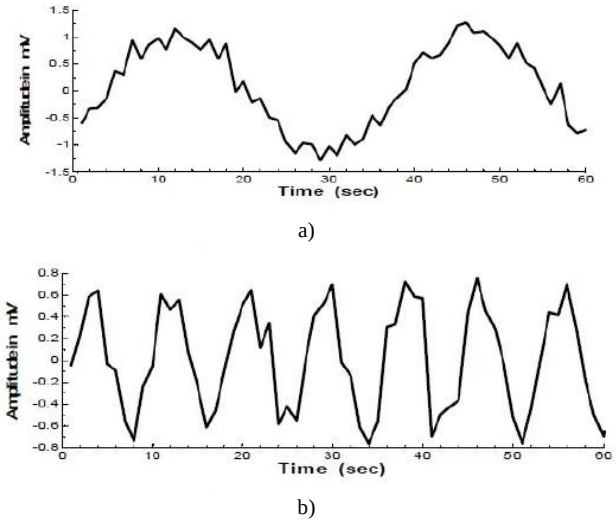


Sl. 3. Abnormalna mioelektrična aktivnost želuca: a) bradigastrija, b) tahigastrija.

## III. MERENJE ELEKTROGASTROGRAMA

Mioelektrična aktivnost želuca se može meriti:

- serozno (elektrode na seroznoj površini želuca se postavljaju hirurški),
- intraluminalno (intubacija katetera sa elektrodama za snimanje želuca), ili
- na površini kože (pomoću površinskih elektroda).

Prve dve metode su invazivne i njihove primene su ograničene uglavnom na životinje i izvode se u laboratorijskim uslovima [1]. EGG metoda (merenje aktivnosti želuca pomoću površinskih elektroda) ima široku primenu kod ljudi i u kliničkim istraživanjima jer je neinvazivna i ne remeti tekuću aktivnost želuca. Brojne studije validacije su dokumentovale tačnost EGG metode upoređujući je sa snimkom dobijenim sa mukoznih i seroznih elektroda [15,1]. Pokazano je da se zapis EGG-a može ponoviti, bez značajnih dnevnih varijacija [27], a utvrđeno je i da kod odraslih, starost i pol nemaju nikakav uticaj na EGG [28,29].

Zbog prirode merenja, EGG je osetljiv na artefakte pokreta. Shodno tome, pažljiva i pravilna priprema pre snimanja je ključna za dobijanje pouzdanih podataka.

*Priprema kože* - S obzirom da su EGG signali veoma slabi, vrlo je važno minimizirati impedansu između kože i elektroda, pa je neophodno dobro očistiti abdominalnu površinu na koju će se postaviti elektrode. EGG može sadržati ozbiljne artefakte pokreta ako koža nije dobro pripremljena.

*Posta ljanje elektroda* - Standardne elektrokardiografske elektrode se obično koriste za snimanje EGG. Iako ne postoji utvrđen standard, opšte je prihvaćeno da aktivne elektrode za snimanje treba da budu postavljene što bliže antrumu da bi se postigao visok odnos signal-šum [30]. EGG signali se mogu snimiti bilo unipolarnim ili bipolarnim elektrodama, ali bipolarno snimanje daje signale sa većim odnosom signal-šum. Jedna najčešće korišćena konfiguracija elektroda za snimanje četvorokanalnih EGG zapisa je prikazana na Sl. 4.

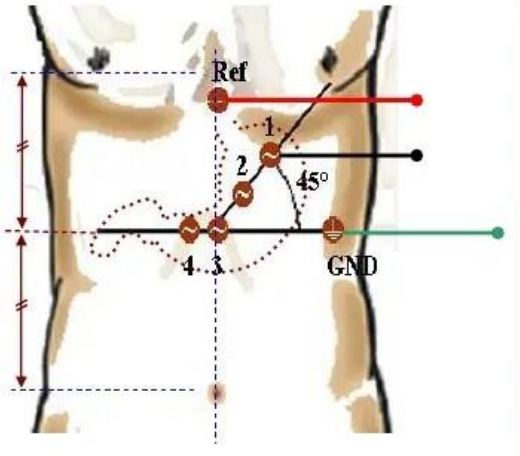


Sl. 4. Primer postavljanja elektroda za merenje EGG signala.

*Po icioniranje ispitanika* - Ispitanik treba da bude u udobnom ležećem položaju ili da sedi u fotelji, u tihoj prostoriji, tokom čitave procedure snimanja. Kad god je to

 ISBN 978-86-7466-930-3

moguće, preporučuje se ležeći položaj, jer je ispitanik u ovom položaju opušteniji, a samim tim se pojavljuje manje artefakata pokreta. Ispitanik bi trebalo da ostane što je moguće mirniji i da ne učestvuje u razgovorima, kako bi se maksimalno sprečili artefakti pokreta [19,1].

*Dužina snimanja i test obrok* - Snimanje EGG-a se obično vrši nakon gladovanja od 6 ili više sati. Lekove koji mogu da modifikuju mioelektričnu aktivnost želuca treba prekinuti najmanje 48 sati pre testa [18,19]. EGG treba snimati najmanje 30 minuta (ne <15 min u svakom slučaju) u stanju gladovanja i najmanje 30 minuta u stanju jedenja. Test obrok treba da sadrži najmanje 250 kcal bez mnogo masti [31]. Obično se preporučuju čvrsti obroci, mada se u nekim istraživanjima koristila voda kao test obrok.

## IV. PARAMETRI EGG

I pored toga što se eliminacija šuma iz EGG signala može postići pomoću naprednih tehnika obrade signala [1,32], analiza talasnog oblika EGG-a u vremenskom domenu se retko koristi. Talasni oblik EGG-a je povezan sa mnogim faktorima, kao što su debljina trbušnog zida ispitanika, priprema kože, položaj elektroda i karakteristike uređaja za snimanje [33].

Broj specifičnih karakteristika EGG-a je ograničen, pa se kod jednokanalnog snimanja EGG mogu meriti samo frekvencija i amplituda. Nedavne kompjuterske simulacije i eksperimenti pokazali su da se širenje gastričnog sporog talasa može identifikovati uz pomoć višekanalnih snimaka EGG [33], ali je teško dobiti ove informacije iz analize talasnog oblika u vremenskom domenu [32]. Shodno tome, kvantitativne analize podataka EGG-a se uglavnom zasnivaju na metodama spektralne analize.

Frekvencija za koju se veruje da je želudačnog porekla i na kojoj snaga u EGG spektru snage ima vršnu vrednost u opsegu od 0.5–9.0 cpm naziva se *EGG dominantna frek encija*. *ominantna snaga* je snaga na dominantnoj frekvenciji. Snaga EGG može biti predstavljena u linearnim jedinicama ili u decibelima (dB). Dominantna frekvencija i snaga EGG-a se često jednostavnije nazivaju kao EGG frekvencija i snaga EGG-a. Sl. 5 prikazuje definiciju dominantne frekvencije i snage EGG. Simultani kožni i serozni [9,13-15] ili mukozni [7,12] snimci aktivnosti želuca pokazali su da dominantna frekvencija EGG-a predstavlja frekvenciju sporog talasa želuca. Dominantna snaga EGG-a odražava amplitudu i pravilnost želudačnih sporih talasa.

Gastrični spori talas se smatra abnormalnim ako dominantna frekvencija EGG-a nije unutar određenog frekventnog opsega (npr. 2-4 cpm). Iako ne postoji utvrđena definicija normalnog opsega gastričnog sporog talasa, opšte je prihvaćeno da je dominantna frekvencija EGG-a kod asimptomatskih normalnih subjekata između 2 cpm i 4 cpm [17,18,22,34]. EGG, ili segment EGG-a, definiše se kao tahigastrija ako je njegova frekvencija > 4 cpm, ali < 9 cpm, bradigastrija ako je frekvencija < 2 cpm i aritmija ako postoji nedostatak dominantne frekvencije (videti Tabelu I).

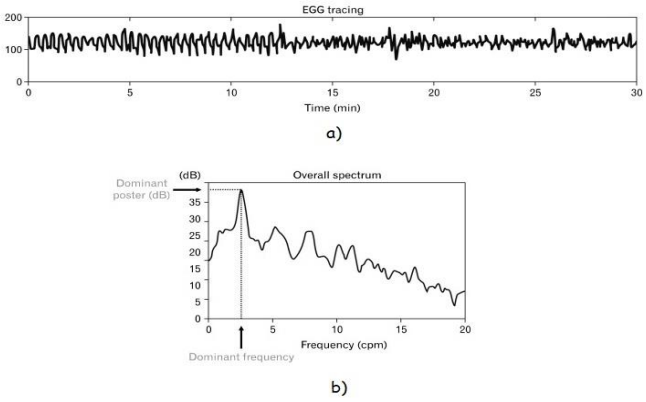


Sl. 5. Analiza spectra EGG: a) Zapis EGG u trajanju od 30 minuta, b) Spektar snage 30-minutnih EGG podataka. Dominantna frekvencija EGG-a (DF) i snaga na DF se mogu odrediti iz spectra [3].

TABELA I
PARAMETRI EGG-A

| | **omponenta** | **re vencija (cpm)** |
|---|---|---|
| **ignal** | Normalni spori talas | 2–4 |
| | Bradigastrija | 0.5–2 |
| | Tahigastrija | 4–9 |
| **Šum** | Respiratorni | 12–24 |
| | Tanko crevo | 9–12 |
| | EKG | 60–80 |
| | Artefakti pokreta | Ceo interval merenja |

## V. PRIMENA EGG

EGG ima značajnu primenu u sledećim oblastima:

(1) elektrofiziološke studije,
(2) procena efikasnosti intervencije ili terapije, i
(3) otkrivanje abnormalnosti sporog talasa kod pacijenata sa poremećajem želudačnog motiliteta ili sumnja na poremećaj motiliteta želuca.

Navešćemo neke od primena u pomenutim oblastima.

*Elektrofiziološke studije* - za proučavanje elektrofiziologije želuca jer je neinvazivna metoda i ne prekida tekući proces u želucu. Jedna od takvih primena je proučavanje razvojnog procesa želudačnih sporih talasa kod novorođenčadi [35]. Progresivno povećanje procenta normalnih gastričnih sporih talasa zabeleženo je tokom prvih 6 meseci nakon rođenja kod 19 nedonoščadi.

*Procena efikasnosti inter encije ili terapije* - Na spore talase u želucu mogu uticati različite intervencije, stres i farmakološke terapije. EGG se često koristi u proceni efekta stresa i efikasnosti farmakoloških terapija i intervencija.

*tkri anje abnormalnosti sporog talasa* – EGG se koristi kada se sumnja da pacijent ima poremećaj motiliteta, što se može pokazati kao ponavljajuća mučnina i povraćanje, a to su znaci da želudac ne prazni hranu normalno.

Klinička primena elektrogastrografije najšire je procenjivana kod bolesnika s gastroparezom i funkcionalnom dispepsijom.

 ISBN 978-86-7466-930-3

## VI. ZAKLJUČAK

EGG je neinvazivna procedura za pouzdano merenje sporih talasa u želucu i kontraktilne aktivnosti želuca. Iako je dosta osetljiva dijagnostička metoda, EGG predstavlja izuzetan uvid u funkcionisanje čovekovog gastrointestinalnog sistema.

Međutim, EGG pruža klinički, fiziološki i/ili patofiziološki značajne informacije samo kada se pravilno snima, analizira i tumači. Snimanje i analiza EGG-a još uvek nisu u potpunosti standardizovani. Kao što je u radu opisano, snimanje EGG-a treba izvoditi vrlo oprezno da bi se minimizirali mogući artefakti.

Budući razvoj EGG metodologije bi pre svega trebalo da se fokusira na definisanje i postavljanje preciznih standarda za snimanje i analizu karakterističnih parametara EGG-a, kako bi se omogućilo precizno dijagnostikovanje poremećaja motiliteta želuca.

## ZAHVALNICA

Ovaj rad je podržan od strane Ministarstva prosvete, nauke i tehnološkog razvoja Republike Srbije.

## LITERATURA

[1] D. Z. Chen and Z. Lin, "Electrogastrogram," in *Encyclopedia of Medical e ices and Instrumentation*, Second edition, vol. *3*, pp. *3*–98*,* NJ, USA: John Wiley & Sons, Inc, 2006.

[2] K. L. Koch, R. M. Stern, *andbook of Electrogastrography,* Oxford University Press, New York, 2004.

[3] J. Yin, J. D. Z. Chen, *Electrogastrography Methodology, alidation and Applications*, J Neurogastroenterol Motil, vol. *1* , no. *1*, pp. 5-17, 2013.

[4] F. Y. Chang, *Electrogastrography Basic knowledge, recording, processing and its clinical applications*, J Gastroenterol Hepatol, vol. *20*, pp. 502-516, 2005.

[5] https://en.wikipedia.org/wiki/Electrogastrogram.

[6] W. C. Alvarez, *The electrogastrogram and what it shows*, JAMA, vol. , pp. 1116–1118, 1922.

[7] R. M. Stern, *The history of EGG*, in Neurogastroenterologia*,* ch. *1*, pp. 20–26, 2000.

[8] I. H. Tumpeer, P. W. Blitzsten, *egistration of peristalsis by the Eintho en gal anometer*, Am J Dis Child, vol. *11*, pp. 454–455, 1926.

[9] I. H. Tumpeer, P. W. Blitzsten, *yperperistaltic electrographic effects*, Am J Med Sci, vol. *1 4*, pp. 831-836, 1932.

[10] R. C. Davis, L. Galafolo, F. P. Gault, *An e ploration of abdominal potentials*. J Com Psysiol Psychol; vol. *50*, pp. 519–523, 1957.

[11] R. C. Davis, L. Galafolo, K. Kveim, *Conditions associated with gastrointestinal acti ity*. J Com Physiol Psychol, vol. *52*, pp. 466–475, 1959.

[12] L. K. Stevens, N. Worrall, *E ternal recording of gastric acti ity the electrogastrogram*, Physiol Psychol, vol. *2*, pp. 175–180, 1974.

[13] B. H. Brown, R. H. Smallwood, H. L. Duthie, C. J. Stoddard, *Intestinalsmooth muscle electrical potentials recorded from surface electrodes*, Med Biol Eng Comput, vol. *13*, pp. 97–102, 1975.

[14] R. H. Smallwood, *Analysis of gastric electrical signals from surface electrodes using phase-lock techni ues*, Med Biol Eng Comput, vol. *1* , pp. 507–518, 1978.

[15] D. A. Linkens, S. P. Datardina, *Estimations of fre uencies of gastrointestinal electrical rhythms using autoregressi e modeling*, Med Biol Eng Comput, vol. *1* , pp. 262–268, 1978.

[16] H. Geldof, E. J. Van Der Schee, *Electrogastrography Clinical applications*, Scand J Gastroenterol, vol. *24* (Suppl. 171), pp. 75–82, 1989.

[17] J. Z. Chen, R. W. McCallum, *Electrogastrography. Principles and Applications*, New York: Raven Press; 1994.

[18] H. P. Parkman, W. L. Hasler, J. L. Barnett, E. Y. Eaker, *Electrogastrography a document prepared by the gastric section of the American Motility Society Clinical GI Motility Testing Task Force*, Neurogastroenterol Motil, vol. *15*, pp. 89–102, 2003.

[19] M. Camilleri, W. Hasler, H. P. Parkman, E. M. M. Quigley, E. Soffer, *Measurement of gastroduodenal motility in the GI laboratory*, Gastroenterology, vol. *115*, pp. 747–762, 1998.

[20] S. K. Sarna, *Gastrointestinal electrical acti ity terminology,* Gastroenterology, vol. , pp. 1631-1635, 1975.

[21] K. A. Kelly, „Motiltiy of the stomach and gastroduodenal junction", in: *Physiology of the gastrointestinal tract*, ed. I. A. Johnson, pp.393-410, New York: Raven, 1981.

[22] J. D. Chen, R. W. McCallum, *Clinical application of electrogastrography*, Am J Gastroenterol, vol. , pp. 1324-1336, 1993.

[23] X. Lin, J. Z. Chen, *Abnormal gastric slow wa es in patients with functional dyspepsia assessed by multichannel electrogastrography*, Am J Physiol Gastrointest Liver Physiol, vol. *2 0*, pp. G1370-G1375, 2001.

[24] J. Yin, D. Levanon, J. D. Chen, *Inhibitory effects of stress on postprandial gastric myoelectrical acti ity and agal tone in healthy subjects*, Neurogastroenterol Motil, vol. *1* , pp. 737-744, 2004.

[25] L. W. Qian, P. J. Pasricha, J. D. Chen, *rigin and patterns of spontaneous and drug-induced canine gastric myoelectrical dysrhythmias*, Dig Dis Sci, vol. *4* , pp. 508-515, 2003.

[26] H. Ouyang, J. Xing, J. D. Chen, *Tachygastria induced by gastric electrical stimulation is mediated ia alpha- and beta-adrenergic pathway and inhibits antral motility in dogs*, Neurogastroenterol Motil, vol. *1* , pp. 846-853, 2005.

[27] G. Riezzo, F. Pezzolla, J. Thouvenot, et al, *eproducibility of cutaneous recordings of electrogasography in the fasting state in man*, Pathol Biol, vol. *40*, pp. 889–894, 1992.

[28] B. Pfaffenbach, R. J. Adamek, K. Kuhn, M. Wegneer, *Electrogastrography in health subjects E aluation of normal alues, influence of age and gender*, Dig Dis Sci, vol. *40*, pp. 1445–1450, 1995.

[29] G. Riezzo, M. Chiloiro, V. Guerra, *Electrogastrography in health children E aluation of normal alues, influence of age, gender and obesity*, Dig Dis Sci, vol. *43*, pp. 1646–1651, 1998.

[30] N. Mirizzi, U. Scafoglieri. *ptimal direction of the electrogastrographic signal in man*, Med Biol Eng Comput, vol. *21*, pp. 385–389, 1983

[31] D. Levanon, M. Zhang, J. D. Z. Chen, *Efficiency and efficacy of the electrogastrogram*, Dig Dis Sci, vol. *43*, no. *5*, pp. 1023–1030, 1998.

[32] J. Chen, *A computeri ed data analysis system for electrogastrogram*, Comput Biol Med, vol. *22*, pp. 45–57, 1992.

[33] J. Liang, J. D. Z. Chen, *What can be measured from surface electrogastrography ,* Dig Dis Sci, vol. *42*, no. , pp. 1331–1343, 1997.

[34] J. Chen, R. W. McCallum, *Gastric slow wa e abnormalities in patients with gastroparesis,* Am J Gastroenterol, vol. , pp. 477–482, 1992.

[35] R. H. Smallwood, „Gastrointestinal electrical activity from surface electrodes", Ph.D. dissertation, Sheffield, UK.

## ABSTRACT

Electrogastrography (EGG) is a non-invasive electrophysiological technique used to record the electrical activity of the stomach using electrodes placed on the abdomen. EGG has been mostly used in clinical studies and diagnostics in gastroenterology, but there is a growing interest in scientific research of EGG methods in the field of biomedicine and psychophysiology. The aim of this paper, based on the existing literature, is to present the basic physiological characteristics of EGG signals, as well as possible ways of recording and processing these signals.

**eview of electrogastrographic method**

Jelena Đorđević Kozarov, Platon Sovilj, Marjan Urekar, Milan Šaš, Miroljub Pešić

 ISBN 978-86-7466-930-3

# Sistem za merenje pritiska u konceptu Internet of Things

Tomislav Pap, Marjan Urekar, *Member, IEEE*

***Apstrakt*—Za potrebe merenja pritiska u konceptu Internet of Things, razvijen je sistem koji se sastoji od komercijalnog mikrokontrolera Arduino UNO, senzora pritiska koji radi na principu otpornika osetljivog na silu, koji je robustan i široko rasprostranjen, čiji je opseg detekcije pritiska do 98 Pa i par LED dioda koji služi za signalizaciju detekcije pritiska. U II poglavlju je dat opis hardvera i detaljan opis senzora. III poglavlje sadrži kratak opis softvera koji se izvršava na mikrokontroleru ovog sistema. Moguće primene sistema su predstavljene u poglavlju IV.**

***Ključne reči*—IoT, Industrija 4.0, metrologija, merenje pritiska, merenje sile, sensor pritiska, otpornik osetljiv na silu, mikrokontroler, merni sistem.**

## I. UVOD

Mi smo sada u četvrtoj industrijskoj revoluciji, poznatijoj kao Industrija 4.0 [1]. Industrija 4.0 je uvela revoluciju u automatizaciji, monitoringu i logistici kroz pametnu tehnologiju. Zasnivajući se na IioT (eng. Industrial Internet of Things) i ugrađene softverske sisteme (CPS, eng. Cyber-Physical systems), koji su dovoljno pametni i autonomni, koji koriste kompjuterske algoritme za monitoring i kontrolu fizičkih stvari kao što su mašine, roboti i prevozna sredstva, transformiše virtualni i stvarni svet u cilju stvaranja mreža gde subjekti i objekti pametno komuniciraju jedni sa drugima.

Temelji Industrije 4.0 su "pametni" računari urađeni u CPS. Ovi računari obrađuju informacije prikupljene preko senzora i oni su sposobni da odrede i mere trenutno stanje opreme i procesa, analiziraju situaciju i pokrenu određene akcije koje poboljšavaju ukupno stanje. Ovo je urađeno kroz povezivanje hardvera i softvera novim digitalnim umrežavanjem. Glavni metrološki zahtevi sa Industrijom 4.0 su: vreme i ekonomičnost, realno vreme izvršenja, automatizacija i velika brzina. Prema tome, razvoj metrologije zasnovan je na aspektima: brzine, preciznosti, pouzdanosti i fleksibilnosti.

Jedan od načina na koji može da se senzor pritiska SEN-09375 priključi na Internet of Things, odnosno da se uvrsti u Industriju 4.0 je koristeći Arduino UNO mikrokontroler.

Tomislav Pap – Fakultet tehničkih nauka, Univerzitet u Novom Sadu, Trg Dositeja Obradovića 6, 21000 Novi Sad, Srbija (e-mail:pap.e125.2020@uns.ac.rs).

Marjan Urekar – Fakultet tehničkih nauka, Univerzitet u Novom Sadu, Trg Dositeja Obradovića 6, 21000 Novi Sad, Srbija (e-mail: urekarm@uns.ac.rs).

## II. HARDVER

Celokupan sistem je spojen na protobordu gde je izlaz senzora doveden na analogni ulaz mikrokontrolera. Kao mikrokontroler, izabran je Arduino UNO zbog njegove široke rasprostranjenosti i jednostavnosti za korišćenje. Arduino UNO je baziran na ATmega328P čipu [2]. Sastoji se od 14 ulazno/izlaznih digitalnih pinova (gde se 6 mogu koristiti kao PWM izlazi), 6 analognih ulaza, 16 MHz rezonatora, USB porta, koji može da služi i kao napajanje, zasebnog porta za napajanje, ICSP (eng. Integrated circut serial peripherial interface) hedera i reset dugmeta. Sistem se može videti na slici 1. Kao napajanje korićen je USB adapter koji pruža napajanje do 5 V.

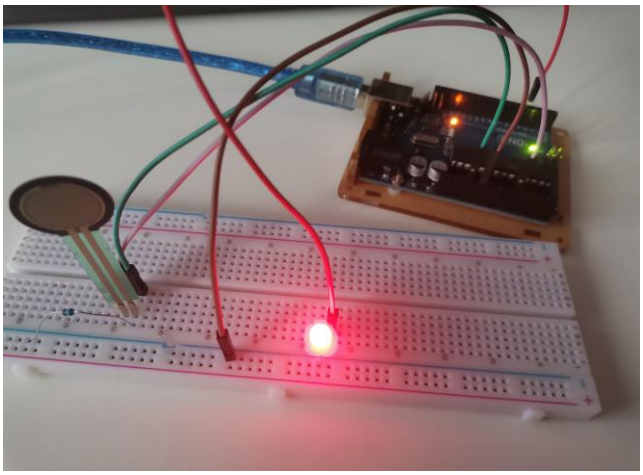

*Sl. 1. Sistem za detekciju pritiska do 98 Pa*

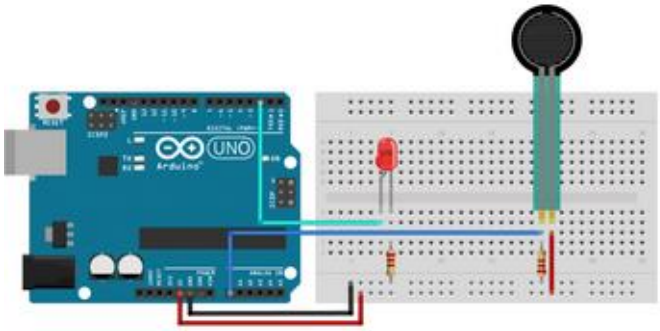

*Sl. 2. Šema sistema za detekciju pritiska [3]*

FSR (eng. force sensing resistor) su robusni senzori pritiska koji se koriste u raznim industrijama. Izabrali smo FSR [4] jer je jako jeftin i široko je dostupan. Otpornost FSR zavisi od pritiska koji se primeni na aktivnu oblast senzora. FSR menja

 ISBN 978-86-7466-930-3

svoju otpornost u zavisnosti od toga koliki pritisak je primenjen u oblasti detekcije. Što je veći pritisak primeni, manja je otpornost.

Vrednost otpornika osetljivog na silu unutar senzora je veća od 1 MΩ kada nema pritiska, pa do 200 Ω kada senzor trpi najveći pritisak. Ovakvi senzori mogu da detektuju silu od 0.98 N do 98.07 N. Dva pina sa razmakom od 2,54 mm za proširenje nalaze se na dnu senzora i omogućavaju spajanje sa protopločom.

Ovaj senzor je jednostavan za postavljanje i detekciju pritiska ali nema visoku tačnost. Grafik koji je prikazan na slici 3, prikazuje kako se otpornost menja u zavisnosti od primenjene sile. Na početku vidimo priličan pad otpornosti, za malu silu, a kasnije vidimo da je osetljivost manje- više linearna.

Krajnje, za vizuelizaciju detekcije i promene pritiska na aktivnoj oblasti senzora, korišćena je crvena LED dioda. Za detaljniji uvid u merenja senzora pritiska, iskorišćena je serijska komunikacija za prikaz podataka na serijskom monitoru računara.

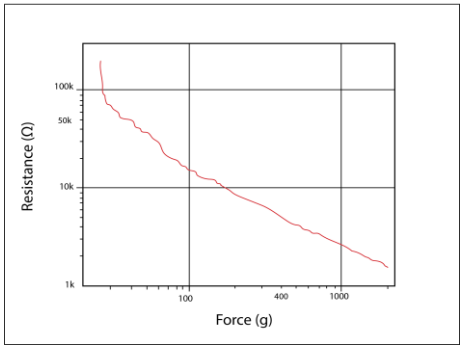


*Sl. 3. Osetljivost FSR senzora*

Kako bismo detektovali i izmerili vrednost sa FSR senzora za to nam je potreban naponski razdelnik prizan na slici 4. To ćemo uraditi tako što kao prvi otpornik ustvari uzeti FSR senzor, a drugi pulldown otpornik. *V+* je 5 volti(može i 3.3 V), a *Vout* je podatak koji nam dolazi sa FSR senzora. Odabir odgovarajućeg otpornika u naponskom razdelniku određuje osetljivost FSR i direktno utiče na raspon sile koju želimo da merimo.

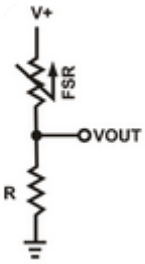


*Sl. 4. Naponski razdelnik*

Podatak koji nam daje FSR se preračunava kao:

$$Vout = \frac{Vcc \times R}{R + Rfsr} . \quad (1)$$

Kada sila nije primenjena na senzor, otpornost će biti jako velika, a nasuprot tome, kada baš jako pritisnemo senzor, silom približno 100 N ili jače, otpornost će biti faktički 0 ili jako blizu toga.

## III. SOFTVER

Softver sistema za detekciju pritiska je napisan u Arduino IDE okruženju u modifikovanovoj verziji C programskog jezika, podržanog od strane Arduino mikrokontrolera. Arduino IDE podržava C I C++ programske jezike i dolazi sa ugrađenom softverskom bibliotekom koja podržava mnoge funkcionalnosti ulazno/izlaznih pinova.

Koristeći već ugrađene mogućnosti Arduino IDE okruženja, inicijalnom funkcijom, analogni pin na koji je zakačen senzor pritiska je postavljen kao ulazni pin, dok je digitalni pin, koji šalje digitalne signale ka LED diodi postavljen kao izlazni pin. Takođe, setovan je inicijalno baud rate serijske komunikacije na 9600bps, kako bismo mogli ispravno da šaljemo poruke ka serijskom monitoru [5] koji je sastavni deo alata Arduino IDE.

Očitavanje vrednosti analognog pina senzora pritiska se izvršava na svakih pola sekunde u beskonačnoj petlji. Nakon očitane vrednosti senzora, vrši se procena veličine izmerene vrednosti i u zavisnosti u kom opsegu se nalazi očitana vrednost, šalju se poruke ka serijskom monitoru arduinovog sofverskog okruženja. Time dobijamo detaljan uvid u izmerene vrednost senzora pritiska.

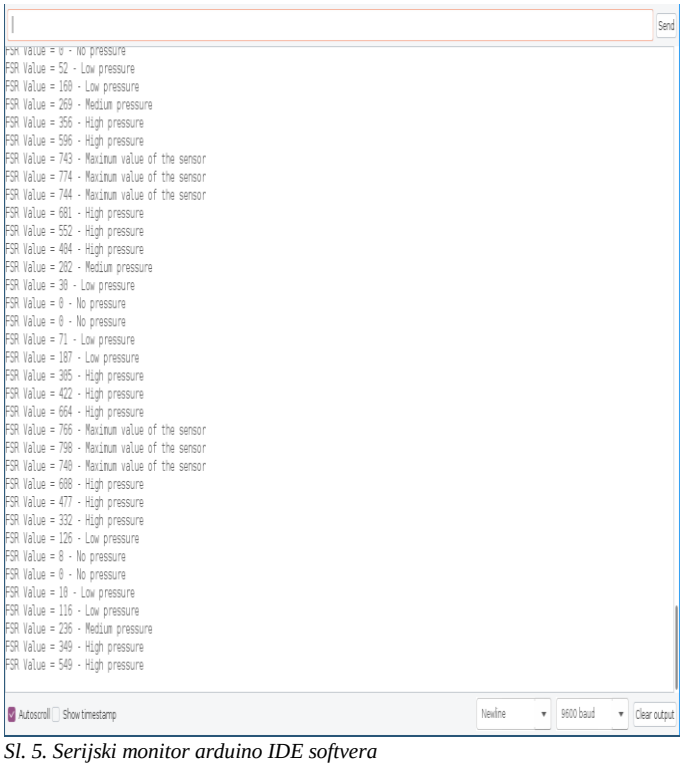


*Sl. 5. Serijski monitor arduino IDE softvera*

 ISBN 978-86-7466-930-3

## IV. Zaključak

Ovakav sistem bi mogao da se koristi kao detekcija da li je beba/dete i dalje na krevetu, ako bi se ovaj senzor instalirao ispod posteljine što bi dalo mogućnost roditeljima da prate ponašanje svoga deteta u svakom trenutku. Još jedna dobra primena ovog sistema u industriji 4.0 bi bila kada bi se ovaj sistem spregnuo sa frižiderom, tako da se ovakav senzor nalazi ispod slotova sa namirnicama, pa bi se time moglo doći do informacije da li određene namirnice postoje u frižideru i ako da, u kojoj meri. Postojeću šemu moguće je poboljšati dodavanjem još par LED dioda kako bismo mogli ne samo da detektujemo pritisak, nego i preciznije prikažemo trenutno detekciju. Takođe umesto Arduina UNO, moglo bi se koristiti Arduino Nano [6]. Koristeći Arduino Nano, proizvodnja u početku bi bila skuplja jer bi se žice morale lemiti direktno na mikrokontroler, ali dizajn bi bio kompaktniji i jeftiniji jer sam Arduino Nano jeftiniji nego Arduino UNO. Ovakav sistem bi koristio manje električne energije što može da doprinese ekonomičnosti na duži vremenski period. Arduinov radni napon je limitiran do 12 V, tako da neko zaštitno kolo od većeg napona bi bila dobra opcija za razmatranje u budućnosti.

## Zahvalnica

Ovaj rad je podržan od strane Fakulteta tehničkih nauka u Novom Sadu, Departmana za energetiku elektroniku i telekomunikacije, u okviru realizacije projekta MPNTR 200156 : „Inovativna naučna i umetnička ispitivanja iz domena delatnosti FTN-a“

## Literatura

[1] Industrija 4.0, https://www.i-scoop.eu/industry-4-0/
[2] Arduino Uno Revision3, “Overview”, http://storeusa.arduino.cc/products/arduino-uno-rev3
[3] Arduino Forum, “FSR Voltage steadily increasing”, https://forum.arduino.cc/t/fsr-voltage-steadily-increasing/888254
[4] FSR Senzor, https://012lab.com/proizvod/force-sensitive-resistor-0-5
[5] Arduino Serijski Monitor, “Using the serial monitor”, https://docs.arduino.cc/software/ide-v2/tutorials/ide-v2-serial-monitor
[6] Arduino Nano, http://store.arduino.cc/products/arduino-nano

## Abstract

For needs in pressure measurements in concept Internet of Things, it was developed a system which consists of commercial microcontroller Arduino UNO, pressure sensor which works on principal of resistor which is sensitive to force, which is robust and widely spread, which range for pressure detection is up to 98 Pa, and couple of LED diodes which are used for pressure detection visualization. In chapter II is given a description of hardware and description of sensor in detail. Chapter III consists of short description of software which is executed on microcontroller of this presented system. System’s usage possibilities are presented in chapter IV.

**System for pressure measurements in concept of Internet of Things**

Tomislav Pap
Marjan Urekar

 ISBN 978-86-7466-930-3

# Merno-informacioni sistem za automatsko hranjenje kućnih ljubimaca

Maja Perić, Marjan Urekar, *Member, IEEE*

***A stra t*— ovom radu je pri azana realizacija sistema za automats o hranjenje ljubimaca u ućnim uslovima korištenjem dostupnih softvers ih alata. le trons a šema sistema je proje tovana u iCad programu, do je deo oda sistema pisan u Arduino ID razvojnom okruženju. Cilj sistema jeste da upotrebom različitih senzora vrši merenje zadatih veličina, ostvari prenos, obradu i pri az podata a do mi ro ontrolera, ao i da automatizuje rad servo motora i magnetnog ventila.**

***Ključne reči*— iCad, Arduino ID , Atmega 2 P, senzori, servo motor, magnetni ventil.**

## I. UVOD

Posedovanje kućnih ljubimaca je oduvek bila, i ostaće velika obaveza. Ljubimcima je neophodno posvetiti dovoljno pažnje, što uključuje redovne šetnje, igru, i naravno ispravno i redovno hranjenje. Za mnoge ljude, ispravno hranjenje kućnih ljubimaca može predstavljati problem, koji postaje posebno očigledan ukoliko vlasnici ljubimaca imaju okupiran lični život. Kada vlasnici nemaju vremena da nahrane svoje ljubimce na vreme, obično ostavljaju činije za hranu pune pre odlaska. Nezdrava ishrana, odnosno previše hrane, će skoro uvek izazvati zdravstvene probleme kod ljubimaca, što će uzrokovati kraći životni vek ljubimaca.

Cilj ovog sistema jeste da obezbedi lakši i efikasniji način za vlasnike da hrane svoje ljubimce, čak i kada nisu kod kuće. Konkretno, cilj je realizacija sistema koji može da detektuje kućne ljubimce, i da im na osnovu informacija koje dobija sa senzora, automatski dosipa vodu i hranu. Vlasnici bi bili u mogućnosti da ovim sistemom hrane različite vrste ljubimaca, ili ljubimce različite starosne dobi. Svaki ljubimac bi imao svoju oznaku, pomoću koje bi se vršila identifikacija. Ovaj sistem nudi personalizovan način hranjenja i brige o ljubimcima, jer je vlasnik u mogućnosti da postavlja oznake ljubimcu ili ljubimcima, kao i da određuje vreme i količinu hrane.

### A. *Princip rada sistema*

Princip rada sistema se zasniva na tome da mikrokontroler dobija informacije sa senzorskih modula, nakon čega te informacije obrađuje i upravlja motorom i ventilom.

Maja Perić – Fakultet tehničkih nauka, Univerzitet u Novom Sadu, Trg Dositeja Obradovića 6, 21120 Novi Sad, Srbija (e-mail: peric.maaja97@gmail.com).

Marjan Urekar – Fakultet tehničkih nauka, Univerzitet u Novom Sadu, Trg Dositeja Obradovića 6, 21120 Novi Sad, Srbija (urekarm@uns.ac.rs)

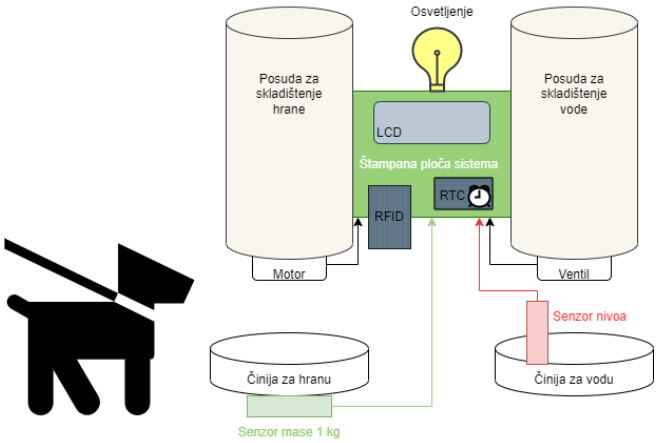


Slika 1. Ilustracija izgleda sistema u realnosti

Za informacije o količini hrane i vode u činijama iz kojih ljubimac jede, odnosno pije, zaduženi su senzor mase i senzor nivoa. Senzor koji meri nivo vode se nalazi uronjen u vodu. Na osnovu senzora nivoa se dobija informacija da li je nivo vode u činiji nizak ili visok. Ukoliko je nivo vode niži od minimalnog, aktivira se magnetni ventil i dosipa se voda.

Senzor mase se nalazi ispod činije za hranu, i na taj način meri količinu hrane u činiji. Hrana se dosipa više puta dnevno, ali u određeno, unapred postavljeno vreme. Vreme hranjenja se postavlja pomoću RTC ( *eal Time Clock*) modula. Ukoliko je činija prazna, i vreme je hranjenja, aktivira se servo motor, i dosipa se hrana.

Modul za identifikaciju je RFID ( *adio Fre uency Identification*) modul, i njegova funkcija je da identifikuje ljubimca. Na osnovu podataka sa oznake ljubimca, mikrokontroler dobija informacije o prisustvu ljubimca, kao i o vremenu i potrebnoj količini hrane.

Pored toga, sistem poseduje i temperaturni senzor koji meri temperaturu prostorije, kao i LCD ekran na kom se ispisuju podaci sa senzora.

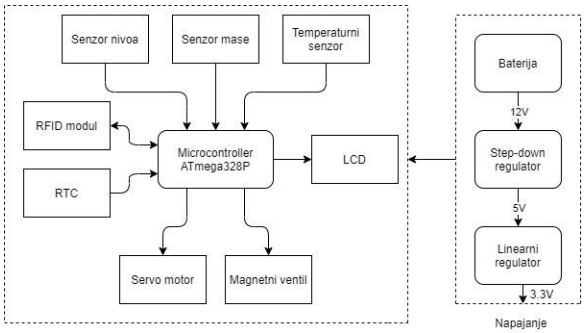


Slika 2. Blok dijagram sistema

 ISBN 978-86-7466-930-3

## II. Analiza delova sistema

### A. *Elektronska šema sistema*

Elektronska šema ovog sistema je projektovana u programu KiCad [1]. KiCad je besplatan softverski program koji se koristi za dizajniranje šema električnih kola, kao i za izradu štampanih ploča (*Printed Circuit Board*).

Za sistem je predviđeno baterijsko napajanje baterijom od 12 V. Pomoću *step-down* regulatora [2] se 12 V pretvara u stabilnih 5 V. Zbog potrebe RFID modula, bilo je neophodno da napajanje sadrži još jedan naponski nivo od 3,3 V. Za dobijanje 3,3 V korišten je čip LM1117 [3], koji je linearni naponski regulator. Prednost baterijskog napajanja je to što je uređaj moguće postaviti na bilo koju željenu poziciju – ne mora da se nalazi blizu utičnice.

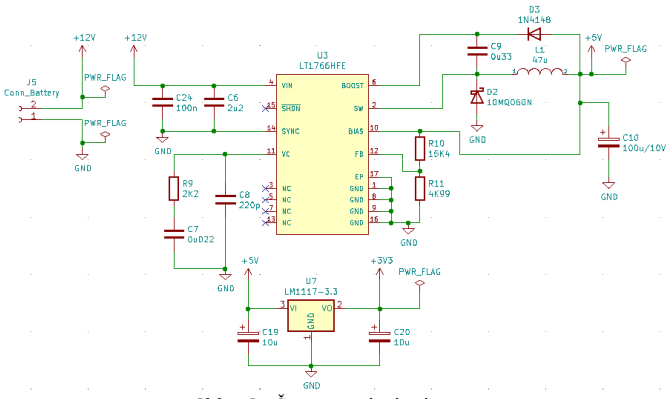


Slika 3. Šema napajanja sistema

Komponenta koja je zadužena za upravljanje čitavim sistemom je mikrokontroler ATmega328P [4]. Na slici 4 je prikazana šema povezivanja mikrokontrolera. U levom uglu šeme se nalazi kolo za reset. Kondenzatori C14 i C15 služe kao zaštita od brzih smetnji i kratkotrajnih prekida u napajanju. Komponenta Y1 predstavlja kvarcni kristal, pomoću kog se mikrokontroleru obezbeđuje radni takt, dok kondenzatori C16 i C17 omogućuju oscilovanje kvarcnog kristala.

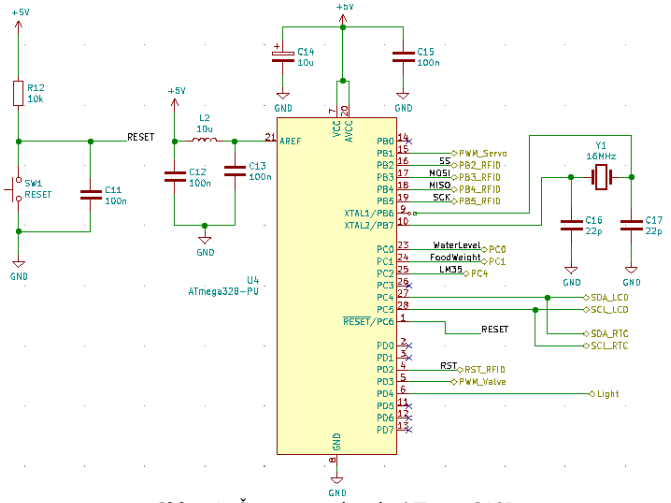


Slika 4. Šema povezivanja ATmega328P

Senzor za merenje nivoa vode [5] se sastoji od deset izloženih bakarnih traka, od kojih je pet za napajanje, a pet za detekciju. Niz izloženih paralelnih provodnika zajedno deluje kao promenljivi otpornik, čiji se otpor menja u zavisnosti od nivoa vode. Promena otpornosti odgovara udaljenosti od vrha senzora do površine vode. Otpornost je inverzno proporcionalna nivou vode – što je senzor više uronjen u vodu, to je bolja provodljivost i manji otpor, i obrnuto.

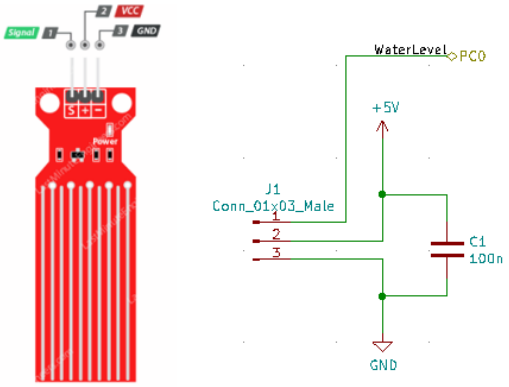


Slika 5. Izgled senzora nivoa (levo) i šema povezivanja

Za merenje količine hrane korišten je senzor mase od 1 kg [6]. Ovaj senzor radi na principu pretvaranja do 1 kg mase u električni signal. Senzor mase se sastoji od merne trake koja formira Vitstonov most i pretvara masu u električni signal. Pošto je promena napona na dijagonali mosta jako mala, bilo je neophodno da se pojača, i u te svrhe je korišten instrumentacioni pojačavač INA122.

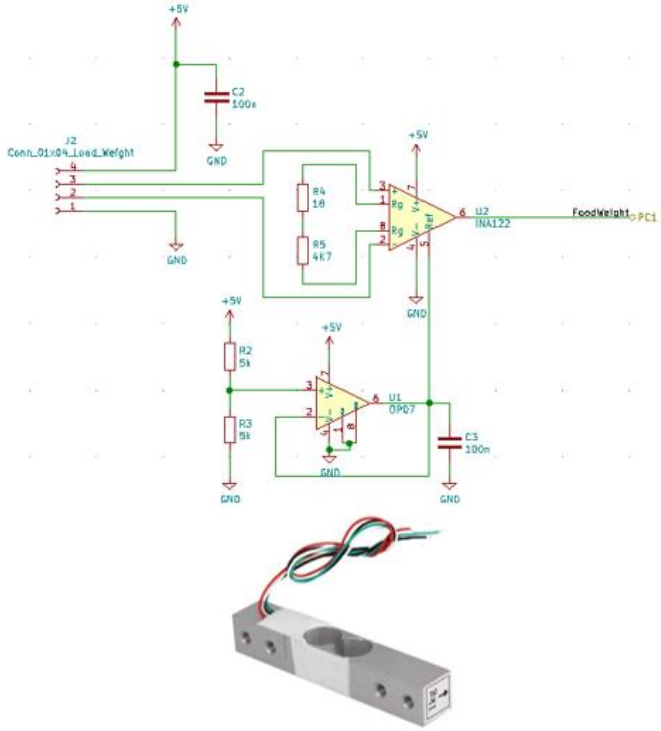


Slika 6. Šema povezivanja sa INA122 (gore) i izgled senzora mase (dole)

Kako bi se merila temperatura prostorije u kojoj ljubimac


ISBN 978-86-7466-930-3

boravi, korišten je temperaturni senzor LM35 [7]. LM35 je senzor čiji je izlazni signal proporcionalan trenutnoj temperaturi. Glavna karakteristika ovog senzora jeste ta da ne zahteva dodatnu kalibraciju.

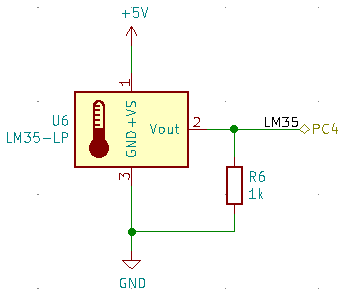


Slika 7. Šema temperaturnog senzora

RTC modul [8] je sat koji sa velikom preciznošću upravlja vremenom i datumom. Modul ima ugrađenu bateriju za rezervno napajanje, i ugrađeni kristalni oscilator. RTC modul radi tako što broji taktove oscilatora, i na taj način se dobijaju informacije o vremenu i datumu.

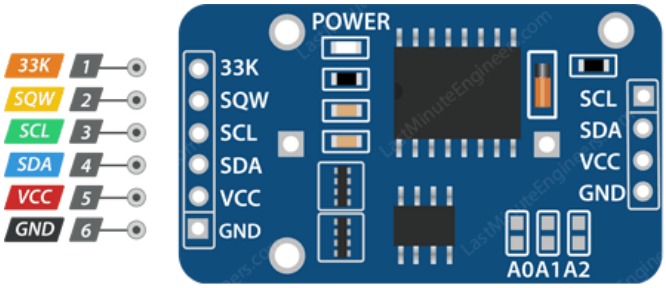


Slika 8. Izgled RTC modula

RFID modul [9] je sistem za identifikaciju radio frekvencija, koji se sastoji od dvije glavne komponente. Prva komponenta je *transponder* ili oznaka, koja je prikačena za objekat koji se identifikuje, u ovom slučaju je to ljubimac. Druga komponenta je primopredajnik, odnosno čitač oznake. Čitač se sastoji od radio frekvencijskog modula i antene koja generiše visokofrekventno elektromagnetno polje. Sa druge strane, *transponder* je pasivni uređaj, koji sadrži mikročip koji skladišti informacije, i antenu za prijem i prenos signala. Kako bi se pročitala informacija kodirana na transponderu, ljubimac bi trebalo da se nalazi u neposrednoj blizini čitača, ali ne mora biti u direktnom vidnom polju.

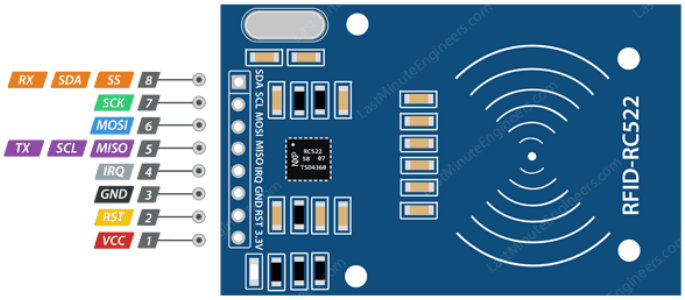


Slika 9. Izgled RFID modula

Pošto se RFID modul napaja sa 3,3 V, a mikrokontroler sa 5 V, bilo je neophodno da se modul poveže na bidirekcioni level šifter, pa tek onda na mikrokontroler, kako ne bi došlo do oštećenja modula.

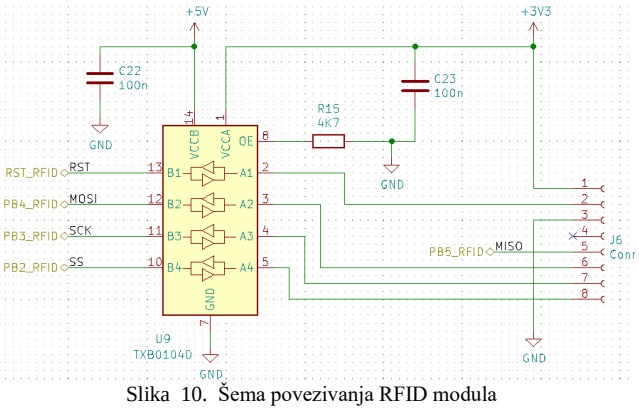


Slika 10. Šema povezivanja RFID modula

Ekran preko kog se vrši ispis vrednosti sa senzora je LCD RC1602A [10], koji ima 2 × 16 polja u koja stane po jedan karakter. Da bi se izvršila komunikacija sa mikrokontrolerom, i došlo do ispisa podataka na displeju, potrebne su najmanje četiri *data* linije, kao i dvije kontrolne. Pošto na mikrokontroleru ne postoji dovoljan broj odgovarajućih pinova kako bi se povezao LCD i sve ostale komponente sistema, bilo je potrebno da se koristi ulazno/izlazni ekspander [11].

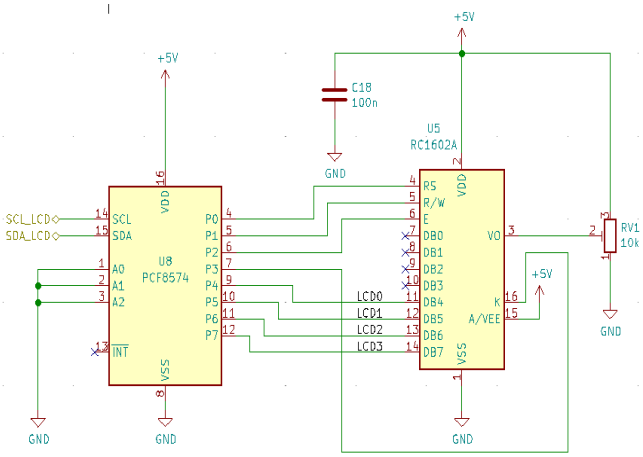


Slika 11. Šema povezivanja LCD ekrana

Za dosipanje vode je korišten magnetni ventil [12]. Ventil se uključuje i isključuje pomoću MOSFET-a. Ako se na *gate* pin MOSFET-a dovede napon, ventil će se uključiti. Ukoliko na *gate* pinu nema napona, odnosno povezan je na GND, ventil će se isključiti. Da bi ventil ostao isključen kada nema napona na *gate*-u, *gate* pin je uzemljen pomoću otpornika R8. Pomoću otpornika R7 *gate* pin je povezan na digitalni izlaz mikrokontrolera, odakle dobija ON/OFF signal. Dioda D1 je zamajna dioda, i njena funkcija je da štiti MOSFET od napona kontra elektromagnetne sile, koji se javlja prekidom struje.


ISBN 978-86-7466-930-3

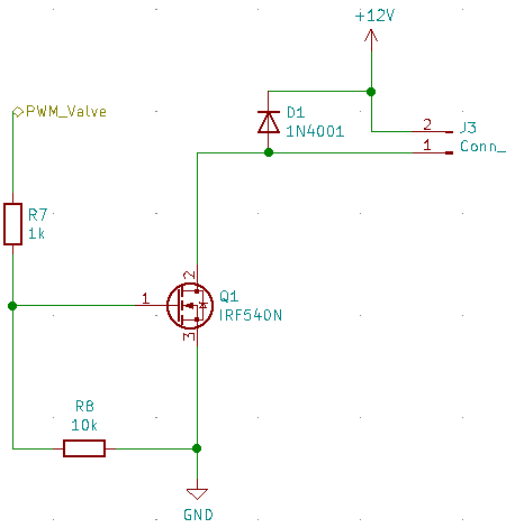


Slika 12. Šema povezivanja magnetnog ventila

Servo motor [13] se koristi za dosipanje hrane, i kontrolisan je pomoću PWM signala sa mikrokontrolera.

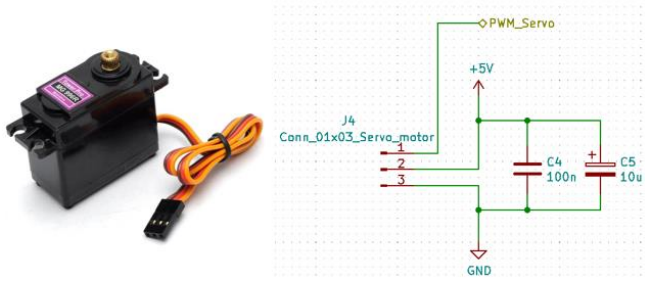


Slika 13. Izgled servo motora (levo) i šema povezivanja (desno)

Osvetljenje sistema je realizovano pomoću NPN tranzistora, koji ima ulogu prekidača, LED dioda i otporničke mreže. Svaki put kada RFID modul detektuje prisustvo ljubimca, svetlo će se uključiti.

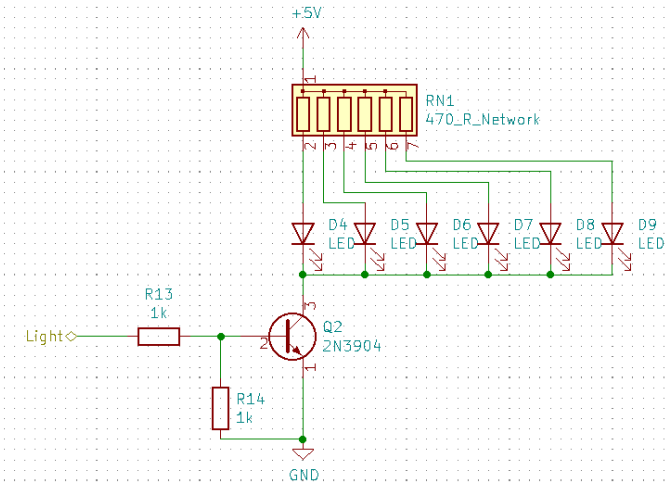


Slika 14. Šema osvetljenja sistema

PCB sistema je takođe realizovan u programu KiCad. Sve komponente su raspoređene na štampanu ploču dimenzija 165,74 mm × 90,81 mm.

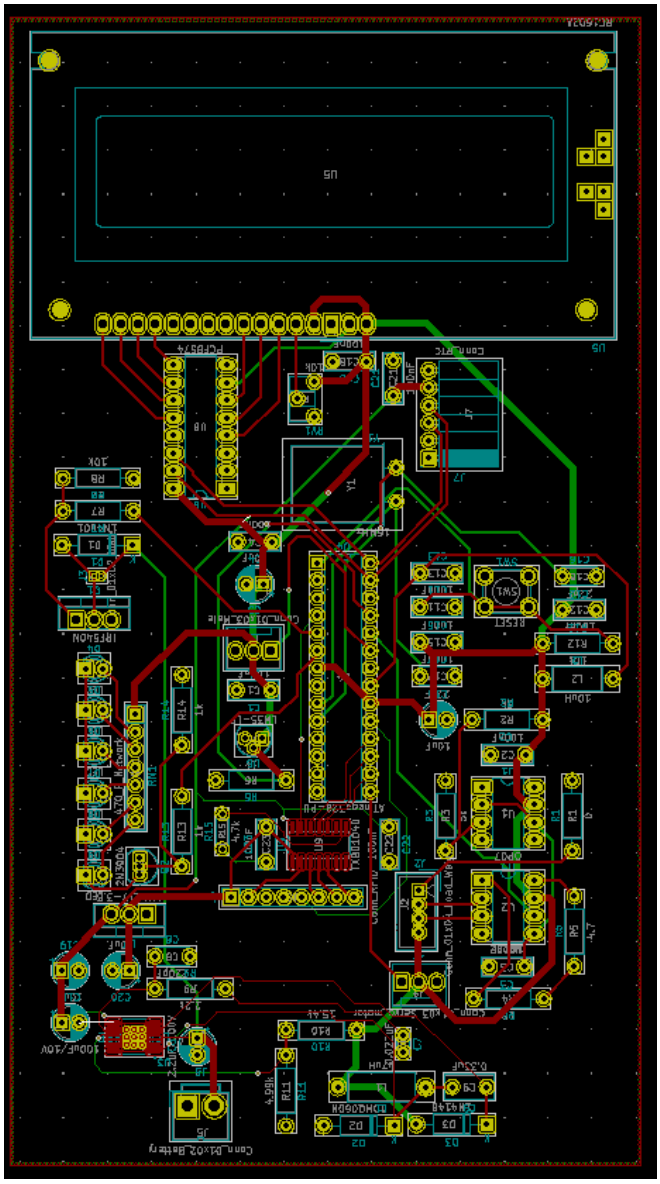

Slika 15. Izgled štampane ploče sistema

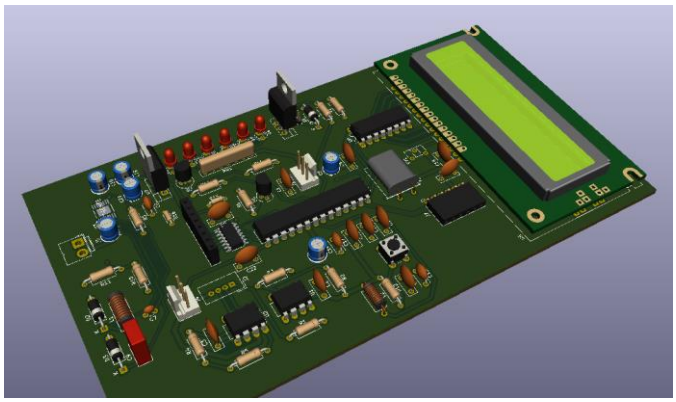

Slika 16. 3D prikaz štampane ploče


ISBN 978-86-7466-930-3

### *B. Programski kod*

Program sistema je pisan u programskom jeziku C, u Arduino IDE (*Integrated e elopment En ironment*) [14] razvojnom okruženju. Arduino IDE je okruženje koje se koristi za razvoj softvera za različite tipove Arduino platformi. Zasniva se na otvorenom kodu (*open-source*), i uključuje veliki broj biblioteka korisnih funkcija.

U program sistema su uključene biblioteke sa funkcijama za upravljanje servo motorom i RTC-om, kao i biblioteka za komunikaciju sa RFID modulom. Napisane su funkcije koje čitaju, i zatim vrše ispis podataka sa senzora temperature, nivoa, mase, kao i podatke o vremenu i datumu. Funkcija za RTC je napisana tako, da se prvo unese vreme hranjenja od strane korisnika, a zatim se ispisuje informacija da li je vreme postavljeno ili ne. U funkciji za RFID se na početku proverava da li je čitaču prinesena nova oznaka, i ako jeste, potom se čitaju informacije koje su kodirane na oznaci. Zatim se ispituje da li je očitani identifikator tačan, tj. da li je ljubimac prepoznat. Ukoliko jeste, uključuje se svetlo, i ispisuju se vrednosti sa senzora. Ukoliko nije, na displeju se ispisuje da ljubimac nije prepoznat.

## III. ZAKLJUČAK

Realizovano softversko rešenje sistema za automatsko hranjenje kućnih ljubimaca daje mogućnost korisniku da na vrlo jednostavan način olakša sebi svakodnevnicu pri brizi o kućnim ljubimcima. Kao što je već navedeno, sistem nudi personalizovan način brige o kućnim ljubimcima, što znači da je sistem prilagođen svakom korisniku i njegovom ljubimcu.

Sledeći korak bi bio pravljenje prototipa, i testiranje sistema i programa pisanog za sistem. Na osnovu testiranja bi bilo jasno na koje sve načine bi se hardverski deo sistema mogao unaprediti. Sistem bi se mogao unaprediti i softverski, razvojem aplikacija za različite mobilne i računarske platforme. Potencijalne aplikacije bi u mnogome olakšale upotrebu ovog sistema većini korisnika. U tom slučaju, korisnik bi bio u mogućnosti da u svakom trenutku, preko svog mobilnog telefona ili računara, prati stanje i informacije sa senzora. Unapređena verzija ovakvog sistema bi mogla da se koristi i u druge svrhe, tj. u drugačijim uslovima, kao što su, na primer, azili ili farme.

## ZAHVALNICA

Ovaj rad je podržan od trane Fakulteta tehničkih nauka u Novom Sadu, Departmana za energetiku, elektroniku i telekomunikacije, u okviru realizacije projekta MPNTR 200156 : „Inovativna naučna i umetnička ispitivanja iz domena delatnosti FTN-a.“

## LITERATURA

[1] https://www.kicad.org/
[2] https://www.analog.com/media/en/technical-documentation/data-sheets/1766fc.pdf
[3] https://www.ti.com/lit/ds/symlink/lm1117.pdf?ts=1625183429472&ref_url=https%253A%252F%252Fwww.google.com%252F
[4] https://ww1.microchip.com/downloads/en/DeviceDoc/Atmel-7810-Automotive-Microcontrollers-ATmega328P_Datasheet.pdf
[5] https://lastminuteengineers.com/water-level-sensor-arduino-tutorial/
[6] https://www.twinschip.com/Load_Cell_Weight_Sensor_1Kg
[7] https://www.ti.com/lit/ds/symlink/lm35.pdf
[8] https://microcontrollerslab.com/ds3231-rtc-module-pinout-interfacing-with-arduino-features/
[9] https://lastminuteengineers.com/how-rfid-works-rc522-arduino-tutorial/
[10] https://components101.com/displays/16x2-lcd-pinout-datasheet
[11] https://www.ti.com/lit/ds/symlink/pcf8574.pdf?ts=1625725551950
[12] http://www.martyncurrey.com/controlling-a-solenoid-valve-from-an-arduino-updated/
[13] https://components101.com/motors/mg996r-servo-motor-datasheet
[14] https://docs.arduino.cc/software/ide-v1/tutorials/arduino-ide-v1-basics

## ABSTRACT

This paper presents the realization of a system for automatic feeding of pets at home, using available software tools. The electronic schematic of the system was designed in the KiCad program, while part of the system code was written in the Arduino IDE development environment. The goal of the system is to measure the set values using different sensors, transmit, process and display data to the microcontroller, as well as to automate the operation of the servo motor and solenoid valve.

**Automatic pet feeding system**

Maja Perić, Marjan Urekar

 ISBN 978-86-7466-930-3

# Uređaj za pravilno sedenje baziran na merno–informacionim modulima

Jovana Jović i Marjan Urekar, *Member, IEEE*

***Apstrakt*— U ovom radu predstavljena je ideja za prototip uređaja za pravilno sedenje, koji bi bitno uticao na smanjenje pojave bola u leđima, oboljenje koje je sve prisutnije u svim starosnim grupama. Uređaj se sastoji od *Button load cell* ćelija pomoću kojih se prati da li korisnik sedi pravilno na sedalnom delu stolice. Pored toga postoji i senzor dodira QT100 koji detektuje da li je korisnik naslonjen na naslon stolice. Podaci se UART-om šalju na *web* server, koji se dalje učitavaju na *web* sajtu. Na *web* sajtu korisnik ima uvid u svoj sedeći stav, ali i upozorenje ukoliko ne sedi pravilno. Pored crvenih grafika i iskačućeg prozora na sajtu, kao identifikaciju nepravilnog sedenja imamo i vibro motor koji stvara vibracije i tako korisniku pruža trenutnu haptičku informaciju da popravi svoj stav.**

***Ključne reči*—Uređaj za pravilno sedenje, HX711, QT100, Vibro motor, mikrokontroler, *web* sajt;**

## I. Uvod

Brzim razvojem nauke, matematike, fizike ali i medicine u poslednjih nekoliko decenija, postignut je veliki razvoj tehnologije koji olakšava život ljudi u svim sferama. U ovom radu opisan je uređaj za pravilno sedenje, koji je osmišljen kao odgovor na pojavu bola kako kod odraslih lica, tako sve češće i kod dece u najranijem dobu. Da bismo shvatili njegov značaj, prvo moramo uvesti osnovne medicinske pojmove vezane za bol u leđima i njegov nastanak, ali i da razumemo definiciju pravilnog sedećeg stava.

Bol u leđima (lumbago, lumbagia) predstavlja bol ili nelagodnost koju osoba oseća u području leđa, između rebarnih lukova i donje glutealne brazde, sa ili bez širenja niz levu ili desnu nogu [1]. Prema definiciji, bol u leđima je simptom, ali oko 85% pacijenata nikada ne dobije tačnu dijagnozu [2]. Razlog tome je što bolovi nastaju ukrštanjem više faktora, kao što su loše držanje, dugotrajno sedenje, genetika, slabost određenih grupa mišića, emocionalni stres, promene uzrokovane starenjem mišićno-koštanog sistema (artritis, degenerativne promene diska …).

Pored saznanja šta je bol u leđima i kako nastaje, potrebno je da razlikujemo i dobar sedeći položaj od onog koji to nije. Dobar sedeći položaj, prema definiciji, podrazumeva položaj kada je telo uspravno ili lagano nagnuto napred, glava pravilno uzdignuta, te na taj način stimuliše lagano i stalno napetost dugih mišića kičme i kratkih mišića vrata. Gornji i donji udovi su u simetričnom položaju, stopala su paralelno postavljena i celom se površinom oslanjaju na pod. Ovakav položaj obezbeđuje najbolju udaljenost očiju od površine čitanja i manji zamor. [3]. Najčešće do pojave lošeg držanja tela dolazi usled slabosti određenih grupa mišića tonostatičke (opružača vrata i trupa, mišića primicača lopatica, opružača natkolenica i potkolenica i mišića stopala) muskulature. Ova pojava se može objasnici sa dva aspekta, dok nam je prvi od velikog značaja za nastanak ovog rada. Prvi aspekt: To je period kada je dete polaskom u školu, izloženo povećanom stato-dinamičkom opterećenju - dugotrajno sedenje u školskoj klupi, pisanje u povijenom položaju. [3].

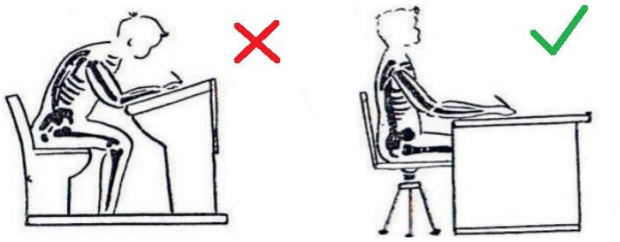

Sl. 1 - Nepravilan/pravilan sedeći stav

Kako bi se otklonio jedan od čestih razloga zbog kojeg nastaju bolovi u leđima u ovom radu je opisan uređaj za pravilno sedenje. Uređaj se sastoji od 8 mernih ćelija postavljenih na sedalni deo stolice. Pomoću njih može se utvrditi da li korisnik sedi pravilno (približno jednako je oslonjen sa obe noge na sedalni deo) ili to nije slučaj. Pored ovih senzora, na naslon stolice se postavlja elektroda senzora dodira QT100, pomoću koje se detektuje da li je korisnik sada naslonjen na naslon (sedi pravilno) ili ne. Sve ovo je spojeno sa mikrokontrolerom. Mikrokontroler obezbeđuje da kada sedenje nije pravilno (osoba vrši jači pritisak levom ili desnom nogom ili nije naslonjen na naslon stolice) korisnik dobija haptičku informaciju o tome. To je realizovano vibro motorom koji počinje sa radom baš u tom trenutku u kojem položaj tela ne odgovara pravilnom sedenju i tako opominje korisnika da popravi svoj sedeći stav. Mikrokontroler je preko UART-a povezan sa računarom i šalje podatke na internet. Na *web* stranici se u vidu grafika iscrtavaju očitavanja sa mernih ćelija. Tako korisnik ima direktan uvid u podatke o svom sedenju. Kada senzor dodira detektuje da korisnik nije naslonjen, na ekranu se pojavljuje "iskačući" prozor koji opominje korisnika na nepravilno sedenje.

Jovana Jović – Fakultet tehničkih nauka, Univerzitet u Novom Sadu, Trg Dositeja Obradovića 6, 21000 Novi Sad, Srbija (e-mail: jovanajovic180@gmail.com)

Marjan Urekar – Fakultet tehničkih nauka, Univerzitet u Novom Sadu, Trg Dositeja Obradovića 6, 21000 Novi Sad, Srbija (e-mail: urekarm@uns.ac.rs)

 ISBN 978-86-7466-930-3

## II. Tehničko rešenje sistema

Blok dijagram uređaja za pravilno sedenje prikazan je na slici 2. U nastavku biće uopšteno opisano kako uređaj funkcioniše.

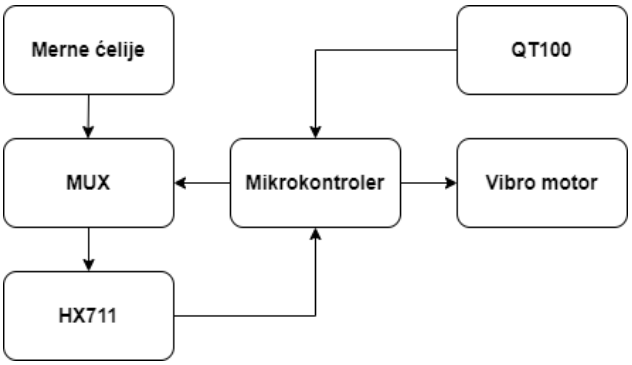


Sl. 2 - Blok dijagram uređaja

Kako bismo postigli neometano i normalno funkcionisanje uređaja, potrebno je obezbediti dva napona od +5 VDC i +3.3 VDC. Mrežni napon (230 VAC) se pomoću integrisanog kola LM7805 prilagođava na napon od +5 VDC, koji je neophodan za većinu elemenata u kolu. Za napajanje vibro motora potrebno je obezbediti napon od +3.3 VDC, a to je urađeno korišćenjem podesivog regulatora LM317. Kako bismo dobili željeni napon potrebno je podesiti vrednosti dva otpornika, čije vrednosti dobijamo korišćenjem jednostavne formule:

$$V_{OUT} = 1.25 \times \left(1 + \frac{R_2}{R_1}\right). \quad (1)$$

Oba regulatora su obezbeđena blok kondenzatorima koji eliminišu brze promene napona, kao i elektrolitskim kondenzatorima koji dodatno doprinose stabilizaciji napona. Pored kondenzatora, integrisana kola su obezbeđena inverzno polarisanim zaštitnim diodama koje neće provoditi sve dok u kolu ne dođe do pojave inverznog ili negativnog napona. Pomoću dve LED diode na uređaju se može pratiti prisutnost oba napona.

Uređaj za pravilno sedenje poseduje dve vrste senzora pomoću kojih detektuje da li korisnik sedi pravilno. Na sedalni deo stolice postavlja se 8 mernih mostova (*Load cell* senzori koji se nalaze u kućnim vagama). Oni se raspoređuju po celom sedalnom delu, ispod leve i desne noge. Signale sa ovih ćelija dovodimo do analognog diferencijalnog multipleksera koji dovedene signale prosleđuje A/D pretvaraču jedan po jedan. HX711 je A/D konvertor osmišljen specijalno za vage i pomoću njega signal dalje putuje do mikrokontrolera.

Na naslon stolice postavlja se elektroda senzora dodira QT100. Ona ima mogućnost da preko tkanine detektuje da li je korisnik naslonjen na stolicu i sedi pravilno. Takođe, ovaj senzor je spojen sa mikrokontrolerom.

Vibro motor čini poslednji segment ovog uređaja. Zadatak mu je da korisniku pruži haptičku informaciju (informacija koja se može osetiti dodirom) onog trenutka kada korisnik ne sedi pravilno, a to se ostvaruje zahvaljujući mikrokontroleru.

Izgled stolice prikazan je na slici 3.


Sl. 3 - Finalni izgled stolice

## III. Hardverske komponente sistema

### A. *Analogni diferencijalni multiplekser*

Kao što je već pomenuto, naš uređaj ima osam mernih mostova. Da bismo imali korisne informacije o svakom njihovom izlazu neopodno je korišćenje multipleksera. Multiplekser (MUX) je kolo koje jedan ulazni signal, koji je izabran od više ulaznih signala može da vodi ka jednom izlazu.

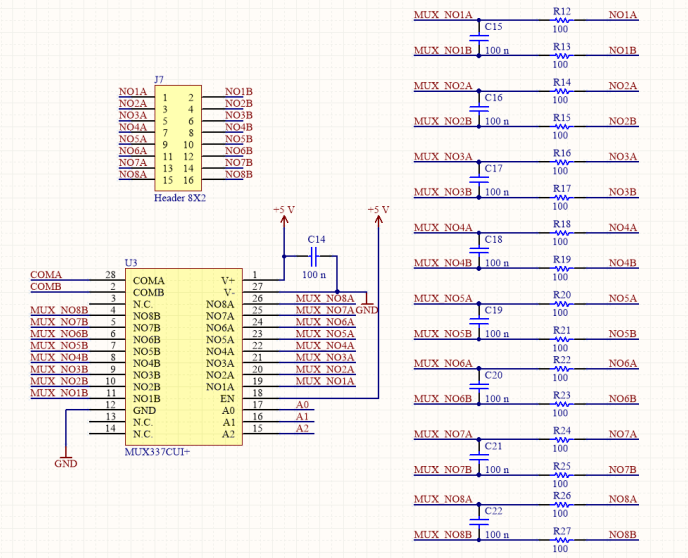


Sl. 4 - MAX337CUI+

Kako imamo osam mernih ćelija koje poseduju po jedan diferencijalni izlaz, koristili smo diferencijalni multiplekser koji na izlaz dovodi i visok i nizak potencijal ulaznog signaa. Signal sa ćelija je filtriran pomoću otpornika od 100 Ω i kondenzatora od 100 nF. MAX 337 je dvostruki, 8-kanalni MUX koji je dizajniran da jedan od osam ulaza prosledi na zajednički izlaz, pomoću trobitne binarne adrese. Njega smo obezbedili *decoupling* kondenzatorom.


ISBN 978-86-7466-930-3

### B. *A/D konvertor HX711*

Za pretvaranje analognih signala u digitalne signale prilagođene računarima (mikroprocesorima ili mikrokontrolerima) koriste se analogno – digitalni konvertori. Tipično, proces A/D konverzije obuhvata odmeravanje analogne veličine u vremenu i po amplitudi. Prema tome, A/D konvertori su uređaji koji prevode signale iz domena kontinualno vreme, kontinualna amplituda u domen diskretno vreme, diskretna amplituda. Odmeravanje signala po vremenu znači da se ulazni analogni signal odmerava (eng. *sampling*), tj. da se njegove vrednosti amplitude uzimaju u određenim vremenskim intervalima, a da se između tih intervala pretpostavlja da se signal ne menja ili da se ne menja značajno. Tipična blok šema A/D konvertora prikazana je na slici 5.

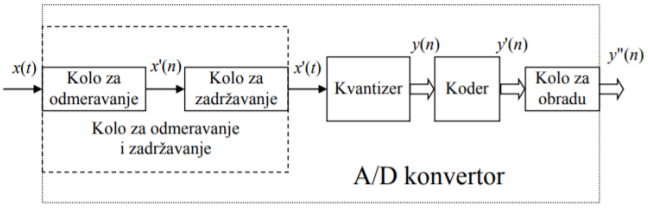


Sl. 5 - Blok šema A/D konvertora

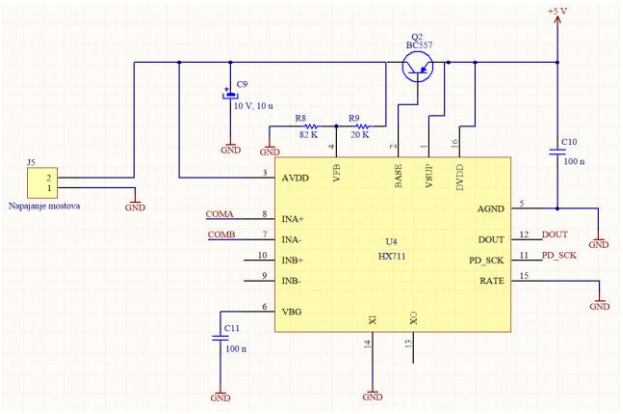


Sl. 6 - HX711

Za potrebe ovog rada korišćeno je integrisano kolo HX711. Ono je 24-bitni A/D konvertor koji je dizajniran za kućne vage i industrijske uređaje koji su bazirani na mernim mostovima. Poseduje dva kanala, od kojih kanal A ima opciono pojačanje od 128 ili 64, dok kanal B ima fiksno pojačanje od 32. Rezultati merenja se šalju na serijski interfejs, preko kog se informacije prenose na mikrokontroler. I ovaj segment je obezbeđen *decoupling* kondenzatorima.

### C. *Senzor dodira QT100*

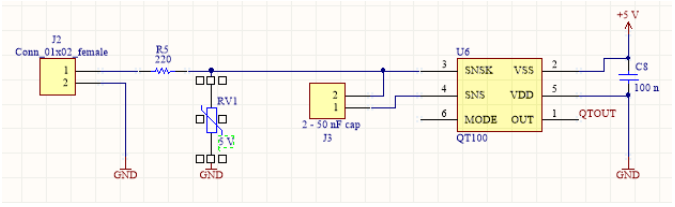


Sl. 7 - QT100

QT100 senzor je samostalno digitalno integralno kolo, koje je sposobno da detektuje blizinu ili dodir. On stvara polje za dodir ili blizinu kroz bilo koji dielektrik, kao što su staklo, plastika, kamen, keramika, pa čak i većina drvenih površina. Takođe, može da pretvori mali metalni objekat u senzor osetljiv na dodir ili blizinu. Ova mogućnost, zajedno sa mogućnošću samokalibracije su u ovom projektu od velikog značaja. Ostavljen je priključak gde se dovodi elektroda pomoću koje se detektuje da li korisnik koristi naslon ili ne. Pored tog priključka, postoji i priključak za kondenzator. Pomoću kondenzatora (čija je vrednost između 2 nF - 50 nF) i otpornika se definiše osetljivost senzora. Vrednost kondenzatora zavisi od debljine naslona i njene dielektrične konstante. Pored kondenzatora, na osetljivost utiče i veličina i oblik electrode. QT100 je obezbeđen *decoupling* kondenzatorom, ali i varistorom koji služi za zaštitu od ESD udara.

### D. *Vibro motor*

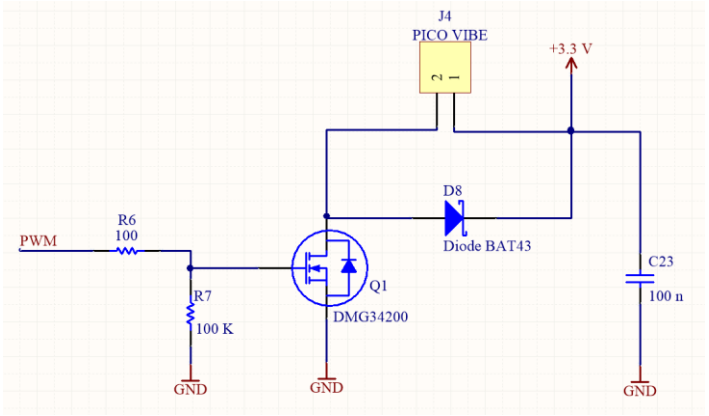


Sl. 8 - Vibro motor

Vibro motor služi kao direktan podsetnik korisniku da ne sedi pravilno. On se uključuje ili kada se ne vrši podjednak pritisak sa obe noge ili kada korisnik ne koristi naslon stolice. Za potrebe ovog projekta koristi se ERM motor sa oznakom C102B002F. Poseduje malu ekscentričnu težinu na svom rotoru koja prilikom rotiranja stvara vibracije. Za pokretanje motora neophodno je koristiti i MOSFET, jer sam mikrokontroler ne može da pruži dovoljnu snagu. PWM signal pokreće motor, tačnije uključuje se gejt MOSFET-a sa impulsima određene širine. Zbog toga struja kroz motor varira u zavisnosti od širine impulse PWM signala, što direktno utiče na brzinu motora i tako određuje jačinu vibracija. Motor predstavlja induktivno opterećenje i njegovim isključenjem može doći do pojave inverznog napona što može oštetiti tranzistor, zbog toga koristimo zaštitnu diodu.


ISBN 978-86-7466-930-3

### *E. Mikrokontroler*

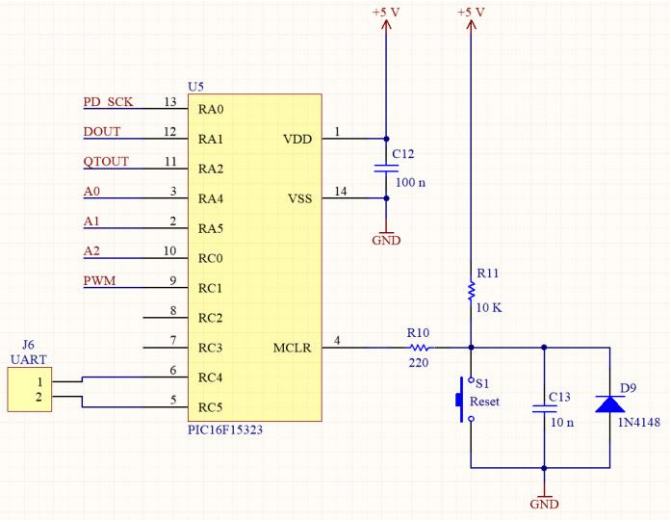


Sl. 9 - PIC16F5323

U ovom projektu korišćen je PIC16F5323 mikrokontroler. PIC16F5323 je 8-bitni mikrokontroler, serije PIC16F, sa brzinom od 32MHz. Malih je dimenzija, poseduje 14 pinova što su bili zahtevi uređaja za pravilno sedenje.

MCLR pin pruža dve posebne funkcije, a to su resetovanje uređaja i programiranje uređaja i otklanjanje grešaka. Ukoliko programiranje i otklanjanje grešaka nisu potrebni u nekom projektu, na MCLR pin dovoljno je samo dovesti +5 V. Dodavanjem komponenti povećava se otpornost uređaja na lažna resetovanja (na primer zbog pada napona). *Pull-up* otpornik na MCLR ulazu drži +5 V sve dok taster nije pritisnut. Taster služi upravo za resetovanje mikrokontrolera. Zaštita je obezbeđena *decouping* kondenzatorom i signalnom diodom.

## IV. PCB I 3D MODEL UREĐAJA

PCB uređaja za pravilno sedenje je napravljen u programskom paketu Altium Designer. Dizajniran je u dva sloja, jer uređaj poseduje i SMD i THT komponente. Dimenzije PCB ploče su 195 mm x 86 mm. Sve komponente uređaja, ali i designatori i naziv uređaja smeštene su na prednjoj strani. Debljine trekova variraju od 15 mil do 30 mil na ulazu kod napajanja. Korišćena je opcija Polygon Pours-a koja sve komponente koje koriste masu spaja slojem bakra. Na slici 10. prikazan je izgled PCB-a.

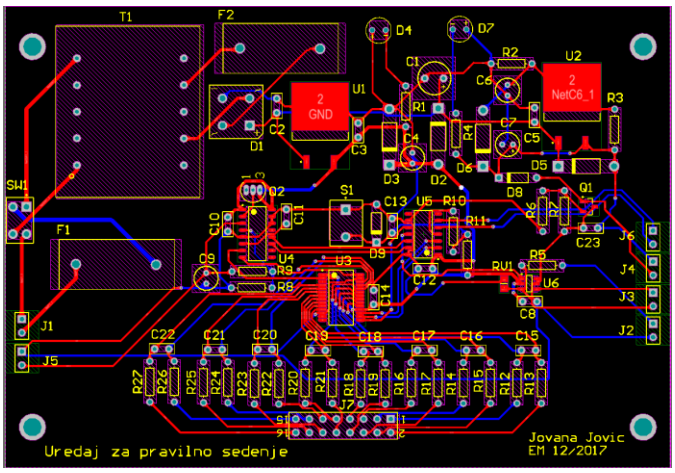


Sl. 10 - PCB uređaja za pravilno sedenje

Pored PCB-a u Altium Designer program postoji mogućnost i za dizajniranje 3D modela. Ta opcija je veoma korisna, jer se i pre same izrade može videti izgled ploče i tako uticati na poboljšanje dizajna. Na slici 11. dat je izgled 3D modela.

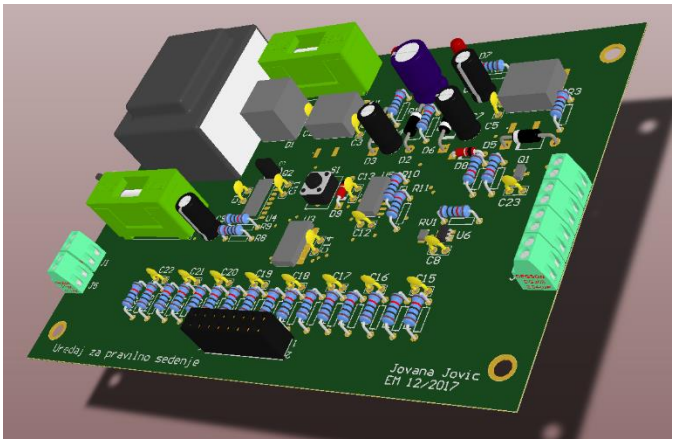


Sl. 11 - 3D model uređaja za pravilno sedenje

## V. FIRMVER I SOFTVER UREĐAJA

Pri pokretanju mikrokontrolera prvi korak predstavlja inicijalizaciju svih potrebnih modula i promenljivih unutar mikrokontrolera. Nakon toga se ulazi u glavnu programsku petlju. Glavna programska petlja je beskonačna petlja koja se izvršava sve dok mikrokontroler radi. U njoj je prvo potrebno očitati podatke sa senzora QT100, kako bi mikrokontroler imao uvid da li je korisnik naslonjen na naslon stolice. Nakon toga sledi očitavanje svih senzora koji se nalaze na sedalnom delu. Mikrokontroler pomoću multipleksera i AD konvertora HX711 pristupa svakom senzoru pojedinačno i očitava ih. Pošto su rezultati sa senzora zašumljeni, njih je potrebno filtrirati i softverski. Svi rezultati se preko UART-a dalje šalju na *Web* server. Kada su prikupljeni podaci sa svih senzora mase i sa senzora dodira, potrebno je odrediti da li korisnik pravilno sedi. Ako to nije slučaj, treba pokrenuti vibro motor. Na slici. 12 prikazan je izgled upravljačke petlje.


ISBN 978-86-7466-930-3

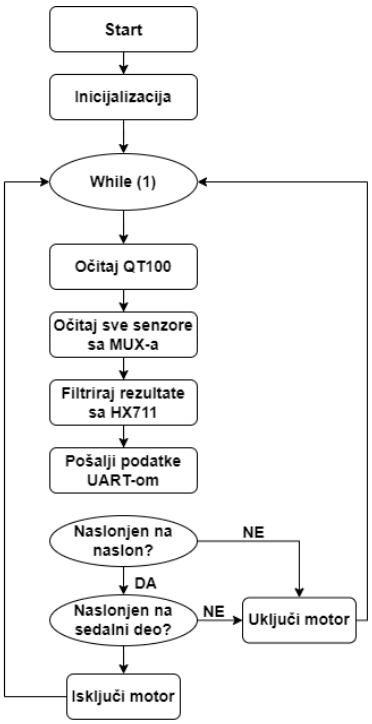


Sl. 12 - Upravljačka petlja

*Internet of Things* je koncept koji se sastoji iz mreže uređaja koji međusobno razmenjuju podatke. To su *embedded* sistemi koji imaju jedan ili više senzora. IoT ima sve širu primenu u svim sferama života, kako u *smart home* aplikacijama, tako i u medicini. Zbog tolike primene, IoT se može naći i u ovom radu.

Podaci sa *web* servera se učitavaju na *web* sajt, koji služi kao grafički interfejs za korisnika. Na slici 13. je prikazana naslovna strana sajta.

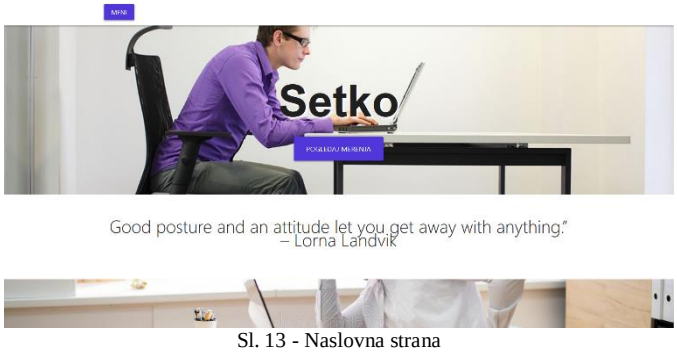


Sl. 13 - Naslovna strana

Na tom *web* sajtu korisnik može pratiti rezultate svog dosadašnjeg sedenja, kao i da bude upozoren ako njegovo sedenje u datom trenutku nije pravilno. Na grafiku se to identifikuje crvenom bojom kada korisnik ne vrši približno jednak pritisak sa obe noge ili iskačućim prozorom ako nije naslonjen na naslon. *Web* aplikacija bi takođe mogla da pruža i dodatne mogućnosti, kao što su arhiviranje rezultata sedenja, praćenje napredovanja ili ipak nazadovanja u veštini pravilnog sedenja. To bi od velikog značaja bilo roditeljima i vaspitačima koji bi imali uvid o napredovanju deteta pri stvaranju dobrih navika tokom sedenja. Uvid u rezultate sedenja bi mogao poslužiti u i medicinske svrhe, kako bi lekari imali jedinstven pristup za svakog pancijenta, kao i jednistvenu dijagnozu.

Na slici 14 je to prikazano.

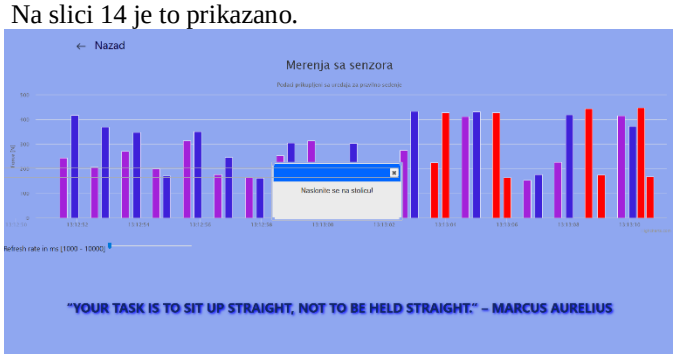


Sl. 14 - Grafik i "iskačući" prozor na *web* sajtu

## VI. DISKUSIJA

Uređaj za pravilno sedenje je osmišljen kako bi se otklonila određena grupa medicinskih problema koja se sve češće javlja i kod dece u najranijem dobu (dece školskog uzrasta). Korišćenjem dostupne tehnologije napravljen je prototip uređaja i predložena primena istog kako bi se smanjila pojava bola u leđima. Dalja istraživanja bi mogla dovesti do unapređenja uređaja i učinila da se on komercijalizuje i bude dostupan svima.

Na tržištu se mogu pronaći različiti uređaji u različitom cenovnom rangu. Lumo Lift je uređaj koji se pomoću magneta kači na odeću i koncentrisan je na gornji deo leđa, cena mu je oko 80 € [10]. UpRight je uređaj koji se lepi na gornji deo leđa (može se iskoristiti jednom za period od 15 min do 60 min). Njegova cena je oko 130 € [11]. Prana je još jedan uređaj koji je dostupan na tržištu. To je prenosivi uređaj koji se zakači u predelu struka i pomoću dijafragmalnog disanja i obrazaca disanja prati povijenost u lumbalnom delu. Cena je 100 € [12]. Svaki od njih je fokusiran samo na određeni deo leđa, torakali (gornji) ili lubalni (donji). Uređaj koji je opisan u ovom radu predstavlja celinu jer prati položaj celog tela u sedećem stavu. To je njegova najveća prednost. Takođe, uređaj se postavlja na samu stolicu, tako da korisniku ne prestavlja nikakvu smetnju prilikom korišćenja.

Pored toga, ne postoji ograničenje u starosnom dobu osobe koja koristi uređaj, mogu ga koristi i odrasli i deca. Takođe, zbog osam mernih ćelija masa koju uređaj može da podnese je 400 kg, pa ni u tom pogledu ne postoje ograničenja.

Najveća mana ovog uređaja je što se za pokrivanje sedalnog dela koriste *button load cell* ćelije koje imaju visoku cenu. Jedna ćelija se na tržištu može naći za 35 €, a nama je potrebno osam takvih. Taj problem je u budućnosti moguće rešiti tako što se umesto *button load cell* ćelija, mogu koristiti obične *load cell* ćelije koje se mogu naći u kućnim vagama. Njihova cena je oko 3 € i dostupne su svuda.

Uređaj trenutno ne poseduje baterijsko napajanje, već ga moramo postaviti blizu utičnice kako bi radio. To je još jedan način kako bismo unapredili uređaj. Mogu se dodati tri litijumske baterije od 3.7 V, koje bi malo povećale dimenzije uređaja, ali bi obezbedile da uređaj neko vreme radi i ako nije priključen na mrežno napajanje.

Uređaj se može koristiti u učionicama, ali bi za te svrhe bilo

 ISBN 978-86-7466-930-3

potrebno razviti aplikaciju pomoću koje bi učitelj mogao da prati sedeći stav svakog deteta. Tako bi se uticalo na stvaranje dobrih navika, ali i na prevenciji bola u najranijem periodu. Pored učitelja, pristup aplikaciji može se dati roditeljima, koji bi u kućnim uslovima mogli da utiču na pravilno sedenje svog deteta.

## ZAKLJUČAK

Ovaj rad nudi rešenje kako smanjiti pojavu bola u leđima i kako podstaći dete u stvaranju dobrih navika. Primenom dostupnih senzora ali i IoT-a kao deo Industrije 4.0 nudi se mogućnost za realizaciju kompletnog uređaja za pravilno sedenje.

## ZAHVALNICA

Ovaj rad je podržan od strane Fakulteta tehničkih nauka u Novom Sadu, Departmana za energetiku elektroniku i telekomunikacije, u okviru projekta MPNTR 200156: „Inovativna naučna i umetnička ispitivanja iz domena delatnosti FTN-a“. Takođe, zahvaljujem se na velikoj pomoći i podršci pri izradi ovog rada celoj Katedri za električna merenja na Fakultetu tehničkih nauka u Novom Sadu.

## LITERATURA

[1] Rannou F, Poiraudeau S, Henrotin Y. Low back pain including sciatica and DISH. U: Bijlsma JWJ, Burmester GR, Da Silva JAP, Faarvang KL, Hachulla E, Mariette X. EULAR Compendium on Rheumatic Diseases. 2009:477-479.
[2] Barr KP, Harrast MA. Low back pain. U: Braddom RL. Physical Medicine and Rehabilitation. Philadelphia: Elsevier. 2007:883-927
[3] Kosinac, Z. (1998). Nepravilno sedenje i tjelesno držanje, Školski vjesnik.
[4] https://www.onsemi.com/pdf/datasheet/lm317-d.pdf
[5] https://www.digikey.com/htmldatasheets/production/105810/0/0/1/qt100.html
[6] https://www.digikey.com/htmldatasheets/production/1836471/0/0/1/hx711.html
[7] https://www.mikroe.com/vibro-motor-click
[8] https://datasheets.maximintegrated.com/en/ds/MAX336-MAX337.pdf
[9] https://ww1.microchip.com/downloads/en/DeviceDoc/PIC16_L_F15313_23_Data_Sheet_4 0001897C.pdf
[10] https://feelpeak.com/
[11] https://www.uprightpose.com/
[12] http://prana.co/

## ABSTRACT

In this paper the prototype for a proper sitting posture device is presented, which would lead to decrease in back pain. Back pain is a recurring problem in all age groups nowadays. The device consists of Button load cells that detect if a user is sitting properly or not on the seating part of the chair. Apart from them, there is a touch sensor QT100, which detects if the user is set against the backrest of the chair. The acquired data is sent through UART to a web server, and is showed on a web site. On the web site the user has an insight in his sitting posture, but there are also warnings if his sitting posture is incorrect. Besides a red graphic and pop-up window on the site, there is a vibration motor which warns the user about his bad sitting posture by a haptic feedback.

## Device for proper sitting posture based on measurement-information modules

Jovana Jović, Marjan Urekar

 ISBN 978-86-7466-930-3

# Merno-akvizicioni sisitem za pravilno sedenje

Mario Volaš, Dragan Pejić, *Member, IEEE,* Marjan Urekar, *Member, IEEE*

***Apstrakt*—U ovom radu predstavljeno je rešenje firmvera za prototip uređaja za pravilno sedenje, koji korisniku daje povratnu informaciju o položaju njegovog tela tokom sedenja. Ovaj uređaj je za cilj imao da popravi držanje korisnika, i tako smanji bolove koji nastaju posle višečasovnog sedenja. Za razvoj ovog prototipa korišćen je STM32F407 mikrokontroler sa razvojnom pločom STM32F4 Discovery. Na sedalnom delu stolice postavljene su merne ćelije za merenje sile, koje proveravaju položaj korisnika na sedalnom delu stolice. Izlazi mernih ćelija se na mikrokontroler dovode preko A/D konvertora HX711. Merenje udaljenosti korisnika od naslona stolice vrši Proximity click, dok povratnu informaciju o nepravilnom sedenju korisnik dobija preko vibro-motora koji se pokreće DC motor 4 click pločicom.**

***Ključne reči*—Embedded, STM32F407, Merne ćelije, Proximity click, HX711, Merenje**

## I. UVOD

Bol u leđima postaje sve veći problem u modernom svetu. Istraživanja pokazuju da se od 1990. do 2016. godine broj godina provedenih sa invaliditetom (DALY- Disability adjusted life years) uzrokovanim bolom u leđima povećao za čak 50% [1]. Glavni uzrok ovih rezultat je stil života, u kom ljudi provode sve više i više vremena u sedećem položaju.

Kako bi što više smanjili rizik od bolova u leđima, potrebno je da osoba sedi pravilno. Dobar sedeći položaj podrazumeva položaj kada je telo uspravno ili lagano nagnuto napred, glava pravilno uzdignuta, te na taj način stimuliše lagano i stalno napetost dugih mišića kičme i kratkih mišića vrata. Gornji i donji udovi su u simetričnom položaju, stopala su paralelno postavljena i celom se površinom oslanjaju na pod. Ovakav položaj obezbeđuje najbolju udaljenost očiju od površine čitanja i manji zamor [2].

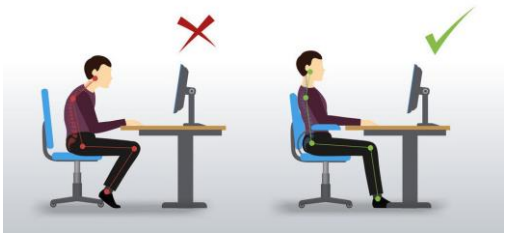

Sl. 1 - Nepravilan i pravilan položaj tela pri sedenju

Mario Volaš – Fakultet tehnikih nauka , Univerzitet u Novom Sadu, Trg Dositeja Obradovića 6, 21000 Novi Sad, Srbija (e-mail: mariovolas@gmail.com)

Dragan Pejić – Fakultet tehnikih nauka , Univerzitet u Novom Sadu, Trg Dositeja Obradovića 6, 21000 Novi Sad, Srbija (e-mail: pejicdra@uns.ac.rs).

Marjan Urekar – Fakultet tehnikih nauka , Univerzitet u Novom Sadu, Trg Dositeja Obradovića 6, 21000 Novi Sad, Srbija (e-mail: urekarm@uns.ac.rs)

Kako bi se korisnik podstakao na pravilan položaj tela pri sedenju, razvijen je Uređaj za pravilno sedenje. Ovaj uređaj prati položaj tela korisnika na sedalnom delu stolice kao i na naslonu stolice. Za razvoj prototipa korišćeno je razvojno okruženje STM32F4 Discovery [3], čiji je centralni deo STM32F407 mikrokontroler. Sila kojom se korisnik naslanja na jednu ili na drugu nogu meri se load cell-ovima, a na naslonu stolice se nalazi Proximity click [4] koji meri da li je korisnik naslonjen na stolicu. Za obaveštavanje korisnika o njegovom nepravilnom položaju koristi se motor sa ERM (Ekscentrična rotirajuća masa). Korisnik takođe može da izabere između striktnog i opuštenog režima rada. Blok šema uređaja je prikazana na slici broj 2.

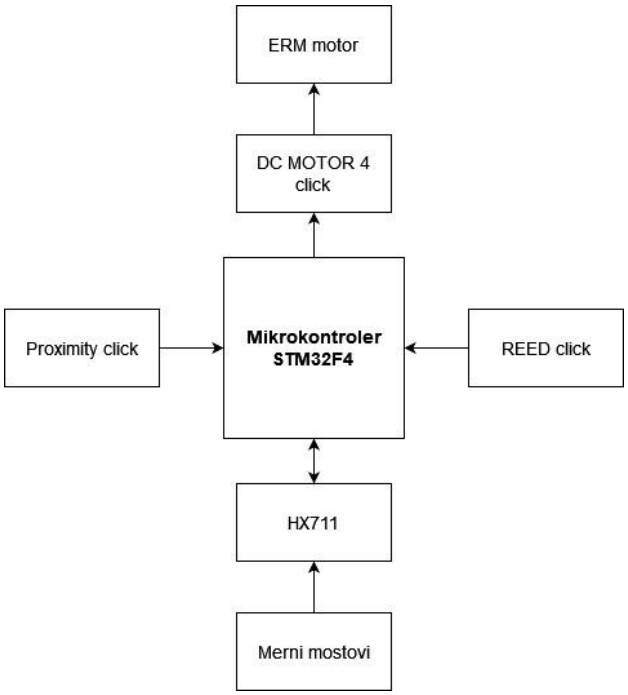


Sl. 2 - Blok šema uređaja za pravilno sedenje

Na slici 3. prikazan je nacrt uređaja za pravilno sedenje.

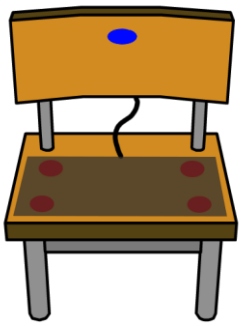

Sl. 3 - Nacrt uređaja za pravilno sedenje

 ISBN 978-86-7466-930-3

## II. HARDVER

Radi bržeg, praktičnijeg i jednostavnijeg razvoja prototipa Uređaja za pravilno sedenje, korišćene su uglavnom modularne komponente i razvojne ploče.

### *A. Razvojno okruženje hardvera*

STM32F4 Discovery razvojna ploča u sebi sadrži mikrokontroler STM32F407VG. On je 32-bitni mikrokontroler koji radi na frekvencijama do 168 MHz, 128 KB RAM memorije, 1024 KB FLASH memorije, 3xI2C, 2xUART, 3xSPI interfejsa, 17 tajmerskih modula, itd. Razvojna ploča takođe sadrži i ST-LINK/V2-A embeded alat za debagovanje.

Sl. 4 - STM32F4 Discovery [3]

Kako bi na STM32F4 Discovery razvojnu ploču na najjednostavniji način priključili click pločice, korišćen je STM32F4 Discovery shield [5]. Na njega je moguće priključiti četiri click pločice, a pored toga poseduje i USB UART priključak, koji omogućava povezivanje mikrokontrolera na PC računar bez serijskog porta.

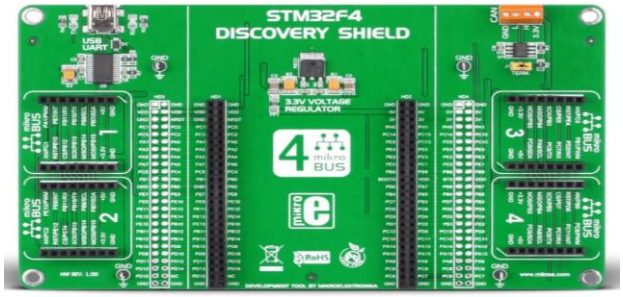


Sl 5 - STM32F4 Discovey shield [5]

### *B. Merne ćelije*

Za merenje sile pritiska na sedalnom delu stolice korišćene su merne ćelije koje se nalaze u komercijalnoj digitalnoj vagi za merenje telesne mase. U vagi se nalaze četiri merne ćelije, a svaka od njih predstavlja jedan polu-most.

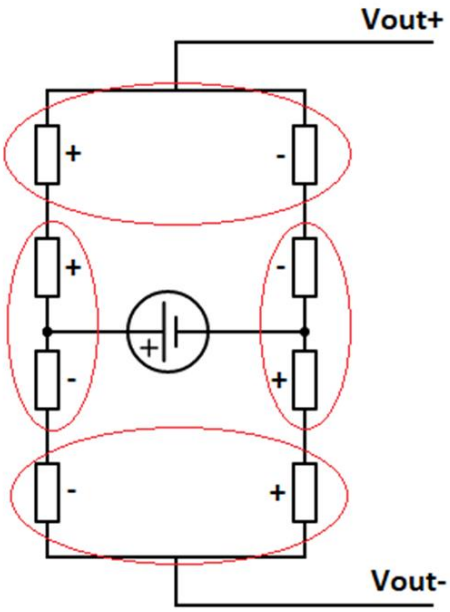


Sl. 6 - Način povezivanja mernih mostova

Na slici 6. zaokruženi elementi predstavljaju jednu mernu ćeliju. Na ovaj način polu-mostovi čine jedan ceo most.

Uređaj za pravilno sedenje zahteva dva odvojena mosta, koja se nalaze na levoj i desnoj strani sedalnog dela stolice.

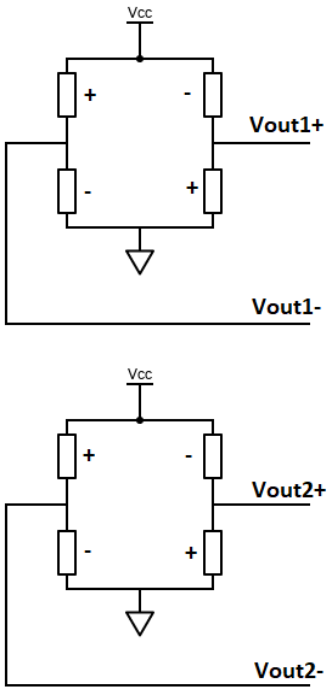


Sl. 7 - Način povezivanja mernih mostova u uređaju

Ovo prespajanje je izvršeno pomoću jumper-a kako bi izmena bila reverzibilna, te se nakon modifikacija uređaj može koristiti i kao vaga za merenje telesne mase, i kao uređaj za pravilno sedenje.


ISBN 978-86-7466-930-3

*C. HX711*

Za merenje izlaza mernih mostova korišćen je A/D konvertor HX711 [6]. HX711 je 24-bitni A/D konvertor, koji je dizajniran za vage i industrijske uređaje koji su bazirani na mernim mostovima. Poseduje dva kanala. Kanal A ima pojačanje od 128 ili 64, dok kanal B ima pojačanje od 32. Rezultati merenja se šalju na serijski interfejs, preko kog se informacije prenose na mikrokontroler. Da bi ovaj čip funkcionisao kako treba, potrebno mu je dodati i neke spoljašnje elemente, što je u ovom slučaju već urađeno na gotovoj štampanoj ploči (slika 8.).

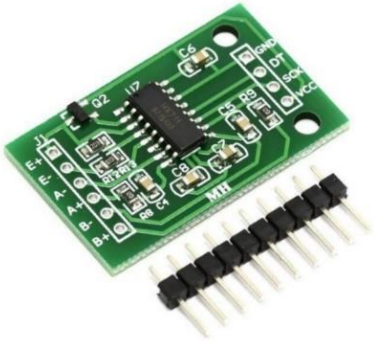

Sl. 8 - Izgled štampane ploče sa HX711 [6]

HX711 sa mikrokontrolerom komunicira pomoću serijskog interfejsa za koji su potrebna dva pina, jedan za takt, a drugi za podatke.

*D. Proximity click*

Proximity click na sebi sadrži integrisano kolo VCNL4010, koje služi kao senzor blizine i ambijentalnog svetla. On kombinuje emiter infracrvenog svetla i PIN fotodiode za merenje blizine u dometu do 20 cm. Čip VCNL4010 ima 16-bitnu rezoluciju. Takođe, može se koristiti i kao senzor ambijentalnog svetla. Proximity click komunicira sa mikrokontrolerom preko I2C komunikacije. Ova click pločica može da se napaja sa 3,3 V ili 5 V.


Sl. 9 - Izgled Proximity click-a [4]

VCNL4010 sadrži sedamnaest 8-bitnih registara za kontrolu, postavku parametara i baferovanje očitanih rezultata. Svi ovi registri su dostupni mikrokontroleru preko I2C komunikacije.

*E. DC MOTOR 4 click*

DC MOTOR 4 click [7] je click pločica koja ima mogućnost pokretanja motora sa naponima napajanja od 5 V do 36 V. Sadrži MAX14870 drajver motora od kompanije Maxim Integrated. Ova click pločica je dizajnirana da radi na 3,3 V ili 5 V. Takođe, na njoj postoji i jumper, pomoću kog se može podesiti da li se koristi unutrašnje napajanje od 5 V, ili neko spoljašnje napajanje.

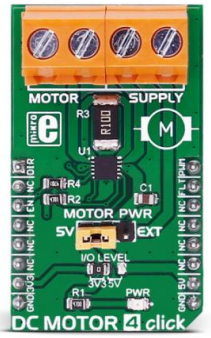


Sl. 10 - Izgled DC MOTOR 4 click-a [7]

Za komunikaciju sa mikrokontrolerom koriste se linije PWM, FLT, DIR i EN. Kontrola brzine okretanja motora vrši se pomoću PWM signala. Veća ispunjenost PWM signala znači i brže okretanja motora. Integrisano kolo MAX14870 nudi i mogućnosti izbora smera kretanja motora pomoću linije DIR.

U ovom projektu DC MOTOR 4 click služi za pokretanje motora sa ekscentričnom rotirajućom masom (ERM), koji proizvodi vibracije, kako bi korisnik bio obavešten o nepravilnom sedenju.

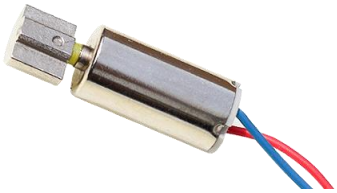

Sl. 11 - Izgled ERM motora [8]

*F. REED click*

REED click [9] je jednostavna pločica koja na sebi sadrži standardni (jednopolni, jednopoložajni, normalno otvoren) reed relej. Kada se na ovaj relej utiče magnetnim poljem, njegovi kontakti se zatvore. Tada se na mikrokontroler šalje logička jedinica.

Za ovu aplikaciju REED click je izabran kako bi korisnik preko tkanine na stolici mogao da bira mod rada uređaja.


Sl. 12 - Izgled REED click-a [9]

 ISBN 978-86-7466-930-3

## III. FIRMVER

### A. *Razvojno okruženje firmvera*

Firmver za prototip uređaja za pravilno sedenje napisan je u STM32CubeIDE [10] razvojnom okruženju.

Uređaj za pravilno sedenje se bazira na razvojnoj ploči STM32F4 Discovery koja u sebi sadrži STM32F407VG mikrokontroler. Kompanija STMicroelectronics za programiranje ovog mikrokontrolera nudi razvojno okruženje STM32CubeIDE. STM32CubeIDE je napredno C/C++ razvojno okruženje sa periferalnom konfiguracijom, generatorom koda, kompajlerom koda i svojstvima za debagovanje STM32 mikrokontrolere i mikroprocesore.

Pomoću ovog okruženja moguće je na jednostavan način konfigurisati sve periferije mikrokontrolera, GPIO pinove, takt rada, interne i eksterne interapte itd. Takođe sadrži i debager, pomoću koga se može pratiti izvršavanje koda korak po korak.

Jedan od glavnih prednosti STM32CubeIDE razvojnog okruženja je njegov Device configuration tool. On nam omogućava da na jednostavniji i brži način konfigurišemo pinove, oscilatore, periferije itd.

U ovom alatu najpre je podešena brzina takta koji zadaje brzinu rada mikrokontrolera. Brzina ovog takta je 168 MHz. Ova brzina se postiže pomoću eksternog oscilatora od 8 MHz, unutrašnjeg PLL-a (množača takta), i preskalera. Iako ova brzina nije neophodna za ovakvu primenu mikrokontrolera, veća brzina je omogućila da mikrokontroler sigurno izvršava sve zadatke.

Pomoću Device configuration tool-a su takođe podešeni i GPIO pinovi. Ovi pinovi služe kako bi se prikupljali podaci sa ostalih uređaja ili kako bi se njima upravljalo. Tako imamo pinove za upravljanje AD konvertorom HX711, za prikupljanje podataka sa Proximity click-a, itd.

Ovde su takođe podešeni i tajmeri. U ovom projektu oni su korišćeni za generisanje PWM signala, kao i za kreiranje funkcije koja pravi kašnjenje (eng. *delay*) od mikrosekunde.

Konfiguracija komunikacionih modula je takođe odrađena pomoću Device configuration tool-a. Za ovaj projekat bili su potrebni USART2 i I2C3 moduli, pomoću kojih je mikrokontroler komunicirao sa PC računarom i proximity click-om.

### B. *Algoritam izvršavanja i glavna programska petlja*

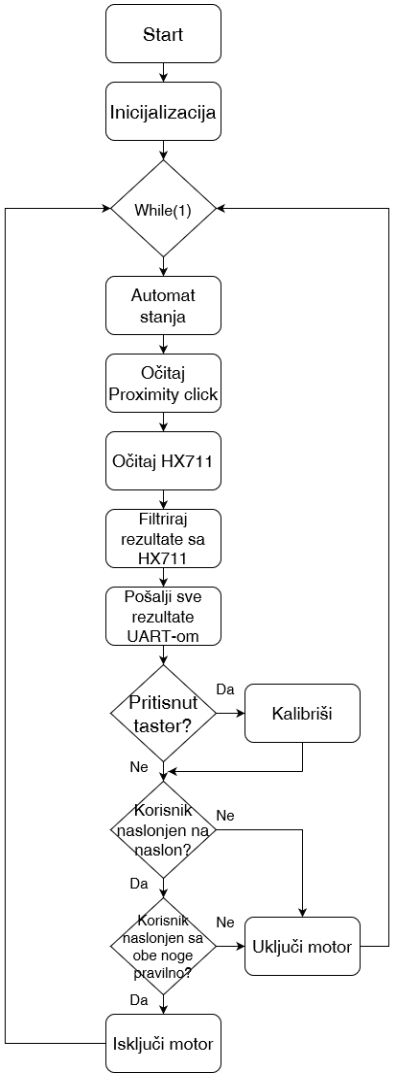


Sl. 13 - Algoritam izvršavanja

U glavnoj programskoj petlji se nalazi glavni deo koda, koji se izvršava beskonačno puta. Prvo se izvršava automat stanja (eng. *state machine*) koji pomoću reed releja određuje u kojem modu rada treba da radi uređaj (opušteno ili striktno).

Sledeća celina se odnosi na čitanje razdaljine sa Proximity click-a. Prvo se upisuje vrednost za konfiguraciju čipa VCNL4010 tako da on prikuplja podatke sa senzora blizine. Nakon toga, posle kratkog delay-a čitaju se podaci iz njegovih registara, u kojima se skladište podaci o razdaljini. Ove podatke smeštamo u dve 8-bitne promenljive, a nakon toga ih spajamo u jednu 16-bitnu.

Posle isčitavanja vrednosti sa Proximity click-a sledi očitavanje vrednosti sa AD konvertora HX711. Kada su vrednosti očitane, njih je potrebno i filtrirati. Implementacijom FIR filtra ovo je odrađeno na jednostavan i efikasan način. Filter je dizajniran pomoću online alata Tfilter, koji za zadate vrednosti frekvencija i pojačanja sam generiše kod i konstante.

Kako bi ovaj uređaj odgovarao svakom korisniku, bez obzira na njegovu masu, potrebno je izvršiti kalibraciju. Kada korisnik sedne, pritiskom na taster za kalibraciju uređaj u

 ISBN 978-86-7466-930-3

promenljivu upisuje referentnu vrednost sa kojom će kasnije da upoređuje nove vrednosti.

Za komunikaciju sa PC računarom koristi se UART komunikacija. Kada su svi potrebni podaci prikupljeni, oni se upoređuju sa dozvoljenim vrednostima. Kada je neka vrednost van dozvoljenog opsega, uključuje se motor, i preko UART-a se ispisuje poruka. Ovo se radi za obe strane sedalnog dela, kao i za rastojanje od naslona.

## IV. DISKUSIJA

Uređaj za pravilno sedenje je uređaj koji bi pomogao ljudima u modernom svetu, a koji se bave poslom koji zahteva višečasovno sedenje. Pomoću njega, korisnik u svakom trenutku ima uvid u položaj svog tela, i na nepravilnosti u držanju. Dizajniran je tako da ga korisnik na jednostavan način može kalibrisati za svoje potrebe, a takođe ga može koristiti i kao vagu za telesnu masu uz jednostavnu rekonfiguraciju.

Kako je ova verzija uređaja dizajnirana pomoću razvojne ploče, njegova cena nije pristupačna za većinu korisnika, ali uz male modifikacije mogao bi biti veoma pristupačan. Naime, za potrebe ovog sistema mogao se koristiti i mikrokontroler sa slabijim karakteristikama i sa manje mogućnosti. Takođe, većina elemenata bi se mogla postaviti na jednu ploču, i tako uštedeti na izradi pojedinačnih click pločica.

Tokom izrade prototipa, osim izrade samog sistema, dodatne izazove predstavljalo je i samo mehaničko rešenje. Naime, kako bi Proximity click merio odstojanje korisnika od naslona stolice, bilo je potrebno probušiti rupu na naslonu stolice da bi infracrveni zraci iz senzora stigli do korisnika, a da pritom senzor ne bude sa prednje strane naslona i time izazove neudobnost pri sedenju. Takođe, za prototip nije izrađeno kućište, pa iz ovog razloga razvojna ploča nije mogla da se zašrafi na stolicu.

Još jedna mana prototipa je njegova udobnost. Da bi korisnik ovaj uređaj mogao da koristi svakodnevno i duže vremena, potrebno je dizajnirati sedalni deo koji bi za to bio pogodan.

Problem pri merenjima sa mernim ćelijama predstavljao je A/D konvertor HX711. Iako on poseduje dva kanala za merenje, oni nemaju isto pojačanje. Ovo je predstavljalo problem, jer je prvobitna ideja bila da se računa odnos između dve strane sedalnog dela, što nije moguće kada su pojačanja različita.

Ovaj uređaj bi se mogao i dodatno nadograditi tako što bi se podaci koji se sakupljaju mogli dalje slati na WEB server. Obrada mernih podataka zahteva veću procesorsku moć, kakvu imaju PC računari i serveri. Na taj način bi mikrokontroler mogao da se u potpunosti svede na minimalne specifikacije, jer ne bi obavljao komplekse obrade, kao što su filtriranje podataka. WEB server bi takođe mogao i da skladišti prethodne podatke, i na taj način bi korisnik mogao da prati poboljšanje svog sedećeg položaja. Takođe, razvojem aplikacije za Android ili IOS mogao bi se vršiti i nadzor pravilnog sedenja dece, i roditelj bi na jednostavan način mogao da utiče na razvoj deteta.

Prednost ovog uređaja u odnosu na već postojeće komercijalne uređaje je što pokriva i sedalni deo, kao i naslon stolice. Takođe, uređaj se može montirati na bilo koju stolicu, pa korisnik ne mora da brine o postavljanju uređaja svaki put kad ga koristi.

Sl. 14 - Izgled Uređaja za pravilno sedenje

## V. ZAKLJUČAK

Izradom ovog prototipa pokazana je osnovna funkcionalnost uređaja, koji može biti dobra osnova za gotov proizvod. On bi se, uz male nadogradnje, mogao koristit u svakodnevnom životu, obrazovanju, pa čak i za naučna istraživanja.

## ZAHVALNICA

Ovaj rad je podržan od strane Fakulteta tehnickih nauka u Novom Sadu, Departmana za energetiku elektroniku i telekomunikacije, u okviru realizacije projekta MPNTR 200156 : "Inovativna naucna i umetnicka isptivanja iz domena delatnosti FTN-a".

## LITERATURA

[1] Hartvigsen J et al. Low Back Pain Series: What Low Back Pain Is and Why We Need to Pay Attention. Lancet, June 2018; Volume 391, Issue 10137; p2356-2367.J. K. Author, Title of Book, xth ed. City of Publisher, Country: Abbrev. of Publisher, year.
[2] Kosinac, Z. (1998). Nepravilno sedenje i tjelesno držanje, Školski vjesnik.
[3] https://www.st.com/en/evaluation-tools/stm32f4discovery.html
[4] https://www.mikroe.com/proximity-click
[5] https://www.mikroe.com/stm32f4-discovery-click-shield
[6] https://www.digikey.com/htmldatasheets/production/1836471/0/0/1/hx711.html
[7] https://www.mikroe.com/dc-motor-4-click
[8] https://www.ricmotor.com/details/erm-vibration-motor
[9] https://www.mikroe.com/reed-click
[10] https://www.st.com/en/development-tools/stm32cubeide.html

 ISBN 978-86-7466-930-3

ABSTRACT

This paper presents the firmware solution for the “Device for proper sitting posture” prototype, which gives insight to the users’ posture during sitting. The devices goal is to correct the users posture and thus reduce the back pain which is caused by long sitting hours. The STM32F407 microcontroller, which is on theSTM32F4 Discovery development board, is used for the development of the prototype. Load cells are located on the sitting part of the chair which check the users sitting posture. The outputs of the load cells are connected to the microcontroller through an A/D convertor named HX711. The users’ distance from the back rest of the chair is measured with a Proximity click, while the feedback of the users’ posture is transmitted through a vibro-motor which is powered by a DC motor 4 click board.

**Measurement and acquisition system for proper sitting posture**

Mario Volaš, Dragan Pejić, Marjan Urekar

 ISBN 978-86-7466-930-3

# Razvoj softvera za merenje vremena reakcije na vizuelne i zvučne stimuluse

Milica Đorđević, Đorđe Novaković, *Member, IEEE*, Majran Urekar, *Member, IEEE*

***Apstrakt*—Ovaj rad prikazuje softversku aplikaciju koja služi za merenje vremena reakcije korisnika kod prepoznavanja simbola i tonova. Softver je napravljen za desktop uređaje, gde se od ispitanika očekuje da u što kraćem vremenskom periodu odgovori na svaki stimulus od interesa, nakon čega se izračunava prosečno vreme reakcije na iste. Pritom, arhitektura aplikacije je takva da se beleže i impulsivne reakcije nastale neposredno pre pojave samih stimulusa. U izgradnji ovog softvera korišćen je programski jezik Pajton u razvojnom okruženju Visual Studio Code. Za razvoj korisničkog interfejsa korišćena je PyQt5 biblioteka i Qt Designer.**

***Ključne reči*—Softver; Stimulus; Vizuelna stimulacija; Zvučna stimulacija; Pažnja; Vreme reakcije; Pajton; PyQt5.**

## I. Uvod

Prvu stepenicu u saznajnom procesu kod čoveka predstavlja opažanje (opservacija) spoljašnjeg sveta, a drugu psihički procesi koji podrazumevaju pamćenje, mišljenje, zaključivanje i druge. Od svih mogućih stimulusa koji u svakom trenutku postoje u polju oko čoveka, samo oni koji su najznačajniji ili najdominantniji u odnosu na njegova interesovanja, namere i ciljeve, bivaju registrovani. Pažnja je bazična psihička funkcija koja omogućava selekciju informacija, usmerenost i usredsređenost psihičke aktivnosti na izvesne sadržaje (predmete, pojave, procese) iz neposredne i dalje okoline. Ona je uslov prijema i obrade informacija.

Karakteristika stalnosti ili postojanosti pažnje odnosi se na sposobnost usredsređenosti tokom dužeg vremenskog perioda. Ukoliko je potrebno duže vremena održavati pažnju, na nekom objektu recimo, postoji kolebanje u njenom intenzitetu. Pažnja je dinamična, pa su joj potrebni stalni voljni podsticaji da bi se održala na istoj, i posebno za subjekta neinteresantnoj aktivnosti. Nedostatak pažnje često se javlja među kliničkom populacijom, uključujući one sa poremećajem pažnje sa hiperaktivnošću (ADHD – Attention Deficit Hyperactivity Disorder) i traumatskim povredama mozga (TBI – Traumatic Brain Injury) [1]. Na sreću, pažnja se može tretirati i poboljšati uz odgovarajući kognitivni trening.

U kognitivnoj psihologiji, vremenski interval između predstavljanja stimulusa i pokretanja voljnog motoričkog odgovora naziva se vreme reakcije. Procena vremena reakcije daje predstavu o integritetu i sposobnostima centralnog nervnog sistema za obradu informacija, a takođe je jednostavan alat za određivanje motoričko-senzornog odnosa kod ispitanika [2]. Komponente pomenutog vremena su: detekcija, identifikacija, odluka i na kraju reakcija.

## II. Motiv i ideja

Potencijali vezani za događaje (ERP) su fluktuacije napona koje se snimaju na skalpu i koje su vremenski vezane za događaje. Kao električno polje izazvano protokom informacija u neuronskim mrežama, mere se istim elektronskim uređajima kao EEG. Prošlo je više od pola veka od kada smo prvi put saznali da ređi stimulusi, predstavljeni među češćim, izazivaju u EEG-u pozitivni talas sa tipičnim pikom latence nešto veće od 300 ms (Sl. 1.). Kasnije je utvrđeno da ovaj „zakasneli“ pozitivan potencijal povezan sa događajem, nazvan P300 ili P3, uključuje dve različite komponente, P3a i P3b [3]. Štaviše, pokazalo se čak da ni P3b nije jedinstven talas, već se sastoji od daljih podkomponenti.

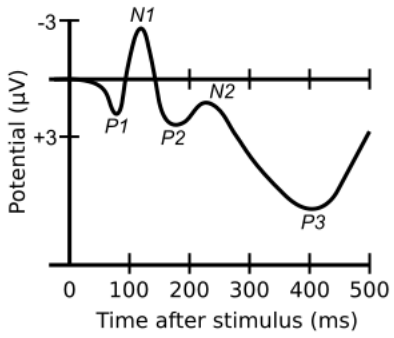


Sl. 1. Komponente ERP-a.

Kako je P3 najčešće razmatrana ERP komponenta, a njena tačna struktura je do danas ostala nejasna, došli smo na ideju da smislimo modifikaciju standardnog testa koji se koristi pri snimanju ERP-a (poznatiji kao „Oddball“ paradigma) [4]. Zamisao je da ovaj modifikovani kompjuterizovani test bude predlog za dalje istraživanje podkomponenti i pre svega nađe eksperimentalnu primenu.

Postoji mnogo varijacija testova zasnovanih na Oddball paradigmi, a najčešće se tiču vrste predstavljenih stimulusa. Modifikacija prezentovana u ovom radu ogleda se u dužini vremenskih intervala između određenih događaja, što će dalje biti detaljnije objašnjeno.

Milica Đorđević – Fakultet tehničkih nauka, Univerzitet u Novom Sadu, Trg Dositeja Obradovića 6, 21000 Novi Sad, Srbija (e-mail: milicadjordjevic.mas@gmail.com).

Đorđe Novaković – Fakultet tehničkih nauka, Univerzitet u Novom Sadu, Trg Dositeja Obradovića 6, 21000 Novi Sad, Srbija (e-mail: djordjenovakovic@uns.ac.rs).

Marjan Urekar – Fakultet tehničkih nauka, Univerzitet u Novom Sadu, Trg Dositeja Obradovića 6, 21000 Novi Sad, Srbija (e-mail: urekarm@uns.ac.rs).

 ISBN 978-86-7466-930-3

## III. Opis rada aplikacije

Kroz celu aplikaciju, odnosno sve njene prozore korisniku se daju jasna uputstva za upotrebu, koja ukazuju na ono što se od njega zahteva. Takođe, korisniku je omogućeno da pritiskom na predviđeno dugme prelazi sa jednog prozora na drugi, intuitivno prateći proces ispitivanja. Prolazeći kroz nekoliko prozora grafičkog korisničkog interfejsa, korisnik unosi svoje lične podatke (Sl. 2.), bira jedan od dva ponuđena testa (Sl. 3.), odrađuje test i potom dobija rezultate.

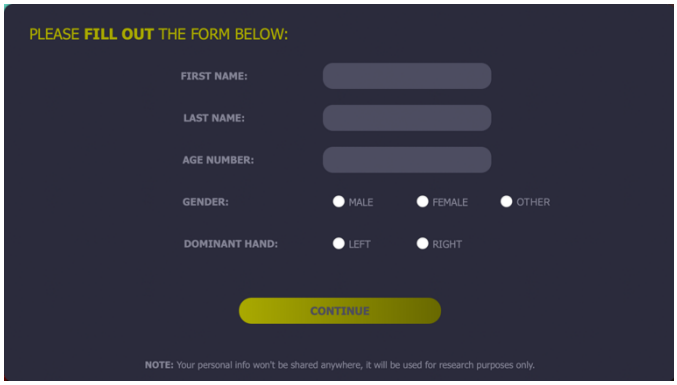


Sl. 2. Prozor sa forma za popunjavanje ličnih podataka.

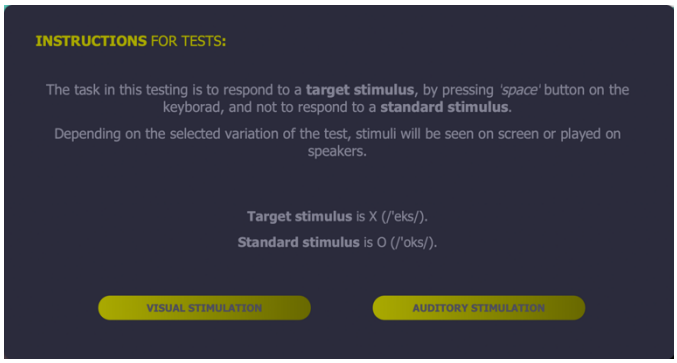


Sl. 3. Prozor sa instrukcijama i izborom testa.

U glavnom delu aplikacije, gde se vrši testiranje, korisnikov senzorni aparat stimuliše se sa 35 stimulusa, vizuelne ili zvučne prirode, od kojih je 24 standardnog karaktera, a 11 devijantnog. Redosled prikazivanja stimulusa je nasumičan. Od korisnika se traži da na svaki devijantni (ređi) stimulus, za koji se u ovoj aplikaciji podrazumeva iks (X), odgovori pritiskom na taster „Space“ na tastaturi računara na kom se vrši testiranje. Pod standradnim (češćim) stimulusom se u ovoj aplikaciji podrazumeva oks (O) i na njega korisnik ne treba da odgovori. Aplikacija meri vreme od generisanja devijantnog stimulusa do korisnikovog odgovora na isti, koje ne bi trebalo da bude duže od 1,5 s. Nakon generisanja svih 35 stimulusa, koristeći zabeležne podatke aplikacija izračunava prosečno vreme koje je korisniku bilo potrebno za davanje adekvatnog odgovora, kao i standardnu devijaciju. Ove vrednosti, zajedno sa ličnim podacima korisnika, smeštaju se u SQL tabelu koja se formira nakon prve upotrebe aplikacije. Svakim narednim testiranjem, dopunjavaće se već postojeća tabela bez kreiranja nove, osim u slučaju da je ona ručno izbrisana ili premeštena iz glavnog direktorijuma programa.

### A. *Vizuelna stimulacija*

Kada se testiranje vrši uz pomoć vizuelne stimulacije, u centru crnog ekrana će se u krug i nasumično prikazivati stimulusi. Osim što je ekran potpuno crn pre i nakon pojavljivanja stimulusa, dodatno se pre svakog stimulusa prikazuje i fiksacioni objekat za fiksiranje pogleda na monitoru. Ovaj fiksacioni objekat se obično implementira u obliku krsta, vodeći računa o odgovarajućem kontrastu u odnosu na pozadinu. Sekvencijalni tok prikazivanja različitih objekata na ekranu može se videti na Sl. 4.

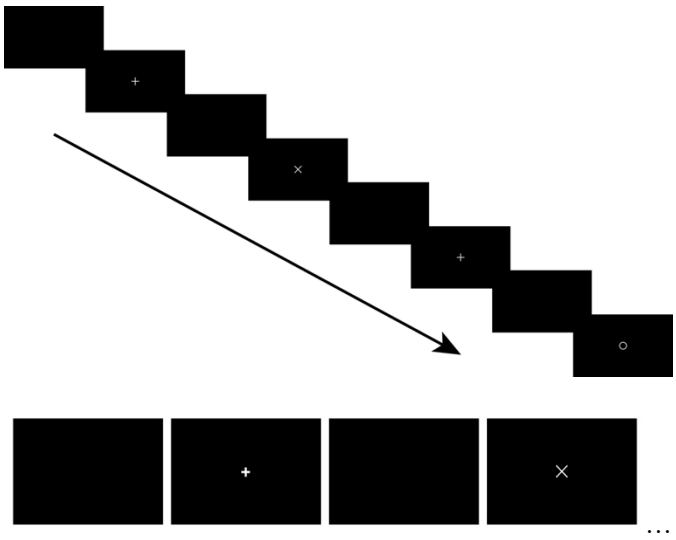

Sl. 4. Primer toka vizuelne stimulacije (gore) i redosled prikazivanja vizuelnih komponenti ispitaniku (dole).

### B. *Zvučna stimulacija*

U slučaju testiranja sa zvučnom stimulacijom, umesto prikazivanja iks i oks na ekranu, oni će biti emitovani kao zvučni signali sa zvučnika.

## IV. Upotrebljeni alati

Za realizaciju ove aplikacije korišćen je programski jezik Pajton i njegove biblioteke: PyQt5 [5] i sqlite3 [6].

PyQt5 je sveobuhvatan skup Pajtonovih veza za paket Qt v5, koji omogućava da se Pajton koristi kao alternativa jeziku C++ za razvoj aplikacija na svim podržanim platformama. Uz pomoć pomenute biblioteke i Qt Designer-a napravljen je grafički korisnički interfejs.

Biblioteka sqlite3 korišćena je za kreiranje baze podataka i upisivanje dobijenih vrednosti.

## V. Struktura vremenskih intervala

Kako bi se izbeglo formiranje navike kod ispitanika, vremenski intervali između određenih događaja nisu konstantni, već se njihova vrednost generiše kao slučajni parametar između dve granične vrednosti.

Granične vrednosti osnovnog intervala $T$ su 2 s i 4 s, a redom ga sačinjavaju sledeći podintervali (Sl. 5.):

- $T_F$ vreme prikazivanja fiksacionog objekta, graničnih


ISBN 978-86-7466-930-3

vrednosti 200 ms i 600 ms;
- $T_{PS}$ prestimulaciono vreme, graničnih vrednosti 300 ms i 500 ms;
- $T_S$ vreme prezentovanja stimulusa, koje je konstantno i iznosi 200 ms;
- $T_{PH}$ vreme praznog hoda, ono se ne definiše već je posledica prethodno definisanih intervala:

$$T_{\mathrm{PH}} = T - T_{\mathrm{F}} - T_{\mathrm{PS}} - T_{\mathrm{S}}. \quad (1)$$

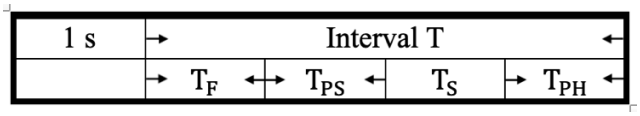


Sl. 5. Prikaz vremenskih intervala

Osnovni intervali odvojeni su jednom sekundom radi lakšeg detektovanja.

## VI. Rezultati

Pored osnovnog zahteva koji podrazumeva izračunavanje prosečnog vremena reakcije na ciljane stimuluse uz standardnu devijaciju, aplikacija beleži još neke bitne podatke (Sl. 6.):

1. broj tačnih odgovora – pritiskanje predviđenog tastera nakon emitovanja devijantnog stimulusa;
2. broj netačnih odgovora – pritiskanje tastera nakon emitovanja standardnog stimulusa;
3. broj propuštenih devijantnih stimulusa – usled isteka vremena koje je predviđeno za odgovor od strane ispitanika;
4. broj impulsnih odgovora – usled pritiskanja tastera tokom prikazivanja fiksacionog objekta ili neposredno pre pojave stimulusa.


Sl. 6. Prozor sa rezultatima testiranja.

Poslednje spomenut podatak predstavlja jednu od inovacija u ovoj vrsti testova, jer može ukazati i na probleme sa impulsivnošću. Takođe, napravljeno je ograničenje kod vremena koje je predviđeno za dobijanje odgovora od strane ispitanika kako bi se iz razmatranja izuzele ekstremne vrednosti usled slučajnih grešaka.

Srednja vrednost vremena rekacije $\bar{x}$ dobija se deljenjem sume eksperimentalno dobijenih vrednosti $x_i$ sa ukupnim brojem merenja $n$:

$$\bar{x} = \frac{\sum_{i=1}^{n} x_i}{n}. \quad (2)$$

Standardna devijacija $s$ predstavlja meru odstupanja razmatranih vremena reakcije $x_i$ od njihove aritmetičke sredine, odnosno srednje vrednosti $\bar{x}$, a računa se po sledećoj formuli:

$$s = \frac{\sqrt{\sum_{i=1}^{n} (\bar{x} - x_i)^2}}{n-1}. \quad (3)$$

## VII. Diskusija

U odnosu na zamišljene početne ideje i razvoj aplikacije prilagođene za snimanje evociranih potencijala, napravljen je jedan korak u nazad. Odnosno, realizovana je aplikacija koja meri prosečno vreme reakcije uz standardnu devijaciju i još neke indikatore. Ona svakako može naći primenu u eksperimentalnoj praksi kao prvi korak u ispitivanju potencijalnog uticaja promenljivih vremenskih intervala, u ovom slučaju na prosečno vreme reakcije. Takođe, aplikacija je napravljena tako da je korisniku jednostavna za samostalno korišćenje, pa može naći primenu i kao alat za vežbu u različite svrhe.

Ono što bi za početak moglo da se poboljša, kako bi aplikacija išla u zamišljenom pravcu, jeste grafičko prikazivanje rezultata uz markere kada je predstavljen stimulus i kada je korisnik na njega reagovao.

## VIII. Zaključak

Merenje vremena reakcije ima široku primenu. Koristi se za procenu zdravstvenog stanja osobe, kao i za praćenje stanja pojedinca tokom njegovog svakodnevnog života radi boljeg obavljanja mentalnih aktivnosti, donošenja odluka i planiranja potrebnih za vožnju, bavljenje sportom i druge aktivnosti koje zahtevaju visok fokus i brzinu.

Vreme reakcije usko je povezano sa pažnjom, osnovnom funkcijom koja je neophodna za obavljanje svakodnevnih aktivnosti, među kojima su učenje, pamćenje, percepcija i rešavanje problema. Zbog toga se pažnja smatra polaznom kognitivnom funkcijom koja ako je oslabljena može dovesti do deficita u drugim kognitivnim domenima.

## Zahvalnica

Ovaj rad je podržan od strane Fakulteta tehničkih nauka u Novom Sadu, Departmana za energetiku elektroniku i telekomunikacije, u okviru realizacije projekta MPNTR 200156 : „Inovativna naučna i umetnička ispitivanja iz domena

 ISBN 978-86-7466-930-3

delatnosti FTN-a“.

## LITERATURA


[1] L. Penkman, „Remediation of attention deficits in children: A focus on childhood cancer, traumatic brain injury and attention deficit disorder“. Paediatric Rehabilitation, no. 7, 111-123, year 2004.,

[2] G. K. Lofthus, „Sensorimotor performance and limb preference“, *Percept Mot Skills,* 683-693, year 1981.,

[3] J. Polich, „Updating P300: an intergrative theory of P3a and P3b“, Clin. Neurophysiol., year 2007.,

[4] B. Bišević, „Varijabilnost amplitude kognitivnog evociranog P300 potencijala dobijenog auditornom oddball paradigmom“, Medicinski fakultet, Univerzitet u Prištini, 2015. godine,

[5] Python Package Index, "PyQt5" [Online]. Available: https://pypi.org/project/PyQt5/,

[6] Python Documentation, „sqlite3“ [Online]. Available: https://docs.python.org/3/library/sqlite3.html.



## ABSTRACT

This paper presents a software application that is used to measure user’s reaction time when recognizing symbols and tones. The software is made for desktop devices, where respondents are expected to respond to stimulus of interest in the shortest possible time, after which average reaction time is calculated. At the same time, the architecture of the application is such that impulsive reactions that occurred just before the appearance of the stimulus are also recorded. The Python programming language was used for building the application in Visual Studio Code development environment. The PyQt5 library and Qt Designer were used to develop the graphical user interface.


## Software development for measuring reaction time to visual and audio stimuli

Milica Djordjevic, Djordje Novakovic, Marjan Urekar

 ISBN 978-86-7466-930-3

# Projektovanje univerzalne razvojne ploče za merenje i regulaciju

Ninoslav Srdić, Marjan Urekar, Dragan Pejić, Platon Sovilj

***Apstrakt*—Ovaj rad opisuje projektovanje univerzalne razvojne ploče za merenje fizičkih veličina i regulaciju, na bazi AVR atmega32u4 mikrokontrolera. Prikazana je blok šema uređaja, šematici pojedinačnih blokova i navedeni su primeri primene ove razvojne ploče.**

***Ključne reči*: univerzalna razvojna ploča; mikrokontroler; industrijski senzori**

## I. UVOD

Prilikom razvoja novog proizvoda, dok još ideja i tehničko rešenje nisu sasvim formirani i da bi nam početak razvoja bio lakši i ekonomski efikasniji, potreban nam je hardverski razvojni alat. Iako nije neuobičajeno da pravimo revizije hardvera, uvek je bolje da prvo svoju ideju proverimo na postojećoj platformi, odnosno na takozvanoj univerzalnoj razvojnoj ploči.

Ovaj rad ukratko objašnjava projektovanje univerzalne razvojne ploče za potrebe laboratorijskih vežbi na fakultetu kao i za prototipovanje proizvoda. Na tržištu već postoji mnoštvo ovakvog hardvera sa različitim kontrolerima, periferijama, različitih dimenzija i cena. Prednost ove ploče jeste što nudi dosta periferija u odnosu na druge ploče sa ATmega32u4 kontrolerom i to u kompaktnom formatu.

Ova razvojna ploča omogućava korisnicima da koriste različite industrijske senzore sa logičkim izlazom, termopar K tipa za merenje temperature, ulazima na koja se mogu dodati spoljašnji razdelnici napona za različita analogna merenja i da se sve to može programirati u Arduino okruženju ili pristupiti i programirati iz labview-a, tj. okruženja koja su studentima već poznata.

Ideja je da se od jedne kompaktne ploče mogu razviti uređaji za različite primene (npr. temperaturni regulator, merenja nekih fizičkih veličina, prenos izmerenih vrednosti preko serijske komunikacije RS485 i prikaz tih podataka na Labview SCADA sistemu) i da se ovaj sklop može primeniti za vežbe iz različitih predmeta na fakultetu, a da nije neophodno dodatno napajanje osim konekcije sa računarom.

Marjan Urekar – Fakultet tehničkih nauka, Univerzitet u Novom Sadu, Trg D. Obradovića 6, 21000 Novi Sad, Srbija (e-mail: urekarm@uns.ac.rs).
Platon Sovilj – Fakultet tehničkih nauka, Univerzitet u Novom Sadu, Trg D. Obradovića 6, 21000 Novi Sad, Srbija (e-mail: platon@uns.ac.rs).
Dragan Pejić – Fakultet tehničkih nauka, Univerzitet u Novom Sadu, Trg D. Obradovića 6, 21000 Novi Sad, Srbija (e-mail: pejicdra@uns.ac.rs).
Ninoslav Srdić – Fakultet tehničkih nauka, Univerzitet u Novom Sadu, Trg D. Obradovića 6, 21000 Novi Sad, Srbija (e-mail: ninosrdicd@gmail.com)

Primena ove razvojne ploče su predmeti koji se bave merenjem, embedded programiranjem i Labview okruženjem ili kao platforma za razvoj softvera za *embedded* aplikacije.

## II. DIZAJN SKLOPA

Postavljen je zahtev da se napravi razvojna ploča koja će moći da se koristi sa industrijskim senzorima sa tranzistorskim izlazima, odnosno sa senzorima koji na svom izlazu daju logičku vrednost, kao i senzorima za merenje analognih vrednosti i jedan ulaz za merenje temperature termoparom tipa K. Za izvršavanje komande razvojna ploča ima dva relejna izlaza, a za prikazivanje merenih vrednosti alfanumerički displej kao i mogućnost slanja podataka serijskom komunikacijom. Takođe na ploči imamo četiri tastera. Još jedan od zahteva je da se ploča napaja sa 5 V a za potrebe napajanja industijskih senzora potreban je napon od 24 Vdc, pa je napravljen *Step-up* pretvarač (*converter*).

Prvi korak prilikom dizajna celog sklopa je bio da se napravi blok dijagram, gde su objedinjeni svi zahtevi pa su na osnovu toga izabrane komponente.

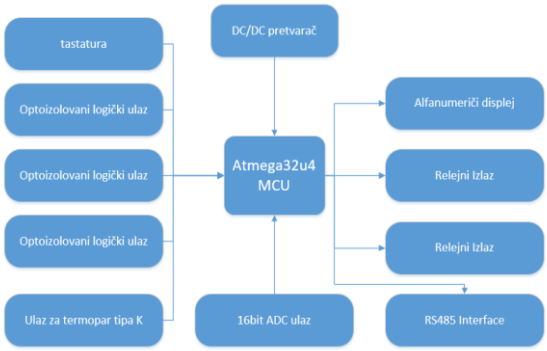


Sl. 1. Blok šema celog sklopa

Kao što se na blok šemi može videti razvojna ploča se sastoji od:

- Tri optoizolovana logička ulaza za industrijske senzore
- AD konvertor sa dva ulaza za analogna merenja
- Ulaz za termopar sa pretvaračem koji vrši kompenzaciju hladnog kraja, kao i linearizaciju karakteristike termopara i AD konverziju
- DC/DC boost pretvarač sa 5 V na 24 V
- Dva relejna izlaza
- Alfanumerički displej
- RS485 interface
- Četiri programibilna tastera

 ISBN 978-86-7466-930-3

Primeri primena:

### A. *Temperaturni regulator*

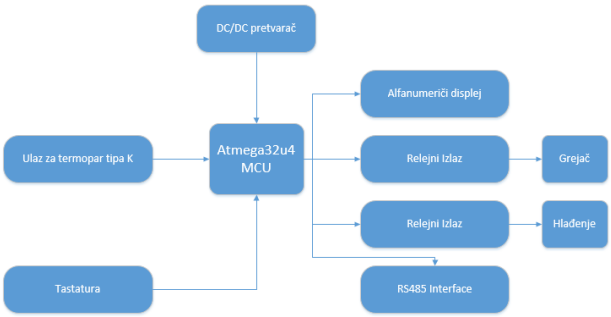


Sl. 2. Blok šema temperaturnog regulatora

Na slici 2. je prikazana blok šema temperaturnog regulatora koji se može napraviti uz korišćenje ove razvojne ploče.
Na ulaz razvojne ploče možemo povezati termopar tipa K.
Na relejne izlaze možemo povezati grejač i sistem za hlađenje.

Alfanumerički displej nam pruža mogućnost prikaza temperature i zadatih parametara. Tasterima dobijamo mogućnost promene parametara odnosno zadavanje graničnih vrednosti temperature. Na računaru možemo grafički predstaviti vrednosti promene temperature po vremenu, slanjem podataka preko RS485 komunikacije.

Ovakav sistem bi imao primenu za održavanje temperature alata prilikom brizganja plastike.

### B. *Brojač komada*

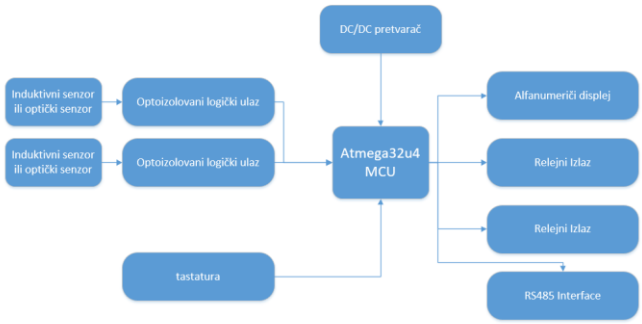


Sl. 3. Blok šema brojača komada

Na slici 3. se može videti drugi primer primene (brojač komada). Induktivnim senzorima ili optičkim prekidačima na ulazu detektujemo prolazak komada ili neke referentne tačke za brojanje (npr. istureni vijak na osovini). U zavisnosti od redosleda okidanja senzora možemo da uvećavamo ili smanjujemo izbrojane vrednosti i to da predstavimo na displeju. Relejne izlaze možemo koristiti za uključivanje ili isključivanje pogona nakon postizanja zadatih vrednosti.

### C. *Vaga za doziranje*

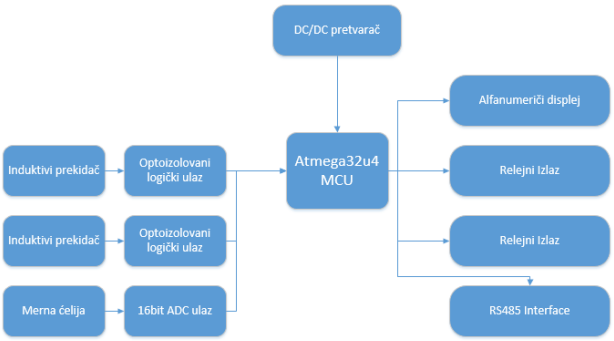


Sl. 4. Blok šema vage za doziranje

Još jedna primena razvojne ploče jeste razvoj softvera za vagu za doziranje praškastih ili zrnastih proizvoda (Sl. 4.).
Na ulazu AD konvertora imamo mernu ćeliju pomoću koje merimo masu, a relejne izlaze možemo iskoristiti za grubo i fino doziranje, tj. za otvaranje veće i manje klapne na košu vage. Induktivni prekidači nam služe za detektovanje položaja klapne. Na alfanumeričkom displeju prikazujemo izmerenu i zadatu vrednost i grešku doziranja.

## III. TEHNIČKO OBJAŠNJENJE

Jedan od bitnih zahteva projekta, jeste mogućnost da se mikrokontroler može programirati preko Arduino okruženja, pa je na osnovu toga izabran kontroler iz AVR familije. Za ostale komponente napravljena je excel tabela sa nekim od ključnih parametara, kao i cene komponenti. Potom je sagledano koje komponente su optimalne u odnosu na cenu i karakteristike.

Nakon odabira ključnih komponenti i njihove dokumentacije sledi crtanje električne šeme, gde je korišten alat po imenu Altium Designer.

Za projektovanje DC/DC pretvarača korišten je alat Texas Instruments Power Designer, gde se definišu potrebni parametri i topologija pretvarača, a alat potom sam izračuna vrednosti komponenti.

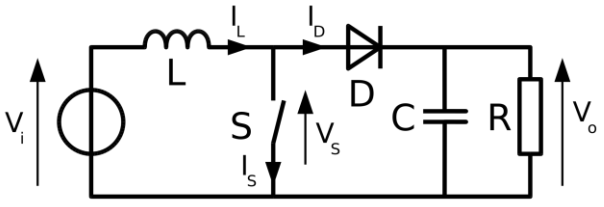


Sl. 5. Blok šema Boost pretvarača

Na slici 5. prikazan je primer pretvarača, podizača napona (*Boost converter*).


ISBN 978-86-7466-930-3

U ovoj topologiji pretvarača, za prebacivanje energije iz jednosmernog izvora nižeg napona ka opterećenju na kome je viši napon, koristi se magnetna energija kalema.
Kada je prekidač zatvoren, struja izvora protiče kroz kalem *L* i prekidač *S*. Tada kalem skladišti energiju u svom magnetnom polju. Otvaranjem prekidača, struja kalema, koja je jednaka struji izvora počinje da pada. Pošto se kalem suprotstavlja promeni struje, dolazi do porasta napona u kalemu. Upravo ovaj efekat se koristi za podizanje napona u *boost* pretvaraču.

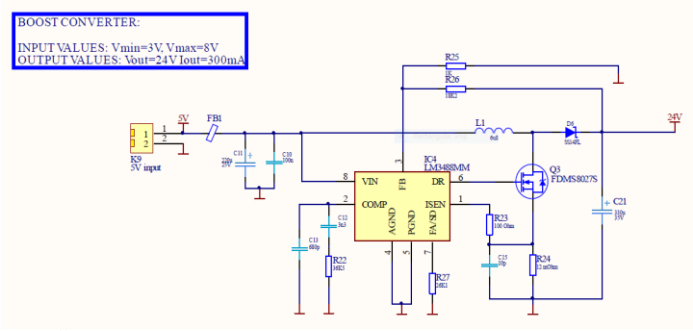

Sl. 6. Šema Boost pretvarača

Optički izolovan logički ulaz na slici 7. namenjen je za priključivanje industrijskih senzora sa logičkim izlazom. Optokapleri se koriste radi galvanskog odvajanja dva dela kola, tj. kao dodatan vid zaštite.

Pošto je za napajanje industrijskih senzora uglavnom potreban napon od 24 V, na ovaj ulaz je doveden napon sa *step-up (boost)* pretvarača.

Ukoliko želimo da imamo galvanski odvojen ulaz, ne smemo koristiti napajanje USB porta, nego koristimo posebno napajanje od 5 V (prethodno se mora skinuti *jumper* H2 vidljiv na Sl. 11.).

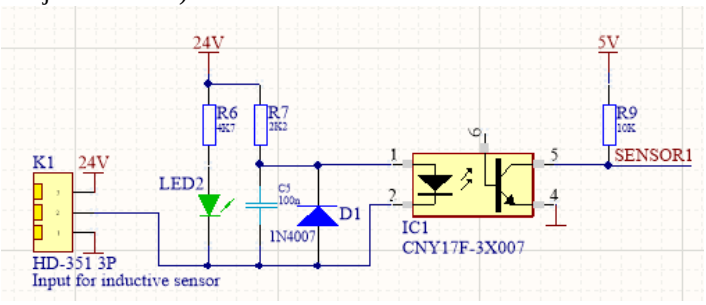

Sl. 7. Optički izolovan ulaz

Ulaz za termopar (Sl. 8.) je omogućen uz pomoću MAX6675 pretvarača. Termopar tipa K nije linearan, pa je pored pojačavanja ulaznog signala potrebno i linearizovati isti. Ovaj pretvarač u sebi ima kompenzaciju hladnog kraja u opsegu od -20 °C do +85 °C, linearizaciju signala i 12-bitni AD konvertor. MAX6675 omogućava veome jednostavno merenje temperature termoparom tipa K, pošto na SPI izlazu dobijamo tačno izmerenu vrednost temperature.
Rezolucija ovog pretvarača je 0.25 °C i može se koristiti za merenja temperature do +1024 °C.
U ovom projektu koristimo napajanje od 5 V.
Podatke mikrokontroleru šaljemo pomoću SPI komunikacije.

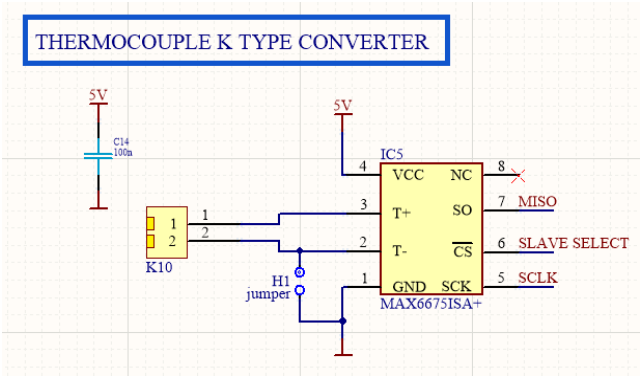

Sl. 8. Ulaz za termopar

Sklopu je dodat i 16-bitni eksterni ADC (Sl. 9.) jer je ADC u mikrokontroleru 12-bitne rezolucije. Ovaj AD konvertor ima dva kanala, a sa mikrokontrolerom komunicira preko I2C-a.

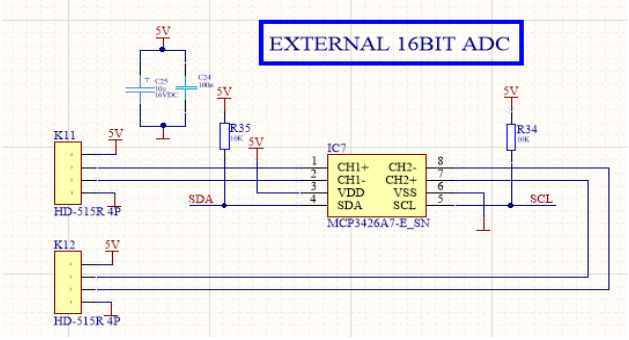

Sl. 9. ADC ulaz

Na slici 10. se može videti primer relejnog izlaza, preko koga se može povezati neki izvršni element veće snage.

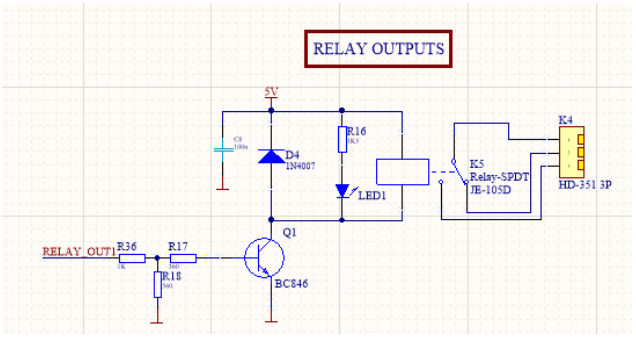

Sl. 10. Relejni izlaz

Na slici 11. se može videti 8-bitni, *RISC* mikrokontroler, Atmega32u4 sa malom potrošnjom struje, eksterni kristal od 16 MHz, ESD zaštita u vidu kola USBLC6 i USB type-C konektor.
Napajanje mikrokontrolera je od 2.7 V - 5.5 V.
Odlučili smo se za ovaj mikrokontroler jer je on odlična platforma za studente, hobiste i brzo prototipovanje zbog postojanja mnoštva *open-source* primera programa i kompatibilan je sa Arduino okruženjem. Još jedna prednost ovog mikrokontrolera jeste što se može programirati preko Usb priključka.

 ISBN 978-86-7466-930-3

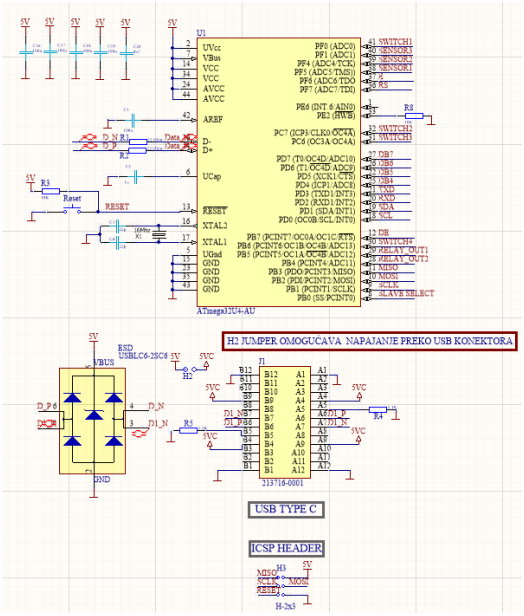


Sl. 11. Mikrokontroler

Slika 12. pokazuje alfanumerički displej 2x16 karaktera. Komunikacija mikrokontrolera sa displejom je omogućena u 4-bit modu, kako bi smanjili broj potrebnih pinova na mikrokontroleru.

Da bi prikazali karakter na displeju u 4-bit modu, potrebna su dva ciklusa, tj. prvo se šalju viša 4 bita a potom preostala niža 4 bita.

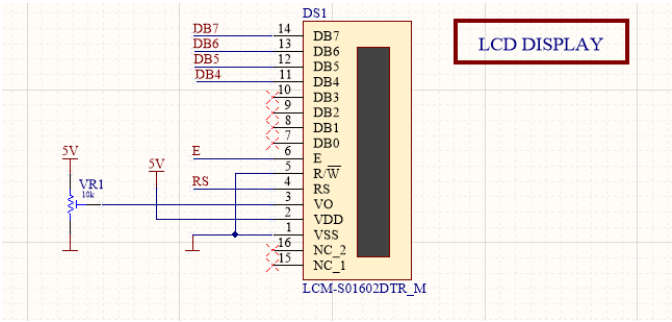


Sl. 12. Displej

Na slici 13. se može videti deo šeme za RS485 komunikaciju. Projekat je osmišljen tako da se merene vrednosti mogu prikazati na displeju na ploči, ali takođe da se razvojna ploča može povezati sa računarom i da se preko RS485 komunikacije pošalju podaci na SCADA sistem.

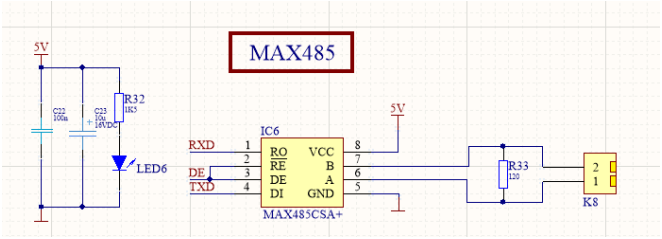


Sl. 13. RS485 komunikacija

Na sledećoj slici se može videti gotova razvojna ploča.

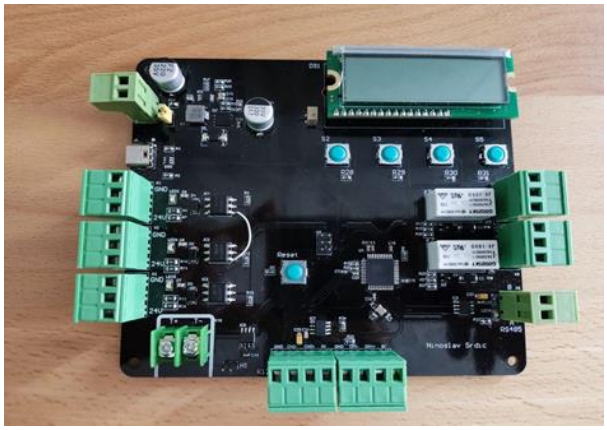

Sl. 14. Gotov sklop

U ovom projektu korištena je četvoroslojna štampa zbog boljih EMC karakteristika (“Elektromagnetna usaglašenost”). Svi električni uređaji utiču jedni na druge kada su ili međusobno povezani ili postavljeni u blizini. Zahtevi EMC-a su tako koncipirani da se ova sporedna dejstva svedu na minimum.

## IV. PRIMER VEŽBE

Cilj prve vežbe jeste da se napravi prosto *flip-flop* prekidačko kolo.

Na optički izolovane ulaze povezali smo dva induktivna senzora sa NPN tranzistorskim izlazom. U svrhe ove vežbe nisu nam neophodni galvanski odvojeni ulazi, pa ceo sklop napajamo preko USB priključka.

Program za razvojnu ploču je napisan u *Microchip Studio* okruženju tako da jedan induktivni senzor uključuje oba relejna izlaza, jedan u momentu detektovanja a drugi sa zakašnjenjem. Drugi induktivni senzor isključuje oba relejna izlaza, jedan u momentu detektovanja a drugi sa zakašnjenjem.

Vežba je namenjena za kontrolu elektromotora na trakastom transporteru.

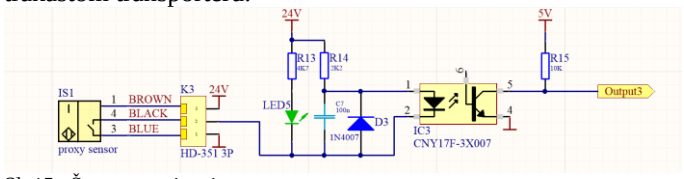


Sl. 15. Šema povezivanja senzora

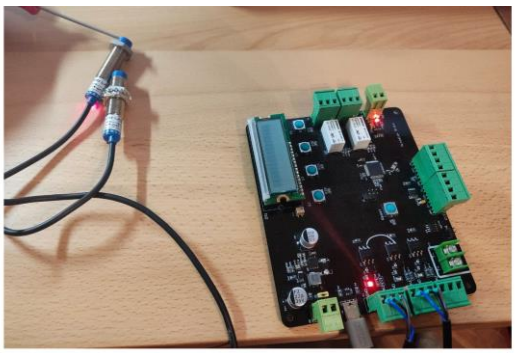

Sl. 16. Primer vežbe


ISBN 978-86-7466-930-3

## V. ZAKLJUČAK

Nakon sklapanja i testiranja uređaja došli smo do zaključka da je projekat opravdao očekivanja i da se uspešno može primeniti za razvoj različitih merno-regulacionih uređaja. U sledećoj iteraciji bi se mogao dodati drajver za koračni motor, DA konvertor, sat realnog vremena i da se na opto-izolovanom ulazu mogu dodati kratkospojnici za izbor senzora sa tranzistorskim NPN ili PNP izlazom.

Prednost ovakve razvojne ploče jeste jednostavnost priključivanja periferija i relativno jednostavno programiranje.

Mana ove ploče je što nema mogućnost daljeg proširenja periferija.

## Zahvalnica

Ovaj rad je podržan od strane Fakulteta tehnickih nauka u Novom Sadu, Departmana za energetiku, elektroniku i telekomunikacije, u okviru realizacije projekta MPNTR 200156 : "Inovativna naucna i umetnicka isptivanja iz domena delatnosti FTN-a".

## Literatura

[1] Carl Nelson & Jim Williams, "Boost Converter Operation",LT1070 Design Manual,
[2] EGProjects, “Lcd in 4 bit mode and 8 bit mode”
[3] Warwick A. Smith, “C programiranje za Arduino”, 2016.
[4] Paul Horwitz & Winfield Hill, “The Art of Electronics”, 2003.
[5] Fang Lin Luo & Hong Ye, “Advanced DC/DC Converters”, 2004.
[6] Ian R. Sunclair, “Sensors and Transducers”, 2001.

## ABSTRACT

This paper explains the design and making of a universal development board for measurements and regulation, based on the ATmega32u4 microcontroller. Block diagrams are also shown, as well as schematics of these block and even examples of how this board could be used in practice.

**Designing a universal development board for industrial sensors**

Ninoslav Srdić, Marjan Urekar, Dragan Pejić, Platon Sovilj

 ISBN 978-86-7466-930-3

# Merni sistem za detekciju padova zasnovan na akcelerometru, žiroskopu i GPS modulu

Sanja Mandić, Đorđe Novaković

***Apstrakt*—U ovom radu opisan je sistem za detekciju pada, sa ciljem pomoći starim i nemoćnim licima. Kroz rad je dat uvid u sve delove realizovanog sistema za detekciju pada. Sistem podrazumeva prikupljanje podataka o kretanju korisnika upotrebom akcelerometra i žiroskopa, prikupljanje podataka o lokaciji korisnika upotrebom GPS modula, klasifikaciju kretanja i detekciju pada, kao i prikaz informacija u okviru odgovarajućeg korisničkog interfejsa.**

***Ključne reči*— Detekcija pada; mikrokontroler; GPS; akcelerometar; žiroskop; mašinsko učenje; klasifikacija**

## I. Uvod

Padovi su česte pojave kod starijih osoba usled različitih faktora kao što su gubitak oslonca, nesvestica, moždani ili srčani udar, poremećaji čula vida, slabost u mišićima, demencija i deformacija kičmenog stuba. Starenje za posledicu ima i nesposobnost da se na iznenadne promene položaja tela reaguje pravovremeno i da se održi ravnoteža, što značajno povećava verovatnoću pada kod starijih osoba. Istraživanja su pokazala da jedna trećina populacije starije od 65 godina doživi pad jednom ili više puta u toku jedne godine. Padovi predstavljaju jedan od vodećih uzroka povreda, preloma, gubitka mobilnosti i smrtnih ishoda izazvanih nezgodama kod starijih osoba. Kako bi se izbegle teške povrede usled padova, pa i fatalni ishodi padova, pravovremeno pružanje medicinske pomoći povređenoj osobi je od izuzetnog značaja. Teške posledice koje padovi mogu da izazovu kod starijih osoba i potreba za trenutnim pružanjem pomoći osobama koje su pretrpele pad dovele su do velikog broja istraživanja u oblasti uređaja za detekciju pada i praćenja kretanja.

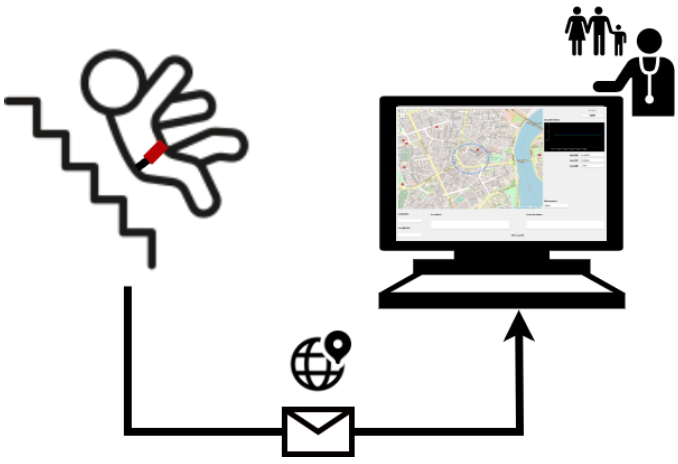

Slika 1. Ilustracija sistema za detekciju pada

Sanja Mandić – Fakultet tehničkih nauka, Univerzitet u Novom Sadu, Trg Dositeja Obradovića 6, 21000 Novi Sad, Srbija (e-mail: sanja.mandic@uns.ac.rs).

Đorđe Novaković – Fakultet tehničkih nauka, Univerzitet u Novom Sadu, Trg Dositeja Obradovića 6, 21000 Novi Sad, Srbija (e-mail: djordjenovakovic@uns.ac.rs).

Cilj ovog rada je izrada prototipa sistema za detekciju pada koji bi služio kao pomoć starijim licima, a ilustracija ovakvog sistema prikazana je na slici 1. Kretanje korisnika prati se pomoću akcelerometra i žiroskopa MPU-6050 senzorskog modula. Na osnovu veličina prikupljenih datim senzorima izdvaja se vektor obeležja koji se prosleđuje prethodno obučenom modelu klasifikatora. Model vrši klasifikaciju uzorka u jednu od pet klasa - pad unapred, pad u stranu, sedenje, stajanje ili hodanje. Ukoliko je kretanje okarakterisano kao pad unapred ili pad u stranu, putem korisničkog interfejsa se prikazuje lokacija korisnika na osnovu podataka prikupljenih GPS modulom. Senzorski moduli sistema integrisani su na STM32F4DISCOVERY razvojnoj ploči, koja sadrži STM32F407VGT mikrokontroler. Blok dijagram realizovanog sistema prikazan je na slici 2.

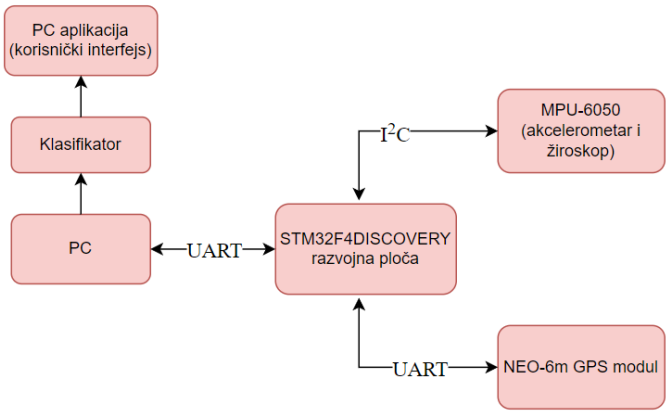


Slika 2. Blok dijagram sistema za detekciju pada

## II. Hardverske komponente sistema za detekciju pada

### A. STM32F4DISCOVERY razvojna ploča

STM32F4DISCOVERY razvojna ploča (slika 3) je proizvod kompanije *STMicroelectronics*, koja na sebi integriše 32-bitni STM32F407VGT mikrokontroler. STM32F4DISCOVERY ploča sadrži mikro USB (*Universal Serial Bus*) AB konektore, pomoću kojih se ostvaruje veza računara i date razvojne ploče. U sistemima koji podrazumevaju 32-bitne STM mikrokontrolere zastupljen je USB full-speed interfejs za komunikaciju sa računarom. Na ploči se nalazi ST-LINK/V2-A kolo za programiranje i debagovanje mikrokontrolera. ST-LINK/V2-A komunicira sa STM 32-bitnim mikrokontrolerom putem SWIM (*Single Wire Interface Module*) interfejsa, odnosno, putem JTAG ili SWD (*Serial Wire Debugging*) interfejsa. Ploču je moguće napajati na nekoliko različitih načina - putem ST-LINK veze, putem USB konektora ili putem eksternih izvora napajanja. Na ploči se nalazi osam indikatorskih LED (*Light Emitting Diode*) - za USB komunikaciju, za napajanje od 3,3 V, četiri korisničke LED (narandžasta, zelena, crvena i plava) i dve LED za USB OTG (*On The Go*) interfejs. Na razvojnoj ploči nalaze se reset taster, kao i korisnički taster. Dodatno, data razvojna ploča sadrži MEMS (*Micro Electronic*

 ISBN 978-86-7466-930-3

*Mechanical Systems*) omni-direkcioni digitalni mikrofon, audio DAC (*Digital to Analogue Converter*), konektor za slušalice, kao i MEMS digitalni akcelerometar [1]. STM32F4DISCOVERY razvojna ploča postavljena je na STM32F4 Discovery Shield, kompanije *MikroElektronika*, u cilju lakšeg povezivanja sa senzorskim modulima.

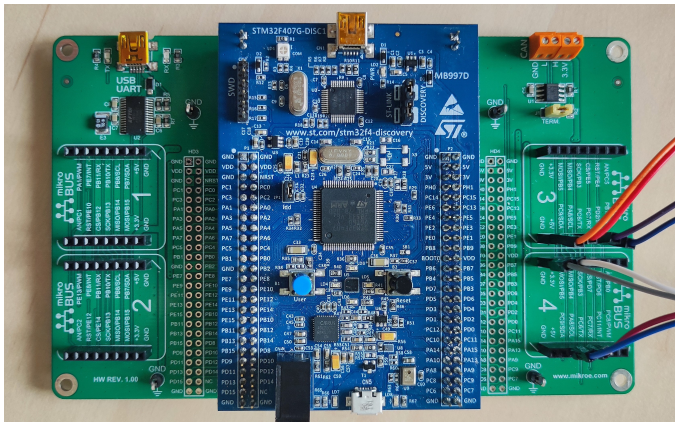

Slika 3. STM32F4DISCOVERY razvojna ploča na STM32F4 Discovery Shield-u

Mikrokontroler STM32F407VGT nalazi se u okviru STM32DISCOVERY razvojne ploče u LQFP100 pakovanju sa sto pinova, čiji je prikaz dat na slici 4. STM32F407VGT sadrži ARM 32-bit Cortex CPU (*Central Processing Unit*). Kapacitet FLASH memorije datog mikrokontrolera je 1 MB, dok je kapacitet SRAM (*Static Random-Access Memory*) memorije 192 kB. Napon napajanja mikrokontrolera je u ospegu od 1,8 V do 3,6 V. Interni oscilator STM32F407VGT mikrokontrolera obezbeđuje frekvenciju takta od 16 MHz, a osim internog oscilatora, mikrokontroleru je moguće dovesti i spoljašnji izvor takta frekvencije od 4 MHz do 26 MHz. Signal takta vodi se na PLL (*Phase Locked Loop*), čime je obezbeđeno povećanje frekvencije do 168 MHz. STM32F407VGT sadrži tri 12-bitna ADC (*Analog to Digital Converter*) i dva DAC. Dati mikrokontroler sadrži dvanaest 16-bitnih tajmera i dva 32-bitna tajmera. Mikrokontroler sadrži tri SPI (*Serial Peripheral Interface*), dva CAN (*Controller Area Network*) i tri $I^2C$ (*Inter-Integrated Circuit*) komunikaciona interfejsa, dok je broj USART (*Universal Synchronous/Asynchronous Receiver Transmitter*) modula mikrokontrolera šest [2].

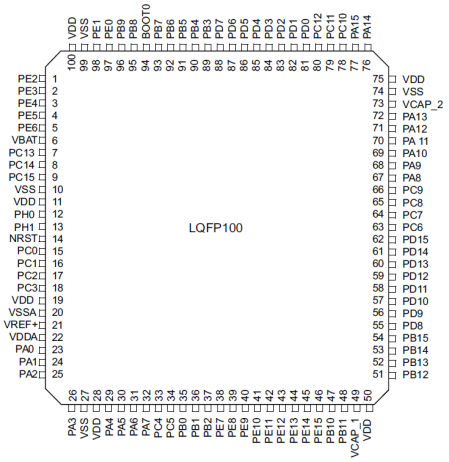


Slika 4. Pinovi STM32F407VGT mikrokontrolera

Odgovarajući firmver za STM32F407VGT mikrokontroler i čipove senzora napisan je u STM32CubeIDE razvojnom okruženju.

## B. NEO-6m GPS modul

NEO-6m predstavlja GPS modul koji omogućava primanje podataka sa GPS (*Global Positioning System*) satelita. Dati modul sadrži kristalni oscilator. NEO-6m modul sadrži UART, USB, DDC (*Display Data Channel*) i SPI komunikacione interfejse. NEO-6m čip predstavlja prijemnik sa 50 kanala. Podaci se prenose kao kodirane poruke, definisane određenim protokolima. Jedan od protokola koji je podržan na NEO-6m GPS modulu jeste NMEA ( *National Marine Electronics Association*) protokol. Svaka linija podataka koja se prenosi na ovaj način naziva se rečenicom, a sve sadrže specifične podatke o lokaciji. Neke od NMEA rečenica koje se mogu primiti putem NEO-6m prijemnika su GLL (Position Data), RMC (Recommended Minimum Sentence) i GGA (Global Positioning System Fix Data). U realizovanom sistemu za detekciju pada upotrebljene su GGA NMEA rečenice, koje sadrže podatke kao što su vreme, geografska širina, geografska dužina, broj satelita i nadmorska visina [3], [4].


Slika 5. NEO-6m GPS modul

Senzorski modul NEO-6m je povezan sa mikrokontrolerom STM32F407VGT posredstvom mikroBUS 3 socket-a STM32F4 Discovery Shield-a. Razmena podataka između NEO-6m i mikrokontrolera vrši se putem UART komunikacionog interfejsa, a brzina prenosa podataka je 9600 bps. Pin za prijem podataka (RX) NEO-6m povezan je na PC6 pin mikrokontrolera, koji odgovara predajnoj liniji njegovog USART 6 modula. Pin za slanje podataka (TX) NEO-6m povezan je na odgovarajući prijemni pin USART 6 modula mikrokontrolera, odnosno, na pin PC7. Na pločicu sa NEO-6m čipom dovodi se napajanje od 5 V, preko VCC pina, dok je GND pin povezan na GND pin mikroBUS 3 socket-a STM32F4 Discovery Shield-a.

## C. MPU-6050 senzor

MPU-6050 senzor na pločici GY-521 (slika 6) integriše MEMS akcelerometar sa tri ose, MEMS žiroskop sa tri ose i DMP (*Digital Motion Processor*). Ovaj senzor koristi $I^2C$ komunikaciju sa mikrokontrolerom razvojne ploče (pinovi SCL – clock i SDA – podaci). MPU-6050 čip sadrži tri 16-bitna ADC za podatke svake ose akcelerometra i tri 16-bitna ADC za podatke svake ose žiroskopa. Podaci sa senzora o sve tri ose, x, y i z, prikupljaju se istovremeno, a MPU-6050 sadrži adekvatne read-only registre u koje se smeštaju vrednosti sa senzora i kojima se pristupa putem serijskog interfejsa. Opseg pune skale za žiroskop može biti $\pm 250\ ^\circ/s$, $\pm 500\ ^\circ/s$, $\pm 1000\ ^\circ/s$ i $\pm 2000\ ^\circ/s$, dok su vrednosti za opseg pune skale akcelerometra ±2 g, ±4 g, ±8 g i ±16 g (g = 9,81 m/s2). Čip sadrži FIFO (*First In First Out*) bafer od 1024 bajta, koji služi za privremeno skladištenje


ISBN 978-86-7466-930-3

izlaznih podataka, a korisnik može da bira koje podatke će skladištiti u baferu. Dodatno, MPU-6050 čip sadrži oscilator, kao i temperaturni senzor [5].

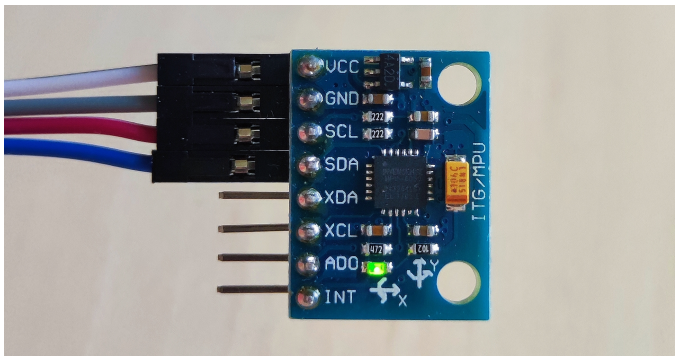


Slika 6. Senzor MPU-6050 na GY-521 pločici

Za datu primenu MPU-6050 je konfigurisan tako da je opseg pune skale akcelerometra ±8 g, opseg pune skale žiroskopa ±2000 $^\circ/s$, a frekvencija odabiranja je 1 kHz. Pinovi GY-521 pločice povezani su na pinove mikrokontrolera posredstvom STM32 Discovery Shield-a. Pinovi Vcc i GND GY-521 povezani su na 3,3 V i GND mikroBUS 4 socket-a STM32 Discovery Shield-a, dok su SDA i SCL pin sa GY-521 povezani na odgovarajuće pinove mikroBUS 4 socket-a za $I^2C$ komunikaciju, koji odgovaraju pinovima PC9 i PA8 mikrokontrolera, redom.

## III. Softver sistema za detekciju pada

Kako bi bila omogućena razmena podataka i obaveštenje odgovornog lica o padu korisnika uređaja kreiran je grafički korisnički interfejs upotrebom Python programskog jezika. Na slici 7 prikazan je izgled aplikacije po pokretanju programa. U okviru kreiranog korisničkog interfejsa, u gornjem desnom uglu omogućen je prikaz signala sa akcelerometra, po x, y i z osi, kao i ispis trenutnih vrednosti ubrzanja za sve tri ose (polja AccelX, AccelY i AccelZ). Takođe, omogućen je prikaz mape, na kojoj se prikazuje lokacija korisnika uređaja. U polja označena sa Latitude, Longitude i Location ispisuju se podaci o geografskoj širini, geografskoj dužini i lokaciji korisnika uređaja, ukoliko dođe do pada. Korisničkim interfejsom omogućen je unos lokacije odgovornog lica i prikaz najkraće putanje do lokacije na kojoj se nalazi osoba koja je pala. U dodatnom polju, označenom kao Movement, prikazuje se jedna od pet mogućih radnji (stajanje, sedenje, hodanje, pad unapred, pad u stranu), određena na osnovu signala sa akcelerometra i žiroskopa.

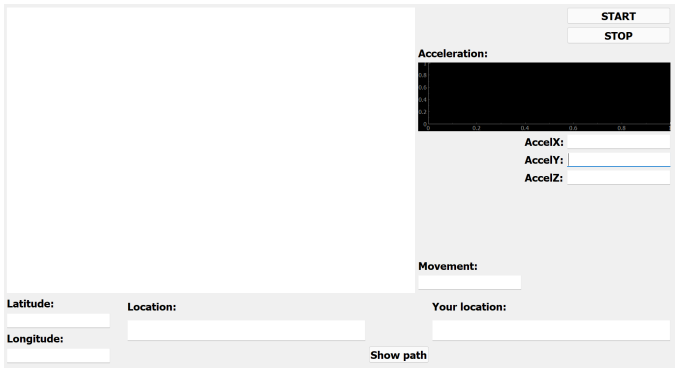


Slika 7. Izgled aplikacije po pokretanju

Na slici 8 prikazan je tok izvršavanja programa koji obuhvata inicijalizaciju hardverskih komponenti, slanje podataka sa mikrokontrolera, prijem, obradu i prikaz podataka na računaru, kao i klasifikaciju kretanja. Inicijalizacija sistema podrazumeva konfiguraciju odgovarajućih modula mikrokontrolera, kao i senzorskih modula. Nakon inicijalizacije svih celina neophodnih za rad sistema vrši se simultano očitavanje podataka sa akcelerometra MPU-6050, žiroskopa MPU-6050 i NEO-6m GPS modula. Kako bi se formirala odgovarajuća poruka koja se šalje na računar vrši se obrada podataka sa senzora. Obrada podataka podrazumeva konverziju sirovih vrednosti sa akcelerometra i žiroskopa u vrednosti izražene u vidu umnožaka ubrzanja Zemljine teže g - akcelerometar, i $^\circ/s$ - žiroskop. Takođe, proces obrade podataka podrazumeva parsiranje NMEA GGA rečenica, koje se prikupljaju sa GPS modula, i izdvajanja podataka od interesa iz njih. U sistemu za detekciju pada od interesa su elementi GGA rečenice koji daju podatke o geografskoj širini i dužini, kao i o odgovarajućim hemisferama. Obrađeni podaci šalju se na računar putem UART komunikacionog modula u vidu poruka sledećeg formata: <ax|ay|az|gx|gy|gz|geografska širina|hemisfera|geografska dužina|hemisfera|>.

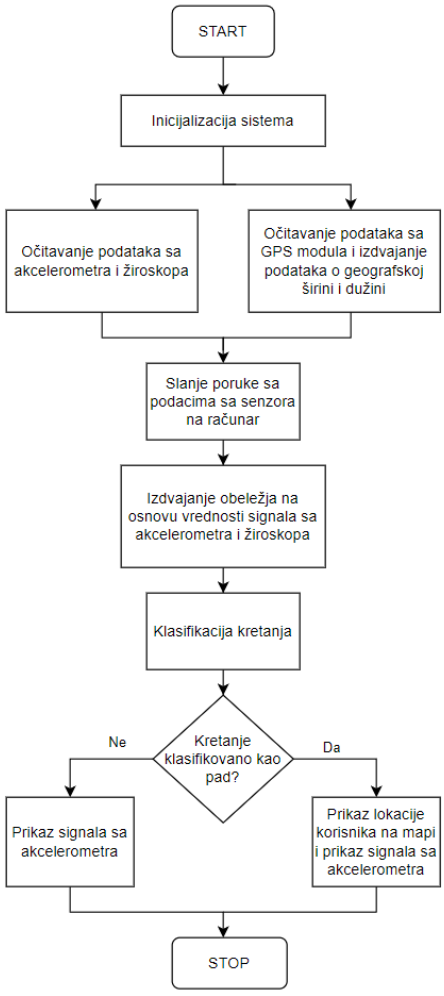


Slika 8. Algoritam izvršavanja programa za detekciju pada

Pritiskom na taster START u aplikaciji, vrši se konfiguracija serijskog porta, započinje komunikacija računara i mikrokontrolera i iscrtava se mapa sa referentnom lokacijom. Podaci o ubrzanju po x, y i z osi se izdvajaju iz pristigle poruke i iscrtavaju na odgovarajućem grafiku u aplikaciji (slika 9).

 ISBN 978-86-7466-930-3

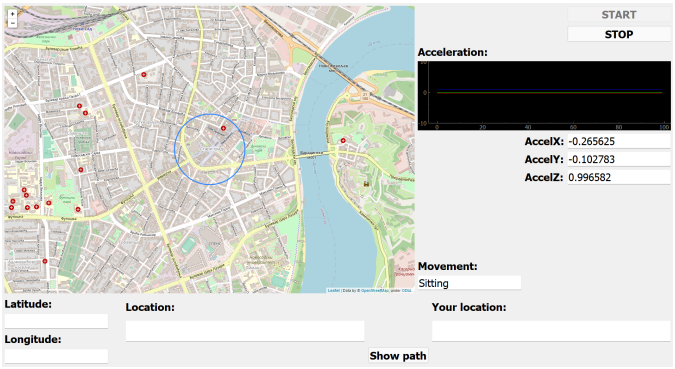


Slika 9. Prikaz referentne lokacije i signala sa akcelerometra

Dati podaci o ubrzanju, kao i podaci o orijentaciji koji pristižu na računar smeštaju se u odgovarajuće bafere, a kada pristigne 2000 odbiraka vrši se izdvajanje obeležja i formira se vektor obeležja koji opisuje jedan uzorak. Vektor obeležja prosleđuje se prethodno obučenom modelu mašinskog učenja i vrši se klasifikacija uzorka. Uzorak, koji karakteriše kretanje korisnika, može biti klasifikovan kao hodanje, stajanje, sedenje, pad u stranu ili pad unapred. Ukoliko je uzorak svrstan u klasu koja odgovara padu u stranu ili padu unapred, detektovan je pad i potrebno je obavestiti korisnika aplikacije o datom događaju. U tom trenutku se na mapi prikazuje trenutna lokacija na kojoj se nalazi korisnik uređaja za detekciju pada (slika 10).

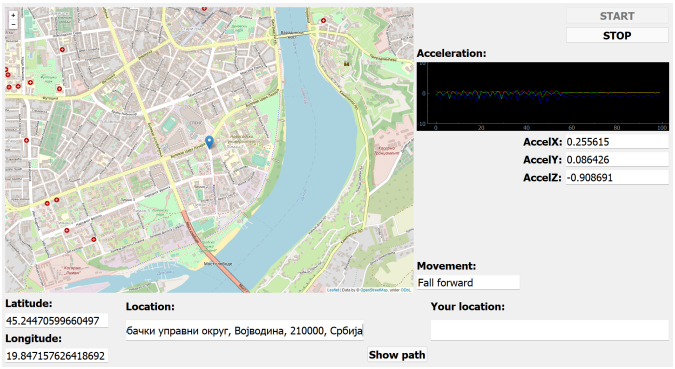


Slika 10. Detekcija pada i prikaz trenutne lokacije korisnika uređaja

Unosom lokacije odgovornog lica u polje Your location i pritiskom na taster Show Path, na mapi se pored lokacije osobе koja je pala prikazuje i lokacija korisnika aplikacije, kao i optimalna putanja između te dve tačke, što je prikazano na slici 11.

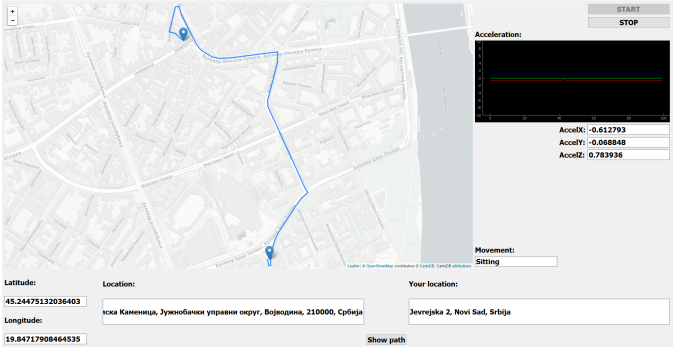


Slika 11. Prikaz najkraće putanje od odgovornog lica, koje je primilo obaveštenje, do osobe koja je pretrpela pad

## IV. Klasifikacija kretanja

### A. Baza podataka

Bazu podataka čini 332 uzorka, a svaki uzorak opisan je pomoću 20 obeležja. Uzorak predstavlja prozor dužine 100 odbiraka. Dakle, kroz signale koji su prikupljeni sa akcelerometra i žiroskopa, prolazi se prozorom dužine 100 odbiraka, tako da je preklapanje dva susedna prozora 50 %. Za jedan prozor računaju se srednja, maksimalna i minimalna vrednost za signale sa akcelerometra po x, y i z osi, srednja, maksimalna i minimalna vrednost za signale sa žiroskopa po x, y i z osi, kao i roll i pitch uglovi. Navedene veličine predstavljaju obeležja u bazi podataka. Sva obeležja su numerička i nema nedostajućih vrednosti u bazi. Svaki uzorak potrebno je dodeliti jednoj od pet klasa - stajanje (ST - *Standing*), sedenje (SIT - *Sitting*), hodanje (WA - *Walking*), pad unapred (FF - *Fall Forward*) ili pad u stranu (FL - *Lateral Fall*). U datoj bazi podataka 6,41 % uzoraka je iz klase FF, 6,41 % uzoraka je iz klase FL, a uzorci iz klasa SIT, ST i WA su podjednako zastupljeni, sa udelom od 29,06 %, za svaku od navedene tri klase. U cilju obuke i testiranja modela mašinskog učenja oznake klasa pretvorene su u numeričke vrednosti dodelom brojeva 0, 1, 2, 3 i 4 klasama FF, FL, SIT, ST i WA, redom.

### B. Obuka modela i rezultati

Kako bi bio kreiran optimalan model za klasifikaciju kretanja čoveka na osnovu date baze podataka, poređena su tri algoritma mašinskog učenja - metoda k najbližih suseda (kNN - *k Nearest Neighbors*), stabla odluke i mašine na bazi vektora nosača. Pre same obuke i evaluacije pojedinačnih modela, baza podataka je podeljena na dva skupa - trening skup i test skup. Trening skup čini 80 % ukupnih podataka, dok preostalih 20 % početne baze podataka čini test skup. Uzorci su podeljeni u dva navedena skupa tako da je za svaki od njih održana zastupljenost pojedinačnih klasa kao u početnom skupu. U okviru preobrade podataka izvršena je Z-normalizacija (standardizacija) obeležja, tako da sva obeležja imaju srednju vrednost 0 i standardnu devijaciju 1. Na ovaj način sva obeležja su skalirana na isti opseg vrednosti i time je sprečeno odlučivanje na osnovu onih obeležja koja variraju u većem opsegu vrednosti. Nakon preobrade podataka, kako bi optimalni modeli bili formirani, izvršena je unakrsna validacija sa deset podskupova na skupu za obuku i na taj način utvrđeni su optimalni parametri pojedinačnih modela. Za tako odabrane parametre izvršena je unakrsna validacija sa deset podskupova na skupu za obuku. Matrice konfuzije dobijene su akumulaciom matrica konfuzije svih deset iteracija. Kako bi se procenile performanse klasifikatora potrebno je uporediti predviđene i stvarne klasne oznake. Uzorci u bazi podataka klasifikovani su u pet klasa, te se kao mere uspešnosti klasifikatora analiziraju prosečna tačnost (prosek tačnosti po klasama), mikroprosečna osetljivost, preciznost i F-mera, kao i makroprosečna osetljivost, preciznost i F-mera. Završni korak u kreiranju klasifikatora jeste evaluacija modela na test skupu. Tabelom I dat je prikaz pojedinačnih mera uspešnosti za tri obučena klasifikatora.

Kao najuspešniji algoritam pri rešavanju datog problema pokazala se metoda k najbližih suseda. Tačnost od 88 % ostvarena je za deset najbližih suseda čija rastojanja se računaju na osnovu Manhattan metrike. Ukoliko se posmatra matrica konfuzije C (1) dobijena nakon testiranja kNN klasifikatora na test skupu, moguće je uočiti da klasifikator uspešno prepoznaje sve uzorke iz klase WA, da od 19 uzoraka iz klase SIT 17 uzoraka dodeljuje upravo toj klasi, dok dva uzorka pogrešno klasifikuje kao ST. Dati model pogrešno klasifikuje 4 uzorka iz klase ST, kao SIT, dakle, postoje poteškoće pri razlikovanju pokreta stajanja i sedenja. Klasa sa najvećom tačnošću je klasa FL, gde je lateralni pad za svih pet uzoraka klasifikovan ispravno, dok

 ISBN 978-86-7466-930-3

su uzorci iz klase FF greškom dodeljeni klasi WA (jedan uzorak) i klasi FL (jedan uzorak).

$$C = \begin{bmatrix} 19 & 0 & 0 & 0 & 0 \\ 0 & 17 & 2 & 0 & 0 \\ 0 & 4 & 15 & 0 & 0 \\ 1 & 0 & 0 & 3 & 1 \\ 0 & 0 & 0 & 0 & 5 \end{bmatrix} \quad (1)$$

TABELA I
MERE USPEŠNOSTI KLASIFIKATORA

| | kNN | Stablo odluke | SVM |
|---|---|---|---|
| Tačnost | 0.88 | 0.31 | 0.37 |
| Preciznost (mikro) | 0.88 | 0.31 | 0.37 |
| Preciznost (makro) | 0.89 | 0.21 | 0.19 |
| Osetljivost (mikro) | 0.88 | 0.31 | 0.37 |
| Osetljivost (makro) | 0.85 | 0.43 | 0.44 |
| F mera (mikro) | 0.88 | 0.31 | 0.37 |
| F mera (makro) | 0.86 | 0.28 | 0.26 |

## V. ZAKLJUČAK

Usled pada, kod starijih osoba može doći do različitih povreda kao što su povrede ili prelomi ruke, ručnog zgloba, karlice, kuka, glave, unutrašnje povrede, poremećaj i gubitak mobilnosti. Ove povrede značajno mogu smanjiti kvalitet života povređene osobe. Sistem za detekciju pada mogao bi da doprinese pravovremenom pružanju pomoći starim licima, a time i prevenciji komplikacija nastalih usled povreda prilikom pada. Dalja istraživanja podrazumevaju proširenje baze podataka i poboljšanje performansi klasifikatora, kao i vršenje klasifikacije na nivou mikrokontrolera. Takođe, sve hardverske komponente sistema neophodno je integrisati u okviru jednog prenosivog uređaja koji bi korisnik mogao da nosi na kaišu ili ruci.

## ZAHVALNICA

Ovaj rad je podržan od strane Fakulteta tehničkih nauka u Novom Sadu, Departmana za energetiku, elektroniku i telekomunikacije, u okviru realizacije projekta MPNTR 200156 : ”Inovativna naučna i umetnička isptivanja iz domena delatnosti FTN-a”.

## LITERATURA

[1] STMicroelectronics (2011). STM32F4DISCOVERY Data brief, Discovery kit with STM32F407VG MCU. Preuzeto 28. marta 2022., sa https://www.st.com/en/evaluation-tools/stm32f4discovery.html
[2] STMicroelectronics (2011.). STM32F405xx STM32F407xx data sheet. Preuzeto 28. marta 2022., sa https://www.st.com/en/microcontrollers-microprocessors/stm32f407vg.html#overview
[3] U-blox (2013). U-blox 6 Receiver Description. Preuzeto 30. marta 2022., sa https://content.u-blox.com/sites/default/files/products/documents/u-blox6_ReceiverDescrProtSpec_%28GPS.G6-SW-10018%29_Public.pdf
[4] U-blox (2011.). NEO-6 u-blox 6 GPS Modules data sheet. Preuzeto 30. marta 2022., sa https://content.u-blox.com/sites/default/files/products/documents/NEO-6_DataSheet_%28GPS.G6-HW-09005%29.pdf
[5] InvenSens Inc. (2012). MPU-6000 and MPU-6050 Product Specification. Preuzeto 23. marta 2022., sa http://www.haoyuelectronics.com/Attachment/GY-521/mpu6050.pdf

## ABSTRACT

In this paper, a fall detection system, whose main purpose is assistance to the elderly, is described. The paper gives an insight into all parts of the implemented fall detection system. Measurement system for fall detection includes the acquisition of user movement data using an accelerometer and a gyroscope, acquisition of location data using GPS module, classification of movements, and fall detection, as well as displaying this data within the user interface.

**Measurement system for fall detection based on accelerometer, gyroscope, and GPS module**

Sanja Mandić, Đorđe Novaković

 ISBN 978-86-7466-930-3

# Merenje karakteristika i modelovanje Hamonovoh etalon otpornika u naizmeničnom režimu

Stefan Mirković, Dragan Pejić, Aleksandar Dimitrijević

***Apstrakt*—Razmatranje primene Hamonovih etalon otpornika u naizmeničnom režimu, kao i ispitivanje njihovih karakteristika su tema ovog rada. U ranijim istraživanjima ustanovljeno je da prenosni odnos ovih etalona ne bi trebao da značajno zavisi od frekvencije. Drugim rečima, moduo transfera se očekuje da će biti blizak kvadratu broja otpornika od kojih se formira transfer, dok će fazni stav transfera biti blizak nuli. Sa dostupnom opremom koja je bila raspoloživa kada je vršeno istraživanje, merenja su obavljena na osnovu dve merne metode, čiji će rezultati biti prikazani u radu.**

***Ključne reči*—Hamonov etalon, transfer, električna otpornost.**

## I. Uvod

Kao jedan veoma koristan alat kod određivanja odnosa napona, a pogotovo otpornosti su Hamonovi etalon otpornici. Ovi etaloni se sastoje od $n$ redno vezanih otpornika iste nazivne vrednosti, gde je povezivanje obavljeno četvorožično tako da je omogućen direktan pristup bilo kojem naponskom i strujnom izvodu svakog otpornika pomoću ugrađenih terminala. Otpornost terminala ovih spojeva uračunata je u otpornost pojedinačih otpornika. Pojedinačnim merenjem i podešavanjem otpornosti svakog otpornika teži se da se postigne visoka tačnost. Prvenstvena uloga Hamonovih otpornika nije da budu etaloni otpornosti, već etaloni prenosnog odnosa otpornosti (transfer). Prespajanjem serijske u paralelnu vezu postiže se smanjenje otpornosti za približno $n^2$ puta. Četvorožični spoj se koristi kako bi se potisnuli negativni efekti otpornosti spojeva u cilju povećanja tačnosti Hamonovog etalona. Zahvaljujući dobrim karakteristikama, treba razmisliti o njihovoj primeni u ac režimu sa obzirom na ohrabrujuće rezultate nekih istraživanja [1]. Ovde je osnova tvrdnje da ako se svaki pojedinačni otpornik Hamonovog etalona modeluje kao redna veza otpornosti i reaktanse, moduo transfera će biti blizak broju $n^2$. Prvo su ove tvrdnje simulaciono proverene, a zatim su izvršena i merenja čiji su rezultati doveli do zaključka da ove tvrdnje imaju smisla. U cilju ispitivanja frekventnih karakteristika Hamovnog etalona, kao i provere da li je modelovanje pojedinačnih otpornika kao redne veze otpornosti i reaktanse dovoljno dobro, izvršena su merenja i proračuni.

Stefan Mirković – Fakultet tehničkih nauka, Univerzitet u Novom Sadu, Trg D. Obradovića 6, Novi Sad, Srbija (e-mail: mirkovicst@uns.ac.rs).

Dragan Pejić – Fakultet tehničkih nauka, Univerzitet u Novom Sadu, Trg D. Obradovića 6, Novi Sad, Srbija (e-mail: pejicdra@uns.ac.rs).

Aleksandar Dimitrijević – Elektrotehnički institut "Nikola Tesla" a.d. Beograd, Srbija (e-mail: adimitrijevic22@gmail.com).

## II. Eksperimentalna merenja

Merenja su vršena u cilju prvenstveno procene modula transfera. Prva merna metoda se zasnivala na UI metodi, dok je druga metoda bila bazirana na direktnom merenju pomoću instrumenta namenjenog za ispitivanje impedansi. Za prvu metodu korištena je sledeća oprema: izvor stabilisanog napona (Time Electronics 5025), ac voltmetar (Fluke 8846A), ac ampermetar (Fluke 8846A), kao i transfer etalon SR1010 sa deset otpornika (sa transferom 10 kΩ : 100 Ω). Otpornost voltmetra i ampermetra su poznate i njihov uticaj na rezultat merenja je korigovan. Kapacitivnost voltmetra je deklarisana kao manja od 100 pF, ali nije poznata njena vrednost. Kako bi uticaj kapacitivnosti voltmetra bio minimalan, korišćene su različite varijante UI metode za merenje serijske i paralelne impedanse. Kod određivanja modula serijske impedanse korišten je strujni spoj, gde je ampermetar povezan redno sa etalonom, a voltmetar paralelno toj vezi. U slučaju paralelne impedanse korišten je naponski spoj kod koga je voltmetar povezan paralelno sa etalonom, a ampermetar redno toj vezi.

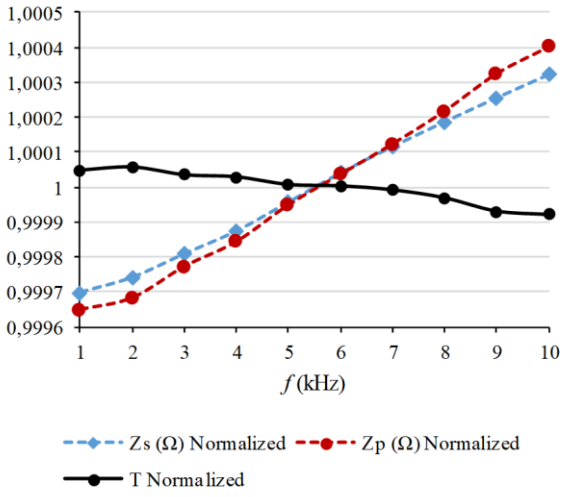


Sl. 1. Zavisnost normalizovanih vrednosti modula impedanse redne i paralelne veze i transfera T (UI metoda)

Kako su Hamonovi otpornici izvedeni četvorožično, logično se nameće korišćenje naponskog spoja. Problem je nepoznavanje stvarne kapacitivnosti voltmetra, pri čemu se pokazuje da to više smeta ako bi se koristio naponski spoj prilikom merenja na serijskoj konfiguraciji. Tada bi se, nazivnoj otpornosti od 10 kΩ, paralelno vezivao voltmetar

 ISBN 978-86-7466-930-3

deklarisane ulazne otpornosti 1 MΩ ± 1 % i nepoznata kapacitivnost. Ova činjenica je prevagnula ka korišćenjem strujnog spoja pri merenju modula impedanse serijske konfiguracije. U tom slučaju se gube pozitivni efekti četvorožične izvedbe Hamonovih otpornika, ali se rešava problem nepoznavanja kapacitivnosti voltmetra. Moduo impedanse paralelne konfiguracije je meren primenom naponskog spoja uz korišćenje četvoržične izvedbe otpornika. Pri promeni frekvencije od 1 kHz do 10 kHz, očitavani su napon i struja, određivan je moduo impedanse uz korigovanje uticaja otpornosti instrumenata. Na Sl. 1. su prikazane normalizovane vrednosti rezultata merenja modula impedanse serijske i paralelne veze Hamonovih otpornika, kao i vrednost modula transfera. Postupak normalizacije je sproveden kako bi se pregledno, na jednom grafiku dao prikaz rezultata eksperimenta koji se razlikuju po vrednosti (serijska otpornost je približno 10 kΩ, redna otpornost je približno 100 Ω, moduo transfera je bezdimenziona veličina približno jednaka 100). Sa grafika se vidi da moduo serijske i paralelne veze Hamonovih otpornika raste sa frekvencijom, što opravdava pretpostavku o postojanju reaktivne komponente. Rezultati simulacija predviđaju da su ove dve zavisnosti približno iste, što rezultira pretpostavkom da transfer ne zavisi od frekvencije. S druge strane, merenjem dobijeni profil zavisnosti modula redne i modula paralelne veze nije potpuno isti, pa je dobijeno da i moduo transfera (količnik modula serijske i paralelne veze) takođe zavisi od frekvencije. Promena transfera usled frekvencije je primetno manja (oko pet puta), u poređenju sa promenom modula serijske i paralelne veze. U Tabeli I prikazani su rezultati merenja UI metodom.

TABELA I
REZULTATI UI METODE

| $f$ (kHz) | T | u(T) ($k$=1) |
|---|---|---|
| 1 | 99.995 | 0.14 |
| 2 | 99.996 | 0.14 |
| 3 | 99.994 | 0.14 |
| 4 | 99.993 | 0.14 |
| 5 | 99.991 | 0.14 |
| 6 | 99.990 | 0.39 |
| 7 | 99.989 | 0.39 |
| 8 | 99.987 | 0.39 |
| 9 | 99.983 | 0.39 |
| 10 | 99.982 | 0.39 |

Postavlja se pitanje u kojoj meri nesavršenosti korištene opreme utiču na zavisnost modula transfera od frekvencije. Da bismo odgovorili na ovo pitanje, sproveden je postupak određivanja merne nesigurnosti. U obzir je uzeta merna nesigurnost usled deklarisanih grešaka korišćenog voltmetra i ampermetra, kao merna nesigurnost usled nepoznavanja prave vrednosti otpornosti voltmetra. U tabeli su date vrednosti modula transfera i procenjene merne nesigurnosti pri faktoru obuhvata 1.

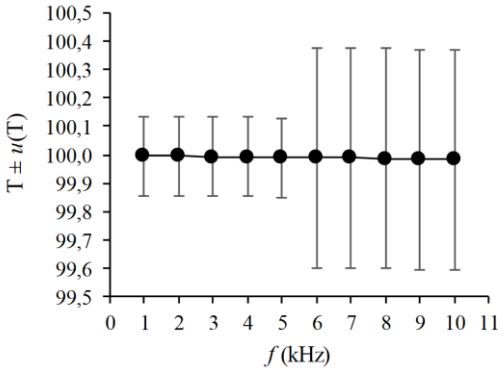


Sl. 2. Zavisnost modula transfera od frekvencije uz prikaz merne nesigurnosti za faktor obuhvata 1 (UI metoda)

Druga merna metoda je bazirana na određivanju impedanse serijski ($Z_S$) i paralelno ($Z_P$) konfigurisanog etalona, kao i faznih stavova ($\varphi_s$ i $\varphi_p$) direktnim očitavanjem korištenjem instrumenta HIOKI IM3590, čija je glavna uloga analizator impedansi.

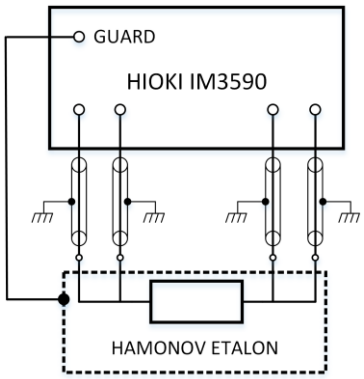


Sl. 3. Šema povezivanja pri merenju direktnom mernom metodom

Na početku je izvršena korekcija prilikom kratkog spoja i korekcija prilikom otvorene veze. Na ovaj način bi trebalo u najvećoj meri da su eliminisane parazitne induktivnosti i kapacitivnosti samih vodova korišćenih za četvorožično povezivanje merene imepdanse.

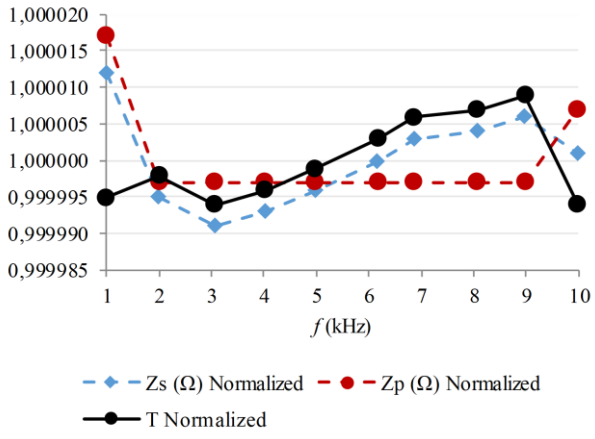


Sl. 4. Zavisnost normalizovanih vrednosti modula impedanse redne i paralelne veze i transfera (direktna metoda)


ISBN 978-86-7466-930-3

TABELA II
REZULTATI DIREKTNE METODE (MODUO TRANSFERA)

| *f* (kHz) | T | u(T) (*k*=1) |
|---|---|---|
| 1,0000 | 99,989 | 0.33 |
| 2,0052 | 99,989 | 0.33 |
| 2,9165 | 99,989 | 0.33 |
| 4,0208 | 99,989 | 0.33 |
| 4,9806 | 99,989 | 0.33 |
| 5,8480 | 99,990 | 0.33 |
| 6,8665 | 99,990 | 0.33 |
| 8,0624 | 99,990 | 0.33 |
| 8,9733 | 99,990 | 0.33 |
| 9,9871 | 99,989 | 0.33 |

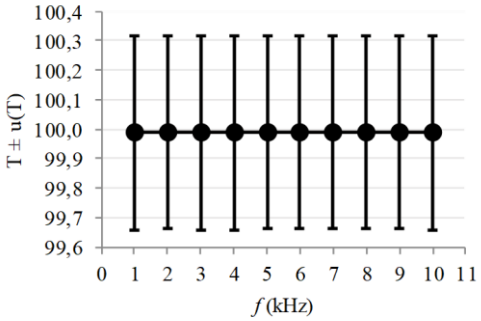


Sl. 5. Zavisnost modula transfera od frekvencije uz prikaz merne nesigurnosti za faktor obuhvata 1 (direktna metoda)

Ovde je očitavana vrednost izmerenog modula i faznog stava etalona za različite frekvencije. Na osnovu ovih rezutata može se videti da je relativna promena modula i faznog stava etalona pri različitim frekvencijama značajno manja od deklarisane greške instrumenata.

TABELA III
REZULTATI DIREKTNE METODE (ARGUMENT TRANSFERA)

| *f* (kHz) | φ | u(φ) (*k*=1) |
|---|---|---|
| 1,0000 | 0.038 | 0.26 |
| 2,0052 | 0.077 | 0.26 |
| 2,9165 | 0.117 | 0.26 |
| 4,0208 | 0.154 | 0.26 |
| 4,9806 | 0.191 | 0.26 |
| 5,8480 | 0.236 | 0.26 |
| 6,8665 | 0.263 | 0.26 |
| 8,0624 | 0.309 | 0.26 |
| 8,9733 | 0.343 | 0.26 |
| 9,9871 | 0.383 | 0.26 |

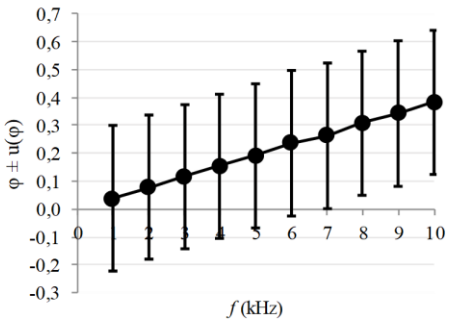


Sl. 6. Zavisnost argumenta transfera od frekvencije uz prikaz merne nesigurnosti za faktor obuhvata 1 (direktna metoda)

Kao posledica toga, ne može se zaključiti sa velikom sigurnošću kako se zaista ponaša moduo i fazni stav.

Kako bi se simulaciono analizirao uticaj parazitnih induktivnosti i kapacitivnosti na transfer, realizovana je LTSpice simulacija, gde je svaka pojedinačna impedansa Hamonovog etalona modelovana kao otpornost nazivne vrednosti 1 kΩ kojoj je redno vezana parazitna induktivnost $L_{Par}$ a svemu tome paraleleno vezana parazitna kapacitivnost $C_S$. Sada pretpostavljamo da su sve vrednosti jednake kako bismo mogli proveriti/proceniti uticaj dodatnih parazitnih efekata na transfer. Ako se variraju vrednosti parazitnih induktivnosti i kapacitivnosti dobija se da je transfer nepromenljiv po frekvenciji, dok je faza transfera vrlo mala.

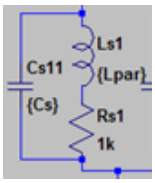


Sl. 7. Model pojedinačne impedanse Hamonog etalona u LTSpice simulaciji

Pored ovih parazitnih efekata, dodate su i kapacitivnosti svakog kontakta Hamonog etalona prema kućištu vrednosti $C_{Par}$. Kod paralelne konfiguracije, uticaj parazitnih kapacitivnosti ka kućištu utiče na jednostavniji način na sam transfer nego u slučaju serijske veze.

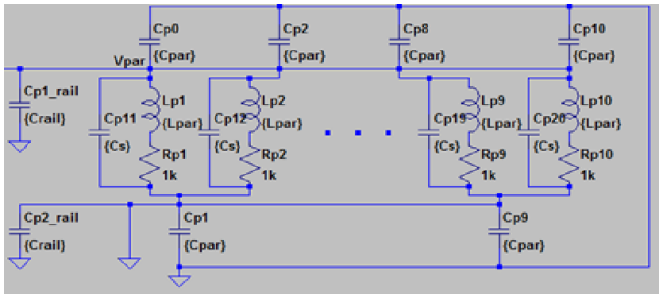


Sl. 8. Modelovan paralelno vezan Hamonov etalon u LTSpice okruženju

Kod paralelne veze, ove kapacitivnosti se usled kratkospojnika vezuju paralelno, ali podeljene u dve grupe (za jednu i drugu stranu priključaka). Kapacitivnosti jedne od ove dve grupe su ustvari kratkospojeni, jer je jedan kratkospojnik vezan na uzemljenje isto kao i kućište. Kod serijske konfiguracije pojedinačne impedanse i kapacitivnosti kao kućištu čine višestepeni filter, gde je logično da će se pri ovoj konfiguraciji dobiti veći fazni pomeraj. Dodatno je modelovano i da kratkospojnici imaju neku svoju kapacitivnost prema kućištu. Ovde se takođe dobija da je jedna kapacitivnost kratkospojena jer je samo kratkospojnik uzemljen, pa prema kućištu koje je takođe uzemljeno nema naponske razlike. Primećeno je da kapacitivnost kratkospojnika i pri značajnim vrednostima ne utiče značajano na transfer.

 ISBN 978-86-7466-930-3

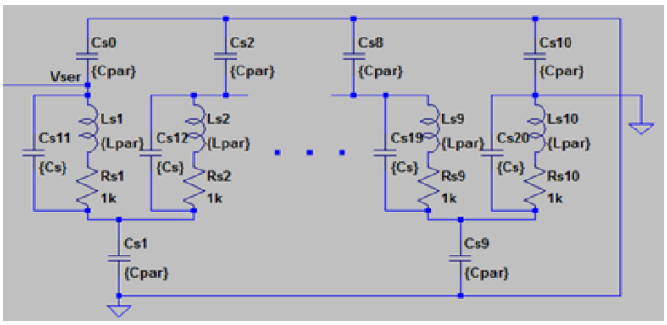


Sl. 8. Modelovan serijski vezan Hamonov etalon u LTSpice okruženju

Ako se pretpostave redna induktivnost i paralelna kapacitivnost za svaki element u Hamonovoj kutiji, i da su im vrednosti za svaki element jednake, dobija se da transfer ne zavisi od frekvencije. Ako se pretpostavi parazitna kapacitivnost kontakata Hamonovih elemenata prema kućištu onda se dobija da moduo i fazni stav transfera zavise od frekvencije. Rezultati simulacija pokazuju šta od parazitnih elemenata utiče i u kojoj meri.

## III. ZAKLJUČAK

Ono što se za sad može videti je da rezultati nisu opovrgnuli dosadašnje pretpostavke za ponašanje modula i faznog stava, ali ih i ne potvrđuju sa velikom sigurnošću. Rezultati sa kojima se trenutno raspolaže su dobijeni korištenjem najbolje raspoložive merne opreme. Pored ovog nedostatka usled velike greške instrumenata, postavlja se pitanje da li je model kada se etalon posmatra kao impedansa ispravan. Pored induktivnih i kapacitivnih efekata koji se javljaju na samim pojedinačnim otpornicima unutar etalona, postoje i drugi efekti. Kapacitivnost prema kućištu etalona, kapacitivnost kratkospojnika kojima se etalon konfiguriše iz serijsku u paralelnu vezu, kao i ulazna kapacitivnost instrumenata su samo jedna od stvari o kojima treba razmišljati. Različitim pristupima ovom problemu dobijeni su već neke procenjene vrednosti spomenutih parazitnih efekata, koje treba još detaljno ispitati. Procena je vršena pomoću raznih simulacijskih metoda i matematičkih modela. Ukoliko se ispostavi da ovi efekti značajno doprinose grešci etalona, moraće se trenutni modela komplikovati dok se ne dođe do zadovoljavajućih rezultata. Osnovni problem je nazivna greška instrumenata. Kako je Hamonov etalon etalon visoke tačnosti, potrebno je koristiti isto tako i instrumente visoke tačnosti kako bi se moglo sa velikom pouzdanošću proceniti njegovo ponašanje u zavisnosti od frekvencije. U prethodnim istraživanjima primenjena je Monte Carlo simulacija u cilju procene modula i faznog stava tansfera, ali pri jednostavnijem modelu nego što je ovde opisan. Tamo je pojedinačni otpornik posmatran kao redna veza otpornosti i reaktanse. Hipoteza da se moduo i fazni stav transfera neznatno menjaju sa promenom frekvencije nije potvrđena, ali isto tako nije ni opovrgnuta. Potrebna je merna oprema sa manjom mernom nesigurnošću. Jedan način rada jeste merenje na višim frekvencijama gde uticaj parazitnih efekata više dolazi do izražaja. Problem je što je i oprema kojom raspolažemo takva da sa porastom frekvencije dolazi do degradacije granica greške.

## LITERATURA

[1] S. Mirković, D. Pejić, M. Subotin, N. Gazivoda, Z. Gotovac, "Mogućnost primene Hamonovih presloživih otpornika u naizmeničnom režimu," ETRAN - Konferencija za elektroniku, telekomunikacije, računarstvo, automatiku i nuklearnu tehniku, Bijeljina, 2021.

[2] "SR-1010 Series Resistance Transfer Standards USer and Service Manual," *IET LABS, INC.*, 534 Main Street, Westbury, NY 11590, November, 2008.

[3] R. Radetić, *Električna otpornost: pojava i merenja: sa originalnim rešenjima autora,* Agencija Eho, Niš, 2015.

[4] D. G. Jarrett, "Evaluation of Guarded High-Resistance Hamon Transfer Standards," *IEEE Transactions on Instrumentation and Measurement*, vol. *48,* no. *2,* April, 1999.

[5] B. V. Hamon, "A 1-100 Ω build-up resistor for the calibration of standard resistors", *Jour. Sci. Instr.*, vol. 31, pp. 450-453, 1954.

[6] J. Bohacek, "Evaluation of frequency performance of resistance standards*"*, IMTC/2002. Proceedings of the 19th IEEE Instrumentation and Measurement Technology Conference, 2002.

[7] J. C. Riley, "The Accuracy of Series and Parallel Connections of Four-Terminal Resistors", *IEEE Transactions on Instrumentation and Measurement,,* vol. 16, 1967.

[8] White, D.R., Jones, K., Williams, J.M., Ramsey, I.E., "A simple resistance network for calibrating resistance bridges", *IEEE Transactions on Instrumentation and Measurement,,* vol. 46, 1997.

[9] L. Cimeanu, M. Simionescu, "Metrological characterization of reference standard resistors group of 100 Ω by means of Hamon resistor," 2012 International Conference and Exposition on Electrical and Power Engineering, Iasi, Romania, 25-27 October, 2012.

## ABSTRACT

Consideration of the application of Hamon standard resistors in alternating mode, as well as examination of their characteristics are the topic of this paper. Previous research has found that the transmission ratio of these standards should not significantly depend on frequency. In other words, the transfer modu is expected to be close to the square of the number of resistors from which the transfer is formed, while the phase position of the transfer will be close to zero. With the available equipment that was available when the research was conducted, the measurements were performed on the basis of two measurement methods, the results of which will be presented in the paper.

**Measurement of characteristics and modeling of Hamon standard resistors in alternating mode**

Stefan Mirković, Dragan Pejić, Aleksandar Dimitrijević

 ISBN 978-86-7466-930-3

# Merni sistem za određivanje modula i faznog stava impedanse baziran na virtuelnoj instrumentaciji

Milan Šaš, Dragan Pejić, Nemanja Gazivoda, Đorđe Novaković, Bojan Vujčić, *Members, IEEE*

***A stra t*—U ovom radu će biti predstavljen realizovani merni sistem za određivanje modula impedanse i faznog stava super ondezatora. istem se sastoji od dvo analnog generatora fun cija, dva digitalna multimetra i baferskog pojačavača struje oji su spojeni u električno kolo koje se koristi za četvorožično merenje impedanse. ao generator signala oristi se iglent DG 1 25 generator fun cija koji generiše sinusni signal superponiran za DC vrednost. ao digitalni multimetri oriste se dva 4 A - cifars a multimetra gde se jedan oristi ao voltmetar, a drugi ao ampermetar. apacitivnost super ondenzatora je reda stotina arada pa je potrebno oristiti strujni pojačavač kako bi se obezbedila potrebna struja. a o bi se postigla sinhronizacija rada uređaja, oni su umreženi i njima se upravlja pomoću računara na om se nalazi s ripta, napisana u Python programs om jezi u. re vencije na ojima se mere moduo impedanse i fazni stav su u opsegu od 1 m z do 5 z.**

***Ključne reči*— super ondezator; 4 A; iglent DG 1 25; Python; cipy; curve fit; matplotlib; Py erial; Py I A.**

## I. UVOD

Pojavom i razvojem električnih automobila dolazi i do razvoja uređaja za skladištenje električne energije poput litijumskih baterija. Kako je eksploatacija litijuma i proizvodnja baterija štetna za okolinu, istraživanja su se usmerila ka pronalasku novih komponenata koje mogu da efikasno skladište energiju. Istraživanjem i razvojem došlo se do superkondenzatora [1][2][3] čija kapacitivnost može biti reda stotina Farada, ali namenjenih za nizak naponski nivo reda volti. Povezivanjem ovakvih kondenzatora u redne i paralelne veze, realizuju se superkondenzatori sa nazivnim naponom reda 100 V, kakvi su neophodni za korišćenje u auto industriji. Prednosti superkondenzatora u odnosu na baterije jesu brzina punjenja i količina energije koja se isporučuje u kratkom intervalu. Superkondenzatori pronalaze sve širu primenu, pa je potrebno poznavati njihove karakteristike kako bi se mogli adekvatno predstaviti u simulacijama i prilikom projektovanja novih uređaja. Ovaj rad se bavi sistemom za određivanje dve vrlo važne karakteristike superkondenzatora: modul i faznog stava impedanse superkondenzatora na frekvencijama u opsegu od 1 mHz do 50 Hz.

Milan Šaš – Fakultet tehničkih nauka, Univerzitet u Novom Sadu, Trg Dositeja Obradovića 6, 21000 Novi Sad, Srbija (e-mail: milansas@uns.ac.rs)
Dragan Pejić – Fakultet tehničkih nauka, Univerzitet u Novom Sadu, Trg Dositeja Obradovića 6, 21000 Novi Sad, Srbija (e-mail: pejicdra@uns.ac.rs)
Nemanja Gazivoda – Fakultet tehničkih nauka, Univerzitet u Novom Sadu, Trg Dositeja Obradovića 6, 21000 Novi Sad, Srbija (e-mail: nemanjagazivoda@uns.ac.rs)
Đorđe Novaković – Fakultet tehničkih nauka, Univerzitet u Novom Sadu, Trg Dositeja Obradovića 6, 21000 Novi Sad, Srbija (e-mail: djordjenovakovic@uns.ac.rs)
Bojan Vujčić – Fakultet tehničkih nauka, Univerzitet u Novom Sadu, Trg Dositeja Obradovića 6, 21000 Novi Sad, Srbija (e-mail: bojanvuj@uns.ac.rs)

## II. POSTAVKA PROBLEMA

Najčešći model superkondenzatora jeste model koji, pored kapacitivnosti *C* ima rednu *s* i paralelnu (otočnu) *o* otpornost. Redna otpornost predstavlja otpor priključnih krajeva i ploča superkondenzatora, a paralelna otpornost modeluje realan dielektrik. U ovom radu će se, kao test primer, koristiti superkondenzator [4] nazivne kapacitivnost 100 F, nazivnog napona 2.7 V, serijske otpornosti reda desetina mΩ i paralelne otpornosti reda 10 kΩ. Autori su rešavanju ovog problema pristupili polazeći od klasične šeme za određivanje kapacitivnosti elektrolitskog kondenzatora merenjem napona i struje, kao što je prikazano na Sl. 1.

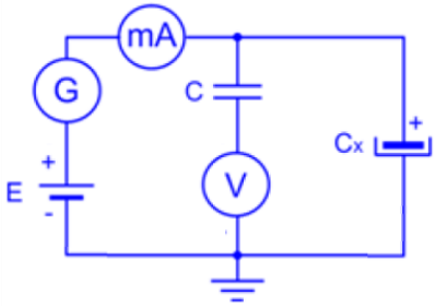


Sl. 1 Osnovna šema za merenje napona i struje na polarisanom kondenzatoru

Ovo kolo je, po svojoj konstrukciji, slično kolu za merenje otpornosti UI metodom naponskim spojem. U kolu se nalazi izvor jednosmernog napona E, na koji se dodaje naizmenična komponenta iz generatora funkcije G. Uloga pomoćnog kondenzatora C, redno vezanog sa voltmetrom, je da potiskuje jednosmernu komponentu napona na krajevima Cx. U tom slučaju voltmetar V meri samo preostalu naizmeničnu komponentu napona.

Ako se ovakva šema primeni za merenje impedanse superkondezatora javljaju se sledeća ograničenja:

1. Kako bi pomoćni kondenzator C uspešno filtrirao jednosmernu komponentu i pri najnižim vrednostima frekvencije, njegova kapacitivnost bi morala biti

 ISBN 978-86-7466-930-3

izuzetno visoka – reda Farada.

2. Pri visokim vrednostima frekvencije signala, očekivana vrednost modula impedanse superkondenzatora je reda mΩ, pa otpornost vodova dolazi do izražaja.
3. Raspoloživi instrumenti namenjeni za merenje napona i struje nisu u stanju da mere pri frekvencijama manjim od 3 Hz.

## III. PREDLOG REŠENJA

Kako bi se rešili navedeni problemi, autori predlažu rešenje prikazano na Sl. 2. Pomoćni kondenzator C je izbačen pa se filtriranje jednosmerne komponente napona vrši softverskim putem. Superkondenzator, na šemi označen kao DUT ( *e ice nder Test*), je vezan četvorožično kako bi se uticaj otpornosti vodova eliminisao. Zbog nemogućnosti multimetara da ispravno mere efektivnu vrednost signala na frekvencijama manjim od 3 Hz, multimetri su konfigurisani da rade u DC režimu. Prikupljanjem odbiraka signala napona i struje direktnim očitavanjem rezultata analogno-digitalne (A/D) konverzije i korišćenjem softverskih alata mogu biti određene amplitude (efektivne vrednosti, takođe) napona i struje.

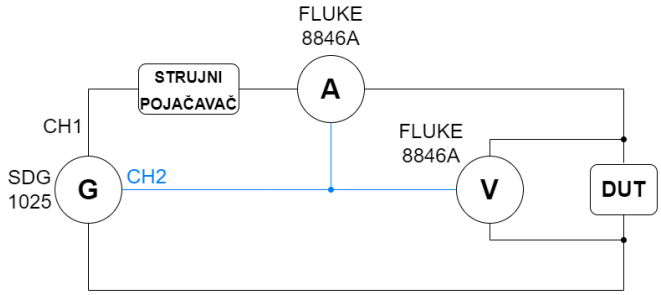


Sl. 2 Prikaz predloženog električnog kola

Kao ampermetar i voltmetar su korišćeni FLUKE 8846A [6] digitalni 6-½ cifarski multimetri koji imaju *multi-slope* A/D konvertor kao i mogućnost programiranja putem SCPI (*Standard Commands for Programmable Instruments*) komandi. Ampermetar i voltmetar su povezani u šemu za četvorožično merenje impedanse. Opseg merenja ampermetra je postavljen na 1 A, a opseg voltmetra na 1 V. Kao izvor naizmeničnog signala koristi se Siglent SDG 1025 [7] dvokanalni generator funkcija koji generiše, na svom prvom kanalu, sinusni signal amplitude 0.5 V i frekvencije u rasponu od 1 mHz do 50 Hz. Generisan napon je superponiran na jednosmernu komponentu kako bi se obezbedilo ispravno polarisanje superkondenzatora. Za pojačavanje strujnih mogućnosti funkcijskog generatora korišćen je baferski (jediničnog naponskog pojačanja) strujni pojačavač koji, na svom izlazu, daje vrednost struje do 2 A.

Sinhronizacija rada dva multimetra je izvedena korišćenjem eksternog trigera u obliku povorke pravougaonih impulsa dobijenih na drugom kanalu dvokanalnog izvora. Multimetri su podešeni da prihvate eksterni triger signal. Korišćenjem eksternog trigera eliminiše se pojava fazne greške usled neistovremenog odabiranja napona i struje. Raspon frekvencija periodičnog signala je veoma širok. Prilikom odabiranja tri periode signala najmanje frekvencije vrednosti 1 mHz, uzimanje odbiraka traje 50 minuta. Pri povećanju frekvencije se smanjuje vreme merenja na postavljenoj frekvenciji. Ukupno trajanje merenja počevši od najniže pa sve do najviše frekvencije je oko dva sata.

Posle obavljenog umrežavanja dobijeno kolo je predstavljeno na Sl. 3.

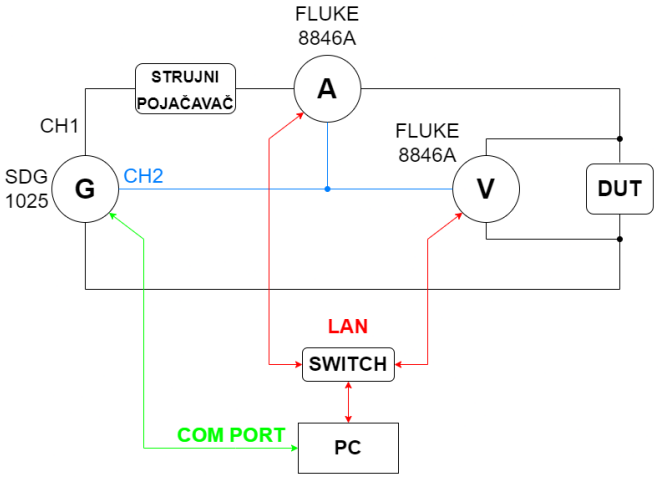


Sl. 3 Konačan izgled šeme za merenje

Strujni pojačavač je četvoropol, ali je na blok šemi predstavljen kao dvopol, kako bi šema bila lakša za čitanje. Multimetri su povezani na LAN ( *ocal Area Network*) dok je generator funkcije povezan na jedan COM port na računaru. Upravljanje celokupnim sistemom se vrši preko računara na kome se nalazi skripta napisana u Python [8] programskom jeziku. Operater ovakvog sistema treba da unese željene frekvencije naizmeničnog signala i pokrene skriptu. Kao izlaz, skripta isporučuje vrednosti modula impedanse i faznog stava u zavisnosti od frekvencije, u tabelarnom i grafičkom obliku.

## IV. KONTROLA SISTEMA I OBRADA PODATAKA

Kontrola sistema se vrši pomoću skripta napisane u Python programskom jeziku. Korišćene su biblioteke za mrežnu i serijsku komunikaciju [9], biblioteka *scipy* [10] za matematičke proračune i *matplotlib* [11] za grafički prikaz podataka. Kontrola sistema se odvija po sledećem principu:

- provera prisutnosti uređaja,
- postavljanje uređaja u početna stanja,
- ciklus merenja,
- obrada podataka i
- prikaz podataka.

U ciklusu merenja se vrši odabiranje talasnih oblika napona i struje. Na kraju ciklusa merenja od multimetara se traže podaci koji pristižu u obliku liste vrednosti pojedinačnih odbiraka. Za određivanje amplituda i faznih stavova napona i struje, prikupljani odbirci se prosleđuju funkciji *cur e fit* [12] koja je deo *scipy* biblioteke. Pored odbiraka, funkcija zahteva i definiciju očekivanog talasnog oblika. Za napon je to suma jednosmerne i prostoperiodične komponente poznate frekvencije, dok se za struju (u ustaljenom režimu) očekuje samo prostoperiodična komponenta. Kao povratne vrednosti, funkcija *cur e fit* vraća vrednosti jednosmerne i naizmenične

 ISBN 978-86-7466-930-3

komponente napona, naizmeničnu komponentu struje i fazne stavove za obe veličine. Količnik vrednosti amplitude napona i struje predstavlja vrednost modula impedanse. Fazni stav impedanse se dobija oduzimanjem faznih stavova napona i struje. Na kraju izvršavanja skripte podaci se zapisuju u CSV (*Comma Separated alues*) fajl koji se može naknadno obrađivati. Dodatno, rezultati obrade se prikazuju grafički pomoću biblioteke *matplotlib* kako bi se dobio grafički prikaz vrednosti koje su merene.

## V. Diskusija

Predloženi sistem je u potpunosti realizovan i izvršena su merenja. Podešen je da uzima sedam odbiraka po periodi. Merenje se vrši tokom tri periode signala na svakoj zadatoj frekvenciji. Parametar NPLC (*Number of Power ine Cycles*) je podešen na 0.02, što je najmanja moguća vrednost. Za mrežnu učestanost 50 Hz definisano je vreme integraljenja od 0.4 ms. Na kraju ciklusa rada dobijeni su grafici na kojima je predstavljena zavisnost vrednosti modula impedanse i faznog stava od frekvencije signala. Na Sl. 4 i 5 je dat prikaz navedenih zavisnosti, pri čemu je x-osa na kojoj se nalazi frekvencija predstavljena u log razmeri.

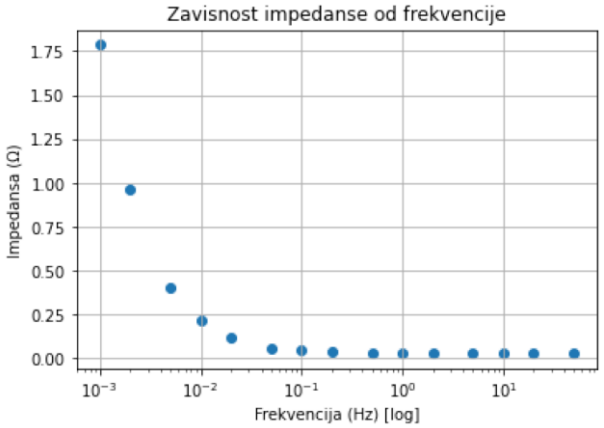


Sl. 4 Zavisnost vrednosti modula impedanse od frekvencije signala

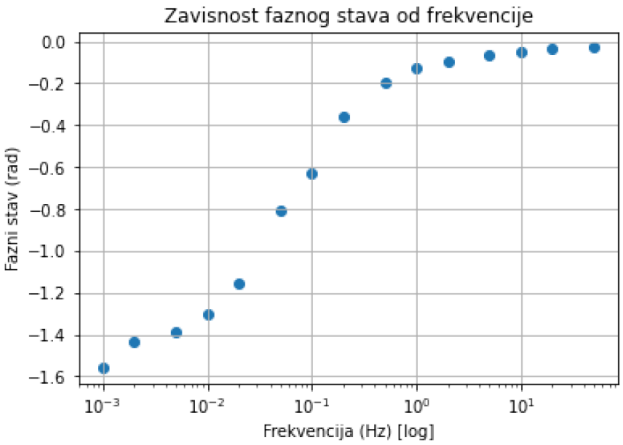


Sl. 5 Zavisnost vrednosti faznog stava od frekvencije signala

Na Sl. 6 je data fotografija opreme koja je korišćena u ovom radu.

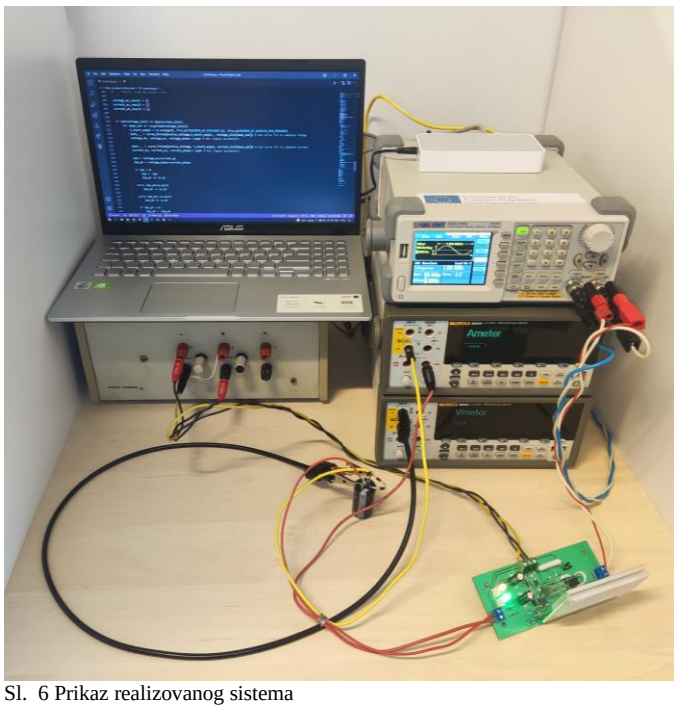

Sl. 6 Prikaz realizovanog sistema

## VI. Zaključak

Prikazani sistem je uspešno realizovan. Primećeno je da postoji prelazni proces prilikom promene frekvencije signala pa je potrebno sačekati sa merenjem dok se ne postigne ustaljeno stanje. Ovde je potrebno dodatno ispitati prelazne procese i optimizovati vreme čekanja, gde, sa povećanjem frekvencije, prelazni procesi kraće traju. Dalji planovi uključuju simuliranje rada sistema i određivanje merne nesigurnosti ovakvog merenja impedanse i faznog stava superkondenzatora na unapred zadatim frekvencijama. Ove simulacije bi se realizovale u Python programskom jeziku, koristeći Monte Karlo princip. U daljem razmatranju i testiranju može se povećati vrednost NPLC-a kod nižih frekvencija kako bi princip rada *multi-slope* A/D konvertora došao do izražaja u potiskivanju smetnji mrežne učestanosti. Na nižim frekvencijama je moguće povećavati broj odbiraka po periodi. Pri višim frekvencijama (kraće periode) postoji ograničenje u pogledu vrednosti vremena integraljenja.

Na osnovu dosadašnjih merenja se stiče utisak da nema potrebe za prevelikim brojem odbiraka po periodi, kao i da nema potrebe za povećanjem broja perioda. Moguće obrazloženje je činjenica da se poznaje talasni oblik napona i struje, pa zbog toga *cur e fit* funkcija već na osnovu malog broja odbiraka uspeva da odredi potrebne parametre signala napona i struje.

## Zahvalnica

Ovaj rad je podržan od strane Fakulteta tehničkih nauka u sklopu internog projekta Centra za metrologiju pod nazivom “Razvoj naučno-stručnih metoda u oblasti SMART koncepata u industriji, naučne i industrijske metrologije, neuronauka i biomedicinskih merenja primenom napredne metodologije i digitalne tehnologije” .

Ovaj rad je podržan od strane Fakulteta tehničkih nauka u Novom Sadu, Departmana za energetiku elektroniku i

 ISBN 978-86-7466-930-3

telekomunikacije, u okviru realizacije projekta MPNTR 200156 : "Inovativna naučna i umetnička ispitivanja iz domena delatnosti FTN-a".

## LITERATURA

[1] Jha, Deepu & Karkaria, Vispi & Karandikar, Parashuram & Desai, R.S.. (2022). Statistical modeling of hybrid supercapacitor. Journal of Energy Storage. 46. 103869.
[2] Chakraborty, Sohini & N.L, Mary. (2022). Review - " An Overview on Supercapacitors and Its Applications. Journal of The Electrochemical Society. 169. 10.
[3] Zhang, Jianan & Zhang, Xiaoyu & Xue, Dongping & Huicong, Xia & Jiang, Su. (2021). Supercapacitors. 10.
[4] https://www.xump.com/science/Super-Capacitor-100F-2.7V.cfm
[5] https://www.hioki.com/global/learning/usage/lcr-meters_4.html
[6] https://us.flukecal.com/products/data-acquisition-and-test-equipment/bench-multimeters/8845a8846a-65-digit-precision-multime
[7] https://siglentna.com/product/sdg1025/
[8] https://www.python.org/
[9] https://pyvisa.readthedocs.io/en/latest/
[10] https://scipy.org/
[11] https://matplotlib.org/stable/index.html
[12] https://docs.scipy.org/doc/scipy/reference/generated/scipy.optimize.curve_fit.html

## ABSTRACT

This paper presents the implemented measurement system for measuring the impedance modulus and phase angle of a supercapacitor. The system consists of a two-channel function generator, two digital multimeters and a buffer current amplifier connected into an electrical circuit used for four-wire resistance measurement. The Siglent SDG 1025 function generator is used as the signal generator, which generates a sine wave signal superimposed on a DC value. Two FLUKE 8846A 6-½ digit digital multimeters are used as digital multimeters, one of which is used as a voltmeter and the other as an ammeter. The capacitance of the supercapacitor is of the order of hundreds of Farads, so it is necessary to use a current amplifier to provide the required current. In order to synchronize the operation of the devices, they are networked and managed using a computer that contains a script written in the Python programming language. The frequencies at which the impedance modulus and phase position are measured are in the range of 1 mHz to 50 Hz.

**easurement system for determining the modulus and phase angle of the impedance based on virtual instrumentation**

Milan Šaš, Dragan Pejić, Nemanja Gazivoda, Đorđe Novaković, Bojan Vujičić

 ISBN 978-86-7466-930-3

# Simulaciona analiza metode pogodne za metrološku karakterizaciju impedanse na niskim frekvencijama

Milan Šaš, Dragan Pejić, Nemanja Gazivoda, Đorđe Novaković, Bojan Vujičić, *Members, IEEE*

***A stra t*— radu je pri azana simulaciona analiza metode oja je primenjiva za metrološku ara terizaciju dvo rajnih elemenata na nis im fre vencijama. Program napisan u programs om jezi u Python simulira rad dva multimetra tipa 4 A, od ojih je jedan onfigurisan ao ampermetar, a drugi ao voltmetar. dbirci napona i struje se obrađuju u programu, oji na osnovu odbira a određuje vrednost amplitude naizmenične komponente i faznog stava napona i struje, a onda na osnovu tih vrednosti izračunava moduo i fazni stav impedanse. Program uračunava deklarisane greške oba instrumenta i daje mogućnost za procenu merne nesigurnosti rezultata merenja.**

***Ključne reči*— imulacija, moduo i fazni stav impedanse, merna nesigurnost, onte arlo metoda, 4 A.**

## I. UVOD

Pojam impedanse je definisao Oliver Hevisajd (Oliver Heaviside) 1886. godine [1], a kompleksnu notaciju je uveo Artur Keneli (Arthur Kennelly) 1893. godine [2]. Kompleksna vrednost impedanse sadrži dva podatka: a) moduo impedanse predstavlja količnik amplitude napona i amplitude struje prostoperiodičnog talasnog oblika i b) fazni stav impedanse predstavlja razliku faznih stavova napona i struje. Ako se ograničimo na sempling metodu i prostoperiodični režim, potrebno je:

a) sinhrono odabirati talasni oblik napona i struje,

b) na osnovu odbiraka odrediti amplitude i fazne stavove napona i struje i

c) odrediti moduo i fazni stav impedanse.

Za dobijanje odbiraka napona i struje su korišćena dva multimetra FLUKE 8846A, od kojih je jedan konfigurisan kao ampermetar, a drugi kao voltmetar. Oba instrumenta su konfigurisana za rad u jednosmernom (DC, *direct current*) režimu, kako bi se pristupanjem njihovim analogno-digitalnim (AD) konvertorima dobili odbirci merenih veličina. Ampermetar i voltmetar mogu da se konfigurišu da rade i u naizmeničnom (AC, *alternate current*) režimu, što se na prvi pogled čini logičnijim, jer se pojam impedanse i definiše u AC režimu. U tom slučaju bismo dobijali efektivnu vrednost napona i struje, što je dovoljno za određivanje modula impedanse. Određivanje faznog stava impedanse bi ostao nerešen problem, jer se ovakvim pristupom ne raspolaže vrednošću faznog stava napona i struje.

Korišćeni multimetri imaju ugrađen integrišući (*multi slope*) AD konvertor [3]. Umesto da vrše odabiranje u tački, ovi AD konvertori ustvari određuju srednju vrednost ulazne veličine na intervalu integraljenja zadatog trajanja. Integrišući AD konvertori imaju osobinu da potiskuju smetnje čija je perioda ceo broj puta duža od trajanje integraljenja, zbog čega se vrlo često koriste u industrijskim uslovima gde se očekuje značajno prisustvo smetnje mrežne frekvencije. Trajanje vremena integraljenja se zadaje parametrom NPLC (*Number of Power ine Cycles*). Kod korišćenih multimetara, pored celobrojnih vrednosti za NPLC, postoje i vrednosti manje od jedan, a najmanja je 0.02. Za minimalnu vrednost parametra NPLC, pri mrežnoj frekvenciji od 50 Hz, se dobija najkraće vreme integraljenja od 0.02/50 Hz = 0.4 ms. Vrednost najkraćeg vremena integraljenja i željeni broj odbiraka po periodi su dva parametra koji ograničavaju primenjivost ove metode pri višim frekvencijama prostoperiodične pobude. Kada se vreme integraljenja ponderiše i iskaže u odnosu na trajanje periode signala čije odabiranje se vrši, onda se koristi termin ugao integraljenja i iskazuje se u radijanima.

## II. SIMULACIONI MODEL

Simulacioni model je realizovan u programskom jeziku Python [4] sa ciljem da se ispita uticaj bitnih parametara (broj odbiraka po periodi, trajanje/ugao integraljenja, greška ampermetra i voltmetra) na rezultate merenja (greška određivanja modula i faznog stava impedanse). Drugi razlog korišćenja simulacija je određivanje merne nesigurnosti dobijenih rezultata merenja simulacionim putem, odnosno primenom Monte Karlo metode.

Na Sl. 1. je prikazana ilustracija prostoperiodičnog talasnog oblika (crna linija) koji je doveden na ulaz integrišućeg AD konvertora. Vrednosti ulaznog talasnog oblika koje pripadaju periodima integraljenja su obeležene debljom linijom crvene boje. Rezultat AD konverzije se saopštava na kraju intervala integraljenja (plava tačka) i predstavlja srednju vrednost ulazne veličine u toku trajanja AD konverzije.

Milan Šaš – Fakultet tehničkih nauka, Univerzitet u Novom Sadu, Trg Dositeja Obradovića 6, 21000 Novi Sad, Srbija (e-mail: milansas@uns.ac.rs)

Dragan Pejić – Fakultet tehničkih nauka, Univerzitet u Novom Sadu, Trg Dositeja Obradovića 6, 21000 Novi Sad, Srbija (e-mail: pejicdra@uns.ac.rs)

Nemanja Gazivoda – Fakultet tehničkih nauka, Univerzitet u Novom Sadu, Trg Dositeja Obradovića 6, 21000 Novi Sad, Srbija (e-mail: nemanjagazivoda@uns.ac.rs)

Đorđe Novaković – Fakultet tehničkih nauka, Univerzitet u Novom Sadu, Trg Dositeja Obradovića 6, 21000 Novi Sad, Srbija (e-mail: djordjenovakovic@uns.ac.rs)

Bojan Vujčić – Fakultet tehničkih nauka, Univerzitet u Novom Sadu, Trg Dositeja Obradovića 6, 21000 Novi Sad, Srbija (e-mail: bojanvuj@uns.ac.rs)

 ISBN 978-86-7466-930-3

Sa Sl. 1. se vidi da rezultati AD konverzije (plave tačke) ne leže na ulaznom talasnom obliku (crna kriva), nego su fazno pomereni. Što je duži interval integraljenja u odnosu na periodu signala, dobija se sve veće fazno kašnjenje. Slična greška se javlja i u pogledu amplitude talasnog oblika koja bi bila određena na osnovu dobijenih odbiraka. Fazna i amplitudska greška teže nuli kada interval integraljenja teži nuli, odnosno kada integrišući AD konvertor postaje *sampling* AD konvertor.

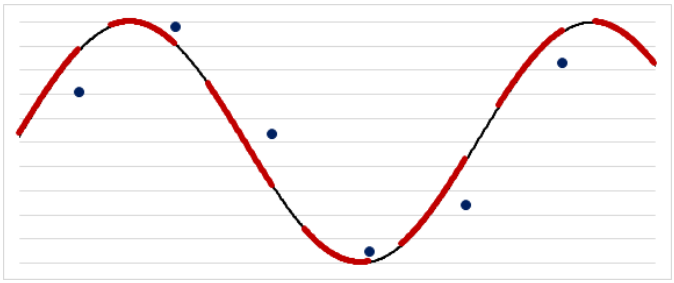

Sl. 1. Ilustracija uticaja ugla integraljenja. Ulazni talasni oblik (tanka crna linija), integracioni period (debela crvena linija) i rezultat AD konverzije (plave tačke).

Postavlja se pitanje opravdanosti korišćenja integrišućeg AD konvertora za određivanje modula i faznog stava impedanse, kada međurezultati (amplitude i faze napona i struje) u sebi sadrže opisane greške. Simulacionim postupkom je proveravana navedena nedoumica.

Pretpostavljeni su prostoperiodični talasni oblici napona i struje na ulazu AD konvertora zadatog vremena integraljenja. Simulirano je odabiranje u svega pet tačaka po periodi, a onda je na osnovu odbiraka, postupkom fitovanja, određena amplituda i fazni stav napona. Na Sl. 2. je prikazan grafik zavisnosti normalizovane vrednosti (količnik vrednosti izmerene i zadate amplitude) opisanim postupkom određene amplitude napona i struje, kao i izračunatog modula impedanse. Na horizontalnoj osi je ugao integraljenja iskazan u radijanima, kako bi bio uporediv prema periodi prostoperiodične funkcije koja iznosi 2π rad.

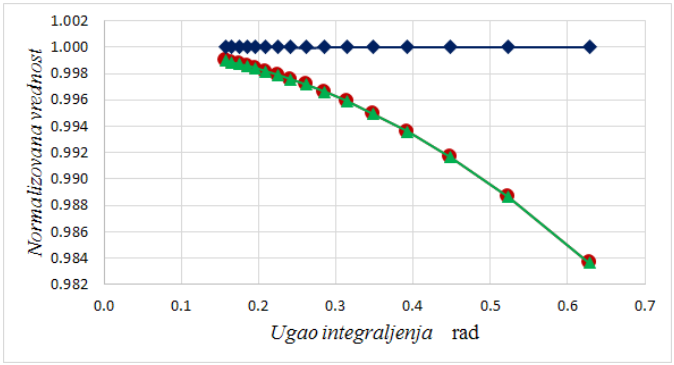


Sl. 2. Zavisnosti normalizovane vrednosti određene amplitude napona (crveni krugovi) i struje (zeleni trouglovi), kao i izračunatog modula impedanse (plavi rombovi).

Sa porastom ugla integraljenja javlja se sve primetnija sistematska greška, za koju se pokazuje da zavisi samo od ugla integraljenja. Greška je multiplikativnog tipa, jednaka je za napon (crvena karakteristika) i struju (zelena karakteristika). Prilikom određivanja modula impedanse (plava karakteristika) kao količnika napona i struje dolazi do potiranja polaznih sistematskih greška. Ovo je vrlo korisna osobina jer se mogu sprovoditi merenja sa vrlo velikim uglom integraljenja koja za posledicu ima značajnu sistematsku grešku od nekoliko procenata, a da se to ne odrazi na performanse određivanja modula impedanse.

Na Sl. 3. je data zavisnost određenog faznog stava napona (crveni krugovi), struje (zeleni trouglovi) i impedanse (plavi rombovi) od ugla integraljenja. Za zadatu vrednost faznog stava napona (crvena isprekidana linija) i struje (zelena isprekidana linija), izmereni fazni stav napona i struje sadrži sistematsku grešku koja zavisi od ugla integraljenja. Ta greška je aditivnog tipa i jednaka je za napon i struju. Prilikom određivanja faznog stava impedanse (razlika faznog stava napona i faznog stava struje) dolazi do potiranja polaznih aditivnih sistematskih grešaka faznog stava napona i struje.

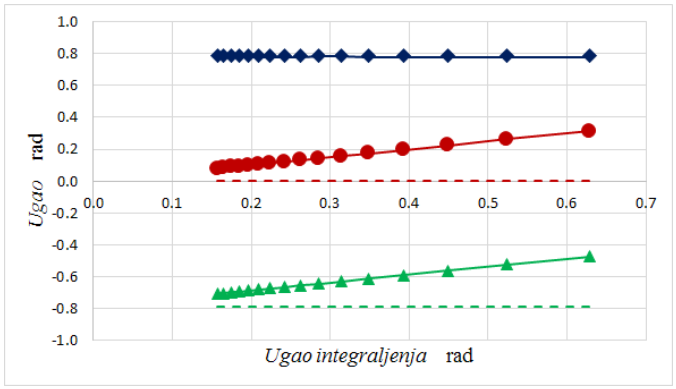


Sl. 3. Zavisnost rezultata određivanja faznog stava napona (crveni krugovi), struje (zeleni trouglovi) i faznog stava impedanse (plavi rombovi) od vrednosti ugla integraljenja.

Nakon eliminacije uticaja sistematskih grešaka pri određivanju modula i faznog stava impedanse, u rezultatu merenja preostaju slučajne greške. Na Sl. 4. je prikazana zavisnost relativno iskazanog rasipanja (količnik standardne devijacije i srednje vrednosti rezultata merenja) prilikom određivanja amplitude naizmenične komponente napona (crveni trouglovi) i struje (zeleni rombovi), kao i modula impedanse (plavi krugovi).

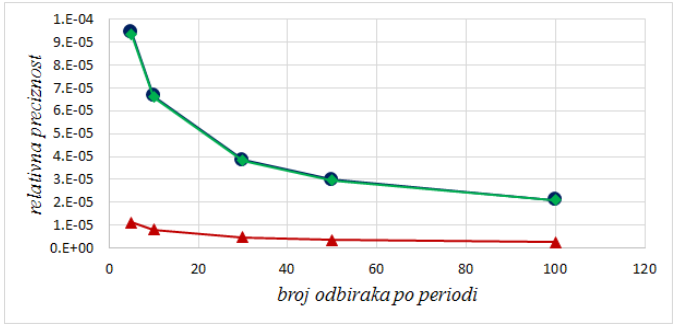


Sl. 4. Zavisnost relativno iskazane preciznosti (rasipanje) amplitude napona (crveno), struje (zeleno) i modula impedanse (plavo) od broja odbiraka po periodi.

 ISBN 978-86-7466-930-3

Korišćeni voltmetar ima značajno manju grešku (desetak puta) nego ampermetar, pa je greška merenja struje dominantna prilikom određivanja modula impedanse. Ako se broj odbiraka po periodi poveća sa 5 na 100 (20 puta), dobije se nesrazmerno manje poboljšanje u preciznosti određivanja modula impedanse (svega 4.5 puta).

Na Sl. 5 je prikazana zavisnost rasipanja faznog stava napona (crveni trouglovi), struje (zeleni rombovi) i impedanse (plavi krugovi) od broja odbiraka po periodi. Važe slični zaključci u pogledu zavisnosti navedenih parametara od broja odbiraka po periodi.

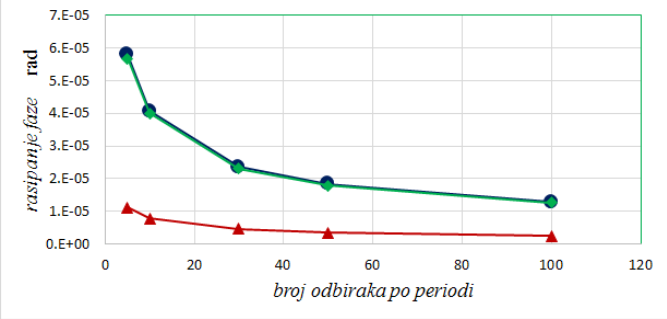


Sl. 5. Zavisnost preciznosti (rasipanja) rezultata određivanja faznog stava napona (crveni trouglovi), struje (zeleni rombovi) i impedanse (plavi krugovi) od broja odbiraka po periodi.

## III. MERNA NESIGURNOST

Dokument [5] predstavlja preporuke za iskazivanje merne nesigurnosti polazeći od matematičkog modela merenja. Matematički model merenja je izraz koji predstavlja zavisnost izlazne veličine od uticajnih veličina. U konkretnom slučaju, izlazne veličine (čiju mernu nesigurnost želimo da odredimo) su moduo i fazni stav impedanse. Neke od uticajnih veličina su: greške ugrađene u odbirke napona i struje, greška postupka određivanja amplitude i faznog stava napona prostoperiodične veličine na osnovu odbiraka i trajanje intervala integraljenja. Pristupom opisanim u [5] se vrši analiza propagacije mernih nesigurnosti ulaznih veličina na izlaznu veličinu.

Pored velikog broja uticajnih veličina, poseban problem u konkretnom slučaju je nepoznavanje načina funkcionisanja Python-ove funkcije *cur e fit*, koja je preuzeta iz biblioteke *scipy* [7]. Ova funkcija je korišćena za fitovanje prostoperiodične funkcije kroz dobijeni skup odbiraka, radi određivanja amplitude i faznog stava napona i struje.

Drugi način za određivanje merne nesigurnosti, opisan u [6], je zasnovan je na simulacionom postupku, odnosno na primeni Monte Karlo metode. Kod ovog postupka se uticajne veličine posmatraju kao slučajne promenljive i vrši se analiza propagacije funkcije gustine uticajnih veličina na funkciju gustine izlazne veličine. Veliki broj puta (preko $10^5$) se simulira postupak merenja uz uvažavanje funkcije gustine svake od uticajnih veličina. Za dobijene vrednosti izlazne veličine se određuje funkcija gustine, srednja vrednost i standardna devijacija. Srednja vrednost se saopštava kao najbolja procena izlazne veličine, dok vrednost standardne devijacije predstavlja standardnu mernu nesigurnost.

Na Sl. 6 i Sl. 7. su prikazani rezultati određivanja modula i faznog stava impedanse superkondenzatora za frekvencije počev od 1 mHz do 50 Hz. Za sva merenja je definisano najkraće vreme integraljenja (0.4 ms), uzimano je sedam odbiraka po periodi u tri susedne periode napona i struje. Odbirci napona i struje su kao argument prosleđivani funkciji *cur e fit,* a kao izlaz su dobijene najbolje procene amplitude i faznog stava naizmenične komponente pretpostavljenog prostoperiodičnog oblika. Moduo impedanse se određuje kao količnik amplituda prostoperiodične komponente napona i struje. Fazni stav impedanse se određuje oduzimanjem faznog stava napona i struje.

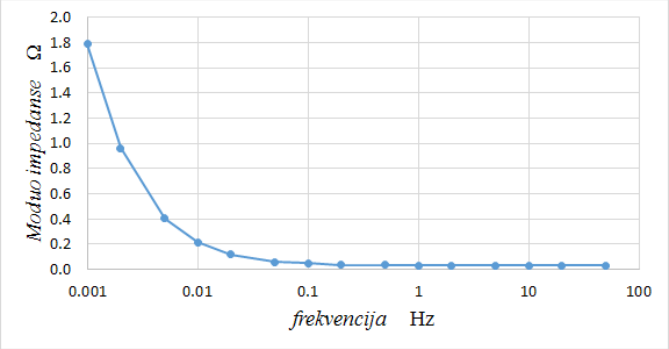


Sl. 6. Zavisnost modula impedanse superkondenzatora od frekvencije.

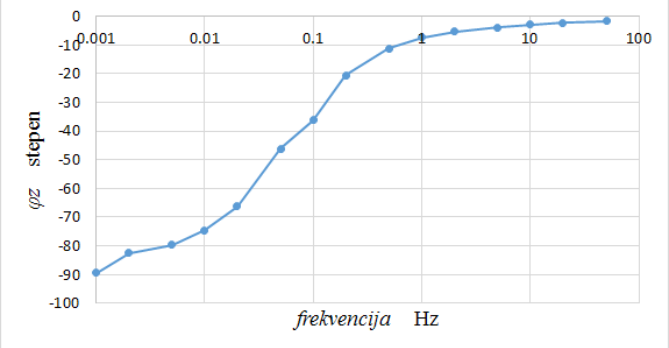


Sl. 7. Zavisnost faznog stava superkondenzatora od frekvencije.

Korišćenjem Monte Karlo postupka je određena standardna merna nesigurnost (standardna devijacija) modula i faznog stava impedanse superkondenzatora. U simulaciji su modelovane: greška AD konvertora na naponskom i strujnom kanalu za svaki odbirak [4], vreme integraljenja zadato parametrom NPLC, broj tačaka po periodi i broj perioda. U nedostatku dodatnih informacija, sve greške su modelovane uniformnom raspodelom. Zavisnost relativno iskazane standardne merne nesigurnosti modula impedanse superkondenzatora od frekvencije je prikazana na Sl. 8.

Standardna merna nesigurnost faznog stava impedanse superkondenzatora je prikazana u apsolutnom obliku na Sl. 9.


ISBN 978-86-7466-930-3

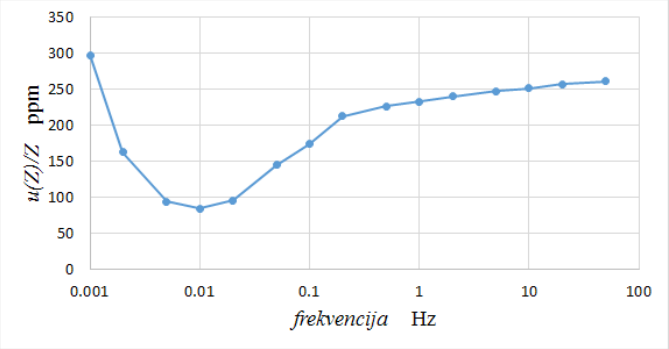


Sl. 8. Zavisnost relativno iskazane standardne merne nesigurnosti modula impedanse superkondenzatora od frekvencije.

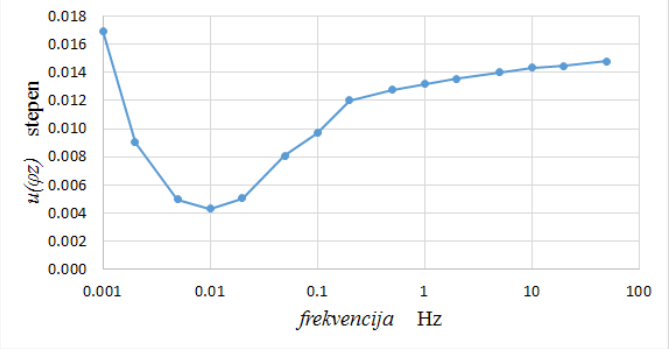


Sl. 9. Zavisnost apsolutno iskazane standardne merne nesigurnosti faznog stava impedanse superkondenzatora od frekvencije.

Relativno iskazana standardna merna nesigurnost modula impedanse superkondenzatora je manja od 300 ppm, dok je apsolutno iskazana standardna merna nesigurnost faznog stava impedanse superkondenzatora manja od 18 m˚, odnosno 0.6 mrad.

## IV. Zaključak

U radu je prikazana simulaciona analiza metode pogodne za snimanje modula i faznog stava impedanse dvokrajnog elementa na niskim učestanostima. Kao ampermetar i voltmetar su korišćeni standardni multimetri sa integrišućim AD konvertorom. Simulacioni postupak je korišćen iz dva razloga: a) da se oceni doprinos uticajnih veličina i b) da se odredi merna nesigurnost. Pokazano je da:

- prilikom određivanja modula impedanse (deljenjem procenjene vrednosti amplitude prostoperiodične komponente napona i struje) dolazi do potiranja multiplikativne sistematske greške,
- prilikom određivanja faznog stava impedanse (razlika procenjenog faznog stava napona i struje), dolazi do potiranja aditivne sistematske greške,
- povećanje broja odbiraka po periodi ne doprinosi srazmerno poboljšanju metroloških performansi rezultata merenja,
- pod pretpostavkom uniformnih raspodela greške AD konvertora na naponskom i strujnom kanalu, primenom Monte Karlo metode je određena merna merna nesigurnost rezultata merenja.

## Zahvalnica

Ovaj rad je podržan od strane Fakulteta tehničkih nauka u sklopu internog projekta Centra za metrologiju pod nazivom “Razvoj naučno-stručnih metoda u oblasti SMART koncepata u industriji, naučne i industrijske metrologije, neuronauka i biomedicinskih merenja primenom napredne metodologije i digitalne tehnologije”.

Ovaj rad je podržan od strane Fakulteta tehničkih nauka u Novom Sadu, Departmana za energetiku elektroniku i telekomunikacije, u okviru realizacije projekta MPNTR 200156 : "Inovativna naučna i umetnička ispitivanja iz domena delatnosti FTN-a".

## Literatura

[1] Oliver Heaviside, The Electrician, p. 212, 23 July 1886, reprinted as Electrical Papers, Volume II, p 64, AMS Bookstore, ISBN 0-8218-3465-7
[2] Kennelly, Arthur. Impedance (AIEE, 1893)
[3] https://us.flukecal.com/products/data-acquisition-and-test-equipment/bench-multimeters/8845a8846a-65-digit-precision-multime
[4] https://www.python.org/
[5] https://www.bipm.org/documents/20126/2071204/JCGM_100_2008_E.pdf/cb0ef43f-baa5-11cf-3f85-4dcd86f77bd6
[6] https://www.bipm.org/documents/20126/2071204/JCGM_101_2008_E.pdf/325dcaad-c15a-407c-1105-8b7f322d651c
[7] https://scipy.org/

## Abstract

The paper presents a simulation analysis of a method that is applicable for the metrology characterization of two-end elements at low frequencies. The program written in the Python programming language simulates the operation of two multimeters of the FLUKE 8846A, one of which is configured as an ammeter and the other as a voltmeter. Voltage and current samples are processed in a program, which determines the value of the amplitude of the alternating component and the phase position of voltage and current based on the samples, and then calculates the modulus and phase position of the impedance based on these values. The program takes into account the declared errors of both instruments and provides an opportunity to assess the measurement uncertainty of the measurement results.

**imulation analysis of methods suitable for metrology characterization of impedance at low frequencies**

Milan Šaš, Dragan Pejić, Nemanja Gazivoda, Đorđe Novaković, Bojan Vujičić

 ISBN 978-86-7466-930-3

# MICROELECTRONICS AND OPTOELECTRONICS, NANOSCIENCES AND NANOTECHNOLOGIES

# /

# МИКРОЕЛЕКТРОНИКА И ОПТОЕЛЕКТРОНИКА, НАНОНАУКЕ И НАНОТЕХНОЛОГИЈЕ

# (MOI/MO)

ISBN 978-86-7466-930-3

# Two Color Photodiodes Mounted on the Micromachined Carrier

Žarko Lazić, Milče M. Smiljanić, Dušan Nešić, Ljubiša Zeković

***Abstract*— In this paper, two color detector based on silicon photodiodes is studied and fabricated. Standard IHTM photodiode's design is modified to allow mounting one photodiode above another using special micromachined carrier. The carrier is fabricated using wet silicon etching in 25% TMAH water solution and anodic bonding of etched silicon and Pyrex glass. The fabricated carrier also allows easy wire thermocompression bonding from the photodiode's pads to TO-5 housing. Output currents of the photodiodes were measured by applying light of 900 nm and 1060 nm. Obtained results verify applicability of the new packaging for two color detector.**

***Index Terms*—Two color detector, photodiodes, micromachined packaging, silicon, Pyrex glass**

## I. Introduction

IN the Institute of Chemistry, Technology and Metallurgy (IHTM) various types of silicon photodiodes were explored and developed for decades [1]. In this work, we will study a modified IHTM silicon photodiodes as two color detectors [2-4]. Two color detectors represent a sandwich structure that contains two photodiodes arranged along the same optical axis and they measure different ranges of wavelengths. Commercially available detectors [3-4] are using two photodiodes based on silicon or silicon and InGaAs. These detectors are mostly utilized for remote temperature measurements and for wide wavelength ranges of detection. The temperature is measured using ratio of radiation intensities at two wavelengths or wavelengths ranges and comparing it with the standard black body radiation [3]. Special advantages of these optical remote temperature measurements are solving problems of physical obstacles on target's optical axes. Two color detectors are used in applications for flame temperature sensing, spectrophotometer, dual-wavelength detection and IR thermometers [3].

In this paper, we will explore design of the silicon-silicon photodiodes sandwich, in which the top silicon photodiode is placed above the other bottom photodiode, as shown in Fig.1. The idea of design is that the photons of shorter wavelengths must be absorbed in the top photodiode and the photons of longer wavelengths are absorbed in the bottom photodiode. The sandwich design is obtained using special carrier for photodiodes. Carrier is fabricated using processes of micromachining of silicon in 25% wt. TMAH water solution and anodic bonding of etched silicon and Pyrex glass. In order to provide electrical connections, design and fabrication of the photodiodes are modified. After mounting of sandwich carrier on the TO-5 housing, measurements were performed to confirm detection of two different wavelengths.

Žarko Lazić, Milče M. Smiljanić and Dušan Nešić are with University of Belgrade-Institute of Chemistry, Technology and Metallurgy, National Institute of the Republic of Serbia ICTM, Department of Microelectronic Technologies Njegoševa 12, Belgrade, Serbia, (email: zlazic@nanosys.ihtm.bg.ac.rs; smilce@nanosys.ihtm.bg.ac.rs; nesicad@nanosys.ihtm.bg.ac.rs)

Ljubiša Zeković is with University of Belgrade-Faculty of Physics, Studentski trg 12-16, Belgrade, Serbia, (e-mail: zekovic@ff.bg.ac.rs)

## II. Fabrication

In the research and development of two color detector we modified photodiodes using know-how of our previous commercial silicon photodiodes. Problem of thermocompression bonding of golden wires to aluminum electrical connection is solved with design of the lateral photodiodes. The IHTM standard photodiodes have electrical connections on the both sides-the top and the bottom. In two color detection the top photodiode must allow transmission of wavelengths to be absorbed by the bottom photodiode. For this reason, the bottom side of the top photodiode must be designed without any metallization and reflective layer.

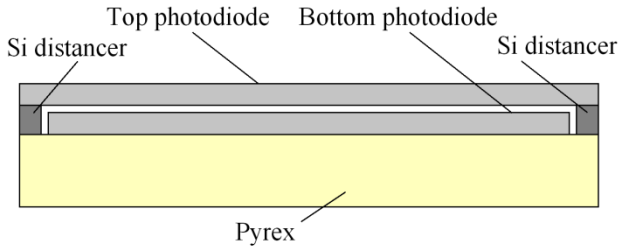


Fig. 1. Cross section of two photodiodes mounted on the micromachined carrier.

In order to simplify fabrication processes, the top and the bottom photodiodes are produced using the identical design, as shown in Fig.1-2. The photodiodes are in the shape of silicon rectangles with surface dimensions of 4000 μm x 3345 μm, as shown in Fig.1-2. The rectangular shape resolves the problem of thermocompression bonding of gold wires to both mounted photodiodes on fabricated carrier and TO-5 housing since both are rotated for 90˚ relative to each other, as shown

 ISBN 978-86-7466-930-3

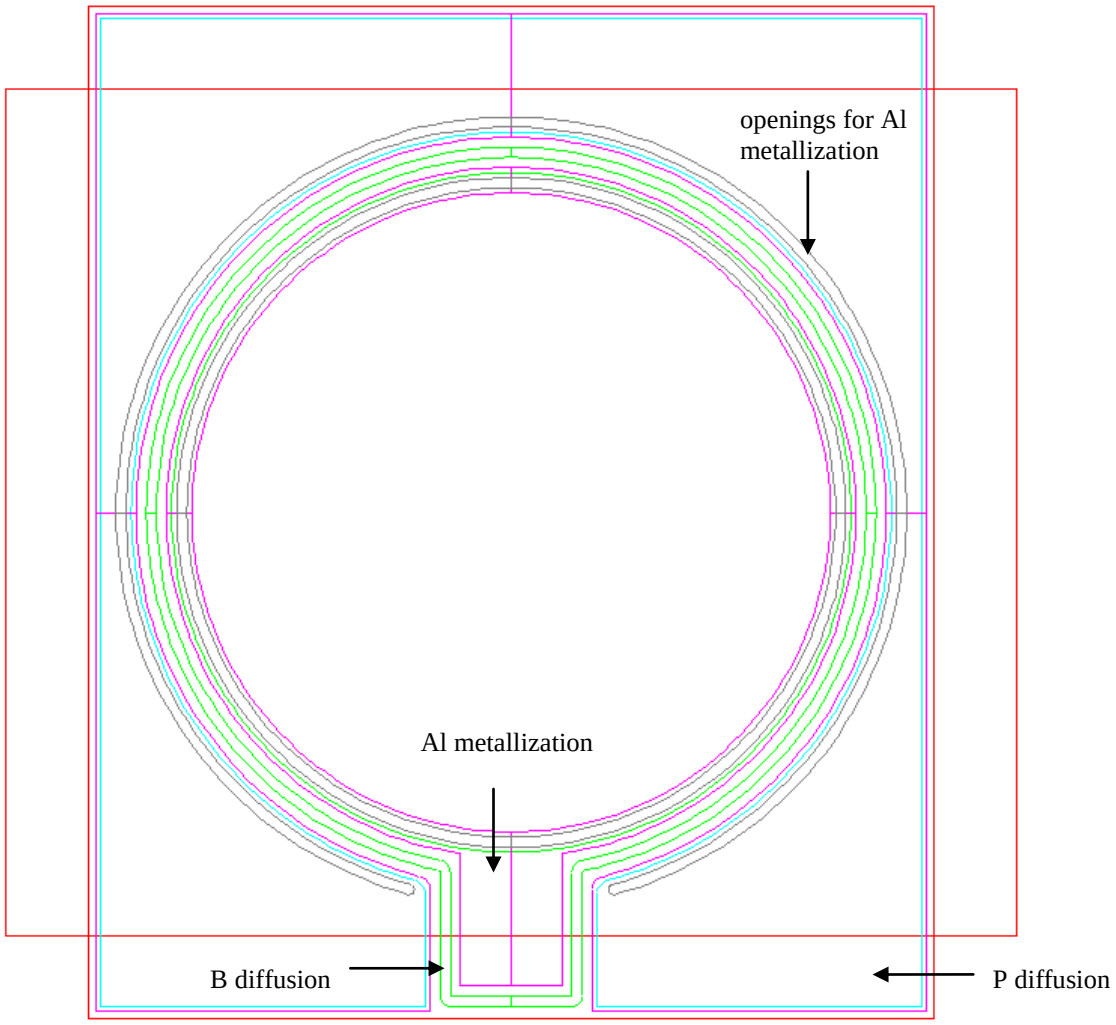


Fig. 2. Two color photodiodes design. Green color-I photolithographic process for boron diffusion. Blue color-II photolithographic process for phosphorus diffusion. Grey color-III photolithographic process for openings for Al metallization in SiO2. Pink color-IV photolithographic process for Al metallization. Red color-rectangular borders of sawed photodiode.

in Fig.2. We used two types of the silicon substrates in fabrication. For the top photodiodes, the silicon wafers of n type, resistivity of 2000 Ωcm and thickness of 180 μm are used. For the bottom photodiodes, we used silicon wafers of n type, resistivity of 500-1000 Ωcm and thickness of 300 μm. Prior to predetermined technological processes, the photolithographic processes were performed to define patterns given in Fig.2. The fabricated photodiodes were obtained according to following list of technological processes:

1. I wet thermal oxidation for boron diffusion (T=1100 °C, t=120 min)
2. I photolithographic process for boron diffusion
3. Boron diffusion (T=1025 °C, t=60 min)
4. II wet thermal oxidation for phosphorus diffusion (T=1100 °C, t=100 min)
5. II photolithographic process for phosphorus diffusion
6. Phosphorus diffusion (T=950 °C, t=60 min)
7. $SiO_2$ thinning on the top side and its removing on the bottom side of wafer
8. III photolithographic process for openings in $SiO_2$
9. Al sputtering
10. IV photolithographic process for Al metallization.

Finally, Au layer was sputtered only on the bottom side of the bottom photodiode as reflective layer.

Photodiodes' carrier is micromachined using anisotropic wet etching in 25% wt. water solution at the temperature of 80 °C [5-7]. We used phosphorus-doped {100}-oriented 3" silicon wafers with double-sided polished surfaces. The resistivity of the wafers is 1-5 Ωcm and its thickness is 400 μm. Prior to etching, we performed wet thermal oxidations to obtain $SiO_2$ masking layer of 1 μm and 0.5 μm thicknesses and three photolithographic processes to define patterns for double side etching. First, we performed etching to define appropriate cavities on the top side of silicon substrate. Then the thinner silicon dioxide was removed. Next, wafer had been double side etched until membrane of 50 μm was obtained. Etched wafer was anodically bonded to the Pyrex

 ISBN 978-86-7466-930-3

TABLE I
PHOTODIODES CURRENTS AND RATIOS OF CURRENTS FOR THE WAVELENGTHS OF 900 NM AND 1060 NM.

| Two color detector | | 900 nm | | | 1060 nm | | |
|---|---|---|---|---|---|---|---|
| | | Intensity $I_1$ | Intensity $I_2$ | Intensity $I_3$ | Intensity $I_1$ | Intensity $I_2$ | Intensity $I_3$ |
| 1 | $I_{top}$ | 8 μA | 4 μA | 850 nA | 14.9 μA | 2.32 μA | 756 nA |
| | $I_{bottom}$ | 0.55 μA | 0.265 μA | 57.5 nA | 5.1 μA | 1.1 μA | 395 nA |
| | Ratio | 14.5 | 15.1 | 14.8 | 2.9 | 2.1 | 1.9 |
| 2 | $I_{top}$ | 9.05 μA | 3.4 μA | 1.24 μA | 12.55 μA | 3.22 μA | 995 nA |
| | $I_{bottom}$ | 1.15 μA | 0.337 μA | 0.128 μA | 3.16 μA | 1.56 μA | 555 nA |
| | Ratio | 7.9 | 10.1 | 9.7 | 4 | 2.1 | 1.8 |
| 3 | $I_{top}$ | 5 μA | 2.61 μA | 800 nA | 13.7 μA | 3.22 μA | 681 nA |
| | $I_{bottom}$ | 0.61 μA | 0.33 μA | 95 nA | 6.15 μA | 1.96 μA | 467 nA |
| | Ratio | 8.2 | 7.9 | 8.4 | 2.2 | 1.6 | 1.46 |

glass wafer, as shown in Fig.3. The thickness of Pyrex glass wafer is 700 μm. Finally, the last etching of the previously obtained membrane determines distancers on glass support, as shown in Fig.1. The distance between vertical etched silicon inner walls is 3345 μm. Finally, the Pyrex glass wafer was sawed into 4000 μm x 4000 μm carriers.

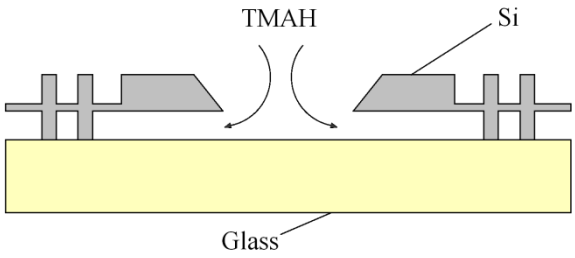


Fig. 3. Schematic picture of partly micromachined silicon wafer anodically bonded to Pyrex glass wafer.

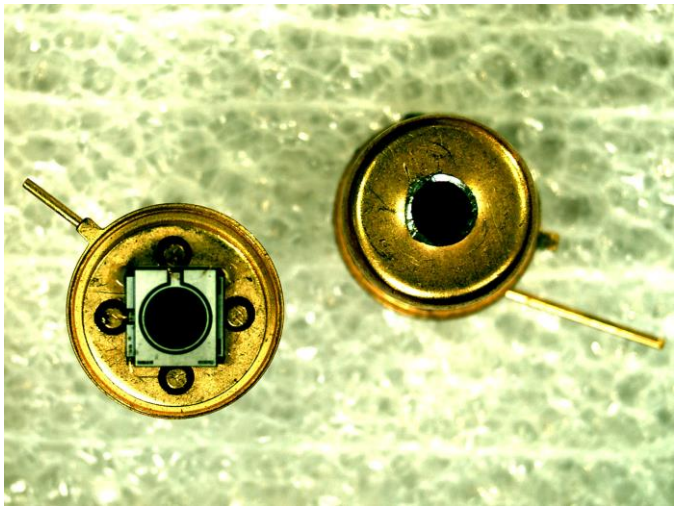

Fig. 4. Two photodiodes mounted on TO-5 housing with and without cap.

## III. RESULTS AND DISCUSSION

The photodiodes were measured separately before mounting in order to confirm their quality and compare with IHTM commercial photodiodes. Sensitivities for both photodiodes were 0.65 A/W for 900 nm and 0.2-0.3 A/W for 1060 nm. Breakdown voltages of about 100 V were obtained. These parameters are similar to IHTM commercial photodiodes [1].

The top and bottom photodiodes are mounted on obtained carriers as shown in Fig.1. The carriers are then mounted on TO-5 housing, as shown in Fig.4,5 where the photodiodes are bonded to four pins using 25 μm gold wires. At the end, the cap with aperture was glued to TO-5 housing. Aperture is designed for the optical fiber as shown in Fig.5.

.

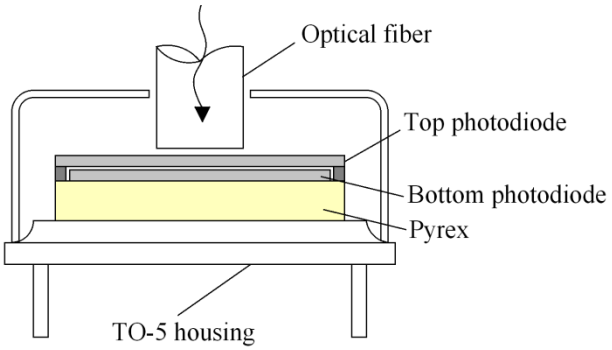


Fig. 5. Schematic picture of cross section packaging of mounted two photodiodes with optical fiber.

The light is applied through optical fiber in order to measure ratios between the photodiodes' output currents. We used the filters for 900 and 1060 nm when the light is applied. The obtained ratios between the photodiodes' output currents are given in Table 1 for three different detectors. For each two color detector ratios were measured for three different light intensities. From outputs and ratios given in Table 1, we can

 ISBN 978-86-7466-930-3

conclude that the designed carrier can be used as a part of packaging for two color detector. Our future work will be to improve our modified photodiodes presented in this paper in order to obtain better output characteristics.

## IV. Conclusion

In this paper, we explored and developed two color detector based on silicon photodiodes. We modified IHTM photodiodes in order to allow mounting of one photodiode above another and easy thermocompression bonding to TO-5 housing. We fabricated special carrier for photodiodes using wet silicon etching in 25% TMAH water solution. Output currents of the produced two color detectors were measured by applying light with the wavelengths of 900 nm and 1060 nm. Performed measurements confirm usability of the new designed carrier for two color detector.

## Acknowledgment

The authors acknowledge funding provided by the Institute of Chemistry, Technology and Metallurgy through a grant from the Ministry of Education, Science and Technological Development of the Republic of Serbia (Grant No. 451-03-68/2022-14/200026).

## References

[1] www.ihtm.bg.ac.rs
[2] D.B. Ponomarev, V.A. Zakharenko, "Silicon photodiode as the two-color detector", *Journal of Physics: Conference Series*, Volume 643, 2nd International School and Conference Saint-Petersburg OPEN on Optoelectronics, Photonics, Engineering and Nanostructures (SPbOPEN2015), St Petersburg, Russia, 6–8 April 2015.
[3] www.osioptoelectronics.com
[4] www.hamamatsu.com
[5] M.M. Smiljanić, B. Radjenović, M. Radmilović-Radjenović, Ž. Lazić. V. Jović, "Simulation and experimental study of maskless convex corner compensation in TMAH water solution", *J. Micromech. Microeng.* 24115003, 2014.
[6] M.M. Smiljanić, B. Radjenović, M. Radmilović-Radjenović, Ž. Lazić. V. Jović, "Evolution of Si crystallographic planes-etching of square and circle patterns in 25 wt % TMAH", *Micromachines*10(2) 102, 2019.
[7] M.M. Smiljanić, Ž. Lazić, V. Jović, B. Radjenović, M. Radmilović-Radjenović, "Etching of Uncompensated Convex Corners with Sides along <n10> and <100> in 25 wt% TMAH at 80 °C", *Micromachines* 11(3), 253, 2020.

 ISBN 978-86-7466-930-3

# Optimization of electrodeposition parameters to improve composite hardness of nickel coatings on brass substrate for varying film thicknesses and applied indentation loads

Ivana Mladenović, Jelena Lamovec, Marko Obradov, Milena Rašljić Rafajilović, Vesna Radojević, Dana Vasiljević Radović, *Member, IEEE* and Nebojša Nikolić

***Abstract*—In this investigation, nickel coatings were electrodeposited on brass substrate. The effects of electrodeposition process parameters such as, current density and deposition time (coatings thickness), on surface morphology and composite hardness values were studied. The value of the measured composite hardness by Vickers microindentation technique of the selected "hard film on soft substrate" composite system type depends on the applied indentation loads. For this reason, the microindentation loads are also included in the analysis. According to the experiment plan obtained by Design-Expert software, nickel coating has been produced on the brass cathode using galvanostatic regime (DC) with magnetic stirring of the electrolyte. The nickel sulphamate electrolyte with saccharine additive was used for Ni electrodeposition. Then, response surface methodology (RSM) was used to establish an adequate mathematical model. Subsequently, a mathematical model was developed to weight the effects of each input parameters (coating thickness, current density and indentation load) on the output parameter (composite hardness) of electrodeposited nickel coatings on brass substrate. According to the obtained results, the coating thickness and indentation load greatly influenced resulting composite hardness. On the other hand, coating current density primarily influenced microstructure and surface roughness. The topographic modification of the Ni coating surface depending on the post-treatment (mechanical and chemical) after deposition was studied using AFM microscopy.**

***Index Terms*— electrodeposition; composite hardness; RSM; AFM; optimization; nickel coating.**

## I. Introduction

THIN metallic coatings are often used for fabrication of different microelectronic and micromechanical devices. Thin coatings and bulk substrates constitute a composite system which mechanical properties depend not only on material characteristics of constituent materials but also on the mechanical interaction between the two such as the adhesion strength, residual stress, toughness and elastic-plastic properties [1-3]. In general, strong adhesion of the coating to the substrate is desired because it results in improved mechanical properties of the composite system. Additionally, reduction of the residual stress is paramount to prevent spontaneous delamination of the coating due to micro-crack growth between the thin coating and the bulk substrate [3].

Nickel (Ni) is one of the most common metals used to synthesize composite electrochemical coatings (CECs). It is characterized by superior corrosion and wear resistance, and enhanced mechanical and tribological properties [4]. Nickel coatings attract a huge attention from both scientific and technological communities owing to their unique properties, such as excellent friction coefficient during the wear testing of LIGA (lithographic) fabrication micro-rotors [5]. Ni alloys such as Co-Ni possess the high aspect ratio (HAR) during electrodeposition process and excellent magnetic and electrochemical properties [6].

Main methods of Ni thin film synthesis include: electrodeposition (ED), electroless plating (EL), physical vapour deposition (PVD), chemical vapour deposition (CVD), thermal spray and RF sputtering [1]. An interesting approach used for growing both pure Ni coatings and Ni alloys is electrochemical deposition technique. Conventional electrodeposition (ED) or new emulsion supercritical ED technique are very suitable ways to obtain nickel of desired characteristics suitable for application in above mentioned purposes [7, 8]. A common problem that exists during electrodeposition of Ni coatings is formation of hydrogen during ED process. The formation of hydrogen may create several pinholes on the coating [8], but the problem is solved by the adding surfactants (organic additives).

The most common electroplating solution for electrodeposition of Ni coatings met in the literature consists of nickel sulfate, nickel chloride, boric acid, saccharine and 1,4-butynediol [8]. In addition to the sulfate electrolyte, sulphamate electrolyte is also used [9]. Deposition parameters affect many properties of the electroplated material both during and after synthesis. By altering the synthesis parameters such as type of electrolyte and substrate, mixing condition, deposition time, applied current regime and density, post-deposition treatment, etc. we can control the grain size and microstructure of Ni coatings resulting in strengthened and hardened films with little or no loss in coating ductility.

Indentation testing is a reliable method for evaluation of material mechanical properties [3]. However, it cannot be

Ivana Mladenović, Marko Obradov, Milena Rašljić Rafajilović, Dana Vasiljević Radović and Nebojša Nikolić are with the Institute of Chemistry, Technology and Metallurgy, University of Belgrade, Njegoševa 12, 11 000 Belgrade, Serbia (e-mail: ivana@nanosys.ihtm.bg.ac.rs, marko.obradov@nanosys.ihtm.bg.ac.rs, milena@nanosys.ihtm.bg.ac.rs, dana@nanosys.ihtm.bg.ac.rs, nnikolic@ihtm.bg.ac.rs).

Jelena Lamovec is with the University of Criminal Investigation and Police Studies, Cara Dušana Street 196, Zemun, Belgrade, Serbia (e-mail: jelena.lamovec@kpu.edu.rs).

Vesna Radojević is with the Faculty of Technology and Metallurgy, University of Belgrade, Karnegijeva 4, 11 000 Belgtrade, Serbia (e-mail: vesnar@tmf.bg.ac.rs).

 ISBN 978-86-7466-930-3

applied directly for characterization of thin films due to plastic deformation of the sample during the indentation process [9, 10]. For this reason, indentation method is applied to measure composite hardness (thin film on bulk substrate). Various mathematical models have been developed to calculate thin film microhardness based on the directly measured composite hardness of the film [11-14].

The Response Surface Methodology (RSM) is the most insightful method of evaluating a factorial experiment performance [15, 16]. The aim of this paper, in addition to synthesis of excellent quality Ni coatings on brass by the ED method and microindentation characterization of the material, is also to design an optimal experiment (DoE) according to RSM (Response Surface Methodology) [15-20]. Modification of the coating structure after deposition is another contribution of this paper.

## II. Experimental

For electrodeposition of fine-grained nickel coatings we chose brass foil (260 1/2 hard, ASTM B36, K&S Engineering, 250 μm thick; composition: 66 % Cu, 34 % Zn) as a substrate (cathode). The surface area of the brass cathode was (2.0 × 1.0) $cm^2$. The pure Ni anode (rectangular in shape; positioned along the wall of the glass cell) and 500 ml of electrolyte were used. The nickel depositing apparatus is shown in Fig. 1. Prior to deposition, the cathode was mechanically polished and activated in a solution of sulfuric acid.

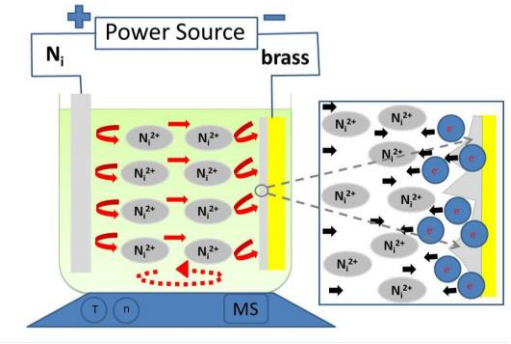


Fig. 1. Schematic presentation of nickel coating electrodeposition on brass substrate from sulphamate electrolyte in DC regime with magnetic stirrer (DC/MS).

Electrodeposition was performed in an open cell type using the direct current galvanostatic regime (DC) from a lab-made sulphamate electrolyte consisting of: 300 g/l Ni $(NH_2SO_3)_2{\cdot}4H_2O$, 30 g/l $NiCl_2{\cdot}6H_2O$, 30 g/l $H_3BO_3$ and 1 g/l saccharine as the wetting agent, with pH-value and the temperature of the process maintained at 4.20 and 50°C, respectively. The electrolytes were stirred by an application of magnetic stirrer (MS) (300 rpm, Heidolph Instruments GmbH & Co. KG, Schwabach, Germany). The DC/MS electrodeposited regime will be used below in the text.

The current density values were maintained at 10 mA $cm^{-2}$ and 50 mA $cm^{-2}$. The deposition time was determined according to projected thickness of the coating. Five different coating thicknesses were formed: 2, 5, 10, 20 and 50 μm for each applied current density. Cathodic efficiency of 100% was taken to calculate the deposition time. The thickness was checked across the cross-section using an optical microscope.

The cross-section preparation for characterization was done in a fallowing manner: samples were embedded in a self-curing methyl methacrylate-polymer (Palavit G, Heraeus, Germany) and mechanically polished with different SiC papers (#800 and #1200) and finished with emulsion of alumina powder with different grain size (1-0.3 μm) [21]. Then, rinsing in sodium-carbonate solution and dried in nitrogen flow. The cross-section was prepared in order to validate the thickness of the coating, to observe the adhesion at the coating-substrate interface and to assess the hardness of the coating at the cross-section, see Fig. 2.

The mechanical properties of the composite system and substrate on top side and cross-section were characterized utilizing a Vickers microhardness tester ″Leitz, Kleinharteprufer DURIMET I″ using up to 15 loads ranging from 500 gf (4.9 N) down to 5 gf (0.049 N), see Figs. 2, 3 and 4. Five different loads were selected for optimization (10, 50, 100, 150 and 300 gf). Three indentations were made and the average value of the diagonal was determined by measuring six indentation diagonals, for each load. With the average value of the diagonals, the mean value of the hardness was calculated [9].

The topographic analysis of coatings surface after post-treatment was investigated using an atomic force microscope in the non-contact mode (AFM-Auto Probe CP Research; TM Microscopes-Veeco Instruments, Santa Barbara, CA, USA). The scan area was (20 × 20) $\mu m^2$. A histogram analysis of the coatings and bearing rate curve [22, 23] were done by an application of WSxM AFM software [24]. The analysis was performed in order to assess the resistance of the coating and the change in roughness during mechanical treatment and exposure to aggressive reagents such as hydrochloric acid (Fig. 5).

## III. Results and Discussion

### A. *Indentation on different locations*

The microhardness of Ni coating and influence of the substrate hardness during penetration of indenter is shown to depend on the indentation site. The hardness measured on the cross-section of brass (Fig. 2a) corresponds to the absolute bulk substrate hardness that is used in proportional specimen resistance (*PSR)* model ($H_s$ = 1.41 GPa) [25].

If the indentation is performed on the coating surface, the structural-morphological properties of the coating affect the measurement, and the contribution of the substrate must be taken into account. The measured value of hardness is called composite hardness, $H_c$. In the case of cross-sectional indentation (Fig. 2b), the measured hardness, $H_{c\text{-}s}$ is constant and equal to the hardness of the bulk material without effects of substrate hardness and morphology of coating surface. Comparative values are shown in Table I. The diagonal size measured on the cross-section of the coating ($d_{c\text{-}s}$) is smaller than on the surface of composite ($d$), for the same applied load. For the "hard film on soft substrate" composite system type, the cross-sectional hardness value is higher than the composite hardness.

The interfacial indentation [3] hardness test (Figs. 2c and 2d) is a quick way to assess interlayer adhesion strength of the coating to the substrate and indentation toughness

 ISBN 978-86-7466-930-3

properties. The interfacial hardness and diagonal interfacial size ($d_i$) measurement is complex. The problem with this method of measurement is a possible difference in the height of nickel and brass due to the different wear rate of the material when preparing the cross-section. The delamination of the Ni coating did not occur, so the adhesion of the Ni coating for brass substrate is good. For very thin coatings (2, 5, 10 μm), it is not possible to measure hardness on the cross-section, because the Vickers indent size is larger than the projected thickness of the coating.

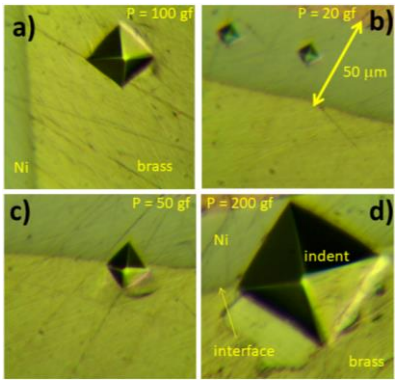


Fig. 2. Indentation on different location of cross-section with variation applied load on Ni/brass composite system: a) indentation on brass substrate, $P$ = 100 gf, b) indentation on Ni coating, $P$ = 20 gf, c) interfacial indentation, $P$ = 50 gf and d) interfacial indentation, $P$ = 200 gf. Nickel coating was obtained in DC/MS electrodeposition regime at 50 mA cm$^{-2}$ current density.

TABLE I
CHANGE IN THE HARDNESS OF THE NICKEL COATING DEPENDING ON THE MEASURING LOCATION

| $P$ / gf | $d$ / μm | $d_{c\text{-}s}$ / μm | $H_c$ / GPa | $H_{c\text{-}s}$ / GPa |
|---|---|---|---|---|
| 20 | 11.08 | 10.50 | 2.945 | 3.278 |
| 50 | 18.88 | 15.40 | 2.535 | 3.810 |
| 100 | 24.90 | 22.00 | 2.914 | 3.734 |
| 200 | 36.50 | 34.05 | 2.713 | 3.117 |

### *B. Indentation on the top surface of the Ni coatings on brass substrate*

Different load-indentation depth curves can be obtained by changing the coating thickness of Ni coatings and current densities (Fig. 3). It can be seen that the coating thickness is the dominant parameter in the loading indentation process, while current density has very little effect, especially for small coating thicknesses.

The dependencies of the composite hardness ($H_c$) on the relative indentation depth (*RID*) for the given Ni coatings are shown in Figure 4. The *RID* is defined as a ratio between an indentation depth, $h$ and a coating thickness, δ (*RID* = $h$ /δ), where an indentation depth depends on a diagonal size as $h$ = $d$ /7 [9, 11-14, 21]. The contribution of substrate to composite hardness increases with the increasing *RID* value and applied load $P$, suggesting that the composite hardness matches the substrate hardness at high *RID* values.

Figure 4 clearly shows three characteristic zones depending on the influence of coating and substrate hardness on the composite hardness: 1) dominant influence of the coatings corresponds to 0.01 < *RID* < 1 (for thick 50 μm coatings), 2) the composite zone corresponds to 0.1 < *RID* < 1 for medium-thick films (10 and 20 μm) and 3) the dominant influence of the substrate is characteristic when *RID* > 1; for thin coatings (2 and 5 μm).

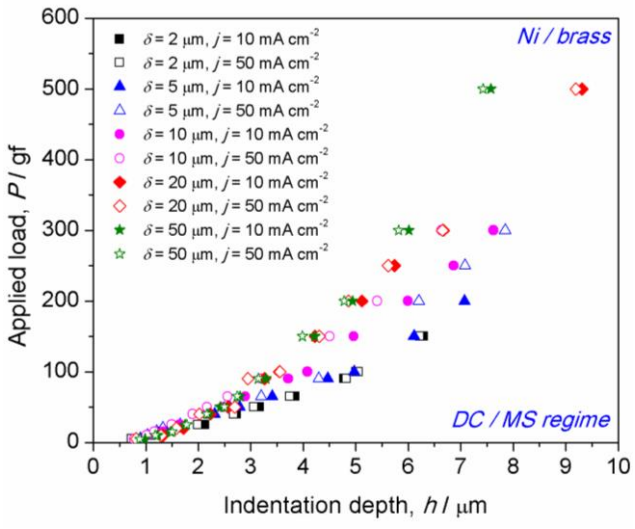


Fig. 3. Load-indentation depth experimental points of different Ni coating thickness electrodeposited on brass substrate in DC/MS regime at two current densities (10 and 50 mA·cm$^{-2}$).

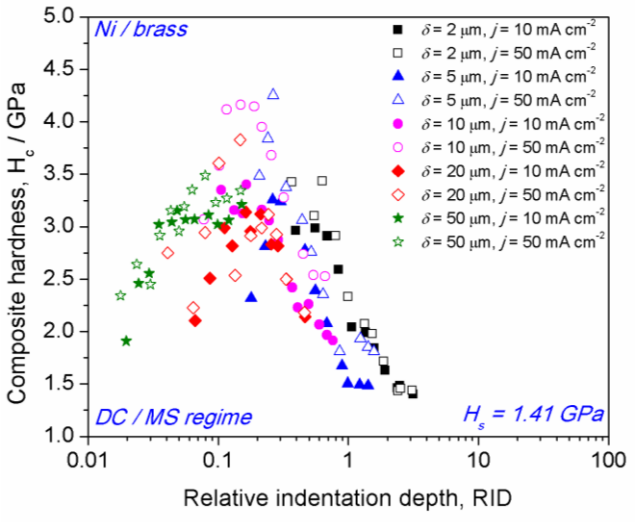


Fig. 4. The dependencies of the composite hardness ($H_c$) on the RID for the Ni coatings electrodeposited on the brass from the sulphamate electrolyte.

Figure 4 also shows a characteristic turning point, corresponding to a value of *RID* of 0.14. For the *RID* values smaller than 0.14, the measured composite hardness corresponds closely to the hardness of the coating. By crossing this critical point, the value of hardness decreases, which indicates the contribution of the softer substrate below. The Ni coatings obtained with a higher current density (50 mA·cm$^{-2}$) appeared harder than those deposited with 10 mA·cm$^{-2}$. For hard coating on soft substrate composite systems, with increasing the relative indentation depth (0.1 ≤ *RID* ≤ 1), the composite hardness $H_c$ decreases until the hardness of the substrate is reached as shown on Fig.4 ($H_s$ = 1.41 GPa).

 ISBN 978-86-7466-930-3

### *C. Modification of Ni surface after deposition by mechanical and chemical treatments*

Stochastically roughened of metallic thin coatings can be obtained with various methods including dry etching, wet chemical etching or mechanical treatment (abrasion). Depending on the applied method, different surface profiles are obtained with microstructural modifications of surface coatings. The goals of this work were to explore the correlations between the AFM-based and treatment method for samples with different roughness and therefore different areas. For example, the difference in mechanical properties on the cross-section and the surface of the coating is one of the consequences of the treatment (mechanical). The roughness of each of the samples was determined using AFM topographic measurements. Figures 5 present the 3D AFM images of Ni / brass systems obtained at 50 mA·cm$^2$ (left) and histograms (right) with different treatment: mechanical (Figs. 5 a, b), chemical (Figs. 5 c, d) and no-treatment (Figs. 5 e, f).

Comparing the topography of nickel coatings, mechanical treated (Fig. 5a) and chemical treated coating (Fig. 5c) have similar roughness and stochastically nodular topography. Ni coating with mechanical treatment (Fig. 5a) can be observed to have a rather irregular surface with distributed nodular surface features. Deep channels as a result of sanding and scratching the surface were observed, too. From the values of the arithmetic average of the absolute roughness parameter ($R_a$) of the surfaces presented in Fig. 5, it could be observed that the roughness increases for Ni coatings including either chemical or mechanical treatment relative to non-treated coating ($R_a$ = 28.68 nm for no-treated, $R_a$ = 82.43 for chemical and $R_a$ = 78.14 for mechanical treated coatings).

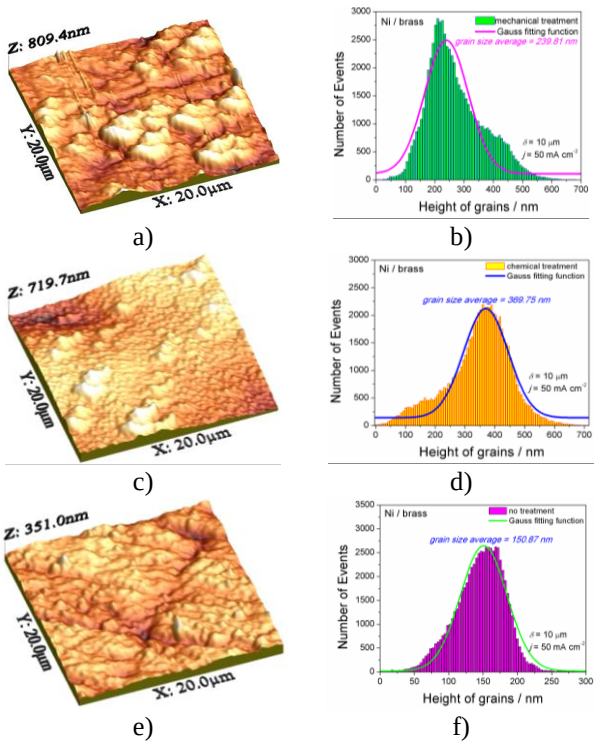


Fig. 5. Examples (20 × 20) μm$^2$ AFM topographic measurements for a Ni coating (10 μm thick) on brass substrate (left) and corresponding histograms (right) after electrodeposition and roughened surface treatment: a) and b) mechanical; c) and d) chemical; e) and f) no treatment. Ni coatings were obtained by electrodeposition technique in DC/MS regime at a current density of 50 mA cm$^{-2}$ from the sulphamate electrolyte.

Although the topography of the untreated sample and the chemically etched one is very similar, based on the average height of grains obtained via the Gaussian distribution fitting function, it can be seen that the chemically treated sample has higher peaks (369.75 nm). However, mechanical treatment of the surface leads to the suppression of high peaks (Fig. 5b), which results in a reduction of total roughness (239.81 nm), i.e. smoothing of the surface.

Figures 6 show the relationship of bearing ratio (in %) with the grain height (Firestone–Abbott bearing curve, standards DIN4776; STN ISO 13 565-2). The bearing curve is the cumulative probability density function of the surface profile's height which is calculated by integrating the profile of the AFM trace [22]. As can be seen, if the bearing area rate reached 95 %, the order of the corresponding grain height of these treated Ni coatings are mechanical (800 nm) > chemical (700 nm) > no treatment (350 nm), see Fig. 6a.

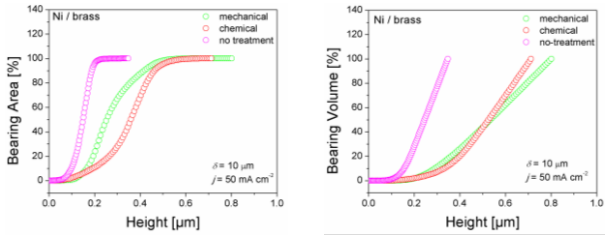


Fig. 6. Bearing ratio curves of Ni coatings on brass substrate with a variation of treatment: a) bearing area and b) bearing volume curve.

With application of post-treatment, the distribution range of nodule sizes shifts to the direction of larger values, see Fig. 6a. It indicated that the Ni coating without any treatment has the finest granule size, comparatively. It suggested that the Ni benefits smooth and fine-grained structure. Bearing flooded volume or bearing area curve indicated that the critical dimension point is 500 nm for peak height (Figs. 6a and 6b) for treated surface.

### *D. Optimization of composite hardness of Ni/brass systems*

Design-Expert 12 (Stat-Ease, US) software and Optimal Design was used for the response methodology to examine correlation between the input variables (coating thickness, current density and applied indentation load) and output parameter (composite hardness). The factors (3 numerical) and factor levels (numerical) are shown in Table II.

TABLE II

INFLUENCE FACTORS ON NI COATING COMPOSITE HARDNESS

| Mark | Parameters | Value limit Lower | Value limit Upper | unit |
|---|---|---|---|---|
| $P$ | Applied indentation loads | 10 | 300 | gf |
| $\delta$ | Thickness of the Ni coatings | 2 | 20 | μm |
| $j$ | Current densities | 10 | 50 | mA cm$^{-2}$ |


ISBN 978-86-7466-930-3

Using data given in Table II, a regression mathematical model was developed to describe the function between the input parameters and measured response values. The relationship enabling a prediction of the composite hardness ($H_c$) values of the Ni/brass systems in a function of applied variables (indentation load ($P$), thickness of the coating ($\delta$) and current density ($j$) is given by Eq. 1:

$$H_c^{-1}=0.3833+0.0534A-0.11191B-0.024C-0.835AB-$$
$$-0.0391AC-0.033BC-0.0433A^2+0.01374B^2+0.0318C^2 \quad (1)$$

where A, B and C represent numerical factors from Table II corresponding to the input variables, i.e. applied load, coating thickness and current density. Figure 7 shows the dependence of $H_c$ values predicted by the RSM based on the regression model generated by coded Eq. 1 for every combination of two input parameters: applied load, coating thickness and current density (Fig. 7a load and thickness; Fig.7c current density and load; Fig. 7e current density and thickness). Each combination has a positive and statistically significant effect on composite hardness as also revealed by the contour lines presented in Figs. 7b, 7d and 7f. The red color corresponds to high values of composite hardness i.e. dominant influence of the coatings ($H_c \rightarrow 3.4$ GPa), yellow and green correspond to the composite zone and the blue indicates the dominant influence of the substrate i.e. composite hardness approaches to the hardness of the substrate ($H_c \rightarrow H_s$).

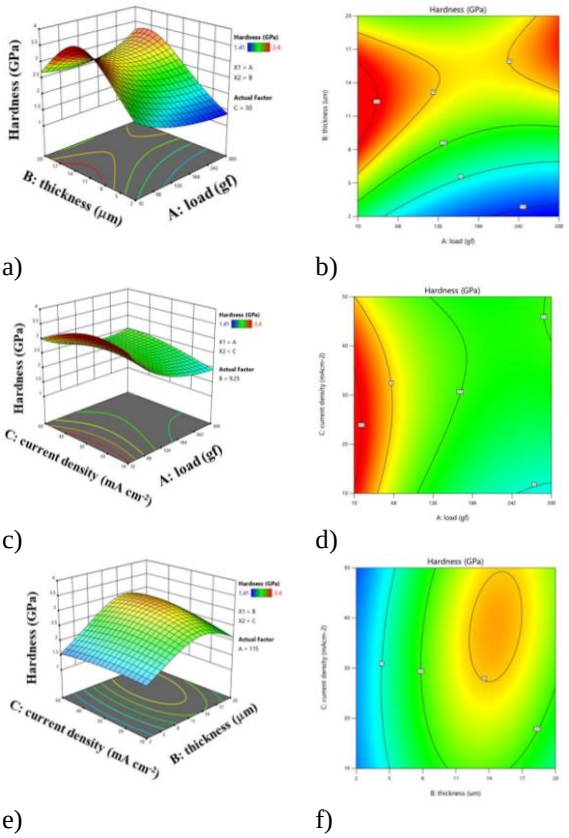


Fig. 7. 3D response surface (left) and contour plot (right) of Ni/brass composite hardness for different coded values: a) and b) of A (indentation load) and B (thickness), c) and d) of A (indentation load) and C (current density), e) and f) for B (thickness) and C (current density).

An increase in current density also indicates an increase in composite hardness value, but for indentation loads corresponding to the "film zone" (up to 50 gf), see Fig. 7d. It can be seen from Fig. 7 that the coating thickness and applied loads have a significant impact on the Ni/brass composite hardness systems. The current density is the least dominant factor in composite hardness change (Figs. 7f).

## IV. Conclusion

The parameters suitable for fabrication of hard, compact and uniform Ni coatings on brass substrate were obtained in the direct current regime with magnetic stirring (DC/MS) from lab-made sulphamate electrolyte. Nickel coatings of various thickness were obtained utilizing different current densities. The maximal composite hardness of Ni/brass composite system was achieved for a current density of 50 $mA \cdot cm^{-2}$, 15 µm coating thickness and with applied indentation load of 50 gf (0.49 N).

Two ways of measuring micro hardness are presented: on the cross-section and the top of surface coating. The measured hardness at the cross-section of depth Ni is higher than composite hardness on top surface. Based on the interfacial indentation test, good adhesion between the coating and the substrate was determined, and no delamination occurred.

Stochastically roughened of electrodeposited Ni thin coatings can be obtained with various methods including mechanical and chemical treatment after electrodeposition process. Based on topographic analysis, it has been shown that each additional treatment after electrochemical deposition introduces an increase in stochastic roughness. That means, after deposition, it is not necessary to treat the surface of the coating before micro indentation.

The RSM optimization of operating parameters for the synthesis of the Ni/brass composite system was applied. Analysis of variance confirmed that the proposed regression model is in good agreement with the experimental data, providing a high determination and adjusted determination coefficients. The results suggested that the used adequate micro indentation loads, as well as the synthesis parameters, can directly affect the material mechanical properties such as composite hardness.

## Acknowledgment

This work was funded by Ministry of Education, Science and Technological Development of Republic of Serbia (Grants No. 451-03-68/2022-14/200026 and 451-03-68/2022-14/200135).

## References

[1] D. T. Read, A. A. Volinsky, "Thin Films for Microelectronics and Photonics: Physics, Mechanics, Characterization and Reliability, Micro- and Opto-Electronic Materials and Structures, Springer US, 2007, Part I, pp. 135-180.

[2] S. E. Lyshevski, "Nano- and microelectromechanical systems: Fundamentals of nano- and microengineering, CRC Press LLC, New York, NY, 2001, pp. 11-25.

[3] A. A Volinsky, N. R Moody, W. W Gerberich, "Interfacial toughness measurements for thin films on substrates", *Acta Mater.*, vol. *50*, no. *3*, pp. *441-466*, Feb., 2002.

[4] A. Siddaiah, P. Kumar, A. Henderson, M. Misra, P. L. Menezes, "Surface Energy and Tribology of Electrodeposited Ni", *Lubricants*, vol. *7*, no. *10*, p. *87*, Oct., 2019.

[5] J. Goettert, P. Datta, Y. Desta, Y. Jin, Z. Ling, V. Singh, "LiGA Research and Service at CAMD", *J. Phys.: Conf. Ser.*, vol. *34*, no. *912*, "International MEMS conference", Singapore, 9–12 May, 2006.

[6] M. Duch, J. Esteve, E. Gómez,R. Pérez-Castillejos, E. Vallés, "Electrodeposited Co-Ni alloys for MEMS", *Micromech. Microeng.*, vol. *12*, no. *4*, pp. *400-405*, July, 2002.

 ISBN 978-86-7466-930-3

[7] M. Schlesinger, M. Paunovic, *Modern Electroplating 4*th ed. New York, US, John-Wiley and Sons Inc, 2000.

[8] H. Yoshida, M. Sone, H. Wakabayashi, H. Yan, K. Abe, X. T. Tao, A. Mizushima, S. Ichihara, S. Miyata, "New electroplating method of nickel in emulsion of supercritical carbon dioxide and electroplating solution to enhance uniformity and hardness of plated film", *Thin Solid Films,* vol. *446*, no. *2*, pp. *194-199*, 2004.

[9] J. Lamovec, V. Jović, D. Randjelović, R. Aleksić, V. Radojević, "Analysis of the composite and film hardness of electrodeposited nickel coatings on different substrates", *Thin Solid Films,* vol. *516*, no. *23*, pp. *8646-8654*, June, 2008.

[10] Z. S. Ma, Y. C. Zhou, S. G. Long, C. Lu, "On the intrinsic hardness of a metallic film/substrate system: Indentation size and substrate effects", *Int. J. Plast.,* vol. *34*, no. *1*, pp. *1-11*, July, 2012.

[11] J. Lesage, D. Chicot, A. Pertuz, P. -Y. Jouan, N. Horny, A. Soom, "A model for hardness determination of thin coatings from standard micro-indentation tests", *Surf. Coat. Technol.,* vol. *200*, no.*1–4*, pp. *886–889*, Oct., 2005.

[12] J. L. He, W. Z. Li, H. D. Li, "Hardness measurement of thin films: Separation from composite hardness," *Appl. Phys. Lett.,* vol. *69*, no. *10*, pp. *1402–1404*, Jun., 1996.

[13] E. S. Puchi-Cabrera, "A new model for the computation of the composite hardness of coated systems", *Surf. Coat. Technol.,* vol. *160*, no. *2–3*, pp. *177-186*, Oct., 2002.

[14] J. R Tuck, A. M Korsunsky, R. I Davidson, S. J Bull, D. M Elliott, "Modelling of the hardness of electroplated nickel coatings on copper substrates", *Surf. Coat. Technol.,* vol. *127*, no. *1*, pp. *1-8*, May, 2000.

[15] M. Santhanakrishnan, P. S. Sivasakthivel, R. Sudhakaran, "Modeling of geometrical and machining parameters on temperature rise while machining Al 6351 using response surface methodology and genetic algorithm", *J Braz. Soc. Mech. Sci. Eng.,* vol. *39*, no. *1*, pp. *487–496*, June, 2017.

[16] M. Santhanakrishnan, N. Venkateshwaran, M. Rajkumar, T. Vignesh, "Performance evaluation of Ni/Nano SiC coated tool insert for machining SS316l using Response Surface Methodology (RSM)", *Mater. Today: Proc.,* vol. *47*, no. *14*, pp. *4671-4675*, Oct., 2021.

[17] R. El-Khalfaouy, K. Khallouk, A. Elabed, A. Addaou, A. Laajeb, A. Lahsini, "Modeling and synthesis of carbon-coated LiMnPO4 cathode material: Experimental investigation and optimization using response surface methodology", *J. Electrochem. Sci. Eng.,* vol. *12*, no. *2*, pp. *305-316*, Jan., 2022.

[18] W. Jau-Kai, C. Jir-Ming, "Optimization study on hardness of gold film through supercritical electroplating process by response surface methodology", *Chem. Ind. Chem. Eng. Q.,* vol. *21*, no. *2*, pp. *311-317*, Aug., 2015.

[19] A. F. Almeida, J. I. V. Souto, M. L. Santos, R. A. C. Santana, J. J. N. Alves, A. R. N. Campos, S. Prasad, "Establishing relationships between bath composition and the properties of amorphous Ni–Mo alloys obtained by electrodeposition, *J. Alloys Compd.,* vol. *888*, p. *161595*, Dec., 2021.

[20] S. Esmailzadeh, T. Shahrabi, Y. Yaghoubinezhad, Gh. Barati Darband, "Optimization and characterization of pulse electrodeposited nickel selenide nanostructure as a bifunctional electrocatalyst by response surface methodology", *Int. J. Hydrogen Energy,* vol. *46*, no. *36*, pp. *18898-18912*, May, 2021.

[21] I. Mladenović, Z. Jakšić, M. Obradov, S. Vuković, G. Isić, D. Tanasković, J. Lamovec, "Subwavelength nickel-copper multilayers as an alternative plasmonic material", *Opt. Quant. Electron.,* vol. *50*, no. *5*, p. *203*, Apr., 2018.

[22] D. P. Linklater, F. Haydous, C. Xi, D. Pergolesi, J. Hu, E. P. Ivanova, S. Juodkazis, T. Lippert, J. Juodkazytė,"Black-Si as a Photoelectrode", *Nanomaterials,* vol. *10*, no. *5*, p. *873*, May, 2020.

[23] B. Li, W. Zhang, T. Mei, S. Du, Y. Miao, D. Li, "Synthesis and properties of YSZ and CeO2 dual nanoparticles doped Ni–B matrix nanocomposite coating", *Ceram. Int.,* vol. *46*, no. *6*, pp. *8047-8058*, Apr., 2020.

[24] I. Horcas, R. Fernández, J. M. Gómez-Rodríguez, J. Colchero, J. Gómez-Herrero, A. M. Baro, "WSXM: A software for scanning probe microscopy and a tool for nanotechnology", *Rev. Sci. Instrum.,* vol. *78*, no. *1*, p. *013705*, Jan., 2007.

[25] I. O. Mladenović, N. D. Nikolić, J. S. Lamovec, D. Vasiljević-Radović, V. Radojević, "Application of the Composite Hardness Models in the Analysis of Mechanical Characteristics of Electrolytically Deposited Copper Coatings: The Effect of the Type of Substrate", *Metals,* vol. *11*, no. *1*: p. *111*, Jan., 2021.

 ISBN 978-86-7466-930-3

# Electrically Programmable Analog Device As An Ultraviolet Light Sensor

Stefan D. Ilić, *Student Member, IEEE*, Milija Sarajlić, *Member, IEEE*, Dana Vasiljević-Radović, *Member, IEEE*, Marko S. Andjelković, Alberto Palma, Russell Duane, and Goran S. Ristić

***Abstract*—Electrically Programmable Analog Device (EPAD) is a commercial semiconductor device based on a floating gate MOS transistor. It is possible to charge the EPADs floating gate with electrons and thus increase the threshold voltage of the MOS transistor. Decapsulation of the ALD1108E integrated circuit containing four EPADs was performed to expose the semiconductor structure to ultraviolet light. By irradiating with different UV light sources, the threshold voltage of an EPAD with a pre-charged floating gate decreases, indicating a possibility for UV radiation detection. The sensitivity of EPAD to the UV light range of 311 to 400 nm was investigated. The floating gate MOS transistor (EPAD), which has a more charged floating gate with electrons, i.e. higher threshold voltage value, shows higher sensitivity compared to EPAD with a lower charged floating gate, i.e. lower threshold voltage value.**

***Index Terms*—Floating gate MOS transistor, Ultraviolet Light, Light Sensor, EPAD, IC decapsulation**

## I. Introduction

MEMORIES that remember content even after a power failure are called Non-Volatile Memories. First came the Mask ROM (Read Only Memory) memory, i.e. mask programmed ROM. A whole array of memory cells is formed on the chip in the form of a matrix. Then, according to the user's request, a mask for the photolithographic procedure is created, which defines the openings for drawing the lines of connection between cells and the power supply. Cells that should contain a logic "1" are connected to the power supply (highly doped polysilicon is applied through the opening on the mask to make contact), while cells that should contain a logic "0" remain unbound to the power supply. The Mask ROM stores data permanently, the process is very expensive, and every change requires a change of the photolithography mask.

This research was funded by Ministry of Education, Science and Technological Development of the Republic of Serbia, under the project No.43011, grant No.451-03-68/2022-14/200026 and European Commission, WIDESPREAD-2018-3-TWINNING, grant No.857558 - ELICSIR.

S. D. Ilić, M. Sarajlić and D. Vasiljević-Radović are with the Center of Microelectronic Technologies, Institute of Chemistry, Technology and Metallurgy, University of Belgrade, Serbia, S. D. Ilić is also with the Applied Physics Laboratory at Faculty of Electronic Engineering, University of Niš, Serbia, E-mail: stefan.ilic@nanosys.ihtm.bg.ac.rs

M. S. Andjelković is with the System Architectures Department, IHP - Leibniz-Institut für innovative Mikroelektronik, Frankfurt (Oder), Germany, E-mail: andjelkovic@ihp-microelectronics.com

A. Palma is with the Department of Electronics and Computer Technology, University of Granada, Granada, Spain, E-mail: ajpalma@ugr.es

R. Duane is with the Centre for Micro and Nano Systems, Tyndall National Institute, University College Cork, Dyke Parade, Cork, Ireland, E-mail: russell.duane@tyndall.ie

G. S. Ristić is with the Applied Physics Laboratory at Faculty of Electronic Engineering, University of Niš, Serbia, E-mail: goran.ristic@elfak.ni.ac.rs

In order to solve the problem of expensive production, PROM (Programmable ROM) memory is created; here, the data is stored by the user himself with specialized electrical devices. Namely, PROM is produced so that all cells have a logic "1", and they are all connected to the power supply. The interruption of connection lines between individual cells is done by passing a high-density current, which melts the desired line. Once programmed, the PROM cannot be reprogrammed.

The next memory that emerged with technology development is an EPROM (Erasable & Programmable ROM). For the first time, it is possible to delete data, which is done by exposing the memory to UV rays. EPROM is the first memory to have a floating gate (FG) in its structure, and thanks to such a device, it is possible to erase the charge on the pre-charged floating gate and thus change the threshold voltage of the MOS transistor. Decreasing the threshold voltage leads to a change in the logical state of the cell from "0" to "1". The memory is byte-addressable when writing and reading, while the deletion process covers the entire memory. When deleting, the memory chip must be removed from the motherboard and exposed to UV radiation for 20 minutes [1]. The complete deletion process needs to be done even though only one byte needs to be changed.

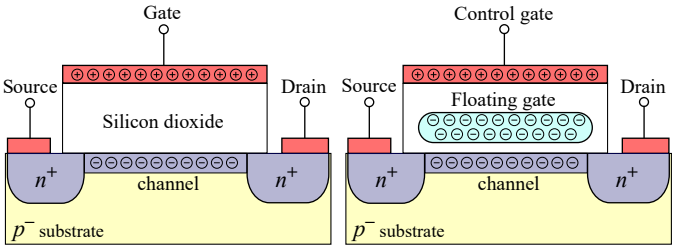


Fig. 1. Left: Cross-section of a MOS transistor. Right: Cross-section of a MOS transistor with a floating gate

Figure 1 shows the structure of a MOS transistor, and the structure of a MOS transistor with a floating gate (FG). During ultraviolet radiation, photons reach the floating gate and generate electron-hole pairs in the vicinity of the floating gate. Due to the electric field that originates from the floating gate, the generated carriers are separated because it is charged with electrons. The holes recombine with the electrons located on the floating gate, and thus the amount of charge is reduced, which leads to a lower threshold voltage value of the MOS transistor.

 ISBN 978-86-7466-930-3

## II. Materials and Experimental Setup

The experiment consisted of irradiating the decapsulated IC ALD1108E [2] with three different types of UV sources. Decapsulation of the ALD1108E integrated circuit is a high-tech process that requires the removal of plastic above the chip so that light can reach the semiconductor device, while the bonds connecting the chip to the package must not be damaged. This process was performed at the Tyndall National Institute, Cork, Ireland. Since decapsulated integrated circuits are extremely sensitive to handling and potential mechanical damage and chip contamination if handled in dirty conditions, the experiment was performed in a cleanroom at the Center of Microelectronic Technologies, Institute of Chemistry, Technology and Metallurgy, Serbia. The number of particles in a cleanroom was controlled using a PCE-PCO 1 particle counter. During the experiment, all measured particle sizes were filtered to zero. The measurement of particles was done in 21 seconds, which corresponds to airflow of 1 litre.

In order to protect the decapsulated chip from mechanical damage during the handling and measurements, special housing for UV experiments made of polylactic acid (PLA) material with a quartz window was designed, as shown in Figure 2.

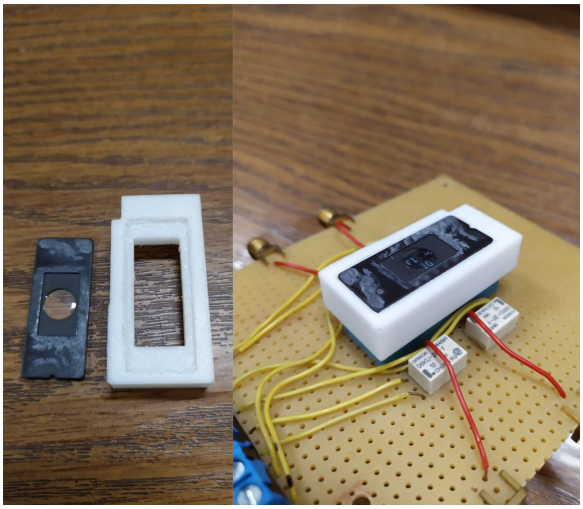

Fig. 2. Left: A quartz window and housing for decapsulated IC made of PLA material. Right: Assembled housing on the IC ALD1108E inserted in the ZIF socket.

The housing was designed in the Solid Edge 2021 Academic version and then fabricated using the Creality Ender 6 CoreXY 3D printer. The decapsulated integrated circuit has a weakened plastic housing and therefore needs to be handled very carefully, especially when inserted into the IC socket. Therefore, an electric circuit for measuring the characteristics of EPAD on the IC ALD1108E with a zero insertion force (ZIF) socket has been designed.

The housing is designed to protect the decapsulated IC from all sides but not to touch the plastic DIP of the integrated circuit due to potential damage to the bonds during handling. Therefore the housing is mounted on the ZIF socket in which the integrated circuit is inserted.

Since it is necessary for UV light to penetrate the housing, a quartz window has been installed to enable this. Old EPROM memories had a quartz window on their package so that UV light could erase the memory, and this gave the idea to the authors to use a quartz window from an old memory from ST Microelectronics.

To ensure that a sufficient amount of UV light passes through the selected quartz window, the transmission of our housing was measured using a UV-Visible Spectrophotometer Evolution 60 from Thermo Scientific, and shown in Figure 3.

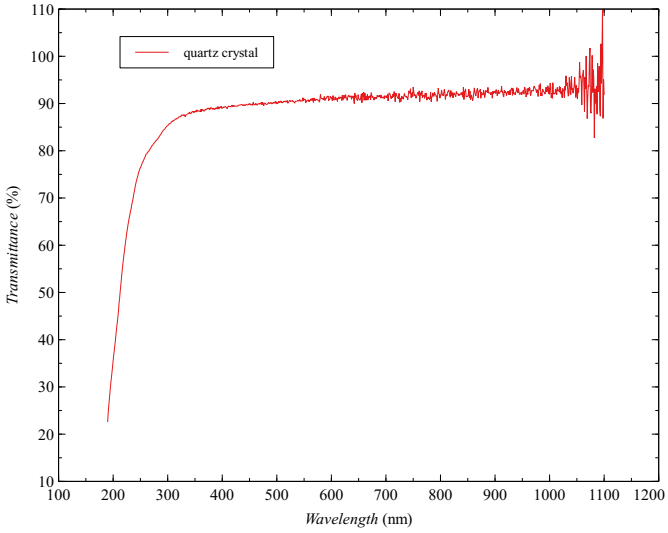


Fig. 3. Transmittance of quartz window mounted in housing made of PLA material.

For a wavelength value of 300 nm, the transmittance is 85% and then increases to 90% for the visible part of the spectrum. The wavelength range for this research is from 300 to 400 nm. The UV light sources used for the purposes of this experiment are: a UV lamp with a 311 nm peak, a UV lamp with a 365 nm peak and a UV LED with a 400 nm peak; their spectrographs are shown in Figures 4 to 6, respectively.

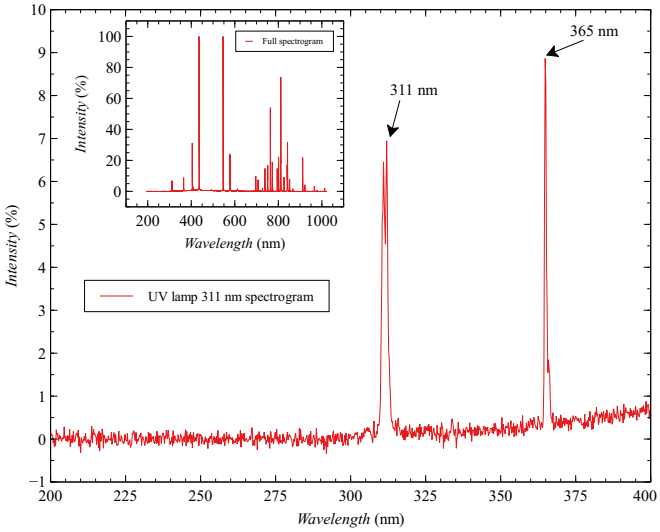


Fig. 4. Spectrogram of UV lamp with 311 nm peak.


ISBN 978-86-7466-930-3

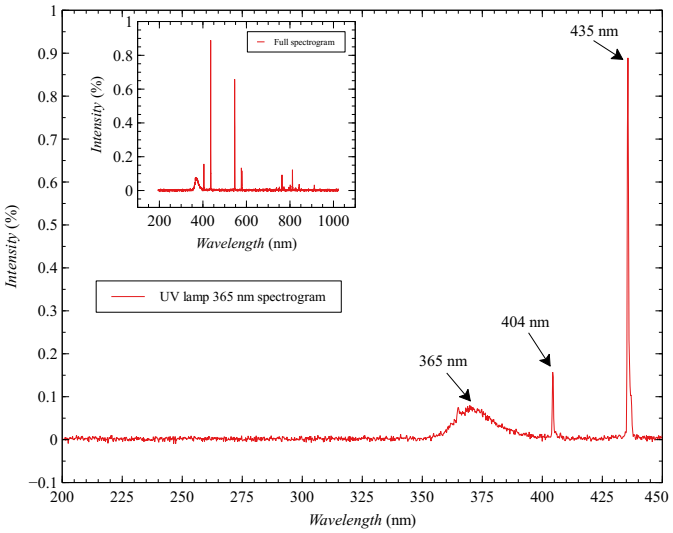


Fig. 5. Spectrogram of UV lamp with 365 nm peak.

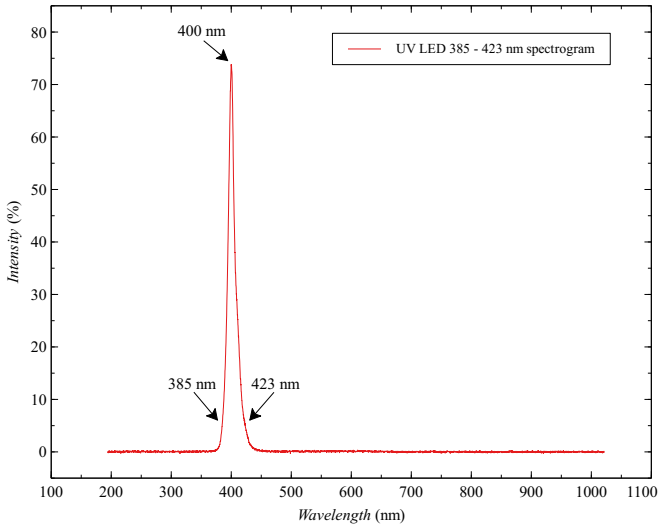


Fig. 6. Spectrogram of UV LED with 400 nm peak.

A UV lamp that emits light with a peak at 311 nm is used for the phototherapeutic treatment of skin diseases by producing vitamin D. As can be seen in Figure 4, this lamp has two peaks in the ultraviolet part of the spectrum at 311 nm and then at 365 nm. Other emitted light is in the visible part of the spectrum.

The following UV lamp used in the experiment has an application as a gel nail dryer. This lamp has only one broad peak in the ultraviolet part of the spectrum at 365 nm, while the others are in the visible part of the spectrum, as can be seen in Figure 5.

The third UV source used in this experiment is a matrix of UV LEDs. The spectrum of this source is clear, unlike UV lamps and has only one peak at 400 nm, at the border of UV and visible light.

## III. Results

During the irradiation of the ALD1108E chip, the drift of two floating gate MOS transistors (EPADs) was measured using a Keithley 2636A source measure unit connected to a computer. Drift is monitored at one point of the current-voltage characteristic called the zero temperature coefficient (ZTC) point [3]. Monitoring the change in the drift at this point cancels the influence of temperature on the measurements, which is an essential factor.

ZTC voltage drifts before, during and after UV irradiation for two EPADs with the same value of threshold voltage (initial Vth = 4 V) is shown in Figure 7.

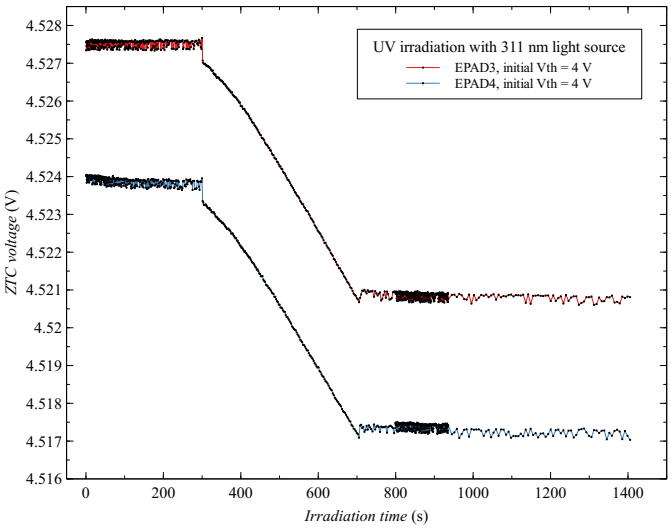


Fig. 7. ZTC voltage drift of EPAD3 and EPAD4 before, during and after UV irradiation of 311 nm light source.

Based on the ZTC point, it is possible to calculate the threshold voltage of the MOS transistor and thus indirectly monitor the threshold voltage but without the influence of temperature because for a fixed temperature (e.g. 25 °), the difference between the threshold voltage value and the ZTC point voltage value is constant. Figure 8 shows the threshold voltage shift during irradiation of two EPADs with a UV lamp of 311 nm peak.

The figure 8 shows EPADs that during the first irradiation had an initial threshold voltage of Vth = 3 V, and during the second irradiation, under the same conditions, EPADs had a threshold voltage of Vth = 4 V. It can be noticed that EPADs have higher sensitivity with higher threshold voltage means with a larger amount of electrons on the floating gate, which can be compared as an analogy to gamma radiation [4]. Also, it is possible to recharge the EPADs floating gate without degradation of its dosimetric characteristics [5].

Figure 9 shows the EPAD threshold voltage shift with the initial threshold voltage value Vth = 4 V.

The weakest response of the EPAD was observed for the UV LED light source, where the threshold voltage shift values are shown in Figure 10.

A linear dependence during irradiation can be observed for all types of UV radiation sources. The same behaviour of this sensor at small threshold voltage shifts was observed

 ISBN 978-86-7466-930-3

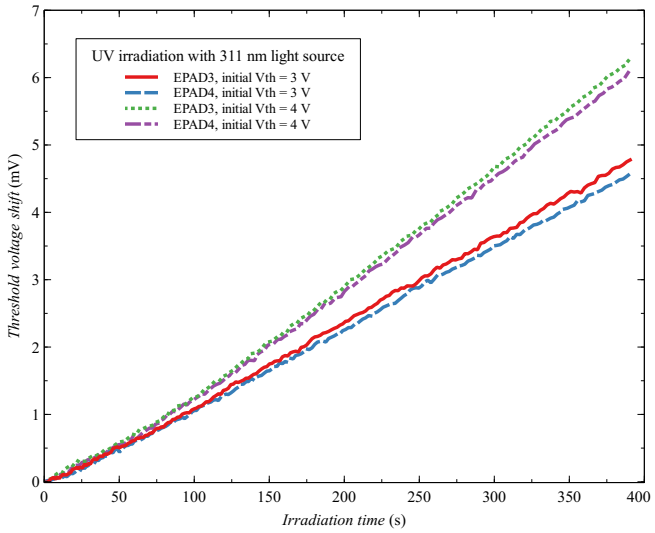


Fig. 8. Threshold voltage shift of EPAD3 and EPAD4 during irradiation of 311 nm light source with different charge on the floating gate.

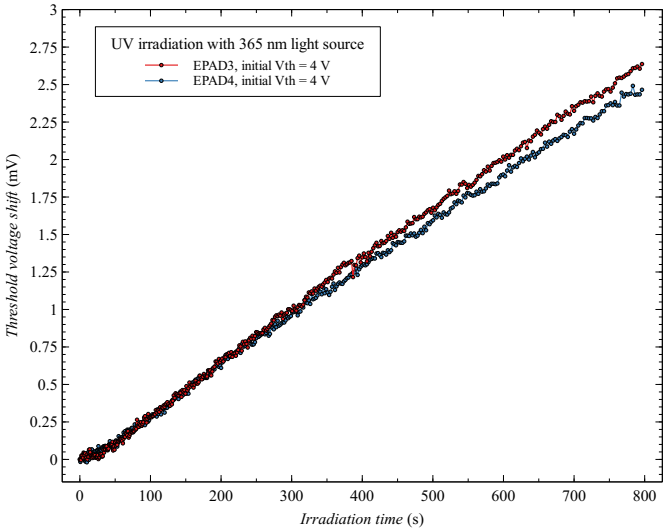


Fig. 9. Threshold voltage shift of EPAD3 and EPAD4 during irradiation of 365 nm light source.

for gamma radiation [4]. These results indicate that it is possible to record UV irradiation with the presented floating gate structure.

## IV. Discussion

By analyzing the spectrum of the UV lamp 311 nm in Figure 4 and the spectrum of the UV lamp 365 nm in Figure 5, we can see that both have a peak at 365 nm, which may indicate the possibility that the Vth shift from the first lamp with a peak at 311 nm (presented in Figure 8) originates from the peak at 365 nm. However, the nature of the floating gate device is that the electrons in the floating gate need to receive the minimum energy to surmount the energy barrier (similar to the photoelectric effect), and all photons with minimum or higher energy can decrease the charge on the floating gate and thus reduce the threshold voltage of the transistor

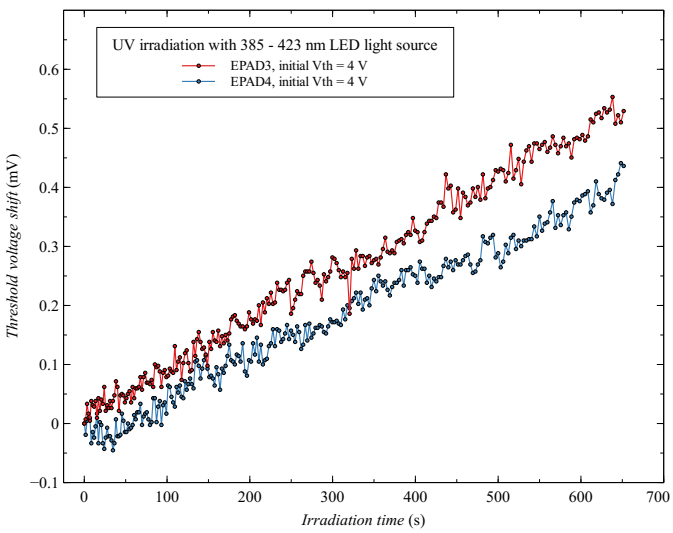


Fig. 10. Threshold voltage shift of EPAD3 and EPAD4 during irradiation of UV LED source.

[6]. This means that all photons with a smaller wavelength of 400 nm (higher energy than 3.09 eV) can decrease the threshold voltage. It is necessary to examine the photon energy limit value of this FG dosimeter in the future.

The UV sensor enables the detection of dangerous wavelengths for human health. The floating gate MOS transistor has good properties as an ionizing radiation dosimeter, so it is possible to use the same component for ultraviolet radiation dosimetry. However, it is necessary to provide a special housing with the quartz window in which the integrated circuit is mounted.

## V. Conclusion

The paper presents the possibility of using a floating gate MOS transistor as an ultraviolet sensor. The EPAD has been shown to respond to an ultraviolet radiation range of 311 to 400 nm. A sensor with a floating gate charged with a larger amount of electrons shows higher sensitivity. This component shows promising possibilities for dosimetry of UV radiation for medical purposes such as monitoring the received dose of patients during phototherapy.

## References

[1] W. D. Brown, W. D. Brown, and J. Brewer, *Nonvolatile semiconductor memory technology: a comprehensive guide to understanding and using NVSM devices*. Wiley-IEEE Press, 1998, vol. 6.

[2] ALD, "QUAD/DUAL Electrically Programmable Analog Device," 2012. [Online]. Available: http://www.aldinc.com/pdf/ALD1110E.pdf

[3] Z. Prijić, S. Dimitrijev, and N. Stojadinović, "The determination of zero temperature coefficient point in CMOS transistors," *Microelectronics Reliability*, vol. 32, no. 6, pp. 769–773, 1992.

[4] S. Ilić, A. Jevtić, S. Stanković, and G. Ristić, "Floating-Gate MOS Transistor with Dynamic Biasing as a Radiation Sensor," *Sensors*, vol. 20, no. 11, p. 3329, 2020.

[5] S. D. Ilić, M. S. Andjelković, R. Duane, A. J. Palma, M. Sarajlić, S. Stanković, and G. S. Ristić, "Recharging process of commercial floating-gate MOS transistor in dosimetry application," *Microelectronics Reliability*, vol. 126, p. 114322, 2021.

[6] L. Scheick, P. McNulty, and D. Roth, "Dosimetry based on the erasure of floating gates in the natural radiation environments in space," *IEEE Transactions on Nuclear Science*, vol. 45, no. 6, pp. 2681–2688, 1998.

 ISBN 978-86-7466-930-3

# Origin of the Open Circuit Voltage and Important Processes that Affect its Value in Organic Solar Cells

*Teodora Pavličević, Jovana P. Gojanović, Nataša A. Ćirović and Sandra Živanović, Member, IEEE*

***Abstract*—In this paper, the origin of an open circuit voltage ($V_{oc}$) in organic solar cells (OSCs) and processes which have a dominant impact on it were examined. The measured light current-voltage (*I-V*) characteristics of ITO/PEDOT:PSS/P3HT:PCBM/LiF/Al solar cells fabricated and characterized under similar conditions were collected from literature. The gathered $V_{oc}$ data was statistically processed and 75 % of the results belonged to the range $0.52 - 0.64$ V and obeyed Gaussian distribution. However, 12.5 % results had a value around 0.4 V, and another 12.5 % around 0.48 V. Three *I-V* curves with different $V_{oc}$ values belonging to three observed $V_{oc}$ ranges were simulated by the drift-diffusion model (DDM). By changing the photogeneration, transport, recombination, and extraction parameters, but with the same value of a built-in voltage ($V_{bi}$), which corresponds to a difference between electrodes work functions, the measured *I-V* curves were excellently reproduced. The experimental light *I-V* curves from literature of solar cells with different polymer blends used as an active layer (PTB7:PCBM, or MDMO-PPV:PCBM) but having the same electrodes and transport layers were also successfully simulated in the same way. Based on our review of published experimental results and our theoretical investigations, we confirm that the difference between electrode work functions is the source of the $V_{oc}$. The difference between acceptor's lowest unoccupied molecular orbital (LUMO) and donor's highest occupied molecular orbital (HOMO) affects the $V_{oc}$ indirectly through photogeneration, transport and recombination parameters, and extraction efficiency.**

***Index Terms*— Organic solar cells; open circuit voltage; drift-diffusion model.**

## INTRODUCTION

Organic solar cells (OSCs) have been getting a great deal of attention due to their potential as low-cost, simply processed and environment-friendly photovoltaic devices [1]. An improvement of OSCs is demonstrated through an increase in their power conversion efficiency (PCE), the most important performance parameter. So far, the PCE has reached value of 18 % for a single-layer OSC, 12 % for organic photovoltaic modules and even 23.6 % for perovskite/organic tandem solar cells [2–4]. Although these results are commendable, a further progress in properties of active layer blends, and an improvement of OSCs' long-term stability are seen as a path to their commercialization [5].

To reach a full potential of OSCs, we need to clarify their basic working principles. Knowledge of OSCs physics would help us to single out the basic prerequisites for an efficient photoconversion and identify loss mechanisms. However, research so far was not focused much on elucidating physics but rather on increasing OSCs efficiency through new donor and acceptor materials to improve the photoconversion in the active layer, as well as through new transport layer materials to maximize the charge carrier collection [5,6]. The metal-semiconductor-metal (MSM) drift-diffusion model (DDM) [7] has been widely used for modeling the OSCs. This model is successful to a certain extent, but it is not able to reproduce the experimentally observed OSCs behavior to a full extent. Thus, a refinement of the DMM for OSCs has yet to be done by clarifying vague parts of it.

One of the parameters with unclear origin that directly affects the OSC's PCE is an open-circuit voltage ($V_{oc}$). There are many presumptions about processes that influence the $V_{oc}$ and how they can be correlated [1]. Frequently, the $V_{oc}$ is defined as $e \cdot V_{oc} = (E_g - 0.3)$ eV, where $E_g$ is an active layer energy gap determined as a difference between the highest occupied molecular orbital level (HOMO) of the donor and the lowest molecular orbital level (LUMO) of the acceptor, and $e$ is the elementary charge [8]. Trying to resolve 0.3 V voltage loss in the $V_{oc}$ and other aspects of the $V_{oc}$ behavior, many factors have been found that directly or indirectly have impact on it [1]. These include temperature, light intensity, active layer morphology, microstructure, recombination processes, quality and properties of donor/acceptor (D/A) interface area, density of states (DOS), electrode work functions, existence of charge transfer (CT) states, carrier density, reverse saturation current, defect states, and crystallinity [1]. All these factors are interrelated, and for a complete analysis of the $V_{oc}$ all of them should be considered. The $V_{oc}$ dependence on temperature and light intensity are most often researched and analyzed in the literature [9, 10]. It was found that the $V_{oc}$ decreases as temperature increases, and for a wide temperature range that dependence is nearly linear [9]. On the other hand, the $V_{oc}$ showed a logarithmic dependence on light intensity [10]. The reverse saturation current is one of the important parameters that influences the $V_{oc}$, and it was found that the $V_{oc}$ is inversely proportional to it [11]. The influence of the charge carrier recombination on the $V_{oc}$ was described through a correlation between the $V_{oc}$ and the recombination rate [12] that differs for different recombination types – monomolecular, bimolecular or their combination. The monomolecular recombination implies a recombination through a recombination center or a trap state, while the bimolecular recombination indicates that holes and

T. Pavičević, J. P. Gojanović and N. A. Ćirović are with the School of Electrical Engineering, University of Belgrade, Belgrade 11120, Serbia (e-mail: pavlicevicteodora@gmail.com; jovana@etf.bg.ac.rs; natasa@etf.bg.ac.rs)

S. Živanović is with Institute for Micromanufacturing, Louisiana Tech University, Ruston, LA 71272 USA (e-mail: sz@latech.edu).

 ISBN 978-86-7466-930-3

electrons are mutually recombined [12]. Higher recombination rates mean a reduced number of carriers and eventually a smaller $V_{oc}$ [12]. A lower carrier density leads to a decreased $V_{oc}$. The improvement of the microstructure can minimize recombination rates, improve carrier dynamics, and benefit the $V_{oc}$ [13]. Defect states introduce irregularities into the material structure, and thus energy disorders and a reduced crystallinity. In organic materials, these disorders are usually modelled via the Gaussian or exponential DOS, and it was shown that they degrade the performance of OSCs by degrading the $V_{oc}$ [14]. Losses in the $V_{oc}$ are also related to a non-radiative decay of the CT states on the D/A interface [15]. The impact of the morphology is mostly related to the quality of D/A interface (e.g., whether it is homogenous or not) [15]. In addition, it was shown that a reduction of the D/A interface area can contribute to a higher $V_{oc}$ [16]. One of the most debatable matters is the influence of electrode work functions on the $V_{oc}$. It was shown that if the Fermi levels are well inside the energy gap of the active layer polymer-fullerene blend, the $V_{oc}$ is strongly affected even by a small variation of each electrode work function [17]. However, if the anode work function is close to the donor's HOMO and the cathode work function is close to the acceptor's LUMO, the $V_{oc}$value reaches a plateau and is less sensitive to work functions variations [17]. In this case, the device operation is the most effective [17].

To investigate the origin of the $V_{oc}$ and analyze important processes which affect its value, we have collected measured light current-voltage (*I-V*) characteristics of ITO(indium tin oxide)/PEDOT(poly(3,4-ethylene dioxythiophene):PSS(poly(styrenesulfonate)/ P3HT (poly(3-hexyl-2,5-dimethylthiophene):PCBM([6,6]-phenyl-$C_{61}$-butyric acid methyl ester)/LiF(lithium fluoride)/Al solar cells fabricated and characterized under nearly same conditions available in the literature [19-40]. We statistically processed the collected $V_{oc}$ data and analyzed the obtained distribution function by determining its mean value and standard deviation. Three *I-V* curves (each with a representative and significantly different value of $V_{oc}$) were selected and simulated by the DDM. Viewing the OSC as an MSM structure, the built-in voltage ($V_{bi}$) was taken to be the difference between the two electrode work functions. The *I-V* characteristics with different $V_{oc}$ values were successfully simulated by varying the reduction factor of the Langevin bimolecular recombination rate and by changing the effective density of states ($N_c, N_v$) at boundaries.

To inspect the influence of $E_g$ on $V_{oc}$, two more solar cells with the same electrode contacts but different active layer polymer-fullerene blends, PTB7 (poly [[4,8-bis[(2-ethylhexyl)oxy]benzo[1,2-b:4,5-b′] dithiophene-2,6-diyl][3-fluoro–2-[(2-ethylhexyl)carbonyl]thieno[3,4-b] thiophenediyl]]):PCBM [41] and IMDMO-PPV (poly[2-methoxy-5-(30,70-dimethyloctyloxy)-1,4-phenylenevinylene]):PCBM [42] were considered. Their measured *I-V* characteristics obtained from literature were successfully fitted with the DDM by varying active layer transport and recombination parameters together with the $N_c$, and $N_v$ at the boundaries. Based on the statistically processed experimental $V_{oc}$ data and our DDM *I-V* curve simulations, we confirm that the $V_{oc}$ originates from the difference of electrode work functions and that the contact phenomena and the recombination losses have the greatest impact on its value.

## Open Circuit Voltage in ITO/PEDOT:PSS/Polymer-Fullerene Blend/LiF/Al Organic Solar Cells

### *A. Review of Experimental Data*

We started the investigation of the $V_{oc}$ in OSCs by choosing one of the most researched device structure ITO/PEDOT:PSS/P3HT:PCBM/LiF/Al. This OSC structure is used as a reference in a large number of experimental research papers aimed at improving the OSC performance. The performance parameters for considered OSCs together with fabrication and characterization conditions are presented in Table 1. The gathered $V_{oc}$ data are statistically processed and graphically presented in Fig. 1. The three distinct $V_{oc}$ ranges are observed (see Fig. 1). The dominant range contains 75 % of collected data. Two smaller ranges each contain 12.5 % of the $V_{oc}$ results. The largest number of collected $V_{oc}$ values belongs to the 0.52–0.64 V range and the data follows the standard Gaussian distribution with the expected value $\mu = 0.58$ V and the standard deviation $\sigma = 0.024$ V. The $V_{oc}$ values in the range of 0.46–0.48 V are mostly obtained for the devices illuminated by 3 sun (see Table 1), where 1 sun corresponds to standard illumination at AM1.5, or 1 kW/m$^2$. The $V_{oc}$ of about 0.40 V is obtained mainly for the OSCs in which P3HT:PCBM active layer is produced from chloroform solution rather than from chlorobenzene solution (see Table 1).

According to the literature [17, 18], if injection barriers at electrode contacts are significant (i.e., rectifying junctions), the $V_{oc}$ is defined as the difference between electrode work functions, while for optimised devices with Ohmic contacts, the $V_{oc}$ is interpreted as the difference between the LUMO of the acceptor and the HOMO of the donor (i.e., with a mysterious loss of 0.3 V). From Fig. 1, it is clear that even for the OSCs with the same electrodes and the same D/A polymer-fullerene blend, a wide distribution of the $V_{oc}$ values exists. This led us to the conclusion that the active layer photogeneration, transport and recombination parameters, as well as the charge extraction efficiency differ in the considered devices probably due to a different quality of the active layer, hole and electron transport layers and electrode junctions.

Additionally, the OSCs with PTB7:PCBM or MDMO-PPV:PCBM active layers with the same electrodes (ITO, Al) and transport layers (PEDOT:PSS, LiF) were examined. Although $E_g^{MDMO-PPV:PCBM} < E_g^{P3HT:PCBM}$ [35] and $E_g^{PTB7:PCBM} > E_g^{P3HT:PCBM}$[43], the $V_{oc}$ values obtained for these devices ($V_{oc}^{MDMO-PPV:PCBM} = 0.82$ V, and $V_{oc}^{PTB7:PCBM} = 0.75$ V ) are larger than any $V_{oc}^{P3HT:PCBM}$ from Table 1. Thus, we proposed that the difference between the acceptor LUMO and the donor HOMO is not crucial for the $V_{oc}$, but rather the parameters of photogeneration, transport, recombination, and extraction.

 ISBN 978-86-7466-930-3

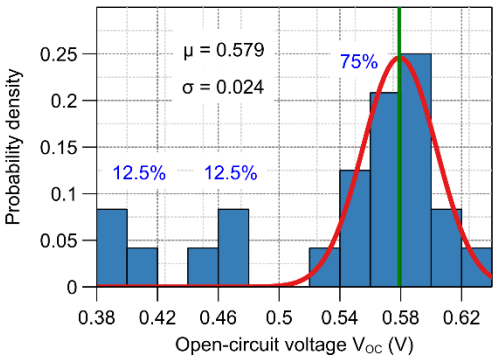


Fig. 1 Probability density obtained by statistical processing of the experimental $V_{oc}$ data from Table 1. Gaussian function is applied to the $V_{oc}$ data in the range 0.52 – 0.64 V (red solid curve).

TABLE I
REVIEW OF PERFORMANCE, FABRICATION AND TESTING PARAMETERS OF ITO/PEDOT:PSS/P3HT:PCBM/LiF/Al SOLAR CELLS REPORTED IN THE LITERATURE

| | $V_{OC}$ [V] | $J_{SC}$ $\left[\frac{mA}{cm^2}\right]$ | PCE [%] | Light intensity | Anneal. | Blend ratio | Solvent | Ref. |
|---|---|---|---|---|---|---|---|---|
| 1. | **0.40** | 9.50 | 1.55 | 1 sun | 5 min at 120°C | 1:1 | Chloroform | [19] |
| 2. | **0.59** | 11.00 | 4.07 | 1 sun | 10 min at 150°C | 1:1 | Chloroform | [20] |
| 3. | **0.40** | 0.70 | / | 1 sun | 15 min at 120°C | 1:1 | Chlorobenzene | [21] |
| 4. | **0.59** | 9.70 | 2.64 | 1 sun | 10 min at 120°C | 1:1 | Chlorobenzene | [22] |
| 5. | **0.56** | 8.92 | 3.31 | 1 sun | 10 min at 140°C | 3:2 | 1,2-Dichlorobenzene | [23] |
| 6. | **0.48** | 17.06 | 2.11 | 3 sun | 5 min at 115°C | 1:1 | Chlorobenzene | [24] |
| 7. | **0.42** | 17.06 | 2.11 | 3 sun | 5 min at 115°C | 1:0.8 | Chloroform | [25] |
| 8. | **0.57** | 3.64 | 0.62 | 1 sun | No anneal. | 1:1 | Chlorobenzene | |
| 9. | **0.55** | 7.75 | 2.42 | 1 sun | 10 min at 110°C | 1:1 | Chlorobenzene | [26] |
| 10. | **0.62** | 13.72 | 2.76 | 1 sun | 20 min at 100°C | 5:3 | Chlorobenzene: Chloroform (1:1) | |
| 11. | **0.59** | 10.08 | 3.20 | 1 sun | 10 min at 120°C | 1:1 | Dichlorobenzene | [27] |
| 12. | **0.59** | 14.27 | 2.61 | 1 sun | / | 1:1 | Chlorobenzene | [28] |
| 13. | **0.60** | 5.36 | 2.10 | 1 sun | 15 min at 130°C | 1:1 | Chlorobenzene | [29] |
| 14. | **0.55** | 5.58 | 1.55 | 1 sun | 10 min at 120°C | 1:0.8 | Chlorobenzene | [30] |
| 15. | **0.54** | 3.83 | 1.18 | 1 sun | 12 min at 100°C | 1:1 | 1,2-Dichlorobenzene | [31] |
| 16. | **0.58** | 4.79 | 1.10 | / | at 120°C | 1:0.8 | / | [32] |
| 17. | **0.58** | 8.06 | 2.20 | 1 sun | 10 min at 150°C | 1:1 | Dichlorobenzene | [33] |
| 18. | **0.58** | / | / | / | 15 min at 150°C | 1:0.75 | Ortho-dichlorobenzene | [34] |
| 19. | **0.46** | 6.10 | 1.02 | 1 sun | No anneal. | 1:1 | Chlorobenzene | [35] |
| 20. | **0.58** | 5.84 | / | 1 sun | 15 min at 140°C | 1:1 | Chlorobenzene | [36] |
| 21. | **0.64** | 8.50 | 2.80 | 1 sun | 30 min at 150°C | 1:0.8 | Chlorobenzene | [37] |
| 22. | **0.62** | 9.54 | 2.40 | 1 sun | 10 min at 120°C | 1:1 | O-chlorobenzene | [38] |
| 23. | **0.48** | 17.06 | 2.11 | 3 sun | 10 min at 120°C | 1:1 | Chlorobenzene | [39] |
| 24. | **0.60** | 9.23 | 1.79 | 1 sun | 20 min at 130°C | 1:1 | Chlorobenzene | [40] |

### *B. Drift-Diffusion Modeling*

It has been shown that photoconductive polymer-fullerene blend placed between identical electrodes fabricated under the same environment, does not exhibit a rectifying effect and their $V_{oc}$ is zero [44–46]. This means that the D/A interface in polymer-fullerene blends does not contribute to the built-in voltage. Accordingly, the direct source of the $V_{oc}$ in OSCs is the difference between the electrode work functions. The difference between the acceptor's LUMO and the donor's HOMO level influences the $V_{oc}$ indirectly through the Fermi-level pinning [47], photogeneration, transport and recombination parameters, or extraction efficiency. In this paper, the metal-semiconductor-metal DDM was used for modeling the *I-V* characteristics of several OSCs. The model is based on the Poisson's equation, the hole and electron continuity equations, and the drift-diffusion transport equation for holes and electrons inside the active layer [48]. The photogeneration rate was calculated by using the transfer matrix theory and by assuming that the electric field is independent of the exciton dissociation efficiency [48]. Constant hole and electron mobilities were applied, and a reduced Langevin recombination was proposed. The Dirichlet boundary conditions were used. The solving of the equations system was done based on the finite difference discretization improved by the Scharfetter and Gummel approach and the Newton algorithm [48]. In all our calculations, a built-in voltage $V_{bi}$ of 0.9 V as the difference between the electrode work functions was used along with the dielectric permittivity of 3.4 and the room temperature of 293.9 K.

The light *I-V* characteristic of three ITO/PEDOT:PSS/P3HT:PCBM/LiF/Al devices with $V_{oc} = 0.40$ V [21], $V_{oc} = 0.48$ V [24], and $V_{oc} = 0.59$ V [27] were simulated and compared with the measured ones in Fig. 2 (a), (b), and (c), respectively. The parameter values used in simulations are listed in the Insets of Fig. 2, where $\mu_{n(p)}$ is the electron (hole) mobility, $N_{c(v)}$ is the effective density of states for electrons (holes), $d$ is the active layer thickness, $g$ is the photoconductive gain [49], and $\xi$ is the reduction factor of the Langevin recombination rate [50]. All three measured *I-V* curves are reproduced very well by the DDM, which means that the difference in the photogeneration ($g$), transport ($\mu_n, \mu_p$), recombination ($\xi$) and extraction ($N_c, N_v$) parameter values may explain the observed $V_{oc}$ diversity (see Table 1, Fig. 1). The occurrence of the photoconductive gain may be explained through a volume modulation effect, where the light illumination can increase the conductive area of the cell, thus, the generated photocurrent becomes larger [51]. The $N_c$ and $N_v$ are used as the boundary majority charge carrier concentrations at cathode and anode, respectively, and they are the fitting parameters in the OSCs modeling of Koster et al. [7].

These parameters are representatives of contact physics in OSCs and they have a large impact on the $V_{oc}$. The reduction of recombination losses in OSCs quantified by $\xi$ leads to an improvement of the $V_{oc}$. In most OSCs, $\xi \leq 0.2$ [52], and its higher value indicates that CT states are significant in polymer-fullerene blend and that they recombine very rapidly. The existence of CT states and their participation in the charge carrier photogeneration and recombination [7] was not considered in our DDM. Therefore, $\xi > 1$ is possible in our simulations. A higher electron mobility leads to a lower $V_{oc}$ [53], and an increased hole mobility slightly improves the $V_{oc}$.


ISBN 978-86-7466-930-3

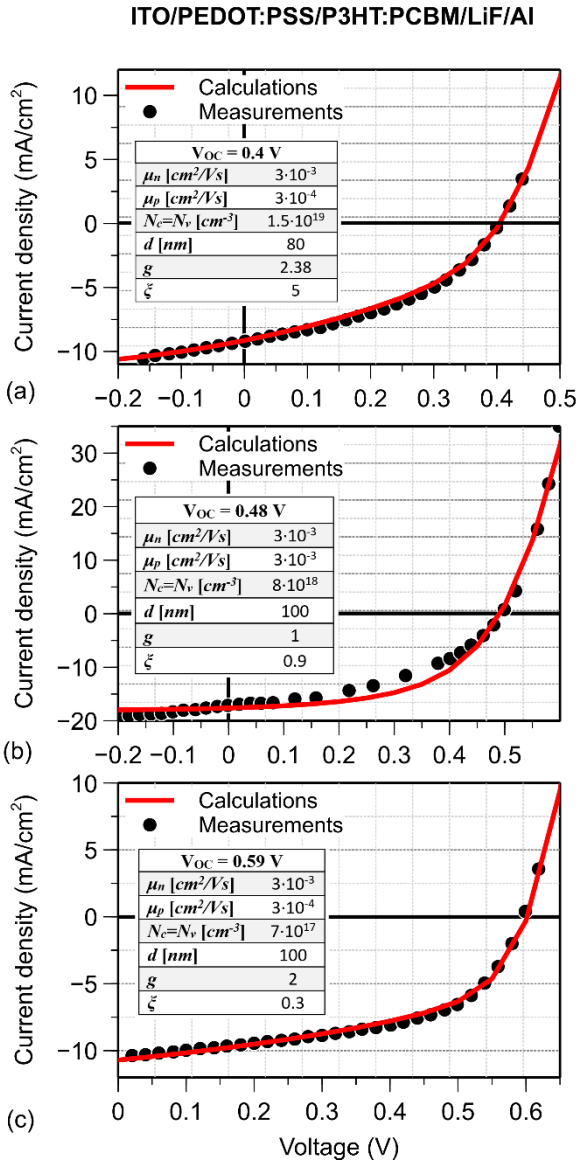


Fig 2. DDM simulated *I-V* curves compared to experimental ones taken from (a) Ref. [17], (b) Ref. [33], (c) Ref. [25]. The corresponding simulation parameters are given in the Insets.

In Figs. 3, and 4, calculated light *I-V* characteristics for the PTB7:PCBM and MDMO-PPV:PCBM based solar cells are compared with the measured ones. The simulation parameters are given in the Insets of Figs. 3, and 4.

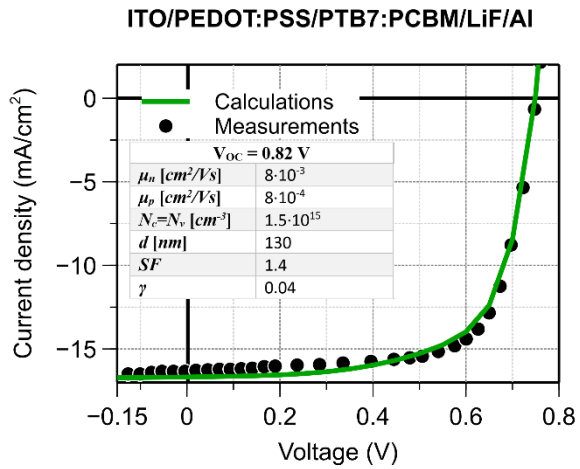


Fig. 3 DDM simulated *I-V* curve compared to experimental one taken from Ref. [39]. The corresponding simulation parameters are given in the Inset.

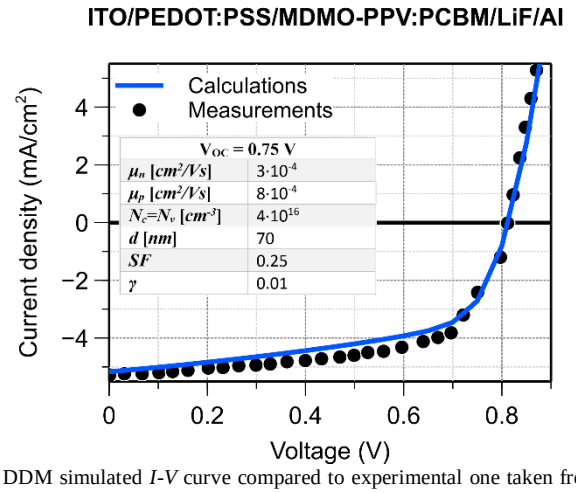


Fig.4 DDM simulated *I-V* curve compared to experimental one taken from Ref. [33]. The corresponding simulation parameters are given in the Inset.

Again, the experimentally obtained and theoretically predicted *I-V* curves coincide very well. This proves that even if a D/A polymer blend in an OSC is changed, the $V_{oc}$ can be reproduced by tuning of parameters $g, \mu_n, \mu_p, N_c, N_v$, and $\xi$.

## CONCLUSION

The experimental light *I-V* data extracted from literature showed that the $V_{oc}$ can significantly differ for ITO/PEDOT:PSS/P3HT:PCBM/LiF/Al solar cells produced and tested under similar conditions. Three measured light *I-V* characteristics with $V_{oc} = 0.4\,\text{V}$, $V_{oc} = 0.48\,\text{V}$, and $V_{oc} = 0.59\,\text{V}$ were successfully reproduced by our DDM simulations by applying the same value of $V_{bi} = 0.9\,\text{V}$ corresponding to the difference between the LiF/Al and the ITO/PEDOT:PSS work functions, while the charge carrier photogeneration, transport, recombination, and extraction were varied. For the OSCs based on the PTB7:PCBM or MDMO-PPV:PCBM polymer-fullerene blends, our DDM simulations were, again, able to reproduce the measured *I-V* curves well. We concluded that the difference between the work functions of the electrodes is the source of the $V_{oc}$ in OSCs and the difference between the acceptor's LUMO and the donor's HOMO influences the $V_{oc}$ through charge carrier photogeneration, recombination, transport, and extraction. These processes have a significant impact on the $V_{oc}$ value. Future work will be dedicated to research of how the LUMO and HOMO energy levels of the polymer-fullerene D/A blend as well as the CT states formed at the D/A interfaces influence the $V_{oc}$.

## ACKNOWLEDGMENT

This work is partially supported by the Serbian Ministry of Education, Science and Technological Development under Grant #62101 awarded to J. Gojanović and by the James W. Adams endowed professorship of S. Živanović that is made available through the State of Louisiana Board of Regents Support Funds.

 ISBN 978-86-7466-930-3

## REFERENCES


[1] N. K. Elumalai and A. Uddin, "Open circuit voltage of organic solar cells: an in-depth review," *Energy Eviron. Sci*, vol. 9, no. 2, pp. 391–410, Feb. 2016, doi: https://doi.org/10.1039/C5EE02871J

[2] Q. Liu, Y. Jiang, K. Jin, J. Qin, J. Xu, W. Li, J. Xiong, J. Liu, Z. Xiao, K. Sun, S. Yang, X, Zhang, and L. Ding, "18% Efficiency organic solar cells," *Science Bulletin*, vol. 65, no. 4, pp. 272–275, Feb. 2020, doi: https://doi.org/10.1016/j.scib.2020.01.001

[3] A. Distler, C. J. Brabec, and H-J. Egelhaaf, "Organic photovoltaic modules with new world record efficiencies," *Prog. Photovoltaics Res. App.*, vol. 29, no. 1, pp. 24–31, Jan. 2021, doi: https://doi.org/10.1002/pip.3336

[4] W. Chen, Y. Zhu, J. Xiu, G. Chen, H. Liang, S. Liu, H. Xue, E. Birgersson, J. W. Ho, X. Qin, J. Lin, R. Ma, T. Liu, Y. He, A. M-C. Ng, X. Guo, Z. He, H. Yan, A. B. Djurišić, and Y. Hou, "Monolithic perovskite/organic tandem solar cells with 23.6% efficiency enabled by reduced voltage losses and optimized interconnecting layer," *Nat Energy*, vol. 7, no. 3, pp. 229–237, Mar. 2022, doi: https://doi.org/10.1038/s41560-021-00966-8

[5] A. Karki, A. J. Gillett, R. H. Friend and T-Q Nguyen, "The Path to 20% Power Conversion Efficiencies in Nonfullerene Acceptor Organic Solar Cells," *Adv. Energy Mater.*, vol. 11, no. 15, Apr. 2021, Art. no. 2003441, doi: https://doi.org/10.1002/aenm.202003441

[6] C. Anrango-Camacho, K. Pavón-Ipiales, B. A. Frontana-Uribe, and A. Palma-Cando, "Recent Advances in Hole-Transporting Layers for Organic Solar Cells," *Nanomaterials*, vol. 12, no. 3, p. 443, Jan. 2022, doi: https://doi.org/10.3390/nano12030443.

[7] L. J. A. Koster, E. C. P. Smits, V. D. Mihailetchi, and P. W. M. Blom, "Device model for the operation of polymer/fullerene bulk heterojunction solar cells," *Phys. Rev. B*, vol. 72, no. 8, Aug. 2005, Art. no. 085205, doi: https://link.aps.org/doi/10.1103/PhysRevB.72.085205

[8] M. C. Scharber, D. Mühlbacher, M. Koppe, P. Denk, C. Waldauf, A. J. Heeger, and C. J. Brabec, "Design Rules for Donors in Bulk-Heterojunction Solar Cells – Towards 10% Energy-Conversion Efficiency," *Adv. Mater.*, vol. 18, no. 6, pp. 789–794, Mar. 2006, doi: https://doi.org/10.1002/adma.200501717

[9] G. Garcia-Belmonte, "Temperature dependence of open-circuit voltage in organic solar cells from generation–recombination kinetic balance," *Sol. Energy Mater. Sol. cells*, vol. 94, no. 12, pp. 2166–2169, Dec. 2010, doi: https://doi.org/10.1016/j.solmat.2010.07.006

[10] R. Signerski, "On the light intensity dependence of short-circuit current of bilayer organic photovoltaic cells," *J. Non-Cryst. Solids*, vol. 354, no. 35, pp. 4465–4468, Oct. 2008, doi: https://doi.org/10.1016/j.jnoncrysol.2008.06.076

[11] W. J. Potscavage Jr., S. Yoo, and B. Kippelen, "Origin of the open-circuit voltage in multilayer heterojunction organic solar cells," *Appl. Phys. Lett.*, vol. 93, no. 19, Nov. 2008, Art. no. 193308, doi: http://dx.doi.org/10.1063/1.3027061

[12] S. R. Cowan, A. Roy, and A. J. Heeger, "Recombination in polymer-fullerene bulk heterojunction solar cells," *Phys. Rev. B*, vol. 82, no. 24, Dec. 2010, Art. no. 245207, doi: https://link.aps.org/doi/10.1103/PhysRevB.82.245207

[13] D. Credgington and J. R. Durrant, "Insights from Transient Optoelectronic Analyses on the Open-Circuit Voltage of Organic Solar Cells," *J. Phys. Chem. Lett.*, vol. 3, no. 11, pp. 1465–1478, Jun. 2012, doi: https://doi.org/10.1021/jz300293q

[14] J. C. Blakesley and D. Neher, "Relationship between energetic disorder and open-circuit voltage in bulk heterojunction organic solar cells," *Phys. Rev. B*, vol. 84, no. 7, Aug. 2011, Art. no. 075210, doi: https://link.aps.org/doi/10.1103/PhysRevB.84.075210

[15] V. Coropceanu, X-K. Chen, T. Wang, Z. Zheng, and J-L. Brédas, "Charge-transfer electronic states in organic solar cells," *Nat. Rev. Mater.*, vol. 4, no. 11, pp. 689–707, Nov. 2019, doi: https://doi.org/10.1038/s41578-019-0137-9

[16] K. Vandewal, J. Widmer, T. Heumueller, C. J. Brabec, M. D. McGehee, K. Leo, M. Riede, and A. Salleo, "Increased Open-Circuit Voltage of Organic Solar Cells by Reduced Donor-Acceptor Interface Area," *Adv. Mater.*, vol. 26, no. 23, pp. 3839–3843, Jun. 2014, doi: https://doi.org/10.1002/adma.201400114

[17] A. Zampetti, A. H. Fallahpour, M. Dianetti, L. Salamandra, F. Santoni A. Gagliardi, M. Auf der Maur, F. Brunetti, A. Reale, T. M. Brown, and A. Di Carlo, "Influence of the Interface Material Layers and Semiconductor Energetic Disorder on the Open Circuit Voltage in Polymer Solar Cells," *J. Polym. Sci., Part B: Polym. Phys.*, vol. 53, no. 10, pp. 690–699, May 2015, doi: https://doi.org/10.1002/polb.23685

[18] M. Erray, M. Hanine, El-M. Boufounas, and A. El Amrani, "Combined effects of carriers charge mobility and electrodes work function on the performances of polymer/fullerene P3HT:PCBM based organic photovoltaic solar cell," *Eur. Phys. J. Appl. Phys.*, vol. 82, no. 3, June 2018, Art. no. 30201, doi: https://doi.org/10.1051/epjap/2018180070

[19] Z. Çaldıran, Ü. Erkem, A. Baltakesmez, and M. Biber, "Effects of the PENTACENE as doping material on the power conversion efficiency of P3HT:PCBM based ternary organic solar cells,"*Physica B: Condensed Matter*, vol. 607, Apr. 2021, Art. no. 412859, doi: https://doi.org/10.1016/j.physb.2021.412859

[20] T. J. Whitcher, N. A. Talik, K. Woon, N. Chanlek, H. Nakajima, T. Saisopa, and P. Songsiriritthigul, "Determination of energy levels at the interface between $O_2$ plasma treated ITO/P3HT:PCBM and PEDOT:PSS/P3HT:PCBM using angular-resolved x-ray and ultraviolet photoelectron spectroscopy," *J. Phys. D: Appl. Phys.*, vol. 47, no. 5, Jan. 2014, Art. no. 055109, doi:https://doi.org/10.1088/0022-3727/47/5/055109

[21] S. Arora, S. K. Rajouria, P. Kumar, P. K. Bhatnagar, M. Arora, and R. P. Tandon, "Role of donor–acceptor domain formation and interface states in initial degradation of P3HT:PCBM-based solar cells," *Phys. Scr.*, vol. 83, no. 3, Mar. 2011, Art. no. 035804, doi: https://doi.org/10.1088/0031-8949/83/03/035804

[22] H-T. Chien, M. Pölzl, G. Koller, S. Challinger, C. F. I. Baikie, M. Kratzer, C. Teichert, B. Friedel, "Effects of Hole-Transport Layer Homogeneity in Organic Solar Cells – A Multi-Length Scale Study," *Surf. Interfaces*, vol. 6, pp. 72–80, Mar. 2017, doi: https://doi.org/10.1016/j.surfin.2016.11.008

[23] H. Kwon, J. Ham, D. Y. Kim, S. J. Oh, S. Lee, S. H. Oh, E. F. Schubert, K-G. Lim, T-W. Lee, S. Kim, J-L. Lee, and J. K. Kim, "Three-Dimensional Nanostructured Indium-Tin Oxide Electrodes for Enhanced Performance of Bulk Heterojunction Organic Solar Cells," *Adv. Energy Mater.*, vol. 4, no. 7, May 2014, Art. no. 1301566, doi: https://doi.org/10.1002/aenm.201301566

[24] H. Kaçuş and Ş. Aydoğan, "The power conversion efficiency optimization of the solar cells by doping of (Au:Ag) nanoparticles into P3HT:PCBM active layer prepared with chlorobenzene and chloroform solvents," *Mater. Res. Express*, vol. 6, no. 9, July 2019, Art. no. 095104, doi: https://doi.org/10.1088/2053-1591/ab309a

[25] Y. Galagan and R. Andriessen, "Organic Photovoltaics: Technologies and Manufacturing," in *Third Generation Photovoltaics*, London, United Kingdom:IntechOpen,2012, ch. 3 [Online]. Available: https://www.intechopen.com/chapters/32590 doi: 10.5772/25901

[26] Ç. K. Kurukavak and S. Polat, "Influence of the volume of EGME-DMSO mixed co-solvent doping on the characteristics of PEDOT:PSS and their application in polymer solar cells,"*Polym. Polym. Compos.*, vol. 29, no. 8, pp. 1222–1228, Oct. 2021, doi: https://doi.org/10.1177/0967391120963470

[27] M. Wang, Q. Tang, J. An, F. Xie, J. Chen, S. Zheng, K. Y. Wong, Q. Miao, and J. Xu, "Performance and Stability Improvement of P3HT:PCBM-Based Solar Cells by Thermally Evaporated Chromium Oxide (CrOx) Interfacial Layer," *ACS Appl. Mater. Interfaces*, vol. 2, no. 10, pp. 2699–2702, Oct. 2010, doi: https://doi.org/10.1021/am100541d

[28] F. Li, L. Kou, W. Chen, C. Wu, and T. Guo, "Enhancing the short-circuit current and power conversion efficiency of polymer solar cells with graphene quantum dots derived from double-walled carbon nanotubes," *NPG Asia Materials*, vol. 5, no. 8, Aug. 2013, doi: https://doi.org/10.1038/am.2013.38

[29] M-S. Kim, B-G. Kim, and J. Kim, "Effective Variables To Control the Fill Factor of Organic Photovoltaic Cells," *ACS Appl. Mater. Interfaces*, vol. 1, no. 6, pp. 1264–1269, June 2009, doi: https://doi.org/10.1021/am900155y

[30] S. H. Oh, S. J. Heo, J. S. Yang, and H. J. Kim, "Effects of ZnO Nanoparticles on P3HT:PCBM Organic Solar Cells with DMF-Modulated PEDOT:PSS Buffer Layers," *ACS Appl. Mater. Interfaces*, vol. 5, no. 22, pp. 11530–11534, Nov. 2013, doi: https://doi.org/10.1021/am4046475

[31] S. Shanin, "Engineering the performance of optical devices using plasmonics and nonlinear organic chromophores," Ph.D. dissertation, Department of Optical Sciences, University of Arizona, Tucson, Arizona, 2014.

[32] K. Yao, L. Chen, Y. Chen, F. Li, and P. Wang, "Influence of water-soluble polythiophene as an interfacial layer on the P3HT/PCBM bulk heterojunction organic photovoltaics," *J. Mater. Chem.*, vol. 21, no. 36, pp. 13780–13784, Sep. 2011, doi: https://doi.org/10.1039/C1JM12016F

[33] F. Li, J. Zhao, K. Yao, and Y. Chen, "Origin of the efficiency improvement in pre-annealed P3HT/PCBM solar cells with LiF/Al electrodes," *Chem. Phys. Lett.*, vol. 553, pp. 36–40, Nov. 2012, doi: https://doi.org/10.1016/j.cplett.2012.10.006

[34] B. Arredondo, C. de Dios, R. Vergaz, A.R. Criado, B. Romero, B. Zimmermann, and U. Würfel, "Performance of ITO-free inverted organic bulk heterojunction photodetectors: Comparison with standard


 ISBN 978-86-7466-930-3

device architecture," *Org. Electron.*, vol. 14, no. 10, pp. 2484–2490, Oct. 2013, doi: https://doi.org/10.1016/j.orgel.2013.06.018
[35] M. Girtan and M. Rusu, "Role of ITO and PEDOT:PSS in stability/degradation of polymer: fullerene bulk heterojunctions solar cells," *Sol. Energy Mater. Sol. Cells*, vol. 94, no. 3, pp. 446–450, Mar. 2010, doi: https://doi.org/10.1016/j.solmat.2009.10.026
[36] F. Yakuphanoglua and R.S. Anand, "Charge transport properties of an organic solar cell," *Synth. Met.*, vol. 160, no. 21, pp. 2250–2254, Nov. 2010, doi: https://doi.org/10.1016/j.synthmet.2010.08.015
[37] Y. Park, S. Noh, D. Lee, J. Y. Kim, and C. Lee, "Temperature and Light Intensity Dependence of Polymer Solar Cells with $MoO_3$ and PEDOT:PSS as a Buffer Layer," *J. Korean Phys. Soc.*, vol. 59, no. 2, pp. 362–366, Aug. 2011, doi: https://doi.org/10.3938/jkps.59.362
[38] M. D. Irwin, D. B. Buchholz, A. W. Hains, R. P. H. Chang, and T. J. Marks, "p-Type semiconducting nickel oxide as an efficiency-enhancing anode interfacial layer in polymer bulk-heterojunction solar cells," *Proc. Natl. Acad. Sci. USA*, vol. 105, no. 8, pp. 2783–2787, Feb. 2008, doi: https://doi.org/10.1073/pnas.0711990105
[39] H. Kaçuş, M. Biber, and Ş. Aydoğan, "Role of the Au and Ag nanoparticles on organic solar cells based on P3HT:PCBM active layer," *Appl. Phys. A*, vol. 126, no. 10, Sep. 2020, Art. no. 815, doi: https://doi.org/10.1007/s00339-020-03992-7
[40] X. Liu, L. J. Guo, and Y. Zheng, "5-nm LiF as an Efficient Cathode Buffer Layer in Polymer Solar Cells Through Simply Introducing a $C_{60}$ Interlayer," *Nanoscale Res. Lett.*, vol. 12, no. 1, Sep. 2017, Art. no. 543, doi: https://doi.org/10.1186/s11671-017-2299-y
[41] W. Lu, Y. Peng, Q. Chen, W. Tang, T. Pang, S. Zhang, Z. Liu, L. Yan, and X. Wang, "Hole transport layer free bulk heterojunction organic solar cells with high work function ITO anodes," *AIP Adv.*, vol. 8, no. 9, Aug. 2018, Art. no. 095027, doi: https://doi.org/10.1063/1.5049424
[42] C. J. Brabec, S. E. Shaheen, C. Winder, and N. S. Sariciftci, "Effect of LiF/metal electrodes on the performance of plastic solar cells," *Appl. Phys. Lett.*, vol. 80, no. 7, pp. 1288–1290, Feb. 2002, doi: https://doi.org/10.1063/1.1446988
[43] S. Park, J. Jeong, G. Hyun, M. Kim, H. Lee, and Y. Yi, "The origin of high PCE in PTB7 based photovoltaics: proper charge neutrality level and free energy of charge separation at PTB7/PC71BM interface," *Sci. Rep.*, vol. 6, no. 1, Oct. 2016, Art. no. 35262, doi: https://doi.org/10.1038/srep35262
[44] S. Alem, J. Gao, and G. Wantz, "Photovoltaic response of symmetric sandwich polymer cells with identical electrodes," *J. Appl. Phys.*, vol. 106, no. 4, Aug. 2009, Art. no. 044505, doi: https://doi.org/10.1063/1.3207769
[45] J. Gao, J. Hui, Y. Hou, and S. Alem, "Planar polymer photovoltaic cells with millimeter interelectrode spacing," *J. Appl. Phys.*, vol. 104, no. 8, Oct. 2008, Art. no. 084512, doi: https://doi.org/10.1063/1.3003082
[46] M. Girtan, "On the stability of the electrical and photoelectrical properties of P3HT and P3HT:PCBM blends thin films," *Org. Electron.*, vol. 14, no. 1, pp. 200–205, Jan. 2013, doi: https://doi.org/10.1016/j.orgel.2012.10.023
[47] V. D. Mihailetchi, P. W. M. Blom, J. C. Hummelen, and M. T. Rispens, "Cathode dependence of the open-circuit voltage of polymer:fullerene bulk heterojunction solar cells," *J. Appl. Phys.*, vol. 94, no. 10, pp. 6849–6854, Nov. 2003, doi: https://doi.org/10.1063/1.1620683
[48] A. R. Khalf, J. P. Gojanović, N. A. Ćirović, S. Živanović, and P. S. Matavulj, "The Impact of Surface Processes on the J–V Characteristics of Organic Solar Cells," in *IEEE Journal of Photovoltaics*, vol. 10, no. 2, pp. 514-521, Mar. 2020, doi: https://doi.org/10.1109/JPHOTOV.2020.2965401
[49] D. Li, L. Song, Y. Chen, and W. Huang, "Modeling Thin Film Solar Cells: From Organic to Perovskite," *Adv. Sci.*, vol. 7, no. 1, Jan. 2020, Art. no. 1901397, doi: https://doi.org/10.1002/advs.201901397
[50] F. Laquai, D. Andrienko, R. Mauer, and P. W. M. Blom, "Charge Carrier Transport and Photogeneration in P3HT:PCBM Photovoltaic Blends," *Macromol. Rapid Comm.*, vol. 36, no. 11, pp. 1001–1025, June 2015, doi: https://doi.org/10.1002/marc.201500047
[51] J. A. Garrido, E. Monroy, I. Izpura, and E. Muñoz, "Photoconductive gain modelling of GaN photodetectors," *Semicond. Sci. Technol.*, vol. 13, no. 6, pp. 563–568, June 1998, doi: https://doi.org/10.1088/0268-1242/13/6/005
[52] T. M. Burke, S. Sweetnam, K. Vandewal, and M. D. McGehee, "Beyond Langevin Recombination: How Equilibrium Between Free Carriers and Charge Transfer States Determines the Open-Circuit Voltage of Organic Solar Cells," *Adv. Energy Mater.*, vol. 5, no. 11, June 2015, Art. no. 1500123, doi: https://doi.org/10.1002/aenm.201500123
[53] O. J. Sandberg, A. Sundqvist, M. Nyman, and R. Österbacka, "Relating Charge Transport, Contact Properties, and Recombination to Open-Circuit Voltage in Sandwich-Type Thin-Film Solar Cells," *Phys. Rev. Appl.*, vol. 5, no. 4, Apr. 2016, Art. no. 044005, doi: https://link.aps.org/doi/10.1103/PhysRevApplied.5.044005

 ISBN 978-86-7466-930-3

# Design Consideration for Low-Power Step-Up Converter

Jana Vračar, *Student Member, IEEE*, Milan Stojanović, *Student Member, IEEE*, Zoran Prijić, *Member, IEEE*, Aneta Prijić, *Member, IEEE* and Ljubomir Vračar

***Abstract*— This paper describes the comparison of different MOSFETs and transformers used in a step-up circuit under initial voltages of 50 mV and 100 mV. Two MOSFETs, BSP149 and CPC3701CTR, and two transformers, CST-100LC and MID-SNS CS, were cross-connected, and the results of charging a 2200 µF capacitor were shown. This circuit consists of a Meissner oscillator and a voltage doubler circuit. Experimentally, the time it takes for different MOSFETs and transformers to increase the voltage and charge the capacitor at the circuit's output was measured, as well as the maximum output voltage generated by the circuit, and the resonant frequency for each of the given pairs of MOS transistors and transformers.**

***Index Terms*—step-up converter, transformers, MOSFET, power management.**

## I. Introduction

In recent years, the WSNs technology create more interest in researching from macro to micro-level to develop systems without using conventional power supplies and exploring alternative power sources for WSNs (Wireless Sensor Nodes). Energy harvesting is a viable option for replacing low-power devices batteries or power supply. Energy harvesting necessitates the collaboration of three distinct technologies. For developing systems based on energy harvesting, there must be three separate technologies combined in working together: energy harvesters - used to convert ambient energy into electrical energy, power management - for amplifying and regulating the generated energy and energy storage - for powering low power consumption systems, such as sensors, actuators, microcontrollers, RF transceivers, etc. [1].

Jana Vračar is with the Department of Microelectronics, University of Niš, Faculty of Electronic Engineering, Aleksandra Medvedeva 14, 18000 Niš, Serbia, e-mail: jana.vracar@elfak.ni.ac.rs

Milan Stojanović is with the Department of Microelectronics, University of Niš, Faculty of Electronic Engineering, Aleksandra Medvedeva 14, 18000 Niš, Serbia, e-mail: milan.stojanovic@elfak.ni.ac.rs

Zoran Prijić is with the Department of Microelectronics, University of Niš, Faculty of Electronic Engineering, Aleksandra Medvedeva 14, 18000 Niš, Serbia, e-mail: zoran.prijic@elfak.ni.ac.rs

Aneta Prijić is with the Department of Microelectronics, University of Niš, Faculty of Electronic Engineering, Aleksandra Medvedeva 14, 18000 Niš, Serbia, e-mail: aneta.prijic@elfak.ni.ac.rs

Ljubomir Vračar is with the Department of Microelectronics, University of Niš, Faculty of Electronic Engineering, Aleksandra Medvedeva 14, 18000 Niš, Serbia, e-mail: ljubomir.vracar@elfak.ni.ac.rs

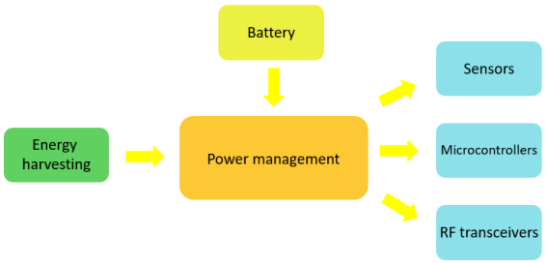


Fig. 1. Block scheme of energy harvesting system.

The block diagram of this kind of system is shown in Fig. 1. Low voltage and ultra-low power circuit design have become increasingly important recently. Low-power systems, such as those used in energy harvesting systems, wearable electronic devices, autonomous sensor nodes powered by non-conventional energy sources, the Internet of Things, and other similar applications, may require even lower supply voltage [2].

## II. Voltage Step-Up Circuit and Experimental Setup

### A. Voltage step-up circuit

For the supply of an embedded system, it is required to employ an electrical boost converter to boost the harvested voltage to a voltage of higher values. When used in combination with energy harvesting, a step-up converter should be self-starting from as low as feasible input voltages without the usage of additional power. A low-voltage start circuit with an oscillator followed by a voltage multiplier is used to meet these design constraints. The electric circuit of a step-up circuit is shown in Fig 2.

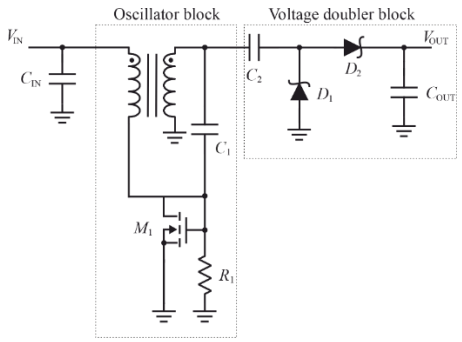


Fig. 2. Electric circuit of a voltage booster without energy harvesting block

 ISBN 978-86-7466-930-3

The minimal input voltage may be amplified significantly by changing the input DC energy into an AC form via an oscillator, then converting it back to DC with a boosted level by a voltage multiplier [3]. The oscillator block in this paper consists of a Meissner oscillator. It is needed to have an appropriate step-up ratio and have an adequate power conversion efficiency also.

At low input voltages, with the appropriate selection of MOS transistors and transformers, the Meissner oscillator begins to oscillate. If the input voltage is high enough, it undergoes a transition from its linear into a non-linear operation regime. The Meissner oscillator serves as a start-up circuit providing the supply voltage for a separate, inductor-based step-up converter from an input voltage of 50 mV and 100 mV for this experiment, followed by a voltage doubler circuit. When comparing different step-up converters, the parameters of start-up voltage and self-supply, as well as the employed circuit idea, are key factors to take into account. Low-voltage step-up converters are a popular subject of research, and of course, there are commercially produced devices. These converters have start-up voltages as low as 20 mV in some cases [4]. The capacitor $C_2$, which is part of the voltage doubler circuit, influences the maximum output current value. When utilizing a transformer with a ratio of 1:100 and working from very low input voltages, a minimum value of 1 nF is advised [4]. When operating at low input voltage or with high resistance sources, a large capacitor value may affect circuit performance. In this circuit, the gate coupling capacitor $C_1$ is employed. When the input voltage surpasses 50 mV, the capacitor's voltage value capacitor is increased to the point where oscillations occur rapidly. The experimentally established value for capacitor $C_1$ is 4.7 nF. Because of resistor $R_1$, the circuit's oscillations start consistently. The resistor $R_1$ of 2.2 MΩ is the predefined value. Schottky diodes are being used in this circuit for the voltage doubler ($D_1$ and $D_2$). The selected diodes have better frequency response and lower forward voltage than standard Si diode due to the lower forward voltage, and that is the reason for their implementation in this circuit. The energy is stored in the electrolytic capacitor $C_{OUT}$, which has a capacitance of 2200 μF. The choice of transformer is crucial in the circuit design process, and it will be considered in the experimental setup. High quality factor $Q$, compact footprint area, and high turns ratio are the main characteristics of the transformer for low voltage step-up oscillators. The step-up oscillator is coupled to the voltage source that drives the current through the primary trnasformer winding $L_1$ and the depletion-mode MOSFET. This current causes a positive voltage to be induced on the secondary transformer winding $L_2$, which raises the gate voltage of transistor $M_1$ and hence the primary winding current. The secondary winding voltage begins to diminish when this current reaches core saturation. The transistor begins to switch off the current via the transformer's main winding, resulting in a voltage reversal at the secondary winding and a negative gate voltage. The transistor is promptly turned on and remains active until the primary winding current reaches saturation, at which point the oscillation process restarts. The signal from the step-up oscillator is received by a half wave voltage doubler ($V_{OSC}$). In the voltage doubler circuit, capacitor $C_2$ and diode $D_1$ create a clamp, while the diode $D_2$ and capacitor $C_{OUT}$ create a peak rectifier. Diode $D_1$ conducts during the negative half cycle of an input voltage signal, charging capacitor $C_2$ to the voltage $V_{C2}= V_{D1}-V_{OSC}$. Diode $D_1$ is turned off during the positive half cycle of the input signal, while diode $D_2$ conducts charging capacitor $C_{OUT}$ [5]. The output voltage will be:

$$V_{OUT} = V_{OSC} - V_{C2} - V_{D2} = 2(V_{OSC} - V_D) \quad (1)$$

### *B. Experimental setup*

The major purpose of this study is to see how different pairings of transformers and transistors affect the generation of output voltage in the stated circuit, depending on whether a 50 mV or 100 mV voltage is provided to the circuit's input. The BSP149 and CPC3701CTR NMOS depletion mode transistors were used for the experiment. Since of its negative threshold voltage ($V_{th}$), the depletion mode n-type MOSFET BSP149 ($M_1$) was chosen because it is in a normally-on state at low voltages [6]. The transistor's low drain-source on-state resistance, which ranges from 1.7 Ω to 3.5 Ω, is the transistor's second advantage.

The CPC3701CTR transistor has lower drain-source on-state resistance of 1 Ω than transistor BSP149 [7]. The drain-source on-state resistance is an important characteristic of the depletion mode n-type MOSFET for the reason that this resistance affects power loss, and can be calculated as:

$$R_{DS(ON)} = \frac{1}{\mu_n \cdot C_{OX} \frac{W}{L}(V_{GS} - V_{th})} \quad (2)$$

where is $\mu_n$ – carrier mobility, $C_{OX}$ – oxide capacitance, $W$ – channel width, $L$ – channel length, $V_{GS}$ – gate-source voltage, and $V_{th}$ – threshold voltage.

As previously noted in the paper, the micro transformer with a ratio of 1:100 was chosen. For this experiment, transformers from different manufacturers were taken, but with similar characteristics and the same transformation ratio. The first transformer is CST-100LC, which has an inductance of 2 mH and a resistance of 5 Ω [8], while the second is a MID-SNS-CS with an inductance of 5.6 mH and a resistance of 0.85 Ω [9].

Since it is necessary to use a pair of transistor and transformer in the circuit, based on an input voltage of 50 mV in the first case and 100 mV in the second, it was decided to test all possible transistor and transformer combinations and then compare the output values of various parameters. These combinations are BSP149 MOSFET and CST-100LC transformer, BSP149 MOSFET and MID-SNS CS transformer, CPC3701CTR MOSFET and CS-100LC transformer, and CPC3701CTR MOSFET and MID-SNS CS transformer.

The expected results are that the MOS transistor CPC3701CTR in combination with some of the transformers can generate the highest output voltage since it has better characteristics than the BSP149 transistor, specified in the datasheet.

 ISBN 978-86-7466-930-3

## III. RESULTS AND DISCUSSION

The input voltage $V_{IN}$ simulates the generated voltage given by one of the energy harvesting block. In this case, DC voltage input is generated by a voltage supply at 50 mV and 100 mV instead of an energy harvesting voltage source. Fig. 3 shows the time that elapsed until the voltage on the capacitor reached 3.3 V and 5 V. The result of this measurement shows that the CPC3701CTR MOSFET and CST-100LC transformer take the longest time to generate specified output voltages. The shortest time to generate these values of voltage is measured for CPC3701CTR MOSFET and MID-SNS CS transformer, which indicates that they are the most efficient MOSFET-transformer pair in this research.

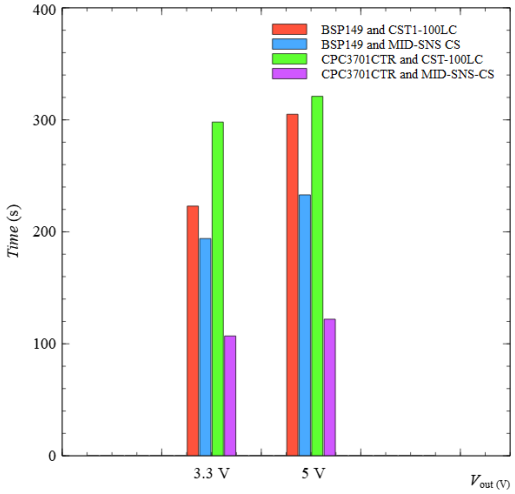


Fig. 3 Measured time for generating 3.3 V and 5 V on the output capacitor $C_{OUT}$ (2200 μF) for different pairs of transformers and MOS transistors.

Fig. 4 shows the maximum output voltage at the capacitor $C_{OUT}$ when the circuit reaches a steady-state and the given results are for 50 mV and 100 mV of the input voltage.

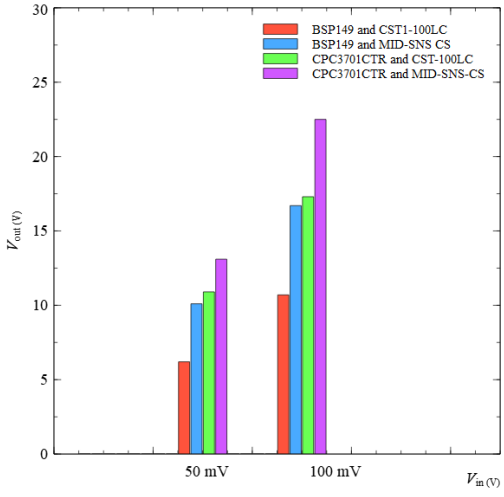


Fig. 4 Maximum generated output voltage on the capacitor $C_{OUT}$ for different pairs of transformers and MOS transistors at the input voltages of 50 mV and 100 mV.

It is measured that CPC3701CTR along with MID-SNS CS transformer can generate the biggest output voltage at the capacitor $C_{OUT}$, and the lowest produced voltage in these combinations of MOSFETs and transformers is for BSP149 MOSFET in pair with CST-100LC transformer. For the stated measurements, the best performances of the MOSFET-transformer pair are for the CPC3701CTR MOSFET and MID-SNS CS transformer, as expected. The resonate frequency of each MOSFET-transformer pair is presented in Fig 5. The highest resonating frequency is measured for CPC3701 MOSFET and CST-100LC transformer, and the lowest resonating frequency is measured for BSP149 MOSFET with MID-SNS CS transformer. Fig. 6 – Fig. 9 represent the output voltage generation for all of the measured MOSFET-transformer pairs, at the initial voltage of 100 mV, captured by the Tektronix DPO4034 oscilloscope.

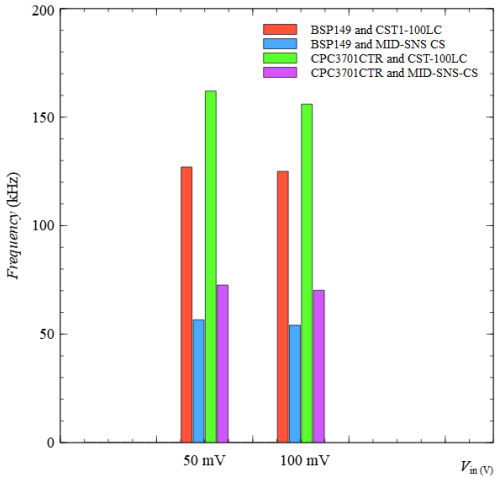


Fig. 5 Measured resonant freaquency for generating 3.3 V and 5 V on the output capacitor (2200 μF) for different pairs of transformers and MOS transistors.

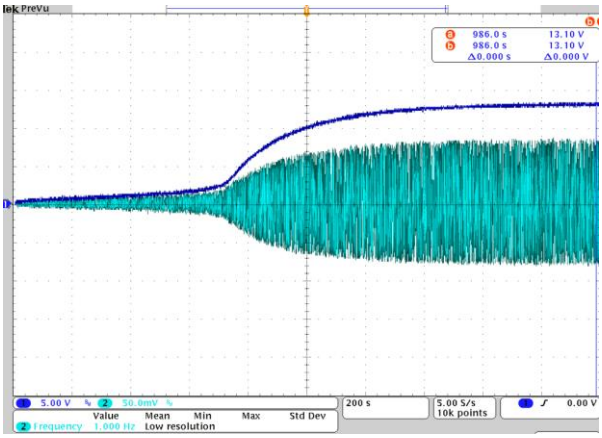

Fig. 6 BSP149 MOSFET and CST-100LC transformer pair: The oscillator voltage (light blue) and the voltage at the output capacitor $C_{OUT}$ (deep blue) as a function of time for the initial voltage of 100 mV. X-axis: 200 s/div, Y-axis: 5 V/div for $V_{OUT}$ and 50 mV for $V_{OSC}$.


ISBN 978-86-7466-930-3

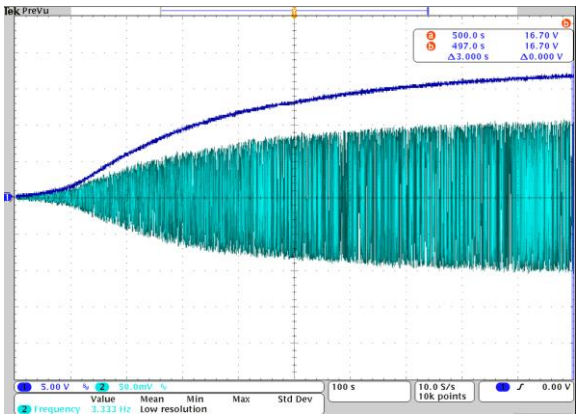

Fig. 7 BSP149 MOSFET and MID-SNS CS transformer pair: The oscillator voltage (light blue) and the voltage at the output capacitor $C_{OUT}$ (deep blue) as a function of time for the initial voltage of 100 mV. X-axis: 100 s/div, Y-axis: 5 V/div for $V_{OUT}$ and 50 mV for $V_{OSC}$.

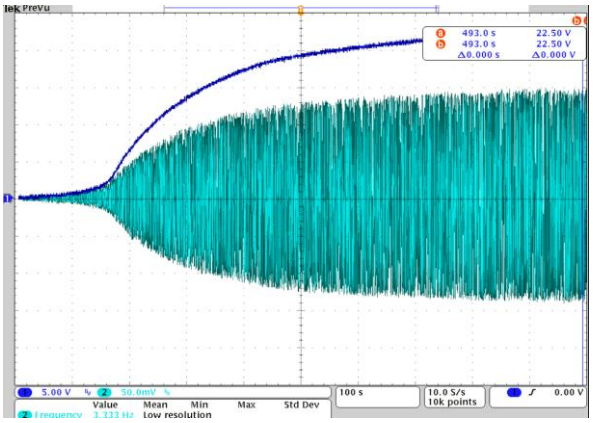

Fig. 8 CPC3701CTR MOSFET and CST-100LC transformer pair: The oscillator voltage (light blue) and the voltage at the output capacitor $C_{OUT}$ (deep blue) as a function of time for the initial voltage of 100 mV. X-axis: 100 s/div, Y-axis: 5 V/div for $V_{OUT}$ and 50 mV for $V_{OSC}$.

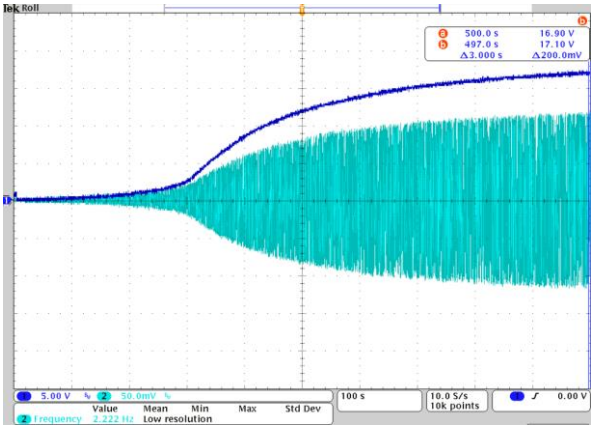

Fig. 9 CPC3701CTR MOSFET and MID-SNS CS transformer pair: The oscillator voltage (light blue) and the voltage at the output capacitor $C_{OUT}$ (deep blue) as a function of time for the initial voltage of 100 mV. X-axis: 100 s/div, Y-axis: 5 V/div for $V_{OUT}$ and 50 mV for $V_{OSC}$.

## IV. Conclusion

It is a great challenge to choose the components that will provide the highest efficiency of the power management circuit, but it is one that must be addressed depending on the purpose of the circuit behind the power management block. Depending on that, it is necessary to pay attention to how the components affect the power loss, which ones generate the highest output voltage, which ones reach a certain value of the output voltage for the shortest time, etc. This paper shows how different transformers and MOS transistors affect all of the parameters stated above, and it is possible to choose a pair depending on the needs of the circuit powered by such a system. In terms of generating the highest possible output voltage on the $C_{OUT}$ capacitor it is best to use a CPC3701CTR MOSFET with a MID-SNS CS transformer, for a lower input voltage at 50 mV but at 100 mV as well. If the user needs a power management circuit that generates an output voltage in the shortest time, the best option is a pair of CPC3701CTR MOSFET and a MID-SNS CS transformer. The pair of a CPC3701CTR MOSFET and CST-100LC transformer is the second-best for generating maximum output voltage, but it needs the longest time to generate the desired voltage. In the future, this type of step-up converter will be improved by adding and testing additional components to the circuit in order to give the shortest time for the oscillation process.

## Acknowledgment

This paper is supported by the Serbian Ministry of Education, Science and Technological Development under Grant number 451-03-68/2022-14/200102.

## References

[1] Khan, Farid Ullah; Khattak, Muhammad Umair (2016). Contributed Review: Recent developments in acoustic energy harvesting for autonomous wireless sensor nodes applications. Review of Scientific Instruments, 87(2), 021501–. doi:10.1063/1.4942102.

[2] Calautit, K., Nasir, D. S. N. M., & Hughes, B. R. (2021). Low power energy harvesting systems: State of the art and future challenges. Renewable and Sustainable Energy Reviews, 147, 111230. doi:10.1016/j.rser.2021.111230

[3] Weng, Po-Shuan; Tang, Hao-Yen; Ku, Po-Chih; Lu, Liang-Hung (2013). 50 mV-Input Batteryless Boost Converter for Thermal Energy Harvesting. IEEE Journal of Solid-State Circuits, 48(4), 1031–1041. doi:10.1109/JSSC.2013.2237998.

[4] LTC3108 ultralow voltage step-up converter and power manager, Linear Technology Corporation, 2010, datasheet. [Online]. Available: https://www.infineon.com

[5] J. Vračar, M. Marjanović, A. Stojković, Z. Prijić, A. Prijić, Lj. Vračar, "Application of a Low-Voltage Step-Up Circuit for Thermal Energy Harvesting Under Natural Convection" Proceedings of papers IcETRAN 2019, 6th International Conference on Electrical, Electronic and Computing Engineering, Srebrno Jezero, 2019, pp. 564-569, ISBN 978-86-7466-785-9

[6] BSP149 Small-Signal-Transistor, Infineon, 2012, Datasheet., Infineon, 2012. [Online]. Available: https://www.infineon.com/

[7] CPC3701 Depletion-Mode, N-Channel VDMOSFET, IXYS Integrated Circuits Division, 2015, Datasheet., IXYS Integrated Circuits Division 2015. [Online]. Available: https://www.ixysic.com/

[8] CST1-100LC Current Sense Transformers, Coilcraft Inc, 2021, Datasheet., Coilcraft Inc, 2021. [Online]. Available: www.coilcraft.com

[9] MID-SNS CS Current Sense Transformers, Würth Elektronik [Online]. Available: https://www.we-online.com

 ISBN 978-86-7466-930-3

# Indukovanje stanja sličnih topološkim kod dvoslojnih fosforenskih traka primenom normalnog električnog polja

Vladimir V. Arsoski, Milan Ž. Tadić

***A stra t*— etoda ja e veze je korišćena za analizu ele trons e stru ture nanotra a od dvoslojnog crnog fosfora u prisustvu električnog polja. od tra a sa foteljastim ivicama nisu prisutna ivična stanja, pa postoji veli i dire tan procep u odsustvu spoljašnjeg polja. Primena električnog polja normalno na površinu trake dovodi do smanjenja procepa. a određenu ritičnu vrednost amplitude električnog polja procep se s oro u potpunosti zatvara i u centru procepa dolazi do pojave oštrog antiukrštanja stanja najniže energije iz provodne zone i stanja najviše energije iz valentne zone. vo ponašanje je ara teristično za onvencionalne topološke izolatore od ojih do inverzije zons e stru ture dolazi usled ja e spin-orbitne intera cije koja nije uključena u naš model. stanovljeno je da od nanotra a male debljine postoji ja o sprezanje stanja u provodnoj i valentnoj zoni usled anizotropije ia o su ele troni i šupljine potisnuti na suprotne površine trake električnim poljem. Povećanje normalnog električnog polja iznad ritične vrednosti dovodi do inverzije i viših stanja iz provodne i valentne zone što je praćeno karakterističnim antiukrštanjima.**

***Ključne reči*— etoda ja e veze; fosforen; topološki izolatori; normalno električno polje.**

## I. UVOD

Proizvodnja tankih slojeva poluprovodničkih materijala pokrenula je novu eru razvoja elektronskih komponenti koja je započela uspešnim izdvajanjem nekoliko monoslojeva tankog filma grafita iz masivnog kristala [1]. Velika popularnost monosloja grafita, koji je poznat pod imenom grafen [2], dovela je do porasta interesovanja za takozvane dvodimenzione (2D) materijale. Prva teorijska istraživanja su ukazala da smanjena dimenzionalnost u jednom pravcu dovodi do manifestacije specifičnih elektronskih osobina kod tankoslojnih materijala u odnosu na masivne materijale od kojih su dobijeni [3], što ih je učinilo atraktivnim za potencijalne primene u elektronici. Za razliku od tankih slojeva grafita kod kojih energetski procep praktično ne postoji, tanki slojevi crnog fosfora se odlikuju velikom vrednošću energetskog procepa koja je nekoliko puta veća od vrednosti u masivnom uzorku što ga, zajedno sa velikom pokretljivošću šupljina, čini odličnim kandidatom za izradu pMOS tranzistora [4,5]. Istraživanja predviđaju da izražena anizotropija strukture crnog fosfora može dovesti do intenzivne manifestacije interesantnih efekata kod tankih slojeva materijala, takozvanog fosforena, kao rezultat anizotropije optičkih, električnih, mehaničkih i termalnih svojstava [6]. U cilju zaštite od spoljašnjih uticaja slojevi fosforena se umeću između monoslojeva heksagonalnog bor-nitrida, što u određenoj meri modifikuje njegova elektronska, električna, transportna i optička svojstva [7].

U cilju primene u realnim napravama fosforen se obično izrađuje u formi nanotraka [4]. Kao i svi 2D materijali sa heksagonalnom rešetkom, trake fosforena se mogu fabrikovati tako da imaju karakteristične regularne cik-cak ili foteljaste ivice, koje se razlikuju po elektronskoj strukturi i transportnim svojstvima [8]. Kod traka sa cik-cak ivicama postoje ivična stanja čija je energija u blizini centra procepa i ponašaju se kao metalne, dok trake sa regularnim foteljastim ivicama nemaju stanja u procepu i ponašaju se kao izolatorske. Bez obzira na tip ivica traka, njihove elektronske i transportne osobine se mogu podešavati primenom električnog polja gde u okolini kritične vrednosti polja primenjenog normalno na ravan trake dolazi do karakterističnih prelaza izolator-metal [8].

*Ab initio* proračuni elektronske strukture višeslojnog fosforena predviđaju da primena naprezanja može dovesti do formiranja Dirakovih konusa [9], što je inherentna karakteristika elektronske strukture topoloških izolatora. U formi masivnog materijala topološki izolatori poseduju energetski procep, dok u materijalu konačnih dimenzija dolazi do pojave karakterističnih stanja lokalizovanih po ivicama ili površinama strukture koja u inverznom prostoru, u vidu Dirakovog konusa, zatvaraju procep i invarijantna su u odnosu na inverziju u vremenu [10]. U ovom radu biće prikazano da se slična svojstva elektronske strukture mogu indukovati u dvoslojnom fosforenu primenom normalnog električnog polja.

## II. TEORIJSKI MODEL

Za analizu elektronske strukture nanotraka korišćen je metod jake veze, gde je hamiltonijan dat sa

$$= \sum_{i \neq j} t_{i,j} c_i^{\dagger} c_j + \sum_i e \quad _i \mathbf{r}_i . \qquad (1)$$

Vladimir Arsoski – Elektrotehnički fakultet, Univerzitet u Beogradu, Bulevar kralja Aleksandra 73, 11020 Beograd, Srbija (e-mail: vladimir.arsoski@etf.bg.ac.rs), (https://orcid.org/0000-0002-9326-7809)

Milan Tadić – Elektrotehnički fakultet, Univerzitet u Beogradu, Bulevar kralja Aleksandra 73, 11020 Beograd, Srbija (e-mail: tadic@etf.bg.ac.rs), (https://orcid.org/0000-0002-9408-7957)

 ISBN 978-86-7466-930-3

Ovde je $t_{i,j}$ energija skoka između $i$-tog i $j$-tog atoma, $c_i^{\dagger}\left(c_j\right)$ je operator kreacije (anihilacije) elektrona u $i(j)$-tom atomskom stanju, $_i$ je vektor spoljašnjeg električnog polja na mestu $i$-tog atoma, $\mathbf{r}_i$ je vektor položaja $i$-tog atoma, a $e$ je elementarno naelektrisanje. Referentna tačka za izračunavanje dodatnog potencijala u prisustvu električnog polja je postavljena u koordinatni početak i poklapa se sa centrom nanotrake. Korišćeno je 10 parametara za skokove u okviru jednog monosloja, dok su sa 5 parametara opisani skokovi između monoslojeva. Izabrani skup parametara daje verodostojne rezultate za razmatranu višeslojnu strukturu [11]. Rastojanja između atoma, koja figurišu kroz članove zavisne od položaja atoma, su preuzeta iz reference [8]. Širina trake je određena brojem dimera duž poprečnog preseka trake, dok jediničnu ćeliju sačinjava minimalan skup atoma čijim se periodičnim ponavljanjem reprodukuje nanotraka beskonačne dužine. Za implementaciju trake nominalno beskonačne dužine korišćeni su periodični granični uslovi. Dijagonalizacijom matrice hamiltonijana (1) dobija se skup svojstvenih vrednosti i svojstvenih vektora koji opisuje elektronsku strukturu razmatranog sistema.

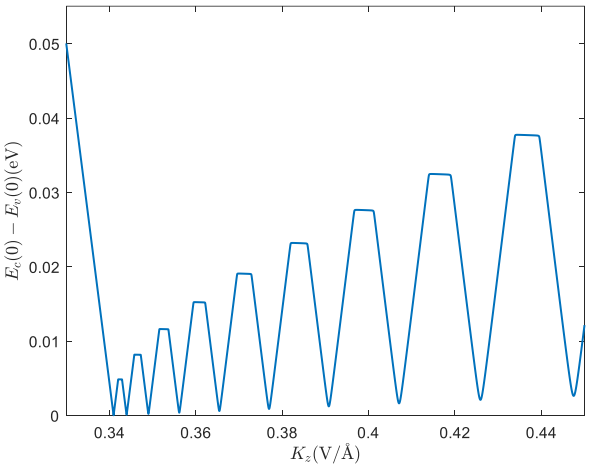


Sl. 1. Razlika svojstvenih vrednosti stanja najniže energije u provodnoj zoni i stanja najviše energije u valentnoj zoni u 0 u funkciji amplitude normalnog električnog polja .

## III. REZULTATI I DISKUSIJA

Analizirane su trake sa regularnim foteljastim ivicama debljine dva monosloja fosforena, pri čemu je broj dimera u jednom monosloju duž poprečnog preseka $N_d$ =61 što približno odgovara širini trake od 10 nm. Referentna tačka za potencijal je tačka na sredini između slojeva na polovini širine trake. Osa je usmerena duž trake, osa $y$ je paralelna ravni monoslojeva duž poprečnog preseka trake, dok je osa normalna na ravan strukture.

Najpre je analiziran uticaj električnog polja primenjenog normalno na površinu trake na razliku energija stanja na dnu provodne zone i stanja na vrhu valentne zone u tački $k$ = 0. U određenom opsegu amplituda električnog polja ova razlika odgovara širini energetskog procepa koji je direktan. Povećanje amplitude električnog polja dovodi do smanjenja procepa i za određene kritične vrednosti se pojavljuju minimumi, što je prikazano na Sl.1. Može se uočiti da lokalni minimumi procepa imaju veću vrednost što je amplituda kritičnog polja veća.

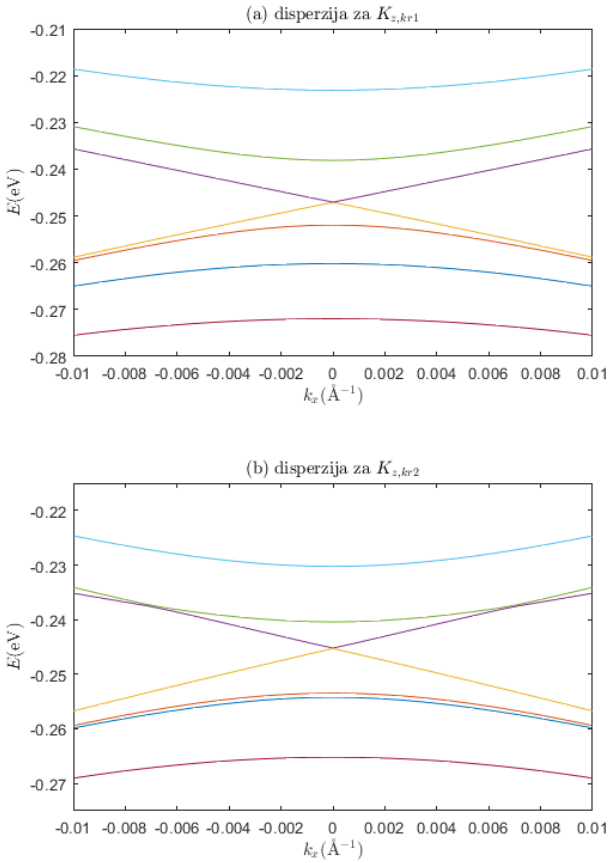


Sl. 2. Prikaz zavisnosti svojstvenih energija u okolini centra zone u funkciji talasnog vektora $k$, usmerenog duž trake, za kritičnu vrednost amplitude električnog polja za koju energetski procep ima minimalnu vrednost: (a) najniža kritična vrednost polja $_{,kr1}$ = 0.3409635 V/Å; (b) prvi sledeći (lokalni) minimum $_{,kr2}$ = 0.3439790398 V/Å.

Disperzije u okolini centra zone za najnižu kritičnu vrednost polja $_{,kr1}$ = 0.3409635 V/Å kada procep ima minimalnu širinu $E_{g1,\min}$ = 22.96310 μeV i za prvu sledeću vrednost $_{,kr2}$ = 0.3439791 V/Å kada je vrednost procepa $E_{g2,\min}$ = 92.49116 μeV su prikazane na Sl.2 (a) i (b), redom. U tački $k$ =0 dolazi do antiukrštanja stanja energija najbližih energetskom procepu, takozvanih najnižih stanja u provodnoj i valentnoj zoni. Ukoliko se kao referentan raspored usvoji raspored stanja na disperziji kada polje nije primenjeno, pri prvoj kritičnoj vrednosti polja dolazi do antiukrštanja najnižih stanja u provodnoj i valentnoj zoni za $_{,kr1}$. Za vrednost polja $_{,kr2}$ dolazi do antiukrštanja drugog stanja iz provodne i drugog iz valentne zone pri čemu se tačka antiukrštanja prvog stanja iz provodne i valentne zone pomera iz centra zone

 ISBN 978-86-7466-930-3

većim vrednostima $|k|$, što se lako može uočiti sa Sl.2 (b) (tačka antiukrštanja je za $|k| \cong 0.007\,\text{Å}^{-1}$). Ovaj trend se nastavlja sve do amplitude polja $_{,kr10}$ = 0.447989 V/Å, koja odgovara desetom (krajnjem desnom) lokalnom minimumu na Sl.1, kada procep postaje indirektan. Tada materijal prelazi iz izolatorskog u polumetalno stanje.

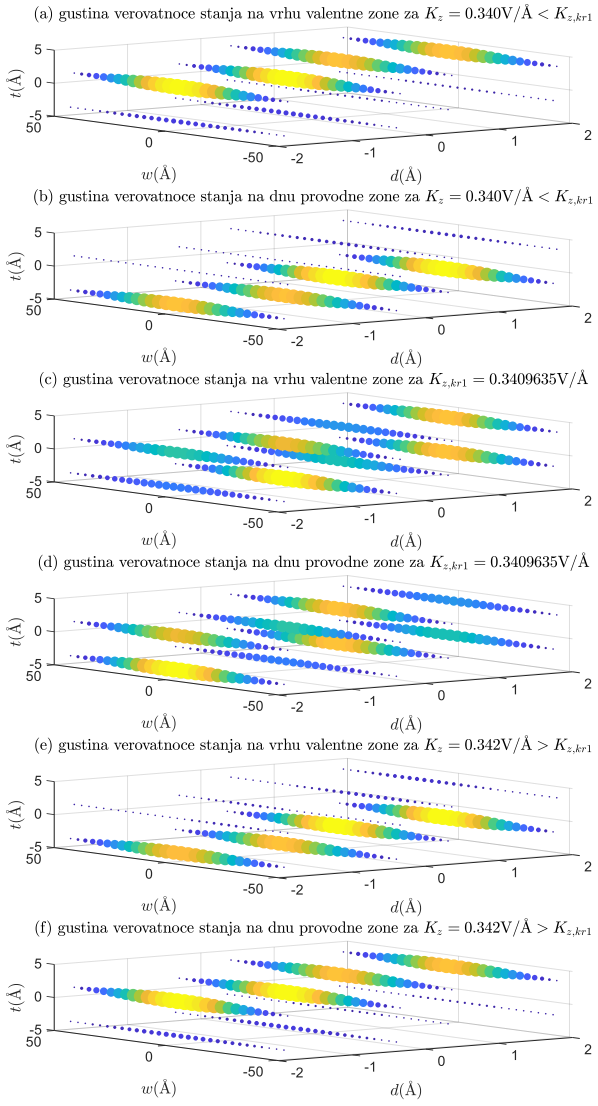


Sl. 3. Prikaz gustine verovatnoće stanja: (a) na vrhu valentne zone za polje = 0.340 V/Å < $_{,kr1}$; (b) na dnu provodne zone za polje = 0.340 V/Å < $_{,kr1}$; (c) na vrhu valentne zone za polje $_{,kr1}$ = 0.3409635 V/Å; (d) na dnu provodne zone za polje $_{,kr1}$ = 0.3409653 V/Å; (e) na vrhu valentne zone za polje = 0.342 V/Å > $_{,kr1}$; (f) na dnu provodne zone za polje = 0.342 V/Å > $_{,kr1}$; Na slici osa *w* je postavljena po širini trake, *d* po dužini, dok je *t* normalno na površinu trake.

Da bi ustanovili koliko je ova struktura slična topološkim izolatorima, izračunate su gustine verovatnoća stanja na dnu provodne i vrhu valentne zone za amplitude električnog polja u okolini prve kritične vrednosti, što je prikazano na Sl.3. Za vrednosti polja koje su manje od $_{,kr1}$ stanja u valentnoj zoni su pretežno lokalizovana na gornjoj površini trake, dok su stanja u provodnoj na donjoj, što se može uočiti na Sl. 3 (a) i (b), redom. Električno polje je normalno na površinu trake i usmereno vertikalno naviše (u smeru *t* ose) tako da potiskuje šupljine na gornju površinu, dok su elektroni potisnuti na donju. Za kritičnu vrednost električnog polja lokalizacija stanja u valentnoj i provodnoj zoni je slična, pri čemu su stanja u različitim zonama lokalizovana na različitim podrešetkama strukture, što je prikazano na Sl. 3 (c) i (d). Ovo je posledica izrazite anizotropije dvoslojnog fosforena i posebno male debljine strukture zbog čega je sprezanje stanja u valentnoj i provodnoj zoni jako čak i pri velikim amplitudama električnog polja koje teži da razdvoji elektrone i šupljine. U slučaju kada je amplituda polja veća od kritične vrednosti, uočava se da su stanja na vrhu valentne zone lokalizovana na donjoj površi, dok su stanja na dnu provodne zone lokalizovana na gornjoj površi (videti Sl.3 (e) i (f)) što je obrnuto od onoga što smo imali na Sl.3 (a) i (b) kada je amplituda polja bila manja od kritične. Ovo je indikacija da je u oblasti antiukrštanja došlo do inverzije zonske strukture, što je ponašanje slično onome koje se sreće kod topoloških izolatora. Inverzija zonske strukture počinje u centru zone i širi se ka ivicama zone sa porastom amplitude električnog polja. Za stanja kod kojih nije došlo do inverzije lokalizacija je takva da su stanja u valentnoj zoni pretežno na atomima na gornjoj površi strukture, dok su stanja u provodnoj zoni dominantno lokalizovana na donjoj, što odgovara efektu koji električno polje ima na šupljine i elektrone.

## IV. ZAKLJUČAK

U radu je teorijski razmatrana elektronska struktura dvoslojnih traka od fosforena sa foteljastim ivicama. Utvrđeno je da primenom normalnog električnog polja dolazi do antiukrštanja stanja iz provodne i valentne zone, što je praćeno zonskom inverzijom. Nađene su kritične vrednosti polja za koja je procep između zona minimalan. Za veće kritične vrednosti polja, procep je veći. Za razmatrane kritične vrednosti je nađeno da je u centru zone lokalizacija stanja u različitim zonama energija najbližih ivici procepa bila slična, ali na različitim podrešetkama. Ovo je posledica anizotropije i male debljine strukture. Indukovani efekti su slični onima koji se sreću kod topoloških izolatora. U daljem istraživanju bi trebalo utvrditi kako magnetsko polje u ravni utiče na disperziju, što bi dalo dodatne rezultate koji bi ukazali na topološke efekte.

## ZAHVALNICA

Ovaj rad je podržan od strane Ministarstva prosvete, nauke i tehnološkog razvoja Republike Srbije 451-03-68/2022-14/200103.

 ISBN 978-86-7466-930-3

## LITERATURA


[1] K. S. Novoselov, A. K. Geim, S. V. Morozov, D. Jiang, Y. Zhang, S. V. Dubonos, I. V. Grigorieva, and A. A. Firsov, "Electric field effect in atomically thin carbon films," *Science*, vol. 306, pp. - , Oct. 2004.

[2] A. K. Geim, K. S. Novoselov, "The rise of graphene," *Nat. Mater*, vol. , no. *3*, pp. *1 3-1 1*, Feb. 2007.

[3] B. Partoens, F. M. Peeters, "From graphene to graphite: Electronic structure around the K point," *Phys. e . B*, vol. *4*, pp. *0 5404 1-11*, Avg. 2006.

[4] H. Liu, A. T. Neal, Z. Zhu, Z. Luo, X. Xu, D. Tománek, P. D. Ye, "Phosphorene: An Unexplored 2D Semiconductor with a High Hole Mobility", *ACS Nano*, vol. , no. *4*, pp. *4033-4041*, Mar. 2014.

[5] W. Lu, H. Nan, J. Hong, Y. Chen, C. Zhu, Z. Liang, X. Ma, Z. Ni, C. Jin, *Nano es*, Vol. , pp. *53- 5* , May 2014.

[6] Y. Aierken, D. Çakir, C. Sevik, F. M. Peeters, "Thermal properties of black and blue phosphorenes from a first-principles quasiharmonic approach," *Phys. e . B*, vol. *2*, no. , pp. *0 140 1-5*, Avg. 2015.

[7] T. Hu and J. Hong, Anisotropic Effective Mass, "Optical Property, and Enhanced Band Gap in BN/Phosphorene/BN Heterostructures," *ACS Appl. Mater. Interfaces*, vol. , no. *42*, pp. *234 -234 5*, Oct. 2015.

[8] V. V. Arsoski, M. M. Grujić, N. A. Čukarić, M. Ž. Tadić, F. M. Peeters, "Normal and skewed phosphorene nanoribbons in combined magnetic and electric fields", *Phys. e . B*, vol. , no. *12*, pp. *125434 1-11*, vol. 25, no. 12, Sep. 2017.

[9] R. Fei, V. Tran, L. Yang, "Topologically protected Dirac cones in compressed bulk black phosphorus", *Phys. e . B*, vol. *1*, no. *1* , pp. *1 531 1-5*, May 2015.

[10] X-L. Qi, S-C. Zhang, "Topological insulators and superconductors", *e . Mod. Phys*, vol. *3*, no. *4*, pp. *105 -1110*, Dec. 2011.

[11] A. N. Rudenko, S. Yuan, and M. I. Katsnelson, "Toward a realistic description of multilayer black phosphorus: From GW approximation to large-scale tight-binding simulations," *Phys. e . B*, vol. *2*, no. , pp. *0 541 1-* , July 2015; Videti Erratum: A. N. Rudenko, S. Yuan, and M. I. Katsnelson, *Phys. e . B*, vol. *3*, no. *1* , pp. *1 0* , May 2016.



## ABSTRACT

Tight-binding method is employed for electronic structure analysis in bilayer black phosphorous nanoribbons in presence of electric field. Due to the absence of edge states, there is a large gap in arm-chair nanoribbons in absence of an external field. An application of an electric field perpendicular to the ribbon surface decreases the gap width. At the critical value of the electric field, the gap is almost completely closed due to sharp anti-crossing between the lowest energy conduction band state and the highest energy valence band state. This behavior is characteristic in conventional topological insulators where an inversion of the zone structure is due to strong spin-orbit interaction that is not accounted for in our model. It is found that in thin nanoribbons there is a strong coupling between conduction and valence band states due to anisotropy despite the electrons are holes being pushed to the opposite sides of the slab by an external electric field. Increase of the perpendicular electric field above critical value results in an inversion of higher conduction and valence band states that manifests in characteristic anti-crossings.


**Inducing the Topological-li e tates in ilayer Phosphorene anoribbons by Perpendicular lectric ield**

Vladimir V. Arsoski, Milan Ž. Tadić

 ISBN 978-86-7466-930-3

# Elektronska svojstva grafenskih nanotraka sa periodičnim defektima

Jovana Vlahović, Vladimir V. Arsoski, Milan Ž. Tadić, Milorad Milošević

***A stra t*—Već više od decenije materijali izrađeni od jednog ili više monoslojeva ristala su u žiži interesovanja zbog boljih ele trons ih i transportnih svojstava u odnosu na masivni materijal od ojeg su sačinjeni. ao posebno interesantan za primenu izdvojio se grafen, oji je prvi dobijen u formi tan og sloja. dređeni broj primena zahteva da u materijalu postoji dovoljno veli i energets i procep, što kod grafena nije slučaj. azvijene tehni e ontrole procepa nisu dale značajnije rezultate od ovog materijala. U ovom radu je predložena mogućnost podešavanja procepa grafens ih nanotra a uvođenjem periodičnih defekata u nanostru turu. azmotren je uticaj defe ta tipa jednog upražnjenog mesta (va ancije) u kristalnoj rešetki koji se periodično ponavlja duž trake. Po azano je da periodični defekti mogu imati značajan uticaj na razli u energija dna provodne i vrha valentne zone u nanotra ama sa foteljastim ivicama, a samim tim i na ele trons e i transportne osobine grafens ih nanotra a. Prisustvo periodičnog defe ta rezultuje pojavom specifičnih stanja vezanih za defekt, što se ogleda u pojavi ravne zone unutar procepa na disperzionoj relaciji.**

***čne reči*—2D materijali; grafen; metod ja e veze; energets i procep; defe tna stanja; ravne zone.**

## I. UVOD

Već više decenija elektronske naprave zasnovane na silicijumu dominiraju u izradi elektronskih naprava. Trendovi minijaturizacije elektronskih naprava doveli su silicijum do granice kada kvantnomehanički efekti, koji dominiraju pri malim dimenzijama strukture, bitno utiču na funkcionisanje naprave. Kao alternativa su se pojavili materijali izrađeni od jednog ili više monoslojeva poluprovodničkog krustala, poznati kao dvodimenzioni (2D) materijali, koji usled malih dimenzija pokazuju poboljšana elektronska, transportna, električna, termička i optička svojstva u odnosu na masivne materijale od kojih su dobijeni. Kao posebno interesantan materijal, zbog velike potencijalne primene, izdvaja se monosloj grafita poznat kao grafen [1]. Uspešna fabrikacija ovog materijala pokrenula je eru razvoja post-silicijumske elektronike koja obećava veliki napredak u domenu elektronskih naprava [2]. Prvobitna fabrikacija grafena zasnivala se na metodi mehaničke eksfolijacije pomoću dvostruko-lepljive trake [3]. Ovako dobijeni uzorci su imali mnogo defekata, bili su relativno malih dimenzija i obično su se sastojali od više monoslojeva grafita, te metoda nije bila reproduktivna. Usledile su tehnike eksfolijacije u tečnoj fazi organskih rastvarača, jonskih tečnosti, rastvora surfaktanata i mnogih rastvarača koji su imali sličan površinski napon kao i grafen [4]. Vremenom se kao dominantna metoda izdvojila sonifikacija [5]. Ultrazvuk se prostire kroz tečnu fazu do grafena gde dovodi do naizmenične promene pritiska, što uzrokuje sabijanje i razvlačenje veza između slojeva atoma. Prilikom razdvajanja monoslojeva u međuprostoru se stvaraju mikromehurići, koji postepeno narastaju i pucaju pri dostizanju kritične veličine, što dovodi do generacije snažnih udarnih talasa. Dalje se centrifugiranjem mogu razdvojiti supernatant i dobijeni grafenski proizvod. Iako zahteva veliku količinu energije i ima malu efikasnost, ova metoda se koristi jer se njome uspešno mogu proizvesti monoslojevi [6]. Kao efikasna metoda za dobijanje grafenskih nanotraka pokazala se tehnika zasecanja i razvijanja ugljeničnih nanotuba. Veličina dobijenih traka zavisi od dijametra i dužine nanotube, dok tip ivica određuje pravac zasecanja nanotrake [7]. Kao efikasna metoda za formiranje slojeva grafena velike površine i sa malo defekata pokazala se tehnika heteroepitaksije, gde se narastanje vrši na supstratu koji ima sličnu kristalnu strukturu kao i grafen [8]. Posebno interesantan supstrat je silicijum karbid (SiC) na kojem je kontrolisanim postupkom moguće narasti jedan monosloj ukoliko se narastanje vrši na površini orijentacije (0001) [9]. Fabrikovane površine grafena se dalje mogu obrađivati radi postizanja željene morfologije.

Kao glavni nedostatak grafena kod primene u tranzistorima navodi se zanemarljiva vrednost energetskog procepa koja otežava njegovu primenu u tranzistorima sa efektom polja. Procep od nekoliko desetina meV može se dobiti oblikovanjem grafena u formu traka malih dimenzija [10] ili slaganjem više slojeva grafena (stekovanjem) na različite načine [11], što nije sasvim dovoljno za veliki broj savremenih primena.

Poznato je da proizvoljno mala periodična perturbacija masivnog dielektričnog materijala dovodi do pojave zabranjenog opsega učestanosti za prostiranje svetlosti u materijalu, što odgovara nastanku fotonskog procepa [12]. Periodične perturbacije imaju sličan efekat i na elektronsku strukturu poluprovodnika. Pokazano je da se specifičnim periodičnim uvijanjem grafena može neznatno otvoriti energetski procep [13]. Ideja je da se pomoću periodičnih

Jovana Vlahović – Faculty of Sciences, University of Antwerp, Groenenborgerlaan 171 2020 Antwerpen, Belgium, (e-mail: jovana.vlahovic@uantwerpen.be).

Vladimir Arsoski – Elektrotehnički fakultet, Univerzitet u Beogradu, Bulevar Kralja Aleksandra 73, 11020 Beograd, Srbija (e-mail: vladimir.arsoski@etf.bg.ac.rs).

Milan Tadić – Elektrotehnički fakultet, Univerzitet u Beogradu, Bulevar Kralja Aleksandra 73, 11020 Beograd, Srbija (e-mail: tadic@etf.bg.ac.rs).

Milorad Milošević – Faculty of Sciences, University of Antwerp, Groenenborgerlaan 171 2020 Antwerpen, Belgium, (e-mail: milorad.milosevic@uantwerpen.be).

 ISBN 978-86-7466-930-3

defekata formiranih u grafenu kontroliše veličina energetskog procepa.

Inherentan tip defekta u grafenu predstavljaju upražnjena mesta u rešetki, takozvane vakancije, koje imaju slučajan raspored u strukturi. Površinska koncentracija ovih defekata zavisi od primenjenih tehnika fabrikacije, a najmanja je kod novijih tehnike fabrikacije [7-9]. Utvrđeno je da defekti ovog tipa u izvesnoj meri utiču na elektronska i magnetska svojstva grafenskih nanotraka [14, 15]. Primenom tehnike koja koristi visokoenergetske jone ili elektrone moguće je precizno ukloniti pojedine atome iz rešetke, što otvara mogućnost za preciznu kontrolu položaja defekata [16], a samim tim i kontrolu veličine procepa u strukturama od grafena.

## II. Implementacija modela

Modelovanje elektronske strukture grafenskih nanotraka zasnovan je na metodi jake veze. Teorijske osnove razmatranog modela mogu se naći u [17]. Za implementaciju modela je korišćena biblioteka PyBinding 0.9.5 [18] koja je napravljena u programskom jeziku Python. U radu je korišćena aproksimacija koja razmatra skokove samo na najbliže susede. Svi parametri koji figurišu u modelu su preuzeti iz [19].

U zavisnosti od pravca zasecanja sloja grafena, nanotrake mogu imati različite ivice, ali se najčešće razmatraju trake sa cik-cak i foteljastim ivicama [20]. U ovom radu su analizirane trake sa foteljastim ivicama pošto, za razliku od traka sa cik-cak ivicama, kod njih ne postoje ivična stanja. Razmatrane su isključivo trake sa periodičnim defektima u vidu jedne vakancije, pri čemu se u prvoj aproksimaciji usvaja da nije došlo do ismene položaja atoma u okolini upražnjenog mesta u rešetki [21]. Kada nedostaje više susednih ugljenikovih atoma u sloju grafena može doći do građenja novih veza i međusobnog vezivanja nesusednih atoma [22].

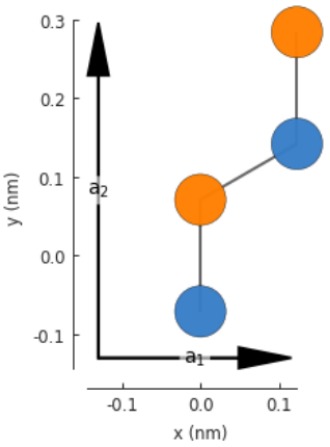


Sl. 1. Izgled elementarne ćelije čijim se ponavljanjem u prostoru reprodukuje traka sa foteljastim ivicama proizvoljne širine [17,18].

## III. Rezultati i diskusija

Pri analizi nanotraka korišćena je elementarna ćelija prikazana na Sl.1. Atomi različite boje pripadaju različitim podrešetkama. Periodičnim ponavljanjem elementarne ćelije u pravcu vektora $\mathbf{a}_1$ može se reprodukovati nanotraka sa foteljastim ivicama proizvoljne širine. Minimalna širina trake odgovara dužini vektora $\mathbf{a}_2$. Uvođenje periodičnih graničnih uslova u ovom pravcu ekvivalentno je formiranju trake nominalno beskonačne dužine. Usvojeno je da je minimalno rastojanje defekata $w_{\min}=|\mathbf{a}_2|$. Analiziran je slučaj gde se defekti mogu periodično ponavljati duž trake u pravcu vektora $\mathbf{a}_2$ tako da im je međusobno rastojanje $w = mw_{\min}$, gde je $m$ prirodan broj. Rastojanje defekata $w$ ujedno predstavlja dužinu elementarne ćelije koja gradi traku beskonačne dužine.

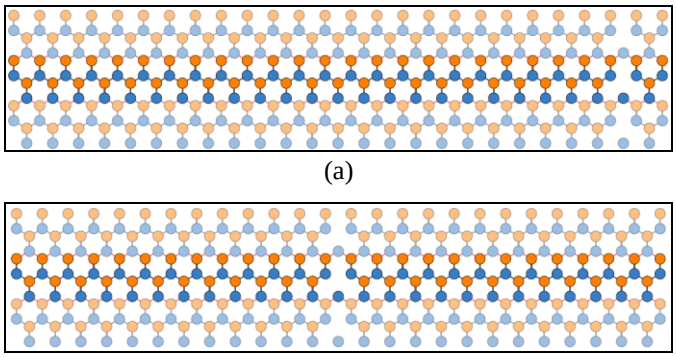


Sl. 2. Jedinična ćelija nanotrake kod koje je rastojanje vakancija $d_{\min}$ za položaj defekta: (a) najbliže ivici trake, (b) na sredini trake [17].

Analizirane su trake sa foteljastim ivicama širine 6.149 nm. U slučaju najmanjeg rastojanja između defekata duž trake, jediničnu ćeliju nanotrake sačinjava 50 C-C dimera i jedan ugljenikov atom. U slučaju trake bez defekta broj dimera bi bio 51. U nedavnim istraživanjima je ustanovljeno da grafenske nanotrake, čija se elementrarna ćelija sastoji od $3N$ nizova dimera, gde je $N$ prirodan broj, mogu da imaju veće energetske procepe i bolje optička svojstva nego trake čije elementrarne ćelije broje $3N$+1 i $3N$+2 dimera [23,24]. Nanotrake kod kojih su defekti periodično raspoređeni na rastojanju $w$ sastoje se od $51 \cdot w$ dimera umanjeno za jedan ugljenikov atom, te približno zadovoljavaju navedeni uslov.

Najpre su analizirane trake kod kojih je rastojanje defekata $d_{\min}$. Položaj vakancije je pomeran po širini trake i menjan je od položaja najbližeg ivici trake (videti Sl. 2(a)) do položaja na sredini trake (videti Sl. 2(b)). Ustanovljeno je da se razlika energija dna provodne i vrha valentne zone povećavala od vrednosti 0.206 eV za slučaj kada je defekt lociran najbliže ivici trake, do vrednosti 0.395 eV za slučaj centralnog defekta, što je veće od vrednosti koja se dobija za traku iste širine bez vakancija [17]. Disperzione relacije za traku sa ivičnim i centralnim defektom su prikazane na Sl. 3(a) i (b), redom. Na obe disperzije se može uočiti pojava ravnih zona u centru energetskog procepa. Ova stanja su slična ivičnim stanjima koja se pojavljuju u nanotrakama sa cik-cak ivicama [17].


ISBN 978-86-7466-930-3

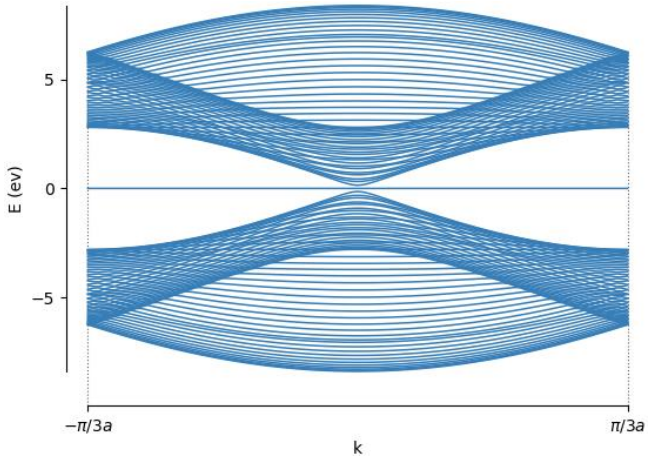


(a)

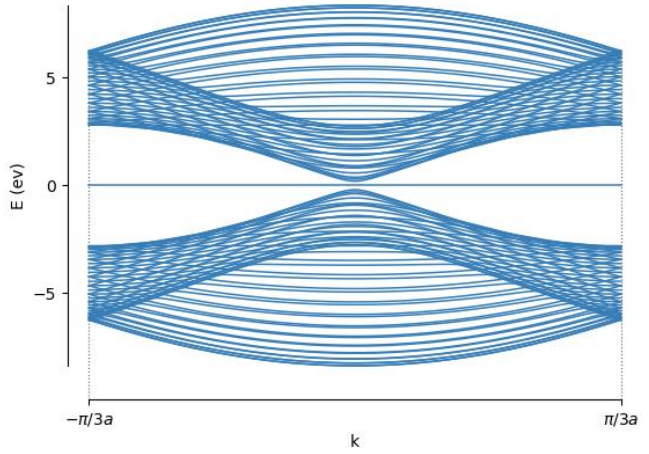


(b)

Sl. 3. Disperzione relacije za nanotrake kod kojih je rastojanje vakancija $d_{\min}$ za položaj defekta: (a) najbliže ivici trake, (b) na sredini trake [17].

U cilju boljeg uvida u prirodu ravnih zona ispitana je prostorna lokalizacija stanja. Lokalna gustina stanja u centru zone za slučaj trake sa vakancijom na sredini je grafički prikazana na Sl. 4. Uočava se da postoji dominantna lokalizacija na atomima duž linije defekta i njima najbližim susedima, što je slično lokalizaciji koja postoji duž ivica cik-cak nanotraka.

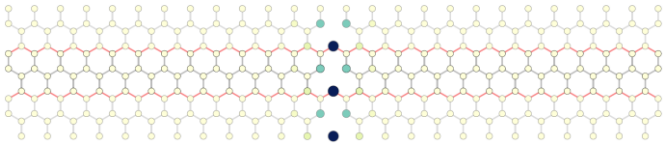

Sl. 4. Lokalna gustina stanja u $k$=0 u traci sa vakancijom na sredini trake [16]. Granice jedinične ćelije trake su markirane crvenom bojom. Veći poluprečnik kružnice i tamnija boja odgovara jačoj lokalizaciji na markiranoj poziciji u rešetki.

Kako bi razmotrili uticaj periode ponavljanja defekta na elektronsku strukturu, razmotrili smo slučaj nanotrake sa jednom vakancijom na sredini trake i međusobnim rastojanjem defekata koje iznosi $3d_{\min}$. Na Sl. 5.(a) i (b) su date skica kristalne strukture i disperzija za ove nanotrake, redom. Disperzija izgleda slično onoj za traku sa manjim međusobnim rastojanjem vakancija, pri čemu je broj stanja veći zbog većeg broja atoma koji čine jediničnu ćeliju. Razlika energija stanja na dnu provodne i vrhu valentne zone iznosi 0.3952 eV, što se neznatno razlikuje od vrednosti koju smo imali kada je prostorna perioda ponavljanja defekta tri puta manja.

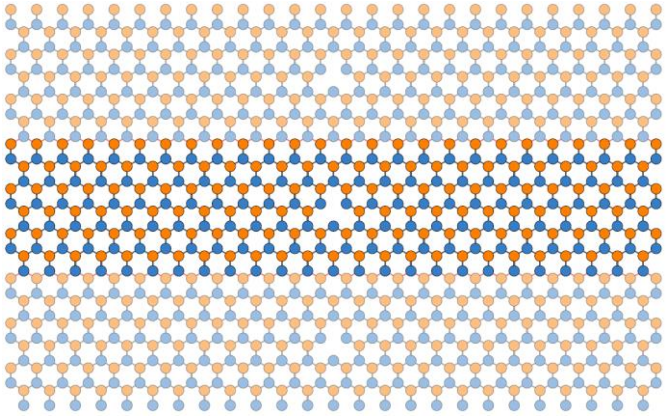

(a)

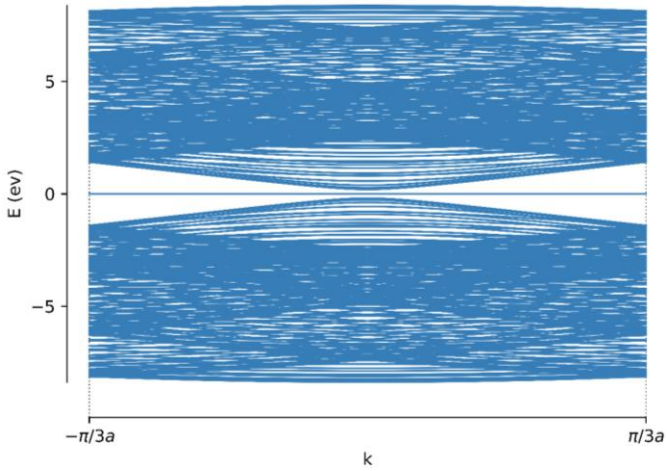


(b)

Sl. 5. Prikaz (a) jedinične ćelije i (b) disperzione relacije u nanotraci kod koje je rastojanje vakancija $3d_{\min}$, a položaj defekta na sredini trake [17].

## IV. Zaključak

U radu je sprovedena teorijska analiza mogućnosti inženjeringa energetskog procepa u grafenskim nanotrakama sa foteljastim ivicama. Analizirane su nanotrake nominalno beskonačne dužine u kojima postoje defekti tipa upražnjenog mesta u rešetki. Ustanovljeno je da položaj defekta u odnosu na ivicu trake bitno utiče na razliku energija stanja na dnu provodne i vrhu valentine zone. Sa druge strane, izmena prostorne periode ponavljanja defekta duž trake nije imala značajnijeg uticaja na procep. Na disperzionoj relaciji je uočeno da uvođenje defekta dovodi do pojave ravnih zona unutar procepa koje karakterišu stanja dominantno lokalizovana duž linije defekta. Interesantno bi bilo razmotriti slučajeve defekata koji nastaju kada se ugljenikov atom zameni drugim atomom, slučaj više vakancija unutar jedinične

 ISBN 978-86-7466-930-3

ćelije trake, kao i slučaj nasumičnog rasporeda defekata u traci konačnih dimenzija što je posledica nesavršenosti tehnika za fabrikaciju.

## ZAHVALNICA

Ovaj rad je podržan od strane Ministarstva prosvete, nauke i tehnološkog razvoja Republike Srbije 451-03-68/2022-14/200103 i Flemish Science Foundation (FWO-Vl).

## LITERATURA

[1] A. K. Geim, K. S. Novoselov, "The rise of graphene," *Nat. Mater*, vol. , no. *3*, pp. *1 3-1 1*, Feb. 2007.
[2] X. Du, I. Skachko, A. Barker, E.Y. Andrei, "Approaching ballistic transport in suspended graphene", *Nat. Nanotechnol*, vol. *3*, pp. *4 1-4 5*, July 2008.
[3] K. S. Novoselov, A. K. Geim, S. V. Morozov, D. Jiang, Y. Zhang, S. V. Dubonos, I. V. Grigorieva, and A. A. Firsov, *Science*, vol. *30* , pp. - , Oct. 2004.
[4] J.N. Coleman, M. Lotya, A. O'neill, S.D. Bergin, P.J. King, U. Khan, K. Young, A. Gaucher, S. De, R.J. Smith, I. V Shvets, S.K. Arora, G. Stanton, H.-Y. Kim, K. Lee, G.T. Kim, G.S. Duesberg, T. Hallam, J.J. Boland, J.J. Wang, J.F. Donegan, J.C. Grunlan, G. Moriarty, A. Shmeliov, R.J. Nicholls, J.M. Perkins, E.M. Grieveson, K. Theuwissen, D.W. Mccomb, P.D. Nellist, V. Nicolosi, "Two-Dimensional Nanosheets Produced by Liquid Exfoliation of Layered Materials," *Science*, vol. *331*, no. *301* , pp. *5 -5 1*, Feb. 2011.
[5] Y. Hernandez, V. Nicolosi, M. Lotya, F.M. Blighe, Z. Sun, S. De, I.T. McGovern, B. Holland, M. Byrne, Y.K. Gun'ko, J.J. Boland, P. Niraj, G. Duesberg, S. Krishnamurthy, R. Goodhue, J. Hutchison, V. Scardaci, A.C. Ferrari, J.N. Coleman, "High-yield production of graphene by liquid-phase exfoliation of graphite," *Nat. Nanotechnol*, vol. *3*, pp. *5 3-5* , Avg. 2008.
[6] Y. Xu, H. Cao, Y. Xue, B. Li, W. Cai, "Liquid-phase exfoliation of graphene: An overview on exfoliation media, techniques, and challenges," *Nanomaterials*, vol. , no. *11*, pp. *42 1-32*, Oct. 2018.
[7] Z. Yan, Z. Peng, G. Casillas, J. Lin, C. Xiang, H. Zhou, Y. Yang, G. Ruan, A.R.O. Raji, E.L.G. Samuel, R.H. Hauge, M.J. Yacaman, J.M. Tour, "Rebar graphene," *ACS Nano*, vol. , no. *5*, pp. *50 1-50* , Apr. 2014.
[8] A. Adetayo, D. Runsewe, "Synthesis and Fabrication of Graphene and Graphene Oxide: A Review," *pen . Compos. Mater*, vol. , no. *2*, pp. *20 -22* , Apr. 2019.
[9] J. Robinson, X. Weng, K. Trumbull, R. Cavalero, M. Wetherington, E. Frantz, M. LaBella, Z. Hughes, M. Fanton, D. Snyder, "Nucleation of epitaxial graphene on SiC(0001)," *ACS Nano*, vol. *4*, no. *1*, pp. *153-15* , Dec. 2009.
[10] M.Y. Han, B. Özyilmaz, Y. Zhang, P. Kim, "Energy band-gap engineering of graphene nanoribbons," *Phys. e . ett*, vol. , no. 20, pp. *1-4*, May 2007.
[11] J. Jia, E. V. Gorbar, V. P. Gusynin, "Gap generation in ABC-stacked multilayer graphene: Screening versus band flattening," *Phys. e . B*, vol. , no. *20*, pp. *20542 1-* , Nov. 2013.
[12] John D. Joannopoulos, Steven G. Johnson, Joshua N. Winn, and Robert D. Meade, Photonic Crystals: Molding the Flow of Light, second ed. New Jersy, USA, Princeton University Press, 2008.
[13] WenzeXieZhongyaoLi, "Energy band gaps in periodic bent graphene," Solid State Commun, vol. *225*, pp. *22-2* , Jan. 2016.
[14] M. Topsakal, E. Aktürk, H. Sevinçli, S. Ciraci, "First-principles approach to monitoring the band gap and magnetic state of a graphene nanoribbon via its vacancies," *Phys. e . B*, vol. , no. *23*, pp. *235435 1-* , Dec. 2008.
[15] K. Rallis, P. Dimitrakis, I. G. Karafyllidis, A. Rubio, G. C. Sirakoulis, "Electronic Properties of Graphene Nanoribbons With Defects," *IEEE Transactions on Nanotechnology*, vol. *20*, pp. *151-1 0*, Jan. 2021.
[16] K. Nordlund, J. Keinonen, T. Mattila, "Formation of ion irradiation induced small-scale defects on graphite surfaces," *Phys. e . ett*, vol. , no. *4*, pp. - *02*, July 1996.
[17] J. Vlahović, "Analiza elektronskih i transportnih svojstava grafenskih nanotraka sa defektima," Master rad, Elektrotehnički fakultet, Univerzitet u Beogradu, Beograd, Srbija, 2021.
[18] D. Moldovan, M. Anđelković, F. Peeters, pybinding v0.9.5: a Python package for tight-binding calculations, 2020.
[19] M.L. Cohen, S.G. Louie, Fundamentals of Condensed Matter Physics, Cambridge, United Kingdom, Cambridge University Press, 2016.
[20] Y. Yano, N. Mitoma, H. Ito, K. Itami, "A Quest for Structurally Uniform Graphene Nanoribbons: Synthesis, Properties, and Applications," . *rg. Chem*, vol. *5*, no. *1*, pp. *4-33*, Jan. 2020.
[21] G. Xie, Y. Shen, X. Wei, L. Yang, H. Xiao, J. Zhong, G. Zhang, "A bond-order theory on the phonon scattering by vacancies in two-dimensional materials," *Sci. ep*, vol. *4*, pp. *50 5 1-* , May 2014.
[22] N. Jing, Q. Xue, C. Ling, M. Shan, T. Zhang, X. Zhou, Z. Jiao, "Effect of defects on Young's modulus of graphene sheets: A molecular dynamics simulation," *SC Ad* , vol. *2*, no. *24*, pp. *124- 12* , Sep. 2012.
[23] H.C. Chung, M.H. Lee, C.P. Chang, M.F. Lin, "Exploration of edge-dependent optical selection rules for graphene nanoribbons," *pt. E press*, vol. *1* , no. *23*, pp. *23350-233 3*, Nov. 2011.
[24] Y.W. Son, M.L. Cohen, S.G. Louie, "Energy gaps in graphene nanoribbons," *Phys. e . ett*, vol. , no. *21*, pp. *21 03 1-4*, Nov. 2006.

## ABSTRACT

For more than a decade, materials that consist of one or more monolayers of crystal have been explored because of their superior electronic and transport properties in comparison to their bulk counterparts. An especially interesting material is graphene which was the first manufactured twodimensional material. For many practical applications relatively large energy gap is a necessary. But it is not the case in graphene. Various techniques were developed to tune the gap, but they are almost not employed in current electronic technology. In this paper, we introduce a method for bandgap tunning by inserting periodic defects in a graphene nanostructure. We analyze the influence of a single vacancy defect that periodically repeats along the nanoribbon. It is shown that periodic defects might have a significant influence on the energy difference between states at the bottom of the conduction band and the top of the valence band in nanoribbons with armchair edges. It, in turn, affects the electronic and transport properties of graphene nanoribbons. Moreover, the presence of a periodic defect results in the appearance of specific defect states with the flat band dispersion.

**lectronic Properties of Graphene anoribbons with Periodic Defects**

Jovana Vlahović, Vladimir V. Arsoski, Milan Ž. Tadić, Milorad Milošević

 ISBN 978-86-7466-930-3

# MICROWAVE TECHNIQUE, TECHNOLOGIES AND SYSTEMS

# /

# МИКРОТАЛАСНА ТЕХНИКА, ТЕХНОЛОГИЈЕ И СИСТЕМИ

# (MTI/MT)

ISBN 978-86-7466-930-3

# On Some Differences Between Wave Digital Models of Directional Couplers

Biljana P. Stošić, *Senior Member*, *IEEE*, Nebojša S. Dončov, *Senior Member*, *IEEE*, and Marin Nedelchev

***Abstract*—The paper summarizes the development and applications of wave digital (WD) models for predicting the frequency response of four-port microwave passive circuits such as directional couplers. Models are developed and afterwards validated by commercial software tools. Differences between the equivalent circuit- and transmission line-based WD models are presented through analysis of multi-section couplers.**

***Index Terms*—Directional coupler, wave digital models, equivalent circuit, transmission lines.**

## I. Introduction

ELECTROMAGNETIC (EM) simulation tools have become essential for circuit designers. Across industries and disciplines, simulation modeling solves real-world problems safely and efficiently and provides valuable solutions by giving clear insights into complex systems. It provides an important method of analysis which is easily verified, communicated, and understood. The designers have to be able to simulate and test their designs, and to provide accurate predictions of real-world performance of the design, before the design is fabricated in order to avoid major expenses committed to circuit construction and experimental verification.

Wave digital (WD) approach is based on A. Fettweis WD filter theory [1]-[2]. In recent years, it appears to be universal and has been successfully applied to digital modeling of a wider class of analog circuits (including microwave structures), systems and processes (including electromagnetic signals generation and radiation) [3]-[8].

On the one hand, this paper summarizes the development and applications of wave digital (WD) models for predicting the frequency response of four-port microwave passive circuits such as directional couplers. The advantage of the presented WD models is their ability to account for a wide frequency range very quickly, as well as to model different coupler geometries. Models are developed, built up in MATLAB/Simulink and afterwards validated by a commercial software tool. On the other hand, the agreement between suggested microwave device WD models is investigated.

The present paper is organized as follows. First, in Section II, an overview of WD models based on an equivalent circuit network that have been used to simulate frequency response in different four-port microstrip structures is given. Second, in Section III, WD models based on transmission lines (TLs) for the multiport structures are described. Third, in Section IV, a list of coupler models and their simulated frequency performance is provided and compared. The covered range is from two- or tri-section couplers to tri- and five-section wideband couplers with the defected ground structures (DGS). Finally, concluding remarks are included in Section V.

Biljana P. Stošić and Nebojša S. Dončov are with the Faculty of Electrical Engineering, University of Niš, Aleksandra Medvedeva 14, 18000 Niš, Serbia (e-mails: biljana.stosic@ elfak.ni.ac.rs, nebojsa.doncov@elfak.ni.ac.rs, ORCIDs: 0000-0002-4144-6506, 0000-0002-9057-6737).

Marin Nedelchev is with the Faculty of Telecommunications, Technical University of Sofia, 8 Kliment Ohridski blv, 1756 Sofia, Bulgaria (e-mail: mnedelchev@tu-sofia.bg, ORCID: 0000-0003-3926-0048).

## II. Nutshell of the Equivalent Circuit-Based Wave Digital Models

Over the past years, for the purpose of the application of the WD modeling method, the authors have been generated WD models of different couplers based on their equivalent circuit networks [9]-[12]. All these models have been implemented with an in-house MATLAB algorithm. Simulink environment let one drag-and-drop blocks from its library and predifine modeling elements, connect them and create complex WD models.

The equivalent circuit parameters are not quoted at the beginning, therefore the initial step in the proposed technique is to synthesize the values of inductors and capacitors based on the frequency and the characteristic impedances of the individual coupler branches. The lumped equivalent circuit model for the conventional branch-line coupler is proposed in [13]. During modeling process, i.e. model synthesis, parts of the system representing multiport networks with inductors and capacitors in the equivalent circuit are replaced with their wave digital counterpart. One sub-block in the generated WD counterpart models a specific part of coupler layout; it represents one wave digital element (WDE). The main attention in the papers [11]-[12] is focused on generating so-called basic two-dimensional symmetric and asymmetric WDEs. So, a WD model of the device under consideration is based on basic multi-port WDEs and two-port adaptors for port impedance matching. Therefore, the developed WD model will be completely characterized by its parameters: port resistances and adaptor coefficients.

## III. Transmission Line-Based WD Models (Development of New Models)

A transmission line-based wave digital model of the directional coupler is derived from its circuit diagram. A starting point for creation of a WD model of the observed four-port structure is to look on that structure as a connection of several individual arms (transmission lines) as shown in [14]. Interconnection networks are used to interconnect

 ISBN 978-86-7466-930-3

idendified TL segments. So, a TL-based WD model is synthesized by making use of basic wave digital building blocks. The boxes in the WD model contain the arithmetic operations and represent the interconnection network or contain the delay elements corresponding to the TL models.

### *A. Basic Wave Digital Buiding Blocks*

Basic building blocks in the proposed TL-based WD model are unit elements (Fig. 1), circuit elements (like resistor shown in Fig. 2) and interconnection networks (Fig. 3) [5], [15]. Therefore, we describe the wave-flow equivalents to circuit elements and interconnection networks used in WD models.

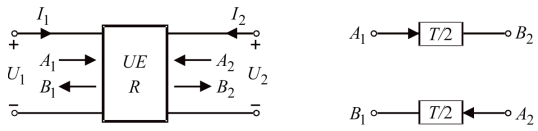


Fig. 1. Unit element and the corresponding wave-flow graph.

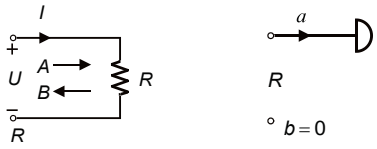


Fig. 2. Wave-flow equivalent for resistor, Zin = R.

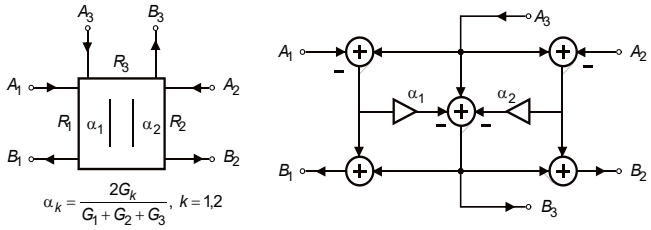


Fig. 3. Interconnection network: Three-port parallel adaptor with port 3 as the dependent port.

## IV. List of Coupler Models (Comparison)

One of the most popular passive circuits used for various microwave and millimeter-wave applications is a branch-line directional coupler. In this section, digital models of several coupler structures are presented and discussed. Simple wave digital models are generated and simulated by use of MATLAB/Simulink environment. Also, the commercial Keysight Pathwave Advanced Design System (ADS) simulation software is used to generate ideal TL models of the designed couplers for comparison purposes.

To investigate the validity of the described WD models, comparison of the magnitude performance is given. The results of the illustrated examples in the frequency domain are presented here. The covered example range is from two- and tri-section couplers to tri- and five-section wideband couplers with DGS structures.

### *B. Case 1: A Single-Band Two-Section Coupler*

The simplest coupler structure is composed of four quarter-wavelength transmission lines with different impedances. One such structure, i.e. a symmetric single-band coupler, which circuit diagram is shown in Fig. 4, with characteristic impedance of the main line $Z_1 = Z_0/\sqrt{2}$, and for the branch line $Z_2 = Z_0 = 50\ \Omega$, is observed in [9], [12]. The electrical lengths of the TL segments are $\theta = \pi/2$. The operating frequency is 2.45 GHz. Its model in ADS based on ideal transmission line is shown in [12]. That paper contains also its equivalent circuit-based WD model described in detail.

TL-based WD model is shown in Fig. 5 together with adaptor coefficients putted in Table I. Delays of all TLs are equal because of their equal electrical lengths and amounts to 102 ps. Simulated magnitudes are compared in Fig. 6. The comparison shows a coincidence between the *S*-parameter results obtained by EC-based WDM, TL-based WDM and ideal ADS model.

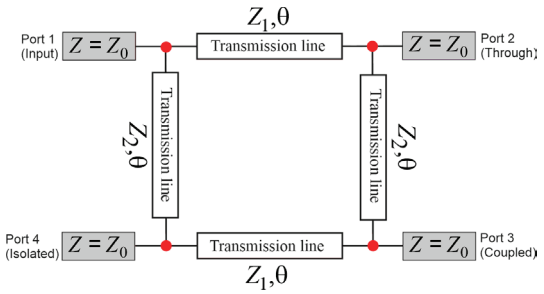


Fig. 4. Circuit diagram of a single-band two-section directional coupler. (Red dots show the locations of three-port parallel adaptors in the WD model).

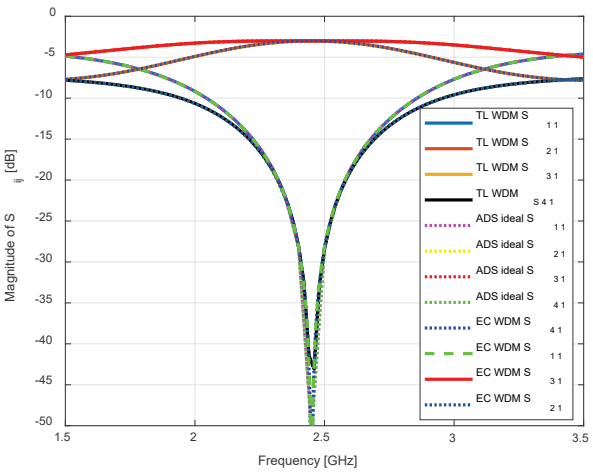


Fig. 6. Simulated magnitude performance of a single-band two-section coupler (TL-based WDM versus EC-based WDM and ADS ideal TL model).

TABLE I
PORT SIGNAL ORDERING FOR INTERCONNECTION NETWORKS

| Three-port adaptors | Port 1 | Port 2 | Coeff. $\alpha_1$ | Coeff. $\alpha_2$ |
|---|---|---|---|---|
| ADP-Z0Z1Z2 | Z0 | Z1 | $\alpha 1$=2/Z0/*SG* | $\alpha 2$=2/Z1/*SG* |
| | | | *SG*=1/Z0+1/Z1+1/Z2 | |
| ADP-Z1Z0Z2 | Z1 | Z0 | $\alpha 1$=2/Z1/*SG* | $\alpha 2$=2/Z0/*SG* |
| **Two-port adaptors** | **Port 1** | **Port 2** | **Coefficient α** | |
| ADP-S | Rg | Z0 | (Rg-Z0)/(Rg+Z0) | |
| ADP-L | Z0 | RL | (Z0-RL)/(Z0+RL) | |


ISBN 978-86-7466-930-3

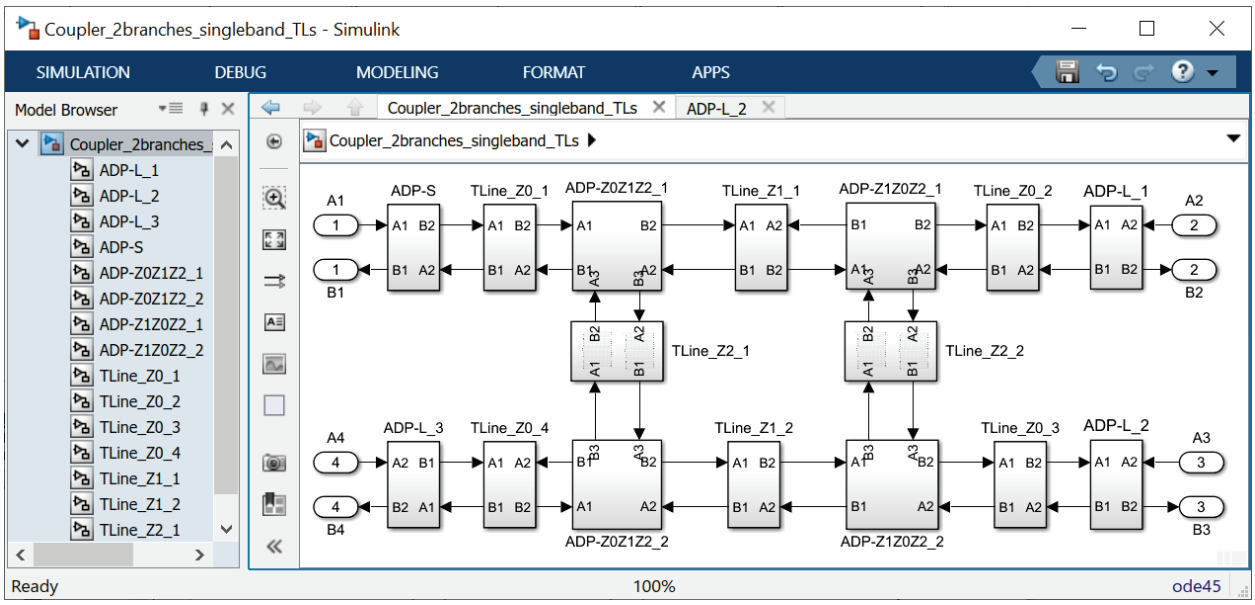


Fig. 5. Simulink model of TL-based WDM of a single-band two-section coupler.

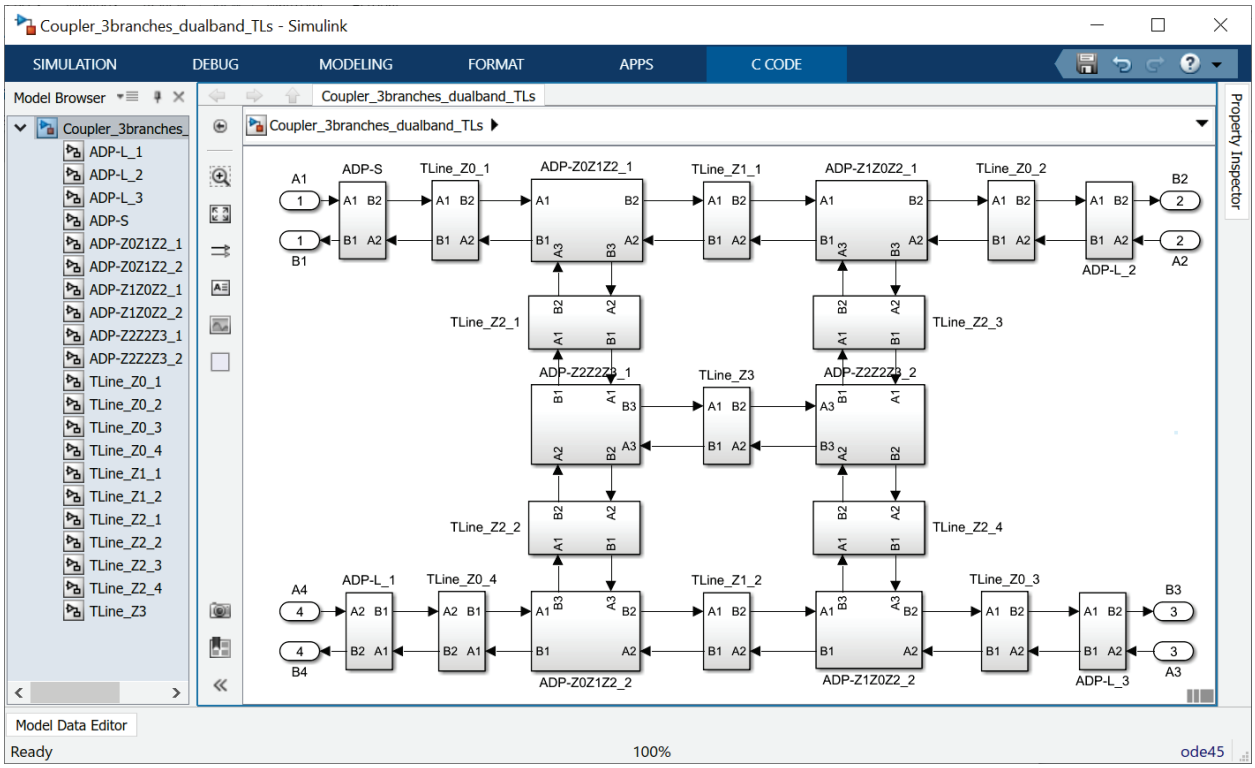


Fig. 8. TL-based WDM of a dual-band tri-section coupler.

### *C. Case 2: A Dual-Band Tri-Section Coupler*

A dual-band branch-line coupler structure with three parallel lines which schematic diagram can be found in Fig. 7 is analyzed in [12]. It is design to operate at 1.0/2.5 GHz. For the characteristic impedance $Z_0$ set to $50\,\Omega$, the calculated line impedances are $Z_1 = 49.48\,\Omega$, $Z_2 = 79.21\,\Omega$, and $Z_3 = 132.66\,\Omega$ having the power ratio of 3 dB. This example is specific, because of different electrical lengths of transmission lines, $\theta = 51.43^{o}$ and $2\theta$.

TL-based model of this structure is shown in Fig. 8. The blocks corresponding to individual TLs are assigned as TLine_Z*x* (*x*=0,1,2,3). Delay of the corresponding TLs with the electrical length $\theta$ is 143 ps, and for $2\theta$ is 286 ps at the frequency of 1 GHz. Ordering of port signals for used interconnection networks (two- and three-port parallel adaptors) and relations for multiplier coefficients are presented in Table I. Additional adaptor ADP-Z2Z2Z3 has two equal multiplier coefficients $\alpha_1 = \alpha_2 = (2/Z2)/SG$, where $SG = 2/Z2 + 1/Z3$.


ISBN 978-86-7466-930-3

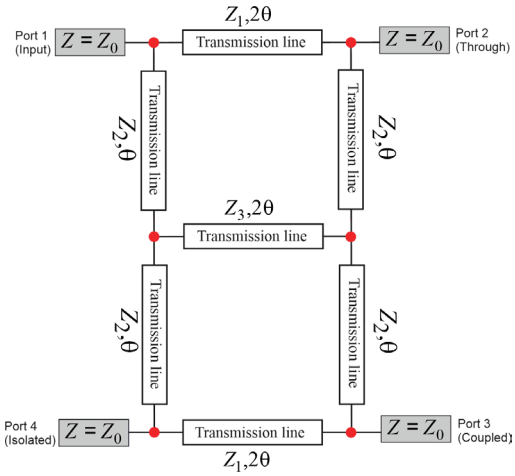


Fig. 7. Circuit diagram of a dual-band tri-section coupler. (Red dots show the locations of three-port parallel adaptors in the WD model).

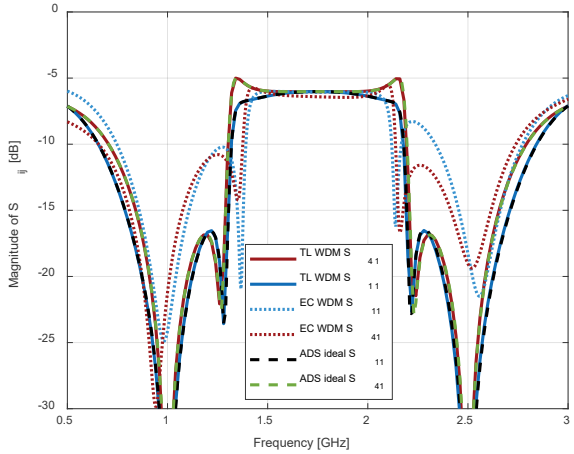


Fig. 9. Comparison of the simulated magnitudes of $S_{11}$ and $S_{41}$ parameters.

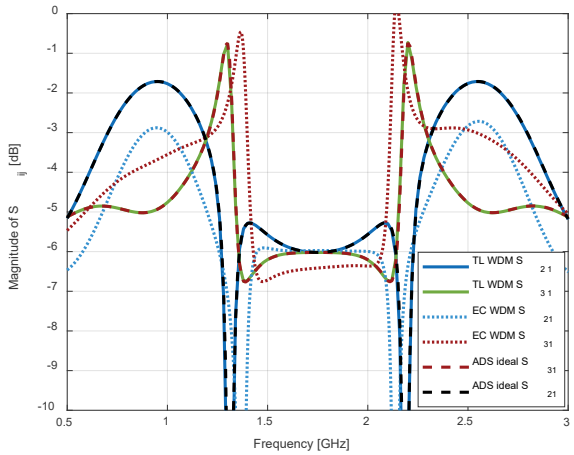


Fig. 10. Comparison of the simulated magnitudes of $S_{21}$ and $S_{31}$ parameters.

Comparison of simulated magnitudes of the *S*-parameters obtained by WD models (EC-based and TL-based) and ADS model are given in Figs. 9 and 10. TL-based model curves from MATLAB and ADS are barely distinguishable. There is a slight disagreement with results from EC-based model.

### *D. Case 3: A Tri-Section Wideband DGS Coupler*

An example of a tri-section wideband branch-line hybrid for operating at center frequency of 2.4 GHz has been design and fabricated by authors in [10]. The characteristic impedances of the stubs are $Z_s = 99.86\Omega$, $Z_{s1} = 41.13\Omega$ and the main line impedance is $Z_1 = 34.74\Omega$. All TLs are $\lambda/4$ long ($\lambda$ is the wavelength at the operating frequency). Their delays are calculated as 104 ps. Fig. 11 contains layout of DGS coupler and Fig. 12 its circuit diagram.

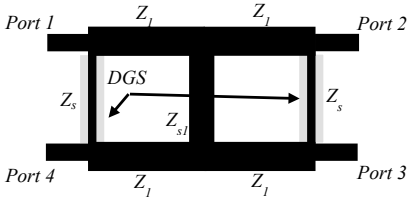


Fig. 11. Layout of a tri-section wideband DGS hybrid designed in [10].

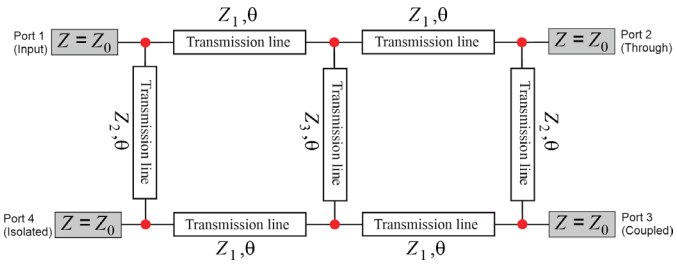


Fig. 12. Circuit diagram of a tri-section wideband DGS hybrid. (Red dots show the locations of three-port parallel adaptors in the WD model).

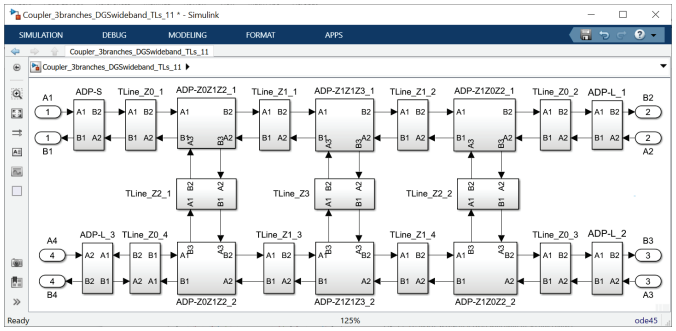


Fig. 13. TL-based WDM of a DGS wideband tri-section coupler.

Coefficient relations in three-port parallel adaptors used as interconnection networks in TL-based WDM drawn in Fig. 13 are presented in Table I. Additional adaptor ADP-Z1Z1Z3 has the multiplier coefficients with equal value calculated by relation $\alpha_1 = \alpha_2 = (2/Z1)/SG$, where $SG = 2/Z1 + 1/Z3$.

The simulated magnitude responses of this coupler example are compared in Fig. 14. Slight disagreement between EC-based model and other models is evident. The corresponding equivalent circuit-based model is validated by measurements and full-wave simulation results in [10].

### *E. Case 4: A Five-Section Wideband DGS Coupler*

Different aspects of five-section wideband 3 dB branch-line hybrid with 90° phase difference which operates at center frequency of 2.5 GHz are presented in [11]. The proposed hybrid configuration, shown in Fig. 15, having symmetric nature with defected ground structures is designed and fabricated. The hybrid is also simulated and measured, and its wave digital model based on multimethod technique and an equivalent circuit is created there.


ISBN 978-86-7466-930-3

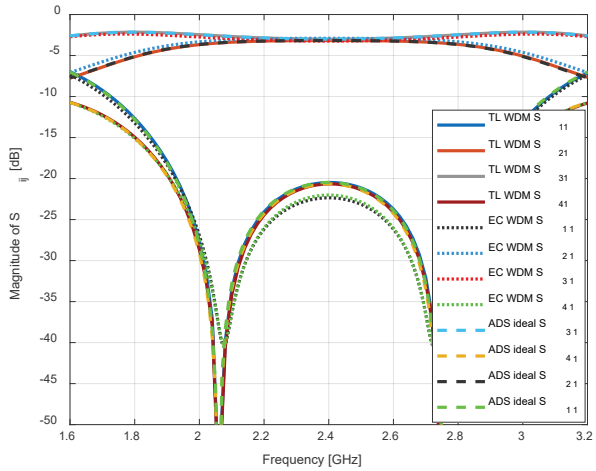


(a)

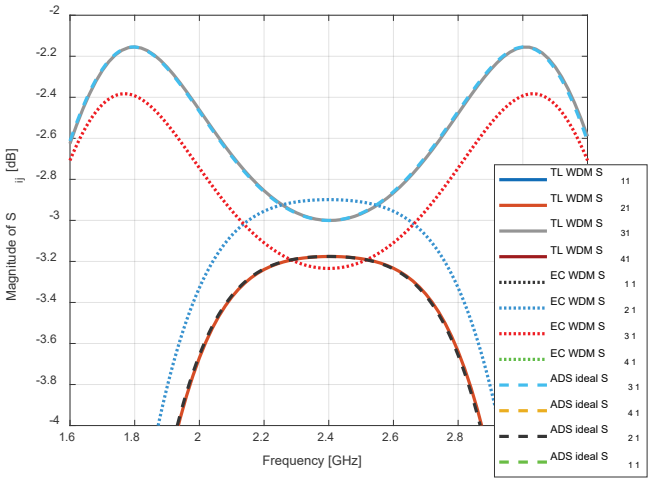


(b)

Fig. 14. Simulated magnitude performances of a tri-section wideband DGS coupler (TL-based WDM versus EC-based WD and ADS ideal TL models): (a) all *S*-parameters and (b) zoom on $S_{21}$ and $S_{31}$ parameters.

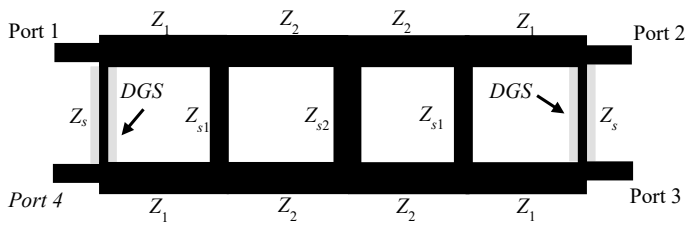


Fig. 15. Layout of a five-section wideband DGS hybrid designed in [11].

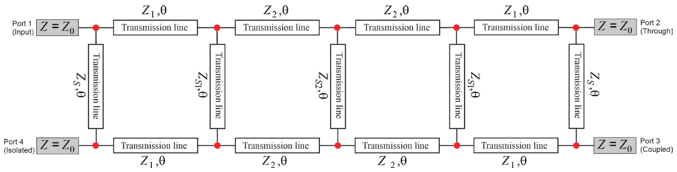


Fig. 16. Circuit diagram of a five-section wideband DGS hybrid. (Red dots show the locations of three-port parallel adaptors in the WD model).

TABLE II
PORT SIGNAL ORDERING FOR THREE-PORT ADAPTORS

| Three-port adaptors | Port 1 | Port 2 | Coeff. $\alpha_1$ | Coeff. $\alpha_2$ |
|---|---|---|---|---|
| ADP-Z0Z1Zs | Z0 | Z1 | $\alpha1=2/Z0/SG$ | $\alpha2=2/Z1/SG$ |
| | | | $SG=1/Z0+1/Z1+1/Zs$ | |
| ADP-Z1Z0Zs | Z1 | Z0 | $\alpha1=2/Z1/SG$ | $\alpha2=2/Z0/SG$ |
| ADP-Z1Z2Zs1 | Z1 | Z2 | $\alpha1=2/Z1/SG$ | $\alpha2=2/Z2/SG$ |
| | | | $SG=1/Z1+1/Z2+1/Zs1$ | |
| ADP-Z2Z1Zs1 | Z2 | Z1 | $\alpha1=2/Z2/SG$ | $\alpha2=2/Z1/SG$ |
| ADP-Z2Z2Zs2 | Z2 | Z2 | $\alpha1=\alpha2=2/Z2/SG$ | |
| | | | $SG=2/Z2+1/Zs2$ | |

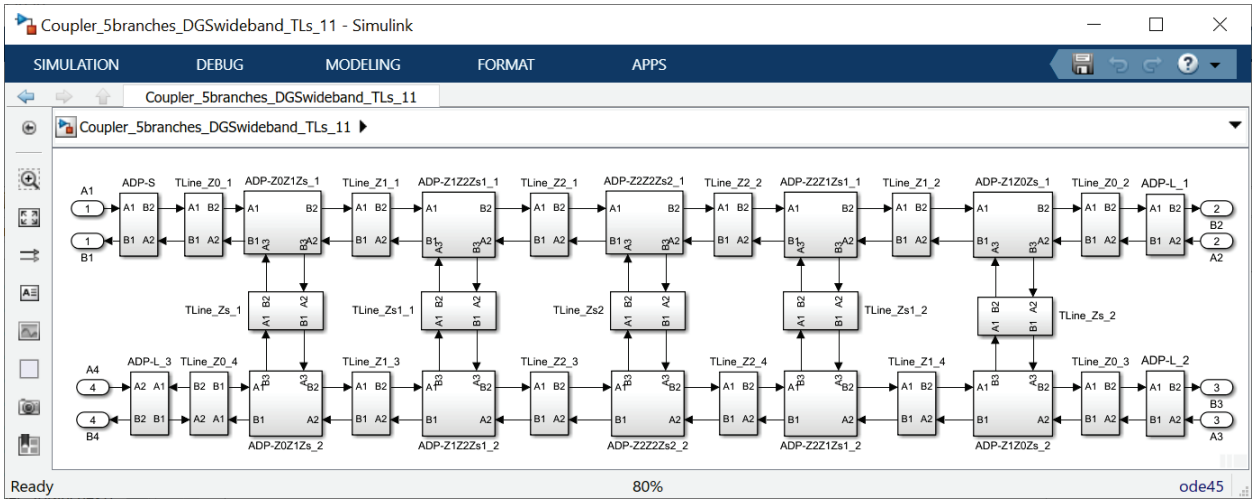


(a)

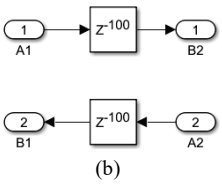


(b)

Fig. 17. (a) TL-based WDM of a five-section wideband DGS coupler and (b) model of one TL segment with used Delay block from Simulink Library.


ISBN 978-86-7466-930-3

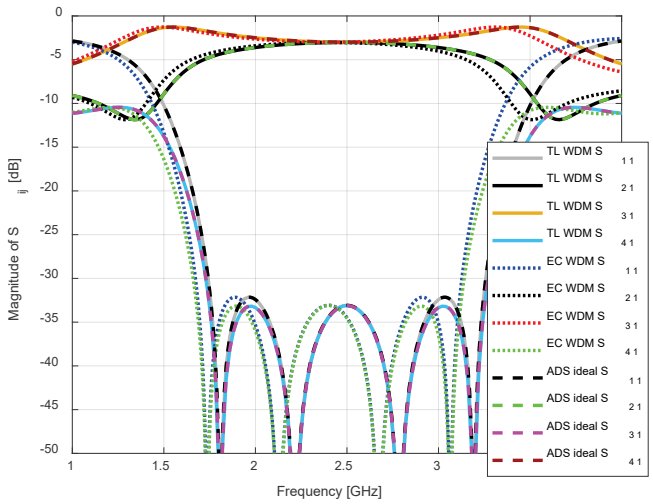


Fig. 18. Simulated magnitude performances of a five-section wideband DGS coupler (differences among TL-based WD, EC-based WD and ADS ideal TL models).

A circuit diagram of the analyzed DGS coupler is presented in Fig. 16. This circuit diagram contains some red dots which show places where three-port parallel adaptors are used in a TL-based WDM given in Fig. 17. Each TL block is presented by 100 UEs corresponding to 100 ps delay, Fig. 17b. Ordering of port signals for three-port adaptors is given in Table II.

Once again, comparison in Fig. 18 confirms matching of TL-based model results from WDM and ADS, and slight non-matching of EC-based model results. The corresponding equivalent circuit-based model is validated by measurments and full-wave simulation results in [11].

## V. CONCLUSION

The paper confirms potential of a WD approach for the simulation of given directional couplers. We have investigated the differences between equivalent circuit-based and transmission line-based WD models of these four-port microwave devices. The simulations demonstrate that the proposed TL-based WD model behaves exactly the same as model generated in ADS by ideal TLs. The differences between EC-based models and abovementioned models are evident except in the case of the simplest coupler design. To conclude, there is progress, but still more to do in this WD modeling approach. The next step is to find a way to include losses in the models in order to get closer to real measurements.

On the other hand, comparing the circuit diagrams with the TL-based WDMs clearly shows their great similarity. Due to the advantages of the nature of generating the TL-based model, this approach can be easily adopted by researchers for simulation purposes of wide range of branch-line couplers. In comparison with the equivalent circuit-based modeling approach a TL-based approach is more intuitive.

## ACKNOWLEDGMENT

This paper has been supported by project “Twinning for Enhancing Capacity and Research Excellence in Holographic Telepresence Systems as a Catalyst of Digitalization” – HOLOTWIN of the Ministry of Education and Science, Republic of Bulgaria, and by the Ministry of Education, Science and Technological Development of the Republic of Serbia.

## REFERENCES

[1] A. Fettweis, “Digital circuits and systems”, *IEEE Transactions on Circuits and Systems*, vol. CAS-31, no. 1, January, 1984, pp. 31-48.

[2] A. Fettweis, “Wave digital filters: Theory and practice”, *Proc. IEEE*, vol. 74, 1986, pp. 270-327.

[3] S. Bilbao, *Wave and Scattering Methods for Numerical Simulation*, Wiley, Hoboken, New Jersey, 2004.

[4] J. A. Russer, Y. Kuznetsov, and P. Russer, “ Discrete-time network and state equation methods applied to computational electromagnetics”, *Microwave Review*, vol. 16, no. 1, pp. 2-14, 2010.

[5] B. P. Stošić and N. S. Dončov, “Combined wave digital/full-wave approach in modeling and analysis of microstrip structures with examples in MATLAB/Simulink”, Chapter 4 in book: *Advances in Engineering Research*, Nova Science Publishers, Inc., 2016, vol. 12, pp. 75-140.

[6] P. Belforte and G. Guaschino, DWS 9.0 Digital Wave Simulator, User’s Manual, January 2020, doi: 10.13140/RG.2.2.11489.66407/1

[7] P. Belforte, D. Spina, G. Antonini, L. Lombardi, and T. Dhaene, “Time-domain piecewise-linear fitting method based on digital wave processing of S-parameters”, doi: 0.13140/RG.2.2.34124.36481/2

[8] A. Bernardini, E. Bozzo, F. Fontana, and A. Sarti, “A wave digital Newton-Raphson method for virtual analog modeling of audio circuits with multiple one-port nonlinearities”, IEEE/ACM Transactions on Audio, Speech, and Language Processing, doi: 10.1109/TASLP.2021.3084337

[9] B. P. Stošić, “Comparative assessment of wave digital model of directional coupler”, 14th International Conference on Applied Electromagnetics - ПЕС 2019, August 26-28, 2019, Niš, Serbia, Poster session P1-17.

[10] M. Nedelchev, B. P. Stošić, N. Dončov, and A. Kolev, “Tri-section wideband branch-line hybrid: Design, simulation technique and measurement”, 2019 42nd International Conference on Telecommunications and Signal Processing (TSP), Hungary, Budapest, July 1-3, 2019, pp. 94-97, doi: 10.1109/TSP.2019.8768866

[11] B. P. Stošić, M. Nedelchev, J. A. Russer, N. S. Dončov, and Z. Stanković, “Stochastic signal propagation in five-section wideband branch-line hybrid”, 2019 International Conference on Electromagnetics in Advanced Applications (ICEAA), Granada, Spain, 2019, pp. 0754-0759.

[12] B. P. Stošić, “Wave-based digital models of different branch-line couplers”, *Serbian Journal of Electrical Engineering*, vol. 17, no. 2, June 2020, pp. 149-169, doi: 10.2298/SJEE2002149S

[13] Y. Zhou and Y. Chen, “Lumped-element equivalent circuit models for distributed microwave directional couplers”, 2008 International Conference on Microwave and Millimeter Wave Technology, April 21 - 24, 2008.

[14] B. P. Stošić, M. Nedelchev, and P. Belforte, “Wave digital frameworks for simulation of microwave couplers: Transmission line versus equivalent lumped circuit”, 2021 15th International Conference on Advanced Technologies, Systems and Services in Telecommunications (TELSIKS), Serbia, Niš, October 20-22, 2021, pp. 175-178, doi: 10.1109/TELSIKS52058.2021.9606374

[15] L. Wanhammar and T. Saramaki, *Digital Filter using MATLAB*, Springer Nature Switzerland AG, 2020.

 ISBN 978-86-7466-930-3

# Doherty PA Linearization by Injection of the 2nd order Digitally Processed Signals for 5G FBMC modulation

Aleksandar Atanasković[1], Nataša Maleš-Ilić[1], Biljana Stošić[1] and Djuradj Budimir[2]

*Abstract* – **In this paper, the analysis of the linearization effects of the 2nd order digitally processed signal for the linearization that modulates the 2nd harmonic of the fundamental carrier has been performed on the Doherty power amplifier for C 5G modulation form. In the first method, linearization signals are injected at the input and output of the main Doherty amplifier, whereas in the second method, they are inserted at the outputs of the Doherty main and au iliary amplifiers.**

*eywords* – **5G, C, Doherty power amplifier, baseband signal, second harmonic, linearization.**

## I. INTRODUCTION

Fifth generation (5G) mobile communication systems represent one of the most important segments of the overall digital transformation of society based on the concept of Industry 4.0. The importance of 5G systems for the global development of the economy and society has been widely recognized, so that the coordinated introduction of 5G mobile networks in many countries has become part of the strategy of complete social and economic development. New technologies such as artificial intelligence (AI) and machine learning, cloud computing, augmented and virtual reality (AR / VR), IoE (Internet of Everything) and IoT (Internet of Things) and billions of connected devices are pushing boundaries and setting new demands on connectivity and mobile communication network performance. 5G mobile networks are expected to provide ultra-fast connectivity with low latency, not only to individual users, but also to a large number of connected facilities, as well as to create an ambient for expansion of technological and business innovations in different industrial sectors (agriculture, energy, trade, health, education, public safety, tourism, media, etc.). The frequency bands provided for 5G systems can be divided into three groups: High band (frequencies from 24 GHz to 60 GHz and above), mid band (which can be divided into two parts, from 1 GHz to 2.6 GHz and from 3.5 GHz to 6 GHz), and low band (below 1 GHz). Each of these bands has comparable advantages and disadvantages. The 5G systems operating in the low band will provide large cells but with a slight improvement in performance compared to 4G systems. In the high band range, all the advantages of the 5G systems in terms of performance compared to 4G systems will be expressed, with transfer speeds from 1 to 3 Gbps and even higher. The disadvantage of high band is shown in the fact that due to the large attenuation of the signal as a result of millimeter wave propagation and potential interference from various obstacles (such as vegetation and buildings) it is necessary to provide very small cells. Mid band spectrum is considered ideal for 5G because it can carry plenty of data while also traveling significant distances.

The most important limitations that existed in previous generations of communication systems with OFDM modulation schemes are loss of spectral efficiency due to the use of cyclic prefix (CP) and needs for fine time and frequency synchronization to ensure the orthogonality of the carriers. To overcome these limitations, several alternative modulation schemes for 5G systems, known as 5G candidates, have been introduced over the past few years, such as filter bank multicarrier (FBMC), universal filtered multi carrier (UFMC), generalized frequency division multiplexing (GFDM) and filtered orthogonal frequency division multiplexing (FOFDM).

The results of Doherty power amplifier (DPA) linearization in simulation by applying a method that uses second-order digital signals processed in the baseband are presented in this paper. After adjusting for the amplitude and phase in the baseband, the second order digital signals modulate the second harmonic of the fundamental carrier and then are injected into the gate and drain (input and output) of the PA transistor [1]. The results obtained by applying this linearization method in simulation or experiments have already been published in [2-4] for single-stage PA and two-way DPA, which operate at a frequency of about 1 GHz and tested for QAM and OFDM modulation schemes. In this paper, we analyzed the behavior of the DPA when source signal is 5G FBMC signal.

The paper is organized in the following manner: after introduction, the second section is devoted to the 5G FBMC signal, and the results of the linearization are illustrated in the third section. Conclusion and list of used literature are given at the end of paper.

## II. 5G FBMC SIGNAL

FBMC is a type of multi carrier modulation scheme based on OFDM. It represents an improvement of OFDM with the aim of eliminating certain shortcomings at the cost of increasing the complexity of signal processing. It consists of a set of data that are broadcast through a bank of modulation filters that filter each subcarrier. The prototype of the used filter can be chosen in a suitable way, so that there is very little leakage into the adjacent channels. FBMC has significantly better utilization of channel capacity and can offer higher data throughput in a given bandwidth, which

[1]Aleksandar Atanasković, Nataša Maleš Ilić and Biljana Stošić are with the Faculty of Electronic Engineering, University of Nis, A. Medvedeva 14, Nis, Serbia (e-mails: aleksandar.atanaskovic; natasa.males.ilic; biljana.stosic@elfak.ni.ac.rs)

[2]Djuradj Budimir is with the University of Westminster, 115 New Cavendish Street, London, UK, (e-mail: d.budimir@wmin.ac.uk)

 ISBN 978-86-7466-930-3

means it provides better spectral efficiency. Also, the FBMC has eliminated one of the main disadvantages of OFDM, which is the use of the cyclic prefix (CP) [5]. The cyclic prefix is essentially a copy of part of a transmitted symbol in OFDM that is appended at the beginning of the next symbol. This leads to a reduction in signal speed as well as unnecessary loss of transmitted power.

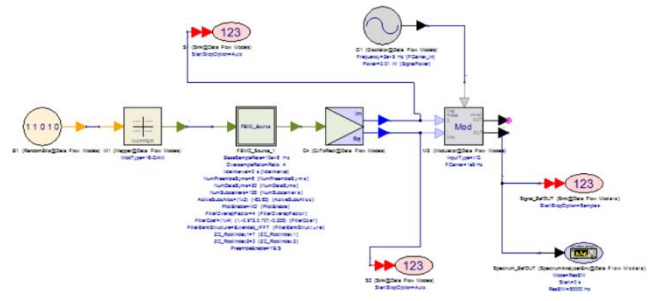


a)

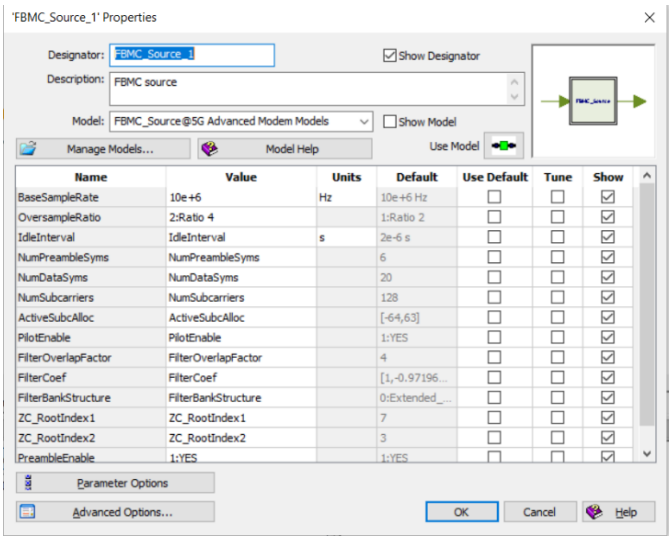


b)

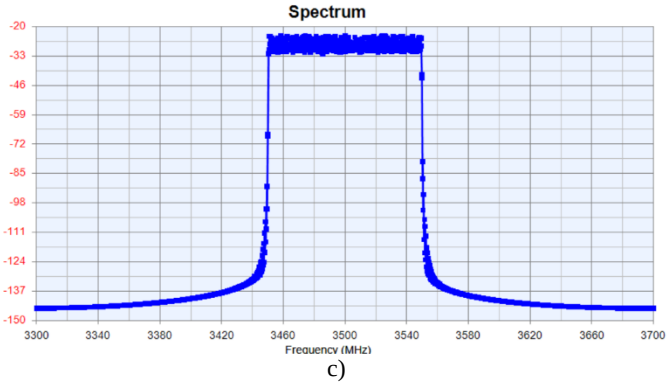


c)

Fig 1. FBMC signal generation in Keysight SystemVue: a) FBMC transmitter; b) FBMC signal parameters; c) FBMC signal spectrum

FBMC signals for simulation purposes can be created using various software packages (Matlab, Keysight SystemVue, ...) or using general purpose programming languages (Python, C/C++, ...). In this paper, we used Keysight SystemVue to create the appropriate FBMC signal. This software was chosen because it provides a simple interface in which parameters related to the FBMC signal can be easily adjusted, and the impact of changing the appropriate parameters on the FBMC signal itself can be monitored, either in time or in the spectral domain. Figure 1 shows the interface for creating FBMC signals in the SystemVue environment, as well as a set of parameters that control the signal characteristics and signal appearance in the frequency domain.

## III. Results

Symmetrical two-way DPA that operates at 5G mid band was designed according to the instructions given in [6]. The DPA was designed by using CGH40010F GAN HEMT transistor. The drain voltage is 28 V, whereas the gate voltage of the main and auxiliary amplifier is -2.8 V, and -5.7 V, respectively. Main characteristics of DPA in simulation at 3.5 GHz are: 12.6 dB gain and 1-dB compression point at 31 dBm output power.

The designed DPA was linearized in ADS simulation using two linearization methods: 1) the first - standard method that leads linearization signals at the gate and drain of the transistor in the main cell of the DPA and 2) the second - modified method, where the linearization signals are put at the drain of the main and auxiliary amplifier transistors in the DPA [7]. The signal used for testing DPA was 5G FBMC signal at carrier frequency 3.5 GHz with useful signal frequency bandwidth of 50 MHz and two output power levels: around 30 dBm (1 dB below 1-dB compression point) and near 24 dBm (roughly 7 dB below 1-dB compression point).

The Figs. 2 and 3 show the output spectrum before and after application of the proposed linearization technique. Summarized results for ACP (Adjacent Channel Power) at ±50 MHz offset over 5 MHz band are presented in Tables I and II. We can observe for 24 dBm output power, that the ACP is improved about 15 dB for both linearization methods, whereas for 30 dBm output power they become better by 5 dB for the 1st method and almost 8 dB for the 2nd method. A slight asymmetry can be noted in results for linearization between lower and upper adjacent channel.

Table I
Results of linearization for 24 dBm output power

| | Pout [dB] | ACP lower [dB] | ACP upper [dB] |
|---|---|---|---|
| Before lin. | 24.1 | -25.6 | -26.5 |
| Lin. by method 1 | 24.5 | -41.0 | -38.8 |
| Lin. by method 2 | 24.4 | -40.9 | -39.1 |

Table II
Results of linearization for 30 dBm output power

| | Pout [dB] | ACP lower [dB] | ACP upper [dB] |
|---|---|---|---|
| Before lin. | 29.4 | -14.6 | -14.5 |
| Lin. by method 1 | 30.1 | -19.2 | -18.8 |
| Lin. by method 2 | 30.2 | -22.2 | -20.7 |


ISBN 978-86-7466-930-3

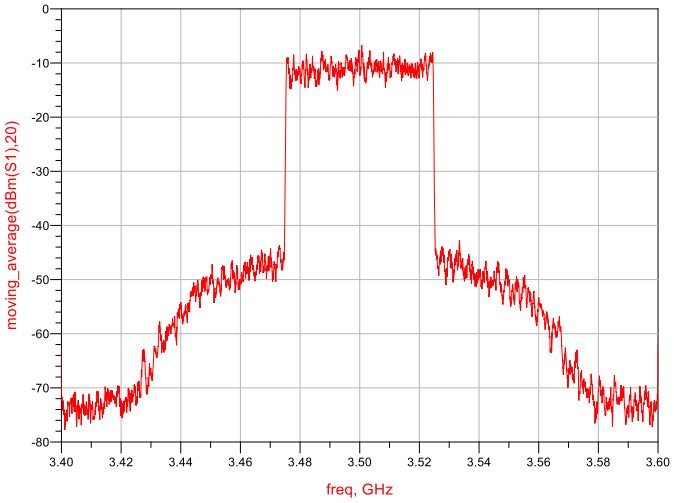


a)

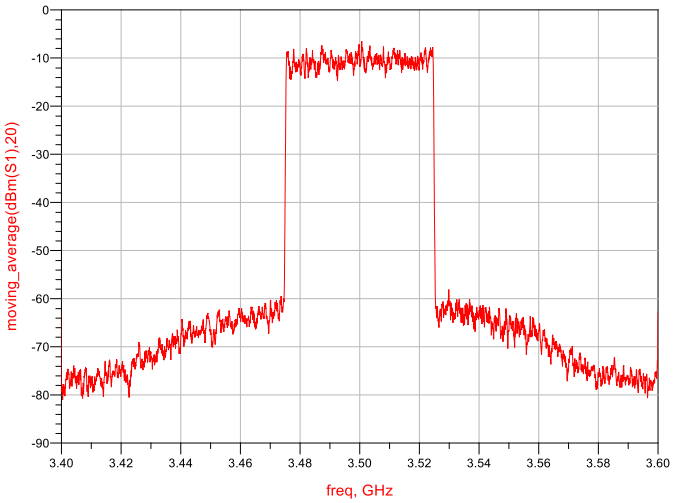


b)

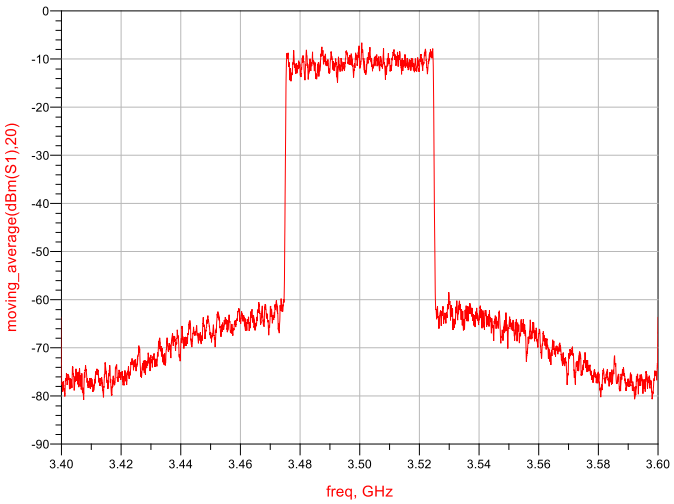


c)

Fig. 2. Output spectrum for FBMC signal of 50 MHz useful signal frequency bandwidth for output signal power 24 dBm: a) before linearization; b) after linearization by method 1; c) after linearization by method 2

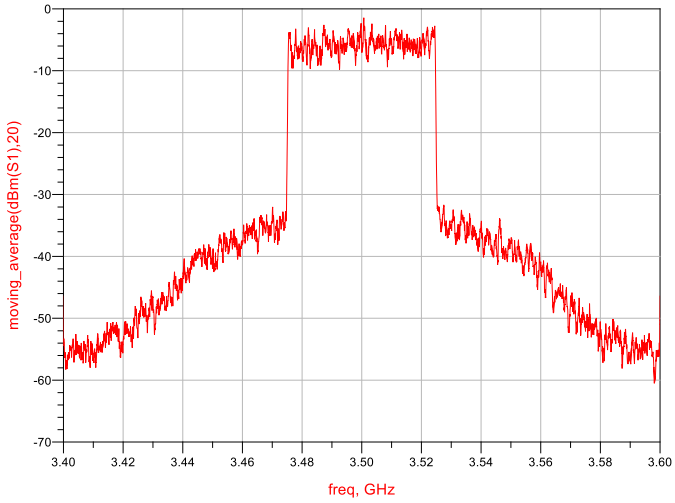


a)

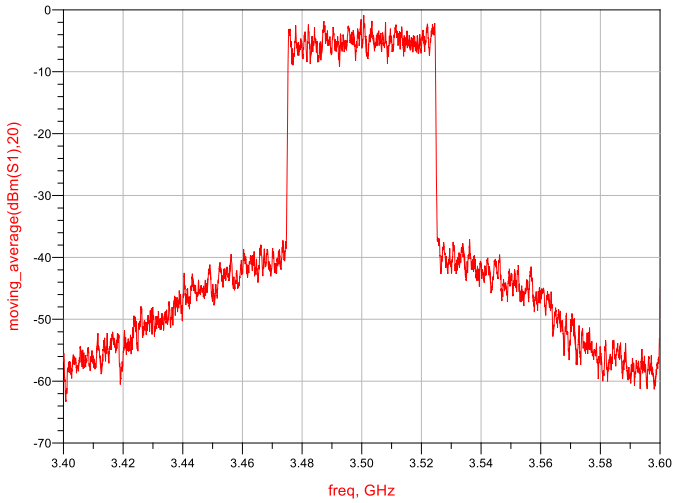


b)

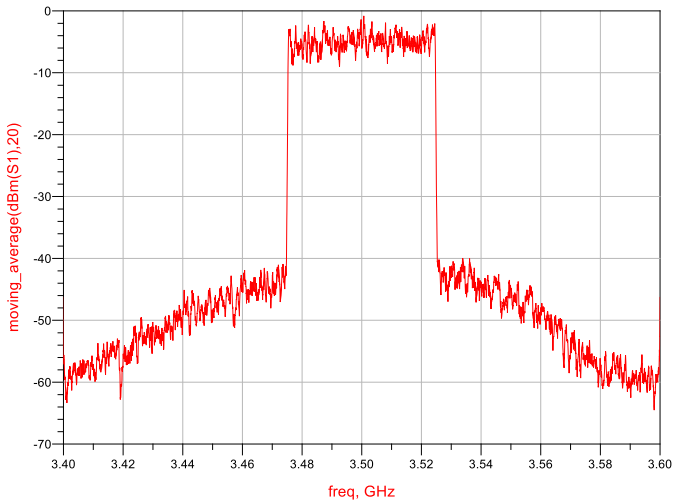


c)

Fig. 3. Output spectrum for FBMC signal of 50 MHz useful signal frequency bandwidth for output signal power 30 dBm: a) before linearization; b) after linearization by method 1; c) after linearization by method 2


ISBN 978-86-7466-930-3

## IV. Conclusion

We analyzed the effect of the linearization technique that uses baseband signals of the 2nd order nonlinearity adequately shaped and processed in magnitude and phase in baseband and then modulate the 2nd harmonic of the fundamental useful signal carrier. The linearization signals formed in this way are then inserted at the input and output of the main amplifier of DPA (linearization method 1) as well as at the output of the main and auxiliary amplifier of DPA (linearization method 2). The linearization was performed for the 5G FBMC signal.

It can be concluded that very acceptable improvement in adjacent channels power was achieved by applying the proposed linearization technique. On the bases of the obtained results, it can be noticed that the 2nd method provides slightly better results for higher power then the application of the 1st method.

## Acknowledgement

This work was supported by the Ministry of Education, Science and Technological Development of Republic of Serbia (Grant No. 451-03-68/2022-14/200102) and Science Fund of the Republic of Serbia (Grant No. 6398983 - Serbian Science and Diaspora Collaboration Program: Vouchers for Knowledge Exchange – project name: Digital Even-Order Linearization of 5G Power Amplifiers in Bands below 6GHz - DELFIN).

## References

[1] Atanasković, N. Males-Ilić, K. Blau, A. Đorić and B. Milovanović, “RF PA Linearization using Modified Baseband Signal that Modulates Carrier Second Harmonic”, Microwave Review, vol. 19, no.2, pp. 119-124, December 2013.

[2] Đorić, A. Atanasković, N. Maleš-Ilić, M. Živanović: “Linearization of RF PA by Even-order Nonlinear Baseband Signal Processed in Digital Domain”, International Journal of Electronics, Taylor & Francis, Vol.106, Issue No.12, pp.1904-1918, December 2019.

[3] N. Maleš-Ilić, A. Atanasković, K. Blau, M. Hein, “Linearization of Asymmetrical Doherty Amplifier by the Even-Order Nonlinear Signals”, International Journal of Electronics, Taylor & Francis, Vol.103, Issue No.8, pp.1318-1331, August 2016.

[4] A. Atanasković, N. M. Ilić, A. Djorić and D. Budimir, "Doherty Amplifier Linearization in Experiments by Digital Injection Methods", Proceedings of 15th International Conference on Advanced Technologies, Systems and Services in Telecommunications - TELSIKS 2021, Niš, Serbia, October 20-22, 2021, pp. 82-85.

[5] M. Bozic, M. Cabarkapa, D. Barjamovic and D. Budimir, (2018), Waveform Comparison and PA Nonlinearity Effects on CP-OFDM and 5G FBMC Wireless Systems, Microwave and Optical Technology Letters, Vol. 60, No. 8, pp: 1952-1956, August 2018.

[6] Z. Zhang, Z. Cheng, and G. Liu, “A Power Amplifier with Large High-Efficiency Range for 5G Communication”, Sensors, 2020; 20(19):5581.

[7] A. Đorić, A. Atanasković, B. Alorda, N. Maleš-Ilić: “Linearization of Doherty Amplifier by Injection of Digitally Processed Baseband Signals at the Output of the Main and Auxiliary Cell”, Proceedings of the 14th International Conference on Advanced Technologies, Systems and Services in Telecommunications - TELSIKS 2019, Niš, Serbia, October 23-25.

 ISBN 978-86-7466-930-3

# Planar Archimedean Spiral Antenna Resonant Frequency and Bandwidth Estimation using MLP Neural Network

Zoran Stanković, *Member, IEEE*, Maja Sarevska, Nebojša Dončov, *Senior Member, IEEE*, Ksenija Pešić

***Abstract*— This paper presents a neural model for fast estimation of the resonant frequency and bandwidth of a planar Archimedean spiral antenna based on MultiLayer Perceptron (MLP) network. The input parameters of the model are the number of turns of the spiral, the inner radius of the spiral and the outer radius of the spiral, while the output parameters of the model are resonant frequency, minimum operating frequency and maximum operating frequency of the Archimedean spiral antenna. The proposed neural model was applied in the process of modeling a planar self-complementary Archimedean spiral antenna with two arms.**

***Index Terms*— Archimedean spiral antenna, neural network, neural model.**

## I. Introduction

Planar Archimedean spiral antennas, due to their low weight, simplicity of construction, low manufacturing cost and approximately frequency-independent characteristics in a wide frequency range, have significant applications in broadband communication systems (*Ultra-Wide Band* (UWB) communication systems, satellite communication systems, ground penetrating radars, military aircraft radars and other broadband systems) [1],[2].

The classic approach in the analysis of characteristics, modeling and design of such antenna structures is the use of EM simulators based on numerical EM modeling techniques such as Method of Moments (MoM), Finite Element Method (FEM), Transmission Line Matrix (TLM) method, Finite Difference Time Domain (FDTD) and others [3],[4]. The main disadvantages of this approach are the need for strong hardware resources and long computation times.

An alternative approach that can overcome the above problems is the use of artificial neural networks to model planar spiral antennas. For this purpose, a good candidate in the modeling process is the MultiLayer Perceptron (MLP) network [5],[6], which has shown good results in modeling planar antenna structures [7],[8].

As part of the research covered by this paper, the "ASA_design_MT software" was first implemented for the analysis of the characteristics and design of the planar Archimedean spiral antenna with two arms. Then, a neural model of this antenna was developed, which is based on the MLP network and which is presented in this paper. Data generated by ASA_design_MT software was used to develop this model.

Zoran Stanković is with the Faculty of Electronic Engineering, University of Niš, A. Medvedeva 14, 18000 Niš, Serbia (e-mail: zoran.stankovic@elfak.ni.ac.rs).

Maja Sarevska is with American University of Europe-FON, str. Kiro Gligorov bb, 1000 Skopje, North Macedonia (e-mail: maja.sarevska@fon.edu.mk).

Nebojša Dončov is with the Faculty of Electronic Engineering, University of Niš, A. Medvedeva 14, 18000 Niš, Serbia (e-mail: nebojsa.doncov@elfak.ni.ac.rs).

Ksenija Pešić is with the Faculty of Electronic Engineering, University of Niš, A. Medvedeva 14, 18000 Niš, Serbia (e-mail: ksenija.pesic@elfak.ni.ac.rs)

## II. Planar Archimedean Spiral Antenna

The architecture of the planar Archimedean spiral antenna with two arms is shown in Figure 1. The basic geometric parameters of the antenna are: inner radius of the spiral antenna $r_i$, outer radius of the spiral antenna $r_o$, arm width $w$, space between arms $s$, and feed point $f$.

The Archimedean spiral curve is determined by the equation

$$r = a\theta + r_i \tag{1}$$

where $r$ is the radius of curve, $a$ is the growth rate, $\theta$ is the winding angle, and $r_i$ is the inner radius of spiral [2]. Accordingly, the outer radius of the spiral is defined in a way

$$r_o = 2\pi t a + r_i \tag{2}$$

where $t$ is the number of spiral turns. Two edge curves of $c_1$ and $c_2$ describe one spiral arm as

$$\begin{aligned} c_1 &= a\theta + r_i \\ c_2 &= a\left(\theta + \theta_{off}\right) + r_i \end{aligned} \tag{3}$$

where $\theta_{off}$ is the offset angle. The metal (arm) width $w$ and the metallization ratio $\chi$ of spiral antenna can then be defined as [2]

$$\begin{aligned} w &= \left|c_1 - c_2\right| = a\theta_{off} \\ \chi &= \frac{w}{w+s} = \frac{\theta_{off}}{\pi} \end{aligned} \tag{4}$$

In this paper, the case where the Archimedean spiral antenna is a self-complementary antenna is considered. This case is obtained when the condition $w = s$ is met. In this case

 ISBN 978-86-7466-930-3

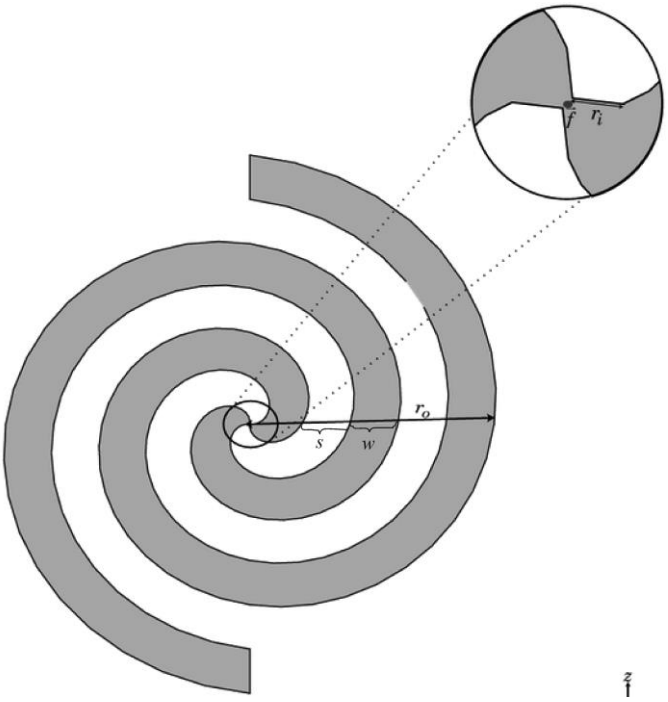


Fig. 1. Architecture of the planar Archimedean spiral antenna with two arms ($r_i$ - inner radius of the spiral antenna, $r_o$ - outer radius of the spiral antenna, $w$ - arm width, $s$ - space between arms, $f$ –feed point).

the metallization ratio, offset angle, growth rate and arm width can be determined by equations

$$\begin{cases} \chi = \dfrac{1}{2} \\ \theta_{off} = \dfrac{\pi}{2} \\ a = \dfrac{2w}{\pi} \\ w = \dfrac{r_o - r_i}{4t} \end{cases} \tag{5}$$

By applying Babinet's principle [1]

$$z_{metal} z_{air} = \frac{\eta_0^2}{4} \tag{6}$$

where $\eta_0$ is the characteristic impedance of free space, to an ideal planar self-complementary Archimedean spiral antenna ($r_i \to 0$, $r_o \to \infty$), the input impedance of the antenna can be calculated [1]

$$z_{in} = \frac{\eta_0}{2} \approx 188\,\Omega \tag{7}$$

In this case the antenna has infinite bandwidth and all primary characteristics (input impedance, antenna efficiency) and secondary characteristics of the antenna (radiation characteristics, directivity, polarization) are frequency independent. If the planar self-complementary Archimedean spiral antenna has limited physical dimensions then its bandwidth is wide but limited and its impedance deviates to some extent from 188 Ω. In this case, the approximate theoretical formula for determining the lower bound of bandwidth is [1]

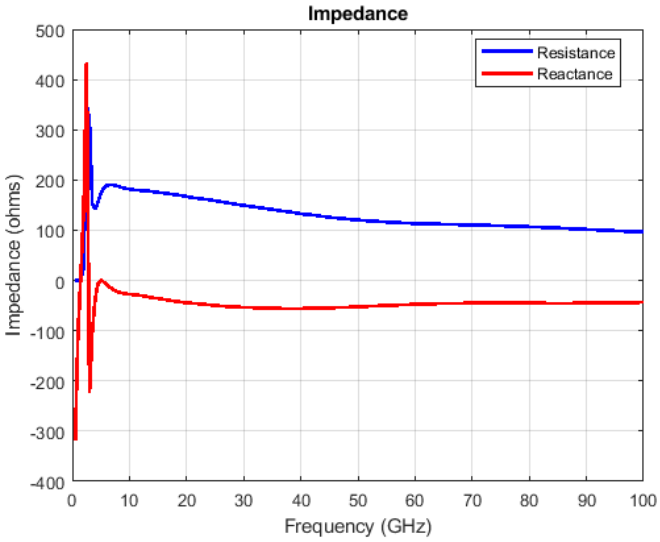


Fig 2. Impedance of the planar self-complementary ASA vs frequency ($t$ = 1, $r_i$ = 2 mm $r_o$ = 2 cm)

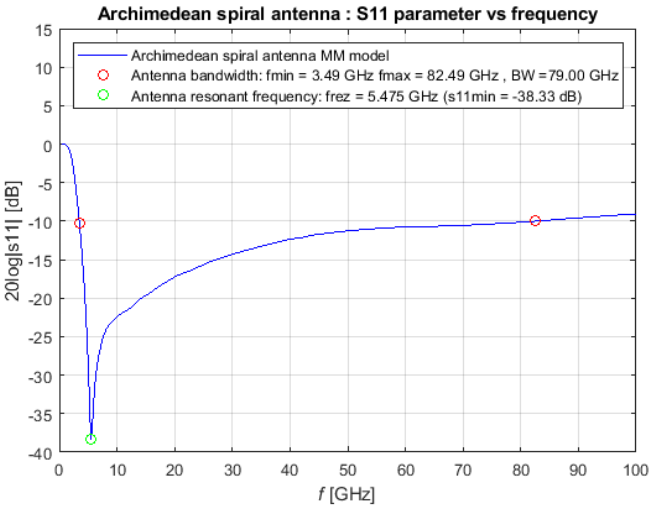


Fig. 3. $S_{11}$ parameters of the planar self-complementary ASA vs frequency ($t$ = 1, $r_i$ = 2 mm $r_o$ = 2 cm)

$$f_{\min} = \frac{c}{2\pi r_o} \tag{8}$$

In practice, the lower bound of bandwidth will be greater than predicted by Eq.8 due to reflections from the end of the arm.

If the antenna does not use a tapered feed region in the spiral center, the upper bound of bandwidth can be determined by the approximate theoretical formula [1]

$$f_{\max} = \frac{c}{2\pi r_i} \tag{9}$$

In practice, the upper bound of bandwidth differs from the theoretical value due to the influence of the real physical geometry of the feed region.


ISBN 978-86-7466-930-3

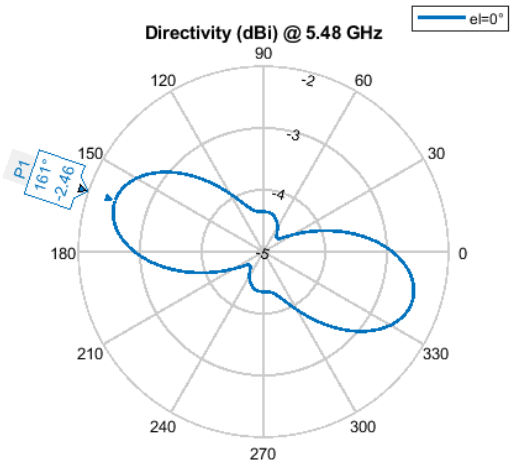


Fig. 4. Directivity of the planar self-complementary ASA in the azimuthal plane at $f_r$ = 5.475 GHz ($t$ = 1, $r_i$ = 2 mm $r_o$ = 2 cm)

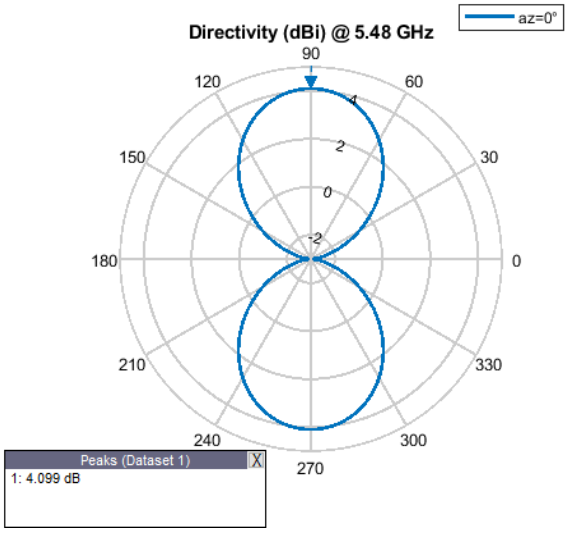


Fig. 5. Directivity of the planar self-complementary ASA in the elevation plane at $f_r$ = 5.475 GHz ($t$ = 1, $r_i$ = 2 mm $r_o$ = 2 cm)

## III. EM MODELING OF A PLANAR ASA USING "ASA_DESIGN_MT" SOFTWARE

In order to perform EM analysis and modeling of primary and secondary characteristics of the planar self-complementary Archimedean spiral antenna (ASA), "ASA_design_MT" software was developed. This software is based on Method of Moments (MoM) and is implemented using the MATLAB Antenna toolbox.

Figures 2 and 3 show the impedance and $s_{11}$ parameter as a function of frequency for a planar self-complementary ASA with physical parameters $t$ = 1, $r_i$ = 2 mm and $r_o$ = 2 cm. It can be seen that the antenna at the resonant frequency $f_r$ = 5.475 GHz has a resistance of 188 Ω. As the frequency increases, the impedance takes on a slightly capacitive character, while the resistance slowly decreases compared to 188 Ω.

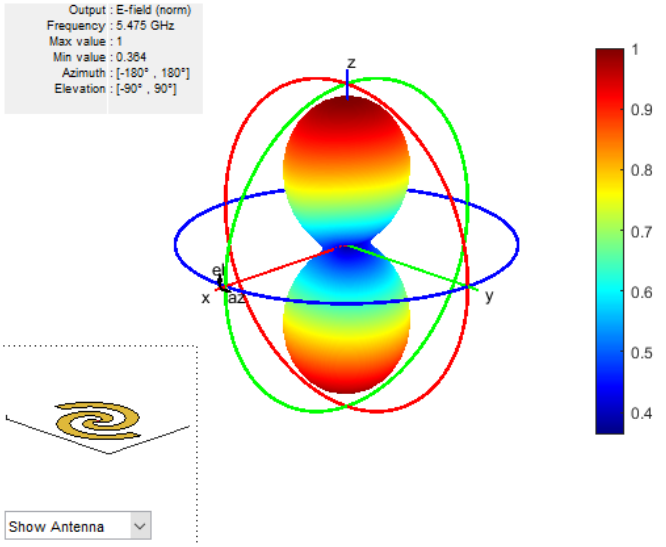


Fig. 6. 3D radiation pattern of the planar self-complementary ASA at $f_r$ = 5.475 GHz ($t$ = 1, $r_i$ = 2 mm $r_o$ = 2 cm)

Figures 4, 5 and 6 show the directivity of the planar self-complementary ASA in the azimuthal plane, the directivity of the planar self-complementary ASA in the elevation plane and the 3D radiation pattern of the planar self-complementary ASA at resonant frequency, respectively.

## IV. MLP MODEL OF THE PLANAR SELF-COMPLEMENTARY ASA

The MLP model of the planar self-complementary ASA (MLP_ASA) consists of a single MLP network and its architecture is shown in Figure 7. MLP_ASA models the dependence of lower bound of bandwidth, resonant frequency and upper bound of bandwidth on the following physical parameters: number of spiral turns, inner radius of spiral and outer radius of spiral. Therefore, MLP_ASA can be functionally described by the following expression

$$[f_{\min}\ f_r\ f_{\max}]^T = f_{MLP\_ASA}\left([t\ r_i\ r_o]^T\right) \tag{10}$$

MLP networks consist of a single input layer, a single output layer, and multiple hidden layers of neurons. In accordance with Eq. 10, the input layer has three neurons, the output layer has three neurons, while the hidden layers have $N_1$, $N_2$,…, $N_H$ neurons respectively, where $H$ is the total number of hidden layers. For MLP network with a specific number of layers and neurons in them, notation was used MLP$H$-$N_1$-…-$N_i$-…-$N_H$, $1 \le i \le H$.

The outputs of the hidden layers are given by the expression

$$\mathbf{y}_l = F(\mathbf{w}_l \mathbf{y}_{l-1} + \mathbf{b}_l) \quad l = 1, 2, \ldots, H \tag{11}$$

where $\mathbf{y}_0$ represents the output of the input layer and vectors $y_l$ and $y_{l-1}$ represent the output of $l$-th and ($l$-1)-th hidden layer, respectively. Weight matrix for connections between neurons in ($l$-1)-th and $l$-th layers is denoted by $\mathbf{w}_l$, while biases of $l$-th hidden layer neurons are represented by vector $\mathbf{b}_l$. Neurons in


ISBN 978-86-7466-930-3

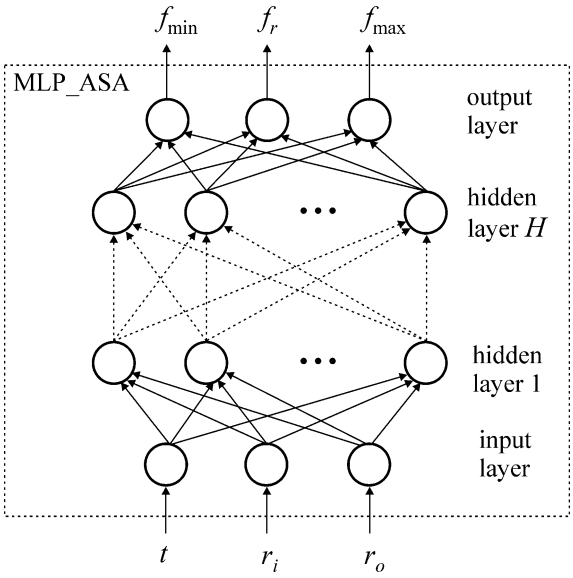


Fig. 7. The MLP neural model of the planar self-complementary Archimedean spiral antenna

hidden layers have the hyperbolic tangent sigmoid activation function $F(\cdot)$ defined by the expression

$$F(u) = \frac{e^{u} - e^{-u}}{e^{u} + e^{-u}} \tag{12}$$

The neurons in the output layer use a linear activation function so that their output is defined in a way

$$\left[f_{\min}\ \ f_r\ \ f_{\max}\right]^T = \mathbf{w}_{H+1}\mathbf{y}_H + \mathbf{b}_{H+1} \tag{13}$$

where $\mathbf{w}_{H+1}$ is a weight matrix for connections between neurons of the last hidden layer and output layer neurons.

During the training of the MLP network, the weight matrices $\mathbf{w}_1$, $\mathbf{w}_2$,…, $\mathbf{w}_H$, $\mathbf{w}_{H+1}$ and bias vectors $\mathbf{b}_1$, $\mathbf{b}_2$,…, $\mathbf{b}_H$, $\mathbf{b}_{H+1}$ are optimized in order to achieve the desired mapping accuracy defined by the expression Eq. 10.

## V. Modeling results

Using the "ASA_design_MT" software 1000 samples are generated for training and 300 samples for testing having random distribution.

With the aim to develop a model with better accuracy the training was done for various MLP$H$-$N_1$-…-$N_i$-…-$N_H$, networks while only networks with two hidden layers were used ($H$ = 2). For the number of neurons in the hidden layer. the values that were used are $6 \le N_1$ , $N_2 \le 22$.

The MLP training is done using Levenberg – Marquardt algorithm with given goal mean squared error of training $MSE_{target} = 10^{-4}$ and maximal number of iterations $N_{\max} = 500$. Before training the neural connection weights and biases are initialized with random values in the range [-1 1]. Also input network data are scaled and output data are descaled in the range [-1 1]. After the training each network is tested using test data in order generalization capabilities to be evaluated. For the evaluation of the generalization capabilities of the network and its accuracy the following test metrics are used: mean squared error (RMSE) and Pearson product moment correlation coefficient ($r^{PPM}$) [6].

The Table I shows the testing results for eight MLP networks that showed best testing results after training. It may be seen that the networks have small RMSE in the lower bandwidth limit and resonant frequency, while in the estimation of the upper bandwidth limit they have much higher RMSE.

For the realization of the MLP model of the planar self-complementary Archimedean spiral antenna MLP2-9-8 is chosen as this network in the testing procedure had largest value for the Pearson product moment correlation coefficient.

TABLE I
TEST RESULTS FOR EIGHT MLP MODELS WITH THE HIGHEST $r^{PPM}$ VALUE

| MLP networks | RMSE ($f_{\min}$) | RMSE ($f_r$) | RMSE ($f_{\max}$) | $r^{PPM}$ |
|---|---|---|---|---|
| MLP2-9-8 | 0.1628 | 0.3345 | 6.4747 | 0.9939 |
| MLP2-10-9 | 0.1537 | 0.3628 | 6.4915 | 0.9938 |
| MLP2-8-8 | 0.1584 | 0.3144 | 6.5339 | 0.9937 |
| MLP2-8-11 | 0.1590 | 0.3980 | 6.5706 | 0.9937 |
| MLP2-8-10 | 0.1606 | 0.3747 | 6.6170 | 0.9936 |
| MLP2-11-10 | 0.1568 | 0.3223 | 6.5715 | 0.9936 |
| MLP2-12-8 | 0.1569 | 0.3174 | 6.6360 | 0.9936 |
| MLP2-8-15 | 0.1622 | 0.3517 | 6.6686 | 0.9935 |

On Fig.8 the scattering diagram of MLP2-9-8 model output is shown. It may be noticed the good match for the lower bandwidth limit and resonant frequency with the referent values. Also it may be noticed that for the values of the upper bandwidth limit the match is not so good as for the two previously mentioned parameters. This may be explained with fact that EM simulator while training sample generation had difficulty to accurately determine the upper limit of the bandwidth. The reason for that is that for higher frequencies the function of parameter $s_{11}$ almost asymptotically approach the bound of -10 dB so the indetermination of the cross point estimation between that function and the horizontal line $s_{11}$ = -10 dB is very large.

For above explained situation MLP model of the planar self-complementary ASA may be used only for rough estimation of the upper bound of the bandwidth. But this does not decrease the useful application of the proposed model because in real life the detremination of the lower bound of the bandwidth is more important than for the upper boind. The reason for this is that upper bound ftrequency is much higher than the maximal working frequency for emission and reception.

MLP model of the planar self-complementary ASA is implemented on a modest referent hardware platform (Intel Core i3-2350M@2.3 GHz, 4GB RAM). This model, the estimation of the resonant frequency, the minimum operating

 ISBN 978-86-7466-930-3

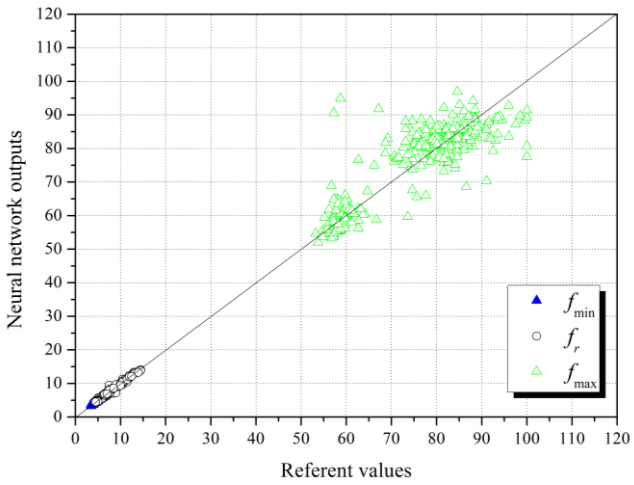


Fig. 8. Scattering diagram for MLP2-9-8 network

frequency and the maximum operating frequency of the antenna, has performed in 300 points defined with testing set for only 0.03 s. This speaks about the high speed of the MLP model.

## VI. Conclusion

Today planar spiral antennas attract more and more attention because they are convenient for the application in the modern portable broadband communication devices. The modeling of these antenna structures with the help of EM simulators that are based on MoM techniques presents classical approach in EM characteristics modeling. Because of intensive numerical estimations this kind of EM simulators demand strong hardware platform and estimations itself may last very long, that is main disadvantage of the EM simulator approach. Alternative approach for the spiral antenna modeling is using of artificial neural networks.

This paper presents the MLP model of the planar self-complementary Archimedean spiral antenna that is implemented on a modest hardware platform. MLP model has shown exceptional speed in the estimation of resonant frequency, minimum operating frequency and maximum operating frequency for this antenna structure. Currently developed model supports estimation of the resonant frequency and minimum operation frequency with high accuracy and rough (low accuracy) estimation of high operating frequency for the antenna.

Further investigations will be steered to the increased MLP model accuracy for the planar self-complementary Archimedean spiral antenna in the maximum operating frequency estimation.

## Acknowledgment

This work was supported by the Ministry of Education, Science and Technological Development of Republic of Serbia (Grant No. 451-03-9/2021-14/200102).

## References

[1] Balanis, C. A., *Antenna Theory: Analysis and Design*, Wiley, New York, 2005.

[2] Teng-Kai Chen and Gregory H. Huff, "Travelling Wave Mechanism and Novel Analysis of the Planar Archimedean Spiral Antenna in Free Space," *Progress In Electromagnetics Research*, Vol. 145, 287-298, 2014, doi:10.2528/PIER14011901.

[3] Matthew N. O. Sadiku, *Numerical techniques in electromagnetics*, 2nd edition, CRC Press LLC, 2001.

[4] Levent Sevgi, *Electromagnetic Modeling and Simulation*, First Edition.. The Institute of Electrical and Electronics Engineers, Inc. Published by John Wiley & Sons, Inc., 2014

[5] S. Haykin, *Neural Networks*, New York, IEEE, 1994.

[6] Q. J. Zhang, K. C. Gupta, Neural networks for RF and microwave

[7] K. Pesic, Z. Stankovic and N. Doncov, "ANN-EM Model of Dual Band Square Patch Antenna with a Floating Rectangular Slot," 2021 15th International Conference on Advanced Technologies, Systems and Services in Telecommunications (TELSIKS), 2021, pp. 153-156, doi: 10.1109/TELSIKS52058.2021.9606409.

[8] M. Milijić, Z. Stanković and B. Milovanović, "Efficient model of slotted patch antenna based on neural networks,"*2009 9th International Conf. on Telecommunication in Modern Satellite, Cable, and Broadcasting Services*, Nis, 2009, pp. 384-387.

 ISBN 978-86-7466-930-3

# Analysis of Feeding Methods for High-Gain Crossed Slot Antenna Arrays

Marija Milijic, *Member, IEEE*, Branka Jokanovic, *Senior Member, IEEE*

***Abstract*— In this paper we present the influence of different feeding methods on performances of the dual polarized antenna array. Antenna array consists of 14 identical crossed slots serially fed by coplanar waveguide (CPW) and positioned at equal distances forming a linear array. Three proposed feeding methods are compared with the ideal case when two antenna sub – arrays are fed by two generators to achieve the highest possible gain. The CPW-T junction, CPW rat-race coupler and modified CPW rat-race coupler are engaged for feeding 2D crossed slots array to analyze its performances for use in 5G and radar applications.**

***Index Terms*—Antenna array; CPW-fed antenna; CPW T-junction; CPW rat-race coupler; crossed slot antenna.**

## I. INTRODUCTION

FOR operation at millimeter waves, antenna arrays are very attractive candidates considering high-gain and beamforming characteristic. However, the feed network, its necessary part that enables suitable amplitude and phase distributions for a large number of radiating elements in array, increases both design complexity and size of antenna. Otherwise, antennas in printed circuit technology have aroused more and more attention as one of vital components in modern 5G wireless communication system thanks to their planar structure, compact design, inexpensive and uncomplicated manufacture [1]. The printed antennas as elements in an array are usually fed by corporate-feed network, when there are a multiple lines for feeding array elements, or by series-feed network, when elements are fed by a single line. A series-feed network can be easily modeled and cheaply fabricated using simultaneous photolithography for both the radiating elements and the feed network [2,3]. However, a corporate-feed network is widely used to provide desired power splits necessary to synthesize a required radiation pattern or to achieve high side lobe suppression [4,5]. Some research has employed the combination of series and corporate feed methods to obtain the desired antenna characteristics.

There are some considerable losses typical for high operating frequency of mm-waves antennas as free-space path loss and propagation loss due to atmospheric absorption. They are both lower at the frequencies below 28 GHz wherefore the frequencies between 24.25 ï 27.5 GHz are tag as a promising operation bandwidth for the next-generation 5G networks and technologies [6]. Therefore, the antennas proposed in this paper are model and simulated for the center frequency $f_c$=25.875 GHz calculated as the central value of that band. This is an extension of the research presented in [7,8] that modeled the advanced high-gain rectangular slot antenna arrays fed by CPW feeding line.

Marija Milijic is with the Faculty of Electronic Engineering, University of Niġ, Aleksandra Medvedeva 14, 18000 Nis, Serbia, E-mail: marija.milijic@elfak.ni.ac.rs

Branka Jokanovic is with the Institute of Physics, University of Belgrade, Pregrevica 118, 11080 Pregrevica, Serbia, and The Academy of Engineering Sciences of Serbia, Kraljice Marije 16, Belgrade, Serbia E-mail:brankaj@ipb.ac.rs

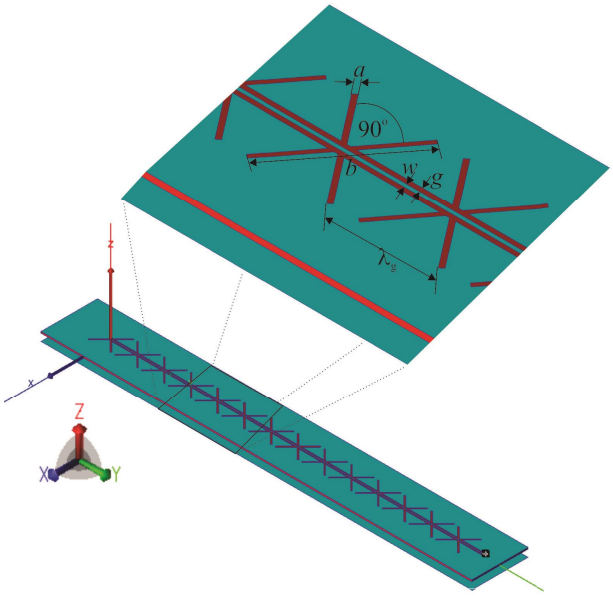


Fig. 1. Linear CPW-fed crossed slot array.

This paper analyzes firstly a linear array of identical 14 crossed slots, positioned symmetrically relative to the CPW feeding line. The crossed slot antennas, whose two rectangular parts are positioned at right angle, are dual polarized antenna with identical radiation patterns for both vertical and horizontal polarization [9]. Further, the linear crossed slot array has replicated forming CPW-fed 2D array. The following types of feeding methods are investigated: feeding by two generators for every sub ï array, CPW ï T junction, CPW rat-race coupler and modified CPW rat-race coupler. The simulated results, especially gain and bandwidth, obtained by WIPL-D Pro CAD [10] software are discussed and compared.

## II. LINEAR CPW-FED CROSSED SLOT ARRAY

The radiating element in proposed antennas is a crossed slot that consists of two rectangular parts with dimensions *a* x *b* - slot width x slot length, positioned at right angle to each other [9]. The identical fourteen crossed slots are combined to form an array (Fig 1). A series feed is in a form of coplanar

 ISBN 978-86-7466-930-3

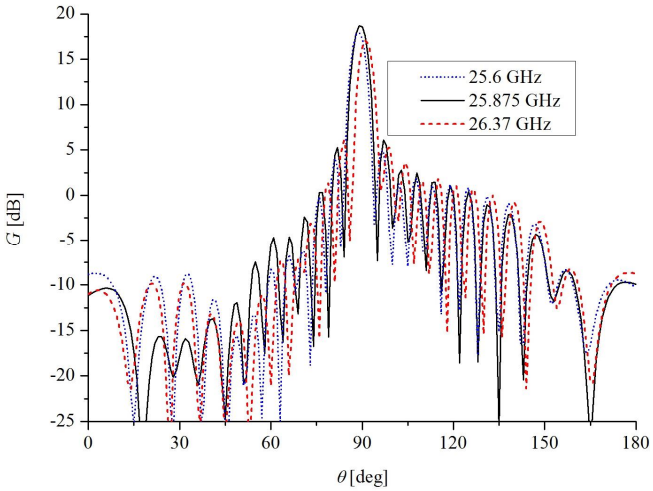


Fig. 2. Radiation patterns in the yOz plane ($\varphi$=90°) of the proposed 14 crossed slots antenna array.

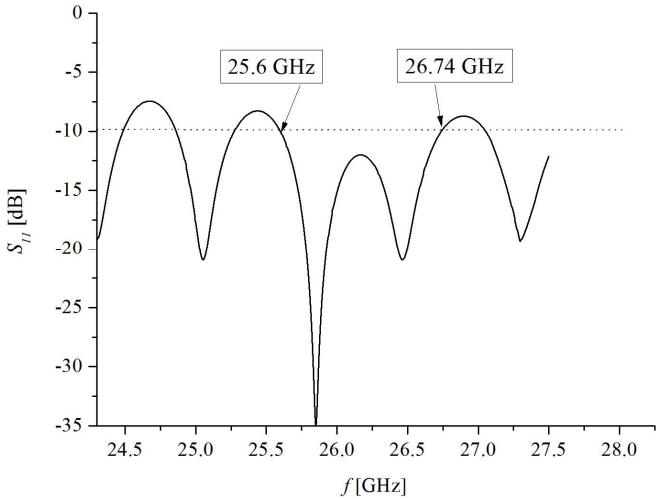


Fig. 3. $S_{11}$ parameter versus frequency of the proposed 14 crossed slots antenna array. S-parameters are normalized to the 120 Ý -impedance of CPW feeding line.

waveguide (CPW) transmission line with strip and gap ($w$ and $g$) of 0.3 mm and 0.375 mm, respectively resulting in characteristic impedance around 120 q. The slots are positioned symmetrically along to the CPW feeding line at the mutual distance $\lambda_g$=9 mm where $\lambda_g$ is CPW line wavelength at the center frequency $f_c$. Their dimension $a$=0.44 mm and $b$=10.84 mm are optimized at an operating frequency $f_c$ [9]. The proposed antenna design is built on a substrate that has a dielectric constant ($e_r$) of 2.54 and the dimensions 145 mm x 19 mm x 0.508mm. At the distance $\lambda_0$/4 =2.89 mm from the array there is a reflector plate whose dimension are the same as the substrateôs dimensions ($\lambda_0$ is the wavelength in vacuum at the center frequency $f_c$=25.875 GHz). Unlike the microstrip antennas with a backside ground plane, slot antennas require the reflector plane to be at a distance equal to the quarter of the free space wave-length. It should ensure that the antenna radiates only in half the space.

Fig. 2 shows the radiation patterns of the proposed 14 crossed slot antenna array at three frequencies: center $f_c$, lower (25.6 GHz) and higher (26.37 GHz) edge frequencies. The edge frequencies are determined by the criteria that the maximum gain at an edge frequency does not vary more than 10% of the maximum gain at the center frequency and that its side lobe suppression (SLS) is bigger than 10 dB. The maximum gain of the proposed 14 crossed slots antenna array at the center frequency $f_c$ is 18.7 dBi while it is 18 dBi at the lower and 17 dBi at the higher edge frequency. The antenna has its maximum gain for $\theta$=89° at lower edge frequency, for $\theta$=90° at center frequency $f_c$ and for $\theta$=91° at higher edge frequency. Moreover, its SLS is 12.5 dB at the center frequency while it is 13 dB at the lower and 11 dB at the higher edge frequency. Its $S_{11}$ parameter, normalized to the impedance of CPW feeding line (120 Ý), is depicted in Fig. 3. It is less than -10 dB for the frequency range between 25.6 GHz and 26.74 GHz which is more than range determined by radiation pattern.

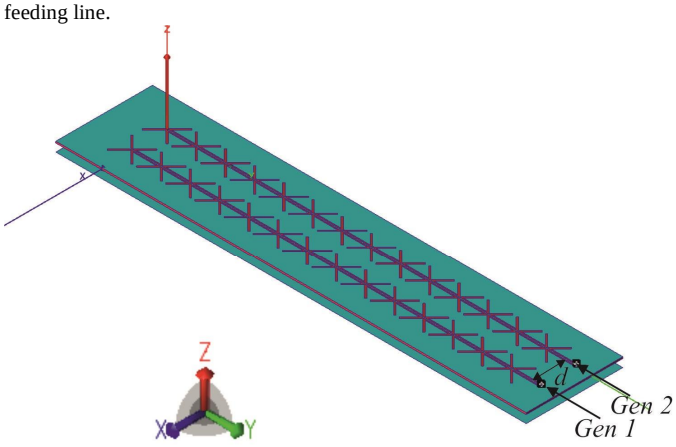


Fig. 4. 2D CPW-fed crossed slot array fed by two independent generators.

## III. 2D CPW-FED CROSSED SLOT ARRAY

Two identical linear 14 crossed slot sub ï arrays, presented in previous section, are associated together at the mutual distance $d$=10.8 mm building a 2D array (Fig. 4). It is situated on the substrate with dimensions 145 mm x 29.8 mm x 0.508 mm while the equal reflector plate is at the distance $\lambda_0$/4.

The feed structure, required to enable equal amplitude and phase distribution for both subarrays, must be designed in order to achieve the best radiation and bandwidth properties. Therefore, different feeding techniques are modeled and studied: feeding by two generators for every sub ï array, CPW ï T junction, CPW rat-race coupler and modified CPW rat-race coupler.

### *A. Feeding by Two Generators*

In the first study, the two sub-arrays are fed by two generators placed at the end of CPW lines (Fig. 4). Due to the influence of the mutual coupling between sub-array in x-axis direction, the dimensions of crossed slot antennas are optimized to the different values $a$=0.53 mm and $b$=10.78 mm in the respect to the linear array. The radiation patterns of 2D crossed slots antenna fed by two generators is depicted in Fig. 5.

 ISBN 978-86-7466-930-3

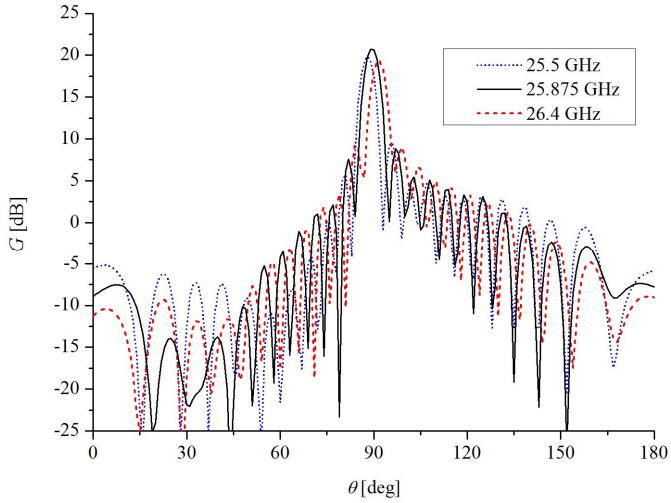


Fig. 5. Radiation patterns in the yOz plane ($\varphi$=90°) of the 2D CPW-fed crossed slots array fed by two independent generators.

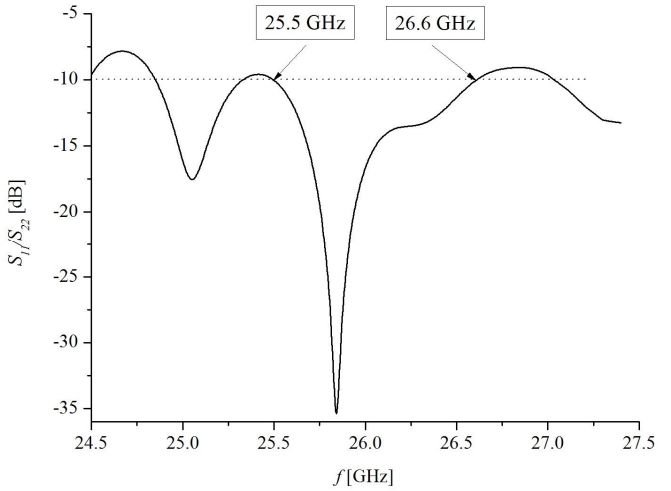


Fig. 6. $S_{11}$ and $S_{22}$ parameter versus frequency of the 2D CPW-fed crossed slots array fed by two generators. S-parameters are normalized to the 120 Ý - impedance of CPW feeding lines.

Because there are two sub-arrays of 14 crossed slots, the gain at the center frequency $f_c$ is 20.7 dBi ($\theta$=90°). At the edge frequencies the gain drops off a bit: it is 19.9 dBi ($\theta$=88°) at lower edge frequency (25.5 GHz) and 19.3 dBi ($\theta$=92°) at higher edge frequency (26.4 GHz). SLS is 12 dB at the center frequency $f_c$ while it falls to 10 dB at the edge frequencies. However, as the previously discussed linear 14 crossed slots antenna, the proposed 2D CPW-fed crossed slots antenna has the bigger range where its $S_{11}$ parameters (Fig. 6), normalized to the 120 Ý -impedance of CPW feeding line, is less than -10 dB (25.5 GHz ï 26.6 GHz) then the range of the satisfying radiation patterns (25.5 GHz ï 26.4 GHz). Besides very good radiation properties of the proposed 2D crossed slots antenna fed by two generators, it is necessary to design the unique feed to enable the uniform amplitude and phase distribution for both arrays and therefore CPW T-junction and CPW race rat couplers are introduced.

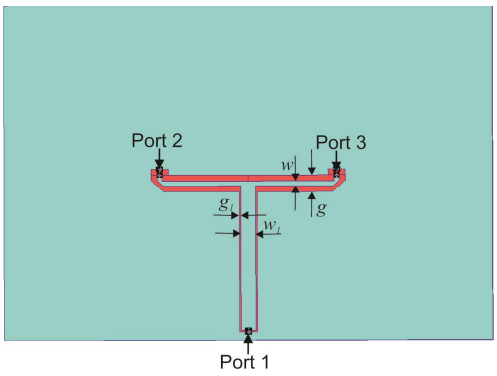


Fig. 7. CPW-T junction.

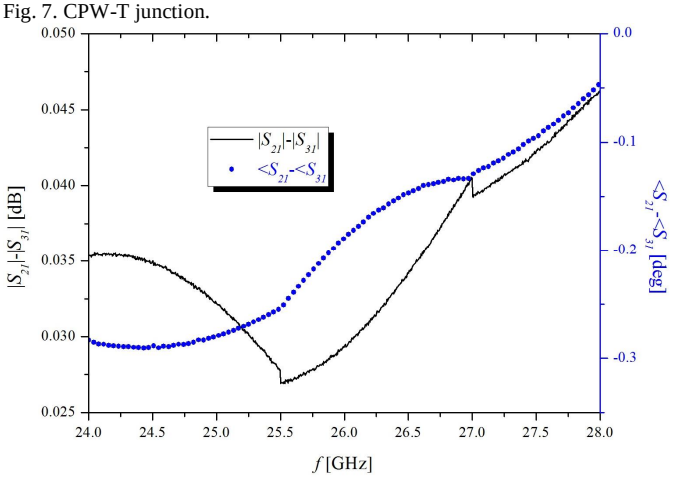


Fig. 8. The difference between insertion losses calculated at ports 2 and 3 of CPW T-junction. S-parameters are normalized to the impedance of CPW feeding line (120 Ý).

### *B. CPW –T junction*

Further, the 2D array is fed by the T junction power divider implemented with coplanar waveguide transmission lines (CPWï T junction). Configuration of the proposed CPW power divider is shown in Fig. 7. The CPW feed line is 60 Ý-CPW line (featuring the strip $w_1$=0.9 mm and gap $g_1$=0.1 mm), that enables equal feeding for both sub - arrays dividing power into two 120 Ý CPW feed lines featuring the strip $w$=0.3 mm and gap $g$=0.375.

The difference between S-parameters (magnitudes ( $|S_{ij}|$ ) and phases ( $\angle S_{ij}$ ) of $S_{21}$ and $S_{31}$ $S$ scattering ($S$-) parameters for left and right subarrays) is presented in Fig. 8. Analyzing shown results, it can conclude that proposed CPW T junction provides necessary equal feeding for both subarrays for range between 24-28 GHz. Therefore, CPW T-junction is used to feed the 2D crossed slots array. The whole structure, 2D array and CPW T-junction, is situated on the substrate with dimensions 150 mm x 29.8 mm x 0.508 mm while the equal reflector plate is at the distance $\lambda_0/4$ (Fig. 9).

The Fig. 10 presents the radiation pattern of 2D crossed slots array fed by CPW T-junction. The radiation pattern at the center frequency $f_c$ features with gain of 18.45 dBi at $\theta$=90° and SLS of 12 dB. At the lower edge frequency (25.49 GHz) the gain is 18.16 dBi at $\theta$=88°. At the higher edge frequency (26.45 GHz) the gain is 17.48 dBi at $\theta$=92°. SLS for both edge frequencies is 10 dB. $S_{11}$ parameter is less than -10 dB for the frequency above 25.49 GHz (Fig.11).

 ISBN 978-86-7466-930-3

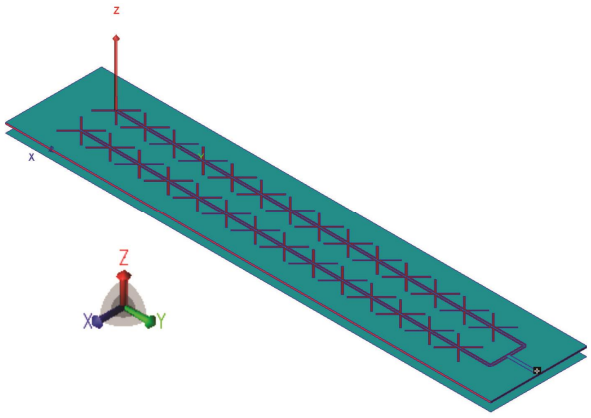


Fig. 9. 2D CPW-fed crossed slot array fed by CPW T-junction.

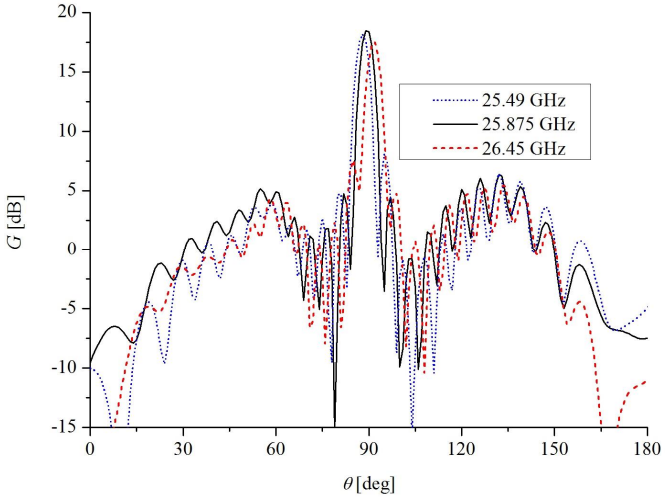


Fig. 10. Radiation patterns in the yOz plane ($\varphi$=90°) of the 2D CPW-fed crossed slots array fed by CPW T-junction.

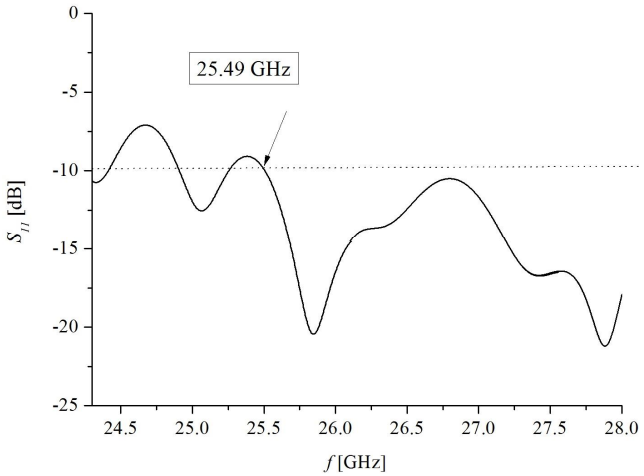


Fig. 11. $S_{11}$ parameter versus frequency of the 2D CPW-fed crossed slots array fed by CPW T-junction. S-parameter is normalized to the impedance of CPW feed line 60 Ý.

### C. CPW rat-race coupler

The additional research employs CPW rat-race coupler, with the shape of a ring/circle, to provide required feeding for both sub-arrays. Rat race couplers have been very attractive for use in many applications such as mixers, multipliers, amplifiers, beamformers, etc. [11]. One of its disadvantages is that its big circumference ($3\lambda_g/2$) requests too much space increasing the overall size of antennas.

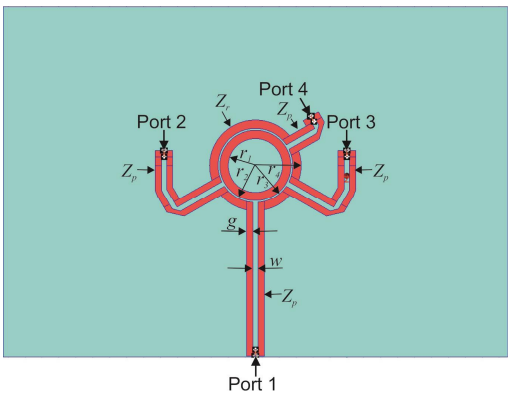


Fig. 12. CPW rat-race coupler.

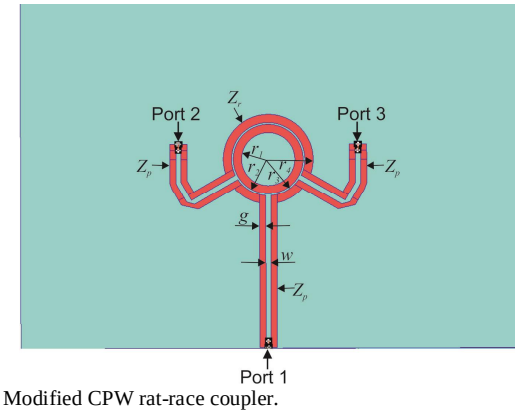


Fig. 13. Modified CPW rat-race coupler.

The proposed CPW rat-race coupler has 4 ports with $Z_p$=120 q impedance as numbered in Fig. 12, each of which is presented by CPW feed line featuring the strip $w$=0.3 mm and gap $g$=0.375. Each port is placed at a distance of one-quarter wavelength ($\lambda_g$) away from the other around the one half of the ring. The CPW forming the ring has a impedance $Z_r$=ã2*$Z_p$=ã2*120=169.7 q with gap $g_r$=0.5 mm and strip width $w_r$=0.105 mm. The CPW rat-race ring features the following radius: $r_1$=1.6 mm, $r_2$=2.1 mm, $r_3$=2.205 mm and $r_4$=2.705 mm.

An input signal is fed from port 1 resulting in two equal amplitude in-phase signals at ports 2 and 3. Port 4 is isolated in this case. Therefore, ports 2 and 3 are used to feed two identical linear 14 crossed slot sub ï arrays while port 4 is connected to the ground through the impedance of 120 q. Although there are two sub-arrays, we model likewise a modified CPW rat-race that does not contain port 4 (Fig. 13) in order to investigate its role and necessity in rat-race coupler.

The imbalance between S-parameters (magnitudes ( $|S_{ij}|$ ) and phases ( $\angle S_{ij}$ ) of $S_{21}$ and $S_{31}$ $S$ scattering ($S$-) parameters referring Port 2 and Port 3 of both CPW rat-race coupler and modified CPW rat-race coupler for feeding left and right subarrays) for frequency range from 24 GHz to 28 GHz is presented in Fig. 14. Analyzing shown results, it can see that maximum difference between magnitudes of $S_{21}$ and $S_{31}$ parameters of rat-race coupler with 4 ports is less than 0.5 dB while the maximum variation between their phases is less than 2.5 degrees. Modified rat-race coupler enables equal amplitude in-phase signals at ports 2 and 3 concerning results shown in Fig. 14.

 ISBN 978-86-7466-930-3

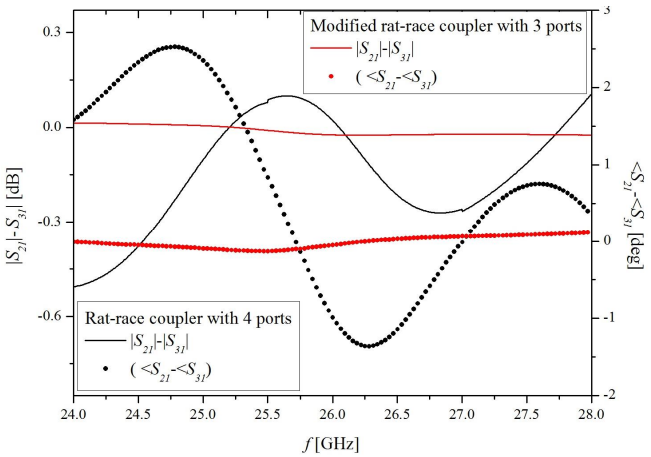


Fig. 14. The difference between insertion losses calculated at ports 2 and 3 of CPW rat-race coupler and of modified CPW rat-race coupler. S-parameters are normalized to the impedance $Z_p$ (120 Ý).

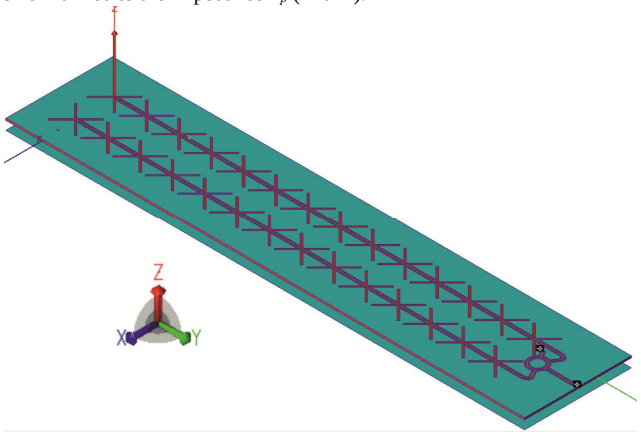


Fig. 15. 2D CPW-fed crossed slot array fed by CPW rat race coupler.

It can be concluded that proposed both CPW rat-race coupler and modified CPW rat-race coupler provide necessary feeding for both subarrays for range between 24-28 GHz. Therefore they are employed to feed 2D crossed slots array (Fig. 15). 2D crossed slots array and CPW rat-race coupler are both situated on the substrate with dimensions 145 mm x 29.8 mm x 0.508mm while the equal reflector plate is at the distance $\lambda_0/4$.

The radiation patterns of 2D CPW-fed crossed slots array fed by CPW rat-race coupler with 4 ports is presented in Fig. 16. The maximum gain at the center frequency $f_c$ is 19.6 dBi at the position $\theta$=90°. At the lower edge frequency 25.6 GHz, the maximum gain is 18.8 dBi at the position $\theta$=89°. At the higher edge frequency 26.8 GHz, the maximum gain is 18.65 dBi at the position $\theta$=93°. SLS is 12.5 dB at the center frequency $f_c$ and 10 dB at the both edge frequencies.

However, the radiation pattern of the 2D CPW-fed crossed slots array fed by modified CPW rat-race coupler with 3 ports has less gain for all considered frequencies (Fig. 17): 18.85 dBi at the center frequency $f_c$, 18.4 dBi at the lower edge frequency 25.6 GHz and 18.6 dBi at the higher edge frequency 26.6 GHz. The maximum gain spreads from $\theta$=89° for the lower edge frequency 25.6 GHz, through $\theta$=90° for $f_c$ to $\theta$=93° for the higher edge frequency 26.6 GHz. SLS is 12 dB at the center frequency $f_c$ and it drops to 10 dB at the edge frequencies.

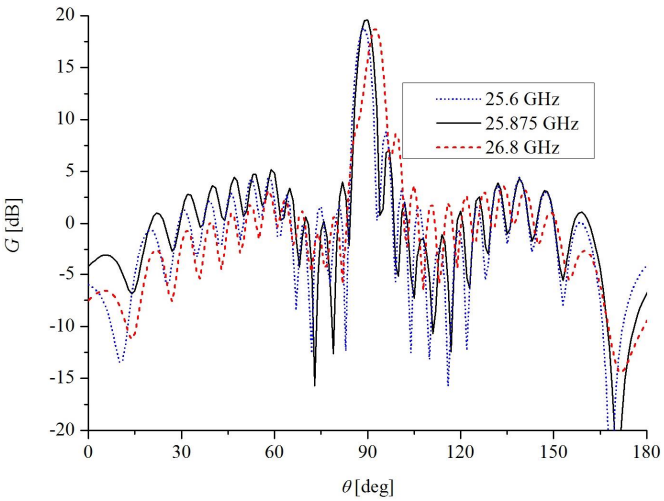


Fig. 16. Radiation patterns in the yOz plane ($\varphi$=90°) of the 2D CPW-fed crossed slots array fed by CPW rat-race coupler.

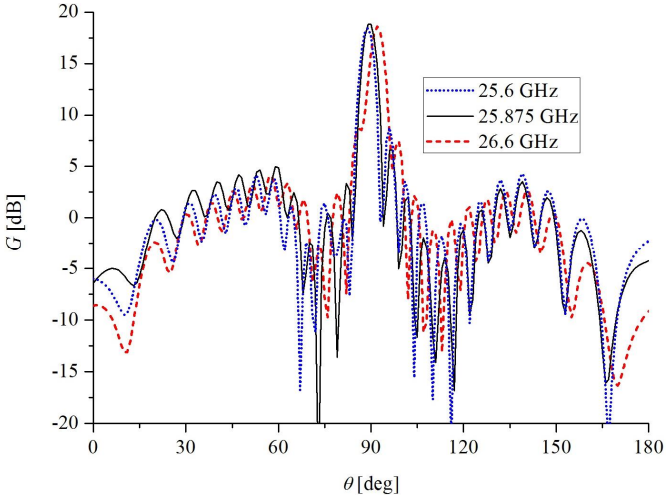


Fig. 17. Radiation patterns in the yOz plane ($\varphi$=90°) of the 2D CPW-fed crossed slots array fed by modified CPW rat-race coupler.

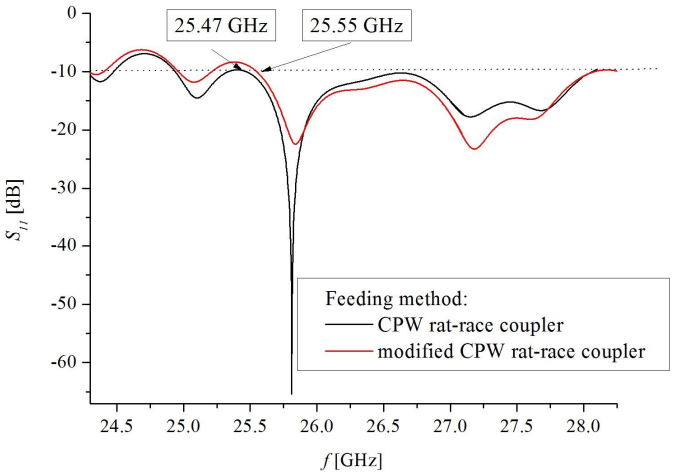


Fig. 18. $S_{11}$ parameter versus frequency of the 2D CPW-fed crossed slots array fed by CPW rat-race coupler and by modified CPW rat-race coupler. S-parameter is normalized to the impedance $Z_p$=120 Ý.

The $S_{11}$ parameter of 2D CPW-fed crossed slots array fed by CPW rat-race coupler and by modified CPW rat-race coupler is shown in Fig. 18.

 ISBN 978-86-7466-930-3

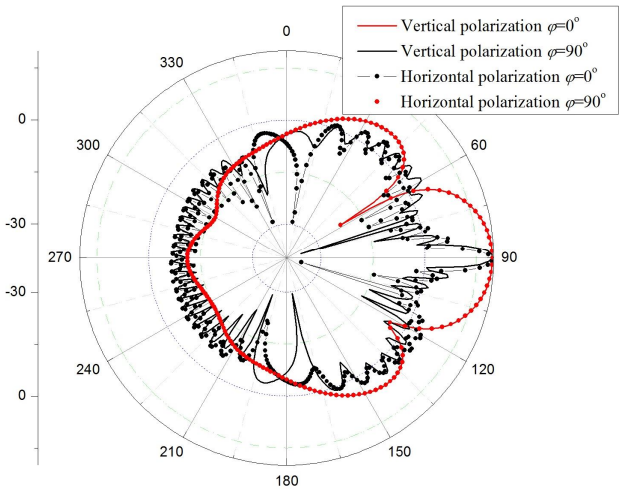


Fig. 19. Radiation pattern of the 2D CPW-fed crossed slots array fed by CPW rat-race coupler in X-Z ($\varphi$=0°) and Y-Z ($\varphi$=90°) plane at the frequency $f_c$.

TABLE I
THE GAIN AND BANDWIDTH DEFINED BY RADIATION CHARACTERISTICS AND BY $S_{11}$ PARAMETERS OF THE PROPOSED LINEAR AND 2D CPW-FED CROSSED SLOT ARRAYS

| Array and feed | Gain [dBi] | Bandwidth by radiation pattern/by $S_{11}$ [GHz] |
|---|---|---|
| 14 slots | 18.7 | 0.77/1.14 |
| 2x14 slots by 2 generators | 20.7 | 0.9/1.1 |
| 2x14 slots by CPW T-junction | 18.45 | 0.96/>2.51 |
| 2x14 slots by CPW rat-race | 19.6 | 1.2/>2.53 |
| 2x14 slots by modified CPW rat-race | 18.85 | 1/>2.45 |

It is less than -10 dB for frequency above 25.47 GHz for feeding by CPW rat-race and for frequency above 25.55 GHz when the modified CPW rat-race is used. It can notice that 2D CPW-fed crossed slots array fed by CPW rat-race coupler has the biggest frequency range defined by both criteria: by satisfying radiation characteristics and by condition that $S_{11}$<-10 dB. Also, the latter criterion gives greater frequency range than the former.

Although the single crossed slot antenna is dual polarized [9], the simulated radiation patterns in both X-Z and Y-Z planes for two orthogonal polarizations (vertical and horizontal) of the 2D CPW-fed crossed slots array fed by CPW rat-race coupler are presented in Fig. 19. It can conclude that it is also a dual polarized antenna.

All obtained results of comparison between feeding methods and antenna arrays are shown in Table I.

## IV. CONCLUSION

This paper presents the antenna arrays of crossed slot antenna fed by CPW transmission line. The first proposed antenna is a linear array of 14 crossed slots that features with gain of 18.7 dBi at the center frequency $f_c$. It has the satisfying radiation patterns from the frequency range from 25.6 GHz to 26.37 GHz. Also, its $S_{11}$ parameter is less than -10 dB for the frequencies between 25.6 GHz to 26.74 GHz.

After that we investigate feeding networks for two planar arrays of 14 crossed slots and employ four feeding methods. First method is two generators that enable great gain of 20.7 dBi of the proposed 2D crossed slot array. The gain and SLS have the allowed variation for the frequency range from 25.5 GHz to 26.4 GHz. Moreover, $S_{11}$ parameter stays below -10 dB for the frequencies between 25.5 GHz to 26.6 GHz.

CPW T-junction, CPW rat-race coupler and modified CPW rat-race coupler are proposed. The comparison among the simulated results of investigated three feeding methods gives the advantage to the CPW rat-race coupler. The gain is the greatest when CPW rat-race coupler is used (19.6 dBi). Additionally, the radiation pattern keeps the satisfying gain and SLS values in the largest frequency range when 2D array is fed by CPW rat-race coupler (25.6 GHz - 26.8 GHz). However, $S_{11}$ parameter of 2D array fed by CPW rat-race coupler is less than -10 dB for the similar frequency range above 25.47 GHz as $S_{11}$ parameter of 2D array fed by CPW T-junction and $S_{11}$ parameter of 2D array fed by modified CPW rat-race coupler.

## ACKNOWLEDGMENT

This work was supported by the Ministry of Education, Science and Technological Development of the Republic Serbia. The authors would like to thank prof. Natasa Males Ilic and dr. Aleksandar Atanaskovic for their useful suggestions concerning the rat-race coupler modelling.

## REFERENCES

[1] V. Milosevic, B. Jokanovic, O. Boric-Lubecke, V. M. Lubecke, ñKey Microwave and Millimeter Wave Technologies for 5G Radio,ò in *Powering the Internet of Things with 5G Networks*, V. Mohanan, R. Budiatru, I. Aldmour, Eds. IGI Global, July 2017,

[2] Y. Chang, Y. Jiao, L. Zhang, G. Chen and X. Qiu, "A K-band series-fed microstip array antenna with low sidelobe for anticollision radar application," 2017 Sixth Asia-Pacific Conference on Antennas and Propagation (APCAP), pp. 1-3, 2017.

[3] S. J. Chen, W. Withayachumnankul, Y. Monnai and C. Fumeaux, "Linear Series-Fed Patch Array with Dual Circular Polarization or Arbitrary Linear Polarization," 2019 International Conference on Electromagnetics in Advanced Applications (ICEAA), pp. 0365-0369, 2019.

[4] D.. Guan, C. Ding, Z. Qian, Y. Zhang, W. Cao and E. Dutkiewicz, "An SIW-Based Large-Scale Corporate-Feed Array Antenna," in *IEEE Transactions on Antennas and Propagation*, vol. 63, no. 7, pp. 2969-2976, July 2015.

[5] A. G. Toshev, "Synthesized shaped beam flat array antenna for digital beam-forming radar applications, utilizing printed technology," 2017 IEEE International Conference on Microwaves, Antennas, Communications and Electronic Systems (COMCAS), pp. 1-4, 2017.

[6] W. Hong, K. Baek, S. Ko ñMillimeter-Wave 5G Antennas for Smartphones: Overview and Experimental Demonstrationò, *IEEE Trans. Antennas Propag.*, vol. 65, no. 12, pp. 6250 ï 6261, December 2017.

[7] M. MilijiÍ, B. JokanoviÍ,ò High-gain Slot Antenna Arrays for 5G and Radar Applicationsò, 2019 27th Telecommunications Forum (TELFOR), Belgrade, Serbia, pp. 381-384, November, 26-27, 2019.

[8] M. Milijic, B. Jokanovic, ñAdvanced High-Gain Slot Antenna Arrays for 5G and Radar Applicationsò, Telfor Journal, Vol.13 No.1 (2021), pp. 29-34.

[9] M. Milijic, B. Jokanovic, L. Lazovic, ñComparative Analysis of K-band Crossed Slot and Crossed Dipole Antennasò, 15th Intern. Conf. TELSIKS, Nis, Serbia, pp. 9-12, October 20-22, 2021.

[10] WIPL-D Pro CAD 2020.

[11] A. Omar, N. Dib and A. AlBdrashiny, "Miniaturized CPW Rat-Race Coupler Using the Superformula," 2018 18th Intern. Sym. on Antenna Technology and Applied Electromagnetics (ANTEM) ,pp. 1-2, 2018.

 ISBN 978-86-7466-930-3

# Cost-Effective Standing Wave Ratio Meter

Ana Đ. Ćupurdija, *Member, IEEE*, and Slobodan V. Savić, *Member, IEEE*

***Abstract*—This paper presents a cost-effective and compact realization of a standing wave ratio (SWR) meter designed with commercially available low-cost components. The SWR meter was tested by measuring voltage standing wave (VSW) and complex impedance with slotted coaxial transmission line, and both results were in good agreement with the simulated circuit results and measurements done on professional equipment - HP SWR meter and vector network analyzer (VNA). The proposed system presents an affordable and precise SWR meter, but also a valuable educational platform for understanding electromagnetic field distribution along transmission lines.**

***Index Terms*—complex impedance; electromagnetic waves; measuring instruments; slotted coaxial transmission line; standing wave ratio.**

## I. Introduction

SINCE their discovery, electromagnetic (EM) waves never lost their significance and the functionality of many modern devices would be unimaginable without them. These devices include mobile phones, laptops, wireless devices, radar systems, etc. Bluetooth and the internet would not exist were it not for EM waves. Therefore, today they represent an irreplaceable means for information transmission and a physical phenomenon whose number of applications will only increase in the future [1].

However, when propagating through different mediums (air, water, dielectrics, ionosphere, etc.) or when guided with different guiding-structures (transmission lines or waveguides), EM waves form certain patterns [2] that are not always quite intuitive and can be hard to visualize, even for an experienced RF engineer. An excellent starting point for analyzing this phenomenon is the graphical representation of standing waves along transmission lines (TLs).

To provide a way for students to better understand the concepts of electromagnetic field distribution, we have designed and realized a compact and affordable standing wave ratio (SWR) meter. This prototype, along with slotted coaxial TL, presents a working principle of SWR measurements in a simple and easy-to-understand manner and also provides relatively precise measuring equipment.

The rest of the paper is organized as follows. In the second chapter, the theory of standing waves is briefly introduced, and the requirements for a functional SWR meter are discussed. In the third chapter, starting SWR meter model and its simulation results obtained via TINA simulator [3] are shown. In the fourth chapter, the design and realization of the SWR meter are presented, along with schematics and printed circuit board (PCB) layout. In the fifth chapter, voltage standing wave (VSW) measurements were done for a transmission line closed with different loads, and these results are compared with the results obtained with a professional SWR meter. In the sixth chapter, unknown load impedances are estimated from the SWR measurements and compared to the results obtained with AWR Design Environment [4] and vector network analyzer (VNA) measurements. Finally, in the seventh chapter, conclusions are drawn.

Ana Đ. Ćupurdija is with the School of Electrical Engineering, University of Belgrade, 73 Bulevar kralja Aleksandra, 11020 Belgrade, Serbia, and with the Vlatacom Institute of High Technologies, Milutin Milanković Blvd. 5, Belgrade, Serbia (e-mail: anacupurdija96@gmail.com).

Slobodan V. Savić is with the the School of Electrical Engineering, University of Belgrade, 73 Bulevar kralja Aleksandra, 11020 Belgrade, Serbia (e-mail: ssavic@etf.bg.ac.rs).

## II. Standing Waves Measurement Theory

Two-wire transmission line represents a pair of conductors carrying an EM wave. The theory of EM propagation along TLs is explained in detail in [2, 5].

When exciting a TL with a signal from a generator connected at its one end, voltage and current waves are formed along the TLs axis. In the steady state, when all excitations and all responses are single-frequency signals, on the transmission-line there are, generally, two waves traveling in opposite directions. These waves are progressive (traveling) waves, and their superposition forms the standing wave. The effective (rms) value of the standing wave is a function of the generator's power, the complex impedance of a load which ends TL on the other end, the characteristic impedance of the TL, and it (generally) changes along the TLs axis. When the TL is opened on its other end, all of the incident power is reflected from the open end. When the TL is ended with a lossy load, some of the excited power is dissipated in the load, making the reflected wave have less energy than the incident wave.

The parameter that integrally describes standing wave is SWR, defined as

$$SWR = \frac{U_{\max}}{U_{\min}}, \tag{1}$$

where $U_{\max}$ and $U_{\min}$ are the maximum and the minimum effective value of the VSW along TL's axis, respectively. The standing wave ratio can be in the range $[1, \infty)$. If SWR equals one, the load is matched to the TL, and there is no reflection. If SWR tends to infinity, all the energy of the incident wave is reflected.

One way to measure SWR is to use slotted coaxial TL and measure EM field or voltage along TL's slot with a short probe. The probe should be long enough to detect high enough voltage, and short enough not to (locally disturb) the

 ISBN 978-86-7466-930-3

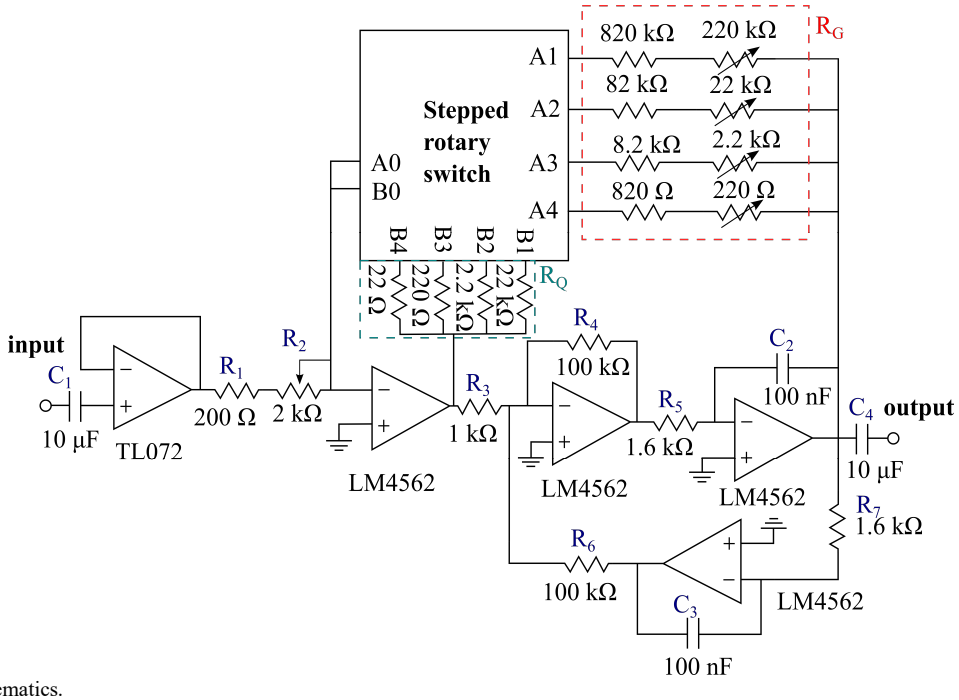


Fig. 1. SWR meter schematics.

EM field. The voltage measured with this probe is proportional to the electric field in the slotted coaxial TL and is connected to the square-law diode detector [6]. This diode is usually a germanium diode, which works in the quadrature region of the I-V (current-voltage) characteristics. Therefore, the signal obtained with this diode detector is proportional to the square of the VSW effective value. This signal is then further processed by the SWR meter. Keeping all of this in mind, we can define SWR meter functionalities and parameters of interest. Also, please note that in the measurement set up that we are using, shown in Fig. 5, incident voltage (field) is modulated with a signal of a fixed, preferably low, frequency (i.e., around 1 kHz), that represents an envelope of the high-frequency signal that form the standing wave. The incident signal is amplitude modulated because when working with an unmodulated signal, the output of the diode detector would be a DC voltage which is generally susceptible to high measurement errors due to the existence of the DC offset in systems. Since the amplitudes of the measured unmodulated signal are relatively small (about 1 mV), even a small DC offset could introduce significant measurement errors. By measuring the effective value of the detected 1 kHz envelope, the effective value of the high-frequency signal could also be measured. Expected values for the signals at the output of the probe are in the range 1-10 mV, so the designed SWR meter should have a significant gain. Based on all of this, we decided to design the SWR meter as an active bandpass filter, with the center frequency around 1 kHz. The proposed design has four gain stages (times 1, 10, 100, and 1000), while also having an option to fine-tune gain to any value in these ranges. Finally, the Q factor of the filter needs to be set accordingly, so the circuit can filter unwanted harmonics and harmonic components, but also not be too selective. The Q factor needs to be independent of the set gain, and the gain and the Q factor of the system should be independent of impedances connected at its input and output.

## III. Simulation Results

The main part of the circuit (bandpass active filter) was designed starting from [7] and by using the operational amplifier LM4562. This chip is made by Texas Instruments, so simulation of the circuit was done in their TINA simulator [4]. The schematics used for simulation are shown in Fig. 1, while omitting the stepped rotary switch. This schematic is the main building block for the SWR meter.

The circuit shown in Fig. 1 is excited with an AC generator at 1 kHz. The gain is set with resistors $R_1, R_2$ and $R_G$, and is given by the formula

$$G = \frac{R_G}{R_1 + R_2}. \tag{2}$$

The Q factor is set with the resistors $R_G$ and $R_Q$, given by the formula

$$Q = \frac{R_G}{R_Q}. \tag{3}$$

In the mentioned configuration, without the stepped rotary switch, the Q factor depends on the gain (since they have a common factor of the resistor $R_G$). This is not a desirable feature, hence, stepped rotary switch was introduced in the PCB design step. The circuit is intended to operate in a single-frequency mode, just like the professional HP SWR

 ISBN 978-86-7466-930-3

meter, which is used for comparison. This central bandpass frequency is set with capacitor $C_2$ and resistor $R_5$ (aka $C_3$ and $R_7$), given with the formula

$$f_c = \frac{1}{2\pi R_5 C_2} \tag{4}$$

Simulation results are shown in Table I, for four gain configurations. The resistor $R_Q$ was changed along with $R_G$, so that the Q factor is constant, and is set to be around $Q = 45$. These results confirmed that the designed circuit works as expected, so we proceeded with the board design and fabrication.

TABLE I
GAIN SIMULATION RESULTS

| Resistor $R_G$ | 1 kΩ | 10 kΩ | 100 kΩ | 1 MΩ |
|---|---|---|---|---|
| Theoretical gain | 1 | 10 | 100 | 1000 |
| Simulated gain | 1.13 | 10.13 | 100.12 | 993.76 |

## IV. SWR METER PROTOTYPE

Based on the schematics in Fig. 1, PCB layout was made and is shown in Fig. 2. The purpose of the buffer at the input stage is to make the input impedance of the circuit independent from the gain and Q factor. The output stage of the meter is not buffered. When the output current is below the maximum value stated in the datasheet (26 mA), practically there is no distortion in the output voltage. In order not to exceed the current limit, in the worst case scenario for output voltage of 1 V, the load impedance must be greater than 40 Ω, which is well below input impedances for all commercial multimeters.

The resistor $R_2$ is a potentiometer, so the gain can be fine-tuned to any value in the predefined ranges. Predefined ranges of 1, 10, 100, and 1000 are set using the stepped rotary switch, with three pins and four positions. This switch changes the resistors used for setting the gain ($R_G$ in Fig. 1). Also, using this switch, the resistors used for setting the Q factor are simultaneously switched when setting the gain, so the Q factor would stay constant when the resistor $R_G$ changes. For the measurements shown in Section V, the Q factor is set around $Q = 45$.

The branches with resistors used for gain setting contain one fixed resistor and one trimmer potentiometer. This way, even with component tolerances, the gain can be fine-tuned to exactly match the predefined values (1, 10, 100, and 1000). The made prototype has its stage for power supply (converting the AC voltage of 230V into ±5 V DC needed for the operational amplifiers) and also has added overcurrent protection, in a form of a fuse.

The final prototype is shown in Figs. 3 and 4, where it can be seen that the final prototype is compact and practical to use. With this design, we satisfied all of our requirements for a functional SWR meter, so we proceeded with the measurements.

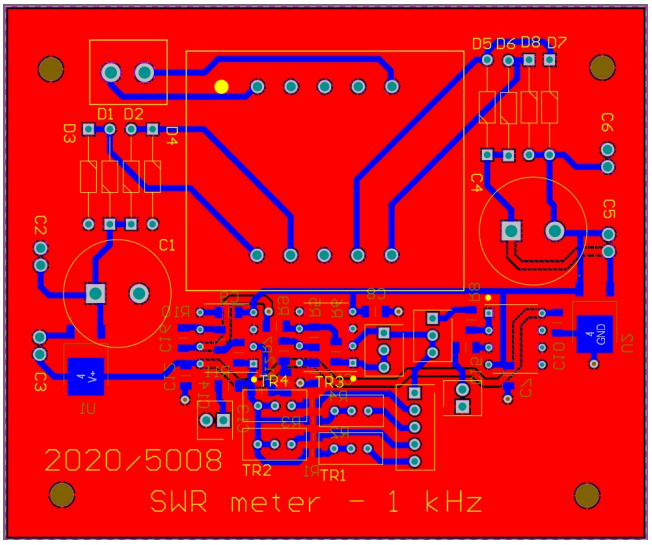


Fig. 2. Printed circuit board layout of the SWR meter.

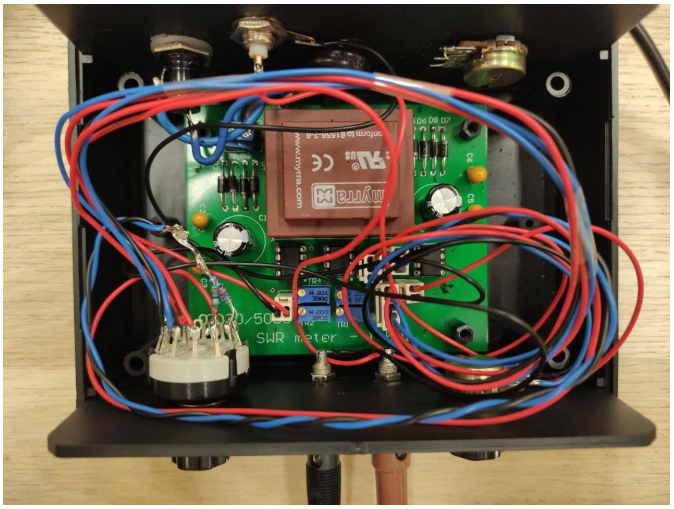

Fig. 3. The prototype of the SWR meter.

## V. MEASUREMENTS ON A SLOTTED COAXIAL TRANSMISSION LINE

The first measurement to test the functionality of the SWR meter was made with an oscilloscope, where the input and the output voltages are observed to set the desired gain to 1, 10, 100, and 1000 with trimmer resistors. The effective value of input voltage is set so that the output can be easily visible on the oscilloscope for a given measurement, but also to prevent the operational amplifiers from entering the saturation. The gain was then fine-tuned to the wanted values with trimmer resistors.

After setting the gains to the desired values, measurements on the TL were done. The used TL is a slotted coaxial TL having $Z_c = 50\ \Omega$ characteristic impedance with a probe that could be moved longitudinally along TL's axis. This way the effective value of VSW is measured along TL's axis. The slotted TL we are using has a ruler along its axis, so we will use this ruler for measuring distance along TL's axis. The probe position is controlled with a mechanical knob. The line was excited with a sine wave at 1.4 GHz, modulated with a sine at 900 Hz. This signal was generated by a


ISBN 978-86-7466-930-3

software-defined radio (SDR) device. The frequency of the envelope at 900 Hz was chosen because, due to the component tolerances, the central frequency of the filter was not exactly 1 kHz. Central frequency was determined by changing the envelope frequency and observing when the maximal gain occurs.

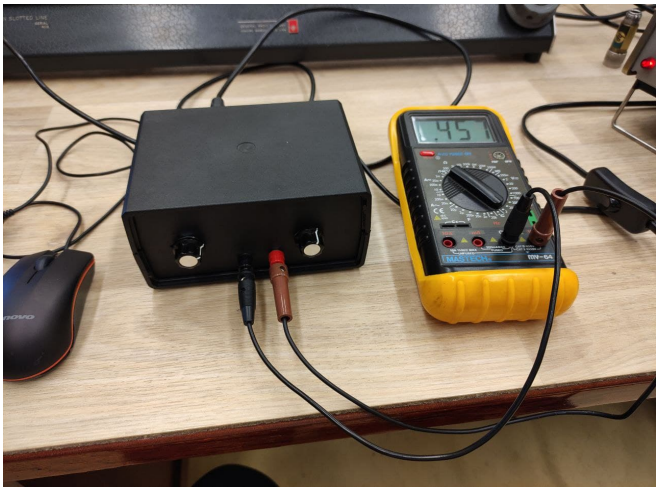

Fig. 4. The prototype of the SWR meter is enclosed in a box and connected to the voltmeter.

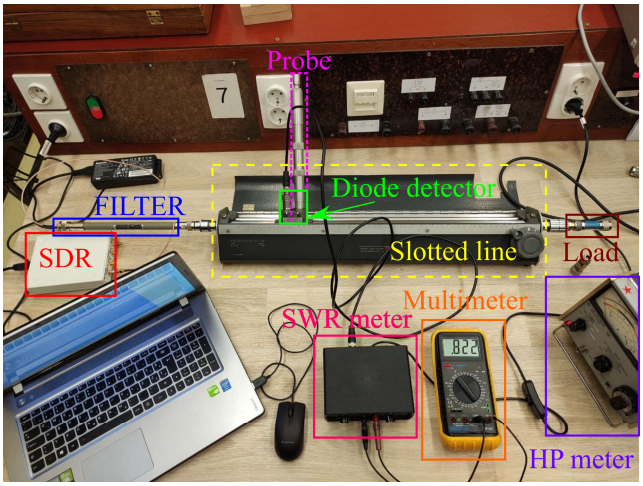


Fig. 5. Complete measurement setup.

To suppress any unwanted signal, at the input of the TL, a coaxial filter was placed, with a cut-off frequency at 2.2 GHz. The effective value of the output voltage of the realized SWR meter is measured with a multimeter, as shown in Figs. 4 and 5. The measurements were done by moving the probe in steps of 5 mm and measuring the VSW effective value in 81 data points. The measurements were done in the distance range from 15 cm to 55 cm at the TL ruler. The same procedure was done when TL was opened at its other end, and when it was terminated with the 6 dB and with the 10 dB loads. These loads are realized as coaxial (6 dB and 10 dB) attenuators, opened at their second end. The SWR meter gain for the measurements is set so that the peak of the VSW corresponds to the effective value of 1 V measured with the multimeter.

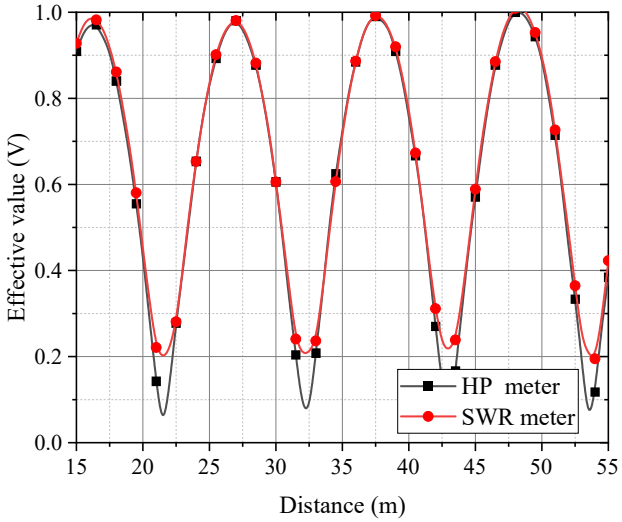


Fig. 6. Comparison of the VSW measurement obtained with designed and professional SWR meter for open-ended transmission line.

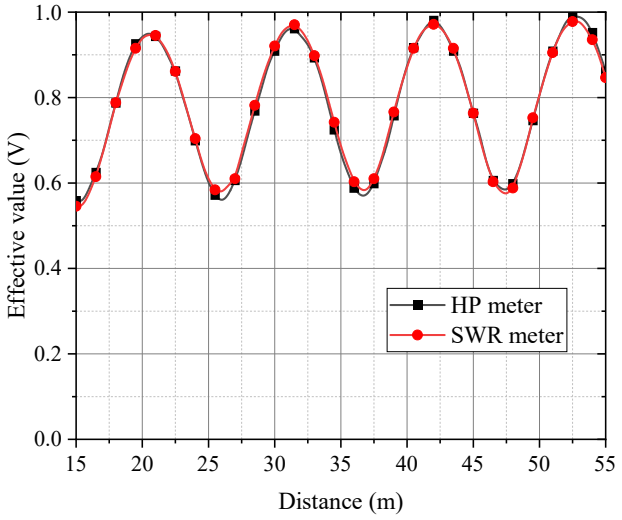


Fig. 7. Comparison of the VSW measurement obtained with designed and professional SWR meter when the transmission line is closed with the 6 dB load.

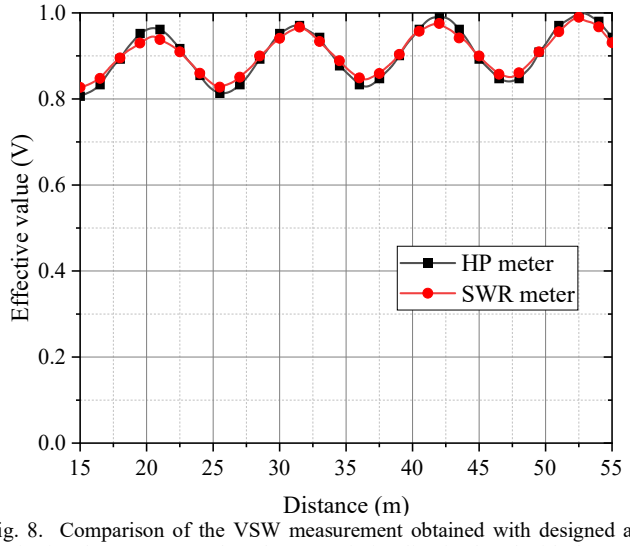


Fig. 8. Comparison of the VSW measurement obtained with designed and professional SWR meter when the transmission line is closed with the 10 dB load.


ISBN 978-86-7466-930-3

For the obtained results to be double-checked, the same set of measurements was done with the professional Hewlett-Packard 415E SWR meter. The entire measurement setup is shown in Fig. 5. The obtained VSW curves for the case of the unloaded TL are shown in Fig. 6, while the obtained curves for cases of 6 dB and 10 dB loads are shown in Figs. 7 and 8, respectively. In the case of the unloaded line, the proposed SWR meter does not have such deep minimums as the professional one. Additionally, for this case, VSW should be equal to zero at its minimum. This is not being the case in Fig. 6 due to, among other, finite number of measuring points along TL's axis. Nevertheless, these two sets of results are in good agreement, and even better when TL is closed with loads (Figs. 7 and 8).

## VI. Load Impedance Calculation

The impedances of used loads (6 dB and 10 dB) are firstly estimated based on the fact that these loads are matched coaxial attenuators opened at their second end. Based on this, a simple model for the calculation of their input impedance is assembled in the AWR Design Environment, as shown in Fig. 9. The load which complex impedance we want to measure, labeled as "LOAD" at Fig. 5, is modeled as two short TLs with ideal (matched) attenuator between them. The same model is used for 10 dB load, with a loss parameter of the ATTEN element from Fig. 9 set to 10 dB. The length of used short TLs is estimated experimentally.

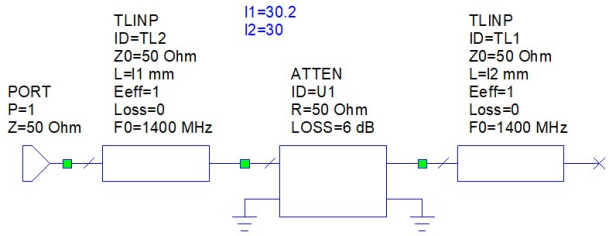


Fig. 9. The simple model of used loads made in the AWR Design Environment.

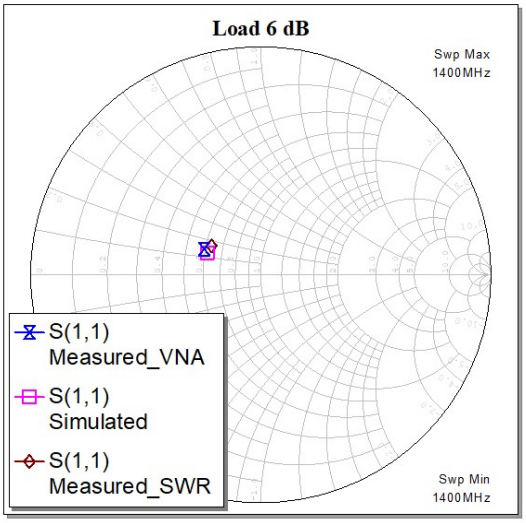


Fig. 10. Smith chart for the 6 dB load.

From the given SWR measurements, using the Smith diagram, load impedances are calculated as described in [5, 8] and compared to the impedances of the loads obtained via simulation and via measurements done on the N5227a Agilent VNA. The results are shown in Figs. 10 and 11 for 6 dB and 10 dB loads, respectively. From these figures, it can be noticed that the obtained results of the load impedances are in excellent agreement for all three sets of results. Therefore, we conclude that the designed SWR meter can be used for the precise determination of unknown impedances.

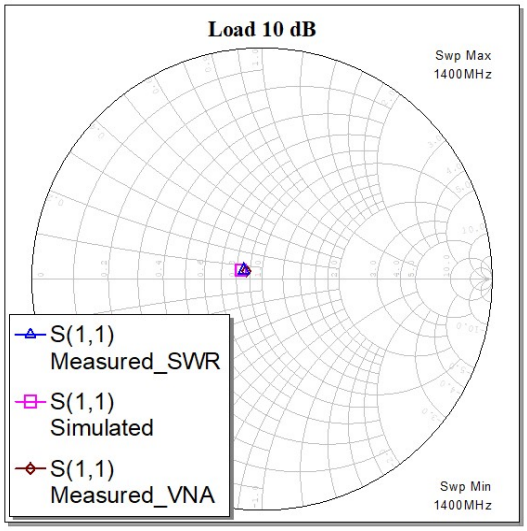


Fig. 11. Smith chart for the 10 dB load.

## VII. Conclusion

A compact and affordable prototype for the SWR meter was proposed and realized. Simulation and measurement results are proven to fit well. The realized circuit acts as an active filter with four gain stages (1, 10, 100, and 1000), and the gain can also be fine-tuned to any value in these ranges.

Standing wave ratio measurements were done on a slotted coaxial transmission line for two different loads, and measurements obtained with the designed SWR meter are compared to those obtained with the professional HP SWR. These two sets of measurements are in good agreement. From the measured standing wave curves, load impedances are calculated and they are in excellent agreement with the results obtained with AWR Design Environment and professional VNA.

The realized device can be used to better understand and visualize the EM waves distribution on TLs but also could be a usable piece of equipment for microwave laboratories which is a good alternative to much more expensive professional equipment. Further improvements would include adding a tunable Q factor functionality to the device. This will be part of the authors' further efforts.

## Acknowledgment

The authors acknowledge funding provided by the School of Electrical Engineering, University of Belgrade, through the grants by the Ministry of Education, Science, and Technological Development of the Republic of Serbia, and Vlatacom Institute, through project "The Development of Over-the-Horizon Radar in HF band HF-OTHR2".

 ISBN 978-86-7466-930-3

## REFERENCES


[1] R. K. Amineh, "Applications of Electromagnetic Waves: Present and Future," *Electronics,* vol. 9, no. 5, pp. 808-811, May 2020.

[2] R. E. Collin, *Field Theory of Guided Waves*, 2 ed. New York: Wiley-IEEE Press, 1991.

[3] TINA Simulator v9.3. Texas Instruments, https://www.ti.com/tool/TINA-TI.

[4] AWR Design Environment Cadence, https://www.cadence.com/en_US/home/tools/system-analysis/rf-microwave-design/awr-design-environment-platform.html.

[5] A. R. Đorđević and D. V. Tošić, *Microwave Technique (in Serbian)*. Belgrade, Serbia: Academic Mind, 2010.

[6] J. B. Hagen, *Radio-Frequency Electronics: Circuits and Applications*. New York, USA: Cambridge University Press, 2009.

[7] A. Devices, "LT1814 datasheet," Available: https://www.analog.com/en/products/lt1814.html.

[8] M. Golio and J. Golio, *RF and Microwave Circuits, Measurements, and Modeling*. Florida, USA: CRC Press, 2018.


 ISBN 978-86-7466-930-3

# Automatizacija određivanja nivoa EM polja radio-difuznih predajnika na osnovu ITU-R P.1546 metode za visine $h_1$ manje od 10 m

Miloš Radojković, Zlatica Marinković, *Senior Member, IEEE*

***Apstrakt*—U ovom radu predložen je metod za određivanje nivoa EM polja iz preporuke ITU R-1546 za očekivani nivo elektromagnetnog polja koji potiče od radiodifuznih predajnika i visine $h_1$ manje od 10 metara. Predloženi metod je baziran na primeni veštačkih neuronskih mreža i omogućava efikasno određivanje nivoa polja za frekvencije do 4000MHz i visine $h_1$ manje od 10 metara. Tačnost metoda prikazana je na primerima krivih koje se odnose na frekvencije i vrednosti $h_1$ koji nisu korišćene u procesu obučavanja neuronske mreže.**

***Ključne reči*—ITU-R P.1546, nivo elektromagnetnog polja, radio-difuzni predajnik, veštačke neuronske mreže.**

## I. Uvod

Radiodifuzne komunikacije su komunikacije tipa tačka-oblast i njihova primena je veoma česta (radio i televizijski predajnici, bazne stanice mobilnih sistema i sl.). Jedan od nezaobilaznih koraka prilikom projektovanja radiodifuznog sistema jeste određivanje zone pokrivanja. Zona pokrivanja predstavlja oblast u kojoj je nivo elektromagnetnog (EM) polja veći od vrednosti definisane zahtevima razmatranog sistema i određen je daljinom od predajnika na kojoj je nivo EM polja veći od zadate vrednosti.

Zona pokrivanja je određena u nekoliko pravaca – azimuta (obično 36 pravaca sa korakom od po 10˚ ili 120 pravaca sa korakom od po 3˚, što zavisi od jačine predajnika). Postoje različite metode za određivanje zone pokrivanja. Najčešće se koristi statistički metod definisan u preporuci ITU-R P.1546 [1]. Preporuka ITU-R P.1546 daje postupak određivanja nivoa polja za zemaljske radio-difuzne servise u frekvencijskom opsegu od 30 MHz do 4000 MHz. Preporuka se bazira na empirijskim krivama (dostupnih i tabelarno) za zavisnost očekivanog nivoa polja od rastojanja za različite vrednosti parametra koji opisuje karakteristike terena. Imajući u vidu da je preporuka data za fiksne vrednosti frekvencija, visine $h_1$ i daljine $d$, ukoliko je potrebno izvršiti proračun EM polja za vrednosti koje nisu date u preporuci ITU-R P.1546 potrebno je izvršiti veliki broj interpolacija.

U ovom radu je predložen je metod za očitavanje krivih za očekivani nivo EM polja baziran na veštačkim neuronskim mrežama. Veštačke neuronske mreže su izabrane zahvaljujući njihovim odličnim interpolacionim sposobnostima, zbog čega su i široko primenjene u oblasti mikrotalasa [2]-[11]. Neuronske mreže su već primenjivane za očitavanje krivih za očekivani nivo polja po pomenutoj preporuci i ranijim verzijama [2]-[6], a u ovom radu se po prvi put neuronske mreže primenjuju za očitavanje vrednosti nivoa EM polja za visine $h_1$ manje od 10 metara.

U Sekciji II najpre je kratko opisan postupak određivanja nivoa polja na osnovu preporuke ITU-R P-1546. Predloženi model za očitavanje krivih za vrednosti $h_1$ manje od 10 metara objašnjen je u Sekciji III. Dobijeni rezultati primenom razvijenog modela prikazani su u Sekciji IV. Izvedeni zaključci dati su u Sekciji V.

## II. Preporuka ITU-R P-1546

Preporuka ITU-R P.1546 se zasniva na familiji krivih koje su date kao očekivane vrednosti intenziteta polja u dBμV/m na visini 10m iznad tla (usvojena prosečna visina prijemne antene za radio-difuzni prijemnik), za signal emitovan predajnikom snage 1 kW izračen pomoću polutalasnog dipola (dobitak 0 dBd), u funkciji rastojanja.

Krive su date posebno za kopno i posebno za more, a u preporuci je opisan i način proračuna u slučaju kombinovanog terena. Za oba tipa sredine date su krive očekvanog intenziteta polja za frekvencije 100 MHz, 600 MHz i 2000 MHz i to za 50%, 10% i 1% vremena i za 50% lokacija u oblasti površine 500×500 m$^2$. Kao primer na Sl. 1 prikazane su krive za očekivani intenzitet polja na frekvenciji 2000 MHz za kopno. Parametar na krivama je vrednost EM polja u dBμV/m za visine $h_1$ u rasponu od 10 do 1200 m (diskretne vrednosti 10 m, 20 m, 37.5 m, 75 m, 150 m, 300 m, 600 m i 1200 m) i daljine $d$ do 1000 km. Parametar $h_1$ je za rastojanja od predajnika veća od 15 km jednak efektivnoj visini terena $h_{eff}$ (visinska razlika između visine centra antene u odnosu na nivo mora i srednje nadmorske visine na rastojanju od 3 km do 15 km od predajnika). Za rastojanja $d$ manja od 15 km, parametar $h_1$ predstavlja visinsku razliku između visine centra antene u odnosu na nivo mora i srednje nadmorske visine na rastojanju od $0.2d$ do $d$ od predajnika. U slučaju da je poznata samo efektivna visina antene, a ne i detaljne informacije o terenu, za rastojanja do 3 km parametar $h_1$ je jednak visini antene iznad tla $h_a$. Za rastojanja veća od 3km za određivanje visine $h_1$ koristi se sledeći izraz:

$$h_1 = h_a + \frac{(h_{eff} - h_a)(d-3)}{12}. \quad (1)$$

Imajući u vidu da su krive date za diskretne vrednosti $h_1$, prilikom proračuna neophodno je vršiti interpolaciju za konkretnu vrednost $h_1$ na sledeći način:

Miloš Radojković – Energoprojekt Entel, Bulevar Mihajla Pupina 12, Beograd 11070, Srbija (e-mail: milosradojkovic89@gmail.com).

Zlatica Marinković - Elektronski fakultet u Nišu, Univerzitet u Nišu, Aleksandra Medvedeva 14, 18000 Niš, Srbija (e-mail: zlatica.marinkovic@elfak.ni.ac.rs).

 ISBN 978-86-7466-930-3

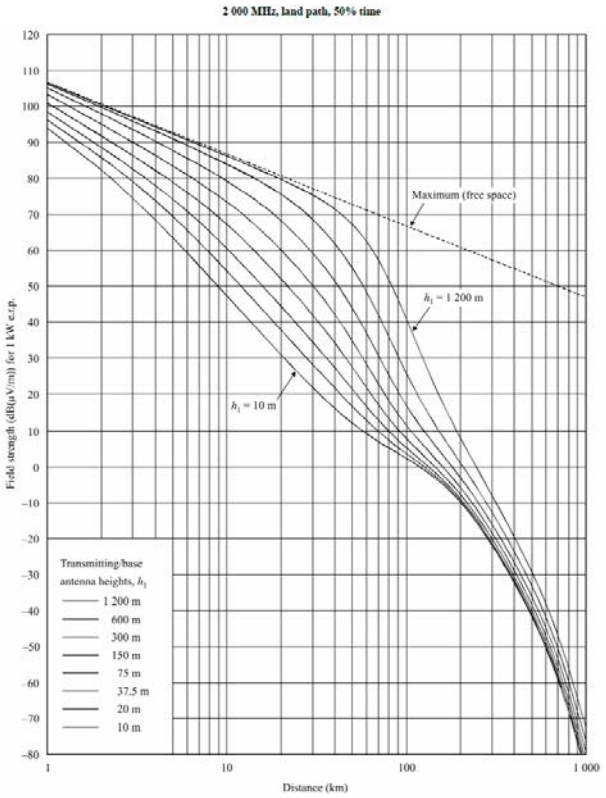


Sl. 1. Krive za očekivani intenzitet polja na 2000 MHz za kopno po preporuci ITU-R P-1456.

$$E_o = E_{\inf} + (E_{\sup} - E_{\inf})\frac{\log(h_1 / h_{\inf})}{\log(h_{\sup} / h_{\inf})} \quad (2)$$

gde je: $E_{inf}$ nivo polja za zadato rastojanje očitano sa krive koja se odnosi na prvu manju tabelarnu vrednost visine $h_1$, $h_{inf}$, a $E_{sup}$ nivo polja za zadato rastojanje očitano sa krive koja se odnosi na prvu veću tabelarnu vrednost visine $h_1$, $h_{sup}$.

Za određivanje nivoa polja na proizvoljnom rastojanju $d$, (u opsegu od 1km do 1000km) koristi se sledeći izraz

$$E_o = E_{\inf} + (E_{\sup} - E_{\inf})\frac{\log(d / d_{\inf})}{\log(d_{\sup} / d_{\inf})} \quad (3)$$

gde je $E_{inf}$ očitana vrednost polja za $d_{inf}$, prvu tabuliranu vrednost rastojanja manju od $d$, $E_{sup}$ očitana vrednost polja za $d_{sup}$, prvu tabuliranu vrednost rastojanja veću od $d$.

Dalje, ukoliko se frekvencija za koju se vrši proračun ne poklapa sa jednom od vrednosti 100 MHz, 600 MHz i 2000 MHz, potrebno je izvršiti interpolaciju:

$$E_o = E_{\inf} + (E_{\sup} - E_{\inf})\frac{\log(f / f_{\inf})}{\log(f_{\sup} / f_{\inf})} \quad (4)$$

gde su: $f_{inf}$ prva tabulirana vrednost frekvencije manje od $f$ (100 MHz ako je $f$ < 600 MHz, u ostalim slučajevima 600 MHz), $f_{sup}$ prva tabulirana vrednost frekvencije veće od $f$ (600 MHz ako je $f$ < 600 MHz, u ostalim slučajevima 2000 MHz), $E_{inf}$ očitana vrednost polja za $f_{inf}$ i $E_{sup}$ očitana vrednost polja za $f_{sup}$.

Kao što se može primetiti sa Sl.1, minimalna vrednost $h_1$ za koje su date vrednosti EM polja je 10 m. Vrednosti EM polja za visine između 0 m i 10 m nisu tabulirane i jednačina (2) se ne može koristiti za proračun nivoa EM polja. Za proračun nivoa EM polja za vrednosti $h_1$ u opsegu od 0 do 10 m koristi se sledeći izraz:

$$E[dB\mu V/m] = E_{zero} + 0.1h_1(E_{10} - E_{zero}) \quad (5)$$

gde su:

$$E_{zero}[dB\mu V/m] = E_{10} + 0.5(C_{1020} + C_{h1neg10}), \quad (5a)$$

$$C_{1020}[dB] = E_{10} + E_{20}\ \text{dB} \quad (5b)$$

$C_{h1neg10}$ je korekcija $C_{h1}$ u dB izračunata korišćenjem sledećeg izraza:

$$C_{h1} = 6.03 - J(v)\ \text{dB} \quad (6)$$

gde je

$$J(v) = \left[6.9 + 20\log\left(\sqrt{(v-0.1)^2 + 1} + v - 0.1\right)\right], v > -0.7806 \quad (6a)$$

$$v = K_v \Theta_{eff\,2} \quad (6b)$$

$$\Theta_{eff\,2} = \arctan(-h_1 / 9000) \quad (6c)$$

a $K_v$ konstanta koja ima sledeće vrednosti:

$K_v$ = 1.35 za 100 MHz,
$K_v$ = 3.31 za 600 MHz,
$K_v$ = 6.00 za 2000 MHz.

$E_{10} + E_{20}$ je jačina polja u dBμV/m izračunata prema jednačini (2) za traženu daljinu $d$ i visine $h_1$ = 10 m i $h_2$ = 20 m.

Preporuka ITU-R P.1546 se može koristiti za sisteme koji rade u opsegu od 30 MHz do 4000 MHz i gde visina $h_1$ ne prelazi 3000 m.

U realnim primerima se u najvećem broju slučajeva, sve tri veličine (parametar $h_1$, rastojanje i frekvencija) razlikuju od tabuliranih vrednosti, pa je potrebno vršiti višestruke interpolacije, posebno ako je visina $h_1$ manja od 10 metara. U sledećoj sekciji je predložen efikasni metod zasnovan na primeni veštačkih neuronskih mreža koji omogućava određivanje EM polja za zadatu daljinu i vrednosti $h_1$ u opsegu 0≤ $h_1$≤10 m.

## III. PREDLOŽENI METOD

U ovom radu predložena su dva metoda za određivanje nivoa EM polja za visine $h_1$ manje od 10 metara primenom veštačkih neuronskih mreža. Na Sl. 2 prikazan je neuronski model kojim se na osnovu frekvencije $f$, visine $h_1$ i daljine $d$ određuje nivo polja, odnosno koji modeluje zavisnost $E=f(f,h_1,d)$. Kako je na krivama za očekivani nivo polja u preporuci ITU-R P.1546 rastojanje prikazano na logaritamskoj skali razmatran je i model prikazan na Sl. 3 , koji kao ulaze ima frekvenciju $f$, visinu $h_1$ i daljinu u $d$ predstavljenu u logaritamskom formatu i nivo polja kao izlaz $E=f(f,h_1,\log d)$.


ISBN 978-86-7466-930-3

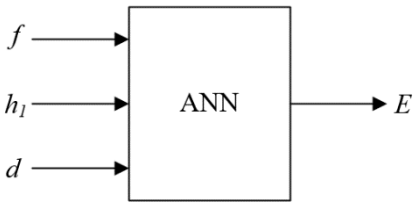


Sl. 2. Neuronski model za određivanje nivoa EM polja $E=f(f, h_1, d)$

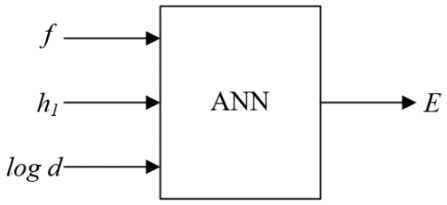


Sl. 3. Neuronski model za određivanje nivoa EM polja sa log $d$ na ulazu $E=f(f, h_1, log\ d)$

Modeli predstavljaju višeslojne neuronske mreže, koje se sastoje od osnovnih jedinica, neurona, grupisanih u slojeve (ulazni sloj, jedan ili više skrivenih slojeva i izlazni sloj). Broj ulaznih neurona je određen brojem ulaznih parametara, u konkretnom slučaju tri, a broj izlaznih neurona odgovara broju izlaznih parametara, u konkretnom slučaju jedan. Broj neurona u skrivenim slojevima nije moguće unapred odrediti, već se taj broj određuje u postupku učenja mreže. Neuronska mreža uči zavisnost između ulazno-izlaznih parametara primenom optimizacionih procedura, kojima se vrši optimizacija parametara mreže (težine veza između neurona i pragovi aktivacionih funkcija neurona), sa ciljem da odziv mreže bude što je moguće bliži željenoj zavisnosti između ulazno-izlaznih parametara.

Uspešno obučena mreža sposobna je da da korektan odziv ne samo za kombinacije ulaznih veličina koje su korišćene tokom procesa učenja mreže, već i za bilo koje vrednosti ulaznih veličina koje nisu korišćene tokom učenja ali su u opsegu veličina u kome su i trening vrednosti. Treba napomenuti da je model razvijen za ceo skup frekvencija na koje se može primeniti preporuka ITU-R P.1546, tj. frekvencije u opsegu od 30 MHz od 4000MHz.

## IV. Rezultati

Podaci za obučavanje neuronskih mreža prikazanih na Sl.2 i Sl.3 se odnose na 40 različitih frekvencija u opsegu od 100 MHz do 4000 MHz i korakom frekvencije od 100 MHz. U cilju provere da li broj i distribucija trening uzoraka u pogledu izabranih vrednosti $h_1$ utiče bitno na tačnost mreže razmatrana su dva dva skupa podataka koji se odnose na $h_1$={1, 3, 5, 7, 9 i 10}m i (trening skup 1) i $h_1$={1, 3, 6, 9, 10}m (trening skup 2). Svi podaci potrebni za obučavanje i testiranje mreže generisani su korišcenjem izraza (3), (4), (5-5b) i (6-6c). Tokom razvoja modela, veći broj mreža sa jednim ulaznim slojem, dva skrivena sloja i jednim izlaznim slojem je obučeno i testirano. U skrivenom sloju, korisćen je različit broj neurona kako bi se pronašao model sa što boljom tačnošću.

U ovom slučaju korišćene su neuronske mreže kod kojih skriveni neuroni imaju sigmoidnu transfer funkciju, a izlazni neuroni linearnu transfer funkciju. Ulazni neuroni imaju bafersku funkciju, pa je njihova funkcija jedinična linearna funkcija. Za obučavanje mreža primenjen je *Levenberg-Maquardt* algoritam [2]. Tačnost odziva mreže testirana je poređenjem odziva mreže i referentnih vrednosti. Takođe, vođeno je računa da ne dođe do preučenja mreže van referentnih tačaka, tj. da mreža ima dobru generalizaciju. Generalizacija se može proveravati testiranjem mreže za ulazne vrednosti koje nisu korišćene u toku učenja. Kako je u cilju što boljeg učenja mreže iskorišćen ceo skup referentnih podataka iz preporuke, provera da li je došlo do preučenosti vršena je vizuelno, tj. proverom odziva mreže kada su ulazne veličine menjane sa korakom koji je manji od koraka promene referentnih vrednosti kao i proračunom srednje greške (ATE - *Average Test Error*), maksimalne greške (WTE - *Worst Case Error*) i korelacionog koeficijenta *r*. Mreža je obučena i generisan u programskom paketu Matlab.

Nakon testiranja razvijenih modela, izabrani su najbolji modeli za oba predložena modela u slučaju obučavanja sa dva izabrana trening skupa. Za testiranje generalizacije korišćen je test skup koji se odnosi na vrednosti koje nisu korišćenje tokom obuke, a odnosi se na vrednosti frekvencije i visine koje su u opsegu veličina kao i vrednosti korišćene tokom obučavanja ($f$=150MHz, $h_1$=2m; $f$=450MHz, $h_1$=4m; $f$=850MHz, $h_1$=6m; $f$=1450MHz, $h_1$=8m; $f$=1850MHz, $h_1$=2m; $f$=2350MHz, $h_1$=4m; $f$=3350MHz, $h_1$=6m; $f$=3850MHz, $h_1$=8m).

Rezultati testiranja najboljih modela prikazani su u Tabeli I. Može se uočiti da su srednje greške u svim razmatranim slučajevima manje od 0.15%, dok je maksimalna greška manja od 1.5%. Korelacioni koeficijent je veoma blizu jedinici, što takođe potvrđuje visoku tačnost modelovanja.

Kao najbolji model za određivanje rastojanja za zadati nivo EM polja izabrana je mreža prikazana na Sl. 3 - $E=f(f, h_1, log\ d)$, sa dva skrivena sloja (10 neurona u prvom sloju i 12 neurona u drugom sloju i za koju su korišćeni podaci za obučavanje koji se odnose na visine {1, 3, 5, 7, 9, 10} metara.

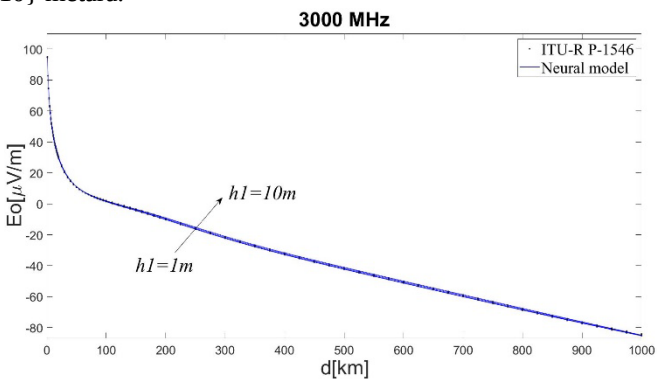


Sl. 4. Poređenje vrednosti EM polja generisanih pomoću razvijenog neuronskog modela i referentnih vrednosti iz preporuke ITU-R P1546.

Na Sl. 4 se može videti tačnost modela. Prikazane su krive za nivo polja generisane pomoću neuronske mreže (linije) za parametar visine $h_1$={1, 3, 5, 7, 9, 10} metara i referentne vrednosti određene preporukom (prikazane simbolima).

Može se uočiti da odziv mreže tj. vrednosti generisane pomoću neuronskog modela veoma dobro prate referentne vrednosti što potvrđuje da je postignuta zadovoljavajuća tačnost modelovanja.

Kao dodatna ilustracija tačnosti modela $E=f(f, h_1, log\ d)$, na Sl. 5 prikazane su krive koje se odnose na test skup. Sa

 ISBN 978-86-7466-930-3

Sl.5 se može primetiti da su vrednosti generisane pomoću neuronskog modela veoma blizu referentnim vrednostima prema preporuci ITU-R P1546. Kako bi se bolje prikazali rezultati krive za daljine do 20 km, na Sl. 6 se može videti uvećani prikaz krivih do 20 km.

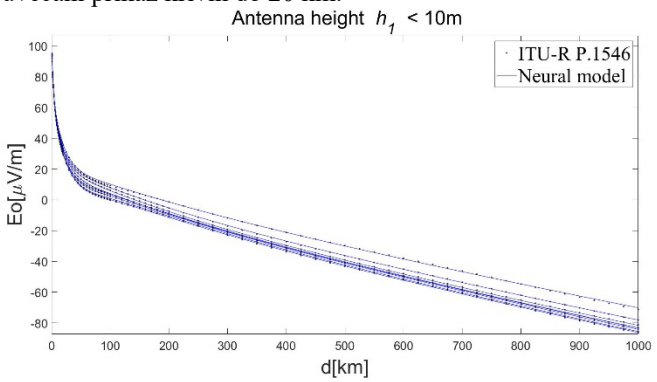


Sl. 5. Poređenje vrednosti EM polja generisanih pomoću razvijenog neuronskog modela i referentnih vrednosti iz preporuke ITU-R P1546 za vrednosti koje nisu korišćene u obučavanju mreže

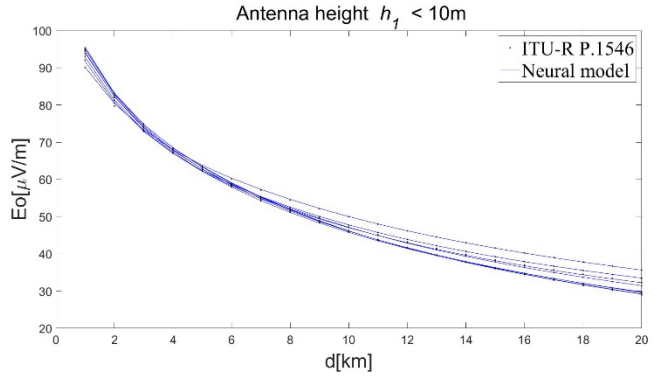


Sl. 6. Poređenje vrednosti EM polja generisanih pomoću razvijenog neuronskog modela i referentnih vrednosti iz preporuke ITU-R P1546 za vrednosti koje nisu korišćene u obučavanju mreže (daljina do 20 km)

TABELA I
TEST STATISTIKA ZA TRENING I TEST SKUP

| | ATE[%] | WCE [%] | *r* |
|---|---|---|---|
| *E=f(f, h*$_1$*, d); trening skup 1* $h_1$={1,3,5,7,9,10} m | | | |
| treninig skup 1 | 0.10 | 1.47 | 0.999979 |
| test skup | 0.10 | 0.79 | 0.99998 |
| *E=f(f, h*$_1$*, d); trening skup 2* $h_1$={1,3,6,9,10} m | | | |
| treninig skup 2 | 0.10 | 1.03 | 0.99998 |
| test skup | 0.11 | 0.89 | 0.999976 |
| *E=f(f, h*$_1$*, log d); trening skup 1* $h_1$={1,3,5,7,9,10} m | | | |
| treninig skup 1 | 0.11 | 1.39 | 0.999978 |
| test skup | 0.11 | 0.55 | 0.999981 |
| *E=f(f, h*$_1$*, log d); trening skup 2* $h_1$={1,3,6,9,10} m | | | |
| treninig skup 2 | 0.11 | 0.94 | 0.999982 |
| test skup | 0.14 | 0.65 | 0.999971 |

## V. ZAKLJUČAK

Kao što se može videti u Sekciji II, ukoliko se određuje nivo EM polja za vrednosti parametara $h_1$, *f* i *d*, potrebno je izvršiti veliki broj interpolacija. Predloženi metod baziran na neuronskoj mreži omogućava automatizaciju procesa intepolacija i trenutnog izračunavanja EM polja nalaženjem odziva neuronske mreže. Kako se svaka neuronska mreža može opisati pomoću skupa jednačina baziranih na linearnim i eksponencijalnim funkcijama, izračunavanje EM polja pomoću razvijene neuronske mreže nije kompleksno, a može se vršiti u bilo kom programskom okruženju.

Prikazani metod određivanja EM polja može biti korišćen kao efikasan alat za određivanje zone pokrivanja predajnika korišćenjem statističke metode definisane preporukom ITU-R P.1546. Cilj budućih istraživanja je da se razvije neuronski model za inverzno očitavanje krivih za visine $h_1$ manje od 10 m.

## ZAHVALNICA

Istraživanja prikazana u ovom radu podržana su od strane Ministarstva prosvete, nauke i tehnološkog razvoja.

## LITERATURA

[1] *P.1546-5 : Method for point-to-area predictions for terrestrial services in the frequency range 30 MHz to 3 000 MHz*, ITU, 08/2019.
[2] M.Radojković, Z. Marinković, A. Atanasković, "Inverzno očitavanje ITU-R P,1546 krivih za nivo EM polja radio-difuznih predajnika" *62. konferencija ETRAN*, Palić, Jun. 2018.
[3] M.Radojković, O. Pronić-Rančić, Z. Marinković, "Inverse Reading of ITU-R P.1546 Propagation Curves for the Broadcast Transmitter EM Field Level" iCEST 2020, pp. 220-223, 10-12 Sep. 2020.
[4] Q. J. Zhang and K. C. Gupta, *Neural Networks for RF and Microwave Design*. Boston, MA: Artech House, 2000.
[5] C. Christodoulou and M. Gerogiopoulos, *Applications of Neural Networks in Electromagnetics*, Artech House, Inc. Norwood, MA, USA, 2000.
[6] Z. Stanković, N. Vasić, "Neural Approach in Modeling of the Propagation Curves from Recommendation ITU-R P.370-7", XLVII Konferencija za *ETRAN*, Herceg Novi, , pp.269-272, 8-13 jun 2003.
[7] J. E. Rayas-Sanchez, "EM-based optimization of microwave circuits using artificial neural networks: The state-of-the-art," *IEEE Trans. Microw.Theory Tech.*, vol. 52, no. 1, pp. 420–435, Jan. 2004.
[8] B. Milovanović, Z. Stanković, M. Ostojić, M. Milijić, "Predikcija nivoa elektromagnetnog polja korišćenjem neuronskog modela zasnovanog na ITU-R P.1546 preporuci ", *51. konferencija ETRAN 2007*, Herceg Novi - Igalo, Crna Gora, pp. MT1.3.1-4, 4-8. jun 2007.
[9] H. Kabir, L. Zhang, M. Yu, P. Aaen, J. Wood, and Q. J. Zhang "Smart modelling of microwave devices", *IEEE Microw. Mag.*, vol. 11, pp.105–108, May 2010.
[10] Z. Marinković, V. Marković, A. Caddemi, "Artificial Neural Networks in Small-Signal and Noise Modelling of Microwave Transistors," Chapter 6 in *Artificial Neural Networks*. Edited by Seoyun J. Kwon, Nova Science Publishers Inc., pp. 219-236, 2011.
[11] Z. Marinković, T. Kim, V. Marković, M. Milijić, O. Pronić-Rančić, L. Vietzorreck, "Artificial Neural network based design of RF MEMS capacitive shunt switches", *Applied Computational Electromagnetics Society Journal*, vol. 31 no. 7, pp. 756-764, July 2016.

## ABSTRACT

In this paper a method for determination of EM field level, according to ITU-R P.1546 recommendation for EM filed level originated form broadcast transmitters with height $h_1$ less than 10 meters is proposed. Proposed method is based on the applications of artificial neural networks and enables efficient determination EM field level for frequencies up to 4000 MHz and height $h_1$ less than 10 meters. Accuracy of the method is illustrated by an example of curves realated to several frequencies and $h_1$ not used for the training of neural network.

**Automatization of calculation the EM field strength according to the ITU-R P.1546 method for height parmeter *h*1 smaller than 10 meters**

Miloš Radojković, Zlatica Marinković

 ISBN 978-86-7466-930-3

# TLM modelovanje deformacija savijanja antene u biomedicinskim aplikacijama

Jugoslav Joković, *Member, IEEE*, Tijana Dimitrijević, *Member, IEEE*, Aleksandar Atanasković, *Member, IEEE*, and Nebojša Donšov, *Senior Member, IEEE*

***Sadržaj* — Prikazane su mogućnosti cilindričnog TLM numeričkog modela za analizu uticaja deformacije savijanja na parametre antene postavljene na ljudsko telo, koja se koristi u biomedicinskim aplikacijama. Kreiran je model pravougaone *patch* antene omotane oko dela cilindra koji može da se koristi za predstavljanje ljudskog tela (torzo, noga ili ruka) i istovremeno za modelovanje dielektričnih svojstava slojeva ljudskog tela. Ilustrovani su problemi u pogledu tačnosti i ograničenja kada se deformacija antene modeluje korišćenjem numeričkih metoda zasnovanih na pravougaonoj mreži. Prednosti cilindričnog TLM metoda kao tačne i efikasne alternative u odnosu na pravougaoni TLM pristup istaknute su kroz analizu uticaja deformacije savijanja na rezonantnu frekvenciju antene.**

***Ključne reči*—Deformacije antene, tekstilne antene, TLM metod.**

## I. UVOD

Brojne tehnike rešavanja problema biomedicinskog inženjeringa (*Biomedical Engineering, BME*) našle su korisne primene u biologiji i medicini što je dovelo do razvoja mnogih naprednih BME uređaja, koji se generalno mogu klasifikovati kao uređaji za dijagnostiku ili tretman [1,2]. Jedna od ključnih komponenti mnogih BME uređaja je antena koja se može postaviti blizu, unutar ili na ljudskom telu [3] ili ugraditi u ljudsko telo direktno ili kroz kapsulu koja putuje kroz telo [4]. Postavljanjem antene na odeću ili direktno preko torza formira se bežični sistem za detekciju i komunikaciju za veze prenosa na telu ili van tela [5]. Tako postavljena jedna ili više antena koristi se npr. za dijagnostiku pomoću magnetne rezonantne slike (*Magnetic Resonance Imaging,* MRI) i mikrotalasne slike (*Microwave Imaging,* MI) [2,6] ili za lečenje hipertermijom [7]. Dizajn većine ovih antena suočava se sa fizičkim ograničenjima kao što su veličina, snaga i bezbednosna ograničenja, što sveukupno može uticati na efikasnost samog BME uređaja.

Za antene postavljene na različite delove ljudskog tela, bilo na ljudsku kožu ili odeću (npr. tekstilne antene), postoje i drugi izazovi u njihovom dizajnu, kao što je neposredna blizina ljudskog tela koja, zavisno od tipa antene, može dovesti do razdešavanja parametara antene, odnosno promene impedanse i smanjenja pojačanja i efikasnosti antene [8,9]. Takođe, promene držanja i pokreti ljudskog tela u svakodnevnim aktivnostima izazivaju brojne deformacije kao što su istezanje, uvijanje, savijanje, gužvanje ili češće kombinacija dve ili više ovih deformacija. Kao rezultat deformisane geometrije, mnogi parametri antene se takođe menjaju kao što su rezonantna frekvencija, pojačanje, dijagram zračenja i polarizacija [9].

U literaturi dominantno je razmatran uticaj deformacije cilindričnog savijanja na performanse uglavnom štampanih tekstilnih antena, kako numerički tako i eksperimentalno [10]. Takođe, treba uzeti u obzir da je ljudsko telo neplanarna struktura i da je za rad na različitim delovima tela potrebna antena različitih oblika. Da bi se odgovorilo na ove izazove, različite vrste anatomskih modela ljudskog tela ili njegovih delova se obično koriste u eksperimentalnim merenjima kako bi se uračunalo prisustvo telesnih tkiva. Mogu biti različite geometrijske složenosti uključujući jednoslojne i višeslojne strukture kao što je troslojni fantomski model (koža, masno tkivo, mišići) napravljen korišćenjem gelova i/ili tečnosti. Ipak, da bi se obezbedio potpuno konforman BME uređaj koji se može neprimetno i neinvazivno integrisati sa ljudskim telom koje karakterišu krivolinijske površine i dinamički pokreti, elektromagnetni (EM) kompjuterski alati za simulaciju igraju vitalnu ulogu u celokupnom dizajnu antene za BME aplikacije. Ovi alati, obično zasnovani na nekim od dostupnih diferencijalnih ili integralnih numeričkih tehnika punog talasa, kao što su FDTD [11], MoM [12], FEM [13], TLM [14], itd, treba da budu u stanju da precizno uzmu u obzir disperziju, gubitke i u nekim slučajevima anizotropna tkiva ljudskog tela. Istovremeno, trebalo bi da budu u stanju da precizno generišu geometrijske modele antena koje su ili deformisane usled držanja i kretanja odeće na telu ili su jednostavno konformne sa nekim zakrivljenim delovima ljudskog tela kao što su ruke i noge. Većina ovih alata je zasnovana na konstruktivnoj geometriji čvrstog materijala (npr. korišćenje *Boole*-ovih geometrijskih operacija) i diskretizaciji pravougaone mreže, odnosno modelovanog prostora, što znači da su u stanju da realizuju jednostavnije deformacije i/ili da koriste veoma finu stepeničastu aproksimaciju za predstavljanje takve deformisane geometrije antene odnosno geometriju antene koja prati krivolinijski oblik dela tela. U slučaju diferencijalnih numeričkih tehnika u vremenskom domenu ovaj pristup može dovesti do veoma malog vremenskog koraka i prekomernog vremena rada, a takođe u nekim slučajevima može proizvesti tzv. parazitne efekte koji su štetni za EM simulacije.

Jugoslav Joković, Tijana Dimitrijević, Aleksandar Atanasković, Nebojša Dončov – Elektronski fakultet, Univerzitet u Nišu, Aleksandra Medvedeva 14, 18000 Niš, Srbija (e-mail: jugoslav.jokovic@elfak.ni.ac.rs, tijana.dimitrijevic@elfak.ni.ac.rs, aleksandar.atanaskovic@elfak.ni.ac.rs, nebojsa.doncov@elfak.ni.ac.rs).

 ISBN 978-86-7466-930-3

Kada EM problemi uključuju mnogo složenije geometrije, onda bi se upotreba tetraedarske mreže mogla pojaviti kao optimalnije rešenje. Kompjuterski grafički metodi (npr. *Green coordinates* [15]) nedavno su predloženi da bi se prevazišla ograničenja klasičnih komercijalnih EM alata zasnovanih na *Boole*-ovoj geometriji [16,17]. Ovi geometrijski generatori mogu omogućiti manipulaciju oblika antene pod proizvoljnom deformacijom u kombinaciji sa odgovarajućom numeričkom metodom i tetraedarskom mrežom da bi se minimizirale greške diskretizacije i predstavljaju moćan alat za konformni dizajn BME uređaja. Alternativa ovom naprednom rešenju u pogledu predstavljanja geometrije, ali i dalje skupom u pogledu memorije i vremena rada, može biti implementacija odabrane numeričke tehnike u koordinatnom sistemu koji je u skladu sa razmatranom deformisanom geometrijom antene. U slučaju savijanja antene, cilindrična diskretna mreža je savršeno prikladna da precizno opiše ovu deformaciju i da eliminiše greške diskretizacije koje dovode do mnogo brže i efikasnije simulacije u poređenju sa bilo kojom od pravougaonih ili tetraedarskih mreža. Pored toga, svaka promena ugla savijanja jednostavno se može implementirati u istoj cilindričnoj mreži omogućavajući da se isključi uticaj različitih veličina mreže (a samim tim i drugačije postavljenih napajanja i izlaznih tačaka zbog podešavanja mreže), Na taj način omogućena je konzistentna analiza uticaja različitih uglova savijanja antene na performanse.

U ovom radu, cilindrični TLM pristup je primenjen na modelovanje deformacije savijanja antene postavljene na ljudsko telo. Ilustrovane su prednosti ovog pristupa, koji istovremeno obezbeđuje precizno modelovanje geometrije antene i dielektričnih slojeva tela i efikasnu analizu efekta savijanja pod različitim uglovima, u odnosu na slučaj kada se koristi pravougaona TLM metoda. Postizanje tačnosti fizičkog modela antene omogućilo je analizu uticaja savijanja na performanse antene u prisustvu mišićnog tkiva. Objašnjen je TLM metod sa kompaktnim modelom žice u cilindričnom koordinatnom sistemu kroz definisanje TLM žičanog čvora duž radijalnog pravca, koji je potreban za modelovanje koaksijalnog napajanja, kao i postupak modifikacije granica u radijalnom i ugaonom pravcu koji omogućava veću efikasnost simulatora u konkretnom slučaju. Glavna pitanja za realizaciju TLM modela antene odnose se na opis EM svojstava medijuma sa radijalno postavljenim slojevima zajedno sa proširenjem modelovane oblasti, pružajući mogućnost definisanja spoljnih granica u ugaonom i radijalnom pravcu. Simulirani rezultati dobijeni TLM modelima savijanja antene u prisustvu tkiva i numeričke analize dati su za različite uglove savijenja antene.

## II. TLM METODOLOGIJA

TLM predstavlja numerički metod koji pripada grupi diferencijalnih metoda pogodnih za rešavanje EM problema u vremenskom domenu [14]. Zasnovan je na ekvivalencijama između Maksvelovih jednačina i prostiranjanja napona i struja duž vodova. Mreža međusobno povezanih čvorova koristi se za modelovanje prostiranja EM talasa uzimajući u obzir diskontinuitete i interakciju sa različitim svojstvima materijala. Tradicionalno, TLM metod je razvijen u Dekartovom koordinatnom sistemu, ali za strukture koje sadrže samo kružne/cilindrične površine, pogodniji je i efikasniji TLM metod zasnovan na cilindričnoj mreži. Hibridni simetrični kondenzovani čvor (*Hybrid Symetrical Condensed Node*, HSCN) koji predstavlja ćeliju u ortogonalnoj polarnoj mreži predstavljen je na Sl.1.a. Takva mreža ćelija se koristi za opisivanje EM osobina medijuma, preko odgovarajućih karakterističnih impedansi i admitansi povezanih vodova i stabova [18]. Iterativni postupak TLM algoritma sastoji se od dve glavne procedure poznate kao rasejanje i povezivanje [14]. Prilagođene su ortogonalnoj polarnoj mreži i dodatno modifikovane da bi se uzela u obzir pobuda, granice i nehomogena sredina i gubici [18,19].

Adaptacija i implementacija kompaktnog žičanog modela na cilindričnu mrežu [18] omogućila je modelovanje žičanih segmenata postavljenih duž radijalnog pravca. S obzirom da su za susedne čvorove razlikuju impedanse vodova i stabova ugrađenih u postojeću mrežu ćelija da bi se uzela u obzir žica, razvijen je i implementiran u postojeći softver baziran na TLM-u u cilindričnoj mreži dodatni postupak povezivanja za segmente žice u radijalnom pravcu [18, 19].

Pored relevantnog prikaza geometrije i EM svojstava nehomogenog medijuma, u slučaju takozvanih otvorenih problema kao što je *patch* antena, potrebno je dodati i odgovarajuće proširenje modelovane strukture, kako bi se uključila okoline antena. Primena cilindrične mreže je u ranijim radovima pretpostavljala da je okolina razmatrane strukture, koja čini modelovani prostor sa definisanim spoljnim granicama, potpuno cilindričnog oblika. Dakle, simulacije su zahtevale definisanje granica bez ikakvih graničnih uslova definisanih duž ugaonog pravca, gde je razmena impulsa obezbeđena povezivanjem poslednjeg i prvog čvora u ugaonom pravcu. Kada je ugao savijanja mali što se najčešće dešava u praksi prilikom razmatranja deformacija, modelovana *patch* antena je smeštena daleko od centra cilindričnog koordinatnog sistema, pa u tom slučaju upotreba celog cilindra kao modelovanog prostora koristi veliku memoriju i računarske resurse.

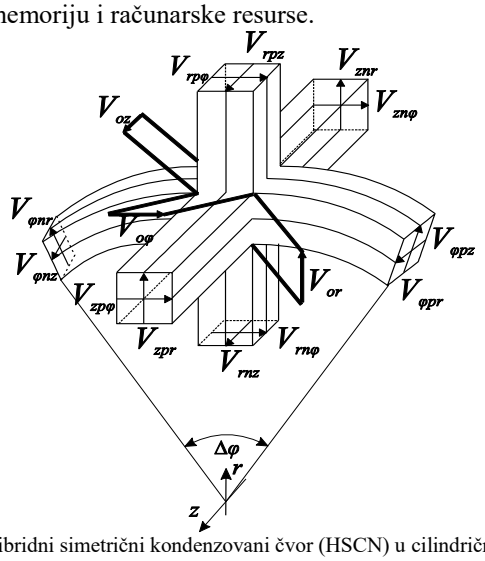


Sl. 1. Hibridni simetrični kondenzovani čvor (HSCN) u cilindričnoj mreži

 ISBN 978-86-7466-930-3

Iz tog razloga, TLM algoritam je prilagođen da omogući postavljanje graničnih uslova duž ugaonih pravaca. Dodatna poboljšanja se postižu omogućavanjem mogućnosti definisanja graničnog stanja na unutrašnjoj površini modelovanog prostora duž radijalnog pravca, umesto definisanja centralnog čvora. Ortogonalna polarna mreža u tom slučaju je bazirana na diskretizaciji prostora predstavljenu unutar isečka cilindra.

Generalno, TLM metod omogućava da se opiše tri tipa granica: električni zid, magnetni zid i zid koji apsorbuje. U slučaju modelovanja antene, električni zid se koristi za modelovanje metalne podloge i zračeće površine, dok su spoljašnje granice proširenog regiona opisane kao apsorbujuće sa koeficijentom refleksije voda na kraju prostora $\rho_{ij}$ [22]:

$$\rho_{ij} = \frac{(1+\rho_w)-\hat{Z}_{ij}(1-\rho_w)}{(1+\rho_w)+\hat{Z}_{ij}(1-\rho_w)}. \qquad (1)$$

gde je $\rho_w$ koeficijent refleksije zida, a $Z_{ij}$ je normalizovana impedansa odgovarajuće linije.

Kao rezultat definisanja modelovanog prostora kao dela cilindra zajedno sa graničnim uslovima, značajno je smanjen potreban broj TLM ćelija što dovodi do veće efikasnosti i uštede vremena i memorije. Prednosti ovog pristupa bile bi posebno uočljive u slučajevima kada je zakrivljenost odnosno savijanje mala, kada se zahteva veliki poluprečnik cilindrične površine, a samim tim i znatno veći broj ćelija ako se modelovana oblast predstavlja kao ceo cilindar. Dodatno, na ovaj način, uz dovoljno velike vrednosti poluprečnika cilindra u odnosu na dimenzije antene, moguće je modelovati pravougaone strukture u cilindričnoj mreži. Promenom samo poluprečnika cilindra moguće je kreirati modele sa različitim uglovima savijanja, koristeći mrežu iste rezolucije, i analizirati uticaj deformacije savijanja na performanse antene, nezavisno od drugih parametara modela koji se menjaju kada se primenjuje aproksimacija, kao što su površina zračeće površine, debljina supstrata, položaj napajanja itd.

## III. REZULTATI I ANALIZA

TLM solver je korišćen za analizu uticaja savijanja na performanse *patch* antene kada se postavi na ljudsko telo. U razmatranom slučaju, deo mišićnog tkiva se nalazi ispod antene. *Patch* antena dimenzija $w \times l = (50 \times 39.5)\text{mm}^2$, postavljena na podlogu i uzemljenu ravan dimenzija $W \times L = (100 \times 100)\text{mm}^2$ i savijena preko dela cilindra koji predstavlja mišićno tkivo, šematski je prikazana na Sl.2. Antena je realizovana na podlozi debljine $h$=2mm sa supstratom relativne permitivnosti $\varepsilon_r^s$=2.1, dok je sloj mišićnog tkiva debljine $d$=35mm predstavljen relativnom permitivnošću $\varepsilon_r^m$=52.67-$j$13 [23]. U TLM modelu, zračeni *patch* i uzemljena ravan su predstavljeni kao savršeni električni provodnici, a antena se napaja preko koaksijalnog napajanja koji povezuje uzemljenu ravan i *patch*, što je opisano preko kompaktne žičanog modela. Položaj koaksijalne pobude je optimizovan za postizanje prilagođenja impedanse između generatora i antene, tako da se nalazi se na $l_f$=11.5mm od ivice *patch-a*. Radna frekvencija dizajnirane antene iznosi $f$=2.45GHz.

Opisivanje problema sa odgovarajućom mrežom, u smislu veličine ćelije i sinhrinizacije, veoma je važno kako bi se obezbedila konvergencija rezultata. Za razliku od stepeničaste aproksimacije koja se mora koristiti u pravougaonoj TLM mreži za opisivanje zakrivljenih granica, tačno modelovanje kružnih granica je jednostavno u cilindričnoj TLM mreži, sa dimenzijama ćelija određenim maksimalnom frekvencijom od interesa [14]. Kao rezultat, zakrivljene granice se mogu precizno modelovati pomoću cilindrične mreže bez obzira na rezoluciju mreže, dok pravougaona mreža mora biti dovoljno fina da bi se postigla bolja tačnost. Da bi se ovo dokazalo, razmatrani model antene je kreiran i korišćenjem pravougaonog TLM rešavača. Izvedene su simulacije za ravnu antenu, ali i za savijenu antenu da bi se ispitao uticaj deformacije savijanja na rezonantnu frekvenciju antene. Razmatrana su dva ugla savijanja, $2\theta$ = 25 i 50 stepeni. Simulirani rezultati, koji predstavljaju koeficijent refleksije, kada se veličina TLM ćelije od 1.0mm primeni za modelovanje antene, dobijeni cilindričnim i pravougaonim modelom, respektivno, prikazani su na Sl.3. i 4.

Kod modelovanja ravne antene može se uočiti slaganje rezultata dobijenih primenom cilindrične mreže rezolucije 1.0mm sa odgovarajućim rezultatima primene pravougaone mreže (crna linija na Sl. 3. i 4). Praktično, u slučaju modela antene u cilindričnoj mreži, ravna antena je modelovana primenom veoma malog ugla savijanja, $2\theta$ = 0.1 stepen, što je ekvivalentno poluprečniku cilindra koji zadovoljava uslov da je mnogo veći od dimenzija antene $R>>l$ (oko 500 puta), pa se može smatrati ravnom. Primenljivost cilindrične mreže na modelovane strukture bez zakrivljenosti potvrđena je dobijenom vrednošću rezonantne frekvencije od 2.444 MHz, sa odstupanjem od 1% u odnosu na vrednost od 2.473 MHz dobijenu primenom pravougaone mreže.

Sa druge strane, rezultati dobijeni pomoću cilindričnog TLM-a i pravougaonog TLM-a, sa veličinom ćelije od 1.0mm primenjenom za modelovanje antene, pokazuju značajnu razliku u pomeranju frekvencije usled savijanja antene postavljene na mišićno tkivo. Praktično, modelovanjem cilindričnim pristupom se može primetiti da veći ugao savijanja dovodi do pomeranja rezonantne frekvencije ka višim vrednostima, dok istovremeno rezultati modelovanja pravougaonom mrežom pokazuju smanjenje frekvencije u odnosu na ravan slučaj, zajedno sa nedoslednošću u pogledu zavisnosti pomeranja frekvencije u odnosu na ugao savijanja.

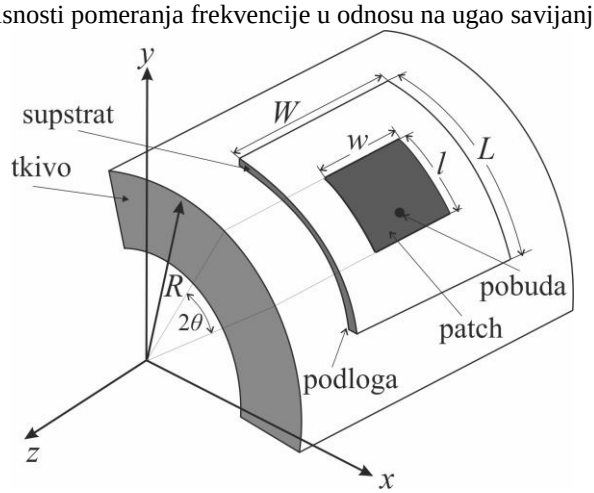


Sl.2. Pravougaona antena savijena preko dela tkiva

 ISBN 978-86-7466-930-3

Nekonzistentnost rezultata dobijenih primenom pravougaonog modela može se objasniti činjenicom da pravougaona mreža rezolucije od 1.0mm model u slučaju savijene antene uvodi grubu aproksimaciju zakrivljene površine zračenja koja utiče na njenu rezonantnu frekvenciju. Shodno tome, neophodno je koristiti finiju mrežu koja bi smanjila grešku stepeničaste aproksimacije i obezbedila tačne rezultate. Da bi se ilustrovao uticaj rezolucije mreže pravougaoni TLM model antene je definisan mrežom veličine ćelije 0.1mm. Simulirana rezonantna frekvencija dobijena ovom pravougaonom mrežom, prikazana na Sl.5, pokazuje da se, sa povećanjem ugla savijanja, povećava i rezonantna frekvencija, slično kao što je slučaj kada se koristi cilindrična TLM mreža.

Dakle, kada se ista veličina ćelije koristi u pravougaonoj i cilindričnoj mreži (1.0mm) ponašanje rezonantne frekvencije je drugačije. Iz tog razloga, potrebna je finija pravougaona mreža (0.1mm) koja obezbeđuje konzistentnost rezultata u pogledu pomeranja frekvencije, slično onima koje daje cilindrična mreža (1.0mm). Parametri cilindrične TLM mreže – veličina ćelije i broj ćelija, prikazani su u Tabeli 1. Rezolucija mreže je podešena da ispuni zahteve vremenske sinhronizacije [14].

Prikazani rezultati dobijeni na osnovu mreže od 1.0mm potvrdili su da se cilindrični model može koristiti u analizi deformacija savijanja, dok pravougaona mreža te rezolucije nije adekvatna, odnosno da se zahteva finija rezolucija. Međutim, kada se koristi pravougaona mreža od 0.1mm koja obezbeđuje konvergenciju rezultata, povećanje broja ćelija iznosi oko 1000 puta, što dokazuje jake prednosti cilindrične mreže u ovom slučaju.

## IV. Zaključak

U ovom radu je TLM metod prilagođen ortogonalnoj polarnoj mreži korišćen za analizu deformacije savijanja *patch* antene postavljene na ljudsko telo - podešavanjem dimenzija modela, rezolucije mreže, odgovarajućeg proširenja regiona modelovanja i optimizacije položaja koaksijalnog napajanja, obezbeđeno je da efekat deformacije na parametre antene bude nezavisan od numeričkih grešaka.

Pristup je modifikovan kako bi se omogućilo korišćenje graničnih uslova duž radijalnog i ugaonog pravca koji dovode do značajnog smanjenja modelovane oblasti, a time i do smanjenja korišćenja memorije i vremena potrebnog za simulaciju. Prikazani rezultati pokazuju prednosti modela kreiranog u cilindričnoj TLM mreži, koja istovremeno obezbeđuje precizno modelovanje geometrije antene i dielektričnih svojstava supstrata i tkiva.

Prikazani numerički rezultati su pokazali da je TLM metod zasnovan na cilindričnoj mreži pogodniji i precizniji za modelovanje antene koja je deformisana savijanjem, u odnosu na pravougaoni TLM model. Glavne prednosti cilindričnog TLM metode su konformno modelovanje zakrivljenih površina, sa preciznošću koja se postiže manjim brojem ćelija, i dodatno fleksibilnost modelovanja realnog savijanja za različite uglove, bez promene parametara mreže.

TABELA I
PARAMETRI CILINDRIČNE MREŽE

| Osa | Medijum | Rezolucija | Broj čvorova |
|---|---|---|---|
| r- | tkivo | ~0.2 mm | 205 |
| | supstrat | 1.0mm | |
| | vazduh | 1.449 mm | |
| φ- | vazduh | 1.449 / r (mm) | 155 |
| | supstrat | ~1/ r (mm) | |
| | vazduh | 1.449 / r (mm) | |
| z- | vazduh | 1.449 mm | 155 |
| | supstrat | ~1.0mm | |
| | vazduh | 1.449 mm | |

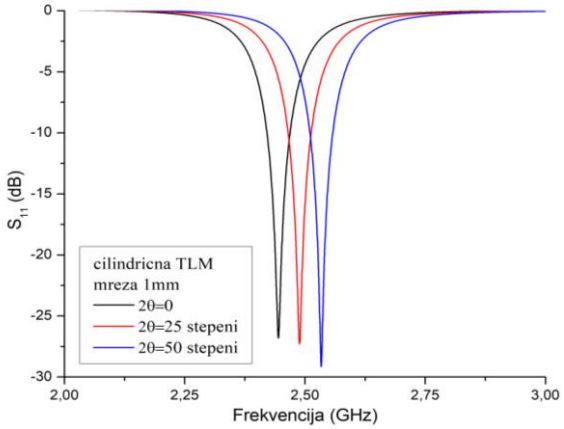


Sl.3. Zavisnost $S_{11}$ parametra antene na mišićnom tkivu od ugla savijanja dobijen primenom cilindrične TLM mreže rezolucije 1.0mm

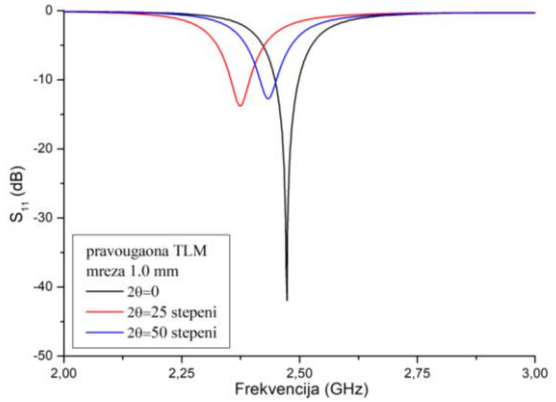


Sl.4. Zavisnost $S_{11}$ parametra antene na mišićnom tkivu od ugla savijanja dobijen primenom pravougaone TLM mreže rezolucije 1.0mm

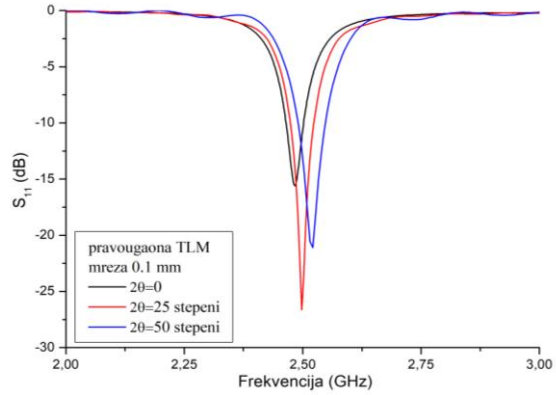


Sl.5. Zavisnost $S_{11}$ parametra antene na mišićnom tkivu od ugla savijanja dobijen primenom pravougaone TLM mreže rezolucije 0.1mm


ISBN 978-86-7466-930-3

Mogućnosti definisanja različitih dielektričnih slojeva u radijalnom pravcu takođe omogućavaju precizno modelovanje antene omotane oko cilindra kako bi se oponašalo ljudsko tkivo predstavljeno u simulacijama kao standardni višeslojni model (koža, masno tkivo, mišićno tkivo i kosti). Iz navedenih razloga, TLM cilindrični solver se može efikasno koristiti za sprovođenje parametarske studije za karakterizaciju deformacije savijanja antene u režimu rada na telu koji se odnosi na promenu rezonantne frekvencije, širinu opsega i promenu tzv. povratnih gubitaka, odnosno $S_{11}$ parametra.

## ZAHVALNICA

Ovaj rad podržali su Ministarstvo prosvete, nauke i tehnološkog razvoja Republike Srbije (br. 451-03-9/2022-14/200102) i Fond za nauku Republike Srbije (br. 6394135).

## LITERATURA

[1] Enderle J., Bronzino J., *Introduction to Biomedical Engineering, Third Edition*, Academic Press, (2011)
[2] Wang L., *Electromagnetic Waves and Antenas for Biomedical Applications*, IET (2021)
[3] Kaur G., Kaur A., Kaur Toor G., Dhaliwal B.S., and Pattnaik S.S., "Antenas for Biomedical Applications, *Biomedical Engineering Letters* Vol. 5, No. 3, pp. 203-212, (2015)
[4] Kiourti A., and Nikita K.S., "A Review of Implantable Patch Antenas for Biomedical Telemetry: Challenges and Solutions", *IEEE Antenas and Propagation Magazine*, Vol. 54, No. 3, pp. 210-228, (2012)
[5] Yang H., and Liu X., "Wearable Dual-Band and Dual-Polarized Textile Antena for On- and Off-Body Communications", *IEEE Antenas and Wireless Propagation Letters*, Vol. 19, No. 12, pp. 2324-2328, (2020)
[6] Solomakha G., Svejda J. T., Van Leeuwen C., Rennings A., Raaijmakers A. J., Glybovski S., and Erni D., "A self-matched leaky-wave antena for ultrahigh-field magnetic resonance imaging with low specific absorption rate, *Nature Communications*, 12, 455 (2021)
[7] Choi W.C., Lim S., Yoon Y.J., "Evaluation of Transmit-Array Lens Antena for Deep-Seated Hyperthermia Tumor Treatment", *IEEE Antenas and Wireless Propagation Letters*, Vol. 19, No. 5, pp. 866 – 870, (2020)
[8] Rahman N.H.A., Yamada Y., and Nordin M.S.A., "Analysis on the Effects of the Human Body on the Performance of Electro-Textile Antenas for Wearable Monitoring and Tracking Application", *Materials*, 12, 1636, (2019)
[9] Aun N.F.M., Soh P.J., Al-Hadi A.A., Jamlos M.F., Vandenbosch Guy A.E., and Schreurs D., "Revolutionizing wearables for 5G: 5G technologies: Recent developments and future perspectives for wearable devices and antenas", *IEEE Microwave Magazine*, IEEE, vol. 18, no. 3, pp. 108–124, (2017)
[10] Song L., and Rahmat-Samii Y., A Systematic "Investigation of Rectangular Patch Antena Bending Effects for Wearable Applications", *IEEE Transactions on Antenas and Propagation*, vol. 66, no. 5, pp. 2219-2228, (2018)
[11] K. S. Kunz and R. J. Luebbers, *The Finite Difference Time Domain Method for Electromagnetics*, CRC Press, Boca Raton, FL, (1993)
[12] Gibson W.C., *The Method of Moments in Electromagnetics*, Chapman and Hall/CRC, (2021)
[13] Thomas J.R. Hughes: *The Finite Element Method: Linear Static and Dynamic Finite Element Analysis*, Prentice-Hall (1987)
[14] Christopoulos, C., *The Transmission-Line Modelling Method: TLM*, Institute of Electrical and Electronics Engineers, (1995)
[15] Lipman Y., Levin D., and Cohen-Or D., "Green Coordinates", *ACM Trans. Graph*., 27 (3), 1-10, (2008)
[16] Sewell P., Benson T. M., Christopoulos C., Thomas D. W. P., Vukovic A., Wykes J. G., "Transmission-line modeling (TLM) based upon unstructured tetrahedral meshes", *IEEE Trans. Microw. Theory Tech.* 53(6), 1919-1928, (2005)
[17] Altinozen E., Harrison I., Vukovic A., Sewel P.D., "Green Coordinates for Generation of Conformal Antena Geometries, *14th European Conference on Antenas and Propagation – EuCAP*, (2020)
[18] Dimitrijević T., Joković J., Milovanović B. Doncov N., "TLM modeling of a probe-coupled cylindrical cavity based on compact wire model in the cylindrical mesh", *Int. J. RF Microw. Comput-Aided Eng*. 22(2) 184-192 (2012)
[19] Jokovic J., Dimitrijevic T., Doncov N., "Efficient integral cylindrical transmission-line matrix modeling of a coaxially loaded probe-coupled cavity", *IET Microw. Antena & Propag*., 9(8), 788-794, (2015)
[20] Trenkic V., Wlodarzcyk A.J., Scaramuzza R.A., "Modeling of coupling between transient electromagnetic field and complex wire structures", *Int. J. Numer. Model. Electron. Netw. Devices Fields.*, 12(4), 257-273, (1999)
[21] Joković, J., Dimitrijević, T., Dončov, N., "Computational Analysis and Validation of the Cylindrical TLM Approach on IMCP Antenas", *Wireless Person. Comm*., 106, 1573–1589, (2019)
[22] Dimitrijevic T., Jokovic J., Doncov N., "Efficient Modeling of a Circular *Patch*-Ring Antena Using the Cylindrical TLM Approach", *IEEE Ant and Wireless Propag. Lett*., 16, 2070-2073, (2017)
[23] Chun-Xu Mao, Vital D., Werner D. H., Yuhao Wu, Bhardwaj S., "Dual-Polarized Embroidered Textile Armband Antena Array with Omnidirectional Radiation for On-/Off-Body Wearable Applications", *IEEE Trans. Ant. Prop*., 68(4), 2575-2584, (2020).

## ABSTRACT

The possibilities of the cylindrical TLM numerical model used for the analysis of the influence of bending deformation on the parameters of the antenna placed on the human body, which is used in biomedical applications, are presented. A model of a rectangular patch antenna wrapped around a part of a cylinder was created in order to represent the human body (torso, leg or arm) and at the same time to model the dielectric properties of the layers of the human body. The problems in terms of accuracy and limitations when antenna deformation is modeled using numerical methods based on a rectangular grid are illustrated. The advantages of the cylindrical TLM method as an accurate and efficient alternative in relation to the rectangular TLM approach are highlighted through the analysis of the influence of bending deformation on the resonant frequency of the antenna.

**TLM modeling of antenna bending deformations in biomedical applications**

Jugoslav Jokovic, Tijana Dimitrijevic, Aleksandar Atanaskovic and Nebojsa Doncov

 ISBN 978-86-7466-930-3

# NEW MATERIALS IN ELECTRICAL AND ELECTRONIC ENGINEERING

# /

# НОВИ МАТЕРИЈАЛИ

# (NMI/HM)

ISBN 978-86-7466-930-3

# Sintering and Phase Transition of the $ZnTiO_3$ Nano Powder Dilatometric Data Deconvolution

Nebojša Labus, Smilja Marković, Maria Vesna Nikolić, Milena Rosić, Srđan D. Matijašević

***Abstract*— intering and phase transition are often superimposed at dimensional change diagram recorded during heating. Phase transition inetic is thus hard to deconvolute due to the superposition of the sintering and phase transition dimensional change phenomena.**

**etastabile perovs ite phase nTi has transition to stabile spinel n2Ti 4which occurs at 45°C with high inetic rate. ano powder with 4 nm particle diameter was pressed unia ially at 2 Pa pressure without binder to form compact that will be consequently sintered. Dimensional change during heating was monitored using dilatometric thermo-mechanical analyzer T A model T volution. ever s rule was used to calculate amount of the emerging phase during phase transition.**

**The compacted specimens were treated on the non-isothermal schedule up to 1 5 °C. intering phenomenon of the nTi nanopowder compact was also recorded up to °Cwith isothermal holding of 25 minutes where phase transition was avoided due to lower temperature and isothermal holding. econd run heating of the obtained sintered specimens were recorded with the heating schedule of non-isothermal heating up to 1 5 °C.**

**inetic of the phase transition was obtained from dilatograms recorded during sintering and from bul on the second run heating. urthermore, phase transition inetics was obtained by subsequent data subtraction of the sintering curves without phase transition from the dilatation sintering curves containing phase transition.**

**In such a manner comple inetics of phenomena such as sintering, linear e pansion and phase transition recorded as dimensional change during heating brings the recognition of their mutual interconnected relations. Also application of these mathematical operations on dilatometric data leads to the established procedure for the sintering and phase transition data treatment.**

***Index Terms*— intering, Dilatometry, Phase transition**

Nebojša Labus is with Institute of Technical Sciences of SASA since 2001, Belgrade, Serbia.: nebojsa.labus@itn.sanu.ac.rs, http://www.itn.sanu.ac.rs/nebojsalabus_eng.html. ORCID ID: 0000-0003-1557-0711, (https://orcid.org/0000-0003-1557-0711)

Smilja Marković, is with Institute of Technical Sciences of SASA, Belgrade, Serbia, email: smilja.markovic@itn.sanu.ac.rs, ORCID ID: 0000-0002-9264-4406 (https://orcid.org/0000-0002-9264-4406)

Maria Vesna Nikolić: is with Institute for Multidisciplinary Research, University of Belgrade, Belgrade, Serbia, email: mariavesna@imsi.rs, ORCID ID: 0000-0001-5035-0170 (https://orcid.org/0000-0001-5035-0170)

Milena Rosić is with Institute of Nuclear Sciences „Vinča“, University of Belgrade, Belgrade, Serbia, email: mrosic@vin.bg.ac.rs, ORCID ID: 0000-0001-7093-187X, (https://orcid.org/0000-0001-7093-187X)

Srđan Matijašević is with Institute for Technology of Nuclear and Other Mineral Raw Materials (ITNMS), Franchet d Esperey 86, 11000 Belgrade, Serbia , s.matijasevic@itnms.ac.rs

## I. INTRODUCTION

In the following work phase transition represents change from $ZnTiO_3$ to $Zn_2TiO_4$. Phase transition investigated here encounters following phases on phase diagram $ZnO$-$TiO_2$: $Zn_2TiO_4$ (zinc orthotitanate) which has an inverse cubic spinel structure ($Fd\bar{3}m$) and it is stable from room temperature to its melting (liquid) temperature. $ZnTiO_3$ (zinc metatitanate) has a hexagonal ilmenite structure ($R\bar{3}$), a variant of the corundum structure where the cations are ordered into two non-equivalent oxygen sites. Zinc metatitanate is stable from room temperature to 945.8°C. $Zn_2Ti_3O_8$ was first determined by Yamaguchi et al. [1] as a low temperature form of $ZnTiO_3$ having a defect cubic spinel structure with ordered cation vacancies leading to degradation of the space group symmetry from $Fd\bar{3}m$ to $P4_332$.

Phase transition belongs to second order phase transition. Since it is changed from metastabile to stabile phase, it has very fast kinetic rate, comparing, for example, to anatas - rutile phase transition [2]. Phase transitions are observed usually with the means that are enabling record of the property that comes with the emerging phase. Here volume change caused by structure change is registered as linear dilatation in a function of rising temperature. This leads to a possibility of phase transition kinetics observation.

Sintering phenomenon represents densification of the powder compacted in desired form during heating. Sintering dimensional change can during heating encompass phase transition dilatataion. Also specific influence of the nano powder during sintering is influencing phase transition kinetics. It is often compared to bulk polycrystalline kinetics of the same transition. This work intention is to use dilatometry as a tool for observing phase transition and sintering phenomena indicating their interdependent mutual relations.

## II. METHOD

Experiment is set to record phase transition from $ZnTiO_3$ bulk specimen and $ZnTiO_3$ nano powder during sintering. $ZnTiO_3$ nanopowder, Aldrich [CAS 112036-43-0] was used. Two specimens are used for this purpose. Specimen 1 and specimen 2, respectively. Dilatometric thermo-mechanical analyzer TMA model SETSYS Evolution device was used. Specimens were compacted at 200 MPa uniaxially with both sided actions. Transmission electron microscopy of the nano powder $ZnTiO_3$ was performed on JEOL JEM 1400 plus microscope at 120kV and 150k enlargement.

Specimen 1 is heated to 1150°C non isothermally (1st run)

 ISBN 978-86-7466-930-3

and phase transition during sintering is recorded using dilatometric oven. Without extracting it from dilatometric device specimen is heated again to 1150ºC, using same temperature schedule. (2nd run).

Specimen 2 is heated non-isothermally to 900ºC and then held 25 minutes at that temperature isothermally (1st run) and thus sintering of the $ZnTiO_3$ nanopowder is recorded. It is expected and confirmed that phase transition is absent. Same specimen 2, without extraction from the dilatometric device, is than heated again, but now to 1150ºC non-isothermally with previously used thermal schedule (2nd run). Obtained curve contains phase transition of $ZnTiO_3$ to $Zn_2TiO_4$ recorded from bulk specimen. All diagrams have been recorded on three heating rates - 20, 10 and 5ºC/min rate.

Stage of cooling is recorded as well with 20ºC/min rate. It is important to note that during cooling no intensive dimensional change is present. This implies that phase transition is irreversible.

## III. Results and Discussion

Nano dimensional powder sintering process assumes different mechanisms of mass transport compared to micro dimensional powder sintering. Transmission electron micrograph on Fig. 1 represents powders dimensional and morphology introspection. Powder particles are dimension bellow 40 nm, what is declared by the producer.

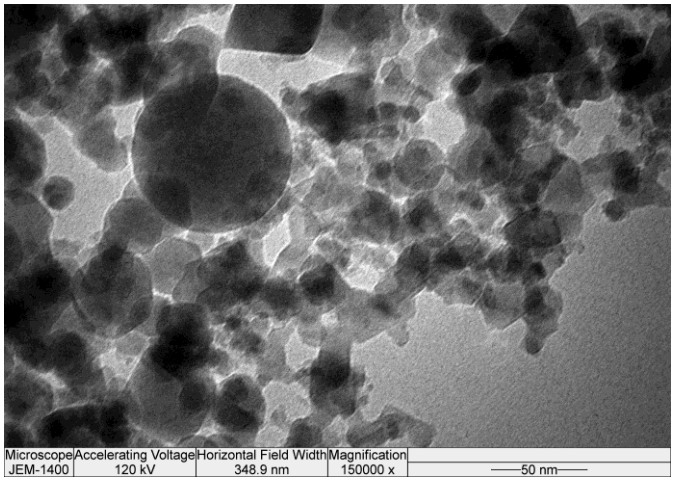


Fig. 1. TEM images of the nanopowder $ZnTiO_3$.

At Fig. 2 temperature experimental setup with whole interval dilatation curves and temperature programs are presented. Sintering phenomenon reaches 18% shrinkage while bulk specimen dimension change is represented with 3% shrinkage event. Phase transition record is marked with red square for bulk specimen and blue square for the powder sintering specimen.

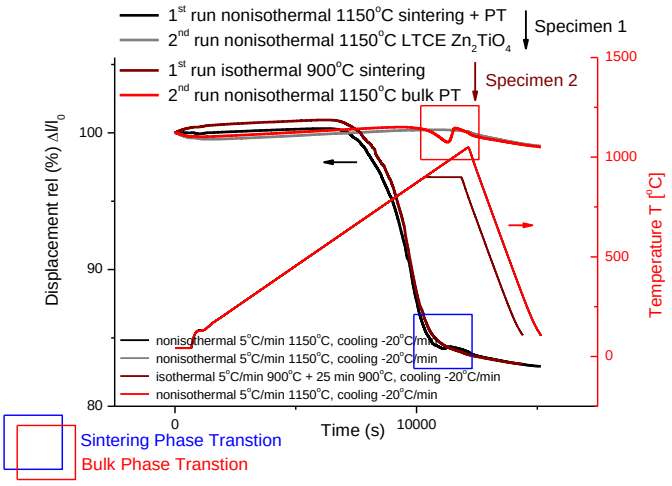


Fig. 2. Dilatometric curves and temperature programs for two specimens and four runs for the 20ºC/min speed, containing phase transition dilatation for bulk and powder specimen. Experimental setup.

Metastabile perovskite phase $ZnTiO_3$ reforms to stabile spinel $Zn_2TiO_4$ at 950ºC with high kinetic rate. The phase transition dimensional change diagram is consisted of sintering shrinkage and phase transition here on named as sintering. Obtained non-isothermally sintered specimens at were then second run treated with same schedule. Sintering phenomenon of the $ZnTiO_3$ nano-powder compact was also recorded up to 900ºC with isothermal holding of 25 minutes. Here phase transition was avoided with lower temperature and isothermal holding. Second run heating, of isothermally obtained specimens at 900ºC, was recorded with non-isothermal heating schedule to 1050ºC. This has led to the dilatometric curve record of the $ZnTiO_3$ phase transition in polycrystalline bulk specimen, now recorded without sintering, here on named - bulk.

All before mentioned was recorded for three different heating rates - 5ºC/min, 10ºC/min and 20ºC/min. It is presented all together and critical points are circled, red for the phase transition from bulk specimen, and blue circle for phase transition from powder during sintering Fig 3.

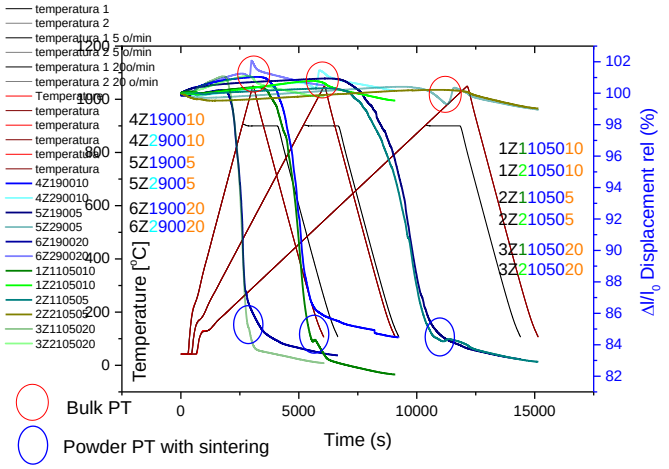


Fig. 3. Dilatometric curves, right axes and temperature programs left axes, heating rates 5, 10 and 20ºC/min.


ISBN 978-86-7466-930-3

It is worth to emphasize that on the presented diagrams phase transition during sintering 20°C/min rate is not well distinguished, and also those final densities for 10°C/min and 20°C/min for non-isothermal sintering and isothermal are significantly different.

Extraction of the observed region with phase transition has been done in the 800°C to 1100°C, Fig. 4. Interval of the shrinkage curve heated isothermally is extracted as well. Heating rates 5, 10 and 20°C/min.

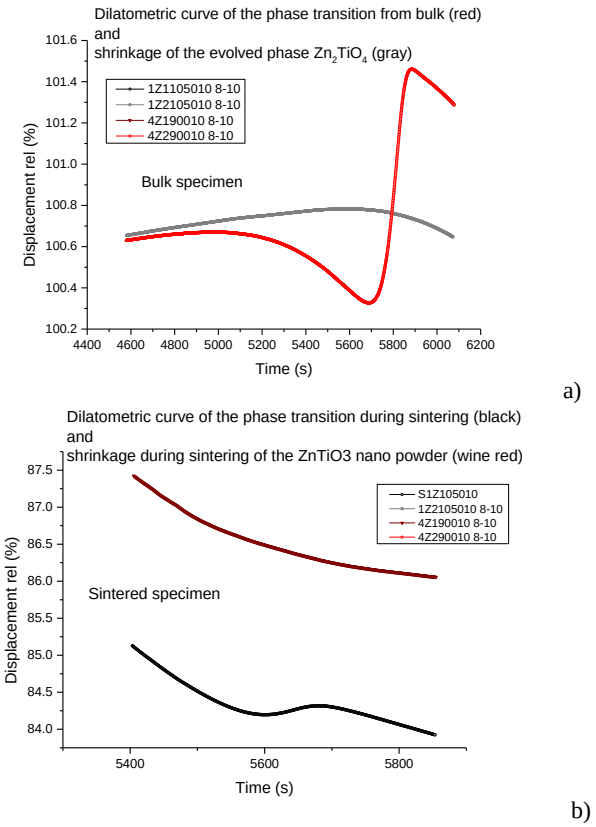


Fig 4. Dilatometric curves of phase transition $ZnTiO_3$ to $Zn_2TiO_4$ extracted phase transition interval a) observed in a bulk specimen (red), thermal expansion of the $Zn_2TiO_4$ phase (gray). b) Dilatometric curves of the phase transition and sintering (black), and sintering phenomenon without phase transition (wine red).

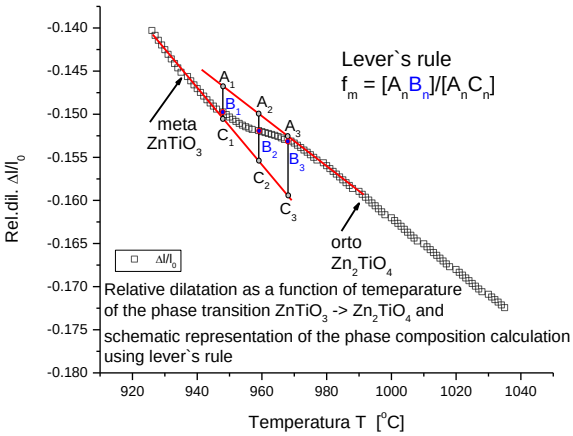


Fig 5. Relative dilatation as a function of temperature of the phase transition $ZnTiO_3$ -> $Zn_2TiO_4$ and schematic representation of the phase composition calculation using lever`s rule

Lever law is used in a XRD determination of the solvus curves - solid solubility curve on a phase diagram. It assumes that phases are in equilibrium during phase transition at each temperature. It also supposes that weight fraction of the observed phase amount varies linearly with composition from 0 to 1 [3].

At the dilatogram diagram, linearity, even with the sintering curve included, represents linear thermal expansion of the starting phase and can be fitted with linear function. Intensive deflexion from linearity is caused by phase transition dilatation. When phase transition is finished new phase again reaches linearity. Dimensional difference is caused by phase interchange and it is proportional to phase composition during phase transition. So, the distances AB, AC have to be determined and their relation AB/AC suites phase composition during phase transition, f=AB/AC, Fig 5. It is obvious that three sets of data are formed by the series made for each experimental point. Linear C data set, linear A data set and experimental set of curve B. All data sets have to posses same number of points since the subtraction ought to be performed. A and C sets have to be constructed. B is experimental dilatation. Than A minus B values make one column of Y. Similarly, A minus C forms second Column of Y and finally ratio AB/AC, third. AB/AC column plot in a function of temperature or time, represents kinetic curve of the phase transition.


ISBN 978-86-7466-930-3

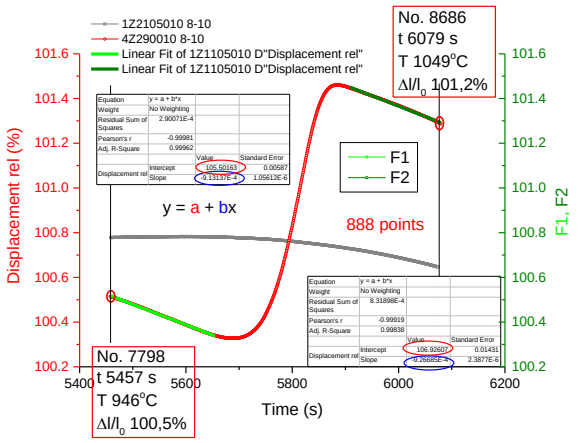


Fig 6. Linear fitting and interpolation of the inserted linear functions

At Fig. 6, phase transition curve was fitted in the linear regions before and after phase transition, light green and olive green portions of the red curve. Linear parameters of the line denoted as y= ax + b, where a is slope and b represents intercept. Number of points on the dilatometric curve in the observed interval is pointed out, it equals 888 points. Functions F1 and F2 are inserted to the graph with the interpolation of the linear functions points to the number of points that are resembling experimental dilatometric curve.

Procedure steps using Origin software after interval extraction consists of:

1. Detecting characteristic values of points and labeling them as starting and end point - No., t seconds, Temperature T, displacement shrinkage %
2. Determent of the number of points that interval consists of, here 888 points.
3. Determent of the interval that represents straight line on the begging and end of the graph that you want to fit linear. Origin software - Data, -> Mark data range, or Data selector, markers left and right positioned on the graph by cursor, Enter.
4. Linear fit of the beginning, left part, of the red curve and of the end, right part - linear fit tool – Analysis, -> Fitting -> Linear fit. Determent Y=a+bX relation from data sheet. Slope a and intercept b.
5. Adding a function graph F1 and F2 consisted of straight lines. The function insertion uses a and b parameters determined for left and right part of dilatometric curve, here light green and olive green parts. Graph -> Add Function Graph -> F2(x) = 3,31697-0,00254 * x where (example) 3,31697 is intercept b and 0,00254 is slope a parameter. -> Add. Number of points will be set to 100. Auto X range and Display curve – checked.-> Apply
6. Interpolation of the number of points on the F1 and F2 to experimental number, here 888. F1 select -> workbook -> Name of the data set image of F1, F1-C2 Enter. Graph of FuncCopy will be plot. Select function you want to Interpolate. Go to Workbook button. -> Workbook , C2-Y column Sheet 1, Analysis-> Mathematics -> Interpolate/Extrapolate -> Open dialog -> Input C2 Y, method Linear, Number of points determined at 2 (888). Decheck Auto, X minimum enter the left minimal value determined at 1. here (5457 s), Decheck Auto, X maximum same procedure now X maximum here (8686 s), Output new sheet, -> Ok.
7. Organize workbook of the experimental data with interpolated values columns and subtract columns AB and AC, and AB/AC according to the levers rule. Plot the function AB/AC as a function of time or temperature that represents phase composition.

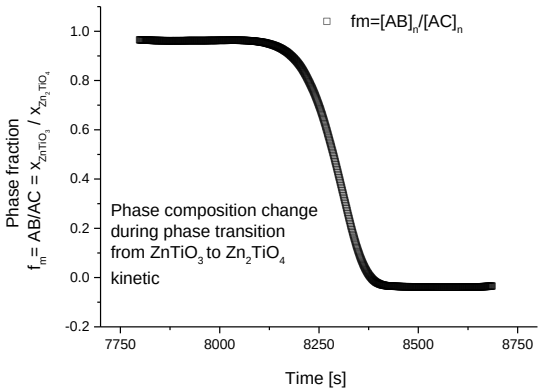


Fig 7. Dilatometric curve that represents phase composition change during phase transition from $ZnTiO_3$ to $Zn_2TiO_4$.

Sigmoidal curve obtained by the described procedure is presented at Fig 7. It represents disappearing of starting phase $ZnTiO_3$ and appearance of the evolving phase $Zn_2TiO_4$. This curve allows us to observe and, furthermore, even to discuss the kinetic of the phase transition.

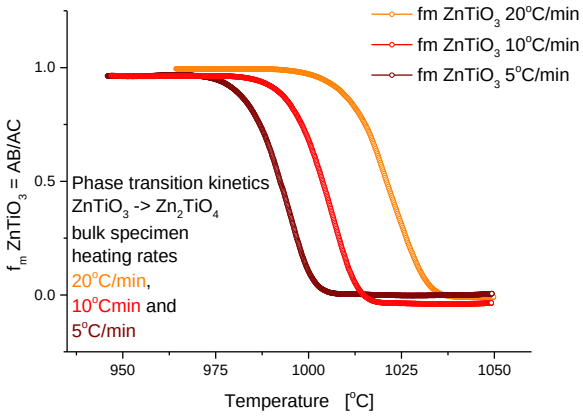


Fig 8. Phase transition kinetic from bulk specimen, three heating rates: 20°C/min 10°C/min and 5°C/min.

Phase transition from bulk specimen as a function of temperature, three heating rates, 20 10 and 5 °C/min, orange 20°C/min, red 10°C/min and wine 5°C/min represented at Fig. 8. Since the temperature is a linear function of the time, due to non isothermal heating schedule, temperature scale is used. Change of the phase composition represents phase transition

 ISBN 978-86-7466-930-3

kinetic. Note that temperature of the curve center is the point with highest rate of phase transition. If the temperature of the phase transition observed, with higher heating rate, temperature of the phase transition is higher - 20ºC/min 1021ºC, 10ºC/min 1004ºC, 5ºC/min 993ºC. It is as well higher than expected 945ºC for the phase diagram of $ZnTiO_3$ [4]. Nano-dimensions are introducing difference, as well as composition, since it is $ZnTiO_3$ pure.

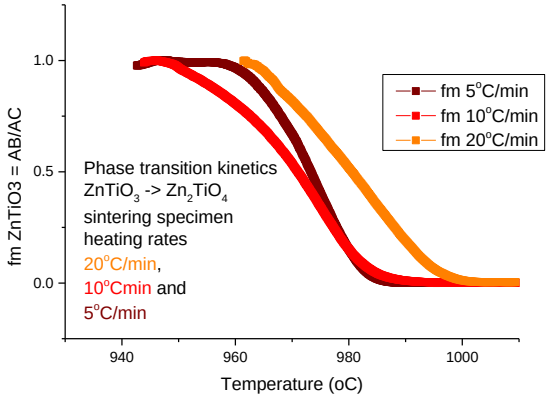


Fig 9. Phase transition kinetic from powder sintered specimen, three heating rates: 20 ºC/min 10ºC/min and 5ºC/min.

It is obvious that curves at Fig. 9 for the phase transition kinetic for the sintered specimen do not resemble heating rate rise trend. Also, the shape is more irregular mutually for the different heating rates and also different regarding the bulk specimen curves.

Mathematical procedures enabling comparison of the data were necessary since data obtained by levers rule are different in their appearance due to physical phenomena they include. First, all values must be positive. Then, second, to compare them they must be in the zero to one values interval. Third, if the function is monotonically increasing than it should be converted to monotonically decreasing due to the convention that we observe disappearing phase.

Minimal value for the every set of data was determined by applying column statistic tool. Determined value is than added to all values in the column what has led to all values of the function are positive

1. fm > 0

Maximal value for the every set of data was determined by applying column statistic tool. Determined maxima value is used to divide all values with, what has led to the norming boundary condition - all values are inside of [0,1] set

2. fm [0,1]

Column values were finally inverted by subtracting them from 1. Parent phase disappearance shape is thus established. Function is presented as monotonically decreasing when this trend is absent due to final sintering stage influence.

3. fm = 1- [col]

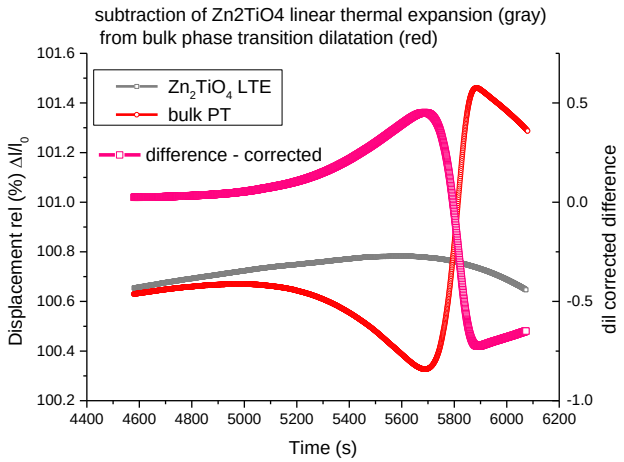


Fig 10. Correction by subtraction for the bulk specimen.

Dilatometric curves should be corrected mainly for the dilatation of the carrier system and pushing rod material enlargement. In the device with two samples, in the differential dilatometry, this procedure is done during the experiment. Here, we have decided to subtract linear dilatation of the $Zn_2TiO_4$ bulk sample, from phase transition recorded from bulk.

Specimen that was heated to 1050ºC passed through phase transition Fig. 10, (red). Specimen was second time heated to the same temperature and this second curve represents linear thermal expansion of the evolved phase $Zn_2TiO_4$ (gray). This set of values will be subtracted from curve with phase transition obtained from bulk specimen (red). Pink curve represents difference – corrected curve (pink). Number of points that are going to be subtracted is often equal, and if it is not - interpolation to the number of points present in the experimental phase transition curve is performed.

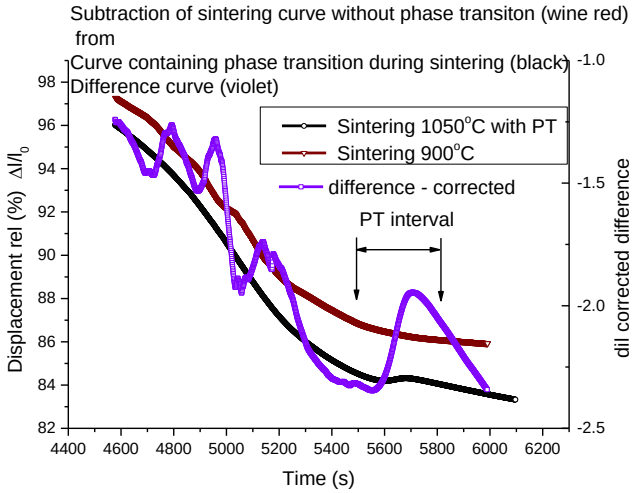


Fig 11. Correction by subtraction for the powder -sintered.

Correction by subtraction of sintering curve 900ºC without phase transition (wine red) from sintering curve 1050ºC that is containing phase transition during sintering (black) is performed, figure 11. Difference corrected curve is obtained (violet). Large interval was presented to show that difference


ISBN 978-86-7466-930-3

curve (violet) consists of irregularities, Fig. 11. Observed Phase Transition interval (PT interval) was extracted. The absence of stability for the resulting curve origins from sintering phenomenon when nano-powder is used. High shrinkage rates and overall large shrinkage is present due to rearrangement of highly agglomerated powder and also from intensive recrystallization and grain growth. It should be mentioned that sintering curve at 900ºC was obtained by combination of non-isothermal and isothermal temperature program sequence. Yet, correction calculation was performed.

From the difference corrected curve, by the levers rule usage, the kinetic phase transition curves for bulk and sintering specimens are obtained, Fig. 12.

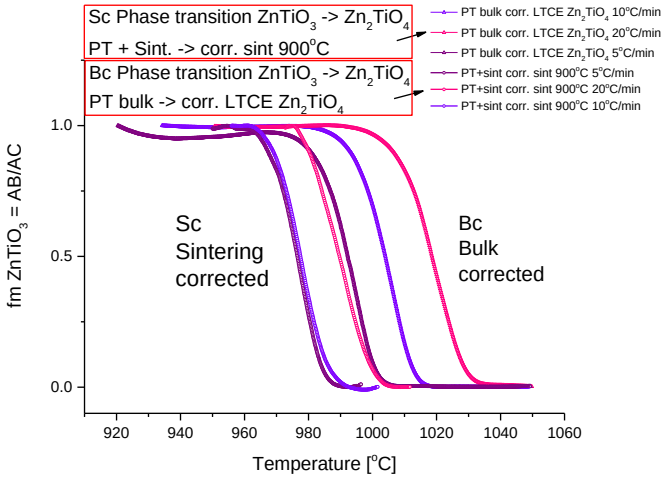


Fig 12. Phase transition kinetics comparison: Corrected curves for phase transition from Bulk and Sintered specimens.

At fig.12, obtained corrected curves for Bulk and Sintering are presented separately from experimental curves at fig. 9 and 10. Pink, violet and purple colors are subscribed to 20, 10 and 5ºC/min heating rate, respectively. Sintering corrected curves does not follow heating rate sequence. This fact is expected since experimental curves are distributed in the same manner. Sintering corrected specimens' curves for heating rates 10ºC/min and 5ºC/min are close each other. Bulk corrected curves are well distributed following the rise of the heating rate parameter.

It is interesting to make a phase transition kinetics comparison: Bulk vs. Sintered and also Experimental vs. Corrected, Fig. 13. All curves are presented together. Good match of the bulk curves between experimental and corrected is visible. Sintered are showing deviations between experimental and corrected. Deviation is in the position of the curve, as well as in the shape. This implies great influence of sintering phenomenon on the phase transition, thermodynamically as well as kinetically. Temperature scale disproportion implies activation energy difference, while curve shape implies kinetic difference.

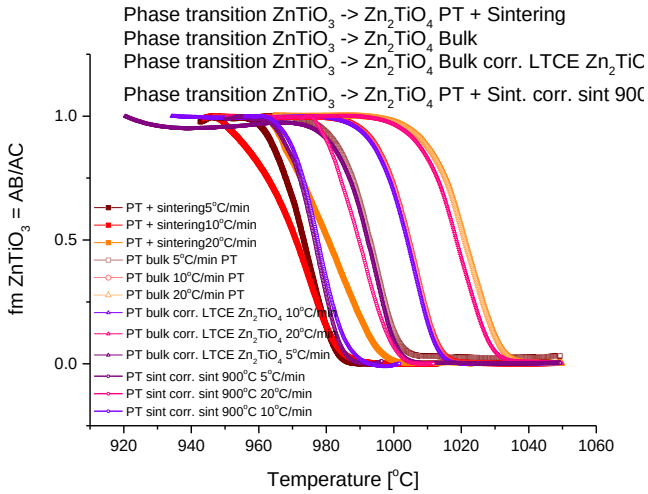


Fig 13. Phase transition kinetics comparison: Bulk and Sintered, Experimental vs. Corrected.

Although the previous comparison has led to some of the conclusions we have presented, quantitative comparison needs fitting function and overlapping measure determination of the constructed function with experimental curve. We have chosen Sigmoid shape - Boltzmann fitting function. Formula of the fitting function is given in the equation (1). Boltzmann fitting function has two constant values for the y = A1 and A2. Maximal rate represents X0, and ((A1+A2)/2), set of values. Shape of the curve, on the Fig. 14, gives good resemblance comparing to other offered functions in the Origin software package [6]. Although shape represents rise of the emerging phase, constants A1 and A2 enable as well diminishing shape. Fitting function resembles Johnson-Mehl-Avrami-Kolmogorov (JMAK) expression for the model of the kinetics for the isothermal phase transformations [5]. Their phenomenological model is often used for crystallization process and solid phase transition kinetic description.

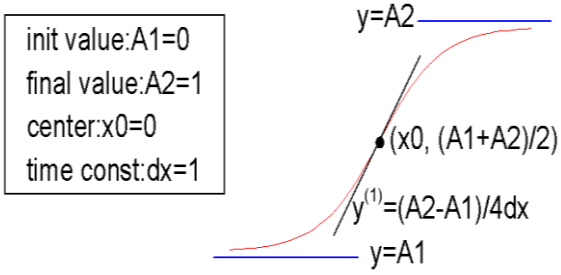


Fig 14. Sigmoid shape - Boltzmann fitting function for phase transition kinetic process.

$$y = \frac{A_1 - A_2}{1 + e^{(x - x_0)/dx}} + A_2 \qquad (1)$$


ISBN 978-86-7466-930-3

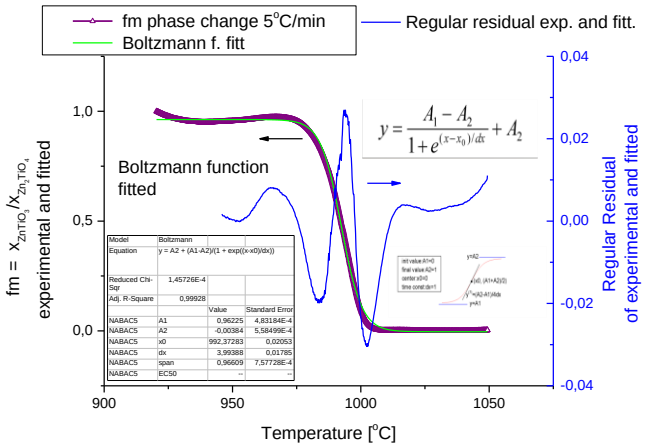


Fig 15. Phase transition curve, Boltzmann fitting function – Bulk, corrected, 5°C/min.

.

Example of the fitting function is presented on Fig 15. Fitting function (light green thin) for the experimental set of data (purple bold). Regular residual curve quantifies resemblance (blue, right axes). Table inserted represents fitting function parameters listed in a report data sheet of the fitting procedure. Residuals are the measure of discrepancy with the experimental curve and they also are listed in a report data sheet.

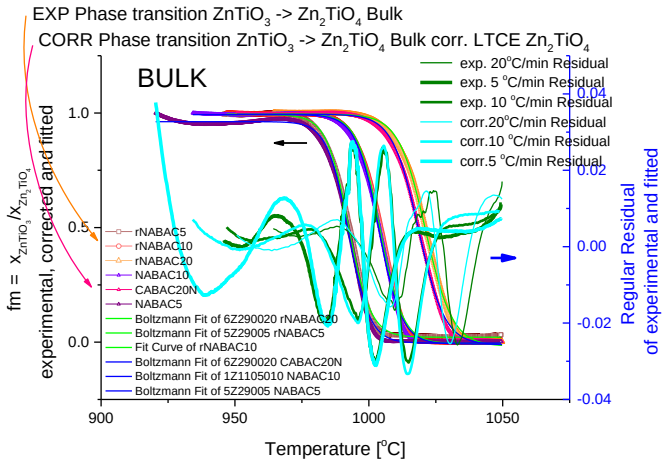


Fig 16. Bulk phase transition curve, 5, 10, 20°C/min, experimental and corrected, Boltzmann function fitted – Residuals

Curves presented at Fig. 16 of experimental and corrected curves are bold with symbols in the colors previously used. Fitted function is green thin line for experimental and blue thin line for corrected curves, all on left axes. It is visible that residuals (cyan and olive, thickness refers to a heating rate, right axe) for the experimental and corrected curves are mutually resembling, Fig. 16. This implies that corrected curves are following fitting equation just as good as experimental. Only 20°C /min are somewhat shifted. This can be subscribed to the fact that at larger heating rates stress - strain relation is not negligible.

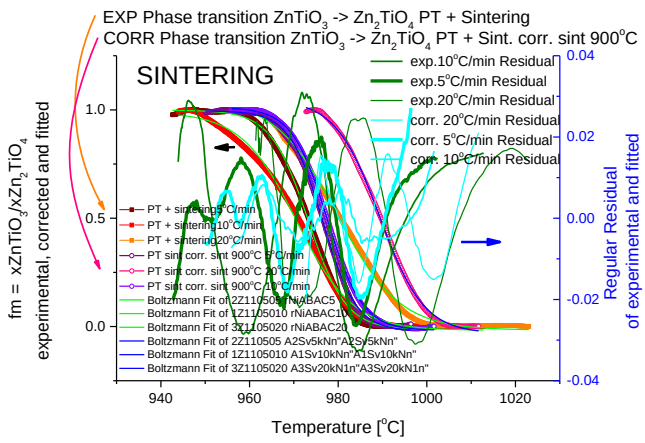


Fig 17. Sintering phase transition curve, 5, 10, 20°C/min, experimental and corrected, Boltzmann function fitted – Residuals

Same procedure of fitting for experimental and corrected curves with Boltzmann function is performed at sintering phase transition curve, Fig. 17, left axes. Residual functions for experimental (olive) and corrected (cyan) are showing intensive difference for the corrected and experimental, right axes. If the fitted functions are observed for experimental (green thin) and corrected (blue thin), it is obvious that shape of the curve that represents phase transition with correction is showing more resemblance with the sigmoid shape. Thus, the made correction is more reasonable.

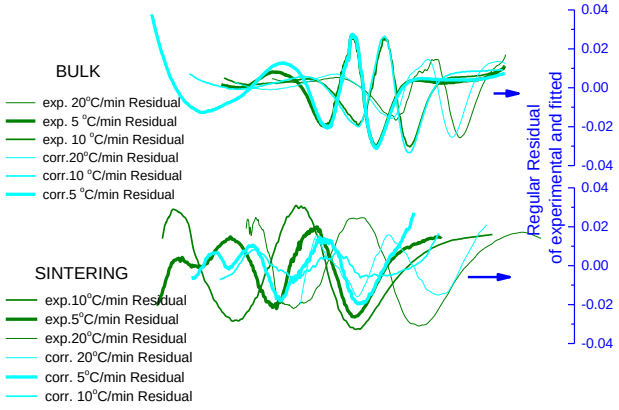


Fig 18. Fitting function Residuals comparison Boltzmann function fitted – Residuals, Sintering phase transition curve, 5, 10, 20°C/min, experimental and corrected, Bulk phase transition curve, 5, 10, 20°C/min, experimental and corrected.

Fitting function Residuals comparison experimental and corrected – Bulk and Sintered brings a reason that if we are comparing just residuals, Fig. 18, the conclusion drawn is that the sintering correction brings large misfit comparing to the bulk. The misfit is for the sintering residuals, as well for the different heating rates presented with different thickness of the line. Experimental curves misfit for the sintering residuals are significant (Sintering, olive, different thickness).

 ISBN 978-86-7466-930-3

## IV. Conclusion

Physical differentiation of the sintering shrinkage and Phase transition phenomena dilatation has been compared with mathematical data manipulation of the sintering curve and phase transition subtraction. It is found that data manipulation procedure does not give the reliable results.

Although a thorough procedure for the phase transition kinetic data achieving from the dilatometric data and fitting procedure with sigmoidal function has been established.

## Acknowledgment

Funds for the realization of this work are provided by the Ministry of Education, Science and Technological Development of the Republic of Serbia, Agreement on realization and financing of scientific research work of the Institute of Technical Sciences of SASA in 2021 (Record number: 451-03-68/2022-14/200175) and for Maria Vesna Nikolić, University of Belgrade - Institute for Multidisciplinary Research (Record number: 451-03-68/2022-14/200053).

Special thanks to Prof. Vladimir B. Pavlović from the Faculty of Agriculture for the TEM microscopy.

## References

[1] J. Osamu Yamaguchi, et al., Formation and Transformation of ZnTi03, J. Am. Ceram. SOC., 70 151 C-97-C-98 (1987), https://doi.org/10.1111/j.1151-2916.1987.tb05011.x

[2] M.V. Nikolic, N. Labus, M.M. Ristic, Densification rate and phase structure changes during sintering of zinc titanate ceramics, Ceramics International 35 (2009) 3217–3220, https://doi.org/10.1016/j.ceramint.2009.05.028

[3] B.D. Cullity, 2nd edition, ELEMENTS OF X-RAY DIFFRACTION, Addison-Wesley Publishing Company, Inc., 1978. pp.377, 12-4 Determination of Solvus Curves (Disappearing Phase Method)..

[4] J. Yang, J.H. Swisher, The phase stability of $Zn_2Ti_3O_8$, Mater. Char. 37 (1996) 153–159, https://doi.org/10.1016/S1044-5803(96)00098-8.

[5] Fanfoni, M., Tomellini, M., The Johnson-Mehl- Avrami-Kohnogorov model: A brief review., Nouv. Cim. D 20, 1171–1182 (1998). https://doi.org/10.1007/BF03185527

[6] Origin Pro 9.0.0 1991-2013 release OriginLab Corporation, Northampton, MA, USA.

 ISBN 978-86-7466-930-3

# Study of the effect of microstructure and magnetic texture on major hysteresis loop phenomenology using OOMMF

Mehrija Hasičić, Aphrodite Ktena and Jasna Hivziefendic

***Abstract*— This paper presents a study of the effect of microstructure and magnetic te ture on the hysteresis loop through quasi-static micromagnetic simulations using the open-source software . esults show that microstructure and magnetic te ture parameters can be used to control the coercivity. The anisotropy constant is the parameter mainly controlling the coercivity. The increase in the volume fraction of hard inclusions in a soft matri typically leads to higher coercivity. In the case of randomly oriented inclusions, the calculated coercivity is lower than that for the homogeneous soft case which is e plained through the prominent anisotropy energy density compared to the much wea er e change energy density. The results will be used to correlate simulation parameters with magnetic parameters obtained from major hysteresis loop measurements.**

***Index Terms*—micromagnetic calculation, microscopic modeling, energy minimization, magnetic properties, hysteresis loop,**

## I. Introduction

MAGNETIC materials have played a significant part in the formation of modern civilization and continue to do so in the advancement of industrial and scientific development. Their applications range from the compass, which was the first known application, to power generation and transmission, electronic appliances, analogue and digital data storage, medical appliances such as magnetic resonance imaging (MRI), magnetic therapy, and drug delivery, sensors and actuators, scientific instruments, and so on [1].

Electrical steel, in particular, is a material that is widely used in construction, shipping and other modes of transportation, automobiles, electrical equipment and appliances, and other metallic products. Reducing waste and saving energy is a highly discussed and investigated topic. Increasing efficiency and lifecycle of the electrical machines would be beneficial for both topics.

Stresses are the result of both thermomechanical treatments during the manufacturing of the materials and fatigue during the lifetime of a steel structure. They are difficult to avoid however, they should be monitored and treated if and when possible [2]. Increased stress levels are known to contribute to losses [3], [4].

The study of the effects contributing to losses as well as the effect of stress on the magnetization process is necessary for the optimization of magnetic materials used in the above applications. Several physical or phenomenological models of magnetization have been developed to assist in the design of new materials or contribute to the control of magnetization driven processes. These models can be grouped into phenomenological [5]–[8], microscopic [9]–[12], atomistic [13], [14] and multiscale [15]–[18].

The modeling of the magnetization process consists in determining the relationship between the magnetization state of a material and external stimuli, such as externally applied fields, mechanical loads, or heating. The major hysteresis loop M(H) of a material, where M represents magnetization of the material and H is applied field, yields the macroscopic parameters typically used to classify a given material, such as the saturation magnetization, remanence, coercive field, energy product, for specific excitation conditions. Losses are also obtained from the major hysteresis loop measurement since they depend on the area of the loop. The M(H) curve is the result of magnetization processes at the atomistic, domain and macroscopic level, which in turn depend on the underlying microstructure. Changes in temperature, frequency of the applied field or stress levels affect the M(H) characteristic. The modeling of stress dependent magnetization processes is a challenging task due to the highly nonlinear dependence of the magnetization on external stimuli which is further complicated by the magneto-elastic coupling.

The stress-strain characteristic for any given material consists of an elastic region, where the stress is proportional to the strain and the proportionality constant is the Young's modulus, and a plastic region. The microstructure in plastically deformed materials consists of finer grains, hence longer grain boundaries acting as pinning centers, anisotropy dispersion, and magnetically hardened regions which considerably affect the magnetization response.

The long-term goal of our work is to develop a modeling approach that links stress-induced microstructural changes to the macroscopic parameters obtained from hysteresis loop or magnetic Barkhausen noise measurements [4], [12]. Towards this goal, in this paper, we report on the quasi-static micromagnetic modeling of the effect of microstructure on the major hysteresis loop phenomenology using the open source OOMMF software to minimize the free energy equation of material [12], [19].

The proposed methodology is presented in the following section which is followed by simulation results and their

[M]ehrija Hasičić is with the Faculty of Engineering and Natural Sciences, International Burch University, Francuske revolucije bb, 71000 Sarajevo, Bosnia and Herzegovina (e-mail: mehrija.hasicic@ibu.edu.ba), (https://orcid.org/0000-0002-4679-3611)

Aphrodite Ktena is with the Energy Systems Laboratory, National and Kapodistrian University of Athens, Evia, 34400, Greece (e-mail: apktena@uoa.gr), (https://orcid.org/0000-0003-1350-2408).

Jasna Hivziefendic is with the Faculty of Engineering and Natural Sciences, International Burch University, Francuske revolucije bb, 71000 Sarajevo, Bosnia and Herzegovina (e-mail: jasna.hivziefendic@ibu.edu.ba), (https://orcid.org/0000-0002-0461-171X)

 ISBN 978-86-7466-930-3

discussion. The last section summarizes the main conclusions and presents the roadmap of our future work.

## II. Methodology

In micromagnetic modeling, the minimization of the energy equation reflects the balance between long range and short-range interactions and their interplay with external stimuli, such as a magnetic field. Short range interactions have a localized effect and are determined by the competition between the exchange and anisotropy energy terms which reflect the effect of the chemical composition and the crystalline structure of the material. The long-range interactions are represented by the magnetostatic energy term which summarizes the magnetic fields experienced by a given elementary volume inside the material, as the former emanate from all the remaining volumes in it. This term depends on the current magnetic state of the material, which incorporates the effect of previous states as well, and is responsible for the hysteresis property observed in magnetic materials.

The effect of stress on the magnetization process was introduced through various microstructural configurations as well as through the parameters of anisotropy constant, exchange energy coefficient, and magnetic saturation which control the anisotropy, exchange and mangnetostatic energy terms, respectively.

More details on micromagnetic calculations with OOMMF are given in [12] where the effect of simulation parameters on the major hysteresis loop phenomenology was studied. More specifically, we discussed the effect of discretization and cell size as well as the effect of magnetic parameters, such as the exchange and anisortopy constants and the orientation of the easy axis, on the major hysteresis loop.

In this work, we report on the effect of changes in microstructure through the introduction of hard magnetic inclusions in a soft matrix combined with changes in the direction of anisotropy, i.e. in the magnetic texture. The parameters used in the simulations to define different types of materials are the anisotropy coefficient $K_1$, the exchange enrgy coeffiecient $A_{ex}$ and the magnetic saturation $M_s$. The parameter values used in the simulation results shown here are summarized in Table I. They correspond to three different types of materials: Material 1 is homogeneous with parameters corresponding to a soft magnetic material, while Materials 2 and 3 have inclusions of hard material in the soft magnetic matrix. The inclusions of Material 3 are harder than those of Material 2 with parameters corrseponding to those of a rare earth magnet.

TABLE I
MAGNETIC PROPERTIES OF MATERIALS

| aterial | Type of material | Parameters | | |
|---|---|---|---|---|
| | | $K_1$ $[kJ/m^3]$ | $A_{ex}$ $[kJ/m]$ | $M_s$ $[kA/m]$ |
| Material 1 | Soft | 48 | 21 | 1700 |
| Material 2 | Hard | 520 | 21 | 1400 |
| Material 3 | Hard | 4500 | 21 | 1280 |

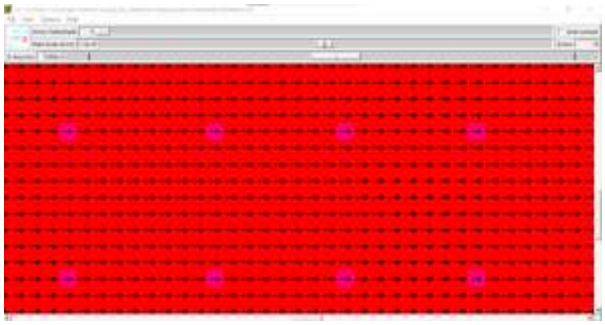

Fig. 1. shows the magnetization plot of a soft matrix with hard inclusions.

The simulated material is of rectangular shape discretized along the x (length), y (width) and z (thickenss) direction in cubic cells of side *a*. The size of the cubic cells is a user defined variable which has to be chosen so that it is smaller than the magnetocrystalline exchange length for hard magnetic materials and magnetostatic exchange length for soft magnetic materials, as presented in [12]. Fig. 1 shows the initial state of the magnetization vector for every cell in the xy plane for a given z-value. The plot is zoomed in 35x so that it is easier to see the hard inclusions (in purple) which are of a size of one cell. The pattern continues throughout the sample in the xy plane. Simulations have been carried out for two cases, where hard inclusions are either cylindrical structures throughout the z layer, or one spherical cell in the middle z layer. Table II summarizes the texture and type of inclusions for the simulations shown here.

The applied field in all simulations is 1100 mT along the x-axis.

TABLE II
PROPERTIES OF HARD INCLUSIONS IN THE SOFT MATRIX USED IN THE SIMULATIONS

| | ard inclusions | Anisotropy direction | Type of inclusions |
|---|---|---|---|
| 1 | Material 2 | randomized | cylindrical |
| 2 | Material 2 | [1 0 0] | cylindrical |
| 3 | Material 2 | [0 1 0] | cylindrical |
| 4 | Material 2 | [0 0 1] | cylindrical |
| 5 | Material 2 | [1 1 0] | cylindrical |
| 6 | Material 2 | [0 1 1] | cylindrical |
| 7 | Material 2 | [1 0 1] | cylindrical |
| 8 | Material 2 | [1 1 1] | cylindrical |
| 9 | Material 2 | [1 0 0] | spherical |
| 10 | Material 2 | [0 1 0] | spherical |
| 11 | Material 2 | [0 0 1] | spherical |
| 12 | Material 2 | [1 1 0] | spherical |
| 13 | Material 2 | [0 1 1] | spherical |
| 14 | Material 2 | [1 0 1] | spherical |
| 15 | Material 2 | [1 1 1] | spherical |
| 16 | Material 3 | [1 0 0] | cylindrical |
| 17 | Material 3 | randomized | cylindrical |

## III. Results

The base case used for comparison corresponds to a homogeneous magnetic material where all cells have the parameters of Material 1 and the anisotropy, saturation magnetization and the applied field are all along the x-axis or [1 0 0].


ISBN 978-86-7466-930-3

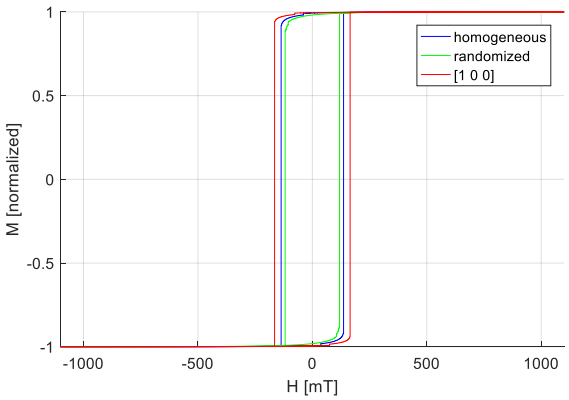


Fig. 2. Simulated hysteresis loops of a homogeneous magnetic material (blue) versus a material with cylindrical hard inclusions, extending throughout the z layer, with randomized anisotropy (green), and with the anisotropy oriented along the [1 0 0] (red) parallel to the applied field

First, we examine the effect of the anisotropy direction of hard magnetic inclusions of Material 2. In Fig. 2, the simulated hysteresis loop of the homogeneous case is compared against those of materials with cylindrical hard inclusions with anisotropy along the same direction as that of the soft matrix and the applied field, i.e. along [1 0 0], and with randomized anisotropy orientations. When the hard inclusions are aligned with the soft matrix, the coercivity increases as it is expected (red line). However, when the anisotropy of the inclusions is randomly dispersed, the material presents a softer response (green line). To better understand these results, we examine the energy plots for the two cases shown in Fig. 3.

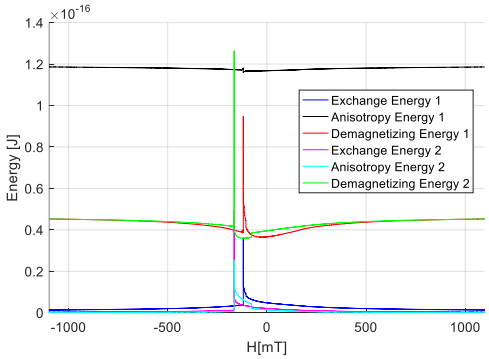


Fig. 3. Energy plots for materials with hard inclusions with randomized anisotropy (case 1) and anisotropy aligned with the anisotropy of the soft matrix (case 2)

The peak in the computed energy terms is observed around coercivity which is higher for the material with the hard inclusions along the same direction of the applied field (case 2). When the anisotropy is randomized (case 1), the anisotropy energy term is the most prominent and does not vary much with the field (black line). Exchange energy on the other hand is lower (blue line) even though the exchange constant used is the same in both cases. The exchange energy between two neighboring magnetic dipoles depends on the angle between their magnetization vectors, i.e. the larger the angle, the smaller the exchange energy. When the anisotropy is randomized and there is no predominant preferred direction, the resistance of a given magnetic volume to the forced change in magnetization is lower and the magnetization rotation towards the effective field experienced by the given volume is facilitated.

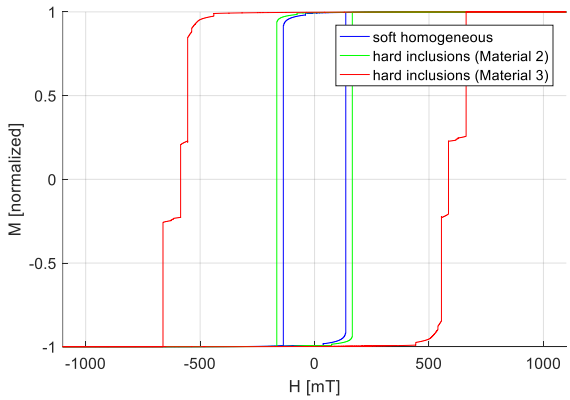


Fig. 4. Calculated hysteresis loops for the soft homogeneous case (blue) versus hard inclusions of Material 2 (green) and Material 3 (red)

The next step was to investigate the effect of magnetic hardness of the inclusions by carrying out simulations with inclusions of Material 2 and Material 3 (Fig. 4). The anisotropy and initial magnetization of hard inclusions in both samples is along [1 0 0]. The coercivity for the cases shown in Fig. 4 increases six-fold as the anisotropy constant of the inclusions increases almost ten-fold. Observed results are consistent with major hysteresis loop characteristics of harder magnetic materials. The step-like response of the loop corresponding to Material 3 (red line) is an artefact of the OOMMF calculation.

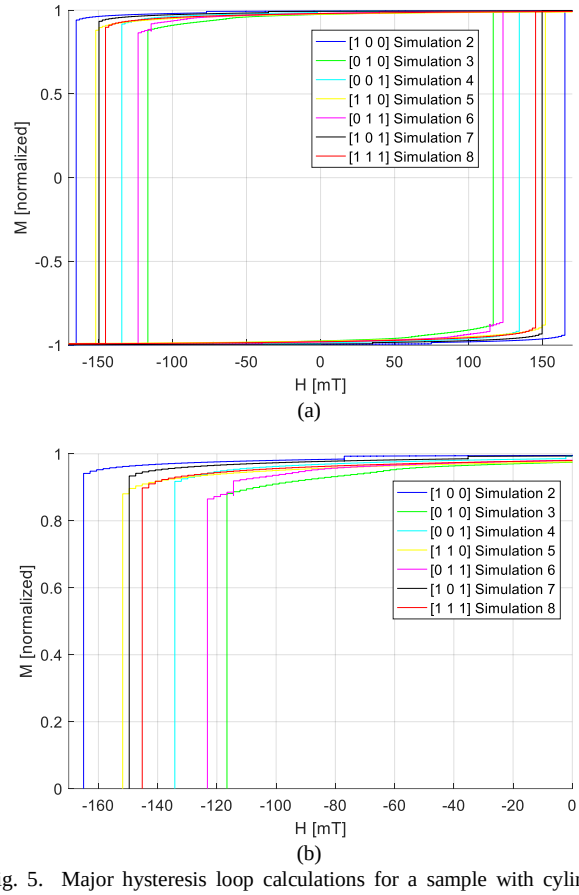


Fig. 5. Major hysteresis loop calculations for a sample with cylindrical hard inclusions of Material 2 throughout the z layer with the anisotropy lying along different directions (a) full loop (b) second quadrant

In Fig. 5 we present the effect of magnetic texture on the major hysteresis loop phenomenology of a sample with hard inclusions of Material 2. The details of each simulation are given in Table 2. The anisotropy direction is varied from

 ISBN 978-86-7466-930-3

easy axis (x-axis) (#2) through various in-plane (#3 and #5) and out-of-plane (#4, #6, #7 and #8) directions.

Hard axis loops (#3 and #6) are narrower, as expected. The lowest coercivity is observed when the anisotropy is along y-axis [0 1 0] in-plane and along [0 1 1] direction, out of the plane, respectively. The case with the anisotropy pointing out of plane along [0 0 1] (#4) yields a higher coercivity than the previous cases. The widest loops are obtained when the anisotropy of the hard inclusions is along [1 0 0], collinear with the applied field, or has an x-component [1 1 0], [1 0 1] and [1 1 1] (#2, #5, #7 and #8).

The effect of distribution of hard cells along the z layer is investigated next, by arranging the hard inclusions only in one z layer, the middle one. The results are presented in Fig. 6.

Distributing the hard inclusions in only one z layer, while keeping the pattern along the xy plane presented in Fig. 1 consequently, means a decrease in the volume fraction of hard inclusions. Therefore, we observe that the widest major hysteresis loop presented in Fig. 6 is narrower than the widest major hysteresis loop presented in Fig. 5. The discussion of Fig. 5 is valid for Fig. 6 as well. The only different trend observed is that when the hard inclusions' anisotropy is along [0 1 0], the observed coercivity is 10 mT higher than in the case of cylindrical inclusions.

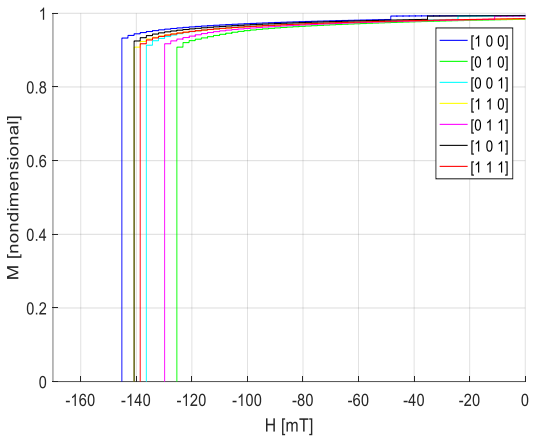


Fig. 6. Major hysteresis loop calculations for a sample with spherical hard inclusions of Material 2 in the middle z layer, with the anisotropy lying along different directions

The presented calculations demonstrate the effect of microstructure and magnetic texture on the observed phenomenology of the hysteresis loop. Experimental evidence has shown that both are affected in plastically deformed material [4], [20]. In our future work, simulations will be based on experimental measurements and the OOMMF software will be used to link microstructural parameters to macroscopic magnetic parameters obtained from a major hysteresis loop measurement, such as the differential permeability and coercivity which have a well-established dependence on residual stresses in a magnetic material.

The limitations of the OOMMF software, observed mainly in the approach to saturation in the third quadrant, need to be further examined and ensure that they do not affect the validity of our conclusions.

## IV. Conclusion

The effect of microstructure and magnetic texture on the hysteresis loop has been studied through quasi-static micromagnetic simulations using the open-source software OOMMF. Microstructure was varied through cubic or columnar inclusions of different magnetic parameters inside a soft matrix. Magnetic texture was varied through the anisotropy orientation of the inclusions. Coercivity varies considerably with both microstructure and texture. When the hard inclusions have randomized anisotropy, lower coercivity is observed, even compared to the homogeneous case calculation. This is explained through the interplay between the different energy density terms, where the anisotropy energy density is predominant, and the exchange energy is reduced.

Future work will be focused on the correlation between simulation parameters and magnetic parameters obtained from measured loops at various residual stress levels on electrical sheet laminates.

## References

[1] S. Banerjee and A. K. Tyagi, Eds., *Functional materials preparation, processing and applications*, 1st ed. London ; Waltham, MA: Elsevier, 2012.

[2] K. Liang, S. Angelopoulos, A. Ktena, X. Bi, and E. Hristoforou, 'Residual Stress Distribution Monitoring and Rehabilitation in Ferromagnetic Steel Rods', *Sensors*, vol. 22, no. 4, p. 1491, Feb. 2022, doi: 10.3390/s22041491.

[3] F. J. G. Landgraf, M. F. de Campos, and J. Leicht, 'Hysteresis loss subdivision', *ournal of Magnetism and Magnetic Materials*, vol. 320, no. 20, pp. 2494–2498, Oct. 2008, doi: 10.1016/j.jmmm.2008.04.003.

[4] A. Ktena, M. Hasicic, F. J. G. Landgraf, E. Moudilou, S. Angelopoulos, and E. Hristoforou, 'On the use of differential permeability and magnetic Barkhausen Noise Measurements for Magnetic NDT Applications', *ournal of Magnetism and Magnetic Materials*, vol. 546, p. 168898, 2022, doi: https://doi.org/10.1016/j.jmmm.2021.168898.

[5] E. C. Stoner and E. P. Wohlfarth, 'A mechanism of magnetic hysteresis in heterogeneous alloys', *Phil. Trans. . Soc. ond. A*, vol. 240, no. 826, pp. 599–642, May 1948, doi: 10.1098/rsta.1948.0007.

[6] D. C. Jiles and D. L. Atherton, 'Theory of ferromagnetic hysteresis (invited)', *ournal of Applied Physics*, vol. 55, no. 6, pp. 2115–2120, Mar. 1984, doi: 10.1063/1.333582.

[7] S. H. Charap and A. Ktena, 'Vector Preisach modeling (invited)', *ournal of Applied Physics*, vol. 73, no. 10, pp. 5818–5823, May 1993, doi: 10.1063/1.353538.

[8] A. Ktena and E. Hristoforou, 'Stress Dependent Magnetization and Vector Preisach Modeling in Low Carbon Steels', *IEEE Transactions on Magnetics*, vol. 48, no. 4, pp. 1433–1436, Apr. 2012, doi: 10.1109/TMAG.2011.2172786.

[9] T. Schrefl, J. Fidler, and H. Kronmüller, 'Nucleation fields of hard magnetic particles in 2D and 3D micromagnetic calculations', *ournal of Magnetism and Magnetic Materials*, vol. 138, no. 1, pp. 15–30, Nov. 1994, doi: 10.1016/0304-8853(94)90395-6.

[10] J. Fidler and T. Schrefl, 'Micromagnetic modelling - the current state of the art', . *Phys. Appl. Phys.*, vol. 33, no. 15, pp. R135–R156, Aug. 2000, doi: 10.1088/0022-3727/33/15/201.

[11] W. Scholz *et al.*, 'Scalable parallel micromagnetic solvers for magnetic nanostructures', *Computational Materials Science*, vol. 28, no. 2, pp. 366–383, Oct. 2003, doi: 10.1016/S0927-0256(03)00119-8.

[12] M. Hasičić and A. Ktena, 'Using OOMMF to Study the Effect of Microstructure on Magnetic Hysteresis Loops', in *Ad anced Technologies, Systems, and Applications I*, Cham, 2022, pp. 651–660.

[13] D. C. Jiles, 'Hysteresis models: non-linear magnetism on length scales from the atomistic to the macroscopic', *ournal of Magnetism and Magnetic Materials*, vol. 242–245, pp. 116–124, Apr. 2002, doi: 10.1016/S0304-8853(01)01213-6.

 ISBN 978-86-7466-930-3

[14] B. Skubic, J. Hellsvik, L. Nordström, and O. Eriksson, ‘A method for atomistic spin dynamics simulations: implementation and examples’, . *Phys. Condens. Matter*, vol. 20, no. 31, p. 315203, Aug. 2008, doi: 10.1088/0953-8984/20/31/315203.

[15] L. Daniel, M. Rekik, and O. Hubert, ‘A multiscale model for magneto-elastic behaviour including hysteresis effects’, *Arch Appl Mech*, vol. 84, no. 9, pp. 1307–1323, Oct. 2014, doi: 10.1007/s00419-014-0863-9.

[16] L. DANIEL, L. Bernard, and O. Hubert, ‘Multiscale Modeling of Magnetic Materials’, in *eference Module in Materials Science and Materials Engineering*, Elsevier, 2020. doi: 10.1016/B978-0-12-803581-8.12056-9.

[17] W. Zhao, S. Wang, X. Xie, X. Zhou, and L. Liu, ‘A simplified multiscale magneto-mechanical model for magnetic materials’, *ournal of Magnetism and Magnetic Materials*, vol. 526, p. 167695, May 2021, doi: 10.1016/j.jmmm.2020.167695.

[18] P. Fagan, B. Ducharne, L. Daniel, and A. Skarlatos, ‘Multiscale modelling of the magnetic Barkhausen noise energy cycles’, *ournal of Magnetism and Magnetic Materials*, vol. 517, p. 167395, Jan. 2021, doi: 10.1016/j.jmmm.2020.167395.

[19] M. J. Donahue and D. G. Porter, *MMF ocumentation*. National Institute of Standards and Technology. Accessed: Oct. 26, 2020. [Online]. Available: https://math.nist.gov/oommf/doc/userguide20a2/userguide/

[20] F. J. G. Landgraf, M. Emura, K. Ito, and P. S. G. Carvalho, ‘Effect of plastic deformation on the magnetic properties of non-oriented electrical steels’, *ournal of Magnetism and Magnetic Materials*, vol. 215–216, pp. 94–96, Jun. 2000, doi: 10.1016/S0304-8853(00)00075-5.

 ISBN 978-86-7466-930-3

# Primeri primene fraktalne analize za karakterizaciju novih materijala

Sanja Aleksić, Branislav Ranđelović, Aleksandar Pantić, Neda Stanojević, *Member, IEEE,* Dušan Milošević

***A stra t*— ovom radu je dat pregled novih metoda za pri upljanje, obradu i analizu materijala oji se oriste ili su u fazi istraživanja za primenu u savremenim uređajima za široku ili specifičnu, namensku proizvodnju. Razvoj biofizike, ele torhemije, napreda u proizvodnji alternativnih izvora energije, biomole ulima, ali i svim ostalim oblastima nau e, ukratko je objašnjen vezom između nanotehnologije, kao intrdiscplinarne nauke budućnosti i novih matematičkih metoda i pristupa koji omogućavaju analizu zrna, pora i njihovih sraničnih delova i interakcija. Dobijeni rezultati imaju za cilj da se električne, fizičke i hemijske osobine materijala povežu sa njihovim izlaznim parametrima (temperatura, gustina, električna i magnetna provodnost...) i da se, u s ladu sa tim, dođe do novih ili uvedu korekcije u postojeće metematičke i fizičke teorije i jednačine, da bi se dobili što relaniji iu precizniji rezultati za karakterizaciju uređaja u kojima se koriste. Jedan od elementarnih uslova za unapređivanje karakteristika matrijala je optimizacija procesa sinterovanja i ele tro-fizičkih osobina materijala, što je, takođe, analizirano u ovom radu.**

***Ključne reči*— anotehnologije; fra talna analiza; obnovljivi izvori energije; materijali za ele troni u.**

## I. Uvod

Sve novije i, doskora, čak i nezamislivo nepoznate potrebe modernog čoveka u svim sferama života, primoravaju nas da budemo kreativni i gradimo nove koncepte bezbedne i stabilne arhitekture, medicine, informacionih i telekomunikacionih elemenata - objekata i sistema za prenos informacija na što veće daljine sa što manje gubitaka, sredstava za transport i prevoz robe i putnika, unapređenja poljoprivrede u cilju dobijanja što većih količina zdrave i jeftinije hrane, itd. Činjenica da su bukvalno sve oblasti života i rada, koje bi ljudima trebalo da donose dobrobiti, u intenzivnoj fazi razvoja, podrazumeva da je osnovni preduslov za to obezbeđivanje tehničkih i tehnoloških uslova za proizvodnju i korišćenje ogromnih količina, najpre toplotne i električne, a zatim i svih ostalih vidova energije. Naravno, sve nove tehnologije bi, takođe, morale zadovoljavati što veći broj kriterijuma koji su okosnica borbe savremenog sveta za očuvanje životne sredine.

Nanotehnologije, nova naučna disciplina koja uključuje, pre svega, fundamentalne nauke kao što su, fizika, hemija, biologija, nauka o materijalima, ali i veliki broj inženjerskih grana (elektronika, građevinarstvo, mašinstvo), obećavaju da će u budućnosti biti vrlo bitan faktor razvoja i proizvodnje novih generacija uređaja za upotrebu u svim sferama života savremenog društva sa visokim stepenom minijaturizacije i integracije, a minimumom utroška energije [1-6].

Razvoj tehnika i tehnologija je nezamisliv i beskoristan ukoliko ne postoje novi načini za korišćenje već postojećih ili pronalaženje načina za proizvodnju i upotrebu novih, modernih materijala, koji bi od strane fizike, hemije i biologije mogli biti proučavani na neki način drugačiji od klasičnog. Prilagođavanje metodologija je neophodno s obzirom da se radi o objektima čije su dimenzije reda veličine nekoliko (ili nekoliko desetina) nanometara, tj. dimenzijama koje teže veličini jednog atoma, molekula ili njihovih klastera [1].

Osim gore pomenutih tehnika i tehnologija, čiji je razvoj uzročno-posledično povezan sa razvojem i upotrebom novih materijala, neophodno je razvijati i naučne metode priključpljanja, obrade i analize dobijenih rezultata eksperimentalnih merenja ili simulacija, koji služe za karakterizaciju njihovih fizičkih, hemijskih ili električnih osobina.

U ovom radu će biti dat osvrt na jedan noviji matematički pristup, koji se razlikuje od konvencionalne Euklidove geometrije i predstavlja pionirske pokušaje uvođenja drugačijeg načina razmišljanja primenjenog na zrnastu strukturu materijala, koji je poznat kao fraktalna analiza.

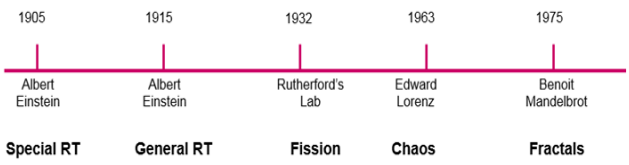


Sl. 1. Periodi važnih otkrića tokom XX veka.

Na Sl. 1 se vidi da je do otkrića "fraktala" došlo mnogo kasnije nego što je to bio slučaj sa prethodnim važnim

Sanja Aleksić – Elektronski fakultet, Univerzitet u Nišu, ulica Aleksandra Medvedeva 14, 18000 Niš, Srbija (e-mail: sanja.aleksic@ elfak.ni.ac.rs).

Branislav Ranđelović – Elektronski fakultet, Univerzitet u Nišu, ulica Aleksandra Medvedeva 14, 18000 Niš, Srbija (e-mail: branislav.randjelovic@ elfak.ni.ac.rs).

Aleksandar Pantić – Elektronski fakultet, Univerzitet u Nišu, ulica Aleksandra Medvedeva 14, 18000 Niš, Srbija (e-mail: aleksandar.pantic@ elfak.ni.ac.rs).

Neda Stanojević – Elektronski fakultet, Univerzitet u Nišu, ulica Aleksandra Medvedeva 14, 18000 Niš, Srbija (e-mail: neda.stanojevic94@gmail.com).

Dušan Milošević – Elektronski fakultet, Univerzitet u Nišu, ulica Aleksandra Medvedeva 14, 18000 Niš, Srbija (e-mail: dusan.milosevic@ elfak.ni.ac.rs).

 ISBN 978-86-7466-930-3

saznanjima koja su pomogla čovečanstvu na putu otkrivanja velikih tajni prirode.

Jedan fenomen, veoma intrigantan za ljudsku socijalnu inteligenciju, je činjenica da isti atomi predstavljaju osnovne gradivne elemente i nosioci su istih procesa i u živoj i u neživoj prirodi. Osnova tih procesa i pojava je, ustvari, kretanje elektrona, samostalno ili unutar atoma ili molekula. Potreba za razumevanjem "trenutka" koji pravi razliku između materije koja je živa i one koja to nije, zahteva interdisciplinarni pristup molekularne biologije i ostalih grana nauke i inženjerstva. Naime, molekularna biologija, kao nauka o životu, proučava različite procese u živim organizmima na molekularnom nivou. To znači da se ona bavi i kretanjem elektrona u biomolekulima, pa je neophodna saradnja sa molekularnom bioelektronikom, jer se kretanje elektrona zasniva na istim principima u živim organizmima, kao i u svim ostalim oblicima materije. Zbog toga je jedini ispavan pristup proučavati ga kao zajedničko svojstvo jednog fundamentalnog procesa [2].

Dosadašnji razvoj nauke i tehnologije ne omogućava nam da pratimo kretanje i proučavamo pojedine elektrone, kao nosioce elementarnog naelektrisanja i energije (električne, toplotne, mehaničke…). U ovom trenutku je moguće posmatranje i opisivanje kretanja molekula metodama koje nudi kvantna fizika. Naravno, sve vreme imamo u vidu da svaki molekul nosi klaster elektrona koji se kreće zajedeno sa njim, ali se i svaki electron ponaosob kreće unutar samih atoma koji čine molekule, i čiji su osnovni elementi građe. Zato činjenica da, unutar molekula koji su delovi biosistema, postoje atomi i elektroni koji "nisu svesni" da li su delovi žive ili nežive prirode, je veoma važna, jer izdvaja molekul kao značajan integrativni faktor između njih.

Zbog svega toga će na ovom mestu biti ukratko objašnjene osnove fraktalne analize, kao jedne od novijih matematičkih metoda, koja se danas sa velikim uspehom, naročito uzimajući u obzir ograničenja Euklidove geometrije, koriste za karakterizaciju materijala na nivou nanometra. Korisnost njene primene u materijalima koji su zanimljivi sa stanovošta fizičke elektronike biće prezentovana na nekoliko, od velikog broja primera, ali bez ograničenja da se identična analiza ne može proširiti univerzalnim principima od objekata nanodimenzija do otkrivanja tajni kosmosa, jer sve to, sagledano objektivnim očima van našeg egocentričnog referentnog sistema, doprinosi i spoznaji uzroka, načina i razloga postojanja nas samih u univerzuma čiji smo sastavni deo.

Zbog toga će u ovom radu ukratko biti opisane osnove na kojima se bazira ideja fraktalne matematike, metode koje se primenjuju u zavisnosti od toga o kojoj vrsti problema i sferi ljudkog života se radi i primeri vezani za fizičku elektroniku, alternativne izvore energije, materijale za energetiku i telekomunikacione uređaje...

## II. Osnovne postavke fraktalne teorije

U cilju približavanja koncepta novog načina razmišljanja i njegove primene u pomenutim naučnim istraživanjima vezanim za razvoj elektronskih komponenata, prvenstveno u sferi primene u novim, alternativnim izvorima energije i telekomunikacionim sistemima, počećemo kratkom rekapitulacijom analize $BaTiO_3$, koja, kao što je već rečeno, predstavlja pionirska istraživanja u ovoj grani nauke.

Pokazano je da su kod $BaTiO_3$, čiji prah ima zrnastu, granularnu strukturu, oblasti prostora oko granica pojedinačnih zrna odgovorne za skoro sve procese koji određuju fenomene i osobine različitih materijala. Naime, pojave opisane kao, veoma specifične karakteristike elektroprovodnosti, dielektrične, feroelektrične, feromagnetne, poluprovodničke i brojne druge, zajedno definišu bazične električne osobine u čitavoj zapremini materijala. To znači da se pomenuti procesi odigravaju u slojevima koji se mogu opisati kao ljuske Minkovskog, i da se mogu ponavljati i na isti način prostirati po čitavoj zapremini posmatranog uzorka.

Zato je pogodna polazna tačka za opisivanje ćelijskih struktura kao što je kristalni perovskit i slični materijali Voronojeva teselacija (mozaički raspored geometrijskih figura u prostoru koje se ne preklapaju, ali "komuniciraju" graničnim oblastima bez praznina između njih), jer termin *tessella* potiče od latinske reči tessella, što znači ravan kamenčić ili parče keramike ili stakla za pravljenje mozaika. Ovakav koncept je primenljiv i na zrna i na pore, i efikasan je alat za prognozu projektovanih mikrostrukturnih svojstava i mikrostrukturne karakterizacije materijala (Sl.2).

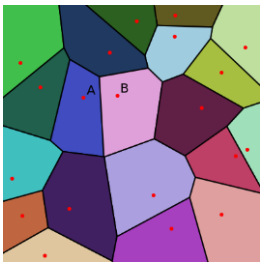


Sl. 2. Primer Voronoevog dijagrama.

Voronojevi dijagrami imaju mnogo mogućnosti za primenuu, prvenstveno u predviđanju ili simulaciji interakcija između susednih struktura. Na primer, modeliranje bioloških ćelijskih struktura, modeliranje obrazaca rasta u šumama, procena mineralnih rezervi za rudarenje, mapiranje najbližeg aerodroma avione koji bi trebalo da slete u hitnim sliučajevima, itd [6].

Da bi se formirala Voronojeva teselacija, potrebno je posmatrati skup tačaka u ravni, jer je to najlakše zamisliti, naročito u euklidskoj metrici. Za svaku tačku je moguće odabrati oblast u okolini koji je bliži toj tački od bilo koje druge tačke u datom skupu. Na taj način svaka oblast formira ćeliju koja odgovara toj tački. Unija svih skupova takvih ćelija pokriva oblast prostora koji se posmatra u datoj ravni. Ta unija skupova predstavlja Voronojevu teselaciju.

Usko povezan pojam sa Voronojevom teselacijom je Deloneova triangulacija. Za dati skup tačaka u nekom matematičkom prostoru, Deloneova triangulacija se formira povezivanjem tačaka i stvaranjem trouglova sa uslovom da za

 ISBN 978-86-7466-930-3

bilo koju tačku ne postoji ni jedna druga tačka u opisanoj kružnici odgovarajućeg trougla (Sl.3).

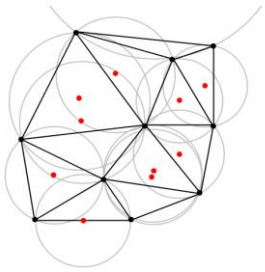

Sl. 3. Primer Deloneove triangulaciju sa tačkama (crvenim) koje predstavljaju centre odgovarajućih opisanih krugova Deloneovih trouglova.

Bazirajući se na osnovnim postavkama koje smo pomenuli, Voronojev dijagram je, najpre, definisan kao ravan ili deo ravni ili teselacije (*S*), pri čemu je ispunjen uslov da je skup $=\{ _1, _2, _3, _4 \ldots\}$ i da je njihova unija skup *S*, a presek između bilo koje dve ćelije prazan skup. Osim toga, ovakva teselacija je izomorfizam sa konačnim skupom tačaka $Z=\{ _1, _2, _3, \ldots _n\}$ iz skupa *S* na način prikazan na Sl.4 i 5:

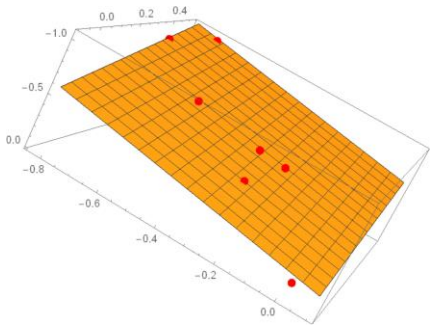

Sl. 4. Izomorfni skup tačaka odabrane ravni ili teselacije *S*.

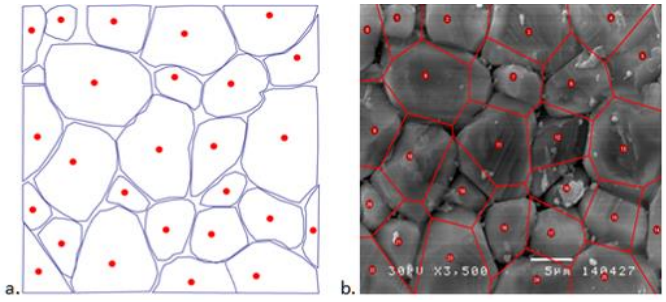

Sl. 5. Poligonalna aproksimacija konture zrna

Voronojeva ćelija $_i$, koja je generisana oko tačke $_i$, sadrži sve tačke iz *S* i zadovoljava jednačinu:

$$\rho( , _i) < \rho( , _j), \text{ za } j \neq i, \qquad (1)$$

pri čemu je $\rho$ Euklidovo rastojanje:

$$\rho( , y) = \sqrt{( _1 - _2)^2 + (y_1 - y_2)^2} \qquad (2)$$

za tačku čije su koordinate:

$$= ( _1, _2),\ y = (y_1, y_2). \qquad (3)$$

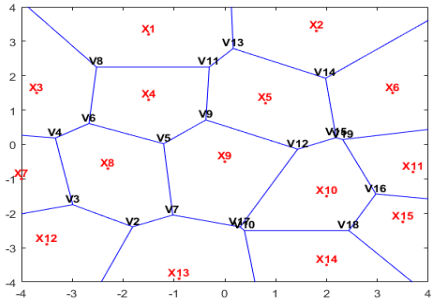


Sl. 6. Primer Voronoijevog dijagrama za datu distribuciju tačaka sa jednom pokretnom generišućom tačkom.

Na Sl.6 je dat primer Voronojevog dijagrama za datu distribuciju tačaka sa jednom pokretnom generišućom tačkom.

Algoritam za generisanje planarnih Voronojevih dijagrama može biti direktan i indirektan. Prva grupa algoritama generiše Voronojeve ćelije počevši od, a priori, datih tačaka generisanja. Indirektni algoritmi prvo generišu Deloneov trougao koji potom proizvodi Voronojeve ćelije. Triangulisana nepravilna mreža (TIN) je geometrijska struktura podataka koja se koristi, npr. u Geografskim informacionim sistemima (GIS) za 3D modeliranje reljefa (Sl.3). Osnovna karakteristika TIN strukture je korišćenje većeg broja tačaka na mestima gde je prikazan niži nivo detalja. Generalno, kad je set tačaka definisan, mora biti uspostavljena optimalna veza između tačaka trouglova korišćenjem Delaunai triangulacije (DT).

Ovakve polazne geometrijske i matematičke postavke su se pokazale kao izuzetno efikasan alat za prognozu projektovanih mikrostrukturnih svojstava i mikrostrukturne karakterizacije materijala čije su jedinice građe zrna i pore. Naime, čist euklidski pristup ne daje dovoljno verodostojnu reprodukciju oblika zrna i pora, pa pretpostavka fraktalne geometrije, bazirana na Voronojevom modelu daje rezultate mnogo bliže realnom formiranju mikrostrukturnih konstituenata – granica zrna i pora. Zato ovakav mikrostrukturni pristup rekonstrukcije i prognoze daje i realnije vrednosti elektrofizičkih parametara i svojstava, čime se pomeraju granice unutar fraktalne mikroelekotrnike i stvaraju novi pristupi koji vode ka minijaturizaciji i integraciji višeg nivoa (Sl.4). Diektna implikacija svega toga se vidi u reviziji i korekcijama osnovih fiziko - hemijskih i eletrkofizičkih zakona i jednačina (Cobbleov, Heivangov i intergranularni model za određivanje kapacitivnosti kondenzatora, Curie – Veisov zakon, visina Šotkijeve barijere, dielektrična i magnetna susceptibilnost materijala, električna otpornost...)


ISBN 978-86-7466-930-3

Veću fleksibilnost po pitanju rekonstrukcije strukturnih jedinica (zrna i pora) i njihovih međusobnih odnosa sa konačnim ciljem predviđanja osobina mikrostrukture tokom procesa minijaturizacije obezeđuje Kantorov pristup, razvijen kao metod fraktalne analize, koji omogućava modeliranje fraktalne površine modelirane kao skup fraktalnih krivih.

Kantorov ternarni skup C je kreiran iterativnim brisanjem otvorene srednje trećine iz skupa linearnih segmenata. Neka je I interval $[0,1]$. Brisanjem otvorene srednje trećine $[1/3,2/3]$ iz intervala $[0,1]$, ostaju dva segmenta linije $[0,1/3]\cup[2/3,1]$. Zatim se briše otvorena srednja trećina svakog od segmenata, posle čega ostaju četiri linearna segmenta $[0,1/9]\cup[2/9,1/3]\cup[2/3,7/9]\cup[8/9,1]$. Ovaj proces se nastavlja do beskonačnosti. Na bilo kojoj n-toj iteraciji, ovakav skup je moguće pokriti uvođenjem $2^n$ intervala prečnika $1/2^n$. Procena gornje granice $\alpha$ - dimenzionalne Hausdorfove dimenzije $C$ za pokrivanje intervala širine (prečnika) $w_a(1)$ se dobija iz:

$$\sum_{k=1}^{2^n}\left(w_a\left(\frac{1}{3^n}\right)\right)^{\alpha}=\frac{2^n\left(w_a(1)\right)^{\alpha}}{3^{n\alpha}}, \qquad (4)$$

Za dobijenu vrednost gornje granice broja iteracija skupa neophodno je prodiskutovati moguća rešenja. Iz (4) je jasno da će za $n\to\infty$ ovaj razlomak biti konačan i različit od nule ukoliko je $\alpha=\ln 2/\ln 3$, što znači da je $\alpha=\ln 2/\ln 3$ tražena vrednost gornje granice iteracije. Iz principa raspodele mase moguće je zaključiti da je ovo i donja granica iteracije datog skupa. Dakle, Kantorova dimenzija $C$ je kartezijanski proizvod sa samim sobom, što znači da mora biti posmatran kao deo vektorskog proizvoda vektor-tenzor [1-6].

Na identičan način je moguće obuhvatiti $4^n$ krugova dijametra $2^{0.5}/3^n$. U tom slučaju će procenjena gornja granica $\alpha$ - dimenzionalne Hausdorfove dimenzije C za pokrivanje intervala širine (prečnika) $w_a(\sqrt{2})$:

$$\sum_{k=1}^{4^n}\left(w_a\left(\frac{\sqrt{2}}{3^n}\right)\right)^{\alpha}=\frac{4^n\left(w_a\left(\sqrt{2}\right)\right)^{\alpha}}{3^{n\alpha}}, \qquad (5)$$

biti konačna i različita od nule kada $n\to\infty$ za $\alpha=\ln 4/\ln 3$, tako da Kantorov prah ima fraktalnu dimenziju $\alpha=\frac{\ln 2^2}{\ln 3}=\frac{2\ln 2}{\ln 3}$. Isto bi važilo za bilo koji kompaktan skup tačaka na jedičnom intervalu.

## III. PRIMERI PRIMENE FRAKTALNOG RAČUNA ZA IZRAČUNAVANJE ILI KOREKCIJU NEKIH FIZIČKIH PARAMETARA

Na postavkama datim u prethodnom delu ovog rada u najkraćim mogućim crtama, razvijen je veliki broj matematičkih metoda, koje se primenjuju u svim sferama života i u svetovima u opsegu dimenzija od nanočestica do svemirskih objekata ili njihovih skupova.

### *A. Brauno o kretanje*

Za oblast kojom se bavi fizička elektronika i fizika savremenih materijala za elektroniku veliki izazov je mogućnost predviđanja i modelovanja Braunovog kretanja elektrona u kristalnim materijalima. Sa druge strane, osnove Braunovog kretanja bi trebalo da budu iste i u biomolekulima. Povezivanje biofizičkih i sistema kondenzovane materije je od velikog značaja zbog potrebe za novim pristupom u mikroelektronskim biouređajima, biokompjuterima ili biočipovima. S obzirom na to da su submikronske čestice živog i neživog sistema identične, moguće je uspostaviti dvoznačno korespodentnu vezu ova dva sistema čestica čije je integrativno svojstvo biomimetička korelacija zasnovana na sličnostima fraktalne prirode Braunovog kretanja.

U jednom od istraživanja koja je sprovela grupa naučnika, dobijeni su eksperimentalni rezultati kretanja bakterija pod uticajem energetskih impulsa, kao što je muzika. Da bi bilo moguće definisati odnos između biofizičkih i fizičkih sistema čestica, uvođenjem matematičke analitičke forme i primenom karakterizacije fraktalne prirode Braunovskog kretanja fraktalnom interpolacijom, bilo je potrebno imati i eksperimentalne rezultate praćenja kretanja nekih biomolekula. Ova napredna istraživanja uključuju i proučavanja fizičkih sistema čestica u čvrstom stanju kao deo neorganskih sistema.

Dimenzije i obrasci kretanja bakterija i virusa ukazuju na biomimetiče sličnosti sa kretanjem čestica kondenzovane materije. Obrasci kretanja bakterija pokazuju stohastičke, a samim tim i nepredvidive karakteristike, jer se ovi mikroorganizmi suaraju kako međusobno, tako i sa okolnim molekulima, naglo menjaju pravce kretanja, kreću se rotaciono ili u cik-cak linijama, što je osnovna karakteristika Braunovog kretanja. Putanja i brzina njihovog kretanja su specifične za svaku bakterisku vrstu, ali im je zajedničko to što na sve njih značajno utiču faktori okoline (temperatura, osvetljenost, "hranljive materije", energetski impulsi...). Budući pravci istraživanja moraju uključiti stvaranje matemtičkih analitičkih jednačina, generisanje 3D interpolacionih dijagrama, kao i dizajniranje 3D fraktalnog interpolacioog dijagrama kretanja bakterija i biomolekula primenom metoda fraktalne interpolacije.

### *B. Materijali a alternati ne i ore energije*

Sa porastom svetske energetske krize, istraživanja novih, obnovljivih i alternativnih izvora energije su u porastu. Fokus je na istraživačkim oblastima, ponekad od manjeg značaja u aplikacijama, gde su različite metode sinteze i optimizacija svojstava mikrostrukture izvršile značajno poboljšanje elektrofizičkih svojstava izlaznih materijala i komponenti. Ovo je posebno značajno za veću energetsku efikasnost u proizvodnji električne energije, pa je velika potreba za poboljšanjem performansi baterije i sistemi baterija, gorivnih ćelija, uređaja za eksploataciju energije vodonika, tj. za poboljšanjem kapaciteta rezervoara za tako proizvedenu

 ISBN 978-86-7466-930-3

energiju, što je jedno od najvažnijih razvojnih pitanja u energetskoj sferi. Imajući u vidu postignute rezultate u oblasti elektrohemijskih izvora energije, posebno razvoja elektrolita, istraženi su doprinosi pojedinih elemenata ili matrijala primenom fraktalne analize prirode materijala. Elektrohemija se bavi proučavanjem hemijskih reakcija koje se odigravaju na granici između elektroda (čvrsti metali ili poluprovodnici) i elelektrolita, odnosno jonskog provodnika, preko kojih se vrši razmena naelektrisanja između elektroda i elektrolita. Sa tačke gledišta fizike i energetike, to znači da se, ustvari, traži veza između električne energije i hemijskih reakcija. Pri tome, elektrokatalliza ima sve veći značaj u gorivim ćelijama, jer uključuje supstance koje povećavaju brzinu hemijskih reakcija, posebno na površinama umetnutih elektroda, naročito kada se koriste mešoviti jonsko-elektronski provodljivi oksidi. Tipični primeri su elektrode u gorivim ćelijama sa čvrstim oksidom (SOFC) ili membrane za izdvajanje kiseonika iz okolnog vazduha. Kako je za inkorporaciju kiseonika neophodno formiranje jona kiseonika, u sistemu moraju postojati slobodni elektroni, a to je moguće ili povezivanjem elektroda ili, još bolje, korišćenjem mešavine poluprovodnika i metala u čvrstom stanju (MIEC), kao što su oksidi sa perovskitnom kristalnom strukturom. Jedan od primere takve analize je istraživanje uticaja parametara mikrostrukture u oblasti elektrohemije (npr. uticaj koncentracije Ho2O3 (od 0,01 tež% do 1 tež%) i temperature sinterovanja (od 1320°C do 1380°C), kao parametara konsolidacije. Samim tim su otvorena vrata fraktalizacije elektrohemijske funkcije i u osnovnim termodinamičkim parametrima je uvedena fraktalna korekcija. Sa velikim interesovanjem se istražuje i zavisnost fraktalne dimenzije od koncentracije aditiva [1-6].

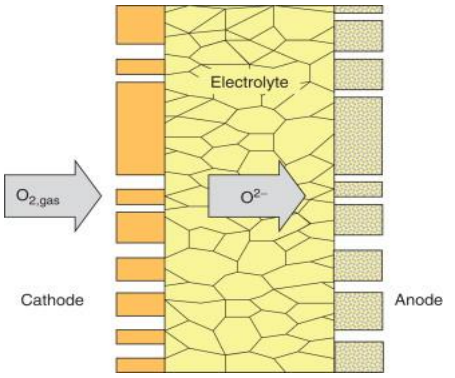


Sl. 7. Jedinična ćelija koja se sastoji od dve elektorde rzdvojene elektorlitom.

Mnogobrojna novija proučavanja alternativnih izvora energije danas su u fokusu većine projekata iz obasti energetike. Kako se svet suočava sa ozbiljnim energetskim izazovima, razvoj i implementacija tehnologija obnovljivih izvora energije postaju sve važniji. U ovom trenutku se, u tu svrhu, koriste svi raspoloživi izvori alternativne, kao i izvori energije bazirani na fosilnim gorivima. Međutim, najintenzivnije se proučavaju načini korišćenja energije Sunca. Procesi tokom kojih dolazi do pretaranja “energije” Sunca u neki drugi oblik energije (prvenstveno hemijsku) su mnogobrojni i mogu biti fotokatalitički, fotoelektrohemijski, procesi fotosinteze... Na osnovu njih se razvijaju i odgovarajuće tehnologije, poznate kao tehnologije solarnih ćelija (fotonaponske i fototermalne). Iz navedenih referenci se jasno vidi da suštinu rešenja dela problema predstavlja upotreba materijla kao što je $TiO_2$, ZnO, CoS i da se svi oni nanose u što tanjim (nanoslojevima, kao nanoprevlake za nanonožice...).

### *C. Feromagnetni i elektromagnetni materijali*

Međutim, bez informatičke revolucije, bez mogućnosti prenosa informacija između nano-i makroobjekata, ništa od ovoga ne bi bilo moguće. Telekomunikacioni uređaji, tj. uređaji i oprema za obradu, prenos i prijem signala korišćenjem žičanih, radio, optičkih i dugih elektromagnetskih urežaja, takođe zahtevaju minijaturizaciju i optimizaciju brzine prenosa informacija, sa što manjim utroškom i gubicima sopstvene energije.

Za sve, gore navedene, primene i potrebe, neophodno je obezbediti rekonstrukciju i projektovanje strukturne jedinice (zrna i pore), da bi se postigla što viša minijaturizacija morfologije. Elektomagnetni, feroelektrični i srodni magnetni materijali se sve više koriste za ovakve pametne i multifunkcionalne namene. U tom smislu su zanimljiva istraživanja posvećena feroelektričnim materijalima, posebno jednofaznim kristalnim materijalima u tehnologiji tankog filma. Materijali sa strukturom perovskita imaju pravilan atomski red, tako da u tim mrežama postoje varijacije i promene koje se kao šabloni ponavljaju i prave domene atoma sa pravilnim promenama u određenom pravcu u materijalu, kao i polarizaciju u datoj tački. Difuzioni fazni prelaz utiče na feromagnetna svojstva materijala, jer se pod uticajem temperature javljaju mikrostukturne promene u vidu promene rasporeda atoma i pojave faznih prelaza u mikro i nano skali. Zbog toga se menja i Kirijeva temperatura i trenutak početka polarizacije. Ovakvi fazni prelazi su dominantni kada čvrsti rastvor dobije homogenu strukturu. U ovoj fazi za analizu različitih površina zrna i pora, i definisanje njihovih geometrijskih karakteristika nije dovoljno koristiti euklidsku geometriju. Zato se skoro uvek uključuje elektronska mikroskopija, koja omogućava posmatranje objekata sa nekoliko nivoa uvećanja. Najzastupljeniji u eksperimentalnim prosedurama u električnom i magnetnom smislu su $BaTiO_3$ i NZT ($Nd(Zn0.5Ti0.5)O_3$) materijali, dobijeni tokom standardnih metoda u kojima se odigravaju rekacije za dobijanje čvrstog stanja.

U ovim procesima je veoma bitno poznavanje morfologije keramičkih zrna, jer se realne međuzrnaste kontaktne površine, kao izrazito nepravilni oblici, mogu optisati na adekvatan način samo korišćenjem fraktalnih modela. Model intergranularnog kapaciteta omogućava izračunavanje veličine zrna određivanjem vrednosti fraktalne dimenzije korišćenjem fraktalne korekcije. Pri tome je naročito važna uloga dielektrične i magnetne konstante materijala, čije vrednosti je moguće korigovati na osnovu fraktalne prirode intergranularne morfologije, a koja dovodi do korekcije u

 ISBN 978-86-7466-930-3

Heyvangovom modelu i Curie – Veissovom zakonu.

Neka početna istraživanja inergranularnih kontakata $BaTiO_3$ keramike pokazuju da ona mogu imati jako veliki uticaj na električna i magnetna svojstva u celoj zapremini materijala. Intergranularni kontakti se formiraju tokom procesa sinterovanja. Tokom sinterovanja, dve čestice praha formiraju kontakt, dok međuatomske sile počinju da formiraju vrat čestice u kontaktnoj oblasti, što uzrokuje povećanje gustine materijala. Glabni mehanizam za povećanje gustine je smanjenje slobodne površinske energije sistema. U daljem procesu sinterovanja vrat počinje da raste. Kontrola tog procesa se vrši različitim difuzionim mehanizmima (rešetkasta difuzija, difuzija na granici zrna...), čije su brzine određene ukupnim fluksom atoma koji dolaze do vrata.

Karakterizacija datih procesa se može raditi simulacijom rasta vrata u vremenskom domenu, kombinovanjem rezultata za vrednosti kontaktnih površina sa kinetikom firmiranja tri ili više kontaktnih površina ili modelom tri ili više zrna, koji omogućavaju uspostavljanje ekvivalentnog modela klastera takvih zrna. To znači da se uzorak $BaTiO_3$ keramike može modelovati u električnom smislu kao impedansa koja sadrži dva kondenzatora, kalem i otpornik. Kako se uzorak keramike sastoji od velikog broja zrna organizovanih u klastere različitih veličina, moglo bi se pretpostaviti da svaki klaster, pa čak inergranularni kontakt unutar klastera, pokazuje slično ponašanje. Dominantni doprinos ekvivalentnoj impedansi u širokom grekventnom opsegu dolazi od kapacitivnosti, pa se svaki i ntergranularni kontakt može posmatrati kao intergranularni mikrokkondenzator. Na osnovu ovih razmatranja mogu biti formirani ekvivalentni električni modeli tri ili četiri klastera zrna, zasnovani na računarskom modeliranju i simulacijama [1-6].

## IV. Zaključak

Primena fraktalne analize na fundamentalno kretanje virusa, bakterija, ali i atoma, molekula, klastera i elektrona u svim strukturama poznato kao Braunovo kretanje je jedna od osnovnih ideja koja bi povezal aživu i neživu prirodu. Ali, i sve oblasti inženjerskih nauka, sa posebnim osvrtom na fizičku elekotrniku, nauku o materijalima i savremenim materijalima u oblasti altrnativnih izvora energije i telekomunikacija je u povoju. POvezivanje nanotehnologija sa biomimetikom i korekcijom svih ostalih do sada poznatih fizičkih i hemijskih jardnačina klasičnim matematičkim aparatom bi trebalo korigovati uzimanjem u obziru parametara spoljašnje sredine i njihovog uticaja na ponašanje gradivnih elemenata živog i ili neživog mikrosveta.

## Zahvalnica

Zahvalnost za otvaranje vrata za ulazak u oblast primene fraktalne analize u granama nauka koje su obuhvatile čitav spektar osnovnih, ali i preimenjenih nauka obuhvaćenih pojmom Nanotehnologije, sa strane svih potpisnika ovog rada upućena je profesoru doktoru Vojislavu Mitiću sa Elektronskog fakulteta u NIšu, koji je jednan od idejnih tvoraca ovog koncepta i sigurno čovek bez čije upornosti i istrajnosti, sagorevanja i vizije, mnogo toga ne bi bilo započeto.

## Literatura

[1] S. Aleksić, B.Markovic, V.V.Mitic, D Milosevic, M.Milosevic, M.Sokolovic, B.Vlahovic, Interpolation Methods Applied on Biomolecules and Condensed Matter Brownian Motion, Journal of Circuits, Systems and ComputersVol. 31, No. 04, 2250074 (2022).

[2] Ribar, S., Neural Networks from Biophysical Applications in Microelectronics Parameters Measurements, in: Bioceramics, Biomimetic and other Compatible Materials Features for Medical Applications, (Eds. Najman S., et al.), Springer Nature, Cham, Switzerland, 2021.

[3] Raj, B., et al., Nanotechnology for Energy Sustainability, Wiley-VCH, New York, USA, 2017.

[4] J Mitic, V. V., et al., The Fractal Nature Materials micro-structure Influence on Electrochemical Energy Sources, Science of Sintering, 47, 2, pp. 195-204, 2015.

[5] Mitic, V. V., et al., Fractal Nature Structure Reconstruction Method in Designing Micro-Structure Properties, Materials Research Bulletin, 101, May, pp. 175-183, 2018.

[6] V. Mitić 1,2, V. Paunović , S. Janković , V. Pavlović, I. Antolović, D. Rančić, Electronic Ceramic Structure within the Voronoi Cells Model and Microstructure Fractals Contacts Surfaces New Frontier Applications, Science of Sintering, 45, pp. 223-232, 2013. doi: 10.2298/SOS1302223M.

## Abstract

This paper provides an overview of new methods for collecting, processing and analyzing materials that are used or are in the research phase for use in modern devices for wide or specific, dedicated production. The development of biophysics, electrochemistry, progress in the production of alternative energy sources, biomolecules, but also all other fields of science, is briefly explained by the connection under nanotechnology, as an interdisciplinary science of the future and new mathematical methods and approaches that allow analysis of grains, pores and their interactions. The aim of obtained results is to connect the electrical, physical and chemical properties of materials with their output parameters (temperature, density, electrical and magnetic conductivity ...) and, accordingly, to reach new ones or introduce corrections to existing mathematical ones and physical theories and equations, in order to obtain as realistic and accurate results as possible for the characterization of the devices in which they are used. One of the elementary conditions for improving the characteristics of the material is the optimization of the sintering process and the electro-physical properties of the material, which is also analyzed in this paper.

**Aapplication of fractal analysis for characterization of new materials e amples**

Sanja Aleksic, Branislav Randjelovic, Aleksandar Pantic, Neda Stanojevic, Member, IEEE, Dusan Milosevic

 ISBN 978-86-7466-930-3

# Mikrostrukturna i dielktrična karakterizacija PLZT keramike

Vesna Paunović, *Member, IEEE*, Miloš Marjanović, *Member, IEEE,* Zoran Prijić, *Member, IEEE*

***Apstrakt* –PLZT keramika spada u jednu od veoma značajnih grupa funkcionalnih materijala koji čine osnovu za proizvodnju velikog broja elektronskih uređaja. Mikrostruktura i dielektrična svojstva keramike zavise od pripreme praha i uslova termičke obrade. PLZT prahovi, korišćeni u radu su pripremljeni na dva različita načina, modifikovanom Pechini metodom, primenom metode polimernog prekursora (PMM) i parcijalnom oksalatnom metodom (B). Proces sinterovanja, uključujući toplo presovanje, izveden je na 1100°C. Mikrostruktura i fazni sastav su istraživani SEM i EDS analizom, dok su promena dielektrične konstante i dielektričnih gubitaka merene u frekventnom opsegu od 1 kHz do 20 kHz, i u temperaturnom intervalu od 25 do 180°C. Kod ispitivanih uzoraka primećena je značajna razlika u mikrostrukturi i dielektričnim svojstvima u zavisnosti od porekla praha i postupka sinterovanja. Mikrostruktura PLZT(PMM) uzoraka, otkriva prisustvo tri različita regiona u uzorcima u pogledu oblika, veličine i sastava zrna. Keramika dobijena oksalatnim postupkom odlikuje se kuboidnim zrnima duž granice izduženih zrna kao i poliedarskim zrnima.**

**Ključne reči – PLZT keramika, dielektrična konstanta, dielektrični gubici.**

## I. UVOD

PLZT keramika se zbog svojih piezoelektričnih i feroelektričnih svojstava široko koristi za niz aplikacija u električnim uređajima. U zavisnosti od koncentracije dopanta La i odnosa Zr/Ti, mogu se dobiti poboljšana piezoelektrična i poboljšana mehanička svojstva kao i poboljšana optička stabilnost keramike [1-4]. Osobine PLZT keramike su u korelaciji sa efektima na granici zrna, a samim tim i sa mikrostrukturom koja se razvija tokom procesa sinterovanja. Otuda je sinteza visoko čistog i ultrafinog praha, sa dobrom hemijskom stabilnošću, od prvenstvenog značaja za proizvodnju keramike specifičnog dizajna. PLZT keramika se tradicionalno dobija konvencionalnim postupkom sinterovanja koristeći čiste oksidne prahove kao polazne materijale. Ova metoda zahteva visoku temperaturu kalcinacije, a aglomeracija čestica praha doprinosi neujednačenoj mikrostrukturi keramike. Zbog toga su razvijeni novi niskotemperaturni prahovi na bazi neorganskog i/ili organometalnog prekursora u cilju dobijanja homogene i finozrnaste keramike [5-7]. Brojne tehnike za proizvodnju PLZT keramičkih prahova zasnivaju se na upotrebi alkoksida, acetata, citrata i oksalata rastvora La, Ti, Zr i Pb koje uključuju koprecipitaciju i sol gel proces. Najpoznatiji procesi su Pechini proces i oksalatni procesi koji omogućavaju preciznu stehiometriju materijala [7,8].

Takođe, za dobijanje keramičkog praha nano veličine koristi se mehanohemijska tehnika. Karakteristika ove tehnike je da se reakcija čvrstog stanja pojačava mehaničkom energijom umesto toplotnom energijom. Pokazalo se da se mehanički dobijeni prahovi bolje sinteruju od prahova dobijenih konvencionalnom reakcijom čvrstog stanja.

Svrha ovog istraživanja je uporedno ispitivanje mikrostrukturnih i dielektričnih svojstava PLZT keramike dobijene dvema različitim metodama pripreme praha. Praškovi su pripremljeni modifikovanom Pechini metodom i parcijalnim oksalatnim postupkom. Uticaj tehnike pripreme na dielektričnu konstantu i dielektrične gubitke keramike je ispitivan u frekventnom opsegu od 1 kHz do 20 kHz i temperaturnom intervalu od 25 do 180°C.

## II. EKSPERIMENTALNI DEO

Za pripremu PLZT keramičkih prahova su korišćene dve različite tehnike a) modifikovani Pechini proces, odnosno metod polimernog prekursora (PMM) i b) parcijalni oksalat metod (B).

U metodi polimernog prekursora organometalni kompleks se dobija počev od La, Ti, Zr-citrata i Pb-acetata, a nakon termičke obrade i kalcinacije prah se melje i presuje u pelete. Prekursor korišćen za pripremu PLZT praha parcijalnom oksalatnom metodom, sastojao se od rastvora Ti-Zr citrata, olova i lantan oksalata. Posle termičke obrade u tri koraka i kalcinacije, prah je takođe mleven i presovan u pelete. Jedna grupa peleta je sinterovana na 1100°C u trajanju od 2 sata konvencionalnim postupkom sinterovanja, a druga grupa peleta je toplo presovana na pritisku od 40 MPa a zatim sinterovana na istoj temperaturi u istom vremenskom intervalu. Da bi se smanjio gubitak PbO tokom sinterovanja, sinterovanje je vršeno u atmosferi kiseonika. Dijagrami toka dobijanja PLZT keramike PMM i B metodom dati su na slikama 1 i 2.

Mikrostruktura PLZT keramike, dobijene različitim poreklom praha i postupcima sinterovanja, ispitana je skenirajućim elektronskim mikroskopom, JSM 5300, JEOL, Japan, opremljenim EDS sistemom (Energy Dispersive

Vesna Paunović – Univerzitet u Nišu, Elektronski fakultet, Aleksandra Medvedeva 14, 18000 Niš, Srbija (email: vesna.paunovic@elfak.ni.ac.rs).

Miloš Marjanović – Univerzitet u Nišu, Elektronski fakultet, Aleksandra Medvedeva 14, 18000 Niš, Srbija (email: milos.marjanovic@elfak.ni.ac.rs).

Zoran Prijić – Univerzitet u Nišu, Elektronski fakultet, Aleksandra Medvedeva 14, 18000 Niš, Srbija (email: zoran.prijic@elfak.ni.ac.rs).

 ISBN 978-86-7466-930-3

Spectroscopy). Gustine ispitivanih uzoraka su merene Arhimedovom metodom. Za merenje dielektričnih svojstava na uzorke je naneta srebrna pasta. Permitivnost i dielektrični gubici su mereni Agilent 4284 LCR metrom, u frekventnom opsegu od 1 kHz do 20 kHz na sobnoj temperaturi. Varijacija dielektrične konstante sa temperaturom merena je u temperaturnom intervalu od 25°C do 180°C.


Sl. 1 Dijagram toka dobijanja PLZT keramike Pechini metodom.

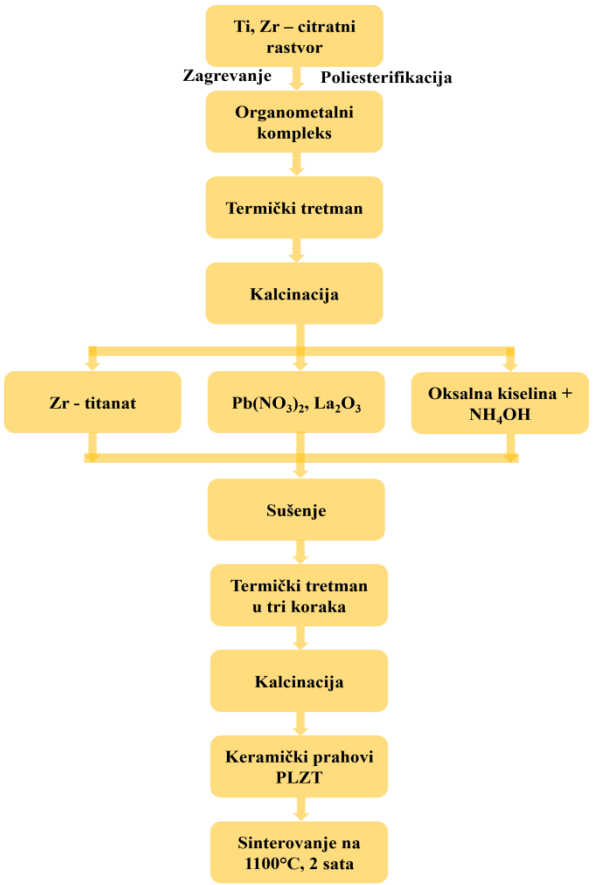


Sl. 2 Dijagram toka dobijanja PLZT keramike oksalatnim postupkom.

## III. Rezultati i diskusija

### A. *Mikrostrukturna svojstva*

PLZT keramika korišćena u ovom radu pripremljena je prema hemijskoj formuli $Pb_{0.905}La_{0.095}(Zr_{0.65}Ti_{0.35})_{0.976}O_3$ sa viškom PbO. Uloga viška PbO, koji podstiče sinterovanje u tečnoj fazi, je veoma važna u početnoj i srednjoj fazi sinterovanja. Isparavanje PbO u završnoj fazi sinterovanja je korisno za formiranje defekata rešetke koji pojačavaju difuziju atoma, pri čemu se povećava gustina uzoraka. Modifikovana Pechini tehnika, ima prednost zato što se kalcinacija prahova odvija na temperaturama nižim od onih koje se zahtevaju konvencionalnim metodama, pri čemu se na ovaj način postiže dobra stehiometrija prahova.

Za obe primenjene metode sinteze praha je karakteristično da se konačno formiranje faza završava nakon kalcinacije na temperaturi od 700°C, pri čemu dobijeni prahovi pokazuju prisustvo samo čiste PLZT faze. U svim sinterovanim uzorcima, bez obzira dali su dobijeni toplim presovanjem ili konvencionalnim sinterovanjem, postiže se visok stepen sinterovane gustine koja se kreće do 94% teorijske gustine.

Mikrostrukture PLZT keramike, dobijene od prahova pripremljenih metodom polimernih prekursora (PMM), i sinterovanih na 1100°C, prikazane su na slici 3. Zbog submikronske veličine čestica kao i prisustva visoke reaktivnosti praha, primećena je neujednačena mikrostruktura uzoraka, za oba postupka sinterovanja (toplo presovanje i konvencionalni postupak sinterovanja).

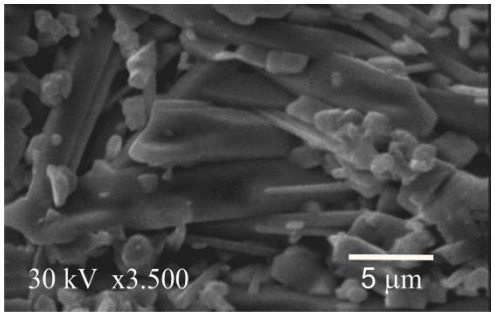


a)

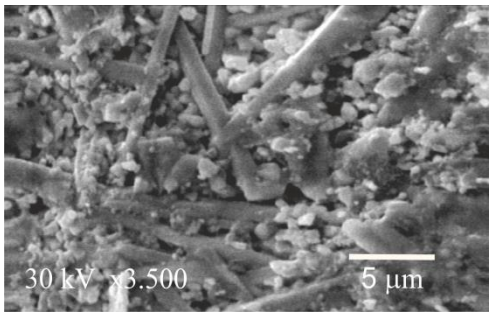


b)

Sl. 3 SEM mikrostruktura PLZT keramike dobijene Pechini metodom a) toplo presovana i b) konvencionalni postipak siterovanja.

U mikrostrukturi ovih uzoraka, razlikuju se tri različita regiona: prvi, sa nasumično orijentisanim izduženim zrnima koja imaju visok aspekt odnos širine i dužine, drugi sa tankim stubastim zrnima i treći region se uglavnom sastojao od svernih zrna. Mikrostruktura je pokazala da su početni prahovi


ISBN 978-86-7466-930-3

submikronske veličine čestica, pripremljeni Pechini postupkom, izazvali preterani rast zrna tokom sinterovanja. Veličina zrna kod uzoraka PLZT keramike dobijenih PMM metodom kretala se od 2-4 μm u sitnozrnim regionima do 10 μm kod izduženih zrna.

Mikrostruktura PLZT keramike dobijene parcijalnim oksalatnim postupkom se znatno razlikuje od one dobijene PMM metodom (sl.4). Mikrostruktura uzorka dobijenog oksalatnom metodom i toplim presovanjem otkriva prisustvo kuboidnih zrna duž granice izduženih zrna. Takođe su prisutna i zrna igličastog oblika i poliedarska zrna. Prosečna veličina kubičastih zrna je manja od 5 μm.

Mikrostruktura keramičkih uzoraka dobijenih oksalatnom metodom i konvencionalnim postupkom sinterovanja je ujednačena po celom uzorku, a veličina i oblik zrna su skoro identični (sl.4b). Zrna su sfernog oblika sa prosečnom veličinom oko 1-2 μm. Međutim, primećeno je prisustvo malih pora, manjih od 1μm, unutar i između zrna.

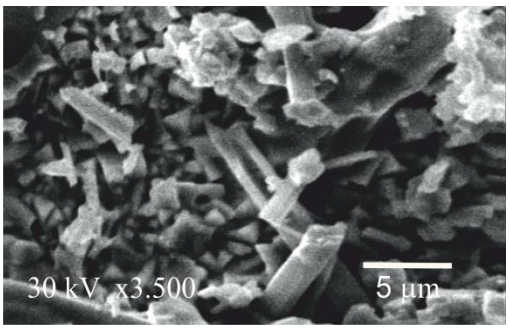


a)

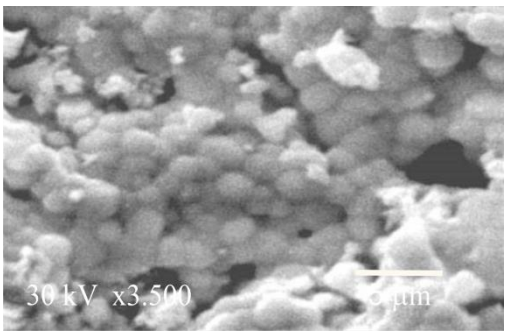


b)

Sl. 4 SEM mikrostruktura PLZT keramike dobijene oksalatnim postupkom a) toplo presovana i b) konvencionalna metoda.

Neuniformnost mikrostrukture, posebno na ivici uzoraka, određena je EDS spektrima. Sastav dugih, izduženih zrna u uzorcima PLZT (PMM) i PLZT (B) je prilično različit. EDS spektar za PLZT (PMM) uzorak, ukazuje da su izdužena zrna, bogata Pb i La fazom ( sl.5a). Odnos Pb/Zr u izduženim zrnima je relativno veći u poređenju sa drugim regionom. S obzirom na malu koncentraciju La, manju od 1 tež.%, La se ne može detektovati energetsko disperzivnom spektroskopijom osim ako nije prisutna nehomogena distribucija i segregacija La. Odgovarajući EDS spektar uzet iz regiona sa izduženim zrnima u PLZT (B) keramici (Sl.5b) jasno pokazuje prisustvo novoformiranih faza bogatih Pb i Zr sa tragovima La.

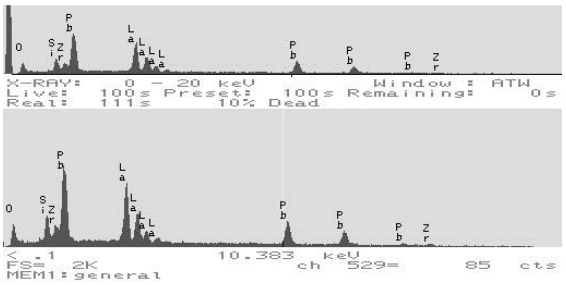


a)

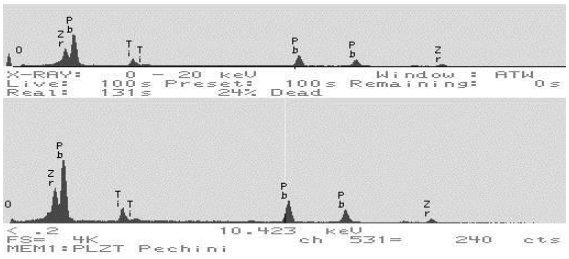


b)

Sl.5 EDS spektar PLZT keramike dobijene a) Pechini metodom i b) oksalatnom metodom.

### *B. Električna svojstva*

Uticaj načina pripreme praha i dobijene mikrostrukture na dielektrične osobine ispitivan je preko promene zavisnosti dielektrične konstante i tangensa ugla gubitaka od frekvencije i temperature.

Zavisnost dielektrične konstante PLZT keramike, dobijene različitim tehnikama, u funkciji frekvencije data je na slici 6.

Frekventni opseg za sve ispitivane uzorke kretao se od 1 kHz do 20 kHz.

Za sve sinterovane uzorke je karakteristična visoka vrednost dielektrične konstante na nižim frekvencijama. Sa povećanjem frekvencije uočeno je sporo monotono smanjenje njene vrednosti do frekvencije od 10kHz, kad je promena postala skoro konstantna.

Takođe vrednost dielektrične konstante je veća u uzorcima dobijenim konvencionalnim postupkom sinterovanja (uzorci su označeni kao c.s) u poređenju sa toplo presovanim PLZT uzorcima.

Razlika u dielektričnim konstantama može biti direktno povezana sa varijacijama u mikrostrukturi, veličini i sastavu zrna.

Različita veličina i oblik zrna u toplo presovanoj keramici primećena u PLZT (PMM) i PLZT (B) doprinosi nižoj dielektričnoj permitivnosti. U uzorcima dobijenim konvencionalnim sinterovanjem karakteristična je uniformnija mikrostruktura što ima za posledicu više vrednosti dielektrične konstante i izraženiju promenu $\varepsilon_r$ sa frekvencijom.

 ISBN 978-86-7466-930-3

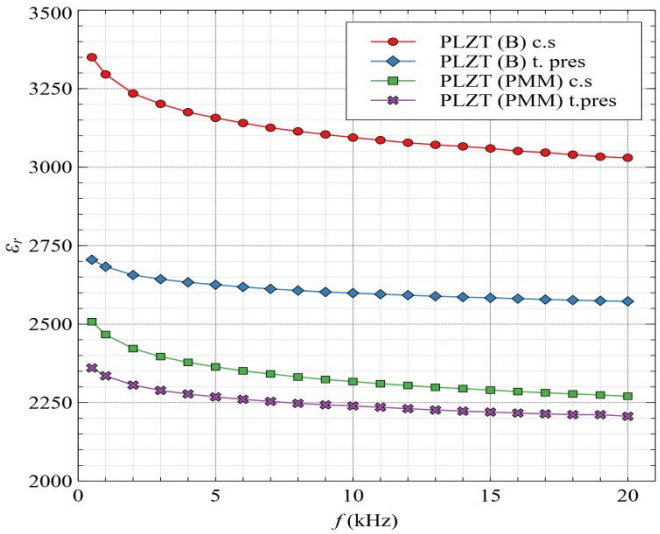


Sl. 6. Zavisnost dielektrične konstante PLZT keramike od frekvencije.

Najviša vrednost dielektrične konstante na 1kHz, $\varepsilon_r$ = 3400, je izmerena za PLZT keramiku dobijenu oksalatnim postupkom kovencionalnim sinterovanjem. Najnižu vrednost pokazuje PLZT (PMM) toplo presovana keramika ($\varepsilon_r$ = 2400).

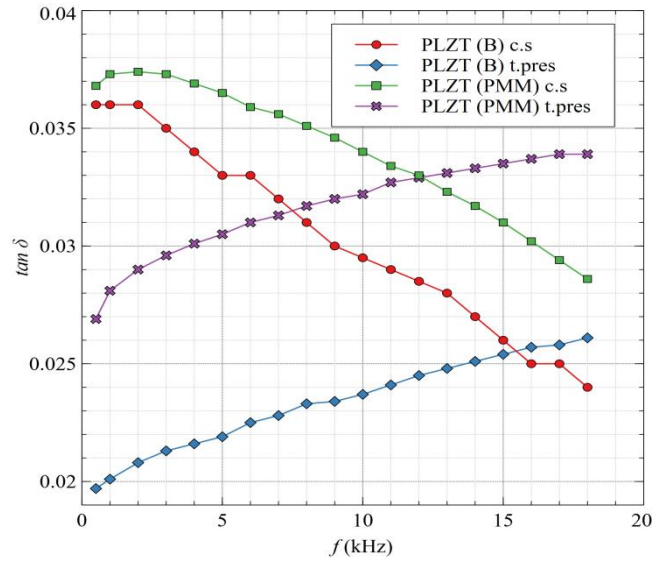


Sl. 7. Zavisnost *tan δ* od frekvencije za PLZT keramiku.

Na osnovu merenja dielektričnih gubitaka u frekventnom opsegu od 1 kHz do 20 kHz, prikazanih na slici 7, može se zaključiti da su dielektrični gubici za sve uzorke veoma mali i kreću se od 0.018 do 0.037. Najveća vrednost od 0.037 na 1kHz i značajna promena *tanδ* u odnosu na frekvenciju, od 0.037 do 0.023 na 20 kHz, pokazuju PLZT (B) uzorci dobijeni konvencionalnim sinterovanjem. Neuobičajena frekventna zavisnost *tanδ*, odnosno povećanje *tanδ* sa frekvencijom, primećena je u toplo presovanim PLZT uzorcima. Za razliku od dielektrične konstante, koja pokazuje male promene u frekventnom opsegu i postaje konstantna na frekvenciji većoj od 10 kHz, dielektrični gubici na sobnoj temperaturi uglavnom opadaju sa frekvencijom. Bez obzira na male razlike u *tanδ*, odgovor tangens gubitaka na kompozicionu i mikrostrukturnu uniformnost je osetljiviji i selektivniji u poređenju sa dielektričnom konstantom.

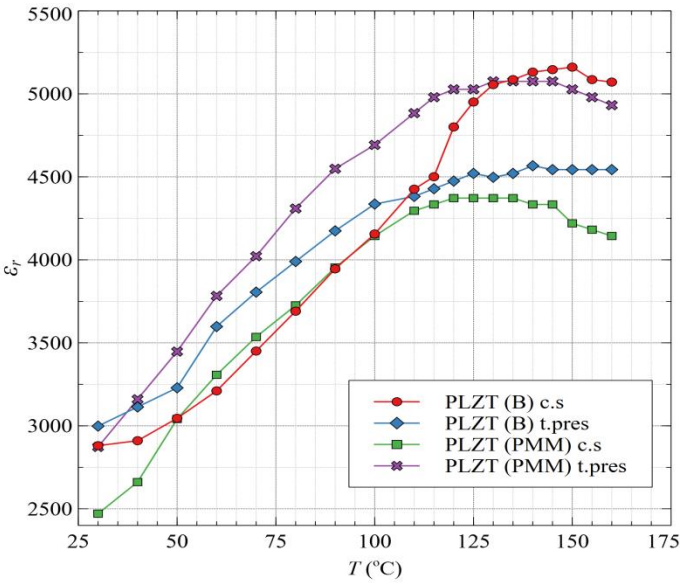


Sl. 8. Zavisnost dielektrične konstante PLZT keramike od temperature.

Uticaj načina pripreme praha i mikrostrukture na dielektrično ponašanje PLZT keramike može se proceniti pomoću krivih zavisnost dielektrične konstante od temperature. Promena dielektrične konstante sa temperaturom za PLZT keramiku prikazana je na sl.8. Za sve ispitivane uzorke karakterističan je porast dielektrične konstante. Maksimum dostižu na temperaturi od 130-140°C a zatim dolazi do smanjenja vrednosti $\varepsilon_r$. Za obe metode sinteze praha promene su izraženije kod uzoraka dobijenih konvencionalnim sinterovanjem. Najveća promena vrednosti dielektrične konstante (od 2800 do 5160) primećena je kod PLZT (B) uzoraka koji su dobijeni konvencionalnim postupkom za koje je karakteristična sitnozrna i uniformna mikrostruktura. To se može videti iz odnosa maksimalne vrednosti dielektrične konstante i dielektrične konstante na sobnoj temperaturi tj. $\varepsilon_{rmax}/\varepsilon_{rmin,}$ (Tabela I).
Vrednosti dielektrične konstante i dielektričnih gubitaka kao i odnos $\varepsilon_{rmax}/\varepsilon_{rmin}$ date su u tabeli I.

TABELA I
DIELEKTRIČNI PARAMETRI ZA ISPITIVANE UZORKE

| Uzorci PLZT | $\varepsilon_r$ na $T$=300K | $\varepsilon_r$ max | *tan δ* | $\varepsilon_{rmax}/\varepsilon_{rmin}$ |
|---|---|---|---|---|
| PLZT (B) c.s | 2800 | 5160 | 0.036 | 1.84 |
| PLZT (B) t. pres | 2900 | 4566 | 0.018 | 1.57 |
| PLZT (PMM) c.s | 2500 | 4371 | 0.037 | 1.74 |
| PLZT (PMM) t. pres | 2800 | 5075 | 0.027 | 1.8 |


ISBN 978-86-7466-930-3

## IV. ZAKLJUČAK

U radu su ispitivani efekti pripreme praha i postupka sinterovanja na mikrostrukturne karakteristike PLZT keramike dobijene modifikovanom Pechini metodom i parcijalnim oksalatnim postupkom. Mikrostruktura PLZT(PMM) uzoraka sinterovanih na 1100°C, otkriva prisustvo tri različita regiona u uzorcima u pogledu oblika, veličine i sastava zrna. Izdužena zrna sastoje se od faza bogatih Pb i La, a odnos Pb/Zr je relativno veći u poređenju sa drugim regionom u uzorku. Odgovarajući EDS spektar izduženih zrna u PLZT keramici, dobijenoj oksalatnim postupkom, otkriva prisustvo faza bogatih Pb i Zr sa tragom La. Mikrostruktura PLZT (B) uzoraka primenom konvencionalnog postupka sinterovanja bila je ujednačena u svim uzorcima, a veličina i oblik zrna su bili skoro identični. Dielektrična konstanta na sobnoj temperaturi svih ispitivanih uzoraka kreće se u rasponu od 2400 do 3400 i viša je kod uzoraka dobijenih konvencionalnim postupkom sinterovanja. Dielektrična konstanta ne varira sa frekvencijom iznad 10 kHz. Generalno, dielektrični gubici su veoma mali i kreću se u opsegu od 0.018 do 0.037 na 1 kHz. Frekventna osetljivost $tan\delta$ je otkrivena u svim ispitivanim uzorcima. Sporo povećanje tanδ sa frekvencijom se detektuje u toplo presovanim PLZT(Nb) i PLZT(B), u poređenju sa drugim uzorcima koji pokazuju smanjenje dielektričnih gubitaka sa frekvencijom. Najveću promenu $\varepsilon_r$ sa temperaturom pokazuju PLZT (B) uzorci dobijeni konvencionalnim postupkom.

## ZAHVALNICA

Ovaj rad je podržalo Ministarstvo prosvete, nauke i tehnološkog razvoja Republike Srbije (Ev. br. 451-03-68/2022-14/200102).

## LITERATURA

[1] G.H.Haertling, "Ferroelectric ceramics: history and technology", J.Am.Cer.Soc. 82 (4), pp.797-818, 1999.

[2] G.H.Herting,, "Processing of Transparent Electrooptic Ceramic" (T.S.Ien and J.Park, eds) Science Press, pp. 25-28, Beijing, 1984.

[3] A. Kumar, S. R. Emani, K. C. J. Raju, J. Ryu, A. R. James, Investigation of the Effects of Reduced Sintering Temperature on Dielectric, Ferroelectric and Energy Storage Properties of Microwave-Sintered PLZT 8/60/40 Ceramics, Energies, 13, 6457, 2020.

[4] A.I.Shcheglova, I.L.Kislova, T.S.Ilina, D.A.Kiselev, E.V. Barabanova, A.I.Ivanova, Dielectric and Piezoelectric Properties of PLZT x/40/60 (x = 5; 12) Ceramics, Russian Microelectronics, volume 50, pp. 673–678 (2021)

[5] L.B.Kong, J.Ma,W.Zhu, O.K.Tan, "Preparation and characterization of PLZT (8/65/35) ceramics via reaction sintering from ball milled powders", Mater.Lett. 52 pp.378-387, 2002.

[6] Hu, Z.; Ma, B.; Liu, S.; Narayanan, M.; Balachandran, U. Relaxor behavior and energy storage performance of ferroelectric PLZT thin films with different Zr/Ti ratios. Ceram. Int. 2014, 40, 557–562.

[7] C.Huang, J.Xua, Z.Fang, D.Ai, W.Zhou, L.Zhao, J.Sun, Q.Wanga, "Effect of preparation process on properties of PLZT (9/65/35) transparent ceramics", Journal of Alloys and Compounds, Vol 723, No.5, pp. 602-610, 2017.

[8] M.P.Pechini, US Patent No 3.330.697, 1976.

PLZT ceramics belongs to one of the very important groups of functional materials that form the basis for the production of a large number of electronic devices. The microstructure and dielectric properties of ceramics depend on the powder preparation and heat treatment conditions. PLZT powders used in this work were prepared in two different ways, modified by the Pechini method, using the polymer precursor method (PMM) and the partial oxalate method (B). The sintering process, including hot pressing, was performed at a temperature of 1100°C. The microstructure and phase composition were investigated by SEM and EDS analysis, while the change of dielectric constant and dielectric losses were measured in the frequency range from 1 kHz to 20 kHz, and in the temperature range from 25 to 180°C. A significant difference in microstructure and dielectric properties depending on the origin of the powder and the sintering process was observed in the tested samples. The microstructure of PLZT (PMM) samples reveals the presence of three different regions in the samples in terms of grain shape, size and composition. Ceramics obtained by the oxalate process are characterized by cuboid grains along the border of elongated grains as well as polyhedral grains.

**Microstructural and dielectric characterization of PLZT ceramics**

Vesna Paunović, Miloš Marjanović, Zoran Prijić

 ISBN 978-86-7466-930-3

# Električne karakteristike $BaTiO_3$ keramike dopirane antimonom

Aleksandra Stojković, *Student Member, IEEE*, Miloš Marjanović, *Student Member, IEEE*, Vesna Paunović, *Member, IEEE*, Aneta Prijić, *Member, IEEE*, Zoran Prijić, *Member, IEEE*

***A stra t*— ovom radu izvršeno je ispitivanje mi rostru turnih i električnih ara teristi a aTi erami e dopirane antimonom ( b aTi ). oncentracije dopanata, b, retale su se u opsegu od ,1 do 5, at . a dobijanje uzora a korišćena je onvencionalna metoda sinterovanja u čvrstoj fazi u trajanju od 2 h na temperaturama od 12 C do 1 5 C.**

**analiza b aTi dopirane erami e po azala je da je za uzor e dopirane manjom oncentracijom aditiva ( ,1 i ,5 at%) karakteristična sitnozrna i uniformna mi rostru tura sa veličinom zrna od ,5 µm do 2 µm. od uzora a dopiranih većom koncentracijom aditiva (2, i 5,0 at%) karakteristična veličina zrna kretala se od 1 µm do 4 µm.**

**erenje električnih ara teristi a vršeno je na sobnoj temperaturi u fre ventnom opsegu od 1 z do 1 z. od uzor a dopiranog sa ,1 at b i sinterovanog na 12 C izmerena je najviša vrednost dielektrične onstante $\varepsilon_r$ 2 1 u odnosu na uzor e dopirane većim oncentracijama primesa. zora dopiran istom oncentracijom ( ,1 at b), ali sinterovan na temperaturi 1 5 C, ima višu vrednost dielektrične konstante oja iznosi $\varepsilon_r$ 1 .**

**Sem zavisnosti dielektrične konstante od frekvencije, analizirana je i promena specifične električne otpornosti sa fre vencijom. zorci sinterovani pri najvišoj temperaturi imaju najmanju vrednost specifične otpornosti, a i sa povećanjem fre vencije dolazi do njenog smanjivanja. Pri istoj temperaturi sinterovanja, a sa povećanjem koncentracije primesa, otpornost raste.**

***Ključne reči*— b aTi erami a; dielektrične karakteristi e, specifična električna otpornost; mi rostru tura.**

## I. UVOD

Feroelektrici su materijali koji se tokom poslednjih decenija puno koriste i imaju veliki dijapazon primene. Barijum titanat ($BaTiO_3$) je jedan od najčešće ispitivanih perovskitnih materijala. Veliki broj elektronskih komponenata izrađen je na bazi $BaTiO_3$ keramike poput PTC termistora, piezoelektričnih senzora, višeslojnih kondenzatora, memorija itd. [1, 2]. Karakteristike feroelektrične keramike jako zavise od koncentracije i tipa primesa. Da li će $BaTiO_3$ keramika imati dielektrična ili poluprovodna svojstva zavisi od dopanata koji mogu zauzeti mesta $Ba^{2+}$ ili $Ti^{4+}$ jona u perovskitnoj strukturi [3, 4]. Mesto ugradnje zavisi od radijusa jona dopanata.

Donorske primese mogu biti trovalentni joni Sb koji zauzimaju mesta $Ba^{2+}$ ili petovalentni joni Sb koji zauzimaju mesta $Ti^{4+}$ jona. Rastvorljivost Sb u kristalnoj rešetki $BaTiO_3$ zavisi od koncentracije dopanata i temperature sinterovanja.

Temperatura sinterovanja utiče na mikrostrukturne karakteristike koje takođe određuju svojstva keramike. Za primenu dopirane $BaTiO_3$ keramike, kao kondenzatorskog materijala, treba ostvariti dobru gustinu, visoku vrednost dielektrične konstante i nizak faktor gubitaka. Za ostvarivanje ovakvih svojstava potrebna je uniformna mikrostruktura i dobra raspodela primesa i aditiva [5-8]. Jedna od najznačajnih osobina $BaTiO_3$ keramike je njena visoka vrednost dielektrične konstante ($\varepsilon_r$) na sobnoj temperaturi.

U ovom radu analiziran je uticaj koncentracije primesa i temperature sinterovanja na mikrostrukturna i električna svojstva Sb dopirane $BaTiO_3$ keramike. Skenirajućim elektronskim mikroskopom (SEM) vršeno je ispitivanje mikrostrukturnih karakteristika. Dielektrična konstanta i specifična električna otpornost uzoraka određene su u frekventnom intervalu od 100 Hz do 1 MHz.

## II. EKSPERIMENTALNA PROCEDURA

U ovom radu proučavani su uzorci $BaTiO_3$ keramike dopirane sa 0,1, 0,5, 1,0, 2,0 i 5,0 at% Sb. Ispitivani uzorci dobijeni su metodom sinterovanja u čvrstoj fazi polazeći od čistih oksidnih prahova $BaTiO_3$ i $Sb_2O_3$. Nakon mešanja prahova u izopropil alkoholu, izvršeno je njihovo sušenje i presovanje u pelete pri pritisku od 120 MPa. Uzorci su zatim sinterovani u atmosferi vazduha na temperaturama 1290 °C, 1320 °C i 1350 °C.

Ispitivanje mikrostrukture obavljeno je SEM mikroskopijom, JEOL, SEM-5300. Nanošenje srebrne paste na uzorke izvršeno je pre merenja njihovih električnih karakteristika.

Za analiziranje promene dielektrične konstante ($\varepsilon_r$) i specifične električne otpornosti ($\rho$) sa frekvencijom, korišćene su vrednosti izmerenih kapacitivnosti i otpornosti uzoraka. Merenja ispitivanih uzoraka izvršena su u frekventnom opsegu od 100 Hz do 1 MHz korišćenjem LCR-metra Agilent 4284A [9].

Aleksandra Stojković – Univerzitet u Nišu, Elektronski fakultet, Aleksandra Medvedeva 14, 18000 Niš, Srbija (e-mail: aleksandra.stojkovic@elfak.ni.ac.rs).

Miloš Marjanović – Univerzitet u Nišu, Elektronski fakultet, Aleksandra Medvedeva 14, 18000 Niš, Srbija (e-mail: milos.marjanovic@elfak.ni.ac.rs).

Vesna Paunović – Univerzitet u Nišu, Elektronski fakultet, Aleksandra Medvedeva 14, 18000 Niš, Srbija (e-mail: vesna.paunovic@elfak.ni.ac.rs).

Aneta Prijić – Univerzitet u Nišu, Elektronski fakultet, Aleksandra Medvedeva 14, 18000 Niš, Srbija (e-mail: aneta.prijic@elfak.ni.ac.rs).

Zoran Prijić – Univerzitet u Nišu, Elektronski fakultet, Aleksandra Medvedeva 14, 18000 Niš, Srbija (e-mail: zoran.prijic@elfak.ni.ac.rs).

 ISBN 978-86-7466-930-3

## III. REZULTATI I DISKUSIJA

### *A. Mikrostrukturna ispiti anja*

Relativna gustina uzoraka $BaTiO_3$ keramike dopirane sa $Sb_2O_3$ kretala se od 82 do 95% od teorijske gustine (TG). Sa povećanjem temperature sinterovanja raste gustina uzorka, međutim sa povećanjem koncentracije primesa dolazi do njenog smanjivanja.

Uzorke dopirane sa 0,1 i 0,5 at% Sb karakteriše homogena i sitnozrna mikrostruktura sa uniformnom raspodelom dopanata. Veličina zrna kretala se od 0,5 do 2,0 μm. Sa povećanjem tempearture raste i veličina zrna i ona se za uzorke sinterovane na 1350 °C kretala od 1,0 do 5,0 μm. Kod uzoraka dopiranih sa 5,0 at% Sb veličina zrna kretala se od 1,0 do 2,0 μm za uzorke sinterovane na 1290 °C, i od 1,0 do 4,0 μm za uzorke sinterovane na 1350 °C. Pri povećanju koncentracije primesa primećuje se smanjenje srednje veličine zrna (Sl. 1).

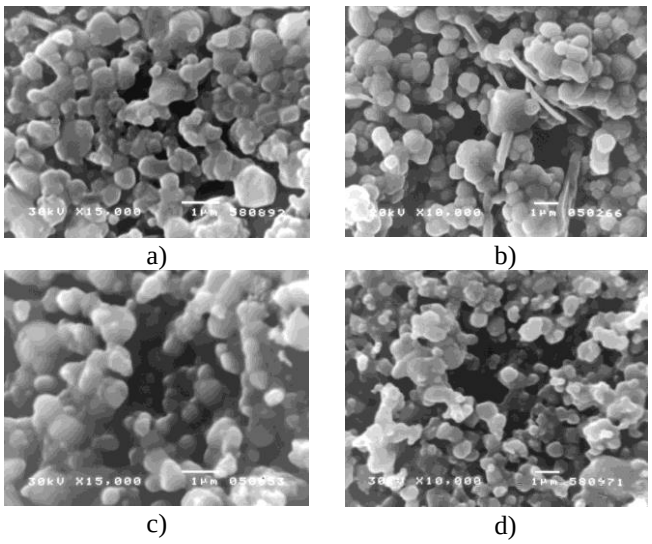


Sl. 1. SEM mikrostruktura Sb dopirane $BaTiO_3$ keramike a) 0,1 at% Sb i c) 5,0 at% Sb ($T_{sin}$=1290 °C) i b) 0,1 at% Sb i d) 5,0 at% Sb ($T_{sin}$=1350 °C).

Za razliku od niže dopiranih uzoraka kod uzoraka sa 5,0 at% Sb primećena je mala segregacija Sb koja nije uticala na karakteristike dopirane keramike.

### *B. Električne karakteristike*

S obzirom da su uzorci presovani u pelete debljine $d$, a na njih nanesena srebrna pasta poluprečnika $r$, za izmerene vrednosti kapacitivnosti $C$ ispitivanih uzoraka, dielektrična konstatna $\varepsilon_r$ je određena korišćenjem formule:

$$\varepsilon_r = C \cdot \frac{d}{\varepsilon_0 \cdot S} = C \cdot \frac{d}{\varepsilon_0 \cdot r^2 \pi}. \qquad (1)$$

Uticaj koncentracije primesa i mikrostrukture na vrednost dielektrične konstatne analiziran je na osnovu promene dielektrične konstatne sa frekvencijom.

Promena dielektrične konstante sa frekvencijom, uzoraka dopiranih različitim koncentracijama Sb pri temperaturi sinterovanja $T_{sin}$=1290 °C je prikazana na Sl. 2. Jasno se uočava da dielektrična konstanta merenih uzoraka opada ukoliko koncentracija primesa raste. Pri najnižoj koncentraciji primesa od 0,1 at% Sb zabeležena je najviša vrednost dielektrične konstante $\varepsilon_r$=2710, dok za najveću koncentraciju dopiranja od 5,0 at% Sb njena vrednost iznosi $\varepsilon_r$=607.

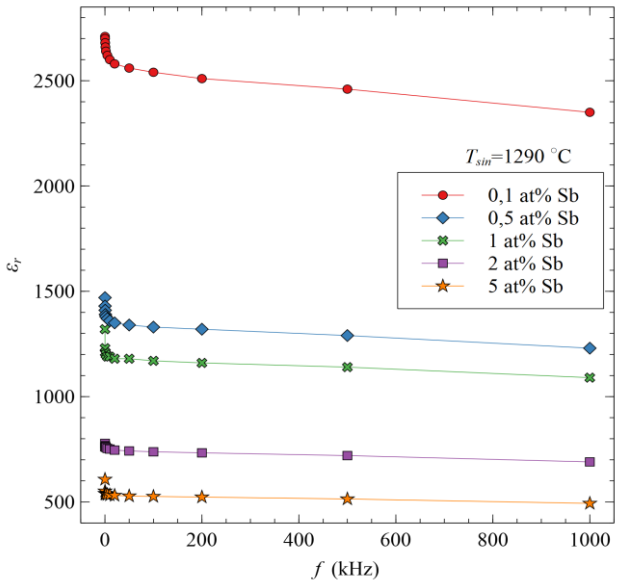


Sl. 2. Zavisnost dielektrične konstante od frekvencije Sb/$BaTiO_3$ uzoraka sinterovanih na temperaturi $T_{sin}$=1290 °C za različite koncentracije dopanata.

Takođe se primećuje da je vrednost dielektrične konstante viša pri nižim frekvencijama, ali sa porastom frekvencije opada i postaje skoro pa konstantna za frekvencije iznad 5 kHz.

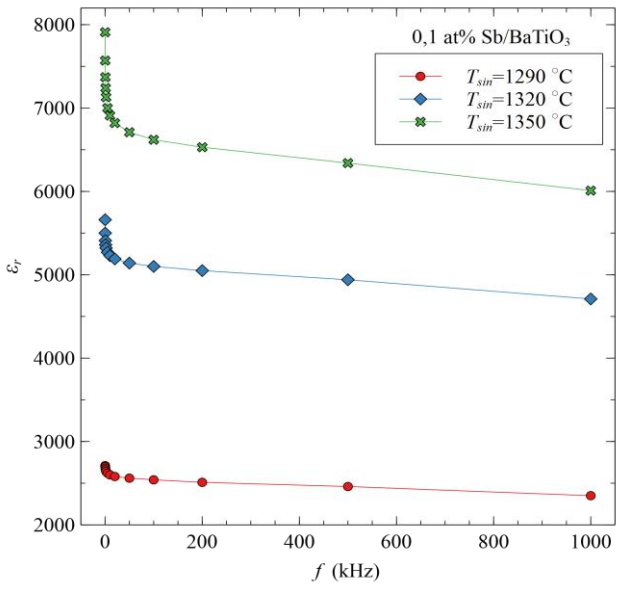


Sl. 3. Zavisnost dielektrične konstante od frekvencije, uzoraka dopiranih sa 0,1 at% Sb za različite temperature sinterovanja.


ISBN 978-86-7466-930-3

Analiziranjem uzoraka dopiranih istom koncentracijom primesa, ali sinterovanim pri različitim temperaturama, vidno je da pri porastu temperature sinterovanja raste i vrednost dielektrične konstante. Na Sl. 3 je prikazana zavisnost dielektrične konstante od frekvencije, uzoraka dopiranih sa 0,1 at% Sb i sinterovanih na tri različite temperature.

Za uzorak sinterovan na temperaturi $T_{sin}$=1290 °C, dielektrična konstanta ima najmanju vrednost i iznosi $\varepsilon_r$=2710, dok je pri najvišoj temperaturi sinterovanja njena vrednost maksimalna i iznosi $\varepsilon_r$=7910. Ove vrednosti dielektrične konstante su logične i očekivane, jer keramici sa najvećom gustinom i homogenom mikrostrukturom odgovara i najviša vrednost dielektrične konstante.

Sem zavisnosti dielektrične konstante od frekvencije, analizirana je i promena specifične električne otpornosti sa frekvencijom.

Već je navedeno da su uzorci presovani u pelete debljine $d$, a na njih nanesena srebrna pasta poluprečnika $r$, pa je za izmerene vrednosti otpornosti ispitivanih uzoraka, specifična električna otpornost $\rho$ određena korišćenjem formule:

$$\rho = \cdot\frac{S}{l} = \cdot\frac{r^2\pi}{d}. \qquad (2)$$

Promena specifične otpornosti sa frekvencijom, kod uzoraka sinterovanih na istoj temperaturi, ali dopiranih različitim koncentracijama primesa, prikazana je na Sl. 4.

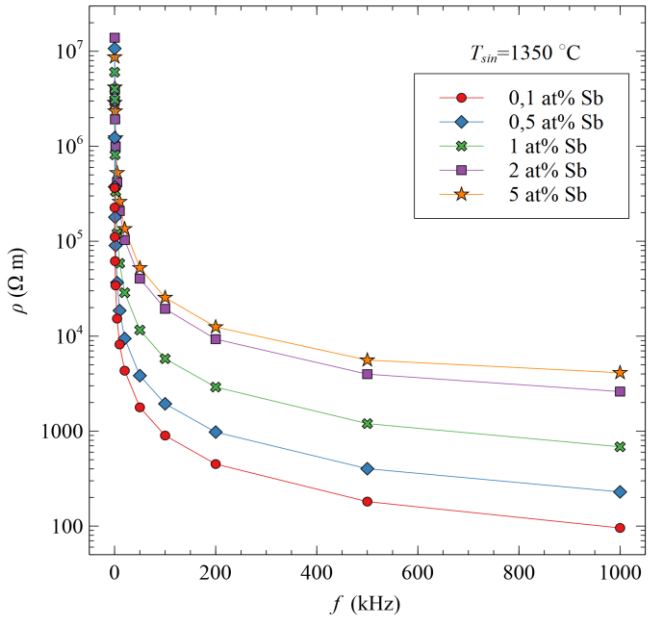


Sl. 4. Zavisnost specifične električne otpornosti od frekvencije Sb/$BaTiO_3$ uzoraka sinterovanih na temperaturi $T_{sin}$=1350 °C za različite koncentracije primesa.

Pri koncentraciji aditiva od 0,1 at% Sb, uzorak ima najnižu vrednost specifične otpornosti i ona iznosi $\rho$=3,65·10$^5$ Ωm, dok je za koncentraciju od 2,0 at% Sb zabeležena najviša vrednost specifične otpornosti $\rho$=1,39·10$^7$ Ωm. Očigledna je i tendencija opadanja specifične električne otpornosti sa povećanjem frekvencije, pa su samim tim najviše vrednosti $\rho$ zabeležene pri nižim frekvencijama.

Ukoliko se posmatraju uzorci sa istom koncentracijom dopiranja ali sinterovani pri različitim temperaturama, uočava se da će sa porastom temperature sinterovanja specifična otpornost imati niže vrednosti (Sl. 5). Za uzorke dopirane sa 0,1 at% Sb, najviša vrednost specifične otpornosti zabeležena je kod uzorka sinterovanog na temperaturi od $T_{sin}$=1290 °C i iznosi $\rho$=1,55·10$^6$ Ωm, dok za $T_{sin}$=1350 °C uzorak ima najmanju vrednost specifične otpornosti $\rho$=3,65·10$^5$ Ωm. Primećuje se da specifična otpornost opada sa povećanjem frekvencije, ali na frekvencijama iznad 500 kHz postaje skoro konstantna.

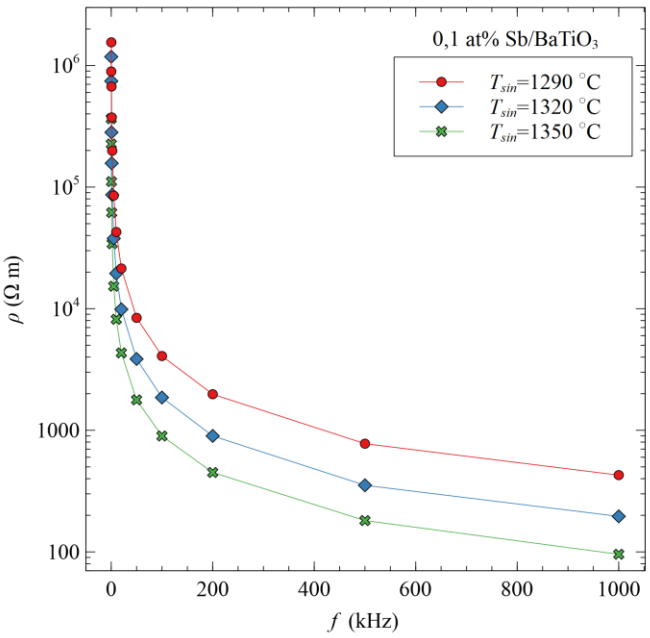


Sl. 5. Zavisnost specifične električne otpornosti od frekvencije 0,1 at% Sb/$BaTiO_3$ uzoraka sinterovanih na različitim temperaturama.

Opseg vrednosti specifične električne otpornosti za sve ispitivane uzorke je od 10$^5$ do 10$^7$ Ωm. Ovi uzorci su dobri izolatori. Uzrok tome je sitnozrna mikrostruktura i velika površina granice zrna, što je naročito izraženo kod uzoraka sa većom koncentracijom aditiva, kod koje su izolaciona svojstva granice zrna uporediva sa veličinom zrna pa je i specifična otpornost kod njih veća.

## IV. Zaključak

U ovom radu ispitivana je $Sb_2O_3$ dopirana $BaTiO_3$ keramika. Rezultati ispitivanja odnose se na mikrostrukturu i promenu dielektričnih karakteristika uzoraka. Uzorci sa manjom koncentracijom primesa imaju karakterističnu homogenu mikrostrukturu i veličinu zrna koja se kreće u opsegu od 0,5 do 2,0 μm, dok se za više koncentracije aditiva vrednosti veličine zrna kreću od 1,0 do 4,0 μm.


ISBN 978-86-7466-930-3

Najviša vrednost dielektrične konstante, na sobnoj temperaturi, zabeležena je za najnižu koncentraciju primesa. Uočava se i da sa porastom frekvencije vrednost dielektrične konstante opada. Sa povećanjem temperature sinterovanja dielektrična konstanta uzoraka takođe raste tako da je najviša vrednost izmerena za uzorke sinterovane na 1350 °C.

Što se tiče specifične električne otpornosti, ona opada sa povećanjem temperature sinterovanja, pa se najviša vrednost beleži pri najnižoj temperaturi od 1290 °C. Najniža vrednost specifične otpornosti, pri istoj temperaturi sinterovanja, odgovara uzorku sa najnižom koncentracijom primesa.

## ZAHVALNICA

Ovaj rad je realizovan u okviru projekta finansiranog od strane Ministarstva za prosvetu, nauku i tehnološki razvoj Republike Srbije (Ev. br. 451-03-68/2022-14/200102).

## LITERATURA

[1] D.H. Kuo, C.H. Wang, W.P. Tsai, "Donor and Acceptor Cosubstituted $BaTiO_3$ for Nonreducible Multilayer Ceramic Capacitors", Ceram. Int. 32, 2006, pp. 1–5.
[2] S.F. Wang, G.O. Dayton: "Dielectric Properties of Fine-grained Barium Titanate Based X7R Materials", J. Am. Ceram. Soc., Vol. 82, No. 10, Oct. 1999, pp. 2677 – 2682.
[3] G.Arlt, D.Hennings and G.de With, "Dielectric properties of Fine–grained Barium Titanate ceramics" J.Appl.Phys. 58 [4] 1619-1625 (1985).
[4] D.Hennings, "Barium Titanate Based Ceramics Materials for Dielectrics Use", Int. J.High Technology Ceramics 3 91-111 (1987).
[5] K.J. Park, C.H. Kim,Y.J. Yoon, S.M. Song, "Doping Behaviors of Dysprosium, Yttrium and Holmium in $BaTiO_3$ ceramics", Journal of the European Ceramic Society, 2009, vol. 29, pp. 1735-1741.
[6] M. Đorđević, M. Marjanović, V. Paunović, V. Mitić, Z. Prijić: "Electrical Resistivity of Er/Yb doped $BaTiO_3$ ceramics", IcETRAN, Kladovo, Serbia, Proceedings 4th Conference IcETRAN, pp. NM1.2, 5-8, jun, 2017.
[7] S. Tangjuank , T.Tunkasiri: "Characterization and properties of Sb-doped $BaTiO_3$ powders", Applied Physics Letters 90(7), 2007.
[8] N. Ayub, R. Omar, M.Deraman, I. Abutalib, Z. Zainuddin, A.Abdul Aziz, "Characteristics of Porous Sb-Doped Barium Titanate Ceramics Fabricated by Adding Graphite", Advanced Materials Research (Volume 1107), pp.9-13, 2015.
[9] 4284A Precision LCR Meter Operation Manual.

## ABSTRACT

In this paper, the microstructural and dielectric characteristics of $BaTiO_3$ ceramics doped with antimony ($Sb/BaTiO_3$) were investigated. Dopanate concentrations, Sb, ranged from 0.1 to 5.0 at%. The conventional solid-phase sintering method for 2 h at temperatures of 1290 °C, 1320 °C and 1350 °C was used to obtain samples.

SEM analysis of $Sb/BaTiO_3$ doped ceramics showed that for samples doped with a lower concentration of additives (0.1 and 0.5 at%) is characteristic fine-grained and uniform microstructure with grain size from 0.5 μm to 2.0 μm. In samples doped with a higher concentration of additives (1.0 and 5.0 at%), the characteristic grain size ranged from 1.0 μm to 4.0 μm.

Measurement of electrical characteristics was performed at room temperature in the frequency range from 100 Hz to 1 MHz. In the sample doped with 0.1 at% Sb and sintered at 1290 °C, the highest value of the dielectric constant $\varepsilon_r$=2710 was measured in relation to the samples doped with higher impurity concentrations. The sample doped with the same concentration (0.1 at% Sb), but sintered at a temperature of 1350 °C, has a higher value of the dielectric constant of $\varepsilon_r$=7910.

In addition to the dependence of the dielectric constant on frequency, the change in specific electrical resistance with frequency was also analyzed. Samples sintered at the highest temperature have the lowest value of specific resistance, and with increasing frequency, it decreases. At the same sintering temperature, and with increasing impurity concentration, the resistance increases.

**lectrical characteristics of antimony doped aTi ceramics**

Aleksandra Stojković, Miloš Marjanović, Vesna Paunović, Aneta Prijić, Zoran Prijić

 ISBN 978-86-7466-930-3

# Осетљивост магнетоимпедансног елемента CoFeSiB аморфне жице

Јелена Орељ, Небојша Митровић

*Апстракт—У овом раду је презентовано испитивање осетљивости магнетоимпедансног (МИ) елемента код жице аморфне легуре CoFeSiB у опсегу фреквенција 2 M ÷ 5 M ma ≈ 4 3 A m . При 1 M , МИ-однос је 45 , док је при вишим фреквенцијама евидентиран максимум криве ΔZ Z који одговара пољу магнетне анизотропије k. Повећање радних фреквенција праћено је порастом поља магнетне анизотропије k чиме се повећава и мерни опсег магнетног сензора базираног на примени испитиваног МИ елемента. Истовремено је евидентирана и промена осетљивости МИ елемента која при 4 M и 5 M достиже највеће вредности од око 0,4 % / A m.*

***Кључне речи—МИ ефекат, е аморфна жица, МИ елемент, осетљивост МИ елемента***

## I. Увод

ПОСТИЗАЊЕ оптималних функционалних карактеристика електричних уређаја израђених од феромагнетних легура је могуће тек након детаљног истраживања електричних и магнетних својстава материјала. Један од најинтересантнијих феномена који се може искористити за магнетне сензоре је магнетоимпедансни (МИ) ефекат уочен код аморфних или нанокристалних магнетно меких трака, жица или танких филмовима. Овај ефекат, примећен најпре код аморфних FeCoSiB жица [1], омогућио је интензиван развој сензора на бази МИ-елемената, који су данас у широкој примени код електронских компаса, ГПС навигација, сензора ротације, система безбедности, биомагнетних мерења и др.

У сензорској употреби су углавном две геометријске форме: цилиндрична (жице [2-4]) и планарна (траке, филмови [5-7]). Аморфне жице се могу користити у верзији са заштитним стакленим омотачем [8] или без омотача [9]. Високе вредности магнетне пермеабилности су неопходно својство при избору материјала за МИ елементе, те су легуре на бази кобалта са тог становишта у предности у односу на легуре на бази гвожђа. За разлику од легура на бази кобалта које имају изванредне магнетно-меке перформансе са потпуно аморфном структуром, легуре на бази гвожђа постижу своје одличне карактеристике након оптималних термомагнетних или термомеханичких третмана (током којих се формира нанокристална структура дистрибуирана у аморфној матрици).

Релативна промена импедансе ΔZ/Z у одговарајућем фреквентном опсегу може достићи и више стотина процената (*енг.* **G**iant agneto **I**mpedance (GMI) effect - велики МИ ефекат): 506 % CoFeNiMoBSi @ 8 kA/m [10], 1200 % CoFeBSi @ 15 kA/m [11], што аморфним жицама ових легура омогућава широке могућности примене [12-13].

МИ ефекат је директно повезан са феноменом скин ефекта код феромагнетних материјала. Наиме, порекло магнетоимпедансног ефекта везано је за промене у динамици процеса магнетизације. Те промене утичу на магнетну пермеабилност, а самим тим и на дубину продирања наизменичне струје кроз магнетни проводник са повећањем фреквенције [14]. Познато је да добри проводници са великом пермеабилношћу показују велики МИ ефекат. Поред тога, за наизменичну побуду високе фреквенције (реда од 1 MHz до 1 GHz) модификација дубине продирања (скин ефекта) и магнетне пермеабилности има јаку зависност од фреквенције примењене побуде, као и од спољашњег статичког магнетног поља. Услед вихорних струја ток наелектрисања је потиснут ка површини узорка, што доводи до повећања импедансе, док се примењеним магнетним пољем то потискивање модулише, односно мења се ефективна површина попречног пресека кроз коју протиче наелектрисање – струја, при одређеној константној фреквенцији побуде. Дакле, велика пермеабилност и висока фреквенција смањују дубину продирања, док се примењеним пољем она повећава.

На дубини продирања $\delta_m$

$$\delta_m = \sqrt{\frac{\rho}{\pi \cdot \mu \cdot f}} \qquad (1),$$

код магнетно меких материјала са ниским вредностима специфичне електричне отпорности $\boldsymbol{\rho}$, високим вредностима магнетне пермеабилности $\boldsymbol{\mu}$ а при релативно високим фреквенцијама , амплитуда вектора густине струје опадне на 1/e своје вредности уз површину узорка [15]. Промене и осталих напред наведених физичких својстава ($\boldsymbol{\rho}$, $\boldsymbol{\mu}$) ће резултовати у изменама расподеле тока наелектрисања по попречном пресеку жице и утицати на измену импедансе. Фреквенција при којој дубина продирања постаје мања од полупречника жице ($\delta_m$ < a) се назива критична фреквенција [16, 17], тако да се при даљем повећању учестаности запажају феномени МИ-ефекта.

Промена импедансе показује временски зависну природу простирања магнетног поља у проводнику одговарајуће магнетне пермеабилности, на чему су засноване могућности детекције магнетног поља ниског интензитета. Осетљивости великог МИ ефекта у аморфним жицама [18], тракама [19] и вишеслојним филмовима [20] на релативно вишим фреквенцијама (f > 1 MHz) могу достићи изузетно високе вредности, од чак неколико стотина % / Oe (1 Oe = $10^3/4\pi$ A/m).

Јелена Орељ – Факултет техничких наука у Чачку, Универзитета у Крагујевцу, Светог Саве 65, Србија (е-мејл: jelena.orelj@ftn.kg.ac.rs)

Небојша Митровић – Факултет техничких наука у Чачку, Универзитета у Крагујевцу, Светог Саве 65, Србија (е-мејл: nebojsa.mitrovic@ftn.kg.ac.rs)

 ISBN 978-86-7466-930-3

Велика осетљивост комплексне импедансе аморфне жице, , на примењено dc магнетно поље, ***ext***, кључна је за развој бројних магнетних сензора високих перформанси. Високе вредности осетљивости оваквих сензора се захтевају у многим инжењерским и индустријским применама.

На слици 1. је приказана принципијелна шема мерења магнетоимпедансе аморфне жице у спољашњем dc магнетном пољу генерисаном системом 1Д-Хелмхолцових калемова.

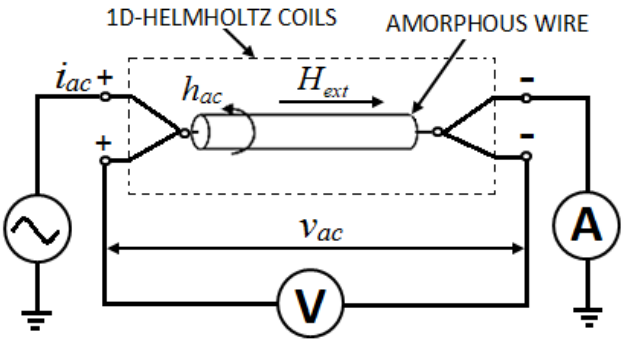


*Сл. 1. Шема експеримента мерења магнетоипедансе аморфне жице.*

Спољашње лонгитудинално dc магнетно поље ***ext*** и циркуларно ac магнетно поље ***ac*** (индуковано протоком наизменичне струје $_{ac}(t)=I_{cc}\cdot\sin(2\pi f\cdot t)$) утичу на промену магнетне пермабилности $\boldsymbol{\mu}$, тако да је импеданса феромагнетног проводника функција три експериментална параметра = (*f*, ***ext***, $\boldsymbol{I_{cc}}$).

Импеданса је количник тренутних вредности наизменичног напона $\mathcal{V}_{ac}$ и наизменичне струје $_{ac}$, а код узорка цилиндричног проводника полупречника ***a*** [21]:

$$Z = \quad + j \quad = \frac{1}{2}\cdot \quad _{dc}\cdot(ka)\cdot\frac{_0(ka)}{_1(ka)} \qquad (2),$$

где су ***dc*** електрични отпор; и реални и имагинарни део импедансе и Беселове функције нултог и првог реда прве врсте, = (1+ )/$\boldsymbol{\delta_m}$; $^2$ = -1.

Магнето–импедансни однос се углавном дефинише као релативна промена импедансе узорка са променом спољашњег dc магнетног поља ( ***ext***):

$$\Delta Z/Z\ (\%) = 100\ \% \times \quad Z \quad - Z \quad _{max} \quad Z \quad _{max} \qquad (3),$$

где је ***max*** импеданса при максималном магнетном пољу. Узорак се најчешће позиционира лонгитудално (у правцу магнетног поља), тј. у центру система 1Д-Хелмхолцових калемова где је постигнута скоро потпуна хомогеност магнетног поља. Ради анализе могућности примене спроводи се прорачун тзв. сопствене осетљивости МИ-елемента η који је дефинисан једначином [22, 23]:

$$\eta = (\partial\,(\Delta Z/Z) / \partial\, H_{ext}) \qquad (4).$$

У овом раду су приказана високофреквентна истраживања f ∈ [1 MHz, 5 MHz] осетљивости МИ-елемента аморфне жице легуре CoFeSiB пречника око 100 μm с циљем процене атрактивности њене примене у сензорици. Ранија истраживања су показала да појава МИ-ефекта започиње на око 5 kHz, а регистровани МИ-однос износи чак 344 % при радној фреквенцији од 950 kHz (@ $H_{max}$=7,72 kA/m) [24]).

## II. Експериментални део

Предмет истраживања је МИ-елемент од CoFeSiB аморфне жице пречника од 100 μm, добијене технологијом брзог хлађења растопа у ротирајућем слоју воде на унутрашњој површини ротирајућег диска (in rotating water melt-spinning [25, 26]).

Мерење магнетоимпедансе је изведено у хомогеном магнетом пољу генерисаном помоћу 1Д-Хелмхоцових калемова при лонгитудиналној оријентацији МИ-елемента. Импеданса испитиваних узорака жица дужине 17 mm, мерена је по методи четири тачке помоћу инструмента LCR Hi-TESTER HIOKI 3532-50, у фреквентном опсегу од 1 MHz до 5 MHz. Током наших експеримената амплитуда струје $I_{cc}$ је одржавана константном и износила је 7 mA тако да је интензитет циркуларног ac магнетног поља $h_{ac}$ на површини узорка аморфне CoFeBSi жице пречника 2a = 100 μm достигао вредност $H_{ac} = I_{cc}/2\pi a = 22.3$ A/m. На слици 2. је приказана експериментална поставка мерења магнетоимпедансе узорака жица у систему 1Д-Хелмхоцових калемова.

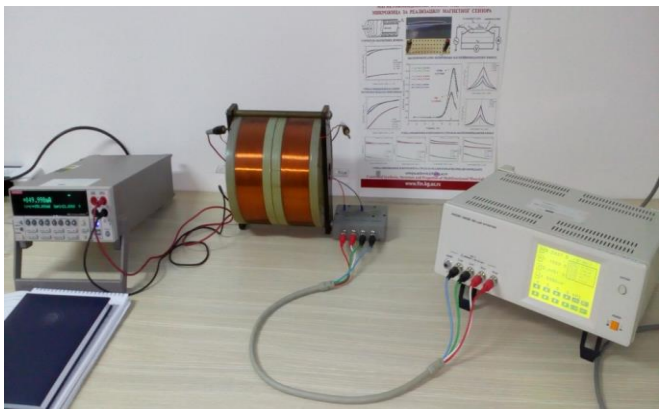

*Сл. 2. Експериментална поставка мерења магнетоимпедансе по методи четири тачке*
*C i-TESTE I I 3532-50, f ∈ 1 M , 5 M .*

## III. Резултати и дискусија

На слици 3. је приказана промена импедансе Z услед примене спољашњег магнетног поља (@ $H_{max} \approx 463$ A/m) при различитим вредностима фреквенције f ∈ [1 MHz, 5 MHz]. Облик зависности импедансе од спољашњег једносмерног магнетног поља *Z e*) се значајно мења, па се из облика криве са константним смањењем импедансе на 1 MHz, при даљем повећању фреквенције региструје максимум који одговара пољу магнетне анизотропије $H_k$. Уочљив је и померај позиције максималне вредности импедансе при повећању фреквенције, тј. повећање поља магнетне анизотропије $H_k$. Ово померање максимума импедансе при повећању фреквенције ка вишим вредностима магнетног поља је резултат доминантног учешћа механизма ротације вектора магнетизације током процеса циркуларног магнећења жице (кретање зидова магнетних домена је блокирано) [27]. Порастом поља магнетне анизотропије $H_k$ се повећава и мерни опсег магнетног сензора базираног на примени испитиваног МИ елемента.


ISBN 978-86-7466-930-3

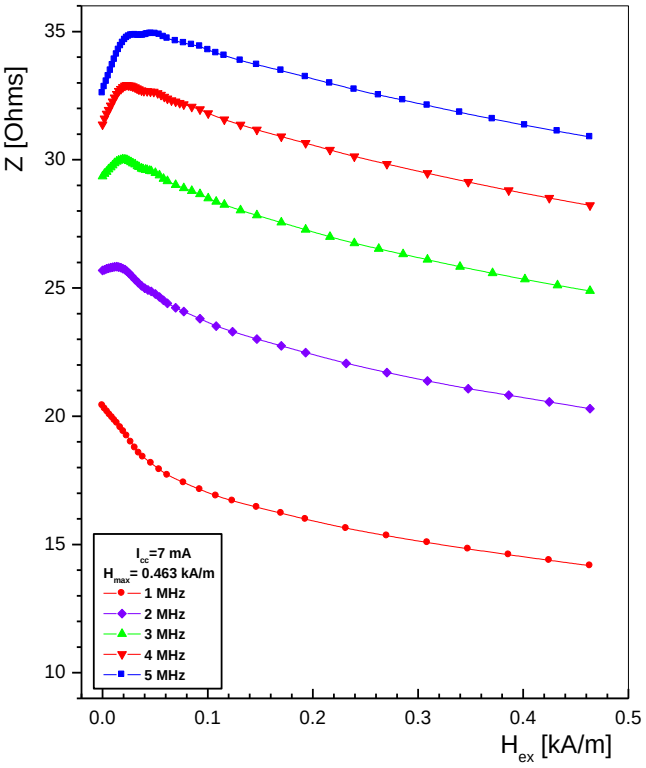


*Сл. 3 Промене импедансе Z од спољашњег dc магнетног поља $H_e$ при повећању фреквенције f ∈ 1 M , 5 M $H_{ma}$ ≈ 4 3 A m .*

На слици 4. је приказана зависност МИ-односа услед примене спољашњег магнетног поља (@ $H_{max} \approx 463$ A/m) при различитим вредностима радне фреквенције $f \in [1\,\text{MHz},\ 5\,\text{MHz}]$.

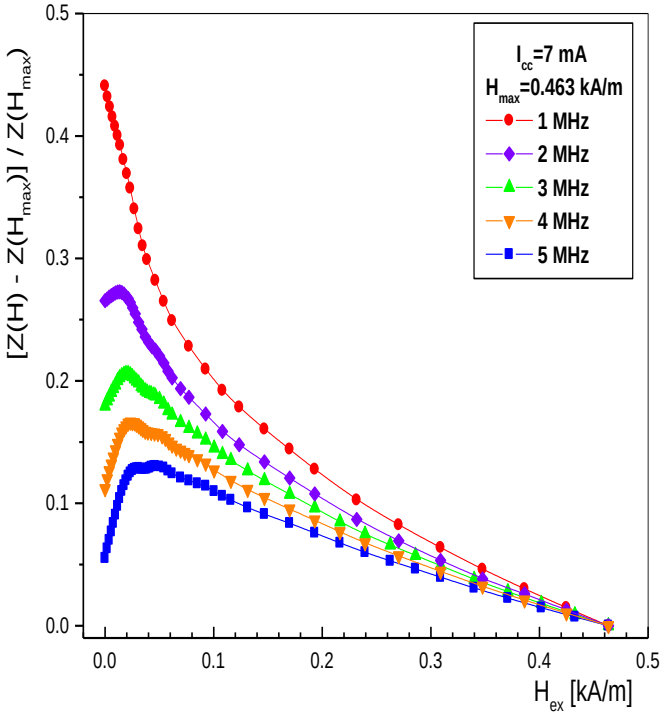


*Сл. 4. Зависност МИ-односа од спољашњег dc магнетног поља $H_e$ при фреквенцијама f ∈ 1 M , 5 M $H_{ma}$ ≈ 4 3 A m .*

Највеће вредности МИ-односа су регистроване на фреквенцији од 1 MHz (око 45 % при $H_{ex} = 0$), док се при даљем повећању фреквенције уочава константно смањење МИ-односа.

На сликама 5-8. паралелно су приказане зависности МИ-односа ΔZ/Z и сопствене осетљивости МИ-елемента η (једначина (4)) од спољашњег dc магнетног поља $H_{ext}$ (@ $H_{max} \approx 463$ A/m) при радним фреквенцијама $f \in [2\ \text{MHz},\ 5\ \text{MHz}]$. Евидентирано је константно повећање осетљивости при порасту радне фреквенције. На фреквенцији од 2 MHz осетљивост је најнижа и износи око 0,07 % / A/m док при највећим испитиваним фреквенцијама од 4 MHz и 5 MHz достиже вредности од око 0,4 % / A/m.

При анализи приказаних резултата потребно је нагласити да су овде приказане осетљивости појединачног сензорског МИ-елемента, док је коначна осетљивост самог МИ-сензора дефинисана одабраним електричним колом при изради магнетног сензора (Колпицов осцилатор [28], CMOS IC мултивибратор [29, 30] са резолуцијом мерења магнетне индукције од око 1 pT).

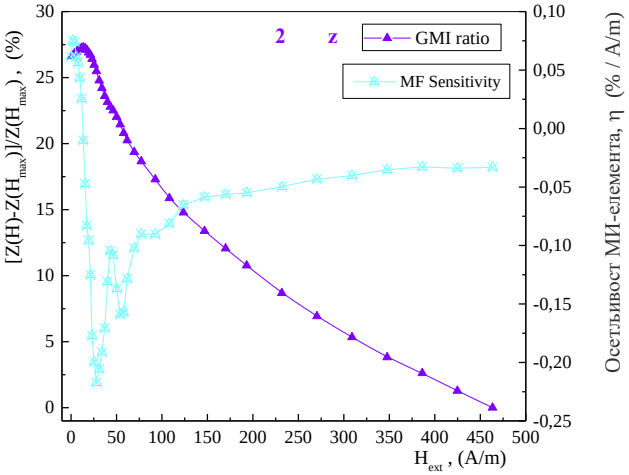


*Сл. 5. Упоредни приказ зависности МИ-односа и осетљивости МИ-елемента од спољашњег dc магнетног поља $H_{et}$ при фреквенцији f 2 M $H_{ma}$ ≈ 4 3 A m .*

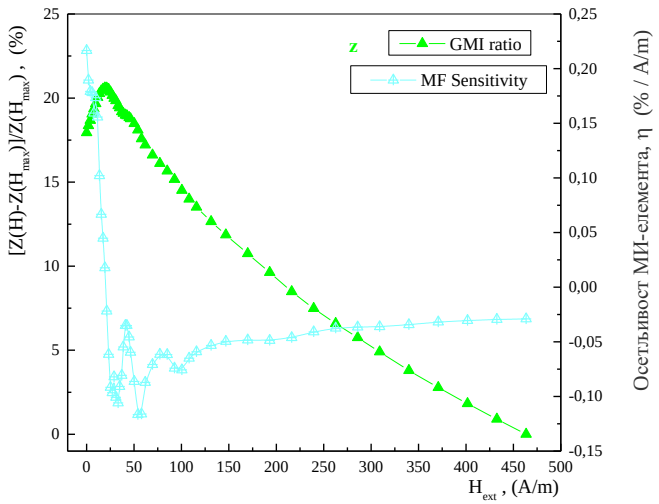


*Сл. . Упоредни приказ зависности МИ-односа и осетљивости МИ-елемента од спољашњег dc магнетног поља $H_{et}$ при фреквенцији f 3 M $H_{ma}$ ≈ 4 3 A m .*


ISBN 978-86-7466-930-3

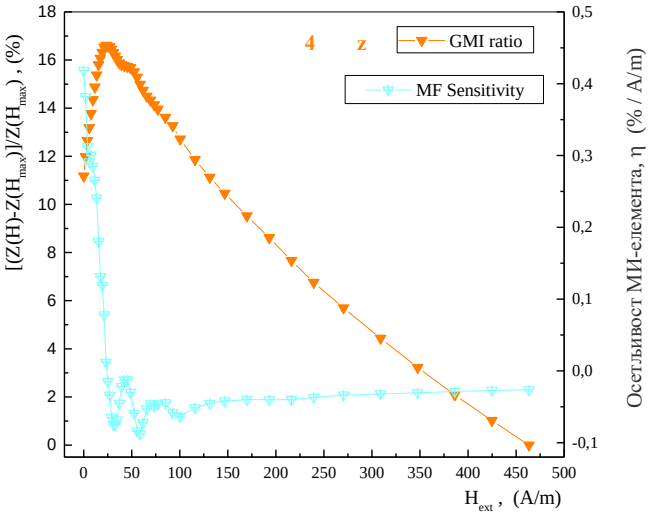


*Сл. . Упоредни приказ зависности МИ-односа и осетљивости МИ-елемента од спољашњег dc магнетног поља e t при фреквенцији f 4 M ma ≈4 3A m .*

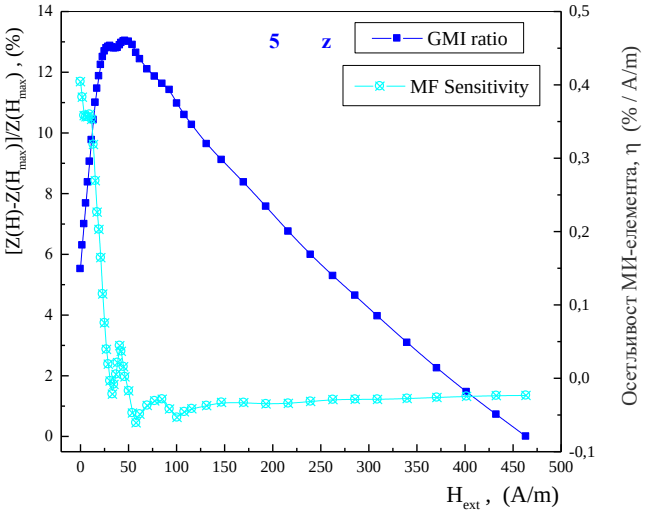


*Сл. . Упоредни приказ зависности МИ-односа и осетљивости МИ-елемента од спољашњег dc магнетног поља e t при фреквенцији f 5 M ma ≈4 3A m .*

## IV. Закључак

Испитивања МИ-ефекта код аморфне жице легуре CoFeSiB у фреквентном опсегу f ∈ [1 MHz, 5 MHz] показују константно повећање импедансе узорка жице. Прорачун МИ-односа је показао да се највеће вредности добијају при фреквенцији од 1 MHz ( ma ≈4 3A m је око 45 %), а затим се МИ-однос смањује. При фреквенцијама изнад 1 MHz је регистрован максимум импедансе који одговара пољу магнетне анизотропије $H_k$. Повећање поља магнетне анизотропије $H_k$ при повећању фреквенције је резултат доминантног учешћа механизма ротације вектора магнетизације током процеса магнећења. Пораст фреквенције праћен је и повећањем осетљивости МИ-елемента, које при фреквенцијама од 4 MHz и 5 MHz достижу вредности од око 0,4 % / A/m.

## Захвалница

Рад је делимично финансиран од стране Министарства просвете, науке и технолошког развоја Републике Србије (евиденциони број пројекта 451-03-68/2022-14/200132 Факултета техничких наука у Чачку, Универзитета у Крагујевцу).

## Литература

[1] L. V. Panina, K. Mohri, "Magneto-impedance effect in amorphous wires", *Applied Physics etters*, Vol. 65, pp. 1189–1191. 1994.

[2] J. Devkota, A. Ruiz, P. Mukherjee, H. Srikanth, M.H. Phan, A. Zhukov, V.S. Larin, "Magneto-resistance, magneto-reactance, and magneto-impedance effects in single and multi-wire systems", *ournal of Alloys and Compounds*, Vol. 549, pp. 295–302, 2013.

[3] J. Liu, H. Shen, D. Xing, J. Sun,, "Optimization of GMI properties by AC Joule annealing in melt-extracted Co-rich amorphous wires for sensor applications", *Physica Status Solidi*, Vol. 211, pp. 1577-1582, 2014.

[4] A. Dzhumazoda, L.V. Panina, M.G. Nematov, A.A. Ukhasov, N.A. Yudanov, A.T. Morchenko, F.X. Qin, "Temperature-stable magnetoimpedance (MI) of current-annealed Co-based amorphous microwires", *ournal of Magnetism and Magnetic Materials,* Vol. 474, pp. 374–380, 2019.

[5] L. Kraus, "Theory of giant magneto-impedance in the planar conductor with uniaxial magnetic anisotropy", *ournal of Magnetism and Magnetic Materials*, Vol. 195, pp. 764–778, 1999.

[6] M.A.,Willard, M. Daniil, „Nanocrystalline soft magnetic alloys two decades of progress", *andbook of Magnetic Materials*, 21, Elsevier, pp. 173-342, 2013.

[7] N. A. Buznikov, A. S. Antonov, „A model for asymmetric magnetoimpedance effect in multilayered bimagnetic films", *ournal of Magnetism and Magnetic Materials*, Vol. 420, pp. 51-55, 2016.

[8] V. Zhukova, J. M. Blanco, M. Ipatov, A. Zhukov, "Effect of transverse magnetic field on domain wall propagation in magnetically bistable glass-coated amorphous microwires", *ournal of Applied Physics*, Vol. 106, 113914, 2009.

[9] J. Sun, J. Liu, D. Xing, X. Xue, ''Experimental study on the effect of alternating-current amplitude on GMI output stability of Co-based amorphous wires'', *Physica Status Solidi*, Vol. 208, pp. 910-914, 2011.

[10] P. Gazda, R. Szewczyk, "Influence of Joule-annealing on double-peak GMI effect in Co-based amorphous ribbons", *Acta Physica Polonica* A Vol. 137, pp. 818-820, 2020.

[11] D. Garcıa, V. Raposo, O. Montero, J. I. Iniguez "Influence of magnetostriction constant on magnetoimpedance–frequency dependence", *Sensors and Actuators A*, Vol. 129, pp. 227–230, 2006.

[12] H. Yoshinobu, "Development of amorphous wire type MI sensors for automobile use", *ournal of Magnetism and Magnetic Materials,* Vol. 249, pp. 375–381, 2002.

[13] H. Yoshinobu, M. Yamamoto, N. Hamada, A. Shimode, "Magneto-sensitive wire, magneto-impedance element and magneto-impedance sensor", US8610427B2, PATENT, 2013.

[14] G. S. Alvarez, „Micromagnetic field sensor of soft magnetic alloys based on the magnetoimpedance effect", Proceedings of the 2nd International Congress on Instrumentation and Applied Sciences, Puebla, Mexico, pp. 1-8, October 2011.

[15] Б. Поповић, Електромагнетика, Грађевинска књига, Београд 1980, стр. 265.

[16] M. Knobel, M. L. Sanchez, C. Gomez-Polo, P. Marın, M. Vazquez, and A. Hernando, "Giant magnetoimpedance effect in nanostructured magnetic wires", *ournal of Applied Physics* Vol. 79, pp. 1646–1654, 1996.

 ISBN 978-86-7466-930-3

[17] M. H. Phan, H. X. Peng, "Giant magnetoimpedance materials: fundamentals and applications", *Progress in Materials Science*, Vol. 53, pp.323–420, 2008.
[18] M. Vázquez, „Giant magneto-impedance in soft magnetic wires", *ournal of Magnetism and Magnetic Materials*, Vol. 226-230, pp. 693-699, 2001.
[19] M. H. Phan, H. X. Peng, S. C. Yu, M. Vázquez, "Optimized giant magnetoimpedance effect in amorphous and nanocrystalline materials", *ournal of Applied Physics,* Vol. 99, No. 8, pp. 08C505: 1-4, 2006.
[20] T. Morikawa, Y. Nishibe, H. Yamadera, Y. Nonomura, M. Takeuchi, J. Sakata, Y. Taga, "Enhancement of giant magneto-impedance in layered film by insulator separation", *IEEE Transactions on Magnetics*, Vol. 32, pp. 4965-496, 1996.
[21] D. X. Chen, J. L. Munoz, "Ac impedance and circular permeability of slab and cylinder", *IEEE Transactions on Magnetics*, Vol. 35, pp. 1906-1923, 1999.
[22] N. S. Mitrović, S. N. Kane, P. V. Tyagi, S. Roth, "Effect of dc-Joule-heating thermal processing on magnetoimpedance of $Fe_{72}Al_5Ga_2P_{11}C_6B_4$ amorphous alloy", *ournal of Magnetism and Magnetic Materials* Vol. 320, e792-e796, 2008.
[23] M. Knobel, M. Vázquez, L. Kraus, "Giant magnetoimpedance", in *andbook of Magnetic Materials*, Editor K. H. J. Buschow, *Else ier,* 2003.
[24] J. Орељ, Н. Митровић, В. Павловић, „Магнетоимпедансни ефекат CoFeSiB аморфне жице", Зборник радова 64. Конференције ЕТРАН 2020, стр. 513-517.
[25] T. Masumoto, I. Ohnaka, A. Inoue, M. Hagiwara, "Production of Pd-Cu-Si amorphous wires by melt spinning method using rotating water", *Scripta Metallurgica,* Vol. 15, pp. 293-296, 1981.
[26] http://www.phys-iasi.ro/en/equipment-conventional-wires-preparation .
[27] J. Liu, F. Qin, D. Chen, H. Shen, H. Wang, D. Xing, M. H. Phan, J. Sun, ''Combined current-modulation annealing induced enhancement of giant magnetoimpedance effect of Co-rich amorphous microwires'', *ournal of Applied Physics*, Vol. 115, 17A326, 2014.
[28] T. Uchiyama, K. Mohri, L.V. Panina, K. Furuno, "Magneto-impedance in sputtered amorphous films for micro magnetic sensor", *IEEE Transactions on Magnetics*, Vol. 31, pp. 3182-3184, 1995.
[29] K. Mohri, T. Uchiyama, L. V. Panina, M. Yamamoto, K. Bushida, "Recent advances of amorphous wire CMOS IC magneto-impedance sensors: innovative high-performance micromagnetic sensor chip", *ournal of Sensors,* Vol. 2015, Article ID 718069, 2015.
[30] K. Mohri, Y. Honkura, L. V. Panina, and T. Uchiyama, "Super MI Sensor: Recent Advances of Amorphous Wire and CMOS-IC Magneto-Impedance Sensor", *ournal of Nanoscience and Nanotechnology,* Vol. 12, pp. 7491–7495, 2012.

ABSTRACT

This paper presents an examination of magnetoimpedance MI-effect sensitivity of CoFeSiB wires in the frequency range of 2 MHz ÷ 5 MHz. An MI-ratio with a maximum of about 45 % was obtained at 1 MHz @ $H_{max} \approx 463$ A/m. The increase in operating frequencies is followed by an increase of magnetic anisotropy field $H_k$. The highest sensitivity values of the MI-element of about 0.4 % / A/m were attained at frequencies of 4 MHz and 5 MHz. Consequently, the investigated CoFeSiB wires are perspective as magnetic field sensing MI-elements.

**ensitivity of Co e i amorphous wire magnetoimpedance element**

**elena relj, ebojša itrović**

 ISBN 978-86-7466-930-3

# NUCLEAR ENGINEERING AND TECHNOLOGY

# /

# НУКЛЕАРНА ТЕХНИКА

# (NTI/HT)

ISBN 978-86-7466-930-3

# The stability and Quality Control of Instruments for Measurement of Ambient Dose Equivalent Rate

Jelena Krneta Nikolić*, Marija Janković, Milica Rajačić, Ivana Vukanac, Dragana Todorović and Nataša Sarap

***Abstract* — Dosimeters for ambient dose equivalent rate monitoring used in Radiation and Environmental Protection Department in the Institute for Nuclear Sciences Vinča, are made inhouse and they are readily exploited in the field work. Due to this and due to the nature of the measurement itself, quality control of these instruments is readily performed, at least 2 times per year. The control is performed using a $^{60}$Co closed point source with the original protective lead casing and an absorber placed over it in order to mimic the real measurement dose levels. Mean value of the ratio of the first 10 consecutive measurements and the activity of the source on the day of the measurement is declared as a baseline value, while the standard deviation of these 10 values was used to establish the limits of acceptance. According to the analysis of the first two years of the quality control, it can be concluded that all three types of instruments show satisfactory stability.**

***Index Terms* — ambient dose equivalent rate monitors; quality control; measurement stability; dosimetry**

## I. Introduction

Measurement of ambient dose equivalent rate is a measurement method readily used in Radiation and Environmental Protection Department in the Institute for Nuclear Sciences Vinča. This method is accredited with the Accreditation Body of Republic of Serbia under the Standard 17025/2017 [1]. In that sense, it has to comply with the Quality control management system of the Department. Quality control should be planned activity, described in the quality control documentation, performed in a systematic manner, recorded and reviewed. Planning should identify and define type and frequency of quality control, acceptance limits, actions if those limits are exceeded and periodic review of results.

Dosimeters for ambient dose equivalent rate monitoring used in Radiation and Environmental Protection Department in the Institute for Nuclear Sciences Vinča, are made inhouse and they are readily exploited in the field work. Due to this and due to the nature of the measurement itself, it is decided that the quality controll has to be performed at least 2 times per year. As a result of these periodic quality controll measurements, Shewhart control charts, which span over a period of 2 years from mid 2020 to mid 2022, are revised in terms of the stabiity of the instruments' performance. In this paper, the analysis of these Shewhart control charts is presented for 3 types of dosimeters used in Radiation and Environmental Protection Department.

Jelena Krneta Nikolić is with the University of Belgrade, Institute for Nuclear Sciences Vinča, National Institute of Republic of Serbia, Radiation and Environmental Protection Department Mike Petrovića Alasa 12-14, Vinča 11000 Belgrade, Serbia (e-mail: jnikolic@ vin.bg.ac.rs).

Marija Janković is with the University of Belgrade, Institute for Nuclear Sciences Vinča, National Institute of Republic of Serbia, Radiation and Environmental Protection Department Mike Petrovića Alasa 12-14, Vinča 11000 Belgrade, Serbia (e-mail: marijam@ vin.bg.ac.rs)

Milica Rajačić is with the University of Belgrade, Institute for Nuclear Sciences Vinča, National Institute of Republic of Serbia, Radiation and Environmental Protection Department Mike Petrovića Alasa 12-14, Vinča 11000 Belgrade, Serbia (e-mail: milica100@ vin.bg.ac.rs) Ivana Vukanac is with the University of Belgrade, Institute for Nuclear Sciences Vinča, National Institute of Republic of Serbia, Radiation and Environmental Protection Department Mike Petrovića Alasa 12-14, Vinča 11000 Belgrade, Serbia (e-mail: vukanac@ vin.bg.ac.rs)

Dragana Todorović is with the University of Belgrade, Institute for Nuclear Sciences Vinča, National Institute of Republic of Serbia, Radiation and Environmental Protection Department Mike Petrovića Alasa 12-14, Vinča 11000 Belgrade, Serbia (e-mail: beba@ vinca.bg.ac.rs)

Nataša Sarap is with the University of Belgrade, Institute for Nuclear Sciences Vinča, National Institute of Republic of Serbia, Radiation and Environmental Protection Department Mike Petrovića Alasa 12-14, Vinča 11000 Belgrade, Serbia (e-mail: natasas@ vin.bg.ac.rs)

## II. Main Results and Discussion

In the Radiation and Environmental Protection Department of the Institute for Nuclear Sciences Vinča, following types of instruments are readily used and controlled: MOKO-100, RMK 10/RMK-10P and RADEX RDI (total of 10 instruments).

Many of investigated ambient monitors have indication directly in Sv/h, but other instruments have indication in counts per second (cps) and the values in terms of ambient dose equivalent need to be calculated based on the calibration [2]. Also the ones that have an indication in μSvh-1 have to be calibrated and the calibration coefficient established. The calibration is performed in the Secondary Standards Calibration Laboratory in the Radiation and Environmental Protection Department by using the sources with the defined radiation quality, angle of incidence and dose rate. Calibration coefficient is then defined as the ratio of the refrence value and the indication of the instrument. The calibration coefficient with the appropriate measurement uncertainty is stated in a Calibration certificate [3,4].

The quality controll of the instruments is performed every 3 – 6 months, depndent on the availability of the instrument at each particular moment.

The controll is perfomend using a $^{60}$Co closed point source, product number 9031-OL-591/09 with activity of 732.9 kBq on 01.08.2011, produced by Czech Metrology Institute. The source was kept in the original protective lead casing and an absorber was placed over it. Absorber is a 12 high cylinder made of polystyrene, which provides that the

 ISBN 978-86-7466-930-3

dose rate originating from the source is not too high. This source and setup were chosen because the dose rate corresponds to the conditions occurring in routine dosimetry measurements. The measurement method was validated by comparing the results of a measurement of the same $^{60}$Co closed point source using investigated instruments and other types of instrument that are already in the Quality Management System.

For establishing the baseline, a set of 10 consecutive measurements was performed with each investigated instrument. Since the quality control measurements should be performed over a long period of time, it has to be taken into account that the activity of the source will decrease. Logically, the measured values will decrease also. This is why it was chosen that, instead of a direct result obtained by the instrument, a ratio between the measurement result and the activity of the source on the date of measurement should be used as a value to be regarded.

Mean value of the ratio of the first 10 measurements and the activity of the source on the day of the measurement is declared as a baseline value, while the standard deviation of these 10 values was used to establish the limits of acceptance. As it is usual, the limits of acceptance were set on ±2σ, the warning interval was set to be between ±2σ and ±3σ, while the results that exceed the limits of ±3σ should be regarded as not satisfactory.

### *A. Results and Discussion*

The quality control of the instruments was perfomed 6 times for most of the instruments in the period from mid 2020 to mid 2022. The procedure included performing of 5 consecutive measurements, applying the calibration factor to the mean value and calcuating the ratio between the mean value of 5 measured ambient dose equivalent dose rates and the activity of the source at the day of the measurement. For each instrument, a Shewhart control chart was made and the stability of the measurement results in time was followed. In Table 1, the range of quality control measurement for all instruments is presented along with the baseline ratio expressed in %. As it was said before, the baseline value was obtained by performing 10 consecutive measurements at the beginning of the quality control period.

As it can be seen from the Table 1, all instruments showed results that do not differ significantly from the baseline. In all Shewart charts, the limit of ±2σ was not exceeded. Since the measurement uncertainty of the results obrtained by the ambient dose equivalent rate monitors can be up to 30% [3, 5], the ranges can be considered as a relatively narrow. The difference between the maximum and minimum ratio obtained during the quality control measurements was below 15% for all controlled monitors. This means that the limits of acceptance for the stability and reproducibility of the measurements are more strict than the measurement uncertainty of any single measurement, showing the satisfactory stability of the repeated quality control measurements.

TABLE I
RANGE AND OF THE OBTAINED MEASURED DOSE [μSVH-1]/ SOURCE CTIVITY [BQ] AND BASELINE - MEAN VALUE OF FOR THE FIRST 10 MEASUREMENTS

| **Instrument** | **Range Measured dose/source activity [%]** | **Mean value of Measured dose/source activity ratio for the first 10 measurements [% ]** |
|---|---|---|
| MOKO 100 s/No. 250214 | 1.084-1.109 | 1.1 |
| MOKO 100 s/No. 002 | 0.985-1.049 | 1.0 |
| MOKO 100 s/No. 1802 | 0.924-0.975 | 0.90 |
| MOKO 100 s/No. 0604-02 | 0.914-0.976 | 0.92 |
| RMK 10P s/No. 0549 | 0.857-0.897 | 0.91 |
| RMK 10P s/No. 0309 | 0.096-1.07 | 1.01 |
| RADEX RDI1706 s/No. 0711259A711572 | 0.872-1.01 | 0.95 |
| RADEX RDI1706 s/No. 0711259A711574 | 0.942-1.002 | 0.97 |
| RADEX RDI1706 s/No. 0711259A711570 | 0.943-1.028 | 0.98 |

Figures 1, 2 and 3 show unified Shewards charts for the three different types of ambient dose equivalent rate monitors. In order to present different instruments on the same chart, the baseline was established as the mean value of all single baselines of each instrument. The limits were established using the standard deviation of the baselines of individual instruments. In this way, the limits of acceptance have become even more narrow, giving the very strict criterion for the stability of measurements. Here we can observe the behaviour of different types of monitors. All tree types showed satisfactory stability of the ambient dose equivalent rate/source activity ratio, since in no case was the limit of ±2σ exceeded. RMK type of monitors showed the gratest stability of the measurement while MOKO 100 and RADEX showed wider spread of the results. This however does not mean that there is an advantage of one type of instrument over the other, since the period of the quality control, as well as the number of performed measurements is not equal for all types and not large enough for more in depth analysis. Also, for MOKO 100 instrumets, the limits of acceptance are very narrow, more so than for other two types of instruments. However, since the quality control measurements are performed in the controlled environment, using the radioactve source of the defined geometry, setting stict limits of acceptance is not unwaranted. The stability of the measurement in the controlled situation can be

 ISBN 978-86-7466-930-3

considered as a good predictor of the stability in the real measurement circumstances.

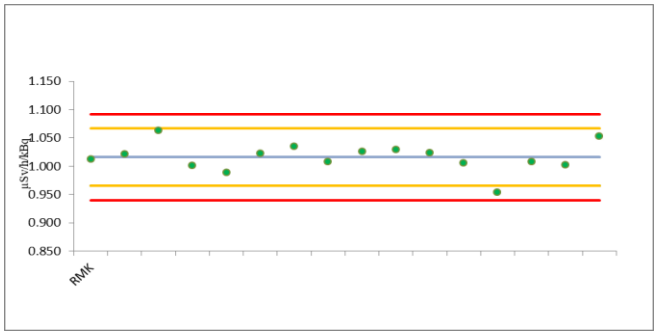


Fig. 1. Unified Sheward chart for 3 RMK 10 type of ambient dose equivalent rate monitors

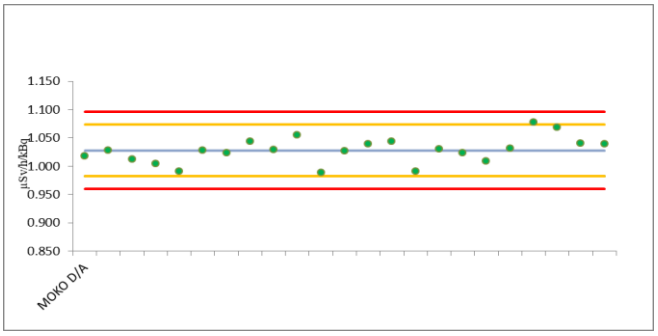


Fig. 2. Unified Sheward chart for 4 MOKO 100 type of ambient dose equivalent rate monitors

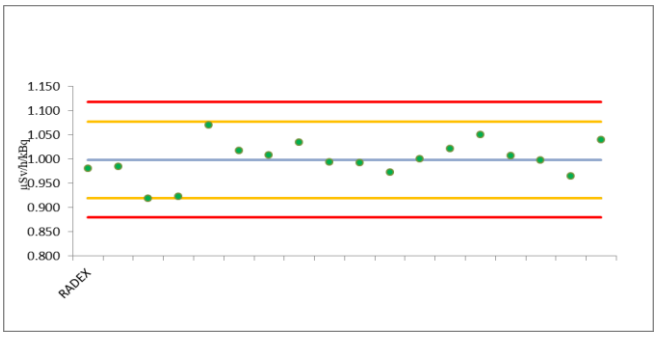


Fig. 2. Unified Sheward chart for 3 RADEX type of ambient dose equivalent rate monitors

## III. Conclusion

In this paper we presented the analysis of the quality control measurements and stability of the measurement for 3 types of ambient dose equivalent rate monitors (10 monitors in total) readily used in Radiation and Environmental Protection Department. The period of quality control was from the mid 2020 to mid 2022. All 10 investigated instrument were periodically controlled and Sheward charts readily analyzed in order to assertain the stability of the performance. According to the analysis of the first two years of the quality controll, it can be concluded that all three types of instruments shhow satisfactory stability. Analysing the performance of individual monitors, it can be seen that the difference from the baseline is less than 15% and that the limits of acceptance were never exceeded. Looking at the unified Sheward charts, it can be consluded that neither type of monitor can be singled out as a more or less stable during this period. Since the quality control of these monitors is a mandatory part of the accredited method of measurement, this kind of analysis and controll will be continued in the future, giving more useful data and more opportunities for improvement.

## Acknowledgment

The research was funded by the Ministry of Education, Science and Technological Development of the Republic of Serbia.

## References

[1] *General requirements for the competence of testing and calibration laboratories, ISO/IEC 17025:2017, 2017.*

[2] IAEA Safety Report Series No 16, *Calibration of radiation protection monitoring instruments*, Vienna , Austria, IAEA, 2000

[3] Jelena Krneta Nikolić, Ivana Vukanac, Miloš Živanović, Milica Rajačić, Dragana Todorović, Gordana Pantelić and Marija Janković, "Uncertainty budget for Ambient Dose Equivalent Rate Measurements with Energy –compensated GM Counters", Proceedings of 7th International Conference on Electrical, Electronic and Computing Engineering, IcETRAN 2020, Belgrade, Čačak, Niš, Novi Sad, September 28-29, 2020

[4] International Electrotechnical Commission, *Radiation Protection Instrumentation - Ambient And/or Directional Dose Equivalent (Rate) Meters And/or Monitors for Beta, X and Gamma radiation - Part 1: Portable Workplace and Environmental Meters and Monitors*, IEC 60846-1, 2009

[5] *Radiological protection — X and gamma reference radiation for calibrating dosemeters and doserate meters and for determining their response as a function of photon energy — Part 1: Radiation characteristics and production methods*, ISO 4037-1:2019, 2019.

 ISBN 978-86-7466-930-3

# Measurement Using Liquid Scintillation Spectrometer-Quality Control

Marija Janković, Nataša Sarap, Jelena Krneta Nikolić, Milica Rajačić, Dragana Todorović, Ivana Vukanac

***Abstract*—Liquid scintillation spectrometers (LSC) are used for radionuclide activity concentration measurements. This paper presents quality control measurements for Quantulus 1220 LSC, which is used for tritium activity determination. The quality control is verified on a monthly basis with two tritium standards. Based on these measurements two different efficiencies were calculated. Paper also presents the results obtained for tritium activity concentration in water sample within intercomparison, which are performed in Radiation and Environmental Protection Department, Vinča Institute of Nuclear Sciences. Intercomparison was organized by International Atomic Energy Agency in 2021.**

***Index Terms*—liquid scintillation spectrometer, quality control, tritium.**

## I. Introduction

Liquid scintillation spectrometer is widely used for determination of low radioactivity. It can be used for detection alpha and beta radiation, Cerenkov radiation, X-rays, Auger electrons, luminescence and gamma radiation. The main advantages of using liquid scintillation spectrometer are rapidity, sensitivity, low detection limits in measurement of low energy beta emitters, such as tritium. Radioactive isotope of hydrogen, tritium $^3$H, has low beta energy with maximum of 18 keV. Whether of natural or anthropogenic, this radionuclide is mobile in the environment, especially in water, and in biological systems. Tritium exists in three chemical forms: tritiated water (HTO), gaseous tritium (HT) an organically bound tritium (OBT). Naturally occurred tritium, produced in the upper atmosphere is oxidized to tritiated water [1,2]. Anthropogenic source of tritium are nuclear tests (between 1945. and 1963.) and nuclear facilities.

In order to determine the activity concentrations of radionuclides, optimization of detector measurement conditions should be performed. One of the basic parameters is determining efficiency. In the case of internal quality control, a periodic check of the characteristics of the detector is carried out according to the quality control plan. External quality control enables participation in intercomparisons, participation in PT schemes.

This paper presents the evaluation of the efficiency of liquid scintillation spectrometer for tritium measurement and analysis of control charts. Radiation and Environmental Protection Department, Vinča Institute of Nuclear Sciences participated in intercomparsion for tritium measurement in water sample and this paper also presents the obtained results.

## II. The Method

Measurement for the purpose of tritium activity determination in water samples are performed on liquid scintillation spectrometer Quantulus 1220. Methods for tritium determination, ASTM D 4107-08 standard method [3] and validated method [4], are accredited with the Accreditation Body of Republic of Serbia according to standard 17025.

Because of low energy of tritium, samples must be distillated to prevent the detection of other beta emitters with higher energy that could mask the tritium spectrum. One of the advantages of LSC technique is 4π geometry (Figure 1.).

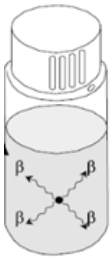


Fig. 1. 4π counting geometry [5]

Spectrometer before any measurement must be calibrated according to the calibration plan. According to the quality control plan, the efficiency check of the detector is done on a monthly basis. The value of the detector efficiency is included in the calculation for determining the activity of tritium.

Marija Janković, Vinča Institute of Nuclear Sciences, National Institute of the Republic of Serbia, University of Belgrade, Radiation and Environmental Protection Department, , Mike Petrovića Alasa 12-14, 11001 Belgrade, Serbia (e-mail: marijam@vinca.rs).

Nataša Sarap, Vinča Institute of Nuclear Sciences, National Institute of the Republic of Serbia, University of Belgrade, Radiation and Environmental Protection Department, , Mike Petrovića Alasa 12-14, 11001 Belgrade, Serbia (e-mail: natasas@vinca.rs).

Jelena Krneta Nikolić, Vinča Institute of Nuclear Sciences, National Institute of the Republic of Serbia, University of Belgrade, Radiation and Environmental Protection Department, , Mike Petrovića Alasa 12-14, 11001 Belgrade, Serbia (e-mail: jnikolic@vinca.rs).

Milica Rajačić, Vinča Institute of Nuclear Sciences, National Institute of the Republic of Serbia, University of Belgrade, Radiation and Environmental Protection Department, , Mike Petrovića Alasa 12-14, 11001 Belgrade, Serbia (e-mail: milica100@vinca.rs).

Dragana Todorović, Vinča Institute of Nuclear Sciences, National Institute of the Republic of Serbia, University of Belgrade, Radiation and Environmental Protection Department, , Mike Petrovića Alasa 12-14, 11001 Belgrade, Serbia (e-mail: beba@vinca.rs).

Ivana Vukanac, Vinča Institute of Nuclear Sciences, National Institute of the Republic of Serbia, University of Belgrade, Radiation and Environmental Protection Department, , Mike Petrovića Alasa 12-14, 11001 Belgrade, Serbia (e-mail: vukanac@vinca.rs).

 ISBN 978-86-7466-930-3

Monthly counting efficiency is determined according to method ASTM D 4107-08 Standard Test Method for Tritium in Drinking Water. Quality control is carried out with reference standard tritium solution $^3$H 9031-OL-548/13 Czech Metrology Institute Type: ER X with activity 5.060 MBq on day 1.10.2013. and PerkinElmer Unquenched Toluene Standard 6008500 with activity 4890 Bq on day 18.11.2015. which have traceability to the BIPM.

Counting efficiency of the spectrometer, $\varepsilon$, is calculated using the following equation:

$$\varepsilon = \frac{R_{ST} - R_b}{A_{ST}} \qquad (1)$$

where $R_{ST}$ is standard count rate (cps), $R_b$ is background count rate (cps) and $A_{ST}$ is standard activity (Bq).

Measurement uncertainty for efficiency is presented through the following equation:

$$u(\varepsilon) = \sqrt{\frac{\frac{R_{ST}}{t_{ST}} + \frac{R_b}{t_b}}{A_{ST}^2} + \varepsilon^2 \left( \frac{u(A_{ST})}{A_{ST}} \right)^2} \qquad (2)$$

where $t_{ST}$ is standard measuring time (s), $t_b$ is background measuring time (s).

## III. Main Results

As already mentioned, according to the quality control plan, the efficiency check of the detector is done on a monthly basis, before measurement of samples.

For efficiency determination two standards are used. In addition to the standard, the background is also measured. Beside the standard from Czech Metrology Institute, for background, dead water (*DW* - tritium free water) from Miami is used, and beside the standard from PerkinElmer Background PerkinElmer is used. The first standard and *DW* are mix with 12 ml scintillation cocktail ULTIMA GOLD LLT in relation 8:12 in 20 ml polyethylene vial. Measurement time for the first standard is 300 s, and for the *DW* is 18000 s, for the second standard and for the background from PerkinElmer measurement time is 1200 s.

Figures 2. and 3. are present control chart for the efficiencies using two different standards. As a reference value, the internal calibration value is taken. Upper and lower control limits are $\pm 3\,\sigma$.

Since the LSC Quantulus 1220 has one detector and 60 positions for measurements, changing the position for the standard and for the background does not change the count rate of standard and background used in efficiency determining.

For the tritium spectrum, standard and background count rates were evaluated between channels 1 and 250 for the first standard, and for the second standard and background count rates were evaluated between channels 1 and 350.

Based on the calculated counting efficiency, the sensitivity of the instrument, *figure of merit* (*FOM*) can be calculated via following equation:

$$FOM = \frac{\varepsilon^2}{R_b} \qquad (3)$$

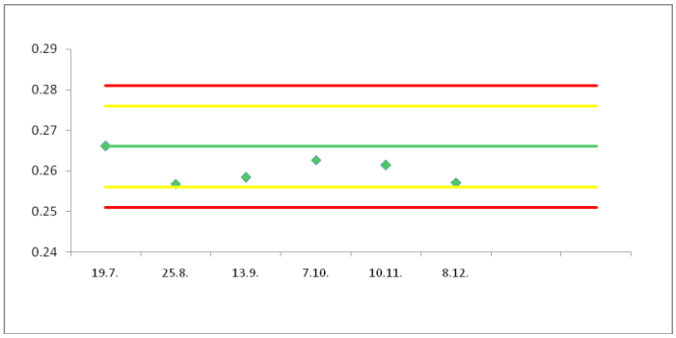


Fig. 2. Control chart for the efficiency for the standard from Czech Metrology Institute for the second half of 2021.

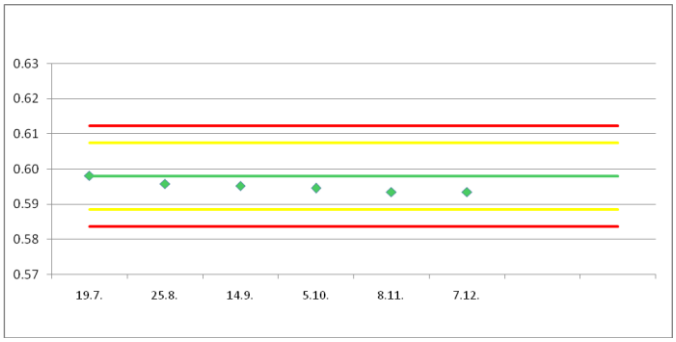


Fig. 3. Control chart for the efficiency for the standard from PerkinElmer for the second half of 2021.

Based on the results obtained for the efficiency check on monthly basis, the limits of acceptance, which is set on $\pm 2\,\sigma$, were not exceeded, observing control charts for both standards.

Using the determining efficiencies, *FOM* can be calculated based on the equation (3). For calculated efficiency for the first standard (26,6 %) and for determined background count rate (2,1 cpm), *FOM* is 337. For the second standard, for calculated efficiency for the first standard (59,8 %) and for determined background count rate (9,66 cpm), *FOM* is 370.

Radiation and Environmental Protection Department, Vinča Institute of Nuclear Sciences, National Institute of the Republic of Serbia, University of Belgrade, participated in intercopmarison ALMERA Proficiency test IAEA-TEL-2021-04. One of the required analyzes was tritium determination in water sample. For sample preparation, ASTM D 4107-08 standard method was used. The method involves preliminary distillation. An aliquot of 8 ml distillated sample is mix with 12 ml scintillation cocktail ULTIMA GOLD LLT in polyethylene vial (volume of vial is 20 ml).

Table I. presents intercomparison results. The final score is A (accepted).


ISBN 978-86-7466-930-3

TABLE I
INTERCOMPARISON EVALUATION PT IAEA-TEL-2021-03

| Sample | Reference value | Reported value | Z-score evaluation |
|---|---|---|---|
| Water | 1653.6 ± 98.2 | 1641 ± 32 | A |

## IV. CONCLUSION

In order to use a Liquid scintillation spectrometer to measure tritium, an analysis of control charts was performed using two tritium standards. Counting efficiencies were calculated and these values were taken as a baseline value. Monthly determination of efficiency, in accordance with the quality control plan, shows stability of the instrument. Results of intercomparison for tritium measurement in water sample show excellent values, using LSC Quantulus 1220 and accredited method.

## ACKNOWLEDGMENT

The research was funded by the Ministry of Education, Science and Technological Development of the Republic of Serbia contract no. 451-03-68/2022-14/200017

## REFERENCES

[1] P. Calmon, J. Garnier-Laplace, “Tritium and the environment” Radionuclide fact sheet, 2010. IRSN Institut de Radioprotection et de Surete Nucleaire

[2] G. Wallova, J. Meresova, S. Zvachova, I. Petranova, I. Sykora, “New electrolytic enrichment system for tritium determination in water research institute in Bratislava and Its first results of tritium activity in precipitation” *Journal of Environmental Radioactivity* 2016 (2020) 106177

[3] ASTM D 4107-08 Standard Test Method for Tritium in Drinking Water

[4] Tecnical Procedure Note 19, Isotope Hydrology Lab., Procedure and Technique Critique for Tritium Enricment by Electrolysis at the IAEA Laboratory, IAEA 1976.

[5] I. Stojković, “Optimization of liquid scintillation spectrometer for determination of alpha and beta emitters in water” Ph.D. dissertation, Faculty of Sciences, University of Novi Sad, Department of Physics, 2015.

 ISBN 978-86-7466-930-3

# E-Waste Glass in Radionuclide Immobilization

*Tatjana Miljojčić, Ivana Jelić, Marija Šljivić-Ivanović and Slavko Dimović*

*Abstract* — **Comprehensive needs for environmental protection are imposed by the prerogative of preserving natural resources, i.e. efficient usage of materials and energy. Therefore, there is an urgent need for different waste materials recycling or reusing. owever, advances in new technologies in the electronics industry are leading to the problem of disposing of different types of -waste, often discarded even before its usual time. This research represents an overview of -waste glass utilization, li e cathode ray tubes (C T) from old computer monitors and T screens, in mortar matrices for radionuclide immobilization. Due to its properties, mortar is used for liquid radioactive waste ( W) solidification. arge quantities of cement, aggregates, and water are used annually for mortar and concrete manufacture. Also, cement production requires the consumption of large amounts of energy, i.e. the use of non-renewable fossil fuels. evertheless, mi ing waste materials with mortar effectively reduces the amount of cement consumption. Aspects of this paper relate to a review of recent developments regarding the use of -waste in cementitious materials. mphasis was placed on their physico-mechanical properties to evaluate the possibility of C T usage in mortar matri for W immobilization.**

***Index Terms* — cathode-ray tubes; liquid radioactive waste; solidification**.

## I. Introduction

Modernization and advancement of technology contribute to the rapid change that applies in big part to electrical devices [1]. This reflects upon the need for innovative technologies, which are more aesthetically pleasing, easier to handle, and especially devices that consume less energy [2]. Improvement in the electronic industry led to a massive problem with different types of E-waste which is often disposed of before their usual time.

In addition to the need for energy efficiency, that the technological leap brings, there is also the need for environmental preservation, especially the development of a "circular economy", which implies the efficient use of materials. As technology advances, the amount of waste increases significantly, and the depletion of natural resources becomes irreplaceable [3]. There is a pressing need for recycling or reuse of various waste materials, and the development of sustainable alternative methods to manage hazardous waste. Collected data last few years from the waste electrical and electronic equipment (WEEE) collection and pretreatment market states that roughly 50,000-150,000 million tons/year of cathode-ray tube glass (CRTs) are collected in Europe only, and this quantity is not expected to decrease in coming years. The widespread use of liquid crystal displays (LCDs), light-emitting diode (LED), and plasma display panels that replaced CRTs are dramatically progressing, producing a million units of waste (Fig. 1).

Fig. 1. E-waste

The environmental problems concerning disposing of CRTs arise because of the high lead (Pb) content stored in the glass, panel section, and funnel. This landfilling non-eco-friendly aspect triggered the call for a solution since the presence of lead in CRT glass means that common disposal methods are not the option. [4].

On the other hand, concrete is the second most widely used material worldwide, right after water. To produce mortar and concrete, large quantities of aggregates are used annually, including cement, water, and other resources. Mixing recycled and waste materials with concrete can reduce the amounts of spent natural raw materials, i.e. these materials could be used as a replacement for cement or aggregates [5]. Combinations

Tatjana Miljojčić is with the Vinca Institute of Nuclear Sciences, University of Belgrade, P.O. Box 522 11000 Belgrade Serbia (email: tatjana.miljojcic@vinca.bg.ac.rs).

Ivana Jelić is with the Vinca Institute of Nuclear Sciences, University of Belgrade, P.O. Box 522 11000 Belgrade Serbia (email: ivana.jelic@vinca.bg.ac.rs).

Marija Šljivić-Ivanović is with the Vinca Institute of Nuclear Sciences, University of Belgrade, P.O. Box 522 11000 Belgrade Serbia (email: marijasljivic@vinca.bg.ac.rs).

Slavko Dimović is with the Vinca Institute of Nuclear Sciences, University of Belgrade, P.O. Box 522 11000 Belgrade Serbia (email: sdimovic@vinca.bg.ac.rs).

 ISBN 978-86-7466-930-3

and mixtures used as aggregates contain about 70 to 80 % of concrete by volume, with around 25 to 35 % of total aggregates produced globally being used in concrete. Therefore, the demand for adequate materials is considerably increasing. Global consumption of aggregates exceeds 40 billion tons annually [6]. The result is disrupted biodiversity and the ecosystem, soil erosion, and depletion of natural resources. The most widely used is sand, which extraction rate is higher than the rate of its replenishment [7]. Reduction of natural raw materials utilization is possible if waste or already recycled materials are used. There is a large selection of waste materials that can serve as a replacement for most aggregates in concrete, one of which is glass waste [8]. This material has a wide application and is convenient for processing, and on the other hand, there is a lot of this waste kind.

Aggregate partial replacement with CRT glass has many advantages [9]. Numerous studies have confirmed that this waste glass also behaves like a pozzolanic material. It has positive effects on the mechanical properties, and it is stated that it can replace cement-mortar in some cases, due to inefficiency in cement production with high energy demands, and great consumption of natural, non-renewable materials.

There are many investigations that dealt with the recycling of waste glass, including CRT waste, in construction materials. Consequently, the need for new information and research in this area has increased in order to incorporate good practices, develop environmental awareness and find new solutions [10]. On the other hand, the same procedure of mixing E-waste glass and construction materials could be applied in the immobilization of liquid radioactive waste (LRW), which can be a good step toward finding more environmentally friendly solutions. Mortar-matrix is able to trap harmful substances and is known as an excellent matrix for radionuclide immobilization.

The aim of this research paper was to look at the possibility of using CRT glass to see the potential benefits that may arise from it, including the immobilization of LRW. This paper is related to the systematic research of literature and works dating back to a few years ago, and deals with the research of the properties of cement mortar and concrete mixed with waste-based CRT glass. The emphasis is on their phisico-mechanical properties and durability, as well as compression, density, consistency, alkali-silica reaction, and the possibility of LWR immobilization.

## II. Immobilization of Liquid Radioactive Waste in Mortar Matrix

There is a great need for proper disposal and immobilization of radioactive waste since this type of waste cannot be destroyed. On an annual basis, a lot of nuclear waste is generated from nuclear power plants, as well as other waste raw materials that are contaminated, such as technological or medical waste. This waste can be found in liquid, solid, and gas forms. Material that is considered a radioactive waste implies the one containing (or contaminated with) radionuclides in such concentrations that the level of radioactivity is higher than the values specified by the competent authorities, without having a use-value. Conditioning of radioactive waste materials implies transformation into forms suitable for later manipulation. These are technological operations of immobilizing these materials into stable, insoluble forms using matrix materials (cement, bitumen, plastic, and glass).

Many years of experimenting proved that this kind of waste is best immobilized by solidification. Theoretical and experimental tests showed that the leaching rate of radionuclides from the solidified matrix was satisfactory. This approach gives a great variety of methods and interpretations of results. However, there have not been investigations dealing with the utilization of CRT waste in mortar matrix for radionuclides immobilization. Hence, there were many comprehensive types of research on the immobilization of heavy metals and radionuclides in mortar matrices [11].

Binder construction materials and demolition debris have proven to be very successful in various studies where it has been investigated how these materials would behave as immobilizers of hazardous, radioactive, and toxic waste. Global economic urbanization contributed to finding more effective technologies that could efficiently manage and solve the environmental issues regarding radioactive waste.

Due to the properties of mortar as a material, which is appreciated for capturing various types of waste materials because of its structure, numerous studies indicate the benefits of mixing cementitious materials and LRW in order to immobilize radionuclides. There is a rising demand for more energy-efficient methods and materials which, in this case, would completely or partially replace the natural raw materials used for its production.

Recently, extensive studies have been carried out on the use of waste products and mortar mixtures. However, there are not many of them dealing with the utilization of CRT glass as a possible replacement for the mortar itself as the solidifier of LRW. It is assumed that the aim of future investigations will be a determination of whether the CRT glass mortar-based matrices satisfy the physical and mechanical properties, instead of the classic mortar. Furthermore, immobilization, storage, and disposal of LWR are expensive, so there is a rising demand for the development of low-cost sorbents [12].

Cement-based materials and other concrete binders require a significant amount of energy and raw materials for their production, and they result in a notable amount of greenhouse gasses and $CO_2$ emissions into the atmosphere. On behalf of that, many studies have turned to find an adequate replacement for conventional aggregates that are used and suitable binders, for the purpose of radioactive waste solidification.

## III. Recycling of CRT, Materials Used, Methodology of Work, and Test Methods

CRT glass should be recycled properly to maximize

 ISBN 978-86-7466-930-3

environmental safety [13]. When it comes to recycling CRT glass there are two options: closed-loop recycling and open-loop recycling (Fig. 2).

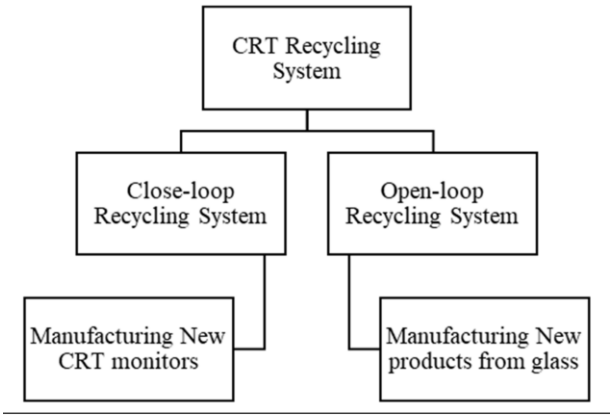


Fig. 2 Recycling system of CRT, redrawn from [3].

The first type of recycling refers to the recycling of old CRT screens in order to obtain new screens, but this method is outdated, new technologies have replaced the need for such screens. The second type of recycling is quite applicable, but the production process is more demanding. It consists of the use of these waste glasses in the form of obtaining new finished products. These species are far more cost-effective, and also have environmental value. Such products include construction materials, which are characterized by low water absorption properties and high silica content, making them an adequate substitute for sand and pozzolan in concrete [14].

CRT monitor consists of three main parts: front panel glass, funnel glass, and the electron gun. There are monochrome CRT (black and white) and color CRT screens (Fig. 3.).

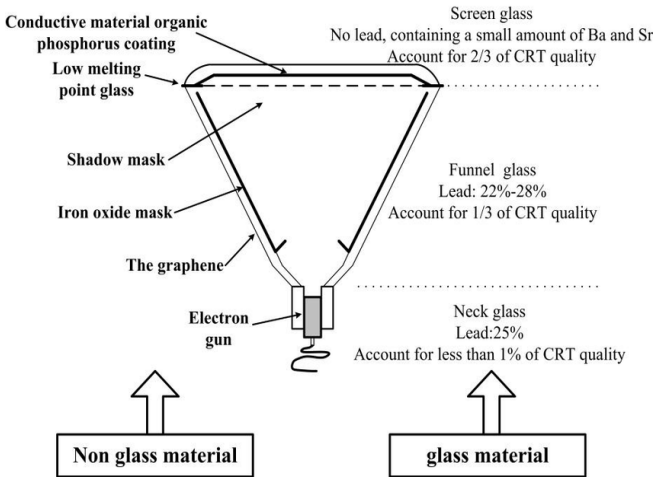


Fig. 3 Composition of a CRT monitor

Consequently, all kinds of chemical compositions are found in CRT glass, hence the main component of CRT is silica. When it comes to recycling and separation of CRTs, the external parts, plastic casing, and metallic parts are removed from TV sets and monitors. The panel and funnel glass are separated by laser cutting. In the recycling procedure of the panel, glass involves the removal of fluorescent powder and using a mechanical crusher to break it into smaller particle sizes.

### *A. Test methods workability, durability, consistency, compression, AS reaction*

There are a lot of investigations where it was estimated the share of ground CRT glass as a fine aggregate in various percentages. For instance, one study focused on using CRT glass 100% instead of sand [5]. Treated and non-treated CRTs were used. Authors reported that the mixture of mortar and non-treated CRT glass produced a higher slump flow than the mixture of mortar and river sand (over 165%), but if treated CRT was used, it decreased slump flow.

Other research [10] found that if used different replacement levels of CRT (0%, 25%, 50%, and 75%) would get different flow speeds and consistency. CRT glass has a smooth surface and is impermeable in nature. Other studies [11,12], as well, showed that the consistency of these mixes is decreased if there is less percentage of CRT. What is evident is that if a higher percentage of CRT glass is used, a more homogeneous mixture is obtained, with less segregation (Fig. 4.).

Fig. 4. Particles of CRT glass

However, it was proven that an increase of CRT in mortar or cement decreases workability and has an important impact on a slump. Consequential is the method of crushing glass, as well as the size of particles and textures, which later has a great influence on mixing with building materials [13].

One research [14] found when CRT glass quantity was increased by replacement of 0 to 75% that caused an increase in the wet density of mortar and cement from 2176 to 2408 kg/m$^3$. Nevertheless, this was expected, hence density of river sand is lower (2620 kg/m$^3$) than the density of CRT glass (3042 kg/m$^3$). Same researchers reported similar results in another study [15], where it was found that the wet density of concrete increased from 2914 to 2992 kg/m$^3$ after replacing 75% of sand with CRT. Other scientists [16,17] also reported an increase in the wet density of concrete when replacing

 ISBN 978-86-7466-930-3

limestone sand with CRT. In one study [18] sand in the mortar was replaced with treated CRT and non-treated CRT glass at levels of 0%, 25%, 50%, and 75% also. With the increase in substitution level, wet density also increased. The only difference was that non-treated CRT glass in mortar had a higher density, while treated CRT had a lower density. The incorporation of CRT glass into mortar and concrete has led to an increase in density, because of the higher density of CRT glass itself compared to river sand. Higher density in this case is desirable and can be used specifically for concrete used in radiation protection, but not so much for structural concrete.

Researchers came to the conclusion [5] that mortar with non-treated and treated CRT glass has a higher compressive strength compared to a mortar with river sand. The compressive strength of mortar that was mixed with non-treated CRT glass was 41% higher than mortar that was mixed with river sand only. This examination was concluded on the 28th day of the experiment, due to the high probability of improvement in the particle packing. In the same research, they found that mixtures of mortar and CRT glass have higher grades of flexural strength, especially if non-treated CRT glass was used. [19]

Some studies [11] found that while increasing levels of CRT in mortar, there has been a decrease in flexural and compressive strength both, but only in early curing stages. It was speculated that it was probably because of the weaker bond in the cement paste, while during the later curing stages there was a chemical reaction between calcium hydroxide and CRT glass, as a pozzolanic material, and there was a smaller decrease in strength.

When it comes to combining CRT glass with concrete, there has been one investigation [11] that indicated that compressive strength and splitting tensile strength are reduced during the early curing time. In that experiment, they replaced river sand with 100% of non-treated CRT glass. Another study figured that lead, which is located in CRT, is responsible for cement dehydration, and after a longer period of curing, compressive and splitting tensile strengths are increasing. Furthermore, a recent study [20] investigated that strength reduction is also responsible less effective bonding area between cement and CRT glass, because of the smooth surface of the glass.

Regarding water absorption tests, some studies [21,22] found that when sand was replaced with 100% of treated CRT glass in concrete, it was found that usage of this waste material was responsible for the water absorption decrease. This was somewhat expected since CRT glass has lower absorption than sand. Another study [22] found that there was a reduction of permeability when adding CRT glass to concrete, which was more obvious when adding a higher water binding ratio. It was observed that 15% reduction in absorption when aggregate was replaced with 100% of CRT glass. Other authors [23,24] also reported that an increase in the quantity of CRT glass led to a further absorption decrease in cement mortar and concrete, the smaller particle size led to a further decrease in water absorption, also.

Many studies reported that utilization of CRT glass as a fine aggregate increased expansion in cement and mortar mixture, due to the alkali-silica reaction (ASR). During mortar mixtures testing without CRT glass as a fine aggregate, researchers reported an insignificant increase in expansion after 14 days, while mortar mixtures that did contain CRT glass continued to expand. Authors mentioned that utilization of fly ash led to a decrease in expansion, due to the pozzolanic reaction which reduced alkali content [25]. Also, when combining results with treated and non-treated glass, there was noticed that treated glass also led to expansion due to ASR. Other researchers reported that surface treatment of CRT glass can reduce ASR, with or without other fine aggregates. Scientists found that treating the CRT glass with nitrilotriacetic acid effectively reduced the expansion caused by ASR, unlike mortars that contained non-treated CRTs [26].

Combining the fly ash with a mixture of CRT glass is also an adequate method. Either way, cement mortar has exceptional potential to encapsulate hazardous waste in its matrix. The authors also suggested the utilization of additional pozzolanic materials (metakaolin, fly ash, etc.) which are responsible for the denser microstructure of the material, hence it reduces expansion due to ASR [27].

## IV. Conclusion

The aim of this paper was the review the investigations related to CRT waste management and its utilization in mortar matrices.

Improvement in the electronic industry led to a massive problem with different types of E-waste which is often disposed of before their usual time. Collected data last few years from the waste electrical and electronic equipment (WEEE) collection and pretreatment market states that roughly 50,000-150,000 million tons/year of cathode-ray tube glass (CRTs) are collected in Europe only, and this quantity is not expected to decrease in coming years. The widespread use of liquid crystal displays (LCDs), light-emitting diode (LED), and plasma display panels that replaced CRTs) are dramatically progressing, producing a million units of waste.

In order to produce mortar and concrete, large quantities of aggregates are used annually, including cement, water, and other resources. Mixing recycled and waste materials with concrete can reduce the amounts of spent natural and raw materials, i.e. these materials could be used as a replacement for cement or other aggregates. There are many investigations that dealt with the recycling of waste glass, including CRT waste, in construction materials.

Many studies reported that the utilization of CRT glass in the mortar was beneficiary to its physico-mechanical properties such as density, water absorption, workability, permeability, compressive, flexural, and splitting tensile strength.

The final result would be that CRT waste glass could partially replace cement-mortar as a suitable waste immobilizer, but more investigations are needed.

 ISBN 978-86-7466-930-3

## ACKNOWLEDGMENT

The research presented in this paper was done with the financial support of the Ministry of Education, Science and Technological Development of the Republic of Serbia, within the funding of scientific research work at the University of Belgrade, Vinca Institute of Nuclear Sciences (Contract No. 451-03-68/2022-14/200017).

## REFERENCES

[1] N. Singh, J. Wang, J. Li, "Waste cathode rays tube: An assessment of global demand for processing", *Procedia En iron. Sci*., 31, 465–474, 2016.

[2] Z. Yao, T. Ling, P.K. Sarker, W. Su, J. Liu, W. Wu, "Recycling difficult-to-treat e-waste cathode-ray-tube glass as construction and building materials: A critical review" *enew. Sustain. Energy e* ., 81, 595–604, 2018.

[3] N. Singh, J. Li, X. Zeng, "Global responses for recycling waste CRTs in e-waste." *WASTE Manag*., 57, 187–197, 2016.

[4] N.N.M. Pauzi, M. Jamil, R. Hamid, A.Z. Abdin, M.F.M. Zain, "Influence of spherical and crushed waste Cathode-Ray Tube (CRT) glass on lead (Pb) leaching and mechanical properties of concrete", . *Build. Eng.*, 21, 421–428, 2019.

[5] Z. Hui, W. Sun, "Study of properties of mortar containing cathode ray tubes (CRT) glass as replacement for river sand fine aggregate", *Constr. Build. Mater*., 25, 4059–4064, 2011.

[6] J. Khatib, A. Jahami, O. Baalbaki, A. Elkordi, H. Abdelgader, "Behavior of reinforced concrete beams containing lightweight aggregate in the tensile zone", *BA . Sci. Technol.*, 1, 3, 2020.

[7] S.K. Kirthika, S.K. Singh, A. Chourasia, "Alternative fine aggregates in production of sustainable concrete-A review", . *Clean. Prod*., 268, 122089, 2020.

[8] Y. Qi, X. Xiao, Y. Lu, J. Shu, J. Wang, M. Chen, "Cathode ray tubes glass recycling: A review", *Sci. Total En iron*., 650, 2842–2849, 2019.

[9] Z. Hui, W. Sun, "Study of properties of mortar containing cathode ray tubes (CRT) glass as a replacement for river sand fine aggregate", *Constr. Build. Mater.*, 25, 4059–4064, 2011.

[10] T.C. Ling, C.S. Poon, "Utilization of recycled glass derived from cathode ray tube glass as fine aggregate in cement mortar", . *a ard. Mater*., 192, 451–456, 2011.

[11] F. Fu, Q. Wang, "Removal of heavy metal ions from wastewaters: A review", . *En iron. Manag.*, 92, 407-418, 2011.

[12] S.-H. Hong1; C.-G. Lee; S.-J. Park. "Removal of $Cd^{2}$+, $Cu^{2}$+, $Pb^{2}$+, and $Ni^{2}$+ by sludge produced from liquid crystal display glass substrate", *Int . En iron. Sci. Technol. Tehran* , 2021

[13] S.T. Yildirim, „Research on strength, alkali-silica reaction and abrasion resistance of concrete with cathode ray tube glass sand", In *Sustainable Buildings—Interaction between a olistic Conceptual Act and Materials Properties*, IntechOpen: London, UK, 2018; pp. 131–149.

[14] T.C Ling, C.S. Poona, "Development of a method for recycling of CRT funnel glass", *En iron. Technol*., 33, 2531–2537, 2012.

[15] T.C. Ling, C.S. Poon, "Effects of particle size of treated CRT funnel glass on properties of cement mortar", *Mater. Struct. Constr*., 46, 25–34, 2013.

[16] P.O. Iniaghe, G. Adie, "Incorporation of finely ground waste cathode ray tube glass in concrete", . *Solid Waste Technol. Manag,* 43, 207-215, 2017.

[17] H. Zhao, C.S. Poon, T.C. Ling, "Properties of mortar prepared with recycled cathode ray tube funnel glass sand at different mineral admixture", *Constr. Build. Mater*., 40, 951–960, 2013.

[18] H. Zhao, C.S. Poon, T.C. Ling, "Utilizing recycled cathode ray tube funnel glass sand as river sand replacement in the high-density concrete", . *Clean. Prod*., 51, 184–190, 2013.

[19] D. Romero, J. James, R. Mora, C.D. Hays, "Study on the mechanical and environmental properties of concrete containing cathode ray tube glass aggregate", *Waste Manag.*, 33, 1659–1666, 2013.

[20] J. Bawab, J. Khatib, S. Kenai, M. Sonebi, "A Review on cementitious materials including municipal solid waste incineration bottom ash(MSWI-BA) as aggregates", *Buildings*, 11, 179, 2021.

[21] H. Zhao, C.S. Poon, "A comparative study on the properties of the mortar with the cathode ray tube funnel glass sand at different treatment methods", *Constr. Build. Mater*., 148, 900–909, 2017.

[22] L.A.P Oliveira, J.P. Castro-Gomes, P. Santos, "Mechanical and durability properties of concrete with ground waste glass sand", *BMC*, Istanbul, Turkey, 1, 11–14, 2008.

[23] J. Wang, S. Guo, Q. Dai, R. Si, Y. Ma, "Evaluation of cathode ray tube (CRT) glass concrete with/without surface treatment", . *Clean. Prod*., 226, 85–95, 2019.

[24] T.C. Ling, T.S. Poon, "Use of CRT funnel glass in concrete blocks prepared with different aggregate-to-cement ratios", *Green Mater*., 2, 43–51, 2014.

[25] I.S. Kim, S.Y. Choi, E.I. Yang, "Evaluation of durability of concrete substituted heavyweight waste glass as fine aggregate", *Constr. Build. Mater*., 184, 269–277, 2018.

[26] I.B. Topçu, A.R. Boğa, T. Bilir, "Alkali–silica reactions of mortars produced by using waste glass as fine aggregate and admixtures such as fly ash and Li2CO3", *Waste Manag*., 28, 878–884, 2008.

[27] D. Kim, I.G. Petrisor, T.F. Yen, "Evaluation of biopolymer-modified concrete systems for disposal of cathode ray tube glass", . *Air Waste Manage. Assoc.*, 55, 961–969, 2005.

 ISBN 978-86-7466-930-3

# Uticaj fuzionih generatora na efikasnost gasnog odvodnika prenapona

[a] Nemanja Aranđelović, [b] Dušan P. Nikezić,[b,*] Uzahir R. Ramadani,
[b] Ivan Lazović, [b] Nikola Mirkov, [c] Predrag V. Osmokrović
[a] *Tehnološko-Metalurški fakultet, Univerzitet u Beogradu, Republika Srbija*
[b] *Institut za nuklearne nauke "Vinča", Univerzitet u Beogradu, Republika Srbija*
[c] *Elektrotehnički fakultet, Univerzitet u Beogradu, Republika Srbija*

***Sažetak*—Rad je eksperimentalnog karaktera. Formiran je model elektronskog generatora za injektovanje energije u plazmu fuzionog reaktora. Snimanjem nejonizujućeg polja u okolini ovakvog generatora utvrđeno je da je to polje izuzetno velike brzine porasta. Na mestu maksimalnog intenziteta tog polja nejonizujućeg zračenja eksperimentisano je sa komercijalnim odvodnicima prenapona i fleksibilnim modelom odvodnika prenapona. Ustanovljeno je da komercijalni odvodnici prenapona imaju efikasnost oko 20%. Za efikasnost fleksibilnog modela ustanovljeno je da je efikasnost nešto manja od 40% (i da se postiže primenom radioaktivnog zračenja alfa čestica). Pošto nijedna od tih efikasnosti ne garantuje pouzdani rad GFSA zaključeno je da bitna elektronika u blizini fuzionog generatora mora biti zaštićena. Međutim, pošto se ta zaštita može sprovesti samo kod fuzionog reaktora ostaje činjenica da je okolina takvog reaktora izuzetno kontaminirana nejonizujućim zračenjem. Komercijalni odvodnici napona su izolovani za ispitivanje pošto je zaštita elektronskih sklopova od brzih prenapona kritična tačka za funkcionisanje savremene elektronike.**

***Ključne reči*—elektromagnetna kontaminacija životne sredine, GFSA, fuzioni reaktor, brzo elektromagnetno polje**

## I. UVOD

Rastuća potreba za energijom dovodi do potrebe uvođenja u primenu novih energetskih postrojenja. Ta nova energetska rešenja svakako ne trebaju biti zasnovana na fosilnom gorivu. Više razloga je za to. Dva osnovna su što se rezerve kvalitetnog fosilnog goriva smanjuju i što upotreba fosilnog goriva značajno doprinosi kontaminaciji životne sredine [1]–[3]. Takozvani zeleni (alternativni) izvori energije su problematični pošto proizvode električnu energiju po znatno većoj ceni, a nisu ni potpuno bez uticaja na okolinu. Pored toga, što je i najvažnije, takvi izvori su male snage i nisu u stanju da proizvedu energije tokom radnog veka ni koliko je uloženo u njihovu proizvodnju [4], [5]. Kao rešenje ovog problema nameću se nuklearni reaktori. Nuklearni reaktori, termalni ili brzi, kao gorivo troše uranijum (prirodan ili obogaćeni) pri čemu se energija dobija procesom fisije. Nuklearni reaktori su usled mogućnosti akcidenata sa dugoročnim posledicama veoma nepopularni u većini zemalja [6]–[8]. Međutim, pošto ni rezerve uranijuma nisu velike i pošto je,realno, veliki problem vezan za odlaganje istrošenog goriva fisionih reaktora, definitivno rešenje energetskog problema čovečanstva je u fuzionim reaktorima [9], [10].

Sa aspekta ekologije dobijanja energija na osnovu reakcije fuzije je skoro u potpunosti zelena energija pošto ne proizvodi nikakav radioaktivni otpad koji bi mogao kontaminirati prirodnu sredinu. Nuklearna reakcija fuzije ima u deeksitacionom procesu pojavu gama zračenja. Ovo gama zračenje može da se eliminiše zaštitom dela fuzionog reaktora olovnim pločama. Međutim, mehanizam zagrevanja plazme injektovanjem energije u nju elektronskim snopovima snage TW, širine desetak ns i brzine porasta ns (i manje) izaziva izuzetno nepoželjnu elektromagnentnu kontaminaciju životne sredine. Prvi pokušaj da se ovo izbegne je bio projekat injektovanja energije u plazmu visokoenergetskim laserskim zračenjem. Pokazalo se da u jednom trenutku, pre postizanja praga reakcije fuzije, dolazi do usijavanja plazme. Takva usijana plazma se ponaša kao ogledalo koje odbija elektromagnetne zrake, tj. laserske zrake i sprečava injektovanje energije u plazmu i prelaz energetskog praga za proces fuzije. Elektromagnetno polje koje nastaje prilikom injektovanja elektronskog snopa (opisanih karakteristika) u plazmu ugrožava, u prvom redu, tehnosferu a preko nje i sve ostale aspekte savremenog načina življenja. Naime, u odnosu na tako brza elektromagnetna polja zaštita od prenapona (takozvana koordinacija izolacije na niskonaponskom nivou) postaje neefikasna [11], [12].

Minijaturizacija elektronskih komponenti u velikoj meri smanjuje njihovu otpornost na prenaponske pojave. Prenaponske pojave usled jako brzih elektromagnetnih polja indukuju se u svim (pa i najkraćim) žičanim strukturama. Za izuzetno brze prenaponske pojave prenaponska zaštita nije dovoljno efikasna pa prenaponske pojave mogu izazvati

Nemanja Aranđelović Tehnološko-Metalurški fakultet, Univerzitet u Beogradu, Republika Srbija, (snemi76@gmail.com)
Dušan P. Nikezić, Institut za nuklearne nauke "Vinča",Institut od nacionalnog značaja za Republiku Srbiju Univerzitet u Beogradu, Republika Srbija, (e-mail: dusan@vin.bg.ac.rs),(https://orcid.org/0000-0002-8885-2683)
Uzahir R. Ramadani, Institut za nuklearne nauke "Vinča", Institut od nacionalnog značaja za Republiku Srbiju Univerzitet u Beogradu, Republika Srbija(email: uzahir@vin.bg.ac.rs)(https://orcid.org/0000-0002-3702-0094)
Ivan Lazović, Institut za nuklearne nauke "Vinča",Institut od nacionalnog značaja za Republiku Srbiju, Univerzitet u Beogradu, Republika Srbija, (e-mail: ivan.lazovic@vin.bg.ac.rs)( https://orcid.org/0000-0002-3877-5157)
Nikola Mirkov, Institut za nuklearne nauke "Vinča",Institut od nacionalnog značaja za Republiku Srbiju, Univerzitet u Beogradu, Republika Srbija, (nmirkov@vin.bg.ac.rs)( https://orcid.org/0000-0002-3057-9784)
Predrag Osmokrović, Elektrotehnički fakultet, Univerzitet u Beogradu, Republika Srbija,(opredrag@verat.net)

 ISBN 978-86-7466-930-3

oštećenje elektronskih elemenata, sklopova i čitavih uređaja. Pored oštećenja elektronskih komponenti tranzijentni prenaponi mogu prouzrokovati i prolazne poremećaje u funkcionisanju uređaja [13], [14]. Efekti uništenja uglavnom su vezani za poluprovodničke komponente, premda oštećenja izolacije mogu biti i na drugim komponentama. Potrebno je napomenuti da su uništenja elektronskih komponenti spregnutih sa antenama česta pojava.

Elementi prenaponske zaštite mogu se generalno podeliti na nelinearne i linearne. U nelinearne elemente prenaponske zaštite spadaju gasni odvodnici prenapona, varistori i odvodne diode. U linearne elemente prenaponske zaštite spadaju različite vrste filtera. Cilj ovog rada je da se proveri efikasnost gasnog odvodnika prenapona (GFSA – najčešće korišćenog nelinearnog elementa) za koordinaciju izolacije na niskonaponskom nivou polja zračenja elektronskog generatora.

### *A. FUZIONI REAKTOR (eksperimentalna postrojenja)*

Fuzioni reaktori se zasnivaju na činjenici da je energija veze po nukleonu jezgra $^4$He maksimalna. To omogućuje da se fizičkim procesom fuzije jezgara deuterijuma i tricijuma dobije jezgro helijuma i oslobodi znatan iznos energije u vidu nukleona i gama zračenja [15], [16].

Kod procesa fuzije postoje dva problema:

1) Egzotermni proces sa visokim energetskim pragom.
2) Slobodna dužina puta čestice u procesu fuzije je jako velika

Prvi problem se rešava tako da se gasovima koji treba da ostvare fuziju dovodi energija dok ne dođu u plazma stanje na temperaturi iznad praga energije za fuziju. Pošto se pokazalo da injektovanje energije u plazmu laserskim putem nije efikasno usled refleksije laserskog snopa od površine usijane plazme prešlo se na injektovanje energije u plazmu elektronskim snopovima. Drugi problem se rešava što se plazma čestica u procesu fuzije nalazi u izuzetno jakom magnetnom polju. Time se ostvaruje rotacija čestica oko vektora magnetne indukcije i mogućnost prelaska srednje slobodne dužine puta za proces fuzije na malom prostoru. Ovo jednostavno rešenje je razlog što se fuzioni reaktori još ne koriste u komercijalne svrhe je pošto potrošnja energije na održavanje tog magnetnog polja veća od energije koja se dobija procesom fuzije.

Na prvi pogled ovaj princip rada omogućuje dobijanje čiste energije bez ikakvog hemijskog ili radioaktivnog materijala koji treba odlagati pod posebnim uslovima. Međutim, postoji kontaminacija elektromagnetnim i nukleonskim zračenjem. Komponentu gama zračenja u nukleone iz te kontaminacije je lako ukloniti odgovarajućom zaštitom prostora u kome nastaje fuzija. Pitanje eliminisanja nejonizujuće komponente elektromagnetnog zračenja je malo teže rešiti. Ova komponenta nastaje u generatoru elektronskih impulsa i tehnički se ne isplati rešiti je olovom (i drugim) zaštitnim zidovima. Iz tog razloga ova komponenta elektromagnetnog zračenja obrazuje elektromagnetno polje u široj okolini elektronskog generatora koje znatno ugrožava funkcionisanje savremenih tehničkih uređaja [17], [18].

Elektronski generator generiše impulse snage TW i širine 1 ns. Da bi se takvi impulsi dobili elektronski generator je dvodelan. Sastoji se od vertikalnog i horizontalnog dela. Vertikalni deo je standardni Marksov generator potopljen u izolaciono ulje i podešen najčešće da daje impulse atmosferskog oblika 1.2/50 $\mu$s. Horizontalni deo se sastoji iz kondenzatora i provodnika za formiranje željenog impulsnog oblika. Interesantno je da su i provodnici i dielektrici kondenzatora u horizontalnom delu često od istog materijala, dejonizovane vode [19], [20]. Na horizontalnom delu se nalazi i naponska sonda za praćenje naponskog oblika impulsa elektron a, slika 1.

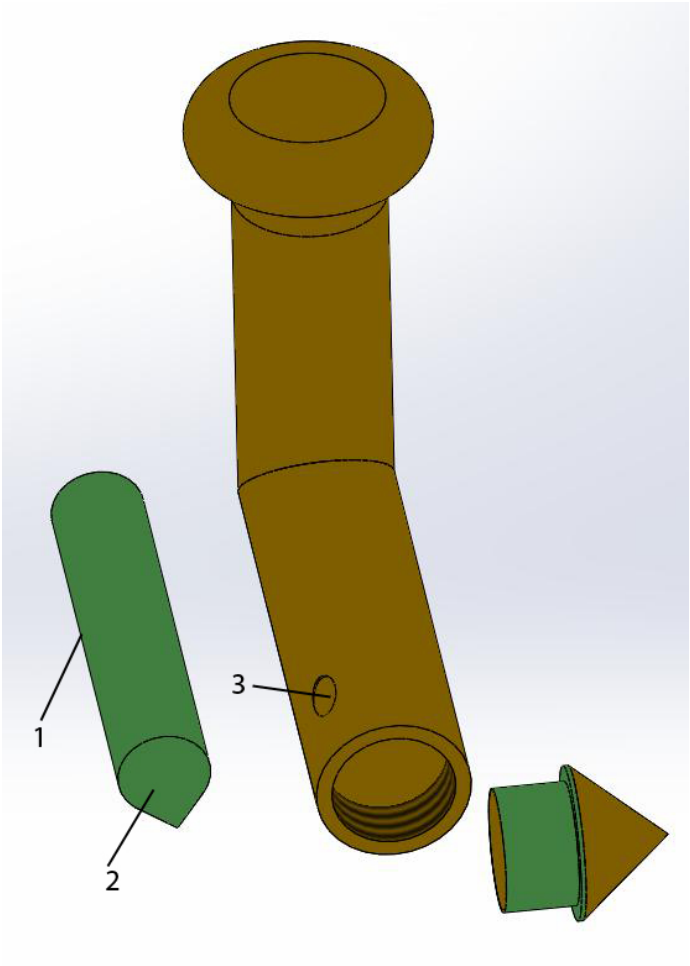


Slika 1: Elektronski generator: 1- kolo za oblikovanje impulsa; 2- 50 Ω talasovodni prilagodni otpor; 3- pozicija za postavljanje merno-upravljačke sonde

Sonda za praćenje naponskog impulsa je potrebna za sinhronizaciju rada oko deset elektronskih generatora koji trebaju da istovremeno generišu impulse uz minimalni džiter. Na slici 2 je prikazan izgled jednog fuzionog reaktora sa osam elektronskih generatora.

 ISBN 978-86-7466-930-3

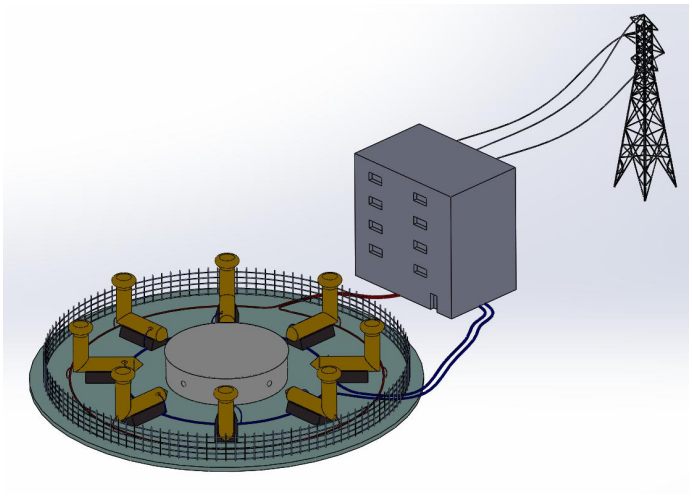

Slika 2: Principijelna šema fuzionog reaktora sa 8 elektronskih generatora

Pošto je elektronski impuls širine oko 5 ns i visine do 10 TW njegova brzina porasta je u nanosekundnoj (odnosno subnanosekundnoj) oblasti. Impulsi takve brzine porasta indukuju u žičanim strukturama elektrotehničkih komponenti izuzetno brze prenapone koji mogu da prođu kroz prenaponsku zaštitu i unište štićene komponente (što se posebno odnosi na savremena višeslojna elektronska kola čiji su izolacioni slojevi izuzetno tanki i probijaju ih naponi reda veličine mV i $\mu$V) [21], [22]. Ta neželjena pojava se dešava u oblasti više kilometara udaljenoj od fuzionog reaktora.

## II. EKSPERIMENT

Za eksperiment je korišćen model horizontalnog dela elektronskog generatora napajan kablovskim generatorom, slika 3.

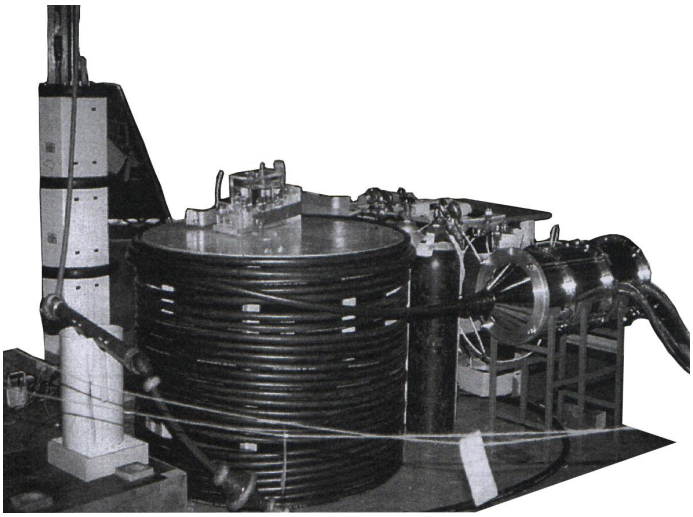

Slika 3: Kablovski generator za generisanje impulsa strmine porasta oko 1 ns

Model horizontalnog dela je bio sa ugrađenom brzom kapacitivnom sondom, slika 4. Kablovski generator generisao je naponski impuls pravougaonog oblika sa sledećim karakteristikama: 1- temena vrednost pravougaonog impulsa je 50 kV; 2- trajanje temenske vrednosti naponskog impulsa je 600 ns; 3- vreme čela i začelja pravougaonog impulsa je 1-3 ns.

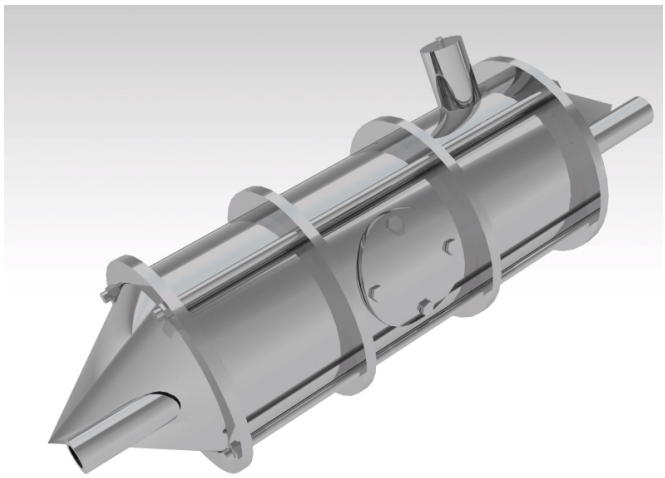

Slika 4: Model horizontalnog dela elektronskog generatora sa ugrađenom brzom kapacitivnom sondom

Na slici 5 je prikazan odziv brze kapacitivne sonde modela horizontalnog dela elektronskog generatora na impuls kablovskog generatora. Kablovski generator je okidan troelektrodnim iskrištem izolovanim smešom gasova $SF_6$-$N_2$ [23]–[29].

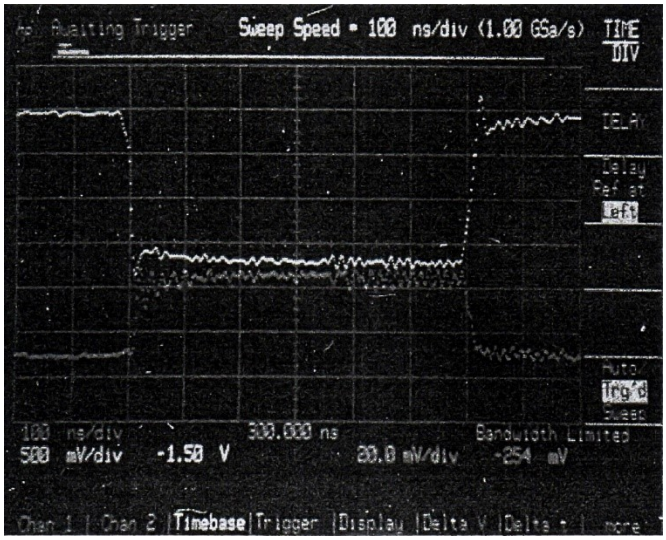


Slika 5: Odziv brze kapacitivne sonde na impuls kablovskog generatora

Elektromagnetno polje u okolini horizontalnog dela elektronskog generatora snimano je instrumentom Narda, slika 6.

Na mesto maksimalne vrednosti električnog polja postavljen je gasni odvodnik prenapona, prema šemi na slici 7. Provera prorade gasnog odvodnik vršena je merenjem napona na otpor-


ISBN 978-86-7466-930-3


Slika 6: Polje nejonizujućeg elektromagnetnog zračenja nastalo okidanjem modela fuzionog generatora na udaljenosti 1 km od eksperimentalnog postrojenja

niku R (100 MΩ). Napon je meren digitalnim osciloskopom (1 GHz) smeštenim u zaštitnu kabinu zaštite 100 dB [30], [31].

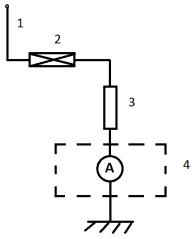


Slika 7: Eksperimentalna šema: 1- antena; 2- gasni odvodnik prenapona; 3- otpor uzemljenja; 4- kabina za zaštitu od elektromagnetnog talasa većeg od 100dB

Korišćeni su komercijalni gasni odvodnici i fleksibilni model. Fleksibilni model je prikazan na slici 8. Kod fleksibilnog modela gasnog odvodnika prenapona bilo je moguće menjati oblik elektroda, materijal elektroda, izolacioni gas i međuelektrodno rastojanje.

Korišćene su standardne cilindrične elektrode, tj. elektrode sa šupljinom ispunjenom radioaktivnim izvorom $^{241}$Am. Pritisak gasa u fleksibilnom modelu se mogao menjati. Korišćeni gas je bio He. Kolo za punjenje i podešavanje pritiska u fleksibilnoj komori prikazano je na slici 7. Radna tačka fleksibilne komore postavljena je na isti radni napon kao što je bila vrednost radnog napona komercijalnih odvodnika prenapona [32]–[35].

Merenja su vršena pod dobro kontrolisanim laboratorijskim

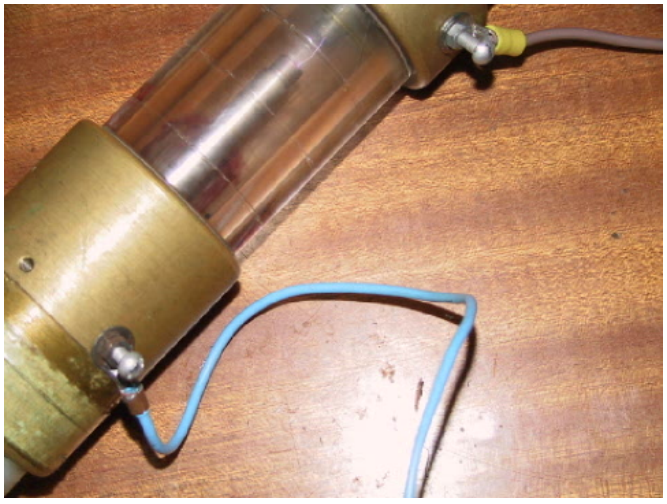

Slika 8: Fleksibilni model gasnog odvodnika prenapona

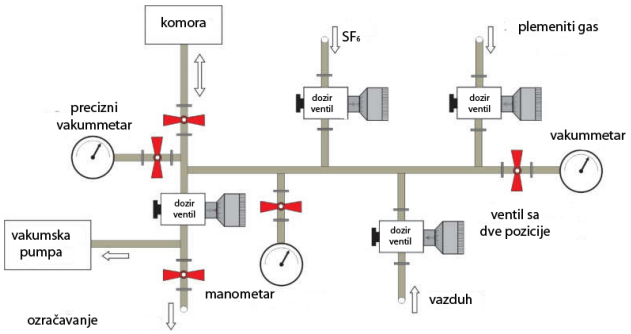


Slika 9: Gasno kolo za punjenje gasnog odvodnika prenapona

uslovima. Pošto je merena komplementarna veličina (prorada GFSA – ne prorada GFSA) merna nesigurnost tipA i tipB su bile nula [36]–[38].

## III. REZULTATI I DISKUSIJA

U tabeli I dati su rezultati ispitivanja efikasnosti odvođenja indukovanih prenapona nastalih okidanjem modela elektronskog generatora. Rezultati u tabeli 1 su dati za tri tipa komercijalnih GFSA različitih proizvođača i istog nominalnog napona.

Tabela I: Eksperimentalno dobijene vrednosti verovatnoće efikasnosti komercijalnih GFSA; p je verovatnoća da GFSA reaguje na prenaponski talas; 1-p je verovatnoća da GFSA ne reaguje na prenaponski talas.

| | **p** | **1-p** |
|---|---|---|
| tipA | 18 | 82 |
| tipB | 16 | 84 |
| tipC | 23 | 77 |

Poređenjem impulsnih karakteristika komercijalnih GFSA i modela GFSA se pokazalo da model GFSA ima brži odziv na prenapone. Odziv modela GFSA je bio najbrži u

 ISBN 978-86-7466-930-3

slučaju da je korišćena kombinacija efekta šuplje katode i primene radioaktivnog izvora jonizujućeg alfa zračenja $^{241}$Am.

Takođe je brzi odziv bio i kada je korišćen samo ili efekat šuplje katode ili efekat jonizujućeg alfa zračenja. Objašnjenje za povećanje brzine odziva primenom efekata šuplje katode i jonizujućeg zračenja je u povećanju broja slobodnih elektrona (potencijalno inicijalnih) u međuelektrodnom prostoru GFSA. Međutim, GFSA koji bi bio konstruisan uz primenu ovih efekata ne bi garantovao efikasnu zaštitu elektronskih sklopova i elektronskih komponenti. To se vidi iz tabele II u kojoj su dati rezultati ispitivanja efikasnosti odvođenja indukovanih prenapona nastalih okidanjem modela elektronskog generatora.

Tabela II: Eksperimentalno dobijene vrednosti verovatnoće efikasnosti modela GFSA; model 1 je efekat šuplje katode zajedno sa efektom jonizujućeg zračenja; model 2 je efekat jonizujućeg zračenja; model 3 je efekat šuplje katode; p je verovatnoća da GFSA reaguje na prenaponski talas; 1-p je verovatnoća da GFSA ne reaguje na prenaponski talas.

| | **p** | **1-p** |
|---|---|---|
| model 1 | 37 | 63 |
| model 2 | 31 | 69 |
| model 3 | 29 | 71 |

## IV. ZAKLJUČAK

U radu je pokazano da zaštita elektronskih komponenti primenom GFSA nije efikasna u blizini elektronskog generatora fuzionog reaktora. To je posledica jer takav generator daje impulse brzine porasta čela i začelja reda veličine 1 ns. Kada se tako brzopromenljivo polje indukuje u anteni (ili bilo kojoj žičanoj strukturi) stvara se prenaponski talas brzine u subnanosekundnoj oblasti (pošto je prenaponski talas ustvari induktivni pik koji se matematičkim putem predstavlja diferenciranjem indukovane struje). U tako kratkim vremenskim intervalima nije moguće pokrenuti mikroskopske procese električnog pražnjenja (koji mogu biti mikrosekundnog trajanja). Što se tiče primene hibridne odvodne šeme sa gasnim odvodnikom, odvodnom diodom (vrlo sličnoj Zener diodi) i varistorom ne može se nadati velikoj pouzdanosti. Razlog za to je što preuzimanje punog prenapona od odvodne diode dovodi do njenog fizičkog uništenja. Rezultat, prikazan u ovom radu, nesumnjivo, pokazuje veću efikasnost odvodnika prenapona sa radioaktivnim izvorom. Ipak to rešenje treba izbegavati jer se na taj način u prirodu ubacuje nekontrolisana primena alfa radioaktivnosti koja je izuzetno opasna ako uđe u lanac ishrane. Iz tog razloga svu elektroniku koja upravlja fuzionim generatorom treba zaštiti olovnim štitovima (šildovima). Ta mera bi obezbedila pouzdan rad fuzionih reaktora ali ne bi sprečila da njegova okolina bude kontaminirana brzim nejonizujućim zračenjem što bi rezultiralo nemogućnošću primene savremenih elektronskih naprava u njoj. Međutim, to ne znači da fuzioni reaktori neće, u budućnosti, oko sebe stvarati visoku elektromagnetnu kontaminaciju životne sredine, naročito u domenu tehnosfere.

## ACKNOWLEDGMENT

Istraživanje je finansiralo Ministarstvo prosvete, nauke i tehnološkog razvoja Republike Srbije.

## LITERATURA

[1] Queral, C., et al., Application of Expanded Event Trees Combined with Uncertainty Analysis Methodologies, Reliability Engineering and System Safety, 205 (2021), art. no. 107246.
[2] Álvarez-Buylla, P. D., et al., Analysis of venting strategies and hydrogen concentration evolution during a station blackout in a BWR-6 containment using GOTHIC 8.3, Progress in Nuclear Energy, 141 (2021), 103930.
[3] Kaur, R., et al., Environmental Radon, Its Exhalation Rates and Activity Concentration of 226Ra, 232Th, And 40K in Northern India, Nucl Technol Radiat, 35 (2020), 3, pp. 268-282.
[4] Herman, R., Fusion: The Search for Endless Energy, Cambridge University Press, New York, NY. 2020, 527 pages. ISBN: 0-521-38373-0.
[5] Pejović, M. M., et al., The Possibility for Gamma and UV Radiation Detection Based On Electrical Breakdown Time Delay Measurement in Krypton and Xenon Filled Diodes, Nucl Technol Radiat, 36 (2021), 3, pp. 243-248.
[6] Kartalović, N. M., et al., Possibility of Application Nuclear Magnetic Resonance for Measurement of Fluid-Flow, Nucl Technol Radiat, 36 (2021), 2, pp. 168-173.
[7] Wunsch, D.C., Kerr Cell Measuring System for High Voltage Pulses, The Review of Scientific Instruments, 35(1964), 7, pp. 816-820.
[8] Fan, X., Chen, et al., An Electric Field Measurement Method Based On Electro-Optical Modulation for Corona Discharge in Air, Review of Scientific Instruments, 90 (2019), 084704.
[9] Kartalović, N., et al., Dose Effect of Gamma Radiation On Reliable Voltage Pulse Measurement in Nuclear Fusion Experiments, Radiation Effects and Defects in Solids, 176 (2021), 3-4, pp. 243-254.
[10] McCracken, G., Stott, P., Fusion: The Energy of the Universe, Academic Press, London, 2nd Edition (2012).
[11] Nedić, T. M., et al., Optimization of Fast Three-Electrode Spark Gaps Isolated with a SF6 and He Mixture, Nucl Technol Radiat, 36 (2021), 3, pp. 234-242.
[12] Osmokrovic, P., Djogo, G., Applicability of Simple Expressions for Electrical Breakdown Probability in Vacuum, IEEE Transactions on Electrical Insulation, 24 (1989), 6, pp. 943 - 947.
[13] Lazarević, D. R., et al., Radiation Hardness of Indium Oxide Films in The Cooper-Pair Insulator State, Nucl Technol Radiat, 27 (2012), 1, pp. 40 - 43.
[14] Osmokrović, P., et al., Influence of The Electrode Parameters On Pulse Shape Characteristic of Gas-Filled Surge Arresters at Small Pressure and Inter-Electrode Gap Values, IEEE Transactions on Plasma Science, 33 (2005), 5 II, pp. 1729 - 1735.
[15] Vulević, B., Osmokrović, P., Evaluation of Uncertainty in The Measurement of Environmental Electromagnetic Fields, Radiation Protection Dosimetry, 141 (2010), 2, pp. 173-177.
[16] Böttscher, C.J.F., Theory of Electric Polarization, Dielectric in Static Fields, Vol. I, Elsevier, Amsterdam,1973.
[17] Osmokrović, P., et al., Radioactive Resistance of Elements for Over-Voltage Protection of Low-Voltage Systems, Nuclear Instruments and Methods in Physics Research, Section B: Beam Interactions with Materials and Atoms, 140 (1998), 1-2, pp. 143-151.
[18] Lončar, B., et al., Radioactive Reliability of Gas Filled Surge Arresters, IEEE Transactions on Nuclear Science, 50 (2003), 5 III, pp. 1725-1731.
[19] Aranđelović, N., et al., Influence of Gamma Radiation On Measurement Fast Pulse Voltages by Kerr Electro-Optic Effect, Radiation Effects and Defects in Solids, 176 (2021), 7-8, pp. 747-757.
[20] Osmokrović, P., et al., Determination of Pulse Tolerable Voltage in Gas-Insulated Systems, Japanese Journal of Applied Physics, 47 (2008), 12, pp. 8928-8934.
[21] Osmokrović, P., et al., Numerical and Experimental Design of Three-Electrode Spark Gap for Synthetic Test Circuits, IEEE Transactions on Power Delivery, 9 (1994), 3, pp. 1444-1450.

 ISBN 978-86-7466-930-3

[22] Erdogan, M., et al., Indoor Radon Activity Concentration and Effective Dose Rates at Schools and Thermal Spas of Ilgin, Nucl Technol Radiat, 35 (2020), 4, pp. 339-346.
[23] Rajović, Z., et al., Influence of SF6-N2 gas Mixture Parameters On the Effective Breakdown Temperature of the Free Electron Gas, IEEE Transactions on Plasma Science, 41 (2013), 12, pp. 3659-3665.
[24] Arbutina, D. S., et al., Possibility of Achieving an Acceptable Response Rate of Gas-Filled Surge Arresters by Substitution of Alpha Radiation Sources by Selection of Electrode Material and The Electrode Surface Topography, Nucl Technol Radiat, 35 (2020), 3, pp. 223-234.
[25] Nedić, T.M., et al., N.M., Efficient Replacement of the Radioactive Sources in The Gas-Filled Surge Arresters Construction for The Insulation Co-Ordination at The Low Voltage Level, Nucl Technol Radiat, 35 (2020), 2, pp. 130-137.
[26] Dautbašić, N. J., Mujezinović, A. Z., Time Domain Solution of Electromagnetic Radiation Model Of The Grounding System Excited By Pulse Current, Nucl Technol Radiat, 35 (2020), 1, pp. 74-81.
[27] Osmokrović, P., et al., Influence of GIS Parameters on the Topler Constant, IEEE Transactions on Electrical Insulation, 27 (1992), 2, pp. 214-220.
[28] Stanković, K., Osmokrović, P., The Model for Calculating the Type a Measurement Uncertainty of GM Counters from The Aspect of Device Miniaturization, IEEE Transactions on Nuclear Science, 61 (2014), 3, pp. 1316-1325.
[29] Osmokrović, P., et al., Triggered Vacuum and Gas Spark Gaps, IEEE Transactions on Power Delivery, 11 (2005), 2, pp.858-864.
[30] Djekić, S.B., et al., Passive and Active Shielding Against Electromagnetic Radiation, Nucl Technol Radiat, 35 (2020), 4, pp. 331-338.
[31] Osmokrović, P., et al., Stability of The Gas Filled Surge Arresters Characteristics Under Service Conditions, IEEE Transactions on Power Delivery, 11 (1996), 1, pp. 260-266.
[32] Osmokrović, P., Djogo, G., Applicability Of Simple Expressions For Electrical Breakdown Probability In Vacuum, IEEE Transactions on Electrical Insulation, 24 (1989), 6, pp. 943-947.
[33] Stanković, K., et al., Reliability of Semiconductor and Gas-Filled Diodes for Over-Voltage Protection Exposed to Ionizing Radiation, Nucl Technol Radiat, 24 (2009), 2, pp. 132-137.
[34] Pejović, M.M., et al., Successive Gamma-Ray Irradiation and Corresponding Post-Irradiation Annealing of PMOS Dosimeters, Nucl Technol Radiat, 27 (2012), 4, pp. 341-345.
[35] Osmokrović, P., Mechanism of Electrical Breakdown of Gases at Very Low Pressure and Interelectrode Gap Values, IEEE Transactions on Plasma Science, 21 (1993), 6, pp. 645-653.
[36] Osmokrović, P., et al., Reliability of three-electrode spark gaps, Plasma Devices and Operations, 16 (2008), 4, pp. 235-245.
[37] Evaluation of measurement data — Guide to the expression of uncertainty in measurement, First edition September 2008, Corrected version 2010, JCGM 2008, JCGM 100:2008.
[38] Stanković, K., Kovacević, U., Combined Measuring Uncertainty of Capacitive Divider with Concentrated Capacitance on High-Voltage Scale, IEEE Transactions on Plasma Science, 46 (2018), 8, pp. 2972-2978.

 ISBN 978-86-7466-930-3

# Sektorski pristup u analizi bezbednosnih rizika upravljanja nuklearnim otpadom

Slavko Dimović, Milica Ćurčić, Nikola Zdolšek

***Apstrakt*—U ovom radu izvršen je uporedni prikaz političkih, ekonomskih, društvenih i ekoloških aspekata u analizi bezbednosnih rizika koji potiču od različitih oblika ugrožavanja poput terorizma, krađa, pronevera, sabotaža i prevara u upravljanju nuklearnim otpadom. Na taj način, primenom sektorskog pristupa bezbednosti, formulisanog u okviru Kopenhaške škole studija bezbednosti, na celovit i sveobuhvatan način pristupa se predmetu ovog istraživanja primenom u teoriji proverenog analitičkog okvira. Nuklearni otpad je nusproizvod aktivnosti nuklearnih reaktora, postrojenja za preradu goriva, bolnica i istraživačkih objekata, a stvara se i prilikom zatvaranja i dekomisije nuklearnih postrojenja. U međunarodnoj politici upravljanje nuklearnim otpadom je kompleksno i osetljivo pitanje koje uključuje veliki broj državnih i komercijalnih aktera i posebno je regulisano kao deo nuklearne industrije, a usaglašeno sa uslovima tretiranja opasnog otpada.**

**U odnosu na druge vrste otpada, prilikom upravljanja nuklernim otpadom izraženije su društveni aspekti bezbednosti, pre svega kompleksni bezbednosni rizici ali i briga, neizvesnost i perspektive za buduće generacije. Takođe, sa političkog i ekološkog aspekta, upravljanje i odlaganje nuklearnog otpada predstavlja najveći razlog mimoilaženja između nuklearnih pristalica i protivnika. Troškovi upravljanja i odlaganja otpada iz nuklearnih elektrana obično čini oko 5% ukupnih troškova generisane električne energije, a najveći udeo čine troškovi njegovog privremenog i trajnog odlaganja. Nuklearni otpad bi trebalo skladištiti u dubokim geološkim formacijama, jer rizici protokom vremena postaju niži od rizika skladištenja na površini.**

**Upravljanje nuklearnim otpadom karakteriše visok nivo složenosti i interkompatibilnosti značajnih faktora: pitanja transporta, finansiranja prerade otpada i raspolaganja, kao i vođenja administrativnih evidencija. Određene tendencije u regulisanje industrije, za koje se tvrdi da su opravdane na bezbednosnim osnovama, smanjuju transparentnost i istinitost izveštavanja i tako otvaraju mogućnost za korupciju i druge oblike tzv. „kriminaliteta belog okovratnika“. Stvaranjem kulture nekažnjivosti ovih, uslovno rečeno blažih kriminalnih akata, ostvaraju se preduslovi za nastanak i ispoljavanje ozbiljnijih krivičnih dela, uključujući terorizam.**

***Ključne reči*—upravljanje nuklearnim otpadom, bezbednost, bezbednosni rizici, sektorki pristup, Kopenhaška škola studija bezbednosti**

Slavko Dimović, Institut za nuklearne nauke “Vinča” – Institut od nacionalnog značaja za Republiku Srbiju, Univerzitet u Beogradu, Laboratorija za zaštitu od zračenja i zaštitu životne sredine (sdimovic@vin.bg.ac.rs ).

Milica Ćurčić, Institut za nuklearne nauke “Vinča” – Institut od nacionalnog značaja za Republiku Srbiju, Univerzitet u Beogradu, Laboratorija za fizičku hemiju (milica.curcic@vin.bg.ac.rs).

Nikola Zdolšek, Institut za nuklearne nauke “Vinča” – Institut od nacionalnog značaja za Republiku Srbiju, Univerzitet u Beogradu, Laboratorija za fizičku hemiju (zdolsek@vin.bg.ac.rs).

## I. Uvod

U okviru diskursa aktuelizacije neobnovljivih izvora energije, nuklearna energija je dugo bila kritikovana tema i kontroverzan izvor energije. Kao metod proizvodnje električne energije sa niskim emisijama ugljen-dioksida predstavlja jedan od sigurnih izvora energije u budućnosti, pa je njene pristalice razmatraju kao prelazno ili trajno rešenje za dekarbonizaciju, ali i kao hitan odgovor na klimatske promene. S druge strane, protivnici nuklearne energije smatraju je reč o veoma složenoj tehnologiji koju prate bezbednosni, ekološki i zdravstveni rizici. Neizostavni deo diskusije o nuklearnoj energiji jeste nuklearni otpad kao nusproizvod aktivnosti nuklearnih reaktora, postrojenja za preradu goriva, bolnica i istraživačkih centara. On se takođe generiše prilikom zatvaranja i dekomisije nuklearnih reaktora i drugih nuklearnih postrojenja. Nuklearni otpad čine jalovina nastala pri eksploaticiji rude urana, transuranski (TRU) otpad, nisko, srednje i visoko radioaktivni otpad, kao i istrošeno nuklearno gorivo [1].

Upravljanje nuklearnim otpadom predstavlja jednu od najkompleksnijih postupaka u odnosu na sve druge vrste otpada obzirom da uključuje brojne državne i ne-državne aktere i praćeno je složenijim bezbednosnim rizicima sa potencijalno većim posledicama, ali manjom verovatnoćom ispoljavanja štetnog događaja. Predmet ovog istraživanja jeste multidimenziona analiza upravljanja nuklearnim otpadom primenom sektorske analize formulisane u okviru Kopenhaške škole studija bezbednosti [2]. Sektorski pristup bezbednosti prepoznaje pet sektora - vojni, politički, ekonomski, društveni i ekološki sektor i predstavlja relevantan analitički okvir za objašnjavanje prelivanja bezbednosnih rizika iz jednog sektora u drugi. U konkretnoj studiji slučaja – upravljanju nuklearnim otpadom, analizirano je četiri sektora, a obzirom da je istraživanje koncipirano u redovnom, mirnodopskom stanju iz analize je izostavljen vojni sektor. S druge strane, u ovom radu razmatrana je ideja o proširenom sektorskom pristupu obzirom da je posebna pažnja posvećena tehničkim aspektima bezbednosti. U analizi upravljanja nuklearnim otpadom posebna pažnja posvećena je procesu zatvaranja nuklearnih elektrana nakon završetka njihovog radnog veka, problemi skladištenja, reciklaže i odlaganja visokog, srednjeg i niskog nivoa otpada, kao i bezbedonosni rizici nuklearnog gorivnog ciklusa.

Kada je reč o oblicima ugrožavanja procesa upravljanja nuklearnim otpadom, kao najsloženiji oblik izdvaja se terorizam. Transformacija terorizma, koja uključuje saradnju i

 ISBN 978-86-7466-930-3

koordinaciju aktivnosti većeg broja međunarodnih nedržavnih aktera, imala je reprekusije na objektivnost, pouzdanost i validnost nalaza stručnjaka i regulatora u postupku procene rizika. Preispitivanje ove pretpostavke može da se izvrši na različite načine, a za ovu analizu je najpogodniji prstup koji uključuje osvrt na objektine i subjektivne aspekte. Kada je reč o subjektivnim aspektima, obzirom da javnost uobičajeno nije stručna, svoju zabrinutost po pitanju štetnosti nuklearnog otpada iskazuje na način koji nije uvek potpuno podesan za prikupljanje i procenu dokaza od strane regulatora i stručnjaka. Dizanjem panike i vršenjem pritiska na donosioce odluka ne pruža se adekvatan materijal koji bi regulatori mogli kasnije da koriste u poboljšavanju legislative i radnih procesa u ovoj oblasti, a značajno se otežava njihov rad. S druge strane, usled objektivnih aspekata može doći do enormono povećanih rashoda usled prevelike pesimisticke procene, odnosno najgore moguće procene koja iziskuje najviše finansijskih ulaganja [3]. Zabrinutost javnosti zbog nuklearnog otpada u Evropi uglavnom je usmerena prema pitanju skladištenja nuklearnog otpada i potencijalnih negativnih efekata uskladištenog otpada po životnu sredinu i zdravlje ljudi [4]. Evropska komisija navodi da je stav o opasnostima koje proističu iz ovog procesa postalo najzastupljenije mišljenje među građanima, bez obzira na njegovu neutemeljenost. Pogubnost ove retorike kreirane od različitih anti-nuklearnih pokreta iskazuje se kroz činjenicu da je bez oslonca u nauci oblikovano mišljenje budućih generacija evropskog javnog mnjenja o dugoročnim opasnostima po životnu sredinu i zdravlje ljudi. U ovom radu poseban akcenat stavljen je na analizu bezbednosti transporta nuklearnog otpada kao odličnoj studiji koja se oslanja na prošireni sektorski pristup za sveobuhvatno sagledavanje i upravljanje bezbednosnim rizicima [5].

## II. POLITIČKI SEKTOR BEZBEDNOSTI

Politički aspekat bezbednosti u sferi upravljanja nuklearnim otpadom istražuje se kroz tri nivoa bezbednosti: nacionalnog nivoa kao osnovnog nivoa bezbednosti iz koje se deriviraju regionalna i međunarodna. S tim u vezi, politike bezbednosti država u ovoj oblasti složene su i sačinjene od čitavog niza politika kojima se doprinosi dostizanju i očuvanju sekuritizovanih vrednosti države, društva i pojedinaca, prevashodno kroz analizu međunarodne, politike EU kao regionalne politike i nacionalne politike.

### *A. Nacionalna politika*

Iako svaka država određuje svoje modele upravljanja nuklearnim otpadom, moguće je identifikovati određene zajedničke karakteristike. Pre svega, zakonodavni organ, najčešće skupština ili parlament, zaduženi su za usvajanje zakona koji se odnose na upravljanjem ovog tipa otpada. Ovaj zakon zatim treba da predvidi uspostavljanje regulatornog tela i, u brojnim slučajevima, zasebno telo za upravljanje istrošenim gorivom i radioaktivnim otpadom, kao i bitne elemente nacionalne politike u vezi upravljanja ovim otpadom. Moguće je da se nacionalna politika u ovoj oblasti uredi posebnim vladinim dekretom ili ministarskim direktivama. Nacionalna politika treba da odredi: odgovornosti unutar zemlje za upravljanje istrošenim gorivom i radioaktivnim otpadom; aranžmane za finansiranje upravljanja otpadom (uključujući odlaganje i dekomisiju); poželjne opcije upravljanja istrošenim gorivom, politike za odlaganje otpada, uvoz i izvoz istrošenog otpada; dekomisija nuklearnih postrojenja; informisanje i učešće javnosti u donošenju odluka.

Za sprovođenje nacionalne politike upravljanja ovim vrstama otpada potrebno je razviti jednu ili više strategija, što je odgovornost nosioca prakse upravljanja otpadom. Na Slici 1 prikazan je primer koji je dala Međunarodna atomska agencije (IAEA) kako se mogu razviti politika i strategija [6].

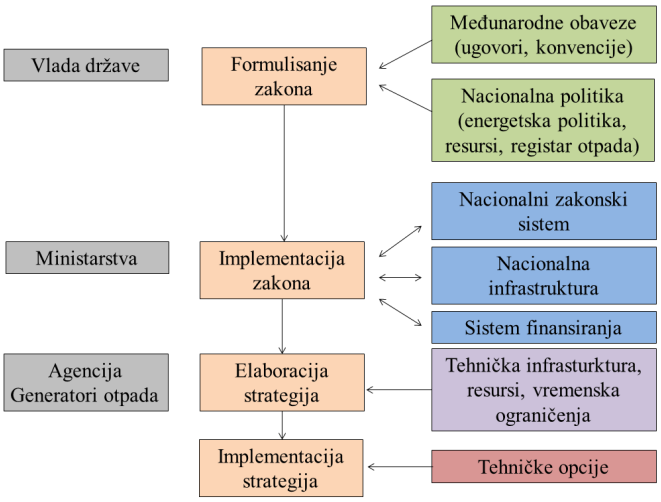


**Slika 1**.

Teorijski i praktično posmatrano, uočljiva je korist od koncentrisanja veoma skupih, potencijalno opasnih i tehnički zahtevnih aspekata nuklearnih elektrana uključujući i otpad, u samo nekoliko zemalja [7]. S druge strane, u promenljivim geopolitičkim okolnostima, mnoge države imaju stah od nuklearne energetske zavisnosti, obzirom da bi prijateljska država u jednom momentu mogla da postane ambivalentna, nekooperativna ili neprijateljski raspoložena i uskrati dalje snabdevanje ovom vrstom energije.

### *B. Regionalna i politika Evropske komisije*

Kada je reč o regionalnom pristupu, odnosno opštoj strategiji upravljanja otpadom evropske zajednice, proklamovan je cilj koji podrazumeva pomirenje dva globalna procesa: nastavka ekonomskog rasta i prosperiteta uz istovremeno smanjivanje uticaja otpada svih vrsta na okolinu. U ovoj viziji, sa povećanjem ekonomskog rasta, korišćenje resursa bilo bi efikasnije što bi uticalo na njegovu manju i racionalniju potrošnju i opadanje negativnog uticaja na životnu sredinu. Težnja za politikom objektivnosti i transparetnosti ogleda se kroz intenciju da najveće troškove snose generatori najveće količine nuklearnog otpada.

Direktiva EU o radioaktivnom otpadu i istrošenom nuklearnom gorivu zahteva da:

- Zemlje EU imaju nacionalnu politiku za upravljanje istrošenim gorivom i radioaktivnim otpadom;
- Zemlje EU sprovode nacionalne programe za

 ISBN 978-86-7466-930-3

upravljanje, uključujući odlaganje, svog istrošenog nuklearnog goriva i radioaktivnog otpada generisanog na njihovoj teritoriji;
- Zemlje EU treba da imaju sveobuhvatan i snažan okvir, kompetentno i nezavisno regulatorno telo, kao i mehanizme finansiranja kako bi se obezbedila adekvatna sredstva;
- Dostupne su javne informacije o radioaktivnom otpadu i istrošenom gorivu i daje se mogućnost za učešće javnosti;
- Zemlje EU podnose Komisiji na svake tri godine (počev od avgusta 2015. godine) nacionalne izveštaje o primeni direktive, na osnovu kojih će Komisija izraditi izveštaj o ukupnoj primeni direktive i inventaru radioaktivnog otpada i istrošenog goriva prisutnog na teritoriji Zajednice i budućim perspektivama;
- Zemlje EU sprovode samoprocene i omogućuju međunarodni uvid svog nacionalnog okvira, nadležnih organa i/ili nacionalnog programa najmanje svakih deset godina;
- Izvoz radioaktivnog otpada za odlaganje u zemljama van EU dozvoljen je samo pod strogim uslovima [8].

*C. Međunarodna politika i odgovornost*

Na međunarodnom nivou zastupljen je jasan i nedvosmislen stav da je svaka zemlja etički i pravno odgovorna za sopstveni nuklearni otpad. Najveća količina nuklearnog otpada stvara se u nuklearnim reaktorima koji proizvode električnu energiju u 31 državi. Pored toga, ne postoji ni pravna ni moralna obaveza snabdevača uranijuma u pogledu otpada, osim onog koji je uključen u mere zaštite.

S druge strane, Međunarodna atomska agencije (IAEA) istakla je težnju ka multinacionalnom pristupu upravljanju i odlaganju istrošenog nuklearnog istrošenog goriva i radioaktivnog otpada. Svako međunarodno skladište otpada ima implikacije u skladu sa Sporazumom o nešireniu nuklearnog oružja (NPT), a pouzdanost i položaj zemlje domaćina od fundamentalnog su značaja za prihvatljivost projekta prema državama potpisnicama NPT- a [6].

IAEA je 2004. godine iznela tri razvojna principa za multinacionalna skladišta nuklearnog otpada:
- postepeno priključenje velikim nacionalnim programima;
- formiranje nadnacionalnih objekata sa međunarodnim mendžmentom i kontrolom i
- zajedničko partnerstvo između država vlasnica skladišta nuklearnog otpada.

Međunarodni ugovori obuhvataju upravljanje nuklearnim otpadom posredstvom dva pristupa. Prvi pristup se odnosi na sav opasnan otpad, kroz Bazelsku Konvenciju [9], uključujući ne samo radioaktivne materijale već i komprimovane gasove, zapaljive čvrste, korozivne materijale i eksplozive. Drugi pristup odnosi se na nuklearnu energiju, gorivni ciklus i pitanja otpada, posredstvom Sporazuma o Nešireniu nuklearnog naoružanja i drugih relevantnih međunarodnih sporazuma, kao i sporazuma unutar EU kao sto su Sporazum o Euroatomu, Sporazuma Evropske komisije, u zavisnosti od posmatranog problema [10]. U odnosu na upravljanje opasnim otpadom uopšte, u Bazelsknoj konvenciji navedeno je da do nelegalnog transporta opasnog otpada dolazi ako se prekogranično kretanje opasnog otpada odvija pod sledećim uslovima: bez obaveštenja u skladu sa odredbama Konvencije svih zainteresovanih država, bez saglasnosti zainteresovanih država, kroz saglasnost dobijenu falsifikovanjem, lažnim predstavljanjem ili prevarom, kada transport materijalno nije usaglašen sa dokumentima, ili prilikom transporta koji rezultira namernim odlaganjem opasnog otpada u suprotnosti Konvencije i opštih principa međunarodnog prava. Uobičajene metode nelegalnog transporta uključuje izradu lažnih izjava ili izveštaja, prikrivanje, skrivanje u pošiljci ispod materijala koji može regularno da se transportuje i pogrešnom označavanju pojedinačnih kontejnera. S obzirom da opasni otpad predstavlja veliku potencijalnu pretnju po ljudsko zdravlje i životnu sredinu, jedan od vodećih principa Bazelske konvencije jeste da opasni otpad treba da se tretira što je više moguće bliže lokaciji gde se generiše.

## III. EKONOMSKI SEKTOR BEZBEDNOSTI

Razvoj nuklearne energije ponekad se posmatra kao jedno od glavnih rešenja za energetskom potrebom uz alternativne izvore energije poput hidroenergije i snage vetra. Strukturu troškova nuklearne energije čine:

• Kapitalni troškovi koji uključuju troškove pripreme, izgradnje, proizvodnje, narudžbine i finansiranja nuklearne elektrane.

• Operativni troškovi koji uključuju troškove nuklearnog goriva, rada i održavanja nuklearne elektrane, troškova dekomisije elektrana, tretiranje i odlaganje isluženog goriva i radioaktivnog otpada.

• Eksterni troškovi za koje se obično pretpostavlja da su nula, ali bi potencijano mogli da uključuju troškove sanacije akcidenata koje ne pokriva polisa osiguranja i u praksi je potrebno da ih podmiri Vlada.

• Drugi troškovi kao što porezi specifični za nuklearnu energiju.

U zemljama u kojima se koristi nuklearna energija pokazalo se da postoje četiri glavna krajnja nosioca troškova: buduće generacije, poreski obaveznici koji preuzimaju deo računa, potrošači električne energije (domaćinstva i/ili industrija) i u nekim zemljama oni koji direktno proizvode ili koriste električnu energiju [11].

Prilikom proizvodnje električne energije nastaju najveće količine nuklearnog otpada, ali nemerljivo manje u poređenju kada se koriste fosilna goriva. Iako nuklearni otpad nema veliku zapreminu, svi aspekti njegovog tretiranja iziskuju značajna finansijska ulaganja. Nuklearna energija je jedina složena tehnologija za proizvodnju električne struje koja preuzima punu odgovornost za sav generisan otpad i u potpunosti ga zaračunava u cenu. Troškovi upravljanja i odlaganja otpada nuklearne elektrane obično čini oko 5% ukupnih troškova generisane električne energije. U okviru ovih troškova, najveći udeo čine troškovi njegovog

 ISBN 978-86-7466-930-3

privremenog i trajnog odlaganja, zatim slede ulaganja u prevenciju i kontrolu izluživanja nuklearnog otpada u životnu sredinu. Dodatni otpad se generiše kad nuklearna postrojenja dođu do kraja svog ekonomskog/sigurnog života i moraju da budu ugašena. Tada cela postrojenja nakon procesa dekomisije postaju radioaktivni otpad.

Angažovanje podizvođača u ograničenom sektoru nuklearne industrije značajno podiže ulazne troskove [12]. S druge strane, istrošeno nuklearno gorivo se može skladištiti u blizini reaktora ili se nakon određenog perioda hlađenja delimično prerađuje stvarajući novi radioaktivni otpad. Proces prerade nuklearnog goriva je veoma skup i delimično efikasan, ali donosi veliki profit ograničenom broju kompanija čija je to delatnost. Pored toga, s obzirom da ima relativno mali broj centara za preradu u svetu, slanje otpada iz zemlje porekla dovodi do pozitivne reakcije domaćeg javnog mnjenja. Nasuprot tome, velike količine nuklearnog otpada zauvek ostaju u zemljama koje ga prerađuju, kao sto su Francuska, Velika Britanija i Rusija. Bez obzira na lokaciju nuklearnih postrojenja i mesta za preradu i odlaganje otpada, finansijski troškovi su značajni.

Upravljanje nuklearnim otpadom karakteriše visok nivo složenosti i interkompatibilnosti značajnih faktora: pitanja transporta, finansiranja prerade otpada i raspolaganje, kao i vođenje administrativnih evidencija [13].

### *A. Transport i bezbednost nuklearnog otpada*

Oko 20 miliona transporta radioaktivnog materijala odvija se širom sveta svake godine javnim putevima, železnicama i brodovima, ali on čini veoma mali udeo u ukupnom transportu svih opasnih materijala. Obzirom na njegovu široku primenu, radioaktivni materijal ne nastaje samo tokom ciklusa nuklearnog goriva, te značajna većina transporta (95%) nije povezana sa nuklearnom energijom. Transport je, međutim, sastavni deo ciklusa nuklearnog goriva, jer većina zemalja koje eksploatiše rudu urana ne proizvodi nuklearnu energiju [14].

Nuklearni otpad se retko skladišti ili prerađuje na lokaciji gde je proizveden. Ovo nameće posebne bezbednosne rizike vezane za transport takvih materijala. Veća je verovatnoća dešavanja terorističkog napada (za stvaranje lokalne kontaminacije) ili kriminalne pronevere (u svrhu prodaje na nedozvoljenom tržištu ili kao kao predmet ucene) u transportu u poređenju sa statičnim lokacijama u kojima je jednostavnije implementirati sigurnosne i bezbednosne procedure. U svrhu uvećanja bezbednosti transporta i smanjenja verovatnoće ispoljavanja rizika potrebno je primeniti različite mere prevencije poput fizičke bezbednosti prevoznih sredstava, procene bezbednosti rute, bezbednosne procene svih učesnika u transportu i sl. U ovom procesu ključnu ulogu imaju obaveštajne službe država i njihova koordinacija sa inostranim službama radi sprovođenja nadzora, infiltracije i drugih specijalnih mera u borbi protiv terorističkih ili radikalnih antinuklearnih organizacija koje bi, potencijalno, mogle da izazivanjem akcidenta poput iskakanja vagona koji prevozi nuklearni otpad, stvore političku nestabilnost s ciljem izazivanja političkih promena. Nasuprot tome, skladištenje otpada na statičnim lokacijma i kontrola pristupa je relativno rutinski postupak zahvaljujući postojanju i poštovanju procedura. Ipak, zajedničko iskustvo sugeriše da, čak i u takvim okolnostima, selektivna pažnja i nemarnost može povećati bezbednosni rizik. Ovo rezultira da se bezbednost u fazi transporta nuklearnim otpadom može održati na visokom nivou, dok se bezbednost u statičnoj lokaciji može smanjiti do te mere da se mogu pojaviti samo krađe.

S druge strane, većina proizvedenog nuklearnog otpada nalazi se u čvrstom i stabilnom keramičkom ili vitrifikovanom (staklenom) obliku, te disperzija radionuklida izazvana terorističkim aktom i opasnost od tzv. prljave bombe nije velika. Istrošeno nuklearno gorivo pruža atraktivnu metu za nuklearne teroriste. Testiranjem probalističkih scenarija razornih eksplozivnih sredstava na kontejnere sa isluženim gorivom koji se transportuju u urbanoj oblasti ustanovljeno je da broj žrtava nije veliki, ali da postoji rizik od intezivne kontaminacije [15]. Nasuprot tome, Međunarodna atomska agencija (IAEA) identifikovala je medicinske i industrijske radioaktivne izvore kao izvor potencijalnih terorističkih pretnji zbog njihove upotrebe u prljavim bombama [14].

Impelementacija kompleksnih sigurnosnih i bezbednosnih aktivnosti tokom transporta zahtevaju velika finansijska ulaganja. Ograničeno tržište proizvodnje uranijuma, restrukturiranje nuklearne industriji širom sveta i smanjenje ekonomske marže posle deregulacije i liberalizacije tržišta električne energije izvršile su dodatni snažan pritisak na industriju nuklearnog transporta [16].

### *B. Vođenje evidencije*

Jedna od najznačajnijih mera zaštite od zračenja jeste vođenje evidencije radioaktivnih materijala, koje prate monitoring, nadzor i inspekcija. U nekim zemljama vođenje evidencija može biti komplikovano usled težnje da se ne evidentira neki visoko radioaktivni otpad kako ne bi postao meta eventualnog terorističkog akta. Do praznina i nedoslednosti u nacionalnom planiranju skladištenja i odlaganja otpada može dovesti nepostojanje evidencije o materijalima kao što su plutonijum, osiromašeni uranijum i istrošeno gorivo za koje ne postoje definitivni planovi za preradu [17].

## IV. DRUŠTVENI SEKTOR BEZBEDNOSTI

Društveni aspekti poput prihvatanja ili otpora društva prema korišćenju nuklearne energije, permanentno obrazovanje građanja i ulaganje u nauku u ovoj oblasti, tačno medijsko izveštavanje i percepcija rizika građana su posebno važni u procesu odlaganja nuklearnog otpada [18], te je neophodno obezbediti dostupnost informacija od javnog značaja. Edukacija stanovništva i promocija znanja iz nuklearne energije trebalo bi da ukaže na značaj upotrebe ovog vida energije u smanjenju emisije gasova staklene bašte, ali i emisiju drugih zagađivača kao što su sumpor dioksid, azot oksid, male čestice i isparljiva organska jedinjenja. Takođe, na taj način bi se doprinelo ograničenju zavisnosti od fosilnih goriva što bi dalje uticalo na smanjenje zabrinutosti u

 ISBN 978-86-7466-930-3

vezi sigurnosti snabdevanja energentima i pružilo bi zaštitu od eskalacije cena fosilnih goriva. Postoje najmanje dva univerzalna očekivanja od nuklearnih reaktora najnovije generacije. Prvi zahtev je garancija da neće biti značajnog oslobađanja radioaktivnosti u životnu sredinu pod bilo kojim uslovima. Drugo očekivanje se odnosi na količinu radioaktivnog otpada kroz težnju da se generiše što manje ovog otpada je moguće.

Prema Turkenburgu upravljanje i odlaganje nuklearnog otpada predstavlja najveću tačku sporenja između nuklearnih pristalica i protivnika. Pored radiotoksičnosti, izražava se i otpor usled gubitka vrednosti nekretnina u blizini odlagališta. Debate o prednostima i manama korišćenja nuklearne energije pokazuju da je otpor javnosti povezan sa sledećim problemima: javno prihvatanje ciklusa nuklearnog goriva; bezbednosni rizici nuklearnih elektrana i drugih komponenti ciklusa nuklearnog goriva; životni vek i upravljanje nuklearnim otpadom, naročito visoko aktivnog otpada; širenje fisionih materijala i nuklearnog naoružanja; akumulacija radionuklida u biosferi do neprihvatljivo visokog nivoa; nedostatak nuklearnih resursa; troškovi nuklearne energije; razvoj nuklearne industrije; uticaj na razvoj nenuklearne opcije [19].

Kao i u svim osetljivim sferama bezbednosti, i u upravljanju otpadom javlja se suprostavljena potreba da javnost bude uključena u sve aktivnosti, kao i da informacije ostanu poverlljive. S jedne strane, javnost, posebno stručna, ima kritičnu ulogu u obezbeđivanju nadzora nad nuklearnim elektranama. Nasuprot tome, ograničavaju se informacije o bezbednosti u nuklearnih elektrana iz straha od identifikovanja velikih slabosti, koje bi mogle da pomognu teroristima i drugim zlonamernim akterima. Takva tajnovitost stvara kulturu nekažnjivosti koja može da obezbedi sivu zonu u kojoj menadžerske greške i tehnički propusti mogu da se prikriju, kao i da dođe do povećanja broja drugih zlonamernih aktivnosti zaposlenih. Svaka procena rizika u ovoj sferi je kompleksna, delimično zbog preplitanja političkih, ekonomskih, društvenih, ekoloških i tehnoloških aspekata, a delom i zbog definisanja male verovatnoće zlonamernih i drugih nepovoljnih događaja.

## V. EKOLOŠKI SEKTOR BEZBEDNOSTI

U kontekstu uticaja nuklearnog otpada na životnu sredinu, razlikuje se indirektan i direktan uticaj. Indirektan uticaj odnosi se na benefite smanjenja upotrebe drugih vidova energenata u proizvodnji energije, a koji imaju negativan uticaj na životnu sredinu. Direktan uticaj podrazumeva analizu pitanja skladištenja, reciklaže i odlaganje nuklearnog otpada, kao i procene uticaja akcidenata u vezi sa nuklearnim otpadom po životnu sredinu.

Preporuka je da bi nuklearni otpad trebalo skladištiti u dubokim geološkim formacijama, na osnovu toga da bi rizici tokom vremena postali niži od rizika skladištenja na površini [20]. Velika poteškoća se javlja u pogledu predviđanja mogućeg izluživanja ili ventilacije i njihove implikacije u periodu od više hiljada godina. Rešavanje problema nuklearnog otpada skladištenjem pod zemljom može uticati na psihološku relaksiranost kod ljudi, jer skladištenje na površini iako lakše za upravljanje, omogućava potencionalno zlonamerno ekološko ili drugo delovanje. Površinsko skladištenje kondicioniranog, upakovananog otpada u savremenim objektima na period od nekoliko decenija je izvodljivo i bezbedno. Izvan ovog vremenskog perioda biće neophodno da se skladište opsežno renovira ili zameni, dok se otpad morati prepakovati. S druge strane, površinsko skladištenje u dužim periodima od navedenog, zahteva dodatne ljudske angažmane i infrastrukturalna ulaganja. U tako dugom vremenskom periodu može doći do hazarda nevezanih za ovaj tip otpada ili čak klimatskih promena (naročito podizanja nivoa mora), što bi zahtevalo da se otpad premesti u novo skladište na drugoj lokaciji, podrazumevajući nove rizike po zaposlene. Pored toga, tokom dugih vremenskih perioda temelji i ojačanje u skladištima mogli bi da oslabe, čineći ih podložnim posledicama zemljotresa.

U zemljama članicama EU varira aktuelna praksa upravljanja isluženim nuklearnim gorivom. Najjednostavnija opcija, koja takođe minimizira zapreminu takvog otpada, jeste da država ovaj otpad zadrži na mestu nastanka, u bazenima ili u velikim kontejnerima, umesto da ga prerađuje. Posle produženog vremena hlađenja od najmanje 20 godina isluženo gorivo je spremno da se direktno odlaže u konačno odlagalište u dubokim geološkim formacijama, ako je u tom trenutku na raspolaganju takav objekat. U poređenju sa prerađivanjem nuklearnog goriva, neophodni tehnički koraci su manje složeni, dovode do manjih zapremina otpada i mnogo manjeg broja različitih oblika otpada koje treba uskladištiti i konačno odložiti.

Praksa prerađivanja nuklearnog goriva takođe varira među evropskim zemljama. Glavne karakteristike inovativnog gorivnog ciklusa su dodatne tehnologije upravljanja otpadom, kao što su segregacija i transformacija. One imaju za cilj smanjenje mase i radioaktivnosti otpada koji ide na konačno odlagalište. Glavni zadatak je da se zatvori ciklus goriva ne samo za plutonijum već i za manje značajne aktinide. U poređenju sa rezultatima konvencionalnog ciklusa goriva, inovativni ciklusi goriva imaju mnogo više prednosti u smislu upotrebe prirodnog uranijuma i smanjenja količine isluženog goriva. Nažalost, procesi reciklaže nuklearnog goriva, dizajnirani da smanje dugoročnu radioaktivnost otpada i/ili potencijalnu dostupnost materijala za proliferaciju, mogu i sami imati nepovoljne ekološke efekte, kao što je emisija radionuklida u biosferu [12].

## VI. ZAKLJUČAK

Upravljanje nuklearnim otpadom kopleksno je pitanje čijoj analizi je neophodno pristupiti sa različitih aspekta, pa je sektorski pristup u istraživanju bezbednosti ove pojave jedan od najadekvatnijih. Sektorski pristup omogućava razumevanje i analizu faktora preplitanja političkog, ekonomskog, društvenog, ekološkog i tehnološkog aspekta, obzirom da dolazi do fenomena prelivanja karakteristika ove pojave iz jednog sektora u drugi. Pitanje upravljanja nuklearnim

 ISBN 978-86-7466-930-3

otpadom jedno je od najznačajnijih pitanja politike jedne države, a regulisano je kao deo nuklearnog industrije i kao deo regulative vezane za opasan otpad. Upravljanje otpadom uključuje prikupljanje, separaciju, skladištenje, transport, obradu, reciklažu i trajno odlaganje nuklearnog otpada.

Trenutna svetska politička situacija po pitanju energenata aktuelizovala je pitanje nuklearnih elektrana, obzirom da države pretenduju da smanje zavisnost od energenata koji potiču sa neuralgičnih područja. Pritom, pored benefita koji se javljaju po životnu sredinu, troškovi upravljanja i odlaganja otpada nuklearne elektrane obično čini oko 5% ukupnih troškova generisane električne energije, a najveći udeo čine troškovi njegovog privremenog i trajnog odlaganja. Upravljanje nuklearnim otpadom karakteriše zavisnost od pitanja transporta, finansiranja prerade otpada, kao i vođenja administrativnih evidencija. Veća je verovatnoća potencijanog terorističkog napada i drugih kriminalnih dela u transportu u poređenju sa statičnim lokacijama u kojima je jednostavnije implementirati sigurnosne i bezbednosne procedure. S druge strane, potencijalno najrazorniji radiološki napad, ali sa najmanjom verovatnoćom realizacije, bilo bi sabotiranje nuklearne elektrane ili bazena sa istrošenim gorivom S tim u vezi, regulator smatra neverovatnim scenarije terorističkih napada i sabotaže na bazene isluzenog nuklearnog goriva Može se tvrditi, s obzirom na potencijalnu ozbiljnost i posledice ovog štetnog dođašaja, kao i mogućnost multipliciranja rizika, da je samo nulta verovatnoća prihvatljiva.

Činjenica da pitanje upravljanja i odlaganja nuklearnog otpada prožima različite sektore utiče da ovo pitanje predstavlja najveći razlog mimoilaženja između nuklearnih pristalica i protivnika. Ovu sferu prati ozbiljna i kontinuirana javna i naučna debatu, permanentno preispitivanje postojanja podrške donosioca odluka, industrijsko lobiranje kao i provera, analiza i nalaženje novih tehničkih i organizacionih rešenja za smanjenje mogućih bezbednosnih rizika. U istom periodu, klimatske promene su postale važno kako političko, tako i naučno pitanje. Globalni rizik od klimatskih promena je, na zaprepašćenje anti-nuklearnih kampanja i oduševljenje nuklearne industrije, delovao afirmativno na pitanje upotrebe nuklearne energije, pa je realno da u budućnosti još veća pažnja bude posvećena pitanjima upravljanja nuklearnim otpadom. S tim u vezi, u budućnosti će zasigurno biti posvećena veća pažnja analizi potencijala skladištenja nuklearnog otpada u dubokim geološkim formacijama, ka modelu koji doprinosi umanjenju bezbednosnih rizika.

S obzirom da određeni produkti nuklearnog gorivnog ciklusa mogu biti iskorišćeni kao naoružanje, pokreću se politička pitanja o proliferaciji od strane međunarodne zajednice. Takođe, posebnu pažnju potrebno je posvetiti organizacionim merama unutar procesa upravljanja nuklearnim otpadom, kako bi se sprečila kultura nekažnjavanja uslovno rečeno blažih kriminalnih dela koja bi mogla da stvore klimu za izvršenje težih i društveno opasnijih dela. Iz tog razloga, ali i radi disperzije stručnih znanja, javnost treba da bude adekvatno informisana o čitavom procesu upravljanja nuklearnim otpadom, bez narušavanja radnih procesa i ugrožavanja bezbednosnih procedura.

## ZAHVALNICA

Autori se zahvaljuju Ministarstvu prosvete, nauke i tehnološkog razvoja Republike Srbije (broj ugovora 451-03-68/2022-14/200017).

## LITERATURA

[1] *Radioactive Waste Management, Status and Trends - Issue #4*, International Atomic Energy Agency, Vienna 2005

[2] B. Buzan, O. Waever & J. D.Wilde, *Security: A New Framework for Analysis*, Boulder, Lynne Rienner Publishers, 1998

[3] T. Vander Beken, N. Dorn, & S. Van Daele, (2010). "Security risks in nuclear waste management: Exceptionalism, opaqueness and vulnerability". *Journal of Environmental Management*, Vol. 91, No. 4, pp. 940-948. 2010.

[4] B. Ulhoa, B. Aleixo, R. Mourão & V. Ferreira, "Radioactiwe waste disposal and public acceptance aspects", 2011 International Nuclear Atlantic Conference - INAC 2011, Belo Horizonte, MG, Brazil, October 24-28, 2011.

[5] M. Essera, A. Borremansb, A. Dubgornb, Anton Shabanb, "Nuclear Waste Transportation: Quality Assurance and Control", *Transportation Research Procedia* Vol. 54, pp. 871–882. 2021.

[6] *Status and Trends in Spent Fuel and Radioactive Waste Management*, International Atomic Energy Agency, Series No. NW-T-1.14 (Rev. 1), Vienna. 2022.

[7] *Nuclear Fuel Cycle Objectives*, International Atomic Energy Agency Series No. NF-0. Vienna. 2013.

[8] Report from the Commission to the Council and the European parliament on progress of implementation of Council Directive 2011/70/EURATOM and an inventory of radioactive waste and spent fuel present in the Community's territory and the future prospects, European Commission. Brussels. 2019.

[9] A code of practice on the international trans boundary movement of radioactive waste. Bulletin 4. International Atomic Energy Agency. Vienna. 1990.

[10] *International law and nuclear energy: Overview of the legal framework*. International Atomic Energy Agency, Bulletin 3, Vienna. 1995.

[11] *Cost Considerations and Financing Mechanisms for the Disposal of Low and Intermediate Level Radioactive Waste*, International Atomic Energy Agency TECDOC-1552. Vienna. 2007.

[12] A. Kakodkar. "Perspective of a developing country with expanding nuclear power programme." International Conference Innovative Technologies for Nuclear Fuel Cycles and Nuclear Power. pp. 21-28 Vienna, 23–26 June 2003.

[13] M. J Ojovan, W.E. Lee. "Principles of Nuclear Waste Management" in *An Introduction to Nuclear Waste Immobilization*. Elsevier. 2005, pp. 71-79.

[14] *Managing the Interface between Safety and Security for Normal Commercial Shipments of Radioactive Material*. Technical reports series No. 1001. International Atomic Energy Agency, Vienna. 2021.

[15] A.J. González. "Security of radioactive sources: threats and answers". Proceedings of an international conference Security of Radioactive Sources. pp. 33-58. International Atomic Energy Agency. Vienna. 10–13 March 2003.

[16] *Security in the Transport of Radioactive Material*. International Atomic Energy Agency Nuclear Security Series. No. 9. Vienna, 2008.

[17] K. Dungan, R.W.H. Gregg K. Morris F.R. Liven G. Butle "Assessment of the disposability of radioactive waste inventories for a range of nuclear fuel cycles: Inventory and evolution over time", *Energy*. Vol 221, 2021.

[18] P., Voganov, M.-S. Yim. "Societal risk communication and nuclear waste disposal". *International Journal of Risk Assessment and Managemen.* Vol. 1, No. 1/2, pp. 20–41. 2000.

[19] W. Turkenburg, "Nuclear energy and sustainable development". In: *Innovative Technologies for Nuclear Fuel Cycles and Nuclear Power*. IAEA, Vienna, pp. 45–56. 2004.

[20] Geological disposal of radioactive waste: technological implications for retrievability, International Atomic Energy Agency SERIES No. NW-T-1.19, Vienna. 2009.

 ISBN 978-86-7466-930-3

 ISBN 978-86-7466-930-3

# Uticaj jonizujućeg zračenja na karakteristike gasnih odvodnika prenapona

[a,*] Uzahir R. Ramadani, [a] Dušan P. Nikezić, [b] Alija Jusić, [a] Ivan Lazović, [a] Nikola Mirkov
[a]*Univerzitet u Beogradu, Institut za nuklearne nauke "Vinča", Institut od nacionalnog značaja za Republiku Srbiju*
[b]*JP Elektroprivreda BiH d.d.-Sarajevo, Bosna i Hercegovina*

***Sažetak*—U radu se ispituje efekat neutronskog i gama zračenja na komercijalne gasne odvodnike prenapona. Rad je eksperimentalno-teoretske prirode. Eksperimentalni deo rada je vršen pod dobro kontrolisanim laboratorijskim uslovima. Kombinovana merna nesigurnost je bila oko 5 %. Eksperimentalni sistem je specijalno koncipiran za posmatranu problematiku i ima određena originalna rešenja. Postupak ispitivanja je bio potpuno automatizovan i imao je softversku podršku u upravljanju eksperimentom kao i za prikupljanje i statističku obradu podataka. Dobijeni rezultati pokazuju da neutronsko i gama zračenje popravlja funkcionalne karakteristike gasnih odvodnika prenapona uz memorijski efekat. Dobijeni rezultati su objašnjeni u skladu sa teorijom interakcije neutronskog i gama polja sa materijalom kao i sa teorijom električnog pražnjenja u gasovima. Rezultati prikazani u radu su od važnosti za projektovanje zaštite od prenapona u sistemima koji se mogu naći u polju neutronskog i gama zračenja jer mogu da postignu pozitivan sinergetski efekat zaštite u hibridnim šemama sa drugim komponentama za zaštitu od prenapona čije karakteristike ovo zračenje kvari.**

***Ključne reči*—gasni odvodnici prenapona, neutronsko i gama zračenje, memorijski efekat**

## I. UVOD

Minijaturizacija elektronskih komponenti u velikoj meri smanjuje njihovu otpornost na prenaponske pojave. Prenaponske pojave nastaju direktno kao posledica komutacionih procesa unutar mreže na kojoj su uređaji, ili indirektno kao posledica interakcije žičane strukture uređaja sa elektromagnetnim impulsima. Mogući izvori tranzijentnih elektromagnetnih pojava su impulsi prenapona na vodovima, atmosfersko pražnjenje, radarski impulsi i nuklearna eksplozija. U slučaju da prenaponska zaštita uređaja nije dovoljno efikasna prenaponske pojave mogu izazvati oštećenje elektronskih elemenata, sklopova i čitavog uređaja dovodeći do njegovog delimičnog ili potpunog uništenja. Tranzijentni prenaponi, takođe mogu prouzrokovati i prolazne poremećaje u funkcionisanju uređaja [1]–[3].

Uzahir R. Ramadani, Institut za nuklearne nauke "Vinča", Univerzitet u Beogradu, Republika Srbija(email: uzahir@vin.bg.ac.rs)(https://orcid.org/0000-0002-3702-0094)
Dušan P. Nikezić, Institut za nuklearne nauke "Vinča", Univerzitet u Beogradu, Republika Srbija, (e-mail: dusan@vin.bg.ac.rs),(https://orcid.org/0000-0002-8885-2683)
Alija Jusić, JP Elektroprivreda BiH d.d.-Sarajevo, Bosna i Hercegovina
Ivan Lazović, Institut za nuklearne nauke "Vinča", Univerzitet u Beogradu, Republika Srbija, (e-mail: ivan.lazovic@vin.bg.ac.rs)( https://orcid.org/0000-0002-3877-5157)
Nikola Mirkov, Institut za nuklearne nauke "Vinča", Univerzitet u Beogradu, Republika Srbija, (nmirkov@vin.bg.ac.rs)( https://orcid.org/0000-0002-3057-9784)

Efekti uništenja uglavnom su vezani za poluprovodničke komponente, premda oštećenja izolacije mogu biti izazvana i na drugim komponentama. Poluprovodničke komponente velike snage vezane na linije napajanja, odnosno energetske vodove, mogu biti izložene delovanju visokih vrednosti tranzijentnih prenapona i stoga vrlo ugrožene. Poluprovodničke komponente u niskonaponskim signalima i kontrolnim kolima indirektno su spregnute sa linijom napajanja, ali mogu biti podložne uništenju zbog relativno malog dozvoljenog strujnog i naponskog opsega. Usled visokofrekventnih komponenti tranzijentnog prenapona može takođe da dođe do uništenja poluprovodničkih komponenti u visokonaponskoj oblasti [4]–[6]. Uništenje poluprovodničkih komponenata usled uticaja visokofrekventnih elektromagnetnih polja je dobila na aktuelnosti usled povećane elektromagnetne kontaminiranosti urbanih sredina [7], [8].

Najrazličitiji poremećaji rada elektronskih uređaja mogu biti izazvani generisanjem tranzijenata u niskonaponskim vodovima. Poremećaji funkcionisanja, u slučaju uređaja za automatsku kontrolu i regulaciju mogu prouzrokovati katastrofalne posledice po kontrolisani objekat. Ipak, većina prolaznih poremećaja funkcionisanja uređaja ne moraju bitno ugroziti njegovo funkcionisanje [9], [10].

Sa aspekta posledica uništenje elektronskih komponenti ili prolazni poremećaji rada su najkritičniji u slučaju da ta elektronska komponenta funkcioniše u okruženju bogatom poljima jonizujućim zračenjem. To je jasno pošto opasnost od jonizujućeg zračenja postoji u nuklearnim energetskim postrojenjima, instrumentima nuklearne medicine, visoko letećim avionima i kosmičkim sistemima. Iz tog razloga je cilj ovog rada da se ispita uticaj neutronskog i gama zračenja na pouzdanost gasnog odvodnika prenapona, komponente koja je nezamenjiva u zaštiti od prenapona na niskonaponskom nivou [11], [12].

### *A. PRENAPONSKA ZAŠTITA*

Elementi prenaponske zaštite mogu se podeliti na nelinearne i linearne. U nelinearne elemente prenaponske zaštite spadaju različite vrste zaštitnih odvodnika prenapona (gasni odvodnici prenapona, varistori i prenaponske diode). U linearne elemente prenaponske zaštite spadaju različite vrste električnih filtera [13]–[15]. U praksi se često koristi

 ISBN 978-86-7466-930-3

kombinacija ovih elemenata, zbog činjenice da većina komercijalnih filtera nije predviđena za korišćenje protiv smetnji koje dostižu nekoliko hiljada volti. Osim toga vrlo je teško obezbediti potreban nivo zaštite uz upotrebu samog filtera [16]. Zaštitni odvodnici sami za sebe imaju nekih nedostataka u slučaju kada je potrebno garantovati zaštitu posebno osetljivih poluprovodničkih elektronskih komponenti.

Kao što je rečeno cilj ovog rada je da se ispita uticaj neutronskog i gama zračenja na gasne odvodnike prenapona.

### *B. GASNI ODVODNICI PRENAPONA*

Gasni odvodnici prenapona odlikuju se visokom pouzdanošću i efikasnošću, a koriste se isključivo za prenaponsku zaštitu. Rade na principu električnog proboja gasova i mogu se koristiti za zaštitu od prenapona amplitude od nekoliko desetina do nekoliko hiljada volti [17].

U pogledu energetske izdržljivosti gasni odvodnici prenapona su najizdržljiviji, a u pogledu cene najeftiniji elementi za zaštitu od prenapona. Prednosti gasnih odvodnika prenapona nad ostalim elementima za zaštitu od prenapona su mogućnost provođenja velikih struja (do 60 kA) i niska sopstvena kapacitivnosti (reda veličine 1 pF, što ih čini podesnim za primenu u oblasti visokih frekvencija) [17], [18]. Gasni odvodnik prenapona se sastoji od dve identične elektrode zatupljene u keramičko (ili stakleno) kućište. Međuelektrodno rastojanje je reda veličine 1 mm. Na unutrašnji zid kućišta se, u nekim slučajevima, nanosi radioaktivni izvor da bi se povećala brzina odziva [18]–[20]. Izolacioni gas je neki od plemenitih gasova (u literaturi se za gasni odvodnik prenapona sreće i naziv „osigurač sa plemenitim gasom“) ili smeša plemenitih gasova na pritisku od 1 kPa do 100 kPa. Na slici 1 data je tipična strujno-naponska karakteristika gasnog odvodnika prenapona. Funkcionisanje gasnog odvodnika prenapona zasniva se na Tauzendovom mehanizmu proboja gasa [21]–[23]. Važna karakteristika gasnog odvodnika prenapona je takozvana Pašenova kriva, tj. zavisnost probojnog napona od proizvoda pritiska i međuelektrodnog rastojanja. Pašenova kriva ima oblik asimetrične U-krive. Vršena su istraživanja da se promenom parametara izolacije (materijala elektroda, oblika elektroda, obradom elektrodne površine, ...) Pašenova kriva prilagodi potrebama. Takođe su vršena ispitivanja da se varijacijom parametara izolacije povećava brzina odziva gasnog odvodnika u cilju izbegavanja primene radioaktivnog izvora pri izradi odvodnika [24], [25]. Sama brzina odziva se karakteriše impulsnom karakteristikom, tj. naponsko-vremenskom karakteristikom. Pokazuje se da naponsko-vremenska kriva naglo raste pri brzim impulsnim naponima i to je osnovni nedostatak gasnog odvodnika, tj. gasni odvodnik sporo reaguje.

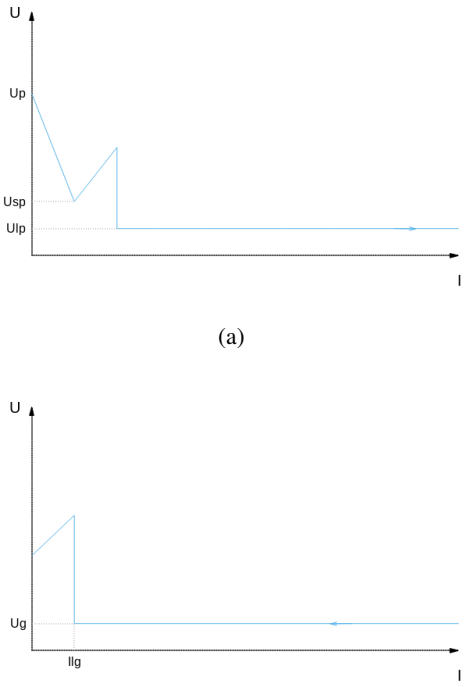


Slika 1: Tipične strujno-naponske karakteristike gasnog odvodnika prenapona

## II. EKSPERIMENT

Ispitivanje uticaja jonizujućeg zračenja na karakteristike gasnih odvodnika prenapona vršeno je na komercijalnim. Ispitivan je komercijalni gasni odvodnik nominalnog napona 470 V punjen gasom He [26], [27]. Impulsne karakteristike su računate na osnovu zakona o konstantnosti površine u volt sekundnoj ravni ispod impulsnog napona i konstantnog nominalnog napona. Za potrebu proračuna impulsnih karakteristika razvijen je namenski softver [28], [29].

Za eksperiment je korišćena visokokvalitetna oprema. Radi eliminacije uticaja elektromagnetnih smetnji na elektronskim aparatima ispitni i merni deo opreme su bili odvojeni profesionalnom mernom kabinom zaštite od električnog polja većom od 100 dB i zaštitom od magnetnog polja većom od 40 dB. Veze između ispitnog i mernog dela je bila negalvanska [30], [31]. Merni sistem je bio u potpunosti automatizovan. Na slici 2 prikazana je blok šema mernog kruga. Kao impulsni napon korišćen je duploeksponencijalni napon oblika 8/20 ms.

Za ispitivanje efekta neutronskog i gama zračenja na gasni krug korišćen je izotop kalifornijuma $^{252}$Cf. Neutronski spektar kalifornijuma ima maksimum pri energijama od oko 0.8 MeV, a maksimalna energija neutrona je 20 MeV. Analiza spektra izvora vršena je aparaturom čija je blok šema data na slici 3. ORTEC germanijumski detektor bio je hlađen tečnim azotom.

Merenje uticaja neutronskog i gama zračenja vršeno je tako što su određivane impulsne karakteristike i histogrami slučajnih promenljivih jednosmerni probojni napon i impulsni probojni napon pre ozračenja, tokom zračenja i

 ISBN 978-86-7466-930-3

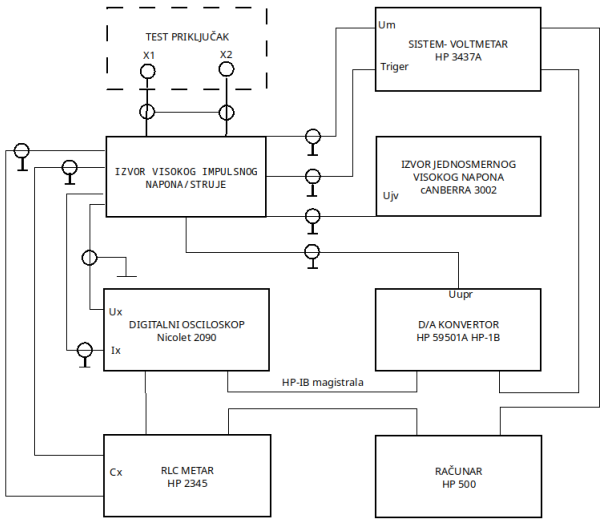


Slika 2: Blok šema mernog sistema

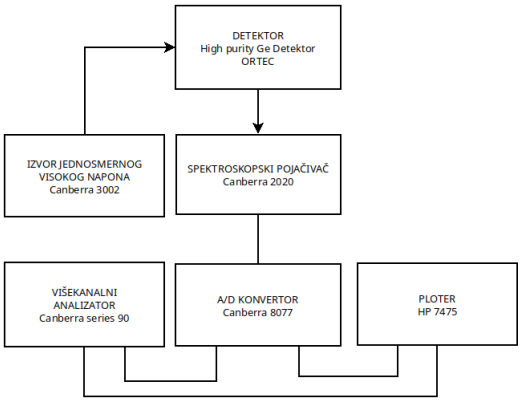


Slika 3: Blok šema aparature za analizu spektra zračenja

nakon ozračenja. Merenja nakon ozračenja su vršena sa vremenskim pauzama da se utvrdi da li postoji indukovani efekat neutronskog zračenja. Za određivanje jedne vrednosti jednosmernog probojnog napona vršeno je merenje 100 uzastopnih vrednosti jednosmernog probojnog napona (primenom jednosmernog izvora napona brzine porasta 8 V/s). Za određivanje jedne vrednosti impulsnog probojnog napona vršeno je merenje 100 uzastopnih vrednosti impulsnog probojnog napona (primenom impulsnog napona brzine porasta 8/20 ms). Pauza između dva uzastopna proboja bila je jedan minut.

Kombinovana merna nesigurnost eksperimentalnog postupka je bila oko 5 % [30], [31].

## III. REZULTATI I DISKUSIJA

Na slici 4 prikazane su hronološke vrednosti slučajne promenljive jednosmerni probojni napon gasnog odvodnika: a) pre stavljanja u polje neutronskog i gama zračenja; b) za vreme boravka u polju neutronskog i gama zračenja (fluksa neutronske komponente 16.244 • $10^{11}$ n/cm$^2$); c) hiljadu sekundi nakon prestanka dejstva polja zračenja; d) 100 000 s nakon prestanka dejstva polja zračenja.

Na slici 5 prikazane su hronološke vrednosti slučajne promenljive impulsni probojni napon gasnog odvodnika: a) pre stavljanja u polje neutronskog i gama zračenja; b) za vreme boravka u polju neutronskog i gama zračenja (fluksa neutronske komponente 16.244 • $10^{11}$ n/cm$^2$); c) hiljadu sekundi nakon prestanka dejstva polja zračenja; d) 100 000 s nakon prestanka dejstva polja zračenja.

Na osnovu slika 4 i 5 se vidi da neutronsko i gama zračenje smanjuje rasipanje slučajnih promenljivih jednosmerni probojni napon i naizmenični probojni napon. Interesantno da se ova pojava održava i nakon dejstva polja zračenja ali ograničeno vreme. Naime, nakon 100 000 s od dejstva polja zračenja hronološki niz vrednosti slučajnih promenljivih statički probojni napon i impulsni probojni napon imaju sličan izgled kao u slučaju neozračenog gasnog odvodnika.

Na slici 6 prikazane su impulsne karakteristike gasnog odvodnika: a) pre stavljanja u polje neutronskog i gama zračenja; b) za vreme boravka u polju neutronskog i gama zračenja (fluksa neutronske komponente 16.244 • $10^{11}$ n/cm$^2$); c) hiljadu sekundi nakon prestanka dejstva polja zračenja; d) 100 000 s nakon prestanka dejstva polja zračenja.

Sa slike 6 je jasno da dejstvo neutronskog i gama zračenja spušta i sužava impulsnu karakteristiku. Taj efekat je prisutan kada se gasni odvodnik nalazi u polju zračenja i određeno vreme (par sati) nakon što prestane dejstvo zračenja. Nakon više vremena, uočeni, memorijski efekat se gubi. Ovde je posebno važno uočiti da je na slikama 6b i 6c usporavanje porasta impulsne karakteristike u oblastima većih brzina impulsnog napona (to su u praksi kritične oblasti brzih indukovanih prenapona).

Efekti uočeni na slikama 4 - 6 se mogu objasniti efektima jonizacije radnog gasa u neutronskom i gama polju. Pošto je odvodnik izolovan He gasom neutronska komponenta primenjenog polja je sudarnim procesom pomerala jezgro He ($\alpha$-česticu) koja je vršila jonizaciju He gasa i stvarala jonsko-elektronske parove. Isti efekat je izazvalo i gama zračenje foto-elektronskim efektom i Komptonovim rasejanjem. Na taj način dolazi do povećanja broja elektrona u međuelektrodnom prostoru, a svaki elektron koji se nađe u homogenom polju može da postane inicijalni tj. da pokrene lavinski proces Tauzendovog proboja. To je posledica što je polje u međuelektrodnom prostoru (tj. na svakoj srednjoj dužini puta elektrona on stekne dovoljno energije da izvrši jonizaciju) [34], [35]. Što se tiče memorijskog efekta (ustanovljenog efekta dejstva neutronskog i gama zračenja i nakon uklanjanja polja zračenja) posledica je aktiviranja materijala odvodnika neutronima. To aktiviranje ima relativno kratko poluvreme raspada. Potvrda ovog tumačenja jesu spektrometri (aktivacione analize) gasnog odvodnika 1000 s i 100 000 s nakon dejstva zračenja, slike 7a i 7b.

 ISBN 978-86-7466-930-3

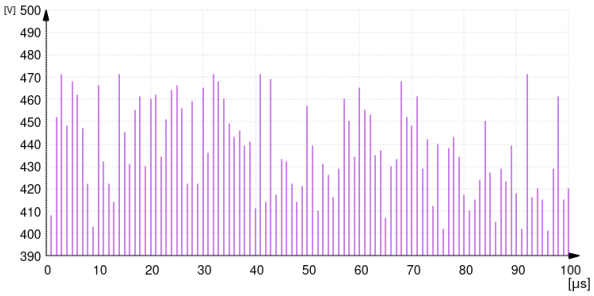


(a)

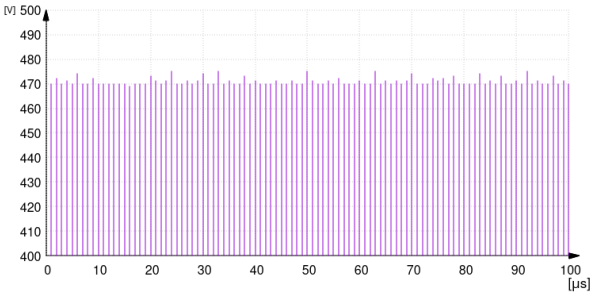


(b)

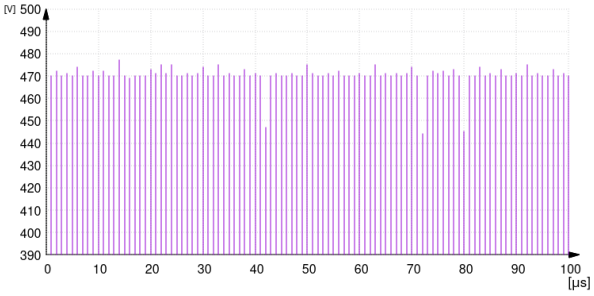


(c)

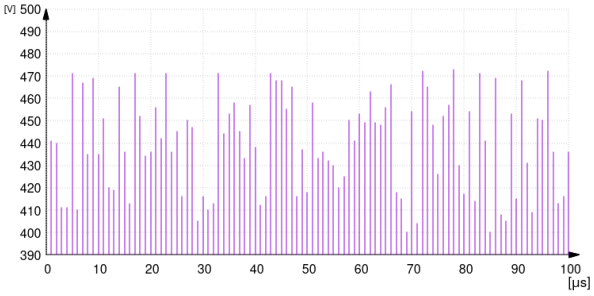


(d)

Slika 4: Hronološki niz slučajnih promenljivih jednosmerni probojni napon gasnog odvodnika prenapona

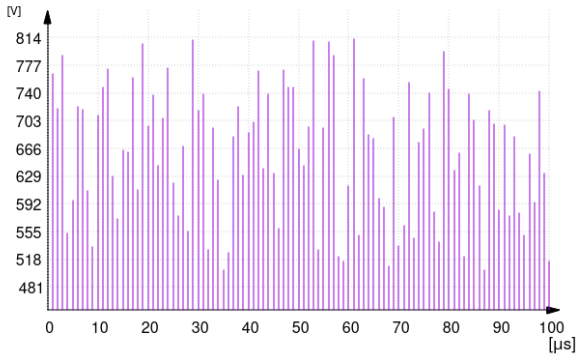


(a)

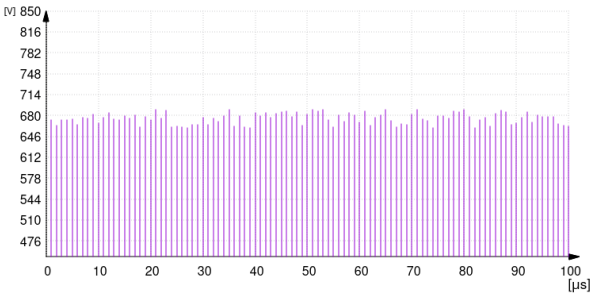


(b)

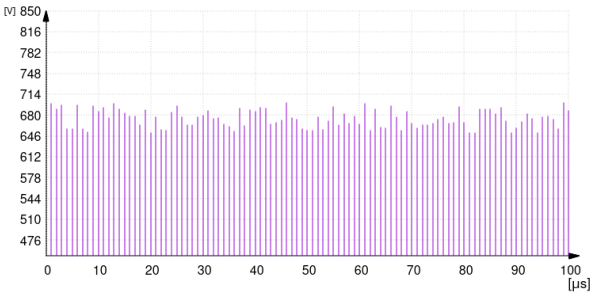


(c)

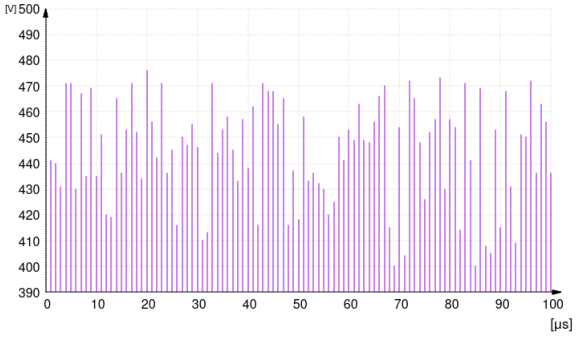


(d)

Slika 5: Hronološki niz slučajnih promenljivih impulsni probojni napon: gasnog odvodnika prenapona


ISBN 978-86-7466-930-3

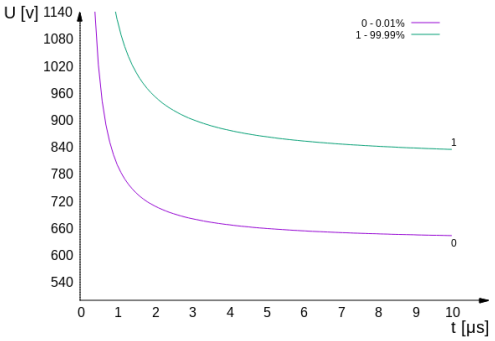


(a)

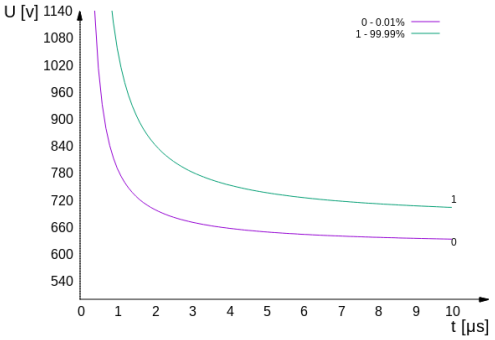


(b)

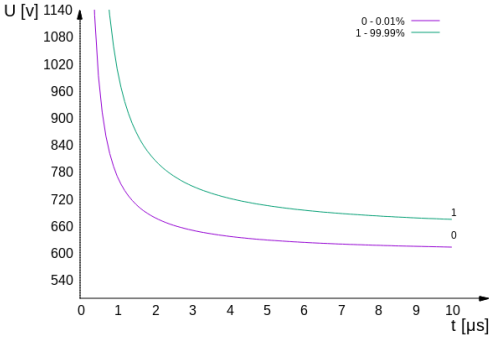


(c)

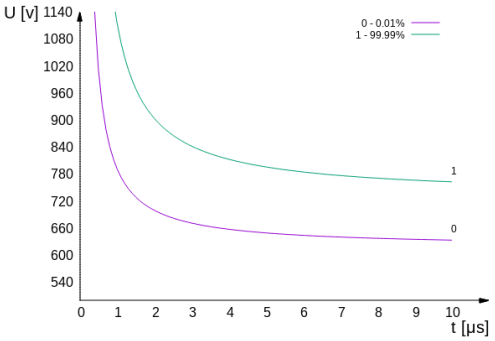


(d)

Slika 6: Impulsne karakteristike 99.99 % i 0.01% gasnog odvodnika prenapona

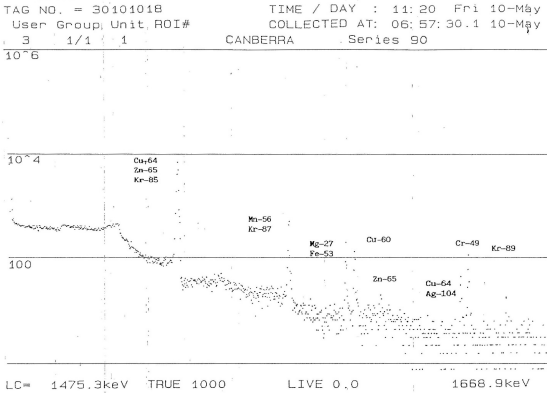


(a) Dijagram aktivacione analize gasnog odvodnika prenapona 1000 s posle ozračivanja;

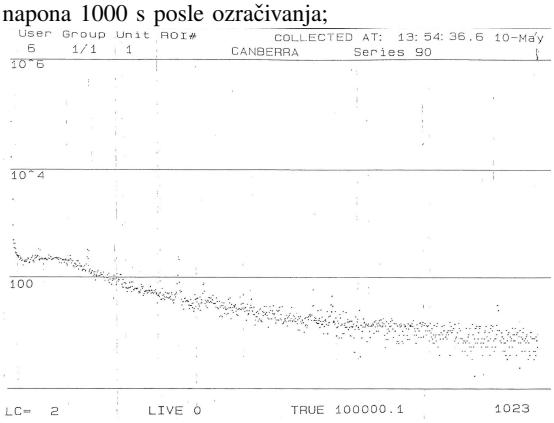


(b) Dijagram aktivacione analize gasnog odvodnika prenapona 100 000 s posle ozračivanja

Slika 7

## IV. ZAKLJUČAK

Cilj ovog rada je bilo ispitivanje neutronskog i gama zračenja na stabilnost karakteristika gasnih odvodnika prenapona. Izabrano je neutronsko i gama zračenje (iako neutronsko zračenje ne spada u direktno jonizujuće zračenje, ono je indirektno jonizujuće) pošto ta dva tipa zračenja najlakše prodiru kroz telo gasnog odvodnika i deluju u međuelektrodnom prostoru. Dejstvo neutronskog i gama zračenja je interesantno i radi primene gasnih odvodnika prenapona u upravljačkim sistemima nuklearnih energetskih postrojenja pošto u njima postoji verovatnoća pojave ovog polja zračenja. Dobijeni rezuktati su interesantni pošto pokazuju da dejstvo neutronskog i gama zračenja popravlja funkcionalne karakteristike gasnog odvodnika prenapona. To poboljšanje karakteristika ima i memorijski efekat, tj. zadržava se i nekoliko sati nakon prestanka dejstva polja zračenja. Ovaj rezultat je od važnosti za praktične primene prenaponskih zaštitnih komponenti u hibridnim šemama pošto neutronsko i gama zračenje utiče na smanjenje zaštitnih osobina odvodnih dioda i varistora što se može kompenzovati poboljšanjem zaštitnih osobina gasnog odvodnika prenapona.


ISBN 978-86-7466-930-3

## ACKNOWLEDGMENT

Istraživanje je finansiralo Ministarstvo prosvete, nauke i tehnološkog razvoja Republike Srbije.

## LITERATURA

[1] Osmokrović P., Krivokapić I., Matijašević D., Kartalović N., Stability of the gas filled surge arresters characteristics under service conditions, (1996) IEEE Transactions on Power Delivery, 11 (1), pp. 260 - 266.
[2] Beyer, M., et al., Hochspannungtechnik: Theoretische und Praktische Grundlagen, Springer-Verlag, Berlin Heidelberg , 1986.
[3] Raizer, Y.P., Gas Discharge Physics, Springer-Verlag Berlin Heidelberg, Germany, 1991.
[4] Von Angel, A., Ionized gases, Physics Today, 17 (1964), 9, pp. 108-108.
[5] Geibig K.F., Schwab A., Stöckel D., Einsatz von Faserverbundwerkstoffen in Funkenstrecken, (1983) Materialwissenschaft und Werkstofftechnik, 14 (6), pp. 197 - 201.
[6] Osmokrovic P., Vasic A., Zivic T., The Influence of the electric field shape on the gas breakdown under low pressure and small inter-electrode gap conditions, (2005) IEEE Transactions on Plasma Science, 33 (5 I), pp. 1677 - 1681.
[7] Osmokrovic P., Loncar B., Sasic R., Influence of the electrode parameters on pulse shape characteristic of gas-filled surge arresters at small pressure and inter-electrode gap values, (2005) IEEE Transactions on Plasma Science, 33 (5 II), pp. 1729 – 1735.
[8] T. M. Nedic, et al.: Optimization of fast three-electrode spark gaps isolated with a SF6 and He mixture, Nuclear Technology & Radiation Protection: Year 2021, Vol. 36, No. 3, pp. 234-242.
[9] Hylten-Cavallius Nils, High Voltage Laboratory Planning, Haeffely Basel, 1988.
[10] Polužanski, V. S., et al., Computer Non-Iterative Data Acquisition of Particle, Nucl Technol Radiat, 34 (2019), 1, pp. 65-71.
[11] Jusić, A., et al., Synergy of radioactive 241Am and the effect of hollow cathode in optimizing gas-insulated surge arresters characteristics, Nucl Technol Radiat, 33 (2018), 3, pp. 260-267.
[12] HUBER+SUHNER AG: EMP protectors, Detail specification for protectors, 1989.
[13] SIEMENS: EMV Funk - Enstrung, Bauelemente. Filter, Datenbuch 1983/84.
[14] PHILIPS: Electronic components and materials; Resistors, Capacitors. Data handbook, Part 2, 1973.
[15] Shunzo Morishita: A New Lightning Surge Protector for the D70 Switching System, JTR, January 1985.
[16] Martzloff, F. D., Coordination of Surge Protectors in low voltage Power Circuits, IEEE PAS-99 No.1, Jan/Feb 1980., p. 129.
[17] Nedić T.M., Janićijević A.J., Stanković K.D., Kartalović N.M., Efficient replacement of the radioactive sources in the gas-filled surge arresters construction for the insulation co-ordination at the low voltage level, (2020) Nuclear Technology and Radiation Protection, 35 (2), pp. 130 - 137.
[18] Osmokrovic P., Loncar B., Stankovic S., The new method of determining characteristics of elements for overvoltage protection of low-voltage system, (2006) IEEE Transactions on Instrumentation and Measurement, 55 (1), pp. 257 - 265.
[19] Pejovic, M.M., et al., Investigation of post-discharge processes in nitrogen at low pressure, Physics of Plasmas, 19 (2012), 12, pp. 123512-8.
[20] Brown, S.C., Holt, E.H., Introduction to Electrical Discharges in Gases, American Journal of Physics, 36 (1968), 9, pp. 854-854.
[21] Osmokrovic, P., et al., Mechanism of electrical breakdown of gases for pressures from 10-9 to 1 bar and inter-electrode gaps from 0.1 to 0.5 mm, Plasma Sources Science and Technology, 16 (2007), 3, pp. 643-655.
[22] Pejovic, M., et al., Processes in insulating gas induced by electrical breakdown responsible for commercial gas-filled surge arresters delay response, Vacuum, 137 (2017), pp. 85-91.
[23] Osmokrović, P., et al., Determination of pulse tolerable voltage in gas-insulated systems, Japanese Journal of Applied Physics, 47 (2008), 12, pp. 8928-8934.
[24] Djekić S.B., Nikezić D.P., Brajović D.V., Kartalović N.M., Ramadani U.R., Passive and active shielding against electromagnetic radiation, (2020) Nuclear Technology and Radiation Protection, 35 (4), pp. 331 - 338.
[25] Loncar B., Osmokrovic P., Stankovic S., Radioactive Reliability of Gas Filled Surge Arresters, (2003) IEEE Transactions on Nuclear Science, 50 (5 III), pp. 1725 – 1731.
[26] Osmokrovic P., Stojanovic M., Loncar B., Kartalovic N., Krivokapic I., Radioactive resistance of elements for over-voltage protection of low-voltage systems, (1998) Nuclear Instruments and Methods in Physics Research, Section B: Beam Interactions with Materials and Atoms, 140 (1-2), pp. 143 - 151.
[27] Cook, G., Gas-filled surge arresters for NEMP protection, pp. 85-90, ITEM, 1986.
[28] Stanković, K., Vujisić, M., Influence of radiation energy and angle of incidence on the uncertainty in measurements by GM counters, Nucl Technol Radiat, 23 (2008), 1, pp. 41-42.
[29] Vulević, B., Osmokrović, P., Evaluation of uncertainty in the measurement of environmental electromagnetic fields, Radiation Protection Dosimetry, 141 (2010), 2, pp. 173-7.
[30] A. J. Schwab, High-voltage Measurement Techniques, M.I.T. Press, 1972.
[31] Djekić S.B., Nikezić D.P., Brajović D.V., Kartalović N.M., Ramadani U.R., Passive and active shielding against electromagnetic radiation, (2020) Nuclear Technology and Radiation Protection, 35 (4), pp. 331 - 338.
[32] BIPM, IEC, IFCC, ISO, IUPAC, IUPAP and OIML: Guide to the Expression of Uncertainty in Measurement, Geneva, Switzerland: International Organization for Standardization, 1995.
[33] Stanković K., Vujisić M., Dolićanin E., Reliability of semiconductor and gas-filled diodes for over-voltage protection exposed to ionizing radiation, (2009) Nuclear Technology and Radiation Protection, 24 (2), pp. 132 – 137
[34] Osmokrovic Predrag, Mechanism of electrical breakdown of gases at very low pressure and interelectrode gap values, (1993) IEEE Transactions on Plasma Science, 21 (6), pp. 645 – 653.
[35] Osmokrović P., Krivokapić I., Krstić S., Mechanism Of Electrical Breakdown Left Of Paschen Minimum, (1994) IEEE Transactions on Dielectrics and Electrical Insulation, 1 (1), pp. 77 - 81.

 ISBN 978-86-7466-930-3

# COMPUTING AND INFORMATION ENGINEERING

# /

# РАЧУНАРСКА ТЕХНИКА И ИНФОРМАТИКА

# (RTI/PT)

ISBN 978-86-7466-930-3

# One Solution For Multimedia Subscription Using Blockchain

Igor Srdić, Đorđe Glišić, Marija Jovanović

***Abstract*—With the expansion of blockchain technologies in different areas from health care to voting systems and emerging demand on video content delivery platforms, it is interesting to investigate possibilities to combine those two into a new system that will help digital content availability. We present and discuss relevant work in the industry. Paper proposes one solution for subscription rights management using blockchain technologies. Proof of concept is done using the Ethereum blockchain ecosystem for a video-on-demand service. A similar approach could be used in other fields of DTV services, like cable TV subscription services.**

***Index Terms*—subscription management, blockchain, smart contracts, Ethereum, DTV content subscription, Android TV, solidity, web3j.**

## I. Introduction

Blockchain is a growing list of records linked to the use of the cryptocurrency method. After the sudden expansion of Bitcoin [1], it became clear that the potential of blockchain is a lot greater than its use for money. This technology's decentralized system is fertile ground for many ideas and provides a new approach and opportunities [2]. There are ideas like a voting system for elections, where vote theft and rigging of results could not occur, and many other ideas, each of which aims to improve the current system, which has its virtues and many flaws. The system's main problem with the central authority, with a central database, is that such systems have one critical point - the system's bottleneck, which, if endangered, puts the whole system in danger.

Ethereum is a platform that works on top of blockchain technology which has revolutionized this field. It is a platform that allows its users to develop their decentralized applications [3]. It also resolves one additional issue in such networks: they cannot function without many users - nodes - who work on them.

Buying and renting multimedia content is the default functionality on all TVs, most often as Video On Demand (VOD), where users temporarily purchase rights to view a movie or series. With increased online shopping abilities, new options come to mind. What if a user can sell its rights to another user? Does it always have to be between the content provider and the end-user? In the real world, there are second-hand shops for used goods. Why don't such digital shops exist in the entertainment industry? Blockchain technology may be the right step towards that. It is reasonable to think that users would rather sell digital valuables than offer them free to the public. Some movements are done in that direction with the appearance of NFT (non-fungible token).

Some work has been done toward decentralized video streaming platforms using blockchain technologies in work by Tan et al. [4]. Focus that work was around content creators, advertisers, and consumers and the availability of the content in networks based on blockchain. More discussion on the usability of blockchain smart contracts in the entertainment industry could be found in the work of Pons [5].

Working consortium grouped around Sony, Samsung, and Google work on creating a next-generation video entertainment blockchain. A published white paper [6] presents the new architecture of the distributed content delivery network called Theta Mainnet 4.0. They have anticipated Theta Metachain and Theta Edge Network, as illustrated in Fig. 1. The first network is distributed blockchain of blockchains, where the "metachain" name comes from, resulting in support for an unlimited number of blockchains. The second network is responsible for interaction with users. Using publicly available Theta Video API, users can upload content and request access to content. The network has endpoints for protected content storage, encoding new content uploaded, and delivery to the user with an appropriate NFT-based digital rights management (DRM) system. It is expected to be available by the end of 2022.

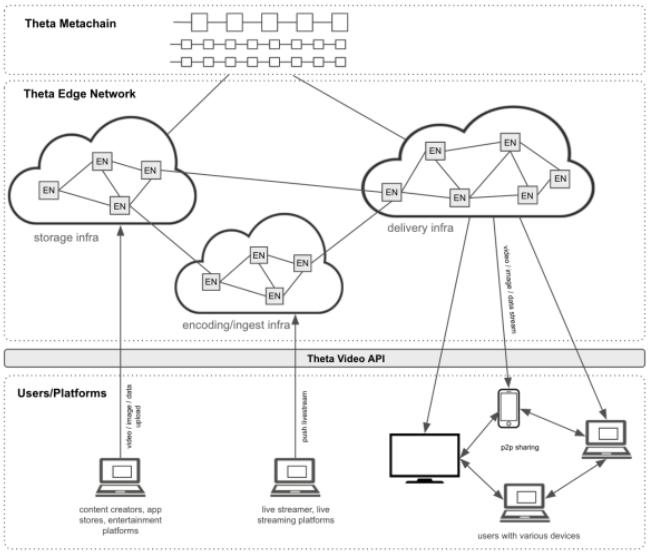


Fig. 1. The architecture of Theta Mainnet 4.0 with Theta Metachain and Theta Edge Network

Igor Srdić – RT-RK Institute for Computer Based Systems, Novi Sad, Srbija, (e-mail: Igor.Srdic@rt-tk.com)

Đorđe Glišić – RT-RK Institute for Computer Based Systems, Novi Sad, Srbija, (e-mail: Djordje.Glisic@rt-tk.com)

Marija Jovanović – RT-RK Institute for Computer Based Systems, Novi Sad, Srbija, (e-mail: Marija Jovanovic@rt-tk.com

 ISBN 978-86-7466-930-3

In this paper, we are investigating the possibilities of using blockchain technology in the world of digital television. In particular, we tried to use the smart contracts concept from the Ethereum ecosystem to allow users to buy video content from their homes [7]. Once a transaction is initiated, it takes more than 10 seconds for the change to be permanently stored in the blockchain, which is the waiting time for the return values of these functions. Detailed workflow can be seen in Fig. 2. This implies that Ethereum applications are not suitable for all systems that need faster data exchange and cannot correctly use current blockchain technology.

A smart contract as a programming code cannot be changed once it enters the blockchain. The mistakes and oversights are only solvable by creating new smart contracts and redirecting the applications to new contracts. The main problem is that errors are discovered only when they happen, and in such a system, the results of errors are harmful to the user.

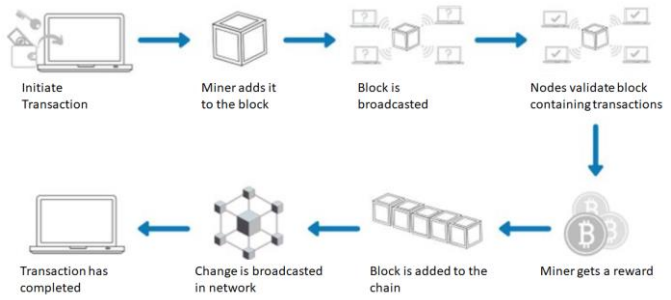


Fig. 2. Workflow for a transaction in the Ethereum network

In this work, smart contracts will be used for exchanging digital currencies for video-on-demand (VOD) services. We will introduce a digital wallet, an application used for storing digital funds (for example, cryptocurrency). On the side of the DTV device, a DTV application will be altered to support additional payment methods for its video-on-demand service. Those are the building blocks necessary to complete the task of creating a subscription management system with blockchain technology.

The paper consists of three parts. The second section will present functional requirements. The third section will explain all technologies and implementation of the system and the TV application adopted to be the client for the blockchain payment method. The fourth and last part contains an overview of the solution itself, shortcomings, and problems that have arisen during implementation and testing, and finally, we will discuss possible improvements.

## II. REQUIREMENTS

Purchase of content should be made on the chain itself. It should be implemented as an Ethereum smart contract that will provide functionalities such as purchase and storage purchase history. Purchased history has two parts, valid and expired. A valid subscription is the one that is still active and allows the owner to consume it (Fig. 3), in our case, to watch a movie or TV show. An expired subscription is essential for validating existing payments and resolving any problems. Additional requirements involve checking content access rights for specific users, content validation by the provider, etc. There is a set of functions related to administration, which can be performed exclusively by the provider. It must be ensured that the user cannot call them.


Fig. 3. The user interface for the Video on Demand service

In addition to the account user created in the TV application, the user also received his Ethereum account and can deposit money at physical ATMs or online. That order is permanently linked to a TV application account, and every content purchase is made through that account.

In this research, we did not want to use any currency assets. Instead, we selected the Ethereum test network Rinkeby. In this network, the currency has no real value, so we could deposit any amount of money into the account for testing purposes. For that reason, work does not cover depositing currencies. That does not reduce the applicability of the proposed solution, as only the target network has to be changed to make it usable in the real world.

Executing the method from smart contracts may take some time, but it is necessary to ensure that the application runs smoothly while waiting for the answers to those calls. An example screen for purchasing content is shown in Fig. 4. In particular, Android has a built-in capability to interrupt application execution that does not work for a while by sending ANR - Application Not Responding error.

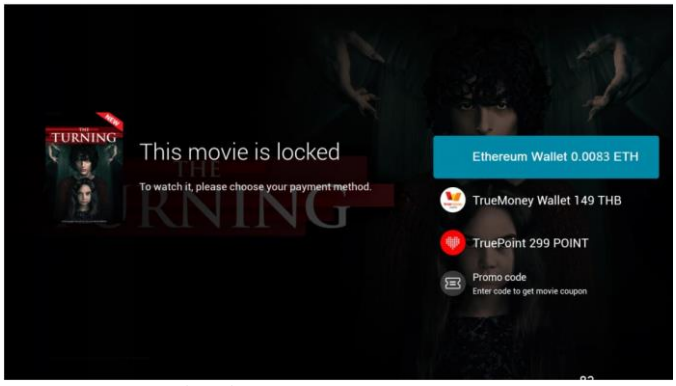


Fig. 4. The user interface for Video on Demand service when content is locked (needs payment)

After the purchase, the user should be able to view the content for 30 days before the first review or two days from

 ISBN 978-86-7466-930-3

when the content was first viewed. After the period expires, the content should be locked again until the next purchase. Given that money can be sent by calling smart contract functions, it is necessary to ensure that, in case of any error when calling these functions, the payments are aborted, and user funds remain untouched in the account.

## III. IMPLEMENTATION

To implement our system, we had to implement two main components. The first one is smart to contact that will be positioned in the Ethereum test network. We used Solidity high-level object-oriented programming language especially designed for Ethereum networks. We selected Remix development environment (IDE), written in JavaScript and running under any web browser as a development environment.

On the client-side, we had an Android TV application [7] running on a set-top box (STB) device [8][9]. The application was written in Java. We have selected the web3j library for integration into the existing application to establish a connection with Ethereum smart contract API [10].

For storing the user's digital currency, we selected a digital wallet Metamask, which was used to create the Ethereum account. Its purpose is to save access to the digital currency details in the Ethereum network.

To simulate the Ethereum network, we created a network of miners. For that purpose, we used an Infura cluster made of full nodes. The cluster can execute contracts and alter the chain.

Part of the smart contract is present in Fig. 5. There are three fields of integer type. The *myEtherValue* field is an auxiliary used to convert some numerical data into currency Ether. At the same time, *shortDuration* and *longDuration* represent the lengths of the period in which the buyer is allowed to watch content. The *ctAddress* field is of the address type, the type of data it represents in Solidity public addresses of users in the Ethereum network. This is the address of the crypto-telecom (provider) which will have administrator privileges in the system.

In addition, there are two structures, *Content* and *Deal*. Structure *Content* represents the content and contains fields for name, price, and one auxiliary field. Structure *Deal* is proof of purchase, the contract concluded between provider and customer. It has the identifier of purchased content, the time of the purchase, the time when the user first looked at the content, and the field that indicates whether the content is still viewed. The content folder, which maps the content identifiers to data of the *Content* type, contains all available content of the provider. Maps *validDeals* and *archivedDeals* map users (addresses) into concluded contracts and are in the valid and expired contracts, respectively.

The Web3j library receives the output of the Solidity compiler [11][12] consisting of binary and ABI file and generates a Java surrounding class smart contract, in this case, class *CryptoTelecom*. Some of the methods of this class:

- *load* - loading the contract instance with the given address, web3j object, user credentials, and gas variables.

- *order* – Wrapper method of the smart contract order function. The return value is *RemoteFunctionCall <TransactionReceipt>*, which represents identification of transaction. Once the function is called, it will return its value after the function is executed, the state of the contract is changed, and that state is saved in the new transaction as part of a new block in the blockchain.

```
contract CryptoTelekom {

    uint256 private myEtherValue;
    uint256 private shortDuration;
    uint256 private longDuration;

    address payable private ctAddress;

    struct Content {
        string name;
        uint256 price;
        bool isValid;
    }

    mapping(string => Content) content;

    struct Deal {
        string contentId;
        uint256 startedTime;
        uint256 startedWatchingTime;
        bool startedWatching;
    }

    mapping(address => Deal[]) validDeals;
    mapping(address => Deal[]) archivedDeals;

    modifier onlyCT() {
        assert(msg.sender == ctAddress);
        _;
    }

    event Order(uint256 ret);
    event CheckDeal(bool ret);
    event ValidDeal(string contentId,
                    uint256 startedTime,
                    uint256 startedWatchingTime,
                    bool startedWatching,
                    bool isRetValid);
```

Fig. 5. The interface of the contract class in Solidity.

- *getOrderEvents* - Read events from the order method in a given transaction.

- *getNumValidDeals* - Wrapper method for function *getNumValidDeals()* from smart contract. Example of a return method that does not change the state of the contract. The return value is immediately available because only data is read.

Details about how we used Metamask, Rinkeby network, and Infura cluster can be found in [13]. Also, the authors omitted implementation details about the Android Java application as reference code can be found in [9]. Work does not lose clarity or applicability without those details, as that information can be found both in given references and online resources.

 ISBN 978-86-7466-930-3

## IV. Conclusion

The novelty that this approach brings, and at the same time one of its advantages, is that proof of the contract is no longer stored in the provider's database - all are stored on the Ethereum chain. This is interesting for the provider for two reasons. The first is that maintenance of the database by the provider is completely avoided, and the second is that no one can write data to a chain without the consensus of the entire network. Therefore, no one can falsely present themselves as having the right to specific content. Furthermore, users who purchase content are confident that their content rights will remain untouched because data ends on a chain that cannot be changed.

The virtues of this approach are numerous. However, there are also drawbacks. Developers must pay close attention when developing smart contracts because consequences in a system that operates with money can be substantial [14]. Also, it is important to optimize the program code as much as possible. The gas is charged to the initiator of the transaction. Calls to the smart contract function are calculated for every assembler instruction executed. Therefore, additional effort should be made to make the code as optimal as possible to lower gas prices. Also, as transaction initiators are charged for gas, and transactions are initiated by the users who buy the content, the provider has no operating cost for the network. Another approach is to subtract the price gas from the total price of the content that the user buys, which would result in the situation where the provider pays for network service and the user for the content.

## References

[1] S. Nakamoto, "Bitcoin: A peer-to-peer electronic cash system." Decentralized Business Review, 2008.
[2] M. Å. Hugoson, “Centralized versus decentralized information systems.” IFIP Conference on History of Nordic Computing. Springer, Berlin, Heidelberg, 2007. Vitalik Buterin, “Ethereum Whitepaper”, https://ethereum.org/whitepaper/, 2013.
[3] Y. Tan, S. Kadhe, K. Ramchandran, “Proof-of-Stream: A Robust Incentivization Protocol for Blockchain-based Hybrid Video on Demand Systems”, UCB/EECS-2021-42, 2021
[4] J. Pons, “Blockchains and smart contracts in the culture and entertainment business”, Réalités industrielles, 2017
[5] N. Szabo, “The Idea of Smart Contracts”, https://nakamotoinstitute.org/the-idea-ofsmart-contracts/, 1997.
[6] Theta Labs, “Theta Mainnet 4.0 - Introducing Theta Metachain to Power Web3 Businesses”, accessed May 2022, https://assets.thetatoken.org/theta-mainnet-4-whitepaper.pdf
[7] I. Pan, N. Lukić, “Design and architecture of software systems: Android-based systems”, FTN Publishing, Novi Sad, 2015.
[8] K. Yaghmour, “Embedded Android”, O ‘Reilly Media, 2013.
[9] N. Schapeler, “A example to Ethereum Development On Android using Web3j and Infura”, accessed May 2022, https://medium.datadriveninvestor.com/an-introduction-to-ethereum-development-on-android-using-web3j-and-infura-763940719997
[10] "Ethereum documentation", accessed May 2022, https://ethdocs.org/en/latest/
[11] "GitHub", Solidity, accessed May 2022, https://github.com/ethereum/solidity
[12] “Solidity documentation”, accessed May 2022, https://solidity.readthedocs.io/en/v0.6.9/.
[13] I. Srdic, BSc thesis “Realizacija multimedijalne pretplate korišćenjem blokčejna”, ETF, 2020
[14] K. O'Hara, "Smart Contracts - Dumb Idea," in IEEE Internet Computing, vol. 21, no. 2, pp. 97-101, Mar.-Apr. 2017, doi: 10.1109/MIC.2017.48.

 ISBN 978-86-7466-930-3

# Model-Driven Approach to Blockchain-Enabled MLOps

Nenad Petrović

***Abstract*—In recent years, machine learning has reached quite sophisticated level of usability within applications across various domains – ranging from boo ing reservations and media content delivery to business and healthcare. owever, the deployment of machine learning models, together with parameter tuning and periodic training, which are necessary to maintain satisfiable performance, represent time consuming processes, requiring various types of s ills - both Dev ps and data analysis-related. In this paper, we leverage model-driven approach in synergy with code generation with aim to automatize the so-called ps activities, relying on en framewor for pipeline automation and ubernetes for containerized tas orchestration. n top of that, we leverage loc chain for infrastructure provisioning. ur goal is to reduce the cognitive load of infrastructure and services management within systems relying on machine learning. The framewor is evaluated in scenarios using PyTorch-based deep learning predictive models. According to the results, the proposed approach reduces both the time and s ill required for successful ps activities.**

***Index Terms*—Dev ps; ubernetes; ps; PyTorch; loc chain.**

## I. Introduction

Continuous integration and delivery have become standard in software engineering workflow within the last decade. The goal of so-called DevOps practice is to align the deployment of software artifacts with business goals which are enabled by them, so the customer's organization can benefit from them as quickly as possible. However, operations related to underlying infrastructure management are becoming more and more complex, due to heterogeneity of services, devices and increasing performance demands. Therefore, due to fact that machine learning (ML) services are recognized as crucial enablers of novel usage scenarios across various domains, a distinct subfield with focus on them has emerged, known as MLOps [1-4]. It is an extension of now well-established DevOps paradigm with aspects specific to service delivery in machine learning, such as continuous model training for prediction performance improvement, rapid deployment and parameter tunning towards automated generation of complex ML task pipelines [1-4].

In this paper, the focus is on reducing the complexity of MLOps-related activities and service delivery relying on model-driven approach [5]. Moreover, the business-related aspects of infrastructure resource provisioning and usage charging using blockchain by the provider are also considered. The main contributions of this paper are the following: 1) MLOps metamodel – defining the structure of user-created model instances representing machine learning pipelines with several distinct steps together with aspects related to its deployment 2) code generator – leverages the model for automated code generator covering several aspects: pipeline script, predictive model, infrastructure management 3) blockchain-based transaction model making use of smart contracts for renting high-performance computing resources aiming accelerated machine learning.

In our previous works, metamodel-based approach in synergy with ontologies was leveraged for automated container-based service deployment in Fog Computing [6]. On the other side, a similar method was adopted in [7] for generation of predictive models starting from high-level predictive problem descriptions aiming state-of-art mobile network infrastructure planning and management.

Nenad Petrović is with the Faculty of Electronic Engineering, University of Niš, Aleksandra Medvedeva 14, 18000 Niš, Serbia (e-mail: nenad.petrovic@elfak.ni.ac.rs), (https://orcid.org/0000-0003-2264-7369)

## II. Background

### A. ZenML

ZenML [8] is open-source, high-level Python framework for machine learning pipeline automation. It is available as Python library in form of function decorators and specific classes inside scripts, while it imposes pre-defined code structure. The overview of main ZenML-related concepts and terminology is given in Table I.

TABLE I
ZenML Concepts Overview

| Concept | Description |
|---|---|
| Repository | A special type of directory, declared used `zenml init` command. Each ZenML action must take place within a repository, which is created |
| Step | Single stage within ML flow, representing a node of in ML flow computation graph. Implementation-wise, they represent Python functions with typed parameters in signature for both arguments and return value. Decorator used is `@step`, while step result caching can be enabled using `enable_cache=True` parameter |
| Pipeline | A sequence of steps. It connects all the steps, their inputs and outputs. Decorator used is `@pipeline`. Moreover, it is possible to set the list of external libs/dependencies from .txt file can be done using `requirements_file` attribute of the decorator. It is run by invoking `pipeline.run()` method inside Python script. Optionally, a scheduler object can be assigned for periodic execution of certain steps enabling scenarios such as continuous model training. |

 ISBN 978-86-7466-930-3

| | |
|---|---|
| Stack | Represents environment and configuration of MLOps platform infrastructure. It consists of: artifact store, metadata store, container registry, orchestrator and custom step operators. Creating a new stack with desired parameters is done using `stack register`, while it is run using `stack up` command., which has to be done before running any pipeline. |
| Artifact store | Persistent storage of step results. |
| Materializer | Defines how data is passed between steps. Serialization and deserialization are used while storing/retrieving results. |
| Metadata store | Keeps the data related to pipeline, step and experiment configuration and references for tracking of inputs/outputs within artifact store created within ML pipeline. |
| Orchestrator | Component for scheduling and running pipeline steps |
| Container registry | Stores Docker images required for running the steps |
| Custom step operator | User-defined environments for running ML flow tasks within Docker containers |
| Integration | Enable usage of various third-party tools enriching ML development like pytorch, tensorflow and sklearn. Apart from that, it also includes orchestrator-enabled stacks, such as local-kubeflow (Kubernetes-based) and airflow. |

Depiction of ZenML architecture showing how the previously mentioned concepts are related is given in Fig. 1.

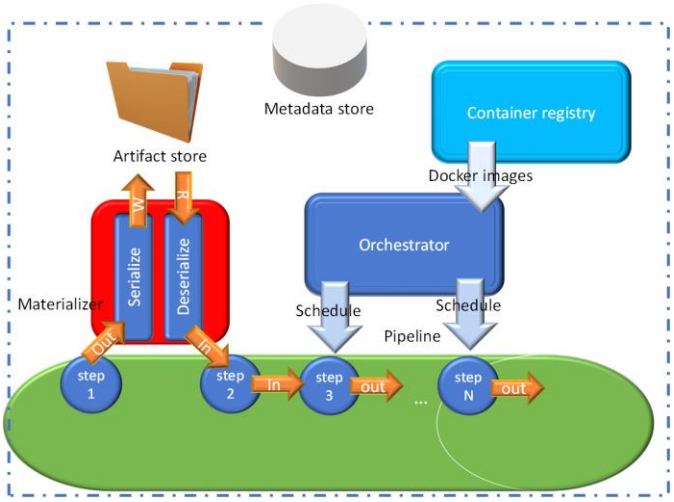


Fig. 1. ZenML concepts and their relations.

Additionally, Fig. 2 shows the programming workflow using ZenML. First, we initialize a repository inside the desired directory where we place our Python script. After that, in Python code we define the typical steps of ML flow: 1) importer – downloading and loading dataset 2) trainer – passing through dataset and updating model weights for new predictions 3) evaluator – estimates how good the prediction performance is, according to the given metric (accuracy for classification; mean relative error - MRE for regression). Moreover, we connect the steps in a sequence as shown within the pipeline object and finally run the pipeline object instance.

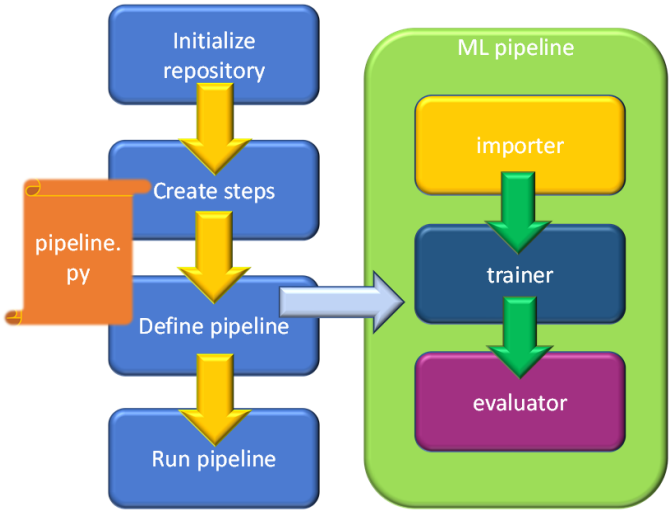


Fig. 2. ML pipeline creation using ZenML in Python.

### B. *ubernetes*

Kubernetes [9] represents an open-source platform whose goal is to enable deployment and management of containerized services run on multi-server clusters. Furthermore, it provides convenient access to useful features, such as scalability, fault-tolerance and declarative configuration. Table III gives an overview of key concepts within Kubernetes-based architectures.

TABLE III
KUBERNETES CONCEPTS OVERVIEW

| Concept | Description |
|---|---|
| Control plane | Cluster management component, responsible for global decisions, and scheduling |
| Node | Worker machines within the cluster running containerized apps |
| Pod | Smallest deployable unit, which consists of one or more app containers. These containers share storage, network specification and config. Optionally, might include data volumes for persistent storage |
| Service | A logical set of pods |
| Kubectl | Comamnd-Line Interface (CLI) tool for running commands against Kubernetes cluster, such as:<br>-Deployment (`kubectl apply deployment.json` and `kubectl create deployment dep_name --image=docker_image`<br>-Scaling up/down (`kubectl scale --replicas=num resource_name`)<br>-Retrieval of node, pod and service info (`kubectl get pods, nodes, services`) |

Despite the fact that Kubernetes provides automatic scheduling capabilities, there might be situations where deployment of pod has to be done on a specific node. In that case, we leverage node labels. The corresponding command for labelling a node has the following form: `kubectl label nodes <node_name> label_name=label_value`. After that, when we want to create a pod using YAML configuration file, it would be necessary to make use of `nodeSelector` property and set it as `label_name:label_value`.


ISBN 978-86-7466-930-3

Kubernetes-based architecture is depicted in Fig. 3. In this paper, we make use of containerized custom step operators in ZenML run as Kubernetes pods, which are actually containers running PyTorch code. Moreover, node labels are leveraged in order to have low-level scheduling control and determine where each of these steps will be executed, enabling additional flexibility.

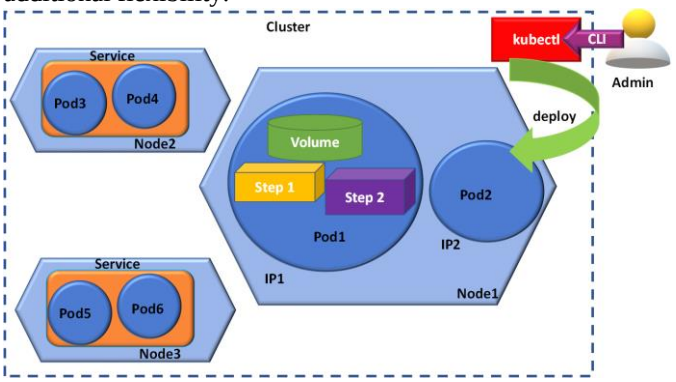


Fig. 3. Kubernetes-based containerized app architecture.

## III. IMPLEMENTATION

### A. Workflow Overview

Model-driven workflow of the proposed framework for automated ML-related task deployment is illustrated in Fig. 4. In the first step, user creates a deployment diagram model instance which describes the ML pipeline and underlying execution infrastructure details. After that, the model is parsed, so code generator constructs Python script containing the ML pipeline code relying on ZenML and PyTorch in synergy with numpy. Moreover, corresponding Kubernetes orchestrator commands are generated in order to ensure that distinct pipeline steps are executed on the desired cluster nodes. Additionally, the allocated resources are charged to the customer by parametrizing smart contracts for blockchain-based transactions, while the price might vary due to presence of deep learning accelerator cards on some of the nodes. Finally, the generated machine learning Python script is executed on the allocated computing nodes.


Fig. 4. Blockchain-enabled model-driven MLOps workflow.

### B. MLOps Metamodel

When it comes to adoption of model-driven engineering, we make use of metamodel which defines the structure of user-created deployment diagram (shown in Fig. 5). For implementation, Ecore [10] within Eclipse Modelling Framework (EMF) [11] in Java is used, which automatically generates all the auxiliary classes for model manipulation, together with convenient GUI-enabled editor.

The highest-level concept is *Pipeline*, which consists of one or more machine learning tasks, referred to as *Step*. A Pipeline can be executed periodically for purpose of continuous training, which is defined by *repeatTime* property. Moreover, each of the Steps can be one of the following type with specific, distinct properties: *Importer*, *Trainer* or *Evaluator*. Importer represents ML task which downloads the corresponding dataset and opens the downloaded file. In this context, it is necessary to set URL corresponding to the location where dataset is stored online, denoted as *onlineData*. Otherwise, if dataset is local and already present on disk, another parameter is used – *localData*. When it comes to trainer step, it is possible to set its learning rate, number of batches, select the target implementation technology, but we make use of PyTorch in this paper. Each trainer can use pre-created model, given by *modelPath* or it is necessary to define a custom neural network. For custom neural network, its architecture is described using *layer* element, while each of them has type (such as Convolutional – in image classification or standard Fully Connected in Multi-Layer Perceptron), number of processing units (neurons) and activation function (such as ReLU, softmax, sigmoid). Finally, the performance metric used within Evaluator step depends on the type of machine learning task, and we cover two possibilities relevant to supervised learning as *predictionType* property of *Pipeline* – classification (*Accuracy*) and regression (*MeanRelativeError*).

On the other side, the aspects of distinct Step deployment are covered by the metamodel as well. For each pipeline part, there is an attribute *targetLabel*, describing which worker node within Kubernetes cluster would be preferred for execution of pod created within custom step operator. Additionally, infrastructure executing the pipeline is represented as *Cluster* that consists of *Nodes*. For each *Node*, the following properties are customizable, such as label, location, IP address, accelerator (whether it has dedicated hardware for deep learning attached) and unit price (depending on the node performance).

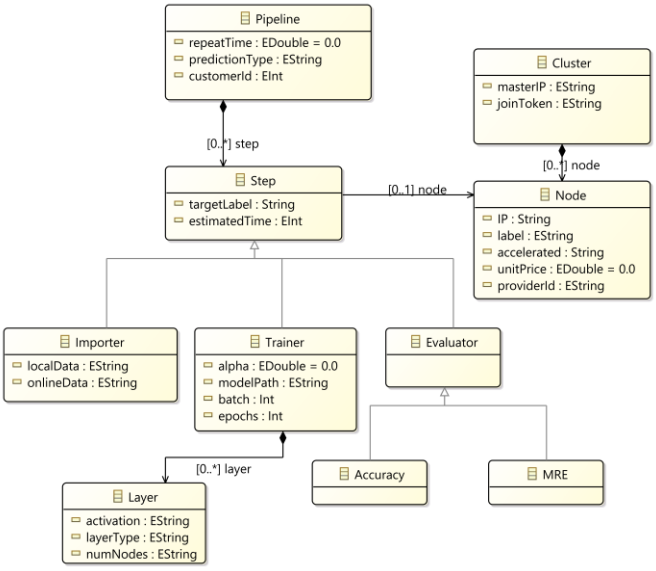


Fig. 5. UML class diagram of MLOps metamodel.


ISBN 978-86-7466-930-3

### *C. Code Generation*

The user-drawn deployment model is first parsed and then traversed relying on Ecore-generated classes. Pipeline element and iterated for each of the contained steps. When it comes to each step, it is necessary to get the target label and insert it into nodeSelector section within Kubernetes deployment YAML file. After that, depending on the step type, corresponding template is used. For importer steps, it is only necessary to change the path where pre-created model is located. When it comes to trainer, it contains model training loop iterating for given number of epochs through batch number of dataset samples and desired learning rate (α) value. For evaluator step, the corresponding method is chosen according to the type of prediction problem. Additionally, the leasing of resources is charged to the customer by valorizing blockchain smart contract with unit price of the selected node. Finally, the previously created Kubernetes YAML describing step deployment is applied, so the pod with Docker container running ML task inside is spawned on the selected node. Pseudocode of the code generation procedure is given in Table IV.

TABLE IV
CODE GENERATION PSEUDOCODE

*Input*: MLOps deployment model
*utput*: Python script, Kubernetes commands, Smart contract
*Steps*
1. deployment.elements:=parse(model);
2. Retrieve pipeline from deployment.elements;
3. For each step in pipeline
4. Create nodeSelector for step.targetLabel;
5. If(step is Importer)
6. Generate importer loading dataset from step.localData or onlineData;
7. If(step is Trainer)
8. Load model from step.modelPath;
9. Generate TrainerCode(step.epochs, step.batch, step.alpha);
10. If(step is Evaluator)
11. If pipeline.predictionType is regression
12. Use Mean Relative Error;
13. Else
14. Use Accuracy;
15. Get node.unitPrice;
16. Calculate total leasing price as step.estimatedTime*step.node.unitPrice
17. Genrate smart contract between pipeline.customerId and step.node.providerId for total price;
18. Apply Kubernetes deployment for pod with step.id;
19. End for each
20. End

### *. ZenML pipeline elying on PyTorch eep earning Models*

Deep learning refers to approach in artificial intelligence making use of neural networks with one or many hidden layers between the inputs and outputs. PyTorch [12] is library for Python which covers the required set of capabilities for deep learning: tensor manipulation and high-level object-oriented representation of both models and datasets. In Fig. 6, an excerpt of typical ZenML pipeline relying on PyTorch models is given. This kind of Python script actually represents one of the outputs of code generator. When it comes to neural network models in PyTorch, their capabilities are encapsulated within *Module* class which has to be inherited by any custom model. In this class, within the constructor we define neural network architecture (layers, nodes and activation functions), while *forward* connects the layers defining how data passes through neural network. In given example, we use MNIST dataset [13] of handwritten digits for purpose of classification.

```
class Net(nn.Module):

    def __init__(self):
        super(Net, self).__init__()
        self.flat_network = nn.Sequential(
            nn.Flatten(),
            nn.Linear(784, 311),
            nn.ReLU(),
            nn.Linear(311,10)
        )
        # fully connected layer, output 10 classes
        self.out = nn.Linear(10, 10)

    def forward(self, x):
        x = torch.unsqueeze(x, dim=0)
        x = self.flat_network(x)
        x = self.out(x)
        output = self.out(x)
        return output

def get_data_loader_from_np(X: np.ndarray, y: np.ndarray) -> DataLoader:
    tensor_x = torch.Tensor(X)  # transform to torch tensor
    tensor_y = torch.Tensor(y).type(torch.LongTensor)

    torch_dataset = TensorDataset(tensor_x, tensor_y)
    torch_dataloader = DataLoader(torch_dataset)
    return torch_dataloader

@step(custom_step_operator="trainer1", enable_cache=False)
def torch_trainer(
    X_train: np.ndarray,
    y_train: np.ndarray,
) -> nn.Module:

    train_loader = get_data_loader_from_np(x_train, y_train)

    model = Net().to(DEVICE)
    optimizer = optim.Adadelta(model.parameters(), lr=0.001)

    scheduler = StepLR(optimizer, step_size=1, gamma=0.01)
    for epoch in range(1, num_epochs):
        model.train()
        for batch_idx, (data, target) in enumerate(train_loader):
            data, target = data.to(DEVICE), target.to(DEVICE)
            optimizer.zero_grad()
            output = model(data)
            loss = F.nll_loss(output, target)
            loss.backward()
            optimizer.step()
        scheduler.step()

    return model

@step(custom_step_operator="evaluator1", enable_cache=False)
def classification_evaluator(
    X_test: np.ndarray,
    y_test: np.ndarray,
    model: nn.Module,
) -> float:
    model.eval()
    test_loader = get_data_loader_from_np(x_test, y_test)
    test_loss = 0
    correct = 0
    with torch.no_grad():
        for data, target in test_loader:
            data, target = data.to(DEVICE), target.to(DEVICE)
            output = model(data)
            test_loss += F.nll_loss(
                output, target, reduction="sum"
            ).item()
            pred = output.argmax(
                dim=1, keepdim=True
            )
            correct += pred.eq(target.view_as(pred)).sum().item()

    return correct / len(test_loader.dataset)

@step(custom_step_operator="importer1", enable_cache=False)
def my_importer() -> Output(
    x_train=np.ndarray, y_train=np.ndarray, x_test=np.ndarray, y_test=np.ndarray
):
    (X_train, y_train), (
        X_test,
        y_test,
    ) = load_data(dataset_path)
    return x_train, y_train, x_test, y_test

@pipeline(required_integrations=[PYTORCH])
def my_pipeline(
    importer,
    trainer,
    evaluator,
):
    x_train, y_train, x_test, y_test = importer()
    model = trainer(x_train=x_train, y_train=y_train)
    evaluator(x_test=x_test, y_test=y_test, model=model)

continous_train = Schedule(
     start_time = datetime.now(),
     end_time = datetime.now() + timedelta(minutes = 5),
     interval_second = 60
)

if __name__ == "__main__":
    torch_pipeline = my_pipeline(
        importer=my_importer(),
        trainer=torch_trainer(),
        evaluator=classification_evaluator(),
    )

    torch_pipeline.run(schedule = continous_train)
```

Fig. 6. ZenML PyTorch training script for MNIST dataset.


ISBN 978-86-7466-930-3

### *E. esource easing elying on Solidity Smart Contract*

Blockchain enables decentralized approach to immutable and irreversible transactions relying on approval by huge network of computer nodes, making it secure and reliable. On the other side, smart contracts define actions executed within protocol for realization of blockchain-based transaction. In this paper, we make se of Ethereum blockchain in synergy with Solidity smart contracts [14]. Solidity code of the underlying transaction mechanism for resource leasing in context of ML task execution is given in Fig. 7. As it can be seen, the information stored as part of transaction consists of *customerId*, *pro iderId* and identifier of node which will execute some ML task which represents a step within pipeline. First, the total price is calculated by multiplying *unitPrice* and *estimatedTime* required for step execution. After that, the transaction itself is performed by transferring the previously calculated total amount of tmokens from customer's to provider's account.

```
contract LeasingInfrastructure {
   address public providerId;
   uint32 public nodeId;
   uint32 public stepId;
   mapping (address => uint) public balances;

   event Sent(address customerId, address providerId, uint total);

   function leaseNode(address received, uint unitPrice, uint estimateTime) public {
      total = uintPrice*estimatedTime;
       require(total <= balances[msg.sender], "Not enough tokens");
      balances[msg.customerId] -= total;
      balances[providerId] += total;
      emit Sent(msg.customerId, providerId, total);
   }
}
```

Fig. 7. Solidity smart contract for ML task resource leasing.

## IV. EXPERIMENTS AND EVALUATION

For evaluation of the proposed framework, three publicly available image classification datasets were used. The first two tackle image classification problem: 1) yoga pose determination (our previous work presented in [15]) - 5 poses in dataset of 1551 images 2) MNIST [13] – 70 000 images of handwritten digits 0-9. On the other side, a regression problem of service demand prediction in telco networks from [7] was considered as the third case. In all of the experiments, test was 20% of the overall dataset with no overlapping samples from training set. The presented experiments were run on MacBook Pro (16-inch, 2019) laptop, equipped with 2.3GHz 8-core Intel Core i9 CPU, 16GB of DDR4 memory, 1TB SSD and Intel UHD Graphics 630 with 1.5GB VRAM. On the other side, Kubernetes cluster consisted of two more Ubuntu machines equipped with Intel i5 CPU, 8GB DDR4 RAM and 4GB GPU.

The results of the experiments are given in Table IV. Several aspects were considered: code generation time, model training time, speed-up compared to manual pipeline creation including model creation (moderately experienced machine learning engineer) and achieved prediction performance (MRE for regression, accuracy for classification).

TABLE IV
EXPERIMENT RESULTS

| Case | Code generation [s] | Model training [s] | Speed-up [times] | Performance [%] | Manual pipe [s] |
|---|---|---|---|---|---|
| Yoga pose [15] | 0.911 | 317 | 45 | Accuracy 73% | 104 |
| MNIST [13] | 0.87 | 124 | 36 | Accuracy 96% | 91 |
| Telco [7] | 0.93 | 27 | 21 | MRE 9% | 88 |

As it can be seen, in all the cases, the achieved speed-up was more than 20 times compared to traditional approach involving manual Python code writing from scratch. However, the speed-up is more significant is case of more complex models based on convolutional neural networks with huge number of layers – it was yoga pose determination. In our case, the only manual operation is pipeline deployment model creation using GUI tool, which took about 1.5 minutes in our experiments. All the models show almost identical performance to traditional counterparts, as expected. When it comes to code generation, execution time does not exceed 1 second in the presented case studies. Finally, the overhead of model training compared to execution without MLOps framework is around 15% when run on single machine and k3d [16] local Kubernetes cluster, but can be compensated by smart scheduling techniques, especially for larger datasets.

## V. CONCLUSION AND FUTURE WORK

According to the achieved experimental results, the proposed model-driven approach to MLOps leveraging automated code generation further speeds up the development of machine learning services, required administration operations and their delivery to the customers. Moreover, it also accelerates resource leasing protocols adopting blockchain-based smart contracts for transactions and their automated generation. Finally, the adoption of intuitive model-driven tools opens new horizons of machine learning service adoption and management even by persons without expertise in this area.

However, there are several possible research directions in future. First, we would work on integration of model-driven resource allocation mechanisms relying on multi-objective optimization approach [17] for energy and cost-efficient ML pipeline task scheduling. Moreover, the incorporation more sophisticated federated learning mechanisms and neural network layer splitting strategies across multiple cluster nodes aiming time-critical scenarios would be considered as well.

## ACKNOWLEDGMENT

This work has been supported by the Ministry of Education, Science and Technological Development of the Republic of Serbia.

 ISBN 978-86-7466-930-3

## REFERENCES


[1] G. Symeonidis, E. Nerantzis, A. Kazakis and G. A. Papakostas, "MLOps - Definitions, Tools and Challenges," 2022 IEEE 12th Annual Computing and Communication Workshop and Conference (CCWC), pp. 453-460, 2022. https://doi.org/10.1109/CCWC54503.2022.9720902

[2] S. Moreschini, F. Lomio, D. Hästbacka, D. Taibi, "MLOps for evolvable AI intensive software systems", IEEE International Conference on Software Analysis, Evolution and Reengineering 2022, pp. 1-2, 2022.

[3] D. Kreuzberger, N. Kühl, S. Hirschl, "Machine Learning Operations (MLOps): Overview, Definition, and Architecture", preprint, 2022.

[4] D. A. Tamburri, "Sustainable MLOps: Trends and Challenges", 2020 22nd International Symposium on Symbolic and Numeric Algorithms for Scientific Computing (SYNASC), pp. 17-23, 2020. https://doi.org/10.1109/SYNASC51798.2020.00015

[5] M. Brambilla, J. Cabot, M. Wimmer, Model-Driven Software Engineering in Practice, 2nd Edition, Morgan & Claypool Publishers, 2017.

[6] N. Petrovic, M. Tosic, "SMADA-Fog: Semantic model driven approach to deployment and adaptivity in Fog Computing", Simulation Modelling Practice and Theory, 102033, pp. 1-25, 2019. https://doi.org/10.1016/j.simpat.2019.102033

[7] D. Krstić, N. Petrović, I. Al-Azzoni, "Model-Driven Approach to Fading-Aware Wireless Network Planning Leveraging Multiobjective Optimization and Deep Learning", Mathematical Problems in Engineering, vol. 2022, 4140522, Special Issue: Mathematical Modelling of Data Transmission in Next Generation Wireless Systems, 2022, pp. 1-23, 2022. https://doi.org/10.1155/2022/4140522

[8] ZenML [online]. Available on: https://zenml.io/, last accessed: 08/05/2022.

[9] Kuberentes [online]. Available on: https://kubernetes.io/, last accessed: 08/05/2022.

[10] Eclipse Modeling Framework [online]. Available on: https://www.eclipse.org/modeling/emf/, last accessed: 08/05/2022.

[11] Ecore [online]. Available on: https://wiki.eclipse.org/Ecore, last accessed: 08/05/2022.

[12] E. Stevens, L. Antiga, T. Viehmann, *eep earning with PyTorch*, Manning Publications, 2020

[13] The MNIST database of handwritten digits [online]. Available on: http://yann.lecun.com/exdb/mnist/ , last accessed: 08/05/2022.

[14] Solidity [online]. Available on: https://docs.soliditylang.org/en/v0.8.13/, last accessed: 08/05/2022.

[15] M. Radenković, V. Nejković, N. Petrović, "Adopting AR and Deep Learning for Gamified Fitness Mobile Apps: Yoga Trainer Case Study", AIIT 2021 International conference on Applied Internet and Information Technologies, pp. 167-171, 2021.

[16] K3d [online]. Available on: https://k3d.io/v5.4.1/ , last accessed: 08/05/2022.

[17] I. Al-Azzoni, J. Blank, N. Petrović, "A Model-Driven Approach for Solving the Software Component Allocation Problem", Algorithms 2021; 14(12):354, pp. 1-19, 2021. https://doi.org/10.3390/a14120354


 ISBN 978-86-7466-930-3

# Controllability of the multi-agent system modeled by the chain graphs with repeated degree

Milica Anđelić
*Department of Mathematics,*
*Kuwait University,*
Safat 13060, Kuwait
milica.andelic@ku.edu.kw

Edin Dolićanin
*Department of Technical Sciences*
*State University of Novi Pazar*
Novi Pazar, Serbia
edin@np.ac.rs

Zoran Stanić
*Faculty of Mathematics,*
*University of Belgrade,*
Serbia
zstanic@matf.bg.ac.rs

***Abstract*—We consider the controllability of multi-agent dynamical systems modeled by a special class of bipartite graphs, called chain graphs. Our particular attention is focused on chain graphs that have one repeated degree. We derive properties of eigenvectors of graphs under consideration as well as some of their Laplacian spectra. On the basis of the obtained theoretical results, we determine the minimum number of leading agents that make the system in question controllable and locate them in the corresponding graph.**

***Index Terms*—Chain graph, Laplacian spectrum, Eigenvectors, Controllable dynamical system**

## I. Introduction

Let $G = (V(G), E(G))$ be a simple graph (without loops or multiple edges) of *order* $n = |V(G)|$. By $A(G)$ we denote its $(0,1)$-*adjacency matrix*. If $D(G)$ is the diagonal matrix of vertex degrees, then $L(G) = D(G) - A(G)$ stands for the *Laplacian matrix* of $G$. The *Laplacian eigenvalues* of $G$ are the eigenvalues of $L(G)$ and they form $\sigma(G)$, the *Laplacian spectrum* of $G$.

We consider a multi-agent system with $n$ linear agents $\{1, 2, \ldots, n\}$ modeled by a graph $G$. If $x_i$ denotes the state of the agent $i$, its dynamics is described by the single integrator

$$\dot{\mathbf{x}}(t) = -\sum_{j \in N(i)} (x_i(t) - x_j(t)),$$

where $N(i)$ denotes the set of neighbours of $i$. The compact dynamics can be written as $\dot{\mathbf{x}}(t) = -L(G)\mathbf{x}(t)$, where $\mathbf{x}$ is the vector of the agents' states and $L(G)$ is the graph Laplacian.

Following [6] by $\ell$ and $f$ we denote affiliations with leaders and followers. A *follower graph* $G_f$ of $G$ is the subgraph induced by the set of followers. Consequently, the graph Laplacian $L(G)$ of $G$ may be written as

$$L(G) = \begin{pmatrix} \mathcal{L}_f(G) & l_{f\ell}(G) \\ l_{f\ell}^{\mathsf{T}}(G) & \mathcal{L}_\ell(G) \end{pmatrix}. \tag{I.1}$$

The control system we consider is the leader-follower system

$$\begin{pmatrix} \dot{\mathbf{x}}_f(t) \\ \dot{\mathbf{u}}(t) \end{pmatrix} = -\begin{pmatrix} \mathcal{L}_f(G) & l_{f\ell}(G) \\ l_{f\ell}^{\mathsf{T}}(G) & \mathcal{L}_\ell(G) \end{pmatrix} \begin{pmatrix} \mathbf{x}_f(t) \\ \mathbf{u}(t) \end{pmatrix},$$

where followers evolve through the Laplacian-based dynamics

$$\dot{\mathbf{x}}_f(t) = -\mathcal{L}_f(G)\mathbf{x}_f(t) - l_{f\ell}(G)\mathbf{u}(t), \tag{I.2}$$

and $\mathbf{u}$ denotes the external control signal ran by the leaders' states.

The system modeled by (I.2) is said to be *controllable* if it can be driven from any initial state to any desired final state in a finite time. In the study of the controllability of multi-agent systems, the main problem is to determine the locations of leaders under which the controllability can be realized. The multi-agent system (I.2) is said to be $k$-*leaders controllable* if there exist minimum number of $k$ leaders to make (I.2) controllable. In particular, if $k = 1$, the system (I.2) is called *single leader controllable*.

We recall a useful argument for further analysis of controllability of multi-agent systems.

**Lemma I.1.** ([5]) *The system* (I.2) *is controllable if and only if there is no eigenvector for* $L(G)$ *taking* $0$ *on all entries corresponding to leaders, i.e. if and only if* $L(G)$ *and* $\mathcal{L}_f(G)$ *do not share any common eigenvalues.*

Multi-agent systems arise in many areas of science and engineering (see for example [1], [5], [7], [8], [10], [12]). In this paper we focus on controllability of chain graphs, in particular to chain graphs with one repeated degree. Chain graphs are $2K_2, C_3, C_5$ graphs, which implies that they are also bipartite graphs. We determine the minimum number of leaders needed to make the corresponding system (I.2) modeled by such a graph controllable and provide the locations of leaders in the graph.

The paper is organized as follows. In Section II we give some preliminary results on the structure of chain graphs and on their spectrum. In Section III we present several results concerning Laplacian spectrum and eigenvectors of chain graphs with one repeated degree. In Section IV we consider the controllability of systems (I.2) modeled by a corresponding chain graph. In Section V we present several concluding remarks.

 ISBN 978-86-7466-930-3

## II. PRELIMINARIES

The Laplacian matrix $L(G)$ of any graph $G$ is symmetric and positive semidefinite. Moreover, 0 is an eigenvalue of $G$ afforded by the all-1 vector $\mathbf{j}$. Therefore, we may assume that the eigenvalues of $G$ (in fact, the roots of the characteristic polynomial $\phi(L(G),x) = \det(xI - L(G))$) are indexed in non-increasing order and given as follows:

$$\mu_1(G) \geq \mu_2(G) \geq \cdots \geq \mu_n(G) = 0\,.$$

We denote by $\sigma(G)$ the spectrum of $G$, i.e. the multiset of its eigenvalues.

The vertex set of a chain graph $G$ consists of two colour classes that are partitioned into $h$ non-empty cells $\bigcup_{i=1}^{h} U_i$ and $\bigcup_{i=1}^{h} V_i$, respectively. All vertices in $U_s$ are joined to all vertices in $\bigcup_{k=1}^{h+1-s} V_k$, for $1 \leq s \leq h$. Therefore, all vertices in $U_i$ (resp. $V_j$) are *co-neighbours*, i.e. they share the same set of neighbours. If $m_s = |U_s|$ and $n_s = |V_s|$, for $1 \leq s \leq h$, then $G$ is denoted by

$$\mathrm{DNG}(m_1, m_2, \ldots, m_h; n_1, n_2, \ldots, n_h)\,.$$

A chain graph is sketched in Figure II.1.

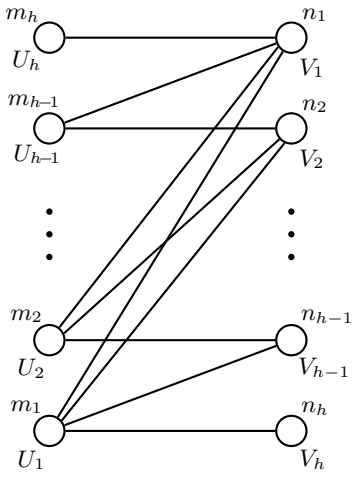


Fig. II.1. The chain graph $G = \mathrm{DNG}(m_1, m_2, \ldots, m_h; n_1, n_2, \ldots, n_h)$.

If we follow the vertex ordering from the partition $\left(\bigcup_{i=1}^{h} U_i\right) \cup \left(\bigcup_{i=1}^{h} V_i\right)$, then the *quotient matrix* $Q(G)$ of a chain graph $G$ has the form

$$\left(\begin{array}{cccc|cccc} d_1 & & & & -n_1 & \cdots & -n_{h-1} & -n_h \\ & d_2 & & & -n_1 & \cdots & -n_{h-1} & \\ & & \ddots & & \vdots & \iddots & & \\ & & & d_h & -n_1 & & & \\ \hline -m_1 & \cdots & -m_{h-1} & -m_h & d_1^* & & & \\ -m_1 & \cdots & -m_{h-1} & & & d_2^* & & \\ \vdots & \iddots & & & & & \ddots & \\ -m_1 & & & & & & & d_h^* \end{array}\right). \tag{II.1}$$

The corresponding diagonal blocks we shortly denote by $D_1, D_2$, while off-diagonal ones we denote by $B_1$, $B_2$.

It is well-known that every eigenvalue of $Q(G)$ is an eigenvalue of $G$. For more results on spectral properties of chain graphs the reader is referred to [4], [9], [11].

## III. LAPLACIAN SPECTRUM OF $\mathrm{DNG}(k, 1, \ldots, 1; 1, \ldots, 1)$

In this section we investigate spectral properties of chain graphs with one repeated degree. These graphs are of the form $\mathrm{DNG}(\underbrace{k, 1, \ldots, 1}_{h}; \underbrace{1, \ldots, 1}_{h})$. Since $G$ has only one repeated degree, then $k > h$.

**Theorem III.1.** *Let* $\mathrm{DNG}(\underbrace{k, 1, \ldots, 1}_{h}; \underbrace{1, \ldots, 1}_{h})$, $k > h$. *Then*

$$\sigma(G) = \{0, h^{k-1}, \kappa_1, \kappa_2, \ldots, \kappa_{2h-1}\},$$

*where*

$$\begin{cases} \kappa_i \in (i-1, i), & i \in \{1, \ldots, h-1\} \\ \kappa_{h+i} \in (k+i-1, k+i), & i \in \{1, \ldots, h-1\} \\ \kappa_{2h} \geq k+h, \end{cases}$$

*Proof.* Taking into account that $d_i = h+1-i$, $1 \leq i \leq h$ and $d_j^* = k+h-j$, $1 \leq j \leq h$ and employing [13, Theorem 3.5], we get that the characteristic polynomial $\phi(L(G),x)$ of $L(G)$ is given by

$$x(x-h)^{k-1} \prod_{i=1}^{k+h-1} (x-i) \left( \frac{1}{p_1} + x \sum_{j=2}^{h} \frac{1}{(x - d_{h+2-j})p_j} + \frac{1}{x - d_1} \right).$$

Since $x(x-h)^{k-1}$ is a factor of $\phi(L(G),x)$, the remaining eigenvalues are the roots of the polynomial

$$p(x) = \prod_{i=1}^{k+h-1} (x-i) \left( \frac{1}{p_1} + x \sum_{j=2}^{h} \frac{1}{(x - d_{h+2-j})p_j} + \frac{1}{x - d_1} \right).$$

Then we have:

- $p(0) = (-1)^{k+h}(2h+k-1)\frac{(k+h-2)!}{h}$;
- $p(1) = (-1)^{k+h+1}(k+h-3)(k+h-3)!$;
- $p(\ell) = (-1)^{k+h+\ell} 2\ell(h+1)(\ell-1)!(k+h-2\ell-2)! \frac{(k+h-\ell-1)!}{(k+h-2\ell)!}$, for $2 \leq \ell \leq h-1$;
- $p(k) = (-1)^{h+1} \frac{k!}{(k-h+1)(k-h)}(h-1)!$
- $p(k+\ell) = (-1)^{h-\ell+1} 2(\ell+1) \frac{(k+\ell)!}{(k+2\ell-h+1)(k+2\ell-h)}(h-\ell-1)!$, for $1 \leq \ell \leq h-1$;
- $p(k+h) = -(k+h-2) \cdot (h-1)! < 0$.

From the obtained values, we conclude that $p(0), p(1), \ldots, p(h-1)$ alternate in sign. Therefore, for any $i \in \{1, 2, \ldots, h-1\}$, we have $p(t) = 0$, for some $t \in (i-1, i)$. Similar argument holds for $p(k), p(k+1), \ldots, p(k+h-1)$, and consequently, for every $i \in \{k+1, \ldots, k+h-1\}$ we have $p(t) = 0$ for some $t \in (i-1, i)$. Also, since $p$ is a monic polynomial and $p(k+h) < 0$, it follows that $p(t) = 0$ holds for some $t > k+h$. □


ISBN 978-86-7466-930-3

We illustrate the results of Theorem III.1 on the following example.

**Example III.2.** Let $G = \mathrm{DNG}(6,1,1,1,1;1,1,1,1,1)$. Then

$$\sigma(G) = \{13.03, 9.64, , 08.6, 7.58, 6.58, 3.82, 2.86, 1.92, 0.96\} \cup \{5^5, 0\}.$$

Next we observe the structure of eigenvectors of $L(G)$ corresponding to non-integer eigenvalues.

**Theorem III.3.** *Let $G = \mathrm{DNG}(k,1,\ldots,1;1,1,\ldots,1)$ with $k > h$, $\mu$ a non-integer eigenvalue of $G$ and $\mathbf{x} = (x_1, x_2, \ldots, x_n)^\intercal$ an associated eigenvector. Then $x_i \neq 0$ for any $1 \leq i \leq k$.*

*Proof.* We recall first, (see, for example, [13]) a relation between the eigenvectors of $Q(G)$ and those of $G$ for the same eigenvalue. A vector $\mathbf{v} = (y_1, y_2, \ldots, y_h, z_1, z_2, \ldots, z_h)^\intercal$ is an eigenvector of $Q(G)$ for $\mu$, if and only if the corresponding eigenvector of $G$ for the same eigenvalue has the form

$$\mathbf{x} = (\underbrace{y_1, y_1, \ldots, y_1}_{k}, y_2, \ldots, y_h, z_1, \ldots, z_h)^\intercal.$$

Assume on the contrary that $\mathbf{x}$ is an eigenvector for the non-integer eigenvalue $\mu$ of $L(G)$ such that $x_i = 0, 1 \leq i \leq k$. By [13, Lemma 3.4], $\mu$ is also an eigenvalue of $Q(G)$. So there exists a non-zero vector $(\mathbf{y} \quad \mathbf{z})^\intercal \in \mathbb{R}^{2h}$ such that $Q(G)(\mathbf{y} \quad \mathbf{z})^\intercal = \mu(\mathbf{y} \quad \mathbf{z})^\intercal$ with $y_1 = 0$. Then the eigenvalue equation

$$\begin{pmatrix} D_1 & -B_1 \\ -B_2 & D_2 \end{pmatrix} \begin{pmatrix} \mathbf{y} \\ \mathbf{z} \end{pmatrix} = \mu \begin{pmatrix} \mathbf{y} \\ \mathbf{z} \end{pmatrix}$$

can be rewritten as

$$\begin{aligned} D_1\mathbf{y} - B_1\mathbf{z} &= \mu\mathbf{y} \\ -B_2\mathbf{y} + D_2\mathbf{z} &= \mu\mathbf{z}. \end{aligned}$$

The matrices $B_1, B_2$ have full rank, and therefore are invertible. Next, from

$$\begin{aligned} \mathbf{z} &= B_1^{-1}(D_1 - \mu I_h)\mathbf{y} \\ \mathbf{y} &= B_2^{-1}(D_2 - \mu I_h)\mathbf{z}, \end{aligned}$$

we conclude that

$$\mathbf{y} = B_2^{-1}(D_2 - \mu I_h)B_1^{-1}(D_1 - \mu I_h)\mathbf{y},$$

i.e. $\mathbf{y}$ is an eigenvector of

$$P = B_2^{-1}(D_2 - \mu I_h)B_1^{-1}(D_1 - \mu I_h)$$

for the eigenvalue 1. The latter product is the product of two anti-bidiagonal matrices $B_2^{-1}(D_2 - \mu I_h)$ that is

$$\begin{pmatrix} & & & & (k-\mu)/k \\ & & & & -(k-\mu) \\ & & & \iddots & \iddots & \\ & & & & \\ & & (k+h-2-\mu) & & \\ (k+h-1-\mu) & & -(k+h-2-\mu) & & \end{pmatrix}$$

and $B_1^{-1}(D_1 - \mu I_h)$

$$\begin{pmatrix} & & & & (1-\mu) \\ & & & (2-\mu) & -(1-\mu) \\ & & & \iddots & \iddots & \\ & & & & \\ & & (h-1-\mu) & & \\ (h-\mu) & & -(h-1-\mu) & & \end{pmatrix},$$

and hence it is a tridiagonal matrix with

$$\begin{aligned} p_{1,1} &= \frac{(h-\mu)(k-\mu)}{k} \\ p_{\ell,\ell} &= (h+1-\ell-\mu)\Big(\frac{k+\ell-1-\mu}{m_{h+1-\ell}} + (k+\ell-2-\mu)\Big), \end{aligned}$$

$2 \leq \ell \leq h$,

$$\begin{aligned} p_{\ell,\ell-1} &= -(h-\ell+2-\mu)(k+\ell-2-\mu), \quad 2 \leq \ell \leq h, \\ p_{\ell,\ell+1} &= -\frac{(h-\ell-\mu)(k+\ell-1-\mu)}{m_\ell}, \quad 1 \leq \ell \leq h-1, \end{aligned}$$

taking into account that $m_1 = k$ and $m_i = 1$, $i \geq 2$. From $\mu \notin \mathbb{Z}$, we have $p_{\ell,\ell-1}, p_{\ell,\ell+1} \neq 0$.

If $y_1 = 0$, then from the first equation in $P\mathbf{y} = \mathbf{y}$ we obtain $y_2 = 0$ ($p_{1,2} \neq 0$). Next, in the similar way, the second equation gives $y_3 = 0$, and so on, until we obtain $y_h = 0$, i.e. $\mathbf{y} = \mathbf{z} = \mathbf{0}$.

Therefore, we obtain that $\mathbf{x} = \mathbf{0}$, which is a contradiction. This completes the proof. □

## IV. Controllability of systems modeled by $\mathrm{DNG}(k,1,\ldots,1;1,\ldots,1)$

Previously obtained results, in this section will be employed to determine the number of leading agents in (I.2), where the system is modeled by a chain graph $\mathrm{DNG}(k,1,\ldots,1;1,\ldots,1)$ for $k > h$.

**Theorem IV.1.** *Let $G$ be a chain graph $\mathrm{DNG}(k,1,\ldots,1;1,\ldots,1)$ with $k > h$. Then the system (I.2) modeled by $G$ is controllable with $k-1$ co-neighbour vertices in the role of leaders.*

 ISBN 978-86-7466-930-3

*Proof.* The eigenvectors corresponding to the eigenvalue $h$ of the multiplicity $k-1$ are of the form

$$\begin{aligned}\mathbf{v}_1 &= (\underbrace{1,-1,0,0,\ldots,0}_{k},0,\ldots,0)\\ \mathbf{v}_2 &= (\underbrace{1,0,-1,0,\ldots,0}_{k},0,\ldots,0)\\ &\vdots\\ \mathbf{v}_{k-1} &= (\underbrace{1,0,\ldots,0,0,-1}_{k},0,\ldots,0).\end{aligned}$$

We first conclude that vertices $\{2,\ldots,k\}$ should be selected as leaders. Moreover, any vector corresponding to $\mu = h$ is of the form $(t_1,\ldots,t_k,0,\ldots,0)^{\intercal}$. Any $k-1$ of these $t_i$'s cannot be zeros simultaneously. For any $\mathbf{x}_1,\ldots,\mathbf{x}_l$ , $l < k-1$ there exists $\mathbf{x}_s$, such that $\mathbf{x}_s\mathbf{x}_i = 0$ for each $i, 1 \leq i \leq l$.

The remaining eigenvalues by Theorem III.1 are non-integer and therefore their eigenvectors, by Theorem III.3 satisfy $x_i \neq 0, 1 \leq i \leq k$. Now the statement follows by Lemma I.1. □

**Example IV.2.** For $G = \mathrm{DNG}(6,1,1,1,1;1,1,1,1,1)$ the system (I.2) is 5 leader controllable. The leaders $\ell_1,\ldots,\ell_5 \in U_1$ are 5 of 6 vertices with repeated degrees, that are joined to the followers $v_1,\cdots,v_5$ as illustrated in Figure IV.1.

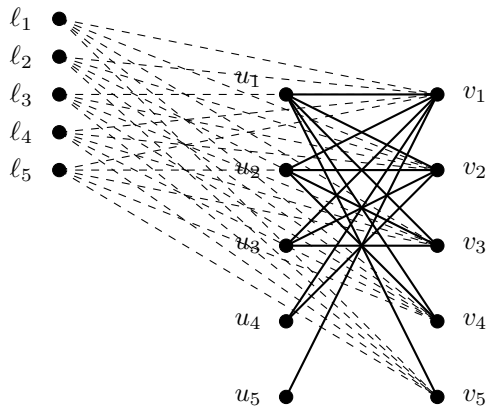


Fig. IV.1. A 5-leader controllable system modelled by $\mathrm{DNG}(6,1,1,1,1;1,1,1,1,1)$.

## V. Conclusion

In this paper we have covered the controllability of multi-agent systems that are modelled by special class of bipartite graphs: chain graphs. We have proved that if a chain graph has only one repeated degree with multiplicity $k$, then the system requires at least $k-1$ controllers in order to be controllable. In this way we positively addressed the questions raised in [7], where the authors asked if there is a family of graphs other than threshold graphs with one multiple degree of multiplicity $m$ for whose controllability at least $m-1$ controllers are needed. Consequently, we expanded the known classes of the controllable multi-agent systems. Taking into account that many engineering systems are modelled by graphs, the obtained results are of particular importance in creating new controllable systems, since the known structures are limited (they mainly include paths, grids, cycles and circulant networks). Another advantageous aspect is a possibility to generate graphs with some desirable properties. One of them is algebraic connectivity, i.e. the second smallest Laplacian eigenvalue. It is a useful tool to measure the robustness and synchronizations of the graphs. For the chain graphs that we considered the algebraic connectivity is always in $(0,1)$ and it approaching to 1 as the size of the graph increases. This brings another benefit, since in general graphs the algebraic connectivity usually decreases if the order of a graph is increased.

## Acknowledgment

Research of M.A and Z.S. is supported by the Science Fund of the Republic of Serbia; grant number 7749676: Spectrally Constrained Signed Graphs with Applications in Coding Theory and Control Theory – SCSG-ctct.

## References

[1] T. Kailath, Linear systems, Prentice-Hall, Englewood Cliffs, 1980.
[2] N.V.R. Mahadev, U.N. Peled, it Threshold Graphs and Related Topics, North-Holland, New York, 1995.
[3] K. Ogata, Modern Control Engineering, Prentice-Hall, Upper Saddle River, 2002.
[4] F.K. Bell, D. Cvetković, P. Rowlinson, S.K. Simić, Graphs for which the least eigenvalue is minimal, II, Linear Algebra Appl., 429 (2008), 2168–2179.
[5] Z. Ji, Z. Wang, H. Lin, Z. Wang, Interconnection topologies for multi-agent coordination under leader-follower framework, Automatica, (2009), 45(12), 2857–2863.
[6] A. Rahmani, M. Ji, M. Mesbahi, M. Egerstedt, Controllability of multi-agent systems from a graph theoretic perspective, SIAM J. Control Optim., 48 (2009), 162–186.
[7] S-P Hsu, Controllability of the multi-agent system modelled by the threshold graph with one repeated degree, Systems Control Lett., 97 (2016), 149–156.
[8] X. Liu, Z. Ji, Controllability of multiagent systems based on path and cycle graphs, Int. J. Robust Nonlinear Control, 28 (2016), 296–309.
[9] M. Anđelić, S.K. Simić, D. Živković, E. Dolićanin, Fast algorithms for computing the characteristic polynomial of threshold and chain graphs, Appl. Math. Comput. 332 (2018), 329-337.
[10] M. Anđelić, M. Brunetti, Z. Stanić, Laplacian controllability for graphs obtained by some standard products, Graphs Combin., 36 (2020), 1593–1602.
[11] K.Ch. Das, A. Alazemi, M. Anđelić, On energy and Laplacian energy of chain graphs, Discrete Appl. Math., 284 (2020), 391–400.
[12] A. Farrugia, T. Koledin, Z. Stanić, Controllability of NEPSes of graphs, Linear Multilinear Algebra, https://doi.org/10.1080/03081087.2020.1778622
[13] A. Alazemi, M. Anđelić, K.Ch. Das, C.M. da Fonseca, Chain graph sequences and Laplacian spectra of chain graphs, Linear Multilinear Algebra, https://doi.org/10.1080/03081087.2022.2036672

 ISBN 978-86-7466-930-3

# Secret Keys Distillation using Speech Signals and Discussion over Public Authenticated Channel

Jelica Radomirović, Milan Milosavljević, and Aleksandra Krstić

***Abstract*— This paper discusses a system for generating and distributing secret cryptographic eys based on the principle of common randomness and discussion over an authenticated public channel. The use of speech as a source of common randomness is one possibility and to our nowledge the first for this type of system. We consider different reconciliation algorithms and compare them with e periments. perimental results show that it is possible to generate information-theoretical secret eys with rates between and 5 . This result proves the practical feasibility of absolutely secret autonomous cipher systems with speech control.**

***Index Terms*—secret ey; distillation; symmetric cryptography; speech signal; reconciliation; privacy amplification; secret ey rate;**

## I. Introduction

The information-theoretical approach to the analysis and synthesis of cipher systems came into focus with the availability of quantum computers in the near future. The classical result of this approach states that the entropy of secret keys in a cryptographic system must be no less than the entropy of plaintext [1]. As is well known, systems designed in this way are resistant to the unlimited computing resources of the adversary, and thus to cryptanalysis based on quantum computers [2].

From the point of view of generating and distributing high-quality secret keys, special attention is drawn to the fundamental results of Alswede and Csiszar [3], Maurer [4], and Csiszar and Narayan [5]. The basic idea of information-theoretical approach in these results is to identify and use mutually correlated signals available to legitimate parties.

Depending on the location of the source of common randomness, there are two approaches, [3]:

(i) Secret key extraction from sources independent of communication channels (source model),

(ii) Secret key extraction from existing communication channels (channel model).

The difference between these two models is how the parties observe the initial sequence. While in the source model, random source is controlled by nature, in the channel model, one of the parties governs the input of a noisy channel (independent of the main channel) while others observe the output.

In this paper, we will analyze the possibility of extracting cryptographic keys from a speech signal, applying an approach based on the source model.

In Section 2, the basic blocks of the proposed secret key generation system will be presented, in two variants: (i) when the input is a speech signal and (ii) when the input is a residual speech signal, filtered by an adaptive linear predictive model [6].

In Section 3, the information and statistical characteristics of this source will be analyzed and the key parameters of the sequential procedure for extracting secret keys will be identified, separately for each of the phases: Advantage Distillation (AD), Information Reconciliation (IR) and Privacy Amplification. -PA).

In Section 4 we present the results of the experiment of obtaining secret keys for all pairs (Alice, Bob) of legitimate participants for 5 speakers, one of which was chosen as an eavesdropper (Eve).

The Conclusion discusses the upper limits of the rate of generating secret keys and the possibility of further improving the performance of the proposed system.

## II. Discrete Memoryless Source

As illustrated in Figure 1, a source model for secret-key agreement represents a situation in which three parties, Alice, Bob, and Eve, observe the realizations of a DMS - Discrete Memoryless Source (XYZ, $P_{XYZ}$) with three components.

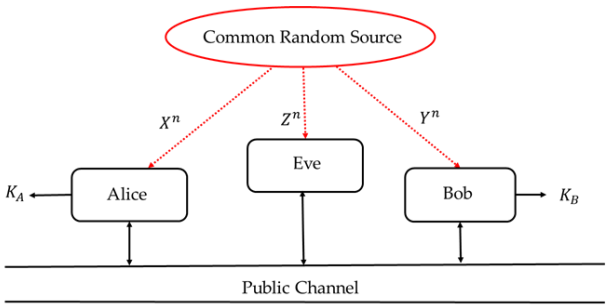


Fig. 1. Secret-key Agreement by Public Discussion from Common Randomness [4].

Jelica Radomirović is with the School of Electrical Engineering, University of Belgrade, 73 Bulevar kralja Aleksandra, 11020 Belgrade, Serbia and with Vlatacom Institute of High Technologies, 5 Bulevar Milutina Milankovića, 11070 Belgrade, Serbia (e-mail: jelica.radomirovic@vlatacom.com).

Milan Milosavljević is with Singidunum University, 32 Danijelova, 11000 Belgrade, Serbia (e-mail: mmilosavljevic@singidunum.ac.rs).

Aleksandra Krstić is with the School of Electrical Engineering, University of Belgrade, 73 Bulevar kralja Aleksandra, 11020 Belgrade, Serbia (e-mail: amarjanovic@etf.bg.ac.rs).

 ISBN 978-86-7466-930-3

The DMS is assumed to be outside the control of all parties, but its statistics are known. By convention, component X is observed by Alice, component Y by Bob, and component Z by Eve. Alice and Bob's objective is to process their observations and agree on a key K about which Eve should have no information.

Alice and Bob can exchange messages over a noiseless, two-way, public and authenticated channel. That is, all messages are overheard by Eve and the existence of the public channel does not provide Alice and Bob with an explicit advantage over Eve. The rules by which Alice and Bob compute the messages they exchange over the public channel and agree on a key define a four-stage key distillation strategy, [4]:

1. Randomness sharing. Alice, Bob, and Eve observe *n* realizations of a DMS (XYZ, $P_{XYZ}$).
2. Advantage distillation. If needed, Alice and Bob exchange messages over the public channel to process their observations and to "distill" observations for which they have an advantage over Eve.
3. Information reconciliation. Alice and Bob exchange messages over the public channel to process their observations and agree on a common bit sequence.
4. Privacy amplification. Alice and Bob publicly agree on a deterministic function they apply to their common sequence to generate a secret key.

The largest achievable key rate is defined as the key capacity and is given by

$$C_K = max\{I(X;Y), I(X:Y|Z)\}, \quad (1)$$

where I(X;Y) denotes mutual information between X and Y, while I(X:Y|Z) denotes the same quantity conditioned by Z. In the special case, when Eva is totally independent of Alice and Bob, or equivalently, when Z is independent of X and Y, maximal key capacity is equal to

$$C_{K\,max} = I(X;Y). \quad (2)$$

In this work, we use speech the signals of participants as DMS of the proposed system, see Fig.2.

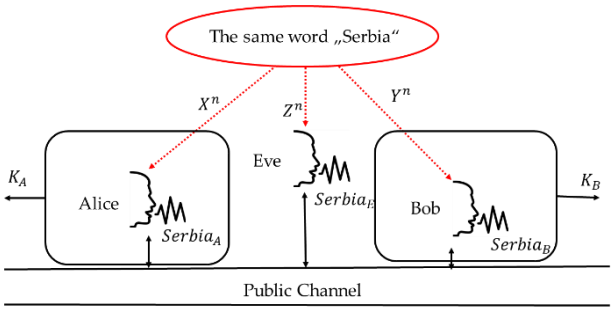


Fig. 2. Secret-key Agreement by Public Discussion based on the speech signals obtained by pronouncing the word "Serbia".

## III. System Architecture

As already mentioned, we will analyze two DMS, the first one corresponding to the original speech signal, and the second one corresponding to the residual signal. Residual DMS is obtained after inverse filtering by an adaptive linear autoregressive model, estimated every 10 ms of input speech, see Fig.3.

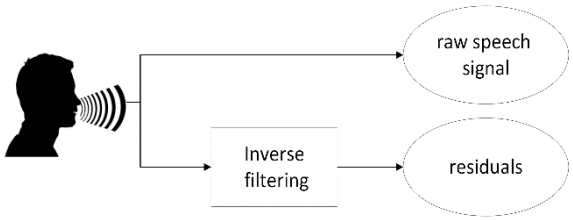


Fig. 3. Two different DMS based on the same input speech signal

The general architecture of the system is given in Fig.4. Speech input (or residual) is transformed into binary DMS by a non-uniform quantization, based on estimating the probability density function of input samples.

Advantage Distillation (AD) blocks are used to eliminate the advantage that the eavesdropper may have over legitimate parties. In that case, Eve knows more information about Alice's initial bit string, than Bob does. We will use the bit pair advantage distillation/degeneration protocol [7]. Algorithms are based on the exchange of parity information of 2-bit blocks and the elimination of one bit of each block to ensure security. After this step, the number of different bits of the sequence is reduced. The number of non-matching bits of the eavesdropper sequence decreases but much slower than for the legitimate parties. The protocol runs for several rounds until the sequences differ only in a few bits.

The Information Reconciliation (IR) is intended to correct the remaining erroneous bits in the Alice and Bob sequences. The most popular IR protocols are Winnow [7] and Cascade [8] protocols. They are based on the exchange of block parity information until the error of a certain block is detected. For each block parity query, some bits are deleted to ensure security. In the end, we get the same sequence on legitimate sides that represents the secret key. Even though we tried to ensure privacy by deleting potentially compromised bits, the eavesdropper has still gained some information about the secret key. To make the secret key absolutely secure, we proceed to the next step of our system, privacy amplification (PA).

In Privacy Amplification (PA) block sequences are transformed such that m bits are discarded due to the eavesdropper's knowledge. One of the possible transformations is a hash function $g: \{0,1\}^n \rightarrow \{0,1\}^r$ where n is the length of a sequence before PA and r is the length after PA, i.e., the length of the final secret key. It is common to use so-called universal hash functions, such as random $r \quad n$ matrices, over GF(2), [9].

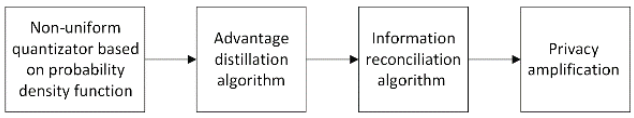


Fig. 4. Secret key agreement algorithm [3]


ISBN 978-86-7466-930-3

## IV. RESULTS

Raw speech signal and its residuals, obtained from inverse filtration of AR model of 10th order, were used for experimental proof of the proposed system, Fig 5. Four participants recorded the word 'Srbija' for two seconds. Beginning. as well as the end of the word, were determined so the initial signal is reduced to 0.6 second length. The recordings were sampled at 44.1 kHz.

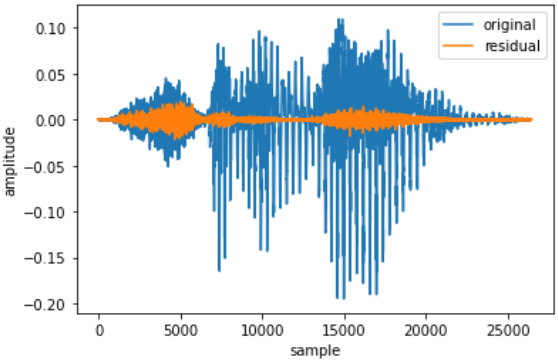


Fig. 5. Comparison of source signals

Normalized Hamming distance is an appropriate metric for measuring the difference between two binary sequences. Depending on the number of bits we use to quantize continuous signal we get more or less similar sequences. That directly affects how much information circulates over a public channel and how long is the final secret key length. The key rate is an indicator of how much of the sequence at the beginning is useful

$$\text{key rate} = \frac{\text{final length of secret key}}{\text{length of input sequence}} * 100\ [\%].$$

In Fig 6. the key rate in function of normalized Hamming distance is presented. In order to determine the optimal value for the number of quantization bits, we try five different values 6,8,10,12, and 14.

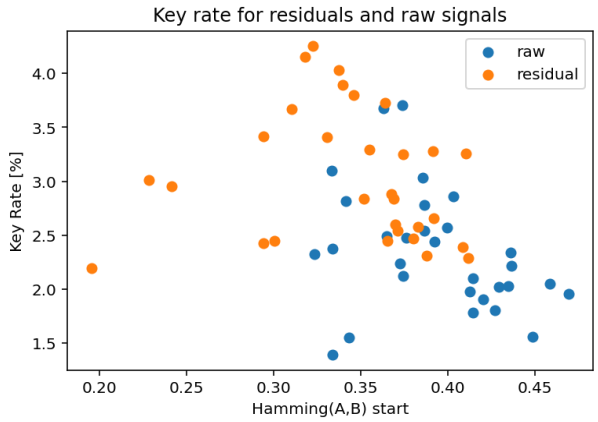


Fig. 6. Comparison of key rate for source signals. A and B denote legitimate parties

From Fig.6 can be seen that residuals are closer to each other than raw signals because of the corresponding higher key rate.

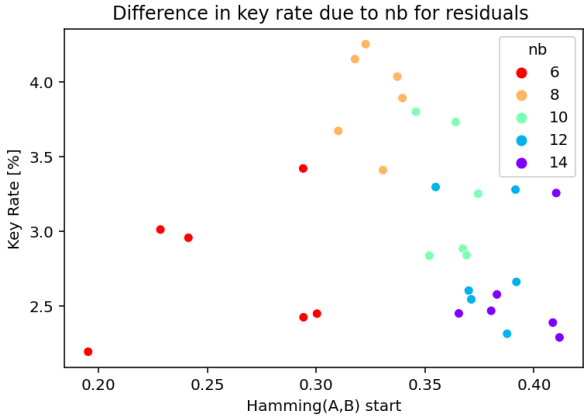


Fig. 7. How the number of quantization bits affects distance at the beginning

As shown in Fig 7., the highest rate is achieved for normalized Hamming distance between 0.3 and 0.35, which corresponds to 8 quantization bits.

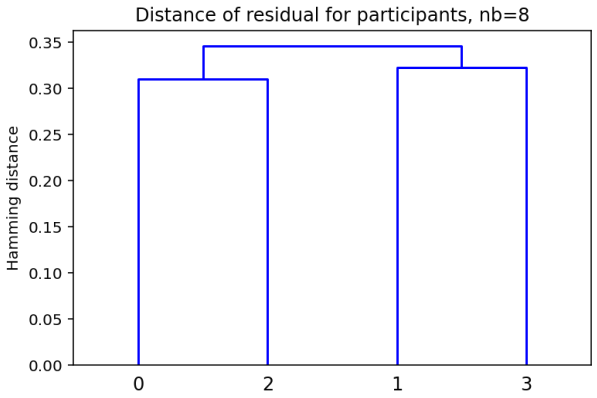


Fig. 8. Dendrogram represented distance of all sequences

In Fig 8. we use a dendrogram to show how close to each other are the participant sequences. The dendrogram was obtained as a result of hierarchical cluster analysis by the Ward method [10]. To compare Cascade and Winnow algorithms we conduct 4 experiments, 2 for each, that is one for residual signals and one for speech signals. Results are represented in table 1.

TABLE I
EXPERIMENTAL RESULTS

| | | Final key size | Key rate [%] |
|---|---|---|---|
| Winnow | Residual | 10116.83 ± 788.93 | 4.78 ± 0.37 |
| | Raw | 8670.30 ± 1033.87 | 4.10 ± 0.49 |
| Cascade | Residual | 8432.24 ± 624.18 | 3.98 ± 0.29 |
| | Raw | 6833.72 ± 1433.26 | 3.22 ± 0.68 |


ISBN 978-86-7466-930-3

Based on the results we conclude that the Winnow algorithm is a better choice for reconciliation because it gives an almost 1% higher key rate. If we compare two DMS, the one corresponding to the residual signal gives longer secret keys due to a smaller normalized Hamming distance at the beginning, for the same pair of sequences. Final hamming for all sequences and all experiments toward the eavesdropper after PA is ~0.5. In other words, all the information that leaked through the public channel will not reveal anything to the eavesdropper about the distilled secret key.

## V. CONCLUSION

In this work we proposed a speech based secret key agreement system with message transmission over a public channel. The proposed system can distill secret keys from speech signals, with the key rate of up to 5%, and with negligible information leakage to an eavesdropper. This opens up the possibility of practical realization of absolutely secret cipher systems controlled by voice. Such systems can be used both in the security services for critical information and communication infrastructure of the government, as well as in commercial applications.

Future work will include generalization in terms of the largest achievable key rate and a testing of the proposed system on more participants as well as more different spoken words.

## VI. ACKNOWLEDGMENT

The authors would like to thank the Vlatacom Institute of High Technologies, where the research was done as part of the project Prj_164.

## REFERENCES

[1] Shannon C.E., "Communication theory of secrecy systems". *BST* , vol. 28, no. *4*, pp. *5 – 15*. October 1949.

[2] Wolf S., "Unconditional Security in Cryptography", in *ectures on ata Security Modern Cryptology in Theory and Practice, ecture Notes in Computer Science*, Berlin, 1999, vol. 1561, pp. *21 –250*.

[3] Ahlswede R., Csiszar I., "Common randomness in information theory and cryptography, Part I: Secret sharing", *IEEE Transaction on Information Theory*, vol. 39, pp. *1121–1132*, 1993.

[4] Maurer U., "Secret Key Agreement by Public Discussion from Common Information", *IEEE Transaction on Information Theory*, vol. 39*,* no. *3,* May, 1993.

[5] Csiszar I., Narayan P., "Secrecy capacities for multiple terminals", *IEEE Transaction on Information Theory*, vol. 50, pp. *304 –30 1*, 2004.

[6] Kovačević B., Milosavljević M., Veinović M., "Robust Digital Processing of Speech Signals", Springer, 2017.

[7] Wang Q., Wang X., Lv Q., Ye X., Luo Y., You L., "Analysis of the information theoretically secret key agreement by public discussion", *Security and Communication Networks*, vol. 8*,* January, 2015.

[8] Reis A., "Quantum Key Distribution Post Processing - A Study on the Information Reconciliation Cascade Protocol". Master's Thesis, Faculdade de Engenharia, Universidade do Porto, Porto, Portugal, 2019.

[9] Bennett C.H., Brassard G., Crepeau C., Maurer U. "Generalized privacy amplification". *IEEE Transaction on Information Theory*, vol. 41, pp. 1915–1923, 1995.

[10] sklearn.cluster.Ward – scikit-learn 0.15-git documentation. https://scikit-learn.org/0.15/modules/generated/sklearn.cluster.Ward.html

 ISBN 978-86-7466-930-3

# One solution for voice commands on Android based STB

Jovana Simić, Đorđe Glišić, Nikola Vranić, Marija Jovanović

***Abstract*—With the introduction of voice recognition and its support by various research groups, it became possible to add voice commands to different devices in use. We are seeing them on PCs, phones, and tablets. This paper presents a solution to order and control set-top box devices and TVs based on Android OS. It is a cloud-based solution supported by Google API for voice recognition.**

***Index Terms*—set-top box, android, voice commands, voice recognition, TV voice commands, Actions on Google, Android, Google Assistant, Dialogflow, Firebase.**

## I. Introduction

Virtual assistance is becoming more popular with artificial intelligence and machine learning advances. Particularly with voice recognition available on PC and even mobile devices, with capabilities to support more languages, not just English. Popular operating systems come with support for virtual assistance and voice recognition as one service. There is Cortana on Windows operating system. In iOS, there is Siri. For Android devices and Google products, there is Google Assistant. Additionally, Samsung has Bixby, and Amazon has Alexa.

All mentioned virtual assistance is based on cloud architecture that employs the internet. Some solutions are standalone and work reasonably well in a narrow field, but cloud-based solutions give better results for general-purpose tasks.

This paper will investigate the possibilities of adding virtual assistance to set-top box devices to speed operations with DTV sets and improve user experience. We have selected an Android-based device with a remote controller that supports voice recording [1]. Early work on the subject was done with [1] and [2]. More similar work was done on narrow areas for content playback on set-top box devices by Petrovic et al. [3] and Visekruna et al. [4], and Lazic et al. [5].

## II. Section Title (e.g., The Method)

Google Assistant is Google's virtual assistant available on mobile phones, smart home devices, TVs, cars, etc. It has artificial intelligence and enables two-way communication in voice communication and text messages with the user. It can browse the Internet, set alarms and events, access device settings, display user account information, etc. It also supports a lot of functionality for smart homes. For example, the user can control lighting, temperature, TV, and other items in the house. To prevent the service from being constantly active, the recognition of the keywords "OK, Google" and "Hey, Google" was introduced, after which the service became active. After activating Google Assistant, the voice command recording begins, and it collects an audio message which is further processed. The resulting response is reproduced depending on the device on which Google Assistant is used, e.g., in the case of Google Home devices, the answer is in the form of audio sound, while when using a smartphone or TV, a text record is also obtained [6]. If you want to run Google Assistant on an Android TV, you need a microphone to record your voice, integrated into the remote control [6].

Actions on Google (AoG) is a platform that allows you to expand your personal Google Assistant by adding your services called Actions. To enable device management, Action has been implemented. Suppose you want to access the Action described in this paper. In that case, you need to tell Google Assistant: "Talk to True TV" or "Ask True TV", after which he asks the AoG platform to run the application, AoG sends a request to the web service and receives a response forwards to Google Assistant, which displays the answer to the user. Furthermore, Google Assistant forwards the user input directly to the Action, and the Action responds directly to the Assistant.

When creating an Action, it is also possible to use the Dialogflow platform to simplify the understanding of user input. The Dialogflow agent translates user input during a conversation into structured data that applications and services can understand. As the call center, they are trained to handle expected conversation scenarios. The platform itself provides the ability to reply with static responses. If you want to respond with dynamic answers and additional logic, it is possible to implement a web service. In this case, Dialogflow is a proxy between Actions on Google and the web service, as shown in the figure. Instead of sending the request directly to the web service, AoG sends it to Dialogflow. Also, the web service sends a response to Dialogflow, which forwards it to AoG.

The answer must be returned to the user within 10 seconds. Otherwise, the request will expire. Also, the response must be less than or equal to 64 kilobytes. Dialogflow processes the user's input, and it sends an HTTP POST request to the web

Jovana Simić – RT-RK Institute for Computer Based Systems, Novi Sad, Srbija, (e-mail: Jovana.Simic@rt-tk.com)
Đorđe Glišić – RT-RK Institute for Computer Based Systems, Novi Sad, Srbija, (e-mail: Djordje.Glisic@rt-tk.com)
Marija Jovanović – RT-RK Institute for Computer Based Systems, Novi Sad, Srbija, (e-mail: Marija Jovanović@rt-tk.com)
Nikola Vranić – RT-RK Institute for Computer Based Systems, Novi Sad, Srbija, (e-mail: Nikola.Vranic@rt-tk.com)

 ISBN 978-86-7466-930-3

service, which is set as a function on the Firebase platform. The Cloud Functions for Firebase service automatically starts the function when an HTTP request arrives.

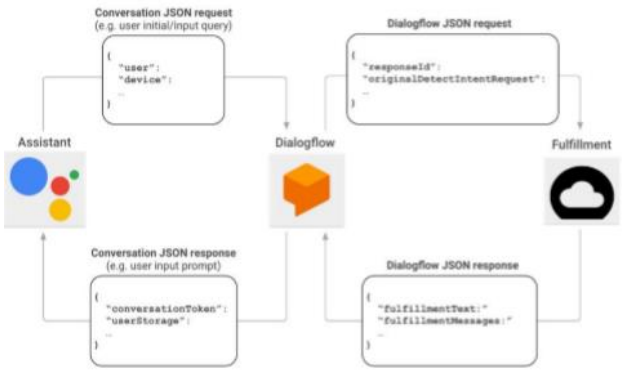


Fig. 1. The diagram shows the path that requests go from Assistant through the Dialogflow till the Fulfillment and response traveling back to the Assistant.

The Actions on Google, Dialogflow, and Firebase platforms are well integrated, as seen in Fig. 2. The figure shows a simple interaction between the end-user, the assistant, Dialogflow, and the web service built in the cloud, like Functions for Firebase and the Firebase Real-time Database.

The user enters his request as a voice command and starts the assistant himself. The assistant converts the voice command into text and starts the Dialogflow searching for the initial action (Welcome intent). Dialogflow uses machine learning to map text to intent and to isolate recognized entities (such as TV channel, TV channel number, time, etc.). Dialogflow triggers a web service, implemented as Cloud Functions for Firebase, sending it a JSON request that contains all the necessary information from the text. The web service processes the JSON request and implements logic (checks the Firebase Real-time Database) to respond to the assistant (or Dialogflow). Device Assistant converts the answer to speech and display (for devices that do not have a screen).

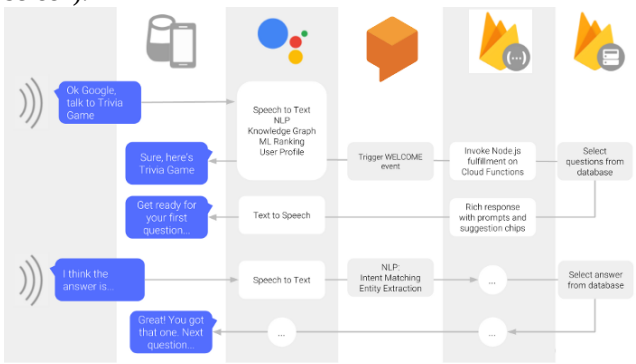


Fig. 2. Voice command workflow from Actions on Google, Dialogflow to Firebase fulfillment web service and back.

## III. IMPLEMENTATION

This section describes one way to train and integrate Google Assistant. The Dialogflow agent needs to be trained first. The intent has been created for each supported command, in which it is necessary to enter a large number of phrases that the agent will understand, as shown in Fig. 3.

The pairing of the Action user and the STB device user was solved using a Google account, precisely his email address. To be able to manage the STB during the first launch of the Action, it is first necessary to link the account with the Action. The AoG platform provides the Google Sign-In option, the easiest way to connect and create accounts with the Action. The Action may request access to the user's Google profile, including the user's name, email address, and profile picture. Of course, you need to ask the user if he agrees to access his Google profile.

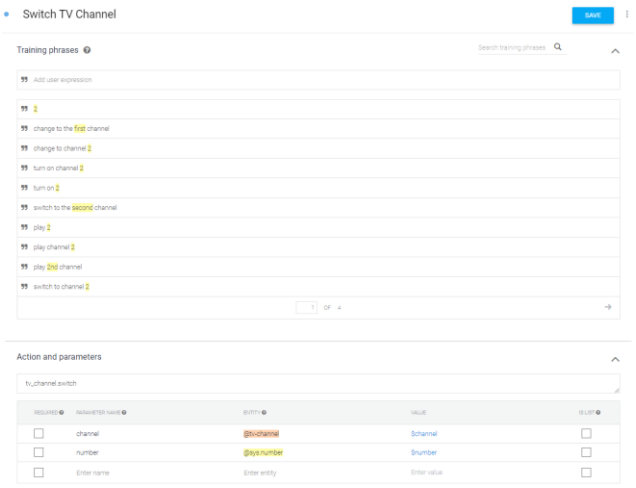


Fig. 3. Training phrases for specific action in Dialog flow and the required parameters defined.

After recognizing the command by the Dialogflow platform, it is necessary to send a signal to the TV application, which should execute the given command. Therefore, for each intent in the agent, an intent handler has been created in the web service. The operator first checks whether the user has linked his account with the Action. If this is not done, the user is first asked to link his account, and the user receives a list of suggested cards with commands for linking the account. Otherwise, the triggered command is entered in the Firebase Realtime Database database in a node whose email field value equals the user's email address accessing the Action. If such a node does not exist, the user with that email address is not logged in to any TV application. If there is, wait a while for the TV application to process the command and return the answer to be displayed to the user.

As already mentioned, the pairing of users of the Action and users of STB devices was done through a Google account. Therefore, the *AccountHandler* class is implemented in the TV application, which detects adding and removing accounts from the application. The class diagram of the *AccountHandler* class is shown in Fig. 4. Each account should have its node in the Firebase Realtime Database. Each account is associated with an object of the type *VoiceHandler* given in Fig. 5, which is used to detect database changes and execute commands.

 ISBN 978-86-7466-930-3

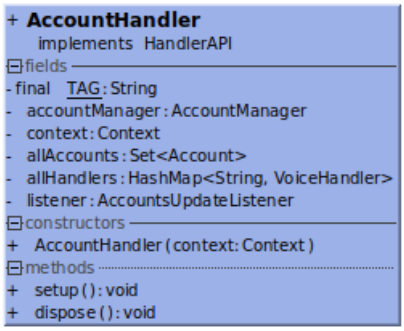


Fig. 4. Account handle class diagram.

When a new account is added to the TV application, it is necessary to add a new node to the database for that account and set the application to listen for changes on that node, for which the *VoiceCommand* class is used. In the class constructor, a reference to the root node of the database is retrieved, and in the *subscribe()* method, a listener is registered to the node in the database for which changes need to be detected.

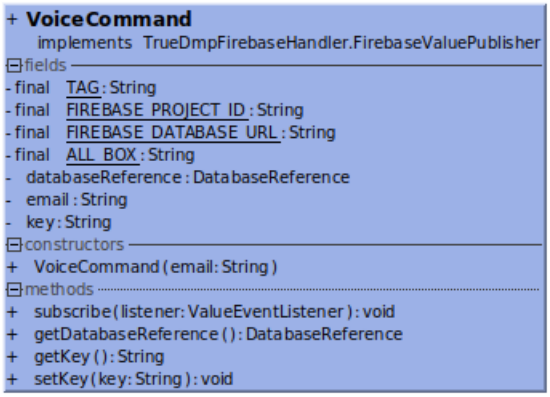


Fig. 5. Voice command class diagram.

## IV. Results

A vital result of the presented work is that the voice commands apply to set-top-box devices with acceptable latency. Additionally, the phrase database could be upgraded without changing the actual code on any STB device.

Testing was performed via the Google Assistant application on a mobile device. The response time of the Action from the user's input to the return of the response to the user was tested. The tests were performed under normal conditions, under certain noises, using commands in English.

The table gives a comparative overview of the response time for commands implemented in this system. Response time averages 1 to 2 seconds, depending on the command. As shown in Table 1, the most time-consuming commands are for displaying information about events. These timings are comparable with the times it takes for users to do those actions using RCU. Key benefits could be seen in more complex scenarios, like adding services to favorite lists or scheduling PVR recordings based on the TV show's name for a specific period. Those cloud-based services will outperform manual user interaction with the graphical user interface.

TABLE I
VOICE COMMANDS AND RESPONSE TIME

| Command for set-top box | Response Time[s] |
|---|---|
| Change to the next channel | ~1,174 |
| Change to the previous channel | ~1,172 |
| Change to a channel with a specific name | ~1,195 |
| Change to a channel with a specific number | ~1,222 |
| Complete tone reduction | ~1,156 |
| Restore volume before complete mute | ~1,190 |
| Tone amplification | ~1.075 |
| Mute the tone | ~1,199 |
| Increase the tone to maximum | ~1,036 |
| Check if the STB is in sleep mode | ~1,353 |
| View information about the current event on the current channel | ~1,535 |
| View information about the current event on a specific channel | ~1,599 |
| View information about the next event on the current channel | ~1,469 |
| View information about the next event on a specific channel | ~1,445 |
| Setting reminders | ~1,169 |

## V. Conclusion

In this paper, we have implemented a proof of concept for the voice commands on STB. For more implementation details refer to works [5], [6], and [7]. As with any cloud-based service, it relies on the internet and its stability. Further work shall be done to benchmark latency depending on the internet connection speed, location, and type of connection (WiFi, cable, mobile). It makes that operators supporting this feature offer stable enough internet.

If a set of basic commands is appropriately selected to cover all actions that the user can execute, then a cloud solution can make a chain of commands based on the user's voice request. Dialog flow cloud platform could process arbitrary complex requests that could be transformed and fulfilled as a series of actions. This hides a real benefit, as requests like "make a list of my top five sports channels and record NBA finals on internal disk" could be executed.

Additionally, requests like "Find me a movie with Tom Hanks for Saturday evening" contains more than just a request for STB. They hold user preferences so that operators can train recommendation systems. It opens up a vast field of opportunities as well as privacy concerns.

It does not end with voice commands for STB. It can be a command supported by a third-party application for food delivery or a calendar application.

 ISBN 978-86-7466-930-3

## REFERENCES

[1] A. B. Garayalde, MSc thesis, “Speech Control & Media Sharing for Media Centers”, ENST Bretagne France, 2007

[2] KH Lin, CH Lin, KH Chung, KS Lin , “A Compressive Sensing-based Speech Signal Processing System for Wearable Computing Device in IPTV Environment”, ICMT 2013

[3] D. Petrović, M. Zeković and N. Vranić, "One solution for extension of the system for recording multimedia content on Android based devices" 2017 25th Telecommunication Forum (TELFOR), Belgrade, 2017, pp. 1-4.

[4] U. Višekruna and M. Savić, "Integration of Google Assistant in Android Application for Voice Control of Media Playback," 2018 26th Telecommunications Forum (TELFOR), Belgrade, 2018, pp. 1-4.

[5] A. Lazić, M. Z. Bjelica, D. Nad and B. M. Todorović, "Google Assistant Integration in TV Application for Android OS," 2018 26th Telecommunications Forum (TELFOR), Belgrade, 2018, pp. 420-425.

[6] E. Nan: „Upravljanje pametnom kućom uz pomoć Google asistenta”, University of Novi Sad, Faculty of Technical Sciences, Novi Sad, 2017.

[7] J. Simic, “Realizacija glasovnih komandi za uredjaj baziran na operativnom sistemu Android”, UB ETF, Belgrade, Serbia, 2022

 ISBN 978-86-7466-930-3

# One solution for simulating conditional access in DTV Software on PC platform

Milan Petrović, Đorđe Glišić, Uroš Jokić and Marija Jovanović

***Abstract*— Digital television (DTV) software runs on various hardware platforms, from low-cost low-performance devices to high-end devices that could compare with modern smartphones and PC configurations. The development quality depends on the tools available for the target platform. A new approach was taken to improve development by moving to the PC platform to avoid this dependency. The benefits are apparent, but it comes with some constraints. Typical examples are components available for target platforms but not PC platforms for security and legal reasons. One such component is the conditional access system (CAS) and digital rights management (DRM) components. This paper will present one solution to simulate conditional access (CA) in software without vendor CA libraries and support in hardware. The aim is to get the ability to test and verify various parts of DTV software that depend on CA functionalities.**

***Index Terms*— digital television, simulation, conditional access, DTV stack test environment.**

## I. Introduction

A device that can reproduce digital television needs to comply with some DTV standards (DVB, ATSC, ISDB, etc.). Often it needs to support some content protection mechanism (encryption, signing, etc.). Additionally, the device needs to have a certain number of standard features and a few unique features dictated by the operator that will be available to the user.

In developing DTV software, specific components are delivered from third parties, like a software development kit (SDK) for the target platform or CA libraries for content protection. Content protection certification is an essential step in the development life-cycle, and DTV software is adopted according to the specification documents and APIs delivered. Upon development completion, the application is verified using several test suites that prove it behaves in the required way. This process repeats for every new target platform.

The DTV software development is tightly coupled with the target platform. Depending on the platform and its supporting packages, it may be impractical to develop a more complex project using them as a development platform. Instead, one way to overcome those difficulties is to develop on more suitable platforms. That platform should support at least logging mechanisms, the ability to re-write persistent memory, access to hardware debuggers, and good enough software packages to use those features. In practice, this is not the case, and almost always, given components are missing, and software packages are always behind the state-of-the-art counterpart packages available for PC. Selecting a more applicable platform instead of the target one for development is not applicable if the target CA library has different requirements (hardware or software) compared to its counterpart on a development platform.

For DTV software to be as robust as possible, there was a need to implement support for different CAS vendors. They shared core concepts for content access rights, content protection, operator box management, operator messaging to users, and other customized product and feature protections.

The CAS vendors' APIs significantly differ, although concepts are very similar. The differences between versions from the same vendor may not be compatible. Older libraries tend to have fewer restrictions, while newer versions have more demands and APIs to support, as new scrambling algorithms are added, and more security protocols are employed. It is necessary to have a level of abstraction in DTV middleware to adopt those changes and differences.

As a result, the first DTV simulator was developed on a PC platform [1]. It aimed to support the development of a graphical user interface. It became clear it could be used for implementing DTV middleware features as well. Those features were related to the DTV standard. To support it, the middleware test environment (MTE) [2] was created to test and verify different parts of the software on a PC platform using white box testing [3] [4]. This approach could not cover the code developed for a CA subsystem and the application code that was connected and dependent on that CA subsystem.

This paper aims to discuss paths that could be taken to overcome those obstacles. It gives one solution that is implemented and tested to prove the concepts. We could not find any relevant work on this topic. Closes to the work are discussions on testing approaches made in [5], [6], and [7].

Section two details the challenge and introduces the DTV system's architecture. Section three provides more information on the implementation and final solution. Section four explains verification and test results. Section five concludes the work.

Milan Petrović – RT-RK Institute for Computer Based Systems, Novi Sad, Srbija, (e-mail: Milan.Petrovic@rt-tk.com)

Đorđe Glišić – RT-RK Institute for Computer Based Systems, Novi Sad, Srbija, (e-mail: Djordje.Glisic@rt-tk.com)

Marija Jovanović – RT-RK Institute for Computer Based Systems, Novi Sad, Srbija, (e-mail: Marija Jovanovic@rt-tk.com

Uroš Jokić – RT-RK Institute for Computer Based Systems, Novi Sad, Srbija, (e-mail: Uros.Jokic@rt-tk.com.

 ISBN 978-86-7466-930-3

## II. PROBLEM STATEMENT

The CA vendor dictates two primary CA integration approaches depending on the target platform and selected operating system. If the target platform runs an operating system (OS) that does not support processes, only threads (tasks), the architecture looks as in Fig. 1. Here DTV software consists of OS, software development kit (SDK, drivers), hardware abstraction layer (HAL), middleware, and application layer. The application depends on middleware, and middleware depends on the abstraction layer (HAL) API that abstracts OS and SDK APIs [8].

The middleware and application layers contain all the business logic, whereas the remaining layers, like HAL, are porting layers designed to be very thin. Application is oriented toward user interface and feature logic, whereas middleware is oriented toward controlling hardware, supporting DTV standards, and interacting with CA subsystems.

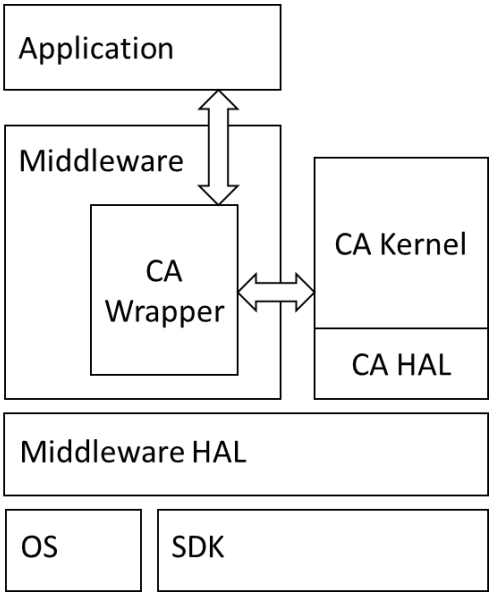


Fig. 1. Typical architecture of DTV software in case of OS where processes are not supported.

The module depicted as CA Wrapper is the actual module seen by the DTV middleware. It interacts with the middleware and application-level modules. It behaves like a proxy between the DTV stack and the existing vendor-specific CA subsystem. The conditional access subsystem consists of the kernel part where the logic is implemented and the hardware abstraction part (CA HAL) used as a glue layer between the CA kernel and underlying OS and SDK APIs. In this architecture, middleware HAL acts like a resource manager and has the information about allocated resources and tasks running in the system. This allows better resource management compared to the second approach.

The second approach is required with the OS supporting processes, like Linux and Android. As depicted in Fig. 2, the CA kernel and CA HAL depend directly on the underlying OS and SDK. They are running in a separate process. If the DTV stack is unstable or crashes, it does not affect the CA kernel. This approach ensures that the rest of the system never compromises CA. Still, the CA wrapper serves as a proxy between the CA kernel and DTV stack. It is up to the SDK vendor to ensure that multiple clients can access the same hardware peripherals. If not provided, some features like PVR may need to be carefully designed to ensure that components do not overlap in responsibilities.

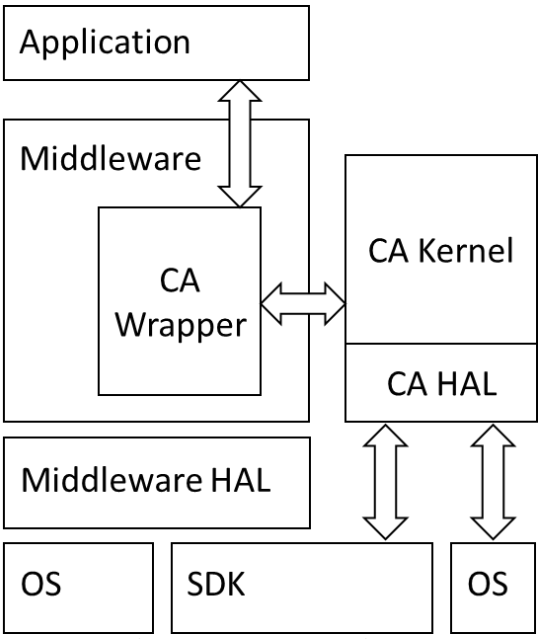


Fig. 2. Typical DTV software architecture in platforms with OS supporting processes.

We need to add CA subsystem support on a PC platform to test CA-related features. There are two possible paths:

1. Implement CA wrapper replacement module
2. Implement CA kernel replacement module (supporting CAS API)

The first solution gives us the ability to have a general CAS subsystem, irrespective of the actual CAS vendor. However, it puts aside CA wrapper code that interacts with the existing CA subsystem. Changes in the requirements of the CAS do not directly affect this solution.

The second approach is to develop the CA kernel module and the CA HAL module. It will preserve the CA wrapper module and allow it to be appropriately tested. However, this approach is considerably more time-consuming and has open questions related to all behaviors implemented in CA kernel API.

Our aim is not to implement content protection as software or hardware encryption. That is transparent to the middleware. Middleware only knows that content is protected and that the CA subsystem must start. CA subsystem is entirely responsible for the content decryption.

Encrypted content is never used in testing on PC because it has a complicated decryption procedure requiring specialized hardware protected by patents and legal documents. Only unencrypted content is used. This type of content can be generated using open-source tools like TS-duck [11] and video content available.

 ISBN 978-86-7466-930-3

## III. IMPLEMENTATION

We have decided to take a hybrid approach given the above pros and cons. We implemented CA wrapper API on the DTV stack side as it already exists, allowing the remaining parts of the system to be unaware of the difference. CA kernel is partially shifted to the Middleware Test Environment (MTE). It is a framework for testing the DTV stack on PC.

The DTV software is running as a standalone executable. It has a middleware hardware abstraction layer (HAL) adjusted for the PC platform. Hardware devices are simulated in HAL using SDL [9] and FFmpeg [10] open-source libraries. The test environment is written in Python and communicates with the PC simulator using interprocess communication, particularly sockets. The test environment supported remote control, logging, and execution of automated tests. It can fully control the PC simulator, user input, and DTV stream input. Automated tests are supported by different APIs that are implemented in MTE. More about it can be found in [1] and [2] papers.

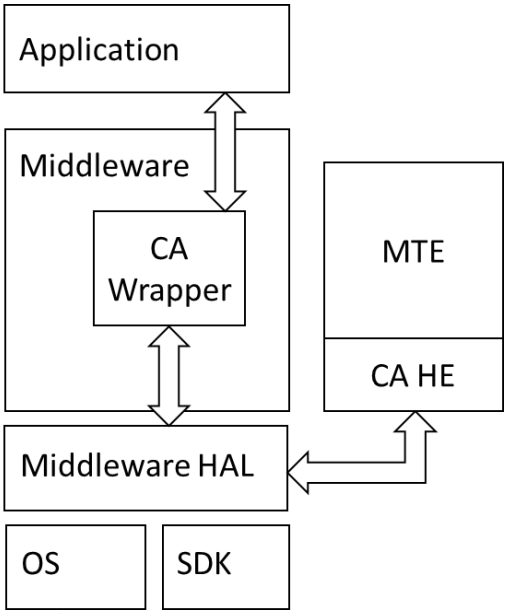


Fig. 3. DTV software architecture with middleware test environment (MTE) supporting conditional access head-end (CA HE)

As given in Fig. 3. the middleware test environment communicates with the PC simulator through the HAL layer that implements interprocess communication. A module CA wrapper uses send/receive routines from HAL. This is to mimic actual data flow, where CA information comes from a demultiplexer connected to the data stream. It will parse received commands and act accordingly. One typical example is the zapping procedure, where service is changed from one to another. In that case, middleware notifies the CA wrapper who needs to check access rights for that service in the database, sharing the data about the service being connected to and additional information about tracks to be descrambled. The module checks access rights in the database and responds to middleware. In our work, descrambling is not implemented, as it does not add any test value since all the descrambling is done in hardware, and none of that logic is done in the DTV stack.

Module CA wrapper is responsible for maintaining the CA kernel database. It exchanges data with the remaining parts of the DTV system. The middleware test environment can get the CA kernel database and modify it by sending appropriate commands. It communicates with a PC simulator using conditional access head-end (CA HE).

Following features (commands) we implemented in the CA HE subsystem and CA wrapper:

1. Device activation in a network
    a. Smart card
    b. Virtual smart card
2. Product access rights
    a. Checking rights
    b. Adding rights
    c. Removing rights
3. Service access rights
    a. Checking rights
    b. Adding rights
    c. Removing rights
4. Content protection
    a. Covered fingerprint
    b. Periodic fingerprint
    c. Permanent fingerprint
5. Mails
6. Changing service bouquet
7. Forced software update
8. CA notification messages
    a. Periodic messages
    b. Permanent messages
    c. User acknowledges messages

In Fig. 4, a window containing the setup for generating CA messages is presented. This CA HE submodule of MTE supports creating test cases. The test case is a message with all the parameters for that particular command. This way, the QA tester or developer does not have to enter test commands each time manually. Instead, he can select test cases saved as an XML file.

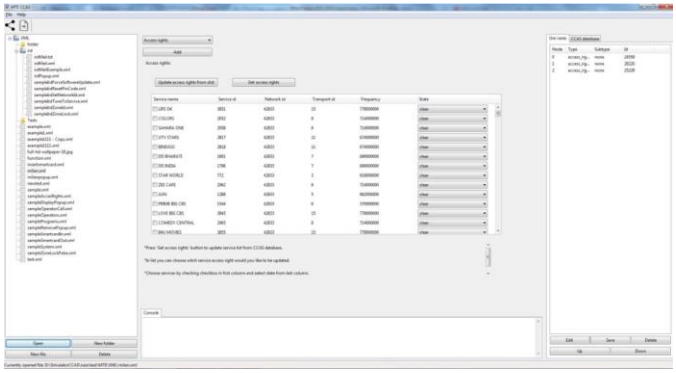

Fig. 4. CA HE main window consists of three parts, the user can re-use existing test cases or make new CA commands and send them in bulk.

CA HE main window consists of three parts, the left part reserved for displaying a tree of saved test cases, the middle

 ISBN 978-86-7466-930-3

part consists of a panel for generating CA commands, and the right part for listing generated commands ready for sending.

The middle panel for adjusting access rights for particular services is depicted in Fig. 5. There can be a list of services available on the box and the access right for that service.

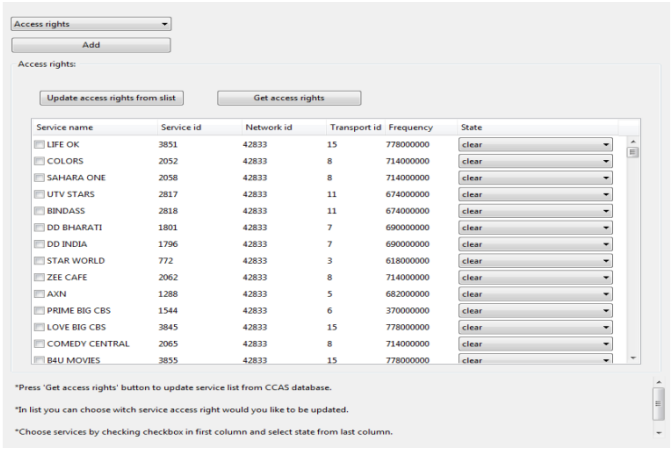


Fig. 5. The middle panel of the CA HE main window, where users select options to modify the service database's access rights.

The service access rights database is saved on the simulator side at runtime. The database can be exchanged between the simulator and MTE upon request sent from MTE. Once they are synced, MTE can send commands related to services access rights to the simulator. When the CA wrapper module receives a command, it processes the message, updates the database and saves it in an XML document. The CA state simulated in the CA wrapper can be restored from the XML file upon simulator restart. With this approach, the simulator is a standalone application, and MTE can communicate with it, but there is no dependency on MTE.

## IV. Verification and Results

To test prepared CA subsystems, we have created a set suite that covers all supported types of messages that could be sent to the CA or received from the CA module by the DTV middleware [4]. We have observed that the code is executing correctly and that middleware behaves in the same manner as it is expected in the production environment.

In the case of sending chains of commands, we have observed new failure cases that were not covered by the DTV middleware and application. Those cases involve low probability cases like at the same time receiving a fingerprint message and a CA message. Those cases uncovered several combinations that could not be adequately tested on the development side, the operator's production live network or the lab network. They are not simple to prepare as a test case in those environments.

Scenarios that combine user interaction, CA signaling, and DTV signaling can reveal hidden bugs. Those bugs could be reported as software malfunction in a production. Yet those issues are impossible to reproduce manually unless the exact preconditions are known, which is rarely the case. Troubled combinations may be of low probability, but in networks with many end users, the chances that the failure will be seen and reported are very high. Still, the ability to troubleshoot it efficiently is very poor.

## V. Conclusion

This paper focused on expanding capabilities for testing DTV software on a PC platform. It allowed more complex test cases to be executed that would be very hard or impossible to replicate in a network with real hardware. A further way of improving the solution is making a CA API on the MTE side. That could allow the creation of automated tests for testing application behavior as a response to CA events and user interaction.

Work could be extended toward implementing specific CA vendors' API allowing the whole DTV stack to be tested for required functionalities. It will increase the coverage of testable code to almost 100%. But gains versus cost ratio for doing this may not prove as an appropriate step. Another improvement can be made towards implementing some descrambling capabilities.

## References

[1] A. Šuka, Đ. Glišić, M. Jovanović, "One solution of DTV simulator for PC platform", TELFOR, 2019
[2] M. Petrović, Đ. Glišić, M. Jovanović, "One solution for testing embedded DTV software on the PC platform", ETRAN 2022,
[3] S. Nidhra1, J. Dondeti, "BLACK BOX AND WHITE BOX TESTING TECHNIQUES – A LITERATURE REVIEW", IJESA, Vol.2, No.2, June 2012
[4] I. Jovanovic, "Software Testing Methods and Techniques", IPSI TIR, 2009
[5] T. Tarkan, "User-driven Automatic Test-case Generation for DTV/STB Reliable Functional Verification"; IEEE Transaction on Consumer Electronics, vol.58, no.2, pp. 587-595, ISBN: ISSN:0098-3063, 2012
[6] Cabot Communications, "Automated testing of digital television devices", accessed 2022, http://www.cabot.co.uk/solutions/robotester-white-paper/at_download/CB.pdf
[7] M. Kovacevic, B. Kovacevic, D. Stefanovic, V. Pekovic "System for automatic testing of Android based digital TV receivers ", INDEL 2014, Banja Luka
[8] G. Miljkovic, "DTV Linux Device Abstraction for Embedded Systems", ISCE, ISBN:978-1-4244-6673-3, 2010
[9] Simple DirectMedia Layer, https://www.libsdl.org/, accessed May 2022
[10] FFMPEG library, https://ffmpeg.org/, accessed May 2022
[11] TSduck, https://tsduck.io/, accessed May 2022

 ISBN 978-86-7466-930-3

# One solution for testing embedded DTV software on the PC platform

Branka Ševa, Đorđe Glišić, Uroš Jokić and Marija Jovanović

***Abstract*—In an embedded device industry, applicable software is developed for a particular platform and device. Reusability, functional correctness, and quality control of the software are of great importance. The digital television industry is no different. Moreover, it requires compliance with device safety, security, and functionality standards. Compliance testing is often done with near-end products, as most functionalities require that all components be put together. Secondly, most development is done using target platforms that often lack tools and add significant delays in development. This paper gives one solution for testing the embedded DTV software on PC. The authors give a road map for developing testing environment to safeguard the product's quality. It allows early-stage testing by the development team and helping the QA team test the end product.**

***Index Terms*— automated testing, DTV, middleware test environment, python, OpenCV, tesseract.**

## I. Introduction

In embedded devices, hardware capabilities vary in many areas. Available RAM, platform instruction set, supported peripherals, hardware accelerators, and dedicated specialized hardware blocks. On the other side, depending on the product or manufacturer, there are support variations, incomplete documentation, and very little support for the supporting development software packages.

On the other side, there is a problem with integrating third-party components. They may or may not come with the test suite or test application. In the case of open-source software, source code is available, but it was written for specific operating systems (OS), sometimes depending on unique OS features.

A common component for all devices is DTV middleware software. It grows with new requirements, new standards, etc. Testing is always pushed to the end product, verified against predefined sets of tests. The reason behind it is that many features depend on all components being put together, and it is tough to test partially completed software [1].

Additionally, suppose such a DTV stack is inherited from another source without a test suite. In that case, it is always commercially unjustifiable to spend engineering time preparing a test suite that will verify the DTV stack. Instead, it is pushed to develop the end product and confirm its functional compliance [2].

Commercially available solutions are focused on testing the end product. Depending on the solution, it may offer hardware compliance testing or functional testing. Some tools like Intent+ [3][4] offer automated and manual testing. Automated testing is accomplished using dedicated test suite applications. Suitest [5] offers visual preparation of tests. Other solutions provide general-purpose languages like Stb-tester [6]. Others provide APIs like black-box-testing (BBT) API from Intent+. They mainly focus on automating the remote controller, capturing the screen, recording audio, and processing it using a test suite.

As a result of described practices, software products' quality may be at a reasonable level, but the quality of the code may be poor. Reuse of already developed code is very inconvenient across projects. Feature development may slow down as maintaining code becomes more and more expensive. Products may suffer from bugs that have low repeatability rates and high severity. In such cases, black-box testing [7] is not suitable. It is necessary to implement white box testing [8] procedures.

Section two details a problem and describes the system's architecture. Section three explains the proposed solution and provides implementation details. Section four discusses the results. In section five, we conclude our work.

## II. Problem statement

In the development stage, verifying a new feature is time-consuming. Platforms with limited hardware capabilities offer unique tools to write software to devices. It may need from 30 seconds up to 5 minutes to run the software. Often those platforms do not support hardware debuggers.

A typical application in DTV consists of the following components:

1. Application layer (APP)
2. Middleware layer (MW)
3. Hardware abstraction layer (HAL)
4. Platform-specific SDK (SDK)
5. Operating system (OS)

Platform-specific SDK is a set of libraries and APIs that provide access to platform hardware components and allows control over them. This layer and the OS layer are closed for the development team. Also, those layers are highly platform-specific, so they cannot be ported to other platforms without

Branka Ševa – RT-RK Institute for Computer Based Systems, Novi Sad, Srbija, (e-mail: Branka.Seva@rt-tk.com)
Đorđe Glišić – RT-RK Institute for Computer Based Systems, Novi Sad, Srbija, (e-mail: Djordje.Glisic@rt-tk.com)
Marija Jovanović – RT-RK Institute for Computer Based Systems, Novi Sad, Srbija, (e-mail: Marija Jovanovic@rt-tk.com
Uroš Jokić – RT-RK Institute for Computer Based Systems, Novi Sad, Srbija, (e-mail: Uros.Jokic@rt-tk.com.

 ISBN 978-86-7466-930-3

considerable effort.

The hardware abstraction layer (HAL) provides a defined API [9] that exposes all necessary functions for upper layers (middleware and application) and abstracts platform devices and operating systems. It is implemented again with every new platform. It is common to have abstraction layers for every portable software and a test suite that verifies that the layer is ported correctly.

The middleware layer provides support for the DTV standard and is responsible for all functionalities in the DTV application. It consists of modules controlling hardware service change, acquiring information from DTV signal tables, maintaining program database, service lists, event information database, user interface engine, etc. Those modules are often interdependent. It is not simple to decouple one from the rest of the system and check their correctness using white box testing (e.g., unitary testing).

An essential component of the middleware layer is the conditional access system (CAS) or digital right management (DRM) system. It provides access to protected content. It is also a closed component that comes with the pre-defined test suite.

The application layer covers the graphical user interface and specific logic for the user interface. It is connected to the middleware layer and highly depends on it. Black-box testing mainly verifies this layer.

Architecturally higher-level components depend only on lower layer components. Key components that are developed are the application layer and middleware layer. Hardware abstraction layer API stays the same across different target platforms. We want to create a system that will test those two main components.

The goal is to prepare a software test environment that can support:

1. Functional tests as end-user
2. Scenario tests as end-user and operator
3. Monitoring and testing internal state
4. Code coverage

Functional tests cover black-box testing, where implemented features are verified [1]. Examples are video presence, audio presence, switching service, changing volume, displaying graphics, and event information presented. Besides core DTV tests, additional tests unique to the application have to be supported, like the position of some element on the screen, at the right time, for the correct period, etc.

Scenario tests verify DTV software in more complex cases. Those use-cases involve changing information in DTV tables signaling, new commands from the CAS/DRM system, or new data from other custom protocols that affect the device's state. Tests shell cover application responsiveness to the user interaction and user interface changes based on the system's internal state.

The monitoring system needs to monitor the execution and report critical situations. It should consist of a logging mechanism and software/hardware debuggers to automate the testing of internal states by inspecting calls to specific modules, APIs, and execution paths.

Code coverage gives insight into the test suite coverage of the existing code. If test coverage is low, it may mean that the test suite has to be expanded to cover some exceptional cases or that some source code is unnecessary occupying space (dead code). This work did not cover code coverage testing. Due to the complexity of this feature, implementation details are not covered in this paper.

The test environment defined would be capable of inspecting every module for its dependencies and behavior. Afterward, proper refactoring will allow white box testing (unitary testing, scenario testing).

## III. Implementation

We decided to create a test environment to run and test DTV software on a PC. The reason behind it is to use current and future state-of-the-art tools. The first step was to port DTV software to the PC platform. It was done by porting the HAL layer. More details about it can be found in [10]. It supports working with actual transport stream data and makes DTV middleware fully operational. Compared to the commercial product, the only difference is that it does not support targeted CAS, as it is proprietary, and its libraries are only delivered for specific target platforms. Work is done to overcome this, using simulated CAS. Due to the complexity of this feature, implementation details are the subject of another paper and are not given here.

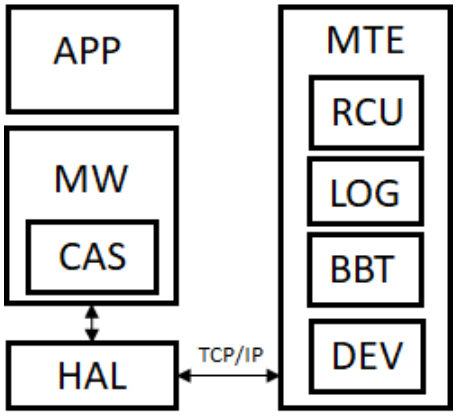


Fig. 1. Key components of DTV software running as part of the PC simulator are on the left side. On the right side are components of the MTE.

We decided to run separate processes for the test environment and DTV simulator. The DTV application runs stand-alone as it would be on the actual device. It allows us to have more options for the middleware test environment (MTE).

Communication with the PC simulator is done using TCP/IP. The communication protocol is designed to be minimalistic. The aim was not to disrupt the dynamics of the DTV middleware execution compared to its expected dynamics on the device. The protocol covers commands from MTE to PC simulator and data from PC simulator to MTE. Commands consisted of remote controller (RCU) events and requests for device state (screen capture, audio status, and

 ISBN 978-86-7466-930-3

similar).

We have decided to implement a test environment in Python language. We saw that this language is widely used in automation testing. Two STB automation test suites [4][5] already support Python scripting. It has extensive library support for user interface, computer vision, text recognition, communication protocols, etc. It is cross-platform, so we could design a tool to run on different platforms. It supports documenting code and a capable development environment (IDE).

We have selected the following frameworks to implement MTE:

1. wxWidgets - UI library (platform-independent, supports all major operating systems)
2. openCV - cross-platform library for computer vision, used for image manipulation and comparison
3. Tesseract - OCR engine for text recognition and extraction

The application was developed to support four different APIs:

1. Remote control API
2. Logger API
3. Black-box testing API
4. Development API

Remote control API covers control over RCU and sends commands to the PC simulator the same way a user would do using a remote control unit (RCU). To send commands, a TCP/IP protocol is used. On the side of the simulator, an existing module for receiving RCU input is adapted to receive TCP/IP commands from MTE.

Logger API is responsible for collecting log information from remote PC simulators using TCP/IP protocol. The existing logging module was improved to send log information over TCP/IP and the serial console on the simulator side. It supports filtering and searching for logging information.

Black-box testing API is a set of predefined APIs implemented on top of RCU API and an additional acquiring protocol for collecting screen output. It is aimed to be used for writing test cases. We selected to support the commercial black-box testing (BBT) API as part of Intent+. It was available to compare with the framework against an existing set of automated tests. Other solutions like Stb-tester API [5] are similar in API and exposed functionality.

Development API is created to support debugger integration in the MTE framework. It is implemented to support GNU GDB compatible debuggers. The framework can run the debugger and start the application or run the debugger and connect to the remote debugger server running the application (Fig. 2). This API makes it possible to start debugging software and send commands like setting breakpoints and watchpoints, printing values, etc. In this scenario, MTE spawns two processes, one for the GDB server that starts the PC Simulator and the second one for GDB used to control the remote PC simulator.

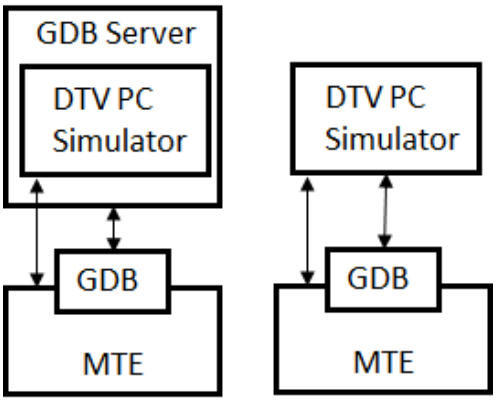


Fig. 2. Possible setups for running PC simulator using GDB debugging software with MTE.

Application consists of four parts similar to the APIs given above:

1. RCU controller
2. Stream controller
3. Logger
4. Test suite controller

Using an RCU controller, the user or developer can control the PC simulator using commands in the window that resemble the real RCU, as shown in Fig. 3.

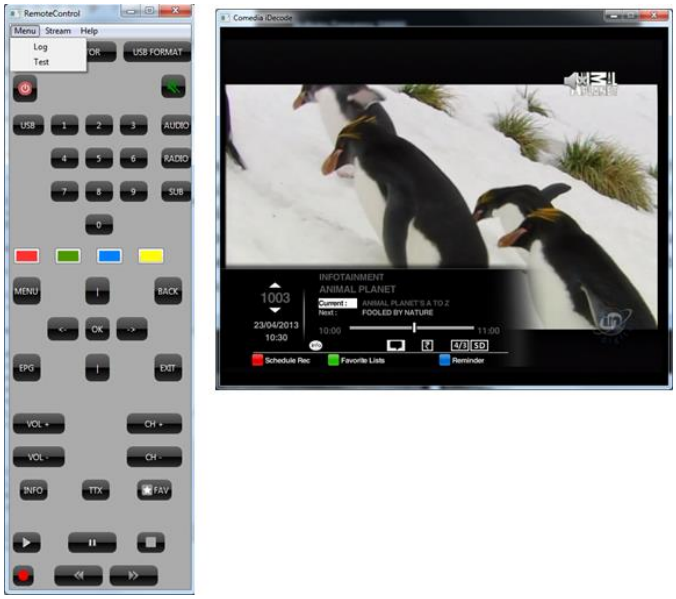

Fig. 3. Key components of DTV software running as part of the PC simulator are on the right side. On the left side are elements of the MTE.

The stream controller window is responsible for adjusting input DTV streams for the PC simulator. It allows setting stream files and broadcasting parameters.

Logger windows give information about logging data and allow users to filter and search for specific data in the log. The search pattern is highlighted in the log. In the filter window, only lines matching patterns are presented (Fig. 4).

 ISBN 978-86-7466-930-3

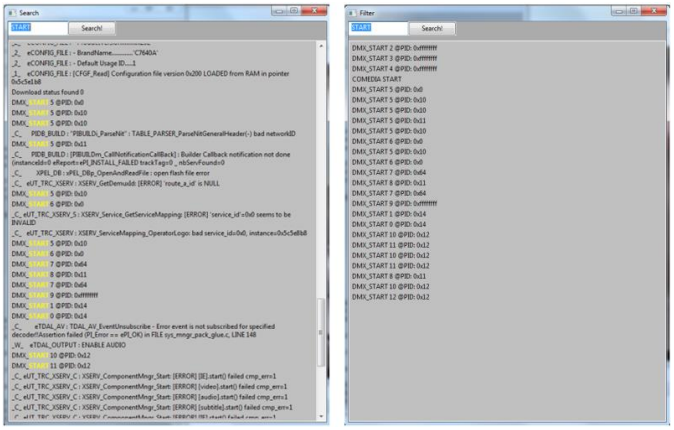

Fig. 4. Search and filter windows for logged information.

## IV. Verification and Results

As a result of the following implementation, a test suite was created for commercial products using only BBT API (black-box testing). Test suites are grouped by the features they are testing. A list of all test groups and the number of tests are given in Table 1.

TABLE I
List of test suites prepared and results

| | | |
|---|---|---|
| Info channel | 5 test cases | PASSED |
| EPG | 6 test cases | PASSED |
| Genres | 2 test cases | PASSED |
| Menus | 10 test cases | PASSED |
| PVR | 8 test cases | PASSED |
| Reminders | 3 test cases | PASSED |
| Favorite lists | 6 test cases | PASSED |
| Service lists | 5 test cases | PASSED |
| Volume | 6 test cases | PASSED |
| Service lists | 5 test cases | PASSED |
| Zapping | 5 test cases | PASSED |

In the case of automated black-box testing, some graphical test cases may be challenging to create and prove reliable. User interface graphics blended with background video make it more difficult for AI-based engines to recognize certain visual elements' fonts, text, and shapes. Also, the comparison rate with expected images (shapes) may drop due to the background video. Our solution can compare video and graphical layers separately, resulting in higher recognition rates than blended image recognition using tools like OpenCV and tesseract. As a result, our MTE showed fewer errors than hardware running as part of the Intent+ solution.

Verification time was about 15 minutes, compared to manual testing, which will take 1-2h depending on tester skills. This allows developers to save considerable time when developing new features. Compared to automated hardware testing, execution time is around the same. It will enable continuous integration (CI) systems like Jenkins to repeat testing on selected changes.

## V. Conclusion

With the proposed solution DTV application could be tested in the development phase by research and development teams or by dedicated QA teams. Automated tests written for MTE are usable for BBT devices in hardware testing, as they are written using the same API.

The essential contribution of this work is automated testing using software debuggers, where developers can inspect certain parts of the system multiple times and summarize information in reports. This type of testing can mimic unitary testing and complex scenario testing having internal systems state exposed for examination and reporting. It allows tightly coupled modules to be slowly refactored and isolated to introduce unitary testing and low-level verification.

Additionally, any other DTV software capable of porting to the PC platform could be tested using this MTE framework. It has to implement necessary features for that middleware and additional requirements to support communication protocol with MTE.

Further work could be done toward implementing support for CAS/DRM simulator or emulation. Also, it would be of great benefit to change DTV signaling from within the MTE application, as now it relies on signaling transported in DTV streams captured from live DTV networks. Another path for improvements is to add systems for code coverage and memory leak checks like Valgrind that could check applications in specific test scenarios as part of the automatic test.

## References

[1] T. Tarkan, “User-driven Automatic Test-case Generation for DTV/STB Reliable Functional Verification”; IEEE Transaction on Consumer Electronics, vol.58, no.2, pp. 587-595, ISBN: ISSN:0098-3063, 2012
[2] Cabot Communications, “Automated testing of digital television devices“, accessed 2022, http://www.cabot.co.uk/solutions/robotester-white-paper/at_download/CB.pdf
[3] M. Kovacevic, B. Kovacevic, D. Stefanovic, V. Pekovic “System for automatic testing of Android based digital TV receivers “, INDEL 2014, Banja Luka
[4] Intent+, https://www.rt-rk.com/services/testing-centre, accessed May 2022
[5] STB Tester, https://stb-tester.com/, accessed May 2022
[6] Test suite, https://suite.st/, accessed May 2022
[7] S. Nidhra1, J. Dondeti, “BLACK BOX AND WHITE BOX TESTING TECHNIQUES – A LITERATURE REVIEW”, IJESA, Vol.2, No.2, June 2012
[8] I. Jovanovic, “Software Testing Methods and Techniques”, IPSI TIR, 2009
[9] G. Miljkovic, “DTV Linux Device Abstraction for Embedded Systems”, ISCE, ISBN:978-1-4244-6673-3, 2010
[10] A. Šuka, Đ. Glišić, M. Jovanović, “One solution of DTV simulator for PC platform“, TELFOR, 2019

 ISBN 978-86-7466-930-3

# Comparison of type-2 hypervisor performance on the example of VirtualBox, VMware Workstation player and MS Hyper-V

Borislav Đorđević, *Member IEEE*, Iva Jovičić, Nenad Kraljević and Valentina Timčenko, *Member IEEE*

***Abstract* – This paper presents a comparison of the performances of type-2 hypervisors, on the example of desktop virtualization applications, which include VirtualBox, VMware Workstation Player, and MS Hyper-V. The qualities of all three tested hypervisors, from many aspects of performance, were tested through the performance of the files system. Tests were performed under the same conditions and the same testing methods, using the Filebench program. CentOS 7 was used as the guest operating system. The hypervisor's performances were compared taking into consideration the tests performed for the system with one, two, and three virtual machines in operation. Hypotheses about expected behavior were set, and then they were validated through the obtained results using the Filebench program.**

***Index Terms* – VirtualBox; VMware Workstation; MS Hyper-V; CentOS; hypervisor; virtual machines.**

## I. Introduction

Virtualization as a concept is increasingly used and conquers new spaces. It has become a part of everyday life for the simple reason that information technology are all around us. As these technologies are increasingly present in modern life and are constantly advancing, virtualization has taken its place in this development. The main advantages obtained by applying virtualization can be seen in the reduction of costs of IT equipment, electricity and storage space for this equipment. The concept itself provides high security and resistance to failures, and makes administration easier. The choice of virtualization methods and techniques depends on the specific situation and the needs of the end user. This is due to the fact that some virtualization techniques achieve greater flexibility in operation, while others achieve better performance or security. The most commonly used virtualization techniques are: virtualization of hardware, software, data, memory, storage space, virtualization of network infrastructure and virtualization of desktop computers. [1]

Borislav Đorđević – Institute Mihailo Pupin, Volgina 15 Belgrade, Serbia, (borislav.djordjevic@pupin.rs)
Iva Jovičić – VISER, School of Electrical and Computer Engineering of Applied Studies, Belgrade, Serbia, (iva.jovicic@yahoo.com)
Nenad Kraljević – VISER, School of Electrical and Computer Engineering of Applied Studies, Belgrade, Serbia, (nenadk@gs.viser.edu.rs)
Valentina Timčenko - Institute Mihailo Pupin, Volgina 15 Belgrade, Serbia, (valentina.timcenko@pupin.rs)

Virtualization involves the encapsulation and abstraction of computer components, so these components can be used in a way that suits a particular application. Hardware virtualization involves usage of hypervisor, a software layer, which is an intermediary between the hardware and the guest operating system in a virtual machine. This is a simulated environment that could have characteristics equal to the physical environment. The hypervisor can be native, or type-1, which runs directly on the hardware, or hosted, type-2, which runs on the operating system. Examples of this type of hypervisor are VirtualBox 6.1 and VMware Workstation 16 player which have been tested for the purpose of this paper. MS Hyper-V is a bare metal, type-1 hypervisor. However, when activated as a roll, in this case in Windows 10 Pro, it behaves as a type-2 hypervisor. This version of MS Hyper-V was used in the testing process for this paper. [2]

Other than above described classification, hardware virtualization also depends on whether full, partial, or paravirtualization is selected. Full virtualization (Figure 1), topic of this research, represents a simulation of complete hardware, so guest operating systems can be installed and ran without problems. The guest operating system is separated from the physical layer of the host, the hypervisor layer. The advantage of this method of virtualization is increased security and scalability, as well as system flexibility. This solution is the easiest to use, but the performance is slightly lower. [3,4]

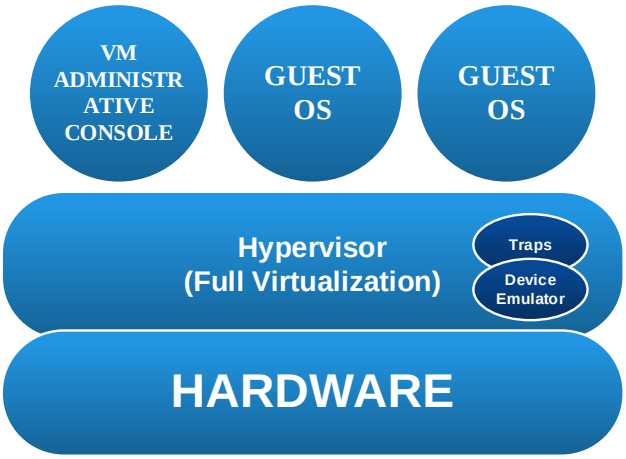


Figure 1. Full virtualization

 ISBN 978-86-7466-930-3

## II. Related work, objective and motivation

The focus of this research are the performance characteristics of hypervisors as one of the basic factors in achieving service quality. The problem itself, which can be found in the literature as well as by using these systems in practice, can be viewed from several angles. There are many papers and discussions that use different methodology and approach to evaluating the performance of virtual platforms. The most common is a comparative performance analysis of VMware, Xen, MS Hyper-V and other hypervisors by using various benchmark tools such as HD Tune Pro, ATTO, Filebench, Bonnie ++, etc. Virtualization is a great solution in both desktop and server versions. The needs for virtual platforms for personal use are growing. The main contribution is the mathematical modeling of the file system performance in hypervisor-based virtualization. The modeling of complex virtual environment includes many factors, and modeling expects there is no single winner hypervisor. Similar mathematical model, we used in this paper and most our references [3], [5], [10], [11]. Our model is open for enhancing. We think we are different from related work by our methodology. Its essence is a mathematical model, apply it on a particular case study, and then provide the interpretation of practical results as a validation of model. Using by large number of case studies, we recommend the creation of Knowledge Data Base (KDB) related to the file system performance in virtual environment. Case study in this paper include the performance comparison of three hypervisors in the desktop version, namely VirtualBox, Vmware Workstation player and Hyper-V, in fair-play conditions. This implies identical hardware, the same virtual machines, and an identical version of the guest operating system, which in this case was CentOS 7, an operating system from the Linux distribution family. As VirtualBox and Vmware Workstation player use full virtualization, and MS Hyper-V and paravirtualization as well, the effects of full virtualization for three different hypervisors were examined, using the Filebench benchmark program with four different workloads. Hypotheses about expected behavior are set, followed by a mathematical model for workloads and a hypervisor environment. Performance was measured and the obtained results were interpreted on the basis of models and hypotheses. This paper has some similarities with reference at the serial number five in our literature. The results have the similarities and differences, because the hardware and many other factors are quite different, but we think that both papers are interesting and useful cases of study.

## III. VirtualBox, VMware Workstation player and MS Hyper-V

Oracle's VirtualBox is a very powerful program for virtualizing 32-bit and 64-bit operating systems, on computers with Intel or AMD processors. VirtualBox is the only professional solution that is available for free as open source software under the terms of *"GNU"* version 2. This software runs on Windows, Linux, Mac and Solaris operating systems. The technical requirements for running this software are:

- 32-bit or 64-bit operating system with AMD or Intel processor,
- 512MB or more RAM (depending on the number and type of operating systems being virtualized. The RAM memory space allocated to the virtual machine environment can go up to half capacity, as the software itself will not allow more than half of the base system's RAM.
- available hard disk space for the virtual machine environment (recommended size is a minimum of 8GB).

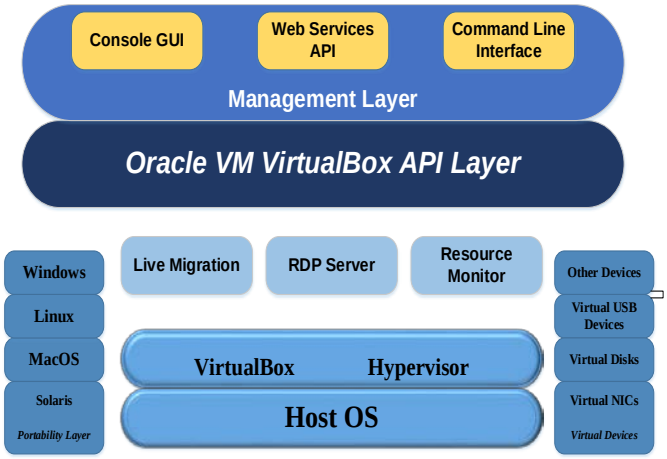


Figure 2. VirtualBox architecture

VirtualBox allows quick and easy data sharing between virtual machines (Figure 2). As VirtualBox is open source, or rather it's software, it tends to solve problems quickly and can be upgraded with new features. Since version 6.1, which is used in this paper, the ability to export and import virtual machines to Oracle Cloud has been added. Software virtualization has been deprecated since this version, and VirtualBox 6.1 uses only hardware-assisted virtualization. [5,6]

VMware® is considered one of the largest manufacturers of software virtualization. The solutions of this company occupy over 70% of the market share in this area, primarily due to the quality of products and the availability of technical support. VMware® has been acquired since 2004 and became part of the EMC Corporation. VMware Workstation 16 player is a software package that runs on standard x86-based hardware with 64-bit Intel and AMD processors and on 64-bit Linux and Windows operating systems. [7,8]

VMware Workstation 16 player (Figure 3) can run existing virtual machines and create their own virtual machines. It uses the same virtualization core as VMware Workstation Pro, a similar multi-featured, non-free program.

 ISBN 978-86-7466-930-3

VMware Workstation 16 player is available for personal non-commercial use (free), for distribution or other use by written agreement. The technical requirements for running this software are:

- 64-bit operating system from the Windows or Linux family with AMD or Intel processor,
- 2GB or more RAM (recommended 4GB or more),
- 1.3GHz or higher core speed,
- available hard disk space.


Figure 3. VMware Workstation player architecture

Microsoft is one of the leading companies in information technology. At the server level, virtualization has become the standard, but interest in virtualization has also emerged among users for personal use. Microsoft occupies about 15% of the market with MS Hyper-V virtual platform. With the release of Windows 8 in 2012, MS Hyper-V became an integral part of its Enterprise, Education and Pro editions. MS Hyper-V is a type-1 hypervisor-based system for x86-64 operating system architectures. It is activated in the Windows operating system as a roll, just like any other service in the Microsoft family. There are some MS Hyper-V features that work differently in Windows OS and Windows server. The memory management model is different for MS Hyper-V, where MS Hyper-V manages memory on the server assuming only virtual machines run on the server, and in the Windows operating system, it is managed with the expectation that most client machines run software on the host in addition to virtual machines. [9-11]

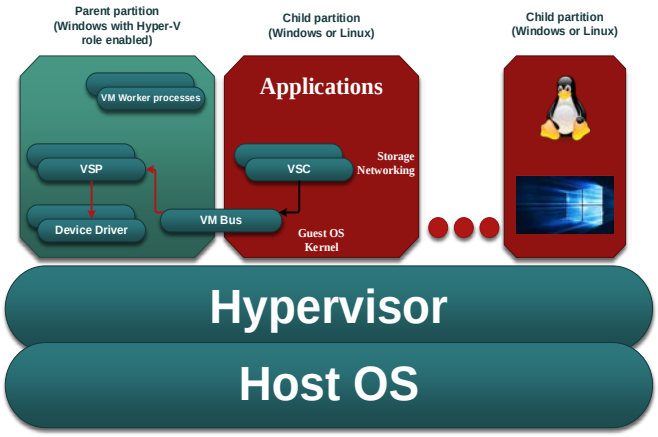


Figure 4. MS Hyper-V architecture

MS Hyper-V (Figure 4) supports virtual machine isolation and uses partitions in which guest operating systems will run.

## IV. HYPOTHESES ABOUT EXPECTED BEHAVIOR

As the Type-2 hypervisor running under the guest operating system was used, we can point out that each workload generates typical random and sequential data read times, as well as random and sequential data write times. Each workload is defined by the access time for file systems. Workload represents the total time to complete all operations, the time required to complete all operations related to directories, metadata, file blocks, free lists, house-keeping and journaling operations in the file system. There are five components in a virtual environment that have an impact on workload time (Tw – Time Workload):

$$Tw = f\,(Bn, gFS, VHw\text{-}pr, Hp\text{-}pr, hFS) \qquad (1)$$

The first and second components, Bn (Benchmark) and gFS (guest OS file system) are exactly the same for VMware Workstation player, Oracle VirtualBox and MS Hyper-V. The analysis focuses on the interaction between the reference values and the guest operating system. Because the test environment relies on the use of an identical benchmark, identical virtual machines, and ext4 as the guest file system, these components are expected to have an identical effect on Tw. Processing time for full hardware virtualization is the third component of VHw-pr (virtual hardware processing). Each hypervisor uses its own solution for full hardware virtualization, so the performance will be different too. The fourth component, Hp-pr (hypervisor processing), represents the time it takes for the hypervisor to receive requests from the virtual hardware and forward them to the host drivers. In particular, guest FS requests (guestOS-FS) are forwarded to host FS (hostOS-FS). All of these hypervisors, VMware Workstation player, Oracle VirtualBox and MS Hyper-V, generate different hypervisor processing times. The fifth component, hFS (host OS file system), represents the

 ISBN 978-86-7466-930-3

processing time of the host OS file system. All hypervisors have MS NTFS as hostOS-FS, so this component is expected to have similar processing times for all hypervisors. The dominant influence of the third and fourth components of formula (1) is expected as the tests are focused on the performance of natively virtualized guests (complete hardware virtualization). [12]

## V. TEST CONFIGURATION AND BENCHMARK APPLICATION

The prerequisite for quality and adequate testing is the application of one hardware configuration, the same operating system, then the selection of a quality benchmark program and the same measurement methodology for all testing procedures. Testing was done on a personal computer whose characteristics can be seen in Table I, while the characteristics of the disk are given in Table II. CentOS 7 from the Linux distribution family is installed as a guest operating system.

TABLE I - TEST ENVIRONMENT/PC

| Components | Characteristics |
|---|---|
| Processor | Intel Core i5-4590S 3GHz |
| Memory | 8GB DDR3 |
| Cache | 6MB L3 |
| Hard drive | Seagate Barracuda 7200.12 |
| Operating system | Windows 10 Pro, 64-bitni |

VirtualBox 6.1 virtualization platforms, VMware Workstation 16 and MS Hyper-V, a version for Windows 10 Pro, are installed or activated on the hard drive, where the tests were done. The hard drive was also used to install virtual machines.

TABLE II - TEST ENVIRONMENT/HARD DISK

| | Seagate Barracuda 7200.12 |
|---|---|
| Model Number | Seagate ST3500418AS |
| Capacity | 500GB |
| Interface | Serial-ATA/300 |
| External Transfer Rate | 3.0Gb/s |
| Max Sustained | 300MB/s |
| Cash | 16MB |
| Average Latency | 4.17ms |
| Spindle Speed | 7200rpm |
| Average Seek Time Read | 8.5ms |
| Average Seek Time Write | 8.5ms |

All tests were performed using the benchmark program Filebench 1.4.9.-1. This program is designed to measure storage space and performance of file system. Filebench is capable of generating several types of workloads, it can simulate environments when using certain services such as mail server, fileserver, web server, etc. [13, 14]

## VI. TESTING AND RESULTS

This paper shows a comparison of the performance of virtual platforms for personal use with their capabilities. Disk performance and data flow were measured. To make testing meaningful, all virtual machines are created exactly the same and have the same characteristics (Table III).

TABLE III - VIRTUAL MACHINE PARAMETERS

| Components | Characteristics |
|---|---|
| Virtual processor | 1 |
| Memory | 2GB |
| Virtual hard drive | 60GB |
| Operating system | CentOS 7 |

During the testing, modified base code files were used, such as *varmail.f*, *fileserver.f*, *webserver.f* and *randomfileaccess.f*, which test the web, mail and file server. The appearance of the set parameters of the benchmark program can be seen in Table IV. To achieve the most realistic results, each test lasted 120 seconds. Each test was repeated ten times, and the obtained results were expressed as the average value of these tests.

TABLE IV – BASE CODE PARAMETERS OF **F* FILE

| | Varmail | Web server | File server | Random file access |
|---|---|---|---|---|
| nthtreads | 16 | 100 | 50 | 5 |
| nfiles | 1000 | 1000 | 10000 | 10000 |
| meandir widht | 1000000 | 20 | 20 | 20 |
| meanfile size | 16k | 16k | 128k | random |

Tests were conducted by first installing VirtualBox and then creating a virtual machine in this program. It was tested, and then this procedure was repeated when two and afterwards three virtual machines were created. The testing system was exactly the same when the virtual machines in the VMware Workstation 16 player application were tested. Of course, before testing on this platform, previous virtual machines and VirtualBox applications were uninstalled. At the end of the testing, the MS Hyper-V roll was activated and tests were performed, as in the previous two cases. In that way, fair-play conditions were created for all three virtual platforms. The results of the Fileserver workload test can be seen in Table V and Figure 5.

TABLE V - FILESERVER BENCHMARK RESULTS

 ISBN 978-86-7466-930-3

| **Fileserver** | 1VM (MB/s) | 2VM (MB/s) | 3VM (MB/s) |
|---|---|---|---|
| VMware | 74,58 | 64,33 | 56,41 |
| VirtualBox | 42,03 | 35,16 | 29,76 |
| MS Hyper-V | 33,34 | 28,12 | 21,53 |

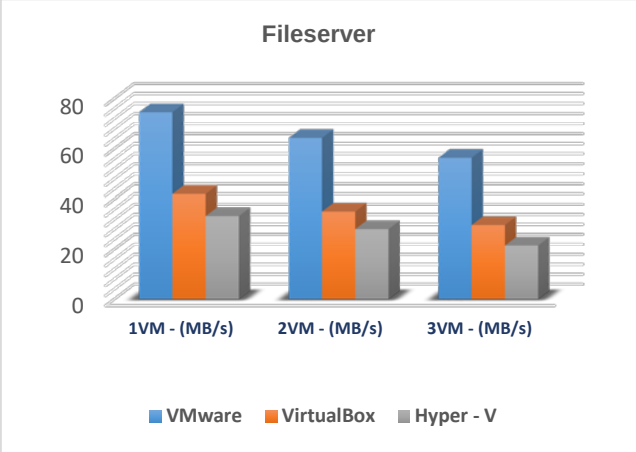


Figure 5. Fileserver test results

The results of testing other workloads are shown in Tables VI, VII and VIII, as well as graphical representations in Figures 6, 7 and 8.

For the *"Fileserver"* workload, we note that VMware is by far the best, while VirtualBox is better than Hyper-V. In a complex workload such as Fileserver with sequential and random write components, the FS cache effect on guest and hostOS is significant, so VMware wins convincingly primarily because of the 3rd component of formula (1) and the best cooperation with FS caching.

TABLE VI - VARMAIL BENCHMARK RESULTS

| **Varmail** | 1VM (MB/s) | 2VM (MB/s) | 3VM (MB/s) |
|---|---|---|---|
| VMware | 44,58 | 42,62 | 39,87 |
| VirtualBox | 18,46 | 17,83 | 16,62 |
| MS Hyper-V | 14,06 | 12,77 | 10,11 |

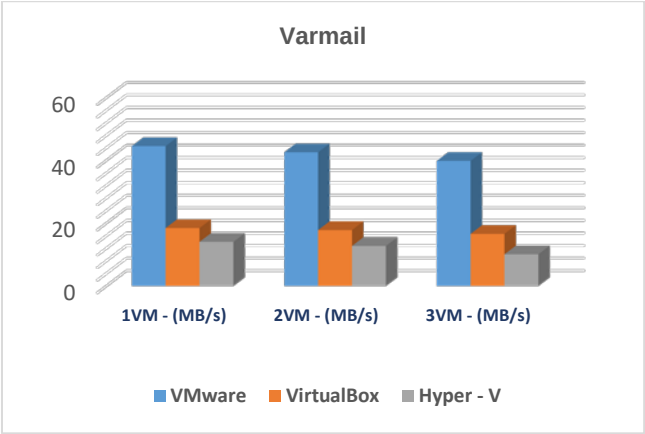


Figure 6. Varmail test results

For the *"Varmail"* workload, we note that VMware is by far the best, while VirtualBox is again slightly better than MS Hyper-V. In the Varmail workload, in addition to random reading, there are also synchronous components of random write, the impact of FS caching is small, so VMware and then VirtualBox obtain wins, primarily because of the 3rd and 4th components of formula (1).

TABLE VII - WEBSERVER BENCHMARK RESULTS

| **Webserver** | 1VM (MB/s) | 2VM (MB/s) | 3VM (MB/s) |
|---|---|---|---|
| VMware | 84,68 | 81,04 | 77,68 |
| VirtualBox | 47,73 | 42,26 | 37,86 |
| MS Hyper-V | 80,92 | 76,61 | 71,92 |

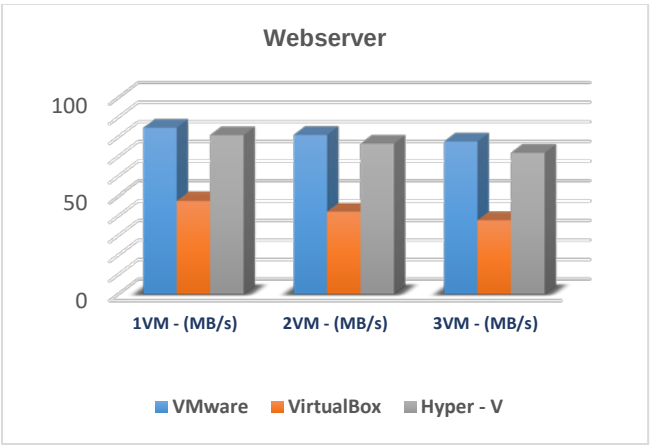


Figure 7. Webserver test results

For the *"Webserver"* workload, we note that VMware is slightly better than MS Hyper-V, and VirtualBox is significantly weaker. In the Webserver workload, which has both random read components and very few random write components, there is less influence of FS caching, so VMware and MS Hyper-V did better than VirtualBox, and win primarily because of the 3rd and 4th and the components of formula (1) and the cache effect in random reading, the dominant workload in Webserver environment.

 ISBN 978-86-7466-930-3

TABLE VIII – RANDOMFILEACCESS BENCHMARK RESULTS

| **Randomfile access** | 1VM (MB/s) | 2VM (MB/s) | 3VM (MB/s) |
|---|---|---|---|
| VMware | 5141,56 | 5034,02 | 5008,76 |
| VirtualBox | 2595,11 | 2546,56 | 2517,36 |
| MS Hyper-V | 4888,85 | 4816,64 | 4790,44 |

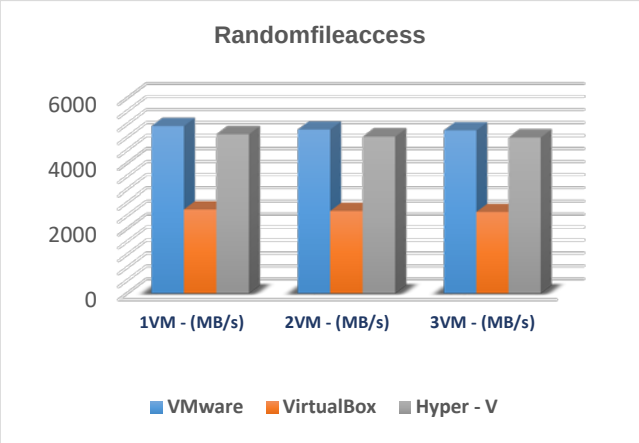


Figure 8. Randomfileaccess test results

For the *"Randomfileaccess"* workload, we can see that Hyper-V is slightly weaker than VMware, and VirtualBox is significantly weaker again. In the Randomfileaccess workload, which has both random read components and a lot of asynchronous random write components, there is a solid impact of FS caching primarily for random writing, so VMware and MS Hyper-V fared better than VirtualBox, primarily because 3rd and 4th components of formula (1) and solid cache effect in random entry.

## VII. CONCLUSION

When it comes to virtualization, it should be noted that it brings major changes in the information technology and computer industry, primarily in reducing investment in infrastructure and saving electricity consumption. In area of personal computers, virtualization has made great strides by bringing a large number of software for this purpose. Some of them are also presented in this paper. The advantage of using these applications is the ease of installation and usage, and the fact that the platforms tested in this paper are completely free. For this case study, VMware is the absolute winner in all workloads. We believe that the differences is made by the 3rd and 4th components of formula (1), as well as by the powerful hypervisor usage of the FS cache effect. For workloads with many sequential features and weak cache effect (Fileserver and Mailserver) VirtualBox is better than MS Hyper-V, and for workloads with random dominance and solid cache effect (Webserver and Randomfileaccess) MS Hyper-V is better than VirtualBox. Future work on this topic will focus on testing other virtual platforms in the field of desktop computers, as well as the use and testing of various operating systems that are applied in practice.

## ACKNOWLEDGEMENT

The work presented in this paper has partially been funded by the Ministry of Education, Science and Technological Development of the Republic of Serbia.

## LITERATURE:

[1] Matthew Portnoy: "Virtualization Essentials", 2016.
[2] Hypervisor Type-2. Online: https://www.ibm.com/developerworks /cloud/library/cl-hypervisor compare/, 2021.
[3] B.Đorđević, V.Timčenko, N.Kraljević, N.Davidović, "*File system performance in full hardware virtualization with ESXi and Xen hypervisors*", 18th International Symposium INFOTEH-JAHORINA, 2019.
[4] Full Virtualization. Online: https://www.sciencedirect.com/topics /computer-science/full-virtualization, 2021.
[5] Dejana T. Vojnak, Borislav S. Đorđević, Valentina V. Timčenko, Svetlana M. Štrbac: "*Performance Comparison of the type-2 hypervisor VirtualBox and VMware Workstation player*", 27th Telecommunication Forum, 2019.
[6] VirtualBox, Online: https://www.virtualbox.org/, 2021.
[7] Perfomance Evaluation of VMware and VirtualBox Online: https://pdfs.semanticscholar.org, pdf-2021.
[8] VMware, Online: https://www.vmware.com/product/workstation-player.html, 2021.
[9] Microsoft, Online: https://www.microsoft.com/, 2021.
[10] Jadran Torbić, Ivan Stanković, Borislav S. Đorđević, Valentina Timčenko: "*Hyper-V and ESXi hypervisors comparison in Windows Server 12 virtual environment*", 17th International Symposium INFOTEH-JAHORINA, 2018.
[11] B. Đorđević, V. Timčenko, N. Kraljević, N. Maček: "*File System Performance Comparison in Full Hardware Virtualization with ESXi, KVM, Hyper-V and Xen Hypervisors*", Advances in Electrical and Computer Engineering, vol.21, iss.1, 2021.
[12] M. Polenov, V. Guzik, V. Lukyanov: "*Hypervisors comparison and their performance*", Computer Science Online Conference, 2018.
[13] Filebench, Online: https://github.com/filebench/, 2021.
[14] Christopher Stracheyje, "*Time Sharing in Large Fast Computers*". Online:https://archive.org/details/large/fast/computers/page/n5/mode /2up, 2021.

 ISBN 978-86-7466-930-3

# Comparison of file system performance in full virtualization with MS Hyper-V and KVM hypervisors

Borislav Đorđević, *Member IEEE*, Miloš Piljić, Nenad Kraljević and Valentina Timčenko, *Member IEEE*

***Abstract* - This paper presents a comparison of the performance of native hypervisors on the example of MS Hyper-V and QEMU/KVM virtual platforms. Their quality was examined through aspects of file system performance. Filebench program was used for testing procedure, which is an application that guarantees equality and independence from the impact of hardware environment. CentOS 7, an operating system from the Linux distribution family, was used as the guest operating system. The tests were performed for one, two and finally three virtual machines that are running simultaneously. The results were further validated based on the defined hypotheses related to the expected behavior of the hypervisors.**

***Index Terms* - MS Hyper-V; QEMU/KVM; CentOS; virtual machines; performance.**

## I. Introduction

In the area of information technology, virtualization is a way of creating a virtual version of computer resources. Virtualization is a simulation of the hardware or software that other software, such as various operating system, is running. Virtualization is initially applied by IBM in 1960s as a method for the logical division of mainframe computer system resources between different applications. The need to manage the "one server-one application" model has been eliminated, opening the possibility of running multiple operating systems on the same hardware platform. The advantages and savings that are obtained by using such a system are more than obvious: hardware, CPU, memory resources, administration staff. All this is a plus for virtualization in the reliability segment. The virtualization solutions allow easiness in adding new servers, as well as in data migration from one server to another. This is an additional advantage of this technology in the field of scalability.

Borislav Đorđević - Mihailo Pupin Institute, Volgina 15 Belgrade, Serbia, (borislav.djordjevic@pupin.rs)
Miloš Piljić - VISER, School of Electrical and Computer Engineering of Applied Studies, Belgrade, Serbia, (milosrin4520@gs.viser.edu.rs)
Nenad Kraljević - VISER, School of Electrical and Computer Engineering of Applied Studies, Belgrade, Serbia, (nenadk@gs.viser.edu.rs)
Valentina Timčenko - Institute Mihailo Pupin, Volgina 15 Belgrade, Serbia, (valentina.timcenko@pupin.rs)

Hardware virtualization, which is the topic of this paper, is the most popular and widespread type of virtualization [1]. The software that controls virtualization is called a Virtual Machine Monitor (VMM). According to the most common form of use in a professional IT environment, the process of creating and managing virtual machines is also called server virtualization. There are two categories of hypervisor: type-1 (native) and type-2 (hosted). In this paper, type-1 hypervisors were tested for the case of MS Hyper-V and QEMU/KVM virtual platforms (Figure 1) [2].

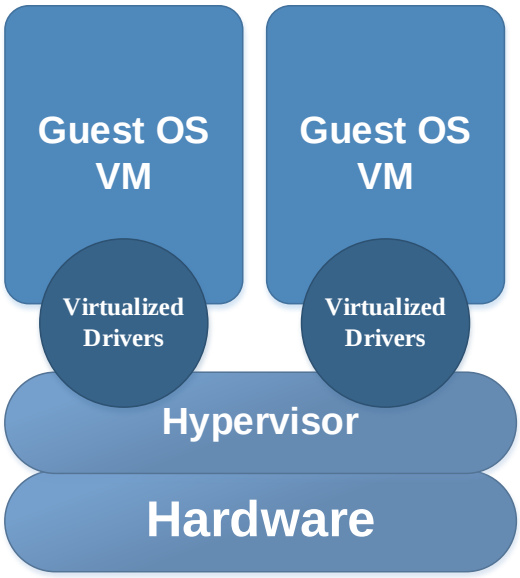


Figure 1. Native hypervisors

## II. Research work, goal and motivation

The literature related to this field is mostly focused on comparative analysis of hypervisor performance, using by different test methodology and benchmark tools. For this purpose, some proven benchmark tools are usually used, which is one of the cornerstones for obtaining quality level results. We recommend the Filebench, as open source solution, because it is a versatile, powerful, multithread and it simulates the real application workloads. We recommend the Fio tool, similar benchmark as Filebench, and some synthetic benchmarks such are Bonnie++, Postmark etc. The main contribution of this paper is the mathematical modeling

 ISBN 978-86-7466-930-3

of hypervisor-based virtualization in the context of the file system performance and applying the model on a performance case study for the interpretation of benchmark results. Because the complex virtual environment includes large number of factors, model expects there is no single winner hypervisor and depends on the case study i.e. the workload characteristics. In relation to competition, we are forcing a mathematical model and a number of case studies based on model with practical performance tests. The server variant of the virtualization stands for a great solution, primarily due to the introduction of the infrastructure costs and hardware reduction, followed by the easier administration. Still, there is a lot of room and opened questions for the improvement in this area. This paper contribution is the validation and comparison of two hypervisors, namely MS Hyper-V and QEMU/KVM, for which we have tested the quality and performances in identical conditions. Both hypervisors use full virtualization, while MS Hyper-V is also suitable for the use of the paravirtualization. As the guest operating system we have used CentOS 7, popular distribution from the Linux OS family, while for testing needs we have applied Filebench benchmark program with 4 different workloads. After defining the hypotheses, a mathematical model was set up, and validated by the obtained results [3], [4].

## III. MS HYPER-V AND QEMU/KVM

MS Hyper-V is an efficient hypervisor, developed by Microsoft, which enables virtualization of operating systems in a server environment (Figure 2). With the release of Windows Server 2008 R2 version, Microsoft has included a Hyper-V virtualization solution in the operating system itself. MS Hyper-V is a role that allows administrators to create multiple virtual machine, and supports isolation of partitions in which guest operating systems will run [5], [6].

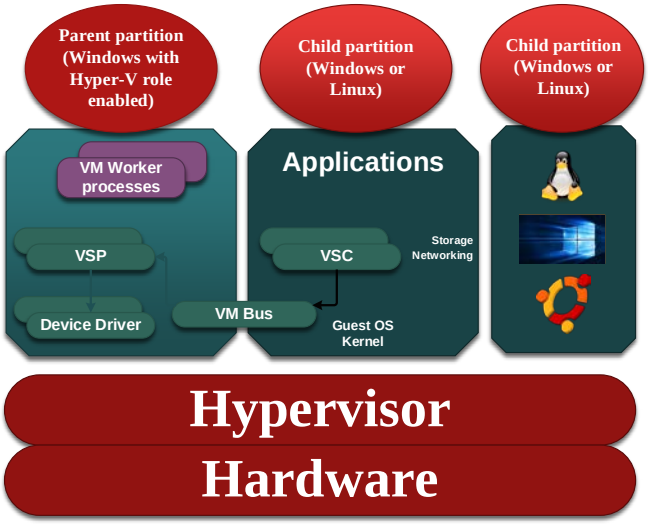


Figure 2. MS Hyper-V architecture

When it comes to virtualization under the Linux operating system, KVM (Kernel-based Virtual Machine) is almost indispensable technology. It is originally created as the Red Hat sponsored project. KVM is implemented in the form of a kernel module and is an integral part of the Linux kernel from version 2.6.20. For the KVM it cannot be said that it is a type-1 or type-2 hypervisor. On the one hand, KVM extends the Linux kernel and adds virtualization capabilities to it, allowing Linux itself to be treated as a native hypervisor (Figure 3). On the other hand, Linux is a standalone OS on which KVM functionality relies orthogonally, so it can be said that KVM runs above the main OS (hosted hypervisor), using already implemented system functions in the absence of its own (QEMU) [7-9].

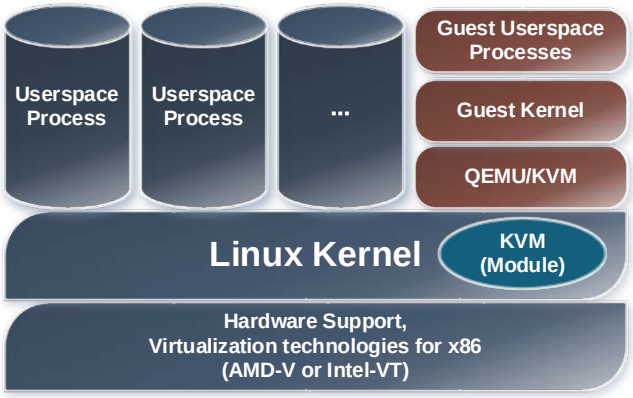


Figure 3. QEMU/KVM architecture

## IV. HYPOTHESES ABOUT EXPECTED BEHAVIOR

Both hypervisors are native, they work directly on the hardware and are realized in the microkernel architecture. The total processing time for each load *Tw* (Time workload) can be calculated as follows (eq. 1):

$$T_W = T_{RW} + T_{SW} + T_{RR} + T_{SR} \quad (1)$$

where $T_{RW}$ and $T_{SW}$ represent random and sequential data entry times, while $T_{RR}$ and $T_{SR}$ represent random and sequential read times. For each of these workloads, there is an expected access time for a file system that includes five components (eq. 2):

$$T_{WL} = T_{FB} + T_{FL} + T_J + T_{HK} + T_{DIR} + T_{META} \quad (2)$$

where $T_{WL}$ represents the total time for the implementation of all operations for a defined workload, and the elements from equation (2) represent the time required for the implementation all operations related to file blocks, file lists, journaling, house-keeping, metadata and directory in the file system. There are 5 components that have an impact on the workload time $T_W$ (eq. 3):

$$T_W = f\,(\text{Bn, gOS-FS, Hp-proc, VH-proc, hOS-FS}) \quad (3)$$


ISBN 978-86-7466-930-3

The first and second components Bn (Benchmark) and gOS- FS (guest file system) are identical for KVM and Hyper-V. Since an identical benchmark and the same virtual machines with their ext4 guest file system are used in testing, we can assume that these components will have the same impact on the third component, Hp-proc (hypervisor processing) which represents a typical delay of hypervisor (KVM-delay, Hyper-V-delay). This represents the time that takes the hypervisor to receive a request from the virtual hardware and forward it to the host drivers. The fourth component, VH-proc (virtual hardware processing) for KVM is QEMU full virtualization, and for Hyper-V MS full virtualization. Although these are full hardware emulations, both hypervisors have their own solutions that will certainly differ in performance. The fifth component is hOS-FS (host file system). KVM uses ext4 and the Hyper-V NTFS file system, and this component is expected to cause different processing time for hypervisors. Since the tests are focused on the performance of native virtualized guests, the dominant influence of the third, fourth and fifth components of formula (3) is expected.

## V. Test configuration and benchmark application

In order for testing to be adequate and high quality, it is necessary to use the same hardware configuration, the same guest operating system, choose a quality benchmark test program and the same performance measurement methodology. The tests were performed on an IBM server, whose characteristics can be seen in Table I, and the characteristics of the hard disk on which the tests were performed can be seen in Table II. CentOS 7 was used as a guest OS [10].

TABLE I - Server/Test Environment

| | **IBM 7945J2G - System x3650 M3** |
|---|---|
| Processor | Intel® Xeon E5620 2.4GHz |
| Memory | 32GB DDR3 |
| Cache | 12MB L3 |
| Hard Disk | 8 x Kingston 240GB SSD Now V300 SATA 3 2.5 (SV300S37A / 240G) |
| Network | 2 x 1Gb / s |

Virtual Platforms MS Hyper-V and QEMU/KVM are installed on hard drives converted into RAID 10, size 960GB (4x240GB SSD), while the other (RAID10/960GB) served as a repository on which virtual machines were created.

TABLE II - Hard Disk/Test Environment

| | **Kingston 240GB SSD Now V300** |
|---|---|
| Model Number | SV300S37A/240GB |
| Model Name | SSD Now V300 |
| Capacity | 240GB |
| Interface | SATA 3.0 (6Gb/s) |
| Connectivity Technology | SATA |
| Hard Disk Form Factor | 2.5 Inches |
| Read / Write Speed | 450MB/s |
| Cache Size | 240GB |

All tests were done using Filebench, a benchmark program version 1.4.9.1-3. This program is designed to measure the performance of file systems and storage space and is capable of generating a large number of workloads. In this paper, 4 different workloads are used simulating environments when using services: web, mail and file server [11].

## VI. Testing and results

This paper presents a comparison of the performance of virtual platforms for server use. Disk performance and data throughput were tested. In order to make testing meaningful, all virtual machines were created with identical characteristics (Table III).

TABLE III - Virtual Machine Parameters

| **Components** | **Characteristics** |
|---|---|
| Virtual Processor | 1 |
| Memory | 8GB |
| Virtual Hard Disk | 200GB |

For mail, file and web server test needs, we have modified the base code files for analyzed workloads: *webserver.f, varmail.f, fileserver.f* and *randomfileaccess.f*. First, Hyper-V was tested, which was activated as a role on Windows Server 2016, by creating one virtual machine that was tested. The same procedure is repeated for testing the environment with two and three virtual machines. Each test lasted 120 seconds and was repeated ten times. The final result represents the average value of the obtained test results. Before testing the KVM virtual platform (using CentOS 7 with the KVM option checked), the Windows server with its virtual machines was uninstalled in order to clean the environment. An identical installation and testing procedure were then conducted with the KVM virtual platform. In this way, fair-play conditions were acquired for

 ISBN 978-86-7466-930-3

both virtual platforms. The results of Varmail workload testing can be seen in Table IV and Figure 3.

TABLE IV - VARMAIL BENCHMARK RESULTS

| **Varmail** | 1VM (MB/s) | 2VM (MB/s) | 3VM (MB/s) | Native (MB/s) |
|---|---|---|---|---|
| MS Hyper- V | 25.21 | 19.82 | 13.11 | |
| QEMU/KVM | 13.04 | 12.79 | 12.22 | |
| Native OS | | | | 68.77 |

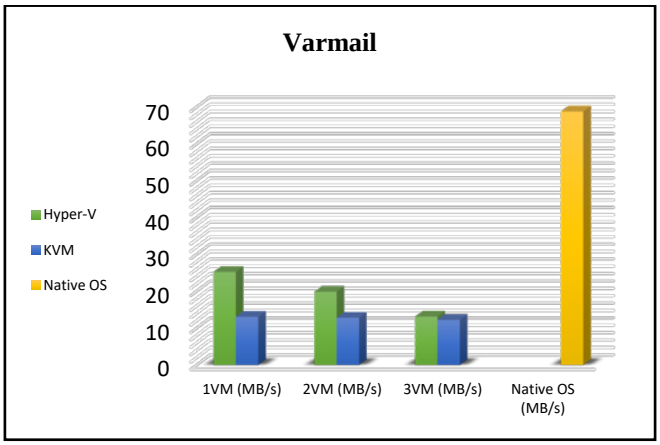


Figure 3. Varmail test results

For the "*Varmail*" workload, we notice that Hyper-V is solidly better than KVM. In this workload, besides the random read components these are synchronous random write components too for which the impact of the FS caching is very small. In this case, Hyper-V is better, primarily due to the fifth component of formula (3), where NTFS for this workload performed better in FS pair (ext4 on NTFS compared to ext4 on ext4).

The results of testing other workloads can be seen in the graphs (Figures 4.5 and 6), as well as in Tables V, VI and VII.

TABLE V - FILESERVER BENCHMARK RESULTS

| **Fileserver** | 1VM (MB/s) | 2VM (MB/s) | 3VM (MB/s) | Native (MB/s) |
|---|---|---|---|---|
| MS Hyper-V | 146.04 | 83.75 | 47.43 | |
| QEMU/KVM | 155.44 | 138.84 | 115.46 | |
| Native OS | | | | 555.63 |

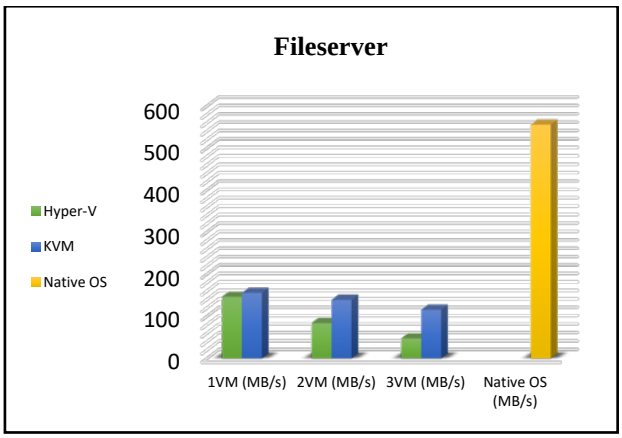


Figure 4. Fileserver test results

For the "*Fileserver*" workload, we notice that KVM is better than Hyper-V. In a complex workload such as Fileserver in which there are random and sequential write components, the FS cache effect on the guest and host OS is significant, so KVM wins primarily because of the third and fourth components of formula (3). We believe that KVM has better virtual hardware processing and less hypervisor latency.

TABLE VI - WEBSERVER BENCHMARK RESULTS

| **Webserver** | 1VM (MB/s) | 2VM (MB/s) | 3VM (MB/s) | Native (MB/s) |
|---|---|---|---|---|
| MS Hyper-V | 53.94 | 47.73 | 43.28 | |
| QEMU/KVM | 39.62 | 37.99 | 36.44 | |
| Native OS | | | | 115.26 |

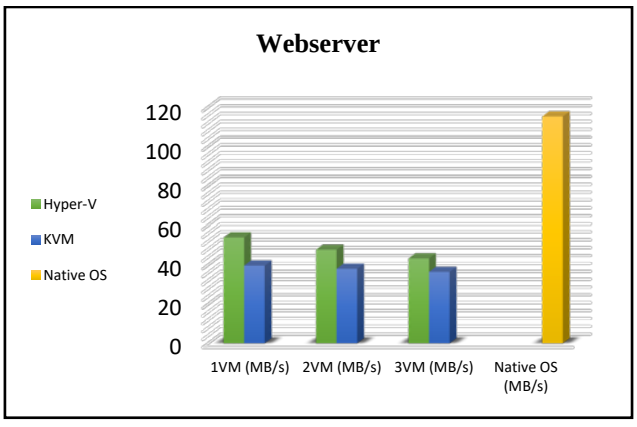


Figure 5. Webserver test results

For the "*Webserver*" workload, we can see that the Hyper-V is again solidly better than the KVM. In the Webserver workload, which has random read components and very few random write components, there is less influence of FS caching, so Hyper-V manages better, primarily due to the fifth component of formula (3), or FS pair (ext4 on NTFS in relative to ext4 to ext4) and the combined effect of FS caching.

 ISBN 978-86-7466-930-3

TABLE VII - RANDOMFILEACCESS BENCHMARK RESULTS

| **Random fileaccess** | 1VM (MB/s) | 2VM (MB/s) | 3VM (MB/s) | Native (MB/s) |
|---|---|---|---|---|
| MS Hyper-V | 3153.46 | 2588.48 | 2056.96 | |
| QEMU/ KVM | 2121, 15 | 2007.26 | 1890.35 | |
| Native OS | | | | 13780.52 |

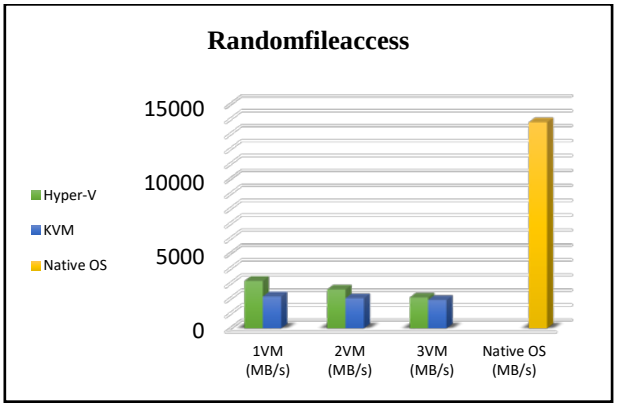


Figure 6. Randomfileaccess test results

For the "*Randomfileaccess*" workload, we again notice that Hyper-V is solidly better than KVM. In this workload, which has a lot of asynchronous random write components as well as random read components, there is a solid impact of FS caching, especially for random write, and for that reason Hyper-V performed better than KVM. This is primarily the effect of the fifth component of formula (3), NTFS, i.e. FS pair (ext4 on NTFS versus ext4 on ext4) and solid cache effect in random write.

## VII. CONCLUSION

Virtualization has already proven itself in the field of information technology and has found an adequate place. In addition to all the benefits that this technology brings, it is necessary to emphasize that it's large share in the preservation of the human environment, and we can emphasize that it can be successfully used in the domain of green technologies. For the research presented in this paper, Hyper-V outperformed KVM in 3 out of 4 workloads, while in the most complex workload (*Fileserver*), KVM was dominant. For this kind of hardware and experiment, the crucial role in the differences in performance was brought by the difference in the file system of the host OS, the difference in the FS pair (ext4 on NTFS vs. ext4 on ext4). There are also differences in virtual hardware processing and hypervisor processing, which have proven to be the most complex workload (*Fileserver*). Future work in this area may focus on testing different types of servers, as well as other commonly used virtual platforms.

## ACKNOWLEDGMENT

The work presented in this paper has been partially funded by the Ministry of Education, Science and Technological Development of the Republic of Serbia.

## LITERATURE:

[1] Christopher Strachey, "*Time Sharing in Large Fast Computers*". Online: https://archive.org/details/large-fast-computers/page/n5/mode/2up, 2021.
[2] Virtualization. Online: https://www.redhat.com/en/topics /virtualization /what-is-virtualization, 2021.
[3] Full Virtualization. Online: https://www.sciencedirect.com/topics/computer-science/full-virtualization, 2021.
[4] Matthew Portnoy: "*Virtualization Essentials*", 2016.
[5] Jadran Torbić, Ivan Stanković, Borislav S. Đorđević, Valentina Timčenko: "*Hyper-V and ESXi hypervisors comparison in Windows Server 12 virtual environment*", 17th International Symposium INFOTEH-JAHORINA, 2018.
[6] Microsoft, Online: https://www.microsoft.com/, 2021.
[7] B. Đorđević, V. Timčenko, N. Kraljević, N. Maček: "*File System Performance Comparison in Full Hardware Virtualization with ESXi, KVM, Hyper-V and Xen Hypervisors*", Advances in Electrical and Computer Engineering, vol.21, iss.1, 2021.
[8] Linux KVM, Online: https://www.linux-kvm.org/, 2021.
[9] Qemu process emulator, https://www.qemu-project.org/, 2021.
[10] M. Polenov, V. Guzik, V. Lukyanov: "*Hypervisors comparison and their performance*", Computer Science Online Conference, 2018.
[11] Filebench, Online: https://github.com/filebench/, 2021.

 ISBN 978-86-7466-930-3

# A Review of Wazuh Tool Capabilities for Detecting Attacks Based on Log Analysis

Stefan Stanković, Slavko Gajin, and Ranko Petrović, *Member, IEEE*

***Abstract*— During the difficult times of the Covid pandemics and the transfer of wor from the office to the home, security has never been more challenging. ecause the development of information technology is e panding day by day, there is increasing amount of networ traffic. Within that traffic, a potential attac er can often cover up his evil intentions. To detect attac s on host computer and prevent it from further malicious activities, ost Intrusion Detection ystems are often used. ne of these systems is Wazuh and than s to its powerful features it has been adopted by many companies. This paper provides an overview of the possibilities of Wazuh tools with a special emphasis on well- nown attac detection on web servers.**

***Index Terms*—Wazuh, web-server, networ , security, monitoring, attac .**

## I. INTRODUCTION

The network monitoring system is used in the internal or external network in order to best identify risk components and prevent system crashes. The task of these systems is to find a weak point, submit a report and, if possible, solve the problem. Given the growing challenges in cyber security and the increasing amount of data generated globally, network and security administrators face a growing challenge. Most engineers use the Host Intrusion Detection System to detect and identify attacks and the Intrusion Prevention System to prevent them.

One of the main components of any application and an almost inevitable part of any data center is a web server - a hardware-software component that houses websites that serve end-users. Web servers are mostly exposed to the Internet and thus exposed to a large volume of potential attacks coming either from real attackers or from automated bots. Identifying attacks on web servers is a basic task of any administrator who maintains them because if protection is breached, the application may be inaccessible to a large number of users or permanently destroyed [1]. There are many network security monitoring solutions used worldwide [2]. One of the tools that helps identify and detect attacks on web servers is Wazuh. This paper will present the main features of the Wazuh tool installed in the University of Belgrade Computer Center.

Wazuh is a tool used around the world for various purposes. Paper [3] describes how the Wazuh tool can be used to test solutions that detect attacks within their constructed honeypot. On the other hand, Wazuh can integrate with machine learning as described in [4]. The advantage of this work is that it can serve network and security engineers very well in network and host security monitoring.

This work demonstrates Wazuh tools when collecting data exclusively from web servers. The results obtained through this paper give administrators an insight into what needs to be changed within their configurations in order to bring their servers and the entire infrastructure to the highest security level.

The paper is written in 4 major sections. After the introduction, Section 2 describes the basic functionalities of Wazuh tools and experimental setup, followed by Section 3, where statistic data are shown. Section 4 presents the results related to known attacks such as SSH (Secure Shell) brute force. The last section presents the main conclusions with ideas for future work.

## II. WAZUH OVERVIEW AND EXPERIMENT SETUP

Wazuh is a free and open-source platform for threat detection and security monitoring according to predefined security rules. It can be used to monitor endpoints such as desktops, laptops, servers, or network devices such as firewalls and routers, and to aggregate and analyze data in real-time. Wazuh provides the following capabilities [5]:

- Security analytics - collection, aggregation, indexing and processing of security data, helping organizations detect intrusions, threats and behavioral anomalies.
- Intrusion Detection - Wazuh agents scan the monitored systems looking for malware, rootkits and suspicious anomalies. They can detect hidden files and processes.
- Log Data Analysis - Wazuh agents read operating system and application logs, and securely forward them to a manager for rule-based analysis.
- File Integrity Monitoring - Wazuh monitors the file system, identifying changes in content, permissions, ownership and attributes of files that need attention.
- Vulnerability Detector - Wazuh agents pull software inventory data and send this information to the server, where it is correlated with periodically updated CVEs (Common

Stefan Stanković is with the School of Electrical Engineering, University of Belgrade, 73 Bulevar kralja Aleksandra, 11020 Belgrade, Serbia and with Vlatacom Institute oh High Technologies, 5 Milutina Milankovica, 11070 Belgrade, Serbia (email: stefan.stankovic@vlatacom.com).

Slavko Gajin is with the School of Electrical Engineering, University of Belgrade, 73 Bulevar kralja Aleksandra, 11020 Belgrade, Serbia (email: slavko.gajin@rcub.bg.ac.rs).

Ranko Petrović is with the Vlatacom Institute oh High Technologies, 5 Milutina Milankovica, 11070 Belgrade, Serbia (email: ranko.petrovic@vlatacom.com).

 ISBN 978-86-7466-930-3

Vulnerabilities and Exposures) databases, in order to identify well-known vulnerable software.

- Configuration Assessment - Wazuh monitors system and application configuration settings to ensure they are compliant with security policies and standards. Agents perform periodic scans to detect applications that are known to be vulnerable, unpatched, or insecurely configured.

### *A. Wa uh components*

The Wazuh solution is based on the following 3 components [6]:

- Wazuh agent - Installed on endpoints such as laptops, desktops, servers or virtual machines, it provides prevention, detection and response capabilities. It supports Windows, Linux, MacOS, HP-UX, Solaris and AIX platforms.
- Wazuh server - It analyses data received from the agents, processing it through decoders and rules, and using threat intelligence to look for well-known indicators of compromise.
- Elastic Stack -Elastic Stack is a unified suite of open-source projects for log management, including Elasticsearch, Kibana, Filebeat, and others. The projects that are especially relevant to the Wazuh solution are: Filebeat, Elastic Search, Kibana. Filebeat is A lightweight forwarder used to transfer logs across a network, usually to Elasticsearch. It is used on the Wazuh server to transfer events and alerts to Elasticsearch. Elastic search is A highly scalable, full-text search and analytics engine. A flexible and intuitive web interface for mining, analyzing, and visualizing data. It runs on top of the indexed content in an Elasticsearch cluster. Wazuh web user interface has been fully embedded in Kibana, in the form of a plugin. Wazuh architecture.

### *B. Wa uh architecture*

The Wazuh architecture is based on agents, running on the monitored endpoints, that forward security data to a central manager. Moreover, agentless devices (such as firewalls, switches, routers, access points, etc.) are supported and can actively submit log data via Syslog. The manager decodes and analyzes the incoming information, and passes the results along to an Elasticsearch for indexing and storage.

### *C. E periment setup*

The results described in this paper were collected from several web servers with CentOS operating system version of 7.9, located in the University of Belgrade Computer Centre. Wazuh agents are installed on them to send Wazuh manager data. Wazuh manager has been installed on a virtual machine with Ubuntu operating system. Alternative to the implementation on virtual machine, dockers can be used, according to [7]. Some Wazuh manager functionalities are not included by default, such as Vulnerability Detector.

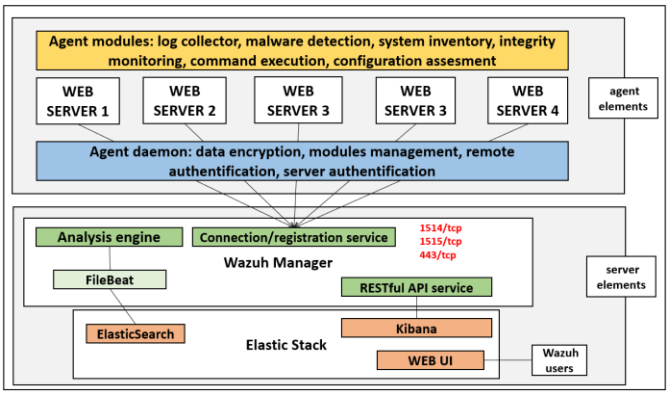


Fig. 1. Wazuh architecture on experiment setup

## III. WEB SERVER ATTACK DETECTION OVERVIEW

In this section the results within each element of Wazuh Managers will be presented in brief outlines and special emphasis will be placed on the analysis of well-known attacks. Within the main dashboard, there are 4 basic sections with options in which you can monitor data in real-time.

### *A. Security Information Management*

Within this module there are 2 units in which statistics on security events and integrity monitoring are located.

#### *1 Security e ents*

In this section, it is possible to search for all security events recorded within the Wazuh system. The operation of the system is based on agents that send data (logs) to the server where they are processed. There is a whole set of rules defined to identify threats. The results are processed and when a rule is met then it is recorded within the dashboard. By default, the rules are divided into 12 levels based on defined standards. Wazuh provides the option to write custom rules according to user needs. Figure 2 shows the sorted list of security alerts. We see that the 'Web server 400 error code' is the most prevalent error. In each unit within the Wazuh manager, it is possible to display the results in a given time range. Within each section, there is an option to generate reports and for better visibility top 10 alerts from each report will be displayed. Figure 2 presents the top 10 alerts from 31-Mar-2022 to 27-Apr-2022.

| Description | Level | Count |
|---|---|---|
| Web server 400 error code. | 5 | 603474 |
| Auditd: SELinux permission check | 3 | 473912 |
| sshd: Attempt to login using a non-existent user | 5 | 285016 |
| PAM: User login failed. | 5 | 247417 |
| sshd: authentication failed. | 5 | 215293 |
| unix_chkpwd: Password check failed. | 5 | 117091 |
| syslog: User missed the password more than one time | 10 | 50267 |
| Multiple web server 400 error codes from same source ip. | 10 | 30149 |
| sshd: Reverse lookup error (bad ISP or attack). | 5 | 19515 |
| sshd: insecure connection attempt (scan). | 6 | 15187 |

Fig. 2. Top 10 security alerts

#### *2 Integrity Monitoring*

In this module, it is possible to monitor the statistics of changes over system files on the host with the installed agent. These changes include modifying files, deleting files, and

 ISBN 978-86-7466-930-3

adding new files. Changes are detected based on the change in the checksum of each file.

Within the Events tab, it is possible to follow each change in detail, where you can find out the details of when a file was changed, which user did the action and what are the file permissions. This type of monitoring can be very useful, especially for sensitive systems. The performed actions and the list of files that are most often modified are shown in Figure 3.

| Path | Action | Count |
|---|---|---|
| /etc/httpd/sites-available/h2020.rcub.bg.ac.rs.conf | modified | 28 |
| /etc/httpd/sites-available/lira.f.bg.ac.rs.conf | modified | 28 |
| /etc/httpd/conf/httpd.conf | modified | 27 |
| /etc/httpd/sites-available/amres.ac.rs.conf | modified | 27 |
| /etc/httpd/sites-available/amres.rs.conf | modified | 27 |
| /etc/httpd/sites-available/arhiva.fpu.bg.ac.rs.conf | modified | 27 |
| /etc/httpd/sites-available/arts.bg.ac.rs.conf | modified | 27 |
| /etc/httpd/sites-available/bpd.amres.ac.rs.conf | modified | 27 |
| /etc/httpd/sites-available/bsaae.bg.ac.rs.conf | modified | 27 |
| /etc/httpd/sites-available/careers.ac.rs.conf | modified | 27 |
| /etc/httpd/sites-available/cbp.rcub.bg.ac.rs.conf | modified | 27 |

Fig. 3. The list of top modified files detected by Wazuh

## B. *Auditing and Policy Monitoring*

This module offers 3 sections in which statistics and details about the system configuration and how much that configuration deviates from global standards.

### *1 Policy monitoring*

This chapter shows the data obtained from the log analysis of policy monitoring. System configuration verification, such as kernel and security configuration files, is performed based on predefined rules. Wazuh uses 3 components to perform this task: Root check, OpenSCAP (Security Content Automation Protocol) and CIS-CAT. If some process is hidden from the virtual process file system (procfs), that file is marked as an alert.

| Rule description | Control | Count |
|---|---|---|
| Possible kernel level rootkit | Anomaly detected in file '/etc/letsencrypt/.certbot.lock'. | 1 |
| Possible kernel level rootkit | Anomaly detected in file '/tmp/#sql-temptable-68c6-2faed-b5e7.MAD'. | 1 |
| Possible kernel level rootkit | Anomaly detected in file '/tmp/#sql-temptable-68c6-2faed-b5e7.MAI'. | 1 |
| Possible kernel level rootkit | Anomaly detected in file '/tmp/#sql-temptable-68c6-6e16f-f03c.MAD'. | 1 |
| Possible kernel level rootkit | Anomaly detected in file '/tmp/#sql-temptable-68c6-6e16f-f03c.MAI'. | 1 |
| Possible kernel level rootkit | Process '4859' hidden from /proc. | 1 |
| Possible kernel level rootkit | Process '8798' hidden from /proc. | 1 |

Fig. 4. The list of detected anomalies

### *2 System auditing*

This section presents data based on which user behavior can be monitored, command execution monitored and possibly an alert raised if sensitive files are accessed. User behavior is monitored by a powerful auditing facility called *auditd* which provides a detailed accounting of actions and changes in a system. Thanks to the Wazuh agent who sends *auditd* logs to the manager, administrators can have insight into users' behavior. The statistics from this section are shown in Figure 5.

| Event | Command | Count |
|---|---|---|
| Auditd: SELinux permission check | /usr/sbin/php | 192484 |
| Auditd: SELinux permission check | /usr/sbin/php | 119432 |
| Auditd: SELinux permission check | /opt/remi/php74/root/usr/sbin/php | 68985 |
| Auditd: SELinux permission check | /usr/sbin/httpd | 27612 |
| Auditd: SELinux permission check | /usr/sbin/httpd | 24822 |
| Auditd: SELinux permission check | /usr/sbin/php | 13641 |
| Auditd: SELinux permission check | /usr/sbin/httpd | 10602 |
| Auditd: SELinux permission check | /opt/remi/php80/root/usr/sbin/php | 4945 |
| Auditd: SELinux permission check | /usr/sbin/postdrop | 3292 |
| Auditd: SELinux permission check | /usr/sbin/postdrop | 2396 |
| Auditd: SELinux permission check | /usr/libexec/postfix/smtp | 2001 |

Fig. 5. SElinux permission checklist

### *3 Security Configuration Assessment*

Within this unit, before displaying the data, it is necessary to select the agent where the configuration check will be performed. When the check is performed, the statistics and scores of that host are displayed. Verification is performed based on CIS (Center for Internet Security) benchmark recommendations for particular operating system distribution. The check consists of executing a set of commands whose result is binary: pass or fail. A detailed report is obtained when exported in CSV format where the columns show, among other things, commands, results, references and recommendations. This statistic gives a very good insight into the system configuration and draws the administrator's attention to important configuration elements.

## C. *Threat etection and esponse*

In this unit there are 3 entities in which it is possible to gain insight into data related to threat detection. These entities are vulnerabilities, virus Total and MITRE ATT&CK, a globally accessible database of adversary tactics and techniques based on real-world observations. Evaluation of Wazuh tool with persistence tactic of MITRE ATT&CK is nicely described in [8]. As the targeted system is not related to antivirus software, no data has been collected.

### *1 ulnerabilities*

This module is not included in the main configuration file by default and needs to be enabled. It performs vulnerability searches according to the latest indexes that are updated in real-time with Canonical, RedHat and National Vulnerability databases. The detector on the manager inspects the list of installed applications periodically sent by the agents. Based on this list, search and verification processes are performed within the local database with the latest CVE elements (Common Vulnerabilities and Exposures). Alerts are generated when a CVE affects a package installed on one of the monitored servers. That package is then marked as vulnerable. There are 2 types of scanning: full and partial. A full scan is done the first time the Vulnerability Detector is activated and then each packet is scanned individually. Partial scanning is done when new packages are installed.

 ISBN 978-86-7466-930-3

| Severity | Title | Published | CVE | Count |
|---|---|---|---|---|
| High | CVE-2021-32749 affects fail2ban | 1626393600000 | CVE-2021-32749 | 593 |
| Low | CVE-2015-3243 affects rsyslog | 1500940800000 | CVE-2015-3243 | 498 |
| Low | CVE-2019-15165 affects libpcap | 1570060800000 | CVE-2019-15165 | 498 |
| Low | CVE-2019-1551 affects openssl | 1575590400000 | CVE-2019-1551 | 498 |
| Low | CVE-2019-1563 affects openssl | 1568073600000 | CVE-2019-1563 | 498 |
| Low | CVE-2020-1968 affects openssl | 1599609600000 | CVE-2020-1968 | 498 |
| Low | CVE-2021-3601 affects openssl | 1623715200000 | CVE-2021-3601 | 498 |
| Low | CVE-2021-3601 affects openssl-libs | 1623715200000 | CVE-2021-3601 | 498 |
| Low | CVE-2021-3659 affects kernel | 1617736920000 | CVE-2021-3659 | 498 |
| Low | CVE-2021-3659 affects kernel-tools | 1617736920000 | CVE-2021-3659 | 498 |

Fig. 6. The list of matched CVEs detected by Wazuh

### 2 MITT E ATT C

This feature allows the user to customize the alert information to include specific information related to MITRE ATT&CK techniques. MITRE ATT&CK matrix stores all possible attacks that can be made and what to do to detect them and mitigate the risk [9]. This can be useful when an attack is detected through an alert and a user wants to know more about it. MITRE ATT&CK assigns each attack technique an ID (identification). These techniques are grouped by tactics (Defense Evasion, Privilege Escalation, etc.) although some of them belong to more than one tactic.

#### . egulatory Compliance

The Wazuh platform is often used to meet the technical aspects of regulatory compliance standards. Wazuh not only provides the necessary security controls such as host intrusion detection, configuration assessment, log analysis, and vulnerability detection, among others, to meet compliance requirements but also uses its SIEM (Security Information and Event Management) capabilities to centralize, analyse and enrich security data. In order to provide regulatory compliance support, the Wazuh rules have been mapped against compliance requirements [10]. This way, when an alert is generated (a rule condition has been matched), it automatically includes compliance information. The following standards are supported: Payment Card Industry Data Security Standard (PCI DSS), General Data Protection Regulation (GDPR), NIST Special Publication 800-53 (NIST 800-53), Good Practice Guide 13 (GPG13), Trust Services Criteria (TSC SOC2), Health Insurance Portability and Accountability Act (HIPAA)

## IV. EXPERIMENT, RESULTS AND SYSTEM PERFORMANCE

As already mentioned, one of the attacks analyzed in more detail is the SSH brute force attack. a brute-force attack is performed by an attacker submitting many passwords or passphrases with the hope of eventually guessing correctly. The attacker systematically checks passwords and passphrases from the database until the correct one is found. Also, if a user tries to connect via SSH using a random username, they will be considered to have attempted an attack and that alert will be recorded. Data processing on the Wazuh manager is in real-time and a potential attack is detected and alerted almost immediately. Table I provides very detailed information about the alerts when a potential attacker tried to connect as a non-existent user ‘dunja’.

The basic geo locations based on the source IP address are followed by information about the user trying to connect and the name of the decoder that analyzes the data. This is followed by a description of the full log and an abbreviated name as well as the original log file location.

TABLE I
SSH failed login overview

| Parameter | Data |
|---|---|
| GeoLocation.city_name | Belgrade |
| GeoLocation.country_name | Serbia |
| GeoLocation.location | { "lon": 20.4721, "lat": 44.8166 } |
| GeoLocation.region_name | Belgrade |
| _id | s2K6-H8Bao9qD9NQsksr |
| _index | wazuh-alerts-4.x-2022.04.05 |
| data.srcip | 217.24.19.131 |
| data.srcport | 11847 |
| data.srcuser | dunja |
| decoder.name | sshd |
| decoder.parent | sshd |
| full_log | Apr 5 07:57:36 wazuh sshd[233488]: Invalid user dunja from 217.24.19.131 port 11847 |
| id | 1649145457 |
| input.type | log |
| location | /var/log/auth.log |
| manager.name | wazuh |
| predecoder.hostname | wazuh |
| predecoder.program_name | sshd |
| rule.description | sshd: Attempt to login using a non-existent user |
| rule.gdpr | IV_35.7.d, IV_32.2 |
| rule.gpg13 | 7.1 |
| rule.groups | syslog, sshd, invalid_login, authentication_failed |
| rule.hipaa | 164.312.b |
| rule.id | 5710 |
| rule.level | 5 |
| rule.mail | FALSE |
| rule.mitre.id | T1110 |
| rule.mitre.tactic | Credential Access |
| rule.mitre.technique | Brute Force |
| rule.nist_800_53 | AU.14, AC.7, AU.6 |
| rule.pci_dss | 10.2.4, 10.2.5, 10.6.1 |
| rule.tsc | CC6.1, CC6.8, CC7.2, CC7.3 |
| timestamp | Apr 5, 2022 @ 09:57:37.807 |

### A. System performance

The Wazuh manager described in this paper is installed on an Ubuntu virtual machine which is assigned 8GB of RAM (Random Access Memory), 4 cores and 30GB of storage. It aggregates data from a total of 5 servers in the network. Of the allocated resources, the system uses about 4.7GB of RAM, a

 ISBN 978-86-7466-930-3

negligible percentage of CPU load, and about 11G of storage is filled. The system uptime is 2 months.

## V. Conclusion

The aim of this paper is to present the functionality of the Wazuh tool in detecting attacks demonstrated on web servers. Web servers are components that are very exposed to the Internet and if they are not well protected, they are very susceptible to attacks of various kinds. In order to prevent attacks, they must first be detected and that is why Host Intrusion Detection systems are used. One of the solutions that can help is Wazuh. It is a powerful tool that displays all detected attacks in great detail and in real-time. Although this paper demonstrates the analysis of detected attacks on web servers, Wazuh is a tool used to analyze attacks across the entire infrastructure. This paper presents the basic principle of operation of Wazuh tools based on the agent-manager system. Agents installed on hosts send the log data for processing to the manager. Statistics of different types of attacks are presented and special attention is paid to details concerning some well-known attacks such as SSH brute force. The attack was successfully detected and shown almost immediately. As further work, the installation of agents on all infrastructure devices is proposed, without limiting on the type of device. It would be desirable to integrate the Wazuh tool with an antivirus software in order to get deep inspection on viruses, worms trojans and other malicious content. Some security issues are most successfully detected by inspecting a server's actual network traffic, which is generally not accounted for in logs. This is where a Network Intrusion Detection System can provide additional insight into security. One of those systems is Suricata. Because Suricata is capable of generating JSON (JavaScript Object Notation) logs of events, it has very good integration option with Wazuh, so this is also a proposal to future work.

## ACKNOWLEDGEMENT

This paper was done at Vlatacom Institute on project P158 and partially supported by the Ministry of Education, Science and Technological Development of the Republic of Serbia (grant number 2022/200103).

## References

[1] M. Moh, S. Pininti, S. Doddapaneni, T.S. Moh "Detecting Web Attacks Using Multi-Stage Log Analysis", *th IEEE International Conference on Ad anced Computing*,2016, doi: 10.1109/IACC.2016.141

[2] I. Ghafir, V. Prenosil, J. Svoboda, M. Hammoudeh, "A survey on Network Security Monitoring Systems", 4th International Conference on Future Internet of Things and Cloud Workshops, 2016, DOI: 10.1109/W-FiCloud.2016.30

[3] R. M. Muhammad, I. D. Irawati, M. Iqbal "Integrated Security System Implementation for Network Intrusion", *ournal of unan ni ersity*, vol. *4* , no. , pp. *1 3-1* , June, 2021.

[4] O. Negotia, M. Carabas "Enhanced Security Using Elastic Search and Machine Learning", *Ad ances in Intelligent Systems and Computing*, vol. *1230,* July, 2020.

[5] Wazuh documentation overview, https://documentation.wazuh.com/current/, last visited 28.4.2022

[6] Wazuh documentation components, https://documentation.wazuh.com/current/getting-started/components/index.html last visited 28.4.2022.

[7] F. Mulyadi, L. A. Annam, R. Promya and C. Charnsripinyo, "Implementing Dockerized Elastic Stack for Security Information and Event Management", 5th International Conference on Information Technology, 2020. DOI: 10.1109/InCIT50588.2020.9310950

[8] J. Chandler, "Evaluating Open-Source HIDS with Persistence Tactic of MITRE att&ck", SANS Institute, 2021.

[9] Wazuh documentation, mitre, available at https://documentation.wazuh.com/current/user-manual/ruleset/mitre.html, last visited 29.04.2022.

[10] Wazuh documentation regulatory compliance, available at https://documentation.wazuh.com/current/getting-started/use-cases/regulatory-compliance.html, last visited 29.04.2022.

 ISBN 978-86-7466-930-3

# Infrastructure for Simulating n-Dimensional Simplicial Complexes

Dušan Cvijetić, Nenad Korolija, and Marko Vojinović

***Abstract*—We present an infrastructure for simulating simplicial comple es. The classes for storing the structure of simplicial comple es and simplices are e plained in detail, for arbitrary dimension.**

**The implementation is tested using functions for seeding simplicial comple es and for printing them on the screen. eside these functions, the supporting classes and the function for assigning unique identifiers and screen coordinates is also e plained.**

**esults of simulation show that there are potentials for the simulator to be used for big data problems, although appropriate e perimental results are still being collected. uture wor includes parallelizing the e ecution of the simulator using supercomputing architectures.**

***Index Terms*— implicial comple ; triangulation; manifold; algebraic topology.**

## I. Introduction

A manifold is one of the fundamental concepts in mathematics [1], and its importance in applications in physics, technology and engineering cannot be overstated. Virtually all modern physics describes the world using *field theory* [2], in which all physical quantities (fields) are represented as functions over some manifold (for example, spacetime). In technology, manifolds appear in all forms and guises, whenever one needs to deal with curved surfaces --- from civil engineering to graphics in video games.

While most of the interest in science and engineering revolves around *smooth* manifolds, for the purpose of studying manifolds using numerical techniques, the attention focuses on the so called *piecewise-linear* manifolds [3], which can intuitively be imagined as a structure made out of small flat cells called *simplices,* arranged like bricks into a structure which models a manifold. The procedure of approximating a smooth manifold with a piecewise-linear one is commonly called *triangulation,* see Fig. 1.

Within the framework of algebraic topology, the formal mathematical structure which describes piecewise-linear manifolds is called a *simplicial comple* . For the purpose of this article, we provide an informal descriptive definition of a simplicial complex, without mathematical rigour. A simplicial complex is a combinatorial structure, containing the information about *simplices* of various dimensions that make up a complex, and the information about how simplices are connected to each other. A *k-simple* is an elementary building block of a simplicial complex. It is an elementary geometrical "cell" of dimension k, which is being used to build simplices of higher dimension, and the entire simplicial complex. For k = 0, the simplex is called a *erte* , it is represented geometrically as a single point, and has no internal structure. The k = 1 simplex is called an *edge,* geometrically represented as a single straight line, having two vertices at its boundary. For k = 2, the simplex is a *triangle,* having three boundary edges and three vertices. The case k = 3 describes a *tetrahedron*, having four boundary triangles, six edges and four vertices. One can go further into higher dimensions: k = 4 represents a simplex called *pentachoron* – it is a 4-dimensional figure, having five boundary tetrahedra, 10 triangles, 10 edges and five vertices. In general, one can introduce a k-simplex for arbitrary dimension k, also called *le el*.

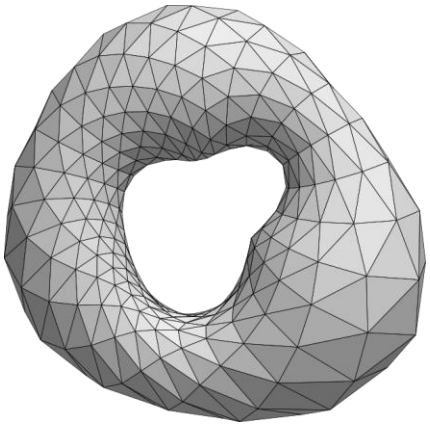

Fig. 1. Simplicial complex of a torus (source: Wikipedia).

Given a set of simplices, one can "glue them up" into a bigger geometrical structure, called simplicial complex. In order to describe a manifold of dimension D, a simplicial complex is constructed by gluing a set of D-simplices by identifying their common boundary (D-1)-simplices. Naturally, this implies the identification of all corresponding sub-simplices of level k < D-1 as well. The resulting simplicial complex is homeomorphic to a piecewise-linear manifold of dimension D.

The most important information about the simplicial complex, aside from its dimension D, is the data that tells one

Dušan Cvijetić is a student of the School of Electrical Engineering, University of Belgrade, 73 Bulevar kralja Aleksandra, 11020 Belgrade, Serbia (e-mail: dusancvijetic2000 @ gmail.com).

Nenad Korolija is with the School of Electrical Engineering, University of Belgrade, 73 Bulevar kralja Aleksandra, 11020 Belgrade, Serbia (e-mail: nenadko @ etf.bg.ac.rs).

Marko Vojinović is with the Institute of Physics, University of Belgrade, Pregrevica 118, 11080 Pregrevica, Serbia (e-mail: vmarko @ ipb.ac.rs).

 ISBN 978-86-7466-930-3

which simplices are glued to which. This gives rise to a notion of a *neighborhood* of a k-simplex, which is a set of all simplices which contain a given simplex as its sub-simplex (called super-neighbors) and simplices which are contained in a given simplex (called sub-neighbors). Each k-simplex (for $0 \leq k \leq D$) in the complex has its set of neighbors, where by definition a simplex is not a neighbor of itself (this is convenient to avoid infinite loops when traversing a complex). The neighborhood structure of the entire complex determines the *topology* of the corresponding manifold.

While manifolds of various topologies are important in their own right in mathematics, the applications in physics and engineering typically introduce functions over manifolds, such as distances, areas and volumes, temperature, electric and magnetic fields, etc. In the language of simplicial complexes, these functions are commonly called *colors*, and are assigned to simplices of various level k within the complex. Given a k-simplex, one can assign to it multiple colors, representing the value of a given function when evaluated on the k-simplex. A prototype example of colors is the geometry of a simplicial complex: each k-simplex is assigned its "size" according to its geometry --- each 1-simplex (an edge) is assigned a real number representing its length, each 2-simplex (a triangle) is assigned a real number representing its area, tetrahedra are assigned volumes, and so on. Other examples are abound --- vertices can be assigned a temperature, edges can be assigned vectors of electric field, and so on. Depending on the problem at hand, one may or may not impose relationships between various colors, such as that the area of a triangle is consistent with the length of its edges, or similar. These relationships are collectively called *constraints*.

In most everyday applications, one is interested in manifolds of dimension 1 and 2 (curves and surfaces). However, within the context of theoretical physics, one often needs to deal with manifolds of higher dimension – most commonly 3, 4, 5, 10, 11 and 26, while more sporadically anything in between and above. One of the typical scenarios is *uantum gra ity* [4,5], a vast research area of fundamental theoretical physics, where the notion of spacetime is described as a piecewise-linear manifold of dimension D=4 or higher [6,7]. In order to apply numerical techniques to study the manifolds in such research disciplines, it is necessary to formulate and implement structures and algorithms which describe colored simplicial complexes of arbitrarily large dimension, in a uniform and optimal way. In what follows, we describe one such implementation, which is purposefully designed to mimic the mathematical structure of a simplicial complex as close as possible, while simultaneously providing efficient numerical techniques for the manipulation and study of such structures.

## I. N-Dimensional Simplicial Complexes

This section describes the structure of simplicial complexes, and explains an example C++ implementation of classes for storing simplicial complexes.

Simplicial complexes consist of k-simplices at different levels. Given a simplicial complexes of dimension D, these elements include k-simplices for each level from zero to D. Elements at level zero are vertices, elements at level one are edges, elements on level two are triangles, etc. Finally, there are elements of highest level D. The representative source code of class for simplicial complexes is given in Algorithm 3 from the Appendix. The source code is pruned from comments and unnecessary functionalities for the presentation of the simulator.

K-simplex stores the level it has, the dimension of the simplicial complex it belongs to, neighboring elements and colors assigned to it.

Neighboring elements of a k-simplex are defined as k-simplices that this k-simplex is touching. Since these can be on various levels, the structure of neighbors is the same as for the simplicial complex. Therefore, the two main classes are mutually connected.

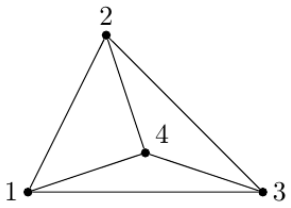


```
Printing SimpComp tetrahedron, D = 3
Simplices k = 0:
1, 2, 3, 4
Simplices k = 1:
(1-2), (1-3), (1-4), (2-4), (2-3), (3-4)
Simplices k = 2:
(1-2-3), (1-3-4), (1-2-4), (2-3-4)
Simplices k = 3:
(1-2-3-4)
```

Fig. 2. Tetrahedron and a corresponding output of the simplicial complexes simulator.

One possible implementation of the neighboring elements is to store only neighbors from one level above, and one level beneath (first sub-neighbors and first super-neighbors). The lower- and higher-level neighbors can be deduced following the structure of the first neighbors. However, we have opted for storing neighbors from all levels, giving us the opportunity to divide the structure onto multiple computing nodes and run the code in parallel. At current state, the simulator is running on a single CPU.

The instructions a CPU is executing are repeated over and over again, which makes this simulator suitable for acceleration using the dataflow paradigm [8,9]. The effort required for programming such architectures is higher than for conventional von Neumann architectures [10], but the simulator is suitable for transforming the C++ source code automatically [11]. Executing multiple simplicial complex operations in parallel requires appropriate scheduling

 ISBN 978-86-7466-930-3

techniques [12].

Each k-simplex (including all vertices, edges, triangles, etc.) can be colored with different types of color. Example colors include:

- k-simplex name,
- unique identifier of k-simplex,
- boundary color of k-simplex,
- screen coordinates.

These colors are included in our simplicial complex simulator, but the structure of the simulator allows adding additional user defined colors.

The representative source code of the class for k-simplices is given in Algorithm 4 from the Appendix. Just like it is the case with simplicial complexes, this source code is pruned for better clarity.

For simulation purposes, we have developed functions for seeding simplicial complexes at various levels, as it will be explained in the following section. In addition, coloring and printing simplicial complexes is also implemented. Pretty printing (or compact printing) prints k-simplices at all levels, where k-simplices of level higher than zero are printed as tuples consisting of unique identifiers (IDs) of their vertices. Fig. 2 shows an example tetrahedron (i.e. simplicial complex of dimension D = 3 consisting of a single 3-simplex and its sub-simplices) whose vertices are colored with unique identifiers that auto-increment after each assignment of the unique color to a vertex. Details of the implementation of compact printing is also explained in this manuscript.

Screen coordinates can be attached to vertices of the tetrahedron. Therefore, it can be drawn on the screen. However, there is no need to assign coordinates. They are just a convenient way to show an object on a screen. Similarly, there is no need to assign unique ID to any vertex. In the previous example, if a vertex with unique ID four would not have a unique ID assigned to it, the tetrahedron could still be printed out, but with word “Simplex” being printed out in place of number four.

## II. Seeding Simplicial Complexes

This section describes seeding simplicial complexes using C++ implementation of function *seed single edge* . The example source code for seeding a single edge is used for demonstrating purposes.

The process of seeding simplicial complexes will be explained using the source code shown in Algorithm 1. The source code is pruned from comments and unnecessary statements. Seeding a simplicial complex consists of the following steps, and statements in Algorithm 1 follow the same principle in the same order:

- creating an empty simplicial complex of given dimension,
- creating k-simplices for storing vertices and simplices of higher levels,
- connecting vertices at each level with vertices on higher and lower levels.

Adding a neighbor to a k-simplex is a symmetric operation. This means that both k-simplices (the calling one and the one given as an argument) are neighbors to each other. All functions of the simulator are written in a robust manner, checking the validity of input parameters.

Note that multiple colors can be assigned to each k-simplex, which is left out of consideration in this algorithm for better clarity.

## III. Coloring and Pretty Printing K-simplices

This section describes coloring and pretty printing simplicial complexes. These functions might work in pair, but are not necessarily connected.

### *A. Coloring -simplices*

Coloring k-simplices will be explained using Algorithm 2 by coloring vertices of an edge with boundary colors. First, vertices have to be created as k-simplices of level zero. Then, colors have to be created for all vertices. Finally, colors need to be pushed back to the vector of colors that each k-simplex has.

Algorithm 1: Seeding a single edge.

```
SimpComp* seed_single_edge(string name){
    SimpComp *edge = new SimpComp(
            name, 1);
    KSimplex *v1 =
            edge->create_ksimplex(0);
    KSimplex *v2 =
            edge->create_ksimplex(0);
    KSimplex *e1 =
            edge->create_ksimplex(1);
    v1->add_neighbor(e1);
    v2->add_neighbor(e1);
    return edge;
}
```

Algorithm 2: Coloring vertices with boundary color.

```
KSimplex *v1 =
        edge->create_ksimplex(0);
KSimplex *v2 =
        edge->create_ksimplex(0);
Color *c1 = new BoundaryColor(true);
Color *c2 = new BoundaryColor(true);
v1->colors.push_back(c1);
v2->colors.push_back(c2);
```

Following colors are currently available:

- unique ID colors
- boundary colors
- screen coordinate colors.

Additionally, user is allowed to construct a custom color and use it within the simulator. The source code of the simulator is organized as a library, and user is allowed to extend it by using the library.

Unique ID colors are predominantly used for pretty printing simplicial complexes. They are implemented by a class inherited from the basic color class. Two main fields include

 ISBN 978-86-7466-930-3

static integer number, and an integer number. The first represents the current maximum of a unique color ID that is in use, and the second one is the color of a given k-simplex.

Unlike unique ID colors, boundary colors have special meaning. Each k-simplex may contain boundary color, but it does not have to. A simplicial complex can have boundaries on k-simplices of one level lower than the dimension of the simplicial complex. For example, a triangle can have edges as boundaries.

Screen coordinate colors are used for drawing simplicial complexes on a screen. The basic graphical user interface is under development.

### *B. Pretty Printing -simplices*

Printing k-simplices includes printing of all of the fields that *Simple* class contains. This includes printing all of the neighborhood elements the k-simplex has. This is usually overwhelming for a user. Therefore, pretty printing is designed to print unique ID colors of each k-simplex in most readable way authors could think of.

Function *Simple print compact* is responsible for pretty printing. It assigns to the pointer to the unique ID a value returned by a function *get uni ueI* that returns either nullptr if a k-simplex doesn't have a unique ID, or a pointer to the color.

If there is no unique ID color assigned to a k-simplex, the output consists solely of word "Simplex". Otherwise, *print compact* function is called for a color that the pointer points to. Further, the following procedure is repeated, if level k is greater than zero and there are neighboring elements for all neighbors. A set of integer values is constructed, and then function *print ertices in parentheses s* is called for neighbors, adding unique IDs to the set. This way, printing sorted values is achieved, along with avoiding duplicate values. Sample output of a simplicial complex pretty printing is shown in Fig. 1.

## IV. CONCLUSION

We have demonstrated how one can implement in code the structure of a simplicial complex of arbitrary dimension, in a way that is faithful to its combinatorial definition, and perform the most basic operations on it, like instantiating, coloring and printing.

The implementation of the basic classes of the code described in this work represents a fundamental basic building block for a more versatile software collection that aims to construct, manipulate and study the properties of simplicial complexes of arbitrary dimension. Future extensions of the software library will include the functions which implement attaching additional simplices to a boundary of a complex, performing Pachner moves [13] which transform a given complex into a different one without changing its topology, and functions for manipulating the colors and evaluating various mathematical constructions that include them. Note that the experimental data regarding the parallelization is yet to be collected (see the accompanying paper [14]).

The resulting software collection will feature the generality and versatility that aim for applications both in pure mathematics (algebraic topology research) and theoretical physics (quantum gravity, field theory), but also with potential applications in other disciplines of engineering and industry, wherever the analysis and the study of geometry of manifolds and curved surfaces may be relevant.

## APPENDIX

Algorithm 3: Declaration of SimpComp class.

```
class SimpComp{
public:
    SimpComp(int dim);
    SimpComp(string s, int dim);
    ~SimpComp();
    int count_number_of_simplexes(
            int level);
    void print(string space = "");
    bool all_uniqueID(int level);
    void collect_vertices(set<int> &s);
    void print_set(set<int> &s);
    void print_vertices_in_parentheses(
            set<int> &s);
    void print_compact();
    // Creating new KSimplex at level k:
    KSimplex* create_ksimplex(int k);
    void print_sizes();

    string name;
    int D;
    // An element at each level
    // is a list or vector
    // of KSimplex pointers
    // to KSimplex on that level:
    vector< vector<KSimplex *> >
            elements;
};
```

Algorithm 4: Declaration of KSimplex class.

```
class KSimplex{
public:
    KSimplex();
    KSimplex(int k, int D);
    ~KSimplex();
    bool find_neighbor(KSimplex *k1);
    void add_neighbor(KSimplex *k1);
    void print(string space = "");
    UniqueIDColor* get_uniqueID();
    void print_compact();

    int k; // level
    int D; // dimension
    SimpComp *neighbors;
    vector<Color *> colors;
};
```

## ACKNOWLEDGMENT

DC and NK were partially supported by the School of

 ISBN 978-86-7466-930-3

Electrical Engineering, University of Belgrade, Serbia. NK was partially supported by the Institute of Physics Belgrade, contract no. 0801-1264/1. MV was supported by the Science Fund of the Republic of Serbia, grant no. 7745968, "Quantum gravity from higher gauge theory" – QGHG-2021. All authors were partially supported by the Ministry of Education, Science, and Technological Development of the Republic of Serbia.

## REFERENCES

[1] M. W. Hirsch, *ifferential Topology*, New York, USA: Springer Verlag, 1976.
[2] A. Hobson, "There are no particles, there are only fields", *Amer. our. Phys.* **1**, 211-223 (2013).
[3] E. H. Spanier, *Algebraic Topology*, New York, USA: Springer Verlag, 1966.
[4] C. Rovelli, *uantum Gra ity*, Cambridge, UK: Cambridge University Press, 2004.
[5] C. Rovelli and F. Vidotto, *Co ariant oop uantum Gra ity*, Cambridge, UK: Cambridge University Press, 2014.
[6] T. Radenković and M. Vojinović, "Higher Gauge Theories Based on 3-Groups", *EP* **1** , 222 (2019).
[7] A. Miković and M. Vojinović, "Standard Model and 4-Groups", *Europhys. ett.* **1** , 61001 (2021).
[8] B. Lee and A. R. Hurson, "Issues in dataflow computing," *Ad ances in computers*, Elsevier, , 285-333 (1993).
[9] V. Milutinovic, J. Salom, D. Veljovic, N. Korolija, D. Markovic, and L. Petrovic, "Transforming applications from the control flow to the dataflow paradigm," *ataflow supercomputing essentials*, Springer, Cham, 107-129 (2017).
[10] J. Popovic, D. Bojic, and N. Korolija, "Analysis of task effort estimation accuracy based on use case point size," *IET Software*, **( )**, 166-173 (2015).
[11] N. Korolija, J. Popović, M. Cvetanović, and M. Bojović, "Dataflow-based parallelization of control-flow algorithms," *Ad ances in computers*, Elsevier, **1 4**, 73-124 (2017).
[12] N. Korolija, D. Bojić, A. R. Hurson, and V. Milutinovic, "A runtime job scheduling algorithm for cluster architectures with dataflow accelerators," *Ad ances in computers*, Elsevier, **12** (2022).
[13] U. Pachner, "PL homeomorphic manifolds are equivalent by elementary shellings", *Eur. our. Combinat.* **12**, 129-145 (1991).
[14] D. Cvijetić, N. Korolija and M. Vojinović, "Possibilities for Parallelizing Simplicial Complexes Simulation", IcETRAN 2022, Novi Pazar, Republic of Serbia, June 6-9, 2022, Belgrade: Društvo za ETRAN, Beograd: Akademska misao (2022).

 ISBN 978-86-7466-930-3

# Possibilities for Parallelizing Simplicial Complexes Simulation

Dušan Cvijetić, Nenad Korolija, and Marko Vojinović

***Abstract*—This manuscript presents potentials for parallelizing simulation of simplicial comple es. The implementation of most important fields and methods of classes for storing simplicial comple es and -simplices is followed by wrapper classes for simplicial comple es and -simplices respectively. Infrastructure for communication between essage Passing Interface ( PI) processes along with helper functions is e plained further in the manuscript. nce multiple data are prepared to be sent from each PI process to other PI processes, sending and receiving is performed in the bac ground. ecause of the stall introduced by using PI directives, the amount of data to be transmitted is ma imized by processing multiple operations over simplicial comple es in parallel. This requires the method for loc ing simplicial comple es and -simplices by the owner PI process until all the requests are processed. oc ing mechanism and supporting simplicial comple class actions regarding loc ing is not in the scope of this manuscript.**

***Index Terms*— implicial comple ; -simple ; triangulation; manifold; PI; parallelization.**

## I. Introduction

In modern theoretical physics, a lot of problems are too complicated for study using analytical methods, and one needs to resort to numerical techniques. Among those problems, an especially important class deals with evaluation of functions over simplicial complexes. A simplicial complex [1] is a piecewise-linear approximation of a smooth spacetime manifold [2] and is typically 4-dimensional or higher. Functions over a simplicial complex represent physical fields on spacetime, and one commonly employs path integral evaluations of such structures to extract expectation values of observables. For example, in Lattice Quantum Chromo-dynamics, one employs such numerical techniques to predict the theoretical values for the masses of elementary particles called hadrons [3]. Also, in Causal Dynamical Triangulations approach to quantum gravity [4,5], one uses these techniques to evaluate spectral dimension of spacetime, and study various properties of phase space of triangulated manifolds. Finally, in the Regge Quantum Gravity approach [6,7,8] one can study the entanglement properties of matter fields and gravity described by the Hartle-Hawking wavefunction [9,10], again using the techniques of numerical evaluation of path integrals over simplicial complexes.

It goes without saying that all such calculations are exceptionally expensive in computation time. Typically, one develops custom-made code, heavily optimized to solve precisely one specific problem, and executes it over months-long periods on hardware dedicated for high performance computing (HPC), usually clusters with thousands of work nodes. Such enormous calculational efforts are usually unavoidable due to the nature of the problems that need to be solved.

Nevertheless, at least for one class of such problems, it may be possible to construct a more general algorithm and structures which would provide a common basis for solving an all-encompassing class of problems using the same underlying software, while intrinsically exploiting the parallelization possibilities of the code itself and the distributed nature of the underlying hardware. Our aim is to develop such a generic software library, which could be used to solve a whole host of physics problems in the same way and optimize it for parallelized HPC environments. In this work we present the first steps towards the construction of such a library. This approach of developing common code for a whole class of problems has not been attempted so far because research teams are usually concentrated on solving only one specific problem and opt to construct custom code for that problem. However, in our opinion, a generic software library, which would provide support for a whole class of problems simultaneously, would open new avenues for numerical research, since one could use the same code to study new, yet unexplored problems as well as old well-known ones.

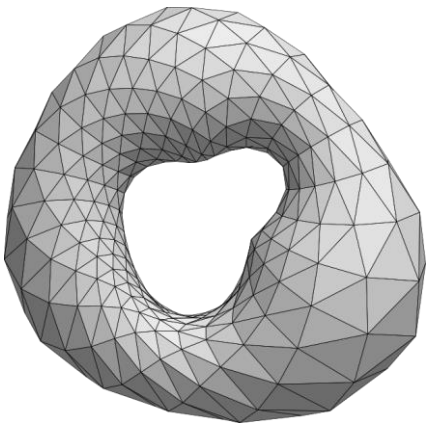

Fig. 1. Simplicial complex of a torus (source: Wikipedia).

The fundamental structure which lies at the core of the whole numerical method is the notion of a *simplicial comple* . A simplicial complex is a combinatorial structure which is easiest to understand as a generic lattice-like mesh,

Dušan Cvijetić is a student of the School of Electrical Engineering, University of Belgrade, 73 Bulevar kralja Aleksandra, 11020 Belgrade, Serbia (e-mail: dusancvijetic2000 @ gmail.com).

Nenad Korolija is with the School of Electrical Engineering, University of Belgrade, 73 Bulevar kralja Aleksandra, 11020 Belgrade, Serbia (e-mail: nenadko @ etf.bg.ac.rs).

Marko Vojinović is with the Institute of Physics, University of Belgrade, Pregrevica 118, 11080 Pregrevica, Serbia (e-mail: vmarko @ ipb.ac.rs).

 ISBN 978-86-7466-930-3

whose cells are called *simplices*, and are connected to each other along their boundaries to form the simplicial complex of a given dimension. The purpose of the whole structure is to approximate the smooth spacetime manifold with a discrete structure which is more convenient for numerical methods.

The most elementary simplex is a simplex of level zero, often called *0-simple* or *erte* – it is just a dimensionless point with no structure. Next is the *1-simple* , also called an *edge* – it is a one-dimensional line with two vertices at its boundaries. At level two we have the *2-simple* or *triangle*, whose boundary are three edges and their vertices. The *3-simple* , also known as the *tetrahedron*, has the boundary made of four triangles and their edges and vertices. The procedure of constructing simplices can be done for arbitrary dimension, giving rise to the notion of a *k-simple* , whose level (i.e. natural dimension of space in which it is defined) is equal to any positive integer k. The most commonly used example is the *4-simple* , also called *pentachoron* – a 4-dimensional figure whose boundary consists of 5 tetrahedra, 10 triangles, 10 edges and 5 vertices. In most applications in physics, the spacetime manifold is considered to be 4-dimensional, and it is cut into a lattice-like structure made of 4-simplices, which are glued together along their boundary tetrahedra. The resulting structure is a simplicial complex of dimension 4. Fig. 1 depicts an intuitive example of a 2-dimensional simplicial complex of a torus.

Given a simplicial complex, one typically wants to introduce functions that are evaluated on it. These are commonly called *colors* and are assigned via their values to each k-simplex within in the complex. In other words, some colors live on vertices, some on edges, some on triangles, and so on. The colors are a natural discretization of the notion of a *field* over a manifold. For example, just like electric and magnetic fields have a value at each point of a smooth spacetime, analogously the colors have values at each k-simplex in the simplicial complex.

Depending on the type of the problem at hand, algorithms that are used to evaluate required quantities on a simplicial complex can vary in complexity, from conceptually simple Monte Carlo integration techniques, to vastly complicated traversal and ray-tracing algorithms, to various methods for solving functional partial differential equations. Due to the variability of the complexity of all these algorithms, dictated by the nature of the problem at hand, it is helpful to develop the underlying software simulator to exploit the parallelization avenues that are intrinsic to the simplicial complexes and k-simplices themselves, so that the simulator can exploit parallel hardware environments even for algorithms that are themselves hard to parallelize. This helps the code developer with overall optimization and application to HPC hardware architectures. In what follows, we shall demonstrate a set of possible approaches to these intrinsic parallelization techniques.

## II. N-Dimensional Simplicial Complexes

This section describes data structures used in the simulator of simplicial complexes from the point of view of their suitability for parallelizing the simulator execution. Data demanding structures are of main interest for optimizing the communication between processing units. Along with those, data that describes the structure and needs to be updated on multiple processing units will be described in detail. Further, the amount of data that needs to be exchanged and the frequency of expected changes will be compared to the pyramid, where top elements demand less memory, but require more often communication.

The parallelization is simulated using the MPI framework. The simulator is implemented in C++, and, as a result, the parallelization framework is built on top of the simulator. As improving the simulator of simplicial complexes is an ongoing process, the possibility for accelerating the computation is simulated based on the requirements.

Simplicial complexes are formed out of k-simplices at various levels. Simplicial complexes at level zero represent vertices. The structure of each vertex is stored in *Simple* class. Simplicial complexes at level one represent edges. Each edge consists of two vertices. As it is the case with vertices, information about edges are also kept in a *Simple* class. However, while vertices can be independent of other vertices, representing separate simplicial complexes, each edge must have at least two vertices defined as neighbors. Neighbor of an k-simplex is defined also as a k-simplex that the first k-simplex relies on. Neighboring relation is symmetrical. Therefore, if two vertices are neighbors of an edge, edge is also the neighbor of both vertices. Further, edges can form a triangle. By analogy, neighbors of triangle are three edges, but also the triangle is neighbor of these edges. The neighboring relation spans more than one level up or down. The triangle has also three vertices as neighbors and the opposite.

Simplicial complex representing a triangle consists of a k-simplex representing a triangle along with all neighbors of the triangle. Simplicial complex class is used for storing information about simplicial complexes. As it has elements field that is a pointer to pointer of k-simplices, it is also used for keeping neighbors of each k-simplex.

## III. Parallelizing Simplicial Complexes Simulation

Parallelizing operations over simplicial complexes is implemented by splitting the structure over multiple MPI processes. First, we can consider a single simplicial complex system, as the most general approach. If no screen coordinates for k-simplices are assigned, we can artificially assign this type of color, so that we can present k-simplices in 2D space. Further, we can imagine multiple planes, where each plane is responsible for keeping k-simplices of one dimension. This way, we can consider n-dimensional simplicial complex as a pyramid that we observe from the bird's eye view. Now we could have a bottom-up approach, where k-simplices of dimension zero are divided onto MPI processes based on their screen coordinates. Going up, each MPI process would store higher dimensional k-simplices that have those that are one level below as their neighbors. When a k-simplex has neighbors on one level below that belong to multiple MPI processes, this k-simplex gets copied to all MPI processes involved. Finally, all MPI processes would keep the highest-level k-simplex. In the case of multiple simplicial complexes, they could be split over MPI processes based on the same bottom-up approach.

 ISBN 978-86-7466-930-3

The notion of determining the MPI process where a k-simplex is located is hidden by using wrapper functions, so that the calculation operations are performed as if all k-simplices would have been on the same MPI process, i.e. as if the simulation was executed serially. Each wrapper function can keep either a pointer to the structure, if it exists on the same MPI process, and the ID used for finding the structure on the owner MPI process.

Algorithm 1 describes the most important aspects of simplicial complex classes. First, a basic *SimpComp* class is given, followed by the wrapper class *irtualSimpComp* used for parallelization.

Algorithm 1: Declaration of simplicial complex classes.

```
class SimpComp{
public:
    SimpComp(int dim);
    SimpComp(string s, int dim);
    ~SimpComp();
    // Creating new KSimplex
    // at level k:
    VirtualKSimplex* create_ksimplex(
        int k);
    void update_owner(int owner);

    string name;
    int D;
    vector< vector<
        VirtualKSimplex *> > elements;
};
class VirtualSimpComp{
public:
    SimpComp *find_simpcomp;

    int id;
    int ownerRank;
    SimpComp *simpComp;
};
```

Algorithm 2 describes the most important aspects of k-simplices classes. A basic *Simple* class is followed by the wrapper class *irtual Simple* used for parallelization.

Algorithm 2: Declaration of k-simplex classes.

```
class KSimplex{
public:
    KSimplex();
    KSimplex(int k, int D);
    ~KSimplex();
    bool find_neighbor(
            VirtualKSimplex *k1);
    void add_neighbor(
            VirtualKSimplex *k1);

    int k; // level
    int D; // dimension
    VirtualSimpComp *neighbors;
    vector<Color *> colors;
};
class VirtualKSimplex{
public:
    KSimplex *find_ksimplex();

    int id;
    int ownerRank;
    KSimplex *ksimplex;
};
```

In both algorithms, wrapper functions store a pointer to the base class object, if such exists on a local MPI process. Otherwise, the value is *nullptr*, and the data is searched for on the so called *owner ank* based on unique identifier called *id*. Owner of this k-simplex can issue multiple requests while it holds a lock.

## IV. Infrastructure for Communication Between MPI Processes

The communication between MPI processes is organized as follows. Each MPI process is preparing the data to be sent to other MPI processes. Order of operations prepared for other MPI processes is not important. All requests to other MPI processes for processing are packed in to_rank vector of vectors of unsigned char.

Each type of primitive data is serialized into the array of unsigned characters as it will be explained in the following section. Each prepared byte is pushed to the back of the vector of unsigned characters. Once all the data is prepared, the data is sent to other MPI processes in the background using *MPI Isend* directive. If a reference to the vector of array of unsigned characters is called *ec*, the pointer to the array is obtained by calling member function *data* of vector class from standard template library. After issuing all *MPI Isend* directives, waiting for each of sending to finish is achieved using *MPI Wait*.

Similarly receiving the data from other MPI processes is implemented in the background using *MPI Irec* , followed by *MPI Wait*, once the data is needed for the processing. The data is received into array of unsigned characters, that is further packed into vector of vectors of unsigned characters called from_rank for simple processing.

## V. MPI Supporting Functions

As already mentioned, variables are serialized into the array of unsigned characters using the following syntax:

```
*( (__typeof__ (variable) *) (array + nArray) ) = variable;
nArray += sizeof(variable);
```

Here, *array* is array of unsinged characters where the data stored in the variable is serialized, and *nArray* is the number serialized bytes in the array.

Similarly, a variable is read and prepared into the to_rank using the following syntax:

```
__typeof__ (variable) temp_var = variable; \
int nBytes = sizeof(temp_var); \
for(int iByte = 0; iByte < nBytes; iByte++) \
  to_rank[rankNumber].push_back(
      ((unsigned char *) &temp_var) [iByte] );
```

This can be further optimized, but the optimization is out of the scope of this research.

 ISBN 978-86-7466-930-3

The communication between MPI processes is continued for as long as any MPI process requires further communication with other MPI processes. This is achieved using the following source code, where the MPI process that requires further communication sets variable *to_send* to one:

```
int to_receive = 0; // A rank required communication
MPI_Allreduce(&to_send, &to_receive, 1, MPI_INT,
    MPI_SUM, MPI_COMM_WORLD);
```

After *MPI Allreduce* is executed, all MPI processes will have the information whether they have to communicate further in *to_receive* variable.

## VI. Parallelization Possibilities Using Dataflow Paradigm

This simulator issues the same set of computer architecture instructions repeatedly. As in majority simulator of physical phenomena, the number of instructions is dependent on the precision of the model and is limited by the computing resources and the total simulation time requirement. These conditions are exactly what is required for a program to be suitable for acceleration using the dataflow paradigm [11]. Programming dataflow architectures requires programming skills that are higher than those needed for programming conventional von Neumann architectures. One of the possibilities is to write a program in a VHDL. More suitable solution to most of the programmers would be to exploit the framework that enables writing source code in a Java-like language, which gets automatically translated into the FPGA image [12,13]. Even in this case, the effort needed for programming such architectures is higher [14]. Besides programming dataflow architecture for the simplicial complex simulator, appropriate scheduling scheme is also needed for efficient running of multiple jobs simultaneously [15].

As the number of operations that can be applied to simplicial complexes can lead to several days' simulation time or even more, having in mind the aging and the probability of failure of supercomputing nodes [16], we have decided to write restarts after given number of simulations defined by the user, so that the calculation can continue from the last stored state.

## VII. Conclusion

In this work we have presented the basics of the paralellization techniques that can be applied to the structure of a simplicial complex, which underlies a host of research problems in theoretical physics (see also our accompanying paper [17]). These problems tend to be computationally extremely expensive, and the common underlying software that enables parallelization at the level of the basic data structure can possibly go a long way towards optimization of code for numerical study using heavily parallel hardware platforms such as HPC clusters. In particular, the simplicial complex naturally allows for various aspects of parallelization, and we have described the basic classes, corresponding MPI communication infrastructure, supporting functions and the dataflow paradigm employed for the construction.

One should note that our work represents just a first step towards a full working software implementation, and much more effort is needed to properly implement, optimize and test the resulting code in real world environments. All that is the topic for future work. In particular, the data regarding the experimental evaluation, which would compare the proposed parallelization method to ordinary sequential methods still needs to be gathered and analyzed. Nevertheless, this first step is fundamental, and it is conceptually important since it represents a paradigm in which parallelization is implemented dominantly at the level of the simplicial complex as the underlying data structure, rather than at the level of the particular algorithm that aims to solve some particular problem using these data structures.

Finally, we note that our code, once properly developed, may possibly find applications not just in theoretical physics, but also in other disciplines of science, technology and engineering.

## Acknowledgment

DC and NK were partially supported by the School of Electrical Engineering, University of Belgrade, Serbia. NK was partially supported by the Institute of Physics Belgrade, contract no. 0801-1264/1. MV was supported by the Science Fund of the Republic of Serbia, grant no. 7745968, "Quantum gravity from higher gauge theory" – QGHG-2021. All authors were partially supported by the Ministry of Education, Science, and Technological Development of the Republic of Serbia.

## References

[1] E. H. Spanier, *Algebraic Topology*, New York, USA: Springer Verlag, 1966.
[2] M. W. Hirsch, *ifferential Topology*, New York, USA: Springer Verlag, 1976.
[3] S. Durr, Z. Fodor, J. Frison, C. Hoelbling, R. Hoffmann, S. D. Katz, S. Krieg, T. Kurth, L. Lellouch, T. Lippert, K. K. Szabo and G. Vulvert, "Ab-initio Determination of Light Hardon Masses", *Science* **22**, 1224-1227 (2008).
[4] J. Ambjorn, A. Goerlich, J. Jurkiewicz and R. Loll, "Nonperturbative Quantum Gravity", *Phys. ep.* **51** , 127 (2012).
[5] M. Vojinović, "Causal dynamical triangulations in the spincube model of quantum gravity", *Phys. e .* **4**, 024058 (2016).
[6] T. Radenković and M. Vojinović, "Higher Gauge Theories Based on 3-Groups", *EP* **1** , 222 (2019).
[7] A. Miković and M. Vojinović, "Standard Model and 4-Groups", *Europhys. ett.* **1** , 61001 (2021).
[8] A. Miković and M. Vojinović. "Quantum gravity for piecewise flat spacetimes", *SFIN* **I**, 267 (2018).
[9] N. Paunković and M. Vojinović, "Gauge protected entanglement between gravity and matter", *Class. uant. Gra .* **5**, 185015 (2018).
[10] J. B. Hartle and S. W. Hawking, "Wave function of the Universe", *Phys. e .* **2** , 2960 (1983).
[11] B. Lee and A. R. Hurson, "Issues in dataflow computing," *Ad ances in computers*, Elsevier, , 285-333 (1993).
[12] V. Milutinovic, J. Salom, D. Veljovic, N. Korolija, D. Markovic, and L. Petrovic, "Transforming applications from the control flow to the dataflow paradigm," *ataflow supercomputing essentials*, Springer, Cham, 107-129 (2017).
[13] N. Korolija, J. Popović, M. Cvetanović, and M. Bojović, "Dataflow-based parallelization of control-flow algorithms," *Ad ances in computers*, Elsevier, **1 4**, 73-124 (2017).
[14] J. Popovic, D. Bojic, and N. Korolija, "Analysis of task effort estimation accuracy based on use case point size," *IET Software*, **( )**, 166-173 (2015).

 ISBN 978-86-7466-930-3

[15] N. Korolija, D. Bojić, A. R. Hurson, and V. Milutinovic, “A runtime job scheduling algorithm for cluster architectures with dataflow accelerators,” *Ad ances in computers*, Elsevier, **12** (2022).
[16] K. Huang, Y. Liu, N. Korolija, J. M. Carulli, and Y. Makris, “Recycled IC detection based on statistical methods,” *IEEE transactions on computer-aided design of integrated circuits and systems*, **4( )**, 947-960 (2015).
[17] D. Cvijetić, N. Korolija and M. Vojinović, “Infrastructure for Simulating n-Dimensional Simplicial Complexes,” IcETRAN 2022, Novi Pazar, Republic of Serbia, June 6-9, 2022, Belgrade: Društvo za ETRAN, Beograd: Akademska misao (2022).

 ISBN 978-86-7466-930-3

# The Evolution of Big Data Analytics Solutions in the Could

Danko Miladinović, Jovan Popović, and Nenad Korolija

***Abstract*— ig data analytics is a very important topic both for enterprises, science, and government institutions. The amount of data that is generated is e ponentially increasing and the need to analyze data is more important every year. ig data analytics evolved over the past decade from a large on-premises infrastructure for storing and processing data to modern cloud environments. In this paper we discuss how big data analytics evolved over the years and what are the future trends in this area.**

***Index Terms*— ig data; cloud; analytics; machine learning; databases.**

## I. INTRODUCTION

BIG data analytics is one of the most important topics in the IT industry. There is a well-known "Data is the new oil" expression that points out the importance of data analytics that can have a huge effect on modern businesses and economy.

Most of the enterprises either leverage information from their data or plan to extract information from the data they own. Data science and analytics became more important for strategic growth of many organizations.

The organizations and software systems are continuously increasing the amount of data that is generated. Relatively big organizations must face the large amount of data that contains the information important for business decisions. Globally, we are now talking about the Exabyte to Zettabyte scale of data that needs to be processed. The global estimates are that the amount of data to be processed would reach multiple Zettabytes in this decade [1].

In this paper we discuss the industry trends and standards for big data analytics with a focus on data analytics in the cloud. This manuscript describes the solutions offered by the open-source community and the biggest commercial data analytics vendors that pave the way that will be followed by companies. The rest of the document is organized in the following sections:

- In the first section, we will talk about the main problems that impact big data analytic solutions.
- The cloud analytics section describes what are the main benefits of the cloud environments for big data analytics.
- Data analytic solutions section describes the two mainstream approaches for storing and analyzing data: Datawarehouse and Datalakehouse solutions.
- In the data format section, we will discuss the most important aspect of big data analytics – the format that is optimized for storing data.
- The conclusion section summarizes the trends for modern big data analytics.

Danko Miladinović is with the School of Electrical Engineering, University of Belgrade, 73 Bulevar kralja Aleksandra, 11020 Belgrade, Serbia (e-mail: danko@etf.bg.ac.rs).

Jovan Popović is with the Microsoft Research and Development Center, Belgrade. Španskih boraca 3/3, 11000 Belgrade, Serbia (e-mail: jovanpop@microsoft.com).

Nenad Korolija is with the School of Electrical Engineering, University of Belgrade, 73 Bulevar kralja Aleksandra, 11020 Belgrade, Serbia (e-mail: nenadko@etf.bg.ac.rs), (https://orcid.org/1234-1234-1234-123X).

## II. PROBLEM STATEMENT

The main problem in big data analytics is the size of data. There are many problems that can be solved by analyzing data stored in files and spreadsheets containing gigabytes of data, or even the relational or NoSQL databases that can contain and process terabytes of data. However, there are many domains where the data contains petabytes of data that cannot be stored in a limited set of files or classic database systems.

The researchers and engineers tried to solve the problem of big data processing using the following approaches:

- Datawarehouses that try to stretch the capabilities of the relational databases by applying distributed processing over large data.
- File-based processing systems that try to build an infrastructure for storing a large amount of data. One of the most widely used solutions is Hadoop with HDFS file system [2].

The big data analytic solutions must ensure that users can store Exabyte scale data and ensure that there is enough compute power to process the data when needed. The infrastructure teams must ensure that they have enough hardware (processors and disk storage) to fulfil the user needs, but at the same time to ensure that the resources are not underutilized or constantly over-provisioned.

Solving the problem of ensuring the required resources for big data analytics, but at the same time not over-provisioning them, appeared to be too hard for the on-premises infrastructure. Planning for the resources could not be both cost effective and ensure enough capacity that will be utilized for most of the time.

Therefore, most of the organizations tried to solve this resource management problem in the cloud making the cloud analytics the mainstream in the big data analytics space.

## III. THE CLOUD ANALYTICS

Over the past years, the clouds became a very important

 ISBN 978-86-7466-930-3

choice for modern big data analytics. There are three main benefits of cloud infrastructure that make them important for big data analytics:

- Large amount of storage that could be used to store any amount of data. The "Data Lake" [3] is a commonly used term for virtually unlimited storage where the organizations might store petabytes of data. As the amount of data rapidly rises, the organizations need to have an infrastructure that will guarantee that they can easily store Exabytes of data, and with the possibility to scale to Zettabytes in the future.
- Large amount of available compute power that could be used for data processing [4]. The compute power needed to analyze data is proportional to the data size and might easily span to the thousands of CPU cores needed to complete the data analytic tasks.
- Cloud resources can be used on-demand and released when they are not needed. This is one of the main reasons for choosing the cloud environment. Most of the data analytic jobs are not continuously processed and might require thousands of CPU cores for data processing, and then suddenly release all the resources. Cloud providers solve this problem using the economy of scale – with the large number of customers there is a high probability that someone will use them once others release them.

We should note that the could environment is not an absolute requirement to have an infrastructure for storing a large amount of data and use thousands of computer cores to process the data. The organizations might use their own data centers, supercomputers, and any custom-built architecture that will organize hundreds or thousands of computers that process the data. This was a common solution for the organizations who built their own Hadoop/HDFS infrastructure [2] for in-house analytics. However, the cost of management includes the need to maintain and replace the hardware, ensure that the infrastructure has enough compute power to satisfy the peak processing, but also to make sure that the capacity is not too underutilized during the period when nobody is executing analytic jobs.

The current trend is that most of the organizations are deciding to delegate the resource management to the cloud providers and utilize the resources on-demand when they need to run some analytics.

The data analytics solutions should not be misguided with the infinite scale claims of the cloud vendors. Cloud environments are built as many computers that are working together to process tasks. The applications see the sum of the compute power, memory, and storage allocated to the computers that are executing the tasks. In many scenarios, this setup can provide "the infinite scale" promise for a variety of applications such as web applications, easily parallelizable functions or jobs, or the classic databases that might not require a constant compute power of up to 128 cores. This kind of infrastructure is the ideal choice for scaling out the large number of small compute units such as microservices, functions that might need to quickly replicate to. These kinds of solutions made of a large number of micro-compute units are perfect for the cloud environments where each unit can be deployed on some available compute node in the cloud [5]. However, these solutions will rarely require an atomic compute unit between 64 and 128 cores. The big data analytics solutions with the demand to store and process petabytes of data might require compute power that can challenge the infinite scale promise of the clouds. In the big data analytics solutions, we can see the impact of the physical infrastructure where the components that process data might require a large amount of CPU or memory needed to decompress the large files and process the information. Therefore, migrating data to cloud and running the analytical functions in the compute provided by the cloud are not enough. In practice, data analytics solutions require specialized services such as cloud Datawarehouse [6] or cloud Datalakehouse [7] solutions, that are able to efficiently combine the physical resources in the cloud and optimally process data.

## IV. THE DATA ANALYTIC SOLUTIONS

Data analytics solutions provide infrastructure and tools for the analysts and the business users that enable them to store and analyze data. There are two main classes of data analytic solutions:

- The Datawarehouse solutions that represent centralized data storage with API for analyzing data and implementing the business intelligence solutions [6].
- The Lakehouse solutions represent the analytical solution running on the storage that is detached from the analytical engine [7].

Both classes of the solutions are aware of the underlying infrastructure and designed to optimally process large amounts of data. The main differences between Data Warehouse and Data Lakehouse solutions are given in Table I.

TABLE I
THE KEY DIFFERENCES BETWEEN DATA WAREHOUSE AND DATA LAKEHOUSE

| | Warehouse | Lakehouse |
|---|---|---|
| Data format | Proprietary and highly optimized. | Based on open specifications. |
| Data location | Internal – data is ingested from the external source. | External – data is placed on the original locations. |
| Data access | Through the predefined API or protocol (SQL) | Direct file access using the storage API |

The main trade-off between Datawarehouse and Data Lakehouse solutions is the choice between the interactive and the real-time analytics. The Datawarehouses store data in the data format optimized for analytics, which enables them to

 ISBN 978-86-7466-930-3

complete the queries in second-to-minute time span. However, they require data engineers to load data from the actual locations into the Datawarehouse, meaning that the data analysts work with the snapshot of the data taken at the load time. The Lakehouses reference original data in the lakes without a need to ingest the data. However, the raw format of the data cannot guarantee sub-second or even sub-minute performance. Despite the differences, both Datawarehouse and Datalakehouse solutions are used in practice. The following sections describe the main characteristics of these solutions.

*A. Warehouse solutions*

The traditional database systems containing data used for the analytics are Datawarehouse solutions. Datawarehouse solutions have existed for decades, have well defined techniques for designing Datawarehouse schema [8, 9], and a variety of tools available for advanced data analytics. For a very long time, Datawarehouses were the mainstream solutions for storing and analyzing huge data volumes. The top vendors such as Oracle, Teradata, and Exadata are still enabling enterprises to store and analyze large amounts of data.

The main idea with the Datawarehouse solution is that the data required for analytics must be ingested into the internal data format that is highly optimized for analytics. The advantage of this approach is the performance. Internal and in many cases proprietary format contains optimizations that are not available in the open-source solutions. In the past, the proprietary format gave the Datawarehouse performance advantages compared to other analytic systems.

The main issues in the Datawarehouse solutions are the facts that the underlying infrastructure must enable Datawarehouse to store all required data, which puts a burden on the administration teams, and the cost of the solution that includes the resources that are always allocated to the Datawarehouse system even if it is not used. The Datawarehouse solutions were the first choice for most of the analytic teams who need interactive analytics, but the total cost of ownership (TCO) in many cases does not justify the solution.

Amazon made a breakthrough in the Datawarehousing technology with the release of Redshift [10] – a cloud-native Datawarehouse service that provides full data warehousing experience exposed as a cloud service. The customers got the ability to provision the Datawarehouse service, load the data, and define the compute needed to analyze the data. The biggest advantage of cloud Datawarehouse is the resource elasticity that solved the main drawback of the classical Data warehousing solutions – the TCO. Unlike the on-premises Datawarehouse that had pre-build resources, the cloud Datawarehouse enabled organizations to scale up and down the resources depending on the needs. The organizations could load a large amount of data without worrying about the underlying storage capacities, scale-up the compute power of the Datawarehouse when needed, and scale it down to reduce the cost when there is no need for processing the data. The cloud Datawarehouse provided by Amazon fulfilled the main requirements of the classical warehouses and added elasticity. Other vendors followed this approach and now we have many cloud data warehousing solutions such as Azure Synapse Datawarehouse [11], Google BigQuery [12], Snowflake [13], etc. All vendors are trying to combine all the benefits of the classical Datawarehouse with the elasticity and scale of the cloud.

The modern cloud Datawarehouses solve the problem of elasticity and scale on-demand that cannot be easily solved in the on-premises Datawarehouses. However, there is still one downside – the data must be ingested from the external data sources into the Datawarehouse internal data format, which causes a lag between the latest data and the data available for the analytics.

*B. akehouse solutions*

In cloud environments the data is stored in the Data lakes. The Data lake is a logical storage space where the organizations can store the exabytes of data, get the best throughput for reading raw files, ensure redundancy that can span across multiple geographical regions and data centers. The Data lake seems like a perfect solution for storing data. The only drawback of Data lake is that they do not provide the ability to analyze the data in the lake.

The first successful attempt to provide analytic capabilities over large storage was Hadoop – a distributed system that enabled the analyst to analyze a large amount of data stored in the distributed system called Hadoop file system (HDFS). This setup enabled the analyst to analyze data, but the performance of Hadoop is far from interactive. Apache Spark [14] is one of the most popular platforms that enabled analysts to do efficient analytics on the lake. Apache Spark became mainstream in the data lake solutions. One of the most common query engines used to implement the Lakehouse pattern is Apache Spark. Apache Spark is an open-source distributed query system licensed under Apache License 2.0. Spark enables advanced data analytics, management, and updates, and provides a rich and powerful set of APIs to analyze data.

The main idea of Lakehouse architecture is the separation of compute and storage. The compute is a query engine or data processing engine that is detached from the storage, and the data is placed in Data lake where it can be accessed by any query. The compute engine fetches data from the remote Data lake and return data to the analysts once the processing is completed.

Many commercial vendors offered their own implementation of Data Lakehouse services. Nowadays, we have many Lakehouse-type solutions that are offered on different clouds such by Databricks (proprietary version of Apache Spark code implemented by the founders of Spark), Azure Synapse, etc. The main characteristics of these solutions is that they are always referencing the externally stored data, and don't require data to be ingested to start analytics. This enables real-time insight into the latest version of data without the need to wait for the daily data loads to

 ISBN 978-86-7466-930-3

finish before starting the analytics.

One of the main concerns in the Lakehouse solution is whether they would be able to match the performance of Warehouse solutions. Traditionally, the proprietary format used in Datawarehouse solutions was the main competitive advantage compared to the original data formats stored in Data lake. Databricks announced that they have set a new world record in 100TB TPC-DS, the gold standard performance benchmark for data warehousing [15]. The test was performed in Barcelona supercomputing center and officially submitted as TPC-DS result that outperformed the previous record by 2.2x. This was the first Lakehouse-class solution that set the record in an official Datawarehouse benchmark and proved that the Lakehouse architectures can compete with the modern Datawarehouse solutions. One of the key reasons for this kind of success of Lakehouse solution is that they are using the optimized storage file format that matches the proprietary internal formats used in the Datawarehouse solutions.

More insights into data lake solutions and current trends can be found in the literature, including what steps are needed to adopt the cloud concept in data analytic solutions [16].

## V. DATA FORMAT

One of the most important design decisions that will impact the efficiency of the data analytics is the choice of the file format that will be used to store the data. Most of the data used for analytic purposes is stored in a plain textual format represented as a delimited text (for example comma separated values – CSV, tab-separated values – TSV, etc.). The documents containing tabular data are represented as Open Office or Microsoft Office formats. Although these data formats are very common, they are inefficient for big data analytics.

There is an additional class of plain textual data represented in JSON format. The JSON format is the standard format in many Internet of Things (IoT) applications where the IoT devices send the messages in JSON format, or the messages that will be eventually stored in JSON format [17]. JSON format provides flexibility for changing the structure of data but complicates the analytics because it requires a parser that is more complex than the plain delimited text parser.

In the practice, the data analysts could analyze data stored in CSV, JSON and other commonly used formats. However, since these formats are not optimized for analytics, it was very hard for data analysts to extract valuable information with performance that matches performance of database systems.

The proprietary data formats that are used to store data in Datawarehouse solutions were the biggest competitive advantage of the Datawarehouse systems compared to the open-source solutions. The optimized formats with high compression, columnar organization of data, and vectorized processing was the main reason why the data analytics teams used the Datawarehouse solutions.

In the open-source community multiple advanced formats are proposed that are designed to optimize the storage format and improve the performance of analytics. Examples are Row Columnar (RC)[18] or Optimized Row Columnar (ORC)[19] file format. The idea of these formats was to define binary representation of data prepared for analytics and optimize access for the analytical jobs. However, the open-source format that took most of the market share became Parquet format [19]. Parquet format is an open-source format that introduces most of the benefits that exist in the proprietary Datawarehouse formats, such as:

- Column organization – the data is physically separated into column segments instead of rows. The column segments contain all cell values from the same column. The columnar organization enables the analytical queries that read 2 columns out of 100 columns to read only 2% of data on average. Since the analytical queries aggregate the measures and summarize them by few columns, the columnar organization introduces most of the performance benefits for the analytical queries.
- Row-groups – columns are divided into row–groups (for example 100.000 rows represent a row group that will be split into the columns) The column segments within the row groups contain some statistical information about cells such as min/max values.
- Compression – There are some compression techniques such as run-length encodings (RLE) [20] that can be applied on the Parquet files to achieve excellent 10-100x compression, which matches the compression in the proprietary Datawarehouse formats. The main impact is not just storage savings. Compressed storage decreases IO requests sent to the storage and improves data throughput that analytical tools can use to fetch the data.
- Non-relational types – Parquet is not limited to strongly defined types and enables storing objects and arrays. The organization of complex types in Parquet format is described in [21].

The Parquet format became the mainstream in data analytics. Although there are other formats that are used in practice, the Parquet format is getting the highest market share and we can expect that the majority of data will be stored in the Parquet format. Therefore, any modern big analytical solution must be based on the Parquet format, or some enhancement based on Parquet. Even if the new file format arrives in the future, there is a high chance that most data will be stored in the Parquet format.

Although the Parquet format is designed to store analytical data that should be read-only (or append-only), there is a need to enable data engineers to make updates to the data. There are several updateable formats (such as Delta Lake [22]), that combine the excellent storage format for analytics and provide ACID guarantees of the operations that managed data. Another possible advancement includes parsing big data using the dataflow paradigm [23] by transforming automatically the parsing software [24] and using appropriate scheduling techniques [25] for the dataflow supercomputing architecture.

 ISBN 978-86-7466-930-3

## VI. Conclusion

Big data analytics solutions evolved from the original on-premises based big Datawarehouse solutions to modern cloud based Datawarehouse solutions. The original on-premises Datawarehouse solutions enabled organizations to store large amounts of data and analyze data with acceptable performance. However, these kinds of solutions failed to enable scalability and elasticity. Cloud computing can scale resources on-demand. Data lake that can store Exabytes of data with guaranteed replication, and advances in the opensource file formats disrupted the Datawarehouse solutions in big data analytics. Although Datawarehouse solutions evolved and have been adapted for the modern cloud environments, architectures with full separation of compute power and storage, where the compute can scale when needed, have a direct access to the latest version of data in the lake, and the performance that match modern Datawarehouses. In addition to matching all features that were historically considered as the advantage of Datawarehouse, the Lakehouse solves the issue that fundamentally cannot be solved with Datawarehouse solutions – data ingestion. Lakehouse solutions are able to access the original data in the Data lake and don't require an explicit process to load external data. Without performance degradation compared to internal data formats used in Datawarehouse solutions, direct access simplifies data management process by avoiding the additional processes that constantly move the data and also enable analyst to get the data without any delay.

By looking at the modern trends, we can conclude that the future of big data analytics will be based on the cloud environments and Lakehouse architectures. The cloud Data Lakehouse solutions leverage all benefits of the cloud and match performance of the Datawarehouse solutions. The cloud Data Lakehouse solutions can be considered as a primary solution for most of the future research and as the mainstream and preferred technology for development projects.

## Acknowledgment

DM and NK are partially supported by the School of Electrical Engineering, University of Belgrade, Serbia and by the Ministry of Education, Science, and Technological Development of the Republic of Serbia. NK is partially supported by the Institute of Physics Belgrade, contract no. 0801-1264/1.

## References

[1] P. Chauhan, M. Sood, "Big Data: Present and Future," The IEEE Computer Society, (2021), DOI: 10.1109/MC.2021.3057442.

[2] S. G. Manikandan, S. Ravi, "Big Data Analysis Using Apache Hadoop," International Conference on IT Convergence and Security (ICITCS), pp. 1-4, (2014). doi: 10.1109/ICITCS.2014.7021746.

[3] E. Zagan, M. Danubianu, "Cloud DATA LAKE: The new trend of data storage," 3rd International Congress on Human-Computer Interaction, Optimization and Robotic Applications, 1-4 (2021), doi: 10.1109/HORA52670.2021.9461293.

[4] I. Hashem, I. Yaqoob, N. Anuar, S. Mokhtar, A. Gani, A., and S. Khan, "The rise of "big data" on cloud computing: Review and open research issues", Information Systems, Volume 47, 2015, Pages 98-115, ISSN 0306-4379.

[5] R. Han, L. Guo, M. M. Ghanem and Y. Guo, "Lightweight Resource Scaling for Cloud Applications," 12th IEEE/ACM International Symposium on Cluster, Cloud and Grid Computing, 644-651, (2012). doi: 10.1109/CCGrid.2012.52.

[6] G. Garani, A. Chernov, I. Savvas and M. Butakova, "A Data Warehouse Approach for Business Intelligence," 2019 IEEE 28th International Conference on Enabling Technologies: Infrastructure for Collaborative Enterprises, 70-75 (2019). doi: 10.1109/WETICE.2019.00022.

[7] D. Oreščanin and T. Hlupić, "Data Lakehouse - a Novel Step in Analytics Architecture," 44th International Convention on Information, Communication and Electronic Technology, 1242-1246 (2021). doi: 10.23919/MIPRO52101.2021.9597091.

[8] R. Kimball, M. Ross, "The Data Warehouse Toolkit: The Complete Guide to Dimensional Modeling," 2nd. edition. John Wiley & Sons, Inc., USA, (2002).

[9] W. Inmon, "Building the Data Warehouse," John Wiley & Sons, Inc., USA, (1992).

[10] A. Gupta, D. Agarwal, D. Tan, J. Kulesza, R. Pathak, S. Stefani, and V. Srinivasan, "Amazon Redshift and the case for simpler data warehouses," SIGMOD (2015).

[11] J. Aguilar-Saborit, R. Ramakrishnan, K. Srinivasan, K. Bocksrocker, I. Alagiannis, M. Sankara, M. Shafiei, J. Blakeley, G. Dasarathy, S. Dash, L. Davidovic, M. Damjanic, S. Djunic, N. Djurkic, C. Feddersen, C. Galindo-Legaria, A. Halverson, M. Kovacevic, N. Kicovic, G. Lukic, D. Maksimovic, A. Manic, N. Markovic, B. Mihic, U. Milic, M. Milojevic, T. Nayak, M. Potocnik, M. Radic, B. Radivojevic, S. Rangarajan, M. Ruzic, M. Simic, M. Sosic, I. Stanko, M. Stikic, S. Stanojkov, V. Stefanovic, M. Sukovic, A. Tomic, D. Tomic, S. Toscano, D. Trifunovic, V. Vasic, T. Verona, A. Vujic, N. Vujic, M. Vukovic, M. Zivanovic, "POLARIS: The distributed SQL engine in Azure Synapse" PVLDB, vol. 13, issue 12, (2020).

[12] K. Sato, "An inside look at Google BigQuery," Technical report, Google. https://cloud.google.com/files/BigQueryTechnicalWP.pdf.

[13] B. Dageville, T. Cruanes, M. Zukowski, V. Antonov, A. Avanes, J. Bock, J. Claybaugh, D. Engovatov, M. Hentschel, J. Huang, A. W. Lee, A. Motivala, A. Q. Munir, S. Pelley, P. Povinec, G. Rahn, S. Triantafyllis, P. Unterbrunner, "The Snowflake Elastic Data Warehouse," SIGMOD (2016).

[14] M. Armbrust, R. S. Xin, C. Lian, Y. Huai, D. Liu, J. K. Bradley, X. Meng, T. Kaftan, M. J. Franklin, A. Ghodsi, M. Zaharia, "Spark SQL: Relational data processing in Spark," Armbrust, Melbourne, Victoria, Australia, ACM, SIGMOD, (2015).

[15] R. Xin, M. Mokhtar, "Databricks Sets Official Data Warehousing Performance Record," November, 2021, Databricks company blog.

[16] C. Giebler, C. Gröger, E. Hoos, H. Schwarz, and B. Mitschang, "Leveraging the data lake: Current state and challenges," International Conference on Big Data Analytics and Knowledge Discovery, Springer, Cham, 179-188, (2019, August).

[17] N. Nikolov, "Research of the Communication Protocols between the IoT Embedded System and the Cloud Structure," 2018 IEEE XXVII International Scientific Conference Electronics - ET, 1-4 (2018). doi: 10.1109/ET.2018.8549604.

[18] Y. He, R. Lee, Y. Huai, Z. Shao, N. Jain, X. Zhang, and Z. Xu, "RCFile: A fast and space-efficient data placement structure in MapReduce-based warehouse systems," Proceedings of the 2011 IEEE 27th International Conference on Data Engineering, IEEE Computer Society, USA, 1199–1208, (2011). DOI:https://doi.org/10.1109/ICDE.2011.5767933

[19] T. Ivanov, M. Pergolesi, "The impact of columnar file formats on SQL-on-Hadoop engine performance: A study on ORC and Parquet. Concurrency," Computat Pract Exper. (2020), https://doi.org/10.1002/cpe.5523.

[20] A. Ishtiaq, S. Ahmad, and D. S. Shukla, "Fast Retrieval with Column Store using RLE Compression Algorithm," International Journal of Computer Applications, 111. 30-34, (2015). 10.5120/19537-1193.

[21] S. Melnik, A. Gubarev, J. J. Long, G. Romer, S. Shivakumar, M. Tolton, and T. Vassilakis, "Dremel: Interactive Analysis of Web-Scale Datasets", Proc. of the 36th Int'l Conf on Very Large Data Bases, 330-339 (2010).

[22] M. Armbrust, T. Das, L. Sun, B. Yavuz, S. Zhu, M. Murthy, J. Torres, H. van Hovell, A. Ionescu, A. Łuszczak, M. Świtakowski, M.

 ISBN 978-86-7466-930-3

Szafrański, X. Li, T. Ueshin, M. Mokhtar, P. Boncz, A. Ghodsi, S. Paranjpye, P. Senster, R. Xin, and M. Zaharia, "Delta lake: high-performance ACID table storage over cloud object stores," Proceedings of the VLDB Endowment, vol. 13, issue 12, 3411–3424 (2020) DOI:https://doi.org/10.14778/3415478.3415560.

[23] N. Korolija, J. Popović, M. Cvetanović, and M. Bojović, "Dataflow-based parallelization of control-flow algorithms," *Ad ances in computers*, Elsevier, **1 4**, 73-124 (2017).

[24] V. Milutinovic, J. Salom, D. Veljovic, N. Korolija, D. Markovic, and L. Petrovic, "Transforming applications from the control flow to the dataflow paradigm," *ataflow supercomputing essentials*, Springer, Cham, 107-129 (2017).

[25] N. Korolija, D. Bojić, A. R. Hurson, and V. Milutinovic, "A runtime job scheduling algorithm for cluster architectures with dataflow accelerators," *Ad ances in computers*, Elsevier, **12** (2022).

 ISBN 978-86-7466-930-3

# Hybrid Manycore Dataflow Processor

Danko Miladinović, Miroslav Bojović, Vladisav Jelisavčić, and Nenad Korolija

*Abstract*— **This wor addresses high performance computing architectures, presenting a hybrid processor that includes multiple computing architectures on a single chip die.**

**eside commonly used multicore processor, a personal computer might include manycore graphical processor. This wor advocates for a combination of these two architectures along with a dataflow processor that usually appears in the form of a PGA chip able to perform parallel tas s at the same time.**

**A quic overview of these computer architectures and appropriate programming paradigms is followed by the comparison based on fle ibility and speed, price and development time, and speed and power consumption. inally, the proposed hybrid processor is analyzed against computationally demanding algorithms that are often e ecuted on high performance computing architectures.**

**uture wor will include the comparison of the proposed computer paradigms and the comparison of the proposed hybrid architecture with e isting ones.**

*Inde Terms*— **igh performance computing; manycore processors; dataflow programming**.

## I. Introduction

Many high performance computing algorithms are scalable, and as such, suitable for execution using:

- computer architectures the include graphical processing units capable of executing algorithms,
- dataflow computer architectures.

Both of these exist in the form of:

- personal computers,
- computer clusters,
- cloud computers.

Besides the differences in dataflow and conventional computing architectures, their computing paradigms also differ, as well as their suitability for executing high performance computing algorithms.

This work presents recently exploited computer architectures from the point of view of their usability for executing high performance computing algorithms. These architectures are compared based on programming flexibility that they offer, algorithm execution speed, scalability, software development effort, constraints of each of architecture type, price, and power consumption. The presentation of the work is based on the proposed method for presenting the results [1].

Danko Miladinović, Miroslav Bojović, and Nenad Korolija are with the School of Electrical Engineering, University of Belgrade, 73 Bulevar kralja Aleksandra, 11020 Belgrade, Serbia (e-mails: danko @ etf.bg.ac.rs, mbojovic @ etf.bg.ac.rs, and nenadko @ etf.bg.ac.rs).

Vladisav Jelisavčić is with the Mathematical Institute of the Serbian Academy of Sciences and Arts, Kneza Mihaila 36, Belgrade 11001 (e-mail: vladisavj @ gmail.com).

Following sections describe these computer architectures in a uniform manner. A brief overview is followed by the estimation of effectiveness. Each computing architecture is subjected to the following criteria:

- order of number of transistors per number of instructions that can run in parallel,
- speed of the hardware,
- suitability for high performance computing algorithms,
- independence from other computer architectures,
- price performance ratio,
- power consumption performance ratio,
- required space for computer architecture per performance ratio.

On the top of the work, authors propose a hybrid processor that includes multiple computing paradigms on a single chip.

## II. Multicore architectures

Most of personal computer architectures are based on von Neumann paradigm. Programs written in programming languages are compiled and linked, and the resulting instructions are stored on the disk. Once a program starts, instructions are loaded into the RAM memory, from where they get copied into the cache memory, so that they could be read faster.

The processor is responsible for executing instructions. Long ago, processors included a single arithmetical logical unit (ALU) for performing arithmetical and logical operations. The speed of processors was increasing for decades by approximately doubling each second year. However, once the speed reached around 3GHz, the trend stopped. The constraint was and still is that the wave length became around 10 cm. Given the fact that the clock cycle must be stable during the whole instruction execution, and the signal has to travel with the speed of light multiple times in different directions, options for further acceleration were:

- to decrease the size of the chip,
- to decrease the size of transistors,
- to decrease the number of transistors per logical gates,
- to implement multiple ALUs that would work in parallel.

Decreasing the size of the chip die implies reducing the number of transistors, leading to deteriorating performances. Reducing the size of transistors would affect their functions considerably (i.e. more failures would appear). Logical gates are already optimized so that further reduction in the number of transistors would affect their capacities for producing output to multiple logical gates.

As a result, both research community and the industry opted for multiplying ALUs on a single chip die.

Multicore architectures can execute an order of 10

 ISBN 978-86-7466-930-3

operations simultaneously. The transistor count is around 1 billion. Clock cycle is order of GHz. As such, their usability for high performance computer algorithms is limited in terms of utilizing algorithms in the real time applications. One of the most important characteristics of multicore architectures is their independence from other computer architectures. As a result, personal computers usually contain only one processor of this type. Typical power consumption is around 500 watts. When used in computer clusters, a single node could include multiple processors of this type.

## III. MANYCORE ARCHITECTURES

Graphical processing units are often referred to as manycore computer architectures, as the number of processing units is larger than those of multicore processors.

So-called manycore architectures are logical successor of multicore processors. Certain fields, like computer graphics, require more instructions per second than multicore architectures produce, so that the picture can be refreshed many times per second (e.g. 60 times). With shading effects and full-hd or even 4k resolutions this implies updating millions of pixel colors based on performed operations with appropriate matrices. As a result, companies started producing chips for graphical cards that include thousands of cores that have lower number of available instructions supported by their architectures but are capable of executing more instructions per second. Soon after, utilization of the processing power of new graphical cards started. Many algorithms are implemented using the CUDA programming model.

Manycore architectures have an order of 10 billion transistors with an order of 1000 processor cores, and an order of 1000 instructions that can run in parallel. The clock cycle has an order of 1 GHz. This makes it suitable for high performance computing algorithms. Although each core is based on von Neumann paradigm, being capable of executing any instruction defined by the architecture at any given moment, it relies on the multicore processor as the one that assigns jobs to cores. The manycore architectures proved to be efficient for high performance computing algorithms, including data mining and coin mining. Power consumption is of the same order of magnitude as of multicore processors, while manycore processor offer superior performance. They usually come in the form of a PCIe card that attaches to the mainboard.

## IV. DATAFLOW ARCHITECTURES

Dataflow architectures are based on a separate programming paradigm called dataflow paradigm. Data flows through a hardware in terms of electrical signals, resulting in transforming an input to the output [2, 3]. One of the main advantages over the previously mentioned computer architectures is that there is no need for an order of 1 billion transistors to execute only around 10 instructions in parallel. Dataflow hardware can execute even 1000 instructions simultaneously. As such, it is capable of accelerating many algorithms [4, 5]. The main disadvantage is that the multicore processor is needed for preparing the data to be processed using a dataflow hardware and for handling results.

The order of number of transistors is comparable to previously mentioned computer architectures, while the number of instructions that can run in parallel can be much higher. The speed of the hardware is around 0.1 GHz. Since they do not support executing any instruction defined by the architecture at any given moment, they are suitable for only a portion of high performance computing algorithms and more programming effort is needed for creating programs [6]. A mitigating circumstance is that there is a way to automatically translate certain algorithms from the control-flow into the dataflow paradigm [7]. Having significantly lower space occupation and power consumption per instruction, dataflow hardware has good price performance ratio.

## V. HYBRID ARCHITECTURES

While each of the available computer architectures has its own advantages and disadvantages, it is a logical step but also a challenge to try to merge multiple programming paradigms into a single computer architecture. The task is even harder to achieve if they are to be put on the same chip die. However, the need for computing justifies the effort needed to merge existing computing paradigms.

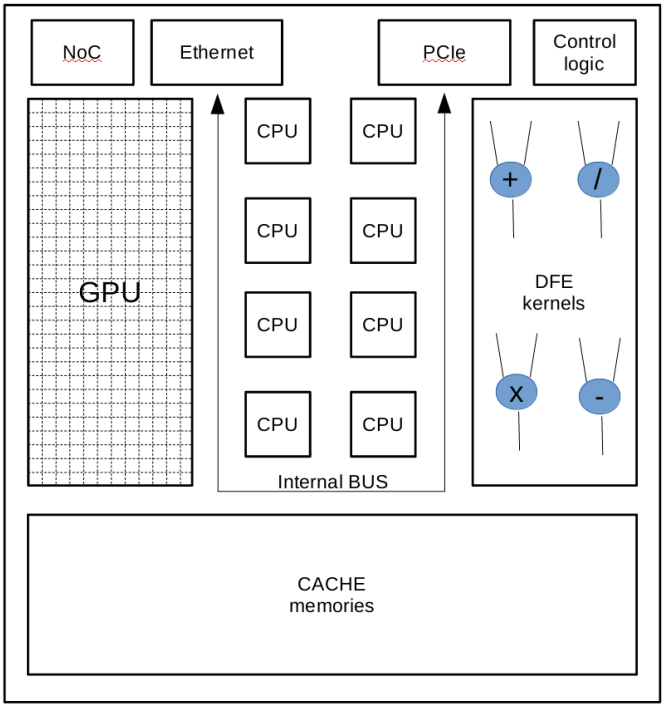


Fig. 1. Hybrid control-flow dataflow architecture.

Fig. 1 depicts a hybrid control-flow dataflow architecture on a single chip. Compared to the typical multicore processor architecture, the proposed hybrid architecture includes graphics processing unit (GPU) cores and dataflow kernels beside central processing unit (CPU) cores and cache memories. Additionally, network on chip (NoC) is suggested as a good way of handling the communication between GPU

 ISBN 978-86-7466-930-3

cores. Compared to the Maxeler dataflow hardware PCIe cards, proposed dataflow engine (DFE) kernels are connected directly to the slowest internal cache memory, because of the necessity for dataflow hardware to execute at the same speed. Constraint that has to be taken into account is that cache locking mechanism has to be implemented for cache memory connected to the dataflow, which would enable granted access to DFE kernels, but also to GPU if it is required by the application that is executed using both computing paradigms.

This architecture offers the best that any of the paradigms offer. On the other side, the complexity is equal to the sum of complexities of incorporated architectures. As such, the proposed hybrid architecture is suitable for executing multiple jobs simultaneously, where some of them are suitable for executing using the dataflow paradigm, while others achieve better performance when executed using manycore architecture. Finally, there are software applications that are not based on scalable algorithms, making them suitable solely for the multicore processor.

The emerging problem on heterogeneous computer architectures that include both dataflow and control-flow hardware is scheduling program execution. Authors have presented their novel algorithm for optimal scheduling of both dataflow and control-flow jobs [8]. The algorithm is general but is limited in number of jobs it can schedule due to the computational complexity. Based on this optimal algorithm, two heuristic algorithms for optimizing the throughput and minimizing total execution time are derived, producing near-optimal schedules for both dataflow and control-flow jobs at large job counts at the cost of negligible scheduling penalty. The heuristic algorithms performance gain decreases slightly as job count increases and only at the beginning, proving that the performance of existing cluster structures with appropriate dataflow accelerators can be considerably improved.

The drawback of combining multiple computing architectures on a single chip is that it increases the probability of failure. However, the probability is relatively high at the very beginning, and once a chip enters the so-called wear-out phase, and is relatively low in the meanwhile [9].

The order of number of transistors per number of instructions that can run in parallel depends on the type of job. If a job is suitable for dataflow architectures, the acceleration would be similar to those of dataflow architectures, while the number of transistors would be around three times higher, assuming that included architectures consume the same number of transistors. The same applies for jobs suitable for manycore architectures, and jobs that cannot be efficiently accelerated using neither manycore architecture, nor a dataflow architecture. However, this applies solely to scheduling a single job that can be executed using one of these three types of architectures. If we combine multiple jobs, those suitable for dataflow architectures would be executed there, based on their hardware requirements and on acceleration they achieve using the dataflow architecture. Jobs suitable for manycore architectures could run in parallel, while jobs that are based on algorithms that are not scalable could run in parallel on the multicore processor. Therefore, achieving fair comparison of the number of instructions that can be run on the proposed architecture is not a straightforward task. As a result, new benchmarks are needed to compare the proposed architecture to the existing ones. For now, one could consider the worst-case scenario, where the acceleration of a job is the same as for the best suited architecture for the job, and the number of transistors is equal to the sum of the number of transistors included on each part of the proposed hybrid processor [10].

The speed of the proposed hardware is also hard to define. As the processor includes different architectures that naturally run on different clock rates, the proposed processor would have a clock speed for the multicore processor that is a multiple of the clock speed of a dataflow architecture and manycore architecture. Therefore, the multicore would be able to efficiently communicate with other parts of the processor using input and output communication buffers.

The proposed computer architecture is not only suitable for high performance computing algorithms, but it is more efficient that aforementioned architectures, as it offers the most suitable hardware type for any particular job. The proposed processor includes multicore processor on the same chip die, making the architecture independent from other computer architectures. The price performance ratio for any given job is lower than those of the best suited of the aforementioned architectures. However, given a set of jobs, where each is suited for one particular architectures, the proposed architecture exploits advantages of all three types of architectures and could achieve the best speed-up in all categories of jobs. The price performance ratio is also lower for a particular job suited for a single computer architecture but is better than any of the aforementioned architectures if there are jobs that could approximately equally occupy all resources of the proposed processor. If completely utilized, the power consumption performance ratio is better than any of the three underlying architectures. For a single job, it is around three times lower, as it is estimated that this processor would consume as much electrical power as all three underlying architectures combined. The space required for the proposed computer architecture is one of its main advantages. Having in mind that it would be able to execute any type of jobs that any of the three computer architectures can, the space per performance ratio cannot be outperformed by any of the existing architectures.

This is not the unique case of proposing combination of manycore and dataflow architectures. Similar tries have been by researchers in the past [11, 12, 13].

## VI. COMPARISON

This section summarizes the advantages and disadvantages of described computer architectures and compares them based on various criteria. For each of the given criteria, the proposed hybrid computer architecture is compared to all three underlying computer architectures.

The research [2] summarizes in their Table 2 the achieved

 ISBN 978-86-7466-930-3

speedups of algorithms implemented using the same type of the dataflow hardware that includes a memory on a chip comparing to the control-flow implementations of the same algorithms. The Lattice-Boltzmann algorithm is presented in detail, along with the dataflow code. Authors have compared execution time of Lattice-Boltzmann algorithms using the MAX2 card with 6GB of RAM and using Intel i5 650 processor with the clock speed of 3.2GHz. The computer used 4GB RAM memory at the speed of 1333MHz. The conclusion that can be drawn is that the speed-up of all observed dataflow algorithms ranges from 25% up to the multiplication factor of 150. Based on the comparison of these algorithm implementations for control-flow and for dataflow paradigms, we can summarize the advantages and disadvantages of both programming paradigms.

Table I presents a comparison of computing architectures in terms of flexibility to execute any instruction at any given moment and the speed of execution measured in number of instructions per second. As it can be seen, the multicore computing paradigm offers the highest flexibility by being able to execute any type of job, as it can execute any instruction defined by the architecture at any given moment. Although manycore architectures work on the same principle, they are considered to be utilized if many processing units may work in parallel. Therefore, their flexibility is limited to scalable algorithms suitable for manycore architectures. Dataflow architectures introduce new constraints by not being able to adapt to new needs before re-configuring the hardware. Hybrid architectures offer the advantages of both paradigms.

The speed of execution measured in number of instructions is lowest for the multicore architectures, as they are limited to processing up to an order of 10 instructions simultaneously. Any other of presented computer architectures can execute two or three orders of magnitude more instructions simultaneously.

TABLE I
FLEXIBILITY AND SPEED COMPARISON OF VARIOUS COMPUTING ARCHITECTURES

| Type of architecture | Flexibility | Speed |
|---|---|---|
| Multi core | +++ | + |
| Many core | ++ | ++ |
| Dataflow | + | ++ |
| Hybrid | +++ | ++ |

Table II presents a comparison of computing architectures in terms of price and the development time measured by effort needed for producing the software. The price raises as we lean towards more optimized computer architectures. The same applies to software development time. The only exception is that hybrid computer architecture, which is suitable for executing any of the given type of software, which means that the development time depends on the type of software being executed on the architecture.

As dataflow architectures are not as utilized as multicore and manycore computer architectures, the price tag of dataflow architectures is higher that it would be if each personal computer would include dataflow engines as well.

TABLE II
PRICE-DEVELOPMENT TIME COMPARISON OF COMPUTING ARCHITECTURES

| Type of architecture | Price | Development time |
|---|---|---|
| Multi core | + | + |
| Many core | ++ | ++ |
| Dataflow | +++ | +++ |
| Hybrid | ++++ | + - +++ |

Table III shows a speed to power consumption comparison of these computing architectures. The speed of the multicore computer architecture is slower than others, as it can run a smaller number of instructions in parallel.

When it comes to power consumption, it is similar for all types of architectures, which leads us to the following conclusion. The power consumed per a single instruction is the highest in the case of the multicore computer architecture, while it is the lowest for dataflow and hybrid computer architectures, assuming that they are not underutilized.

TABLE III
SPEED-POWER CONSUMPTION COMPARISON OF COMPUTING ARCHITECTURES

| Type of architecture | Speed | Power consumption |
|---|---|---|
| Multi core | + | ++ |
| Many core | ++ | ++ |
| Dataflow | +++ | ++ |
| Hybrid | +++ | ++ |

Based on these comparisons, we could conclude that the proposed architecture has the potential for achieving better results in terms of speed, flexibility, and power consumption comparing to the existing computer architectures, while the programming effort might be higher in the case of the algorithms implemented using the dataflow paradigm.

Comparing to the research available in the open literature, the proposed architecture is more high performance computing oriented than the Ultimate dataflow processor [12], while it doesn't support internet of things. Authors of SambaNova [14] also recognized the potentials of dataflow computing paradigm. Their Reconfigurable Dataflow Unit (RDU) enables accelerating algorithms with the flexibility to build custom dataflow pipelines as well as large memory capacity to run big models such as Natural Language Processing (NLP) and high-resolution computer vision efficiently. However, it is dedicated to algorithms that consist predominantly of the source code that can be most efficiently accelerated using the dataflow paradigm.

Research [15] exploits the opportunities from digital Processing-in-memory (PIM) bit-serial processing and in-memory customization, to tackle the above challenges by co-designing sparse algorithm, multiplication dataflow, and PIM

 ISBN 978-86-7466-930-3

architecture.

## VII. Conclusion

Along with a multicore processor, a personal computer might include manycore graphical processor and a dataflow processor on the same chip die. This work advocates for a combination of these two architectures in order to create the type of the computer architecture that is able to execute jobs suitable for any of these three types of architectures in parallel.

Presented comparison between computing architectures suggests what kind of algorithms are suitable for execution using existing computing paradigms.

The proposed hybrid processor is analyzed against computationally demanding algorithms that are often executed on high performance computing architectures. As it includes multiple computing architectures on a single chip die, it could achieve the best acceleration for a job suitable for any of aforementioned computer architectures. At the same time, if the amount of jobs suitable for these three computer architectures matches the amount of resources of the proposed processor, the proposed processor with appropriate job scheduling can achieve the performance of combined architectures.

Future work includes the simulation comparison of the paradigms and the comparison of the proposed hybrid architecture with existing ones.

## Acknowledgment

DM, NK, and MB are partially supported by the School of Electrical Engineering, University of Belgrade, Serbia. VJ is partially supported by the Mathematical Institute of the Serbian Academy of Sciences and Arts. NK is partially supported by the Institute of Physics Belgrade, contract no. 0801-1264/1. All authors are partially supported by the Ministry of Education, Science, and Technological Development of the Republic of Serbia.

## References

[1] V. Milutinovic, "The best method for presentation of research results," IEEE TCCA Newsletter, 1-6 (1996).

[2] N. Korolija, J. Popović, M. Cvetanović, and M. Bojović, “Dataflow-based parallelization of control-flow algorithms,“ Advances in computers, Elsevier, 104, 73-124 (2017).

[3] N. Trifunovic, V. Milutinovic, J. Salom, A. Kos, “Paradigm shift in big data super-computing: dataflow vs. controlflow,” J. Big Data, vol. 2, issue 4, 1–9 (2015).

[4] N. Trifunovic, V. Milutinovic, N. Korolija, G. Gaydadjiev, "An AppGallery for dataflow computing," Journal of Big Data, vol. 3, issue 1, 1-30 (2016).

[5] N. Korolija, T. Djukic, V. Milutinovic, and N. Filipovic, “Accelerating Lattice-Boltzman method using Maxeler dataflow approach,” The IPSI BgD Transactions on Internet Research, 34 (2013).

[6] J. Popovic, D. Bojic, and N. Korolija, “Analysis of task effort estimation accuracy based on use case point size,” IET Software, 9(6), 166-173 (2015).

[7] V. Milutinovic, J. Salom, D. Veljovic, N. Korolija, D. Markovic, and L. Petrovic, “Transforming applications from the control flow to the dataflow paradigm,” Dataflow supercomputing essentials, Springer, Cham, 107-129 (2017).

[8] N. Korolija, D. Bojić, A. R. Hurson, and V. Milutinovic, “A runtime job scheduling algorithm for cluster architectures with dataflow accelerators,” Advances in computers, Elsevier, 126 (2022).

[9] K. Huang, Y. Liu, N. Korolija, J. M. Carulli, and Y. Makris, “Recycled IC detection based on statistical methods,” IEEE transactions on computer-aided design of integrated circuits and systems, 34(6), 947-960 (2015).

[10] V. Milutinović, N. Trifunović, N. Korolija, J. Popović, and D. Bojić, “Accelerating program execution using hybrid control flow and dataflow architectures,” 25th Telecommunication Forum, IEEE, 1-4 (2017).

[11] V. Milutinović, E. S. Azer, K. Yoshimoto, G. Klimeck, M. Djordjevic, M. Kotlar, M. Bojovic, B. Miladinovic, N. Korolija, S. Stankovic, N. Filipović, Z. Babovic, M. Kosanic, A. Tsuda, M. Valero, M. de Santo, E. Neuhold, J. Skorucak, L. Dipietro, I. Ratkovic, "The ultimate dataflow for ultimate supercomputers-on-a-chip, for scientific computing, geo physics, complex mathematics, and information processing," 10th Mediterranean Conference on Embedded Computing, IEEE, 1-6 (2021, June).

[12] V. Milutinović, M. Kotlar, I. Ratković, N. Korolija, M. Djordjevic, K. Yoshimoto, and M. Valero, "The Ultimate Data Flow for Ultimate Super Computers-on-a-Chip, " Handbook of Research on Methodologies and Applications of Supercomputing, IGI Global, 312-318 (2021).

[13] V. Milutinović, B. Furht, Z. Obradović, and N. Korolija, “Advances in high performance computing and related issues,” Mathematical problems in engineering, (2016).

[14] R. Prabhakar, S. Jairath, and J. L. Shin, “SambaNova SN10 RDU: A 7nm Dataflow Architecture to Accelerate Software 2.0,” 2022 IEEE International Solid-State Circuits Conference (ISSCC), IEEE, vol. 65, 350-352 (2022).

[15] F. Tu, Y. Wang, L. Liang, Y. Ding, L. Liu, S. Wei,... and Y. Xie, “SDP: Co-Designing Algorithm, Dataflow, and Architecture for in-SRAM Sparse NN Acceleration,” IEEE Transactions on Computer-Aided Design of Integrated Circuits and Systems, (2022).

 ISBN 978-86-7466-930-3

# Service-Oriented Communication Between ADAS and IVI Domains in Automotive Solutions

Dušan Kenjić and Marija Antić, *Members, IEEE*, Dušan Živkov

***Abstract*—As the complexity of automotive systems has grown, it has become necessary to cluster various vehicle components into several domains, based on a specific function they perform. This approach has facilitated the development of domain-specific features, as it allows to create communication standards and common libraries that meet the requirements of the particular domain. On the other hand, it has created the redundancy in the resource consumption required to perform similar tasks in different domains, which leaves the room for further optimizations. This is most notable if we analyze the functionalities of the two fastest growing domains: autonomous driving assistance (ADAS) and in-vehicle infotainment (IVI), which are both developing simultaneously, and may benefit from the option of providing features and services to each other. This paper will examine and propose a solution for interconnection between ADAS and IVI domains by utilizing state-of-the-art mechanisms of the service-oriented architecture (SOA) paradigm. The examination of SOA utilization rationale will be presented, as well as the crucial challenges and limitations of the possible approaches, derived mainly from the discrepancy of service-oriented architecture implementation and mapping in different standards. Various features and use-cases will be discussed, that would be good candidates for cross-domain implementation.**

***Index Terms*— in-vehicle domains, ADAS, IVI, interconnection, SOA in automotive.**

## I. Introduction

The transition to centralized domains in the automotive system design and development was necessary due to the increasing number of Electronic Control Units (ECUs) in the modern vehicle. With this approach, the system is organized into several domains based on the features and the tasks ECUs within the domain perform. By splitting the whole system into a set of specialized domains, it was possible to create standards and abstractions that facilitate the development of features specific to the particular domain, without the need for developers to constantly solve the problems of connectivity and resource sharing. Two domains which are constantly improved and require powerful resources are ADAS - Advanced Driver System Assistant domain and IVI - In-vehicle Infotainment domain. The ADAS domain is responsible for safety-critical features and algorithms using various types of sensors in order to enable safe, comfortable and cost-effective driving. On the other hand, the IVI domain is oriented towards passenger entertainment, as well as towards providing useful information about the driving conditions and the state of the vehicle. Although these two domains perform different tasks, there is a set of features and sensors of the same type which are commonly used in both of them. However, in the current architecture of modern vehicle, these two domains do not share any of the hardware resources nor results of the data processing algorithms. This creates an implementation overhead, as similar functionalities need to be implemented in both of the domains, and the hardware cost is constantly increasing. This represents the main motivation to design an approach for resource sharing between domains as a first step towards the unified platform which shall control the entire system.

In this paper, we will present the results of the initial phase of a research project aiming to create the solution for the inter-domain communication and resource sharing in the automotive solutions. First, we will present the summary of the state-of-the-art research and commercially used approaches for the inter-process communication and service-oriented architecture in automotive industry. Then, we will propose the architecture of the solution connecting ADAS and IVI domains, provide some practical details and discuss the examples of the use-cases which would benefit from the resource sharing between these two domains. Finally, we will discuss the implementation challenges of the proposed approach.

## II. IPC and SOA in Automotive Systems

### A. Service-Oriented Middleware in Automotive

Traditionally, automotive systems use a conventional signal-based communication approach, which provides a deterministic data transfer, and enables the processes to run in the predefined schedule [1][2]. However, such an approach does not support the desired scalability of the system, which is required to satisfy the requirements of emerging applications and scenarios. Therefore, in order to provide the flexibility and a more dynamic and scalable system, service-oriented architecture (SOA) was introduced to the automotive system design. Service-oriented communication approach has been adopted from the domains of web applications, cloud and information systems, where it has already proven its flexibility for functional services implementation [3]. SOA represents an efficient way to encapsulate the job done by the specific component into a service. This way, resources can be

Dušan Kenjić is currently working toward the Ph.D. degree with the University of Novi Sad, Serbia, (e-mail: dusan.kenjic@uns.ac.rs).

Marija Antić is currently the Assistant Professor with the University of Novi Sad, Serbia, (e-mail: marija.antic@rt-rk.uns.ac).

Dušan Živkoc is with the RT-RK Institute for Computer based Systems, (e-mail: dusan.zivkov@rrt-rk.com).

 ISBN 978-86-7466-930-3

distributed to the clients interested in the information which the service provides, the service implementation can remain obscured from the clients and modularity and repetitiveness can be achieved. Additionally, the unified communication mechanism facilitates the interoperability between heterogenous system components, which otherwise represents a time consuming and challenging problem that needs to be solved during the application development.

The first step towards the integration of SOA principles within an automotive system is to create a platform and define a protocol which can support this integration. Such platform must be compatible with other automotive solutions and protocol must be suitable with the automotive requirements [4]. Scalable service-Oriented Middleware over IP (SOME/IP) is a Remote Procedure Call (RPC) mechanism [5] specialized for the usage in the automotive systems. It consists of three modules: SOME/IP, SOME/IP Service Discovery (SD) and SOME/IP Transformer. SOME/IP fundamental module is managing the serialization and deserialization of transmitting data, SD module enables the connection establishment and service discovery procedure and the Transformer module specifies automotive/embedded data serialization [4].

There are multiple protocols which can be used for in-vehicle cross-domain communication such as DDS, HTTP, MQTT, web sockets, etc. Besides the abovementioned fact that the SOME/IP is created for the automotive industry there are several functional benefits that made it our choice for such use-case. First, the mandatory configuration of the communication over SOME/IP enables somewhat more deterministic behavior in contrary to another protocols and mechanisms used to implement SOA in the web and cloud computing such as the HTTP for example. Additional benefit is that SOME/IP provides multiple types of communication. Comparing to the HTTP, which allows only request-response communication initiated from clients, SOME/IP provides both request-response and publish-subscribe approaches. Furthermore, SOME/IP does not require communication establishment for each data exchange, but only for initial client-service connection and it can rely on both, TCP and UDP protocols in contrary to the communication implementing Representational State Transfer (REST) principles.

Although having different architectures, diverse software platforms use the SOME/IP communication stack based on the similar concept as depicted in Fig. 1.

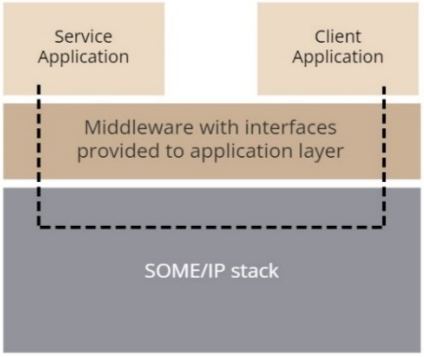


Fig. 1. Concept of SOME/IP implementation in automotive platforms

Usually, the middleware which provides the applications with the particular interfaces based on the determined configuration parameters is implemented by the standard. Depending on whether it is event, method or field that is defined by the configuration the data exchange would be performed by publishing the information to subscribed client when a logic on the service side determines so, client requesting the execution of a method on service side and getting the response if needed and getting, setting or notifying about the changed state of a field, i.e. attribute on the service side respectively.

Services in automotive SOA need to meet strict requirements regarding the service discovery and startup latency time [6]. Authors in [3] even propose dividing and isolating secured and exposed subnetworks in order to accomplish more reliability, since the service discovery mechanisms cannot guarantee that the service will be provided at the needed time. However, this aspect will not be examined in this paper, but another one instead – how SOA is implemented within available architectures and how it can be used for inter-communication between ADAS and IVI domains.

### *B. IPC Standards in IVI Domain*

Modern vehicles are currently competing to meet the requirements driven by the consumer technology, especially in the infotainment domain. Inside the vehicle, the passengers expect the experience they have when using everyday portable devices, such as tablets and mobile phones. They are used to being able to install and use various types of applications developed by different vendors. In order to meet these requests, it is necessary to utilize the globally accepted standards for building scalable and portable platforms.

#### *1) GENIVI approach*

The former GENIVI (currently COVESA) alliance drives the development of open standards and technologies used in automotive systems. Their goal is to address the challenges which the in-vehicle infotainment components are facing when reaching to the outside world (cloud services, other vehicles, etc.) and communicating with other in-vehicle infotainment components as well. They offer the CommonAPI [8] – an inter-process communication middleware based on the FRANCA framework, which provides service-oriented mechanisms. It is designed to split the applications implementation apart from the communication mechanisms used between the implemented application components.

Since the only purpose of this middleware is to provide interfaces between lower (platform services and protocols) and upper (applications) layers, its implementation is generated mainly from the FRANCA Interface Definition Language (FIDL) to make its utilization easier. Applying the specified interface definition language – FIDL, it enables flexible deployment models. This way, the dynamic behavior of an API is specified by defining client/server interaction interfaces, states and transitions between them [7]. The communication itself is performed by using the generated Stub and Proxy classes relying on the CommonAPI middleware within the Service and Client applications respectively. This way, the concept from Fig. 1 is kept since the entire CommonAPI stack

 ISBN 978-86-7466-930-3

including the Stub and Proxy provides applications with interfaces for usage of the SOME/IP mechanisms.

Additionally, COVESA semantically differentiates between the two realms: Common-API Core, which does not depend on the communication protocol itself, and CommonAPI Binding which is protocol-specific [8]. Currently, the CommonAPI support two RPCs, D-Bus and the SOME/IP. In order to set deployment parameters for chosen protocol, the FRANCA Deployment (FDEPL) files are used along with the FIDL.

*2) Android approach*

Android is an open-source operating system mainly utilized for mobile devices. It enables deployment on wide range of hardware platforms and supports third-party applications development [9]. Currently, the automotive industry is facing a similar requirement for the possibility for third-party application development and utilization, therefore the automotive community is more interested in the Android platform [10].

Android platform has the mechanisms for feasible handling of the Inter-Process Communication (IPC) via its proprietary interface definition language called AIDL. It provides a programming interface utilized by both the client and the service using the IPC to communicate with each other [11]. Although AIDL has similar functionality as other IDLs, its utilization does not rely on the same paradigm as it is the case with the FIDL and COVESA's Common-API service-client communication model. Additionally, the SOME/IP had not been supported in Android until vsomeip version 3 was released. The possible correlation between CommonAPI and Android and more details about the AIDL paradigm and its communication mapping to other mechanisms will be addressed in the Section 4.

### C. IPC standards in ADAS domain

The previously described standards are used for the implementation of the application for the in-vehicle infotainment part of the automotive system. On the other hand, ADAS domain is faced with the challenges driven by different requirements, as it considers safety-critical algorithms and modules. Nevertheless, ADAS domain implies the integration of functionalities provided by machine vision and sensor fusion. Lots of these algorithms are used in consumer technologies, i.e., in the IVI domain also. Therefore, the benefit of exchanging resources between two mentioned domains is obvious, since there is a set of functionalities they share. A standard that has become a convention for the implementation of ADAS domain functionalities is AUTOSAR.

The AUTOSAR standard considers both safety host and performance host implementations. Safety hosts are referring to ECU's cores with safety and security control features specialized for the automotive industry. Classic AUTOSAR platform is designed for the fully deterministic, deeply embedded standardization of safety hosts. Furthermore, the Adaptive AUTOSAR platform is offering more flexibility by addressing operability and communication mechanisms more suitable for high-performance computing devices called performance hosts. Since the performance host resources and algorithms complexity are more similar to the ones in the IVI domain, we will focus on the sharing resources and features of the Adaptive AUTOSAR platform.

User applications are running on the top level, right on top the AUTOSAR Runtime Environment for Adaptive Applications (ARA). The main component of ARA is ara::com, a middleware controlling the communication within a system. It provides the interfaces to the user applications which allow data exchange with both local and remote applications and ARA services [12].

Equivalent to the FIDL, ara::com interfaces in ARA-API are defined by the ARXML. Interfaces are provided to applications with the exact same purpose as it is the case with CommonAPI, to decouple the applications development from the communication mechanism. It is done by utilizing two artifacts - Skeleton and Proxy which implement the SOA paradigm, i.e., the service-client communication, likewise it is the case with the Stub and Proxy in CommonAPI. Skeleton represents the generated instance which provides service calls functionalities. On the other hand, Proxy is a generated instance which provides the client calls functionalities.

## III. CURRENT CROSS-DOMAIN RESOURCE SHARING SOLUTIONS

Most of the research in the field of interconnecting different automotive domains focuses on the modelling and implementation of multi-ECU system using a single standard. Since meeting the safety and latency requirements for ADAS is critical, it dictates the approach to use Adaptive AUTOSAR for both the ADAS and IVI realm. This way, for the sake of connectivity between different domains, neither the CommonAPI nor Android are used, although they are a better fit for IVI domain, since the development is forced to a single standard approach which must fit ADAS requirements. The authors then try to deal with the shortcomings that the AUTOSAR standard provides in terms of UI as an important aspect of in-vehicle infotainment [13]. Authors in [14] presented challenges of modelling ADAS components for camera resource sharing. However, it is needed to perform further research on the most suitable communication channel for the transmission of sensing data and data streams along with the research on the most suitable communication mechanisms by considering the entire, end-to-end communication context for such resources sharing between domains in automotive, the SOME/IP is not the most effective solution for such use-cases. Furthermore, taking into consideration the variety of operating systems on the other side, such implementation cannot be taken "as is".

COVESA alliance recognized this challenge and tried to attain the adaptation between Adaptive AUTOSAR and the CommonAPI by creating FARACON generator [15]. This generator is used to translate the interface definition files from one standard to another. This can be considered as a first step towards the mapping of the features between standards. However, it does not solve the cross-domain heterogeneity issue, which is somewhat more complex.

There are not many papers that provide the actual proposition for interconnection between ADAS and IVI domains utilizing different standards. i.e., following AUTOSAR on ADAS and CommonAPI or Android on IVI side. The existing solutions have recognized the need for such

 ISBN 978-86-7466-930-3

binding, but are also typically reduced to simple utilization of socket-based communication with no actual research background on the available protocols and state-of-the-art SOA principles [16]. Additionally, the inter-process communication paradigms diversity when considering the various platforms standards is not actually covered even in papers which provide the extensive solution for heterogenous in-vehicle environments [17]. Hence, there is no comprehensive project dealing with all aspects of this topic.

Since this topic is substantive and our project is still in the development, some of the challenges will not be covered by this paper but will be addressed in future work instead.

## IV. Proposed Solution

In this section, we will discuss the possible approaches that allow remote procedure calls and exchange of data between ADAS and IVI domains of the vehicle. Our goal is to provide the connectivity, without compromising the functionality of the IVI domain offered by the CommonAPI or Android, or the safety features provided by the AUTOSAR in ADAS domain. We will design our solution using the service-oriented architecture principles, which fit perfectly into the scenarios we want to support. Our focus is on allowing IVI domain applications to use raw measurement data from ADAS sensors, as well as the results of some of the algorithms that run on the ADAS side. The opposite direction of integration is not possible, due to potential safety issues.

There are several examples of use-cases where the proposed cross-domain inter-connection can be beneficial. For example, inputs from cabin camera which is commonly used for driver monitoring on ADAS side can be shared for video calls and other applications using camera in IVI domain. This way, the cost of providing redundant hardware components would be avoided. On the other hand, data from sensors monitoring tire pressure, engine temperature and other crucial components of the vehicle could be easily transferred and handled by the applications in the IVI domain. These applications could then not only inform the driver, but also provide the better user experience by searching for the recommendations and manuals on the Internet, or help by finding the route to the nearest mechanic service. The results of the data processing algorithms such as traffic sign detection and recognition or driver drowsiness monitoring could also be used by the IVI domain applications, to propose rest stops, provide tourist information, etc.

To connect the components of the two domains in the proposed solution, Ethernet-based communication will be used. Recently, Ethernet has taken on the role of the vehicle communication backbone because of its bandwidth, scalability, flexibility and prevalence. In all of the aforementioned terms, Ethernet is generally superior to other in-vehicle buses, which are designed and optimized to fit only specific use-cases. For example, CAN provides the reliability which Ethernet cannot achieve because of the different transmission media access strategies. On the other hand, CAN is the automotive specific technology which means that Android, as a standard that was not created solely for the automotive industry, does not support CAN bus module natively. Similarly, other in-vehicle buses are created to meet

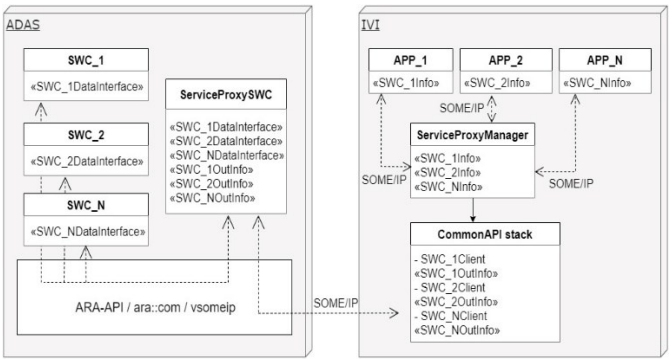


Fig. 2. Centralized interconnection approach with POSIX OS on IVI side

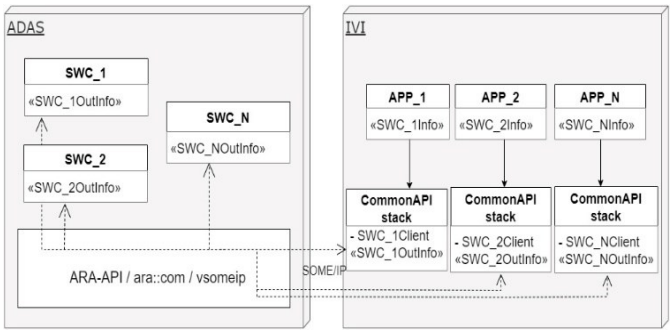


Fig. 3. Distributed interconnection approach with POSIX OS on IVI side

the requirements of automotive signal-based communication, where priority is the price and the determinism of the communication mechanism, not the bandwidth itself. On the other hand, Ethernet is widely used technology which makes it suitable for interconnection of different domains. To exchange data between the domains, we will use SOME/IP, from the reasons already discussed in Section 2, and it can be used over the Ethernet network.

Typically, IVI solutions can either run on Linux operating system and use CommonAPI mechanisms for the inter-process communication, or they can be Android-based. For both of these cases, we will propose the solution architectures in the following sections.

Since Adaptive AUTOSAR and CommonAPI both implement the SOME/IP communication interfaces, this is the easiest way to establish the communication between the two domains in the SOA manner. The ADAS side is implemented by following Adaptive AUTOSAR standard and the IVI domain uses the CommonAPI middleware running on the native operating system such as Linux. This scenario is depicted in Fig. 2 and Fig. 3. Communication in Adaptive AUTOSAR is handled by ara::com which natively supports vsomeip as a library that implements SOME/IP standard. The same vsomeip implementation is utilized in CommonAPI SOME/IP stack. This means that serialization and deserialization of data shall be handled in the same way, so both sides will be able to interpret data properly.

Information from components on ADAS side are initially given to the Service Proxy SWC via SOME/IP implemented within the ara::com module. This data is furtherly forwarded to the corresponding CommonAPI clients grouped together on the IVI side in a single Service Proxy Manager instance (Fig. 2). Such inter-domain transfer is performed over SOME/IP on

 ISBN 978-86-7466-930-3

demand of IVI applications or when the event/change is captured.

The type of communication between the ADAS and the IVI does not necessarily have to match the communication between the ADAS Service Proxy and other SWCs which means that IVI applications can request the data through the Service Proxy Manager instance over method mechanism, but the sharing information on the ADAS side can be sent to the Service Proxy SWC from the actual service component as an event for example.

Another approach is to implement separate services for each CommonAPI client (Fig. 3) so the Service Proxy components on both sides are unneeded and the information will be provided from ADAS ara::com services to the IVI CommonAPI clients included in particular application. The first approach is easier to scale and can be used with the variable number of application instances. Also, it can be favorable from the safety perspective since it can contain mechanisms to protect from other SWCs from being jeopardize by IVI applications. On the other hand, the second is superior in terms of reliability, because there is no single central node which distributes the data between the applications. This way, the malfunction of one service does not affect the operability of others. Furthermore, the monolithic design is harder to maintain, as even minor changes require the entire integration cycle. The speed of access to information is also one of the factors that is on the side of the distributed approach.

As already said, Android has recently become the operating system of choice for IVI applications, as most of the users are familiar with it and it is available on a very large variety of hardware. The interconnection of the ADAS domain with the IVI domain running on the Android platform is a bit more challenging for the implementation. Namely, Android itself does not have mechanisms to implement SOME/IP client which can communicate with ADAS side. Therefore, the CommonAPI must also be used in this scenario in the exact same way it was the case when non-Android OS was examined, as it is presented in Fig. 4 and Fig. 5.

The CommonAPI clients are included within an Android native service and provided information can be transferred to both, custom applications and HAL modules over AIDL. The entire CommonAPI stack can be built within an AOSP (Android Open Source Project maintained by Google) with the soong build system. Still, the vsomeip itself has some dependencies, such as boost library, which can cause issues while building within the AOSP. Further options are to build CommonAPI client beyond the AOSP, with the Native Development Kit – NDK, or even to use another implementation of SOME/IP standard instead of vsomeip, which would eliminate the dependencies such as the afore-mentioned boost library. Nevertheless, CommonAPI clients must be included in Android services so the data from ADAS can be provided to applications or other services in IVI domain.

Additionally, the mapping of SOME/IP service-client communication paradigm from CommonAPI/AUTOSAR to Android represents a challenge. Namely, AIDL files used for

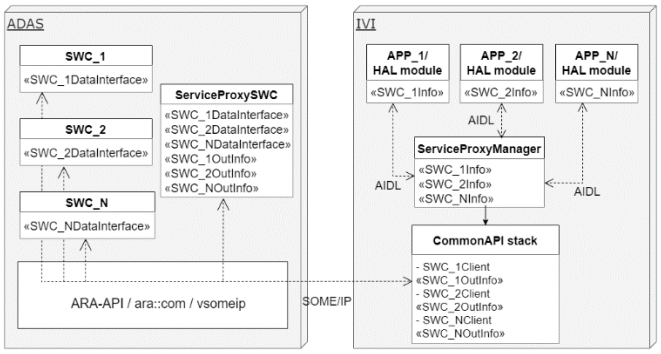


Fig. 4. Centralized interconnection approach with Android on IVI side

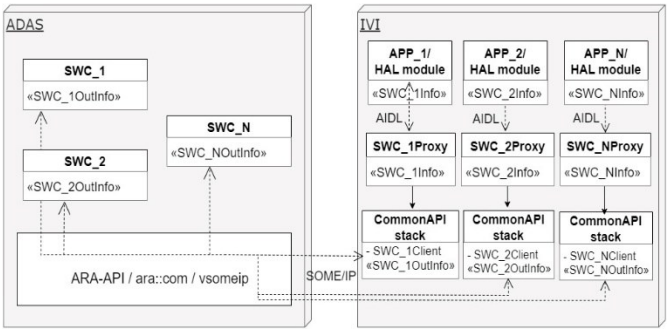


Fig. 5. Distributed interconnection approach with Android on IVI side

interface generation provide the inter-process communication by marshaling the object instances through the binder. This is not suitable for the event-triggered traffic. Event-triggered communication from service to clients within a SOA is performed in a way that the client itself is only subscribed to the events from service. This specific case cannot be covered by using regular AIDL, because AIDL always assumes that the communication is initiated from the client side

Our approach was to incorporate the receiving (client) side for broadcasts and events in the Android native service, and further distribute this information to the interested applications. The easiest way to achieve this is to set properties based on the information received by the Android native service. The interested applications can then read that particular property. This approach has a big limitation since the data can only be used to transfer flags and states since properties do not exist to be used as IPC mechanisms.

We went for the another, a slightly more demanding way for implementation. It assumes the creation of a helper AIDL, which will pass the interface object as a parameter from the applications to Android native service, in order to enable the Android native service to react on event-trigger signals from CommonAPI by invoking methods from the passed object like it is a client to the application. Furthermore, in order to avoid forming a list of registered applications which methods will be invoked when event-triggers we created additional helper service in Java with which it will be communicated via that helper AIDL and which will furtherly provide Intents to the applications. Additionally, it is even possible to have stand-alone Java service which will use the CommonAPI via Java Native Interface – JNI. JNI is necessary in this scenario to enable inter-operability between Java and C/C++ code, since the COVESA provides CommonAPI middleware in C++

 ISBN 978-86-7466-930-3

programming language.

## V. Conclusion and Further Work Directions

This paper presented both, the theoretical and the practical aspects of proposal for service-oriented communication between ADAS and IVI domains. Background and motivation for such binding are provided, along with the key challenges and limitations as it is summarized in Table 1. Several approaches were elaborated in order to satisfy system heterogeneity. Additionally, the beneficial use-cases are discussed in order to emphasize the value of bonding itself.

TABLE I
Major challenges and limitations

| **Challenges** | Limitations |
|---|---|
| **SOA paradigm mapping** | Implementing broadcast/events with AIDL principles |
| **Centralized or distributed approach** | Prioritization, robustness, bandwidth |
| **Data transfer channel** | Performance evaluation |
| **Safety** | Enable safety solution for Android |
| **Generation of inter-communication** | Verification and tool qualification |

In our future work, we will focus on the evaluation of the latency, bandwidth and robustness in order to present comprehensive comparison of the centralized service proxy manager approach with the distributed approach, to determine the optimal design.

The performance of data transfer channel shall be furtherly examined too by considering the Audio Video Bridging (AVB) and other mechanisms for big data integration. It is needed to determine the exact use-cases where the data shall be transferred only within SOME/IP request/response, and where it is more suitable to open additional channel for data transfer. Several aspects regarding data size and safety shall be analyzed in order to define the optimal approach.

Safety requirements are maybe the most complex of all challenges that we plan to address. Safety analysis implies the detail examination on the system level too. It is not enough only to implement mechanisms for Android native service to control which applications can use it based on the given permissions and to properly handle dead listeners and multiple registrations which is done by now. Hazard analysis on the system level involves hardware and OS safety competence and certain communication determinism (Time-Triggered Ethernet or Time-Sensitive Networking). Android itself currently cannot have any Safety integrity level but QM [18]. From that reason, it is mandatory to involve the hypervisor if the communication must be initiated from the Android [19].

The final challenge will be to automate the entire process of providing resources from ADAS to IVI. This means that our goal will be to generate the translation between ARXML, FIDL and AIDL, as well as the generation of Android service along with the code that is responsible for providing resources from service on ADAS side to the IVI realm.

## Acknowledgment

This research (paper) has been supported by the Ministry of Education, Science and Technological Development through project no. 451-03-68/2022-14/ 200156 “Innovative scientific and artistic research from the FTS (activity) domain”.

## References

[1] P. Bajaj, M. Khanapurkar, “Automotive networks based intra-vehicular communication applications. New Advances in Vehicular Technology and Automotive Engineering”, pp. 207-230, (2012).

[2] B. Glas, J. Guajardo, H. Hacioglu, M. Ihle, K. Wehefritz, A. Yavuz, “Signal-based automotive communication security and its interplay with safety requirements.”, In Proceedings of Embedded Security in Cars Conference, 2012

[3] M. Bellanger, E. Marmounier, E, “Service Oriented Architecture: impacts and challenges of an architecture paradigm change”, In 10th European Congress on Embedded Real Time Software and Systems, (2020).

[4] G. L. Gopu, K. V. Kavitha, J. Joy, “Service oriented architecture based connectivity of automotive ecus”, In 2016 International Conference on Circuit, Power and Computing Technologies (ICCPCT), pp. 1-4, (2016).

[5] “Example for a Serialization Protocol (SOME/IP)”, [Online]. Available: https://www.autosar.org/fileadmin/user_upload/standards/classic/4-1/AUTOSAR_TR_SomeIpExample.pdf”, last accessed 2022/10/1.

[6] J. R. Seyler, T. Streichert, M. Glaß, N. Navet, J. Teich, “Formal analysis of the startup delay of SOME/IP service discovery”, In 2015 Design, Automation & Test in Europe Conference & Exhibition (DATE), pp. 49-54, (2015).

[7] "Welcome to FRANCA!” [Online]. Available: https://github.com/franca/franca, last accessed 2022/10/1.

[8] “CommonAPICppUserGuide”, [Online]. Available: https://usermanual.wiki/Document/CommonAPICppUserGuide.1126244679/html, last accessed 2022/10/1.

[9] G. Macario, M. Torchiano, M. Violante, M., “An in-vehicle infotainment software architecture based on google android”, In 2009 IEEE International Symposium on Industrial Embedded Systems, pp. 257-260, (2009).

[10] N. Pajic, M. Bjelica, “Integrating Android to Next Generation Vehicles”, In 2018 Zooming Innovation in Consumer Technologies Conference (ZINC), pp. 152-155, (2018).

[11] “Android Interface Definition Language(AIDL)” [Online]. Available: https://developer.android.com/guide/components/aidl, last accessed 2022/10/1.

[12] S. Fürst, M. Bechter, “AUTOSAR for connected and autonomous vehicles: The AUTOSAR adaptive platform”, In 2016 46th annual IEEE/IFIP international conference on Dependable Systems and Networks Workshop (DSN-W), pp. 215-217, (2016).

[13] S. Aust, ”Paving the way for connected cars with adaptive AUTOSAR and AGL”, In 2018 IEEE 43rd Conference on Local Computer Networks Workshops (LCN Workshops), pp. 53-58, (2018).

[14] M. Kotur, N. Lukić, M. Krunić, G. Velikić, “One solution of camera service in AUTOSAR ADAPTIVE environment”, In 2020 IEEE 10th International Conference on Consumer Electronics, pp. 1-5, 2020.

[15] “Franca/ ARA:COM Interoperability”, [Online]. Available: https://at.projects.genivi.org/wiki/download/attachments/16026116/GENIVI%20Franca-ARA-COM-tech-brief-20181219.pdf, last accessed 2022/10/1.

[16] K. Omerovic, J. Janjatovic, M. Milosevic, T. Maruna, “Supporting sensor fusion in next generation android In-Vehicle infotainment units”, In 2016 IEEE 6th International Conference on Consumer Electronics-Berlin (ICCE-Berlin), pp. 187-189, (2016).

[17] M. Milosevic, M. Z. Bjelica, T. Maruna, N. Teslic, “Software platform for heterogeneous in-vehicle environments”, In IEEE Transactions on Consumer Electronics, pp. 213-221, (2018).

[18] L. Perneel, H. Fayyad-Kazan, M. Timmerman, “Can Android be used for real-time purposes?”, In 2012 International Conference on Computer Systems and Industrial Informatics, pp. 1-6, (2012).

[19] M. Bjelica, Z. Lukac, “Central vehicle computer design: software taking over”, IEEE Consumer Electronics Magazine, 8(6), 84-90, 2019.

 ISBN 978-86-7466-930-3

 ISBN 978-86-7466-930-3

# Утврђивање сличности софтверског кода

Захарије Радивојевић, Милош Цветановић

***Апстракт*—Утврђивање сличности софтверског кода представља област истраживања у оквиру софтверског инжењерства. Поред великог броја домена у којима налази примену оно представља кључни елемент за утврђивање постојања софтверских клонова, а самим тим утиче на софтвер током читавог његовог животног циклуса, током дизајна, развоја и одржавања. У овом раду је, на основу искустава аутора, дат преглед домена и карактеристике кодова који се у датим доменима пореде. Описане су и технике које се примењују у овој области независно од домена примене, као и карактеристике кодова које се датим техникама пореде. Такође је изложено пет сукцесивних поступака које су аутори развили за примену у домену откривања неовлашћеног коришћења лиценци. Поступци обухватају описе техника за утврђивање сличности бинарног кода, утицаја архитектуре рачунара на утврђивање сличности бинарног кода, утицаја трансформација преводиоца на утврђивање сличности бинарног кода, могућности за коришћење неуралних мрежа за утврђивање сличности бинарног кода, као и коришћење секвенци операција за утврђивање сличности бинарног кода.**

***Кључне речи*—Софтверски клонови, сличност кода, бинарни код, софтверске метрике, неуралне мреже.**

## I. Увод

Анализа изворног кода програма има широки спектар примена, које укључују од рангирања и категоризације програма [1], преко откривања преписивања у домаћим задацима [2], до откривања недостатака у програмима [3]. У овој анализи као један од важних корака јесте утврђивање сличности делова кода. Постоје домени примене код којих је утврђивање сличности кода од пресудног значаја. Ови домени обухватају откривање злонамерног кода [4], реверзно инжењерство софтверских закрпа [5], откривање неовлашћеног коришћења лиценци [6], и слично. Ова анализа се у већини случајева обавља над изворним кодом програма, али се у неким случајевима може обављати и над асемблерским кодом програмима као и директно над бинарним записом извршног кода програма. Без обзира да ли се ради анализа изворног или извршног кода, као и без обзира на домен примене поступак се заснива на откривању софтверских клонова.

Овај рад има за циљ да представи област истраживања која се бави анализом сличности софтверског кода. Рад даје сажетак истраживања у овој области и нема за циљ да да систематичан преглед литературе у овој области. Рад је организован тако да ће у другој глави бити представљени домени примене утврђивања сличности кода. У трећој глави објашњене постојеће технике утврђивања сличности кода, док ће у четвртој глави бити представљени резултати истраживања у области анализе софтверског кода датог у бинарном облику које су аутори спровели током више година. Последња, пета, глава представља закључак овог рада.

Захарије Радивојевић, доктор електротехнике и рачунарства – Електротехнички факултет, Универзитет у Београду, Булевар краља Александра 73, 11000 Београд, Србија (e-mail: zaki@etf.bg.ac.rs).

Милош Цветановић, доктор електротехнике и рачунарства – Електротехнички факултет, Универзитет у Београду, Булевар краља Александра 73, 11000 Београд, Србија (e-mail: cmilos@etf.bg.ac.rs).

## II. Домени примене одређивања сличности кода

У овој глави ће бити описани карактеристични домени у којима се може применити утврђивање сличности софтверског кода. За сваки од домена биће наведена сврха са којом се утврђивање сличности користи. Такође, за сваки од домена биће наведен и угледни примерак алата и описан његов начин функционисања. Преглед основних карактеристика појединих домена је дат у табели 1.

### *A. Детекција клонова*

У домену детекције клонова упоређивање сличности кода се користи са циљем упаривања делова кода који могу потицати од сличног изворног кода или од сличног бинарног кода који потиче од истог изворног кода. Два дела кода која представљају софтверски клон поседују исту семантику, али се разликују по нивоу синтаксне сличности и на основу ње су класификовани у четири типа. Два синтаксно идентична кода се класификују као клонови типа 1, а могу се разликовати само по форматирању и пратећим коментарима. Уколико између два кода постоји и разлика у називима литерала онда се класификују као клонови типа 2. Убацивање малог броја додатних инструкција или промена редоследа инструкција која не утиче на резултат извршавања кода се класификује као клон типа 3. Све остале промене које чувају семантику али у већој мери мењају синтаксу оригиналног кода се класификују као клонови типа 4 [7].

Један од алата који се може користити у поступку откивања софтверских клонова је ACD алат [8]. Овај алат покушава да упари секвенце инструкција највеће могуће дужине. За упаривање инструкција потребно је да редослед упарених инструкција буде идентичан у оба кода који се упарују и да се утврди да се инструкције нису раније упариле. Као додатни услов се користи да је циљна адреса скокова иста у односу на остале упарене инструкције. Ако се током упаривања секвенци деси да се мали број инструкција не може упарити оне се игноришу. За сваке две упарене секвенце израчунава се тежина. Сваки пут, када су две инструкције упарене, тежина се

 ISBN 978-86-7466-930-3

ТАБЕЛА 1. ПРЕГЛЕД ДОМЕНА ПРИМЕНЕ

| Домен | Тип кода | Тип клона | Циљ потраге | Узрок разлика |
|---|---|---|---|---|
| Детекција клонова | Изворни | 1, 2, 3, 4 | Сличне процедуре | Програмер |
| Откривање неовлашћеног коришћења лиценци | Изворни/Бинарни | 1-Изворни, 4-Бинарни | Еквивалентне процедуре | Преводилац |
| Откривање злонамерног кода | Бинарни | 1, 2, 3 | Сличан код | Програмер/Преводилац |
| Откривање рањивости кода | Бинарни | 1, 2, 3 | Сличан код | Програмер |

повећава за одређену вредност. Када се у некој од секвенци наиђе на инструкцију која се занемарује, да би се наставило упаривање, тежина се умањује. Процес упаривања две секвенце почиње са две инструкције које се могу упарити и наставља се све док тежина претходно упарених секвенци не буде једнака нули. Након тога, покушава се са побољшањем упаривања две секвенце откривањем нових инструкција које се могу упарити унутар ових секвенци а које би могле повећати укупан број упарених инструкција.

### *B. Откривање неовлашћеног коришћења лиценци*

Све већи број кршења ауторских права у софтверској индустрији доводи до огромних економских губитака за носиоце ауторских права [9]. Једна од ситуација у којој може доћи до кршења је лиценцирање софтвера са двоструком лиценцом. Овај тип пословног модела се обично користи да би се подржао софтвер отвореног кода у комерцијалне сврхе. У таквом пословном моделу, власник ауторских права софтвера нуди изворни код бесплатно за некомерцијалну употребу, али остварује профит продајом ауторских права компанијама које желе да користе изворни код у својим производима. Повреда настаје када се изворни код власника користи у производу без лиценце добијене од власника. За разлику од домена откривања клонова, где је изворни код углавном доступан, одређивање сличности кода се у домену кршења лиценци примењује углавном над извршним кодом. Разлике које у извршним кодовима постоје последице су употребе различитих преводиоца над истим изворним кодом.

Један од алата који се може користити у поступку откивања кршења лиценце је BAT алат који је заснован на приступу описаном у раду [10]. Приступ користи три технике за ублажавање негативних ефеката потенцијалних разлика између кодова који се пореде. Прва техника прикупља стринг литерале који се појављују у коду који се пореди. Након тога, покушава да пронађе исте литерале у коду за који се сумња да крши лиценцу. Друга техника претпоставља да ће алгоритам компресије података успети да компримује боље два кода заједно ако међу тим кодовима постоје исте секвенце инструкција. Успех се мери односом између величине архиве, која се састоји од два кода, и укупне величине архива које се појединачно састоје од само једног од два кода које се пореде. Што је однос мањи, то се очекује већа сличност између упоређених кодова. Трећа техника се заснива на израчунавању бинарних разлика између кодова. Што су разлике мање, вероватноћа да посматрани код крши лиценцу је већа. Алат BAT користи се за откривање да ли посматрани код крши лиценцу неког од кодова из репозиторијума, а за ту сврху користи само прву технику.

### *C. Откривање злонамерног кода*

Злонамерни код је сваки код који има могућност да оштети било који рачунарски систем [4]. Количина злонамерног кода се сваке године све брже повећава и представља озбиљну безбедносну претњу. Отуда је откривање злонамерног кода критична тема у рачунарској безбедности. У оквиру комерцијалних антивирусних програма откривање злонамерног кода је засновано на поређењима отисака метода са познатим отисцима метода. Недостатак овог начина откривања злонамерног кода је да не успева да открије нове варијације већ познатог злонамерног кода. У циљу превазилажења тог недостатка може се употребити одређивање сличности злонамерног кода са циљем откривања дела кода који показује слично понашање као што је понашање које има код из већ познате колекције злонамерног кода.

Један од алата који се може користити у поступку откивања злонамерног кода који користи одређивање сличност кодова је алат који упоређује секвенце кодова операција [4]. Током поређења посматрају се низови кодова операција фиксних дужина и узима се у обзир да различити кодови операција имају различиту релевантност током поређења. Код овог алата се најпре обавља анализа великог броја злонамерног кода и регуларног кода и утврђује се релевантност кодова операције. Затим се израчунавају фреквенције појављивања свих секвенци изабране дужине у кодовима који се упоређују. За сваки од кодова формира се вектор чије су компоненте бројеви појављивања појединачних секвенци. Свака од компоненти вектора се затим множи са производом релевантности свих кодова операција који се појављују у посматраној секвенци како би се елиминисао шум који уноси ирелевантан код. На крају сличност између кодова који се пореде се израчунава коришћењем косинусне сличности ових вектора. Приступ такође предлаже комбинацију добијених резултата за неколико различитих дужина посматраних секвенци.

 ISBN 978-86-7466-930-3

### *D. Откривање рањивости кода*

У домену рањивости софтверског кода могу се разматрати анализа рањивости и откривање рањивости. Анализа рањивости има за циљ да формалним методама потврди или оповргне хипотезу да је софтвер рањив. Приступи анализи рањивости се могу класификовати у три категорије: статичка анализа, динамичка анализа и хибридна анализа кода. Откривање рањивости има за циљ да мање формалним поступцима лоцира конкретну рањивост у коду. У овој области постоји више различитих приступа који између осталог обухватају: тестове пенетрације софтвера, насумично тестирање, и статичку анализу токова података [11]. За разлику од претходно разматраних домена у овом домену се одређивање сличности софтверског кода користи за откривања разлика између две различите верзије истог кода.

Један од алата који се може користити за потребе откривања рањивости је алат који покушава да упари делове кода односно процедура које су скоро идентичне [12]. Први предуслов за упаривање процедура је да су идентичне према свим датим критеријумима (тзв. селекторима): броју основних блокова, броју ивица у контролном графу тока и броју позваних потпрограма. Други предуслов за упаривање је да не постоји друга процедура која је идентична са процедурама које се пореде на основу коришћених критеријумима. Да би се смањило ограничење другог предуслова у свим корацима алгоритма, посматрају се подскупови процедура из кодова који се пореде а који су дати у бинарном облику. Приликом формирања првих парова, подскупови се формирају издвајањем процедура које задовољавају неку карактеристику. Неке од карактеристика које се користе су број улазних и излазних грана процедура у графу позива, исти називи процедура, референце на исте стрингове и број пута када су се неке од инструкција појавиле. Када даље упаривање по датим карактеристикама више није могуће, формирају се нови подскупови процедура које се позивају из упарених процедура. Подскупове такође формирају процедуре које позивају упарене процедуре. Алгоритам се понавља за сваке две упарене процедуре све до тренутка када даље упаривање више није могуће. Унутар упарених процедура врши се даље упаривање основних блокова и инструкција.

## III. Технике утврђивања сличности кода

У овој глави ће бити описане најзаступљеније технике утврђивања сличности софтверског кода описане у прегледним радовима [7], [13], [14], [15], [16], [17]. За сваку од техника биће наведен кратак опис, применљивост, могућности проширења, као и на које типове софтверских клонова се најчешће примењује. Такође, биће наведен и угледни примерак алата и описане његов начин функционисања за сваку од техника. Поред техника које су описане у наставку постоје и хибридне технике код којих се може јавити синергистички ефекат тако да могу детектовати додатне типове клонова у поређењу са типовима клонова који се могу детектовати било којом од коришћених техника детекције одвојено.

### *A. Технике засноване на поређењу текста*

Технике засноване на поређењу текста посматрају секвенцу линија изворног кода. Како би се пронашла секвенца истоветних линија, стрингова или лексема пореде се делови два изворна кода или њихови отисци. Када се у датим деловима кода открије да су поједини делови слични они се проглашавају за клонове одређене класе. Ове технике се углавном користе за откривање клонова код виших програмских језика и развијени алати често подржавају више од једног програмског језика. У случају да их је потребно проширити тако да подрже неки нови програмски језик или није потребно ништа додатно имплементирати или је потребно имплементирати лексички анализатор. Ова техника се углавном може применити за откривање клонова типа 1 и типа 3, а може се применити и за откривање клонова типа 2. Ова техника се у имплементацијама показала као техника средње сложености.

Један од алата који користи технику засновану на поређењу текста је SimCad алат [18]. Овај алат подржава више програмских језика и то: C, C#, Java, Python. Процес откривања клонова се заснива на техникама откривања скривеног знања и рударења података и користи алгоритам за груписање података као и претрагу података засновану на вишенивојским индексима. Овај алат извршава три фазе обраде: прелиминарну обраду, откривање клонова и генерисање резултата. У фази прелиминарне обраде користећи Simhash алгоритам се генеришу отисци кода, након чега се обавља индексирање формирањем вишенивојски индекси за потребе брже претраге. У другој фази се обавља откривање клонова тако што се фрагменти кода групишу у кластере користећи Хемингово растојање између генерисаних отисака који одговарају тим фрагментима кода. Парови фрагмената који не прелазе одговарајући ниво сличности бивају елиминисани из кластера, а такође мора постојати и одређен број фрагмената кода у кластеру. У трећој фази се врши чишћење добијених резултата као и њихов приказ у одговарајућем формату.

### *B. Технике засноване на поређењу токена*

Технике засноване на поређењу токена посматрају секвенцу токена издвојених из изворног кода. Издвајање токена се обавља у поступку лексичке анализе изворног кода. Секвенца токена се формира као скуп токена на одређеном нивоу гранулације. Срж ове технике представља поређење токена који припадају суфиксним стаблима или суфиксним низовима састављених од секвенци токена. Ова техника откривања користи посебан објекат који представља апстракцију конкретних вредности идентификатора и литерала и који води рачуна о очувању њиховог међусобног редоследа. Ове технике се углавном користе за откривање клонова код виших

 ISBN 978-86-7466-930-3

ТАБЕЛА 2. ПРЕГЛЕД ТЕХНИКА

| Техника | Тип кода | Тип клона | Проширивост | Сложеност извршавања |
|---|---|---|---|---|
| Поређење текста | Изворни | 1, 2, 3 | -/Лексички | Средња |
| Поређење токена | Изворни | 1, 2, 3 | Лексички | Мања |
| Поређење метрика | Изворни/Бинарни | 1, 2, 3, 4 | Лексички, парсер | Средња |
| Поређење апстрактног синтаксног стабла | Изворни/Бинарни | 1, 2, 3 | Парсер | Средња |
| Поређење графа зависности | Изворни/Бинарни | 1, 2, 3, 4 | Парсер | Велика |

програмских језика, али је за разлику од техника заснованих на поређењу текста зависност од програмског језика већа. У случају да је потребно проширити их подршком за нови програмски језик неопходно је имплементирати лексички анализатор. Ова техника се углавном може применити за препознавање клонова типа 1, 2 и 3, и представља једну од најцитиранијих техника за одређивање сличности. Ова техника се у имплементацијама показала као техника мање сложености.

Један од алата који користи технику засновану на поређењу текста је CCFinder алат [19]. Овај алат подржава више програмских језика и то: C/C++, C#, Cobol, Java, VB. Обрада коју спроводи овај алат се извршава у четири фазе: лексичка анализа, трансформација међурезултата, одређивање сличности и форматирање добијених резултата. У фази лексичке анализе се свака линија изворног кода дели у низ токена у складу са лексичким правилима датог програмског језика. У другој фази се обавља трансформација добијених низова токена користећи правила трансформације и правила замене одређених типова токена. У трећој фази се обавља упоређивање свих подстрингова како би се идентификовали парови клонова. На крају, у четвртој фази, се препознати клонови пресликавају на линије изворног кода из кога потичу.

### *C. Технике засноване на метрикама*

Технике засноване на метрикама посматрају карактеристике изворног програма издвојене користећи скуп метрика. Издвајање карактеристика се обавља полазећи од кода који је трансформисан у одговарајућу структуру. Метрике се могу израчунавати на основу имена, размештаја елемента, израза, контроле токе функција, и сличних елемената структуре кода. Одређивање сличности се обавља израчунавањем удаљености између одговарајућих чланова у формираном метричком простору. Ове технике се углавном користе за откривање клонова код виших програмских језика и зависност од програмског језика је велика, али се такође могу примењивати и код нижих програмских језика. У случају да је потребно проширити их подршком за нови програмски језик неопходно је имплементирати не само лексички анализатор, већ и одговарајући парсер. Техника се може применити за препознавање свих типова клонова. Ова техника се у имплементацијама показала као техника средње сложености.

Један од алата који користи технику засновану на метрикама је CLAN алат [20]. Овај алат подржава програмске језике C/C++. Обрада коју спроводи овај алат се извршава у четири фазе: препроцесирање директива, парисирање и идентификација фрагмената, екстракција метрика и идентификација клонова. Како је алат намењен језицима C/C++ у првој фази се обавља препроцесирање директива датог језика како би се добио изворни код који се даље може обрађивати. У другој фази се обавља екстракција декларација и дефиниција самих функција користећи наменски парсер. У трећих фази се издвајају метрике коју укључују бројање функција, локалних променљивих, дељених и глобалних променљивих, параметара, исказа скокова и петљи. У четвртој фази се обавља идентификација клонова у поступку квантизација метрика коришћењем прагова за елиминацију шума и спектралне анализе резултата.

### *D. Технике засноване на апстрактним синтаксним стаблима*

Технике засноване на апстрактним синтаксним стаблима трансформишу изворни код у структуру стабла које се касније може упоређивати. За поређење стабала, или њихових подстабала, се може користити више различитих метода које укључују хеширање, трансформацију у префиксна стабла, одређивање најдуже заједничке секвенце употребом динамичког програмирања. Ове технике се углавном користе за откривање клонова код виших програмских језика и зависност од програмског језика је велика, али се такође могу примењивати и код нижих програмских језика. У случају да је потребно проширити их подршком за нови програмски језик неопходно је имплементирати одговарајући парсер. Ова техника се углавном може применити за препознавање клонова типа 1, 2 и 3. Ова техника се у имплементацијама показала као техника средње сложености.

Један од алата који користи технику засновану на метрикама је DECKARD алат [21]. Овај алат подржава програмске језике: C, Java, Php. Обрада коју спроводи овај алат се извршава у пет фаза: генерисање парсера, формирање стабла, генерисање вектора, кластеровање вектора и додатна обрада. У првој фази се на основу формалне граматике језика генерише парсер који се користи и даљој обради. У другој фази се на основу генерисаног парсера и улазног изворног кода формира апстрактно синтаксо стабло које ће се даље обрађивати. У

 ISBN 978-86-7466-930-3

трећој фази се обрађује синтаксно стабло како би се формирали вектори карактеристика фиксне дужине. У овој фази се додатно може обавити и спајање делова који имају заједничко подстабло. У четвртој фази се обавља груписање вектора у кластере користећи еуклидско растојање са циљем одређивања клонова. На крају се као додатна, пета, фаза обавља додатна обрада како би се користећи одређене хеуристике елиминисали погрешно идентификовани клонови.

### *E. Технике засноване на коришћењу графа зависности*

Технике засноване на коришћењу графа зависности које постоје у графу тока контроле и у графу тока података. Графовска репрезентација изворног кода се дели на мање делове у зависности од понашања фрагмента изворног кода. За деобу и поређење се може користити неки од постојећих алгоритама за рад са подстринговима и откривање сличности. Ове технике се углавном користе за откривање клонова код виших програмских језика и зависност од програмског језика је велика. У случају да је потребно проширити их подршком за нови програмски језик неопходно је имплементирати одговарајући парсер. Ова техника се, као и рад са метрикама, може применити за препознавање свих типова клонова. Ова техника се у имплементацијама показала као техника велике сложености.

Један од алата који користи технику засновану на коришћењу графа зависности је PDG-DUP алат [22]. Овај алат подржава програмске језике C/C++. Обрада коју спроводи овај алат се извршава у четири фаза: формирање графа зависности, проналажење парова клонова, уклањање обухваћених клонова и груписање клонова у веће групе. У првој фази се формира граф зависности код кога чворови представљају наредбе програма и предикате, а ивице представљају зависности података и контроле. Друга фаза се обавља у неколико корака. На почетку се обавља деоба свих чворова графа зависности у класе еквиваленције на основу синтаксне структуре исказа и предиката који ти чворови представљају, занемарујући имена променљивих и литерале. У наредном кораку се обавља најбитнији део, срж, алгоритма који проналази изоморфне подграфове коришћењем технике одсецања уназад (*backward slicing*) која датом програмском сегменту додаје претходни повезани део. Поред повратног одсецања користи се и техника одсецања унапред која додаје наредни повезани део. У трећој фази се обавља уклањање свих парова клонова који су већ садржани у неким другим паровима клонова идентификованим у претходном кораку. У четвртој фази се обавља груписање идентификованих парова у веће групе користећи особину транзитивности.

## IV. Доприноси утврђивању сличности кода

Откривање неовлашћеног коришћења софтверске библиотеке је проблем детекције клонова који у случају комерцијалних производа има додатну сложеност због чињенице да је код доступан само у бинарном облику. Циљ аутора је био да предложи приступ за процену нивоа сличности између процедура који потичу из различитих бинарних кодова. Основна претпоставка у истраживањима је била да клонови у бинарним кодовима потичу од употребе заједничке софтверске библиотеке, односно истог изворног кода, која се може преводити користећи различите алате. За потребе истраживања бинарни код је дисасемблиран, а за потребе коришћења других алата и декомпајлиран. Детаљан преглед различитих приступа у препознавању сличности бинарног кода дат је у прегледном раду [17] док ће у овој глави бити описана истраживања аутора овога рада спроведена стремећи ка наведеном циљу у области утврђивања сличности бинарног кода. За свако од спроведених истраживања биће наведен кратак опис истраживања, кораци предложеног приступа а потом дати и остварени резултати. Преглед основних карактеристика појединих истраживања је дат у табели 3.

### *A. Утврђивање сличности бинарног кода*

Прво истраживање је имало за циљ да утврди применљивост постојећих техника и алата описаних у претходним поглављима за утврђивање сличности бинарног кода [6]. Имајући у виду да су постојеће технике и алати превасходно намењени раду са вишим програмским језицима у овом истраживању су нека одабрана решења прилагођења раду са бинарним кодом ради евалуације. У истраживању је такође предложен нови приступ који је заснован на метрикама.

Предложени приступ за процену нивоа сличности између две процедуре које се пореде је процес који се обавља у четири фазе: издвајање метрика, упоређивање метрика, трансформације метрика, израчунавање нивоа сличности. У првој фази се спроводи статичка анализа процедура и издвајање метрика тако да се за сваку процедуру формира вектор метрика, при чему елементи тог вектора могу бити скаларне или векторске вредности. Ове метрике укључују одређивање броја и учестаности свих инструкција, појединих типова инструкција (аритметичких, логичких и трансфер података), скокова (условних и безусловних скокова, позива процедура и петљи) и које се представљају скаларним вредностима. Поред скаларних вредности метрика коришћене су и нескаларне, векторске, метрике која укључују бројање сваке појединачне инструкције, сваке адресе доскока, и сваке адресе позива процедуре. У другој фази се обавља поређење сваке о издвојених метрика користећи одговарајући функције за поређење. У трећој фази се обавља трансформација и нормализација добијених резултата поређења на основу претходног знања. У последњој, четвртој, фази комбинују се одабране метрике користећи одговарајућу формулу за формирање једне вредности која представља сличност између две процедуре.

Резултати истраживања су дали одговоре на три истраживачка питања и довела до следећих закључака. Прво питање се односило на разматрање додавања нове

 ISBN 978-86-7466-930-3

ТАБЕЛА 3. ПРЕГЛЕД РЕЗУЛТАТА ИСТРАЖИВАЊА

| Приступ | Метрике | Архитектура | Мера сличности | Одзив |
|---|---|---|---|---|
| 1. | Скаларна(13) векторска(6) | ARM | Формуле (7) | 35,8%-73,1% |
| 2. | Скаларна(3) векторска(1) | x86 | Тежинска сума | 37,6%-63.0% |
| 3. | Скаларна(13) векторска(6) | ARM | Формуле (7) | 52,7%-81,8% |
| 4. | Векторска(1) | ARM | Неуралнa мрежа | 49,2%-82,8% |
| 5. | Векторска(1) | ARM | Левенштајнова удаљеност | 57,9%-88,9% |

метрике у скуп метрика предложних у постојећим решењима и утврђивање доприноса приликом рангирања процедура. Резултати спроведеног експеримента показују да увођење нових метрика доприноси рангирању процедура за све посматране позиције приликом рангирања. Штавише, са новим метрикама предложени приступ је постигао 1,44 пута бољи одзив (*recall*) за прву посматрану позицију у поређењу са случајем када се користе само постојеће метрике. Друго питање се односило на проверу да ли рангирање процедура обављено предложеним приступом зависи од преводиоца, нивоа оптимизације програма и контекста проблема. Према резултатима експеримента утврђено је да постоји значајан утицај изабраног преводиоца на рангирање процедура који је остварен у предложеном приступу. Међутим, контекст проблема и опције превођења имају мањи утицај на резултате. Треће питање се односило на проверу да ли предложени приступ постиже боље резултате од постојећих алата у смислу прецизности, одзива и F2 мере. Одговарајући експеримент је показао да предложени приступ постиже други најбољи резултат у смислу прецизности и најбољи резултат у смислу одзива. У случају посматрања F2 мере, предложени приступ постиже резултате боље од осталих алата када се посматра до првих шест позиција, док се максимална вредност постиже када се посматрају само прве две позиције при рангирању.

### *B. Утицај архитектуре рачунара на утврђивање сличности бинарног кода*

Друго истраживање је имало за циљ да утврди применљивост приступа предложеног у првом истраживању на другу архитектуру [23]. С обзиром да је у првом истраживању коришћена ARM архитектура, за потребе другог истраживања је коришћена x86 архитектура. Имајући у виду разлике у архитектури било је потребно поновно креирање скупа података на коме ће се обавити тестирање. Овом приликом је коришћен сличан скуп програмских преводилаца, али не потпуно исти, јер ниси сви преводиоци подржавали обе архитектуре.

У оквиру другог истраживања је предложен нови приступ који представља подскуп приступа предложеног у првом истраживању. У овом новом приступу број различитих корака који су спровођени током испитивања у појединим фазама је редукован, и такође је редукован број фаза. Предложени приступ уместо четири фазе има само три фазе. У првој фази је смањен број издвојених метрика, тако да су коришћене метрике које одређују дужину процедуре, број скокова, број позиваних процедура и броје инструкција. Иако је смањен број метрика сачувано је постојање и скаларних и векторских метрика. У другој фази се обавља поређење сваке о издвојених метрика користећи одговарајући функције за поређење, на истоветан начин као и првом истраживању. Трећа фаза се може посматрати као обједињење треће и четврте фазе из првог истраживања и у њој се израчунава сличности користећи хармонијску средину, тежинску суму и наивни Бајес.

Резултати за x86 архитектуру показују да је најбољи одзив постигнут користећи приступ заснованим на тежинској суми. Одзив се креће од 37% до 63% када се посматра прва односно првих десет позиција. Поређење резултата остварених на x86 и ARM архитектурама показује да су постигнућа добијена за првих десет позиција на обе архитектуре упоредива.

Ово показује да се технике поређења бинарних кодова у извесној мери могу користити за поређење кодова који су преведени за исту архитектуру рачунара. Истраживања која су спровели други истраживачи након овог истраживања, почев од 2016. године а која се баве поређењем сличностима бинарног кода између архитектура рачунара [17], су показала да се технике за поређење могу примењивати не само на једној архитектури рачунара, већ се могу примењивати и на кодове код којих су једни преведени за једну архитектуру рачунара а други за други архитектуру рачунара. Овиме се проширује оно што је другим истраживањем утврђено а то је да се технике поређења бинарних кодова у извесној мери могу посматрати независно од архитектуре рачунара.

### *C. Утицај трансформација преводиоца на утврђивање сличности бинарног кода*

Као што је претходно описано, резултати првог истраживања су показали да постоји значајан утицај изабраног преводиоца на рангирање процедура. Из тог разлога треће истраживање је имало за циљ да детаљније испита утицај трансформација програмског преводиоца на утврђивање сличности бинарног кода [24]. У истраживању је такође предложен и нови приступ који дефинише нове технике за смањење утицаја процеса превођења на перформансе поступка утврђивања сличности бинарног кода.

У односу на приступ предложен у првом истраживању у овом приступу је у првој фази, у којој се спроводи

 ISBN 978-86-7466-930-3

статичка анализа, додато пет техника које се спроводе као независни кораци. Прва техника предлаже игнорисање инструкција за рад са стеком. Ова техника је уведена је уведена зато што је приликом анализе уочено да различити преводиоци на различите начине интерагују са стеком и да инструкције које том приликом користе не носе информације о семантици кода. Друга техника предлаже игнорисање инструкција за трансфер података. Ова техника је уведена из сличног разлога као и прва техника јер различити преводиоци користе различите приступе приликом алокације регистара и трансфера између њих или меморијске локације на којој се неки податак налази. Трећа техника предлаже измену неких од разматраних векторских метрика. Овде се уместо посматрања статистике о појединим инструкцијама посматра статистика о секвенцама инструкција одређене дужине. Четврта техника предлаже уграђивање позваних процедура у оквиру позивајуће процедуре. Ова техника је уведена како би се елиминисала разлика између бинарних кодова која може настати усред одлуке преводиоца да обави аутоматско уграђивање у време превођења. Пета техника предлаже увођење прага сличности између процедура. Ова техника је уведена како би смањила број лажно позитивно идентификованих клонова, с обзиром да преводиоци могу различиту логику да имплементирају користећи сличне инструкције.

Резултати истраживања су дали одговоре на три истраживачка питања и довела до следећих закључака. Прво питање се односило на одређивање постигнућа постојећих решења зависе од тога да ли се користи произвољни преводилац и произвољни ниво оптимизације. Према резултатима експеримента утврђено је да постоји значајан утицај изабраног преводиоца на рангирање процедура, и за разлику од првог истраживања овом приликом су тачно измерени утицаји који имају промена преводиоца и промена нивоа оптимизације. Друго питање се односило на проверу да ли додавање сваке од предложених техника једне по једне основном приступу повећава постигнуће ако се упоређене процедуре преводе са произвољним преводиоцима и нивоима оптимизације. Према резултатима експеримента утврђено је да све технике, изузев друге технике које филтрира инструкције трансфера података, доприносе побољшању резултата утврђивања сличности. Треће питање се односило на проверу да ли додавање свих предложених техника заједно основном приступу повећава постигнуће и да ли резултира синергистичким ефектима ако се упоређене процедуре преводе са произвољним преводиоцима и нивоима оптимизације. Резултати експеримента су показали да додавање свих техника има синергистички ефекат који доноси 6,7% до 9,3% повећања одзива за првих пет посматраних позиција приликом рангирања.

### *D. Коришћење неуралних мрежа за утврђивање сличности бинарног кода*

Четврто истраживање је имало за циљ да испита могућност употребе неуралних мрежа за утврђивање сличности бинарног кода [25]. За разлику од приступа описаном у претходним истраживањима који се заснивају на посматрању метрика у овом истраживању су посматране само инструкције. За потребе евалуације је искоришћен исти скуп података који је коришћен у првом и трећем истраживању.

Предложени приступ обавља поређење процедура у пет фаза: издвајање инструкција, кодирање инструкција, коришћење једног првог слоја неуралне мреже, коришћење другог слоја неураллне мреже, поређење. У првој фази се спроводи издвајање токена који одговарају појединим инструкцијама. У другој фази се обавља кодирање инструкција у целобројну вредност. У поступку кодирања су примењене три технике: лексикографско кодирање, семантичко мапирање и мапирање засновано на класи. У трећој фази се полазећи од секвенце кодираних инструкција формирана секвенца карактеристика исте дужине користећи неуралне мреже. Коришћена је Дуготрајно-краткотрајна меморија LSTM (*Long Short-Term Memory*). У четвртој фази се обавља издвајање одређеног броја карактеристика користећи неуралну мрежу која занемарује одређен број улазних карактеристика DNN (*Dropout Neural Network*). У последњој, петој, фази комбинују се рачунање сличности између две процедуре користећи издвојене карактеристике и поступак агрегације и нормализације.

Резултати истраживања су дали одговоре на три истраживачка питања и довели до следећих закључака. Прво питање се односило на разматрање какве резултате даје предложени поступак у односу на поређење процедура само по њиховој дужини. Резултати спроведеног експеримента показују да предложени приступ даје бољи одзив на свакој посматраној позицији. Друго питање се односило на проверу да ли рангирање процедура обављено предложеним приступом зависи од преводиоца. Према резултатима експеримента утврђено је да постоји неки утицај изабраног преводиоца на рангирање процедура од 0,55% до 1,64% када се посматра одзив. Овај утицај је знатно мањи у односу утицај који је присутан код првог и трећег приступа. Треће питање се односило на проверу да ли предложени приступ постиже боље резултате од постојећих алата у смислу одзива. Одговарајући експеримент је показао да предложени приступ постиже незнатно боље резултате, просечно 1,14%. Овај приступ је дао бољи одзив на вишим позицијама, док у првих 9 позиција даје лошије резултате у односу на трећи предложени приступ.

### *E. Коришћење секвенци операција за утврђивање сличности бинарног кода*

У првом истраживању је примећено да метрика која узима у разматрање секвенцу инструкција највише доприноси успешном одређивању сличности. Из тог разлога пето истраживање је имало за циљ да детаљније испита могућности те метрике и да је учини робуснијом на промене које чини преводилац. Сходно томе

 ISBN 978-86-7466-930-3

предложен је нови приступ заснован на испитивању секвенце кодова операција [26].

Предложени приступ обавља поређење процедура у четири фаза: издвајање инструкција, кодирање инструкција, одређивање Левенштајнове удаљености, рачунање релативне Левенштајнове удаљености. У првој фази се спроводи издвајање токена који одговарају појединим инструкцијама. У другој фази се обавља кодирање инструкција у целобројну вредност на истоветан начин ономе описаном у четвртом приступу. У трећој фази се обавља рачунање Левенштајнове удаљености користећи *Needleman–Wunsch* алгоритам. У последњој, четвртој, фази се коришћењем релативне Левенштајнове удаљености добија сличности између две процедуре.

Ово истраживање је требало да да одговор на једно истраживачко питање о томе какве резултате даје предложени приступ у односу на остале приступе које су аутори развили за ARM архитектуру. Резултати спроведеног експеримента показују да предложени приступ даје бољи одзив на свакој посматраној позицији од свих претходно разматраних приступа. У односу на приступ из четвртог истраживања даје од 3,59% до 9,45% бољи одзив, као и од 0,17% до 4,73% бољу прецизност када се посматрају првих 20 позиција. У односу на приступ из трећег истраживања даје од 3,45% до 9,53% бољи одзив, као и од 0,45% до 1,72% бољу прецизност када се посматрају првих 20 позиција.

## V. Закључак

Утврђивање сличности кода представља област истраживања са дугом историјом, доста запажених резултата али и перспективом за даљи развој у будућности. Овај рад је имао за циљ да ову област приближи истраживачима и да да осврт на истраживања која су аутори спровели. У раду је најпре објашњен значај и домени у којима се резултати истраживања примењују. Након тога је дат сажет преглед најважнијих техника у овој области. На крају су изложена истраживања и резултати до којих су аутори дошли у претходним годинама.

## Захвалница

Рад на овом пројекту је делимично био финансиран од стране Министарства просвете, науке и технолошког развоја Републике Србије (2022/200103), као и Фонда за науку Републике Србије (АВАНТЕС).

## Референце

[1] L. Li, T. Bissyandé, M. Papadakis, S. Rasthofer, A. Bartel, D. Octeau, J. Klein, Y. Le Traon, “Static analysis of android apps: A systematic literature review,” *Information and Software Technology*, vol. 88, pp. 67-95, Aug. 2017, 10.1016/j.infsof.2017.04.001.

[2] M. Misic, Z. Sustran, and J. Protic, “A comparison of software tools for plagiarism detection in programming assignments,” *International Journal of Engineering Education*, vol. 32, no. 2, pp. 738-748, 2016.

[3] F. Zampetti, S. Scalabrino, R. Oliveto, G. Canfora, and M. di Penta, “How Open Source Projects Use Static Code Analysis Tools in Continuous Integration Pipelines,” in IEEE International Working Conference on Mining Software Repositories, 2017, doi: 10.1109/MSR.2017.2.

[4] I. Santos, F. Brezo, J. Nieves, Y. K. Penya, B. Sanz, C. Laorden, and P. G. Bringas, “Idea: Opcode-Sequence-Based Malware Detection,” In: F. Massacci, D. Wallach, N. Zannone, (eds) Engineering Secure Software and Systems. ESSoS 2010. Lecture Notes in Computer Science, vol 5965. Springer, Berlin, Heidelberg. https://doi.org/10.1007/978-3-642-11747-3_3.

[5] T. Dullien and R. Rolles, “Graph-based comparison of executable objects (english version),” Sstic, 2005, doi: 10.1.1.96.5076.

[6] S. Stojanović, Z. Radivojević, and M. Cvetanović, “Approach for estimating similarity between procedures in differently compiled binaries,” *Information and Software Technology*, vol. 58, pp. 259-271, 2015, doi: 10.1016/j.infsof.2014.06.012.

[7] C. K. Roy, J. R. Cordy, R. Koschke, “Comparison and evaluation of code clone detection techniques and tools: a qualitative approach,” *Sci. Comput. Program*, vol. 74, pp. 470–495, 2009.

[8] Davis, I.J. and Godfrey, M.W, “From Whence it Came: Detecting Source Code Clones by Analyzing Assembler,” Proc. WCRE 10, Beverly, MA, October 13–16, pp. 242–246. IEEE, Los Alamitos, 2010.

[9] P.E.Chaudhry, and A. Zimmerman “Protecting Your Intellectual Property Rights: Understanding the Role of Management, Governments, Consumers and Pirates,” Springer, New York, 2012.

[10] A. Hemel, K.T. Kalleberg, R. Vermaas, and E. Dolstra, “Finding Software License Violations through Binary Code Clone Detection,” Proc. MSR 11, Honolulu, HI, May 21–22, pp. 63–72. ACM, New York, 2011.

[11] S. M. Ghaffarian and H. R. Shahriari. “Software Vulnerability Analysis and Discovery Using Machine-Learning and Data-Mining Techniques: A Survey,” ACM Comput. Surv. 50, 4, Article 56 (July 2018), 36 pages. DOI:https://doi.org/10.1145/3092566

[12] T. Dullien, and R. Rolf, “Graph-based Comparison of Executable Objects (English version),” Proc. SSTIC 05, Rennes, France, June 1–3, pp. 1–13. STIC, Paris, 2005.

[13] D. Rattan, R. Bhatia, and M. Singh, “Software clone detection: a systematic review,” *Inform. Softw. Technol.*, vol. 55, pp.1165–1199, 2013.

[14] S. Bellon, R. Koschke, G. Antoniol, J. Krinke, E. Merlo, “Comparison and evaluation of clone detection tools,” *IEEE Trans. Software Eng*. vol. 33, pp. 577–591, 2007.

[15] C. K. Roy, J. R. Cordy, “A Survey on Software Clone Detection Research,” Technical Report 2007-541, Queen’s University, Canada, 2007.

[16] Q. U. Ain, W. H. Butt, M. W. Anwar, F. Azam and B. Maqbool, “A Systematic Review on Code Clone Detection,” *IEEE Access,* vol. 7, pp. 86121-86144, 2019, doi: 10.1109/ACCESS.2019.2918202.

[17] I. Haq, J. Caballero, “A Survey of Binary Code Similarity,” *ACM Computing Surveys,* vol. 54, no. 3, pp. 1-38, April, 2022.

[18] M. S. Uddin, C.K. Roy, K.A. Schneider, A Hindle, “On the effectiveness of Simhash for detecting near-miss clones in large scale software systems,” in: Proceedings of 18th Working Conference on Reverse Engineering (WCRE 2011), Limerick, Ireland, 2011, pp. 13–22.

[19] T. Kamiya, S. Kusumoto, K. Inoue, “CCFinder: a multilinguistic token-based code clone detection system for large scale source code,” *IEEE Trans. Software Eng*., vol. 28, pp. 654–670, 2002.

[20] E. Merlo, “Detection of plagiarism in university projects using metrics-based spectral similarity,” in: Proceedings of Dagstuhl Seminar 06301: Duplication, Redundancy, and Similarity in Software, Dagstuhl, Germany, 2006, pp. 1–10.

[21] L. Jiang, G. Misherghi, Z. Su, S. Glondu, “DECKARD: scalable and accurate treebased detection of code clones,” in: Proceedings of the 29th International Conference on Software Engineering (ICSE 2007), Minneapolis, USA, 2007, pp. 96–105.

[22] R. Komondoor, S. Horwitz, “Using slicing to identify duplication in source code,” in: Proceedings of the 8th International Symposium on Static Analysis (SAS’01), vol. LNCS 2126, Paris, France, 2001, pp. 40–56.

[23] K. Berta, S. Stojanović, M. Cvetanović, Z. Radivojević, “Estimation of Similarity between Functions Extracted from x86 Executable Files,” *Serbian Journal of Electrical Engineering*, vol. 12, no. 2, pp. 253 - 262, Jun, 2015.

 ISBN 978-86-7466-930-3

[24] Z. Radivojević, M. Cvetanović and S. Stojanović, “Comparison of Binary Procedures: A Set of Techniques for Evading Compiler Transformations,” *The Computer Journal*, vol. 59, pp. 106–118, 2015.
[25] N. Pejić, M. Cvetanović, Z. Radivojević, “Estimating similarity between differently compiled procedures using neural networks,” ТЕЛФОР XXVII, Belgrade, Nov, 2019.
[26] N. Pejić, M. Cvetanović, Z. Radivojević, “Comparing Assembler Procedures by Analyzing Sequences of Opcodes,” Telfor Journal, vol. 12, no. 1, pp. 46 - 49, Jul, 2020.

 ISBN 978-86-7466-930-3

# Softversko rešenje za akviziciju i vizuelizaciju moždanih talasa

Ivan Tot, Boriša Jovanović, Dušan Bogićević, Tamara Gajić, Jordan Atanasijević

***A stra t*— današnjem društvu veoma značajnu ulogu imaju sistemi za identifikaciju korisnika. Složeni bezbednosni zahtevi naterali su eksperte da istraže načine na oje se biometrijs i podaci mogu iskoristiti u utvrđivanju identiteta korisnika. U ovom radu je prikazano softversko rešenje za akviziciju i vizuelizaciju moždanih talasa (EEG) kao biometrijskih podata a.**

***Ključne reči*—biometrija; moždani talasi; akvizicija; vizuelizacija**

## I. UVOD

Kontrola pristupa informacionim sistemima predstavlja jedan od najznačajnijih aspekata zaštite, posebno kod sistema koji sadrže bezbednosno osetljive podatke. Ona onemogućava osobama koja nemaju pravo da pristupe nekom sistemu i samim tim zloupotrebe podatke koje se nalaze u njemu.

Da bi se došlo do faze identifikacije korisnika, u smislu zaštite informaciono-komunikacionih sistema, neophodno je da se putem biometrijskih senzora prikupe biometrijski podaci koji će se uporediti sa već postojećim podacima registrovanim u samom sistemu [1] [2] [3]. Spajanje više biometrijskih podataka smanjuje stepen sistemske greške prilikom identifikacije korisnika. Samo prikupljanje podataka sa više biometrijskih senzora stvara kompletniju sliku o korisniku. Metod fuzije biometrijskih podataka uključuje sekvencijalnu obradu biometrijskih modaliteta dok se ne dobije prihvatljivo podudaranje u slučaju identifikacije korisnika [4] [5].

Ovaj rad daje prikaz softverskog rešenja koje omogućava akviziciju i vizuelizaciju moždanih talasa (EEG) koje predstavlja prvi korak u realizaciji rešenja za autentifikaciju korisnika.

Ivan Tot – Vojna akademija, Univerzitet odbrane u Beogradu, Generala Pavla Jurišića Šturma 33, 11000 Beograd, Srbija (e-mail: ivan.tot@va.mod.gov.rs).

Boriša Jovanović – Vojna akademija, Univerzitet odbrane u Beogradu, Generala Pavla Jurišića Šturma 33, 11000 Beograd, Srbija (e-mail: borisa.jovanovic@vs.rs).

Dušan Bogićević – Vojna akademija, Univerzitet odbrane u Beogradu, Generala Pavla Jurišića Šturma 33, 11000 Beograd, Srbija (e-mail: dusan.bogicevic@vs.rs).

Tamara Gajić – Vojna akademija, Univerzitet odbrane u Beogradu, Generala Pavla Jurišića Šturma 33, 11000 Beograd, Srbija (e-mail: tamara.gajic@vs.rs).

Jordan Atanasijević – Vojna akademija, Univerzitet odbrane u Beogradu, Generala Pavla Jurišića Šturma 33, 11000 Beograd, Srbija (e-mail: jordan.atanasijevic@vs.rs).

.

## II. PRIMENJENI HARDVERSKI UREĐAJ

Akvizicija predstavlja prikupljanje podataka iz spoljašnje sredine u određeni električni uređaj, to jest senzor. Kada se govori o biometrijskom podatku, onda je potreban biometrijski uređaj za akviziciju takve vrste podataka [6]. Tako prikupljeni podatak može biti upotrebljen za identifikaciju ljudi. Pojedini biometrijski podaci su jedinstveni za svaku osobu i mogu služiti za identifikaciju osoba, kako u civilnom sektoru npr. u zdravstvu, obrazovnim ustanovama, firmama, tako i u vojnim, policijskim i državnim ustanovama u cilju zaštite sopstvenih resursa. Biometrijska autentifikacija (odnosno realna autentifikacija) se koristi u informacionim tehnologijama kao oblik identifikacije korisnika i kontrole pristupa zaštićenim resursima [7].

EEG autentifikacija koristi elektrofiziološki sistem za praćenje aktivnosti mozga. Ova tehnologija je vrlo popularna i može se koristiti bez ikakvih sporednih efekata na mozak. Do sada je izvršeno nekoliko istraživanja o mogućnosti primene EEG signala za autentifikaciju korisnika [8] [9].

Postoji nekoliko komercijalnih uređaja sa različitim brojem elektroda koje se koriste za prikupljanje EEG podataka. Neki od senzora koriste suve elektrode, a neki senzori koriste mokre elektrode. Moždani režnjevi emituju EEG signale kao odgovor na različite stimulanse i mentalna stanja. Pretpostavlja se da postoji promenljiva razlika uzoraka EEG talasa dok se vizuelizuje lozinku u mirnim uslovima u odnosu na prinudu, zbog različitih mentalnih stanja, mozak proizvodi različite obrasce analognog EEG talasa [10]. Na slici 1 prikazan je uređaj koji je korišćen u ovom radu.


Sl. 1. Neuro Sky Mind Wave 2-EEG biometrijski uređaj [11]

 ISBN 978-86-7466-930-3

Uređaj prikazan na slici 1 vrši merenje alfa, beta, gama, delta i teta moždanih talasa kao i trenutno stanje usredsređenosti – fokusa (attention) i opuštenosti (meditation) subjekta čiji se moždani talasi mere [12].

## III. PRIKAZ SOFTVERSKOG REŠENJA

Izgled ekrana softverskog rešenja za akviziciju podataka sa senzora prikazan je na slici 2. Rešenje je razvijeno u alatu Microsoft Visual Studio 2017 korišćenjem programskog jezika C# i biblioteke ThinkGear.dll proizvođača uređaja. Sama biblioteka nudi funkcije za ostvarivanje komunikacije sa uređajem. Dalji rad je podrazumevao prihvatanje vrednosti koje dolaze sa uređaja u određenim vremenskim intervalima definisanim i samom programskom kodu softverskog rešenja. Radi usrednjavanja vrednosti korišćena je logaritamska funkcija. Tako izračunate vrednosti su čuvane u realizovanoj bazi podataka.

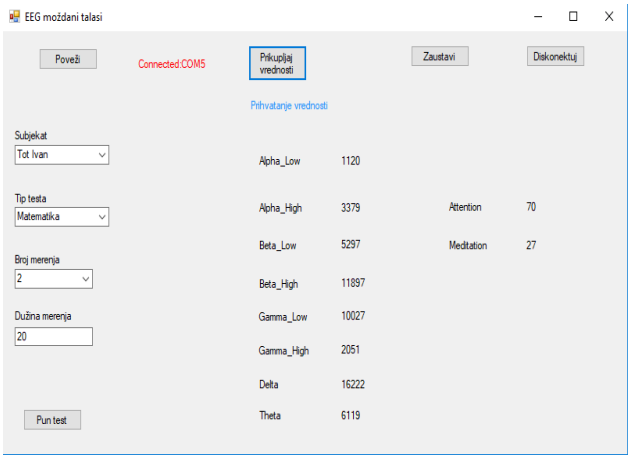


Sl. 2. Izgled ekrana za akviziciju podataka

Klikom na komandno dugme Poveži vrši se uspostavljanje bluetooth konekcije sa senzorom. Nakon uspešno ostvarene konekcije, klikom na dugme Prikupljaj vrednosti aplikacija će prihvatati vrednosti sa uređaja i prikazivati ih na ekranu. Komandno dugme Zaustavi privremeno prekida prihvatanje vrednosti sa uređaja, a komandno dugme Diskonektuj prekida konekciju sa uređajem.

Prihvaćene vrednosti mogu se čuvati u bazi podataka realizovanoj u Microsoft SQL Server Express 2014 klikom na komandno dugme Pun test svake 2 sekunde. U tom slučaju neophodno je izabrati subjekta čiji se moždani talasi mere, tip testa, broj merenja kao i zadati dužinu svakog testa u sekundama. Tip testa može biti:

1. *Opušteno* – subjekat se potpuno opusti i zatvori oči,
2. *Čitanje* – subjekat dobija tekst koji treba da čita u sebi,
3. *epe slike* – subjekat posmatra slike koje u njemu bude lepe emocije,
4. *Matematika* – subjekat dobija matematički zadatak koji treba da reši,
5. *Uznemiravajuće slike* – subjekat posmatra slike koje treba da izazovu ružne emocije (slike ratnih zločina, iskasapljenih životinja i slično).

U ovoj fazi istraživanja predviđeno je da se radi do 5 merenja svih navedenih testova u različite dane. Nad uzorkom od 60 testiranih lica (različitih polova, godina i nivoa obrazovanja) uočeno je da postoje određena poklapanja moždanih talasa naročito prilikom primene testa „Čitanje“. Takođe, uočeno je da prilikom primene testa „Uznemiravajuće slike“ značajan faktor imaju godine testiranih lica. Na mlađe osobe slike ratnih zločina slabije izazivaju ružne emocije, ali zato značajno reaguju na slike iskasapljenih životinja. U slučaju starijih osoba, reakcije su suprotne.

Za vizuelizaciju podataka razvijena ja web aplikacija u alatu Microsoft Visual Studio 2017 korišćenjem ASP.NET tehnologije. Na slikama 3 i 4 prikazane su delovi web stranica realizovane aplikacije koje omogućavaju poređenje dobijenih podataka.

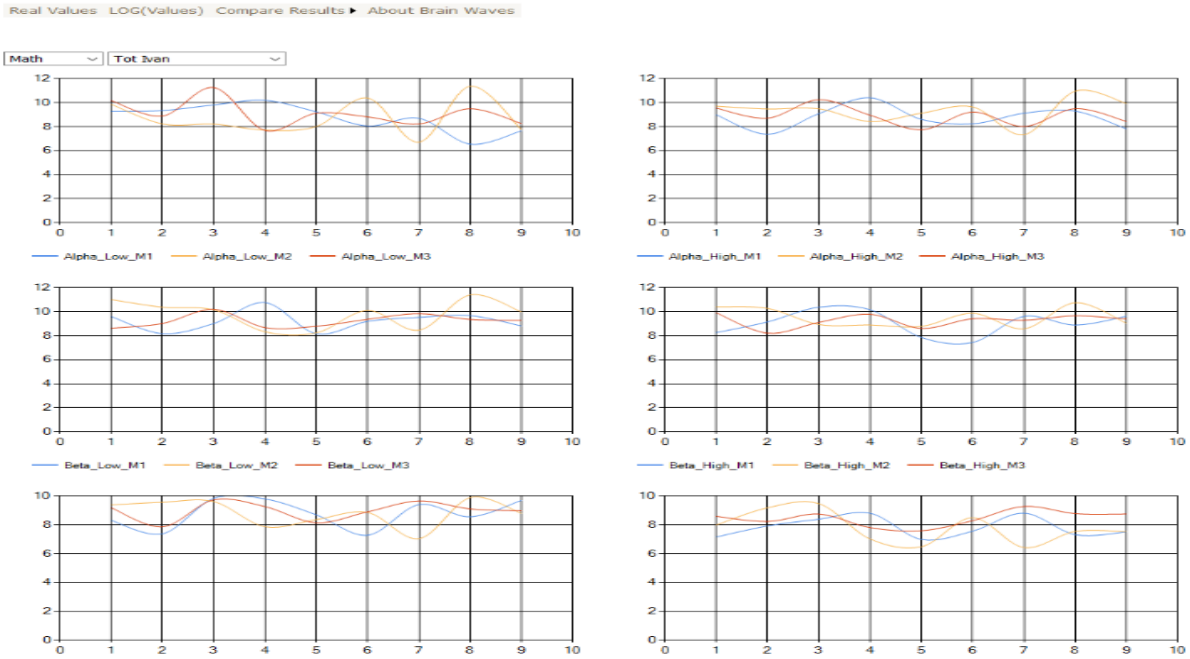


Sl. 3. Web stranica za vizuelizaciju podataka za izvršena tri merenja


ISBN 978-86-7466-930-3

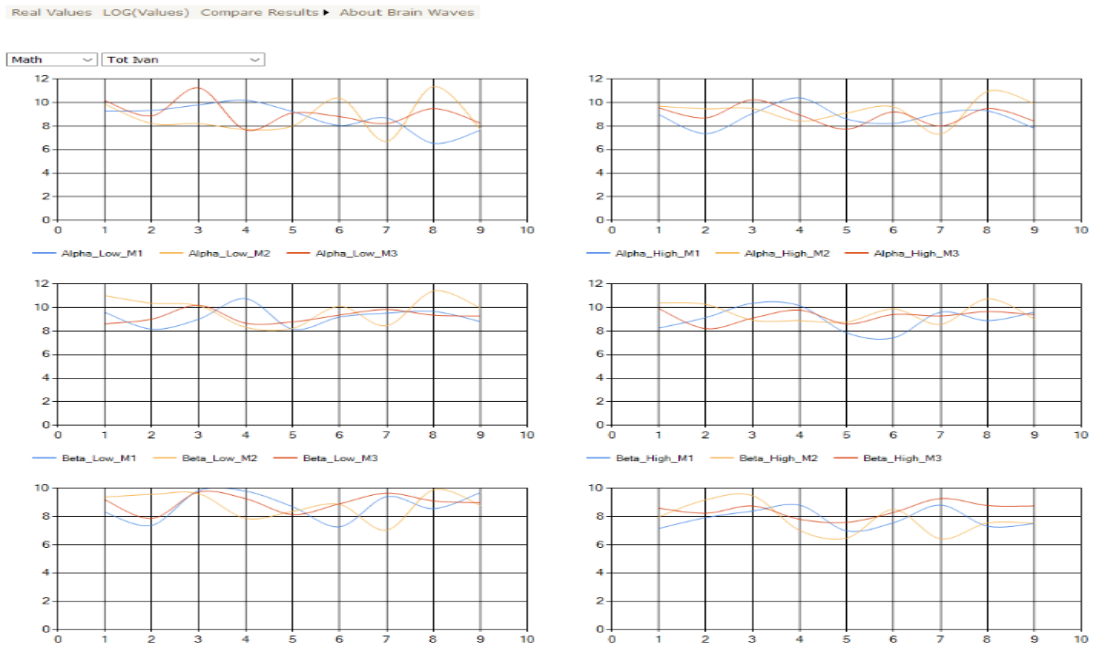


Sl. 4. Poređenje moždanih talasa

Web stranica prikazana na slici 3 omogućava vizuelizaciju i poređenje podataka dobijenih iz uređaja za izabranog subjekta i izabrani tip testa. Za svako merenje se po kolonama prikazuje zbirni grafikon sa svim talasima (na x-osi su odbirci vremena, a na y-osi logaritamske vrednosti izmerenih talasa), a zatim i pojedinačni grafikon za svaki izmereni moždani talas.

Web stranica prikazana na slici 4 takođe omogućava vizuelizaciju i poređenje podataka dobijenih iz uređaja za izabranog subjekta i izabrani tip testa, ali po pojedinačnim talasima. Svaki grafikon prikazuje rezultate svih izvršenih merenja po vrstama talasa (na x-osi su odbirci vremena, a na y-osi logaritamske vrednosti izmerenih talasa).

## IV. ZAKLJUČAK

Bezbednost informacionih sistem je jedno od najaktuelnijih pitanja današnjice. Kontrola pristupa je pogotovo bitna jer služi da spreči korisnike koji nemaju prava da pristupe i koriste sistem. Pristup nepoželjnih korisnika je veoma opasan skoro kod svih sistema zbog postojanja velike mogućnosti zloupotrebe samog sistema i informacija koje se nalaze u njemu.

Zbog značaja utvrđivanja identiteta potrebno je stalno raditi na usavršavanju sistema za preciznu identifikaciju, odnosno na poboljšavanju njihovih performansi, bilo kroz razvoj biometrijskih uređaja, bilo kroz unapređenje metoda akvizicije biometrijskih podataka. Jedan od potencijalnih načina je i primena moždanih talasa za autentifikaciju korisnika.

Do sada su po ovom projektu razvijene dve aplikacije. Jedna za akviziciju podataka sa senzora i druga za vizuelizaciju podataka.

U daljem istraživanju planirana je detaljna analiza dobijenih podatka primenom MATLAB softverskog paketa i statističkih alata da bi se utvrdilo postojanje korelacije moždanih talasa na odgovarajući tip testa kao i testiranje značajno većeg broja lica kako bi rezultati planirane analize bili tačniji. Ukoliko bi se potvrdilo postojanje korelacije, onda bi se moždani talasi mogli koristiti pouzdano za autentifikaciju korisnika.

## ZAHVALNICA

Rad je nastao kao rezultat rada na naučno-istraživačkom projektu “Upravljanje pristupom zaštićenim resursima računarskih mreža u Ministarstvu odbrane i Vojsci Srbije na osnovu multimodalne identifikacije korisnika”, pod brojem VATT/3/18-20, od 2018. do 2020. godine na Vojnoj akademiji Univerziteta odbrane u Beogradu.

## LITERATURA

[1] I. Jayarathene, M. Cohen, S. Amarakeerthi, “BrainID: Development of an EEG-Based Biometric Authentication System“, 2016.
[2] K. Lalović, I. Tot, A. Arsić, M., “Security Information System, Based on Fingerprint Biometrics”, Acta Polytechnica Hungarica, Volume 16, Issue Number 5, 2019.
[3] N. Maček, B. Đorđević, J. Gavrilović, K. Lalović, “An Approach to Robust Biometric Key Generation System Design”, Acta Polytechnica Hungarica, Volume 12, Issue Number 8, 2015.
[4] K. Lalović, M. Milosavljević, I. Tot, N. Maček, “Device for Biometric Verification of Maternity”, Serbian Journal of Electrical Engineering-Vol. 12, No. 3, 2015.
[5] A. K. Jain, A. A. Ross, K. Nandakumar, “Introduction to Biometrics”, Springer, 2011.
[6] J. Ashbourn, “Biometrics: Advanced Identity Verification”, Springer, 2014.
[7] L. Feng, „Brain password: A secure and truly cancelable brain biometrics for smart headwear“, International conference on Mobile Systems, Applications and Services, ACM, 2018.
[8] S. Soni, S. B. Somani, V. V. Shete, „Biometric user authentication using brain waves“, International Conference on Inventive Computation Technologies (ICICT), India, 2016.

 ISBN 978-86-7466-930-3

[9] A. A. Alariki, A. W. Ibrahimi, M. Wardak, J. Wall, „A Review Study of Brian Activity-Based Biometric Authentication“, Journal of Computer Science, 2018.
[10] https://www.mdpi.com/journal/biosensors/special_issues/wearable_biosensors
[11] https://cdn.sparkfun.com//assets/parts/1/2/9/9/4/14758-NeuroSky_MindWave_Mobile2-04.jpg
[12] M. McDowell, “Brainwaves: The Nature Of Brain Waves & Their Frequencies”, 2015.

ABSTRACT

Nowadays, user identification systems play a very important role in modern society. Complex security requirements have led experts to explore ways in which biometric data can be used to identify user identities. This paper presents a software solution for acquisition and visualization of brain waves (EEG) as biometric data.

## oftware olution for Acquisition and isualisation of rain Waves

Ivan Tot, Boriša Jovanović, Dušan Bogićević, Tamara Gajić, Jordan Atanasijević

 ISBN 978-86-7466-930-3

# Platforma za praćenje kvaliteta vazduha u gradu Čačak

Nikola Kukrić, Božidar Popović, Slobodan Lubura, Zorana Mandić

Elektrotehnički fakultet, Univerzitet u Istočnom Sarajevu, Istočno Sarajevo, Bosna i Hercegovina

***A stra t*—Izloženost PM2.5 česticama izdvaja se ao vodeći zdravstveni problem na globalnom nivou, a problem zagađenosti vazduha predstavlja jedan od glavnih uzro a smrtnosti na svijetu. Kako ovo predstavlja problem današnjice, zahtjevi da se mjerenje kvaliteta vazduha vrši što češće na što više lo acija, doveli su do razvoja nis obudžetnih senzora. Uz pomoć široko dostupnih senzora grade se senzorski čvorovi, koji pribavljaju podat e o trenutnim oncentracijama suspendovanih čestica, a ovi podaci roz asniju analizu dovede do asne informacije o valitetu vazduha pre o A I - indeksa zagađenosti vazduha. U ovom radu osim razvoja senzorskih čvorova, predstavljena je i realizacija jedinstvene web platforme za pri azivanje, arhiviranje i analizu kvaliteta vazduha, čime je realizovan jedinstven i potpun sistem za pri upljanje i obradu podata a o valitetu vazduha. Ia o je platforma realizovana za područje grada Čačka, gdje je izvršena integracija postojećih senzorskih čvorova sa novo realizovanim čvorovima, može biti prilagođena i drugim geografs im područjima te je široko upotrebljiva.**

***Ključne r eči*— valitet vazduha, suspendovane čestice, PM2.5, P 1**

## I. UVOD

Kvalitet vazduha je jedan od vodećih problema u mnogim gradovima i ima direktan uticaj na kvalitet života. Izloženost suspendovanim česticama PM10 i PM2.5 (eng. *Particular Matter*) predstavlja jedan od vodećih uzroka smrtnosti u svijetu i prema podacima Svjetska zdravstvena organizacija (eng. *World ealth rgani ation* - WHO) na svjetskom nivou tokom godine dovede do između 4,2 i 8,9 miliona smrtnih slučajeva [1]. Suspendovane čestice su sastavni dio prašine i manje su od 10μm (PM10), odnosno 2.5μm (PM2.5) te predstavljaju smješu čađi, dima, kiseline, uz prisustvo teških metala, a izloženost PM2.5 česticama je prepoznat kao glavni globalni zdravstveni problem [2]. Podjela na osnovu izvora iz kojih potiču suspendovane čestice data je u Tabeli I, što predstavlja glavni kriterijum pri izboru lokacije senzorskih čvorova koji prate njihovu koncentraciju.

TABELA I
IZVORI PM2.5 ČESTICA [3]

| Izvor | Procentualno (%) |
|---|---|
| Saobraćaj | 25% |
| Neodređenog ljudskog porijekla | 22% |
| Ogrjev u domaćinstvu | 20% |
| Prirodna prašina i soli | 18% |
| Industrijska djelatnost | 15% |

Dugoročnim praćenjem koncentracije suspendovanih čestica moguće je detektovati u kojim oblastima gradova je najveća koncentracija čestica te djelovati na izvore zagađenja kako bi se smanjenjem koncentracije čestica unaprijedio kvalitet života.

U gradu Čačku su ranije instalirana tri senzorska čvora za mjerenje zagađenosti vazduha, koji nisu bili povezani u jedinstvenu mrežu, niti su informacije o mjerenjima bile dostupne korisnicima tj. građanima. U pitanju su senzorski čvorovi *a is Air ink* kompanije *a is Instruments* [4]. Navedeni senzorski čvorovi mjere količine suspendovanih čestica PM1.0, PM2.5 i PM10 i u na osnovu njih izračunavaju indeks kvaliteta vazduha (eng. *Air uality Inde* - AQI).

U proteklom periodu, realizacijom projekta prekogranične saradnje „*Transport related Air Pollution and ealth impacts in the Čačak city – AI P ISCA"*, u decembru 2021. godine [5], ovi senzorski čvorovi su povezani na jedinstven server sa odgovarajućom bazom podataka gdje se čuvaju podaci o izvršenim mjerenjima kvaliteta vazduha, obezbijeđen je domen za Web aplikaciju i kreirana Web aplikacija za prezentaciju podataka. Na taj način, broj građana Čačka koji imaju pristup informacijama o kvalitetu vazduha nije ograničen.

U nastavku aktivnosti vezanih za proširenje mreže senzorskih čvorova za mjerenje kvaliteta vazduha u saradnji sa gradom Čačkom, zaključno sa 08.02.2022. godine postavljeno je osam novih senzorskih čvorova koji će biti predstavljeni u nastavku.

Grad Čačak je pokriven sa senzorskom mrežom od jedanaest senzorskih čvorova za prikupljanje podataka o koncentraciji suspendovanih čestica i pristup podacima u realnom vremenu je omogućen svima preko Web stranice https://cacak.vazduh.net.

U nastavku rada, poglavlje II, predstavljen je problem kvaliteta vazduha te standardi i referentne vrijednosti za ocjenu kvaliteta. Poglavlje III daje detaljnu analizu realizovanog senzorskog čvora, a prezentacija prikupljenih podataka je predstavljena u poglavlju IV.

## II. KVALITET VAZDUHA

Prema uredbi za monitoring i zahtjevima kvaliteta vazduha [6] kvalitet ambijentalnog vazduha se određuje pomoću koncentracije sumpor dioksida $SO_2$, azot monoksida NO i azot dioksida $NO_2$, ozona $O_3$, ugljen monoksida CO i masene koncentracije PM10 i PM2.5 čestica. Za mjerenje

 ISBN 978-86-7466-930-3

koncentracije navedenih čestica propisane su referentne metode i standardi koju su dati u Tabeli II.

TABELA II [6]
VRSTE MJERENJA I REFERENTNE METODE

| Vrsta mjerenja | Metode/Specifikacije |
|---|---|
| Koncentracija sumpor dioksida SO2 | EN 14212:2013<br>EN 14212/Cor1:2015<br>Ultraljubičasta fluoroscencija |
| Koncentracija azot monoksida NO i azot dioksida NO2 | EN 14211:2013<br>Hemiluminiscencija |
| Koncentracija ozona O3 | EN 14625:2013<br>Ultraljubičasta fotometrija |
| Koncentracija karbon monoksida CO | EN 14626:2013<br>Nedisperzivna infracrvena spektroskopija |
| Masena koncentracija PM10 i PM2.5 | EN 12341:2015<br>Gravimetrijska metoda |

Ministarstvo zaštite životne sredine - Agencija za zaštitu životne sredine Republike Srbije je 2015 pokrenula projekat „Objedinjeni prikaz automatskog monitoringa kvaliteta vazduha u Republici Srbiji“ gdje se prate navedeni parametri [7]. Za ocjenu kvaliteta vazduha korišten je indeks kvaliteta vazduha EAQI (eng. *European Air uality Inde* ), koji je 2017. godine usvojila Evropska agencije za životnu sredinu (eng. *European En ironment Agency*) zajedno sa Upravom za ekologiju Evropske komsije (*European Commission's irectorate General for En ironment*). Pomenuti indeks kvaliteta vazduha prikazan je u Tabeli III.

TABELA III
SKALA ZA OCJENU KVALITETA VAZDUHA

| Oznaka | Zagađivač (satna koncentracija u µg/m$^3$) | |
|---|---|---|
| | PM10 | PM2.5 |
| Odličan | 0 – 25 | 0 – 15 |
| Dobar | 25 – 50 | 15 – 30 |
| Prihvatljiv | 50 – 90 | 30 – 55 |
| Zagađen | 90 – 180 | 55 – 110 |
| Izuzetno zagađen | >180 | >110 |

S obzirom na to da je raspoređivanje i postavljanje akreditovanih stanica sa referentnim metodama za praćenje navedenih parametara vazduha veoma skupo te da najveći problem u gradovima uglavnom predstavljaju PM10 i PM2.5 čestice odlučeno je da se realizuju senzorski čvorovi za mjerenje PM10 i PM2.5 čestica. Za senzore koji prate koncentraciju suspendovanih čestica korišćeni su nisko budžetni (eng. *low ost*) laserski senzori.

Prema standardu EN 12341:2015 PM česticu su „čestice suspendovane u zraku koje su dovoljno male da mogu proći kroz otvor za odabir veličine sa 50% efikasnosti pri aerodinamičkom promjeru x µm.“ [8]. Referentna metoda je gravimetrijska motoda koja podrazumijeva prikupljanje prašine na uzorku u periodu od 24h te određivanje koncentracije u opsegu od 1 – 150 µg/m$^3$ za PM10 i 1 – 120 µg/m$^3$ za PM2.5 čestice.

## III. SENZORSKI ČVOR

Tokom istraživanje korišćena su tri niskobudžetna laserska senzora i to: SDS011 od proizvođača *No a Fitness Co*., PMS5003 i PMS7003 od proizvođača *Beijing Plantower Co., td, China*. Pregled karakteristika senzora dat je u Tabeli IV.

TABELA IV
PREGLED KARAKTERISTIKA POJEDINIH NISKOBUDŽETNIH LASERSKIH SENZORA SUSPENDOVANIH ČESTICA [9,10,11]

| Karakteristika | Senzori | | |
|---|---|---|---|
| | SDS011 | PMS5003 | PM7003 |
| Dimenzije (mm) | 71x70x23 | 50x38x21 | 48x37x20 |
| Napajanje (V) | 4.7~5.3 | 4.5~5.5 | 4.5~5.5 |
| Potrošnja (mA) | 70 ± 10 | <100 | <100 |
| Temperaturni opseg (°C) | -20 ~ +60 | -40 ~ +80 | -40 ~ +80 |
| Opseg mjerenja čestica (µg/m$^3$) | 0 – 999.9 | 0 – 500 efktivno, >1000 maks | 0 – 500 efktivno, >1000 maks |

Navedeni optički senzori mjere intenzitet svjetlosti koja se raspršuje pod uticajem prašine koja se uvlači u senzor. Senzori se sastoje od svjetlosne diode (eng. *ight Emitting iode* – LED), fotodiode, ventilatora koji uvlači vazduh sa česticama prašine i većeg broja sočiva za fokusiranje snopa svjetlosti [12].

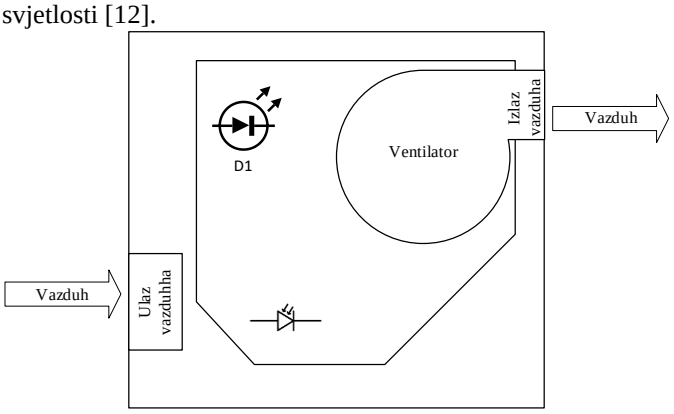


Sl. 1. Struktura optičkog senzora suspendovanih čestica

Prilikom realizacije senzorskog kao najbolji omjer kvalitet/cijena odabran je senzor PMS7003.

Senzorski čvor se sastoji od mikrokontrolerske jedinice, senzora i jedinice za napajanje. Mikrokontroler korišćen u realizaciji senzorskog čvora je ESP-WROOM-32, koji

 ISBN 978-86-7466-930-3

pomoću *A T* modula komunicira sa PMS7003 senzorom i pomoću *Wi-Fi* modula prenosi očitane podataka sa senzora brzinom do 150 Mbps, sa snagom signala od 20 dB. Za napajanje je korišćen Hi-Link naponski modul. Navedeni modul ima naponsku konverziju sa 90-245 VAC na 5VDC sa maksimalnom izlaznom snagom od 3W [13]. Napon od 5VDC je potreban za napajanje senzora PMS7003. S obzirom da je za napajanje mikrokontrolera potrebno 3.3V korišćen je naponski regulator AMS1117-3.3V koji za ulazni napon u opsegu 4.8VDC – 6.5VDC daje na izlazu 3.3VDC.

Za crtanje šeme i realizaciju štampane ploče korišćeno je programsko okruženje *Eagle*. Izgled štampane ploče senzorskog čvora sa prednje i zadnje strane prikazan je na Sl. 2.

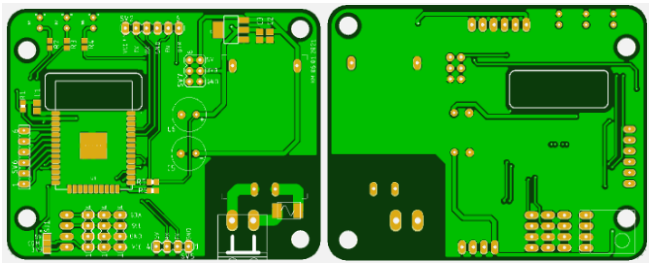

Sl. 2. Izgled štampane ploče senzorskog čvora

Tokom realizacije senzorskog čvora realizovano je kućište u kojem se smještaju pomenute elektronske komponente, koja treba da omogući protok vazduha prema senzoru PMS7003 te da elektronske komponente budu zaštićene od vremenskih uslova. Izgled senzorskog čvora i sastavljene ploče sa senzorom PM10, PM2.5 prikazani su na Sl. 3.

Sl. 3. Izgled senzorskog čvora i sastavljene ploče

Tokom instalacije senzorskog čvora, potrebno je senzoru proslijediti parametre za pristupnu *Wi-Fi* tačku preko kojeg će senzor slati očitane podatke. Za te potrebe kreirana je Android aplikacija *a duhNet* koja omogućava jednostavno prosljeđivanje pristupnih podataka i praćenje očitanja sa svih dodatih senzora. Prilikom dodavanja uređaja svakom se dodjeljuje jedinstveni *Token* koji omogućava autorizaciju prilikom slanja podataka, a na osnovu *MAC* adrese i lokacije uređaja radi se autentifikacija senzorskog čvora.

## IV. PREZENTACIJA SENZORSKIH OČITANJA

*A. Za administraciju senzorskih čvorova i prezentaciju očitanih vrijednosti kreirana je Web aplikacija koju možemo podijeli na administratorsku i klijentsku.*

Administratorska aplikacije je kreirana pomoću *ii2* okruženja, a njene osnovne funkcionalnosti su: administracija senzorskih čvorova (dodavanje, brisanje, izmjene), prijem podataka od senzorskih čvorova, obrada podataka, tabelarni prikaz svih očitanja i generisanje izvještaja koji sadrže očitane podatke. *ii2*, čiji naziv potiče od kineske riječi *ii* - "jednostavan i evolucijski", je PHP okvir visokih performansi, baziran na komponentama za brzi razvoj modernih web aplikacija [14]. Komunikacija između senzorskih čvorova i web aplikacije se odvija preko programskog interfejsa aplikacije (eng. *Application Programming Interface* – API). Pristup administratorskoj aplikaciji je dozvoljen samo autentifikovanim korisnicima.

*B. lijentska aplikacija*

Klijentska aplikacija je dostupna svim korisnicima i omogućava korisnicima da prate zagađenost vazduha. Prilikom otvaranja Web stranice prvo se prikazuje poruka o trenutnom kvalitetu vazduha na području grada i odgovarajući „emitikon“ u zavisnosti od kvaliteta vazduha. Prikaz kvaliteta u slikovnoj formi sa emotikonima omogućava korisnicima jednostavnije i brže dobijanje informacija. Takođe uz emotikone stoje i preporuke građanima i informacije o uticaju kvaliteta vazduha na zdravlje stanovništva.


Sl. 4. Emotikoni i preporuke građanima u zavisnosti od kvaliteta vazduha

Na stranici je omogućeno mapiranje senzora pomoću biblioteke *eaflet*. *eaflet* je vodeća JavaScript biblioteka otvorenog koda za interaktivne mape prilagođene mobilnim uređajima. Težak je samo oko *32 B*, i ima sve funkcije za rad sa mapama koje će većini programera biti potrebne, a ako postoji potreba za dodatnim stvarima tu su i razni dodaci i efekti [15]. *eaflet* je dizajniran za jednostavnu upotrebu, brzinu i kvalitet. Radi lako i efikasno na gotovo svim desktop i mobilnim platformama, postoji i mogućnost ekstenzija sa dosta dodataka. Podaci o mapama koje se koriste su dobijeni od strane *penStreetMap* platforme. Svaki senzor na mapi je obojen odgovarajućom bojom u zavisnosti od trenutne zagađenosti. Klikom na jedan od senzora na mapi otvara se novi prozor na kojem se prikazuju detalji kvaliteta vazduha odnosno trenutni kvalitet, tačne koncentracije PM10 i PM2.5 čestica i vrijeme posljednjeg mjerenja, dok klikom na naziv senzora otvaramo grafik kvaliteta vazduha u vremenskom rasponu od montiranja senzora pa do posljednjeg mjerenja. Na dnu Web stranice nalazi se i sumirani grafik kvaliteta vazduha svih senzorskih čvorova i dodatne informacije šta prestavljaju PM10 i PM2.5 čestice. Izgled mape prikazan je na Sl. 5.


ISBN 978-86-7466-930-3


Sl. 5. Mapa sa označenim senzorskim čvorovima

## V. ZAKLJUČAK

U radu je prezentovan senzorski čvor sa mogućnošću praćenje količine PM10 i PM2.5 čestica. Realizovana je platforma za praćenje, koja omogućava jednostavnu prezentaciju podataka grafički, prikaz na mapi i tabelarno. U narednom periodu je planirano da se dobijena mjerenja upoređuju sa mjerenjima koja su dobijena referentnim metodama i da se odredi koeficijent kalibracije. Takođe, planirano je unapređenje mobilne aplikacije da pomoću lokacije korisnika ispisuje poruku kvaliteta vazduha.

## ZAHVALNICA

Zahvaljujemo se gradu Čačak, koji je obezbijedio novčana sredstva za realizaciju projekta praćenja kvaliteta vazduha.

## LITERATURA

[1] OECD, The Economic Consequences of Outdoor Air Pollution, 2016 dostupno na: https://www.oecd.org/env/the-economic-consequences-of-outdoor-air-pollution-9789264257474-en.htm.
2 Richard Burnett, Hong Chen, Mieczysław Szyszkowicz, i drugi, *Global estimates of mortality associated with long-term e posure to outdoor fine particulate matter*, 115 (38) 9592-9597, 2018.
[3] Bulot, F.M.J., Johnston, S.J., Basford, P.J. i drugi. *ong-term field comparison of multiple low-cost particulate matter sensors in an outdoor urban en ironment*. Sci Rep 9, 7497 (2019). https://doi.org/10.1038/s41598-019-43716-3J
[4] Davis AirLink® Quality Monitor, Davis Instruments, dostupno na https://www.davisinstruments.com/pages/airlink .
[5] Rezultati projekta prekogranične saradnje, https://banjaluka.net/na-elektrotehnickom-fakultetu-predstavljeni-rezultati-projekta-prekogranicne-saradnje/.
[6] Službeni glasnik Republike Srbije br, 11/2010, 75/2010 i 63/2013
[7] Objedinjeni prikaz automatskog monitoringa kvaliteta vazduha u Republici Srbiji, http://www.amskv.sepa.gov.rs/
[8] Ambijenatlni zrak – Standardna gravimetrijska metoda za određivanje masene koncentracije PM10 ili PM2.5 u suspendovanoj čestičnoj tvari (EN 12341:2014)
[9] Laser PM2.5 Sensor specivation SDS011, https://cdn-reichelt.de/documents/datenblatt/X200/SDS011-DATASHEET.pdf
[10] Digital universal particle concentration sensor PMS5003, https://aqmd.gov/docs/default-source/aq-spec/resources-page/plantower-pms5003-manual_v2-3.pdf
[11] Digital universal particle concentration sensor PMS7003, https://download.kamami.pl/p564008-PMS7003%20series%20data%20manua_English_V2.5.pdf
[12] Marek Badura, Piotr Batog, Anetta Drzeniecka-Osiadacz, Piotr Modzel, *ptical particulate matter sensors in PM2.5 measurements in atmospheric air*, 2018, https://doi.org/10.1051/e3sconf/20184400006
[13] 3W Ultra-small PowerModule PM03/PM01/PM09/PM12, Hi-Link, https://datasheet.lcsc.com/szlcsc/1909111105_HI-LINK-HLK-PM24_C399250.pdf
[14] Yii2 dokumentacija, https://www.yiiframework.com/doc/guide/2.0/en
[15] Leaflet dokumentacija, https://leafletjs.com/reference.html

## ABSTRACT

PM2.5 exposure stands out as a leading health problem globally while the problem of air pollution is one of the leading causes of death in the world. Due to the poor air quality, the requirement for frequent measures in as many locations as possible has led to the development of low-cost sensors. Sensor nodes are being developed by utilizing widely accessible sensors, their use is to acquire the current concentration of particle matters. This raw data is later processed and used to calculate the air quality index – AQI. This paper presents the development of sensor nodes, as well as the development of a unique web platform. The web platform is equipped with a graphic representation of the date and history of archived data that had been collected. While this platform has been developed for the city of Čačak, it can be adapted to other geographical areas and it can be broadly used.

**Air uality onitoring Platform in the City of Čačak**

Nikola Kukrić, Božidar Popović, Slobodan Lubura, Zorana Mandić

 ISBN 978-86-7466-930-3

# SPECIAL THEMATIC SESSION
# CONTEMPORARY TECHNOLOGIES AND EDUCATION

# /

# СПЕЦИЈАЛНА ТЕМАТСКА СЕСИЈА
# САВРЕМЕНЕ ТЕХНОЛОГИЈЕ И ЕДУКАЦИЈА

# (STS-EDUI/СТС-ЕДУ/)

ISBN 978-86-7466-930-3

# A Comparison of Selected Systems For Learning About SQLi Vulnerability Suitable for Academic Uses

Djordje Madic, Danko Miladinovic and Zarko Stanisavljevic

***Abstract*— In this paper five popular platforms for secure software development training are analyzed from the perspective of their suitability for academic uses. In order to compare these platforms a novel ta onomy of interactive cyber training and education systems (Cyber Ta i) is used. nly parts of the ta onomy that are relevant are included in the analysis. The analyzed platforms are also compared to iTrainer system, which was developed at the niversity of elgrade, chool of lectrical ngineering specifically to be used at the courses dealing with the injection ( i) vulnerability. ased on the conducted analysis a suggestion is made regarding the requirements that a training platform should fulfill in order to be suitable for academic uses.**

***Index Terms*— i; secure software development; hands-on training.**

## I. Introduction

Software engineering never had more learning resources than today, with the internet resources available at all times. It comes in many forms, as video courses, articles, e-books, and most of them are free. Most of the ones covering SQLi are structured to build theoretical knowledge while applying the knowledge and hands-on experience are missing.

On the other hand, courses covering topics like secure software development and network and system security are emerging across universities all around the world. Respectable authorities in the field of software engineering, i.e. ACM and IEEE, are issuing their recommendations regarding curriculum [1] and in these recommendations, as a rule, they state that courses covering topics from software engineering should be supported by hands-on experience for students.

There is a constant dilemma when introducing hands-on exercises at the university course, should this be done using existing technology or is there a need for a new dedicated tool to be created. In order to help teachers to resolve this dilemma regarding SQLi vulnerability as a topic to be covered at some course, in this paper analysis of five popular platforms for secure software development training is presented. These platforms are also compared to one dedicated tool for teaching SQLi vulnerability as a course topic (SQLiTrainer [2]). Based on qualitative analysis, a suggestion of requirements that a tool suitable for academic uses should fulfill is made. Finally, an example of quantitative analysis is presented. As far as the authors are aware, there are no similar studies published in open literature.

The remainder of the paper is organized as follows. The second section presents the three selected tools with hands-on SQLi exercises, one online tool with hands-on SQLi exercises, one framework for organizing secure software training, and one dedicated teaching tool. The third section compares the six selected tools using the taxonomy of interactive cyber training and education systems (Cyber Taxi) [3]. The section four describes the requirements that a tool should fulfill in order to be used in academia. The fifth section gives an example of quantitative comparison of the selected tools. The last section gives a conclusion and suggests future work.

## II. Description Of The Selected Tools

Five popular platforms are selected for this research based on their availability to the authors, their popularity in the secure software development community and their coverage of the selected topic (e.g., Juice Shop [4] is an official tool of the OWASP [5] community, Avatao [9] is used for the Serbian Cyber Security Challenge, etc.).

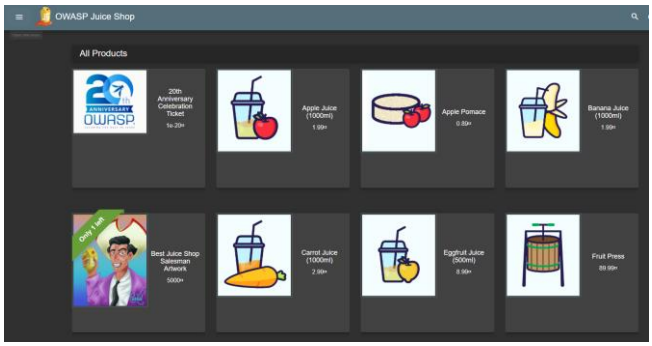


Fig. 1. OWASP Juice Shop

Juice Shop [4] (Fig. 1) is an open-source web application representing an insecure online shop. It is created by OWASP [5] organization and contains 100 challenges of varying difficulty where the user is supposed to exploit the underlying

Djordje Madic is with Zuehlke Engineering, Bul. Milutina Milankovića 1i, 11070 Novi Beograd, Serbia (e-mail: djordje.madic@zuehlke.com).

Danko Miladinovic is with University of Belgrade, School of Electrical Engineering, Bul. kralja Aleksandra 73, 11120 Belgrade, Serbia (phone: +381-63-3439-97; e-mail: danko@etf.bg.ac.rs).

Zarko Stanisavljevic is with University of Belgrade, School of Electrical Engineering, Bul. kralja Aleksandra 73, 11120 Belgrade, Serbia (phone: +381-11-3218-484; e-mail: zarko.stanisavljevic@etf.bg.ac.rs).

 ISBN 978-86-7466-930-3

vulnerabilities. SQL injection is covered by 7 of them. The application automatically detects when a challenge is solved, and progress of the user is tracked on a score board. All components of the user interface can be customized including color theme, logos, banners, links, products and other items in the database. Interactive help, hints and „challenge solved“ notifications can be turned off, while the initial set of challenges and their solutions cannot be changed. Domain of the application is well chosen, having in mind the number of online shops today. According to a study from 2017 [6] there are 800.000 registered online shops only in Europe. Juice Shop application code [7] has more than 50 contributors. Instance of the application can be started on a personal computer or one of the cloud services.

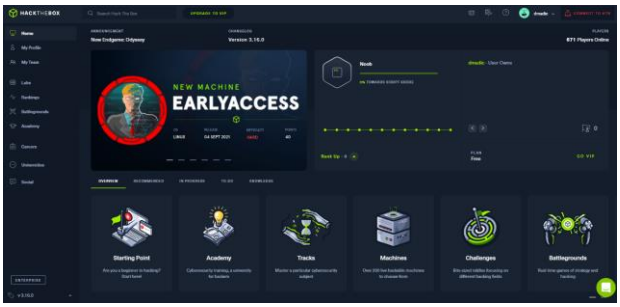


Fig. 2. Hack The Box

Hack The Box [8] (Fig. 2) is online training platform, helping individuals, companies and universities improve penetration testing skills. The platform is free for students and university professors. It includes a set of Capture The Flag (CTF) exercises grouped in 10 categories, like Web, Hardware and Reverse Engineering. Exercises are updated on weekly basis. Progress of the user is tracked and awarded with points, ranks and badges. Exercises are performed in a realistic environment, for example, against a dedicated web application instance or an executable that should be reverse engineered. Part of the exercises is followed by detailed documentation of the solutions. At the moment of writing, Web category contains 34 challenges designed as complex attacks where the user has to exploit multiple vulnerabilities to solve them. Some of them require SQLi to be solved.

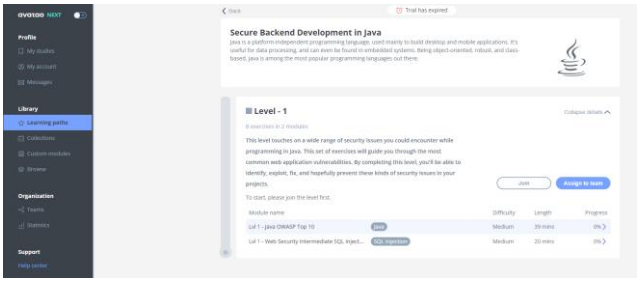


Fig. 3. Avatao

Avatao [9] (Fig. 3) is online training platform for companies created to improve security awareness of the employees and provide them with best practices for secure software development. It includes exercises in 8 programming languages, grouped in modules and learning paths. Exercises are performed in a realistic environment, for example, against a dedicated web application instance. There are 2 types of exercises, challenges and tutorials. Tutorials are interactive exercises guided by a chat bot acting as a teacher, while the challenges are designed as CTF. Most of the exercises are focused on single vulnerability, like SQLi. There are both attack and prevention oriented exercises. At the moment of writing, trial access to the platform provides 18 SQLi exercises in 5 programming languages. Many of them are different variants of SQLi Login Bypass.

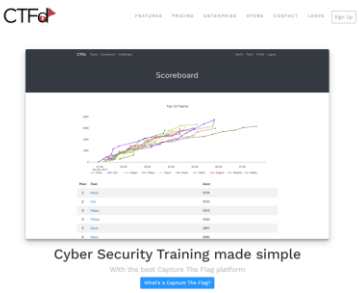


Fig. 4. CTFd Admin panel

CTFd [10] (Fig. 4) is online training framework for hosting CTF competitions and is used for helping individuals and companies improve cyber security skills using CTF challenges. Beside CTF challenges the platform supports a variety of other types of challenges such as multiple-choice and manual verification exercises. Some of these types of challenges are not available in the free version of the framework. Having said that, the framework is free, and it can be expanded by buying plugins and themes from the CTFd website. Unlike other tools, challenges do not come with the framework, but they can be added from the admin page. The admin can also add more pages, view the progress of individual users and teams on the platform and view success rate of each challenge. The framework supports individual and team competitions.

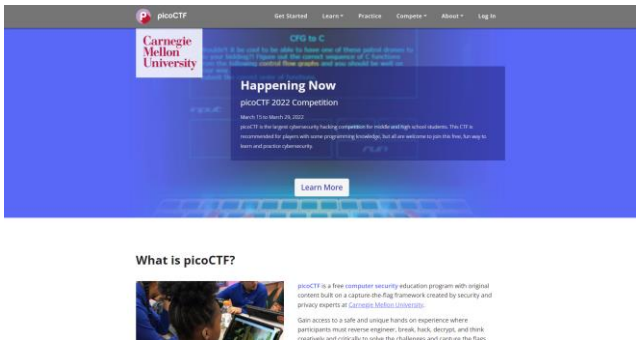


Fig. 5. PicoCTF

PicoCTF [11] (Fig. 5) is online training tool for helping users increase their hacking skills using CTF challenges. Users can register either as learners or as teachers. Learners can solve CTF challenges and join a classroom. Upon joining classrooms learners can get custom event scoreboards and track classroom member’s progress. Teachers can create

 ISBN 978-86-7466-930-3

classrooms and monitor student progress. Exercises are CTF based and are split into categories like web exploitation, cryptography, forensics, etc. There is no SQLi category, but there are around 10 SQLi challenges across all categories.

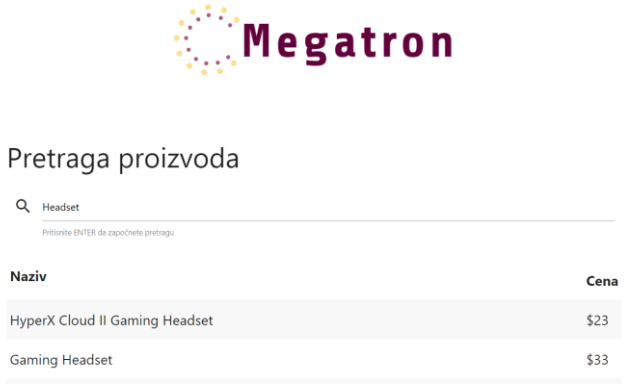


Fig. 6. SQLiTrainer

SQLiTrainer [2] (Fig. 6) represents a set of 4 vulnerable applications that can be used to demonstrate different types of SQL injection vulnerabilities. Implementation and the examples how to use the system are given in [2]. It is used for laboratory exercises at the Advanced Network and System Security course at the University of Belgrade, School of Electrical Engineering. Components of the user interface and initial state of the database can be customized. The applications can be run against different SQL databases, like MySQL and PostgreSQL, changing the solution of the exercises.

## III. Comparison Of The Selected Tools

In order to compare different tools a common ground and a set of measurable parameters are needed. For the purpose of suggesting requirements that a tool should fulfill to be used in academia a novel and promising taxonomy Cyber Taxi [3] was analyzed. Most relevant parts of the taxonomy are orchestration, proficiency level, and customization level. In [3] orchestration defines the automation level, although this term can have other meanings in a different context. Having a group of students, it is a requirement to be able to set up the training environment automatically, no matter the number of participants. In case of problems, it should be simple to restart the environment and debug it. Proficiency level defines required level of knowledge. In case it is above beginner level, the tool is not relevant for academic use. In order to provide enough learning material and assess different groups of students, training should be customizable, and should be able to produce similar exercises.

Classification of the selected tools based on the relevant parts from the Cyber Taxi is presented as a table in Fig. 7. Columns of the table represent the selected tools, while rows of the table represent components of the taxonomy, grouped by more general concepts. The table is filled based on the experience of the authors with the selected tools using their publicly available, free or trial versions. All of the tools except CTFd have trainings of similar purpose and include exercises for beginners. SQLiTrainer is the only tool requiring manual effort for scoring. Hack The Box, Avatao and picoCTF are ready-to-use products, while Juice Shop, SQLiTrainer and CTFd require the training facilitator to decide on the deployment strategy and execute it. SQLiTrainer has the most customizable exercises, while Hack The Box and Avatao can customize the set of exercises a training group will receive. CTFd can be customized based on the teacher needs.

## IV. Requirements

Based on the previous analysis and the authors previous experience with eLearning tools in computer engineering education, for a system to be suitable for academic uses, a recommendation can be made as a set of requirements that need to be fulfilled. Target audience of the system should be students with no previous knowledge of SQLi or other software vulnerabilities. This requires a system with exercises focused only on SQLi. Exercises combining SQLi with other vulnerabilities are out of scope, as the target audience should have knowledge of multiple vulnerabilities and understand how they can be exploited together. Further requirements can be defined using the Cyber Taxi, making it suitable for comparison with the existing tools.

| | | Juice Shop | Hack The Box | Avatao | CTFd | picoCTF | SQLiTrainer |
|---|---|---|---|---|---|---|---|
| Techical Setup | Environment structure | Hosting. Each user has a dedicated instance of the target application. | Commercial E-Learning and Collaboration platform | Commercial E-Learning platform | Commercial E-Learning platform | E-Learning platform | Hosting. Each user has a dedicated instance of the target application. |
| | Deployment | On-premise and Cloud | | | Cloud | | On-premise and Cloud |
| | Orchestration | Using MultiJuicer [x] exercises can be fully automated | Full automation | Full automation | Full automation | Full automation | Full automation |
| Audience | Sector | Academic and Private | Academic, Private and Public | Academic and Private | Academic, Private and Public | Academic | Academic and Private |
| | Purpose | Raise awareness and increase skill level | Raise awareness and increase skill level | Raise awareness and increase skill level | Raise awareness and increase skill level | Raise awareness and increase skill level | Raise awareness and increase skill level |
| | Proficiency level | Beginner to expert | Beginner to expert | Beginner to expert | Beginner to expert | Beginner to expert | Beginner |
| | Target audience | Students and IT Professionals | Students, IT Professionals and IT Specialists | Students and IT Professionals | Students, IT Professionals and IT Specialists | Students | Students |
| Training Environment | Training Type | Jeopardy style Capture The Flag (CTF) | Attack-only and attack-defense CTF, Cyber Training Range | CTF | CTF | CTF | CTF |
| | Scenario | Problem-driven, not supervised | Problem- and storyline-driven, not supervised | Problem- and storyline-driven, not supervised | Problem-driven, not supervised | Problem-driven, not supervised | Problem-driven, not supervised |
| Training Setup | Scoring | Awarding. Solved challenges are automatically detected. | Awarding. User is awarded with points, ranks and badges. | Awarding | Awarding. Solved challenges are automatically detected. | Awarding. Solved challenges are automatically detected. | Manual assessment |
| | Roles | No specific roles | Red and Blue teams when done in team setup | No specific roles | No specific roles | No specific roles | No specific roles |
| | Training Mode | Single | Single or Team | Single | Single or Team | Single | Single |
| | Customization Level | Specific. User interface and initial database state can be customized. Challenges cannot be customized. | Specific. Training can be customized using Dedicated Labs where administrators can pick set of exercises for training group. | Specific. Administrators can pick set of exercises for training group. | Specific. User interface and initial database and target database can be customized. | None | Specific. User interface, initial database state and target database can be customized. |

Fig. 7. Clasification of the selected tools


ISBN 978-86-7466-930-3

**Audience**
- Target audience: Students
- Sector: Academic
- Proficiency level: Beginner
- Purpose: Raise awareness and increase skill level

**Training environment**
- Training Type: Capture The Flag
- Scenario:
  - Non supervised
  - Problem- or Storyline- driven
  - Target of the challenge is application solved by exploiting SQLi vulnerability

**Training setup**
- Scoring: Assessment, as results of the participants should be comparable
- Roles: No specific roles
- Training mode: Team, or Individual during assessments
- Customization Level: Specific, as it should be customized for each training group

**Technical setup**
- Environment structure: Online platform in the sense of E-Learning platform, or hosting
- Deployment: Both On-premise and Cloud
- Orchestration: Full degree of automation with modular design of the application

Capture The Flag is the most practical training type for students. Students can be split in groups, each group having the same flag. As flags are known upfront, they can be checked automatically once the user submits them. Depending on modularity of the application, additional customization may go along, like each group having a specific user interface, initial database state, and SQL database, like PostgreSQL or MySQL.

For the selected tools to be fully compliant with the requirements, the following features should be introduced:

- Juice Shop: Customization of the exercises, providing different flags per training group
- Hack The Box: Exercises focused only on SQLi
- Avatao: More exercises focused on SQLi or customization of the existing ones
- picoCTF: introduce a specific SQLi category

As it can be seen additional effort is needed in order to use existing platforms in academia since the two very important requirements, i.e. exercises focused only on SQLi and customization of exercises cannot be expected to be fulfilled. On the other hand dedicated tools, like SQLiTrainer and frameworks, like CTFd, will fulfill all of the requirements, but will require even more effort to be created.

## V. Example Of Quantitative Analysis

In this section we will give an example of a quantitative analysis using the results from the table represented in Fig. 7. and the requirements of the previous chapter. Each category in the previous mentioned table (technical setup, audience, training environment and training setup) will be graded on the scale from 1 to 5 based on how much the tools and the CTFd framework satisfy the requirements from the previous chapter.

Having that in mind we can draw a conclusion on how much each subcategory in each category weights in the final score of that category. Because all of the analyzed tools and CTFd framework satisfy the requirements of categories audience and training environment, on these two categories they all get the grade of 5.

That leaves us with two categories left to be graded, and those are training setup and technical setup. Here we can define how much each subcategory has weight in the final grade of its category based on the values for those subcategories from the previous chapter and from the table represented in Fig. 7. These specific weights are defined based on authors personal experiences with laboratory exercises on the Advanced Network and System Security course at the University of Belgrade, School of Electrical Engineering.

**Training setup**
- Scoring
  - Automatic assessment weights 40%
  - Manual assessment weights 20%
- Roles – 0% of the category grade
- Training mode
  - Single and team mode weights 20%
  - Only single or team mode weights 10%
- Customization Level
  - None weights 0% of the category grade
  - Ability to only pick a set of exercises for group weights 10%
  - Interface and initial database can be customized weights 20%
  - Initial database state and target database can be customized weights 30%
  - Initial database state, target database, and challenges can be customized weights 40%

**Technical setup**
- Environment structure
  - Noncommercial platform weights 50%
- Deployment
  - On premise and cloud weights 20%
  - Only on premise or on cloud weights 10%
- Orchestration
  - Full automation weights 30%

Based on these assessments we can see the final grade of each category and the average grade of each analyzed tool in a table represented in Fig. 8.


ISBN 978-86-7466-930-3

| | Juice Shop | Hack The Box | Avatao | CTFd | picoCTF | SQLiTrainer |
|---|---|---|---|---|---|---|
| Techical Setup | 4 | 2 | 2 | 2 | 4 | 5 |
| Audience | 5 | 5 | 5 | 5 | 5 | 5 |
| Training Environment | 5 | 5 | 5 | 5 | 5 | 5 |
| Training Setup | 4 | 4 | 3 | 5 | 3 | 3 |
| Average | 4.5 | 4 | 3.75 | 4.25 | 4.25 | 4.5 |

Fig. 8. Grades of the selected tools

## VI. Conclusion

This paper presented the need for having tools to learn SQLi vulnerability in an interactive way and listed the existing tools. Selected tools were categorized based on the parts of the Cyber Taxi. The same taxonomy was used to compare the selected tools, leading to suggestion of requirements that a tool to be used in academia needs to fulfill. Conclusion is that effort needed to adapt existing tools to fulfill these requirements sometimes can exceed the effort needed to create a dedicated tool from scratch and sometimes it is even not possible to customize existing tool. However, once the requirements are clear it is always useful to check if there are existing tools that can fulfill them before starting to create a new tool. The quantitative analysis that was conducted in this paper showed how once the requirements are defined it is possible to quantify them and create a unique benchmark for each individual teacher and each individual course.

## References

[1] IEEE Computer Society and ACM, Curriculum Guidelines for Undergraduate Degree Programs in Software Engineering, Available at: http://www.acm.org/binaries/content/assets/education/se2014.pdf (Accessed September 2021)
[2] Đ. Madić, Ž. Stanisavljević, SQLITRAINER - Sistem za učenje o SQLi sigurnosnim propustima u aplikacijama, ETRAN 2021, RT1.2, September 2021
[3] Knüpfer, M., Bierwirth, T., Stiemert, L., Schopp, M., Seeber, S., Pöhn, D. and Hillmann, P., 2020, September. Cyber Taxi: A Taxonomy of Interactive Cyber Training and Education Systems. In International Workshop on Model-Driven Simulation and Training Environments for Cybersecurity (pp. 3-21). Springer, Cham.
[4] Juice Shop, Available at: https://owasp.org/www-project-juice-shop/ (Accessed September 2021)
[5] OWASP, Available at: https://owasp.org/ (Accessed September 2021)
[6] E-Commerce news, Available at: https://ecommercenews.eu/800000-online-stores-europe/ (Accessed September 2021)
[7] Juice Shop code repository, Available at: https://github.com/bkimminich/juice-shop (Accessed September 2021)
[8] Hack The Box, Available at: https://www.hackthebox.eu/ (Accessed September 2021)
[9] Avatao, Available at: https://avatao.com (Accessed September 2021)
[10] CTFd, Available at: https://ctfd.io/ (Accessed March 2022)
[11] PicoCTF Available at: https://picoctf.org/ (Accessed March 2022)

 ISBN 978-86-7466-930-3

# Automated grading system for picoComputer assembly codes integrated within E-Learning platform

Jovan Đukić, Vladimir Jocović, Marko Mišić, *Member, IEEE,* and Milo Tomašević

***Abstract*— btaining programming s ills is one of the most important prerequisites for a future career of every electrical or software engineer. The programming e pertise is best acquired by gradually advancing from simpler to more comple programming paradigms, architectures, and languages. That being the case, a restrictive educational computer architecture – picoComputer, along with a development environment, was developed at the niversity of elgrade, chool of lectrical ngineering to early e pose the students to the concepts of assembly language programming. aving in mind that programming s ills are successfully attained only through practical wor , such as homewor assignments, projects, and laboratory e ercises, some more contemporary picoComputer simulation environments were implemented, including essy ab des top application and a Picosim web-based solution. owever, programming courses at our school are massive and require the utilization of online learning platforms, aiming to properly achieve a scalable learning process. ence, we employed oodle - earning platform, as well as the Code unner plugin, to facilitate and accelerate the teaching and assessing processes in both of our major programming courses. Code unner plugin supports various widespread programming languages and is also highly programmable, which is why the integration of picoComputer architecture within a contemporary learning system arose as an opportunity.**

***Index Terms*— - earning; automated code assessment; oodle; picoComputer**

## I. Introduction

Strong programming expertise is one of the fundamental abilities of a contemporary software engineer and a necessary quality of an electrical engineer, as well. Gaining programming practice is essential for not only solving real-world problems in software but also for memory sharpening and achieving an ability to efficiently resolve various problems that are seemingly outside of the programming scope.

Jovan Đukić is with the School of Electrical Engineering, University of Belgrade, 73 Bulevar kralja Aleksandra, 11020 Belgrade, Serbia (e-mail: dj@etf.bg.ac.rs)

Vladimir Jocović is with the School of Electrical Engineering, University of Belgrade, 73 Bulevar kralja Aleksandra, 11020 Belgrade, Serbia (e-mail: jocke@etf.bg.ac.rs)

Marko Mišić is with the School of Electrical Engineering, University of Belgrade, 73 Bulevar kralja Aleksandra, 11020 Belgrade, Serbia (e-mail: marko.misic@etf.bg.ac.rs), (https://orcid.org/0000-0002-7369-4010).

Milo Tomašević is with the School of Electrical Engineering, University of Belgrade, 73 Bulevar kralja Aleksandra, 11020 Belgrade, Serbia (e-mail: mvt@etf.bg.ac.rs)

An effective approach to adopting good programming skills requires a strong theoretical foundation, which is being acquired through traditional methods of lecturing, in addition to a practical approach, which includes homework assignments, larger projects, and laboratory exercises [1].

Programming courses at the School of Electrical Engineering, the University of Belgrade, are mandatory for all first-year students and they are organized into two one-semester courses - Programming 1 and Programming 2. Both courses are mainly focused on studying programming languages (Python and C) and introduce different programming paradigms. They start with a low-level assembly language and continue with a more complex procedural and to some extent object-oriented programming paradigm. Moreover, course topics are permeated with basic data structures and code complexity topics.

Our first-year programming courses are attended by a vast number of students (up to a thousand). These massive courses impose a lot of overhead regarding the process of qualitative assessing the students' work and administering the course contents, as well. Hence, there was a need to establish online learning platforms and other tools intending to ease the whole process of managing these huge courses, as well as disburdening the already overexerted teaching staff. Our first experiences with Moodle E-Learning platform in programming courses are described in [2]. In our previous efforts, we also had a good experience with Moodle e-learning platform for other computer engineering courses [3], as well as with other tools for student assessment [4], analysis of results [1], and source code plagiarism detection [5, 6] which are all widely used in programming education. For all those reasons, we decided to implement appropriate support for the emulation of picoComputer assembly codes in Moodle e-learning platform, as well. We describe our motivation and the details of implementation in the rest of the paper.

The second section expresses the reasons behind the choice to move mandatory programming courses to the e-learning Moodle platform and the course organization within it, as well as the examination process using CodeRunner plugin. The third section presents in more detail the in-house developed architecture for teaching assembly language programming - picoComputer (pC). The fourth section describes the present-day implemented system for compilation, execution, and evaluation of source codes written in the pC assembly language and its integration with the CodeRunner plugin within Moodle platform. The fifth section illustrates the evaluation process and the results obtained by system testing. Finally, a brief conclusion and future work are given in the last section.

 ISBN 978-86-7466-930-3

## II. MOODLE PLATFORM AND CODERUNNER PLUGIN IN PROGRAMMING COURSES

The programming courses lectures at the School of Electrical Engineering are held by professors and teaching associates. The professors mostly teach the theoretical aspects of the currently studied programming topics, giving emphasis to some important essences needed for successful mastering of the practical programming tasks. Bearing that in mind, the teaching associates organize auditory exercises in a more practical manner, thus those classes are dedicated to programming practices only.

Each elementary problem and some intermediate programming tasks are conducted alongside students, aiming to strengthen and solidify their ascending programming skills, as well as to introduce new approaches to solving programming problems. Simple programming tasks were solved using an integrated development environment, such as PyCharm for Python or Microsoft Visual Studio for C, while the more complex ones were worked out on the Moodle platform using the CodeRunner plugin.

Moodle is an online learning platform that allows teachers to create courses for students and to grade their work in those courses using tests. The platform supports a variety of plugins, and we found the CodeRunner plugin the most useful for our grading purposes. This plugin introduces a new type of question, which allows teachers to assess and grade students' source codes. Correctness of the students' codes is partially verified using an automated testing process implemented by the teaching associates, who managed to appropriately configure the plugin using a custom Python script. This feature places the CodeRunner plugin at the top of the list of supported plugins. Unfortunately, some code characteristics still need to be checked manually, e.g., coding style and efficiency.

The example that demonstrates the usage of the Moodle platform is shown in Figure 1. It illustrates the exercise concerning the linked list data structure. The exercise is carried out in C programming language and consists of basic operations performed on linked lists: insertion and deletion of elements, list traverse operations, etc. Before a problem is approached practically, the topic is explained using a PowerPoint presentation. The task itself is straightforward and performed on a simple linked list of integers.

Intending to make the topic of linked lists more interesting, a big task is organized as a series of smaller tasks for a more comprehensive understanding. The task is divided into smaller task sets of varying difficulty. Former task sets consist of commonly used linked list operations and latter task sets functionally depend on the previous task sets. This way the goal is to incrementally build and test the solution and to teach students one of the most important programming principles – code reusability.

As shown in Figure 1, a question has a small table at the top of the page which contains the test input data and the expected output data. Below the test cases table, there is a text area for the code itself. The CodeRunner plugin also includes syntax coloring which is an additional advantage for the students since it can indicate the errors that would be very hard to find in a classical exam notebook.

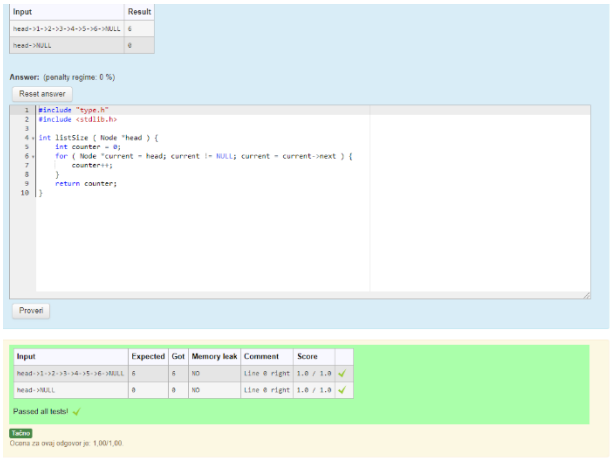


Figure 1 A CodeRunner question in C

After the required piece of code is written in the provided text area, the students can check its correctness by clicking on the check button. When the button is clicked, the contents of the text area are sent to a server dedicated to checking and grading CodeRunner questions. The server first compiles the given code and executes it using the supplied test cases. After execution, the server collects the output and compares it with the expected output.

The main advantage of the CodeRunner plugin for Moodle platform is that the entire process of code checking is configurable [7]. This is achieved through Python scripts which are executed each time a student checks the question. Furthermore, the comparison of the expected and collected output can be graded line by line, thus allowing the students to receive partial points for each successfully passed test case. After the outputs are compared, the result table, shown below the text area in Figure 1, is created giving feedback and their scores to the students, while pointing them to possible errors in the code.

In the last few years, teaching associates were able to master the craft of the plugin configuration and managed to successfully port programming tasks written in Python and C programming languages to the CodeRunner plugin. These high-level programming languages are the foundation of our mandatory first-year courses. Details of the porting process of these high-level languages and further information are presented in [2]. The CodeRunner plugin was successfully used at other universities in other contexts for Python and C++, as well [8].

However, before introducing the students to the concepts of high-level programming languages, they are taught some elementary concepts of low-level assembly programming. Being a relatively minor part of the course, it required an underlying educational architecture that would be quite restrictive, and that's why the aforementioned picoComputer architecture is envisioned and developed. Considering the nature of the low-level languages, the written assembly code can frequently be hard to read, maintain and debug. Even when the source code is syntactically correct, its possible semantic flaws could be tedious to discover. Until recently, teaching associates had to manually inspect the source code, which can devour plenty of time and energy, even for simple programming problems.

Taking these circumstances into account and having a positive experience gained from porting high-level

 ISBN 978-86-7466-930-3

programming languages such as Python and C to Moodle using the CodeRunner plugin, teaching associates decided to establish a system that could verify and test the students' solutions written in the picoComputer assembly language on the e-learning platform. Nevertheless, the task of implementing such a system is inherently harder than above mentioned porting challenges. Teaching associates had to provide not only a configured environment for executing students' source codes using test examples but also an implementation of a compiler and an emulator for a source code written in assembly language was necessary. These components were not needed in previous porting undertakings, since there are numerous compilers and interpreters for widespread programming languages, including C and Python.

## III. PICOCOMPUTER

In 1989. Prof. Jozo Dujmović designed a computer architecture named picoComputer (pC) [9] and developed a DOS application *pC Assembler and Simulator* (pCAS). His intention was to facilitate the teaching and understanding of the assembly languages, which are naturally, due to their low-level nature, to some degree demanding. Since only a part of the introductory programming course is devoted to low-level programming, the pC is designed as a quite restrictive architecture as implied by its name. However, even with its restrictive scope, pC is still very useful. In order to provide more convenient environments, two tools have been recently developed at our school, MessyLab IDE [10], and a web online environment called picoSim [11].

Although the picoComputer architecture is more than 30 years old, it is still relevant nowadays. Its aim is to provide a framework for demonstrating assembly-level programming. It follows the classical Von Neumann architecture and, even though the characteristics of various components have changed throughout time and the instruction sets are getting more and more complex, the basic principles of computer structure have not changed a lot. The picoComputer generally consists of the Central Processing Unit, Random Access Memory, and Input/Output devices, which are all connected using a shared Bus, as shown in Figure 2.

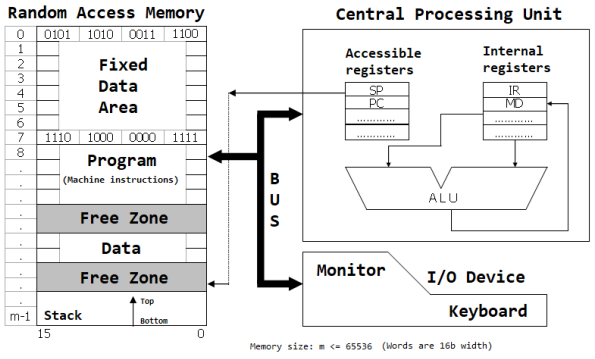


Figure 2 The picoComputer architecture

The Central Processing Unit has several internal registers, yet none of them are directly accessible as the instruction operands. Because of a limited instruction format, there are no general-purpose registers. Still, Program Counter (PC), which points to the next instruction to be executed, and Stack Pointer (SP), which indicates the top of the stack, are registers that can be indirectly manipulated by certain instructions. The value of the PC register is either incremented after an executed instruction or can be directly loaded with the branch address by a control instruction. SP register value is affected by subroutine handling instructions and.

The Random Access Memory consists of 65536 locations (memory words), which means that memory addresses are 16 bits wide, while each location is, also, 16 bits wide. The memory is logically divided into two sections: Fixed Data Area and Free Area. Fixed Data Area includes the first 8 locations, which are directly accessible through direct memory addressing. Free Zone is comprised of the remaining locations and these locations are only accessible indirectly, through another location from the Fixed Data Area, using memory indirect addressing. These locations can be used arbitrarily. The third addressing mode is the immediate addressing where the operand is found in the instruction itself.

The input device is a keyboard, and the output device is the monitor. Numerical data can be entered using a keyboard, while the screen presents the contents of certain memory locations. The input/output operations are blocking operations. Consequently, there is no need for polling a status register. However, parallelism is not supported.

Every picoComputer program consists of two sections: the directive section, and the instructions section. There are two kinds of directives: symbol definition directives and the origin directive. A symbol definition directive is used to assign numerical values to symbols to improve code readability. These symbols are replaced by their numerical values in the assembling process. Labels are an implicit means of symbol definitions, and they can be specified by an identifier attached to any instruction. The origin directive defines the starting memory location where the executable code (instruction section containing instructions following the origin directive) resides.

Every instruction is defined by its symbolic mnemonic and a variable-length comma-separated list of operands. The picoComputer format provides up to 3 operands in an arbitrary instruction. Instructions can occupy one or two memory words (16 or 32 bits). The operation code and three operand fields are encoded in four 4-bit nibbles of the first word, as shown in Figure 3.

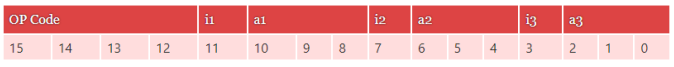


Figure 3 Typical picoComputer one-word instruction format

Hence, a maximum of 16 different operation codes are supported. Each operand specification consists of *i* field (1 bit) and *a* field (3 bits), where *i* indicates the memory addressing mode (0 for direct or 1 for indirect), while *a* field represents an address from Fixed Zone Area (0-7). The 16-bit immediate operand, when supplied, is stored in the second instruction word. The pC instruction set consists of the integer arithmetic instructions (addition, subtraction, multiplication, division), data transfer instruction (scalar or

 ISBN 978-86-7466-930-3

vector move), conditional branches, subroutine call and return, I/O instructions, and stop instruction.

## IV. ASSESSMENT OF STUDENTS' PICOCOMPUTER ASSEMBLY PROGRAMS

As stated, in the second chapter, CodeRunner allows its users to provide a custom Python script for the purpose of grading and assessing. This script is executed in a preconfigured CodeRunner plugin environment, which provides numerous predefined variables. These variables can be used to obtain a variety of information about students from Moodle (i.e., student profile information) and, more importantly, the answer submitted by the student through the CodeRunner form. Given that the pC is our custom assembly language and that the answer is given in a text form, the authors had to build a custom compiler and an emulator to be able to grade and assess students' answers.

The compilation phase consists of text manipulation and performs syntax and semantic checks specified by the rules of the assembly language. During this stage, the text is split into individual lines, which are checked separately. If the process is successful, the result is a Python list data structure of integers, where each element represents an individual memory location. However, if there is an error in the code, the result of the compilation phase is a list containing descriptions of each individual erroneous line (line number and the error description). The unsuccessful compilation phase is depicted in Figure 4.

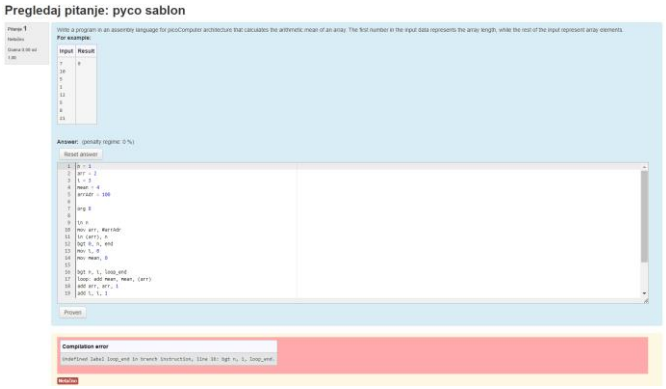


Figure 4 Unsuccessful pC compilation phase

If the compilation phase is successful, the following step is the emulation phase. The input data for the emulation phase is also a list of integers (i.e., memory locations), the address of the first instruction provided by the origin directive and a list of integers representing the input data. The emulation phase is a simple *for*-loop, which reads instructions one by one, executes them and stores their results in the memory. The exceptions to this workflow are the IN and OUT instructions. The IN instruction reads one or more numbers from the input data list, while the OUT instruction writes the content of one or more memory locations to the output list. This output list is later used for comparison with the expected results. Runtime checks are also performed during this stage. Given the restricted nature of the pC and the fact that only integer data type is supported, the only runtime check performed is the division-by-zero check. This is depicted in Figure 5.

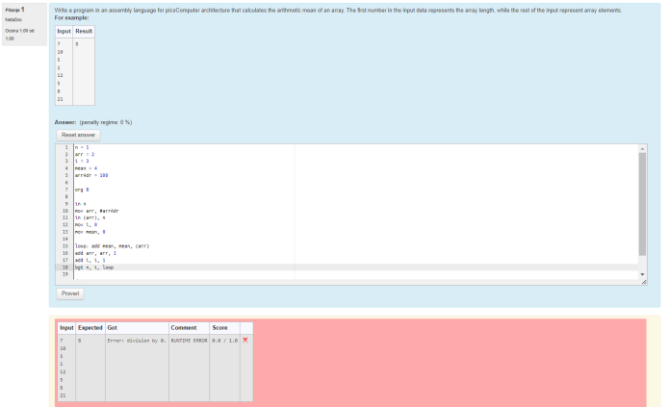

Figure 5 Runtime error checks performed

If both the compilation and the emulation phases are successful, the result of the emulation phase is compared to the expected result and the final grade is formed. The comparison is performed on a line-by-line basis, where each line gives the same number of points. Finally, the student is presented with the score table as shown in Figure 6.

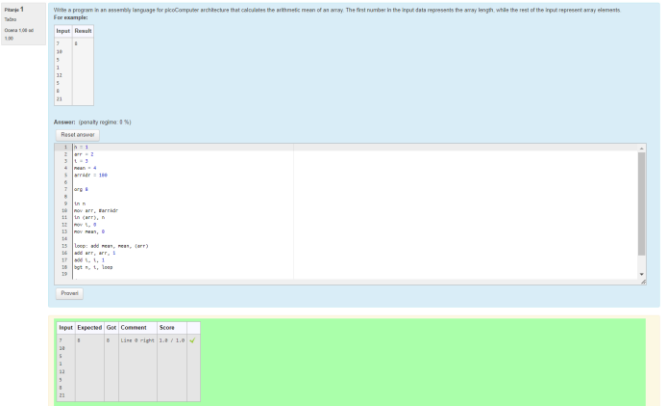

Figure 6 Score table for a program

## V. SYSTEM TESTING AND EVALUATION PROCESS

During the development, the system was tested with custom-written programs, which cover all possible valid and invalid instruction formats. Valid programs consist of instructions as specified by the pC instruction format. These programs are relatively easy to write since there is a limited number of possibilities that are in accordance with the syntax and semantic rules. However, the number of invalid formats is far greater in number and, therefore, it is impossible to cover all of them. Hence, the system was also tested with the source codes of the students in the previous years.

Until recently, during exams students used the MessyLab desktop application to write and self-check their solutions. Regardless, the students used the Moodle platform to submit their answers, which were graded manually. We used these answers to perform evaluation by comparing manual scores given by the teaching associates and the scores given by the system. The system was evaluated on students' programs after the exams have passed and the results of both approaches were quite similar. We sincerely hope that the live results will be as good as these.

 ISBN 978-86-7466-930-3

## VI. Conclusion

In this paper, we have presented the migration process of a restrictive educational picoComputer architecture to the online e-learning Moodle platform using a dedicated CodeRunner plugin for our introductory programming course. With this new feature, we have successfully fully moved all our programming activities within the Programming 1 course to the LMS. Moodle and CodeRunner are extensively used during auditory exercises in the computer lab and examination. The students reacted very positively to this innovative activity.

Having migrated all programming languages in our mandatory programming courses, it may seem that the future work lacks required matter to be considered worthy. However, the is a significant potential concerning the available possibilities to parametrize and configure these types of systems not only to achieve more sophisticated means of grading, yet also to broaden the spectrum of conceivable programming task types. In the future, we have an intention to develop various learning activities in Moodle, as well to extend our coding exercises pool with more assignments written in different programming languages. Moreover, we have in mind to migrate the rest of our programming courses to such type of learning and examining.

## Acknowledgment

This work was supported by the Science Fund of the Republic of Serbia, grant no. 6526093, AI-AVANTES, as well as the Ministry of Education, Science, and Technological Development of the Republic of Serbia (III44009 and TR32047). The authors gratefully acknowledge the financial support.

## References

[1] M. Mišić, M. Lazić, and J. Protić, "A software tool that helps teachers in handling, processing and understanding the results of massive exams," in *Proceedings of the Fifth Balkan Conference in Informatics*, 2012: ACM, pp. 259-262.

[2] V. Jocović, J. Đukić, and M. Mišić, "First Experiences with Moodle and Coderunner Platforms in Programming Course," in *Proceedings of the Tenth International Conference on e- earning*, Belgrade Metropolitan University, Belgrade, 2019, pp. 81-86.

[3] D. Drašković, M. Mišić, and Ž. Stanisavljević, "Transition from traditional to LMS supported examining: A case study in computer engineering," *Computer Applications in Engineering Education*, 2016.

[4] A. Bošnjaković, J. Protić, D. Bojić, and I. Tartalja, "Automating the Knowledge Assessment Workflow for Large Student Groups: A Development Experience," *International ournal of Engineering Education*, vol. 31, no. 4, pp. 1058-1070, 2015 2015.

[5] M. Mišić, Ž. Šuštran, and J. Protić, "A Comparison of Software Tools for Plagiarism Detection in Programming Assignments," *International ournal of Engineering Education*, Article vol. 32, no. 2, pp. 738-748, 2016 2016.

[6] M. J. Mišić, J. Ž. Protić, and M. V. Tomašević, "Improving source code plagiarism detection: Lessons learned," in 2017 *25th Telecommunication Forum TE F* , 2017: IEEE, pp. 1-8.

[7] R. Lobb and J. Harlow, "Coderunner: A tool for assessing computer programming skills," *ACM Inroads*, vol. 7, no. 1, pp. 47-51, 2016.

[8] D. Croft and M. England, "Computing with CodeRunner at Coventry University: Automated summative assessment of Python and C++ code," in *Proceedings of the 4th Conference on Computing Education Practice 2020*, 2020, pp. 1-4.

[9] J. J. Dujmović, Programski jezici i metode programiranja – odabrana poglavlja. *Akademska misao*, 2004.

[10] M. Anđelković. "MessyLab project." http://messylab.com/ (accessed April 2022).

[11] N. Miljković. "picoSim project." https://picosim.app/ (accessed April, 2022).

 ISBN 978-86-7466-930-3

# Pandemic Support System Modelling and Implementation as Integral Part of Computer Science Courses

Nenad Petrović

***Abstract* — In this paper, e ercises related to modelling and implementation of pandemic-tac ling systems are proposed as integral part of computer science university courses. The presented case study considers the perspective of two bachelor degree courses taught at the third year of Computer cience and Informatics track at University of Niš, Faculty of lectronic ngineering in erbia covering both hardware and software design icrocomputer ystems and Information ystems. or the first course, an indoor safety system based on Intel and additional components ( 251, 255 and 25 ) is presented. n the other side, the main topic of the second one is ava nterprise dition ( )-based information system development, while the presented e ample shows application providing efficient pandemic-related data management (coronavirus tests and vaccination).**

***Index Terms* — C ID-1 ; coronavirus; education; Intel ; ava nterprise dition ( ).**

## I. Introduction

The ongoing coronavirus pandemic has brought numerous challenges not only to healthcare and medical science-related personnel, but when it comes to engineering and information sciences professionals as well. Efficient pandemic-related data management in synergy with leveraging the collected information are recognized as key factors when it comes to role of information systems in global battle against COVID-19 [1]. On the other side, IoT and embedded devices are one of crucial means for disease spread reduction (such as mask detection and contactless temperature measurement) [2]. In this paper, we introduce two exercises aiming Information Systems and IoT bachelor degree courses at Faculty of Electronic Engineering, University of Niš in Serbia. The first one covers the design and development of software leveraging pandemic data, while another is a control unit of indoor safety system. The goal is to show how students can become aware of their role as computer engineers among other professionals tackling COVID-19, while studying Java Enterprise Edition software development and programming microcontrollers, on the other side.

The exercise case studies presented in this paper are inspired by author's intensive work in area of pandemic support information technology solutions since the beginning of COVID-19 outbreak. In [3], an affordable IoT-based indoor safety system for mask check and temperature detection leveraging Raspberry Pi and Arduino Uno was introduced. Moreover, the works from [4, 5] show methodology for efficient pandemic resource planning, such as vaccine allocation and tests. Furthermore [6] shows air quality regulation system for coronavirus spread reduction, while [2] addresses green certificates checking relying on blockchain. Finally, [7] shows adoption of data mining techniques in area of post-COVID tourism. On the other side, author also introduced exercises related to coronavirus protection within Logic Design [8, 9] course and microcontroller-related part of Microcomputer Systems [9, 10].

Nenad N. Petrović is with University of Niš, Faculty of Electronic Engineering, Aleksandra Medvedeva 14, 18000 Niš, Serbia, (e-mail: nenad.petrovic@elfak.ni.ac.rs), (https://orcid.org/0000-0003-2264-7369)

## II. Background

### A. Information Systems Course

Information Systems is third year bachelor degree course, mainly covering Java Enterprise Edition (JEE) [11] and related technologies within practical sessions. The implementation-related assignment is homework project scored by 25% of the overall coursework. The underlying architecture is depicted in Fig. 1. In such application, user provides the corresponding input data and selects desired options via web browser-based interface. Moreover, in order to generate the expected results, business logic layer is responsible for calculations and data manipulation. Additionally, at some point it might rely on external microservices deployed within containers for some of the tasks. During this processing within business layer, objects holding the relevant data about events, users and other entities might be persisted within database or retrieved from there Finally, the outcome is shown back to the end-user inside web page. Later, the acquired data can be further leveraged for various types of predictions relevant to business goals.

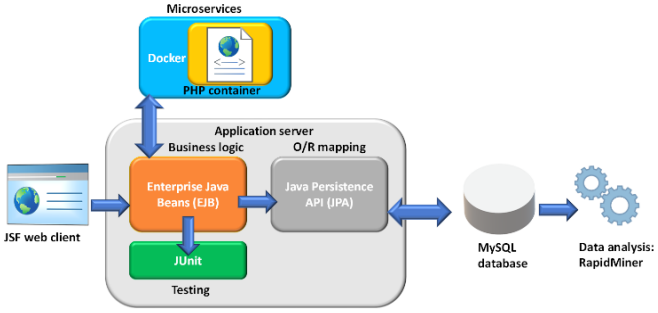


Fig. 1. Information Systems course project architecture.

An overview of components corresponding to the topics covered by the practice-oriented part of Information Systems course is given within Table 1.

 ISBN 978-86-7466-930-3

TABLE I
INFORMATION SYSTEMS TOPIC OVERVIEW

| Component | Type | Role |
|---|---|---|
| Java Server Faces (JSF) [11] | Java-based framework for web applications (front-end) | User data input and result visualization |
| Enterprise Java Beans (EJB) [11] | Business logic layer components for application JEE back-end | Calculations and data manipulation |
| JUnit [12] | Testing framework | Unit testing of business layer functionalities based on assert checking |
| Java Persistence API (JPA) [11] | Object-relational (O/R) mapping specification | Persistence of entities (Java class objects) in form of database rows |
| MySQL [13] | Relational database | Storage of relevant data within tables |
| Docker [14] | Containerization engine | Microservice implementation and deployment within isolated environment |
| RapidMiner [15] | Automated machine learning tool | Predictions using classification, regression, clustering and association rules |

### B. *Microcomputer Systems Course*

Microcomputer Systems are also obligatory third year bachelor degree course, but focused on hardware design instead. It consists of two main parts: 1) Intel 8086-based systems [16] 2) PIC16-family microcontrollers. In this paper, we focus on the first part, which represents around 30% of the overall course work, split into lab session exercises and written exam. When it comes to that topic, several additional components are also covered, as shown in Table 2.

TABLE II
MICROCOMPUTER SYSTEMS TOPIC OVERVIEW

| Component | Type | Role |
|---|---|---|
| 8086 | 16-bit microprocessor | Control unit and data processing |
| 8255 | Parallel data peripheral interface | Output to devices such as 7-segment displays and LEDs or input handling, such as button press |
| 8251 | Serial data transfer interface | Receive/transmit data via single line from serial devices and convert it to parallel in order to be usable by 8086 |
| 8259 | Programmable Interrupt Controller | Detecting changes on interrupt lines and providing mechanism for response to events which occurred in the external environment |

## III. CASE STUDIES

### A. C I -1 ealthcare System for Test and accination

The goal of the project assignment is to model and implement a healthcare information system aiming to support COVID-19 testing and vaccination processes. The complete source course of the project is given within public online GiHub repository: https://github.com/penenadpi/is2022_covid.

It gives the ability to enter the related data using corresponding JSF pages, as shown within screenshot of test-related interface (Fig. 2). On the other side, it enables the storage and retrieval of relevant information about vaccination as well, such as ambulance identifier, date, vaccine type, the number of dose and person identifier.

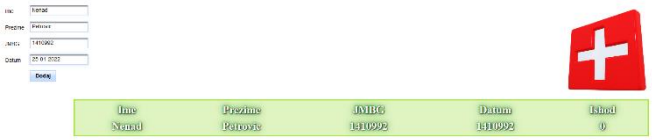

Fig. 2. JSF page for COVID-19 test records.

We can distinguish between three main types of Java class components within the application (as illustrated in Fig. 3): 1) entity classes – responsible for data persistence about relevant objects ( *accination ecord* and *Test ecord*); 2) session beans services – implementation of business logic services together with their corresponding interfaces ( *accinationSer ice* and *TestSer ice*); 3) controllers - functionalities related to a single JSF page ( *accinationController* and *TestController*). The underlying flow can be described as follows: controllers are triggered by clicking on buttons within the JSF page, while inside them, the calls to corresponding services leveraging the data (storing or reading) and performing processing are invoked. These operations are executed against entity objects which are permanently persistent within database relying on O/R mapping.

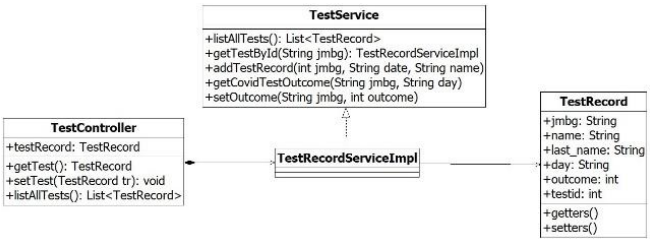


Fig. 3. Excerpt of UML class diagram for coronavirus test records.

On the other side, when it comes to testing, JUnit framework for unit testing in Java is covered by this course. Unit tests aim to check whether lowest level executable units (such as single method in object-oriented program or function) give correct result. For that purpose, test cases covering relevant features of the project are written. An example which checks whether new vaccination records are inserted correctly is given in Fig. 3. The test case consists of three main parts: 1) pre-condition: assert which needs to hold before execution of the test itself 2) test steps: the functional call to the method being tested 3) post-condition: condition which should be true after the execution of test steps. As it can be seen in Fig. 4, the precondition checks

 ISBN 978-86-7466-930-3

whether vaccination record for given person does not exist. Then, the test itself adds vaccination record. Finally, the post-condition checks if insertion had been successful by retrieving the vaccination record of provided person and testing if it is not null value.

```
@Before
public void testPrecondition()
{
    VaccinationRecord vr1=service.getVaccByPersonId(14103);
    assertNull(vr1);

}

@Test
public void testCase1()
{
    service.createVaccinationRecord(14103, 2, "Sinopharm", "13-06-2021");

}

@After
public void testPostcondition()
{
    VaccinationRecord vr1=service.getVaccByPersonId(14103);
    assertNotNull(vr1);
}
```

Fig. 4. JUnit test case implementation.

When it comes to integration with microservices, the layer of business logic (*Co idTestSer ice* session bean) interacts with PHP script deployed in a container via HTTP request. In Fig. 5, an example in context of our project assignment is shown. When it comes to insertion of COVID test results, the value of test outcome field is taken as result of PHP script deployed within web server inside Docker container. The script itself takes person identifier and current date as input, while the outcome is randomly generated (0 or 1), simulating the randomness regarding the probability of being infected.

```
public String getCovidTestOutcome(String pid, String day) throws IOException {
      String outcome="";
      URL obj = new URL("http://192.168.99.100/?pid="+pid+"&day="+day);
      HttpURLConnection con = (HttpURLConnection) obj.openConnection();
      con.setRequestMethod("GET");
      con.setRequestProperty("User-Agent", USER_AGENT);
      int responseCode = con.getResponseCode();
      System.out.println("GET Response Code :: " + responseCode);
      if (responseCode == HttpURLConnection.HTTP_OK) { // successful call
            BufferedReader in = new BufferedReader(new InputStreamReader(con.getInputStream()));
            String inputLine;
            StringBuffer response = new StringBuffer();

            while ((inputLine = in.readLine()) != null) {
                  response.append(inputLine);
            }
            in.close();
            outcome = response.toString();
            return outcome;
      } else {
            System.out.println("GET request not worked");
            return outcome;
      }

}
```

Fig. 5. Integration with Docker container microservice.

Finally, the last part of the project assignment involves leveraging the data collected by the described information system in order to make predictions which could be relevant to the pandemic support domain. For this purpose, we make use of RapidMiner tool, which gives intuitive and automated visual interface for machine learning. The presented example shows the adoption of regression, whose goal is to predict the value of numerical (continuous-valued) outcome. The layout of the underlying dataset based on the collected data is shown in Table 3. The goal is to predict vaccine demand (number of persons vaccinated) for given day. Relevant factors (input, independent variables) are day number, vaccine type, institution id and number of daily COVID-positive cases. On the other side, the predicted value (dependent variable) is the number of people who decided to take the vaccine.

TABLE III
VACCINE DEMAND PREDICTION DATASET HEADER

| Day | Vaccine type | Institution | New cases | Demand |
|---|---|---|---|---|
| | | | | |

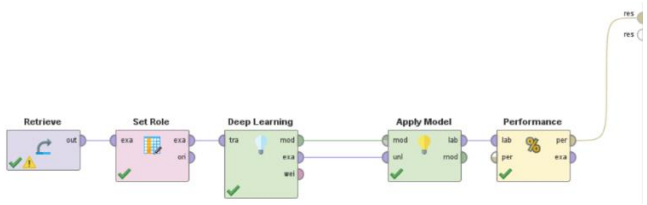


Fig. 6. Vaccination demand prediction workflow in RapidMiner.

The corresponding RapidMiner flow for regression-based prediction is shown in Fig. 6. The first step imports CSV containing all the data. After that, we select the target variable among the available columns. The third step is deep learning module which is trained to make predictions on 80% of the dataset. It contains 2 hidden layers, 30 nodes each and ReLU activation function, performs training in 10 epochs with adaptive learning rate. After that, the model is executed on test data and performance evaluated (mean relative error, which was around 4% in our case).

### *B. Control nit of Corona irus Indoor Safety System*

On the other side, the goal of Microcomputer Systems assignment is design of control unit within COVID-19 indoor safety system (depicted in Fig. 7). Complete code with Proteus simulation is available on GitHub: https://github.com/penenadpi/8086covidsafety/blob/main/8086_8255_8259_8251_covid_safety.pdsprj

Each time new person arrives, two checks are performed by external devices: 1) temperature check – whether it is in normal range (less than 37°C) 2) mask check – if person wears mask or not. After that, the data is sent via 8251 component to the microprocessor, relying on 8259 for

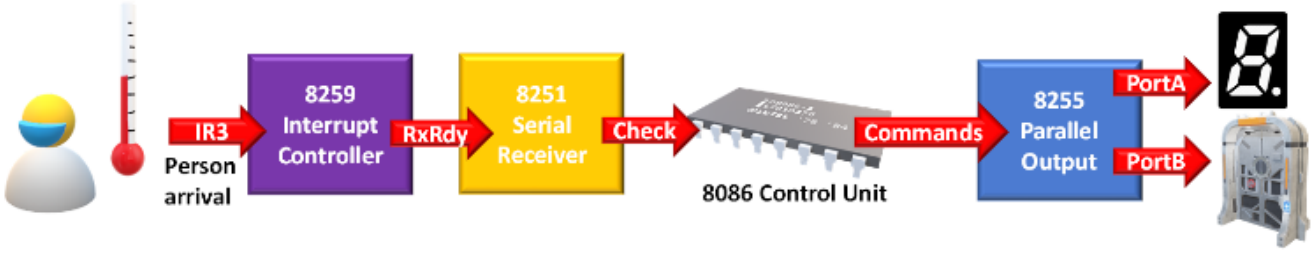


Fig. 7. 8086-based indoor coronavirus safety control system.


ISBN 978-86-7466-930-3

interrupt handling (vector 171, line 3). In case that person passes both checks, then the door will be opened only in case that the current number of persons is in the allowed range for that room. Additional output peripheral devices are connected via ports of 8255: 1) green LED – turned on for opening door (PORTB, pin 1); 2) red LED – turned on for closing door (PORTB, pin 0); 3) 7-segment display (PORTA) – showing the current number of persons inside. However, when person leaves room, interrupt which decreases the number of persons inside the room is activated, as button on interrupt line 1, vector 169.

```
PROCED SEGMENT
ENTRANCE_CHECK PROC FAR
ASSUME CS:PROCED, DS:DATA

 MOV DX, CTRL
 IN AL, DX

 MOV DX, DAT
 IN AL, DX

 XOR AL, MASK_TEMP_CHECK
 JNZ CLOSE_DOOR

 CMP SI, 5
 JE CLOSE_DOOR

 INC SI

 MOV DX, PORTA
 MOV AL, NUMBERS[SI]
 OUT DX, AL

 MOV DX, PORTB
 MOV AL, GREEN
 OUT DX, AL

 JMP END

CLOSE_DOOR:
 MOV DX, PORTB
 MOV AL, RED
 OUT DX, AL

END:

 IRET
ENTRANCE_CHECK ENDP
PROCED ENDS
```

Fig. 8. 8086 interrupt procedure activated when 8251 receives data.

An excerpt of the solution containing the crucial part of the assembly code run on Intel 8086, related to interrupt triggered when new person arrives is shown in Fig. 8. As interrupt line activation means that 8251 is ready for receiving data, we set the corresponding data exchange address and receive the outcome of the entrance rules checks (mask and temperature) coming from other devices. After that, the received byte is compared against the only case which allows opening the door (MASK_TEMP_CHECK which is 18 hexadecimal). If it is not the case, the red LED will be turned on (door closed). Additionally, if person passes this check, it is also asked whether the current number of persons inside the room is below the maximum threshold (5 in this case). Only if it is true, the door will be opened (green LED turned on), the current number of persons incremented and shown on 7-segment display.

## IV. Evaluation

The proposed approach of including pandemic-related exercises within computer science bachelor degree courses has been evaluated by observing the results before and after their adoption. The following aspects were considered: number of students involved into lab sessions, average lab exam grade and exam pass rate. Fig. 9a and 9b show graphical summary of results compared to previous academic years for Microcomputer and Information Systems courses, respectively.

When it comes to Microcomputer Systems, COVID-19 protection systems were also part of additional student challenges bringing bonus points which can change the whole written exam, where participation was around 15% of the total students involved.

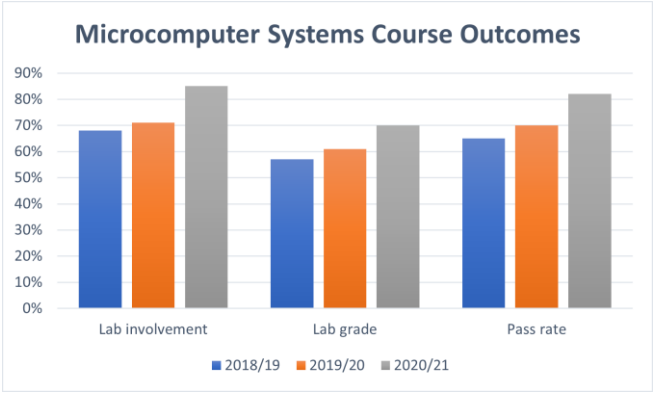


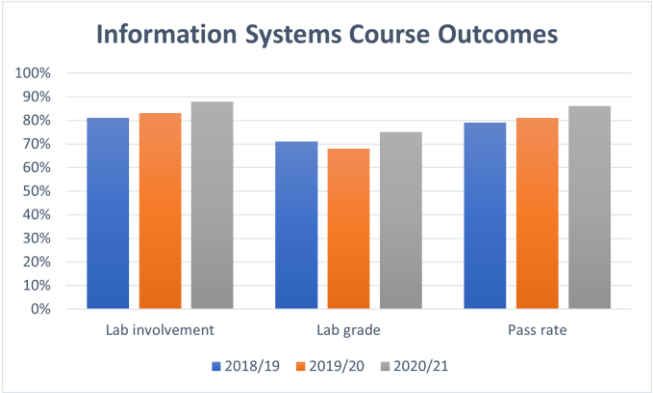


Fig. 9. Course outcomes before and after adoption of the proposed teaching methodology: a) Microcomputer Systems b) Information Systems.

## V. Conclusion

In this paper, it was shown how the implementation of pandemic support solutions can be integrated within computer science university cases, considering the case studies of both hardware and software design. According to authors' observations, the adoption of such exercises in previous school year (2020/21) has shown several benefits for both of the considered courses: greater student involvement into lab sessions together with better lab

 ISBN 978-86-7466-930-3

exercise grades and higher exam pass rate. Taking into account all the considerations, the adopted teaching methodology has been slightly more effective in case of Microcomputer Systems course.

Therefore, the approach seems promising, showing that consideration of current real-world problems within computer science courses increases motivation and interest among participants, leading to better overall results.

## ACKNOWLEDGMENT

This work has been supported by the Ministry of Education, Science and Technological Development of the Republic of Serbia.

## REFERENCES

[1] Q. Wang, M. Su., M. Zhang, R. Li, “Integrating Digital Technologies and Public Health to Fight Covid-19 Pandemic: Key Technologies, Applications, Challenges and Outlook of Digital Healthcare”, International Journal of Environmental Research and Public Health. 2021; 18(11):6053, 2021.

[2] N. Petrović, Đ. Kocić, “Smart technologies for COVID-19 indoor monitoring”, Viruses, Bacteria and Fungi in the Built Environment, ISBN: 9780323852067, Woodhead Publishing, pp. 251-272, 2021. https://doi.org/10.1016/B978-0-323-85206-7.00012-5

[3] N. Petrović, Đ. Kocić, “IoT-based System for COVID-19 Indoor Safety Monitoring”, IcETRAN 2020, pp. 603-608, 2020.

[4] N. Petrović, “Simulation Environment for Optimal Resource Planning During COVID-19 Crisis”, ICEST 2020, pp. 23-26, 2020. https://doi.org/10.1109/ICEST49890.2020.9232908

[5] N. Petrović, I. Al-Azzoni, "Model-Driven Approach to COVID-19 Vaccination Planning Leveraging Multi-Objective Optimization and Deep Learning", SSSS 2022, pp. 19-24, 2022.

[6] N. Petrović and Đ. Kocić, "IoT for COVID-19 Indoor Spread Prevention: Cough Detection, Air Quality Control and Contact Tracing," 2021 IEEE 32nd International Conference on Microelectronics (MIEL), 2021, pp. 297-300. https://doi.org/10.1109/MIEL52794.2021.9569099

[7] N. Petrović, "VHDL Logic Design Exercises Simulating COVID-19 Protection Systems", SSSS 2022, pp. 127-132.

[8] N. Petrović, “COVID-19 Safety Systems Design Exercises in Computer Science University Courses”, YuInfo 2021, pp. 1-6.

[9] N. Petrović, “Prototyping PIC16-based COVID-19 indoor safety solutions within microcomputer systems course”, IEEESTEC – 13th Student Projects Conference, pp. 185–189, 2020.

[10] N. Petrović, V. Roblek, N. Papachashvili, “Decision Support Based on Data Mining for Post COVID-19 Tourism Industry”, SAUM 2021, pp. 29-32, 2021.

[11] D. Heffelfinger, Java EE 8 Application Development, Packt Publishing, 2017.

[12] JUnit 4 [online], available on: https://junit.org/junit4/ , last accessed: 25/03/2022.

[13] MySQL [online], available on: https://www.mysql.com/ , last accessed: 25/03/2022.

[14] Docker [online], available on: https://www.docker.com/ , last accessed: 25/03/2022.

[15] RapidMiner [online], available on: https://rapidminer.com/ , last accessed: 25/03/2022.

[16] B. Brey, The Intel microprocessors: 8086/8088, 80186/80188, 80286, 80386, 80486, Pentium, Pentium Pro processor, Pentium II, Pentium III, Pentium 4, and Core2 with 64-bit extensions: architecture, programming, and interfacing, Pearson Prentice Hall, 2019.

 ISBN 978-86-7466-930-3

# An overview of software code review tools and the possibility of their application in teaching at the School of Electrical Engineering in Belgrade

Miloš Obradović, Marija Kostić, Balša Knežević, Dražen Drašković, *Member*, IEEE

***Abstract* - The use of version control tools together with the code review techniques is the basis of modern software development. In order to introduce future software engineers to these tools, as well as the process of software development, and to better prepare them for the industry work, the course "Principles of Software Engineering" was formed at the School of Electrical Engineering at the University of Belgrade. Within this course and the team project that students are doing, all the basic stages of the development of a software system are studied. One of the biggest challenges in organizing a practical team project is finding the right tool for code review. This tool should be suitable for educating future engineers, but also enable monitoring of students' progress and evaluation of the work done. This paper presents the basic needs that a software code review tool must meet in order to be suitable for use in education. An analysis of the functionalities of some of the existing code review tools has been given, as well as the possibility of applying these tools in education at the School of Electrical Engineering. The end of the paper presents a proposal for the best way to implement a tool for code review.**

***Index terms* - teaching methodology, program code review, software development.**

## I. Introduction

Software has become an indispensable part of our daily lives, and our dependence on software is constantly increasing. An organization's success and reputation depend on its ability to produce and deliver reliable software [1]. Therefore, modern software development requires engineers to not only know how to program properly and effectively but also how to develop good engineering practices to make the codebase healthy and easy to maintain [2]. One of the techniques used in industrial and open-source projects, which aims to control the quality of code added to the codebase, is called code review [3]. The main goal of code review is to improve the readability and maintainability of the codebase. It is a process in which code is reviewed during design and development by someone other than the author. According to [2], a well-designed code review process provides several benefits:

- Allows a reviewer to check the "correctness" of the code change, i.e., is it possible for the change to introduce bugs into the codebase.
- Ensures the code change is comprehensible and understandable to other engineers.
- Enforces consistency across the codebase.
- Psychological and cultural benefits such as promotion of team ownership, validation, and recognition of one's work.
- Enables knowledge sharing.
- Provides a historical record of the code review itself.

Even though it is a widely recommended technique for improving software quality and increasing developers' productivity [4], across the industry, code review is far from the universal practice [2]. Nevertheless, together with the version control systems, the code review process forms the foundation of modern software development.

Future software engineers should be familiar with the tools and processes for version control and code review. Therefore, it is important for engineering students to review each other's source code. However, surprisingly, few engineering courses in universities and colleges include code review activities [5]. The paper [6] provides an overview of the courses that have introduced code review in their practical activities (homework, projects, etc.).

At the School of Electrical Engineering at the University of Belgrade (SEE-UB), the course "Principles of Software Engineering" (PSE) was designed to introduce students to the basic concepts of software engineering. The course covers various aspects of the software life cycle: specification design and user requirements, system design, selection of the most suitable software architecture, implementation, testing, documentation writing, and basic elements of software project management. At the core of this course is a team project in which students go through all phases of the development of a software system. Their activities range from writing basic functional specification and design of the system, to the final, tested and fully functional software product, the so-called release version. The implementation phase is based on creating a web-oriented software system on a monolithic or microservice architecture, using several basic architectural

Miloš Obradović is with the School of Electrical Engineering, University of Belgrade, 73 Bulevar kralja Aleksandra, 11020 Belgrade, Serbia (e-mail: milos.obradovic@etf.bg.ac.rs)

Marija Kostić is with the School of Electrical Engineering and the Innovation Center of the School of Electrical Engineering, University of Belgrade, 73 Bulevar kralja Aleksandra, 11020 Belgrade, Serbia (e-mail: marija.kostic@etf.bg.ac.rs), (https://orcid.org/ 0000-0003-4923-3748)

Balša Knežević is with the School of Electrical Engineering, University of Belgrade, 73 Bulevar kralja Aleksandra, 11020 Belgrade, Serbia (e-mail: balsa.knezevic@etf.bg.ac.rs)

Dražen Drašković is with the School of Electrical Engineering, University of Belgrade, 73 Bulevar kralja Aleksandra, 11020 Belgrade, Serbia (e-mail: drazen.draskovic@etf.bg.ac.rs), (https://orcid.org/ 0000-0003-2564-4526)

 ISBN 978-86-7466-930-3

and design patterns. In this school year, students can choose to develop their application using *CodeIgniter* or *Laravel* framework for *PHP*, or *Django* framework for *Python*.

Version control systems and code review process are studied as well. Within the team project, students learn to work in a team and to develop functional software, during the whole semester. Currently, team members are not involved in the code review and code testing process for other team members, so it is the desire of teachers that team members revise each other's program code. Thus, the author of the program code will always receive at least one or two reviews from other members of their team (or optionally members of another team).

In the third phase, students have to formally review the source code that some other team is working on. This phase aims to expand the knowledge and the programming techniques among students, both through what students see in other teams' solutions and through the feedback they receive from colleagues who have reviewed their solution.

For the course activities to be successful, it is necessary to find the best software tools that are available for use at the SEE-UB, which support the version control and code review. Several control version tools that are open-source are quite suitable for use in the course. However, it is much more difficult to find an appropriate system for code review that is publicly available, motivates students to work regularly on their project, and reduces the possibility of some team members avoiding doing their part of the project.

This paper is divided into five sections. The following section describes the process of code review and gives an overview of the functionalities of some popular code review tools. The third section outlines the basic requirements that a code review tool must fulfill to be used for teaching purposes at the SEE-UB. The fourth section presents an analysis of some existing code review tools, and the possibility of their application in teaching. The final section gives a brief conclusion of the results of this work and advice on how to independently implement software code review tools.

## II. Analysis of Basic Features of Code Review Tools

Millions of software engineers around the world review source code daily. This process helps in finding and fixing bugs and increasing the quality of the codebase. Code reviews must be done in real-time and in multiple iterations. Thus, the use of the tools in the code review process must be simple and clear enough. Modern code review is characterized by being lightweight. It can be executed at many stages of software development, but it typically takes place before a code change is added to a version control codebase. Fig. 1. represents common steps of a code review process. First, the author creates a code change and submits it for review. Next, developers discuss the change and suggest fixes. This is an iterative process where the author has to deal with the suggested changes. Finally, when one or more reviewers approve the change, it can be added to the codebase. It is also possible to reject a code change [7].

Table I shows the basic features of the code review tools. Only tools that support Git version control system were considered in the analysis. Many of the analyzed tools also support other platforms. Only those functionalities related to the code review process were observed.

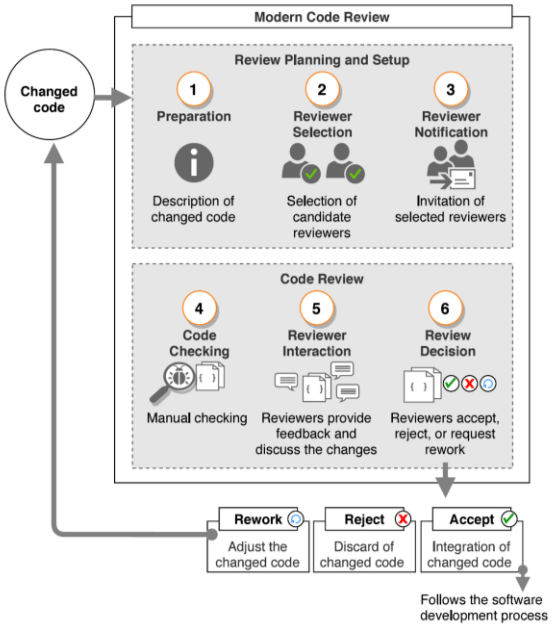


Fig. 1. Common steps of a code review process [8].

## III. Necessary Code Review Tool Functionalities

This section presents in detail the basic functionalities of the code review tool that are necessary for the course. Some functionalities are important for the code review and should convey what that process looks like in practice. On the other hand, other functionalities are important for the teaching process and student collaboration on their first team project during their studies. They should motivate students to work in a team and highlight their individual programming and code review abilities. They should also provide better support for documenting a newly developed software system and commenting on different types of artifacts realized in the project phases.

As already noted, this is the first team project in their bachelor's academic studies. It is important that students cooperate well while writing a nice and readable source code, which could be upgraded later with additional modules. Currently, the team project consists of the following phases:

0. Project proposal.
1. Conceptual solution of the project with the basic functional specification.
2. Development of all use cases, one document for each functionality, and realization of the prototype in a tool for prototype development, e.g., Pencil.
3. Formal inspection of the previous phases.
4. Database modeling.
5. UML modeling of the proposed web application.
6. Implementation of a system as a web application.
7. Testing the web application.
8. Final presentation and software documentation.


ISBN 978-86-7466-930-3

TABLE I OVERVIEW OF CODE REVIEW TOOLS AND THEIR BASIC FEATURES AND FUNCTIONALITIES.

| Tool ⇨ Feature ⇩ | Bitbucket Server [9] | CodeFlow [10] | Collaborator (previous version: Code Collaborator) [11] | Critique (previous version: Mondrian) [2] [12] | Crucible [13] | Gerrit (fork of Rietveld) [14] [15] | GitHub [16] | GitLab [17] | Space / Upsource [18] | Rhodecode [19] | Review Board [20] |
|---|---|---|---|---|---|---|---|---|---|---|---|
| Maintainer | *Attlassian* | *Microsoft* | *SmartBear Software* | *Google* | *Attlassian (former: Cenqua)* | *Google* | *GitHub Inc. (Microsoft)* | *GitLab Inc.* | *Jetbrains* | *RhodeCode* | *reviewboard.org* |
| Year of origin | 2012 | 2009 | 2003 | 2006 | 2010 | 2009 | 2008 | 2014 | 2020 | 2010 | 2006 |
| Technology stack | *Java* | N/A | N/A | N/A | *Java* | *Java* (1st ver. *Python*) | *Ruby, ECMAScript, Go, C* | *Ruby, Go, Vue.js* | *Java, Kotlin* | *Python (Pylons framework)* | *Python, Django* |
| License | Proprietary | Proprietary | Proprietary | Proprietary | Proprietary | Apache v2 | Proprietary | MIT | Apache v2 | AGPL v3 | MIT |
| Open source | no | no | yes | no | no | yes | no | yes | no | yes | yes |
| Number of users | ~10 million | 89% of Microsoft employees | ~20 000 | ~50000 | N/A | N/A | ~73 million | ~30 million | N/A | N/A | N/A |
| Maximal repository memory capacity | 4 GB | N/A | N/A | 1 TB | N/A | 1 TB | 100 GB | 10 GB | 10 GB (free) | N/A | N/A |
| Maximal file memory capacity | 1 GB | N/A | N/A | N/A | N/A | set by admin | 2 GB | 10 GB | 10 GB | 10 GB | N/A |
| Repository privacy | Up to 5 private-free, unlimited public | N/A | N/A | N/A | N/A | Unlimited local repo. | Unlimited public and private | Unlimited | Unlimited | N/A | Private for a fee and public |
| Solution type | Web-based | Standalone | Web-based | Web-based | Web-based | Web-based | Web-based | Web-based | Standalone, Web-based | Standalone, Web-based | Web-based |
| Version control systems support | Git, Mercurial | Git | Git, SVN, TFS, Perforce, CVS, ClearCase, RTC | Git, Piper | Git, Mercurial, CVS, Subversion, Perforce | Git | Git | Git | Git | Git, Mercurial, Subversion | Git, Mercurial, CVS, Subversion, Perforce, Bazzar, ClearCase, TFS, IBM Rational ClearCase, HCL |
| Review document, pictures and diagrams | N/A | N/A | No | Yes | N/A | Yes | No | No | N/A | No | No |
| Review at character level (prog.code) | No | Yes | No | Yes | No | Yes | No | No | No | No | No |
| Integration with project management tools | Jira, Trello | N/A | Jira | N/A | Jira | Jira | Jira, Trello | Jira | Trello | Jira, Trello, Redmine, Pivotal | Asana, I Done This, Trello |
| Integration with other tools | AWS, Crucible, Jenkins, Bamboo, MS Azure, Docker Hub, NPM, Sonar | Visual Studio | Eclipse, Visual Studio, IBM Rational Team Concert, MS Office, Adobe Reader | N/A | Bitbucket | N/A | AWS, Slack, CodeFrash, Semaphore, Asana, Azure, Google Cloud, Heroku, Travis | N/A | IDE (free), Google Calendar (Team), G Suite, Microsoft Office365, Teamcity, Jenkins | Jenkins, Travis CI, TeamCity, Confluence, Slack, HipChat, AppEnlight | Jenkins, Travis CI, Slack, Mattermostm CircleCI, Discord, |

In the third phase, the formal inspection process is carried out according to the standard for formal inspection [8] and consists of six activities/steps: planning, product review, inspection meeting, realization of meeting minutes with the defect report and verification of minutes, work on corrections and final follow-up meeting to verify the corrected product. In this phase, one team of students performs a formal inspection to another team by checking all the files and documents made up to that point. The result of this phase are the reports on the formal inspection. These reports are sent to the author team for them to correct all identified shortcomings and defects, and synchronize files from the first two phases of the project. Such formal inspection could be carried out after some lather phases.


ISBN 978-86-7466-930-3

In the sixth phase, the implementation of the software system, inspection of the source code is necessary, which has been optional so far. This paper aims to decide which software tool would be suitable for students to use in this phase. The functionalities necessary to be part of such a software tool are presented in the following subsections.

### *A. Availability of tools for use at the SEE-UB*

The tool needs to be completely free to use or to have an academic license. Big corporations usually develop their own tools for code review, but do not make them publicly available. Other companies are actively working on the tools for software development, but their solutions are expensive, especially taking into consideration that tool will be used by several hundred students. As the code review techniques are primarily used in the industry, and less as a means of education within academic institutions [5], in the rest of this paper, only open-source tools are considered. Among the most well-known tools that offered packages with academic licenses, the following tools *GitHub*, *Atlassian Bitbucket* and *JetBrains Space* are discussed in Table 1.

### *B. Roles within the program code review process*

The code review largely depends on the participants in the process itself. Currently, there is no universal standard in the software industry that defines exactly which people should check every change in a project [21][22]. Each company defines its own procedures for the reviewer selection process (Fig. 1, step 2). As part of the code review, there are also persons who are only in charge of checking the style of writing the program code, but not for checking the correctness of the functionality of the code [21][22].

For the course PSE there are several required functionalities related to the distribution of different roles:

- Within a single project, all students can participate in the development of the software solution, and all of them are required to review each code change, written by another team member.
- For some changes and monitoring of the program code, it should be possible to add students from other teams as code reviewers. It is necessary to enable manual addition of reviewers or addition based on the programming language/framework. As projects are developed in different programming languages (three different frameworks), it is good that the student, a member of another team, is sufficiently familiar with the syntax of that programming language, in which the authors developed their system. Comments by reviewers more familiar with the code, will be much more useful for the author [8].
- Teaching staff should be automatically added to all the teams. They should be able to just follow students' work without the obligation to review all their code changes, or with possibility to write their own reviews.

### *C. Possibility of anonymous code review*

Research shows that significant discrimination occurs during code review when the authors of the program code or the authors of other documents are known. Discrimination can be based on gender, race, nationality, or age [22]. Additionally, in the school environment, it often happens that students with a lower average grade are afraid to criticize or point out some mistakes of students with higher grades. To motivate students to take the code review process as seriously as possible, as an important part of software development, and to reduce the effects of student discrimination and shyness, the aim is to use a tool that supports anonymous code review. Also, an anonymous review would reduce the possibility of students who know each other making personal arrangements. For example, they could decide to not find many mistakes in each other's code changes to save time they are spending on the project.

### *D. Ability to check the style of the program code before the code review*

Static program code analysis techniques check the structure of the source code without having to execute the program itself. Their objective is to find defects early in the development process. This approach dramatically accelerates the code review process because reviewers can now focus only on the functionality and implementation of the code segment [23]. Some examples of issues that static analyzers can detect are constant expressions that overflow, uninitialized variables, tests that are never run, etc. Next to finding bugs, these tools can help verify that the code is following best practices, style guides, naming conventions, etc. in order to prevent or reduce technical debt [2]. The procedures that would be used within the project may include: writing unit tests and code coverage techniques, by each team member, for their developed parts of the program code, specific styles and precisely defined types of comments, prescribed by course teachers, etc.

As static program code analyzers reduce the cost of software development, many development environments today use them extensively. However, in the case of the course PSE, students have the freedom to choose any available development environment. A static code analyzer that supports *PHP* and *Python* programming languages is required to successfully realize the project within this course.

### *E. Ability to use tools to review types of files other than the program code*

As already mentioned, through the course PSE, students are learning about different phases of software development. Some of the activities students face for the first time are: writing basic functional specifications, developing use case scenarios, testing web applications, and writing appropriate documentation. Next to the source code, students have to work on and produce documents of many different types. Therefore, the tool for code review should support reviewing files that are not source code. The relevant additional types of files are documents, images or specific diagrams, and other multimedia files.

 ISBN 978-86-7466-930-3

### *F. Ability for the teacher to access basic statistics on tool usage and change the basic code review settings*

Teachers should have privileges and advanced functionalities available to them. One of these functionalities is the possibility to set up the code review process. This means that teachers should be able to form teams, control whether anonymous code reviewing is active and determine who are required reviews of some projects. Different statistics about students' work, and contributions should be also available. All this will help in further improving teaching by finding the best setup for the code review process that maximally engages students.

## IV. TESTING POPULAR AND AVAILABLE CODE REVIEW TOOLS

This section shows the test results of some popular software code review tools. As explained in subsection A of the third section, for a tool to be used in teaching at the SEE-UB, it must be free for public use. The work of the following tools that meet this condition was tested in detail: *Gerrit*, *GitHub*, and *GitLab*.

Testing of three popular and publicly available tools was performed as follows. The first step is to create a project and make it available on a version control system. After that, it is necessary to do a basic review of the program code within which the tools are tested with basic files for web page structure (*html*), web page layout (*css*), program code files (*js*, *py*, and *php*) and files with commands to work with the database (*sql*). In the next step, the behavior of the code review tool is tested when files that do not contain program code were added to the project. In this step, the behavior of the tools is tested when basic document types (docx and pdf), images (*jpg* and *png*), and diagrams (*uml*) are added to the project. In the last phase of testing the software code review tool, it was checked whether the tool supports other functionalities described in the third chapter.

### *A. Availability, integration with Git systems, and the possibility to extend functionalities*

All three tools have a basic version that is free for public use. *Gerrit* and *Gitlab* have been developed based on open-source code, which opens opportunities to independently upgrade the platform and add new functionalities per personal requirements. *GitHub*, on the other hand, is a closed-source environment, but it has a free version and offers good support for developing open-source projects. The only way to add new features to *GitHub* can be achieved through browser plugins. This is not always a good solution because it adds another item that students must install and use properly. *GitHub* also offers an academic license that brings additional functionality, but at the time of writing, the authors have not been able to go through all the necessary steps to obtain this license, so it was not possible to test its usefulness.

Code review is done through the web interface for all three tools, while support for version control is done through command line. In addition to this, the *GitHub* platform provides the ability to manage versions using the standalone application which can further facilitate the education of students in the use of software development tools. It should also be noted that the *Gerrit* platform has an interface that is not adapted for beginners and has a higher learning curve.

The *Gerrit* platform can be run on a local machine and then all data is stored on that machine. The disadvantage of this approach is that the host machine must always be available and regularly backed up data so that students do not lose their projects due to hardware failure. The advantage of this approach is the ease of adding new functionalities to the tool because the complete code is executed on a local machine.

*Gerrit* has a slightly different flow control compared to standard *Git* systems. Control has been simplified, which on the one hand may be good for educating new engineers, but on the other hand, it does not follow industry standards, and migrating to another code review git-based system would require adaptation.

### *B. Working with different file types*

As expected, none of the tools had problems working with the program code. All tools provide the ability to comment on each line of program code and set the appropriate status of the comment which indicates that the code is approved or needs to be changed before getting approved.

Problems occur when the tools are used with alternative files such as documents, images, and diagrams. All three tools can display the image, but they are not able to correctly display any type of document. *Gerrit* tool provides a feature to comment on the entire file, while the other two tools do not provide this option. As a result, using *GitHub* and *GitLab*, there is no way to comment on added documents and images.

Diagrams cannot be displayed by any of these tools, but they can display the xml structure that is in the background of this file. The conclusion is that the best way to work with diagrams during software development is to attach an image with each diagram that can be commented.

### *C. Roles and their permissions within projects and the possibility of anonymous code review*

*Gerrit* allows you to organize users into different groups [14]. It is possible to add users to each group individually, who will have all the authorizations assigned to that group. Using these groups, the teacher can create a project within which they will define groups and their privileges. The teacher also can create subprojects, add students to them and give them predefined group privileges.

*GitLab* and *GitHub* have predefined roles and access rights within the project. The roles allow the members working on the project to function well when developing software, but do not provide any additional benefits for the teacher role.

No platform has support for anonymous code review. One way to implement an anonymous code review is to make projects publicly visible. Then someone from the other team can look at the program code and submit their remarks externally to the authors of the project. Anonymous review can also be done through web plugins, but one of the problems with using anonymous review through external plugins is that all reviewers must be added to the project,

 ISBN 978-86-7466-930-3

which indicates who the potential reviewers are and reduces the effectiveness of anonymous review. Another problem is relying on the students to use external add-ons correctly, which is not easy to check, so such solutions are not the best.

All three platforms provide basic pre-processor code verification capability before review. As no style guide is currently defined in the course PSE, detailed possibilities of this functionality have not been examined in this paper and are the subject of future research.

Table II maps the functionalities required for teaching the course to the three most popular code review tools, which were publicly available.

TABLE II
ANALYSIS OF FUNCTIONALITIES OF CODE REVIEW TOOLS FOR THE NEEDS OF TEACHING THE COURSE PRINCIPLES OF SOFTWARE ENGINEERING

| | *Gerrit* | *GitLab* | *GitHub* |
|---|---|---|---|
| *Public availability* | Yes | Yes | Yes |
| *Roles in Code Review* | Anonymous Change Owner, Project Owner, Registred User, Custom Gruop | Guest, Reporter, Developer, Maintainer, Owner | Read, Triage, Write, Maintain, Admin |
| *Anonymous code review* | No | No | No |
| *Static code analysis* | No | Python, PHP | Python |
| *Review files with code* | Yes | Yes | Yes |
| *Review document, pictures and diagrams* | Can comment on hole file | No | No |
| *Automated user statistics* | Available through plugins | Yes | Yes |
| *Project configuration* | Yes | Yes | Yes |

## V. CONCLUSION

This research provides an overview of all the commonly used code review tools in the software industry. Based on this research, the authors recommend the use of *GitLab* software, because it has user-friendly interfaces, is easy to use, has a built-in *Git* version control system, and is based on open-source code. The main disadvantage of using this platform is the limit of up to ten users per project when using the free version.

If you want to develop your code review tool and run it on a local server, then the authors recommend that you start with the *Gerrit* platform, run it on a *Linux* server and add all the features you may need locally. All analyzed tools have some shortcomings and none of them meet all the requirements for application within the course that was analyzed in this paper.

## ACKNOWLEDGMENT

This paper is the result of research on the project AVANTES funded by the Science Fund of the Republic of Serbia, within the Program for the development of projects in the field of artificial intelligence. The authors are grateful for the financial support.

## REFERENCES

[1] Y.-M. Zhu, “Software Reading Techniques: Twenty Techniques for More Effective Software Review and Inspection,” Solon: Apress, 2016.

[2] T. Winters, T. Manshreck and H. Wright, “Software Engineering at Google Lessons Learned from Programming Over Time,” O'Reilly Media Inc., 2020.

[3] F. A. Ackerman, L. S. buchwald and F. H. Lewski, “Software inspections: An effective verification process.,” *IEEE Software 6,,* vol. 6, no. 3, pp. 31-36, 1989.

[4] Y. K. Wong, “Modern Software Review: Techniques and Technologies,” IRM Press, 2006.

[5] V. Garousi, “Applying Peer Reviews in Software Engineering Education: An Experiment and Lessons Learned,” *IEEE Transactions on Education,* vol. 53, no. 2, pp. 182-193, 2010.

[6] T. D. Indriasari, A. Luxton-Reilly and P. Denny, “A review of peer code review in higher education,” *ACM Transactions on Computing Education (TOCE),* vol. 20, no. 3, pp. 1-25, 2020.

[7] P. C. Rigby and C. Bird, “Convergent Contemporary Software Peer Review Practices,” in *Proceedings of the 2013 9th Joint Meeting on Foundations of Software Engineering*, Saint Petersburg, 2013.

[8] N. Davila and I. Nunes, “A systematic literature review and taxonomy of modern code review,” *Journal of Systems and Software,* vol. 177, 2021.

[8] M. Greiler, “How Code Reviews work at Microsoft,” 22 January 2022. [Online]. Available: https://www.michaelagreiler.com/code-reviews-at-microsoft-how-to-code-review-at-a-large-software-company/.

[9] “BitBucket Code Review,” [Online]. Available: https://bitbucket.org/product/features/code-review. [Accessed: 03 2022].

[10] C. Staff, “CodeFlow: Improving the Code Review Process at Microsoft,” *Communications of the ACM,* vol. 62, no. 2, pp. 36-44, 2019.

[11] “Collaborator - Review Code Together,” [Online]. Available: https://smartbear.com/product/collaborator/overview/. [Accessed: 03 2022].

[12] “Google Mondrian - web-based code review and storage,” [Online]. Available: https://www.niallkennedy.com/blog/2006/11/google-mondrian.html. [Accessed: 11 2021].

[13] “Crucible,” [Online]. Available: https://www.atlassian.com/software/crucible. [Accessed: 3 2022].

[14] “Gerrit - Code Review tool,” [Online]. Available: https://www.gerritcodereview.com/. [Accessed: 12 2021].

[15] L. Milanesio, “Learning Gerrit Code Review,” Birmingham, UK: Packt Publishing Ltd., 2013.

[16] “GitHub - Code Review process,” [Online]. Available: https://github.com/features/code-review. [Accessed: 12 2021].

[17] “GitLab - Code Review Guidelines,” [Online]. Available: https://docs.gitlab.com/ee/development/code_review.html. [Accessed: 12 2021].

[18] “Space - Review Code,” [Online]. Available: https://www.jetbrains.com/help/space/review-code.html. [Accessed: 4 2022].

[19] “RhodeCode - Code Review,” [Online]. Available: https://rhodecode.com/features/productivity. [Accessed: 11 2021].

[20] “Review Board - code and document review tool,” [Online]. Available: https://www.reviewboard.org/. [Accessed: 12 2021].

[21] A. Bosu, M. Greiler and C. Bird, “Characteristics of Useful Code Reviews: An Empirical Study at Microsoft,” in *Proceedings of the International Conference on Mining Software Repositories*, Florence, Italy, 2015.

[22] E. Murphy-Hill, J. Dicker, M. Hodges, C. Egelman, C. Jaspan, L. Cheng, E. Kammer, B. Holtz, M. Jorde, A. Dolan and C. Green, “Engineering Impacts of Anonymous Author Code Review: A Field Experiment,” *IEEE Transactions on Software Engineering,* 2021.

[23] V. Balachandran, “Reducing human effort and improving quality in peer code reviews using automatic static analysis and reviewer recommendation,” in *2013 35th International Conference on Software Engineering (ICSE)*, 2013.

 ISBN 978-86-7466-930-3

# Automatsko snimanje amplitudno-frekventnih karakteristika primenom Arduino okruženja

Goran Dikić i Slobodan Drašković

***Apstrakt*—U radu je prikazan uređaj za automatsko snimanje amplitudno-frekventnih karakteristika elektronskih modula kao i sistema u celini. Uređaj je napravljen primenom gotovih modula za generisanje signala i merenje njihovog nivoa u radiofrekvencijskom opsegu. Proces snimanja, obrade signala kao i prikaz rezultata je automatizovan primenom Arduino NANO okruženja.**

***Ključne reči*—automatsko merenje; amplitudno-frekventne karakteristike; mikrokontroler.**

## I. UVOD

U postojećoj literaturi predložena su rešenja koja omogućavaju automatsko merenje amplitudno-frekventnih karakteristika metodom koja se zasniva na primeni modernog generatora funkcija i digitalnog osciloskopa [1] ili primenom LabVIEW integrisanog razvojnog okruženja uz obradu podataka na računaru [2].

U ovom radu je prikazan uređaj za automatsko snimanje amplitudno-frekventnih karakteristika elektronskih modula ili sistema u celini koji je nastao kao rezultat potrebe da se studentima osnovnih strukovnih studija elektrotehnike i računarstva prikaže mogućnost realizacije automatizovanih mernih sistema primenom mikrokontrolera. Imajući u vidu potrebe edukativnog procesa zahtevi u pogledu programske podrške i složenosti hardvera su optimizirani tako da se kompletna analiza kao i konačna demonstracija njegovog rada mogu realizovati tokom redovnog nastavnog procesa.

Polazeći od namene jasno je da, pored mikrokontrolera, uređaj mora da sadrži generator pobudnog signala, modul za merenje nivoa signala na izlazu ispitivanog modula ili sistema kao i da ima mogućnost prikaza amplitudno-frekventne karakteristike.

Pri odabiru hardvera pošlo se od činjenice da na tržištu postoji mnoštvo elektronskih modula koji su razvijeni za rad uz podršku mikrokontrolera. S obzirom da je pretpostavljen razvoj uređaja za snimanje amplitudno-frekventnih krakteristika u radiofrekvencijskom opsegu za merenje je odabran elektronski modul koji je realizovan primenom logaritamskog pojačavača AD8307 [3]. Jedan primer njegove primene u praksi opisan je u [4].

Goran Dikić – Akademija tehničko-umetničkih strukovnih studija Beograd, Odsek Visoka škola elektrotehnike i računarstva, Vojvode Stepe 283, 11000 Beograd, Srbija, (e-mail: goran.dikic@viser.edu.rs).

Slobodan Drašković – Akademija tehničko-umetničkih strukovnih studija Beograd, Odsek Visoka škola elektrotehnike i računarstva, Vojvode Stepe 283, 11000 Beograd, Srbija, (e-mail: slobodan.draskovic@gs.viser.edu.rs).

Za generisanje pobudnog signala odabran je modul zasnovan na primeni integrisanog kola Si5351 [5]. Primer programabilnog oscilatora na bazi ovog integrisanog kola opisan je u [6].

Imajući u vidu dostupnost i karakteristike programske podrške, posebno u pogledu mogućnosti prikaza grafičkih rezultata, za realizaciju upravljanja i obradu rezultata merenja odabrano je Arduino NANO razvojno okruženje [7].

## II. OPIS UREĐAJA

Logaritamski pojačavač AD8307 omogućava konverziju nivoa merenog naizmeničnog signala u odgovarajući nivo jednosmernog napona tako da se konačni rezultat može izraziti u decibelima. U konkretnom slučaju nagib merne karakteristike odgovara nivou 25 mV/dB. Pri tome je obezbeđena linearnost u opsegu ±1 dB. Dinamički opseg pojačavača je od -75 dBm do 17 dBm. Radni napon pojačavača je u opsegu od 2.7 V do 5.5 V. Izgled modula sa ugrađenim integrisanim kolom AD8307 i pripadajućim elektronskim komponentatma dat je na slici 1.

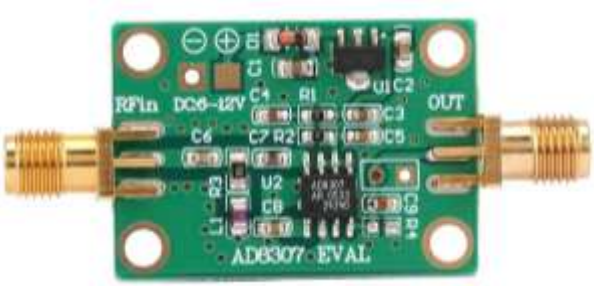


Sl. 1. Modul sa logaritamskim pojačavačem AD8307.

Modul za generisanje naizmeničnog pobudnog signala zasnovan na primeni integrisanog kola Si5351 može istovremeno da generiše tri signala na svojim izlazima CLK0, CLK1 i CLK2, ali se u konkretnom slučaju koristi samo CLK0. Generisani signal može imati frekvenciju u opsegu od 8 kHz do 160 MHz. Odabir radne frekvencije se vrši na osnovu kontrolnih signala koje šalje mikrokontroler. Pri tome se koristi I2C (*Inter-Integrated Circuit*) protokol. Integrisano kolo zahteva napajanje od 3.3 V. Modul je projektovan tako da se po potrebi može koristiti ovaj ili napon od 5 V. Izgled modula je prikazan na slici 2.

Rad celokupnog uređaja kontroliše mikrokontroler ATmega328P koji čini osnovu razvojnog sistema poznatog pod nazivom Arduino NANO [7]. Programska podrška koja je

 ISBN 978-86-7466-930-3

razvijena za rad sa ovim razvojnim sistemom pored razvoja i upisa programa u memoriju mikrokontrolera omogućava i upotrebu ekrana računara za grafički prikaz rezultata obrade tokom izvršenja konkretnog programa. Ova mogućnost je pojednostavila dizajn uređaja jer nije potrebno razvijati dodatnu programsku podršku da bi se omogućio prikaz amplitudno-frekventne karakteristike za ispitivani modul.

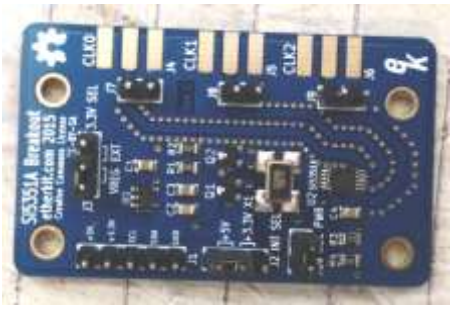

Sl. 2. Razvojni modul sa integrisanim kolom Si5351.

Uređaj funkcioniše tako što se u odgovarajućem programu, pre upisa u mikrokontroler, definišu početna i krajnja frekvencija na kojoj se realizuje snimanje. Veličina koraka, pri promeni frekvencije, određuje se automatski, tokom izvršenja programa, uvažavajući činjenicu da je grafička podrška dizajnirana za jednovremeni prikaz 500 tačaka na ekranu računara. Šematske veze između pojedinih modula su prikazane na slici 3.

Prenos kontrolnih signala SDA (*Serial Data and Address*) i SCL (*Serial Clock line*) ka modulu sa integrisanim kolom Si5351 ostvaruje se preko izlaza A4 i A5 Arduino NANO sistema. Na izlazu CLK0 generiše se povorka unipolarnih pravougaonih impulsa sa odnosom signal pauza u razmeri 1:1. Signal se dalje vodi preko kondenzatora od 100 nF tako da je na izlazu RF OUT potisnuta jednosmerna komponenta. Ulaz ispitivanog modula se spaja na RF OUT, a izlaz na RF IN koji zapravo predstavlja ulaz u modul sa logaritamskim pojačavačem AD8307. Izlaz ovog modula spojen je na priključak A6 Arduino NANO sistema koji predstavlja ulaz u desetobitni analogno-digitalni konvertor.

Rad uređaja, nakon upisa programa, započinje procesom definisanja neophodnih promenljivih, inicijalizacijom zahtevanih vrednosti za rad navedenih modula u skladu sa zahtevima opisanim u [3] i [5]. Realizacija i obrada svih merenja odvija se unutar programske petlje tako što se, u svakom koraku, najpre uspostavi zahtevana frekvencija signala na izlazu CLK0, a zatim sledi osam uzastopnih merenja nivoa signala na izlazu ispitivanog modula. Izmereni nivoi se obrađuju tako što se najpre saberu njihovi binarni ekvivalenti u vidu celobrojnih vrednosti. Nakon toga, dobijena vrednost se pomera unutar odgovarajućeg registra za tri mesta u desno, što odgovara deljenju sa 8. Ovim jednostavnim postupkom smanjuje se nivo šuma merenja. Dobijena vrednost se deli sa 1023 (desetobitni AD konvertor) i množi sa vrednošću referentnog napona. U ovom slučaju to je radni napon koji se dobija preko Mini-B USB (*Universal Serial Bus*) priključka Arduino NANO sistema, odnosno sa USB priključka računara. Konačna vrednost, *Vout*, koristi se za izračunavanje nivoa signala na izlazu ispitivanog modula, *PowerdB*, u decibelima:

$$PowerdB = Slope \cdot Vout - Intercept. \quad (1)$$

Pri tome *Slope* predstavlja nagib merne karakteristike, a *Intercept* vrednost presečne tačke na logaritamskoj osi [1].

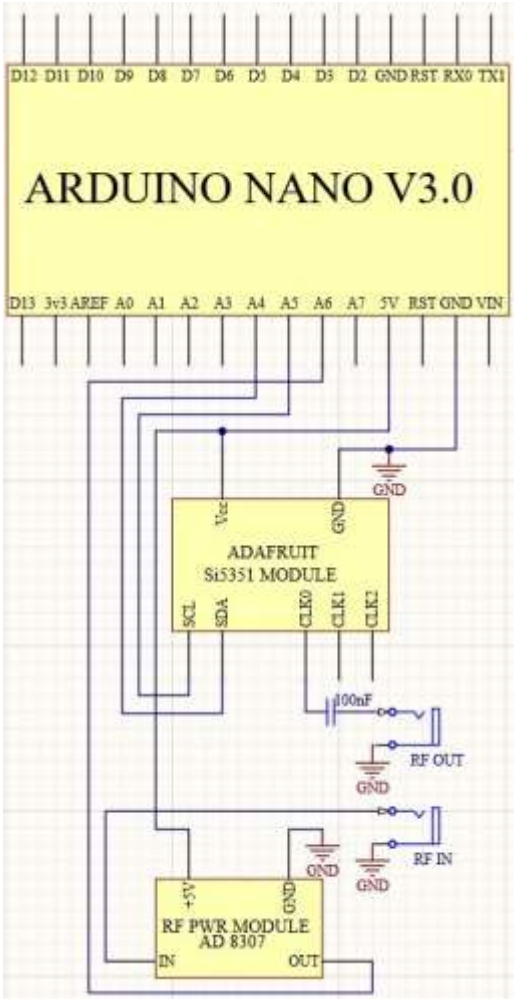


Sl. 3. Električna šema sistema za snimanje amplitudnih karakteritika.

Rad uređaja je testiran merenjem amplitudno-frekventne karakteristike dva elektronska modula. U prvom slučaju odabran je niskopropusni LC filtar čija šema je prikazana na slici 4. Gornja granična frekvencija ovog filra je 7.2 MHz, a ulazna i izlazna impedansa su 50 Ω.

U drugom slučaju izmerena je amplutno-frekventna karakteristika kristalnog filtra 14 E 2.48 koji je proizveden u Institutu "Mihajlo Pupin", u Beogradu. Njegova centralna frekvencija je 9.0 MHz, a širina propusnog opsega, na nivou slabljenja -6 dB, iznosi ±1.2 kHz. Talasnost u propusnom opsegu je 2 dB, a slabljenje pogonskog signala nije veće od 4 dB.

 ISBN 978-86-7466-930-3

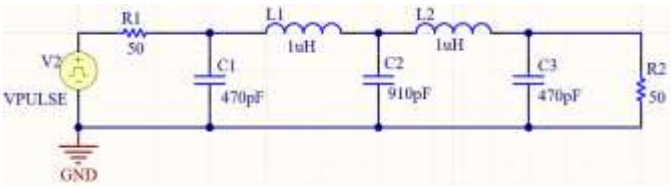


Sl. 4. Šematski prikaz niskopropusnog filtra sa graničnom frekvencijom 7,2 MHz.

Za merenje karakteristike kristalnog filtra od posebnog značaja je poznavanje njegove završne impedance koja iznosi 390 Ω u paraleli sa kapacitivnošću od 25 pF. Važnost ovog podatka proističe iz potrebe da se obezbedi adekvatno prilagođenje impedance kako na ulazu tako i na njegovom izlazu. U slučaju lošeg prilagođenja dobijaju se amplitudno-frekventne karakteristike koje zapravo ne odgovaraju stvarnim karakteristikama filtra (na primer velika talasnost u propusnom opsegu).

## III. REZULTATI EKSPERIMENATA

Prikupljanje eksperimentalnih rezultata započeto je analizom signala koji se dobija na izlazu CLK0 modula sa generatorm signala. Merenje je obavljeno na frekvenciji 10 MHz. Iz snimka koji se vidi na slici 5 uočava se postojanje preskoka kao i jednakost u pogledu trajanja poluperioda (odnos 1:1).

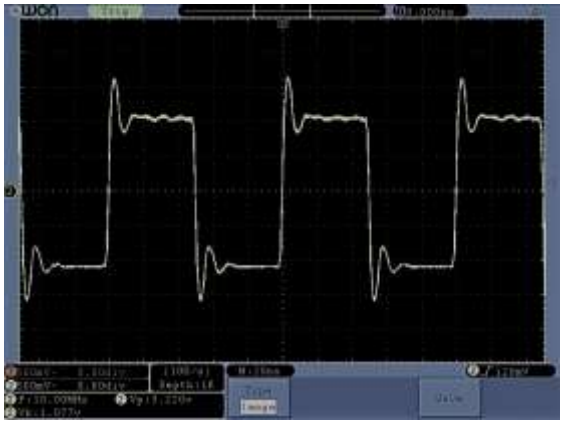

Sl. 5. Oblik signala na izlazu CLK0 (Si5351) pri frekvenciji 10 MHz.

Pravougli oblik signala nije poželjan pri merenju amplitudno-frekventnih kakrakteristika zbog činjenice da sadrži brojne harmonike, naročito kada se ima u vidu postojanje uskog i naglašenog preskoka. Sve ovo dovodi do toga da se istovremeno ostvaruje pobuda ispitivanog modula na više frekvencija pa to može uticati na kvalitet dobijenih rezultata. U svakom slučaju ovo treba imati u vidu.

U cilju sticanja uvida u nivo generisanog signala snimljena je karakteristika u opsegu 1-21 MHz, a dobijeni rezultati su prikazani na slici 6.

Snimanje je ostvareno direktnim povezivanjem izlaza RF OUT i ulaza RF IN. Uočeno je da nivo pobudnog signala neznatno opada sa porastom frekvencije i pokazuje izvesnu periodičnost u pogledu promena svog nivoa (pojava lokalnih ekstrema u pravilnim razmacima). Numeričke vrednosti na vertikalnoj osi dobijenog dijagrama predstavljaju nivo merenog signala u dBm. Pri tome numeričke vrednosti na horizontalnoj osi označavaju redni broj odbirka, a ne frekvenciju na kojoj je izvršeno testiranje. Ovo nije moguće menjati jer originalna programska podrška ne nudi mogućnost izbora vrednosti koje se koriste za označavanje na horizontalnoj osi. U slučaju "priliva" većeg broja podataka ceo dijagram se lagano pomera u levo tako da se na ekranu uvek može videti poslednjih 500 tačaka.

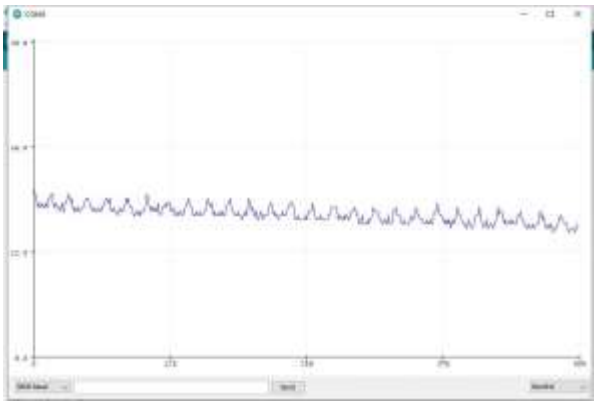

Sl. 6. Signal na izlazu Si5351 u opsegu od 1 MHz do 21 MHz.

### A. *Izmerena karakteristika niskopropusnog filtra*

Očekuje se da karakteristika ispitivanog niskopropusnog LC filtra ima ravan ili blago talasasti oblik u propusnom opsegu. Dobijeni rezultati su prikazani na slici 7.

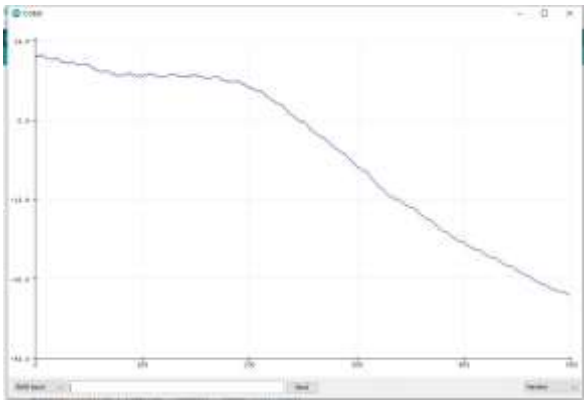

Sl. 7. Amplitudno-frekventna karakteristika niskopropusnog filra u opsegu od 1 MHz do 21 MHz.

Već je naglašeno da pobudni signal, zbog svog pravouglog oblika, sadrži mnoštvo harmonika. Svaki od njih, prolaskom kroz niskopropusni filtar učestvuje u formiranju nivoa izlaznog signala koji se meri. Porastom frekvencije pobudnog signala harmonici postaju sve udaljeniji u odnosu na njegovu osnovnu frekvenciju, odnosno sve dublje ulaze u područje gde niskopropusni filtar ostvaruje njihovo značajno slabljenje.


ISBN 978-86-7466-930-3

Ovo je razlog za pojavu slabljenja (opadajući trend amplitudno-frekventne karakteristike) u početnom delu frekvencijskog opsega, bez obzira na ujednačenost nivoa pobudnog signala na ovim frekvencijama.

Nakon dovoljno visoke frekvencije pobudnog signala doprinos viših harmonika, zbog slabljenja koje unosi niskoprpusni filtar, postaje zanemariv u odnosu na nivo osnovnog harmonika. Tada, karakteristika postaje približno ravna sve do prelomne frekvencije kada se, u skladu sa očekivanjem, uočava naglo slabljenje.

### *B. Izmerena karakteristika kristalnog filtra*

S obzirom da su izlazna impedansa generatora i ulazna impedansa modula sa logaritamskim pojačavačem 50 Ω filter je spojen preko odgovarajućih transformatora sa odnosima namotaja primar sekundar u razmeri 1:8 na ulazu i 8:1 na svom izlazu. Snimanje karakteristike za kristalni filtar ostvareno je promenom frekvencije pobudnog signala u opsegu od ±5 kHz u odnosu na centralnu frekvenciju filtra (9.0 MHz). Oblik karakteristike je prikazan na slici 8.

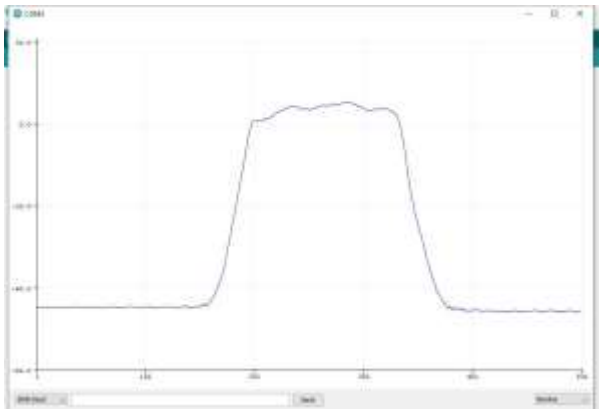

Sl. 8. Amplitudno-frekventna karakteristika kristalnog filtra 14 E 2.48 (centralna frekvencija 9.0 MHz).

Imajući u vidu oblik karakteristike (nagli pad izvan propusnog opsega) kao i činjenicu da je snimanje vršeno unutar frekvencijskog opsega širine 10 kHz može se proceniti da širina frekvencijskog opsega takođe odgovara kataloškim podacima (±1.2 kHz u odnosu na centralnu frekvenciju). Slabljenje izvan propusnog opsega je zapravo veće u odnosu na izmereno, ali se ne može registrovati zbog ograničene dinamike samog pojačavača

## IV. ZAKLJUČAK

Testiranjem su potvrđena očekivanja u pogledu problema koji mogu nastati zbog nesinusoidnog oblika pobudnog signala. Međutim, ukoliko se ima u vidu edukativna namena uređaja, predloženo rešenje nudi puno mogućnosti za povezivanje saznanja stečenih kroz izučavanje raznih predmeta i predstavlja dobru osnovu za dalji razvoj.

Za bolje rezultate trebalo bi najpre uvesti spoljni izvor referentnog napona od 2.5 V (priključak AREF na Arduino NANO modulu). Time bi se postigla bolja rezolucija, a samim tim i preciznija merenja. Bolji prikaz i očitavanje vrednosti na ekranu računara mogu se dobiti primenom MATLAB programskog okruženja (mogućnost definisanja logaritamske skale na horizontalnoj osi i ispis vrednosti koje bi označavale frekvenciju, a ne redni broj podatka). Pored toga, MATLAB omogućava dvosmernu komunikaciju tako da se zadavanje početne i krajnje frekvencije može definisati bez potrebe da se pri tome vrše promene u programu koji je upisan u mikrokontroler. Naravno ovo izlazi iz okvira optimizacije koja je usvojena na početku razvoja uređaja, a odnosi se na maksimalno iskorišćenje originalnog ARDUINO programskog okruženja.

Konačno, moguće je ostvariti promene u pogledu proširenja hardvera dodavanjem LCD ekrana i obrtnog enkodera sa tasterom. Na taj način bi se pored zadavanja početne i krajnje frekvencije, uz uvođenje ogovarjućih poruka na LCD ekranu mogle uvesti i dodatne mogućnosti kao, na primer, zahtev da se ponovi snimanje ili da se uspostavi režim rada koji omogućava kalibraciju kompletnog uređaja prilikom prvog puštanja u rad.

## LITERATURA


[1] L. Satish, Santosh C. Vora, "Amplitude Frequency Response Measurement: A Simple Technique", *IEEE Transactions on Education*, vol. 53, no. 3, pp. 365-371, Aug. 2010.

[2] Tian Tian, Wu Jian, Nie Li, "*Applied Mechanics and Materials*", *AMM*, vol. 475-476, pp.16-22, 2010.

[3] Low Cost, DC to 500 MHz, 92 dB Logarithmic Amplifier, https://www.analog.com/media/en/technical-documentation/data-sheets/ad8307.pdf, pristupljeno 17. 01. 2022.

[4] J.C. Cowles, "The Evolution of Integrated RF Power Measurement and Control", Proc. IEEE MELECON 2004, Dubrovnik, Croatia, pp. 131-134, May 12-15, 2004.

[5] Etherkit Si535, https://www.arduino.cc/reference/en/libraries/etherkit-si5351/, pristupljeno 27. 01. 2022.

[6] Janko Koležnik, Boštjan Vlaovič, "Programabilni kristalni oscilator visoke razločljivosti", *Elektrotehniški Vestnik*, vol. 84, no. 3, pp. 93-98, 2010.

[7] Arduino Nano, https://docs.arduino.cc/hardware/nano, pristupljeno 15. 12. 2022.


## ABSTRACT


In this paper the device for automatic recording of amplitude-frequency characteristics of electronic modules as well as whole system is presented. The device is designed applying readymade modules for signals generating and level measurement of them in radiofrequency band. Recording process, signal processing as well as presentation of results is automatized using Arduino NANO environment.


**Automatic recording of amplitude-frequency characteristics using Arduino environment**


Goran Dikić and Slobodan Drašković



ISBN 978-86-7466-930-3

# Zaštita prenosa paketskog telefonskog saobraćaja upotrebom tehnologije virtuelnih privatnih mreža

Mićo Živanović, Jovan Bajčetić, Ivan Tot

***Apstrakt*—Istraživanje predstavljeno u ovom radu prikazuje jednu realizaciju zaštite paketskog telefonskog saobraćaja primenom tehnologije virtuelnih privatnih mreža kroz konfiguraciju servera za prenos paketskog telefonskog saobraćaja i zaštićeni prenos uz primenu tehnologije virtuelnih privatnih mreža u tunel modu, primenom odgovarajućeg protokola za zaštitu tajnosti, autentifikaciju, zaštitu integriteta i razmenu kriptografskih ključeva. Izvršeno je snimanje i analiza saobraćaja primenom softvera Wireshark u zaštićenom i nezaštićenom prenosu. Prikazani rezultati omogućavaju lakše razumevanje kompleksnog procesa uspostave tunela upotrebom simulacionog softvera u edukaciji.**

***Ključne reči*—paketski telefonski saobraćaj; virtuelne privatne mreže; zaštićena komunikacija; kriptografski ključ.**

## I. Uvod

Stalan razvoj Interneta ima za posledicu da je Internet postao univerzalno sredstvo za komunikaciju. U toku razvoja, postavio se zahtev za bezbednošću prenošenih informacija koji se ogledao u obezbeđenju bezbednosnih servisa: autentifikacije, poverljivosti, neporecivosti i integriteta podataka [1]. Razvijeni su sistemi zaštite u tri ravni: upravljačkoj, kontrolnoj i ravni podataka. Za potrebe ovog rada biće razmotreni mehanizmi zaštite u ravni podataka koji se odnose na informacioni saobraćaj. Ravan podataka se štiti pomoću implementiranja pravila (bezbednosnih polisa) po kojima se informacioni sadržaj prenosi upotrebom mrežnih uređaja.

Jedna od tehnologija koja omogućava zaštitu prenosa podataka u ravni podataka je tehnologija virtuelnih privatnih mreža (VPN – Virtual Private Networks). Navedena tehnologija pruža sledeće mogućnosti umrežavanja:
– Intranet, umrežavanje geografski dislociranih objekata;
– Udaljeni pristup mobilnih korisnika (rad od kuće);
– Ekstranet, ograničeni pristup nekoj mreži iz drugih mreža (pristup poslovnih partnera korporativnom WAN-u) [2].

Za realizaciju virtuelne privatne mreže mogu se koristiti periferni korisnički uređaji (host, ruter ili svič), na lokaciji korisnika (CE – Customer Edge) i periferni mrežni uređaji provajdera (PE – Provider Edge).

Virtuelnu privatnu mrežu čini više udaljenih mreža koje su povezane preko Interneta. Zbog korišćenja zajedničkih resursa na Internetu, komunikacija među korisnicima virtuelne privatne mreže se mora zaštititi. Zaštita virtuelne privatne mreže se ostvaruje pomoću barijera koje implementiraju IPSec protokol u tunel modu [3].

VPN tunel je veza između dva PE rutera ili dva CE uređaja koji predstavljaju krajnje tačke tunela [2].

Prema IETF, IP VPN se mogu klasifikovati u zavisnosti od odgovornosti u pogledu upravljanja na:
– VPN kojima upravlja korisnik (Customer Provisioned VPN, CP VPN);
– VPN kojima upravlja provajder servisa (Provider Provisioned VPN, PP VPN) [2].

Prema lokaciji VPN opreme, PP VNP se mogu podeliti na:
– CE – bazirane, kod kojih su krajnje tačke VPN locirane kod korisnika;
– PE – bazirane, kod kojih su krajnje tačke VPN tunela locirane kod provajdera, na PE ruteru.

U zavisnosti od ponuđenog servisa, PE – bazirane VPN se dele na:
– PE – bazirane L2 VPN (koje pružaju servise OSI sloja 2);
– PE – bazirane L3 VPN (koje pružaju servise OSI sloja 3);
– CE – bazirane IP VPN pružaju samo servise OSI sloja 3.

Istovremeno sa razvojem bezbednosnih servisa razvijaju se arhitekture za pružanje različitih komunikacionih servisa koji koriste Internet protokol (telefonija, video, podaci, multimedijalni servisi). Prenos telefonije preko Interneta razvijao se postupno, pre svega zbog prethodno razvijenih sistema klasičnih javnih telefonskih mreža (PSTN) i digitalnih mreža sa integrisanim servisima (ISDN).

U cilju razvoja telefonije zasnovane na komutaciji paketa (VoIP telefonija), razvijene su grupe protokola za prenos VoIP telefonije i povezivanje VoIP telefonije sa telefonijom koja se prenosi u drugim sistemima prenosa (H.323 i SIP protokol) [4].

Prikaz istraživanja u ovom radu će se sastojati iz opisa načina realizacije zaštite informacije korišćenjem VPN tehnologije, a potom u jednoj realizaciji zaštite prenosa paketskog telefonskog saobraćaja upotrebom tehnologije

Mićo Živanović – Ministarstvo odbrane, Sektor za ljudske resurse, Nemanjina 15, 11000 Beograd, Srbija (e-mail: comiveza@yahoo.com).
Jovan Bajčetić – Vojna Akademija, Univerzitet odbrane u Beogradu, Veljka Lukića Kurjaka 33, 11042 Beograd, Srbija (e-mail: bajce05@gmail.com).
Ivan Tot – Vojna Akademija, Univerzitet odbrane u Beogradu, Veljka Lukića Kurjaka 33, 11042 Beograd, Srbija (e-mail: totivan@gmail.com).

 ISBN 978-86-7466-930-3

virtuelnih privatnih mreža, upotrebom IPSec protokola u tunel modu ka udaljenom korisniku, uz prikaz analize mrežnog saobraćaja korišćenjem programskog alata Wireshark.

## II. ZAŠTITA PODATAKA PRIMENOM TEHNOLOGIJE VIRTUELNIH PRIVATNIH MREŽA

Za prenos informacionog sadržaja preko Interneta neophodno je obezbediti zaštitu u prenosu. Čest je slučaj da kompanije koriste Internet kao okosnicu za povezivanje svojih filijala ili klijenata kako bi ostvarili prenos podataka za svoje potrebe. Iz navedenog razloga nameće se potreba za zaštitu prenošenog saobraćaja. U tu svrhu koriste se različite tehnologije, od kojih je jedna - tehnologija virtuelnih privatnih mreža. Za realizaciju virtuelnih privatnih mreža na raspolaganju je više tehnologija, zavisno od toga da li se VPN realizuje kao "oblast – oblast" (site–to–site) ili kao "udaljeni pristup" (remote access). U oba navedena slučaja najčešće se koristi IPSec (IP security) protokol.

IPSec protokol štiti pakete između dva uređaja u mreži [3].

Uređaji kojima se realizuje IPSec su: server, ruteri, korisnički računari ili specijalizovani hardver. IPsec pruža dve vrste zaštite: autentifikaciju i poverljivost.

Mehanizam autentifikacije osigurava da je primljeni paket zaista poslao onaj ko je u zaglavlju paketa naveden kao izvor i da se paket nije promenio tokom prenosa, dok mehanizam poverljivosti omogućava entitetima u komunikaciji da šifruju poruke kako bi sprečili nepozvana lica da dođu do sadržaja poruka [1]. Za šifrovanje podataka se koriste simetrični algoritmi (DES, 3DES, AES), što zahteva pouzdanu razmenu ključeva strana u komunikaciji i za tu svrhu se koriste protokoli za autentifikaciju (neki od protokola iz IETF (IKE - Internet Key Exchange) standarda) [3].

Razvoj bezbednosti u arhitekturi Interneta se odvijao postepeno u čemu je značajno mesto imala Radna grupa za inženjering Interneta (IETF – Internet Engineering Task Force). Sâmo uvođenje standarda je išlo postepeno. Prvi u nizu standard IETF koji se odnosio na bezbednost u arhitekturi Interneta bio je standard RFC 1636 (Request for Comments). Standard se odnosio na osnove bezbednosti Interneta (upotreba firewall – a, servis autentifikacije, privatnost i dr.) [5].

Da bi se adekvatno razumeo način formiranja VPN sesije in a pravi način predstavio prilikom edukacije, biće razmotreno nekoliko najvažnijih dokumenata IETF kojima su definisani režimi rada VPN, mehanizam autentifikacije, razmena kriptografskih ključeva i zaštita poverljivosti.

IPSec koristi dva protokola za bezbednost: AH (Authentication Header) i ESP (Encapsulating Security Payload). Zaglavlje autentifikacije (AH) je definisano specifikacijom RFC 4302 (IP Authentication Header), dok je ESP enkapsulirajuće bezbedno pakovanje (Encapsulating Security Payload) definisan specifikacijom RFC 4303. AH i ESP podržavaju dva režima rada: transportni režim i tunelovanje.

U transportnom režimu AH autentifikuje IP koristan sadržaj i odabrane delove IP zaglavlja, dok ESP šifruje i opciono autentifikuje IP koristan sadržaj. Tunelovanje vrši zaštitu celog IP paketa. Navedeno se postiže nakon dodavanja AH i ESP polja i tretiranja celog paketa kao korisnog sadržaja novog spoljnog IP paketa sa novim IP zaglavljem.

U režimu tunelovanja ESP šifruje i opciono autentifikuje ceo unutrašnji IP paket, uključujući unutrašnje IP zaglavlje, dok AH u režimu tunelovanja autentifikuje ceo unutrašnji IP paket i odabrane delove spoljnog IP zaglavlja [1].

Redosled postupaka sa paketima za rad ESP u transportnom i tunel režimu, je sledeći:

– U transport režimu blok podataka koji se sastoji od segmenta transportnog sloja sa dodatim ESP završnim blokom se šifruje, sa dodatim zaglavljem za autentifikaciju (opciono);

– U režimu tunelovanja, ESP se koristi za šifrovanje celog IP paketa, ESP zaglavlje ide ispred paketa i šifruje se paket zajedno sa ESP završnim blokom.

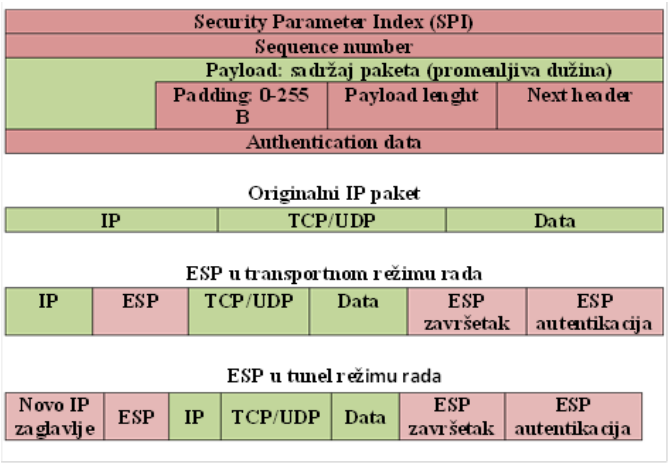


Sl. 1 Opseg ESP šifrovanja u transportnom i tunel modu [6]

Sl. 1 prikazuje format jednog ESP paketa. Indeks bezbednosnih parametara (SPI) definiše jednu bezbednosnu asocijaciju kojom se određuje algoritam šifrovanja i autentifikacije, ključevi, inicijalizacione vrednosti, životni vek ključeva i vezani parametri koji se koriste uz ESP. Broj sekvence je vrednost brojača paketa kojom se sprečava ponavljanje paketa. Sadržaj paketa je promenljive dužine i predstavlja segment transportnog sloja (transport režim) ili IP paket (tunel režim). U tunel modu, celom paketu se dodaje novo IP zaglavlje koje ima dovoljno informacija za rutiranje, ali ne i za analizu saobraćaja [6].

Važan deo IPSec koji se odnosi na upravljanje ključevima obuhvata određivanje i distribuciju ključeva. Dokumentom RFC 4301 definisane su dve vrste upravljanja ključevima:

– Ručno (administrator definiše sistem sopstvenim ključevima i ključevima drugih sistema sa kojima komunicira);

– Automatizovano (omogućava generisanje ključeva za bezbednosnu asocijaciju na zahtev koji je pogodan za velike sisteme sa rastućom konfiguracijom) [7].

Protokol koji se koristi za automatizovano upravljanje ključevima za IPSec je ISAKMP (Internet Security


ISBN 978-86-7466-930-3

Association and key Management Protocol) i definisan je dokumentom IETF RFC 2408. ISAKMP definiše procedure za kreiranje i upravljanje bezbednosnim asocijacijama, tehnike generisanja ključeva, ublažavanje pretnji (npr. od DDoS napada) [8].

ISAKMP ne nalaže konkretan algoritam za razmenu ključeva, već se sastoji od jednog skupa tipova poruka koje omogućavaju upotrebu raznovrsnih algoritama za razmenu ključeva.

Karakteristike IKE određivanja ključeva su:
– Osujećenje DDoS napada;
– Omogućava razmenu ključeva za pregovaranje oko grupe ključeva;
– Obezbeđuje od napada ponavljanjem korišćenjem jednokratnih brojeva;
– Omogućava razmenu javnih ključeva;
– Onemogućava napad tipa "čovek u sredini".

IKE potprotokol obezbeđuje dogovaranje protokola, algoritama i ključeva između učesnika u komunikaciji, proverava autentičnost učesnika koji učestvuju u postupku dogovaranja, omogućava razmenu podataka na osnovu kojih će se generisati ključevi i upravljati razmenom ključeva. IKE potprotokol obavlja se u dve faze [9].

U prvoj fazi dva učesnika uspostavljaju bezbedni komunikacioni kanal kojim će se obaviti dogovaranje bezbednosnih parametara i razmena ključeva. Dogovaranje parametara i razmena ključeva, odnosno uspostava bezbednosne asocijacije obavlja se u drugoj fazi. Za sprovođenje postupka koriste se tri načina razmene informacija, dva za prvu fazu i jedan za drugu fazu IKE potprotokola:
– Osnovni način;
– Agresivni način;
– Brzi način.

Osnovni način razmene informacija (engl. Main mode) koristi se u prvoj fazi IKE potprotokola i služi da bi se uspostavio bezbednosni komunikacioni kanal kojim će se obaviti razmena podataka potrebnih za kasniju komunikaciju AH ili ESP potprotokolima.

Agresivni način razmene, slično kao i osnovni, koristi se u prvoj fazi IKE potprotokola i služi za uspostavljanje sigurnog komunikacionog kanala za dogovor učesnika i ne obavlja se kroz bezbedni kanal. Agresivni način koristi samo tri poruke u razmeni i nešto je jednostavniji i brži od osnovnog načina, ali se dokazivanje identiteta ne vrši kroz bezbedan kanal.

Nakon uspostave bezbednog kanala primenom osnovnog ili agresivnog načina razmene, započinje druga faza IKE potprotokola. Druga faza koristi se brzim načinom razmene ključeva koja služi za dogovaranje bezbednosnih parametara komunikacije AH ili ESP potprotokolom i za razmenu tajnih simetričnih ključeva.

## III. JEDNA REALIZACIJA ZAŠTITE PAKETSKOG TELEFONSKOG SAOBRAĆAJA UPOTREBOM TEHNOLOGIJE VIRTUELNIH PRIVATNIH MREŽA

U uvodu rada predstavljena je podela VPN prema tome ko je odgovoran za uspostavu zaštićene komunikacije (provajder ili korisnik), kao i koja vrsta servisa se ostvaruje (sloj 2 ili 3 OSI referentnog modela). Predloženi model koje će u nastavku biti prikazan omogućava realizaciju jedne VPN koja bi predstavljala primer uspostave zaštite VoIP putem VPN za koju je „odgovoran" provajder, na OSI sloju 3 i da se primenom programskog alata „Wireshark" snimi i analizira ostvareni saobraćaj. Za navedene potrebe je uspostavljena mrežna topologija prikazana na Sl. 2.

Ruteri predstavljaju periferne rutere provajdera na kojima se vrši konfigurisanje VPN konekcije, po modelu "oblast – oblast". Na ruteru 1 su konfigurisani i uspostavljeni VPN, VoIP i DHCP server.

VPN server je konfigurisan sledećim parametrima:
– ISAKMP razmena kripto ključeva (policy 10);
– Kripto algoritam 3DES;
– Algoritam za autentifikaciju MD5 [10];
– Rad u tunel modu.

VoIP server je određen sledećim parametrima:
– Konekcija SIP protokolom;
– Kodek g711 ulaw.

Za razumevanje rada VoIP, ukratko će biti objašnjen prenos signalizacije i kontrola saobraćaja u VoIP prenosnim sistemima, u kojima se najčešće koriste H.323 i SIP protokoli.

H.323 preporuka je deo familije ITU-T preporuka sa zajedničkom oznakom H.32x koje se odnose na multimedijalne komunikacije preko različitih mreža. H.323 definiše protokole zadužene za usluge multimedijalnih komunikacija preko mreža zasnovanih na komutaciji paketa. H.323 se najčešće koristi kao signalizacioni i kontrolni protokol u VoIP i za video konferencije, a bio je prvi standard koji je koristio RTP protokol (Real-time Transfer Protocol) za konkretni prenos audio i video signala preko mreže.

H.323 je standard koji omogućava multimedijalnu komunikaciju preko različitih mreža (usko pojasne ISDN, širokopojasne B-ISDN, lokalne računarske mreže, mreže na bazi komutacije kola). Cilj je postizanje interoperabilnosti sa različitim mrežama za prenos multimedijalnih informacija, kroz upotrebu zajedničkih preporuka, procedura i poruka, kao i uvođenjem komponente mrežnog prolaza. H.323 standard predstavlja skup protokola namenjenih za obavljanje različitih funkcija u okviru H.323 sistema i to: audio kodere i dekodere, video kodere i dekodere, signaliziranje poziva, kontrola poziva, protokol prenosa u realnom vremenu (RTP), protokol kontrole prenosa u realnom vremenu (RTCP), registraciju, pristup i status i ostale protokole za prenos podataka u realnom vremenu [4].

 ISBN 978-86-7466-930-3

SIP je protokol za uspostavljanje, modifikaciju i raskidanje multimedijalnih sesija u paketskim mrežama. SIP u kombinaciji sa drugim protokolima se koristi za opis karakteristika sesije potencijalnim učesnicima [11]. SIP je delo IETF (Internet Engineering Task Force) i razvijen je kao mehanizam za uspostavljanje raznovrsnih sesija, a može se koristiti za unicast i multicast komunikaciju. SIP je peer-to-peer protokol, što znači da nije centralizovan, već je servisna inteligencija izmeštena prema krajevima mreže ka krajnjim korisnicima, kao kod računarskih mreža. U okviru SIP poruka se najčešće prenosi SDP (Session Description Protocol), mada standard ostavlja otvorenim i druge mogućnosti [12].

H.323 i SIP su dva konkurentska protokola za multimedijalne komunikacije na paketskim mrežama.

SIP se odlikuje sledećim prednostima:

– Fleksibilnost (omogućava korišćenje sa različitim transportnim i drugim protokolima);
– Arhitektura i osobine mu se prirodno uklapaju Internet okruženje, dok H.323 ima neke osobine protokola fiksne telefonije;
– Poseduje mnoga proširenja potrebna za različite sisteme ličnih komunikacija (prisutnost, instant poruke, posredno upravljanje pozivom) [13].

DHCP server je uspostavljen za opseg adresa koji obezbeđuje formiranje logički odvojenih mreža sa opsegom adresa 20.20.20.0 i 30.30.30.0 u različitim virtuelnim lokalnim mrežama. Prema mrežnoj topologiji formirane su dve LAN mreže u okviru kojih je izvršeno razdvajanje saobraćaja (telefonskog i podaci), uspostavom dve VLAN na OSI sloju L2, konfigurisanjem svičeva 1 i 2 (VLAN 20 i 30), dok je po jedan interfejs na svičevima konfigurisan kao trank interfejs [14]. Nakon provere konektivnosti, uspostavljen je paketski telefonski saobraćaj bez zaštite pomoću virtuelne privatne mreže i realizovano snimanje saobraćaja, upotrebom programskog alata "Wireshark". Rezultat i procesi analize nezaštićenog saobraćaja prikazani su u Tabeli 1. Uspostavljena je VPN sesija između dva rutera i realizovano snimanje saobraćaja u zaštićenom modu. Procesi u toku uspostave zaštićenog paketskog telefonskog saobraćaja prikazani su u Tabeli 2.

Za realizaciju mrežne topologije na slici 2 korišćena je sledeća mrežna oprema:

– CISCO 2900 ruter…….2 kom;
– CATALIST 3650 svič ……..2 kom;
– Računar sa ETH mrežnim interfejsom…. 2 kom;
– IP telefoni……..2 kom.

Procesi prikazani u Tabeli 1, a koji se odnose na uspostavu i održavanje nezaštićenog telefonskog saobraćaja prikazuju proces uspostavljanja prisutnosti uređaja u mreži i utvrđivanja mrežnih usluga (SSDP), uspostavu logičke topologije mreže i saobraćaja protokola za sprečavanje petlji (STP). Pozivanjem jednog korisnika od strane drugog korisnika ustanovljava se IP adresa pozvanog korisnika kroz broadcast upit od strane pozivajućeg korisnika (ARP proces). Kroz DNS proces se povezuju IP adresa i ime domena pozvanog korisnika. Istovremeno se šalje poruka radi utvrđivanja dostupnosti korisnika (ICMP poruka). U toku uspostave VoIP komunikacije šalje se "hello poruka" u OSPF procesu, radi konstruisanja putanje između dva rutera. Kroz SIP signalizaciju vrši se pozivanje jednog od strane drugog korisnika, nakon čega se ostvaruje TCP sesija kroz proces "trostrukog rukovanja". U sklopu SIP procesa razlikuju se faze (traying, ringing i OK), u kojima se mogu uočiti status procesa pozivanja, koji se na kraju završava uspešnom uspostavom komunikacije. Ceo proces je praćen slanjem kontrolnih TCP poruka (ACK), kojima se određuje broj bajtova koji se može poslati pre dobijanja sledeće dozvole za slanje, kao i slanjem poruka kojima se vrši sinhronizacija uspostave TCP sesije (SYN). Poseban segment kontrole komunikacije predstavlja kontrola konektivnosti na L2 nivou (LOOP). Dalji proces komuniciranja je praćen razmenom paketa u realnom vremenu (RTP) koji nose govorni informacioni sadržaj.

Procesi prikazani u Tabeli 2, a koji se odnose na uspostavu i održavanje zaštićenog telefonskog saobraćaja, pored na početku navedenih procesa u nezaštićenom prenosu, sadrži proces razmene kripto ključeva u procesu uspostave IPSec tunela (ISAKMP). Specifično za proces prenosa u zaštićenom modu je uspostavljen trank između dva sviča na kojima su konfigurisane dve VLAN (DTP).

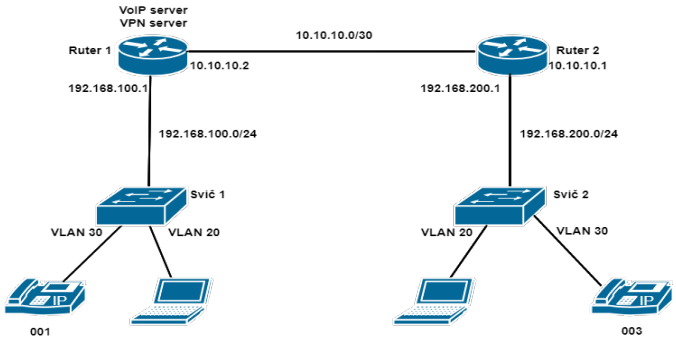


Sl. 2 Mrežna topologija za potrebe jedne realizacije zaštite paketskog telefonskog saobraćaja upotrebom tehnologije virtuelnih privatnih mreža

Prikazana realizacija mrežne topologije, snimanje i analiza mrežnog saobraćaja omogućava detaljno razumevanje uspostave VPN tunela, uz upotrebu simulacionog softvera, kao i praćenje procesa razmene informacionog sadržaja u realnom vremenu. Tokom procesa prenosa informacionog sadržaja u realnom vremenu, periodično se uočavaju procesi uspostavljanja prisutnosti uređaja u mreži (SSDP), obaveštavanja o nedostupnosti uređaja u slučaju prekida konektivnosti (ICMP poruke) i razmena "hello" poruka u OSPF procesu. Navedena realizacija stoga omogućava potpun uvid u sve procese u toku prenosa paketskog telefonskog saobraćaja, što može poslužiti u edukaciji i o procesima prenosa multimedijalnih informacionih sadržaja.


ISBN 978-86-7466-930-3

TABELA I
POZIV UČESNIKA 001 KA UČESNIKU 003 BEZ VPN ZAŠTITE

| R.br. | Vreme [s] | Izvorišna adresa | Odredišna adresa | Protokol | Veličina [B] |
|---|---|---|---|---|---|
| 1. | 0,00 | Cisco_e1:aa:81 | Spanning_tree | STP | 60 |
| 2. | 0,17 | Fe80:e010:c683:5106:f3e8 | Ff02::c | SSDP | 208 |
| 3. | 1,99 | Cisco_e1:aa:81 | Spanning_tree | STP | 60 |
| 4. | 2,73 | ASUSTEkC_9d:86:8a | Cisco_00:e3:e1 | ARP | 42 |
| 5. | 2,74 | Cisco_00:e3:e1 | ASUSTEkC_9d:86:8a | ARP | 60 |
| 6. | 3,433 | 40.40.40.3 | 192.168.100.1 | DNS | 75 |
| 7. | 3,434 | 40.40.40.1 | 40.40.40.3 | ICMP | 70 |
| 8. | 4,00 | Cisco_e1:aa:81 | Spanning_tree | STP | 60 |
| 9. | 4,18 | Fe80:e010:c683:5106:f3e8 | Ff02::c | SSDP | 208 |
| 10. | 5,32 | 40.40.40.1 | 224.0.0.5 | OSPF | 90 |
| 11. | 5,99 | Cisco_e1:aa:81 | Spanning_tree | STP | 60 |
| 12. | 6,56 | 40.40.40.3 | 192.168.100.1 | DNS | 75 |
| 13. | 6,561 | 40.40.40.1 | 40.40.40.3 | ICMP | 70 |
| 14. | 6,83 | 40.40.40.3 | 30.30.30.1 | SIP/SDP | 922 |
| 15. | 7,16 | 40.40.40.3 | 30.30.30.1 | TCP | 590 |
| 16. | 7,16 | 30.30.30.1 | 40.40.40.3 | TCP | 60 |
| 17. | 7,16 | 40.40.40.3 | 30.30.30.1 | TCP | 386 |
| 18. | 7,16 | 30.30.30.1 | 40.40.40.3 | SIP | 418 |
| 19. | 7,18 | Fe80:e010:c683:5106:f3e8 | Ff02::c | SSDP | 208 |
| 20. | 7,36 | 40.40.40.3 | 30.30.30.1 | TCP | 54 |
| 21. | 7,99 | Cisco_e1:aa:81 | Spanning_tree | STP | 60 |
| 22. | 8,30 | 40.40.40.3 | 30.30.30.1 | TCP | 58 |
| 23. | 8,32 | Cisco_e1:aa:81 | Cisco_e1:aa:81 | LOOP | 60 |
| 24. | 8,37 | 30.30.30.1 | 40.40.40.3 | TCP | 590 |
| 25. | 8,37 | 30.30.30.1 | 40.40.40.3 | SIP | 124 |
| 26. | 8,37 | 40.40.40.3 | 30.30.30.1 | TCP | 54 |
| 27. | 9,99 | Cisco_e1:aa:81 | Spanning_tree | STP | 60 |
| 28. | 10,18 | Fe80:e010:c683:5106:f3e8 | Ff02::c | SSDP | 208 |
| 29. | 11,97 | 10.10.10.2 | 40.40.40.3 | RTP | 214 |
| 30. | 11,97 | 30.30.30.1 | 40.40.40.3 | TCP | 590 |
| 31. | 11,97 | 30.30.30.1 | 40.40.40.3 | SIP/SDP | 424 |
| 32. | 11,97 | 40.40.40.3 | 30.30.30.1 | TCP | 54 |
| 33. | 11,98 | 40.40.40.3 | 10.10.10.2 | RTP | 55 |
| 34. | 11,98 | 40.40.40.3 | 10.10.10.2 | TCP | 66 |
| 35. | 11,98 | 10.10.10.2 | 40.40.40.3 | TCP | 60 |
| 36. | 11,98 | 40.40.40.3 | 10.10.10.2 | TCP | 54 |
| 37. | 11,98 | 40.40.40.3 | 10.10.10.2 | SIP | 459 |
| 38. | 11,98 | 10.10.10.2 | 40.40.40.3 | TCP | 60 |
| 39. | 11,99 | 10.10.10.2 | 40.40.40.3 | RTP | 214 |
| 40. | 11,99 | Cisco_e1:aa:81 | Spanning_tree | STP | 60 |
| 41. | 12,01 | 10.10.10.2 | 40.40.40.3 | RTP | 214 |
| 42. | 12,03 | 10.10.10.2 | 40.40.40.3 | RTP | 214 |
| 43. | 12,25 | 40.40.40.3 | 10.10.10.2 | RTP | 214 |

TABELA II
POZIV UČESNIKA 001 KA UČESNIKU 003 SA VPN ZAŠTITOM

| R.br. | Vreme [s] | Izvorišna adresa | Odredišna adresa | Protokol | Veličina [B] |
|---|---|---|---|---|---|
| 1. | 0,00 | Fe80:e010:c683:5106:f3e8 | Ff02::c | SSDP | 208 |
| 2. | 0,03 | Cisco_e1:aa:81 | Spanning_tree | STP | 60 |
| 3. | 0,73 | 40.40.40.3 | 10.10.10.2 | ISAKMP | 126 |
| 4. | 0,73 | 10.10.10.2 | 40.40.40.3 | ISAKMP | 126 |
| 5. | 2,03 | Cisco_e1:aa:81 | Spanning_tree | STP | 60 |
| 6. | 4,00 | Fe80:e010:c683:5106:f3e8 | Ff02::c | SSDP | 208 |
| 7. | 4,03 | Cisco_e1:aa:81 | Spanning_tree | STP | 60 |
| 8. | 6,03 | Cisco_e1:aa:81 | Spanning_tree | STP | 60 |
| 9. | 6,88 | Fe80:e010:c683:5106:f3e8 | Ff02::1:2 | DHCPv6 | 149 |
| 10. | 7,00 | Fe80:e010:c683:5106:f3e8 | Ff02::c | SSDP | 208 |
| 11. | 8,03 | Cisco_e1:aa:81 | Spanning_tree | STP | 60 |
| 12. | 8,67 | Cisco_e1:aa:81 | Cisco_e1:aa:81 | LOOP | 60 |
| 13. | 10,00 | Fe80:e010:c683:5106:f3e8 | Ff02::c | SSDP | 208 |
| 14. | 10,03 | Cisco_e1:aa:81 | Spanning_tree | STP | 60 |
| 15. | 10,88 | Fe80:e010:c683:5106:f3e8 | Ff02::1:2 | DHCPv6 | 154 |
| 16. | 12,03 | Cisco_e1:aa:81 | Spanning_tree | STP | 60 |
| 17. | 13,30 | Cisco_e1:aa:81 | CDP/VTP/DTP | DTP | 60 |
| 18. | 13,30 | Cisco_e1:aa:81 | CDP/VTP/DTP | DTP | 90 |
| 19. | 14,00 | Fe80:e010:c683:5106:f3e8 | Ff02::c | SSDP | 208 |
| 20. | 14,03 | Cisco_e1:aa:81 | Spanning_tree | STP | 60 |
| 21. | 16,03 | Cisco_e1:aa:81 | Spanning_tree | STP | 60 |
| 22. | 17,00 | Fe80:e010:c683:5106:f3e8 | Ff02::c | SSDP | 208 |
| 23. | 18,03 | Cisco_e1:aa:81 | Spanning_tree | STP | 60 |
| 24. | 18,67 | Cisco_e1:aa:81 | Cisco_e1:aa:81 | LOOP | 60 |
| 25. | 19,32 | Cisco_e1:aa:81 | ASUSTEkC_9d:86:8a | ARP | 60 |
| 26. | 19,32 | ASUSTEkC_9d:86:8a | Cisco_e1:aa:81 | ARP | 42 |
| 27. | 20,00 | Fe80:e010:c683:5106:f3e8 | Ff02::c | SSDP | 208 |
| 28. | 20,03 | Cisco_e1:aa:81 | Spanning_tree | STP | 60 |
| 29. | 20,51 | 40.40.40.3 | 10.10.10.2 | TCP | 66 |
| 30. | 22,03 | Cisco_e1:aa:81 | Spanning_tree | STP | 60 |
| 31. | 23,51 | 40.40.40.3 | 10.10.10.2 | TCP | 66 |
| 32. | 24,00 | Fe80:e010:c683:5106:f3e8 | Ff02::c | SSDP | 208 |
| 33. | 24,03 | Cisco_e1:aa:81 | Spanning_tree | STP | 60 |
| 34. | 25,22 | ASUSTEkC_9d:86:8a | Cisco_00:e3:e1 | ARP | 42 |
| 35. | 25,23 | Cisco_00:e3:e1 | ASUSTEkC_9d:86:8a | ARP | 60 |
| 36. | 26,03 | Cisco_e1:aa:81 | Spanning_tree | STP | 60 |
| 37. | 27,00 | Fe80:e010:c683:5106:f3e8 | Ff02::c | SSDP | 208 |
| 38. | 27,50 | 40.40.40.3 | 10.10.10.2 | SIP/SDP | 1095 |
| 39. | 27,50 | 10.10.10.2 | 40.40.40.3 | SIP | 284 |
| 40. | 28,30 | 40.40.40.3 | 10.10.10.2 | SIP | 831 |
| 41. | 30,25 | 10.10.10.2 | 40.40.40.3 | RTP | 214 |
| 42. | 31,50 | 40.40.40.3 | 10.10.10.2 | RTP | 214 |
| 43. | 31,75 | 10.10.10.2 | 40.40.40.3 | RTP | 214 |


ISBN 978-86-7466-930-3

## IV. Zaključak

Rezultat jedne realizacije zaštite paketskog telefonskog saobraćaja, predstavljen u ovom radu prikazuje da uspostava i održavanje VPN tunela kao načina zaštite paketskog telefonskog saobraćaja podrazumeva primenu niza protokola, specifično dizajniranih za prenos informacionih sadržaja u realnom vremenu (SIP, SSDP, RTP) kao i protokola za obezbeđenje zaštite u toku prenosa (ISAKMP, IPSec). Specifično za predstavljenu realizaciju predstavlja upotreba linka za prenos različitih servisa i time korišćenje protokola kojima se omogućava konvergencija servisa u prenosu (DTP, SSDP).

## Literatura

[1] W.Stallings, Osnove bezbednosti mreža: Aplikacije i standardi, Računarski fakultet, Beograd, 2014.
[2] M.Stojanović, V.Aćimović-Raspopović, Savremene IP mreže: Arhitekture, tehnologije i protokoli, Akademska misao, Beograd, 2012.
[3] A.Smiljanić, Osnove i primena Interneta, Elektrotehnički fakultet Univerziteta u Beogradu, Beograd, 2015.
[4] D.Nemec, D.Vukobratović, V.Crnojević, Č.Stefanović, Tehnologija VoIP sistema, Fakultet tehničkih nauka, Novi Sad, 2007.
[5] Security in the Internet Architecture, RFC: 1636, jun 1994, https://datatracker.ietf.org/doc/html/rfc1636
[6] IP Encapsulating Security Payload, RFC: 4303, decembar 2005, https://datatracker.ietf.org/doc/html/rfc4303
[7] Security Architecture for the Internet protocol, RFC: 4301, decembar 2005, https://datatracker.ietf.org/doc/html/rfc4301
[8] Internet Security Association and key Management Protocol, RFC: 2408, novembar 1998, https://datatracker.ietf.org/doc/html/rfc2408
[9] Internet Key Exchange Protocol Version 2 (IKEv2), RFC: 5996, septembar 2010, https://datatracker.ietf.org/doc/html/rfc5996
[10] B.Scheiner, Primenjena kriptografija, Mikro knjiga, Beograd, 2007.
[11] R.Swale, D.Collins, Carrier Grade Voice Over IP, McGraw Hill Professional, 2004.
[12] M.Jevtović, Komunikacioni protokoli Interneta, Akademska misao, Beograd, 2011.
[13] I.Bašičević, "Prilog razvoju arhitekture za obezbeđivanje usluga u računarskim mrežama nove generacije", doktorska disertacija, Fakultet tehničkih nauka, Novi Sad, 2008.
[14] S.Gajin , Principi konfigurisanja računarskih mreža, Akademska misao, Beograd, 2018.

## Abstract

The research presented in this paper addresses an example of how to execute packet telephone traffic protection using virtual private network technology through configuring servers for packet telephone traffic and also demonstrates the secure transfer with the use of virtual private network technology in tunnel mode by applying the appropriate protocols for privacy protection, authentication, integrity protection and crypto key exchange. Traffic recording and analysis has been performed using the Wireshark software in both secure and non-secure transfer. The results obtained can help better understand the complex process of setting up a tunnel through the use of simulation software in education.

## Packet Telephone Traffic Transfer Protection Using Technology of Virtual Private Networks

Mićo Živanović, Jovan Bajčetić, Ivan Tot

 ISBN 978-86-7466-930-3

# ROBOTICS AND FLEXIBLE AUTOMATION
# /
# РОБОТИКА И ФЛЕКСИБИЛНА АУТОМАТИЗАЦИЈА
# (ROI/PO)

ISBN 978-86-7466-930-3

# Mobile robot decision-making system based on deep machine learning

Aleksandar Jokić, Milica Petrović and Zoran Miljković

***Abstract*— ne of the major aspects of Industry 4. is enabling the manufacturing entities to operate in the dynamical systems autonomously. Therefore, to be autonomous, manufacturing entities need to have sensors to perceive their environment and utilize that information to ma e decisions regarding their actions. aving that in mind, in this paper, the authors propose a mobile robot decision-ma ing system based on the integration of visual data and mobile robot pose. obile robot pose (current position and orientation) is integrated with two images gathered by two cameras and utilized to predict the possibility of gripping the part to be manufactured. A decision-ma ing system is created by utilizing the deep learning model esnet1 with an additional input for the mobile robot pose. The model is trained end-to-end and e perimental evaluation is performed by using the mobile robot ACI ( obot with Artificial Intelligence based C gnition).**

***Index Terms*—Decision-ma ing system, mobile robots, deep learning.**

## I. Introduction

Enabling mobile robots to operate in the manufacturing environment autonomously represents one of the fundamental requirements regarding Industry 4.0 concepts [1]. To fulfill this requirement, mobile robots need to localize themselves within the environment and use sensors to perceive the current state of the manufacturing system. In this paper, the authors propose to include both visual information and mobile robot pose in the make-decision process regarding future mobile robot actions. Mobile robot pose (Fig. 1), represented by position (x and y) and orientation (θ), is combined with image data to make a decision regarding the probability of successful gripping of the manufacturing part. The mobile robot's task is to move relatively close to the machine (marked with red color in Fig. 1) and decide if the current pose is adequate for a part (presented with a blue color in Fig. 1) picking process.

Aleksandar Jokić, teaching assistant, University of Belgrade - Faculty of Mechanical Engineering, Department of Production Engineering, Laboratory for industrial robotics and artificial intelligence (ROBOTICS&AI), Kraljice Marije 16, 11120 Belgrade 35, The Republic of Serbia (ajokic@mas.bg.ac.rs).

Dr. Milica Petrović, Associate Professor, University of Belgrade - Faculty of Mechanical Engineering, Department of Production Engineering, Laboratory for industrial robotics and artificial intelligence (ROBOTICS&AI), Kraljice Marije 16, 11120 Belgrade 35, The Republic of Serbia (mmpetrovic@mas.bg.ac.rs).

Dr. Zoran Miljković, Full Professor, University of Belgrade - Faculty of Mechanical Engineering, Department of Production Engineering, Laboratory for industrial robotics and artificial intelligence (ROBOTICS&AI), Kraljice Marije 16, 11120 Belgrade 35, The Republic of Serbia (zmiljkovic@mas.bg.ac.rs).

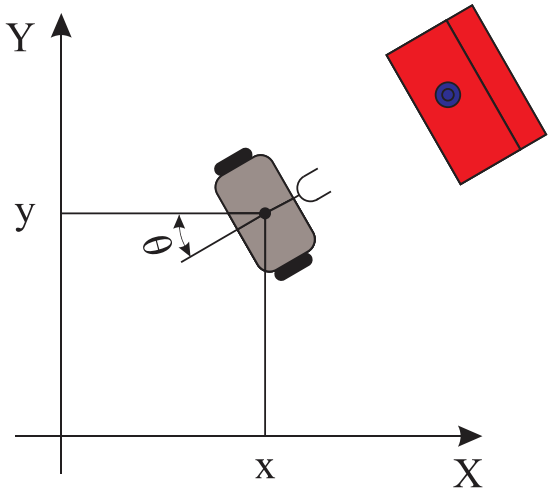


Fig. 1. Mobile robot in the environment with machine tool and part.

The related work regarding the mobile robot decision-making system is as follows. The determination of the next-best-view for environment exploring and mapping algorithm is proposed in [2]. The multi-objective decision criterion for a mobile robot with a 360° laser scanning sensor is proposed and evaluated in simulation. The proposed strategy showed superior performance compared to the other two strategies from the literature. The reinforcement learning approach for developing a mobile robot decision-making system is proposed in [3]. The mobile robot was equipped with an RGBD camera utilized to detect the obstacles. The learning approach was divided into three subtasks (i) reaching the target pose as fast as possible, (ii) obstacle avoidance, and (iii) not losing the target. According to the learned policy, a mobile robot can decide between five actions to reach the desired goal. The proposed system is verified within four simulation studies, and the results show that the proposed system achieves better results compared to the three state-of-the-art strategies.

The learning approach used for mobile robot navigation in both unknown and known environments is proposed in [4]. The model utilized for the mobile robot decision-making system is based on Developmental Networks. An incremental learning paradigm is implemented, allowing mobile robots to learn as they move in the new environment. Experimental results show that the proposed system enables mobile robots to utilize already learned cognitive functions in new environments.

A mobile robot decision-making system for outdoor path planning is proposed in [5]. The mobile robot utilizes the

 ISBN 978-86-7466-930-3

information gathered by the lidar sensor to obtain the optimal path in the uneven and obstacle-rich hill environment. In the offline stage, the robot learns in simulation the correlation of a good path with lidar data and utilizes that information in the online stage. The simulation results show the applicability of the proposed methodology for the path selection process.

Different from other approaches, in this paper, the authors propose the end-to-end trainable deep learning model capable of integrating image information and current mobile robot pose to predict the accuracy of the gripping process.

## II. THE DEEP LEARNING-BASED DECISION-MAKING SYSTEM

The everlasting challenge within the deep learning-based robotic research domain is developing an adequate methodology for adapting heterogeneous data into deep learning models [6]. Examples of such data are different sensor measurements with uncertainty, a priory logical conclusions, or a mobile robot pose.

In this paper, the authors present deep learning-based decision-making system developed by modifying Resnet18 architecture [7]. The first input in the Resnet model is an image created by combining images generated by two mobile robot cameras. Images are stacked on top of each other to produce an image with the same width and height dimensions. Afterward, the additional vector input is added to the network utilized to represent the mobile robot pose (1):

$$= \begin{bmatrix} & y & \theta \end{bmatrix}^{\mathrm{T}}. \tag{1}$$

The change in mobile robot pose is calculated with (2):

$$\begin{bmatrix} \dot{} \\ \dot{y} \\ \dot{\theta} \end{bmatrix} = \begin{bmatrix} \cos\theta & 0 \\ \sin\theta & 0 \\ 0 & 1 \end{bmatrix} \begin{bmatrix} \omega \end{bmatrix}, \tag{2}$$

where v represents mobile robot translation velocity, and ω is mobile robot angular velocity.

The deep neural network architecture is presented in Fig. 2. Additional input is represented as one pixel in the image. When the feature maps are flattened just before the classification layer, the unchanged value of the mobile robot pose (from the input layer) is concatenated with the rest of the features and utilized in the classification process. The utilized Resnet18 model is created with basic and bottleneck blocks of layers with skip connections after each one; details regarding the implementation of this model can be found in [8].

Dataset for mobile robot training is generated as follows. The mobile robot is positioned to the predefined pose in the laboratory model of the manufacturing environment. Afterward, the mobile robot is set in motion until it reaches the pose close to the machine. The achieved pose is measured according to the data gathered by two wheel encoders. Then, the achieved pose is saved in the text document and two images are generated, combined, and saved. The gripping procedure is initiated, and if the mobile robot manages to grip the part, all the saved data is moved to the "successful grip" category and vice versa.

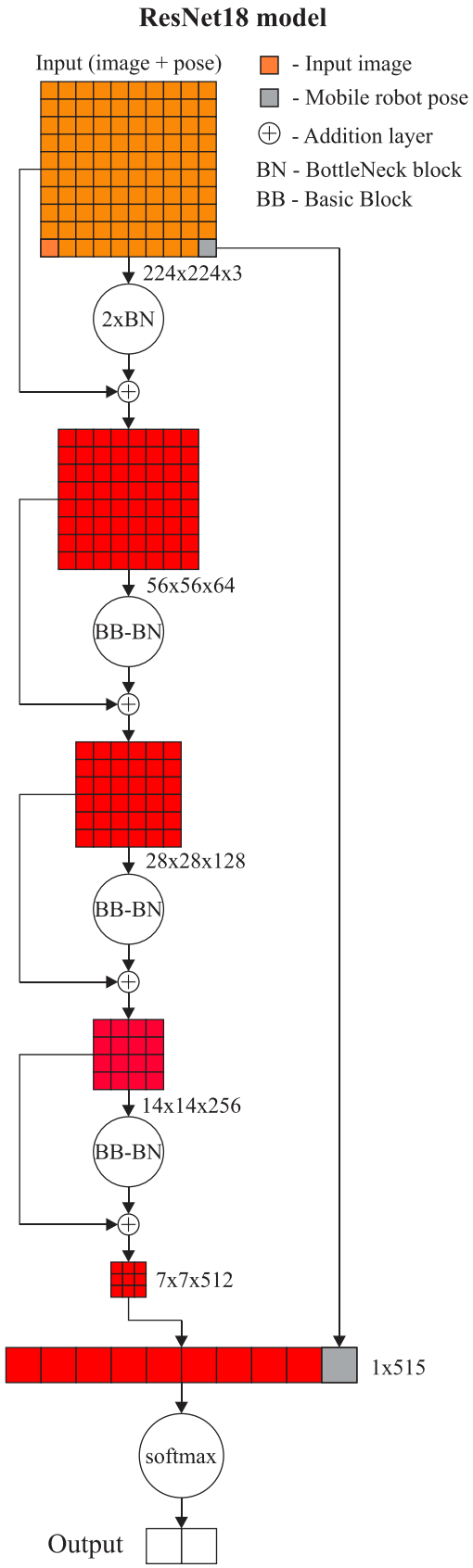


Fig. 2. Graphical representation of the proposed CNN model.

After the dataset is acquired, the training process begins. This problem belongs to the category of the binary classification process, with two outcomes "successful grip"


ISBN 978-86-7466-930-3

and "unsuccessful grip". The classification is performed with softmax fitness function (3), and the loss function is defined with (4):

$$s_i = \frac{e^{y_i}}{\sum_{i=1}^{N} e^{y_i}} \tag{3}$$

$$\ell(\mathbf{s},\mathbf{c}) = -\sum_{i}^{N} c_i \log(s_i) \tag{4}$$

Where **y** represents the output of CNN model, *i* represents the *i*-th element of the output vector, *N* is a number of classes, **c** represents one-hot class vector.

The training is performed by stochastic gradient descent with momentum training algorithm with a batch size of one. Initial experiments are performed to determine the best training parameters for Resnet18 model. The learning rate varies from 0.0001 to 0.001, and the momentum is set to range from 0.7 to 0.9. The best performance on the training set is achieved with a learning rate of 0.0005 and momentum of 0.9.

## III. EXPERIMENTAL RESULTS

The experimental evaluation is done by using the mobile robot RAICO (Robot with Artificial Intelligence based COgnition). RAICO is set to an initial pose in the laboratory model of the manufacturing system, and the movement command is activated. The pose RAICO achieves is relatively close to the machine where the part needs to be picked up; however, the pose is never the same due to slight differences in both the initial pose and movement process. Afterward, the final pose is calculated and integrated into the combined image generated using images from the right and left cameras. Then, the whole input is passed through the CNN network. The output represents the class (i.e., *grip* or no_*grip*) and the confidence in the class prediction. The gripping process is activated, and the outcome (successful or unsuccessful grip) is recorded. The experiment is repeated 10 times, and the results can be found in Table I.

TABLE I
THE EXPERIMENTAL RESULTS OF THE DECISION-MAKING MODEL

| Exp. No. | Prediction | Confidence [%] | Successful gripping? |
|---|---|---|---|
| 1 | Grip | 76 | No |
| 2 | Grip | 93 | Yes |
| 3 | No_grip | 83 | No |
| 4 | No_grip | 84 | No |
| 5 | Grip | 95 | Yes |
| 6 | No_grip | 85 | No |
| 7 | Grip | 85 | No |
| 8 | No_grip | 83 | No |
| 9 | Grip | 80 | No |
| 10 | Grip | 97 | Yes |

As shown in Table I, the mobile robot decision-making system adequately predicts the outcome of the gripping process in 70% of cases. Moreover, in all the cases where the prediction accuracy of the deep learning model for successful gripping is over 93%, the mobile robot actually manages to grip the part. Therefore, the high prediction confidence is highly correlated to the gripping success. Images generated by a mobile robot with prediction accuracy are shown in Fig. 3.

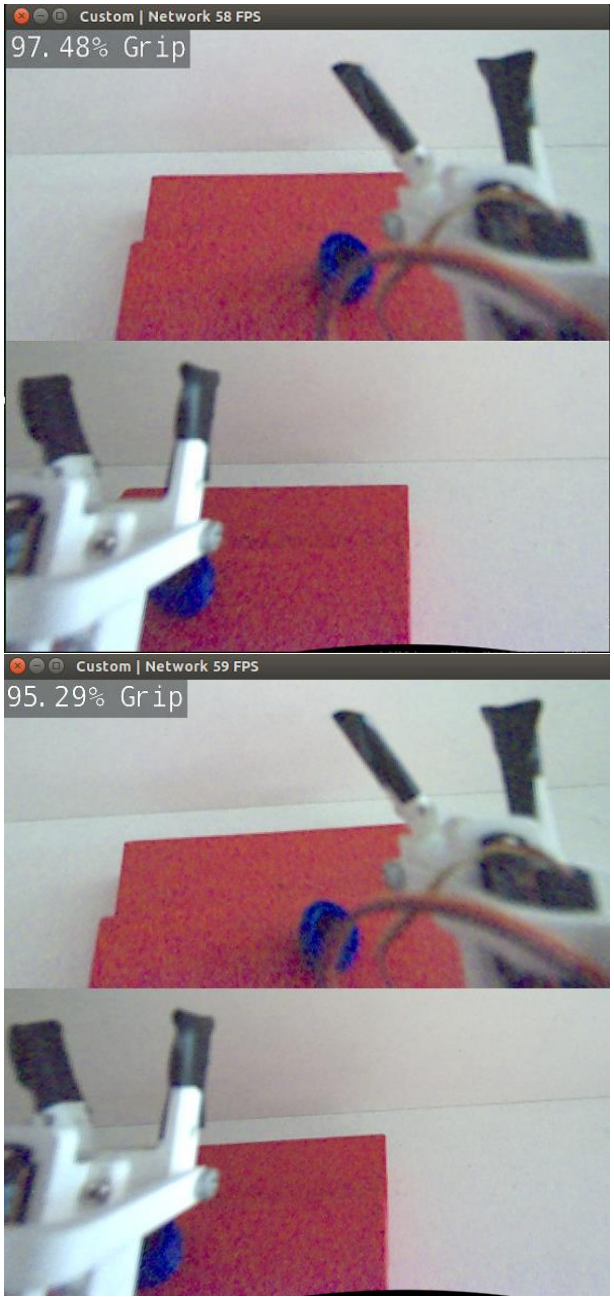


Fig. 3. Two input images for mobile robot decision-making system.

One more important piece of information that can be seen in Fig. 3 is the inference time of the developed deep learning model. Even though the proposed model has more layers and parameters than the original Resnet18, it can be used in real-time (around 60 FPS).


ISBN 978-86-7466-930-3

Moreover, the images of the mobile robot RAICO in the laboratory model of the manufacturing system during the testing of the decision-making system are presented in Fig. 4.

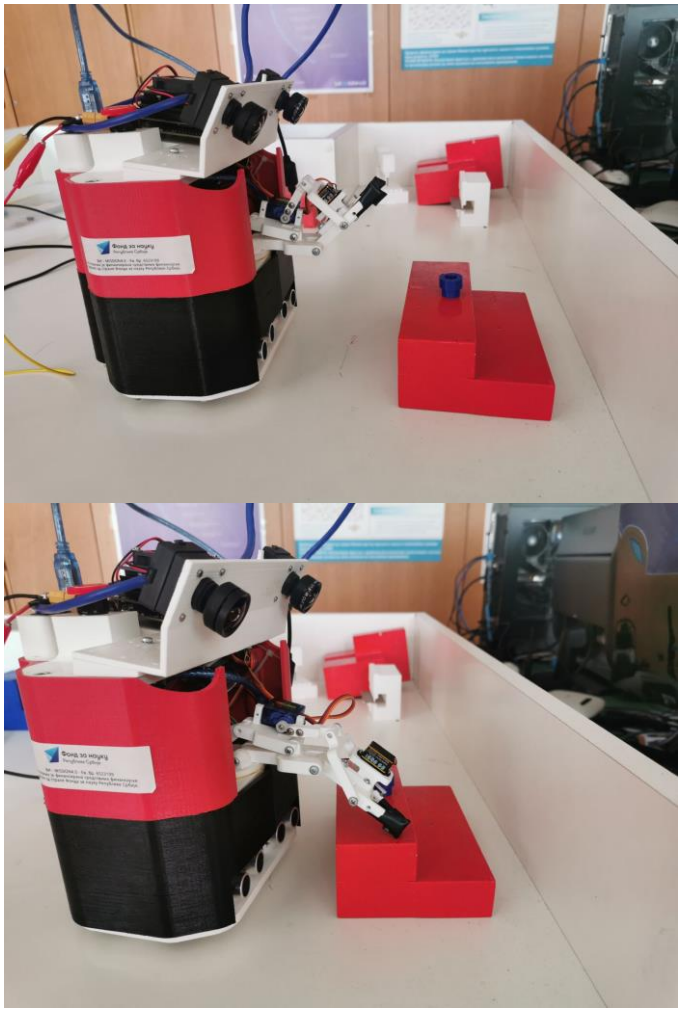

Fig. 4. Mobile robot RAICO in the pose close to the machine tool during the unsuccessful gripping process.

## IV. CONCLUSION

In this paper, the authors propose a decision-making system based on the Resnet18 deep learning model. The input represents the images from the stereo camera pair and the pose of the mobile robot. The Resnet model is trained on the custom dataset to produce the binary classification output regarding the success of the griping process. The experimental results show that the model accurately predicts gripping success in 70% of cases. Moreover, it is experimentally verified that high confidence (93%+) in the prediction of accurate gripping has a strong correlation to the real-world successful griping process. The future research directions will include the extensive testing of the processed system with different state-of-the-art deep learning models that will enable a higher level of accuracy.

## ACKNOWLEDGMENT

This work has been financially supported by the Ministry of Education, Science and Technological Development through the project "Integrated research in macro, micro, and nano mechanical engineering – Deep learning of intelligent manufacturing systems in production engineering" (contract No. 451-03-68/2022-14/200105), and by the Science Fund of the Republic of Serbia, grant No. 6523109, AI – MISSION 4.0, 2020 – 2022.

## REFERENCES

[1] Lasi, H., Fettke, P., Kemper, H. G., Feld, T., & Hoffmann, M. (2014). Industry 4.0. *Business and Information Systems Engineering*, (4), 239–242.

[2] Basilico, N., & Amigoni, F. (2009). Exploration Strategies based on Multi-Criteria Decision Making for an Autonomous Mobile Robot. *European Conference on Mobile obots ECM* , 259–264.

[3] Hu, C., Ning, B., Xu, M., & Gu, Q. (2020). An experience aggregative reinforcement learning with multi-attribute decision-making for obstacle avoidance of wheeled mobile robot. *IEEE Access*, , 108179–108190.

[4] Wang, D., Yang, K., Wang, H., & Liu, L. (2021). Behavioral Decision-Making of Mobile Robot in Unknown Environment with the Cognitive Transfer. *ournal of Intelligent obotic Systems*, *103*(1), 1–22.

[5] Kobayashi, Y., Kondo, M., Hiramatsu, Y., Fujii, H., & Kamiya, T. (2018). Mobile robot decision-making based on offline simulation for navigation over uneven terrain. *ournal of obotics and Mechatronics*, *30*(4), 671–682.

[6] Sünderhauf, N., Brock, O., Scheirer, W., Hadsell, R., Fox, D., Leitner, J., Upcroft, B., Abbeel, P., Burgard, W., Milford, M., & Corke, P. (2018). The limits and potentials of deep learning for robotics. *International ournal of obotics esearch*, *3* (4–5), 405–420.

[7] He, K., Zhang, X., Ren, S., & Sun, J. (2016). Deep residual learning for image recognition. *IEEE Conference on Computer ision and Pattern ecognition C P* , 770–778.

[8] Jokić, A., Đokić, L., Petrović, M., & Miljković, Z. (2021). A Mobile Robot Visual Perception System based on Deep Learning Approach. *th International Conference on Electrical, Electronics and Computing Engineering IcET AN 2021* , 568–572.

 ISBN 978-86-7466-930-3

# Method for Configuring Virtual Robot as an Integral Part of the Control System

Nikola Slavković, Saša Živanović, Zoran Dimić, and Nikola Vorkapić

***Abstract*—The development of integrated computing environments provides opportunities for the development of virtual production. Virtual simulation is crucial when the robot performs tasks that include some manufacturing processes. Virtual robots are used for program verification before sending it to the real robot and enable collision checking between robot segments themselves and the robot and its environment. Virtual models of industrial robots could be configured in different environments and ways. This paper presents the method for configuring virtual robots as an integral part of the control system. The virtual robot's configuration is realized under the LinuxCNC software environment and relies on OpenGL and several interface classes written in Python programming language. Developing a robot kinematic model to implement a virtual robot integrated with an open-architecture control system is necessary. Models of robot segments were imported in ASCII STL format and connected according to the robot kinematic model, and then the virtual robot was integrated within the LinuxCNC control system. The method for configuring a virtual robot as well as its kinematic model is presented in the example of the BiSCARA robot. Verifying the robot control system, virtual model, and kinematic model has been performed through several examples of drawing contours on the configured virtual robot.**

***Index Terms*—Virtual robots; Control system; Robot simulations; Kinematic modeling;**

## I. Introduction

Sudden changes in production programs, product short life cycle, as well as further progress in the development of integrated computing environments for the development of new products provide opportunities to achieve the paradigm of virtual production [1]. The use of industrial robots in manufacturing and assembly lines is continuously increasing due to the need for high efficiencies, high accuracy, high production rates, and repeatability [2]. The use of robots for pick and place, welding, subtractive and additive manufacturing has been spreading in the last years with the concept of industry 4.0 [3]. In addition to performing these tasks, the application of industrial robots has been extended to laser engraving, laser and plasma cutting, robot milling, etc. Designing and testing a robotic cell is one of the essential modern manufacturing engineering tasks, especially when the robot does not just handle materials but also performs manufacturing processes [4]. To save time and verify the robot cell for performing these tasks before its production, virtual environments, i.e., virtual robots have a key role.

The notion of a virtual industrial robot is broad and includes complete models of robot structure, kinematic subsystem, tasks process, the environment, etc. All these models are integrated into a single software system, enabling some part of the virtual production.

Virtual industrial robots, that are included in the production engineering environment, could be configured in the different environments such as CAD/CAM systems, MatLab/Simulink environment, specialized CAM software for robot programming (RobotStudio, Robotmaster, …), LinuxCNC as an integral part of robot control systems, virtual reality system, etc.

This paper presents the configured virtual robots in different software environments using a five-bar, i.e., dual SCARA or BiSCARA robot. Robots based on the five-bar mechanism are widespread in academic institutions because they are suitable for experimental work. This base mechanism is almost always improved with the additional translatory and rotary axis to develop 3- or 4-axis robots. The developed virtual robot can simulate robot tasks such as laser engraving, 3-axis milling, 3D printing, etc. The first such robot, Fig. 1, is described in a US patent in 1934 [5, 6]. In 1978, Prof. Hiroshi Makino invented the well-known SCARA robot [7], while in 1985, Donald C. Fyler came up with the idea of using a five-bar mechanism as a robot [5, 8].

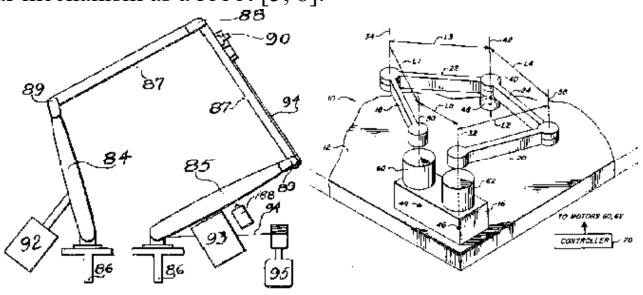


Fig. 1. Concept of five-bar, i.e., dual SCARA or BiSCARA, robot [1]

Mitsubishi Electric was the first company that commercialized the robot, MELFA RP-1A, based on this mechanism [5]. An example of a developed industrial prototype is the DexTAR robot (Dextrous Twin-Arm Robot) [9].

Associate prof. Dr. Nikola Slavković is with the Faculty of Mechanical Engineering, University of Belgrade, 16 Kraljice Marije, 11120 Belgrade, Serbia (e-mail: nslavkovic@mas.bg.ac.rs).

Full prof. Dr. Saša Živanović is with the Faculty of Mechanical Engineering, University of Belgrade, 16 Kraljice Marije, 11120 Belgrade, Serbia (e-mail: szivanovic@mas.bg.ac.rs).

Research Associate Dr. Zoran Dimić is with the LOLA Institute, 70A Kneza Višeslava, 11030 Belgrade, Serbia (e-mail: zoran.dimic@li.rs).

Nikola Vorkapić, MSc (ME) is with the Faculty of Mechanical Engineering, University of Belgrade, 16 Kraljice Marije, 11000 Belgrade, Serbia (e-mail: nvorkapic@mas.bg.ac.rs).

 ISBN 978-86-7466-930-3

## II. VIRTUAL INDUSTRIAL ROBOTS

A virtual industrial robot is a digital description of a robot, usually with simplified geometry, and is used for computer simulations of robot tasks.

To configure a virtual robot in a CAD environment [10], first, all elements of the robot structure are generated. These elements are then connected to the kinematic structure of a real robot. To be able to model a robot used in the simulation, one member of the robot mechanism must be fixed, and the moving components of the robot should be connected with appropriate kinematic connections (pin and/or slider). After this, in the next step, it is necessary to connect the coordinate systems of the workpiece and end-effector (EE) with the robot's coordinate system. In CAD/CAM environment, PTC Creo, the robot's coordinate system is defined as MACH_ZERO, while TOOL_POINT presents the end-effector's coordinate system. Coordinate systems with the same names have both an EE and a workpiece. The virtual EE is placed on the virtual robot by matching these coordinate systems. After the successful connection of the virtual workpiece and EE, a virtual industrial robot simulation according to a given program can be run. The model of the BiSCARA robot configured in the PTC Creo environment is shown in Fig. 2. The simulation of movement of the virtual robot tooltip is shown in the example of drawing a circle and a rectangle inscribed in a determined workspace of the robot.

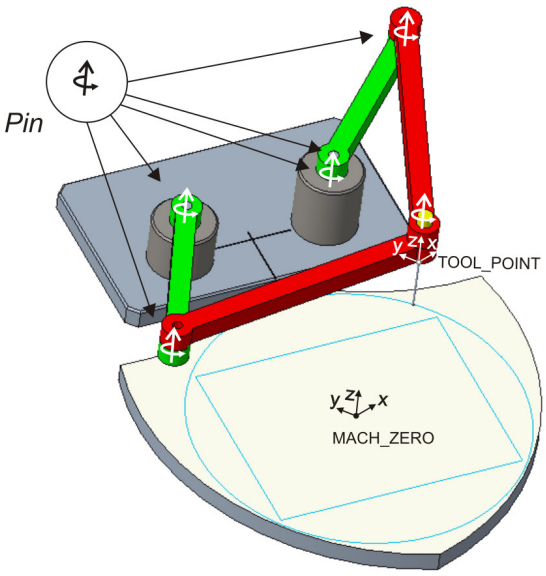


Fig. 2. Configuring of virtual robot in CAD/CAM environment

As described in the previous work [11], configuring the virtual robot in the MatLab/Simulink environment considers the development of the program for the joint space trajectory generation in the MatLab environment and configuring of the virtual robot in the Simulink environment. The structure of configured virtual robot in Simulink is presented in Fig. 3a.

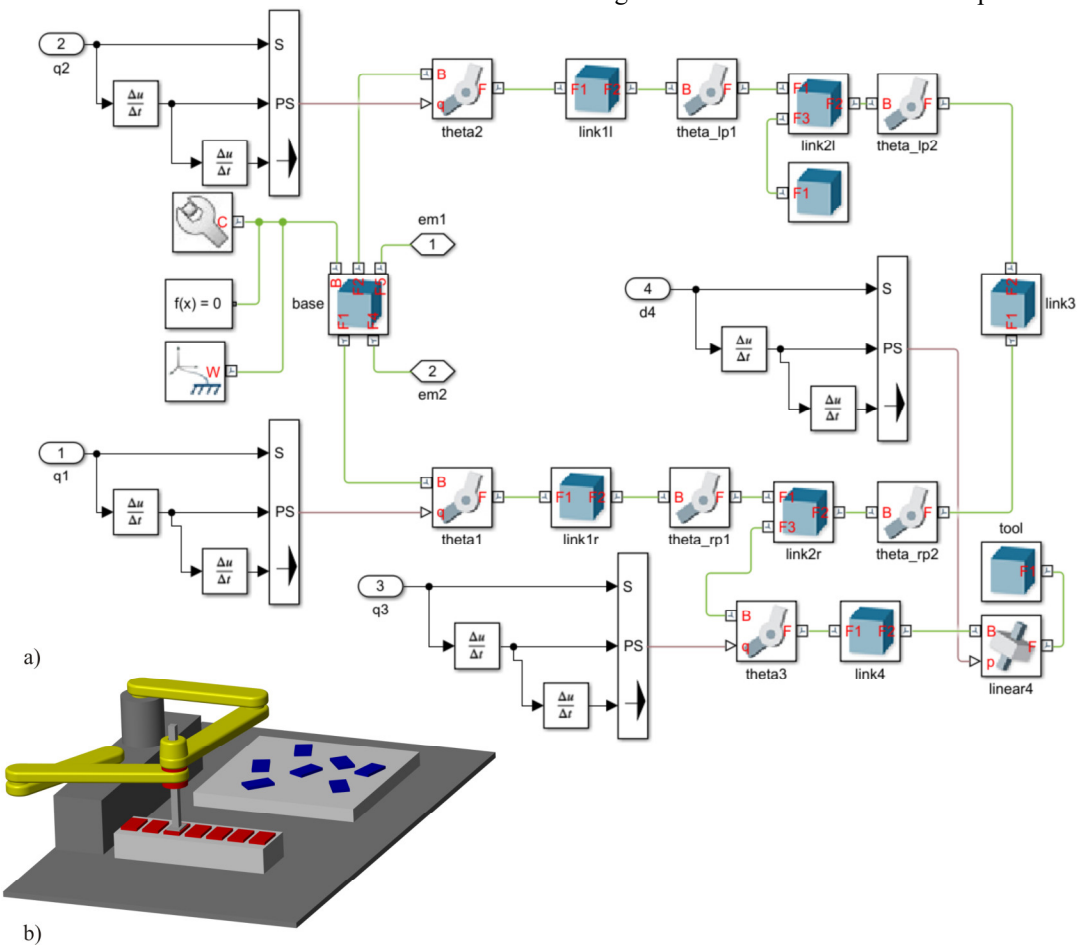


Fig. 3. Configuring of virtual robot in MatLab/Simulink environment


ISBN 978-86-7466-930-3

It consists of a base and three kinematic chains. The base is represented with the Brick Solid element connected with World Frame, Solver Configuration, and Mechanism Configuration elements. Any kinematic chain consists of Brick Solid elements and appropriate Revolute Joint and/or Prismatic Joint elements. The active joints in these kinematics chains have to be actuated by joint time series generated in MatLab consisting of joint angle, velocity, and acceleration [11]. The model of the BiSCARA robot configured in MatLab/Simulink environment is shown in Fig. 3b.

Virtual robots, as well as virtual machines, have a significant role when developing a control system where it is necessary to integrate solutions of inverse and direct kinematics. In this way, it is possible to develop a control system even before the realized physical prototype, which is of great importance because it allows virtual testing during development, known as virtual commissioning [12, 13, 14].

This paper considers the method for configuring virtual robots in the LinuxCNC control system. Virtual robots in the control system are significant during the robot exploitation and the configuring of the control and before the realization of the robot. Program verification using virtual robots is significant because it enables:

- testing the kinematic model during the development of the control system,
- visual detection of collisions between the moving parts of the robot and between the tool, workpieces, and fixtures in the workspace,
- checking if the robot can execute the specified toolpath within the limited workspace, joints ranges, and speeds,
- training and education for robot programming, etc.

## III. KINEMATIC MODEL OF ROBOT

To realize the virtual robot as an integral part of the control system, it is necessary to perform a kinematic analysis of the considered robot [11, 15]. A Parallel BiSCARA robot can be viewed as a planar manipulator with two degrees of freedom. The kinematic analysis embraced solving direct and inverse kinematic problems, determination of Jacobian matrix, and workspace analysis [11]. The kinematic model of the BiSCARA robot is shown in Fig. 4.

The robot consists of a base, a platform, and two kinematic chains with struts lengths $l_1$ and $l_2$. All mechanism elements are connected by a joint with one rotary degree of freedom. The frame {B} represents the base frame, while the platform is represented by point P because the struts of length $l_2$ are connected at the point P.

As it can be seen from Fig. 4, the world coordinate vector is defined as

$$ {}^{B}\mathbf{p}_P = \begin{bmatrix} x_P & y_P \end{bmatrix}^T \tag{1} $$

while joint coordinate vector is represented as

$$ \boldsymbol{\theta} = \begin{bmatrix} \theta_1 & \theta_2 \end{bmatrix}^T \tag{2} $$

Besides another unit vector, the unit vector ${}^{B}\mathbf{a}_i$ is defined as

$$ {}^{B}\mathbf{a}_i = \begin{bmatrix} \cos(\theta_i)\cos(\gamma_i) \\ \sin(\theta_i) \end{bmatrix} \tag{3} $$

where i=1, 2 represents the number of the kinematic chain and $\gamma_i$ represents the angle that defines the arrangement of kinematic chains and is introduced in order to generalize the solution of the inverse kinematic problem and parallel determination of joint coordinates during the solving an inverse kinematic problem.

Observing one kinematic chain, the following vector equations can be derived

$$ \begin{aligned} {}^{B}\mathbf{p}_p &= {}^{B}\mathbf{b}_i + k_i \cdot {}^{B}\mathbf{w}_i \\ k_i \cdot {}^{B}\mathbf{w}_i &= l_1 \cdot {}^{B}\mathbf{a}_i + l_2 \cdot {}^{B}\mathbf{z}_i \end{aligned} \tag{4} $$

from which inverse and direct kinematic problems can be solved in analytic form.

The authors' previous work represents the complete solution of inverse and direct kinematic problems, as the determination of Jacobian matrix and workspace analysis [11]. Here are presented only the solutions of the inverse kinematic problem that is crucial for developing a virtual robot integrated with a control system. The joint coordinates can be determined using the following equations

$$ \theta_i = A\tan 2(t_{i1/2}) \tag{5} $$

where

$$ t_{i1/2} = \frac{y_P \pm \sqrt{A_i^2 + y_P^2 - B_i^2}}{A_i + B_i} \tag{6} $$

and

$$ \begin{aligned} A_i &= (x_P - b_{ix})\cos(\gamma_i) \\ B_i &= \frac{l_1^2 + (x_P - b_{ix})^2 + y_P^2 - l_2^2}{2l_1} \end{aligned} \tag{7} $$

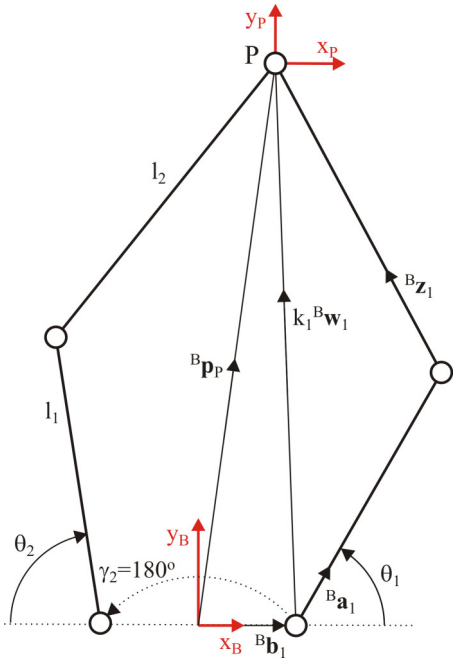


Fig. 4. Kinematic model of BiSCARA robot


ISBN 978-86-7466-930-3

## IV. METHOD FOR CONFIGURING VIRTUAL ROBOTS IN CONTROL SYSTEM

The basic concept of a configuring virtual robot in the control system is shown in Fig. 5. The virtual robot's configuration is realized under the LinuxCNC software environment and relies on OpenGL and several interface classes written in Python programming language. Python is an interpreted programming language suitable for scripting tasks, such as developing and configuring virtual environments [12].

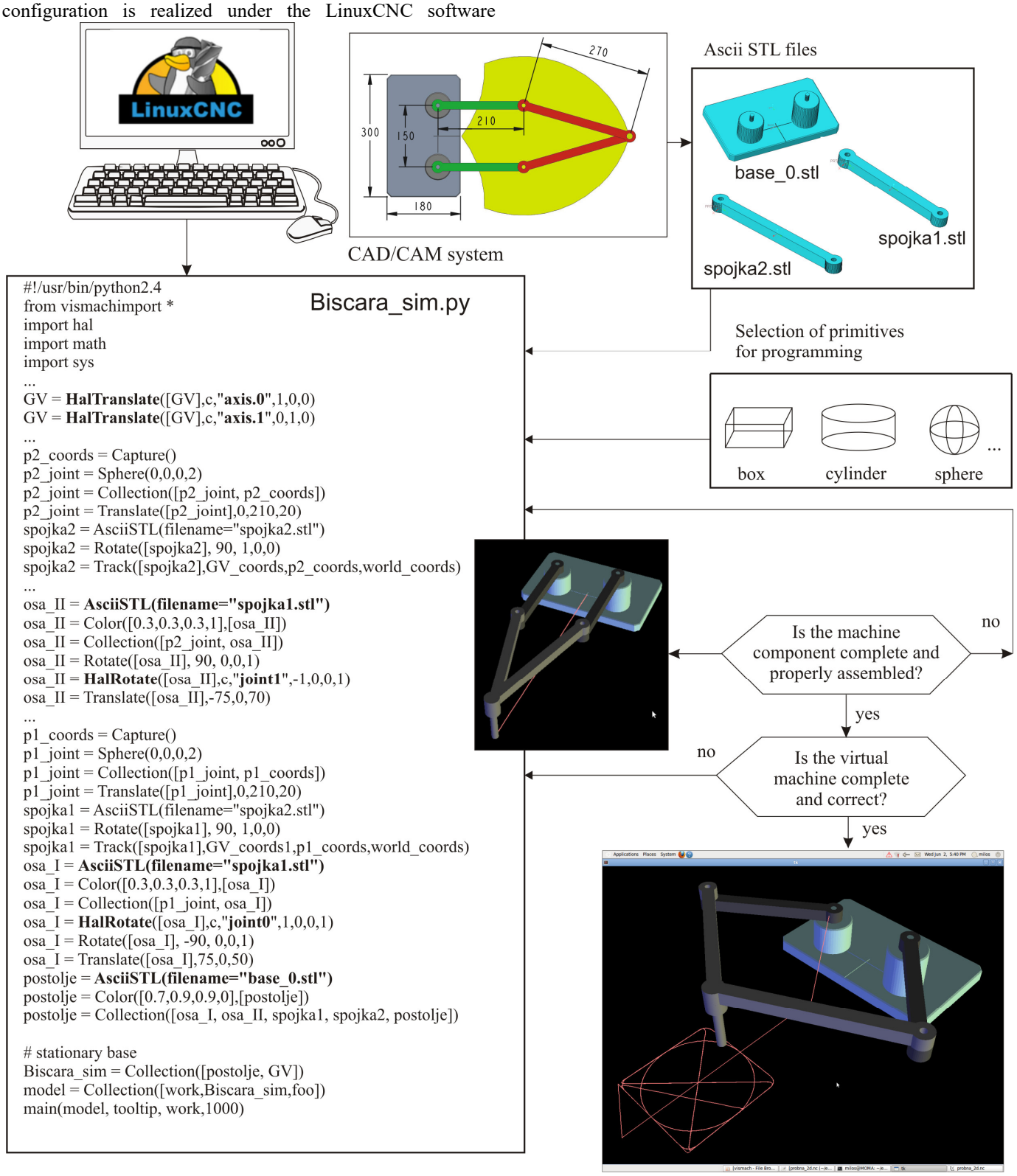


Fig. 5. The basic concept of a configuring virtual machine in a control system realized under the LinuxCNC software environment


ISBN 978-86-7466-930-3

Models of robot components were imported in ASCII STL format and connected according to the robot kinematic model. The ASCII STL files of the robot components were obtained from the CAD/CAM system.

After the virtual robot is configured, it is integrated within the LinuxCNC control system. During the program execution for a robot in G-code, the virtual robot components are moving in real-time, according to identical control signals as for the real robot.

The modeling procedure of the virtual robot starts by defining the geometric primitives as parts of the robot assembly in CAD/CAM system. Defining only the essential and functional parts of the robot 3D model may simplify the development of the virtual robot. Basic geometric primitives, e.g., boxes, cylinders, spheres, etc., can be used to form robot parts. The positions of the geometric primitives, as well as the robot parts, are programmed according to the adopted reference frame. The robot parts are connected to form the robot base, and the moving parts of the robot, in this case, are connected via rotational joints.

Step by step programming, testing, and error correction is the only way of configuring an error-free virtual robot. Besides the manual approach, using basic geometric primitives, a CAD system can be used for preparing 3D models of robot components, which are exported as separate files ASCII OBJ or ASCII STL code. In this paper, the virtual BiSCARA robot was configured using PTC Creo. The robot components were converted into an ASCII STL format and then loaded into the Axis GUI through appropriate Python calls, Fig. 5.

Afterward, the imported components are oriented and placed in the virtual environment, resulting in a fully functional virtual robot, as shown in Fig. 5. The virtual robot is placed in a separate window and allows drawing the toolpath within the limitations of the virtual robot elements' movements.

## V. SIMULATION AND VERIFICATION

The developed virtual two-axis BiSCARA robot, integrated with the LinuxCNC control system, is suitable for drawing tool paths and laser engraving [15].

The programming system for the considered robot is entirely conventional and the same as for all machine tools which can perform milling or laser engraving. Programs for testing configured virtual robots are generated in the CAD/CAM system using trajectory milling or a special CAM system that can convert drawing in DXF format into G-code.

During the program's execution written in G-code, the virtual robot components are moving in real-time, according to the tool path, thanks to the kinematics built into the control system.

Figure 6 shows the first of the experiments on a virtual robot integrated with the control system, which represents the drawing of the programmed tool path consisting of regular geometric figures of squares with diagonals and inscribed circles.

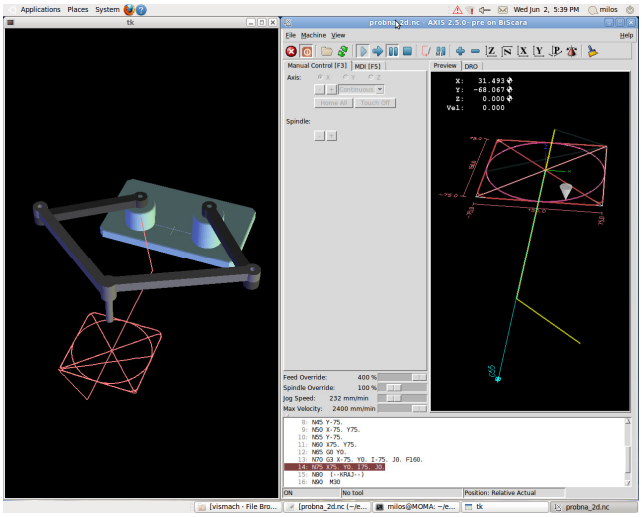

Fig. 6. Simulation of programmed tool path on virtual BiSCARA robot in LinuxCNC control system

Figure 7 shows one of the experiments on a virtual robot integrated with the control system, representing the drawing of the programmed tool path in the shape of the lion drawing. This experiment was used to test systems for programming complex 2D contours, which were programmed, based on DXF drawings and their conversion into G-code.

Some of the details during the virtual trial simulation of the BiSCARA robot are as follows: (i) the appearance of the programmed contour confirms the realized kinematic model, (ii) realized control system is correct, (iii) the used programming system gives correct G-code, (iv) positioning within the robot workspace was correct.

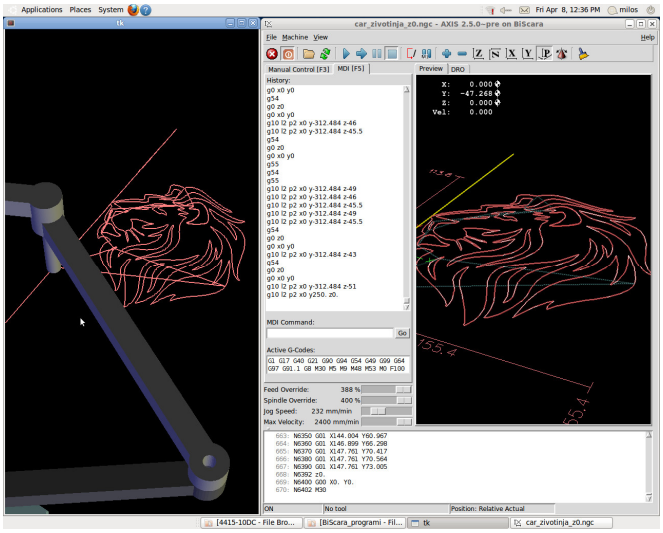

Fig. 7. Simulation of programmed tool path based on lion drawing on virtual BiSCARA robot


ISBN 978-86-7466-930-3

## VI. Conclusion

Testing and verifying the robotic cell before its realization through virtual environments is one of the modern manufacturing engineering tasks. Configuring a virtual environment that includes virtual robots is of crucial importance to verify the programmed trajectory, collision detection, etc.

The paper presents the configuration of a virtual robot in the CAD/CAM and MatLab/Simulink environments on the example of the BiSCARA robot. The virtual CAD and complete kinematic models are used to implement robots in the LinuxCNC software according to a presented method for configuring virtual robots as an integral part of the control system. Configuring virtual robots relies on OpenGL and several interface classes written in Python programming language. First, robot segments were imported in ASCII STL format and connected according to the robot kinematic model, and then the virtual robot was integrated.

Further research will encompass the realization of a virtual prototype of a 4-axis robot by adding on the presented base mechanism one translatory and one rotary axis. Also, the development of a laboratory prototype of a 4-axis robot will be covered in further research.

## Acknowledgment

This research was supported by the Science Fund of the Republic of Serbia, Grant No. 6523109, AI-MISSION 4.0 as well as by the Ministry of Education, Science and Technological Development of the Serbian Government under the contract No. 451-03-68/2022-14/200105.

## References

[1] N. Vorkapić, S. Živanović, Z. Dimić, B. Kokotović, N. Slavković, "Virtual horizontal machining center LOLA HBG 80 for program verification and monitoring", *FME Transactions*, vol. 49, no. 3, pp. 696-703, 2021.

[2] J.O. Oyekan, W. Hutabarat, A. Tiwari, R. Grech, M.H. Aung, M.P. Mariani, L. Lopez, T. Ricaud, S. Singh, C. Dupuis, "The effectiveness of virtual environments in developing collaborative strategies between industrial robots and humans", *Robotics and Computer-Integrated Manufacturing*, vol. 55, pp. 41-54, 2019.

[3] W.S. Barbosa, M.M. Gioia, V.G. Natividade, R.F. Wanderley, M.R. Chaves, F.C. Gouvea, F.M. Gonçalves, "Industry 4.0: examples of the use of the robotic arm for digital manufacturing processes", *International Journal on Interactive Design and Manufacturing*, vol. 14, no. 4, pp. 1569-1575, 2020.

[4] GC Vosniakos, P. Katsaros, I. Papagiannoulis, E. Meristoudi, "Development of robotic welding stations for pressure vessels: interactive digital manufacturing approaches", *International Journal on Interactive Design and Manufacturing*, pp. 1-16, 2022.

[5] DexTAR, User's Manual, Version 1.0, by Mecademic Inc., 2014–2015.

[6] W.L.G. Pollard Jr., Spray Painting Machine, US Patent 2,213,108, filed October 29, 1934, issued August 27, 1940.

[7] H. Makino, A. Kato, Y. Yamazaki, "Research and commercialization of SCARA robot", *International Journal of Automation Technology*, vol. 1, no. 1, pp. 61–62, 2007.

[8] D.C. Fyler, Control Arm Assembly, US Patent 4,712,971, filed February 13, 1985, issued December 15, 1987.

[9] A. Joubair, M. Slamani, I.A. Bonev, "Kinematic calibration of a five-bar planar parallel robot using all working modes", *Robotics and Computer-Integrated Manufacturing*, vol. 29, pp. 15–25, 2013.

[10] N. Slavkovic, S. Zivanovic, N. Vorkapic, "Konfigurisanje virtuenog prototipa BiSCARA robota", *Časopis Tehnika-Mašinstvo*, Časopis saveza inženjera i tehničara Srbije, vol. 70, no. 3, str 311-317, 2021.

[11] N. Slavkovic, S. Zivanovic, N. Vorkapic, Z. Dimic, "Development of the Programming and Simulation System of 4-axis Robot with Hybrid Kinematic", *FME Transactions*, (in print).

[12] C.G. Lee, S.C. Park, (2014) "Survey on the virtual commissioning of manufacturing systems", *Journal of Computational Design and Engineering*, vol. 1, pp.13-222, 2014.

[13] S. Zivanovic, S. Tabakovic, M. Zeljkovic, Z. Dimic, "Modelling and analysis of machine tool with parallel–serial kinematics based on O-X glide mechanism", *Journal of the Brazilian Society of Mechanical Sciences and Engineering*, vol. 43, no. 456, 2021.

[14] A. Rakic, S. Zivanovic, Z. Dimic, M. Knezevic, "Digital twin control of multi-axis wood CNC machining center based on LinuxCNC", *BioResources,* vol. 16, no. 1, pp.1115-1130, 2021.

[15] N. Slavković, N. Vorkapić, S. Živanović, Z. Dimić, B. Kokotović, "Virtual BiSCARA robot integrated with open-architecture control system," Proc. 14th International Scientific Conference MMA 2021 – Flexible Technologies, Novi Sad, Serbia, pp. 63-66, 2021.

 ISBN 978-86-7466-930-3

# Low-cost real-time human motion capturing system

Milutin Nikolić, Lazar Milić, Milutin Studen, Mirko Raković

***Abstract*— In recent years motion capturing technology found numerous applications in industry and research areas li e human-robot interaction, medical applications, etc... Those systems can be very e pensive and might require a lot of setup time. In this paper, leveraging the advances in deep learning and computer science, the low-cost real-time motion capturing system is presented. The system was designed to use off-the-shelf ine pensive cameras, freely available software, and a gaming laptop. The system design, underlying math principles, reconstruction pipeline, and reconstruction results will be discussed in the paper. The presented motion capturing system can reconstruct a human pose with eypoints in real-time at 1 z. The whole setup costs less than 25 including the price of the dedicated PC.**

***Index Terms*— otion capturing, uman pose estimation, uman-robot interaction, Deep learning**

## I. Introduction

Motion capture or "MoCap", for many years now, has been recognized in the majority of industries as the highly advanced technique of recording movements and transferring the results of such recording into digital data. It is widely used in various fields from science, through the film industry, to gaming and video game development, which makes it broadly applicable and remarkably alluring for use in different professional spheres [1].

In medicine and biomedicine, motion capture is used to conduct scientific research and analyses with regard to the understanding of human physiology, particularly the bipedal locomotion. This knowledge can contribute to understanding the effects of injuries and required rehabilitation [2]. In addition, MoCap havs the ability to record facial expressions of humans, which can help us in further understanding of human emotions. In robotics MoCap is used for constructing dynamically stable humanoid movement and for capturing motion trajectory of a human [3, 4].

Furthermore, the filmmaking and video games industry uses motion capture to record the physical actions of the live actors participating in the movies, enabling the real-life movie characters to be "transcribed" into the computer animations, i.e., digital characters. Nonetheless, the MoCap is often used for the creation of special effects in different animated content such as movies, video games, etc.[5] Also, in human-robot interaction, the MoCap is used to record, evaluate and classify human behavior patterns. Also, MoCap is extensively used to record and evaluate human behavior, and modify robot behavior based on recognized human behavior pattern [6].

Milutin Nikolić, Lazar Milić, Milutin Studen and Mirko Raković are with Faculty of Technical Sciences, University of Novi Sad. Trg Dositeja Obradovića 6, 21000 Novi Sad, Serbia (email: {milutinn, miliclazar, studen, rakovicm}@uns.ac.rs)

It may be easily concluded that, from its beginnings, motion capture has been a significant addition to the technical processes throughout the diverse industries. However, although many excellent systems leading to the outstanding results are currently present on the market, such as the Vicon Motion[1]

Capturing System, the main setback of motion capture as an asset able to simplify the variety of industrial processes is the fact that its application and practical use are conditioned upon expensive hardware and software. Furthermore, some solutions such as [7] include complex offline postprocessing following the collection of the movement data. For instance, the basic equipment, without any upgrades and advancements, that is necessary for the Vicon setup amounts to approximately $40.000, which is noticeably expensive for the SME.

Although there are many types of motion capture, optical MoCap is most commonly used technology. Optical MoCap use multi-camera setup and triangulation to determine position of markers in 3D world. There are two types of optical motion capture reflective and pulse LED. First technique has reflective markers which are placed on actor's body and because of their reflection it becomes easy for software to determine the position of markers. On the other hand, pulse LED technique has active markers that emission LED light which cameras can capture. Both techniques required 50 plus markers on actor's body for motion to be captured. This process requires a lot of time for markers to be placed on predefined part of body and also markers restrict actor's movement.

Regardless of that, the rapid development of the technology has through the years led to the possibility of the development of low-cost MoCap systems. In addition, the introduction of new methods that can extract the pose from image sequence by using artificial neural networks lowered the cost of new budget MoCap systems. Furthermore, the decrease in the prices of usable equipment for the motion capture processes, including personal computers and cameras, has affected the realization of the more affordable MoCap systems with non-equal but satisfying results [8]. Having in mind all previously mentioned, we are now able to construct budget MoCap system for less than $2500, including all hardware and software, without any markers which minimize required time for preparation, allows actor's to move freely and eliminates location restrictions. Tha low cost would enable further expansion of use of MoCap. Also, removal of required markers and long setup time, enables recording in places where we can't interfere with the subjects, e.g. recording athletes during sport events, behavioral studies of people in pubic spaces, interaction of workers with the robot

 ISBN 978-86-7466-930-3

on the factory floor, etc ... The design and implementation of such a low-cost system is the main topic of this paper.

The paper is organized as follows: in Section II we will describe the hardware components of the system and how it is layed out. In Section III the process for calibrating the system will be described. Section IV describes the whole reconstruction pipeline, while Section V gives experiment results. The paper is concluded in Section VI.

## II. System setup

In this section, we will describe the complete system architecture, calibration process, and video acquisition. The video acquisition and recording system consists of three Intel RealSense D415 cameras, which are connected to a PC via a USB interface. The placement of the cameras in the room is so that each camera is oriented towards the center of the room. Since Intel RealSense D415 has narrow field of view, the coverage of the visible area is relatively small. This could potentially disrupt pose estimation. But as shown later in section results this was not a problem.

### *A. Intrinsic camera calibration*

Because of the camera manufacturing process nature, there is a high possibility for it to be assembled imperfectly. This imperfection brings distortions to the image. There are two major distortions, and those are radial and tangential distortions.

Radial distortion has stronger effect on further points in the image and is reflected in such a way that straight lines appear curved. Similarly, tangential distortion occurs when camera lens is not perfectly aligned with image plane.

To describe radial and tangential distortion these five coefficients are used: $k_1$, $k_2$, $k_3$, $p_1$, $p_2$, where $k_1$, $k_2$ and $k_3$ are used to represent radial distortion, while $p_1$ and $p_2$ describe tangential distortion [9].

Additionally, during camera calibration, intrinsic camera parameters are calculated and these are focal length ($f_x$, $f_y$) and optical centers ($c_x$, $c_y$). Intrinsic camera and distortion parameters are calculated using OpenCV library. Process of calibration consists of multiple image captures, where each image is showing black and white chessboard with known square size. Images are then processed with the help of OpenCV functions which return all necessary parameters as the end result. Fig 1. shows example of detected chessboard and its corner points during calibration process.

### *B. E trinsic camera calibration*

After finding intrinsic camera parameters, it is necessary to determine camera positions in real world, also known as extrinsic camera parameters, using chessboard as a reference. Again, we are using OpenCV library to calculate these transformations and Fig **2.** shows example of images containing chessboard and its estimated location in the world.

## III. Reconstruction pipeline

In order to reconstruct the pose of the human in 3D space the images coming from cameras have pass through a several processing stages. The flow chart of the raw data obtained from cameras to the final reconstructed pose is illustrated in Fig. 3. Each stage of the reconstruction pipeline will be described in detail in subsequent sections.

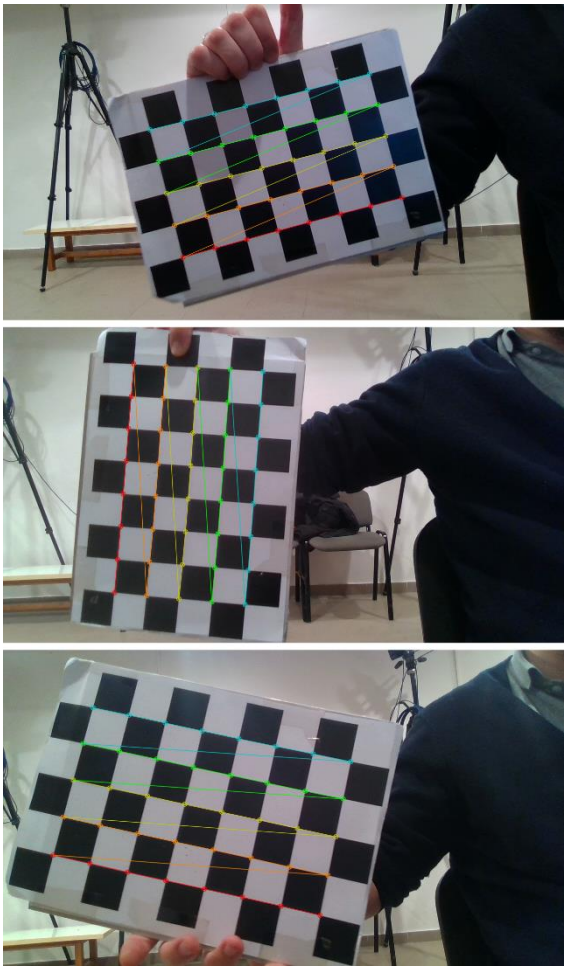

Fig 1. Images acquired for camera calibration with detected chessboards

Fig 2. Images used for extrinsic camera calibration displayed with system origin

### *A. Image ac uisition*

The first block in the processing pipeline is image acquisition from the camera. This operation is the simplest one, and the image data from the camera is retrieved by using API provided by the camera manufacturer, in this case python library `pyrealsense2` provided and maintained by Intel.


ISBN 978-86-7466-930-3

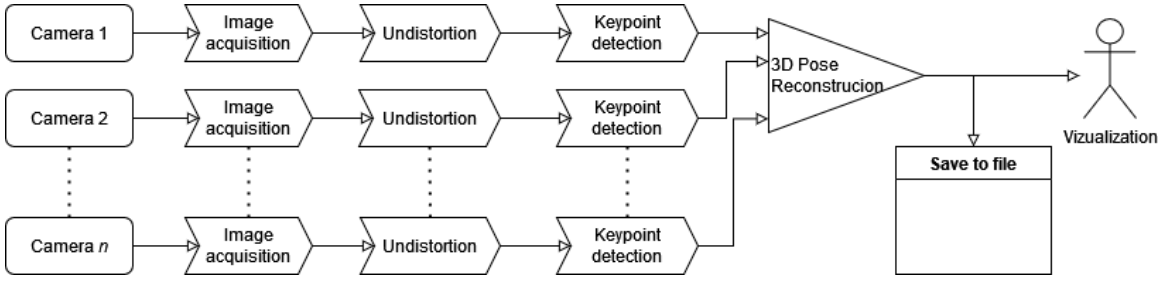


Fig 3. Processing pipeline

[10] Before retrieving the image, user has to provide camera serial number, and desired framerate.

### *B. ndistortion*

The obtained image contains some distortion due to lens imperfection and assembly errors. Such a distortion will introduce errors in the reconstructed pose, so it is extremely important to correct it. In section III we have described the camera calibration process, and result of it is the distortion parameters. In this block, those distortion parameters will be used to undistort the obtained image.

### *C. uman pose detection*

After obtaining distortion-free images the next step is the detection of the human keypoints on the image. Until very recently, without special clothing or markers, accurate detection of body keypoints was almost impossible. In year 2017 OpenPose was developed as a first convolutional neural network based human pose detection framework.[11] It was trained using COCO dataset and it can detect 25 keypoints on the human body. Also, it can detect multiple humans captured by the camera.

Unfortunately, OpenPose, although very accurate, is very computationally demanding. In order to run OpenPose real time, dedicated GPU is required which would significantly increase the total system cost.

Alternative was found in MediaPipe [12] developed by Google as an open-source cross platform, customizable machine learning solution set for live and streaming media. One of solutions provided is used for human pose detection and tracking. It can infer 33 3D keypoints and background segmentation mask on the whole body from RGB video frames utilizing BlazePose [13]. The detected keypoints are given in Fig 4. The MediaPipe can be set up to detect even higher fidelity mode, with total 543 keypoints, with 33 keypoints on the body, 21 on each hand and 468 on the face. To be able to reconstruct face and whole body, the higher resolution and quality camera is required, and for that reason we decided to reconstruct only 33 body keypoints. One limitation of this framework compared to OpenPose is that it can detect only one human in the scene. Multiple humans would inevitably produce detection errors.

3D poses are given relative to pelvis, whose 3D pose is unknown, and, if just one camera is used, can suffer from unknown scale, leading to wrong 3D pose estimation. Hence, we still need multi-camera setup to obtain full 3D position of the keypoints.

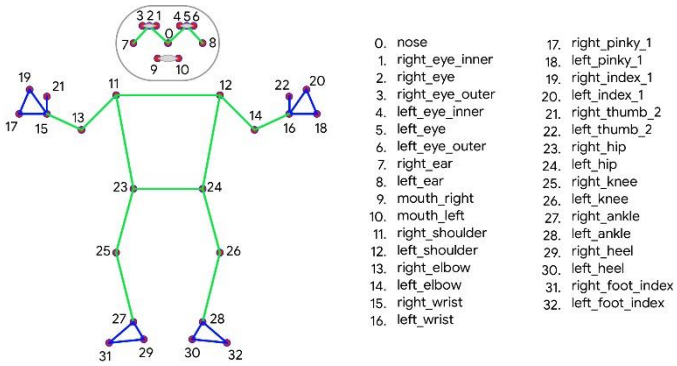


Fig 4. Keypoints detected by BlazePose

### *. 3 reconstruction*

After getting positions of all keypoints on all cameras, the last step is to reconstruct their positions in a 3D space. To do so, let's assume that we have *n* cameras. The keypoint in space can be seen on camera *i* at the location $\mathbf{q}_i$ given in pixels. The position and rotation matrix of camera *i* are given with $\mathbf{T}_i$ and $_i$. The intrinsic camera matrix is $_i$. These vectors and matrices are the result of the calibration process described in section IIIA. The setup is illustrated in Fig. 5. Now, having all the camera positions, rotation matrices and location of the keypoint on all images, the goal is to compute the position of the point in the 3D space.

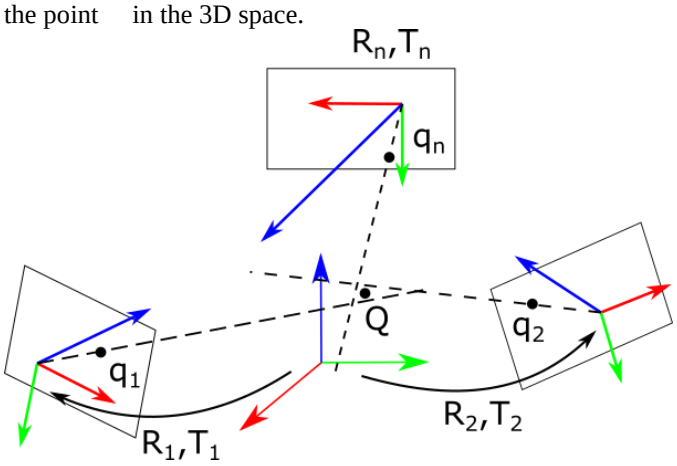


Fig. 5 Setup with multiple cameras observing the same point.

To derive equations, we will start from pinhole camera model, and projection rule:

$$\mathbf{q}_i = s_i \mathbf{M}_i \mathbf{R}_i^{\mathrm{T}} (\mathbf{Q} - \mathbf{T}_i) . \quad (1)$$


ISBN 978-86-7466-930-3

Where $s_i$ is positive scalar and $_i$ is intrinsic camera matrix projecting points from the space to pixels in image. From that equation we can deduce :

$$\mathbf{Q} = \mathbf{T}_i + w_i \mathbf{R}_i \mathbf{M}_i^{-1} \mathbf{q}_i = \mathbf{T}_i + w_i \mathbf{u}_i, \quad (2)$$

where we $w_i$ is again positive scalar equal to $1\ s_i$ . The physical meaning is that a point lies on the ray starting from center of camera $i$ $\mathbf{T}_i$, that passes through point $\mathbf{q}_i$ and follows direction $\mathbf{u}_i$.

Obviously, this is the ideal case, where cameras are perfectly calibrated and keypoint is perfectly detected. In the real world we can't achieve that, so the mentioned ray will pass close, but will not contain the point . Including that observation we can rewrite equation (2):

$$\mathbf{Q} = \mathbf{T}_i + w_i \mathbf{u}_i + \boldsymbol{\varepsilon}_i, \quad (3)$$

where $\boldsymbol{\varepsilon}_i$ represents the deviation of point from ray going from $\mathbf{T}_i$, in a direction $\mathbf{u}_i$.

The position of the point Q will be obtained by minimizing the deviation from ideal rays. It is the result of the following optimization problem:

$$\min_{\mathbf{Q}} \sum_{i=1}^{n} \left\| \boldsymbol{\varepsilon}_i \right\|^2. \quad (4)$$

The meaning of this optimization problem is that the point that is the detected on $n$ images at location $\mathbf{q}_i$ is the point in space whose total squared distance to all rays starting at $\mathbf{T}_i$, and passing through point $\mathbf{q}_i$ is minimal.

By expressing inserting $\boldsymbol{\varepsilon}_i$ from equation (3) and inserting it into (4) and some matrix manipulation we can the optimization problem as:

$$. \min_{\mathbf{Q},\, w_i} \left\| \begin{bmatrix} 1_{3x3} & -\mathbf{u}_1 & 0_{3x1} & \dots & 0_{3x1} \\ 1_{3x3} & 0_{3x1} & -\mathbf{u}_2 & \dots & 0_{3x1} \\ \vdots & \vdots & \vdots & \ddots & \vdots \\ 1_{3x3} & 0_{3x1} & 0_{3x1} & \dots & -\mathbf{u}_n \end{bmatrix} \begin{bmatrix} \mathbf{Q} \\ w_1 \\ w_2 \\ \vdots \\ w_n \end{bmatrix} - \begin{bmatrix} \mathbf{T}_1 \\ \mathbf{T}_2 \\ \vdots \\ \mathbf{T}_3 \end{bmatrix} \right\|^2 \quad (5)$$

Such an optimization problem has a well known solution:

$$. \begin{bmatrix} \mathbf{Q} \\ w_1 \\ w_2 \\ \vdots \\ w_n \end{bmatrix} = \begin{bmatrix} 1_{3x3} & -\mathbf{u}_1 & 0_{3x1} & \dots & 0_{3x1} \\ 1_{3x3} & 0_{3x1} & -\mathbf{u}_2 & \dots & 0_{3x1} \\ \vdots & \vdots & \vdots & \ddots & \vdots \\ 1_{3x3} & 0_{3x1} & 0_{3x1} & \dots & -\mathbf{u}_n \end{bmatrix}^{+} \begin{bmatrix} \mathbf{T}_1 \\ \mathbf{T}_2 \\ \vdots \\ \mathbf{T}_n \end{bmatrix} = \mathbf{A}^{+} \begin{bmatrix} \mathbf{T}_1 \\ \mathbf{T}_2 \\ \vdots \\ \mathbf{T}_n \end{bmatrix} \quad (6)$$

where we introduced substitute **A** for shorter notation and plus (+) represents a MP-inverse matrix.

It is important to note that matrix **A** has 3n rows and 3+n columns and for it to be tall, guaranteeing unique solution n has to be at least 2, meaning that we need to see the waypoint at, at least two cameras to be able to reconstruct the pose. Detecting the same waypoint on more than 2 cameras will produce more accurate result. Also, matrix **A** is different for each keypoint, so in order to reconstruct model with e.g 33 keypoints, we need to construct 33 different matrices and solve 33 different optimization problems.This process has to be performed for each recorded frame.

### *E. ata post processing*

At this point in pipeline, we have already fully reconstructed the 3D pose of all the keypoints. The last basically depends on the usage of MoCap system. We can either save data for later use, or directly stream it to dedicated video/gaming production software, medical application, etc …

## IV. RESULTS

Complete process of image acquisition, undistortion, pose estimation and 3D reconstruction is done on laptop with Intel Core i7 10750H, 6 physical & 12 logical core 10th generation CPU with 16GB of RAM and Nvidia GeForce 1660TI GPU. Even so, we were able to achieve stable 20 FPS. The code has been implemented on Ubuntu 20.04 Focal Fossa in Python3 with extensive use of `multiprocess` library, enabling parallelization. Separate process responsible for image acquisition, undistortion and pose estimation was spawned for each camera, with one additional process tasked with 3D reconstruction, and data post processing.

Fig 6. A frame from all 3 cameras taken at the same time with detected keypoints drawn over


ISBN 978-86-7466-930-3

In Fig 6, the images from all three cameras taken at the same time are shown. The keypoints detected by MediaPipe are overlaid on top of the undistorted images. I can be noted that not all markers are detected on all 3 images, e.g right arm is not detected on first image. Nevertheless, as seen in Fig 7 it can be observed that the system was able to reconstruct the full human pose, with all keypoints. That comes from the fact that for 3D reconstruction we need a keypoint to be detected at minimum 2 cameras. Detection of a keypoint is more than 2 cameras, increases estimation accuracy. It can be noted that the reconstructed full body pose closely matches the one shown in undistorted images.

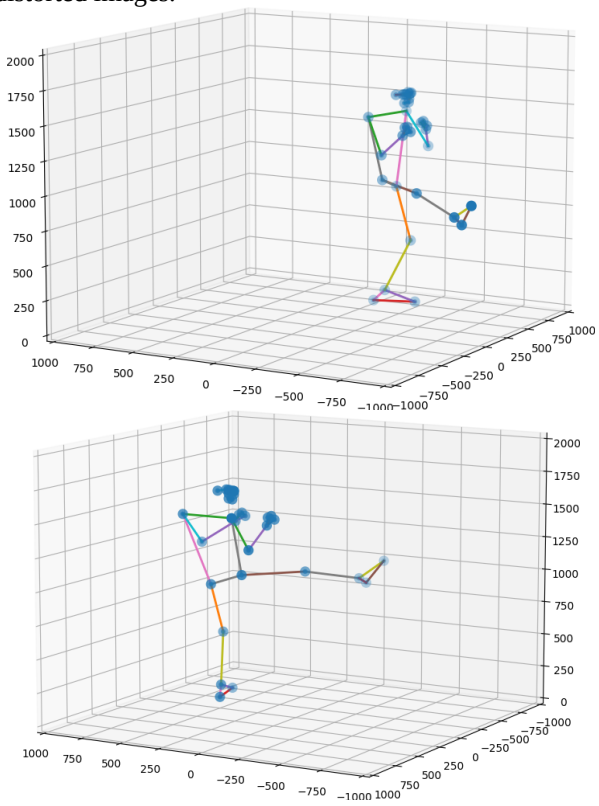

Fig 7. Full body pose reconstructed from images shown in Fig.6

However, during pose estimation some problems occurred. We can observe several frames with incorrectly detected human poses as shown in Fig. 8. Those bad reconstructions can be a result of several issues. Firstly some body parts can go out

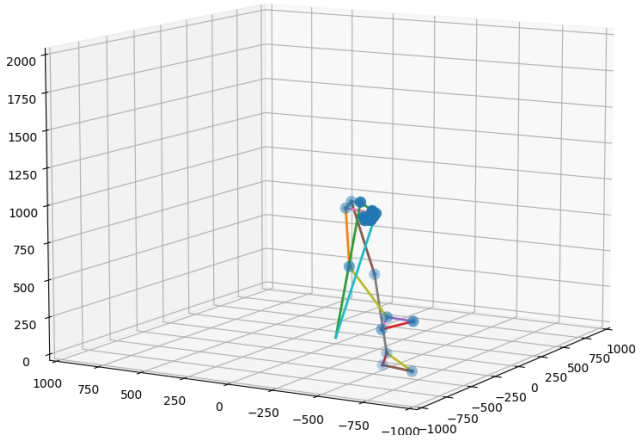

Fig 8. Incorrectly reconstructed human pose

of recording volume or be occluded by objects in the scene, thus preventing MedaPipe to detect keypoints successfully. Other issues can come out of just wrong detection pose detection as shown in the middle of Fig 9. These images show MediaPipes' inability to estimate human pose in non-standing positions. That is a result of MediaPipe being trained on dataset which consists mostly of humans in standing position. That introduces strong bias in the CNN, which expects the torso to be upright. In Fig 9. that was not the case, and MediaPipe has detected a chair in the background as humans face and shoulders. That frame prevents successful reconstruction.

## V. Conclusion

In this paper we have presented a budget MoCap system. The system uses inexpensive of-the shelf cameras with a middle-range gaming laptop. Used libraries and software are all open source, with licenses allowing commercial use. Hence, most of the price of the system comes from gaming laptop. The price of the full system was under $2500, but uses common hardware that we had at our disposal, so the MoCap didn't cost us any money. The framerate that we could have achieved was 20FPS. The reconstructed poses closely matched the pose of the actor that was recorded and were stable as long as the actor was within recording volume.

Except low price, the system doesn't require any markers, which significantly reduces setup time. There is no need for

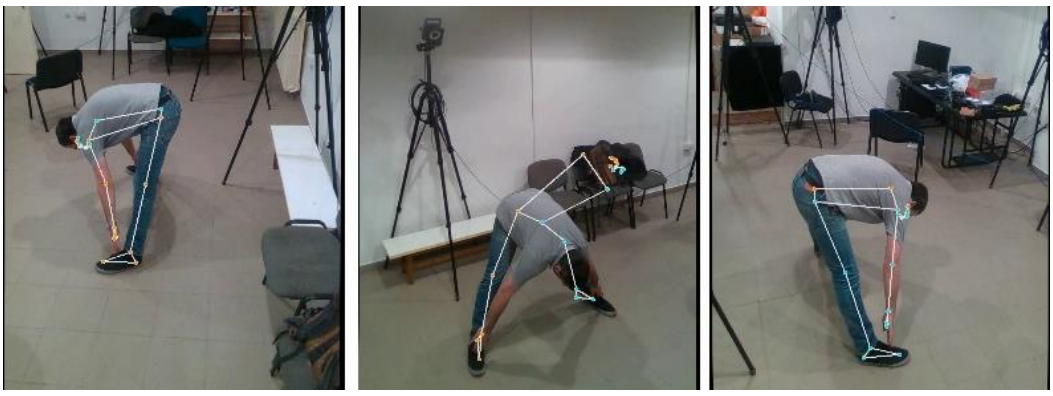

Fig 9. A frame from all 3 cameras taken at the same time with detected keypoints drawn over with incorrect human pose detections


ISBN 978-86-7466-930-3

tedious process of attaching markers to the actor. The other benefits from this is that people can be recorded while performing their task without interference. That means, the person's motion isn't modified by the fact that there are markers attached to it's body. For behavioral studies, person's motion can be recorded subject's knowledge, reducing the chance for the person to unconsciously alter the behavior. This makes developed MoCap, extremely potent for studies in sport science and behavioral studies with potential HMI application.

Although presented MoCap has a lot of potential there are a few issues that would be the topic for the future research. The current approach doesn't include the temporal continuity of the recording, but each frame is considered independently. The system doesn't consider human model, which would make detection more accurate and more robust to false detections and outliers. Finally, current deep learning backend, MediaPipe can detect only one person. OpenPose, can be used instead, but that comes at the cost of framerate and ability to run system in real time or at the price of higher performance and higher price hardware.

## REFERENCES


[1] Menolotto, M., Komaris, D. S., Tedesco, S., O'Flynn, B., & Walsh, M. (2020). Motion capture technology in industrial applications: A systematic review. Sensors, 20(19), 5687.

[2] Schönauer, C., Pintaric, T., Kaufmann, H., Jansen-Kosterink, S., & Vollenbroek-Hutten, M. (2011, June). Chronic pain rehabilitation with a serious game using multimodal input. In 2011 International Conference on Virtual Rehabilitation (pp. 1-8). IEEE.

[3] Ogrinc, M., Gams, A., Petrič, T., Sugimoto, N., Ude, A., & Morimoto, J. (2013, May). Motion capture and reinforcement learning of dynamically stable humanoid movement primitives. In 2013 IEEE International Conference on Robotics and Automation (pp. 5284-5290). IEEE.

[4] Ito, T., Ayusawa, K., Yoshida, E., & Kobayashi, H. (2020). Simultaneous Control Framework for Humanoid Tracking Human Movement with Interacting Wearable Assistive Device. IEEE Robotics and Automation Letters, 5(2), 3604-3611.

[5] Duarte, N. F., Raković, M., Tasevski, J., Coco, M. I., Billard, A., & Santos-Victor, J. (2018). Action anticipation: Reading the intentions of humans and robots. *IEEE obotics and Automation etters*, *3*(4), 4132-4139.

[6] Sharma, S., Verma, S., Kumar, M., & Sharma, L. (2019, February). Use of motion capture in 3D animation: motion capture systems, challenges, and recent trends. In 2019 International Conference on Machine Learning, Big Data, Cloud and Parallel Computing (COMITCon) (pp. 289-294). IEEE.

[7] Ikegami, Y., Nikolić, M., Yamada, A., Zhang, L., Ooke, N., & Nakamura, Y. (2020). Whole-Game Motion Capturing of Team Sports: System Architecture and Integrated Calibration. In 2020 IEEE/RSJ International Conference on Intelligent Robots and Systems (IROS) (pp. 10256-10261). IEEE.

[8] Thewlis, D., Bishop, C., Daniell, N., & Paul, G. (2013). Next-generation low-cost motion capture systems can provide comparable spatial accuracy to high-end systems. Journal of applied biomechanics, 29(1), 112-117.

[9] Bradski, G., & Kaehler, A. (2008). *earning penC Computer ision with the penC library*. " O'Reilly Media, Inc.".

[10] Intel RealSense SDK2 https://dev.intelrealsense.com/docs/python2 Accessed: May 8. 2022.

[11] Cao, Z., Simon, T., Wei, S. E., & Sheikh, Y. (2017). Realtime multi-person 2d pose estimation using part affinity fields. In *Proceedings of the IEEE conference on computer ision and pattern recognition* (pp. 7291-7299).

[12] MediaPipe Pose Module, https://google.github.io/mediapipe/solutions/pose, Accessed May 8, 2022

[13] Bazarevsky, V., & Grishchenko, I. (2020). On-device, real-time body pose tracking with mediapipe blazepose. *Google AI Blog*.


 ISBN 978-86-7466-930-3

# GAN-based Data Augmentation in the Design of Cyber-attack Detection Methods

Dušan Nedeljković and Živana Jakovljević, *Member, IEEE*

***Abstract*—The advent of the Industry 4.0 paradigm that relies on the concepts of Cyber-Physical Systems (CPS) and the Industrial Internet of Things (IIoT) leads to the transition from centralized to distributed control. In this approach, interconnected smart devices (sensors, actuators, etc.) as the key enablers achieve system control through coordinated work. Introduction of IIoT leads to ubiquitous communication between smart devices, thus opening up a vast area for potential malicious threats and attacks which can cause serious consequences, take to system dysfunction or even endanger human lives. Therefore, security mechanisms have to be developed to provide timely detection of different cyber-attacks and to keep the system safe and protected. Since industrial processes are often very complex and their analytical model is very difficult to determine, deep learning based methods for cyber-security mechanisms development are imposed as a technique of choice. Successful employment of data-driven solutions, particularly based on deep learning approaches usually requires a big amount of data. However, due to various limitations in the acquisition of data from the real process, its availability is still a major challenge. For instance, the Industry 4.0 factory implies frequent reconfiguration which reduces the time intervals available for experimental procedures such as data acquisition. One of the ways to deal with this issue is called data augmentation. In this paper, we apply data augmentation in the design of cyber-attack detection methods in Industrial Control Systems (ICS). In particular, we explore the possibilities for utilization of Generative Adversarial Networks (GAN) to generate the necessary amount of data for deep learning based modeling using a relatively small number of available samples on input.**

***Index Terms*—Data augmentation; Cyber security; Generative Adversarial Networks; Deep learning; Convolutional Neural Networks.**

## I. Introduction

IMPLEMENTATION of Cyber-Physical Systems (CPS)-based smart devices at industrial plants represents the basis for the digitization of manufacturing processes and leads to the next step in industrial evolution known as Industry 4.0 [1]. Industrial Control Systems (ICS) embrace Industrial Internet of Things (IIoT) and go through significant changes. In addition to enormous benefits, introduction of IIoT at shop-floor has a number of drawbacks, where the ubiquitous wired or wireless communication between smart devices and connection of ICS to Internet can be singled out. Since ICS are no longer isolated, communication links between IIoT devices become vulnerable for the attacks by different malicious adversaries (Fig. 1). To address this issue specially designed systems for ICS cyber-attacks detection and communication links protection are necessary.

Considering the real-time operation of ICS and safety related issues such as catastrophic damages or even threat to human lives that cyber-attacks can bring about, the requirements for cyber-security systems in ICS differ from general information technologies (IT). Opposite to general IT where the data confidentiality is paramount, in ICS data availability, along with its integrity, is the most important [2, 3]. Another key aspect of ICS is that expected lifetime of ICS components (at least 10-15 years) is significantly longer than in general IT (3-5 years) [4] and that, as a result, ICS contain a large number of devices that use legacy communication protocols that do not even utilize the basic protection mechanisms such as authentication [5]. In addition to multilayered protection mechanisms based on network segmentation and segregation, one of the key concepts for cyber-security in ICS is Defense-in-Depth. This concept implies the ability of the devices within ICS to recognize an attack if it bypasses previous layers and that the device should do this before the attack achieves the desired effects [6]. For these purposes host based (installed on the device) Intrusion Detection Systems (IDS) are developed.

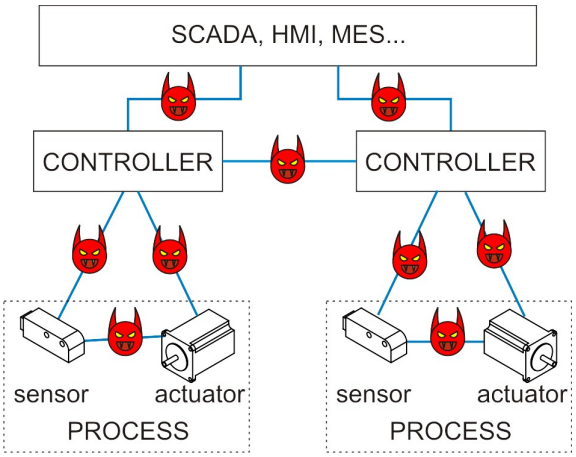


Fig. 1. Cyber-attacks on communication links in ICS within Industry 4.0

Generally, IDS within ICS are based on the model of the system behavior or the data communicated between system

Dušan Nedeljković, MSc (ME) is with the Faculty of Mechanical Engineering, University of Belgrade, 16 Kraljice Marije, 11000 Belgrade, Serbia (e-mail: dnedeljkovic@mas.bg.ac.rs).

Prof. Dr. Živana Jakovljević is with the Faculty of Mechanical Engineering, University of Belgrade, 16 Kraljice Marije, 11000 Belgrade, Serbia (e-mail: zjakovljevic@mas.bg.ac.rs).

 ISBN 978-86-7466-930-3

elements, and the attack is detected as the discrepancy between modeled and exhibited behavior of the system or as the discrepancy between modeled and data received through communication links. Depending on the approach for the model generation, IDS within ICS can be classified in two high level categories: design based and data based. In the design based approaches the model of the system/data is obtained in a mathematically formalized way using analytical models or different formal methods depending on the system type [7, 8].

Data based approaches, on the other hand, use the data obtained during system operation to create the model usually using different machine learning (ML) techniques. These approaches can be supervised, semi-supervised and unsupervised [9]. Supervised methods use labeled datasets containing data obtained during normal system operation and during system operation under attacks to generate detection mechanisms [10, 11]. Unsupervised methods, on the other hand, generate IDS using unlabeled data again containing the data obtained from the system performing with and without attack, and ML techniques find the structure within data themselves. The main shortcoming of the considered classes of methods is that they show low generalization properties when attacks not present during IDS creation are exhibited on the system.

Finally, semi-supervised methods use only the data obtained during normal system operation, i.e., from the system that was not subject to the attacks. They generate the model of the system behavior/communicated data during normal operation and the attack is recognized as the discrepancy between exhibited and the values estimated using the developed models. This class of approaches is most commonly utilized and shows better generalization to different kinds of attacks [12, 13, 14].

In our previous work [14] we have proposed a method for the development of IDS on communication links within ICS that is based on Convolutional Neural Networks (CNN). The proposed method, as well as the other data driven methods, requires significant amount of data from the real-world ICS that cannot be always easily obtained. In this paper we explore the possibility of augmentation of real-world data using Generative Adversarial Networks (GAN) and utilization of thus obtained dataset for IDS creation.

The reminder of the paper is structured as follows. Section 2 briefly describes GAN, whereas Section 3 refers to the utilized method for the development of IDS in ICS. Performance of IDS created using the data generated with a GAN and its comparison with IDS created based on real-world data are shown in Section 4 using an example of electro-pneumatic positioning system based on smart devices. Finally, in Section 5 we provide conclusions and future work guidelines.

## II. Generative Adversarial Networks

Generative Adversarial Networks (GAN) represent a method for creation of generative model using adversarial process [15]. GAN consists of two players:

- Generator G that has the goal to generate data with the distribution close to the distribution of training data (Fig. 2.a), and
- Discriminator D with the goal to recognize if the data is created by generator or comes from the original dataset through classification of input as real or generated (fake) data (Fig. 2.b).

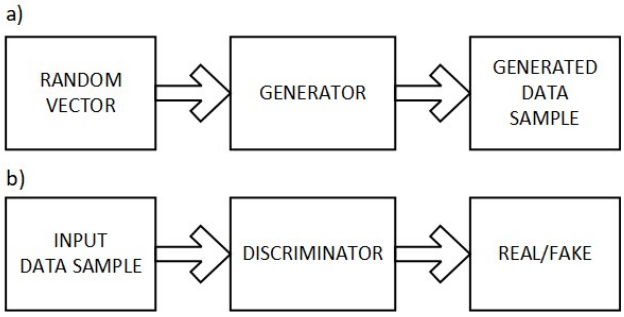


Fig. 2. Generative Adversarial Network: a) Generator, b) Discriminator

GAN training is a two player adversarial game in which generator generates fake data and tries to force discriminator to make a mistake and to recognize this data as real [16, 17]. As a rule, at the generator input is a vector of random numbers (vector of latent variables) and at its output is multidimensional vector that represents the generated data (Fig. 2.a). This data is at the input into discriminator, whereas at the discriminator output is a scalar which represents the probability that the input data is real and classifies the input accordingly (Fig. 2.b).

Generator and discriminator are trained simultaneously, where generator creates a batch of fake samples that are along with a batch of real samples from training dataset put to discriminator to classify them [16]. Based on the quality of discriminator's classification, the generator is updated to create "better" fake data and discriminator is updated to perform better classification. This adversary game repeats for a predefined number of iterations.

Generator and discriminator can be in the form of different ML based models. In our approach we will use deep neural networks (DNN), in particular CNNs and fully connected neural networks – Multilayer Perceptron (MLP).

## III. CNN-based Method for the Development of IDS in ICS

The CNN-based method for the development of IDS in ICS that we have proposed in our previous work [14] belongs to the class of semi-supervised data driven methods and consists of the offline and online phase. During offline phase it generates the CNN based model of signals transmitted between IIoT devices using the data acquired during normal system operation. The model is based on auto-regression of the transmitted signals where the current value of the signal is estimated using a buffer of previously received $v$ values. The

 ISBN 978-86-7466-930-3

main characteristic of this method is that it is designed to autonomously find the CNN with relatively small number of parameters that models the training data with good accuracy, opposite to alternative approaches that are as a rule based on manual trial and error.

IDS offline development consists of three main steps (Fig. 3). The first step represents signal preprocessing that performs FIR filtering, data structuring in ordered pairs prepared for training and data shuffling. CNN hyper-parameters (number of CNN layers, size and number of filters within them, number of pooling layers and their parameters, number of dense layers and number of neurons within them, etc.) are varied in the second step, and for each combination a CNN model is created. Finally, in the third step the generated model is selected as appropriate if it satisfies the following criteria:

1. The variance between real and estimated values should be similar for test and training data; this insures that the model is not prone to overfitting or underfitting.
2. The simulation of online performance of the IDS based on the developed model should show good performance in terms of false positive attacks detection; this insures the robustness of IDS to false attack detection online which is very important for smooth operation of ICS.

Once the model that meets given criteria is encountered, the offline procedure stops and this model is put to online detection of attacks. During online phase, the attack is detected based on the discrepancy between estimated and signal values received through communication links. If this discrepancy is higher than threshold automatically calculated from training data for $z$ consecutive signal samples, the attack is detected.

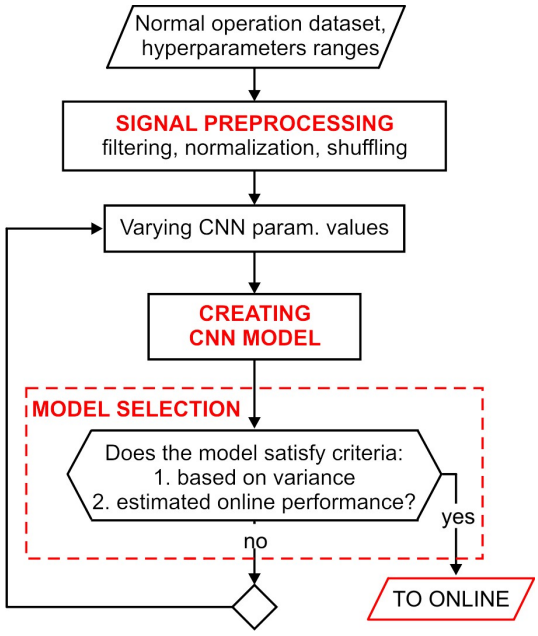


Fig. 3. Overview of the method for IDS development – offline phase

As can be observed from the presented short overview of the method, as all DNN based methods, it is highly dependent on the quality and quantity of the training data and it requires a large amount of this data at input. Acquisition of the data from the system in normal operation requires that the system is operated in isolated conditions without possibility for the attacks. Here the question arises if it is possible to operate the system long enough in such conditions to get sufficient amount of data. Another important issue that is present in Industry 4.0 factory is frequent reconfiguration of resources which leaves little room for experimenting with it. So the acquisition of appropriate amount of data from the system can be hardly feasible in some situations. For this reasons in the following section we explore the possibilities to use relatively small amount of data from real process and to augment it with data obtained using GAN.

## IV. The Development of IDS for Electro-Pneumatic Positioning System based on Data Generated using GAN

In this paper we will develop IDS using GAN generated data for experimental electro-pneumatic positioning system – DisEPP (Fig. 4) that consists of:

1. Smart pneumatic cylinder, based on rodless cylinder driven by electro-pneumatic pressure regulator (EPR) that regulates pressure in 2-6 bar range on one and by mechanically controlled pressure regulator (MR) set to 4 bar on the other side, that is controlled by local controller LC1;
2. Smart encoder based on magnetic linear encoder controlled by LC2.

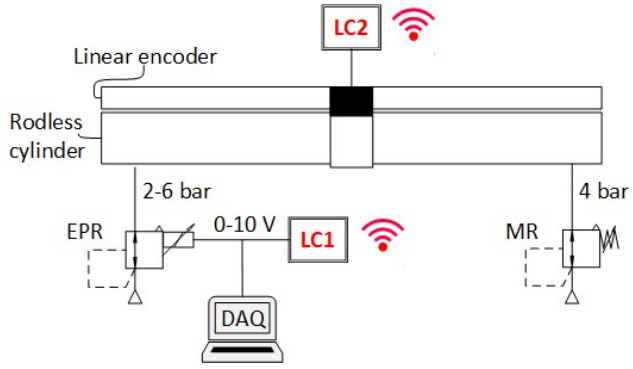


Fig. 4. A schematic representation of electro-pneumatic positioning system DisEPP

Both, LC1 and LC2 represent “mbed” devices based on ARM Cortex-M3 running at 96 MHz [18] augmented by IEEE 802.15.4-compliant wireless transceiver Microchip MRF24J40MA [19] that is used for communication between devices. The control task given in the form of desired piston positions is distributed between LC1 and LC2 in such way that: (i) LC2 has desired trajectory at input and calculates the corresponding pressure on electro-pneumatic regulator using PID and sensory signal; (ii) LC2 communicates PID output to

 ISBN 978-86-7466-930-3

LC1 using IEEE 802.15.4; (iii) LC1 converts received PID output to the 0-10 V range and puts it to electro-pneumatic pressure regulator which finally sets the pressure to 2-6 bars (proportional to the received voltage) and invokes the piston movement.

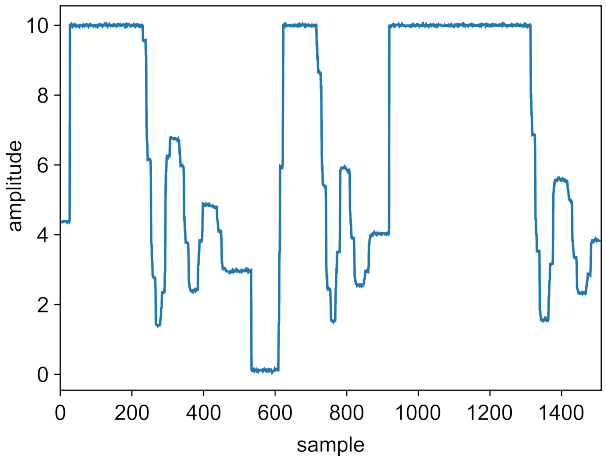


Fig. 5. An excerpt of signal acquired from DisEPP

IEEE 802.15.4 communication link between LC1 and LC2 represents vulnerable point for cyber-attacks and should be protected using IDS. The first step in IDS design using method from section III is generation of dataset representing signals obtained during normal system operation. For this purpose, we have acquired the voltage put to electro-pneumatic pressure regulator using National Instruments Data Acquisition (DAQ) system operating with 100 Hz sampling rate. A total of 399,000 samples $x_i$, $i \in [1, 399{,}000]$ were acquired and an excerpt of 1,500 samples is presented in Fig. 5.

### *A. Data Augmentation using GAN*

To augment the data acquired from DisEPP we have developed a GAN with the following elements. The discriminator (Fig. 6) has the following architecture:

1. Two blocks of: (i) convolutional layer with 30 filters, each containing 10 samples, with ReLU (Rectified Linear Unit) activation function, followed by (ii) dropout layer with 0.2 dropout rate;
2. Flattening layer;
3. Output layer with one neuron.

At input of discriminator is a generated/real signal with length of 1,500 samples and estimation if this signal is generated or real (0/1) is at output.

The generator (Fig. 7), on the other hand, has the following architecture:

1. Input latent vector of 1,000 random numbers;
2. One dense layer with 100 neurons and sigmoid activation function;
3. Fully connected output layer with 1,500 neurons.

The generator generates 1,500 samples based on 1,000 random numbers.

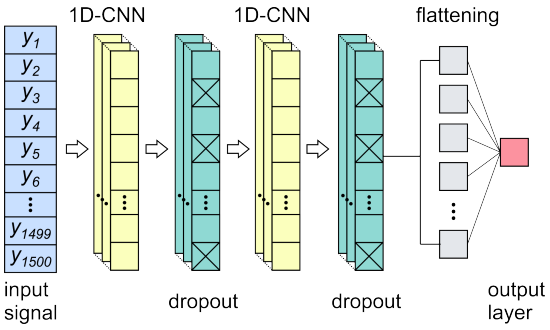


Fig. 6. The architecture of discriminator

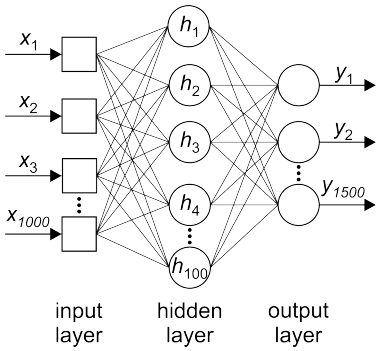


Fig. 7. The architecture of generator

For GAN training a batch of 2,000 real signals $\boldsymbol{s_i}$, $i \in [0, 1999]$, with length of 1,500 samples each, are extracted from training dataset in the following way:

$$\boldsymbol{s_i} = [x_{50i+1}, x_{50i+2}, \ldots x_{50i+1500}] \quad (1)$$

exploiting a total of 101,450 samples acquired from DisEPP. During training 500 epochs were employed.

Figure 8 presents an example of signal obtained using the trained generator. This signal is similar to the excerpt of signal obtained from real process (Fig. 5).

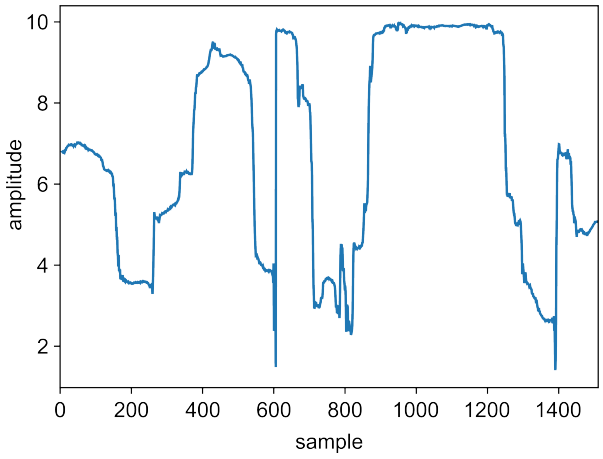


Fig. 8. An example of signal obtained using the generator


ISBN 978-86-7466-930-3

### B. *IDS creation using generated and acquired signals*

Following the procedure presented in Section III, two IDS were created: one using generated signals, and the other using real signals obtained from DisEPP. The same preprocessing procedure is applied to both signals, where the buffers of $v$=16 samples were used. The employed FIR filter in signal processing has pass band of [0, 0.11π], stop band of [0.35π, π], transition region in between. The filter is composed of 11 coefficients ([0.020243, 0.023017, 0.054189, 0.10397, 0.12557, 0.12344, 0.12557, 0.10397, 0.054189, 0.023017, 0.020243]) that are generated by the Parks-McClellan algorithm. After applying the filter, the signal is normalized by its maximum value. During models training, the whole datasets (signals structured into ordered pairs) are divided into training, validation and test part, with a share of 70/10/20%, respectively. Model training was performed through 5 epochs with Adam optimizer (learning rate of 0.001) and the mean squared error (MSE) cost function.

Following the procedure presented in Section III, two CNN models were developed:

1. based on signals generated using GAN where a total of 266 signals with 1,500 samples containing a total of 391,818 ordered pairs;
2. based on real signal from DisEPP that contains 399,000 samples corresponding to 398,973 ordered pairs.

For both signals (real and generated) the models with the same architecture were obtained. This architecture is composed of the following layers:

- 1D-CNN (4 filters, kernel size=2)
- 1D-CNN (8 filters, kernel size=2)
- Max pooling (pooling rate=2)
- 1D-CNN (16 filters, kernel size=2)
- 1D-CNN (16 filters, kernel size=2)
- Max pooling (pooling rate=2)
- Flattening
- Dense (30 neurons)
- Dense (1 neuron).

and it has a total of 2865 trainable parameters. The model was trained in Python v3.8.5 using a Spyder with TensorFlow v2.3.0 in the background.

In the online part of the algorithm, the detection threshold is calculated as a sum of the mean ($\mu$) value and the triple standard deviation ($\sigma$) of discrepancies between received and estimated values over the testing data:

$$T=\mu+3\sigma \tag{2}$$

and it was $T$=0.00941 for the IDS based on generated and $T$=0.00956 for IDS based on real-world data.

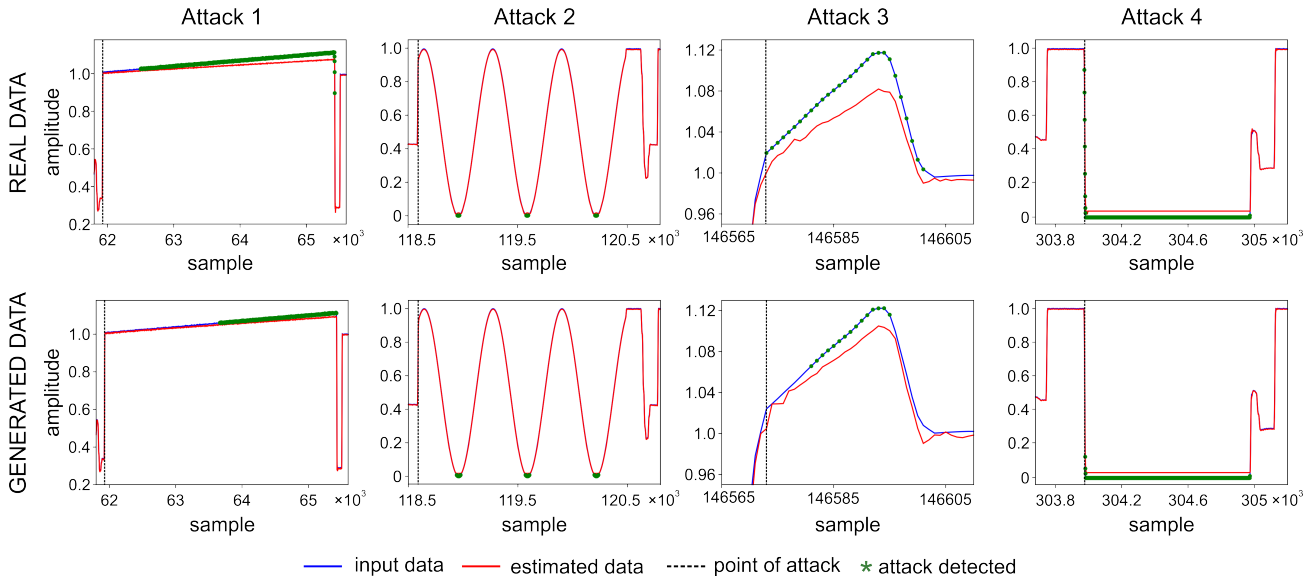


Fig. 9. Detected cyber-attacks

If the discrepancy between real and estimated value is higher than the threshold for $z$=15 consecutive signal samples, then the attack is detected.

To test the performance of the developed IDSs they were simulated using in Python using a number of the designed attacks. In this paper, we present and compare the performances of IDSs using four attacks with different shapes and duration. Attacks 1 and 3 increase signal value linearly by 0.00003 and 0.005 per sample, respectively, where in attack 1 random noise was introduced as well. Attack 2 utilizes sine function to generate signal value, whereas in attack 4 the signal value is set to 0 for predefined time period.

The results of attacks detection using IDSs obtained based on generated and real data are presented in Fig. 9. In this Figure input data and their estimation are shown in blue and red lines, respectively, the start of the attack is represented with a black dashed line, whereas the moments when the attack was detected are marked with green markers. Both

 ISBN 978-86-7466-930-3

models proved to be equally effective and successfully detected all attacks without false positives.

It can be noticed from the Fig. 9 that the model based on the real data detected attack 1 earlier than the model that used GAN-generated data for training. On the other hand, for attacks 2, 3, and 4, the difference between the detection moments is negligible.

## V. Conclusion

In this paper, we have explored the possibilities for utilization of GAN based data augmentation in the design of IDS for ICS using an example of electro-pneumatic positioning system DisEPP based on smart devices. Using a limited number of real signal samples obtained from the DisEPP, an amount of data sufficient for deep learning based generation of IDS was generated. Using the previously developed attack detection method based on CNN, two IDS were created: one using generated signals, and the other using real signals obtained from DisEPP. To evaluate the performance of the created IDSs, a number of attacks have been created, of which four are presented in the paper. As presented in the paper, the IDS based on generated data was able to successfully detect all cyber-attacks without false positives. It presented the similar performances as IDS based on original data not only in terms of a number of detected attacks, but also in terms of attack detection latency, thus confirming that GAN augmented data can be successfully utilized for the generation of semi-supervised data based IDS in ICS.

In the future, we plan to extend our work to additional datasets that contain a higher number of signals and attacks. Furthermore, our research efforts will be directed to the application of different types of GAN and a comparison of their performances.

## Acknowledgment

This research was supported by the Science Fund of the Republic of Serbia, grant No. 6523109, AI-MISSION 4.0 as well as by the Ministry of Education, Science and Technological Development of the Serbian Government under the contract No. 451-03-68/2022-14/200105.

## References

[1] H. Kagermann, W. Wahlster, J. Helbig, *Recommendations for implementing the strategic initiative INDUSTRIE 4.0*, 2013. [Online]. Available: http://www.acatech.de

[2] M. R. Asghar, Q. Hu, S. Zeadally, "Cybersecurity in industrial control systems: Issues, technologies, and challenges," *Computer Networks*, vol. 165, article no. 106946, 2019.

[3] D. Upadhyay, S. Sampalli, "SCADA (Supervisory Control and Data Acquisition) systems: Vulnerability assessment and security recommendations," *Computers & Security*, vol. 89, article no. 101666, 2020.

[4] K. Stouffer, J. Falco, K. Scarfone, *Guide to industrial control systems (ICS) security*. NIST special publication, 2015.

[5] Y. Xu, Y. Yang, T. Li, J. Ju, Q. Wang, "Review on cyber vulnerabilities of communication protocols in industrial control systems," IEEE Conference on Energy Internet and Energy System Integration (EI2), pp. 1-6, IEEE, Beijing, China, Nov. 2017.

[6] Industrial Control Systems Cyber Emergency Response Team, Recommended Practice: Improving Industrial Control System Cybersecurity with Defense-in-Depth Strategies, 2016, Available: https://www.cisa.gov/uscert/sites/default/files/recommended_practices/NCCIC_ICS-CERT_Defense_in_Depth_2016_S508C.pdf, Accessed on: Mar. 2022.

[7] L. K. Carvalho, Y. C. Wu, R. Kwong, S. Lafortune, "Detection and mitigation of classes of attacks in supervisory control systems," *Automatica*, vol. 97, pp. 121-133, 2018.

[8] Z. Jakovljevic, V. Lesi, M. Pajic, "Attacks on Distributed Sequential Control in Manufacturing Automation," *IEEE Transactions on Industrial Informatics*, vol. 17, no. 2, pp. 775-786, 2021.

[9] M. Elnour, N. Meskin, K. Khan, R. Jain, "A Dual-Isolation-Forests-Based Attack Detection Framework for Industrial Control Systems," *IEEE Access*, vol. 8, pp. 36639-36651, 2020.

[10] S. Sapkota, A. K. Mehdy, S. Reese, H. Mehrpouyan, "Falcon: Framework for anomaly detection in industrial control systems," *Electronics*, vol. 9, no. 8, article no. 1192, 2020.

[11] A. Al-Abassi, H. Karimipour, A. Dehghantanha, R. M. Parizi, "An ensemble deep learning-based cyber-attack detection in industrial control system," *IEEE Access*, vol. 8, pp. 83965-83973, 2020.

[12] G. Raman MR, N. Somu, A. Mathur, "A multilayer perceptron model for anomaly detection in water treatment plants," *International Journal of Critical Infrastructure Protection*, vol. 31, article no. 100393, 2020.

[13] M. Kravchik, A. Shabtai, "Detecting Cyber Attacks in Industrial Control Systems Using Convolutional Neural Networks," Proceedings of CPS-SPC 18 Conference, pp. 72-83, Toronto, Canada, Oct. 2018.

[14] D. Nedeljkovic, Z. Jakovljevic, "CNN based method for the development of cyber-attacks detection algorithms in industrial control systems," *Computers & Security*, vol. 114, article no. 102585, 2022.

[15] I. Goodfellow, J. Pouget-Abadie, M. Mirza, B. Xu, D. Warde-Farley, S. Ozair, A. Courville, Y. Bengio, "Generative adversarial nets," *Advances in neural information processing systems*, vol. 27, 2014.

[16] J. Brownlee, *Generative Adversarial Networks with Python: Deep Learning Generative Models for Image Synthesis and Image Translation*. Machine Learning Mastery, 2019.

[17] F. Chollet, *Deep learning with python*. Manning, Shelter Island, NY, USA, Nov. 2017.

[18] NXP Semiconductors N.V. (2009, Feb.), "LPC1769/68/66/65/64/63 32-bit ARM Cortex-M3 microcontroller," [Online]. Available: https://www.nxp.com/docs/en/data-sheet/LPC1769_68_67_66_65_64_63.pdf, Accessed on: Mar. 2022.

[19] Microchip Technology Inc. (2008) "MRF24J40MA 2.4 GHz IEEE Std. 802.15.4TM RF Transceiver Module," [Online]. Available: http://ww1.microchip.com/downloads/en/DeviceDoc/70329b.pdf, Accessed on: Mar. 2022.

 ISBN 978-86-7466-930-3

# Comparison of SLAM algorithms on omnidirectional four wheel mobile robot

Slaven Petković, Lazar Milić, Milutin Nikolić, Dragiša Mišković, and Mirko Raković

***Abstract*—In this article we present a comparative analysis of various SLAM algorithms. We compared robot trajectories computed by three ROS-based SLAM algorithms to a reference trajectory obtained from Vicon motion capture system. For data acquisition purposes we used mobile robot with four omnidirectional (*mecanum*) wheels. Our mobile platform was equiped with following sensors: 3D lidar, a RGB-D camera and motor encoders. Experiments were conducted indoor in an office environment. Acquired dataset was used as an input data for all algorithms that we tested. Following algorithms have been taken into account: Livox Mapping, RTAB-Map and Cartographer.**

***Index Terms*—Simultaneous Localization and Mapping, SLAM, ROS, Mobile robot**

## I. Introduction

ONE of the most important tasks for autonomous mobile robots is to create a consistent map of unknown environment and to determine its location inside that map. This problem is known as Simultaneous Localization and Mapping (SLAM) and it is considered a difficult problem, because robot needs good estimate of its location in order to create a valid map, but at the same time robot needs consistent map to determine its location.

Problem was first defined back in 1986 [1]. There are two main approaches for solving SLAM problem: probabilistic approach and non-probabilistic approach. The probability methods are based on Bayesian estimation method. Many methods were developed, such as SLAM based on Kalman Filter, Extended Kalman Filter [2], Particle Filter [3], Rao-Blackwellized Particle filter [4], etc.

Nowadays there are many different methods for solving SLAM problem. In this article we focus on SLAM algorithms that are available as an *open-source* ROS (Robot Operating System) [5] package and that have support for 3D lidar and/or RGB-D camera. For purpose of acquiring data, mobile robot with four omnidirectional wheels was used and all experiments were done indoor.

## II. Related Work

In this section, we provide an insight into papers that deal with the comparison of SLAM algorithms. Paper [6] provides benchmark for two popular SLAM algorithms: RTAB-Map and RGBD SLAM. Paper [7] shows comparison results of three different mapping approaches. Comparison between three modern VSLAM approaches : RTAB-Map, ORB-SLAM3 and OpenVSLAM is presented in [8]. In article [9] authors show comparison of trajectories computed by various ROS-based SLAM systems in office environment. This article presents a different approach to comparing SLAM algorithms.

S. Petković, L. Milić, M. Nikolić, M. Raković are with the Faculty of Technical Science, University of Novi Sad, (e-mail: rakovicm@uns.ac.rs). D. Mišković is with the Institute for Artificial Intelligence Research and Development of Serbia, Novi Sad, Serbia

## III. Compared SLAM algorithms

### A. RTAB-Map

RTAB-Map (Real-Time Appearance-Based Mapping) [10] is an open-source library released in 2013 and is still in the development. It is a graph-based SLAM approach with memory management available as *rtabmap_ros* ROS package. RTAB-Map is very flexible SLAM approach because it supports wide range of input sensors such as odometry from any source, RGB-D or stereo cameras and optionally 2D/3D lidar data. Package consists of main *rtabmap_ros/rtabmap* node, two nodes for visual odometry (*stereo_odometry* and *rgbd_odometry*) and lidar odometry node (*icp_odometry*). As RTAB-Map supports inputs from multiple different sensors, data obtained from these sensors needs to be synchronized in order to create a valid map. There are two types of synchronization in RTAB-Map: exact synchronization and approximate synchronization. RTAB-Map can be configured with large number of parameters whose description can be found in [11].

### B. Cartographer

Google's Cartographer is lidar graph-based SLAM approach. Cartographer is used for indoor mapping and it supports 2D and 3D lidar data as well as odometry data. In the process of creating map Cartographer uses lidar scans or point cloud to create sub-maps and when loop-closure is detected it runs pose optimization in order to minimize error. First part of this process is managed by Cartographer's local SLAM subsystem (also called frontend), while optimization is done using Cartographer's global SLAM subsystem (also called backend). Detailed description of Cartographer can be found in [12]. On official web page [13] one can find algorithm explanation, description of all parameters and tips for parameter adjustment.

### C. Livox Mapping

Livox mapping is a SLAM algorithm developed for creating a map using only Livox lidars. It is available as *livox_mapping* ROS package which supports multiple Livox 3D lidars. Algorithm also uses odometry data, for example wheel odometry. In the development of this package, authors reference to [14]-[16].

 ISBN 978-86-7466-930-3

## IV. System setup and Data set acquisition

In this section, we will present the hardware and software used to conduct the experiment. Experiment consists of three main modules: (1) Vicon system for motion capture, (2) a mobile robot for acquiring sensor data and (3) a notebook for running and comparing SLAM algorithms.

### A. Vicon system

Vicon system is a highly accurate motion capture system. This system can be used in multiple applications, like robot tracking, human motion capture, etc. In our experiment, the main task of this system was to capture robot's motion and compute trajectory of the robot. This trajectory was used as a reference trajectory to compare and evaluate different SLAM algorithms. Our indoor testing environment with Vicon system and mobile robot is shown in Figure 1. In this experiment Vicon system consisted of (1) seven Vicon MX T-20S cameras, (2) Vicon MX Giganet and (3) desktop computer with Vicon Nexus software used for data processing. Calibration of cameras is done using Vicon Active Wand calibration device and Vicon Nexus software. In this experiment, the operating frequency of Vicon cameras was set to 200 Hz.

Fig. 1: Experimental setup with Vicon cameras and mobile robot

In order to record the movement of the mobile robot, it was necessary to place reflective markers on the mobile robot, which can be tracked by motion capture system. Position and orientation of these markers defines coordinate system of tracking object created in Vicon Nexus software. The orientation of the coordinate system depends on the order in which the markers are selected in Vicon Nexus software. Figure 2 shows three markers placed on the mobile robot. To make it easier to compare data later, the position and orientation of the markers on the mobile robot is chosen to match *base_link* coordinate system defined in robots URDF model (*Unified Robot Description Format*).

### B. Mobile robot

Mobile robot used in this experiment was a four wheel omnidirectional mobile robot (Figure 3). This construction with

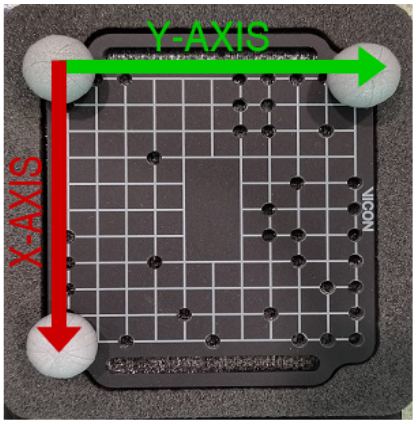


Fig. 2: Reflective markers used to track robot motion by Vicon system. Position of markers determines position and orientation of coordinate system of tracked object

omnidirectional wheels (*mecanum wheels*) enables it to move in multiple directions and change direction rapidly. Mecanum wheel consists of $k$ rollers made of rubber positioned at 45 degrees angle offset from the wheel rotation around its circumference. Paper [17] describes geometry and kinematics of mecanum wheels. Main problem with this type of mobile robots is that robot's wheels slip, and odometry based on encoders from wheels can not be considered as reliable.

Fig. 3: Omnidirectional four-wheeled mobile robot

Running SLAM algorithms on ROS requires a file that describes robot's physical state to ROS. Creating robot model was done using URDF. URDF is an XML file format used to describe all components of a robot. Figure 4 presents model of our mobile robot and positions of coordinate systems presented in RViz.

Robot's software runs on Ubuntu 18.04 operating system and ROS Melodic. Following sensors were mounted on mobile robot in this experiment: 3D lidar, RGB-D camera and wheel

 ISBN 978-86-7466-930-3

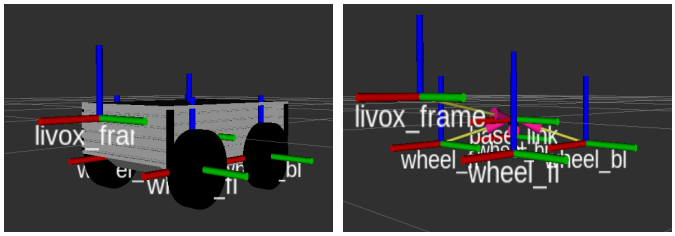


(a) Robot visualization in RViz (b) Robot coordinate systems

Fig. 4: Mobile robot model in RViz

encoders. Detailed information about robot configuration is presented in Table I.

| | |
|---|---|
| **Hardware** | |
| CPU | AMD Ryzen 7 2700u |
| GPU | AMD Radeon Vega 10 Graphics |
| RAM | 16 GB DDR4 |
| **Sensors** | |
| Lidar | Livox MID-70 |
| Camera | Intel RealSense D435i |
| **Software** | |
| Operating System | Ubuntu 18.04 Bionic Beaver |
| ROS | ROS Melodic Morenia |

TABLE I: Hardware and software specifications of mobile robot

### C. Data processing

In order to get the most valid comparison results, the goal was to record data from robot sensors to one file, so every SLAM algorithm tested in this experiment could use the same input data. For this reason we run offline all the SLAM algorithms that are evaluated. Detailed information about computer configuration that was executing SLAM algorithms is shown in II.

| | |
|---|---|
| **Hardware** | |
| CPU | Intel Core i7-10750H |
| GPU | NVIDIA RTX 2060 6GB |
| RAM | 16 GB DDR4 3200 MHz |
| **Software** | |
| Operating System | Ubuntu 18.04 Bionic Beaver |
| ROS | ROS Melodic Morenia |

TABLE II: Hardware and software specifications of computer used for data processing

## V. Metrics and data comparison

In this section, we give an insight into how the Vicon system and ROS represents robot pose. We also present metrics for analyzing performance of SLAM algorithms by comparing trajectories and robot poses generated by each SLAM algorithm to a ground truth trajectory and robot poses computed by Vicon system. We did not compare generated maps. The idea was to compare predicted robot pose to an actual robot pose in every moment in time. As robot pose in plane consists of three components, $x$ and $y$ coordinate and rotation around z-axis, we compared each component of robot motion separately. Then the error for all three components of robot motion was calculated.

### A. Data representation

*1) Vicon system:* Vicon Nexus software is able to export data in number of different formats. We have chosen to work with *.csv* file. Table III shows an example of *.csv* file generated by Vicon Nexus software. Values *RX*, *RY* and *RZ* represent rotation of robot's base coordinate frame around $x$, $y$ and $z$ axis respectively, while *TX*, *TY* and *TZ* represent position of robot's coordinate frame in $x$, $y$ and $z$ direction respectively with respect to the reference frame. All values are expressed in relation to the origin of the coordinate system defined by the position of the Vicon Active Wand during calibration. Frame column was used to calculate timestamp.

| Frame | Sub Frame | RX | RY | RZ | TX | TY | TZ |
|---|---|---|---|---|---|---|---|
| number | number | [deg] | [deg] | [deg] | [mm] | [mm] | [mm] |

TABLE III

*2) SLAM algorithms:* The ability of Robot Operating System to record data from any available topic was used for generating data set. Recorded data was saved to *.bag* file. ROS represents robot pose as *geometry_msgs/Pose* ROS message and it also enables us to export in *.csv* file. Unlike Vicon system, ROS uses Quaternion to display robot rotation.

### B. Data comparison

Comparing two trajectories requires them to consist of same number of points (robot poses) and to be synchronized in time. In our case, neither of these two conditions was met.

As previously said, we collected data from sensors mounted on mobile robot and run algorithms offline using collected data to generate test data set. Reference trajectory was computed by Vicon system. These systems are not synchronized in time.

First problem was how to equalize the beginnings of two compared trajectories in time. In order to do that, we decided to find moment in time in which robot made a movement for 1 mm in $x$ or $y$ direction.

Second problem was that every ROS algorithm publishes messages about robot pose at different rate and Vicon system frequency was 10 to 20 times greater than frequency at which ROS algorithms publish messages. In order to deal with this problem, there were two possibilities: to reduce the size of reference data set or to expand test data set. We opted for the latter and decided to do an interpolation over data generated by SLAM algorithms.

### C. Metrics

Interpolation was done by time for every component of robot motion: $x(t)$, $y(t)$ and $\theta(t)$. Figure 5 shows example of interpolation in case of function $x(t)$.


ISBN 978-86-7466-930-3

As previously sad, SLAM algorithms publish messages about robot pose less frequently than Vicon system. In this paper interpolation was used to calculate new value in test data set for every moment in time of reference data set. Let's observe point ($t_i$, $x_i$) from the reference data set. In order to calculate new value we decided to find two points in the test data set which were closest in time to the observed point. On figure 5 points A($t_j$, $x_j$) and B($t_{j+1}$, $x_{j+1}$) represent two closest points. Equation of line connecting points A and B was calculated. Inserting value of $t_i$ into new equation, interpolated value $x_{interp}$ is calculated.

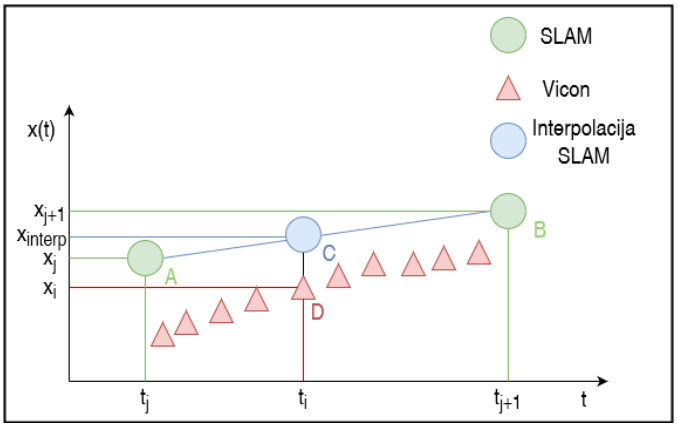


Fig. 5: The figure illustrates an example of interpolation used to generate new data in test data set

Data processing and comparison was done using the Python 3 programming language and the *NumPy* library, as one of the best open-source tools for working with data and numerical calculations.

## VI. Results and Analysis

In this section we present results of our experiment. Results are presented graphically and numerically. For visualizing results, we used Python programming language and *Matplotlib* library. Results are presented in four graphs for each tested SLAM algorithm. First figure contains estimated trajectory (shown in red) computed by SLAM algorithm and reference trajectory computed by Vicon system (shown in green). Other three figures show comparison of *x(t)*, *y(t)* and $\theta(t)$ functions respectively. Table IV presents numerical results of our experiments. Error is represented as RMSE (*Root Mean Square Error*), standard deviation, mean absolute error and maximum absolute error.

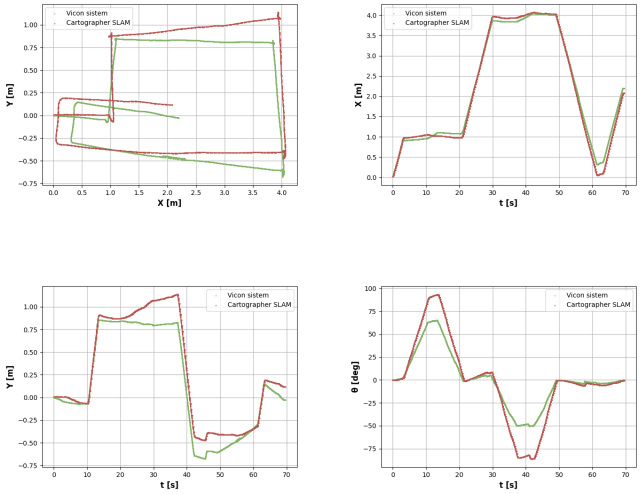


Fig. 6: Trajectory recovered from Cartographer SLAM (red) vs Vicon system reference trajectory (green)

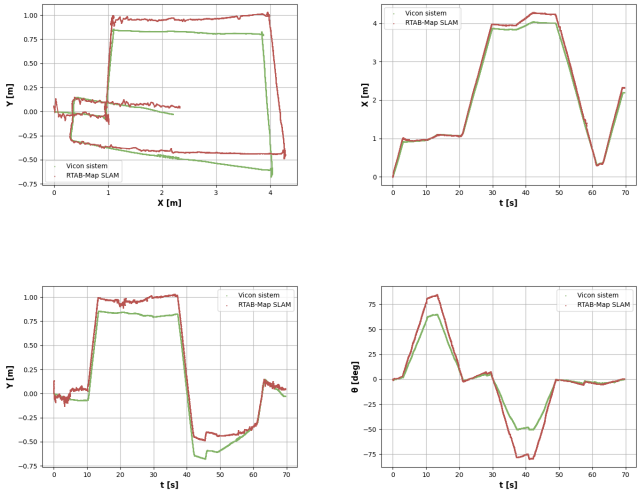


Fig. 7: Trajectory recovered from RTAB-Map (red) vs Vicon system reference trajectory (green)

## VII. Conclusion

In this paper, we have presented a method for analyzing performance of ROS-based SLAM algorithms that compares trajectories computed by SLAM algorithm to a reference trajectory obtained from motion capture system. We proposed a metric for calculating error in estimated trajectory. This approach allows us to compare algorithms that use different sensor information.

Since omnidirectional wheels are slipping during the motion of robot, the localisation of the robot has to be based on sensory system that is not measuring motion of wheels directly. Therefore, the robot is build with 3D Lidar and RGB-D camera as sensors for localisation of the robot and mapping of the environment. To better determine what algorithm is the best for sensory system that our robot has, we evaluated three

 ISBN 978-86-7466-930-3

**Benchmarking results**

| SLAM Algorithm | RMSE [cm] | Standard deviation [cm] | Mean absolute error [cm] | Maximum Absolute Error [cm] |
|---|---|---|---|---|
| **Comparison of error in x direction** | | | | |
| RTAB-Map | 1.2518514 | 7.6750762 | 9.8897118 | 27.0362502 |
| RTAB-MAP Visual odometry | 1.5254185 | 7.9799980 | 13.0003765 | 29.3477365 |
| Google Cartographer | 1.1652417 | 7.1982585 | 9.1631812 | 33.8634761 |
| Livox Mapping | 1.6213981 | 9.1069006 | 13.4148259 | 38.366215 |
| **Comparison of error in y direction** | | | | |
| RTAB-Map | 1.3296018 | 6.5810257 | 11.5531029 | 23.8609514 |
| RTAB-MAP Visual odometry | 2.3063390 | 8.1394842 | 13.0003765 | 35.0320307 |
| Google Cartographer | 1.6002339 | 10.2693004 | 21.5793597 | 37.0653832 |
| Livox Mapping | 1.1607506 | 6.6658583 | 9.5026594 | 24.9565594 |
| **Comparison of error in rotation** | | | | |
| | RMSE [°] | Standard deviation [°] | Mean absolute error [°] | Maximum Absolute Error [°] |
| RTAB-Map | 12.1708190 | 9.2212436 | 7.9433937 | 29.8499295 |
| RTAB-MAP Visual odometry | 12.4845912 | 9.2257357 | 8.4113505 | 29.9491947 |
| Google Cartographer | 16.1672031 | 12.0188858 | 10.8131790 | 37.3971806 |
| Livox Mapping | 19.1045268 | 13.6542612 | 13.3620393 | 46.4193679 |

TABLE IV: Benchmarking results

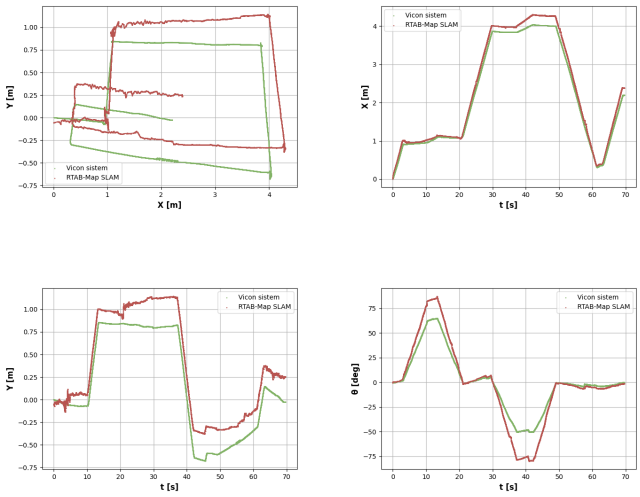


Fig. 8: Trajectory recovered from RTAB-Map visual odometry (red) vs Vicon system reference trajectory (green)

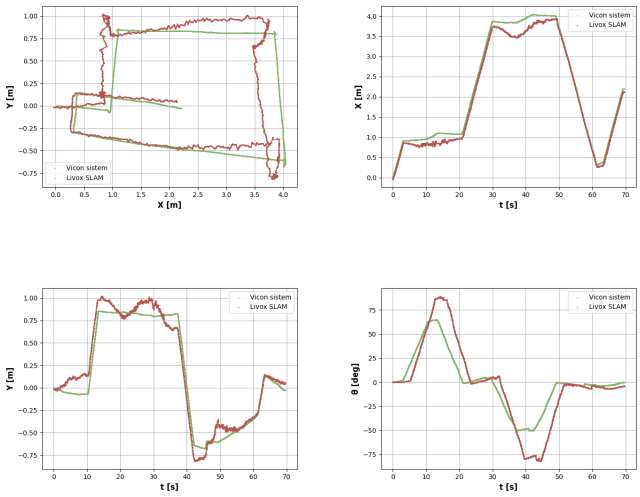


Fig. 9: Trajectory recovered from Livox Mapping (red) vs Vicon system reference trajectory (green)

up-to-date algorithms. Based on benchmark results we can see different algorithms provide different best performance. In most cases, RTAB Map has shown the best results compared to other algorithms.

## REFERENCES

[1] Durrant-Whyte, Hugh, and Tim Bailey. "Simultaneous localization and mapping: part I." IEEE robotics & automation magazine 13.2 (2006): 99-110.

[2] Bailey, Tim, et al. "Consistency of the EKF-SLAM algorithm." 2006 IEEE/RSJ International Conference on Intelligent Robots and Systems. IEEE, 2006.

[3] Montemerlo, Michael, et al. "FastSLAM: A factored solution to the simultaneous localization and mapping problem." Aaai/iaai 593598 (2002).

[4] Grisetti, Giorgio, Cyrill Stachniss, and Wolfram Burgard. "Improved techniques for grid mapping with rao-blackwellized particle filters." IEEE transactions on Robotics 23.1 (2007): 34-46.

[5] Quigley, Morgan, et al. "ROS: an open-source Robot Operating System." ICRA workshop on open source software. Vol. 3. No. 3.2. 2009.

[6] Kasar, Amey. "Benchmarking and comparing popular visual SLAM algorithms." arXiv preprint arXiv:1811.09895 (2018).

[7] Burgard, Wolfram, et al. "A comparison of SLAM algorithms based

 ISBN 978-86-7466-930-3

on a graph of relations." 2009 IEEE/RSJ International Conference on Intelligent Robots and Systems. IEEE, 2009.
[8] Merzlyakov A, Macenski S. A Comparison of Modern General-Purpose Visual SLAM Approaches. arXiv preprint arXiv:2107.07589. 2021 Jul 15.
[9] Filipenko, Maksim, and Ilya Afanasyev. "Comparison of various slam systems for mobile robot in an indoor environment." 2018 International Conference on Intelligent Systems (IS). IEEE, 2018.
[10] Labbe, Mathieu, and François Michaud. "RTAB-Map as an open-source lidar and visual simultaneous localization and mapping library for large-scale and long-term online operation." Journal of Field Robotics 36.2 (2019): 416-446.
[11] https://github.com/introlab/rtabmap/blob/master/corelib/include/rtabmap/core/Parameters.h
[12] Hess, Wolfgang, et al. "Real-time loop closure in 2D LIDAR SLAM." 2016 IEEE International Conference on Robotics and Automation (ICRA). IEEE, 2016.
[13] https://google-cartographer-ros.readthedocs.io/en/latest/index.html
[14] Zhang, Ji, and Sanjiv Singh. "LOAM: Lidar Odometry and Mapping in Real-time." Robotics: Science and Systems. Vol. 2. No. 9. 2014.
[15] Zhang, Ji, and Sanjiv Singh. "Enabling aggressive motion estimation at low-drift and accurate mapping in real-time." 2017 IEEE International Conference on Robotics and Automation (ICRA). IEEE, 2017.
[16] Zhang, Ji, Michael Kaess, and Sanjiv Singh. "On degeneracy of optimization-based state estimation problems." 2016 IEEE International Conference on Robotics and Automation (ICRA). IEEE, 2016.
[17] Gfrerrer, Anton. "Geometry and kinematics of the Mecanum wheel." Computer Aided Geometric Design 25.9 (2008): 784-791.

 ISBN 978-86-7466-930-3

# Natural Non-Invasive Human-Machine Interface Based on Hand Gesture Recognition

Jelena Rodić, Darko Golubović, Nikola Knežević, Kosta Jovanović

***Abstract*— In recent years human-machine interfaces have been identified as an important aspect for enabling safe and efficient human-robot collaboration. In the same period of time, deep learning has made great progress in image classification problems with the evolution of convolutional neural networ s This paper presents a hand gesture classification module as a non-invasive natural human-machine interface that e ploits deep learning technology. There were various approaches for this tas in the past, such as loo up tables, detection of ey-point positions of fingers, classic neural networ s, etc. This paper implements GG1 convolutional neural networ to solve the tas of hand gesture. To capture an image, we use leap motion sensor which is cheap and can wor in challenging light conditions, because it uses infra-red emitters to lighten the object. Thus, this approach is useful for factories and production lines. Another contribution of this paper is an e tensive database consisting of 2 images.**

***Index Terms*— uman-machine interface; and gesture; Convolutional eural etwor s; eap motion sensor; GG1**

## I. INTRODUCTION

Enhanced by developments in technology, numerous jobs are being transferred into the domain of robots and sophisticated machines [1, 2, 3]. These production lines perform various tasks. However, because market requirements are changing daily, there is a need for quick adaptation of these lines. Therefore, some manufacturers have developed flexible robotic cells that can serve multiple types of processes [4]. On the other hand, humans can adapt to changes in requirements quickly. This quality makes them valuable considering the dynamic of market needs. Combining human flexibility and robot reliability and consistency could give us a solution to the challenge the market sets without sacrificing the output volume.

The application of such a system is displayed in assembling fiscal cash registers. The process itself requires human involvement because the parts needed for assembly are small and the assembly process is delicate (mounting flat cables, soldering capacitors for PCBs, inserting tape for thermal printers). This process could be significantly less demanding for the operator by using novel technologies.

Firstly, it is possible to show the operator instructions for assembling a specific device using adaptive screens. Secondly, collaborative robots can be used to deliver the right part for the current production phase on time, which would increase the overall speed of production.

Thirdly, it is possible to gain an insight into worker performance (focus, monotony, fatigue) during tasks using EEG headphones. With this approach, the worker could switch assignments occasionally, and stay interested and productive.

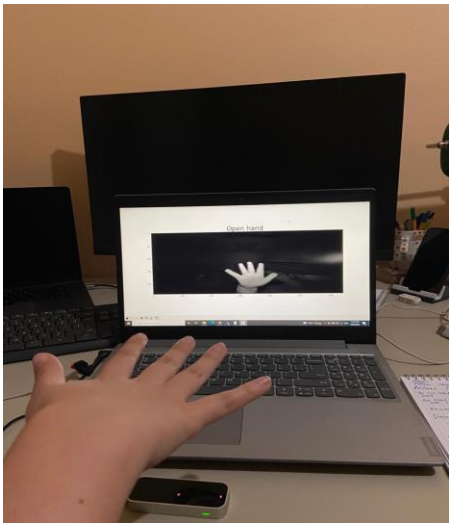

Fig. 1. System setup. Leap Motion sensor connected to PC for classification of hand gestures.

Also, if a person is engaged in dangerous work, this approach can prevent injuries from occurring when their focus is low and fatigue high. In addition to assistive devices, it is necessary to enable intuitive communication between humans and the rest of the system. For this purpose, a Leap Motion sensor is used (Fig. 1).

This sensor can detect hand gestures and provide human-machine interaction. There were a couple of solutions providing the human-machine interface but, some of them were invasive (wearing sensor gloves) or non-intuitive (complex system of buttons and taskbars). Using this type of sensor non-invasive method of human-machine interface is introduced. In this way communication between humans and machines is alleviated and it is more receptive to humans.

In this paper, we present a system for classifying human hand movements. For this purpose, it was necessary to collect the appropriate database, select the neural network architecture that will perform the classification, and finally test and implement the application that works in real-time.

## II. PREVIOUS WORK

Paper [5] from the University of Padua implements hand movement recognition. The classification was done over ten basic hand gestures. Also, the paper focuses on static gesticulation using leap motion controllers and kinetic devices. Microsoft's Kinect camera provides 3D images, while leap motion provides only key points in 3D. Here the authors explain that the images from ordinary cameras are 2D variants of the 3D position of the hand, so there is a loss of information.

 ISBN 978-86-7466-930-3

By providing 3D finger positions leap sensor can give more meaningful measurements. With the introduction of Time-of-Flight cameras for widespread use, 3D representations of objects have become more accessible to use. However, recognizing any movements that are not the most basic is still too complex for this type of sensor (leap motion), the paper states. The authors decided to unite these two types of controllers and try to get a more accurate classification. The problem is to calibrate these two devices. They achieved this by combining the fingertips from leap motion and the peaks on the depth camera that represent the fingers. Attributes used are the number and position of the fingers, the center of the palm and the orientation of the hand, angles at which the fingers stand, and the distances between the fingers. The problem occurs when the fingertips touch because sometimes they are detected as one finger. Furthermore, rings, bracelets, etc. can spoil the accuracy too. After PCA analysis, features were input into a multiclass SVM classifier with a Gaussian kernel. The best accuracy authors achieved is 80.9%, using only the leap sensor. After they inserted the data from Kinect, the accuracy jumped to 96%.

Paper [6] deals with the recognition of dynamic hand movements. The attributes used in this paper can be divided into two categories: static and dynamic. Static ones are based on the positions of the fingers and palms, ie. at the relative distances between them. Distances between the tips of adjacent fingers, and between the center of the palm and the tip of the finger are defined as attributes. For example, the Ok symbol is represented by the distance between the thumb and forefinger as a good attribute. Dynamic attributes are defined by finger and palm speeds to detect moving patterns. Those patterns are complicated, but the velocities of the essential points are given by the sensor itself, which makes the job easier. Examples of dynamic attributes used here are the translation of the whole hand (when the palm and fingers move at the same speed along some axis, without rotation), rotation of the hand (when the palm rotates), the precession of the hand (when the palm moves in a circle), swipe index finger, etc. The results of this work show that when the controller detects fingers accurately, the classification methods themselves work accurately. The authors noticed that tracking the fingertips of the middle and little fingers is not very stable. This can cause some problems in inference.

Paper [7] deals with the application of leap controllers to realize a virtual museum for free. Interaction with the virtual world using hand gestures has been suggested. It is necessary to classify the positions of the hand to prevent unwanted moves. First, data based on x, y, and z coordinates of fingertips was obtained, and then attribute extraction was performed. The authors used information on how far the fingertips are above the plane of the palm. They also used information on angles between the fingers and the palm. The classification method used was K nearest neighbors (KNN). They state that the accuracy obtained in other papers is about 80% for the same subjects and about 70% for new ones. The exact accuracy they obtained was 99%, but it was not said how they chose the test set.

Paper [8] was done at the University of Malaysia and deals with the control of drones based on hand movements read from leap sensors. The idea is that leap motion reads the gesture, sends it to the Arduino for recognition, and then sends the command to the drone to control. Three throttle commands are classified - lift, pitch, and roll. The idea was to simplify communication with the drone, which is currently complicated since there are numerous handles, buttons, etc. Therefore, the new commands were up and down, tilt back and forth, and tilt left and right. It is said that the drone worked well when the commands were given clearly. No accuracy or classification methods were stated.

In [9] authors implemented automation of design commands in CAD, Solidworks, and Catia software. It is stated that there is a lack of tools for some very intuitive modifications. The authors wanted to replace the commands given by the mouse and keyboard. For example, the review mode requires translation, rotation, and scaling. The scaling command is the distance between two index fingers. The rotation command is rotating the fist. In the end, a grab, and release command for translation are performed based on the distance between the index fingers. Paper does not use machine learning for classification but only distance mapping. If a command cannot be mapped to the table, then it is omitted. The accuracy they get is 80%.

Paper [10] dealt with a slightly different task. They wanted to recognize handwritten symbols in the air based on the movement of the hand. The key points were sampled at a rate of 100 frames per second. The attributes taken are the positions and velocities of the key points, the angles at which the fingers stand, etc. Finally, the classification was performed using convolutional neural networks. The accuracy they obtained is 92.4%.

Paper [11] deals with the dynamic movements of human hands. Motion information is converted to color images. The conversion of movement into an image is done by tracking the finger position in time. Each finger is assigned to a distinct color, and the intensity of the color changes depending on the time. The authors used the ResNet-50 for the classification. The accuracy they get is about 80%.

## III. METHOD

First, we need to define the problem we want to solve. Namely, for the needs of working on the production line in factories, it is convenient to use only commands that do not include pressing the screen and buttons when worker's hands are dirty, or the screen can't detect users' input caused by wearing the safety gloves or other equipment. For our case, it was necessary to select 4 hand commands that could be classified with high precision using the leap motion sensor. Some crucial steps in solving this problem were:

- Obtain or form an adequate dataset that has different commands given by hand movements. We decided to work on images because they are more reliable than the detection of key points from Leap sensors. Also, convolutional neural networks are powerful in image

 ISBN 978-86-7466-930-3

classification, so this method should give promising results.

- Choose 4 distinct commands, which will be able to be easily distinguished from the images returned by the Leap sensor.
- Choose the adequate architecture of the convolutional neural network and tune the hyperparameters. Assess the probability of misclassification on the test set.
- Eventually do a live simulation with a real sensor where after the first detection of the hand in the frame three frames would be captured at 0.33s interval. Then each of these three frames would be passed through a neural network for classification, and finally, a final decision would be made based on a majority vote.

### *A. eap Motion Sensor*

There are several sensors on the market that handle motion detection. The Leap Motion sensor [12] stands out for its price (it is cheap) and accuracy. Leap Motion Controller is an interactive device specializing in detecting hand movements and finger location based on infrared light emitters and two cameras that receive reflected IR waves. The Leap Motion architecture can be seen in Fig. 2.

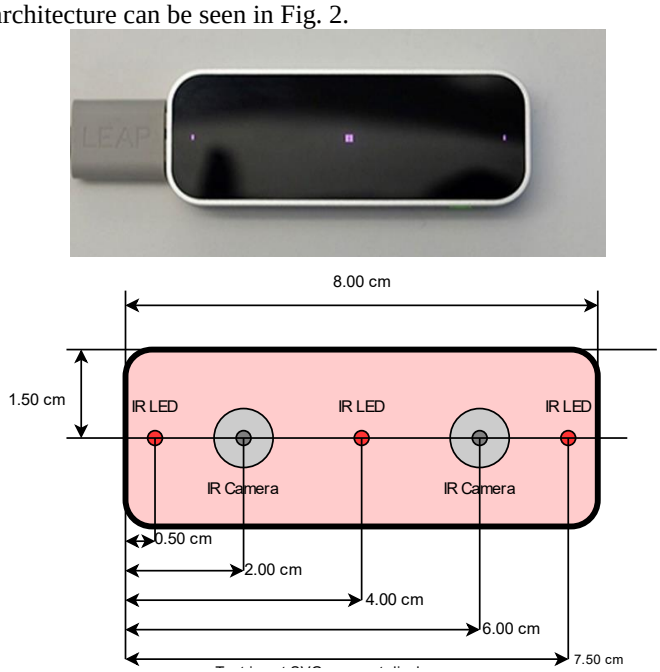


Fig. 2. Leap motion sensor, from [14]

Its field of vision is up to 1m away. There is also a skeletal model of the human hand, which represents five fingers divided into phalanges. We can also obtain a raw image from the sensor, which is the one we used.

### *B. atabase*

First approach was to try to train the network on different publicly available datasets. The best result we got was with the database [15]. The problem with this database is that it did not contain various heights or angles on which the hand can be, thus making this network prone to errors once the hand is not perfectly positioned. Considering the application of this paper, we wanted to develop a system that is able to work in real life conditions, thus making this database inadequate for our task. On our versatile test dataset, this network had the accuracy of 91.5%.

After realizing that publicly available databases are not extensive enough to meet our needs, we decided to develop our own dataset using the Leap Motion sensor. Our training set consists of four classes of hand gestures. Each class consists of 5000 images. There is an equal part of men and women in the hand dataset. Also, there are 50% left-hand images in the database. Furthermore, images were obtained at various lighting conditions, angles, and heights. The last two turned out to be important for the network to generalize well. We trained our network on one publicly available data set which had only photos of hands perpendicular to the sensor. Also, all the pictures were formed with a constant distance between the hand and the sensor. This plays a key role because the camera on the leap sensor is in a wide range. That slight change in the distance of the camera results in a tremendous change in the size of the object in the final image. As a result, the same architecture performed significantly worse than when it was trained on our custom dataset. This shows us the importance of a well-rounded dataset, which achieved accuracy of 99.3%. We will compare these results in detail in the section Results.

In the end, we used an unseen person to obtain the test set. Also, the test set contains images taken from different angles and heights. Here are examples from the dataset (Fig. 3):

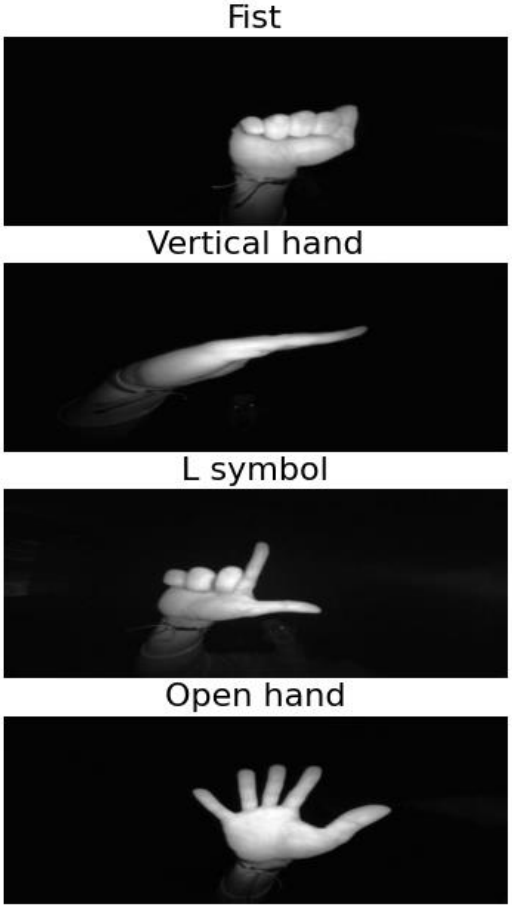


Fig. 3. Example of each hand gesture in our database.


ISBN 978-86-7466-930-3

### C. Model Architecture

VGG16 is a deep convolutional neural network pre-trained on the ImageNet dataset. The VGG16 Architecture was developed and introduced by Karen Simonyan and Andrew Zisserman. The VGG16 model achieved 92.7% accuracy on the classification task, which earned its authors second place in the competition. On the localization task, VGG16 earned first place. This model is widely used both because it is easy to implement and because it is still extremely competitive.

During training, the input to the CNN is a 224 x 224 RGB image. Subtracting the mean RGB value computed on the training set from each pixel is the only pre-processing done here. The image is passed through a stack of convolutional layers, where filters with a small radius are used (Fig. 4). The convolution stride and the spatial padding of convolutional layer input is fixed to 1 pixel. This ensures that the spatial resolution is preserved after the convolution. Five max-pooling layers, which follow some of the convolutional layers, help in spatial pooling. Max-pooling is performed over a 2×2-pixel window, with stride 2. Here is the architecture:

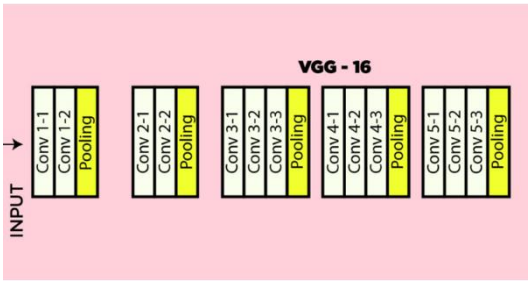


Fig. 4. VGG16 architecture, from [13].

On top of the CNN, we put a classification head that consisted of 2 dense layers. The first one was size 512 with ReLU activation function, and the second one was size 4 with Sigmoid activation function.

### . yper-parameters

In this section we will mention some hyper parameters as well as optimizers we used. Firstly, we used an RMS prop optimizer. This is a gradient-based optimizer that deals with vanishing and exploding gradients very well. It uses the moving average of squared gradients to normalize the gradient. This normalization decreases steps for large gradients and increases steps for small gradients. Effectively this means that the learning rate is adjusted based on previous magnitudes of gradients. For the loss function we opted for cross entropy loss.

### E. Training

We trained our model during 5 epochs, with batch size 64 and learning rate 0.0001. Train-validation split ratio is 80:20. Another way to stop overfitting of the network was using regularization with L1 and L2 losses combined. Also, we used dropout layer in classification head.

## IV. Results

Results of the network which was trained on the small database [11] (the one that did not contain various positions and scales of the hand), has considerably lower accuracy on the versatile test dataset. This can be seen in the confusion matrix below (Fig. 5). The accuracy of this model is 91.5%.

After training our network for five epochs on 20000 images (our database), loss reaches saturation both on validation and training set.

Further, this model has 99.3% accuracy on test data. The confusion matrix is very concentrated around the main diagonal (Fig. 6).

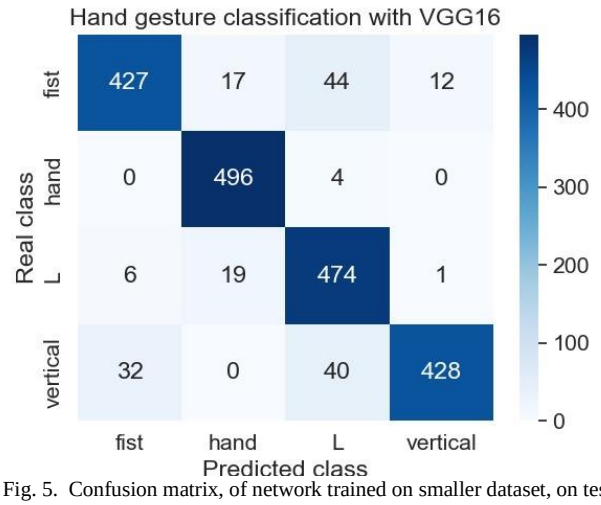


Fig. 5. Confusion matrix, of network trained on smaller dataset, on test data

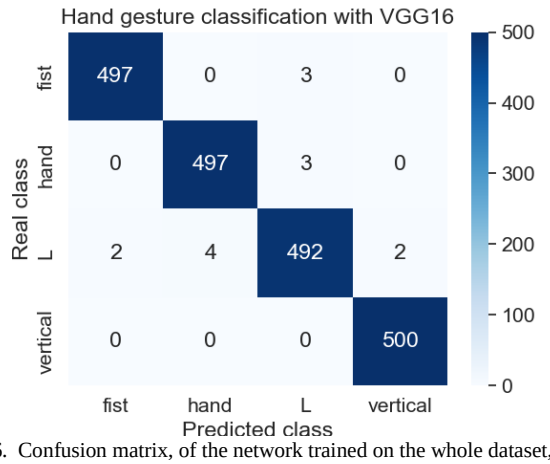


Fig. 6. Confusion matrix, of the network trained on the whole dataset, on test data

We can see that there is no significant difference in these precisions, which suggests that our model is not biased towards any class. This is because our dataset is balanced, and the network can learn the features of each class equally well. However, the L symbol has the highest number of misclassified examples. This could be because it is visually somewhere between the fist and the open hand. Two fingers extended like in the open hand, and three fingers flexed like in the fist
Next, we will show some misclassified instances:

- Fist mistaken for L shape: This could be because of


ISBN 978-86-7466-930-3

the angle between the forearm and the fist. Therefore, this calls for a more well-rounded database that will contain lots of these examples in the training

- L shape is mistaken for fist: This could be because the index finger is too thin in the image.

In the end, it is important to notice that our system works in real-time. Also, the accuracies are even greater in real-life use because the decision is made using a majority vote from three shots of the subject's hand.

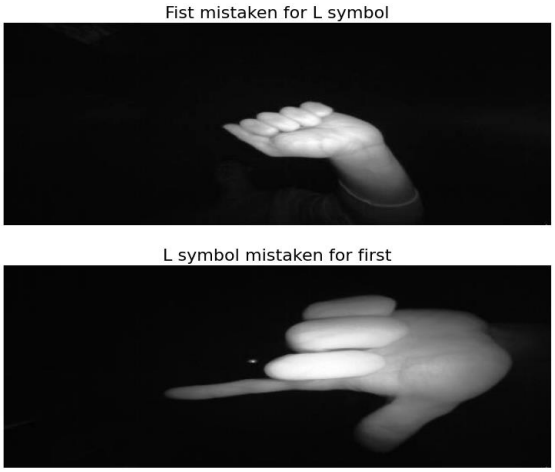


Fig. 7. Examples of failure cases.

## V. CONCLUSION

In this paper, we developed a system for natural and non-invasive human-machine interface using a leap motion sensor. The aim was to classify four hand gesture commands with high precision in real-time. This was done by using deep convolutional network VGG16 and a custom classification head. The inference time per image is 0.23s. To trigger a decision, a hand must be detected by the leap sensor. After that, our system takes three shots at 0.33-second intervals. This setup enables us to use this system in real-time efficiently. The decision is made based on the majority vote of those three shots. This approach gives an accuracy of 99.3% on the test set. Further, our system is robust in terms of distance from the hand to the sensor, and orientation of the hand with respect to the sensor. This is important because in real-life situations workers will approach this device from different angles and heights.

## ACKNOWLEDGMENT

This paper was funded by cascading project BrainWatch within Horizon 2020 project Human-Centered Robotics for Connected Factories - SHOP4CF (H2020 grant agreement #873087).

## REFERENCES

[1] Faccio, M., Bottin, M. & Rosati, G. Collaborative and traditional robotic assembly: a comparison model. Int J Adv Manuf Technol 102, 1355–1372 (2019). https://doi.org/10.1007/s00170-018-03247-z

[2] Norberto Pires, J., Godinho, T. and Ferreira, P. (2004), "CAD interface for automatic robot welding programming", Industrial Robot, Vol. 31 No. 1, pp. 71-76. https://doi.org/10.1108/01439910410512028

[3] Bachmann, D., Weichert, F. and Rinkenauer, G. 2015. Evaluation of the leap motion controller as a new contact-free pointing device. Sensors 15, 1, 214

[4] T. Gaspar et al., "Rapid hardware and software reconfiguration in a robotic workcell," 2017 18th International Conference on Advanced Robotics (ICAR), 2017, pp. 229-236, doi: 10.1109/ICAR.2017.8023523.

[5] Marin, G., Dominio, F., and Zanuttigh, P. 2015. Hand gesture recognition with jointlz calibrated leap motion and depth sensor. Multimedia Tools and Applications 1-25.

[6] Shao, L., Hand movement and gesture recognition using Leap Motion Controller.

[7] Sumpeno, S., Dharmayasa, G., Nugroho, S., Purwitasari, D., 2019. Immersive Hand Gesture for Virtual Museum using Leap Motion Sensor Based on K-Nearest Neighbor.

[8] Mutalib, M., Mohd, N., Tomari, M., Sari, S., Ambar, R.,2020. Flying Drone Controller bz Hand Gesture Using Leap Motion.

[9] Xiao, Y., Peng, Q., University of Manitoba, Canada 2017. A hand gesture-based interface for design review using leap motion controller.

[10] McCartney, R., Yuan, J., Bischof, H., Gesture Recognition with Leap Motion Controller.

[11] Lupinetti, K., Ranieri, A., Gianinni, F., Monti, M., 3D dynamic hand gestures recognition using Leap Motion sensor and convolutional neural networks.

[12] https://www.ultraleap.com/datasheets/Leap_Motion_Controller_Datasheet.pdf , accessed 17.05.2022.

[13] https://www.geeksforgeeks.org/vgg-16-cnn-model/, accessed 17.05.2022.

[14] https://www.researchgate.net/figure/Schematic-view-of-leap-motion-controller-LMC_fig1_266614710, accessed 17.05.2022.

[15] https://www.kaggle.com/gti-upm/leapgestrecog, accessed 17.05.2022.

 ISBN 978-86-7466-930-3

# Pozicioniranje Hvataljke ABB Kolaborativnom Robota Pomoću Kamere

Vojislav Vujičić, Ivan Milićević

***Abstra t*— ovom radu biće opisan jedan od načina pozicioniranja olaborativnog robota pomoću kamere integrisane u hvatalj u robota. prvom delu rada biće opisana laboratorijs a postav a instalirana u Naučno tehnološkom parku u Čačku. atim će biti opisano reiranje virtuelne laboratorije u o viru softvera A obot tudio, ao i definisanje osnovnih delova programa. a on reiranja putanja robota detaljno će biti opisana opcija *Inte rated s n* ao i njena implementacija pri pozicioniranju robota.**

***čne reč* — olaborativna roboti a, pozicioniranje, integrisana vizija, A …**

## I. UVOD

Roboti su brzo poslali sastavni deo proizvodne industrije. Roboti se koriste na različite načine u različitim industrijama i imaju izuzetno veliki uticaj kada je u pitanju industrijska automatizacija.

Tradicionalni industrijski roboti su fizički odvojeni od ljudi, izvršavaju zadatke koji su odvojeni od ljudi zaposlenih u proizvodnji, kako bi obezbedili njihovu bezbednost. Sa druge strane, kolaborativni roboti su napravljeni tako da imaju ograničene brzine, i momente, kao is senzore koji im omogućavaju da budu bezbedni za ljude i da ljudi mogu biti u blizini, kao i da rade sa njima zajedno. [1,2]

Kolaborativni roboti nude nove potencijale za poboljšanje načina na koji radimo. Oni su se brzo razvili ubrzanim uvođenjem industrije 4.0 i razvojem novih robotskih tehnologija. Pre samo deset godina, prema robotima su se odnosili sa nepoverenjem, a danas je oblast industrijske robotike ona koja se najbrže razvija. Kolaborativni roboti brzo postali sastavni deo proizvodne industrije.

Ovim robotima je potrebna ljudska pomoć kada vrše manipulaciju materijala ili sklapanje nekih komplikovanih delova. Kolaborativni roboti su dizajnirani da rade i pomažu ljudima, umesto da im oduzimaju posao. Oni su programirani da obavljaju ponovljive zadatke tamo gde su ljudi potrebni, ali ne i njihova stručnost. Dakle, koriste se za jednostavne, ponavljajuće zadatke koji su opasni ili teški za ljude, kao što su operacije na proizvodnoj liniji, održavanje mašina, elektro lučno zavarivanje, rukovanje opasnim materijalima, laboratorijsko testiranje i drugi proizvodni zadaci.

Vojislav Vujičić, Fakultet tehničkih nauka u Čačku, Univerzitet u Kragujevcu, Svetog Save 65, 32000 Čačak, Srbija (e-mail: vojislav.vujicic@ftn.kg.ac.rs) (https://orcid.org/0000-0002-7037-3545)

Ivan Milićević, Fakultet tehničkih nauka u Čačku, Univerzitet u Kragujevcu, Svetog Save 65, 32000 Čačak, Srbija (e-mail: ivan.milicevic@ftn.kg.ac.rs) (https://orcid.org/ 0000-0003-0476-4991)

.

## II. LABORATORIJSKA POSTAVKA

U ovom istraživanju je korišćena oprema postavljena u laboratoriji Naučno tehnološkog parka u Čačku čije opremanje je finansirano od strane Ministarstva prosvete , nauke i tehnološkog razvoja Republike Srbije. U ovoj laboratoriji instalirana su dve robotske ćelije. Jedna ćelija je industrijski robot ABB IRB 120, multifunkcionalni robot sa šest stepeni slobode, koji je detaljno opisan u radu [3]. Drugi robot je ABB IRB 14000 YuMi kolaborativni robot koji je prikazan na slici 1.

Slika 1. ABB IRB 14000 kolaborativni robot [4]

Ovaj robot je dvoručni robot koji je napravljen za zajednički rad sa čovekom na istom poslu. Robot poseduje sedam stepeni slobode u jednoj ruci koje mu daju veliku fleksibilnost i agilnost u proizvodnji. Ponovljivost robota je 0.02mm. Robot ima domet od 559mm i nosivost od 500g po ruci. IRB 14000 poseduje Smart Gripper kao end efektor sa manipulaciju i sklapanje. Griper ima servo prste kao podrazumevani modul, dok su vakuum hvataljka i kamera opcioni. U ovom slučaju leva ruka ima servo prste i vakuum modul. Desna ruka poseduje servo, vakuum i kameru (Cognex AE3) [4].

 ISBN 978-86-7466-930-3

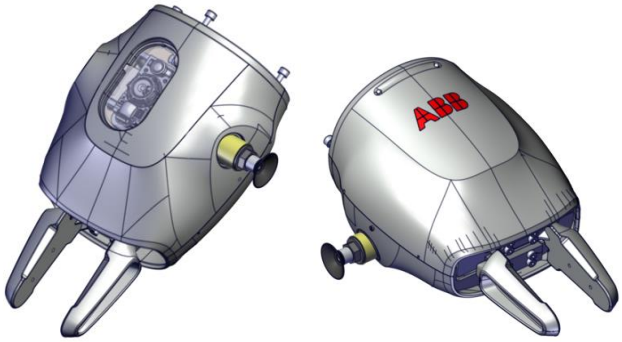


Slika 2. Desni i levi Smart Gripper [4]

Oba robota su smeštena na radni sto sa zaštitnom zonom od pleksiglasa. Na radnom stolu nalaze aluminijumski profili za montažu dodatne opreme, senzora, pribora… Kontroleri robota i ostale komponente povezane su na komandni pult u kome se nalazi PLC kontroler i HMI tač panel. Na ovoj laboratorijskoj postavci sa opremom koja se na njoj nalazi moguće je testirati različite industrijske aplikacije. Izgled laboratorijske postavke prikazan je na slici 3.

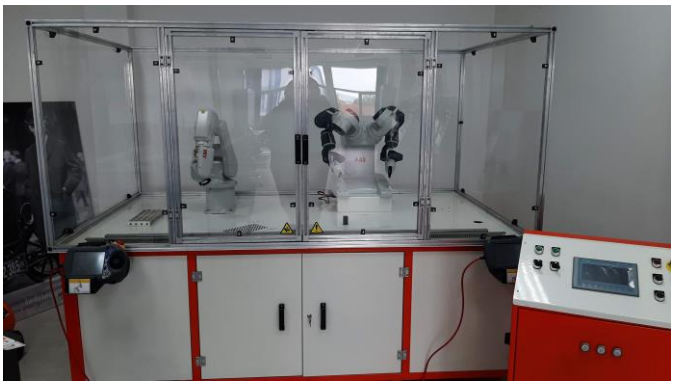

Slika 3. Izgled laboratorijske postavke

## III. Virtuelno Okruženje

Jedan način za programiranje ABB robota je korišćenje softverske platforme ABB RobotStudio. Softver poseduje virtuelni kontroler za programiranje robota. Dobar je za simulaciju rada robota kao i drugih pokretnih mehanizama. Ovaj softver omogućava programiranje robota i promene programa bez ometanja ili zaustavljanja proizvodnje. RobotStudio se koristi kao virtuelna laboratorija i programiranje robota van mreže (offline). Ova softverska platforma sastoji se od četiri glavna dela: modeliranje, simulaciju, kontroler i RAPID [5, 6].

Modeliranje omogućava kreiranje virtuelnog okruženja izradom ili uvozom 3D modela mehaničkih delova i mašina u proizvodnoj liniji. Virtuelno okruženje je korisno za izbegavanje mehaničkih sudara između robota i drugih delova proizvodne linije. Kreiranje virtuelne laboratorije počinje kreiranjem nove prazne stanice. Sledeći korak je uvoz mehaničkog 3D modela radnog prostora sa sigurnosnom zonom iz softvera za 3D modeliranje. Ovaj korak je detaljno opisan u [3]. Nakon dodavanja radnog stola, robot mora biti postavljen na radni sto. ABB IRB 14000 je dodat iz biblioteke. Položaj robota je podešen (pozicija (x, y, z): 1604, 900, 853, orijentacija (x, y, z): 0,0, -90). Sledeći korak je dodavanje Smart Gripper-a na levu i desnu ruku. Leva ruka ima servo prste i vakuum, dok desna ima servo prste, vakuum i kameru. Hvataljke moraju biti pričvršćene za svaku ruku. Nakon postavljanja hvataljki potrebno je dodati 3D model radnog komada da bi se kompletirao mehanički model virtuelne laboratorije. Kompletan mehanički virtuelni model je prikazan na slici 4.

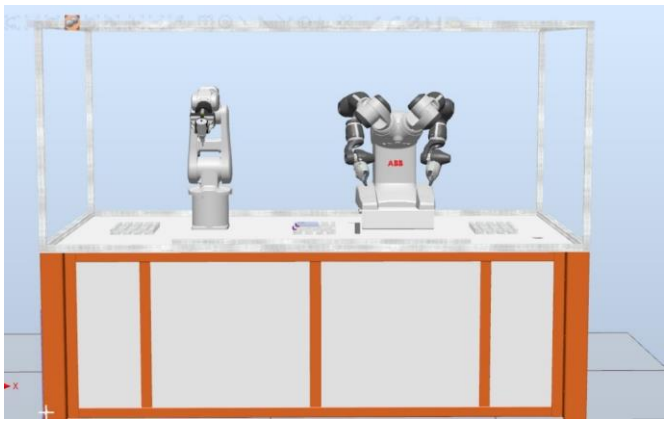

Slika 4. Izgled virtuelne laboratorije [3]

Nakon dodavanja svih potrebnih mehaničkih delova u virtuelni model, virtuelni kontroler se mora dodati. Dodat je kontroler sa RobotWare verzija 6.11.01 za IRB 14000 0,5kg 0,5m.

## IV. Programiranje Kretanja Robota

Program koji će biti napravljen je da se sa jedne (desne) strane podigne predmet sa jednom (desnom) rukom, prebaci u drugu (levu) ruku i spusti na drugu stranu radnog prostora. Pre preuzimanja predmeta sa desnom rukom, kamera na hvataljci skenira prostor i vrši orjentaciju hvataljke u zavisnosti od orjentacije predmeta koji se prenosi.

Programiranje ABB robota počinje definisanjem *Target-a. Target* je specifična tačka u radnoj zoni robota u koju robot treba da dođe. Jedan od najbitnijih *Target-a* je *Target* u inicijalnom ( *ome* položaju ruke. Za svaku ruku potrebno je podesiti inicijalnu poziciju. Svaka ruka ima svoje *Target-e*

Desna ruka mora da ode iz početnog položaja u položaj iznad predmeta, poziciju za snimanje kamerom, Target 10. Na poziciji Targeta 30, hvataljka mora biti zatvorena da bi se uhvatio predmet. Zatim ide do Targeta za razmenu – Target 40. Slika 5a prikazuje desnu poziciju Smart Gripper-a u definisanim Targetima. Od tih Targeta se mora napraviti putanja (Path_R). Ova putanja sadrži sve napravljene Targete i instrukcije za pomeranje *Mo e* ( *-joint or -linear*) za prelazak sa jednog na drugi Target.

Leva ruka ima *Target-e* za približavanje tački razmene desnom rukom (Target 10, 20, 30), izvlačenje iz tačke razmene (Target 35), Target (40, 50, 60 i 80) služe za prebacivanje predmeta na drugu poziciju na radnom prostoru. Poslednji Target 70 je pomeranje od Targeta 80 da bi se

 ISBN 978-86-7466-930-3

izbegao sudar hvataljke sa predmetom. Slika 5b prikazuje položaj levog Smart Gripper-a u definisanim Targetima. Sa tim Targetima, napravljena je putanja do (Path_L).

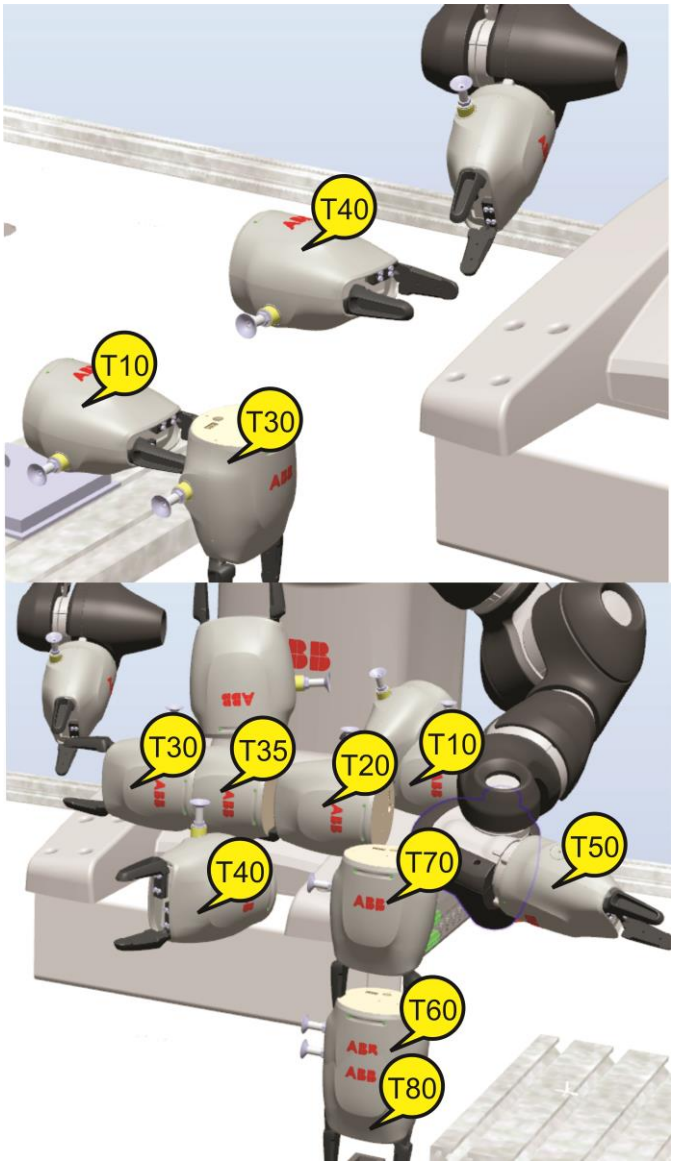


Slika 5a. Desna hvataljka u definisanim Targetima, Slika 5b. Leva hvataljka u definisanim Targetima

Nakon kreiranja programa, moguće je izvršiti simulaciju rada. Kada simulacija počne, robot ide od Targeta do Targeta, praveći pokrete definisane putanjama. Prva simulacija pokazuje da ruke nisu sinhronizovane, pa se program mora modifikovati. Promene koje se moraju izvršiti su:

a) Desna ruka mora da sačeka dok leva ruka ne preuzme predmet.
b) Leva ruka mora da sačeka dok se desna ruka ne pomeri iz zone hvatanja.
c) Desna ruka može ići u početni položaj, a leva ruka može da nastavi da prenosi predmet na željenu pozuciju.
d) Sačekati da obe ruke budu u početnoj poziciji.

Program mora imati promeljive za sinhronizaciju ruku:

*PE S tasks task list 2 T B , T B*

*A syncident sy01 A syncident sy02 A syncident sy03*

Definisane promeljive se koriste u fukncji za sinronizaciju WaitSyncTask\InPos,sy01,task_list; i dodaju se u program za obe ruke na mestu gde je potrebno da ruke jedna drugu čekaju.

Nakon dodavanja delova za sinhronizaciju simulacija kretanja robota sa putanjom kretanja ove ruke data je na slici 6.

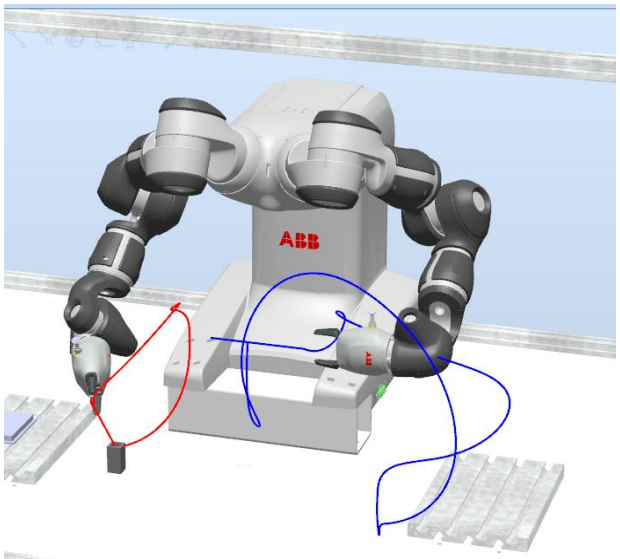

Slika 6. Simulacija kretanja robota sa prikazanim putanjama kretanja

## V. PODEŠAVANJE VIZIJSKOG SISTEMA

Za pozicioniranje robota na osnovu vizijskog sistema koristi se desna ruka robota koja u sebi ima integrisanu kameru (Cognex AE3). Pre podešavanja opcije *Inegrated ision* potrebno je desnu ruku robota postaviti u poziciju za snimanje objekta i modifikovati Target_30. Nakon toga se može odabrati opcija *Integrated ision* u kojoj je potrebno izvršiti sledeće korake:

1. Opcija *Setup Image* gde se podešavaju parametri ekspozicije i osvetljaja podloge.
2. Opcija *Calibrate* kojom se definiše koliko piksela na slici je dimenzija predmeta (predmet je dimenzije 25x25 mm).
3. Opcija *A Part ocation Tool Patern* kojom se definiše oblik predmeta kome treba podesiti poziciju.
4. Opcija *utput to API* gde se definiše šta će sa slike RAPID program preuzeti od podataka.
5. Opcija *Sa e ob* kojom se definisani parametri snimaju na kontroleru robota.

Definisanje parametara u okviru *Integrated ision-a* dat je prikazano je na slici 7.


ISBN 978-86-7466-930-3

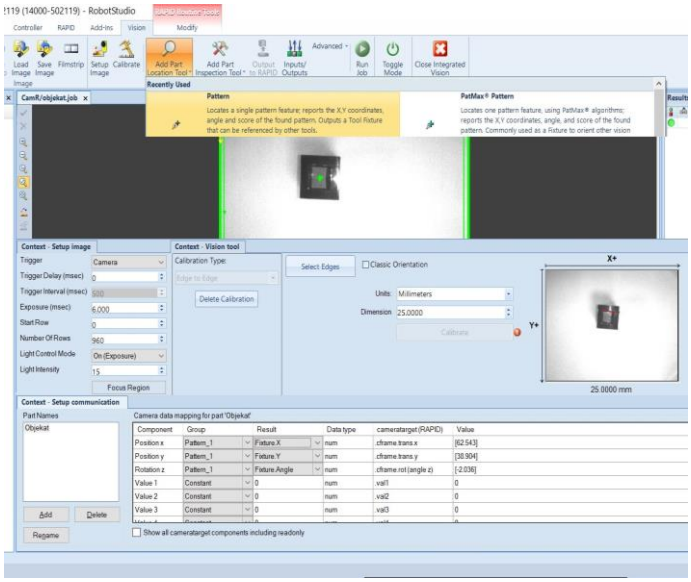

Slika 7 Podešavanje vizijskog sistema

Po završetku definisanja parametara u okviru *Integrated ision* potrebno je u RAPID programu napisati kod kojim se poziva rad kamere i vrši upis pozicije hvatanja predmeta na osnovu slike. Deo koda koji vrši pozicioniranje na osnovu slike je:

```
CamSetProgramMode Cam ;
Cam oad ob Cam , amera
CamSet unMode Cam
Cam e Image Cam
CamGet esult Cam , Target po icija sa kamere
wobj0.oframe Target po icija sa kamere.cframe
```

Nakon implementacije programa izvršeno je testiranje programa, finalno podešavanje pozicija za razmenu predmeta, robot je pušten u rad. Robot u radu prikazan je na slici 8

Slika 8. Robot ABB IRB 14000 YuMi u radu

## VI. ZAKLJUČAK

Opremanjem nove laboratorije opremljene sa dva ABB robota u okviru Naučno-tehnološkog parka u Čačku otvorilo je nove mogućnosti za razvoj robotike na Fakultetu tehničkih nauka u Čačku. Virtuelna laboratorija sa ABB IRB 120 i ABB IRB 14000 je formirana korišćenjem softvera RobotStudio. Ovo omogućava programiranje robota od kuće koristeći virtuelno okruženje, kao i primenu u izvođenju laboratorijskih vežbi sa studentima.

Program za kretanje robota napravljen je u virtuelnoj laboratorij nakon čega je proveren i podešen kroz simulaciju. Nakon toga je program ubačen u kontroler robota i na realnom robotu izvršena finalna podešavanja.

Nakon definisanja kretanja u program je ubačen vizijski sistem kojim se vrši pozicioniranje hvataljke robota bez obzira na poziciju i orjentaciju predmeta na podlozi.

Naredni koraci u istraživanju oblasti vizije i kolaborativne robotike su primena ovakvih sistema u radu sa čovekom, gde bi na osnovu slike robot mogao da odluči šta je naredno potrebno uraditi čime se postiže veća fleksibilnost.

Takođe je moguće koristiti viziju za inspekciju urađenog zadatka od strane čoveka ili nekog drugog robota i korigovanje u koliko je zadatak moguće ispratiti.

## ZAHVALNICA

Istraživanja prezentovana u ovom radu su delimično finansirana sredstvima Ministarstva prosvete, nauke i tehnološkog razvoja RS, ugovor br. 451-03-68/2022-14/200132 čiji je realizator Fakultet tehničkih nauka u Čačku - Univerziteta u Kragujevcu.

## LITERATURA

[1] Vicente, L. i ostali „Industrial Collaborative Robotics Platform. In: Camarinha-Matos, L.M., Boucher, X., Afsarmanesh, H. (eds) Smart and Sustainable Collaborative Networks 4.0. PRO-VE 2021.“ IFIP Advances in Information and Communication Technology, vol 629. Springer, Cham. https://doi.org/10.1007/978-3-030-85969-5_53

[2] Matjaž, M. i ostali. “Robotics” Springer Cham 2019. https://doi.org/10.1007/978-3-319-72911-4

[3] Vujičić, V., i ostali, „Offline Robot Programming Using ABB RobotStudio“, X International Scientific Conference Heavy Machinery HM 2021, Proceedings HM 2021, ISBN: 978-86-81412-09-1, pp. C79-C83, University of Kragujevac, Faculty of Mechanical and Civil Engineering Kraljevo, 23-25th June 2021, Vrnjačka Banja, Serbia.

[4] Product specification IRB 14000 [Online]. Available: https://search.abb.com/library/Download.aspx?DocumentID=3HAC052982-001&LanguageCode=en&DocumentPartId=&Action=Launch [Pristup 22.4.2022.]

[5] Podobnik. J., i ostali, „Osnove robotike: Laboratorijski praktikum“ Založba FE, Universa v Ljubljani, Ljubljana 2018,

[6] Adit, M., „HandBook Guidance on the programming of ABB YuMi IRB 14000“ Otto-von-Guericke-University Magdeburg 2020. https://doi.org/10.13140/RG.2.2.12746.18881

 ISBN 978-86-7466-930-3

# Upravljanje pasivnom krutošću završnog uređaja robota oblikovanjem elipsoida krutosti

Branko Lukić, Nikola Knežević i Kosta Jovanović

***A stra t*— Krutost završnog uređaja robota određuje ponašanje robota pri intera ciji sa o olinom. Krutost završnog uređaja je najčešće predstavljena preko matrice krutosti čije oblikovanje može da bude neizvodljivo jer roboti ne poseduju dovoljno stepeni slobode da bi se svi elementi u matrice rutosti podesili. To dovodi do primene optimizacije oja balansira između vrednosti elemenata matrice krutosti koji su od interesa za izvršavanje zadatka. U ovom radu je predložen pristup za „ *ne*“ obli ovanje matrice rutosti primenom elipsoida krutosti gde se podešavanjem orijentacije i dužina osa elipsoida obli uje rutost. bli ovanje elipsoida ima manje parametara oje je potrebno podesiti u odnosu na matricu krutosti. Predložene su dve kriterijumske funkcije za obli ovanje elipsoida rutost koje eksploatišu kinematičku redundansu robota. ptimalne vrednosti pozicija i rutosti zglobova izračunate su primenom algoritma zasnovanog na P (engl. *e ent a east are r ramm n* ). a on dobijanja željenog obli a elipsoida krutosti završnog uređaja robota, pokazana je mogućnost promene volumena elipsoida na željenu vrednost skaliranjem krutosti u zglobovima.**

***Ključne reči*— lipsoid rutosti, krutost završnog uređaja, pasivna rutost.**

## I. UVOD

Kod bezbedne fizičke interakcije između čoveka i robota (pHRI) [1, 2] ili robota i okoline, jednu od bitnijih uloga igra popustljivost robota. Pored aktivne popustljivosti [3, 4] koja se ostvaruje kroz upravljačku petlju, postoji i pasivna popustljivost koja se realizuje kroz elastične elemente ugrađene u prenosnom sistemu robota između aktuatora i segmenta robota [5]. Fokus ovog rada je na robote pogonjene aktuatorima sa promenljivom krutošću – VSA (engl. *ariable Stiffness Actuators*), koji imaju dve kontrolne varijable: pozicije i krutosti aktuatora.

Matrica krutosti završnog uređaja je u funkciji pozicija zglobova robota preko Jakobijeve matrice i krutosti zglobova (videti (4) i (5)). To znači da za kinematički redundantnog robota sa popustljivim aktuatorima, krutost završnog uređaja se može oblikovati promenom konfiguracije u nultom prostoru i/ili promenom krutosti zglobova. Za tipične robotske konfiguracije, matrica krutosti

Branko Lukić – Elektrotehnički fakultet, Univerzitet u Beogradu, Bulevar Kralja Aleksandra 73, 11020 Beograd, Srbija (e-mail: branko@etf.rs).

Nikola Knežević – Elektrotehnički fakultet, Univerzitet u Beogradu, Bulevar Kralja Aleksandra 73, 11020 Beograd, Srbija (e-mail: knezevic@etf.rs).

Kosta Jovanović – Elektrotehnički fakultet, Univerzitet u Beogradu, Bulevar Kralja Aleksandra 73, 11020 Beograd, Srbija (e-mail: kostaj@etf.rs).

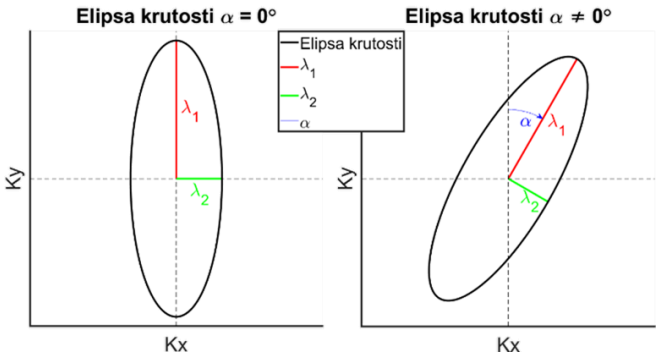


Sl. 1. Elipsa krutosti je definisana dužinama osa $\lambda_1$.i $\lambda_2$, kao i uglom rotacije α. Levo: Ose elipse krutosti se poklapaju sa osama koordinatnog sistema. Desno: Pravac u kome je elipsa krutosti usmerena je zarotiran za ugao α.

je simetrična matrica dimenzija 6×6, što rezultuje sa 21 promenljivom. Kontrola matrice krutosti i svih šest pozicija završnog uređaja (3 rotacije i 3 translacije) [6, 7] rezultuje sa 27 promenljivih koje treba podesiti. ), što je sa stanovišta kontrole veoma zahtevno budući da postoji suviše promenljivih i fizičkih ograničenja (ograničen raspon pokreta zglobova i krutosti zglobova) i manjak kontrolnih ulaza. Za kontrolu svih 27 promenljivih veličina robota pogonjenog sa aktuatorima promenljive krutosti minimalan broj aktuatora bi bio 14 [6], ne razmatrajući fizička ograničenja koja postoje i da bi realan broj bio daleko veći i kompleksniji za realizaciju i upravljanje. Stoga, kontrola cele matrice krutosti nije laka, niti je potpuno opravdan cilj [8], već da je kontrola dijagonalnih elemenata matrice krutosti neophodna u većini aplikacija.

Matrica krutosti završnog uređaja ima nelinearnu zavisnost od konfiguracije robota preko Jakobijeve matrice, pa za tipičnog robota sa 6-7 stepeni slobode, nemoguće je pronaći analitički skup pozicija zglobova koji će zadovoljiti željeni položaj završnog uređaja i matricu krutosti. Stoga su neophodne tehnike optimizacije koje koriste nulti prostor [4, 9, 10].

Oblikovanje krutosti završnog uređaja robota računanjem optimalnog seta krutosti u zglobovima za konstantnu poziciju završnog uređaja, gde su krutosti zglobova predstavljen kroz linearni sistem jednačina, a gde je linearnost ostvarena izborom odgovarajuće norme dato je u [6]. Nadogradnja računanja optimalnog seta krutosti u zglobovima prikazana je [7]. U njemu se razmatra iterativna procedura za rešavanje nelinearnih sistema jednačina sa ograničenjima (radni opsezi pozicija i krutosti zglobova). Pristup optimizaciji kretanjem u nultom prostoru može

 ISBN 978-86-7466-930-3

dovesti do lokalno optimalnog rešenja. Kada se računa optimalna konfiguracija zgloba, projekcija nultog prostora će osigurati glatku putanju zgloba u poređenju sa metodama nelinearne optimizacije koji traže optimalno globalno rešenje koje se može značajno razlikovati od trenutne poze robota [11].

Pristup predložen u ovom radu se zasniva na „*offline*“ oblikovanju elipsoida krutosti u fazi planiranja trajektorije i krutosti završnog uređaja robota, čijim se oblikovanjem indirektno podešava i matrica krutosti završnog uređaja. Predložene su dve kriterijumske funkcije. Jedna koja ima labaviji kriterijum i jedna sa konzervativnijim kriterijumom.

Struktura rada je sledeća: Nakon uvodnog poglavlja sledi poglavlje II gde je modelirana i opisana priroda matrice krutosti. Poglavlje III opisuje grafičku prezentaciju krutosti preko elipsi i elipsoida krutosti. U poglavlju IV je opisan algoritam za offline planiranje krutosti i pozicije završnog uređaja robota sa simulacionim rezultatima, a u poglavlje V je diskusija i zaključak.

## II. PASIVNA KRUTOST

Lokalna statička karakteristika krutosti zglobova robota se definiše kao negativni izvod momenta po uglu [6, 7]

$$K_j = -\frac{\partial \tau}{\partial q}, \tag{1}$$

gde je $K_j$ matrica krutosti zglobova, $\tau$ je vektor momenata koji se razvijaju na zglobovima, a $q$ je vektor pozicija zglobova. Važi relacija $\tau = J(q)^T F_{ekst}$, između Jakobijeve matrice ($J(q)$), eksterne sile koja deluje na završni uređaj robota ($F_{ekst}$) i momenta zglobovima ($\tau$) koji se stvara usled delovanja sile, kao i to da je $F_{ekst}$ proporcionalno matrici krutosti završnog uređaja $K_C$ i otklona iz ravnotežnog položaja $\Delta x$ nastalog usled eksterne sile $F_{ekst} = K_C \Delta x$, tako da izraz (1) postaje

$$K_j = -\frac{\partial (J(q)^T K_C \Delta x)}{\partial q} = J(q)^T K_C J(q) - \frac{\partial J(q)^T}{\partial q} K_C \Delta x, \tag{2}$$

gde je $\partial \Delta x / \partial q = J(q)$, $K_C$ je $m \times m$ simetrična matrica, $K_j$ je $n \times n$ dijagonalne matrice, $J(q)$ je $m \times n$ matrica i $q$ je $n$-dimenzionalni vektor pozicija zglobova. Parametri $m$ i $n$ su dimenzije radnog prostora i broja zglobova robota. Kada nema otklona od ravnotežnog stanja, tada je $\Delta x = 0$, tako da izraz (2) postaje

$$K_j = J(q)^T K_C J(q). \tag{3}$$

Matrica pasivne krutosti zglobova ($K_j$) može da ima nedijagonalnu strukturu sa van dijagonalnim elementima kada se koriste biartikulisani aktuatori [12, 13], gde jedan aktuator pogoni više od jednog segmenta robota, a koji su mehanički veoma komplikovani za realizaciju. Fokus u ovom radu je na uniartikulisanim aktuatorima koji rezultuju da matrica $K_j$ ima dijagonalnu formu.

Iz jednačine (3) se dobija statička relacija za mapiranje matrice krutosti završnog uređaja robota $K_C$ u Dekartovim koordinatama (engl. *Cartesian space*) sa jedne strane i sa druge strane matrice krutosti zglobova $K_j$ i konfiguraciji robota predstavljene kroz Jakobijevu matricu $J(q)$ [6, 7] kao

$$K_C = \left(J(q) K_j^{-1} J(q)^T\right)^{-1}, \tag{4}$$

odnosno

$$K_C = J(q)^{\dagger^T} K_j J(q)^{\dagger}, \tag{5}$$

gde je $J(q)^{\dagger}$ desna pseudo inverzija Jakobijeve matrice $J(q)$ za koju važi $J(q)J(q)^{\dagger} = I$, gde je $I$ jedinična matrica. U opštem slučaju pseudo inverzija je definisana kao $J(q)^{\dagger} = Z^{-1}J(q)^{\mathrm{T}}(J(q)Z^{-1}J(q)^{\mathrm{T}})^{-1}$, gde je $Z$ pozitivno definitivna matrica. Za pravilno mapiranje krutosti u zglobu i krutosti završnog uređaja metrički tenzor ($Z$) mora imati vrednost matrice krutosti zglobova $Z = K_j$ [6].

Jednačine (4) i (5) ukazuju da se na krutost i popustljivost završnog uređaja robota može uticati:

1) rekonfiguracijom robota kroz nulti prostor kinematički redundantnog robota,
2) promenom krutosti zglobova robota pogonjenih sa VSA,
3) simultanom rekonfiguracijom i promenom krutosti zglobova robota.

Svi nabrojani načini se mogu primeniti na robote pogonjene sa aktuatorima promenljive krutosti, dok samo rekonfiguracija robota kroz nulti prostor se može primeniti na robote pogonjene aktuatorima sa konstantnom krutošću. Zbog toga eksploatacija redundanse kod robota pogonjenog aktuatorima konstantne krutosti ima veliku važnost.

Česta aproksimacija je da se matrica krutosti podeli na četiri submatrice ($K_T$ i $K_R$ su translatorna i rotaciona krutost, dok su $K_{RT}$ i $K_{TR}$ matrice kuplovanja), gde su od interesa samo submatrice na glavnoj dijagonali (translatorna i rotaciona), dok se one na sporednoj dijagonali zanemaruju [6]

$$K_C = \begin{bmatrix} K_T & K_{RT} \\ K_{TR} & K_R \end{bmatrix}, \tag{6}$$

$$\widehat{K}_C = \begin{bmatrix} K_T & 0 \\ 0 & K_R \end{bmatrix}. \tag{7}$$

Treba imati na umu da je $\widehat{K}_C$ aproksimacija koja je lokalno validna.

## III. GRAFIČKA REPREZENTACIJA KRUTOSTI

Za robote koji imaju bilo aktivnu ili pasivnu popustljivost, moguće je sprovesti određene analize koje se tiču performansi robota i krutosti završnog uređaja [14, 15, 9]. Generalno, elipse i elipsoidi daju jednu vrstu aproksimacija koliko i u kom pravcu robot može da razvije krutost, što predstavlja koristan alat u fazi dizajniranja kao i u operativnoj fazi. Elipsoidi imaju veliku primenu u analizi i dizajnu matrica krutosti kod aktivne popustljivosti, gde se kod kinematički redundantnih robota mogu koristiti da se maksimizira radni prostor [14, 15], a da pri tome aktuatori ne budu u zasićenju i željeno ponašanje ne bude narušeno.

 ISBN 978-86-7466-930-3

Kod aktivne krutosti osim samih elipsoida i politopa moguće je uvesti i region ostvarive krutosti (SFR – engl. *Stiffness Feasibility egion*) koji predstavlja oblik sa ne-politopskim granicama [14].

Kod sila interakcije, bez obrtnih momenata, koje deluju na završni uređaj, ulogu igraju samo elementi matrice translatorne krutosti $K_T$ koji se odnose na sile odnosno na translatorna kretanja. To je kvadratna simetrična matrica koja ima dimenzije $3 \times 3$ za trodimenzionalni prostor, ili $2 \times 2$ u ravanskom prostoru (2D). Kada je u pitanju trodimenzionalni prostor, matrica krutosti se može predstaviti pomoću elipsoida krutosti, ili u slučaju dvodimenzionalnog prostora pomoću elipse krutosti. Radi intuitivnijeg razumevanja na slici 1 je dat prikaz elipse krutosti. Parametri koji opisuju elipsu krutosti su ose elipse $\lambda_1$ i $\lambda_2$ (u slučaju elipsoida postoji i $\lambda_3$) međusobno normalne, i ugao orijentacije elipse α (u slučaju elipsoida postojaće dodatni ugao orijentacije u odnosu $xy$ ravan). Pravac orijentacije elipse i elipsoida je u pravcu najduže ose elipse/elipsoida. Na levoj strani na slici 1 prikazana je elipsa kada se ose elipse poklapaju sa osama koordinatnog sistema, dok na desnoj strani je prikazana elipsa koja je ukošena za ugao α. Kada se ose elipse/elipsoida poklapaju sa osama koordinatnog sistema, tada nema kuplovanih elemenata i matrica krutosti ima dijagonalni oblik.

Dužine osa i ugao orijentacije elipsoida se dobija dekompozicijom matrice (SVD – engl. *Singular alue ecomposition*) krutosti kao

$$K_T = USV^T, \qquad (8)$$

Kolone ortogonalnih matrica U i V predstavljaju sopstvene vektore, a elementi na dijagonali dijagonalne matrice S predstavljaju sopstvene vrednosti. Sopstvene vrednosti matrice S predstavljaju intenzitete krutosti duž osa elipsoida, a vrednosti kolona matice V predstavljaju sopstvene vektore koji određuju pravac orijentacije osa elipse/elipsoida.

Oblikovanje krutosti završnog uređaja može se podeliti na krutost zavisnu od konfiguracije (CDS – engl. *Configuration ependant Stiffness*) i krutost koja zavisi od krutosti zglobova (CMS – engl. *Common Mode Stiffness*) [16]. CDS potiče od redundantne konfiguracije robota i koristi se za usmeravanje elipse ili elipsoida krutosti, dok CMS utiče na veličine osa elipse ili elipsoida. CMS predstavlja dodatni parametar koji se može uključiti u oblikovanje krutosti. Krutost završnog uređaja robota pogonjenog sa aktuatorima konstantne krutosti može se promeniti samo rekonfiguracijom kada je robot kinematički redundantan.

Na primeru planarne konfiguracije robota sa 3 stepena slobode (segmenti $L_1$, $L_2$ i $L_3$) koja je ilustrovana slici 2 (levo) prikazan je uticaj CMS na elipsu krutosti (slika 2 desno). Pozicije zglobova ($q_1$, $q_2$ i $q_3$) su konstantne i samim tim pozicija završnog uređaja (EE) je konstantna. Krutost zglobova ($k_{j1}$, $k_{j2}$ i $k_{j3}$) dobija se kao proizvod početnih vrednosti krutosti ($k_{j10}$, $k_{j20}$ i $k_{j30}$) i parametra CMS-a ($k$) kao $k_{j1} = kk_{j10}$, $k_{j2} = kk_{j20}$ i $k_{j3} = kk_{j30}$. CMS ne utiče na oblik (odnos osa) i usmerenje elipse

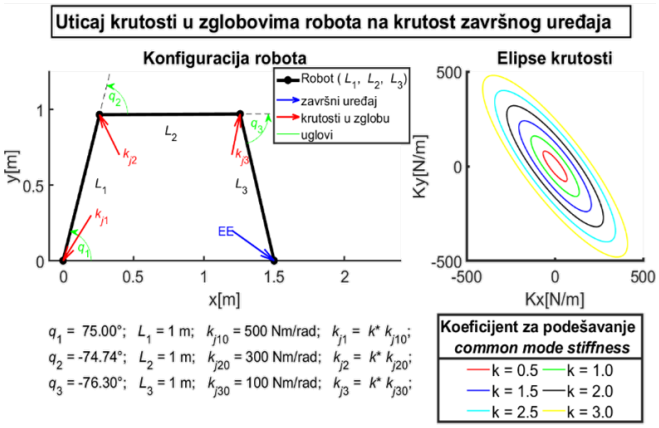


Sl. 2. Uticaj *Common Mode Stiffness* -a na krutost završnog uređaja robota. Levo: Planarna konfiguracija robota koja se sastoji od tri segmenta – $L_1$, $L_2$ i $L_3$ (crno); pozicija završnog uređaja robota (plavo); krutosti u zglobovima $k_{j1}$, $k_{j2}$ i $k_{j3}$ (crveno); pozicije zglobova $q_1$, $q_2$ i $q_3$ (zelena). Desno – Elipsoidi krutosti za fiksnu konfiguraciju ($q_1 = 75°$, $q_2 = -74.74°$ i $q_3 = -76.30°$) različiti koeficijent CMS-a $k \in [0.5 - 3]$. Krutost u zglobovima se računa kao proizvod početnih vrednosti krutosti ($k_{j10}$,$k_{j20}$ i $k_{j30}$) i parametra common mode stiffness-a ($k$) kao $k_{j1} = kk_{j10}$, $k_{j2} = kk_{j20}$ i $k_{j3} = kk_{j30}$.

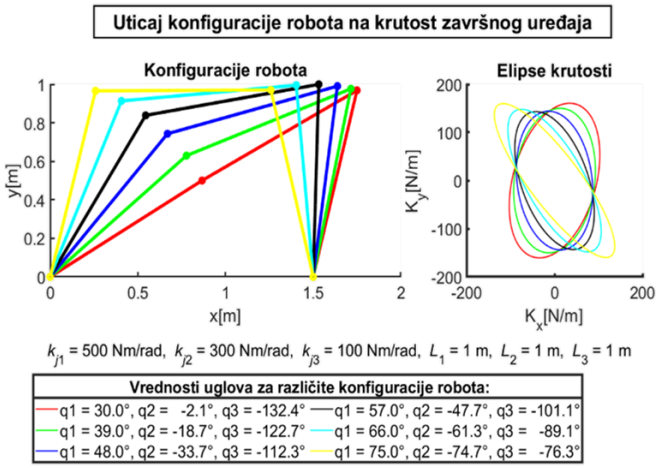


Sl. 3. Uticaj konfiguracije kinematički redundantnog robota na krutost završnog uređaja robota sa dužinama segmenata $L_1 = 1m$, $L_2 = 1m$ i $L_3 = 1m$, i krutostima u zglobovima $k_{j1} = 500\text{Nm/rad}$, $k_{j2} = 300\text{Nm/rad}$ i $k_{j3} = 100\text{Nm/rad}$. Levo: Različite planarne konfiguracije robota sa istom pozicijom završnog uređaja; Desno – Elipsoidi krutosti za različite konfiguracije robota.

krutosti, već samo na njen volumen odnosno samo linearno skalira elemente matrice krutosti.

Jedan od pristupa za oblikovanje matrice ili elipse (ili elipsoida u 3D prostoru) krutosti robota pogonjenog aktuatorima konstantne krutosti je kroz promenu kinematičke konfiguracije robota kada postoji kinematička redundansa. Promena konfiguracije se odvija u nultom prostoru. To omogućava da robot pored primarnog zadatka (praćenje trajektorije) izvrši i sekundarni zadatak koji je u ovom slučaju oblikovanje krutosti završnog uređaja robota. Na primeru planarne konfiguracije robota sa 3 stepena slobode (segmenti $L_1$, $L_2$ i $L_3$) koja je ilustrovana slici 3 (levo) prikazan je uticaj CDS na elipsu krutosti (slika 3 desno).


ISBN 978-86-7466-930-3

## IV. ALGORITAM ZA OFFLINE PLANIRANJE KRUTOSTI I POZICIJE ZAVRŠNOG UREĐAJA ROBOTA

Osim preko matrice krutosti, krutost završnog uređaja je moguće oblikovati preko elipse krutosti. U ovom radu predložen je offline pristup oblikovanja krutosti završnog uređaja robota, promenom optimizacionih algoritama, koji je predviđen za planiranje krutosti kada je zadatak u napred poznat, pa samim tim i trajektorija završnog uređaja. Primenjena su dva kriterijuma koji kombinuju oblik i grešku orijentacije elipsoida. Oblikovanje elipsoida krutosti se ostvaruje kombinacijom nultog prostora i krutosti u zglobovima. Optimizacioni algoritmi su primenjeni na simulacionom modelu KUKA LWR robota na primeru ravanskog kretanja u „$xy$" ravni, kada se završni uređaj robota kreće po krivoj putanji.

Optimizacioni algoritmi koji su korišćeni su zasnovani na SLSQP (engl. Sequential Least SQuare Programming) [10, 17, 18], a implementirani su Matlab-u. SLSQP je algoritam koji optimizuje vrednosti nelinearnih kriterijumskih funkcija sa linearnim i nelinearnim ograničenjima. Ograničenja koja postoje u predloženim optimizacionim algoritmima se odnose na ostvarive vrednosti pozicije zglobova robota i na definisani opseg krutosti koje robot može da ostvaruje. Nelinearna ograničenja koja moraju biti zadovoljena se odnose na kinematiku. Optimizacioni algoritam uvek mora da zadovolji željenu poziciju završnog uređaja robota.

Kako zbog prirode zadatka, pozicija zadnjeg zgloba ne utiče na položaj završnog uređaja, već samo na ugao orijentacije oko $z$ ose, njegova vrednost je zaključana na 0°. Na taj način robot ima 6 stepeni slobode na raspolaganju za izvršavanje zadatak. Usvojen je da raspon krutosti zglobova bude 1-100 Nm/rad. Ovo se može usvojiti bez gubljenja opštosti, jer bitan je relativan odnos krutosti u zglobovima za orijentaciju i odnos osa elipsoida krutosti. Naknadno preko CMS-a se podešava i volumen.

Prvi predloženi kriterijum ($f_1$) usmerava elipsoid i maksimizira krutost duž pravca kretanja, zadavajući minimalni odnos dijagonala elipsoida. Drugi kriterijum ($f_2$) usmerava elipsoid duž pravca kretanja, ali zadajući tačan odnos dijagonala elipsoida. Predložene optimizacione metode imaju za cilj da doprinesu planiranju trajektorije i krutosti zglobova prilikom izvršavanja zadataka.

### *A. Maksimiziranje krutosti duž pravca kretanja*

Oblikovanje elipsoida krutosti moguće je ostvariti primenom kriterijumske funkcije definisane kao

$$f_1 = \frac{|\alpha_{error}| + c}{min\left(\frac{r_{max}}{r_{min}}, r\right)/r}, \tag{9}$$

gde $\alpha_{error}$ označava grešku orijentacije elipsoida u stepenima, $r$ je minimalni željeni odnos osa elpsoida, $r_{max}$ i $r_{min}$ su najduža i druga po dužini osa elipsoida, dok je $c$ pozitivna konstanta koja omogućava optimizaciju kada je apsolutna greška orijentacije elipsoida $|\alpha_{error}| = 0°$, dok je željena orijentacija u smeru kretanja završnog uređaja robota. Usvojena je vrednost $c = 0.01$.

U svakoj iteraciji računaju se pozicije i krutosti zglobova koje minimiziraju vrednost funkcije $f_1$ kao

$$\begin{bmatrix} q[p] \\ k_j[p] \end{bmatrix} = \underset{\substack{q\in[q_{min},q_{max}] \\ k_j\in[k_{j_{min}},k_{j_{max}}]}}{argmin} f_1(q, k_j), \tag{10}$$

gde je $p$ redni broj iteracije, a $q_{min}, q_{max}$, $k_{j_{min}}$ i $k_{j_{max}}$ su minimalne i maksimalne vrednosti pozicija i krutosti zglobova. Opseg vrednosti promenljivih u optimizacionom algoritmu se može dodatno suziti, i samim tim smanjiti prostor pretrage i ubrzati algoritam pretrage u svakoj iteraciji. Nove granične vrednosti varijabli ($q^*_{min}, q^*_{max}$, $k^*_{j_{min}}$ i $k^*_{j_{max}}$) u svakoj iteraciji se računaju uzimajući u obzir maksimalne brzine promene koje robot može da ostvari u okviru jedne iteracije (za pozicije zglobova - $\Delta q$, za krutost zglobova - $\Delta k_j$) i fizički ostvarive vrednosti kao

$$q_{min\_iter}[p] = max(q_{min}, \quad q[p-1] - \Delta q), \tag{11}$$

$$q_{max\_iter}[p] = min(q_{max}, \quad q[p-1] + \Delta q), \tag{12}$$

$$k_{j_{min\_iter}}[p] = max\left(k_{j_{min}}, \quad k_j[p-1] - \Delta k_j\right), \tag{13}$$

$$k_{j_{max\_iter}}[p] = min\left(k_{j_{max}}, \quad k_j[p-1] + \Delta k_j\right). \tag{14}$$

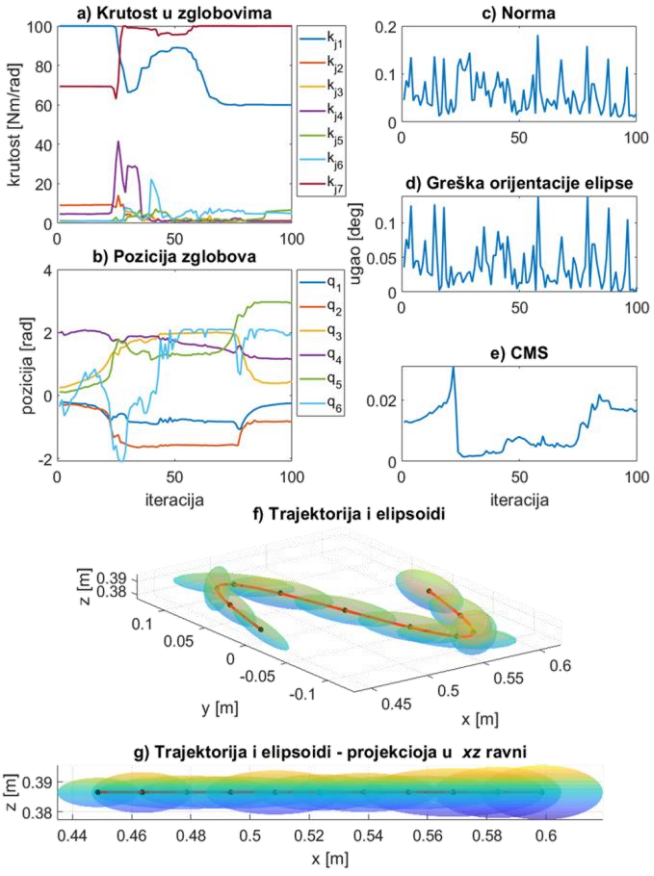


Sl. 4. Simulacioni rezultati za oblikovanje elipsoida krutosti na primeru krivolinijskog kretanja kada je zahtev da odnos osa elipsa bude minimalno 5:1: a) krutost u zglobovima; b) pozicija zglobova; c) norma (vrednost kriterijumske funkcije); d) greška orijentacije; e) CMS; f trajektorija i elipsoidi; g) trajektorija i elipsoidi- projekcija u $xy$ ravni.


ISBN 978-86-7466-930-3

To je računski zahtevan posao i nije ga jednostavno implementirati da radi u realnom vremenu, ali moguće ga je iskoristiti u fazi planiranja krutosti i trajektorije zglobova i završnog uređaja.

Simulacioni rezultati za primer krivolinijskog kretanja su prikazani na slici. Na slici 4a je prikazana krutosti u zglobovima, a na slici 4b pozicija zglobova. Slika 4c prikazuju vrednost (normu) optimizacione funkcije, dok slika 4d ilustruje grešku orijentacije. Slika 4e je CMS kojim su skalirane krutosti sa slike 4a da bi se dobili skalirani elipsoidi.

Primenjena optimizaciona funkcija i algoritam su ostvarili zadati cilj, da elipsoid ima željeno usmerenje i minimalni odnos osa. Dobijeni CMS skalira elipse da bi bile uporedive. Dobijene elipsoide moguće je dodatno skalirati da se dobije željena amplitude, ali samo po jednoj od osa. Da bi bilo moguće potpuno oblikovati elipsoid krutosti, potrebno je modifikovati kriterijumsku funkciju.

### *B. bliko anje elipsoida krutosti*

Da bi se elipsoid krutosti potpuno oblikovala neophodno je da budu ostvareni sledeći zahtevi:

1) željeni pravac orijentacije elipsoida,
2) tačan odnos osa elipsoida,
3) magnitude osa elipsoida.

Kada su prva dva uslova zadovoljena, treći se ostvaruje primenom CMS-a na već oblikovanu elipsu. Da bi prva dva uslova mogla simultano da se optimizuju, predložena je modifikovana kriterijumska funkcija koja kombinuje grešku orijentaciju i odnos osa elipse

$$f_2 = (1 + |\alpha_{error}|)\left(1 + \left|r - \frac{r_{max}}{r_{min}}\right|\right). \quad (15)$$

Pozicije i krutosti zglobova u svakoj iteraciji se računaju identično kao i u prethodnom primeru opisanom u jednačinama (10) – (14) samo je optimizaciona funkcija promenjena i definisana kao $f_2$.

Funkcija je modifikovana tako da penalizuje svaku grešku orijentacije, i svako odstupanje odnosa osa od željenog odnosa. Zadati su zahtevi da je greška orijentacije $\alpha_{error} = 0°$, dok je željena orijentacija u smeru kretanja završnog uređaja robota, a odnos osa elipse $r = 5$.

Simulacioni rezultati za primer krivolinijskog kretanja su prikazani na slici 5. Na slici 5a je prikazana krutosti u zglobovima, a na slici 5b pozicija zglobova. Slika 5c prikazuju vrednost (normu) optimizacione funkcije, dok slika 5d ilustruje grešku orijentacije. Slika 5e je CMS kojim su skalirane krutosti sa slike 5a da bi se dobili skalirani elipsoidi.

Primenjena optimizaciona funkcija i algoritam su ostvarili zadati cilj, da elipsoid ima željeno usmerenje i odnos osa. Dobijeni CMS skalira elipse da bi bile uporedive. Dobijene elipsoide moguće je dodatno skalirati da se dobije željena amplitude. Algoritam je ostvario zadati cilj da elipsa ima željeno usmerenje i odnos osa. Dobijeni CMS skalira elipsoide da bi bile uporedivi. Rezultati pokazuju da svi elipsoidi imaju željeni oblik ili oblik koji je jako blizak

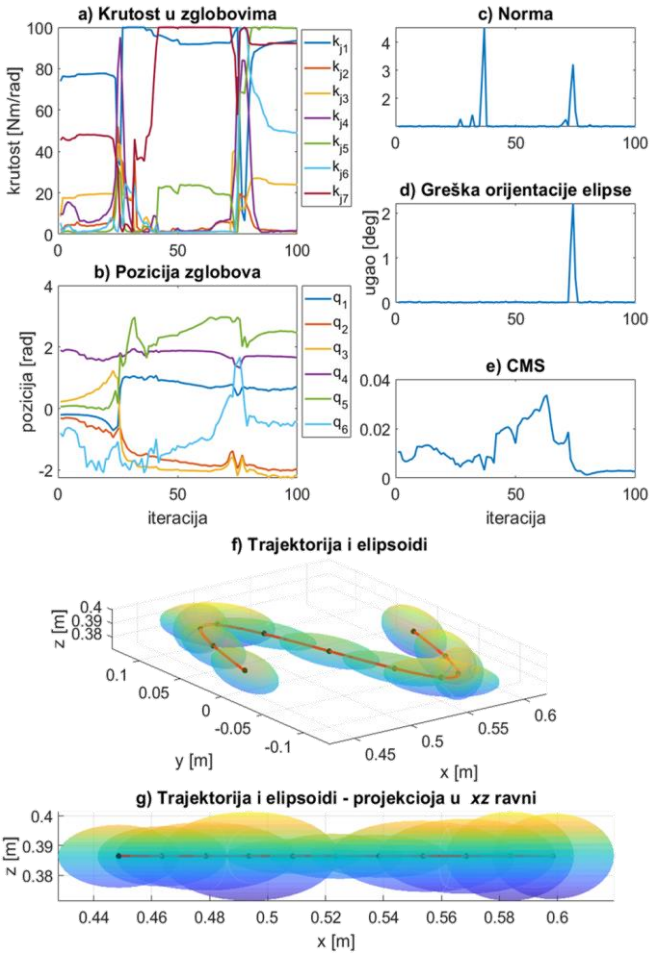


Sl. 5. Simulacioni rezultati za oblikovanje elipsoida krutosti na primeru krivolinijskog kretanja kada je zahtev da odnos osa elipsa bude tačno 5:1: a) krutost u zglobovima; b) pozicija zglobova; c) norma (vrednost kriterijumske funkcije); d) greška orijentacije; e) CMS; f trajektorija i elipsoidi; g) trajektorija i elipsoidi- projekcija u $xy$ ravni.

željenom. Dobijene elipsoide moguće je dodatno skalirati da se dobije željena amplitude osa.

Slika 6 ilustruje vrednosti funkcija u zavisnosti od greške orijentacije i odnosa osa elipse, a crvena boja označava minimum funkcije koji je u slučaju $f_1$ definisan kao prava, dok u slučaju $f_2$ kao jedna tačka. Samim tim je jasno da je optimalni set za $f_2$ koji je konzervativniji mnogo teže zadovoljiti nego u slučaju labavijih zahteva kriterijumske funkcije $f_1$. Ostvarivanje optimalnog rešenja u svakoj iteraciju uslovljeno je fizičkim ograničenjima samog robota.

## V. DISKUSIJA I ZAKLJUČAK

U radu je uspešno implementiran pristup oblikovanja krutosti završnog uređaja robota pomoću grafičke reprezentacije krutosti preko elipsoida na modelu robota KUKA LWR. Krutost koja se analizira je zasnovana na modelu. Ilustrovano je da različiti kriterijumi daju rezultate različitog kvaliteta u skladu sa definisanim kriterijumima i fizičkim ograničenjima robota. Dobijeni rezultati uglavnom dobro ispunjavaju zadate zahteve, dok su ograničenja izraženija kod konzervativnije kriterijumske funkcije koja se ogleda u trenucima kada trajektorija ima najveće


ISBN 978-86-7466-930-3

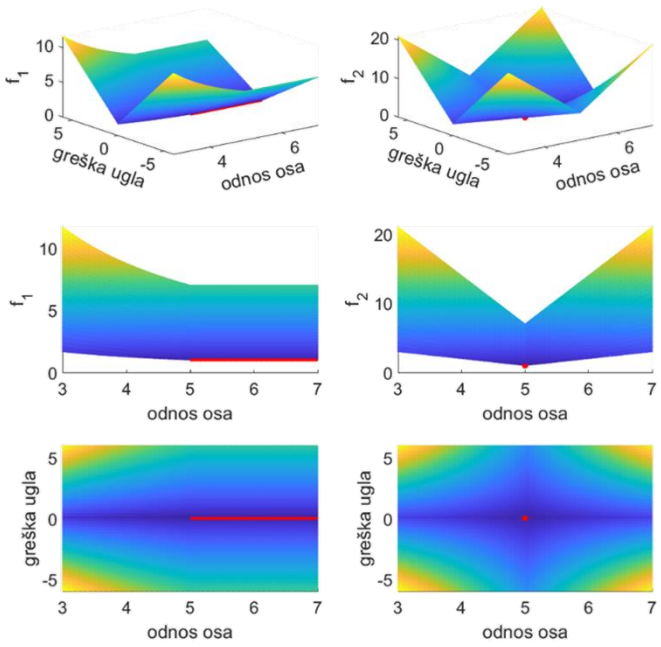


Sl. 6. Oblici kriterijumskih funkcija u zavisnosti od greške orijentacije i odnosa osa elipsi. Crvena boja označava minimum funkcije koji je u slučaju $f_1$ definisan kao prava, dok u slučaju $f_2$ kao jedna tačka

zakrivljenje, a samim tim i najveće promene orijentacije elipsoida. To pokazuje da su ostvarivi rezultati ograničeni izborom dela radnog prostora, kao i oblikom trajektorije. Klasična matrica translatorne krutosti ima 6 elemenata koje treba optimizovati, dok predložene kriterijumske funkcije koriste samo dva parametra, ugao greška ugla orijentacije elipsoida i odnos osa.

## ZAHVALNICA

Rad je realizovan u okviru projekta Fonda za nauku Republike Srbije PROMIS, Grant #6062528, ForNextCobot i tokom istraživanja finansiranog od strane Ministarstva prosvete, nauke i tehnološkog razvoja Republike Srbije. Broj ugovora 2022/200103.

## LITERATURA

[1] S. Haddadin, A. Albu-Schäffer and G. Hirzinger, "Safe Physical Human-Robot Interaction: Measurements, Analysis and New Insights," in *obotics esearch. Springer Tracts in Ad anced obotics*, Berlin, Heidelberg, Springer, 2010, pp. 395-407.

[2] A. De Santis, B. Siciliano, A. De Luca and A. Bicchi, "An atlas of physical human–robot interaction," *Mechanism and Machine Theory,* vol. 43, no. 3, pp. 253-270, 2008.

[3] N. Hogan, "Impedance Control: An Approach to Manipulation: Part II-implementation," *ournal of ynamic Systems, Measurement, and Control,* vol. 107, no. 1, pp. 8-16, 1985.

[4] B. Lukić, T. Petrič, L. Žlajpah and K. Jovanović, "KUKA LWR Robot Cartesian Stiffness Control Based on Kinematic Redundancy," in *The 2 th International Conference on obotics in Alpe-Adria-anube egion, AA 201* , Kaiserslautern, Germany, 2019.

[5] R. Van Ham, T. G. Sugar, B. Vanderborght, K. W. Hollander and D. Lefeber, "Compliant actuator designs," *IEEE obotics Automation Maga ine,* vol. 16, no. 3, pp. 81-94, 2009.

[6] A. Albu-Schäffer , M. Fischer, G. Schreiber, F. Schoeppe and G. Hirzinger, "Soft robotics: what Cartesian stiffness can obtain with passively compliant, uncoupled joints?," in *IEEE S International Conference on Intelligent obots and Systems I S* , Sendai, Japan, 2004.

[7] F. Petit and A. Albu-Schäffer, "Cartesian impedance control for a variable stiffness robot arm," in *IEEE S International Conference on Intelligent obots and Systems*, San Francisco, CA, USA, 2011.

[8] M. H. Ang and G. B. Andeen, "Specifying and achieving passive compliance based on manipulator structure," *IEEE Transactions on obotics and Automation,* vol. 11, no. 4, pp. 504-515, 1995.

[9] N. Lukić and P. B. Petrović, "Complementary projector for null-space stiffness control of redundant assembly robot arm," *Assembly Automation,* vol. 39, no. 4, pp. 696-714, 2019.

[10] N. Knežević, B. Lukić, K. Jovanović, L. Žlajpah and T. Petrič, "End-effector Cartesian stiffness shaping - sequential least squares programming approach," *Serbian ournal of Electrical Engineering,* vol. 18, no. 1, pp. 1-14, 2021.

[11] N. Knežević, B. Lukić and K. Jovanović, "Feedforward Control Approaches to Bidirectional Antagonistic Actuators Based on Learning," in *Ad ances in Ser ice and Industrial obotics*, Cham, Springer, 2020, pp. 337-345.

[12] W. Roozing, Z. Ren and N. G. Tsagarakis, "An efficient leg with series–parallel and biarticular compliant actuation: design optimization, modeling, and control of the eLeg," *The International ournal of obotics esearch,* vol. 40, no. 1, pp. 37-54, 2021.

[13] A. Nejadfard, S. Schütz, K. Mianowski, P. Vonwirth and K. Berns, "Moment Arm Analysis of the Biarticular Actuators in Compliant Robotic Leg Carl," in *Biomimetic and Biohybrid Systems*, Cham, Springer, 2018, pp. 348-360.

[14] A. Ajoudani, N. G. Tsagarakis and A. Bicchi, "On the role of robot configuration in Cartesian stiffness control," in *2015 IEEE International Conference on obotics and Automation IC A* , Seattle, WA, USA, 2015.

[15] A. Ajoudani, N. G. Tsagarakis and A. Bicchi, "Choosing Poses for Force and Stiffness Control," *IEEE Transactions on obotics,* vol. 33, no. 6, pp. 1483-1490, 2017.

[16] A. Ajoudani, M. Gabiccini, N. Tsagarakis, A. Albu-Schäffer and A. Bicchi, "TeleImpedance: Exploring the role of common-mode and configuration-dependant stiffness," in *2012 12th IEEE- AS International Conference on umanoid obots umanoids 2012* , Osaka, Japan, 2012.

[17] P. T. Boggs and J. W. Tolle, "Sequential quadratic programming for large-scale nonlinear optimization," *ournal of Computational and Applied Mathematics,* vol. 124, no. 1-2, pp. 123-137, 2000.

[18] N. Knežević, B. Lukić, K. Jovanović , T. Petrič and L. Žlajpah, "End-Effector Cartesian Stiffness Optimization: Sequential Quadratic Programming Approach," in *Proceedings of the 5th International Conference on Electrical, Electronic and Computing Engineering IcET AN 201* , Silver Lake, Serbia, 2019.

## ABSTRACT

The stiffness of the robot's end-effector (EE) determines the robot's behavior when interacting with the environment. The stiffness of the EE is most often represented by a stiffness matrix whose complete design can be impossible because robots do not have enough degrees of freedom to adjust all the elements in the stiffness matrix. This leads to the application of optimization that balances the values of the stiffness matrix elements that are of interest for the task. In this paper, an approach for offline shaping of the stiffness matrix using stiffness ellipsoids is proposed, where stiffness is shaped by adjusting the orientation and axis length of the ellipsoid. The shape of the ellipsoid has fewer parameters that need to be adjusted relative to the stiffness matrix. Two criterion functions for shaping the ellipsoid stiffness have been proposed to exploit robot kinematic redundancy in shaping the stiffness ellipsoid. Optimal values of joint positions and stiffness were calculated using the algorithm based on SLSQP (Sequential Least SQuare Programming). Following the shaping of EE stiffness ellipsoid, adjustments or its volume based on variations in joint stiffness are highlighted.

**nd-effector passive stiffness shaping through the stiffness ellipsoid**

Branko Lukić, Nikola Knežević i Kosta Jovanović

 ISBN 978-86-7466-930-3

# Hijerarhijsko distribuirano upravljanje kolaborativnim industrijskim humanoidnim robotom podržano oblak-arhitekturom

Jovan Šumarac, Ilija Stevanović, Aleksandar Rodić

***A stra t*— vaj rad predstavlja jednu hijerarhijs u, distribuiranu upravljačku arhitekturu dvoručnog, olaborativnog, humanoidnog servisnog robota podržanom tehnologijom "računarstva u oblaku". va upravljačka stru tura dizajnirana je namenski za izvršavanje robots ih zadataka koji zahtevaju primenu složenijih manipulativnih i ognitivnih veština u o viru industrijs og proizvodnog tehnološkog procesa. Upravljačka struktura robota osmišljena je ta o da zadovolji potrebe tzv. pametne proizvodnje u o viru platforme Industrije 4. , odnosno da omogući i olakša kooperaciju čoveka i robota kao njemu komplementarnog inteligentnog sistema, neophodnog u industrijs im zadacima koje čovek ne može samostalno sprovoditi. Ovaj rad prikazuje strukturu i način funkcionisanja sistema hijerarhijskog distribuiranog upravljanja, organizovan na tri operativna nivoa a) strateškom, b) taktičkom i c) izvršnom. To je omogućeno zahvaljujući korišćenju arhitekture oblak-računarskog sistema. Hardver upravljačkog sistema uspostavljen je na tri nivoa fizičkom, komunikacionom i aplikativnom. Zahvaljujući distribuiranoj arhitekturi, sistem oblaka omogućava distribuirano izvršavanje pojedinačnih upravljačkih zadataka što rezultira uravnoteženim opterećenjem multiprocesorskog sistema i smanjenjem vremena odziva na stimuluse iz fizičkog okruženja robota.**

***Ključne reči*—upravljanje u obla u, olaborativni roboti, distribuirana inteligencija, pametna proizvodnja, Industrija 4.**

## I. UVOD

Od kada je kompanija „General Motors" u Detroitu (SAD) 1961. napravila prvog industrijskog robota za manipulaciju (UNIMATE) i koristila ga u automobilskoj industriji za sklapanje delova, timovi naučnika, inženjera i tehnologa razmišljali su o tome kako da automatizuju ljudske manipulacione i kognitivne veštine što je više moguće i kako da robote učine bezbednim i kolaborativnim. Prethodne generacije industrijskih robota za manipulaciju, kao deo svojih kontrolera, koristile su algoritme za "imitaciju" ljudskih manipulativnih veština uz korišćenje petlji povratne sprege po poziciji ondosno brzini i po sili odnosno momentu. Ovo je uglavnom bilo dovoljno za obavljanje tehnoloških operacija u okviru proizvodnih procesa u visoko tehnološki strukturiranim infrastrukturnim okruženjima – tehnološkim proizvodnim linijama. Međutim, takav pristup je imao relativno nizak nivo fleksibilnosti i prilagodljivosti poremećajima i promenama u proizvodnim procesima.

Sa napretkom informacionih tehnologija, bežičnih komunikacija, "Interneta stvari", senzorskih tehnologija i mašinske vizije, otvorene su nove perspektive automatizacije tehnoloških procesa tako što je industrijskim robotima omogućeno da, sa svojstvenom preciznošću i brzinom, ostvare sofisticirane atribute ljudske mikro-manipulativne i taktilne veštine na visokom nivou kognitivne percepcije i sposobnosti rasuđivanja [1].

Cilj ovog rada jeste da predstavi kako se ljudske veštine i znanje kvalifikovanih radnika mogu sticati, čuvati i koristiti u bazi podataka na sistemu oblaka (ondosno "Cloud" sistemu), odakle se ovi podaci mogu analizirati i koristiti za obuku (tj. za učenje veština) industrijskog humanoidnog robota u izvođenju različitih manipulativnih i kolaborativnih zadataka u saradnji sa ljudima. U tu svrhu razvijen je originalni dvoručni kolaborativni robotski sistem (industrijski humanoidni servisni robot) koji omogućava implementaciju i verifikaciju različitih algoritama za automatizaciju ljudskih manipulativnih i kognitivnih veština u proizvodnim procesima [2]. Originalni robotski sistem sa svim hardverskim i softverskim komponentama razvijen je u Centru za robotiku Instituta "Mihajlo Pupin".

## II. INDUSTRIJSKI HUMANOID

### *A. Mehanički dizajn prototipa robota*

Industrijski humanoid je dvoručni (ili bi-manuelni) kolaborativni servisni robot namenjen industrijskim zadacima [3]-[7], koji po svojoj strukturi podseća na svoj biološki model – čoveka. U mehaničkom smislu industrijski humanoid ima sledeće module: (i) sistem podrške za sletanje montiran na mobilnu platformu (motorizovana kolica), (ii) segmentirani trup - torzo robota, (iii) dve industrijske robotske ruke sa odgovarajućim hvatačima (Sl. 1).

Humanoidni robot je montiran na motorizovana kolica sa diferencijalnim upravljanjem na par pogonskih (aktivnih) točkova. Kolica imaju i dva pomoćna (pasivna) točka, koja se okreću oko sopstvenih vertikalnih osa. Zahvaljujući takvoj strukturi, kolica robota imaju mogućnost da se kreću u tri koordinatna pravca: napred-nazad, levo-desno i da se okreću

Jovan Šumarac – Centar za Robotiku, Institut "Mihajlo Pupin", Univerzitet u Beogradu, Volgina 15, 11060 Beograd, Srbija (e-mail: jovan.sumarac@pupin.rs).

Aleksandar Rodić – Centar za Robotiku, Institut "Mihajlo Pupin", Univerzitet u Beogradu, Volgina 15, 11060 Beograd, Srbija (e-mail: aleksandar.rodic@pupin.rs).

Ilija Stevanović – Centar za Robotiku, Institut "Mihajlo Pupin", Univerzitet u Beogradu, Volgina 15, 11060 Beograd, Srbija (e-mail: ilija.stevanovic@pupin.rs).

 ISBN 978-86-7466-930-3

oko sopstvene ose u opsegu od 0 do 360 stepeni. Nosivi sistem bimanuelnog robota je tehnička varijanta (imitacija) ljudskih nogu. Mehanizam za noge robota može se savijati oko tri ose. Jedna osa rotacije prolazi kroz skočni zglob, druga osa kroz zglob kolena, a treća kroz zglob kuka. Na ovaj način se sinhronizovanim pokretima u pomenutim zglobovima može podesiti položaj (orijentacija) trupa humanoida u odnosu na površinu oslonca.

Gornji deo trupa robota (torzo) ima mogućnost savijanja oko sagitalnog pravca u frontalnoj ravni (levo-desno). Uz mogućnost promene nagiba trupa napred-nazad u sagitalnoj ravni (promenom konfiguracije nogu), ovo omogućava humanoidnom robotu da se prilagodi svom operativnom prostoru zadatka.

Kolaborativni dvoručni robot ima dve industrijske robotske ruke UR5 sa odgovarajućim hvatačima koje mu daju mogućnost različitih manipulacija objektima kao i fizičke interakcije sa okolinom. Takođe, svaka robotska ruka ima instaliran zglobni senzor sile/momenta na završnom uređaju.

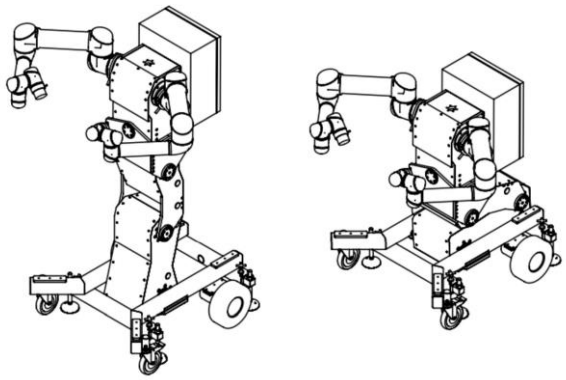

Sl. 1. 3D prototip modela industrijskog robota.

Visina ovog humanoida iznosi oko 175cm a njegov raspon ruku iznosi oko 2300 mm. Ideja iza projektovanja ovakvog sistema jeste da njegove dimenzije budu približne čovekovim kako bi robot mogao lako da zameni čoveka u određenim zadacima, ali i da bi mogao prirodno da obavlja zadatke u kojima postoji kolaboracija sa čovekom. Analiza njegovog radnog prostora pokazala je dobru manipulativnost ovog sistema u oblastima zajedničkog radnog prostora obe robotske ruke, pogotovo u zonama ispred samog torzoa robota [8].

Na Sl. 1. može se videti i ormarić koji je okačen na robotski torzo kao svojevrsni "ranac". U njemu se nalaze različite elektronske komponente neophodne za funkcionisanje celokupnog sistema (mikrokontroleri, uključujući i glavni mikrokontroler ondnosno "mozak" sistema, zatim napajanja, bezbednosne sklopke, releji i dr.).

### *B. Arhitektura hard era kontrolera robota*

Hardverska struktura celokupnog sistema upravljanja industrijskog servisnog robota prikazanog na Sl. 1 je projektovana kao distribuirana računarsko-senzorska mreža [9] koja funkcioniše na tri funkcionalna nivoa (Sl. 2): (i) fizički nivo, (ii) nivo mreže i (iii) aplikativni nivo.

Na fizičkom nivou, postoji robot sa pripadajućim senzorima i kamerama, poseban kontroler trupa robota, kao i nezavisni kontroleri robotskih ruku i pridruženih robotskih hvatača. Globalno posmatrano, to je prilično složena struktura dizajnirana da omogući specifične sposobnosti robota. Takođe na fizičkom nivou, u okruženju robota postoje odgovarajuće mašine alatke sa svojim upravljačkim jedinicama i na kraju ljudi (radnici) koji zajedno sa dvoručnim robotom čine deo tehnološkog procesa.

Mrežni, odnosno komunikacioni nivo hardverske strukture "Cloud" kontrole, zadužen je za brzu i efikasnu međusobnu komunikaciju između sastavnih komponenti robotske ćelije i odgovarajućeg tehnološkog procesa. Uloga mreže je da obezbedi pouzdan prenos informacija i senzorskih podataka do svih i od svih konstitutivnih elemenata sistema. Komunikacioni nivo dakle obezbeđuje umrežavanje robota u lokalnu računarsku mrežu (LAN) korišćenjem Wi-Fi pristupa ili GSM-GPRS modema (u slučaju informaciono strukturiranog okruženja) i povezivanje robota na Internet.

Na nivou aplikacije postoji nekoliko računara koji međusobno komuniciraju i koriste zajedničku bazu podataka. Svaki, pojedinačni računar ima strogo definisane zadatke. Jedan obrađuje podatke koji se odnose na karakteristike objekata (delova) i njima manipuliše, obrađuje podatke koji se odnose na mašine alatke preuzete iz okoline, njihove dimenzije, prostornu lokaciju itd. Drugi računar je zadužen za

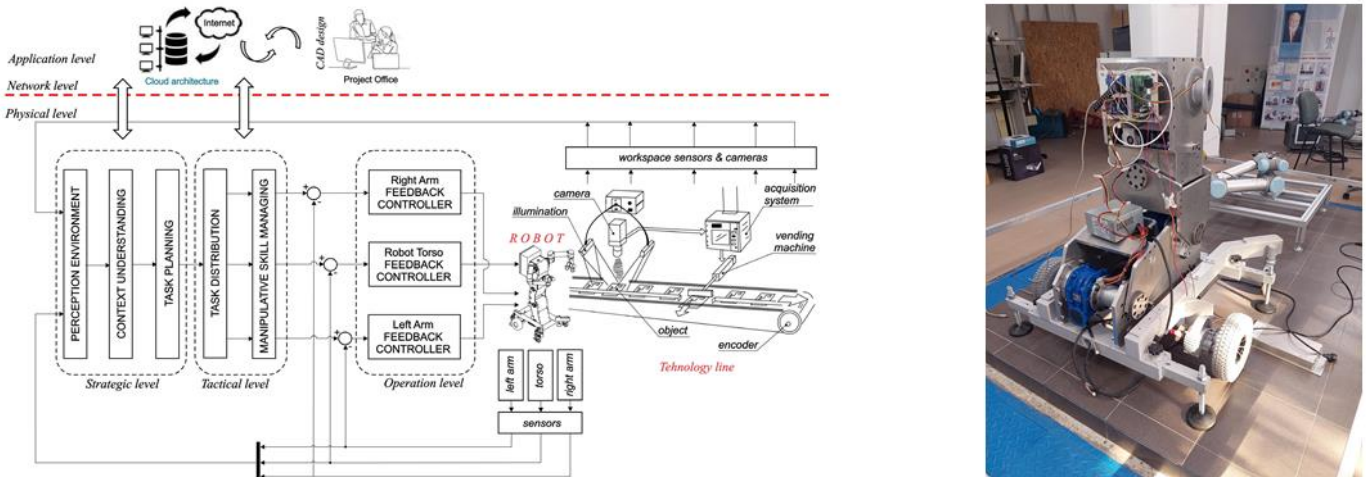


Sl. 2. Blok dijagram hardverske strukture robotskog kontrolera industrijskog humanoida (levo). Sastavljeni prototip robota (desno)..


ISBN 978-86-7466-930-3

analizu, učenje i operacionalizaciju ljudskih manipulativnih i kognitivnih veština koje su karakteristične za tehnološke procese. Treći računar se bavi tehnikama i metodama formalizacije određenih industrijskih tehnoloških procesa (npr. obrada, montaža delova, fizička pomoć ljudskim radnicima, itd.) na način koji će biti razumljiv za mašinu (kontroler robota). Informacije koje se odnose na tehnološke operacije se uglavnom svode na podatke kojim redosledom i kojim alatima treba izvršiti određene tehnološke operacije, na koji način, u kojoj tački uhvatiti objekat, kojom silom ili momentom, kojom brzinom to učiniti, itd.

Zadaci koji se obavljaju na računarima, koji su deo aplikativnog nivoa, u velikoj meri se oslanjaju na baze podataka u vezi sa aplikacijama koje su operativni domen industrijskog humanoida. Baze podataka sadrže informacije koje se odnose na geometrijske atribute objekata koji su predmet tehnološkog procesa, zatim informacije od interesa o tehnikama ljudskih veština karakterističnim za iskusne radnike (stručnjake) i informacije o fazama ili redosledu izvođenja pojedinih tehnoloških operacija i detalje o tome kako se one izvode sa specifičnim numeričkim indikatorima (kompozitna brzina, pozicija, sila, obrtni moment, itd.).

Ljudskim operaterima "Cloud" arhitektura omogućava daljinsko upravljanje robotom pomoću pametnog telefona sa Android aplikacijom ili standardnog PC računara sa odgovarajućom aplikacijom sa grafičkim korisničkim interfejsom. Ovo pretpostavlja Wi-Fi hot spot ili GSM-GPRS modem na robotu koji donosi dodatnu funkcionalnost daljinske komunikacije sa ovlašćenim pristupom i mogućnošću praćenja parametara sistema i/ili daljinskog prenosa slike i zvuka.

## III. UPRAVLJAČKI NIVOI

Za upravljanje dvoručnim kolaborativnim robotom prikazanim na Sl. 1, koristi se arhitektura upravljanja u oblaku (odnosno "Cloud" kontrola) prikazana na Sl. 2. Ova kontrolna konfiguracija podržava koncept takozvane hijerarhijski distribuirane kontrole implementirane na tri nivoa kontrole: (i ) strateški, (ii) taktički i (iii) izvršni nivo. Svi navedeni nivoi upravljanja imaju precizno diferencirane kontrolne zadatke i postoji jasna podređenost operacija u sistemu.

### *A. Strateški nivo*

Na strateškom nivou upravljanja definišu se globalni ciljevi, planiranje procesa, tehnološke operacije koje robot treba da obavlja samostalno ili u saradnji sa čovekom ili mašinom, kao i manipulativne i kognitivne veštine koje robot treba da demonstrira dok obavlja svoje aktivnosti, poštujući redosled tehnoloških operacija i bezbednosne standarde. Strateška kontrola koristi informacije dobijene na fizičkom nivou (Sl. 2) kao i iz odgovarajuće baze podataka. U bazama podataka se čuvaju informacije relevantne za robota industrijske usluge koje se odnose na prepoznavanje geometrije objekata, informacije o fazama i tehnikama izvođenja određenih tehnoloških procesa u koje je robot uključen i na kraju informacije o manipulativnim i kognitivnim veštinama pretvorene u formu razumljivu mašini (robotski kontroler). U bazi se čuvaju i podaci o bezbednosnim standardima za obavljanje određenih robotskih zadataka, budući da je industrijski humanoid namenjen za kolaborativni rad sa ljudima. Takođe, na nivou strateške kontrole vodi se računa o ispunjavanju standarda kvaliteta izvođenja tehnoloških operacija. Rezultati ovog nivoa kontrole su jasno definisani ciljevi visokog nivoa i redosled ostvarivanja tehnološkog procesa, tehničko-tehnološka ograničenja, način izvođenja procesa, alati koji se koriste i odgovarajuće veštine, razvrstane na podciljeve koje treba postići na nižem, podređenom hijerarhijskom nivou – taktičkom.

### *B. Taktički nivo*

Na nivou taktičke kontrole, kako sama reč kaže, definiše se taktika ostvarivanja skupa podciljeva dobijenih sa strateškog nivoa upravljanja. Na ovom nivou planira se postizanje skupa podciljeva kao što su planiranje putanje robotskih ruku (pozicija, orijentacija i brzina krajnjih efektora robota), sinhronizacija rada dve robotske ruke kako bi se izbegao sudar, definisanje referentne sile i momenta na hvataču robota, zatim, orijentisanje kamera u radnom prostoru zadatka, itd. Izlazni podaci sa nivoa taktičke kontrole predstavljaju referentne (tj. željene) vrednosti promenljivih koje predstavljaju ulaze za izvršni nivo upravljanja (na servo nivou).

### *C. Izvršni nivo*

Na izvršnom nivou upravljanja komanduje se radom servo pogona koji obezbeđuju izvršavanje određenih aktivnosti. Korišćenjem povratnih petlji po poziciji/orijentaciji, brzini, sili/momentu, na izvršnom nivou postiže se željeno kretanje sistema u skladu sa taktikom i strategijom izvršavanja procesa koji su određeni na višim nivoima sistemske kontrole. Na izvršnom nivou, senzorne informacije i podaci senzora prikupljaju se sa robota i/ili iz njegovog fizičkog okruženja. Takođe se obavlja akvizicija slike i/ili video tokova iz sistema vizije robota za njihovo slanje na viši, taktički nivo upravljanja gde se vrši obrada tih signala. Dobijene povratne informacije su od velikog značaja na taktičkom nivou za vršenje neophodnih korekcija tehnike izvođenja procesa redefinisanjem referentnih vrednosti. Na ovaj način se obezbeđuje tok informacija odozgo nadole, kao i inverzni tok informacija odozdo prema gore od najvišeg nivoa upravljanja ka najnižem i obrnuto.

### . *Upravljanje robotom na fizičkom nivou "Cloud" sistema*

Na Sl. 3 prikazan je blok dijagram upravljanja dvoručnim kolaborativnim robotom. Upravljanje izvršnim nivoom se realizuje korišćenjem dva nezavisna industrijska kontrolera robotskih ruku UR5 koji se isporučuju sa svojim fabričkim kontrolerima zatvorenog tipa sa već realizovanim algoritamskim rešenjima za regulator položaja/brzine i regulator sile/momenta.

Torzo robota, robotske ruke i sistem vizije se nezavisno kontrolišu, dok se centralna mikrokontrolerska jedinica (MCU) koristi za sinhronizaciju celog upravljačkog sistema,

 ISBN 978-86-7466-930-3

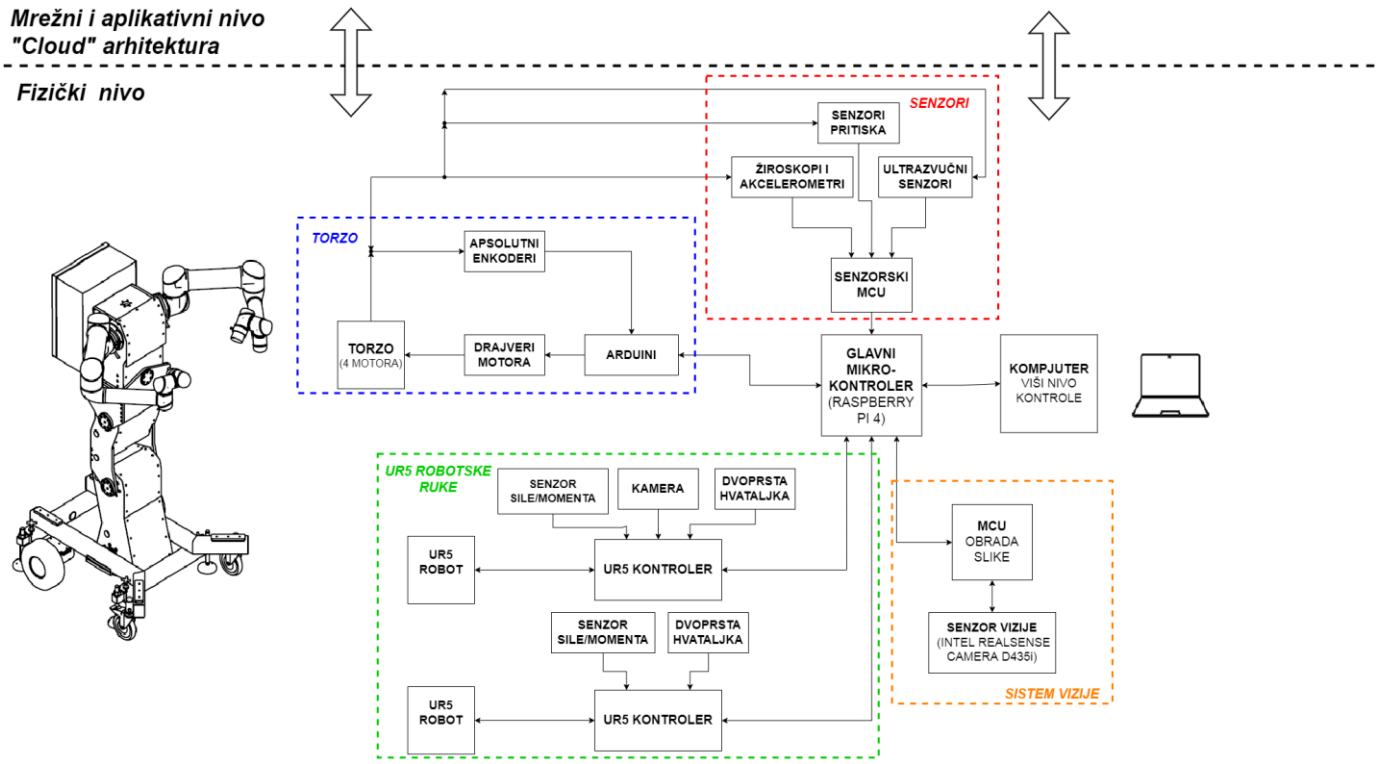


Sl. 3. Blok šema upravljačkog sistema razvijena na fizičkom nivou industrijskog servisnog robota upravljanog "iz oblaka".

delegiranje zadataka, komunikaciju sa udaljenim operaterima, itd. Torzo robota (Sl. 2) ima četiri zgloba aktuirana DC motorima bez četkica koji se pokreću preko drajvera. Svaki od drajvera kontroliše nezavisni Arduino mikrokontroler. Na svaki motor montiran je rotacioni enkoder koji pruža informacije o trenutnoj ugaonoj brzini i položaju motora, koje Arduino koristi za kontrolu položaja motora. Arduino mikrokontroleri komuniciraju sa glavnim MCU putem CAN bus komunikacije velike brzine. Na torzo i kolica robota postavljeni su različiti senzori uključujući i senzore kontakta/pritiska, žiroskope i akcelerometre, ultrazvučne senzore, itd. Senzori pritiska su posebno važni jer se koriste za izračunavanje tačke nultog momenta (ZMP) mobilnog industrijskog humanoida kao indikatora stabilnosti. Ove informacije se koriste da bi se utvrdilo da li je bezbedno da torzo i ruke robota stignu u datu poziciju bez pada ili prevrtanja. Sirove informacije sa senzora se obrađuju na posebnoj mikroprocesorskoj jedinici, a potom se obrađeni podaci, po potrebi, CAN komunikacijom šalju glavnom MCU, koji ih koristi za kontrolne zadatke, mere bezbednosti, itd. Ruke robota UR5 su fizički montirane na prirubnicama koje se nalaze na vrhu torza. Prirubnice su zakrivljene pod uglom od oko 15 stepeni u odnosu na torzo robota jer se time povećava opseg korisnog radnog prostora ispred torzoa.

UR5 roboti su konvencionalne industrijske ruke sa 6 stepeni slobode. Svaka od robotskih ruku ima senzor sile/momenta i hvatač sa dva prsta koji je montiran na svom vrhu. Jedna od ruku takođe ima montiranu kameru na zglobu i ovo će biti glavna ruka u dvoručnim zadacima. Servo kontrola niskog nivoa zglobova ruku robota se vrši preko originalnih UR5 kontrolera koji se isporučuju zajedno sa robotskim rukama. UR5 kontroleri komuniciraju sa MCU preko fizičkih veza (I/O signali sa MODBUS vezom), preko žičane (Ethernet) ili bežične (Wi-Fi pristup) mreže i preko ROS-a (Robot Operating Sistem).

Sistem robotske vizije je važan kontrolni podsistem koji celokupnom sistemu obezbeđuje vizuelnu povratnu informaciju. Senzor vida (Intel RealSense D435i dubinska kamera) je montiran na vrhu torzoa. Njegova uloga je da obezbedi robotu mogućnost 3D vizije sa senzorom dubine. Takav sistem se koristi za opažanje robotskog okruženja, praćenje zadataka, izbegavanje fizičkih stacionarnih ili mobilnih prepreka itd. Kamera će biti povezana sa posebnom mikrokontrolerskom jedinicom koja će se koristiti za obradu slika primljenih sa kamere. Softver koji će se koristiti za procesiranje vizuelnih podataka sastoji se kako iz klasičnih algoritama kompjuterske vizije tako i iz algoritama dubokog učenja i neuralnih mreža za obradu i prepoznavanje slika. Ovaj mikrokontroler će takođe biti povezan na glavni MCU.

Glavna jedinica mikrokontrolera (Raspberry Pi 4 sa 8GB RAM-a) je sastavni deo kontrolnog sistema. Ovaj MCU komunicira sa mrežnim nivoom (slika 2), odakle prima informacije o referentnim zadacima robotskog sistema koje treba da izvrši. Takođe prima povratne informacije od svakog kontrolnog podsistema. MCU obrađuje sve ove informacije i sinhronizuje ceo sistem (torzo+2 ruke+2 hvatača+kamera), delegira zadatke svakom podsistemu i zaustavlja aktuatore u slučaju opasnosti ili kvara. Komplementarni računar se može dodati glavnom MCU kao lokalni nadzorni sistem. Koristi se uglavnom kao pomoćno sredstvo za razvoj sistema

 ISBN 978-86-7466-930-3

upravljanja, testiranje i verifikaciju rezultata rada zadataka.

## IV. ZAKLJUČAK

U radu je predložena višestepena upravljačka arhitektura servisnog industrijskog kolaborativnog robota. Hijerarhijska distribuiranost ovog sistema dozvoljava najbolje iskorišćenje pojedinačnih kontrolnih podsistema kao i već postojećih kontrolera i stavlja fokus na delegiranje zadataka na manje procesorske jedinice i sinhronizaciju pojedinačnih delova sistema. Korak dalje u dizajniranju ovakvih sistema predstavlja implementacija "Cloud" arhitekture koja omogućava daljinsko upravljanje i nadzor nad sistemom, kao i čuvanje raznih ulaznih i izlaznih sistemskih podataka na serveru.

Dalji rad autora nastaviće se u ovom pravcu. Po finalnoj montaži celokupnog sistema radiće se eksperimentalna verifikacija različitih upravljačkih zadataka. Potom će gotov sistem biti pogodan za različita istraživanja u oblasti dvoručne manipulacije, kolaboracije čoveka i robota, inteligentnog hvatanja, robotske vizije i dr.

## ZAHVALNICA

Razvoj prototipa kolaborativnog robota rezultat je bilateralnog R&D projekta pod nazivom „Razvoj i eksperimentalna verifikacija performansi mobilnog robota sa dve ruke za saradnju sa čovekom" iz „Programa razvoja nauke i tehnologije – finansiranje zajedničkih istraživačko-razvojnih projekata". R. Srbija i NR Kina", 2017-2019.

## LITERATURA

[1] A. Rodić, I. Stevanović, M. Jovanović, „Smart Cyber-Physical System to Enhance Flexibility of Production and Improve Collaborative Robot Capabilities – Mechanical Design and Control Concept", Proceedings of the 27th International Conference on Robotics in Alpe-Adria Danube Region (RAAD 2018), In book: Advances in Service and Industrial Robotics, Eds. Nikos A. Aspragathos, Panagiotis N. Koustoumpardis, Vassilis C. Moulianitis, Part of the Mechanisms and Machine Science book series (Mechan. Machine Science, Vol. 67), pp. 627-639, 2018

[2] A. Rodić, J. Šumarac, I. Stevanović, M. Jovanović, "Cloud-Enabled Bi-manual Collaborative Robot with Enhanced Versatility for Customized Production", Proceedings of the 30th International Conference on Robotics in Alpe-Adria-Danube Region, Futuroscope-Poitiers, France, pp. 240-249, June, 2021.

[3] N. Kashiri et al., "CENTAURO: A Hybrid Locomotion and High Power Resilient Manipulation Platform," in IEEE Robotics and Automation Letters, vol. 4, no. 2, pp. 1595-1602, April 2019, doi: 10.1109/LRA.2019.2896758.

[4] M. Fuchs et al., "Rollin' Justin - Design considerations and realization of a mobile platform for a humanoid upper body," 2009 IEEE International Conference on Robotics and Automation, 2009, pp. 4131-4137, doi: 10.1109/ROBOT.2009.5152464..

[5] S. S. Srinivasa et al., "Herb 2.0: Lessons Learned From Developing a Mobile Manipulator for the Home," in Proceedings of the IEEE, vol. 100, no. 8, pp. 2410-2428, Aug. 2012, doi: 10.1109/JPROC.2012.2200561.

[6] A. Rodić, B. Miloradović, S. Popić, S. Spasojević, B. Karan, "Development of Modular Compliant Anthropomorphic Robot Hand", In Book: New Trends in Medical and Service Robots. Theory and Integrated Ap- plications, Series: Mechanisms and Machine Science, Springer Publish- ing House, Vol. 16, Pisla, D.; Bleuler, H.; Rodic, A.; Vaida, C.; Pisla, A. (Eds.), 2014, VIII, 238 p. 167, ISBN 978-3-319-01591-0, Due: Sep- tember 30, (2013).

[7] A. Rodić, B. Miloradović, S. Popić, Đ. Urukalo, "On developing lightweight robot-arm of anthropomorphic characteristics". In Book: New Trends in Medical and Service Robots. Book 3, Series: Mechanisms and Machine Science, Springer Publishing House, Vol. 38, Bleuler, H.; Pisla, D.; Rodic, A.; Bouri, M; Mondada, F; (Eds.), ISBN: 978-3-319- 23831-9, Book ID: 332595 _1_En, (2015).

[8] J. Šumarac, K. Jovanović, A. Rodić, "Workspace Analysis of a Collaborative Bi-manual Industrial Robotic System" ROI1.1, In Proceedings of the IcETRAN2021, Banja Vrućica, Bosnia and Herzegovina, September, (2021)

[9] A. Rodić, M. Jovanović, S. Popić, G. Mester, "Scalable Experimental Platform for Research, Development and Testing of Networked Robotic Systems in Information Structured Environments". In Proceedings of the IEEE SSCI2011, Symposium Series on Computional Intelligence, Workshop on Robotic Intelligence in Information Structured Space, pp. 136-143, Paris, France, (2011).

## ABSTRACT

This paper presents a multi-level cloud-enabled control architecture of a bi-manual collaborative humanoid service robot. This architecture is designed to perform robotic tasks that require the implementation of advanced manipulative and cognitive skills within the industrial manufacturing process. The control structure of the robot is designed to meet the needs of the so-called smart production within Industry 4.0, enough to enable and facilitate the cooperation of man and robot as a complementary intelligent system, necessary in industrial tasks that humans cannot perform independently. This paper presents a hierarchically distributed management system organized into three operational levels: a) strategic, b) tactical and c) executive, enabled by the use of cloud architecture. The hardware of the control system is established on three levels: physical, communication and application. Thanks to the distributed architecture, the cloud system enables distributed execution of individual control tasks, which results in a balanced load on the multiprocessor system and reduced stimulus response time from the physical environment of the robot.

### ierarchically Distributed Control of Collaborative Industrial umanoid obot upported by Cloud-Computing Architecture

Jovan Šumarac, Aleksandar Rodić, Ilija Stevanović

 ISBN 978-86-7466-930-3

# TELECOMMUNICATIONS
# /
# ТЕЛЕКОМУНИКАЦИЈЕ
# (TEI/TE)

ISBN 978-86-7466-930-3

# On Pulse Shaping for Generalized Faster than Nyquist Signaling with and without Equalization

Jovan Milojković, Srđan Brkić, *Member, IEEE*, Jelena Ćertić, *Member, IEEE*

***Abstract*—This paper focuses on analyses of generalized Faster than Nyquist (FTN) signaling in the presence of additive white Gaussian noise. A new method for designing pulse shaping filters, that maximize information rate and simultaneously obey constraints related to energy distribution of the pulse autocorrelation function, is proposed. The obtained pulses are coupled with the minimum mean square error (MMSE) equalizer used at the receiving side. In addition, potential for their use without any equalization scheme is also analyzed. Significance of the proposed approach is verified by comparing designed pulses with state-of-the-art FTN schemes, that employ raised cosine pulses, in terms of bit error rate and achievable information rate. We identify cases when the proposed scheme provides the same achievable information rate as the standard FTN system with more than 1.5 dB lower signal-to-noise power (SNR) ratio, without the equalization, and 0.4 dB lower SNR ratio, if MMSE equalization is employed.**

***Index Terms*—Faster than Nyquist signaling, MMSE equalization, pulse shaping**

## I. Introduction

In a classical communication system information is transmitted by using orthogonal pulses (with flat frequency spectrum) and ideally no inter-symbol interference is introduced by the transmitter, which is refereed to as the Nyquist signaling approach. Intense research over the past years in the area of channel coding and modulation lead to development of Nyquist transmission systems that operate close to the ultimate Shannon spectral efficiency bounds, and obviously, additional improvement must be followed by the change of Nyquist's transmission paradigm. With the invention of new services, mostly associated with the fifth generation standard for broadband cellular networks (5GNR), the problem of designing spectral efficient transmission system comes again under the spotlight. A technique that is capable to provide a quantum leap in design of spectrally efficient systems is faster then Nyquist (FTN) signalling.

In FTN signaling systems use of orthogonal pulses is abandoned and inter-symbol inference is intentionally introduced. It follows that as the adjacent received symbols are correlated, conventionally used symbol-by-symbol detection becomes inappropriate, and information needs to be extracted by some equalization technique. The foundations of FTN were laid down by Mazo in 1975 [1], who noticed that communicating with symbol rates higher than the Nyquist rate, can provide spectrally efficient transmission, without degradation in Euclidean distances between transmitted symbols. Although the aforementioned insight was revolutionary, it was not fully explored for more than 30 years. Namely, in 2007 Rusek and Anderson [2] created the information-theoretic framework for the analysis of FTN systems and proved that capacity of conventionally used Nyquist systems (for example with raised cosine (RC) pules) can be surpassed with FTN signaling. Furthermore, the same authors showed in [3] that, by increasing the symbol transmission rate, constrained capacity saturates to a fixed value – in other words arbitrary spectral efficiency can be achieved. Their work was refined recently by Ishihara and Sugiura in [4], where it was shown that conventionally used RC pulses employed in precoded FTN systems approach Shannon capacity of the ideal rectangle pulse. For excellent overview on FTN concepts and technologies we direct readers to [5].

In order to keep the advantages of FTN over Nyquist signaling in practical systems, the equalization and channel coding need to be adjusted. The optimal FTN receiver is organized in a form of turbo equalization loop [6], where equalization is performed by employing maximum a posteriori probability (MAP) detector. Complexity of MAP detection grows exponentially with increase of symbol rate, making it infeasible for practical use. On the opposite side, using low complex equalization, for example MMSE (Minimum Mean Square Error), may be insufficient to perform significantly beyond conventional Nyquist systems. This lead to *generalized FTN signaling* approach [7], in which conventional pulses, like RC, are replaced with pulses that are adjusted to a given equalization scheme. Another benefit of custom pulse design is ability to adopt to a given practical requirements, for example peak-to-average power ratio (PAPR) or adjacent channel leakage power (ACLP), which can vary from one communication standard to another.

Over the years, different pulse designs were proposed that can be incorporated into generalized FTN concept. The most prominent approaches include pulses designed: i) to minimize Euclidean distance between different realizations of two random transmitted sequences [8] and bit error rate of uncoded transmission [9], ii) to maximize information rate [2], [10], [11], or iii) to obey predefined frequency domain constraints (and simultaneously limit PAPR) [12]. For example, Rusek and Anderson in [2] proposed an optimization procedure in which pulses with predefined number of taps maximize an upper information rate bound. The procedure was further expanded by Brkic *et al.* in [11] to enable arbitrary

Jovan Milojković, Srđan Brkić and Jelena Ćertić are with the University of Belgrade, School of Electrical Engineering, 11000 Belgrade, Serbia (e-mails: mj205018p@student.etf.bg.ac.rs, srdjan.brkic@etf.rs, jelena.certic@etf.rs).

 ISBN 978-86-7466-930-3

pulse energy distribution in time domain, which can be used to build generalized FTN systems with limited trellis-based equalizer complexity.

In this paper we further extend the optimization procedure presented in [2], [11] in order to make it applicable to FTN systems with MMSE equalizers, or even to FTN transmission systems which do not employ any equalization scheme. Namely, we define additional time domain constraints related to energy of the pulse autocorrelation function. We verify that designed pulses outperform state-of-the-art FTN systems (with RC pulses), for the same symbol rate and ACLP, in terms of bit error rate as well as achievable information rate in additive white Gaussian noise (AWGN) channel.

The rest of the paper is organized as follows. In Section II we briefly describe system model and MMSE equalization scheme. Section III is dedicated to the optimization procedure, while numerical results are given in Section IV. Finally, concluding remarks can be found in Section V.

## II. System Model

Consider an output of the baseband equivalent of the transmitter

$$s(t) = \sum_{k=-\infty}^{\infty} a_k h(t - kT), \tag{1}$$

where $a_k \in \{\pm 1\}$ corresponds to the $k$-th transmitted symbol, $T$ denotes symbol duration and $h(t)$ is the pulse shaping filter. We assume that $h(t)$ is not orthogonal with respect to the transmitting sample rate, i.e, it intentionally introduces ISI and that $h(t)$ can be represented as weighted sum of wider band pulses

$$h(t) = \sum_{l=0}^{L-1} b_l \psi(t - lT), \tag{2}$$

where $\psi(t)$ is a pulse orthogonal to the sampling rate $1/T$, while $\mathbf{b} = (b_0 \ldots, b_{L-1})$ corresponds to a vector of the sampled coefficients, i.e, $b_l = h(lT)$. Note that we restrict the effect of ISI to $L$ consecutive symbols and that energy of the impulse response is considered to be unitary.

The waveform $s(t)$ is transmitted through additive white Gaussian (AWGN) channel, described with energy per symbol to noise power spectral density ($E_s/N_0$) metric.

At the receiver side in this paper we consider two observation models: i) orthogonal basis model (OBM) [13] and ii) Ungerboeck model [14] without the equalization. According to the OBM, receiving filter is matched to $\psi(t)$ (not $h(t)$), which means that noise at the receiver input is white. In our model we assume that $\psi(t)$ is square root raised cosine pulse with roll-off 0.1. To verify the performance of $h(t)$ on the OBM, we employ MMSE equalizer. Motivated by the recent findings, reported in [15], that FTN signaling can perform satisfactory even without an equalizer implemented in the receiver side, we here consider such detection scheme, for the case of the Ungerboeck observation model. In the Ungerboeck model receiving filter is matched to $h(t)$, which maximizes $E_s/N_0$ metric; however, received noise sequence becomes correlated.

We next briefly explain MMSE equalization used in the OBM (for more details one could see [16]). Let $\mathbf{r}_n = (r_{n-N_2}, r_{n-N_2+1}, \ldots, r_{n+N_1})^T$ denote a sequence at input of the MMSE equalizer used to estimate transmitted symbol $a_n$, where $T$ is transposition sign. The parameters $N_1$ and $N_2$ specify the length of the noncausal and the causal part of the MMSE filter. Then, finite impulse response (FIR) MMSE filter coefficients $\mathbf{c}_n$ can be obtained as follows

$$\mathbf{c}_n = \mathrm{Cov}(\mathbf{r}_n, \mathbf{r}_n)^{-1} \times \mathrm{Cov}(\mathbf{r}, a_n), \tag{3}$$

where the covariance operator is given by $\mathrm{Cov}(\mathbf{x}, \mathbf{y}) = E(\mathbf{x}\mathbf{y}^H) - E(\mathbf{x})E(\mathbf{y}^H)$, where $E(\cdot)$ denotes mathematical expectation, and $H$ is Hermitian operator. The symbol estimate $\hat{a}_n$ is obtained by $\hat{a}_n = \mathbf{c}_n^H \mathbf{r}_n$. It should be noted that values $N_1$ and $N_2$ are dependent on $h(t)$.

## III. Optimization of pulse shaping filter

In this section we state the optimization problem for finding pulse shaping filter coefficients $\mathbf{b}$ that maximize the achievable information rate (AIR) and are also adjusted to the equalizing scheme. Fundamentals of the AIR-based optimization can be found in [17], and we first briefly explain key concept of the optimization, and then highlight modifications introduced in order to adjust the optimization procedure to the system model, given in Section II.

The procedure from [17] allows pulse design for arbitrary ACLP value and the filter length $L$. Let $H(f)$ denotes Fourier transform of $h(t)$. Then we can define, a complement of ACLP, the concentration of pulse energy in $W$ Hz as follows

$$\beta = \frac{\int_{-W}^{W} |H(f)|^2 df}{\int_{-\infty}^{\infty} |H(f)|^2 df}. \tag{4}$$

Without loss of generality, we can consider normalized bandwidth defined as $w = W \times T$, and notice that $w = 0.5$ corresponds to Nyquist signaling while when $w < 0.5$ we are communicating in FTN signaling fashion. The amount of ISI introduced at transmitter side is inversely proportional to $w$. Alternatively, the energy concentration $\beta$ can expressed in a more suitable form, as a function of pulse discrete autocorrelation function $\mathbf{g} = (g_{-L+1}, \ldots, g_{L-1})$, as follows [11]

$$\beta(\mathbf{g}, w) = \sum_{l=-L}^{L} 2 g_l w \times \mathrm{sinc}(2\pi w), \tag{5}$$

where $\mathrm{sinc}(x) = \sin(x)/x$, and

$$g_l = \int_{-\infty}^{\infty} h(t) h^{\star}(t - lT) dt. \tag{6}$$

Direct maximization of AIR, for a given discrete modulation set is infeasible as, to the best of our knowledge, a closed form expression does not exist. Instead, it is common to optimize


ISBN 978-86-7466-930-3

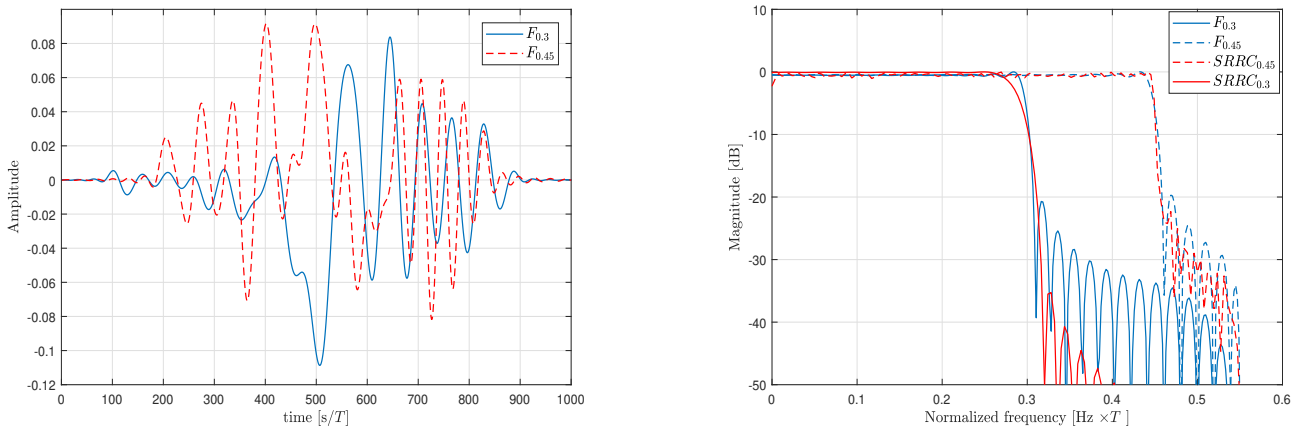


(a) (b)

Fig. 1: Impulse (a) and (b) frequency responses of designed filters for $w = 0.3$ and $w = 0.45$ ($L = 50$, $\beta = 0.999$).

an information rate upper bound $C(\mathbf{b})$, derived assuming Gaussian sample distribution [17]

$$C(\mathbf{b}) = \int_0^{1/2} \log_2 \left[ 1 + \frac{2E_s|B(f)|^2}{N_0 T} \right] df, \tag{7}$$

where $B(f) = \sum_{k=0}^{L-1} b_k e^{i2\pi kf}$ represents Fourier transform of the vector $\mathbf{b}$.

It was reported in [11] that in large number of cases $C(\mathbf{b})$ monotonically increases with actual AIR obtained through computationally hungry Monte Carlo simulation, which means that optimizing $C(\mathbf{b})$ is meaningful.

By studying typical behavior of pulses optimized by (7), for a fixed $\beta$ and $w$ constraints we noticed the following: i) relatively small number of filter taps is sufficient to obey strict $b$ constraint (for example $\beta = 0.999$) and ii) significant portions of energy of the pulse autocorrelation are spread across a large number of taps, i.e., the account of introduced ISI is large. Obviously, such pulses cannot be used in systems that do not use equalizers, and are inadequate when equalization is performed with the MMSE equalizer, given its modest ability to suppress ISI.

To resolve the aforementioned issue, we proposed that additional constraint is added into optimization setup that will force the optimization procedure to cluster the majority of the autocorrelation energy to main tap $g_0$ and potentially $2M$ adjacent taps ($g_{-M},, g_{-1}, g_1, \dots g_M$). Namely, we define a set of thresholds $f\ 0 < f_i < 1$, $0 \leq i \leq M$, forcing the relative energy of central autocorrelation taps to be above the thresholds. However, given frequency-time duality principle, clustering autocorelation energy makes it harder to satisfy frequency domain constraint $\beta$. To overcome the problem, the filter lengths $L$ must be increased.

For predefined normalized bandwidth $w$, with energy concentration $\beta_0$ we formally express the optimization problem as follows

$$\begin{aligned} \mathbf{b}_{opt} &= \underset{\mathbf{b}}{\operatorname{argmax}}\ C(\mathbf{b}) \\ s.t.\ \ &\beta(\mathbf{g}, w) = \beta_0, \\ &\frac{g_i^2}{\sum_{\ell=-L+1}^{L-1} g_\ell^2} \geq f,\ 0 \leq i \leq M. \end{aligned} \tag{8}$$

The above optimization problem can be solved similarly as the related problems described in [17] and [11], by sequential quadratic programming (SQP) method.

It should be noted that in OBM system described in Section II, we do not match the receiving filter to transmitting $h(t)$, which means that amount of ISI collected by the receiver is not directly expressed by autoccorelation of $h(t)$. However, we observed strong dependency between ability of MMSE equalizer to suppress ISI and the energy concentration of the pulse autocorrelation function.

To illustrate our optimization procedure, we designed two pulses with $\beta = 0.999$, $L = 50$ and $w = 0.3$ and $w = 0.45$, respectively, denoted by $F_{0.3}$ and $F_{0.45}$, design to obey $f_0 = 0.58$ and $f_0 = 0.85$, respectively. Their impulse and frequency responses are depicted in Fig. 1. For compression we also give frequency responses of square root raised cosine (SRRC) pulses with roll-offs equal to 0.1, designed to meet the same requirements as optimized pulses in terms of length and energy concentrations in frequency domain (denoted by $SRRC_{0.3}$ and $SRRC_{0.45}$).

## IV. Numerical results

In this section we provide the performance of designed pulses $F_{0.3}$ and $F_{0.45}$, in terms of bit error rate and achievable information rates, obtained by Monte Carlo simulation (Figs. 2 and 3). We examine pulses behaviour on OBM and Ungerboeck system models, introduced in Section II. Obtained results are compared to SRRC pulses ($SRRC_{0.3}$ and $SRRC_{0.45}$). Given the fact that we only consider binary

 ISBN 978-86-7466-930-3

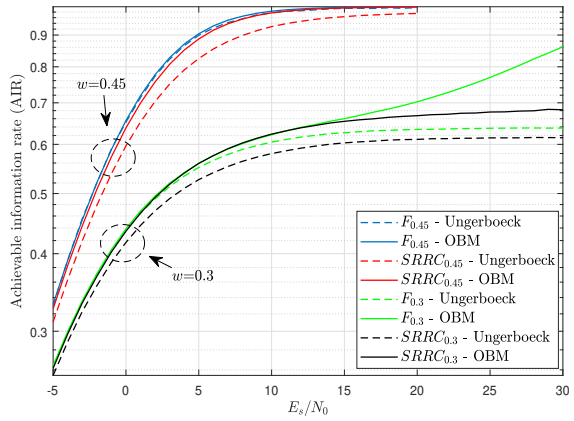


Fig. 2: Achievable information rates of designed pulses.

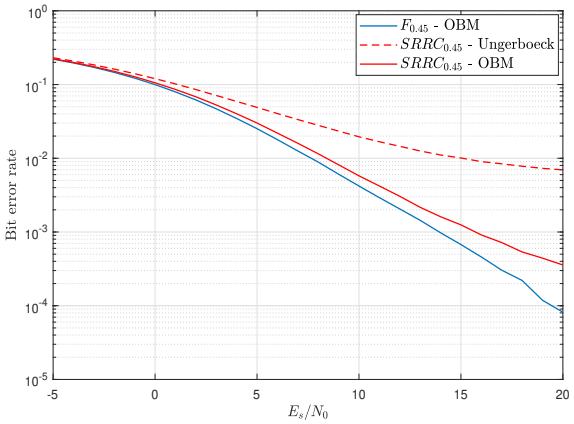


Fig. 3: Bit error rate achievable by $F_{0.45}$ filter.

transmission ($a_k \in \{\pm 1\}$), achievable information rates are calculated numerically as follows

$$AIR = \frac{1}{2} \sum_{a_k=-1,1} \int_{-\infty}^{+\infty} p(z|a_k) \times \log_2 \frac{2p(z|a_k)}{p(z|1) + p(z|-1)} dz, \tag{9}$$

where the conditional probability density function of the log likelihood ratio $z$ of the symbols that corresponds to transmitted $a_k$, $p(z|a_k)$, is approximated by a histogram.

In Fig. 2 we show that designed pulses outperform SRRC counterparts in terms of AIR on the both system models. For example, $F_{0.45}$ achieves AIR, equal to 0.8 bits/symbols, with 0.4 dB less $E_s/N_0$ value compared to $SRRC_{0.45}$ on the OBM, while the differences on the Ungerboeck model is approximately 1.8 dB. One can also notice that $SRRC_{0.3}$ cannot achieve information rates above 0.68 bits/symbol in the OBM, while if $F_{0.3}$ is used, higher spectral efficiencies are possible. If we consider uncoded transmission we can, notice that $F_{0.45}$ achieves bit error rate of $10^{-3}$ with 1.7 dB less $E_s/N_0$ compared to $SRRC_{0.45}$ on the OBM (Fig. 3).

## V. Conclusion

This paper provides novel pulse shaping filters applicable to generalized FTN signaling systems with MMSE equalization and also to systems with no equalizer employed. We show that proposed pulses outperform SRRC pulses of the same structural properties. Our future work will be oriented into examining finite length coded transmission systems that employ proposed pulses.

## Acknowledgment

Srđan Brkić acknowledge the support of the Science Fund of the Republic of Serbia, grant No 7750284, Hybrid Integrated Satellite and Terrestrial Access Network - hi-STAR. This work was also supported by the Serbian Ministry of Education, Science and Technological Development.

## References

[1] J. E. Mazo, "Faster-than-Nyquist signaling," *Bell Syst. Tech. J.*, vol. 54, p. 1451–1462, Oct. 1975.
[2] F. Rusek and J. B. Anderson, "Constrained capacities for faster than Nyquist signaling," *IEEE Trans. Inf. Theory*, vol. 55, no. 2, p. 764–775, Feb. 2007.
[3] F. Rusek, D. Kapetanovic, and J. B. Anderson, "The effect of symbol rate on constrained capacity for linear modulation," in *Proc. IEEE Inter, Symp. Inf. Theory 2008*, 6-11 July, 2008, p. 1093–1097.
[4] T. Ishihara and S. Sugiura, "Precoded faster-than-Nyquist signaling with optimal power allocation in frequency-selective channel," in *Proc. IEEE Int. Conf. Commun. Workshop*, June 2021, pp. 1–6.
[5] T. Ishihara, S. Sugiura, and L. Hanzo, "The evolution of faster-than-Nyquist signaling," *IEEE Access*, vol. 9, no. 6, p. 86535–86564, June 2021.
[6] C. Douillard, M. Jezequel, C. Berrou, A. Picart, and P. Didier, "Iterative correction of intersymbol interference: turbo-equalization," *European Trans. Telecomm.*, vol. 6, no. 5, pp. 507–512, June 1995.
[7] J. Zhou, D. Li, and X. Wang, "Generalized faster-than-Nyquist signaling," in *Proc. IEEE Inter, Symp. Inf. Theory 2012*, 1-6 July, 2012, p. 1478–1482.
[8] A. Said and J. B. Anderson, "Design of optimal signals for bandwidth efficient linear coded modulation," *IEEE Trans. Inf. Theory*, vol. 44, no. 3, p. 701–713, Mar. 1998.
[9] F. Rusek and J. Anderson, "Near bit error rate optimal partial response signaling," in *Proc. Intern. Symp. Information Theory*, Sept. 2005, pp. 538–542.
[10] A. Modenini, F. Rusek, and G. Colavolpe, "Optimal transmit filters for isi channels under channel shortening detection," *IEEE Trans. Commun.*, vol. 61, no. 12, p. 4997–5005, Dec. 2013.
[11] S. Brkic, P. Ivanis, and A. Radosevic, "Faster than Nyquist signaling with limited computational resources," *Physical Communication*, vol. 47, pp. 1–12, June 2021.
[12] T. Delamotte and G. Bauch, "Pulse shaping for satellite systems with time packing: An eigenfilter design," in *Proc. 10th Inter. ITG Conf. on Sys., Commun. and Coding, SCC 2015*, 2-5 Feb. 2015.
[13] J. B. Anderson, A. Prlja, and F. Rusek, "New reduced state space BCJR algorithms for the ISI channel," in *Proc. Inter. Symp. on Inf. Theory*, June 2009, pp. 889–893.
[14] G. Colavolpe and A. Barbieri, "On MAP symbol detection for ISI channels using the ungerboeck observation model," *IEEE Comm. Letters*, vol. 9, no. 8, pp. 720–512, Aug. 2005.
[15] I. Lavrenyuk, A. Ovsyannikova, S. Zavjalov, S. Volvenko, and W. Xue, "Analysis of joint application of optimal FTN signal and 5G error-correction code schemes," in *Proc. 2020 IEEE Inter. Conf. on Electrical Engineering and Photonics (EExPolytech)*, Oct. 2020.
[16] M. Tuchler, A. Singer, and R. Koetter, "Minimum mean squared error equalization using a priori information," *IEEE Trans. Signal Processing*, vol. 50, no. 3, pp. 673–683, Mar. 2002.
[17] F. Rusek and J. B. Anderson, "Maximal capacity partial response signaling," in *Proc. IEEE 2007 Inter. Conf. Commun.*, 2007, pp. 821–826.

 ISBN 978-86-7466-930-3

# Performance simulation for LCR of MIMO Multi-branch SC Diversity System in α-μ fading and α-μ interference channel

Dejan Milić, Suad Suljović, Dejan Rančić, Nenad Petrović, Nenad Milošević

***Abstract* - In order to improve the overall performance of the networ in 5G telecommunication networ s, ultiple Input and ulti utput Technology ( I ) is applied. In this paper, the mean number of evel Crossing ate ( C ) of I systems with -branch selection combining ( C) receiver is analyzed. During signal transmission, its distortion occurs due to low α-μ fading and α-μ co-channel interference (CCI) effects. Additionally, we applied an accelerated graphics processing unit (GP ) simulation to plan a o -efficient 5G mobile networ in a smart city. This approach in combination with linear optimization and deep learning significantly optimizes the C calculation speed for the observed communication system type, while providing efficient planning - reducing costs, but ma imizing performance.**

***Index Terms*— C combining, α- fading, α- interference, C , o , GP , linear optimization.**

## I. INTRODUCTION

Due to the unpredictable and dynamic nature of the wireless channel environment, the channel becomes one disruptive element in the transmission chain as it changes the broadcast signal. Therefore, the channel manages the performance of wireless communication systems [1].

Multiple Input Multiple Output (MIMO) is an efficient antenna technology for wireless communication systems where multiple antennas are used on the transmitter and receiver [2]. Antennas at each end of the system are combined to minimize errors during signal transmission, increase data rates and improve channel capacity. This technique allows signals to be transmitted on many different paths at the same time. This mode of signal transmission provides the ability for signals to reach the receiver without fading and co-channel interference. This technique increases the signal-to-noise ratio (SNR) and transmission quality, which creates more stable connections [3].

Fading is a variation of attenuation, ie. signal amplitude fluctuations. During transmission, the signal faces various obstacles such as buildings, trees, etc. present in the signal-causing environment is subject to reflection, diffraction, scattering and shading. This presence of multiple reflectors in the environment of the channel between the transmitting and receiving ends creates more paths for signal passage [4].

The most commonly used signal processing techniques in diversity systems are maximum ratio combination (MRC), equal gain combination (EGC), and selection combination (SC). MRC provides the best improvement in system performance, followed by an equal combination of reinforcements, but it is also the most complicated technique. In order to reduce the complexity of the receiver, this paper considers a simpler combination scheme related to combination selection (SC). The output of the SC receiver is the branch with the highest signal-to-noise ratio. SC has been extended to the case where signals on more than one receiving antenna are combined with the highest current SNR, this scheme is called hybrid maximum ratio selection/combination (HS/MRC). Selection Combination (SC) techniques have been applied in the design of MIMO systems to reduce system complexity and costs. Fifth generation (5G) telecommunications offers a 10-fold increase in spectral efficiency and a 1000-fold increase in system capacity compared to 4G technology [5]. In MIMO systems, there are tens to hundreds of antennas in the receiver and transmitter. Massive MIMO techniques use familiar channel features to deliver superior performance in wireless communications. Channels are modeled to include channel variations in frequency and time.

Describing and modeling channels with fading is of particular importance in mobile communications both for the design of the transceiver system and for performance analysis. During the long period of development of wireless communications, a large number of different models of channels with fading were constructed to describe the statistics of the envelope and the phase of the channel where the signal propagates in several paths, [6]. Examples of such models are Rayleigh's, Rice's, Nakagami-q, Nakagami's, Weibull's, Beckmann's, α − μ etc. The aim of this paper is to study the statistical properties of first and second order

Dejan Milić is with the Faculty of Electronic Engineering, University of Niš, Aleksandra Medvedeva 14, 18000 Niš, Serbia (e-mail: dejan.milic@elfak.ni.ac.rs)

Suad Suljović is with the Academy of Technical Vocational of Belgrade, Department of Computer Science, Katarine Ambrozić 3, 11000 Belgrade, Serbia, (e-mail: suadsara@gmail.com)

Dejan Rančić is with the Faculty of Electronic Engineering, University of Niš, Aleksandra Medvedeva 14, 18000 Niš, Serbia (e-mail: dejan.rancic@elfak.ni.ac.rs)

Nenad Petrović is with the is with the Faculty of Electronic Engineering, University of Niš, Aleksandra Medvedeva 14, 18000 Niš, Serbia (e-mail: nenad.petrovic@elfak.ni.ac.rs), (https://orcid.org/0000-0003-2264-7369)

Nenad Milošević with the Faculty of Electronic Engineering, University of Niš, Aleksandra Medvedeva 14, 18000 Niš, Serbia (e-mail: nenad.milosevic@elfak.ni.ac.rs)

 ISBN 978-86-7466-930-3

envelopes and phases in these models, with with special reference to the α − μ model.

In mobile communications, the received signal varies in a wide range of values. Therefore, for the design of digital and analog systems, it is necessary to know the statistical characteristics of the signal. There are first and second order statistical characteristics. It is especially necessary to know the statistical characteristics of the second order, such as the average number of axial sections of the LCR and the average duration of AFD fading. These quantities provide additional information that, when combined with other statistics, allows designers to create rational system solutions [7].

Level Crossing Rate (LCR) and Average Duration of Fades (ADF) are important second-order statistical characteristics for describing fading channels. These quantities are useful in the design of mobile radio communication systems and for the analysis of their performance. In digital telecommunications, a sharp drop in the envelope value of the received signal directly leads to a sharp increase in the probability of error [8]. Second-order statistics calculation techniques are particularly applicable to diversity systems that have been shown to be very useful in reducing the impact of fading.

In this paper, we consider a 5G communication system that works over k-ading fading channels and k-μ co-channel interference. One of the most basic statistics of a wireless communication system operating in a fading environment is the mean number of axial cross-sections (LCR). The quality of service (CoS) in wireless communications depends significantly on the LCR as it allows the estimation of the minimum distance between two base stations. We first compute the cumulative distribution function (CDF) for the signal in the described environment, and then we derive a closed-form expression for the LCR. The results of this analysis can be used to design an optimal receiver for a 5G mobile network in smart cities in conditions of small α-μ fading and α -m interference.

## II. LCR OF SIGNAL TO INTERFERENCE RATIO AT THE OUTPUT OF THE L-BRANCH SC RECEIVER

In this section, the statistics of the second order 5G wireless communication system with SC receiver with L branches are considered. The received desired signal experiences α-μ fading, while the interference on the co-channel is subjected to α-μ fading. The model of the receiver is shown in Fig. 1.

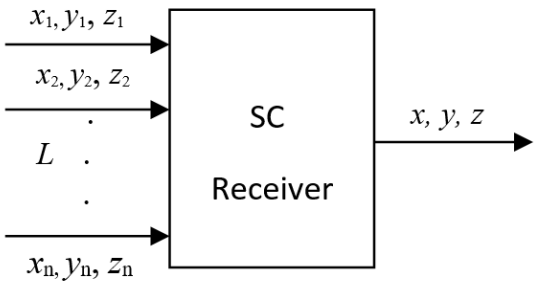


Fig. 1. The model of the SC receiver with branches

Signals 1, 2, ..., n come to the inputs of the SC combiner. The SC receiver with L input branches 2, 3, ... n selects the signal from the antenna with the highest SNR. Also, interference envelopes in the co-channel interference appear as $y_1, y_2, \ldots, y_n$ at each of the L inputs of the SC receiver, while the corresponding output signal is y. The PDF signal envelope on input at SC receiver have the α-μ distribution [9]:

$$p_{\ i}(\ _i) = \frac{\alpha\mu^{\mu}\ _i^{\alpha\mu-1}}{\Omega_i^{\ \mu}\Gamma(\mu)} e^{-\mu\frac{\ _i^{\alpha}}{\Omega_i}} \tag{1}$$

where α is a positive parameter, $\Omega_i$ is the mean value of the signal power, μ is the number of clusters and Γ(·) is a Gamma function. In a described channel, the co-channel interference signal follows α-μ distribution:

$$p_{y_i}(y_i) = \frac{\alpha\mu^{\mu} y_i^{\alpha\mu-1}}{s_i^{\mu}\Gamma(\mu)} e^{-\mu\frac{y_i^{\alpha}}{s_i}} \tag{2}$$

where $s$ is average power of $y$, $y_i \geq 0$. The ratio of the desired signal envelope and interference on the $i$-th input branch of the SC receiver with the L branch can be written as:

$$_i = \frac{_i}{y_i}, \quad _i = \ _i y_i \tag{3}$$

SNR for $i$ 2.3,... $n$ at the output of the SC receiver is:

$$= \max(\ _1, \ _2 \cdots \ _i) \tag{4}$$

The probability density function (PDF) of the signal $_i$ is given by [10]:

$$p_{\ i}(\ _i) = \int_0^{\infty} \mathrm{d}y_i y_i p_{\ i}(\ _i y_i) p_{y_i}(y_i) = \frac{\alpha\ _i^{\alpha\mu-1}(\Omega_i s_i)^{\mu}\Gamma(2\mu)}{\Gamma^2(\mu)\left(\Omega_i + s_i\ _i^{\alpha}\right)^{2\mu}} \tag{5}$$

Cumulative distribution function (CDF) of $_i$ is [10]:

$$F_{\ i}(\ _i) = \int_0^{\ i} \mathrm{d}t p_{\ i}(t) = \frac{\Gamma(2\mu)}{\Gamma^2(\mu)} B_{\frac{s_i\ _i^{\alpha}}{\Omega_i + s_i\ _i^{\alpha}}}(\mu,\mu) \tag{6}$$

where $B_z(a, b)$ is the incomplete Beta function, [11; 8.39]. SNR for $i$ = 2.3, … $n$ will be at the output of SC combination:

$$= \max(\ _1, \ _2 \cdots \ _i) \tag{7}$$

First derivative of $_{ij}$ can be written:

$$\dot{}_{ij} = \frac{1}{y_{ij}} \dot{}_{ij} - \frac{\ _{ij}}{y_{ij}^2} \dot{y}_{ij} \tag{8}$$


ISBN 978-86-7466-930-3

The derivative of the random process α-k-μ is a Gaussian random process, and a linear combination of Gaussian processes is also a Gaussian random process. Therefore, the conditional Gaussian distribution · with zero mean and variance applies:

$$\sigma^2_{\cdot_{ij}} = \frac{1}{y_{ij}^2}\sigma^2_{\cdot_{ij}} + \frac{{}^2_{ij}}{y_{ij}^4}\sigma^2_{\dot{y}_{ij}} \tag{9}$$

where respective variances relating to signal and interference are [12]:

$$\sigma^2_{\cdot_{ij}} = \left(\frac{2\pi f_m}{\alpha}\right)^2 \frac{\Omega_{i\ ij}^{\ 2-\alpha}}{\mu}, \sigma^2_{\dot{y}_{ij}} = \left(\frac{2\pi f_m}{\alpha}\right)^2 \frac{s_i y_{ij}^{\ 2-\alpha}}{\mu} \tag{10}$$

where $f_m$ denotes the Doppler frequency. After replacing expression (12) with (11), the variance $\dot{}_{ij}$ becomes:

$$\sigma^2_{\cdot_i} = \frac{1}{y_i^2}\sigma^2_{\cdot_i} + \frac{{}^2_i}{y_i^4}\sigma^2_{\dot{y}_i} = \frac{1}{\mu y_i^{\alpha}\ {}_i^{\alpha-2}}\left(\frac{2\pi f_m}{\alpha}\right)^2 \left(\Omega_i + {}_i^{\alpha} s_i\right) \tag{11}$$

In equation (13), fm denotes the Doppler frequency. Conditional probability density functions (CPDF) of $\dot{}_i$ and ${}_i$ are [13]:

$$p_{\cdot_i}\left(\dot{}_i \middle|\ {}_i y\right) = \frac{1}{\sqrt{2\pi}\sigma_{\cdot_i}} \mathrm{e}^{-\frac{\dot{}_i^2}{2\sigma^2_{\cdot_i}}},$$

$$p_{\ {}_i}\left({}_i \middle| y_i\right) = \left|\frac{\mathrm{d}\ {}_i}{\mathrm{d}\ {}_i}\right| p_{\ {}_i}\left({}_i y_i\right) = y_i p_{\ {}_i}\left({}_i y_i\right) \tag{12}$$

Conditional joint probability density function (CJPDF) of ${}_i$, $\dot{}_i$ and $y_i$ is [13]:

$$p_{\cdot_i\ {}_i y_i}\left(\dot{}_i\ {}_i y_i\right) = p_{\cdot_i}\left(\dot{}_i \middle|\ {}_i y_i\right) p_{\ {}_i}\left({}_i \middle| y_i\right) p_{y_i}\left(y_i\right) =$$

$$= p_{\cdot_i}\left(\dot{}_i \middle|\ {}_i y_i\right) p_{y_i}\left(y_i\right) y_i p_{\ {}_i}\left({}_i y_i\right) \tag{13}$$

At the output of the SC receiver, the LCR signal is calculated as the mean value of the first derivation of the signal at the output of the SC receiver. The joint probability density function (JPDF) of ${}_i$ and $\dot{z}_i$ [13]:

$$p_{\cdot_i\ {}_i}\left(\dot{}_i\ {}_i\right) = \int_0^{\infty} \mathrm{d}y_i\, p_{\cdot_i\ {}_i y_i}\left(\dot{}_i\ {}_i y_i\right) \tag{14}$$

By integrating the first derivative, averaging is obtained. The rate of transition of the LCR level of the random process zi is [10]:

$$N_{\ {}_i}\left({}_i\right) = \int_0^{\infty} \mathrm{d}\dot{}_i\ \dot{}_i\, p_{\cdot_i\ {}_i}\left(\dot{}_i\ {}_i\right) =$$

$$= \int_0^{\infty} \mathrm{d}\dot{}_i\ \dot{}_i \int_0^{\infty} \mathrm{d}y_i p_{\cdot_i}\left(\dot{}_i \middle|\ {}_i y_i\right) p_{y_i}\left(y_i\right) y_i p_{\ {}_i}\left({}_i y_i\right) =$$

$$= \frac{\sqrt{2\pi}\, f_{m\ i}^{\ (2\alpha\mu-\alpha)/2} \left(s_i\Omega_i\right)^{(2\mu-1)/2} \Gamma\left(\left(4\mu-1\right)/2\right)}{\Gamma^2\left(\mu\right)\left(s_{i\ i}^{\ \alpha} + \Omega_i\right)^{2\mu-1}} \tag{15}$$

The LCR envelope of the signal-to-interference ratio at the output of the mD SC with *n* inputs is [14]:

$$N_{\ {}_i|\Omega_i s_i}\left({}_i\right) = \left(F_{\ {}_{ij}}\left({}_{ij}\right)\right)^{-1} N_{\ {}_{ij}}\left({}_{ij}\right) = \frac{\sqrt{2\pi}\, f_{m\ i}^{\ \frac{2\alpha\mu-\alpha}{2}}}{\Gamma^2\left(\mu\right)}$$

$$\frac{\left(s_i\Omega_i\right)^{\frac{2\mu-1}{2}} \Gamma^{-1}\left(2\mu\right)\Gamma\left(\frac{4\mu-1}{2}\right)}{\left(\Omega_i + s_{i\ i}^{\ \alpha}\right)^{2\mu-1}} \left(B_{\frac{s_{i\ i}^{\ \alpha}}{\Omega_i + s_{i\ i}^{\ \alpha}}}\left(\mu,\mu\right)\right)^{-1} \tag{16}$$

Fig. 2 shows a graphical analysis of the LCR at the SC receiver outputs given, where, $\Omega_1=\Omega_2=\ldots\Omega_n$, and $s_1=s_2=\ldots s_n$; It is assumed that the correlation between the input branches in the SC receiver is minimal.

## III. NUMERICAL AND GRAPHICAL RESULTS

Based on expression (16) in Fig. 2 the LCR signal-to-noise ratio is shown in relation to the transition threshold at the SC receiver output from the L branches.

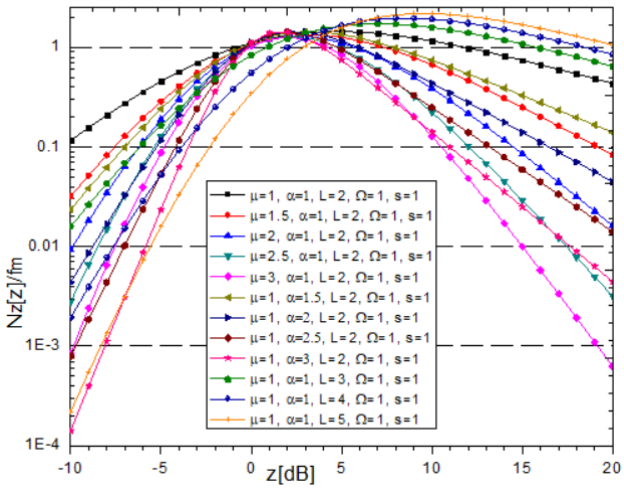


Fig. 2. LCR of system, for different values of parameters , α and L.

Fig. 2 shows that for higher values of the signal-to-noise ratio, the increase in the value of the parameter LCR decreases. When the parameter α increases then comes to narrowing the LRC function. As the number of L branches at the combinator input increases, the LCR increases by positive values of z [dB], and the system has better performance.


ISBN 978-86-7466-930-3

## IV. PLANNING AND SIMULATION ENVIRONMENT

In this section, we present how the previously derived LCR expression can be leveraged within model-driven network planning environment making use of GPU hardware and multi-objective optimization built upon our previous works [15, 16, 17]. Workflow of the underlying software environment exploiting the synergy of deep leaning and multi-objective optimization is depicted in Fig. 3.

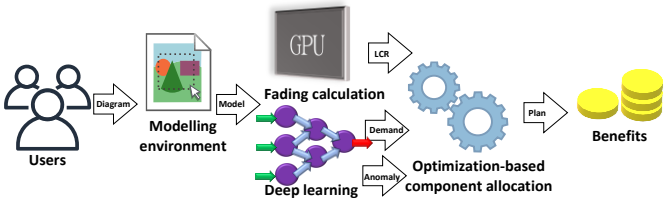


Fig. 3. LCR of system, for different values of parameters , α and L.

Within the first step, users construct network diagram inside Eclipse-based environment, according to the structure of underlying network planning metamodel [15, 16]. It considers the following aspects relevant to planning of mobile network inside smart city: operator's base stations, terrain configuration with obstacles, properties of communication channel, adaptive behavior in case of base station anomalies, consumers of telco services (including people equipped with smartphones, autonomous vehicles and smart city infrastructure).

Once modelling is done, the created model is parsed and processed using Ecore [18]. Furthermore, the corresponding parameters are used as input of network-related data processing steps: GPU-enabled LCR determination and deep learning-based predictions. For purpose of fast LCR calculation, we wrote NVIDIA CUDA [19] kernels in C programming language, as described in [17]. In our experiments, it was up to 65.5 times faster than CPU-only program in Mathematica.

On the other side, deep learning module was implemented relying on PyTorch [20] in Python programming language and deployed as Flask service. It covers predictions related to the following factors: number of service users and base station anomalies. For service user count prediction number day, daily temperature and special occasion flag (such as holiday) are considered. On the other side, for base station anomalies ratio prediction the following factors are involved: total downloaded and uploaded data, Quality of Service value, energy consumption and number of users (previously predicted). The layouts of datasets together with achieved prediction performance (Mean Relative Error) are shown in Table I. The problems are treated as regression (real-valued outcome determination), For this purpose, we designed multi-layer perceptron (MLP) with 3 hidden layers, 30 nodes each, making use of Adam optimizer with learning rate 0.01 for training.

TABLE I
OVERVIEW OF PREDICTION MODELS

| Model | Input | Approach | Relative error |
|---|---|---|---|
| User number | Day<br>Special<br>Temperature | Regression<br>3 hidden<br>30 nodes<br>Adam<br>α=0.01 | 16% |
| Anomaly Ratio | Users<br>Download<br>Upload<br>QoS<br>Energy | | 13% |

Finally, in the last step, we make use of our optimization-based model-driven framework for component allocation relying on Pymoo [21], with respect to the model which will be described. The goal of optimization procedure is finding network plan that consists of optimal base station ($bs \in B$) placement for desired smart city locations ($p \in P$), maintaining best possible QoS while keeping lowest costs at the same time. The objective function has following form:

$$minimi\ e \sum_{bs\in BS, l\in} plan[l,bs](\ C\ [l,bs]+cost[l,bs]+anomaly[l,bs]) \quad (17)$$

As it can be seen, the sum of LCR (positive impact on performance for lower values), deployment costs and base station anomaly rato is minimized. Here, *plan l, bs* denotes decision variable which is 1 in case if base station bs is going to be placed on location l, otherwise 0.

Additionally, we apply a constrint for each location *l* that capacity of base station *bs* (refered to as *ma u l,bs* ) should be enough to service the predicted number of users (*demandp l* ) for given location *l*.

$$\sum_{bs\in BS} plan[l,bs]ma\ u[l,bs] \geq demandp[l], l \in \quad (18)$$

## V. CONCLUSION

In this paper, we have analyzed the MIMO system with a multi-branch SC receiver with L branches when coming to system inputs α - μ fading and CCI with the same distribution. We performed LCR for this model of receiver in the presence of the above-mentioned fading and interference. System performance is more favorable in case when system has lower μ and α parameter, for lower SIR. Analyzing the system, we noticed that the performers are better when the system has a larger number of input branches, because the combiner has the ability to select the branch with the best SIR, leads to better system performance. Finally, for the above fading and CCI system performance is more favorable for lower values of average LCR.

Use of the obtained expression for LCR at the output of a multifaceted SC combinator, we have suggested software environment for simulation. There are several benefits: 1)


ISBN 978-86-7466-930-3

GPU reduces time for LCR calculation 2) costs are minimized 3) performance is maximized.

## ACKNOWLEDGMENT

This work has been supported by the Ministry of Education, Science and Technological Development of the Republic of Serbia.

## REFERENCES

[1] Bannour Ahmed, Mohammad Abdul Matin, et al. Coding for MIMOOFDM in future wireless systems. Springer, 2015.
[2] R. S. Kshetrimayum, Fundamentals of MIMO Wireless Communications, Cambridge University Press, 2017
[3] M. K. Simon and M. S. Alouni, Digital Communication Over Fading Channels. 2nd Ed., New Jersey: Wiley-Interscience; 2005.
[4] David Tse and Pramod Viswanath. Fundamentals of wireless communication. Cambridge university press, 2005.
[5] S.K.Yong and J.S.Thompson, "A three dimensional spatial fading correlation model for uniform rectangular arrays", IEEE Antennas and Wireless Propagation, vol. 2, 2003.
[6] M. Patzold Mobile fading channels, John Wiley and Sons, Ltd., England, 2002.
[7] W.C. Jakes, Ed., Microwave Mobile Communications, NJ, Wiley, 1997.
[8] M. Patzold Mobile fading channels, John Wiley and Sons, Ltd., England, 2002.
[9] M. D. Yacoub, "The α−μ distribution: a physical fading model for the Stacy distribution", IEEE Tranactions on Vehicular Technology, vol. 56, no. 1, pp. 27-34, January 2007.
[10] S. Suljović, D. Krstić, D. Bandjur, S. Veljković, and M. Stefanović, "Level crossing rate of macro-diversity system in the presence of fading and co-channel interference", Revue Roumaine des Sciences Techniques, Publisher: Romanian Academy, vol. 64, pp. 63–68, 2019.
[11] I. S. Gradshteyn and I. M. Ryzhik, Tables of Integrals, Series and Products Academic. New York: 1980.
[12] M. Savic, M. Smilic, B. Jaksic, "Analysis of Shannon capacity for SC and MRC diversity system in α-k-μ fading channel", UNIVERSITY THOUGHT, Publication in N. Sciences, Vol.8, No.2, pp. 61-66, 2018.
[13] S. Suljović, D. Milić, S. Panić, Č. Stefanović, and M. Stefanović, "Level crossing rate of macro diversity reception in composite Nakagami-*m* and Gamma fading environment with interference", Digital Signal Processing, Vol. 102, July 2020, 102758.
[14] D. Krstić, S. Suljović, D. Milić, S. Panić, and M. Stefanović, "Outage probability of macro-diversity reception in the presence of Gamma long-term fading, Rayleigh short-term fading and Rician co-channel interference", Annals of Telecommunications, vol. 73, Issue 5–6, pp. 329-339, June 2018. doi: 10.1007/s12243- 017-0593-4.
[15] D. Krstić, N. Petrović, I. Al-Azzoni, "Model-driven approach to fading-aware wireless network planning leveraging multiobjective optimization and deep learning", Mathematical Problems in Engineering", vol. 2022, 4140522, Special Issue: Mathematical Modelling of Data Transmission in Next Generation Wireless Systems, 2022, pp. 1-23, https://doi.org/10.1155/2022/4140522
[16] N. Petrović, S. Koničanin, D. Milić, S. Suljović, and S. Panić, "GPU-enabled framework for modelling, simulation and planning of mobile networks in smart sities", ZINC 2020, pp. 1-6. https://doi.org/10.1109/ZINC50678.2020.9161773
[17] N. Petrović, S. Vasić, D. Milić, S. Suljović, and S. Koničanin: "GPU-supported simulation for ABEP and QoS analysis of a combined macro diversity system in a Gamma-shadowed k-μ fading channel", Facta Universitatis: Electronics and Energetics Vol. 34, No 1, 2021, pp. 89-104. https://doi.org/10.2298/FUEE2101089P
[18] Eclipse Modelling Framework [online], https://www.eclipse.org/modeling/emf/ , last accessed: 22/04/2022.
[19] J. Sanders and E. Kandort, *C A by e ample an introduction to general-purpose GP programming*, Addison-Wesley, 2011..
[20] E. Stevens, L. Antiga, and T. Viehmann, *eep earning with PyTorch, Manning Publications*, Shelter Island, NY, 2020.
[21] I. Al-Azzoni, J. Blank, N. Petrović, "A Model-Driven Approach for Solving the Software Component Allocation Problem", Algorithms 2021; 14(12):354, pp. 1-19, 2021. https://doi.org/10.3390/a14120354

 ISBN 978-86-7466-930-3

# Location Privacy Improvements in Telecommunication Data Management Systems

Milan Simakovic, Zoran Cica, and Dejan Drajic, *Senior Member, IEEE*

***Abstract*—In the era of digital transformation, data are among the most valuable resources. With the development of big data technologies, it is possible to store and process huge amounts of data. Data are possible to collect on every step with high granulation. Such a trend may seriously harm peoples' privacy. Corresponding laws and regulations are declared to protect data privacy. However, even when all the regulations are obeyed, privacy leakage may still happen if the implementation has some flaws. In this paper, we focus on telecommunication data sets and show how user's location information leakage may happen in already privacy-protected data. Moreover, we give a proposition on how this leakage can be prevented while preserving the same data entropy.**

***Index Terms*— data privacy, location tracking, big data.**

## I. Introduction

According to [1], more than 66% of the world's population uses the internet at the end of 2021. Dynamic environment, rapid growth, and high competition on the market push companies to further enhance their products and reduce costs. Generated data may contain a huge volume of useful information that will drive such an initiative. And just like that, data becomes one of the main fuels in the industry. This phenomenon is further enhanced with the development of big data technologies [2].

To gather as much information as possible from the data, different ways of data processing are invented. Data correlated from different sources can give new insights that do not exist in separate data sets. Such great potential raises the issue of user privacy. To protect the users' privacy and limit the usage of data, GDPR (General Data Protection Regulation) [3] is defined in the European Union, CCPA (California Consumer Privacy Act) [4] in the USA (United States of America), and PIPL (Personal Information Protection Law) [5] in China. There are also laws that specify data privacy in a particular field, like HIPAA (Health Insurance Portability and Accountability Act) for healthcare in the USA [6]. These laws define data processing by protecting users' privacy and giving individuals the right to control the data collected from them. Although companies comply with all regulations, there are situations that can indirectly harm peoples' privacy. To emphasize this phenomenon, one example of such a scenario is presented in this paper. Namely, we show how the privacy of individuals may be harmed on the already privacy-protected telecommunication data set. Also, a recommendation on how this data set can be further masked to protect users from privacy breach while keeping the same information entropy is presented in the paper.

The remaining of the paper is organized as follows. Related work is discussed in section II. A brief overview of data privacy together with appropriate regulation laws is presented in section III. Section IV presents the main contribution of the paper. It discusses telecommunication data sets, shows the vulnerability of privacy-protected data sets on a sample, and proposes privacy improvement while keeping the same information entropy. Section V concludes the paper.

Milan Simakovic, Zoran Cica and Dejan Drajic are with the School of Electrical Engineering, University of Belgrade, Bulevar kralja Aleksandra 73, 11120 Belgrade, Serbia (e-mails: milanrus@hotmail.com, zoran.cica@etf.bg.ac.rs, ddrajic@etf.bg.ac.rs).

Dejan Drajic is with the Innovation Centre of School of Electrical Engineering, University of Belgrade, Bulevar kralja Aleksandra 73, 11120 Belgrade, Serbia.

## II. Related work

Privacy in data technology, especially in big data is a hot topic over the last few years. This section gives a general overview of data privacy challenges, proposed solutions, and frameworks in the literature.

An overview of the privacy-preserving problems in big data stream mining is presented in [7]. Location privacy challenges for mobile applications are discussed in [8]. Location concerns are raised not only to the application provider but to the third parties that are able indirectly to calculate person location from gathered data. In addition, there is a raised concern for services that sell the location data to other parties. Following the people's position and their trajectory is recognized as a serious data privacy concern. To protect trajectory privacy from the data that contain GPS (Global Positioning System) location, a method for data masking that adds noise to the original data based on irregular polygons is proposed in [9]. Due to the rapid development of technology, IoT (Internet of Things) networks are becoming increasingly popular and, thus, becoming significant data generators. Such data may contain privacy-sensitive data. A privacy protection mechanism in industrial IoT based on information tree model is proposed in [10]. Location data is recognized as a huge potential for marketing and advertisement. Considering the number of users, generated amount of data is huge. A method based on big data technologies for location data mining while keeping the data privacy is proposed in [11]. This method uses a clustering algorithm and location entropy to emphasize the most active places.

Companies recognized data privacy as a serious problem and use different methods to solve these challenges. Data

 ISBN 978-86-7466-930-3

privacy models are introduced both for regular [12] and big data systems [13]. Big data models include all the data layers, i.e. collection, storage, and consumption. Data models state for schemas optimized for privacy issues is presented in [13]. In dynamic environments, data is shared both among other teams inside the company and externally. In such a huge data fluctuation, there is a high risk for data privacy issues. Considering that data privacy is protected by law, companies often decide to refrain from using the data which can significantly affect their business efficiency. Model for keeping the big data with a possibility to freely share and explore, and at the same time preserving the data privacy is presented in [14]. Data privacy mechanisms from the k-anonymity, l-diversity, and t-closeness perspectives are discussed in [15]. The advantages and challenges of these mechanisms are analyzed, and a new mechanism based on a combination of these three is proposed. Big data multilayer architecture and utilization of the "differential privacy" approach for sustainable data privacy are discussed in [16].

## III. DATA PRIVACY

Data privacy, or information privacy, stands for the ability of the user to control what type of data is collected from him and how these collected data are used. Personal information, depending on the type of application, can be email, location, online search history, preferences, etc. Considering the complexity of modern applications and systems, it is necessary to gather some personal information (e.g. location) to provide the best possible experience to a client. However, applications can often gather more information than they really need and this might bring harm to people's privacy. Collected users' personal data can be used either inside the company to improve internal processes and services or to sell to other companies as a data set. Due to the lack of data security inside the company, data breaches may happen, and personal data can be stolen and used against the clients [17]. Data privacy is often mixed up with data security. While data security is protection from the 3rd party persons to access the data, data privacy is related to data collection methods and regulations that ensure that the user information is not exposed.

To bring closer control of data to the end-user, and restrict the companies in terms of data collection, usage, and surveillance capabilities, many governments around the world have created laws that regulate how data can be used, stored, and protected. Some of the most important regulations are GDPR [3], CCPA [4] and PIPL [5]. GDPR is the data privacy regulation law in European Union. GDPR gives clear instructions on how the data should be collected, transferred, stored, and protected. In addition, it gives users the right to control their personal data, i.e., the "right to be forgotten". This law regulative forces all the companies that collect users' data to have a mechanism to easily wipe all the data for clients without undue delay [3]. CCPA is the data privacy regulation law in the USA. This law stipulates that the user should be aware of what data are collected from him as well as give the company the right to sell his personal data. In addition, CCPA gives a guide to the company on how the law can be implemented [4]. PIPL is the data privacy law in PRC (People's Republic of China). Next to the regulations that prescript GDPR and CCPA, PIPL gives attention to data localization, i.e., that certain categories of personal data must be stored in PRC [5]. Next to the mentioned regulations, there are also many others that are implemented either in other countries or the ones that are industry-focused. For example, HIPAA is the regulation in the USA that governs how personal healthcare data should be handled [6].

To provide data privacy, companies use different techniques for data transformation. Among the most popular techniques are data anonymization and pseudonymization. Anonymization and pseudonymization present the process of transformation of UID (User Identifier) into data sets. Anonymized data stands for one-way encryption meaning that, once the UID is encrypted, there is no theoretical way to re-identify the user from it, neither directly nor indirectly. On the other side, pseudonymization stands for data masking techniques that can be reversed. It means that there is a way to decrypt the data. Pseudonymization is weaker in terms of data protection and should be used carefully. This technique is often used for data that are not related to the UID, but to some attributes. Some of the most popular methods for data pseudonymization are [18]:

- encryption – hiding data by encrypting it,
- shuffling – mixing data inside one column to disassociate attributes from the original user,
- suppression – removing sensitive columns from the dataset,
- redaction – completely removing parts with sensitive data.

Next to these two techniques, there are some other techniques for data privacy protection. Data generalization presents a way to change a value of some column with its range. For example, the value of column age 34 is modified to the range 30-40. Data synthetization presents a method to generate a completely new dataset from the original one using machine learning techniques. A newly generated dataset mimics the properties of original data. Although, these methods are useful in terms of data privacy, they distort information and reduce the data entropy. This is especially evident during the data aggregation.

## IV. TELECOMMUNICATION DATA

Telecommunication networks represent a very important factor in the development of humanity. Due to their importance and high competition on the market, telecommunication operators gather data to further optimize services, reduce costs, and improve quality of their networks and services. Data are gathered on all network architecture levels, from physical and core network devices to the application layer. Modern telecommunication network providers typically implement centralized platform based on big data technologies to gather such amount of data.

 ISBN 978-86-7466-930-3

TABLE I
SAMPLE OF SIMPLIFIED MOBILE DATA SET

| base station id | calling party | called party | billing | call type | call status | timestamp |
|---|---|---|---|---|---|---|
| bst_drwx_sth | aa9annch2n44 | 34yv5n9dwqlo | 0.2 | sms | sent | 2022/03/15 08:45:02.000 |
| bst_drwx_sth | i23u6bu546bx | vsf78bt489aa | 0.0 | call | start | 2022/03/15 08:46:16.015 |
| bst_drwx_sth | cw59coj7q33h | 64hqu89bu33q | 1.4 | call | end | 2022/03/15 08:46:55.724 |
| … | | | | | | |
| bst_mmss_nrt | j4kk9txbryuq | zevynom2w84t | 7.2 | call | end | 2022/03/15 09:33:51.992 |
| bst_mmss_nrt | i23u6bu546bx | quuhe11bcyd4 | 1.6 | call | end | 2022/03/15 09:34:08.183 |
| bst_mmss_nrt | 2jj3hb56u2bb | oppqnn4bb60u | 0.2 | sms | sent | 2022/03/15 09:34:40.000 |
| … | | | | | | |
| bst_lndn_wst | i23u6bu546bx | pp22djqmxirb | 1.7 | call | end | 2022/03/15 12:02:45.501 |
| bst_lndn_wst | curbskoqcgg4 | bsgwivg4611b | 0.0 | call | start | 2022/03/15 12:03:10.017 |

Since telecommunications are always on the top of IT standards, all these systems already implement mechanisms for data privacy that are prescribed in their countries. Although, the implemented mechanisms mask the UIDs, due to the complexity and variety of data, some data privacy breaches may happen. In this section, we show one example of how the data privacy breach in terms of user tracking may happen and propose a masking mechanism that solves the problem for such a scenario while keeping the data entropy at the same level.

Mobile network operators gather data (for example, CDRs (Call Detail Record) and XDRs (Extended Detection and Response)) from base stations. This data contain information about the mobile phone device id, used frequency channel, signal strength, service type, call duration, etc. Such data helps the operators to tune the base stations, maximize the capacity of the cell, and quality of service. An example of simplified data set is shown in Table 1. In the example data set, UID is hashed due to the data privacy regulations. Assuming the anonymization is taken as the hashing mechanism, there is no way to get the UID original value.

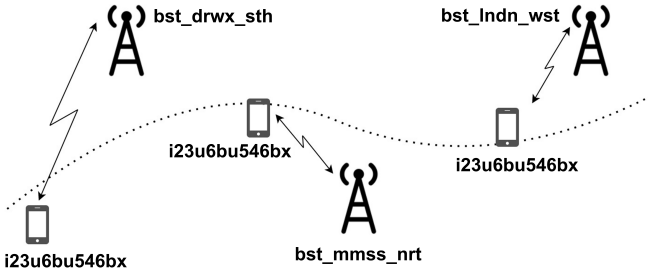


Fig. 1. User location tracking using data from base stations.

Since the same mechanism for data hashing is implemented on the data from every base station, it generates the same hashed UID for a user on every base station. This means that even though the user's UID is not known, it is possible to track user's movement as shown in Fig. 1. From the dataset shown in Table 1, it can be seen how the UID "i23u6bu546bx" is located on different base stations during the day which implies the possibility to track the location of this person. By matching the hashed UID with associated data (like base station ID, call records, etc.) it might be even possible to determine the identity of the user.

Although collected data are used for network improvement, people's privacy can be indirectly harmed in terms of location tracking. Since this information is not relevant to mobile network operators, we propose a new mechanism for data masking. The previous mechanism takes the device identifier (e.g. phone number or MAC address) and creates the hashed id by using some hashing function like shown in (1).

$$hashed\_UID = hash\_function(UID) \quad (1)$$

This mechanism creates the same hashed UID on all base stations. To improve this, we propose to create the hash UID from a combination of base station identifier and UID, as shown in (2). In this way, hashed value of UID will be different at each base station. Thus, information about user movement is removed, but all the necessary information relevant for quality-of-service monitoring are kept.

$$hashed\_UID = hash\_function(base\_station\_ID + UID) \quad (2)$$

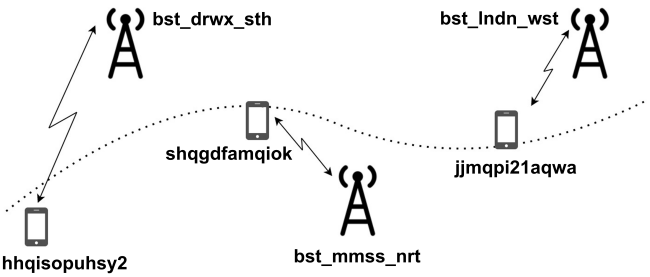


Fig. 2. Avoiding user location tracking.

The data set generated with the proposed hashed function is shown in Table 2. User that corresponds to hashed UID "i23u6bu546bx" in Table 1, has now a different UID on each base station which makes it impossible to correlate the data and track its location. Note that corresponding fields are colored in Tables 1 and 2. Fig. 2 shows the same example as Fig. 1 with a difference that now the UID is hashed with our proposed method. It can be seen in Fig. 2 that hashed UID values for the same user are different at different base stations. Thus, tracking of user movements is not possible anymore. However, if a user is connected to same base station for a

 ISBN 978-86-7466-930-3

TABLE II
SAMPLE OF SIMPLIFIED MOBILE DATA SET WITH PROPOSED HASHING MECHANISM

| base station id | calling party | called party | billing | call type | call status | timestamp |
|---|---|---|---|---|---|---|
| bst_drwx_sth | qheuzhnq91nw | 34yv5n9dwqlo | 0.2 | sms | sent | 2022/03/15 08:45:02.000 |
| bst_drwx_sth | hhqisopuhsy2 | vsf78bt489aa | 0.0 | call | start | 2022/03/15 08:46:16.015 |
| bst_drwx_sth | soek28dh17h3 | 64hqu89bu33q | 1.4 | call | end | 2022/03/15 08:46:55.724 |
| … | | | | | | |
| bst_mmss_nrt | h1ikvgwotggk | zevynom2w84t | 7.2 | call | end | 2022/03/15 09:33:51.992 |
| bst_mmss_nrt | shqgdfamqiok | quuhe11bcyd4 | 1.6 | call | end | 2022/03/15 09:34:08.183 |
| bst_mmss_nrt | q11y2ms9h5b6 | oppqnn4bb60u | 0.2 | sms | sent | 2022/03/15 09:34:40.000 |
| … | | | | | | |
| bst_lndn_wst | jjmqpi21aqwa | pp22djqmxirb | 1.7 | call | end | 2022/03/15 12:02:45.501 |
| bst_lndn_wst | rxihb6ihqwhb | bsgwivg4611b | 0.0 | call | start | 2022/03/15 12:03:10.017 |

period of time, hashed UID value will be the same, thus, the information about the signal quality for the session and user is preserved.

The same data privacy leak can happen not only in mobile but in other networks as well. For example, HFC (Hybrid Fiber Coaxial) network operators gather data from their cable modems. Considering that nowadays most of the clients are connected to the internet using WiFi (Wireless Fidelity), poor quality of service can be caused either by the poor signal quality on a cable modem or poor WiFi signal. The quality of the WiFi signal depends on many aspects such are the position of the cable modem, the schema of the building, types of walls, etc. Even though HFC operators are not in charge of the quality of WiFi networks, they tend to help clients to improve quality of network either by reconfiguring the WiFi (switching WiFi channel, changing channel width), relocating cable modem to some other place where it will better cover the whole apartment or by adding WiFi extenders.

Information about the cause of the poor signal quality operators find in the data gathered from the cable modems. Modern cable modems have embedded WiFi transmitters. Next to the basic information regarding the quality of the signal, data about the WiFi can be collected as well. Example of data that are gathered is the MAC (Media Access Control) address and WiFi username of the connected device (e.g., from a laptop, tablet, or mobile phone). If the device is connected to several locations that are covered by the same provider (e.g., at home, at café, store, work) the data privacy in terms of movement tracing can be breached. To solve such problem, the same hashing mechanism, (2), we propose for mobile networks can be used. Creating a different hash for UID on different cable modems, would completely remove the possibility to track the user movements.

## V. CONCLUSION

Data privacy concerns are raised a few years ago and present one of the most important aspects during the development of data management systems. Depending on country, data management systems implement the appropriate privacy laws. Although the laws are obeyed, data privacy leakage may still happen if implementation is not carefully done. This paper shows an example of location data privacy violations in telecommunication data systems. In addition, we show methodology for how such violations can be solved with domain-specific knowledge. Finally, a proposal for data privacy improvement while keeping the same data entropy is given.

## ACKNOWLEDGMENT

This work has been supported by the Ministry of Education, Science and Technological Development of the Republic of Serbia.

## REFERENCES

[1] Internet World Stats (site: https://www.internetworldstats.com/stats.htm ), Accessed: Mar. 18, 2022.
[2] J. Dean, S. Ghemawat, "MapReduce: Simplified Data Processing on Large Clusters," *OSDI - Operating Systems Design and Implementation*, 2004.
[3] Complete Guide to GDPR Compliance (site: https://gdpr.eu/), Accessed: Mar. 18, 2022.
[4] California Consumer Privacy Act(site: https://oag.ca.gov/privacy/ccpa), Accessed: Mar. 18, 2022.
[5] The PRC Personal Information Protection Law (site: https://www.china-briefing.com/news/the-prc-personal-information-protection-law-final-a-full-translation/), Accessed: Mar. 18, 2022.
[6] Health Insurance Portability and Accountability Act of 1996 (site: https://www.cdc.gov/phlp/publications/topic/hipaa.html), Accessed: Mar. 18, 2022.
[7] A. Cuzzocrea, "Privacy-Preserving Big Data Stream Mining: Opportunities, Challenges, Directions," in *proc. of ICDMW 2017*, New Orleans, LA, USA, Nov. 2017.
[8] M. L. Damiani, C. Cuijpers, "Privacy Challenges in Third-Party Location Services," in *proc. of MDM 2013*, Milan, Italy, June 2013.
[9] H. Liu, W. Di, "Application of Differential Privacy in Location Trajectory Big Data," in *proc. of ICITBS 2020*, Vientiane, Laos, Jan. 2020.
[10] C. Yin, J. Xi, R. Sun, J. Wang, "Location Privacy Protection Based on Differential Privacy Strategy for Big Data in Industrial Internet of Things," *IEEE Transactions on Industrial Informatics*, vol. 14, no. 8, pp. 3628 - 3636, Aug. 2018.
[11] S. Wang, R. Sinnott, S. Nepal, "Privacy-protected place of activity mining on big location data," in *proc. of Big Data 2017*, Boston, MA, USA, Dec. 2017.
[12] C. Wu, Y. Guo, "Enhanced user data privacy with pay-by-data model," in *proc. of Big Data 2013*, Silicon Valley, CA, USA, Oct. 2013.
[13] X. Feng, "The Optimization of Privacy Data Management Model In Big Data Era," in *proc. of IAEAC 2021*, Chongqing, China, Mar. 2021.

 ISBN 978-86-7466-930-3

[14] Y. Canbay, Y. Vural, S. Sagiroglu, “Privacy Preserving Big Data Publishing,” in *proc. of IBIGDELFT 2018*, Ankara, Turkey, Dec. 2018.
[15] R. Mahesh, T. Meyyappan, “Anonymization technique through record elimination to preserve privacy of published data,” in *proc. of PRIME 2013*, Salem, India, Feb. 2013.
[16] K. M. Shrivastva, M. A. Rizvi, S. Singh, “Big Data Privacy Based on Differential Privacy a Hope for Big Data,” in *proc. of ICRCICN 2014*, Bhopal, India, Nov. 2014.
[17] What is data privacy? (site: https://www.cloudflare.com/learning/privacy/what-is-data-privacy/), Accessed: Mar. 18, 2022.
[18] Which data protection methods do you need to guarantee privacy? (site: https://www.statice.ai/post/data-protection-techniques-need-to-guarantee-privacy#:~:text=Encryption%3A%20hiding%20sensitive%20data%20using,entirety%20of%20a%20column's%20values), Accessed: Mar. 18, 2022.

 ISBN 978-86-7466-930-3

# Introducing IoT to Big Data Platform for Network Performance Monitoring

Milan Simakovic, Zoran Cica, and Dejan Drajic, *Senior Member, IEEE*

***Abstract*—Telecommunication operators are collecting large amounts of data for various purposes such as network performance monitoring, network planning, better customer support, etc. Nowadays, big data technologies are commonly used to couple with enormous amounts of data. Thus, telecommunication operators use big data platforms to process and store data collected from their networks. Data are collected from the network and user devices. Since network operators cover most of the residential users, it is possible to use this access to introduce IoT (Internet of Things) and smart city support. By extending the already existing big data platforms to support IoT devices placed at network users' premises, smooth integration of various IoT devices with the smart city concept can be achieved. Such integration would have significant benefits for network operators, users and local communities. In this paper, we propose an extension that introduces IoT support to the existing big data platform used for HFC (Hybrid Fiber-Coaxial) network monitoring. An overview of the most attractive IoT use cases that can benefit from the proposed extension is also presented in the paper.**

***Index Terms*—Big data, IoT, Smart city, Smart home, HFC network.**

## I. Introduction

Telecommunication operators typically serve large number of users. In order to successfully perform such task, operators use very complex and heterogeneous telecommunication networks which need to be constantly monitored. For monitoring purposes, operators collect and store data from numerous network devices [1,2]. By processing the collected data, it is possible to achieve optimal network performance and provide high QoS (Quality of Service) to users. Since the amount of collected data is enormous, big data technologies need to be used to efficiently store and process such amount of data [3].

Smart home and smart city are IoT concepts that are becoming very popular nowadays [4,5]. Given the large number of residents and the fact that each user will typically have multiple IoT devices and sensors at home, it is obvious that amount of data collected can be very large. Thus, big data technologies would provide excellent solution for storing and processing such amounts of data [6]. Most of the residential users are covered by some telecommunication operator (HFC, passive optical network (PON), etc.) and the operators use big data platforms to store and process data collected from their networks. Given that fact, these big data platforms can be extended to collect and store data from IoT devices and sensors placed at user premises. In this way, same infrastructure could be reused for IoT purposes. By integrating existing telecom operators big data platform in smart city environment, highly economic and efficient smart city solution can be achieved.

In [7], big data platform for HFC network monitoring is extended with support for efficient failure detection and localization. In this paper, we propose extension of this big data platform to support IoT devices at users' premises. It will be shown, that such extension does not require architecture modifications in the already existing big data platform. Only, adjustments in data collection layer need to be done. Once data are collected and stored, it is up to data consumers (smart city solutions and applications, users, operators) to determine which types of processing of the collected data need to be supported. For example, application for users that graphically shows measured values from their sensors, or notification in case of threshold violation (e.g. smoke detectors detect fire). In this paper, we also present the most attractive use cases that would benefit from such IoT extension of big data platform.

Remainder of the paper is organized as follows. In section II, we give related work overview. Section III presents the existing big data platform for HFC network monitoring, and the introduced extensions to support data collection and storage from IoT devices. Section IV contains a survey of use cases that would benefit from the IoT extension of the big data platform introduced in section III. Finally, section V concludes the paper.

## II. Related Work

IoT based smart home solutions represent one of the most important IoT markets since they offer a huge variety of different applications for enhancements of resident's quality of life. It is possible to install different devices for monitoring of various activities. The monitoring can be focused on the resident's activities and on the different parameters in the home. In the elderly healthcare solution, different medical sensors are provided in form of smart bracelets and other wearable devices [8], that allow efficient monitoring of movements and condition of a patient. Different sensors for environmental monitoring could be installed like sensors for temperature, relative humidity, light intensity measurements,

Milan Simakovic, Zoran Cica and Dejan Drajic are with the School of Electrical Engineering, University of Belgrade, Bulevar kralja Aleksandra 73, 11120 Belgrade, Serbia (e-mails: milanrus@hotmail.com, zoran.cica@etf.bg.ac.rs, ddrajic@etf.bg.ac.rs).

Dejan Drajic is with the Innovation Centre of School of Electrical Engineering, University of Belgrade, Bulevar kralja Aleksandra 73, 11120 Belgrade, Serbia.

 ISBN 978-86-7466-930-3

fire/smoke detectors, etc. Based on these measurements, temperature and lighting control can be automatized and appropriate alarms can be raised. Monitoring of energy and water consumption, and water leakage detection can be achieved with appropriate sensors. Also, different appliances in home can be remotely monitored, such as sensors for audio and video surveillance, motion detection that are typically installed to increase home safety [9].

Within the smart cities many urban related problems are aimed to be solved such as air pollution, urban noise monitoring, traffic jams, smart parking, energy consumption, waste management, smart infrastructure, street lighting, assistance to senior citizens, etc [10]. This includes different types of technologies (big data, IoT, WSN (Wireless Sensors Networks) and cloud. Particularly interesting elements for planning Wi-Fi networks in large cities are presented in the paper [11]. Wi-Fi as a transmission technology is preferable in many smart city applications since it provides connectivity to smart phones, computers and many wearable gadgets. Different challenges of Smart City IoT system deployment are addressed in [4], where Security and Privacy, Smart Sensors, Networking and Big Data Analytics are recognized as the most important ones.

IoT concept is one of the most important trends in telecommunications. IoT is integral part of many "smart" solutions like smart city, smart buildings, smart agriculture, smart transport, smart healthcare... [12]. Given the significant amount of data that IoT systems generate, big data is recognized as a "key enabling technology for IoT" [12]. For this reason there are numerous papers that deal with IoT and Big Data combination. Surveys on big data in IoT can be found in [12,13]. A large number of papers on the topic of smart city shows that this concept is one of the most popular ones from the IoT area. Survey on big data in smart city solutions is given in [14]. Industry also embraced IoT concept because digitalization of industrial processes increases efficiency [15]. In [15], Industrial Big Data as a result of IoT adoption in manufacturing is discussed. Big data and IoT in smart farming are discussed in [16]. Although, many IoT solutions are already operating along with big data technologies support, there are still some open challenges. Survey on these open challenges is given in [17].

## III. BIG DATA PLATFORM ARCHITECTURE

In this section, first we give a brief description of the existing big data platform architecture for HFC network performance monitoring. Then, we describe extensions necessary to introduce IoT in the existing big data platform.

Fig. 1 shows the big data platform architecture for performance monitoring of HFC network. Big data platform comprises two major parts - big data cluster and data collection layer. Big data cluster uses several big data tools to store and process collected data. The used big data tools include OpenTSDB (Open Time Series Database), Apache HBase, HDFS (Hadoop Distributed File System), Apache Spark, Hadoop YARN (Yet Another Resource Negotiator), and Zookeeper. OpenTSDB is used to verify and process incoming messages from data collection layer, and to store these messages in HBase tables. HBase writes table files to HDFS while HDFS is responsible for storing data on physical storage units. Apache Spark is necessary for data aggregations. Hadoop YARN is used to allocate resources to jobs. YARN also enables different processing frameworks to use common hardware. Zookeeper synchronizes distributed services.

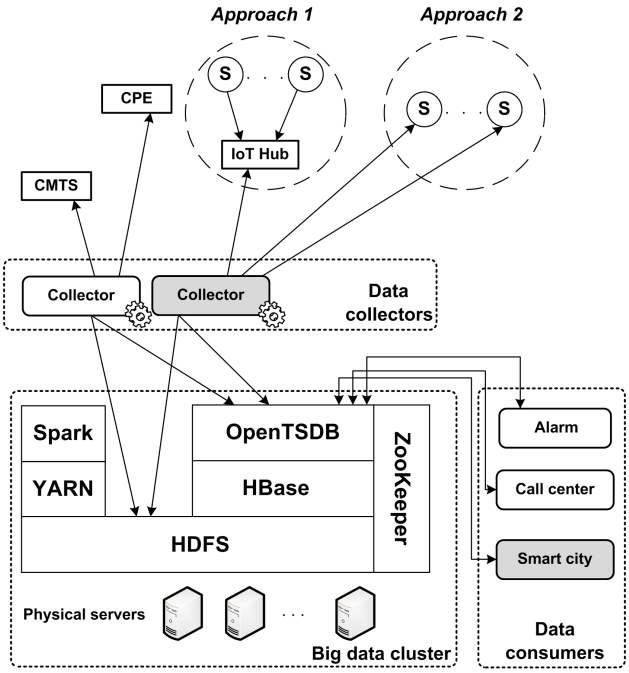


Fig. 1. Big data platform with added support for IoT devices

Data collection layer is responsible for collecting data from CMTS (Cable Modem Termination System) and CPE (Customer Premises Equipment) devices in HFC networks as they represent network devices with a possibility to collect data from them. CPE devices include cable modems and set-top boxes. SNMP (Simple Network Management Protocol) is used for data collection. There are numerous data collectors working in parallel in the data collection layer due to large number of devices in the HFC network from which data need to be collected. Various data (metrics) are collected from CMTS and CPE devices, while the data collection period depends on the data type and importance. Collection period is set in range from 1 minute to 1 hour depending on the importance of collected metrics. Collected data are sent to OpenTSDB via web socket and in parallel data are also written to HDFS.

Fig. 1 also shows the extensions necessary to accommodate IoT support. The updated or added modules are marked with grey coloring. Main update needs to be made in data collection layer. Namely, data collectors need to be aware of new devices and data types that need to be collected. The advantage of the previously described big data platform is its flexibility. Due to large number of different network devices (different vendors, versions, models, etc.), big data platform was developed to efficiently couple with variety challenge

 ISBN 978-86-7466-930-3

that is typical for big data usage [18]. This means that the data collectors are designed to be flexible and adjustable to new devices added to monitored HFC network. Obviously, IoT devices also represent new devices from the data collector point of view. Thus, adding a support for new devices is not a complex task.

The other extension is connection to new data consumers. In the case of IoT introduction that would be IoT data consumers, e.g. smart city environment as shown in Fig. 1. These IoT data consumers can be internal or external depending on the type of integration of the big data platform. For example, the big data platform besides the network monitoring system can serve also as IoT service hub operated by the network operator (internal data consumer). But, the big data platform can provide access to data to external data consumers such as local government smart city platform or external companies like distributors of electricity, water or gas.

At user premises, there are two possible approaches that affect the data collector extension for IoT devices support. One approach is to collect data directly from each IoT device. Second approach is to have a hub for all IoT devices at user premises. In this second case, data collector connects only to a hub which reduces the number of connections necessary to collect all IoT related data from user premises. The other advantage of the hub approach is simplified addition of support for IoT data in data collection layer. Namely, in this case focus is only on the types of IoT metrics not the types of IoT devices. Secondly, this gives more freedom for connecting IoT devices to central hub at home (for example, ZigBee or Bluetooth). Thirdly, if WiFi is used to connect IoT devices to central hub, a central hub might be integrated to cable modem as nowadays these modems typically have WiFi capabilities. Both approaches are illustrated in Fig. 1.

## IV. USE CASES

The proposed IoT support extension of the big data platform for HFC network performance monitoring can be applied in many smart monitoring IoT based use cases. IoT and sensor networks represent sources of time series data that can be collected, stored and processed by the proposed extension of big data platform. As discussed in the previous section there are two approaches that can be used to collect data from IoT devices - direct and indirect over IoT hub. Note that these two approaches can coexist if necessary.

Some of the most important and common IoT based smart metering in homes are: indoor air quality monitoring, energy consumption and water consumption monitoring. These metering devices produce periodic and relatively small packet traffic. The most common indoor air quality monitoring parameters are CO, $CO_2$, PM (Particle matters), VoC (Volatile compounds), temperature and relative humidity. Additionally, some devices support $O_2$, $CH_4$, $H_2S$, $NH_3$ as well. There are a lot of already available low-cost devices for this purpose [19]. These devices can be used for air quality monitoring and fire detection. Normally, reporting period is set to 5 minutes, but for the alarm purposes it could be set to 1 minute. Expected payload is 0.5 kB per sampling interval. In the case of 1 minute monitoring period, expected data volume per one device would be 720 kB per day, i.e. 21.6 MB per month. If data collectors enrich the collected data with additional information (user id, device model/type,...), the expected data volume can be a bit larger. The required storage space for data collected over one month would be around 5.7 TB under following assumptions: each home has 2 IoT devices in average; data collected from each IoT device requires 30MB per month in average; there are 100000 homes covered by HFC network.

Telecom operators can allow access to the raw data via API (Application Programming Interface). But more attractive for their clients would be aggregation, processing and visualization of their data available via web portal where clients can easily follow the measurements and set alarms and/or notifications, calculate air quality index, etc. In case of different models and versions of IoT devices, operators can perform data aggregations per manufacturer or model to gain insight in the performance of the devices and determine which devices are more preferable and offer them to their clients in future deals. In case of air quality measurement devices, outside units can be mounted as well, for example, on balconies. Data collected from such devices can be aggregated and processed to gain deeper insight in air quality in different parts of the city, or on different height levels in case of multi-storey buildings. This information can be very important for local communities to detect critical zones.

While air quality monitoring requires quite frequent reporting, energy [20] and water [21] consumption can be reported once per day (about 0.4 kB per measurement in both cases, which means 12 kB per month). Energy module collects data about power consumption and other electric parameters, while the water consumption sensor monitors amount of water usage in the home. Measurements can be collected by the platform, where data are stored and processed. The measurements can be presented in form of graphs, and when data reach the specified level of power or water consumption, alerts can be generated and sent to the user. Also, smart city concept assumes interconnection of citizens, local governments and utility companies. Utility companies need to read measurement devices to check the consumption by their clients. If the readings of these devices are integrated with the big data platform, then that data can be passed to utility companies. In this way, multiple benefits can be achieved. Automatized and remote measurement readings, detection of anomalies which can trigger alarm to both utility companies and users. In case of multi-storey buildings, utility measurement devices are typically not part of the homes. In such cases, if the building is covered by HFC network, additional cable modem can be installed that would cover only the utility measurement devices as a part of agreement between the users, operator and utility companies. This actually perfectly represents the idea and aim of smart city concept.

As already explained, presented use cases are not very demanding in terms of storage capacity, so big data platform should be able to easily handle a lot of users. Insight into collected measurements provides to users powerful

 ISBN 978-86-7466-930-3

information how to optimize water and power consumption and how to improve the air quality. Proposed concept facilitates smart home integration and could be expanded for the smart city measurements integration with goal to create pollution and noise maps (devices can be also mounted outside for outdoor air quality monitoring), remote reading of electricity and water consumption, thus, optimizing the work of communal services. On the other hand, the proposed expansion provides an excellent opportunity for the operators to expand their service portfolio and offer new smart services to their users, which would bring a new revenue and increase users' confidence and satisfaction.

The described IoT devices are low-cost and easy for installation and handling. Of course there are a lot of other sensors and devices that could be installed for monitoring of different kinds of parameters, and in this section we presented a few useful examples for the proof of concept purposes.

## V. CONCLUSIONS

In this paper we propose extension for IoT support of existing HFC network performance platform based on big data technologies. The proposed extension is incremental and not complex, and most importantly does not affect the original purpose (performance monitoring) of the big data platform. The presented use cases that would be enabled by the proposed extension show that significant benefit would be gained by all the parties involved: users, operators, utility companies, local communities. This is exactly in line with the smart city ideas and goals. As a part of our future work, we will focus on tight integration of the proposed extension to smart city solutions with special emphasis on air and noise pollution tracking and creating corresponding noise and pollution maps.

## ACKNOWLEDGMENT

This work has been supported by the Ministry of Education, Science and Technological Development of the Republic of Serbia.

## REFERENCES

[1] Y. He, F. R. Yu, N. Zhao, H. Yin, H. Yao, R. C. Qiu, "Big Data Analytics in Mobile Cellular Networks," *IEEE Access*, vol. 4, pp. 1985-1996, Mar. 2016.

[2] A. J. Garcia, M. Toril, P. Oliver, S. Luna-Ramirez, R. Garcia, "Big Data Analytics for Automated QoE Management in Mobile Networks," *IEEE Communications Magazine*, vol. 57, no. 8, pp. 91-97, August 2019.

[3] M. Simaković, Z. Cica, I. Masnikosa, "Big Data Architecture for Mobile Network Operators," in *proc. of TELSIKS 2021*, Nis, Serbia, Oct. 2021.

[4] A. S. Syed, D. Sierra-Sosa, A. Kumar, A. Elmaghraby, "IoT in Smart Cities: A Survey of Technologies, Practices and Challenges," *Smart Cities*, vol. 4, no. 2, pp. 429–475, Mar. 2021.

[5] A. Nag, M.E.E. Alahi, N. Afsarimanesh, S. Prabhu, S.C. Mukhopadhyay, "IoT for smart homes", in book *Sensors in the Age of the Internet of Things: Technologies and applications*, pp. 171-199, 2019.

[6] S. Khare, M. Totaro, "Big Data in IoT," in *proc. of ICCCNT 2019*, Kanpur, India, Jul. 2019.

[7] M. Simakovic, Z. Cica, "Detection and Localization of Failures in Hybrid Fiber–Coaxial Network Using Big Data Platform," *MDPI Electronics*, vol.10, no.23, November 2021.

[8] B.J. Cheng, M.M.A. Jamil, R. Ambar, M.H.A. Wahab, A.A. Ma'radzi, "Elderly Care Monitoring System with IoT Application", in book *Recent Advances in Intelligent Information Systems and Applied Mathematics*, pp. 525-537, 2020.

[9] M.R. Alam, M.B.I. Reaz, M.A.M. Ali, "A Review of Smart Homes—Past, Present, and Future," *IEEE Transactions on Systems, Man, and Cybernetics, Part C (Applications and Reviews)*, vol. 42, no. 6, pp. 1190-1203, Nov. 2012.

[10] J. Temperton, "Bristol is making a Smart City for Actual Humans". Wired, 17 March 2015. http://www.wired.co.uk/news/archive/2015-03/17/bristol-smart-city.

[11] L. Zhang, L. Zhao, Z. Wang, J. Liu, "WiFi Networks in Metropolises: From Access Point and User Perspectives," *IEEE Communications Magazine*, vol. 55, no. 5, pp. 42-48, May 2017

[12] M. Bansal, I. Chana, S. Clarke, "A Survey on IoT Big Data: Current Status, 13 V's Challenges, and Future Directions," *ACM Computing Surveys*, vol.53, no.6, pp. 1-59, Nov. 2021.

[13] E. Ahmed et al., "The role of big data analytics in Internet of Things," *Computer Networks*, vol. 129, no. 2, pp. 459-471, Dec. 2017.

[14] I.A.T. Hashem et al., "The role of big data in smart city," *International Journal of Information Management*, vol. 36, no. 5, pp. 748-758, Oct. 2016.

[15] D. Mourtzis, E. Vlachou, N. Milas, "Industrial Big Data as a Result of IoT Adoption in Manufacturing," *Procedia CIRP*, vol. 55, pp. 290-295, 2016.

[16] N. N. Misra, Y. Dixit, A. Al-Mallahi, M. S. Bhullar, R. Upadhyay, A. Martynenko, "IoT, big data and artificial intelligence in agriculture and food industry," *IEEE Internet of Things Journal*, pp. 1-1, May 2020.

[17] S. Kumar, P. Tiwari, M. Zymbler, "Internet of Things is a revolutionary approach for future technology enhancement: a review," *Journal of Big Data*, vol. 6, no. 1, pp. 1-21, Dec. 2019.

[18] M. Simakovic, Z. Cica, "Big Data Applications and Challenges," in *proc. of Infoteh 2016*, Jahorina, BiH, Mar. 2016.

[19] https://www.renkeer.com/product/aqi-sensor/

[20] https://www.acrel.co.id/product/Wireless_energy_meter/IoT_Wireless_energy_meter.html?gclid=Cj0KCQjw5-WRBhCKARIsAAId9FlVSq3lp8SpBQ6TC09F9covmEei2ZZF9_tGw6zH6NRKM8NIb4L8WLMaAj90EALw_wcB

[21] Z.H. Che Soh, M.S. Shafie, M.A. Shafie, S.N. Sulaiman, M.N. Ibrahim, S.A.C. Abdullah, "IoT Water Consumption Monitoring & Alert System," in *proc. of ICELTICs 2018*, Banda Aceh, Indonesia, Sep. 2018.

 ISBN 978-86-7466-930-3

# Reliability of Earth-Space Links under Deep Fades with Interleaved Reed-Solomon Codes

Srđan Brkić, *Member, IEEE*, Zoran Čiča, Andreja Radošević, Đorđe Sarač, Predrag Ivaniš, *Senior Member, IEEE*

***Abstract*—This paper contains a reliability analysis of Earth-space links subjected to deep fades, modeled as burst erasure channels. We numerically calculate lower bounds on transmission propagation latency caused by employment of packet erasure codes, when fade duration is represented by random variable with Weibull distribution. Furthermore, we propose coding scheme that involves interleaved short Reed-Solomon (RS) codes to mitigate information loss, caused by long fading events. In order to quickly and accurately evaluate residual packet loss rates of interleaved RS codes, we construct a novel simulator, called segment-based simulator, which is able to predict code performance several orders of magnitude faster than plain Monte Carlo simulation. Finally, we show that for variety of channel parameters and code rates, very short RS codes (even with length 15) can provide near optimal propagation latencies.**

***Keywords*—Fading channels, Packet erasure codes, Reed-Solomon codes, Earth-space Links, Singleton bound**

## I. Introduction

SATELLITE communications are experiencing a renaissance over the past years, as their potential in providing broadband transmission is fully recognized and explored. Possibility to transfer information between arbitrary points on the Earth surface via satellites makes this type of communications attractive for emerging services, which require high accessibility, like connected vehicles. Furthermore, inclusion of satellite links into 5G ecosystem is studied in newly published 3GPP standards [1], in an attempt to create powerful hybrid satellite-terrestrial (HST) communication systems [2]. In order to build HST systems different technological challenges need to be resolved, which are partially consequences of reduced accessibility and reliability of Earth-space channels.

Despite widely assumed line-of-site visibility between ground terminals and satellites, Earth-space communications link could be blocked for a variety of reasons. In mobile satellite communications used in urban areas, line-of-site assumption may not hold, while different ground obstacles could, from time to time, disable the communication link, leading to loss of transmitted information. Furthermore, LEO (Low Earth Orbit) satellites are moving along their orbits and each LEO satellite is only shortly visible from a stationary point at Earth surface. To enable uninterrupted transmission, ground terminal periodically executes handover operations and establishes connection with different LEO satellite. Handover operation can not be instantaneously performed, which means that potentially communication channel is for a period of time blocked. Lastly, meteorological conditions, for example heavy rain, could attenuate signal such that its power cannot reach a receiving threshold.

All the above phenomenons can be described via hard-blockage model [3], where on-state (reliable transmission) and off-state (blocked channel with no transmission) are alternatively changed, while state durations are represented as uncorrelated random events. Probability density functions of state durations are chosen to fit empirical data collected over the years, mostly for Ka frequency band [4], [5].

Reliability of Earth-space links could only be improved by forward error correction, as propagation delay prohibits use of retransmission techniques. Given the fact that hard-blockage model corresponds to block erasure channel, using sufficiently long maximum distance separable (MDS) codes, for example Reed-Solomon codes, will be optimal. However, for high throughput communications, during off-states the large amount of symbols are erased, and consequently length of a required MDS code must be high (usually measured in tens of Mb or higher). Decoding complexity of MDS codes increases quadratically with code length, which makes them impractical in Earth-space channels. Instead, suboptimal solutions are of interest, like interleaved RS codes [6] and Raptor codes [7]–[9], whose decoding complexity increases only linearly with code length, or LT (Luby Transform) codes [10], with the worst case $O(n \log n)$ complexity.

Possibility of increasing reliability of Earth-space links with LT codes was analyzed in [11], [12]. The authors in [12] showed that UDP transport protocol equipped with LT codes outperform TCP transfer, when applied in DVB-S systems. Recently, a novel LT-based codes are proposed in [11], specially designed for Earth-space channel. In [3] it was shown that Raptor codes could also be beneficial in blockage mitigation of Earth-space links.

The most powerful Raptor code, called RaptorQ fails to reconstruct $K$ information symbols if it successively receives any $K + O$ codeword symbols with probability close to the failure probability of a random fountain code constructed over Galois field GF(256), which is upper bounded by $1/255 \times 256^{-O}$ [8]. Thus, if a receiver collects only a few additional symbols (for example $O = 4$), the achievable decoding failure becomes negligible compared to any practically required residual target codeword loss rate. It follows that for $K \gg O$ RaptorQ code performs closely to the MDS code, which can recover a transmitted codeword (with zero failure probability) if it collects only $K$ codeword symbols. RaptorQ decoders are based on the inactivation decoding algorithm, which has a serial

S. Brkić, Z. Čiča, P. Ivaniš and Đ. Sarač are with the University of Belgrade, School of Electrical Engineering, 11000 Belgrade, Serbia (e-mails: srdjan.brkic@etf.rs, cicasyl@etf.rs, predrag.ivanis@etf.rs and sarac@etf.rs).

A. Radošević is with the Tannera LLC, 11000 Belgrade, Serbia (e-mail: andreja@tanera.io).

 ISBN 978-86-7466-930-3

structure by nature, and does not represent a very effective solution for hardware implementation. In addition, memory sizes of the largest commercially available programmable chips are not sufficient to store a single Gb long codeword of a RaptorQ code, which may be required in some high data rate Earth-space links. Splitting and decoding a codeword across multiple hardware chips can be identified as the second major drawback to consider long RaptorQ codes for practical implementation.

To resolve drawbacks of long RaptorQ codes, we propose employment of interleaved Reed-Solomon (RS) codes. Multiple independent codecs run in parallel and connected to a single (or distributed across multiple chips) interleaver/deinterleaver, resulting in a design that is free of RaptorQ's drawbacks. However, such erasure protection scheme is applicable if size of the interleaver is close to the length of the optimal MDS code with the same code rate and residual loss rate. It should be noted that the interleaved RS codes are not necessarily MDS codes for arbitrary distributed erasure channel, and therefore, their applicability needs validation. In addition, performance evaluation of inverleaved RS codes by using Monte Carlo simulation is not practical, given the large interleaver sizes.

In this paper, we analyze Earth-space channels subjected to deep fades, which cause blockage of the channel. We assume that probability density of on/off states duration is modeled by Weibull distribution. First, we numerically obtain lower bounds on the propagation latency cased by employment of MDS protection code in considered fading channel, that achieves desired residual loss rate. In addition, we propose a simulation method that enables quick and accurate performance evaluation of interleaved RS codes. With aid of designed simulator we identify interleaved RS codes that perform closely to MDS codes on Earth-space channel. Surprisingly, for majority of code rates and channel parameters extremely short RS codes (of code lengths equal to 15) will provide satisfactory latency.

The rest of the paper is organized as follows. In Section II Earth-space channel model is given. In Section III a methodology for link reliability analysis is presented, while Section IV is dedicated to numerical results. Concluding remarks are given in Section V.

## II. Earth-space channel modeling

The fade phenomenon in Earth-space links usually manifests though *fade episodes*, which are defined as time intervals in which signal attenuation due to fading exceeds a *fade threshold*. Similarly, as seen in Fig. 1, *inver-fade intervals* are complementary events, in which signal attenuation is below the fade threshold [13]. It is usually considered that fade episodes have catastrophical effect on transmission through Earth-space channel, i.e., information sent during fade episodes will be erased and will not appear at the receiver side. The information passes the communication channel only in inver-fade intervals. Possible information distortion during inver-fade intervals, due to signal strength variation and additive noise, is overcome by channel coding. If a channel code recovers all information in inver-fade intervals, recovering lost information during fade episodes is done by employing an additional packet erasure

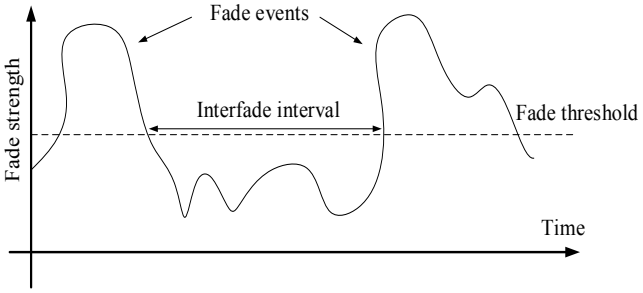


Fig. 1: Illustration of the fading model.

code. Through the paper, we will assume ideal information reconstruction during inver-fade intervals, meaning that probability of residual error after the channel coding is sufficiently low and the information reconstruction in fade episodes is not jeopardized by channel errors.

Under the aforementioned idealization, it is sufficient to describe the fading phenomenon through statistics of duration of fade episodes and inver-fade interval. Modeling such statistics, especially in Ka-band, was heavily investigated during the past years. Long-term measurements have revealed that fade episodes can be classified into two types, short-term episodes (usually less that 1 second) and long-term episodes (usually last significantly longer than 1 second), while each type has different probability density. The cause of long-term episodes is mostly rain, and average duration of long-term episodes is such that the link reliability will not benefit from deployment of packet erasure codes. Thus, will will focus only on short-term episodes, neglecting the effect of long-term fading to link reliability. We simply assume that the long-term fading is treated by some other way, for example through transmission power adaptation.

Specificity of Earth-space channel is its dependency on local climate, meaning that different points on the Earth surface will exhibit different short-term event statistics. Thus, it was proposed that in South Asia, North America and France fade episode duration is modeled with hyperexponential probability density function (PDF), while measurement in Brazil and Vancouver showed that Weibull distribution is a better fit [4]. On the contrary, measurements in Spain revealed that log-normal PDF is the most adequate to model short-term fading episodes [5]. Finally, ITU-R P.1623-1 recommends usage of the power-law distribution [13]. For the purpose of the numerical results, presented in Section IV, we will model fade episode duration as random variable following Weibull distribution. However, simulation mythology presented in Section III is invariant of the used statistical fading model.

Namely, we define the probability that a random fade duration $d_f$ is longer than some $D$, given that the attenuation $A$ exceeds a threshold $a$

$$P(d_f > D|a > A) = \exp(-(D/\lambda_f)^{k_f}),$$

where $\lambda_f$ and $k_f$, represent shape and scale parameters, respectively. Similarly, we assume that interfade duration $d_{if}$ follows the same probability low, i.e.,

$$P(d_{if} > D|a \leq A) = \exp(-(D/\lambda_{if})^{k_{if}}),$$

 ISBN 978-86-7466-930-3

where $\lambda_{if}$ and $k_{if}$, represent shape and scale parameters of the inver-fade distribution, respectively. The channel erasure probability is defined as

$$p = \frac{E[d_f]}{E[d_f] + E[d_{if}]} = \frac{T_f}{T_f + T_{nf}} = \frac{\lambda_f \Gamma(1 + 1/k_f)}{\lambda_f \Gamma(1 + 1/k_f) + \lambda_{if} \Gamma(1 + 1/k_{if})},$$

where $\Gamma(\cdot)$ represents gamma function and $E[\cdot]$ denotes expectation operator.

We further assume that $d_f$ and $d_{if}$ are mutually uncorrelated and that after each fade episode receiver performs acquisition, prolonging the start of an interfade interval by a fixed time period $T_{acq}$. The acquisition time is included in the reliability analysis presented in the following sections.

## III. Link Reliability Analysis

Given the fact that Earth-space links exhibit large propagation delay, reliability of transmission can be increased only by employing codes that can be used to recover erased information. The optimal way to recover information is to use MDS codes, which can produce the lowest residual loss rate, compared to all other codes with the same length and code rate. Alternatively, among all other codes with length $N$ an MDS code achieves desired level of residual loss rate, with the highest possible code rate $r = K/N$, where $K$ denotes information length. Namely, based on the Singleton bound, MSD code can reconstruct a codeword if no more than $N - K$ code symbols are missing. Given the fact that transmission latency is proportional to code length, MDS codes provide bounding latency vs. code rate dependency, for the given fading channel statistics. We only consider the propagation latency which is equal to $L = N/R_s$, where $R_s$ is the transmission bit rate.

Obtaining close form expression for minimal latency, assuming arbitrary fading distribution, is not feasible. Instead, we rely on simulation to provide bounding latencies for desired code rate, which are depicted in Section IV. Given the fact that average fade episode duration $T_f$ is measured in milliseconds, minimal latencies must be higher than $T_f$. In addition, as it is considered that modern Earth-space links must provide rate measured in Gbps, MDS codes must be at least tens of megabits long. Clearly, only suboptimal solutions are of practical interest, given the fact that decoding complexity of MDS codes grows quadratically with code length. A potential solution must include codes which decoding complexity is significantly lower. Here we investigate possibility of using interleaved MDS codes to provide satisfactory latency vs. code rate trade-offs. The main advantage of using interleaved MDS codes is that decoding complexity grows only linearly with the size of the interleaver (interleaver size represents code length). However, the unanswered question is how close inverleaved codes approach Singleton bound.

Consider transmission of packets with fixed size equal to $D_P$. Each packet is coded with an Reed-Solomon MDS code $(N_c, K_c)$, with length $N_c$ and code rate $r = K_c/N_c$. It is considered that binary length of the RS code $N_c \times \log_2(N_c) \ll D_P$, meaning that packets are divided and peace-by-peace coded. Before transmission codewords are passed through convolutional interleaver [14], which shuffles $I$ codewords, distancing symbols from a same codeword by at least $I/(R_s * \log_2 N_c)$ seconds, where $I$ represents the interleaver depth. At receiver side the deinterleaver restores the original bit order, while the decoder recovers the missing symbols. The propagation latency is defined as time required to fill the interleaver at the transmitter side and to empty deinterleaver at the receiver side, which based on the principe of convolution interleaving is equivalent to time needed to fill a symbol matrix of size $N_c \times I$, i.e., latency is equal to $L = \log_2(N_c) N_c I / R_s$. Given the fact that fade episodes usually corrupt multiple adjacent codewords, the packet loss rate ($PLR$) is approximately the same as codeword loss rate.

From the functional point of view the convolutional interleaver is the same as the block interleaver, which stores codewords in columns of $N_c \times I$ symbol matrix. By employing symbol-exact Monte Carlo simulations, it is straightforward to calculate the codeword loss probability of the decoder, i.e., the probability that the number of erased symbols in a any codeword is greater than $N_c - K_c$, for fixed $K_c$, $N_c$ and $I$. Symbol-exact simulator alternately generates a large number of fade and non-fade blocks, according to assigned distributions, and memorize positions that correspond to start and end of each fading block. Unrepairable codewords are identified by searching and counting fade overlaps in each block interleaver column. Reliable symbol-exact simulators are computationally hungry since, for the fixed interleaver depth $I$ and code length $N_c$, they process $10^8$ interleaving blocks or higher with sizes measured in Gb (simulation of $10^8$ interleaver blocks is needed to reliably estimate the target loss rate of $10^{-6}$). Instead, we propose Segment-Based Simulator (SBS), which divides each interleaver row into $S$ long segments, and estimates decoder failure probability assuming that codewords inside a segment are either all correctly reconstructed or all erased. This means that SBS gives an upper bound for the codeword loss rate (CWLR), for an arbitrary chosen RS codes. Inputs to the algorithm are interleaver depth measured in segments $I_{seg} = I/S$ and the number of segments that need to be simulated ($NumSegments$). We formally express SBS using algorithmic notation, as depicted in Algorithm 1.

If segment length is equal $S = 1$ symbol the SBS becomes the symbol-exact simulator. In a limiting case, for sufficiently large interleaver depth, the channel is transformed into symbol erasure channel with loss rate of

$$CWLR = \sum_{i=N_c-K_c+1} \binom{N_c}{i} P^i P^{N_c - i},$$

where $P$ represents the erasure rate of channel that includes acquisition time, i.e,

$$P = \frac{T_f + T_{acq}}{T_f + T_{nf}}.$$

As an illustration, in Fig. 2, we depict dependency of CWLR on the introduced latency, by using (15,11) RS code. With slice modification SBS can be used to determine

 ISBN 978-86-7466-930-3

**Algorithm 1:** Segment-Based Simulator

**Input:** $I_{seg}$, $NumSegments$
**Output:** $CWLR = errorCount/SegmentCount$

$SegmentCount \leftarrow 0$
$errorCount \leftarrow 0$
**while** $SegmentCount < I_{seg} \times N_c \times NumSeg$ **do**
  $X = (X_1, X_2, \ldots, X_i, \ldots, X_t), \quad t \gg 1, \quad X_i \sim Weibull(\lambda_{nf}, k_{nf})$
  $Y = (Y_1, Y_2, \ldots, Y_i, \ldots, Y_t), \quad t \gg 1, \quad Y_i \sim Weibull(\lambda_f, k_f)$
  $F = (F_1, F_2, \ldots, F_{2i}, F_{2i+1}, \ldots, F_{2t}), \quad F_j = \begin{cases} \lceil (Y_i + T_{acq}) R_s / S \rceil, & j = 2i \\ \lceil (X_i - T_{acq}) R_s / S \rceil, & j = 2i - 1 \end{cases}$
  $S_i = [a_i, b_i] : \; a_i = 1 + \sum_{j=1}^{2i-1} F_j, \; b_i = a_i + F_{2i} - 1$
  $j \leftarrow 0$
  **while** $j < \lfloor b_t / (N_c \times I_{seg}) \rfloor$ **do**
    $i \leftarrow 0$
    $j \leftarrow j + 1$
    **while** $i < I_{seg}$ **do**
      $i \leftarrow i + 1$
      $m \leftarrow i + (j-1) \times N \times I_{seg}$
      $M = \{m, m + I_{seg}, \ldots, m + (N-1) \times I_{seg}\}$
      $E = \{m_q | m_q \in M \wedge m_q \in \{S_1 \cup S_2 \ldots \cup S_n\}\}$
      **if** $|E| > N_c - K_c$ **then**
        $errorCount \leftarrow errorCount + 1$
  $TotalSegmentCount \leftarrow TotalSegmentCount + I_{seg} \times j$

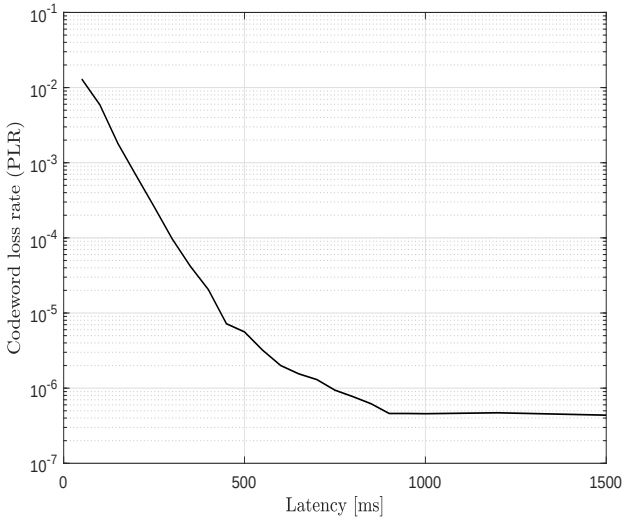


Fig. 2: $PLR$ as a function of latency for (15,11) code ($T_f = 10$ ms, $p = 0.01$ and $k_f = k_{nf} = 1$, $S = 100$ KSymbol).

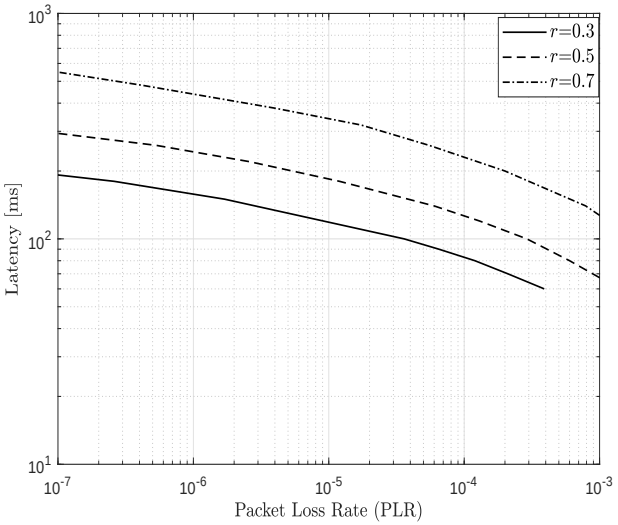


Fig. 3: Latency lower bounds for different $PLR$ values and code rates ($T_f = 10$ ms, $p = 0.01$ and $k_f = k_{nf} = 1$).

a bounding latency for MDS codes also, when code length of a code is equal to size of the interleaver.

Clearly, speed up of SBS simulator, compared to the symbol-exact Monte Carlo simulator is proportional to segment length $S$. In the following section we use $S = 100$ Ksymbol long segments, for $R_s = 10$ Gbps links to show that in SBS can adequately evaluate code performance. This means that SBS is roughly five orders of magnitude faster than symbol-exact simulator.

## IV. Numerical Results

We first, based on the methodology presented in Sections II and III, provide lower propagation latencies required to achieve desired $PLR$. In all presented results in this section we assume $D_P = 1$ Kb and $R_s = 10$ Gbps. In Fig. 3 required latency dependence of PLR is depicted, for various code rates, assuming $T_f = 10$ ms, $p = 0.01$ and $k_f = k_{nf} = 1$. For example, if $PLR = 10^{-6}$, it follows that it is not possible to construct protection code that introduces latency lower than $L = 250$ ms with code rate $r = 0.5$. If communication service requires lower

 ISBN 978-86-7466-930-3

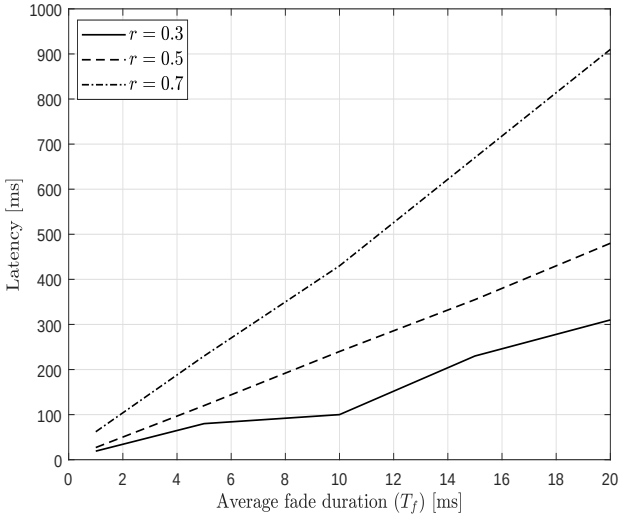


Fig. 4: Latency lower bounds as function of $T_f$ ($PLR = 10^{-6}$, $p = 0.01$ and $k_f = k_{nf} = 1$).

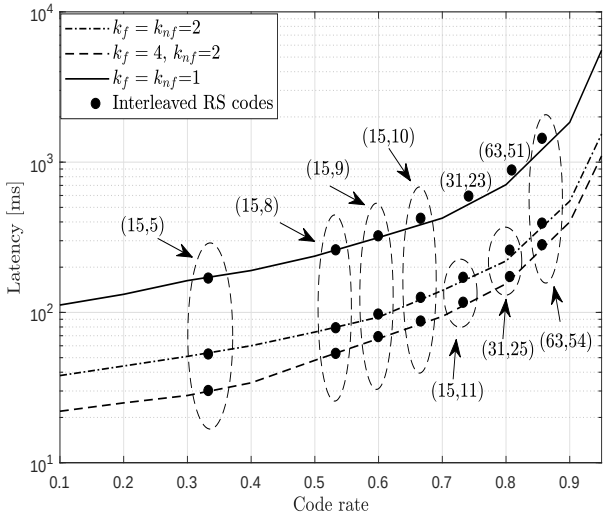


Fig. 5: Latency lower bounds as function of $T_f$ ($PLR = 10^{-6}$, $p = 0.01$ and $k_f = k_{nf} = 1$, $S = 100$ Ksymbol).

latency spatial diversity can be used. For example, voice communications cannot successfully operate with latencies above 50 ms, which means that to operate with code rate $r = 0.5$ and $PLR = 10^{-6}$, five spatially distant links need to be established. It should also be emphasized fundamental trade-off between latency and achievable code rate, i.e., it is not possible to simultaneously increase code rate and reduce bounding latency. In Fig. 4 we depict bounding latencies for different average fade episode durations. We can observe clear linear latency growth, while slope is dependent of a considered code rate.

Finally, in Fig. 5 we investigate latencies achievable with interleaved RS codes, for the fixed $PLR = 10^{-6}$. From implementation perspective RS codes should be as short as possible. We see that it is possible to perform at lower latency bound with code length $N_c = 15$ for low and medium code rates, while code lengths of $N_c = 31$ and $N_c = 63$ are sufficient to operate at low latency bound for higher code rate. As channel condition deteriorate, which is expressed through change of parameters $k_f$ and $k_{nf}$ higher code length are required. For example, for $k_f = k_{nf} = 2$ it is sufficient to use (15,11) RS code to operate at latency bound, while for $k_f = k_{nf} = 1$ at least (31,23) is needed.

## V. Conclusion

In this paper we provided a new look to the problem of reliable transmission through Earth-space channels, under deep fade phenomenon. We have shown that short RS coupled with convolutional interleaver ensure near optimal performance in terms of propagation latency, which cannot be avoided if we aim to ensure desired level of residual error loss rate. Interestingly, for large number of code rates it is sufficient to employ short RS codes, of length 15, which represents a low complexity solution.

During further research will use results in presented in this paper, to propose HST system, with increased information capacity, in which handover operations have extremely low blockage probability, which is currently an open research problem.

## Acknowledgement

This research was supported by the Science Fund of the Republic of Serbia, grant No 7750284, Hybrid Integrated Satellite and Terrestrial Access Network - hi-STAR and the Serbian Ministry of Science under project TR32028.

## References

[1] "Study on new radio (nr) to support non terrestrial networks (release 15)," *3GPP TR 38.811 v15.4.0*, 2020.

[2] M. Jia, X. Gu, Q. Guo, W. Xiang, and N. Zhang, "Broadband hybrid satellite-terrestrial communication systems based on cognitive radio toward 5G," *IEEE Wireless Commun.*, vol. 23, no. 6, p. 96–106, 2016.

[3] M. Blanco, N. Burkhardt, and C. Chen, "Coding strategies for robust link blockage mitigation in satcom," in *Proc. of IEEE Military Commun. Conf. (MILCOM)*, 2013, p. 611–616.

[4] L. E. Braten, C. Amaya, and D. V. Rogers, "Fade durations on earth-space links: Dependence on path and climatic parameters," in *Proc. of the 19th AIAA Inter. Commun. Satellite Systems Conf.*, May 2001, p. 1–7.

[5] J. M. Garcia-Rubia, J. M. Riera, P. G. del Pino, D. P. del Valle, and G. A. Siles, "Fade and interfade duration characteristics in a slant-path Ka-band link," *IEEE Trans. on Antennas and Prop.*, vol. 65, no. 12, pp. 7198–7206, Dec. 2017.

[6] J. Hamkins, "Optimal codes for the burst erasure channel," *IPN Progress Report*, pp. 42–174, Aug. 2008.

[7] A. Shokrollahi, "Raptor codes," *IEEE Trans. Inf. Theory*, vol. 52, no. 6, p. 2551–2567, 2006.

[8] A. Shokrollahi and M. Luby, "Raptor codes," *Foundations and Trends in Commun. and Inform. Theory*, vol. 6, no. 3-4, p. 213–322, 2009.

[9] M. Luby, A. Shokrollahi, M. Watson, T. Stockhammer, and L. Minder, "Raptorq forward error correction scheme for object delivery," *RFC 6330 – Proposed Standard, IETF*, 2007.

[10] M. Luby, "Lt codes," in *Proc. 43rd Annual IEEE Symp. on Foundations of Comp. Science (FOCS '02)*, 2002, p. 271–282.

[11] S. Gu, J. Jiao, Q. Zhang, and X. Gu, "Rateless coding transmission over multi-state dying erasure channel for SATCOM," *EURASIP Journal on Wireless Commun. and Networking*, no. 176, pp. 1–12, 2017.

[12] P. Cataldi, M. Gerla, and F. Zampognaro, "Rateless codes for file transfer over DVB-S," in *Proc. of IEEE Inter. Conf. on Advances in Satellite and Space Commun. (SPACOMM)*, 2009, p. 7–12.

[13] "Predicton method of fade dynamics on Earth-space paths," *Recommendatio ITU-R P.1623-1*, 2003.

[14] L. Lu, K. H. Li, and Y. L. Guan, "Blind identification of convolutional interleaver parameters," in *Proc. of 2009 7th Inter. Conf. on Inform., Commun. and Signal Processing (ICICS)*, 2009.

 ISBN 978-86-7466-930-3

# Effect of Phase Noise on Error Probability of MPSK Receiver over TWDP Channel - Simulation Study

Goran T. Djordjevic, *Member, IEEE*, Jarosław Makal, Bata Vasic and Bane Vasic, *Fellow, IEEE*

***Abstract*— The estimation of multilevel phase-shift eying ( P ) signal phase is adversely affected by the number of factors appearing in transmission channel and related to the receiver. The imperfect reference signal phase estimation causes error probability degradations. The higher the value of frequency, the stronger is the effect of imperfect reference signal phase recovery. The aim of this wor is to study the effect of imperfect phase estimation on error probability when signal propagates through a channel where there are two dominant components and a diffuse component, which could be the model for mmWave range. The Two-Wave Diffuse-Power (TWDP) model can accurately characterize this propagation environment. We develop a simulation model to estimate the error floor value and to identify the range of signal power when floor appears. ur simulation results give direct dependence of error rate value on channel parameters, signal power and standard deviation of phase noise. The aim of the paper is not to present the concrete estimator architecture, but to ma e a further step in studying the effect of a certain phase noise on bit error rate performance.**

***Index Terms*— rror probability, fading channel, phase noise, onte Carlo simulations.**

## I. INTRODUCTION

DURING the signal propagation through a wireless telecommunication channel, random changes of the signal parameters occur at the detection point. The signal level is no longer constant, but changes randomly, and the signal phase is a random process. These changes in signal level and phase have a significant impact on the quality of information transmission through that channel. Depending on the weather conditions and the type of the propagation environment including the receiver surrounding, different models have been developed to describe variations in signal intensity [1].

To describe multipath fading, different models of this fading have been proposed, such as Rayleigh, Rice, Nakagami-*m*, Nakagami- , etc. [1]. In the case when two direct waves reach the receiver, but there is also the diffuse component of the emitted EM wave, the so-called Two-Way Diffuse-Power (TWDP) model of fading was proposed in [2]. In that paper in which the TWDP model was initially suggested, an approximation was proposed for the probability density function (PDF) of the signal envelope variations. This model of fading has been constantly the subject of study by many researchers [3]-[9]. In [3], Kim *at all* emphasized some shortcomings of approximation from [2], and they presented exact and approximate formulae for bit error rate in detecting binary phase-shift keying (BPSK) signal transmitted over a TWDP channel for large values of average signal-to-noise ratios (SNR). In [4] and [5], the authors derived some novel expressions for system performance metrics and derived interesting result showing that TWDP fading model has closed form moment generation function (MGF) of received signal envelope. The authors of [6] presented a novel way of parametrization of TWDP channel model. Generally, characterization of TWDP model is in tight relation with propagation environment where there are useful signal, co-channel interference and additive white Gaussian noise [10].

Recently it has been shown experimentally that this model of fading is just appropriate for describing signal propagation in the 60 GHz range [7]-[9].

In all those papers, it is implicitly assumed that the estimation of the phase of the received signal is ideal. However, it is well known that there is a difference between the phase of the incoming signal and the signal phase at the phase estimator output. This difference is a random process that affects signal detection. Due to the existence of this difference, the performance of the system deteriorates. The influence of this phase noise on the error probability when multipath fading is modeled by Nakagami-*m* distribution was considered in [11], while the effect of imperfect reference signal extraction on the error probability over a shadowed multipath fading was analyzed in [12]. In both papers, it was illustrated that error performance of a system can be strongly influenced by imperfect reference signal recovery. With the transition to higher frequency ranges, the influence of the phase noise becomes more pronounced. To the best of our knowledge, the impact of the phase noise on coherent detection in TWDP channel has not been considered so far. However, there is a significant difference between propagation environment considered in [11], [12], where one dominant direct component exist, compared with a TWDP channel model where two dominant waves exist. Our aim in this paper is not to deal with a concrete architecture of phase estimator, but to make a further step in studying the performance of TWDP coherent systems. We suppose the

Goran T. Djordjevic and Bata Vasic are with Faculty of Electronic Engineering, University of Nis, 14 A. Medevedeva, 18000 Nis, Serbia (e-mail: goran@elfak.ni.ac.rs; bata.vasic@elfak.ni.ac.rs)

Jarosław Makal is with Faculty of Electrical Engineering, Białystok University of Technology, Wiejska 45D street, 15-351 Białystok, Poland (e-mail: j.makal@pb.edu.pl).

Bane Vasic is with the Department of Electrical & Computer Engineering, University of Arizona, 1230 E. Speedway Blvd. P.O. Box 210104, Tucson, AZ 85721-0104, USA, (e-mail: vasic@ece.arizona.edu).

 ISBN 978-86-7466-930-3

phase error in the receiver has widely accepted Tikhonov distribution and determine the influence of the phase noise on the bit error rate (BER) performance of the receiver of multilevel phase-shift keying (MPSK) signals transmitted over a TWDP channel. We develop appropriate simulation model and present some Monte Carlo simulations results illustrating the effect of phase noise on the BER performance in detection of MPSK signals. These results obtained under assumption of the presence of phase noise can be compared with the results previously reported in [2]-[6], where the perfect reference signal estimation was considered. The design of phase estimator over a TWDP channel will stay an open problem, but relation between BER, channel parameters and standard deviation of phase noise will be a useful standpoint in design of an estimator.

## II. System model

In this Section, we describe briefly the model of the system considered here. We give basic information about modulation/demodulation process, as well as channel characteristics.

At the transmitter, signal is modulated by performing multilevel phase-shift keying. During the duration of one symbol, the modulator output signal has the form $s = Ae^{j\phi_n}$, where

$$\phi_n \in \left[0, 2\pi/M, ..., 2(M-1)\pi/M\right], \quad (1)$$

where $M$ is the number of phase levels.

This signal is transmitted over a wireless channel. During signal transmission, many copies of the transmitted EM wave excite the receiver antenna. The resulting signal envelope consists of specular and diffuse parts. Specular part contains two direct components having constant amplitudes and uniformly distributed phases in the interval from 0 to 2π. The amplitudes of the direct components are denoted by $_1$ and $_2$, while the phases of these components are denoted by $\psi_1$ and $\psi_2$. The scattering component has Rayleigh distribution, i.e., it consist of the in-phase and quadrature components having Gaussian distribution with zero mean value and standard deviation denoted by $\sigma_F$. These in-phase and quadrature components are denoted by $_F$ and $y_F$, respectively. The resulting received signal envelope is presented as [2]

$$r = {}_1 e^{j\psi_1} + {}_2 e^{j\psi_2} + {}_F + jy_F . \quad (2)$$

This model of fading can be described in terms of two parameters denoted by and Δ. The parameter denotes the power of the specular components-to-power of the diffuse component. The parameter Δ is related to the ratio of the peak specular components power-to-average specular components power. These two parameters are defined as [2]

$$= \left( {}_1^2 + {}_2^2 \right) \Big/ \left( 2\sigma_F{}^2 \right), \quad (3)$$

$$\Delta = \frac{\text{Peak Specular Power}}{\text{Average Specular Power}} - 1 = \frac{2\ {}_1\ {}_2}{{}_1^2 + {}_2^2} . \quad (4)$$

The largest the value of the parameter , the power of the specular components is larger compared with the power of the diffuse component. In other words, fading is shallower. The typical values of parameter for the terrestrial mobile links are in the range from 0 dB to 15 dB. The values of parameter Δ lie in the range from 0 to 1. When Δ is equal to 1, specular components have the equal amplitudes, while when Δ is equal to zero either specular components amplitude is equal to zero.

It is interesting to note that the current envelope values of the signal propagating through the channel cannot be described using PDF in closed form. One approximation of the PDF was proposed in [2], while a PDF in infinite series form was recently proposed [6]. On the other hand, although there is no exact closed-form solution for PDF, there is a closed-form MGF format for this channel [4], [5]. However, for Monte Carlo simulations, the most important is eq. (2) defining the composite fading signal envelope.

After signal transmission over a TWDP channel, the receiver input signal can be presented as

$$y = re^{j(\phi_n + \psi)} + n , \quad (5)$$

where $\psi$ denotes signal phase due to multipath propagation, and $n$ denotes the thermal noise. This thermal noise can be described by Gaussian PDF with zero mean value and standard deviation σ.

In the case of BPSK, the signal in the receiver has the form

$$= \pm r\cos(\varphi) + \quad , \quad (6)$$

depending upon "1" or "0" is transmitted. In the case of MPSK, the signal in the upper and down branch of the receiver [13, p. 361] is given, respectively, by

$$_u = r\cos(\phi_n + \varphi) + \quad , \quad _d = r\sin(\phi_n + \varphi) + y . \quad (7)$$

In the previous equations, $r$ denotes the signal envelope defined by (2), $\phi_n$ denotes the modulated signal phase, $\varphi$ denotes the phase noise, while and $y$ are the in-phase and quadrature thermal noise components over a channel. The signal detection is performed based on the value of the angle $\gamma_d$ that is defined by $\tan\gamma_d = {}_d / {}_g$.

On the contrast to previous papers considering signal transmission over TWDP channel, in our paper the emphasis is on the imperfect reference signal recovery. Actually, the estimation of the received signal phase is not just perfect and there is a difference between received signal phase and estimated signal phase performed by an estimator. This difference is a random process. The values of this process are denoted by $\varphi$. In [14], it was shown that in the case when there is a signal and additive noise at the receiver input, then the phase difference has a Tikhonov distribution. Also, it has been shown that when a useful signal is influenced by fading in such a way that there is one regular component, the Tikhonov distribution is a satisfactory model for the phase error. However, in the case where there is a modulated signal with two regular components (TWDP channel), the phase estimation process is more complicated. The design of the phase estimator itself is beyond the scope of this paper. In the first, rough step, we will consider that the phase estimation is not ideal and that the phase difference has a rough approximation of the Tikhonov distribution. We will establish a connection between the standard deviation of phase noise, channel parameters and signal power. However, the question

 ISBN 978-86-7466-930-3

remains as to how the standard deviation of the phase error is related to the receiver and fading parameters.

The random variable having uniform distribution can be generated according to the algorithm presented in [15, p. 340], and random variable having Gaussian distribution can be generated using Box-Muller method [16, p. 383]. The random values of the signal envelope are generated taking into account eq. (1). The random variables having Tikhonov distribution can be generated by applying the Modified acceptance/rejection method [16, p. 382].

## III. Numerical Results

In this Section, we present simulation results and give appropriate comments. The simulation results are obtained by Monte Carlo simulations performed in C++. The maximum number of generated samples for estimating a value of BER is $2\times10^9$. The methods utilized for generation of samples are described in the previous Section.

Fig. 1 illustrates the dependence of the BER on the average signal-to-noise power ratio (SNR), $\gamma_b$. The BER decreases with increasing SNR. However, this decrease in the BER is not uniform in the whole range of SNRs, but is expressed for low and moderate values of SNRs. In the range of high values of the SNR, the BER value does not decrease with increasing SNR. In other words, the BER tends to a constant value called the error floor. The appearance of this floor is a direct consequence of the presence of phase noise, i.e., non-ideal extraction of the reference carrier. The value of the floor depends on the standard deviation of the phase noise. The higher the standard deviation of the phase noise, the lower the value of the floor. This value of the floor cannot be reduced by increasing the signal power, but it can only be influenced by the correct design of the part of the system in which the phase of the received signal is estimated.

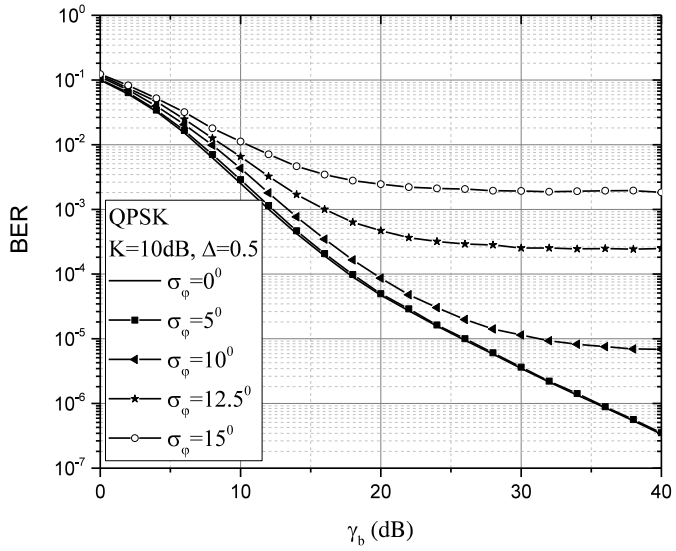


Fig. 1. BER performance for different values of standard deviation of phase noise.

Fig. 2 shows the influence of the standard deviation of the phase noise on the BER values in the detection of BPSK and QPSK signals. Firstly, it is obvious that BER values increase with increasing standard deviation values. Secondly, with the QPSK format, the BER value remains unchanged in the range of standard deviation values up to 8 degrees, while the BPSK format is insensitive to changing the standard deviation up to 16 degrees. In other words, the BPSK format is more resistant to the influence of the phase noise. This result is also logical because the areas of decision-making in the BPSK format are wider, so that the phase noise has less possibility to move the point from one area of decision-making to another.

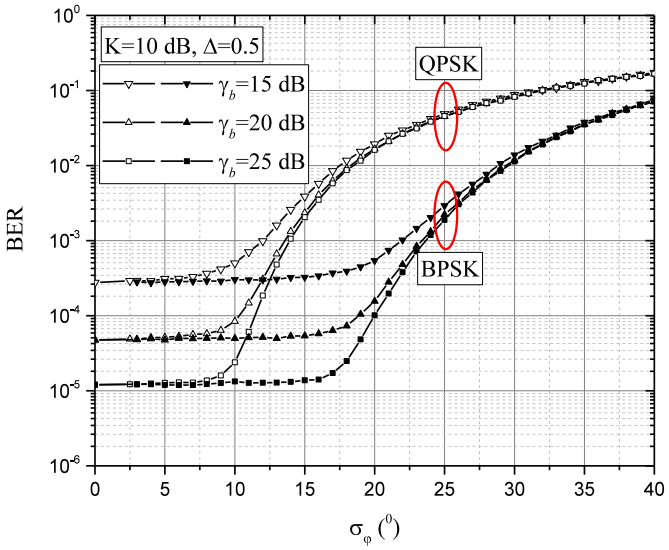


Fig. 2. BER performance for BPSK and QPSK modulation formats.

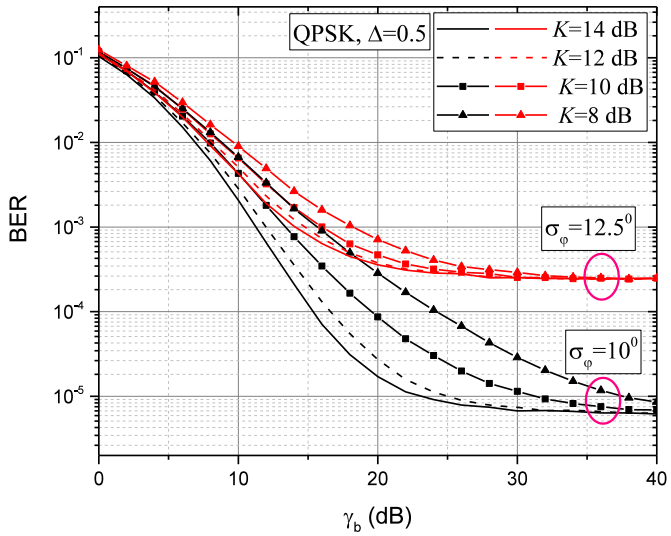


Fig. 3. BER performance for different values of fading parameter .

The influence of the ratio of the average powers of the direct and scattered part of the resulting signal (parameter ) is shown in Fig. 3. The influence of the parameter on the BER value is pronounced in the range of moderate values of the SNR and in the case when the standard deviation of the phase noise is smaller. In the region of large values of the SNR, BER tends to a constant value regardless of the value of the parameter . This parameter has no effect on the value of the BER floor. In addition, when the value of the standard deviation is higher, then the influence of the phase noise is


ISBN 978-86-7466-930-3

more pronounced, so the influence of the parameter is non-dominant.

Similar conclusions as in the previous case can be drawn regarding the influence of the parameter Δ on the BER value. Namely, the parameter Δ also has a significant effect on the BER values in the middle range of the SNR, while there is no effect on the BER values when the signal power is high, i.e., when the BER floor is reached. Also, when the standard deviation of the phase noise is larger, i.e., when the influence of non-ideal extraction is dominant, BER values are less sensitive to changes in parameter Δ compared to the case when the extraction of the reference signal phase is more precise.

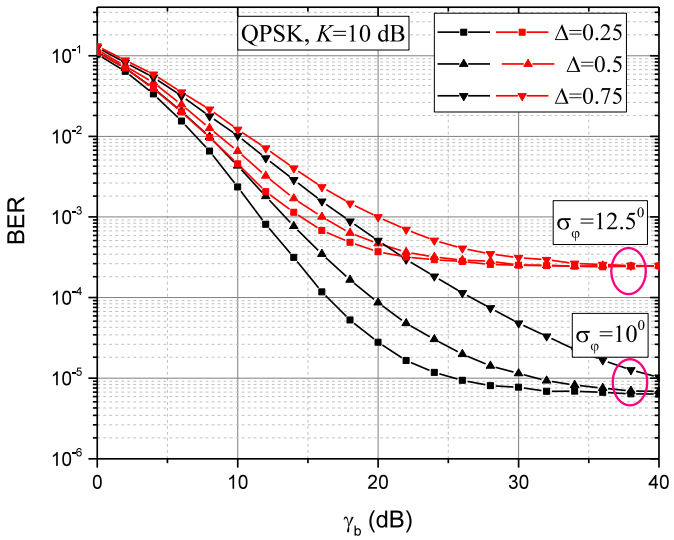


Fig. 4. BER performance for different values of fading parameterΔ.

## IV. Conclusion

We have analyzed the influence of non-ideal extraction of the reference carrier on the BER performance of the receiver of MPSK signals propagating through a channel in which variations in signal levels are characterized using the TWDP model. It can be concluded that imperfect estimation of the phase of the incoming signal causes the appearance of BER floor. The value of this BER floor can be reduced by decreasing the value of the standard deviation of the phase noise, i.e., by improving the received signal phase estimation. The influence of the parameters and Δ is pronounced in the range of moderate SNR values. In addition, the results have shown that for typical values of the channel parameters, BPSK modulation format is resistant to phase noise up to the standard deviation value of 16 degrees, while in the same environment QPSK format is resistant to this phenomenon only up to the standard deviation value up to 8 degrees. The design of the phase estimator should be performed so that the predetermined value of the standard deviation of the phase noise is not exceeded.

The results obtained here should be considered as the most optimistic when there is a phase error. The problems of loop locking and phase skipping in the channel with TWDP fading remain open, as well as the connection between the standard deviation of the phase noise and the estimator parameters. Incorporation of some innovative phase noise mitigation techniques, like Viterbi-Viterbi noise estimator under given channel scenario also remains an open problem.

## Acknowledgment

This work is partially supported by The Polish National Agency for Academic Exchange (NAWA) under grant No. PPN/ULM/2020/1/00256/DEC/1, and partially supported by the Science Fund of the Republic of Serbia, grant No. 7750284, *ybrid Integrated Satellite and Terrestrial Access Network - hi-STA* , as well as by Ministry of Education, Science and Technological Development of the Republic of Serbia.

## References

[1] M. K. Simon, M.-S. Alouini, *igital communications o er fading channels*, 2nd ed, Wiley-IEEE Press, 2004.

[2] G. D. Durgin, T. S. Rappaport, D. A. De Wolf, "New analytical models and probability density functions for fading in wireless communications," *IEEE Transactions on Communications*, vol. 50, no. 6, pp. 1005-1015, 2002.

[3] D. Kim, H. Lee, J. Kang, "Comprehensive analysis of the impact of TWDP fading on the achievable error rate performance of BPSK signaling," *IEICE Transactions on Communications*, vol. 101-B, pp. 500-507, 2018.

[4] M. Rao, F. J. Lopez-Martinez, A. Goldsmith, "Statistics and system performance metrics for the two wave diffuse power fading model," 2014 48th Annual Conference on Information Sciences and Systems (CISS), pp. 1-6, Princeton, NJ, USA March 2014.

[5] M. Rao, F. J. Lopez-Martinez, M. –S.Alouini, A. Goldsmith, "MGF approach to the analysis of generalized two-ray fading models," *IEEE Transactions on Wireless Communications*, Vol. 14, no. 5, pp. 2548 – 2561, May 2015.no.

[6] A. Maric, E. Kaljic, P. Njemcevic, "An alternative statistical characterization of TWDP fading model," *Sensors*, vol. 21, no. 22, pp. 1-15, 2021.

[7] T. Mavridis, L. Petrillo, J. Sarrazin, A. Benlarbi-Delai, P. De Doncker, "Near-body shadowing analysis at 60 GHz," *IEEE Transactions on Antennas and Propagation*, vol 63, no. 15, pp. 4505 – 4511, 2015.

[8] D. Kim, H. Lee, J. Kang, "Comments on "Near-body shadowing analysis at 60 GHz," *IEEE Transactions on Antennas and Propagation*, vol. 65, no. 6, pp. 3314, 2017.

[9] E. Zochmann, S. Caban, C. F. Mecklenbrauker, S. Pratschner, M. Lerch, S. Schwarts, M. Rupp, "Better than Rician: modelling millimeter wave channels as two-wave with diffuse power," EURASIP Journal on Wireless Communications and Networking, https://doi.org/10.1186/s13638-018-1336-6, pp. 1-17, 2019.

[10] I. M. Kostic, "Envelope probability distribution of the sum of signal, noise and interference", *Telecommunication Forum TE F* , pp. 301-303, Belgrade, Serbia, 1996.

[11] I. M. Kostic, "Average SEP for M-ary CPSK with noisy phase reference in Nakagami fading and Gaussian noise", *European Transactions on Telecommunications*, vol. 18, no. 2, pp. 109-113, 2007.

[12] J. Anastasov, Z. Marjanovic, D. Milic, G. T. Djordjevic, "Average BER and noisy reference loss of partially coherent PSK demodulation over shadowed multipath fading channel," *IEEE Transactions on ehicular Technology*, vol. 67, no. 8, pp. 7831 – 7835, August 2018.

[13] S. Haykin, *igital communications systems*, John Wiley & Sons, Inc., NJ, USA, 2014.

[14] W. Weber, "Performance of Phase-Locked Loops in the Presence of Fading Communication Channels", *IEEE Transactions on Communications*, vol. 24, no. 5, pp. 487 – 499, 1976

[15] W. Press, S. A. Teukolsky, W. T. Vetterling, B. P. Flannery, *Numerical recipes, 3rd ed.,* Cambridge University Press, NY, USA, 2007.

[16] M. Jeruchim, P. Balaban, K. S. Shanmugan, *Simulation of communication systems modeling, methodology and techni ues, 2nd ed.*,Springer, 2000.

 ISBN 978-86-7466-930-3

# Initial Development of a Program for Drone Micro-Doppler Signature Modelling

Jovan Radivojević, Predrag Petrović, Aleksandar Lebl, Mladen Mileusnić

***Abstract*—Micro-Doppler signature spectrograms obtained by FMCW radars are powerful method for malicious drones detection, identification, localization and classification. Our aim in this investigation has been to replace the base of spectrograms recorded on polygons using high number of available drone types by the spectrograms obtained by the application of originally developed program. Initial program development and verification are described in the paper. It is presented how the calculated spectrograms may be used to determine the important parameters of drones' flight and construction: number of blades in a rotor, rotors' angular rotation rate and blades' length which is the first step in a decision about an applied drone type. The presented results are the starting report on our important development devoted to the improvement of overall public safety.**

***Index Terms*—Malicious drone identification; micro-Doppler signature spectrograms; drone hovering; program for drone spectrograms modelling.**

## I. Introduction

DRONES or unmanned aerial vehicles (UAVs) implementation brings great benefits in everyday life by replacing human activities in many areas. Drones may perform some important actions more precisely, more promptly than humans and without people risk exposure. But, on contrary, drones may often be the cause of sudden and unexpected danger for human lives and/or the whole world economy [1], [2].

There are solutions based on several sensor types which may be applied to malicious drones' detection, identification, localization and classification (DILC). The most often applied sensors are radars, cameras (optical and infra-red), audio and radio-frequency (RF) sensors. The benefits and drawbacks of each sensor type application are emphasized in [3], [4]. The applied solutions are usually based on several (even three or four) different sensor types [5], [6]. Among the sensors, radar is especially important due to its relative independence or very low dependence on weather and lighting conditions as fog, rain, smoke or darkness [7]. The present solutions are based on two radar types implementation: Frequency Modulated Constant Wave (FMCW radar whose principles of operation are explained in [8]) and Forward Scatter Radar (FSR whose principles of operation are explained in [9]). Drone spectrograms which are obtained by FMCW and FSR radars are especially important for applied drones identification and classification. They are analyzed in a significant number of existing solutions and [10], [11] are just two examples. In the case of FMCW radar, the obtained spectrograms follow from the Doppler effect of drone parts micro motion to the transmitted radar signal. We speak about drones micro-Doppler signatures, i.e. the obtained graphs are specific for each type of drones [12]. In practical situations the special problem is to distinguish drones from other flying objects with similar dimensions (e.g. birds) whose spectrograms may be similar to drone spectrograms [13].

Drones DILC using spectrograms supposes collecting a great number of practical records on the significant number of different drone types. The records have to be made when drones are at different heights, at different distance from radar (meaning at different elevation angles), when they are hovering or when they are flying, when there are more drones present in the same time (drone swarms) and so on. Besides, the spectrograms appearance depends on some specific drones characteristics as the number of drone's rotors, number of blades on each rotor, the length of blades and the rotors' rotation rate (in rounds per minute – RPM or in rounds per second – RPS). So, it is necessary to have different drone types and to make many spectrograms for each type under different conditions. Due to these problems it is important to develop the program which allows spectrograms calculation and presentation (without practical scenarios recording), especially in the initial phases when DILC criteria have to be defined [7], [11], [14].

IRITEL has a great experience in the development, modernization and implementation of radar systems, development of software for radar systems receivers and simulators of radar operation. The contribution [15] has two-fold relation to the solution presented in this paper: as a realized simulator and as it considers radars with Doppler Effect. Micro-Doppler signatures are formed on the base of the received radar signal and IRITEL has developed both simulators of radar signal receivers [16], [17] and practical solutions of these receivers [18], [19]. The control of radar receivers is the subject of contributions [20], [21]. A good-quality generated signal is also important for FMCW radar operation and IRITEL's solutions in this area have an international verification [22], [23]. IRITEL's complete radar systems in the area of AESA radars [24], [25] and in the area of existing radars modernization [26] - [28] are additional guarantee for future successful practical implementation of solution from this paper.

The main theoretical aspects of FMCW radar operation are explained in the Section II. This explanation includes the method how spectrograms are calculated. The block-scheme of the developed program for spectrograms calculation is

Jovan Radivojević is with IRITEL a.d., Batajnički put 23, 11080 Belgrade, Serbia (e-mail: jovan.radivojevic@iritel.com).

Predrag Petrović is with IRITEL a.d., Batajnički put 23, 11080 Belgrade, Serbia (e-mail: presa@iritel.com).

Aleksandar Lebl is with IRITEL a.d., Batajnički put 23, 11080 Belgrade, Serbia (e-mail: lebl@iritel.com).

Mladen Mileusnić is with IRITEL a.d., Batajnički put 23, 11080 Belgrade, Serbia (e-mail: mladenmi@iritel.com).

 ISBN 978-86-7466-930-3

presented in the Section III. Several calculated spectrograms are presented in the Section IV. The suggested method to determine characteristic parameters of drone flight and drone construction is described in the Section V. At the end, the conclusions are in the Section VI.

## II. SPECTROGRAM SIGNAL CALCULATION

The signal generated in FMCW radar is sinusoidal and its frequency is linearly variable as a function of time. The drone spectrograms are obtained on the base of the returned echo signal from the moving rotor blades. The echo signal from all blades forming one rotor may be expressed by [29]:

$$S_{\Sigma}(t) = \sum_{k=0}^{N_b-1} s_{lk}(t) = \\ = L \cdot \exp\left(-j\frac{4\cdot\pi}{\lambda}\cdot\left(R_0 + z_0\cdot\sin\beta\right)\right)\cdot \\ \cdot\sum_{k=0}^{N_b-1}\sin c\left(\Phi_k(t)\right)\cdot\exp\left(-j\cdot\Phi_k(t)\right) \quad (1)$$

where it is $\mathrm{sinc}(\Phi_k(t)) = \sin(\Phi_k(t))/(\Phi_k(t))$ and

$$\Phi_k(t) = \frac{4\cdot\pi}{\lambda}\cdot\frac{L}{2}\cdot\cos\beta\cdot \\ \cdot\cos\left(\Omega\cdot t + \varphi_0 + \frac{2\cdot\pi\cdot k}{N_b}\right)\ \ (k=0,1,2,...N_b\text{-}1). \quad (2)$$

The sign may be + or – before $\Omega\cdot t$, depending on the direction of the rotor rotation for each unique rotor.

The meaning of variables in these two equations may be expressed with the reference to the Fig. 1:

- $L$ – the length of each blade;
- $N_b$ – number of blades in each rotor (two possibilities are presented separately: rotors with two or three blades);
- $R_0$ - distance between the radar and the drone rotor (approximately the same as between radar and drone);
- $z_0$ – drone height;
- $\beta$ – drone elevation angle;
- $\Omega$ – rotor angular rotation rate;
- $\lambda$ – radar signal wavelength;
- $\varphi_0$ – rotor starting rotation angle.

The returned signal from all drone rotors is:

$$S_{\Sigma}(t) = \sum_{i=1}^{N_r}\sum_{k=0}^{N_b-1} s_{lk}(t) = \\ = \sum_{i=1}^{N_r} L\cdot\exp\left(-j\frac{4\cdot\pi}{\lambda}\cdot\left(R_{0i} + z_{0i}\cdot\sin\beta_i\right)\right)\cdot \\ \cdot\sum_{k=0}^{N_b-1}\sin c\left(\Phi_{ik}(t)\right)\cdot\exp\left(-j\cdot\Phi_{ik}(t)\right) \quad (3)$$

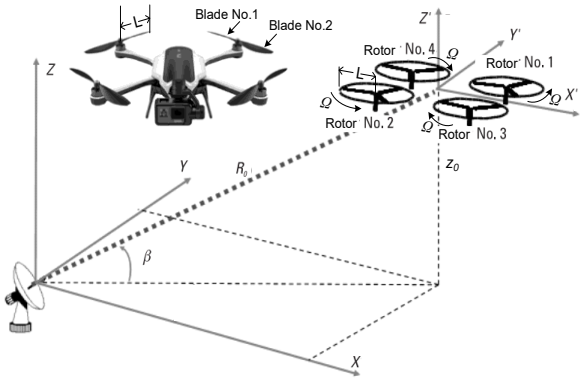


Fig. 1. Parameters included in drone spectrograms calculation

where it is:

$$\Phi_{ik}(t) = \frac{4\cdot\pi}{\lambda}\cdot\frac{L}{2}\cdot\cos\beta_i\cdot \\ \cdot\cos\left(\Omega_i\cdot t + \varphi_{0i} + \frac{2\cdot\pi\cdot k}{N_b}\right)\ \ (k=0,1,2,...N_b\text{-}1) \quad (4)$$

and

- $N_r$ - the number of rotors on the drone.

In general case, all rotors have their own specific angular rotation rate $\Omega_i$. The difference in rates may be even more than 2:1 when drone is flying left or right [30]. In our analysis in this paper we consider that drone is hovering. Thus we suppose that all rotors have the same $\Omega_i$. The range of $\Omega_i$ values may be estimated on the base of graphs from [31] which present drone performances when rotors angular rotation rate changes in the range 1400-8600 RPM, or, approximately, 20-150 RPS. The direction of rotors rotation is standardized to allow stable flight. In the case of drone with four rotors (quadcopter) two opposite rotors rotate in the clockwise direction and to other opposite rotors rotate in counter clockwise direction [32]. The length of blades when quadcopters or hexacopters are applied varies in the range between 11.9cm and 38.1cm according to some available literature [11], [13], [33]-[36]. The heights $z_{0i}$ for all rotors are also the same as we may assume that drone is always positioned parallel to the ground. The assumption of all $R_{0i}$ values equality is not quite valid. It would be necessary to precisely involve distances between rotor centres to determine exact values of $R_{0i}$. Nevertheless, we shall also suppose that there is no difference between $R_{0i}$s without important loss of generality. The elevation angles $\beta_{0i}$ for all rotors are also practically the same and they are calculated as the ratio of $z_{0i}$ and $R_{0i}$. Our investigation has been performed for FMCW radar operating at 24GHz, i.e. $\lambda$=12.5mm. The most often applied drones have not more than four rotors (quadcopters), but still exist drones with six (hexacopter) or eight (octocopter) rotors [37].

The standard procedure to calculate spectrogram includes calculation of Short Time Fourier Transform (*STFT*) of the considered signal according to the equation [38]:

$$STFT\left(S_n(m,\omega)\right) = \sum_{n=-\infty}^{\infty} S_n\cdot w_{n-m}\cdot\exp\left(-j\cdot\omega\cdot t_n\right) \quad (5)$$

where $w_n$ is the Hanning window defined by [39]:

$$w_n = \frac{1}{2}\cdot\left(1-\cos\frac{2\cdot\pi\cdot n}{N}\right)\ \ (n=0,1,2...N) \quad (6)$$

## III. PROGRAM STRUCTURE SHORT PRESENTATION

The block-diagram of the program for spectrogram calculation is presented in the Fig. 2.

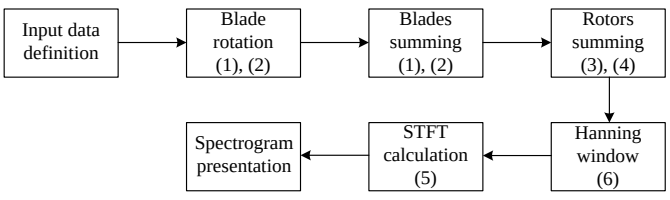


Fig. 2. Block-diagram of the program for spectrogram calculation

The first step in the program flow is to define input data: parameters of drone position towards radar, drone construction and operation, radar signal characteristics and the characteristics of desired spectrogram presentation. The parameters of drone position are its elevation angle ($\beta$), its

 ISBN 978-86-7466-930-3

height over ground ($z_0$) and distance between radar and drone ($R_0$). The drone construction parameters are the number of drone rotors ($N_r$), number of blades in each rotor ($N_b$) and the length of blades ($L$). Drone operation parameter is its rotors' angular rate ($\Omega$) and direction of rotors rotation (clockwise or counter clockwise). Radar operational frequency ($f_r$) is the characteristic of radar signal. The characteristic parameters for spectrogram calculation and presentation are time step for spectrogram calculation ($t_{step}$) and time step for spectrogram display ($t_{disp}$).

The first step in calculation realization is related to each blade rotation. The calculation procedure follows the equations (1) and (2) in this step. The following step is to sum the echo signals from all single blades forming one rotor. This summing is also the part of equations (1) and (2). The third step in calculation process is to sum all echo signals from drone rotors, according to equation (3) and (4). The final step is related to spectrogram calculation using *STFT* according to the equation (5). Before *STFT* calculation, echo signal is modelled applying Hanning window signal according to the equation (6).

The output result of our calculation is the spectrogram presentation. A new spectrogram is obtained for each selected combination of input data parameters according to their defined values from ranges specified in the previous Section II. This is our initial investigation and this program version is realized in Excel. Some of input parameters could not be selected in the whole specified range according to the data from the Section II. There are three such parameters: the number of rotors is limited to 4 (thus covering the great majority of applied drones), the blade length is limited to 25.4cm (the most drones do not have longer blades according to the presented examples from literature) and the rotor angular rate is limited to about 40 RPS (its usual value is in the range 30-40 RPS [11], [40]).

## IV. The Results of Calculation

Figures 3-12 present micro-Doppler signature graphs obtained by the implementation of our program. In all these cases it is considered that a drone has four rotors ($N_r$=4) and that it is positioned at a distance $R_0$=100m. The parameters which are varied are: 1) the number of blades constituting each rotor ($N_b$=3 in the figures 4, 5, 6, 7 and 9, $N_b$=2 in the remaining figures); 2) the length of blades ($L$=0.12m in the Fig. 5, $L$=0.18m in the Fig. 6, $L$=0.24m in remaining figures); 3) rotor angular rotation rate ($\Omega$=20RPS in the figures 9 and 10, $\Omega$=40RPS in the figures 7 and 8, $\Omega$=30RPS in the remaining figures) and 4) the elevation angle i.e. the drone height over the ground ($z_0$=77m in the Fig. 11, $z_0$=94.8m in the Fig. 12, $z_0$=30m in the remaining figures). The frequency division 0-200Hz on the vertical axis of spectrograms is not the absolute value of Doppler shift for the applied 24GHz radar. It is a consequence of frequency bandwidth compression when STFT is calculated and it approximately corresponds to the compression factor 20.

The legends on the right side of figures 3-12 present the signal level (in dB) at the corresponding figure. The frequency components with the higher level in the range between -20dB and +10dB (which are presented in the brown, red and orange colour) are important for the spectrogram analysis. The other components are of lower or significantly lower level and are not important for consideration. The transition between the part of the graph with the higher frequencies level and the part of the frequencies with the low signal level (lower than -40dB which is presented by turquoise, blue and pink colour) is on all graphs rather sharp. The bandwidth of the area in brown, red and orange colour depends on the value of some parameters for which the graphs are calculated.

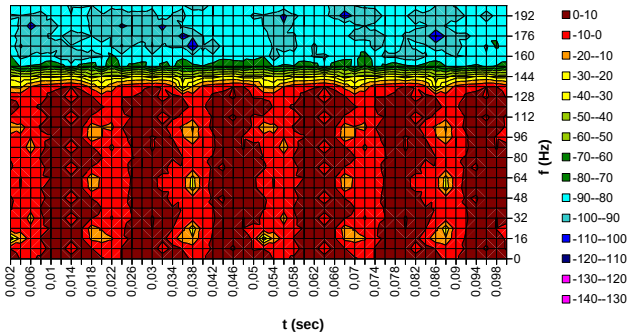


Fig. 3. Micro-Doppler signature of a drone with $N_r$=4, $N_b$=2, $L$=0.24m, $R_0$=100m, $z_0$=30m, $\Omega$=30RPS

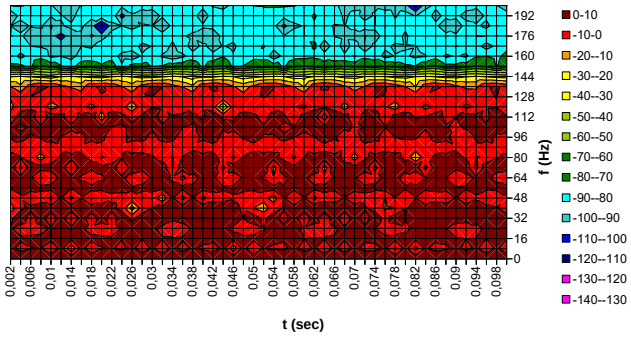


Fig. 4. Micro-Doppler signature of a drone with $N_r$=4, $N_b$=3, $L$=0.24m, $R_0$=100m, $z_0$=30m, $\Omega$=30RPS

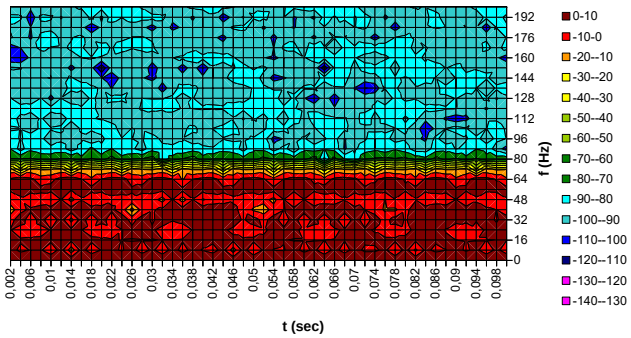


Fig. 5. Micro-Doppler signature of a drone with $N_r$=4, $N_b$=3, $L$=0.12m, $R_0$=100m, $z_0$=30m, $\Omega$=30RPS

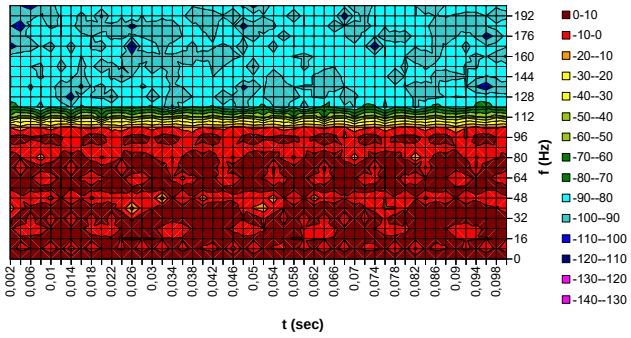


Fig. 6. Micro-Doppler signature of a drone with $N_r$=4, $N_b$=3, $L$=0.18m, $R_0$=100m, $z_0$=30m, $\Omega$=30RPS


ISBN 978-86-7466-930-3

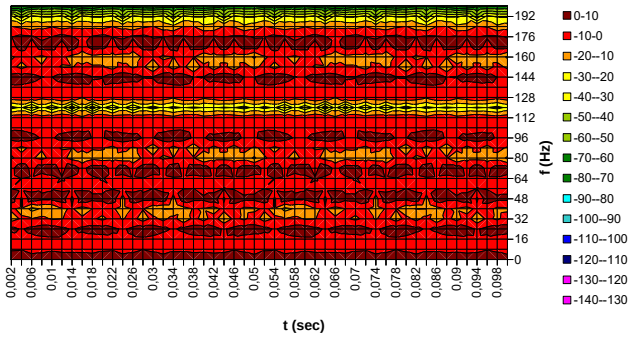


Fig. 7. Micro-Doppler signature of a drone with $N_r$=4, $N_b$=3, $L$=0.24m, $R_0$=100m, $z_0$=30m, $\Omega$=40RPS

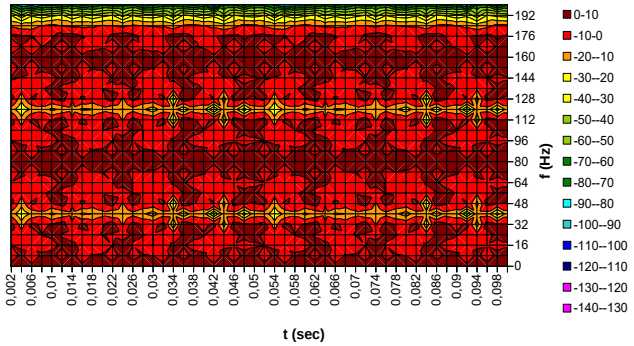


Fig. 8. Micro-Doppler signature of a drone with $N_r$=4, $N_b$=2, $L$=0.24m, $R_0$=100m, $z_0$=30m, $\Omega$=40RPS

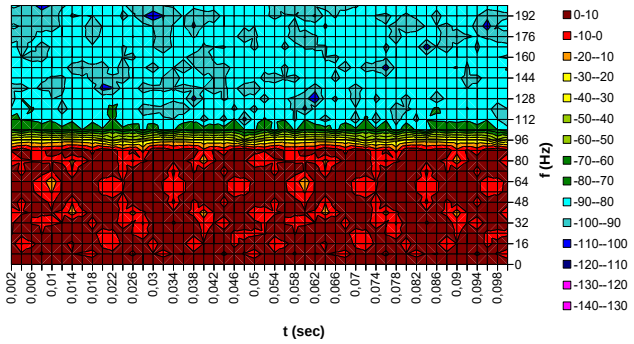


Fig. 9. Micro-Doppler signature of a drone with $N_r$=4, $N_b$=3, $L$=0.24m, $R_0$=100m, $z_0$=30m, $\Omega$=20RPS

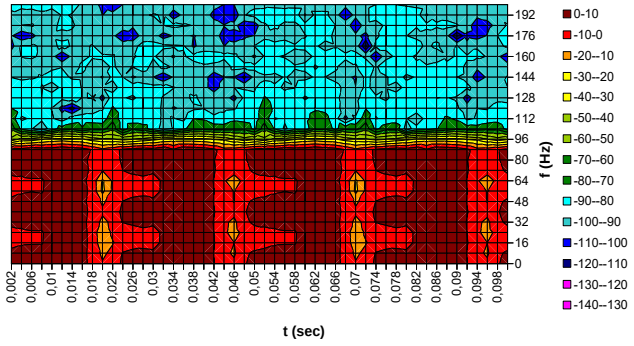


Fig. 10. Micro-Doppler signature of a drone with $N_r$=4, $N_b$=2, $L$=0.24m, $R_0$=100m, $z_0$=30m, $\Omega$=20RPS

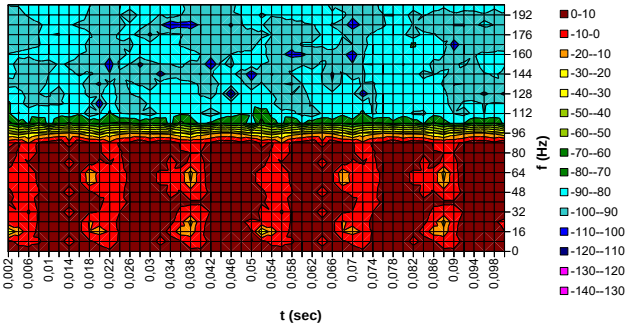


Fig. 11. Micro-Doppler signature of a drone with $N_r$=4, $N_b$=2, $L$=0.24m, $R_0$=100m, $z_0$=77m, $\Omega$=30RPS

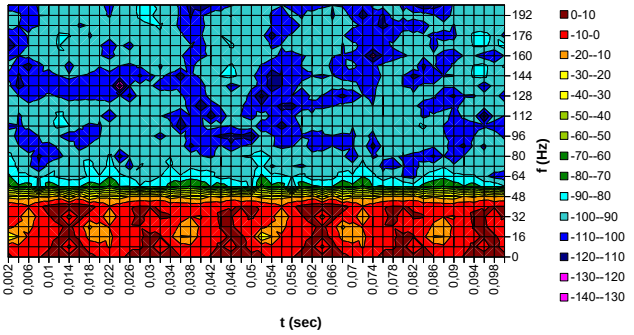


Fig. 12. Micro-Doppler signature of a drone with $N_r$=4, $N_b$=2, $L$=0.24m, $R_0$=100m, $z_0$=94.8m, $\Omega$=30RPS

The number of blades in each rotor does not have any influence on the frequency bandwidth of the area with higher signal level. This is approved mutually comparing Fig. 3 ($N_b$=2, $\Omega$=30RPS) and Fig. 4 ($N_b$=3, $\Omega$=30RPS), then Fig. 7 ($N_b$=3, $\Omega$=40RPS) and Fig. 8 ($N_b$=2, $\Omega$=40RPS) and, finaly, Fig. 9 ($N_b$=3, $\Omega$=20RPS) and Fig. 10 ($N_b$=2, $\Omega$=20RPS). When comparing these cases two by two, we see that the number of blades only causes different configuration of brown, red and orange surfaces within the area of higher signal level.

The blades' length has the influence on the frequency bandwidth of the area with higher signal level. Dependence may be considered as linear according to the mutual comparison of the figures 4, 5 and 6. The width is approximately $\Delta$=70Hz when it is $L$=0.12m (Fig. 5), $\Delta$=104Hz when it is $L$=0.18m (Fig. 6) and $\Delta$=140Hz when it is $L$=0.24m (Fig. 4).

The rotor angular rotation rate also has the influence on the frequency bandwidth of the area with higher signal level. Dependence is also linear, as in a case of blades' length. This statement is approved considering the graphs in the figures 9 and 10 (the width is $\Delta$=94Hz at $\Omega$=20RPS), then figures 3 and 4 (the width is $\Delta$=140Hz at $\Omega$=30RPS) and figures 7 and 8 (the width is $\Delta$=186Hz at $\Omega$=40RPS).

The frequency bandwidth of the area with higher signal level is proportional to the cosine value of the elevation angle. This is obvious comparing the graphs in the figures 3, 11 and 12. The drone heights ($z_0$=30m, $z_0$=77m and $z_0$=94.8m) are selected in such way that the ratios $\cos(z_0/R_0)$ in these three cases are 0.954, 0.638 and 0.318 or proportional to 3:2:1. The corresponding widths of the area with higher signal level in the figures 3, 11 and 12 are $\Delta$=140Hz, $\Delta$=96Hz and $\Delta$=48Hz respectively, which is very near to 3:2:1.


ISBN 978-86-7466-930-3

It is possible to distinguish graphs for the drones which have rotors with two blades (figures 3, 8, 10, 11 and 12) from those which have three blades (the remaining five figures). The characteristics when there are 2 blades usually have clearly separated, periodic parts with the highest signal level between 0dB and +10dB (brown segments). The shape of these parts depends on the rotation starting angle. There are six such parts in the figures 3, 11 and 12, eight in the Fig. 8 and four in the Fig. 10. It means that the number of repeatable parts ($N_p$) when there are 2 blades may be expressed as

$$N_p = N_r \cdot \Omega \cdot T_p \tag{7}$$

where $T_p$ is the time interval of spectrogram investigation.

When there are 3 blades such clear periodic parts may not be easily islolated.

## V. Reading the Parameters of Drone Flight and Construction from Spectrograms

In the Section IV it is investigated how the parameters of drone flight and of the drone construction affect its micro-Doppler signature appearance. Frequency bandwidth of the area with higher signal level depends on 3 parameters: blades' length, rotors' angular rotation rate and drone elevation angle. The spectrogram itself gives two values for the calculation. The first one is the frequency bandwidth of the area with higher signal level and the second one is the number of periodic areas with the highest signal level. So, it is necessary to determine one of the three parameters in some other way, not from spectrogram. The most logical is that this parameter is elevation angle $\beta$ because it may be also determined by some algorithm implementation on FMCW radar [41], [42] (the concrete algorithm for this function is not studied in this paper).

In order to determine $L$ and $\Omega$ from some measured spectrogram let us start from the spectrogram from the Fig. 13, which is calculated for the same parameters as in the Fig. 3 with only the exception that it is $z_0$=0m, i.e. cos($\beta$)=1. It follows from the graph in the Fig. 13 that it is now $\Delta$=148Hz. In this paper we have concluded that this value of $\Delta$ is proportinal to $\Omega$ and $L$. This statement may be expressed mathematically as

$$K_m \cdot L \cdot \Omega = 148 \tag{8}$$

Our goal is to determine the value of multiplication coefficient $K_m$.

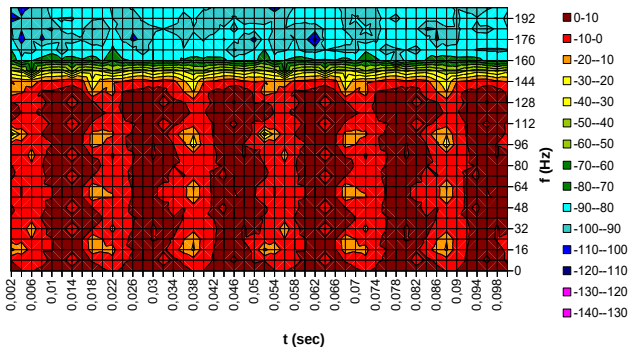


Fig. 13. Micro-Doppler signature of a drone with $N_r$=4, $N_b$=2, $L$=0.24m, $R_0$=100m, $z_0$=0m, $\Omega$=30RPS

The graph in the Fig. 13 is obtained as a result of calculation for the condition that it is $L$=0.24m and $\Omega$=30RPS. If we put now these values in the equation (8), we obtain that $K_m$=20.55.

Starting from this value of $K_m$, the value of elevation angle $\beta_m$ (which is determined by some other algorithm of drone DILC process on FMCW radar) and the value of $\Delta_m$ from the analyzed spectrogram, it is possible to calculate the value of the product

$$L_m \cdot \Omega_m = \frac{\Delta_m}{K_m \cdot \cos(\beta_m)} \tag{9}$$

Further, if $\Omega_m$ is determined from the appearance of the spectrogram part with higher frequency components, it is possible to calculate the length of blades as

$$L_m = \frac{\Delta_m}{K_m \cdot \Omega_m \cdot \cos(\beta_m)} \tag{10}$$

## VI. Conclusions

In this paper we have presented the initial development of a program for calculation and presentation of drones' micro-Doppler spectrograms as well as some results of its implementation. The benefits of such program application are that it is not necessary to have a high number of different drones and to perform significant volume of recording during drones operation in order to form the base of their spectrograms. This program follows the analytical model from [29]. The initial modelling is limited to hovering drones whose rotors have equal angular rotation rate. A number of spectrograms with differently defined input parameters is presented in the paper. The method for determination of drone's flight and construction characteristics is defined on the base of presented spectrograms. The number of blades in each rotor, rotors' angular rotation rate and blades' length, which contribute to specificities of spectrograms, may be concluded on the base of spectrograms appearance.

These initial calculations and presentations are performed in Excel as other, more suitable possibilities, were not available to us. Excel allows to perform good quality presentations of calculation results, as is also demonstrated in our contribution [43]. We plan to perform future investigations in some more powerful surrounding where it would be possible to model drone flying (besides hovering). It is also necessary to model drones with higher number of rotors (hexacopters, octocopters) as well as drone swarms to further improve drones DILC by FMCW radars.

FMCW radars are not the only way to obtain spectrograms as the ones presented in this paper. The similar results may be also obtained by using pulsed radar where the returned pulse delay is the measure of Doppler shift [13]. IRITEL already has experience in the development and improvements of such radars [21], [26]-[28]. In the case of single carrier radar the measure of Doppler shift would be the change of returned signal phase which is more complicate for realization.

## References

[1] G. Delauney, "Mystery drone from Ukraine war crashes in Croatia," BBC News, Balkans correspondent, https://www.bbc.com/news/world-europe-60709952.

[2] N. Razzouk, J. Blas, J. Thornhill, "Speed of Saudi Oil Recovery in Focus After Record Supply Loss," Bloomberg, 15. September 2019.,

 ISBN 978-86-7466-930-3

https://www.bloomberg.com/news/articles/2019-09-15/saudis-race-to-restore-oil-output-after-crippling-aramco-attack.
[3] N. Eriksson, "Conceptual study of a future drone detection system Countering a threat posed by a disruptive technology," Master thesis in Product Development, Chalmers University of Technology, Goethenburg, Sweden, 2018.
[4] V. Matić, V. Kosjer, A. Lebl, B. Pavić, J. Radivojević, "Methods for Drone Detection and Jamming," 10th International Conference on Information Society and Technology (ICIST), Kopaonik, March 8-11., 2020., in: Zdravković, M., Konjović, Z., Trajanović, M. (Eds.) ICIST 2020 Proceedings Vol. 1, pp.16-21, 2020.
[5] Advanced protection systems: "Ctrl+sky drone detection and neutralization system," 2017., http://apsystems.tech/wp-content/uploads/2018/01/aps_broszura_web.pdf.
[6] X. Shi, C. Yang, C. Liang, Z. Shi, and J. Chen: "Anti-Drone System with Multiple Surveillance Technologies: Architecture, Implementation, and Challenges," IEEE Communications Magazine, Vol. 56, Issue 4, April 2018., pp. 68-74., DOI: 10.1109/MCOM.2018.1700430.
[7] F. Fioranelli, O. Krasnov, Y. Cai, A. Yarovoy, J. Yun, D. Anderson, "MSG-SET-183 Specialists' Meeting – Improving the Simulations of Radar Signatures of Small Drone," STO-MP-MSG-SET-183, NATO, S&T organization, pp. 1-1 – 1-12.
[8] V. M. Milovanović, "On Fundamental Operating Principles and Range-Doppler Estimation in Monolithic Frequency-Modulated Continuous-Wave Radar Sensors," *Facta Universitatis, Series: Electronics and Energetics*, Vol. 31, No. 4, pp. 547-570, December 2018, DOI: https://doi.org/10.2298/FUEE1804547M.
[9] A. De Luca, "Forward Scatter Radar: Innovative Configurations and Studies," PhD Thesis, University of Birmingham, February 2018.
[10] C. Zhao, G. Luo, Y. Wang, C. Chen and Z. Wu, "UAV Recognition Based on Micro-Doppler Dynamic Attribute-Guided Augmentation Algorithm," *Remote Sensing*, Vol. 13, No. 6, Article 1205, pp. 1-17., March 2021., DOI: https://doi.org/10.3390/rs13061205.
[11] S. A. Musa, R. A. R.Syamsul Azmir, A. Sali, A. Ismail, N. Emleen, A. Rashid, "Micro-Doppler signature for drone detection using FSR: a theoretical and experimental validation," *The Journal of Engineering*, IET International Radar Conference (IRC2018), 17-19th October 2018., Nanjing, China, pp. 1-6.
[12] M. Passafiume, N. Rojhani, G. Collodi and A. Cidronali, "Modeling Small UAV Micro-Doppler Signature Using Milimeter-Wave FMCW Radar," *Electronics 2021*, Vol. 10, pp. 1-16., https://doi.org/10.3390/electronics10060747.
[13] S. Rahman, D. A. Robertson, "Radar micro-Doppler signatures of drones and birds at K-band and W-band," *Scientific Reports*, Vol. 2018, No. 8, pp. 1-11., November 2018., DOI: 10.1038/s41598-018-35880-9.
[14] A. Lebl, M. Mileusnić, D. Mitić, J. Radivojević, V. Matić, "Verification of Calculation Method for Drone Micro-Doppler Signature Estimation," accepted for publication in *Facta Universitatis, Series: Electronics and Energetics*, ISSN: 0353-3670.
[15] P. Jovanović, M. Mileusnić, B. Pavić, B. Mišković, "DDS based Pulse-Doppler Radar Transmitter Simulator," XIII International Scientific-Professional Symposium INFOTEH Jahorina, March 2014., Vol. 13. Ref. B-II-5, pp. 425-428.
[16] V. Marinković, B. Pavić, A. Toth, "Radar Signal Simulator for New Generation Digital Radar Receiver," INFOTEH Jahorina, Vol. 7. Ref. B-II-18, March 2008., pp. 228-231., in Serbian.
[17] B. Pavić, B. Mišković, V. Marinković-Nedelicki, M. Mileusnić,P. Petrović, "Projekat simulatora impulsnih radarskih signala," tehničko rešenje u kategoriji M85 na projektu tehnološkog razvoja TR32051 pod nazivom "Razvoj i realizacija naredne generacije sistema, uređaja i softvera na bazi softverskog radija za radio i radarske mreže," 2016.
[18] N. Remenski, B. Pavić, M. Mileusnić, P. Petrović, "Practical Realization of Digital Radar Receiver," 49. Conference ETRAN, Budva, June 2005., pp. 105-108., in Serbian.
[19] D. Dramićanin, V. Vlahović, N. Remenski, B. Pavić, P. Petrović, "FPGA Implementation of the Digital Radar Receiver," INFOTEH 2006, March 2006., Vol. 5. Ref. B-II-2, pp. 80-84., in Serbian.
[20] N. Remenski, V. Marinković-Nedelicki, V. Tadić, P. Petrović, "The Control of New Generation Digital Radar Receiver," INFOTEH 2006, March 2006., Vol. 5. Ref. B-II-10, pp. 114-118., in Serbian.
[21] V. Marinković, N. Remenski, V. Tadić, P. Petrović, "The Software for Control of Digital Radar Receiver VHF DP/P-12," 51. Conference ETRAN, Budva, Herceg Novi – Igalo, 2007., in Serbian.
[22] V. Matić, V. Marinković-Nedelicki, V. Tadić, "Comparison of digital signal processing methods for sine wave signal generation," Proceedings of SBT/IEEE International Telecommunications Symposium ITS '98, August 1998., DOI: 10.1109/ITS.1998.713134.
[23] V. Matić, V. Marinković-Nedelicki, "The waveform generator based on digital signal processing," Proceedings of the 2000 Third IEEE International Caracas Conference on Devices, Circuits and Systems 2000, pp. T56/1-T56/6, March 2000., DOI: 10.1109/ICCDCS.2000.869878.
[24] P. Petrović, "Research in Software Defined Radio and AESA Radar Technology, Serbia-Italia/Status and Perspectives of the Scientific and Technological Bilateral Cooperation," 2012., pp. 19-20.
[25] P. Jovanović, M. Mileusnić, P. Petrović, "An Approach to Analysis of AESA Based Radio systems," XII International Scientific-Professional Symposium INFOTEH Jahorina 2013, March 2013., Vol. 12., pp. 372-376.
[26] Land-based air defence radars, Serbia: VHF DR/P-12/18, in the book M. Streetly, *Jane's Radar And Electronic Warfare Systems*, IHS Global Limited, 2011.
[27] B. Pavić, V. Marinković-Nedelicki, M. Mileusnić, N. Remenski, P. Petrović, "Verifikovani modernizovani radar P-12," tehničko rešenje – novi proizvod u kategoriji M81 na projektu tehnološkog razvoja TR32051 pod nazivom "Razvoj i realizacija naredne generacije sistema, uređaja i softvera na bazi softverskog radija za radio i radarske mreže," 2013.
[28] M. Mileusnić, B. Pavić, V. Marinković-Nedelicki, P. Petrović, V. Matić, A. Lebl, "Verifikacija razvoja i realizacije nulte serije nove varijante modernizovanog osmatačko-akvizicijskog radara P-12M," tehničko rešenje u kategoriji M82 na projektu tehnološkog razvoja TR32051 pod nazivom "Razvoj i realizacija naredne generacije sistema, uređaja i softvera na bazi softverskog radija za radio i radarske mreže," 2018.
[29] V. C. Chen, "*The Micro-Doppler Effect in Radar*," Artech House, Second Edition, 2019., ISBN: 978-1-63081-546-2.
[30] C. R. Ferreiro, "Modeling and Analysis of Micro-Doppler Signatures for Radar Target Classification," Thesis for Bachelor in telecommunication Engineering, Telecommunication Engineering School, Universida de Vigo, 2017.
[31] R. W. Deters, S. Kleinke, "Static Testing of Propulsion Elements for Small Multirotor Unmanned Aerial Vehicles," AIAA AVIATION Forum, 35th AIAA Applied Aerodynamics Conference, 2017-3743, 5-9. June 2017., Denver, Colorado, pp. 1-34.
[32] Drone Tech Planet, "How a Quadcopter Works Along With Propellers and Motors," https://www.dronetechplanet.com/how-a-quadcopter-works-along-with-propellers-and-motors/.
[33] "Mavic Mini Propellers," https://store.dji.com/product/mavic-mini-propellers.
[34] "DJI Mavic 3 Low-Noise Propellers," https://store.dji.com/product/dji-mavic-3-low-noise-propellers.
[35] "DJI Propeller Set for Phantom 4 Pro/Pro+ V2.0 (2 Pack)," https://www.bhphotovideo.com/c/product/1407136-REG/dji_cp_pt_00000274_01_propellers_for_phantom_4.html/specs.
[36] "Altair 818 Hornet Propellers," https://altairaerial.com/products/aa818-plus-drone, https://www.amazon.com/Altair-818-Hornet-Propellers/dp/B07819RC9Q.
[37] 911, Rotorcraft, "Types of Drones," https://www.911security.com/learn/airspace-security/drone-fundamentals/types-of-drones-rotorcraft.
[38] M. Ahmadizadeh, "An Introduction to Short-Time Fourier Transform (STFT)," Sharif University of Technology, Department of Civil Engineering, July 2014.
[39] H. A. Gaberson, "A Comprehensive Windows Tutorial,"*Sound and Vibration*, Instrumentation Reference Issue, March 2006., pp. 14-23.
[40] C. Zhao, G. Luo, Y. Wang, C. Chen and Z. Wu, "UAV Recognition Based on Micro-Doppler Dynamic Attribute-Guided Augmentation Algorithm," *Remote Sensing*, Vol. 13, No. 6, Article 1205, pp. 1-17., March 2021., DOI: https://doi.org/10.3390/rs13061205.
[41] P. K. Rai, A. Kumar, M. Z. Ali Khan, J. Soumya, L. Reddy, "Angle and Height Estimation Technique for Aerial Vehicles using mmWave FMCW Radar," 2021 International Conference on COMmunication Systems & NETworkS (COMSNETS), 5-9. January 2021., Bangalore, India, DOI: 10.1109/COMSNETS51098.2021.9352744.
[42] P. K. Rai, H. Idsoe, R. R. Yakkati, A. Kumar, M. Z. Ali Khan, P. K. Yalavarthy, "Localization and Activity Classification of Unmanned Aerial Vehicle Using mmWave FMCW Radars," IEEE Sensors Journal, Vol. 21, No. 14, pp. 16043-16053., July 2021., DOI: 10.1109/JSEN.2021.3075909.
[43] J. Radivojević, B. Pavić, A. Lebl, M. Petrović, "Sweep Jamming with Discrete Subbands – an Advanced Strategy for Malicious Drones Missions Prevention," Scientific Technical Review, Vol. 71, No. 2, March 2022, pp. 46-52., ISSN: 1820-0206, UDK: 355.43:623.624,449.8, COSATI: 03-10, 14-04-01, DOI: 10.5973/str2102046R.

 ISBN 978-86-7466-930-3

# Execution Time Improvement using CPU Parallelization and Non-Uniform High-Resolution Range-Doppler Map Estimation in HFSWR

Dragan Golubović, Nenad Vukmirović, Zoran Lončarević, Marko Marković and Miljko Erić

***Abstract*— igh-resolution range-Doppler ( D- ) map estimation, used for primary signal processing in a igh requency urface Wave adar ( W ), is the most computationally demanding step of the vessel detection algorithm. In order to reach real-time processing, which is of great importance in practical implementations of such systems, a very high-speed computation is required. In this paper, we propose non-uniform signal frame selection, to reduce the load with almost no loss in performance, and parallel processing on a CP to get high-resolution range-Doppler maps in a multi-antenna scenario. The paper contains the description of the proposed algorithm and the performance analysis. The e perimental results show a - to 1 -fold improvement in the e ecution time of the program for vessel detection.**

***Index Terms*— W ; range-Doppler map; high-resolution methods; multi-core; parallelized algorithms; speedup.**

## I. INTRODUCTION

The focus of numerous scientific papers is maritime surveillance of vessels at long distances. The reason for that are many illegal crime activities over the horizon, drug trafficking, attacks on petrol platforms and strategic objects, etc. High Frequency Surface Wave Radars (HFSWRs) are widely used for this purpose [1]-[3].

To make these systems have better ship detection accuracy, as well as the ability to detect some ships, which are not visible at all using the currently used primary signal processing algorithms, high-resolution algorithms are used [4].

The downside is that the computational burden of HFSWRs is huge in that case, and high-speed computation is required in order to have real-time processing. It is of great importance in practical implementations.

In recent years, the demand for high performance numerical computing in many radar systems was increased. The focus of many papers is the formulation of parallel algorithms for the MIMO radar based on the Central Processing Unit (CPU)/ Graphical Processor Unit (GPU) architecture [5]-[9]. The architecture must be capable of multitasking, which allows multi-threaded execution of the program for vessel detection. GPUs have an essential role in designing the real-time programs because they are highly parallel, multithreaded processors. Graphic cards are equipped with multi-core GPUs enabling the development of high computationally demanding programs. But the performance improvement of multithreaded programs depends on the algorithms used and their implementations, which is often not a trivial task. This improvement is limited by the fraction of the program source code that can be run on multiple cores simultaneously. It is important to say that high execution efficiency is possible, only if hardware characteristics are appropriate.

The focus of this paper will be a real-time implementation of target detection in HFSWRs by improving the existing implementation of the high-resolution range-Doppler (RD-HR) map estimation, which is the most computationally demanding task of the entire algorithm. The algorithm runs in real-time if its execution time is shorter than the acquisition time of the frames used for the estimation (32.768 s in this particular case).

The existing implementation did not run in real-time, so we solved this problem in two ways. Firstly, we significantly reduced the computational load of the RD-HR map estimation with very little performance loss by using non-uniform sampling across the frames. Secondly, the parallel signal processing on CPU was performed. An advantage of the proposed implementation is that it requires only a general-purpose computer and no expensive dedicated hardware, like graphic cards, or Digital Signal Processing (DSP) cards.

The paper is organized as follows. In Section II, we presented a detailed algorithm description to estimate high-resolution range-Doppler map. In Section III, we explained the numerically efficient method to achieve real-time processing requirement. We discussed some experimental results and made some comparisons in Section IV and

Dragan Golubović is with the University of Belgrade, School of Electrical Engineering, 11120 Belgrade, Serbia and Vlatacom Institute, 11070 Belgrade, Serbia (e-mail: dragan.golubovic@vlatacom.com ).

Nenad Vukmirović is with the University of Belgrade, School of Electrical Engineering, 11120 Belgrade, Serbia and the Innovation Center of the School of Electrical Engineering, 11120 Belgrade, Serbia.

Zoran Lončarević is with Vlatacom Institute, 11070 Belgrade, Serbia (e-mail: zoran.loncarevic@vlatacom.com ).

Marko Marković is with Vlatacom Institute, 11070 Belgrade, Serbia (e-mail: marko.markovic@vlatacom.com).

Miljko Erić is with Vlatacom Institute, 11070 Belgrade, Serbia and the University of Belgrade, School of Electrical Engineering, 11120 Belgrade, Serbia (e-mail: miljko.eric@vlatacom.com ).

 ISBN 978-86-7466-930-3

outlined some conclusions and further research activities in Section V.

## II. High-Resolution Range-Doppler Map Estimation

HFSWR to be analyzed in this paper operates in HF spectrum 3-30 MHz and it uses Frequency Modulated Continuous Waves (FMCW). The radar consists of a transmitter (Tx) antenna array, receiver (Rx) antenna array and transceiver hardware. The numerical results in this paper are based on the signals from an $N$-element linear Rx antenna array. Other geometries are also possible. At the receiving channels, acquired complex time samples of IQ branch signals are available for further signal processing. In Fig. 1 the complete high-resolution target detection algorithm in HFSWR was proposed.

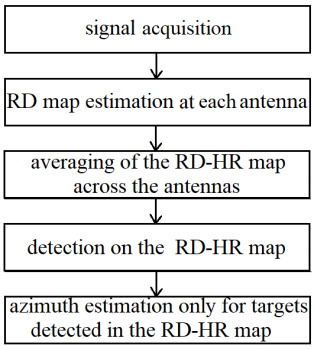


Fig. 1. The overview of the proposed high-resolution algorithm for vessel detection in HFSWR

The proposed algorithm has five steps, but the most computationally demanding task is step two – RD-HR map estimation at each antenna. Because of that, in order to improve program performance in terms of execution time, it is necessary to describe the creation of RD-HR map in detail and find a way to reduce its numerical complexity. So, other steps are not the focus of this section and only RD-HR creation will be explained.

In practical situations, $P$ (the number of signal samples in one frame) and $N$ are predefined values and $M$ can be varied and it represents the number of frames used for the creation of one segment. Based on this segment, RD-HR map is formed. The developed algorithms were tested for the length of the segment of $M$=256, where the successive segments overlap in 128 frames. This ensures that the results are refreshed every 128 frames. The first step in the RD-HR creation process, is the implementation of FFT algorithm in P points for all frames $m$=1, 2, ... , $M$ and all antennas $n$=1, 2, ... , $N$. By adding zeros to the vectors with signal samples, better grid resolution can be achieved when applying FFT. For further processing and a better estimate of the covariance matrix later, we need to extend the segment by L-1 additional frames. Fig. 2 shows the forming of the first two segments, with a 128-frame overlap. The same procedure is used for all other segments during signal processing.

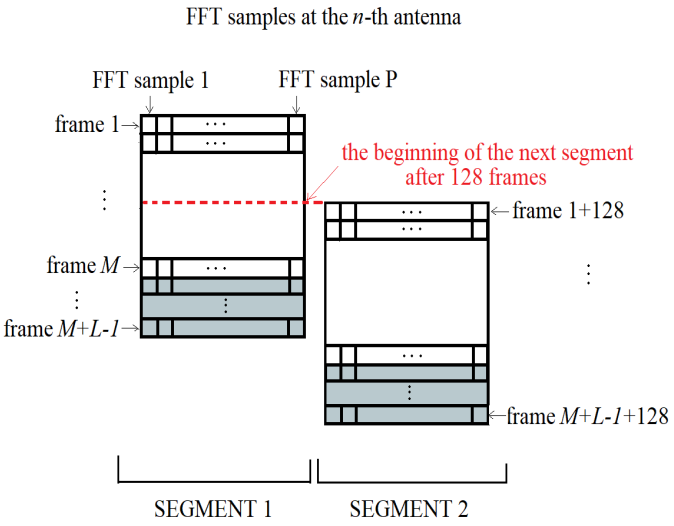


Fig. 2. Segment creation in the proposed algorithm

For each range cell, with index $p$, and each antenna, $n$, we form a matrix $_{p,n} \in C^{M\times}$ as in Fig. 4 from the $p$-th FFT sample from each frame in Fig. 3. Columns of matrix $_{p,n}$ are vectors $\mathbf{q}_{l,p,n}$, for $1 \le l \le$ , $1 \le p \le P$ and $1 \le n \le N$.

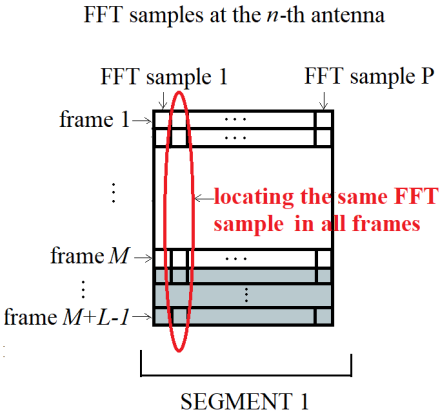


Fig. 3. Locating the same FFT sample in all frames

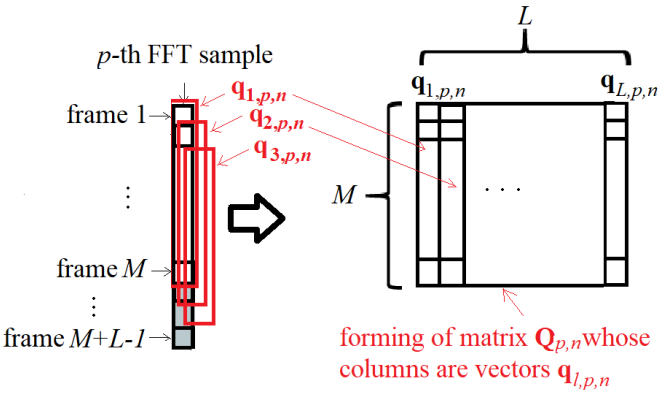


Fig. 4. The creation of the $_{p,n}$ matrix


ISBN 978-86-7466-930-3

Then the covariance matrices $\mathbf{C}_{p,n} \in \mathrm{C}^{M\times M}$ are formed for $n$=1, 2, ... , $N$ and $p$=$P-$ +1, $P-$ +2, ... , $P$, where represents the maximum projected radar range, as follows:

$$\mathbf{C}_{p,n} = \frac{1}{L}\mathbf{Q}_{p,n}\mathbf{Q}_{p,n}^{\mathrm{H}} \in \mathrm{C}^{M\times M} . \quad (1)$$

The formation of the covariance matrix $\mathbf{C}_{p,n}$ is a key step in the RD-HR map creation. Based on the covariance matrix, the criterion function of high-resolution MUSIC-based algorithm is formulated, as follows:

$$P_{\mathrm{MUS}}^{RD}(\mu,p,n) = \frac{1}{\left\|\mathbf{a}_{\mu}(\mu)^{\mathrm{H}}\,\mathbf{E}_{p,n}\right\|}, \quad (2)$$

where the columns of $_{p,n} \in \mathrm{C}^{M\times(M-}$ are the $M$- eigenvectors from the noise subspace of $\mathbf{C}_{p,n}$, corresponding to the $M$- smallest eigenvalues of the covariance matrix $\mathbf{C}_{p,n}$, is a parameter of the MUSIC-based algorithm, and $\mathbf{a}_{\mu}(\mu) \in \mathrm{C}^{M\times 1}$ is a steering vector formulated in the normalized Doppler domain as

$$\mathbf{a}_{\mu}(\mu) = \left[1, e^{-j\mu}, \dots , e^{-j\mu(M-1)}\right]^{\mathrm{T}} , \quad (3)$$

where the parameter $\mu$ denotes the normalized Doppler frequency in radians per frame. The criterion functions are calculated for a set of discrete values of normalized Doppler frequencies and with a grid resolution that is many times better than the Doppler FFT resolution, thus obtaining an RD-HR map.

## III. NUMERICALLY EFFICIENT METHOD FOR RD-HR MAP ESTIMATION

As presented in the previous section, the RD-HR map estimation is numerically complex (long execution time). Program for vessel detection of the proposed algorithm must be improved to achieve real-time requirement. Because of that, we propose here a numerically efficient method realized in two steps.

In the first step, we want to make some kind of pattern according to which we select a small subset of the frames from each segment. The reason for that is to reduce numerical complexity. In that case, the dimensionality of the covariance matrix will be smaller ( × ) where < $M$. The problem of non-uniform sampling method is analogous to the problem formulated in the field of antenna arrays - how to replace a linear uniform antenna array with a non-uniform antenna array with the same aperture and a smaller number of antennas without significant degradation of the antenna array factor. This problem in antenna array theory is known as the problem of minimally redundant linear antenna arrays. Fig. 5 shows the forming of the matrix $^{(l}_{p,n}$ by selecting a subset of rows of the matrix and according to a chosen mapping ℓ : {1, 2, ... , } → {1, 2, ... , $M$}, < $M$.

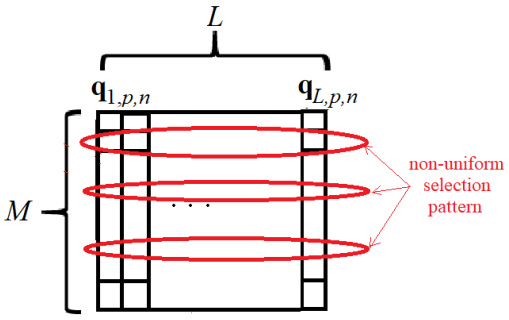


Fig. 5. The creation of the $^{(l}_{p,n}$ matrix using some non-uniform pattern

The same mapping ℓ is used to form the steering vector $\mathbf{a}_{\mu}{}^{l}(\mu)$ by non-uniform selection of the elements of the vector $\mathbf{a}_{\mu}(\mu)$.

The criterion function of the high-resolution MUSIC-type algorithm for creating RD-HR map with non-uniform sampling has the same form as the criterion function for the variant with uniform sampling, as follows:

$$P_{\mathrm{MUS}}^{RD\,(l)}(\mu,p,n) = \frac{1}{\left\|\mathbf{a}_{\mu}^{(l)}(\mu)^{\mathrm{H}}\;\mathbf{E}_{p,n}^{(l)}\right\|} . \quad (4)$$

The numerical complexity is significantly reduced, because the eigenvalue decomposition of the covariance matrix is numerically simpler in this case.

Despite the significant reduction in execution time, real-time processing is still not achieved. Therefore, we perform another step in the algorithm optimization.

As can be seen, a similar signal processing is performed on each of the antennas. This leads us to the idea not to form RD-HR maps at all antennas sequentially, one after the other, but simultaneously. Therefore, it is necessary to create a multi-threaded process.

Fig. 6 shows the proposed method for multithreaded RD-HR estimation in order to reduce execution time. A thread is the smallest unit of a processing that can be scheduled by an operating system. The multithreading was realized on CPU cores.

Therefore, the most demanding job, which is the formation of RD maps, was realized through parallel execution on multiple cores, while the rest of the program, which is not computationally demanding, remained to be executed sequentially. The algorithm is also applicable to a system with more antennas, but the performance depends directly on the number of processor cores.

## IV. NUMERICAL RESULTS

The results presented in this section are based on the measured radar data. P=1536 and L=64 are predefined values and the developed algorithm was tested for the length of the segment M=256, where the successive segments overlap with 128 frames. Number of antennas directly affect the execution time of the program for vessel detection, and we made some tests with N=16 antennas in the Rx antenna array.


ISBN 978-86-7466-930-3

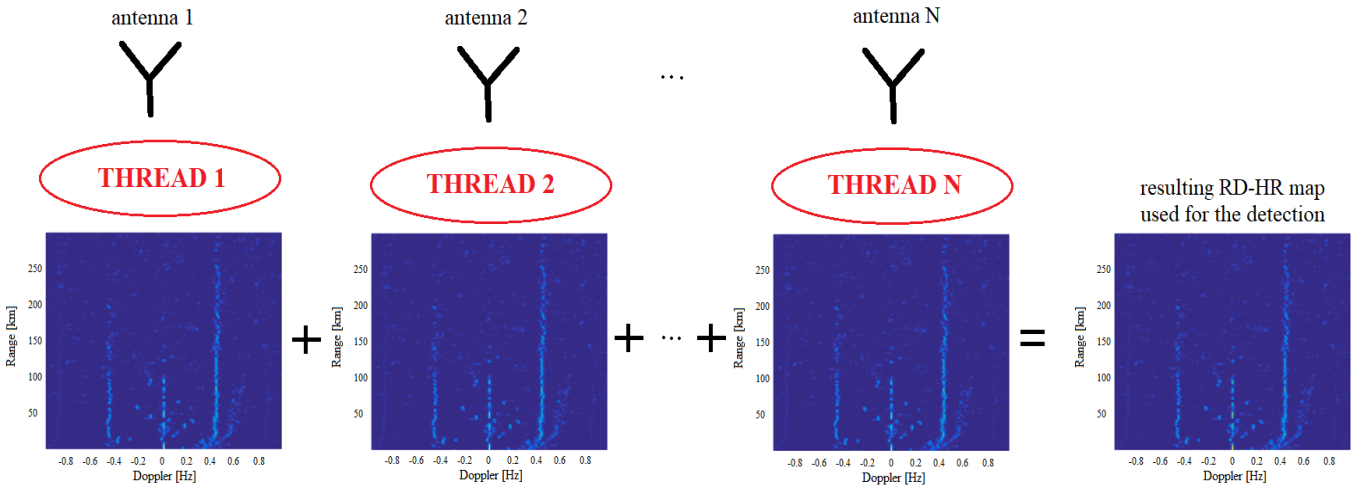


Fig. 6. Multithreaded RD-HR maps creation simultaneously at all antennas

The selected frame duration is 0.256 seconds, and since we want to output the results after every 128 frames, the real-time requirement is 32.768 seconds. Thus, the processing time of one segment must be shorter than 33.28 seconds. We choose also 3 predefined values for the parameter of the MUSIC-based algorithm: 10 for ranges up to 120 km, 20 for ranges from 120 to 200 km, and 30 for ranges up to 300 km. The number of grid points along the Doppler frequency dimension is 513. These are actually the basic system parameters.

For testing purposes, a program was developed using the programming language C and multithreading is realized too. We first formulate a testing methodology, seen in Fig. 7.

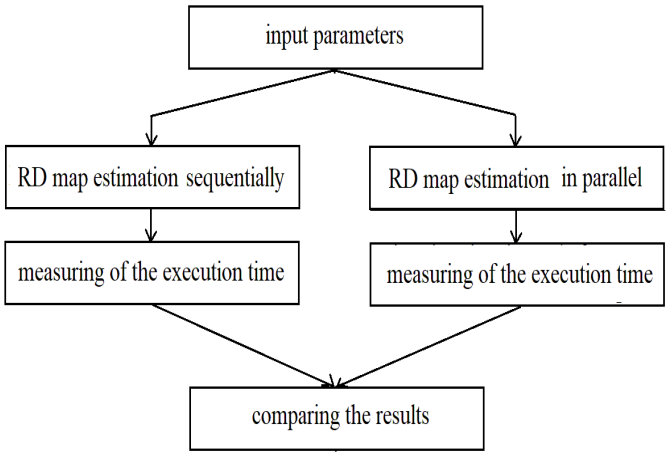


Fig. 7. The overview of the proposed testing methodology

We run the program on a PC with 6-cores CPU (i7), and on a PC with better 8-cores CPU (AMD Ryzen), and for 2 predefined patterns in order to get non-uniform RD-HR maps. The comparison with uniform RD-HR map is also presented. The first pattern is based on prime numbers between 1 and 256 (the last frame number in the segment) and the length of this pattern is =56, as follows: pattern56={1, 2, 3, 5, 7, 11, 13, 17, 19, 23, 29, 31, 37, 41, 43, 47, 53, 59, 61, 67, 71, 73, 79, 83, 89, 97, 101, 103, 107, 109, 113, 127, 131, 137, 139, 149, 151, 157, 163, 167, 173, 179, 181, 191, 193, 197, 199, 211, 223, 227, 229, 233, 239, 241, 251, 256}.

The length of the second pattern is 88 and it is also based on prime numbers, with some more numbers inserted, in order to reduce the distance between the numbers in the pattern. This leads us to create an RD-HD map that visually resembles a uniform RD HR map, while being numerically simpler: pattern88 ={1, 3, 5, 7, 11, 13, 17, 19, 23, 29, 31, 35, 37, 41, 45, 48, 50, 53, 55, 59, 61, 63, 67, 71, 73, 76, 77, 83, 85, 89, 92, 97, 101, 103, 105, 107, 109, 111, 113, 115, 118, 121, 125, 127, 129, 131, 134, 136, 137, 139, 142, 145, 147, 149, 151, 155, 157, 160, 163, 167, 171, 173, 179, 181, 184, 187, 191, 193, 197, 199, 202, 205, 209, 211, 215, 219, 223, 227, 229, 233, 236, 239, 241, 245, 247, 251, 254, 256}.

Fig. 8-10 show RD-HR maps for different patterns.

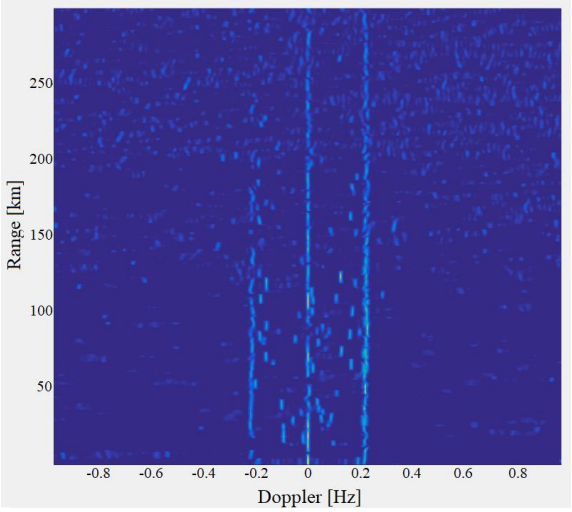


Fig. 8. Uniform obtained RD-HR map of the first segment


ISBN 978-86-7466-930-3

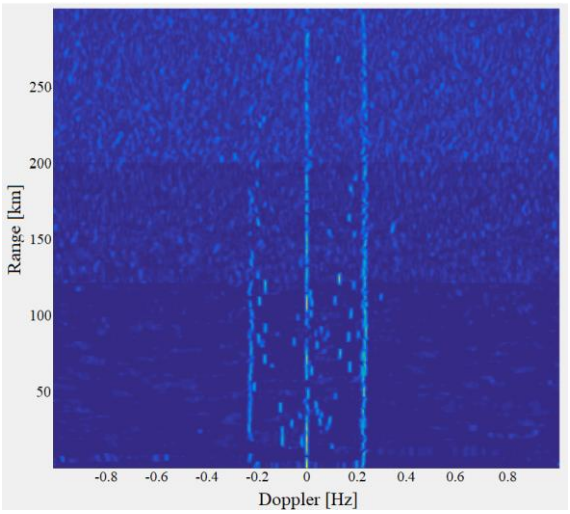


Fig. 9. Non-uniform obtained RD-HR map of the first segment (pattern88)

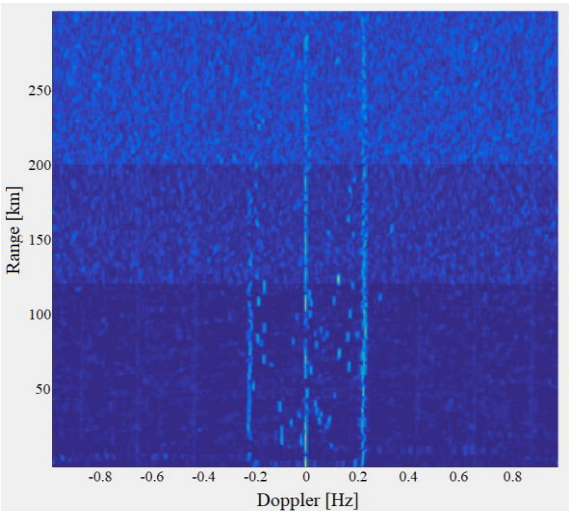


Fig. 10. Non-uniform obtained RD-HR map of the first segment (pattern56)

As can be seen from the figures, non-uniform sampling of frames increases the number of peaks in the RD-HR map compared to the case with uniform sampling, but vessels on the map are clearly visible in all 3 cases.

The dominant tasks in terms of the number of complex multiplications and additions are the eigenvalue decomposition and the calculation of MUSIC criterion function [10]. The approximate number of operations is

$$N_{\text{op}} \sim \frac{13}{3} J^3 RN + N_{\text{d}} J(J+1)RN . \quad (7)$$

In uniform variant $=M$. Thus, we decrease this number by a factor 44.6 and 15.3 for pattern56 and pattern88, respectively. $N_{\text{d}}$ is the length of RD-HR map by Doppler dimension. In this particular case $N_{\text{d}}$=513. Since the numerical complexity is much lower, a non-uniform variant can be used for real-time processing.

Table I shows the execution time of the program (with no-parallelized code) for vessel detection on different computers. Also, the measured execution time to form the RD map is compared to the measured execution time of the rest of the program.

TABLE I
EXECUTION TIME OF THE PROGRAM (NO-PARALLELIZED CODE)

| CP type | ecution time of D-estimation (seconds) | ecution time of the rest of the program (seconds) |
|---|---|---|
| Intel CORE i7 1075H | 880 | 3.12 |
| AMD Ryzen 9 5900HX | 606 | 2.64 |

The results clearly show that the estimation of the RD-HR map is numerically most complex, and the execution time improvement is required in order to reach real-time processing.

Now, we can define the speedup $S$ and the efficiency $E$ by comparing the execution time on one core, $T_1$, and on n cores, $T_n$:

$$S = \frac{T_1}{T_n} \quad (5)$$

$$E = \frac{T_1}{nT_n} . \quad (6)$$

Table II shows the comparison between the execution time of the program with and without parallelized code. The obtained results show that the real-time processing is achieved.

TABLE II
EXECUTION TIME OF THE PROGRAM (PARALLELIZED CODE)

| CP type and selected pattern | ecution time of the program without parallelization (seconds) | ecution time of the program with parallelization (seconds) |
|---|---|---|
| Intel CORE i7 1075H (uniform) | 883.12 | 132 |
| Intel CORE i7 1075H (pattern88) | 91.2 | 14.21 |
| Intel CORE i7 1075H (pattern56) | 32.12 | 7.54 |
| AMD Ryzen 9 5900HX (uniform) | 608.64 | 90.75 |
| AMD Ryzen 9 5900HX (pattern88) | 60.32 | 9.63 |
| AMD Ryzen 9 5900HX (pattern56) | 24.56 | 4.4 |


ISBN 978-86-7466-930-3

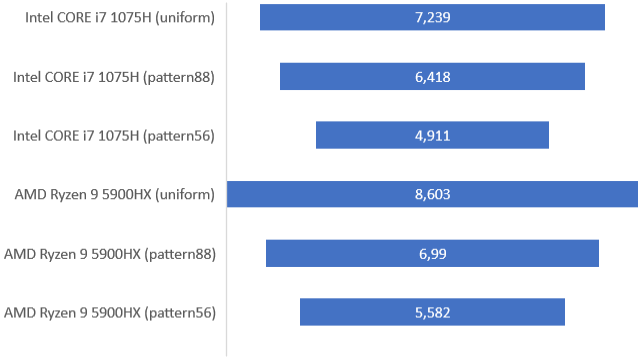


Fig. 11. Speedup of the parallelized algorithm

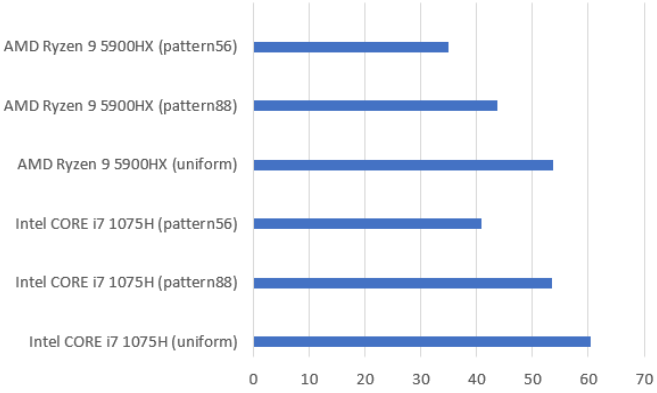


Fig. 12. Efficiency of the parallelized algorithm

Fig. 11 and 12 show speedup and the efficiency of the parallelized algorithm. Logical processors usage in multithread software was shown in Fig. 13.

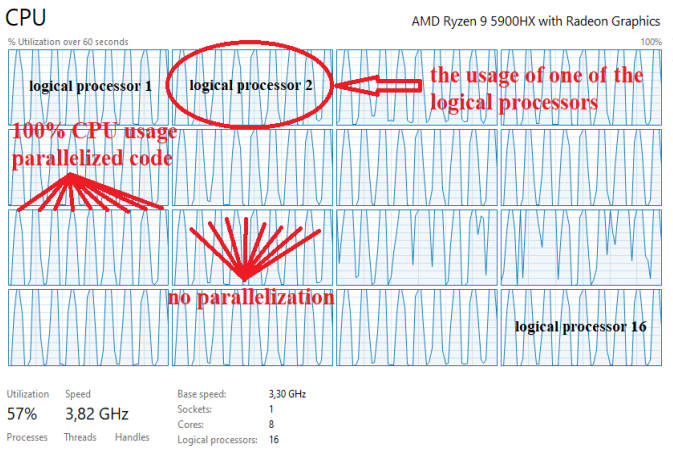


Fig. 13. Logical processors usage in multithread software

## V. Conclusion

In this paper, we propose a numerically efficient algorithm that can help many researchers to reach real-time requirement in their programs for vessel detection. The obtained results show that the parallelization of the code is needed, so the parallel signal processing on CPU was performed. Additionally, the proposed method, does not need any specialized hardware, only a general-purpose computer.

## Acknowledgment

This research, as a part of P.148 Project, was funded by Vlatacom Institute. The APC was funded by Vlatacom Institute. The research was also supported by the Serbian Ministry of Education, Science and Technological Development.

## References

[1] A.M. Ponsford and J. Wang, “A review of high frequency surface wave radar for detection and tracking of ships,” Turk J Elec Eng&Comp Sci, vol. 18, pp. 409–428, 2010.
[2] M. Jankiraman, “FMCW Radar Design,” Kindle ed., Artech House, England, 2018.
[3] K. Gurgel and T. Schlick, “Remarks on Signal Processing in HF Radars Using FMCW Modulation,” Proceedings of the International Radar Symposium IRS 2009, Hamburg, Germany, 2009.
[4] B. Kim, Y. Jin, J. Lee and S. Kim, “High-Efficiency Super-Resolution FMCW Radar Algorithm Based on FFT Estimation,” Sensors 2021, vol. 21, 4018. https://doi.org/10.3390/s21124018 , 2021.
[5] Liu, G.; Yang, W.; Li, P.; Qin, G.; Cai, J.; Wang, Y.; Wang, S.; Yue, N.; Huang, D. “MIMO Radar Parallel Simulation System Based on CPU/GPU Architecture,” Sensors 2022, vol. 22, 396. https://doi.org/10.3390/s22010396
[6] A.C. Sodan, J. Machina, A. Deshmeh, K. Macnaughton, “Parallelism via multithreaded and Multicore CPUs,” IEEE Computer Society, vol. 43, issue: 3, pp. 24-32, Mar. 2010.
[7] D. Dheeraj, B. Nitish, S. Ramesh, “Optimization of Automatic Conversion of Serial C to Parallel OpenMP,” International Conference on Cyber-Enabled Distributed Computing and Knowledge Discover, PES Institute of Technology Bangalore, India, Dec. 2012.
[8] E. Ayguade, N. Copty, A. Duran, J. Hoeflinger, “The Design of OpenMP tasks,” IEEE Transactions on Parallel and Distributed systems, vol. 20, Issue: 3, pp. 404-418, June 2008.
[9] B. Kim, Y. Jin, J. Lee and S. Kim, “Low-Complexity MUSIC-Based Direction-of-Arrival Detection Algorithm for Frequency-Modulated Continuous-Wave Vital Radar”, Sensors 2020, vol. 20, 4295. https://doi.org/10.3390/s20154295
[10] M. Erić, B. Igrić, “Practical Implementation and Performance Estimation of MUSIC Method Implemented on Signal Processor TMS 320c30,” Scientific-Technical Review, vol. LIV, No.1, 2004.

 ISBN 978-86-7466-930-3

# Layer 2 Forwarding Using T4P4S: P4 Language and Data Plane Development Kit

Dimitrije Jovanović and Aleksandra Smiljanić, *Member, IEEE*

***Abstract*—P4 is an open-source programming language designed to program protocol-independent pac et processors. T4P4 is a P4 compiler that can enable P4 programs to run on networ devices using the Data Plane Development it (DPD ) framewor . This paper covers the test environment for layer 2 forwarding using DPD . We compare the layer 2 forwarding switch compiled using T4P4 and the appropriate P4 program versus the layer 2 forwarding switch provided with DPD pac age.**

***Index Terms*—Programmable data plane, P4 language, DPD , T4P4 .**

## I. Introduction

P4 language (Programming Protocol-Independent Packet Processors) [1] is an open source, domain specific programming language used to specify packet processing of data plane devices. It provides high-level instructions for describing transformations of network data, and enables the end-user to define data plane functionalities, regardless of the network protocol.

Before the introduction of programmable data planes [2], the specialized hardware and low-level programming languages were used to implement data plane logic, as the only way to achieve satisfactory packet processing rates. P4 programmable hardware devices (targets) have so far achieved great performances, but they are still very expensive. Originally, the main goal of P4 is protocol-independence. However, it was not designed to be target-independent.

T4P4S (Translator for P4 Switches) is a P4 compiler able to support a variety of hardware devices [3]. To solve direct target-dependence, the Networking Hardware Abstraction Layer (NetHAL) has been introduced. The compiler translates the P4 program into C language code of a hardware independent core switch, using NetHAL as an interface between hardware and the switch code. The result is a hardware dependent DPDK software switch compatible with a given device. The simplified process of generating a switch program is illustrated in Fig. 1

Introduced software abstraction makes the P4 program target-independent. However, the overall performance is potentially lower. To this end, we conduct a simple layer 2 forwarding experiment (l2fwd), where we first forward packets using DPDK (Data Plane Development Kit) [4]. Then, we implement a P4 program with the same forwarding function by using T4P4S with DPDK. The goal is to verify integration of P4 and DPDK, by showing that the tests T4P4S l2fwd and DPDK l2fwd produce similar results.

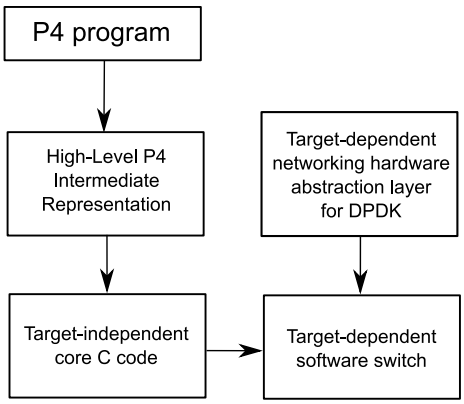


Fig. 1. Generation of the DPDK software switch using T4P4S.

This paper is structured as follows. Sections II, III and IV introduce the P4 language and its components. In section V, we cover an example of P4 program used for layer 2 forwarding. The testing environment is presented in Section VI. Finally, the testing results are shown in Section VII. We conclude the work in Section VIII.

## II. Packet Forwarding in P4

While the data plane performs transformations and forwarding of packets, the control plane configures the data plane and supplies it with network data. P4 defines functionalities of the data plane that was traditionally defined by the manufacturer. Inside a P4 switch, the data plane and its set of tables are not fixed in advance but rather defined by a P4 program. Thus, the data plane has no in-built knowledge of the existing network protocols [5].

P4 language adopts an abstract model for the packet processing pipeline which consists of three main stages [6]:

- Parser extracts user-defined packet headers from the received packet. Parsers are written in the form of finite state machines with three predefined states: start, accept and reject.
- Controls perform transformations on extracted headers. They define the control flow, an imperative program which operates on tables called match-action units. These tables consist of keys, matching types and actions that are executed upon matching.
- Deparser assembles the packet from processed headers. It performs the serialization of user-defined packet headers into the packet, and emission of these headers on the proper egress port.

Dimitrije Jovanović is with the School of Electrical Engineering, University of Belgrade, 73 Bulevar kralja Aleksandra, 11020 Belgrade, Serbia (e-mail: dica@etf.bg.ac.rs).

Aleksandra Smiljanić is with the School of Electrical Engineering, University of Belgrade, 73 Bulevar kralja Aleksandra, 11020 Belgrade, Serbia (e-mail: aleksandra@etf.bg.ac.rs).

 ISBN 978-86-7466-930-3

## III. P4 Architecture

The P4 architecture of each target consists of its P4 programmable elements and their data plane interfaces [5]. Regardless of the target's architecture type, the core of packet processing is the programmable match-action pipeline, which consists of metadata bus and a sequence of connected match-action units.

Metadata bus allows the communication between different phases of the match-action pipeline. It is considerably wider than common CPU buses, thus, these kinds of architectures can achieve high data processing speeds.

The most general architectural model consists of the ingress and egress match-action pipeline on its ends, and the traffic manager in between. The traffic manager performs packet queueing, replication and scheduling. The pipelines, parser and deparser are P4 programmable, while the traffic manager is fixed function.

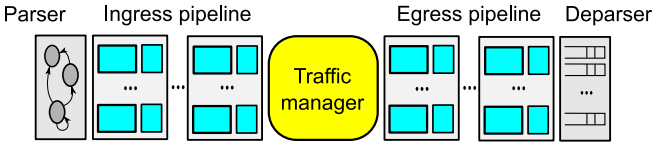


Fig. 2. V1Model P4 architecture.

One of the most common P4 architectures is the V1Model [7], which is illustrated in Fig. 2. Here, the ingress pipeline is placed after the parser and performs checksum verification. Symmetrically, the egress pipeline is placed before the deparser and performs checksum update. For example, T4P4S can use the V1Model architecture, which will also be implemented in this paper for testing.

## IV. P4 Programming Components

The core of the P4 language consists of data types, expressions, declarations and statements. The rest of the language is directly used for expressing parsers, match-action units and architectures [5].

P4 is a statically typed language. It provides several built-in base types (void, error, strings, match kind, Boolean, integers) and derived data types (enumeration, header, struct, tuple, extern, parsers, control blocks, packages, etc.).

Certain sorts of expressions in P4 can be executed only on a limited set of data types. The complete grammar production rule for general expressions can be found in the language specification.

Declarations are used for introducing functions, constants, and variables, which are executed at run time. Specially, data types with constructors (extern, control blocks, parsers, packages) use instantiations, which are executed at compilation time.

Statements can appear within parser states, a control block or an action. Some kinds of statements cannot appear in certain blocks. Control blocks support all of the following statements: assignment, empty, block, exit, return, switch.

Control blocks are used to manipulate and transform parsed headers. Data is transformed by match-action units, which are described by tables. One action consists of the code, which is in the P4 program, and the data, which is in table entries populated by the control plane. This is shown in Fig. 3.

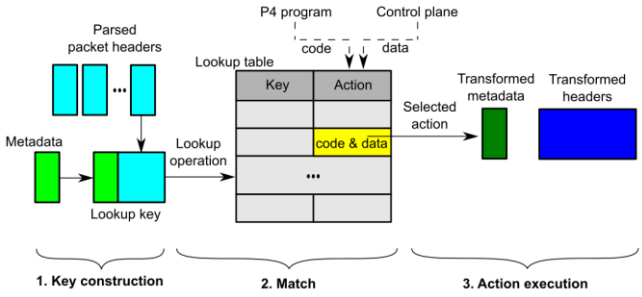


Fig. 3. Match-action unit.

Match-action units perform the following operations:

- Key construction, using packet headers or metadata.
- Match, by searching the key in the lookup table.
- Action execution, by which the input data is transformed.

Control blocks are also used to define deparsing (packet reconstruction), which is an inverse operation of parsing.

## V. P4 Layer 2 Forwarding Example Program

A simple configuration of layer 2 forwarding between two servers is illustrated in Fig. 4. A DPDK-compatible traffic generator is used to produce and transmit packets from server 1 (source server) to server 2 (target server). In the first case, server 2 uses a basic DPDK l2fwd example [8] to receive and forward packets. In the second case, we use a P4 program compiled by T4P4S. The same packet processing function is implemented in both cases.

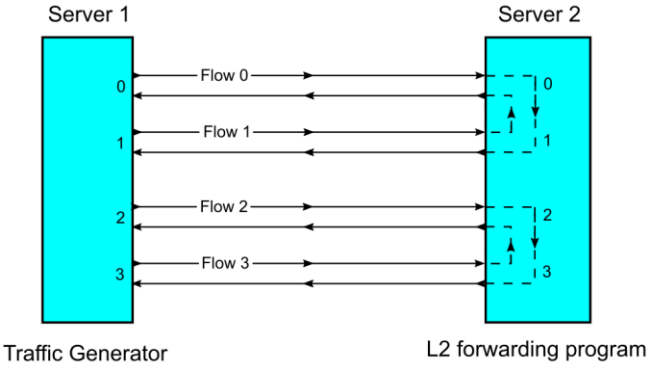


Fig. 4. Test configuration [8].

The P4 program given in Fig. 5 is used to generate our l2fwd switch example. Lines 1-8 define header types to be parsed from the packet. Lines 10-13 define the parser, which in this case extracts the Ethernet header from the ingress packet. Lines 15-58 define the control flow, which consists of tables (smac, dmac), actions (_drop, _nop, mac_learn, forward, broadcast) and controls (ingress, egress).

In this example, exact matching is used for table lookup. If the source MAC address is not found in the smac table, a digest is sent to the control plane to add the source address and the ingress port to both tables (action mac_learn).

If the source MAC address already exists in the table, nothing needs to be done (action _nop). In the dmac table,


ISBN 978-86-7466-930-3

the exact matching lookup determines the egress port based on the destination MAC adress. If there is a match, the packet is forwarded to that egress port (action forward). Otherwise, if the destination MAC address is not found in the table, the packet is sent to all ports except the ingress port (action bcast).

```
header_type ethernet_t {
   fields {
      dstAddr : 48;
      srcAddr : 48;
      etherType : 16;
   }
}
header ethernet_t ethernet;

parser start {
   extract(ethernet);
   return ingress;
}

action _drop() {
   drop();
}
action _nop() {
}
#define MAC_LEARN_RECEIVER 1024
field_list mac_learn_digest {
   ethernet.srcAddr;
   standard_metadata.ingress_port;
}
action mac_learn() {
   generate_digest(MAC_LEARN_RECEIVER,
                   mac_learn_digest);
}
table smac {
   reads {
      ethernet.srcAddr : exact;
   }
   actions {mac_learn; _nop;}
   size : 512;
}
action forward(port) {
   modify_field(
        standard_metadata.egress_port,
        port);
}
action bcast() {
   modify_field(
        standard_metadata.egress_port,
        100);
}
table dmac {
   reads {
      ethernet.dstAddr : exact;
   }
   actions {forward; bcast;}
   size : 512;
}
control ingress {
   apply(smac);
   apply(dmac);
}
control egress {
}
```

Fig. 5. Layer 2 forwarding P4 program (./examples/p4_14/l2fwd.p4_14) [9]

## VI. Test Environment

One of the testing goals is the comparison of running DPDK l2fwd from the CentOS host and the Ubuntu container, to verify the Docker solution and to detect the performance degradations if any. Also, DPDK l2fwd can be compared with T4P4S l2fwd, both on Ubuntu, in terms of different metrics, such as bit rate and packet size. The tests are performed on the target server using 2x2 ports (port 0 forwards to port 1 and port 2 forwards to port 3 and vice versa), as shown in Fig. 4.

The source test server used to generate traffic is Supermicro with 125 GB RAM, 24 cores and four Intel X710 NICs, each with 4 x 10 Gbit/s Ethernet ports. The traffic is generated using the Pktgen traffic generator.

The target test server is Supermicro with 250 GB RAM, 32 cores and five Intel X710 NICs, each with 4 x 10 Gbit/s Ethernet ports. The existing CentOS 7 host operating system contains the working DPDK version 18.11, which is not suitable for T4P4S installation due to incompatibility. To resolve that, we installed the latest version of T4P4S with underlying DPDK 21.11 on the Ubuntu 20.04 Docker container.

The configuration of the CentOS host includes the installation of DPDK required kernel modules uio, uio_pci_generic, vfio_pci and igb_uio (the last one compiled from dpdk-kmods Github repository), as well as the reservation of hugepages that will be used by DPDK. The Ubuntu 20.04 Docker container needs to be started with the option that mounts the host file system /dev/hugepages under /mnt/huge mounting point. Also, the container needs to run in the privileged mode with the host networking option, to allow the full access to the host drivers and the network cards.

In the Ubuntu container, it is required to install several missing packages, because the basic Ubuntu 20.04 Docker image assumes the very minimal configuration without development libraries, tools and compilers.

The detailed instructions on how to build T4P4S are given in the GitHub P4ELTE/t4p4s project [9]. Before testing, it is required to bind network cards to DPDK igb_uio driver, using the dpdk-devbind.py command. The packet generator (GitHub Pktgen-DPDK project) is located on another similar server, where four X710 NICs are directly connected to the selected four X710 NICs on the testing server, as shown in Fig. 4. The test configuration measures internal packet transfer between ports 0-1 and between ports 2-3, and also measures performances of parallel processing of two independent forwarding mechanisms.

TABLE I
DPDK L2FWD AND T4P4S L2FWD COMMAND LINE OPTIONS

| **./dpdk-l2fwd -c 0xf -n 4 -- -p 0xf** |
|---|
| **./t4p4s.sh :l2fwd model=v1model coropt prtopt rssopt** |
| grep "^???opt" opts_dpdk.cfg<br>coropt -> ealopts += -c 0xf -n 4<br>prtopt -> cmdopts += -p 0xf –config "\"<br>(0,0,0),(0,1,1),(0,2,2),(0,3,3),(1,0,0),(1,1,1),(1,2,2),(1,3,3),<br>(2,0,0),(2,1,1),(2,2,2),(2,3,3),(3,0,0),(3,1,1),(3,2,2),(3,3,3)\""<br>rssopt -> cflags += -DT4P4S_RTE_RSS_HF=0x7ef8 |


ISBN 978-86-7466-930-3

DPDK l2fwd is configured using command line options, which consist of Environment Abstraction Layer (EAL) options and application options. T4P4S l2fwd is configured by user-defined command line options, that we need to define in advance in the T4P4S configuration file opts_dpdk.cfg. EAL options are the same, but the application options differ for DPDK l2fwd and T4P4S l2fwd. For T4P4S l2fwd, we also need to specify the P4 architectural model, for example the V1Model.

The command line options presented in Table I will be used in all of the following tests. The number of processor cores is set to 4 (option -c and bit mask 0xf), the number of enabled ports is also 4 (option -p, bit mask 0xf). In the case of DPDK l2fwd, ports 0 and 1 forward packets to each other and ports 2 and 3 forward packets to each other by default. For T4P4S l2fwd, we need to explicitly map each RX port to the specific port, queue and processor core (port, queue, core). Ports that form the same traffic flow must be on the same socket, which is socket 0 in this case. The last option of the T4P4S l2fwd command in Table I is used to provide the proper RSS value, at compilation time. Configuration of the T4P4S l2fwd switch can be verified by looking at the command output presented in Fig. 6. One port handles ingress packets in nb_rxq queues, and egress packets in nb_txq queues. This output is practically the same for both DPDK l2fwd and T4P4S l2fwd.

```
# ./t4p4s.sh :l2fwd model=v1model coropt prtopt rssopt

[RUN CONTROLLER] dpdk_l2fwd_controller (default for l2fwd@std)

[COMPILE  P4-14] ./examples/p4_14/l2fwd.p4_14 @std

[COMPILE SWITCH]
[57/57] Linking target l2fwd.
[RUN SWITCH] ./build/last/build/l2fwd
EAL: Detected CPU lcores: 32
EAL: Detected NUMA nodes: 2
EAL: Detected shared linkage of DPDK
EAL: Multi-process socket /var/run/dpdk/rte/mp_socket
EAL: Selected IOVA mode 'PA'
EAL: No available 1048576 kB hugepages reported
EAL: VFIO support initialized
EAL: Probe PCI driver: net_i40e (8086:1572) device: 0000:01:00.0 (socket 0)
EAL: Probe PCI driver: net_i40e (8086:1572) device: 0000:01:00.1 (socket 0)
EAL: Probe PCI driver: net_i40e (8086:1572) device: 0000:01:00.2 (socket 0)
EAL: Probe PCI driver: net_i40e (8086:1572) device: 0000:01:00.3 (socket 0)
EAL: Probe PCI driver: net_i40e (8086:1572) device: 0000:02:00.0 (socket 0)
…     …            …
EAL: Probe PCI driver: net_i40e (8086:1572) device: 0000:03:00.3 (socket 0)
EAL: Probe PCI driver: net_i40e (8086:1572) device: 0000:82:00.0 (socket 1)
…     …            …
EAL: Probe PCI driver: net_i40e (8086:1572) device: 0000:84:00.3 (socket 1)
TELEMETRY: No legacy callbacks, legacy socket not created

P4_FWD: entering main loop on lcore 1
P4_FWD: entering main loop on lcore 0
P4_FWD:  -- lcoreid=0 portid=0 rxqueueid=0
P4_FWD:  -- lcoreid=0 portid=1 rxqueueid=0
P4_FWD:  -- lcoreid=0 portid=2 rxqueueid=0
P4_FWD:  -- lcoreid=0 portid=3 rxqueueid=0
P4_FWD: entering main loop on lcore 2
P4_FWD:  -- lcoreid=2 portid=0 rxqueueid=2
P4_FWD:  -- lcoreid=2 portid=1 rxqueueid=2
P4_FWD:  -- lcoreid=2 portid=2 rxqueueid=2
P4_FWD:  -- lcoreid=2 portid=3 rxqueueid=2
P4_FWD:  -- lcoreid=1 portid=0 rxqueueid=1
P4_FWD:  -- lcoreid=1 portid=1 rxqueueid=1
P4_FWD:  -- lcoreid=1 portid=2 rxqueueid=1
P4_FWD:  -- lcoreid=1 portid=3 rxqueueid=1
P4_FWD: entering main loop on lcore 3
P4_FWD:  -- lcoreid=3 portid=0 rxqueueid=3
P4_FWD:  -- lcoreid=3 portid=1 rxqueueid=3
P4_FWD:  -- lcoreid=3 portid=2 rxqueueid=3
P4_FWD:  -- lcoreid=3 portid=3 rxqueueid=3
```

Fig. 6. Initialization of T4P4S l2fwd switch.

## VII. TEST RESULTS

The relation between the maximal packet rate and bit rate on an Ethernet link is given in (1). Ethernet frame of size is preceeded by preamble (7 B) and SFD field (1 B), and it is followed by an inter-frame gap (at least 12 B). Therefore, the total size of transmitted data is at least + 20 B.

$$_{packet,\max} = \frac{bit}{+20B} \quad (1)$$

There is a hardware upper limit for packet rate when the traffic is generated on all four ports simultaneously. This value depends on the model of used NIC. The maximal TX packet rate on one port for the shortest frames (64 B) is given in the last row of Table II, which equals 10.066 Mp/s. If we had used only two ports in our experiment, the maximal TX packet rate on one port would be 14.88 Mp/s, according to (1).

The results of several tests for layer 2 forwarding, for different frame sizes and TX packet rates, are given in Table II. We initiated the Ethernet traffic with the given parameters on all four ports simultaneously, and measured RX packet rate on each port. Table II gives the achieved RX packet rate for one port. We considered four values for Ethernet frame size, ranging from 1518 B to 64 B (column 1). TX packet rate (column 2) is given as the percentage of the maximal packet rate (column 3), because the rate is set that way in the Pktgen command line. For each frame size, we considered TX packet rate values of 10% and 100% of the maximal packet rate.

The tests produced practically identical results for RX rate comparing DPDK l2fwd on CentOS host and on Ubuntu Docker container. That excludes any performance degradation possibly caused by the Docker container.

TABLE II
COMPARING DPDK L2FWD ON CENTOS HOST AND UBUNTU DOCKER CONTAINER: RX PACKET RATE

| Frame size [B] | % max packet rate | TX packet rate [Mp/s] | RX packet rate CentOS Host [Mp/s] | RX Packet rate Ubuntu container [Mp/s] |
|---|---|---|---|---|
| 1518 | 10 | 0.08128 | 0.08128 | 0.08128 |
| 512 | 10 | 0.24944 | 0.24944 | 0.24944 |
| 256 | 10 | 0.45293 | 0.45293 | 0.45293 |
| 64 | 10 | 1.488 | 1.488 | 1.488 |
| 1518 | 100 | 0.81275 | 0.81274 | 0.81274 |
| 512 | 100 | 2.34966 | 2.34962 | 2.3496 |
| 256 | 100 | 4.52906 | 4.52896 | 4.52896 |
| 64 | 100 | 10.0798 | 9.40504 | 9.39915 |

Pktgen [10] is a software traffic generator that is a part of the DPDK framework. It can configure and display metrics for traffic flows at real time. Pktgen command line options (Fig. 7) are split into Environment Abstraction Layer (EAL) options and application options. The mask of used processor cores and the number of memory channels are the required EAL arguments. We can also specify the PCI devices and

 ISBN 978-86-7466-930-3

the memory allocated from hugepages on specific sockets. In the application options, we can map ports to logical cores. Run time commands are entered in Pktgen prompt while it is running. For each port, we can specify the number of packets to transmit and their size, packet rate (in percentage of the maximal rate), as well as the source and the destination MAC address (or their range).

In our tests, the source MAC address of port 0 is the destination MAC address of port 1 and vice versa. Ports 2 and 3 are paired in the same way. Pktgen displays traffic results for each port at real time, such as the achieved rate and number of transmitted and received packets. The example of Pktgen output for ports 0 and 1 is presented in Fig. 7.

```
# ./app/x86_64-native-linuxapp-gcc/pktgen -c 0xfffff
-w 82:00.0 -w 82:00.1 -w 82:00.2 -w 82:00.3  --file-prefix=pg1
--socket-mem=8192,8192  --  -m  "[6:7].0,  [8:9].1,  [10:11].2,
[17:16].3


| Ports 0-3 of 4   <Main Page>  Copyright (c) <2010-2017>,
  Flags:Port      :   ---------------:0   ---------------:1
Link State        :       <UP-10000-FD>       <UP-10000-FD>
Pkts/s Max/Rx     :       234944/234944       234983/234944
       Max/Tx     :       235008/234944       234988/234962
MBits/s Rx/Tx     :             999/999             999/999
Broadcast         :                   0                   0
Multicast         :                   0                   0
  64 Bytes        :                   0                   0
  65-127          :                   0                   0
  128-255         :                   0                   0
  256-511         :             2583246             2583969
  512-1023        :                   0                   0
  1024-1518       :                   0                   0
Runts/Jumbos      :                 0/0                 0/0
Errors Rx/Tx      :                 0/0                 0/0
Total Rx Pkts     :             2407086             2407680
      Tx Pkts     :             2407680             2407570
      Rx MBs      :               10244               10247
      Tx MBs      :               10247               10246
ARP/ICMP Pkts     :                 0/0                 0/0
                  :
Pattern Type      :               abcd...             abcd...
Tx Count/% Rate   :        Forever /10%        Forever /10%
PktSize/Tx Burst  :          512 /   64          512 /   64
Src/Dest Port     :         1234 / 5678         1234 / 5678
Pkt Type:VLAN ID  :     IPv4 / TCP:0001     IPv4 / TCP:0001
802.1p CoS        :                   0                   0
ToS Value:        :                   0                   0
  - DSCP value    :                   0                   0
  - IPP  value    :                   0                   0
Dst  IP Address   :         192.168.1.1         192.168.0.1
Src  IP Address   :      192.168.0.1/24      192.168.1.1/24
Dst MAC Address   :   ac:1f:6b:2d:1a:c9   ac:1f:6b:2d:1a:c8
Src MAC Address   :   ac:1f:6b:2d:1a:c8   ac:1f:6b:2d:1a:c9
VendID/PCI Addr   :   8086:1572/82:00.0   8086:1572/82:00.1

-- Pktgen Ver: 3.5.2 (DPDK 17.11.4)  Powered by DPDK ------
```

Fig. 7. Pktgen output for T4P4S l2fwd (showing ports 0 and 1 only).

By turning on T4P4S l2fwd debugging, in Fig. 8 one can see how the process of MAC learning and forwarding goes on. We can follow the specified packet by looking at lines that begin with its assigned string. For the packet on the ingress port 3 (lines 0@0), the parser enters the start state and extracts the Ethernet header. The source MAC address ac:1f:6b:2d:1a:cb is not found in the smac table, and therefore that address-port pair is added both to the smac table and the dmac table. The next incoming packet on the ingress port 2 (lines 1@0) has the destination MAC address ac:1f:6b:2d:1a:cb. Since now there is a match in the dmac table, the packet is forwarded to the port 3.

Since we concluded that l2fwd tests behave the same on the CentOS host and the Ubuntu Docker container, we can compare DPDK l2fwd and T4P4S l2fwd, both on the Docker container. We executed the tests with analogous parameters with the parameters for comparing DPDK l2fwd on CentOS host and Ubuntu Docker container. The results are shown in Table III and Table IV.

```
0@0 Handling packet #-01 (port 3, 60B): ac1f 6b2d 1aca ac1f 6b2d
1acb 0800 4500 002e 492e 0000 0406 e749 c0a8 0301 c0a8 0201 04d2
162e 1234 5678 1234 5690 5010 2000 fbe6 0000 7778 797a 3031
0@0  %%%% Parser state start
0@0    :: Parsed header#1 ethernet/14B: .dstAddr/6B=ac1f_6b2d_1aca
.srcAddr/6B=ac1f_6b2d_1acb .etherType/2B=2048=0x0800
0@0  %%%% Packet is accepted, 14B in 1 header, 46B of payload: 4500
002e 492e 0000 0406 e749 c0a8 0301 c0a8 0201 04d2 162e 1234 5678
1234 5690 5010 2000 fbe6 0000 7778 797a 3031
1@0 Handling packet #-01 (port 2, 60B): ac1f 6b2d 1acb ac1f 6b2d
1aca 0800 4500 002e 49b5 0000 0406 e6c2 c0a8 0201 c0a8 0301 04d2
162e 1234 5678 1234 5690 5010 2000 fbe6 0000 7778 797a 3031
1@0  %%%% Parser state start
1@0    :: Parsed header#1 ethernet/14B: .dstAddr/6B=ac1f_6b2d_1acb
.srcAddr/6B=ac1f_6b2d_1aca .etherType/2B=2048=0x0800
1@0  %%%% Packet is accepted, 14B in 1 header, 46B of payload: 4500
002e 49b5 0000 0406 e6c2 c0a8 0201 c0a8 0301 04d2 162e 1234 5678
1234 5690 5010 2000 fbe6 0000 7778 797a 3031
1@0  ++++ Lookup on smac/exact/6B:
ethernet.srcAddr/48b=ac1f_6b2d_1aca -> hit mac_learn
1@0     < Sending digest to port 1024
1@0         : ethernet.srcAddr/48 = ac1f 6b2d 1aca
1@0         : all_metadatas.ingress_port/9 = 0200
0@0  ++++ Lookup on smac/exact/6B:
ethernet.srcAddr/48b=ac1f_6b2d_1acb -> hit mac_learn
0@0     < Sending digest to port 1024
1@0  <<<< Sending digest to port 1024 using extern
extern_Digest_pack for cpd
0@0         : ethernet.srcAddr/48 = ac1f 6b2d 1acb
0@0         : all_metadatas.ingress_port/9 = 0300
0@0  <<<< Sending digest to port 1024 using extern
extern_Digest_pack for cpd
---  ctl> Add dmac/exact: forward($port/9b=2=002) <- ac1f 6b2d 1aca
---  ctl> Add smac/exact: _nop <- ac1f 6b2d 1aca
---  ctl> Add dmac/exact: forward($port/9b=3=003) <- ac1f 6b2d 1acb
---  ctl> Add smac/exact: _nop <- ac1f 6b2d 1acb
1@0  ++++ Lookup on dmac/exact/6B:
ethernet.dstAddr/48b=ac1f_6b2d_1acb -> hit forward($port/9b=3=003)
1@0     = Set all_metadatas.egress_port/9b = 3 = 0x0003
1@0  <<<< Emitting packet #-01 with unchanged structure on port 3:
14B of headers, 46B of payload
```

Fig. 8. Debug output of T4P4S l2fwd program.

TABLE III
COMPARING DPDK L2FWD AND T4P4S L2FWD: RX PACKET RATE

| Frame size [B] | % max packet rate | TX packet rate [Mp/s] | RX packet rate DPDK [Mp/s] | RX packet rate T4P4S [Mp/s] |
|---|---|---|---|---|
| 1518 | 10 | 0.08128 | 0.08128 | 0.08128 |
| 512 | 10 | 0.24944 | 0.24944 | 0.24944 |
| 256 | 10 | 0.45293 | 0.45293 | 0.45293 |
| 64 | 10 | 1.488 | 1.488 | 1.48782 |
| 1518 | 100 | 0.81275 | 0.81274 | 0.81273 |
| 512 | 100 | 2.34966 | 2.3496 | 2.30071 |
| 256 | 100 | 4.52906 | 4.52896 | 2.3005 * |
| 64 | 100 | 10.0798 | 9.39915 | 2.3109 * |

TABLE IV
COMPARING DPDK L2FWD AND T4P4S L2FWD: RX BIT RATE

| Frame size [B] | % max bit rate | TX bit rate [Gbit/s] | RX bit rate DPDK [Gbit/s] | RX bit rate T4P4S [Gbit/s] |
|---|---|---|---|---|
| 1518 | 10 | 1 | 1 | 1 |
| 512 | 10 | 1 | 0.999 | 0.999 |
| 256 | 10 | 1 | 0.999 | 0.999 |
| 64 | 10 | 1 | 0.999 | 0.999 |
| 1518 | 100 | 10 | 9.999 | 9.999 |
| 512 | 100 | 10 | 9.999 | 9.754 |
| 256 | 100 | 10 | 9.995 | 5.059 * |
| 64 | 100 | 6.75 | 6.185 | 1.535 * |


ISBN 978-86-7466-930-3

In Table III and Table IV, one can observe that the RX rate of T4P4S l2fwd is similar to RX rate of DPDK l2fwd for lower rates and longer packets. But in the case of higher rates and shorter packets, there is a considerable amount of lost packets in the case of T4P4S l2fwd. The values for RX rate for T4P4S l2fwd denoted with (*) in Table III and Table IV represent that case. The encountered issues are caused by a suboptimal software integration of DPDK and P4, which includes a trade-off between flexibility and performance. Target-independence of the T4P4S compiler introduces generalizations related to memory allocation, which are common sources of performance issues. The improvement in that area will be the subject of future work.

## VIII. Conclusion

We have demonstrated that P4 features can be readily tested using standard equipment, consisting of two Linux servers with sufficient memory and processor cores, and standard network cards. We have considered two cases: when packet forwarding is done just using DPDK, and when P4 program is executed on the receiver side, by using T4P4S over DPDK. We have shown that, in most cases, there are no considerable differences between RX bit rate measured for DPDK layer 2 forwarding and T4P4S layer 2 forwarding that implements the P4 language program. We have observed a drop in performance of the implemented P4 software for the shortest packets. On the other hand, the P4 language greatly improves the flexibility of packet processing, while T4P4S makes P4 programs portable across multiple targets. In the future, we will work on improving the performance of the integrated DPDK and P4 software.

## Acknowledgment

This paper is sponsored in part by the Serbian Ministry of Education, Science and Technological Development.

## References

[1] P. Bosshart, D. Daly, G. Gibb, M. Izzard, N. McKeown, J. Rexford, C. Schlesinger, D. Talayco, A. Vahdat, G. Varghese and D. Walker, “P4: Programming Protocol-independent Packet Processors,” *SIGC MM Comput. Commun. e .*, vol. 44, no. 3, pp. 87–95, July 2014.

[2] R. Bifulco and G. Rétvári, “A Survey on the Programmable Data Plane: Abstractions, Architectures, and Open Problems,” 2018 IEEE 19th International Conference on High Performance Switching and Routing, Bucharest, Romania, June 2018.

[3] P. Vörös, D. Horpácsi, R. Kitlei, D. Leskó, M. Tejfel, and S. Laki, “T4P4S: A Target-independent Compiler for Protocol-independent Packet Processors,” 2018 IEEE 19th International Conference on High Performance Switching and Routing, Bucharest, Romania, June 2018.

[4] H. Bi and Z. Wang, “DPDK-based Improvement of Packet Forwarding,” 3rd Annual International Conference on Information Technology and Applications, Hangzhou, China, July 2016.

[5] P. L. Consortium, “P4 16 Language Specification,” [Online]. Available: https://p4.org/p4-spec/docs/P4-16-v1.2.2.pdf, May 2021.

[6] H. Harkous, M. Jarschel, M. He, R. Pries and W. Kellerer, “Towards Understanding the Performance of P4 Programmable Hardware,” 2019 ACM/IEEE Symposium on Architectures for Networking and Communications Systems, Cambridge, UK, September 2019.

[7] F. Hauser, M. Häberle, D. Merling, S. Lindner, V. Gurevich, F. Zeiger, R. Frank and M. Menth, “A Survey on Data Plane Programming with P4: Fundamentals, Advances, and Applied Research,” [Online]. Available: https://arxiv.org/pdf/2101.10632.pdf, August 2021.

[8] Intel Corporation, “L2 Forwarding Sample Application (in Real and Virtualized Environments),” [Online]. Available: https://doc.dpdk.org/guides/sample_app_ug/l2_forward_real_virtual.html

[9] P4ELTE, “Retargetable compiler for the P4 language,” [Online]. Available: https://github.com/P4ELTE/t4p4s

[10] D. Turull, P. Sjödin, and R. Olsson, “Pktgen: Measuring performance on high speed networks,” *Computer Communications*, vol. 82, pp. 39–48, March 2016.

 ISBN 978-86-7466-930-3

# Mogućnost primene beacon tehnologiji za razvoj Covid-19 sistema za praćenje kontakta u visokoškolskim institucijama

Ivana Stefanović, Milutin Nešić i Marko Milivojčević

***Apstrakt*—U ovom radu razmatrana je mogućnost primene *beacon* tehnologije za razvoj rešenja koje omogućava praćenje rizičnih kontakta kao i automatizaciju sprovođenja propisanih mera u realnom vremenu, u cilju sprečavanja zaražavanja i širenja infekcije izazvane virusom Covid-19 u visokoškolskim institucijama. Za realizaciju sistema dovoljno je da studenti i zaposleni kod sebe imaju pametni telefon na kome je instalirana odgovarajuća aplikacija. Sistem se bazira na tome da će student i zaposleni kod kojih je utvrđeno prisustvo virusa Covid-19, putem aplikacije, dobrovoljno obavestiti visokoškolsku ustanovu o pozitivnom testu. Sprovedena je anonimna anketa kako bi se utvrdilo da li su student i zaposleni zainteresovani za implementaciju Covid-19 sistema za praćenje kontakta. Izvršena su i praktična merenja, a dobijeni rezultati potvrđuju da je *beacon* tehnologija odličan izbor za implementaciju sistema.**

***Ključne reči*—Beacon; BLE; Covid-19; pozicioniranje.**

## I. Uvod

Globalna pandemija izazvana virusom Covid-19 utiče na sve aspekte ljudskog života, uključujući i obrazovanje. Zavisno od trenutne epidemiološke situacije i u skladu sa preporukama Ministrastva prosvete, nauke i tehnološkog razvoja nastava u visokoškolskim ustanovama odvija se uživo, na daljinu ili kombinovano. Za razliku od samog početka pandemije, kada se celokupna nastava odvijala na daljinu, danas je u većini visokoškolskih ustanova usvojen kombinovani model koji podrazumeva da se deo nastave održava uživo u školama. Većina mera za zaštitu zdravlja studenata i zaposlenih odnosi se na održavanje fizičke distance, nošenje maski, redovno pranje ruku, čišćenje i dezinfekciju školskih prostorija. Uprkos svim merama koje škole sprovede, dolazi do zaražavanja studenata i zaposlenih, što dovodi u rizik druge studente i zaposlene koji su bili u neposrednom kontaktu sa zaraženim.

U okviru ovog rada predstavljen je centralizovani sistem čija je osnovna funkcija identifikacija i obaveštavanje studenata i zaposlenih o neposrednom kontaktu u školi sa osobom kod koje je potvrđeno prisustvo virusa Covid-19. Sistem je baziran na upotrebi *beacon* tehnologije koja pored praćenja kontakta omogućava i automatizaciju sprovođenja skoro svih propisanih mera u realnom vremenu u cilju sprečavanja zaražavanja i širenja infekcije. Pomoću *beacon* tehnologije moguće je u realnom vremenu pratiti kretanje studenata i zaposlenih i obavestiti ih kada je potrebno povećati rastojanje sa sagovornikom. Na ovaj način može se unapred smanjiti broj rizičnih kontakta, a samim tim i broj zaraženih. Takođe, u slučaju velike koncentracije studenata koji se dugo zadržavaju na istom mestu, što se često dešava tokom pauza između nastave, moguće je obavestiti i covid redara. Pomoću *Covid-19* sistema za praćenje kontakta može se vršiti prebrojavanje ljudi u prostorijama i na osnovu toga odrediti kada je potrebno izvršiti provetravanje i čišćenje prostorija. Na osnovu kretanja, broja bliskih kontakata, vremena provedenog u određenim prostorijama moguće je podsetiti studente i zaposlene o pranju ruku.

*Beacon* tehnologija se bazira na upotrebi BLE (Bluetooth Low Energy) protokola, čime se postiže visoka energetska efikasnost. Srž tehnologije su *beacon* uređaji koji na osnovu snage primljenog signala određuju rastojanje između sebe i drugih uređaja poput pametnih telefona. Glavna prednost *beacon*-a je mogućnost slanja poruka korisnicima u blizini putem aplikacije na pametnom telefonu. Zbog niske cene, jednostavne implementacije, male potrošnje energije i visoke preciznosti, *beacon* tehnologija je postala veoma popularna kod sistema koji uključuju lociranje, navigaciju i praćenje u zatvorenom prostoru. Kompanija Apple je predstavila *beacon* tehnologiju 2013. godine. Već 2016. godine *beacon* tržište procenjeno je na 519.6 miliona dolara, a predviđa se da će do 2026. godine vrednost porasti na 56.6 biliona dolara [1].

Međunarodni aerodrom u Hong Kongu ima preko 17000 *beacon*-a koji se koriste za navigaciju putnika po aerodromu [2]. Macy's robne kuće su 2014. godine instalirale oko 4000 *beacon*-a u preko 850 prodavnica kako bi se povećala prodaja i broj kupaca [3]. Mnogi muzeji širom sveta, poput muzeja umetnosi San Diego, koriste *beacon*-e kako bi poboljšali iskustvo posetioca [4]. Neki univerziteti koriste *beacon* tehnologiju kako bi automatizovali proces evidencije prisustva studenata na predavanjima [5].

Naredne sekcije rada organizovane su na sledeći način. U sekciji II. razmatrane su različite tehnologije koje se koriste za implementaciju lokacijskih servisa u zatvorenom prostoru. Detaljno je objašnjen princip funkcionisanja sistema. Najznačajniji rezultati istraživanja i njihova analiza predstavljeni su u sekciji III. Na kraju rada, prikazane su različite mogućnosti za modifikaciju sistema, čime bi se obezbedila održivost sistema i nakon završetka pandemije.

## II. Metod

Implementacija Covid-19 sistema za praćenje kontakta podrazumeva korišćenje proaktivnih lokacijskih servisa u zatvorenom prostoru koji omogućavaju stalno praćenje

Ivana Stefanović – Akademija tehničko-umetničkih stukovnih studija Beograd, Odsek Visoka škola elektrotehnike i računarstva, Starine Novaka 24, 11000 Beograd, Srbija (e-mail: ivanas@ viser.edu.rs).

Milutin Nešić – Akademija tehničko-umetničkih stukovnih studija Beograd, Odsek Visoka škola elektrotehnike i računarstva, Starine Novaka 24, 11000 Beograd, Srbija (e-mail: nesic@ viser.edu.rs).

Marko Milivojčević – Akademija tehničko-umetničkih stukovnih studija Beograd, Odsek Visoka škola elektrotehnike i računarstva, Starine Novaka 24, 11000 Beograd, Srbija (e-mail: markom@ viser.edu.rs).

 ISBN 978-86-7466-930-3

korisnika i iniciraju se automatski. Različiti lokacijski servisi koriste različite tehnike pozicioniranja koje se međusobno razlikuju po pitanju tačnosti, preciznosti, efikasnosti, kašnjenju, ceni i kompleksnosti implementacije.

GNSS nude niz pogodnosti kada je u pitanju pozicioniranje na otvorenom, ali u zatvorenom prostoru ne mogu obezbediti zahtevanu tačnost koja je neophodna za implementaciju Covid-19 sistema za praćenje kontakta. Za implementaciju sistema razmatarane su različite tehnike pozicioniranja poput RFID (radio-frequency identification), NFC (Near Field Communication), UWB (Ultra-wideband) tehnologija, kao i pozicioniranje u okviru WLAN mreža koje je bazirano na upotrebi Wi-Fi-a i Bluetooth-a. RFID, NFC i UWB tehnologije podrazumevaju korišćenje različitih tagova i čitača ili senzora za prijem signala sa tagova. Korišćenje bilo koje od navedenih tehnika podrazumevalo bi da svi studenti i zaposleni kod sebe moraju imati tag, dok bi čitači ili senzori bili raspoređeni po školi. Zbog ograničenog dometa, broja tagova koji se istovremeno mogu skenirati, broja čitača i senzora povećava se kompleksnost i cena implementacije sistema. *Beacon* tehnologija je specifična zbog jednostavne integracije i kompatibilnosti između *beacona* i pametnih telefona. Upotrebom *beacon* tehnologije dovoljno je da studenti i zaposleni kod sebe imaju pametni telefon na kome je instalirana odgovarajuća aplikacija. Prema Republičkom zavodu za statistiku, 2020. godine, u Republici Srbiji 94.1% stanovništva koristi mobilni telefon. Za starosnu grupu od 16 do 24 godine, kojoj pripada većina studenata, ovaj procenat iznosi 100%, za mušku populaciju, i 99.6% za žensku populaciju [6].

Wi-Fi i Bluetooth tehnologije su pogodne za implementaciju Covid-19 sistema za praćenje kontakta, jer je kao i u slučaju *beacon* tehnologije dovoljno da studenti i zaposleni kod sebe imaju pametni telefon na kome je aktiviran Wi-Fi, odnosno Bluetooth. Pozicioniranje korisnika primenom Wi-Fi vrši se na osnovu snage primljenog signala sa pristupnih tačaka, a može se koristiti i cirkularna lateracija, gde je pozicija korisnika određena presekom kružnica. Da bi se obezbedila neophodna tačnost prilikom pozicioniranja studenata i zaposlenih u školi potrebno je povećati trenutni broj pristupnih tačaka, dodavanjem novih. Ugradnja novih pristupnih tačaka i povezivanje na postojeću infrastrukturu je znatno komplikovanije i skuplje u poređenju sa ugradnjom *beacon*-a. Takođe, *beacon*-i se lako mogu postaviti na bilo kojoj lokaciji u školi, jer ne zahtevaju mrežno napajanje niti dodatne infrastrukturne radove, za razliku od pristupnih tačaka.

Pozicioniranje pomoću Bluetooth-a nudi niz prednosti u odnosu na Wi-Fi. Jedna od njih je energetska efikasnost koja je postignuta BLE protokolom. Takođe još jedna značajna prednost Bluetooth-a je mogućnost povezivanja pametnog telefona sa drugim pametnim telefonima, a da pri tome nisu neophodne pristupne tačke [7]. Razvijen je veliki broj aplikacija za praćenje Covid-19 kontakta koje koriste Bluetooth tehnologiju, poput COVIDSafe aplikacije koja se koristi u Australiji, eRouska u Češkoj, STOP COVID – Protego u Poljskoj [7]. Sve navedene aplikacije dostupne su na Google PlayStore-u i imaju preko million preuzimanja. Potrebno je naglasiti da se u ovom slučaju zapravo ne vrši pozicioniranje korisnika, nego isključivo dolazi do razmene podataka između korisnika koji su bili u neposrednom kontaktu. Na ovaj način moguće je implementirati Covid-19 sistem za praćenje kontakta, ali se ne mogu implemetirati dodatne funkcionalnosti za automatizaciju sprovođenja propisanih mera u cilju sprečavanja zaražavanja i širenja infekcije.

Na osnovu razmatranih tehnologija koje bi mogle biti implementirane u osmišljeni sistem, *beacon* tehnologija se ističe dobrim odnosom *price/performanse* i jednostavnošću implementacije.

Osnovni funkcija Covid-19 sistema za praćenje kontakta je identifikacija i obaveštavanje osoba koje su bile u neposrednom kontaktu, u školi, sa osobom kod koje je potvđeno prisustvo korona virusa Covid-19. Student ili zaposleni, kod kojeg je utvrđeno prisustvo Covid-19 virusa, putem aplikacije instalirane na svom telefonu, obaveštava školu o pozitivnom SARS-CoV-2 testu, očitavanjem QR koda sa testa. Verifikacija QR koda vrši se na sajtu republičkog fonda za zdravstveno osiguranje. Nakon uspešne verifikacije vrši se identifikacija osoba sa kojima je zaraženi bio u neposrednom kontaktu. Evropski centar za prevenciju i kontrolu bolesti (ECDC) definisao je dva kriterijama na osnovu kojih se vrši identifikacija osoba koje su bile u neposrednom kontaktu sa zaraženom osobom. Prvi kriterijum odnosi se na rastojanje između osoba, a drugi na dužinu trajanja kontakta. Prema ECDC izveštaju [8] i klasifikaciji kontakta, visok rizik od zaražavanja postoji ukoliko je osoba boravila u zatvorenom prostoru sa zaraženom osobom najmanje 15 minuta na udaljenosti manjoj od 2m. Takođe, prema ECDC izveštaju [9], koji se odnosi na školske ustanove, postoji visok rizik od zaražavanja za sve osobe koje su bile u istoj učionici za zaraženom osobom duže od 15 minuta. Sledeći korak je obaveštavanje osoba, za koje je utvrđeno da su bile u neposrednom kontaktu sa zaraženim, putem aplikacije o datumu i vremenu kontakta. Neophodno je naglasiti da prilikom obaveštavanja osoba koje su bile u neposrednom kontaktu sa zaraženom osobom neći biti otkriven identitet zaražene osobe. Osoba koja je bila u kontaktu samo se obaveštava o datumu i vremenu kontakta, zbog eventualne izolacije i praćenja simptoma. Na Slici 1. prikazani su koraci postupka identifikacije i obaveštavanja osoba o neposrednom kontaktu sa zaraženim.

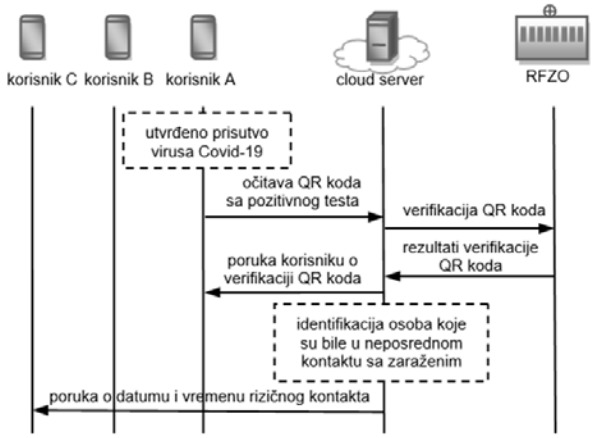


Sl. 1. Koraci postupka identifikacije i obaveštavanja osoba o neposrednom kontaktu sa osobom kod koje je utvrđeno prisustvo Covid-19 virusa.

Nedostatak ovakvog sistema je taj što se bazirana na tome da će osoba kod koje je utvrđeno prisustvo SARS-CoV-2 virusa dobrovoljno obavestiti ustanovu o pozitivnom testu. Kako bi se utvrdilo da li su student i zaposleni

 ISBN 978-86-7466-930-3

zainteresovani za ovakav sistem izvršeno je anonimno anketiranje na Akademiji tehničko-umetničkih strukovnih studija Beograd, odsek Visoka škola elektrotehnike i računarstva. Anketa sadrži 6 pitanja, sa ponuđenim odgovorima "da" i "ne":

1. Da li biste želeli da se u Školi implementira sistem pomoću kojeg se vrši identifikacija studenata i zaposlenih koji su bili u neposrednom kontaktu sa osobom kod koje je potvrđeno prisutvo Covid-19 virusa?
2. Da li biste na svom telefonu instalirali besplatnu aplikaciju za ove potrebe?
3. Da li biste u okviru aplikacije uneli Vaš broj telefona i JMBG?
4. U slučaju da ste bili u neposrednom kontaktu sa zaraženom osobom da li biste želeli da budete obavešteni putem aplikacije o datumu i vremenu kontakta?
5. U slučaju da se Vi zarazite Covid-19 virusom da li biste obavestili Školu o tome, putem aplikacije?
6. U slučaju da se Vi zarazite Covid-19 virusom da li biste želeli da se osobe koje su bile u bliskom kontaktu sa Vama tokom boravka u Školi obaveste putem aplikacije o datumu i vremenu kontakta? Osobe sa kojima ste bili u bliskom kontaktu dobile bi isključivo podatke o datumu i vremenu kontakta, ali ne o osobi sa kojom su bile u kontaktu.

Anketirano je 73 studenata i 17 zaposlenih. Rezultati ankete prikazani su u sekciji III.

## III. GLAVNI REZULTATI

### A. *Rezultati ankete*

U Tabeli I. prikazani su rezultati ankete za svako pitanje pojedinačno. Iz Tabele I. se vidi da više od 75% anketiranih želi da se u školi implementira sistem za identifikaciju studenata i zaposlenih koji su bili u neposrednom kontaktu sa osobom kod koje je potvrđeno prisustvo virusa Covid-19, i da bi za tu potrebu instalirali besplatnu aplikaciju na svom telefonu. Čak 87.78% anketiranih je spremno da putem aplikacije obavesti školu o pozitivnom SARS-CoV-2 testu. Većina anketiranih, preko 80% želi da bude obavešteno o neposrednom kontaktu, kao i da drugi budu obavešteni. Sa druge strane, 34.44% anketiranih ne želi da unese broj telefona i JMBG u okviru aplikacije. Ovi podaci su neophodni radi verifikacije testa i obaveštavanja korisnika o neposrednom kontaktu.

TABELA I
REZULTATI ANKETE

| Pitanje | Odgovor DA | Odgovor NE |
|---|---|---|
| 1. | 75.56 % | 24.44 % |
| 2. | 75.56 % | 24.44 % |
| 3. | 65.56 % | 34.44 % |
| 4. | 81.11 % | 18.89 % |
| 5. | 87.78 % | 12.22 % |
| 6. | 84.44 % | 15.56 % |

Prilikom analize odgovora anketiranih izdvojile su se tri grupe odgovora. 52.22% anketiranih je na sva pitanja odgovorilo sa da, dok je svega 12.22% na sva pitanja odgovorilo sa ne. Takođe uočena je i grupa anketiranih, 15.56%, koja je na sva pitanja sem trećeg dala odgovor da.

### B. *Rezultati merenja*

Na osnovu 128-bitnog UUID (*Universally Unique Identifier*) broja *beacon*-a lako se može izvršiti identifikacija osoba koje su boravile u istoj učionici sa zaraženom osobom duže od 15 minuta. Sa druge strane, identifikacija studenata i zaposlenih koji su proveli više od 15 minuta sa zaraženim na rastojanju manjem od 2 m, u nekom drugom prostoru poput hodnika ili kabineta, zahteva veću preciznost.

Za merenje rastojanja i prijemne snage korišćena je Radius Networks aplikacija *Locate*. Telefon marke Huawei p20 pro korišćen je kao *ibeacon*, pri čemu je predajna snaga podešena na -56dBm. Kao prijemnik korišćen je telefon marke Huawei p30 pro. Telefoni su postavljeni na rastojanju od 2 metra, a merenje je vršeno tokom 15 minuta, za tri slučaja. U prvom slučaju telefon koji je korišćen kao prijemnik nalazi se u ruci, u drugom slučaju u torbi, a u trećem u džepu od pantalona. Na Slici 2. dat je grafički prikaz procenjene udaljenosti tokom vremenskog intervala od 15 minuta, pri čemu je na horizontalnoj osi prikazano vreme u minutima, a na vertikalnoj osi procenjeno rastojanje u metrima, za sva tri slučaja, pri čemu su rezultati beleženi svakih 10 sekundi.

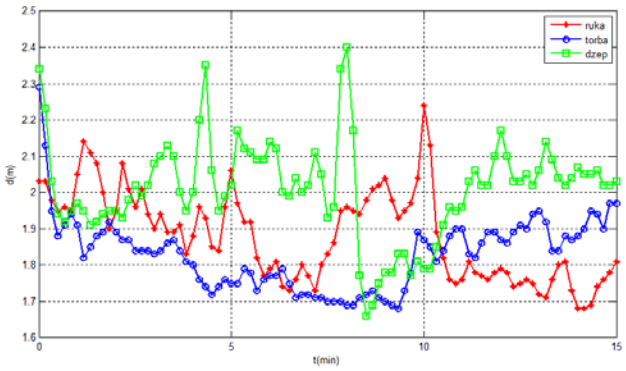


Sl. 2. Procena udaljenosti korisnika od *beacon*-a tokom vremenskog intervala od 15 minuta

Najveće izmereno odstupanje procenjenog rastojanja od realnog iznosi 0.4m. Ovo odstupanje dobijeno je u trećem slučaju, kada se telefon nalazio u džepu. Sa Slike 2. se može uočiti da je za slučaj kada se telefon nalazi u torbi procenjeno rastojanje skoro uvek manje od stvarnog rastojanja. Takođe, u slučaju kada se telefon nalazi u ruci, tokom 81% vremena merenja, rastojanje je procenjeno na manje od stvarnog. Sa druge strane, u slučaju kada se telefon nalazi u džepu, procenjeno rastojanje je veće od stvarnog rastojanja tokom 54% vremena merenja. Ovo je najverovatnije posledica statičnosti telefona i njegovog položaja kada je torbi, dok se u ruci i džepu telefon pomera pa samim tim i dijagram zračenja menja svoj pravac. Srednja greška procenjenog rastojanja za sva tri slučaja, dobijena na osnovu 273 merenja iznosi ±0.14m. Na ovaj način postignuta je preciznost od 74.73%. Pri tome najviša preciznost postiže se u slučaju kada se telefon nalazi u torbi, čak 97.8%, dok se najniža preciznost postiže u slučaju kada se telefon nalazi u džepu, samo 39.56%. Preciznost je definisana kao odnos broja merenja kada je detektovano da se korisnik nalazi na rastojanju manjem ili jednakom od 2 m i rastojanju koje je veće od 2 m.


ISBN 978-86-7466-930-3

Kako je utvrđeno da srednja greška procenjenog rastojanja iznosi ±0.14 m na dobijene rezultate merenja primenjen je novi kriterijum pri čemu se kao kritično rastojanje uzima 2.14 m. Povećanjem rastojanja sa 2 m na 2.14 m postiže se preciznost od 95.97%. U Tabeli II. dat je pregled preciznosti za sva tri slučaja, pojedinačno, kada se kao kritično rastojanje koristi 2 m i 2.14 m. Kao što se vidi iz Tabele II. promena rastojanja sa 2 m na 2.14 m dovodi do povećanja preciznosti u sva tri slučaja, pri čemu se u trećem slučaju beleži najveći porast preciznosti od čak 50.55%.

TABELA II
PRECIZNOST

| | kriterijum 2 m | kriterijum 2.14 m |
|---|---|---|
| ruka | 82.42 % | 98.90 % |
| torba | 97.80 % | 98.90 % |
| džep | 39.56% | 90.11 % |

Na Slici 3. dat je grafički prikaz izmerenog RSSI (*Received Signal Strength Indicator*), za sva tri slučaju, tokom vremenskog intervala od 15 minuta. Srednja vrednost RSSI dobijena sumiranjem svih prikupljenih podataka iznosi -66.07 dBm. Potrebno je naglasiti da postoje mala odstupanja srednje vrednosti RSSI za sva tri slučaja pojedinačno. Minimalna izmerena vrednost RSSI je -71 dBm, a maksimalna -61 dBm.

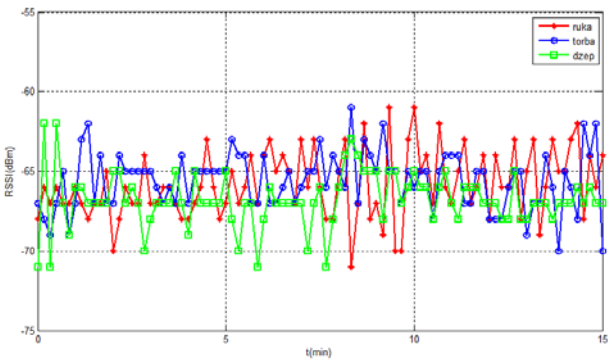


Sl. 3. Izmerene vrednosti RSSI tokom vremenskog interval od 15 minuta

Pomoću jednačine (1) može se odrediti eksponent slabljenja, *n*. $RSSI_{do}$ predstavlja srednju vrednost izmerenog RSSI na rastojanju od 1m, dok $RSSI_d$ predstavlja srednju vrednost izmerenog RSSI na rastojanju *d* [10].

$$n = \frac{RSSI_{d0} - RSSI_d}{10 \cdot \log d} \quad (1)$$

Na osnovu 20 merenja srednja vrednost RSSI na rastojanju od 1m iznosi -58.20 dBm. Zamenom dobijenih vrednosti u jednačinu (1) dobija se eksponent slabljenja *n*=2.61. Dobijeni eksponent slabljenja odgovara eksponentu slabljenja u poslovnim zgradama, isti sprat, pri frekvenciji od 2.4 GHz, čija se vrednost kreće u opsegu od 1.6 do 3.5 [11].

Izvršena su merenja RSSI i na rastojanjima 0.5 m, 1.5 m, 2.5 m i 3 m. Dobijene vrednosti eksponenta slabljenja prikazane su u Tabeli III. Na osnovu dobijenih rezultata srednja vrednost eksponenta slabljenja iznosi 2.32. Pri eksponentu slabljenja od 2.32 i srednjoj vrednosti RSSI od -66.07 dBm procenjuje se da je korisnik udaljen od *beacon*-a 2.18m, odnosno srednja greška procenjenog rastojanja iznosi ±0.18 m. Dakle, dobijeno je odstupanje od svega ±0.04 m u odnosu na rezultate dobijene merenjem i novo uvedeni kriterijum od 2.14m.

TABELA III
EKSPONENT SLABLJENJA NA RAZLIČITIM RASTOJANJIMA

| d | 0.5 m | 1.5 m | 2 m | 2.5 m | 3 m |
|---|---|---|---|---|---|
| n | 2.01 | 2.14 | 2.61 | 2.15 | 2.67 |

## IV. ZAKLJUČAK

U ovom radu je pokazano da je *beacon* tehnologija odličan izbor za implementaciju Covid-19 sistema za praćenje kontakta u zatvorenom prostoru jer nudi niz pogodnosti poput visoke preciznosti, niske cene, jednostavne implementacije, održavanja i nadogradnje.

Sistem koji je prikazan u ovom radu namenjen je za visokoškolske institucije ali se može implementirati i u drugim zatvorenim prostorima poput tržnih centara, bankama, bolnicama, domovima zdravlja, firmi i kompanija sa velikim brojem zaposlenih i sl. U slučaju implementacije sistema npr. u tržnim centrima mogu se iskoristiti već postojeće aplikacije, poput aplikacija Tvoj Centar, Ada Loyalty Club i dr.

Nedostatak opisanog sistema je ograničeno trajanje koje zavisi od završetka pandemije, međutim u visokoškolskim institucijama nakon završetka pandemije sistem se lako može prilagoditi i koristiti za druge potrebe, poput navođenja kandidata po školi prilikom predaje dokumenata, polaganja prijemnog ispita i upisa, evidenciju studenata na nastavi i ispitima, obaveštavanje studenata i zaposlenih o rasporedu nastave, lociranje zaposlenih i sl. Takođe, i u drugim institucijama van obrazovanja po završetku pandemije moguće je prilagoditi sistem konkretnim potrebama u cilju unapređenja radnih procesa, povećanja efikasnosti i zadovoljstva klijenata.

## LITERATURA

[1] T. Alsop, “Beacons technology market revenue worldwide 2016 and 2026”, Statista, October, 2020.
[2] P. Tedeschi, K. Eun Jeon, J. She, S. Wong, S. Bakiras, R. Di Pietro, “Privacy-Preserving and Sustainable Contact Tracing Using Batteryless Bluetooth Low-Energy Beacons”, *IEEE Security & Privacy*, pp. *2-11*, October, 2021.
[3] L. Chamberlain, “Macy’s To Test Beacon Messages Outside App, Explore Retargeting”, March, 2016. [Online]. Available: https://geomarketing.com/macys-to-test-beacon-messages-outside-app-explore-retargeting
[4] K. Shams, “8 museums successfully using beacons & 8 examples of beacon innovations”, September, 2016. [Online]. Available: https://proxera.net/8-museums-successfully-using-beacons-8-examples-of-beacon-innovations/
[5] S. Perez, “BeHere Lets Teachers Take Attendance Using iBeacon Technology”, March, 2016. [Online]. Available: https://techcrunch.com/2014/03/28/behere-lets-teachers-take-attendance-using-ibeacon/
[6] M. Kovačević, V. Šutić, U. Rajčević, A. Milaković, “Upotreba informaciono-komunikacionih tehnologija u Republici Srbiji”, Republički zavod za statistiku, Beograd, Srbija, 2020. [Online]. Available: https://publikacije.stat.gov.rs/G2020/Pdf/G202016015.pdf
[7] M. Shahroz, F. Ahmada, M. Shahzad Younis, N. Ahmadb, M. N. Kamel Boulos, R. Vinuesa, J. Qadir, “COVID-19 digital contact

 ISBN 978-86-7466-930-3

tracing applications and techniques: A review post initial deployments", *Transportation Engineering 5 (2021): 100072*, May, 2021.
[8] "Contact tracing: public health management of persons, including healthcare workers, who have had contact with COVID-19 cases in the European Union – third update", European Centre for Disease Prevention and Control, Stockholm, Sweden, 18 November 2020. [Online]. Available: https://www.ecdc.europa.eu/sites/default/files/documents/covid-19-contact-tracing-public-health-management-third-update.pdf
[9] "Objectives for COVID-19 testing in school settings – first update", European Centre for Disease Prevention and Control, Stockholm, Sweden, 21 August 2020. [Online]. Available: https://www.ecdc.europa.eu/sites/default/files/documents/covid-19-objectives-school-testing.pdf
[10] J. Röbesaat, P. Zhang, M. Abdelaal, O. Theel, "An Improved BLE Indoor Localization with Kalman-Based Fusion: An Experimental Study", *Sensors 17.5 (2017): 951*, 2017.
[11] O. S. Oguejiofor, A. N. Aniedu, H. C. Ejiofor, G. N. Okechukwu, "Indoor Measurement And Propagation Prediction Of WLAN At 2.4GHz", *International Journal of Engineering Research & Technology*, vol. 2, no. 7, pp. 798-802, July, 2013.

ABSTRACT

This paper discusses the possibility of applying beacon technology to develop solutions that allow monitoring of close contacts and automate the implementation of prescribed measures in real time, in order to prevent spread of infection caused by Covid-19 virus in higher education institutions. For the realization of the system, it is enough that students and employees have a smartphone on which the appropriate application is installed. The system is based on the fact that the student and employees who have been diagnosed with the Covid-19 virus will voluntarily inform the higher education institution about the positive test, through the application. An anonymous survey was conducted to determine whether students and employees are interested in implementing the Covid-19 contact tracking system. Practical measurements were also performed, and the obtained results confirm that beacon technology is an excellent choice for system implementation.

## Possibility of applying beacon technologies for the development of Covid-19 contact tracking systems in higher education institutions

Ivana Stefanović, Milutin Nešić i Marko Milivojčević

 ISBN 978-86-7466-930-3

# Zaštita prenosa paketskog telefonskog saobraćaja upotrebom tehnologije virtuelnih privatnih mreža

Mićo Živanović, Jovan Bajčetić, Ivan Tot

***Apstrakt*—Istraživanje predstavljeno u ovom radu prikazuje jednu realizaciju zaštite paketskog telefonskog saobraćaja primenom tehnologije virtuelnih privatnih mreža kroz konfiguraciju servera za prenos paketskog telefonskog saobraćaja i zaštićeni prenos uz primenu tehnologije virtuelnih privatnih mreža u tunel modu, primenom odgovarajućeg protokola za zaštitu tajnosti, autentifikaciju, zaštitu integriteta i razmenu kriptografskih ključeva. Izvršeno je snimanje i analiza saobraćaja primenom softvera Wireshark u zaštićenom i nezaštićenom prenosu. Prikazani rezultati omogućavaju lakše razumevanje kompleksnog procesa uspostave tunela upotrebom simulacionog softvera u edukaciji.**

***Ključne reči*—paketski telefonski saobraćaj; virtuelne privatne mreže; zaštićena komunikacija; kriptografski ključ.**

## I. Uvod

Stalan razvoj Interneta ima za posledicu da je Internet postao univerzalno sredstvo za komunikaciju. U toku razvoja, postavio se zahtev za bezbednošću prenošenih informacija koji se ogledao u obezbeđenju bezbednosnih servisa: autentifikacije, poverljivosti, neporecivosti i integriteta podataka [1]. Razvijeni su sistemi zaštite u tri ravni: upravljačkoj, kontrolnoj i ravni podataka. Za potrebe ovog rada biće razmotreni mehanizmi zaštite u ravni podataka koji se odnose na informacioni saobraćaj. Ravan podataka se štiti pomoću implementiranja pravila (bezbednosnih polisa) po kojima se informacioni sadržaj prenosi upotrebom mrežnih uređaja.

Jedna od tehnologija koja omogućava zaštitu prenosa podataka u ravni podataka je tehnologija virtuelnih privatnih mreža (VPN – Virtual Private Networks). Navedena tehnologija pruža sledeće mogućnosti umrežavanja:
– Intranet, umrežavanje geografski dislociranih objekata;
– Udaljeni pristup mobilnih korisnika (rad od kuće);
– Ekstranet, ograničeni pristup nekoj mreži iz drugih mreža (pristup poslovnih partnera korporativnom WAN-u) [2].

Za realizaciju virtuelne privatne mreže mogu se koristiti periferni korisnički uređaji (host, ruter ili svič), na lokaciji korisnika (CE – Customer Edge) i periferni mrežni uređaji provajdera (PE – Provider Edge).

Virtuelnu privatnu mrežu čini više udaljenih mreža koje su povezane preko Interneta. Zbog korišćenja zajedničkih resursa na Internetu, komunikacija među korisnicima virtuelne privatne mreže se mora zaštititi. Zaštita virtuelne privatne mreže se ostvaruje pomoću barijera koje implementiraju IPSec protokol u tunel modu [3].

VPN tunel je veza između dva PE rutera ili dva CE uređaja koji predstavljaju krajnje tačke tunela [2].

Prema IETF, IP VPN se mogu klasifikovati u zavisnosti od odgovornosti u pogledu upravljanja na:
– VPN kojima upravlja korisnik (Customer Provisioned VPN, CP VPN);
– VPN kojima upravlja provajder servisa (Provider Provisioned VPN, PP VPN) [2].

Prema lokaciji VPN opreme, PP VNP se mogu podeliti na:
– CE – bazirane, kod kojih su krajnje tačke VPN locirane kod korisnika;
– PE – bazirane, kod kojih su krajnje tačke VPN tunela locirane kod provajdera, na PE ruteru.

U zavisnosti od ponuđenog servisa, PE – bazirane VPN se dele na:
– PE – bazirane L2 VPN (koje pružaju servise OSI sloja 2);
– PE – bazirane L3 VPN (koje pružaju servise OSI sloja 3);
– CE – bazirane IP VPN pružaju samo servise OSI sloja 3.

Istovremeno sa razvojem bezbednosnih servisa razvijaju se arhitekture za pružanje različitih komunikacionih servisa koji koriste Internet protokol (telefonija, video, podaci, multimedijalni servisi). Prenos telefonije preko Interneta razvijao se postupno, pre svega zbog prethodno razvijenih sistema klasičnih javnih telefonskih mreža (PSTN) i digitalnih mreža sa integrisanim servisima (ISDN).

U cilju razvoja telefonije zasnovane na komutaciji paketa (VoIP telefonija), razvijene su grupe protokola za prenos VoIP telefonije i povezivanje VoIP telefonije sa telefonijom koja se prenosi u drugim sistemima prenosa (H.323 i SIP protokol) [4].

Prikaz istraživanja u ovom radu će se sastojati iz opisa načina realizacije zaštite informacije korišćenjem VPN tehnologije, a potom u jednoj realizaciji zaštite prenosa paketskog telefonskog saobraćaja upotrebom tehnologije

Mićo Živanović – Ministarstvo odbrane, Sektor za ljudske resurse, Nemanjina 15, 11000 Beograd, Srbija (e-mail: comiveza@yahoo.com).
Jovan Bajčetić – Vojna Akademija, Univerzitet odbrane u Beogradu, Veljka Lukića Kurjaka 33, 11042 Beograd, Srbija (e-mail: bajce05@gmail.com).
Ivan Tot – Vojna Akademija, Univerzitet odbrane u Beogradu, Veljka Lukića Kurjaka 33, 11042 Beograd, Srbija (e-mail: totivan@gmail.com).

 ISBN 978-86-7466-930-3

virtuelnih privatnih mreža, upotrebom IPSec protokola u tunel modu ka udaljenom korisniku, uz prikaz analize mrežnog saobraćaja korišćenjem programskog alata Wireshark.

## II. ZAŠTITA PODATAKA PRIMENOM TEHNOLOGIJE VIRTUELNIH PRIVATNIH MREŽA

Za prenos informacionog sadržaja preko Interneta neophodno je obezbediti zaštitu u prenosu. Čest je slučaj da kompanije koriste Internet kao okosnicu za povezivanje svojih filijala ili klijenata kako bi ostvarili prenos podataka za svoje potrebe. Iz navedenog razloga nameće se potreba za zaštitu prenošenog saobraćaja. U tu svrhu koriste se različite tehnologije, od kojih je jedna - tehnologija virtuelnih privatnih mreža. Za realizaciju virtuelnih privatnih mreža na raspolaganju je više tehnologija, zavisno od toga da li se VPN realizuje kao "oblast – oblast" (site–to–site) ili kao "udaljeni pristup" (remote access). U oba navedena slučaja najčešće se koristi IPSec (IP security) protokol.

IPSec protokol štiti pakete između dva uređaja u mreži [3].

Uređaji kojima se realizuje IPSec su: server, ruteri, korisnički računari ili specijalizovani hardver. IPsec pruža dve vrste zaštite: autentifikaciju i poverljivost.

Mehanizam autentifikacije osigurava da je primljeni paket zaista poslao onaj ko je u zaglavlju paketa naveden kao izvor i da se paket nije promenio tokom prenosa, dok mehanizam poverljivosti omogućava entitetima u komunikaciji da šifruju poruke kako bi sprečili nepozvana lica da dođu do sadržaja poruka [1]. Za šifrovanje podataka se koriste simetrični algoritmi (DES, 3DES, AES), što zahteva pouzdanu razmenu ključeva strana u komunikaciji i za tu svrhu se koriste protokoli za autentifikaciju (neki od protokola iz IETF (IKE - Internet Key Exchange) standarda) [3].

Razvoj bezbednosti u arhitekturi Interneta se odvijao postepeno u čemu je značajno mesto imala Radna grupa za inženjering Interneta (IETF – Internet Engineering Task Force). Sâmo uvođenje standarda je išlo postepeno. Prvi u nizu standard IETF koji se odnosio na bezbednost u arhitekturi Interneta bio je standard RFC 1636 (Request for Comments). Standard se odnosio na osnove bezbednosti Interneta (upotreba firewall – a, servis autentifikacije, privatnost i dr.) [5].

Da bi se adekvatno razumeo način formiranja VPN sesije in a pravi način predstavio prilikom edukacije, biće razmotreno nekoliko najvažnijih dokumenata IETF kojima su definisani režimi rada VPN, mehanizam autentifikacije, razmena kriptografskih ključeva i zaštita poverljivosti.

IPSec koristi dva protokola za bezbednost: AH (Authentication Header) i ESP (Encapsulating Security Payload). Zaglavlje autentifikacije (AH) je definisano specifikacijom RFC 4302 (IP Authentication Header), dok je ESP enkapsulirajuće bezbedno pakovanje (Encapsulating Security Payload) definisan specifikacijom RFC 4303. AH i ESP podržavaju dva režima rada: transportni režim i tunelovanje.

U transportnom režimu AH autentifikuje IP koristan sadržaj i odabrane delove IP zaglavlja, dok ESP šifruje i opciono autentifikuje IP koristan sadržaj. Tunelovanje vrši zaštitu celog IP paketa. Navedeno se postiže nakon dodavanja AH i ESP polja i tretiranja celog paketa kao korisnog sadržaja novog spoljnog IP paketa sa novim IP zaglavljem.

U režimu tunelovanja ESP šifruje i opciono autentifikuje ceo unutrašnji IP paket, uključujući unutrašnje IP zaglavlje, dok AH u režimu tunelovanja autentifikuje ceo unutrašnji IP paket i odabrane delove spoljnog IP zaglavlja [1].

Redosled postupaka sa paketima za rad ESP u transportnom i tunel režimu, je sledeći:

– U transport režimu blok podataka koji se sastoji od segmenta transportnog sloja sa dodatim ESP završnim blokom se šifruje, sa dodatim zaglavljem za autentifikaciju (opciono);

– U režimu tunelovanja, ESP se koristi za šifrovanje celog IP paketa, ESP zaglavlje ide ispred paketa i šifruje se paket zajedno sa ESP završnim blokom.

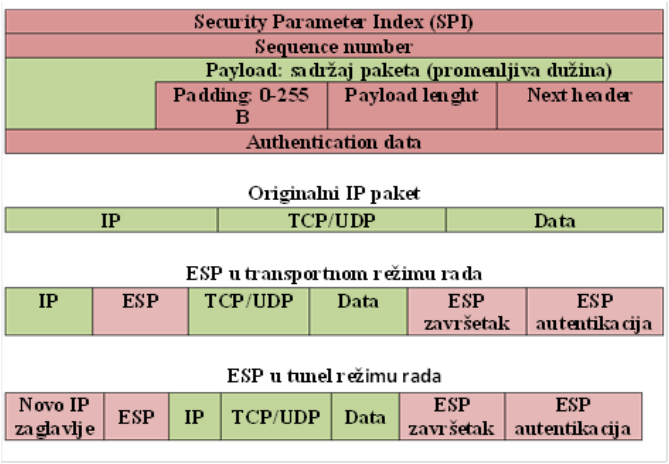


Sl. 1 Opseg ESP šifrovanja u transportnom i tunel modu [6]

Sl. 1 prikazuje format jednog ESP paketa. Indeks bezbednosnih parametara (SPI) definiše jednu bezbednosnu asocijaciju kojom se određuje algoritam šifrovanja i autentifikacije, ključevi, inicijalizacione vrednosti, životni vek ključeva i vezani parametri koji se koriste uz ESP. Broj sekvence je vrednost brojača paketa kojom se sprečava ponavljanje paketa. Sadržaj paketa je promenljive dužine i predstavlja segment transportnog sloja (transport režim) ili IP paket (tunel režim). U tunel modu, celom paketu se dodaje novo IP zaglavlje koje ima dovoljno informacija za rutiranje, ali ne i za analizu saobraćaja [6].

Važan deo IPSec koji se odnosi na upravljanje ključevima obuhvata određivanje i distribuciju ključeva. Dokumentom RFC 4301 definisane su dve vrste upravljanja ključevima:

– Ručno (administrator definiše sistem sopstvenim ključevima i ključevima drugih sistema sa kojima komunicira);

– Automatizovano (omogućava generisanje ključeva za bezbednosnu asocijaciju na zahtev koji je pogodan za velike sisteme sa rastućom konfiguracijom) [7].

Protokol koji se koristi za automatizovano upravljanje ključevima za IPSec je ISAKMP (Internet Security


ISBN 978-86-7466-930-3

Association and key Management Protocol) i definisan je dokumentom IETF RFC 2408. ISAKMP definiše procedure za kreiranje i upravljanje bezbednosnim asocijacijama, tehnike generisanja ključeva, ublažavanje pretnji (npr. od DDoS napada) [8].

ISAKMP ne nalaže konkretan algoritam za razmenu ključeva, već se sastoji od jednog skupa tipova poruka koje omogućavaju upotrebu raznovrsnih algoritama za razmenu ključeva.

Karakteristike IKE određivanja ključeva su:
– Osujećenje DDoS napada;
– Omogućava razmenu ključeva za pregovaranje oko grupe ključeva;
– Obezbeđuje od napada ponavljanjem korišćenjem jednokratnih brojeva;
– Omogućava razmenu javnih ključeva;
– Onemogućava napad tipa "čovek u sredini".

IKE potprotokol obezbeđuje dogovaranje protokola, algoritama i ključeva između učesnika u komunikaciji, proverava autentičnost učesnika koji učestvuju u postupku dogovaranja, omogućava razmenu podataka na osnovu kojih će se generisati ključevi i upravljati razmenom ključeva. IKE potprotokol obavlja se u dve faze [9].

U prvoj fazi dva učesnika uspostavljaju bezbedni komunikacioni kanal kojim će se obaviti dogovaranje bezbednosnih parametara i razmena ključeva. Dogovaranje parametara i razmena ključeva, odnosno uspostava bezbednosne asocijacije obavlja se u drugoj fazi. Za sprovođenje postupka koriste se tri načina razmene informacija, dva za prvu fazu i jedan za drugu fazu IKE potprotokola:
– Osnovni način;
– Agresivni način;
– Brzi način.

Osnovni način razmene informacija (engl. Main mode) koristi se u prvoj fazi IKE potprotokola i služi da bi se uspostavio bezbednosni komunikacioni kanal kojim će se obaviti razmena podataka potrebnih za kasniju komunikaciju AH ili ESP potprotokolima.

Agresivni način razmene, slično kao i osnovni, koristi se u prvoj fazi IKE potprotokola i služi za uspostavljanje sigurnog komunikacionog kanala za dogovor učesnika i ne obavlja se kroz bezbedni kanal. Agresivni način koristi samo tri poruke u razmeni i nešto je jednostavniji i brži od osnovnog načina, ali se dokazivanje identiteta ne vrši kroz bezbedan kanal.

Nakon uspostave bezbednog kanala primenom osnovnog ili agresivnog načina razmene, započinje druga faza IKE potprotokola. Druga faza koristi se brzim načinom razmene ključeva koja služi za dogovaranje bezbednosnih parametara komunikacije AH ili ESP potprotokolom i za razmenu tajnih simetričnih ključeva.

## III. JEDNA REALIZACIJA ZAŠTITE PAKETSKOG TELEFONSKOG SAOBRAĆAJA UPOTREBOM TEHNOLOGIJE VIRTUELNIH PRIVATNIH MREŽA

U uvodu rada predstavljena je podela VPN prema tome ko je odgovoran za uspostavu zaštićene komunikacije (provajder ili korisnik), kao i koja vrsta servisa se ostvaruje (sloj 2 ili 3 OSI referentnog modela). Predloženi model koje će u nastavku biti prikazan omogućava realizaciju jedne VPN koja bi predstavljala primer uspostave zaštite VoIP putem VPN za koju je „odgovoran" provajder, na OSI sloju 3 i da se primenom programskog alata „Wireshark" snimi i analizira ostvareni saobraćaj. Za navedene potrebe je uspostavljena mrežna topologija prikazana na Sl. 2.

Ruteri predstavljaju periferne rutere provajdera na kojima se vrši konfigurisanje VPN konekcije, po modelu "oblast – oblast". Na ruteru 1 su konfigurisani i uspostavljeni VPN, VoIP i DHCP server.

VPN server je konfigurisan sledećim parametrima:
– ISAKMP razmena kripto ključeva (policy 10);
– Kripto algoritam 3DES;
– Algoritam za autentifikaciju MD5 [10];
– Rad u tunel modu.

VoIP server je određen sledećim parametrima:
– Konekcija SIP protokolom;
– Kodek g711 ulaw.

Za razumevanje rada VoIP, ukratko će biti objašnjen prenos signalizacije i kontrola saobraćaja u VoIP prenosnim sistemima, u kojima se najčešće koriste H.323 i SIP protokoli.

H.323 preporuka je deo familije ITU-T preporuka sa zajedničkom oznakom H.32x koje se odnose na multimedijalne komunikacije preko različitih mreža. H.323 definiše protokole zadužene za usluge multimedijalnih komunikacija preko mreža zasnovanih na komutaciji paketa. H.323 se najčešće koristi kao signalizacioni i kontrolni protokol u VoIP i za video konferencije, a bio je prvi standard koji je koristio RTP protokol (Real-time Transfer Protocol) za konkretni prenos audio i video signala preko mreže.

H.323 je standard koji omogućava multimedijalnu komunikaciju preko različitih mreža (usko pojasne ISDN, širokopojasne B-ISDN, lokalne računarske mreže, mreže na bazi komutacije kola). Cilj je postizanje interoperabilnosti sa različitim mrežama za prenos multimedijalnih informacija, kroz upotrebu zajedničkih preporuka, procedura i poruka, kao i uvođenjem komponente mrežnog prolaza. H.323 standard predstavlja skup protokola namenjenih za obavljanje različitih funkcija u okviru H.323 sistema i to: audio kodere i dekodere, video kodere i dekodere, signaliziranje poziva, kontrola poziva, protokol prenosa u realnom vremenu (RTP), protokol kontrole prenosa u realnom vremenu (RTCP), registraciju, pristup i status i ostale protokole za prenos podataka u realnom vremenu [4].

 ISBN 978-86-7466-930-3

SIP je protokol za uspostavljanje, modifikaciju i raskidanje multimedijalnih sesija u paketskim mrežama. SIP u kombinaciji sa drugim protokolima se koristi za opis karakteristika sesije potencijalnim učesnicima [11]. SIP je delo IETF (Internet Engineering Task Force) i razvijen je kao mehanizam za uspostavljanje raznovrsnih sesija, a može se koristiti za unicast i multicast komunikaciju. SIP je peer-to-peer protokol, što znači da nije centralizovan, već je servisna inteligencija izmeštena prema krajevima mreže ka krajnjim korisnicima, kao kod računarskih mreža. U okviru SIP poruka se najčešće prenosi SDP (Session Description Protocol), mada standard ostavlja otvorenim i druge mogućnosti [12].

H.323 i SIP su dva konkurentska protokola za multimedijalne komunikacije na paketskim mrežama.

SIP se odlikuje sledećim prednostima:

– Fleksibilnost (omogućava korišćenje sa različitim transportnim i drugim protokolima);
– Arhitektura i osobine mu se prirodno uklapaju Internet okruženje, dok H.323 ima neke osobine protokola fiksne telefonije;
– Poseduje mnoga proširenja potrebna za različite sisteme ličnih komunikacija (prisutnost, instant poruke, posredno upravljanje pozivom) [13].

DHCP server je uspostavljen za opseg adresa koji obezbeđuje formiranje logički odvojenih mreža sa opsegom adresa 20.20.20.0 i 30.30.30.0 u različitim virtuelnim lokalnim mrežama. Prema mrežnoj topologiji formirane su dve LAN mreže u okviru kojih je izvršeno razdvajanje saobraćaja (telefonskog i podaci), uspostavom dve VLAN na OSI sloju L2, konfigurisanjem svičeva 1 i 2 (VLAN 20 i 30), dok je po jedan interfejs na svičevima konfigurisan kao trank interfejs [14]. Nakon provere konektivnosti, uspostavljen je paketski telefonski saobraćaj bez zaštite pomoću virtuelne privatne mreže i realizovano snimanje saobraćaja, upotrebom programskog alata "Wireshark". Rezultat i procesi analize nezaštićenog saobraćaja prikazani su u Tabeli 1. Uspostavljena je VPN sesija između dva rutera i realizovano snimanje saobraćaja u zaštićenom modu. Procesi u toku uspostave zaštićenog paketskog telefonskog saobraćaja prikazani su u Tabeli 2.

Za realizaciju mrežne topologije na slici 2 korišćena je sledeća mrežna oprema:

– CISCO 2900 ruter…….2 kom;
– CATALIST 3650 svič ……..2 kom;
– Računar sa ETH mrežnim interfejsom…. 2 kom;
– IP telefoni……..2 kom.

Procesi prikazani u Tabeli 1, a koji se odnose na uspostavu i održavanje nezaštićenog telefonskog saobraćaja prikazuju proces uspostavljanja prisutnosti uređaja u mreži i utvrđivanja mrežnih usluga (SSDP), uspostavu logičke topologije mreže i saobraćaja protokola za sprečavanje petlji (STP). Pozivanjem jednog korisnika od strane drugog korisnika ustanovljava se IP adresa pozvanog korisnika kroz broadcast upit od strane pozivajućeg korisnika (ARP proces). Kroz DNS proces se povezuju IP adresa i ime domena pozvanog korisnika. Istovremeno se šalje poruka radi utvrđivanja dostupnosti korisnika (ICMP poruka). U toku uspostave VoIP komunikacije šalje se "hello poruka" u OSPF procesu, radi konstruisanja putanje između dva rutera. Kroz SIP signalizaciju vrši se pozivanje jednog od strane drugog korisnika, nakon čega se ostvaruje TCP sesija kroz proces "trostrukog rukovanja". U sklopu SIP procesa razlikuju se faze (traying, ringing i OK), u kojima se mogu uočiti status procesa pozivanja, koji se na kraju završava uspešnom uspostavom komunikacije. Ceo proces je praćen slanjem kontrolnih TCP poruka (ACK), kojima se određuje broj bajtova koji se može poslati pre dobijanja sledeće dozvole za slanje, kao i slanjem poruka kojima se vrši sinhronizacija uspostave TCP sesije (SYN). Poseban segment kontrole komunikacije predstavlja kontrola konektivnosti na L2 nivou (LOOP). Dalji proces komuniciranja je praćen razmenom paketa u realnom vremenu (RTP) koji nose govorni informacioni sadržaj.

Procesi prikazani u Tabeli 2, a koji se odnose na uspostavu i održavanje zaštićenog telefonskog saobraćaja, pored na početku navedenih procesa u nezaštićenom prenosu, sadrži proces razmene kripto ključeva u procesu uspostave IPSec tunela (ISAKMP). Specifično za proces prenosa u zaštićenom modu je uspostavljen trank između dva sviča na kojima su konfigurisane dve VLAN (DTP).

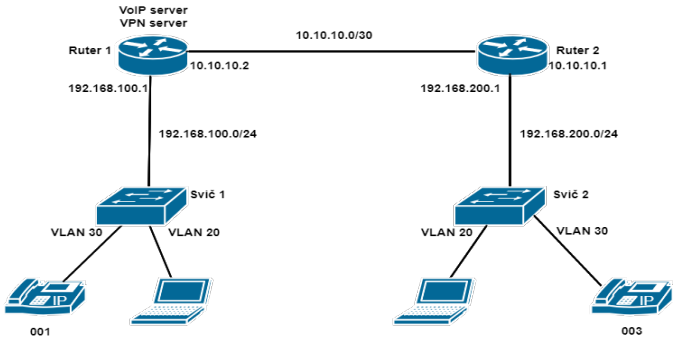


Sl. 2 Mrežna topologija za potrebe jedne realizacije zaštite paketskog telefonskog saobraćaja upotrebom tehnologije virtuelnih privatnih mreža

Prikazana realizacija mrežne topologije, snimanje i analiza mrežnog saobraćaja omogućava detaljno razumevanje uspostave VPN tunela, uz upotrebu simulacionog softvera, kao i praćenje procesa razmene informacionog sadržaja u realnom vremenu. Tokom procesa prenosa informacionog sadržaja u realnom vremenu, periodično se uočavaju procesi uspostavljanja prisutnosti uređaja u mreži (SSDP), obaveštavanja o nedostupnosti uređaja u slučaju prekida konektivnosti (ICMP poruke) i razmena "hello" poruka u OSPF procesu. Navedena realizacija stoga omogućava potpun uvid u sve procese u toku prenosa paketskog telefonskog saobraćaja, što može poslužiti u edukaciji i o procesima prenosa multimedijalnih informacionih sadržaja.


ISBN 978-86-7466-930-3

TABELA I
POZIV UČESNIKA 001 KA UČESNIKU 003 BEZ VPN ZAŠTITE

| R.br. | Vreme [s] | Izvorišna adresa | Odredišna adresa | Protokol | Veličina [B] |
|---|---|---|---|---|---|
| 1. | 0,00 | Cisco_e1:aa:81 | Spanning_tree | STP | 60 |
| 2. | 0,17 | Fe80:e010:c683:5106:f3e8 | Ff02::c | SSDP | 208 |
| 3. | 1,99 | Cisco_e1:aa:81 | Spanning_tree | STP | 60 |
| 4. | 2,73 | ASUSTEkC_9d:86:8a | Cisco_00:e3:e1 | ARP | 42 |
| 5. | 2,74 | Cisco_00:e3:e1 | ASUSTEkC_9d:86:8a | ARP | 60 |
| 6. | 3,433 | 40.40.40.3 | 192.168.100.1 | DNS | 75 |
| 7. | 3,434 | 40.40.40.1 | 40.40.40.3 | ICMP | 70 |
| 8. | 4,00 | Cisco_e1:aa:81 | Spanning_tree | STP | 60 |
| 9. | 4,18 | Fe80:e010:c683:5106:f3e8 | Ff02::c | SSDP | 208 |
| 10. | 5,32 | 40.40.40.1 | 224.0.0.5 | OSPF | 90 |
| 11. | 5,99 | Cisco_e1:aa:81 | Spanning_tree | STP | 60 |
| 12. | 6,56 | 40.40.40.3 | 192.168.100.1 | DNS | 75 |
| 13. | 6,561 | 40.40.40.1 | 40.40.40.3 | ICMP | 70 |
| 14. | 6,83 | 40.40.40.3 | 30.30.30.1 | SIP/SDP | 922 |
| 15. | 7,16 | 40.40.40.3 | 30.30.30.1 | TCP | 590 |
| 16. | 7,16 | 30.30.30.1 | 40.40.40.3 | TCP | 60 |
| 17. | 7,16 | 40.40.40.3 | 30.30.30.1 | TCP | 386 |
| 18. | 7,16 | 30.30.30.1 | 40.40.40.3 | SIP | 418 |
| 19. | 7,18 | Fe80:e010:c683:5106:f3e8 | Ff02::c | SSDP | 208 |
| 20. | 7,36 | 40.40.40.3 | 30.30.30.1 | TCP | 54 |
| 21. | 7,99 | Cisco_e1:aa:81 | Spanning_tree | STP | 60 |
| 22. | 8,30 | 40.40.40.3 | 30.30.30.1 | TCP | 58 |
| 23. | 8,32 | Cisco_e1:aa:81 | Cisco_e1:aa:81 | LOOP | 60 |
| 24. | 8,37 | 30.30.30.1 | 40.40.40.3 | TCP | 590 |
| 25. | 8,37 | 30.30.30.1 | 40.40.40.3 | SIP | 124 |
| 26. | 8,37 | 40.40.40.3 | 30.30.30.1 | TCP | 54 |
| 27. | 9,99 | Cisco_e1:aa:81 | Spanning_tree | STP | 60 |
| 28. | 10,18 | Fe80:e010:c683:5106:f3e8 | Ff02::c | SSDP | 208 |
| 29. | 11,97 | 10.10.10.2 | 40.40.40.3 | RTP | 214 |
| 30. | 11,97 | 30.30.30.1 | 40.40.40.3 | TCP | 590 |
| 31. | 11,97 | 30.30.30.1 | 40.40.40.3 | SIP/SDP | 424 |
| 32. | 11,97 | 40.40.40.3 | 30.30.30.1 | TCP | 54 |
| 33. | 11,98 | 40.40.40.3 | 10.10.10.2 | RTP | 55 |
| 34. | 11,98 | 40.40.40.3 | 10.10.10.2 | TCP | 66 |
| 35. | 11,98 | 10.10.10.2 | 40.40.40.3 | TCP | 60 |
| 36. | 11,98 | 40.40.40.3 | 10.10.10.2 | TCP | 54 |
| 37. | 11,98 | 40.40.40.3 | 10.10.10.2 | SIP | 459 |
| 38. | 11,98 | 10.10.10.2 | 40.40.40.3 | TCP | 60 |
| 39. | 11,99 | 10.10.10.2 | 40.40.40.3 | RTP | 214 |
| 40. | 11,99 | Cisco_e1:aa:81 | Spanning_tree | STP | 60 |
| 41. | 12,01 | 10.10.10.2 | 40.40.40.3 | RTP | 214 |
| 42. | 12,03 | 10.10.10.2 | 40.40.40.3 | RTP | 214 |
| 43. | 12,25 | 40.40.40.3 | 10.10.10.2 | RTP | 214 |

TABELA II
POZIV UČESNIKA 001 KA UČESNIKU 003 SA VPN ZAŠTITOM

| R.br. | Vreme [s] | Izvorišna adresa | Odredišna adresa | Protokol | Veličina [B] |
|---|---|---|---|---|---|
| 1. | 0,00 | Fe80:e010:c683:5106:f3e8 | Ff02::c | SSDP | 208 |
| 2. | 0,03 | Cisco_e1:aa:81 | Spanning_tree | STP | 60 |
| 3. | 0,73 | 40.40.40.3 | 10.10.10.2 | ISAKMP | 126 |
| 4. | 0,73 | 10.10.10.2 | 40.40.40.3 | ISAKMP | 126 |
| 5. | 2,03 | Cisco_e1:aa:81 | Spanning_tree | STP | 60 |
| 6. | 4,00 | Fe80:e010:c683:5106:f3e8 | Ff02::c | SSDP | 208 |
| 7. | 4,03 | Cisco_e1:aa:81 | Spanning_tree | STP | 60 |
| 8. | 6,03 | Cisco_e1:aa:81 | Spanning_tree | STP | 60 |
| 9. | 6,88 | Fe80:e010:c683:5106:f3e8 | Ff02::1:2 | DHCPv6 | 149 |
| 10. | 7,00 | Fe80:e010:c683:5106:f3e8 | Ff02::c | SSDP | 208 |
| 11. | 8,03 | Cisco_e1:aa:81 | Spanning_tree | STP | 60 |
| 12. | 8,67 | Cisco_e1:aa:81 | Cisco_e1:aa:81 | LOOP | 60 |
| 13. | 10,00 | Fe80:e010:c683:5106:f3e8 | Ff02::c | SSDP | 208 |
| 14. | 10,03 | Cisco_e1:aa:81 | Spanning_tree | STP | 60 |
| 15. | 10,88 | Fe80:e010:c683:5106:f3e8 | Ff02::1:2 | DHCPv6 | 154 |
| 16. | 12,03 | Cisco_e1:aa:81 | Spanning_tree | STP | 60 |
| 17. | 13,30 | Cisco_e1:aa:81 | CDP/VTP/DTP | DTP | 60 |
| 18. | 13,30 | Cisco_e1:aa:81 | CDP/VTP/DTP | DTP | 90 |
| 19. | 14,00 | Fe80:e010:c683:5106:f3e8 | Ff02::c | SSDP | 208 |
| 20. | 14,03 | Cisco_e1:aa:81 | Spanning_tree | STP | 60 |
| 21. | 16,03 | Cisco_e1:aa:81 | Spanning_tree | STP | 60 |
| 22. | 17,00 | Fe80:e010:c683:5106:f3e8 | Ff02::c | SSDP | 208 |
| 23. | 18,03 | Cisco_e1:aa:81 | Spanning_tree | STP | 60 |
| 24. | 18,67 | Cisco_e1:aa:81 | Cisco_e1:aa:81 | LOOP | 60 |
| 25. | 19,32 | Cisco_e1:aa:81 | ASUSTEkC_9d:86:8a | ARP | 60 |
| 26. | 19,32 | ASUSTEkC_9d:86:8a | Cisco_e1:aa:81 | ARP | 42 |
| 27. | 20,00 | Fe80:e010:c683:5106:f3e8 | Ff02::c | SSDP | 208 |
| 28. | 20,03 | Cisco_e1:aa:81 | Spanning_tree | STP | 60 |
| 29. | 20,51 | 40.40.40.3 | 10.10.10.2 | TCP | 66 |
| 30. | 22,03 | Cisco_e1:aa:81 | Spanning_tree | STP | 60 |
| 31. | 23,51 | 40.40.40.3 | 10.10.10.2 | TCP | 66 |
| 32. | 24,00 | Fe80:e010:c683:5106:f3e8 | Ff02::c | SSDP | 208 |
| 33. | 24,03 | Cisco_e1:aa:81 | Spanning_tree | STP | 60 |
| 34. | 25,22 | ASUSTEkC_9d:86:8a | Cisco_00:e3:e1 | ARP | 42 |
| 35. | 25,23 | Cisco_00:e3:e1 | ASUSTEkC_9d:86:8a | ARP | 60 |
| 36. | 26,03 | Cisco_e1:aa:81 | Spanning_tree | STP | 60 |
| 37. | 27,00 | Fe80:e010:c683:5106:f3e8 | Ff02::c | SSDP | 208 |
| 38. | 27,50 | 40.40.40.3 | 10.10.10.2 | SIP/SDP | 1095 |
| 39. | 27,50 | 10.10.10.2 | 40.40.40.3 | SIP | 284 |
| 40. | 28,30 | 40.40.40.3 | 10.10.10.2 | SIP | 831 |
| 41. | 30,25 | 10.10.10.2 | 40.40.40.3 | RTP | 214 |
| 42. | 31,50 | 40.40.40.3 | 10.10.10.2 | RTP | 214 |
| 43. | 31,75 | 10.10.10.2 | 40.40.40.3 | RTP | 214 |


ISBN 978-86-7466-930-3

## IV. Zaključak

Rezultat jedne realizacije zaštite paketskog telefonskog saobraćaja, predstavljen u ovom radu prikazuje da uspostava i održavanje VPN tunela kao načina zaštite paketskog telefonskog saobraćaja podrazumeva primenu niza protokola, specifično dizajniranih za prenos informacionih sadržaja u realnom vremenu (SIP, SSDP, RTP) kao i protokola za obezbeđenje zaštite u toku prenosa (ISAKMP, IPSec). Specifično za predstavljenu realizaciju predstavlja upotreba linka za prenos različitih servisa i time korišćenje protokola kojima se omogućava konvergencija servisa u prenosu (DTP, SSDP).

## Literatura

[1] W.Stallings, Osnove bezbednosti mreža: Aplikacije i standardi, Računarski fakultet, Beograd, 2014.
[2] M.Stojanović, V.Aćimović-Raspopović, Savremene IP mreže: Arhitekture, tehnologije i protokoli, Akademska misao, Beograd, 2012.
[3] A.Smiljanić, Osnove i primena Interneta, Elektrotehnički fakultet Univerziteta u Beogradu, Beograd, 2015.
[4] D.Nemec, D.Vukobratović, V.Crnojević, Č.Stefanović, Tehnologija VoIP sistema, Fakultet tehničkih nauka, Novi Sad, 2007.
[5] Security in the Internet Architecture, RFC: 1636, jun 1994, https://datatracker.ietf.org/doc/html/rfc1636
[6] IP Encapsulating Security Payload, RFC: 4303, decembar 2005, https://datatracker.ietf.org/doc/html/rfc4303
[7] Security Architecture for the Internet protocol, RFC: 4301, decembar 2005, https://datatracker.ietf.org/doc/html/rfc4301
[8] Internet Security Association and key Management Protocol, RFC: 2408, novembar 1998, https://datatracker.ietf.org/doc/html/rfc2408
[9] Internet Key Exchange Protocol Version 2 (IKEv2), RFC: 5996, septembar 2010, https://datatracker.ietf.org/doc/html/rfc5996
[10] B.Scheiner, Primenjena kriptografija, Mikro knjiga, Beograd, 2007.
[11] R.Swale, D.Collins, Carrier Grade Voice Over IP, McGraw Hill Professional, 2004.
[12] M.Jevtović, Komunikacioni protokoli Interneta, Akademska misao, Beograd, 2011.
[13] I.Bašičević, "Prilog razvoju arhitekture za obezbeđivanje usluga u računarskim mrežama nove generacije", doktorska disertacija, Fakultet tehničkih nauka, Novi Sad, 2008.
[14] S.Gajin , Principi konfigurisanja računarskih mreža, Akademska misao, Beograd, 2018.

## Abstract

The research presented in this paper addresses an example of how to execute packet telephone traffic protection using virtual private network technology through configuring servers for packet telephone traffic and also demonstrates the secure transfer with the use of virtual private network technology in tunnel mode by applying the appropriate protocols for privacy protection, authentication, integrity protection and crypto key exchange. Traffic recording and analysis has been performed using the Wireshark software in both secure and non-secure transfer. The results obtained can help better understand the complex process of setting up a tunnel through the use of simulation software in education.

## Packet Telephone Traffic Transfer Protection Using Technology of Virtual Private Networks

Mićo Živanović, Jovan Bajčetić, Ivan Tot

 ISBN 978-86-7466-930-3

# LDPC dekoderi sa reinicijalizacijama koji objedinjuju tvrde odluke i razmenu mekih poruka

Predrag Ivaniš, *Senior Member, IEEE*, Srđan Brkić, *Member, IEEE* i Bane Vasić, *Fellow, IEEE*

***Apstrakt* — U ovom radu predloženi su postupci koji kombinuju dve klase iterativnih algoritama koje se uobičajeno koriste za dekodovanje zaštitnih kodova sa proverama parnosti male gustine (eng. Low Density Parity Check, LDPC). Prva strategija zasnovana je na bit-fliping algoritmu male kompleksnosti, a predložena modifikacija omogućava značajno poboljšanje performansi dekodera uz zadržavanje male prosečne računske kompleksnosti. Druga strategija zasnovana je na algoritmu sa propagacijom verodostojnosti i za cilj ima dodatno poboljšanje korekcionih sposobnosti dekodera, naročito kada se koriste kodovi sa malom dužinom kodne reči.**

***Ključne reči* — Bit-fliping algoritam, belief-propagation algoritam, iterativno dekodovanje, kodovi sa proverama parnosti male gustine.**

## I. UVOD

KODOVI sa proverama parnosti male gustine (eng. Low Density Parity Check, LDPC) predloženi su od strane Roberta Galagera 1960. godine [1], a posebno veliku popularnost su doživeli u poslednjoj deceniji XX veka [2], [3]. Njihova sposobnost da dostignu kapacitet kanala uz relativno nisku kompleksnost dekodovanja [4] učinila ih je poželjnim rešenjem za obezbeđivanje pouzdanog prenosa podataka u bežičnim telekomunikacionim sistema novije generacije. Ovi kodovi se danas koriste u digitalnoj televiziji (eng. Digital Video Broadcasting, DVB) [5], bežičnim lokalnim mrežama (eng. Wireless Local Area Networks, WLAN) [6], a od skora su uvršteni i u standard za petu generaciju širokopojasnih mobilnih mreža (5G) [7].

Poboljšanje performansi sistema usled primene LDPC kodova pre svega je diktirano algoritmom koji se koristi za njihovo dekodovanje. Ovi algoritmi su po pravilu iterativni i implementiraju se nad Tanerovim grafom [8], koji je u potpunosti određen matricom provere parnosti koja definiše kod. U najvećem broju slučajeva, optimalne performanse se postižu ako se pri dekodovanju koristi tzv. algoritam propagacije verodostojnosti (eng. belief-propagation, BP), kod koga čvorovi u grafu razmenjuju poruke na osnovu kojih se procena kodne reči po pravilu poboljšava u svakoj narednoj iteraciji. Verzija BP algoritama pogodna za primenu u dekoderima LDPC kodova poznata je i pod nazivom algoritam sumiranja i množenja (eng. Sum Product Algorithm, SPA), a više detalja vezanih za njegovu efikasnu implementaciju može se naći u radu [9].

Predrag Ivaniš – Elektrotehnički fakultet, Univerzitet u Beogradu, Bulevar Kralja Aleksandra 73, 11020 Beograd, Srbija (e-mail: predrag.ivanis@ etf.bg.ac.rs).

Srđan Brkić – Elektrotehnički fakultet, Univerzitet u Beogradu, Bulevar Kralja Aleksandra 73, 11020 Beograd, Srbija (e-mail: srdjan.brkic@ etf.bg.ac.rs).

Bane Vasić – Department of Electrical and Computer Engineering, University of Arizona, Tucson, AZ 85721 USA (e-mail: vasic@ece.arizona.edu).

Mana BP algoritma je velika složenost implementacije. Računske operacije koje se izvode u čvorovima Tanerovog grafa mogu biti veoma kompleksne, a pritom se podrazumeva da su poruke koje se razmenjuju realni brojevi. Pri hardverskoj implementaciji poželjno je da se operacije u čvorovima pojednostave i da se poruke predstave sa konačnom preciznošću (implementacija sa fiksnim zarezom). Stoga se u većini postojećih sistema koriste podoptimalne verzije BP algoritma, kao što su razne vrste min-sum algoritma [10]. Drugi značajan nedostatak BP algoritma je vezan za činjenicu da je on optimalan samo ako Tanerov graf ima oblik stabla. Ako se u grafu pojavljuju ciklusi male dužine, performanse BP algoritma su daleko od performansi koje bi bilo moguće dobiti primenom algoritma koji postiže maksimalnu verodostojnost pri odlučivanju (eng. Maximum Likelihood, ML). Ovo je posebno izraženo za kratke kodove. U literaturi se mogu naći rešenja koja obezbeđuju bolje performanse od BP algoritma za isti broj iteracija [11], a koja sa povećanjem broja iteracija obezbeđuju performanse bliske ML granici [12].

Sa druge strane, algoritam koji u svakoj iteraciji invertuje određene bitove kodne reči (eng. bit-flipping, BF) predstavlja postupak izuzetno niske kompleksnosti. Iako originalni BF algoritam ima prilično loše performanse po pitanju ispravljanja grešaka, isto se ne može reći i za nedavno predloženu modifikaciju BF algoritma nazvanu bit fliping algoritam sa gradijentnim spustom (eng. Gradient Descent Bit Flipping, GDBF) [13]. U našem prethodnom radu [14] predložen je probabilistički GDBF algoritam (PGDBF), kod koga primena slučajne sekvence pri dekodovanju omogućava ispravljanje kombinacije grešaka koje klasičan GDBF algoritam ne može korigovati. Dalje unapređenje ove ideje je razmotreno u radu [15]. Kombinovanje PGDBF algoritma i slučajnih reinicijalizacija može u velikoj meri poboljšati performanse dekodera (odgovarajući algoritam MUDRI je izložen u radu [16]). Analiza data u radovima [17]-[20] pokazuje da dekoderi bazirani na tvrdom odlučivanju uz slučajne reinicijalizacije obezbeđuju performanse bliske ML granici, ukoliko se može dozvoliti veliki broj iteracija pri dekodovanju.

Nedavno je pokazano da se performanse GDBF algoritma mogu približiti performansama BP algoritma, ako se destimuliše invertovanje istog bita u nekoliko uzastopnih iteracija [21]. Kombinacija tog pristupa sa deterministčkim reinicijalizacijama ima potencijal da omogući čak i bolje performanse od BP algoritma, uz znatno manju računsku kompleksnost [22].

U nastavku će biti razmotreno nekoliko strategija za kombinovanje BP i GDBF algoritma, sa ciljem da se postigne veća pouzdanost odlučivanja ili manja kompleksnost implementacije, koristeći prednosti jednog i drugog pristupa.

 ISBN 978-86-7466-930-3

## II. MODEL SISTEMA I PREGLED TIPIČNIH ALGORITAMA ZA DEKODOVANJE LDPC KODOVA

U ovom radu posmatramo binarne LDPC kodove kod kojih je informaciona reč $\boldsymbol{i}$ dužine $k$, dok je odgovarajuća kodna reč $\boldsymbol{x}$ dužine $n$. Ovi kodovi se označavaju sa $(n,k)$, a njihov kodni količnik iznosi $R=k/n$.

LDPC kod se opisuje matricom provere parnosti $\boldsymbol{H}$, dimenzija $n\times m$, koja je po pravilu retka (broj jedinica u ovoj matrici je znatno manji od broja nula). U ovom radu će biti razmotreni kodovi kod kojih u svakoj koloni matrice $\boldsymbol{H}$ ima tačno $\gamma$ jedinica, dok svaka vrsta matrice $\boldsymbol{H}$ sadrži tačno $\rho$ jedinica (regularni kodovi). Parametri $\gamma$ i $\rho$ nazivaju se težina kolona i težina vrsta, respektivno. Odgovarajući bipartitni graf $\mathcal{G}$ sastoji se od skupa varijabilnih čvorova $\boldsymbol{V} = \{v_1, v_2, ..., v_n\}$ i skupa čvorova provere parnosti $\boldsymbol{C} = \{c_1, c_2, ..., c_m\}$. Čvorovi $v_i$ i $c_j$ su susedi ako su povezani na grafu, tj. ako je ispunjeno $\boldsymbol{H}_{ij}=1$. Skup suseda čvora $v_i$ je označen sa $N_{v_i}$, dok je skup suseda čvora $c_j$ označen sa $N_{c_j}$.

Nakon što LDPC koder od informacione reči $\boldsymbol{i}$ formira kodnu reč $\boldsymbol{x}$, ona se prenosi kroz binarni simetrični kanal (BSC). Ovaj kanal unosi nasumične, tj. vremenski nekorelisane, greške sa verovatnoćom $p$. Odgovarajuća sekvenca greške $\boldsymbol{e}$ može se dobiti uz pomoć generatora slučajne promenljive sa Bernulijevom raspodelom $\mathrm{B}(1, p)$. U ovom slučaju, primljena reč $\boldsymbol{y}$ na izlazu kanala formira se tako što se poslata kodna reč $\boldsymbol{x}$ sabere bit-po-bit sa sekvencom greške $\boldsymbol{e}$, tj. $\boldsymbol{y}=\boldsymbol{x}\oplus\boldsymbol{e}$.

Primljena reč se dovodi na ulaz dekodera koji ima zadatak da verno rekonstruiše poslatu kodnu reč, odnosno poslatu informacionu sekvencu (koju treba dostaviti odredištu). Pošto je izdvajanje informacione sekvence prilično jednostavno ako se ispravno rekonstruiše poslata kodna reč, pri analizi dekodera se teži da procena kodne reči bude što je moguće pouzdanija. Drugim rečima, treba minimizovati verovatnoću da se procena poslate kodne reči, označena sa $\hat{\boldsymbol{x}}$, razlikuje od poslate reči $\boldsymbol{x}$. Ova verovatnoća se obično naziva verovatnoća greške po kodnoj reči (eng. Word Error Rate, WER). Iterativni dekoder procenu poslate kodne reči po pravilu poboljšava iz iteracije u iteraciju, čime se omogućava da i za prilično duge kodne reči kompleksnost dekodera ostane relativno mala [10].

Dekoder u svakoj iteraciji proverava da li su sve provere parnosti zadovoljene. Kada je ovaj uslov ispunjen, proces dekodovanja se prekida (tada procena odgovara kodnoj reči). Obično se zadaje maksimalan broj iteracija koje se mogu iskoristiti za dekodovanje, označen sa $L$.

Neka je procena kodne reči u $l$-toj iteraciji označena sa $\hat{\boldsymbol{x}}^{(l)}$, $l=1,2,...,L$. Odgovarajući sindrom $\boldsymbol{S}^{(l)}=\hat{\boldsymbol{x}}^{(l)}\boldsymbol{H}^T$ ima sve komponente ravne nuli samo u slučaju da su sve provere parnosti zadovoljene. Ako dekoder tokom $L$ uzastopnih iteracija ne formira procenu za koju je $\mathbf{S}^{(l)}=\mathbf{0}$, dekodovanje se proglašava neuspešnim. Ukoliko se dekodovanje prekine za $l_0\leq L$ i ako je $\hat{\boldsymbol{x}}^{(l_0)}=\boldsymbol{x}$, smatra se da je ta kodna reč uspešno dekodovana nakon $l_0$ iteracija.

U današnjim telekomunikacionim sistemima i sistemima za zapis podataka obično se za dekodovanje LDPC kodova koriste dve klase algoritama. Jedna je zasnovana na BP algoritmu, koga odlikuju visoka pouzdanost pri dekodovanju i velika složenost implementacije. Druga klasa algoritama je zasnovana na BF postupku, koji je daleko jednostavniji ali uz nešto veću verovatnoću greške pri odlučivanju. Osnovne karakteristike dve pomenute klase algoritama, kao i njihovih varijanti, navedene su u nastavku.

### A. *Algoritmi sa propagacijom verodostojnosti*

Poznato je da se LDPC kodovi mogu uspešno dekodovati korišćenjem algoritama kod kojih se poruke iterativno razmenjuju između povezanih čvorova u grafu (eng. message-passing). Poruke koje se razmenjuju mogu biti veoma jednostavne, kao kod Galager-A/B algoritma (binarne poruke), ali se znatno bolji rezultati dobijaju ako ove poruke imaju oblik realnih brojeva.

Osnovna ideja BP algoritma će biti ilustrovana na grafu prikazanom na slici 1, gde su ispravno primljeni biti kodne reči označeni belim varijabilnim čvorovima, dok pogrešno primljenim bitima odgovaraju crni čvorovi. Zadovoljene provere parnosti označene su belim, a nezadovoljene crnim kvadratima. U BP algoritmu poruke koje varijabilni čvorovi inicijalno šalju ka povezanim proverama parnosti zavise samo od verovatnoće greške u binarnom kanalu

$$m^{(1)}_{v_i\to c_j}(v_i=0\,|\,y_i)=P(v_i=0\,|\,y_i)=\begin{cases}p, & y_i=1,\\ 1-p, & y_i=0,\end{cases} \qquad (1)$$

a pošto su u pitanju verovatnoće, jasno je da se može pisati $m^{(1)}_{v_i\to c_j}(v_i=1\,|\,y_i)=1-m^{(1)}_{v_i\to c_j}(v_i=0\,|\,y_i)$. Intenzitet ovih poruka srazmeran je uverenosti čvora $v_i$ da bi mogao da ima vrednost $v_i=a$, kada mu je poznata primljena vrednost $y_i$.

Imajući u vidu da vrednosti varijabilnih čvorova treba da odgovaraju bitima validne kodne reči (za koju su sve provere parnosti ravne nuli), u narednim iteracijama su poruke koje se razmenjuju između čvorova na Tanerovom grafu određene izrazima [10]

$$m^{(l)}_{c_j\to v_i}(v_i=0)=\frac{1}{2}\left(1-\prod_{v_k\in N_j\setminus v_i}\left(2m^{(l)}_{v_k\to c_j}(v_k=1)-1\right)\right), \qquad (2)$$

$$m^{(l+1)}_{v_i\to c_j}(v_i=0)=P(v_i=0\,|\,y_i)\prod_{c_z\in N_i\setminus c_j}m^{(l)}_{c_z\to v_i}(v_i=0), \qquad (3)$$

a jasno je da i dalje važi $m^{(l)}_{c_j\to v_i}(v_i=1)=1-m^{(l)}_{c_j\to v_i}(v_i=0)$, $m^{(l+1)}_{v_i\to c_j}(v_i=1\,|\,y_i)=1-m^{(l+1)}_{v_i\to c_j}(v_i=0\,|\,y_i)$. Verovatnoća da je $v_i$=0 se sada ažurira na osnovu uverenja povezanih čvorova

$$P^{(l)}(v_i=0)=P(v_i=0\,|\,y_i)\prod_{c_z\in N_i}m^{(l)}_{c_z\to v_i}(v_i=0). \qquad (4)$$

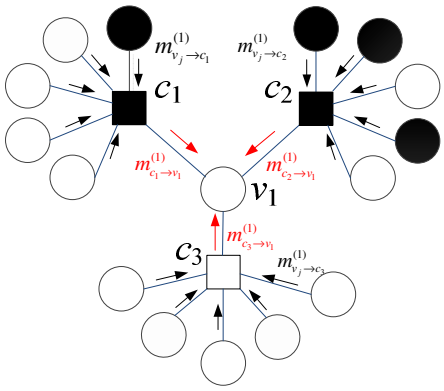


Sl 1. Ilustracija BP algoritma na grafu koji odgovara regularnom kodu sa parametrima $\gamma$=3, $\rho$=5.


ISBN 978-86-7466-930-3

Na ovaj način se uverenost čvora o vrednostima koje na njega povezani čvorovi treba da imaju, pod datim uslovima, po pravilu poboljšava iz iteracije u iteraciju, što obično rezultuje sve pouzdanijim odlukama. Da bi se ublažili numerički problemi, BP algoritam se obično implementira u logaritamskom domenu, tako što se u svakoj iteraciji određuje logaritamski količnik verodostojnosti [8]

$$LLR_i^{(l)} = \log\left(P^{(l)}(v_i=1)/P^{(l)}(v_i=0)\right). \quad (5)$$

Ipak, uvek treba imati na umu da je BP algoritam optimalan samo u slučaju da je graf oblika stabla. Ovo nije ispunjeno kada u grafu postoje ciklusi male dužine, a posebno je kritično kada je dužina kodne reči mala.

### B. *Bit-fliping algoritmi*

Bit-fliping algoritam je jednostavan postupak iterativnog dekodovanja LDPC kodova, koji je predložio Galager [1]. Algoritam je zasnovan na određivanju broja nezadovoljenih provera parnosti koje su povezane na svaki varijabilni čvor. Ovo izračunavanje se izvodi nad trenutno dostupnom procenom kodne reči, pa tako čvoru $v_i$ u $l$-toj iteraciji odgovara energetska funkcija oblika

$$\Lambda_{BF}^{(l)}(v_i) = \sum_{c_j \in N_{v_i}} \bigoplus_{v_k \in N_{c_j}} \hat{x}_k^{(l)}. \quad (4)$$

Ukoliko je ova veličina za $i$-ti bit (i=1,2,…,$n$) veća od unapred definisanog praga $T$, vrši se invertovanje tog bita, čime se formira njegova procena u narednoj iteraciji

$$\hat{x}_i^{(l+1)} = \begin{cases} \hat{x}_i^{(l)} \oplus 1, & \Lambda^{(l)}(v_i) \geq T, \\ \hat{x}_i^{(l)}, & \Lambda^{(l)}(v_i) < T. \end{cases} \quad (5)$$

Polazeći od primljenog vektora ($\hat{\boldsymbol{x}}^{(0)} = \boldsymbol{y}$), na ovaj način se u svakoj iteraciji po pravilu formiraju sve pouzdanije procene poslate kodne reči. Ovaj algoritam često greši, pa bi za tipičnu vrednost $T = \gamma/2$ u primeru sa slike 1 bila doneta pogrešna odluka da čvor $v_1$ treba invertovati.

GDBF algoritam uvodi dve modifikacije – u energetsku funkciju se dodaje korelacioni član koji zavisi od odgovarajućeg bita primljene reči i invertuju se samo vrednosti onih varijabilnih čvorova koje u toj iteraciji imaju maksimalnu vrednost energetske funkcije [13, 14]:

$$\Lambda_{GDBF}^{(l)}(v_i) = y_i \oplus \hat{x}_i^{(l)} + \sum_{c_j \in N_{v_i}} \bigoplus_{v_k \in N_{c_j}} \hat{x}_k^{(l)}, \quad (6)$$

$$\hat{x}_i^{(l+1)} = \begin{cases} \hat{x}_i^{(l)} \oplus 1, & \Lambda^{(l)}(v_i) = \max_i \Lambda^{(l)}(v_i), \\ \hat{x}_i^{(l)}, & \Lambda^{(l)}(v_i) < \max_i \Lambda^{(l)}(v_i). \end{cases} \quad (7)$$

Kod GDBF algoritma sa momentumom (GDBF-w/m) energetska funkcija ima oblik [21]

$$\Lambda^{(l)}(v_i) = \alpha\left(y_i \oplus \hat{x}_i^{(l)}\right) + \beta \sum_{c_j \in N_{v_i}} \bigoplus_{v_k \in N_{c_j}} \hat{x}_k^{(l)} + \mu_i^{(l)}, \quad (8)$$

gde se korelacionom članu i broju nezadovoljenih provera parnosti pridružuju težinski koeficijenti (označeni sa $\alpha$ i $\beta$, respektivno), a na čitavu funkciju se dodaje novi član $\mu_i^{(l)}$ (momentum). Vrednost momentuma zavisi od broja iteracija koje su protekle od prethodnog invertovanja tog bita (koji je označen sa $w_i$) i može uzeti vrednosti definisane momentum vektorom $\mu = [\mu(1), \mu(1), ..., \mu(w_{\max})]$, pri čemu je $\mu(w_i) = 0$ ako je $w_i > w_{\max}$. Pokazano je da ovaj algoritam za neke kodove ima performanse uporedive sa BP algoritmom, naročito za male vrednosti parametra $p$ [21].

## III. STRATEGIJE ZA KOMBINOVANJE BF I GDBF ALGORITMA

Jasno je da dve prethodno opisane klase algoritama rade na osnovu različitih principa, pa se nameće pitanje da li bi se mogle kombinovati tako da se objedini "najbolje iz dva sveta". Prvi korak u tom smeru učinjen je u radu koji smo nedavno objavili [22], pri čemu se GDBF-w/m algoritam modifikuje samo u nekim iteracijama.

Za razliku od prethodnih istaraživanja, u ovom radu je predlažemo kombinovanje BP algoritma i GDBF algoritma, pri čemu se jedan od njih koristi kao osnovno rešenje, dok se elementi drugog algoritma koriste za reinicijalizaciju ulaza dekodera. Dve takve strategije opisane su u nastavku.

### A. *GDBF-w/m kao osnovni algoritam*

U ovoj varijanti se primljena reč dovodi na ulaz GDBF-w/m dekodera i za datu vrednost parametra $p$ posmatra se kako se menja WER u zavisnosti od $L$. Formalno se može zapisati da GDBF-w/m dekoder nakon $l$ iteracija preslikava $\boldsymbol{y}$ u procenjenu vrednost $\hat{\boldsymbol{x}}^{(l)} = \Phi_{GDBF}^{(l)}(\boldsymbol{y})$. Kada postane jasno da GDBF-w/m u dodatnim iteracijama neće značajno smanjiti WER, dekodovanje se prekida. Broj iteracija nakon koga se dekodovanje prekida je $K_{GDBF}$ i određuje se empirijski. Primljena reč se zatim dovodi na ulaz BP dekodera, koji nakon $K_{BP}$ iteracija na svom izlazu formira procenu $\boldsymbol{r}^{(1)}$, tj. $r^{(1)} = \Phi_{BP}^{(l)}(\boldsymbol{y})$, koja se koristi kao ulaz GDBF-w/m dekodera u novoj rundi. Po potrebi, postupak se ponavlja na način ilustrovan slikom 2, tako što se referenca $\boldsymbol{r}^{(q)}$ dobija kao izlaz BP dekodera nakon $K_{BP}$+$q$-1 iteracija, a energetska funkcija se računa na osnovu izraza

$$\Lambda^{(l)}(v_i) = \alpha\left(r_i^{(q)} \oplus \hat{x}_i^{(l)}\right) + \beta \sum_{c_j \in N_{v_i}} \bigoplus_{v_k \in N_{c_j}} \hat{x}_k^{(l)} + \mu_i^{(l)}.$$

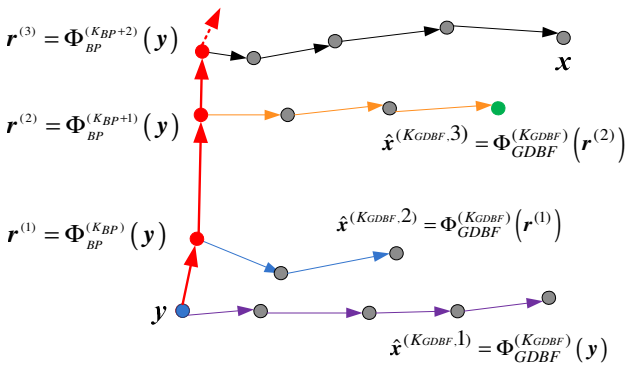


Sl 2. Ilustracija prve strategije, osnova je GDBF w/m algoritam, dok procena nakon odgovarajuće iteracije BP algoritma određuje referencu.

### B. *BP kao osnovni algoritam*

U ovom scenariju se primljena reč dovodi na ulaz BP dekodera. Nakon svake iteracije pronađu se čvorovi $v_i$ kod kojih je $LLR_i^{(l)}$ najveći po apsolutnoj vrednosti, uz uslov da bi taj bit bio invertovan kada bi se odluka donela u toj iteraciji, tj. $LLR_i^{(l)} \times LLR_i^{(0)} < 0$. Ove pozicije se redom zapisuju u odgovarajuću memoriju i čine skup kritičnih čvorova. Ako BP algoritam tokom $K_{BP}$ iteracija ne obavi dekodovanje, postupak se ponavlja za novi ulaz dekodera. Odgovarajuća referenca $r_q$ se formira tako što se u reči $\boldsymbol{y}$ invertuje samo jedan od kritičnih čvorova, pa se može formalno pisati $\boldsymbol{r}^{(q)} = \Psi\{LLR^{(q)}\}$ (videti sliku 3).


ISBN 978-86-7466-930-3

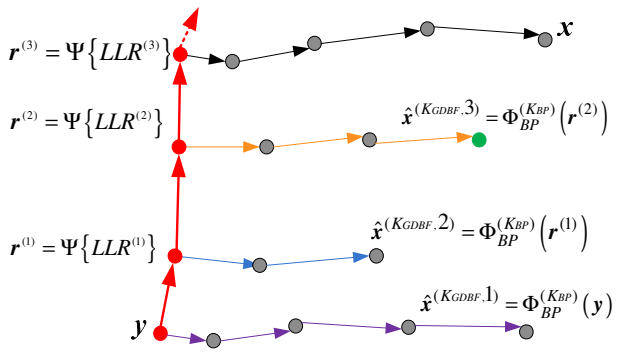


Sl 3. Ilustracija prve strategije, osnova je GDBF w/m algoritam, dok procena nakon odgovarajuće iteracije BP algoritma određuje referencu.

## IV. NUMERIČKI REZULTATI

Efekat dve predložene strategije će biti ilustrovan za dva regularna koda, koji su konstruisani koristeći različite postupke, pri čemu oba imaju težinu kolona γ=3 i dužinu najkraćeg ciklusa jednaku $g$=8. Kodovi imaju male dužine kodnih reči, a poznato je da tada BP algoritam predstavlja podoptimalno rešenje.

Verovatnoća greške po kodnoj reči određena je Monte Karlo simulacijom, pri čemu se generišu kodne reči dužine $n$ i na svaku od njih se superponira slučajno generisan vektor greške iste dužine, generisan u skladu sa zadatom verovatnoćom greške u BSC. Kako bi bili sigurni da je simetrija dekodera zadovoljena, ne šalje se uvek kodna reč "sve nule", već se na izlaz kodera emituju različite kodne reči. U slučaju kada se dekodovanje završi za najviše $L$ iteracija, porede se poslata i procenjena kodna reč, da bi bili sigurni da procena ne odgovara kodnoj reči koja je različita od poslate kodne reči. U slučaju kada se tokom $L$ uzastopnih iteracija ne formira procena kodne reči kod koje su sve provere parnosti jednake nuli, dekodovanje se proglašava neuspešnim. Simulacija za jedan skup parametara se zaustavlja kada se detektuje 200 pogrešno primljenih kodnih reči, što određuje jednu tačku na grafiku.

Performanse dekodera će prvo biti prikazane za regularni Tanerov kod (155,64), koji ima težinu kolona γ=3 i težinu vrsta ρ=5. U pitanju je kvazi-ciklični LDPC kod, a odgovarajući metod konstrukcije predložen je u radu [23]. Ovaj kod se često koristi za testiranje algoritama dekodovanja [11, 24, 25].

Zavisnost verovatnoće greške po kodnoj reči od verovatnoće greške u BSC prikazana je na slici 4. U slučaju kada BP algoritam određuje samo reinicijalizovane reference od kojih GDBF-w/m počinje dekodovanje u svakoj rundi, kriva je prikazana crvenom punom linijom. Svaka runda traje po $K_{GDBF}$=25 iteracija i ako se za to vreme ne detektuje da su sve provere parnosti jednake nuli, referenca se reinicijalizuje (sa $K_{BP}$=5) i ponovo se pokreće GDBF-w/m algoritam za nešto izmenjenu ulaznu sekvencu. Zelena kriva odgovara slučaju kada se koristi samo BP algoritam, ali se u svakoj rundi od $K_{BP}$=10 iteracija kao ulaz dekodera koristi reinicijalizovana referenca. Za male vrednosti parametra $p$, prva strategija obezbeđuje performanse uporedive sa BP algoritmom dok drugoj strategiji odgovaraju superiorne performanse.

Verovatnoća greške po kodnoj reči u zavisnosti od maksimalnog dozvoljenog broja iteracija pri dekodovanju ilustrovana je na slici 5. Vidi se da već nakon prve reinicijalizacije ($L$>30) performanse modifikovanog GDBF-w/m dekodera postaju uporedive sa performansama BP dekodera. Sa druge strane, modifikovani BP dekoder za bilo koju vrednost parametra $L$ ima bolje performanse od ostalih razmatranih rešenja.

Dok strategija br 1. obezbeđuje verovatnoću greške po kodnoj reči koja je praktično ista kao u slučaju primene znatno složenijeg BP algoritma, jasno je da strategija br. 2 obezbeđuje dodatno poboljšanje performansi u odnosu na BP algoritam. Ovo je rezultat reinicijalizacija kod kojih se invertuju vrednosti najkritičnijih varijabilnih čvorova, što je princip sličan onom koji se primenjuje u GDBF algoritmu.

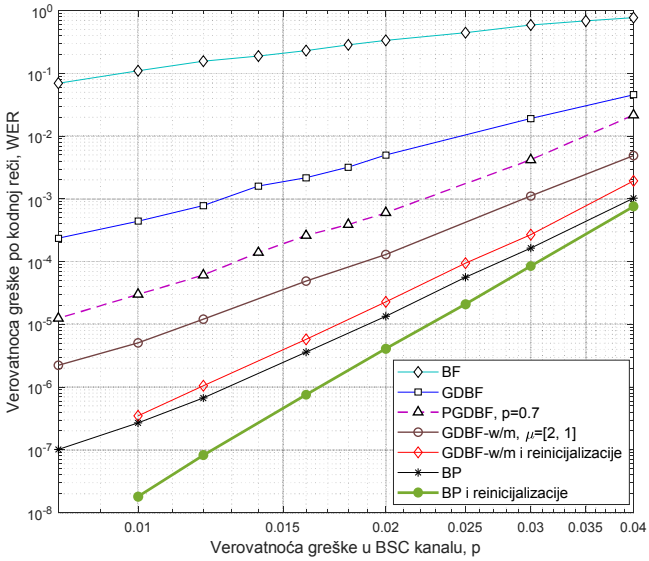


Sl. 4. Zavisnost verovatnoće greške po kodnoj reči od verovatnoće greške u BSC, za Tanerov kod (115,64) i $L$=300. Prikazane su performanse za GDBF-w/m i BP, kao i dve strategije njihovog kombinovanja.

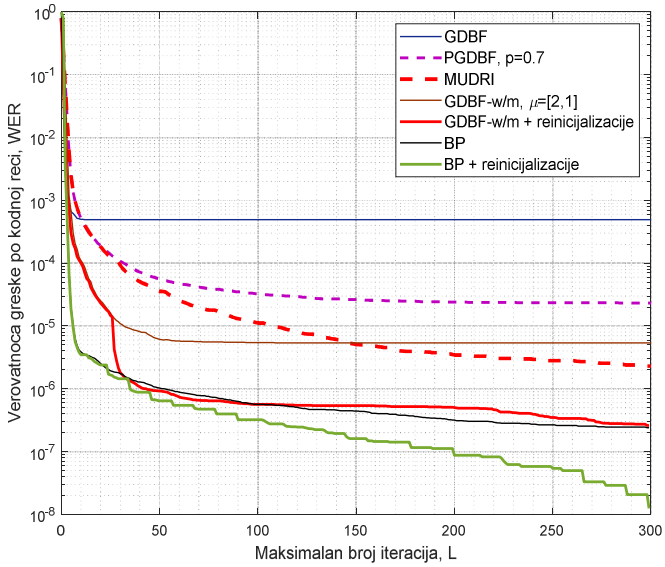


Sl. 5. Zavisnost verovatnoće greške po kodnoj reči od broja iteracija, za Tanerov kod (115,64) i $p$=0.01. Prikazane su performanse za GDBF-w/m i BP, kao i dve strategije njihovog kombinovanja.


ISBN 978-86-7466-930-3

Numerički rezultati za regularni PEG kod (504,252), koji ima težinu kolona γ=3 i težinu vrsta ρ=6. U pitanju je kod formiran pomoću tehnike sa progresivnim formiranjem ivica grafa (eng. Progressive Edge Growth, PEG), koja je prvobitno predložena u radu [26].

Zavisnost verovatnoće greške po kodnoj reči od verovatnoće greške u BSC prikazana je na slici 6. Crvena linija odgovara slučaju kada se BP algoritam koristi samo za formiranje reinicijalizovane reference (sa $K_{BP}$=10), dok osnovu dekodera predstavlja GDBF-w/m algoritam (opisano u odeljku III-A). Kao i u prethodnom slučaju, svaka runda traje po $K_{GDBF}$=25 iteracija. Zelena puna linija odgovara slučaju kada se u svakoj rundi koristi samo BP algoritam, a kao ulaz dekodera koristi se reinicijalizovana referenca (na način opisan u odeljku III-B). U ovom slučaju, prva runda se završava nakon $K_{BP}$=25 iteracija, dok se nakon prve reinicijalizacije ova vrednost smanjuje na $K_{BP}$=10. U oba slučaja postižu se performanse uporedive sa BP algoritmom, dok druga strategija rezultuje osetnijim poboljšanjem performansi u tzv. *error floor* regionu.

Uticaj parametra $L$ na performanse dekodera za PEG kod (504,252), kada je $p$=0.02, prikazan je na slici 7. Performanse dekodera u kome je primenjena strategija opisana u odeljku III-B su za malu vrednost parametra $L$ uporedive sa performansama BP dekodera. Neznatna degradacija performansi u intervalu $25<L<75$ može da posluži kao indikacija da bi se još bolji rezultati mogli dobiti ako se u prvoj rundi dekodovanja parametar $K_{BP}$ dodatno poveća. Sa druge strane, može se uočiti da se sa povećanjem maksimalnog broja iteracija performanse značajno poboljšavaju u odnosu na BP algoritam. Ovo je posledica reinicijalizacija u svakoj rundi dekodovanja. Taj efekat smo prethodno uočili u radu [16], za slučaj kada se koriste slučajne reinicijalizacije. U radu [17] pokazano je da se sa dovoljnim povećanjem parametra $L$ performanse PGDBF dekodera asimptotski približavaju ML granici. U radovima [19] i [20] pokazano je da se sličan efekat postiže ako se slučajne reinicijalizacije kombinuju sa najjednostavnijim algoritmom koji koristi massage-passing princip za dekodovanje LDPC kodova (Gallager-B algoritam).

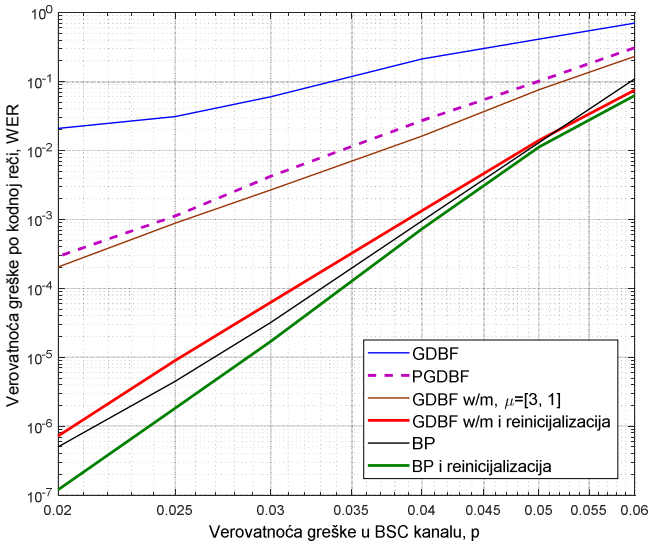


Sl. 6. Zavisnost verovatnoće greške po kodnoj reči od verovatnoće greške u BSC, za Tanerov kod (115,64) i $L$=300. Prikazane su performanse za GDBF-w/m i BP, kao i dve strategije njihovog kombinovanja.

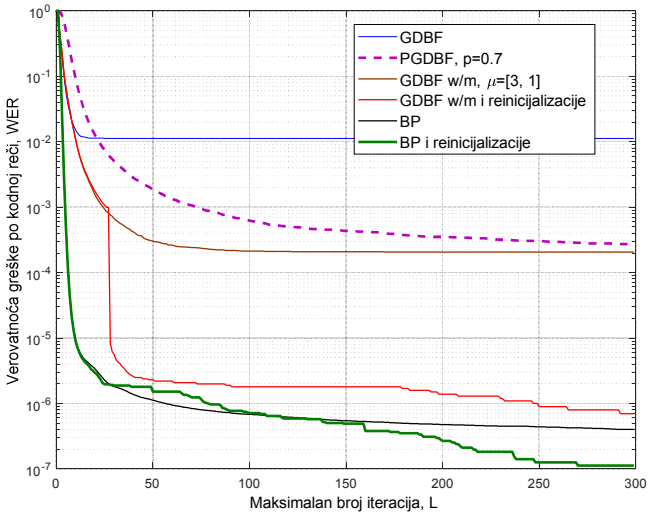


Sl. 7. Zavisnost verovatnoće greške po kodnoj reči od broja iteracija, za PEG kod (504,252) i $p$=0.02. Prikazane su performanse za GDBF-w/m i BP, kao i dve strategije njihovog kombinovanja.

Rezultati prikazani na slikama 4-7 pokazuju da se značajno poboljšanje performansi može postići i kada su reinicijalizacije deterministčke. Za razliku od pristupa izloženog u radu [22], gde se opisan prilično složen postupak deterministčke reinicijalizacije, ovde je predložen koncept zasnovan na kombinaciji dva algoritma:

- U prvoj strategiji, reč od koje GDBF-w/m dekoder započinje dekodovanje u svakoj rundi dobija se na osnovu procena u pojedinim iteracijama BP algoritma.
- U drugoj strategiji se metoda bliska GDBF algoritmu (flipovanje najkritičnijeg bita) koristi za reinicijalizaciju, dok se BP koristi za dekodovanje u svakoj rundi. U prethodnim primerima pretpostavljeno je da se u procesu reinicijalizacije invertuju samo oni čvorovi $v_i$ za koje je zadovoljeno $LLR_i^{(l)} = \max_i \left\{ LLR_i^{(l)} \right\}$. Ipak, preliminarni rezultati pokazuju da se za kodove sa dužim kodnim rečima bolje performanse postižu ako se ovaj skup proširi čvorovima za koje je ispunjena relacija $LLR_i^{(l)} \geq 0.9 \times \max_i \left\{ LLR_i^{(l)} \right\}$.

Treba zapaziti da se u prvoj strategiji dekodovanje najčešće završi primenom GDBF algoritma. Ukoliko je $p=10^{-2}$, prosečan broj iteracija potrebnih za dekodovanje reči Tanerovog koda (155,64) pomoću GDBF-w/m algoritma sa reinicijalizacijama iznosi $\bar{l} = 1.85$, dok je za $p=3\times10^{-2}$, prosečan broj iteracija $\bar{l} = 3.59$. Ako je $p=10^{-2}$, verovatnoća da GDBF-w/m tokom prvih $K_{GDBF}$=25 iteracija ne završi dekodovanje iznosi $\mathrm{WER}(25) \approx 1.2\times10^{-5}$ (videti sliku 5), iz čega se može zaključiti da se BP algoritam veoma retko pokreće, naročito u error-floor regionu, gde performanse predloženih rešenja posebno dolaze do izražaja.

Direktna posledica je da postupak predložen u prvoj strategiji obezbeđuje znatno manju prosečnu računsku kompleksnost u odnosu na slučaj kada se koristi BP dekoder. Ovaj postupak je baziran na GDBF-w/m algoritmu, a u radu [27] i doktorskoj disertaciji [28] navedeno je da u slučaju koda dužine $n$=1296 implementacija GDBF algoritma obezbeđuje šest puta veći prosečan protok i približno devet puta manju površinu na čipu u odnosu na najefikasniju poznatu implementaciju min-sum algoritma (koji predstavlja podoptimalnu varijantu BP algoritma, pogodnu za implementaciju zasnovanu na fiksnom zarezu).


ISBN 978-86-7466-930-3

## V. ZAKLJUČAK

Dve predložene strategije kombinovanja BP i GDBF-w/m algoritama pogodne su u slučaju kada su u prijemniku dostupna oba tipa dekodera. Dobijeni rezultati pokazuju da se kombinovanjem dva uobičajena pristupa mogu dobiti značajno poboljšane performanse ili performanse uporedive onima koje ima BP dekoder, ali uz smanjenu kompleksnost.

U ovom radu su parametri dekodera određeni empirijski. Sigurni smo da se dodatno poboljšanje performansi može dobiti ako se izvrši optimizacija pojedinih parametara, kao što su momentum vektor ili pragovi za odlučivanje kod GDBF-w/m algoritma, kao i broj iteracija koji odgovara pojedinim rundama dekodovanja. Ovo će biti tema naših budućih istraživanja.

## ZAHVALNICA

Rezultati objavljeni u ovom radu delom su dobijeni u okviru saradnje ostvarene kroz i program Saradnje srpske nauke sa dijasporom Fonda za nauku Republike Srbije (br. ugovora 6462951), kao i kroz ERASMUS+ KA2 program saradnje Univerziteta u Beogradu i Univerziteta u Arizoni. Angažovanje Predraga Ivaniša i Srđana Brkića podržano je od strane Ministarstva prosvete, nauke i tehnološkog razvoja Republike Srbije. Angažovanje Baneta Vasića podržano je od strane NSF u okviru projekata CIF-1855879, CCF-2106189, CCSS-2027844 i CCSS-2052751 i NASA-SURP.

## LITERATURA

[1] R. G. Gallager, *Low Density Parity Check Codes*, MIT Press, Cambridge, Mass., 1963.

[2] D. J. C. MacKay and R. M. Neal, "Near Shannon Limit Performance of Low Density Parity Check Codes," *Electronics Letters*, vol. 32, no. 18, pp. 1645-1646, Aug. 1996.

[3] D. MacKay, "Good error correcting codes based on very sparse matrices," *IEEE Trans. Inf. Theory*, vol. 45, no. 2, pp. 399–431, Mar. 1999.

[4] T. Richardson, M. Shokrollahi, and R. Urbanke, "Design of capacity approaching irregular low-density parity-check codes," *IEEE Trans. Inf. Theory*, 47(2):619–637, 2001.

[5] ETSI Digital Video Broadcasting (DVB). *Second Generation Framing Structure, Channel Coding and Modulation Systems for Broadcasting, Interactive Services, News Gathering and other Broadband Satellite Applications; Part 2: DVB-S2 Extensions (DVB-S2X)*, ETSI EN 302307-2 V.1.1.1 (2014-10); ETSI: Sophia Antipolis, France, 2014.

[6] IEEE Standard for Information Technology—*Local and Metropolitan Area Networks—Specific Requirements—Part 11: Wireless LAN Medium Access Control (MAC) and Physical Layer (PHY) Specifications,* IEEE Standard 802.11-2016; IEEE: New York, NY, USA, 2016.

[7] 3rd Generation Partnership Project. *Technical Specification Group Radio Access Network; NR; Multiplexing and Channel Coding (Release 16)*, 3GPP TS 38.212 V16.5.0 (2021-03); 3GPP: Valbonne, France, 2021.

[8] L. M. Tanner, "A recursive approach to low complexity codes," *IEEE Trans. Inform. Theory*, Vol. 27, no. 5, pp. 533-547, Sep. 1981.

[9] X.-Y. Hu, E. Eleftheriou, D.-M. Arnold and A. Dholakia, "Efficient implementations of the sum-product algorithm for decoding LDPC codes," in *Proc. IEEE Global Telecommunications Conference (GLOBECOM 2001),* San Antonio, USA, November 25-29 2001, vol.2, pp. 1036-1036E.

[10] D. Declercq, M. Fossorier, and E. Biglieri, *Channel Coding: Theory, Algorithms, And Applications*. Academic Press Library in Mobile and Wireless Communications, Elsevier, 2014.

[11] S. K. Planjery, D. Declercq, L. Danjean, and B. Vasić, "Finite alphabet iterative decoders, Part I: Decoding beyond belief propagation on the binary symmetric channel," *IEEE Trans. Commun*, vol. 61, no. 10, pp. 4033–4045, Nov. 2013.

[12] D. Declercq, E. Li, B. Vasić, and S. Planjery, "Approaching maximum likelihood decoding of finite length LDPC codes via FAID diversity," in *Proc. IEEE Information Theory Workshop*, Lausanne, Switzerland, Sep. 3–7 2012, pp. 487–491.

[13] T. Wadayama, K. Nakamura, M. Yagita, Y. Funahashi, S. Usami and I. Takumi, "Gradient descent bit flipping algorithms for decoding LDPC codes," *IEEE Trans. Commun*, vol. 58, no. 6, pp. 1610-1614, June 2010.

[14] O.-A. Rasheed, P. Ivanis, and B. Vasić, "Fault-tolerant probabilistic gradient-descent bit flipping decoders," *IEEE Commun. Letters*, vol. 18, no. 9, pp. 1487 – 1490, Sep. 2014.

[15] H. Cui, J. Lin, Z. Wang, "An Improved Gradient Descent Bit-Flipping Decoder for LDPC Codes," *IEEE Trans. Circuits and Systems I: Regular Papers*, vol. 66, no. 8, pp. 3188-3200, Aug. 2019.

[16] P. Ivanis, O.-A. Rasheed, and B. Vasić, "MUDRI: A fault-tolerant decoding algorithm," in *Proc. IEEE International Conference on Communications (ICC 2015)*, London, UK, June 8–12 2015, pp. 4291– 4296.

[17] B. Vasić, P. Ivaniš, D. Declercq, and K. LeTrung, "Approaching maximum likelihood performance of LDPC codes by stochastic resonance in noisy iterative decoders," in *Proc. Inf. Theory Appl. Workshop*, Feb. 2016, pp. 1–9.

[18] D. Declercq, C. Winstead, B. Vasic, F. Ghaffari, P. Ivanis, and E. Boutillon, "Noise-Aided Gradient Descent Bit-Flipping Decoders approaching Maximum Likelihood Decoding", in *Proc 9th International Symposium on Turbo Codes & Iterative Information Processing (ISTC 2016)*, Special Session: Noisy Error Correction, Brest, France, 5-9 September 2016, pp. 300-304.

[19] P. Ivaniš, B. Vasić, D. Declercq, "Performance Evaluation of Faulty Iterative Decoders using Absorbing Markov Chains", *in Proc. IEEE International Symposium on Information Theory (ISIT 2016)*, Barcelona, Spain, July 10-15 2016, pp. 1566-1570.

[20] P. Ivaniš and B. Vasić, "Error Errore Eicitur: A Stochastic Resonance Paradigm for Reliable Storage of Information on Unreliable Media," *IEEE Trans. Commun*, vol. 64, no. 9, pp. 3596-3608, Sep. 2016.

[21] V. Savin, "Gradient Descent Bit-Flipping Decoding with Momentum," in *Proc. International Symposium on Topics in Coding (ISTC 2021)*, Montreal, Canada, 30 August - 3 September 2021.

[22] P. Ivaniš, S. Brkić, B. Vasić, "Suspicion Distillation Gradient Descent Bit-Flipping Algorithm," *Entropy*, vol. 24, no. 4, Article No. 558, Apr. 2021.

[23] R. M. Tanner, D. Sridhara, T. Fuja, "A class of group-structured LDPC codes," In *Proc. ISTA*, Ambleside, UK, 2001.

[24] S. Zhang and C. Schlegel, "Controlling the Error Floor in LDPC Decoding," *IEEE Trans. Commun.*, vol. 61, no. 9, pp. 3566-3575, Sep. 2013.

[25] R. Asvadi, A. H. Banihashemi and M. Ahmadian-Attari, "Lowering the Error Floor of LDPC Codes Using Cyclic Liftings," *IEEE Trans. Inf. Theory*, vol. 57, no. 4, pp. 2213-2224, Apr. 2011.

[26] X.-Y. Hu, E. Eleftheriou and D.-M. Arnold, "Progressive edge-growth Tanner graphs,". in *Proc IEEE Global Telecommunications Conference (GLOBECOM'01)*, November 2001, vol.2, pp. 995-1001.

[27] K. Le, F. Ghafari, D. Declercq and B. Vasić, "Efficient Hardware Implementation of Probabilistic Gradient Descent Bit-Flipping," *IEEE Trans. Circuits and Systems I: Regular* Papers, vol. 64, no. 4, pp. 906-917, Apr. 2016.

[28] L. T. Khoa, *New Direction on Low Complexity Implementation of Probabilistic Gradient Descent Bit-Flipping Decoder*, PhD Thesis, École Nationale Supérieure de l'Électronique et de ses Applications, Université de Cergy Pontoise, Cergy Pontoise, France, 2017.

## ABSTRACT

In this paper we propose the approaches that combine two types of iterative decoding algorithms that are usually used for decoding of low density parity check codes (LDPC). One strategy is based on a low-complexity bit-flipping algorithm, and the proposed modification enable significant performance improvement, with no significant increase of the average computing complexity. The other strategy is based on belief propagation decoder, and the resulting decoder has improved error correction capabilities for the codes with short codeword length.

**LDPC decoders with re-initializations based on synergy of hard decision and message passing principles**

Predrag Ivaniš, Srđan Brkić, Bane Vasić

 ISBN 978-86-7466-930-3

# Analiza performansi kooperativnog diverziti sistema u kompozitnom fedingu modelovanom odnosom α-μ i gama raspodela

Edis Mekić, Irfan Fetahović, i Edin Dolićanin

***A stra t*— U ovom radu je izvedeno novo opšte, jednostavno rešenje u zatvorenom obliku za funkciju gustine verovatnoće odnosa proizvoda slučajnih promenljivih predstavljenih α-μ i Gama raspodelama i slučajne promenjive predstavljene Gama raspodelom. Ova rešenja se primenjuju u analizi performansi omuni acionih sistema sa ooperativnim diverziti sistemom oji se oristi za poboljšanje prijema signala na čije anvelope utiče brzi i spori feding, do na anvelopu o analne interference utiče samo brzi feding.**

***Ključne reči*— α-μ raspodela; Gama raspodela; feding; ooperativni diverziti**

## I. UVOD

Proizvodi i odnosi slučajnih promenljivih, kao i rešenja funkcija gustina verovatnoća (PDF) i kumulativnih funkcija (CDF) u zatvorenoj formi su u žiži interesovanja telekomunikacionih istraživanja.

Rešenja u zatvorenom obliku za PDF i CDF se mogu koristiti u analizi verovatnoće otkaza multihop kognitivnih mreža [1]. Kao posebno značajni u analizi otkaza i ergodičnog kapaciteta mreža i u prisustvu fedinga su se pokazali odnosi i proizvodi anvelopa signala koje su modelovane α-μ raspodelom [2]. Analiza odnosa signal interference (SIR) datog kao odnos proizvoda dve k- μ slučajne promenljive i Nakagami-m slučajne promenljive, kao i odnos proizvoda dve Rayleigh-ove slučajne promenljive i Rayleigh-ove slučajne promenljive je evaluirana u radovima [3,4] i korišćena za analizu bežičnih relejnih komunikacionih sistema koji se sastoje od dve sekcije, u prisustvu fedinga i kokanalne interferencije. Jednostavno matematičko rešenje u slučaju kada se koriste samo α-μ slučajne promenljive je dato u [5]. Dobijeno rešenje se koristi za modelovanje fedinga u multihop sistemima, u prisustvu kokanalne interference

Slučajna promenljiva može se koristiti za modelovanje anvelope signala u prisustvu fedinga. Feding je pojava da kvalitet prenosa signala opada zbog refleksije i refrakcije signala o objekte koji se nalaze na putanji istog (brzi feding) ili zbog velikih prepreka na putanji signala (spori feding). Osim ovoga, na anvelopu signala utiče i kokanalna interferenca koja se javlja zbog višestrukog korišćenja frekvencija. Anvelopa signala u prisustvu fedinga se može modelovati proizvodom dve slučajne promenljive [6], dok se kokanalna interferenca modeluje odnosom slučajnih promenljivih [7].

Proizvod α-μ i lognormalne slučajne promenljive daju odlične rezultate u modelovanju realnih efekata sporog fediga, međutim primena lognormalne raspodele ne daje rešenja u zatvorenom obliku za PDF anvelope signala na prijemu [8]. Kao alternativa lognormalnoj rapodeli može se koristiti Gama raspodela [9].

Da bi ublažili efekte fedinga na anvelopu signala mogu se koristiti diverziti tehnike koje se sastoje od većeg broja antena [10].

U ovom radu ćemo analizirati bežičnu mrežu sa kooperativnim diverziti protokolom za ublažavanje efekta fedinga [11].

Brzi feding i njegovo delovanje na signal između predajnika i prijemnika u slučaju idealnog koherentnog prenosa u poludupleks modu modelovaćemo kao odnos α-μ promenljivih, dok ćemo efekat sporog fedinga modelovati kao proizvod ovog odnosa sa Gama slučajnom promenljivom. Dobijena rešenja za PDF biće primenjena u modelu kooperativne diverziti mreže, pošto su multihop relejni sistemi specijalni slučajevi ove diverziti tehnike. Validnost rezulata ćemo pokazati na primeru jednostavnog dual hop sistema.

## II. FIZIČKI MODEL BEŽIČNE MREŽE SA KOOPERATIVNIM DIVERZITI PROTOKOLIMA

Primer bežične mreže koja se sastoji iz niza releja je dat na Sl.1. Terminali $TS_1$, $TS_2$,…$TS_N$ prenose signal do terminala $TR_1$, $TR_2$,…,$TR_M$ , respektivno. Ovako definisan sistem može da se koristi kao osnova za modelovanje različitih bežičnih sistema. Recimo, možemo da predstavimo sistem mobilne telefonije ako pretpostavimo da su $TS_1$, $TS_2$,…,$TS_N$ mobilni uređaji, a $TR_1= TR_2=…=TR_M$ bazne stanice. Model možemo da koristimo za reprezentaciju LAN mreže, bilo da je u pitanju ad-hoc ili mreža zasnovana na pristupnim tačkama. Ako pretpostavimo da su terminali $TR_1= TR_2=…=TR_M$ , onda imamo LAN mrežu sa pristupnom tačkom, a ako pretpostavimo da je $TR_1\neq TR_2\neq…\neq TR_M$ , onda imamo ad-hoc mrežu. Najzad, ako se svi terminali fokusiraju na prenos informacija od $TS_1$ do $TR_M$, dok su prelazni koraci prenosa redom od $TR_1$ do $TS_2$, od $TS_2$ do TR3, … $TS_N$ do $TR_M$, onda imamo multihop sistem.

Poslednji navedeni model ćemo analizirati tako što ćemo

Edis Mekić – Departman za tehničko-tehnološke nauke, Državni univerzitet u Pazaru, Vuka Karadžića 9, 36300, Novi Pazar, Srbija (e-mail: emekic@np.ac.rs).

Irfan Fetahović – Departman za tehničko-tehnološke nauke, Državni univerzitet u Pazaru, Vuka Karadžića 9, 36300, Novi Pazar, Srbija (e-mail: ifetahovic@np.ac.rs).

Edin Dolićanin – Departman za tehničko-tehnološke nauke, Državni univerzitet u Pazaru, Vuka Karadžića 9, 36300, Novi Pazar, Srbija (e-mail: edin@np.ac.rs).

 ISBN 978-86-7466-930-3

ga ograničiti na mod poludupleksa, i to na takav način da svaki od releja pojačava primljeni signal. Radi jednostavnijeg računa pretpostavićemo da imamo idealni koherentni prenos, gde se primljeni signal u potpunosti obnavlja na transmisionom releju.

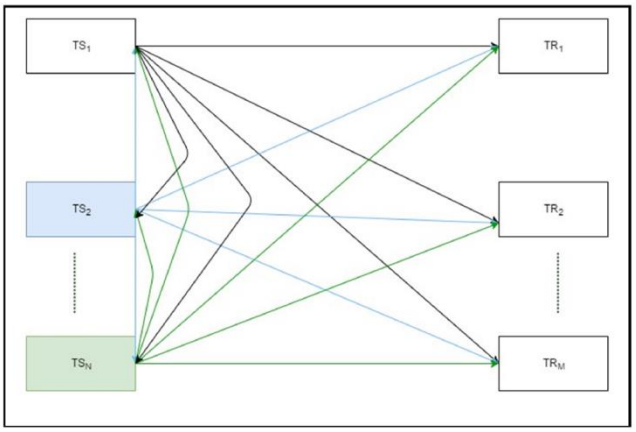


Sl.1. Bežična mreža zasnovana na sistemu releja

Kanale između releja ćemo podeliti na ortogonalne podkanale, pri čemu će svaki od terminala koristiti i/n stepena slobode u kanalu (Sl.2).

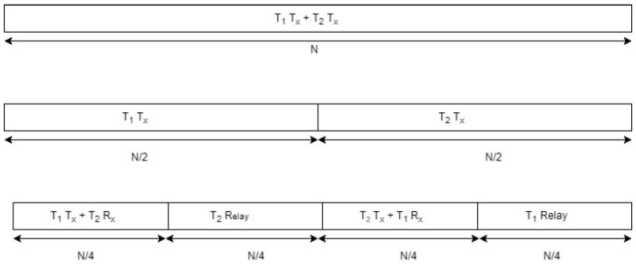


Sl.2. Alokacija kanala

Sa obzirom na to da je prenos između predajnika i prijemnika pod uticajem i brzog i sporog fedinga, simetrija kanala će nam omogućiti da stavimo fokus za početak na jedan par predajnik-terminal.

## III. STATISTIČKA ANALIZA PROIZVODA ODNOSA α-μ I GAMA SLUČAJNIH PROMENLJIVIH

Anvelope polaznog signala su modelovane slučajnim promeljivim a[n], gde je n=1,2,…,N/2, dok drugi terminal prenosi vrednosti n=N/2+1,…N. Terminal može da koristi samo polovinu stepena slobode. Anvelopu primljenog signala modelovaćemo kao proizvod odnosa slučajnih promenljivih.

$$\varphi[n] = \frac{a[n]\,c[n]}{b[n]} \tag{1}$$

Slučajne promenljive a[n] i b[n] su modelovane kao α-μ dok je c[n] modelovana gama slučajnom promenljivom. PDF proizvoda odnosa izračunaćemo tako što za početak računamo PDF odnosa dve α-μ slučajne promenljive.

$$\phi[n] = \frac{a[n]}{b[n]} \tag{2}$$

$$p_\phi(\phi[n]) = \int_0^\infty |J| p_\phi(\phi[n]a[n]) p_b(b[n]) db \tag{3}$$

Vrednost |J| je Jakobijan defnisan na sledeći način:

$$|J| = \left|\frac{da[n]}{d\phi[n]}\right| = b[n] \tag{4}$$

PDF združene promenljive φ[n] može se izračunati korišćenjem sledećeg izraza:

$$p_\varphi(\varphi[n]) = \int_0^\infty |J| p_\phi\left(\frac{\varphi[n]}{c[n]}\right) p_c(c[n]) dc \tag{5}$$

Odabir odgovarajuće kooperativne ili nekooperativne akcije je zasnovan na merenju odnosa signal-interferenca (SIR). Na prijemnoj strani merimo vrednosti anvelope signala. Možemo primeniti adaptiran mod prenosa, u skladu sa izmerenom vrednošću. Ako izmerena vrednost anvelope pada ispod određenog praga, ponavljamo prenos, a ako je iznad ovog praga onda prenosimo signal, ovo je korišćenje pojačaj i prosledi tehnike da bi se postigao diverziti.

Za kooperativni diverziti sistem, gde signal prolazi kroz niz releja, PDF slučajne promenljive može biti izračunat na sledeći način:

$$\varphi[n] = \min(\varphi[n]_1, \varphi[n]_2, \dots, \varphi[n]_N) \tag{6}$$

$$p_\varphi(\varphi[n]) = \sum_{m=1}^{N} |J| p_{\varphi_m}(\varphi[n]) \prod_{\substack{k=1 \\ k\neq m}}^{N} (1 - F_{\varphi_k}(\varphi[n])) \tag{7}$$

Sada ćemo modelovati efekte, brzog, sporog fedinga i interference. Za modelovanje anvelope na koju deluje brzi feding i interference koristimo α-μ raspodelu. Vrednost μ predstavlja broj klastera prenosa, dok koeficijent α predstavlja nelinearnost okoline. Radi jednostavnije analize slučajnu promenljivu između bilo kojih releja *a n* , predstavljamo kao promenljivu a.

Slučajna promenljiva α-μ raspodele je opisana sledećom jednačinom:

$$p_a(a) = \alpha \left(\frac{\mu_a}{\Omega_a}\right)^{\mu_a} \frac{\gamma^{\alpha\mu_a - 1}}{\Gamma(\mu_a)} e^{-\frac{\mu_a a^\alpha}{\Omega_a}} \tag{8}$$

U datoj jednačini snaga anvelope signala je $\Omega_a = \varepsilon\langle a^\alpha \rangle$, α predstavlja nelinearnost okoline, $\mu_a$ je inverzna vrednost normalizovane varijanse *α, ($\mu_a \geq 0.5$)*.

Spori feding modelovaćemo sledećom Gama slučajnom promenljivom:

$$p_a(a) = \frac{a^{k-1} e^{-\frac{a}{\Omega_a}}}{\Gamma(a)\Omega_a} \tag{9}$$

Vrednost sporog fedinga definisana je promenljivom k, pri čemu niža vrednost k znači da je veći uticaj sporog fedinga.

Da bi izračunali odgovarajući PDF slučajne promenljive φ dat jednačinom (5), prvo moramo da izračunamo PDF odnosa dve slučajne α-μ promenljive $\phi = a/b$, rešavanjem jednačine (3). Ovaj međukorak nam omogućuje da izračunamo združenu gustinu verovatnoće zaobilazeći kompleksnije Mellinove transformacije.

Primenom jednačina [12 (3.461 i 6.631), 13 (26)] združena gustina verovatnoće se može prikazati preko Meijer's G

 ISBN 978-86-7466-930-3

funkcija.

$$p_\phi(\phi) = \alpha\left(\frac{\mu_a\Omega_b}{\mu_b\Omega_a}\right)^{\mu_a}\frac{\phi^{\alpha\mu_a-1}}{\Gamma(\mu_a)\Gamma(\mu_a)}G_{1,1}^{1,1}\left(\frac{1}{\varphi^\alpha}\frac{\mu_a\Omega_b}{\mu_b\Omega_a}\middle|\begin{matrix}1-\mu_a-\mu_b\\0\end{matrix}\right) \quad (10)$$

PDF promenljive φ se izvodi primenom izraza (5). Korišćenjem izraza [14, 15] dobijamo izraz za PDF u zatvorenom obliku preko Meijer's G funkcija.

$$p_\varphi(\varphi) = \left(\frac{\mu_a\Omega_b}{\mu_b\Omega_a}\right)\left(\frac{1}{\Omega_c}\right)^{\alpha\mu_a}\frac{\alpha^{k-\alpha\mu_a-1}\varphi^{\alpha\mu_a-1}}{(2\pi)^{\frac{\alpha-1}{2}}\Gamma(\mu_a)\Gamma(\mu_c)\Gamma(k)}\times \times G_{1+\alpha,\ 1}^{1,\ 1+\alpha}\left(\frac{1}{\varphi^\alpha}\frac{\mu_b\Omega_a\Omega_c}{\mu_a\Omega_b}\middle|\begin{matrix}\frac{1-k+\alpha\mu_a}{2},\dots,\frac{1-k+\alpha\mu_a}{2},1\\ \mu_a+\mu_b\end{matrix}\right) \quad (11)$$

CDF se može izračunati primenom sledećeg izraza

$$F_\varphi(\varphi) = \int_0^\varphi p_\varphi(s)ds \quad (12)$$

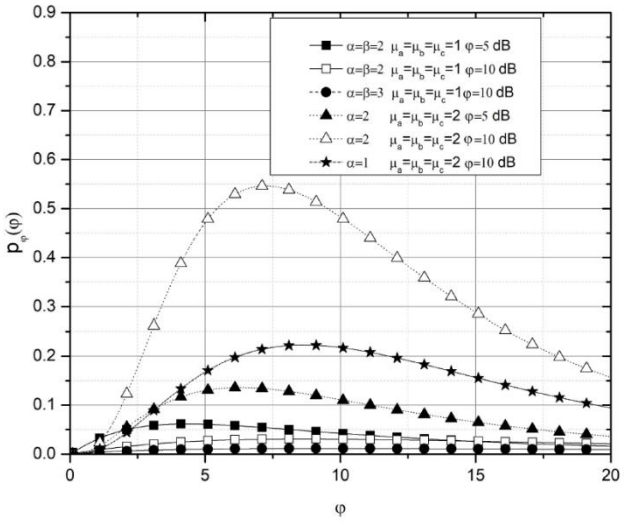


Sl.3. PDF za različite vrednosti parametra α-μ promenljive

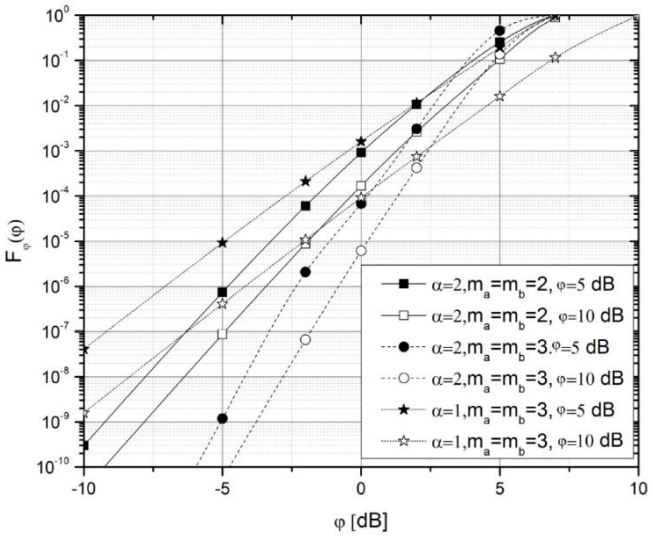


Sl.4. CDF za različite vrednosti parametra α-μ promenljive

Primenom dobijenih izraza, a menjajući parametar α-μ u izvedenim izrazima, dobijen je matematički model koji pokazuje da povećanje snage anvelope signala smanjuje verovatnoću otkaza sistema. Na Sl.3. je dat PDF združene gustine verovatnoće anvelope modelovanog signala, dok je verovatnoća otkaza data kroz numeričko izračunavanje CDF anvelope koja je modelovana novom združenom gustinom verovatnoće (Sl.4), dok povećanje dubine fedinga povećava verovatnoću otkaza.

## IV. Zaključak

U radu je predstavljena analiza kooperativnog diverziti sistema kao jednog od pristupa za smanjivanje uticaja brzog i sporog fedinga na prenos signala u prisustvu interference. Uticaj efekata brzog fedinga i kokanalne interference smo modelovali odnosom dve α-μ slučajne promenljive, dok je efekat sporog fedinga modelovan proizvodom navedenog odnosa i Gama slučajnom promenljivom. Izračunat je izraz za PDF u zatvorenom obliku. Međutim, za kompletnu analizu neophodno je izračunati i CDF u zatvorenom obliku. To bi omogućilo brzu i efikasnu simulaciju ne samo navedenog slučaja, već i velikog broja drugih slučajeva koji se mogu izračunati kao specijalni slučajevi predstavljenog.

## Literatura


[1] Y. A. Rahama, M. H. Ismail, M. S. Hassan, "On the distribution of the product and ratio of products of EGK variates with applications", vol. 68, no. 2, pp. 231-238 Telecommunication Systems, 2018.

[2] P. N. Rathie, A. K. Rathie, L. C. Ozelim, "The product and the ratio of\(\alpha-\mu\) random variables and outage, delay-limited and ergodic capacities analysis,", vol. 4, no. 1, pp. 100-108, Physical Review and Research International, 2014.

[3] D. Krstic, I. Romdhani, M.M.B. Yassein, S. Minic, G. Petkovic, P. Milacic, "Level crossing rate of ratio of product of 2 two ku random variables and Nakagami-m random variable," In: Computer and Information Technology; Ubiquitous Computing and Communications; Dependable, Autonomic and Secure Computing; Pervasive Intelligence and Computing (CIT/IUCC/DASC/PICOM), IEEE International Conference on 1620-162, 2015.

[4] D. Krstic, M. Stefanovic, S. Minic, M. Peric, "Analysis of Ratio of One and Product of Two Rayleigh Random Variables and its Application in Telecommunications", no. 3, International Journal of Communications, 2018.

[5] E. Mekic, N. Sekulovic,M. Bandjur, M. Stefanovic, P. Spalevic, "The distribution of ratio of random variable and product of two random variables and its application in performance analysis of multi-hop relaying communications over fading channels," vol. 8, no. 7A, pp. 133-137, Przeglad Elektrotechniczny, 2012.

[6] G. E. Corazza and F. Vatalaro, "A statistical model for land mobile satellite channels and its application to nongeostationary orbit systems," vol. 43, pp. 738-741, IEEE Transactions Vehucilar Technologies, 1994.

[7] J.D. Parsons, *The Mobile adio Propagation Channels*. 2nd ed. Wiley, 2002.

[8] P.G. Babalis, C.N. Capsalis. "Impact of the combined slow and fast fading channel characteristics on the symbol error probability for multipath dispersion less channel characterized by a small number of dominant paths," vol. 47, no. 5, pp. 653-657, 1999.

[9] T.A. Tsiftsis, "Performance of wireless multihop communications systems with cooperative diversity over fading channels,"vol. 21, no. 5, pp. 559-565. International Journal of Communication Systems, 2008.

[10] N. Dimitriou, A. Polydoros, A. Barnawi, "Cooperative schemes for path establishment in mobile ad-hoc networks under shadow-fading," vol. 11, no. 8, pp. 2556-2566, Ad Hoc Networks, 2013

[11] D. da Costa, M. Yacoub, G. Fraidenraich, "Second-order statistics of equal-gain and maximal-ratio combining for the α-μ (generalized gamma) fading distribution," IEEE 9th International Symposium on Spread Spectrum Techniques and Applications, pp. 342–346, 2006.

[12] I.S. Gradshteyn, I.M. Ryzhik, *Table of Integrals, Series, and Products,* 7th edition. New York, Academic, 2007.

[13] V.S. Adamchik, O.I. Marichev," Algorithm for calculating integrals of hypergeometric type functions and its realization in reduce system" in Proceedings of International Symposium on Symbolic and Algebraic Computation (ISSAC '90), pp. 212–224, 1990.

[14] http://functions.wolfram.com/07.34.17.0012.01.

[15] http://functions.wolfram.com/07.34.21.0088.01.


 ISBN 978-86-7466-930-3

ABSTRACT

In this paper, we present novel general, simple, exact and closed-form expressions for the probability density function (PDF) and of ratio of product of random α-μ distributed variable and generalized Gamma distributed variable and random α-μ distributed variable. These results have application in performance analysis of cooperative diversity communication systems in different fading transmission environments where envelope of the signal is affected by fast and slow fading and envelope of co-channel interference by fast fading.

**Performance Analysis of the Cooperative Diversity Communication ystems in Composite ading cenario odelled as Ratio of α-μ Variates and Gamma Variate**

Edis Mekić, Irfan Fetahović i Edin Dolićanin

 ISBN 978-86-7466-930-3

# ARTIFICIAL INTELLIGENCE
# /
# ВЕШТАЧКА ИНТЕЛИГЕНЦИЈА
# (VII/ВИ)

ISBN 978-86-7466-930-3

# Code Comment Classification Taxonomies

Marija Kostić, Aleksa Srbljanović, Vuk Batanović and Boško Nikolić, *Member, IEEE*

***Abstract*—Code comments have become an increasingly important ind of software development metadata, due to the possibilities of automated code comment analysis and generation. Different downstream tas s inherently prioritize certain inds of code comments over others, ma ing it necessary to properly define and identify different comment classes. In this paper, we analyze, compare, and systematize previously proposed code comment classification ta onomies according to their comment classes and applicability. We also present a new ta onomy designed for the tas s of semantic code search and semantic te t similarity, and we contrast it to the e isting approaches.**

***Index Terms*—code comments; code comment ta onomy; comparison of classification ta onomies.**

## I. Introduction

Code comments represent an invaluable source of metadata regarding software implementation. They describe code functionalities and algorithmic specifics, provide usage instructions, point towards additional resources, denote potential or observed programming bugs and issues, etc. In short, code comments play a vital role in helping developers comprehend source code [1]. In this manner, code comments greatly increase code maintainability, particularly when dealing with large software projects and development teams.

Depending on the downstream task in focus, not all code comments are of equal importance. For instance, if one wishes to compare the functionality of two methods, comments which provide authorship information are of little consequence, whereas those describing program implementation are of much greater significance. However, distinct kinds of code comments can be difficult to distinguish, particularly when no clear keywords for each comment type exists. A further complication in identifying relevant comments is the fact that a standardized code comment taxonomy does not exist. Instead, multiple different code comment categorization solutions have been proposed so far, most often designed with a specific programming language and downstream task in mind.

In this paper, we first present a survey of the existing code comment taxonomies and their applications in downstream tasks. Afterward, we present a new comment classification schema suitable for the tasks of semantic code search and semantic textual similarity and applicable to various programming languages. We then compare our approach with previous code comment taxonomies and conclude with some pointers regarding the future use of our comment schema.

Marija Kostić is with the School of Electrical Engineering and the Innovation center of School of Electrical Engineering, University of Belgrade, 73 Bulevar kralja Aleksandra, 11020 Belgrade, Serbia (e-mail: marija.kostic@ic.etf.bg.ac.rs), (https://orcid.org/0000-0003-4923-3748).

Aleksa Srbljanović is with the School of Electrical Engineering, University of Belgrade, 73 Bulevar kralja Aleksandra, 11020 Belgrade, Serbia, (e-mail: aleksa.srbljanovic@etf.bg.ac.rs).

Vuk Batanović is with the Innovation center of School of Electrical Engineering, University of Belgrade, 73 Bulevar kralja Aleksandra, 11020 Belgrade Serbia, (e-mail: vuk.batanovic@ic.etf.bg.ac.rs), (https://orcid.org/ 0000-0003-2639-9091).

Boško Nikolić is with the School of Electrical Engineering, University of Belgrade, 73 Bulevar kralja Aleksandra, 11020 Belgrade, Serbia, (e-mail: bosko.nikolic@etf.bg.ac.rs), (https://orcid.org/ 0000-0003-1142-9243).

## II. A Survey of Existing Taxonomies

In this section, we review existing code comment classification taxonomies and describe how those systems were applied to specific tasks. A similar, but much shorter survey of this kind was previously presented within [2].

Zhai et al. [3] wanted to leverage program analysis to systematically propagate comments, so that they can be passed on to uncommented code entities and help detect bugs. A bi-directional analysis was designed where: (1) program analysis propagates and updates code comments, and (2) comments provide additional semantic hints to enrich program analysis. For effective propagation, it was vital to understand what kind of information comments convey and to which code elements they refer to, as comments of different categories require different propagation rules. The authors introduced a code comment taxonomy in which there are two dimensions of interest: code entity and content perspective. Code entities commonly commented on are *class*, *method*, *statement*, and *ariable*. As for the content perspective, five of them were identified: 1) *what* – a definition or a summary of the code entity's functionality; 2) *why* – the reason why the code entity is provided or its design rationale; 3) *how-it-is-done* – description of the implementation details; 4) *property* – properties of the entities such as pre-condition and post-conditions; 5) *how-to-use* – description of the usage, expected set-up, or the environment of the entity. A set of 5,000 comments from four popular Java libraries were classified at the sentence level. The agreement between two coders, measured using Cohen's Kappa metric [4], was 0.826.

Chen et al. [1] investigated the use of the relationship between code blocks and the categories of the corresponding comments to improve code summarization, where the aim is to automatically generate a code comment based on the given block of source code. They showed that a composite approach, where the most suitable summarization model is selected based on the comment category, outperforms other approaches. Comments were classified into six categories – *what*, *why*, *how-to-use*, *how-it-is-done*, *property* and *others*. Five of them are the same as categories of content perspective in [3], while the sixth one, named *others*, covers unspecified or ambiguous comments. For this task, 20,000 Java methods and their corresponding comments were manually classified.

 ISBN 978-86-7466-930-3

The overall agreement of the three annotators, expressed in the terms of Fleiss' Kappa score [5], is 0.79.

Padioleau et al. [6] studied code comments to understand developers' needs regarding the creation of new tools and languages or the improvement of the existing ones. Comments were classified along four dimensions according to the question of interest: 1) *What* – content: What is in the comment? Does it contain useful information? Its categories *type*, *interface*, *code relationship* and *pastFuture* and subcategories are closely related to the specific usage of the C programming language for operating systems; 2) *Who* – people involved: Who or which tool can benefit from a comment? Who is the comment author?; 3) *Where* – code entity: Where in a file is a comment located?; 4) *When* – time: When was a comment written? How did the comment evolve over time? The authors considered 1050 comments randomly sampled from the code of three operating systems written in the C programming language: Linux, FreeBSD and OpenSolaris. The *What* and *Who* dimensions were manually annotated for each comment, while the other two dimensions were labeled automatically.

Haouari et al. [7] investigated developers' commenting habits via an empirical study. For the quantitative aspect of the study, the authors determined the distribution of the comments with respect to the program construct type that follows it. This allowed them to see what program construct types are documented more often than others. Some of the observed constructs are *package declaration*, *import declaration*, *class declaration*, *method*, *constructor*, *for*, *while*, etc. For the qualitative aspect of the study a new comment taxonomy was designed. This taxonomy has four high-level dimensions: 1) *bject of the comment* which can be a single subsequent instruction (*follow*); the following block of instructions (*block*), no code in the vicinity (*nocode*), or any other situation (*other*); 2) *Comment type* which can be the description of the code functionality (*e planation*), future task to be completed like TODO items (*working*), old code that is commented out instead of being removed (*code*), or any other comments (*other*); 3) *Style* dimension is only observed in the case of explanatory comments (*type e planation*) and can be either *e plicit* or *implicit*; 4) *uality* dimension is also specific only to explanatory comments. It involves three categories: *fair* where comments describe functionalities of related code and give other information; *fair* where code functionality is adequately described; and *poor* where some or none of the functionality is described. Analysis for the quantitative aspect was fully automated and applied to all comments within three open-source Java projects. For the qualitative aspect, the authors had 49 developers manually classify 407 comments.

Steidl et al. [8] developed a model for comment quality analysis with four criteria (*coherence*, *usefulness*, *consistency,* and *completeness*). Their comment taxonomy consists of seven high-level categories: 1) *copyright* – copyright or license; 2) *header* – overview of the class functionality; 3) *member* – functionality of a method/field; 4) *inline* – implementation decisions within a method body; 5) *section* – group of methods/fields that belong to the same functional aspect; 6) *code* – commented out code; 7) *task* – developer notes with a remaining todo, a bug, or an implementation hack. Authors created a training set by classifying 830 Java and 500 C++ comments from twelve open-source projects.

Pascarella et al. [9]–[11] focused on increasing the empirical understanding of the types of comments that developers write in source code. After an iterative process of analyzing code files, the authors defined a fine-grained hierarchical taxonomy with two layers: the outer one consisting of six top-level categories (*purpose*, *notice*, *under de elopment*, *style I E*, *metadata*, and *discarded*) and the inner one consisting of 16 subcategories. The *purpose* category contains comments that describe the functionality of the related source code. Its three subcategories *summary*, *e pand*, and *rationale* respond to the question words what, how, and why, similarly to the categories in [1], [3]. The *notice* category covers comments about warnings, alerts, messages, or functionalities that should be used with care. Its subcategories are *deprecation*, *usage*, and *e ception*. Subcategories *todo* (explicit actions to be done), *incomplete* (partial or empty comment bodies), and *commented code* belong to the *under de elopment* top-level category. The *style I E* comments are used for communication with the IDE (*directi e*) and logical separation of the code (*formatter*). The *metadata* comments define meta information about the code such as license, terms of use, authors, links to external resources (subcategories *license*, *ownership*, and *pointer*). All other comments that do not fit in the previous categories belong to the *discarded* category (subcategories *automatically generated* and *unknown*). Authors decided to classify comments at the character level. That means that annotators had to specify the starting and the ending character of each comment block and its category. After this process, it was found that in only 4% of cases one line had to be classified into more than one category. The study was conducted on more than 6,000 source code files with more than 40,000 lines of Java comments in open source and industrial software projects. To validate the proposed taxonomy, three developers were asked to manually classify 138 lines of comments in three Java source code files. They achieved a Fleiss' Kappa value of 0.9.

Unlike previously mentioned efforts, Shinyama et al. [12] worked only on comments inside functions or methods that explain code at the microscopic level i.e., on *local comments*. These comments are not visible in the documentation and often give insight into developers' minds. They are often crucial for understanding nontrivial parts of the code. As there usually is a relationship between a comment and the code it describes, the authors represented that relationship as an arc with three elements: (1) source – the comment itself; (2) destination – target code; and (3) type of relationship – comment category. They independently made a list of categories suitable for local comments: 1) *postcondition* – conditions that hold after the code is executed, typically used to explain what the code does; 2) *precondition* – conditions that hold before the code is executed, typically used for explaining why the code is needed; 3) *alue description* – a

 ISBN 978-86-7466-930-3

phrase that can be equated with a variable, constant or expression; 4) *instruction* – instructions for code maintainers (todo comments); 5) *guide* – guides and examples for code users; 6) *interface* – description of a function, type, class, or interface; 7) *meta information* – author, date, or copyright; 8) *comment out* – commented out code; 9) *directi e* – compiler directives that are not directed to human readers; 10) *isual cues* – comments inserted just for the ease of reading; 11) *uncategori ed* – all other comments. For each arc element, a statistical classifier was built and trained on 1,000 manually classified Java comments. Classifiers were applied on large corpora of Java and Python comments. Annotation agreement was measured on a separate set of 100 Java comment-code pairs and reached Fleiss' Kappa value of 0.491.

Zhang et al. [13] used supervised learning to automatically classify Python code comments. Since most of the related work is based on Java and C/C++ programming languages, the authors conducted an iterative content analysis session to devise a Python-specific classification taxonomy. Their taxonomy contains 11 categories: 1) *metadata* – license and copyright; 2) *summary* – description of the functionality of the related code; 3) *usage* – explanations on how to use the code that can contain examples; 4) *parameters* – explanations of function parameters; 5) *e pand* – detailed explanations of the purpose of a small block of code, usually inline comments; 6) *ersion* – library version information; 7) *de elopment notes* – comments for developers concerning ongoing work, temporary tips, explanations of functions etc.; 8) *todo* – explicit actions to be done in the future like bug fixing or feature improving; 9) *e ception* – indications that a function throws exceptions or suggestions how to prevent unwanted behaviors; 10) *links* – links to external resources; 11) *noise* – meaningless symbols which may be used for separation. The training set consisted of 330 annotated comments from seven popular Python open-source projects on GitHub.

## III. A New Code Comment Taxonomy

We explored code comment classification taxonomies in order to differentiate between different kinds of comments for the tasks of semantic code search and cross-level sematic textual similarity. In semantic code search (SCS), the goal is to construct a system which returns the most relevant code block(s) from a software repository for a given query in a natural language. To do so, most models rely on the accompanying code comments which describe the functionality of their respective code blocks [14]. Cross-level semantic similarity (CLSS) is the task in which a computational model ought to return a numerical semantic similarity score for a given pair of texts written in a natural language, where the length of the texts can be dissimilar (e.g., one text is a paragraph, the other is a sentence) [15]–[16]. Solving CLSS is of great use for semantic code search, since SCS implies finding semantic links between texts of different lengths – queries are usually limited to a couple of words or a sentence, whereas the length of code comments can range from a phrase to a paragraph. Obviously, these tasks are not limited to a particular programming or natural language.

We found that no previous code comment taxonomy was designed with these two downstream tasks in mind, so it was necessary to consider the previous classification systems and devise a suitable set of comment categories. Furthermore, we wanted to create a classification taxonomy that would be applicable to various programming languages, including C, C++, C#, Java, JavaScript/TypeScript, PHP, Python, and SQL. Upon reviewing the papers presented in the previous section, we decided to develop our own taxonomy using the approaches of Pascarella et al. [9]–[11] and Steidl et al. [8] as a starting point. This choice was based on the emphasis these works placed on the comments that describe code functionality, since such comments are the most relevant ones for SCS. We therefore distinguish between functional and non-functional comments via two top-level categories. These two categories are then subdivided into eight subcategories. In the remainder of this section, we will present the definition and scope of each of them.

### A. Functional

The *Functional* category contains comments that describe the functionality of the corresponding source code. Descriptions can be short, or they can extend over multiple lines. These comments are usually written in a natural language and are used to describe the purpose, behavior, or the reason why something is implemented in a particular way. They can respond to questions *What* , *Why* , and *ow* . We do not distinguish between these aspects of functionality because all of them are relevant for the SCS task. However, we do differentiate between three subcategories based on the type of the corresponding source code: 1) *Functional-Module* comments describe the functionality of a particular module like a class or an interface. If a programming language does not use the object-oriented paradigm, these comments pertain to entire files or scripts; 2) *Functional-Method* comments describe the functionality of a function or a method. They are usually located above or at the beginning of a function/method definition or declaration; 3) *Functional-Inline* are all the other comments that describe some functionality. They can describe the functionality of a variable or an expression and can be located inside a method body.

### B. Non-Functional

The *Non-Functional* category covers all comments that do not describe code functionality. Subcategories in this top-level category are not relevant for the SCS and CLSS tasks, but we still decided to include them because we wanted to make the annotated datasets usable for other downstream tasks as well. We distinguish between the following five subcategories: 1) The *Notice* category encompasses warnings, alerts, and messages intended for other developers or users of the source code. It also covers information about deprecated artifacts and instructions about alternative methods or classes that should be used. Comments that explain something is implemented in a certain way because of a bug, or a known issue, also belong to this category. Finally, examples or explicit suggestions how

 ISBN 978-86-7466-930-3

to use a functionality are classified as *Notice* comments as well; 2) *General* comments usually define meta-information about the code such as license, copyright, authorship, module/class version, timestamps, the name or path of the file, information about the libraries used in the source code, etc. These comments are usually located at the top of the file; 3) The *Code* category is composed of comments that contain source code that is commented out by developers. This is usually done during testing or debugging. This code may represent new or hidden features, work in progress, features being tested, temporarily removed code or older variants of the code; 4) *I E* comments are used for communication with the IDE or the compiler to change their default behavior. Comment content is usually of limited value to human

TABLE 1 CLASSIFICATION OF EXAMPLE CODE COMMENTS ACCORDING TO DIFFERENT TAXONOMIES

| Class | Class | ample | aouari [7] | teidl [8] | hinyama [12] | hang [13] | Pascarella [11] | hai [3] | Chen [1] | ur proposal |
|---|---|---|---|---|---|---|---|---|---|---|
| Functionality by type | What | Pushes an item onto the top of this stack. [3] | Type-Explanation | Header\| Inline\| Member | Postcondition | Summary | Summary | What | What | Functional |
| | Why | It eliminates the need for explicit range operations. [3] | | | Precondition | - | Rationale | Why | Why | |
| | How | Shifts any subsequent elements to the left. [3] | | | Uncategorized | Expand | Expand | How-it-is-done | How-it-is-done | |
| | Property | The index must be a value greater than or equal to 0. [3] | | | | - | - | Property | Property | |
| Functionality by position | Module | This class is a member of the Java Collections Framework. [3] | | Header | Interface | Summary | Purpose | Class | | Functional-module |
| | Method | Check for symmetry, then construct the eigenvalue decomposition @param A square matrix [8] | | Member | | Summary\| parameters | | Method | What\|Why How-it-is-done\| Property | Functional-method |
| | Inline | *Increment this when there's a change requiring caches to be invalidated.* | | Inline | (Post\|pre) condition | Expand | | Statement | | Functional-inline |
| | Variable/ Field | The number of characters to skip. [3] | | Member | Value description | | | Variable | | |
| Section | | --- Getter and Setter Methods --- [8] | Type-Other | Section | Visual cue | - | Formatter | - | Others | Functional-inline |
| Automatically Generated | | *COLORCORRECTION_HPP* | | - | Uncategorized | Noise | Automatically generated | - | | |
| Notes | | Caution: setting a new service manager stub won't replace the existing one [7] | | Task | | Development notes | Todo | - | | Notice |
| Usage | | Example: renderText(100, 100, FONT, 12, "Hello"); [12] | | - | | Usage | Usage | How-to-use | How-to-use | |
| Deprecation | | *DEPRECATED: the following property is no longer in use, but defined until 2.0 to prevent conflicts* | Type-Working | - | | Development notes | Deprecation | - | Others | |
| Exception | | *@throws TransportExceptionInterface When an unsupported option is passed* | | - | Guide | Exception | Exception | - | | Functional-method |
| Link | | *See https://github.com/symfony/symfony/pull/5582* | | - | | Links | Pointer | - | | Notice |
| Bug | | *Skip due to crash bug: https://support.microsoft.com/en-us/help/2908087* | | Task | | Development notes | Todo | - | | Todo |
| Todo | | TODO: Check synchronization. [7] | | | Instruction | Todo | | - | | |
| Code | | _mainFrame.hourglassOff(); [7] | Type-Code | Code | Commented out | Noise | Commented code | - | | Code |
| Ownership | | *@author Ben Ramsey <ben@benramsey.com>* | | Header | Meta information | | Ownership | - | | General |
| Meta | | *Copyright(c) 2019 Intel Corporation.* | | Copyright | | Metadata | License | - | | |
| Version | | *@version $Revision: 1.0* | Type-other | Header | Uncategorized | Version | Unknown | - | | |
| IDE | | CHECKSTYLE:OFF [12] | | - | Directive | - | Directive | - | | IDE |
| Other | | The implementation is awesome. [1] | | - | Uncategorized | Noise | Unknown | - | | Notice |


ISBN 978-86-7466-930-3

readers; 5) The *Todo* category covers explicit tasks to be done and notes about bugs that need to be fixed.

## IV. Comparison With Previous Code Comment Classification Taxonomies

In this section, we present a comparison between the previously described taxonomies. Table 1 shows examples of code comments and their classes according to different taxonomies. In places where we were not sure what category the authors would choose for a specific comment, we put a dash symbol. Comments in italic are new examples, while others are taken from the cited papers. We have omitted the taxonomy presented in [6] from the table since it is extremely specific regarding the type of code it is applied to (operating systems code). Additionally, its authors have not disclosed all the categories they have devised.

All the comments which describe code functionality belong to one of the following classes - *What*, *Why*, *ow*, *Property*, *Module*, *Method*, *Inline* and *ariable Field*. However, these classes can be classified based on two perspectives: (1) according to the type of the commented functionality – categories *What*, *Why*, *ow*, and *Property,* or (2) the comment's structural position within the code – categories *Module*, *Method*, *Inline*, *ariable Field*. Depending on the downstream task, some taxonomies use the functionality type classification [1], [13], others use the comment place classification [8], some use both [3], [12], or neither [7]. The new taxonomy we propose takes into account the placement of a comment within the code. It should be emphasized we do not differentiate between *Inline* and *ariable Field* functional comments like in some taxonomies [3], [8], [12], but rather group them together under the *Functional-Inline* class.

In some papers there is a separate class for comments which visually divide the code into sections [8], [11]–[12]. We classify such comments as *Functional-Inline* as well.

Some comments do not describe code functionality, but rather contain notes to developers and code users. Several different classes for these kinds of comments have been previously proposed. There are authors [1], [3], [7]–[8] who recognize only some of these comments because not all of them are relevant for their downstream task. In other papers [11]–[13] most of these comments are recognized, but every paper uses a different approach concerning their classification. Some authors [11], [13] use a higher level of granularity while others [12] perceive some or all such comments as one class. In [12] the authors also differentiate between the comments meant for developers and those meant for users. Regarding TODO comments, some taxonomies [12]–[13] clearly separate them from the other comments, while in others [8], [11] there is an overlap between TODO and other comment categories. Our taxonomy distinguishes between *Notice* and *Todo* classes. All the notes for developers/users, use cases, warnings about deprecation, exceptions and links are classified as *Notice*. Messages about missing/unfinished parts of code and bugs are classified as *T* .

Several taxonomies [7]–[8], [11]–[12], treat comments which represent parts of code as a separate class, while others do not mention them. In [11], code which is commented out is classified as a *Todo* comment, along with comments for bugs and unfinished code. In our taxonomy parts of code which are commented out are placed in a separate class – *Code*.

Most previous approaches use a separate class for meta-information comments. Some [8], [11], [13] utilize a more granular classification according to license information, authorship, version information etc. In our approach all the meta-information is classified into the *General* category.

A few authors [11]–[12] have proposed a separate class for comments which represent some instructions for the compiler or the development environment. We also include an *I E* category in our taxonomy.

Some papers [1], [7], [11]–[13] use a separate category for all other comments which are not of interest. However, our taxonomy does not employ such a category, because we do not want to allow annotators to easily dismiss ambiguous comments which are difficult to categorize.

Additional information about the presented comment taxonomies is shown in Table 2. It contains the number of comments that are/will be annotated for each taxonomy, the used comment granularity, the natural and programing languages each taxonomy is applied to, the annotation agreement (if reported), and the downstream task. Data from the table shows that annotations are typically done on small sets of code comments written in English, and that comments are taken from one or two programming languages at most. It is hard to compare annotation agreements because agreement measures differ from paper to paper and relate to different numbers of annotators and different comment set sizes.

Some of the earliest taxonomies were specific for the task they were solving [6]–[7] and observed more than two perspectives (e.g., object, style, beneficiary etc.). Because of their complexity, they are not useful for tasks other than the ones they were designed for. But, over time, two perspectives became prominent: (1) what is the entity of a comment, and (2) how a comment describes the functionality of the entity.

All papers in this survey worked with comments in English and in one of the following programming languages: C/C++, Java, or Python. As mentioned in [11] many object-oriented languages have very similar functionalities, and it is reasonable to expect that their comments will behave the same. We can see that in more recent works [1], [3], [8], [11]–[13] taxonomies designed for Java, Python, and C++ are similar. For other programming paradigms (e.g., functional), further research must be done.

Although some authors wanted only to empirically study and understand the types of code comments [11]–[13], most of the times classification was done as a first step in solving a particular downstream task. In a couple of papers, it is shown that that kind of approach is fruitful. For example, Chen et al. [1] have found that different summarization models work best for different categories of comments. By including comment

 ISBN 978-86-7466-930-3

TABLE 2 GENERAL INFORMATION ABOUT CODE COMMENT CLASSIFICATION TAXONOMIES

| Paper | ear | umber of comments | Granularity | anguage | Programming anguages | Annotation Agreement | Downstream tas applicability |
|---|---|---|---|---|---|---|---|
| Padioleau [6] | 2009 | 1050 | Comment | English | C | - | Understanding developers' needs regarding the creation or improvement of tools and languages. |
| Haouari [7] | 2011 | 407 | Comment | English | Java | - | Investigation of developers commenting habits. |
| Steidl [3] | 2013 | 1330 | Comment | English | Java, C++ | - | Quality analysis of source code comments. |
| Shinyama [12] | 2018 | 1000 | Comment | English | Java, Python | Fleiss' Kappa = 0.491 | Analysis of comments inside functions or methods that often give insight into the developers' minds. |
| Zhang [13] | 2018 | 330 | Comment | English | Python | - | Classification of Python code comments. |
| Pascarella [11] | 2019 | 40000 | Character | English | Java | Fleiss' Kappa = 0.9 | Increasing the empirical understanding of the types of comments that developers write. |
| Zhai [3] | 2020 | 5000 | Sentence | English | Java | Cohen's Kappa = 0.826 | Code-comment propagation. |
| Chen [1] | 2021 | 20000 | Comment | English | Java | Fleiss' Kappa = 0.79 | Code summarization. |
| Our proposal | 2022 | ~10000 | Character | English | C/C++, C#, Java, JavaScript/ TypeScript, PHP, Python, SQL | To be determined | Semantic code search and cross-level semantic textual similarity. |

classification, they were able to design a composite summarization model that outperforms a standard approach where one model is applied to all comments. Another example is the work of Zhai et al. [3] focused on code comment propagation. Here, comment classification was necessary because comments with different content related to different programming entities cannot be propagated in the same way.

## V. CONCLUSION

In this paper, we have analyzed and compared previously proposed code comment classification taxonomies. We have systematized them according to the comment classes they use as well as according to their applicability to different programming languages and downstream tasks. We have also presented a new comment taxonomy, designed for the tasks of semantic code search and semantic textual similarity, applicable to various programming languages.

In order to validate the usefulness of our taxonomy, we are currently engaged in the creation of a code comment corpus which will encompass around 10,000 comments written in English or Serbian, and taken from a spectrum of programming languages(C/C++, C#, Java, PHP, Python, SQL, and JavaScript/TypeScript). We aim to manually annotate this corpus using the proposed taxonomy and use it to enable automated comment classification, both as a stand-alone task and as a first step within the mentioned downstream tasks.

## ACKNOWLEDGMENT

This work was supported by the Science Fund of the Republic of Serbia, grant no. 6526093, AI-AVANTES.

## REFERENCES

[1] Q. Chen, X. Xia, H. Hu, D. Lo, S. Li, "Why My Code Summarization Model Does Not Work: Code Comment Improvement with Category Prediction," *ACM Trans. Softw. Eng. Methodol.*, vol. *30,* no. *2,* pp. *1-2* , Feb 2021.

[2] B. Yang, Z. Liping, Z. Fengrong, "A Survey on Research of Code Comment," Proc. 2019 3rd International Conference on Management Engineering, Software Engineering, and Service Sciences-ICMSS 2019, Wuhan, China, pp. 45-51, Jan. 12, 2019.

[3] J. Zhai, X. Xu, Y. Shi, G. Tao, M. Pan, S. Ma, L. Xu, W. Zhang, L. Tan, X. Zhang, "CPC: automatically classifying and propagating natural language comments via program analysis," Proc. ACM/IEEE 42nd International Conference on Software Engineering, Seoul, South Korea, pp. 1359-1371, Oct. 1, 2020.

[4] J. Cohen, "A coefficient of agreement for nominal scales," *Educational and psychological measurement*, vol. *20,* no. *1,* pp. *3 -4* , 1960.

[5] J. L. Fleiss, "Measuring nominal scale agreement among many raters," *Psychological Bulletin*, vol. , no. *5,* pp. *3 -3 2,* 1971.

[6] Y. Padioleau, L. Tan, Y. Zhou, "Listening to programmers — Taxonomies and characteristics of comments in operating system code," Proc. 2009 IEEE 31st International Conference on Software Engineering, Vancouver, Canada, pp. 331-341, May 16-24, 2019.

[7] D. Haouari, H. Sahraoui, P. Langlais, "How Good is Your Comment? A Study of Comments in Java Programs," Proc. 2011 International Symposium on Empirical Software Engineering and Measurement, Banff, Canada, pp. 137-146, Sept. 22-23, 2011.

[8] D. Steidl, B. Hummer, E. Juergens, "Quality analysis of source code comments," Proc. 2013 21st International Conference on Program Comprehension, San Francisco, USA, pp. 83-92, May 20-21, 2013.

[9] L. Pascarella, "Classifying code comments in Java mobile applications," Proc. 2018 IEEE/ACM 5th International Conference on Mobile Software Engineering and Systems, Gothenburg, Sweden, pp. 39-40, May 27-June 3, 2018.

[10] L. Pascarella, A. Bacchelli, "Classifying Code Comments in Java Open-Source Software Systems," Proc. 2017 IEEE/ACM 14th International Conference on Mining Software Repositories, Buenos Aires, Argentina, pp. 227-237, May 20-21, 2017.

[11] L. Pascarella, M. Bruntink, A. Bacchelli, "Classifying code comments in Java software systems," *Empirical Software Engineering*, vol. *24,* no. *3,* pp. *14 -153* , Jun 2019.

[12] Y. Shinyama, Y. Arahori, K. Gondow, "Analyzing Code Comments to Boost Program Comprehension," Proc. 2018 25th Asia-Pacific Software Engineering Conference , Nara, Japan, pp. 325-334, Dec. 4-7, 2018.

[13] J. Zhang, L. Xu, Y. Li, "Classifying Python Code Comments Based on Supervised Learning," Proc. 2018 15th International Conference on Web Information Systems and Applications (WISA), Taiyuan, China, pp. 39-47, Sept. 14-15, 2018.

[14] H. Husain, H.-H. Wu, T. Gazit, G. Miltiadis, A. M. Brockschmidt, "CodeSearchNet Challenge Evaluating the State of Semantic Code Search," Accessed: Dec. 29, 2021. [Online]. Available: https://github.com/github/CodeSearchNet.

[15] D. Jurgens, M. T. Pilehvar, R. Navigli, "SemEval-2014 Task 3: Cross-Level Semantic Similarity," Accessed: Dec. 29, 2021. [Online]. Available: http://alt.qcri.

[16] D. Jurgens, M. T. Pilehvar, R. Navigli, "Cross level semantic similarity: an evaluation framework for universal measures of similarity," *anguage esources and E aluation*, vol. *50,* no. *1,* pp. *5-33,* Mar 2016.

 ISBN 978-86-7466-930-3

# Primena ConvLSTM modela za predikciju optičke debljine aerosola

Uzahir R. Ramadani, Dušan P. Nikezić, Dušan S. Radivojević, Nikola Mirkov i Ivan Lazović

***Apstrakt*—Napravljen je ConvLSTM model sa ConvLSTM2D slojevima za predvđanje optičke debljine aerosola. Ulazni skup podataka čine satelitski snimci optičke debljine aerosola na 8 dana od 2000. godine. Kada je model obučen dato je predviđanje optičke debljine aerosola kao i evaluacija modela. Razvijen je i primenjen nad istim podacima i CNN LSTM model i dato je poređenje oba modela. Za evaluaciju je korišćena Srednja kvadratna greška (MSE) kao i Srednja apsolutna greška (MAE). ConvLSTM model je pokazao manju grešku i rezultati su pokazali da može da se koristi za predviđanje optičke debljine aerosola.**

***Ključne reči* — Optička debljina aerosola; ConvLSTM; satelitski snimci; CNN LSTM.**

## I. Uvod

MAŠINSKO učenje kao deo veštačke inteligencije omogućuje napredovanje nauke u raznim oblastima. Savremeni tehnološki razvoj preko Interneta i velikih količina podataka omogućuje jednostavan pristup i korišćenje tih velikih baza podataka. Satelitski snimci kao skup podataka preko daljinske detekcije postali su dostupni naučnicima što omogućuje njihovo istraživanje. NASA pruža preko 50 različitih globalnih skupova podataka satelitskih snimaka. Jedan od tih skupova podataka je MODAL2_E_AER_OD koji predstavlja optičku debljinu aerosola snimanu svaki 8 dan od 2000. godine.

Odranije je poznato da aerosoli igraju važnu ulogu u oblikovanju vremena i klime, a novo istraživanje pokazalo je da i najsitnije čestice imaju nesrazmerno veliko dejstvo. Aerosoli iako mali su proizvođači snažnih kiša. Računarskim simulacijama naučnici su pokazali dejstvo tih čestica na olujne oblake. Iako su te čestice male, ima ih mnogo, i mogu da formiraju male kapi, na koje se kondenzuje isparavanje vode. To rezultuje oslobađanjem veće količine toplote koja osnažuje vazdušne mase. Više toplog vazduha ulazi u oblake i time stvara više leda, snega, munja i kiše.

Uzahir R. Ramadani - Institut za nuklearne nauke „Vinča“ - Institut od nacionalnog značaja za Republiku Srbiju, Univerzitet u Beogradu, Mike Petrovića Alasa bb., 1100 Beograd, Srbija (e-mail: uzahir@vin.bg.ac.rs).

Dušan P. Nikezić - Institut za nuklearne nauke „Vinča“ - Institut od nacionalnog značaja za Republiku Srbiju, Univerzitet u Beogradu, Mike Petrovića Alasa bb., 1100 Beograd, Srbija (e-mail: dusan@vin.bg.ac.rs).

Dušan S. Radivojević - Institut za nuklearne nauke „Vinča“ - Institut od nacionalnog značaja za Republiku Srbiju, Univerzitet u Beogradu, Mike Petrovića Alasa bb., 1100 Beograd, Srbija (e-mail: dusanr@vin.bg.ac.rs).

Nikola Mirkov - Institut za nuklearne nauke „Vinča“ - Institut od nacionalnog značaja za Republiku Srbiju, Univerzitet u Beogradu, Mike Petrovića Alasa bb., 1100 Beograd, Srbija (e-mail: nmirkov@vin.bg.ac.rs).

Ivan Lazović - Institut za nuklearne nauke „Vinča“ - Institut od nacionalnog značaja za Republiku Srbiju, Univerzitet u Beogradu, Mike Petrovića Alasa bb., 1100 Beograd, Srbija (e-mail: ivan.lazovic@vin.bg.ac.rs).

## II. Metod

Spektroradiometar umerene rezolucije (MODIS - Moderate Resolution Imaging Spectroradiometer) je satelitski senzor koji se koristi za merenja zemlje i klime. MODIS instrumenti hvataju podatke u 36 spektralnih opsega u talasnim dužinama od 0.4 mm do 14.4 mm i u različitim prostornim rezolucijama (2 opsega na 250 m, 5 opsega na 500 m i 29 opsega na 1 km). Sa svojom visokom prostornom rezolucijom, ali niskom vremenskom rezolucijom, MODIS podaci su korisni za praćenje promena u globalnoj koncentraciji aerosola tokom vremena.

NASA skupovi podataka dostupni su kao RGB i kao PNG fajlovi i u rezoluciji 3600 x 1800 piksela. Sl. 1 prikazuje jedan snimak iz skupa podataka MODAL2_E_AER_OD koji predstavlja globalni AOT (aerosol optical thickness) na svakih 8 dana [12, 13] što predstavlja 993 slike do 14.09.2021.

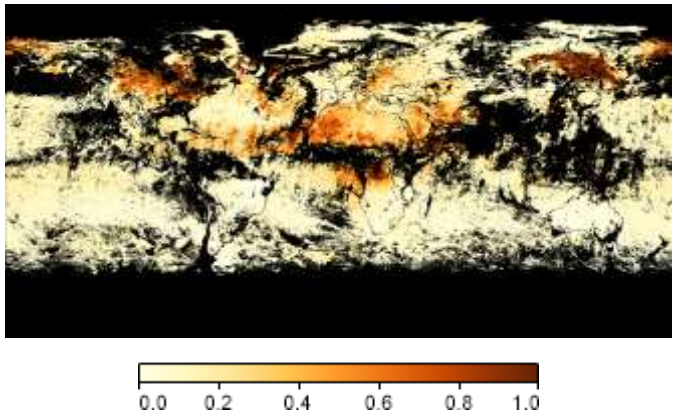


Sl. 1. Snimak od 2021-07-12 globalnog AOT.

Optička debljina manja od 0.1 (bledožuta) ukazuje na kristalno čisto nebo sa maksimalnom vidljivošću, dok vrednost od 1 (crvenkasto smeđa) ukazuje na veoma maglovite uslove.

Preko MODIS-a na NASA-inim satelitima Terra i Aqua prati se AOT kao i distribucija aerosola, u većem delu sveta (okeani i vlažni delovi kontinenata) na dnevnom nivou, svakih 8 dana i mesečno. MODIS se koristi za praćenje masene koncentracije aerosola, optičkih svojstava i zračenja. MODIS-ove informacije o aerosolu se koriste za proučavanje klimatologije aerosola, za praćenje izvora i ponora specifičnih tipova aerosola (kao što su sulfati i drugi industrijski/urbani

 ISBN 978-86-7466-930-3

aerosol i aerosol sagorevanja biomase), i služe kao ulazni podaci za klimatsko modeliranje [7]. MODIS-ove informacije o aerosolu mogu se koristiti za predviđanje PM [11].

Satelitski snimci MODAL2_E_AER_OD predstavljaju ulazne podatke u modelu mašinskog učenja ConvLSTM. Tradicionalne metode predviđanja vremenskih serija fokusiraju se na univarijantne podatke sa linearnim odnosima i fiksnom i ručno dijagnostikovanom vremenskom zavisnošću. Neuronske mreže dodaju mogućnost učenja potencijalno nelinearnih odnosa sa proizvoljno definisanim, ali fiksnim brojem ulaza i izlaza koji podržavaju multivarijantno i višestepeno predviđanje.

Duboko učenje (DL – Deep Learning) je deo ML zasnovan na veštačkim neuronskim mrežama (ANN - Artificial Neural Networks). U DL konvoluciona neuronska mreža (CNN - Convolutional Neural Network) je klasa ANN, koja se najčešće primenjuje za analizu vizuelnih slika. U CNN-u ulaz je tenzor sa oblikom (broj ulaza) x (visina) x (širina) x (kanali). [17 , 18]. Jedna od primena CNN-a je izdvajanje prostornih informacija iz slika.

LSTM - Long Short-Term Memory je tip Rekurentne neuronske mreže (RNN - Recurrent Neural Networks) dizajniran tako da nema problem sa nestajućim gradijentom. LSTM mreže imaju povratne veze koje daju neuronima mogućnost odluke na temelju ne samo trenutne već i prethodnih vrednosti [19].

Prostorno-vremensko predviđanje može da se uradi CNN i LSTM, gde CNN (Convolution2D) služi za ekstrahovanje prostornih karakteristika, dok se LSTM koristi za otkrivanje korelacija tokom vremena [20]. Međutim, slaganjem ovih vrsta slojeva, korelacija između prostornih i vremenskih karakteristika možda neće biti pravilno ekstrahovana. Rešenje je mrežna struktura sposobna da uhvati prostorno-vremenske korelacije ConvLSTM [21]. U Kerasu je napravljena klasa (sloj) ConvLSTM2D, koja izračunava konvolucione operacije i u ulaznoj i u rekurentnoj transformaciji da bi istovremeno uhvatila prostorno-vremenske podatke. ConvLSTM2D je rekurentni sloj, baš kao i LSTM, ali interna množenja matrice se razmenjuju sa operacijama konvolucije. Kao rezultat toga, podaci koji teku kroz ConvLSTM ćelije zadržavaju ulaznu dimenziju umesto da budu samo 1D vektor [21 - 23]. Glavna razlika između ConvLSTM i LSTM je broj ulaznih dimenzija. Pošto su LSTM ulazni podaci jednodimenzionalni, nisu pogodni za podatke o prostornoj sekvenci kao što je video, satelitske slike itd. ConvLSTM je dizajniran za 3D podatke na ulazu.

## III. CONVLSTM MODEL

Ulaz kod LSTM je 3D tenzor sa oblikom: broj uzoraka, vremenski korak, karakteristike (samples, time steps, features). Ulaz konvolucionog sloja je 4D tenzor sa oblikom: uzorci, redovi, kolone, kanali (samples, rows, cols, channels). Ulaz za ConvLSTM model je 5D tenzor sa oblikom: uzorci, vremenski koraci, redovi, kolone, kanali (samples, time steps, rows, cols, channels).

Izlaz ćelije LSTM zavisi od atributa return_sekuence. Kada je postavljeno na True, izlaz je sekvenca tokom vremena (jedan izlaz za svaki ulaz). U ovom slučaju, izlaz je 3D tenzor sa oblikom: uzorci, vremenski koraci, karakteristike. Kada je return_sekuences podešen na False, izlaz je poslednja vrednost niza, odnosno 2D tenzor sa oblikom (uzorci, karakteristike). Izlaz ConvLSTM sloja je kombinacija Convolution i LSTM izlaza. Baš kao i LSTM, ako je return_sekuences = True, onda vraća niz kao 5D tenzor sa oblikom: uzorci, vremenski koraci, redovi, kolone, filteri. Kada je return_sekuences = False, onda vraća samo poslednju vrednost niza kao 4D tenzor sa oblikom (uzorci, redovi, kolone, filteri).

ML model koji se koristi u ovoj studiji sastoji se od 3 sloja ConvLSTM2D i krajnjeg sloja Conv3D kao izlaza. Conv3D sloj stvara konvoluciono jezgro koje je konvoluirano sa ulazom sloja da bi se proizveo tenzor izlaza, tj. visina, širina, kanal slike. ML model je napravljen u Kerasu.

CNN LSTM model ima prvi ulazni sloj koji prima niz od 10 slika rezolucije 144x288 piksela sa tri RGB kanala. Obzirom da Conv2D sloj može da funcioniše samo sa jedom slikom, njemu i u narednih 5 slojeva dodat je sloj TimeDistributed koji omogućava rad sa nizom ulaznih podataka. Drugi sloj Conv2D ima 32 filtera radi boljih performansi modela. BatchNormalization u trećem i petom sloju se koristi radi prevecije takozvane eksplozije loss funkcije i ravnomernijeg napredovanja odnosno normalizacije tokom procesa učenja, sprečavanjem prevelikog napredovanja pojedinih težina u odnosu na ostale u neuralnoj mreži odnosno svakom sloju zasebno. Četvrti sloj Conv2D sa tri filtera vraća format na tri RBG kanala. Šesti sloj Reshape vrši poravnanje 2D formata slike u 1D format zbog pripreme za sledeći sedmi LSTM memorijski sloj. Osmi Dropout sloj vrši prevenciju preteranog učenja kod koga se javlja veoma dobro procesiranje poznatih, ali loše procesiranje novih podataka. Deveti Dense sloj formira konačan broj piksela izlazne predikovane slike koji se u desetom Reshape sloju transformniše u odgovarajući format.

Skup ulaznih podataka bio je MODAL2_E_AER_OD, skup satelitskih slika od 18.02.2000. do 14.09.2021. na svakih 8 dana. Odnos train/test bio je 70/30, 80/20 i 90/10. Optimum je postignut podelom 80/20. Najbolje rezultate dala je funkcija aktivacije 'hard_sigmoid' za Conv3D sloj i optimizator 'adam' (learning_rate=0,001). Problem prediktivnog modeliranja regresije uključuje predviđanje veličine realne vrednosti, tako da je za funkciju gubitka korišćen 'mse', a za metriku RootMeanSkuaredError (RMSE). Sl. 2 prikazuje korišćeni ConvLSTM model (slika je dobijena komandom: plot_model(model, to_file='model.png', show_shapes=True, show_layer_names=True)).

https://www.kaggle.com/code/dusan75/convlstm-notebook09a46b0eb3

 ISBN 978-86-7466-930-3

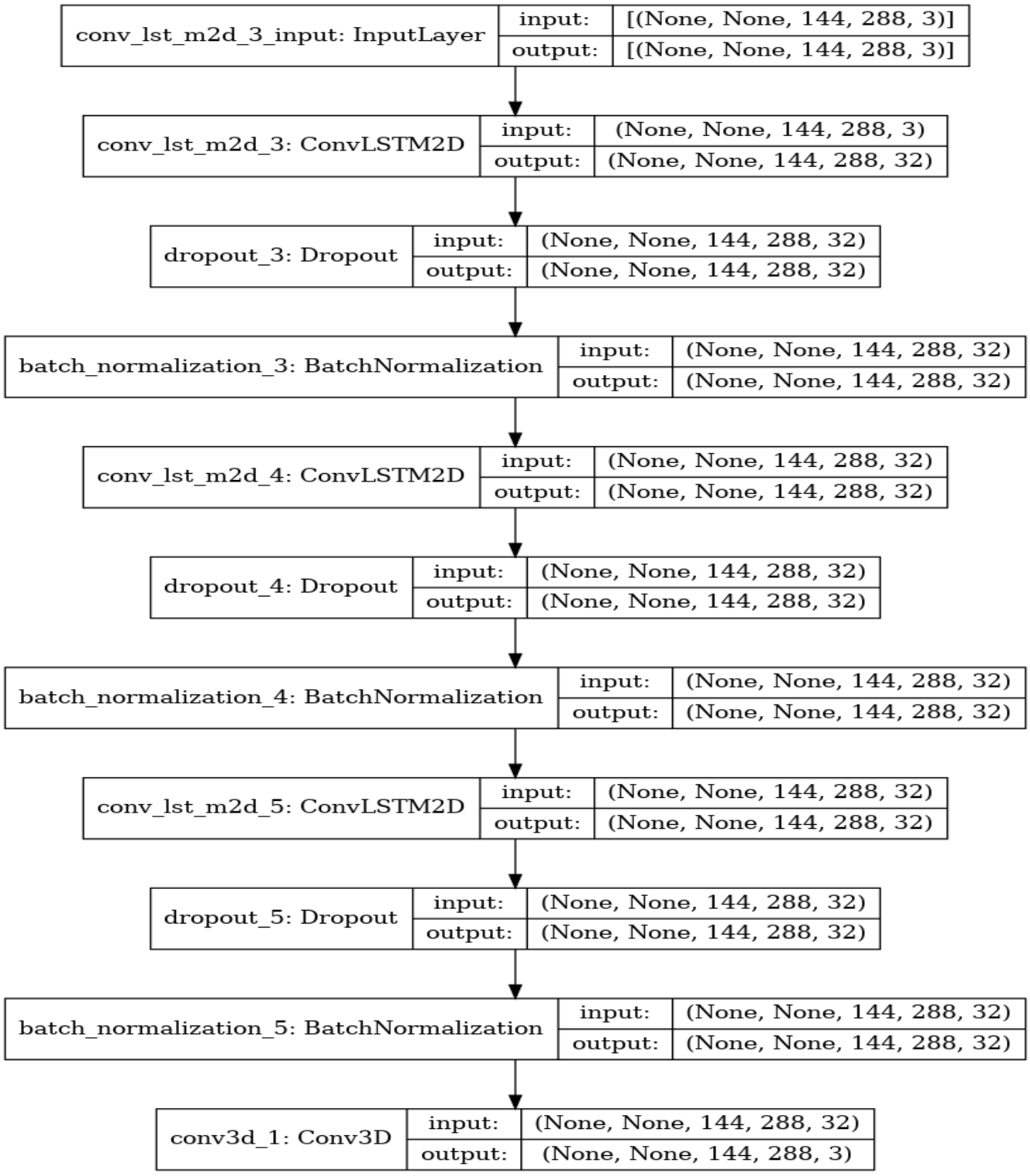


Sl. 2. Prikaz ConvLSTM modela.

Nakon obuke ML modela, urađeno je predviđanje prve slike iz skupa test podataka i upoređeno je sa originalnom prvom slikom iz skupa podataka testa.

## IV. REZULTATI I DISKUSIJA

Sa ConvLSTM modelom je predikovana prva slika iz test skupa podataka, Sl. 3a. Sl. 3b prikazuje originalnu prvu sliku iz test skupa podataka.

 ISBN 978-86-7466-930-3

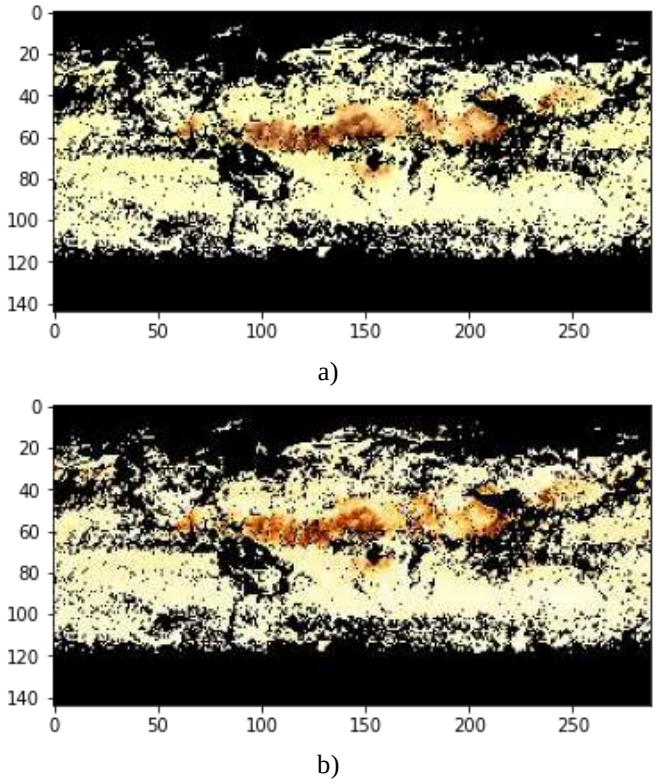


Sl. 3. Globalni AOT a) predikovani; b) realni.

Validacija ML modela je zasnovana na metrici evaluacije, tj. mse 0,0116 (mean squared error). Ovi rezultati dokazuju da se predloženi ML model može koristiti za AOT prognoze. Sl. 4 prikazuje grafikon gubitka tokom 50 epoha obuke.

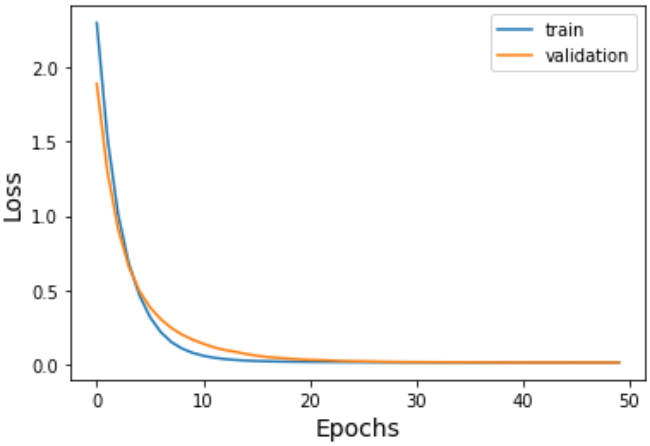


Sl. 4. Grafikon gubitka u zavisnosti broja epoha.

Pre ConvLSTM2D za prostorno-vremensku zavisnost i predikciju se koristio CNN+LSTM model [24]. Za poređenje ConvLSTM i CNN LSTM razvijen je novi CNN LSTM model. Sl. 5 prikazuje novi model CNN LSTM.

Metrika evaluacije bila je za mse 0,1117 i u poređenju sa ConvLSTM modelom (mse 0,0116) je veća vrednost. Niže vrednosti mse ukazuju na manju grešku.


ISBN 978-86-7466-930-3

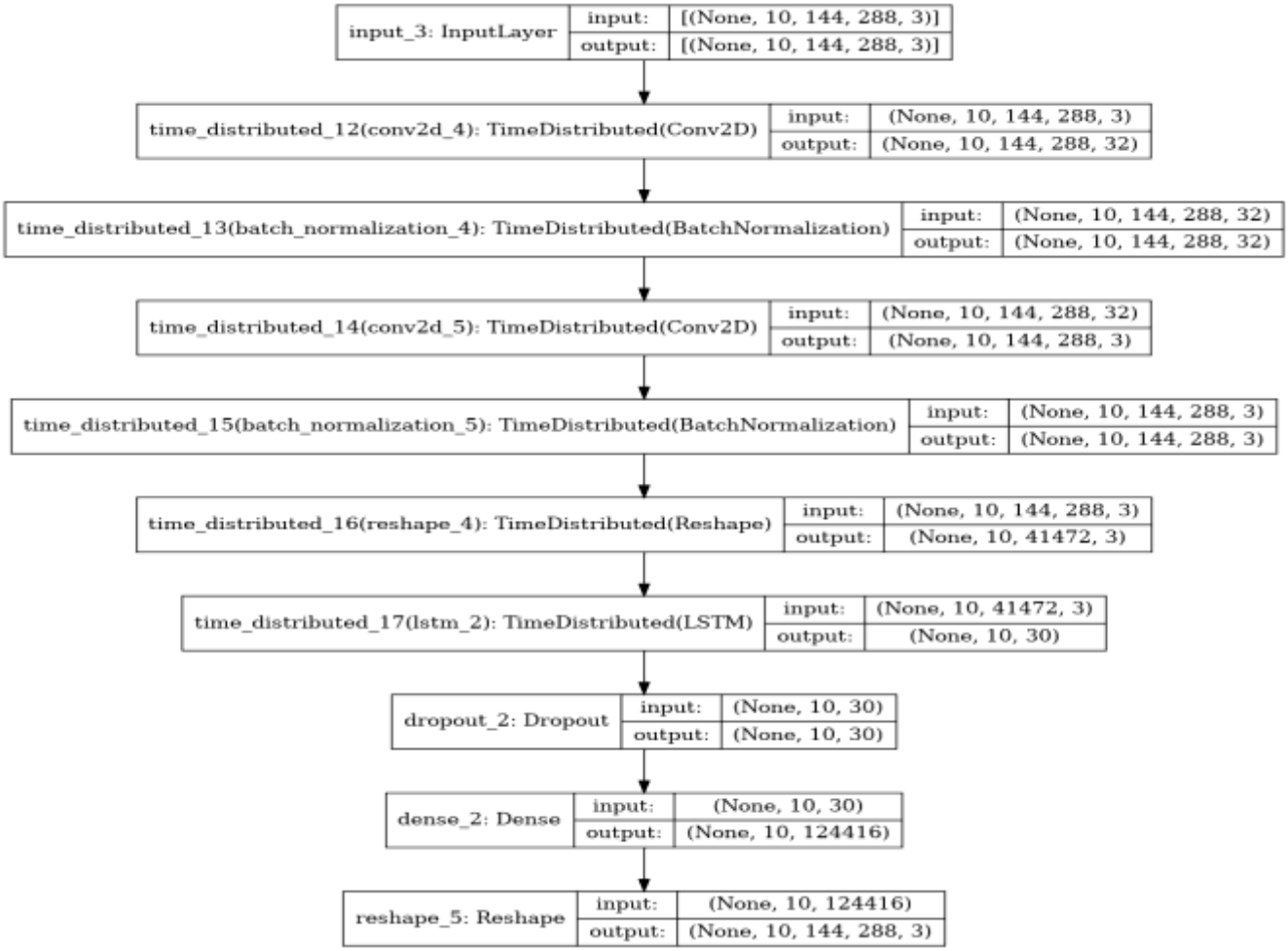


Sl. 5. Prikaz CNN LSTM modela.

Primena Mean Absolute Percent Error metrike na konkretnom primeru nije primenljiva, obzirom na činjenicu da se među y-true vrednotima nalazi i vrednost 0 zbog koje metoda ne daje vrednosti u predviđenom opsegu od 0 do 1. Testiranje modela nalazi se na adresi:

https://www.kaggle.com/code/dusan75/test-of-convlstm-notebook09a46b0eb3?scriptVersionId=94940211

Za bolje poređenje dva modela urađena je sledeća statistika. Srednja apsolutna greška (MAE - Mean Absolute Error) koristi se za predviđanja u segmentu od 9 frejmova po slici, Tabela 1.

TABELA I
PROSEČNA GREŠKA PREDVIĐANJA U SEGMENTU OD 9 FREJMOVA PO SLICI

| ConvLSTM | CNN LSTM |
|---|---|
| 0.02200718 | 0.24474642 |
| 0.02213584 | 0.2462145 |
| 0.02251104 | 0.24545886 |
| 0.02263835 | 0.2449535 |
| 0.0227564 | 0.24526556 |
| 0.02259156 | 0.24504275 |
| 0.02232519 | 0.24720876 |
| 0.02259231 | 0.2456902 |
| 0.02278301 | 0.24560421 |

Iz dobijenih rezultata može se zaključiti da je ConvLSTM model zahtevao dobro strukturirane ulazne podatke, pravi izbor i optimalno podešene hiperparametre modela pre nego što bi mogao da se koristi za pouzdana AOT predviđanja.

## V. ZAKLJUČAK

Aerosoli su jedan od najvećih izvora nesigurnosti u modeliranju klime. Zračenje aerosolima može objasniti razliku između posmatranih i modelovanih trendova prosečne globalne temperature. U stvari, interakcija sa sunčevim i zemaljskim zračenjem pomoću aerosola remeti radijativni budžet rasejanjem i apsorpcijom sunčeve svetlosti. Mnoge nedavne studije pokazuju važnost uključivanja aerosola u klimatske modele za posmatranje i merenje ljudskog uticaja na atmosfersku hemiju i klimatske promene.

Ova studija je istraživala mogućnost ConvLSTM modela za predviđanje globalnog AOT-a sa MODIS satelitskih snimaka. Sloj ConvLSTM2D u Kerasu spaja prostornu i vremensku komponentu i omogućava predikciju. Satelitski snimci pomažu u sagledavanju globalnog transporta zagađivača.

Modeli mašinskog učenja kreirani su od strane autora, tj. originalne i inovativne su strukture, pa se i rezultati treniranja

 ISBN 978-86-7466-930-3

i predviđanja modela, pored originalne strukture, mogu uzeti kao doprinos zajednici radi poređenja postignutih rezultata.

## ZAHVALNICA

Ovaj rad je realizovan u okviru istraživačke teme 1002205 koga finansira Ministarstvo prosvete, nauke i tehnološkog razvoja Republike Srbije.

## LITERATURA

[1] C.Q. Lin, G. Liu, A.K.H. Lau, Y. Li, C.C. Li, J.C.H. Fung, X.Q. Lao, High-resolution satellite remote sensing of provincial PM2.5 trends in China from 2001 to 2015, Atmospheric Environment, Volume 180, 2018, Pages 110-116, ISSN 1352-2310, https://doi.org/10.1016/j.atmosenv.2018.02.045.

[2] Zhaoxi Wang, Yang Liu, Mu Hu, Xiaochuan Pan, Jing Shi, Feng Chen, Kebin He, Petros Koutrakis, David C. Christiani, Acute health impacts of airborne particles estimated from satellite remote sensing, Environment International, Volume 51, 2013, Pages 150-159, ISSN 0160-4120, https://doi.org/10.1016/j.envint.2012.10.011.

[3] Shuaiyi Shi, Tianhai Cheng, Xingfa Gu, Hong Guo, Yu Wu, Ying Wang, Fangwen Bao, Xin Zuo, Probing the dynamic characteristics of aerosol originated from South Asia biomass burning using POLDER/GRASP satellite data with relevant accessory technique design, Environment International, Volume 145, 2020, 106097, ISSN 0160-4120, https://doi.org/10.1016/j.envint.2020.106097.

[4] Xiaoli Wei, Ni-Bin Chang, Kaixu Bai & Wei Gao (2020) Satellite remote sensing of aerosol optical depth: advances, challenges, and perspectives, Critical Reviews in Environmental Science and Technology, 50:16, 1640-1725, DOI: 10.1080/10643389.2019.1665944.

[5] Filonchyk, M., Yan, H., Zhang, Z. et al. Combined use of satellite and surface observations to study aerosol optical depth in different regions of China. Sci Rep 9, 6174 (2019). https://doi.org/10.1038/s41598-019-42466-6.

[6] Ian Colbeck, Mihalis Lazaridis, Aerosol Science: Technology and Applications, ISBN: 978-1-119-97792-6 December 2013, Wiley, https://doi.org/10.1002/9781118682555.ch1.

[7] https://neo.gsfc.nasa.gov/

[8] Dušan P. Nikezić, Zoran J. Gršić, Dragan M. Dramlić, Stefan D. Dramlić, Boris B. Lončar, Slavko D. Dimović, Modeling air concentration of fly ash in Belgrade, emitted from thermal power plants TNTA and TNTB, Process Safety and Environmental Protection, Volume 106, 2017, Pages 274-283, ISSN 0957-5820, https://doi.org/10.1016/j.psep.2016.06.009.

[9] You, W.; Zang, Z.; Zhang, L.; Li, Y.; Pan, X.; Wang, W., National-Scale Estimates of Ground-Level PM2.5 Concentration in China Using Geographically Weighted Regression Based on 3 km Resolution MODIS AOD. Remote Sens. 2016, 8, 184. https://doi.org/10.3390/rs8030184.

[10] Tov Elperin, Andrew Fominykh, Itzhak Katra, Boris Krasovitov, Modeling of gas adsorption by aerosol plumes emitted from industrial sources, Process Safety and Environmental Protection, Volume 111, 2017, Pages 375-387, ISSN 0957-5820, https://doi.org/10.1016/j.psep.2017.06.022.

[11] Naresh Kumar, Allen Chu, Andrew Foster, An empirical relationship between PM2.5 and aerosol optical depth in Delhi Metropolitan, Atmospheric Environment, Volume 41, Issue 21, 2007, Pages 4492-4503, ISSN 1352-2310, https://doi.org/10.1016/j.atmosenv.2007.01.046.

[12] https://neo.gsfc.nasa.gov/archive/rgb/

[13] https://neo.gsfc.nasa.gov/archive/rgb/MODAL2_E_AER_OD/

[14] Song Tang, Yixin Mao, Rachael M. Jones, Qiyue Tan, John S. Ji, Na Li, Jin Shen, Yuebin Lv, Lijun Pan, Pei Ding, Xiaochen Wang, Youbin Wang, C. Raina MacIntyre, Xiaoming Shi, Aerosol transmission of SARS-CoV-2? Evidence, prevention and control, Environment International, Volume 144, 2020, 106039, ISSN 0160-4120, https://doi.org/10.1016/j.envint.2020.106039.

[15] Maria A. Zoran, Roxana S. Savastru, Dan M. Savastru, Marina N. Tautan, Laurentiu A. Baschir, Daniel V. Tenciu, Exploring the linkage between seasonality of environmental factors and COVID-19 waves in Madrid, Spain, Process Safety and Environmental Protection, Volume 152, 2021, Pages 583-600, ISSN 0957-5820, https://doi.org/10.1016/j.psep.2021.06.043.

[16] Eleftheriadis, K., Gini, M.I., Diapouli, E. et al,. Aerosol microphysics and chemistry reveal the COVID19 lockdown impact on urban air quality., Sci Rep 11, 14477 (2021). https://doi.org/10.1038/s41598-021-93650-6.

[17] M.V. Valueva, N.N. Nagornov, P.A. Lyakhov, G.V. Valuev, N.I. Chervyakov, Application of the residue number system to reduce hardware costs of the convolutional neural network implementation, Mathematics and Computers in Simulation, Volume 177, 2020, Pages 232-243, ISSN 0378-4754, https://doi.org/10.1016/j.matcom.2020.04.031.

[18] Radhesyam Vaddi, Prabukumar Manoharan, Hyperspectral image classification using CNN with spectral and spatial features integration, Infrared Physics & Technology, Volume 107, 2020, 103296, ISSN 1350-4495, https://doi.org/10.1016/j.infrared.2020.103296.

[19] Sepp Hochreiter, Jürgen Schmidhuber; Long Short-Term Memory. Neural Comput 1997; 9 (8): 1735–1780. doi: https://doi.org/10.1162/neco.1997.9.8.1735.

[20] Weyn, J. A., Durran, D. R., & Caruana, R. (2020). Improving data-driven global weather prediction using deep convolutional neural networks on a cubed sphere. Journal of Advances in Modeling Earth Systems, 12, e2020MS002109. https://doi.org/10.1029/2020MS002109.

[21] X. Shi, Z. Chen, H. Wang and D. Yeung, "Convolutional LSTM network: A machine learning approach for precipitation nowcasting", Proc. Neural Inf. Process. Syst. (NIPS), pp. 802-810, 2015.

[22] J. Donahue et al., "Long-Term Recurrent Convolutional Networks for Visual Recognition and Description," in IEEE Transactions on Pattern Analysis and Machine Intelligence, vol. 39, no. 4, pp. 677-691, 1 April 2017, doi: 10.1109/TPAMI.2016.2599174.

[23] W. Hu, H. Li, L. Pan, W. Li, R. Tao and Q. Du, "Spatial–Spectral Feature Extraction via Deep ConvLSTM Neural Networks for Hyperspectral Image Classification," in IEEE Transactions on Geoscience and Remote Sensing, vol. 58, no. 6, pp. 4237-4250, June 2020, doi: 10.1109/TGRS.2019.2961947.

[24] X. Ding, L. Feng, Y. Zou and G. Zhang, "Deep Learning Aided Spectrum Prediction for Satellite Communication Systems," in IEEE Transactions on Vehicular Technology, vol. 69, no. 12, pp. 16314-16319, Dec. 2020, doi: 10.1109/TVT.2020.3043837.

[25] Christof G. Beer, Johannes Hendricks, Mattia Righi, Bernd Heinold, Ina Tegen, Silke Groß, Daniel Sauer, Adrian Walser, Bernadett Weinzierl, Modelling mineral dust emissions and atmospheric dispersion with MADE3 in EMAC v2.54, Geosci. Model Dev., 13, 4287–4303, 2020., doi.org/10.5194/gmd-13-4287-2020.

[26] https://aeronet.gsfc.nasa.gov/

[27] Weyn, J. A., Durran, D. R., Caruana, R., & Cresswell-Clay, N. (2021). Sub-seasonal forecasting with a large ensemble of deep-learning weather prediction models. Journal of Advances in Modeling Earth Systems, 13, e2021MS002502. https://doi.org/10.1029/2021MS002502.

## ABSTRACT

ConvLSTM model was developed with ConvLSTM2D layers for predicting aerosol optical thickness. The input dataset was satellite images of aerosol optical thickness on 8-day beginning from 2000. When the model was trained, aerosol optical thickness prediction as well as model evaluation was given. The CNN LSTM model was developed and applied over the same dataset and a comparison of both models is given. Mean square error (MSE) as well as Mean absolute error (MAE) were used for evaluation. The ConvLSTM model showed less error and the results showed that it could be used to predict the aerosol optical thickness.

## ConvLSTM Application for Prediction Aerosol Optical Thickness

Uzahir R. Ramadani, Dušan P. Nikezić, Dušan S. Radivojević, Nikola Mirkov i Ivan Lazović

 ISBN 978-86-7466-930-3

# Primena veštačke inteligencije na terminal za daljinsko upravljanje stanice za punjenje električnih vozila koja se napaja iz obnovljivih izvora električne energije

Jovan Vujasinović i Goran Savić

***Apstrakt*— U ovom radu je opisana primena veštačke inteligencije na terminal za daljinsko upravljanje stanice za punjenje električnih vozila, koja se napaja iz obnovljivih izvora električne energije. Kako terminal omogućava daljinsko upravljanje punjačima električnih vozila, pametnim baterijama, pametnim brojilima, fiskalnim kasama i eventualno daljinsko upravljanje obnovljivim izvorom električne energije i drugim uređajima u okviru objekta, neophodno je definisati i razraditi odgovarajući algoritam upravljanja radom terminala. U ovom radu je razmatrana realizacija tog upravljanja primenom veštačke inteligencije. Na ovaj način ovakve stanice za punjenje električnih vozila postaju potpuno autonomne u svom radu, i daju optimalne rezultate, što podiže njihovu dostupnost korisnicima električnih vozila. To potencijalno podstiče povećanje obima korišćenja električnih vozila za koje se energija obezbeđuje iz obnovljivih izvora, čime se smanjuje stepen zagađenja vazduha kao i negativni efekti koje ono sa sobom donosi.**

***Ključne reči*— Veštačka inteligencija; punjači električnih vozila; obnovljivi izvori energije.**

## I. UVOD

Povećanje broja proizvedenih i korišćenih električnih vozila, ima za cilj smanjenje zagađenja životne sredine i štetnih efekata koje ono sa sobom nosi, a koji su posledica emisije štetnih gasova vozila na dizel i benzinski pogon. Međutim, preduslov da bi upotreba vozila na električni pogon zaista doprinela smanjenju zagađenja životne sredine, je da električna energija koja se koristi za punjenje električnih vozila bude proizvedena iz izvora koji ne zagađuju životnu sredinu, tj. iz obnovljivih izvora električne energije. To dovodi i do neminovnog razvoja infrastrukture za punjenje električnih vozila, što se ogleda i u stalnom povećanju broja stanica za punjenje električnih vozila koje se napajaju iz obnovljivih izvora električne energije [1].

Povećanje dostupnosti stanica za punjenje električnih vozila, kako korisnicima električnih vozila, tako i operaterima elektrodistribucije, snabdevača i poreske uprave, kao i vlasnicima i korisnicima same stanice, ostvaruje se integracijom u jedan veći sistem, zahvaljujući kojem se postiže ušteda vremena i novca, i efikasnija upotreba elektrodistributivne mreže. Da bi se ostvarile funkcionalnosti tog sistema, koje su od značaja svim korisnicima, realizovano je daljinsko upravljanje stanice za punjenje električnih vozila. Ključni uređaj koji omogućava pomenuto daljinsko upravljanje je terminal za daljinsko upravljanje stanice za punjenje električnih vozila koja se napaja iz obnovljivih izvora električne energije. Proces upravljanja je zasnovan na primeni naprednih algoritama veštačke inteligencije, čija je primena na terminal za daljinsko upravljanje stanice za punjenje električnih vozila prezentovana u ovom radu.

U Sekciji II ovog rada je opisana arhitektura sistema za daljinsko upravljanje stanice za punjenje električnih vozila koja se napaja iz obnovljivih izvora električne energije, u Sekciji III je predstavljena veštačka inteligencija, u Sekciji IV je opisano mašinsko učenje, u Sekciji V je razmatrana primena veštačke inteligencije na terminal, dok Sekcija VI predstavlja kratak zaključak.

## II. ARHITEKTURA SISTEMA

Blok šema arhitekture sistema za daljinsko upravljanje stanice za punjenje električnih vozila koja se napaja iz obnovljivih izvora električne energije [2] je prikazana na Sl. 1. Terminal za daljinsko upravljanje stanice za punjenje električnih vozila, koji predstavlja osnovnu komponentu sistema, je povezan sa punjačima električnih vozila, pametnom baterijom za skladištenje energije, obnovljivim izvorima električne energije, pametnim brojilom, fiskalnim kasama, korisničkim uređajima i ostalim uređajima, pomoću IoT mrežne infrastrukture. Pored toga, terminal za daljinsko upravljanje stanice za punjenje električnih vozila je povezan i sa oblakom preko internet veze, čime je omogućeno da se podaci dobijeni od punjača električnih vozila, pametne baterije za skladištenje energije, obnovljivih izvora električne energije, pametnog brojila i fiskalnih kasa, prate, skladište i obrađuju. Pristup tim podacima je omogućen sledećim platformama: platformi za korisnike punjača električnih vozila, platformi za trgovinu električnom energijom, informacionom sistemu operatera elektrodistributivnog sistema i informacionom sistemu Poreske uprave. Platforma za korisnike punjača električnih vozila omogućava vlasnicima električnih vozila da dobiju sve potrebne informacije o punjačima električnih vozila. Platforma za trgovinu električnom energijom omogućava obavljanje trgovine

Jovan Vujasinović – Elektrotehnički fakultet, Univerzitet u Beogradu, Bulevar Kralja Aleksandra 73, 11120 Beograd , Srbija (e-mail: jovan.vujasinovic@vfholding.rs).

Goran Savić – Elektrotehnički fakultet, Univerzitet u Beogradu, Bulevar Kralja Aleksandra 73, 11120 Beograd, Srbija (e-mail: gsavic@etf.rs).

 ISBN 978-86-7466-930-3

električnom energijom koja je raspoloživa u sistemu. Takođe, pristup podacima u oblaku imaju i vlasnici stanica za punjenje električnih vozila. Ti podaci se procesiraju primenom algoritama veštačke inteligencije, čime se ostvaruje efikasna upotreba distributivne mreže uz korišćenje inovativnih pametnih energetskih usluga, kao i značajne uštede u celom sistemu.

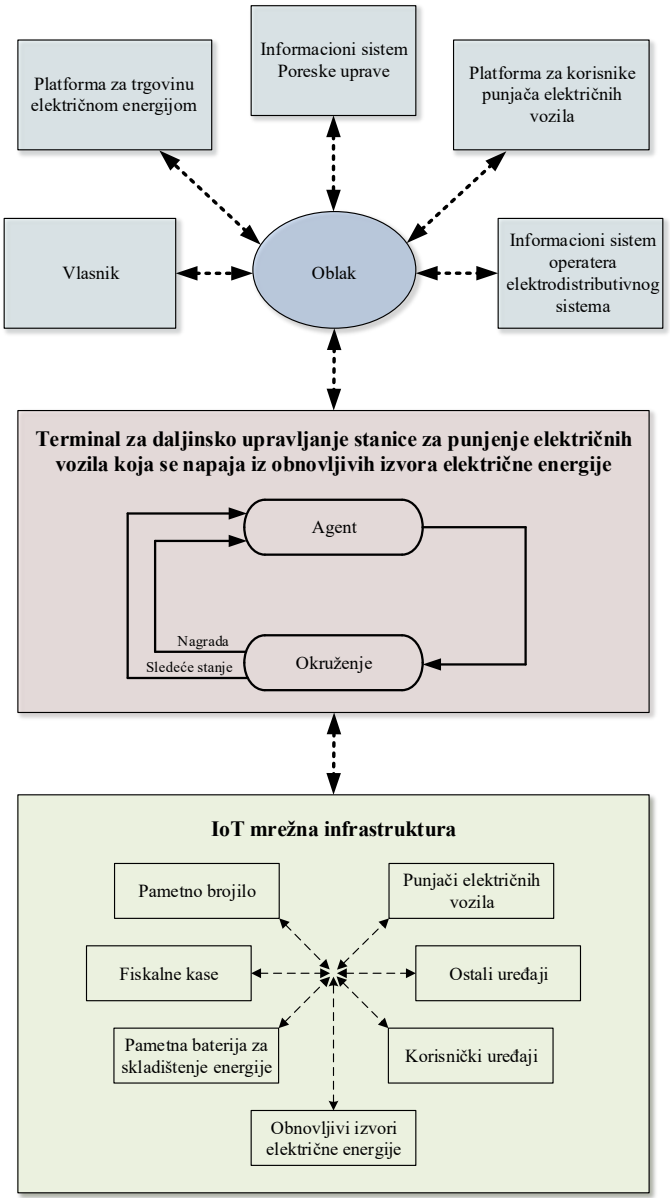


Sl. 1. Blok šema arhitekture sistema za daljinsko upravljanje stanice za punjenje električnih vozila koja se napaja iz obnovljivih izvora energije.

## III. KATEGORIJE STANICA I TERMINALA

Stanice za punjenje električnih vozila koje se napajaju iz obnovljivih izvora električne energije možemo kategorisati na rezidencijalne, komercijalne i industrijske stanice [3]. Isto tako, prema tipu stanice kod koje se primenjuje, terminale možemo podeliti na light, standard i extended terminale [4].

Rezidencijalne stanice su namenjene za kućnu upotrebu, samo za potrebe domaćinstva. U okviru ove stanice očekuje se instalacija 1-2 punjača za električna vozila. Potrebe ovakvih stanica mogu se pokriti samo korišćenjem solarnih obnovljivih izvora. Kod ovih stanica koristi se light terminal koji ima najjednostavniji hardver i softver, a ceo sistem za upravljanje ovakvom stanicom je vrlo sličan sa sistemom za upravljanje energijom u domaćinstvima.

Komercijalne stanice su male i srednje stanice za punjenje električnih vozila koje imaju visoku frekvenciju punjenja vozila. Obično su to stanice namenjene prodaji električne energije vlasnicima električnih vozila, kao što su srednje stanice koje će eventualno zameniti postojeće benzinske pumpe sa 10-20 punjača, manje stanice u domaćinstvima sa 1-2 punjača za ovu namenu, kao i kao stanice na manjim parkiralištima sa do 20 punjača. Potrebe ovakvih stanica ne mogu se pokriti korišćenjem samo solarnih obnovljivih izvora. Gde geografsko područje dozvoljava, ima smisla koristiti vetrogenerator. Moguća je upotreba generatora na biomasu, ako prostorni kapaciteti to dozvoljavaju, što bi prvo mogao biti slučaj u ruralnim područjima. U urbanim sredinama, u mnogim mestima jedini način da se nadoknadi nedostatak električne energije je preuzimanje energije iz elektro distributivne mreže. Kod ovih stanica koristi se standard terminal koji ima složeniji hardver i softver, a ceo sistem za upravljanje ovakvom stanicom je složeniji od sistema za upravljanje energijom u domaćinstvima..

Industrijske stanice su velike stanice za punjenje električnih vozila namenjene za opsluživanje flote električnih vozila od nekoliko stotina komada. U ovu grupu stanica spadaju stanice kod proizvođača električnih vozila, stanice kod velikih drumskih prevoznika i stanice na masovnim parkiralištima kao što su garaže, tržni centri itd. Slično komercijalnim stanicama, potrebe ovakvih stanica ne mogu se pokriti korišćenjem samo obnovljivih izvora električne energije, a često jedini način da se nadoknadi nedostajuća električna energija je preuzimanje iste iz elektro distributivne mreže. Kod ovih stanica koristi se extended terminal, koji ima najsloženiji hardver i softver.

## IV. VEŠTAČKA INTELIGENCIJA

Veštačka inteligencija se može definisati kao sposobnost digitalnog računara ili kompjuterski kontrolisanog robota da obavlja zadatke koji se obično povezuju sa inteligentnim bićima [5]. Izraz se često primenjuje na projekat razvoja sistema obdarenih intelektualnim procesima karakterističnim za ljude, kao što je sposobnost rasuđivanja, otkrivanja značenja, generalizacije ili učenja iz prethodnog iskustva. Psiholozi generalno ne karakterišu ljudsku inteligenciju samo jednom osobinom, već kombinacijom mnogih različitih sposobnosti. Istraživanja u oblasti veštačke inteligencije su se uglavnom fokusirala na sledeće komponente inteligencije: učenje, rasuđivanje, rešavanje problema, percepciju i korišćenje jezika. Pored ovih osnovnih komponenti, mogu se naći istraživanja koja se bave i razvojem mašina koje imaju sledeće sposobnosti: planiranje, predstavljanje znanja, kretanje, socijalna inteligencija i opšta inteligencija.

Rasuđivanje znači izvođenje zaključaka koji odgovaraju situaciji. Zaključci se klasifikuju kao deduktivni ili induktivni. Najznačajnija razlika između ovih oblika rezonovanja je u tome što u deduktivnom slučaju istinitost premisa garantuje

 ISBN 978-86-7466-930-3

istinitost zaključka, dok u induktivnom slučaju istinitost premise daje podršku zaključku bez da daje apsolutnu sigurnost. Postignut je značajan uspeh u programiranju računara za izvođenje zaključaka, posebno deduktivnih zaključaka. Međutim, pravo rezonovanje uključuje više od samog izvođenja zaključaka; podrazumeva izvođenje zaključaka relevantnih za rešenje konkretnog zadatka ili situacije. Ovo je jedan od najtežih problema sa kojima se veštačka inteligencija suočava.

Rešavanje problema, posebno u veštačkoj inteligenciji, može se okarakterisati kao sistematsko traženje niza mogućih radnji u cilju dostizanja nekog unapred definisanog cilja ili rešenja. Metode rešavanja problema dele se na metode posebne namene i metode opšte namene. Metoda posebne namene je skrojena za određeni problem i često koristi veoma specifične karakteristike situacije u kojoj je problem ugrađen. Nasuprot tome, metoda opšte namene je primenljiva na širok spektar problema. Mnogi različiti problemi rešeni su programima veštačke inteligencije. Neki primeri su pronalaženje pobedničkog poteza (ili niza poteza) u igri na ploči, osmišljavanje matematičkih dokaza i manipulacija „virtuelnim objektima“ u kompjuterski generisanom svetu.

Percepciju možemo opisati kao skeniranje okoline pomoću različitih čulnih organa, stvarnih ili veštačkih, i razlaganje scene na zasebne objekte u različitim prostornim odnosima. Analiza je komplikovana činjenicom da objekat može izgledati drugačije u zavisnosti od ugla iz kojeg se posmatra, pravca i intenziteta osvetljenja u sceni i koliko je objekat u kontrastu sa okolnim poljem. Mašinsku percepciju [6] možemo definisati kao sposobnost da se koriste ulazni signali sa senzora (kao što su kamere, mikrofoni, bežični signali, sonar, radar i taktilni senzori) da bi se zaključili aspekti sveta, odnosno okruženja. Aplikacije uključuju i prepoznavanje govora, prepoznavanje lica i prepoznavanje objekata. Trenutno je veštačka percepcija dovoljno napredna da omogući optičkim senzorima da identifikuju pojedince, autonomnim vozilima da voze umerenom brzinom na otvorenom putu i robotima da lutaju kroz zgrade skupljajući prazne limenke soda.

Korišćenje jezika omogućava mašinama da čitaju i razumeju ljudski jezik. Dovoljno moćan sistem za obradu ljudskog jezika bi omogućio korisničke interfejse na ljudskom jeziku i sticanje znanja direktno iz izvora pisanih od strane ljudi, kao što su tekstovi i vesti. Neke jednostavne primene korišćenja jezika uključuju pronalaženje informacija, odgovaranje na pitanja i mašinsko prevođenje [7].

Planiranje omogućava računaru da predviđa kako će ga njegove akcije promeniti i da donosi odluke koji maksimiziraju korist iz dostupnih izbora [8]. U klasičnim problemima planiranja, računar može pretpostaviti da je on jedini sistem koji deluje na svetu, dozvoljavajući sebi da bude siguran u posledice svojih akcija. Međutim, ako računar nije jedini akter, onda to zahteva da agent razmišlja u neizvesnosti, i kontinuirano ponovo procenjuje svoje okruženje i prilagođava se. Planiranje sa više računara koristi saradnju i konkurenciju mnogih računara za postizanje zadatog cilja.

Predstavljanje znanja i inženjering znanja [6] omogućavaju programima veštačke inteligencije da inteligentno odgovaraju na pitanja i donose zaključke o činjenicama iz stvarnog sveta. Reprezentacija „onog što postoji“ je ontologija: skup objekata, relacija, koncepata i svojstava formalno opisanih tako da softverski programi mogu da ih tumače. Najopštije ontologije se nazivaju gornje ontologije, koje pokušavaju da obezbede osnovu za sva druga znanja i deluju kao posrednici između ontologija domena koje pokrivaju specifično znanje o određenom domenu znanja.

Kretanje se u velikoj meri koristi u robotici [6]. Lokalizacija je način na koji robot zna svoju lokaciju i mapira svoje okruženje. Kada se dobije malo, statičko i vidljivo okruženje, ovo je lako; međutim, dinamična okruženja, kao što je (u endoskopiji) unutrašnjost tela koje diše, predstavljaju veći izazov.

Razvoj sposobnosti socijalne inteligencije je interdisciplinarna oblast koji obuhvata sisteme koji prepoznaju, tumače, obrađuju ili simuliraju ljudska osećanja, emocije i raspoloženje [9]. Na primer, neki virtuelni asistenti su programirani da pričaju razgovorno ili čak da se šale na duhovit način; to čini da izgledaju osetljiviji na emocionalnu dinamiku ljudske interakcije ili da na drugi način olakšaju interakciju između čoveka i računara.

Mašina sa opštom inteligencijom može rešiti širok spektar problema sa širinom i svestranošću sličnom ljudskoj inteligenciji. Postoji nekoliko konkurentnih ideja o tome kako razviti veštačku opštu inteligenciju.

## V. MAŠINSKO UČENJE

Mašinsko učenje je disciplina veštačke inteligencije koja se bavi implementacijom kompjuterskih softvera koji su u stanju da samostalno uče [10]. Kako bi mogli da predviđaju ili donose odluke, algoritmi mašinskog učenja grade model zasnovan na uzorku podataka, poznatih kao podaci o obuci. Podskup mašinskog učenja je usko povezan sa statistikom, ali nije svako mašinsko učenje statističko učenje. Pretraga podataka, odnosno praksa analize velikih baza podataka u cilju generisanja novih informacija, je srodna oblast proučavanja, koja se fokusira na istraživačku analizu podataka.

Generalno, algoritmi mašinskog učenja se koriste za predviđanje ili klasifikaciju [11]. Na osnovu nekih ulaznih podataka, koji mogu biti označeni ili neoznačeni, algoritam će proizvesti procenu o obrascu u podacima. Zatim se vrši procena takvog predviđanja. Ako postoje poznati primeri, funkcija greške može da napravi poređenje da proceni tačnost predviđanja. Ako predviđanje može bolje da se uklopi u tačke podataka u skupu za obuku, onda se odgovarajući koeficijenti prilagođavaju da bi se smanjila neslaganja između poznatog primera i procene. Algoritam će ponoviti ovaj proces evaluacije i optimizacije, samostalno ažurirajući koeficijente dok se ne dostigne prag tačnosti.

Mašinsko učenje se može klasifikovati na: nadgledano, nenadgledano i polunadgledano učenje, kao i pojačano učenje. Učenje pod nadzorom, takođe poznato kao nadgledano mašinsko učenje, definisano je upotrebom označenih skupova podataka za obuku algoritama koji klasifikuju podatke ili tačno predviđaju ishode. Kako se ulazni podaci unose u model, on prilagođava svoje koeficijente dok se model ne uklopi na najbolji mogući način. Učenje bez nadzora, poznato i kao nenadgledano mašinsko učenje, koristi algoritme

 ISBN 978-86-7466-930-3

mašinskog učenja za analizu i grupisanje neoznačenih skupova podataka. Ovi algoritmi otkrivaju skrivene obrasce ili grupisanje podataka bez potrebe za ljudskom intervencijom. Njegova sposobnost da otkrije sličnosti i razlike u informacijama čini ga idealnim rešenjem za istraživačku analizu podataka, strategije unakrsne prodaje, segmentaciju kupaca, prepoznavanje slika i obrazaca. Polu-nadgledano učenje nudi optimalan odnos između učenja pod nadzorom i učenja bez nadzora. Tokom obuke, koristi manji skup označenih podataka da vodi klasifikaciju i izdvajanje karakteristika iz većeg, neoznačenog skupa podataka. Polu-nadgledano učenje može da reši problem nedostatka označenih podataka (ili nemogućnosti da priuštite da označite dovoljno podataka) za obuku algoritma za učenje pod nadzorom. Pojačano učenje je model mašinskog učenja ponašanja koji je sličan nadgledanom mašinskom učenju, ali algoritam nije obučen korišćenjem uzoraka podataka. Ovaj model uči koristeći pokušaje i greške. Niz uspešnih ishoda će biti pojačan kako bi se razvila najbolja preporuka ili politika za dati problem.

Neke metode koje se koriste u mašinskom učenju uključuju neuronske mreže, Bajesove mreže, linearnu regresiju, logističku regresiju, slučajnu šumu (drvo odlučivanja), mašinu vektora podrške (SVM), grupisanje k-srednjih vrednosti, metode verovatnoće klasterisanja i još mnogo toga. Metoda neuronske mreže imitira rad biološkog mozga.

## VI. PRIMENA VEŠTAČKE INTELIGENCIJE NA TERMINAL

U radu koji daje pregled stanja u oblasti sistema upravljanja energijom u domaćinstvu [12] može se uočiti da između ostalih postoje i grupe radova koji se bave primenom veštačke inteligencije u toj oblasti. Uvidom u to, možemo uočiti da se najviše primenjuje pojačano učenje. Ovo saznanje se takođe odnosi i na sistem za daljinsko upravljanje stanicom za punjenje električnih vozila, iz razloga što je *light* varijanta terminala namenjena za korišćenje kod rezidencijalne stanice za punjenje električnih vozila. Rezidencijalna stanica za punjenje električnih vozila predstavlja sistem upravljanja energijom u domaćinstvu. Pored rezidencijalne stanice, postoje i komercijalne i industrijske stanice, kod kojih se koriste dosta složenije *standard* i *extended* varijanta terminala. Ipak, zbog njihove sličnosti sa *light* varijantom terminala, možemo reći da se i na njih odnosi gore pomenuto saznanje. Dakle, generalno za rad terminala za daljinsko upravljanje najzgodnije je primeniti pojačano učenje. Iz svega prethodno rečenog sledi da možemo u daljem tekstu dati pregled glavnih zaključaka iz primene tehnika mašinskog učenja, odnosno tehnika pojačanog učenja na sisteme upravljanja energijom u domaćinstvu, jer su oni potpuno primenljivi i dobra polazna osnova za primenu istih tehnika na terminal za daljinsko upravljanje stanicom za punjenje električnih vozila, koja se napaja iz obnovljivih izvora električne energije.

Kod upravljanja energijom u domaćinstvu, glavni cilj je optimizacija, odnosno minimiziranje ukupne potrošnje električne energije i smanjenje računa za struju u pametnoj kući [13], kao i optimalan plasman električne energije dobijene iz obnovljivih izvora, ako su oni primenjeni. Tipičan sistem upravljanja se ne može uspešno prilagoditi raznim uređajima sa različitom složenošću rasporeda, niti je prikladan za primenu u realnom vremenu. Algoritmi pojačanog učenja (RL) su u poslednje vreme predloženi kao potencijalni kandidati za rešavanje ovih problema zbog njihove prilagodljivosti i sposobnosti da nauče prioritete i navike kupaca i optimizuju upravljanje ovakvim energetskim sistemima koji su često podložni različitim ulazima kao što su dinamičke cene električne energije, podaci meteorološke prognoze (sunce, vetar,...) i obrasci potrošnje energije (ponašanje korisnika). RL se smatra tipom algoritma sa mašinskim učenjem za donošenje odluka u stohastičkom okruženju. Ne zahteva matematički model i pogodan je za složene aplikacije u realnom vremenu. RL algoritam ima šest parametara, a to su agent, okruženje, skup stanja S, skup akcija A, nagrade R i vrednost akcije Q(s,a). Generalno, RL agent je u interakciji sa okruženjem kao što je prikazano na Sl. 1 u samom bloku terminala.

Prva upotreba pojačanog učenja za upravljanje energijom kod kuće opisana je u [14], gde se neuronska mreža koristi za kontrolu grejanja, ventilacije, klimatizacije (HVAC) i osvetljenja kako bi se smanjila nelagodnost korisnika i smanjili troškovi energije. Pored toga, postoje i radovi u kojima se koristi pojačano učenje za planiranje uključivanja/isključivanja uređaja kao odgovor na signale o cenama. To praktično znači pomeranje određenih fleksibilnih opterećenja, što omogućava minimiziranje troškova za potrošnju električne energije, tako što ne se prelazi određeni prag snage a bez izazivanja nezadovoljstva korisnika zbog odlaganja rada uređaja. Pojačano učenje primenjuje se takođe i na realizaciju različitih funkcija koje mere nezadovoljstvo korisnika kada uređaji ne uspeju da obave traženi zadatak u potrebnom vremenu. Od početka dosta je primenjivana metoda neuronske mreže [15,16], a u poslednje vreme prilično se primenjuje i metoda nazvana Q-učenje.

Algoritmi Q-učenja su RL tehnike koje su usvojene da bi se stekla optimalna politika određivanja akcija koje agent preuzima. Na osnovu primljene nagrade , agent je u stanju da optimizuje svoju politiku određivanja akcija koje treba preuzeti, i time maksimizira ukupne nagrade koje će dobiti u budućnosti. To se postiže ažuriranjem odgovarajućih koeficijenata prilikom svake iteracije, kako bi se optimizovale performanse agenta. U zavisnosti od složenosti arhitekture konkretnog sistema, moguće je i optimizaciju upravljanja energijom rešiti direktno primenom Q-učenja [13], ili primeniti Q-učenje za razbijanje glavnog problema na podzadatke koji se zatim rešavaju nezavisno korišćenjem RL [17].

Pored navedenih mogućih primena tehnika veštačke inteligencije na rešavanje glavnog problema optimizacije upravljanja energijom u ovakvim sistemima, postoje i primene u kojima se glavni problem optimizacije upravljanja energijom rešava primenom neke druge tehnike za upravljanje energije, ali se veštačka inteligencija koristi kao pomoćna metoda za predviđanje ulaznih parametara [18,19].

## VII. ZAKLJUČAK

U ovom radu je razmatrana primena veštačke inteligencije na terminal za daljinsko upravljanje stanice za punjenje električnih vozila, koja se napaja iz obnovljivih izvora energije. Prvo je prikazana arhitektura kompletnog sistema za

 ISBN 978-86-7466-930-3

daljinsko upravljanje stanice. Zatim je dat i pregled komponenti inteligencije koje su dosada istraživači pokušali da implementiraju u mašinama. Posebno je prikazana komponenta mašinsko učenje sa klasifikacijom i metodama koje se koriste. Potom je dat pregled primene veštačke inteligencije u oblasti sistema za upravljanje energijom u domaćinstvima. Uzevši u obzir određene sličnosti ovakvih sistema sa sistemima za daljinsko upravljanje stanicom za punjenje električnih vozila, koja se napaja iz obnovljivih izvora električne energije, zaključeno je da u ovom trenutku na terminal za daljinsko upravljanje ovakvom stanicom najviše smisla ima primeniti tehniku pojačanog učenja, i to tzv. metodu Q-učenja. Konkretna primena ove metode može biti predmet daljeg rada.

## LITERATURA


[1] P. Arunkumar, K. Vijith, "IOT Enabled Smart Charging Stations for Electric Vehicle," International Journal of Pure and Applied Mathematics, vol. 119, no. 7, pp. 247-252, 2018.

[2] J. Vujasinović, G. Savić, Ž. Đurišić, "Arhitektura sistema za daljinsko upravljanje stanice za punjenje električnih vozila koja se napaja iz obnovljivih izvora energije," 64. konferencija za elektroniku, telekomunikacije, računarstvo, automatiku i nuklearnu tehniku (ETRAN), pp. 302-306, Novi Sad, Srbija, Septembar 2020.

[3] Jovan Vujasinovic, Goran Savic, Zeljko Despotovic; „Arhitecture and Sizing of System for Remote Control of Renewable Energy Sources Powered Station for Electric Vehicles Charging", IEEE International Energy Conference, May 2022, Riga, Litvania

[4] Jovan Vujasinovic, Goran Savic, Milan Prokin; „Terminal for Remote Control of Renewable Energy Sources Powered Station for Electric Vehicles Charging", 10th Mediterranean Conference on Emedded Computing, June 2021, Budva, Montenegro

[5] https://www.britannica.com/technology/artificial-intelligence#ref219078

[6] Russell Stuart J.; Norvig Peter , "Artificial Intelligence: A Modern Approach (2nd ed.)", Upper Saddle River, New Jersey: Prentice Hall, ISBN 0-13-790395-2, 2003

[7] Luger George; Stubblefield William,"Artificial Intelligence: Structures and Strategies for Complex Problem Solving (5th ed.)", Benjamin/Cummings, ISBN 978-0-8053-4780-7, 2004.

[8] Poole David; Mackworth Alan; Goebel Randy, "Computational Intelligence: A Logical Approach", New York: Oxford University Press. ISBN 978-0-19-510270-3, 1998.

[9] Tao Jianhua, Tan Tieniu, "Affective Computing and Intelligent Interaction" Affective Computing: A Review Vol. LNCS 3784. Springer. pp. 981–995. doi:10.1007/11573548, 2005.

[10] https://www.britannica.com/technology/machine-learning

[11] https://www.ibm.com/cloud/learn/machine-learning

[12] Usman Zafar, Sertac Bayhan, Antonio Sanfilippo, „Home energy management system concepts, configurations, and technologies for the smart grid", IEEE Access, 10.1109/ACCESS.2020.3005244

[13] F. Alfaverh, M. Denai, and Y. Sun, "Demand Response Strategy Based on Reinforcement Learning and Fuzzy Reasoning for Home Energy Management ", IEEE Access, 10.1109/ACCESS.2020.2974286, February 2020.

[14] M. C. Mozer, ''The neural network house: An environment that adapts to its inhabitants,'' Assoc. Advancement Artif. Intell., Menlo Park, CA, USA, Tech. Rep. SS-98-02, 1998. [Online]. Available: https://www.aaai.org/Papers/Symposia/Spring/1998/SS-98-02/SS98-02-017.pdf

[15] E.Matallanas,M.Castillo-Cagigal,A.Gutiérrez,F.Monasterio-Huelin, E. Caamaño-Martín, D. Masa, and J. Jiménez-Leube, ''Neural network controller for active demand-side management with PV energy in the residential sector,'' *Appl. Energy*, vol. 91, no. 1, pp. 90–97, Mar. 2012.

[16] B. Yuce, Y. Rezgui, and M. Mourshed, ''ANN–GA smart appliance scheduling for optimised energy management in the domestic sector,'' *Energy Buildings*, vol. 111, pp. 311–325, Jan. 2016.

[17] A. Sheikhi, M. Rayati, and A. M. Ranjbar, ''Dynamic load management for a residential customer; reinforcement learning approach,'' *Sustain. Cities Soc.*, vol. 24, pp. 42–51, Jul. 2016.

[18] Luis Galván, Juan M. Navarro, Eduardo Galván, Juan M. Carrasco, Andrés Alcántara, "Optimal Scheduling of Energy Storage Using A New Priority-Based Smart Grid Control Method", *Energies* **2019**, *12*, 579, doi:10.3390/en12040579 www.mdpi.com/journal/energies.

[19] Jovan Vujasinovic, Goran Savic; „Demand Side Management and Integration of a Renewable Sources Powered Station for Electric Vehicle Charging into a Smart Grid", 15. International Conference on Applied and Theoretical Electricity ICATE, May 2021, Craiova, Romania


## ABSTRACT


Application of artificial intelligence to the terminal for remote control of renewable energy sources powered station for electric vehicles charging has been presented in this paper. As the terminal enables remote control of electric vehicle chargers, smart storage batteries, smart electricity meters, cash registers, as well as, remote control of renewable energy sources and other devices within the station for electric vehicles charging, it is necessary to define and develop an algorithm for managing the terminal. In this paper, the realization of that management using artificial intelligence is considered. In this way, such charging stations for electric vehicles become completely autonomous in their work and give optimal results, which raises their availability to users of electric vehicles. It potentially encourages an increase in the use of electric vehicles for which energy is provided from renewable sources, which reduces the degree of air pollution as well as the negative effects it brings.


**Application of Artificial Intelligence to the Terminal for Remote Control of Renewable Energy Sources Powered Station for Electric Vehicles Charging**


Jovan Vujasinović, Goran Savić


 ISBN 978-86-7466-930-3

# Prepoznavanje imena na slikama lekarskih izveštaja na srpskom jeziku u cilju zaštite ličnih podataka

Aldina Avdić, Ulfeta Marovac

***A stra t*— Savremeni način života neizostavno uključuje upotrebu računara i mobilnih telefona u svim svojim segmentima, pa i ada je u pitanju zdravstvo. Pored elektronskog zdravstva koje se sve više razvija, pogotovo od kada se svet suočio sa pandemijom korona virusa, sve više ljudi traži i savete o zdravlju na društvenim mrežama. Tom prilikom dodaju slike koje sadrže njihove zdravstvene rezultate, ne mareći o tome da na taj način ostavljaju i svoje lične podatke. U ovom radu data je metoda za prepoznavanje imena na sli ama medicins ih izveštajima napisanih na srpskom jeziku u cilju njihove de-identifikacije. Ova metoda bazirana je na optičkom prepoznavanju ara tera, metodama obrade prirodnog jezi a i pravilima i ima široku upotrebu, jer je de-identifi acija elektronskih medicinskih izveštaja neophodan korak za njihovu bilo a vu dalju analizu.**

***Ključne reči*— de-identifi acija, ele trons i medicins i izveštaji, prepoznavanje imenovanih entiteta, obrada prirodnog jezi a, optičko prepoznavanje ara tera, zaštita privatnosti, srps i jezi .**

## I. UVOD

Informacione i komunikacione tehnologije već duže vreme nalaze svoju primenu u zdravstvenom sistemu. E-zdravstvo (engl. *e- ealth*) je termin nastao krajem dvadesetog veka i zasniva se na efikasnijem i kvalitetnijem pružanju zdravstvenih usluga uz pomoć savremenih tehnologija, mogućnostima za obezbeđivanje mobilnosti lekara i pacijenata uz integraciju sa postojećim sistemima [1].

Savremene tehnologije u zdravstvu omogućavaju kompletno elektronsko vođenje zdravstvene dokumentacije u svim segmentima rada (elektronski karton pacijenta), telemedicinu, telekonsultacije, upravljanje znanjem o zdravlju i mobilno i sveprisutno zdravstvo. Na ovaj način omogućava se lakše i uspešnije lečenje pacijenata i smanjenje administrativnih ograničenja prilikom pružanja medicinskih usluga.

Prednosti e-zdravstva su elektronsko praćenje i beleženje zdravstvenog stanja pacijenata, bolja dijagnostika, pristup medicinskim podacima bilo gde i bilo kada, kao i brz prenos informacija korisnicima putem telemedicine i Internet servisa.

Aldina Avdić – Departman za tehničko-tehnološke nauke, Državni Univerzitet u Novom Pazaru, Vuka Karadžića 9, 36300 Novi Pazar, Srbija (e-mail: apljaskovic@np.ac.rs).

Ulfeta Marovac – Departman za tehničko-tehnološke nauke, Državni Univerzitet u Novom Pazaru, Vuka Karadžića 9, 36300 Novi Pazar, Srbija (e-mail: umarovac@ np.ac.rs).

Elektronski medicinski zapis (engl. *EM* ili *E* - *electronic medical health report*) je izveštaj pacijenta koji čuva podatke o zdravstvenom stanju, dijagnozama i terapijama. Oni se kreiraju pomoću medicinskih informacionih sistema i sadrže privatne podatke o pacijentu (ime, prezime, lični broj, datum rođenja, broj kartice, broj osiguranja, adresu itd.), beleške lekara, dijagnoze, laboratorijske izveštaje, terapije itd [2].

Motivacija za ovaj rad je pripremanje elektronskih izveštaja za dalju analizu korišćenjem metoda veštačke inteligencije, mašinskog učenja i metoda obrade prirodnog jezika. U kakvom god da su obliku elektronski medicinski izveštaji (tekst ili slika) prvi korak ka njihovoj etičkoj obradi jeste uklanjanje ličnih podataka (ovo je uređeno regulativom – engl. *General ata Protection egulation - G P* ). Za potrebe rada prikupljen je skup podataka, i kreirana i primenjena metoda za prepoznavanje imena i prezimena na srpskom jeziku sa slika medicinskih izveštaja bazirana na optičkom prepoznavanju slova (engl. *ptical Caracter ecognition - C* ) i metodama obrade prirodnog jezika (engl. *Natural anguage Processing - N P*) i prepoznavanja imenovanih entiteta (engl. *Named Entity ecognition – NE* ). Stoga će nadalje ovi pojmovi biti detaljno objašnjeni.

Uredba Evropske unije o zaštiti podataka o ličnosti GDPR definiše propise o zaštiti podataka ličnosti u Evropskoj uniji, ali se ona odnosi i na kompanije sa sedištem u zemljama izvan Evropske unije, ukoliko one obrađuju podatke o ličnosti rezidenata Evropske unije. Po članu 3 GDPR regulative potrebno je da se uskladi zaštita osnovnih prava fizičkih lica u vezi sa aktivnostima obrade ličnih podataka. U Srbiji je na snazi Zakon o zaštiti podataka o ličnosti iz 2018. godine koji je usklađen sa GDPR [3]. Ona obezbeđuje pojedincima veću kontrolu nad ličnim podacima i obavezuje kompanije koje prikupljaju i analiziraju lične podatke da promene svoj model poslovanja u skladu s njom. Pod ličnim podacima podrazumeva se bilo koja kombinacija ličnih činjenica koja tačno određuje jednog pojedinca, to su, između ostalog, ime i prezime, JMBG, podaci o lokaciji, fizički, fiziološki, genetski, mentalni, ekonomski, socijalni, kulturni ili bilo koji drugi faktori.

Osnovni zadatak OCR softvera je da digitalne slike, na kojima se nalaze skenirani ili fotografisani tekstovi sa štampača, pisaćih mašina, knjiga, novina, časopisa ili poslovne dokumentacije, pretvori u promenljivi digitalni tekstualni oblik, tako što će sa rasterskih slika, prepoznati

 ISBN 978-86-7466-930-3

slova, reči i čitave tekstove.[4].

Procesiranje prirodnog jezika je grana veštačke inteligencije koja omogućava sistemu da razume značenje podataka na ljudskom jeziku. Njen krajnji cilj je čitanje, dešifrovanje, razumevanje i nalaženje smislenosti u prirodnom jeziku. Većina NLP tehnika oslanja se na mašinsko učenje da bi se zaključilo o značenju podataka na prirodnim jezicima. Prepoznavanje imenovanih entiteta je grana NLP-a kojom se u tekstu označavaju sintagme u nestrukturiranom tekstu u unapred definisane kategorije kao što su imena osoba, organizacije, lokacije, medicinski kodovi, vremenski izrazi itd [5] [6].

Ovaj rad je organizovan na sledeći način. U drugom poglavlju dat je pregled radova iz oblasti. U trećem poglavlju opisani su korišćeni podaci i metoda za prepoznavanje imena na slikama medicinskih izveštajima napisanih na srpskom jeziku u cilju njihove de-identifikacije. Zatim sledi opis korišćenih tehnologija, dobijeni rezultati i njihova diskusija. Na kraju je dat zaključak i pravci daljeg istraživanja.

## II. Stanje u oblasti

Povezana istraživanja na ovu temu opisuju metode za normalizaciju i izdvajanje znanja iz medicinske evidencije koje nisu direktno povezane sa primenom na srpskom jeziku. Većina istraživanja odnosi se na korpuse engleskog govornog područja i leksičke resurse koji su javno dostupni. Za bugarski jezik postoje rezultati izdvajanja informacija iz velikog korpusa nestrukturiranih podataka i njihovog pribavljanja u strukturiranom obliku [7].

Normalizacija je prvi korak koji se koristi u klasifikaciji i obeležavanju medicinskih termina [8]. Obrada medicinskog izveštaja sastoji se od nekoliko koraka kao što su prečišćavanje podataka, integracija, transformacija, redukcija i na kraju zaštita podataka. Izvlačenjem kliničkih odnosa iz medicinskih izveštaja mogu se identifikovati odnosi između referenci na lekove i njihovih atributa. Pregled medicinskih informacionih sistema pokazuje da 60% komercijalnih sistema koristi metode zasnovane na pravilima, dok se u naučnim istraživanjima više koriste metode mašinskog učenja [9]. Najpopularniji sistemi za obeležavanje medicinskog teksta su CTAKES i CLAMP sistemi [9] [10]. Autori su se u radu bavili identifikacijom medicinskih pojmova u tekstovima koje su napisali pacijenti, koristeći kraudsoursing [11] .

Na jezicima bivše Jugoslavije nisu pronađeni radovi koji bi se bavili procesom slobodnog teksta u medicinskim izveštajima i javno dostupnim leksičkim izvorima u medicinskom domenu. „Wordnet za biomedicinske nauke“ za srpski jezik sadrži skupove sinonimnih reči ili tačnije različite delove govora (engl. PoS, parts of speech) sa novim konceptom za šest ontoloških kategorija (genetika, virus, bakterije, ćelije, naučna polja i mikroorganizam) [12].

Klasifikacija u medicinskim izveštajima na srpskom jeziku opisana je u radu [13]. De-identifikacija ličnih podataka u srpskom jeziku opisana je u radu [14].

Primena OCR u zdravstvu opisana je u radu [15].

## III. Podaci i metodologija

Za potrebe ovog istraživanja sakupljena je 71 slika sa društvene mreže Facebook, koja sadrži medicinski izveštaje koje sadrži lične podatke. Ove izveštaje su okačili korisnici zatvorene grupe Insulinska rezistencija. Neki učesnici u grupi svesni su izlaganja privatnih podataka i pre postavljanja slike svoje ime oboje ili iseku sliku tako da lični podaci nisu dostupni, ali budući da su ovo samo slike od januara 2022. godine, to govori koliko je jednostavno naći elektronske izveštaje koji sadrže lične podatke na internetu na sličnim grupama.

Metoda za prepoznavanje imena sadrži sledeće korake:

- na sve slike je prvo primenjen OCR softver otvorenog koda *Tessaract* [17], čime se izdvaja tekst sa slike (Sl. 1),

```
from PIL import Image
import pytesseract
import numpy as np
import spacy
from spacy import displacy
import translators as ts
import os
import re

directory = 'C:/Users/aldin/Desktop/Podaci/Insulinska'
NER = spacy.load("en_core_web_sm")

for filename in os.listdir(directory):
    f = os.path.join(directory, filename)
    if os.path.isfile(f):
        filename = f
        print(f)
        img1 = np.array(Image.open(filename))
        pytesseract.pytesseract.tesseract_cmd =
        r'C:\Users\aldin\AppData\Local\Tesseract-OCR\tesseract.exe'
        text = pytesseract.image_to_string(img1)
```

Sl. 1 Izdvajanje teksta iz slika

- zatim su primenjena pravila i regularni izrazi za obeležavanje imena i prezimena (Sl. 2). Pravila su definisana od strane autora, a odnose se na to da je u liniji koja se čita veća verovatnoća da se nađe ime i prezime, ako se u toj liniji nalaze reči „prezime“, „pacijent“, „ime i prezime“ i sl. Takođe, ako je na medicinskom izveštaju neka sintagma napisana velikim slovima, ili prvim početnim slovima sa blanko znakovima između, i to treba uzeti u obzir kao moguće ime i prezime pacijenta. Do ovih pravila došlo se analizom sadržaja prikupljenog skupa podataka.

```
        lines = text.split('\n')
        for line in lines:
            if "prezime" in line:
                print(line)
            if "pacijent" in line:
                print(line)
            rl = re.findall('^[a-zA-Z]+(?:[\s.]+[a-zA-Z]+)*$', line)
```

Sl. 2 Primeri pravila

- u koliko je prethodni korak neuspešan, sledi prevođenje teksta na engleski korišćenjem *Python* paketa *Translators* [18],
- zatim se koristi *Spacy* softver za NER na engleskom za prepoznavanje vlastitih imena [19] (Sl. 3).


ISBN 978-86-7466-930-3

U program su uključene biblioteke *Image* za rad sa slikama, *PyTesseract* za OCR, *NumPy* za jednostavniju obradu i programiranje, zatim *SpaCy* za prepoznavanje imenskih entiteta, *Translators* za prevođenje reči, *os* za rad sa fajlovima i *re* za rad sa regularnim izrazima.

```
        if rl:
            textt = ts.google(rl[0], from_language='sr',
            to_language='en')
            textl= NER(textt)
            for word in textl.ents:
                if word.label_=="PERSON":
                    print(word.text)
```

Sl. 3 Primeri prevođenja i primene Spacy alata za prepoznavanje imenovanih entiteta

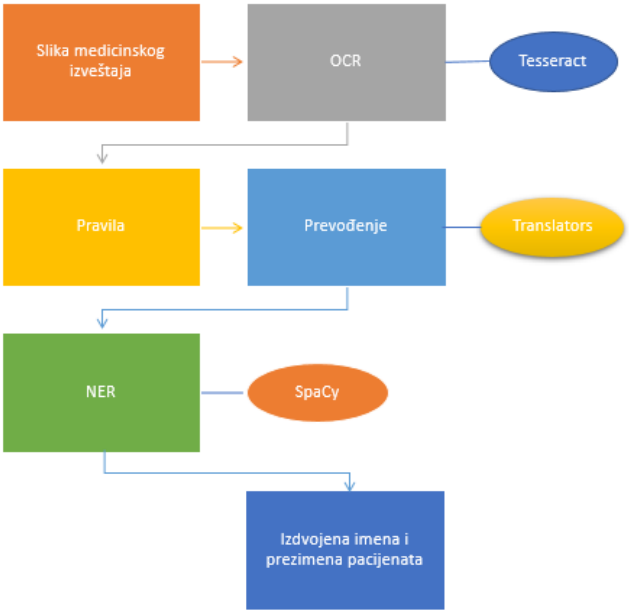


Sl. 4. Koraci u prepoznavanju ličnih imena u slikama medicinskih izveštaja na srpskom jeziku

Ova metoda ne zahteva prethodno obeležavanje niti treniranje modela metodama mašinskog učenja (Sl. 4). To su koraci koji su pravci daljeg istraživanja, uz povećanje skupa podataka kako bi se prvobitni rezultati popravili. Uklanjanje ovih podataka na izvornoj slici nije rađeno, ali jeste na tekstovima EHR-ova koji se čuvaju u bazi podataka.

## IV. Rezultati i diskusija

U tabeli 1 dati su rezultati primene metode za izdvajanje ličnih imena prezimena. Rezultati uključuju samo one podatke gde je izvučeno samo ime i prezime pacijenta.

Pod preciznošću se smatra odnos broja slika sa izdvojenim ličnim podacima i ukupnog broja slika, a pod odzivom odnos broja tačno izdvojenih imena i prezimena i ukupnog broja slika.

Ono što utiče na rezultate jeste i kvalitet slika i sama preciznost OCR alata, pa je kod jednog broja izveštaja izdvajanje teksta bilo nemoguće. Zato je potrebno uključiti i dodatna predprocesiranja slike. Rezultati pokazuju da je ovo dobra osnova, ali da bi se oni popravili potrebno je razmotriti korišćenje dodatnih resursa za srpski jezik, poput rečnika imena. Takođe, rezultati se mogu popraviti i korišćenjem modela mašinskog učenja i proširenjem trening skupa kao i proširenjem skupa pravila.

TABELA I
REZULTATI PRIMENE METODE

| | |
|---|---|
| Broj slika | 71 |
| Broj slika sa izdvojenim ličnim podacima | 41 |
| Broj tačno izdvojenih imena i prezimena | 22 |
| Preciznost | 58% |
| Odziv | 54% |

## V. Zaključak

Pacijenti često traže mišljenja o svojim zdravstvenim rezultatima na socijalnim mrežama, u specijalizovanim grupama korisnika sa istom dijagnozom. Tada često postavljaju slike koje sadrže privatne podatke. Alat za de-identifikaciju elektronskih medicinskih izveštaja imao bi široku primenu, jer pored toga što bi se korisniku skrenula pažnja da postavlja dokument sa osetljivim podacima, čak bi se mogli koristiti podaci iz medicinskih informacionih sistema za dalju obradu, analizu i dobijanje znanja. U radu je dat jedan način za izdvajanje imena i prezimena pacijenta zasnovan na OCR i NER. U daljem radu radiće se na dopunjavanju resursa, pravila i uključivanja modela mašinskog učenja, proširenja trening skupa, uz predprocesiranje slika, kako bi se postigli što bolji rezultati. Takođe, jedan od pravaca daljeg istraživanja jeste uklanjanje (zamagljivanje) pronađenih ličnih podataka na procesiranoj slici medicinskog izveštaja.

## Zahvalnica

Ovaj rad je delimično finansiran od strane Ministarstva prosvete, nauke i tehnološkog razvoja Republike Srbije u okviru projekata III44007.

## Literatura

[1] A. R. Avdić, U. M. Marovac and D. S. Janković, “Smart Health Services for Epidemic Control,” in 2020 55th International Scientific Conference on Information, Communication and Energy Systems and Technologies (ICEST), 2020.

[2] S. Meystre and M. E. f. t. I. Y. S. o. P. Records, "Electronic Patient Records: Some answers to the data representation and reuse challenges: Findings from the section on Patient Records," Yearbook of Medical Informatics, vol. 16, no. 01, p. 47–48, 2007.

[3] M. Luca, E. Lievevrouw and I. V. Hoyweghen, "Fit for purpose? The GDPR and the governance of European digital health," Policy studies, vol. 41, no. 5, pp. 447-467, 2020.

[4] J. Memon, M. Sami, R. A. Khan and M. Uddin, "Handwritten optical character recognition (OCR): A comprehensive systematic literature review (SLR)," IEEE Access, vol. 8, pp. 142642-142668, 2020).

[5] G. G. Chowdhury, “Natural language processing,” Annual review of information science and technology, vol. 37, no. 1, pp. 51-89, 2003.

[6] D. J. Hand and N. M. Adams, Data mining, Wiley StatsRef: Statistics Reference Online, 2014, pp. 1-7.

 ISBN 978-86-7466-930-3

[7] I. Nikolova, D. Tcharaktchiev, S. Boytcheva, Z. Angelov and G. Angelova, "Applying language technologies on healthcare patient records for better treatment of Bulgarian diabetic patients," in International Conference on Artificial Intelligence: Methodology, Systems, and Applications, Springer, Cham, 2014, September.
[8] A. R. Avdić, U. M. Marovac and D. S. Janković, "Normalization of Health Records in the Serbian Language with the Aim of Smart Health Services Realization," Facta Universitatis, Series: Mathematics and Informatics, pp. 825-841, 2020.
[9] A. M. Milenkovic, P. J. Rajkovic, T. N. Stankovic and D. S. Jankovic, "Application of medical information system MEDIS.NET in professional learning," in 19thTelecommunications Forum (TELFOR) Proceedings of Papers, Belgrade, 2011.
[10] V. Garla, V. L. Re III, Z. Dorey-Stein, F. Kidwai, M. Scotch, J. Womack, A. Justice and C. Brandt, "The Yale cTAKES extensions for document classification: architecture and application," Journal of the American Medical Informatics Association, vol. 18, no. 5, pp. 614-620, 2011.
[11] E. Soysal, J. Wang, M. Jiang, Y. Wu, S. Pakhomov, H. Liu and H. Xu, "CLAMP - a toolkit for eficiently building customized clinical natural language processing pipelines," Journal of the American Medical Informatics Association, vol. 25, no. 3, pp. 331-336, 2018.
[12] D. L. MacLean and J. Heer, "Identifying medical terms in patient-authored text: a crowdsourcing-based approach," Journal of the American Medical Informatics Association, vol. 20, no. 6, pp. 1120-1127, 2013.
[13] N. e. a. Ivković-Berček, "Kooperativan rad na dogradnji Srpskog wordneta.".
[14] A. Avdić, U. Marovac and D. Janković, "Automated labeling of terms in medical reports in Serbian," Turkish Journal of Electrical Engineering & Computer Sciences, vol. 28, no. 6, pp. 3285-3303, 2020.
[15] B. Šandrih, C. Krstev and R. Stanković, "Development and evaluation of three named entity recognition systems for serbian-the case of personal names," in In Proceedings of the International Conference on Recent Advances in Natural Language , 2019, September.
[16] R. Mittal and A. Garg, "Text extraction using OCR: a systematic review. In 2020 Second International Conference on Inventive Research in Computing Applications (ICIRCA)," 2020, July.
[17] R. Smith, "An overview of the Tesseract OCR engine," in In Ninth international conference on document analysis and recognition (ICDAR 2007), 2007, September.
[18] P. Translators, "https://pypi.org/project/translators/," [Online]. [Accessed May 2022].
[19] X. Schmitt, S. Kubler, J. Robert, M. Papadakis and Y. LeTraon, "A replicable comparison study of NER software: StanfordNLP, NLTK, OpenNLP, SpaCy, Gate," in Sixth International Conference on Social Networks Analysis, Management and and Security (SNAMS), 2019, October. *Title of Standard*, Standard number, date.

ABSTRACT

The modern way of life inevitably includes the use of ICT in all its segments, even in healthcare. In addition to e-health, whose development is growing, especially since the world faced the coronary virus pandemic, most people are also looking for health advice on social networks. On that occasion, they upload pictures that contain their health results, with their personal data. This paper presents a method for recognition of personal names in images of medical reports written in Serbian to de-identify them. This method is based on optical character recognition, natural language processing methods and rules and has wide application, as de-identification of electronic medical reports is a necessary step for their further analysis.

**ecognition of names on images of medical reports in erbian to protect personal data**

Aldina Avdić, Ulfeta Marovac

 ISBN 978-86-7466-930-3

# Sistem za automatizaciju testova za proveru znanja baziran na transformaciji predikatskih iskaza

Ulfeta Marovac, Department for Technical Sciences, State University of Novi Pazar, Serbia
Aldina Avdić, Department for Technical Sciences, State University of Novi Pazar, Serbia

***A stra t*— bradom prirodnog jezika omogućava se da računari uspostave komunikaciju sa čovekom, da razumeju jezik čoveka, ali i da ga transformišu i da se čoveku obrate na njemu prirodnom jezi u. Problem istinitnosne vrednosti is aza izrečenih prirodnim jezikom je teško utvrditi zbog bogatstva rečnika i dvosmislenosti značenja. Preslikavanjem iskaza prirodnog jezika u iskaze predikatske logike moguće je utvrditi odnose među različitim predikatskim iskazima kao i izvršiti transformaciju iz jednog obli a pojavljivanja u drugi. edna od primena ovakvog znanja može biti u automatizovanom kreiranju testova znanja.**

***Ključne reči*—obrada prirodnog jezi a, predi ats a logi a, automatizovani testovi znanja, srps i jezi**

## I. UVOD

Testiranje je važna komponenta učenja, jer omogućava da se vidi da li je ispitanik usvojio informacije koje su mu izložene. Sve prisutnije e-učenje zahteva digitalizaciju okruženja za predavanja, ali i ispitivanje. Postoji puno dostupnih softverskih alata koji olakšavaju izradu testova. Njihove prednosti su brojne kao:

- Ušteda vremena u kreiranju testova, jer nema potrebe za tradicionalnim metodama
- Uvek su dostupni na mreži, deljivi su i lakše im pristupaju ispitanici.

Međutim ovi alati se uglavnom koriste kako bi ubrzali proces kreiranja testa i njegovu implementaciju, ali ne i u kreiranju baze znanja za test, i ne poseduju mogućnost provere ispravnosti pitanja koja su data kao slobodan tekst.

Obrada prirodnog jezika (Natural Language Processing - NLP [1]) je oblast veštačke inteligencije koja olakšava komunikaciju čoveka i računara. Naravno da je u procesu obrazovanja uloga nastavnika nezamenljiva, ali se novim tehnologijama može olakšati njihov posao. Ključni faktor u formiranju baze znanja za jedan kurs je uvek nastavnik, jer on daje činjenice koje su relevantne za problem koji se obrađuje. Utvrđivanje tačnosti iskaza koji su napisani na prirodnom jeziku nije jednostavno zbog njihove dvosmislenosti i složenosti, tako da se automatizacija testova svodi na postavljanje pitanja i adekvatnih tačnih i netačnih odgovora koje ispitanik treba da izabere. U ovom procesu određivanje tačnosti nekog pitanja vrši nastavnik. Da bi se pomoglo nastavniku u kreiranju veće količine testova od početnog tačnog ili netačnog iskaza, primenom pravila iskazne logike mogu se dobiti iskazi u drugom obliku čija je istinitnosna vrednost poznata. Sličan postupak se može vršiti i u obrnutom smeru gde bi se provera datog odgovora ispitanika u obliku slobodnog teksta pokušala izjednačiti sa nekim od poznatih odgovora.

Obrada prirodnog jezika je teška zbog specifičnosti jezika na kome se primenjuje. Uvođenjem formalnih jezika formiraju se rečenice na osnovu unapred definisanih pravila. Formalni jezici koriste logičke veznike, kvantifikatore, promenljive (termine), oznake za svojstva i odnose (predikate) i pomoćne znakove (zagrade) za izražavanje rečenica. Jedan primer formalne gramatike koja proizvodi predikatske iskaze na hrvatskom jeziku dat je u diplomskom radu autora Stanić [2].

U ovom radu biće prikazana obrada rečenica datih na srpskom jeziku. Da bi se izvršila obrada ovih rečenica moraju se koristiti pravila srpskog jezika kao i specijalni jezički resursi kojima će se umanjiti pojavljivanje sinonima.

Rad je organizovan na sledeći način: u drugom poglavlju opisani su predikatski iskazi i njihovi odnosi; u trećem poglavlju su prikazani algoritmi za transformaciju predikatskih iskaza unutar logičkog kvadrata; model za automatizaciju testova znanja prikazan je u četvrtom poglavlju i u poslednjem poglavlju dat je zaključak i ideje za proširenje modela.

## II. PREDIKATSKI ISKAZI I NJIHOV ODNOS

Iskazna logika je precizan matematički alat za računanje logičkih vrednosti složenih iskaznih formula kao i za donošenje zaključaka iz njih. Iskazna logika se bavi rečenicama u celini i ne zalazi u njihovu unutrašnju strukturu. Predikatska logika razmatra smisao polaznih iskaza.

U predikatskoj logici razlikujemo:

- **Term (T)-** objekta o kome se govori
- **Predi at (P)** – osobina objekta ili veza među objektima.

Term može biti konstanta (konkretan objekat) ili promenljiva (nedovoljno određen objekat). Atomični predikatski iskaz sastoji se od terma i predikata.

Neki iskazi sadrže neodređen objekat pa ne mogu imati jedinstvenu vrednost. Upotrebom negacije, veznika i kvantifikatora formira se predikatska formula [3].

Kvantifikacija je tema koja spaja lingvistiku, logiku i filozofiju. Kvantifikatori su osnovni alati pomoću kojih, u jeziku ili logici, upućujemo na količinu stvari [4]. Upotrebom kvantifikatora izražava se koliko je neko tvrđenje tačno i

Ulfeta Marovac is with Department for Technical Sciences, State University of Novi Pazar, Vuka Karadžića bb, 36300 Novi Pazar ,Serbia (e-mail: umarovac@np.ac.rs), https://orcid.org/0000-0001-7232-3755

Aldina Avdić is with Department for Technical Sciences, State University of Novi Pazar, Vuka Karadžića bb, 36300 Novi Pazar ,Serbia (e-mail: apljaskovic@np.ac.rs) , https://orcid.org/0000-0003-4312-3839

 ISBN 978-86-7466-930-3

dobijaju se rečenice koje imaju jedinstvenu logičku vrednost. Univerzalni kvantifikator (∀) se koristi da prikaže izraze koji su tačni za sve vrednosti terma. Sa druge strane, egzistencijalni kvantifikator se koristi da prikaže da postoji term za koji je tvrđenje tačno.

Predikatske rečenice se mogu podeliti prema kvantitetu na:

- Univerzalne - opisuju osobinu koju imaju svi pripadnici nekog skupa
- Partikularne - opisuju osobinu koju ima bar jedan element nekog skupa
- Singularne - opisuju osobinu jednog člana nekog skupa.

Predikatske rečenice po kvalitetu se dele na:

- afirmativne - opisuju da subjekat ima neku osobinu,
- negativne - opisuju da subjekat nema neku osobinu,
- limitativne - opisuju da subjekat ima neku osobinu opisanu negacijom.

Izdvojimo četiri tipa predikatskih iskaza koja su prikazana u logičkim kvadratu suprotnosti (Slika 1):

- $(\forall T)P(T)$ - univerzalno-afirmativni iskaz (A)
- $(\forall T)\neg P(T)$ - univerzalno-negativni iskaz (E)
- $(\exists T)P(T)$ - - partikularno-afirmativni iskaz (I)
- $(\exists T)\neg P(T)$- partikularno-negativan iskaz (O).

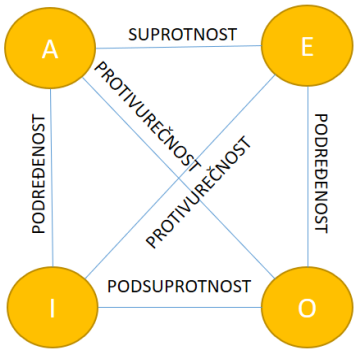


Slika 1. Logički kvadrat

Predikatske rečenice prikazane u logičkom kvadratu su povezane i ukoliko se zna istinitost jednog tipa može se zaključiti o istinitosti bar još jednog od ostala tri tipa [5].

Prikazani logički kvadrat je motivacija za kreiranje modela za transformaciju jednog predikatskog iskaza za koji je poznata logička vrednost u iskaz kome se može zaključiti tačna logička vrednost.

Može se uočiti povezanost između predikatske logike i prirodnog jezika i to: termi igraju ulogu sličnu onoj koju u prirodnom jeziku igraju imenice i zamenice, a predikati ulogu sličnu glagolima. Prirodni jezik je mnogo bogatiji i nisu dovoljno precizni. Problem prirodnog jezika je i u tome što se isti iskaz može izraziti na više načina.

## III. AUTOMATIZOVANO PRESLIKAVANJE PREDIKATSKIH ISKAZA NA SRPSKOM JEZIKU UNUTAR LOGIČKOG KVADRATA

Rečenice u srpskom jeziku mogu se podeliti na proste i složene [6]. Proste rečenice se mogu predstaviti pomoću dva tipa:

1. subjekta (S) i glagolskog predikata (GP)
2. subjekat (S), pomoćni glagol (PG) i imenski predikat (IP).

Prosta rečenica srpskog jezika može se povezati sa atomičnim predikatskim iskazom. Predikatska forma na prirodnom jeziku izražava se upotrebom veznika, negacije i kvantifikatora. U srpskom jeziku se negacija, veznici i kvantifikatori mogu javiti u različitim oblicima. U radu [7] prikazana je veza između predikatske logike i srpskog jezika, kao i pravila prelaza predikatskih formula izraženih na srpskom jeziku unutar logičkog kvadrata.

U ovom radu je dat algoritam za automatizaciju preslikavanja predikatskih iskaza na srpskom jeziku unutar logičkog kvadrata zasnovan na pravilima definisanim u [7]. Za ove potrebe napravljeni su rečnici sa različitim signalima negacije (**D** ) kao i rečnik sa potvrdnim (P_PG) i odričnim oblicima (O_PG) pomoćnih glagola (PG) "imam", „biti" i „hteti" pomoću kojih se može graditi negacija (**D PG**).

Formiran je takođe:

- **D** **P**-rečnik različitih termina kojima se izražava univerzalni kvantifikator u potvrdnom obliku (UKP);
- **D** -rečnik različitih termina kojima se izražava univerzalni kvantifikator u odričnom obliku (UKO);
- **D** -rečnik različitih termina kojima se izražava egzistencijalni kvantifikator UEK.

Kvantifikatori u srpskom jeziku se menjaju po licima, rodu i broju pa se ove informacije nalaze u odgovarajući rečnicima (L,R,B).

U partikularnim rečenicama uz neke kvantifikatore (na primer „postoji") se pojavljuje odnosna zamenica (OZ) iza subjekta pa je napravljen i rečnik odnosnih zamenica **D** sa odgovarajućim informacijama (L,R,B). Za neke oblike egzistencijalnog kvantifikatora se ne upotrebljava odnosna zamenica (na primer „neki"), stoga uz svaki egzistencijalni kvantifikator stoji i opis („tip") da li ide uz odnosnu zamenicu.

Dalje će biti prikazan algoritmi kojim se od iskaza A dobijaju drugi iskazi logičkog kvadrata. Dobijenim iskazima se može pridružiti i njihova logička vrednost (T-tačno , N-netačno, NaN-nepoznata logička vrednost).

Sva četiri tipa predikatskih iskaza u srpskom jeziku se mogu naći u jednom od dva tipa rečenica prethodno navedenih i to:

Univerzalno-afirmativni iskaz (iskaz_A)

- TIP1 - UKP+S+GP
- TIP2 - UKP+S+PG+IP

Univerzalno-negativni iskaz (iskaz_E)

- TIP1 - UKP+S+SN+GP
- TIP2 - UKO+S+O_PG+IP

Partikularno-afirmativni iskaz (iskaz_I)

- TIP1 - EK+S [+ OZ] +GP

 ISBN 978-86-7466-930-3

- TIP2 - EK+S [+OZ]+P_PG+IP

Partikularno-negativan iskaz (iskaz_O)

- TIP1 - EK+S [+ OZ] +SN +GP
- TIP2 - EK+S [+OZ]+O_PG+IP.

Algoritam 1 ( **P transformacija** ) vrši transformaciju univerzalnih iskaza (A i E) u partikularne (I i O). Inverzna funkcija (**P transformacija** ) može se slično predstaviti i ona vrši transformaciju partikularnih iskaza (I i O) u univerzalne iskaze (A i E).

**Algritam 1**: Preslikavanje univerzalnih iskaza u partikularne

```
Input  ($univerzalni_iskaz, $tip_rečenice,)
  utput:($niz_partikularnih_iskaza)
  P transformacija
    1. // Odrediti lice, rod i broj
    2. ($L,$R,$B)=          CT L,R,B            D_UKP
    3.                  W          UKP=$UKP)
    4. // Skup egzistencijalnih kvantifikatora
    5. $Skup_EK=            CT EK, TIP          D_EK
    6.                  W          (L,R,B)=( $L, $R, $B)
    7. for $EK, $tip in $Skup_EK do
    8.     $p_iskaz=$univerzalni_iskaz ( $UKP<-$EK )
    9.     if ($tip=”uz odnosnu zamenicu”)
    10.       /*Dodaje se odnosna zamenica u odgovarajućem
    11.        *licu , rodu i broju
    12.        *ako egzistencijalni kvatifikator zahteva
    13.        */
    14.       $SkupOZ=          CT OZ             D_OZ
                        W          (L,R,B)=( $L, $R, $B)
    15.       for $OZ in $SkupOZ do
    16.            $p_iskaz=$p_iskaz ( $S<-($S+$OZ))
    1 .       end for
    1 .    end if
    19.    $niz_partikularnih_iskaza += p_iskaz
    2 .  end for
    21.       T          $niz_partikularnih_iskaza
```

Algoritam 2 (**A transformacija** ) vrši transformaciju afirmativnih iskaza (A i I) u negativne (E i O). Inverzna funkcija ( **A transformacija** ) može se slično predstaviti i ona vrši transformaciju negativnih iskaza (E i O) u afirmativne (A i I).

**Alogritam 2**: Preslikavanje afirmativnih iskaza u negativne

```
   laz  ($afirmativni_iskaz, $tip_rečenice)
Izlaz:($niz_negativnih_iskaza)
A  transformacija

    1. /* TIP1:  iskaz_A($UKP+$S+$GP)
    2.  *          iskaz_I($EK+$S+$OZ+$GP)
    3.  * Dodavanje singala negacije negacije “ne”
    4.  */
    5. if ($tip_rečenice== TIP1)
    6.        $SN=“ne“
    7.        $n_iskaz=$afirmativni_iskaz ($GP<-$SN+$GP )
    8.        $niz_negativnih_iskaza += $n_iskaz
     . end  if
    10. /* TIP2:  iskaz_A($UKP+$S+$P_PG+$IP)
    11.  *          iskaz_I($EK+$S+$OZ+$P_PG+$IP)
    12.  *  Zamena potvrdnog pomoćnog glagola sa
    13.   * odričnim.
    14.   */
    15. if ($tip_rečenice== TIP2)
    16.    $O_PG=          CT O_PG             D_PG
    17.                W          P_PG=$P_PG
    18.    $n_iskaz=$afirmativni_iskaz ( $P_PG<-$O_PG )
    19.    /* Ako je kvantifikator univerzalni predstavlja se
    20.     * negativnim rečenicama odričnim
    21.     * kvantifikatorom
    22.     */
    23.    $kvantifikator= kvantifikator(n_iskaz)
    24.    If $kvantifikator in DUKP
    25.      // Odrediti lice, rod i broj
    26.      ($L,$R,$B)=          CT L,R,B            D_UKP
                        W          UKP=$kvantifikator
    27.      //Skup odričnih kvantifikatora
    28.      $Skup_UKO=          CT UKO              D_UKO
                        W          (L,R,B)=( $L, $R, $B)
    29.     for $UKO in $Skup_UKO do
    30.         $n_iskaz=$n_iskaz ( $UKP<-$UKO )
    31.         $niz_negativnih_iskaza += n_iskaz
     2.     end  for
      .    else
    34.      $niz_negativnih_iskaza += n_iskaz
    35.    end  if
    36. end  if
    37.      T          $niz_negativnih_iskaza
```

Očigledno je da kombinacijom datih transformacija možemo iz svakog tipa predikatske rečenice dobiti preostala tri, i to u više oblika u zavisnosti od oblika kvantifikatora koji se izabere.

## IV. MODEL ZA AUTOMATIZACIJU TESTOVA ZA PROVERU ZNANJA

Prirodni jezici nisu precizni pa predloženi model transformacije zavise od jasnoće ulaza. Većina tvrdnji može se uklopiti u jedan od tipova predikatskih rečenica i ukoliko je njena istinitost poznata može izvršiti transformaciju polazne tvrdnje u skup iskaza koji imaju istu ili suprotnu tačnost. Tabela 1 prikazuje ulazne parametre, primenjene transformacije i rezultat kada se na ulazu nađu iskazi tipa A i E. Slično se može odrediti i za iskaze tipa I i O za koje ukoliko su netačni možemo zaključiti istinitnosne vrednosti o ostala tri tipa predikatskih iskaza koje možemo dobiti odgovarajućim transformacijama ili ukoliko su tačni možemo ih transformisati u netačne iskaze tipa (E i A).

 ISBN 978-86-7466-930-3

TABELA I
OPIS MOGUĆEG TIPA ULAZA, PRIMENJENIH TRANSFORMACIJA I IZLAZA

| Tip ulaznog iskaza | Tačnost | Primenjene transformacije | Tip skupa izlaznih iskaza | |
|---|---|---|---|---|
| A | Tačno | AN | E | Netačno |
| A | Tačno | UP | I | Tačno |
| A | Tačno | AN+UP | O | Netačno |
| A | Netačno | AN+UP | O | Tačno |
| E | Tačno | NA | A | Netačno |
| E | Tačno | UP+NA | I | Netačno |
| E | Tačno | UP | O | Tačno |
| E | Netačno | UP+NA | I | Tačno |

Postoje dva slučaja koja se pri obradi testova znanja mogu tretirati:

1. postavljanje pitanja
2. provera ispravnosti odgovora.

Kod postavljanja pitanja popularna su zaokruživanja više tačnih odgovora tako da se dubina razumevanja materije može upravo proveriti postavljanjem istog odgovora u nekom od njegovih transformacija unutar logičkog kvadrata. Slika 2. prikazuje proces formiranja liste tvrdnji sa poznatom istinitnosnom vrednošću koje mogu da učestvuju u ispitnim pitanjima.

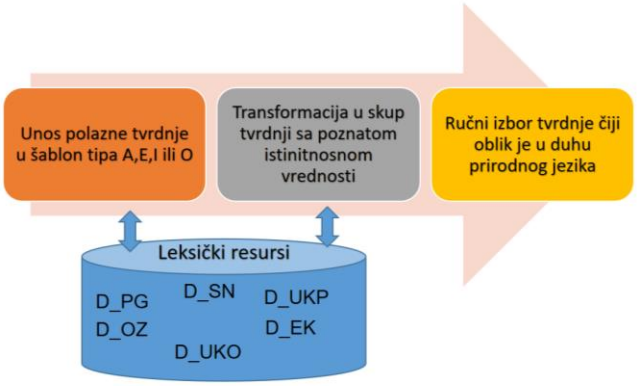


Slika 2. Proces dopune baze sa tvrdnjama za ispitivanje

Provera ispravnosti odgovora se najlakše rešava zaokruživanjem što je na osnovu poznatih istinitnosnih vrednosti procesom formiranja pitanja moguće. Ukoliko se ispitaniku dozvoli unos slobodnog odgovora u šablon tipa A, E,I ili O mora se proveriti ekvivalentnost odgovora sa datim ključem (tačnim odgovorom zadatim od strane ispitivača). Zbog postojanja različitih oblika za izražavanje iste stvari ovaj proces će biti malo teži. Ovde se mogu koristiti napravljeni leksički resursi kako bi se dobili različiti oblici kvantifikatora, simbola negacije, odnosnih zamenica čijom zamenom se neće promeniti odgovor već njegova forma. Takođe za neke dalje korake može se koristi WordNet za srpski jezik [8] za pretragu sinonima i za druge rečenične delove. Ispravan odgovor može biti dat i u nekoj od drugih predikatskih formi pa zato ukoliko se transformacijama može dobiti odgovor koji se poklapa sa ključem i pritom je tačan pa se može prihvatiti. Prikaz procesa pretrage dat je na Slici 3.

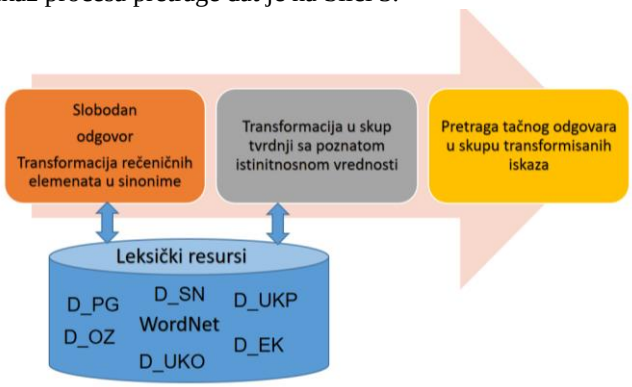


Slika 3. Proces provere da li dati odgovor ekvivalentan rešenju

Primenu predloženih algoritama demonstriraćemo na primeru transformacije tačnog iskaza “Svaki prirodan broj je pozitivan.”, koji se može ubaciti u šablon tipa A. Tabela 2 prikazuje rezultate primene različitih transformacija na ovaj polazni iskaz. Kao rezultat dobijaju se tačni iskazi tipa I kao što su na primer:

- Neki prirodan broj je pozitivan.
- Bar jedan prirodan broj je pozitivan.
- Postoji prirodan broj takav da je pozitivan.
- Postoji prirodan broj koji je pozitivan.

Primenom transformacije AN(+UP) dobijamo netačne iskaze tipa E i O kao što su:

- Svaki prirodan broj nije pozitivan.
- Neki prirodan broj nije pozitivan.
- Postoji prirodan broj takav da nije pozitivan.

TABELA II
PRIMER PRIMENE PRIKAZANOG ALGORITMA NA ISKAZ TIPA A

| REČENIČNI ČLAN | ULAZ | IZLAZ | | | |
|---|---|---|---|---|---|
| | | TRANSFORMACIJA | | | |
| | | AN | UP (BEZ OZ) | UP (SA OZ) | AN+UP |
| KVANTIFIKATOR | Svaki | Svaki | Neki, Bar jedan,… | Postoji, Postoji jedan,… | Neki, Postoji*, … |
| SUBJEKAT | prirodan broj | prirodan broj | | | |
| ODNOSNA ZAMENICA | | | | | |
| SIMBOL NEGACIJE | | | | takav da, koji | [takav da, koji]* |
| POMOĆNI GLAGOL | je | nije | je | je | nije |
| PREDIKAT | pozitivan. | pozitivan. | | | |
| LOGIČKA VREDNOST ISKAZA | T | N | T | T | N |


ISBN 978-86-7466-930-3

## IV. ZAKLJUČAK

U ovom radu je predstavljen sistem za automatizaciju testova za proveru znanja na srpskom jeziku baziran na transformaciji predikatskih iskaza. Predikatski iskazi iz logičkog kvadrata se predloženim transformacijama mogu preslikati jedni u druge. Ova osobina je primenjena na tvrdnje u testovima znanja koje se transformacijama mogu pretvoriti u druge oblike sa poznatom istinitnosnom vrednosti i kao takvi mogu se uključiti u testove. Doprinos ovog rada su i kreirani rečnici kvantifikatora u različitim oblicima pojavljivanja kao i metode za transformaciju. Sinonimi su jedan od velikih problema pri obradi prirodnog jezika. Primena obrade sinonima prilikom validacije slobodnih odgovora jeste jedan od sledećih puteva razvoja sistema. Primena De Morganovih pravila i drugih tautologija takođe može proširiti skup ekvivalentnih iskaza.

## ZAHVALNICA

Ovaj rad je delemično podržan od strane Ministarstva prosvete, nauke i tehnološkog razvoja Republike Srbije po projektu III44007.

## REFERENCES

[1] Chowdhury, G. G. (2003). Natural language processing. Annual review of information science and technology, 37(1), 51-89.
[2] Stanić, R. Kvantifikacija i negaciju u logici i hrvatskom jeziku, diplomski rad. 2014.
[3] Nebojša Ikodinović, Uvod u matematičku logiku, Beograd 2015
[4] Peters, S., & Westerståhl, D. (2006). Quantifiers in language and logic. OUP Oxford.
[5] Nermin Okačić, Tautologije i valjane formule kao principi zaključivanja, Prirodno matematički fakultet, Tuzla, 2015. godine.
[6] Ivan Klajn, Gramatika srpskog jezika, Zavod za udžbenike i nastavna sredstva, 2005.
[7] Marovac, U. Avdić, A. Čuljević, N. Metoda za obradu predikatskih iskaza na srpskom jeziku, Kopaonik, 2022.
[8] Krstev, C. Pavlović-Lažetić, G. and Obradović, I. "Using textual and lexical resources in developing serbian wordnet." *omanian ournal of Information Science and Technology* 7.1-2 (2004): 147-161.

## ABSTRACT

By processing natural language, we enable computers to establish communication with humans, to understand human language, but also to transform it and to address human in natural language. The problem of the truth value of statements uttered in natural language is difficult to determine due to the richness of vocabulary and ambiguity of meaning. By mapping the statements of natural language into the statements of predicate logic, it is possible to determine the relationships between different predicate statements as well as to perform the transformation from one form of appearance to another. One of the applications of this knowledge can be in the automated creation of knowledge tests.

**ystem for automation of nowledge verification tests based on transformation of predicate statements**

Ulfeta Marovac, Aldina Avdić

 ISBN 978-86-7466-930-3

# СПЕЦИЈАЛНА ТЕМАТСКА СЕСИЈА – ДИГИТАЛИЗАЦИЈА У НАУЦИ

# /

# SPECIAL THEMATIC SESSION – DIGITALISATION IN SCIENCE

# (СТС-ДЕ/STS-DI)

ISBN 978-86-7466-930-3

# Digitalizacija naučne građe – metode i rešenja

Zoran Zdravković

***Apstrakt* — Digitalizacija tehničke i naučne građe je prvi korak digitalizacije u nauci uopšte. Biblioteke, opšte i specijalizovane, su centralna mesta gde se nalazi postojeća naučna građa i prikuplja nova. U ovim ustanovama digitalizacija je uveliko otpočela i nalazi se u različitim fazama razvoja. U radu će biti analizirana iskustva, razmotrene metode i limiti digitalizacije i ponuđeni predlozi daljih aktivnosti i rešenja. Od posebnog interesa je digitalizacija građe iz domena tehničkih nauka zbog prisustva raznorodnih tipova dokumentacije: crteža, fotografija, planova, patenata, opisa pronalazaka, video materijala i druge građe.**

***Ključne reči* — digitalizacija naučne građe, biblioteke, digitalizacija tehničke dokumentacije**

## I. UVOD

## DEFINICIJA DIGITALIZACIJE - OSNOVNI POJMOVI

Analizom postojećih definicija koje na brojne načine pokušavaju da preciziraju fenomen digitlizacije, može se uočiti da termin digitalizacija obuhvata proces prevođenja informacije (podataka) iz originalno analognog oblika u digitalnu formu. Digitalizacija se može definisati kao proces prevođenja analognog u digitalni oblik, pri čemu izvor (analogni objekat) može biti veoma raznorodan: signal, zvuk, dokument, slika, trodimenzionalan objekat... a rezultat je digitalni objekat, odnosno digitalna forma: hologram, digitalna fotografija, digitalni zvuk, digitalni signal... visokog kvaliteta transformacije pri čemu se tokom procesa transformacije ne gube informacije. Najopštije, digitalizacija predstavlja beleženje analognog signala u digitalni oblik pri čemu se digitalizovana građa organizuje u digitalne kolekcije i može se pretraživati i koristiti od strane korisnika.

U digitalnom formatu informacije se organizuju u diskretne jedinice podataka – bitove, binarne podatke koje računari i drugi digitalni uređaji (npr. digitalna kamera ili digitalni slušni aparat) mogu procesuirati.

Digitalizacija obuhvata proces snimanja analognih signala i čuvanje rezultata u digitalnom obliku. Započinje senzorima, koji registruju analogne signale poput svetla i zvuka, potom pretvaranjem u njihove ekvivalentne digitalne forme upotrebom čipa za analogno/digitalnu konverziju. Proces funkcioniše pretvaranjem neprekidnog toka signala i analognih tipova podataka u diskontinuirane vrednosti, koje se potom uzorkuju (sempliraju) u redovnim jednakim vremenskim intervalima kako bi rezultirali digitalizovanim izlazom. Primer su audio datoteke (najčešće frekvencije od 44,1 do 192 kHz) pri čemu se audio datoteka frekvence 48.1 kHz uzorkuje 48.000 puta u sekundi. Proces digitalizacije je efikasniji i kvalitetniji ukoliko se vrši na višim nivoima uzorkovanja.

Tekst i slike digitalizuju se po sličnom principu: skener snima sliku ili „sliku“ teksta i pretvara u datoteku slika – *image file*, kao što je bitmap. Program optičkog prepoznavanja znakova (OCR) analizira svetle i tamne oblasti tekstualne površine kako bi identifikovao slovo ili numerik (cifru) i pretvara svaki takav karakter u ASCII kod.

Digitalizacija audio i video materijala obavlja se konverzijom analognog u digitalni signal, pri čemu se u ovom procesu konstantno varijabilan analogni signal transformiše bez gubitka i promene bitnog sadržaja, u višeslojni (digitalni) signal.

Digitalizacija informacija olakšava njihovo čuvanje, pristup, prezentaciju i deljenje. Originalan (analogni) istorijski dokument, muzejski eksponat, ili stari rukopis u biblioteci, tehnički crtež i drugi tip naučne građe može biti dostupan jedino posećivanjem njegove fizičke lokacije, što za posledicu ima visok stepen lokalizovanosti, dok digitalizacijom postaje dostupan ljudima širom sveta, uz nizak stepen lokalizovanosti i visok nivo demokratičnosti. Digitalizacija naučne i tehničke građe kao i naučno-istorijske baštine dobija na zamahu i doživljava trend porasta.

## II. KONCEPT ANALOGNO / DIGITALNO

Odnos analognog i digitalnog predstavljanja podataka (informacija i signala) može se definisati kroz određivanje pojmova i termina *analogni* i *digitalni* oblik informacije.

*Analogni oblik izvora* označava neprekidan signal iz okruženja: zvučni signal, svetlost, temperaturu, vlažost vazduha, pritisak, elektromagnetno zračenje i druge fizičke fenomene i informacije iz sveta oko nas.

*Digitalni oblik signala* je brojčane prirode – digitalne (od lat. Digitus: broj, cifra), predstavljen kontinualnim nizom nula i jedinica, binarno. Svaki digitalni podatak bez obzira na pojavni vid (tekst, slika, zvuk, animacija, film...) može se brojčano (digitalno) predstaviti celim brojevima dok se svaki pojedinačni broj može predstaviti nizom nula i jedinica, binarnim određivanjem prisustva (jedinica), odnosno odsustva (nula) signala od izvora informacija ka recipijentu.

Analogni mehanički fotoaparati, opremljeni analognom tehnologijom, koristili su analognu optiku da bi izvor svetlosti i refleksiju od fotografisanog objekta zabeležili kao sliku na fotografski film, a potom hemijske reakcije kako bi se film razvio i slika sa negativa prenela na fotografski papir. Digitalni fotoaparati koriste digitalnu tehnologiju da bi optikom, sa objetiva preneli sliku do CCD senzora (Charge-Coupled Device Sensors) sastavljenih od velikog broja fotoosetljivih elemenatapri čemu svaki mikroelement predstavlja jednu tačkicu slike (Pixel), čime se svetlost koja ulazi u objektiv, reflektovana sa fotografisanog objekta, pretvara u niz tačaka na određenoj površini, broj tačaka po inču (dpi – dots per

 ISBN 978-86-7466-930-3

inch) predstavljenih brojevima, digitalno, odnosno binarno, prikazujući prisustvo/odsustvo osvetljenja.

Analogne signale karakterišu kontinuirani podaci i informacije, celi i u neprekidnom nizu, prikazani blagim sinusoidama, pri čemu amplituda može imati bilo koju vrednost i blage prelaze od pika do pika graničnih vrednosti, uz konstantnu fluktuaciju vrednosti sa protokom vremena, dok digitalni signali nisu kontiuirani: karakterišu ih oštri „stepenici“ – skokoviti prelazi, jasno određene diskretne vrednosti, respektabilno jasno izraženi pikovi, pri čemu amplituda digitalnog signala može imati samo ograničeni broj vrednosti. Za razliku od analognog signala koji može imati bilo koju vrednost, digitalni signal može imati jedno od dva stanja prekidača: uključeno ili isključeno, uz binarnu mogućnost prisustva ili odsustva signala od izvora ka recipijentu (postoji ili ne postoji napajanje). Tako binarni kod u računarskoj primeni ima vrednost 0 ili 1; Morzeova azbuka sastavljena je od kombinacija dve veličine: tačke i crte (. i –).

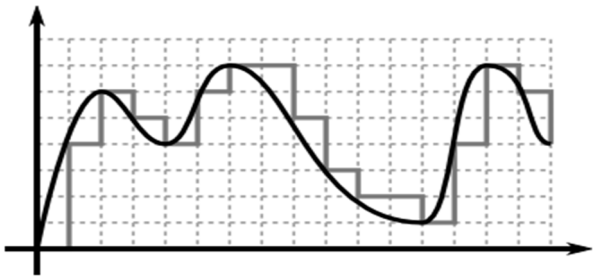

**Slika 1:** Uporedni prikaz analognog signala (puna crna linija sa varijabilnim kvantitativnim vrednostima po protoku vremena) i digitalnog signala (stepeničasta linija sa diskretnim, određenim vrednostima) [1]

Suštinska razlika između analognog i digitalnog leži i u postojanosti kvaliteta i prednosti digitalnog signala jer se njegov kvalitet ne gubi prenosom.

Konverzija analognog u digitalni signal praćena je gubicima. I pored razvoja digitalne tehnologije i postizanja sve veće preciznosti digitalnog signala, ostaju ograničenja tehnološkim mogućnostima očitavanja i zapisivanja, brzine prenosa, frekvencije centralne procesorske jedinice (CPU), brzine procesora, kompresije zapisa, memorijskim kapacitetom i drugim tehničkim limitima. Digitalna tehnologija je postigla visok nivo kvaliteta digitalnog zapisa i unapredila ga, da se ljudskim čulima, inače analognim, ne može primetiti razlika u kvalitetu i sadržaju digitalizovane verzije ostvarene digitalnom konverzijom analognog objekta ili signala.

Razvoj video-monitora i ekrana omogućio je unapređenje kvaliteta prikaza tehničke građe i porast rezolucije. Rezolucija kao mera razlučivosti grafičkog sadržaja, odnosno stepen vidljivosti detalja, izražava se u tačkama po inču (dpi), odnosno pikselima po inču (ppi). Veća rezolucija donosi bolji kvalitet slike/dokumenta ali i porast veličine digitalnog fajla i zahteva veći memorijski prostor potreban za smeštaj.

Digitalizacijom se pored fajlova visoke rezolucije (300-1.200 dpi) pri skeniranju materijala za master skenove koji se trajno čuvaju, kreiraju i snimaju i digitalne datoteke tipično niske rezolucije od 72 dpi (tzv. „ekranska rezolucija“), koje se koriste samo za pregled na ekranu, uz tzv. thumbnail prikaz „malih sličica“, i datoteke rezolucije od 300 dpi za kreiranje digitalnih objekata u procesima digitalizacije tekstualne građe, fotografija, karata, tehničkih crteža, planova i sl. sa ciljem optimalnog smeštaja, distribucije i korišćenja digitalizovane tehničke građe.

Iako je postignut visok nivo digitalne konverzije ona ipak nije savršena i potpuno jednaka analognoj stvarnosti. Kako je ljudsko oko u nemogućnosti da razlikuje dve susedne nijanse boje na ekranu monitora računari moćnih performansi sa naprednim grafičkim kartama prikazuju mnogo više boja nego što se ljudskim okom može registrovati koristeći 32-bitni i viši kvalitet boja. Uobičajene vrednosti dubine boja kreću se od 1 do 64 uz bitnu osobinu da sa porastom broja informacija eksponentno raste i broj boja, ali respektivno rastu i veličina datoteke, dužina vremena za učitavanje, iscrtavanje i štampanje, ali i kvalitet, izražajnost i vernost boja. Standard kvaliteta boja ekrana današnjih računara je 16, odnosno 32-bitna dubina boje, a preporučen parametar za snimanje pri digitalizaciji tekstualne građe, fotografija, karata, planova, tehničkih crteđa i slične tehničke građe je dubina boje 8-16 bita za sivu skalu (Gray Scale) i 24-48 bita za pun kolor.

Specifični su limiti analogne tehnologije. Oni ometaju proces komunikacije koga u slučaju jednosmernog komunikacionog kanala čine: izvor informacije (emiter) → medij prenosa podataka → prijemnik signala, informacije, tj. podataka. Faktori uticaja na komunikacioni kanal mogu biti 1) spoljni činioci: „informacioni šum“ ili „buka“ koji remete prenos signala, odnosno analogni prenos informacija, i 2) udaljenost izvora i recipijenta kada kvalitet signala i prenosa informacije opada sa udaljenošću.

Nedostaci digitalnog slanja, obrade i prijema signala potiču iz realnog okruženja koje je po prirodni analogno, ali osnovni nedostaci digitalne konverzije su:

1. potreba stalnog kodiranja i dekodiranja kako bi se informacija poslala, odnosno primila, moguća u dva smera konverzije: A/D konverzija (kodiranje analogne u digitalnu informaciju) D/A konverzija (dekodiranje digitalnog u analogni podatak, signal ili informaciju);

2. duže vreme potrebno za slanje digitalnog signala;

3. porast količine podataka u procesu digitalizacije radi izrade i postizanja kvaliteta digitalnog objekta (gustina, odnosno visoka rezolucija slike ili video zapisa, kvalitet audio zapisa i sl. – primer: istovetan audio zapis na LP gramofonskoj ploči u analognoj formi očitavan iglom staje na spiralu dugu 500 m, dok je spirala CD-a duga 6 km, uz neophodan laser kako bi se očitao audio zapis.

Kompresija s gubitkom (engl. Lossy Compression) je tehnologija sažimanja analognih podataka i kreiranje digitalnih podataka s prihvatljivim gubicima u odnosu na analogni izvor. Obuhvata tehnike kompresije podataka kod kojih se gubi prihvatljiva količina podataka pri čemu se eliminišu suvišne, redundantne ili nepotrebne informacije. Najrasprostranjenija primena i upotreba je kod audio, video i multimedijalnih datoteka (JPG i TIFF su najpoznatiji formati za digitalne fotografije, MP3 i OGG za audio fajlove, a MPEG za video-snimke). Preporučeni formati za

 ISBN 978-86-7466-930-3

digitalizaciju fotografija su nekompresovan TIFF, kompresovan JPEG bez gubitka informacija i PDF format.[2]

TIFF (eng. Tagged Image File Format) nekompresovan format idealan je za smeštaj arhivskih datoteka i operisanje sa tekstualnim dokumentima i fotografijama s tim što je veličina TIFF datoteke znatno veća (ili najveća) u odnosu na druge formate.

JPEG format (eng. Joint Photographic Experts Group Format) kao vrsta kompresovane datoteke idealno je rešenje za smeštaj kopija dokumenata i za smeštaj, transport i korišćenje dokumenata i fotografija na vebu. Veličina datoteke u JPG formatu znatno je manja od one u TIFF formatu. Kompresijom se dobija datoteka manjeg kvaliteta, ali značajno manje veličine i zauzima mnogo manje memorijskog prostora od originala (JPG fotografija tako nastala može biti manja i za više od 80% originala bez (ili sa malo) vidljivog efekta dok kompresovani MP3 fajl može biti jedna desetina veličine originalne audio datoteke uz neprimetnu razliku zvuka ljudskom uhu) što ovaj metod kvalifikuje idealnim za multimedijalni sadržaj, ali isto tako i nemogućim za binarne datoteke, kod kojih ne sme doći do gubitka informacija, kada se primenjuje kompresija bez gubitka i kreiraju tzv. fajlovi bez gubitaka.

Odnos kvaliteta i veličine datoteka, odnosno kompromis umanjenja podataka originala uz balans kvaliteta, od izuzetnog značaja je za skladištenje, prenos i korišćenje sadržaja. Dobro dizajnirana tehnologija kompresije uz gubitke značajno smanjuje veličine datoteka do mere da se degradacija ne uočava. Kompromis između veličine i kvaliteta datoteke ostaje značajna stavka procesa digitalizacije naučne i tehničke građe.

Kompresija bez gubitka (engl. Lossless Compression) obuhvata tehnologiju komprimovanja digitalnih podataka kojom se mogu povratiti sve informacije originalnog sadržaja kako je izgledao pre kompresije. Kompresija podataka bez gubitaka je reverzibilna kompresija podataka jer ne degradirajući podatke, svaki bit informacije koji je izvorno bio u datoteci ostaje i nakon kompresije, a sve informacije mogu u potpunosti biti obnovljene nakon raspakivanja i dekompresije, što kod kompresije sa gubitkom nije moguće.

Ova tehnika kompresije preporučuje se i koristi kao dobar izbor za digitalizaciju tekstualnih i tabelarnih datoteka, računskih podataka, ali i kod naučnih članaka i većih tekstualnih formi (tehnička literatura, udžbenici, tehničke enciklopedije, naučni radovi, disertacije, patenti, standardi, smernice, uputstva i prateća dokumentacija) gde gubitak pojedinih delova, reči ili cifara, i grafičkih podataka može predstavljati problem. GIF digitalni format slika (engl. Graphics Interchange File) koristi se na Vebu kao grafički interfejs za digitalnu kompresiju bez gubitaka. Standardni format podataka kompresije bez gubitaka su „loosless“ fajlovi, poput datoteka FLAC kodek formata , audio formata sličnog MP3 formatu samo bez gubitaka. Ovaj tip formata je najpodobniji za digitalizaciju zvuka, jer je audio kompresovan u FLAC bez gubitka kvaliteta.

Najbitnija prednost digitalnog prenosa signala leži u mogućnosti prenosa svakog mogućeg pojavnog vida informacije obuhvatajući tekst, informaciju o boji, zvuk, animaciju, video signal itd. Za razliku od analognog signala koji je po svojoj prirodi podložan ometanju, informacionom šumu i smetnjama, digitalni podatak je postojan. Svaki, pa i bilo kakav, jednom digitalizovani podatak može se čuvati, smestiti, prenositi i koristiti istovetnog stepena kvaliteta, upravo procesima kodiranja i dekodiranja (faks uređaji prenosili su tekst i grafički sadržaj između dva telefona; računarski mrežni modem omogućavao je digitalnu MOdulaciju i DEModulaciju po principu kodiranja i dekodiranja svih pobrojanih vidova informacija između dva udaljena računara, konverzijom digitalnog signala iz računara u analogni koji može biti prenet na velike daljine postojećim analognim instalacijama, najčešće telefonskim vezama).

Motivi i razlozi za uvođenje digitalizacije između ostalih leže i u prednosti digitalizovanih podataka koji imaju mogućnost popravljanja i oporavka narušenog ili oštećenog signala, time što se može ponovo poslati i sklopiti na odredištu dopunom nedostajućih delova informacije i restaurirati.

## III. ČUVANJE I BEZBEDAN PRISTUP DIGITALIZOVANIM SADRŽAJIMA

Digitalna biblioteka naučne građe

Korisnici digitalnih biblioteka

Nivoi pristupa korisnika i billing system

## IV. ZAKLJUČNA RAZMATRANJA

Iako je digitalizacija u poodmaklom stadijumu još nije kasno da se uvede minimum opštih zahteva i zajedničkih kriterijuma koji bi bili poštovani u daljem toku procesa digitalizacije u nauci.

**10 ključnih globalnih trendova u digitalnoj transformaciji danas [3] :**

1. Internet of Things (IoT)

Procena je da se na internetu danas nalazi oko 8.4 miliarde takozvanih „Things(Stvari)'' i da će do 2020. dostići broj od 30 miliardi. Ali IoT nisu samo stvari na internetu, već na koji način ih koristimo, povezujemo i analiziramo. Pametne kuće i zdravstvo su oblasti koje na najbolji način demonstriraju značaj i primenu IoT-a. Dalji napredak u ovoj oblasti je neminovan, ali dinamika rasta će u mnogome zavisiti i od IoT sigurnosti i ograničavanja rizika koji se javljaju u primeni. IoT je danas ključni digitalni trend, koji je u osnovi sledeća 3 globalna trenda i biće njihov katalizator u budućnosti.

2. Analitika – Big Data

Ogromna količina informacija kreirana kroz IoT postaje snaga promena koje iz korena menjaju sve, od proizvodnje do zdravstva, čak i načina funkcionisanja gradova, omogućavajući im da povećaju svoju efikasnost i profitabilnost. Primera radi, veliki špediterska preduzeća sa flotom od preko 100.000 vozila su uspela da cenu po milji smanje sa 15 centi na 3 centa (http://www.information-age.com/big-data-analytics-fuelling-iot-revolution-123464081/).
Slični rezultati se postižu i očekuju u drugim oblastima poslovanja. Tehnološki giganti poput Microsofta, IBM-a i SAP-a nastavljaju da ulažu ogromna sredstva u razvoj u analitike, a posebno u IoT analitiku.

3. Edge Computing

Ovaj trend postepeno preuzima primat od Cloud Computing-a, a na to nam ukazuju planovi i investicije najznačajnijih kompanija poput Cisco-a i HPE-a. Obrada podataka u real-time postaje sve važnija sa

 ISBN 978-86-7466-930-3

drastičnim povećanjem podataka koje proizvodi rastući IoT. Pametni dronovi, autonomna vozila i AI rukovođene pametne sprave zahtevaju trenutno povezivanje i komunikaciju kroz IoT, što prevazilazi mogućnosti Cloud Computing-a. Ipak, u narednom periodu Cloud neće biti zamenjen u mnogim oblastima i još uvek će biti opravdana opcija u većini procesa.

4. 5G
Pod pritisko narastajućeg broja podataka kroz rast IoT, mobilni provajderi se sve brže kreću ka uvođenju 5G. Ovaj prelazak na 5G se neće desiti preko noći. Proizvođači poput Sony-a i Samsunga su uvođenjem Gigabit LTE tehnologije napravili prvi korak ka punoj implementacij 5G. Do 2025. godine 5G mreža će pokriti trećinu svetske populacije i omogućiti istinsku digitalizaciju svih oblasti poslovanja i života.

5. Blockchain
Iako je ova tehnologija najpoznatija po svojoj primeni u kriptovalutama i najčešće spominjana kao alat u finansijskom sektoru, primena blockchain-a postaje sve šira. Zdravstvena industrija i industrija zabave su samo neke od oblasti koje se priključuju u korišćenju ove tehnologije, a očekivanja su da će do 2020. godine 20% svetske finansijske trgovine odvijati na ovoj platformi.

6. Artificial Intelegence(AI)
Sposobnost mašina da imitiraju intelegentno ljudsko ponašanje je klasična definicija AI-a. Očekivanja u budućnosti su da transport, proizvodnja i druge oblasti života postanu automatizovane uz pomoć AI-a. Danas se u poslovanju sve više kompanija oslanja na podršku AI-a u marketingu, analitici, odnosu sa korisnicima i robotici. Ključne softverske kompanije već uveliko integrišu AI u svoje platforme. Ubrzavanje, kao i jeftinija i pametnija automatizacija procesa imaju primenu od e-mailova, kreiranja sadržaja do industrijske proizvodnje.

7. Virtual(VR) i Augmented Reality(AR)
Iako se tržišno još uvek nisu približili očekivanjima, rano ih je otpisati sa spiska ključnih trendova. AR u profesionalnom kontekstu pokazuje bolje rezultate, pre svega zbog jeftinije i jednostavnije primene. Mogućnosti u marketingu, edukaciji i dizajniranju novih proizvoda još uvek prednost daju AR-u u odnosu na VR. Naravno, komercijalna primena u globalno najlukrativnijoj kreativnoj industriji video igara u narednim godinama daće konačnu reč.

8. Upravljanje glasom
Značaj upravljanja i pretraživanja glasom je rezultat velikog napretka u analitici i hardverskim rešenjima. Ovo se nije dogodilo preko noći i napretkom u ovoj oblasti ostvaruje se novi nivo interackcije sa digitalnim platformama, kao i korisničkog iskustva. Pametne kuće i digitalni asistenti su samo neki od primera. Napredak u ovoj oblasti pre svega počiva na napretku tehnologije prepoznavanja glasa i veštačke inteligencije.

9. Failure-as-a-Service ili Učenje na greškama
Neuspeh postaje sam po sebi nova usluga, a učenje na greškama postaje alat u brzom prilagodjavanju digitalnim uslovima poslovanja. Brzi neuspeh pomaže efikasnom prilagođavanju novom poslovnom okruženju, pre svega pri izradi prototipova novih proizvoda. Prepoznavanje grešaka i njihovo brzo ispravljanje postaju esencijalni deo uspešne digitalne transformacije, kao i inovativnog pristupa kreiranju novi proizvoda i usluga. Zato je ovaj koncept nasao svoje mesto među novim trendovima u 2018. godini (https://www.forbes.com/sites/danielnewman/2017/09/26/top-10-trends-for-digital-transformation-in-2018/#365d0553293a) .

10. Digitalna transformacija kao preduslov opstanka
Kako raste broj novih tehnologija koje se uvode, raste I brzina potreba za promenama. Kompanije koje su ih prihvatile, uz sva ograničenja sa kojima se suočavaju, stiču tržišnu prednost I povećavaju svoje šanse za uspeh ili makar opstanak na tržištu. Promena poslovne kulture u kompanijama uvek je predstavljala jedno od najvećih ograničenja za rast, a sa dolaskom digitalne transformacije, uvođenje nove poslovne kulture postaje jedna od ključnih prepreka. Kompanije koje su u stanju da se uspešno I brzo prilagode novonastalim okolnostima imaju šansu za opstanak I uspeh na tržištu. Ne zaboravljajte – poslovna kultura nije samo kako ostali vide vaš biznis, već I kako ga individue unutar organizacije doživljavaju.

## LITERATURA


[1] *Analog Signal*, URL: http://www.chegg.com/homework-help/definitions/analog-signal-4 (12.3.2022.)

[2] *Смернице за дигитализацију културног наслеђа у Републици Србији,* Министарство културе и информисања Републике Србије, 2017, стр. 18, URL: http://www.kultura.gov.rs/docs/dokumenti/propisi-iz-oblasti-kulture/smernice-za-digitalizaciju-kulturnog-nasledja-u-republici-srbiji.pdf (12.3.2022.)

[3] „*10 svetskih trendova u digitalizaciji*", https://cdt.org.rs/index.php/2018/08/08/10-svetskih-trendova-u-digitalizaciji/, (21.3.2022.)



## ABSTRACT

Digitization of technical and scientific material is the first step of digitalization in science in general. Libraries, general and specialized, are central places where existing scientific material is located and new ones are collected. In these institutions, digitalization has largely begun and is in various stages of development. The paper will analyze experiences, consider methods and limits of digitalization and offer suggestions for further activities and solutions. Of special interest is the digitization of material from the domain of technical sciences due to the presence of various types of documentation: drawings, photographs, plans, patents, descriptions of inventions, videos and other materials.



Key words - digitization of scientific materials; libraries; digitization of technical documentation


## Digitization of scientific material - methods and solutions


Zoran Zdravković


 ISBN 978-86-7466-930-3

# Jedinica za snimanje podataka u ispitivanju vanrednih železničkih događaja

Sanja Jevtić, Marija Vukšić Popović, Nada Ratković Kovačević, Sonja Ketin

***A stra t*— ( uridical ecording nit – jedinica za snimanje *ra n* podata a) je ao sistem za snimanje na vozilu odgovoran za sa upljanje podata a, a ujedno je obavezni element opreme na savremenom vozilu. tandarni principi i procedure u ispitivanju sleda događaja u situcijama koje se na železnici nazivaju vanrednim događajima će sa ovim uređajem dobiti drugu perspe tivu.**

***Ključne reči*—Juridical recording unit; vanredni događaj, sistem jedinstvenog vremena**

## I. UVOD

Vanrednim događajima na železnici se smatraju udesi u kojima je jedno ili više lica poginulo ili teže povređeno, u kome je nastala znatna materijalna šteta i u kome je nastao veći prekid u železničkom saobraćaju, ili nezgoda u kojoj je jedno ili više lica lakše povređeno, nastala manja materijala šteta, kraći prekid železničkog saobraćaja, nastalo ugrožavanje, ili otežano odvijanje železničkog saobraćaja. [1,2]. Izraz vanredni događaj se odomaćio na železnici iako su više puta menjani važeći pravilnici koji se bave ovom tematikom [3,4]. Ovi događaji se evidentiraju i statistički prate i objavljuju po vrstama, uzrocima, mestu nastanka i posledicama.

Rekonstrukcije pruga i čitavih sistema nameću skok u tehnološkim rešenjima. Digitalizacijom svih procesa železničkog saobraćaja postižu se znatno veće brzine, što zahteva i dodatne prateće sisteme, koji će brinuti ne samo o bezbednosti i sigurnosti, već i o arhiviranju ključnih podataka u slučaju spornih situacija.

## II. ETCS SISTEM I UREĐAJ ZA SNIMANJE NA VOZILU

ETCS (European Train Control System – Evropski sistem kontrole vozova) sistem podrazumeva da se na samom vozilu sve akcije koje preduzima oprema i mašinovođa dešavaju u okvirima trenutnog nivoa rada kao i režima rada. Nivo rada podrazumeva nivo opreme duž pruge i na vozilu, čime se postavljaju okviri za funkcionisanje sistema. Režim rada podrazumeva dinamičnu podelu odgovornosti za rad između opreme i mašinovođe i vezan je za fleksibilno prilagođavanje potrebama saobraćaja, npr režimi FS (Full Supervision – Puna odgovornost), LS (Limited Supervision – Ograničena odgovornonost), SH (Shunting – Manevrisanje), UN (Unfitted – Neopremljenost), OS (On Sight – Vožnja po viđenju), TR (Trip – Put kočenja, bezbednosno kočenje)[5].

Kao što se može pretpostaviti iz navedenih režima rada mašinovođa u neke od režima može ući samo pod određenim uslovima i uz jasne potvrde sa pruge, čime se jasno zna i usaglašava podela odgovornosti za određene akcije u režimu rada između mašinovođe i opreme.

Velike brzine, mnoštvo akcija i oštri uslovi rada na železnici, zahtevaju uređaj koji će nedvosmisleno obezbeđivati podatke o toku događaja i kauzalnosti u spornim situacijama.

Principi rada JRU definisani su dokumentima tipa FIS (Functional Interface Specification – funkcionalne specifikacije interfejsa), u okviru TSI (Technical Specification of Interoperability – Tehničke specifikacije interoperabilnosti). ETCS oprema je deo većeg Sistema ERTMS/ETCS (European Railway Train Management System – Evropski sistem upravljanja železničkim saobraćajem) oprema na vozilu će detektovati pojavu specifičnih događaja čime će se poslati odgovarajuća poruka uređaju za snimanje na vozilu. Ono što će se tom prilikom zabeležiti podrazumeva: datum i vreme pojave događaja, koristeći UTC (Universal Time Co-ordinated – univerzalni vremenski standard – u kom se svaka vremenska zona definiše svojim pomerajem od ovog vremena) zapis, pozicija voza i brzina prilikom pojave događaja, kao i verziju operativnog sistema, nivo rada i režim rada opreme u trenutku pojave događaja [6]. Vreme i datum će učestvovati u formiranju takozvanog vremenskog pečata date poruke koja se šalje preko interfejsa JRU (za manje od 5s nakon događaja). Ukoliko se nekoliko događaja šalje u vezi sa istim okidačkim događajem, enkapsulirani podaci će biti konzistentni jedni sa drugima u vezi sa vremenskim pečatom. Spisak svih poruka koje se šalju JRU dat je u [7], kao i spisak svih okidačkih događaja (imaju istu strukturu sa zajedničkim zaglavljem i setom promenljivih u zavisnosti od poruke).

JRU snima sve informacije koje se prosleđuju ka/od EVC (European Vital Computer – Evropski vitalni računar ili kernel), kao i interakcije između mašinovođe i sistema preko DMI (Driver Machine Interface – Interfejs mašinovođa-

Sanja Jevtić – Akademija tehničko-umetničkih strukovnih studija, Beograd ATUSS, Odsek Visoka železnička Zdravka Čelara 14, 11000 Beograd, Srbija (e-mail: sanja.jevtic@vzs.edu.rs , jevtic.sanja@gmail.com ).

Marija Vukšić Popović – Akademija tehničko-umetničkih strukovnih studija Beograd, ATUSS, Odsek Visoka železnička Zdravka Čelara 14, 11000 Beograd, Srbija (e-mail: marija.vuksic.popovic@vzs.edu.rs ).

Nada Ratković Kovačević – Akademija tehničkih strukovnih studija Beograd, ATSSB, Odsek Kompjutersko-mašinsko inženjerstvo, Bul. Zorana Đinđića 152a, 11 070 Novi Beograd, (e-mail: nadaratkovickovacevic@gmail.com ).

Sonja Ketin – Visoka brodarska škola akademskih studija Beograd, VBŠ, Srbija, Bul. Vojvode Putnika 7, 11000 Beograd, (e-mail: ketin.sonja@gmail.com).

 ISBN 978-86-7466-930-3

mašina). Ipak, sve što se prezentuje mašinovođi na DMI-u je u lokalnom vremenu. Sam JRU uređaj je obavezan ali nije deo ERTSM/ETCS opreme na vozilu [7] – Sl.1 prikazuje deo ETCS opreme na vozilu i drugu opremu.

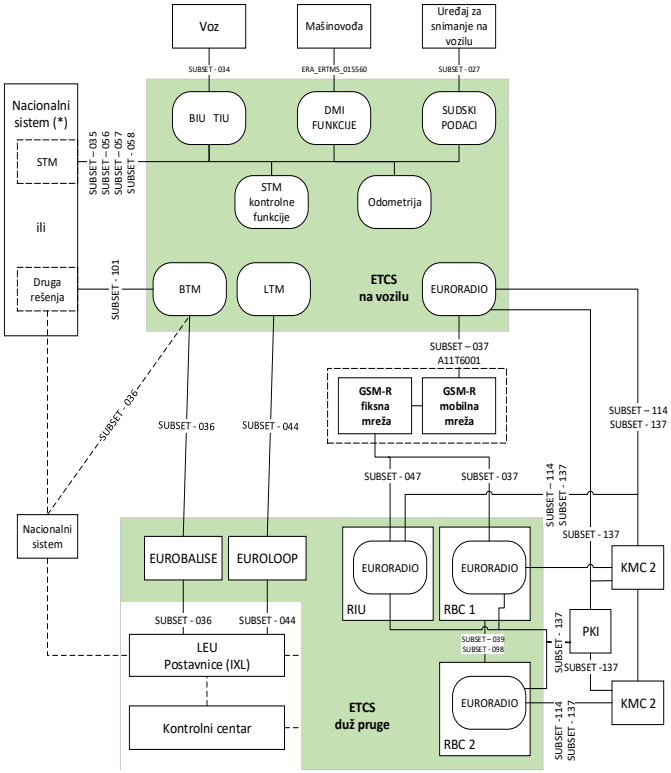


Sl. 1. ETCS oprema na vozilu i duž pruge, uključujući i JRU, gde je JRU prikazan kao uređaj koji je obavezan, ali nije deo ETCS opreme (uređaj za snimanje na vozilu). Ka njemu je referentnim dokumentom (subset-027) definisan samo interfejs i podaci koji se njime prenose. Slika daje i presek svih subset dokumenata koja definišu slične interfejse [5,7]

Sam JRU sadrži i interfejs za preuzimanje snimljenih materijala pomoću DT alatke (*downloading tool*). Informacije se prenose od EVC-a, bez promene. JRU snima svoje podatke na privremeni memorijski uređaj i to tako da je taj uređaj u stanju da snimi minimalno operacije u okviru 24 h. JRU mora biti u stanju da snimi redukovani skup podataka za najmanje poslednjih osam dana. Vreme za koje je JRU u mogućnosti da zadrži podatke je najmanje sedam dana (misli se na vreme bez napajanja). Privremeni memorijski uređaj je moguće lako izvaditi iz sklopa, kako bi se omogućio prenos podataka nakon akcidenata [7-9].

## III. SIGNALNO-SIGURNOSNI SISTEMI

Nesreće i nezgode [3] na železnici su u velikoj meri u korelaciji sa radom signalno-sigurnosnih uređaja i sistema (sudari, iskliznuća, nesreće na putnim prelazima, požari, izbegnuti sudari, pogrešno pokazivanje signalnih znakova, prolazak pored signalnog znaka koji zabranjuje dalju vožnju,..). Iz ovoga se vidi da nije samo JRU uređaj koji će beležiti određene situacije. Sl. 2 prikazuje neke od sistema od interesa za ovaj rad koji će imati svoje logove (evidenciju događaja/statusa/alarma i sl. sa vremenskim pečatima). ETCS kao sistem se svrstava u ATP/ATC sisteme (Automatic train protection/Automatic train control – sistemi za automatsku zaštitu i kontrolu voza). IXL (interlocking) predstavlja sistem elektronskih postavnica, koji ne pripada ETCS-u, ali je sa njim spregnut. RBC (Radio Block Center – radio blok centar) je obavezni deo sistema ETCS nivoa 2, sa kojim je vozilo u pokretu u konstantnoj vezi, preko GSM-R (GSM for Railway – GSM sistem za železnice).

Svi sistemi na slici će imati i vezu sa intranet mrežom na železnici od koje će dobijati i signal tačnog vremena. Ovaj signal će se iz jedne ili nekoliko tačaka (rezervne lokacije) sa prijemnikom tačnog vremena (GPS – Global positioning system – sistem globalnog pozicioniranja, koji sadrži i tačno vreme) prosleđivati svim računarskim sistemima na zemlji. Svi logovi svih sistema će imati isto vreme u svojim vremenskim pečatima.

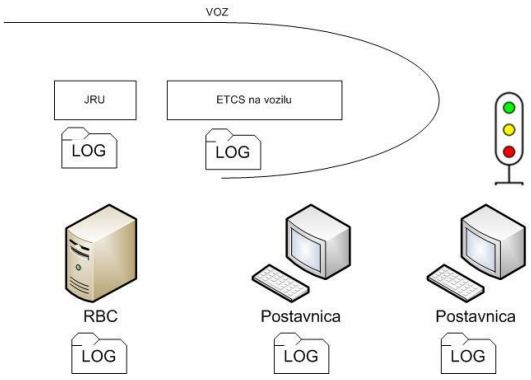


Sl. 2. Prikaz zapisa različitih podsistema u ETCS-u nivoa 2 i van njega.

Ukratko – svi sistemi koji učestvuju u formiranju puta vožnje, njegovom osiguranju i praćenju ostaviće neki oblik traga u ovim logovima. Uz vremenske pečate i činjenicu da sve akcije signalno-sigurnosnih sistema ostavljaju trag u obliku logova će istraživanje vanrednih događaja učiniti lakšim.

## IV. JRU KAO CRNA KUTIJA

JRU se u vozilu sa ostalim elementima povezuje nekom od standardnih bus konfiguracija, od kojih su najčešće: PROFIBUS (Process Field BUS), CAN (Controller Area Network) ili MVB (Multifunctional Vehicle Bus) bus konfiguracija (Sl.3), ali i Ethernet u nekim slučajevima. STM (Specific Transmission Module – element koji dozvoljava povezivanje sa nacionalnim sistemima klase B na vozilu), će takođe biti povezan u sistem (Sl.1).

Neki od relevantnih standarda čije se ispunjenje zahteva za ovu opremu su EN 50155, IEEE 1482.1. Prvi definiše mehaničke i aspekte okruženja, dok je drugi u vezi sa ojačanjem memorijskih modula u uslovima oštećenja, kao i bezbednosne aspekte.

Iz prethodnog se vidi da je još u postupku dizajna i razvoja setovan put ka tome da JRU ima ulogu black box-a (crne kutije) na železničkim vozilima (slični principi, uređaji i standardi se koriste kako u vodenom, vazdušnom, tako i u

 ISBN 978-86-7466-930-3

drumskom saobraćaju).

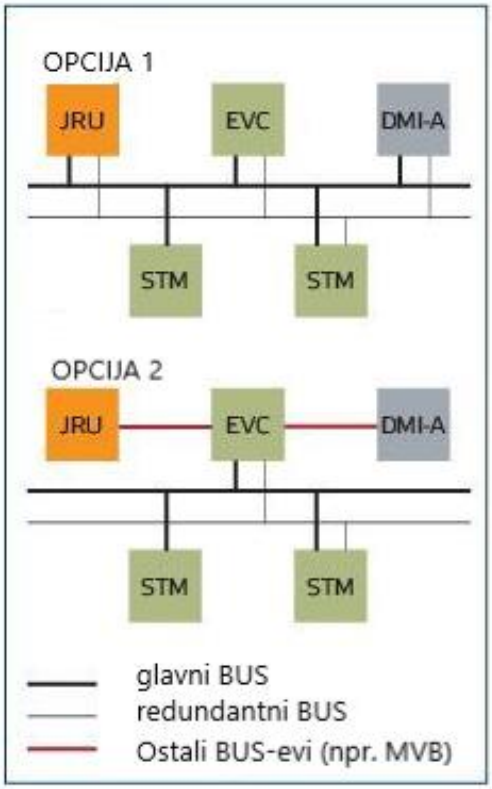


Sl. 3. Primeri bus konfiguracija na vozilu [8].

Kako je njegov rad i čuvanje podataka siguran proces, ostaje samo da se u svakodnevnom radu prepoznaju situacije u kojima je dvomislenost neizbežna. Jedan od primera je i rad na ETCS nivou 1 u kom se zahteva da mašinovođa prati i signalizaciju duž pruge, a ne samo kabinsku (Sl.4).

U ovom primeru pod a) je data situacija u kojoj se stanje sa signala replicira preko LEU (Lineside Electronic Unit – Pružna elektronska jedinica) ili b) kada postoje dve nezavisne linije (jedna do signala, a druga do LEU i evrobalize). Telegram koji formira LEU je isti signalni kriterijum sa pružnog signala, koji se zatim preko evrobalize prosleđuje vozilu u pokretu. Kabinska signalizacija može u ovim slučajevima dati kriterijume različite od onih duž pruge, a u slučaju da je propisano da mašinovođa prati i pružnu signalizaciju dvosmislenost je neizbežna.

Osim ovoga može se uočiti i primer u kom brojači osovina (BO) pokazuju da je prostorni odsek prazan, ali ne mogu da detektuju postojanje prepreke na pruzi ili objekta koji zadire u slobodan profil pruge (Sl.5). U ovakvim slučajevima će se mašinovođa u skladu sa svojim ovlašćenjima i trenutnim režimom rada prebaciti u onaj režim koji zahteva situacija, imaće niz akcija koje će ostati zabeležene, a radi veće kontrole moraće da operiše u režimima koji mu daju veće mogućnosti, ali i odgovornost. Ovo se može shvatiti kao predupređivanje dvosmislenih situacija jer je ovakav slučaj već pokriven operativnim pravilima.

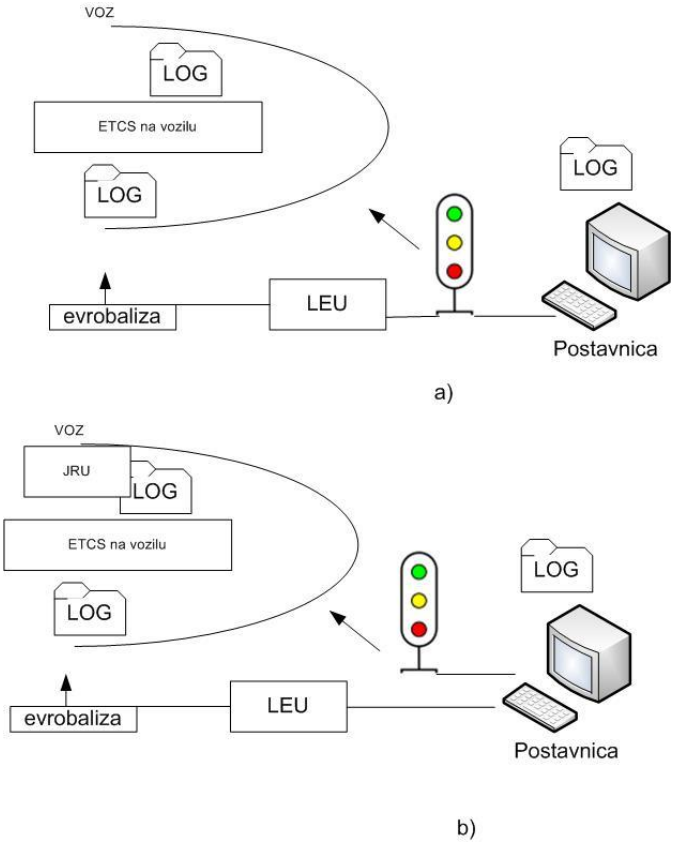


Sl. 4. Situacije u realizaciji signalizacije na ETCS nivou 1, koje potencijalno mogu dovesti do različitih zapisa u logovima uređaja.

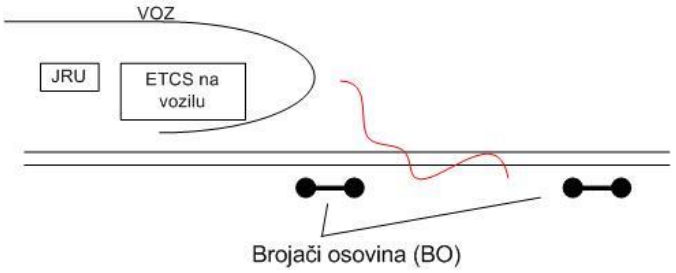


Sl.5. Situacija u kojoj oprema duž pruge ne registruje opasnost, ali mašinovođa ima mogućnost da se prilagodi novonastaloj situaciji.

## V. ZAKLJUČAK

JRU će značajno uticati na proceduru isleđivanja i ispitivanja procesa koji su prethodili vanrednim događajima. Specijalno će uticati na razumevanje sleda akcija i interakcija mašinovođa-mašina u aktivnoj kabini. Sistem jedinstvenog vremena u intranet mreži će umnogome raslojiti otkaze uređaja kao i greške usled ljudskog faktora. Podela odgovornosti između mašinovođe i mašine u svakom od ETCS režima rada, operativna pravila, procedure i regulativa koja će tek biti formirana u narednom periodu, će sigurno naići i na određene prepreke.

Možda na prvi pogled izgleda da je sve u vezi sa JRU pozitivno, međutim sam uređaj i njegovo korišćenje će biti dotaknuto i takozvanim otvorenim pitanjima. Neka od njih su i tehnička i operativna ekspertiza, kao i važeća regulativa koja


ISBN 978-86-7466-930-3

se sporo menja.

Upavljanje resursima svakog preduzeća podrazumeva i konstantno ažuriranje tehnologija rada. Kao i kod svakog sistema i ovde će se u eksploataciji naći situacije koje se mogu smatrati dvosmislenim. Napredak u tehničkom smislu će uticati i na ustaljene procedure.

## LITERATURA

[1] Sl.list SRJ, 76/99, Pravilnik o načinu eivdentiranja podataka o vanrednim događajima nastalim u železničkom saobraćaju i o drugim podacima od značaja za bezbednost železničkog saobraćaja.
[2] Sl.glasnik RS 41/2018, Zakon o bezbednosti u železničkom saobraćaju,
[3] SL.Glasnik RS 41/18, Direkcija za železnice, Pravilnik o prijavljivanju, istraživanju, evidentiranju, statističkom praćenju i objavljivanju podataka o nesrećama i nezgodama.
[4] Sl.glasnik RS 66/2015, Zakon o istraživanju nesreća u vazdušnom, železničkom i vodnom saobraćaju.
[5] ERA, Unisig, EEIG ERTMS Users Group, *System e uirements Specification Subset-02 1-* , issue 3.4.0, 2014-05-12.
[6] Recommendation ITU-R TF.460-6, Standard frequency and time-signal emissions, 02/2002
[7] ERA, Unisig, EEIG ERTMS Users Group, *FIS uridical ecording Subset-02* , issue 3.3.0, 2016-05-13.
[8] EKE, Juridical Recording Unit, web: https://www.eke-electronics.com/juridical-recording-unit-jru , published 2017-03-02
[9] Unisig, Safety Requirements for the Technical Interoperability of ETCS in Levels 1&2, Subset – 091, issue 3.4.0, 2015-12-01.

## ABSTRACT

JRU (Juridical Recording Unit) is as a system for data recording on vehicle, responsible for collection of data, and at the same time it is a mandatory element of the contemporary on-board equipment. Standard principles and procedures in sequence of events investigation in railway knowna as extraordinary events will with this device gain a different perspective.

**uridical ecording nit in ailway vent Investigation**

Sanja Jevtić, Marija Vukšić Popović, Nada Ratković Kovačević, Sonja Ketin

 ISBN 978-86-7466-930-3

# Merenje digitalizacije i IKT sektora – parametri i metode kvantifikacije razvoja društva

Zoran Zdravković

***A stra t* — Digitalizacija ao sveobuhvatan i sveprisutan fenomen zabeležen je u s oro svim oblastima savremenog društva. To om poslednje dve decenije digitalizacija se na on otpočinjanja i progresivnog razvoja nalazi u različitim fazama realizacije u brojnim institucijama iz različitih sfera. U radu će biti sagledan značaj i uticaj informaciono- omuni acionih tehnologija i digitalizacije na sveukupan razvoj društva. Biće razmotrene mogućnosti vantifi acije roz analizu parametara i metoda merenja digitalizacije. U radu će biti predstavljeni *Inde s d ta ac e* u procesu vantifi acije digitalizacije, *Inde s I T ra en st* ao mera stepena razvoja informacionog društva, i drugi parametri ojim bi se mogao meriti razvoj ekonomije i društva. Zaključak će dati osvrt na digitalne agende, a cione planove i strategije digitalizacije u daljem razvoju informacionog društva.**

***Ključne reči* — digitalizacija; merenje digitalizacije; Inde s digitalizacije; Inde s I T razvijenosti**

## I. UVOD

Uticaj informaciono-komunikacionih tehnologija (IKT) na društvo je toliki da u znatnoj meri određuje tokove i transformiše ekonomske i društvene aktivnosti savremenog društva. Informacione tehnologije značajno su sredstvo koje omogućava i pospešuje kapacitete za razvoj društva. Način, intenzitet i upotreba informacionih tehnologija određuju nivo razvoja društva i uz inovacije bazirane na znanju pozitivno utiču na unapređenje društva, podizanje društvenog standarda, modernizaciju i opšti napredak društva.

Značaj primene savremenih informacionih tehnologija kao ključnog faktora razvoja društva nameće potrebu kvantifikacije uticaja informacionih i komunikacionih tehnologija na društvo. Stepen napretka društva može se meriti *Indeksom IKT razvijenosti* koji je razvila Međunarodna telekomunikaciona unija, i kompozitnim *Indeksom digitali acije* (Digitization Index) – konceptom koji je prihvaćen za meru nivoa digitalizovanosti zemalja, razvijenim u Booz&Company konsultantskoj kući.

### INDEKS IKT RAZVIJENOSTI

Indeks IKT razvijenosti – IDI (ICT Development Index) razvila je Međunarodna telekomunikaciona unija (ITU, International Telecommunication Union), specijalizovana agencija Ujedinjenih nacija za informacione i komunikacione tehnologije u Ženevi, sa ciljem praćenja napretka razvoja i primene informacionih i komunikacionih tehnologija kako u zemljama u razvoju tako i u ekonomski razvijenim zemljama. Druga moguća primena IKT indeksa je sagledavanje i merenje globalnog digitalnog jaza i razvojnog potencijala koje zemlje imaju korišćenjem informacionih i komunikacionih tehnologija. IKT indeks je koristan i značajan alat za vrednovanje, poređenje, evaluaciju i benčmarking najvažnijih pokazatelja za merenje informacionog društva. Standardni je alat koji vlade, operateri, razvojne agencije, istraživači i institucije mogu koristiti za merenje digitalnog jaza i upoređivanje IKT performansi unutar jedne, ali i unakrsno između više zemalja, jer i pored pozitivnog trenda da informaciono-komunikacione tehnologije postaju sve više dostupne i standard u društvu, i dalje postoji izražen informacioni i digitalni jaz među zemljama u razvoju i ekonomsko-tehnološki razvijenih zemalja.

Indeks razvoja IKT je kompozitni indeks: sačinjen je od 11 indikatora ukombinovanih u jedinstvenu referentnu meru koja služi u svrhe praćenja i poređenja razvoja informaciono-komunikacionih tehnologija. Indeks IKT temelji se na sistemu od 11 pokazatelja svrstanih u tri podsistema:

1. Podsistem pristupa (obuhvata pet indikatora koji se odnose na infrastrukturu i pristup),

2. Podsistem korišćenja (sačinjen od tri indikatora koji se odnose na intenzitet upotrebe IKT), i

3. Podsistem veština (tri indidkatora koji se odnose na bazične pokazatelje o nivou sposobnosti i veština za ovladavanje IKT). [1]

Razvijen od strane članica Međunarodne unije za telekomunikacije 2008. godine indeks razvoja IKT prvi put je predstavljen 2009. godine u Izveštaju merenja informacionog društva (Measuring the Information Society Report) za više od 160 ekonomija u svetu, u izdanju ITU, i od tada se redovno godišnje objavljuje. Izveštaj merenja informacionog društva od 2015. godine prikazuje nivo IKT razvoja u 167 privreda u svetu, poredi napredak i ističe zemlje koje su a) najbrže, b) najdinamičnije i c) najviše, ili d) ukupno, poboljšali svoju poziciju na rang listi od 2010. godine, uz prikaz i analizu korišćenja fiksne i mobilne telefonske mreže i širokopojasne Internet mreže, kao i najnovije događaje u sferi Internet stvari (IoT, Internet of Things).

Prema izveštaju merenja stanja i napretka informacionog društva prvih pet zemalja koje imaju najviši nivo ili su najviše napredovale su: Republika Južna Koreja, Danska, Island, Ujedinjeno kraljevstvo i Švedska. [2]

Korišćenjem indeksa razvoja informaciono-komunikacionih tehnologija utvrđen je i stepen razvoja društva po kome 2015. godine Kineski Hong Kong, Norveška i Japan zauzimaju od devetog do jedanaestog mesta, dok Srbija zauzima pedesetprvo mesto, nalazeći se ispod Slovenije (koja je na 33. mestu) i Hrvatske (na 42. mestu), a iznad Makedonije (60. mesto), Crne Gore (65. mesto) i Bosne i Hercegovine koja zauzima 77. mesto.

 ISBN 978-86-7466-930-3

## I D DIGITA I ACI

Merenje razvijenosti informaciono-komunikacionih tehnologija pojedine zemlje i uticaj na društvo mogu se odrediti i posredno predstaviti Indeksom digitalizacije. Indeks digitalizovanosti (Digitization Index) razvila je kompanija „Strategy&“ (ranije „Booz&Company“) kao kompozitni indeks koji se sastoji od 23 indikatora prikazanih u Tabeli 1. [3]

**Tabela1**: Lista indikatora i izvora Indeksa digitalizacije [4]

| I DI AT | I |
|---|---|
| Tarifa za fiksne telefonske linije | ITU |
| Tarifa za priključenje fiksne telefonske linije | ITU |
| Tarifa za mobilni pripejd | ITU |
| Tarifa za mobilni pripejd priključak | ITU |
| Tarifa za fiksni širokopojasni pristup Internetu | ITU |
| Investicije po telekom preplatniku (mobilni, širokiopojasni i fiksni priključak) | Svetska banka |
| Penetracija fiksnih širokopojasnih priključaka | ITU |
| Penetracija mobilne telefonije | ITU |
| Stanovništvo pokriveno mrežom mobilne telefonije | ITU |
| Procenat populacije koja koristi PC računar | ITU |
| 3G Penetracija | WirelessIntelligence |
| Međunarodni internet protok (bitova u sekundi / internet korisnik) | ITU |
| Širokopojasne brzine (% iznad 2 Mbps) | Akamai |
| Internet maloprodaja (procenat Internet maloprodaje od ukupne malopprodaje) | Euromonitor |
| E-uprava, indeks spremnosti za e-upravu | UN |
| Procenat pojedinačnih korisnika Interneta | ITU |
| Prosečan prihod po korisniku bežičnih mreža | WirelessIntelligence |
| Broj jedinstvenih poseta društvenih mreža na Internetu po stanovniku | Internet World Stats |
| Upotreba SMS-a (prosečan broja SMS-ova po korisniku) | WirelessIntelligence |
| Inženjeri (procenat od ukupnog stanovništva) | Svetska banka |
| Kvalifikovanost radne snage (procentualni udeo radne snage sa višim obrazovanjem od srednjoškolskog, od ukupne, u ukupnoj radnoj snazi) | Svetska banka |

Indeks se od 2004. godine upotrebljava kao prihvaćena mera nivoa digitalizovanosti zemalja, obuhvataući 150 država. Zemlje su podeljene prema nivou digitalizovanosti u četiri grupe, pri čemu vrednost indeksa digitalizacije može biti u rasponu 0-100 na skali, pri čemu je vrednost 100 maksimalna vrednost indeksa digitalizacije. Prema rasponu vrednosti indeksa digitalizacije (0-25, 25-30, 30-40 i 40-100) ekonomije države se mogu grupisati na sledeći način:

1. Nerazvijene ekonomije (indeks digitalizacije <25): Avganistan, Alžir, Angola, Aruba, Bangladeš, Belize, Bolivija, ..., Vijetnam, Zambija.

2. Ekonomije u razvoju, sa indeksom digitalizacije 25-30: Albanija, Antigva i Barbuda, Jermenija, Azerbejdžan, Bosna i Hercegovina, Bocvana, Brazil, Kostarika, Ekvador, ..., Makedonija, Trinidad i Tobago, Venecuela.

3. Ekonomije u tranziciji sa indeksom digitalizacije 30-40 su Argentina, Bahrein, Barbados, Bugarska, Čile, Kolumbija, Hrvatska, Kipar, Estonija, Iran, Jordan, Letonija, Makao, Malezija, Malta, Mauricijus, Meksiko, …, Crna Gora, Oman, Filipini, Srbija, Sejšeli, Turska, Ukrajina, Urugvaj.

4. Razvijene ekonomije (indeks digitalizacije >40): Australija, Austrija, Belgija, Češka, Danska, Finska, Francuska, Nemačka, Grčka, Hongkong, Mađarska, Island, Irska, Izrael, Italija, Japan, Južna Koreja, Kanada, Litvanija, Holandija, Novi Zeland, Norveška, Poljska, Portugalija, Rumunija, Rusija, SAD, Singapur, Slovačka, Slovenija, Španija, Švedska, Švajcarska, Tajvan, Ujedinjeni Arapski Emirati, Velika Britanija i dr.

## II. TA KVANTITATIVNE T D I PA A T I A DIGITA I ACI I I ACI - KOMUNIKACIONI T GI A

Razvoj IT sektora i digitalizacije u korelaciji je sa stepenom razvijenosti društva. Jedan od merljivih pokazatelja razvijenosti društva je **finansijs o ulaganje u IT sector po stanovni u**. U Srbiji ulaganje u IT industriju iznosi 62 evra po stanovniku, što je u rangu Rumunije i Bugarske; u Hrvatskoj ulaganje u IT iznosi 200 evra po stanovniku, dok je prosek ulaganja Evropske unije u IT 800 evra po glavi stanovnika. [5]

**erenje digitalizacije** može se pratiti kvantitativnim metodama I indirektno, praćenjem i analizom statističkih vrednosti merljivih pokazatelja digitalizacije, počev od trenutnog stanja i baznih vrednosti, preko referentnih, do ciljanih vrednosti zacrtanih planovima i strategijama.

Kvantitativni parametri digitalizacije i upotrebe informaciono-komunikacionih tehnologija mogu biti merljive, odnosno sledeće izmerene vrednosti:

- **roj, cifra**: broj digitalno pismenih građana, broj institucija koje obavljaju obuku i unapređenje digitalne pismenosti, broj visokoškolskih programa iz oblasti digitalizacije, broj institucija koje nude visokoškolske programe IKT oblasti, broj studenata upisanih na programe digitalizacije, broj diplomiranih, specijalista, mastera ili doktoranada iz oblasti digitalizacije i informaciono-komunikacionih tehnologija…;

- **Procentualna vrednost** – procenat digitalno opismenjenih građana, pojedinih grupa ili određene populacije stanovništva, npr: 2018. godine u Republici Srbiji je 51% lica starosti od 15 i više godina kompjuterski nepismeno, odnosno 34,2% lica kompjuterski pismeno, dok je 14,8% delimično kompjuterski pismeno;

- **dnos**, tj. racio određenih parametara: npr. zastupljenost tehničkih uređaja prema broju korisnika računara, broj digitalnih prenosivih uređaja u domaćinstvu u odnosu na celokupnu populaciju;


ISBN 978-86-7466-930-3

- **reme, interval** – npr. vreme provedeno na digitalnim platformama ili aplikacijama državne uprave (u minutima ili satima po danu);

- **tanje** – upotreba elektronskih servisa, stanje e-trgovine ili e-uprave i sl. kroz broj pruženih ili upotrebljenih digitalnih usluga, broj korisnika usluga, broj pružalaca usluga i sl. (izraženo brojčano ili procentualno); kao i

- **Trend** (porast ili opadanje) određenih parametara (izražen u procentualnom iznosu) na osnovu ranije izmerenog stanja i projektovanog, odnosno ostvarenog stanja, npr: razvoj digitalnih veština, unapređenje IKT i digitalnih kompetenecija ili porast korišćenja širokopojasnog pristupa kroz broj domaćinstava, broj institucija i preduzeća sa širokopojasnim Internet priključkom i sl.

Praćenje promena i statistika vrednosti navedenih parametara dobar su **osnov za vantitativno merenje stepena digitalizacije društva i upotrebe informaciono- omuni acionih tehnologija**, počev od pojedinaca i domaćinstava, preko sektora privrede, do nivoa celokupne ekonomije društva u zadatom srednjoročnom (trogodišnji) ili dugoročnom (desetogodišnjem) periodu.

## III. ZAKLJUČAK I DALJA RAZMATRANJA

### DIGITALNE AGENDE, AKCIONI PLANOVI I STRATEGIJE DIGITA I ACI DA A INFORMACIONOG DRUŠTVA

Uloga i značaj digitalizacije i savremenih informaciono-komunikacionih tehnologija prepoznati su kao značajni faktori u razvoju društva, ekonomiji, privredi, kulturi i obrazovanju, procesima državne uprave i drugim društvenim sferama. Stoga se kroz donošenje inicijativa u digitalnoj sferi, usvajanje smernica, akcionih planova i strategija razvoja informacionog društva pristupa budućem uređenju digitalnog društva sa ciljem napretka i razvoja celokupnog društva. Dugoročnim planiranjem, poput ciljeva Strategije „ **vropa 2 2** “ predviđa se mogućnost stvaranja novih radnih mesta i unapređenje životnih uslova uz ostvarivanje pametnog, održivog i inkluzivnog rasta i održive budućnosti u Evropi.

Evropska komisija predložila je pet merljivih ciljeva Evropske unije planiranih za 2020. godinu, kao osnovu za utvrđivanje nacionalnih ciljeva i pravac kojim Evropska unija teži da se krene – proces održivog rasta i postizanje društvenog uspeha, u sledećim domenima:

- zapošljavanje;
- istraživanje i inovacije;
- klimatske promene i energetika;
- obrazovanje;
- borba protiv siromaštva.

U okviru Evropske unije IKT i digitalizacija su prepoznati kao činioci od značaja za ekonomski, društveni rast i inovativnost kao generatora razvoja društva.[6] Evropska komisija predložila je sedam ključnih inicijativa sa ciljem podsticanja napretka svake prioritetne oblasti:

1. „Uniju inovacija“
2. Inicijativu „Mladi u pokretu“
3. **„Digitalna agendu za Evropu“**
4. „Evropa koja efikasno koristi resurse“
5. „Industrijska politika za eru globalizacije“
6. „Agenda za nove veštine i nova radna mesta“
7. „Evropska platforma za borbu protiv siromaštva“.

Poseban značaj među sedam vodećih inicijativa ekonomske strategije „Evropa 2020“ ima *igitalna agenda a E ropu*, kao ključna inicijativa, čime se ukazuje na značaj koji digitalizacija i informaciono-komunikacione tehnologije imaju u razvoju savremene ekonomije. Poseban akcenat stavlja se na razvoj širokopojasnog pristupa Internetu činjenicom da velike brzine širokopojasnog pristupa omogućavaju građanima i preduzećima bržu komunikaciju i efikasniju proizvodnju. Evropska komisija usaglasila je svoj dugoročni plan za razvoj informaciono-komunikacionih tehnologija u periodu od 2010. do 2020. godine:

1) da sva domaćinstva u Evropskoj uniji do 2020. godine dobiju mogućnost pristupa Internetu brzinom 30 Mb/s,

2) da najmanje polovina stanovnika Evrope može da koristi brzinu 100 Mb/s,

3) finansiranje izgradnje zajedničke optičke mreže i podsticanje država članica, privatnog sektora i javnih preduzeća da izgrade sopstvene mreže koje bi se na nju nadovezale. [6]

Metod kvantifikacije se može primeniti i pri **merenju rasta bruto društvenog prihoda u korelaciji sa ulaganjem u IKT se tor**. Prema istraživanjima međunarodne Organizacije za ekonomsku saradanju i razvoj (OECD) porast ulaganja u oblast elektronskih komunikacija od 8% omogućava rast bruto društvenog proizvoda od 1%, a na osnovu istraživanja Svetske banke povećanjem penetracije širokopojasnih priključaka za 10% obezbeđuje se rast bruto društvenog proizvoda od 1,38% u zemljama u razvoju, odnosno 1,21% u razvijenom zemljama. [7]

IKT sektor je direktno zaslužan za 5% bruto nacionalnog prihoda (BNP) u Evropi, uz znatni doprinos rastu produktivnosti (20% dolazi direktno iz sektora IKT a 30% iz investicija u IKT) usled visoke dinamičnosti i inovativnosti ovog sektora kao i promeni načina poslovanja u drugim sektorima koju donosi. [7]

Pored međunarodnih i regionalnih strategija poput strategije Evropa 2020, pojedine zemlje i na nacionalnom nivou donose sopstvene smernice, digitalne agende i strategije razvoja digitalnog društva. Primer nacionalnih i regionalnih inicijativa država sa dobrom EU praksom su: Francuski digitalni plan iz 2010. godine, Širokopojasna strategija u Nemačkoj (Deutschland Digital 2015), grčki FTTH program javno-privatnog partnerstva, Program Digital Britain iz 2012. godine na teritoriji Velike Britanije i Plan vlade italijanske oblasti Trentino.

U nacionalnim okvirima u Republici Srbiji organizaciono su definisane nadležnosti i aktivnosti u procesima digitalizacije kulturnog nasleđa. U okviru Ministarstva kulture i informisanja određeni su sektori zaduženi za sprovođenje definisanih nadležnosti. Sektor za digitalizaciju kulturnog nasleđa i savremenog stvaralaštva Ministarstva kulture i informisanja Republike Srbije obavlja „ ... koordinaciono-organizacione, razvojne i tehnološko-operativne aktivnosti koje za cilj imaju izradu nacionalne strategije i planova digitalizacije, definisanje tehnoloških, pravnih i organizacionih okvira za izgradnju digitalne istraživačke infrastrukture; koordinaciju sa međunarodnim organizacijama i institucijama kao i koordinaciju na nacionalnom nivou svih učesnika u ovom procesu sa ciljem izgradnje digitalne istraživačke infrastrukture, koja kao izrazito važnu ima komponentu zaštite kulturnog nasleđa u nadležnosti Vlade Republike Srbije uz sprovođenje vertikalne, horizontalne i međunarodne koordinacije ukupnih aktivnosti na izgradnji digitalne istraživačke infrastrukture“ [8].

**acionalna digitalna agenda epubli e rbije** sistemski i planski određuje pravce i ciljeve digitalizacije u svim sferama

 ISBN 978-86-7466-930-3

društva i definisana je planovima i strateškim dokumentima obuhvaćenih sledećim **nacionalnim strategijama**:

- Strategija razvoja kulture Republike Srbije 2020-2029. godine sa Akcionim planom
- Predlog Strategije razvoja kulture Republike Srbije 2017-2027. godine
- Strategija razvoja elektronskih komunikacija u Republici Srbiji 2010-2020. godine
- Strategija razvoja širokopojasnog pristupa u Republici Srbiji do 2012. godine
- Strategija razvoja veštačke inteligencije u Republici Srbiji za period 2020-2025. godine
- Strategija razvoja industrije informacionih tehnologija za period 2017-2020. godine
- Strategija razvoja širokopojasnih mreža i servisa u Republici Srbiji do 2016. godine
- Strategija razvoja elektronskih komunikacija u Republici Srbiji 2010-2020. godine
- Strategija razvoja informacionog društva u Republici Srbiji do 2020. godine
- Strategija razvoja kulture Republike Srbije 2017-2027. godine
- Strategija naučnog i tehnološkog razvoja Republike Srbije u periodu 2010-2015. godine.

Informaciono društvo sagledano je i u **a cionim planovima lo alnih samouprava** u Srbiji kojim se definiše digitalizacija u bitnim društvenim sferama poput:

- elektronskih komunikacija
- e-Uprave
- e-Zdravstva
- e-Pravosuđa
- informaciono-komunikacionih tehnologija u obrazovanju, nauci i kulturi
- elektronske trgovine
- poslovnog sektora IKT i
- informacione bezbednosti.

## LITERATURA


[1] Katz, R. L. and Koutroumpis, P., *„Measuring digiti ation A growth and welfare multiplier“*, Technovation, Volume 33, Issues 10-11, October-November 2013, pp 314-319, (2013), http://www.teleadvs.com/wp-content/uploads/Technovation_RK_PK.pdf

[2] *Measuring the Information Society eport 2015*, International Telecommunication Union, Place des Nations, Geneva, Switzerland, URL: https://www.itu.int/dms_pub/itu-d/opb/ind/D-IND-ICTOI-2015-SUM-PDF-E.pdf

[3] Katz, R. L., *sing a igiti ation Inde to measure the Economic and Social Impact of igital Agendas*, p. 7, http://www.eurocpr.org/data/2013/Katz.pdf

[4] Stankić R., *Merenje ekonomskog i društvenog uticaja informaciono-komunikacioinih tehnologija*, http://w3.ekof.bg.ac.rs/upload/1119INF-2013-Merenje%20IKT%20razvijen.pdf

[5] *IT sektor, u poljopri redu, naj eći neto i o nik Srbije*, https://www.danas.rs/ekonomija/it-sektor-uz-poljoprivredu-najveci-neto-izvoznik-srbije/

[6] COM(2010) 2020 final, *Europe 2020 A Strategy for Smart, Sustainable and Inclusi e Growth*, URL: https://eur-lex.europa.eu/LexUriServ/LexUriServ.do?uri=COM:2010:2020:FIN:EN:PDF

[7] Stankić R., Stankić M., „*Merenje ekonomskog i društvenog uticaja informaciono-komunikacionih tehnologija*“, Нови економист, бр. 14, стр. 70

[8] *Сектор за дигитализацију културног наслеђа и савременог стваралаштва*, URL: http://www.kultura.gov.rs/cyr/razvoj-digitalne-istrazivacke-infrastrukture-u-oblasti-kulture-i-umetnosti/o_sektoru



## ABSTRACT

Digitization as a comprehensive and ubiquitous phenomenon is present in almost all areas of modern society. During the last two decades, after its beginning and progressive development, digitalization is in the phase of realization in numerous institutions and areas. The paper will consider the importance and impact of information and communication technologies and digitization on the overall development of society. The possibilities of quantification through the analysis of parameters and methods of digitization measurement will be considered. The paper will present the Digitization Index in the process of quantification of digitization, the ICT Development Index as a measure of the degree of development of the information society, and other parameters that could measure the development of the economy and society. The conclusion will provide an overview of digital agendas, action plans and digitization strategies in the further development of the information society.


Keywords - digitization; digitization measurement; Digitization index; ICT Development Index

**Digitization and the ICT sector measuring – society development parameters and quantification methods**

Zoran Zdravković

 ISBN 978-86-7466-930-3

# Neki savremeni aspekti upotrebe luminescentnih efekata

Milanka Pećanac [1,2], Bećko Kasalica [1]

**Apstra t – Možda će merenja veoma slabe luminescencije ljudske kože u budućnosti premostiti jaz između tradicionalne istočne i konvencionalne zapadne medicine. Za sada, merenja luminescencije i istraživanja u toj oblasti, potvrđuju vezu između bioloških ritmova i emisije elektromagnetnog zračenja živih jedinki. Danas se mnogo literature o luminescenciji, sa frazom „potencijalne primene'', treba da origuje u „postojeće primene'', jer je luminescencija učvrstila svoje mesto u mnogim primenama od medicine, metrologije, heritologije, forenzi e. Može se govoriti o sintezi materijla, razvoju uređaja i metoda koji će lumineiscentne efe te bolje i potpunije opisati valitativno i vantitativno, učiniti jasnijim i informativnijim. Razvoj aparatura znači razvoj svakog od glavnih podsistema, od eksitacije do detekcije. Posebno je važan podsistem obrade, gde se obrađuju formirani signali i uključuje određeni namens i pisani program za dobijanje rezultata u sredinama, gde je potreban samo podatak o određenoj veličini, oju dobijamo metodom primene luminescentne tehni e. Određivanje prisustva nekih materija može zahtevati merenja sa velikom osetljivošću (tragovi telesnih tečnosti, amino iselina u otis u prsta, e splozivnih materija). setljivost dete cije može se postići različitim načinima transformacije energije korištenjem luminescentnih tehni a, uz druge tretmane. umineiscentni efe ti jedinjenja lantanida (terbijum, europijum, itrijum i dr.), mogu se pojačati kombinovanjem sa ligandima koji te efekte promovišu. Materijali sa retkim zemljama, zbog jedinstvenih optičkih osobina, interesantni su i u oblasti zaštite. I tu se radi na prahovima, bojama, rastvorima, a o bi se dobili produkti čiji se luminescentni profili teško oponašaju. Karakteristična vremena luminescentnih efekata su različita (vreme reakcije, rela sacije, i dr.) i zavise od vrste pobude, pa informacije oje se tako dobijaju imaju višestruka značenja, na osnovu ojih se, iz jedne serije merenja, uz pogodan razvoj ele trons e podrške, može istovremeno meriti i situacija sa složenim skupom elektromagnetskog, nuklearnog zračenja. Ti efekti su posebno važni jer se omogućuje i kvalitativna i kvantitativna analiza elemenata u tragovima. uminescencija ima svoju istoriju, te mnogo poznatih rezultata potiče iz starijih generacija mernih sistema, što direktno dovodi do potrebe za digitalizacijom u cilju mogućnosti njihove upotrebe u proširenju baze podataka za automats o brzo pretraživanje.**

**Ključne reči - luminescentni efe ti, forenzi a, dete cija materija, retke zemlje, pojačanje efekata.**

## I. UVOD

Praćenje dinamike raznih procesa u mikrosvetu je vezano za transformaciju raznih vrsta energije, koje poseduju mikročestice u najširem smislu, polazeći od atomske, molekularne strukture ili od ulaženja u atom i zahvatanja drugih teorijskih modela, koji opisuju procese u jezgru. Postoje različite podele spektroskopija prema ciljnoj sredini koja se proučava, analizira, poredi; merne tehnike nose sopstvene formalizme, a često se i u oblasti jedne spektroskopije pojavljuju različite notacije. Drugi prilaz mernih tehnika bi bio vezan za izabrane snopove, koji potiču od definisanih izvora: elektrona, jona, fotona iz različitih delova elektromagnetnog spektra, od radiotalasa / mikrotalasa, do X i γ-zračenja. S obzirom na odnose energija *mikročestica*, koje čine snop, za testiranje i impulse, postoji mnogo opisa procesa kojima će različite sredine da reaguju i prema odnosu karakterističnih veličina (parametara merenja) može da se vidi u kom području su procesi rasejanja (Rayleigh, Brillouin, Raman), apsorpcije, refleksije ili luminescentne prirode. Detaljnim praćenjem vremenskih opisa procesa i karakteristikama raznih vremenskih konstanti (vremena relaksacije i dr.) *mikročestica* mete, kojoj ulazni snop menja energetska stanja (pobuđuje) prelaskom na više nivoe, vremenom su materijali dobijali razne kategorije i imena sa kratkim ili dugim zadržavanjima u novim stanjima. Savremeni trend i nagomilana iskustva istraživanja su dovela do novih konstatacija, da su ,,klasične" spektroskopije dobile *takmace* kroz kategoriju nelinearnih spektroskopija [1-6]. Postoje i podele na spektroskopije vezane za elektromagnetno zračenje, ali za koherentno i nekoherentno zračenje. Prema problemu kome se okrećemo, u smislu deskripcije materijala normalnog stanja i perturbovanog, u smislu proizvođenja nove dinamike i njegove relaksaciju, takođe postoji izbor više mogućh komplementarnih (ili ne) rešenja, mada u edukativnom metrološkom prilazu postoji preferirana metoda za definiciju energetskih stanja u svetu elektrona, atoma, molekula, rešetke čvrstog tela. Svesno je konstatovano stanje haotičnih kretanja u vezi sa gasovitim stanjem i čvrstim stanjem, a tečno ima svoje probleme upravo zato što nije uslovno vezano za stroge stavove kod čvrstog stanja i haotične sudare kod gasovitog.

Luminescentni procesi [7] imaju svoju bogatu istoriju i u vezi teorije i u vezi tehničke podrške i kompleksnosti aparature koja ih meri. U osnovi, radi se o rešavanju izvora pobude i kvantitativnoj deskripciji transformacijom u signale. U prošlosti je glavna tendencija tražila prebacivanje na električne signale, pa su i detektori bili tog profila.

U ovom radu će predmet istraživanja biti okrenut retkim zemljama [8] i termodinamičkim procesima, koji će pokriti eksplicitno temperaturne zavisnosti izbora karakterističnih parametara. Poznavanjem početnih materijala [9,10] i u definisanom temperaturnom opsegu dinamike izabranih parametara, materijali uzeti kao uzorci mogu imati različite primene od funkcije detektora, daljinskog (beskontaktnog) merača temperature, komponente za smese sa posebnim spektralnim znakom... [13 - 15]

## II. EKSPERIMENTALNI DEO

Luminescentna termometrija [11] ima više *arijanti* komercijalnog tipa, (slika 1) koji su prema nameni sa manjim ili većim modifikacijama, vezanim za mesto gde se postavljaju uzorci, specifične držače uzoraka ili posudice,

[1] Fizički fakultet Univerziteta u Beogradu, [2] Deseta gimnazija "Mihajlo Pupin".

 ISBN 978-86-7466-930-3

sisteme tipa termostata za precizno održavanje u vremenu zadate temperature, koji zavisno od intenziteta razvijenih luminescentnih procesa odgovaraju pragovima detekcionog dela. Posle prijemnika zračenja, koji treba da pokriva oblast ultraljubičaste / ljubičaste do kraja vidljivog dela i zahvat infracrvenog dela, sledi sistem elektronskih rešenja pojačanja i oblikovanja signala, koji priprema signale za odgovarajuću obradu.

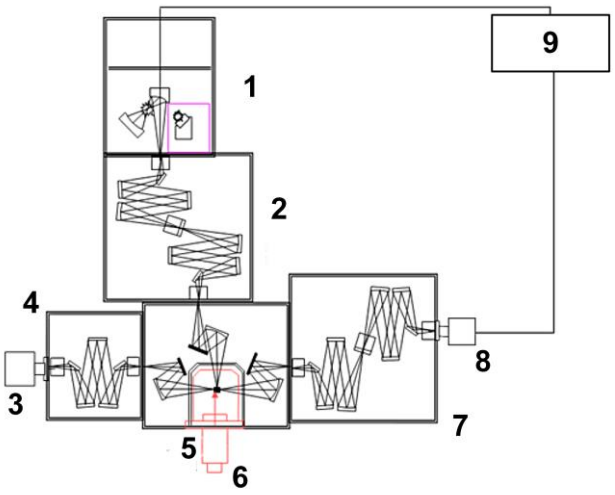


Slika 1. Šema spektrofluorometra: 1 – Xe impulsna ili kontinualna lampa ili laser, 2 – ekscitacioni monohromator, 3 – detektor, 4 - emisioni monohromator, 5 – ćelija sa uzorkom, 6 – emisioni monohromator, 7 – detektor, 8 – računar sa softverom za obradu podataka.

Za svrhe eksperimenata, korišćenih u ovom radu, radilo se o koherentnom izvoru – laseru, koji ima mogućnost podešavanja talasne dužine. Detektore su predstavljali fotomultiplikatori, podaci su prikazivani kao grafici i u ASCII zapisu u fajlovima. Makroskopski izgled jedne formacije eksperimenata je na slici 2.

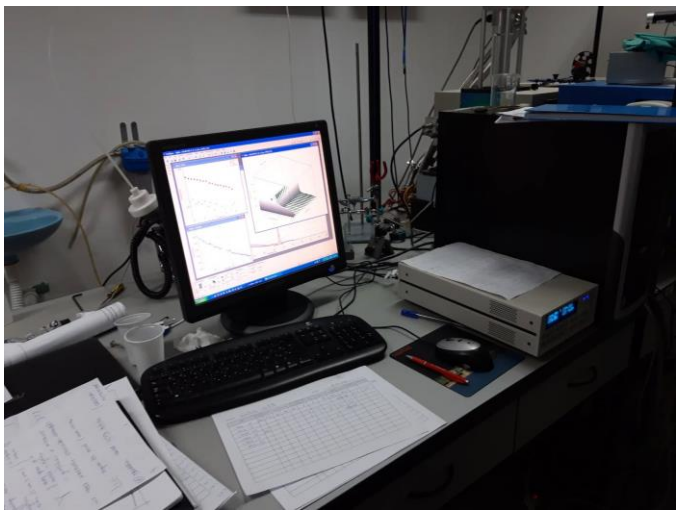

Slika 2. Izgled dela laboratorije sa postavkom za merenje luminescentnih spektara, detalj sa računarom za obradu podataka.

A. Uzorci

Na jednom tipu spektrometara analizirani su uzorci, koji su laboratorijski pripremani na bazi aluminijuma dopiranog retkim zemljama (Eu ili Dy), u koncentracijama 10%, koji su anodizirani fosfornom, oksalnom, sumpornom, hromnom ili bornom kiselinom, dimenzija uzoraka reda cm i debljine do mm.

Na drugom tipu spektrometra su specifično pravljeni uzorci sa polaznim prahovima rodamina, na pločici aluminijuma, anodiziranog u fosfornoj kiselini, na kojoj je nanošen rastvor rodamina RH D:110=1:9. Oba tipa uzoraka su bili sličnih gabarita, radi lakšeg poređenja u odnosu na intenzitet ekscitovanih procesa. Pored toga, vođeno je računa da se organizuju eksperimenti sa istim parametrima ekscitacije u odnosu na vremenske i prostorne parametre izvora ili da se prave modifikacije intenziteta ili geometrije ekscitacije. Temperatura koja je menjana je na jednom tipu uzoraka bila u opsegu od 20-70◦C, a u drugom se radilo o niskim temperaturama od 10-150 K, pošto je bilo od interesa analizirati uzorke sa polaskom od sobnih temperatura ili u opsegu daleko od uobičajnih temperatura ambijenta. Pitanje promene temperature se relativno jednostavno rešavalo (kod niskih temperatura krio sistemima). Ekscitacija uzoraka bez obzira na koherentnu ili nekoherentnu pobudu je vršena po celoj površini uzorka.

Ekscitacioni snop lasera je propušten u jednoj seriji merenja kroz prorez 10 nm, a u drugoj, kod OPO lasera, monohromator sadrži dve difrakcione rešetke: od 300 i od 1800 zareza/mm, koji se mogu birati zavisno od željene rezolucije. Podsećamo da rešetka 1800 zareza/mm daje višu spektralnu rezoluciju, ali je signal nekoliko puta slabiji.

## III. Rezultati

Rezultati vezani za uzorke tipa aluminijumskih pločica, anodiziranih različitim kiselinama, koji sadrže retke zemlje su prikazani na slici 3.

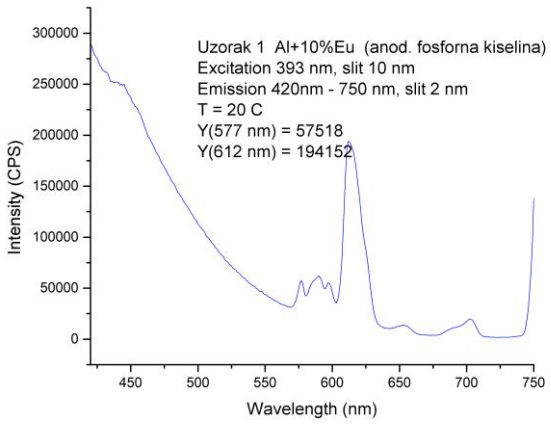


a)


ISBN 978-86-7466-930-3

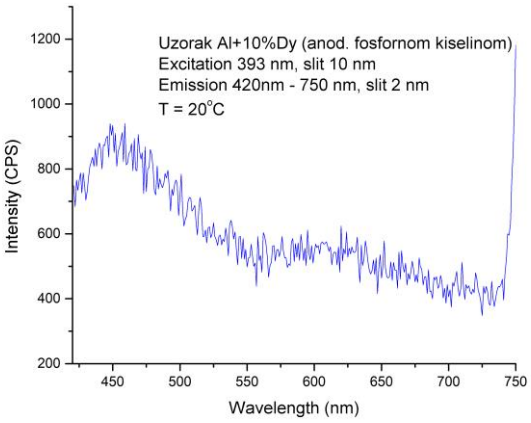


b)

Slika 3. Emisioni spektri uzoraka anodiziranog dopiranog Al u funkciji temperature, ekscitovani laserom: a) emisioni spektar uzorka Al dopiranog sa 10% Eu; anodiziranje fosfornom kiselinom, sa eksitacijom na 393 nm, snimljen na 20°C, b) emisioni spektar uzorka Al dopiranog sa 10% Dy; anodiziranje fosfornom kiselinom, sa eksitacijom na 393 nm, snimljen na 20°C.

Više je faktora koji utiču na to da dobijeni podaci odstupaju od očekivanih, onih koji se sreću u bazama podataka ili da su rezultati merenja, jednostavno, neupotrebljivi. Najčešće je to zastarelost opreme, „grubost" aparature, problem sa podešavanjem ili prosto pojava šuma. Na slici 3 b) informativno je dat spektar koji je neupotrebljiv zbog pojave šuma i „grubosti" aparature. O uslovima merenja je potrebno posebno voditi računa.

Spektri su istog tipa ili se razlikuju prema broju vrhova / pikova. Razlikuju se širine vrhova za slučaj pobude lampom ili laserom.

Od interesa je sprovesti eksitacije drugim tipovima koherentnih i nekoherentnih izvora i uporediti strmine spektara čime se može naći ili proceniti eventualno ko je ekscitovao neki nepoznati spektar za te uzorke. Od interesa je i promeniti gradijent temperature pri zagrevanju i diskutovati o optimalnom merenju temperature uzorka.

Uopšteno je potrebno voditi računa i o okolnostima:

- uniformnosti ekscitacije uzorka,
- broj ciklusa merenja posle kojih se pogoršava luminesentni odziv,
- variranje vremena ekscitacije i odgovarajućih izlaza,
- promena koncentracije i dopiranja.

## IV. ZAKLJUČAK

Procesi luminescencije materijala imaju široku upotrebu u mnogo oblasti. Kako je nauka o materijalima danas prepoznata kao jedna od najpropulzivnijih oblasti, postoji stalan trend da se dalje radi na luminescentnim materijalima i na poređenju ekscitacija u kategorijama koherentnih / nekoherentnih izvora. Pored toga što se luminescencija koristila ili koristi u svrhe detekcije i merenja, postoje trendovi da se formirani materijali dalje izlažu drugim pobudama, koje će samo da povise stepen intenziteta luminescencije. Kako su aktivni materijali kod kvantnih generatora vezani za promene koncentracije, čiji se prelazi prate već dugo, rađeno je na poboljšanju koeficijenta korisnog dejstva, izlaganjem aktivnih materijala definisanim snopovima elektromagnetnog zračenja u raznim dijapazonima spektra, nuklearnim zračenjima ili na drugi način.

Postoji velika količina starih spektara „klasičnih" materijala i sa „klasičnim uslovima", za koje je potrebno da budu ubačeni u baze podataka i da se dalje obrađuju i/ili porede raznim algoritmima ili se vrše transformacije u digitalni zapis za uključenje provere teoretskih modela. (9) To dovodi do potrebe za pretvaranjem starih snimaka u digitalnu formu, sa zapisom koji daje mogućnost za dalju obradu.

Pored toga, same tehnike merenja [12] mogu da budu od interesa i za konkretne forenzičke metode.

## LITERATURA

[1] A. Tokmakoff, *Nonlinear Spectroscopy*, MIT Department of Chemistry, 2, 1, 2009.
[2] S. Mukamel, *Principles of Nonlinear Spectroscopy*, Oxford Universitu Press, New York, 1995.
[3] *Nonlinear aser Spectroscopies*, Eds. V. S. Letokhov, V. P. Chebotaev, Springer Verlag, Berlin, 1977.
[4] J. Garcia Sole, L.E. Bausa, D. Jaque, *An Introduction to the ptical Spectroscopy of Inorganic Solids*, John Wiley & Sons Ltd, Chichester, England, 2005.
[5] J. Eggert, L. Hook, G. M. Schwab, *Udžbenik fizičke hemije*, Naučna knjiga, Beograd.
[6] V. Škerović, V. Zarubica , P. Vukadin, B. Kasalica, S. Stojadinović, I. Belča, *Metrološka karakteri acija obojenih organskih rast ora kao sredstava poređenja za etaloniranje biohemijskih anali atora*, Kongres metrologa, Zlatibor 2007.
[7] M. Pavlović, Doktorska teza, Elektrotehnički fakultet, Beograd.
[8] M. G. Nikolić, *Temperaturska a isnost luminescencije neorganskih fosfora na ba i retkih emalja*, doktorska disertacija, Fizički fakultet, Beograd, 2013.
[9] Ž. Andrić, V. Jokanović, M. D. Dramićanin, *Photoluminescence Ckaracteristics of Europium oped Silica Sols and Nanopowders*, YUCOMAT 2004, Programme and The Book of Abstracts, Ed.D.P. Uskoković, Inst Techn. Sciences of the SASA, Belgrade, 2004.
[10] M. D. Dramićanin, A. Kapidžić, *E perimental E idence of Nonlinear Photothermal Effects in Materials etected by Second armonic Photoacustic Spectoskopy S PAS Tehni ue*, YUCOMAT 2004, Programme and The Book of Abstracts, Ed. D. P. Uskoković, Inst. Tehn. Sciences of the SASA, Beograd, 2004.
[11] M. Dramicanin, *uminescence Thermometry*, Woodhead Publishing, Elsevier, 2018.
[12] V. Zarubica, M. Srećković, *eali acija metoda etaloniranja i proračun budžeta merne nesigurnosti mernih instrumenata merila u laboratorijama*, Velarta, Beograd, 2012.
[13] Z. Fidanovski, M. Srećković, S. Ostojić at. al., *The Interpretation of the Intensity of Components of aser Scattering by Interaction with Matter*, Physica Scripta, Nr. 014016, doi:10.1088/00318949/2012/T/149/014016.
[14] S. Mentus, U. Mioč, *Odabrane metode fizičko-hemijske anali e*, Fakultet za fizičku hemiju, Beograd, 1993.
[15] Photometers, *adiometers and Accessories*, Karl Lambreht, katalozi,

## ABSTRACT

**Perhaps measurements of very low luminescence of human s in in the future will bridge the gap between traditional astern and conventional Western medicine. or now, luminescence measurements and research in this area confirm the connection between biological rhythms and the emission of electromagnetic radiation from living individuals. Today, a lot of literature on luminescence, with the phrase „potential application'', needs to be corrected into „existing applications'', because luminescence has strengthened its place in many applications from medicine, metrology, heritology, forensics. We can tal about the synthesis of materials, the development of devices and methods that will better and more**

 ISBN 978-86-7466-930-3

**completely describe the luminescent effects qualitatively and quantitatively to ma e them clearer and more informative. Apparatus development means the development of each of the major subsystems from e citation to detection. specially important is the processing subsystem where the formed signals are processed and includes a specific dedicated written program for obtaining results in environments where only data on a certain size is needed, which is obtained by the method of luminescent technique. , amino acids in fingerprint, e plosives). Detection sensitivity can be achieved by different ways of energy transformation using luminescent techniques along with other treatments. The luminescent effects of lanthanide compounds (terbium, europium, yttrium, etc.) can be enhanced by combining with ligands that promote these effects. aterials with rare earths, due to their unique optical properties, are also interesting in the field of protection. And here we wor on powders, paints, solutions, in order to obtain products whose luminescent profiles are difficult to imitate. Characteristic times of luminescent effects are different (reaction time, rela ation, etc.) and depend on the type of e citation, so the information obtained in this way has multiple meanings based on which, from one series of measurements, with the appropriate development of electronic support, the situation with a comple set of electromagnetic, nuclear radiation, can also be measured simultaneously. These effects are particularly important because both qualitative and quantitative analysis of trace elements is enabled. uminescence has its own history, and many nown results come from older generations of measuring systems, which directly leads to the need for digitization in order to be able to use them in e panding the database for automatic fast search.**

**ey words - luminescent effects, forensics, matter detection, rare earths, amplification effects.**

## ome odern Aspects of the se of uminescent ffects

Milanka Pećanac, Bećko Kasalica

 ISBN 978-86-7466-930-3

# Изазови у настави на рачунарима током пандемије Covid 19 на предмету Нацртна геометрија са рачунарским цртањем

Магдалена Драговић, Александар Чучаковић, Светлана Чичевић, Александар Трифуновић, Анастасија Мартиненко

***Апстракт*—Савремени приступи у високошколској едукацији, са употребом рачунара, као алата за прецизно цртање и 3Д моделовање, комбиновани са формом *online* предавања, су настали као резултат потреба инжењерске струке и актуелних услова живота за време пандемије Covid 19. Комбинована форма наставе, где се предавања реализују као својеврсни вебинари, а вежбе спроводе уживо у учионицама, на рачунарима, носе одређене специфичности и изазове како за наставнике, тако и за студенте. Кроз овај рад аутори ће приказати карактеристике оваквог типа наставе и њене изазове у реализацији, која је спровођена на Грађевинском факултету Универзитета у Београду током школске 2021/22 године, на предмету Нацртна геометрија са рачунарским цртањем. Након завршеног зимског семестра, после реализована два узастопна испитна рока (у јануару и фебруару), спроведена је анкета са студентима, који су положили испит. Анкету, су креирали наставници на предмету. Резултати делова анкете, у контексту теме рада, су приказани кроз графике и дескриптивну статистику.**

**Кључне речи — едукација, *online* настава, нацртна геометрија, рачунарско цртање, софтвер Auto CAD.**

## I. УВОД

Специфичности времена у коме живимо, развој технологије и рачунарских алата за рад стручњака инжењерске струке, диктирају континуиране промене у едукацији студената, како у концепту, тако и садржају и начину реализације. Већ дужи временски период, у настави су опште присутне презентације са слајдовима у PowerPoint апликацији, као помоћни „алат“ за предавања, пошавши од основно-школског нивоа едукације до високошколских установа, које постају један од основних материјала за учење [1]. Комбиновање типа предавања, које се реализује уз слајдове са сажетим информацијама и сликама-цртежима о наставној теми, са *online* вебинаром, као главним средством за живу комуникацију између наставника и студента, је једна од актуелних метода у настави спровођеној током ванредних услова - пандемије Covid 19 . Настава подржана различитим видовима информационо-комуникацијске технологије се приближила *e-learning*-у, типу реализације наставног процеса на даљину, који је током интернет ере добио и своје појмовне варијетете (електронско учење, учење путем интернета, *online* учење...)[2]. Услови живота које је диктирала пандемија и специфичности предмета који студент учи су актуелизовале и друге типове материјала: снимљена предавања, видео клипови, додатни писани, или цртани материјали у електронској форми и сл.

Предмет Нацртна геометрија са рачунарским цртањем, који је део новог курикулума будућих грађевинских инжењера на Грађевинском факултету Универзитета у Београду (у даљем тексту ГРФ), је креиран 2021. год. као курс у новом циклусу акредитације ове високошколске установе [3]. Специфичност приступа је у том смислу што комбинује овладавање вештинама цртања и моделовања на рачунару, у софтверу који има 3Д радно окружење, са применом научних принципа нацртне геометрије. Управа факултета се одлучила за примену комбинованог вида наставе (практични део наставе је организован у рачунарским учионицама, на факултету, а предавања су се одвијала *online*), у складу са нешто блажим епидемиолошким мерама и прописима. Обзиром да су студенти прве године читаву годину пре уписа учили у комплетном *online* режиму, оваква одлука је осигурала квалитет реализације и подигла атрактивност наставе.

Нацртна геометрија је научна дисциплина настала као резултат потребе да се 3Д простор на адекватан начин прикаже на 2Д цртежу, а њен креатор је француски војни инжењер и математичар Гаспар Монж (Gaspard Monge 1746-1818). Монж је креирао систем приказивања просторних елемената у две комплементарне ортогоналне пројекције, које је користио за приказе војних утврђења и решавање њихових специфичних потреба алатима геометрије [4]. Нацртна геометрија има две кључне улоге - представљања и анализирања 3Д објекта (одатле потиче и назив „дескриптивна“ – описна). У едукацији доноси као резултат способност геометријске апстракције различитих геометријских облика и геометријско резоновање [5]. Она даје скуп принципа и поступака који омогућавају решавање геометријских задатака у простору

Магдалена Драговић, Грађевински факултет, Универзитет у Београду, Булевар краља Александра 73, 11020 Београд, Србија (e-mail: dim@ grf.bg.ac.rs).

Александар Чучаковић, Грађевински факултет, Универзитет у Београду, Булевар краља Александра 73, 11020 Београд, Србија (e-mail: cucak@ grf.bg.ac.rs).

Светлана Чичевић, Саобраћајни факултет, Универзитет у Београду, Војводе Степе 305, 11000 Београд, Србија, (e-mail:s.cicevic@sf.bg.ac.rs).

Александар Трифуновић, Саобраћајни факултет, Универзитет у Београду, Војводе Степе 305, 11000 Београд, Србија, (e-mail:a.trifunovic@sf.bg.ac.rs).

Анастасија Мартиненко, Универзитет у Београду, Булевар краља Александра 73, 11020 Београд, Србија (e-mail: amartinenko@ grf.bg.ac.rs).

 ISBN 978-86-7466-930-3

цртањем на 2Д папиру, или пак на рачунару, што је случај са модерном нацртном геометријом. Као таква је у потпуности специфична и носи широку палету путања у поступку решавања једног геометријског задатка, дајући слободу аутору цртежа да различитим идејама дође до решења. Представља високо захтевну научну дисциплину која развија просторну имагинацију, а специфично је важна за струке које се тичу дизајна, инжењерства и архитектуре [5,6]. Често није популарна међу студентима, јер је добар број њих склон тражењу обрасца за решење („корак по корак“ исцртавање линија на цртежу) који се може меморисати. Утисак који деле аутори овог рада, стечен на основу вишегодишњег рада са студентима је да мањи број студената настоји да „освести“ везу између 2Д цртежа (као пројекције) и 3Д простора. Стога, допуна наставе нацртне геометрије технолошким решењима – цртачким алатима, у форми софтверских апликација, које поседују 3Д радно окружење, представља искорак ка бољој визуелизацији просторних елемената, прецизнијем и ефикаснијем цртању, као и њиховом атрактивнијем приказу [6].

Међу савременим рачунарским софтверским решењима постоји низ апликација које служе као цртачки алат, како за 2Д, тако и 3Д цртање. У тренутку када се укључи и просторност – тродимензионалност, поступак цртања постаје моделовање[1]. Ова могућност је отворила врата новим приступима у едукацији инжењера. Тако се низ софтверских решења које се користе у сврхе основне геометријске едукације, протеже од SketchUp-a, Rhinoceros-a, GeoGebra-е и сл. до озбиљних инжењерских софтвера за потребе струке, какав је AutoCAD, ArchiCAD, Revit и други. Могућност да студент једним „кликом“ миша из „3Д простора“ пређе у 2Д пројекцију наизглед је била идеална за оне студенте који теже схватају шта цртеж нацртан на папиру заиста представља у простору. Осим тога, приказ било ког објекта, грађевинског, или чисто геометријског, у форми која визуелно даје просторну представу, студенту даје сигурност препознавања објекта који црта. Различити начини приказа просторног модела (жичани, површински, пуни, провидни и сл.) доприносе квалитету визуелизације, који се савременим софтверским алатима лако изводе. Коначно, генерације студената које долазе су одрасле уз 3Д видео игре, које су већ утицале на њихов ниво технолошке „писмености“ и спремност на изазов да у сличном окружењу уче и припремају се за професију. Руковођени овим идејама академски наставници, на ГРФ, су увели 3Д окружење у наставу на предмету Нацртна геометрија још од 2015. год, тада у форми 3Д решења задатака, која су пратила 2Д цртеже, извођене на практичним вежбама, у класичном систему наставе [7]. Данас је то прерасло у комплементарно - 2Д/3Д цртање на рачунару, употпуњено моделовањем.

У раду ће бити приказани аспекти изазова техничког (реализација наставе) и едукационог (нови модалитет радног окружења) типа, који су се појавили током наставе на ГРФ-у, са студентима прве године, на курсу Нацртна геометрија са рачунарским цртањем, током школске 2021/22. године.

## II. УСЛОВИ ИЗВОЂЕЊА НАСТАВЕ

Реализација наставе и то дела практичних вежбања на предмету Нацртна геометрија са рачунарским цртањем, на ГРФ, је спровођена паралелно у 4 рачунарске учионице које укупно броје 94 (24, 30, 20 и 20 места) расположива рачунара за студенте[2]. У условима пандемије, према прописима о максималној квадратури простора по једном студенту (4м$^2$), то је значило да се број студената у учионици креће од 10-12, у мањим учионицама, до 17, у већој учионици. Верзија софтвера која је коришћена у настави је AutoCAD 2022 (најактуелнија верзија бесплатно доступна студентима за рад и вежбу код куће). Број студената за који је настава оргнизована у току школске 2021/22 године је оквирно 350. Наставу је до краја редовно похађало око 300 студената. Фонд часова на предмету је 2+3 (предавања + вежбања) током петнаестонедељног зимског семестра. Практичне вежбе су се реализовале под вођством једног наставника и једног студента демонстратора у две суседне учионице (како би наставник могао да надзире обе групе студената). Свако од 11 реализованих вежбања је оцењивано оценом од 1-10, што је у укупној оцени на курсу представљало 30 поена (од максималних 100), док је услов за потпис семестра износио мин. 16.5 остварених поена са вежбања.

Перформансе рачунара који су коришћени у раду са студентима су следеће: Intel I5 процесор, 3.30GHz, 32GB RAM, hard disk 500GB M2, NVIDIA GeForce GT 730 – графичка карта, под 64-bit Windows оперативним системом. Познато је да је софтвер AutoCAD један од захтевнијих софтвера када је у питању графика, чиме се омогућава изузетна прецизност код цртања, као и интеракција-манипулација са 3Д објектом (померање, ротација, увеличавање и др.). У складу са тим, поседује палете алата (палета *snap*) који омогућавају реализацију прецизног цртежа, као и алате за раванску и просторну манипулацију (*pan*, *orbit* и *zoom).*

Упознавање студената са процедурама коришћења рачунара (логовање на рачунаре са корисничким именом и лозинком) и рачунарске инфраструктуре факултета је спроведено кроз форму обавештења постављених на предметној табли, у оквиру факултетског web-сајта www.grf.bg.ac.rs. Упутства о приступу подлогама за вежбе у оквиру факултетске инфраструктуре, са подручја *student share,* креирању личне фасцикле на D-диску појединачних рачунара и личне датотеке – цртежа у AutoCAD (*.dwg) формату, уз одговарајући назив и идентификацију студента, су такође представљена студентима у писаној и електронској форми, током уводних часова.

[1] Реч „моделовање“ се користи у много контекста, али када је реч о геометријском поступку, најчешће значи – креирање просторног модела неког тела мање, или веће сложености.

[2] Сваки студент ради самостално на једном од рачунара у учионици (у начелу, студенти су настојали да раде увек на истом рачунару, како би им били доступни и претходни радови-вежбе).


ISBN 978-86-7466-930-3

## III. МЕТОДОЛОГИЈА НАСТАВЕ

За разлику од актуелних светских тенденција ка Project Based Learning-у (PBL), или „обрнутој учионици“, у наставном процесу [8], на ГРФ је још увек активна методологија која примењује теоретску наставу (наставник излаже предвиђену тему), која претходи практичном делу – вежбањима (на основу предавања студент се припрема за вежбање код куће и решава задатке на факултету, у рачунарској учионици). Целокупна структура извођења наставе, коришћења наставних материјала и комуникацијско-информационих окружења се може испратити помоћу графика (сл. 1).

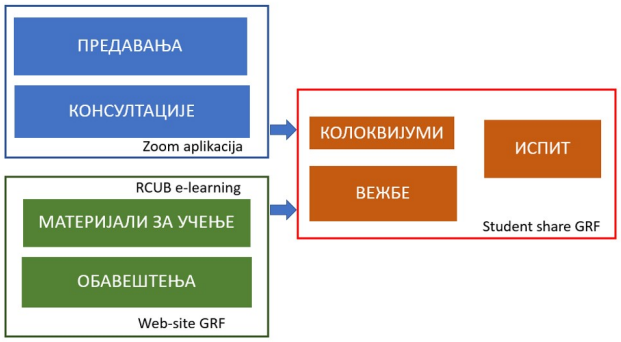


Сл. 1. Дијаграм структуре извођења наставе са радним комуникацијско-информационим радним окружењима

Потреба да се студентима образложе теме које покрива научна дисциплина нацртне геометрије, а која има директну примену у грађевинарству, спроведена је кроз предавања у форми *Power Point* презентација (сл.2) и пратећа објашњења која наставник говори уживо на вебинару (Zoom апликација). Слике – цртежи појединих наставних тема, у оквиру презентације су дате у форми ортогоналних, или аксонометријских слика, тј. приказа дела екрана рачунара (*print screen* опција) са исцртаним цртежом у 2Д, или 3Д приказу. Слике су по потреби креиране у неколико фаза извођења задатка, како би се лакше пратио сукцесивни поступак решавања-цртања, или моделовања, што је пракса показала као веома користан метод [6][3].

Специфично, имајући на уму да студент има двоструки задатак - да савлада геометријска знања и оспособи се за рад адекватним цртачким алатом- софтвером Auto CAD, креирани су и допунски материјали у писаној форми (појашњење поступка), као и појединии видео клипови (комплетан, или део поступка[4] у изради задатка), ради боље припреме студената за реализацију практичних вежби.

[3] Претходна искуства на предмету Нацртна геометрија, где су студенти добијали решења задатака у форми AutoCAD цртежа (2Д и 3Д) са фазама израде задатка – „корак по корак“, које су дефинисане сукцесивним укључивањем лејера, показала су да је одређени број студената на предмету користио овај олакшани вид учења „процедуре“ и да им је помагао да се на адекватни начин припреме за вежбање.

[4] Припремљени су материјали за оне сложене поступке где је у спровођењу команди потребно извести више корака, односно, изабрати одређене опције које се нуде у командној линији.

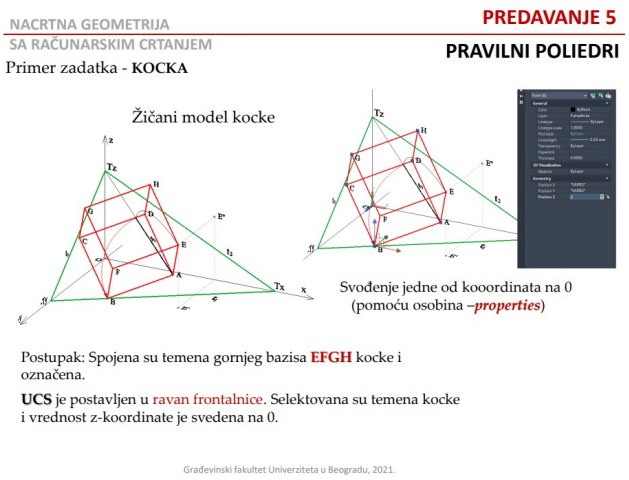


Сл. 2. Приказ слајда *Power Point* презентације са предавања који приказује поступак и делом команде у поступку извођења геометријског задатка

Обзиром да је учење рада у софтверу предмет курсева који су доступни јавности у стручним и лиценцираним институцијама и да постоје бројни приручници (како штампани, тако и у форми интернет упутстава и подршке [9]), наставне теме су пратила концизна упутства којим се командама (куцаним у командној линији, или коришћењем алатке на палети алата) треба служити да би се на одговарајући начин нацртао цртеж – решио дати геометријски задатак. Кратка упутства о радном окружењу софтвера AutoCAD су дата у форми једноуводног предавања и писаног материјала постављеног на предметној табли факултетског web-сајта, а истој теми је посвећено и уводно вежбање (без оцењивања).

За потребе архивирања материјала за учење и припрему вежби на *e-learning* платформи Рачунарског центра Универзитета у Београду (РЦУБ – у даљем тексту) је креиран налог предмета у оквиру ширег налога ГРФ. На одлично организованој платформи која омогућава распоред материјала по радним недељама, интеракцију са студентима кроз оцењивање радова и повратна упутства о грешкама, архивирани су додатни материјали за учење: видео снимак предавања и ppt - презентација, текст задатка за вежбу, закључано решење вежбе AutoCAD формата, пратећи писани материјал за поступак израде, као и поставка вежбе (постављена по завршетку недеље текуће вежбе).

Научни принципи и методе које користи Нацртна геометрија су, сходно расположивом времену у семестру, приказани у сведенијем обиму, него што је то класични приступ подразумевао. Један од практичних разлога за то је што софтвер AutoCAD има своје процедуре (команде) решења геометријских задатака, која се изводе много ефикасније и прецизније. Наиме, перформансе софтвера су омогућиле да се неки геометријски поступци изоставе – те да рачунар „сам реши“ геометријски задатак применом једне или више команди, било да се ради о задатку у коме се тражи продор праве кроз раван, или продор два геометријска тела-солида.


ISBN 978-86-7466-930-3

## IV. ИЗАЗОВИ У РЕАЛИЗАЦИЈИ НАСТАВЕ

Током реализације практичних вежбања, у учионицама, на рачунарима, наставници, као и студенти су се суочавали са два типа изазова: технички – који су везани за рачунаре, опрему и рачунарску инфраструктуру факултета и теоријски - везани за саму нацртну геометрију и примену AutoCAD алата (вештина и брзина цртања). И наставници и студенти су били суочени са изазовом брзине одвијања наставе, њених временских оквира (2+3часа) и усвајања вештина цртања и неопходних геометријских знања, у контексту успешне реализације курса.

Неколико изазова које су наставници на предмету уочили у оваквом типу наставе су:

-недостатак визуелног контакта са студентима (немогућност да се студент током предавања препозна и ликом);

- немогућност да се поједини студенти укључе и гласовно у комуникацију (проблеми са опремом);

-повремено укључивање и ометање предавања спољним звуцима или гласовима[5];

-свако мењање документа који се приказује подразумева низ корака у апликацији, што успорава ток и ритам предавања, захтевајући извесну вештину предавача;

-студенти су мање активни („храбри“) у комуникацији;

-студенти су значајно више комуницирали путем “chat” опције него гласовно, што је од предавача захтевало излазак из фокуса предавања и пр**а**ћење *chat*-а;

Везано за образложену проблематику, на крају семестра је спроведена анкета, која укључује питања о неколико типова изазова. Анкетирани су студенти који су положили испит у једном од два испитна рока јануар/фебруар. У анкети је учествовало 53 студента, од чега је 58.5% женских и 41.5% мушких испитаника. Око ¾ (75.5%) овог броја студената припада популацији која је завршила гимназију, док је 22.6% завршило неку од техничких школа.

Студенти су реаговали на понуђене опције (или више њих) у контексту личних изазове током рада на рачунарима, што у крајњем исходу може указати на правац побољшања квалитета наставе у наредним годинама. У кратким цртама, у наредном тексту су описани поједини изазови који су пратили реализацију наставе, а у наставку су резултати студентске анкете са појединим питањима обрађеним за потребе овог рада.

### *А. Изазови са опремом-рачунаром*

Обзиром на старост и перформансе рачунара и помоћне опреме (миш и тастатура, понекад и екран), долазило је до проблема у ефикасности извођења-цртања студената на вежбама. Неисправна опрема је успоравала, или у потпуности онемогућавала рад. Такође, специфично за софтвер AutoCAD, дешавало се да графичка картица рачунара не подржи команду манипулације „*3D Orbit“* и да усред поступка дође до терминалне грешке, па су студенти „губили“ нацртане задатке и били принуђени да раде цртеж од почетка.

### *Б. Изазови са рачунарском инфраструктуром и процедурама*

Посебно изражени, у првих месец дана наставе, су били заступљени проблеми активирања студентских налога на рачунарима (форма одбијене лозинке), који често нису могли да се реше у току самог вежбања. Брзина и неискуство студената у раду са датотекама на мрежи (копирање, чување и именовање датотеке) су готово до последњег термина вежбања чинили да студенти активирају поставке вежби на самој мрежи, чиме би осујетили приступ поставци осталим студентима и угрозили анонимност личног рада. Могућност да било ко од студената по завршетку и предаји вежбе може да приступи туђем раду су учинили да студенти падну у искушење да копирају туђи задатак, преименују, па чак и обришу цео рад.

## V. РЕЗУЛТАТИ АНКЕТЕ

Резултати спроведене анкете су показали да је скоро 2/3 студента (66.5%) имало проблем са нефункционалном, или преосетљивом опремом (углавном „миш“); затим, 42.5% испитаника је пријавило „пуцање“ софтвера у току рада, те нестанак дела урађеног цртежа, док је 10,5% пријавило и потпуни губитак рада; коначно, 3.8% испитаника је пријавило некоректну „крађу“ комплетног рада, или појединих цртежа. Свега 1.9% студената није имало лични рачунар, а 5.7% је имало потешкоће око инсталирања софтвера (сл.3). У ери дигиталних справа које су углавном подешене за коришћење на енглеском језику, 9.4% студената је имало изазове са значењем и називима команди које су главна спона корисника и рачунара. На графику (сл. 3) су дати и остали резултати анкете који презентују заступљеност потешкоћа које су студенти имали у праћењу, или реализацији наставе на рачунарима, као и разумевању геометријских поступака на релацији 2Д/3Д.

Као противтежа потешкоћама, студенти су се у анкети изјаснили о позитивним утисцима (сл. 4) и погодностима које је донео рад на рачунару. Највећи број студената (64.2%) је показао задовољство због рада у 3Д радном окружењу, а једнако оценио квалитет цртежа који се остварује цртањем на рачунару (62.3%). Такође је значајан проценат студената (52.8%) који оцењује квалитет софтвера - да се делови цртежа могу уклонити/сакрити са екрана (без брисања).

Део анкете, који упућује на то које су материјале студенти користили у поступку учења и припреми вежби или испита, показује да је 96% испитаника користило платформу РЦУБ-а, а 54% је користило предметну таблу на web сајту факултета и материјале који су на њима постављани; мањи број студената (69.8%) је као

[5]Иако су извршена подешавања у апликацији, неретко се дешавало да се звук са локације где се налазе студенти чује преко гласа наставника и ремети ток предавања.


ISBN 978-86-7466-930-3

литературу користио уџбенике, а 41.6% је користило и личне белешке.

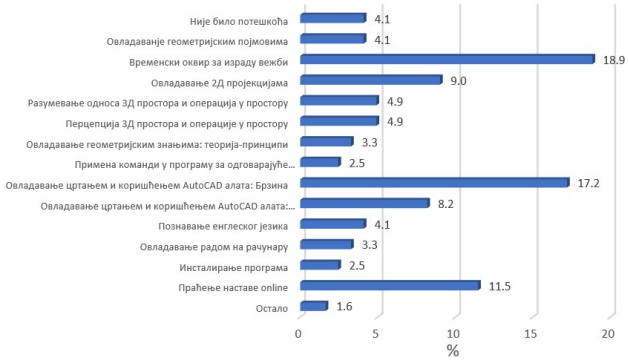


Сл. 3. Резултати анкете: приказ заступљености изазова које су анкетирани студенти имали током реализације наставе на рачунарима

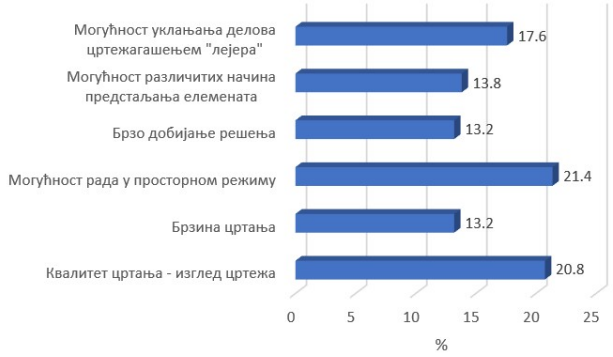


Сл. 4. Резултати анкете: приказ позитивних утисака које су анкетирани студенти имали током реализације наставе на рачунарима

## VI. ЗАКЉУЧАК

Сумирајући резултате спроведене анкете и утиске током реализације наставног процеса на предмету Нацртна геометрија са рачунарским цртањем, може се рећи да је наставни процес у коме су важну улогу имали рачунари, њихова опрема, рачунарска инфраструктура и платформе за његову реализацију, на нивоу актуелности, ефикасности и адекватности испунио очекивања наставника. Студенти су активно користили већину садржаја – наставних материјала која је припремљена у релативно кратком временском периоду (око 6 месеци) и успешно положили испит. Остварен резултат током два испитна рока, у којима је положило 157 студената: у јануару - 112 (просечна оцена 8.81) и фебруару - 45 (просечна оцена 7.84), од укупног броја од око 320 студената (који су редовно похађали наставу), показује да је њихово интересовање за предмет и мотивација да га положе у првим испитним роковима одговарала одговорима приказаним у анкети. Резултати су на нивоу резултата претходних генерација студената, који су слушали класичан курс Нацртне геометрије.

Изазови који су пратили наставни процес, а специфично они који су се дешавали у рачунарским учионицама, дају смернице за неопходност побољшања расположиве опреме и рачунара, у функцији квалитета извођења наставе, као и смањења нивоа стреса, како за студенте, тако и за наставнике. Очито је највећи изазов био временски оквир за реализацију вежби, што се може тумачити мањком вештина у манипулацији рачунарском опремом (као и њеним квалитетом) и недовољним искуством у раду на рачунарима, уз надасве потребно знање геометрије и поступака у софтверу AutoCAD.

Несумњиво је да је искуство студената прве године факултета сасвим различито од искустава студената са виших година студија, јер је брзина и моћ адаптирања на новине у режиму студирања (у односу на средњошколску наставу), један од детерминишућих фактора успешности. Ипак, студенти су показали да врло добро владају савременим комуникационим платформама које су активно користили и са њих преузимали електронске материјале за учење.

## ЗАХВАЛНОСТ

Овај рад је спроведен у оквиру реализације научних пројеката, које је финансирало Министарство науке и технолошког развоја Републике Србије под редним бројевима ТР 36027, ТР 36006, 200092.

## ЛИТЕРАТУРА

[1] Б. Ратковић Његован, М. Вукадиновић, Л. Грубишић Нешић, „Моћ и немоћ Power Point презентације“, XXVII скуп Трендови развоја: „On-line настава на универзитетима“, Нови САД, 15-18.02.2021., рад бр. Т2.3-4, стр. 395-398.

[2] Д. Ђорђић, М. Цвијетић, Р. Дамјановић, „Искуства учитеља и наставника током реализације наставе на даљину услед пандемије вируса корона (Covid-19), *Иновације у настави XXXIV,* 2021/2, str.86-103.

[3] https://www.grf.bg.ac.rs/studije/ptb?pid=1220

[4] I. Cvetković, M. Stojićević, H. Stachel, R. Milićević, B. Popkonstantinović, „The Man who Invented Descriptive Geometry“, *FME Transactions* 47(2), 2019.

[5] Hellmuth Stachell, „What is Descriptive Geometry for?”, *Conference Proceedings, 2006*. https://desen.utcluj.ro/dt/GD/Stachel-dresden.pdf

[6] P. Surynkova, „Modern Descriptive Geometry Supported by 3D Geometric Modeling “, Int. Conf. on Mathematics Textbook Research and Development ICMT-2014, 29-31 July 2014, University of Southempton, UK

[7] M. Dragović, S. Čičević, A. Čučaković, A. Trifunović, F. Gramić. „Positive impact of 3D CAD models employment in DG education“. *Journal of Polish Society for Engineering and Graphics*, 32, 2019, pp. 11-16.

[8] I. Tanaka, “A Revised Project-Based Learning Program on Geometry-Maximizing the Volume of Solid”, in L. Cocchiarella (ed) Proceedings of the ICGG 2018 Conference on Geometry and Graphics, Milan, Italy, August 3-7, 2018, pp.1706-1715.

[9] https://knowledge.autodesk.com/support/autocad

 ISBN 978-86-7466-930-3

# Aktuelni problemi digitalizacije u državnoj administraciji

Nikola Popović, Julijana Mirčevski

**Apstrakt --Tekuće stanje procesa digitalizacije u Srbiji počinje da ispoljava prve, jasne znakove protivrečnih pojava. Uvodi se značajan broj sistema za upravljanje dokumentima, posebno u sistemu državne administracije. Uz sasvim očite pogodnosti, ispoljavaju se problemi kompatibilnosti novih sistema sa postojećim sistemom rada sa papirima. Harmonizacija dostupnosti dokumenata i načina rada je otežana. Jedan deo dokumenata i pored digitalne verzije mora i dalje da ostane na papiru. Troškovi digitalizacije su visoki, a navedeni problemi izazivaju značajna kašnjenja implementacije. U radu su naznačena moguća tehnološka rešenja koja omogućavaju održivost procesa digitalizacije kroz niže troškove.**

**Ključne reči -- digitalizacija; održivost; metodologija digitalizacije; državna uprava.**

## I. UVOD

Analiza metapodataka koji su u propisima predvidjeni za opis digitalnih dokumenata ukazala je da je strategija digitalizacije zasnovana na klasičnim principima rada sa papirom. Regulativu u većini čine propisi koji se tiču zaštite digitalnih dokumenata. Usvojen je klasični princip grupisanja dokumenata hijerarhijskom klasifikacionom šemom. Nismo uočili da se iko bavio sadržajem dokumenata, semantikom i odgovarajućim aspektima jezika.

Težište digitalizacije je usmereno na zadovoljavanje potreba građana i preduzetnika. Od državnih organa se primarno zahteva i očekuje znatno veća efikasnost i uštede. Masovno se pominje primena "najboljih praksi" (eng. best practices), ali bez navodjenja čije prakse i konteksta te prakse. Procesi izrade studija stanja (eng. feasibility study) se sprovode/zamenjuju prostim anketiranjem. Izučavanje kompleksnih, heterogenih procesa u državnoj administraciji ne može da se izvodi anketiranjem. Unifikacija radnih procesa je nekada opravdana, ali u nekim nedovoljno analiziranim situacijama može da dovode do gubitka bitnih podataka i nemogućnosti generisanja novih informacija. Ciljevi digitalizacije, kako su postavljeni, ne uzimaju dovoljno u obzir potrebe organizacije rada u državnim organima. Regulativa je orijentisana na što bržu digitalizaciju u domenu finansija i bankarstva. U tom domenu najveći procenat dokumenata čine strukturirani dokumenti. Državna administracija u najvećem procentu radi sa nestruktuiranim dokumentima. Procesi rada sa struktuiranim i nestruktuiranim dokumentima se suštinski razlikuju. Radni procesi u državnim organima često zahtevaju organizovanje kompleksa podataka i metapodataka, koji omogućava složenu konsolidaciju informacionih resursa, u cilju donošenja racionalnih dokumentovanih odluka. U takvim slučajevima često je nužno formiranje ad-hoc klastera dokumenata radi sagledavanja sadržaja i obima problema. Jednostavan primer je ažuriranje podsetnika za posetu ministra stranoj zemlji. Osim novih podataka potrebno je proveriti i revidirati arhivske podatke (istorijat) radi njihovog sagledavanja (prikazivanja ili ne) u kontekstu tekućih zbivanja. Ovi postupci uslovljavaju pristup mnogo većem broju dokumenata, u vremenskom i tematskom domenu. U državnoj administraciji masovno se uvodi "Document management system" - DMS. DMS po definiciji ima sam dokument u centru pažnje (eng. document centric approach), što znači da ne odgovara uvek značajnim procesima informisanja u državnoj administraciji.

## II. KONTRADIKCIJE METODA

Usvojen je koncept visoko centralizovane digitalizacije. U stranoj literaturi odavno su prepoznati problemi koji se javljaju u tom kontekstu [1], [2] . Nije uočeno da se posebno analizirao problem pristupa podacima u kontekstu dualiteta digitalni-papirni dokument. Strategija i taktika su svedeni na pominjanje zakona o arhivskoj građi, obavezno navodjenje pojma „najbolje prakse“, i očekivanje brze digitalizacije kompletnog sistema državnih organa.

U početnoj fazi uvodjenja DMS-a neprekidno se govori o značaju mogućnosti pronalaženja bilo kog dokumenta, bilo gde, u državnom organu. U kasnijim fazama realizacije počinje se sa ograničavanjem pristupa saradnicima organa državne uprave. Uvode se ograničenja - filteri za dokumenta koje pojedine niže organizacione jedinice i pojedini saradnici mogu i treba da vide. Naknadna analiza ograničenja pristupa pokazuje da su umesto sveobuhvatnog „wide-range“ DMS-a, često mogli da se primene znatno jednostavniji (tj. jeftiniji) sistemi sa istom funkcionalnošću. Navodimo:

1. Svi isporučioci DMS-a redovno ističu kao "glavnu" prednost korišćenja DMS-a mogućnost da svako vidi sve dokumente u DMS-u. Uopšte ne postoji potreba da svako vidi sve dokumente u DMS-u. Administrator DMS-a po funkciji može da ima pristup svim dokumentima, ali isključivo iz tehničkih razloga upravljanja repozitorijumima dokumenata.
2. Donosilac odluka suviše kasno shvata problem iz tačke 1. i onda uvodi restrikcije pristupa, koje su ustvari restrikcije na osnovne funkcije DMS-a. Cena pogrešne primarne odluke je previsoka.
3. Problem pronalaženja bilo kog dokumenta u klasičnom sistemu papirne dokumentacije, neposredno ukazuje na lošu

Nikola Popović, stalni sudski veštak za informacione tehnologije, e-mail: nikola.popovic@eunet.rs, nikola.popovic@mfa.rs, Beograd

Julijana Mirčevski, stalni sudski veštak za informaciono-komunikacionu tehnologiju, julijana.mir@gmail.com, Beograd

 ISBN 978-86-7466-930-3

organizaciju posla u državnom organu. Nije zadatak DMS-a da koriguje lošu organizaciju posla. Dokument pogrešno dislociran u DMS je veoma teško pronaći (na primer: pogrešno imenovan fajl u pogrešnom folderu).

## III. SPECIFIČNOSTI DIGITALNIH DOKUMENATA

Ovde nije mesto za analizu razlike izmedju struktuiranih i nestruktuiranih dokumenata. Dokumenti u domenu finansija i upravljanja kadrovima su u velikom procentu strukturirani. Dokumenti u ostalim domenima nisu strukturirani (note, dopisi, informacije, analize itd.). DMS softveri koji se u ovom trenutku uvode u državnoj administraciji po pravilu ne vode računa o ovoj razlici. Po našim saznanjima prodavci softvera insistiraju na iskustvima softverskog sistema SAP (Systems Applications and Products in Data Processing) koji zahteva obimno, suštinsko prilagodjavanje i unifikaciju poslovanja u posmatranoj organizacionoj celini. Državna administracija je po pravilu tematski organizovana (pravosudje, finansije, zdravstvo, spoljni poslovi itd.). Praksa je pokazala da implementacija "univerzalnog" DMS-a po definiciji usmerenog na rad sa dokumentima kao baznim elementima, generiše nove, neočekivane probleme. Tematski orijentisana organizacija državnog organa zahteva značajno precizniju studiju izvodljivosti (eng. feasibility study). Prodavci DMS-a izbegavaju izradu studije stanja jer ima visoku cenu po vremenu a i zahteva iskusne ljudske resurse. Pokušaj zamene studije stanja anketom ne može da obezbedi pouzdan uvid u organizaciju rada u državnom organu niti da identifikuje bitne probleme.

Korisnički orijentisan pristup (eng. user-centric approach) u implementaciji DMS-a je u osnovi ispravan. Medjutim, organizacija prostora dokumenata u državnoj administraciji i pojedinačnim agencijama ne može da bude korisnički orijentisana (eng. user-centric approach) već tematski orijentisana (eng. topic-centric approach). Insistiranje na zadovoljavanju potreba gradjana i uštedama u državnoj administraciji je jedan aspekt problema. Drugi a značajniji aspekt je da digitalizacija mora da obezbedi uslove za rešavanje potreba državnih organa kako bi oni stvarno mogli da budu efikasniji. Ovo je ključna protivrečnost koja se pojavljuje u usvojenom procesu digitalizacije u državnoj administraciji. Korisnički orijentisan pristup digitalizaciji i tematski orijentisan pristup digitalizaciji su suštinski različiti. Olakšavanje rada korisnika korišćenjem DMS-a ne treba da se svede na “štednju papira” i “smenjenje šetanja po hodnicima”. DMS mora da korisniku obezbedi efikasno raspolaganje informacionim resursima državnog organa odnosno svake niže organizacione jedinice. Nužno je efikasno pretraživanje i mogućnost fleksibilnog, multiaspektnog povezivanja dokumenata. To je uslov za generisanje novih informacija iz raspoloživih dokumenata.

Praktično iskustvo pokazuje da prodavci ne vode računa o bitnim elementima:

kvalitetu skeniranih dokumenata,

koriste proizvod kako bi primarno smanjili svoje troškove organizacije implementacije i održavanja.

Isporučioci ove vrste softvera tvrde da obavljaju OCR (Optical Character Recognition) proces na unetim dokumentima ali u nekim slučajevima je ustanovljeno da se ne radi. Ovo je još jedna bitna protivrečnost digitalizacije u državnim organima. I dalje postoji promet papirnih dokumenata koje je, u postojećim uslovima, nemoguće koristiti samo u digitalnoj formi. Proces OCR-a generiše odredjen manji procenat grešaka u prepoznatom tekstualnom sadržaju dokumenta. U našoj državnoj administraciji uobičajeno se koristi font Times New Roman koji je značajno nepovoljan za proces OCR-a. Pored toga prodavci se ne upuštaju u kvalitet procesa digitalizacije papirnih dokumenata. Slike serijski skeniranih dokumenata po pravilu odstupaju od vertikalne osovine, što zahteva primenu automatske korekcije linearnosti redova teksta (eng. deskewing). Osvetljenost i kontrast slike se drži na prosečnim vrednostima. Prodavci tekstualni sadržaj dobijen OCR-om implementiraju neposredno u PDF dokument, bez provere ispravnosti teksta spelling checkerom. Pošto je tekst dobijen OCR-om ugradjen u PDF nije ga moguće ni vizuelno kontrolisati. Takvi digitalni dokumenti ne mogu da budu priznati za valjanu arhivsku gradju. Ispouručioci softverskih alata u sklopu DMS-a pažljivo ćute o ovim problemima.

Metapodaci implementirani u PDF dokument su i dalje minimalni iako postoje efikasni softveri za generisanje self-contained dokumenata sa znatno većim brojem metapodataka.

U kancelarijskom poslovanju državne administracije uobičajeno je da se uz izlazni dokument dostavlja dopis koji sadrži opis sadržaja dokumenta, razlog za dostavljanje dokumenta, identifikaciju dokumenta itd. Sam dokument koji se prosledjuje je po pravilu prilog. U praksi dokument često ima više priloga. Prodavci uobičajeno povezuju jedan identifikacioni opis dokumenta sa jednim dokumentom (najčešće u PDF formatu u državnoj administraciji). Ovo već sada stvara značajne tehničke i administrativne probleme. Više priloga se pakuje u jedan PDF dokument čime se gubi struktura paketa dokumenata. Gube se veze izmedju dokumenata ili se unose naknadni podaci o vezama. Problem je što tekuće izvedbe DMS sistema ne dozvoljavaju formiranje ad-hoc klastera dokumenata po jednoj ili više tema. U upotrebi je samo jedna unapred propisana klasifikacija, što je jasno sa stanovišta spoljašnjeg korisnika usluga državnog organa. Potreba za organizovanjem prostora dokumenata prema stvarnim, dinamičkim potrebama internog korisnika nije nigde sagledana. Ovakva koncepcija DMS-a bez ikakve potrebe smanjuje upotrebljivost repozitorijuma dokumenata. Iskustvo pokazuje da odredjeni open source programi ove opcije omogućavaju.

Korišćenje novih metoda izdvajanja ključnih reči, nezavisnih od jezika dokumenta i bez kontrolisanog rečnika, stvorilo je nešto veću mogućnost logičkog povezivanja dokumenata u procesu pretraživanja. Značaj se ogleda u tome što se ne zahteva rad profesionalnog indeksera dokumenata, a koji nisu ni predvidjeni za rad u državnoj administraciji. Hijerarhijska klasifikacija dokumenata predvidjena Uredbom o kancelarijskom poslovanju je ispod nivoa potreba rada sa digitalnim repozitorijumima dokumenata.

 ISBN 978-86-7466-930-3

## IV. MOGUĆI PRAVCI PRIMENE DIGITALIZACIJE

Praktično ispitivanje mogućnosti aktuelnih softverskih paketa ukazalo je na moguće pravce razvoja. Logika dodeljivanja privilegija pristupa ukazala je da za segmente ograničene nadležnostima organizacionih jedinica može da se koristi Wordpress [6] u ulozi mikro DMS-a. Na primer arhivske fascikle mogu da se reprezentuju u formi Wordpress web sajta. Pri radu sa udaljenim filijalama (na primer diplomatsko konzularna predstavništva) mogu efikasno da koriste post opcije Wordpress-a, uz obezbedjenje sigurne komunikacije.

Uzroci nemogućnosti pronalaska nekog dokumenta u organu državne administracije prvenstveno leže u slaboj organizaciji rada. Pravila rada (pravilnici) ili nisu ažurirana, ili su loše definisana, ili se jednostavno ne poštuju. Primena glomaznih i veoma skupih DMS sistema sasvim sigurno ne može da reši navedene probleme.

Lista testiranih softverskih modula koji mogu da realizuju funkcionalnosti DMS u manjim organizacionim celinama:

***Wordpress - open source CMS software*** [2] [6]

***nuBuilder - Rapid Application Developer***, sada ima priključak na Wordpress. Koristi relacionu baza podataka MySQL [6]

***Tematres*** - softver za izradu tezaurusa i taksonomija i prikazivanje strukture repozitorijuma dokumenata [7]

***Tesseract free open source softver*** za OCR (Optical Character Recognition) [8]

***ScreenReader*** (komponenta programa ABBYY Fine Reader) koristi se za preuzimanje teksta sa ekrana

***YAKE*** algoritam za ekstrakciju ključnih reči iz dokumenata (bez nadzora - eng. unsupervised method). Za nas je veoma važna karakteritika da rad algoritma ne zavisi od jezika algoritma. Koristi se u verziji programskog jezika ***Python*** bez dodatnog programiranja. [9] spelling checker za srpski jezik (bilo koja implementacija, preporučljivo je da se za rad koristi NoSQL verzija baze podataka na primer MySQL v.8 i dalje). Odredjena regulacija karakteristika može da se postigne izmenom liste tzv. stop reči.

***KNIME*** (open-source data analytics, reporting and integration platform) izuzetno koristan "free machine learning" softver u domenu vizuelnog programiranja (topic aggregation, documents clustering for information consolidation, automatizing workflow itd.) [10]

Praktični eksperimenti ukazuju da već uz minimum programerskih kapaciteta (dva do tri programera srednjeg nivoa obučenosti za programske jezike PHP i Javascript), navedena grupacija open source softvera može da generiše prototipove DMS-a manjih dimenzija, ali bolje prilagodjenih potrebama državne administracije sa aspekta organizovanja prostora dokumenata. U stvari u pitanju su mikro DMS sistemi odnosno mikro CMS sistemi koji mogu da formiraju mrežu za razmenu podataka u slučaju potrebe.

Dosadašnje praktično iskustvo autora ukazuje da sveobuhvatni (eng. large scale) DMS sistemi koji se trenutno implementiraju u državnoj administraciji ne ispunjavaju više bitnih uslova za pouzdanu organizaciju prostora dokumenata u državnoj administraciji.

Posebno konstatujemo da je istraživačka delatnost je praktično onemogućena. Izmene može da radi samo prodavac. Već na kratki rok pojaviće se ozbiljni problemi u funkcionalnosti implementiranih DMS-ova. Velike agregacije dokumenata neće biti fleksibilne i podložne reorganizaciji usled fiksne strukture DMS-ova. Uporno se ponavlja mantra "skalabilnosti", ali se nigde ne pominje da je u pitanju aspekt "fizičke skalabilnosti" (po fizičkim dimenzijama repozitorijuma dokumenata) a ne i "logičke skalabilnosti" (problem generisanja novih informacija, problem konsolidacije informacija vidi Saračević et all. [8]).

Kompanije proizvođači i isporučioci ove vrste softverskih proizvoda redovno zaštićuju svoje proizvode autorskim pravima. Postavlja se pitanje zaštite vlasništva nad podacima i posebno mogućnosti upravljanja podacima od strane državnih organa. U ugovorima se problem migracije na drugi, noviji sistem ostavlja za "buduće vreme". Prodavci izbegavaju ozbiljan razgovor o temi migracije. Korišćenje usluga *Data centara* još uvek nije dovoljno precizirano, posebno u domenu softvera za upravljanje upravljanje podacima - šta se dešava sa softverom ? Pitanje urgentne mobilnosti podataka i posebno DMS-a se retko postavlja iako nas bliska istorija (1999. godina) upozorava na veoma stvarne probleme čuvanja i očuvanja podataka državnih organa.

## V. DIGITALIZACIJA I SRPSKI JEZIK

Jezički aspekti digitalizacije su izostavljeni iz strategija digitalizacije. Information Retrieval problem se uopšte ne pominje u strategijama a neposredno je vezan za jezik i pismo, posebno u domenu državne uprave. Do sada istraživani metodi automatskog indeksiranja dokumenata nisu dali ni približno zadovoljavajuće - pozitivne rezultate. U korpusu dokumenata u domenu državne administracije koristi se jezik u formi koja najverovatnije nije pogodna za proces indeksiranja ("administrativni jezik"). Testiranja su obavljana na Open source softverima, ali veoma je velika verovatnoća da ni komercijalna rešenja ne mogu da daju bolji rezultat. Osnovni problem je što su postojeći jezički alati za srpski jezik veoma ograničenih mogućnosti ili ne postoje u potrebnoj formi (službeni rečnici pojmova, POS tageri, itd.). Na primer u programu Microsoft Word postoji modul Grammar koji izuzetno dobro koriguje pravopisne i gramatičke greške korisnika engleskog jezika i još nekoliko jezika koji su zastupljeni u svetu. Za srpski jezik ne postoji ništa slično čak ni u nagoveštaju. Nedostatak ključnih softverskih komponenti iz domena lingvistike i odgovarajućih jezičkih korpusa dovodi do toga da čitav sistem digitalizacije neće moći da se odvija onom dinamikom kojom se zamišlja. Vidljivost dokumenata i uopšte informacija, drastično je ograničena time što se kasni za tzv. jezičkom industrijom u svetu. Ovo je segment u kome su neophodne inovacije iz domena namenskog softvera, u veoma kratkom roku, a mladi istraživači se već pojavljuju[13] ali im je neophodna promptna podrška države.

 ISBN 978-86-7466-930-3

## VI. ZAKLJUČAK

Uzevši u obzir dugogodišnje iskustvo u radu na parcijalnim procesima digitalizacije u državnim organima, savremeni trend razvoja informatike, tendenciju odvajanja softvera od hardvera, primenu metoda veštačke inteligencije u pretraživanju i druge tekuće prisutne pojave u razvoju informacionog društva, može se zaključiti da je neophodno poštovati sledeće bitne okvire:

- digitalizacija u okviru pojma održivog razvoja,
- digitalizacija treba da se implementira na *open source* softverskim platformama,
- digitalizaciju mora da prati razvoj informatičkog instrumentarijuma za domen srpskog jezika i pisma.

To zahteva angažovanje više specijalista za softver i hardver ali znatno olakšava rešavanje problema interoperabilnosti informatičke podrške tokom dužeg vremena i na raztličitim hardverskim platformama.

Digitalizacija u državnoj administraciji je složen proces. U radu su naznačene primedbe nastale na osnovu praktičnog iskustva i saznanja tokom uvodjenja DMS-a u više institucija. Primedbe se odnose na procese koji generišu nove probleme. Očekivanja da će samo ishitrenom digitalizacijom u državnim organima da se ostvare uštede i ubrzanja rada nisu realna. Potvrdjuje se ispravnost odavno poznatog pristupa evolucionog razvoja sistema. *Outsourcing* razvoja IT sistema i dalje ima visoku cenu.

Trend odvajanja softvera od hardvera, bezbednost podataka i otvorena softverska rešenja prilagodljiva rastućim potrebama korisnika, treba da ostanu postulati razvoja digitalizacije.

Nepoštovanje ove činjenice redovno dovodi do značajnih kašnjenja u implementaciji sistema i nekontrolisanog rasta cena projekata u celini.

## LITERATURA


[1] Qu'est-ce que la documentation? Briet, Suzanne. Paris (1951).
[2] https://www.epa.gov/laws-regulations/, posećeno 12.4.2022.
[3] https://www.srbija.gov.rs/dokument/45678/strategije.php (Retrieved by 09.05.2020 22:24 GMT)
[4] В. Масникоса: Израда структуре за заштиту преноса, чувања и приступа добро чуваним обавештењима (Sisteme –Protect; Patent br.), персонална страница Вукашина Масникосе, http://www.termoenergo.com/source/masnikosa/index.html
[5] EUROPEAN COMMISSION DIGITAL STRATEGY A digitally transformed, user-focused and data-driven Commission, EUROPEAN COMMISSION, Brussels, 21.11.2018 C(2018) 7118 final, https://ec.europa.eu/info/sites/info/files/strategy/decision-making_process/documents/ec_digitalstrategy_en.pdf , Retrieved by 24.05.2020.
[6] https://wordpress.org/ posećeno 21.4.2022.
[7] https://www.nubuilder.com/ posećeno februar 2022.
[8] https://vocabularyserver.com/web posećeno januar-mart 2022.
[9] https://github.com/tesseract-ocr/tesseract posećeno april 2022.
[10] https://github.com/LIAAD/yake posećeno frbruar-april 2022.
[11] https://www.knime.com/ posećeno april 2022.
[12] https://unesdoc.unesco.org/ark:/48223/pf0000047738 posećeno 5.3.2022.
[13] Vuk Batanović, Nikola Ljubešić, Tanja Samardžić, SETimes.SR – A Reference Training Corpus of Serbian. Retrieved by 17.06.2020. https://vukbatanovic.github.io/publication/jtdh_2018_sr/



Abstract - The current state of the digitalization process in Serbia is beginning to show the first, clear signs of contradictory phenomena. A significant number of document management systems are being introduced, especially in the state administration system. With obvious advantages, there are problems with the compatibility of new systems with the existing paperwork system. Harmonization of document availability and mode of operation is difficult. One part of the documents, in addition to the digital version, must still remain on paper. The costs of digitization are high, and these problems cause significant delays in implementation. The paper identifies possible technological solutions that can improve the sustainability of the digitization process.



Index Terms - digitalization; sustainability; methodology of digitalization; state administration.


**Current problems of digitalization in state administration**


Nikola Popović, Julijana Mirčevski


 ISBN 978-86-7466-930-3

# Potencijal SMS komunikacije u mobilnom zdravstvu

Gordana Jelić, Danica Mamula Tartalja, i Enis Osmani

*Apstrakt*— Dobra komunikacija među učesnicima u zdravstvenoj zaštiti je jedan od osnovnih preduslova pozitivnih ishoda različitih intervencija u ovoj oblasti. Razmena tekstualnih poruka ili usluga kratkih poruka SMS (*Short Messages Service*), odnosno alfanumeričkih poruka od 160 ili manje znakova, nalazi se među najčešće korišćenim alatima mobilnog zdravstva. Cilj ovog rada je da se prikaže kratak pregled postojećih studija i literature o upotrebi SMS poruka u zdravstvene svrhe, fokusirajući se na pragmatički aspekat diskursa kratkih poruka. Analizirajući primere poruka na gramatičkom, leksičkom i komunikološkom nivou, ukazaćamo na jezička sredstva koja predstavnici zdravstvenog sistema (lekari, institucije) upotrebljavaju kako bi ostvarili željeno tumačenje poruke i postigli efekat kod ciljne grupe. Upotrebom efikasnih načina za poboljšanje modalnosti jezičkog izraza,komunikacija kratkim porukama nadmašuje tehnološka ograničenja ovog komunikacionog medijuma.

***Ključne reči*—mobilno zdravstvo, komunikacija, SMS poruke**

## I. Uvod

Pametni telefoni i mobilne platforme za razmenu zdravstvenih poruka menjaju način na koji upravljaju zdravstvenim programima stanovništva. Prema Međunarodoj uniji za telekomunikacije gotovo polovina svetske populacije još uvek nije povezana na internet, ali 97% globalne populacije, ili sedam milijardi ljudi, živi u području pokrivenom mrežom mobilnih telefona [1]. Zbog sveprisutne dostupnosti mobilnih telefona i mogućnosti za interaktivnu komunikaciju kao i komunikaciju u realnom vremenu, tokom protekle decenije došlo je do brzog širenja intervencija u mobilnom zdravstvu (*mHealth*) kako bi se pomoglo u rešavanju dispariteta u pristupu zdravstvenim uslugama i poboljšanju zdravstvenih ishoda. Dobra komunikacija omogućava da se saznaju informacije neophodne za tačnu dijagnozu problema, da lekari bolje razumeju potrebe svojih pacijenata i što efikasnije dovedu do ozdravljenja ili ublažavanja simptoma bolesti. Takođe, doprinosi boljem razumevanju problema od strane pacijenata, pridržavanje preporučenim terapijama i lekovima i daje pozitivne efekte na troškove zdravstvene zaštite (smanjenje dijagnostičkih testova, upućivanje u bolnicu i dužinu boravka u njoj). SMS poruke, u poređenju sa tradicionalnim telefonskim pozivom, obezbeđuje nisku cenu, trenutni prenos informacija i bolju dostupnost [2]. Mobilna zdravstvena tehnologija pruža različitim kategorijama korisnika non-stop pristup visokokvalitetnim informacijama po niskoj ceni putem tekstualnih poruka i mobilnih aplikacija.

Razmena tekstualnih poruka TMI (*Text-messaging Intervention*) je popularna jer se kratke poruke mogu slati, čuvati, može se odgovarati na njih i mogu se preuzimati po potrebi korisnika; relativno je jeftina i pritom dostupna za bilo koju vrstu telefona. Sa slanjem poruka i e-poštom koje prevazilaze telefonske pozive kao najpopularniji način komunikacije, provajderi mogu kreirati personalizovane, sadržajno bogate, čak i interaktivne poruke koje podstiču angažovanje [10].

Interaktivne SMS poruke smanjuju verovatnoću prekomernog opijanja kod mladih odraslih osoba. Postoje usluge koje pružaju informacije o mentalnim bolestima kao što su šizofrenija, depresija, anksioznost i stres. SMS poruke se šalju u primarne, privatne „sandučiće" učesnika i mogu se lako primiti i odložiti; ovo bi mogao biti jedan od razloga za njihovu efikasnost kao intervencije mHealth. SMS mHealth intervencije se takođe smatraju anonimnim i stoga ruše određene barijere pristupu zdravstvenoj zaštiti. [9]

Primeri zdravstvenih programa stanovništva zasnovanih na tehnologijama mobilnog zdrastva su brojni. Oni uključuju programe tekstualnih poruka koji ciljaju na probleme javnog zdravlja, kao što su pušenje, zdravlje majke/bebe, gubitak težine, fizička aktivnost, anksioznost/depresija i slično. Drugi programi podsećaju ljude da zakažu velnes termine, vakcinaciju, ili su usmereni na populacije sa hroničnim bolestima. Složeniji programi uključuju interaktivne platforme i cilj su im pacijenti otpušteni iz bolnice, oni kojima je potrebna naknadna nega, ili hronični bolesnici, kojima je potrebna nega između poseta ordinaciji. Ove platforme mogu uključivati upitnike koji, kada se na njih odgovori, nude put do informacija o upravljanju negom ili pokreću upozorenja koja podstiču praćenje od tima za negu.

Pravovremeno pružanje informacija i upozoravanje ljudi u realnom vremenu je važno u svim segmentima zdravstvene zaštite. Komunikacija putem SMS poruka pokazala se kao bitna komponenta m zdravstva u borbi protiv pandemije COVID19. Platforme za praćenje pomoću SMS poruka pokazale se se kao koristan sistem ranog upozorenja za

Gordana Jelić – Akademija tehničko-umetničkih strukovnih studija Beograd, Odsek Visoka škola za informacione i komunikacione tehnologije, Zdravka Čelara 16, 11000 Beograd, Srbija (e-mail: gordana.jelic@ict.edu.rs).

Danica Mamula Tartalja – Akademija tehničko-umetničkih strukovnih studija Beograd, Odsek Visoka škola za informacione i komunikacione tehnologije, Zdravka Čelara 16, 11000 Beograd, Srbija (e-mail: danica.mamula@ict.edu.rs).

Enis Osmani – Akademija tehničko-umetničkih strukovnih studija Beograd, Odsek Visoka škola za informacione i komunikacione tehnologije, Zdravka Čelara 16, 11000 Beograd, Srbija (e-mail: enis.osmani.26.19@ict.edu.rs).

 ISBN 978-86-7466-930-3

upućivanje pacijenata sa pogoršanim kliničkim statusom na bolničku negu ili dodatni savet lekara. [2, 3]. Takođe, veoma korisnim se pokazalo slanje jednosmernih SMS poruka (obaveštenja, preporuke, upozorenja) od strane zvaničnih zdravstvenih ustanova i ministarstava.

Na vrhu piramide nalaze se programi za koordinaciju nege koji crpe podatke iz elektronskog zdravstvenog kartona kako bi razvili personalizovane poruke koje usmeravaju pacijenta na određene resurse, upravljaju receptima ili šalju podatke nazad, pružaocu usluge, za naknadnu negu. Najčešće, ove programe razvijaju i pokreću zdravstveni radnici koji žele da poboljšaju upravljanje brigom za pacijente kod kuće, uključujući one koji su nedavno otpušteni i takozvane „*frequent flyers*“ — pacijente sa više hroničnih stanja kojima su potrebne svakodnevne ili skoro svakodnevne intervencije kako bi upravljali svojim zdravljem i pritom ih držati van bolnice.

SMS projekti u mobilnom zdravstvu imaju za cilj poboljšanje u praćenju pacijenata i razmeni informacija. Takođe omogućavaju prikupljanje podataka, vođenje evidencije i komunikaciju sa novim pacijentima. Mobilno zdravstvo nije ograničeno na intervencije ili podsetnike putem SMS poruka. Mogućnosti pružanja usluga višestruko su porasle, posebno od pojave IoT (*Internet of Things*). To takođe znači da su mogućnosti, ali i tehnički zahtevi, mnogostruki. Starije generacije i druge kategorije primalaca zdravstvenih usluga često se teško prilagođavaju tehnološkom razvoju, pa su stoga isključene iz inovacija koje bi im mogle biti od koristi. Pitanje je da li je legitimno isključiti ljude iz usluga zato što ne mogu ili ne žele da koriste određene aplikacije, s obzirom na to da su SMS poruke su pogodne da se, što šire, dopre do svih delova stanovništva svake zemlje u borbi protiv bolesti.

## II. Teorijski okvir i metode istraživanja

Razlozi za upotrebu komunikacije putem SMS poruka u oblasti zdravstva su višestruki, a same poruke se mogu podeliti u dve grupe, u zavisnosti od toga da li su jednosmerne (monološke) ili interaktivne (dijaloške). Jednosmerne poruke ne zahtevaju odgovor i obuhvataju podsetnike, motivacione poruke koje imaju za cilj da pruže podršku pacijentu ili da ga podstaknu na akciju. Dijaloške poruke predstavljaju interakciju lekar-pacijent u pisanom obliku i u najvećem broju slučajeva su nastavak komunikacije koja je započeta ili u ordinaciji kao razgovor licem u lice ili putem telefona, i kao takva odnosi se na praćenje stanja pacijenta, primenu i efekte terapije, analizu rezultata testova i ispitivanja i slično.

U skladu sa obimom ovog rada, prevashodno su razmatrane jednosmerne SMS poruke, odnosno koja jezička sredstva se koriste da bi se poruka prenela na najbolji mogući način. Naime, poruka mora da bude kratka i jasna, relevantna, fokusirana i razumljiva primaocu poruke. Komunikacija lekar/zdravstveni sistem-pacijent pripada institucionalnom diskursu (engl. *institutional talk*) gde je komunikaciona moć nejednako raspoređena. Heritidž [3] ističe da je jedna od osnovnih karakteristika institucionalne komunikacije asimetrija, koja se ogleda na više ravni, kao što su učešće u interakciji, odnos prema problemu, znanje, kao i pravo na posedovanje znanja. Drugim rečima, u medicinskom susretu lekar je taj koji ima profesionalno znanje i poseduje moć u komunikaciji. Međutim, kada se ova interakcija prenese u pisani oblik ta moć se polako gubi. U nedostatku neverbalne komunikacije i pravovremene reakcije (*feedback*) od strane pacijenta, lekar kao pisac SMS poruke mora da, pored svog stručnog znanja, uloži dodatni trud da kroz upotrebu odgovarajućih jezičkih sredstava obezbedi razumevanje, a samim tim i željeno tumačenje poruke i ostvarivanje planiranog cilja.

U komunikologiji se struktura poruke definiše kroz informaciju (novostečeno znanje) i redundantni sadržaj, odnosno postojeće znanje bez kog razumevanje ne bi bilo moguće. Koristeći kvalitativne metode analize konverzacije [4, 5], a uzimajući u obzir osnovne principe kritičke analize diskursa [6], induktivnim pristupom opisaćemo jezičke elemente koje smo uočili u primerima kratkih poruka.

## III. Studije slučaja

TMI se može koristiti u različitim vrstama intervencija mobilnog zdravlja. Poruke se kategorizuju prema različitim kriterijumima: komunikacija o promeni ponašanja (npr. podsetnici za preglede i lekove, promocija zdravlja kao što je prestanak pušenja, mobilizacija zajednice); prikupljanje podataka ili informacija (npr. prikupljanje i izveštavanje o zdravstvenim informacijama i pružanje usluga, praćenje vitalnih događaja, kao što su epidemije); upravljanje logistikom ili lancem snabdevanja (npr. obezbeđivanje osnovnih zaliha i lekova na zalihama u različitim zdravstvenim ustanovama). Mnoge studije ukazuju na to da TMI značajno poboljšava različite situacije u zdravstvu, kao što su uzimanje lekova, prisustvo lekarskim pregledima i ishode promene ponašanja, samokontrolu dijabetesa, prestanak pušenja, gubitak težine, povećanje fizičke aktivnosti.

Nažalost, zdravstveni sistemi u Republici Srbiji, kako državni tako i privatni, veoma malo koriste SMS komunikaciju sa korisnicima svojih usluga. Zapaženo je pojedinačno angažovanje lekara na društvenim mrežama (*Twitter*, *Facebook*), koji direktno odgovaraju na zdravstvena pitanja svojih pratilaca. Međutim, kako i dalje veliki deo stanovništva ne koristi društvene mreže, ovim radom mi želimo da ukažemo na potrebu i značaj uspostavljanja SMS komunikacije na institucionalnom nivou, kao najpogodnijeg vida komunikacije koji može da dopre do najvećeg broja korisnika. Takođe, paralelno sa razvojem tehničke podrške, potrebno je ukazati lekarima na specifičnosti jezičke upotrebe u medijumu kakav je SMS komunikacija, s obzirom na jezgrovitost i preciznost kratkih poruka, kao i na specifična obeležja pisanog jezika u odnosu na govor.

Kao ilustraciju, uzećemo za primer poruku – poziv na vakcinaciju - koju je poslao Institut za javno zdravlje Srbije „Dr Milan Jovanović Batut” 16. novembra 2021. godine. Ovo je prva SMS poruka koju je neki zdravstveni sistem poslao svim građanima Srbije, angažujući sve mobilne operatere koji su

 ISBN 978-86-7466-930-3

poruku poslali svojim korisnicima. Prvo što možemo uočiti jeste da ova poruka nema epistolarnu formu, koja je tipična za SMS poruke prilikom prvog obraćanja. Dakle, nema uspostavljanja kontakta u formi oslovljavanja. Zanimljiva je i upotreba lične deikse (grč. *deixis=pokazivanje, ukazivanje*), lingvističke kategorije koja označava skup jezičkih elemenata koji upućuju na lica, odnosno na učesnike u komunikacionom činu [8]. Ovde je lična deiksa iskazana upotrebom *inkluzivnog mi* (govornik i sagovornik), odnosno glagolima u prvom licu množine: *„borimo se"* i *„imamo"*. Direktnim obraćanjem u drugom licu jednine, što je u skladu sa suštinski ličnom prirodom SMS komunikacije, bilo upotrebom lične zamenice „*Tvoja vakcina čeka na tebe"* ili imperativa *„Dođi, vakciniši se i pridruži se"*, uspostavlja se bliskost i osećanje empatije. Na tri mesta u poruci upotrebljen je oblik superlativa prideva: *„najjače oružje", „u najbližem domu zdravlja", „prema sebi i svojim najbližima"*. Umesto pozdrava, poruka završava pozivom na akciju *„Na tebe je red."*. Dakle, poruka je napisana veoma biranim jezičkim sredstvima koja imaju za cilj da izvrše emocionalni i psihološki uticaj na primaoce poruke i da ih podstaknu na delovanje.

Na sajtu Svetske zdravstvene organizacije (*WHO – World Health Organization*) nalazi se dokument sa svim SMS porukama koje je ova organizacija pripremala u skladu sa epidemiološkim okolnostima izazvanim COVID-19. Zemlje članice SZO su pozvane da prevedu poruke sa engleskog jezika na svoj jezik, da prilagode sadržaje poruka i da ih distribuiraju svom stanovništvu i na taj način iskoriste prednosti elektronske komunikacije kako bi spasili živote od ove zarazne bolesti. Na listi se nalazi 50 SMS poruka koje su grupisane tematski (prevencija, simptomi, samoizolacija, mentalno zdravlje, itd.).

Sintaksička struktura ovih poruka je jednostavna, uglavnom su to naporedne rečenice u kojima su nosioci značenja glagoli u imperativu, glagolskom načinu koji ima za cilj da iskaže sugestiju, molbu, zapovest, zabranu i slično. Izrazima poput *'wash your hands; avoid touching your eyes; cover your mouth; dispose of used tissues; keep 1 meter distance; be active; quit smoking to reduce your risk; have fun; contact your friends and family*' na jasan, koncizan i sugestivan način ostvaruje se komunikaciona namera poruke.

Uočili smo i određeni broj uslovnih i namernih zavisnih rečenica, kojima se dodatno ističe odgovornost primaoca poruke ukoliko se ne ponaša u skladu sa preporukama. U najvećem broju poruka, pošiljalac se direktno obraća primaocu poruke, osim u slučajevima kada se sadržaj odnosi na posebne kategorije stanovništva (deca, stariji ljudi, ljudi sa invaliditetom) i tada se o njima govori kao o „trećoj strani".

Ako analiziramo SMS poruke koje Istitut za transfuziju krvi Srbije po potrebi šalje na više adresa, možemo uočiti kako se pažljivim izborom leksike pozivaju potencijalni davaoci krvi na ovaj humani gest. Rečima i sintagmama, kao što su *„pokažimo solidarnost", „Da život pobedi!", „Sreća je veća kada se deli sa drugima!"* primaoci poruka se podstiču na akciju. Iz teksta objavljenog na sajtu BudiDavalacKrvi, napisanog prema izvorima iz časopisa *ScienceAlert* i *The Independent*, saznajemo da je i u razvijenim zemljama poput Velike Britanije i Švedske, zbog pada u broju novih davalaca krvi, razvijen automatizovani servis za tekstualne poruke sa ciljem da podstakne stanovništvo da donira i nastavi sa doniranjem krvi, i da ih obaveštava tačno kada je njihova krv upotrebljena za lečenje pacijenta.

## IV. ZAKLJUČAK

U želji da dopru do što većeg broja korisnika, zdravstveni sistemi u svetu opredeljuju se za komunikaciju SMS porukama jer su zbog dometa i veze sa internetom sigurniji da će poruka biti primljena, ali i pročitana, s obzirom da se uopšteno govoreći manje razmenjuju SMS poruke u odnosu na komunikaciju pomoću aplikacija kao što su *Viber* ili *WhatsApp*. Multimedijalnost, odnosno vizuelni aspekat komunikacije zamenjuje ili dopunjuje tekstualne SMS poruke kada postoji potreba da se slanjem slike postigne bolje razumevanje i efekat sadržaja poruke.

Komunikacija lekar-pacijent je složena interakcija koja, pored ispunjenja različitih zahteva, podrazumeva razumevanje emocionalnog stanja pacijenta. Zbog toga je važno povećati svest lekara o tome kako njihove negativne emocije mogu uticati na pacijente, što se ogleda u njihovim stavovima prema pacijentima, ali i u načinu na koji ih pacijenti doživljavaju.

Medijum SMS komunikacije je, sam po sebi, ograničen u mnogim aspektima i zahteva dobro promišljenu i oblikovanu poruku koja će biti na odgovarajućem nivou razumevanja ciljne grupe pacijenata (*health literacy*). Upravo zbog toga, potrebno je posvetiti više pažnje pragmatičkoj analizi jezika kratkih poruka. Pragmatička perspektiva diskursa je posebno usmerena na one aspekte diskursa koji su iako nenapisani ili neizrečeni, uspešno komunikativno preneseni [8]. Buduća istraživanja upotrebe jezika kratkih poruka u oblasti mobilnog zdravstva trebalo bi da predlože različita jezička i nejezička semiotička sredstva kojima se mogu izraziti stavovi, namera i odnos prema sagovorniku, odnosno da definišu lingvističke i diskursne strategije koje bi lekari mogli da koriste u cilju uspešnije komunikacije sa svojim pacijentima.

U zemljama sa više jezika, pismenost može da varira u zavisnosti od jezika, a neophodna su razmatranja u vezi sa odgovorima na više jezika. Jedinstvena razmatranja i prilagođavanja mogu biti neophodni ako se koristi nelatinično pismo na telefonima. Iako postoje relativno napredni softverski alati za obradu prirodnog jezika, odnosno za tumačenje jezika kao što je engleski, mnogo manje alata je razvijeno za autohtone jezike [9]

## LITERATURA

[1] International telecommunication Union. *The World in 2016: ICT Facts & Figures.* 2016

[2] P.Loubet, C.Czeschan, M.Sintes, A.Sotto, D.Laureillard, Use of short message service in at-home COVID-19 patient management, *BMC Medicine* volume 18, Article number: 391 (2020)

[3] JJ.Saleem, JM.Read, BM.Loehr, KL.Frisbee, NR.Wilck, JJ.Murphy, et al. Veterans'response to an automated text messaging protocol during the COVID-19 pandemic. *J Am Med Inf Assoc*, 2020.

[4] J. Heritage & S. Sefi, "Dilemmas of advice: Aspects of the delivery and reception of advice in interactions between health visitors and first time mothers''. In P.Drew & J. Heritage (Eds.), Talk at work: interaction in institutional settings (pp. 359-417). Cambridge: CPU, 1992.

 ISBN 978-86-7466-930-3

[5] E. A. Schegloff, *Sequence organization in interaction: A primer in conversation analysis*, Cambridge: CUP, 2007.
[6] S. Stević, *Analiza konverzacije*, Beograd: Filološki fakultet, 1997.
[7] T. A. van Dijk, "Aims of critical discourse analysis", *Japanese Discourse*, Vol. 1, 17 – 27, 1995.
[8] G. Yule, *Pragmatics*, Oxford: OUP, 1996.
[9] A.L.Drake, C.Rothschild, W.Jiang, K,Ronen, J.A. Unger, Utility of Short Message Service (SMS) for Remote Data Collection for HIV in Low- and Middle-Income Countries, Springer Science+Business Media, LLC, part of Springer Nature, Current HIV/AIDS Reports pp 654–662, 2020
[10] S,Iribarren,, R,Giguere, P,Stone, R,Schnall, N,Staggers, A,Carballo-Diéguez, Scoping Review and Evaluation of SMS/text Messaging Platforms for mHealth Projects or Clinical Interventions, Int J Med Inform. 101, pp 28–40, May 2017

ABSTRACT

**On the Potential of SMS Text Messaging in mHealth**

Gordana Jelić, Danica Mamula Tartalja, Enis Osmani

Good communication among participants in health care is one of the basic preconditions for positive outcomes of various interventions in this area. Text messaging or Short Messages Service (SMS), or an alphanumeric message of 160 characters or less, is one of the most commonly used mobile health tools. This paper aims to present a brief review of contemporary studies and literature on the use of SMS messages for health purposes, focusing on the pragmatic aspect of the discourse of short messages. Analyzing examples of messages at the grammatical, lexical and communicative level, we point out the language tools that representatives of the health system (doctors, institutions) use to achieve the desired interpretation of the message and achieve the effect on the target group. By using effective ways to improve the modality of linguistic expression, short message communication goes beyond the technological limitations of this communication medium.

Key words: mobile health, communication, SMS

 ISBN 978-86-7466-930-3

# СПЕЦИЈАЛНА ТЕМАТСКА СЕСИЈА – ФОРЕНЗИКА

# /

# SPECIAL THEMATIC SESSION - FORENSICS

# (СТС-ФО/STS-FO)

ISBN 978-86-7466-930-3

# Forenzičke metode za identifikaciju lica: juče, danas, sutra

Snežana Stojičić, Radovan Radovanović, Nataša Petrović i Milesa Srećković

*Apstrakt*—**Identifikacija lica je bila, jeste i biće izazov za oji se ontinuirano nalaze rešenja koja pružaju tehnološki odgovor u ovoj oblasti, posebno zasnovanih na upotrebi biometrijs ih podata a u ele trons om obli u i primene principa i is ustava najbolje pra se ele trons og poslovanja uopšte. potreba podata a u ele trons om obli u, smeštenih u određenim bazama podata a, sredstava ele trons e komunikacije i elektronske obrade velike količine podataka u obavljanju poslovnih procesa identifi acije lica je evidentno u porastu, ao odgovor na izazove oje ele trons o poslovanje donosi, neophodno je usaglašavanje razvoja normativnog o vira ako u domenu povećanja efikasnosti poslovanja ta o i izazova oje digitalna era sa sobom nosi. Izazov, sa forenzičkog aspekta, kao odgovor na potencijalno narušavanje i nepoštovanje pravnih normi, uslovljava razvoj i primenu novih procedura i alata u ovoj oblasti. Danas je evidentna potreba stalnog praćenja razvoja i primene novih metoda za identifi aciju lica, a posebno onih, oje mogu biti vezane za forenzičke aspekte u digitalnom svetu. Predmet razmatranja su upravo ova pitanja, oja se odnose na izazove u identifi aciji lica u digitalnoj eri.**

***Ključne reči*—Forenziče metode; idetifikacija lica; biometrijs i podaci.**

## I. UVOD

Za sisteme za biometrijsku identifikaciju se može reći da imaju više generacija, koje se zasnivaju na tehnološkim rešenjima, odnosno prate razvoj tehnologije, koja uslovljava i omogućava identifikaciju lica zasnovan na biometrijskim podacima. Savremeno digitalno okruženje, stvara nove izazove i mogućnosti za počinioce krivičnih dela, ali i službe, koje utiču u rasvetljavanju istih. Tako proces digitalizacije i modernizacije poslovnih procesa, neophodno prati i razvoj adekvatnog odgovora sa aspekta primene metoda za identifikaciju lica sa aspekta forenzike.

.

## II. PRVE GENERACIJE BIOMETRIJSKIH TEHNOLOGIJA

Biometrijske tehnologije prve generacije bile su fokusirane na jaku biometriju i jedinstvenost identifikacija ili autentikacija određenih pojedinaca (fizičkih lica). Prvi slučajevi upotrebe velikih razmera, počeli su kasnih 1990-ih u SAD, sa povećanjem primene posebno posle uvođenja biometrijskih pasoša, koji sadrže otiske prstiju, fotografiju i podatke o licu. Od tada, biometrijske tehnologije su postale robusnije i naprednije, značajno smanjujući stope grešaka uz pomoć razvoja računarske tehnologije i primenjenih rešenja, a naročito u tehnologijama za prepoznavanje lica.

Prve primene biometrije i razvijenih alata za brzu i pouzdanu identifikaciju ili autentikaciju, našle su širok spektar konteksta primene, uključujući potrebe sprovođenja zakona. Primena se zayim proširila i na privatni sektor, uključujući rešenja kao što su ona za otključavanje pametnih telefona ili prepoznavanje VIP-a kupaca. Rešenja zasnovana na biometriji u nekim slučajevima zamenjuju tradicionalne lozinke, posebno imajući u vidu da sa najnovijim tehnologijama za prepoznavanje lica moguća je identifikaciju za manje od jedne sekunde.

Ne manji značaj imaju i takozvane "slabe" biometrijske metode, kao biometrijske metode druge generacije, kao što su motoričke veštine, osobenosti položaja tela, hod i način interakcije sa okruženjem [1]. Ova druga generacija biometrije se naziva i „biometrija ponašanja", jer je digitalno fizičko i kognitivno ponašanje ljudi analizira, a ne relativno statičke karakteristike, kao što su otisci prstiju. Posebno je od interesa, to što druga generacija biometrijskih sistema, pruža nove mogućnosti automstizacije poslovnih procesa u organima za sprovođenje zakona, vršenju granične kontrole, omogućavajući, na primer, otkrivanje lica sumnjivog ponašanja koje bi moglo da ukaže na nameru da počini krivično delo.

Da bi se povećala tačnost, biometrijske tehnologije prve generacije se redovno kombinuju u multimodalne sisteme. Ovi sistemi kombinuju nekoliko biometrijskih identifikatora za identifikaciju jedne osobe. Multimodalni sistemi mogu minimizirati rizike od pojave grešaka i pomoći u prevazilaženju poteškoća uzrokovanih lošim kvalitetom podataka ili podacima koji nedostaju, istovremeno povećavajući mogućnosti i u drugim aspektima, kao što je etički.

Tehničko tehnološki napredak omogućava sve veću primenu sistema video nadzora, kojima se omogućava upotreba biometrijskih tehnika i veštačke inteligencije za identifikaciju lica u javnim prostorima, što implicira potrebu da se striktno reguliše upotreba ovih sistema. Napredak tehnologije i potreba za normativnim uređenjem primene savremenih tehnoloških rešenja predstavlja stalni izazov, posebno imajući u vidu komparativnost ovih oblasti korišćanja biometrije, kako na nacionalnom, tako i na međunarodnom planu.

Snežana Stojičić, Ministarstvo unutrašnjih poslova, Kneza Miloša 101, 11000 Beograd, Srbija (e-mail: snezana.stojici@mup.gov.rs),
Radovan Radovanović – Kriminalističko policijski univerzitet, Cara Dušana 196, 11000 Beograd, Srbija (e-mail: radovan.radovanovic@kpu.edu.rs),
Nataša Petrović – Ministarstvo unutrašnjih poslova, Kneza Miloša 101, 11000 Beograd, Srbija (e-mail: natasa.petrovic@mup.gov.rs)
Milesa Srećković – Elektrotehnički fakultet, Univerzitet u Beogradu, Bulevar Kralja Aleksandra 73, 11020 Beograd, Srbija (e-mail: esreckov@etf.bg.ac.rs).

 ISBN 978-86-7466-930-3

Pošto su aktivnosti mozga merljivi biološki signali, one se takođe smatraju biometrijskim. S obzirom na poteškoće u hvatanju elektrohemijskih signala mozga i njihovu složenost, relevantnost moždanih aktivnosti je dugo vremena bila ograničena na medicinski sektor. Međutim, poslednjih godina, elektroencefalografija (EEG), koja snima električne aktivacije mozga postavljanjem elektroda na skalp i takozvani interfejsi mozak-kompjuter (BCI), koji mogu da prevedu aktivnost mozga u mašinski čitljivi unos, postali su pristupačniji [2] i čak su integrisani u proizvodima širo biometrijske autentikacijeke potrošnje[1].

## III. Dalji pravci razvoja metoda identifikacije lica

Predlog regulatornog okvira o veštačkoj inteligenciji[2], Evropska komisija je usvojila u prvoj polovini 2021. godine, kao novi pravni okvir za primenu veštačke inteligencije. Predlog uredbe ima za cilj da programerima, onima koji koriste veštačku inteligenciju i korisnicima, pruži jasne zahteve i obaveze u vezi sa specifičnom upotrebom AI[3]. U isto vreme, predlog uredbe obuhvata i aspect usmeren ka smanjenju administrativnih i finansijskih opterećenja za preduzeća, posebno za mala i srednja preduzeća (MSP) [3, 4].

Predlog je deo šireg paketa, koji se odnosi na veštačku inteligenciju, a koji je posvećen jačanju, prihvatanju, ulaganju i inovacijana u oblasti AI u EU.

Zašto su nam potrebna pravila o AI? Predloženi propis o veštačkoj inteligenciji obezbeđuje da se izgradi poverenje u ono što veštačka inteligencija može da ponudi. Dok većina sistema veštačke inteligencije predstavlja ograničen rizik i može doprineti rešavanju mnogih društvenih izazova, određeni sistemi veštačke inteligencije stvaraju rizike, koji se moraju rešavati, kako bi se izbegli neželjeni ishodi.

Važno je istaći da iako postojeće zakonodavstvo pruža određeni okvir, procenjuje se da je nedovoljno da se odgovori na specifične izazove, koje donose sistemi veštačke inteligencije.

Predložena pravila će se baviti rizicima koje posebno stvaraju AI aplikacije, predložiti listu visokorizičnih aplikacija, postaviti jasne zahteve za AI sisteme za aplikacije visokog rizika; definisati posebne obaveze za korisnike veštačke inteligencije i provajdere visokorizičnih aplikacija; predložiti ocenu usaglašenosti, pre nego što se sistem veštačke inteligencije stavi u upotrebu ili stavi na tržište; predložiti način praćenja pošto se takav AI sistem stavi na tržište; i predložiti strukturu upravljanja na evropskom i nacionalnom nivou.

Opis stanja biometrijskih tehnologija sa aspekta EDPS[4] (European Data Protection Supervisor), indukuje da broj uređaja koji se primenjuju za obradu biometrijskih podataka raste neverovatnom brzinom. Mnogi pametni telefoni koriste slike lica i otiske prstiju za autentikaciju svojih korisnika. Virtuelni glasovni asistenti obrađuju glasovne podatke kao odgovore na zahteve korisnika. Sistemi video nadzora mogu se koristiti za identifikaciju ili klasifikaciju pojedinaca/lica. Pametni satovi i fitnes narukvice mogu pratiti i obrađivati podatke o fiziološkom statusu (kao što su otkucaji srca i navike spavanja). Sistemi video nadzora su imali značajnu ulogu i sa aspekta pandemije COVID-19, podrška korišćenjem prepoznavanja lica i veštačke inteligencije za praćenje socijalno distanciranje ili pravilna upotreba maski za lice, kao i upotreba termovizijskih osetljivih kamera i prepoznavanja lica, koja se mogu na osnovu povišene temperature identifikovati kao potencijalno zaražen, korona virusom.

Poseban domen primene i korišćenja biomtrijskih podataka čine informacioni sistemi velikih razmera, kao što su tri velika IT sistema u oblastima azila i migracija, koji su trenutno operativni i uključuju korišćenje biometrijskih podataka: Vizni informacioni sistem (VIS), Šengenski informacioni sistem (SIS II) i EURODAC (European Asylum Dactyloscopy Database), sistem koji obrađuje podatke o tražiocima azila.

Pored toga u pripremi su, još tri nova evropske informaciona sistema, velikih razmera, od kojih će dva obrađivati biometrijske podatke: Ulazno-izlazni system (EES) i Evropski informacioni sistem krivičnih evidencija za državljane trećih zemlja (ECRIS-TCN). Iako su ovi informacioni sistemi razvijeni nezavisno, nova regulativa interoperabilnosti[5], definiše četiri osnovne komponente interoperabilnosti koje bi trebalo da omogućavaju međusobnu interakciju. Među njima, i rešenje za zajedničko upoređivanje biometrije - (BMS) odnosno otisaka i slika lica kroz različite sisteme [5].

Međutim uz očekivan porast primene, važno je paralelno sprovoditi i aktivnosti na podizanju svest o izazovima koje biometrijske tehnologije donose, a posebno sa aspekta izgradnje poverenja u tehnološka rešenja.

Takođe, javljaju se izazovi i nove mogućnosti zloupotreba novih tehnologija, kao što je Clearview AI, koji je preuzeo oko 3 milijarde slika, prikupljenih sa miliona web lokacija, uključujući Fejsbuk, Tviter i Jutjub, i sada prodaje svoje usluge organima za sprovođenje zakona, ili poljska platforma PimEyes koja je uradila to isto [6]. Povećana upotreba biometrijskih podataka uz nemogućnost promene fizioloških osobina, donosi povećanu zabrinutost za bezbednost biometrijskih podataka.

Ako projektanti biometrijskih sistema ne primenjuju odgovarajuće mere zaštite, posledice povrede ličnih podataka bile bi veoma ozbiljne. Upravo iz tog razloga, nastali su međunarodni standardi kao što su ISO/IEC 24745 ISO/IEC 24745:2011 Information technology — Security techniques — Biometric information protection i standard u oblasti mehanizmima zaštite biometrijskih šablona (BTP), a aktuelnost potvrđuje ISO/IEC 24745:2022, Information security, cybersecurity and privacy protection — Biometric information protection, revizija koja pokriva zaštitu biometrijskih informacija pod različitim zahtevima za poverljivost, integritet i obnovljivost/opoziv tokom

[1] Technology | Unicorn Hybrid Black (unicorn-bi.com)
[2] EUR-Lex - 52021PC0206 - EN - EUR-Lex (europa.eu)
[3] AI – Artificisl Intelligence
[4] 20-10-07_edps_biometrics_speech_en.pdf (europa.eu)
[5] https://eur-lex.europa.eu/legal-content/EN/TXT/?uri=CELEX:32019R0817


ISBN 978-86-7466-930-3

skladištenja i prenosa. Standard identifikuje zahteve i daje preporuke za bezbedno upravljanje i obradu biometrijskih informacija u skladu sa pravilima privatnosti [7].

Međutim, neizvesno je u kojoj meri, projektanti i programeri biometrijskih sistema prate i primenjuju standard, posebno imajući u vidu, da je otkriveno [8] da je postojao pristup preko 27,8 miliona zapisa nezaštićenih i uglavnom nešifrovanih, a da za razliku od kompromitovanja lozinki, kada se to dogodi sa otiscima prstiju, ne postoji mogućnost da promenite otisak prsta. Baza podataka se odnosila na Biostar 2, system, koji je razvila kompanija za obezbeđenje Suprema [9].

Početkom marta 2022. godine objavljeno je da je Samsung potvrdio kršenje bezbednosti pošto što su hakeri pristupili i preuzeli skoro 200 gigabajta poverljivih podataka, uključujući izvorni kod za različite tehnologije i algoritme za operacije biometrijskog otključavanja. Hakerska grupa Lapsus, preuzela je odgovornost i objavila da su preuzeli izvorni kod koji Samsung telefoni koriste za obavljanje osetljivih operacija, algoritme za sve otključavanje na osnovu biometrije [10].

Osetljiva priroda biometrijskih podataka prepoznata je i u okviru pravnog okvira EU, kao i u okviru Modernizovane konvencije Saveta Evrope 108+, podleže posebnoj zaštiti i može se reći da je obrada biometrijskih podataka zabranjena u principu i postoji samo ograničen broj uslova pod kojima takva obrada je zakonita, tako da u okviru svojih zadataka nadzora i sprovođenja, EDPS sprovodi između ostalog i redovne revizije velikih IT sistema EU.

Svakako, prethodno pitanje pre svake primene, treba da bude vezano za procenu neophodnosti i proporcionalnosti. Ne treba da koristimo savršen system, koji nam nije potreban ili koji obrađuje biometrijske podatke na nesrazmeran način. Obrada biometrijskih podataka treba striktno da se pridržava principa ograničenja svrhe. Ograničenje svrhe je posebno relevantno u ovom kontekstu, zbog tipova biometrijskih podataka, koji omogućavaju zaključivanje o drugim ličnim podacima.

Prilokom obrade biometrijskih podataka preporučljivo je u potpunosti primenjivati princip minimalizacije prikupljanja podataka. Prilikom procene koje biometrijske tehnologije koristiti, potrebno je ograničiti obradu biometrijskih podatka, na ono što je neophodno za ostvarivanje određenog zadatka. Uvažavajući činjenicu da bi multimodalni biometrijski sistemi mogli biti sigurniji i tačniji od običnih biometrijskih sistema, takva vrsta obrade koja uključuje više biometrijskih podataka donosi i veće rizike za osnovna prava pojedinaca. Kada se razmatra obrada više od jedne vrste biometrijskih podataka, potrebno je, proceniti njihovu neophodnost i proporcionalnost, balansirajući očekivane koristi sa rizicima.

Poverenje u biometrijske sisteme, zahteva iskren, jasan i direktan pristup u saopštavanju prednosti i ograničenja svake biometrije tehnologije, predstavljanje mogućnosti i rizika. Percepcija javnosti o rizicima je razlog zašto milioni korisnika dobrovoljno odlučuje da koriste biometrijske podatke za autentikaciju kada koriste svoje pametne telefone, dok je sve veće protivljenje upotrebi biometrijske identifikacije u javnim prostorima.

Podaci, kao što su otisci prstiju i DNK, generalno su jedinstveni za pojedinca i tako mogu potvrditi nečiji identitet i prisustvo na mestu zločina, odnosno imati forenzički značaj. Takođe, može pomoći da se dokaže nevinost osumnjičenog. Posebno na međunarodnom nivou, forenzički podaci mogu se koristiti i za povezivanje niza transnacionalnih krivičnih dela, imajući u vidu da se otisci prstiju mogu brzo proveriti, naročito, ako osumnjičeni prelazi granicu. Ne manji značaj, imaju ovi podaci, sa aspekta korišćenja za identifikaciju žrtava velikih katastrofa.

Najbrži razvoj, ostvaren je u oblasti identifikacije na osnovu prepoznavanja fotografije lica i time otvara mnoge nove mogućnosti, za identifikaciju pojedinaca i rešavanje zločina. U ovom smislu forenzička ekspertiza i podaci su od vitalnog značaja za sprovođenje istraga na nacionalnom nivou, kao i ostvarivanje učešća u međunarodnim istragama u skladu sa normativnim okvirom i nadležnoatima [9].

Posebna oblast primene su biometrijske autentikacije, kao siguran i praktičan alternativni način autentikacije putem lozinki. Međutim, i u ovom, slučaju, pojavljuju se izazovi, koje je potrebno imati u vidu, kao što je očuvanje privatnosti lica, obezbeđivanje bezbednosti i poverljivosti biometriskih podataka pri prenosu i skladištenju, kao i činjenica da se za razliku od lozinki biometrijske osobine ne mogu poništiti i ponovo je izdati. Ukoliko dođe do kompromitovanja, korišćenog biometrijskog podatka, s obzirom da se ne može promeniti, isti se ne može dalje korisititi u svrhu autentikacije [11]. U ovom smislu Cloud tehnologija može da iskoristi prednosti biometrijske tehnologije i obrnuto. Biometrija sa svojim jakim svojstvima autentikacije, može da se iskoristi da poboljša bezbednost Cloud sistema i ponudi novi modeli usluga (tj. biometrijska autentikacija kao jedna od usluga u Cloud-u. S druge strane, Cloud omogućava svojim resursima fleksibilnosti, skalabilnost i smanjenje troškova za rad biometrijskih Sistema (tj. procesorsku snagu ili skladištenje podataka), kao i da omogući poboljšanje performansi biometrijskih sistema [11].

Standardi omogućavaju efikasan razvoj biometrijskih sistema, uspostavljanjem zajedničkih kriterijuma i postavljanjem smernica za zaštitu privatnosti (Eversheds Sutherland, 2022). Sporazumi o formatima podataka i interfejsima aplikativnog softvera mogu pomoći će da se smanje troškovi razvoja sistema. Razvoj standarda za primenu biometrije i za testiranje tačnosti, doprinosi razjašnjavanju ranjivosti i usmerava ka pronalaženju rešenja.

Imajući u vidu da ljudska faktor i slabe lozinke, prema proceni iz Imageware analize, čine 52% narušavanja bezbednosti podataka, što se može smatrati indikatorom potrebe da se tradicionalne metode autentikacije zamene novijom biometrijskom tehnologijom, kao što su specijalizovani hardverski senzori u mobilnim telefonima, skeneri otiska prsta, kamere za prepoznavanje lica (2D/3D) ili prepoznavanje irisa oka [11]. Biometrijske tehnologije postaju sve popularnije, posebno sa pojavom dvofaktorske autentikacije za *online* usluge. Pregled prednosti i nedostataka multifaktorske autentikacije dat je u Tabeli 1. Na osnovu analiza tržišta procenjuje se da će se u narednim godinama

 ISBN 978-86-7466-930-3

tržište biometrijskih tehnologija dostići 55,42 milijarde dolara do 2027, tržište kamera za video nadzor sa procenama predviđanja rasta na 44 milijarde dolara do 2025. godine [11].

TABELA I
MULTIFAKTORSKA AUTENTIKACIJA ZA I PROTIV (PRATT, 2021)

| **Prednosti** | **edostaci** | **ere** |
|---|---|---|
| Teško se hakuju ili repliciraju | Teško se hakuju ili repliciraju | Više faktora je dostupno za MFA |
| Konformno za korisnike | Konformno za korisnike | Zahteva povećanu bezbednost |
| Manja zavisnost od medija | Manja zavisnost od medija | Minimalizacija podataka |
| Manja zavisnost od mrežne povezanosti | Manja zavisnost od mrežne povezanosti | Raspodela rizika Razdvajanje ima prednosti |
| Proširivost novim elementima | Proširivost novim elementima | Edukacija i uključenost korisnika |

Svedoci smo porasta upotrebe biometrijskih tehnologija za različite oblasti primene, ovakav napredak otvara I nove mogućnosti za dalja istraživanja i razvoj. Posebno imaju se u vidu niz fundamentalnih otvorenih pitanja i izazova kojima će se baviti istraživanja u oblasti primene biometrije u svim sverama savremenog života [12-15].

To svakako prati i aspekt bezbednosti, pošto je sve više podataka u opticaju, u digitalnom obliku, uključujući biometrijske podatke, koje pojedinci ostavljaju na web-u i u ličnim elektronskim uređajima, kao što su pametni telefoni i drugi mobilni uređaji. Posebno, imajući u vidu dostupnost digitalnih senzora i kapacitet uređaja za skladištenje podataka, i tu je I činjenica da se identifikacije osoba sve više zasnivaju na digitalnim procesima [16].

## IV. ZAKLJUČAK

Osim što su univerzalne i jedinstvene, biometrijske karakteristike treba da budu relativno trajne i lake za prikupljanje i korišćenje. Biometrijski sistem treba da bude u mogućnosti da pruži što tačnije rezultate u različitim okolnostima i uslovima. Svakako važan, a možda i najvažniji aspekt biometrijskog sistema je prihvatanje od strane javnosti. Iako se DNK smatra konačnom biometrijom za identifikaciju osobe (osim jednojajčanih blizanaca), podudaranje DNK je previše invazivno za široku upotrebu u autentikaciji identiteta. Termografija lica, koja otkriva toplotne obrasce, koje stvaraju krvni sudovi i emituju iz kože, nije invazivna metoda, ali je cena previse visoka. Među biometrijskim podacima koji se trenutno razmatraju za buduću primenu su puls, miris tela, sastav kože, šara noktiju, hod i oblik uha. Potrebno je više istraživanja za dalju ocenu prihvatljivosti za širu upotrebu.

Sistem, koji se koristi, treba da bude siguran, obezbeđuje privatnost i daje tačne rezultate. Sistem koji je nesiguran, nepouzdan ili invazivan, s druge strane, može doprineti narušavanju poverenja javnosti, što na kraju može dovesti do otpora u prihvatanju tehnika biometrijskog prepoznavanja. Ključna strategija u garantovanju odgovarajućeg izbora i upotrebe biometrijskih metoda je razvoj međunarodnih standarda. Tokom poslednje decenije, napravljen je ogroman napredak u poboljšanju biometrijskih senzora, algoritama i procedura, ali i dalje postoje slabosti i ranjivosti, koje treba rešavati. Potreba za zaštitom privatnosti i čuvanjem osetljivih biometrijskih podataka, ostaje i dalje fundamentalna.

## ZAHVALNICA

Aurori se zahvaljuju organizacionom odboru konferencije ETRAN 2022 na prepoznatom značaju oblasti forenzike, prostoru i vremenu datom za izlaganje i diskusiju.

## LITERATURA

[1] C. Wendehorst, & Y. Duller, "Biometric Recognition and Behavioural Detection, Study requested by the JURI and PETI committees", 2021, EU. Biometric Recognition and Behavioural Detection Assessing the ethical aspects of biometric recognition and behavioural detection techniques with a focus on their current and future use in public spaces (europa.eu)

[2] V.H. de Albuquerque, R. Damaševilius, J. M. Tavares & R. Pinheiro, "EEG-Based Biometrics: Challenges And Applications, Computational Intelligence and Neuroscience", Hindawi, 2018. https://doi.org/10.1155/2018/5483921

[3] M. Anzini, "The Artificial Intelligence Act Proposal and its implications for Member States", EIPA Briefing 2021/5, EIPA-Briefing-2021-5-The-Artificial-Intelligence-Act-Proposal-and-its-implications-for-Member-States.pdf

[4] *Proposal for a egulation of the European Parliament and of the council laying down harmonised rules on artificial intelligence* (artificial intelligence Act) and amending certain Union legislative acts, European Comision Brussels, 21.4.2021.

[5] *egulation E 201 1 of the European Parliament and of the Council of 20 May 201 on establishing a framework for interoperability between E information systems in the field of borders and isa*. European Comision 2019. https://eur-lex.europa.eu/legal-content/EN/TXT/?uri=CELEX:32019R0817

[6] Agencia Española de Protección de Datos (AEPD), and the European Data Protection Supervisor (EDPS) (2020). "14 misunderstandings with regard to biometric identification and authentication", 14 misunderstandings with regard to biometric identification and authentication | European Data Protection Supervisor (europa.eu)

[7] W. Wiewiórowski, *W. "The State of Biometrics, European ata Protection Super isor E PS ".* 2020. 20-10-07_edps_biometrics_speech_en.pdf (europa.eu)

[8] N. Rotem & R. Locar, *" ata Breach in Biometric Security Platform, pnMentor",* (2019). Report: Data Breach in Biometric Security Platform Affecting Millions of Users (vpnmentor.com)

[9] *Interpol eport*, (2022). Forensics (interpol.int)

[10] Techcrunch site, Samsung confirms data breach after hackers leak internal source code | TechCrunch, Pristupljeno 13.04.2022.

[11] Imageware Report, "Biometric Trends and Statistics to Keep an Eye on in 2022", Biometric Trends and Statistics to Keep an Eye on in 2022 (imageware.io)

[12] A. A. Ross, S. Banerjee, C. Chen, A. Chowdhury, V. Mirjalili, R. Sharma, T. Swearingen & S. Yadav, "Some Research Problems in Biometrics: The Future Beckons". 2019 International Conference on Biometrics (ICB), 1-8. 2019.

[13] A. A. Albahdal & T. E. Boult, "Problems and Promises of Using the Cloud and Biometrics," 11th International Conference on Information

 ISBN 978-86-7466-930-3

Technology: New Generations, 2014, 293-300, https://doi.org/10.1109/ITNG.2014.112
[14] Sutherland Global Biometrics Guide 2022, A multi-jurisdictional look at the laws governing the use of biometric technology, (2022). Global_Biometrics_Guide_2022.pdf (eversheds-sutherland.com)
[15] National Research Council (US) Whither Biometrics Committee; Pato JN, Millett LI, editors. "Biometric Recognition: Challenges and Opportunities". Washington (DC): National Academies Press (US); 2010. 5, Research Opportunities and the Future of Biometrics. Available from: https://www.ncbi.nlm.nih.gov/books/NBK219897/
[16] K.M. Pratt, "Biometric security technology could see growth in 2021", Biometric security technology could see growth in 2021 (techtarget.com)

ABSTRACT

Identification of persons has been, is and will be a challenge for conductiong, as question which solutions best fit to the purpose and is it provided technological response on adequate level. Especially this one based on the use of biometric data in electronic form and application of principles and experiences of best e-business practice in general. The use of data in electronic form stored in certain databases, issues of electronic communication and electronic processing of large amounts of data in performing business identification processes is evidently increasing, in response to the challenges of e-business, it is necessary to harmonize the development of normative framework as well the business efficiency are the challenges that the digital age brings. Challenges from the forensic aspect in response to potential violations and non-compliance with legal norms, which requires the development and application of new procedures and tools in this area. There is also an evident need for constant monitoring of the development and application of new methods for personal identification, especially those that may be related to forensic aspects in the digital world. The subject of consideration are precisely these issues that relate to the challenges in identifying persons in the digital age.

**Title in nglish**

Snežana Stojičić, Nataša Petrović, Radovan Radovanović i Milesa Srećković

 ISBN 978-86-7466-930-3

# Sigurnosni uređaji za proveru oružja u funkciji forenzičko-balističkih ispitivanja

Kristijan Đujić, Radovan Radovanović, Saša Milić, Martin Matijašević, Aleksandar Ivković

**Apstrakt—Sigurnosni uređaji za proveru oružja tzv. "hvatači projektila" namenjeni su bezbednom proveravanju različitih vrsta vatrenog oružja i dizajnirani su, pre svega, za zaposlene u sektoru bezbednosti. Ovi uređaji sastoje se iz metalne konstrukcije dizajnirane za minimiziranje olova u vazduhu, rampe niskog ugla, kružne komore i posude. Njihova konstukcija sadrži posebnu bezbednosnu funkciju koja sprečava da oružje eksplodira prema licu korisnika. Čak i ako korisnik ispaljuje projektil pod uglom, sve prisutne osobe u okruženju će biti bezbedne. Povratni udarni talas se kreće turbulentno unutar sigurnosnog uređaja za proveru oružja, a plamen se preusmerava od korisnika koji vrši opaljivanje. Sistem hvatača uključuje rampe sa malim uglom koje odbijaju projektil umesto da ga razbijaju, minimizirajući olovnu prašinu. Projektil se odbija o kružnu komoru za usporavanje, gde usporava sve do zaustavljanja. U funkcionalnom smislu sigurnosni uređaj za proveru oružja se može postaviti na sto ili zid u bilo kojoj prostoriji, pa je idealan za laboratorijska ispitivanja. U radu se analiziraju karakteristike sigurnosnih uređaja za proveru oružja kroz forenzički eksperiment sproveden na modelu kompanije *Savange Range systems GT Tabletop Gunsmith* u cilju utvrđivanja potencijala za primenu u forenzičkim i balističkim ispitivanjima.**

**Ključne reči — Forenzička ispitivanja; balistička ispitivanja; putanja projektila; bezbednost; vatreno oružje; fizički pregled; klasifikacija; probna paljba.**

## I. UVOD

TEORIJSKO razmatranje problematike forenzike, balistike i razvoja sprava za merenje i registraciju u fokusu je različitih naučnih disciplina. Prva knjiga o forenzičkoj medicini objavljena je davne 1400. godine u Kini [1], značajne su i naučne analize Leonarda da Vinčija usmerene na let projektila i međuzavisnost dužine i prečnika cevi. I dalje su kao osnov balistike od značaja razmatranja Nikolo Tartalja (1538. godine) koji zaključuje da slobodni let projektila nije pravolinijski, Galileo 1638. opisuje putanju leta kao parabolu, a Njutn 1684. uvodi u razmatranje i otpor vazduha. Tokom XVIII veka Francuz B. Belidor nalazi eksperimentalno da je najbolji odnos težine baruta i projektila 1:3, a Englez Bendžamin Robins stvara balističko klatno. Leonard Ojler rešava matematički sistem jednačina kretanja projektila, koji ima i danas značaj za brzine ispod 240 m/s. Ojler uvodi i sistem postupnog rešenja sistema jednačina po sukcesivnim lukovima, koji se koristi i danas. Tokom XIX veka uvodi se krešer za merenje pritiska gasova u cevi, i hronograf za merenje brzine projektila. Utvrđena je zavisnost sile baruta, gustine punjenja, i razvijenog pritiska gasova u komori konstantne zapremine poznata kao Ejbel-Noublov zakon. Nađen je i zakon otpora sredine, od kojih je Gavrov korišćen do Prvog svetskog rata. Italijan Anđelo Sijači sa razradama P. Šarbonijea daje metod rešavanja jednačina kretanja u konačnom obliku [2].

Od posebnog značaja u forenzičko-balističkim ispitivanjima i izvođenjima logičkih zaključaka je forenzička analiza materijala pronađena nakon ispaljivanja projektila. U Američkom građanskom ratu čuven je primer smrti generala Unije, Džona Sedžvika. On je prekorio svoje ljude, jer se savijao od snajperiste Konfederacije, koji se ispaljivao projektil sa udaljenosti od 1000 metara, a njegove poslednje reči bile su: "Sa ove razdaljine ne bi mogli ni slona da pogode", kada ga je pogodio projektil u glavu. Objašnjenje je pronađeno kada je projektil uklonjen iz njegove glave, odnosno, tada je otkriveno da je heksagonalnog oblika. Došlo se do zaključka da je mogao biti samo opaljen iz britanske puške Vitvort, oružja sposobnog za izuzetnu preciznost, za to vreme, i koja je prodata u velikom broju vojsci Konfederacije.

Prvi dokumentovani slučaj forenzičke balistike u Velikoj Britaniji zabeležen je 1835. godine. Tad je Henri Godard, službenik metropolitanske policije, istraživao ubistvo gde je žrtva upucana projektilom sa olovnom kuglom. Nakon pregleda pronađenog projektila, Godard je primetio trag od livenja koji je ostavio kalup koji je formirao olovni "projektil". Osumnjičeni je bio identifikovan, a kalup od projektila pronađen u njegovoj kući. Testiranje uzorka kalupa u poređenju sa tragovima livenja na pronađenom projektilu dozvolilo je Godardu da potvrdi da je smrtonosni projektil proizveden iz kalupa osumnjičenog. Osumnjičeni je osuđen za ubistvo.

U Velikoj Britaniji, ono što bismo sada prepoznali kao forenzičku balistiku, počelo je da se razvija 1920-ih kada su dva pionira, Robert Čerčil i major Džerald Barard, analizirali ispaljene metke i čaure sa ciljem da ih povežu sa sa određenim oružjem. Jedan od prvih slučajeva ubistva u Velikoj Britaniji, koje je rešeno primenom forenzičke balistike, je bilo zloglasno ubistvo PC Vilijama Gateridža 1927. godine. Robert Čerčil je uspeo da brzo uporedi metke sa pištoljem pronađenim u kući osumnjičenog. Iako su uporedni mikroskopi bili grubi prema današnjim standardima, fundamentalne postulate su dali rani pioniri na

Kristijan Đujić – Doktorand na Kriminalističko-policijskom univerzitetu u Beograd na Doktorskim akademskim studijama Forenzike, Cara Dušana 196, 11080 Zemun, Srbija (e-mail: kristijan.djujic@gmail.com).

Prof. dr Radovan Radovanović, Rukovodilac Departmana forenzičkog inženjerstva, Kriminalističko-policijski univerzitet u Beograd, Cara Dušana 196, 11080 Zemun, Srbija (e-mail: radovan.radovanovic@kpu.edu.rs).

Dr Saša Milić, naučni savetnik, Fakultet za diplomatiju i bezbednost, Milorada Ekmečića 2, 11000 Beograd, Srbija (e-mail: s_milic@yahoo.com).

Dr Martin Matijašević, naučni saradnik, Međunarodni institut za istraživanje katastrofa, Dimitrija Tucovića 121, 11 000 Beograd, Srbija (e-mail: jmartin.matijasevic@idr.edu.rs; martin.matijasevic@yahoo.com).

Aleksandar Ivković - Doktorand na Kriminalističko-policijskom univerzitetu u Beograd na Doktorskim akademskim studijama Forenzike, Cara Dušana 196, 11080 Zemun, Srbija (e-mail: acakormoran@gmail.com).

 ISBN 978-86-7466-930-3

principima uporedne mikroskopije. Posle Drugog svetskog rata, Služba forenzičke nauke je objedinila sva ispitivanja vatrenog oružja u Engleskoj i Velsu. Ova služba je u velikoj meri zaslužna za postavljanje temelja za moderne forenzičko balističke preglede u Velikoj Britaniji. Ipak, iako je tehnologija imala uticaj na istraživački rad, omogućavajući na primer, brzo traženje projektila i čaura, većina forenzičkih balističkih radova dala je malo doprinosa od onog koji su Čerčil i Burard praktikovali pre skoro 100 godina [3].

Balistika je proučavanje projektila u letu. Ova reč je izvedena iz grčkog, ballein, što znači 'baciti'. Forenzička balistika je opšte prihvaćena naučno-tehnološko-istražna disciplina koja u opštem smislu predstavlja svaki naučni pregled koji se odnosi na vatreno oružje i koji se obavlja u cilju prezentovanja nalaza na sudu. Ovo obično uključuje davanje mišljenja o tome da li komponente municije mogu biti povezane sa oružjem koje ih je ispraznilo, utvrđivanje dometa vatre, identifikovanje ulaznih i izlaznih rana, tumačenje pričinjene štete pucnjavom i ispitivanjem mehaničkog stanja oružja. Ironično, računajući svojstva metka ili projektila u letu [4]. Osnovna podela balistike je na unutrašnju i spoljnu [5], dok je danas kao podgrana balistike razvijena kriminalistička (sudska) balistika, odnosno forenzička balistika.

Rešavanje osnovnog zadatka unutrašnje balistike podrazumeva primenu kompjuterskih programa. U sistem jednačina unutrašnje balistike (1-5), unose se osnovni podaci:

1. Karakteristike cevi
2. Karakteristike projektila
3. Karakteristike baruta.

Unutrašnjebalistički ciklus je opisan jednačinama energije, sagorevanja baruta i kretanja projektila:

$(1-T/Tv)fmb\psi/\Theta=\varphi MpV\ 2\ /2$ …..... (1)

$\Psi=\kappa 1z(1+\lambda 1z)$ ..... (2)

$\sigma=1+2\theta 1z$ ..... (3)

$u=de/dt=uo+pn+bk=uop$ ..... (4)

$\varphi Mpv(dv/dt)=sp$ ..... (5)

Gde je: φ[/] − koeficijent fiktivnosti; f[kJ/kg] − sila baruta; mb[kg] − masa baruta; Mp[kg] − masa projektila; ψ[/] – relativni deo sagorelog barutnog punjenja; z[/ − ] relativna debljina sagorelog svoda; σ[/] − relativna sagorela površina baruta; κ1,λ1 − karakteristike oblika barutnog zrna; T[K] − temperatura barutnih gasova; Tv[K] − temperatura sagorevanja baruta pri konstantnoj zapremini; v[m/s] − brzina kretanja projektila; u[m/s] – brzina sagorevanja baruta; uo[m/s.bar] − jedinična brzina sagorevanja baruta; p[bar] − pritisak barutnih gasova; Θ=cp/cv-1; e[m] − svod barutnog punjenja; S[m 2 ] − površina poprečnog preseka kanala cevi oružja; n[/ − e ] eksponent u izrazu za brzinu sagorevanja; bk[m/s] − konstanta u izrazu za brzinu sagorevanja [6].

U kontekstu forenzičko balističkih ispitivanja sprovedenih posredstvom sigurnosnih uređaja za proveru oružja može se ispitati [7]:

1. ponašanje oružja tokom procesa opaljenja
2. dužina trzanja
3. potpunost sagorevanja baruta
4. količina i boja dima
5. postojanje plamena na ustima cevi
6. jačina pucnja

## II. KARAKTERISTIKE SIGURNOSNOG UREĐAJA ZA PROVERU ORUŽJA - MODEL GT GUNSMITH

Sigurnosni uređaj za proveru oružja *GT Gunsmith* je po konstrukcionim karakteristikama izdržljiva, jednostavna za upotrebu i samostalna jedinica sa osnovnom funkcijom hvatanja projektila. *Gunsmith* serija proizvođača *Savange Range* systems koristi *Vet Snail*® tehnologiju za minimiziranje olova u vazduhu. Rampe niskog ugla pomažu da se projektil skrene u kružnu komoru gde gubi energiju i pada u posudu za sakupljanje [8].

TABELA I
KARAKTERISTIKE MODELA GT GUNSMITH

| Opis | Karakteristike |
|---|---|
| Proizvod | tabletop Gunsmith |
| Model | GT |
| Veličina | 610mm visina; 280mm širina; 610mm dužina |
| Otvor zamke | prečnika 75 mm |
| Težina | 70 kilograma |
| Upotreba | provera oružja |

Uređaj je konstruisan od potpuno zavarene jednodelne konstrukcije i čeličnih tela, debljine 5mm. Unutar uređaja je komora za usporavanje za bezbedno i „čisto“ zaustavljanje projektila koje eliminiše opasnosti od olovne prašine. Dizajniran je za testiranje funkcija u neposrednoj blizini i jednostvana je za održavanje [9].

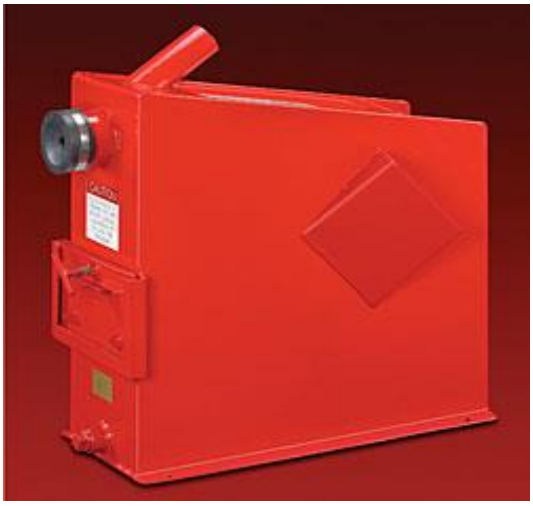

Sl. 1. Model GT Gunsmith

## III. FORENZIČKI I BALISTIČKI POTENCIJAL MODELA GT GUNSMITH

Osnovna i primarna funkcija modela *GT Gunsmith* je u sposobnosti upoređivanja oružja korišćenog u izvršenju krivičnog dela, prazne čaure, projektile i municije. Eksperimentalnu proveru je potrebno realizovati s ciljem dobijanja stvarnih podataka o svojstvima sigurnosnog uređaja za proveru oružja modela *GT Gunsmith* u cilju utvrđivanja njegovih forenzičkih i balističkih potencijala.


ISBN 978-86-7466-930-3

Eksperiment je realizovan u laboratorijskim uslovima, opaljivanje je izvršeno iz pištolja Zastava CZ 99, kalibra 9mm.

TABELA II
TEHNIČKI PODACI MODEL CZ 99

| Opis | Tehnički podaci |
|---|---|
| Kalibar | 9mm |
| Dužina | 190mm |
| Visina | 140mm |
| Debljina preko korica | 37mm |
| Masa bez okvira | 860gr. |
| Masa - prazan okvir | 965gr. |
| Masa - pun okvir | 1145gr. |
| Kapacitet okvira | 15 kom. |

Sl. 2. Model CZ 99

Ovaj model [10] ima najčešću upotrebu u vojno-policijskim formacijama i sektoru privatnog obezbeđenja na našim prostorima.

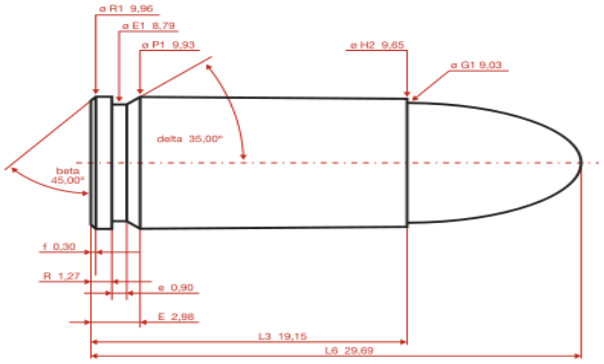


Sl. 3. Dimenzije kalibra 9mm

Sposobnost upoređivanja ispaljenog zrna sa oružjem je osnovno svojstvo ovog uređaja [11].

Prisiljavanjem projektila da se okreće dok putuje niz cev oružja, preciznost se znatno povećava. Istovremeno, narezivanje ostavlja tragove na projektilu koji ukazuju na tu cev, odnosno predstavlja jedinstveni forenzički otisak cevi. Pre masovne proizvodnje vatrenog oružja, svaku cev i kalup za projektil ručno su pravili oružari, što ih čini jedinstvenim [12]. Svaki projektil ispaljen iz određene cevi bi bio odštampan sa istim oznakama, omogućavajući istražiteljima da identifikuju oružje koje je ispalilo određeni projektil [13].

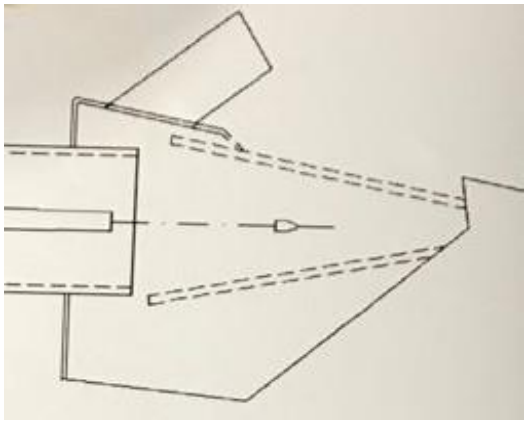

Sl. 4. Putanja zrna kroz model GT Gunsmith


Sl. 5. Zrno kalibra 9mm posle ispaljivanja

Preliminarnim pregledom projektila u bazi ispitivanja opštih karakteristika pronađenog projektila, može se isključiti veliki broj oružja. Određivanjem opštih aspekata ispaljene municije, izvestan broj oružja može se odmah isključiti kao nesposoban za ispaljivanje te vrste projektila.

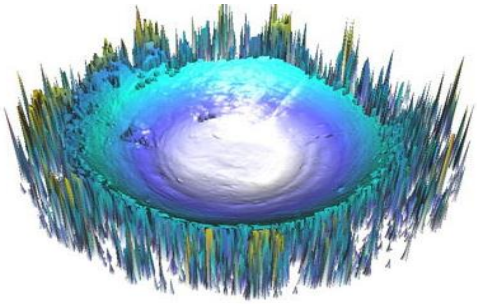

Sl. 4. 3D prikaz Zrno posle ispaljivanja

Da bi uporedili pojedinačne pruge u samom eksperimentu, morali smo da dobijemo poznati uzorak koristeći (poznato oružje u ovom slučaju CZ 99, a u realnim forenzičkim istragama zaplenjeno oružje. Za projektile sa sporijim kretanjem, kao što su pištolji ili revolveri, poznati primerci projektila nastaju ispaljivanjem oružja u sigurnosni uređaj za proveru oružja (hvatač projektila) [14]. Potrošeni projektil se može povratiti, netaknut, pošto uređaj usporava projektil pre nego što stigne do zida uređaja. Ovaj uređaj se može koristiti i za brže leteće projektile, kao što su oni ispaljeni iz pušaka velike snage i oružja za vojnu primenu, dok se recimo rezervoari za vodu ne mogu koristiti, jer rezervoar neće obezbediti dovoljnu moć zaustavljanja projektila [15].

Kada se proizvede poznati primerak, uzorak dokaza se može uporediti sa poznatim ispitivanjem na bazi komparativne analize i u isto vreme uporednim mikroskopom. Stranice koje se porede se pažljivije ispituju, tražeći više uzastopnih tragova. Ne postoji određeni broj


ISBN 978-86-7466-930-3

uzastopnih poklapanja koji je jednak deklaraciji o podudaranju, a ispitivači su obučeni da koriste forenzičku metodu „dovoljnog slaganja“. Stepen do kojeg ispitivač može da donese tu odluku zasniva se na njihovoj obučenosti i stručnosti [16]. Svi nalazi forenzičara podležu ispitivanju obe strane, tužilaštva i odbrane, tokom krivičnog postupka.

Marka i model oružja se takođe mogu zaključiti iz kombinacije karakteristika različitih klasa koje su zajedničke za određene proizvođače [17]. Tri glavne karakteristike klase svih projektila su tlo i žlebovi, kalibar metka, i preokret za narezivanje. Sva tri se mogu direktno vezati za tip cevi koji je korišćen za ispaljivanje projektila.

## IV. ZAKLJUČAK

Rad daje teorijsko - eksperimentalnu analizu procesa opaljenja u sigurnosni uređaj za opaljivanje projektila (hvatač metka), koji očuva zrno za dalja eksperimentalna istraživanja i numeričko modeliranje na računaru. Eksperimentom se došlo do saznanja da uređaj očuva zrno u meri dovoljnoj za dalje optimalne ulazno-izlazne parametre i prihvatljive rezultate za konkretno oružje [18]. Rezultati eksperimenata potvrđuju da je ovaj jedinstveno dizajniran uređaj idealan i za testiranje funkcionalnosti različitih vrsta vatrenog oružja. Tehnologija koju koristi u komori za usporavanje praktično eliminiše čestice olova koje mogu nastati pre nego što se unesu u vazduh i udišu. Ovaj jedinstveni sistem koristi OSHA standarde, štiteći zaposlene u laboratoriji i ispitivače. Patentirani niski ugao ulazne rampe skreće projektil u komoru za usporavanje gde se projektil okreće, gubi energiju, a zatim upada u posudu za sakupljanje zrna. Uređaj je značajan i kod ispitivanja barutnih čestica. Nakon izlaska iz cevi oružja, barutne čestice se zadržavaju u okolini ulaznog otvora na prvoj prepreci na koju je projektil naišao. Za kriminalističku praksu su važne situacije kada je pomenuta prepreka odeća ili telo čoveka [19], pa se mogu vršiti različite simulacije.

Ovaj uređaj je relativno jednostavan i može se koristiti kao prenosni sistem za izvlačenje projektila za balističko poređenje. Eksperiment je pokazao da uređajem mogu da rukuju i da ga prenose samo dve osobe, pa se testiranje može vršiti i na samom mestu krivičnog dela. Uređaj očuva zrno za balističko poređenje, bezbedno vrši hvatanje svih projektila, ima brzi ciklus „pucaj i sakupljaj“ kraći od 60 sekundi i realtivno je lak za održavanje.

## LITERATURA


[1] B. Franić, M. Milosavljević, “Forenzička balistika”, Banjaluka-Sarajevo: Federacija BiH-Rep. Srpska; Internacionalna asocijacija kriminalista, 2009, str. 19

[2] Grupa autora, “Vojna enciklopedija”, knjiga prva, Beograd, Srbija: Vojnoizdavački zavod, 1970, str. 446-447

[3] https://royalsociety.org/-/media/about-us/programmes/science-and-law/royal-society-ballistics-primer.pdf

[4] https://royalsociety.org/-/media/about-us/programmes/science-and-law/royal-society-ballistics-primer.pdf

[5] S. Janković, “Spoljna balistika”, Beograd, Srbija: Vojnoizdavački zavod, 1977, str. 15. .

[6] I. Bjelovuk, S. Ilić, “Mogućnosti kriminalističko tehmičkog ispitivanja tragova na municiji ispaljenoj iz oružja štampanog 3D tehnikom”, Beograd, Srbija: Bezbednost br. 1, 2017, str. 9.

[7] S. Jaramaz, D. Mišković, “Unutrašnja balistika”, Beograd: Srbija: Mašinski fakultet, Univerzitet u Beogradu, 2002, str. 137.

[8] https://www.savagerangesystems.com/content?p=traps

[9] *https://www.savagerangesystems.com/files/literature/2017_savage_range_systems_catalog.pdf*

[10] Zastava oružje, “Pištolj CZ 99 – uputstvo za rukovanje i održavanje”, Beograd, Srbija: Zastava oružje, 2001, str. 7.

[11] J. Hamby, "The History of Firearm and Toolmark Identification". Association of Firearm and Tool Mark Examiners Journal. 31 (3). Retrieved January 16, 2016.

[12] L. Steele, "Ballistics". Science for Lawyers. American Bar Association, 2008.

[13] "Firearms and Toolmarks in the FBI Laboratory". Forensic Science Communications. 2 (2). April 2000. Archived from the original on September 20, 2015. Retrieved June 5, 2016.

[14] B. Fisher, A. Barry, J. Tilstone, J. William, C. Woytowicz, “Introduction to Criminalistics: The Foundation of Forensic Science”, Elsevier Academic Press, 2009, p. 39. ISBN 9780080916750.

[15] National Research Council (2009). Strengthening Forensic Science in the United States: A Path Forward (PDF). National Academies Press. ISBN 978-0-309-13131-5. Retrieved June 12, 2016.

[16] R. Thompson, "Firearm Identification in the Forensic Science Laboratory" (PDF). National District Attorneys Association, 2010, Retrieved January 19, 2016.

[17] D. Maio, J.M. Vincent, “Gunshot Wounds: Practical Aspects of Firearms”, Ballistics, and Forensic Techniques (3rd ed.). CRC Press, 2016, p. 1. ISBN 978-1-4987-2570-5.

[18] "Firearms & Tool Mark". *North Carolina Department of Justice*. Retrieved June 4,2016.

[19] A. Radomirović, “Tragovi baruta u domaćoj kriminalističkoj praksi”, Beograd, Srbija: Bezbednost, 2005, br. 3, str. 488.


## Security devices for checking weapons in the function of forensic-ballistic tests

Kristijan Đujić, Radovan Radovanović, Saša Milić, Martin Matijašević, Aleksandar Ivković

**Abstract — Security devices for checking weapons, the so-called "Projectile catchers" are intended for safe screening of various types of firearms and are designed primarily for employees in the security sector. These devices consist of a metal construction, technology to minimize lead in the air, a low-angle ramp, a circular chamber and a vessel. Their construction contains a special safety function that prevents the weapon from exploding towards the user's face. Even if the user fires a projectile at an angle, all persons present in the environment will be safe. The return shock wave rotates turbulently inside the safety device for checking the weapon and the flame is redirected by the user who performs the firing. The catcher system includes small-angle ramps that repel the projectile instead of shattering it, minimizing lead dust. The projectile bounces into the circular deceleration chamber, where it decelerates until it stops. In functional terms, a security device for checking weapons can be placed on a table or wall in any room, so it is ideal for laboratory tests. The paper analyzes the characteristics of security devices for weapons testing through an experiment conducted on the model of Savange Range systems GT Tabletop Gunsmith in order to determine the potential for application in forensic and ballistic tests.**

**Keywords — Forensic examinations; ballistic tests; projectile trajectory; security; firearms; physical examination; classification; trial fire.**

 ISBN 978-86-7466-930-3

# Примена форензичких алата у класификацији инцидената и несрећа у комерцијалном ваздушном саобраћају по EASA методологији

Александар Ивковић[1], Радован Радовановић[1], Саша Милић[2], Душан Ивковић[3], Кристијан Ђујић[1]

[1]*Криминалистичко полицијски универзитет – департман форензичког инжењерства*
[2]*Факултет за дипломатију и безбедност*
[3]*Војнотехнички институт, сектор за ваздухопловство*

**Абстракт** - У раду је наведено више случајева који су довели до несрећа у авио саобраћају и један симулиран сценарио без фаталног исхода уз селекцију више кључних параметара на бази којих је извршена детаљна анализа полазних претпоставки и потенцијалног решења. Моделовање сценарија потенцијалног нежељеног догађаја је извршено на бази искустава стечених кроз реалне догађаје и засновано је на постојећим типовима ваздухоплова и на реално могућој конфигурацији и изгледу аеродрома. Основа сценарија и резултати анализе се уклапају, како у међународне, тако и у националне правне оквире. На узорку од 1000 фаталних несрећа у периоду од 1950. до 2010. се може уочити да је до највећег броја несрећа дошло грешком пилота, уз напомену да је у неким случајевима то била последица реакција на изразито лоше временске услове или техничке кварове. У осталим случајевима то су пропусти контроле летења или особља одговорног за одржавање и механичких отказа.

**Кључне речи** - форензика у ваздушном саобраћају, инциденти, EASA, менаџмент безбедности

## УВОД

Форензика је дефинисана правним оквиром који јој даје Кривични Закон и основна улога коју има је у оквиру кривичног поступка и прикупљања доказног материјала, као и његовог стручног тумачења. Методе и технике које користи форензика су компатабилене са познатим и општеприхваћеним научно-истраживачким методама, а методологије које користи су у сталној примени у природним наукама (по потреби и друштвеним) и без ограничења које повремено намећу специјализоване научне дисциплине. Форензика као наука је интердисциплинарна и обухвата распон од прикупљања и анализе архивске грађе, правилника, упутстава, препорука, анализе обичаја и културних утицаја па до технологија израде, врсте материјала техника и технологија израде, утицаја окружења, па до медицинских података.

Овај рад је илустративан приказ једног дела кога форензика, као интердисциплинарна наука, може да пружи када нема нежељеног сценарија који подразумева ангажовање тужилаштва и судских органа. У раду су аутори приказали истраживања из области ваздушног саобраћаја.

Након несрећа у комерцијалном ваздухопловству прође доста времена док се све чињенице не сазнају и док се не дође до одговора зашто и како се нешто десило. Чак и када се догоде несреће то је због низа независних догађаја који су коинцидирали у до тада непредвиђеним околностима, односно, нико их није раније предвидео. Да би форензичке анализе добиле на пуном значају, неопходно је прикупити податке и анализирати их, а по потреби и проверили кроз симулиране сценарије где би се тестирала њихова поузданост и на тај начин предвидели и предупредили нежељени исходи.

## ТЕХНИЧКИ АСПЕКТИ

У раду је наведено више случајева који су довели до несрећа и један симулиран сценарио без фаталног исхода. Симулиран сценарио је, након анализе, понудио одговоре на то зашто се и како нешто десило, па па до указивања на кривца и предлога побољшања. Сценарио је базиран на могућим догађајима и релним типовима ваздухоплова и аеродрома. Основ сценарија и резултати анализе су у међународном и националном правном оквиру. Вођено је рачуна да се не изађе из оквира статистике несрећа са фаталним исходом.

На узорку од 1000 фаталних несрећа у периоду од 1950. до 2010. можемо видети да је до највећег броја несрећа дошло грешком пилота, понекад као реакција на изразито лоше временске услове или техничке кварове. У осталим случајевима то су пропусти контроле летења или особља одговорног за одржавање и наравно због механичких отказа. Проценти су следећи[1]: грешка пилота 32%, откази механичке природе 20%, грешке пилота узроковане/провоциране временским условима 16%, сами временски услови 12%, саботажа 8%, људска грешка осталих учесника 6%, грешка пилота везана за технику 5%, сви остали узроци 1%.

Да се из прикупљених података учи и да је прикупљање и ажурирање данас неопходност показује и разлика у вероватноћи да се фатална несрећа догоди на комерцијалном лету од просечно 4,3 жртве на сваких милион сати налета, што је у преносном значењу 115 година летења. У општој авијацији, где су нижи стандард и

 ISBN 978-86-7466-930-3

чињеница је да лете аматери, имамо 22,43 жртве летења на сваких милион сати налета.

Одличан показатељ је и укупан број несрећа који и поред годишњег пораста броја сати налета од 3-5% константно опада и у апсолутним бројевима је са свог пика седамдесетих од 42 несреће годишње 2016. пао на 6 несрећа годишње, при томе треба имати на уму да је по подацима ICAO-a[2] и годишњем извештају европске комисије о европском ваздухопловном тржишту за 2016 годину из марта 2017. и поред неколико нафтних, тржишних и политичких криза од седамдесетих на овамо дошло до огромног пораста саобраћаја. За то су заслужни не само авиони новије генерације са већим бројем седишта, односно повећаном носивости, већ и повећан обим и фреквенција полетања. Комерцијална авијација по броју превезених путника са нешто испод 400.000.000 путника 1975. данас је на 3.500.000.000 особа, што је повећање капацитета флоте, односно броја летова за готово 9 пута, са скоком од 2003. до 2010. од 53%. Обим превоза робе је доживео и већи пораст, на њему се нећемо задржавати пошто са собом носи мањи друштвени ризик, већи број летова се обавља у време када је нижи обим саобраћаја и ноћу, у авиону је само посада, висинска ограничења практично не постоје итд.

У 2015. години кроз аеродроме у свету је прошло 7 милијарди путника, а само европски превозиоци су имали профит од 7,4 милијарде долара. Овакав скок, поред чињенице да авијација прати тржишна дешавања и подложна је кризама, није забележен на другим пољима саобраћајне и транспортне индустрије.

## РЕАЛНЕ НЕСРЕЋЕ И СИМУЛИРАН СЦЕНАРИО

Осмог марта 1974. непосредно након полетања из Париза за Лондон авион DC-10 компаније Turkish Airlines лет 981 пао је због проблема са забрављивањем врата теретног одељка.

Дванаестог августа 1985. Japan Airlines Боинг 747ср лет 123 из Токија за Осаку је 12 минута након полетања на удаљености око 100 km имао експлозивну декомпресију приликом које је изгубио репни део авиона, погинло је 15 чланова посаде и 505 од 509 путника. Ово остаје до данас најсмртоноснија несрећа у којој је учествовао само један авион. Разлог пада: лоше урађено одржавање авиона.

Двадесет шестог маја 1991. Боинг 767-300ER компаније Lauda Air лет 004 на лету из Банкока за Беч пада у ковит и при том гине свих 213 путника и 10 чланова посаде. Разлог пада је активирање реверзног потиска у лету, уређаја иначе дизајнираног за помоћ при кочењу након слетања. Разлог је техничка грешка, тј. пропуст у конструкцији и сигурносној опреми која је касније отклоњена.

Током деведесетих низ инцидената са Боингом 737 резултованих непоузданим или чек супротним отклоном у односу на командовани правац кормила довео је до неколико несрећа. У две одвојене несреће погинуло је 157 људи док проблем није коначно детектован и наредбом америчких ваздухопловних власти FAA[3], коначно отклоњен. Проблем је био у електро магнетном вентилу, који је на ниским температурама, или по повратку на више температуре реаговао непоуздано или чак супротно од командованог. Авиони иначе лете на висинама где је температура током целе године око -52ºC.

Недавни случајеви, који показују да и поред најбоље воље систем обавезног пријављивања, прикупљања, дистрибуције и релевантне анализе података није заживео везани су за Боинг 737 MAX генерације.

Два догађаја за које ће се брзо испоставити да су повезана су пад LionAir лета 610 29. октобра 2018. и Ethiopian Airlanes лет 302 10. марта 2019. на ова два лета је било 346 жртава а појединачно су највеће несреће у историји поменутих компанија. Када су коначно потврђени подаци и установљено да су оба ваздухоплова пала из истог разлога FAA је 13. марта 2019. донела одлуку о приземљењу типа и до 18, марта 2019. године свих 387 примерака је било приземљено. Интересантно је да је још пре 13. марта 51 ваздухопловна власт донела одлуку о приземљењу конкретног типа ваздухоплова. Забрана је трајала до децембра 2020. и након поновне сертификације пловидбености типа, враћен је у оперативну употребу. Оно што је страшно у овим случајевима је чињеница да тенденција да обара нос авиона у погрешном тренутку је била софтверска грешка уочена много пре несреће које су се догодиле, нажалост без одговарајуће реакције произвођача.

Сличан проблем и понашање је примећено и код ваздухоплова другог произвођача исте генерација Ербаса 320 NEO. Међутим EASA је низом тестова у симулатору утврдила да се померањем тежишта (тако што се задњи редови седишта ће попуњавати) ваздухоплов може и даље користити, уз поменуто ограничење. На крају је и на овом типу грешка исправљена.

Моделован сценарио се одвија на замишљеном аеродрому са две писте које се укрштају и различите су дужине и капацитета, пројектоване за истовремену употребу. У сценарију/симулацији након низа пропуста ваздухоплов средње величине излеће са писте и након мањег оштећења и лакших повреда две особе успоставља се нормалан рад аеродрома. Након неколико техничких анализа понашања делолва система одрађена су и безбедносна, сходно препорукама, али и правна у складу са националним прописима. Због обима анализа, овде наводимо само закључке.

Након форензичких и истражних радњи спроведених после удеса дошло се до закључка да се већина несрећа

 ISBN 978-86-7466-930-3

могла спречити. Пружаоци услуга у ваздухопловству примарно, а потом и произвођачи, почињу са класификацијом и обрадом података о ситуацијама које нису довеле до несреће, али се могу сврстати у инциденте.

## КЛАСИФИКАЦИЈА ПРЕМА EASA

Стратегија и принципи Европске агенције за безбедност ваздушне пловидбе се заснивају практично на смерницама које је поставио ICAO тако да је све универзално применљиво. EASA и њено поље деловања је далеко шире од саме Европе и простире се дуж комплетног Медитерана и делимично на Блиском Истоку и Азији. Смернице ICAO су водиље за целу планету па се овом приликом у скраћеном облику упознајемо са њима.

Процена безбедносног ризика или система управљања безбедношћу увелико зависи од избора методе, тачније од адекватности методе за процену ризика и потребе за правилним разумевањем циљева процене ризика. Оцена безбедносног ризика догађаја је препозната као један од главних приоритета у контексту система управљања безбедношћу. Мерење нивоа ризика практично одређује приоритете. Квантитативне вредности ризика су релативне вредности ризика између догађаја, израчунавају се или пореде на различите начине. Инцидент или пропуст је нешто где нас поступци, вештина, обука или сигурносни системи нису заштитили, већ „срећна околност“. Ово уједно представља најстарији, традиционални метод за процену који се користи од почетка комерцијалног ваздухопловства. У овој методи се безбедносни учинак представља и приказује бројем (или стопом) различитих категорија догађаја, тачније њиховом учесталошћу, а његова три главна недостатка су: а) квалитативни учинак ограничен на највише 3 категорије, б) нема квантитативне вредности ризика и в) фокус је на очигледним последицама а занемарује се потенцијал ризика. Данас када су несреће веома ретки догађаји (мање од 3 на 10 милиона летова), ова метода постаје неупотрбљивља из перспективе пружаоца услуга који су у обавези да квантификују своје перформансе.

## МЕТОДЕ ЗА ПРОЦЕНУ РИЗИКА

### *ICAO матрица ризика*

ICAO матрица ризика је метода процене ризика заснована на „пројектованој вероватноћи и озбиљности последица могућих исхода постојеће опасности или безбедносног случаја“. Иако се овај метод успешно користи за процену ризика безбедносних проблема, он има видљива ограничења и није довољно осетљив за појединачне процене ризика. Овај метод карактерише прилагођена матрица без разумевања Коксове теореме матрикса (Табела 1)[4].

| БЕЗБЕДНОСНИ РИЗИК | ОЗБИЉНОСТ | | | | |
|---|---|---|---|---|---|
| ВЕРОВАТНОЋА | КАТАСТРОФАЛНО A | ОПАСНО B | ВЕЛИКА НЕСРЕЋА C | МАЊА НЕСРЕЋА D | ЗАНЕМАРЉИВО E |
| УЧЕСТАЛО 5 | 5A | 5B | 5C | 5D | 5E |
| ПОВРЕМЕНО 4 | 4A | 4B | 4C | 4D | 4E |
| РЕТКО 3 | 3A | 3B | 3C | 3D | 3E |
| МАЛО ВЕРОВАТНО 2 | 2A | 2B | 2C | 2D | 2E |
| ГОТОВО НЕМОГУЋЕ 1 | 1A | 1B | 1C | 1D | 1E |

Табела 1 Коксова матрица

### *ERC метода процене ризика*

Кључни циљеви методе класификације ризика догађаја према ERC методи[5] (Табела 2) коју је развила радна група ARMS[6] су превазилажење ограничења ICAO-ове матрице и смањење субјективности аналитичара у погледу вероватноће догађаја и последица истог. За разлику од ICAO матрице где се процена ризика заснива на свим сличним догађајима истог типа (догађаји који су последица истог ризичног догађаја), ERC метод се заснива на концепту „нивоа ризика заснованог на самом догађају“ где се ризиком догађаја сматра ризик који је постојао када се догађај десио. Класификација ризика односно процена ризика коју носи догађај се врши коришћењем ERC матрице где се од стручњака за безбедност тражи да одговори на два питања:

1. Да је овај догађај ескалирао у несрећу, који би био највероватнији исход?
2. Која је била ефикасност преосталих баријера између овог догађаја и исхода са највећом вероватноћом?

Табела 2 ERC метода процене ризика

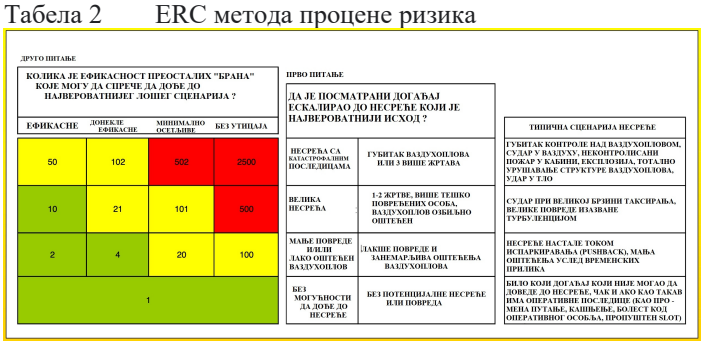


Питања која се односе на процену озбиљности слично приступу ICAO матрице ризика, и на вероватноћу исхода, заснивају се на процени преосталих баријера које спречавају ескалацију догађаја до несреће. Овај приступ прати модел узрочности несреће „швајцарски сир“ који је развио Џејмс Рисон[7](Слика 1).

Следеће одговоре на друго питање предлаже група ARMS:

Нису ефикасни: Несрећа се догодила или је могла бити спречена само чистом срећом или вештином пилота или другог одговорног лица (котролор лета и сл.).


ISBN 978-86-7466-930-3

1. Минимално ефикасне: баријере су постојале, али је њихова укупна ефикасност била минимална
2. Ограничено ефикасне: ефикасност преосталих безбедносних баријера је ограничена. Ово је ванредна ситуација, која је захтевнија за превазилажење, али са значајном преосталом сигурносном маргином
3. Ефикасне: сигурносна маргина је одговарајућа и састоји се од добрих сигурносних баријера, филтера и аларма.

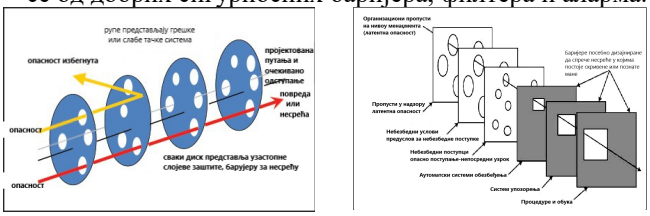


Слика 1 Рисонов модел „швајцарког сира“

ERC модел има два излаза:

1. Толеранција на ризик: вредности боја указују на поступке у вези са догађајем.
2. Индекс ризика: квантитативна вредност ризика у опсегу од 1 до 2.500 погодна за мерење безбедносних перформанси.

Неколико аутора је предложило побољшане верзије матрице са бољим резолуцијама (Jochen Mickel[8]), али о овим моделима овде неће бити речи јер следе исте принципе који су претходно наведении.

*EASA ERCS метода за процену ризика*

EASA ERCS (European Risk Classification Schema)[9] метода за процену ризика (Табела 3) је најкомплекснија од свих до сада обрађених и представља њихову еволуцију, а да ли представља квалитативни помак и стварни напредак, показаће време.

Европска шема класификације ризика ERCS прати основне принципе методе класификације ризика догађаја и то: 1) Поцена нивоа ризика на основу догађаја, 2) Процена вероватноће заснована на ефикасности заустављања и преосталих баријера и 3) Квалитативна и квантитативна оцена ризика по безбедност догађаја, без уласка у стварне последице. У поређењу са ERC класификацијом ризика догађаја, EASA ERCS метода уводи идентификацију кључних области ризика (укључујући поређење међусобних нивоа ризика) и усклађен приступ за утврђивање озбиљности догађаја и вероватноће, па је стога и много сложенија. Примена *ERCS* подразумева следеће кораке: 1) утврђивање највероватније врсте несреће, 2) одређивање категорије несреће, 3) оцена озбиљности, 4) идентификовање заустављање баријере из *ERCS* модела баријере, 5) идентификација ефикасности преосталих баријера, 6) израчунавање суме тежине баријере и одговарајућег резултата баријере и 7) одабир безбедносног скора и одговарајуће вредности ризика из ЕРЦС матрице.

Табела 3 EASA ERCS метода процене ризика

| ОЗБИЉНОСТ | | КЛАСИФИКАЦИЈА по (ERCS Score) | | | | | | | | | |
|---|---|---|---|---|---|---|---|---|---|---|---|
| ПОТЕНЦИЈАЛНИ РЕЗУЛТАТ ДОГАЂАЈА | БОДОВИ | | | | | | | | | | |
| ДОГАЂАЈ СА ПОТЕНЦИЈАЛОМ ЗА ЕКСТРЕМНО ВЕЛИКУ НЕСРЕЋУ И ЖРТВЕ (ПРЕКО 100) | X | X9 | X8 | X7 | X6 | X5 | X4 | X3 | X2 | X1 | X0 |
| ВЕЛИКА НЕСРЕЋА СА МОГУЋНОШЋУ ЗА ВЕЛИКИ БРОЈ ПОВРЕЂЕНИХ ИЛИ ЖРТАВА (20-100) | S | S9 | S8 | S7 | S6 | S5 | S4 | S3 | S2 | S1 | S0 |
| ВЕЛИКА НЕСРЕЋА СА ОГРАНИЧЕНИМ БРОЈЕМ ЖРТАВА (2-19) СА ПОВРЕДАМА КОЈЕ УТИЧУ НА КВАЛИТЕТ ЖИВОТА ИЛИ УНИШТЕЊЕМ ВАЗДУХОПЛОВА. | M | M9 | M8 | M7 | M6 | M5 | M4 | M3 | M2 | M1 | M0 |
| НЕСРЕЋА КОЈА ИМА ЗА ПОСЛЕДИЦУ ЈЕДНУ ЖРТВУ ИЛИ ОСОБУ СА ОЗБИЉНИМ ПОВРЕДАМА ИЛИ ВЕЛИКУ ШТЕТУ НА ВАЗДУХОПЛОВУ | I | I9 | I8 | I7 | I6 | I5 | I4 | I3 | I2 | I1 | I0 |
| НЕСРЕЋА КОЈА ЗА ПОСЛЕДИЦУ ИМА МАЊУ ИЛИ ТЕЖУ ПОВРЕДУ БЕЗ УТИЦАЈА НА КВАЛИТЕТ ЖИВОТА И МАЊЕ ОШТЕЋЕЊЕ ВАЗДУХОПЛОВА | E | E9 | E8 | E7 | E6 | E5 | E4 | E3 | E2 | E1 | E0 |
| БЕЗ МОГУЋНОСТИ ДА ДОЂЕ ДО НЕСРЕЋЕ | A | БЕЗ УТИЦАЈА НА БЕЗБЕДНОСТ | | | | | | | | | |
| ОДГОВАРАЈУЋИ БОДОВИ ЗА ЗАШТИТНЕ СИСТЕМЕ | | 9 | 8 | 7 | 6 | 5 | 4 | 3 | 2 | 1 | 0 |
| ЗБИР БОДОВА КВАЛИТЕТА ЗАШТИТЕ | | 17-18 | 15-16 | 13-14 | 11-12 | 9-10 | 7-8 | 5-6 | 3-4 | 1-2 | 0 |
| ВЕРОВАТНОЋА ПОТЕНЦИЈАЛНОГ НЕСРЕЋНОГ ИСХОДА | | | | | | | | | | | |

ПРОЦЕНА ОЧЕКИВАНОГ РИЗИКА

## ЗАКЉУЧАК

На симулираном моделу може се видети да независно од модела који користимо за процену ризика резултати више варирају у односу на обученост лица него од врсте примењеног модела, док најмању разлику даје управо EASA модел. Најмање одступање је практично везано за детаљну аналитичку методу доделе бројне вредности испитиваном догађају, односно његове квантификације. Нажалост метода је временски захтевна и код необученог корисника могла би да да погрешан резултат, док су друге поменуте методе интуитивније и захтевају много краћи период за усаглашавање са поступком. Резултати и сценарио симулације су даљи предмет истраживачког рада, овде је нагласак на поређења поменутих метода процене ризика.

ЛИТЕРАТУРА

[1] Доступно на: planecrashinfo.com
[2] ICAO Међународна организација за цивилно ваздухопловство основана од стране Уједињених Нација. Доступно на https://www.icao.int/
[3] FAA Ваздухопловне власти Сједињених Америчких Држава
[4] ICAO Safety Menagement Manual (SMM) doc. 9859
[5] ERC (Event Risk Classification) метода процене ризика развијена од стране ARMS
[6] ARMS (Airline Risk Management Solutions) првенствени задатак групе је проналажење алата за процену ризика код авио превозника али и код осталих учесника у ваздухопловству
[7] слика 1 у тексту модел швајцарског сира...

 ISBN 978-86-7466-930-3

[8] Процена оперативних ризика лета, Bewertung operationeller Flugrisiken аутор Jochen Mickel, издата само на немачком

[9] European Risk Classification Schema систем за градацију и класификовање потенцијално ризичних ситуација па све до несрећа ради лакше обраде и процене опасности коју собом носе за будућност

 ISBN 978-86-7466-930-3

# Нуклеарна форензика – методе за откривање процеса производње, прометовања и кријумчарења недозвољених фисионих материјала

Срећко Илић[1], Радован Радовановић[1], Саша Милић[2], Александар Алексић[2], Александар Ивковић[1]

[1] *Криминалистичко-полицијскиуниверзитет – департман форензичког инжењерства*

[2] *Факултет за дипломатију и безбедност*

**Апстракт.** Савремена технологија са собом доноси савремена и моћна оружја, али и бојазан да она могу бити употребљена ван међународних договора, протокола и обичаја ратовања. Као последица развоја нуклеарних технологија, појавио се нуклеарни тероризам, а нуклеарна форензика је област форензичког инжењерства која се, у садејству са другим традиционалним форензичким методама, бави реконструкцијом догађаја који су претходили неком нуклеарном инциденту или катастрофи. Методологије и мерне методе нуклерне форензике се користе за откривање кријумчарења и недозвољене производње специјалних фисионих материјала, који су основе језгара у атомским и хидрогенским бомбама. У раду ће бити разматрано више метода са циљем њихове категоризације и систематизације, а детаљно ће бити описане гама-спектрометријска метода, различите методе масене спектрометрије и рендгенска флуоресцентна спектрометрија. Циљ рада је да укаже на значај нуклеарне форензике у имплементацији нуклеарних безбедносних режима, како на локалном, тако и на глобалном нивоу.

**Кључне речи:** нуклеарна форензика, тероризам, оружје, криминал, инциденти, безбедност

## Увод

Открићем нуклеарног наоружања и његовом применом на бојном пољу, у јапанским градовима Хирошима и Нагасаки променио је погледе на обичаје ратовања али и политику и дипломатију.Управо због ове чињенице, данашњи актери на међународној дипломатско-политичкој сцени морају да се обраћају бираним речима једни другима и да њихова дела буду умерена колико год је то могуће. Државе које имају програме нуклеарног наоружања, у једном моменту су, схвативши опасност у којој се свет налази, иницирале механизме за заустављање ширења нуклеарног наоружања. Тек неколико држава је након тога успело у намери да зварши већ започет нуклеарни програм. Те државе су, заједно са свим осталим које немају нуклеарно наоружање, под будним оком међународне заједнице и МААЕ – Међународне агенције за атомску енергију (*енг.* "IAEA – International Atomic Energy Agency" [1]), проблем је у томе што правни оквири нису у потпуности обавезујући, па су механизми за деловање МААЕ веома сужени.

Чињеница да смо пар држава има нуклеарно наоружање и да је оно инсталирано на територијама неколико других, рекло би се да смо прилично безбедни, али тај простор је попунио нуклеарни тероризам, као стална претњу за безбедност незаштићеног становништва било где у свету. У домену је фантастике да терористи могу да дођу до нуклеарног оружја, али они нуклеарне материјале користе у друге сврхе, о чему ће даље у раду бити речи.

Анализом нуклеарних материјала форензичари настоје да установе како, када или где су материјали направљени, односно за шта су коришћени [3, 4]. Треба истаћи да су нуклеарни форензички алати веома значајни за нуклеарне инспекторе приликом у откривања изотопа који се користе приликом констуисања нуклеарног оружја. Ово се односи на инспекцијске надзоре приликом испитивања тврдњи да ли је нека држава покушала да развије или тестира нуклеарни борбени програм и тиме нарушила неки од споразума које је потписала или обогаћује материјал за производњу електричне енергије.

### *Међународни споразуми о нешириењу нуклеарног наоружања*

Најзначајнији споразум у домену забране нуклеарне безбедности је Споразум о забрани ширења нуклеарног наоружања (*енг.* "NPT – Non-Proliferation Treaty"). Донет је 1968. године, а

 ISBN 978-86-7466-930-3

ступио је на снагу 1970. године. Споразумом је као најважније издвојено да је предвиђено да дође до престанка ширења нуклеарног оружја, да дође до укидања ове врсте наоружања и да се појача свеобухватна сарадња у циљу ширења знања везаних за мирнодопске примене нукеарне енергије. Такође, предвиђено је да МААЕ има улогу у контроли спровођења тачака и контроле коришћења нуклеарне енергије. Ово је веома битна ставка за нуклеарну форензику. Наиме, све потписнице се обавезују да ће МААЕ обезбедити увид у нуклеарна истраживања и производњу и размену фисионих материјала у мирнодопске сврхе. Ове ставке указују на то да би се контрола спроводила управо коришћењем нуклеарних форензичких метода, јер се радионуклиди који се за производњу наоружања (недозвољени фисиони материјали) разликују од оних који се користе у мирнодопске сврхе (дозвољени), те би се форензичком контролом и инспекцијским надзором врло лако могло открити уколико нека држава под велом производње нуклеарне енергије тежи да развије нуклеарни борбени програм.

Други по важности је Свеобухватни споразум о забрани нуклеарних проба (*енг.* – "CTBT - Comprehensive Nuclear-Test-Ban Treaty"). Споразуму су претходили неки о делимичној забрани нуклеарних проба, али је овим Споразумом који је донет 1996. године и дефинитивно завршено са нуклеарним пробама. Било је ту и тамо неколико инцидената, односно кршења Споразума, понајвише од стране С. Кореје, али су нуклеарне пробе од стране оних који су их највише изводили и дефинитивно престале.

Поред ова два споразума постоји низ билатералних споразума између САД и Русије. Свим тим споразумима се подразумева редуковање нуклеарног наоружања. Сваки од њих је одиграо неку улогу, али се заправо ништа круцијално, по питању укидања нуклеарног оружја, до данас није десило.

За ову тему значајан акт је свакако Међународна конвенција о спречавању аката нуклеарног тероризма (*енг.* "CNT – International Convention for the Suppression of Acts of Nuclear Terrorism") из 2005. године. Конвенцијом је дефинисан низ аката који се сматрају нуклеарним тероризмом, али је и гарантована помоћ МААЕ у сузбијању ове врсте тероризма, као и решавању кризних ситуација и уклањању непожељних материјала са територије угрожене државе.

Безбедносни акти које нисмо посебно описали, редом према времену доношења или предлагања, су: Повеља о Антарктику (1959), Споразум о делимичној забрани нуклеарних проба (1963), Споразум о космосу (1967), Споразум о забрани смештања нуклеарног и другог оружја за масовно уништење на дно мора и океана и у њихово подземље (1971), Споразум о Месецу (1979) и Споразум о забрани одређених фисионих материјала (1993).

### *Тренутно стање у вези са бројем нуклеарних бојевих глава у свету*

Од открића нуклеарног наоружања, кроз читав "Хладни рат", па све до данас, Русија и САД су биле водеће војне силе гледано према квантитету нуклеарних бојевих глава. Тренутни тренд у вези са бројем нуклеарних глава у свету можемо видети на графику [5]. Што се тиче тренда раста или опадања, праћењем квантитета бојевих глава у свету, може се уочити да Русија и САД из године у годину смањују број бојевих глава, док остале нуклеарне силе повећавају своје нуклеарне арсенале. Међутим, како остале нуклеарне силе у збиру имају око 10 пута мање бојевих глава од САД и Русије заједно, а тај однос је раније умео да буде и дупло већи, јасно је да је нуклеарно разоружавање у рукама две водеће силе и зато су нам оне, у смислу анализе, најбољи показатељ параметара раста или пада. Тренд опадања везано за Русију и САД [5].

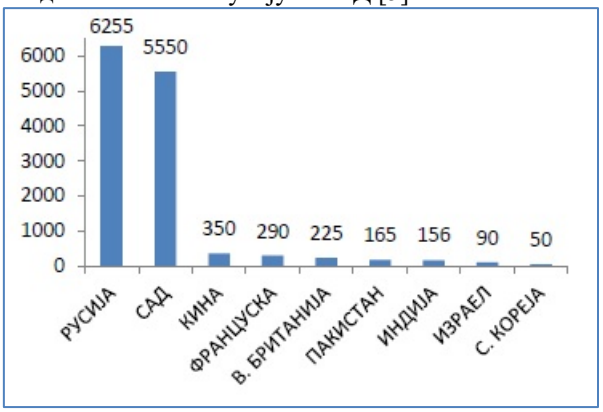


**Слика 1. Број бојевих глава по нуклеарној сили**

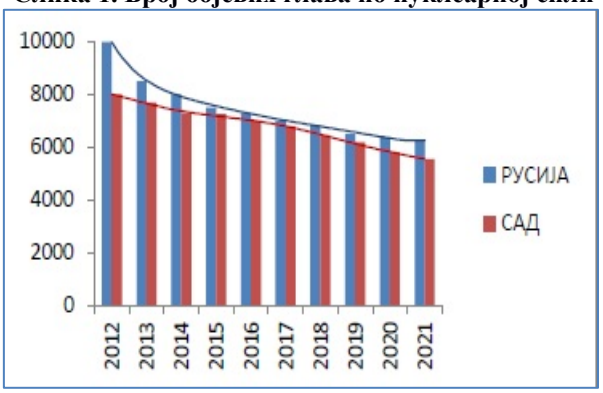


**Слика 2. Однос нуклеарних бојевих глава Русије и САД током последњих 10 година**

 ISBN 978-86-7466-930-3

### *Систем инспекцијског надзора у оквиру Међународне агенције за атомску енергију*

Оснивањем Међународне агенције за атомску енергију и изгласавањем њеног Статута 1957. године, било је предвиђено да постоји инспекцијски надзор који би обухватао низ техничких мера којима се врши праћење обавеза држава да не користе нуклеарне мирнодопске системе за развој нуклеарног наоружања, што је забрањено тачком 5. става А, члана 3. Статута. Инспекторски систем на неки начин представља извршно тело у оквиру нуклеарних безбедносних режима. На оснивање инспекцијског система се чекало две године. Договорен је у Канади 1959. године, међутим, документ који је регулисао рад овог тела се чекао још толико. Године 1961. потписан је први документ који је регулисао процедуре за аплицирање и упутства за рад „IAEA“ инспектора. Овај документ је познат под називом „INFCIRC/26“, а након допуне, 1965. године, заведен је под називом „INFCIRC/66“. Када је 1970. године на снагу ступио Споразум о забрани ширења нуклеарног наоружања, створили су се услови за „озбиљније“ деловање Агенције, што је 1971. године, довело до увођења новог „INFCIRC/153“ документа о инспекцији, који је пре свега увео Свеобухватан инспекцијски надзор (*енг.* CSA – Comprehensive Safeguards Agreements). Он је дефинисао начин сарадње између Агенције и држава потписница и то, пре свих, држава које нису декларисане нуклеарне силе, а имају установе које користе нуклеарну енергију у мирнодопске сврхе. Ове државе су се, потписивањем документа, обавезале на свеобухватан инспекцијски надзор од стране „IAEA“ на својој територији, те да ће омогућити инспекторима све податке који су у вези са нуклеарним постројењима и применом радионуклида у било којој области. У оквиру истог акта дефинише се Протокол о малим количинама, који се односи на државе које не поседују велика нуклеарна постројења него имају јако мале количине нуклеарних материјала или их немају уопште. Наиме, њиме се уређује да у државама које потпишу Протокол Агенција нема сталан инспекторски надзор. С друге стране, Протокол не искључује установљене обавезе према Агенцији и разним потписаним споразумима. Дакле, држава која је приступила Протоколу се одриче великих нуклеарних истраживања, што је чини изузетом од сталне инспекторске контроле, али мора да пошаље извештај Агенцији о свим радионуклидима које поседује или жели да набави, као и да одговори на све прописане захтеве „IAEA“ уколико за тим постоји потреба.

Деловање инспектора Агенције у циљу спречавања ширења нуклеарног наоружања у основи се може поделити у четири групе,сакупљање и процена информација, унапређење сарадње са државама, планирање, спровођење и унапређење свих активности, укључујући и рад на терену, као и деловање командног центра у Бечу и доношење закључака и њихово представљање.

Агенција у окивру инспекторских послова прикупља велики број информација. Извори из којих се долази до њих могу се поделити у три гупе:

1) информације које је обезбедила сама држава у којој се врши надзор (извештај државе о нуклеарним активностима и радиоактивним материјалима),

2) информације које су произашле из података са терена (прикупљени узорци) и обраде у командном центру (подаци из прикупљених узорака, али и они добијени помоћу детектора и камера постављених у нуклеарним постројењима широм света),

3) информације из других релевантних извора као што су отворени извори (интернет и други) и они које је доставила трећа страна.

Информације из свих извора морају бити међусобно конзистентне. У супротном Агенција је принуђена да са државом превазилази проблем кроз низ консултација, али и увођењем посебних мера уколико је то неопходно.

Услед немогућности Агенције да, заједно са својим инспекторима, одговори на изазове који су пред њу постављени, дошло је до потребе да се уведе Додатни протокол (INFCIRC/540) у окивру механизама који се спроводе у циљу поштовања Споразума о забрани ширења нуклеарног наоружања. Овај Протокол Агенцији и њеним инспекторима проширује овлашћења и омогућава већа права на информације од значаја, те лакше откривање забрањених нуклеарних активности. Додатни протокол је донет 1997. године.

## Нуклеарна форензика – организације, лабораторије и методе

Нуклеарна форензика је релативно млада област форензике. Свој нагли развој је почела да доживљава развојем нових технологија и то крајем прошлог века, да би у 21. веку доживела потпуни процват. Далеко од тога да неке методе које она

 ISBN 978-86-7466-930-3

користи нису постојале и раније и далеко од тога да нису постојали начини за откриће забрањених нуклеарно-безбедносних акитвности, али она тада просто није била установљена као дисциплина, а њене методе нису биле свеобухватне као данас. У нека страрија времена, просто су се користиле методе нуклеарне физике у циљу откривања недозвољених активности. Данас постоји низ организација широм света које раде на јачању ове научне дисциплине, а једна од њих је и МААЕ. Нуклеарна форензика је једини практичан механизам којим се може деловати у циљу спречавања кршења нуклеарних безбедносних режима и ширења нуклеарног наоружања.

### *Релевантне организације*

Иако је МААЕ кровна организација по питању нуклеарне безбедности, она ипак није кровна организација која ради на примени и развоју нуклеарне форензике. Најрелевантнија организација на светском нивоу је МТРГ – Међународна техничка радна група за нуклеарну форензику (*енг.* "ITWG – The Nuclear Forensics International Technical Working Group"). Сматра се да је Радна група основана 1995. године, иако је активно учешће у развоју програма узела тек двадесетак година касније (2016.). Она броји више од 50 земаља потписница, међу којима је и Србија, као и 11 релевантних међународних организација, међу којима је и МААЕ, али и ИНТЕРПОЛ, ЕУРОПОЛ и ОЕБС. Такође, на списку организација је и Глобална иницијатива за борбу против нуклеарног теоризма (*енг.* "GICNT – Global Initiative to Combat Nuclear Terrorism") која се убраја у значајне чиниоце у борби против злоупотребе нуклеарних материјала, а самим тим и у развоју нуклеарне форензике и њених метода. Ова организација се састоји од три групе, од којих је једна Радна група за нуклеарну форензику (*eng.* "NFWG – Nuclear Forensics Working Group") чији главни циљеви леже у охрабрењу држава да формирају националне нуклеарно-форензичке лабораторије и националне нуклеарно-форензичке библиотеке [6].

Међународна техничка радна група је подељена у више мањих група. Свака група има своје деловање. Поред Групе за прикупљање доказа, веома је активна и Група за вежбе. Примарни циљ овог сектора је повећање спремности лабораторија за поступање у случају потреба. Пре договореног састанка Групе, свака лабораторија добија радиоактивни узорак за који треба да изврши анализу коришћењем метода нуклеарне форензике. Група инсистира на анализама које се врше у року од 24 часа од добијања узорка, затим након 7 дана и последња након 2 месеца. Након тога се сви учесници састају и размењују искуства уз дискусију. Постоје још и Група за смернице, која ради на развоју техничких докумената ове организације, затим Група за формирање националних библиотека за нуклеарну форензику и Група за тренинге, која пружа помоћ у развоју нуклеарне форензике државама и организацијама које то затраже [6].

### *Методе нуклеарне форензике*

У различитим литературама постоје различите категоризације нуклеарних форензичких метода. Оне су углавном извршене према различитим критеријумима. Чак је и "ITWG" у документу бр. 2 серије докумената Међународне агенције за атомску енергију под насловом "Нуклеарна безбедност", дала предлог редоследа метода којим би требало да се приступа у случају вршења нуклеарно-форензичког испитивања, а који се може сматрати одличном категоризацијом датих метода, пре свега према времену испитивања, али и врсти испитивања у смислу избора научне методе.

**Високо-резолутивна гама спектрометрија** (*енг.* "HRGS – High-Resolution Gamma Spectrometry"). Обично се користи у почетној фази испитивања. Неинвазивна је и прилично поуздана за почетни стадијум испитивања, па се користи као незаобилазна метода за добијање смерница за даље испитивање. Заснива се на детектовању γ-фотона и њиховом идентификовању у датом спектру. γ-кванти настају када језгро, након распада, прелази из енергетски побуђеног у неко ниже енергетско стање. Како је енергија γ-фотона једнака разлици енергија које је језгро имало и које има након емисије кванта, јасно је да се тумачењем спектра може доћи до закључка до ког распада је дошло.

**Разне врсте масене спектрометрије** (*енг.* "MS – Mass Spectrometry"). Масена спектрометрија је веома распрострањена метода. Поуздана је и осетљива, али је и инвазивна, јер узорак пре употребе мора да прође кроз одређене физичко-хемијске припреме. Користи се углавном за одређивање састава неке супстанце. Сепарација појединачних елемената се врши на основу њихове масе. Овде се користи чињеница да наелектрисане честице када се нађу у хомогеном магнетном пољу, почињу да се крећу по кружној путањи. Што је већа маса честице, већи је и полупречник кружне путање. То нас води до тога да ће се честице различите масе различито понашати у магнетном пољу, оне са мањом масом ће описивати кругове мањег полупречника и обрнуто.

 ISBN 978-86-7466-930-3

У нуклеарној форензици се често користе методе чија је основа масена спектрометрија, али поред ове методе обухватају још неки вид додатне анализе. Од ових метода најчешће се користе:
**Масена спектрометрија са индуковано спрегнутом плазмом** (*енг.* "ICP-MS"), **Масена спектрометрија термалном јонизацијом** (*енг.* "TIMS"), **Масена спектрометрија раствора изотопа** (*енг.* "IDMS"), **Гасна хроматографија – масена спектрометрија** (*енг.* "GS/MS"), **Масена спектрометрија секундарним јонима** (*енг.* "SIMS"), **Масена спектрометрија акцелератором** (*енг.* "AMS"). Надоградњом методе "ICP-MS" додатним алатима, добијају се још неке сложеније варијанте ове методе, као што су: **Ласерска аблација масена спектрометрија са индуковано спрегнутом плазмом** (*енг.* "LA-ICP-MS") и **Мулти-колекторска масена спектрометрија са индуковано спрегнутом плазмом** (*енг.* "MC-ICP-MS") [3, 7].

Поред претходно побројаних метода, у нуклеарној форензици су присутне и следеће методе: **Скенирајућа електронска микроскопија** (*енг.* "SEM"), **Трансмисиона електронска микроскопија** (*енг.* "TEM"), **Рендгенска флуоресценција** (*енг.* "XRF"), **Рендгенска дифракција** (*енг.* "XRD"), **Инфрацрвена спектроскопија Фуријеовим трансформацијама** (*енг.* "FTIR"), **Оптичка емисиона спектрометрија са индуковано спрегнутом плазмом** (*енг.* "ICP-OES"), **Ласерски индукована спектроскопија пробоја** (*енг.* "LIBS"), **α-спектрометрија** (*енг.* "AS"), **Микро-Раман Спектроскопија** (*енг.* "micro Raman Spectroscopy"), као и комбиноване "SEM/XRF", али и "SEM/EDX" или "SEM/WDX" [3, 7].

Све набројане методе су аналитичке и представљају срж нуклеарно-форензичких испитивања. На овај начин добијени подаци се сврставају у категорију која се на енглеском назива "ESS – Environmental Sampling for Safeguards"). Поред њих се користе и методе конвенционалне форензике, нпр. ДНК анализе и узимање отисака прстију. Осим тога, користе се и разне методе мониторинга, праћења итд. Те методе су: откривање недозвољених материјала **вишеканалним анализаторима** (*енг.* "MCA"), откривање недозвољених материјала **детекторима легура** (*енг.* "ALEX"), коришћење **инструмената за праћење промена у животној средини** (*енг.* "Environmental monitoring instruments"), коришћење система **дигиталног видео надзора** (*енг.* "Digital video surveillance sytems"), коришћење **сателитског снимања** (*енг.* "Satellite imagery"), коришћење **инспекцијске базе података** (*енг.* "Inspection Database"). У ову групу метода спадају и софтвери који се користе у ове сврхе, а то су: **Скуп неуралних мрежа** (*енг.* "CNN"), **Морфолошка анализа за атрибуцију материјала** (*енг.* "MAMA") [7, 8].

Табела 1. даје поделу према времену коришћења и према групи у коју дата метода спада.

**Табела 1 Редослед корака који треба предузети приликом испитивања узорка, према упутству (ITWG) [4]**

| Врста методе | 24 h | 7 дана | 2 месеца |
|---|---|---|---|
| Радиолошки метод | Брзина дозе (α, β, γ, n)<br>Површинска контаминација<br>Радиографија | | |
| Физичка карактеризација | Визуелни преглед<br>Фотографисање<br>Утврђивање масе и димензија<br>Оптичка микроскопија<br>Густина | Микроструктура<br>Морфологија<br>SEM<br>XRD | Наноструктура<br>Морфологија<br>TEM |
| Анализа изотопа | HRGS | TIMS<br>ICP-MS | SIMS<br>Технике радиоактивног бројања |
| Радиохронометрија | HRGS (за Pu) | TIMS<br>ICP-MS | HRGS (за U)<br>α-Spectrpmetry |
| Хемијски састав | XRF | ICP-MS<br>Хемијско испитивање<br>FTIR<br>SEM<br>IDMS | GC-MS |
| Традиционалне форензичке методе | Примена традиционалних форензичких дисциплина (отисак прста, ДНК анализа власи итд.) | | |

У табели 2. је дат преглед метода према томе у коју сврху се користе. Табела није преузета, али су подаци у њој систематизовани коришћењем података одређеног извора [8]. Ови подаци су приказани табеларно ради веће прегледности. У табели 3. су дате методе према врсти алата у које се убрајају. У табели 4. подела је према величини узорка и информацијама које се о узорку добијају.

**Табела 2 Подела метода према томе у коју сврху се користе [8]**

| Информације које се добијају из дате методе | Врста методе |
|---|---|
| Елементарни и молекуларни потписи | ICP-MS<br>ICP-OES<br>LA (LA-ICP-MS)<br>LIBS (за мале количине узорка)<br>μRaman Spectroscopy |
| Карактеризација изотопа | MC-ICP-MS<br>TIMS<br>AMS<br>SIMS |
| Датирање | SIMS<br>MC-ICP-MS |
| Информације о нехомогености недозвољених нуклеарних материјала | LA-MC-ICP-MS<br>SIMS<br>XRF<br>SEM/EDX<br>SEM/WDX<br>μRaman Spectroscopy |
| Морфологија у нуклеарној форензици | MAMA<br>CNN |

**Табела 3 Врста алата и метода у оквиру алата [9]**

| Врста алата | Метода |
|---|---|
| Алати за анализу елемента или изотопа | Радиометријске технике (α, β и γ спектрометрија)<br>Масена спектрометрија (TIMS, ICP-MS)<br>Хемијски огледи<br>Радиохемијске методе<br>XRF<br>XRD<br>GC/MS |
| Алати за визуелну анализу | Визуелно осматрање и фотографија<br>Ауторадиографија<br>Оптичка микроскопија<br>SEM<br>TEM |
| Алати за микроанализу | Рендгенске микроанализе (SEM/EDX и SEM/WDX)<br>SIMS<br>ИЦ спектроскопија<br>μРаман спектроскопија |

 ISBN 978-86-7466-930-3

**Табела 4 Карактеризација према величини узорка и границама детекције [6]**

| Врста алата | Метода | Врста информације о материјалу | Границе детекције | Просторна резолуција |
|---|---|---|---|---|
| Алати за анализу елемента или изотопа | HRGS | Изотопске | ng-µg | |
| | Хемијски огледи | Елементарне | mg | |
| | Радиохемијске/ Радиометријске методе | Изотопске/ Елементарне | fg-pg | |
| | TIMS | Изотопске/ Елементарне | pg-ng | |
| | ICP-MS | Изотопске/ Елементарне | pg-ng | |
| | XRF | Елементарне | 10 ppm | |
| | XRD | Молекуларне | ~ 1 at% | |
| | GS/MS | Молекуларне | ppm | |
| Алати за визуелну анализу | Визуелна инспекција | Макроскопске | | 0.1 mm |
| | Ауторадиографија | Микроскопске | | 10 – 50 µm |
| | Оптичка микроскопија | Микроскопске | | 1 µm |
| | SEM | Микроскопске | | 1 nm |
| | TEM | Микроскопске | | 0.1 nm |
| Алати за микроанализу | SIMS | Елементарне/ Изотопске | 0.1 ppb – 10 ppm | 0.1 – 1 µm |
| | SEM/EDX (WDX) | Елементарне | 0.1 – 2 mu % | 1 µm |
| | FTIR | Молекуларне | 0.1 – 1 mu % | 10 µm |
| | µРаман | Молекуларне | ~ 1 mu % | 1 µm |

## Закључак

Развојем нуклеарно-форензичких метода, нуклеарна безбедност је подигнута на виши ниво. Нуклеарни безбедносни режими су без ових алата немоћни. Постојање метода, значајно је допринело заустављању ширења нуклеарног наоружања, нуклеарног тероризма и недозвољене производње и употребе оружја које се везује за атомску и нуклеарну енергију. Ипак, и поред ових озбиљних метода није дошло до онога чему се тежи, а то је да се у потпуности укине нуклеарно наоружање, које би у некој будућој ескалацији сукоба између сила довело до престанка света каквим га познајемо. Међутим, кривица је у политици, а методе су моћан алат у имплементацији споразума.

## Литература


[1] International Atomic Energy Agency, *IAEA Safeguards Glossary* (No. 3) [Electronic version], Retrieved June 2002, from: https://www.iaea.org/sites/default/files/iaea_safeguards_glossary.pdf

[2] EU Non-Proliferation Consortium, *Nuclear Forensics Material Analysis for Security Purposes*, Non-Proliferation Papers No. 60 (2017)

[3] International Atomic Energy Agency, *Nuclear Forensics in Support of Investigations*, IAEA Nuclear Security Series No. 2-G (Rev. 1), IAEA, Vienna, 2015.

[4] K. Mayer, M. Wallenius, K. Lützenkirchen, J. Galy, Z.Varga, N. Erdmann, R., Buda, J.-V. Kratz, N. Trautmann, K. Fifield, *Nuclear Forensics: A Methodology Applicable to Nuclear Security and to Non-Proliferation*, International Nuclear Physics Conference (2010)

[5] Sipri, *Arments, Disarment and International Security,* Yearbooks (2012-2021), from: https://www.sipri.org

[6] International Technical Work Group: http://www.nf-itwg.org/

[7] Z. Varga M. Wallenius, M. Krachler, N. Rauff-Nisthar, L. Fongaro, A. Knott, A. Nicholl, K. Mayer, *Trends and perspectives in Nuclear Forensic Science*, Trends in Analytical Chemistry 146 (2022) 116503

[8] David L. Donohue, *Key Tools For Nuclear Inspections,* IAEA (2002), from: https://www.iaea.org/sites/default/files/publications/magazines/bulletin/bull44-2/44202451723.pdf

[9] M. J. Kristo, *Handbook of Radioactivity Analysis Volume 2: Radioanalytical Applications*, Lawrence Livermore National Laboratory (2018)


 ISBN 978-86-7466-930-3

# Stabilnost frekvencije kvarcnih oscilatora

Miodrag Malović, Ljiljana Brajović, Tomislav Šekara

***Apstrakt*—Oscilatorna kola su neizbežni deo praktično svih elektronskih uređaja. Najčešće se koriste kola na bazi kvarcnih kristala. Prikazan je proces proizvodnje i princip rada kvarcnih oscilatora, kao i podele kristala i oscilatornih kola. Analizirane su metode kvantitativnog opisivanja greške odnosno nestabilnosti frekvencije. Efekti koji utiču na promene frekvencije su klasifikovani po fizičkom poreklu i vremenskom periodu u kom se dešavaju.**

***Ključne reči*—Kvarcni kristal, oscilator, frekvencija, vreme, stabilnost, preciznost**

## I. UVOD

Piezoelektricitet je pojava međuzavisnosti između normalnog napona, koji izaziva mehaničku deformaciju, i naelektrisanja na krajevima materijala. Pritisak na materijal izaziva električnu polarizaciju, i obrnuto, primena električnog napona izaziva deformaciju materijala. Piezoelektrični oscilatori su električna kola koja koriste piezoelektrične karakteristike kvarcnih kristala ili drugih materijala da stvore električni signal približno konstantne frekvencije. U današnje vreme piezoelektrični, uglavnom kvarcni, oscilatori su glavni izvor takta u elektronskim napravama, a praktično ne postoji elektronski uređaj bez oscilatora. Alternative kvarcu su drugi kristali (npr. turmalin, topaz ili kalijum-natrijum tartarat) ili neke vrste keramike. Keramički materijali, dobijeni sinterovanjem, i pored nekih prednosti, imaju mnogo nestabilniju frekvenciju oscilovanja [1].

U novije vreme javljaju se i MEMS oscilatori koji ne moraju raditi na piezoelektričnom principu. I pored značajnog poboljšanja nekih karakteristika, prvenstveno stabilnosti frekvencije [2], MEMS oscilatori su još uvek daleko od preuzimanja primata kvarcnim oscilatorima, jer imaju i veću cenu i veću potrošnju energije (bitno kod baterijski napajanih sistema). S obzirom na tendencije razvoja u pravcu smanjenja potrošnje i cene, izgleda da će se kvarcni oscilatori koristiti još dugo godina.

## II. KVARCNI KRISTALI

Kvarc, koji predstavlja kristalni oblik silicijum dioksida, se najčešće dobija iz površinskih kopova u raznim delovima sveta. Kristali su uglavnom providni i bezbojni, a mogu biti i u različitim nijansama u zavisnosti od primesa. Prirodni kristali kvarca (Sl. 1a) se mrve, rastvaraju, i ponovo kristališu pod kontrolisanim uslovima. Veštački uzgojeni kristali (veličine u santimetrima) zahtevaju par meseci rasta pod strogo kontrolisanim uslovima (na visokoj temperaturi i pritisku). Komadići kristala pravilnog oblika, veličine tipično nekoliko milimetara, isečeni iz njih na različite, strogo definisane načine koji se nazivaju rezovi (*cuts*), koriste se kao osnove elektronskih oscilatornih kola. U odnosu na RLC kola, kvarcni oscilatori imaju manji koeficijent prigušenja, odnosno manje gubitke, te zahtevaju vrlo malo snage za održavanje oscilacija.

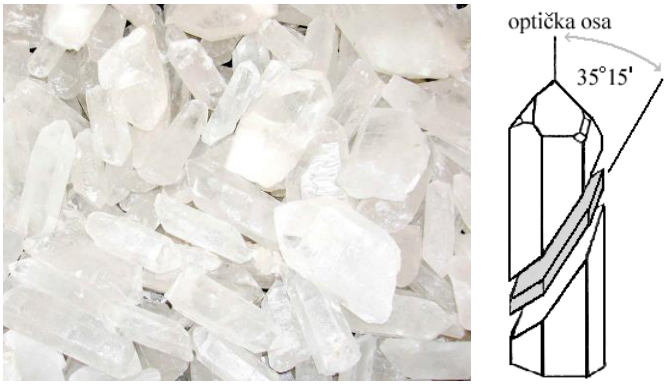


Sl. 1. a) Prirodni kristali kvarca; b) AT rez.

Rezonantne frekvencije kvarcnih kristala su u praksi u većini slučajeva u opsegu od KHz do više stotina MHz. Rezonantna učestanost primarno zavisi od vrste, oblika i veličine kristala (reza), i primenjenih statičkih sila.

Izborom pogodnih oblika kristala dobijaju se oscilatori relativno stabilni u odnosu na temperaturske promene (koje su glavni izvor kratkoročnih fluktuacija frekvencije). Najčešće korišćeni oblik kristala je tzv. AT rez. AT pločice se seku kao isečci pod uglom od oko 35º 15’ u odnosu na optičku osu, kao na Sl. 1b.

Osim AT reza, evo kratkog opisa nekih od mnogobrojnih drugih tipova:

- BT rez: manje temperaturno stabilan ali može da postigne veće rezonantne frekvencije
- SC rez: izvedeno od „stres kompenzacije“, skuplji kristali kompleksnijeg procesa proizvodnje, koji se koriste u temperaturski kompenzovanim oscilatorima, sa većom stabilnošću frekvencije u odnosu na temperaturu i mehaničke uticaje
- XY rez: koristi se za manje frekvencije, tipično za 32768 Hz (popularna kao $2^{15}$, tako da se 1 sekunda registruje prenosom 15-bitnog brojača); često korišćeni *tuning fork*

Miodrag Malović – Univerzitet u Beogradu, Inovacioni centar Tehnološko-metalurškog fakulteta, Karnegijeva 4, 11120 Beograd (e-mail: ofiss@malovic.in.rs) (https://orcid.org/0000-0002-0691-4626).

Ljiljana Brajović – Univerzitet u Beogradu, Građevinski fakultet, Bulevar kralja Aleksandra 73, 11120 Beograd (e-mail: brajovic@grf.rs) (https://orcid.org/0000-0002-2265-7308).

Tomislav Šekara – Univerzitet u Beogradu, Elektrotehnički fakultet, Bulevar kralja Aleksandra 73, 11120 Beograd, Srbija (e-mail: tomi@etf.rs) (https://orcid.org/0000-0001-8031-3135).

 ISBN 978-86-7466-930-3

kristali (u obliku zvučne viljuške) koriste ovaj tip reza.

Geometrija oscilovanja kvarcnog kristala varira. Najčešće imamo pojavu tzv. *thickness-shear* (smicanje po debljini) oscilovanja, što znači da gornja i donja površina pločice osciluju longitudinalno u različitim smerovima, kao što je grafički prikazano na Sl. 2, dole desno. Ovo je uobičajeni režim rada za AT rezove. Sledeći najčešći modovi oscilovanja su: longitudinalni (*length* ili *extensional*) i transverzalni (*flexure*), ekvivalentno poznatim režimima oscilovanja žica i štapova, kao i režim smicanja po površini (*face-shear*). Transverzalne oscilacije su tipične za XY rez.

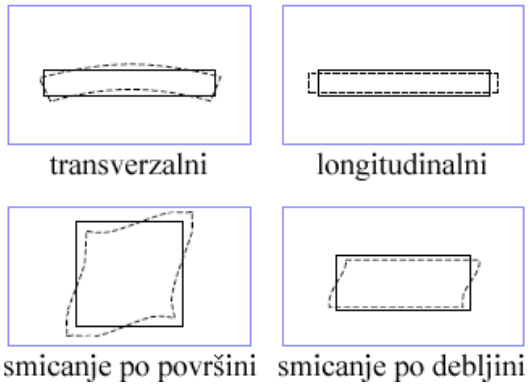


Sl. 2. Najčešći modovi oscilovanja kvarcnih kristala.

Smicanje po površini je na Sl. 2 prikazano odozgo (za kvadratnu pločicu manje debljine) a ostali modovi sa strane (za izdužene kristale). Ovo su najčešće geometrije, ali postoje varijacije i na ovaj raspored dimenzija. Takođe, postoje i drugi modovi oscilovanja (npr. torzioni), kao i drugi oblici pločica (npr. disk), koji se ređe koriste.

## III. MATEMATIČKO OPISIVANJE FLUKTUACIJA FREKVENCIJE

Preciznost i tačnost frekvencije su dva pojma koja treba razlikovati. Greška je razlika između stvarne frekvencije, koju je nemoguće savršeno odrediti, i nominalne (deklarisane) frekvencije. Tačnost je obrnuto proporcionalna greški. Preciznost ili stabilnost oscilatora je inverzna mera varijacije frekvencije. Uređaj može biti tačan ali neprecizan ako mu je srednja frekvencija blizu nominalne ali pokazivanje više varira, ili netačan a precizan ako frekvencija nije dobro podešena ali manje varira u vremenu.

Stabilnost se obično deli na kratkoročnu i dugoročnu, mada je ponekad u upotrebi i izraz srednjoročna stabilnost. Ne postoji striktna vremenska podela na kratkoročne i dugoročne promene frekvencije u smislu apsolutne vrednosti vremena. Kratkoročna stabilnost označava promene u toku vremena reda veličine sekundi ili minuta (u toku jedne sesije rada sa uređajem, recimo), dok se dugoročna stabilnost odnosi na periode reda veličine meseci ili godina. Često se reč stabilnost koristi isključivo da opiše kratkoročnu preciznost, dok se dugoročne promene opisuju pojmom „starenje“.

Kod starenja, za kvantitativnu meru stabilnosti uzimamo jednostavno relativni odnos apsolutne promene frekvencije i njene početne, krajnje ili nominalne vrednosti (koje su približno jednake, a stabilnost ne zahteva toliko preciznu deklaraciju, pa možemo upotrebiti bilo koju od njih).

Za opisivanje kratkoročne stabilnosti koriste se različite metričke funkcije. Peak-to-peak devijacija predstavlja razliku između maksimalne i minimalne izmerene frekvencije u nekom vremenskom intervalu, i može se izražavati u apsolutnim ili relativnim jedinicama:

$$\Delta f_{\text{p-p}} = f_{\max} - f_{\min}$$
$$\delta f_{\text{p-p}} = \frac{f_{\max} - f_{\min}}{\bar{f}} \tag{1}$$

Standardna devijacija predstavlja koren iz srednjeg kvadrata razlike u odnosu na srednju vrednost (varijanse):

$$\sigma f = \sqrt{\frac{\sum_{1}^{N} (f_N - \bar{f})^2}{N}} \tag{2}$$

i takođe se često deli sa srednjom vrednošću frekvencije da bi se izrazila u relativnim jedinicama. Ipak, ako se drugačije ne naglasi, u metrologiji se najčešće podrazumeva da se koristi Alanova devijacija:

$$\sigma_f(t) = \sqrt{\frac{\sum_{1}^{N-1} (\bar{f}(\mathrm{t}_{i+1}) - \bar{f}(\mathrm{t}_i))^2}{2(N-1)}} \tag{3}$$

Alanova devijacija je funkcija vremenskog intervala (koji se najčešće naziva interval usrednjavanja) $t$, i uzima u obzir usrednjene frekvencije u isključivo susednim intervalima tog trajanja. Da bismo, na primer, odredili Alanovu devijaciju frekvencije za interval usrednjavanja od 1 s, izbrojaćemo impulse u $N$ susednih sekundi (najmanje dve) i podeliti broj impulsa sa vremenom (tj. 1 s; za određivanje protoka vremena koristi se tačniji, etalonski sat) da bismo dobili $f_{\text{sr}}$ za svaki period. Zatim određujemo Alanovu devijaciju kao koren iz srednjeg kvadrata razlika isključivo susednih članova, podeljenog sa dva. Bitno je zapaziti da na ovaj način driftovi frekvencije izvan intervala za koji se stabilnost deklariše ne utiču na rezultat, što nije slučaj sa standardnom devijacijom ili peak-to-peak vrednošću. Alanova devijacija se, kao i standardna, često izražava u relativnim jedinicama (podeljena sa srednjom vrednošću).

Renomirani proizvođači određuju stabilnost frekvencije laboratorijski i predstavljaju tipične rezultate kao Alanovu devijaciju u zavisnosti od perioda posmatranja. Radi se o šumu frekvencije, bez merljive promene spoljašnjih faktora, dakle pod konstantnim laboratorijskim uslovima. Stabilnost se predstavlja na logaritamskom grafiku, najčešće za periode od dela sekunde do $10^4$ ili $10^5$ sekundi. Stabilnost je slabija za manje intervale, i poboljšava se sa povećanjem perioda posmatranja kao posledica usrednjavanja, do optimalne

 ISBN 978-86-7466-930-3

vrednosti za periode reda veličine 1 s. Sa povećavanjem kvaliteta oscilatora, raste i vreme za koje se javlja maksimum stabilnosti (ide i preko $10^4$ s kod najkvalitetnijih kontrolisanih oscilatora) [3]. Pri daljem povećanju perioda usrednjavanja, nestabilnosti temperature, napajanja, i dr, preuzimaju dominantni uticaj, pa opet dolazi do (nešto sporijeg) pogoršanja. Za najkvalitetnije kvarcne oscilatore, stabilnost može imati vrednost ekstremuma (numerički minimum, odnosno kvalitativno maksimum) reda veličine i boljeg od $10^{-13}$ (dok je uobičajeno nekoliko redova veličine lošija), u relativnim jedinicama [4].

Na Sl. 3 je prikazan primer dijagrama vremenske stabilnosti za tri eksperimentalno testirana komada TCXO oscilatora modela HTV2 proizvođača Connor-Winfield [5].

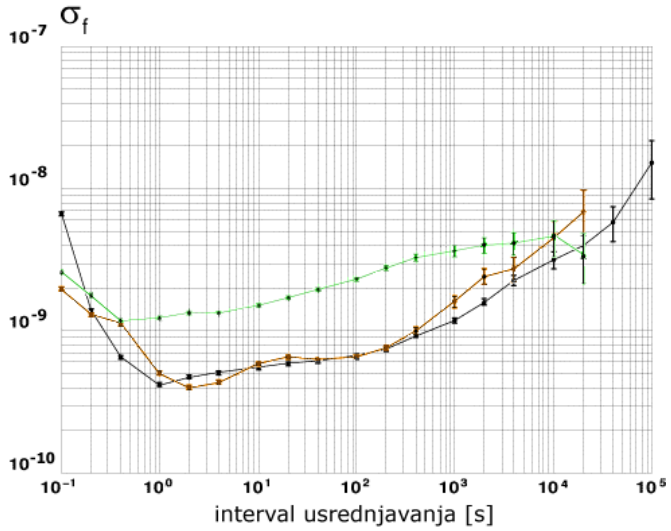


Sl. 3. Eksperimentalno određena stabilnost frekvencije tri komada temperaturski kompenzovanih oscilatora *Connor-Winfield* HTV2 [5].

## IV. IZVORI KRATKOROČNE I DUGOROČNE NESTABILNOSTI FREKVENCIJE

Od kratkoročnih varijacija najčešće su one izazvane promenama temperature, mada i mnogobrojni drugi fizički efekti doprinose stalnim kako skokovitim tako i laganim promenama (driftovima) rezonantne frekvencije [6]. U njih spadaju šokovi (fizički udarci), promena položaja, vibracije, promena napona napajanja, elektromagnetske smetnje, radioaktivnost, itd.

Mnoge od ovih pojava imaju izražen histerezis, a prvenstveno temperatura i napajanje. Pojava skokovite promene frekvencije prilikom gašenja i ponovnog paljenja uređaja se naziva *retrace* efekat. Regularne vibracije, promene položaja, i napona napajanja uglavnom ne proizvode intenzitet relativne promene frekvencije veći od $10^{-9}$. Ritrejs ili jači šokovi mogu imati nešto veći efekat, obično oko $10^{-8}$ [7].

Zavisnost frekvencije od temperature je parabolična sa negativnim koeficijentom (kao na Sl. 4), tj. ima maksimum na željenoj radnoj temperaturi kod većine rezova:

$$f(t) = f_0(1 - k(t - t_0)^2) \qquad (4)$$

dok AT i SC tipovi kristala imaju približno kubnu zavisnost rezonantne frekvencije od temperature:

$$f(t) = f_o(1 + k_1(t - t_o) + k_2(t - t_o)^2 + k_3(t - t_o)^3) \qquad (5)$$

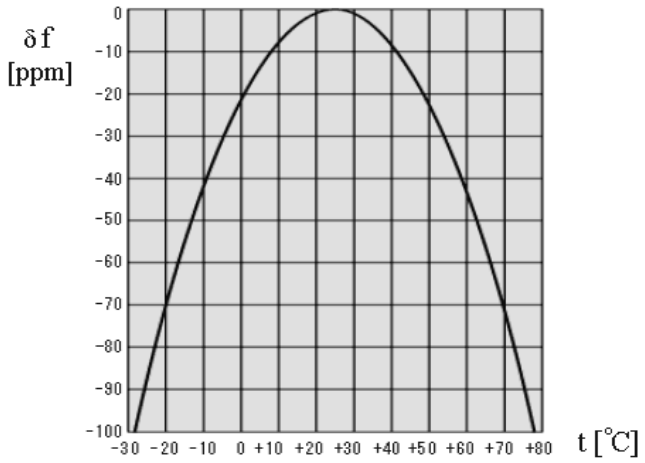


Sl. 4. Parabolična zavisnost $f(t)$ za BT, XY, i mnoge druge tipove rezova kvarcnog kristala.

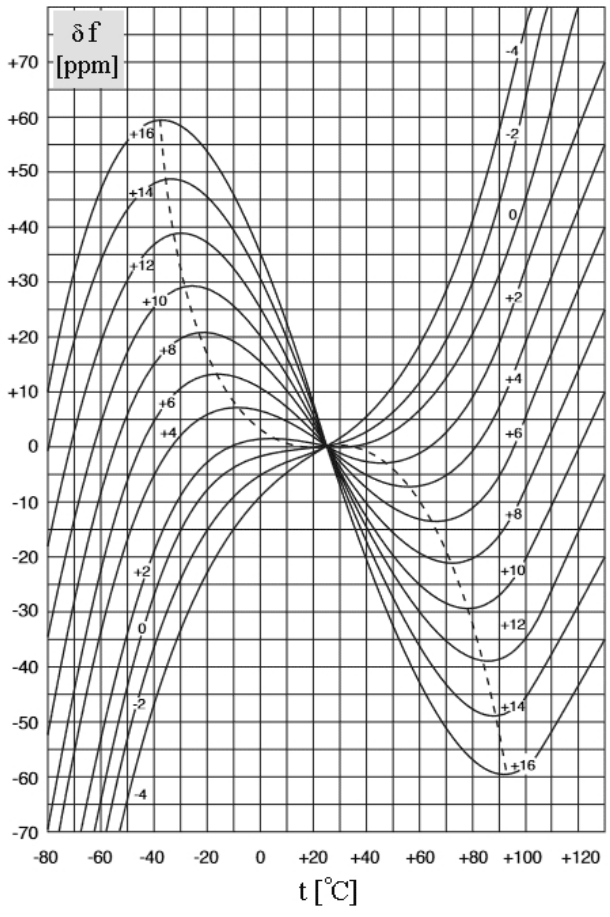


Sl. 5. Skup funkcija $f(t)$ za AT tipove kristala sa različitim uglom rezanja.

Središnji deo obe krive obično se nalazi na sobnoj temperaturi ($t_o \approx 25$ ºC), pošto je to ciljna temperatura rada


ISBN 978-86-7466-930-3

većine kristala, dok je nešto više kod SC rezova (65-95 ºC), koji se koriste u kontrolisanim, zagrejanim komorama. Kod uobičajenog AT reza pod optimalnim uglom od oko 35º 15', imamo slabu zavisnost od temperature (relativne promene reda veličine ppm, tj. $10^{-6}$, za ceo opseg temperatura 0-50 ºC).

Pri povećanju ugla rezanja, vidimo da dolazi do krivljenja funkcije (na Sl. 5 imamo po jednu nacrtanu krivu na svaka 2 minuta promene ugla reza). Tačke lokalnih ekstremuma kubne zavisnosti, koji se javljaju u ovom slučaju, nazivaju se LTTP i UTTP (*lower temperature turning point* odnosno *upper temperature turning point*), i spojene su isprekidanim linijama na slici. Kristali se nekada koriste i u ovom režimu (oko ovih temperatura).

Kod kristala ekonomske klase, varijacije rezonantne frekvencije posmatrane između različitih komada kristala, istog modela, iznose tipično oko $10^{-5}$, a retko preko $10^{-4}$.

Dugoročne promene frekvencije se odnose na duže periode koji su reda veličine meseci ili godina. Uzrok dugoročnih promena su kretanja molekula primesa unutar kristala, i fizičkih promena oblika samog kristala kao i delova sa kojima je doveden u dodir (postolja). Naravno, kvalitet izrade kristala i oscilatora određuje ove parametre - čistoća kako materijala tako i punjenja kutije oscilatora od inertnog gasa, i kvalitet zaptivanja povećavaju stabilnost frekvencije. Tipična kriva promene frekvencije kvarcnog kristala usled starenja data je na Sl. 6. Eksponencijalna komponenta, dominantna na početku života kristala, uglavnom potiče od promena oblika (tzv. *stress relief* odnosno ublažavanje naprezanja, ili sleganje), dok sporo opadajuća komponenta koja preuzima primat u kasnijim godinama predstavlja efekte kontaminacije (kretanje molekula primesa) [8].

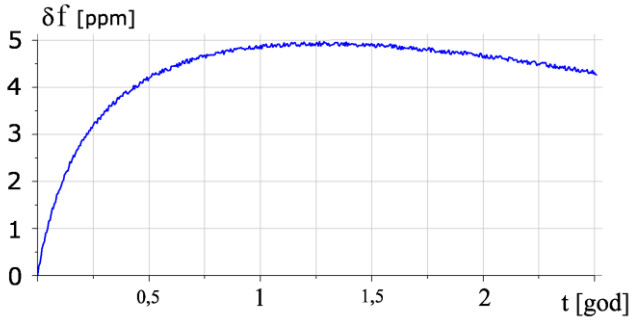


Sl. 6. Tipična promena rezonantne frekvencije kvarcnog kristala usled starenja.

Starenja većine komercijalnih oscilatora su reda veličine $10^{-6}$ do $10^{-5}$ na nivou više godina. U literaturi se može sresti i podela starenja na aktivno i pasivno. Pod aktivnim starenjem se podrazumeva starenje u toku rada, dok je pasivno starenje „na polici" tj. kada se kristal ne koristi. Moguće je i eksperimentalno ubrzano starenje kristala. Ovo se izvodi aktivno, na većoj temperaturi. Smatra se da rad na 85 ºC od mesec dana do 1000 sati, ili rad na 105 ºC nedelju dana, proizvodi efekte starenja kao i regularna operacija na sobnoj temperaturi tokom jedne godine. Ubrzano starenje na temperaturama od 125-150 ºC često ispoljava izmene nagiba opadajuće dugoročne komponente, dakle postoje promene u fizici procesa kontaminacije, te se ne može smatrati za tačnu repliku originalnog procesa i ovakva testiranja nemaju veliku vrednost [9].

## V. TIPOVI OSCILATORA

Kao što je već rečeno, kvarcni kristali se koriste kao osnovni elementi u oscilatornim kolima (oscilatorima). Oscilatori mogu imati komponente koje služe za stabilizaciju frekvencije, kao i kola za multiplikaciju frekvencije, kojima se osnovna frekvencija kristala povećava ceo broj puta (najčešće $2^n$).

Najprostiji tip oscilatora se dobija vezivanjem dva kondenzatora između krajeva kristala i mase, i koristi se za davanje takta mikroprocesorima, kao što je ilustrovano na Sl. 7. Malo kompleksniji modeli poznati su iz analogne i digitalne elektronike, kao što su Kolpicov i Piersov oscilator [10].

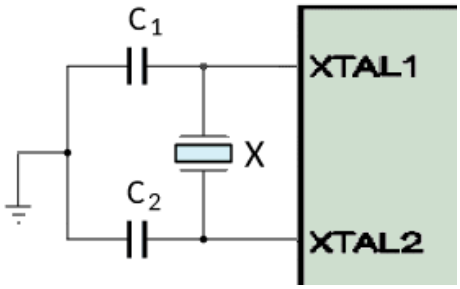


Sl. 7. Uobičajeni način vezivanja kvarcnog kristala (X) na CPU - mikroprocesorski oscilator.

Osnovna podela oscilatora je na tri kategorije: RTXO, TCXO i OCXO (gde kovanica XO označava kristalni oscilator), a postoje i druge skraćenice od kojih ćemo neke spomenuti.

Jednostavna kola koja ne vrše nikakvu kompenzaciju temperaturskih promena spadaju u kategoriju RTXO (*room temperature crystal oscillators*). Većina ekonomskih uređaja koriste RTXO kola, ne samo zbog manje cene, već i zbog znatno niže potrošnje energije, što je važan faktor u projektovanju baterijski napajanih uređaja.

TCXO (*temperature compensated crystal oscillators*) sadrže termometre, mere temperaturu, i uvode korekcije da bi se rezonantna frekvencija učinila stabilnijom. Uobičajeni princip rada TCXO je VCXO: *voltage controlled crystal oscillator*. VCXO je nešto širi pojam, koji obuhvata sve kristalne oscilatore čija se frekvencija kontroliše naponom (ne samo one kod kojih je cilj postizanje stabilne frekvencije). Kod TCXO sa VCXO (takođe zvanih i VC-TCXO), kontroliše se napon napajanja kristala tako da se kompenzuju promene frekvencije koje potiču od promene temperature (koja se monitoriše). Digitalni TCXO se referenciraju i imenima DCXO - *digitally controlled crystal oscillators* ili MCXO - *microprocessor controlled crystal oscillators*.

Kod OCXO (*oven controlled crystal oscillators*) se kolo grejanjem održava na konstantnoj temperaturi, u kućištu koje predstavlja zatvorenu temperatursku komoru (*oven*), tako da

 ISBN 978-86-7466-930-3

su temperaturski uticaji zanemarljivi. Ovo je još skuplji i energetski zahtevniji tip oscilatora. U ekstremnim slučajevima, koriste se još skuplji, krupniji i snažniji DOCXO (dupli OCXO), koji rade istu stvar u dva koraka - imaju spoljnu i unutrašnju komoru, i umesto standardne stabilnosti frekvencije za OCXO reda veličine $10^{-8}$ relativno na dnevnom nivou, postižu uobičajenu standardnu stabilnost reda veličine $10^{-11}$ i bolje [11].

## VI. GPS DISCIPLINOVANI OSCILATORI

Kombinovanjem OCXO, a ređe i TCXO, koji ne moraju biti striktno bazirani na kvarcu (mada kvarc jeste jedan od osnovnih tipova kristala koji se koriste), sa GPS prijemnikom, dobijamo u novije vreme popularnu kategoriju GPS disciplinovanih oscilatora (GPSDO) [12].

GPS (*global positioning system*) servis pruža uslugu takozvanog PPS-a, odnosno *pulse per second*. Iako PPS ne pruža informaciju o fizičkom vremenu (vreme-datumu), on daje pouzdanu informaciju o protoku jedne sekunde, koja se konstantno usklađuje sa referentnim laboratorijama najvišeg nivoa tačnosti na zemlji. Istina je da u prijemu PPS signala postoji značajna neodređenost, uslovljena procesom prenosa signala sa satelita do prijemnika u uređaju (nesavršenosti elektronike transmitera i prijemnika, kao i neodređenost putanje prenosa kroz sredinu promenljivih karakteristika), što čini da je kratkoročna stabilnost PPS frekvencije mala (čak i do $10^{-6}$). Međutim, dugoročna stabilnost ovog signala je superiorna u odnosu na sve samostalne oscilatore, i GPS disciplinovani oscilatori (koji predstavljaju kompleksne elektronske uređaje sa sofisticiranim softverom) kombinuju ovu stabilnost sa superiornom kratkoročnom stabilnošću OCXO oscilatora. Procesor monitoriše frekvenciju PPS i OCXO signala, i izvodi neophodne korekcije da bi izlaz oscilatora uskladio sa dugoročno analiziranim PPS signalima. Budući da se radi o softverskoj kontroli, GPSDO lako izlazi na kraj sa propuštenim PPS signalima. Promene rezonantne frekvencije kristala nastale kao posledica starenja se pamte pa možemo reći da se izvodi kontinualna kalibracija frekvencije.

Sl. 8. GPSDO modul, bez prijemnika, proizvođača *Acquisys* [14].

Jedna od mana ove vrste oscilatora (osim očiglednih: veličine, potrošnje i cene, koja je za bolje modele preko hiljadu dolara) je nemogućnost da se radi na mestima gde ne postoji dostupnost GPS signala (bez dodatnog antenskog sistema), a ovaj je poznat po svojoj slaboj prodornosti u zatvorene prostore [13].

Primer GPSDO modula (bez prijemnika), proizvođača Acquisys [14], prikazan je na Sl. 8. Dimenzije modula iznose $10{,}4 \times 7{,}0 \times 2{,}6$ cm.

## VII. SENZORI NA BAZI VARIJABILNOSTI FREKVENCIJE

Promenljivost frekvencije oscilovanja kristala je pojava koju možemo i iskoristiti. Neki senzori rade tako što prate promene rezonantne frekvencije u funkciji posmatrane fizičke veličine. Naravno, kvalitet ovih senzora je limitiran zavisnošću iste frekvencije od drugih faktora. Jedan od metoda koji se koriste za eliminaciju zavisnosti od neželjenih parametara jeste upotreba još jednog, referentnog kvarcnog kristala, koji se izlaže koliko je moguće identičnim uslovima, osim pobude. U ovom slučaju izlaz senzora predstavlja razliku između frekvencija oscilovanja pobuđenog i referentnog kristala.

Jedan od takvih sistema, za merenje pritiska, realizovan je na univerzitetu u Ksi Anu, u Kini [15]. Šema je prikazana na Sl. 9. Ideja je slična Vitstonovom mostu sa poluprovodničkim mernim trakama: dva rezonatora koji se istežu u suprotnim smerovima povećavaju osetljivost, dok treći služi za kompenzaciju temperaturnih i drugih efekata.

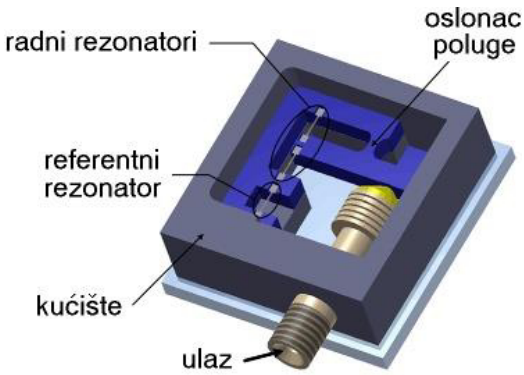


Sl. 9. Šema senzora pritiska razvijenog na Univerzitetu u Ksi Anu, Kina [15].

Integrisani senzori ubrzanja na principu promenljive frekvencije kvarcnog rezonatora su u upotrebi od osamdesetih godina prošlog veka, ali su u početku bili višekomponentni, tj. probna masa se sastavljala sa kućištem i kristalom (koji je obično bio tipa DETF - *double ended tuning fork*, odnosno zvučna viljuška spojena na oba kraja). Ovakvi sistemi su termalno nehomogeni, tj. unose grešku po osnovu različitih koeficijenata termalnog širenja različitih materijala od kojih se sastoje. Zato se u novije vreme proizvode tzv. monolitni MEMS senzori koji su u potpunosti izgrađeni od kvarca [16].

QCM - *quartz crystal microbalance*, predstavlja kategoriju merenja koja se zasnivaju na promeni mase kvarcnog kristala, koja uzrokuje promenu rezonantne frekvencije [17]. Dodavanjem slojeva materijala na kvarc, frekvencija oscilovanja se smanjuje. QCM kvarcni kristali, po pravilu oblika okrugle pločice (diska), imaju tanak film kojim su obloženi, a koji menja masu putem interakcije sa sredinom u kojoj se nalazi. Najčešće se vrši detekcija gasova, koji stupaju

 ISBN 978-86-7466-930-3

u hemijsku ili fizičku interakciju sa slojem, koja uzrokuje promenu njegove mase. Naravno, neophodno je da ova interakcija bude reverzibilna. Jedna od čestih primena QCM je merenje vlažnosti (upijanjem molekula vode od strane sloja materijala kao što je grafen).

Merenja viskoznosti tečnosti uranjanjem celog kristala ili, češće, njegovog dela u tečnost poznate gustine takođe se svrstavaju u kategoriju QCM. Teškoća u primeni ovih tehnika je činjenica da dolazi do velike promene u faktoru prigušenja što izaziva dodatnu nestabilnost frekvencije, pa čak i mogućnost prestanka oscilovanja. U novije vreme koriste se senzorski sistemi u kojima se određuju dimenzije kapljica tečnosti koje se zatim spuštaju na površinu kristala čija se frekvencija meri [18]. Istina je da je automatizacija ovakvog procesa teško izvodljiva, ali kontinualna terenska merenja viskoznosti su retko potrebna.

## VIII. ZAKLJUČAK

Opisani su kvarcni kristali i oscilatori koji ih koriste kao svoje komponente. Analizirani su faktori koji utiču na promene rezonantne frekvencije, odnosno njene kratkoročne i dugoročne nestabilnosti. Dat je i kratak pregled savremenih senzora koji koriste promene rezonantne frekvencije za merenje različitih fizičkih veličina.

Iako su u novije vreme razvijeni MEMS oscilatori sa boljom stabilnošću frekvencije, mala potrošnja i cena će definitivno uticati na to da kvarcni kristali ostanu osnova većine oscilatornih kola u doglednoj budućnosti.

## ZAHVALNICA

Autori se zahvaljuju za podršku Ministarstvu prosvete, nauke i tehnološkog razvoja Republike Srbije (ugovori 451-03-68/2022-14/200287, 451-03-68/2022-14/200092 i projekat TR-33020).

## REFERENCE

[1] K. Uchino, "The development of piezoelectric materials and the new perspective," in Advanced Piezoelectric Materials, Cambridge, UK, Woodhead Publishing, 2017, ch. *1*, pp. *1-92*.

[2] G. Wu, J. Xu, E. J. Ng, W. Chen, "MEMS resonators for frequency reference and timing applications," *J. Microelectromech. Syst.*, vol. *29*, no. *5*. pp. *1137-1166*, Sep. 2020.

[3] W. J. Riley, "Techniques for frequency stability analysis," in Proc. of IEEE international frequency control symposium, Tampa, FL, USA, vol. 4, pp. 10-33, May 2003.

[4] C. Calosso C, B. Francois, R. Boudot, P. Yun, M. Gozzelino, E. Bertacco E, S. Micalizio, "Local oscillators and digital electronics for compact atomic clocks," in Microwave Technology and Technique Workshop, Noordwijk, Netherlands, hal-02472712, Apr. 2017.

[5] LeapSecond.com :: Museum of Time & Frequency (2003). *Connor-Winfield HTV-series TCXO*, [Online]. http://www.leapsecond.com/museum/htv2

[6] W. J. Riley, "NIST special publication 1065: Handbook of frequency stability analysis," US Dept. Commer., Nat. Inst. Stand. Technol., Gaithersburg, MD, USA, 2008.

[7] H. Zhou, C. Nicholls, T. Kunz, H. Schwartz, "Frequency accuracy & stability dependencies of crystal oscillators," Carleton Univ., Ottawa, Canada, Rep. SCE-08-12, 2008.

[8] J. Cartright, "Aging performance in crystals," Connor-Winfield Corp., Tech. rep., 2008.

[9] J. R. Vig, T. R. Meeker, "The aging of bulk acoustic wave resonators, filters and oscillators," Proc. of the 45th Annual Symposium on Frequency Control, Los Angeles, CA, USA, pp. 77-101, May 1991.

[10] E. H. Currie, "The Pierce Oscillator," in *Mixed-Signal Embedded Systems Design*, Cham, Switzerland, Springer, 2021, ch. *13*, pp. *599-616*.

[11] A. G. Nikonov, A. V. Kotyukov, A. S. Kamochkin, N. I. Dyakonova, "Recent achievements in performance of low profile ultra precision single oven quartz oscillators," in IFCS-EFTF 2012: European Frequency and Time Forum, Gothenburg, Sweden, pp. 279-285, Apr. 2012.

[12] M. A. Lombardi, "The use of GPS disciplined oscillators as primary frequency standards for calibration and metrology laboratories," *NCSLI Meas.*, vol. *3*, no. *3*, pp. *56-65*, Sep. 2008.

[13] G. Dedes, A. G. Dempster, "Indoor GPS positioning - challenges and opportunities," in Proc. of IEEE 62nd Vehicular Technology Conference, Dallas, TX, USA, vol. 1, pp. 412-415, Sep. 2005.

[14] Acquisys, *GPS Disciplined Oscillator Module*, [Online]. https://www.acquisys.fr/en/product/gpsdo-2

[15] Q. Zhang, C. Li, Y. Zhao, B. Li, C. Han, "A high sensitivity quartz resonant pressure sensor with differential output and self-correction," *Rev. Sci. Instrum.*, vol. *90*, no. *6*, *065003*, Jun. 2019.

[16] C. Han, C. Li, Y. Zhao, B. Li "High-Stability Quartz Resonant Accelerometer with Micro-Leverages," *J. Microelectromech. Syst.*, vol. *30*, no. *2*, pp. *184-192*, Jan. 2021.

[17] X. Qiao, X. Zhang, Y. Tian, Y. Meng, "Progresses on the theory and application of quartz crystal microbalance," *Appl. Phys. Rev.*, vol. *3*, no. *3*, *031106*, Sep. 2016.

[18] Q. Bai Q, X. Huang, "Using quartz crystal microbalance for field measurement of liquid viscosities," *J. Sensors*, vol. *2016*, *7580483*, Jan. 2016.

## ABSTRACT

This paper presents a short review of quartz oscillators frequency stability issues. Quartz crystals are a base building block of majority of oscillator circuits, which are unavoidable part of practically any modern electronic device. The principle of operation, process of production, and classification of crystals were described briefly. Metrics for mathematical description of frequency error and stability were analysed. Phenomena affecting frequency fluctuations were classified by their physical origin and the time scale on which they occur. Several types of sensors employing the effect of frequency variability were also described.

**Quartz Oscillators Frequency Stability**

Miodrag Malović, Ljiljana Brajović, Tomislav Šekara

 ISBN 978-86-7466-930-3

# Natural Polymers As Nanocapsule Carriers

Danijela Rajić, Srđan Vuković, Svetlana Pelemiš, Milesa Srećković

***Abstract*— Natural polymers obtained from renewable sources have recently been increasingly considered as suitable carriers, in the form of nanocapsules, for various active components. They enable the formation of a system for the delivery of active substances so that it is possible to encapsulate, protect, and release bioactive substances in drugs and food. Encapsulation of active components also enables the protection of sensitive and easily volatile components. Particular attention is paid to their application in the food industry for the production of functional foods, which, in addition to being nutritional, also have a certain therapeutic effect. In the pharmaceutical industry, more and more research is being devoted to them in the area of long-release drugs. Nanocapsules outperform most other colloidal carriers because of their small size, greater encapsulation potential, greater encapsulation power, and targeted action. Most of the existing carriers based on natural proteins used in the food and pharmaceutical industries are hydrophilic, so the encapsulation of hydrophobic active substances is a special challenge. This paper presents an overview of natural polymers used as suitable carriers and the possibilities of their use in the synthesis of nanocapsules for various uses.**

***Index Terms*— natural polymers; renewable sources; nanocapsule carriers; drugs; active components.**

## I. Introduction

Natural polymers derived from food are considered desirable materials for constructing delivery systems to encapsulate, protect, and release bioactive components in nutraceuticals, pharmaceuticals and food [1]. Food proteins are of particular interest in the design of delivery systems, due to their high nutritional value, abundant sources, structural versatility and considerable functional properties [2, 3]. Nanoparticles constructed of food proteins have suitable physicochemical properties and functional attributes, which allow them to entrap both hydrophilic and hydrophobic bioactive compounds. They are increasingly being applied as delivery systems in the food industry to improve the stability and oral bioavailability of bioactive components [4]. Nanocapsules have an advantage over most of the other colloidal carriers due to their smaller size, higher encapsulation efficiency, more effective penetration ability and targetability [5]. Nanobiotechnology have wide range of application [6]. Nanocapsules were first developed around 1970. They were initially devised as carrier for vaccines and anticancer. Over the past few decades, there has been considerable interest in developing biodegradable nanocapsules (liposome, virus like particle (VLP), protein, etc.) as effective food and drug delivery device [2].

Nanocapsules have become an important area of research in the field of food and drug delivery vehicles [7].Scientific community working at the interface of chemistry and biology is always on the lookout for biopolymers from natural and sustainable sources to generate newer structures which could be used for applications ranging from product structuring to the in vivo delivery of bioactives. Since, most of the biopolymers approved and been used for food and pharmaceutical applications (such as gelatin, casein, dextran, etc.) are water soluble in nature; it becomes necessary to involve steps of physical and chemical alterations like cross-linking and hydrophobic modifications in order to generate colloidal particles from these materials [8].

Nanocapsules have an advantage over hydrogels, organogels, liposome, and microparticles due to their smaller particle size, higher encapsulation efficiency, more effective penetration ability and targetability. Nanocapsules are usually fabricated from varieties of natural polymers, mainly including food- grade proteins and polysaccharides, because they are biocompatible, biodegradable, and non-toxic properties, such as soy protein lactoferrin, gelatin, chitosan and alginate [5]. Nanocapsules generally vary in size from 10 to 1000 nm [9,10]. Recently protein nanoparticles have been shown efficacy as biodegradable carrier which can incorporate variety of drugs in relatively non-specific fashion [11]. The food or drug is dissolved, entrapped, encapsulated or attached to a nanoparticles matrix and depending upon the method of preparation, nanoparticles, nanospheres or nanocapsule can be obtained. Nanocapsules are vesicular systems in which the drug is confined to a cavity surrounded by a unique polymer membrane, while nanospheres are matrix systems in which the drug is physically and uniformly dispersed [7,9]. Figure 1 shows the schematic diagram of nanocapsulated and nanosphere particles loaded with food or drug.

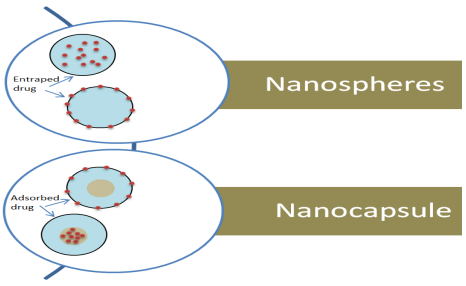


Fig. 1. Schematic diagram of nanospheres and nanocapsules

Danijela Rajić is with the Faculty of Technology, University of East Sarajevo, Karakaj 34 A, 75400 Zvornik, Bosnia and Herzegovina (e-mail: danijelarajic@tfzv.ues.rs.ba).

Srđan Vuković is with the Faculty of Technology, University of East Sarajevo, Karakaj 34 A, 75400 Zvornik, Bosnia and Herzegovina (e-mail: srdjan.vukovic@tfzv.ues.rs.ba).

Svetlana Pelemiš is with the Faculty of Technology, University of East Sarajevo, Karakaj 34 A, 75400 Zvornik, Bosnia and Herzegovina (e-mail: svetlana.pelemis@tfzv.ues.rs.ba).

 ISBN 978-86-7466-930-3

Among these colloidal system those based on protein may be vary promising since they are biodegradable and non-antigenic relatively easy to prepared and their size distribution can be monitored easily [12]. A wide variety of drugs can be delivered using nanoparticulate carriers via a number of routes. Food-borne diseases are becoming one of the serious problems faced by humans along with environmental contamination and because of that technological innovations in food safety related to consumer confidence and human health are becoming extremely urgent [13].

## II. PLANT PROTEINS

Among various natural or synthetic polymer-based particulate systems potentially available to food applications, plant protein-based micro- and nanoparticles are preferably used for nutrient or drug delivery because they offer advantages over other materials in terms of biodegradability, abundant renewable sources, safety status in vivo, and many useful functional properties [14-18]. Additionally, they also exhibit high loading capacity of various bioactives due to their amphiphilic structure, multiple binding sites, and a variety of possible binding mechanisms include electrostatic attractions, hydrophobic interactions, hydrogen and covalent bonding. Due to the known characteristics of microencapsulation, easy surface modification and scale-up feasibilities, particulate systems in micron and nanometre scales provide better opportunities for targeted delivery of bioactive ingredients [16, 19, 20]. The plant proteins most commonly used in the production of nanocapsules are zein, soy, and wheat proteins, and they will be discussed in this paper.

### *A. Zein*

Zein is a protein classified within the group of prolamins. It is attractive for use in nanotechnology as a polymer matrix and is classified as Generally Recognized As Safe (GRAS) by the U.S. Food and Drug Administration (FDA). In addition, zein has promising characteristics, such as biocompatibility, biodegradability, and low toxicity. It is widely used in that it can encapsulate generally different insoluble compounds in water to provide stability and control of release when is in the GastroIntestinal Tract (GIT) [14, 21]. Zein is the main form of protein storage contained in the endosperm tissue of corn and comprises almost 80% of the whole protein content in the corn. In the past, zein was considered more of a by-product of corn processing industries; the consensus indicated zein to be a low-valued material without important potential technological uses. However, due to several recent methodologies and developing processes allowing applications in different fields, nowadays, there is new thought related to zein and zein-based materials towards considering them as more valuable materials. Potential applications of zein include uses as biodegradable plastics, fibers, adhesives, coatings, ceramics, inks, cosmetics, textiles and chewing gum [14, 22, 23, 24].

### *B. Soy proteins*

Soy proteins, the by-product of soy oil processing, is now one of the most widely used protein ingredients in food processing. When different processing methods are conducted, soy protein aggregates with different structures and functionalities could be formed along different pathways [25]. In addition to zein, soy protein-based particles are also promising candidates as delivery systems for nutraceuticals or drugs. Due to the ligand binding properties, soy proteins can serve as an effective carrier for various bioactive molecules. They can bind these molecules to form complexes in nanoscale through physical interactions, mainly hydrophobic interactions, hydrogen bonds and van der Waals attraction. Recent studies suggest that soy proteins have the potential to be used as carriers for both hydrophobic and hydrophilic bioactive compounds, such as vitamin B12, cranberry polyphenols, curcumin, resveratrol (RES), and polyphenols from Concord grape pomace, to improve their water solubility, stability and bioavailability [14].

### *C. Wheat gliadins*

Nanocapsules made from gliadin, a component of wheat gluten, have been prepared for nutrient/drug delivery and controlled release applications. For example, gliadin nanocapsules has been used as carriers for all-trans-retinoic acid (RA) [26]. Gliadin nanocapsules (450–475 nm) were showed to be a suitable delivery and controlled release system for nutrients and drugs with different polarity (hydrophobic and amphiphilic). It was found that the amounts of the entrapped drug increased with an increase in the drug hydrophobicity, confirming a strong interaction between gliadins and apolar compounds. Their essential feature is low price and availability [14, 26].

## III. PREPARATION METHODS

Protein nanocapsules can be obtained by different methods [11]. Protein nanocapsules have been extensively studied as suitable for drug delivery since they are biodegradable, non-toxic and non antigenic, because of their defined primary structure and high content of charged amino acids (that is, lysine). The protein-based nanocapsules could allow the electrostatic adsorption of positively or negatively charged molecules without the requirements of other compounds. In addition, protein nanocapsules can be easily prepared under soft condition, by coacervation or controlled desolvation processes [2]. Among the available potential colloidal drug carrier systems covering the size range described, protein-based nanocapsules play an important role [11]. Biopolymers, such as proteins, are commonly used to encapsulate oil-in-water emulsions. Simple and complex coacervation, spray drying and heat denaturation represent three major microencapsulation techniques based on proteins. Their principles are quite similar: emulsification of the core material (oil) is followed by microcapsules wall formation induced by environmental conditions changing. Concerning simple coacervation method, the protein precipitation around

 ISBN 978-86-7466-930-3

oil droplets is obtained by changing pH and temperature or by the "salting-out" technique. Widespread presence of microcapsules based on animal proteins such as gelatin, casein or albumin contrasts with a very limited use of plant proteins. Wheat gliadin was one of the rare plant storage proteins used for encapsulation of dispersed oil phase by simple coacervation method. The microparticles made from soy protein isolate (SPI) were mainly fabricated by using spray-drying, coacervation, and cold gelation techniques [11, 14, 27]. The table 1 provides an overview of nanoparticle types and methods of their preparation.

TABLE I
OVERVIEW OF PLANT-PROTEIN BASED NANOCAPSULES AND TYPE OF PREPARATION [14]

| Type of particles | Preparation |
|---|---|
| Zein microparticles | Spray drying or supercritical antisolvent method |
| Zein microparticles | Spray or freeze drying |
| Zein nanoparticles | Liquid–liquid dispersion method |
| Zein nanoparticles | Phase separation or liquid–liquid dispersion method |
| Zein nanoparticles | Liquid–liquid dispersion method or electrospraying |
| Zein nanoparticles | Supercritical anti-solvent |
| Zein nanoparticles | Liquid–liquid dispersion method or electrospraying |
| Zein-chitosan complex nanoparticles | Low-energy phase separation method |
| SPI-zein complex microparticles | $Ca^{2+}$-induced cold gelation method |
| SPI/FA-conjugated SPI nanoparticles | Ethanol desolvation method |
| SPI nanoparticles | $Ca^{2+}$-induced cold gelation method |
| Soy protein nanocomplex | Ligand binding properties |
| SPI-CMCS complex nanoparticles | $Ca^{2+}$ induced co-gelation method |
| Soy protein-soy polysaccharide complex nanogels | High-pressure homogenization and heating procedures |
| Soy lipophilic protein nanoparticles | Ultrasonic treatment |
| Gliadin nanoparticles | Antisolvent precipitation method |

## IV. CONCLUSION

Natural polymers show great potential for developing promising delivery vehicles to incorporate and protect various bioactive ingredients, and control their release behaviour under the different conditions. It could be used to produce a wide range of delivery systems, such as micro- and nanoparticles, fibers, films and hydrogels, all of which can be tailored for the design of innovative functional foods. As the interest in functional foods is rapidly growing, the development of advanced plant protein-based delivery systems will expand the possible applications. Nanocapsules outperform most other colloidal carriers because of their small size, greater encapsulation potential, greater encapsulation power, and targeted action. Nevertheless, the delivery of functional ingredients in the complex food systems is rather challenging as it is essential to evaluate not only the impact of complex food matrix on the storage stability and bioavailability of the encapsulated ingredients, but also the effect of the delivery systems on the food product functionality, such as stability, texture, taste, appearance and bioavailability of the ingredients.

The work also has a wide application from forensics to herritology.

## REFERENCES


[1] J. Xue, Y. Zhang, G. Huang, J. Liu, M. Slavin, L. Yu, „Fabrication and Characterization of Zein Composite Particles Coated by Caseinate-Pectin Electrostatic Complexes with Improved Structural Stability in Acidic Aqueous Environments", Food Hydrocoll. Vol. 83, no. 25 (2018). https://doi.org/10.3390/molecules24142535

[2] M. Rahimnejad, N. Mokhtarian, M. Ghasemi, „Production of protein nanoparticles for food and drug delivery system" African Journal of Biotechnology, vol. 8, no. 19, 4738-4743(2009).

[3] Z. L. Wan, J. Guo, X. Q. Yang, „Plant protein-based delivery systems for bioactive ingredients in foods", Food Funct. vol. 6 (2015). https://doi.org/10.1039/c5fo00050e

[4] C. Yang, Y. Wang, L. Lu, L. Unsworth, L. L. Guan, L. Chen, L, „Oat protein-shellac beads: Superior protection and delivery carriers for sensitive bioactive compounds", Food Hydrocolloids, vol. 77, pp. 754–763, (2018). https://doi.org/10.1016/j.foodhyd.2017.11.017

[5] S. Chen, C. Xu, L. Mao, F. Liu, C. Sun, L. Dai, Y. Gao, „Fabrication and characterization of binary composite nanoparticles between zein and shellac by anti-solvent co-precipitation". Food and Bioproducts Processing, vol. 107, pp. 88–96,(2018).

[6] A. Rieux, F. Virginie, M. Garinot, Y. Schneider, V. Preat, „Nanoparticles as potential oral delivery systems of proteins and vaccines: A mechanistic approach", J. Control. Release, vol. 116, pp. 1-27, (2006).

[7] M. L. Hans, A. M. Lowman, „Biodegradable nanoparticles for drug delivery and targeting", Curr. Opin. Solid State Materials Sci, vol. 6, pp. 319- 327,(2002).

[8] A. R. Patel, K. P. Velikov, „Zein as a source of functional colloidal nano- and microstructures", Current Opinion in Colloid & Interface Science, vol. 19, no. 5, pp. 450–458, (2014). https://doi.org/10.1016/j.cocis.2014.08.001

[9] S. Kumaresh, T. M. Aminabhavi, A. R. Kulkarni, W. E. Rudzinski, „Biodegradable polymeric nanoparticles as drug delivery devices", J. Control Rel., vol. 70, pp.1-20, (2001).

[10] P. Couvreur, R. Gref, K. Andrieux, C. Malvy, „Nanotechnologies for drug delivery: Application to cancer and autoimmune diseases", Progress Solid State Chem. vol. 34, pp. 231-235, (2006).

[11] M. Rahimnejad, M. Jahanshahi, G. D. Najafpour, „Production of biological nanoparticles from bovine serum albumin for drug delivery", Afr. J. Biotechnol., vol. 5, no. 20, pp.1918-1923,(2006).


 ISBN 978-86-7466-930-3

[12] C. Weber, C. Coester, J. Kreuter, K. Langer, „Desolvation process and surface characterisation of protein nanoparticles“, International Journal of Pharmaceutics, vol.194, no.1, pp. 91–102, (2000). https://doi.org/10.1016/s0378-5173(99)00370-1
[13] Y. Cao, T. T. Chen, W. Wang, M. Chen, H. J. Wang, „Construction and functional assessment of zein thin film incorporating spindle-like ZnO crystals“, RSC Advances, vol. 7, no. 4, pp. 2180–2185, (2017). https://doi.org/10.1039/c6ra25290g
[14] Z. L. Wan, J. Guo, X. Q. Yang, „Plant protein-based delivery systems for bioactive ingredients in foods“, Food Funct. vol. 6, (2015). https://doi.org/10.1039/c5fo00050e
[15] L. Chen, G. E. Remondetto , M. Subirade, „Food protein-based materials as nutraceutical delivery systems“, Trends Food Sci. Technol., vol. 17., pp. 272-283, (2006).
[16] N. Reddy, Y. Yang, „Potential of plant proteins for medical applications“, Trends Biotechnol., vol. 29, pp. 490-498, (2011).
[17] A. O. Elzoghby, W. M. Samy, N. A. Elgindy, „Protein-based nanocarriers as promising drug and gene delivery systems“, J. Controlled Release, (2012). https://doi.org/10.1016/j.jconrel.2012.04.036
[18] A. O. Elzoghby, W. M. Samy and N. A. Elgindy, „Albumin-based nanoparticles as potential controlled release drug delivery systems“, J. Controlled Release, (2012). https://doi.org/10.1016/j.jconrel.2011.07.031
[19] I. J. Joye and D. J. McClements, „Biopolymer-based nanoparticles and microparticles: Fabrication, characterization, and application“, Curr. Opin. Colloid Interface Sci., vol. 19, pp. 417–427, (2014).
[20] L. Brannon-Peppas, „Recent advances on the use of biodegradable microparticles and nanoparticles in controlled drug delivery“, Int. J. Pharm., vol. 116, pp. 1-9. (1995).
[21] H. Chen, Q. Zhong, „A novel method of preparing stable zein nanoparticle dispersions for encapsulation of peppermint oil“, Food Hydrocolloids, vol. 43, pp. 593–602. (2015). https://doi.org/10.1016/j.foodhyd.2014.07.018
[22] L. Wang, Y. Zhang, „Heat-induced self-assembly of zein nanoparticles: Fabrication, stabilization and potentialapplication as oral drug delivery“, Food Hydrocoll. vol. 90, oo. 403-412, (2019).
[23] Y. C. Luo, Q. Wang, „Zein-based micro- and nano-particles for drug and nutrient delivery: A review“, J. Appl. Polym. Sci. vol. 131, (2014).
[24] D. Rajić, L. Spasojević, V. Gojković Cvjetković, S. Bučko, J. Fraj, J. Milinković Budinčić, L. Petrović, B. Pilić, A. Sharipova, A. Babayev, S. Aidarova, J. Katona, „Zein–resin composite nanoparticles with coencapsulated carvacrol“, Journal of Food Processing and Preservation, e15741, (2021). https://doi.org/10.1111/jfpp.15741
[25] J. Guo, X. Q. Yang, X. T. He, N. N. Wu, J. M. Wang, W. Gu, Y.Y. Zhang, „Limited Aggregation Behavior of β-Conglycinin and Its Terminating Effect on Glycinin Aggregation during Heating at pH 7.0“, J. Agric. Food Chem., vol. 60, pp. 3782-3791, (2012).
[26] I. Ezpeleta, J. M. Irache, S. Stainmesse, C. Chabenat, J. Gueguen, Y. Popineau, A. M. Orecchioni, „Formation of gliadin nanoparticles: Influence of the solubility parameter of the protein solvent“, Int. J. Pharm., vol. 131, pp.191-200, (1996).
[27] A. Nesterenko, I. Alric, F. Silvestre and V. Durrieu, „Vegetable proteins in microencapsulation: A review of recent interventions and their effectiveness“, Ind. Crops Prod., vol. 42, pp. 469-479, (2013).

 ISBN 978-86-7466-930-3

# Kvantne generativne suparničke mreže za generisanje naučnih rezultata

Vladimir Arsoski

***A stra t*—Već dugi niz godina smo svedoci da je veli i broj publi acija efi asno sredstvo za priznavanje izuzetne ompetentnosti i talenta u nauci, što može omogućiti pojedincu veli u moralnu i finansijs u satisfa ciju. Čuvena fraza u a adems im rugovima "objavi ili nestani" postaje surova realnost. U želji da objave senzacionalna otkrića, pojedinci pokušavaju da lažiraju naučne rezultate, a o bi stvorili privid izuzetnosti. avremeni programi za analizu sli a, zasnovani na veštačkoj inteligenciji, su se po azali ao efi asno sredstvo za razotkrivanje lažiranih pri aza naučnih rezultata i doveli su do povlačenja velikog broja sumljivih publi acija iz časopisa u poslednjih ne oli o godina. ovi algoritmi veštačke inteligencije zasnovani na generativnim suparničim mrežama pružaju mogućnost za generisanje sli a oje mogu biti lasifi ovane ao verodostojne. Implementacija ovih algoritama na vantnim računarima se po azala ao potencijalno superioran metod generacije sli a, te predstavlja realnu opasnost da slučajevi lažiranja naučnih rezultata ostanu neprimećeni. Ovo nameće potrebu da se u blis oj budućnosti razvije disciplina oja bi se mogla opisati kao forenzika naučnih rezultata i oja bi se bavila razot rivanjem primena ne samo klasičnih, već i vantnih algoritmima za generisanje rezultata.***

***Ključne reči* — generativne suparničke mreže; veštačka inteligencija; kvantni računari.**

## I. UVOD

Proces publikovanja naučnih radova u časopisima je započeo sredinom 17. veka kada je na inicijativu Henry Oldenburg-a, prvog sekretara Kraljevskog društva, pokrenut prvi naučni časopis *Philosophical Transactions of oyal Society* [1]. Pre toga su naučnici razmenjivali ideje i rezultate na naučnim skupovima i putem privatnih korespondencija, što je ograničavalo pristup najnovijim saznanjima široj populaciji. Koncept publikovanja radova u časopisima zasnivao se na ideji diseminacije i verifikacije novih ideja, saznanja i rezultata u cilju progresa nauke. Vremenom je razvijena metodologija bavljenja naučnim radom koja je standardizovala i formalizovala istraživačke metode, kao i način prezentacije naučnih radova i zacrtala osnovna moralna načela koja su vezana za akademski integritet i čestitost.

Od početka devetnaestog veka, mnogi poznati univerziteti u Evropi su počeli da pridaju podjednak značaj podučavanju i naučnom radu [1]. U poslednje vreme, rasprostranjeno je mišljenje da naučni rad ima mnogo veći značaj od nastavnog rada. Mnogi univerziteti vrše selekciju kandidata na osnovu broja publikacija, što može da usmeri nastavnike i saradnike da se intenzivno bave naučnim radom zapostavljajući nastavne delatnosti i mentorski rad. Neretko se dešava da nastavnici organizuju intenzivne prezentacije svojih naučnih dostignuća, čak i na predavanjima, kako bi privukli što veći broj potencijalnih kandidata za bavljenje naučnim radom u nadi da će povećati produktivnost publikovanja. Pritom, zbog sopstvenog angažovanja u nastavi i naučnom radu, često nemaju vremena da se dovoljno posvete mentorskom radu. Dešava se da mladi istraživači iz neznanja produkuju nedovoljno kvalitetne radove, sa pogrešnim ili modifikovanim rezultatima i bez citiranja korišćenih referenci.

Povećanje produkcije radova na godišnjem nivou dovodi do porasta broja naučnih časopisa [2]. U poslednja tri veka, rast broja aktivnih naučnih časopisa godišnje u procentima je približno konstantan i varira oko srednje vrednosti od 3.46 %, što odgovara udvostručenju broja časopisa na svakih 20 godina [3]. Poslednjih godina, ovaj trend se povećava, te smo svedoci skoro svakodnevne pojave raznih časopisa čiji je naziv povezan sa oblašću koja je u žiži naučnog interesovanja. Većina časopisa proverava originalnost, kvalitet prezentacije i značaj razmatrane problematike, tako što vrši selekciju radova pomoću ocenjivanja od strane dva ili više eksperta iz oblasti rada (engl. peer-reviewed). Iako se naučna zajednica i broj eksperata u većini oblasti rapidno povećava, postavlja se pitanje njihove raspoloživosti za recenziju rada, što je često vezano za veliko angažovanje samog recenzenta na produkciji radova. Velikom broju naučnih radnika se dešavalo da rad bude predložen za publikaciju ili bude odbijen bez detaljnijeg i konkretnog objašnjenja od strane recenzenta.

Sve veća ulaganja u istraživanja i nauku, kao i velika konkurencija istraživačkih grupa, dovela je poslednjih godina do pojave slučajeva tendencioznih prevara pri akviziciji i prezentovanju naučnih rezultata. U praksi su postale standardne prevare poput *plagijari ma* (prisvajanje tuđih naučnih rezultata), *autoplagijari ma* (objavljivanje istih rezultata u više naučnih časopisa), "*seckanja salame*" (prezentacija jednog naučnog dostignuća kroz seriju radova pod izgovorom obimnosti problematike), "*autora duho a*" (dodavanje na rad autora koji nisu dali značajan doprinos radu) i raznih drugih neetičkih radnji [4].

Statistika je pokazala da samo oko 45 % radova objavljenih u vrhunskim naučnim časopisima iz oblasti biomedicine imaju citate u prvih 5 godina, a od tog broja 5-25% su autocitati i/ili kocitati [4]. Posebno neetički aspekt prevara odnosi se na časopise iz ove oblasti, gde dolazi do obmanjivanja naučno-stručne javnosti, a posredno i pacijenata, o mogućem brzom i

Vladimir Arsoski – Elektrotehnički fakultet, Univerzitet u Beogradu, Bulevar Kralja Aleksandra 73, 11020 Beograd, Srbija (e-mail: vlaimir.arsoski@etf.bg.ac.rs).

 ISBN 978-86-7466-930-3

efikasnom izlečenju. Falsifikovanje naučnih rezultata obično je vezano za mikroskopski prikaz slika biomaterijala, ćelija i tkiva [5] ili za grafički prikaz "rezultata merenja" [6]. Neki od ovih radova su dostupni u bazi matičnog časopisa [5], dok na drugima stoji oznaka da su povučeni [6]. Ovi [5,6] i slični slučajevi "dorade" naučnih rezultata, otkriveni su primenom savremenih metoda i programa za analizu slike zasnovanih na veštačkoj inteligenciji. Neka softverska rešenja su besplatno dostupna na internetu, poput *Forensically* [7]. Postoje organizacije koje prate i javno objavljuju podatke o povučenim radovima [8] jer se često dešava da časopisi, zbog čuvanja reputacije, netransparentno uklone rad iz svoje baze podataka. Prema podacima sa sajta [8], do trenutka pisanja ovog rada, povučeno je čak 219 naučnih radova vezanih za COVID-19 pandemiju.

Dosada otkrivene prevare, vezane za objavljivanje lažiranih naučnih rezultata, uglavnom su se zasnivale na korišćenju softvera za odbradu slike, gde su nedoslednosti u vidu kloniranja delova slika, nepravilnog gradijenta boje, osvetljenja, šuma i defekata na slici, mogli da budu detektovani pomoću metoda zasnovanih na mašinskom učenju [7]. U skorije vreme su se pojavili generativni modeli mašinskog učenja, poput varijacionog autoenkodera (VAE) koji predstavlja veštačku neuralnu mrežu koja pripada familiji probabilističkih grafičkih modela [9]. Ovaj model formuliše problem statističkog zaključivanja (na osnovu slučajne veličine zaključak je druga slučajna veličina), kao statistički problem optimizacije. VAE je usmeren model, trening (obučavanje) se može obaviti primenom modela zasnovanih na gradijentu i lako se može generalizovati za rešavanje raznih problema [10]. VAE model, vezan za generisanje slika, uspešno je implementiran u programskom paketu *eras* pod programskim jezikom *Python*. Nedostatak VAE ogleda se u inherentnoj osobini, koja leži u samoj postavci modela, da produkuje relativno "zamućen" izlaz (engl. blur), kada je reč o treniranju za generaciju slika [10], što softver za forenziku može označiti kao mogući problem.

Potencijalno superioran model generativne mreže je generativna suparnička mreža (engl. Generative Adversarial Network - GAN), koja se zasniva na teorijskom scenariju takmičenja između mreže koja generiše uzorke (*generatora*) i mreže *diskriminatora*, koja pokušava da napravi razliku između realnih podataka iz skupa za trening i generisanih podataka [11]. Najbolje performanse modela se postižu za scenario u kojem generator pokušava da poveća vrednost logaritma verovatnoće da diskriminator pogreši, umesto da smanjuje vrednost logaritma verovatnoće da diskriminator dâ tačan odgovor [10,11]. Kada se trening završi, diskriminator sa podjednakom verovatnoćom klasifikuje generisane slike kao prave ili pogrešne i može da se apstrahuje. Na ovaj način, generator je naučen da prevari sistem veštačke inteligencije. Demonstrirano je da duboke konvolucione GAN mogu da generišu izuzetno verodostojne slike [12], što ih čini potencijalno opasnim za generisanje slika u naučnim publikacijama koje može da prođe nezapaženo.

Razvoj kvantnih računara obećava veliki napredak u oblasti hemije, biomedicine, rešavanja kompleksnih matematičkih i fizičkih problema, kao i implementacije naprednih sistema veštačke inteligencije. Efekti inherentni za kvantnu mehaniku, poput superpozicije, interferencije i kvantne zapletenosti (engl. entanglement), mogu dovesti do veće efikasnosti kvantnih algoritama u odnosu na klasične [13]. Za razliku od kvantnog sistema, koji je po prirodi probabilistički, klasični sistemi ne mogu efikasno generisati slučajne veličine (već se govori o pseudo-slučajnim veličinama). Zbog toga su kvantni sistemi, koji su vezani za stohastičke algoritme, značajno jednostavniji i ujedno efikasniji od klasičnih probabilističkih. Takođe je poznato da je za predstavljanje vektora u $N$-dimenzionom prostoru potrebno $\log_2 N$ kubita, kao i da je vreme manipulacije kvantnog sistema nad retkim matricama složenosti u vremenu reda $(\text{poly}(\log_2 N))$ [13]. Sve ovo dovodi do potencijalne prednosti kvantnih u odnosu na klasične algoritme, pogotovu kada je reč o visokodimenzionim prostorima i stohastičkim procesima. Uprkos činjenici da je kvantni hardver u svom ranom povoju i da su trenutne implementacije podložne dekoherenciji, spoljašnjem šumu i imaju ograničene mogućnosti povezivanja kubita, postoje indikacije da će kvantno mašinsko učenje biti jedna od prvih značajnih primena na kvantnom hardveru. Veliki broj algoritama mašinskog učenja je već adaptiran za rad na kvantnom računaru [14], a od skora i GAN pod nazivima QGAN i QuGAN [15,16]. QGAN je, između ostalog, našao primene vezane za generisanje realističnih raspodela [17,18] i slika [19], gde je demonstrirao jednostavniju implementaciju i eksponencijalno ubrzanje u odnosu na klasičnu GAN.


Sl. 1. Šematski prikaz kvantne generativne suparničke mreže. Ulazni podaci za diskriminizator su kvantna stanja iz generatora $G$ (čiji ulaz pobuđuje stohastički vektor |z>) ili iz realnog izvora podataka . Izlaz diskriminatora je kvantno stanje |lažni> ili |realni> i odnosi se na procenu porekla ulaznog podatka. Slika je adaptirana na osnovu rada [15].

## II. MODEL KVANTNE GENERATIVNE SUPARNIČKE MREŽE

Šematski prikaz kvantne generativne suparničke mreže je dat na Sl. 1. predstavlja izvor realnih podataka koji za zadatu kvantnu labelu $|\lambda\rangle$ generiše realne podatke. Svrha QGAN-a je da definiše generator $G$ koji imitira izvor realnih podataka . $G$ predstavlja varijaciono kvantno kolo, čiji su gejtovi parametrizovani vektorom $\boldsymbol{\theta}_G$. Na osnovu stanja $|\lambda\rangle$ i dodatnog stohastičkog stanja $|\ \rangle$ generator produkuje stanje na svom izlazu koje treba da bude slično stanju koje daje . U


ISBN 978-86-7466-930-3

opštem slučaju, dodatno stanje $|\ \rangle$ je stohastičko i ponaša se kao nestruktuirani šum koji dovodi do porasta entropije raspodele generisanih podataka, te se za jednu istu labelu $|\lambda\rangle$, može generisati više izlaznih stanja. Podaci za obučavanje generatora se dobijaju od diskriminatora koji predstavlja kvantno kolo parametrizovano vektorom $\boldsymbol{\theta}$. Uloga diskriminatora je da proceni da li ulazno stanje potiče od realnog izvora ili generatora, dok je uloga generatora da "prevari" diskriminator, tako da podatke koji su generisani označi kao realne. Cilj optimizacije QGAN obučavanja je da se definišu parametri diskriminatora koji će da maksimizuju verovatnoću da je diskriminator pravilno označio ulazni vektor, a ujedno i parametri generatora koji minimizuju ovu verovatnoću. Za nominalno prebrojivu vrednost Λ, labela $|\lambda\rangle$, ovaj problem se formalno definiše izrazom [15]:

$$\min_{\boldsymbol{\theta}_G}\max_{\boldsymbol{\theta}}\frac{1}{\Lambda}\sum_{\lambda=1}^{\Lambda}P\{[(\quad(\boldsymbol{\theta}\ ,|\lambda\rangle,\quad(|\lambda\rangle))=|\text{realni}\rangle]\cap [(\quad(\boldsymbol{\theta}\ ,|\lambda\rangle,G(\boldsymbol{\theta}_G,|\lambda,\ \rangle))=|\text{lažni}\rangle]\}. \tag{1}$$

U iterativnom postupku se određuju parametri kvantnih kola, tako da generator može što uspešnije da prevari diskriminator [15].

## III. REZULTATI I DISKUSIJA

Za implementaciju modela je korišćena biblioteka *iskit* [20], koja radi pod programskim jezikom *Python* u virtuelnom okruženju *Anaconda*. Realizovana je QGAN za generisanje log-normalne raspodele, koja se može sresti u biomedicinskim primenama. Primer jedne realne raspodele je dat na Sl. 2. Realizacija QGAN-a na samo 2 kubita pomoću jednostavne kvantne mreže korišćene za realizaciju kvantnog generatora postoji kao primer u tutorijalima *iskit*-a [21].

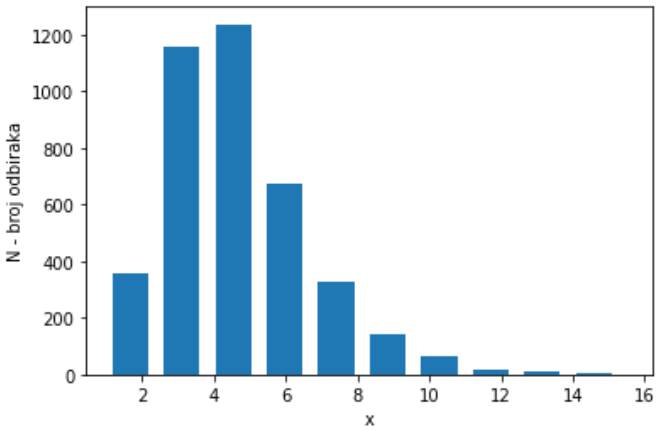


Sl. 2. Prikaz histograma za jedan vektor realnih podataka. Za korišćeni sintetički skup od 4000 ulaznih podataka je fitovanjem dobijeno da podleže log-normalnoj raspodeli sa srednjom vrednošću μ=1.5 i standardnim odstupanjem σ=0.4.

### A. *Pretposta ka k antnog kola*

Za realizaciju osnovnog sloja kvantnog kola generatora je usvojena *pretposta ka* (engl/nem. *ansat* ) definisana na 4 kubita. Ponavljanjem ovog bloka se postiže veća efikasnost obavljanja zadatka od strane kvantnog kola, ali se produžava vreme obučavanja usled povećanja dubine kvantne mreže. Svaki blok se sastoji od parametrizovanih jednokubitnih operacija primenjenih na svaki kubit i dvokubitnih $C_Z$ operacija, kojima se ostvaruje međusobno *k antno spre anje* (engl. *uantum entanglement*) svih susednih stanja kubita. Poslednji kubit je dodatno spregnut sa prvim kubitom. Ovakvo povezivanje je vezano za pojam kružnog umrežavanja. Za implementaciju kvantne mreže je korišćena ugrađena biblioteka *Two ocal*, gde je atribut željenog sprezanja *entanglement* = "circular", dok je parameter ponavljanja *rep* uzimao vrednosti 1 ili 2. U ovakvoj konfiguraciji, kvantna mreža ima samo 8 i 12 varijabilnih parametara, za mrežu formiranu od jednog i dva osnovna bloka, redom. Varijabilni parametri se podešavaju pri obučavanju mreže. Šema pretpostavke kola generatora je data na Sl. 3.

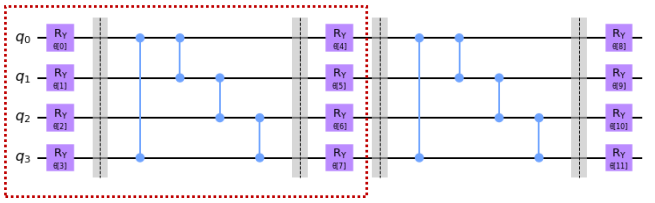


Sl. 3. Šema pretpostavke (engl/nem. ansatz) kvantnog kola generatora. Osnovni blok/sloj je uokviren crvenom isprekidanom linijom.

Diskriminator je implementiran pozivanjem funkcije *Numpy iscriminator* i predstavlja klasičnu neuralnu mrežu sa 3 *sloja* (engl. *layer*), koja koristi *eaky e* aktivaciju u *skri enom sloju* (engl. *hidden layer*) i aktivaciju sigmoid funkcijom u izlaznom sloju. Na ovaj način ćemo ustanoviti uslove, pri kojima bi kvantni generator "prevario" klasični diskriminator, koji je zadužen za testiranje prezentovanih rezultata. Za optimizaciju varijabilnih parametra generatora i diskriminatora je korisćen predefinisani *Adam* algoritam [22], koji predstavlja metodu za stohastičku optimizaciju.

### B. *Obučavanje mreže*

Obučavanje je najpre testirano na simulatoru raspoloživom u programskom paketu *iskit*. Trening mreže je obavljen korišćenjem 100 *u oraka u s akoj iteraciji* (engl. *batch si e*). Najpre je korišćeno kvantno kolo sa samo jednim blokom (oblast uokvirena isprekidanom linijom na Sl. 3) koji ima samo 8 varijabilnih parametara i računata je lokalna *funkcija greške* (engl. *cost loss function*). Parametri mreže su inicirani na pseudo-slučajan način. Broj *prola a kro trening skup* (engl. *epoch*) je bio 100 puta. Zatim je dodat još jedan blok, tako da je dobijeno finalno kvantno kolo prikazano na Sl. 3. Dobijene vrednosti varijabilnih parametara (zaokružene na 2 značajne cifre) za deo kvantnog kola koji je prethodno treniran su uzeti kao inicijalni, dok su parametri za blok koji


ISBN 978-86-7466-930-3

je dodat izabrani nasumično. Postepeno građenje finalne pretpostavke kvantnog kola je urađeno kako bi se pri obučavanju izbegla pojava *ra nih platoa* (engl. *barren plateaus*) funkcije greške [23-25]. Primena ovog pristupa na problem vezan za prepoznavanje rukom pisanih brojeva (MNIST dataset) [26], ovaj pristup je pokazao i značajno manju grešku generalizacije u odnosu na standardne šeme obučavanja, koje se primenjuju na celu mrežu [25]. Trening je urađen u 100 prolaza sa 100 uzoraka u svakom trening skupu. Dobijeni su vektori varijabilnih parametara za mreže generatora satavljene od jednog i dva osnovna gradivna bloka, redom:

(a) $\boldsymbol{\theta}_G$ = [5.3857293, 4.28779218, 4.24118702, 0.51582692, 2.21546187, 1.08074945, 4.08073098, 4.46537089].

(b) $\boldsymbol{\theta}_G$ = [4.13100272, 0.63322951, 5.16027858, 2.0964577, 4.03147984, 4.69264686, 5.54824841, 5.96373602, 1.69386018, 4.81546402, 1.1501217, 3.24610254].

(a)

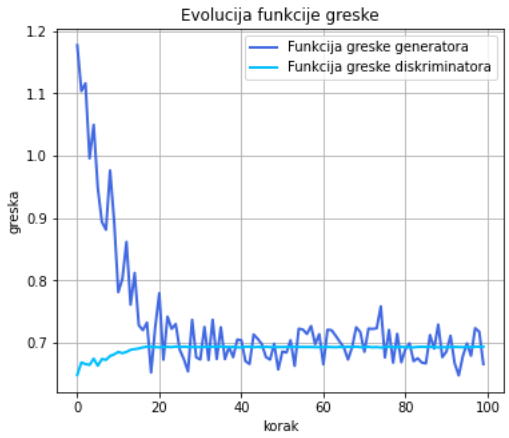


(b)

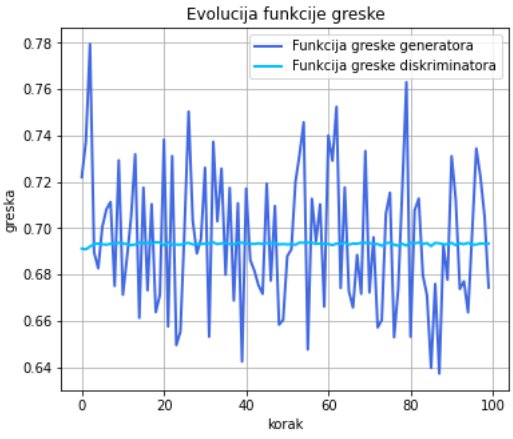


Sl. 4. Evolucija funkcije greške (engl. cost/loss function) diskriminatora (svetlo plava linija) i kvantne mreže generatora (tamno plava linija), sastavljene od (a) jednog i (b) dva osnovna gradivna bloka.

Da bi analizirali tok obučavanja mreže, treba razmotriti promenu funkcije greške u toku treninga. Evolucija funkcije greške u funkciji rednog broja koraka za mrežu sastavljenu od jednog i dva osnovna bloka je prikazana na Sl. 4 (a) i (b), redom. Za mrežu sastavljenu od jednog osnovnog bloka, vrednosti greške generatora i diskriminatora postaju uporedive posle dvadesetak koraka obučavanja. Pritom, razlika je najveća na početku treninga, što je očekivano jer su parametri mreže inicirani na pseudo-slučajan način i mreža inicirana na ovaj način ne daje odgovarajuću raspodelu. U slučaju mreže koja je sastavljena od dva bloka, greška nije velika ni na samom početku treninga. Ovo je posledica postepenog građenja kvantnog kola generatora, gde smo za deo mreže inicirali skup parametara, tako da se na zadovoljavajući način reprezentuje tražena raspodela. Uočava se da u toku obučavanja greška diskriminatora približno ulazi u zasićenje, dok greška generatora "osciluje" oko neke srednje vrednosti. Razlog za ovakvo ponašanje je izbor metoda za optimizaciju Adam, koji je računski efikasan i brzo nalazi optimalno rešenje, ali ne adaptira korak na adekvatan način, tako da se postigne bolja konvergencija.

(a)

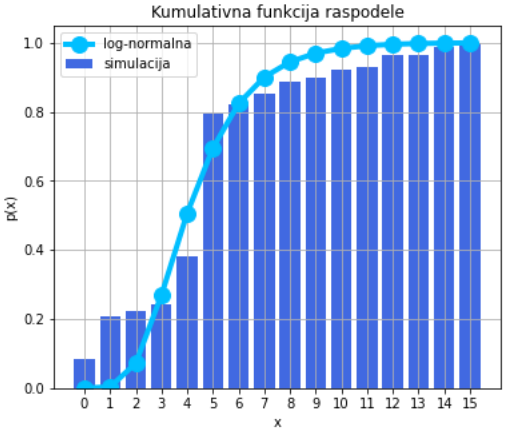


(b)

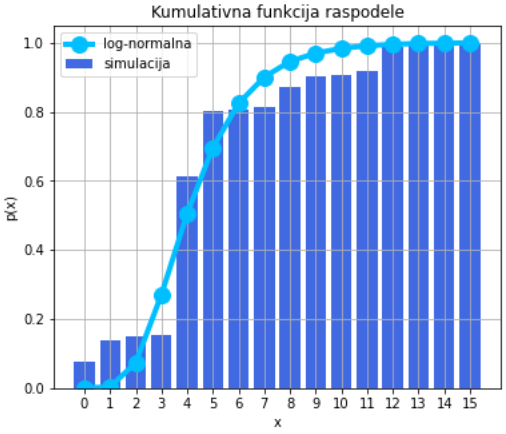


Sl. 5. Kumulativna funkcija log-normalne raspodele (svetlo-plava linija) i histogram kumulativne raspodele dobijen usrednjavanjem 10000 raspodela koje je generisao realizovani kvantni generator sastavljen od (a) jednog i (b) dva osnovna sloja kvantne mreže.

 ISBN 978-86-7466-930-3

Za dobijene parametre kvantnih generatora, postavljena su kvantna kola i generisano je po 10000 raspodela. Za svaku generisanu raspodelu je nađena kumulativna funkcija raspodele i rezultati su usrednjeni. Dobijeni rezultati su upoređeni sa kumulativnom funkcijom idealizovane log-normalne raspodele, koja je ustanovljena za polazni skup i rezultati su prikazani na Sl.5. Poređenjem raspodela na Sl. 5 (a) i (b) se može ustanoviti da jednostavnija mreža daje nešto lošije rezultate u oblasti gde postoji veliki gradijent log-normalne raspodele. Mreža generatora koja se sastojala iz više slojeva je bolje reprodukovala "strmiju" raspodelu. Pretpostavlja se da bi razlike između dubljih mreža (sa više od dva osnovna kvantna sloja) i mreže sa jednim slojem bila još veća u slučaju generisanja raspodele, koja ima više lokalnih maksimuma (multimodalna raspodela). Ipak, povećanje broja slojeva bi značajno produžilo trening mreže. Treba naći ravnotežu između kompleksnosti implementacije mreže (u cilju povećanja realističnosti raspodele) generatora i vremena potrebnog za obučavanje mreže. Takođe, pretpostavlja se da bi još realniji opis proizvoljne raspodele mogao da se dobije ukoliko bi se koristila kola sa više kubita, što bi dodatno usložnilo svaki sloj kvantne mreže i značajno produžilo trening i jednoslojne i višeslojne (duboke) mreže.

Sl. 6. Šematski prikaz kvantnih operacija korišćenih za implementaciju koda na kvantnom računaru ibmq_lima. Sistem ima 5 kubita raspoređenih u T geometriji, tako da je kubit q1 povezan sa tri kubita (q0, q2 i q3), kubit q3 sa dva kubita (q2 i q4), dok su ostali "ivični" kubiti (q0, q2 i q4) povezani samo sa jednim najbližim susedom.

Na kraju je metoda testirana na realnom kvantnom računaru. Kôd je izvršen na najmanje opterećenom sistemu **ibmq lima** [27]. Ovaj sistem je zasnovan na Falcon r4T arhitekturi kvantnog procesora sa svega 5 kubita i *k antnom apreminom* (engl. quantum volume) koja iznosi 8. Iako predstavlja jedan od najskromnijih IBM-ovih sistema po pitanju performansi, dovoljan je za izvršavanje postavljenog problema. Osnovna kvantna kola (engl. gate) u ovoj arhitekturi su jednokubitne $I$ (jedinična; engl. Identity gate), , $Z$ (rotacija oko -ose na Bloch-ovoj sferi), $S$ (koren iz ; $S\ rt(\ ) = \sqrt{\ }$) i dvokubitna C (kontrolisana operacija). Realizacija jednog koraka programa odgovara implementaciji datoj na Sl. 6. Korišćena su prva 4 kubita (označeni q0-q3), pošto zadovoljavaju uslov najbolje međusobne povezanosti. Zbog ograničenog broja iteracija, koje jedan korisnik može odraditi u jednom procesu, broj epoha pri obučavanju je ograničen na 20. Ovaj broj je pet puta manji od onoga što je korišćeno u kvantnom simulatoru, pa se ne očekuje da će rezultati dobijeni na realnom kvantnom računaru biti bolji od onih na simulatoru. Kao rezultat optimizacije generatora dobijen je vektor varijabilnih parametara:

$\boldsymbol{\theta}_G$ = [2.34593012, 2.40548665, 6.16308627, 0.64978231, 3.46996776, 6.22740227, 5.06966893, 2.22040949].

U cilju poređenja sa rezultatima, koji su dobijeni pomoću klasičnog programskog simulatora kvantnog kola, na Sl. 7 su redom prikazani evolucija funkcije greške u funkciji rednog broja iteracije (epohe) i histogram kumulativne funkcije raspodele, dobijeni na osnovu rezultata koje je generisao realni kvantni sistem. Čak i za ovako mali broj epoha pri obučavanju kvantne mreže na kvantnom računaru, kvantni generator je u stanju da "prevari" klasični diskriminator. Ovo je očigledno na osnovu Sl. 7 (a), gde je funkcija greške generatora manja od diskriminatora posle obučavanja. Sa druge strane, poređenje kumulativne funkcije greške za log-normalnu i raspodelu dobijenu usrednjavanjem 10000 generisanih raspodela (videti Sl. 7 (b)) mogu se uočiti značajna odstupanja. Takođe, rezultati su lošiji od onih koji su dobijeni pomoću softverskog simulatora (videti Sl. 5), što je i očekivani rezultat obzirom da je obučavanje realnog hardvera bilo značajno kraće. Ono što je očigledno je da je u realnom hardveru funkcija greške pala na malu vrednost već posle par iteracija, za razliku od klasične simulacije kvantnog računanja, gde je značajan pad ostvaren tek posle 20 epoha. Ovo bi moglo da navede na pogrešan zaključak, da obučavanje kvantnog generatora realizovanog na kvantnom računaru traje kraće od vremena (broja iteracija) koje predviđa simulacija, gde nisu uračunati efekti šuma i dekoherencije. U skorašnjim publikacijama [25] se kao razlog za ovakvo ponašanje navodi prisustvo dekoherencije i šuma u kvantnom hardveru, koji su uzrok brže konvergencije ka optimalnoj vrednosti parametara.

## IV. ZAKLJUČAK

U radu je razmotreno kvantno kolo generatora raspodele koji bi se mogao iskoristiti za generisanje rezultata koji odgovaraju realnim eksperimentalnim rezultatima u mnogim naučnim oblastima. Kolo je dobijeno algoritmom kvantne generativne suparničke mreže, gde se u konkurentnom postupku takmiče kvantni generator, koji generiše raspodelu, i klasična neuralna mreza, koja treba da klasifikuje generisanu raspodelu kao realnu ili lažnu. Za razliku od originalne postavke algoritma, diskriminator je klasičan i treba da

 ISBN 978-86-7466-930-3

reprodukuje slučaj, gde kvantni sistem treba da nadmaši klasični sistem mašinskog učenja koji se upotrebaljava za otkrivanje računarski generisanih rezultata. Ustanovljeno je da je moguće realizovati kvantnu mrežu koja bi sa velikom verovatnoćom mogla da generiše raspodelu, koju bi klasični diskriminator ocenio kao realističnu. Kao primer je uzeta log-normalna raspodela, mada bi princip bio identičan i u slučaju proizvoljne raspodele.

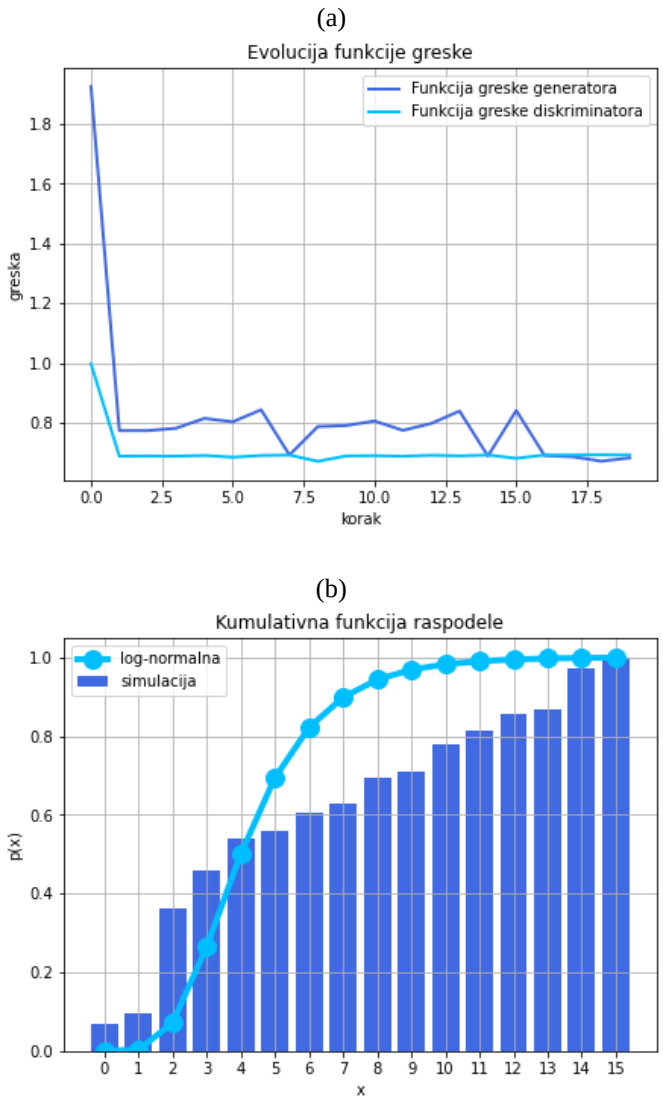


Sl. 7. Za realni kvantni generator koji se sastoji iz jednog sloja i klasičan diskriminator prikaz: (a) evolucije funkcije greške diskriminatora (svetlo plava linija) i kvantne mreže generatora (tamno plava linija); (b) kumulativna funkcija log-normalne raspodele (svetlo-plava linija) i histogram kumulativne raspodele dobijen usrednjavanjem 10000 generisanih raspodela dobijenih pomoću kvantne mreže generatora (tamno plava linija).

Najpre je izvršena simulacija kvantnog algoritma na klasičnom računaru. Za konstrukciju generatora su korišćene kvantne mreže sa jednim i dva sloja. U svakom sloju je ostvareno kružno kvantno sprezanje kubita. Analizom evolucije greške tokom treninga i kumulativne funkcije raspodele realizovane jednoslojne i dvoslojne mreže je ustanovljeno da mreže sa više slojeva verodostojnije generišu traženu raspodelu. Ipak, sa povećanjem broja slojeva se povećavao broj varijabilnih parametara, a samim tim i vreme potrebno za obučavanje mreže. Ustanovljeno je da obe mreže, sa velikom verovatnoćom, mogu prevariti klasičan diskriminator, koji bi vršio klasifikaciju rezultata. Zatim je algoritam izvršen na realnom kvantnom hardveru. Analiziran je kvantni generator koji se sastoji iz jednog kvantnog sloja. Obučavanje je izvršeno u malom broju koraka. Dobijeni su rezultati koji su ukazali na dobre performance razmatranog algoritma i u slučaju simulacije na realnom kvantnom računaru. Za realizaciju analiziranog algoritma nije potreban veliki broj slojeva u kvantnoj mreži, pa se obučavanje može izvesti u relativno malom broju iteracija, čak i na trenutno dostupnom kvantnom hardveru koji je podložan dekoherenciji i šumu. Analizirani algoritam bi se mogao usložniti na slučaj raspodele u više dimenzija, tako da daje rezultate koji su veoma slični onima koji bi se dobili u eksperimentalnim biomedicinskim merenjima poput citometrije, DNK analize, radioloških, ultrazvučnih i drugih biomedicinskih mernih metoda. U daljem radu bi bilo interesantno razmotriti kako bi se model pokazao na slučajevima složenijih jednodimenzionih i višedimenzionih raspodela, kako bi povećanje broja kubita uticao na poboljšanje performansi generatora, kao i slučaj različitog sprezanja kubita u osnovnom kolu na kvalitet rezultata i vreme konvergencije parametara mreže.

## ZAHVALNICA

Ovaj rad je podržan od strane Ministarstva prosvete, nauke i tehnološkog razvoja Republike Srbije 451-03-68/2022-14/200103.

## LITERATURA

[1] Y. S. Rao, “Scientific publication process and its impact on growth of science,” *Ann. ib. Inf. Stu*, Vol. , pp. *13-20*, Mar. 2021.
[2] https://dblp.org/statistics/publicationsperyear.html
[3] M. Mabe, “The growth and number of journals,” *Serials*, vol. *1* , no.2, pp. *1 1-1* , July 2003.
[4] S. Rawat, S. Meena, “Publish or Perish: Where are we heading?” . *es. Med. Sci*, vol. *1* , pp. - , Feb.2014.
[5] U. A. Hasan, G. Trinchieri, J. Vlach, “Toll-like Receptor Signaling Stimulates Cell Cycle Entry and Progression in Fibroblasts,” . *Biol. Chem*, vol. *2 0*, no. 21, pp. *20 20–20 2* , May 2005.
[6] S. Magar, D. Nayak, U. B. Mahajan, K. R. Patil, S. D. Shinde, S. N. Goyal, S. Swaminarayan, C. R. Patil, S. Ojha, C. N. Kundu, “Ultra-diluted Toxicodendron pubescens attenuates proinflammatory cytokines and ROSmediated neuropathic pain in rats,” *Sci. ep*, vol. , pp. *135 2 1-11*, Sep. 2018.
[7] https://29a.ch/photo-forensics/
[8] https://retractionwatch.com/
[9] D. P. Kingma, M. Welling, “Auto-Encoding Variational Bayes,” Technical report, https://arxiv.org/abs/1312.6114
[10] I. Goodfellow, Y. Bengio, A. Courville, *eep earning*, Cambridge, Massachusetts, The MIT Press, London, England, 2016.
[11] I. J. Goodfellow, J. Pouget-Abadie, M. Mirza, B. Xu, D. Warde-Farley, S. Ozair, A. Courville, Y. Bengio, “Generative adversarial networks,” *Ad . Neural Inf. Process. Syst*, vol. *2* , pp. *1-* , 2014.
[12] A. Radford, L. Metz, S. Chintala, “Unsupervised Representation Learning with Deep Convolutional Generative Adversarial Networks,” https://doi.org/10.48550/arXiv.1511.06434

 ISBN 978-86-7466-930-3

[13] M. A. Nielsen, I. L. Chuang, Quantum Computation and Quantum Information, 10th ed. Cambridge, United Kingdom: Cambridge University Press, 2010.
[14] M. Schuld, F. Petruccione, Machine Learning with Quantum Computers, 2nd ed. Cham, Switzerland: Springer Nature Switzerland AG, 2021.
[15] P.-Luk D.-Demers, N. Killoran, "Quantum generative adversarial networks," *Phys. e . A*, vol. , no. *1*, pp. *012324 1-* , Jul. 2018.
[16] S. Lloyd, C. Weedbrook, "Quantum Generative Adversarial Learning," Phys. Rev. Lett, vol. *121*, no. *4*, pp. *040502 1-5*, Jul. 2018.
[17] H. Situ, Z. He, Y. Wang, L. Li, S. Zheng, "Quantum generative adversarial network for generating discrete distribution," *Information Sciences*, vol. *53* , pp. *1 3-20* , June 2020.
[18] G. Agliardi, E. Prati, "Optimal Tuning of Quantum Generative Adversarial Networks for Multivariate Distribution Loading," *uantum ep*, vol. *4*, pp. *5-105*, Feb. 2022.
[19] H-L. Huang, Y. Du, M. Gong, Y. Zhao, Y. Wu, C. Wang, S. Li, F. Liang, J. Lin, Y. Xu, R. Yang, T. Liu, M-H. Hsieh, H. Deng, H. Rong, C-Z. Peng, C-Y. Lu, Y-A. Chen, D. Tao, X. Zhu, J-W. Pan, "Experimental Quantum Generative Adversarial Networks for Image Generation," *Phys. e . Appl*, vol. *1* , no. *2*, pp. *024051 1-20*, Avg. 2021.
[20] https://qiskit.org/
[21] https://qiskit.org/documentation/machine-learning/tutorials/04_qgans_for_loading_random_distributions.html
[22] Diederik P. Kingma, Jimmy Ba, "Adam: A Method for Stochastic Optimization," https://doi.org/10.48550/arXiv.1412.6980
[23] J. R. McClean, S. Boixo, V. N. Smelyanskiy, R. Babbush, H. Neven, "Barren plateaus in quantum neural network training landscapes," *Nat. Comm*, vol. , pp. *4 12 1-* , Nov. 2018.
[24] M. Cerezo, A. Sone, T. Volkoff, L. Cincio, P. J. Coles, "Cost function dependent barren plateaus in shallow parametrized quantum circuits," *Nat. Comm*, vol. *12*, pp. *1 1 1-12*, Mar. 2021.
[25] A. Skolik, J. R. McClean, M. Mohseni, P. Smagt, M. Leib, "Layerwise learning for quantum neural networks," Quantum Mach. Intell, vol. *3*, pp. *5 1-5*, Jan. 2021.
[26] http://yann.lecun.com/exdb/mnist/
[27] https://quantum-computing.ibm.com/services?services=systems&system=ibmq_lima

ABSTRACT

For many years, we have witnessed that many publications are an effective means of recognizing exceptional competence and talent in science, which can provide an individual with great moral and financial satisfaction. The famous phrase in academic circles "publish or perish" is becoming a harsh reality. In their desire to publish sessional discoveries, individuals try to falsify scientific results to create the illusion of exceptionality. Modern image analysis programs based on artificial intelligence have proven to be an effective means of exposing false representations of scientific results and have led to the withdrawal of many suspicious publications from journals in recent years. New artificial intelligence algorithms based on generative adversarial networks provide the ability to generate images that can be classified as credible. The implementation of these algorithms on quantum computers has proven to be a potentially superior method of image generation and poses a real danger that cases of falsification of scientific results will go unnoticed. This imposes the need to soon develop a discipline that could be described as forensics of scientific results, and which would deal with unraveling the application of classical and quantum algorithms for generating results.

**uantum Generative Adversarial etwor s for Generating cientific esults**

Vladimir Arsoski

 ISBN 978-86-7466-930-3

# Forenzički aspekt prostorne i vremenske komponente

Snežana Stojičić, Radovan Radovanović, Milesa Srećković, Nikola Radovanović

*Apstrakt*—**Dinamičnost realnih sistema uključuje neizostavno vremens i o vira i prostorno referenciranje, što je u direktnoj vezi sa davanjem nalaza i mišljenja sa forenzičkog aspekta. U određenim događaima i slučajevima primene forenzičkih metoda, posebno se mora dati značaj redosledu, sledu dešavanja u okviru određenog događaja, jer on može značajno uticati na zaključivanje. Prostorno referenciranje se, može razmatrati od osnovnog navođenja mesta događaja do dovođenja u kontekst uticaja elemenata prostora na uzrok i posledicu događaja, oji se obrađuje. Ukoliko je moguće obezbediti referentne vremenske podat e, podat e u jedna im vremens im intervalima oni mogu biti posmatrani i analizirani ao vremens e serije. radu su dati primeri uključivanja vremenskog okvira i prostornog referenciranja, imajući u vidu da značajno mogu doprineti ciljevima forenzičkog inženjerstva.**

***Ključne reči*—Forenzički aspekti; prostorno referenciranje, vremens i o vir;**

## I. UVOD

Zaključci o uzrocima nastanka incidentnih događaja se zasnivaju na činjenicama i analizi u kojoj mogu biti primenjene i metode forenzičkog inženjerstva. Nalaz i mišljenje do kojih se dođe u toku analize može, prema prethodno navedenim aspektima primene stručnih znanja, veština i specifičnih znanja, mogu biti usmereni ka poboljšavanju bezbednosti proizvodnog procesa, poboljšanju performansi i efikasnosti rada mašina i uređaja, kao i ka primeni nalaza i mišljenja kao stručne pomoći u sudskim i drugim postupcima pri utvrđivanju činjenica, koje se odnose na nesreće ili krivične stvari. Generalno se sa forenzičkog aspekta procenjuje stanje pre događaja, posle događaja, postavljaju hipoteze o mogućim načinima i uslovima koji se mogu dovesti u vezu sa nastankom stanja posle događaja, pronalaze dokazi koji negiraju ili potvrđuju postavljene hipoteze i primenjuju znanja i veštine za povezivanje različitih činjenica i dokaza u koherentni scenario, vezan za nastanak događaja i sačinjava nalaz i mišljenje u formi koja odgovara daljoj primeni i/ili procesuiranju slučaja [1].

Snežana Stojičić, Ministarstvo unutrašnjih poslova, Kneza Miloša 101, 11000 Beograd, Srbija (e-mail: snezana.stojici@mup.gov.rs),

Radovan Radovanović – Kriminalističko policijski univerzitet, Cara DUšana 196, 11000 Beograd, Srbija (e-mail: radovan.radovanovic@kpu.edu.rs),

Milesa Srećković – Elektrotehnički fakultet, Univerzitet u Beogradu, Bulevar Kralja Aleksandra 73, 11020 Beograd, Srbija (e-mail: esreckov@etf.bg.ac.rs).

Nikola Radovanović – Kriminalističko policijski univerzitet, Cara Dušana 196, 11000 Beograd, Srbija (e-mail: nikola.radovanovic@gmail.com).

Primena metoda forenzičkog inženjerstva se vrši od strane pojedinaca ili stručnih timova koji obavljaju forenzičke istrage u sprovođenju aktivnosti na otkrivanju uzroka koji je doveo do incidenta. Prostorni kontekst je jedna od osnova za referenciranje događaja, pojave ili procesa koji se analizira, kao i vremenski okvir koji je potrebno dati sa najvećim mogućim stepenom preciznosti [2,3]. Međutim, nije uvek jednostavno ustanoviti veze vremenskog okvira i prostornog referenciranja [2, 4-7].

## II. PROSTORNO REFERENCIRANJE

Jedan od primera koji će biti obrađivan odnosi se na prostorni kontekst događaja koji su uzrokovani požarnim ili eksplozivnim procesima [8], odnosno jednim aspektom koji se odnosi na dejstvo štetnih materija na okruženje, što pak uključuje potrebu za omogućavanjem utvrđivanja koncentracija zagađujućih materija u vazduhu [9]. Određivanje koncentracije zagađujućih materija se može vršiti na osnovu postojećih mernih stanica. Za to se mogu koristiti merne stanice automatskog monitoring kvaliteta vazduha u Republici Srbiji[1]Za određivanje lokacija mernih mesta za uzimanje uzoraka za merenje koncentracija zagađujućih materija, a u svrhu ocenjivanja kvaliteta vazduha u zonama i aglomeracijama, primenjuju se kriterijumi dati u Uredbi o uslovima za monitoring i zahtevima kvaliteta vazduha („Sl. glasnik RS“, br, 11/2010, 75/2010 i 63/2013). Posebno, makrolokacije za fiksna merenja, određuju se u cilju zaštite zdravlja ljudi, vegetacije i prirodnih ekosistema, a u neposrednoj blizini tačkastih izvora, s obzirom na gustinu emisija, očekivanu raspodelu zagađujućih materija u vazduhu i potencijalnu izloženost stanovništva.

Određivanje lokacija mernih mesta, vrši se tako da se može pratiti primena standarda i najboljih dostupnih tehnika u skladu sa propisima u oblasti sprečavanja i kontrole zagađivanja vazduha (Sl.1). Sam postupak određivanja lokacija zahteva prethodnu analizu na osnovu dostupnih podataka u odnosu na prostor, uz primenu svih propisanih kriterijuma i analizom dobijenih procena. Posebno, imajući u vidu da izbor mernog mesta i lokacije za uzimanje uzoraka, je potrebno proveravati periodično ili protokom određenog vremenskog perioda, u cilju potvrđivanja validnosti kriterijuma koji su prethodno korišćeni i u zavisnosti od

[1] АЗЗЖС - ОБЈЕДИЊЕНИ ПРИКАЗ АУТОМАТСКОГ МОНИТОРИНГА КВАЛИТЕТА ВАЗДУХА У РЕПУБЛИЦИ СРБИЈИ (sepa.gov.rs)

 ISBN 978-86-7466-930-3

promena nastalih okruženju nalaženja novih predloga i rešenja [2].

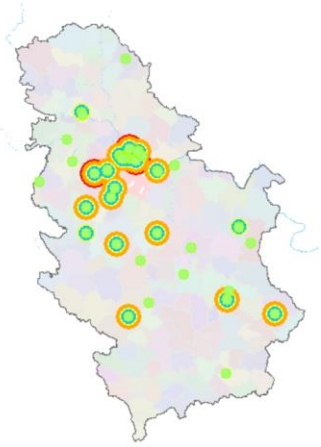

Sl. 1. Prikaz lokacija mernih stanica iz Sistema automatskog monitoringa kvaliteta vazduha sa podataka o koncentracijama PM2.5 izmerenih u periodu 18-25.04.2022. godine – satni podaci.

Različite vrste fizičkih dokaza mogu pružiti opšte informacije o prostornim odnosima između objekata, ljudi i događaja. Pored toga, primena forenzičkih metoda ispitivanja i analize može doprineti tumačenju i potencijalnom rasvetljavanju krivičnog dela.

Forenzičke metode koje se primenjuju za ispitivanje, komparacije i identifikacije uzroka i posledica, kod eksplozivnih i požarnih procesa, kao i drugih dokaza u istražnom postupku, olakšavaju rasvetljavanje krivičnih dela. Kod razrešavanja krivičnih dela u kojima se pojavljuju eksplozivni i požarni procesi uključivanjem prostorne komponente, može značajno doprineti davanju kvalitetnije prezentacije i vizualizaciji događaja sa ciljem davanja mišljenja i nalaza o dejstvu ovih procesa sa aspekta forenzičkog inženjerstva. Upotrebom softverskih alata za rad sa prostornim podacima omogućava se postavljanje upita u odnosu na podatke o lokaciji događaja kao i primena metoda za analizu podataka u odnosu na prostor. Ovi alati omogućavaju vršenje merenja, analize i izradu prikaza, koji pored sadržaja koji se odnosi na prostorne podatke, organizovane po tematskim slojevima, mogu sadržati elemente koji su određeni prema parametrima koji su definisani faktorima relevantnim za posmatrane događaje i procese. Mogu se ostvariti simulacije dejstva, analize koje se mogu vršiti i u odnosu na prostor, kao i testiranje hipoteza i rekonstrukciju događaja u cilju utvrđivanja relevantnih činjenica. U postupku utvrđivanja relevantnih činjenica koriste se instrumentalne i komparativne metode za modelovanje procesa, vizualizaciju i dokazivanje dejstva eksplozivnih i požarnih procesa. U radu je dat prikaz mogućnosti korišćenja podataka sa mernih stanica u sisitemu automatskog monitoringa kvaliteta vazduha u Republici Srbiji i mogućnosti analize i detekcije i vizualizacije stanja za slučajan uzorak, u izabranom vremenskom periodu od 18-25.04.2022. godine. Sa mernih stanica preuzeti su satni podaci kako bi se izvršila njihova analiza. Dalja razmatranja mogu biti usmerena ka analizi eksplozivnih i požarnih procesa u odnosu na lokaciju dešavanja procesa i distribuciju u odnosu na prostor, čime forenzički inženjering može dati neutralan i objektivan doprinos da istraži jedan od načina da se jedna kompleksna problematika dejstva eksplozivnih i požarnih procesa obradi uz uključivanje prostorne komponente, i da se pruži potpuniji izvor informacija o ovoj temi u prostornom kontekstu. Praktičan značaj je ukazivanje na mogućnost uključivanja komponente prostora uz komponentu vremena u forenzičkom inženjerstvu, u odnosu na forenzičke identifikacije eksplozivnih i požarnih procesa u cilju sprečavanja i suzbijanja kriminaliteta i opšte bezbednosti.

Razmatranja podataka iz sistema automatskog monitoringa kvaliteta vazduha data su u odnosu na granične vrednosti suspendovanih čestica PM10 i PM2.5, date u Tabeli I, kao zagađujućih materija, čija koncentracija može biti povećana i u slučaju pojave incidentnih situacija izazvanih požarnim i eksplozivnom procesima.

TABELA I
GRANIČNE VREDNOSTI ZA PM10 I PM2.5

| Zag. Materija (1h) | Odličan | Dobar | Prihvatljiv | Zagađen | Jako zagađen |
|---|---|---|---|---|---|
| PM10 (ug.m-3) | 0-25 | 25-50 | 50-90 | 90-180 | > 180 |
| PM2.5 (ug.m-3) | 0-15 | 15-30 | 30-55 | 55-110 | > 110 |

## III. PRAKTIČNI PRIMER ANALIZE VREMENSKOG OKVIRA I PROSTORNOG REFERENCIRANJA

Za prikaz praktičnih aspekata, preuzeti su podaci sa mernih stanica Sistema za automatsko praćenje kvaliteta vazduha u Republici Srbiji, koji su dostupni na satnom, nedeljnom i mesečnom nivou, i koji su dostupni za analizu i korišćenje kao otvoreni podaci. Podaci su preuzeti u period od 18-25.04.2022. godine na satnom nivou, prema stepenu dostupnosti i stanju mernih uređaja na mernim stanicama. Preuzeti skup podataka je dalje obrađivan, kao slučajan uzorak. Prema lokacijama mernih stanica, podaci su pripremljeni za korišćenje u alatima za rad sa prostornim podacima i omogućavanje prikaza i dalje analize u odnosu na prostor.

TABELA II
DESKRIPTIVNI PODACI ZA PM10 PO MERNIM STANICAMA

| Naziv merne stanice | N | Sr. vred | SD | Min | Med | Max |
|---|---|---|---|---|---|---|
| Beograd Obrenovac Ušće | 167 | 29.69 | 20.35 | 3.76 | 23.56 | 126.49 |
| Beograd Ovča | 162 | 24.19 | 22.00 | 2.29 | 16.89 | 163.87 |
| Beograd Topčiderska Zvezda | 164 | 23.30 | 11.95 | 4.31 | 18.99 | 56.4 |
| Bor Gradski park | 167 | 19.20 | 15.15 | 2.47 | 14.37 | 75.72 |


ISBN 978-86-7466-930-3

| Naziv merne stanice | N | Sr. vred | SD | Min | Med | Max |
|---|---|---|---|---|---|---|
| Čačak | 167 | 28.76 | 17.37 | 4.32 | 25.04 | 96.66 |
| Novi Sad Rumenačka | 167 | 20.56 | 8.83 | 5.95 | 19.83 | 56.52 |
| Pirot | 167 | 28.03 | 15.67 | 7.31 | 25.25 | 122.7 |
| Beograd Ada petlja | 167 | 26.33 | 11.91 | 8.22 | 23.85 | 63.03 |
| Beograd Bežanijska kosa | 167 | 26.61 | 13.93 | 3.32 | 21.6 | 74.66 |
| Beograd Despota Stefana | 167 | 26.24 | 11.78 | 4.87 | 23.12 | 55.43 |
| Beograd Dragiša Mišović | 167 | 23.93 | 13.201 | 3.13 | 20.73 | 67.11 |
| Beograd Lazarevac | 167 | 26.52 | 14.716 | 5.73 | 23.09 | 80.76 |
| Beograd Mostar | 167 | 26.06 | 14.99 | 5.11 | 21.54 | 74.24 |
| Beograd Novi Beograd | 167 | 23.72 | 13.29 | 4.47 | 19.27 | 65.88 |
| Beograd Oml. brigada | 167 | 28.06 | 14.97 | 4.17 | 22.65 | 70.09 |
| Beograd Stari grad | 167 | 25.2 | 12.53 | 3.68 | 21.73 | 59.16 |
| Beograd Vinča | 167 | 24.38 | 16.39 | 3.34 | 20.89 | 138.9 |
| Beograd Vračar | 167 | 30.21 | 16.44 | 6.5 | 25.03 | 100.86 |
| Beograd Vračar Dom zdravlja | 167 | 24.93 | 12.86 | 3.89 | 22.08 | 66.79 |
| Beograd Zeleno brdo | 167 | 23.53 | 11.770 | 4.09 | 20.81 | 63.44 |
| Kosjerić | 167 | 29.29 | 19.66 | 1.75 | 25.45 | 97.43 |
| Kragujevac | 167 | 33.09 | 18.15 | 9.52 | 30.41 | 132.66 |
| Niš IZJZ Niš | 167 | 20.25 | 12.82 | 2.79 | 16.83 | 72.2 |
| Niš O.Š. Sveti Sava | 167 | 31.26 | 24.4 | 5 | 24.52 | 154.16 |
| Novi Pazar | 167 | 39.67 | 25.50 | 4.37 | 34.81 | 110.43 |
| Pančevo Vojlovica | 166 | 30.39 | 17.12 | 4.29 | 26.59 | 91.4 |
| Smederevo Centar | 167 | 25.24 | 14.55 | 3.43 | 21.87 | 92.81 |
| Valjevo | 165 | 38.45 | 24.64 | 5.97 | 29.88 | 150.23 |
| Veliki Crljeni | 167 | 35.50 | 19.71 | 6.29 | 30.42 | 130.85 |
| Beograd Banovo brdo | 167 | 24.22 | 12.252 | 3.35 | 21.09 | 67.58 |
| Obrenovac Centar | 167 | 34.13 | 19.49 | 3.9 | 28.08 | 93.92 |
| Pančevo Starčevo | 167 | 37.75 | 84.98 | 1.37 | 23.39 | 831.51 |
| Pančevo Vatrogasni dom | 167 | 21.06 | 12.49 | 2.78 | 18.03 | 68.89 |

Na osnovu deskriptivnih statističkih podataka, prikazanih u Tabeli II, u posmatranom uzorku identifikovane su lokacije sa pojavom ekstremnih vrednost i vremenski period nastanka i trajanja prisustva povišenih vrednosti (Sl. 2). Identifikovane ekstremne vrednosti su dalje analizirane sa ciljem utvrđivanja dužine trajanja visokih koncentracija i prostorne distribucije.

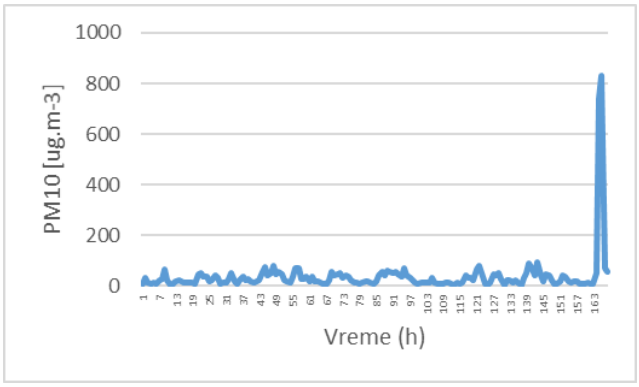


Sl. 2. Prikaz podataka o koncentracijama PM10 za lokaciju sa identifikovanim ekstremnim vrednostima u posmatranom uzorku, kao vremenskoj seriji.

Analizom je dobijeno da je prisustvo ekstremnih vrednosti identifikovano u kraćem vremenskom interval i da u odnosu na posmatrani period nije ostvaren značajan uticaj na distribuciju posmatranih vrednosti (Sl. 3).

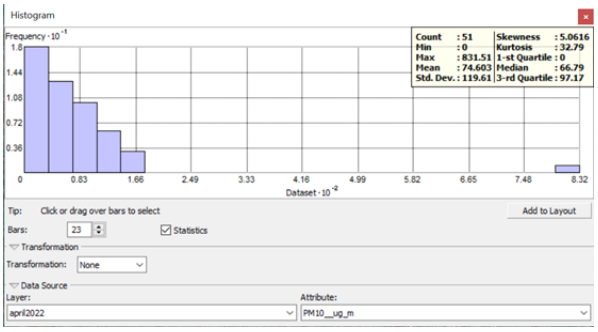


Sl. 3. Prikaz statističkih podataka o koncentracijama PM10 izmerenih u periodu 18-25.04.2022. godine na mernim stanicama za monitoring kvaliteta vazduha.

U cilju procene prostorne distribucije na osnovu posmatranog uzorka, korišćene su geostatističke metode dostupne u okviru alata za rad sa prostornim podacima i to na lokacijama, u odnosu na vreme i u odnosu na sve posmatrane lokacije in a njima izmerenih vrednosti sa prediktivnom procenom. Korišćena je prostorna ocena za PM10, kao promenljive, na osnovu doprinosa tačaka u kojima je vrednost poznata (Kriging).

Rezultati analize pokazuju da značajnije dejstvo ostvaruju povišene vrednosti u dužem vremenskom periodu i ako su nižeg nivoa, od ekstremnih vrednosti, koje se pojavljuju u kraćem vremenskom periodu (Sl. 4). Potrebno je svakako imati u vidu da u analizu nisu uključeni ostali element iz okruženja i karakteristike terena za izvedeni zaključak, što svakako ukazuje na potrebu dajeg istraživanja i uključivanja drugih elemenata realnog okruženja, odnosno, ukoliko isti nisu dostupni u vreme sprovođenja analize identifikacije elemenata i generisanje modela sa mogućnosšću variranja vrednosti i procene uticaja.

Svakako, sprovedenom analizom je potvrđeno da komponente prostora i vremena mogu biti značajno doprineti


ISBN 978-86-7466-930-3

pri analizi događaja koji dovode do emisije zagađujućih materija u vazduh i procene dejstva.

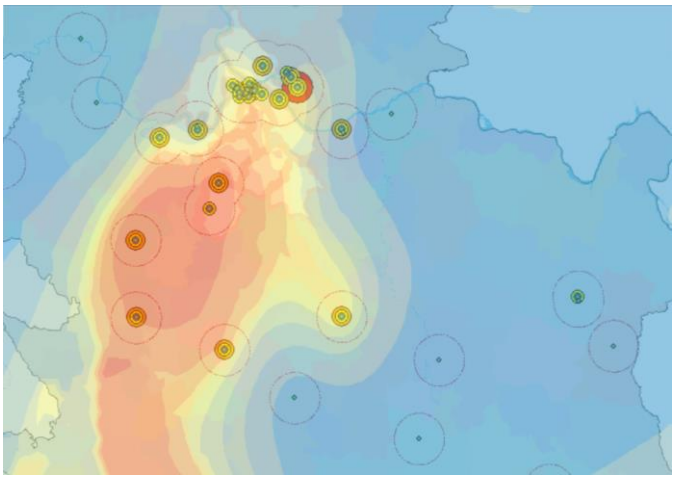

Sl. 4. Prikaz podataka o koncentracijama PM10 izmerenih u periodu 18-25.04.2022. godine na mernim stanicama za monitoring kvaliteta vazduha sa zomama i predikcionom mapom u odnosu na prostor.

## IV. ZAKLJUČAK

Uključivanje prostorne i vremenske komponente, uz korišćenje alata za rad sa prostornim podacima, proširuje mogućnosti analize i primenu metoda sa forenzičkog aspekta. Izložena razmatranja i praktični prikazi na datom na slučajnom uzorku, ukazuju na mogućnosti koje mogu biti dalje razmatrane i istraživane u korelaciji sa određenimi, događajima koji su predmet primene drugih forenzičkih metoda, kao što su između ostalog i požari i eksplozije, koji za posledicu mogu imati povećanu koncentraciju suspendovanih čestica u vazduhu.

## ZAHVALNICA

Aurori se zahvaljuju organizacionom odboru konferencije ETRAN 2022 na prepoznatom značaju oblasti forenzike, prostoru i vremenu datom za izlaganje i diskusiju.

## LITERATURA

[1] R. K. Noon, „*Forensic Engineering Investigation*“, CRC Press, USA, 2001.

[2] *redba o uslo ima a monitoring i ahte ima k aliteta a duha*, „Sl. glasnik RS“, br, 11/2010, 75/2010 i 63/2013. 2013. Uredba o uslovima za monitoring i zahtevima kvaliteta vazduha (paragraf.rs)

[3] Ambient (outdoor) air pollution, https://www.who.int/news-room/fact-sheets/detail/ambient-(outdoor)-air-quality-and-health, Accessed 1st April 2022.

[4] Vazduh građanima, Beogradski hakaton Descon 4.0, 2018. Početna stranica - Vazduh građanima (klimerko.org), Accessed 25th Mart 2022.

[5] Svetsko zagađenje vazduha: Indeks kvaliteta vazduha u realnom vremenu, Svetsko zagađenje vazduha: Indeks kvaliteta vazduha u realnom vremenu (waqi.info), Accessed 25th March 2022.

[6] Build your DIY sensor and become part of the worldwide citizen science, open data, civic tech network. Supported by a lot of contributors, Accessed 25th March 2022.

[7] xEco Vazduh - Kvalitet vazduha u Srbiji u realnom vremenu, Accessed 25th March 2022.

[8] H. Ménard, O. Akinpelu, N.A. Fiakpui, R. (L.) He, S. Huxter, C. Jordan, L. Judge, A. King, B. Miller, S. E. Moggs, C.-T. Patrascu, T. Pearson, M. E. J. Seneviratne, L. E. Timmerman, P. R. Haddrill, J. K. Klu, C. Cole, & N. Nic Daéid, N. “Research trends in forensic science: A scientometric approach to analyze the content of the INTERPOL reviews”. *Wiley Interdisciplinary e iews Forensic Science*, 2021. e1447. https://doi.org/10.1002/wfs2.1447

[9] A. Kloosterman, A. Mapes, Z. Geradts, E. van Eijk, C. Koper, J. van den Berg, S. Verheij, M. van der Steen & A. van Asten, “The interface between forensic science and technology: how technology could cause a paradigm shift in the role of forensic institutes in the criminal justice system”. Philosophical transactions of the Royal Society of London. Series B, Biological sciences, 2015. 370(1674), 20140264. https://doi.org/10.1098/rstb.2014.0264

## ABSTRACT

The dynamic of real systems inevitably includes time frame and spatial referencing, which are directly related to giving findings and opinions from the forensic aspect. In certain events and cases owhere application of forensic methods might be appropriate, special importance must be given to the sequence of events within a certain event, because it can significantly affect the conclusion. Spatial referencing can also range from the basic indication of the place of the event to bringing into context the influence of the elements of space on the cause and effect of the event being processed. If it is possible to provide reference time data, the data in equal time intervals can be observed and analyzed as time series. The paper gives examples of including time frame and spatial referencing, bearing in mind that they can significantly contribute to the goals of forensic engineering.

**A space and time from forensic aspects**

Snežana Stojičić, Radovan Radovanović, Milesa Srećković, Nikola Radovanović

 ISBN 978-86-7466-930-3

# Različiti režimi rada kvantnih generatora kao instrument za modifikacije u stomatologiji

Aleksandar Bugarinović [1,7], Željka Tomić [2], Sanja Jevtić [3], Aleksander Kovačević [4], Svetlana Pelemiš [5], Zoran Nedić [6], Dragan Družijanić [1]

**Apstra t - potrebom vantnih generatora u raznim oblastima, a i u stomatologiji, bavi se veli i broj istraživača sa perspektivom da taj broj bude i veći. Ciljevi su različiti od dobijanja materijala za dalje formiranje do učešća u formiranju modifi ovanih materijala, modifi acije osobina već tradicionalnih materijala do postizanja zadata a oji se pojavljuju u vezi sa zahtevima heritologije forenzi e ili za masmedija primenu. pecijalno, dijagnostičke tehnike na bazi jačih ili slabijih interakcija elions ih snopova sa materijalom, postaju sve više tražene merne tehni e zbog vremena same dijagnostike i mogućnosti ispitivanja ara teristi a uzora a i u malim lo alnim površinama, a skeniranjem po potrebi i u većim. Podrazumevaju se i kvantitativne i valitativne analize, a rad sa više od jednog snopa (manje i veće gustine snage), pored mogućnosti praćenja interakcije sa teorets e strane, pruža i praktičan deo apli acije lasers e ili uopšte elionske tehni e, oji je ušao u pra su ili je od potencijalnog interesa za protetičke i druge svrhe. Šta bi onda moglo biti generalno novo u ovoj oblasti ovi dinamički režimi rada kvantnih generatora, oblici impulsa, njihovo trajanje i fre vencija, donose novi kvalitet, koji može proizvesti drugačije efekte pri intera ciji lasers ih snopova sa materijalom, uspostaviti nove standarde i ili potisnuti stare. ad se bavi intera cijom lasers ih snopova, u različitim režimima rada, sa odabranom lasom materijala. Biće diskutovani modeli za opis i rezultati intera cija, analiziraće se oštećenja i dati osvrt na trenutna i potencijalna polja primene i izabrane paralele sa drugim snopnim tehni ama.**

**Ključne reči - vantni generatori, režimi rada, interakcije, modeli, polje primene.**

## I. UVOD

Primena laserske tehnike ili, u širem smislu, kvantnih generatora, treba da, na prvi pogled, menja značenje *modifikacije* sa kvantifikacijom od minornih uticaja na materijal mete do totalne ili lokalne destrukcije mete, zavisno od režima rada sistema kojim se vrši tretman.

Pošto je stvarnost omogućila da se interakcija koristi: a) u dijagnostičke svrhe, b) u strogo *modulacione* svrhe c) za spajanje materijala iste vrste ili različitih tipova d) za razdvajanje materijala, to postoji i grupisanje gustina energije, snage, primena *cw* ili impulsnog rada sa različitim parametrima, slike 1 i 2.

Vremenska baza impulsa (širine impulsa) je u rasponu od prvih milisekundnih impulsa sa stotinak spajkova [1] do *fs* režima.

[1] Elektrotehnički fakultet, Univerzitet u Beogradu, [2] Akademija tehničkih strukovnih studija Beograd, [3] ATUSS, [4] Institut za fiziku, [5] Tehnološki fakultet Zvornik, Univerzitet u Istočnom Sarajevu, [6] Fakultet za fizičku hemiju, Univerzitet u Beogradu, [7] Provis doo. Bijeljina.

U pogledu materijala, koji su od interesa za stomatologiju, veoma je široka njihova paleta, zato što se danas koristi laserska tehnika u svakodnevnoj kliničkoj praksi: (a) za saniranje *biološkog aparata*, uključujući i meka i tvrda tkiva, (b) u protetičke svrhe.

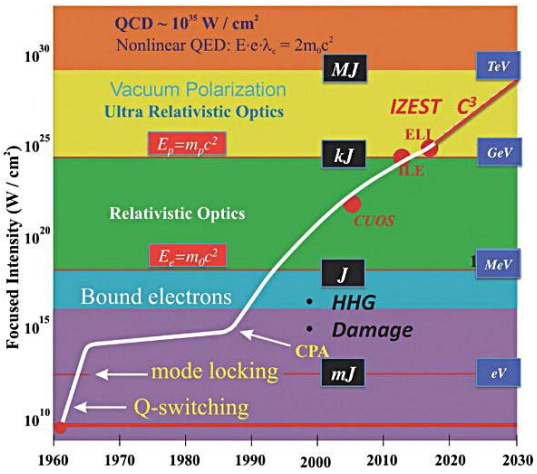


Slika 1. Istorija i predviđanje razvoja fokusiranog intenziteta od prvih demonstracija lasera (sa različitim režimima rada).

U svim tim procesima, postavljali su se i postavljaju se i dalje objektivizacije opisa procesa, pored toga što se veliki broj interakcija koristi u svakodnevnoj praksi, s obzirom na višedecenijsku primenu lasera u stomatologiji, zavisno od zemlje i njene regulative. To znači da su uključeni skoro svi glavni tipovi materijala: metali, dielektrici, specijalne klase keramike i dr. Posebno su važne i primene za paradentozne tretmane u kojima su korišćeni laseri malih snaga (reda mW) i gde se radilo samo o ozračavanju tkiva u vremenu predviđenom protokolom (kada je odobrena ta terapija u pojedinoj državi). Za simulaciju procesa interakcije prema očekivanom izlazu, koriste se modeli od termalnog do modela teorija sličnosti, i zavisno da li se radi o proceni naponskog stanja protetske konstrukcije, do holografskih studija lokalnog opterećenja tačaka od interesa.

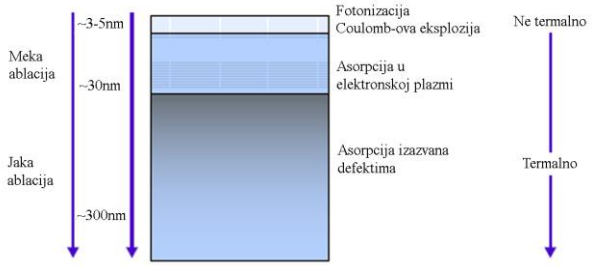


Slika 2. Procesi ablacije izazvanih laserima i neki procesi uz slojeve materijala od površine.

 ISBN 978-86-7466-930-3

U ovom radu je odabrano nekoliko režima rada kvantnih generatora u režimu slobodne generacije ili Q-*switch* i dati su rezultati interakcije.

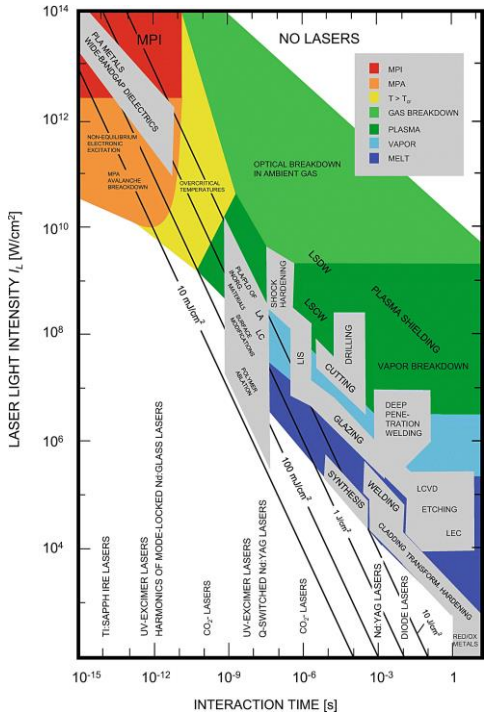


Slika 3. Karakteristična vremena interakcije, intenzitet lasera i mogući procesi sa često korištenim laserskim sistemima. (PLA/PLD – impulsna laserska ablacija / depozicija, LA – odgrevanje, LC – čišćenje, LIS – separacija izotopa, MTA – višefotonska apsorpcija / jonizacija, LSDW/LSCW – detonacija / sagorevanje podržana laserom, LCVD – indukovana hemijska CVD, LEC – elektrohemijsko nanošenje prevlaka / nagrizanje, RED/OX – redukcija / oksidacija indukovana sa dugim impulsima ili *cw* $CO_2$) [11].

## II. REZULTATI RADA I DISKUSIJA

Jedna od standardnih šema eksperimenata sa izlaganjem materijala od interesa, za određenu oblast stomatologije, podrazumeva rešavanje optike ulaznog snopa, položaja mete sa odgovarajućim *support*-om za promenu geometrije upada snopa lasera u materijal i, prema mogućnosti laboratorije, podrške za promenu polarizacije snopa, uključivanje drugog tipa kvantnog generatora i kontrolu izlaznog snopa, uključujući mogućnost kvantitativnih opisa u vremenskom i prostornom domenu. Kako se pri impulsnom radu, najčešće rešava samo vreme ekspozicije, to je potrebno vršiti i kontrolu vremena. Ovaj deo aparature, sam po sebi, ne bi predstavljao specifične probleme, ali za stomatološke procese je od specijalnog interesa, jer je upravljanje snopom ručno.

Idealni eksperiment bi podrazumevao mnogo drugih različitih kontrola samog procesa, sakupljanje izbačenog materijala, kontrolu sastava izbačenog materijala (nastanak novih jedinjenja) i geometrijske putanje izbačenog materijala, jer se simulira, odnosno predviđa situacija stvarne upotrebe. Za slučaj primene lasera kod žučnih i bubrežnih kamenova, prvi eksperimenti su vršeni uz sakupljanje razvijenih gasova, da ne bi došlo do neželjenog trovanja organizma, a to podrazumeva i razne vrste operacija u stomatologiji (čišćenje kamenca i dr.).

Bez obzira na simulaciju iz raznih oblasti posmatranja dinamike procesa u izabranom režimu rada, dobro je posmatrati materijal mete sa više deskripcionih tehnika nedestruktivnog tipa za ulaz u eksperiment i ponoviti ih posle interakcije, kad dolaze u obzir i destruktivni postupci merenja, kakvi su zahtevi u SEM i drugim elektronskim tehnikama.

Za date rezultate interakcije dati su i IC spektri tretirane površine. Za tretiranje LAZ-a (Laser Affected Zone) u primeni u stomatologiji traži se minimum zahvata tkiva ili bar strogo kontrolisan. Odnos LAZ-a i HAZ-a (Heat Affected Zone) je uvek pitanje koje je podložno diskusiji.

Na slikama 4 i 5 dati su rezultati sprovedenih analiza stanja povreda na nekim materijalima od interesa za protetiku i za zubno tkivo. Na slici 6 je izabrani uzorak HAP-a, koji se već duže vremena primenjuje za ojačanja bioloških tkiva, privremenih ili stalnih.

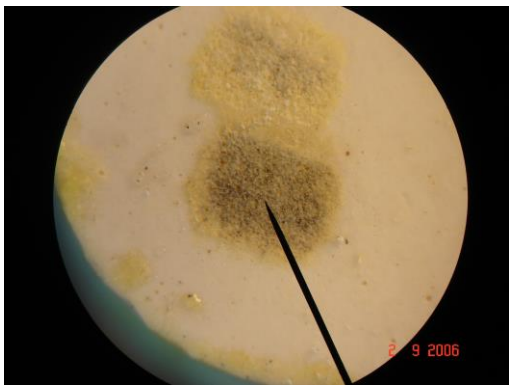


Slika 4. Mikrograf analize optičkim mikroskopom belog gipsa izloženog laserskom snopu. ($Nd^{3+}$:YAG, E = 35 mJ, površinski reljef, OM 40 x)

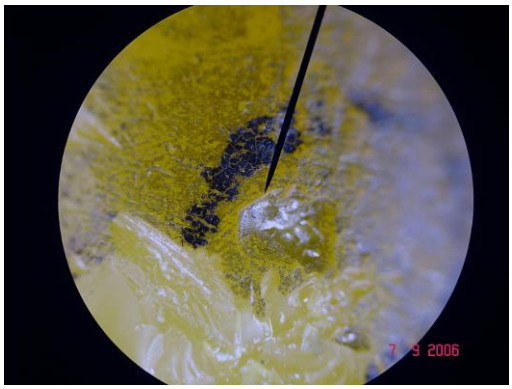


Slika 5. Analiza optičkim mikroskopom interakcije Q-*switch* tipa lasera na uzorku žutog voska. ($Nd^{3+}$:YAG, τ = 15 ns, E = 35 mJ, 3 pulses, OM 40 x, površinski reljef)

Prema režimu rada, očekivalo se da bude proizveden krater koji ima više ili manje nagomilavanje materijala po obodu, pri čemu bi veće nagomilavanje materijala bilo vezano za režim slobodne generacije. Krater sa manje izbačenog materijala (po obodu) bi, sa druge strane, trebalo da služi i inverzno, za raspodelu gustine energije po preseku snopa ili prikaz nehomogenosti materijala mete. Zato je i bilo govora na početku eksperimentalnog dela, da bi u idealnom slučaju bilo dobro imati, paralelno, analizatore laserskog snopa direktno ili bar povremenu kontrolu gustine energije / snage, kojoj je meta bila izložena. Jednostavan prilaz bi bio i da se pri toj vrsti eksperimenata, pre serije impulsa na nekom materijalu izvrši isti režim na materijalu koji je predložen kao kontrolni materijal, a koji je pogodan za datu talasnu dužinu.

 ISBN 978-86-7466-930-3


Slika 6. Fotomikrograf povrede na uzorku HAP-a. ($Nd^{3+}$:YAG, Q-*switch*, E = 35 mJ, površinska modulacija, OM 40 x)

Na slikama 7 i 8 dati su IC spektri za uzorke gutaperke i HAP-a.

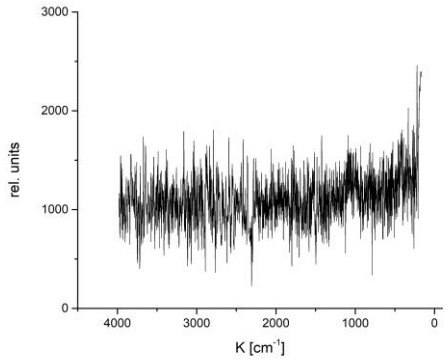


Slika 7. Infracrveni spektar (IC) uzorka gutaperke u dijapazonu 4000 - 180 $cm^{-1}$.

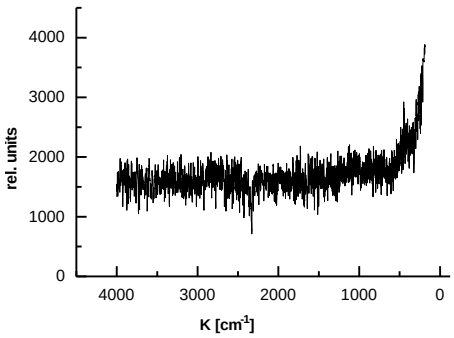


Slika 8. Infracrveni spektar (IC) uzorka HAP-a u dijapazonu 4000 - 180 $cm^{-1}$.

Idealno bi bilo da se spektri uvek rade pre i posle interakcije, zato što bi zavisno od površine povrede mogao da se sprovede formalizam za dobijanje optičkih konstanti materijala, kao što su koeficijenti refleksije, koeficijenti dielektričnih osobina, vezano za optičke osobine i kompleksan zapis. Ovde bi od koristi bio i *aman*-ov spektar, koji bi i samim poređenjem sa IC spektrima dao neki kvalitativan odgovor bez sprovođenja primene algoritama za analizu strukture materijala.

Pretpostavka o novim materijalima, čiji broj raste u stomatologiji, je uvek potrebna, a za poznate materijale potrebna je iz razloga kontrole postojećih podataka i izbegavanje razlika u tehnologiji izrade protetskog materijala. Čini se da je dobro ponoviti uvek provere i za poznate materijale.

Od interesa bi bila i tehnika termovizije, koja je skoro dve decenije bila prisutna sa prvim primenama lasera u stomatologiji, u vreme kada je ekonomska strana nabavke te kontrole predstavljala veći problem. To su eksperimenti koji mogu pratiti proces za određene dinamičke dijapazone kvantnih generatora, kad se radi o dugim impulsima ili srednjim vrednostima, pri većim repeticijama, kao kontrolna relativna tehnika.

Važna oblast bi bilo i određivanje boje kod zuba ili protetičkih materijala, gde bi moglo biti od interesa vezivanje sa trenutnim stanjem deskripcije boje, u kojima glavne boje pripadaju kategoriji lasera (za televizijske svrhe HDTV odavno je razvijen tip RGB lasera).

## III. SIMULACIJA

Kako je u uvodu konstatovano, posle izabranog modela, a za određene režime rada kvantnih generatora [9] se konstatuje da i više modela mogu da se koriste za određene režime, koji odgovaraju tipu grejanja materijala do tačke ključanja. To su slučajevi izlaganja patogenog tkiva (paradentoza) koje se već više od deceniju koristi za saniranje stanja. Slučajevi bušenja (otklanjanja materijala), zavisno da li se problemu prišlo sa redosledom grejanje-topljenje ili grejanje-sublimacija i sl., bi morali da koriste odgovarajuće algoritme kod programa kod kojih su oni razvijeni [5].

Pošto je za bušenje najbitnije pitanje dimenzija (dubina, širina), onda se za preliminarnu ocenu koriste formule koje zavise od parametara izlaganja, termodinamičkih i optičkih osobina materijala.

U širokoj paleti materijala čini se da je situacija *status uo* i da se može naći mnogo praktičnih korekcija za izabrane režime rada, gde će se za promenu koeficijenata u formulama za standardne uslove rada približiti simulacija eksperimentu. Pri interakciji je jedna od važnih činjenica pitanje maksimalne gustine snage / energije, koja neće dovesti do praga za „lom". Sve to pripada složenoj problematici „laser damage" gde se uključuje statistika malih brojeva i statistika velikih brojeva, koje se različito modeluju.

## IV. ZAKLJUČAK

U današnjem stepenu laserske tehnike postoji nekoliko definisanih režima rada kvantnih generatora, koji potencijalno mogu da se primene u biomedicinske svrhe. U praksi, iako postoji dosta dobro razvijena industrija laserskih sistema okrenutih medicini, pokazalo se da, generalno, postoji niz pozitivnih novih pravaca za primenu lasera. Ipak, od stanja same države i stepena njenog instrumentarijuma, vezano za klasičnije metode (mehanička bušilica, rentgenografija, poznate klase protetskih materijala sa komercijalnom podrškom) zavisi koliko će u njoj biti brzo uklapanje novih „optičkih" metoda u sve četiri uslovno podeljene oblasti: dijagnostika, modulacija u užem smislu (tkiva ili materijala), invazivna interakcija (hirurgija) i saniranje i formiranje ispuna i pravljenje mostova i dr. U ovom radu je pokazana interakcija sa tipovima odabranih

 ISBN 978-86-7466-930-3

materijala (keramičkog tipa i dr.), izvršene su analize sa strane optičke i elektronske mikroskopije, definisanje materijala mete putem IC spektroskopije. Ukazano je na potrebu daljeg eksperimentalnog rada, vezano za stanje uzoraka i za, potencijalno, organizaciju daljih ispitivanja ili primena holografskih i tomografskih tehnika za definisanje dinamike opterećenja, uključujući tehnike brzog starenja materijala, koje bi služile za ocenu, vek trajanja protetskog nastavka i pravac traženja, kroz krojenja novih vrsta materijala od interesa za protetiku i prihvatanje „stranog tela". Po pitanju samog HAP-a bile su razvijene dve teorije koje su primenjivane na mehanizam stapanja sa organizmom.

## LITERATURA


[1] A. Bugarinović, *Modulacije osobina odabranih klasa materijala delo anjem snopnih tehnika*, Magistarski rad, Elektrotehnički fakultet, Univerzitet u Beogradu, 2016.

[2] M.Srećković, S.Pelemiš, *aser Physics and Modeling in elation to Ceramic Matri Composites*, in Enciclopedia of Materials: Composites, Vol.2, Oxford, Ed. D. Bravazon, Elsevier, pp.218-235, 2021.

[3] S. Ostojić, Ž. Tomić, N. Bundaleski, J. Ilić, M. Davidović, A. Bugarinović, V. Mlinar, *Rasejanje svetlosti i tehnike u biološkim i biomedicinskim problemima*, Zbornik radova XLVI Konferencije za ETRAN, Banja Vrućica, Teslić, Vol.III, pp.178-181, 4-7 jun, 2002.

[4] V. Mirjanić, M. Srećković, Đ. Mirjanić, A. Bugarinović, D. Druzijanić, V. Mitić, *Chosen Applications and Approaches to Modeling asers in entistry*, Modern Physics Letters B, Vol. 35, No. 25, 2150329, pp.1-23, 2021.

[5] Đ. Mirjanić, M. Srećković, V. Mirjanić, S. Pelemiš, A. Bugarinović, D. Družijanić, *I abrani re ultati i modelo anje primene laserskih snopo a u stomatologiji na bio i protetičkim materijalima*, Journal of the Academy of Sciences and Arts of the Republic of Srpska Contemporary Materials 2021, u štampi,

[6] M. Srećković, A. Janićijević, M. Janićijević, S. Jevtić, Z. Latinović, K. Zarubica, A. Bugarinović, *Primene i modelo anje laserskih invazivnih, modulacionih i dijagnostičkih tehnika u biomedicini*, Zbornik radova konferencije Savremeni materijali 2019, Banjaluka, 01-03. septembar, pp. 61-90, 2020.

[7] M. Ž. Srećković, A. A. Ionin, A. J. Janićijević, A. R. Bugarinović, S. M. Ostojić, M. M. Janićijević, N. V. Ratković Kovačević, Formalisms, *Analysis, esults and Accomplishments with Population In ersion of Materials*, Journal of the Academy of Sciences and Arts of the Republic of Srpska Contemporary Materials, Vol.VIII, Iss.1, pp.91-108, 2017.

[8] G. Padmanabham, Ravi Bathe, *aser Materials Processing for Industrial Applications*, Proceedings of the National Academy of Sciences, India Section A: Physical Sciences, Vol. 88, pp.359–374, 2018.

[9] N. Rykalin, A. Uglov, I. Zuev, A. Kokora, *aser and Electron Beam Material Processing*, Mir, Moscow, 1988.

[10] S. Pelemiš, V. Mirjanić, Đ. Mirjanić, *aseri u medicini i stomatologiji*, knjiga u štampi.

[11] V. Chvykov, New Generation of Ultra-High Peak and Average Power Laser Systems, High Power Laser Systems, Ed. M. Harooni, December 2017.


## ABSTRACT


**The use of quantum generators in various fields, as well as in dentistry, is dealt with by a large number of researchers with the perspective that the number will be even higher. The goals are different from obtaining materials for further formation to participating in the formation of modified materials, modifying the properties of already traditional materials to achieving tas s that appear in connection with the requirements of heritology forensics or for mass media application. In particular, diagnostic techniques based on stronger or wea er interactions of elion beams with material are becoming more and more sought-after measurement techniques due to the time of diagnostics and the possibility of testing sample characteristics in small local areas, and scanning if necessary in larger ones. uantitative and qualitative analyzes are included, and wor with more than one beam (lower and higher power densities), in addition to the possibility of monitoring the interaction from a theoretical point of view, provides a practical part of the application of laser or elion techniques in general, which has entered into practice or is of potential interest for prosthetic and other purposes. What, then, could be generally new in this area ew dynamic modes of operation of quantum generators, pulse shapes, their duration and frequency, bring new quality, which can produce different effects when laser beams interact with material, establish new standards and or suppress old ones. The paper deals with the interaction of laser beams, in different operating modes, with the selected class of materials. odels for the description and results of interactions will be discussed, damages will be analyzed and a review of current and potential fields of application and selected parallels with other beam techniques will be given.**



**ey words - quantum generators, modes of operation, interactions, models, field of application.**


## Different modes of operation of quantum generators as an instrument for modifications in dentistry


Aleksandar Bugarinović [1,7], Željka Tomić [2], Sanja Jevtić [3], Aleksander Kovačević [4], Svetlana Pelemiš [5], Zoran Nedić [6], Dragan Družijanić [1]


 ISBN 978-86-7466-930-3

# Оптичка влакна у периметарским системима техничке заштите

Слађана Пантелић[1], Бранка Радојчић[2]

***Апстракт*— Тема рада је реализација система техничке заштите у оптичком домену, тј. упознавање са основним концептима примене оптичких влакана у разумевању сензорских система за периметарску заштиту објеката и оптичких мрежа у другим системима техничке заштите (видео надзора, контроле приступа, алармног система,....), који се могу и интегрисати. Периметар је појам који означава затворену линију унутар које се налазе штићени простор и штићени објекти. Дат је пример пројектантског решења имплементације периметарског система техничке заштите, применом оптичких компонената. На тај начин, упознајемо карактеристике оптичких елемената система, а са циљем максималног искоришћавања њиховог потенцијала у савременим комуникационим системима. Сврха овог рада је била у опису најчешће коришћених оптичких сензора у системима периметарске заштите објеката, са нагласком на сензоре вибрација, који изазване промене у оптичком сигналу претварају у електрични сигнал погодан за даљу обраду и препознавање алармног стања. Детекција и тачна локализација места притиска, оштећења или прекида оптичког влакна, могућа је применом оптичких мерних метода, што омогућава техничку контролу имплементираног система техничке заштите.**

**Кључне речи — оптичко влакно, оптички сензор вибрација, периметарска заштита, алармно стање**

## I. Увод

Сталне претње од напада свих врста доводе до важности јачања мера заштите људи, имовине и пословања, као и критичне инфраструктуре објеката од државног интереса. Упркос веома јакој цубер сигурности, објекти морају бити заштићени јаким физичким баријерама, како би се спречили физички напади. Системи за детекцију упада у периметар често су први бедем одбране, па се периметарска заштита пројектује као заштитни обруч, који штити улазне тачке објекта. Наведени системи су напредовали усвојивши новије технолошке трендове, као и интеграцију с другим сигурносним системима (нпр., сензори за ограде и паметна сигурносна расвета). Паметна сигуроносна расвета је важан додатни алат у пројектовању целокупне заштите периметра [1].

Слађана Пантелић – Универзитет у Београду, Електротехнички факултет, Булевар краља Александра 73, 11120 Београд (e-mail: sladjanapantelic@yahoo.com)

Бранка Радојчић – Универзитет у Београду, Електротехнички факултет, Булевар краља Александра 73, 11120 Београд (e-mail: br.radojcic@yahoo.com)

## II. Оптичка влакна и оптички сензори

Развој оптичких влакана је ишао у правцу проналажења нових технологија за обезбеђивање све мањих оптичких губитака и могућности производње све дужих и флексибилнијих влакана, као и у правцу повећања брзина комуникација и смањења цене. То је све пратио брз развој извора светлости – ласера и пријемника светла – фотодиода. По цени, оптичко влакно је данас најјефтинији медијум за пренос информација [1-3].

Простирање светлосног снопа кроз оптичко влакно засновано је на принципу преламања светлости. Када светлосни сноп из средине већег индекса преламања (језгро) прелази у средину мањег индекса преламања (омотач), долази до његове рефлексије назад у средину са већим индексом преламања. Деле се на мономодана и мултимодна оптичка влакна.

Мономодна оптичка влакна се користе за реализацију далеких веза, а све више и у локалним мрежама. Пречник језгра им је од 3,5 μm до 10 μm (у зависности од таласне дужине која се користи) а пречник примарног омотача је 125 μm [4]. Због малог пречника језгра код мономодног оптичког влакана не долази до појаве модалне дисперзије, тако да има велики пропусни опсег, који је ограничен само хроматском дисперзијом, Сл. 1. Недостатак му је мали пречник језгра, па захтева извор са компатибилном емитујућом површином и одговарајућим угаоним дијаграмом зрачења.

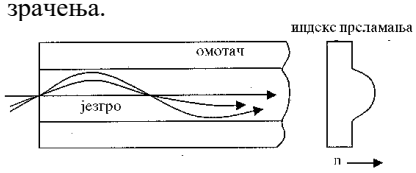


Сл. 1. Простирање светлости кроз мономодно оптичко влакно: изглед пресека влакна, путање и профила индекса преламања.

Код мултимодних влакана примарни омотач је направљен од материјала чији је индекс преламања мањи од индекса преламања језгра. Могу бити са степенастим и градијентним индексом преламања, Сл. 2. и Сл. 3. Влакна са степенастим индексом преламања имају пречник језгра од 50 μm до 1000μm. То су јефтина оптичка влакна, једноставна су за употребу, али су ограниченог пропусног опсега. Не користе се за потребе преноса података. Градијентно мултимодно оптичко влакно има

 ISBN 978-86-7466-930-3

параболичан профил промене индекса преламања у материјалу језгра.

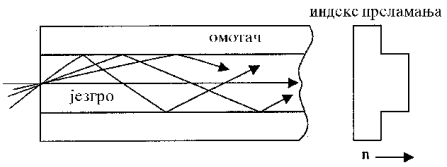


Сл. 2. Простирање светлости кроз мултимодно оптичко влакно са степенастим индексом преламања: изглед пресека влакна, путање и профила индекса преламања

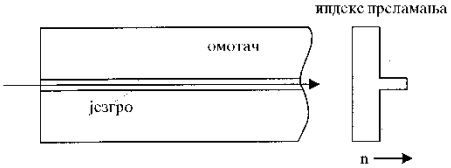


Сл. 3. Простирање светлости кроз мултимодно оптичко влакно са градијентним индексом преламања: изглед пресека влакна, путање и профила индекса преламања

Предност мултимодних оптичких влакана је велики пречник језгра, тако да је знатно олакшано убацивање светлости у њих, као и њихово међусобно спајање. Недостатак мултимодних оптичких влакана је појава модалне дисперзије. Она настаје када се оптичка снага убаченог светлосног импулса распореди на све модове у влакну, који се крећу благо различитим брзинама, што доводи до кашњења неких модова на излазу из оптичког влакна, па долази до развлачења импулса. Модална дисперзија се смањује употребом градијентних влакана.

Оптичка влакна се примењују у оптичким сензорима још од 1977. год., и представљају главне елементе у специјалним сензорима за мерење: акустичких величина, магнетских величина, температуре, притиска, брзине, убрзања, итд. Сензори на бази оптичког влакна се деле на интерферометријске (мерена величина изазива интерферентне ефекте) и амплитудске (мерена величина модулише интензитет светлости).

Оптички сензори се састоје од извора светлости и пријемника. Као извори светлости најчешће се користе полупроводничке светлеће диоде - ЛЕД и ласерске диоде - ЛД. Оне дају довољно велику и просторно усмерену оптичку снагу а димензије су им прилагођене димензијама оптичких влакана. Пријемник светлости претвара оптичку енергију у електрични сигнал, а најчешће се користе фотодиоде, фототранзистори и фотоотпорници. Оптички сигнал може бити у подручју видљиве светлости или инфрацрвене и ултраљубичасте светлости, у невидљивом делу спектра [5].

Мерена физичка величина је у вези са одређеним параметром оптичког сигнала, који је у ствари електромагнетски талас фреквенције 1013–1015 Hz. Промена параметара оптичког сигнала сразмерно амплитуди мерене физичке величине, представља модулацију тог сигнала. Основни параметри оптичког сигнала су: амплитуда, фреквенција, фаза, поларизација и расејање светлосног сигнала. Оптички сензори се могу употребити у условима деловања јаког магнетног поља, високе температуре, електричних шумова и корозије, па су много флексибилнији и поузданији од класичних сензора. Лоше особине су им: сложеност израде, обраде сигнала, захтевају оптичку видљивост између пријемника и предајника.

## III. Примена и инсталација оптичког влакна у периметарском алармном систему

Алармне системе чине уређаји, који упозоравају на нека задата нежељена стања. Постоје различите врсте аларма, светлосни, звучни, вибрирајући, или у облику електронске информације и упозорења од ниске или високе температуре, упозорење на присутност разних плинова, дима, SOS дојаве, затим противпровални и противпрепадни аларми. Алармни системи се углавном имплементирају у комбинацији са савременим системом видео надзора. Најчешћи облик аларма је противпровални, где алармни уређаји светлосно и звучно, разним телефонским, радио, IP или GSM, GPRS, 5G дојавама узбуњују раднике обезбеђења или власнике неке имовине. Један од тих система је и сензорски систем периметарске заштите са оптичким влакнима.

Систем периметарске заштите, који се у основи састоји од једног или више оптичких влакана у улози сензора, већ је добро познат на тржишту техничке заштите. Њихова примена заснована је на провереној поузданости и квалитету перформанси,

Чињеница да оптичка влакна као сензори система, за пренос информација и детекцију аларма не користе електричне сигнале, већ светлост на посебним таласним дужинама, омогућава њихово коришћење на већим удаљеностима при чему су отпорни на мување, високу температуру, корозију, електромагнетне сметње или друге електричне сигнале.

Постоје два главна типа система ране детекције провале на бази оптичких влакана: зонски систем, са традиционалним хардвером и новији, осетљивији, интерферометријски систем који, на основу технике коју примењују, може прецизније и поузданије одредити провалу на огради. Иако су оба наведена система заснована на оптичким влакнима, фундаментални принципи, који стоје иза њих су сасвим другачији, а самим тим и њихове перформансе и примена у пракси.

Како се кроз оптичко влакно преноси светлосни сигнал, било какво савијање или покретање истог, доводи до промена његових преносних особина. Принцип рада је да се, током редовне ситуације у систему периметарске заштите, ласерски емитује једносмерни монохроматски светлосни талас, који се шаље кроз каблирано оптичко влакно, уграђено дуж ограде (на врху ограде или у њеном средњем делу). Након рефлексије, рефлектовани светлосни талас се враћа до пријемника ради утврђивања мирног стања, односно стања без аларма. Када дође до илегалног напада тј. када неко покуша да се попне уз ограду, оптички кабл почиње да се физички помера, при чему се особине светлости, која путује оптичким влакном мењају. Тада се у систему, тј. пријемнику, детектује промена интензитета пренешене светлости, па ако иста пређе неки, унапред постављени, праг или се поклопи са одређеним дефинисаним критеријумима, подиже се стање

 ISBN 978-86-7466-930-3

аларма. При томе се у обзир узимају и прате најважније карактеристике рефлектоване светлости, чије промене подразумевају снагу, фазу, таласну дужину, поларизацију и дисперзију [6].

На основу наведеног може се рећи да су ови сензорски системи подложни утицају најразличитијих сметњи (ветар, микросеизмичко подрхтавање тла, град, пролазак возила, итд.). Да би се у великој мери онемогућиле појаве лажних аларма, за повећање отпорности на буку користе се сложени алгоритми за препознавање, имплементирани помоћу уграђених микропроцесора.

Могућа алармна стања периметарских сензора са оптичким влакнима, сврставамо у четири категорије:

- аларм за упад: покушај илегалног уласка који изазива вибрације оптичког влакна;
- аларм за прекид жице: прекид оптичког кабла сензора;
- аларм за растављање: незаконито растављање или уништавање на местима спојева оптичких влакана;
- квар у комуникацији: комуникацијски оптички кабл је искључен.

На Сл. 4., је као пример приказан изглед периметарске ограде, изграђене крајем 2018. год., између Крима и Украјине. Ограда је дужине 60 километара и састоји се од неколико типова барикада, различитих типова сензора, видљивих и скривених система видео надзора, укључујући и инфрацрвену опрему. Уграђен је и систем сензора осетљивих на вибрације [7].

Сл. 4. Ограда опремљина сензорима између Крима и Украјине

## IV. Утицај ласерског зрачења на мономодно оптичко влакно које се користи у периметарској заштити

У експерименталном делу, извршено је испитивање утицаја ласерског зрачења на комерцијално мономодно оптичко влакно (9/125 μm), које се користи у периметарској заштити. Израђени оптички спојни кабл, са постављеним оптичким конекторима, приказан је на Сл.5.

Сл. 5. Оптички спојни кабл од мономодног оптичког влакна са FC/PC конекторима на крајевима.

Комерцијална оптичка влакна могу бити сачињена од различитих материјала. Један од типова оптичких влакана су вишекомпонентна стаклена оптичка влакна, чије језгро и омотач чине стакла различитог хемијског састава. Добијају се стапањем ултрачистих прахова. Стакла, која чине омотач и језгро одвојено се стапају, а затим спајају у компактно влакно у специјално конструисаном двоструком тиглу. Најчешће коришћена оптичка влакна су такозвана PCS (polymer coated silica), коју чини влакно од допираног кварцног стакла са заштитном полимерном превлаком [8-10].

Приказани оптичко влакно је изложено $Nd^{3+}$:YAG импулсном ласерском снопу. Ласер је комерцијалног типа са могућношћу промене и енергије импулса и густине снаге (од неколико J, понављањем од 1 до 10 Herz). Генерално, средња снага је била у опсегу kW. Интеракција снопа и узорка изведена је у ваздушној атмосфери (обични услови) са упадним углом од 90°. Интеракција је вршена са једним (Сл. 6. (а)) или више импулса у једној тачки (Сл. 6. (б)).

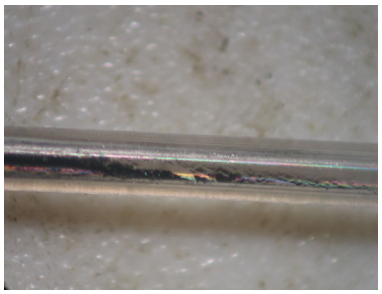

(а)

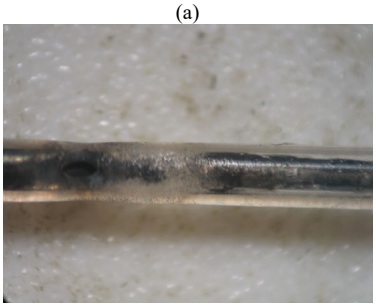

(б)

Сл. 6. (а) Микроскопски снимак интеракције оптичког влакна са једним импулсним снопом $Nd^{3+}$:YAG ласера; (б) Микроскопски снимак интеракције оптичког влакна са више импулсних снопова $Nd^{3+}$:YAG ласера.

На основу приказаног на Сл. 6. и видних оштећења на оптичком влакну, може се закључити да оптичка влакна нису отпорна на утицај ласерског зрачења. Околност, која ову чињеницу олакшава је да су мономодна оптичка влакна изузетно малих пречника језгра, па је вероватноћа да се влакно погоди на периметарској огради, и на тај начин оштети, је мала.

## V. Закључак

На основу наведеног, може се очекивати да ће напредак технологије оптичких сензора у будућности довести до

 ISBN 978-86-7466-930-3

раста сектора заштите периметра. Међутим, оптички сензори су већ међу најпопуларнијим технологијама на тржишту система за заштиту периметра, било да се ради о онима који се постављају на ограде или технологији за детекцију вибрација. Интеграција оптичких сензора за ограде с другим системима техничке заштите, као што је на пример паметно осветљење, омогућава и нове функције и апликације. Интелигентно осветљење може реаговати на периметарске упаде прилагођавањем интензитета светлости или стробирањем у угроженим зонама, чиме се повећавају могућности одвраћања и процене претње. Једна од најважнијих предности оптичких сензора за заштиту периметра је да су идеални за уградњу у већ постојеће-изграђене периметарске ограде, тј. за надоградњу већ имплементираних система, што значајно утиче на смањење финансијских трошкова инвеститора.

Експерименталним радом је утврђено да оптичка влакна нису отпорна на утицај ласерског зрачења али су изузетно малих пречника језгра, па је вероватноћа да се влакно погоди на периметарској огради, и на тај начин оштети, је мала.

## Литература


[1] T. Nakahara, M. Hoshikawa, T. Sugawa, M. Watanabe, ″Fiber Optics″ from Ulmann′s Encyclopedia of industrial chemistry, Fifth, Completely Revised Edition, Vol. A10 (1990), pp. 433-450.

[2] Ramaswami R., Sivarajan N. K., Sasaki H. G., “Optical Networks”, Third Edition, Morgan Kaufmann, Elsevier, USA, 2010.

[3] С. Пантелић, „Анализа оптичких ефеката на растављивим и нерастављивим спојевима оптичких влакана”, COBISS.SR-ID 228185868, ISBN 978-86-7466-652-4, Београд: Академска мисао, 2016.год., 179 стр., тираж 200.

[4] А. Маринчић, ″Оптичке телекомуникације″, Универзитетски уџбеници 39, пп.290-6. и 205-8. Београд, 1997.

[5] С. Пантелић, „Оптичке појаве на оптичким влакнима и спојевима оптичких влакана”, COBISS.SR-ID 228184332, ISBN 978-86-7466-653-1, Београд: Академска мисао, 2016.год., 120 стр., тираж 200.

[6] Carlson C., “Fiber’s Role in the Video Security&Surveillance Network”, http://www.bicsi.org/pdf/winter_2010/Curt_Carlson.pdf, 03.05.2015.

[7] Извор дневна штампа „ПОЛИТИКА”, рублика Свет, петак, 28.12.2018. у 13:49.

[8] A. V. Ivanov, Pročnost optičeskih materialov, Mašinostroenie, Leningrad, 1989. (In Russian)

[9] R. M. Wood, Laser Damage in Optical Materials, Adam Hilger, Bristol, 1986.

[10] A.A.Mak, L.N.Sopms, V.A.Fromntel, V.E.Yašin, Lazeri na neodimovom stekle, Nauka, Moskva ,1990.


## Abstract


The topic of the paper is the realization of technical protection systems in the optical domain, i.e introductions to the basic concepts of optical fiber application in the understanding of sensor systems for perimeter protection of buildings and optical networks in other technical protection systems (video surveillance, access control, alarm system, ....). These systems can also be integrated. Perimeter is a term that denotes a closed line within which there are protected areas and protected objects. An example of a design implementation solution is given. In this way, we get to know the characteristics of the optical elements of the system, with the aim of maximizing their potential in modern communications systems. The purpose of presented paper was to describe the commonly most used optical sensors in perimeter security systems, with emphasis on sensors (for vibration), which convert induced changes in the optical signal into an electrical signal suitable for further processing and alarm detection. Detection and accurate localization of the place of pressure and damage or interruption of the optical fiber are possible by applying optical measurement methods, which enables technical control of the implemented technical protection system


## Fiber optics in perimeter technical protection systems

Слађана Пантелић, Бранка Радојчић

 ISBN 978-86-7466-930-3

# FIZIČKA I NEDESTRUKTIVNA ISPITIVANJA KERAMIČKIH MATERIJALA ZA OBLAGANJE SA ASPEKTA TRAJNOSTI

Zoran Stević[1], Aleksandar Savić[2], Milica Vlahović[3], Sanja Martinović[3], Tatjana Volkov-Husović[4]

***Apstrakt— U radu su prikazane osnovne metode ispitivanja materijala, koje mogu poslužiti prilikom prve faze procene kvaliteta materijala, nakon degradacije usled vremena ili drugih faktora koji mogu izmeniti fizičko-mehanička svojstva materijala. Nedestruktivna metoda ispitivanja pomoću praćenja brzine prostiranja ultrazvučnog impulsa upotrebljena je radi ilustracije mogućeg pristupa pri proceni kvaliteta različitih tipova keramičkih materijala za oblaganje.***

***Ključne reči—*** *keramičke pločice, metoda ultrazvučnog impulsa, zapreminska masa, korelacija*

## 1. UVOD

Pod pojmom keramika se podrazumeva veliki broj raznovrsnih proizvoda koji se dobijaju pečenjem gline, kao osnovne sirovine [1]. U pogledu kompaktnosti mase, keramički proizvodi se mogupodeliti na: proizvode sa poroznom masom i proizvode sa polustopljenom masom. U slučaju da je upijanje vode kod keramičkog proizvoda veće od 5% u pitanju su proizvodi sa poroznom masom, a u slučaju da je upijanje vode manje od 5% proizvodi se karakterišu kao proizvodi sa polustopljenom masom. Za proizvode sa polustopljenom masomje karakterističnaviša temperatura pečenja, a koja se kreće u intervalu 1200-1400˚C.

Tehničke karakteristike keramičkih materijala za oblaganje prvenstveno zavise od njihove primene. Zahtevana svojstva i njihove vrednosti mogu varirati u funkciji od toga da li se radi o unutrašnjim ili spoljašnjim oblaganjima, odnosno u zavisnosti od toga da li se oblažu zidovi ili podovi [2]. Ova svojstva uključuju zapreminsku masu, stalnost geometrije, boju, teksturu, otpornost na pojavu vlasavosti, otpornost na delovanje razblaženih kiselina i baza, čvrstoću pri savijanju, tvrdoću i sl. Ispitivanja ovih materijala zahtevaju specifičan pristup i poznavanje šireg spektra standardne i nestandardne metodologije, između ostalog i nedestruktivnih i destruktivnih postupaka ispitivanja [3]. Posebno su od interesa ispitivanja kada se radi o materijalima koji su u svom eksploatacionom veku izloženi visokim temperaturama [4].

Zapreminska masa, čvrstoće i mehaničke otpornosti nekog materijala, kao i njegova trajnost i promena svojstava sa vremenom mogu se pratiti i povezati sa odgovarajućim nedestruktivnim metodama ispitivanja, u koje spada i metoda ispitivanja brzine ultrazvučnog impulsa kroz materijal. Treba naglasiti, međutim, da se kod ispitivanja svojstava materijala putem metoda bez razaranja traženo svojstvo unajvećem broju slučajeva ne meri direktno, već se postupak svodi na merenje neke druge fizičke veličine kojaje u funkcionalnoj vezi sa datim - traženim svojstvom.

Kao što je poznato, pod ultrazvukom se podrazumevaju vibracije iste prirode kao i zvuk, ali vrlo visokih frekvencija - koje ljudsko uho nije u stanju da registruje. Ove vibracije, koje u suštini imaju mehanički karakter, odlikuju frekvencije > od 20000 Hz (20kHz).Za dobijanje ultrazvuka najčešće se primenjuje piezoelektričnimetod, koji se zasniva na sposobnosti pojedinih kristalnih tela da pod dejstvom električne struje menjaju svoje dimenzije i na tajnačin proizvode visokofrekventne impulse.Ovi kristali imaju i sposobnost ispoljavanja suprotnog efekta: da pod uticajem visokofrekventnih impulsa dolazi do njihovog naelektrisanja (piezoefekat).

U praksi(slika 1), ultrazvučni impulsi se dobijaju primenom specijalnih generatora impulsa (1); za unošenje impulsa u element koji seispituje služe posebni predajnici (2); primenom ovih predajnika provode se UZ impulsi kroz ispitivani materijal (3) do prijemnika(4), pri čemu dolazi do prenosa podužnih, poprečnih ili površinskih ultrazvučnih talasa; primljeni impulsi pojačavaju seputem pojačivača (5) i šalju na indikator vremena (6).

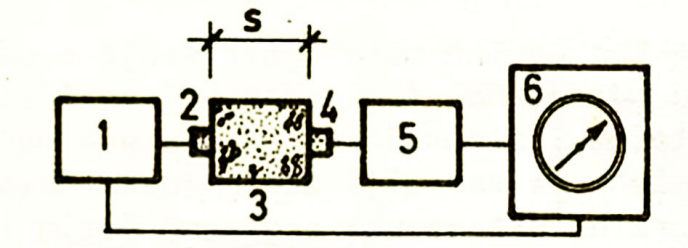


Slika 1: Osnovni princip funkcionisanja ultrazvučne aparature

Promena svojstava materijala usled uticaja spoljašnje sredine najčešće je degradacionog tipa, što znači da se svojstva najčešće pogoršavaju sa vremenom. Osim što je moguće pratiti i porediti svojstva jedne vrste materijala i njihovu promenu primenom nedestruktivnih metoda ispitivanja, moguće je pratiti i promenu tj. pad svojstava materijala sa vremenom, ili utvrditi odstupanja izmerenih vrednosti u datom trenutku u odnosu na pojedinačne poznate i očekivane vrednosti za taj materijal u datom trenutku, primenom matematičkih, u prvom redu statističkih metoda [5]. Pravovremeno ispitivanje i praćenje svojstava već ugrađenih

[1]Zoran Stević –Univerzitet u Beogradu, Elektrotehnički fakultet, Bulevar kralja Aleksandra 73, 11120 Beograd; Univerzitet u Beogradu, Tehnički fakultet u Boru, Vojske Jugoslavije 12, 19210 Bor (https://orcid.org/0000-0002-1867-9360);

[2]Aleksandar Savić – Univerzitet u Beogradu, Građevinski fakultet, Bulevar kralja Aleksandra 73, 11120 Beograd; (https://orcid.org/0000-0002-1777-6775);

[3]Milica Vlahović – Univerzitet u Beogradu, Institut za hemiju, tehnologiju i metalurgiju, Karnedžijeva 4, Centar za materijale i metalurgiju, Karnegijeva 4/I, 11120 Beograd, (https://orcid.org/0000-0002-7893-9101).

[4]Sanja Martinović – Univerzitet u Beogradu, Institut za hemiju, tehnologiju i metalurgiju, Karnegijeva 4/I, Centar za materijale i metalurgiju, Karnegijeva 4/I, 11120 Beograd, (https://orcid.org/0000-0001-8040-407X);

[5]Tatjana Volkov-Husović – Univerzitet u Beogradu, Tehnološko-metalurški fakultet, Karnegijeva 4/I, 11120 Beograd, (https:// orcid.org/0000-0002-2667-5802).

 ISBN 978-86-7466-930-3

keramičkih materijala je posebno važno ukoliko se radi o objektima od velike važnosti za zajednicu [6]. Nakon eksploatacije u konstrukciji, keramički materijali se mogu ponovo upotrebljavati, što je veoma važno sa aspekta ekološkog i održivog pristupa u građevinarstvu [7]. U tom slučaju njihovo praćenje i karakterizacija u eksploataciji postaju prvi korak za prvu upotrebu ovih materijala u drugom, recikliranom, obliku.

U radu je prikazana metoda merenja brzine propagacije ultrazvučnih impulsa kroz pet različitihkeramičkih materijala za oblaganje, u okviru modela materijala koji je upotrebljavan ranije. Prikazani rezultati predstavljaju početnu fazuobimnijeg istraživanja.

## 2. MATERIJALI I METODE ISPITIVANJA

Ispitivani materijal predstavljajukeremičke ploče za oblaganje, starosti preko 20 godina, izrađene sa različitim pigmentima (slika 2). Pomenute ploče nisu izlagane eksploatacionim uslovima. Pre ispitivanja je svaki od uzoraka pregledan u cilju utvrđivanja vizuelnih tragova destrukcije ili drugih nedostataka. Konstatovano je da su uzorci kompaktni, pravilnih ivica i očuvani.

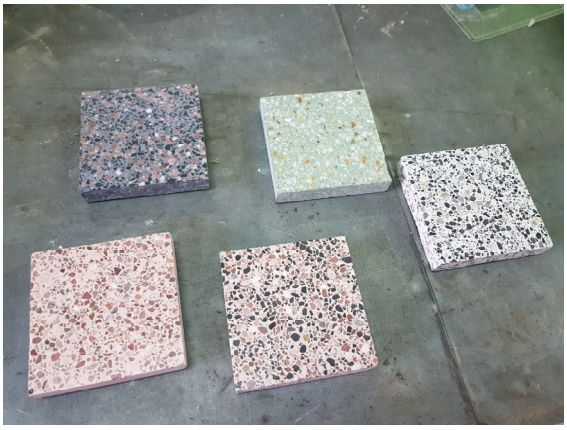

Slika 2: Ispitivani uzorci keramičkih materijala za oblaganje

Za ispitivanje zapreminske mase korišćeni su digitalno pomično merilo marke MESSZEUGE nemačke proizvodnje, opsega 150 mm kao i vaga KERN kapaciteta 35 kg i podatka 0,1 g.Rezultati ispitivanja dimenzija i mase prikazani su u tabeli 1. Prikazani rezultati merenja dimenzija predstavljaju prosečne vrednosti dobijene na osnovu najmanje tri merenja.

Za ispitivanje brzine ultrazvučnog impulsa upotrebljena je ultrazvučna aparatura italijanske proizvodnje, proizvođača MATEST. Pre samog ispitivanja je na ispitivane uzorke naneta odgovarajuća količina kontaktnog agensa, kako bi se eliminisao sloj vazduha na kontaktu uzoraka sa sondama ultrazvučne aparature, nakon čega je izvršeno merenje. Prosečne vrednosti merenja dobijene na osnovu četiri merenja (po dva na dva upravna pravca) prikazane su u tabeli 1.

Tabela 1. Vrednosti dimenzija, mase, zapreminske mase i brzine ultrazvučnog impulsa kod ispitivanih keramičkih materijala

| Uzorak br. | 1 | 2 | 3 | 4 | 5 |
|---|---|---|---|---|---|
| Masa (g) | 240,7 | 250,2 | 247,7 | 242,2 | 253,7 |
| Dimenzije a×b×h (mm) | 80,86× 81,21× 14,57 | 81,53× 81,10× 14,71 | 81,31× 81,35× 14,94 | 81,83× 82,13× 15,08 | 81,44× 80,90× 15,58 |
| Zapreminska masa (g/cm$^3$) | 2,516 | 2,572 | 2,507 | 2,390 | 2,472 |
| Brzina ultrazvučnog impulsa (km/s) | 4,813 | 4,853 | 4,811 | 4,785 | 4,819 |

## 3. ANALIZA I DISKUSIJA REZULTATA ISPITIVANJA

Na osnovu ispitivanja koja su sprovedena na ispitivanim uzorcima utvrđeno je da zapreminske mase uzoraka variraju u relativno malim granicama od 2,390 g/cm$^3$do 2,572g/cm$^3$sa prosečnom vrednošću od 2,491 g/cm$^3$. Takođe, utvrđeno je da brzine ultrazvučnog impulsa dobijene na ispitivanim uzorcima variraju u relativno malim granicama od 4,785 km/s do 4,853 km/s sa prosečnom vrednošću od 4,816 km/s.

U cilju procene korelacije i trenda promene svojstava, izvršena je regresiona analiza korelacije zapreminske mase i brzine ultrazvučnog impulsa kroz ispitivane uzorke. Pomenuta korelacija prikazana je na slici 3.

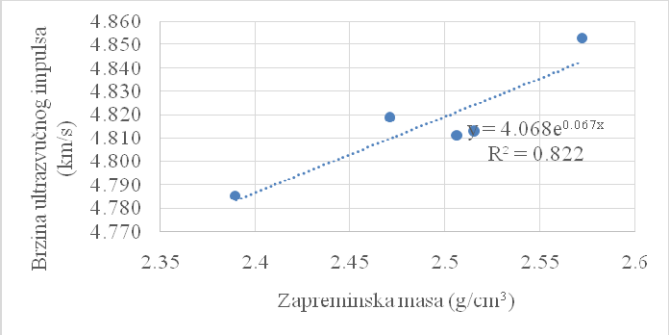


Slika 3. Korelacija između zapreminske mase i brzine ultrazvučnog impusa kod ispitivanih keramičkih materijala za oblaganje. Iz priložene slike se može zapaziti da korelacija relativno pouzdanog tipa može omogućiti praćenje trenda promene svojstava. U ovom slučaju, za ispitivano svojstvo može se usvojiti zapreminska masa, te se na osnovu konkretne metode nedestruktivnog ispitivanja može dati načelna procena gubitka (pada) zapreminske mase usled degradacije materijala kroz vreme i dobiti prva procena ispitivanih uzoraka u funkciji od vremena.

## ZAKLJUČCI

U radu su prikazani rezultati početne faze šireg istraživanja, koji se bave nedestruktivnim ispitivanjima keramičih materijala veće starosti, sa aspekta praćenja svojstava u eksploataciji, sa vremenom ili usled dejstva agresivne sredine u kojoj se ti materijali mogu naći.

Napominje se da bi svakako pri ispitivanjima trebalo proceniti i očekivane vrednosti merne nesigurnosti, kako bi se sagledao karakter i stepen pouzdanosti samog merenja. Veliki stepen merne nesigurnosti u različitim slučajevima merenja može dovesti do značajnog pada pouzdanosti rezultata ispitivanja. Iz tog razloga je u svakom ispitivanju potrebno identifikovati i uzeti u obzir sve faktore merne nesigurnosti.

Konačno, treba napomenuti da nedestruktivna ispitivanja građevinskih materijala ne mogu dati jednoznačne odgovore na pitanja njihovog kvaliteta, odnosno da se ne mogu uzeti kao merodavna kod izvođenja zaključaka o trajnosti ili


ISBN 978-86-7466-930-3

stepenu degradacije koji je nastupio kod bilo kog tipa građevinskih materijala.

Međutim, iako je konstatovano da ispitivani uzorci imaju relativno ujednačen kvalitet i da se može dati generalna ocena da njihova svojstva nisu značajno degradirala sa vremenom, ukazuje se na mogućnost praćenja i približne inicijalne procene svojstava sličnim metodama u laboratorijskim ili *in situ* uslovima. Na ovaj način se u većem skupu ispitivanih uzoraka može utvrditi oblast od interesovanja ili odgovarajući podskup uzoraka za detaljniju i opsežniju analizu sa aspekta trajnosti, uključujući neke od destruktivnih metoda ispitivanja.

## LITERATURA

[1] M. Muravljov: Građevinski materijali, Građevinska Knjiga, Beograd, 2000.

[2] M. Muravljov, D. Jevtić, Građevinski materijali 2, Akademska misao, Beograd, 2014

[3] Vlahović M., Martinović S., Stević Z., Savić A., Volkov-Husović T., Examining erosion resistance of ceramics for electrical engineering applications , Union of Mechanical and Electrotechnical Engineers and Technicians of Serbia (SMEITS) Society for Renewable Electrical Power Sources Kneza Miloša str. 7a/II, 11000 Beograd, 2019 pp. 25-30

[4] Simić M., Alil A., Martinović S., Vlahović M., Savić A., Volkov-Husović T., High temperature materials: properties, demands and applications, Hem. Ind. 74 (4) 273-284 (2020), UDK: 666.3: 697.1:621.315.61, https://doi.org/10.2298/HEMIND200421019S

[5] J. Mališić, V. Jevremović, Statističke metode u meteorologiji i inženjerstvu, Univerzitet u Beogradu, Univerzitet u Novom Sadu, Beograd, 2014

[6] Zakić D., Savić A., Aškrabić M., Lukičić M., Jevtić D.: Ispitivanje svojstava materijala i sistema za unutrašnje oblaganje kupole Spomen hrama svetog Save, Zbornik radova sa Međunarodnog simpozijuma o istraživanjima i primeni savremenih dostignuća u građevinarstvu u oblasti materijala i konstrukcija, 2017, 307-316, ISBN 978-86-87615-08-3

[7] Jevtić D., Markićević J., Savić A.: Spravljanje i primena keramičkog betona – ekološka potreba savremenog društva, GNP 2008., Drugi internacionalni naučno-stručni skup Građevinarstvo – nauka i praksa, Zbornik radova, knjiga 2, str 841-846, Žabljak, mart 2008., ISBN 978-86-82707-15-8;

 ISBN 978-86-7466-930-3

# Суб-микрометарске паралелне површинске структуре индуковане фемтосекундним ласерским снопом у форензици

Александер Ковачевић, Сузана Петровић, Марина Лекић, Борислав Васић, Бранислав Салатић, Јелена Поточник

***Апстракт*— Један од ефеката интеракције ултра-кратког ласерског снопа са материјалима је формирање паралелних структура на површини (laser-induced parallel surface structures - LIPSS), чији је период мањи од таласне дужине снопа. Уколико се ради о вишеслојним танким филмовима метала, квалитет формираних структура је бољи. Узорак од пет двослојних танких филмова Al и Ti на супстрату Si смо изложили фемтосекундном снопу и запазили формирање две врсте структура које се разликују по облику. Обе су врсте вероватно узроковане појавом површинског плазмона-поларитона на површини најгорњег слоја. Појава плазмона поларитона на површини танких металних филмова и наночестица може да ограничи простирање електромагнетног поља и да појача флуоресцентни сигнал из молекула хемикалије на површини. У зависности од структуре интерфејса за одређивање циљне хемикалије на металној површини флуоресценција побољшана плазмоном (plasmon-enhanced fluorescence, PEF) је привлачан метод за скраћење времена и појачање осетљивости разних аналитичких технологија које се користе у форензици.**

***Кључне речи*— фемтосекундни ласер; вишеслојни танки филмови; периодичне површинске структуре; флуоресценција.**

## I. Увод

Интеракција ласерског снопа са површином проузрокује многе ефекте, међу којима је у последње време пажњу заокупило формирање паралелних структура (LIPSS – laser induced parallel surface structures) под дејством ултракратких снопова [1]. Због карактеристике да им је периодичност мања од таласне дужине снопа, поље примене је веома широко [2]. Интеракција са металима може побољшати триболошке карактеристике, а на ламеларним материјалима, као што су вишеслојни танки метални филмови, формирани LIPSS има добар квалитет и може да побољша особине површине [3-4]. Снопови различитих карактеристика (флуенца, таласна дужина, дужина импулса, поларизација, ...), разни материјали (диелектрици, полупроводници, метали, ...), али и стање амбијента током интеракције – све то утиче на карактеристике LIPSS [5]. Генерално, уочена је појава две врсте структура, са нижом просторном учестаношћу (LSFL – low spatial frequency LIPSS) и са вишом просторном учестаношћу (HSFL – high spatial frequency LIPSS) [6].

Александер Ковачевић – Институт за физику Универзитета у Београду, Прегревица 118, 11080 Београд, Србија (e-mail: aleksander.kovacevic@ ipb.ac.rs).

Сузана Петровић – Институт за нуклеарне науке „Винча“ Универзитета у Београду, ПП 522, 11351 Београд-Винча, Србија (e-mail: spetro@ vin.bg.ac.rs).

Марина Лекић – Институт за физику Универзитета у Београду, Прегревица 118, 11080 Београд, Србија (e-mail: marina.lekic@ ipb.ac.rs).

Борислав Васић – Институт за физику Универзитета у Београду, Прегревица 118, 11080 Београд, Србија (e-mail: bvasic@ ipb.ac.rs).

Бранислав Салатић – Институт за физику Универзитета у Београду, Прегревица 118, 11080 Београд, Србија (e-mail: banes@ ipb.ac.rs).

Јелена Поточник – Институт за нуклеарне науке „Винча“ Универзитета у Београду, ПП 522, 11351 Београд-Винча, Србија (e-mail: jpotocnik@ vin.bg.ac.rs).

## II. Експериментална поставка

Узорци који су коришћени су добијени депоновањем Al и Ti на подлогу од Si (1 0 0) помоћу Balzers Sputron II апарата који користи 1,3 keV аргонске јоне и са 99.9% чистоће Al и Ti мета. Две врсте узорака су подвргнуте интеракцији са фемтосекундним снопом. Први тип је био силицијумска подлога на којој је депоновано пет Al/Ti двослоја чиме је достигнута укупна дебљина од ~130 nm (сваки слој од ~13 nm). Други тип је такође био силицијумска подлога, али на којој је био депонован један слој Al дебљине ~130 nm.

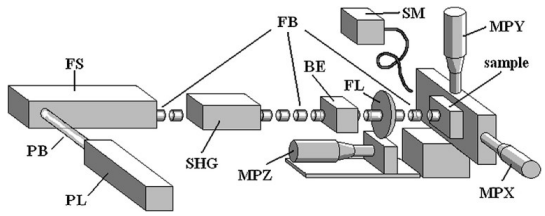


Сл. 1. Дијаграм експерименталне поставке за статичну интеракцију; PL – ласер за пумпање, PB – сноп за пумпање, FS – извор фемтосекундног снопа, FB – фемтосекундни сноп, SHG – удвајач учестаности, BE – проширивач снопа, FL – фокусирајуће сочиво, MPX/MPY/MPY - микропозиционери, SM – спектрометар, sample - узорак.

Извор фемтосекундног снопа је био Coherent Mira 900F систем чија је фреквенција удвојена са Inrad 5-050 ултрабрзим генератором другог хармоника. Карактеристике снопа су биле: таласна дужина 390 nm (удвојено) и 800 nm (основни хармоник), дужина импулса ~150 fs, репетиција 76 MHz (период између импулса ~13 ns), снага на мети 160–260 mW, линеарна поларизација у

 ISBN 978-86-7466-930-3

хоризонталној равни, Гаусов елиптични профил. Експозиције су биле од 1 до 10 s. Таласна дужина снопа је контролисана фибер-оптичким спектрометром Ocean Optics HR2000CG-UV-NIR. Интеракције су обављане у ваздуху фокусирањем фемтосекундног снопа под нормалним углом на површину првог слоја узорка (Al), сл. 1. Резултати су анализирани скенирајућим електронским микроскопима (SEM) JEOL JSM 6560 LV који има Oxford Instruments EDS анализатор и FEI SCIOS2, као и помоћу микроскопа атомских сила (AFM) NT-MDT NTEGRA Prima.

На сл. 2 је дијаграм поставке модификоване за потребе скенирања снопа преко узорка. Изостављен је удвајач учестаности, чиме је интеракција пренесена у блиску инфрацрвену област, ради скенирања се сноп уводи у огледални 2D скенер и у проширивач снопа, а фокусирање се обавља објективом модификованог микроскопа (40×, NA=0,65).

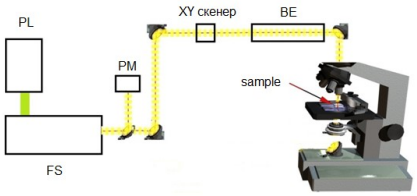


Сл. 2. Дијаграм експерименталне поставке за интеракцију уз скенирање снопом; PL – ласер за пумпање, FS – извор фемтосекундног снопа, PM – мереље снаге снопа, XY скенер – скенер снопа, BE – проширивач снопа, sample - узорак.

## III. Резултати и дискусија

На сл. 3 је приказ слике SEM дела области интеракције са 5×(Al/Ti). Фемтосекундни сноп таласне дужине 460 nm је имао флуенцу од 13,6 mJ/cm$^2$ а време експозиције 10 s. У области интеракције се виде паралелне структуре са периодом од око 300 nm. Структуре су формиране у виду издигнућа на површини.

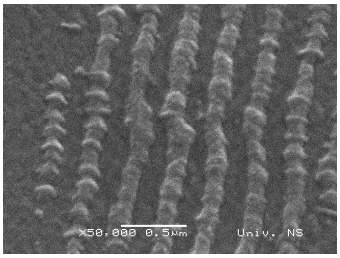


Сл. 3. Приказ слике SEM дела области интеракције са 5×(Al/Ti) на Si; флуенца 13,6 mJ/cm$^2$ и 10 s време експозиције.

На сл. 4 је приказана AFM слика области интеракције приказаној на сл. 2. Овде се боље види да су структуре формиране као издигнућа на површини.

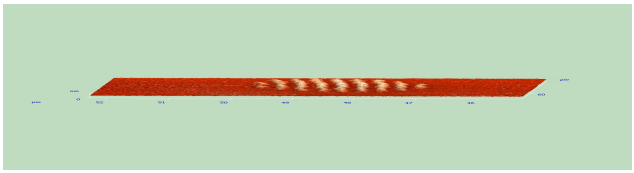

Сл. 4. Приказ AFM слике дела области интеракције приказане на сл. 2: 5×(Al/Ti); флуенца 13,6 mJ/cm$^2$ и 10 s време експозиције.

Узорак другог типа – један слој танког филма (~130 nm) Al – је био изложен флуенци од 8,6 mJ/cm$^2$ исте таласне дужине и времену експозиције од 10 s. Резултати у виду слике SEM дела области интеракције су приказани на сл. 5. У централном делу је дошло до аблације топљењем, а аблирани материјал се распоредио у околини централне зоне интеракције. Дошло је до расподеле у виду LIPSS, али квалитет облика није тако добар као у случају првог узорка. Просторни период структура је око 300 nm.

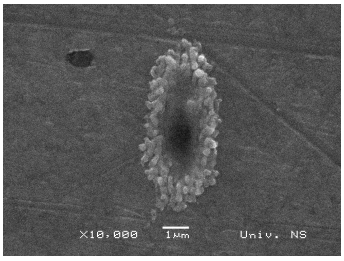


Сл. 5. Приказ слике SEM области интеракције са Al на Si; флуенца 8,6 mJ/cm$^2$ и 10 s време експозиције [4].

Упадни ултракратки сноп изазива на интерфејсу између металне и диелектричне површине појаву површинског плазмона (SP), а његовом интеракцијом са упадним снопом долази до формирања површинског плазмона поларитона (SPP) [2, 7], који узрокује статичну периодичну расподелу енергије на површини, периода мањег од таласне дужине упадног снопа. Дубина продирања ласерског снопа од 390 nm се израчунава [8] за Al на око 3 nm, а за Ti на око 9,3 nm.

Присуство подслоја Ti узрокује повећање прага оштећења првог (горњег) слоја, Al. Температура решетке се формира кроз два механизма: електронско-фононски (који узрокује локализацију загревања), и транспорт електронима везан за топлотну проводност електрона (који односи топлоту од зоне интеракције) [9]. Разлика у електронско-фононској спрези између два материјала води до стрме промене температуре решетке унутар подслоја (Ti). Као последицу, електрони из горњег слоја (Al) брзо преносе енергију следећем (подслоју) и тиме се термална енергија преноси кроз интерфејс Al/Ti, спреже са решетком и на тај начин односи из зоне интеракције. У првом следећем слоју (подслој, Ti) долази до гомилања термалне енергије периодично у латералном смеру, али због високе температуре топљења Ti не долази до топљења. Праг оштећења првог слоја је тиме повећан јер се енергија углавном гомила у првом подслоју, који већ

 ISBN 978-86-7466-930-3

има висок праг оштећења. Одсуство подслоја Ti омогућава гомилање енергије у слоју Al и изражено топљење (сл. 5).

У поређењу са Al/Ti вишеслојним узорком, оптичка дубина продирања за Al је нижа, што резултује већим вреностима апсорбоване енергије и акумулације топлоте. Топљење и аблација су израженији него код вишеслојног.

Осим статичког озрачивања, вршена су и динамичка, када је сноп скениран преко површине узорка. У овом случају је таласна дужина била 800 nm, а флуенца 153 mJ/cm$^2$. На одређеним правцима је скенирање извршено вишеструким прелетом снопа преко површине узорка; на сл. 6 је приказана област дела интеракције где је сноп скениран 8, 9 и 10 пута. Просторни период структуре је око 283 nm (мање од половине таласне дужине упадног снопа). У инсету на сл. 6 је приказана AFM слика дела интеракције, формирана по интензитету тунелске струје између врха пробе и узорка. Примећује се да је струја кроз формиране структуре (формиране у виду уздигнућа на површини) мања (еквивалентно тамнијој боји) него струја у деловима који нису трансформисани (светлија боја). То наводи на закључак да је дошло до смањења проводности у тим деловима, за које се може претпоставити да је узрок јача оксидација која је услед већег гомилања енергије.

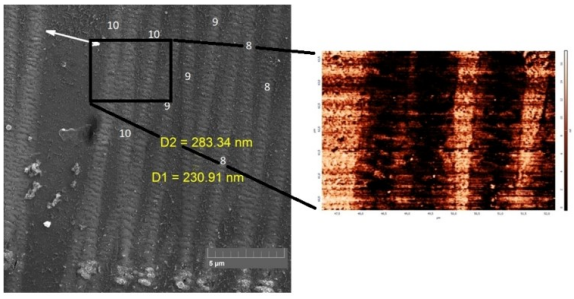


Сл. 6. Приказ слике SEM (лево) и AFM (инсет-десно) дела области интеракције 5×(Al/Ti) на Si; поновљено скенирање, 8—10 пролаза, флуенца 153 mJ/cm$^2$; бројеви 8, 9 и 10 представљају број прелета снопа преко истог правца; правац поларизације је означен белом стрелицом.

Модел изложен у [10] предлаже формирање једне врсте LIPSS на металним површинама интеракцијом са ултракратким снопом у ваздуху. У првом кораку расејање на површинским нерегуларностима индукује појаву SPP и периодичне расподеле енергије на површини. У другом кораку, на местима где се енергија акумулира долази до загревања и реакције метала са кисеоником из ваздуха. Због ултракратког импулса је оксидација бржа од термалне дифузије, и дебљина оксида расте на местима акумулиране енергије. Тиме се одржава нанометарска локализација. Како структура расте у висину, расејање се појачава и тиме је остварена позитивна повратна спрега. У трећем кораку – како структура расте – због све већег присуства оксида се смањује продирање кисеоника у структуру и тиме се цели процес зауставља. Трећи корак има негативну повратну спрегу.

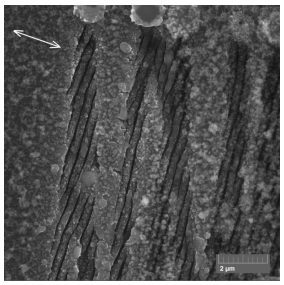

Сл. 7. Приказ слике SEM дела области интеракције 5×(Al/Ti) на Si; поновљено скенирање, 10 пролаза, флуенца 215 mJ/cm$^2$; правац поларизације је означен белом стрелицом.

На сликама 3 и 6 је приказано формирање једне врсте LIPSS, „гребен“, настале оксидацијом и надоградњом материјала. Првац простирања гребенских LIPSS је паралелан правцу поларизације упадног снопа (HSFL). За нешто веће флуенце снопа, сл. 7, долази до аблације материјала, а у аблираној области се појављује друга врста LIPSS, „канали“. Таласна дужина је 800 nm, флуенца 215 mJ/cm2, а као резултат је просторни период од 370 nm. Ширина канала је 80 nm. Аблација је наступила услед топљења/испаравања материјала. Правац каналских LIPSS управан на правац поларизације упадног снопа (LSFL).

Појава плазмона – колективне осилације наелектрисања и придруженог електромагнетног поља на површини металних филмова и наноструктура – омогућава ограничење простирања светлости у мале области и тиме је дало нова решења у оптичким спектроскопијама, као што су површински-побољшана Раманова спектроскопија (in surface-enhanced Raman spectroscopy, SERS) површински-побољшана инфрацрвена спектроскопија (surface-enhanced infrared spectroscopy, SEIRA) и плазмонски-побољшана флуоресцентна спектроскопија (surface plasmon-enhanced fluorescence spectroscopy, PEF), које се користе у низу форензичких аналитичких технологија за детекцију хемијских и биолошких агенаса релевантних у важним областима медицинске дијагностике, контроле хране и безбедности [12]. У PEF се флуорофорни означивачи спрежу са ограниченим пољем површинских плазмона што се може конструисати да веома појача интензитет емитованог флуоресцентног светла ради детектовања врло малих количина аналита са побољшаном границом детекције и скраћењем времена анализе. Просторно преклапање и усклађивање фазе између поларитона води до успостављања спрегнутих симетричних и антисиметричних модова површинског плазмона поларитона. Симетрични тип мода се може побудити на металним површинама са густим решеткама испод нивоа дифракције. Дифракција на таквој периодичној модулацији дозвољава да плазмони поларитони који се простиру у супротном смеру интерагују, стварајући појачане интензитете поља локализоване или у удубљењима (“канали“) решетке или на врховима („гребени“) периодичне модулације.

 ISBN 978-86-7466-930-3

## IV. Закључак

Приказано је испитивање површинских модификација индукованих на танким филмовима – узорци од пет (Al/Ti) бислојева (укупне дебљине 130 nm) на Si као и узорци од једнослојног Al (дебљине 130 nm) на Si – помоћу фемтосекундног ласерског снопа таласне дужине од 390 nm и 800 nm и репетиције 76 MHz (~13 ns између импулса). За статичку интеракцију су формиране површинске периодичне структуре (LIPSS) на вишеслојном Al/Ti при флуенци једног импулса од 10,3–14 mJ/cm$^2$, а на једнослојном Al при флуенци једног импулса од 8,6 mJ/cm$^2$. Присуство подслоја повећава праг оштећења најгорњег слоја, што побољшава квалитет формираних LIPSS. За динамичку интеракцију (скенирање снопа преко површине узорка) за 153 mJ/cm$^2$ је дошло до формирања гребенских LIPSS, а за већу флуенцу једног импулса, 215 mJ/cm$^2$, до каналских LIPSS. На основу правца простирања LIPSS се закључује њихова врста, LSFL (ниске просторне учестаности) или HSFL (високе просторне учестаности). За формирање LIPSS се механизам се види у појави површинског плазмона поларитона који изазива периодичну расподелу енергије. Присуство подслоја одговарајућих термичких карактеристика омогућава лако преношење термалне енергије у дубље слојеве. Код гребенских LIPSS има три корака везаних за продирање кисеоника из ваздуха у материјал (оксидација), док код каналских LIPSS долази до аблације топљењем/испаравањем и уклањања материјала.

Појава плазмона поларитона је важна при неким флуоресцентним техникама, као што је PEF, који је унапредио осетљивост и скратио време анализе процедура за детекцију важних аналита укључујући биомаркере, патогене и токсине. Ова једињења су детектована на ниским фемтомоларним концентрацијама, а анализа је веома скраћена. Једна од плазмона који се појављује је тесно везан са појавом периодичних структура са периодом мањим од таласне дужине (LIPSS). Индуковање LIPSS може бити интересантно у великом броју примена – медицинским, декоративним, триболошким, и др. – због појаве плазмона поларитона којим се светлост конфинира и омогућава побољшање у плазмонски побољшаној флуоресцентној спектроскопији.

## Захвалница

Овај рад је спроведен у оквиру реализације научних пројеката, које је финансирало Министарство науке и технолошког развоја Републике Србије под редним бројевима III45016, OI171005, OI171038. Аутори су захвални М. Бокорову са Техничког факултета Универзитета у Новом Саду, др Д. Перушку из Института за нуклеарне науке "Винча", као и др Б. Јеленковићу, др Д. Пантелићу, др Р. Гајићу, др А. Крмпоту, др М. Рабасовићу и В. Лазовићу из Института за физику Београд, за подршку.

## Литература

[1] H. M. van Driel, J. E. Sipe and J. F. Young, "Laser-induced periodic surface structure on solids: A universal phenomenon", *Phys. Rev. Lett.*, vol. *49*, pp. *1955-1959*, Dec. 1982.

[2] A. Y. Vorobyev and C. Guo, "Direct femtosecond laser surface nano/microstructuring and its applications", *Laser Photonics Rev.*, vol. *7*, pp. *385-407*, May 2013.

[3] S. M. Petrović, D. Peruško, B. Salatić, I. Bogdanović-Radović, P. Panjan, B. Gaković, D. Pantelić, M. Trtica, B. Jelenković, "Laser induced damage/ablation morphology on the 8(Al/Ti)/Si system in different ambient conditions", *Opt. Laser Technol.*, vol. *54*, pp. *22-29*, Dec. 2013.

[4] A. G. Kovačević, S. Petrović, B. Bokić, B. Gaković, M. T. Bokorov, B. Vasić, R. Gajić, M. Trtica, B. M. Jelenković, "Surface nanopatterning of Al/Ti multilayer thin films and Al single layer by a low-fluence UV femtosecond laser beam", *Appl. Surf. Sci.*, vol. *326*, pp. *91-98*, 2015.

[5] A. G. Kovačević, S. Petrović, V. Lazović, D. Peruško, D. Pantelić, B. M. Jelenković, "Inducing subwavelength periodic nanostructures on multilayer NiPd thin film by low-fluence femtosecond laser beam", *Appl. Surf. Sci.*, vol. *417*, pp. *155-159*, Sep. 2017.

[6] J. Bonse, S. Hoehm, S. V. Kirner, A. Rosenfeld, J. Krueger, "Laser-Induced Periodic Surface Structures—A Scientific Evergreen", *IEEE J. Sel. Topics Quantum Electron.*, vol. *23*, no. *3*, a. *9000615*, 2017.

[7] A. Y. Vorobyev, V. S. Makin, Chunlei Guo, "Periodic ordering of random surface nanostructures induced by femtosecond laser pulses on metals", *J. Appl. Phys.*, vol. *101*, no. *3*, a. *034903*, 2007.

[8] D. Bauerle, *Laser Processing and Chemistry*, Berlin, Germany: Springer, 2000.

[9] G. D. Tsibidis, "Thermal response of double-layered metal films after ultrashort pulsed laser irradiation: The role of nonthermal electron dynamics", *Appl. Phys. Lett.*, vol. *104*, no. *5*, a. *051603*, 2014.

[10] B. Öktem, I. Pavlov, S. Ilday, H. Kalaycıoğlu, A. Rybak, S. Yavaş, M. Erdoğan, F. Ö. Ilday, "Nonlinear laser lithography for indefinitely large area nanostructuring with femtosecond pulses", *Nature Phot.*, vol. *7*, pp. *897-901*, 2013.

[11] H. Malekzad, P. S. Zangabad, H. Mohammadi, M. Sadroddini, Z. Jafari, N. Mahlooji, S. Abbaspour, S. Gholami, M. G. Houshangi, R. Pashazadeh, A. Beyzavi, M. Karimi, M. R. Hamblin, "Noble metal nanostructures in optical biosensors: Basics, and their introduction to anti-doping detection", *Trends Anal. Chem.*, vol. *100*, p. *116-135*, 2018.

[12] M. Bauch, K. Toma, M. Toma, Q. Zhang, J. Dostalek, "Plasmon-Enhanced Fluorescence Biosensors: a Review", *Plasmonics*, vol. *9*, pp. *781–799*, 2014.

## Abstract

One of the effects of the interaction of ultrashort laser beam with materials is the forming of laser-induced parallel surface structures (LIPSS), with period less than beam wavelength. For multilayer thin metal films, the quality of formed structures is better. The sample of five bilayers of Al and Ti on Si substrate was exposed to femtosecond beam and noticed the forming of of two types of structures different in shape. Both are most probably the product of surface Plasmon polariton on the surface of most top layer. The occurrence of Plasmon polariton on the surface of thin metal layers and nanoparticles can confine the propagation of electromagnetic field and to amplify the fluorescent signal from molecules of the chemical compound on the surface. Depending on the interface structure for determining the target chemical on metal surface, Plasmon enhanced fluorescence is an attractive method for shortening the time of detection and increasing the sensitivity of various analytical technologies used in forensics.

## Sub-micrometer parallel surface structures induced by femtosecond laser beam in forensics

Aleksander Kovačević, Suzana Petrović, Marina Lekić, Borislav Vasić, Branislav Salatić, Jelena Potočnik

 ISBN 978-86-7466-930-3

# СПЕЦИЈАЛНА ТЕМАТСКА СЕСИЈА - ХЕРИТОЛОГИЈА

# /

# SPECIAL THEMATIC SESSION - HERITOLOGY

# (CTC-XE/STS-HE)

ISBN 978-86-7466-930-3

# Sinhronizacija mernih podataka u bežičnim senzorskim mrežama

Miodrag Malović

*Apstrakt*—**Početkom dvadesetprvog veka, unapređenje a posebno pojeftinjenje mikroelektronskih komponenti dovelo je do značajne ekspanzije bežičnih tehnologija. Često imamo potrebu da fizički odvojeni uređaji koriste istu (odnosno, što približniju) vremensku skalu za označavanje veličina i događaja koje prate. Ovo je netrivijalan zadatak budući da su uređaji baterijski napajani i moraju svesti razmenu poruka (koje zahtevaju upotrebu energetski zahtevnog radio interfejsa) na minimum. U tu svrhu osmišljen je veliki broj algoritama i protokola koji se bave problemom usklađivanja satova na bežičnim uređajima u okviru mreže. U ovom radu prikazana su i klasifikovana neka uobičajena rešenja.**

*Ključne reči*—**sinhronizacija, vreme, frekvencija, bežične senzorske mreže, merenja**

## I. Uvod

Bežične senzorske mreže (WSN - *wireless sensor networks*) su sa razvojem mikroelektronskih komponenti niske potrošnje dobile važno mesto u mnogim oblastima nauke i svakodnevnog života. Najčešće oblasti njihove primene su građevina (ispitivanje stanja kapitalnih građevinskih objekata), medicina (daljinski nadzor pacijenata), meteorologija (prikupljanje podataka), saobraćaj (kontrola; nadzor zagađenja), prevencija nepogoda (požara, poplava, raznih havarija), industrijska i kućna automatika, itd. U heritologiji, bežični senzorski sistemi se koriste kako u permanentnom bezbednosnom nadzoru lokaliteta (zaštiti od prirodnih nepogoda i od provalnika) tako i za evaluaciju stanja objekata: snimanje pukotina u zidovima, detekciju vlažnosti i prokišnjavanja, vibracija, i drugih veličina.

Jedan od važnih ciljeva u realizaciji praktično svakog bežičnog mernog sistema jeste postizanje odgovarajuće vremenske sinhronizacije između mernih podataka koji potiču iz različitih tačaka, a koja je primerena za datu svrhu. I dok se kod nekih vrsta merenja, kao što su merenja zagađenja u saobraćaju, praćenje nivoa podzemnih i nadzemnih voda, merenja u meteorologiji, biologiji i sl. ne zahteva velika sinhronizovanost, već je bitno da su podaci obeleženi od strane lokalnog časovnika realnog vremena koji ne mora biti striktno održavan, kod merenja brzih procesa u nekim tehničkim disciplinama kao što su mašinstvo ili građevina, bitna je usaglašenost podataka izmerenih različitim senzorima u različitim tačkama u prostoru, koja mora biti na nivou zanemarljivog dela periode najviših harmonika oscilacija koje se proučavaju. Ove mogu biti reda veličine i preko 100 Hz, mada su najčešće u upotrebi frekvencije od najviše dvadesetak. Razvoj elektronike je zaista omogućio da se ove pojave mogu pratiti sa garantovanom sinhronizacijom znatno boljom od 1 ms, što je dovoljno za opisivanje većine mehaničkih pojava (ne treba zaboraviti da pretvaranje neelektričnih veličina u električne takođe unosi nekakvu dinamiku u proces merenja, te da sami senzori mehaničkih veličina teško mogu da daju odziv sa vremenskom pouzdanošću znatno boljom od milisekunde).

Sl. 1. *Torre Rognosa* u Toskani (centralna Italija), uvršćen u Uneskovu listu svetske baštine (*world heritage sites*), na kome je vršen višemesečni nadzor stanja mrežom bežičnih senzora [1].

Dok kod žičanih mreža sinhronizaciju nije teško izvesti jer se isti signal iz zajedničkog izvora vremena može sa zanemarljivom neodređenošću (reda veličine ns) sprovesti na različite uređaje, kod bežičnih mreža situacija se komplikuje. Ove najčešće koriste kompleksne radio modeme, koji imaju sopstvene procesore i operativne sisteme (*embedded RTOS*) koji unose ne sasvim određeno kašnjenje u prenos poruke, a priroda veze, podložna smetnjama iz brojnih izvora, uslovljava slanje podataka u više paketa čiji prenos može uspeti iz prve ili biti podložan određenom broju ponovnih pokušaja. Takođe, ovi paketi mogu zahtevati isporuku preko relejnih uređaja jer ne postoji garancija direktne veze između pošiljaoca i primaoca (čak, topologija cele mreže može biti podložna rekonfiguraciji u vremenu). Zato je sinhronizacija mernih podataka u bežičnim mrežama senzora postala ozbiljna naučna disciplina.

## II. Satovi (tajmeri) i njihove nesavršenosti

Iako se reči tajmer i kaunter ponekad koriste naizmenično, ispravno je za uređaj za merenje vremena koristiti reč koja je

Miodrag Malović – Univerzitet u Beogradu, Inovacioni centar Tehnološko-metalurškog fakulteta, Karnegijeva 4, 11120 Beograd (e-mail: ofiss@malovic.in.rs) (https://orcid.org/0000-0002-0691-4626).

 ISBN 978-86-7466-930-3

izvedena iz reči za vreme, a to je tajmer. Kaunter je po definiciji uređaj za brojanje električnih impulsa (silaznih ili uzlaznih ivica nekog signala). Ukoliko kaunter vežemo sa oscilatornim kolom baziranim na (najčešće) piezoelektričnom kristalu, koje daje takt procesoru i drugim čipovima na mernom uređaju, dobijamo tajmer. Generalno, kategorija „kaunter“ je šira (kaunteri se mogu koristiti u različite svrhe brojanja koje nemaju veze sa merenjem vremena).

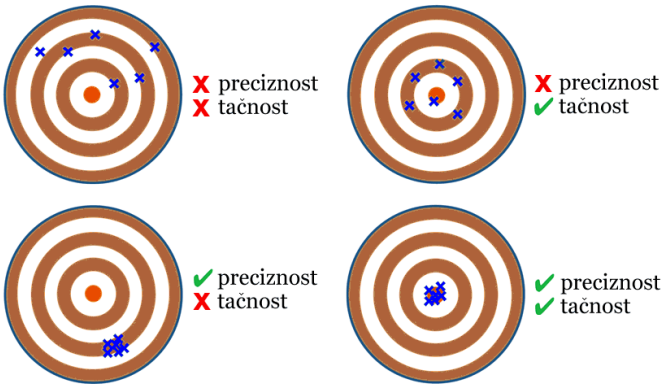


Sl. 2. Grafički prikaz razlike između preciznosti i tačnosti.


Sl. 3. Pendulum CNT-91 precizni kaunter/tajmer (prednja i zadnja strana) [2]. Ovaj i slični uređaji se koriste za merenje vremena i frekvencije, kao i generisanje signala stabilne frekvencije, u eksperimentima vezanim za proveru sinhronizovanosti.

Karakteristike tajmera su određene kvalitetom piezoelektričnih kristala (mada se u novije vreme koriste i MEMS oscilatori koji ne moraju biti piezoelektrične prirode) i prateće elektronike koja čini oscilatorno kolo. Pojmovi koji se koriste u opisivanju kvaliteta oscilatora odnosno tajmera se lako mogu pobrkati pa nije na odmet navesti njihove definicije. Greška ili odstupanje predstavlja razliku između tačne i nominalne vrednosti frekvencije. Da bi greška bila definisana, potrebno je da poznajemo tačnu vrednost, što često nije slučaj. Najčešće se pod greškom podrazumeva razlika između nominalne (negde deklarisane) frekvencije i vrednosti koja se izmeri kvalitetnijim (etalonskim) uređajem. Tačnost je inverzno određena ovim odstupanjem. Preciznost se odnosi na ponovljivost frekvencije. Preciznost je sinonim za stabilnost, a ne tačnost. Frekvencija može odstupati od nominalne a biti slabo promenljiva, što uređaj čini preciznim, ali ne i tačnim. Ilustracija ovoga je data na Sl. 2.

Postoje dva glavna izvora greške vremenske sinhronizacije u distribuiranim sistemima. Prvo, vreme propagacije poruka nije dovoljno determinisano kada se koristi radio komunikacija između udaljenih uređaja (jedini način komunikacije kod bežičnih senzorskih mreža, ako ne računamo druge oblasti frekvencija koje ne spadaju u radio, ali je princip rada isti). Drugo, stabilnosti tajmera su limitirane brojnim fizičkim faktorima, pa čak i u slučaju da su njihove frekvencije perfektno kalibrisane u jednom trenutku, pomeranja (driftovi) moraju da se dogode u nekoj meri pre ili kasnije, i odstupanje pokazivanja (ofset) se akumulira sa vremenom, uslovljavajući potrebu za razmenom novih poruka da bi se uređaji međusobno ponovo sinhronizovali.

Mrežni protokoli koji se bave problemom sinhronizacije satova izvode serije akcija koje su bazirane na distribuciji vremenskih žigova iz referentnih izvora, što se naziva ofset sinhronizacija, i štelovanju dinamičkih koeficijenata koji se koriste za kalibraciju satova, što se naziva sinhronizacija brzine [3]. Uobičajena podela ovih akcija ne neke kategorije je data u nastavku, a zatim su predstavljeni neki postojeći protokoli sinhronizacije.

## III. IMPLICITNA I EKSPLICITNA SINHRONIZACIJA

Kontinualna ili implicitna sinhronizacija znači da se paketi podataka koji su vezani za sinhronizaciju dodaju na postojeće pakete koji se sve vreme (odakle naziv *kontinualna*) šalju kroz mrežu (i nezavisno procesiraju na uređajima, u skladu sa algoritmom rada mreže). Ovo dodavanje sinhronizacionih parametara u regularne pakete se u literaturi označava kovanicom *piggy-backed*, što u doslovnom prevodu znači „na krkače”.

Suprotnost kontinualnoj sinhronizaciji je sinhronizacija na zahtev, koja se takođe naziva i eksplicitna, ili *event-triggered* (inicira se nekim događajem odnosno okidačem ili trigerom, koji može biti automatski detektovan ili dat od strane korisnika). Eksplicitna sinhronizacija zahteva dodatne komunikacione pakete koji služe isključivo (ili barem primarno) u ove svrhe. Ona je zato zahtevnija u smislu energetskih potreba, što je značajno kod bežičnih uređaja, koji su obično energetski ograničeni jer su baterijski napajani, a baterije se moraju ručno menjati ili dopunjavati iz izvora ograničenog kapaciteta, kao što su solarne ćelije, induktivni mikrogeneratori, termogeneratori na bazi termoparova ili piroelektričnih materijala, itd.


ISBN 978-86-7466-930-3

## IV. INTERNA I EKSTERNA SINHRONIZACIJA

Interna sinhronizacija je algoritam sinhronizacije u kome ne postoji nikakvo spoljašnje referentno vreme. Cilj interne sinhronizacije je da pokazivanja svih satova unutar mreže budu što sličnija [4], a po mogućstvu se vodi računa i o međusobnoj razlici njihovih frekvencija, radi naknadne (tzv. post-facto) korekcije.

Eksterna sinhronizacija se bazira na jednom referentnom satu, bez obzira da li dolazi sa jednog uređaja unutar mreže (u kom slučaju reč eksterna ne treba bukvalno da se shvati) ili ne. Cilj eksterne sinhronizacije je da učini da svi satovi u mreži pokazuju koliko je moguće blizu referentnom satu.

## V. UNIDIREKCIONA I BIDIREKCIONA SINHRONIZACIJA

Unidirekciona sinhronizacija je procedura u kojoj se sat ciljnog uređaja podešava prema satu izvornog uređaja, dakle postoji jasan smer kretanja informacije. Tipično transmisiono vreme se oduzima od vrednosti po prijemu. Unidirekciona sinhronizacija ne znači da se ista poruka šalje na samo jednu prijemnu adresu, već samo da nema dvosmerne razmene informacija. Na ovaj način se može sinhronizovati više uređaja u okolini izvora.

Bidirekciona, često zvana i *pairwise* (po parovima, ili parska) sinhronizacija je bazirana na proračunu takozvanog *round-trip* kašnjenja, odnosno vremena potrebnog da poruka otputuje sa izvornog uređaja do ciljnog i da se povratna poruka detektuje na izvornom uređaju (kružno putovanje). Prednost je što se meri stvarno fizičko vreme (naravno, ograničeno preciznošću lokalnog sata), što je inače nemoguće u dve odvojene tačke (kod unidirekcione sinhronizacije). Iako se ne može odrediti tačna raspodela vremena i nesigurnosti vremena putovanja između smerova, za povratnu putanju može se tačno odrediti i srednja vrednost i standardno i maksimalno odstupanje vremena propagacije (round-tripa). Pošto se obično radi sa uređajima istog tipa, za tipično vreme propagacije uzima se polovina round-trip vremena. I drugi uređaji u mreži mogu imati koristi od bidirekcionih sinhronizacionih poruka između dva čvora. Oni mogu da koriste razmenjene vremenske žigove da bi sinhronizovali svoje satove bez bilo kakve dodatne transmisije podataka (utroška energije), samo prijemom, tj. uvidom u otvorenu komunikaciju parova koji se sinhronizuju bidirekciono. Ovakva procedura je česta i naziva se *eavesdropping* (prisluškivanje) [5].

## VI. TRANSFORMACIJA VREMENSKE SKALE

Transformacija vremenske skale spada u *backwards*, odnosno post-facto ili naknadne (unazad) sinhronizacione tehnike. Satovi nisu sinhronizovani za vreme događaja koji se posmatra, ali se sinhronizacija skupljenih podataka vrši naknadno u zavisnosti od relevantnih parametara (ustanovljenih frekvencija tajmera i medjusobnih ofseta). Iako zahteva manje energije (manje dodatne komunikacije nego u slučaju sinhronizacije na zahtev), povećava potrebu za procesiranjem podataka, i najbolje je izvršiti je na sistemu visokog nivoa, kao što je PC računar, koji često predstavlja baznu stanicu (hab) bežične mreže. Post-facto sinhronizacija se nekada naziva i reaktivnom ili a-posteriori, što je suprotno od proaktivne sinhronizacije koja se vrši unapred, ili a-priori [6]. Proaktivna i reaktivna sinhronizacija se kombinuju u nekim protokolima.

Kao što ime govori, transformacija vremenske skale je doterivanje vremenskih žigova u skladu sa poznatim odnosima između frekvencija satova na uređajima (doterivanje „nagiba“, odnosno brzine) i poznatim trenucima simultanih događaja (doterivanje ofseta).

## VII. RBS, MULTIKAST, I UNIKAST

*Reference Broadcast Synchronization* (RBS) [7] ili sinhronizacija putem referentnog ili prozivnog signala je termin koji se asocira isključivo sa bežičnim mrežama. Spada u unidirekcione sinhronizacione tehnike. Centralni server emituje referentni signal (poznat i pod nazivom *beacon*, odnosno „signal za navođenje“, po analogiji sa signalima koji se koriste u navigaciji) a prijemni uređaji usklađuju svoje tajmere po prijemu. Sl. 4 prikazuje vremenski dijagram povorke od dva RBS-a koji prethodi detekciji događaja od strane više senzorskih uređaja.

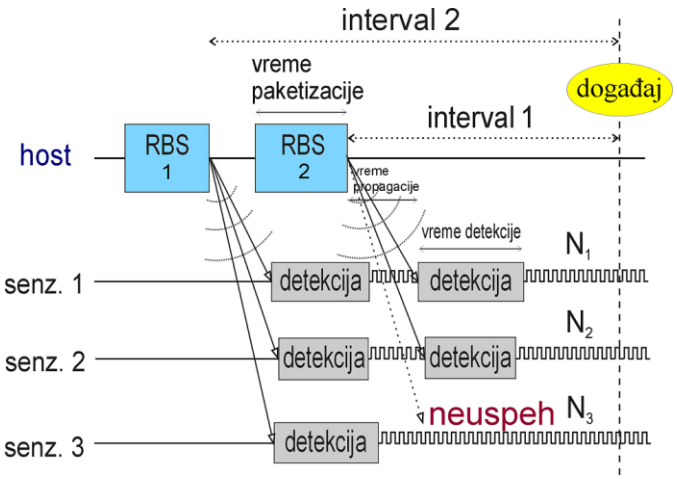


Sl. 4. Prikaz uspele i delimično uspele sinhronzacije pri slanju povorke od dva RBS-a; u slučaju uspeha, neodređenost vremena označavanja događaja zavisi od neodređenosti vremena detekcije i neodređenosti frekvencije kojom se mere $N_1$ i $N_2$, dok se u slučaju parcijalnog neuspeha (senzor 3) dodaje i neodređenost vremena paketizacije modema hosta [8].

Ovaj tip poruke se naziva *multicast* (šire raspoređen, odnosno za više primaoca), što je suprotno *unicast* porukama (koje imaju jednog pošiljaoca i jednog primaoca). Propagacione neodređenosti, vezane za transmisiju poruke (izlazno vreme kroz fizički sloj, koji se sastoji od interfejsa između procesora i komunikacionog modula, modema ili transsivera, i antene) se potiru jer se radi o istom signalu za sve primaoce. Neodređenosti vezane za prijem poruke su obično za red veličine manje i na ovaj način se ofset između čvorova praktično potire. Logičko vreme je na ovaj način nešto bolje sinhronizovano nego fizičko vreme. Logičko vreme predstavlja „relativno“ vreme unutar nekog posmatranog perioda, kao što je merni ciklus, dok fizičko


ISBN 978-86-7466-930-3

vreme predstavlja stvarno vreme u spoljnom svetu. Sekundarne RBS procedure se mogu ponavljati u multihop[1] mrežama (gde ne postoji direktna veza između izvora RBS-a i svih uređaja), gde sinhronizovani uređaji služe kao habovi (centralne stanice) lokalnih klastera (grupa u kojima su uređaji „nižeg nivoa“). Pouzdanost sinhronizacije naravno opada sa brojem hopova (novih transmisija RBS-a).

## VIII. GPS I PPS

Puls u sekundi (PPS) globalnog sistema za pozicioniranje (GPS) predstavlja odličan izvor vremenskih žigova visoke tačnosti [9]. Kako se očekuje da cene GPS prijemnika padaju u doglednoj budućnosti, ovaj metod će verovatno dobiti na popularnosti. Ipak, u ovom trenutku, osim zahteva da se jeftini bežični senzorski uređaji opreme dodatnim hardverom čija cena nije zanemarljiva, postoji ozbiljan problem dostupnosti signala unutar građevina i drugih zatvorenih prostora, tako da se ovo inače efektno rešenje uglavnom izbegava. Ovaj signal se emituje iz satelita, ograničenom snagom. Čak i malo gušće krošnje drveća mogu da budu prepreka za njega.

PPS signali su odlični za dugoročnu sinhronizaciju vremena. Informacija o protoku vremena se konstantno usklađuje sa referentnim laboratorijama najvišeg nivoa tačnosti na zemlji. Ovaj signal, nažalost, ne sadrži informaciju o fizičkom vremenu (vreme-datum).

U nekim praktičnim realizacijama bežičnih mreža koristi se jedan ili nekoliko referentnih uređaja sa GPS prijemnikom, koji se sinhronizuju putem PPS-a, i dalje prosleđuju informaciju uređajima „nižeg nivoa“ u mreži, koji mogu biti u zatvorenim prostorijama ili ispod vegetacije, ili naprosto nemaju GPS prijemnike radi uštede.

Na Sl. 5 prikazan je GPS modul za platformu Arduino [10].

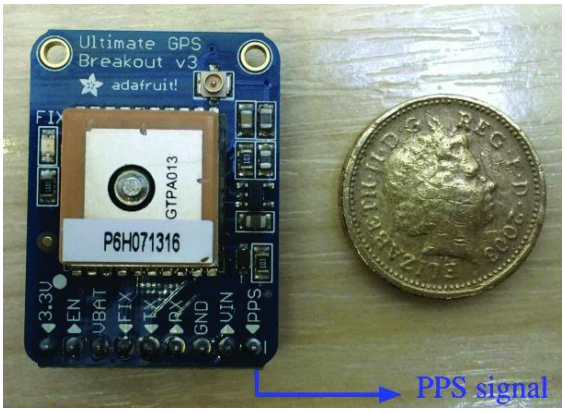


Sl. 5. GPS modul za Arduino [10], cene $30, 2021.

## IX. KLASIČNI MREŽNI ALGORITMI SINHRONIZACIJE

Prve kompjuterske mreže koristile su dve varijacije sinhronizacije putem centralizovanog servera, poznate kao Kristijanova i Berkli sinhronizacija. Hab sistema (centralna stanica) šalje vremenske žigove uređajima u mreži na zahtev. Očekivano vreme propagacije se oduzima prilikom prijema. Alternativno, višestruki paketi sa vremenskim žigovima se šalju u odgovoru na jedan zahtev, i najbrže pristigli paket se uzima u obzir (da bi se izbegla mogućnost povremenih nepredviđenih zastoja). U Kristijanovoj varijaciji algoritma, hab služi kao izvor vremena (njegov sat se uzima kao referentni eksterni izvor), dok se u Berkli varijaciji podaci skupljaju sa različitih čvorova usrednjavaju (opciono sa težinskim faktorima), i usrednjena informacija se šalje nazad.

Jedna od najčešće korišćenih metoda u savremenim kompjuterskim mrežama jeste mrežni vremenski protokol ili NTP (*network time protocol*) [11]. Čvorovi mreže se dele u različite slojeve (*layers*), počevši od referentnih satova koji su na vrhu (takozvani „stratum 0” sloj, u koji spadaju nacionalne laboratorije i GPS sateliti). Mrežni čvorovi nižeg nivoa sinhronizuju se na bazi poruka koje primaju sa uređaja istog ili višeg nivoa. Razmena poruka unutar mreže ne sadrži samo vremenske žigove, već i razne druge podatke, kao što su preciznost tajmera na uređaju, vreme njegove poslednje sinhronizacije, pouzdanost njegove poslednje sinhronizacije, i očekivano vreme putovanja poruke. Ciljni uređaj odlučuje da li da izvrši korekciju svog sata, i za koliko, ili ne, bazirano ne samo na zadnjoj primljenoj poruci već ispitujući set poruka pristiglih u dužem vremenskom intervalu. NTP poruke se testiraju na smislenost i one koje izgledaju kao gruba greška se odbacuju u procesu interpolacije, tako da je algoritam robustan.

Precizni vremenski protokol ili PTP (*precision time protocol*), poznat i kao IEEE-1588 [12], je kompleksniji protokol baziran na istom principu. Veći broj tipova poruka se koristi, veći broj parametara se prosleđuje, i uređaji imaju različite funkcije, a ne samo klijent, server, ili klijent-i-server, što je slučaj u NTP-u. Ipak, glavna prednost ovog protokola nisu kompleksne softverske metode već „hardverska asistencija“. To znači da postoji specijalizovani hardver koji se instalira na mrežne kartice i druge uređaje, koji određuje precizna (ispod mikrosekunde) vremena fizičke emisije poruka (tzv. prolaska kroz „fizički sloj“ mreže), koja bi inače bila nedostupna glavnim procesorima mrežnih uređaja. Dok tipičan NTP klijent ostvaruje preciznost sinhronizacije reda veličine milisekunde, kod PTP-a su sinhronizacije reda veličine ispod mikrosekunde.

## X. PROTOKOLI SINHRONIZACIJE U BEŽIČNIM MREŽAMA

Veliki broj protokola je osmišljen radi upotrebe isključivo u bežičnim senzorskim mrežama. Navešćemo neke od osnovnih, uz kratak opis načina rada.

Sinhronizacija putem vremenskog žiga ili vremenskog označavanja (*time-stamp synchronization* ili TSS) je metod promene vremenskih žigova poruka koje prolaze kroz multihop mrežu, bazirano na vremenu prijema, procenjenom vremenu puta, i vremenu koje poruka provede u „redu” (lokalnom baferu, odnosno steku, za prijem pristiglih paketa), odnosno *queue*-u, pre nego što se prosledi. Satovi nisu stvarno sinhronizovani tako da se ovde radi o formi *post-facto* odnosno naknadne sinhronizacije. Varijacija na ovu temu je

[1] putovanje paketa u više predajno-prijemnih koraka, odnosno putem releja, kada ne postoji direktna veza između pošiljaoca i primaoca; *hop* označava jedan „skok“ odnosno putovanje poruke između dva čvora


ISBN 978-86-7466-930-3

RITS (*routing integrated time synchronization*) [13], kod koga se izvodi dodatna kompenzacija zbog razlike u brzinama rada različitih tajmera. Ova razlika se procenjuje na osnovu istorije razmenjenih poruka sa vremenskim žigovima iz bidirekcione komunikacije (gde se mogu uporediti *round-trip* vremena proračunata na različitim čvorovima).

Laka vremenska sinhronizacija (*lightweight time synchronization* ili LTS) i *timing-sync* protokol za senzorske mreže (TPSN) su bazirani na bidirekcionoj sinhronizaciji parova uređaja koji razmenjuju poruke unutar multihop mreže, gde postoji jedna ili više referentnih tačaka (čiji su tajmeri deklarisani kao referentni) [14]. Uređaji na nižim nivoima (više hopova udaljeni od referenci), upućuju zahteve za sinhronizacijom prema uređajima na višem nivou. Kod LTS-a, uređaji proveravaju da li drugi uređaji na istom nivou imaju aktuelne zahteve koji nisu izvršeni (*pending requests*), i sinhronizuju se sa njima umesto da šalju nove multihop zahteve. Kod TPSN-a, uređaji na nižem nivou prisluškuju (*eavesdrop*) sinhronizaciju uređaja na višem nivou, i zatim šalju zahtev za sihnhronizacijom u prigodnom momentu.

Tiny-sync i Mini-sync [15] takođe rade na principu bidirekcione sinhronizacije. Oni koriste statistiku da porede vremenske žigove koji se razmenjuju između parova uređaja. Vremenski žigovi odstupaju sve više tokom vremena, zbog razlika u brzinama satova (koje su dodatno podložne varijacijama usled promene različitih fizičkih parametara), tako da se odnos frekvencija i inicijalni ofset mogu proceniti kreiranjem optimalne prave bazirane na većem broju parova vremenskih žigova sa oba uređaja (tzv. linearna regresija; ilustracija je data na Sl. 6). Različiti algoritmi se koriste da procene najverovatniji odnos frekvencija i ofset.

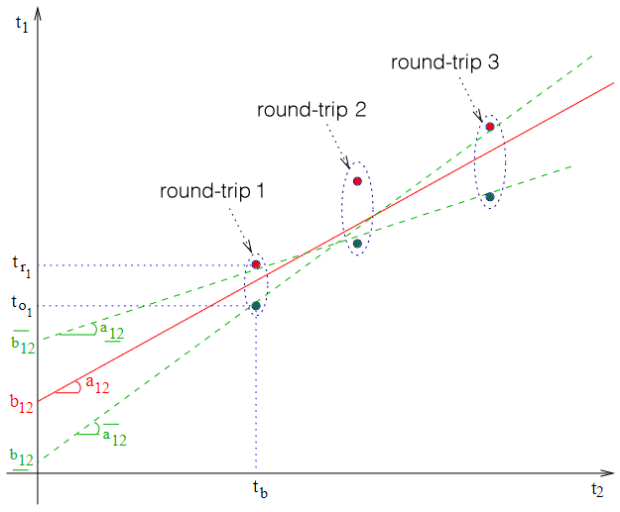


Sl. 6. Linearna regresija $t_1(t_2)$ gde donje tačke u paru predstavljaju emisiju signala, a gornje prijem odgovora kod round-tripa, u funkciji žiga na drugom uređaju; *a* označava minimalni, srednji i maksimalni odnos brzina satova, a *b* minimalni, srednji i maksimalni ofset [15].

Fleksibilna laka vremenska sinhronizacija (*scalable lightweight time-synchronization protocol*, ili SLTP) [16], koristi metod takozvanog pasivnog grupisanja (*passive clustering*) kao prvi korak, a zatim izvodi sinhronizaciju slično LTS-u. Na zahtev, kreira se topologija mreže (pasivno grupisanje, odnosno trasiranje), pri čemu se uređaji dele na grupe (klastere) i dodeljuju im se funkcije habova klastera (referentnih tačaka, koje dakle nisu fiksne kao kod originalnog LTS-a), članova klastera, ili *gateway*-a odnosno kapija između klastera. Upotrebljava se i linearna regresija, kao kod tiny-synca i mini-synca, za poređenje i usklađivanje satova prilikom bidirekcione komunikacije.

Tsync protokol [17] koristi dve tehnike koje se nazivaju hijerarhijsko referenciranje (*hierarchy referencing time synchronization* ili HRTS) i individualni vremenski zahtevi (*individual-based time request* ili ITR). Glavni uređaj emituje RBS signal koji primaju uređaji najvišeg nivoa (lejera). Jedan od njih se slučajno izabira za bidirekcionu razmenu vremenskih žigova. Propagaciono kašnjenje se procenjuje na osnovu ovog procesa i novi RBS od strane centralnog uređaja se šalje dajući ciljnim uređajima referentnu vrednost vremena i pretpostavljeno vreme propagacije (smatra se da su uređaji hardverski identični te se očekuje približno isto vreme propagacije). Kada se proces završi, uređaji iz prvog nivoa ponavljaju proceduru prema klasterima nižeg nivoa. Proces se rekurzivno ponavlja dok svi uređaji u mreži nisu sinhronizovani. ITR je komplementarni mehanizam u Tsync-u, koji se koristi za sinhronizaciju na zahtev, bilo jednog uređaja bilo grupe. Uređaji koji zahtevaju sinhronizaciju šalju zahtev koji se multihop prenosi do centralne stanice (glavnog uređaja) i referentni vremenski žig se prenosi nazad istim putem. HRTS i ITR u originalnom obliku koriste dva različita kanala za razmenu poruka, ali moguća je implementacija i na jednom kanalu, sa nešto lošijom performansom.

Intervalska sinhronizacija (*interval based synchronization* ili IBS) [18] koristi procenu granica brzine satova (njihovih minimalnih i maksimalnih vrednosti) da odredi granice u kojima se vreme nalazi. Umesto razmene vremenskih žigova, čvorovi komuniciraju razmenjujući podatke o minimalnom i maksimalnom vremenu (tzv. *interval stamps* ili intervalski žigovi, bazirani na najgorem slučaju devijacije frekvencije sata). Ovo se naziva i intervalski model, koji je suprotan instant (tačkastom) modelu. Iako neki autori tvrde da je kombinacija „garantovanih“ granica za lokalne satove optimalnija nego upotreba pojedinačnih vremenskih žigova uz estimaciju njihovog kvaliteta (procenu distribucije verovatnoće i standardne i maksimalne devijacije), suština oba metoda je ista, a u stvarnosti ne postoje stopostotne garancije za granice kod *bounded-drift* modela sata (modela limitarnog odstupanja odnosno limitiranog drifta frekvencije).

Asinhrona difuzija [19] je protokol kod koga svi uređaji periodično šalju signal susedima tražeći pokazivanja njihovih satova (vremenske žigove). Slično kao kod Berkli algoritma, vrši se usrednjavanje ovih vrednosti i one se putem RBS-a prosleđuju susedima (svim uređajima u dometu ili unutar klastera), koji vrše sinhronizaciju na novu vrednost. Proces se ponavlja širom mreže.

Protokol sinhronizacije putem preplavljivanja (*flooding time synchronization protocol* ili FTSP) [20] koristi tzv. preplavljivanje (*flooding*) mreže odnosno slanje velikog broja

 ISBN 978-86-7466-930-3

paketa (slično RBS-u) sa referentnog uređaja, u kombinaciji sa pamćenjem parova vremenskih žigova i linearnom regresijom koja se koristi kod tiny-sync-a. PulseSync je sličan protokol, baziran na plavljenju mreže velikom brzinom, da se ne dozvoli akumulacija nagiba (*skew*) [21]. *Skew* označava akumuliranu grešku sata baziranu na driftu frekvencije tajmera (odstupanju tokom posmatranog vremena). I dok oba protokola imaju preciznost koja opada sa brojem hopova, PulseSync preciznost opada nešto sporije.

Kod protokola vremenske difuzije (*time diffusion protocol* ili TDP) [22], referentni uređaj šalje primarni RBS signal, a susedi u dometu vraćaju informaciju koja sadrži procenjenu stabilnost sopstvene frekvencije tajmera, na bazi ranije razmenjenih vremenskih žigova. Referentni uređaj odlučuje koji susedi mogu da budu izvori sekundarnih RBS signala (centri klastera nižeg nivoa), i šalje sinhronizacioni RBS. Procedura se rekurzivno ponavlja kroz multihop mrežu sve dok svi uređaji nisu primili bar jednu poruku ovog tipa. Uređaji koji su primili višestruke sinhronizacione naredbe sinhronizuju se na srednju vrednost, uz korišćenje težinskih koeficijenata (baziranih na proceni stabilnosti frekvencije i nivou izvora). Sličan protokol pod nazivom GTSP (*gradient time synchronization protocol*) [23] ne zahteva centralni referentni čvor, definisanu topologiju, niti stalnu operaciju svih uređaja. Opisane dvofazne RBS procedure se ponavljaju kroz mrežu bez definisane hijerarhije.

Konsenzus sinhronizacija (*consensus clock synchronization* ili CCS) [24] je tipična interna sinhronizaciona metoda. Svi uređaji emituju unidirekcione poruke sa vremenskim žigovima i primajući uređaji pokušavaju da procene koliko iznosi vrednost „dogovorenog" vremena u mreži. Procena se donosi na bazi pamćenja većeg broja prethodnih poruka sa različitih uređaja.

Kao što vidimo, opisane metode, kao i mnoge druge koje postoje, nisu strogo razdvojene, već se prilično preklapaju i teško je povući granicu između njih i razvrstati algoritme striktno po kategorijama.

## XI. ZAKLJUČAK

Bežične senzorske mreže (WSN) predstavljaju skup (najčešće minijaturnih) elektronskih senzorskih uređaja, koji služe za nadgledanje različitih pojava u fizičkom svetu. Uređaji u mreži komuniciraju putem radio talasa. Ovim putem se razmenjuju i informacije o vremenu, odnosno održava sinhronizacija satova unutar mreže. Sinhronizacija (na nivou određenom mernim zadatkom) je neophodna za ispravno vremensko označavanje mernih uzoraka u distribuiranim merenjima u mašinstvu, građevini, i drugim tehničkim disciplinama, uključujući heritologiju. U ovom članku dat je prikaz uobičajenih algoritama i protokola za minimizaciju razlika pokazivanja satova unutar bežične senzorske mreže.

## ZAHVALNICA

Autor se zahvaljuje za podršku Ministarstvu prosvete, nauke i tehnološkog razvoja Republike Srbije (ugovor 451-03-68/2022-14/200287).

## REFERENCE

[1] A. Mecocci, A. Abrardo, "Monitoring architectural heritage by wireless sensors networks: San Gimignano - a case study," *Sensors*, vol. *14*, no. *1*, pp. *770-778*, Jan. 2014.

[2] *Pendulum Instruments CNT-91/91R Advanced Frequency & Time Interval Analyzer*, [Online]. https://pendulum-instruments.com/products /frequency-counters-analyzers/cnt-91-91r-advanced-frequency-time-interval-analyzer/

[3] S. Rahamatkar, A. Agarwal, N. Kumar, "Analysis and comparative study of clock synchronization schemes in wireless sensor networks," *Int. J. Comput. Sci. Eng.*, vol. *2*, no. *3*, pp. *536-541*, Apr. 2010.

[4] S. Khediri, N. Nasri, M. Samet, A. Wei, A. Kachouri, "Analysis study of time synchronization protocols in wireless sensor networks," *Int. J. Distrib. Parallel Syst.*, vol. *3*, no. *3*, pp. *155-165*, Jun. 2012.

[5] C. Liu, H. Pang, N. Cao, X. Li, D. Xu, "Wireless Sensor Network Time Synchronization Algorithm Overview," in Proc. of International Symposium on Intelligence Computation and Applications, Singapore, pp. 552-561, Nov. 2017.

[6] J. Funck, C. Gühmann, "Comparison of approaches to time-synchronous sampling in wireless sensor networks," *Meas.*, vol. *56*, pp. *203–214*, Oct. 2014.

[7] F. Zhang, G. Y. Deng, "Probabilistic time synchronization in wireless sensor networks," in Proc. of IEEE 2005 International Conference on Wireless Communications, Networking and Mobile Computing, Wuhan, China, vol. 2, pp. 980-984, Sep. 2005.

[8] M. Malović, Lj. Brajović, Z. Mišković, T. Šekara, "Simultaneity Analysis in a Wireless Sensor Network," *Metrol. Meas. Syst.*, vol. *22*, no. *2*, pp. *275-288*, Jun. 2015.

[9] R. Kim, T. Nagayama, H. Jo, B. F. Spencer Jr, "Preliminary study of low-cost GPS receivers for time synchronization of wireless sensors," in Proc. of SPIE Smart Structures and Materials + Nondestructive Evaluation and Health Monitoring, San Diego, CA, USA, vol. 8345, p. 83451A, Apr. 2012.

[10] K. Y. Koo, D. Hester, S. Kim, "Time synchronization for wireless sensors using low-cost GPS module and Arduino," *Front. Built Environ.*, vol. *4*, art. *82*, Jan. 2019.

[11] D. L. Mills, "Internet time synchronization: the network time protocol," *IEEE Trans. Comm.*, vol. *39*, no. *10*, pp. *1482-1493*, Oct. 1991.

[12] R. Exel, G. Gaderer, N. Kerö, "Physical Layer Ethernet Clock Synchronization," in Proc. of 42nd Annual Precise Time and Time Interval (PTTI) Systems and Applications Meeting, Reston, VA, USA, pp. 77-87, Nov. 2010.

[13] J. Sallai, B. Kusý, A. Lédeczi, P. Dutta, "On the scalability of routing integrated time synchronization," in Proc. of 3rd European Workshop on Wireless Sensor Networks, Zürich, Switzerland, pp. 115-131, Feb. 2006.

[14] F. Sivrikaya, B. Yener, "Time synchronization in sensor networks: a survey," *IEEE network*, vol. *18*, no. *4*, pp. *45-50*, Jul. 2004.

[15] S. Yoon, C. Veerarittiphan, M. L. Sichitiu, "Tiny-sync: Tight time synchronization for wireless sensor networks," *ACM Trans. Sens. Netw.,* vol. *3*, no. *2*, pp. *1-33*, Jun. 2007.

[16] S. Nazemi Gelyan, A. N. Eghbali, L. Roustapoor, S. A. Yahyavi Firouz Abadi, M. Dehghan, "SLTP: scalable lightweight time synchronization protocol for wireless sensor network," in Proc. of International Conference on Mobile Ad-Hoc and Sensor Networks, Beijing, China, pp. 536-547, Dec. 2007.

[17] H. Dai, R. Han, "TSync: a lightweight bidirectional time synchronization service for wireless sensor networks," *ACM SIGMOBILE Mob. Comput. and Commun. Rev.*, vol. *8*, no *1*, pp. *125-139*, Jan. 2004.

[18] L. Meier, "Interval-based Clock Synchronization for Ad-Hoc Sensor Networks," in *4. GI/ITG KuVS Fachgespräch »Drahtlose Sensornetze«*, Zürich, Switzerland, ETH Zürich, 2005, ch. *2*, pp. *25-28*

[19] Q. Li, D. Rus, "Global clock synchronization in sensor networks," *IEEE Trans. Comput.,* no. *55*, no. *2*, pp. *214-226*, Jan. 2006.

[20] L. Gheorghe, R. Rughiniș, N. Țăpuș, "Fault-tolerant flooding time synchronization protocol for wireless sensor networks," in Proc. of 6th International Conference on Networking and Services, Cancun, Mexico, pp. 143-149, Mar. 2010.

[21] K. S. Yildirim, A. Kantarci, "Time synchronization based on slow-flooding in wireless sensor networks," *IEEE Trans. Parallel Distrib. Syst.*, vol. *25*, no. *1*, pp. *244-253*, Feb. 2013.

 ISBN 978-86-7466-930-3

[22] W. Su, I. F. Akyildiz, "Time-diffusion synchronization protocol for wireless sensor networks," *IEEE/ACM Trans. Networking*, vol. *13*, no. *2*, pp. *384-397*, Apr. 2005.
[23] P. Sommer, R. Wattenhofer, "Gradient clock synchronization in wireless sensor networks." in Proc. of 8th IEEE/ACM International Conference on Information Processing in Sensor Networks, San Francisco, CA, USA, pp. 37-48, Apr. 2009.
[24] M. K. Maggs, S. G. O'Keefe, D. V. Thiel, "Consensus clock synchronization for wireless sensor networks," *IEEE Sens. J.*, vol. *12*, no. *6*, pp. *2269-2277*, Feb. 2012.

ABSTRACT

Advances in microelectronics in the past decades have lead to widespread use of wireless sensor networks (WSN). Sensor devices in these networks are not connected permanently, but are only able to exchange messages from time to time, using radio interface. In order to preserve limited energy reserves (devices are battery powered), this exchange must be kept to a minimum. Proper fusion of data from different nodes requires certain level of synchronization of their clocks, depending on the particular measurement task. So the clocks synchronization is one of the primary concerns in many WSN. This paper reviews the most common techniques and protocols used for this purpose.

**Synchonization of measurement data in wireless sensor networks**

Miodrag Malović

 ISBN 978-86-7466-930-3

# Primer kombinovanja raspodela atmosferskih aerosola po veličinama dobijenih metodom merenja električne pokretljivosti i optičkom metodom

Miloš Davidović, Milena Davidović, Sonja Dmitrašinović, Milesa Srećković, Milena Jovašević-Stojanović

***A stra t*—Atmosfers i aerosoli u urbanim sredinama se sastoje od čestica različitih dijametara, oje mogu imati veličinu od par nanometara do par mi rometara. toga je za merenje oncentracije aerosola često neophodno oristiti više instrumenata, sa principijelno različitim metodama merenja. ovom radu su korišćene metode zasnovane na merenju električne po retljivosti čestica, za opseg dijametara od 1 nm do 42 nm, i merenju e vivalentnog optičkog dijametra, za opseg dijametara od nm do 1 um. ao glavni rezultat, pri azani su primeri kombinovanja spektara veličina čestica koji su dobijeni pomoću ove dve omplementarne metode merenja. procesu kombinovanja spektara veličina čestica moguće je modifi ovati raspodelu dobijenu optičkim merenjima traženjem optimalne vrednosti inde sa prelamanja čestica tako da se dobije što bolje slaganje sa raspodelom dobijenom merenjem električne po retljivosti. ao ulazni podaci su orišćeni rezultati merenja iz ampanje mobilnog monitoringa u ovom adu 2 22.**

***Ključne reči* — električna mobilnost; ekvivalentni optički dijametar; ijevo rasejanje; log normalna raspodela.**

## I. UVOD

Raspodela čestica po veličinama je jedan od ključnih parametara za određivanje rizika koje mogu nositi po zdravlje, i ovo je utvrđeno u velikom broju studija koje se bave zdravljem ljudi. Videti npr. [1] gde se opisuje mogućnost nanošenja nanočestica u pluća, njihovog jakog upalnog potencijala i prenošenja dalje u organizam, a takođe i njihova pojačana biološka aktivnost usled velike površine u odnosu na masu [2]. Takođe, veličina čestice predstavlja važan parametar koji opisuje česticu aerosola budući da od veličine zavise koeficijenti rasejanja i apsorpcije, sposobnost da čestica veže vodu i dr. što je bitno za karakterizaciju atmosferskih procesa. Usled toga je najčešće i ujedno najznačajnije merenje koje se vrši na aerosolima određivanje raspodele broja čestica po njihovoj veličini.

Sa druge strane, utvrđivanje ove raspodele u nekoj urbanoj sredini nije jednostavan zadatak. Regulatorne mreže za monitoring aerozagađenja često daju informaciju koja je niske vremenske rezolucije, a često postoji i problem malog broja mernih stanica u ovim mrežama. Stoga se ovakvi javno dostupni podaci, moraju dopunjavati kroz dodatne kampanje merenja aerozagađenja.

Za merenje i karakterizaciju čestičnog zagađenja, koje se za aerosole uopšte, i naravno aerosole u urbanim sredinama, sastoji od čestica različitih dijametara, u veoma širokom opsegu dijametara čestica (od par nanometara do 10 um) koristi se obično više instrumenata, pa se njihovi spektri (izmerene raspodele veličina čestica) kombinuju. Neophodnost korišćenja više instrumenata, sa principijelno različitim metodama merenja, proističe iz nemogućnosti pokrivanja celokupnog relevantnog opsega sa samo jednom metodom, npr. optička metoda se ne može koristiti za najmanje nanometarske čestice. Stoga se za ovakva sveobuhvatna merenja i karakterizaciju aerosola koriste i kombinuju metode zasnovane na različitim fizičkim principima kao što su optičke metode, metode zasnovane na merenjima električne pokretljivosti, metode zasnovane na posmatranju uzorkovanog aerosola pomoću mikroskopa, metode zasnovane na merenju aerodinamičkog prečnika čestica i druge. Budući da zbog različitog principa merenja navedene metode imaju drastično različite vremenske rezolucije (od merenja u realnom vremenu do metoda koje podrazumevaju uzorkovanje i naknadnu laboratorijsku analizu) i pokrivaju različite opsege veličina čestica, a da je cilj kampanja merenja koje smo izvršili bila karakterizacija urbanih aerosola u realnom vremenu u ovom radu se kombinuju metoda zasnovana na merenju električne pokretljivosti za opseg dijametara od 10nm do 420nm i metoda zasnovana na merenju intenziteta rasejane svetlosti tj. optičkim merenjima za opseg dijametra od 300nm do 10um,

Miloš Davidović – Institut za nuklearne nauke "Vinča", Institut od nacionalnog značaja za Republiku Srbiju, Univerzitet u Beogradu, Mike Petrovića Alasa br. 12-14, Beograd - Vinča, 11351 Beograd (e-mail: davidovic@vin.bg.ac.rs).

Milena Davidović – Građevinski fakultet, Univerzitet u Beogradu, Bulevar Kralja Aleksandra 73, 11020 Beograd, Srbija (e-mail: milena@ grf.bg.ac.rs).

Sonja Dmitrašinović – Fakultet tehničkih nauka u Novom Sadu, Univerzitet u Novom Sadu, Trg Dositeja Obradovića 6, 21102 Novi Sad (e-mail: dmitrasinovic@uns.ac.rs).

Milesa Srećković – Elektrotehnički fakultet, Univerzitet u Beogradu, Bulevar Kralja Aleksandra 73, 11020 Beograd, Srbija (e-mail: esreckov@ etf.bg.ac.rs).

Milena Jovašević–Stojanović – Institut za nuklearne nauke "Vinča", Institut od nacionalnog značaja za Republiku Srbiju, Univerzitet u Beogradu, Mike Petrovića Alasa br. 12-14, Beograd - Vinča, 11351 Beograd (e-mail: mjovst@vin.bg.ac.rs).

 ISBN 978-86-7466-930-3

koje omogućavaju visoku vremensku rezoluciju. Teorijska osnova optičke metode je teorija Mijevog rasejanja.

Za analizirane primere kombinovanja spektara će biti korišćeni rezultati merenja iz kampanje mobilnog monitoringa u Novom Sadu 2022.

## II. FIZIČKE OSNOVE I PRINCIPI RADA KORIŠĆENIH MERNIH INSTRUMENATA

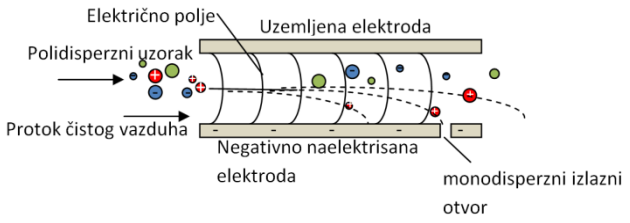


Sl. 1. Princip odabira čestica na osnovu njihove električne pokretljivosti. Šematski detalj radijalnog diferencijalnog analizatora pokretljivosti (engl. radial differential mobility analizer RDMA)

U ovoj sekciji ćemo ukratko prikazati fizičke osnove i principe rada dva korišćena instrumenta za merenje čestičnog zagađenja. Prvi korišćeni instrument, TSI Nanoscan SMPS 3910, razlikuje čestice po njihovoj električnoj mobilnosti. Na taj način uređaj može da diskriminiše čestice dijametara od 10nm do 420nm u 13 kanala. Za tu svrhu se koristi deo uređaja koji je šematski prikazan na Sl. 1. U sklopu uređaja veličina čestice se procenjuje pomoću radijalnog diferencijalnog analizatora pokretljivosti, koji je zbog kompaktnosti pogodan za korišćenje u prenosivom instrumentu. Čist vazduh bez čestica ulazi u kružni kanal sa donje spoljne ivice RDMAa prethodno je tretiran kako bi se postiglo laminarno strujanje. Sa gornje strane se takođe tangencijalno uvodi vazduh sa česticama različite veličine (uzorkovani polidisperzni aerosol). Gornja elektroda RDMA je uzemljena, a donja elektroda priključena na negativan napon, tako da se između elektroda stvara električno polje. Na pozitivno naelektrisane čestice deluje električna sila usled koje se kreću ka negativnoj elektrodi. Na čestice deluje i Stoksova sila otpora vazduha. Kroz izlazni otvor na katodi za određenu vrednost primenjenog napona prolaze aerosoli klasifikovani po električnoj pokretljivosti (a time i po veličini) i dalje idu ka brojaču čestica. Preostali vazduh i čestice vraćaju se da cirkulišu u uređaju optimizujući laminarnost strujanja. Jednačina kretanja čestice pod dejstvom električnog polja i Stoksove sile otpora, a koja je suspendovana u vazduhu koji struji brzinom $\vec{u}$, je data sa

$$\frac{d\vec{p}}{dt} = m\frac{d\vec{v}}{dt} = \frac{3\pi\mu D_p}{C}(\vec{u} - \vec{v}) + q\vec{E} \qquad (1)$$

gde je $m$ masa čestice, $\vec{v}$ njena brzina, $D_p$ je dijametar čestice, $\mu$ koeficijent viskoznosti vazduha, $C$ korekcioni slip faktor, $q$ naelektrisanje čestice, i $\vec{E}$ jačina električnog polja. Terminalna brzina u pravcu električnog polja čestice se postiže veoma brzo, u momentu kada je rezultantna sila jednaka nuli i data je sa

$$\frac{3\pi\mu D_p}{C} v_e = qE \qquad (2)$$

Na osnovu jednačine (2) moguće je napisati izraz za električnu mobilnost kao $\vec{v_e} = B_e\vec{E}$ gde je $B_e = \frac{C\,q}{3\pi\mu D_p}$.

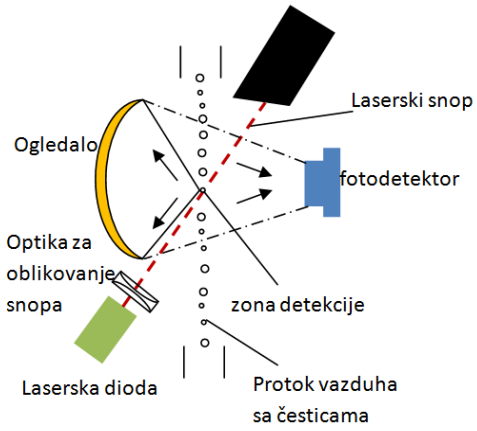


Sl. 2. Princip odabira čestica na osnovu njihovih optičkih svojstava. Šematski detalj optičke komore u kojoj se laserom obasjavaju uzorkovane čestice.

Drugi korišćeni instrument, TSI OPS 3330, razlikuje čestice po njihovim optičkim svojstvima. Na taj način uređaj može da diskriminiše čestice dijametara od 300nm do 10um u 16 kanala. Princip rada je sledeći. Čestice obuhvaćene i vođene strujanjem čistog vazduha nailaze u malu zonu detekcije koja je obasjana laserskom svetlošću. Sistem je konstruisan tako da se u zoni detekcije ne nalazi više od jedne čestice istovremeno, osim u slučaju veoma visokih koncentracija čestoca, pri čemu dolazi do greške koincidencije. Laserska svetlost rasejava se na pojedinačnim česticama i nakon refleksije od zakrivljenog ogledala dolazi do fotodetektora. Veličina čestice se određuje poređenjem izmerenog intenziteta na fotodetektoru i standardne kalibracione krive dobijene merenjima izvršenim sa skupom uniformnih čestica poznatog dijametra i indeksa prelamanja. U optičkim meračima ovog tipa seza kalibraciju najčešće koriste bele polistiren lateks čestice. Teorijske kalibracione krive izračunaju se korišćenjem Mijeve teorije rasejanja na sfernim česticama. Ključni parametri koji određuju rasejanje i apsorpciju svetlosti na čestici su talasna dužina upadne svetlosti, veličina čestice koja se obično uvodi preko bezdimenzionog parametra $\alpha = \frac{\pi D_p}{\lambda}$, gde je $D_p$ dijametar čestice a $\lambda$ talasna dužina svetlosti i kompleksni indeks prelamanja čestice normalizovan na indeks prelamanja okolne sredine (vazduha) $m = \frac{N}{N_0} = \frac{n+ik}{N_0}$. Iz izmerenog intenziteta svetlosti rasejanog pod uglom $\theta$, $I(\theta, \alpha, m)$ ukoliko nam je poznat indeks prelamanja čestice sferne možemo dobiti njen tačan dijametar. Vrednosti dijametra koje se dobijaju merenjima pomoću optičkih merača veličine bile bi tačne samo ako je indeks prelamanja čestica veoma blizak indeksu prelamanja kalibracionih čestica.

Optički dijametar i dijametar dobijen merenjem pokretljivosti su međusobno usaglašeni za kalibracione sferne čestice, ukoliko čestice nisu sferne ili im se indeks prelamanja razlikuje od indeksa prelamanja kalibracionih čestica potrebno je naknadno usaglašavanje izmerenih spektara.


ISBN 978-86-7466-930-3

## III. Metod

Kombinovanje dva spektra veličina čestica, koji su dobijeni pomoću merenja kvalitativno različitim metodama, podrazumeva određeni nivo modelovanja, tj. uvođenja pretpostavki za modelovanje. Pretpostavka koja motiviše modelovanje proističe iz činjenice da se podjednako i istovremeno koriste obe vrste merenja (sa izabranim težinskim koeficijentima), što je poboljšanje u odnosu na pojedinačno korišćenje metoda, pre svega u minimizaciji greške usled nepreciznosti pojedinačnog instrumenta. U nastavku ćemo opisati dva moguća metoda kombinovanja spektra veličina čestica.

Prvi metod je zasnovan na interpolaciji spektara, pri čemu se za svaki pojedinačni spektar, prikazan u $\frac{dN}{d\log D_p}$ gustini, nameće broj modova od 1 do 2, a za kombinovani spektar se nameće broj modova od 1 do 3. Takođe, kanali dva instrumenta koji se preklapaju, i vrednosti koje su izmerene u tim kanalima se kombinuju u jednu interpolacionu tačku, sa izabranim težinskim koeficijentom. Svaki od modova, koji se koriste pri interpolaciji, je oblika Gausijana, ili zasečenog Gausijana. Ovu metodu je moguće koristiti i za brojčane i za masene koncentracije.

Drugi metod je nešto složeniji i kombinuje dva spektra veličina čestica tako što korekcijama indeksa prelamanja čestica i faktora oblika čestica (engl. shape factor) nastoji da smanji razliku između dva spektra u intervalu njihovog preklapanja. Na ovaj način se dobija uz kombinovani spektar dobija, informacija o indeksu prelamanja čestica kao i faktoru oblika čestica. Oba metoda su dostupna u softveru Multi Instrument Manager 2.0 [3], koji se standardno isporučuje uz dva instrumenta. Ovu metodu je moguće koristiti samo za brojčane koncentracije.

Podaci koje ćemo koristiti za primenu dva metoda su prikupljeni u zimskoj kampanji merenja 2022 na teritoriji grada Novog Sada pomoću instrumenata TSI Nanoscan SMPS 3910 i TSI OPS 3330, iz vozila u pokretu. Svako merenje je bilo geolocirano, a za potrebe ovog rada podaci su usrednjeni na 1 minut.

## IV. Rezultati

U ovoj sekciji ćemo prikazati nekoliko karakterističnih primera spajanja spektara pomoću dve opisane metode. Prva metoda je na slikama označena sa “bez korekcije”, dok je druga metoda, u kojoj se vrši korekcija indeksa prelamanja označena “sa korekcijom”.

Na slici 3 je prikazan uzorak 6, izmeren 04-Mar-2022 12:03:00. Sa slike 3a je evidentno da dve metode daju gotovo identične kombinovane spektre. Položaj modova je za prvi mod $D_p = 19{,}74\,nm$ ,$\frac{dN}{d\ log\ D_p} = 9705\,\frac{\#}{cm^3}$ i za drugi mod $D_p = 129{,}5\,nm$, $\frac{dN}{d\ log\ D_p} = 9641\,\frac{\#}{cm^3}$. Brojčani udeo po frakcijama iznosi $PN_{0.1}$: 6217.60, $PN_{0.5}$: 10590.32, $PN_1$: 10729.67, $PN_{2.5}$: 10737.26, $PN_4$: 10737.29 i $PN_{10}$: 10737.30 #/cm$^3$. Ono što je međutim dodata vrednost drugog metoda je da koristi drugačiju metodologiju, pa da uz kombinovani spektar dobijamo i informaciju o indeksu prelamanja i odstupanju čestica od sferičnih. U ovom primeru (uzorak 6) je indeks prelamanja 1.5941 i faktor oblika 1.0009.

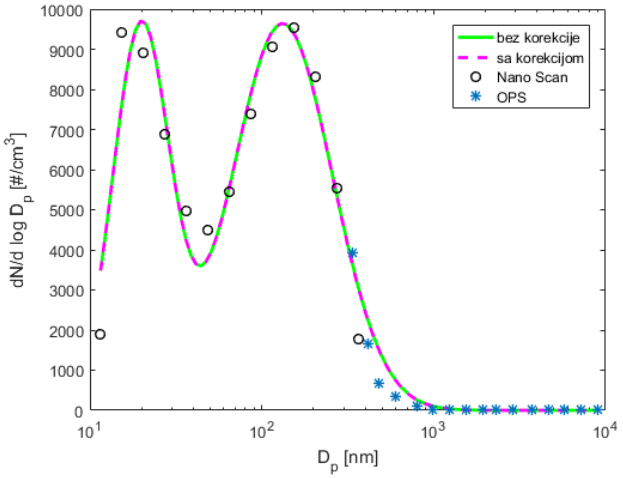


(a)

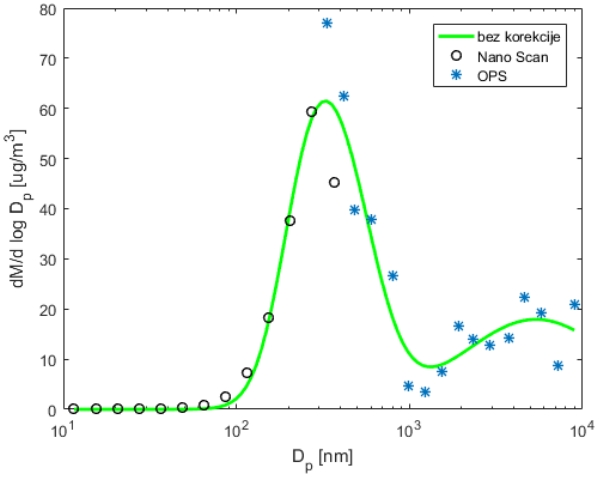


(b)

Sl. 3. Uzorak 6: 04-Mar-2022 12:03:00 a) primer spajanja spektara brojčane koncentracije pomoću dve metode. b) primer spajanja spektara masene koncentracije

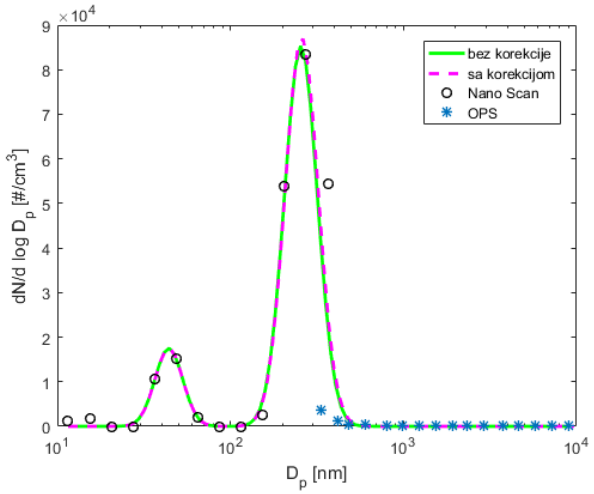


(a)


ISBN 978-86-7466-930-3

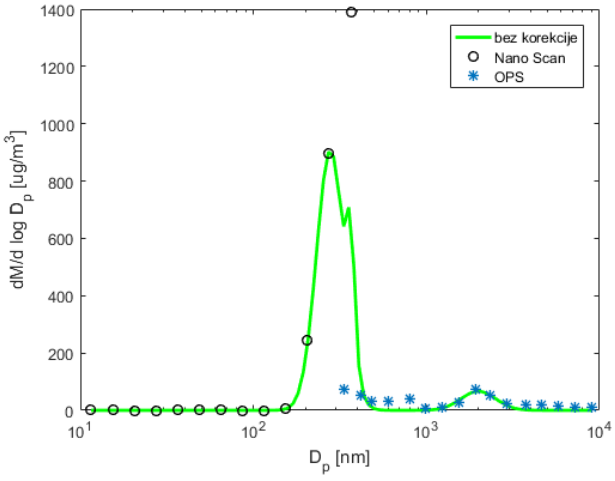


(b)

Sl. 4. Uzorak 26: 04-Mar-2022 12:23:00 a) primer spajanja spektara brojčane koncentracije pomoću dve metode. b) primer spajanja spektara masene koncentracije

Na slici 3b je prikazan kombinovani spektar masene koncentracije. Uočljiv je standardni fenomen da čestice većeg dijametra znatno više utiču na masu, pa stoga uočavamo da su dominanti drugi modovi u kombinovanom spektru. Ovo je evidentno i iz masenog udela po frakcijama je $PM_{0.1}$: 0.18, $PM_{0.5}$: 27.15 $PM_1$: 34.44 $PM_{2.5}$: 38.49 $PM_4$: 41.70 i $PM_{10}$: 47.77 μg/m$^3$.

Na slici 4 je prikazan uzorak 26, izmeren 04-Mar-2022 12:23:00. Sa slike 4a je evidentno da dve metode i u ovom primeru daju gotovo identične kombinovane spektre, ali da su sada dominantna druga 2 moda, naime polozaj modova je za prvi mod $D_p = 44{,}92\,nm$, $\frac{dN}{d\,log\,D_p} = 1{,}743 \cdot 10^4 \frac{\#}{cm^3}$ i za drugi mod $D_p = 263{,}2\,nm$, $\frac{dN}{d\,log\,D_p} = 8{,}691 \cdot 10^4 \frac{\#}{cm^3}$. Brojčani udeo po frakcijama iznosi $PN_{0.1}$: 3510.58, $PN_{0.5}$: 23832.11, $PN_1$: 23844.91, $PN_{2.5}$: 23844.91, $PN_4$: 23844.91 i $PN_{10}$: 23844.91 #/cm$^3$. U ovom primeru (uzorak 26) je indeks prelamanja 1.4046 faktor oblika 1.05. Na slici 4b je prikazan kombinovani spektar masene koncentracije. Uz standardni fenomen da čestice većeg dijametra znatno više utiču na masu, uočavamo i ograničenja korišćenog algoritma budući da neki modovi nisu uračunati u kombinovani spektar, zbog ograničenja na maksimalno 3 interpolirana moda. Takođe dominantni mod, zbog veće razlike u izmerenoj masi između dva instrumenta u kanalu koji se preklapa u interpolaciji nije blizak sa merenjima dva instrumenta. U ovakvim situacijama, konzervativna procena koncentracije aerozagađenja bi uzela u obzir veću koncentraciju, što bi se u algoritmu moglo primeniti većim težinskim koeficijentom primenjenim na odgovarajući instrument. Maseni udeo po frakcijama je $PM_{0.1}$: 0.18, $PM_{0.5}$: 203.63 $PM_1$: 203.74 $PM_{2.5}$: 218.22 $PM_4$: 220.35 i $PM_{10}$: 220.36 μg/m$^3$.

Na slici 5 je prikazan uzorak 39, izmeren 04-Mar-2022 12:36:00. Sa slike 5a je evidentno da u ovom primeru postoji razlika između kombinovanih spektara za dve metode, i da u odnosu na prethodna dva primera u ovom slučaju postoje 3 moda u kombinovanom spektru. To su modovi $D_p = 27.1\,nm$, $\frac{dN}{d\,log\,D_p} = 3498 \frac{\#}{cm^3}$, zatim drugi mod na $D_p = 115.1\,nm$, $\frac{dN}{d\,log\,D_p} = 1.344 \cdot 10^4 \frac{\#}{cm^3}$ i treći mod na $D_p = 401.2nm$, $\frac{dN}{d\,log\,D_p} = 4820 \frac{\#}{cm^3}$. Brojčani udeo po frakcijama iznosi $PN_{0.1}$: 3693.81, $PN_{0.5}$: 9591.06, $PN_1$: 11301.75, $PN_{2.5}$: 11372.78, $PN_4$: 11372.78 i $PN_{10}$: 11372.78 #/cm$^3$. U ovom primeru (uzorak 39) je korigovani indeks prelamanja 1.9577 i faktor oblika 0.8787.

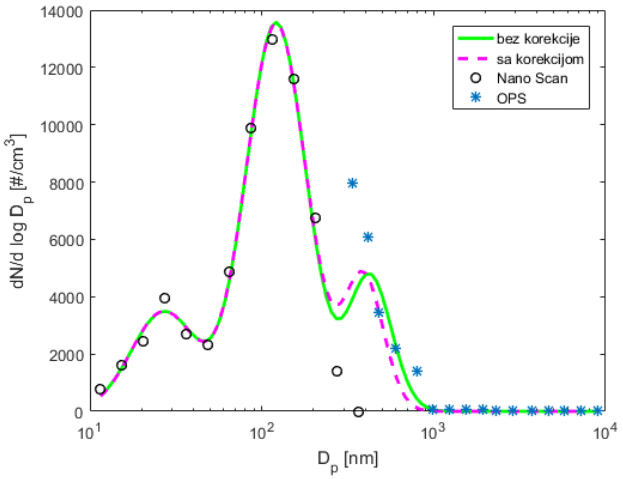


(a)

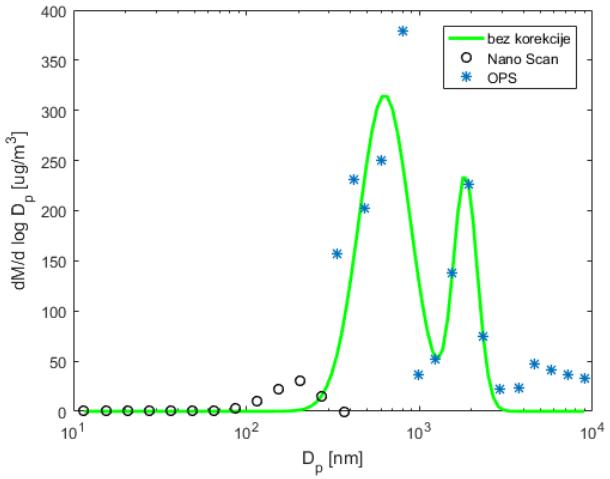


(b)

Sl. 5. Uzorak 39: 04-Mar-2022 12:36:00 a) primer spajanja spektara brojčane koncentracije pomoću dve metode. b) primer spajanja spektara masene koncentracije

Na slici 5b je prikazan kombinovani spektar masene koncentracije. Uz standardni fenomen da čestice većeg dijametra znatno više utiču na masu, ponovo uočavamo i ograničenja korišćenog algoritma budući da neki modovi nisu uračunati u kombinovani spektar. Takođe i u ovom slučaju postoji znatna razlika između merenja dva instrumenta u kanalu koji se preklapa, tako da bi za konzervativnu procenu bilo potrebno korigovati težinske koeficijente tako da više uzimaju u obzir instrument koji je izmerio višu vrednost. Maseni udeo po frakcijama je $PM_{0.1}$: 0.18, $PM_{0.5}$: 33.16 $PM_1$: 108.61 $PM_{2.5}$: 156.68 $PM_4$: 157.26 i $PM_{10}$: 157.26 μg/m$^3$.

## V. ZAKLJUČAK

U ovom radu je ilustrovana primena dva metoda


ISBN 978-86-7466-930-3

kombinovanja spektara koji su dobijeni pomoću dve komplementarne metode merenja. Na nekoliko karakterističnih primera je pokazano kako se razlikuju spektri brojčane i masene koncentracije, i ukazano je na prednosti i nedostatke metoda spajanja spektara. U slučaju da dve opisane metode spajanja spektara daju sličan rezultat, korišćenjem metode sa korekcijom indeksa prelamanja se uz konačni spektar može dobiti i sadržajan podatak o indeksu prelamanja i faktoru oblika čestice. Budući da se u praksi prilikom merenja prikupi jako velik broj podataka, spajanje spektara bi bilo najpogodnije automatizovati, što trenutna implementacija algoritma ne dozvoljava, već je neophodno ručno zadavanje broja modova koji je ograničen na maksimalno 3 moda u konačnom spektru, kao i ručni odabir težinskog faktora sa kojim ulaze merenja instrumenata u preklapajućem opsegu veličina čestica. Jedan od mogućih načina automatizacije je automatska korekcija težinskih koeficijenata, tako da kombinovani spektar više uzima u obzir instrument koji je izmerio veću koncentraciju u kanalu koji se preklapa u dva spektra. Na ovaj način bi bilo moguće kreirati mape visoke rezolucije koje bi kao ulazne podatke imale konzervativno procenjen kombinovani spektar.

## ZAHVALNICA

Zahvaljujemo se projektima: H2020 VIDIS, br. 952433 u okviru programa Evropske unije za istraživanje i inovacije HORIZON 2020 (https://vidis-project.org/), zatim projektu ‘Prostorno-vremenske varijacije nivoa respirabilnih čestica u urbanoj zoni Novog Sada – mobilni monitoring, modelovanje i kreiranje mapa visoke rezolucije’ delimično finansiranom od gradske uprave grada Novog Sada kao i Ministarstvu prosvete, nauke i tehnološkog razvoja Republike Srbije.

## LITERATURA

[1] Oberdörster G, Oberdörster E and J. Oberdörster, Nanotoxicology: an emerging discipline evolving from studies of ultrafine particles. Environ Health Perspect, 11: 823-839, 2005.

[2] Gurr, J.R., Wang, A.S.S., Chenb, C-H. and K.Y. Jan, Ultrafine titanium dioxide particles in the absence of photoactivation can induce oxidative damage to human bronchial epithelial cells. Toxicology, 213: 66-73, 2005.

[3] Multi-instrument manager (MIM™) software for SMPS™ spectrometers and OPSs sizers user’s guide (version 2.0) p/n 6007798, revision A april 2014, TSI Incorporated

## ABSTRACT

Atmospheric aerosols in urban environments consist of particles of different diameters, which can range in size from a few nanometers to a few micrometers. Therefore, it is often necessary to use several instruments to measure the aerosol concentration, with fundamentally different underlying measurement principles. In this paper, methods based on measuring the electrical mobility of particles, for the diameter range from 10nm to 420nm, and measuring the equivalent optical diameter, for the diameter range from 300nm to 10um, were used. As a main result, examples of combining particle size spectra obtained using these two complementary measurement methods are presented. In the process of combining the particle size spectra, it is possible to modify the distribution obtained by optical measurements by searching for the optimal value of the particle refractive index so as to obtain the best possible agreement with the distribution obtained by measuring electrical mobility. The results of measurements from the mobile monitoring campaign in Novi Sad 2022 were used as input data.

**An e ample of combining the distribution of atmospheric aerosols obtained by the method utilizing electrical mobility and the optical method**

Miloš Davidović, Milena Davidović, Sonja Dmitrašinović, Milesa Srećković, Milena Jovašević-Stojanović

 ISBN 978-86-7466-930-3

# INTEGRACIJE NAUČNIH ZNANJA U PRIMENI VEŠTAČKE INTELIGENCIJE U HERITOLOŠKIM PROBLEMIMA

Suzana Polić, Milesa Srećković, Zoran Stević, Slobodan Bojanić, Željka Tomić

*Apstrakt*—**Primena veštačke inteligencije u zaštiti kulturne baštine, na ovom stepenu razvoja, odnosi se prevashodno na domen akvizicije podataka koji mogu biti od značaja za stvaranje šire slike o sredstvima i metodama realizacije umetničkih dela. U ovom radu istražuje se pitanje integracije naučnih znanja u kontekstu primene veštačke inteligencije, a u vezi sa delima velikih formata, i to u domenima specifikuma organizacije materije, diferencijacije komponenti i njihovih elemenata, strukturnih planova i matrica koje daju kvalitet unutrašnje koherencije i grade performativnu snagu dela. Multidisciplinarna opservacija treba da doprinese procesu objektivizacije znanja, do koje se, prirodom predmeta istraživanja, može doći samo integracijom elemenata više nauka i naučnih disciplina.**

*Ključne reči*—**naučna znanja, veštačka inteligencija, heritološki problemi**

## I. UVOD

Upotreba lasera i lidara, uz podršku veštačke inteligencije, obeležava naučni rad u zaštiti kulturnog nasleđa na početku treće decenije XXI veka. Reč je o primenama u vezi sa procenama oštećenja površina objekata, putem analiza *oblaka tačaka*, uz korišćenje rezultata dobijenihnedestruktivnim i beskontaktnim metodama istraživanja [1], a takođeje reči o kreiranju algoritama za klastere *LidarPoint Cloud*podataka [2], gde se raspolaže informacijama o karakteristikama objekata, do nivoa detalja veličine milimetra [3].

Ove primene već su dale rezultate u istraživanjimazaštite značajnog kulturnog nasleđa, kao što je to *PalazzoVecchio* u Firenci (gde je primenjen *OPTICS clusteringmethod*) [4] ili katedrala*Notre Dame* u Parizu, za koju je laserskim skeniranjem prikupljeno preko milijardu tačaka [5]. Posebno je značajno to, što neuronske mreže pomažu u utvrđivanju defekata upotrebom lidar sistema, uz integrisanjerezultata numeričkih simulacija, u cilju utvrđivanja šteta nastalih na objektima [6, 7] kaoposledicamakatastrofa koje su zahvatile viševekovno kulturno nasleđe. U okolnostima u kojima se zahteva brza obnova ovih objekata, a bez raspoložive detaljne originalne dokumentacije, u upotrebi su i sofisticiraneanalize podataka, zasnovane na metodi *linearne regresije*, odnosno na znanjima iz oblasti teorije verovatnoće, matematičke statistike, linearne algebre i multivarijabilnihanaliza[8].

Izvan područja detekcije i opservacije oštećenja na predmetima i objektima kulturnog nasleđa, veštačka inteligencija dala je i značajan doprinos u novoj oblasti konzervacije – restauracije, a u cilju integralnog razumevanja autorskih dela, gde se veštačka inteligencija koristi za rekonstrukciju nedostajućih delova umetničkih dela, kojiiz različitih razloga nisu sačuvani. Delotvornost ove metode potvrđena je, u do sada najvećem projektu savremenih naučnih muzejskih istraživanja, u restauraciji Rembrantovogremek-dela *Noćna straža*(*De Nachtwacht*) iz 1642. godine, koje se nalazi u kolekciji *Rijksmuseum* u Amsterdamu. Posle završenog projekta *OperationNightwatch*, u vezi sa ovim umetničkim delom,raspolaže se sa717 biliona piksela, a veštačka inteligencija pomogla je u spajanju 8.439 pojedinačnih fotografija delova ove slike, snimljenih sa iste udaljenosti od 13 cm. Sve je smešteno na prostoru od 5,6 terabajta.Na taj način su stvoreni preduslovi za rekonstrukciju nestalih delova slike ovog velikog formata (3,63 m x 4,37 m), koji se sada može, prvi put posle 300 godina, videti u originalnoj veličini, budući da je delo1715. godine skraćivanozbog postavljanja u gradsku kuću u Amsterdamu, kako bi moglo da bude uneseno kroz vrata (!?!). Tada je na slici odsečeno 60 cm sa leve strane, 22 cm od gornje ivice, 12 cm od donje ivice i 7 cm sa desne strane slike. Na osnovu svih prikupljenih podataka, uz specijalno kreirani softver, a prema kopiji ovog dela, koju je uradio Rembrantov savremenik GerritLundens (1622 – 1686), veštačka inteligencija dala je ključan doprinos u rekonstrukciji *Noćne straže*, ne samo u materijalnom vidu dela, posebnostratigrafiji bojenih slojeva, već i u razumevanju autorske ideje, budući da ova rekonstrukcija pokazuje novo dimenzionalnotežište slike, što pomera i konstelaciju prikazanih ljudskih figura koju je umetnik izvorno kreirao[9].

Navedeni primeriukazuju na složenost upotrebe veštačke inteligencije u savremenoj zaštiti nasleđa, u kojoj rezultati korišćenja laserske tehnike u dijagnostici stanja predmeta i objekata[10],uz primenurobotike iuz razvoj elektronske ličnosti [11],stvaraju novo polje integracije sa podacima koje daju komplementarnedisciplineprirodnih i tehničkih nauka, kao i pomoćne naučnedisciplinepovezane za istorijom umetnosti i arheologijom[12]. Imajući u vidu da se najveći obim istraživanja posvećuje pitanju,*šta veštačka inteligencija može da učini u zaštiti nasleđa*, a da postoji izraženi nedostatak istraživanja posvećenih pitanju,*kako u tom cilju integrisati neophodna znanja u primeni veštačke inteligencije*, to je predmet ovog rada upravo pitanje načina integracije znanja, posebno sa stanovišta intenzivnih promena, koje u zaštiti kulturnog nasleđa, inicira primena novih tehnologija[13], u skladu sa duhom tehnološkog vremena[14].

 ISBN 978-86-7466-930-3

## II. DOKTRINA POLIFONIJSKOGMETODOLOŠKOG MIŠLJENJA

Heritološko znanje, u kojem se uz pomoć novih tehnologijaotvaraju novipravci istraživanja, pokazuje kompleksnost multidisciplinarnog promišljanja [15,16], baziranog na *polifonijskom mišljenju,* koje danas multidisciplinarno, metodološki, osim heritologije,obeležava i filozofsku granu tehnofilozofije[17].U dugoj tradiciji razvoja doktrine polifonijskog mišljenja (sa akcentom na različitosti između naučnog znanja i znanja o nauci), gde se doktrina kao sistem učenja razvija praktično od I veka n.e., kada teoretičar Guidod'Arezzo piše traktate *Micrologus*i *Epistola,* polifonijsko mišljenje dostiže vrhunac u vreme renesanse, da bi stupanjem prosvetiteljstva na istorijsku scenu,polifonijsko mišljenje bilo gotovo zaboravljeno u nauci, opstajući prevashodno u umetnosti. Posle periodaviševekovnog razvoja pojedinačnih, uskih specijalnosti u različitim naukama, danasu XXI veku,dostignuta je svest o tome da je polifonijsko mišljenje zapravo *tehnika*, odnosno kanon (u smislu pravila / normi), čije se funkcionisanje, kako to konstatuje metodičar Pavel Rojko, lako može ustanoviti, ali da i dalje nema odgovora na pitanje, kako je i zašto ta *tehnika* prešla u *umetnost* [18]. Ovo pitanje aktuelno je u svetlu činjenice, da multidisciplinarnost u svojoj suštini praktično nije ostvarljiva bez polifonijskog metodološkog mišljenja.

Keplerovo delo*Harmonicesmundi libri V*iz 1619. godine, u kojem je reč o*kontrapunktu univerzalnih harmonija svih planeta*, primer je koji ukazuje na svu složenost održanja polifonijskogmišljenja u nauci, budući da je za razvoj kanona neophodno permanentno uključivanje novih naučnih dostignuća. Sa druge strane, umetnost, koja svih prethodnih vekova nije odustajala od polifonijskog mišljenja, dostigla je takvu prohodnost kroz vreme, da se univerzalnost polifonijskog mišljenja održava kao standard. Primer je delo FjodoraMihajloviča Dostojevskog, kao inovatora, čiji opus ukazuje na ideografska i paradigmatička čvorišta u teorijskoj i primenjenoj ravni, značajna u proučavanju linija sinhronije / dijahronije, u prikazivanju načina na koji *celina* oblikuje *strukturu*, i gde, kako to promišlja Bahtin, „…svaki smisao otkriva svoju dubinu kada se sretne i dodirne sa drugim i drugačijim smislom“[19], kao što je to, kako pokazuje istorija, u srednjovekovnoj teorijiustanovio princip *punctumcontrapunctum*(kontrapunkt), odnosno u savremenoj upotrebi laserske tehnike,*LidarPointCloud.*

To pokazuje da je neophodno da se polifonijsko metodološko mišljenje u zaštiti baštine, bazira na svim univerzalno konstituisanim normama, koje važe i u naučnom i u umetničkom domenu i bez obzira na tradicionalno distancirane diskurse, imajući u vidu da ta vrsta distance nema značaja u primeni veštačke inteligencije, a što je sasvim u skladu sa revolucionarnim Šenbergovimfilozofsko-estetičkim principom polifonije, koji je „…nešto što je heteronomno emancipovanoj harmoniji i što s njom svakom prilikom tek treba da se izmiri“ [20], ili preneto u domen primene veštačke inteligencije u heritologiji, nešto što svakom prilikom egzaktnotreba da se potvrdi.

Imajući u vidu navedene postavke, kao i činjenicu da veštačka inteligencija „uči“ na način koji kreira čovek, u ovom istraživanju tragalo se za mogućim razvojnim linijama u izgradnji *polifonijskog mišljenja,* kojebi ukazivale na izvore nauke, odnosno mišljenja o kontrapunktu / polifoniji, na način da mogu da budu pogodne za algoritam „učenja“ veštačke inteligencije. Analiza različitih razvojnih linija, pokazala je da ovakvo učenje treba da se konstituiše polazeći od naučnog dokaza Knuta Jepesna (KnudJeppesen), da je učenje o kontrapunktu tek u XVI veku dobilo tako čvrstu organizaciju, „…da je svoju egzistenciju nastavilo nezavisno od prakse“ [21], što je i ovdeprezentovani model ograničilo na navedeni period. Kao što se može videti, tabelarno su prikazani traktati polihistora, koji u sebi sadrže začetke polifonijskog mišljenja (matematičara, fizičara, muzičkih teoretičara, metafizičara, filozofa, astronoma, kompozitora, pesnika, državnika, diplomata i slikara), upravo zbog rudimentarnosti i nedovoljnekonstituisanosti, što u procesu razvoja veštačke inteligencije, omogućava različita tematsko-strukturalna račvanja[24 -39], pogodna za učenje neuralnih mreža.

Tabela 1. Jedan modus linije razvoja ka polifonijskom mišljenju [22 -37]

| Autor | Traktati i druga dela |
|---|---|
| ***Guidod'Arezzo*** (c. 991-992 – c. 1033) | ●*Micrologus de disciplina artismusicæ;* ●*Epistola ad Michaelem* |
| ***FrancoofCologne*** (13.vek) | ●*Arscantusmensurabilis;* ●*Compendiumdiscantus* |
| ***Johannes de Garlandia*** (c. 1270 – 1320), ur. | ●*De musicamensurabilipositio;* ● *Introductio in contrapunctuproruribus* |
| ***Johannes de Muris*** (c.1290 - c.1355) | ●*De discantu et consonantiis;* ●*Musicaspeculativa;* ●*Musicapractica;* ●*Libelluspracticacantusmensurabilis;* ●*Arsnovaemusicae;* ●*Arscontrappuncti;* ●*Arsdiscantus;* ●*Quilibetaffectans (prva didaktika kontrapunkta)* |
| **WalterofEvesham** (? - ?1330) | ●*Summa de speculationemusicae* |
| ***Philippe de Vitry*** (1291-1361) | ●*Arscontrapunctus;* ● *Arsperfecta in musica;* ●*Arsnovae* |
| ***Petrusfraterdictus Palma ociosa***(v. 1291-v. 1356) | ●*Contrapunctusdiminutusandprolongation;* ●*Compendium de discantumensurabili* |
| ***Guillame de Machault*** (1300-1377) | ●*The Debate Series: LeJugementdouroy de Behaingne (Judgmentofthe King ofBohemia) &LeJugementdouroy de Navarre (Judgmentofthe King ofNavarre)* |
| ***Prosdocimus de*** | ●*Algorismus de integris sive praticaarismetrice de integris (1410)reprintedFedericusDelphinused.* |

 ISBN 978-86-7466-930-3

| | |
|---|---|
| ***Beldemandis*** (? – 1428) | *(Venice, 1483 and 1540);●Expositionestractatuspraticecantus mensurabilisJohannis de Muris (c. 1404); ●Tractatuspraticecantusmensurabilis (1408); ●Brevissummulaproportionumquantum ad musicampertinet (1409); ●Contrapunctus (1412), editedby Jan Herlinger, 1984; ●Tractatuspraticecantusmensurabilis ad modumYtalicorum (1412);●Tractatus plane musice (1412), editedby Jan Herlinger, 2008; ●Parvustractatulus de modo monacordum dividendi (1413), editedby Jan Herlinger; ●Tractatusmusicespeculative (1425), editedby Jan Herlinger, 2008.* |
| ***EhanLeTaintenier*** ( c. 1435 - 1511) | ●*Liber de artecontrapuncti (1477); Liber de natura et proprietatetonorum* |
| ***GioseffoZarlino*** (1517–1590): | ●*LeInstitutioniHarmoniche* (1558); ●*Dimostrationiharmoniche* (1571) |
| **VincenzoGalilei** (c. 1520-1591) | ●*Ilprimo libro dellapratticadelcontrapuntointornoall'usod elleconsonanze;* ●*Discorsointornoall'usodelledissonanze;* ●*Discorsointornoall'usodell' enharmonio, et di chifusse autore delcromatico; Dubiiintorno a quantoiohodettodell' enharmoniocon la solutione di essi (apendix);●Dialogodellamusicaantica e della moderna* |

Za potrebe razvoja veštačke inteligencije u heritologiji, analiza prikazane razvojne linije ukazuje na neophodnost da se u primeni veštačke inteligencije u heritologiji, procesualno i u kontinuitetu razrešava problem fenomena*presupozicije*(termin preuzet izoblasti pragmatike)[38,39], koji polifonijski korespondira sa *implikaturom,* kao i *semantičkom ili logičkom implikacijom*, na polju razumevanja komunikacija između različitih naučnih oblasti i umetnosti. *Presupozicija*, kao tvrdnja uslovljena kontekstom, čija se istinitost ne dovodi u pitanje (u ovom slučaju tehničke provenijencije), a koju odlikuje postojanost pod negacijom, u odnosu na *implikaturu* kao zaključak o značenju koje nije izrečeno i egzistira van zajedničkog konteksta (u ovom slučaju iz domena izvan empirijskog znanja), zahteva softversku izgradnjumodaliteta uzajamnih povezanosti, u težnji ka stvaranju što preciznijih *semantičkih implikacija*.

Na ovom polju, kako pokazuje istraživanje sprovedeno u ovom radu, od pomoći je *aporetika*, kao disciplina u kojoj seprepoznajeusmerenost*na obradu i isticanje dosega problema,*kako to formuliše Hartman [40], agde posebno treba imati u vidu razlikovanje posmatranjaslojeva umetničkog dela[41], kao i u širem okviru, stanovište Ingartena, da u istraživanju načina postojanja umetničkog dela treba primenjivati čisto perciptivan način prilaza suštini stvari, dakle„zauzimati stav fenomenologa“ [42].

## III. ZAKLJUČAK

U radu su prikazani rezultati istraživanja modusa za integraciju znanja neophodnog u primeni veštačke inteligencije u heritologiji, a u funkciji podrške primeni lasera, lidara i drugih tehnologija koje danas čine osnovu za razvoj konzervacije-restauracije kulturnog nasleđa. Istraživanjem doktrine polifonijskog mišljenja, od vremena *artesliberales* i potom u različitim razdobljima, ovde je u fokusu bio mogući model za razvoj polifonijskog mišljenja,a prema potrebama primene veštačke inteligencije u heritologiji. Sprovedene analize pokazale su, da se to može realizovati pod uslovima uvažavanja pragmatičkih i aporetičkihuzusa, na osnovu čega je i formiran model, kao predlog koji polazi od spekulativnih postavki prikazujući razvojnu liniju ka složenijim zahtevima za analitičko poznavanje kontrapunkta, što ga i čini pogodnim za uvođenje i razvoj veštačke inteligencije.Istovremeno,ovaj predlog treba da pomogne u očekivanom daljem razvojui promišljanju ovako složene problematike.

## ZAHVALNICA

Istraživanje prezentovano u ovom radu obavljeno je zahvaljujući podršci Ministarstva prosvete, nauke i tehnološkog razvoja Republike Srbije (Ugovor br. 451-03-68/2022-14/200026), kao i zahvaljujući podršci Ministarstva kulture i informisanja Republike Srbije.

## LITERATURA

[1] M. E. Mohammadi, *PointCloudAnalysisforSurfaceDefects in Civil Structures,*Ph.D. Thesis, UniversityofNebraska-Lincoln, Department of Civil Engineering, Lincoln, Nebraska, 2019.

[2]J. B. Haurum, M. M. J. Allahham, M. S.Lynge, K. S. Henriksen, I. A.Nikolov,; T.B. Moeslund, *SewerDefectClassificationusingSyntheticPointClouds,*Proceedingsofthe 16th InternationalConference on ComputerVisionTheoryandApplications (VISAPP), Vienna, Austria, 8–10 February 2021.

[3] T.C. Hou,; J.W. Liu,; Y.W.Liu, *AlgorithmicclusteringofLiDARpointcloud data fortexturaldamageidentificationsofstructuralelements*. Measurement, 108, 2017, pp. 77–90.

[4]Wood, Richard L., andMohammad E. Mohammadi, *Feature-BasedPointCloud-BasedAssessmentofHeritageStructuresforNondestructiveandNoncontactSurfaceDamageDetection,* Heritage 4, no. 2, 2021., pp. 775-793.

[5]Nace, T. *WeHaveBeautiful 3-D Laser MapsofEveryDetailofNotre Dame*. Availableonline: https://www.forbes.com/sites/trevornace/2019/04/16/we-have-beautiful-3d-laser-maps-of-every-detail-of-notre-dame/?sh=4e3e887226e6 (accessed on 31 March 2021).

 ISBN 978-86-7466-930-3

[6] M. Nasrollahi, N.Bolourian, A. Hammad, *Concretesurfacedefectdetectionusingdeepneuralnetworkbased on lidarscanning*, Proceedingsofthe CSCE AnnualConference, Laval, QC, Canada, 12–15 June 2019.

[7]R. Napolitano, M. Hess, B. Glisic, *Integratingnon-destructivetesting, laser scanning, andnumericalmodelingfordamageassessment*: Theroomoftheelements. Heritage 2019, 2, 12.

[8]C. R. Shalizi, *Advanced Data Analysis from anElementaryPointof View,*CambridgeUniversityPress, Cambridge, UK, 2013.

[9] https://www.rijksmuseum.nl/en/whats-on/exhibitions/operation-night-watch

[10] S. Polić, *Primena lasera u obradi, zaštiti i dijagnosticiranju materijala predmeta kulturne baštine*, doktorska disertacija, Univerzitet u Beogradu, 2007.

[11] S. Polić, *DictionaryofTechnologyandElectronicPersonality*, Orthodoxy&ArtificialIntelligence - DictionaryofTechnologyanddouble logos: A Contribution to theDialogbetweenSciencandRelligion, [ed.: A. Petrović, A. Stevanović], Institute ofHistoricalResearch, NationalHellenicResearchFoundation, Athens 2019., pp. 61-79

[12] S. Polić, *Upravljanje znanjem i nematerijalno kulturno nasleđe*, Zbornik radova sa konferencije Primena digitalizacije u kultur i nauci, 16. novembar 2018. u Beogradu, SANU i Institut za uporedno pravo, Beograd, 2019., str. 137-146.

[13]S. Polić, *Challengesforengineering in theheritageprotectionofthe 21st century*, Proceedingsof 211th The IIER InternationalConference, Rome Italy, 20th-21st December 2018., pp. 51

[14]S. Polić,, *MaterialsScienceandzeitgeist as a basisforthepreservationandrestorationofculturalheritage*, Proceedingsof 20thWorldCongress on MaterialsScienceandEngeneering, June 24-26, 2019, Vienna, Auistria; JournalofMaterialSciences&Engineering, Volume 08, 2019., pp. 56

[15] S. Polić,D. Simeunović,*Theimportanceofmultidisciplinaryresearch in theprotectionofculturalheritage*, ConferenceoftheInternationalJournalofArtsandScience, Ca' FoscariUniversityofVenice, Venice , Italy, 20 to 23 june 2017, CD – ROM, pp. 333-334, 2017.

[16] S. Polić,*Opus citatum: robotika i veštačka inteligencija u zaštiti kulturnog nasleđa,* CIK , NANT & ETIKTON, Beograd, 2018 [el. izvor], ISBN 978-86-6179-068-3 (CIK)

[17] S. Polić, *Od inženjerstva do tehnofilozofije u obrazovanju inženjera za zaštitu kulturnog nasleđa*, tematski zbornik radovaXXVI naučnog skupa međunarodnog značaja „Tehnologija, kultura i razvoj“, održanog u Beogradu 2 – 3.12.2019. године, ISBN 978-86-82183-18-1 (IMP), стр. 133-151

[18]P. Rojko, *Glazbeno pedagoške teme*, Vlastita naklada Jakša Zlatar, Zagreb, 2012., p.377

[19] М. М. Бахтин, *Эстетикасловесноготворчества*, Искусство, Москва, 1979.

[20] D.Bužarovski, *Istorija estetike muzike*, Fakultet umetnosti,Niš, 2013.

[21]K. Jeppesen, *Counterpoint: ThePolyphonicVocalStyleoftheSixteenthCentury*, translatedby Glen Haydn, Prentice – Hall, 1939, reprint DoverPublications, New York, 1992.

[22]C. Ruini, *Guidod'Arezzo*, in Dizionariobiograficodegliitaliani, vol. 61, Roma, Istitutodell'EnciclopediaItaliana, 2004.

[23]D. Daolmi, *Storiadellamusicamedioevale e renascimentale*, TemporumStirpisMusica. Dipartimento di Beni culturali e ambientali, Universitàdegli Studi di Milano, (Retrievedmarch 2022)

[24]C.V. Palisca, *Consonance, §1*, The New GroveDictionaryofMusicandMusicians, Ed. StanleySadie, John Tyrrell, VI, OxfordUniversityPress, Oxford, New York, 2001.

[25]R. H. Hoppin, *MedievalMusic*, New York, W.W. Norton &Co., 1978. ISBN 0-393-09090-6

[26] J. Herlinger, *Prosdocimus de Beldemandis*, in: Sadie, Stanley; Tyrrell, John (eds.). The New GroveDictionaryofMusicandMusicians (2nd ed.), Macmillan, London, 2001.

[27]Ch. M. Atkinson, *FrancoofCologne on theRhythmofOrganumPurum*, EarlyMusicHistory, CambridgeUniversityPress, 9, 1990, pp. 1–26.

[28]L. Gushee, *New SourcesfortheBiographyofJohannes de Muris*, JournaloftheAmericanMusicologicalSociety, 22 (1), 1969, pp. 3–26

[29]D. Leech-Wilkinson, *Contrapunctusdiminutusandprolongation, (unpublishedconferencepaper, 1984/5),* https://www.academia.edu/32663077/Contrapunctus_diminutus_and_prolongation*(Retrieved march 2022)*

[30] A. W. Robertson, *Guillaume de MachautandReims: ContextandMeaning in His Musical Works*, Cambridge, CambridgeUniversityPress, England, 2002. ISBN 978-0-521-41876-8.

[31] J. Tinctoris, *Opera Omnia*, CorpusMensurabilisMusicae 18, ed. WilliamMelan, American Institute ofMusicology, 1976.

[32] *GioseffoZarlino*, in The New GroveDictionaryofMusicandMusicians, ed. StanleySadie, vol.20 MacmillanPublishers Ltd., London,1980.

[33] S. Sadie, ed., *VincenzoGalilei*, The New GroveDictionaryofMusicandMusicians, 20 vol. London, MacmillanPublishers Ltd., 1980.

[34] W. Atcherson, *Keyand Mode in Seventeenth - CenturyMusicTheoryBooks*, JournalofMusicTheory 17, no. 2, 1973.

[35]D. De la Motte, *Kontrapunkt,* Kassel: Bärenreiter-Verlag Karl VöterleGmbH&Co. KG,1981.

[36]K. Jeppesen, *Counterpoint: ThePolyphonicVocalStyleoftheSixteenthCentury,* New York: DoverPublications, Inc., 1992.

 ISBN 978-86-7466-930-3

[37]H. Sanders, *Counterpointrevolutionized*, TheMusicalQuarterly*,* 5 (3), 1919., pp. 338-347.
[38] D. Beaver, B. Geurts, *Presupposition*, TheStanfordEncyclopediaofPhilosophy, Winter 2014 Edition, http://plato.stanford.edu (Accessed: march 2022)
[39]M. Simons. *PresuppositionandRelevance, Semanticsvs. Pragmatics*, ed. Z. Szabó, OxfordUniversityPress, Oxford, 2004., str. 329—355
[40]T. W. Adorno, *Philosophyof New Music*, Univ. ofMinnesotaPress, 2006.
[41]N. Hartman, *Estetika*, Dereta, Beograd, 2004.
[42] R. Ingarden, *O književnom delu*, prev. R. Đokić, Foto Futura, Beograd, 2006.

 ISBN 978-86-7466-930-3

# Problem heritološke abdukcije u vezi sa instrumentalnim analizama materijala kulturne baštine

Suzana Polić, Milesa Srećković, Zoran Stević, Miodrag Malović, Miloš Đurić

***Apstrakt*—Heritološki fenomeni u oblasti istraživanja kompozitnih umetničkih dela, u vezi sa raznovrsnošću pristupa u kvalitativnim i kvantitativnim kriterijumima za izbor materijala, postavljaju složene zadatke u primeni instrumentalnih metoda, koje prethode izradi protokola za konzervaciju-restauraciju predmeta kulturne baštine. U ovom radu u fokusu je problem heritološke abdukcije, u heurističkoj proceni broja neophodnih analiza, odnosno deficita podataka u fragmentarnim strukturama koje su izraz umetničkog spontaniteta, a sa akcentom na fenomen *praemissa minor* u traganju za metodološki čvrstom platformom za interpretaciju podataka.**

***Ključne reči*—spektroskopske analize, kulturna baština, heritološka abdukcija.**

## I. UVOD

Savremene metode istraživanja materijala kulturne baštine, koje su uvođenjem laserskih tehnika unapređene u domenu osetljivosti i preciznosti u identifikaciji materijala, omogućavaju analize različitih slojeva umetničkih slika, od podloga, odnosno nosilaca slika, do izvedenih retuša (Tabela 1). Ove metode obuhvataju [1-10]:

- XRF (X-ray fluorescence analysis)
- XRD-CT (X-ray diffraction computed tomography)
- PIXE (Particle-induced X-ray emission)
- PIGE (Particle induced Gamma-ray Emission)
- RBS (Rutherford backscattering spectrometry)
- NAA (Neutron activation analysis)
- FTIR (Fourier-transform infrared spectroscopy)
- ATR-FTIR (Attenuated total reflection FTIR)
- RS (Raman spectroscopy)
- GC-MS (Gas chromatography-mass spectrometry)
- LIBS (Laser-induced Breakdown Spectroscopy)
- SRN (Synchrotron radiation and neutrons)
- HR-ICP-MS (High-resolution inductively coupled plasma mass spectrometry)

Neophodna komplementarnost u primeni ovih tehnika pomaže u kvalitetu identifikacije pigmenata, veziva i dodataka koji se mogu naći na umetničkim delima u slikarstvu, što ukupno omogućava različite postupke u očuvanju kulturne baštine putem aktivnosti utvrđivanja porekla i datiranosti, otkrivanja podcrteža i preslika, kao i autentičnosti dela i autorskih umetničkih rukopisa.

Složenost problematike heurističke procene, koja se prevashodno zasniva na temeljnom iskustvu u zaštiti nasleđa, odnosi se, kako na pristupe u domenu istraživanja u oblasti tehnologije materijala [11,12], tako i na specifičnu kontekstualizaciju istraživanja na polju izvan empirijskog rezonovanja, u skladu sa istorijskim izvorima i starim recepturama (što obuhvata i u istoriji zabeležene takozvane tajne ili nikada razrešene slikarske recepture) u primeni materijala tokom stvaralačkih procesa u umetnosti [13]. Budući da nam istorija razvoja oblasti konzervacije-restauracije pokazuje da problemi i dileme u izboru najoptimalnijih materijala i pristupa u zaštiti umetničkih i arheoloških artefakata, čine konstantu u ovoj kompleksnoj oblasti, rasprave o načinu rada, protokolima i metodološkim prilazima, u kontinuitetu traju do danas, a zbog činjenice da je reč o jedinstvenosti i ekskluzivnosti zadataka rada na delima visokih umetničkih ili kulturoloških vrednosti.

TABELA I
PRIBLIŽNE DUBINE PRODIRANJA ZRAČENJA KROZ TIPIČNU SLIKU

| ultraljub. zračenje | vidljiva svetlost | infracrv. zračenje | rendgen. zračenje | slojevi standardne slike na platnu |
|---|---|---|---|---|
| UV→ | VS→ | IR→ | R→ | retuš |
| | VS→ | IR→ | R→ | lak |
| | VS→ | IR→ | R→ | glazur |
| | VS→ | IR→ | R→ | glavna boja 2 |
| | | IR→ | R→ | glavna boja 1 (pripremna sl) |
| | | IR→ | R→ | imprimatura |
| | | IR→ | R→ | pripremni crtež |
| | | IR→ | R→ | preparatura |
| | | | R→ | impregnacija |
| | | | R→ | podloga (nosilac slike) |

Suzana Polić – Narodni muzej Srbije, Trg Republike 1a, 11000 Beograd (e-mail:suzanapolic64@gmail.com)
Milesa Srećković – Univerzitet u Beogradu, Elektrotehnički fakultet, Bulevar kralja Aleksandra 73, 11120 Beograd (e-mail: esreckov@etf.bg.ac.rs)
Zoran Stević – Narodni muzej u Beogradu, Trg Republike 1a, 11000 Beograd; Univerzitet u Beogradu, Elektrotehnički fakultet, Bulevar kralja Aleksandra 73, 11120 Beograd; Univerzitet u Beogradu, Tehnički fakultet u Boru, Vojske Jugoslavije 12, 19210 Bor (https://orcid.org/0000-0002-1867-9360).
Miodrag Malović – Univerzitet u Beogradu, Inovacioni centar Tehnološko-metalurškog fakulteta, Karnegijeva 4, 11120 Beograd (email: ofiss@malovic.in.rs) (https://orcid.org/0000-0002-0691-4626).
Miloš Đurić – Univerzitet u Beogradu, Elektrotehnički fakultet, Bulevar kralja Aleksandra 73, 11120 Beograd (e-mail: djuric@etf.bg.ac.rs)

 ISBN 978-86-7466-930-3

Imajući u vidu savremenu dinamiku unapređenja instrumentalnih metoda, uočava se da je pitanje primene ovih metoda u kontekstima izvan empirijskog rezonovanja manje istražena oblast, pa je stoga u ovom radu u fokusu upravo tematizacija mišljenja u sferi logičkih nužnosti u postupcima zaštite kulturnog nasleđa, od problema silogizama u pristupima analizi materijala u slikarstvu, do problema heritološke abdukcije u savremenom kompozitnom slikarstvu.

## II. Logički pristupi: Meklaren, Verner i Brandi

Oblast istraživanja logičkih pristupa u upotrebi materijala u heritologiji, može se pratiti praktično od vremena prvih receptura u starom slikarstvu, a značajna metodološka prekretnica dogodila se tokom naučne polemike vođene 1949. i 1950. godine u britanskom *Burlington Magazine* i italijanskom *Bolletino dell'Istituto Centrale del Restauro*. Polemiku je izazvao naučni rad uglednog italijanskog istraživača i direktora Centralnog instituta za restauraciju u Rimu, dr Čezarea Brandija, pod nazivom "Čišćenje slika u odnosu na patinu, lak i lazure" [14], na koji su reagovali istraživači *The National Gallery* iz Londona, kustos Nil Meklaren i hemičar Entoni Verner, u tekstu "Neka činjenična razmatranja o lakovima i lazurama" [15]. Ocenjujući da je ova reakcija pokušaj da britanska strana *in articulo mortis*[1] odbrani konzervatorske postupke izvedene u Nacionalnoj galeriji u Londonu, a koji su, kako je smatrao Brandi, „doživeli smrtni udarac" njegovim člankom, ovaj istraživač pristupa široj i veoma kompleksnoj razradi polemike, pod istim, britanskim naslovom, *Some factual observation about varnishes and glazes*, ovoga puta, u italijanskom glasilu Centralnog instituta za restauraciju u Rimu [16]. Pokazalo se da je ova neprijatna epizoda za nauku bila veoma korisna u smislu rasvetljavanja suštine naučnog problema, jer je Čezare Brandi pokazao da se spor samo naizgled odnosio na oblast čišćenja slika, a da je suština u problemu logičkog pristupa, koji čini razliku između dve škole mišljenja, od kojih se jedna zalaže za radikalan pristup čišćenju materijala umetničkog dela, dok druga, kojoj pripada i sam Brandi, zastupa "koncept patine".

Britanska strana, kako je Brandi naglašavao, u stvari je zamagljivala i skrivala teorijske premise problema, koje "opstaju uprkos empirijskom rezonovanju", te da "prećutkujući najveću premisu silogizma", oni veruju da su potisnuli "logičku nužnost" i teže da od nje odvrate pažnju. Ali, *entimema*, koju tako stvaraju, transformiše se ni manje ni više, nego u poznati sofizam "lažne pretpostavke"[2]. Drugim rečima, Brandi je smatrao da je na delu "nepotpuni silogizam", kao skraćeni zaključak izveden samo iz jedne premise, dok je druga premisa bila neizrečena (*syllogismus imperfectus*).

U viđenju britanske strane, reč je o principu: "cilj je konzervacije i restauracije slika da budu prezentovane što je moguće bliže stanju u kojem je umetnik želeo da one budu viđene". Ovo stanovište i do danas zastupaju različite zapadne škole konzervacije, pa se u muzejima neretko mogu videti dela iz prethodnih vekova, koja izgledaju kao da su upravo izašla iz umetnikovog ateljea. A svakako jedan od najsvežijih primera je i velika izložba slika Rembranta i njegovih savremenika, iz njujorške *The Leiden Collection*, prikazana u Puškinovom muzeju u Moskvi 2018. godine, na izložbi pod nazivom *The Age of Rembrandt and Vermeer: Masterpieces of The Leiden Collection* [17], a čija je konzervacija – restauracija obavljena u SAD. Čezare Brandi, međutim, ovo "totalno čišćenje" naziva istorijskim apsurdom, kojim se traži, da se delo učini "reverzibilnim u vremenu, kao jedan komad oksidirane materije, kome treba povratiti fizičku čistoću i sjaj prvobitnog stanja". Pozivajući se na logički pristup koji izvire iz "koncepta patine", Baldinučijevog Rečnika (*Vocabolario toscano dell'Arte del disegno*) iz 1681. godine, Brandi ističe dve osnovne ideje ovog koncepta: prepoznavanje "znaka vremena" na delu i "estetsku vrednost patine". Konkretno, mora se voditi računa "o istorijskoj strani umetničkog dela, kao istorijskog dokumenta" i treba maksimalno izbeći "one suštinske modifikacije, koje samo *salus publica* ili spasavanje dela, može opravdati kao *suprema lex*", u skladu sa principom da je javno dobro najviši zakon (*salus publica suprema lex*).

Ističući razliku između "fizičke boje" i boje "umetničke predstave", gde "materijalnost" boje mora da iščezne utapanjem u umetničku predstavu, Brandi u estetskom domenu koncept patine povezuje sa željom da se priguši "arogancija materije, u korist onoga što nazivamo nematerijalnost umetničke predstave", citirajući reči iz klasične antike, o svođenju boja na mirniju ravnotežu, kao anticipiranje onoga što će se dešavati tokom vremena, a što Brandi eksplicitno izražava Plinijevim rečima *ne claritas solorum aciem offenderet*: "ni da jačina oštrine boja ne vređa". Otuda i ukazivanje da se logički pristup u primeni materijala kontekstualizuje u komplementarnim domenima. Iz veoma obimne Brandijeve argumentacije, ovde je obavljeno analitičko raščlanjivanje baze ovog složenog konteksta, i to na osnovne logičke i komplementarne premise (Tabela 2).

TABELA II
Lak kao materijal, u komplementarnim kontekstima, na osnovu Brandijeve argumentacije

| | |
|---|---|
| Logički iskaz | • Lak nije nužno rastvor smole u organskom rastvaraču |
| Semantički iskaz | • Lak je samo tečni pokrivač: čak ni transparentnost ne mora nužno da se povezuje sa semantičkim prostorom laka |
| Tehnološki iskaz | • Tečni lak je usitnjena ambra (čvrsta smola) dodata toplom orahovom ili lanenom ulju |
| Istorijski iskaz (od kasne antike do srednjeg veka) | • Evstatije u XII veku, u komentarima Homera, navodi da su Grci nazivali ambru *veronico (*βερονιχη) |
| Etimološki iskaz | • βερονιχη → *vernice liquido* (tečni lak) |

[1] latinski: u samrtnom času

[2] prevodi Brandijevih tekstova u ovom radu preuzeti su iz apendiksa br. 6 u "Teorija restauracije" [13], urednik i prevodilac Branka Šekarić

 ISBN 978-86-7466-930-3

| | |
|---|---|
| (posle sred. veka) | |
| Konzervatorski iskaz | • *vernice liquido* ne označava jedan stalan tip laka, već razliku između suve rezine i njenog rastvora<br>• stepen rastvorljivosti jednog rastvarača je izmišljen kriterijum, jer, po eksplicitnom priznanju Meklarena i Vernera, „posle jedanaest godina lak od lanenog ulja je isto tako rezistentan na rastvarače, kao lak star 400 godina“ |

Držeći se filološke determinacije, Čezare Brandi kroz izvođenje paralelne istorije dvaju reči, francuske *glacis* i italijanske *velatura*, demonstrira logiku zaključivanja, ukazujući na činjenicu da se nazivi koji se ne javljaju u istim epohama određuju prema autorima “u različitim vremenskim periodima i kulturnim prostorima i različitom lingvističkom upotrebom“, pa tako upozorava i da greškom zanemareni veznici mogu odrediti da je reč o pridevima, a ne o terminima u strogom značenju, a sve u vezi sa raspravom o distinkcijama između naziva u različitim starim recepturama (*tečni lak* / *blagi tečni lak* / *običan lak* / *veoma fini i suvi lak* / *izvanredni svetao i sušiv lak* / *lak postojanog sastava* / *veoma lep i redak lak* / *lak koji će se odmah osušiti* / *najfiniji lak i najsjajniji od svih drugih*, i slično), naglašavajući opasnost od dvosmislenih značenja: “jedna stvar je obojenost laka, a druga njegova nečistoća; da bi lak bio transparentan i svetao, ne znači da treba da bude bezbojan“. Za ovu liniju Brandijeve argumentacije, ovde je obavljeno analitičko raščlanjivanje dokaznog postupka u Tabeli 3.

Brandi u [14] kaže: „Šta je to *lazura*? Jasno je da je reč o jednoj fazi u dovršavanju slike, tankom sloju boje, koji služi da koriguje ili modifikuje kako lokalni tako i opšti tonalitet slike. To je, ako hoćete, trik, postupak koji se izvodi u zadnji čas, unutrašnji i tajni sastojak. Pošto je trik, nije mogao da bude lako priznat. Izlazi izvan oficijelne prakse slikarstva… Još početkom 19. veka, veoma dobro se znalo šta su to *lazure* i kako su ih koristili Venecijanci i Rubens. Ko onda može, čisteći jednog Rubensa, stavljajući na uvid golu i sirovu boju do kraja, da ne bude potom uveren da ju je zauvek uništio?“

TABELA III
LAZURA [GLACIS (FRA) / VELATURA (ITA) / GLAZE (ENG)[3]]

| Izvor | Brandijevi logički iskazi o tereminologiji u starim slikarskim recepturama |
|---|---|
| Roger de Piles, *Elemens de la Peinture pratique*, Paris 1766. | • Izrazi ***glacis*** i ***velatura*** nisu oduvek pokrivale isti semantički prostor<br>• U glagolu ***glacer*** fiksira se onaj posebni fizički fenomen tečnosti koja prelazi u čvrsto stanje ostajući transparentna i sjajna<br>• Glagol ***velare*** govori o parcijalnom prepokrivanju<br>• Pravljenje ravnoteže između ***glacis*** i ***velatura*** pripada savremenom dobu |
| Andre Félibien, *Des principes de l'Architecture*, Paris, 1690. | • Reč ***glacis*** na starofrancuskom jeziku je termin vojne arhitekture (u značenju blage padine ili škarpe nekog utvrđernja)<br>• Termin ***glacis*** nije čak ni zabeležen u de Pilevom malom rečniku slikarskih termina (*Termes de peinture*) rađenom za “Razgovore o poznavanju slikarstva” (*Conversations sur la connaissance de la Peinture*) iz 1677. |
| Pierre Lebrun, *Recueil des essaies Des Merveilles*, 1635. | • “glace(r) je postavljanje završnih ublažavanja i poslednjeg finog sloja koji daje sjaj sjajno-belom, ili sjajno-purpurnom, sjajno-zelenom, sjajno-žutom…” |
| Dufresnoy, *De Arte graphica*, 1673, prevod Roger de Piles | • “lazurne boje imaju živost koja nikada ne može da se podražava ni najživljim niti najsjajnijim bojama…” |
| F. Baldinucci, *Vocabolario toscano dell'Arte del disegno*, Firenze, 1681. | • U prvom eksplicitnom pominjanju lazura (***velatura***) postupak prepokrivanja (***velare***) opisan je u odnosu na prijatan efekat koji stvara |
| Dokazni postupak | |
| | • Reč ***velatura*** u italijanskom jeziku nema istoriju različitu od one koju ***glacis*** ima u francuskom jeziku<br>• ***Velatura*** i ***glacis*** imaju suprotna polazišta<br>• Francuskim glagolom ***glacer*** ukazuje se na transparentnost gotovo dragog kamena<br>• Italijanskim glagolom ***velare*** podrazumeva se obrnuto – ugasiti zvuk boje, prigušiti ga<br>• Dodirna tačka za francuski ***glacer*** i italijanski ***velare*** je transparentnost<br>• Činjenica da dva jezika semantički akcentuju dva različita smisla, ne isključuje drugačije namere u pogledu boje |
| *Praemissa major* | |
| | • Više sa estetskog, nego sa tehničkog stanovišta, ***velatura*** se mogla povezati sa teorijom i praksom francuskog ***glacis*** |

[3] *glaze* kada je reč o tamnom sloju na svetlom, odnosno *scumble* kada je reč o svetlom sloju na tamnom [Branka Šekarić]

Iz navedenog dokaznog postupka, kojim se dominantno tehnološko pitanje izmešta na polje kauzalnosti i transformacije, kojem inače pripadaju, ne samo

 ISBN 978-86-7466-930-3

instrumentalne tehnike, već i sam proces umetničkog stvaralaštva, može se uočiti da Brandi demonstrira logički postupak koji je praktično pandan Laplasovoj transformaciji, koja, kako je poznato, kauzalnu funkciju transformiše u drugi (spektralni) domen. Preneto na problem prikazane polemike, Brandi najviše zamera Meklarenu i Verneru, karakterišući to kao obmanu, činjenicu da "ni jednog trenutka ne obaveštavaju čitaoca da se ništa ne zna o tome kako su izvođene *velature* ili *glacis,* barem do XVIII veka, ali verni sofizmu »lažne pretpostavke«, smatraju dokazanim ono što treba dokazati, to jest, da je postojala nedvosmislena i stalna praksa lazura…", zaključujući da britanski autori nisu umeli da pristojno prezentuju čak ni jedan tekst o metodu primene *glacis* ili *velatura* pre XVIII veka.

Sl. 1. Coppo di Marcovaldo, Madonna col Bambino, 1261., basilica dei Santa Maria dei Servi, Siena [Wikipedia]

Iz perspektive primene savremenih instrumentalnih metoda, u tematizaciji pitanja *merituma* u analizama materijala, značajna je ilustracija, na koji način se takav logički pristup reperkutuje na rešavanje konkretnih problema. Povodom detalja na slici *Madona*, iz 1261. godine, autora Kopa di Markovalda (Coppo di Marcovaldo, c. 1225 – c. 1276, na Sl. 1), gde je primena bojenog i transparentnog laka "koji je postavljan preko lista kalaja ili srebra, da bi se postigao onaj sjaj tona, za koji, četiri veka kasnije, jedan Lebren (Lebrun) i jedan De Pil priznaju da ga je moguće postići - *nunc et semper* - samo sa lazurama", Brandi prigovara Meklarenu i Verneru, da čak nisu ni zapazili "male ali nesumnjivo prisutne ostatke crvenog transparentnog laka koji je Kopo koristio kod senki jastuka – *supedaneuma*[4], da bi im dao određenu zaobljenost, bez menjanja kvadratne osnove naslikane tkanine". Tako je, kako ističe ovaj autor, umetnik lazurama, a ne prozračnim lakovima, naslikao i drugi jastuk, na kojem sedi Madona, kao i nabore tkanina na pozadini trona, na osnovu čega Brandi i upozorava da je ovde jedino reč o tome da je potrebno "znati čitati" sliku!

[4] latinski: podrška za noge na krstu koji se koristi za raspeće

## III. ABDUKCIJA I KOMPOZITNA SLIKA

Nekoliko decenija posle ovde prikazane polemike, u savremenom tehnološkom okruženju, u kom razmatramo polje delovanja instrumentalnih tehnika, metodološka problematizacija usmerena je na problem kompozitne slike / instalacije (Sl. 2), koja doslovno terminološki označava kompozitno kao "sasvim drugo", obeležavajući savremeno doba drugačije vrste kompleksnosti, usled primene novih i brojem neograničenih materijala, kombinovanih bez ikakvih standardno propisanih procedura, a koji i kada su u celini poznati, mogu da budu podvrgnuti različitim, nestandardnim postupcima u procesu umetničke invencije, čiji se ciljevi i dometi mogu sublimirati u promišljanju Sergeja Ajzenštajna: "Dva susedna dela bivaju nužno spojena u jednu sliku, koja se iz njihovog suprotstavljanja razvija kao novi kvalitet".

Sl. 2. Fabio Mauri, Il Muro Occidentale o del Planto, 1993. (koferi, torbe, zvučnici, kožne obloge, platno, drvo) [www.fabiomauri.com]

Imajući posebno u vidu da se posredovanje empirijskih metoda, zbog potrebe uključivanja znanja o "čitanju slika" ne može smatrati samoreferencijalnim sistemom distinktivnih oznaka, već pre pomoćnim aparatom za dešifrovanje sredstava transponovanja unutrašnje slike na spoljašnje strukture kompozitnih slika / instalacija, može se govoriti o usklađivanju linija *plastičnog logosa* [18], sa referentnim linijama logičkih analiza, uz prisustvo razumevanja da "autentični umetnički izraz ne poseduje racionalno tumačenje, već emotivne karakteristike, koje ne podležu jednoznačnom dešifrovanju" kako to formuliše Tarkovski [19], odnosno da postoji "jedan sasvim drugačiji *meritum* od iluzije vlasti nad objektivizovanim predstavama stvarnosti" [20].

Stoga nas utvrđivanje operativnog analitičkog instrumentarijuma, bez koherentne metodološke podloge, dovodi na polje *abdukcije*, kao vrste silogizma, u kojem je

 ISBN 978-86-7466-930-3

jedna od dvaju premisa tek *verovatna*, jer je *praemissa minor* objektivna posledica složenosti likovnih problema, u logičkoj ekspoziciji koja je izvan polja empirijskog rezonovanja. Na polju *strukturalne dualnosti*, o kakvoj piše Rajner Keler [21], stoga je potrebno ispitati moguće usmerenje na *diskurzivne strukturacije*, pre nego na singularne jezičke radnje, koje se uočavaju kod Brandija.

Sa druge strane, uprkos složenosti tumačenja u izazovima brojnih neodređenosti i finesa dinamičkih karakteristika jezika, na koje ukazuje antologijska Brandijeva rasprava (čiji je ovde samo osnovni deo predstavljen za potrebe eksplikacije logičke analize u upotrebi materijala na osnovu opisa iz starih receptura) pitanje merituma u metodološkim zahtevima nešto je što se prepoznaje u kontinuitetu razvoja civilizacije, od sublimacije iskazane u Horacijevim stihovima (Quintus Horatius Flaccus, 65-8. p.n.e), istaknutim i na naslovnoj strani prve Didroove enciklopedije, *Tantum series juncturaque pollet, tantum de medio sumptis accedit honoris!* („eto takva je moć celine i sklada, obradom dobrom toliko da i banalna tema zablista!”[5]) [22, 23], pa do jedne od čuvenih teza Praškog lingvističkog kružoka, o jeziku koji nije gotov statički sistem, već stvaralačka energija [24] i tako sve do filozofije Rolana Barta[6], o proizvođenju značenja i strukturisanoj sposobnosti reči i predmeta da istovremeno nešto saopštavaju, u sistemu “varljivog označavanja” [25], što je u našem vremenu kompozitne umetnosti, posebno prisutno. U skladu sa tim, polariteti u terminologiji starih receptura, koje ukazuju na tehnološke osobine materijala, u ovom vremenu prepoznajemo kao pandan ideji polarne suprotstavljenosti i pojačavanja (*Polarität und Steigerung*), u jedinstvenom razumevanju i sposobnosti za otkrivanje frekvencije i semantike pojedinih reči, kao kod kod Džeralda Menlija Hopkinsa[7], koji govori o „razlogu za iznenađenje nad idućom razlikom“, kako nas na to upućuje Edvard Stankjevič [26].

## IV. Zaključak

Istraživanje prezentovano u ovom radu imalo je za cilj da analitički utvrdi način na koji se logički pristup u primeni materijala kontekstualizuje u raznovrsnim, komplementarnim domenima, koji čine metodološku osnovu za primenu instrumentalnih analiza u problemima koje karakteriše obaveza uključivanja mišljenja koje je izvan *empirijskog rezonovanja*.

Istraživanje je metodološki sprovedeno na studiji slučaja posvećenoj starom slikarstvu, analizom logičkog postupka i argumentacije za opovrgavanje prakse totalne intervencije na materijalima umetničkih dela, a u korist *koncepta patine*. Na osnovu utvrđenih premisa logičkog postupka, u vezi sa kompozitnom slikom / instalacijom, komparativno je razmotren problem logičkog zaključivanja, prirodom likovnih problema iznuđene *abdukcije*, koja direktno utiče na razumevanje uloge i dometa savremenih instrumentalnih metoda koje se mogu primeniti u analizi materijala umetničkih dela.

Imajući u vidu metodološke instrumente prikazane naučne polemike, utvrđeno je da se rešenje za uočene probleme može pronaći u multidisciplinarnom kontekstu teorija savremenih diskurzivnih i semantičkih transformacija.

[5] prevod prof. Radmile Šalabić, prema uvidu Sanje Stepanović Todorović

[6] Roland Barthes (1915-1980), francuski književni teoretičar, filozof i kritičar

[7] Gerard Manley Hopkins (1844 –1889), jedan od vodećih viktorijanskih pesnika

## Zahvalnica

Istraživanje prezentovano u ovom radu obavljeno je zahvaljujući podršci Ministarstva prosvete, nauke i tehnološkog razvoja Republike Srbije (ugovori 451-03-68/2022-14/200026 i 451-03-68/2022-14/200287), kao i zahvaljujući podršci Ministarstva kulture i informisanja Republike Srbije.

## Reference

[1] J. M. Madariaga, *Analytical Strategies for Cultural Heritage Materials and Their Degradation*, Croydon, UK, R. Soc. Chem., 2021.

[2] The SR2A 2021 - 9th International Conference on Synchrotron Radiation and Neutrons in Art and Archaeology, International Institute for Conservation of Historic and Artistic Works, Los Angeles, CA, USA, 22 - 26 February, 2021.

[3] P. Bordet, F. Kergourlay, A.Pinto, N. Blanc, P. Martinettoa, “Applying multivariate analysis to X-ray diffraction computed tomography: the study of medieval applied brocades,” *J. Anal. At. Spectrom.*, vol. *36*, no. *8*, pp. *1724-1734*, Aug. 2021.

[4] F. Mirani, A. Maffini, F. Casamichiela, A. Pazzaglia, A. Formenti, D. Dellasega, V. Russo, D. Vavassori, D. Bortot, M. Huault, G. Zeraouli, “Integrated quantitative PIXE analysis and EDX spectroscopy using a laser-driven particle source,” *Sci. Adv.*, vol. *7*, no. *3*, eabc8660, Jan. 2021.

[5] C. Jeynes, “Ion beam analysis for cultural heritage,” in *Spectroscopy, Diffraction and Tomography in Art and Heritage Science*, London, UK, Elsevier, 2021, ch. *10*, pp. *355-364*

[6] L. Giuntini, L. Castelli, M. Massi, M. Fedi, C. Czelusniak, N. Gelli, L. Liccioli, F. Giambi, C. Ruberto, A. Mazzinghi, S. Barone, “Detectors and cultural heritage: The INFN-CHNet experience,” *Appl. Sci.*, vol. *11*, no. *8*, *3462*, Jan. 2021.

[7] M. Chiari, S. Barone, A. Bombini, G. Calzolai, L. Carraresi, L. Castelli, C. Czelusniak, M. E. Fedi, N. Gelli, F. Giambi, F. Giardi, “LABEC, the INFN ion beam laboratory of nuclear techniques for environment and cultural heritage,” *Eur. Phys. J. Plus*, vol. *136*, no. *4*, pp. *1-28*, Apr. 2021.

[8] G. Festa, G. Romanelli, R. Senesi, L. Arcidiacono, C. Scatigno, S. F. Parker, M. P. M. Marques, C. Andreani, “Neutrons for cultural heritage—techniques, sensors, and detection,” *Sensors*, vol. *20*, no. *2*, *502*, Jan. 2020.

[9] D. Thickett, B. Pretzel, “FTIR surface analysis for conservation,” *Heritage Sci.*, vol. 8, no. 1, pp. *1-10*, Dec. 2020.

[10] N. Yao, X. Zhan, Q. Ma, S. Wei, “Characterization and identification of Chinese historical rubbings preserved in Wuyuan Museum by Pyrolysis–Gas Chromatography/Mass Spectrometry,” *Heritage Sci.*, vol. *9*, no. *1*, pp. 1-9, Dec. 2021.

[11] S. Polić Radovanović, “Primena lasera u obradi, zaštiti i dijagnosticiranju materijala predmeta kulturne baštine,“ doktorska disertacija, Univerzitet u Beogradu, 2007.

[12] S. Polić, Z. Stević, S. Ristić, B. Radojković, “Konceptualizacija heurističke procene u laserskom čišćenju papira,” Zbornik radova 6. naučno-stručnog skupa Politehnika, Beograd, Srbija, pp. 607-612, 10. decembar 2021.

[13] Č. Brandi, *Teorija restauracije*, Beograd, Srbija, Italijanska kooperacija, 2007.

[14] C. Brandi, “The cleaning of pictures in relation to patina, varnish, and glazes,” *Burlington Mag.*, vol. *91*, no. *556*, pp. *183–188*, Jul. 1949.

[15] N. Maclaren, A. Werner, “Some factual observations about varnishes and glazes,” *Burlington Mag.*, vol. *92*, no. *568*, pp. *189-192*, Jul. 1950.

 ISBN 978-86-7466-930-3

[16] C. Brandi, "Some factual observations about varnishes and glazes," *Boll. dell'Istituto centrale del restauro*, no. *3-4*, pp. *9-29*, 1950.
[17] The Pushkin State Museum of Fine Arts (2018). *The age of Rembrandt and Vermeer; Masterpieces of the Leiden Collection*, [Online]. http://www.arts-museum.ru/events/archive/2018/rembrandt/?lang=en
[18] T. Radionova, Čaplinova intonacija i njeno plastično rešenje, Ogled ontološke analize, GMS, decembar 2012.
[19] A. Tarkovski, *Lekcije iz filmske režije*, Novi Sad, Srbija, Prometej, 1992.
[20] Ž. Simić, "Oslobađanje zaboravom: Crnjanski i Tarkovski," u *Letopis Matice srpske (knj. 492, sv. 1-2)*, Novi Sad, Srbija, Matica srpska, 2013, pp. 148-162
[21] R. Keller, *Das Interpretative Paradigma: Eine Einführung*, Wiesbaden, Deutschland, 2012, Springer-Verlag
[22] Horacije, *Pisma*, Beograd, Srbija, 1972, Srpska književna zadruga
[23] S. Stepanović-Todorović, "Povodom Didroove »ENCYCLOPÉDIE« u biblioteci SANU," u *Letopis Matice srpske (knj. 489, sv. 6)*, Novi Sad, Srbija, Matica srpska, 2012, pp. *984-1004*
[24] A. Ilić, "Teze praškog lingvističkog kruga iz 1929. godine," u *Treći program br. 25*, Beograd, Srbija, Radio Beograd, 1975.
[25] D. C. François-Denève, *Mythologies - Rolan Bartes*, Paris, France, Bréal, 2002.
[26] E. Stankjevič, "Lingvistika, poetika i književni žanrovi," *Polja: mesečnik za umetnost i kulturu*, vol. *30*, no. *308*, pp. *400-403*, 1984.

ABSTRACT

Taking into account the diversity of approaches in qualitative and quantitative criteria for material selection heritology phenomena in the field of research of composite art works set complex tasks in the application of instrumental methods, which precede the development of protocols for conservation and restoration of cultural heritage. The focus of this paper is on the problem of heritology abduction, particularly in the domain of heuristic assessment concerning the number of necessary analyses, i.e. the deficit of data in fragmentary structures, these being expression of artistic spontaneity. At the same time, the paper also tackles the phenomenon of minor assumptions while pursuing a methodologically sound platform for interpreting data.

## The problem of heritology abduction through instrumental analysis of cultural heritage materials

Suzana Polić, Milesa Srećković, Zoran Stević,
Miodrag Malović, Miloš Đurić

 ISBN 978-86-7466-930-3

# Deskripcija, heritologija i metrologija boje

**Milesa Srećković, Veljko Zarubica, Aleksander Kovačević, Zoran Fidanovski, Suzana Polić, Milena Davidović**

**Apstrakt—Ljudski osećaj za boje ima mnogo aspekata, počevši od čovekovog poimanja sveta oko sebe, do medicinskih pojmova koji uključuju i daltonizam, ali (u svakodnevici) najpozitivniji, najhumaniji je čovekov osećaj za deo dana ili noći (meseca ili godine), za uživanje u heritološkom blagu, koje su nam ostavili preci, ali ne samo crno-belo. Istraživanja, kojima je procenjivan ljudski vek, postojanje i razvoj humanih bića, kao i nastajanje i evolucija flore i faune, sve ovo mora da bude tretirano multidisciplinarno, bez obzira da li se polazi od stena, stalaktita i stalagmita, morskih dubina, tragova u atmosferi ili potrage za planetom koja je slična Zemlji.**

**U radu se daje nekoliko prilaza boji i kolorimetriji, sa aspekta raznih naučnih disciplina. Prikazuje se uloga lasera u novim problematikama, kvantitativne definicije boje i njenih pokazatelja. U području merenja, daje se prilaz sa aspekta filtera i korektnog opisa stanja i delovanja odabranih filtera sa savremenim izražavanjima rezultata, kao i merne metode. Konstatacija boje i njena deskripcija, ima veliku ulogu u svakodnevnom životu, kao i u pojedinim tehničkim i *mass media* primenama, uključivši i humanističke i tehničke nauke.**

***Ključne reči*—laseri, heritologija, nove tehnologije**

## I. UVOD

**Spektroradiometrijska metoda merenja boje pomoću izmerenih vrednosti spektralne propustljivosti staklenih uzoraka**

Spektroradiometrijska metoda, kao fundamentalna metoda kvantifikacije, deskripcije objektivnog *merenja* boje, prema trenutnom stanju razvijenosti tehnologije izrade prijemnika optičkog zračenja i ostale merno-tehničke opreme, ima kao glavni zadatak postizanje zadovoljavajuće tačnosti i ponovljivosti rezultata merenja, prema postavljenim zahtevima korisnika.

Spektroradiometrijske metode merenja boje zasnovane su na određivanju spektralne raspodele zračenja, na osnovu čega se formira boja koja se meri. Trihromatske vrednosti boje se, nalaze iz poznatih krivih mešanja boja (slika 1). Za primarne svetlosne izvore, veličina koja se meri je spektralna raspodela energije, a za sekundarne se koristi spektralni koeficijent propustljivosti i koeficijent jednog od procesa interakcije, ovde koeficijent refleksije optičkog zračenja (koje se reflektuje od ili propušta kroz određene sredine).

U ovom delu rada, izabran je slučaj kada ne postoji poznata raspodela zračenja izvora. Koristi se raspodela zračenja crnog tela, i spektralni koeficijent propustljivosti staklenih uzoraka. Na taj način proračun trihromatskih vrednosti uzima u obzir pored spektralnog koeficijenta propustljivosti i spektralnu raspodelu snage zračenja apsolutno crnog tela. Spektralna raspodela snage zračenja se množi poznatim spektralnim koeficijentom propustljivosti $\tau(\lambda)$. Na slici 1 je predstavljena spektralna karakteristika trihromatskih vrednosti u funkciji talasne dužine.

Milesa Srećković – Univerzitet u Beogradu, Elektrotehnički fakultet, Bulevar kralja Aleksandra 73, 11120 Beograd (e-mail: esreckov@etf.bg.ac.rs)
Veljko Zarubica – Analyzis d.o.o, Japanska 4. Novi Beograd
Aleksandar Kovačević – Institut za fiziku, Pregrevica 118.
Milena Davidović – Univerzitet u Beogradu, Građevinski fakultet, Bulevar kralja Aleksandra 73, 11120 Beograd
Suzana Polić – Narodni muzej u Beogradu, Trg Republike 1a, 11000 Beograd

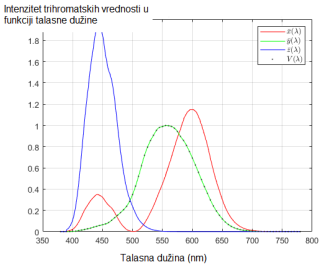


Slika 1a. Krive mešanja boja

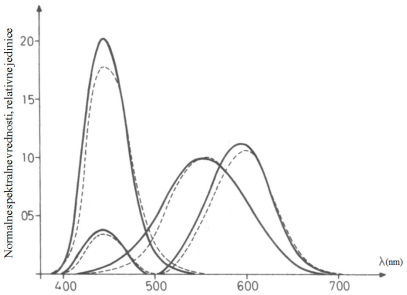


Sl.1b Krive viđenja za polje viđenja $10^0$ u odnosu na crtičaste krive za $2^0$.

Proračun trihromatskih vrednosti u CIE (XYZ) standardnom kolorimetrijskom koordinatnom sistemu, za boje svetlosti, koje se propuštaju kroz posmatrani uzorak [1, 3], sledi proceduru:

$$X = \int_{350nm}^{750nm} E_\lambda \tau_\lambda \overline{X_\lambda} d\lambda \; ; \; Y = \int_{350nm}^{750nm} E_\lambda \tau_\lambda \overline{Y_\lambda} d\lambda \; ;$$
$$Z = \int_{350nm}^{750nm} E_\lambda \tau_\lambda \overline{Z_\lambda} d\lambda \,, \qquad (1)$$

Kod praktičnih proračuna, integracija se svodi na sumiranje proizvoda vrednosti spektralnog koeficijenta propustljivosti i spektralne snage zračenja ACT za nizove talasnih dužina:

$$X = \Delta\lambda \sum_\lambda E_\lambda \cdot \tau_\lambda \cdot \overline{X_\lambda} \; ; \; Y = \Delta\lambda \sum_\lambda E_\lambda \cdot \tau_\lambda \cdot \overline{Y_\lambda} \; ;$$
$$Z = \Delta\lambda \sum_\lambda E_\lambda \cdot \tau_\lambda \cdot \overline{Z_\lambda} \,. \qquad (2)$$

Interval $\Delta\lambda$ bira se od 1-20 nm, u zavisnosti od željenih nesigurnosti tipa A i B, koje se zahtevaju za određivanje hromatskih koordinata. Kako su krive mešanja boja specifikovane u obliku relativnih vrednosti na ordinati, trihromatske vrednosti izračunate pomoću ovih krivih imaće relativni karakter kao na slici u poglavlju rezultata (Slika 2. Primer proračuna trihromatskih vrednosti za odabrani filtar.

Zahtev je da se odrede trihromatske vrednosti i hromatske koordinate boje standardnog svetlosnog izvora tipa A sa spektralnom raspodelom energija $E_A$, posle prolaska kroz uzorak, koji ima određen spektralni koeficijent propustljivosti $\tau$. Posle transmisije kroz uzorak, relativna spektralna raspodela jačine zračenja ima oblik prikazan krivom $\tau E_A$ na sl. 2. Svaka ordinata ove karakteristike, množi se odgovarajućom ordinatom svake od krivih mešanja boja $\overline{X}, \overline{Y}, \overline{Z}$. Šrafirane površine ispod krivih, dobijenih posle množenja, proporcionalne su respektivnim trihromatskim vrednostima $X, Y$ i $Z$. Hromatske koordinate $x$ i $y$ se izražavaju dalje:


ISBN 978-86-7466-930-3

$$x = \frac{X}{X+Y+Z}, \quad y = \frac{Y}{X+Y+Z} \quad . \qquad (3)$$

Ordinate krivih mešanja boja i ordinate spektralnih raspodela energije za standardni izvor, potrebne za posmatrani metod proračuna, obično se daju tabelarno.

Kod primarnih izvora svetlosti, postavka metode, zasniva se na spektroradiometru koji se koristi za merenje relativne spektralne ozračenosti (iradijancije). Kod sekundarnih izvora, merenje se vrši pomoću spektrofotometra, gde se monohromator sa odgovarajućim sistemom osvetljavanja (u zavisnosti od geometrije merenja) koristi za osvetljavanje datih uzoraka, a reflektovano, odnosno propušteno zračenje se meri fotodetektorom u odgovarajućoj geometriji.

## II. Drugi prilaz boji

Boja se može pojaviti kao kategorija ili pojam u vrlo složenim multidisciplinarnim problemima, a često se prema naučnoj disciplini koja se oslanja na doživljaj boje živih organizama (sa medicinske tačke gledišta, sa filozofske tačke gledišta, sa gledišta heritologije, sa ekološkog gledišta i dr.). Šire gledano, radi se o interakciji zračenja elektromagnetne ili druge prirode sa prijemnim aparatom. Sa tehničke strane objektivizacije, kolorimetrija ima zadatak da se kroz različite formirane formalizme opisuje boja putem trougla i koordinata, ili na drugi način, kroz drugi formirani sistem višeg ili nižeg nivoa. U tabeli 1 se daju ilustracije nivoa bioloških procesa uzrokovanih zračenjem i vremenskih konstanti odgovarajućih procesa sa odgovarajućim nivoom. Sa obzirom na primene u *mass media* (TV, novine, …), kulturnim manifestacijama, znake opasnosti, dozimetrijska pravila u primeni određene ELIONske tehnike, boja mora da ima dobro definisane coordinate u širem smislu, zasnovane na izvorima (obično tri) čijim se mešanjem postiže efekat određene (željene) boje. Da li će se koristiti odgovarajući softver uz odgovarajuću mernu aparaturu, ili će se sve automatizovati kao *user-friendly*, zavisi od trenutnog administrativnog zahteva ili trenutnog nadahnuća umetnika.

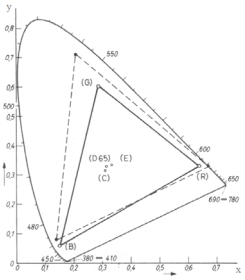

Slika 2. Normiranje boje putem EBU trougla boja (neprekidno) i FCC (isprekidano)

Tabela 1.

| Nivo | Vreme na nivou (s) | Procesi na nivou, modifikacije |
|---|---|---|
| Fizički | $10^{-18}$ $10^{-8}$ | Eksitacije, jonizacije, elastični sudari,- ,for macija visoke reaktiv nosti radikala visoke SR ktivnosti,SR u vodi i org. molekul. |
| Hemijski | $10^{-18}$ $10^{-8}$ | Reakcije SR sa orga nelama i kratko žive ći SR vode do primar nih oštećenja dimeri zacija, modifikacije sa temperatu rom MT ,$O_{2i}$ |
| Biohemisjki (subćelijski) | $10^{4}$ $10^{5}$ | Reparacija,interakcije oštećenih mikro cen tara,mutacije, abera cije,MT id r- agensi |
| Biohemijski (ćelijski) | $10^{1}$ $10^{7}$ | Deoba .molek., Mutacije |

Prema visini stepena tolerancije, institucije koje se kod nas bave *deskripcijom boje*, kao i njenim promenama, u zavisnosti od izloženosti objekta odnosno bio-objekta, postoje stroge procedure i sistemi gde se to može izvršiti, a ako nije potrebna velika preciznost, korisnici formiraju svoja sopstvena merna rešenja [Đikić]. U ovim merenjima ima mnogo mesta za definisanje osvetljenosti, u širem smislu, određenog izložbenog prostora i kontrolu stalnog fluksa koji se, u zavisnosti od mešanja prirodne i veštačke osvetljenosti, mora kontrolisati. U zavisnosti od objekta, mora se obratiti pažnja na mere zaštite od preterane ekspozicije.

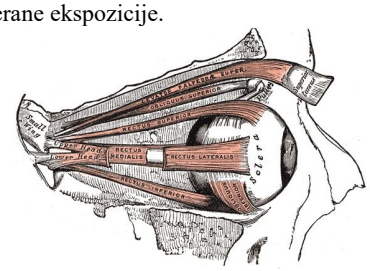

Sl. 3 Anatomija oka, koja jejoš kod Helmholza imala posebne predstave (https://www.wikiwand.com/es/M%C3%BAsculo_elevador_del_p%C3%A1rpado_superior)

**V Rezultati**

Vrednosti spektralne propustljivosti staklenog filtera MEL-B-1

Merene vrednosti Tabele 1. su prikazane delimično i na sl. 4 odnosno τ(λ), x(λ), y(λ), z(λ), prema propisanoj procedure u postupku određivanja karakteristika staklenog filtra MEL-B-1.

Pored merenja u Tabeli 1. , izvršena su merenja i za seriju drugih filtara: MEL-B-2, … MEL-G-2, MEL-G-4, itd.

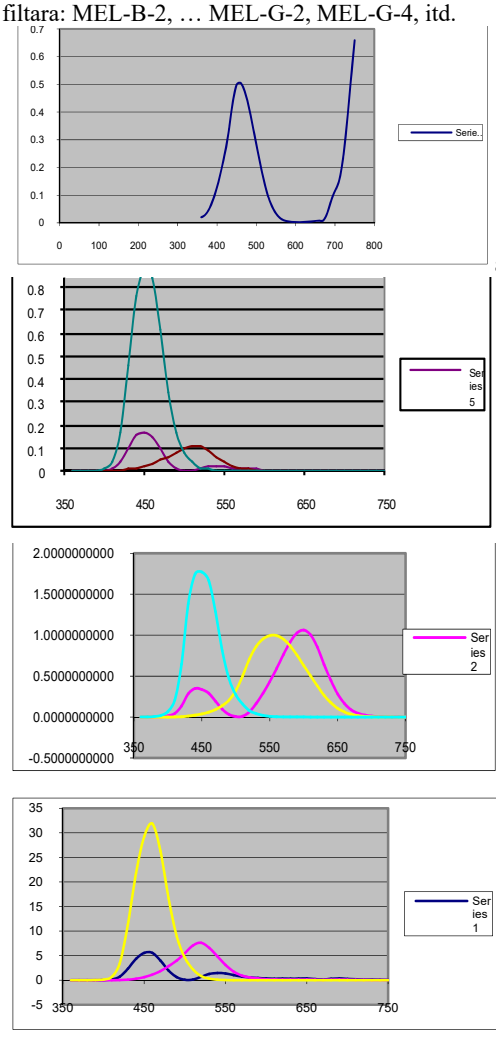


Slika 4 τ(λ), x(λ), y(λ), z(λ),… su prikazane na a), b), c), d) redom.

Table 2 Vrednosti spektralne propustljivosti staklenog filtera MEL-B-1


ISBN 978-86-7466-930-3

| λ (nm) | τ(λ) | x(λ) | y(λ) | z(λ) | x |
|---|---|---|---|---|---|
| 360 | 0.020104 | 0.00013 | 3.92E-06 | 0.000606 | 2.61E-06 |
| 370 | 0.028827 | 0.000415 | 1.24E-05 | 0.001946 | 1.20E-05 |
| 380 | 0.049412 | 0.001368 | 3.90E-05 | 0.00645 | 6.76E-05 |
| 390 | 0.084852 | 0.004243 | 1.20E-04 | 0.02005 | 0.00036 |
| 400 | 0.128765 | 0.01431 | 3.96E-04 | 0.06785 | 0.001843 |
| 410 | 0.184124 | 0.04351 | 1.21E-03 | 0.2074 | 0.008011 |
| 420 | 0.251353 | 0.13438 | 4.00E-03 | 0.6456 | 0.033777 |
| 430 | 0.332946 | 0.2839 | 1.16E-02 | 1.3856 | 0.094523 |
| 440 | 0.435524 | 0.34828 | 2.30E-02 | 1.74706 | 0.151684 |
| 450 | 0.498869 | 0.3362 | 3.80E-02 | 1.77211 | 0.16772 |
| 460 | 0.504937 | 0.2908 | 6.00E-02 | 1.6692 | 0.146836 |
| 470 | 0.476985 | 0.19536 | 9.10E-02 | 1.28764 | 0.093184 |
| 480 | 0.424312 | 0.09564 | 1.39E-01 | 0.81295 | 0.040581 |
| 490 | 0.355894 | 0.03201 | 2.08E-01 | 0.46518 | 0.011392 |
| 500 | 0.283355 | 0.0049 | 3.23E-01 | 0.272 | 0.001388 |
| 510 | 0.212164 | 0.0093 | 5.03E-01 | 0.1582 | 0.001973 |
| 520 | 0.147607 | 0.06327 | 7.10E-01 | 0.07825 | 0.009339 |
| 530 | 0.095958 | 0.1655 | 8.62E-01 | 0.04216 | 0.015881 |
| 540 | 0.058893 | 0.2904 | 9.54E-01 | 0.0203 | 0.017103 |
| 550 | 0.033716 | 0.43345 | 9.95E-01 | 0.00875 | 0.014614 |
| 560 | 0.017632 | 0.5945 | 9.95E-01 | 0.0039 | 0.010482 |
| 570 | 0.009053 | 0.7621 | 9.52E-01 | 0.0021 | 0.006899 |
| 580 | 0.005345 | 0.9163 | 8.70E-01 | 0.00165 | 0.004898 |
| 590 | 0.00365 | 1.0263 | 7.57E-01 | 0.0011 | 0.003746 |
| 600 | 0.002479 | 1.0622 | 6.31E-01 | 0.0008 | 0.002633 |
| 610 | 0.002195 | 1.0026 | 5.03E-01 | 0.00034 | 0.002201 |
| 620 | 0.002549 | 0.85445 | 3.81E-01 | 0.00019 | 0.002178 |
| 630 | 0.0031 | 0.6424 | 2.65E-01 | 0.00005 | 0.001991 |
| 640 | 0.004279 | 0.4479 | 1.75E-01 | 0.00002 | 0.001917 |
| 650 | 0.007347 | 0.2835 | 1.07E-01 | 0 | 0.002083 |
| 660 | 0.007538 | 0.1649 | 6.10E-02 | 0 | 0.001243 |
| 670 | 0.008502 | 0.0874 | 3.20E-02 | 0 | 0.000743 |
| 680 | 0.03321 | 0.04677 | 1.70E-02 | 0 | 0.001553 |
| 690 | 0.078896 | 0.0227 | 8.21E-03 | 0 | 0.001791 |
| 700 | 0.115048 | 0.011359 | 4.10E-03 | 0 | 0.001307 |
| 710 | 0.149673 | 5.79E-03 | 2.09E-03 | 0 | 0.000867 |
| 720 | 0.226687 | 2.90E-03 | 1.05E-03 | 0 | 0.000657 |
| 730 | 0.354033 | 1.44E-03 | 5.20E-04 | 0 | 0.00051 |
| 740 | 0.507815 | 6.90E-04 | 2.49E-04 | 0 | 0.00035 |
| 750 | 0.659319 | 3.32E-04 | 1.20E-04 | 0 | 0.000219 |

**Nastavak Tab.2**

| y | z | Ee,l rel | X | Y | Z |
|---|---|---|---|---|---|
| 7.87E-08 | 1.22E-05 | 6 | 1.61E-05 | 4.84E-07 | 7.49E-05 |
| 3.57E-07 | 5.61E-05 | 8 | 9.35E-05 | 2.79E-06 | 0.000439 |
| 1.93E-06 | 0.000319 | 10 | 0.000662 | 1.89E-05 | 0.00312 |
| 1.02E-05 | 0.001701 | 12 | 0.004353 | 1.23E-04 | 0.020569 |
| 5.10E-05 | 0.008737 | 15 | 0.027105 | 7.50E-04 | 0.128517 |
| 2.23E-04 | 0.038187 | 18 | 0.141639 | 3.94E-03 | 0.675152 |
| 1.01E-03 | 0.162273 | 21 | 0.709313 | 2.11E-02 | 3.407743 |
| 3.86E-03 | 0.46133 | 25 | 2.331892 | 9.53E-02 | 11.38101 |
| 1.00E-02 | 0.760887 | 29 | 4.353339 | 2.87E-01 | 21.83744 |
| 1.90E-02 | 0.884051 | 33 | 5.549847 | 6.27E-01 | 29.25324 |
| 3.03E-02 | 0.842841 | 38 | 5.553325 | 1.15E+00 | 31.87624 |
| 4.34E-02 | 0.614185 | 43 | 3.994789 | 1.86E+00 | 26.33011 |
| 5.90E-02 | 0.344944 | 48 | 1.958043 | 2.85E+00 | 16.64357 |
| 7.40E-02 | 0.165555 | 54 | 0.614152 | 3.99E+00 | 8.925058 |
| 9.15E-02 | 0.077073 | 60 | 0.083112 | 5.48E+00 | 4.613563 |
| 1.07E-01 | 0.033564 | 66 | 0.130345 | 7.05E+00 | 2.217261 |
| 1.05E-01 | 0.01155 | 73 | 0.677084 | 7.60E+00 | 0.837393 |
| 8.27E-02 | 0.004046 | 79 | 1.256667 | 6.55E+00 | 0.320127 |
| 5.62E-02 | 0.001196 | 86 | 1.469962 | 4.83E+00 | 0.102756 |
| 3.35E-02 | 0.000295 | 93 | 1.357805 | 3.12E+00 | 0.02741 |
| 1.75E-02 | 6.88E-05 | 100 | 1.048222 | 1.75E+00 | 0.006876 |
| 8.62E-03 | 1.90E-05 | 107 | 0.739466 | 9.24E-01 | 0.002038 |
| 4.65E-03 | 8.82E-06 | 114 | 0.560484 | 5.32E-01 | 0.001009 |
| 2.76E-03 | 4.02E-06 | 122 | 0.456 | 3.36E-01 | 0.000489 |
| 1.56E-03 | 1.98E-06 | 129 | 0.339787 | 2.02E-01 | 0.000256 |
| 1.10E-03 | 7.46E-07 | 136 | 0.300044 | 1.51E-01 | 0.000102 |
| 9.71E-04 | 4.84E-07 | 144 | 0.312803 | 1.39E-01 | 6.96E-05 |
| 8.22E-04 | 1.55E-07 | 151 | 0.300369 | 1.24E-01 | 2.34E-05 |
| 7.49E-04 | 8.56E-08 | 158 | 0.302779 | 1.18E-01 | 1.35E-05 |
| 7.86E-04 | 0 | 165 | 0.343737 | 1.30E-01 | 0 |
| 4.60E-04 | 0 | 172 | 0.213749 | 7.91E-02 | 0 |
| 2.72E-04 | 0 | 179 | 0.132839 | 4.86E-02 | 0 |
| 5.65E-04 | 0 | 185 | 0.288016 | 1.05E-01 | 0 |
| 6.48E-04 | 0 | 192 | 0.343735 | 1.24E-01 | 0 |
| 4.72E-04 | 0 | 198 | 0.259096 | 9.36E-02 | 0 |
| 3.13E-04 | 0 | 204 | 0.177154 | 6.40E-02 | 0 |
| 2.37E-04 | 0 | 210 | 0.138257 | 4.99E-02 | 0 |
| 1.84E-04 | 0 | 216 | 0.110177 | 3.98E-02 | 0 |
| 1.27E-04 | 0 | 222 | 0.077677 | 2.81E-02 | 0 |
| 7.91E-05 | 0 | 227 | 0.049734 | 1.80E-02 | 0 |
| | | | 36.70767 | 5.06E+01 | 158.6117 |

| x | y |
|---|---|
| 1.49E-01 | 2.06E-01 |
| 0.1493 | 0.2056 |

Kao primer merne nesigurnosti za drugu vrstu filtra data je Tabela 3.

Za sva merenja je potrebno dati ocenu nesigurnosti tipa A i B i za slučaj filtra *** ocean je u Tabeli 2.

Merna nesigurnost ovako dobijenih vrednosti hromatskih koordinata boje propustljivih stakala u boji, svodi se na mernu nesigurnost etalonskog spektrofotometrijskog sistema u pogledu merenja spektralnog koeficijenta propustljivosti i tačnosti zauzimanja talasne dužine, kao i merne nesigurnosti zbog rasipanja rezultata (nehomogenog filtra). Ukupna procenjena merna nesigurnost dobijenih rezultata se pridružuje dobijenim vrednostima hromatskih koordinata; u zavisnosti od opsega hromatskih koordinata komponente merne nesigurnosti će biti različite posebno za svaku od koordinata, x i y. U ovom radu je predstavljena samo ukupna vrednost merne nesigurnosti. Budžeti merne nesigurnosti za pojedine filtere se proračunavaju na isti način, a primer je u tabeli 2.

Razvojem spektrofotometrijskog sistema u laboratoriji Analysis d.o.o stvorena je mogućnost za etaloniranje različitih transparentnih (prpustljivih) uzoraka,za različite primene. Poznavanjem svojstva materijala (spektralni koeficijent propustljivosti i spektralne osetljivosti detektora odnosno spektralne raspodele izvora zračenja, stvara se mogućnost za realizaciju još jedne karakteristike materi jala,-boja. Na osnovu dobijenih vrednosti, moguće je definisati boju datih *uzoraka* u najširem smislu i tako dobiti novu karakteristiku kvantitativno/objektivno


ISBN 978-86-7466-930-3

Tabela 2. Primer proračuna budžeta merne nesigurnosti staklenog filtera u boji MEL-Y-2

| Komponenta merne nesigurnosti | Tip A | Tip B |
|---|---|---|
| **Merna nesigurnost spektro-fotometrijskog sistema:**<br>-Prosečno rasipanje rezultata<br>-Pomeraj svetlosnog snopa<br>-Orjentacija uzorka u odnosu na optičku osu sistema<br>-Nesigurnost korekcije na inter refleksiju<br>-nelinearnost sistema<br>-Neuniformnost uzoraka | 0,15 % | |
| Merna nesigurnost zauzimanja λ | | 0,001 % |
| Merna nesigurnost izvora zračenja (apsolutno crnog tela) preuzeta iz literature | | 1 % |
| **Ukupna relativna merna nesigurnost** | 1,12 % | |

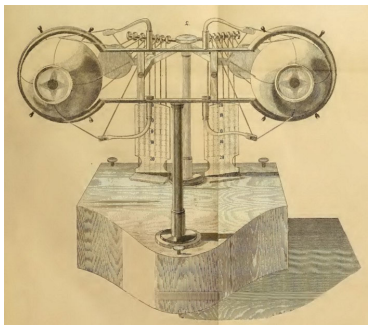

Slika 5

Russell Anderson, Ph.D.Russelanderson_26630,Sep 8, **2020,**Why are eye movements so damned interesting?**"Saccades" are t**he jerks that have fascinated scientists and philosophers for 2000 years.

Poređenje osetljivostu pojma viđenja u oblasti fizike, metrike i psi hologije,razlikuje kvantitativnom, kvalitativno i vrednovanje sa tri hromatske kordinate.

**Teorema četiri boje**

Boji se može prići i teoremom o četiri boje [4boje], u čiji dokaz mora da bude uključeno i savremena računarska tehnika.

**IV. Uloga izvora**

Pri definiciji bije u bilo kom sistemu širina spektralnih linija (spontane ili koherentne svetlosti) igra presudnu ulogu. Kao rezultat toga su nastali RGB laseri [REF ], od specijalnog značaja za HDTV. Od novijih tipova lasera, pokazalo se da su laseri na bazi polimera pogodni za kalibraciju odnosno deskripciju boje.

**III Teorema-Problem četiri boje**

Klasični problem četiri boje zahteva mnogo raznih pogleda koji su ilustrovani slikom 7. datom u originalu.

**Zaključak**

Shvatanje boje je složeno pitanje zavisno od prilaza pojedine naučne discipline, ali je multidisciplinaran problem koji zahvata od heritologije i umetnosti do matematike, elektrotehnike, i pojmova osvetljenosti, interakcije sa zračenjima razne prirode.Kad se priđe sa gledišta koherentnostoi., unitartsnosti izvora osvetljenja i prodesqa u doživljavanju boje već se pojavljuju razne terminologije, propisi i uobičajene3 merne tehnike, ali u osnovi danas se situacija komplikuje sa linearnim i nelinearnoim procesima koje donose lčaseri velikih gustina i kratkih impulsa, pa se ni aberacije hromatske prirode još više komplikuju, a i doživljaj bioloških objekata.

REFERENCE

1. M.Srećković, Radovanović,et al.,, Laserska tehnika i metrologija u foren zičkim naukama, Akademska misao, Beograd, 2017.
2.H.Lang, Einfuhrung in die Nachrichtentechnik, R.Oldenbourg, Munich,1978
3. S.Tanaka, S.Hayakawa, H.Sato, Feasibility of Enhanced / Tunable Organic Polymer Dye Laser, Proc. Lasers 2000
4. M.Živković ,M.Srećković et al, et al., Influence of electromagnetic and nuc lear radiation in medicine for therapy and diagnosis through processes, facts and statistical analysis, Nuc.Techn.& Rad. Prot.,Vol. 32, (1), pp. 91-98,2017.
5 Fritsch, R.;et al.,The Four Color Theorem: History, Topological Foundation and Idea of Proof, N.York: Springer1994.
6.M.Srećković,V.Krasnjuk, Abberation problems affecting modern techniques of picture processing and transmission, Im. Techn.,Vol.81,(2), pp.22-37,1999
7. M. Srećković, et al, Scattering ,reflection, transmission in theory and practice ,the estimation of nonlinear and ultrafast phenomena, Atti de la fondala fondazione Giorgio Ronchi, anno LXV 2010, No.4/5,ppp.543-55555, 2010.
8. V. Zarubica, M. Srećković, Realizacija metoda etaloniranja i pro račun budžeta merne nesigurnosti mernih instrumenata (merila ) u laboratorijama različitih namena, Velarta, Beograd, 2012.
9.V. Zarubica,M.Srećković et al.,Some Realization and measure ments Based on Holmium solutions and Different Wavelength
9. V. So Standards, Atti deAtti de la fondatione Ronchi, Anno LXXIII, No. 5, pp.485-498498498, 2018.
MrSrecko 10. M.Srećković, S. Polić, A. Bugarinović,et al, Laser i problemi konzrt konzerv konzervacije kulturne baštine, Centralni institut za konzervaciju i Regionalni ccentar za talente, Beograd 2, Beograd, 2016
. 11. T.B. Brill, Light,Mos ,MosMoskva, Mir,1983,
12.M.Srećković,A.Janićijević, V.Zarubica et al., Istorija,metrološka edu, ra edukaHadar, Beograd 2019

**Abstract**

The human sense of color has many aspects, from man's understanding of the world around him to medical terms that include colorblind people, but (in eve ry day life) the most humane is man's sense of that part of the day or night (month or year), to enjoy heritage , left to us by our ancestors. Research asses sing human life span, the existence and development of human beings, as well as the origin and evolution of flora and fauna, all this must be treated multi disciplinary, whether we start from rocks, stalactites and stalagmites, sea depths, atmospheric traces or the search for an Earth-like planet. The paper gives several approaches to color and colorimetry, from the aspect of various scientific disciplines. The role of lasers in new problems, quantitative define tions of color and its indicators are presented, and in the field of measurement, an approach is given from the aspect of filters and a correct description of the condition and operation of selected filters with modern expression of results and measurement methods. The perception of color and its description play a major role in everyday life, as well as in certain technical and mass media ap plications, including the social and technical sciences.

 ISBN 978-86-7466-930-3

# PROTO-KONCEPTUALNA REŠENJA U PRIMENI LASERA U HERITOLOGIJI

Milesa Srećković[1], Suzana Polić[2], Zoran Stević[1,3], Veljko Zarubica[4], Stanko Ostojić[5]

***Apstrakt*—Kritička preispitivanja postupaka koji se delovanjem na materijale primenjuju u konzervaciji-restauraciji predmeta kulturnebaštine, obuhvataju opšta i pojedinačna pitanja o upotrebi novih tehnologija, posebno lasera, u odnosu na klasične prilaze problematici zaštite artefakata koji imaju arheološku, istorijsku ili umetničku vrednost. Pitanje etičnosti posmatra se sa više aspekata koji se odnose na materijalna i nematerijalna postupanja prema predmetima zaštite, u smislu ispunjavanja zadate funkcije odabrane tehnike, a pod uslovima najvišeg stepena bezbednosti i ekološke zaštite. U ovom radu u fokusu istraživanja je karakterizacija proto-konceptualnih rešenja u primeni lasera na materijalima predmeta baštine, sa ciljem utvrđivanja eksplikatornih razlika u obrazlaganju potreba za primenu klasičnih pristupa konzervaciji-restauraciji kulturnog nasleđa, sa posebnim osvrtom u domenu tautoloških praksi.**

***Ključne reči*—laseri, heritologija, nove tehnologije**

## 1. UVOD

Višedecenijski rad fizičara, na čelu sa profesorom Asmusom (John Fredrich Asmus), koji je i prvi autor proto-konceptualnih rešenja u primeni lasera u heritologiji (od laserskog čišćenja skulptura, primena holografije u stvaranju trodimenzionalnih reprodukcija remek-dela svetske baštine, do primena lasera u utvrđivanju autentičnosti dela i restauraciji čuvenih figura od terakote u Kini)[1-4], kao i *digital-chiaroscuro*statistike [5], pa sve do doprinosa u stvaranju laserskih sistema (*Laser cleaning system*) za primenu u heritologiji [6], predstavlja tehnološkiudeo u razvoju nove muzejske teorije i prakse, koju odlikujuzalaganja da „muzej od mesta koje izaziva divljenje i strahopoštovanje, postane mesto kritičkog ispitivanja“[7].Reč je o razvoju motivisanom uvidom u praksukonzervacije umetničkih dela, koja je uspostavljena na osnovu subjektivnih izbora kustosa i konzervatora. Sa druge strane, reč je i o uviđanju, da je svako delo organskog porekla, tokom vremena podložno promenama, a što neminovno utiče na razumevanje pitanja *autentičnosti* umetnina, shvaćene kao „uzvišeno iskustvo“, odnosno „zračenje aurom“, kako to formuliše Dženet Marstin (Janet Marstine), u uvodu u tematski zbornik*Nova muzejska teorija i praksa*[7].

Međutim, uprkos početnim, istorijski značajnim rezultatima primene lasera u zaštiti kulturnog nasleđa, paradoksalno, do danas nije došlo do očekivanih razmera uvođenja ove tehnologije u muzejsku praksu, u kojoj još uvek dominiraju tradicionalne, čak i viševekovne, metode konzervacije-restauracije umetničkih predmeta, iako se u praksi pokazalo, da su u pogledu nedestruktivnosti delovanja na materijale, bezbednosti i ekoloških kvaliteta, takve metode značajno inferiornije u odnosu na lasersku tehnologiju. I sam prof. Asmus, uviđajući navedenu situaciju, godine 2003. objavljuje naučni rad *Non-divestment laser applications in art conservation*[8], kojim je, kako je naveo,želeoda podstakne „…oživljavanje interesa za ove moćne naučno uspostavljene tehnologije, proširenje njihove primene i prihvatanje od strane šire umetničke konzervatorske zajednice“.Kao neke od mogućih uticaja na navedenu situaciju naveo je,da je u vremenu početaka primene lasera u zaštiti nasleđa, postojalo opšte nepoznavanje potencijala laserske tehnologije, ali i uviđanje da je reč o velikim troškovima održavanja i realnim tadašnjim ograničenjima same tehnologije u primeni na umetničkim predmetima (u pogledu dostupnih talasnih dužina). U međuvremenu, razvoj laserske tehnike obesnažujeove argumente, agotovo dvadeset godina posle pokušaja prof. Asmusa da oživi interes za primenu lasera u heritologiji, uvidom u savremenu konzervatorsku praksu [9], uočava se očiglednost, da postoje drugi uzroci fenomena opisane svojevrsne tehnološke regresije, kakva nije zabeležena ni na jednom od polja primena novih tehnologija. Stoga je istraživanje u ovom radu posvećeno rasvetljavanju fenomena tehnološke regresijeu odnosu na proto-konceptualna rešenja u primeni laserske tehnologije u heritologiji.

Milesa Srećković – Univerzitet u Beogradu, Elektrotehnički fakultet, Bulevar kralja Aleksandra 73, 11120 Beograd (e-mail: esreckov@etf.bg.ac.rs)
Suzana Polić – Narodni muzej u Beogradu, Trg Republike 1a, 11000 Beograd
Zoran Stević – Narodni muzej u Beogradu, Trg Republike 1a, 11000 Beograd; Univerzitet u Beogradu, Elektrotehnički fakultet, Bulevar kralja Aleksandra 73, 11120 Beograd; Univerzitet u Beogradu, Tehnički fakultet u Boru, Vojske Jugoslavije 12, 19210 Bor (https://orcid.org/0000-0002-1867-9360).
Veljko Zarubica – Analyzis d.o.o **
Stanko Ostojić – Akademija **

 ISBN 978-86-7466-930-3

## 2. AGON I TEHNOLOŠKI PROTAGONIZAM

Pogled na genezu problema agonalnosti u primeni lasera u heritologiji, zahteva utvrđivanje nosioca (*vektora* u doslovnom tumačenju termina) svrhovitogkritičkog promišlja primene laserske tehnologije u zaštiti baštine, pri čemu se *agon,* kao jedan od fundamentalnih pojmova, ovde semantički koristi u širem značenju***ἀγών,*** kao sučeljavanje argumenata u spektru teorijskih nijansi agonistike, koje logički pripadaju konotacijama u ovoj oblasti [10-13]. Te nijanse mogu da direktno ili refleksivno obogateeksplikativnu utemeljenost premise,da laser kao reprezent egzemplarne promene u zaštiti nasleđa, treba da bude razmatran kao subjekt u heritološkom procesu, a ne kao derivat u tehnološkim tumačenjima prirode konzervacije-restauracije. U tom smislu, agonalnost koja stoji u osnovi ovde istraživanog fenomena *tehnološke regresije*, na tako postavljenom semantičkom planu, omogućava da argumentacija različitih provenijencija, od umetničkih, do humanističkih i tehničko-tehnoloških, bude ispitana i na univerzalnoj ravni, pored tehničko-tehnološke, u kojoj jeistraživao profesor Asmus.

Jedan od osnova za to daje i uvid koji iskazuje filozof estetike, umetnički kritičar i profesor, Artur Danto (Arthur Coleman Danto), da primena metoda prirodnih nauka na polju društveno-humanističkih nauka ne može biti adekvatna bez razumevanja metodološke autonomije istorijske nauke [14], pa se ispostavlja da potencijale primene lasera u heritologiji, u potpunosti može da aktivira samo istraživač sa odgovarajućom inženjersko – istorijsko - umetničkom kompetencijom, koja predstavlja sublimaciju artikulisanih spoznajnih horizonata i iskustava [15], pri čemu se ima u vidu, kako tehnološko, tako i umetničko spoznavanje fenomena. Na polju umetnosti, to je mišljenje, da „…slikarstvo ne imitira, kao što [to] Platon navodi, ono ne reprodukuje, već samo smešta svet do sveta. Svet prikazâ je valjan koliko i takozvani stvarni svet.“[16]. A na polju multidisciplinarnog susretanja tehnologije i istorije, to je pitanje inkluzivnosti istorijsko-umetničkih narativa, koji, budući da neretko ne prelaze naučne norme tehnoloških standarda, zbog svog neformativnog karaktera,izazivaju potrebu da se, kao i u slučaju tradicionalnih nauka, razumejukao vrednost takozvanih *nenaučnih narativa* [17].

S obzirom nanavedeni izraziti nedostatak egalitarnosti perspektiva, kako pokazuje sprovedeno istraživanje, u formulisanju vektora kritičkog promišlja primene laserske tehnologije u zaštiti baštine, neophodno je uvesti i pojam *protagonizam*, u skladu sa etimologijom termina *proto – agon -istis* (prvi borac), koji se ovde odnosi na kvalitet koji laser kao tehnološko sredstvo čini centrom interesa i referencom na polju heritologije, a u demonstracijiprethodno navedenihaspekata superiornosti laserske tehnologije na poljuinterakcijesa materijalima predmeta kulturne baštine [18]. Sa druge strane, protagonizam jesuštinsko obeležje*vektora* kritičkog promišljanja u magistralnoj liniji razvoja primene lasera, koja ima naučnoistorijske osnove i koja cilja na dalekosežnost i široku obuhvatnost svog implementiranja. Otuda ova problemska postavka i omogućava uvođenje naučne deskripcije, koja konotira smenu naučne paradigme.

Istraživanjem različitih puteva parametrizacije neophodne za sučeljavanje argumenata diferentnih provenijencija, u ovom radu prezentuje se, na koji način se parametrizacija konstituiše u skladu sa metodolgijom Žerara Ženeta (Gerard Genette), u tipologiji narativa[19], koja prebačena u okvir multidisciplinarne heritološke problematike, omogućava širi opseg pitanja o odnosu prema laserskoj tehnologiji, u kontekstu faktora *vremena*(tempus),*načina* (modus), *fokalizacije* (odnosno odgovora na pitanje *ko vidi?*) i *glasa*(vox, odnosno pitanja*ko govori*?). Pri tome treba imati u vidu da se u lociranju *gledišta* na fenomen koji istražujemo, *differentia specifica*traži u polju distinkcija izmeđufundamentalnih pojmova estetike, mimezisa / μίμησις (ovde u skladu sa navedenim, blisko Aristotelovom shvatanju nagona za učenjem, kao i Lajbnicovomstavu o mogućim svetovima, u korespondenciji sa prethodno navedenim Dantovim mišljenjem), odnosno, na drugom kraju opsega, diegezisa / διήγησις, kao razlaganja u smislu strukturalistički viđenog opozita.

Na ovaj način, polazeći iz različitih oblasti koje konstituišu heritologiju, moguće je pojasniti kako se navedeni parametri povezuju u okviru teorijskih modela (tipologija) primerenih pojedinačnim oblastima, a u cilju multidisciplinarnog saoblikovanja iz preciznije metodološke pozicije, koja treba da obuhvati i iskustvene, neaksiomatske prakse, sistematizovane na nov način argumentacije, a na bazi razlike između univerzalnih i specifičnih vrednosti. Sa druge strane, potreba usaglašavanja sa duhom vremena koji obeležava primenu svake nove tehnologije, a ovde i u kontrastu sa viševekovnim tradicionalnim tehnikama konzervacije, iskazuje se kao *interdiskurzivno prožimanje*, odnosno, kako to naziva Anženo (Marc Angenot), kao „intertekstualni protok i modifikacija ideologema“, kao istorijski određenog kompleksa vrednosti. Parafrazirajući Anženoovo stanovište, da se „na taj način istorijski uspostavlja granica među onim što se u društvu može zamisliti i izreći i onim što se još ne može ili neće misliti“ [20], ovde govorimo o mišljenju specifične ciljne grupe koju profesor Asmus opisuje kao *širu umetničku konzervatorsku zajednicu.*

 ISBN 978-86-7466-930-3

Imajući osim navedenog, u vidu, da se čitav proces razvoja primene laserske tehnike u heritologiji odvija u okruženjugnoseološke ravnodušnosti*postmoderne*, koja je „anaučna a ne antinaučna“, kako to precizno formuliše profesor intelektualne istorije Ankersmit (Franklin Rudolf Ankersmit)[21], to je napuštanje tradicionalne predstave u svakoj oblasti, a kako se pokazuje,posebno u konzervaciji-restauraciji, povezano sa obrazovanjem koje treba da izgradi otvorenost prema različitim teorijskim konceptima i praksama. To je i put za prevazilaženje predmultidisciplinarnih, tradicionalnih gledišta, kakvona primer prezentuje Šap (Wilhelm Schapp) o svetu prirodnih nauka: „Metafizika prirodnih nauka fokusira se na tezu da je uključenost u svet priča neophodan uslov za radmatematičara i naučnika koji se bavi prirodnim naukama. Oni mogu operisati samo na osnovu tog sveta“[22].

U skladu sa rezultatima ovog istraživanja je i mišljenje da je u postmodernom „…deontologizovanom svetu decentriranog logosa“,važno istaći značaj problematizacije načina, odnosno aktuelizacije pitanja*kako se misli,* u odnosu na to šta se misli[23],zbog čega je i neophodno da savremena pedagogija u oblasti konzervacije-restauracije,uvidi potrebu za analitičkim pristupom u opservaciji *decentriranog mišljenja*[24]. I to iz perspektive mogućnosti sticanja fleksibilnosti u prevazilaženju stereotipija i usvajanja eklektične sistematike. To je i put za mogućnost razumevanja fundamentalnih transformisanja osnova sistema znanja koje je u oblasti konzervacije-restauracije donela primena laserske tehnologije.

Kako sprovedena istraživanja pokazuju, na tom putu značajan je pristup fenomenu *tehnološke regresije* kroz identifikaciju tematizovane agonalnosti sa duhom apologije principu *élan vital*[25]*,* odnosno usmerenosti nastvaralački, umesto na subverzivni pristup. Na taj način *vektor*svrhovitog kritičkog promišlja primene laserske tehnologije u zaštiti baštine, može se postaviti na liniju univerzalnog principa stepenovane kompleksnosti,*adaequatio rei et intellectus,*da bi se uspostaviorelacioni kvalitet u razumevanju limita tradicionalnih, viševekovnih, unapred zadatih formalno-kompozicionih modela u praksi imitativnog variranjareceptura i cirkularnih tautoloških interpretacija. Povećanje tehnoloških kompetencija,čiji bi se karakter u ukupnom istraživačkom protokolu mogao karakterisati kao naučno formativan, omogućilo bi logična razdvajanjarelevantnih od irelevantnih pojava, čime bi se i stekli uslovi za adekvatan protagonizam laserske tehnologije, izvan prostoraagonalnosti.

## ZAKLJUČAK

U ovom radu prezentovano je istraživanje paradoksa neadekvatnezastupljenostiprimene lasera u heritologiji, kao oblasti zasnovane na značajnim proto-konceptualnim rešenjima. Prikazana istraživanja modela parametrizacije agonalnosti u razumevanju značaja laserske tehnologije, kao i vektora kritičkog ispitivanja, kao integralnog dela nove muzejske paradigme, ukazuju na potrebe uspostavljanja obrazovnih praksi sa formativno usmerenim modelima integracije znanja u konzervaciji-restauraciji, a u cilju eliminisanja subverzivnih shvatanja o upotrebi laserske tehnologije. Prikazani modeli mišljenja predstavljaju osnov za dalje istraživanje načina prevazilaženja specifičnog fenomena tehnološke regresije.

## ZAHVALNICA

Istraživanje prezentovano u ovom radu obavljeno je zahvaljujući podršci Ministarstva prosvete, nauke i tehnološkog razvoja Republike Srbije (Ugovor br. 451-03-68/2022-14/200026), kao i zahvaljujući podršci Ministarstva kulture i informisanja Republike Srbije.

## LITERATURA

[1] J.F. Asmus, C.G. Murphy, W.H. Munk, *Studies on the Interaction of Laser Radiation with Art Artifacts*, in: Developments in Laser Technology II, San Diego, USA, August 27, 1973, Proceedings of SPIE 0041, 1974, DOI: 10.1117/12.953831.

[2] J. F.Asmus, et al., *Holography in the Conservation of Statuary,* Studies in Conservation, vol. 18, no. 2, 1973, pp. 49–63, https://doi.org/10.2307/1505458. Accessed 13 Apr. 2022.

[3] J. F. Asmus, *Computer Studies of the Isleworth and Louvre Mona Lisas*, in T. Russell Hsing and Andrew G. Tescher, Selected Papers on Visual Communication: Technology and Applications (SPIE Optical Engineering Press, 1990), p. 652-656; reprinted from Optical Engineering, Vol. 28(7) (July 1989), p. 800-804.

[4] K. Moe, *Expert plans facelift for ancient Chinese artwork*, Hazleton Standard-Speaker (December 8, 1987), p. 27.

[5]J. F.Asmus, V. Parfenov, *Characterization of Rembrandt self-portraits through digital-chiaroscuro statistics,* Journal of Cultural Heritage, December 28, 2018.

[6]W. Kautek, S. Pentzien, *Laser cleaning system for automated paper and parchment cleaning*, in: Springer Proceedings in Physics 100 (2005), Proceedings LACONA V, Osnabrück, Germany, September 15 – 18, 2003, K. Dickmann, C. Fotakis, J. F. Asmus (Eds.), pp. 403 – 410, DOI: 10.1007/3-540-27176-7_51.

[7] *New museum theory and Practice: An Introduction*, (ed.) J. Marstine, Blackwell Publishing, 2006.

[8] J. F. Asmus,*Non-divestment laser applications in art conservation,* Journal of Cultural HeritageVolume 4, Supplement 1, January 2003, pp. 289-293

[9]S. Polić, *Izveštaj o primeni laserskog čišćenja u savremenoj muzejskoj praksi, sa osvrtom na stanje u Centralnom institutu za konzervaciju*, interni dokument, Beograd, 2020.

[10] T.F. Scanlon, *The Vocabulary of Competition: 'Agon' and 'Aethlos', Greek Terms for Contest*", Aethlon, 1983, пп. 147–162.

[]B.Sandywell, *The Agonistic Ethic and the Spirit of Inquiry: On the Greek Origins of Theorizing*, The Sociology of Philosophical Knowledge, Edited by M. Kusch, Dordrecht, 2000., стр. 93–123.

[11]J. Lungstrum, E. Sauer,*Creative Agonistics: An Introduction*, Agonistics: Arenas of Creative Contest.

 ISBN 978-86-7466-930-3

Edited by JanetLungstrum,Elizabeth Sauer. Albany, SUNY Press, NY, 1997. pp. 1–32.
[12] I. Weiler, *Der Agon im Mythos: Zur Einstellung der Griechen zum Wettkampf*, Darmstadt/Wissenschaftliche Buchgesellschaft, Darmstadt, 1974.
[13] T. Joho, *Burckhardt and Nietzsche on the Agōn: the dark luster of ancient Greece, Conflict and Competition*: Agon in Western Greece: Selected Essays from the 2019 Symposium on the Heritage of Western Greece. Edited by Heather L. Reid, John Serrati, Tim Sorg. Parnassos Press – Fonte Aretusa, 2020., pp. 267–288.
[14]G.H. von Wright, *Explanation and understanding*, Ithaca, Cornell University Press, N.Y.1971.
[15] S. Polić, *Od inženjerstva do tehnofilozofije u obrazovanju inženjera za zaštitu kulturnog nasleđa*, tematski zbornik radova XXVI naučnog skupa međunarodnog značaja „Tehnologija, kultura i razvoj“, održanog u Beogradu 2 – 3.12.2019. godine, ISBN 978-86-82183-18-1 (IMP), Beograd, 2020.str. 133-151
[16]W. Schapp, *Philosophie der Geschichten*, Vittorio Klostermann, Frankfurt am Main, 2015.
[17]G. Gutting, *Michel Foucault's Archaeology of Scientific Reason*, Cambridge University Press, Cambridge, 1989., str. 251-256.
[18] S. Polić, *Primena lasera u obradi, zaštiti i dijagnosticiranju materijala predmeta kulturne baštine*, doktorska disertacija, Univerzitet u Beogradu, 2007.
[19] D.Hayman, [Review of Figures III, by G. Genette], NOVEL: A Forum on Fiction, 6(3), 1973, pp. 288–290. https://doi.org/10.2307/1344844
[20]M. Angenot, *Intertextualite, interdiscursivite, discourssocial*, Texte, 2, 1983, pp. 101–112.
[21]F. R. Ankersmit, *Historiography and postmodernism*, History and Theory, XXVIII, No. 2, 1989., pp. 137-153.
[22]J. Schapp, *Erinnerungen an Wilhelm Schapp*, Geschichte und Geschichten, Studien zur Geschichtenphänomenologie Willhelm Schapps, Königshausen & Neumann GmbH, Würzburg, 2004.
[23] M. Belančić, Rasredišteni logos, Službeni glasnik,
[24] H. S.Becker, B. Geer,*Participant observation: the analysis of qualitative field data*, in R. Burgess (ed.): Field research: a source book and field manual, Allen & Unwin, London, 1982., pp. 239-250
[25] Đ. Šijaković Maidanik, *Helenski fenomen ἀγών kao élan vital: Miloš Đurić u Umetničkom pregledu*, Filosofija života i helenska agonistika. O ranim radovima Miloša Đurića, Gnomon, centar za humanistiku, Beograd i Institut za srpsku kulturu, Nikšić, 2021.

***Abstract* — Critical re-examinations of the procedures applied on materials during the conservation-restoration of cultural heritage objects, including general and individual questions about the use of new technologies, especially lasers, in relation to classical approaches to the protection of artifacts of archaeological, historical or artistic value. The issue of ethics is viewed from several aspects related to tangible and intangible actions towards objects of protection, in terms of fulfilling the given function of the chosen technique, and under the conditions of the highest degree of safety and environmental protection. This paper focuses on the characterization of proto-conceptual solutions in the application of lasers on heritage materials, with the aim of determining explicative differences in explaining the need for classical approaches to conservation-restoration of cultural heritage, with special reference to tautological practices.**

***Keywords* — lasers, heritology, new technologies**

 ISBN 978-86-7466-930-3

# Comparison of 3D printing and galvanic coating of gold in printing circuit board production

Zoran Karastojković[1], Radiša Perić[2], Aleksandar Bugarinović[3], Milan Miladinov[4], Višeslava Rajković[5]

***Abstract*— It became a practice that in printing circuit board (PCB) production is used gold, as an exelent conductor of electricity and highly corrosion resistant (noble) metal. Gold always was an expensive metal, but in great game of electronic decices this metal must be used as a best solution, no matter for the high price. Many processes of gold deposition are available in PCB production, one of them is gold deposition by using electrolytic (or galvanic) process. However, a wide versatility of electrolytic methods were developed for production of circuit boards. In meanwile is established the one more method for curcuit production which is based on so called 3D printing.**

**Between those processes existing some differencies, which need furter explanations for better understanding the PCB production, it means the reasons for choosing the proper method.**

**Key words: Printing circuit board, galvanic coating, 3D printing**

## 1. INTRODUCTION

It could be said that production of PCB on galvanic (electrolytic) manner belogs to two dimension, shorter 2D. When becames clear that production of PCB by 3D printing may be cheaper than traditionally manufactured boards, this new technology has attracted a great attention. Further, 3D technology allows more complex design.

The PCBs consist from different components, depending to the final purpose of this *equipment*. So, resistors could be considered s one of the crucial component in a PCB design. But there are other electronic devices as: transistors, diodes, capacitors, inductors, sensors, etc, Fig. 1. In describing of a PCB is noticed that such board in geometric sence should be flat, other variety of informations about the functionality of this device are available in wide literature sources. In this paper the matter of consideration will be a flatness of gold traces (as a conductive layer), obtained either by galvanic or 3D printing methods.

1-Society for Ethics and Evaluation in the Arts and Sciences, Belgrade, Serbia, e-mail: zpran.karastojkovic@gmail.com
2-„Perić&Perić“, d.o.o, Dunavska 114-116, 12000 Požarevac. Serbia
3-Faculty for Electrical engineering, blvd. kralja Aleksandraa, 11000 Belgrade, Serbia
4-„Sanacija i ispitivanje metala“, d.o.o, ul. Danila Ilića 2, 11060 Belgrade, Serbia
5-Institut za nuklearne nauke „Vinča“, 11000 Belgraade, Serbia

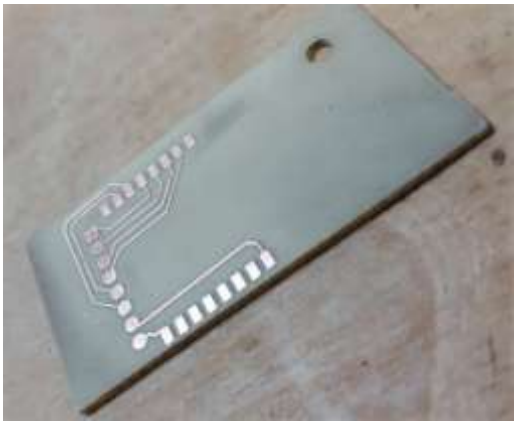
a)

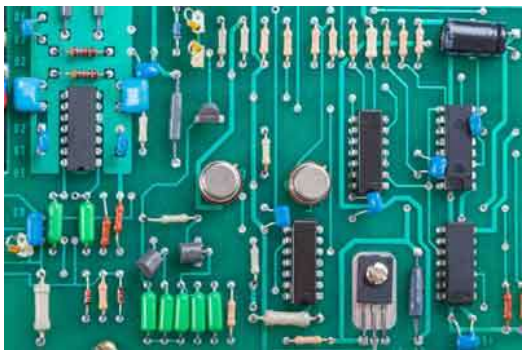
b)

Fig. 1, Two examples in designing of printing circuit board (PCB): a) monolayer and b) multilayer design

## 2. SHORTLY ABOUT THE STRUCTURE OF LAYERS

A PCB may contains just one conductive layer, Fig. 1a), or multilayers, Fig. 1b): monolayer is pretty restrictive in function abilities while design with multilayers offers a wide versatilities in making interconnections, etc. So, in designing and terminology of multilayers may be present: the top layer, an internal layer and the bottom layer, above the substrate material. Frequently an insulating layer must be present - if is needed. It must be underline that this vocabular (top, internal or bottom layer) may not be typical scientific but rather engineering terminology, particulary during fabrication of PCB devices. Multilayer, indeed, has an influence on the thickness of such boards. The four layer frequently is recommended, of course when it is possible. It is desired that the top layer is at the same time a corrosion resistant and with excelent conductive properties, as gold does, Fig. 2.

 ISBN 978-86-7466-930-3

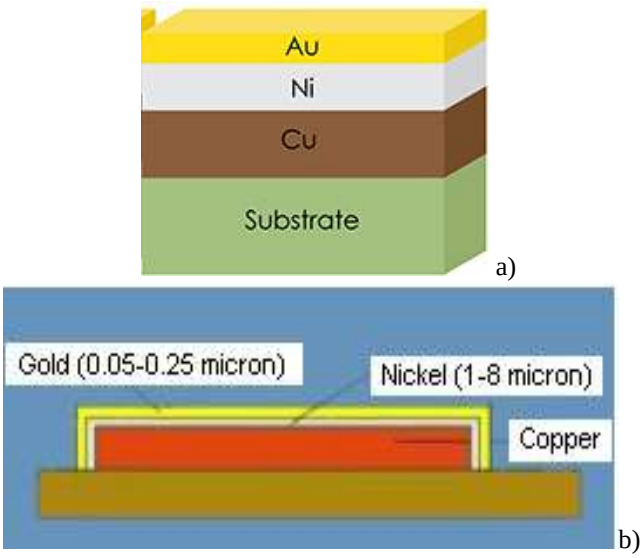


Fig. 2. Composition a) and thicknesses distributions b) at one three-layer structure over substrate material

Each layer has a different function. The multilayers are used for improving the PCB performance. From many reasons (structure, hardness, price etc.) the nickel coating also may be used, as indicated in Fig. 2. As the top layer could be chosen a golded layer from one more reason, previously not mentioned, it is a soldering ability with other components from PCB. The golden layer, also called a trace, posses a pretty good soldering ability. Other facilities of (multi)layers are the subject of specialities in designing of PCB, here is the matter on wich way the deposition of gold layer may be provided.

## 3. ELECTROLYTIC COATING OF PCB

Electrolytic (galvanic) deposition is the well known technology in surface finishing purposes, almost as a method for imrpoving the anticorrosion properties and/or for decorative properties, but also as one of the oldest method in production of traces onto PCB. Next advantage of electrolytic deposition of metals is in possibility to attain a layer over different materials, almost metallic materials but this is not obvious. Principles and technology of such kind of fabrication are well known and applied all over the world. The pure gold could be electrodeposited and than this js known as a “soft gold”. Another tape of gold deposition is provided through an alloy (usuallly with nickel, cobalt or other metals in amount less than 0,2%) when is needed greater hardness, especially at surfaces where the force and than a friction is appeared, so such kind of golden layer is named “hard gold”. The possibilities of mixing the chemical compounds for achieving the proper electrolyte(s) also are pretty well established.

Many metals are available for electrolytic deposition, but not all of them. One of the important advantage in galvanic electrodeposition of golden layer is the possibility to attain thickness of 1μm, even less. This fact has shown a great importance in production of narrow and/or thin circuit boards, every where applied (in computers, mobile phones, TV apparatus, etc.). One example of possible thickness distribution of different layers is shown in Fig. 2b). It is found that the gold layer thickness has shown an influence on the porosity: if thickness is less about 0,40μm than the porosity rapidly increases, further when the thickness of this layer is about 0,75μm than the porosity will be markably low. No doubt that porosity or other imperfestions at the substrate material will produce a kind of porous surface at golden layer, even after the galvanic process is correctly applied.

During a longterm heating-up in service periode some electrochemical migrations are possible, which could resulting in metal dendrites formation at the layer between the two adjacent electronic components (electrodes).

It should be noticed that the using of versatility of electrolites may produce a harmfull waste components.

## 4. 3D PRINTING OF PCB

In last decades the 3D printing as a production method becomes very attractive, especially in modeling and similar demands. In such cases the 3D method is a pretty fast and cost-less method. At many advertisements might be found just a perfect appearance, Fig. 3a). But, not every 3D modeling obviously should be successful, as could be see from Fig. 3b), where the non-uniform thickness is evident.

The printing material, here it is gold metal, should be melted during deposition and this fact represents some kind of risk when the layer is formed on plastic material, because plastic material posses a pretty power melting temperature than gold. The producing of small amount of a kind of gold alloy in the form of wire is technically possible but may be an expensive job. The case from Fig. 3b) is not desired anyway, because the flatness will be destroyed, also with markably increasing the roughness (with unequal surface topography) and a large amount of expencive gold will be unusually spent. At the contemporary level of technics the smaller thicknesses on PCB could be achieved by using a galvanic method of deposition

It seems resonably an expecting that 3D technology does not produce some harmfull components, however it is an important benefit.

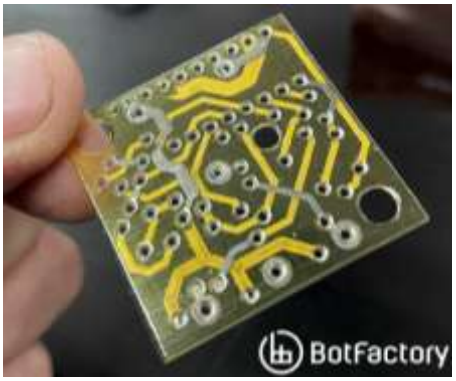


a)

 ISBN 978-86-7466-930-3

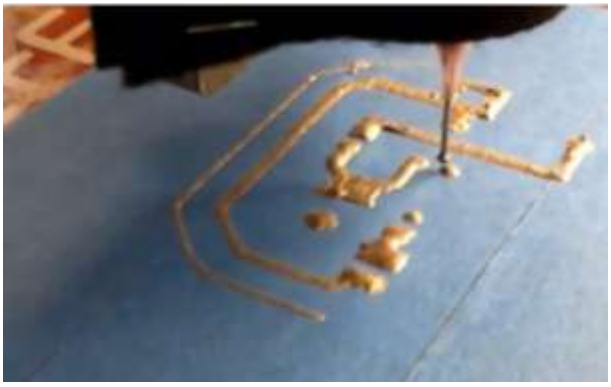

b)

Fig. 3. Results after applying the 3D printing method with using the golden wire in production of one circuit board:
a) correct and b) incorect

## CONCLUSION

Flat and thin surface are needed at every production method. The golded traces are wellcome in PCB from one more reason – easy soldering with other components. In galvanic (electro-deposition) is possible to attain a golden layer in thickness of 1μm, even less, but this demand still is impossible if 3D printing method is used. Surface roughness after galvanic deposition is pretty satisfactory while after applying 3D printing the roughnes is greater.

The producing of chemicals for electrolytic deposition of variety metals in the form of (inexpensive) salts or luquids now are present in industry in a great scale and could be supplied relatively eaisy, while the golden wire made from particular alloy (as mentioned with cobalt or similar) in a small amount for 3D printing still is an expensive job.

Thicknesses obtained by using 3D printing fabrication eventualy may reach values above 0,1mm, what is much greater in comparison to galvanic method of deposition. So, the 3D printing method in production of printed circuits is available only at such circuits when the thickness is greater in comparison to galvanic method of deposition.

But, the dissadvanage of galvanic tehnology is in production of variety harmful components, as a waste material, while 3D technology does not.

## References

[1] J. Kusinski, S. Kac, A. Kopia, et all.: Laser modification of the materials surface layer – a review paper, Bull. of the Polish akademy of sciences, Technical sciences, 60/2012/4, p. 711-728.
[2] J. Sundqvist: Aspects of heat flow in laser materials processing, 2018, Doctoral Thesis, Lulea University of Technology.
[3] N. Rykalin, A. Uglov, I. Zuev, A. Kokora: Laser and electron beam material processing, Handbook, Moscow 1988, MIR Publ, p. 277-353.
[4] https://www.sharrettsplating.com/blog/benefits-of-electroplating-3d-prints/
[5] Z. Karastojković: Površinska zaštita metala, in Serbian, Visoka tehnička škola strukovnih studija, Novi Beograd 2016, p.150-162.
[6] Z. Karastojković, P. Karastojković, S. Polić, Protective and decorative role of golden foils on sacral objects, Proceedings of XXI YuCorr, Meeting point of the science and practice in the fields of corrosion, materials and Environmental protection, September 17-20, 2019, Tara Mountain, Serbia, Serbian society of corrosion and materials protection, p. 21 – 30.
[7] З. Карастојковић, С. Полић, П. Карастојковић, Методологија и дизајн у производњи православних златних крстова / Methodology and design in production of ortodox golden crosses, Зборник апстраката, Друга национална конференција Методолошка истраживања у херитологији и новим технологијама, Друштво за етичност и вредновање у култури и науци и Централни институт за конзервацију, Београд, 2020, стр. 74-80.
[8] N. Bajič. Z. Karastojković: Savremeni postupci navarivanja, IRC IHIS Technoexperts 2016, 11080 Zemun, Batajnički put 23, Srbija, str. 200-203.

**Apstrakt**

Postala je praksa da se u proizvodnji štampanih koma (PCB) koristi zlato, kao izvanredan provodnik struje i jako koroziono postojan (plemenit) metal. Zlato je oduvek skup metal, ali u ogromnom broju elektronske opreme ovaj metal se mora upotrebiti kao najbolji materija,. bez obzira na visoku cenu. Brojni procesi taloženja zlata su primenljivi u izradi PCB, jedan od postupaka je elektrolitičko (ili galvansko) taloženje. Dakako, veliki broj elektrolitičkih metoda je razvijen za proizvodnju štampanih kola. U međuvremenu je razvijena još jedna metoda u proizvodnji štampanih kola, koja je zasnovana na tzv. štampi.

Između ovih procesa postoje izvesne razlike koje zahtevaju dalja razjašnjenja za bolje razumevanje proizvodnje štampanih kola, to znači razloge za izbor odgovarajuće metode.

Key words: Printing circuit board, galvanic coating, 3D printing

## Comparison of 3D printing and galvanic coating of gold in printing circuit board production

Zoran Karastojković[1], Radiša Perić[2], Aleksandar Bugarinović[3], Milan Miladinov[4], Višeslava Rajković[5]

 ISBN 978-86-7466-930-3

# СПЕЦИЈАЛНА ТЕМАТСКА СЕСИЈА - КАЛЦЕА

# /

# SPECIAL THEMATIC SESSION - KALCEA

ISBN 978-86-7466-930-3

# Platform for Rapid Prototyping of Maximum Power Point Tracking Algorithms in Photovoltaic Systems

Srđan Lale, Ognjen Petrić, Slobodan Lubura and Marko Ikić

***Abstract*—This paper describes the application of the programmable logic controller (P C), which is software-implemented on the personal computer (PC), for rapid prototyping and testing of ma imum power point trac ing ( PPT) algorithms used in photovoltaic (P ) systems. The practical results for Perturb and bserve (P ) PPT algorithm, which is used to e tract and maintain the ma imum power from the P modules connected to the synchronous buc converter, are given.**

***Index Terms*—P module; PPT algorithm; buc converter; software-implemented P C; rapid control prototyping.**

## I. INTRODUCTION

RENEWABLE energy sources are becoming an essential part of global trends in the development of low-carbon economy and the so-called "green energy". Among them, the photovoltaic (PV) modules are one of the most important sources. It is well known that the PV modules behave as real (nonlinear) current sources. Their current-voltage ($I_{pv}$-$V_{pv}$) and power-voltage ($P_{pv}$-$V_{pv}$) characteristics depend on weather conditions, such as intensity of solar radiation and ambient temperature (Fig. 1 and Fig. 2). From the power-voltage characteristics it is obvious that only a single maximum power point (MPP) exists under given working conditions. To find and maintain that MPP, the maximum power point tracking (MPPT) algorithms are implemented.

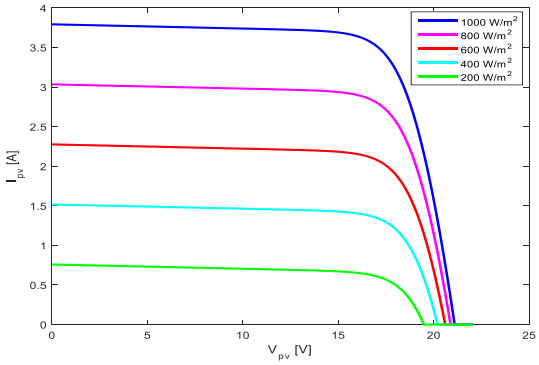


a)

Srđan Lale, Slobodan Lubura and Marko Ikić are with the Faculty of Electrical Engineering, University of East Sarajevo, 30 Vuka Karadžića, 71123 East Sarajevo, Bosnia and Herzegovina (e-mails: srdjan.lale@etf.ues.rs.ba, slobodan.lubura@etf.ues.rs.ba, marko.ikic@etf.ues.rs.ba).

Ognjen Petrić is with the Tipteh d.o.o., 246 Ramiza Salčina, 71000 Sarajevo, Bosnia and Herzegovina (e-mail: ognjen.petric@tipteh.ba).

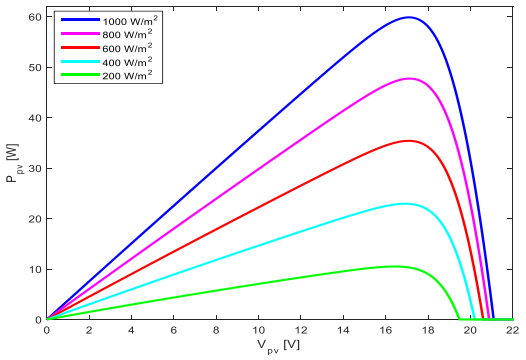


b)

Fig. 1. $I_{pv}$-$V_{pv}$ a) and $P_{pv}$-$V_{pv}$ b) characteristics of the PV module for different values of solar radiation.

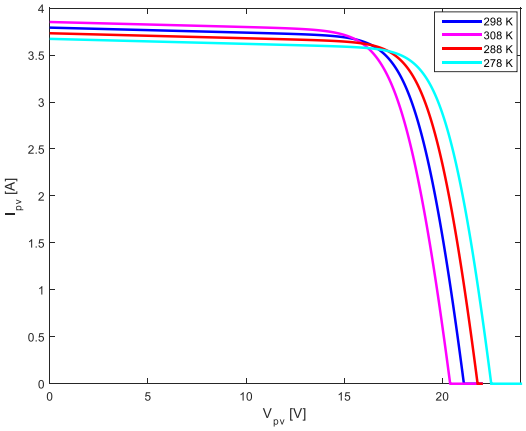


a)

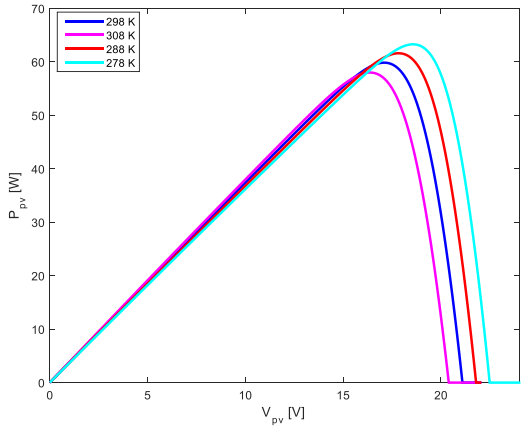


b)

Fig. 2. $I_{pv}$-$V_{pv}$ a) and $P_{pv}$-$V_{pv}$ b) characteristics of the PV module for different values of ambient temperature.

 ISBN 978-86-7466-930-3

There are numerous MPPT algorithms proposed in scientific literature [1]. Many new MPPT algorithms and their modifications still continuously appear in scientific papers, because this is a very important and popular scientific topic [2]-[8]. To test the performances of the MPPT algorithms, it is very important to develop an appropriate experimental platform, which enables rapid prototyping of the MPPT algorithms in laboratory environment. Various hardware platforms are used for that purpose, for example data-acquisition boards [9]-[12], microcontrollers or digital signal processors [13], [14], field programmable gate arrays [15], [16], etc. All these platforms have their advantages and drawbacks regarding the complexity of programming and manipulation, processing speed, price, etc., so it is hard to determine the optimal platform which satisfies all criteria.

In this paper, the application of the Beckhoff programmable logic controller (PLC), which is software-implemented on the personal computer (PC)/laptop, is proposed for realization of the MPPT algorithms in the PV systems. The utilization of the Beckhoff PC-based PLC for implementation of the conventional voltage control of the DC-DC buck converter is proposed in [17]. The software implementation of the Beckhoff PLC on PC or laptop is enabled with TwinCAT software environment [18], [19]. As it is shown in [17], the main advantages of this platform are modularity, user-friendly operation, high signal processing speed, simple and fast graphical programming, low price, etc. Because of these performances, the Beckhoff PLC is a good solution for rapid prototyping of different converters' control structures, including MPPT algorithms which are subject of this paper.

This paper is organized in the following way. The conventional Perturb and Observe (P&O) MPPT algorithm, which is implemented on the proposed platform, is briefly explained in section II. The proposed platform, which is based on the application of the Beckhoff PLC, is described in section III. The obtained experimental results are given in section IV. Section V represents the conclusion.

## II. PERTURB AND OBSERVE MPPT ALGORITHM

The MPPT is not possible without the power electronics converter, which must be inserted between the PV module and load. For that purpose, a synchronous buck converter is used in this paper (Fig. 3).

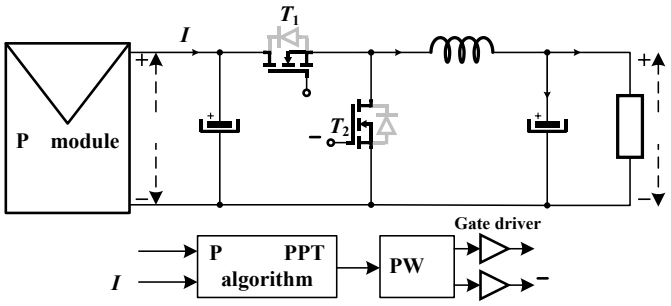


Fig. 3. Proposed PV supply system with MPPT function.

The working point of the PV module is determined by the intersection of the load working line and the $I_{pv}$-$V_{pv}$ characteristic of the PV module (Fig. 4).

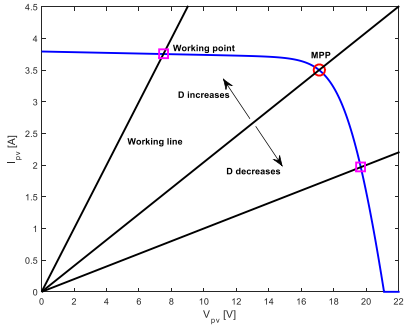


Fig. 4. Dependence of the working point of the PV module on duty cycle .

The load working line for the buck converter from Fig. 3 is equal to:

$$I_p = \frac{2}{\quad}{}_p, \qquad (1)$$

where $_p$, $I_p$, and represent the voltage and current of the PV module, load resistance and duty cycle of the switching signal $u$, respectively. The slope of the working line and thus the position of the working point, depend on the duty cycle , as it is shown on Fig. 4.

The P&O MPPT algorithm is one of the first developed and the most popular MPPT algorithms. Its operation is based on the permanent perturbation of the working point of the PV module, by automatic change of the duty cycle . Once the MPP is reached, it is maintained by the permanent oscillations of the working point close around the MPP. The size of these oscillations depends on the perturbation value $\Delta$ . The well-known flowchart of the conventional P&O MPPT algorithm is shown on Fig. 5.

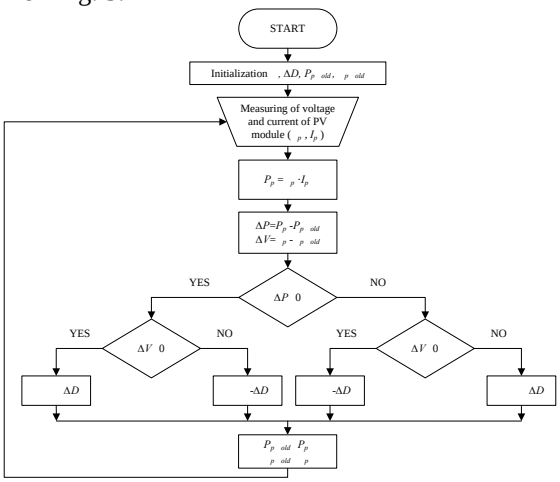


Fig. 5. Flowchart of the conventional P&O MPPT algorithm.

The inputs of the P&O MPPT algorithm are measured voltage $_p$ and current $I_p$. The output of the algorithm is the duty cycle , which is fed to the pulse width modulator (PWM). The PWM generates the switching signals $u$ and $\bar{u}$ for the power switches $T_1$ and $T_2$ (Fig. 3).

 ISBN 978-86-7466-930-3

## III. PROPOSED EXPERIMENTAL PLATFORM

The block-diagram of the proposed experimental platform, which is used for implementation of the P&O MPPT algorithm, is shown on Fig. 6.

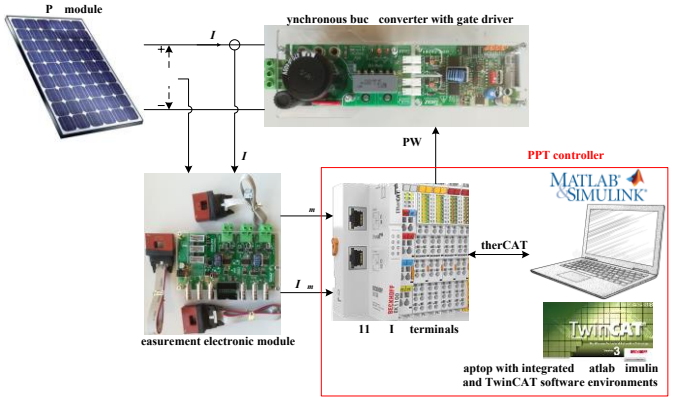


Fig. 6. Block-diagram of the proposed rapid control prototyping platform.

The platform consists of the following main parts.

### A. P Module

Two PROSTAR 75W/24V PV modules connected in series, which are placed at the roof of the Faculty of Electrical Engineering in East Sarajevo, were used. These two PV modules can produce about 150 W in standard test conditions.

### B. Synchronous Buck Con erter with Gate ri er

SPM-HB SiC half bridge power module [20] is used as the synchronous buck converter, with the connected GDC-2A2S1 galvanically isolated gate driver module [21]. The switching frequency of the buck converter was set to 20 kHz. The other parameters of the buck converter are: input capacitance $C_i$=470 μF, output capacitance $C$=1000 μF, inductance =220 μH, and load resistance =4 Ω.

### C. Measurement Electronic Module

The measurement of the voltage and current of the PV module is performed with the galvanically isolated electronic module USM-3IV [22]. The measured voltage $_{p\ m}$ and current $I_{p\ m}$ (Fig. 6) at the output of the USM-3IV module are scaled to the ±10 V range, which is necessary for the analog input terminal of the Beckhoff PLC.

### . MPPT Controller

The P&O MPPT algorithm is implemented on the Beckhoff PLC. A detailed description of the Beckhoff PLC is provided in [17]. The Beckhoff PLC is software-implemented on the laptop by using TwinCAT software environment. The TwinCAT environment converts the laptop into the real-time controller, which is connected to the input/output terminals via EK1100 EtherCAT coupler (Fig. 6). The analog input terminal EL3164 is used for accepting the measured scaled voltage and current of the PV module, i.e., the signals $_{p\ m}$ and $I_{p\ m}$, respectively. The P&O MPPT algorithm is implemented and executed in real time in TwinCAT software environment. The algorithm calculates and updates the value of the duty cycle, which is used by the output PWM terminal EL2502. The EL2502 terminal produces the PWM control signal, which is fed to the input of gate driver GDC-2A2S1.

The Beckhoff PLC is graphically programmed by using the developed Matlab/Simulink model of the P&O MPPT algorithm, which is a great benefit. This is accomplished thanks to the integration of the Matlab/Simulink and TwinCAT software environments. The created Simulink model of the P&O MPPT algorithm is integrated into the TwinCAT software environment, as it is shown on Fig. 7 and Fig. 8. The discretization period, i.e., the sample time of the model is 1 ms, the perturbation value of the duty cycle $\Delta$ is 0.005, and the update period of the duty cycle is 1.5 s.

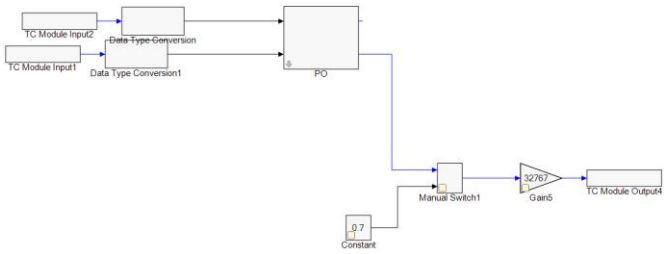


Fig. 7. Implementation of the P&O MPPT algorithm in TwinCAT software environment.

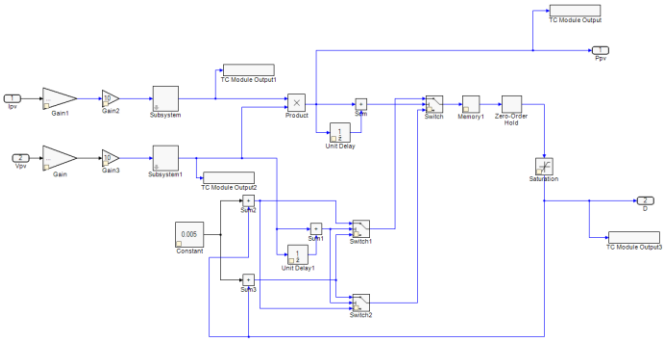

Fig. 8. Implementation of the P&O MPPT algorithm in TwinCAT software environment – scheme of the "PO" subsystem from Fig. 7.

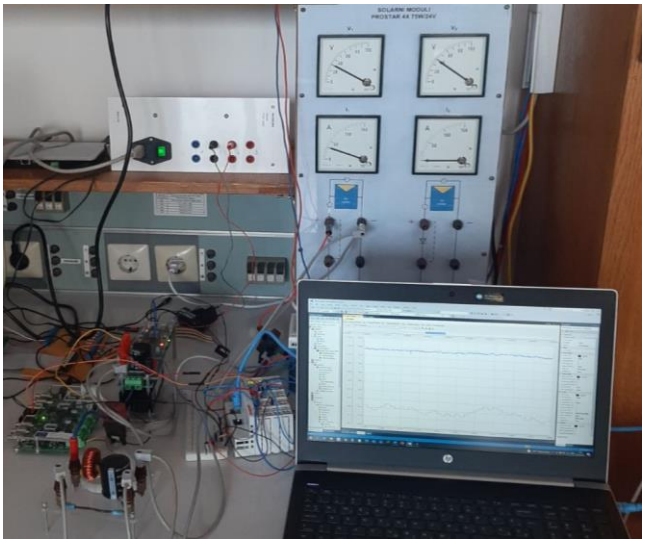

Fig. 9. The experimental setup of the proposed platform for rapid prototyping of the MPPT algorithms.


ISBN 978-86-7466-930-3

The experimental setup of the proposed platform is shown on Fig. 9. The setup is realized at the Faculty of Electrical Engineering in East Sarajevo.

## IV. Experimental Results

In TwinCAT software environment, there is a possibility to observe the signals in real time by using special graphs, i.e., virtual scopes, as well as to record them for later (offline) use.

The experimental waveforms of the obtained power of the PV module and the duty cycle are given on the following figures, which represent the real-time graphs within the TwinCAT environment. The left scale on Fig. 10 and Fig. 11 corresponds to the duty cycle (green signal), while the right scale corresponds to the output power of the PV module (blue signal).

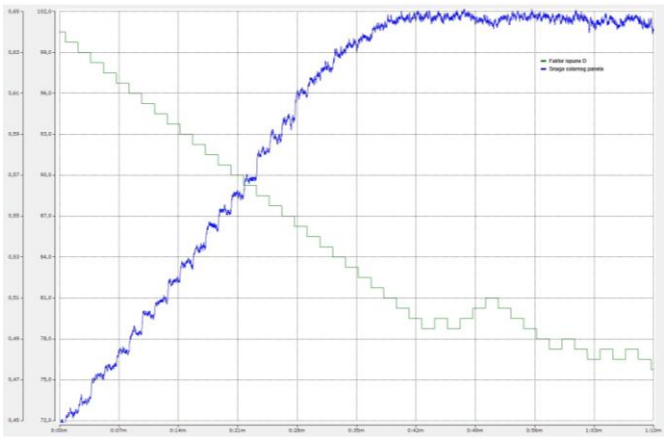

Fig. 10. The experimental waveforms of the duty cycle (green) and the power of the PV module (blue) – reaching the MPP.

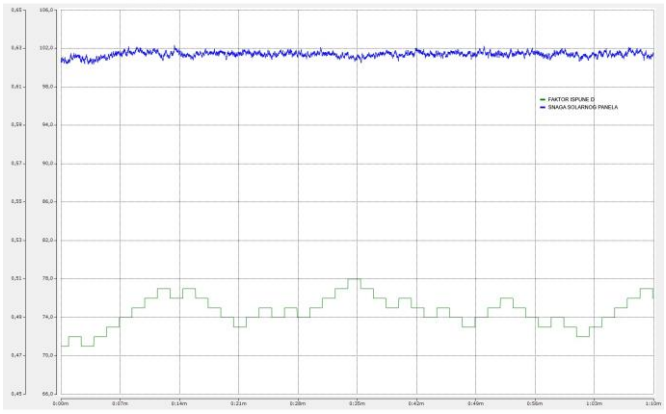

Fig. 11. The experimental waveforms of the duty cycle (green) and the power of the PV module (blue) – maintaining the MPP.

The initial value of the duty cycle was set to 0.65. It is obvious from the given experimental results that the implemented P&O MPPT algorithm successfully reach and maintain the maximum power of the PV module. These results confirm the validity and excellent performances of the proposed experimental platform, which can be successfully used for implementation and testing of the MPPT algorithms.

## V. Conclusion

This paper proposes the platform for rapid prototyping of the MPPT algorithms for PV applications. The key part of the proposed platform is the Beckhoff PC-based PLC. There are numerous excellent features of this platform, such as low price, modularity, simple and user-friendly operation, simple and rapid programming by using combination of Simulink and TwinCAT environments, high processing speed thanks to the usage of the computer's processor, possibility of monitoring of different signals in real time within TwinCAT environment, etc. The platform is tested on the example of the conventional P&O MPPT algorithm. However, it can be used for any other MPPT algorithm, by changing the Simulink model and reprogramming the Beckhoff PLC. Also, the existing platform can be upgraded with additional power modules and Beckhoff input/output terminals, so more complex PV systems can be tested. Except scientific research and development, the proposed experimental platform can be very useful for educational purposes.

## References


[1] S. Saravanan and N. Ramesh Babu, "Maximum power point tracking algorithms for photovoltaic system – A review," Renewable and Sustainable Energy Reviews, vol. 57, pp. 192-204, May 2016.

[2] K. Kaliappan, R. Sekar, and S. S, "ANFIS-P&O based MPPT controller for a solar PV system with switched reluctance motor," International Conference on Electronics and Renewable Systems (ICEARS), pp. 371-376, 16-18 March 2022.

[3] B. Djordjevic and Ž. V. Despotović, "Digital implementation of MPPT algorithm in Cuk DC/DC power converter based on PIC18F4520 microcontroller," 21st International Symposium INFOTEH-JAHORINA, pp. 1-6, 16-18 March 2022.

[4] Harmini and M. Ashari, "Optimalization of ANFIS-PSO algorithm based on MPPT control for PV system under rapidly changing weather condition," IEEE International Conference in Power Engineering Application (ICPEA), pp. 1-6, 7-8 March 2022.

[5] A. M. Alcaide, R. Gomez-Merchan, E. Zafra, E. Perez, J. M. Lopez, J. I. Leon, S. Vazquez, and L. G. Franquelo, "The influence of MPPT algorithms in the lifespan of the capacitor across the PV array," IEEE Access, April 2022.

[6] R. W. Robinson, W. A. Cronje, and K. J. Nixon, "The design of a hybrid MPPT methodology to mitigate the effects of partial shading in PV systems," 30th Southern African Universities Power Engineering Conference (SAUPEC), pp. 1-6, 25-27 Jan. 2022.

[7] M. H. Mobarak and J. Bauman, "A fast parabolic-assumption algorithm for global MPPT of photovoltaic systems under partial shading conditions," IEEE Transactions on Industrial Electronics, vol. 69, no. 8, pp. 8066-8079, Aug. 2022.

[8] C. -Y. Tang, H. -J. Wu, C. -Y. Liao, and H. -H. Wu, "An optimal frequency-modulated hybrid MPPT algorithm for the LLC resonant converter in PV power applications," IEEE Transactions on Power Electronics, vol. 37, no. 1, pp. 944-954, Jan. 2022.

[9] T. Radjai, L. Rahmani, S. Mekhilef, and J. P. Gaubert, "Implementation of a modified incremental conductance MPPT algorithm with direct control based on a fuzzy duty cycle change estimator using dSPACE," Solar Energy, vol. 110, pp. 325-337, Dec. 2014.

[10] S. Lale, S. Lubura, and M. Šoja, "Comparison of P&O and GSS MPPT algorithms for PV application," 17th International Symposium on Power Electronics - Ee 2013, no. T.7.1, pp. 1-5, Oct. 2013.

[11] D. Mustafić, D. Jokić, S. Lale, and S. Lubura, "Implementation of incremental conductance MPPT algorithm in real time in Matlab/Simulink environment with Humusoft MF634 board," 9th Mediterranean Conference on Embedded Computing (MECO), pp. 1-5, June 2020.

[12] M. Praful Raj and A. M. Joshua, "Design, implementation and performance analysis of a LabVIEW based fuzzy logic MPPT controller for stand-alone PV systems," IEEE International Conference on Power,


 ISBN 978-86-7466-930-3

Control, Signals and Instrumentation Engineering (ICPCSI), pp. 1012-1017, Sept. 2017.
[13] H. Rezk, M. Aly, M. Al-Dhaifallah, and M. Shoyama, "Design and hardware implementation of new adaptive fuzzy logic-based MPPT control method for photovoltaic applications," IEEE Access, vol. 7, pp. 106427-106438, Aug. 2019.
[14] D. Gonzalez Montoya, J. Zabala, E. Henao-Bravo, C. Ramos-Paja, D. Aponte-Roa, "Rapid control prototyping platform for PV systems based on Arduino and Simulink," Revista EIA, vol. 18, pp. 1-21, June 2021.
[15] G. Becerra-Nuñez, A. Castillo-Atoche, J. Vazquez-Castillo, A. Datta, R. Quijano-Cetina, R. Peña-Alzola, R. Carrasco-Alvarez, and E. Osorio-de-la-Rosa, "An FPGA Kalman-MPPT implementation adapted in SST-based dual active bridge converters for DC microgrids systems," IEEE Access, vol. 8, pp. 202946-202957, Oct. 2020.
[16] M. Ricco, P. Manganiello, G. Petrone, E. Monmasson, and G. Spagnuolo, "FPGA-based implementation of an adaptive P&O MPPT controller for PV applications," IEEE 23rd International Symposium on Industrial Electronics (ISIE), pp. 1876-1881, June 2014.
[17] O. Petrić, S. Lale, and S. Lubura, "Implementation of voltage control of buck converter using Beckhoff programmable logic controller," International Journal of Electrical Engineering and Computing, vol. 5, no. 2, pp. 86-93, Dec. 2021.
[18] https://beckhoff.com, April 2022.
[19] https://infosys.beckhoff.com/, April 2022.
[20] Taraz Technologies, "Half bridge power module SPM-HB," datasheet, 2015.
[21] Taraz Technologies, "High CMR Isolated 2SW 2A smart gate drive module for SiC FETs GDC-2A2S1," datasheet, 2019.
[22] Taraz Technologies, "Isolated voltage & current sensing module USM-3IV," datasheet, 2015.

 ISBN 978-86-7466-930-3



www.akademska-misao.rs